Paul A. Iaizzo *Editor*

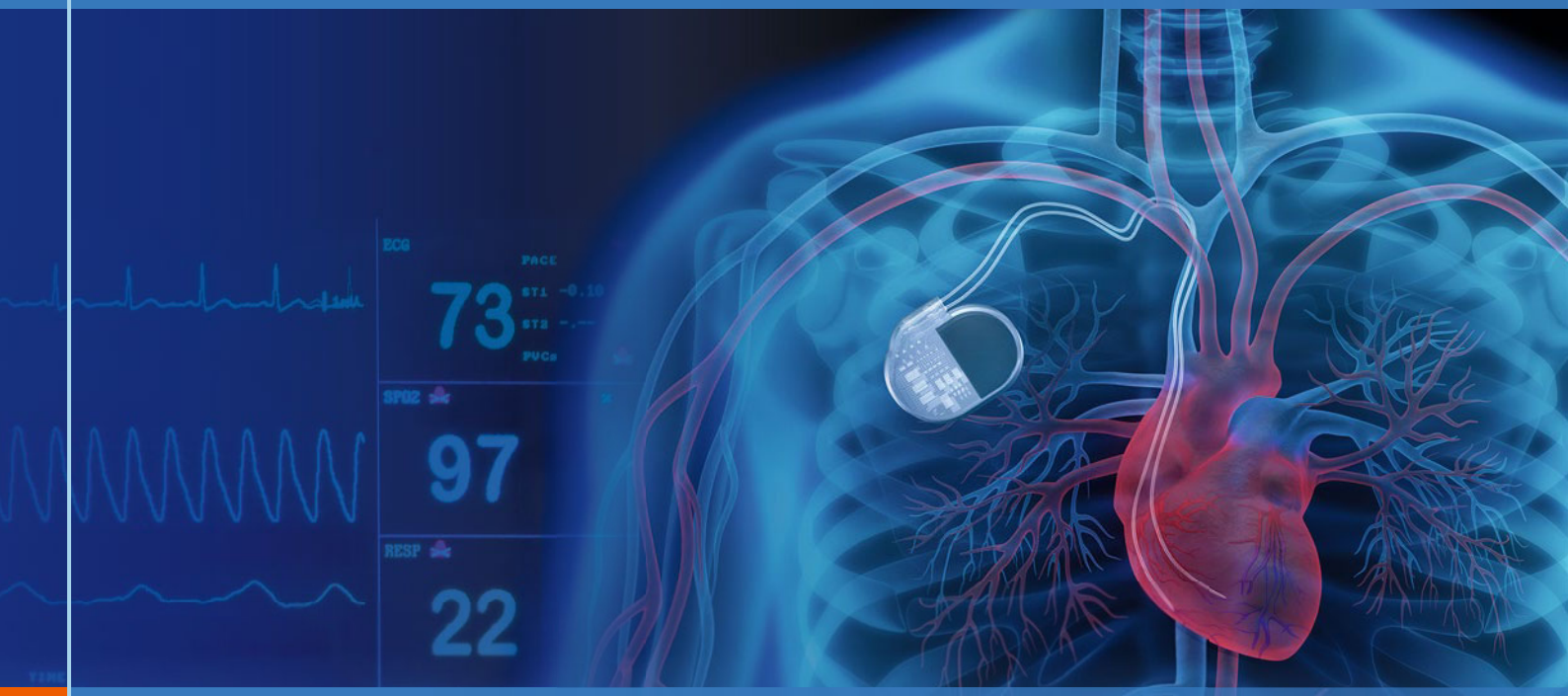

Handbook of Cardiac Anatomy, Physiology, and Devices

Third Edition

EXTRAS ONLINE

Springer

Handbook of Cardiac Anatomy, Physiology, and Devices

Paul A. Iaizzo
Editor

Handbook of Cardiac Anatomy, Physiology, and Devices

Third Edition

Springer

Editor
Paul A. Iaizzo
University of Minnesota
Department of Surgery
Minneapolis, MN, USA

Additional material to this book can be downloaded from http://extras.springer.com

ISBN 978-3-319-19463-9 ISBN 978-3-319-19464-6 (eBook)
DOI 10.1007/978-3-319-19464-6

Library of Congress Control Number: 2015950854

Springer Cham Heidelberg New York Dordrecht London
1st edition: © 2005 Humana Press Inc.
2nd edition: © 2009 Springer Science+Business Media, LLC

Printed on acid-free paper

Springer International Publishing AG Switzerland is part of Springer Science+Business Media (www.springer.com)

Foreword

In the course of one's professional life, you may be fortunate to encounter an opportunity that brings new clarity to your approach to business. I had such an experience in 1997, when three people—Dr. Paul A. Iaizzo, Tim Laske, and Mark Hjelle—walked into my office and started talking about reanimating porcine hearts on the bench, as a training tool for engineers and scientists working on medical devices. I had no idea what they were talking about, and I did not really know Dr. Paul A. Iaizzo, a professor at the University of Minnesota. But I did know Tim Laske and Mark Hjelle, who are two of the most creative engineers I have ever met. I trust their judgment and their skills. The trio's story, vision, and declaration of what could be achieved were compelling. I was cautious, however, because, to that point in time, our ability to work effectively in partnership with universities was nothing to write home about…except to complain.

Nonetheless, we were always looking for better ways to educate our employees engaged in research, design, or manufacturing of medical products. Clinical applicability is the name of the game for any medical product, but it is very easy for scientists and engineers to design without fully understanding the environment in which their products are being used. This is true in all industries. Lack of understanding of the specific application creates mediocrity in performance. Because of the increasing complexity of the products required to support the rapidly growing tachycardia and resynchronization therapies, we were feeling the pressure to "up our game." If Tim and Mark believed that Dr. Iaizzo could do what he was proposing, I had no choice but to say yes, and we provided the seed money to get the Visible Heart® laboratory off the ground. Little did I realize at the time what "the trio" and the University of Minnesota team were about to accomplish.

Throughout this book, you will see many images and videos of what the heart prep at the University of Minnesota's Visible Heart Lab can produce. The results of Professor Iaizzo and his research team exceeded my most optimistic projections of the value of the investment. The Visible Heart Lab brings a new depth of understanding to what actually is going on inside beating animal and human hearts. It has helped to reshape how the industry designs and evaluates products. It changed how we made decisions on products to fund or not fund and impacted how we ran our business. In advocating for the investment, Tim Laske, Mark Hjelle, and I made one mistake—we underestimated what Dr. Iaizzo and his team were capable of accomplishing. We would not make that mistake again. I do not believe failure is ever considered as an option by his team.

However, as fantastic as the Visible Heart prep is by itself, it is not the most valuable product of the Visible Heart Lab. I am in awe of Dr. Iaizzo, his team, and industry partners who worked so hard to master the reanimation of hearts. The quality and educational value of the videos and images that they produce are amazing and unbelievably impactful. But the real "gems" of the Visible Heart Lab are the students who graduate every year and go out into the world. The heart prep experience is the core of their training. It is where the students get a chance to "put it all together" in their minds. The training they receive along the way in physiology, biochemistry, instrumentation, tissue engineering, genetics, core biology, and many other related disciplines is unparalleled in my experience. You will see both the basic and applied nature of their education and research as you read this book.

It was clear to me the first time we brought one of these students into our company that they were not the "normal" new graduates. Within weeks after graduating and coming to work at Medtronic, they were providing advice on cardiac anatomy and function to seasoned scientists and engineers who had been designing complex products and bringing them to market for years. These graduates had an uncanny ability to visualize products in the final application and judge how they would perform. They quickly became integrated and valuable contributors to our team, months to years ahead of our expectations. Once we experienced the quality of these graduates, we hired as many as we could. At one time we had hired all but one of the fourteen Ph.D. students; we would have hired that one too, if there had been an opening. Unfortunately, one of our competitors hired this individual.

Years later, these graduates are still breaking new ground and raising the bar for others. They are establishing incubators in New York and computer modeling centers in California, running clinical study departments, managing product development for Fortune 500 companies, starting new companies, and providing leadership in many notable organizations. Most significantly, some of them are teaching, and all of them are both teachers and students. That is because Dr. Iaizzo ingrained in them the value and importance of continual learning and passing on knowledge to others. As a result, they are collaborators by nature, and they make a difference.

Finally, I have to give credit to Dr. Iaizzo and his academic partners for the role they played in creating a new environment between the University of Minnesota and the medical device industry. Their response to the educational needs of the industry over the past 20 years has been more than notable—it is remarkable!!

My experience with this dynamic group started with a casual comment made to Dr. Iaizzo in a hallway conversation almost 20 years ago regarding the need for training of industry scientists and engineers on anatomy and physiology. That hallway conversation sparked the annual "Advanced Cardiac Physiology and Anatomy" course, creating what has become the gold standard for training on the basics of anatomy and physiology for medical device professionals. Additionally, Dr. Iaizzo participates in the "New Product Design and Business Development" course, which was developed to pair business people with students to work in partnership with companies to solve real-world new product issues. Importantly, he created the Visible Heart Lab which represents the first major collaborative breakthrough in several years that initiated a change in the dynamic between the industry and the University. Subsequently, the University approved the establishment of the Medical Devices Center that has broken new ground in working in close partnering relationships with the industry. Building upon such work, the team of Professors Art Erdman, Will Durfee, and Paul Iaizzo founded the Design of Medical Devices Conference that is already a large and globally recognized annual conference. Last year the University announced a new policy governing intellectual property, which makes it easier for companies to license technology and enhances the University's ability to capitalize on its research. This year a master's degree in medical devices was offered for the first time. For years the University of Minnesota and the device industry did not partner well. Today they have set the standard for what collaborations between industry and academia can be, and it gets better every year.

I am amazed and in admiration of what a team of creative people can do when they decide to do what most think is impossible. Enjoy the book; it gives you a sense of the quality of the people involved.

LifeScience Alley and the BioBusiness Alliance of Minnesota Dale Wahlstrom
Minneapolis, MN, USA

Preface

Personalized medicine, clinical imaging, and the medical device industry continue to grow at an incredibly rapid pace. Further, our overall understanding of the molecular basis of diseases steadily increases, as does the number of available therapies to treat specific health problems. This remains particularly true in the field of cardiovascular care. With this rapid growth rate in cardiac medicine, clinicians and biomedical engineers alike have been challenged to either retool or continue to seek out sources of concise information.

The major impetus for this third edition was to update this resource textbook for interested students, residents, clinicians, and/or practicing biomedical engineers. A secondary motivation was to promote the expertise, past and present, in the areas of cardiovascular science at the University of Minnesota. As Director of Education for the Lillehei Heart Institute and Associate Director for Education of the Institute for Engineering in Medicine at the University of Minnesota, I feel that this book also represents a unique outreach opportunity to carry on the legacy of Drs. C. Walton Lillehei, M.D., Ph.D., and Earl Bakken, M.D., Ph.D. (Hon.) through the twenty-first century. Interestingly, the completion of this textbook coincides with two recent important anniversaries in cardiovascular medicine and engineering at the University of Minnesota. First, it was 61 years ago, in 1954, that Dr. C. Walton Lillehei performed the first cross-circulation procedures at the University. One year ago in January, Earl Bakken (the cofounder of Medtronic) turned 90 years old; Dr. Bakken has five implanted Medtronic devices and continues to be an inspiration to those working in this field.

For the past 15 years, the University of Minnesota has presented the week-long short course *Advanced Cardiac Physiology and Anatomy*, which was designed specifically for the biomedical engineer working in the industry; this serves as the course textbook. Thus there was a need to update the textbook to include state-of-the-art information on a variety of topics related to cardiac anatomy, physiology, and devices. For example, six new chapters were added to this third edition, and all other chapters were carefully updated and/or greatly expanded. One last historical note that I feel is interesting to mention once again is that my current laboratory, where isolated heart studies are performed weekly (the Visible Heart® laboratory), is the same laboratory in which C. Walton Lillehei and his many esteemed colleagues conducted the majority of their cardiovascular research studies in the late 1950s and early 1960s. It is also the laboratory where Earl Bakken, along with Drs. Vincent Gott and Lillehei, first tested the wearable battery-powered pacemaker on an animal with an induced heart block. After being tested on an animal, the prototype pacemaker was very quickly (later the same day) used by Dr. Lillehei on one of his cardiac surgical patients.

With this new edition, complimentary materials (e.g., movies and images) that will enhance this textbook's utility can be accessed online. Additionally, my laboratory continues to support the online, free access website *The Atlas of Human Cardiac Anatomy* (www.vhlab.umn.edu/atlas) which also contains many tutorials and unique movie clips of functional cardiac anatomy. These images were obtained from human hearts made available via LifeSource (St. Paul, MN, USA), through the generosity of families and individuals who made the final gift of organ donation for research (their hearts were not deemed viable for transplantation).

I would especially like to acknowledge the exceptional efforts of our Lab Coordinator, Monica Mahre, who for a third time (1) assisted me in coordinating the efforts of contributing authors, (2) skillfully incorporated my editorial changes, (3) verified the readability and formatting of each chapter, (4) pursued additions or missing materials for each chapter, (5) contributed as a coauthor, and (6) kept a positive outlook throughout. I would also like to thank Gary Williams for his computer expertise and assistance with numerous figures; Tinen Iles and Charles Soule who made sure the laboratory kept running smoothly while many of us were busy writing or editing; the Chairman of the Department of Surgery, Dr. David Rothenberger, for his support and encouragement; the Institute for Engineering in Medicine at the University of Minnesota, headed by Prof. Bin He, who helped support this project via educational funds; and the Lillehei Heart Institute at the University of Minnesota, headed by Dr. Daniel Garry, who also generously supported educational outreach efforts.

I would like to thank Medtronic, Inc., for their continued support of the Visible Heart® laboratory for the past 18 years, and I especially acknowledge the commitment, partnership, and friendship of Tim Laske, Mark Hjelle, Alex Hill, Michael Eggen, Nick Skadsberg, Mark Borash, Rick McVenes, and Dale Wahlstrom for making our collaborative research possible.

It is also my pleasure to thank the past and present graduate students or residents who have worked in my laboratory and who were contributors to this third edition including Sara Anderson, Michael Bateman, James Coles, Michael Eggen, Kevin Fitzgerald, Alexander Hill, Brian Howard, Stephen Howard, Tinen Iles, Jason Johnson, Ryan Lahm, Timothy Laske, Anna Legreid Dopp, Michael Loushin, Lars Mattison, Jason Quill, Maneesh Shrivastav, Daniel Sigg, Julianne Spencer, Eric Richardson, Nicholas Skadsberg, and Sarah Vieau. I feel extremely fortunate to have the opportunity to work with such a talented group of scientists and engineers, and I continue to learn a great deal from each of them.

Finally, I would like to thank my family and friends for their continued support of my career and their assistance over the years. Specifically, I would like to thank my wife, Marge; my three daughters, Maria, Jenna, and Hanna; my mom Irene; and my sisters Chris and Susan, for always being there for me. On a personal note, it has been a difficult couple of years as both of my brothers passed away, as well as my longtime laboratory scientist Bill Gallagher. Furthermore, I myself dealt with some health issues that provided me with a much greater appreciation for cardiac medicine, medical advances, and what is feels like to be a patient. I am truly inspired by all individuals who dedicate their lives to all aspects of cardiovascular science and technology.

Minneapolis, MN, USA Paul A. Iaizzo

Contents

Part I

Introduction

General Features of the Cardiovascular System

1

Paul A. Iaizzo

Abstract

The purpose of this chapter is to provide a general overview of the human cardiovascular system, to serve as a quick reference on its underlying physiological composition. The rapid transport of molecules over long distances between internal cells, the body surface, and/or various specialized tissues organs is the primary function of the cardiovascular system. This body-wide transport system is composed of several major components: blood, the blood vessels, the heart, and the lymphatic system. When functioning normally, this system adequately provides for the wide-ranging activities that a human can accomplish. Failure in any of these components can lead to pathological or even grave consequences. Subsequent chapters will cover, in greater detail, the anatomical, physiological, and pathophysiological features of the cardiovascular system.

Keywords

Cardiovascular system • Blood • Blood vessels • Blood flow • Heart • Coronary circulation • Lymphatic system

1.1 Introduction

Currently, more than 85 million individuals in the United States have some form of cardiovascular disease. More specifically, heart failure continues to be an increasing problem in our society. Coronary bypass surgery, angioplasty, stenting, the implantation of pacemakers and/or defibrillators, and valve replacement are currently routine treatment procedures, with growing numbers of these procedures being performed worldwide each year. However, such treatments often provide only temporary relief of the progressive symptoms of cardiovascular disease. Nevertheless, optimizing therapies and/or the development of new treatments continue to dominate the cardiovascular biomedical industry (e.g., coated or biodegradable vascular or coronary stents, left ventricular assist devices, biventricular pacing, implantable monitors, and transcatheter-delivered valves).

The purpose of this chapter is to provide a general overview of the cardiovascular system, so to serve as a quick reference relative to its underlying physiological mechanisms. More details concerning the pathophysiology of the cardiovascular system and state-of-the-art treatments can be found in subsequent chapters. In addition, the reader should note that a list of source references is provided at the end of this chapter.

1.2 Components of the Cardiovascular System

The principle components considered to make up the cardiovascular system include: blood, blood vessels, the heart, and the lymphatic system (Fig. 1.1).

P.A. Iaizzo, PhD (✉)
Department of Surgery, University of Minnesota,
420 Delaware St. SE, B172 Mayo, MMC 195, Minneapolis,
MN 55455, USA
e-mail: iaizz001@umn.edu

P.A. Iaizzo (ed.), *Handbook of Cardiac Anatomy, Physiology, and Devices*, DOI 10.1007/978-3-319-19464-6_1

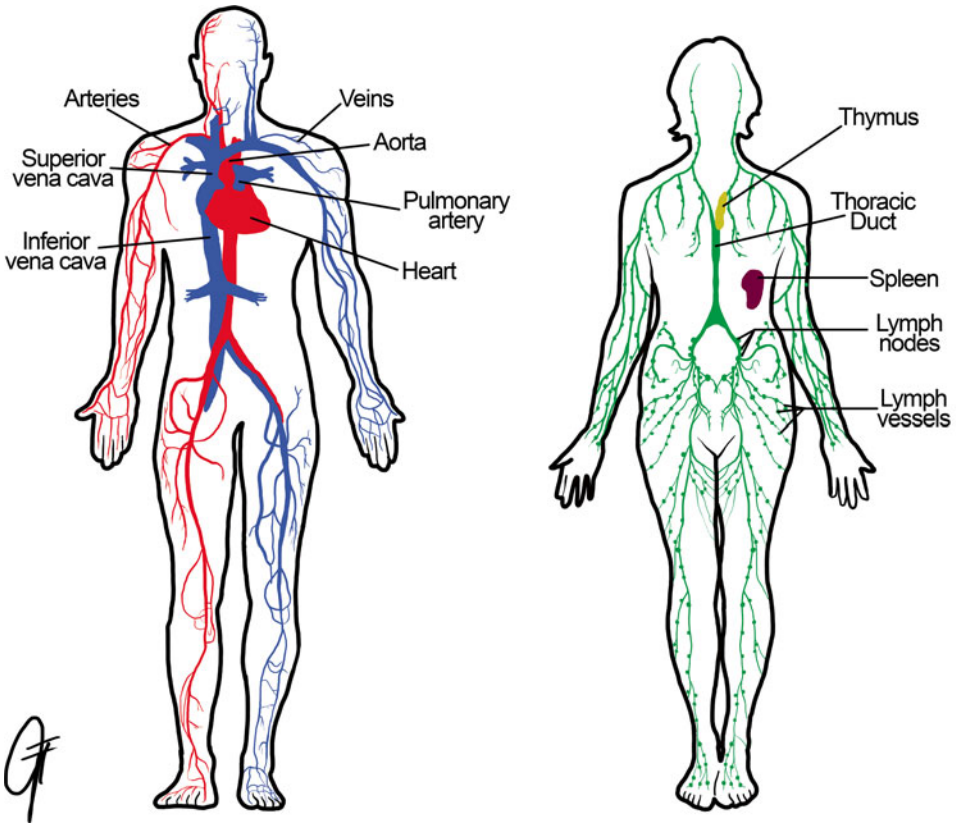

Fig. 1.1 The major components of the cardiovascular system: circulating blood, the blood vessels, the heart, and the lymphatic system. (*Left*) Major vessels that return deoxygenated blood to the heart (*blue*) and major arteries carrying oxygenated blood that leave the heart (*red*). (*Right*) Shown is the relative extent of the lymphatic system within the human body

1.2.1 Blood

Blood is composed of formed elements (cells and cell fragments) which are suspended in the liquid fraction known as plasma. Blood, often considered as the only liquid connective tissue in the body, has three general functions: (1) transportation (e.g., O_2, CO_2, nutrients, waste, hormones), (2) regulation (e.g., pH, temperature, osmotic pressures), and (3) protection (e.g., against foreign molecules and diseases, as well as for clotting to prevent excessive loss of blood). Dissolved within the plasma are many proteins, nutrients, metabolic waste products, and various other molecules being transported between multiple organ systems.

The formed elements in blood include red blood cells (erythrocytes), white blood cells (leukocytes), and the cell fragments known as platelets. These are all formed in bone marrow from a common stem cell. In a healthy individual, the majority of bloods cells are red blood cells (~99 %) which have a primary role in O_2 exchange. Hemoglobin, the iron-containing heme protein which binds oxygen, is concentrated within the red cells; hemoglobin allows blood to transport 40–50 times the amount of oxygen that plasma alone could carry. The white cells are required for the immune process, e.g., to protect against infections and also cancers. Platelets play a primary role in blood clotting. In a healthy cardiovascular system, the constant movement of blood helps keep these various cells and plasma constituents well dispersed throughout the larger-diameter vessels.

The *hematocrit* is defined as the percentage of blood volume that is occupied by the red cells (erythrocytes). It can be easily measured by centrifuging (spinning at high speed) a sample of blood, which forces these cells to the bottom of the centrifuge tube. The leukocytes remain on the top and the platelets form a very thin layer between the cell fractions (other more sophisticated methods are also available for such analyses). Normal hematocrit is approximately 45 % in men and 42 % in women. The total volume of blood in an average-sized individual (70 kg) is approximately 5.5 L; hence, the average red cell volume would be roughly 2.5 L. Since the fraction containing both leukocytes and platelets is normally relatively small or negligible, in such an individual, the plasma volume can be estimated to be 3.0 L. Approximately 90 % of plasma is water which acts: (1) as a solvent, (2) to suspend the components of blood, (3) in the absorption of molecules and their transport, and (4) in the transport of thermal energy. Proteins make up 7 % of

the plasma (by weight) and exert a colloidc osmotic pressure. Protein types include albumins, globulins (antibodies and immunoglobulins), and fibrinogen. To date, more than 100 distinct plasma proteins have been identified, and each presumably serves a specific physiologic function. The other main solutes in plasma include: electrolytes, nutrients, gases (some O_2, large amounts of CO_2 and N_2), regulatory substances (enzymes and hormones), and waste products (urea, uric acid, creatine, creatinine, bilirubin, and ammonia).

1.2.2 Blood Vessels

Blood flows throughout the body's tissues within blood vessels via bulk flow (i.e., all constituents together and in one direction). An extraordinary degree of vascular branching exists within the human body, which ensures that nearly every cell in the body lies within a short distance from at least one of the smallest branches of this system—a capillary. Nutrients and metabolic end products move between the capillary vessels and the surroundings of the cell through the interstitial fluid by diffusion. Subsequent movement of these molecules into a cell is accomplished by both diffusion and mediated transport. Nevertheless, blood flow through all organs can be considered as somewhat passive and occurs only because arterial pressure is kept higher than venous pressure via the pumping action of the heart.

In an individual at rest at any given moment, approximately 5 % of the total circulating blood is actually within the capillaries. Yet, this volume of blood can be considered to perform the primary functions of the entire cardiovascular system, specifically the supply of nutrients and removal of metabolic end products. The cardiovascular system, as reported by the British physiologist William Harvey in 1628, is a closed-loop system, such that blood is pumped out of the heart through one set of vessels (arteries) and then returns to the heart in another (veins).

More specifically, one can consider that there are two closed-loop systems which both originate and return blood to the heart—the pulmonary and systemic circulations (Fig. 1.2). The pulmonary circulation is composed of the right heart pump and the lungs, whereas the systemic circulation includes the left heart pump which supplies blood to the systemic organs (i.e., all tissues and organs except the gas exchange portion of the lungs). Because the right and left heart pumps function in a series arrangement, both will circulate an identical volume of blood in a given minute (one's cardiac output, normally expressed in liters per minute).

In the systemic circuit, blood is ejected out of the left ventricle via a single large artery—the aorta. All arteries of the systemic circulation branch from the aorta (this is the largest artery of the body, with a diameter ranging from 2 to 4 cm) and divide into progressively smaller vessels. The aorta's four principle divisions are the ascending aorta (begins at the aortic valve where, close by, the two coronary artery branches have their origin), the arch of the aorta, the thoracic aorta, and the abdominal aorta.

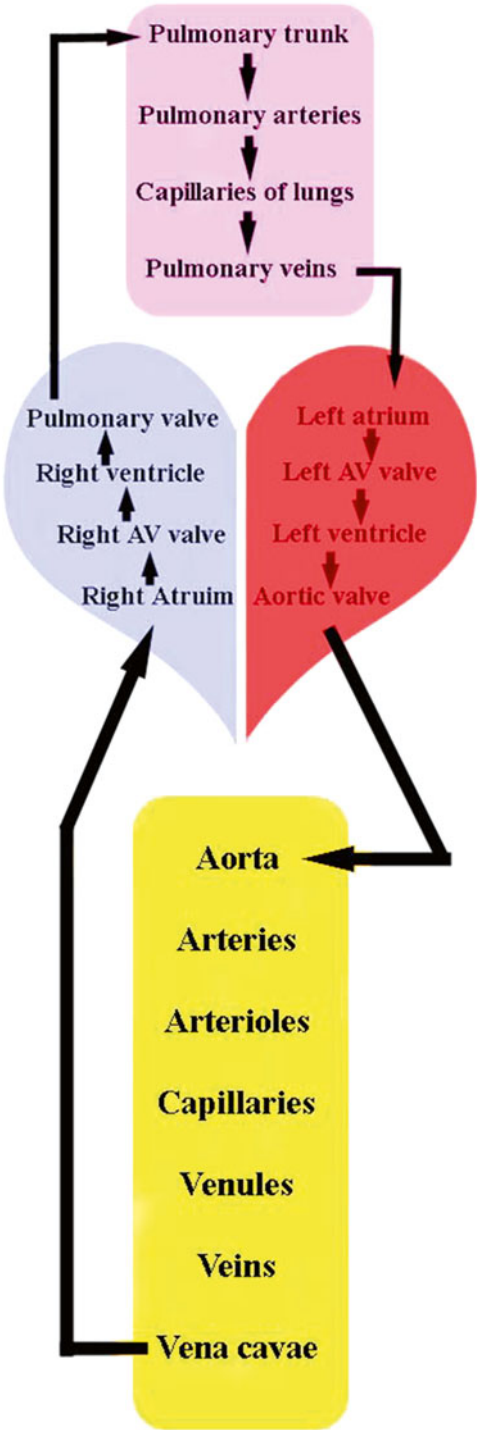

Fig. 1.2 The major paths of blood flow through pulmonary and systemic circulatory systems. *AV* atrioventricular

The smallest of the arteries eventually branch into arterioles. They, in turn, branch into an extremely large number of the smallest diameter vessels—the capillaries (with an estimated

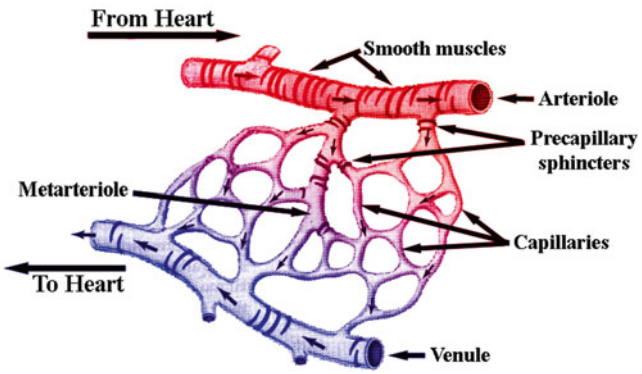

Fig. 1.3 The microcirculation including arterioles, capillaries, and venules. The capillaries lie between, or connect, the arterioles to the venules. They are found in almost every tissue layer of the body, but their distribution varies. Capillaries form extensive branching networks that dramatically increase the surface areas available for the rapid exchange of molecules. A metarteriole is a vessel that emerges from an arteriole and supplies a group of 10–100 capillaries. Both the arteriole and the proximal portion of the metarterioles are surrounded by smooth muscle fibers whose contractions and relaxations regulate blood flow through the capillary bed. Typically, blood flows intermittently through a capillary bed due to the periodic contractions of the smooth muscles (5–10 times per minute, vasomotion), which is regulated both locally (metabolically) and by autonomic control (Figure modified from [5])

ten billion in the average human body). Next, blood exits the capillaries and begins its return to the heart via the venules. Microcirculation is a term coined to collectively describe the flow of blood through arterioles, capillaries, and the venules (Fig. 1.3).

Importantly, blood flow through an individual vascular bed is profoundly regulated by changes in activity of the sympathetic nerves innervating the arterioles. In addition, arteriolar smooth muscle is very responsive to changes in local chemical conditions within an organ (i.e., those changes associated with increases or decreases in the metabolic rate of that given organ).

Capillaries, which are the smallest and most numerous blood vessels in the human body (ranging from 5 to 10 μm in diameter and again numbering around ten billion), are also the thinnest walled vessels; an inner diameter of 5 μm is just wide enough for an erythrocyte to squeeze through. Further, it is estimated that there are 25,000 miles of capillaries in an adult, each with an individual length of about 1 mm.

Most capillaries are little more than a single cell layer thick, consisting of a layer of endothelial cells and a basement membrane. This minimal wall thickness facilitates the capillary's primary function, which is to permit the exchange of materials between cells in tissues and the blood within. As mentioned above, small molecules (e.g., O_2, CO_2, sugars, amino acids, and water) are relatively free to enter and leave capillaries readily, promoting efficient material exchange. Nevertheless, the relative permeability of capillaries varies from body region to body region, with regard to the physical properties of their formed walls.

Based on such differences, capillaries are commonly grouped into two major classes: continuous and fenestrated capillaries. In the continuous capillaries, which are more common, the endothelial cells are joined together such that the spaces between them are relatively narrow (i.e., narrow intercellular gaps). These capillaries are permeable to substances having small molecular sizes and/or high lipid solubilities (e.g., O_2, CO_2, and steroid hormones) and are somewhat less permeable to small water-soluble substances (e.g., Na^+, K^+, glucose, and amino acids). In fenestrated capillaries, the endothelial cells possess relatively large pores that are wide enough to allow proteins and other large molecules to pass through. In some such capillaries, the gaps between the endothelial cells are even wider than usual, enabling quite large proteins (or even small cells) to pass through. Fenestrated capillaries are primarily located in organs whose functions depend on the rapid movement of materials across capillary walls, e.g., kidneys, liver, intestines, and bone marrow.

If a molecule cannot pass between capillary endothelial cells, then it must be transported across the cell membrane. The mechanisms available for transport across a capillary wall differ for various substances depending on their molecular size and degree of lipid solubility. For example, certain proteins are selectively transported across endothelial cells by a slow, energy-requiring process known as *transcytosis*. In this process, the endothelial cells initially engulf the proteins in the plasma within capillaries by *endocytosis*. The molecules are then ferried across the cells by vesicular transport and released by *exocytosis* into the interstitial fluid on the other side. Endothelial cells generally contain large numbers of endocytotic and exocytotic vesicles, and sometimes these fuse to form continuous vesicular channels across the cell.

The capillaries within the heart normally prevent excessive movement of fluids and molecules across their walls, but clinical situations have been noted where they may become "leaky." For example, *capillary leak syndrome* may be induced following cardiopulmonary bypass and might last from hours up to days. More specifically, in such cases, the inflammatory response in the vascular endothelium can disrupt the "gatekeeper" function of capillaries; their increased permeability will result in myocardial edema.

From capillaries, blood throughout the body then flows into the venous system. It first enters the venules which then coalesce to form larger vessels—the veins (Fig. 1.3). Then veins from the various systemic tissues and organs (minus the gas exchange portion of the lungs) unite to form two major veins—the inferior vena cava (lower body) and superior vena cava (above the heart). By way of these two great vessels, blood is returned to the right heart pump, specifically into the right atrium.

Like capillaries, the walls of the smallest venules are very porous and represent the sites where many phagocytic white blood cells emigrate from the blood into inflamed or infected tissues. Venules and veins are also richly

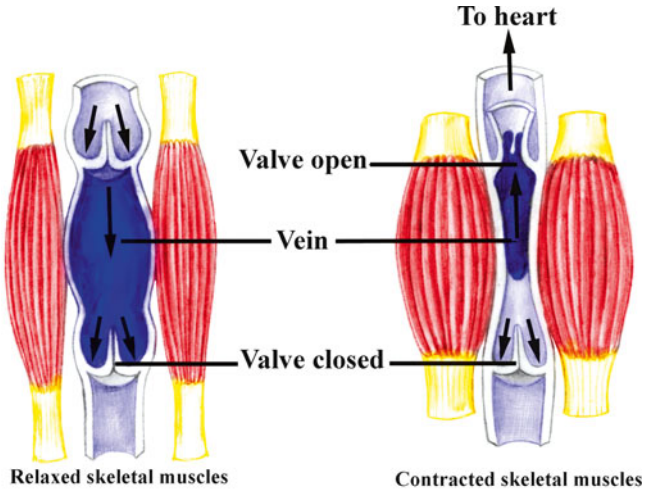

Fig. 1.4 Contractions of the skeletal muscles aid in returning blood to the heart—skeletal muscle pump. While standing at rest, the relaxed vein acts as a reservoir for blood; contractions of limb muscles not only decrease this reservoir size (venous diameter) but also actively force the return of more blood to the heart. Note that the resulting increase in blood flow due to the contractions is only toward the heart due to the valves that are present within the veins

innervated by sympathetic nerves and thus the smooth muscles within constrict when these nerves are activated. Therefore, increased sympathetic nerve activity is associated with a decreased venous volume, which results in increased venous return and hence cardiac filling and ultimately an increased cardiac output (via Starling's law of the heart).

Many veins, especially those in the limbs, also feature abundant valves (which are notably also found in the cardiac venous system) which are thin folds of the intervessel lining that form flap-like cusps. The valves project into the vessel lumens and are directed toward the heart, thus promoting unidirectional flow of blood. Because blood pressure is normally low in veins, these valves are important for aiding venous return, by preventing the backflow of blood (which is especially true in the upright individual). In addition, contractions of skeletal muscles (e.g., in the legs) also play a role in decreasing the size of the venous reservoir and thus the return of blood volume to the heart (Fig. 1.4).

The pulmonary circulation is comprised of a similar circuit. Blood leaves the right ventricle in a single great vessel, the pulmonary artery (trunk), which, within a short distance (centimeters), divides into the two main pulmonary arteries, one supplying the right lung and another the left. Once within the lung proper, the arteries continue to branch down to arterioles and then ultimately form capillaries. From there, the blood flows into venules, eventually forming four main pulmonary veins which empty into the left atrium. As blood flows through the lung capillaries, it picks up oxygen supplied to the lungs by breathing air; hemoglobin within the red blood cells is loaded up with oxygen (oxygenated blood).

1.2.3 Blood Flow

The task of maintaining an adequate interstitial homeostasis (the nutritional environment surrounding cells) requires that blood flows almost continuously through each of the millions of capillaries within the human body. The following is a brief description of the parameters that govern flow through a given vessel. All blood vessels have certain lengths (L) and internal radii (r) through which blood flows when the pressure in the inlet and outlet are unequal (P_i and P_o, respectively); in other words, there is a pressure difference (ΔP) between the vessel ends, which supplies the driving force for flow. Because friction develops between moving blood and the stationary vessel walls, this fluid movement has a given resistance (vascular), which is the measure of how difficult it is to create blood flow through a vessel. One can then describe a relative relationship between vascular flow, the pressure difference, and resistance (i.e., the basic flow equation):

$$\text{Flow} = \frac{\text{pressure difference}}{\text{resistance}} \text{ or } Q = \frac{\Delta P}{R}$$

where Q = flow rate (volume/time), ΔP = pressure difference (mmHg), and R = resistance to flow (mmHg × time/volume).

This equation may be applied not only to a single vessel but can also be used to describe flow through a network of vessels (i.e., the vascular bed of an organ or the entire systemic circulatory system). It is known that the resistance to flow through a cylindrical tube or vessel depends on several factors (described by Poiseuille) including: (1) radius, (2) length, (3) viscosity of the fluid (blood), and (4) inherent resistance to flow, as follows:

$$R = \frac{8L\eta}{\pi r^4}$$

where r = inside radius of the vessel, L = vessel length, and η = blood viscosity.

It is important to note that a small change in vessel radius will have a very large influence (4th power) on its resistance to flow; e.g., decreasing vessel diameter by 50 % will increase its resistance to flow by approximately 16-fold. If one combines the preceding two equations into one expression, which is commonly known as the Poiseuille equation, it can be used to better approximate the factors that influence flow though a cylindrical vessel:

$$Q = \frac{\Delta P \pi r^4}{8L\eta}$$

Nevertheless, flow will only occur when a pressure difference exists. Hence, it is not surprising that arterial blood pressure is perhaps the most regulated cardiovascular variable in the human body, and this is principally accomplished

by regulating the radii of vessels (e.g., arterioles and metarterioles) within a given tissue or organ system. Whereas vessel length and blood viscosity are factors that influence vascular resistance, they are not considered variables that can be easily regulated for the purpose of the moment-to-moment control of blood flow. Regardless, the primary function of the heart is to keep pressure within arteries higher than those in veins, hence a pressure gradient to induce flow. Normally, the average pressure in systemic arteries is approximately 100 mmHg and decreases to near 0 mmHg in the great caval veins.

The volume of blood that flows through any tissue in a given period of time (normally expressed as mL/min) is called the *local blood flow*. The velocity (speed) of blood flow (expressed as cm/s) can generally be considered to be inversely related to the vascular cross-sectional area, such that velocity is slowest where the total cross-sectional area is largest. Shown in Fig. 1.5 are the relative pressure drops one can detect through the vasculature; the pressure varies in a given vessel also relative to the active and relaxation phases of the heart function (see below).

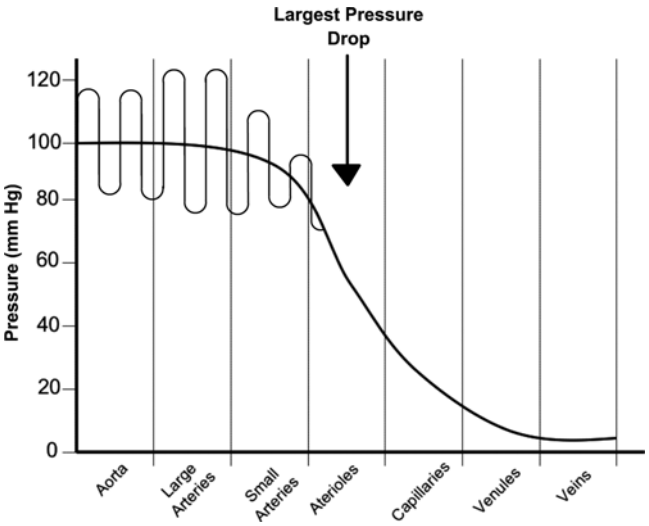

Fig. 1.5 Relative pressure changes one could record in the various branches of the human vascular system due to contractions and relaxation of the heart (pulsatile pressure changes). Note that pressure may be slightly higher in the large arteries than that leaving the heart into the aorta due to their relative compliance and diameter properties. The largest drops in pressures occur within the arterioles which are known as the active regulatory vessels. The pressures in the large veins that return blood to the heart are near zero

1.2.4 The Heart

The heart lies in the center region of the thoracic cavity and is suspended by its attachment to the great vessels within a fibrous sac known as the *pericardium*; note that humans have relatively thick-walled pericardiums compared to those of the commonly studied large mammalian cardiovascular models (i.e., canine, porcine, or ovine; see also Chap. 9). A small amount of fluid is present within the sac, *pericardial fluid*, which lubricates the surface of the heart and allows it to move freely during functioning (i.e., cycles of contractions and relaxations). The pericardial sac extends upward enclosing the great vessels (see also Chaps. 4 and 5).

The pathway of blood flow through the chambers of the heart is indicated in Fig. 1.6. Recall that venous blood returns from the systemic organs to the right atrium via the superior and inferior venae cavae. It next passes through the tricuspid valve into the right ventricles and from there is pumped through the pulmonary valve into the pulmonary artery. After eventually passing through the pulmonary capillary beds, the oxygenated pulmonary venous blood returns to the left atrium through the pulmonary veins. The flow of blood then passes through the mitral valve into the left ventricle and is pumped through the aortic valve into the aorta.

In general, the gross anatomy of the right heart pump is considerably different from that of the left heart pump, yet the pumping principles of each are primarily the same. The ventricles are closed chambers surrounded by muscular walls, and the valves are structurally designed to allow flow in only one direction. The cardiac valves passively open and close in response to the direction of the pressure gradient across them.

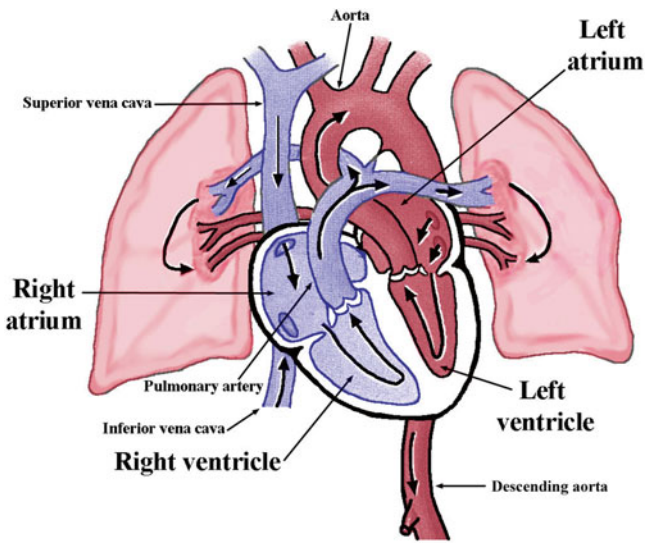

Fig. 1.6 The pathway of blood flow through the heart and lungs. Note that the pulmonary artery (trunk) branches, within a few centimeters, into left and right pulmonary arteries. There are commonly four main pulmonary veins that return blood from the lungs to the left atrium (Modified from [5])

The myocytes of the ventricles are organized primarily in a circumferential orientation; hence, when they contract, the tension generated within the ventricular walls causes the pressure within the chamber to increase. As soon as the ventricular pressure exceeds the pressure in the pulmonary artery (right) and/or aorta (left), blood is forced out of the given ventricular chamber. This active contractile phase of the cardiac cycle is known as *systole*. The generated pres-

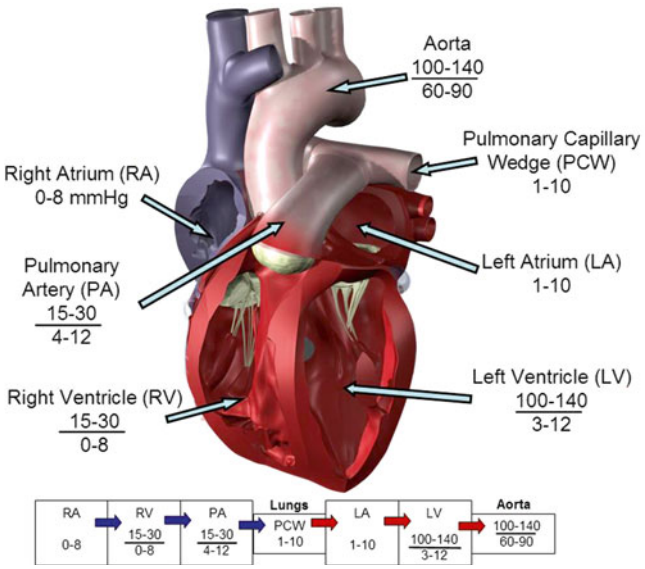

Fig. 1.7 Average relative pressures within the various chambers and great vessels of the heart. During filling of the ventricles, the pressures are much lower and, upon active contraction, they will increase dramatically. Relative pressure ranges that are normally elicited during systole (active contraction; ranges noted above lines) and during diastole (relaxation; ranges noted below lines) are shown for the right and left ventricles, right and left atria, pulmonary artery and pulmonary capillary wedge, and aorta. Shown at the bottom of this figure are the relative pressure changes one can detect in a normal healthy heart as one moves from the right heart through the left heart and into the aorta; this flow pattern is the series arrangement of the two-pump system

sures are higher in the ventricles than the atrium during systole; hence, the tricuspid and mitral (atrioventricular) valves are closed. When the ventricular myocytes relax, the pressures in the ventricles fall below those in the atria, and the atrioventricular valves open; the ventricles refill and this phase is known as *diastole*. The aortic and pulmonary (semilunar or outlet) valves are closed during diastole because the arterial pressures (in the aorta and pulmonary artery) are greater than the intraventricular pressures. Shown in Fig. 1.7 are the average pressures within the various chambers and great vessels of the heart. For more details on the cardiac cycle, see Chap. 20.

The effective pumping action of the heart requires that there be a precise coordination of the myocardial contractions (millions of cells), and this is accomplished via the conduction system of the heart. Contractions of each cell are normally initiated when electrical excitatory impulses (action potentials) propagate along their surface membranes. The myocardium can be viewed as a functional syncytium; action potentials from one cell conduct to the next cell via the gap junctions. In the healthy heart, the normal site for initiation of a heartbeat is within the sinoatrial node, located in the right atrium. For more details on this internal electrical system, refer to Chap. 13.

The heart normally functions in a very efficient fashion and the following properties are needed to maintain this effectiveness: (1) the contractions of the individual myocytes must occur at regular intervals and be synchronized (not arrhythmic), (2) the valves must fully open (not stenotic), (3) the valves must not leak when closed (not insufficient or regurgitant), (4) the ventricular contractions must be forceful (not failing or lost due to an ischemic event), and (5) the ventricles must fill adequately during diastole (no arrhythmias or delayed relaxation).

1.2.5 Regulation of Cardiovascular Function

Cardiac output in a normal individual at rest ranges between 4 and 6 L/min, but during severe exercise, the heart may be required to pump three to five times this amount. There are two primary modes by which the blood volume pumped by the heart, at any given moment, is regulated: (1) by the intrinsic cardiac regulation, in response to changes in the volume of blood flowing into the heart, and (2) by the control of heart rate and cardiac contractility via the autonomic nervous system. The intrinsic ability of the heart to adapt to changing volumes of inflowing blood is known as the *Frank–Starling* mechanism (law) of the heart, named after two great physiologists of a century ago.

In general, the Frank–Starling response can simply be described—the more the heart or myocytes are stretched (e.g., via an increased blood volume), the greater will be the subsequent force of ventricular contraction and, thus, the amount of blood ejected through the aortic valve. In other words, within its physiological limits, the heart will pump out all the blood that enters it without allowing excessive damming of blood in veins. The underlying basis for this phenomenon is related to the optimization of the lengths of sarcomeres, the functional subunits of striated muscle; in other words, there is optimization in the potential for the contractile proteins (actin and myosin) to form crossbridges. It should also be noted that "stretch" of the right atrial wall (e.g., due to increased venous return) can directly increase the rate of the sinoatrial node by 10–20 %; this also aids in the amount of blood that will ultimately be pumped per minute by the heart. For more details on the contractile function of heart, refer to Chap. 12.

The pumping effectiveness of the heart is also effectively controlled by the sympathetic and parasympathetic components of the autonomic nervous system. There is extensive innervation of the myocardium by such nerves (for more details on innervation, see Chap. 14). To understand how effective the modulation of the heart by this innervation is, investigators have reported that cardiac output often can be increased by more than 100 % by sympathetic stimulation and, by contrast, output can be nearly terminated by parasympathetic (vagal) stimulation.

Cardiovascular function is also modulated through reflex mechanisms that involve baroreceptors and the chemical composition of the blood and via the release of various hormones. More specifically, baroreceptors, which are located in the walls of some arteries and veins, exist to monitor one's relative blood pressure. Those specifically located in the carotid sinus help to reflexively maintain normal blood pressure in the brain, whereas those located in the area of the ascending arch of the aorta help to govern general systemic blood pressure (for more details, see Chaps. 14, 18, and 20).

Chemoreceptors that monitor the chemical composition of blood are located close to the baroreceptors of the carotid sinus and arch of the aorta, in small structures known as the carotid and aortic bodies. The chemoreceptors within these bodies detect changes in blood levels of O_2, CO_2, and H^+. Hypoxia (low availability of O_2), acidosis (increased blood concentrations of H^+), and/or hypercapnia (high concentrations of CO_2) can all stimulate the chemoreceptors to increase their action potential firing frequencies to the brain's cardiovascular control centers. In response to this increased signaling, the central nervous system control centers (hypothalamus), in turn, cause an increased sympathetic stimulation to arterioles and veins, producing vasoconstriction and a subsequent increase in blood pressure. In addition, the chemoreceptors simultaneously send neural input to the respiratory control centers in the brain, to induce the appropriate control of respiratory function (e.g., increase O_2 supply and reduce CO_2 levels). Features of this hormonal regulatory system include: (1) the renin-angiotensin-aldosterone system, (2) the release of epinephrine and norepinephrine, (3) antidiuretic hormones, and (4) atrial natriuretic peptides (released from the atrial heart cells). For details on this complex regulation, refer to Chap. 15.

The overall functional arrangement of the blood circulatory system is shown in Fig. 1.8. The role of the heart needs be considered in three different ways: as the right pump, as the left pump, and as the heart muscle tissue which has its own metabolic and flow requirements. As described above, the pulmonary (right heart) and system (left heart) circulations are arranged in a series (see also Fig. 1.7). Thus, cardiac output increases in each at the same rate; hence, an increased systemic need for a greater cardiac output will automatically lead to a greater flow of blood through the lungs (greater potential for O_2 delivery).

In contrast, the systemic organs are functionally arranged in a parallel arrangement; hence, (1) nearly all systemic organs receive blood with an identical composition (arterial blood), and (2) the flow through each organ can be and is controlled independently. For example, during exercise, a typical circulatory response is to increase blood flow through some organs (e.g., heart, skeletal muscle, brain) but not others (e.g., kidney and gastrointestinal system). The brain, heart, and skeletal muscles typify organs in which blood flows solely to supply the metabolic needs of the tissue; they do not recondition the blood.

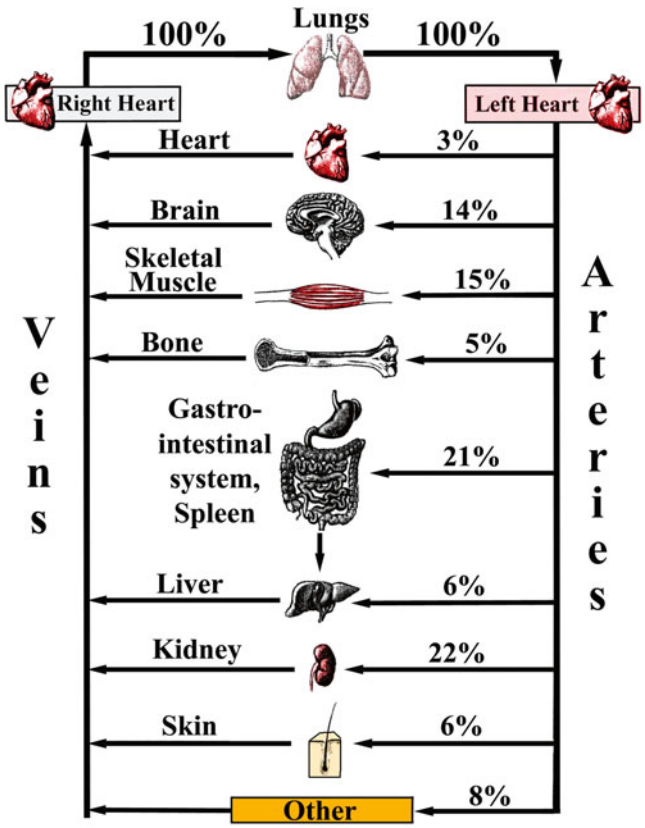

Fig. 1.8 A functional representation of the human circulatory system. The numbers indicate the approximate relative percentages of the cardiac output that is delivered, at a given moment in time, to the major organ systems within the body

The blood flow to the heart and brain is normally only slightly greater than that required for their metabolism; hence, small interruptions in flow are not well tolerated. For example, if coronary flow to the heart is interrupted, electrical and/or functional (pumping ability) activities will noticeably be altered within a few heartbeats (as can be detected by a 12-lead electrocardiogram or ECG; see Chap. 19. Likewise, stoppage of flow to the brain will lead to unconsciousness within a few seconds, and permanent brain damage can occur in as little as 4 min without flow. The flow to skeletal muscles can dramatically change (flow can increase from 20 to 70 % of total cardiac output) depending on use and thus their metabolic demand.

Many organs in the body perform the task of continually reconditioning the circulating blood. Primary organs that perform such tasks include the (1) lungs (O_2 and CO_2 exchange), (2) kidneys (blood volume and electrolyte composition, Na^+, K^+, Ca^{2+}, Cl^-, and phosphate ions), and

(3) skin (temperature). Blood-conditioning organs can often withstand, for short periods of time, significant reductions of blood flow without subsequent compromise.

1.2.6 The Coronary Circulation

In order to sustain viability, it is not possible for nutrients to diffuse from the internal wall chambers of the heart (endocardium) through all the layers of cells that make up the heart tissue. Thus, the coronary circulation is responsible for delivering blood to the heart tissue itself (the myocardium). The normal heart functions almost exclusively as an aerobic organ with little capacity for anaerobic metabolism to produce energy. Even during resting conditions, 70–80 % of the oxygen available within the blood circulating through the coronary vessels is extracted by the myocardium.

It then follows that because of the limited ability of the heart to increase oxygen availability by further increasing oxygen extraction, increases in myocardial demand for oxygen (e.g., during exercise or stress) must be met by equivalent increases in coronary blood flow. Myocardial ischemia results when the arterial blood supply fails to meet the needs of the heart muscle for oxygen and/or metabolic substrates. Even mild cardiac ischemia can result in anginal pain, focal electrical changes, and the cessation of regional cardiac contractile function. Sustained ischemia within a given myocardial region will most likely result in an infarction (cell death).

As noted above, as in any microcirculatory bed, the greatest resistance to coronary blood flow occurs in the arterioles. Blood flow through such vessels varies approximately with the fourth power of these vessels' radii; hence, the key regulated variable for the control of coronary blood flow is the degree of constriction or dilatation of coronary arteriolar vascular smooth muscle. As with all systemic vascular beds, the degree of coronary arteriolar smooth muscle tone is normally controlled by multiple independent negative feedback loops. These mechanisms include various neural, hormonal, local non-metabolic, and/or local metabolic regulators.

It should be noted that the local metabolic regulators of arteriolar tone are usually the most important for coronary flow regulation; these feedback systems involve oxygen demands of the local cardiac myocytes. In general, at any point in time, coronary blood flow is determined by integrating all the different controlling feedback loops into a single response (i.e., inducing either arteriolar smooth muscle constriction or dilation). It is also common to consider that some of these feedback loops are in opposition to one another. Interestingly, coronary arteriolar vasodilation from a resting state to one of intense exercise can result in an increase of mean coronary blood flow from approximately 0.5–4.0 mL/min/g. For more details on metabolic control of flow, see Chaps. 15 and 21.

As with all systemic circulatory vascular beds, the aortic or arterial pressure (perfusion pressure) is vital for driving blood through the coronaries and thus needs to be considered as another important determinant of coronary flow. More specifically, coronary blood flow varies directly with the pressure across the coronary microcirculation, which can be essentially considered as the aortic pressure since coronary venous pressure is typically near zero. However, since the coronary circulation perfuses the heart, some very unique determinants for flow through these capillary beds may also occur; during systole, myocardial extravascular compression causes coronary flow to be near zero, yet it is relatively high during diastole (note that this is the opposite of all other vascular beds in the body). For more details on the coronary vasculature and its function, refer to Chap. 8.

1.2.7 Lymphatic System

The lymphatic system represents an accessory pathway by which large molecules (proteins, long-chain fatty acids, bacteria, etc.) can reenter the general circulation and thus not accumulate in the interstitial space. If such particles do accumulate within the interstitial spaces, then filtration forces exceed reabsorptive forces and edema occurs. Almost all tissues in the body have lymph channels that drain excessive fluids from the interstitial space (exceptions include portions of skin, the central nervous system, the endomysium of muscles, and bones which have pre-lymphatic channels).

The lymphatic system begins in various tissues with blind-end specialized lymphatic capillaries that are roughly the size of regular circulatory capillaries, but they are less numerous (Fig. 1.9). However, the lymphatic capillaries are very porous and thus can easily collect the large particles within the interstitial fluid known as *lymph*. This fluid moves through the converging lymphatic vessels and is filtered through lymph nodes where bacteria and particulate matter are removed. Foreign particles that are trapped in the lymph nodes are destroyed (phagocytized) by tissue macrophages which line a meshwork of sinuses that lie within. Lymph nodes also contain T and B lymphocytes which can destroy foreign substances by a variety of immune responses. There are approximately 600 lymph nodes located along the lymphatic vessels; they are 1–25 mm long (bean shaped) and covered by a capsule of dense connective tissue. Note that lymph flow is unidirectional through the nodes (Fig. 1.9).

The lymphatic system is also one of the major routes for absorption of nutrients from the gastrointestinal tract (particularly for the absorption of fat and lipid-soluble vitamins A, D, E, and K). For example, after a fatty meal, lymph in the thoracic duct may contain as much as 1–2 % fat.

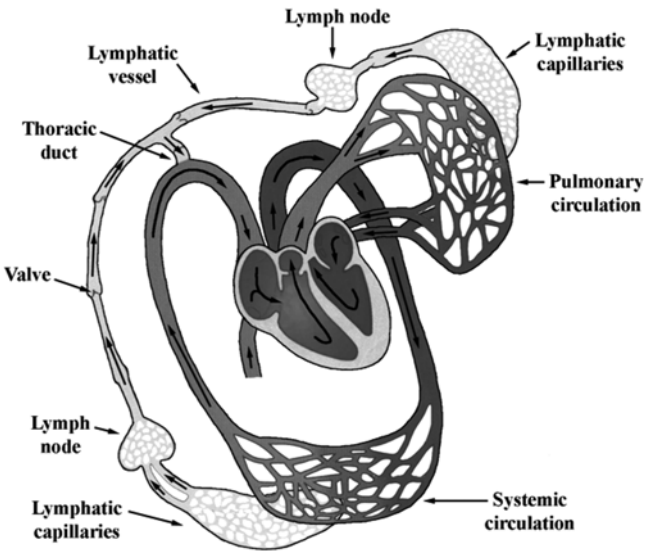

Fig. 1.9 A schematic diagram showing the relative relationship between the lymphatic system and the cardiopulmonary system. The lymphatic system is unidirectional, with fluid flowing from interstitial space back to the general circulatory system. The sequence of flow is from blood capillaries (systemic and pulmonary) to the interstitial space, to the lymphatic capillaries (lymph), to the lymphatic vessels, to the thoracic duct, and into the subclavian veins (back to the right atrium) (Modified from [5])

The majority of lymph reenters the circulatory system via the thoracic duct which empties into the venous system at the juncture of the left internal jugular and subclavian veins (which then enters into the right atrium; see Chaps. 4 and 5). The flow of lymph from tissues toward the entry point into the circulatory system is induced by two main factors: (1) higher tissue interstitial pressures and (2) the activity of the lymphatic pumps (contractions within the lymphatic vessels themselves, contractions of surrounding muscles, movement of parts of the body, and/or pulsations of adjacent arteries). In the largest lymphatic vessels (e.g., thoracic duct), the pumping action can generate pressures as high as 50–100 mmHg. Valves located in the lymphatic vessel, like in veins, aid in the prevention of the backflow of lymph.

Approximately 2.5 L of lymphatic fluid reenters the general blood circulation (cardiopulmonary system) each day. In the steady state, this indicates a total body net transcapillary fluid filtration rate of 2.5 L/day. When compared with the total amount of blood that circulates each day (approximately 7000 L/day), this seems almost insignificant; however, blockage of such flow will quickly cause serious tissue edema. Therefore, the lymphatic circulation plays a critical role in keeping the interstitial protein concentrations low and also in removing excess capillary filtrate from tissues throughout the body.

1.3 Summary

The primary function of the cardiovascular system is rapid transport of molecules over long distances between internal cells, the body surface, various specialized tissue and/or organs. This body-wide transport system is composed of several major components: blood, the blood vessels (arteries and veins), the heart, and the lymphatic system. When functioning normally, this system adequately provides for the wide-ranging activities that a human can accomplish. Failure in any of these components can lead to grave consequence. Many of the subsequent chapters in this book will cover, in greater detail, the anatomical, physiological, and pathophysiological features of the various components of the cardiovascular system. The normal and abnormal performance of the heart and various clinical treatments to enhance function will also be discussed within the following chapters.

References

1. Alexander RW, Schlant RC, Fuster V (eds) (1998) Hurst's the heart, arteries and veins, 9th edn. McGraw-Hill, New York
2. Germann WJ, Stanfield CL (eds) (2002) Principles of human physiology. Pearson Education, Inc./Benjamin Cummings, San Francisco
3. Guyton AC, Hall JE (eds) (2000) Textbook of medical physiology, 10th edn. W.B. Saunders Co., Philadelphia
4. Mohrman DE, Heller LJ (eds) (2003) Cardiovascular physiology, 5th edn. McGraw-Hill, New York
5. Tortora GJ, Grabowski SR (eds) (2000) Principles of anatomy and physiology, 9th edn. Wiley, New York. http://www.vhlab.umn.edu/atlas

Part II

Anatomy

Attitudinally Correct Cardiac Anatomy

2

Alexander J. Hill

Abstract

Anatomy is one of the oldest branches of medicine, dating back as far as the third century BC. Throughout time, the discipline has been served well by a universal system for describing structures based on the *anatomic position*. Unfortunately, cardiac anatomy has been a detractor from this long-standing tradition and has commonly been incorrectly described using confusing and inappropriate nomenclature. This is most likely due to the examination of the heart in the *Valentine position*, in which the heart stands on its apex, as opposed to how it is actually oriented in the body. The description of the major coronary arteries, such as the *anterior descending* and *posterior descending,* is attitudinally incorrect; as the heart is oriented in the body, the surfaces are actually superior and inferior. An overview of attitudinally correct human anatomy, the problem areas, and the comparative aspects of attitudinally correct anatomy will be presented in this chapter.

Keywords

Cardiac anatomy • Attitudinally correct nomenclature • Comparative anatomy

2.1 Introduction

Anatomy is one of the oldest branches of medicine, with historical records dating back at least as far as the third century BC. Cardiac anatomy has been a continually explored topic throughout this time, and there are still publications on new facets of cardiac anatomy being researched and reported today. One of the fundamental tenets of the study of anatomy has been the description of the structure based on the universal orientation, otherwise termed the *anatomic position* (Fig. 2.1). The anatomic position depicts the subject facing the observer and is then divided into three orthogonal planes. Each plane divides the body or individual structure within the body (such as the heart) into two portions. Thus, using all three planes, each portion of the anatomy can be localized precisely within the body. These three planes are called (1) the *sagittal* plane, which divides the body into right and left portions; (2) the *coronal* plane, which divides the body into anterior and posterior portions; and (3) the *transverse* plane, which divides the body into superior and inferior portions. Each plane can then be viewed as a slice through a body or organ and will also have specific terms that can be used to define the structures within. If one is looking at a sagittal cut through a body, the observer would describe structures as being anterior or posterior and superior or inferior. On a coronal cut, the structures would be described as superior or inferior and right or left. Finally, on a transverse cut, anterior or posterior and right or left would be used to describe the structures. This terminology should be used regardless of the actual position of the body. For example, assume an observer is looking down at a table and does not move. If a body is lying on its back on this table, the anterior surface would be facing upward toward the observer. Now, if the body is lying on its left side, the right surface of the body would be facing

A.J. Hill, PhD (✉)
Medtronic,
8200 Coral Sea Street NE, Mounds View, MN 55112, USA

Department of Surgery, University of Minnesota,
Minneapolis, MN 55432, USA
e-mail: alex.hill@medtronic.com

P.A. Iaizzo (ed.), *Handbook of Cardiac Anatomy, Physiology, and Devices*, DOI 10.1007/978-3-319-19464-6_2

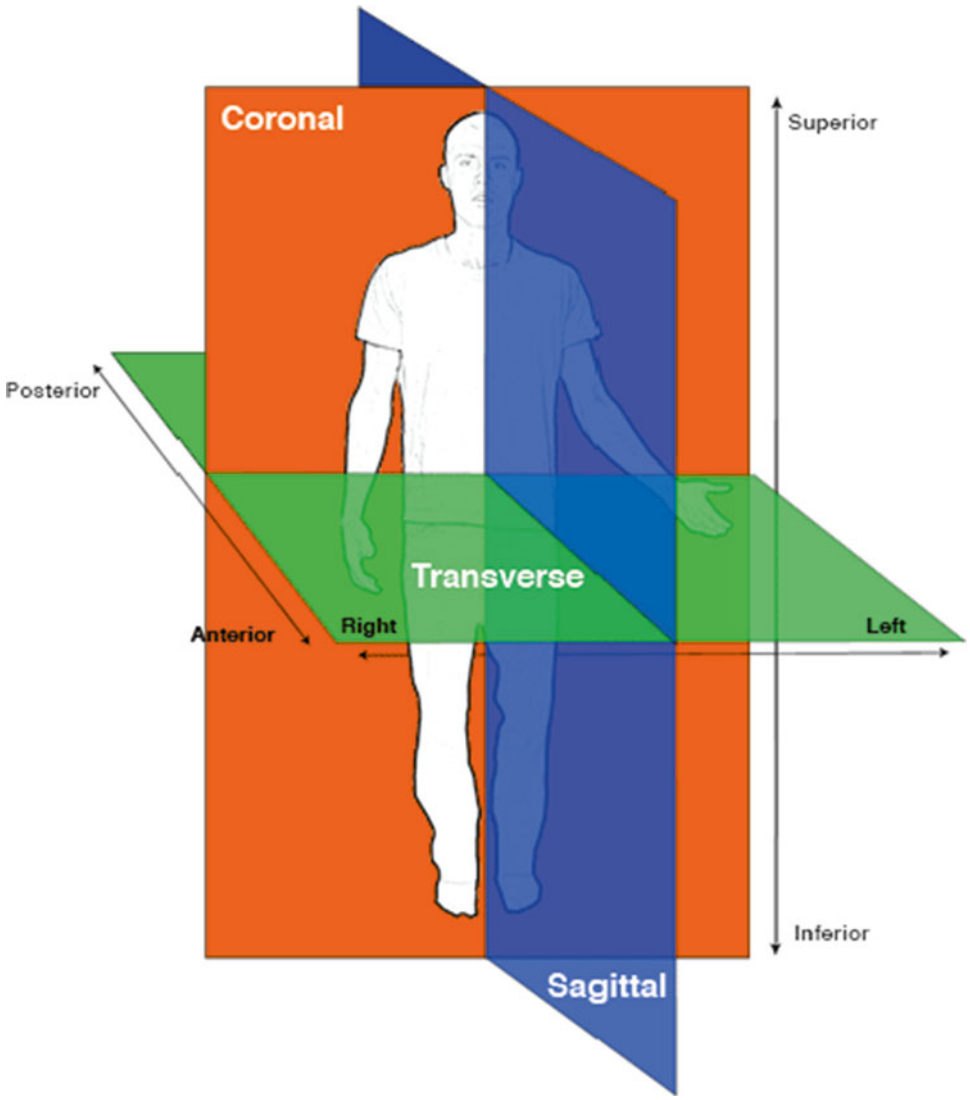

Fig. 2.1 Illustration showing the anatomic position. Regardless of the position of the body or organ upon examination, the anatomy of an organ or the whole should be described as if observed from this vantage point. The anatomic position can be divided by three separate orthogonal planes: (1) the sagittal plane, which divides the body into right and left portions; (2) the coronal plane, which divides the body into anterior and posterior portions; and (3) the transverse plane, which divides the body into superior and inferior portions

upward toward the observer, and the anterior surface would be facing toward the right. Regardless of how the body is moved, the orthogonal planes used to describe it move with the body and do not stay fixed in space. The use of this position and universal terms to describe structure have served anatomists well and have led to easier discussion and translation of findings among different investigators. It continues to be emphasized that there remains a strong need in the fields of cardiovascular science and medicine to promote the use of attitudinally correct cardiac anatomic nomenclature [1, 2].

2.2 The Problem: Cardiac Anatomy Does Not Play by the Rules

As described above, the use of the *anatomic position* has stood the test of time and is still used to describe the position of structures within the body. However, within approximately the last 50 years, descriptions of cardiac anatomy have not adhered to the proper use of these terms; rather they have been replaced with inappropriate descriptors. There are two major reasons for this: (1) many descriptions of heart anatomy have been made with the heart removed from the body and incorrectly positioned during examination, and (2) a *heart-centric* orientation has been preferred to describe the structures. These two reasons are interrelated and negatively affect the proper description of cardiac anatomy. Typically, when the heart is examined outside the body, it has been placed on its apex into the so-called Valentine position, which causes the heart to appear similar to the common illustration of the heart used routinely in everything from greeting cards to instant messenger icons (Fig. 2.2). It is the author's opinion that this problem has been confounded by the comparative positional differences seen between humans and large mammalian cardiac models used to help understand human cardiac anatomy and physiology. As you will see in the following

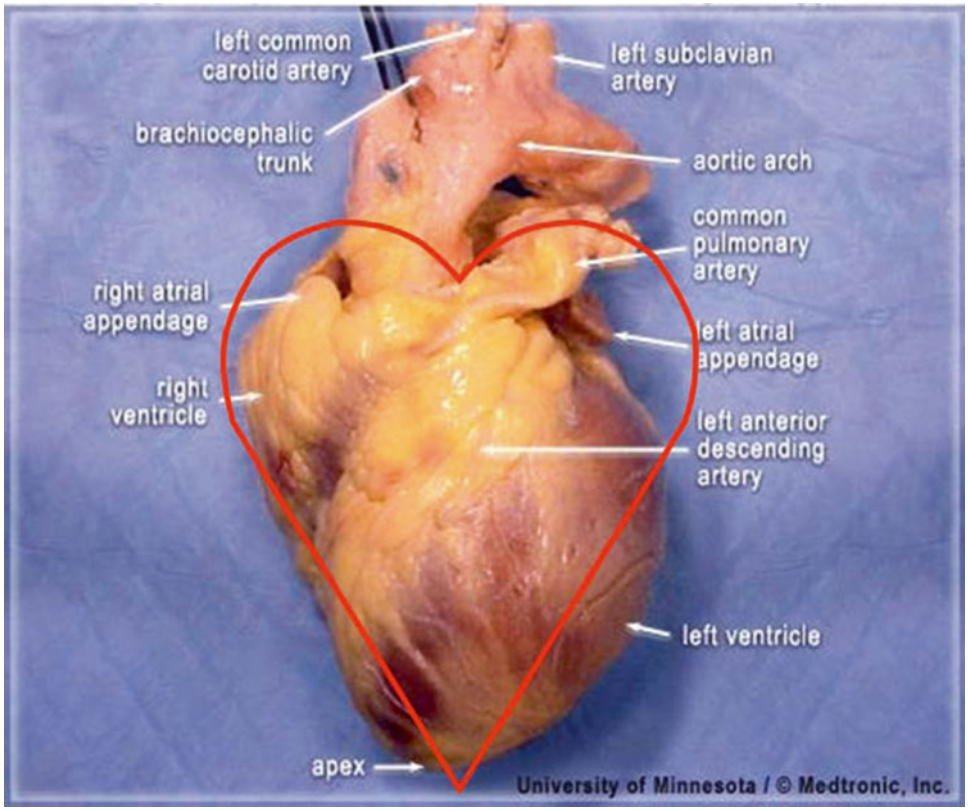

Fig. 2.2 A human heart viewed from the so-called anterior position, demonstrating the Valentine heart orientation used by many to incorrectly describe anatomy. The *red line* surrounding the heart is the characteristic symbol, which was theoretically derived from observing the heart in the orientation

sections, the position of the heart within a sheep thorax is very similar to the Valentine position used to examine human hearts. I will point out that I have been guilty of describing structures in such a manner, as is evidenced by some of the images available in the Visible Heart® Viewer CD (Fig. 2.2), as have countless others as seen in the scientific literature and many textbooks (even including this one). Regardless, it is a practice I have since given up and have reverted to the time-honored method using the *anatomic position*.

Further impacting the incorrect description of cardiac anatomy is the structure of the heart itself. A common practice in examining the heart is to cut the ventricular chambers in the short axis, which is perpendicular to the long axis of the heart which runs from the base to the apex. This practice is useful in the examination of the ventricular chambers, but the cut plane is typically confused as actually being transverse to the body when it is, in most cases, an oblique plane. The recent explosion of tomographic imaging techniques, such as magnetic resonance imaging (MRI) and computed tomography (CT), in which cuts such as the one just described are commonly made, has further fueled the confusion.

Nevertheless, this incorrect use of terminology to describe the heart can be considered to impact a large and diverse group of individuals. Practitioners of medicine, such as interventional cardiologists and electrophysiologists, are affected, as are scientists investigating the heart and engineers designing medical devices. It is considered here that describing terms in a more consistent manner, and thus using the appropriate terminology, would greatly increase the efficiency of interactions between these groups.

It should be noted that there have been a few exceptions to this rule, in that attempts have been made to promote proper use of anatomic terminology. Most notable are the works of Professor Robert Anderson [3–6], although he will also admit that he has been guilty of using incorrect terminology in the past. Other exceptions to this rule are Wallace McAlpine's landmark cardiac anatomy textbook [7] and an excellent textbook by Walmsley and Watson [8].

In addition to these exceptions, a small group of scientists and physicians has begun to correct the many misnomers that have been used to describe the heart in the recent past; this is the major goal of this chapter. A description of the correct position of the heart within the body will be presented along with specific problem areas, such as the coronary arteries, where terms such as left anterior descending artery are most obviously incorrect and misleading.

2.3 The Attitudinally Correct Position of the Human Heart

The following set of figures used to describe the correct position of the heart within the body was created from 3D volumetric reconstructions of magnetic resonance images of

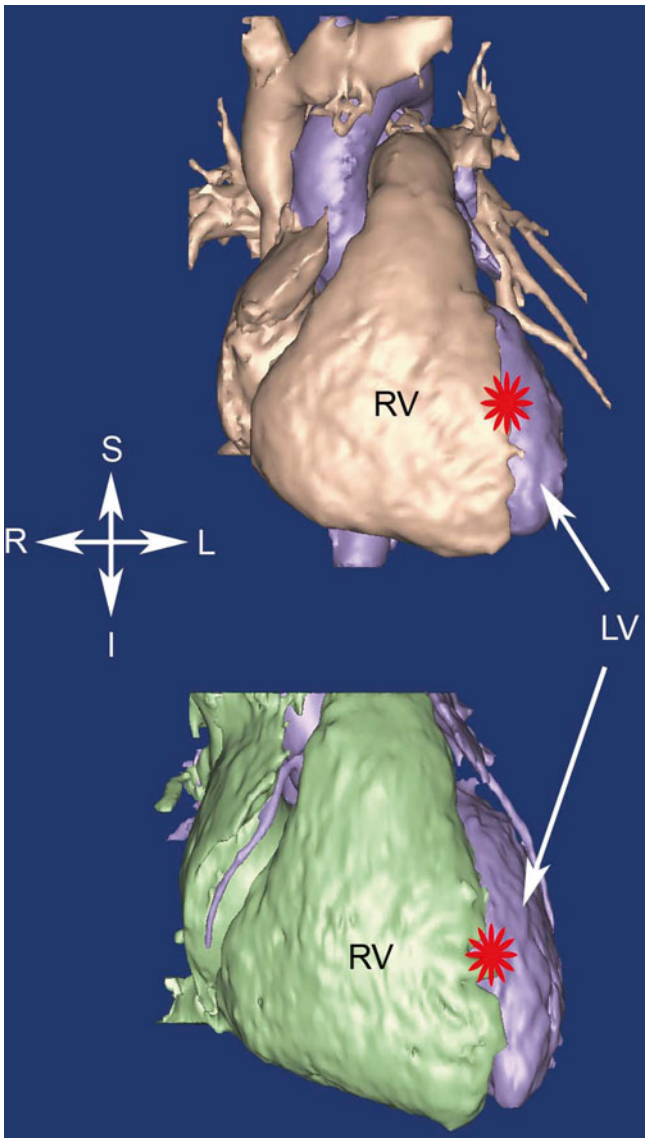

Fig. 2.3 Volumetric reconstructions from magnetic resonance imaging showing the anterior surfaces of two human hearts. The major structures visible are the right atrium and right ventricle. The apex of the heart is positioned to the left and is not inferior as in the Valentine position. The so-called anterior interventricular sulcus (shown with a *red star*) in fact begins superiorly and travels to the left and only slightly anteriorly. *I* inferior, *L* left, *LV* left ventricle, *R* right, *RV* right ventricle, *S* superior

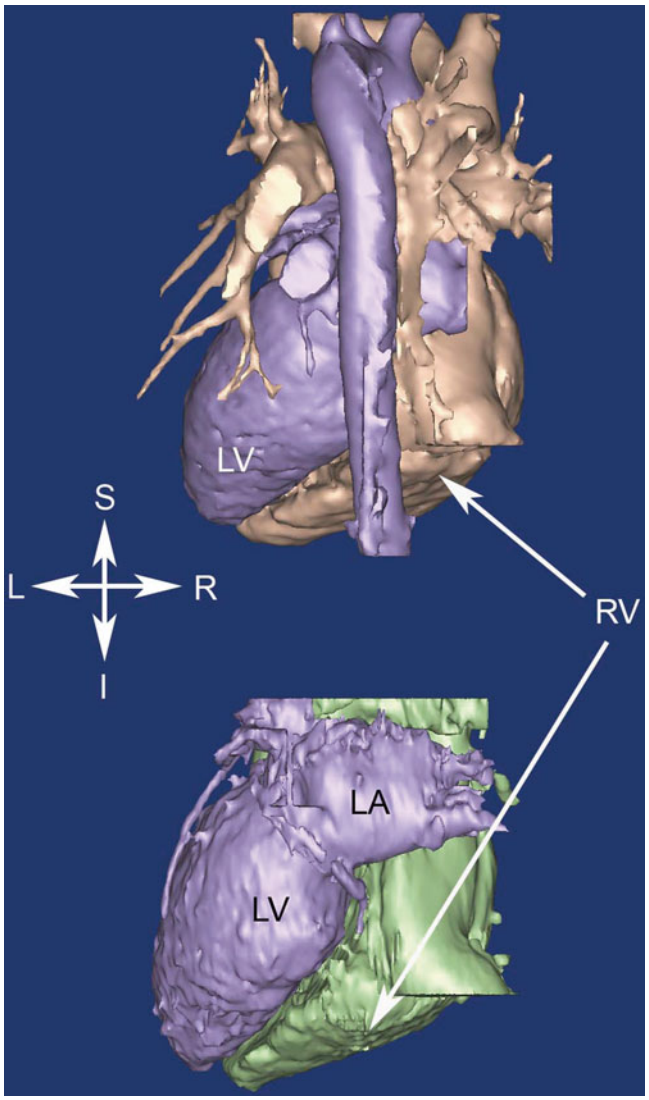

Fig. 2.4 Volumetric reconstructions from magnetic resonance imaging showing the posterior surfaces of two human hearts. The major structures visible are the right and left atrium and the descending aorta (*top* image only). The apex of the heart is positioned to the left and is not inferior as in the Valentine position. *I* inferior, *L* left, *LA* left atrium, *LV* left ventricle, *R* right, *RV* right ventricle, *S* superior

healthy humans with normal cardiac anatomy. In Fig. 2.3, the anterior surfaces of two human hearts are shown. Note that in this view of the heart, the major structures visible are the right atrium and right ventricle. In reality, the right ventricle is positioned anteriorly and to the right of the left ventricle. Also, note that the apex of the heart is positioned to the left and is not inferior, as in the Valentine position. Furthermore, note that the so-called anterior interventricular sulcus (shown with a red star), in fact, begins superiorly and travels to the left and only slightly anteriorly. Figure 2.4 shows the posterior surfaces of two human hearts, in which the first visible structure is the descending aorta. Anterior to that are the right and left atria. Figure 2.5 shows the inferior or diaphragmatic surfaces of two human hearts, commonly referred to as the posterior surface, based on Valentine positioning. The inferior caval vein and descending aorta are cut in the short axis; in this region of the thorax, they tend to travel parallel to the long axis of the body. Note that the so-called posterior interventricular sulcus is actually positioned inferiorly (shown with a red star). Figure 2.6 shows a superior view of two human hearts. In this view, the following

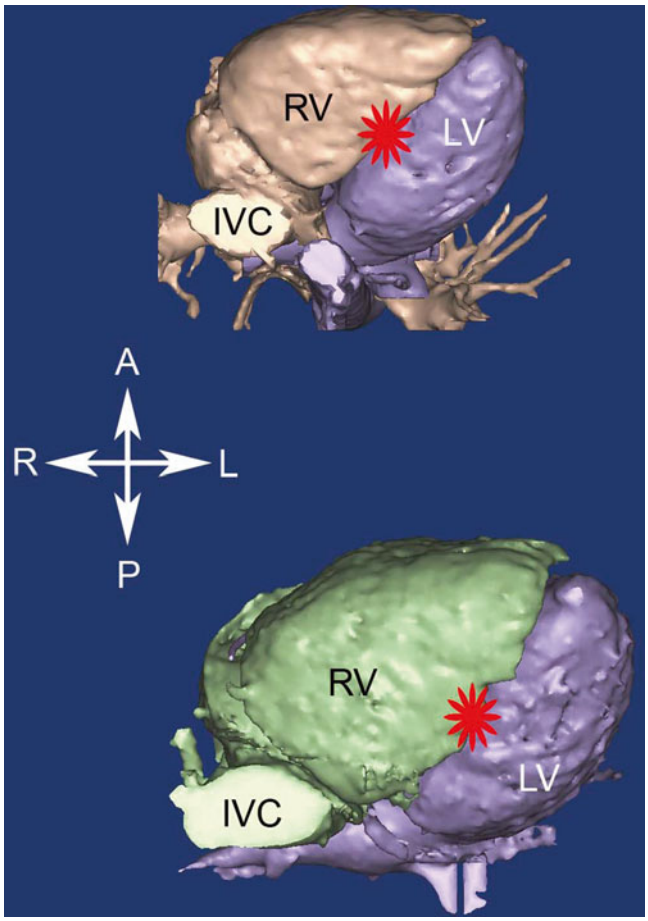

Fig. 2.5 Volumetric reconstructions from magnetic resonance imaging showing the inferior or diaphragmatic surfaces of two human hearts. This surface is commonly, and incorrectly, referred to as the posterior surface, based on Valentine positioning. The inferior caval vein (IVC) and descending aorta are cut in the short axis; in this region of the thorax, they tend to travel parallel to the long axis of the body. The so-called posterior interventricular sulcus is actually positioned inferiorly and is denoted by a *red star*. *A* anterior, *L* left, *LV* left ventricle, *P* posterior, *R* right, *RV* right ventricle

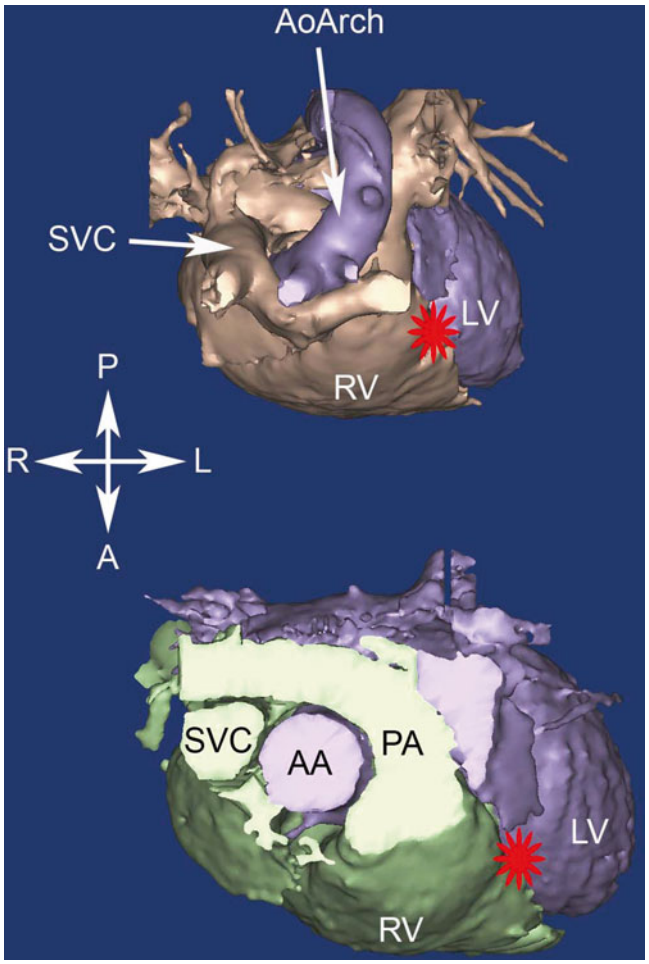

Fig. 2.6 Volumetric reconstructions from magnetic resonance imaging showing the superior surfaces of two human hearts. In this view, the following structures are visible: the superior caval vein (SVC), the aortic arch (AoArch), and the major arteries arising from it, the free portion of the right atrial appendage, and the pulmonary trunk (PA) which, after arising from the right ventricle, runs in the transverse plane before bifurcating into the right and left pulmonary arteries. Also, note that the position of the "anterior" interventricular sulcus (shown with a *red star*) is more correctly termed superior. *A* anterior, *AA* ascending aorta, *L* left, *LV* left ventricle, *P* posterior, *R* right, *RV* right ventricle

structures are visible: (1) the superior caval vein, (2) the aortic arch and the major arteries arising from it, (3) the free portion of the right atrial appendage, and (4) the pulmonary trunk which, after arising from the right ventricle, runs in the transverse plane before bifurcating into the right and left pulmonary arteries. Also, note that the position of the *anterior* interventricular sulcus (shown with a red star) is more correctly termed *superior*.

2.4 Commonly Used Incorrect Terms

This section will specifically describe a few obvious problem areas in which attitudinally incorrect nomenclature is commonly used: the coronary arteries, myocardial segmentation for depiction of infarction, and cardiac valve nomenclature.

In the normal case, there are two coronary arteries which arise from the aortic root, specifically from two of the three sinuses of Valsalva. These two coronary arteries supply the right and left halves of the heart, although there is considerable overlap in supply, especially in the interventricular septum. Nevertheless, the artery which supplies the right side of the heart is aptly termed the *right coronary artery*, and the corresponding artery which supplies the left side of the heart is termed the *left coronary artery*. Therefore, the sinuses in which these arteries arise can be similarly named the right coronary sinus and left coronary sinus, and for the sinus with no coronary artery, the noncoronary sinus; this convention is commonly used. These arteries then branch as they continue their path along

the heart, with the major arteries commonly following either the atrioventricular or interventricular grooves, with smaller branches extending from them. It is beyond the scope of this chapter to fully engage in a description of the nomenclature for the entire coronary arterial system. However, there are two glaring problems which persist in the nomenclature used to describe the coronary arteries, both which involve the interventricular grooves. First, shortly after the left coronary artery arises from the left coronary sinus, it bifurcates into the *left anterior descending* and the *left circumflex* arteries. The *left anterior descending artery* follows the so-called "anterior" interventricular groove, which was described previously as being positioned superiorly and to the left and only slightly anteriorly (Fig. 2.3). Second, depending on the individual, either the right coronary artery (80–90 %) or the left circumflex artery supplies the opposite side of the interventricular septum as the left "anterior" descending. Regardless of the parent artery, this artery is commonly called the "posterior" descending artery. However, similar to the so-called "anterior" descending artery, the position of this artery is not posterior but rather inferior (Fig. 2.5).

Now that the courses of the two main coronary arteries are clear, the description of myocardial segmentation needs to be addressed. It is rather interesting that, although clinicians typically call the inferior interventricular artery the posterior descending artery, they often correctly term an infarction caused by blockage in this artery as an inferior infarct. Current techniques used to assess the location and severity of myocardial infarctions include MRI, CT, and 2D, 3D, or 4D cardiac ultrasound. These techniques allow for the clinician to view the heart in any plane or orientation; due to this, a similar confusion in terminology arises. Recently, an American Heart Association working group issued a statement in an attempt to standardize nomenclature for use with these techniques [9]. Upon close examination, this publication correctly terms areas supplied by the inferior interventricular artery as inferior but incorrectly terms the opposite aspect of the heart as anterior.

Finally, nomenclatures commonly used to describe the leaflets of the atrioventricular valves—the tricuspid and mitral valves—are typically not attitudinally correct. For example, the tricuspid valve is situated between the right atrium and right ventricle and is so named because, in the majority of cases, there are three major leaflets or cusps. These are currently referred to as the anterior, posterior, and septal leaflets and were most likely termed in this manner due to examination of the heart in the Valentine position. Figure 2.7 shows an anterior view of a human heart in an attitudinally correct orientation, with the tricuspid annulus shown in orange. The theorized locations of the commissures between the leaflets are shown in red. In order for the "anterior" leaflet to be truly anterior, the tricuspid annulus would need to be orthogonal to the image. However, the actual location of the annulus is in an oblique plane as shown in the figure, and therefore the leaflets would be more correctly termed anterosuperior, inferior, and septal.

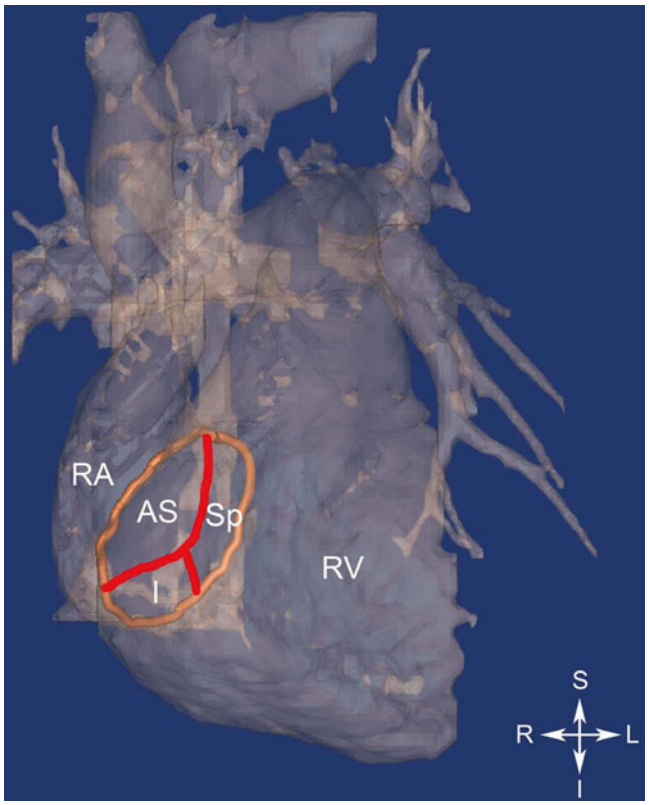

Fig. 2.7 Volumetric reconstruction from magnetic resonance imaging (MRI) showing the anterior surfaces of the right ventricle and atrium of a human heart. The tricuspid annulus is highlighted in *orange* and was traced on the MRI images. The theorized positions of the commissures between the leaflets are drawn in *red*, and the leaflets are labeled appropriately. *AS* anterosuperior, *I* inferior, *L* left, *R* right, *RA* right atrium, *RV* right ventricle, *S* superior, *Sp* septal

The same is true for the mitral valve, although the terms used to describe it are a bit closer to reality than the tricuspid valve. The mitral valve has two leaflets, commonly referred to as the anterior and posterior. However, Fig. 2.8 shows that the leaflets are not strictly anterior or posterior, or else the plane of the annulus (shown in orange) would be perpendicular to the screen. Therefore, based on attitudinal terms, one would prefer to define these leaflets as anterosuperior and posteroinferior. It should be noted that these leaflets have also been described as aortic and mural, which is less dependent on orientational terms and also technically correct.

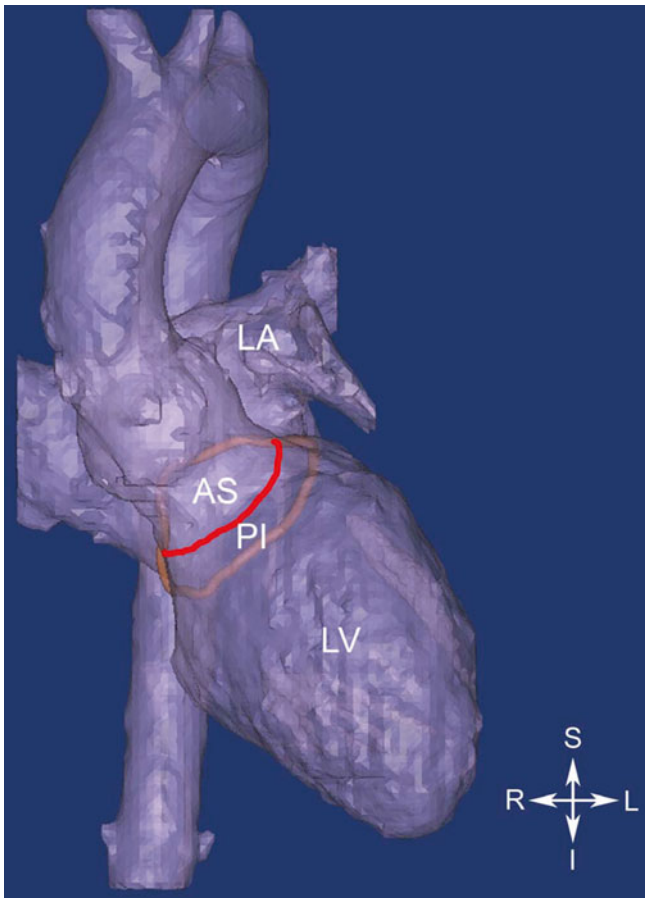

Fig. 2.8 Volumetric reconstruction from magnetic resonance imaging (MRI) showing the anterior surfaces of the left ventricle and atrium of a human heart. The mitral annulus is highlighted in *orange* and was traced on the MRI images. The theorized positions of the commissures between the leaflets are drawn in *red*, and the leaflets are labeled appropriately. *AS* anterosuperior, *I* inferior, *L* left, *LA* left atrium, *LV* left ventricle, *PI* posteroinferior, *R* right, *S* superior

2.5 Comparative Aspects of Attitudinally Correct Cardiac Anatomy

In addition to the incorrect terminology used to describe the human heart, translation of cardiac anatomy between human and other species is often further complicated due to differences in the orientation of the heart within the thorax. Compared to the human heart, the commonly used large mammalian heart is rotated so that the apex is aligned with the long axis of the body. Furthermore, the apex of the heart is oriented anteriorly and is commonly attached to the posterior (dorsal) aspect of the sternum. Further confounding the differences is varying nomenclature. The terms inferior and superior are rarely used and rather are replaced by cranial and caudal. Likewise, the terms anterior and posterior are commonly replaced with ventral and dorsal. Also see Figs. 6.10 and 6.11 in Chap. 6 for more information on the relative position of a sheep heart compared to a human heart.

2.6 Summary

As the field of cardiac anatomy continues to play an important role in the practice of medicine and the development of medical devices, it benefits all involved to adopt commonly used terminology to describe the heart and its proper location in the body. Furthermore, it may be of great utility to describe the cardiac anatomy of major animal models using the same terminology as that of humans, at least when comparisons are being made between species. Finally, due to advances in 3D and 4D imaging and their growing use in the cardiac arena, a sound foundation of attitudinally correct terms will benefit everyone involved.

References

1. Iaizzo PA, Anderson RH, Hill AJ (2013) The importance of human cardiac anatomy for translational research. J Cardiovasc Transl Res 6:105–106
2. Anderson RH, Spicer DE, Hlavacek AJ, Hill AJ, Loukas M (2013) Describing the cardiac components–attitudinally appropriate nomenclature. J Cardiovasc Transl Res 6:118–123
3. Anderson RH, Becker AE, Allwork SP et al (eds) (1980) Cardiac anatomy: an integrated text and colour atlas. Churchill Livingston, New York
4. Anderson RH, Razavi R, Taylor AM (2004) Cardiac anatomy revisited. J Anat 205:159–177
5. Cook AC, Anderson RH (2002) Attitudinally correct nomenclature. Heart 87:503–506
6. Cosio FG, Anderson RH, Kuck KH et al (1999) Living anatomy of the atrioventricular junctions. A guide to electrophysiologic mapping. Circulation 100:e31–e37
7. McAlpine WA (1975) Heart and coronary arteries: an anatomical atlas for clinical diagnosis, radiological investigation, and surgical treatment. Springer, New York
8. Walmsley R, Watson H (1978) Clinical anatomy of the heart. Churchill Livingstone, New York
9. Cerqueira MD, Weissman NJ, Dilsizian V et al (2002) Standardized myocardial segmentation and nomenclature for tomographic imaging of the heart: a statement for healthcare professionals from the Cardiac Imaging Committee of the Council on Clinical Cardiology of the American Heart Association. Circulation 105:539–542

Cardiac Development

3

Brad J. Martinsen and Jamie L. Lohr

Abstract

The first heart field (FHF), second heart field (SHF), cardiac neural crest (CNC), and proepicardial organ (PEO) are the four major embryonic regions involved in vertebrate heart development. They each make an important contribution to overall cardiac development with complex developmental timing and regulation. This chapter describes how these regions interact to form the final structure of the heart in relationship to the developmental timeline of human embryology.

Keywords

Human heart embryology • First heart field • Second heart field • Cardiac neural crest • Proepicardial organ • Cardiac development

3.1 Introduction to Human Heart Embryology and Development

The first heart field (FHF), second heart field (SHF), cardiac neural crest (CNC), and the proepicardial organ (PEO) are the four major embryonic regions involved in the process of vertebrate heart development (Fig. 3.1). They each make an important contribution to cardiac development with their own complex developmental timing and regulation (Table 3.1) [1, 2]. The heart is the first internal organ to form and function during vertebrate development, and many of the mechanisms of heart formation are molecularly and developmentally conserved [3–6]. The description presented here is based on development research from the chick, mouse, frog, and human model systems. Research conducted in the last decade has redefined the FHF which gives rise to the left ventricle and parts of the atria; furthermore, it has led to the exciting discovery of the SHF which gives rise to the outflow tract, right ventricle, and parts of the atria of the mature heart [7–18]. These discoveries were critical steps in helping us understand how the outflow tract of the heart forms, a cardiac structure where many congenital heart defects arise, and thus has important implications for the understanding and prevention of congenital heart disease [6, 15–19]. Great strides have also been made in understanding the contributions of both the CNC [20] and the PEO [15, 21, 22] to overall heart development.

B.J. Martinsen, PhD (✉) • J.L. Lohr, MD
Division of Pediatric Cardiology, Department of Pediatrics, University of Minnesota School of Medicine, East Building, MB 560, 2450 Riverside Avenue, Minneapolis, MN 55454, USA
e-mail: brad.martinsen.phd@gmail.com

3.2 First Heart Field Contribution to the Linear Heart Tube, Left Ventricle, and Atria

The cells that will become the heart are among the first cell lineages formed in the vertebrate embryo [23, 24]. By day 15 of human development, the primitive streak has formed [1] and the first mesodermal cells to migrate (gastrulate) through the primitive streak are also the cells fated to become myocytes or heart cells [25, 26] (Fig. 3.2). These mesodermal cells dedicated for heart development migrate to an anterior and lateral position where they initially form a bilateral FHF and a more medially located SHF [10, 11, 15, 16, 27]

P.A. Iaizzo (ed.), *Handbook of Cardiac Anatomy, Physiology, and Devices*, DOI 10.1007/978-3-319-19464-6_3

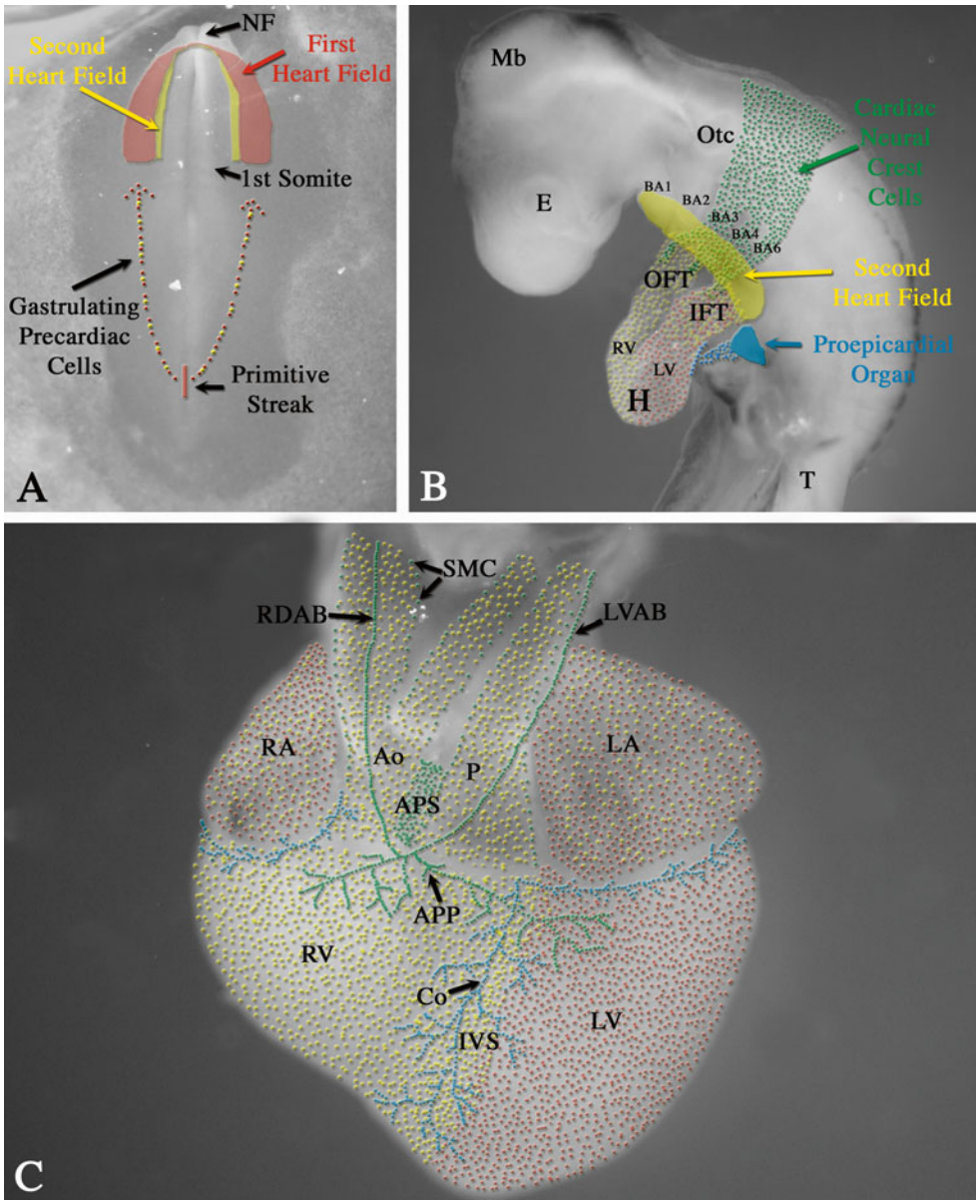

Fig. 3.1 The four major contributors to heart development illustrated in the chick model system: first heart field, second heart field, cardiac neural crest, and the proepicardial organ. (**A**) Day 1 chick embryo (equivalent to day 20 of human development). *Red* denotes first heart field cells and *yellow* denotes second heart field cells. (**B**) Day 2.5 chick embryo (equivalent to approximately 5 weeks of human development). Color code: *green* = cardiac neural crest cells; *red* = first heart field cells; *yellow* = second heart field cells; *blue* = proepicardial cells. (**C**) Day 8 chick heart (equivalent to approximately 9 weeks of human development). Color code: *green* = derivatives of the cardiac neural crest; *yellow* = derivatives of the second heart field; *red* = derivatives of the first heart field; *blue* = derivatives of the proepicardial organ. *Ao* aorta, *APP* anterior parasympathetic plexus, *APS* aorticopulmonary septum, *BA* branchial arch, *Co* coronary vessels, *E* eye, *H* heart, *IFT* inflow tract, *IVS* interventricular septum, *LA* left atrium, *LV* left ventricle, *LVAB* left ventral arterial branch of the Xth (vagal) cranial nerve, *Mb* midbrain, *NF* neural folds, *OFT* outflow tract, *Otc* otic placode, *P* pulmonary artery, *RA* right atrium, *RDAB* right dorsal arterial branch of the Xth (vagal) cranial nerve, *RV* right ventricle, *SMC* smooth muscles cells, *T* trunk

(Fig. 3.1A). Specifically, the posterior border of the bilateral FHF reaches down to the first somite in the lateral mesoderm on both sides of the midline [8, 28] (Fig. 3.1A). At day 18 of human development, the lateral plate mesoderm is split into two layers—somatopleuric and splanchnopleuric [1]. It is the splanchnopleuric mesoderm layer that contains the myocardial, smooth muscle, and endocardial cardiogenic precursors in the region of the FHF and SHF, as defined above. Presumptive endocardial cells delaminate from the splanchnopleuric mesoderm in the FHF and coalesce via vasculogenesis to form two lateral endocardial tubes [29]. During the third week of human development, two bilateral layers of

Table 3.1 Developmental timeline of human heart embryology

Human development (days)	Developmental process
0	Fertilization
1–4	Cleavage and movement down the oviduct to the uterus
5–12	Implantation of the embryo into the uterus
13–14	Primitive streak formation (midstreak level contains precardiac cells)
15–17	Formation of the three primary germ layers (gastrulation): ectoderm, mesoderm, and endoderm; midlevel primitive streak cells that migrate to an anterior and lateral position form the bilateral **first heart field** and a more medially located the **second heart field**
17–18	Lateral plate mesoderm splits into the somatopleuric mesoderm and splanchnopleuric mesoderm; splanchnopleuric mesoderm contains the myocardial and endocardial cardiogenic precursors in the region of the **first heart field** and **second heart field**
18–26	Neurulation (formation of the neural tube)
20	Cephalocaudal and lateral folding brings the bilateral endocardial tubes into the ventral midline of the embryo
21–22	Heart tube fusion
22	Heart tube begins to beat
22–28	Heart looping and the accretion of cells from the first and **second heart fields; proepicardial cells** invest the outer layer of the heart tube and eventually form the epicardium and coronary vasculature; neural crest migration starts
32–37	**Cardiac neural crest** migrates through the aortic arches and enters the outflow tract of the heart
57+	Outflow tract and ventricular septation complete
Birth	Functional septation of the atrial chambers, as well as the pulmonary and systemic circulatory systems

Most of the human developmental timing information is from *Larsen's Human Embryology* [1], except for the human staging of the second heart field and proepicardium which was correlated from other model systems [7–9, 30]

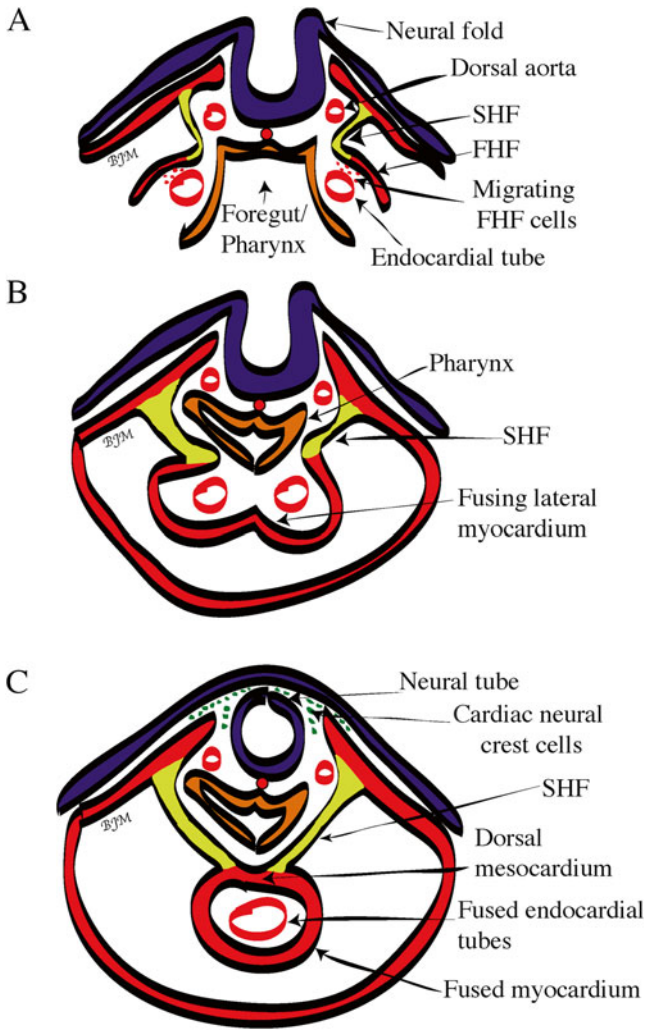

Fig. 3.2 Cross-sectional view of human heart tube fusion. (**A**) Day 20, cephalocaudal and lateral folding brings bilateral endocardial tubes into the ventral midline of the embryo. (**B**) Day 21, start of heart tube fusion. (**C**) Day 22, complete fusion, resulting in the beating primitive heart tube. Color code of the embryonic primary germ layer origin: *blue/purple* = ectoderm; *red* = mesoderm; *orange* = endoderm; *yellow* = second heart field. *FHF* first heart field, *SHF* second heart field

myocardium surrounding the endocardial tubes are brought into the ventral midline during closure of the ventral foregut via cephalic and lateral folding of the embryo [1] (Fig. 3.2A). The lateral borders of the myocardial mesoderm layers are the first heart structures to fuse, followed by the fusion of the two endocardial tubes which then form one endocardial tube surrounded by splanchnopleuric-derived myocardium (Fig. 3.2B, C). The medial borders of the myocardial mesoderm layers are the last to fuse [30]. Thus, the early heart is continuous with splanchnopleuric mesoderm across the dorsal mesocardium (Fig. 3.2C). This will eventually partially break down to form the ventral aspect of the linear heart tube with a posterior inflow (venous pole) and anterior outflow (arterial pole), as well as the dorsal wall of the pericardial cavity [18, 30]. During the fusion of the endocardial tubes, the myocardium secretes an extracellular (acellular) matrix (enriched in chondroitin sulfate, versican, heparan sulfate, hyaluronic acid, hyaluronan, and proteoglycans), forming the cardiac jelly layer separating the myocardium and endocardium [31]. By day 22 of human development, the linear heart tube begins to beat. As the human heart begins to fold and loop from day 22 to day 28 (described below), epicardial cells from the PEO will invest the outer layer of the heart tube (Figs. 3.1B and 3.3A), resulting in a heart tube with four primary layers: endocardium, cardiac jelly, myocardium, and epicardium [1] (Fig. 3.3B).

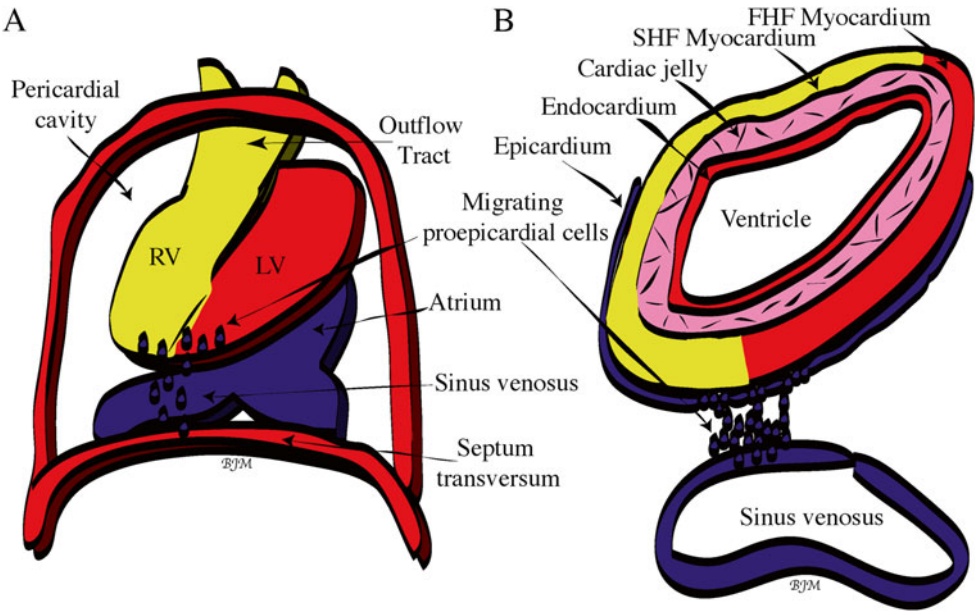

Fig. 3.3 Origin and migration of proepicardial cells. (**A**) Whole mount view of the looping human heart within the pericardial cavity at day 28. Proepicardial cells (*blue dots*) emigrate from the sinus venosus and possibly the septum transversum and then migrate out over the outer surface of the ventricles, eventually surrounding the entire heart. (**B**) Cross-sectional view of the looping heart showing the four layers of the heart: epicardium, myocardium, cardiac jelly, and endocardium. Color code: *yellow* = second heart field (SHF)-derived cells; *red* (within heart) = first heart field (FHF)-derived cells. *LV* left ventricle, *RV* right ventricle

3.3 Second Heart Field Contribution to the Outflow Tract, Right Ventricle, and Atria

A cascade of signals identifying the left and right sides of the embryo is thought to initiate the process of primary linear heart tube looping [32]. The primary heart tube loops to the right of the embryo and bends to allow convergence of the inflow (venous) and outflow (arterial) ends between day 22 and day 28 of human development (Fig. 3.4). This process occurs prior to the division of the heart tube into four chambers and is required for proper alignment and septation of the mature cardiac chambers. During the looping process, the primary heart tube increases dramatically in length (by four- to fivefold) on both the outflow and inflow poles via the addition of progenitor cells originating from the SHF (pharyngeal mesoderm) [7–18]. These multipotent progenitor cells within the developing heart give rise to myocardium, smooth muscle, and endothelial cells [12]. Previous experiments in the 1970s already revealed that the distal right ventricle and outflow tract (OFT) are added later to the looping heart by addition of cells lying outside the early heart [12, 33]. Researchers at that time, however, still assumed that the primary linear heart tube already contained all the cell lineages to build the adult heart. It was not until the rediscovery of these progenitor cells in 2001 (at the time termed *anterior heart field* or *secondary heart field*) that the clinical relevance of congenital heart defects was correlated to cells in this heart field—a big step in truly understanding heart development [7–9, 12]. The terms *anterior heart field* and *secondary heart field* are now considered to be a subpopulation of the SHF, a larger field of progenitor cells in pharyngeal mesoderm [12, 34]. The SHF is then contained within a larger field of multipotent cranial mesoderm (cardiocraniofacial field) that plays a critical role in development of both the arterial pole of the heart and craniofacial morphogenesis [12]. Specifically, the SHF (Figs. 3.1b and 3.2c) is located along the splanchnopleuric mesoderm (beneath the floor of the foregut) at the attachment site of the dorsal mesocardium [7–18]. During looping, the anterior SHF (previously termed *anterior heart field* or *secondary heart field*) cells undergo epithelial-to-myocardial transformation at the outflow (arterial) pole and add additional myocardial cells onto the then developing outflow tract, creating the great vessels (aorta and pulmonary trunk) and the right ventricle. This lengthening of the primary heart tube appears to be an important process for the proper alignment of the inflow and outflow tracts prior to septation. If this process does not occur normally, ventricular septal defects and malpositioning of the aorta may occur [30]. Recent evidence also indicates that the posterior SHF contributes to the inflow tract, creating parts of the left and right atria. Thus, the SHF contains two primary regions: (1) an anterior region or compartment that contributes to the outflow tract and (2) a posterior region or compartment that contributes to the inflow tract, as well as possibly the PEO [10, 15, 17, 35–37]. Defects in posterior SHF development result in conotruncal, atrial, and atrioventricular septal defects, major forms of congenital heart defects in humans [12].

By day 28 of human development, the chambers of the heart are in position and are demarcated by visible constrictions and expansions which denote the sinus venosus, common atrial chamber, atrioventricular sulcus, ventricular chamber, and conotruncus (proximal and distal outflow tract) [1, 30] (Fig. 3.4).

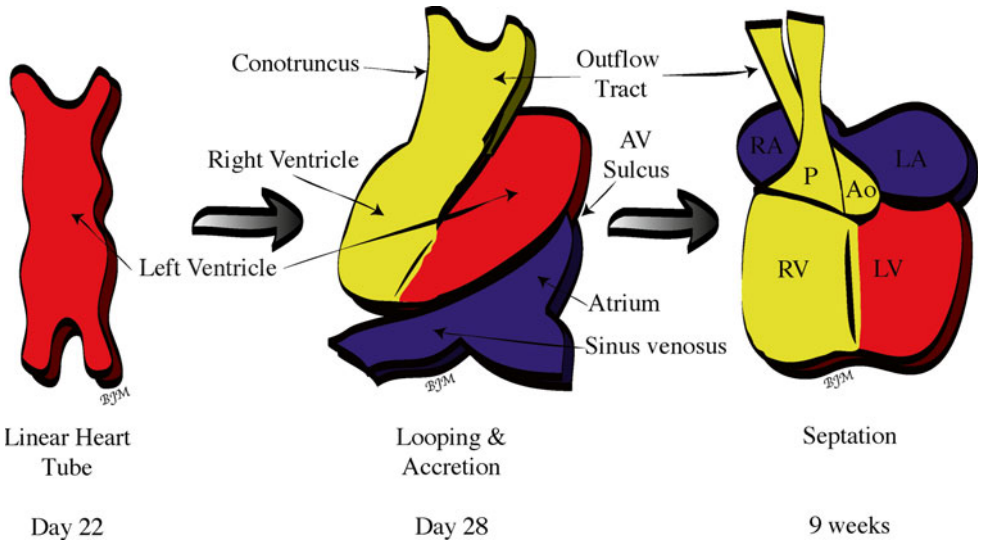

Fig. 3.4 Looping, accretion, and septation of the human primary linear heart tube. *Blue* (first heart field- and second heart field-derived cells) and *yellow* (second heart field-derived cells) regions represent tissue added during looping; *red* = first heart field-derived cells. *Ao* aorta, *AV* atrioventricular, *LA* left atrium, *LV* left ventricle, *P* pulmonary trunk, *RA* right atrium, *RV* right ventricle

3.4 Cardiac Neural Crest Contribution and Septation of the Outflow Tract and Ventricles

Once the chambers are in the correct position after looping, extensive remodeling of the primitive vasculature and septation of the heart can occur. The CNC is an extracardiac population of cells (from outside of the first or SHFs) that arise from the neural tube in the region of the first three somites up to the midotic placode level (rhombomeres 6, 7, and 8) (Fig. 3.5) [2, 38, 39]. CNC cells leave the neural tube during weeks 3–4 of human development and then migrate through aortic arches 3, 4, and 6 (Fig. 3.1b) and eventually into the developing outflow tract of the heart (during weeks 5–6). These cells are necessary for complete septation of the outflow tract and ventricles (completed by week 8 of human development), as well as the formation of the anterior parasympathetic plexus which contributes to cardiac innervation and regulation of heart rate [1, 2, 20, 38–42]. Recent evidence shows that CNC cells migrate to the venous pole of the heart as well and that their role is in the development of the parasympathetic innervation, the leaflets of the atrioventricular valves, and possibly the cardiac conduction system [43–45]. The primitive vasculature of the heart is bilaterally symmetrical but, during weeks 4–8 of human development, there is remodeling of the inflow end of the heart so that all systemic blood flows into the future right atrium [1]. In addition, there is also extensive remodeling of the initially bilaterally symmetrical aortic arch arteries into the great arteries (septation of the aortic and pulmonary vessels) that is dependent on the presence of the CNC [30, 46]. The distal outflow tract (truncus) septates into the aorta and pulmonary trunk via the fusion of two streams or prongs of CNC that migrate into the distal outflow tract. In contrast, the proximal outflow

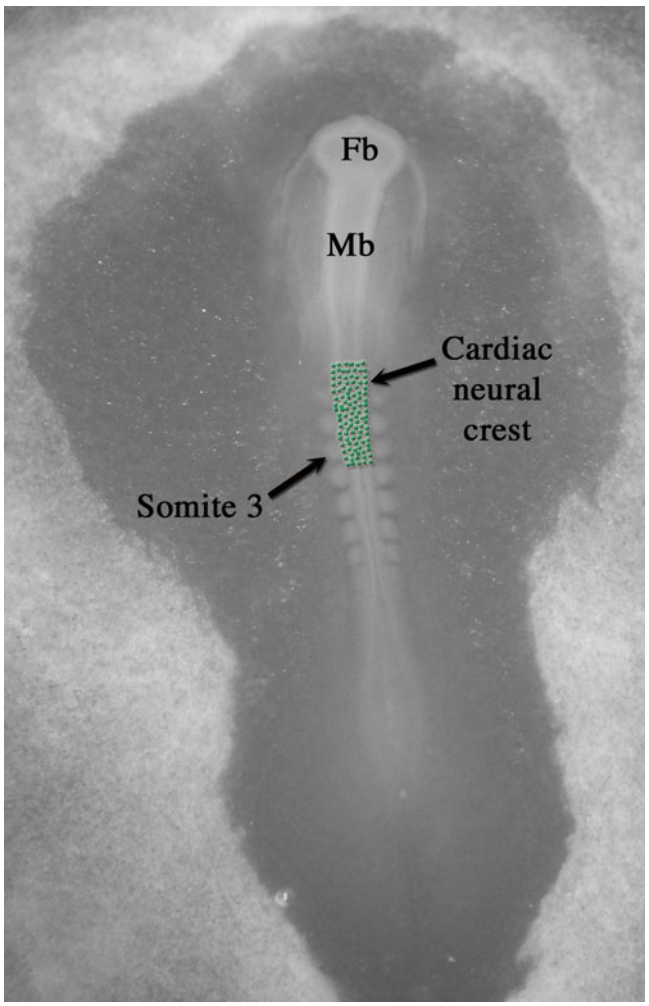

Fig. 3.5 Origin of the cardiac neural crest within a 34-h chick embryo. *Green dots* represent cardiac neural crest cells in the neural folds of hindbrain rhombomeres 6, 7, and 8 (the region of the first three somites up to the midotic placode level). *Fb* forebrain, *Mb* midbrain

tract septates by fusion of the endocardial cushions and eventually joins proximally with the atrioventricular endocardial cushion tissue and the ventricular septum [47, 48]. The endocardial cushions are formed by both atrioventricular canal and outflow tract endocardial cells that migrate into the cardiac jelly, forming bulges or cushions.

Despite its clinical importance, to this date, almost nothing is known about the molecular pathways that determine cell lineages in the CNC or regulate outflow tract septation [30, 49, 50]. However, it is known that if the CNC is removed before it begins to migrate, conotruncal septa completely fail to develop, and blood leaves both the ventricles through what is termed a *persistent truncus arteriosus*, a rare congenital heart anomaly that can be seen in humans [20, 40]. Failure of outflow tract septation may also be responsible for other forms of congenital heart disease including transposition of the great vessels, high ventricular septal defects, and tetralogy of Fallot [1, 20, 38, 40]. Additional information on these congenital defects can be found in Chap. 10.

The septation of the outflow tract (conotruncus) is tightly coordinated with the septation of the ventricles and atria to produce a functional heart [1, 51, 52]. All of these septa eventually fuse with the atrioventricular (AV) cushions that also divide the left and right AV canals and serve as a source of cells for the AV valves. Prior to septation, the right atrioventricular canal and right ventricle expand to the right, causing a realignment of the atria and ventricles so that they are directly over each other. This allows venous blood entering from the sinus venosus to flow directly from the right atrium to the presumptive right ventricle without flowing through the presumptive left atrium and ventricle [1, 30]. The new alignment also simultaneously provides the left ventricle with a direct outflow path to the truncus arteriosus and subsequently to the aorta.

Between weeks 4 and 7 of human development, the left and right atria undergo extensive remodeling and are eventually septated. Yet, during the septation process, a right-to-left shunting of oxygenated blood (oxygenated by the placenta) is created via a series of shunts, ducts, and foramens (Fig. 3.6). Prior to birth, the use of the pulmonary system is not necessary, but eventually a complete separation of the systemic and pulmonary circulatory systems will be required for normal cardiac and systemic function [1]. Initially, the right sinus horn is incorporated into the right posterior wall of the primitive atrium, and the trunk of the pulmonary venous system is incorporated into the posterior wall of the left atrium via a process called *intussusception*. At day 26 of human development, a crescent-shaped wedge of tissue called the septum primum begins to extend into the atrium from the mesenchyme of the dorsal mesocardium. As it grows, the septum primum diminishes the ostium primum, a foramen allowing the shunting of blood from the right to left atrium. However, programmed cell death near the superior edge of the septum primum creates a new foramen, the ostium secundum, which continues the right-to-left shunting

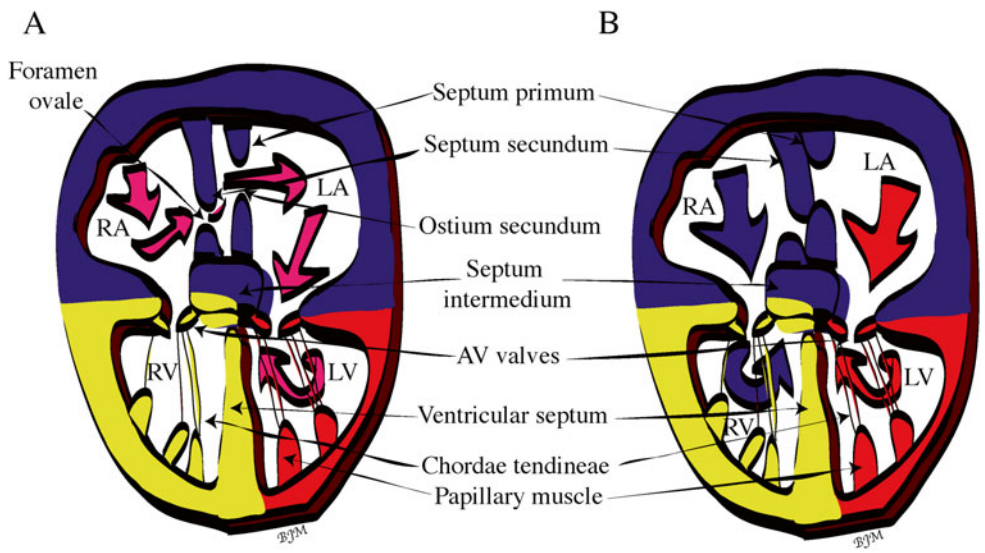

Fig. 3.6 Transition from fetal dependence on the placenta for oxygenated blood to self-oxygenation via the lungs. (**A**) Circulation in the fetal heart before birth. *Pink arrows* show right-to-left shunting of placentally oxygenated blood through the foramen ovale and ostium secundum. (**B**) Circulation in the infant heart after birth. The first breath of the infant and cessation of blood flow from the placenta cause final septation of the heart chambers (closure of the foramen ovale and ostium secundum) and thus separation of the pulmonary and systemic circulatory systems. *Blue arrows* show the pulmonary circulation and *red arrows* show the systemic circulation within the heart. Color code: *Blue* (first heart field- and second heart field-derived cells), *red* (first heart field-derived cells), and *yellow* (second heart field-derived cells). *AV* atrioventricular, *LA* left atrium, *LV* left ventricle, *RA* right atrium, *RV* right ventricle

of oxygenated blood. An incomplete, ridged septum secundum with a foramen ovale near the floor of the right atrium forms next to the septum primum, both of which fuse with the septum intermedium of the AV cushions [1]. At the same time as atrial septation is beginning, about the end of the fourth week of human development, the muscular ventricular septum begins to grow toward the septum intermedium (created by the fusion of the atrioventricular cushions), creating a partial ventricular septum. By the end of the ninth week of human development, the outflow tract septum has grown down onto the upper ridge of this muscular ventricular septum and onto the inferior endocardial cushion, completely separating the right and left ventricular chambers.

It is not until after birth, however, that the heart is functionally septated within the atrial region. At birth, dramatic changes in the circulatory system occur due to the transition from fetal dependence on the placenta for oxygenated blood to self-oxygenation via the lungs. More specifically, during fetal life, only small amounts of blood (about 5 % of the cardiac output) are flowing through the pulmonary system because the fluid-filled lungs create high flow resistance, resulting in low-volume flow into the left atrium from the pulmonary veins. This allows the high-volume blood flow coming from the placenta to pass through the inferior vena cava into the right atrium, where it is then directed across the foramen ovale into the left atrium. The oxygenated blood then flows into the left ventricle and directly out to the body of the fetus via the aorta. At birth, the umbilical blood flow is interrupted, stopping the high-volume flow from the placenta. In addition, the alveoli and pulmonary vessels open when the infant takes its first breath, dropping the resistance in the lungs and allowing more flow into the left atrium from the lungs. This reverse in pressure difference between the atria pushes the flexible septum primum against the ridged septum secundum and closes off the foramen ovale and ostium secundum, resulting in the complete septation of the heart chambers [1] (Fig. 3.6). For more information on defects and repairs of the foramen ovale, see Chap. 37.

3.5 Proepicardial Organ and Coronary Artery Development

The last major contributor to vertebrate heart development discussed in this chapter is the PEO [15, 21, 22]. Prior to heart looping, the primary heart tube consists of endocardium, cardiac jelly, and myocardium. It is not until the start of heart looping that epicardial cells from the PEO surround the myocardium, forming the fourth layer of the primary heart tube called the epicardium [15, 53] (Fig. 3.3). This population of cells will eventually give rise to the coronary vasculature. A neural crest origin of the coronary vessels was originally hypothesized, but recent lineage tracing studies have shown that the neural crest gives rise to cells of the tunica media of the aortic and pulmonary trunks but not the coronary arteries [29, 54]. These experiments eventually showed that the coronary vasculature is derived from the PEO, a nest of cells in the dorsal mesocardium of the sinus venosus or septum transversum. These cells, which are derived from an independent population of splanchnopleuric mesoderm cells, migrate onto the primary heart tube (Fig. 3.3) between days 22 and 28 of human development, just as the heart initiates looping [1, 30]. Prior to migration, these cells are collectively called the PEO (or proepicardium). Interestingly, three lineages of the coronary vessel cells (smooth muscle, endothelial, and connective tissue cells) are segregated in the PEO prior to migration into the heart tube [29, 55]. These cells will coalesce to form coronary vessels de novo via the process of vasculogenesis [56]. Recently, it has also been shown that the epicardium provides a factor needed for normal myocardial development and is a source of cells forming the interstitial myocardium and cushion mesenchyme [30, 36]. It is considered that understanding the embryological origin of the vascular system and its molecular regulation may help to explain the varying susceptibility of different components of the vascular system to atherosclerosis [29, 57]. Recently, it has also been suggested that epicardium-derived cells may provide a source of cells for myocardial regeneration after a myocardial infarction [22]. Lastly, among the different stem cell populations identified in the later heart, Isl1-positive cells may be a population of resident cardiovascular stem cells derived from residual SHF cells [12, 58, 59]. Thus, approaches aimed at cardiac repair by manipulation of cardiac progenitor cells will depend on properly understanding how lineage choices are regulated in the SHF and PEO [12, 60].

3.6 Cardiac Maturation

Although the embryonic heart is fully formed and functional by the 11th week of pregnancy, the fetal and neonatal heart continues to grow and mature rapidly, with many clinically relevant changes taking place after birth. During fetal development or from the time after the embryo is completely formed in the first trimester of pregnancy until birth, the heart grows primarily by the process of cell division [61–64]. Within a few weeks after birth, the predominant mechanism of cardiac growth is cell hypertrophy, so that most existing cardiac cells become larger, rather than increasing significantly in number [61–63]. The exact timing of this process and the mechanisms regulating this change are not yet completely elucidated. It has classically been thought that mature cardiac cells lose their ability to divide; however, recent work suggests that limited amounts of cell division do occur in adult hearts that have been damaged by ischemia [65–67].

This finding has led to a renewed interest in understanding the regulation of cell division during cardiac maturation. Additional maturational changes in the fetal and neonatal heart include (1) alterations in the composition of the cardiac myocytes, (2) differences in energy production, and/or (3) maturation of the contractile function. These changes, along with physiologic changes in the transitional circulation, as discussed earlier, significantly affect the treatment of newborns with congenital heart disease, particularly those requiring interventional procedures or cardiac surgery.

The hemodynamic changes associated with birth include significant increases in left ventricular cardiac output to meet the increased metabolic needs of the newborn infant. This improvement in cardiac output occurs despite the fact that the neonatal myocardium has less muscle mass and less cellular organization than the mature myocardium. The newborn myocardium consists of 30 % contractile proteins (mass) and 70 % noncontractile mass (membranes, connective tissues, and organelles). This is in contrast to the adult myocardium which is 60 % contractile mass [63]. The myocardial cells of the fetus are rounded, and both the myocardial cells and myofibrils within them are oriented randomly. As the fetal heart matures, these myofibrils increase in size and number and also orient themselves to the long axis of the rows of cells, which will likely contribute to improved myocardial function [61]. In general, the fetal myocardial cell contains higher amounts of glycogen than the mature myocardium, suggesting an increased dependence on glucose for energy production. In experiments using nonprimate model systems, the fetal myocardium is able to meet metabolic needs with lactate and glucose as the primary fuels [68]. In contrast, the preferred substrate for energy metabolism in the adult heart is long-chain fatty acids, although the adult heart is able to utilize carbohydrates as well [68, 69]. This change is presumably triggered in the first few days or weeks of life by an increase in serum long-chain fatty acids with feeding, yet the timing and clinical impact of this change in ill or nonfeeding neonates with cardiovascular disease remain unknown.

In addition to the changes described above, maturing myocardial cells undergo changes in their expression of many innate contractile proteins, which may be responsible for some of the maturational differences in cardiovascular function. For example, the gradual increase in expression of myosin light chain 2 (MLC 2) in the ventricle from the neonatal period through adolescence is considered to be important in humans. In the fetal ventricle, two myosin light chain forms, MLC 1 and MLC 2, are expressed in equal amounts [63, 70]; MLC 1 is associated with increased contractility and has been documented to increase contractility in isolated muscle from patients with tetralogy of Fallot [71]. After birth, there is a gradual increase in the amount of MLC 2 or the "regulatory" myosin light chain, which has a slower rate of force development, but can be phosphorylated to increase calcium-dependent force development in mature cardiac muscle [63, 72]. There is also variability in actin isoform expression during cardiac development. More specifically, the human fetal heart predominantly expresses cardiac alpha-actin, while the more mature human heart expresses skeletal alpha-actin [61, 73]. Furthermore, actin is responsible for interacting with myosin crossbridges and regulating ATPase activity; work done in the mouse model system suggests that the change to skeletal actin may be one of the mechanisms of enhanced contractility in the mature heart [61, 74, 75]. There are also developmental changes of potential functional significance in the regulatory proteins of the sarcomere. Initially, the fetal heart expresses both alpha- and beta-tropomyosin, a regulatory filament, in nearly equal amounts. After birth, the proportion of beta-tropomyosin decreases and alpha-tropomyosin increases, possibly optimizing diastolic relaxation [61, 76, 77]. In contrast, expression of high levels of beta-tropomyosin in the neonatal heart is associated with early death due to myocardial dysfunction [78]. Lastly, the isoform of the inhibitory troponin, troponin I, changes after birth. The fetal myocardium contains mostly the skeletal isoform of troponin I [61, 79]. After birth, the myocardium begins to express cardiac troponin I, and by approximately 9 months of age, only cardiac troponin I is present [61, 80, 81]. Importantly, cardiac troponin I can be phosphorylated to improve calcium-binding dynamics and contractility, which correlates with improved function in the more mature heart. It is thought that the skeletal form of troponin I may serve to protect the fetal and neonatal myocardium from acidosis [63, 74, 82]. The full impact of these developmental changes in contractile proteins and their effect on cardiac function or perioperative treatment of newborns with heart disease remain unclear at the present time.

Two of the most clinically relevant features of the immature myocardium are its requirement for high levels of extracellular calcium and a decreased sensitivity to beta-adrenergic inotropic agents. The neonatal heart has a decrease in both volume and amount of functionally mature sarcoplasmic reticulum, which is the intercellular storage site for calcium [61]. This paucity of intracellular calcium storage and release via the sarcoplasmic reticulum in the fetal and neonatal myocardium increases the requirement of the fetal myocardium for extracellular calcium, so that exogenous administration of calcium can be used to augment cardiac contractility in the appropriate clinical setting. In addition, neonates and infants are significantly more sensitive to calcium channel-blocking drugs than older children or adults and thus may be at risk for severe depression of myocardial contractility with the administration of these agents [61, 63, 83]. Lastly, although data in humans are limited, there appears to be significantly decreased sensitivity to beta-agonist agents in the immature myocardium and also in older children with con-

genital heart disease [63, 84–86]. This altered sensitivity may be due to: (1) a paucity of receptors, (2) sensitization to endogenous catecholamines at birth or with heart failure, or (3) some combination of these or additional factors. Due to this decreased responsiveness to beta-agonists, there are common requirements for higher doses of beta-agonist inotropic agents in newborns and infants. Note that alternative medications, including phosphodiesterase inhibitors, are often useful adjuncts to improve contractility in newborns with myocardial dysfunction [63].

Although the structure of the heart is complete in the first trimester of pregnancy, cardiac growth and maturation continue to occur in the fetus, newborn, and child. Many of these developmental changes, particularly decreased intracellular calcium stores in the immature sarcoplasmic reticulum and a decreased responsiveness to beta-agonist inotropic agents, significantly impact the care of newborns, infants, and children with congenital heart disease, particularly those requiring surgical intervention early in life.

3.7 Summary of Embryonic Contribution to Heart Development

The contribution of the four major embryonic regions to heart development—FHF, SHF, CNC, and PEO—illustrates the complexity of human heart development. Each of these regions has a unique contribution to the heart, but they ultimately depend on each other for the creation of a fully functional organ. Furthermore, a better understanding of the mechanisms of human heart development will provide clues to the etiology of congenital heart disease. The genetic regulatory mechanisms of these developmental processes are just beginning to be characterized. A molecular review of heart development is outside the scope of this chapter, but several informative molecular heart reviews have been recently published [6, 16, 30, 87, 88]. A better understanding of the embryological origins of the heart, combined with the characterization of the genes that control heart development, will likely lead to many new clinical applications to treat congenital and/or adult heart disease.

References

1. Schoenwolf GC, Bleyl BB, Brauer PR, Francis-West PH (eds) (2009) Larsen's human embryology, 4th edn. Churchill Livingstone Elsevier, Philadelphia
2. Martinsen BJ (2005) Reference guide to the stages of chick heart embryology. Dev Dyn 233:1217–1237
3. Srivastava D, Olson EN (2000) A genetic blueprint for cardiac development. Nature 407:221–226
4. Jensen B, Wang T, Christoffels VM, Moorman AFM (2013) Evolution and development of the building plan of the vertebrate heart. Biochim Biophys Acta 1833:783–794
5. Sperling SR (2011) Systems biology approaches to heart development and congenital heart disease. Cardiovasc Res 91:269–278
6. Fahed AC, Gelb BD, Seidman JG, Seidman CE (2013) Genetics of congenital heart disease: the glass half empty. Circ Res 112:707–720
7. Kelly RG, Brown NA, Buckingham ME (2001) The arterial pole of the mouse heart forms from Fgf10-expressing cells in pharyngeal mesoderm. Dev Cell 1:435–440
8. Mjaatvedt CH, Nakaoka T, Moreno-Rodriguez R et al (2001) The outflow tract of the heart is recruited from a novel heart-forming field. Dev Biol 238:97–109
9. Waldo KL, Kumiski DH, Wallis KT et al (2001) Conotruncal myocardium arises from a secondary heart field. Development 128:3179–3188
10. Xin M, Olson EN, Bassel-Duby R (2013) Mending broken hearts: cardiac development as a basis for adult heart regeneration and repair. Nat Rev Mol Cell Biol 14:529–541
11. Kodo K, Yamagishi H (2011) A decade of advances in the molecular embryology and genetics underlying congenital heart defects. Circ J 75:2296–2304
12. Kelly RG (2012) The second heart field. Curr Top Dev Biol 100:33–65
13. Van den Berg G, Abu-Issa R, de Boer BA et al (2009) A caudal proliferating growth center contributes to both poles of the forming heart tube. Circ Res 104:179–188
14. De Boer BA, van den Berg G, de Boer PAJ et al (2012) Growth of the developing mouse heart: an interactive qualitative and quantitative 3D atlas. Dev Biol 368:203–213
15. Brade T, Pane LS, Moretti A et al (2013) Embryonic heart progenitors and cardiogenesis. Cold Spring Harb Perspect Med 3:a013847
16. Lin CJ, Lin CY, Chen CH et al (2012) Partitioning the heart: mechanisms of cardiac septation and valve development. Development 139:3277–3299
17. Francou A, Saint-Michel E, Mesbah K et al (2013) Second heart field cardiac progenitor cells in the early mouse embryo. Biochim Biophys Acta 1833:795–798
18. Kelly RG, Buckingham ME (2002) The anterior heart-forming field: voyage to the arterial pole of the heart. Trends Genet 18:210–216
19. Degenhardt K, Singh MK, Epstein JA (2013) New approaches under development: cardiovascular embryology applied to heart disease. J Clin Invest 123:71–74
20. Keyte A, Hutson MR (2012) The neural crest in cardiac congenital anomalies. Differentiation 84:25–40
21. Pérez-Pomares JM, de la Pompa JL (2011) Signaling during epicardium and coronary vessel development. Circ Res 109:1429–1442
22. Smart N, Riley PR (2012) The epicardium as a candidate for heart regeneration. Future Cardiol 8:53–69
23. Hatada Y, Stern CD (1994) A fate map of the epiblast of the early chick embryo. Development 120:2879–2889
24. Yutzey KE, Kirby ML (2002) Wherefore heart thou? Embryonic origins of cardiogenic mesoderm. Dev Dyn 223:307–320
25. Garcia-Martinez V, Schoenwolf GC (1993) Primitive-streak origin of the cardiovascular system in avian embryos. Dev Biol 159:706–719
26. Psychoyos D, Stern CD (1996) Fates and migratory routes of primitive streak cells in the chick embryo. Development 122:1523–1534
27. DeHaan RL (1963) Organization of the cardiogenic plate in the early chick embryo. Acta Embryol Moprhol Exp 6:26–38
28. Ehrman LA, Yutzey KE (1999) Lack of regulation in the heart forming region of avian embryos. Dev Biol 207:163–175
29. Harvey RP, Rosenthal N (eds) (1999) Heart development, 1st edn. Academic, San Diego
30. Kirby ML (2002) Molecular embryogenesis of the heart. Pediatr Dev Pathol 23:537–544

31. Nandadasa S, Foulcer S, Apte SS (2014) The multiple, complex roles of versican and its proteolytic turnover by ADAMTS proteases during embryogenesis. Matrix Biol 35:34–41
32. Lohr JL, Yost HJ (2000) Vertebrate model systems in the study of early heart development: Xenopus and zebrafish. Am J Med Genet 97:248–257
33. De la Cruz MV, Sánchez Gómez C, Arteaga MM, Argüello C (1977) Experimental study of the development of the truncus and the conus in the chick embryo. J Anat 123:661–686
34. Dyer LA, Kirby ML (2009) The role of secondary heart field in cardiac development. Dev Biol 336:137–144
35. Kelly RG (2005) Molecular inroads into the anterior heart field. Trends Cardiovasc Med 15:51–56
36. Gittenberger-de Groot AC, Vrancken Peeters MP, Bergwerff M et al (2000) Epicardial outgrowth inhibition leads to compensatory mesothelial outflow tract collar and abnormal cardiac septation and coronary formation. Circ Res 87:969–971
37. Lie-Venema H, van den Akker NMS, Bax NAM et al (2007) Origin, fate, and function of epicardium-derived cells (EPDCs) in normal and abnormal cardiac development. Scientific World Journal 7:1777–1798
38. Kirby ML, Gale TF, Stewart DE (1983) Neural crest cells contribute to normal aorticopulmonary septation. Science 220:1059–1061
39. Kirby ML, Stewart DE (1983) Neural crest origin of cardiac ganglion cells in the chick embryo: identification and extirpation. Dev Biol 97:433–443
40. Kirby ML, Turnage KL, Hays BM (1985) Characterization of conotruncal malformations following ablation of “cardiac” neural crest. Anat Rec 213:87–93
41. O’Rahilly R, Müller F (2007) The development of the neural crest in the human. J Anat 211:335–351
42. Porras D, Brown CB (2008) Temporal-spatial ablation of neural crest in the mouse results in cardiovascular defects. Dev Dyn 237:153–162
43. Hildreth V, Webb S, Bradshaw L et al (2008) Cells migrating from the neural crest contribute to the innervation of the venous pole of the heart. J Anat 212:1–11
44. Poelmann RE, Jongbloed MRM, Molin DGM et al (2004) The neural crest is contiguous with the cardiac conduction system in the mouse embryo: a role in induction? Anat Embryol (Berl) 208:389–393
45. Poelmann RE, Gittenberger-de Groot AC (1999) A subpopulation of apoptosis-prone cardiac neural crest cells targets to the venous pole: multiple functions in heart development? Dev Biol 207:271–286
46. Bockman DE, Redmond ME, Kirby ML (1989) Alteration of early vascular development after ablation of cranial neural crest. Anat Rec 225:209–217
47. Waldo K, Miyagawa-Tomita S, Kumiski D, Kirby ML (1998) Cardiac neural crest cells provide new insight into septation of the cardiac outflow tract: aortic sac to ventricular septal closure. Dev Biol 196:129–144
48. Waldo KL, Lo CW, Kirby ML (1999) Connexin 43 expression reflects neural crest patterns during cardiovascular development. Dev Biol 208:307–323
49. Martinsen BJ, Groebner NJ, Frasier AJ, Lohr JL (2003) Expression of cardiac neural crest and heart genes isolated by modified differential display. Gene Expr Patterns 3:407–411
50. Martinsen BJ, Frasier AJ, Baker CVH, Lohr JL (2004) Cardiac neural crest ablation alters Id2 gene expression in the developing heart. Dev Biol 272:176–190
51. Anderson RH, Webb S, Brown NA et al (2003) Development of the heart: (2) Septation of the atriums and ventricles. Heart 89:949–958
52. Lamers WH, Moorman AFM (2002) Cardiac septation: a late contribution of the embryonic primary myocardium to heart morphogenesis. Circ Res 91:93–103
53. Komiyama M, Ito K, Shimada Y (1987) Origin and development of the epicardium in the mouse embryo. Anat Embryol (Berl) 176:183–189
54. Noden DM, Poelmann RE, Gittenberger-de Groot AC (1995) Cell origins and tissue boundaries during outflow tract development. Trends Cardiovasc Med 5:69–75
55. Mikawa T, Gourdie RG (1996) Pericardial mesoderm generates a population of coronary smooth muscle cells migrating into the heart along with ingrowth of the epicardial organ. Dev Biol 174:221–232
56. Noden DM (1990) Origins and assembly of avian embryonic blood vessels. Ann N Y Acad Sci 588:236–249
57. Hood LC, Rosenquist TH (1992) Coronary artery development in the chick: origin and deployment of smooth muscle cells, and the effects of neural crest ablation. Anat Rec 234:291–300
58. Bu L, Jiang X, Martin-Puig S et al (2009) Human ISL1 heart progenitors generate diverse multipotent cardiovascular cell lineages. Nature 460:113–117
59. Laugwitz K-L, Moretti A, Lam J et al (2005) Postnatal isl1+ cardioblasts enter fully differentiated cardiomyocyte lineages. Nature 433:647–653
60. Musunuru K, Domian IJ, Chien KR (2010) Stem cell models of cardiac development and disease. Annu Rev Cell Dev Biol 26:667–687
61. Anderson PAW (2000) Developmental cardiac physiology and myocardial function. In: Moller JH, Hoffman JIE (eds) Pediatric cardiovascular medicine. Churchill Livingstone, New York, pp 35–57
62. Huttenbach Y, Ostrowski ML, Thaller D, Kim HS (2001) Cell proliferation in the growing human heart: MIB-1 immunostaining in preterm and term infants at autopsy. Cardiovasc Pathol 10:119–123
63. Kern FH, Bengur AR, Bello EA (1996) Developmental cardiac physiology. In: Pediatric intensive care, 3rd edn. Lippincott, Williams and Wilkins, Baltimore, pp 397–423
64. Kim HD, Kim DJ, Lee IJ et al (1992) Human fetal heart development after mid-term: morphometry and ultrastructural study. J Mol Cell Cardiol 24:949–965
65. Beltrami AP, Urbanek K, Kajstura J et al (2001) Evidence that human cardiac myocytes divide after myocardial infarction. N Engl J Med 344:1750–1757
66. Anversa P, Leri A (2013) Innate regeneration in the aging heart: healing from within. Mayo Clin Proc 88:871–883
67. Rota M, Leri A, Anversa P (2014) Human heart failure: is cell therapy a valid option? Biochem Pharmacol 88:129–138
68. Vick GW, Fisher DA (1998) Cardiac metabolism. In: Garson A (ed) The science and practice of pediatric cardiology. Williams and Wilkens, Baltimore, pp 155–169
69. Opie LH (1991) Carbohydrates and lipids. In: Opie LH (ed) The heart: physiology and metabolism, 2nd edn. Raven, New York, pp 208–246
70. Price KM, Littler WA, Cummins P (1980) Human atrial and ventricular myosin light-chains subunits in the adult and during development. Biochem J 191:571–580
71. Morano M, Zacharzowski U, Maier M et al (1996) Regulation of human heart contractility by essential myosin light chain isoforms. J Clin Invest 98:467–473
72. Morano I (1999) Tuning the human heart molecular motors by myosin light chains. J Mol Med (Berl) 77:544–555
73. Boheler KR, Carrier L, de la Bastie D et al (1991) Skeletal actin mRNA increases in the human heart during ontogenic development and is the major isoform of control and failing adult hearts. J Clin Invest 88:323–330
74. Anderson PAW, Kleinman CS, Lister G, Talner N (1998) Cardiovascular function during normal fetal and neonatal development and with hypoxic stress. In: Polin RA, Fox WW (eds) Fetal and neonatal physiology, 2nd edn. Saunders, Philadelphia, pp 837–890

75. Hewett TE, Grupp IL, Grupp G, Robbins J (1994) Alpha-skeletal actin is associated with increased contractility in the mouse heart. Circ Res 74:740–746
76. Muthuchamy M, Grupp IL, Grupp G et al (1995) Molecular and physiological effects of overexpressing striated muscle beta-tropomyosin in the adult murine heart. J Biol Chem 270:30593–30603
77. Palmiter KA, Kitada Y, Muthuchamy M et al (1996) Exchange of beta- for alpha-tropomyosin in hearts of transgenic mice induces changes in thin filament response to Ca^{2+}, strong cross-bridge binding, and protein phosphorylation. J Biol Chem 271:11611–11614
78. Muthuchamy M, Boivin GP, Grupp IL, Wieczorek DF (1998) Beta-tropomyosin overexpression induces severe cardiac abnormalities. J Mol Cell Cardiol 30:1545–1557
79. Kim SH, Kim HS, Lee MM (2002) Re-expression of fetal troponin isoforms in the postinfarction failing heart of the rat. Circ J 66:959–964
80. Hunkeler NM, Kullman J, Murphy AM (1991) Troponin I isoform expression in human heart. Circ Res 69:1409–1414
81. Purcell IF, Bing W, Marston SB (1999) Functional analysis of human cardiac troponin by the in vitro motility assay: comparison of adult, foetal and failing hearts. Cardiovasc Res 43:884–891
82. Morimoto S, Goto T (2000) Role of troponin I isoform switching in determining the pH sensitivity of Ca(2+) regulation in developing rabbit cardiac muscle. Biochem Biophys Res Commun 267:912–917
83. Tanaka H, Sekine T, Nishimaru K, Shigenobu K (1998) Role of sarcoplasmic reticulum in myocardial contraction of neonatal and adult mice. Comp Biochem Physiol A Mol Integr Physiol 120:431–438
84. Buchhorn R, Hulpke-Wette M, Ruschewski W et al (2002) Beta-receptor downregulation in congenital heart disease: a risk factor for complications after surgical repair? Ann Thorac Surg 73:610–613
85. Schiffmann H, Flesch M, Häuseler C et al (2002) Effects of different inotropic interventions on myocardial function in the developing rabbit heart. Basic Res Cardiol 97:76–87
86. Sun LS (1999) Regulation of myocardial beta-adrenergic receptor function in adult and neonatal rabbits. Biol Neonate 76:181–192
87. Dees E, Baldwin HS (2002) New frontiers in molecular pediatric cardiology. Curr Opin Pediatr 14:627–633
88. McFadden DG, Olson EN (2002) Heart development: learning from mistakes. Curr Opin Genet Dev 12:328–335

Anatomy of the Thoracic Wall, Pulmonary Cavities, and Mediastinum

4

Mark S. Cook and Anthony J. Weinhaus

Abstract

This chapter will review the mediastinum and pulmonary cavities within the thorax and discuss their contents. The wall of the thorax and its associated muscles, nerves, and vessels will be covered in relationship to respiration. The surface anatomical landmarks that designate deeper anatomical structures and sites of access and auscultation will be reviewed. The goal of this chapter is to provide a complete picture of the thorax and its contents, with detailed anatomy of thoracic structures excluding the heart.

Keywords

Thorax • Cardiac anatomy • Thoracic wall • Superior mediastinum • Middle mediastinum • Anterior mediastinum • Posterior mediastinum • Pleura • Lungs

4.1 Introduction

The thorax is the body cavity, surrounded by the bony rib cage, that contains the heart and the lungs, the great vessels, the esophagus and trachea, the thoracic duct, and the autonomic innervation for these structures. The inferior boundary of the thoracic cavity is the respiratory diaphragm, which separates the thoracic and abdominal cavities. Superiorly, the thorax communicates with the root of the neck and the upper extremity. The wall of the thorax contains the muscles that assist with respiration and those connecting the upper extremity to the axial skeleton. The wall of the thorax is responsible for protecting the contents of the thoracic cavity and for generating the negative pressure required for respiration. The thorax is covered by muscle, superficial fascia containing the mammary tissue, and skin. A detailed description of cardiac anatomy is the subject of Chap. 5.

M.S. Cook, PT, PhD (✉) • A.J. Weinhaus, PhD
Program in Human Anatomy Education, Department of Integrative Biology and Physiology, University of Minnesota, 6-125 Jackson Hall, 321 Church St. SE, Minneapolis, MN 55455, USA
e-mail: cookx072@umn.edu

4.2 Overview of the Thorax

Anatomically, the thorax is typically divided into compartments—the pleural cavities and the mediastinum. The two pleural cavities contain the lungs and their pleural coverings. The space between the pleural cavities is the mediastinum, which contains all the other structures found in the thorax (Fig. 4.1). The mediastinum is divided into the superior and inferior compartments by a plane referred to as the *transverse thoracic plane*, passing through the mediastinum at the level of the sternal angle and the junction of the T4 and T5 vertebrae (Fig. 4.1). The superior mediastinum contains the major vessels supplying the upper extremity, the neck, and the head. The inferior mediastinum, the space between the transverse thoracic plane and the diaphragm, is further divided into the anterior, middle, and posterior mediastinum. The middle mediastinum is the space containing the heart and pericardium. The anterior mediastinum is the space between the pericardium and the sternum. The posterior mediastinum extends from the posterior pericardium to the posterior wall of the thorax.

The inferior aperture of the thorax is formed by the lower margin of the ribs and costal cartilages and is closed off from the abdomen by the respiratory diaphragm (Fig. 4.1).

P.A. Iaizzo (ed.), *Handbook of Cardiac Anatomy, Physiology, and Devices*, DOI 10.1007/978-3-319-19464-6_4

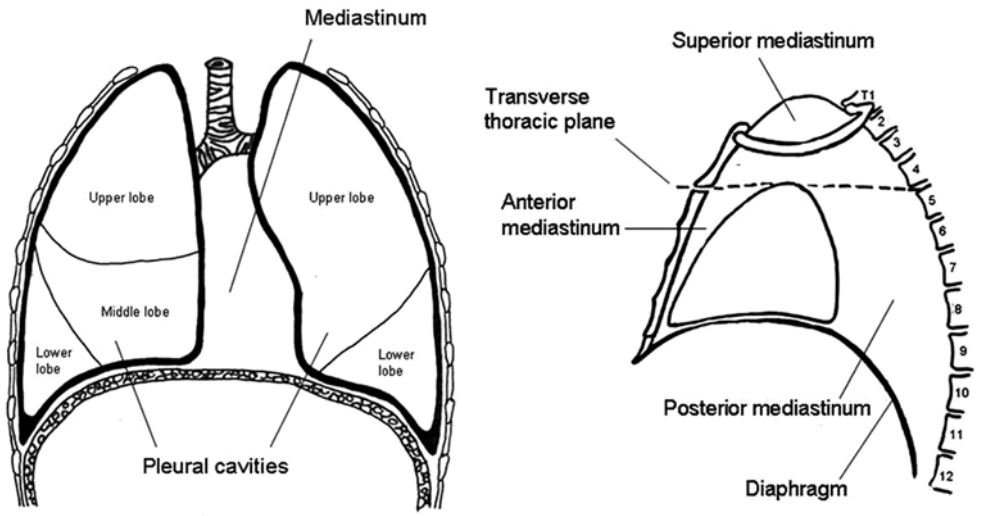

Fig. 4.1 The *left panel* is a diagrammatic representation of pulmonary cavities on each side of the thorax with the mediastinum in between. The *right panel* illustrates the divisions of the mediastinum. Figure adapted from Grant's Dissector, 12th edn. by EK Sauerland (Fig. 1.14, left; Fig. 1.24, right)

The superior aperture of the thorax leads to the neck and the upper extremity; it is formed by the first ribs and their articulation with the manubrium and first thoracic vertebra. The superior aperture of the thorax, or root of the neck, allows for the passage of structures between the neck and thoracic cavity. The clavicle crosses the first rib at its anterior edge close to its articulation with the manubrium. Structures exiting the superior thoracic aperture and communicating with the upper extremity pass between the first rib and clavicle. Anatomists often refer to the superior thoracic aperture as the *thoracic inlet* due to the entrance of air and food through the trachea and esophagus, respectively. However, clinicians may refer to the superior thoracic aperture as the *thoracic outlet* due to the fact that arteries and nerves leave the thorax through this area to enter the neck and upper extremities.

4.3 Bones of the Thoracic Wall

4.3.1 The Thoracic Cage

The skeleton of the thoracic wall is composed of the 12 pairs of ribs, the thoracic vertebra (and intervertebral disks), and the sternum. Articulating with the thorax are the bones of the pectoral girdle, the clavicle and the scapula (Fig. 4.2). Nerves and blood vessels entering the upper extremity pass between the clavicle and first rib.

The 12 thoracic vertebrae, which comprise the midline of the posterior wall of the thorax, articulate with the 12 pairs of ribs. Each thoracic vertebra has a body anteriorly and a neural arch which form a vertebral foramen. Extending from the neural arch posteriorly is an elongated, inferiorly slanting, spinous process and extending bilaterally are transverse processes. The transverse processes of thoracic vertebrae become progressively shorter from superior to inferior. The parts of the neural arch between the body and transverse processes are the *pedicles*, while the parts between the transverse processes and spinous process are the *laminae* (Fig. 4.3). Thoracic vertebrae have several articular surfaces, called *facets*. Superior and inferior articular facets form facet joints with vertebrae above and below, respectively. Costal facets are sites of articulation with ribs. Generally, each rib articulates with two adjacent vertebrae such that the head fits between adjacent bodies and the tubercle (slightly distal to the neck of the rib) articulates with the transverse process of the vertebra below. Therefore, a rib articulates with its corresponding thoracic vertebrae through the body and transverse process and with the vertebra above through its body. The articular surfaces on transverse processes are called *costal facets*, while those on the bodies, which generally share rib articulation with the vertebra above, are referred to as *costal demifacets*.

There are a few exceptions to this general relationship between thoracic vertebrae and ribs. The first thoracic vertebra shares the articulation with the second rib, but receives all of the articulation of the first rib superiorly. Ribs 10, 11, and 12 only articulate with their corresponding vertebrae.

The ribs form the largest part of the bony wall of the thorax (Fig. 4.2). Each rib articulates with one or two thoracic vertebrae, and the upper ten ribs articulate directly or indirectly with the sternum anteriorly. The upper seven ribs are referred to as *true* ribs because each connects to the sternum via its own costal cartilage. Ribs 8–10 are referred to as *false* ribs because they connect to the sternum (indirectly) by joining the articular cartilage of the seventh rib. Ribs 11 and 12

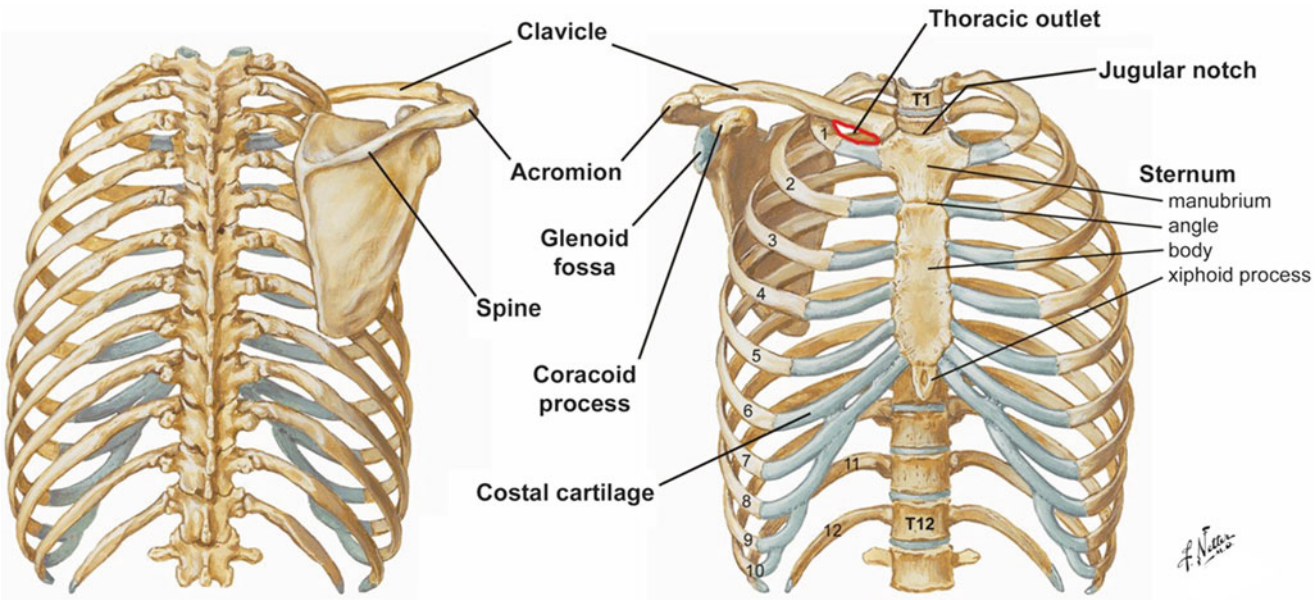

Fig. 4.2 The *left panel* illustrates the bones of the thorax from an anterior view. The *right panel* is a posterior view of the bony thorax. ©1998 Elsevier Inc. All rights reserved. www.netterimages.com, Frank Netter

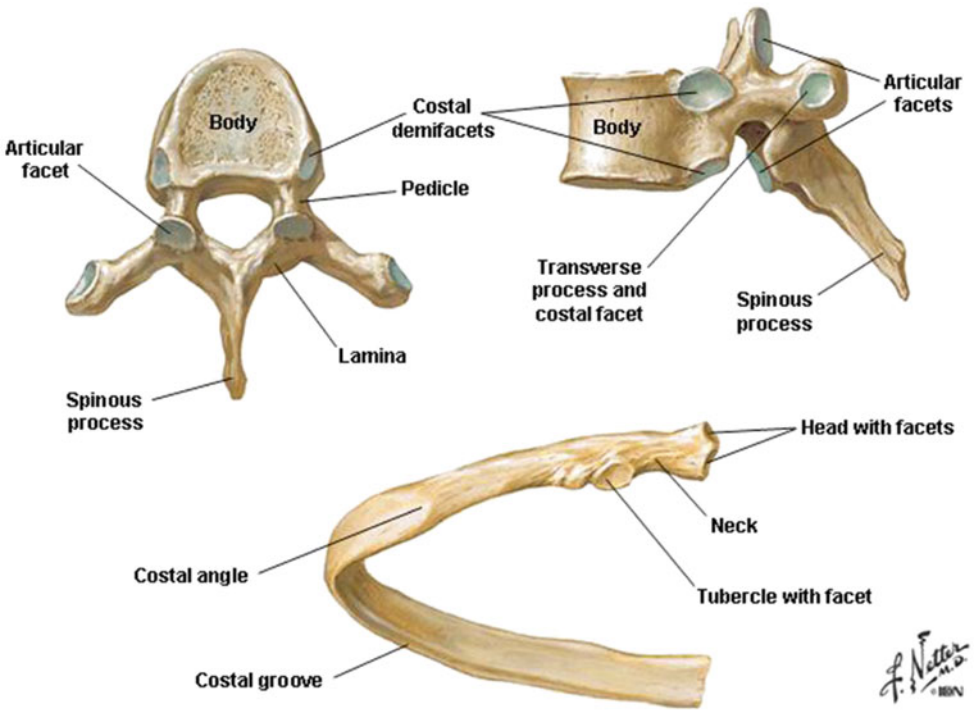

Fig. 4.3 The T6 vertebra as viewed from above (*upper left*) and laterally (*upper right*), and a typical rib (*lower*). ©1998 Elsevier Inc. All rights reserved. www.netterimages.com, Frank Netter

are referred to as *floating* ribs because they do not connect to the sternum, but end in the musculature of the abdominal wall. Each rib has a head that articulates with the thoracic vertebra and a relatively thin flat shaft that is curved (Fig. 4.3). The costal angle, the sharpest part of the curved shaft, is located where the rib turns anteriorly. At the inferior margin of the shaft, the internal surface of each rib is recessed to form a costal groove. This depression provides some protection to the intercostal neurovascular bundle, something that must be considered when designing devices for intercostal access to the thorax. The heads of ribs 2–9 have two articular facets for articulation with the vertebra of the same level and the vertebra above. The heads of ribs 1, 10, 11, and 12 only articulate with the vertebra of the same number and, consequently, have

only one articular facet. In ribs 1–10, the head is connected to the shaft by a narrowing called the *neck*. At the junction of the head and the neck is a tubercle that has an articular surface for articulation with the costal facet of the transverse process. Ribs 11 and 12 do not articulate with the transverse process of their respective vertebra and do not have a tubercle or, therefore, a defined neck portion.

The sternum is the flat bone making up the median anterior part of the thoracic cage (Fig. 4.2). It is composed of three parts—the manubrium, body, and xiphoid process. The manubrium (from the Latin word for *handle*, like the handle of a sword) is the superior part of the sternum; it is the widest and thickest part of the sternum. The manubrium alone articulates with the clavicle and the first rib. The sternal heads of the clavicle can be readily seen and palpated at their junction with the manubrium. The depression between the sternal heads of the clavicle above the manubrium is the suprasternal, or jugular, notch. The manubrium and the body of the sternum lie in slightly different planes and thus form a noticeable and easily palpated angle, the sternal angle (of Louis), at the point where they meet. The second rib articulates with the body of the sternum and the manubrium at the sternal angle. The body of the sternum is formed from the fusion of segmental bones (the sternebrae). The remnants of this fusion may be seen in the transverse ridges of the sternal body, especially in young people. The third through sixth ribs articulate with the body of the sternum, and the seventh rib articulates at the junction of the body and xiphoid process. The xiphoid process is the inferior-most part of the sternum and is easily palpated. It lies at the level of T9–T10 vertebrae and marks the inferior boundary of the thoracic cavity anteriorly. It also lies at the level even with the central tendon of the diaphragm and the inferior border of the heart. When a median sternotomy is performed on a patient, typically a sternal saw is used to cut through the manubrium, the sternal body, and the xiphoid process. For more details, refer to Chap. 33.

4.3.2 The Pectoral Girdle

Many of the muscles encountered on the wall of the anterior thorax are attached to the bones of the pectoral girdle and the upper extremity. Since movement of these bones can impact the anatomy of vascular structures communicating between the thorax and upper extremity, it is important to include these structures in a discussion of the thorax.

The clavicle is a somewhat "S"-shaped bone that articulates at its medial end with the manubrium of the sternum and at its lateral end with the acromion of the scapula (Fig. 4.2). It is convex medially and concave laterally. The scapula is a flat triangular bone, slightly concave anteriorly, that rests upon the posterior thoracic wall. It has a raised ridge posteriorly called the *spine* that ends in a projection of bone called the *acromion* that articulates with the clavicle. The coracoid process is an anterior projection of bone from the superior border of the clavicle that serves as an attachment point for muscles that act on the scapula and upper extremity. The head of the humerus articulates with the shallow glenoid fossa of the scapula forming the glenohumeral joint. The clavicle serves as a strut to hold the scapula in position away from the lateral aspect of the thorax. It is a highly mobile bone, with a high degree of freedom at the sternoclavicular joint that facilitates movement of the shoulder girdle against the thorax. The anterior extrinsic muscles of the shoulder pass from the wall of the thorax to the bones of the shoulder girdle.

4.4 Muscles of the Thoracic Wall

4.4.1 The Pectoral Muscles

Several muscles of the thoracic wall, including the most superficial ones that create some of the contours of the thoracic wall, are muscles that act upon the upper extremity. Some of these muscles form important surface landmarks on the thorax, and others have relationships to vessels that communicate with the thorax. In addition to moving the upper extremity, some of these muscles also can play a role in movement of the thoracic wall and participate in respiration. The pectoralis major muscle forms the surface contour of the upper lateral part of the thoracic wall (Fig. 4.4). It originates on the clavicle (clavicular head), the sternum, and ribs (sternocostal head), and inserts near the greater tubercle of the humerus. The lower margin of this muscle, passing from the thorax to the humerus, forms the major part of the anterior axillary fold. The pectoralis major muscle is a powerful adductor and medial rotator of the arm.

The pectoralis minor muscle is a much smaller muscle and lies immediately deep to the pectoralis major muscle (Fig. 4.4). It originates on ribs 3–5 and inserts upon the coracoid process of the scapula. This muscle forms part of the anterior axillary fold medially. It acts to depress and stabilize the scapula when upward force is exerted on the shoulder.

The anterior part of the deltoid muscle also forms a small aspect of the anterior thoracic wall. This muscle has its origin on the lateral part of the clavicle and the acromion and spine of the scapula (Fig. 4.4). It inserts upon the deltoid tubercle of the humerus and is the most powerful abductor of the arm. The anterior deltoid muscle borders the superior aspect of the pectoralis major muscle. The depression found at the junction of these two muscles is called the *deltopectoral groove*. Importantly, within this groove, the cephalic vein can consistently be found. The muscles diverge at their origins on the clavicle, creating an opening bordered by these two muscles

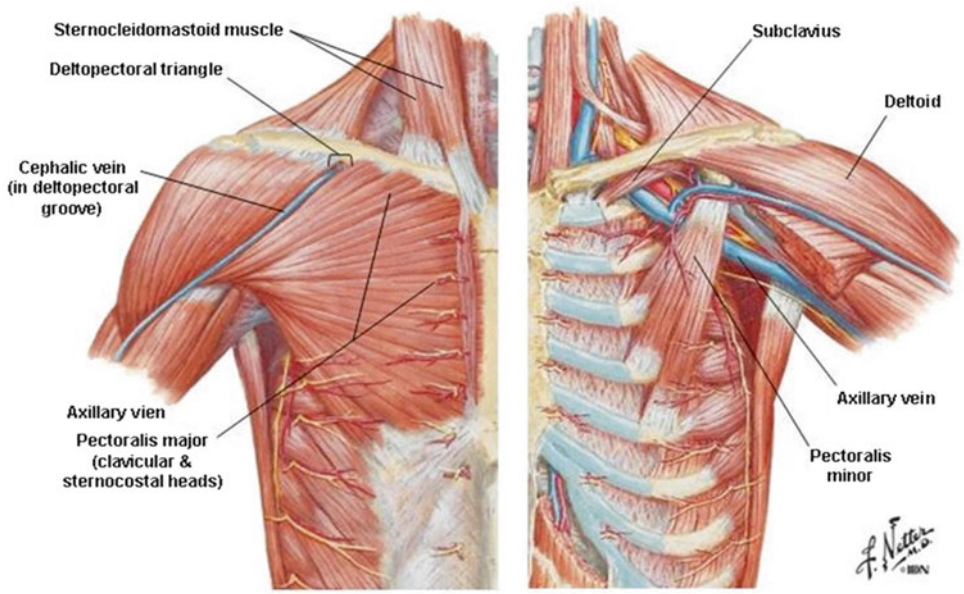

Fig. 4.4 The musculature of the anterior thoracic wall. The *left panel* shows the superficial muscles intact. The *left panel* shows structures deep to the pectoralis major muscle. ©1998 Elsevier Inc. All rights reserved. www.netterimages.com, Frank Netter

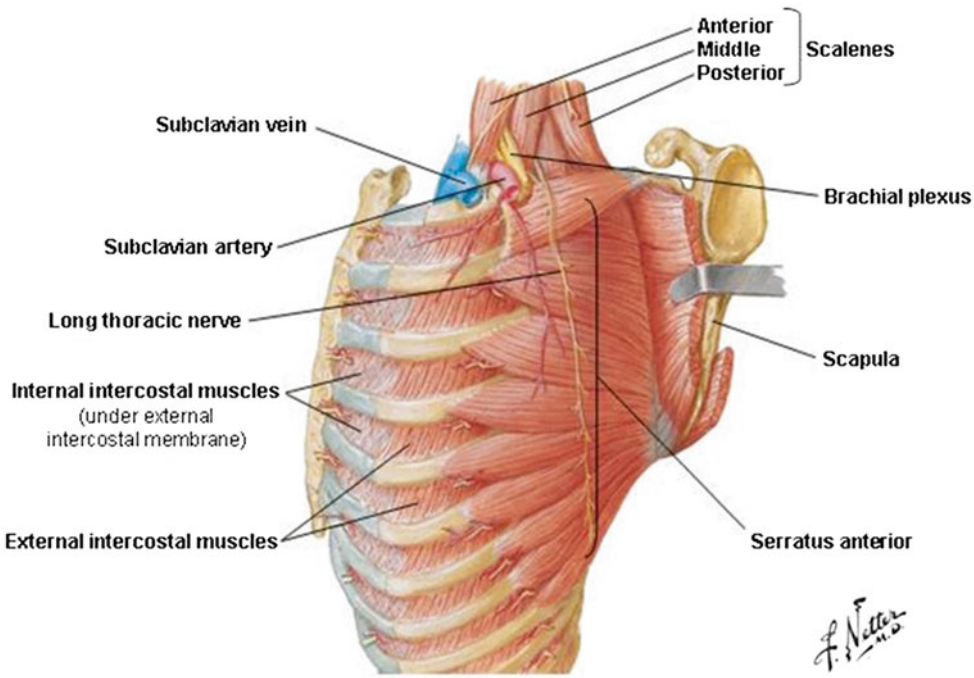

Fig. 4.5 A lateral view of the musculature of the thoracic wall. ©1998 Elsevier Inc. All rights reserved. www.netterimages.com, Frank Netter

and the clavicle known as the *deltopectoral triangle*. Through this space the cephalic vein passes to join the axillary vein.

The subclavius is a small muscle originating on the lateral inferior aspect of the clavicle and inserting on the sternal end of the first rib (Fig. 4.4). This muscle depresses the clavicle and exerts a medial traction on the clavicle that stabilizes the sternoclavicular joint. In addition to these actions, the subclavius muscle provides a soft surface on the inferior aspect of the clavicle that serves to cushion the contact of this bone with structures passing under the clavicle (i.e., nerves of the brachial plexus and the subclavian artery) when the clavicle is depressed during movement of the shoulder girdle and especially when the clavicle is fractured.

The serratus anterior muscle originates on the lateral aspect of the first eight ribs and inserts upon the medial aspect of the scapula (Fig. 4.5). This muscle forms the *serrated* contour of the lateral thoracic wall in individuals with good muscle definition. The serratus anterior forms the medial border of the axilla and acts to pull the scapula forward (protraction) and to stabilize the scapula against a posterior force on the shoulder; it also assists with cranial rotation of the scapula with elevation.

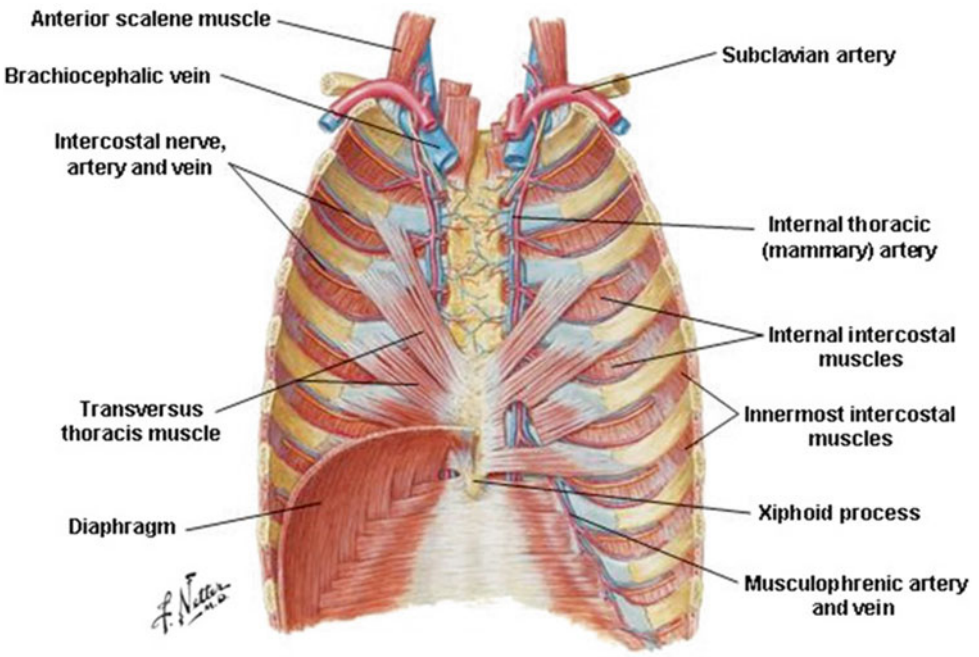

Fig. 4.6 The deep musculature of the anterior thoracic wall viewed from the posterior side. ©1998 Elsevier Inc. All rights reserved. www.netterimages.com, Frank Netter

4.4.2 The Intercostal Muscles

Each rib is connected to the one above and below by a series of three intercostal muscles. The external intercostal muscles are the most superficial (Fig. 4.5). These muscles course in an obliquely medial direction as they pass from superior to inferior between the ribs. Near the anterior end of the ribs, the external intercostal muscle fibers are replaced by the external intercostal membrane. Deep to the external intercostals are the internal intercostals (Figs. 4.5 and 4.6). The direction of the internal intercostal muscle fibers is perpendicular to the external intercostals. Near the posterior end of the ribs, the internal intercostal muscle fibers are replaced by the internal intercostal membrane. The deepest layer of intercostal muscle is the innermost intercostal muscle (Fig. 4.6). These muscles have a fiber direction similar to the internal intercostals, but they form a separate plane. The innermost intercostal muscles become membranous near the anterior and posterior ends of the ribs. The intercostal nerves and vessels pass between the internal and innermost intercostal muscles, which help to distinguish between the two muscular layers. There are two additional sets of muscles in the same plane as the innermost intercostals—the subcostals and the transversus thoracic muscles. The subcostal muscles are located posteriorly and span more than one rib. The transversus thoracic muscles are found anteriorly and pass from the internal surface of the sternum to ribs 2–6, extending superiorly and laterally (Fig. 4.6).

The intercostal muscles, especially the external and internal intercostals, are involved with respiration by elevating or depressing the ribs. The external intercostal muscles and the anterior interchondral part of the internal intercostals act to elevate the ribs. The interosseous parts of the internal intercostal muscles depress the ribs. The innermost intercostals likely have an action similar to the internal intercostals. The subcostal muscles probably help to elevate the ribs. The action of transversus thoracis is not well understood. It may, by virtue of its attachments, help to depress the ribs with forced exhalation or play a role in proprioception. In so-called less or minimally invasive surgical procedures performed to gain access to the heart, one needs to transect through the intercostal muscles (see Chap. 35).

4.4.3 Respiratory Diaphragm

The respiratory diaphragm is the musculotendinous sheet separating the abdominal and thoracic cavities (Figs. 4.6 and 4.7). It is considered the primary muscle of respiration. The diaphragm originates along the inferior border of the rib cage, the xiphoid process of the sternum, the posterior abdominal wall, and the upper lumbar vertebra. The medial and lateral arcuate ligaments are thickenings of the investing fascia over the quadratus lumborum (lateral) and the psoas major (medial) muscles of the posterior abdominal wall that serve as attachments for the diaphragm (Fig. 4.7). The right and left crura of the diaphragm attach to lumbar vertebrae. They originate on the bodies of lumbar vertebrae 1–3, their intervertebral disks, and the anterior longitudinal ligament spanning these vertebrae. The diaphragm ascends from its origin to form a right and left dome, the right dome being typically higher than the left. The muscular part of the

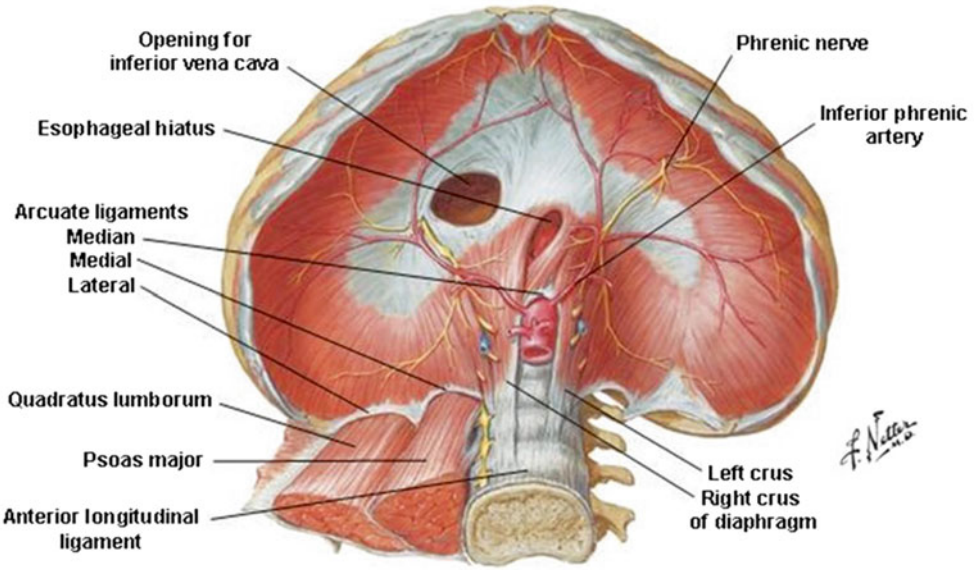

Fig. 4.7 The abdominal side of the respiratory diaphragm illustrating the origins of the muscle. ©1998 Elsevier Inc. All rights reserved. www.netterimages.com, Frank Netter

diaphragm is dome-shaped at rest. Contraction (during inhalation) causes the dome of the diaphragm to flatten (downward), increasing the volume of the thoracic cavity. The aponeurotic central part of the diaphragm, called the *central tendon*, contains the opening for the inferior vena cava (Fig. 4.7). The esophagus also passes through the diaphragm, and the hiatus for the esophagus is created by a muscular slip originating from the right crus of the diaphragm. The aorta passes from the thorax to the abdomen behind the diaphragm, under the median arcuate ligament created by the intermingling of fibers from the right and left crura of the diaphragm. The inferior vena cava, esophagus, and aorta pass from the thorax to the abdomen at thoracic vertebral levels 8, 10, and 12, respectively.

4.4.4 Other Muscles of Respiration

The scalene muscles and the sternocleidomastoid muscle in the neck also contribute to respiration, especially during deep inhalation (Figs. 4.4 and 4.5). Collectively, the scalene muscles have their origin on the transverse processes of cervical vertebra 2–7. The anterior and middle scalenes insert on the first rib and the posterior scalene on the second rib. As its name suggests, the sternocleidomastoid originates on the sternum and medial clavicle and inserts on the mastoid process of the skull. Although the primary action of sternocleidomastoid is on the head and neck, it is also capable of exerting an upward force on the thorax with forced respiration. The muscles of the anterior abdominal wall are also involved with respiration. These muscles, the rectus abdominis, external and internal abdominal obliques, and the transverses abdominis, act together during forced exhalation to depress the rib cage and to increase intra-abdominal pressure forcing the diaphragm to expand upward, reducing the volume of the pulmonary cavities. The mechanics of respiration are explained in detail in Sect. 4.11.2.

4.5 Nerves of the Thoracic Wall

The wall of the thorax receives its innervation from intercostal nerves (Fig. 4.8). These nerves are the ventral rami of segmental nerves, leaving the spinal cord at the thoracic vertebral levels. Intercostal nerves are mixed nerves, carrying both somatic motor and sensory fibers, as well as autonomics to the skin. The intercostal nerves pass out of the intervertebral foramina and run inferior to the ribs. As they reach the costal angle, the nerves pass between the innermost and the internal intercostal muscles. The motor innervation to all the intercostal muscles comes from the intercostal nerves. These nerves give off lateral and anterior cutaneous branches that provide cutaneous sensory innervation to the skin of the thorax (Fig. 4.8). The intercostal nerves also carry sympathetic nerve fibers to the sweat glands, smooth muscle, and blood vessels. However, the first two intercostal nerves are considered atypical. The first intercostal nerve divides shortly after it emerges from the intervertebral foramen. The larger superior part of this nerve joins the brachial plexus to provide innervation to the upper extremity. The lateral cutaneous branch of the second intercostal nerve is large and typically pierces the serratus anterior muscle to provide sensory innervation to the floor of the axilla and medial aspect of the arm. The nerve associated with the 12th rib is the subcostal nerve and, since there is no rib below this level, is considered a nerve of the abdominal wall.

The pectoral muscles receive motor innervation from branches of the brachial plexus of nerves (derived from

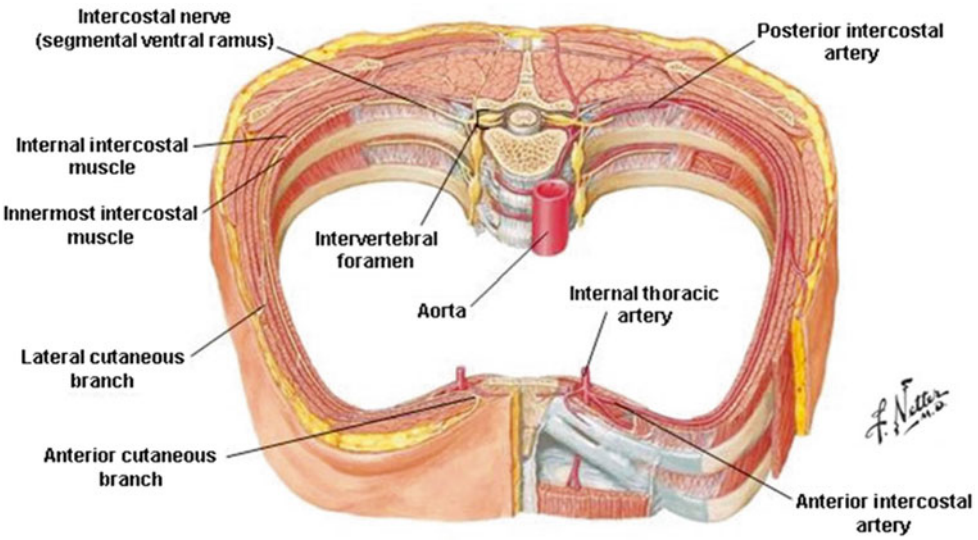

Fig. 4.8 A typical set of intercostals arteries and nerves. ©1998 Elsevier Inc. All rights reserved. www.netterimages.com, Frank Netter

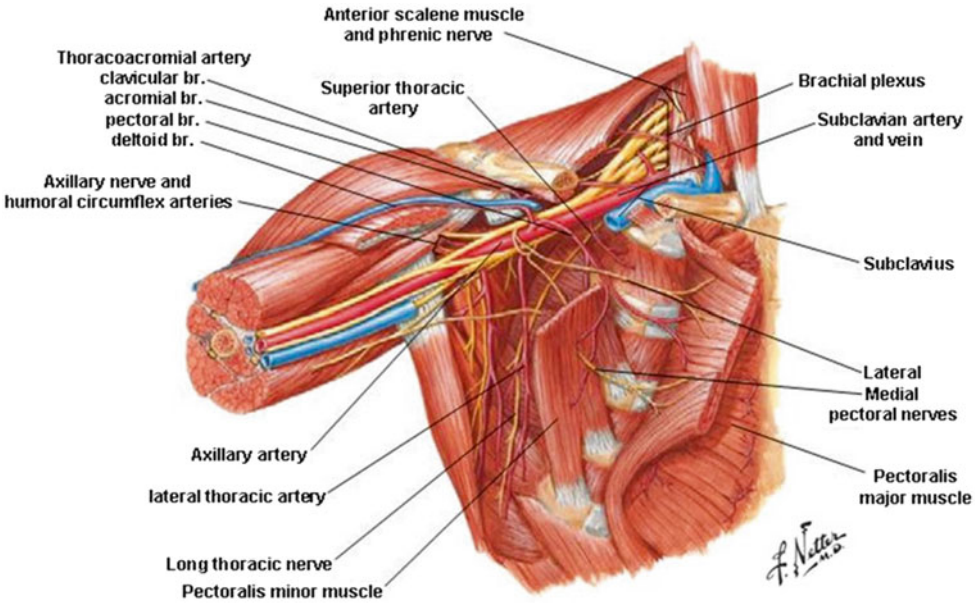

Fig. 4.9 The nerves and arteries of the axilla viewed with the pectoralis major and minor muscles reflected. ©1998 Elsevier Inc. All rights reserved. www.netterimages.com, Frank Netter

cervical levels 5–8 and thoracic level 1) which supply the muscles of the shoulder and upper extremity. The lateral and medial pectoral nerves, branches of the lateral and medial cords of the brachial plexus, supply the pectoralis major and minor muscles (Fig. 4.9). The pectoralis major muscle is innervated by both nerves and the pectoralis minor muscle by only the medial pectoral nerve, which pierces this muscle before entering the pectoralis major. The serratus anterior muscle is innervated by the long thoracic nerve which originates from ventral rami of C5, C6, and C7 (Figs. 4.5 and 4.9). The deltoid muscle is innervated by the axillary nerve, a branch of the posterior cord of the brachial plexus (Fig. 4.9). Finally, the subclavius muscle is innervated by its own nerve from the superior trunk of the brachial plexus.

4.6 Vessels of the Thoracic Wall

The intercostal muscles and the skin of the thorax receive their blood supply from both the intercostal arteries and the internal thoracic artery (Figs. 4.6 and 4.8). Intercostal arteries 3–11 (and the subcostal artery) are branches directly from the thoracic descending aorta. The first two intercostal arteries are branches of the supreme intercostal artery, which is a branch of the costocervical trunk from the subclavian artery. The posterior intercostals run with the intercostal nerve and pass with the nerve between the innermost and internal intercostal muscles. The intercostals then anastomose with anterior intercostal branches arising from the internal thoracic artery descending lateral to the sternum. The internal thoracic arteries are anterior branches from the subclavian

arteries. The anterior and posterior intercostals anastomoses create an anastomotic network around the thoracic wall. The intercostal arteries are accompanied by intercostal veins (Fig. 4.6). These veins drain to the azygos system of veins in the posterior mediastinum. The anatomy of the azygos venous system is described in detail in Sect. 4.10.2. Anteriorly, the intercostal veins drain to the internal thoracic veins which, in turn, drain to the subclavian veins in the superior mediastinum (Fig. 4.7).

The intercostal nerves, arteries, and veins run together in each intercostal space, just inferior to each rib. They are characteristically found in this order (vein, artery, and nerve) with the vein closest to the rib.

The diaphragm receives blood from the musculophrenic arteries and terminal branches of the internal thoracic arteries, which runs along the anterior superior surface of the diaphragm (Fig. 4.6). There is also a substantial blood supply to the inferior aspect of the diaphragm from the inferior phrenic arteries, the superior-most branches from the abdominal aorta that branch along the inferior surface of the diaphragm (Fig. 4.7).

The muscles of the pectoral region get their blood supply from branches of the axillary artery. This artery is the continuation of the subclavian artery emerging from the thorax and passing under the clavicle (Fig. 4.9). The first branch of the axillary artery, the superior (supreme) thoracic artery, supplies blood to the first two intercostal spaces. The second branch forms the thoracoacromial artery or trunk. Subsequently, this artery gives rise to four branches (pectoral, deltoid, clavicular, acromial) that supply blood to the pectoral muscles, the deltoid muscle, the clavicle, and the subclavius muscle. The lateral thoracic artery, the third branch from the subclavian artery, participates along with the intercostal arteries in supplying the serratus anterior muscle. Additional distal branches from the axillary artery, the humeral circumflex arteries, also participate in blood supply to the deltoid muscle. Venous blood returns through veins of the same names to the axillary vein.

4.7 The Superior Mediastinum

The superior mediastinum is the space behind the manubrium of the sternum (Fig. 4.1). It is bounded by parietal (mediastinal) pleura on each side and the first four thoracic vertebrae behind. It is continuous with the root of the neck at the top of the first ribs and with the inferior mediastinum below the transverse thoracic plane, a horizontal plane that passes from the sternal angle through the space between the T4 and T5 vertebrae. The superior mediastinum contains several important structures including the branches of the aortic arch, the veins that coalesce to form the superior vena cava, the trachea, the esophagus, the vagus and phrenic nerves, the cardiac plexus of autonomic nerves, the thoracic duct, and the thymus (Fig. 4.10).

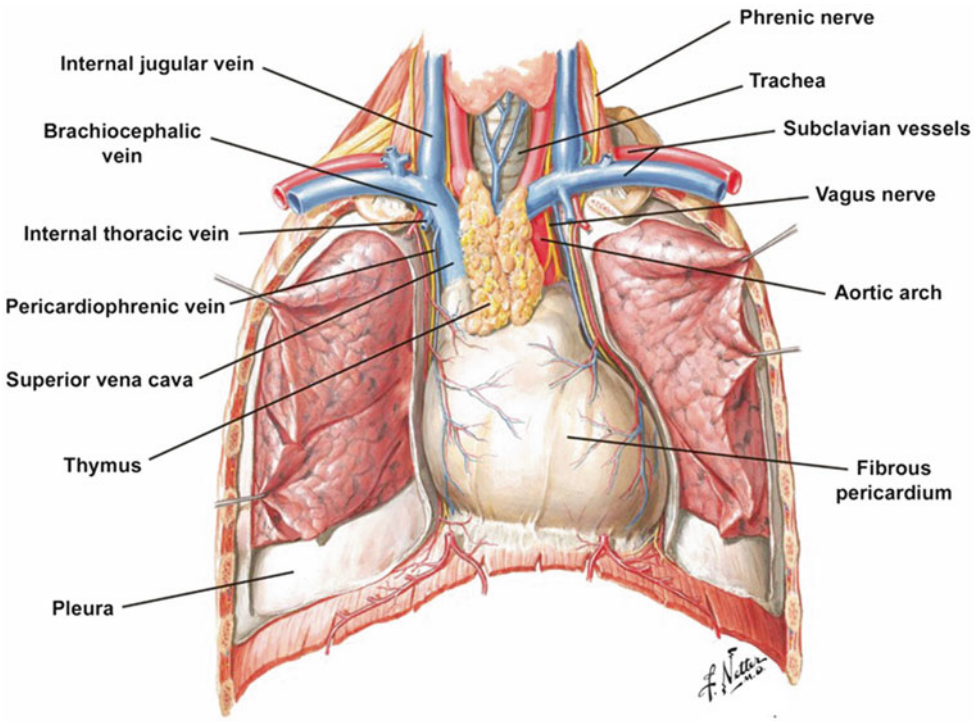

Fig. 4.10 Contents of the superior and middle mediastinum. ©1998 Elsevier Inc. All rights reserved. www.netterimages.com, Frank Netter

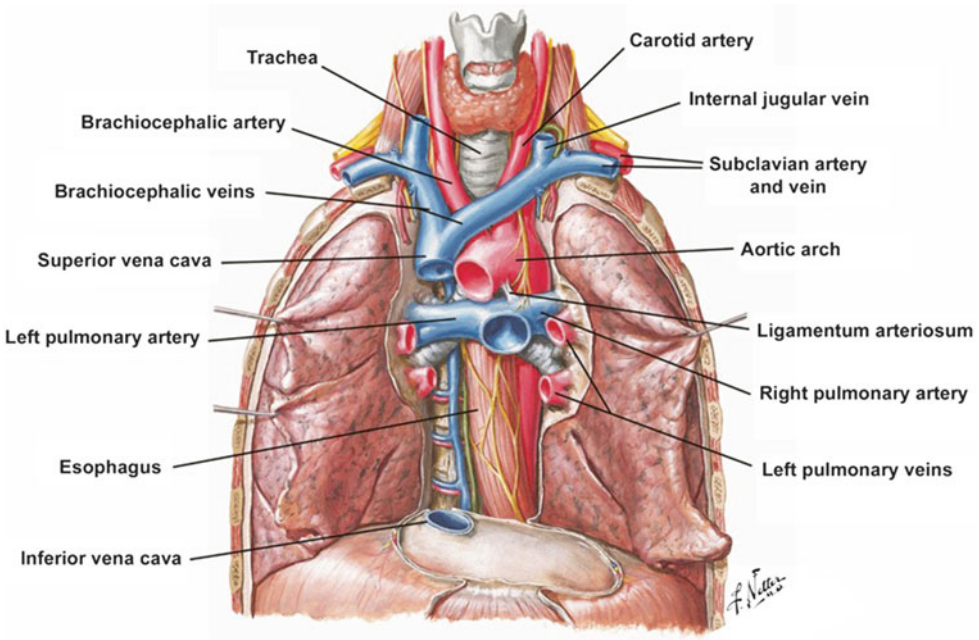

Fig. 4.11 Vessels of the superior and middle mediastinum. ©1998 Elsevier Inc. All rights reserved. www.netterimages.com, Frank Netter

4.7.1 Arteries in the Superior Mediastinum

As the aorta emerges from the pericardial sac, it begins to arch posteriorly and to the left (Fig. 4.11). At the level of the T4 vertebra, the aorta has become vertical again, descending through the posterior mediastinum. The aortic arch passes over the right pulmonary artery and ends by passing posterior to the left pulmonary artery. The trachea and esophagus pass posterior and to the right of the aortic arch. The arch of the aorta gives off the major arteries that supply blood to the head and to the upper extremity. This branching is asymmetrical. The first (from the right) and most anterior branch from the aorta is the brachiocephalic trunk. This arterial trunk bends toward the right as it ascends, and as it reaches the upper limit of the superior mediastinum, it bifurcates into the right common carotid and right subclavian arteries. The next two branches from the aortic arch are the left common carotid and the left subclavian arteries. These two arteries ascend almost vertically to the left of the trachea. The common carotid arteries will supply the majority of the blood to the head and neck. The subclavian arteries continue as the axillary and brachial arteries and supply the upper extremity. The arch of the aorta and its branches make contact with the upper lobe of the right lung, and their impressions are normally seen on the fixed lung after removal. Neither the brachiocephalic trunk, left common carotid, nor the left subclavian gives off consistent branches in the superior mediastinum. However, the subclavian arteries at the root of the neck give off the internal thoracic arteries which reenter the superior mediastinum and descend along each side of the sternum. On occasion there will be an artery branching from either the aortic arch, the right common carotid, or one of the subclavian arteries, and supplying the thyroid gland in the midline. This variant artery is called a *thyroid ima*. Since this artery is often found crossing the region where a tracheostomy is performed, it is important to remember that this artery is present in ~10 % of individuals.

4.7.2 Brachiocephalic Veins

The bilateral brachiocephalic veins are formed by the merging of the internal jugular vein and the subclavian vein on both sides at the base of the neck (Figs. 4.10 and 4.11). The right brachiocephalic vein descends nearly vertically, while the left crosses obliquely behind the manubrium to join the right and form the superior vena cava. The superior vena cava continues inferiorly into the pericardial sac. The brachiocephalic veins run anteriorly in the superior mediastinum. The left brachiocephalic vein passes anterior to the three branches of the aortic arch and is separated from the manubrium only by the thymus gland (Fig. 4.10). The brachiocephalic veins receive blood from the internal thoracic veins, the inferior thyroid veins, and the small pericardiacophrenic veins. They also receive blood from the superior intercostal veins from behind.

4.7.3 The Trachea and Esophagus

The trachea is a largely cartilaginous tube that runs from the larynx inferiorly through the superior mediastinum and ends by branching into the main bronchi (Fig. 4.11). It serves as a

conduit for air to the lungs. The trachea can be palpated at the root of the neck, superior to the manubrium in the midline. The esophagus is a muscular tube that connects the pharynx with the stomach. The upper part of the esophagus descends behind the trachea and, in contact with it, through the superior mediastinum (Fig. 4.11). The esophagus continues through the posterior mediastinum behind the heart, pierces the diaphragm at the level of T10, and enters the stomach at the cardia. Both the trachea and esophagus are crossed on the left by the arch of the aorta. The impression of the aorta on the esophagus can usually be seen on a posterior to anterior radiograph of the esophagus coated with barium contrast. The trachea and esophagus are crossed on the right side by the azygos vein at the lower border of the superior mediastinum. Both the trachea and esophagus come into contact with the upper lobe of the right lung. The esophagus also contacts the upper lobe of the left lung. The arch of the aorta and its branches shield the trachea from the left lung.

4.7.4 Nerves of the Superior Mediastinum

The vagus and phrenic nerves pass through the superior mediastinum on either side.. The phrenic nerve originates from the ventral rami from cervical levels 3, 4, and 5. This nerve travels inferiorly in the neck on the surface of the anterior scalene muscle, entering the superior mediastinum behind the subclavian vein and passing under the internal thoracic artery (Fig. 4.12). The right phrenic nerve passes through the superior mediastinum lateral to the subclavian artery and the arch of the aorta. The left phrenic nerve passes lateral to the brachiocephalic vein and the superior vena cava. The phrenic nerves then enter the middle mediastinum where they pass anterior to the root of the lung, across the pericardium, finally piercing the diaphragm lateral to the base of the pericardium. Throughout their course, the phrenic nerves pass under the mediastinal pleura. The phrenic nerve is the motor innervation to the diaphragm ("C-3-4-5 keeps your

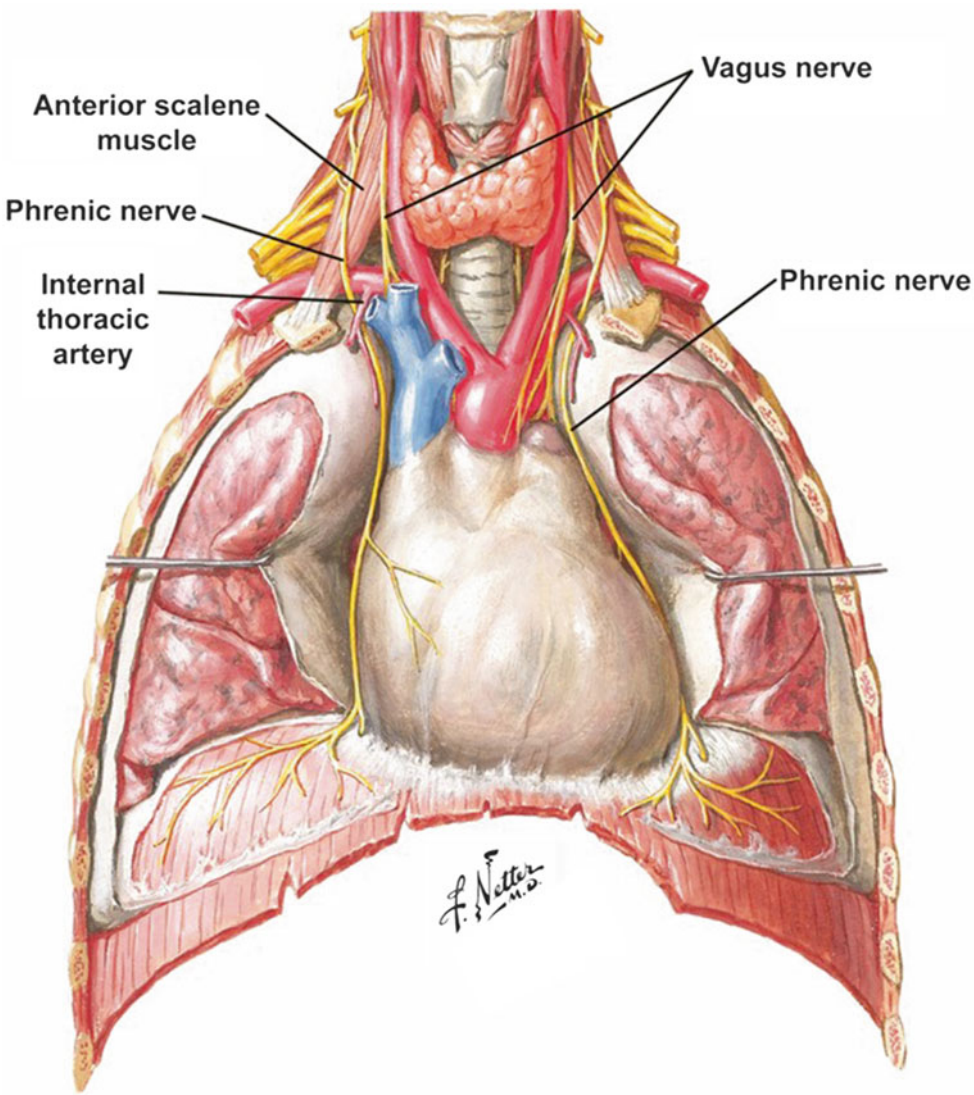

Fig. 4.12 Course of the phrenic nerve and the vagus nerve in the superior and middle mediastinum. ©1998 Elsevier Inc. All rights reserved. www.netterimages.com, Frank Netter

diaphragm alive"), and it also provides sensory innervation to the pericardium, mediastinal, and diaphragmatic pleura and to the diaphragmatic peritoneum on the inferior surface of the diaphragm. The course of the phrenic nerves adjacent to the heart makes them susceptible to stimulation (via leak currents from a pacing lead within the cardiac veins) or damage (temporary or permanent) during cardiac ablation procedures.

The vagus nerves pass out of the skull via the jugular foramen and descend through the neck in the carotid sheath, just lateral to the common carotid arteries. These nerves are the parasympathetic supply to the thorax and most of the abdomen. On the right, the vagus crosses anterior to the subclavian artery and then turns posterior to pass behind the root of the lung and onto the esophagus. Before the right vagus enters the superior mediastinum, it gives off a recurrent laryngeal branch that passes behind the subclavian artery and ascends into the neck. On the left, the vagus passes lateral to the arch of the aorta and then turns posterior to pass behind the root of the lung and onto the esophagus (Fig. 4.12). At the level of the aortic arch, it gives off the left recurrent laryngeal nerve that passes under the aorta, just posterior to the ligamentum arteriosum, and ascends into the neck. The recurrent laryngeal nerves are motor to most of the muscles of the larynx. It should be noted that an aneurism in the arch of the aorta can injure the left recurrent laryngeal nerve and manifest as hoarseness of the voice due to unilateral paralysis of the laryngeal musculature. The right and left vagi contribute to the esophageal plexus of nerves in the middle mediastinum. The right and left vagus nerves give off cardiac branches in the neck (superior and inferior cardiac nerves) and a variable number of small cardiac nerves in the superior mediastinum (thoracic cardiac branches) that provide parasympathetic innervation to the heart via the cardiac nerve plexus.

Sympathetic innervation to the heart is also found in the superior mediastinum. The heart receives postganglionic branches from the superior, middle, and inferior cardiac nerves, each branching from their respective sympathetic ganglia in the neck (Fig. 4.13). There are also thoracic cardiac nerves emanating from the upper 4 or 5 thoracic sympathetic

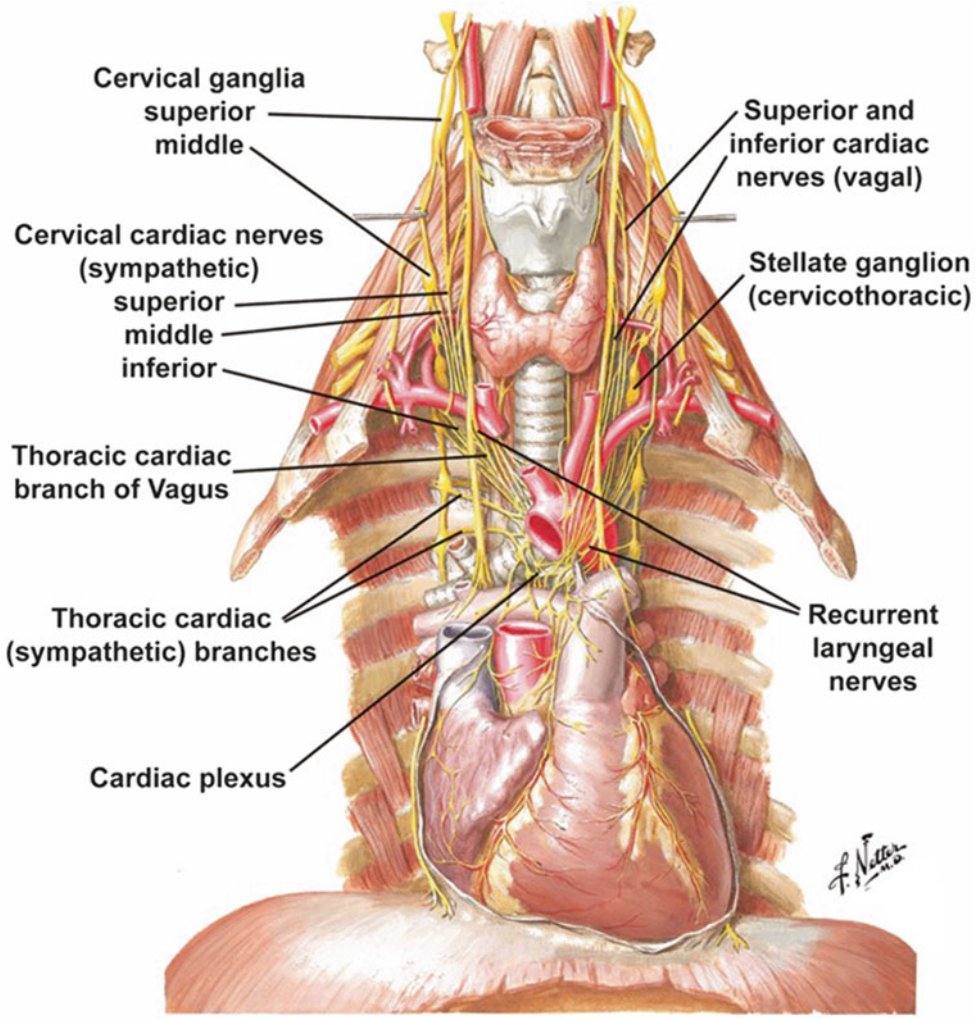

Fig. 4.13 Pattern of innervation in the superior mediastinum. ©1998 Elsevier Inc. All rights reserved. www.netterimages.com, Frank Netter

ganglia. The uppermost thoracic ganglion and the inferior cervical ganglion are often fused to form an elongated ganglion called the *cervicothoracic* (or stellate) ganglion which will give off the inferior cardiac nerve.

The cardiac plexus is located between the trachea, the arch of the aorta, and the pulmonary trunk (Fig. 4.13). It is a network of sympathetic and parasympathetic nerves derived from the branches described above and provides autonomic innervation to the heart. Nerves from the plexus reach the heart by traveling along the vasculature and primarily innervate the conduction system and the atria. The sympathetic components cause the strength and pace of the heart beats to increase, while the parasympathetics counter this effect. Pain afferents from the heart travel with the sympathetic nerves to the upper thoracic and lower cervical levels. This distribution accounts for the pattern of referred heart pain to the upper thorax, shoulder, and arm.

4.7.5 The Thymus

The thymus is found in the most anterior part of the superior mediastinum (Fig. 4.10). It is considered an endocrine gland but is actually more important as a lymphoid organ. The thymus produces lymphocytes that populate the lymphatic system and bloodstream. It is particularly active in young individuals and becomes much less prominent with aging. The thymus is located directly behind the manubrium and may extend up into the neck and inferiorly into the anterior mediastinum. It lies in contact with the aorta, the left brachiocephalic vein, and trachea.

4.8 The Middle Mediastinum

4.8.1 The Pericardium

The middle mediastinum is the central area of the inferior mediastinum occupied by the great vessels, pericardium, and the heart (Fig. 4.14). Within this space, the heart is situated with the right atrium on the right, the right ventricle anterior, the left ventricle to the left and posterior, and the left atrium entirely posterior. The apex, a part of the left ventricle, is projected inferiorly and to the left. The pericardium is the closed sac that contains the heart and the proximal portion of the great vessels. It is attached to the diaphragm inferiorly. The pericardium is a serous membrane, with both visceral and parietal layers into which the heart projects such that there is a potential space within pericardial sac called the *pericardial cavity*. The visceral pericardium, also called the *epicardium*, covers the entire surface of the heart and base of the great vessels, reflecting from the great vessels to become parietal pericardium. The parietal pericardium is characterized by a thickened, strong

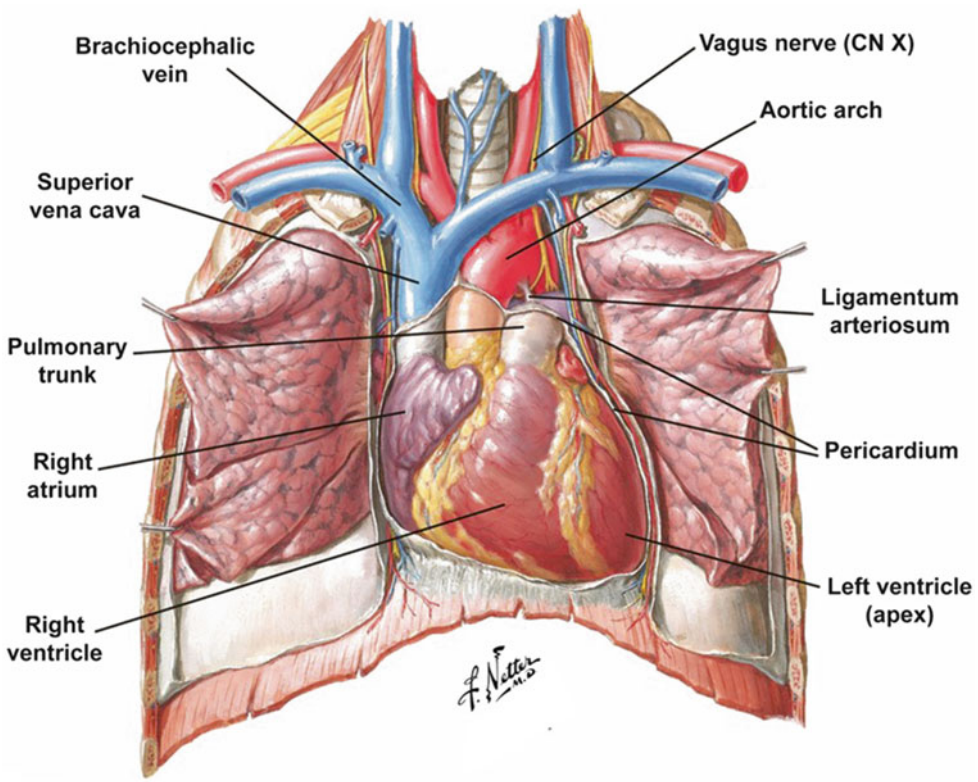

Fig. 4.14 The position of the heart in the middle mediastinum and the relationship of the pericardium to the heart and great vessels. ©1998 Elsevier Inc. All rights reserved. www.netterimages.com, Frank Netter

outer layer called the *fibrous pericardium*. The fibrous pericardium is fused to the layer of parietal serous pericardium, creating a single layer with two surfaces. The fibrous pericardium has little elasticity and, by its fusion with the base of the great vessels, effectively creates a closed space in which the heart beats. The pericardial cavity can accumulate fluids under pathological conditions and create pressure within the pericardium, a condition known as cardiac *tamponade*. For a complete description of the pericardium and its features, see Chap. 9.

4.8.2 The Great Vessels

Great vessels is a composite term used to describe the large arteries and veins directly entering and exiting the heart (Figs. 4.11 and 4.15). They include the superior and inferior vena cava, the aorta, pulmonary trunk, and pulmonary veins. All of these vessels, except for the inferior vena cava, are found within the superior mediastinum. The inferior vena cava and the pulmonary veins are the shortest of the great vessels. The inferior vena cava enters the right atrium from below almost immediately after passing through the diaphragm. The pulmonary veins (there are normally two emerging from each lung) enter the left atrium with a very short intrapericardial portion. The superior vena cava is formed from the confluence of the right and left brachiocephalic veins. It also receives the azygos vein from behind and empties into the superior aspect of the right atrium. The pulmonary trunk ascends from the right ventricle on the anterior surface of the heart at an oblique angle to the left and posterior, passing anterior to the base of the aorta in its course. As the pulmonary trunk emerges from the pericardium, it bifurcates into left and right pulmonary arteries which enter the hilum of each lung (Fig. 4.11). The right pulmonary artery passes under the arch of the aorta to reach the right lung. The left pulmonary artery is connected to the arch of the aorta by the ligamentum arteriosum, the remnant of the ductus arteriosus—the connection between the aorta and pulmonary trunk present in the fetus. The aorta ascends from the left ventricle at an angle to the right and then curves back to the left and posterior as it becomes the aortic arch. As the aorta exits the pericardium, it arches over the right pulmonary trunk, passing to the left of the trachea and esophagus and entering the posterior mediastinum as the descending aorta (Fig. 4.15). Backflow of blood from both the aorta and the pulmonary trunk is prevented by semilunar valves. The semilunar valves, each with a set of three leaflets, are found at the base of each of these great vessels. Immediately above these valves are the *aortic and pulmonary sinuses*, which are regions where the arteries are dilated. The coronary arteries branch from the right and left aortic sinuses (see Chap. 5).

Also passing through the middle mediastinum are the phrenic nerves and the pericardiacophrenic vessels (Fig. 4.10). The phrenic nerves pass out of the neck and through the superior mediastinum. They travel through the middle mediastinum on the lateral surfaces of the fibrous pericardium and under the mediastinal pleura to reach the diaphragm. The phrenic nerve on each side is accompanied by a pericardiacophrenic artery, a branch from the proximal internal thoracic artery, and a pericardiacophrenic vein, which empties into the subclavian vein. These vessels, as

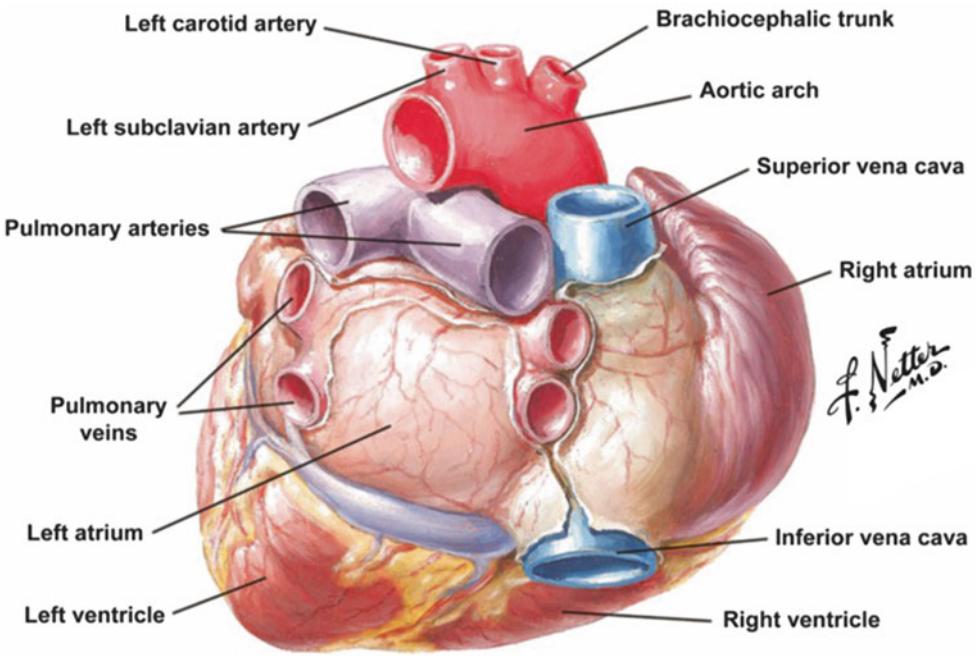

Fig. 4.15 The great vessels as viewed from the posterior side of the heart. ©1998 Elsevier Inc. All rights reserved. www.netterimages.com, Frank Netter

their name implies, supply the pericardium and the diaphragm, as well as the mediastinal pleura.

4.9 The Anterior Mediastinum

The anterior mediastinum is the subdivision of the inferior mediastinum bounded by the sternum anteriorly and the pericardium posteriorly (Fig. 4.1). It contains sternopericardial ligaments, made up of loose connective tissue, the internal thoracic vessels and their branches, lymphatic vessels and nodes, and fat. In children the thymus often extends from the superior mediastinum into the anterior mediastinum.

4.10 The Posterior Mediastinum

The posterior mediastinum is the division of the inferior mediastinum bounded by the pericardium anteriorly and the posterior thoracic wall posteriorly (Fig. 4.1). Structures found in the posterior mediastinum include the descending aorta, azygos system of veins, thoracic duct (common drainage of the lymphatic system; see below), esophagus, esophageal plexus, thoracic sympathetic trunk, and thoracic splanchnic nerves.

4.10.1 The Esophagus and Esophageal Plexus

The esophagus descends into the posterior mediastinum, passing along the right side of the descending aorta (Fig. 4.11). It passes directly behind the left atrium and veers to the left before passing through the esophageal hiatus of the diaphragm at the level of T10. Because of the juxtaposition of the esophagus to the heart, high-resolution ultrasound images of the heart can be obtained via the esophagus. It should be noted that it is possible to damage the esophagus during cardiac ablative procedures (see Chap. 29). As the vagus nerves approach the esophagus, they divide into several commingling branches forming the esophageal plexus (Fig. 4.16). Toward the distal end of the esophagus, the plexus begins to coalesce into an anterior and a posterior vagal trunk that pass with the esophagus into the abdomen. The left side of the esophageal plexus (from the left vagus nerve) contributes preferentially to the anterior vagal trunk and likewise for the right vagus and the posterior vagal trunk, reflecting the normal rotation of the gut (during development). The parasympathetic branches of the anterior and posterior vagal trunks comprise the innervation to the abdominal viscera as far as the splenic flexure.

4.10.2 The Azygos System of Veins

The azygos venous system in the thorax is responsible primarily for draining venous blood from the thoracic wall to

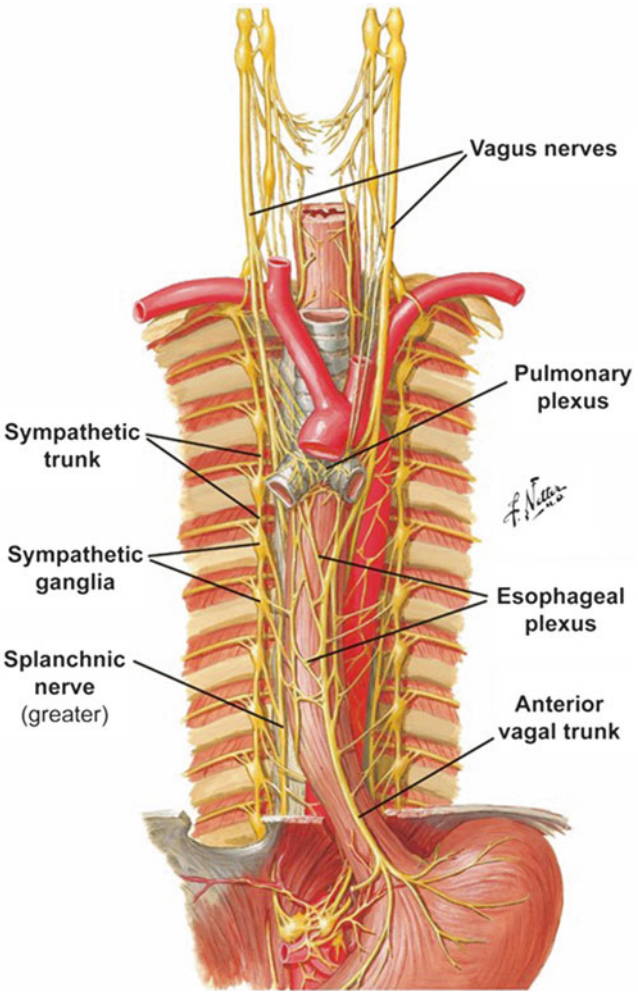

Fig. 4.16 Course of the esophagus in the posterior mediastinum and the esophageal plexus of nerves. ©1998 Elsevier Inc. All rights reserved. www.netterimages.com, Frank Netter

the superior vena cava (Fig. 4.17). The azygos veins also receive venous blood from the viscera of the thorax, such as the esophagus, bronchi, and pericardium. The term azygos means *unpaired* and describes the asymmetry in this venous system. The system consists of the azygos vein on the right and the hemiazygos and accessory hemiazygos veins on the left. Both the azygos and hemiazygos veins are formed from the lumbar veins ascending from the abdomen uniting with the subcostal vein. On the right, the azygos vein is continuous, collecting blood from the right intercostal veins before arching over the root of the lung to join the superior vena cava. On the left, the hemiazygos vein ends typically at the level of T8 by crossing over to communicate with the azygos vein on the right. Above the hemiazygos vein, the accessory hemiazygos vein collects blood from the posterior intercostal veins. It typically communicates with the hemiazygos vein and crosses over to communicate with the azygos vein. On both sides, the second and third intercostal spaces are drained to a superior inter-

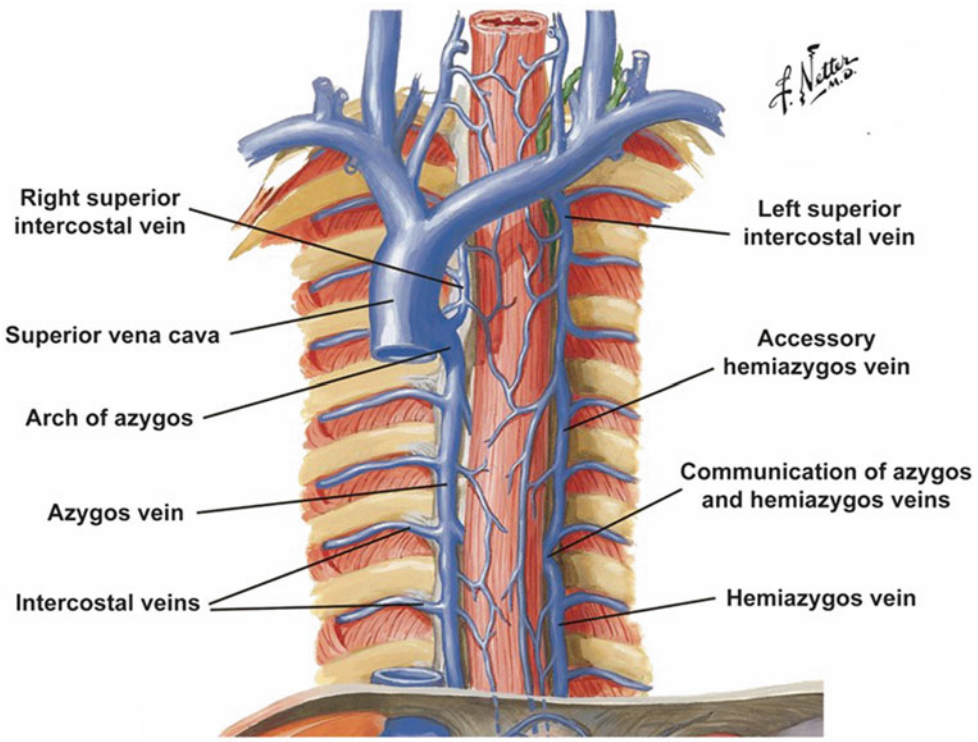

Fig. 4.17 The azygos venous system in the posterior mediastinum. This figure illustrates a "typical" pattern of the azygos and hemiazygos veins. ©1998 Elsevier Inc. All rights reserved. www.netterimages.com, Frank Netter

costal vein that drains directly to the subclavian vein but also communicates with the azygos and accessory hemiazygos veins on their respective sides. The first intercostal vein drains directly to the subclavian vein. There is a tremendous amount of variation in the azygos system of veins, all of which is functionally inconsequential. However, it should be noted that the azygos system can be quite different in some of the large animal models used to study cardiac function (see Chap. 6).

4.10.3 The Thoracic Duct and Lymphatics

The thoracic duct is the largest lymphatic vessel in the body (Fig. 4.18). It conveys lymph from the cisterna chyli, which is the collection site for all lymph from the abdomen, pelvis, and lower extremities back to the venous system. The thoracic duct enters the posterior mediastinum through the aortic hiatus and travels between the thoracic aorta and the azygos vein behind the esophagus. It ascends through the superior mediastinum to the left and empties into the venous system at or close to the junction of the internal jugular and subclavian veins. The thoracic duct often appears white due to the presence of chyle in the lymph and beaded due to the many valves within the duct. The thoracic duct also receives lymphatic drainage from posterior mediastinal lymph nodes

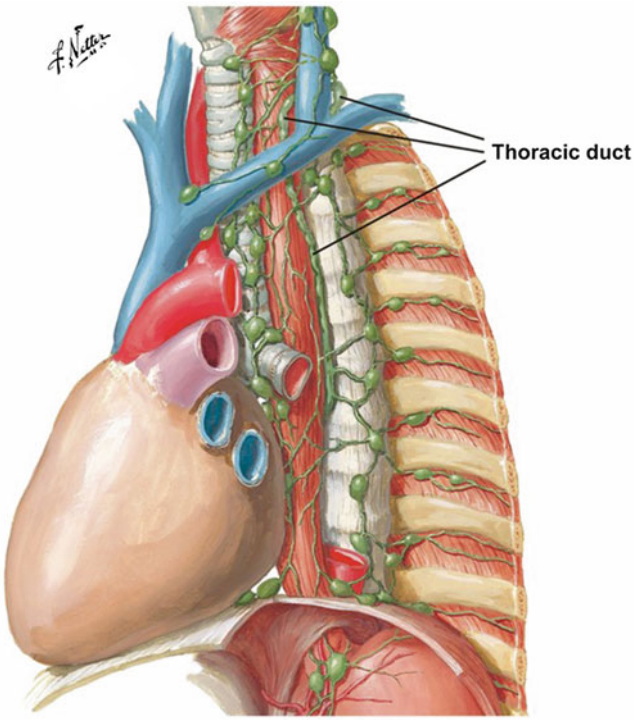

Fig. 4.18 The course of the thoracic duct in the posterior mediastinum through the superior mediastinum and ending at the junction of the internal jugular and subclavian veins. ©1998 Elsevier Inc. All rights reserved. www.netterimages.com, Frank Netter

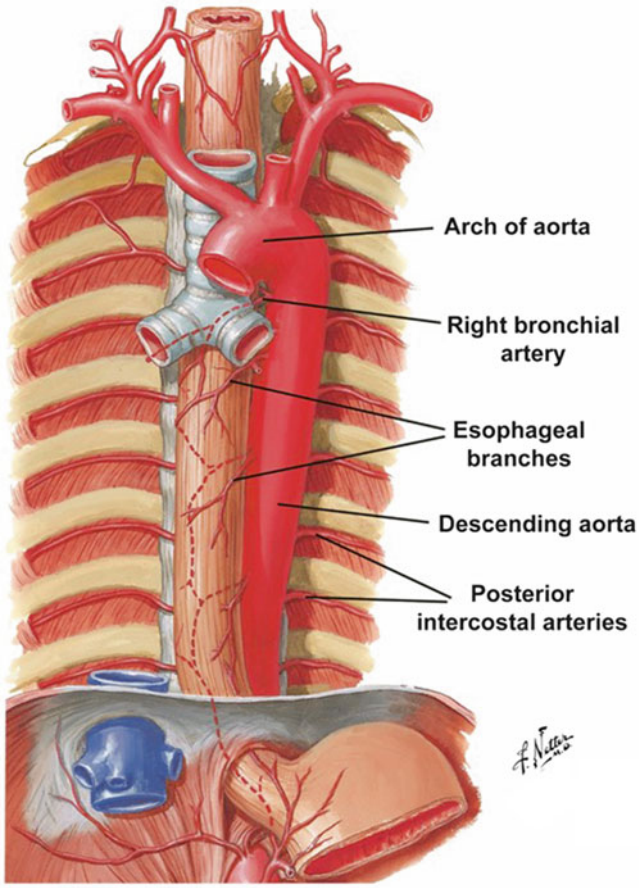

Fig. 4.19 Course of the descending aorta in the posterior mediastinum with posterior intercostals branches and branches to the esophagus and bronchi. ©1998 Elsevier Inc. All rights reserved. www.netterimages.com, Frank Netter

that collect lymph from the esophagus, posterior intercostal spaces, and posterior parts of the pericardium and diaphragm. Approximately 2.5 L of lymph fluid return to the general circulation via this drainage daily.

4.10.4 The Descending Thoracic Aorta

The descending thoracic aorta is the continuation of the aortic arch through the posterior mediastinum (Fig. 4.19). It begins to the left of the T5 vertebra and gradually moves to the middle of the vertebral column as it descends. It passes behind the diaphragm, under the median arcuate ligament (the aortic hiatus), and into the abdomen at the level of T12. The thoracic aorta gives off the 3rd through 11th posterior intercostal arteries and the subcostal artery. It also supplies blood to the proximal bronchi and the esophagus via bronchial and esophageal branches. The superior phrenic arteries supply the posterior aspect of the diaphragm and anastomose with the musculophrenic and pericardiacophrenic branches of the internal thoracic artery.

4.10.5 The Thoracic Sympathetic Nerves

The sympathetic chain of ganglia, or *sympathetic trunk*, extends from the pelvic cavityto the cervical spine. It is also called the thoracolumbar division of the autonomic nervous system because preganglionic neurons of this system have their cell bodies in the thoracic and lumbar segments of the spinal cord, from T1 to L2. The thoracic portion of the sympathetic trunk is found in the posterior mediastinum (Fig. 4.16). It is composed of sympathetic ganglia, located along the spine at the junction of the vertebrae and the heads of the ribs, and the intervening nerve segments that connect the ganglia. These sympathetic ganglia also called *paravertebral sympathetic ganglia* due to their position alongside the vertebral column (see Chap. 5).

There is approximately one sympathetic chain ganglion for each spinal nerve. There are fewer ganglia than nerves because some adjacent ganglia fuse during embryologic development. Such fusion is most evident in the cervical region where there are eight spinal nerves but only three sympathetic ganglia—the superior, middle, and inferior cervical ganglia (Fig. 4.13). The inferior cervical ganglion and the first thoracic (T1) ganglion are often fused, forming the cervicothoracic, or stellate (star-shaped) ganglion.

An axon of the sympathetic nervous system that emerges from the spinal cord in the thorax travels with the ventral nerve root to a ventral ramus (in the thorax, this would be an intercostal nerve) (Fig. 4.20). After traveling a short distance on this nerve, this presynaptic (preganglionic) neuron enters the chain ganglion at its level (Fig. 4.21). Within the ganglion, it either synapses or travels superiorly or inferiorly to synapse at another spinal cord level (C1 to S4). After synapsing, the postsynaptic (postganglionic) neuron travels out of the ganglion and onto the ventral ramus to its target structure or organ. Presynaptic sympathetic neurons travel from the ventral ramus to the chain ganglion, and postsynaptic neurons travel back to the ventral ramus, via small connections called *rami communicantes* (so named because they communicate between the ventral ramus and the sympathetic ganglion). The presynaptic neuron has a myelin protective coating and the postsynaptic neuron does not. This pattern of myelination is true of all nerves in the autonomic system. The myelin coating appears white and thus the presynaptic (myelinated) rami communicantes form *white rami communicantes*, and the postsynaptic (unmyelinated) neurons form *gray rami communicantes*. The gray and white rami communicantes can be seen spanning the short distance between the intercostal nerves and the sympathetic ganglia in the posterior mediastinum (Fig. 4.8).

Also present in the posterior mediastinum are the thoracic splanchnic nerves which are seen leaving the sympathetic trunk and running inferiorly toward the midline (Fig. 4.20). Splanchnic nerves are mainly preganglionic sympathetic neu-

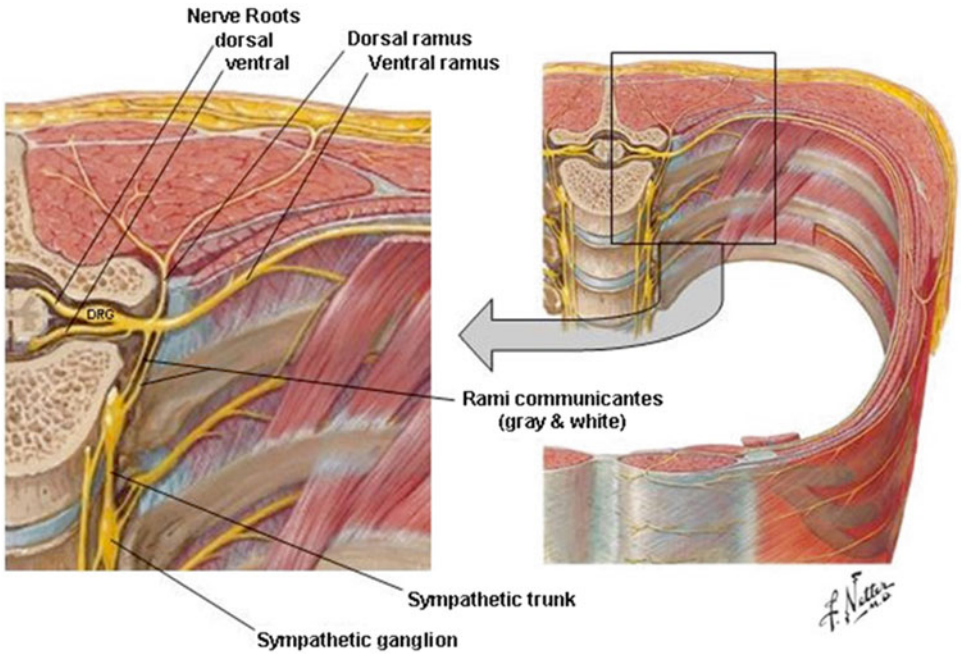

Fig. 4.20 A typical spinal nerve showing the communication of sympathetic nerves with the chain ganglia via *white* and *gray* rami communicantes. ©1998 Elsevier Inc. All rights reserved. www.netterimages.com, Frank Netter

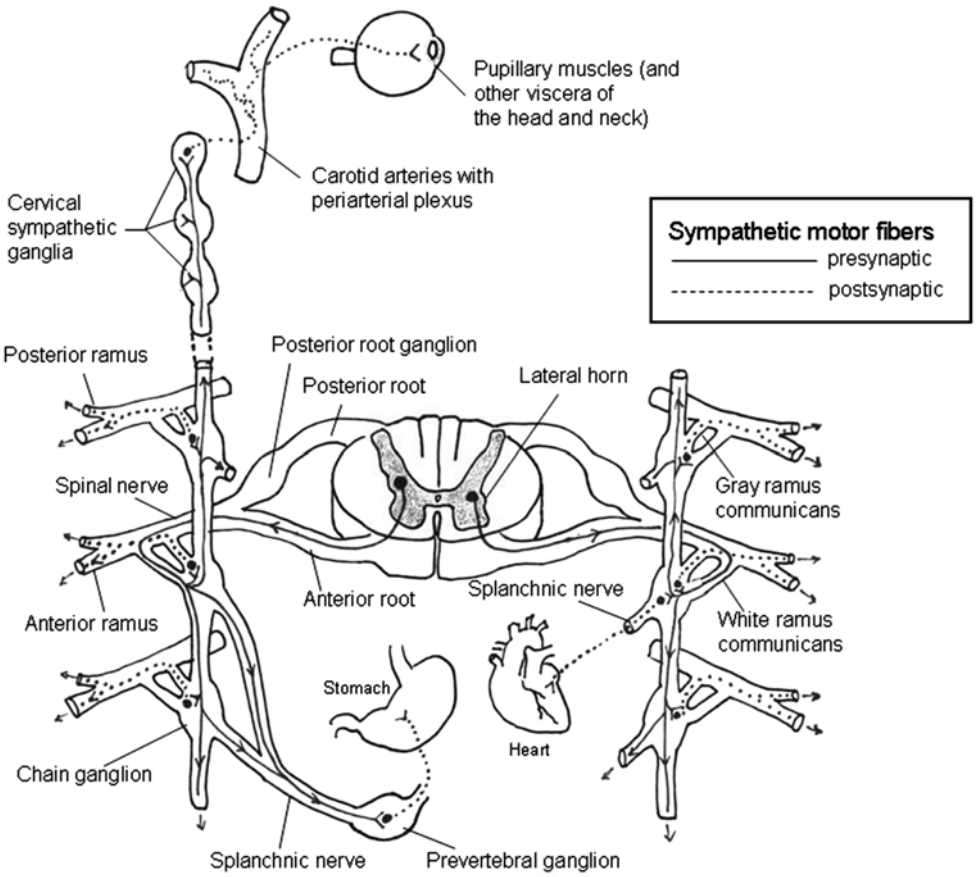

Fig. 4.21 The three options taken by presynaptic sympathetic fibers are illustrated. All presynaptic nerves enter the sympathetic trunk via *white* rami communicans. They can synapse at their level and exit via *gray* rami communicantes and travel up or down the chain before synapsing, or they can exit before synapsing in the splanchnic nerves. Figure adapted from Clinically Oriented Anatomy, 4th edn. by KL Moore and AF Dalley (Fig. 1.32)

rons that emerge from the spine and pass through the chain ganglion without synapsing (Fig. 4.21). In the thorax, these preganglionic splanchnic nerves emerge from spinal cord segments T5 to T12 and travel into the abdomen where they synapse in collateral ganglia called *prevertebral ganglia*, located along the aorta. The postganglionic fibers then innervate the abdominal organs. There are three splanchnic nerves that emerge in the thorax. The greater splanchnic nerves

emerge from spinal cord segments T5 to T9, although a few studies report that they can emerge from T2 to T10. The axons of the lesser and least splanchnic nerves emerge from segments T10, T11, and T12, respectively.

4.11 Pleura and Lungs

4.11.1 The Pleura

The bilateral pulmonary cavities contain the lungs and the pleural membranes (Fig. 4.1). The pleural membrane is a continuous serous membrane forming a closed pleural cavity within (Fig. 4.10). The relationship of the lung to this membrane is the same as a fist (representing the lung) pushed into an under inflated balloon (representing the pleural membrane). The fist becomes covered by the membrane of the balloon, but it is not "inside" the balloon. In the case of the lung, the pleura that is in contact with the lung is the visceral pleura, and the outer layer, which is in contact with the inner wall of the thorax and the mediastinum, is the parietal pleura (Fig. 4.22). The space within the pleural sac is the pleural cavity. Under normal conditions, the pleural cavity contains only a small amount of serous fluid and has no open space at all. It is referred to as a *potential space* because a real space can be created if outside materials, such as blood, pathologic fluids, or air, are introduced into this space.

The parietal pleura is commonly subdivided into specific parts based on the part of the thorax it contacts (Figs. 4.10 and 4.22). Costal pleura overlies the ribs and intercostal spaces. In this region, the pleura is in contact with the endothoracic fascia, the fascial lining of the thoracic cavity. The mediastinal and diaphragmatic pleura are named for their contact with these structures. The cervical pleura extends over the cupola of the lung, above the first rib into the root of the neck; it is strengthened by the suprapleural membrane, an extension of the endothoracic fascia over the cupola of lung.

The lines of pleural reflection are the lines along which the parietal pleura transitions from one region to the next (Fig. 4.23). The sternal line of reflection is the point where costal pleura transitions to mediastinal pleura on the anterior side of the thorax. The costal line of pleural reflection lies along the origin of the diaphragm where the costal pleura transitions to diaphragmatic pleura. Both the costal and sternal lines of reflection are very abrupt. The vertebral line of pleural reflection lies along the line where costal pleura becomes mediastinal pleura posteriorly. This angle of reflection is shallower than the other two. The surface projections of the parietal pleura are discussed in Sect. 4.12.2.

The parietal pleura reflects onto the lung to become the visceral pleura at the root of the lung. A line of reflection descends from the root of the lung, much like the sleeve of a loose robe hangs from the forearm, forming the pulmonary ligament (Fig. 4.24). The visceral pleura covers the entire surface of each lung, including the surfaces in the fissures, where the visceral pleura on one lobe is in direct contact with the visceral pleura of the other lobe.

The pleural cavity is the space inside the pleural membrane (Fig. 4.22). It is a potential space that, under normal conditions, contains only a small amount of serous fluid that lubricates the movement of the visceral pleura against the parietal pleura during respiration. During expiration, the lungs do not entirely fill the inferior-most aspect of the pulmonary cavity. This creates a region, along the costal line of reflection, where the diaphragmatic and costal pleura come into contact with each other, with no intervening lung tissue. This space is known as the *costodiaphragmatic recess*.

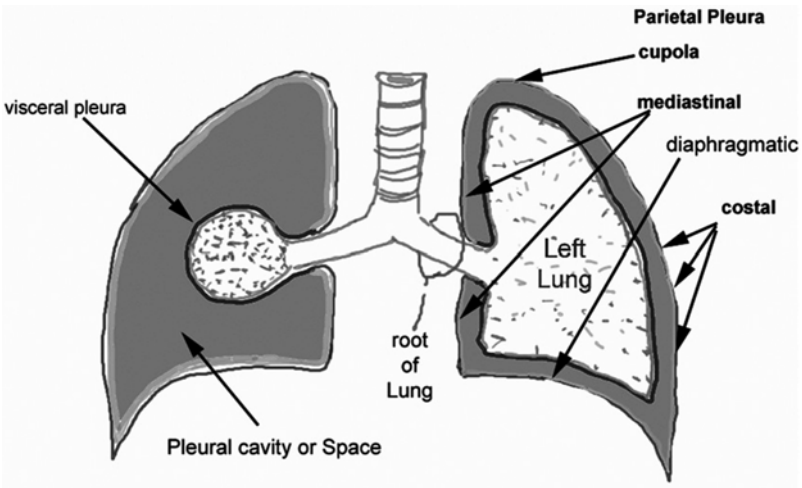

Fig. 4.22 Relationship of the lungs and walls of the thoracic cavity to the pleural membrane. Figure adapted from Grant's Dissector, 12th edn. by EK Sauerland (Fig. 1.15)

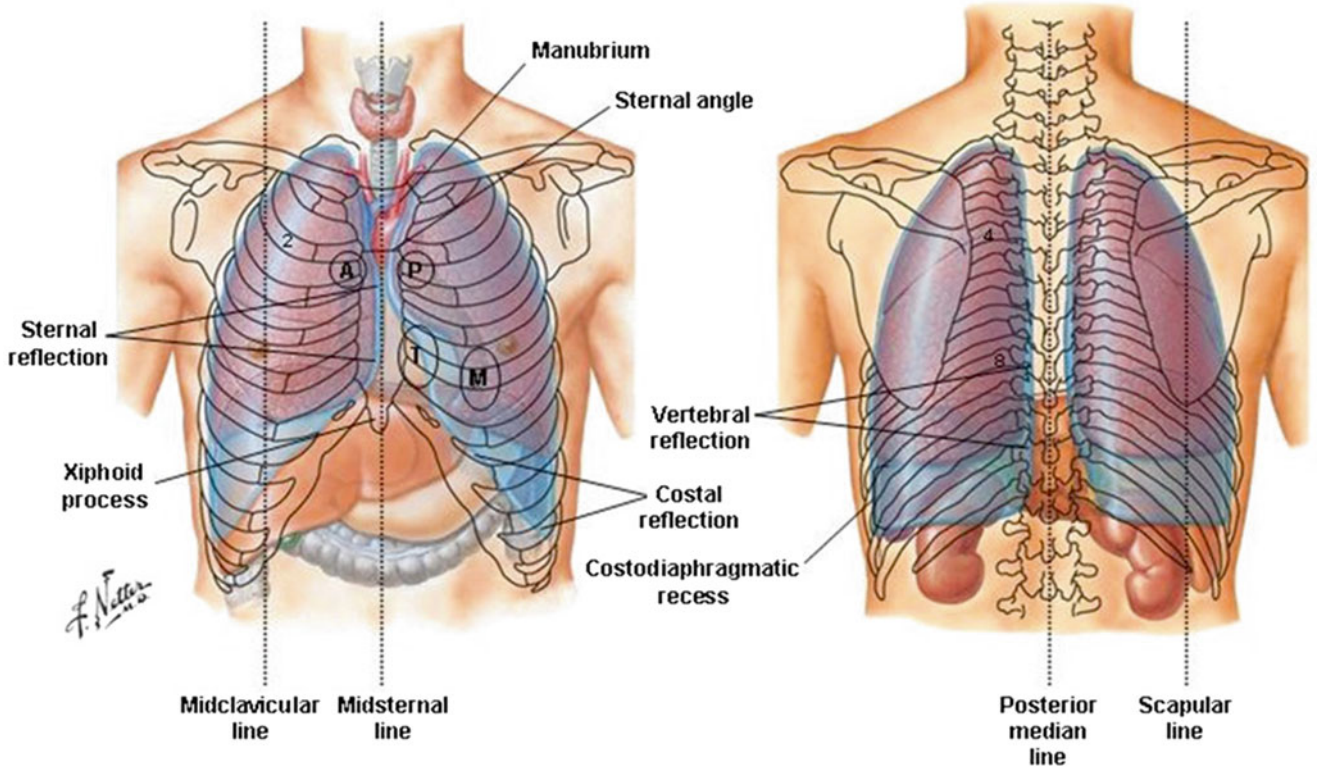

Fig. 4.23 Surface anatomy and important surface landmarks on the anterior and posterior thorax. ©1998 Elsevier Inc. All rights reserved. www.netterimages.com, Frank Netter

4.11.2 The Lungs

The primary function of the lungs is to acquire O_2, required for metabolism in tissues, and to release CO_2, which is the metabolic waste product from tissues. The lungs fill the pulmonary cavities and are separated from each other by structures in the mediastinum. In the living, the lung tissue is soft, light, and elastic, filling the pulmonary cavity and accommodating surrounding structures that impinge on the lungs. In the fixed cadaveric lung, the imprint of structures adjacent to the lungs is easily seen. Blood and air enter and exit the lung at the hilum or root of the lung via the pulmonary vessels and the bronchi.

Each lung is divided into a superior and inferior lobe by an oblique (major) fissure (Fig. 4.24). The right lung has a second horizontal (minor) fissure that creates a third lobe called the *middle lobe*. Each lung has three surfaces—costal, mediastinal, and diaphragmatic—and an apex extending into the cupula at the root of the neck. The costal surface is smooth and convex while diaphragmatic surfaces are smooth and concave. The mediastinal surface is concave and is the site of the root of the lung, where the primary bronchi and pulmonary vessels enter and exit the lungs. The mediastinal surface has several impressions created by structures in the mediastinum. The left lung has a deep impression accommodating the apex of the heart called the *cardiac impression*. There is also a deep impression of the aortic arch and the descending thoracic aorta behind the root of the lung. At the superior end of the mediastinal surface, there are impressions from the brachiocephalic vein and the subclavian artery and a shallow impression from the esophagus and trachea. On the right side, there are prominent impressions of the esophagus, behind the root of the lung, and the arch of the azygos vein, extending over the root of the lung. An impression of the superior vena cava and the brachiocephalic vein appear anterior and above the root of the lung. An impression of both the trachea and esophagus are seen close to the apex of the lung. Descending from the root of both lungs, the pulmonary ligament can be seen.

The lungs also have three borders where the three surfaces meet. The posterior border is where the costal and mediastinal surfaces meet posteriorly. The inferior border is where the diaphragmatic and costal surfaces meet. The inferior border of the lung does not extend to the costal pleural reflection. The anterior border is where the costal and mediastinal surfaces meet anteriorly. On the left lung, the cardiac impression creates a visible curvature on the anterior border called the *cardiac notch*. Below the cardiac notch, a tongue-like segment of lung called the *lingula* protrudes around the apex of the heart.

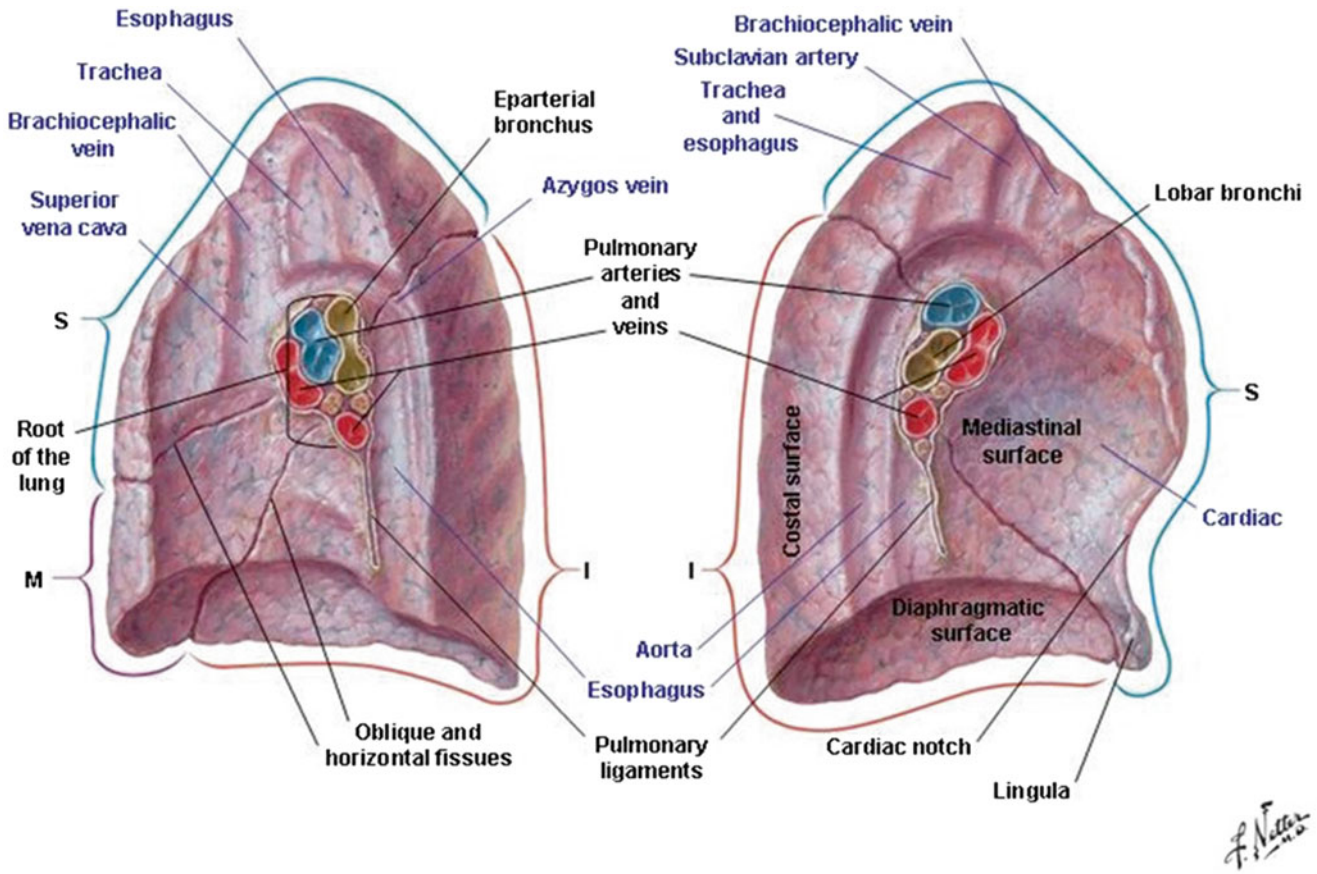

Fig. 4.24 Surface anatomy of the right (*right*) and left (*left*) lungs. ©1998 Elsevier Inc. All rights reserved. www.netterimages.com, Frank Netter

The main bronchi are the initial right and left branches from the bifurcation of the trachea that enter the lung at the hilum (Fig. 4.25). They, like the trachea, are held open by C-shaped segments of hyaline cartilage. The right main bronchus is wider and shorter and enters the lung more vertically than the left main bronchus. This is the reason aspirated foreign objects more often enter the right lung than the left. The left main bronchus passes anterior to the esophagus and under the aortic arch to enter the lung. Once in the lung, the main bronchi branch multiple times to form the bronchial tree (Fig. 4.25). The first branching supplies each lobe of the lung. These are the secondary or lobar bronchi. There are three lobar bronchi on the right and two on the left supplying their respective lobes. The lobar bronchi branch into several segmental bronchi, each of which supplies air to a subpart of the lobe called a *bronchopulmonary segment*. Each bronchopulmonary segment has an independent blood supply and can be resected without impacting the remaining lung. The segmental bronchi then further divide into a series of intersegmental bronchi. The smallest intersegmental bronchi branch to become bronchioles, which can be distinguished from bronchi in that they contain no cartilage in their wall. The terminal bronchioles branch into a series of respiratory bronchioles, each of which contain alveoli. The respiratory bronchioles terminate by branching into alveolar ducts that lead into alveolar sacs, which are clusters of alveoli. It is in the alveoli where gasses in the air are exchanged with the blood.

Each lung is supplied by a pulmonary artery that carries deoxygenated blood (thus they are colored blue in anatomical atlases) from the right ventricle of the heart (Fig. 4.25). Each pulmonary artery enters the hilum of the lung and branches with the bronchial tree to supply blood to the capillary bed surrounding the alveoli. The arterial branches have the same names as the bronchial branches. Oxygenated blood is returned to the left atrium of the heart via the paired pulmonary veins emerging from the hilum of both lungs. The pulmonary veins do not run the same course as the pulmonary arteries within the lung. At the hilum of the lung, the pulmonary artery is typically the most superior structure with the main bronchus immediately below. On the right, the main bronchus is somewhat higher and the superior lobar bronchus crosses superior to the pulmonary artery; it is referred to as the *eparterial bronchus*. The pulmonary veins exit the hilum of the lung inferior to both the main bronchus and the pulmonary artery.

Lymphatic drainage of the lungs is to tracheobronchial lymph nodes located at the bifurcation of the trachea (Fig. 4.26). A subpleural lymphatic plexus lies under the vis-

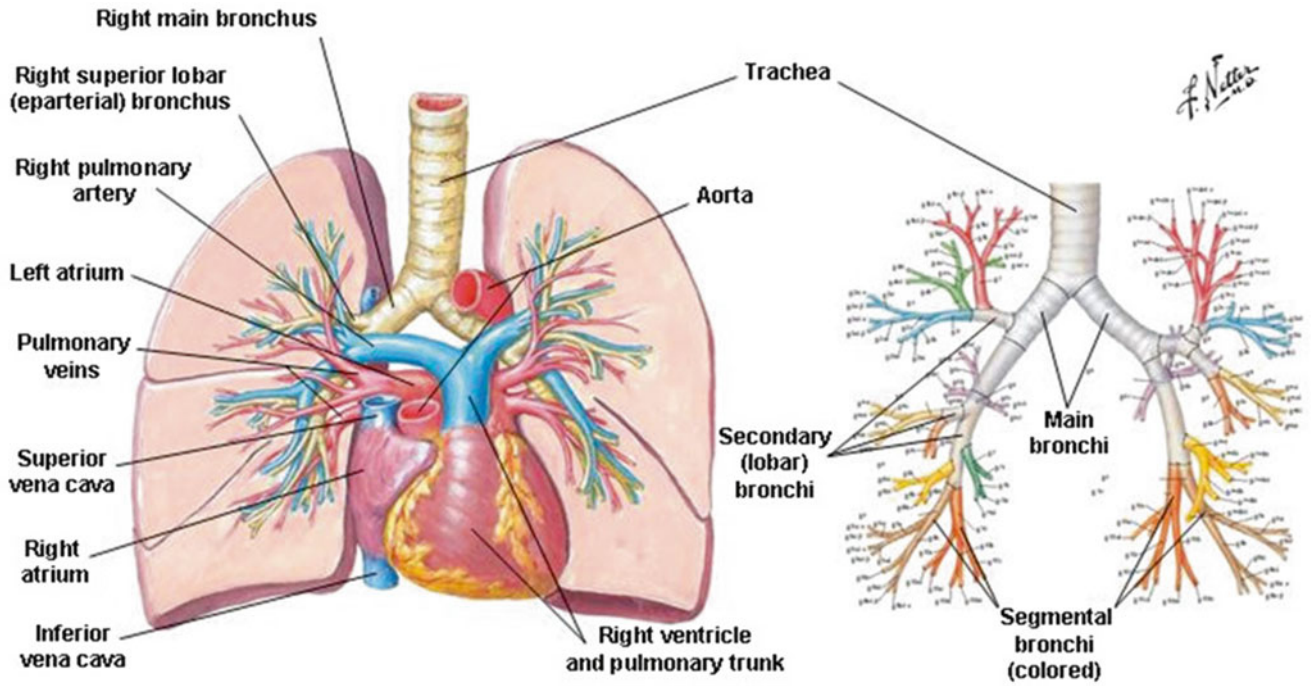

Fig. 4.25 Pattern of structure entering and leaving the root of the lung (*left*) and the branching pattern of the bronchi (*right*). ©1998 Elsevier Inc. All rights reserved. www.netterimages.com, Frank Netter

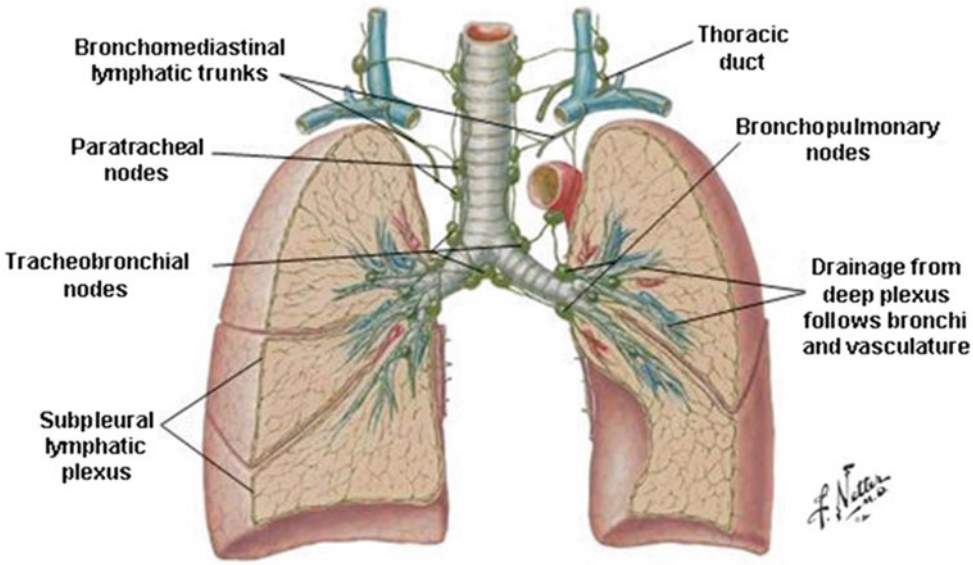

Fig. 4.26 Pattern of lymphatic drainage from the lungs. ©1998 Elsevier Inc. All rights reserved. www.netterimages.com, Frank Netter

ceral pleura and drains directly to the tracheobronchial nodes. A deep lymphatic plexus drains along the vasculature of the lungs to pulmonary nodes along the bronchi, which communicate with bronchopulmonary nodes at the hilum and from there to the tracheobronchial nodes. The lymphatic drainage from the lungs may drain directly to the subclavian veins via the bronchomediastinal trunks or into the common thoracic duct.

The lungs receive innervation from the pulmonary plexus (Fig. 4.16). The parasympathetic nerves are from the vagus (CN X), and they are responsible for the constriction of the bronchi and vasodilatation of the pulmonary vessels. They are also secretomotor to the glands in the bronchial tree. The sympathetics act opposite to the parasympathetics. Pain afferents from the costal pleura and the outer parts of the diaphragmatic pleura are derived from the intercostal nerves. The phrenic nerves contain sensory afferents for the mediastinal pleura and the central part of the diaphragmatic pleura.

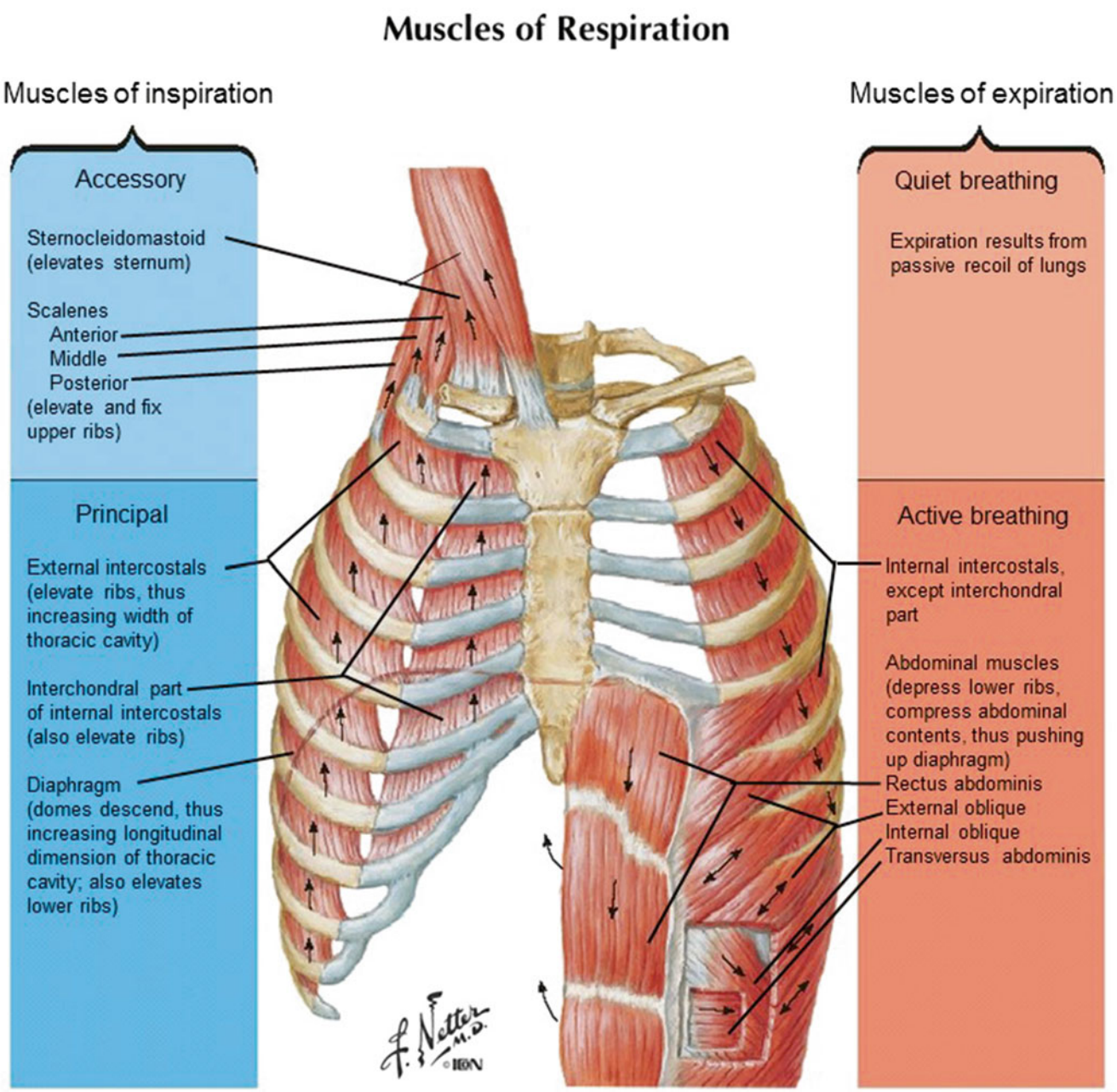

Fig. 4.27 The participation of muscles in respiration. ©1998 Elsevier Inc. All rights reserved. www.netterimages.com, Frank Netter

4.11.3 Mechanics of Respiration

Respiration is controlled by: (1) the muscles of the thoracic wall, (2) the respiratory diaphragm, (3) the muscles of the abdominal wall, and (4) the natural elasticity of the lungs (Fig. 4.27). The diaphragm contracts during inspiration, causing the dome of the diaphragm to descend and the vertical dimension of the thoracic cavity to increase. Simultaneously, the ribs are elevated by the contraction of external intercostal muscles and the interchondral parts of the internal intercostals. During deep inspiration, the ribs are further elevated by the contraction of muscles in the neck. Elevation of the ribs increases the diameter of the thoracic cavity. The net result is the expansion of the pulmonary cavities. When the walls of the thorax expand, the lungs expand with them due to the negative pressure created in the pleural cavity and the propensity of the visceral pleura to maintain contact with the parietal pleura due to the surface tension of the liquid between these surfaces (somewhat like two plates of glass sticking together with water in between them). The resultant negative pressure in the lungs forces the subsequent intake of air.

Quiet expiration of air is primarily caused by the elastic recoil of the lungs when the muscles of inspiration are relaxed. Further expiration is achieved by the contraction of the lateral internal intercostal muscles, depressing the ribs, and the contraction of abdominal muscles, causing increased abdominal pressure which pushes up on the diaphragm. At rest, the inward pull of the lungs (trying to deflate further) is at equilibrium with the springlike outward pull of the thoracic wall.

4.12 Surface Anatomy

4.12.1 Landmarks of the Thoracic Wall

There are several defined vertical lines that demark regions of the anterior and posterior thoracic wall (Fig. 4.23). These lines are used to describe the location of surface landmarks and the locations of injuries or lesions on or within the thorax. The anterior median line runs vertically in the midline; it is also referred to as the *midsternal line*. The midclavicular line bisects the clavicle at its midpoint and typically runs through, or close to, the nipple. Three lines demarcate the axilla. The anterior axillary line runs vertically along the anterior axillary fold, and the posterior axillary line runs parallel to it along the posterior axillary fold. The midaxillary line runs in the midline of the axilla, at its deepest part. The scapular line runs vertically on the posterior thorax, through the inferior angle of the scapula. The posterior median line, also called the *midvertebral or midspinal line*, runs vertically in the midline on the posterior thorax.

The sternum lies subcutaneously in the anterior median line and can be palpated throughout its length. The jugular notch is found at the upper margin of the sternum, between the medial ends of the clavicle. The jugular notch is easily palpated and can usually be seen as a depression on the surface. The jugular notch represents the anterior junction of the superior mediastinum and the root of the neck. It lies at the level of the T2 vertebra posteriorly. The manubrium intersects with the body of the sternum about 4 cm inferior to the jugular notch, at the manubriosternal joint; this joint creates the sternal angle which is normally visible on the surface of the thorax. The sternal angle(of Louis) demarcates the inferior border of the superior mediastinum and lies at the level of the intervertebral disk between T4 and T5. The second rib articulates with the sternum at the sternal angle, making this site an excellent landmark for determining rib number. Immediately adjacent to the sternal angle is rib 2; the other ribs can be found by counting up or down from rib 2. Intercostal spaces are numbered for the rib above. On the posterior thorax, the fourth rib can be found at the level of the medial end of the spine of the scapula and eighth rib at the inferior angle.

The manubrium overlies the junction of the brachiocephalic veins to form the superior vena cava (Fig. 4.23). The superior vena cava passes at the level of the sternal angle and at (or slightly to the right of) the border of the manubrium. The superior vena cava typically enters the right atrium behind the costal cartilage of the third rib on the right and is sometimes accessed for various procedures; knowledge of this surface anatomy is critical.

The xiphoid process is the inferior part of the sternum and lies in a depression called the *epigastric fossa* at the apex of the infrasternal angle formed by the convergence of the costal margins at the inferior border of the thorax (Fig. 4.23). Note that the location of the xiphisternal joint is used as a landmark to determine hand position for cardiopulmonary resuscitation.

The breasts are also surface features of the thoracic wall. In women, the breasts vary greatly in size and conformation, but the base of a breast usually occupies the space between ribs 2 and 6, from the lateral edge of the sternum to the midaxillary line. The nipples, surrounded by an area of darker pigmented skin called the *areola*, are the prominent features of the breast. In men, the nipple is located anterior to the fourth intercostal space in the midclavicular line. Because of the variation in breast anatomy in the female, the location of the nipple is difficult to predict.

4.12.2 The Lungs and Pleura

The pleural sac is outlined by the parietal pleura as it projects onto the surface of the lungs (Fig. 4.23). From the root of the neck, these projections follow the lateral edge of the sternum inferiorly. On the left, the border of the parietal pleura moves laterally at the level of fourth costal cartilage to accommodate the cardiac notch within the mediastinum. The pleura follows a line just superior to the costal margin, reaching the level of the tenth rib at the midaxillary line. Posteriorly the inferior margin of the plural cavity lies at the level of T12, and the medial margin follows the lateral border of the vertebral column to the root of the neck. In the superior parts of the pleural cavity, the visceral pleura of the lungs is in close contact with the parietal pleura, with the lungs consequently filling the plural cavity. Both lungs and parietal pleura (cervical part) extend above the clavicles into the supraclavicular fossae, at the root of the neck. At the inferior reaches of the pleural cavities, the lungs stop short of filling the plural cavity, reaching only to the level of the sixth rib in the midclavicular line, the eighth rib in the midaxillary line, and the tenth rib posteriorly, creating the costodiaphragmatic recesses. The major (oblique) fissures of the lungs extend along a line from the spinous process of T2 to the costal cartilage of the sixth rib. The minor (horizontal) fissure of the right lung lies under the fourth rib.

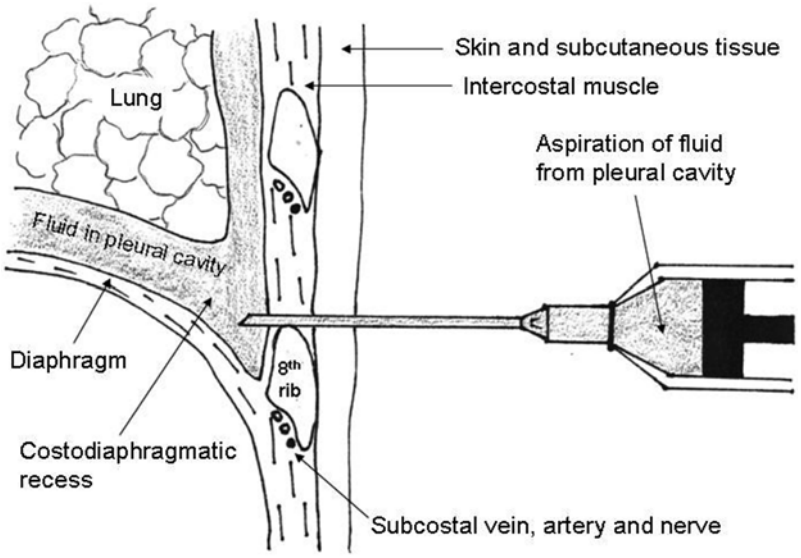

Fig. 4.28 Illustration of thoracocentesis. Figure adapted from Grant's Dissector, 12th edn. by EK Sauerland (Fig. 1.16)

Under pathologic conditions, fluid can accumulate in the pleural cavity. This fluid normally drains inferiorly and accumulates in the costodiaphragmatic recess. Thoracocentesis refers to the procedure used to drain such fluid (Fig. 4.28). To do so, a needle is commonly inserted into the costodiaphragmatic recess by passing it through the middle of the intercostal space, being careful to avoid the primary intercostal neurovascular bundle immediately below the rib above and collaterals above the rib below.

4.12.3 The Heart

The heart and great vessels are covered by the sternum and central part of the thoracic cage (Fig. 4.23). The apex of the heart usually lies in the fifth intercostal space just medial of the midclavicular line. The upper border of the heart follows a line from the inferior border of the left second costal cartilage to the superior border of the right costal cartilage. The inferior border of the heart lies along a line from the right sixth costal cartilage to the fifth intercostal space at the midclavicular line, where the apex of the heart is located. The right and left borders follow lines connecting the right and left ends of the superior and inferior borders. All four heart valves, the closing of which account for the heart sounds, lie well protected behind the sternum. The sounds of the individual valves closing are best heard at auscultatory sites to which their sounds are transmitted (see Chap. 18). The bicuspid (mitral) valve is heard at the apex of the heart in the region of the fourth or fifth intercostal spaces on the left near the midclavicular line. The tricuspid valve can be heard along the left margin of the sternum at the level of the fourth or fifth intercostal space. The pulmonary valve is heard along the left border of the sternum in the second intercostal space. The aortic valve is heard at the second intercostal space on the right sternal border.

4.12.4 Vascular Access

Understanding the surface landmarks relative to the axilla and subclavian region is critical for the successful access of the venous system via the subclavian vein. The subclavian vein passes over the first rib and under the clavicle at the junction of its middle and medial thirds; it courses through the base of the neck where it passes anterior to the apex of the lung and the pleural cavity (Fig. 4.29). The subclavian vein is immediately anterior to the subclavian artery and is separated from the artery medially by the anterior scalene muscle. To access the subclavian vein, a needle is inserted approximately 1 cm inferior to the clavicle at the junction of its medial and middle thirds and aimed toward the jugular notch, parallel with the vein to minimize risk of injury to adjacent structures. The most common complication of subclavian venous access is puncture of the apical pleura with resulting pneumothorax or hemopneumothorax. In addition, the subclavian artery, lying behind the vein, also has the potential to be injured by this procedure. If subclavian access is attempted on the left, one must also be aware of the junction of the thoracic duct with the subclavian vein. Injury to the thoracic duct can result in chylothorax, the accumulation of lymph in the plural cavity. This is difficult to treat and has an associated high morbidity. When access of the subclavian is attempted for cardiac lead placement, care must be taken to avoid piercing the subclavius muscle or costoclavicular ligament. Passing the lead through these structures tethers it to the highly mobile clavicle which may cause premature breakage of the lead.

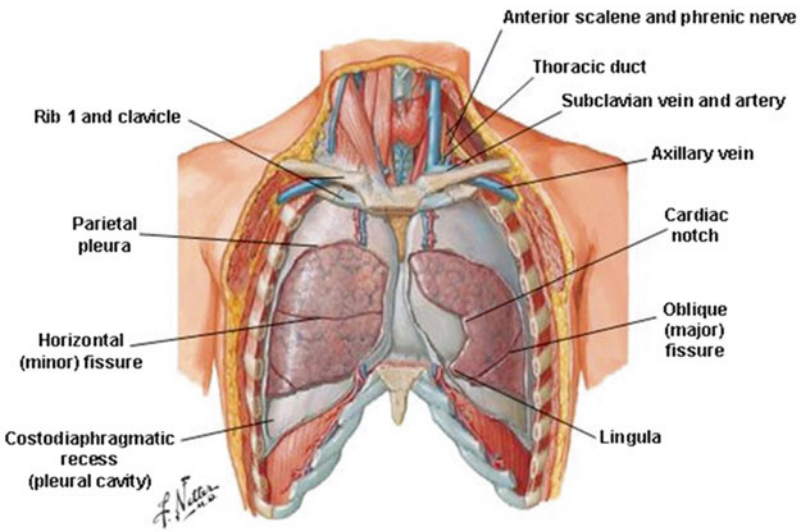

Fig. 4.29 Anatomy of the subclavian veins and surrounding structures.

4.13 Summary

Options for accessing the heart, in a minimally invasive fashion, are limited by the vascular anatomy of the superior mediastinum and the axilla. Percutaneous access strategies are limited by the bony anatomy of the thoracic cage. How a device interacts with the thorax, and accommodates basic thoracic movements and movements of the upper extremity and neck, must be understood in order for design devices that will endure in the body. Thus, a thorough understanding of the thoracic anatomy surrounding the heart is important to those seeking to design and deploy devices for placement and use in the heart. With an understanding of the important thoracic anatomical relationships presented in this chapter, the engineer should be able to design devices with an intuition for the anatomical challenges that will be faced for proper use and deployment of the device.

References

1. Moore KL, Dalley AF (1999) Thorax. In: Moore KL, Dalley AF (eds) Clinically oriented anatomy, 4th edn. Lippincott Williams & Wilkins, Philadelphia, pp 62–173
2. Hollinshead WH, Rosse C (1985) Part IV: thorax. In: Hollinshead WH, Rosse C (eds) Textbook of anatomy, 4th edn. Harper & Row, Philadelphia, pp 463–575
3. Netter FH (ed) (2003) Atlas of human anatomy, 3rd edn. Icon Learning Systems, Teterboro
4. Sauerland EK (1999) The thorax. In: Sauerland EK (ed) Grant's dissector, 12th edn. Lippincott Williams & Wilkins, Philadelphia, pp 1–39
5. Weinberger SE (1998) Pulmonary anatomy and physiology–the basics. In: Weinberger SE (ed) Principles of pulmonary medicine, 3rd edn. Saunders, Philadelphia, pp 1–20
6. Magney LE, Flynn DM, Parsons JA, Staplin DH, Chin-Purcell MV, Milstein S, Hunter DW (1993) Anatomical mechanisms explaining damage to pacemaker leads, defibrillator leads, and failure of central venous catheters adjacent to the sternoclavicular joint. Pacing Clin Electrophysiol 16:445–457

Anatomy of the Human Heart

5

Anthony J. Weinhaus

Abstract

This chapter covers the internal and external anatomy of the heart, its positioning within the thorax, and its basic function. Briefly, the heart is a muscular pump, located in the protective thorax, which serves two functions: (1) collect blood from the tissues of the body and pump it to the lungs and (2) collect blood from the lungs and pump it to all the tissues of the body. The heart's two upper chambers (or atria) function primarily as collecting chambers, while two lower chambers (ventricles) are much stronger and function to pump blood. The right atrium and ventricle collect blood from the body and pump it to the lungs, and the left atrium and ventricle collect blood from the lungs and pump it throughout the body. There is a one-way flow of blood through the heart which is maintained by a set of four valves (tricuspid, bicuspid, pulmonary, and aortic). The tissues of the heart are supplied with nourishment and oxygen by a separate vascular supply committed only to the heart; the arterial supply to the heart arises from the base of the aorta as the right and left coronary arteries, and the venous drainage is via cardiac veins that return deoxygenated blood to the right atrium.

Keywords

Cardiac anatomy • Mediastinum • Pericardium • Atrium • Ventricle • Valves • Coronary artery • Cardiac veins • Cardiac skeleton • Cardiopulmonary circulation

5.1 Introduction

The heart is a muscular pump which serves two functions: (1) collect blood from the tissues of the body and pump it to the lungs and (2) collect blood from the lungs and pump it to all of the tissues of the body. The human heart lies in the protective thorax, posterior to the sternum and costal cartilages, and rests on the superior surface of the diaphragm. The heart assumes an oblique position in the thorax, with two-thirds to the left of midline. It occupies a space between the pleural cavities called the *middle mediastinum*, defined as the space inside of the pericardium, the covering around the heart. This serous membrane has an inner and an outer layer, with a lubricating fluid in between. The fluid allows the inner visceral pericardium to "glide" against the outer parietal pericardium.

The internal anatomy of the heart reveals four chambers composed of cardiac muscle or myocardium. The two upper chambers (or atria) function mainly as collecting chambers; the two lower chambers (ventricles) are much stronger and function to pump blood out of the heart. The role of the right atrium and ventricle is to collect blood from the body and pump it to the lungs. The role of the left atrium and ventricle is to collect blood from the lungs and pump it throughout the body. There is a one-way flow of blood through the heart; this flow is maintained by a set of four valves. The atrioventricular or AV valves (the right tricuspid and left bicuspid or

A.J. Weinhaus, PhD (✉)
Department of Integrative Biology and Physiology, University of Minnesota, 6-125 Jackson Hall, 321 Church St. SE, Minneapolis, MN 55455-0328, USA
e-mail: weinh001@umn.edu

P.A. Iaizzo (ed.), *Handbook of Cardiac Anatomy, Physiology, and Devices*, DOI 10.1007/978-3-319-19464-6_5

mitral) allow blood to flow only from atria to ventricles. The semilunar valves (pulmonary and aortic) allow blood to flow only from the ventricles out of the heart and through the great arteries.

A number of structures that can be observed in the adult heart are remnants of fetal circulation. In the fetus, the lungs do not function as a site for the exchange of oxygen and carbon dioxide, and the fetus receives all of its oxygen from the mother. In the fetal heart, blood arriving to the right side of the heart is passed through specialized structures to the left side. Shortly after birth, these specialized fetal structures normally collapse, and the heart takes on the "adult" pattern of circulation. However, in rare cases, some fetal remnants and defects can occur (see Chap. 37).

Although the heart is filled with blood, it provides very little nourishment and oxygen to the tissues of the heart. Instead, the tissues of the heart are supplied by a separate vascular supply committed only to the heart. The arterial supply to the heart arises from the base of the aorta as the right and left coronary arteries (running in the coronary sulcus). The venous drainage is via cardiac veins that return deoxygenated blood to the right atrium (see Chap. 8).

It is important to note that besides pumping oxygen-rich blood to the tissues of the body for exchange of oxygen for carbon dioxide, the blood also circulates many other important substances. Nutrients from digestion are collected from the small intestine and pumped through the circulatory system to be delivered to all cells of the body. Hormones are produced from one type of tissue and distributed to all cells of the body. The circulatory system also carries waste materials (salts, nitrogenous wastes, and excess water) from cells to the kidneys, where they are extracted and passed to the bladder. The pumping of interstitial fluid from the blood into the extracellular space is an important function of the heart. Excess interstitial fluid is then returned to the circulatory system via the lymphatic system.

5.2 Position of the Heart in the Thorax

The heart lies in the protective thorax, posterior to the sternum and costal cartilages, and rests on the superior surface of the diaphragm. The thorax is often referred to as the thoracic cage because of its protective function of the delicate structures within. The heart is located between the two lungs which occupy the lateral spaces called the *pleural cavities*. The space between these two cavities is referred to as the *mediastinum* ("that which stands in the middle"; Fig. 5.1).

The mediastinum is divided first into the superior and inferior mediastinum by a midsagittal imaginary line called the *transverse thoracic plane*. This plane passes through the sternal angle (junction of the manubrium and body of the sternum) and the space between thoracic vertebrae T_4 and T_5. This plane acts as a convenient landmark as it also passes

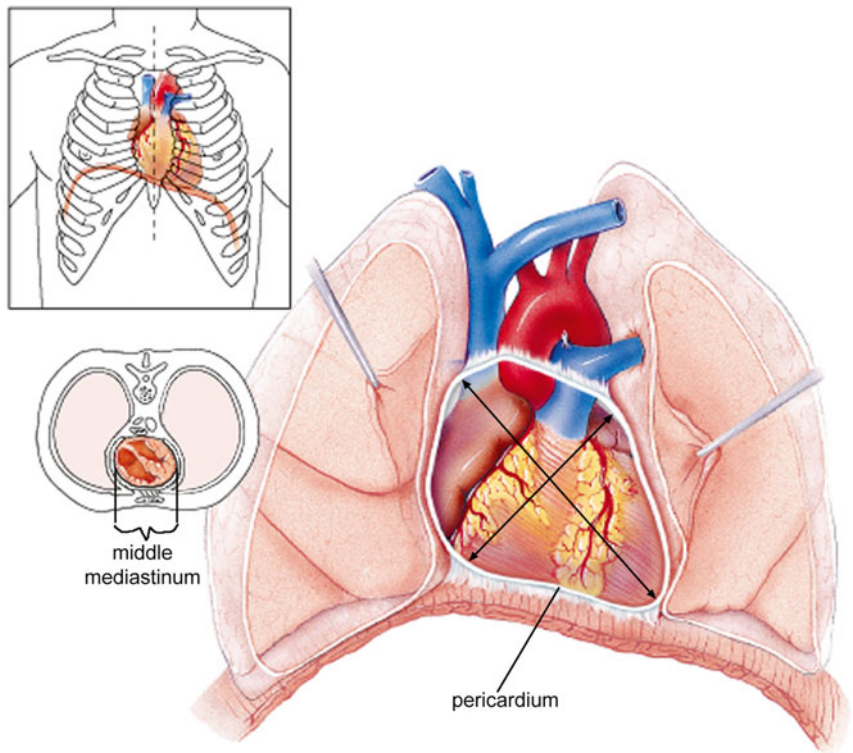

Fig. 5.1 Position of the heart in the thorax. The heart lies in the protective thorax, posterior to the sternum and costal cartilages, and rests on the superior surface of the diaphragm. The heart assumes an oblique position in the thorax, with two-thirds to the left of midline. It is located between the two lungs which occupy the lateral spaces called the pleural cavities. The space between these two cavities is referred to as the mediastinum. The heart lies obliquely in a division of this space, the middle mediastinum, surrounded by the pericardium. Marieb, Elaine N.: Wilhelm, Paticia Brady; Mallatt, Jon B., Human Anatomy, 7th, © 2013. Printed and electronically reproduced by permission of Pearson Education, Inc., New York, New York

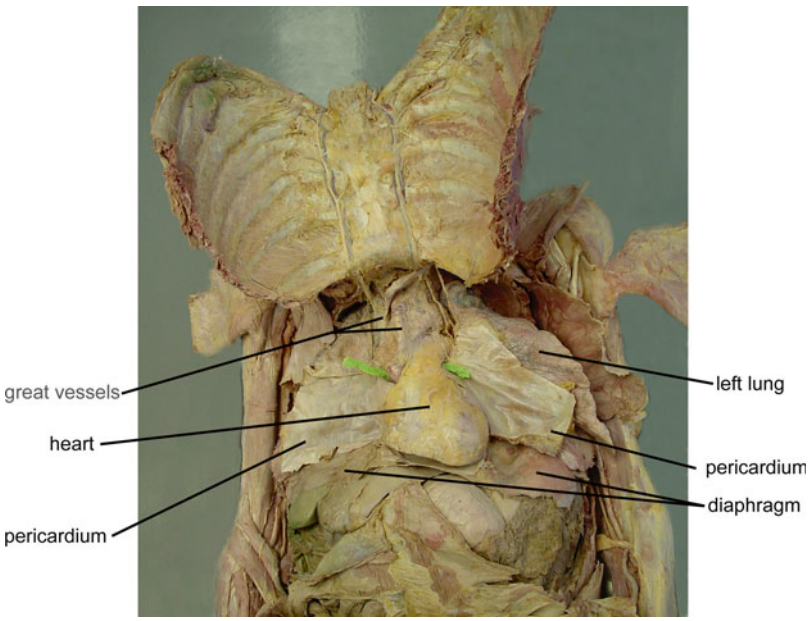

Fig. 5.2 Human cadaver dissection in which the ribs were cut laterally and the sternum and ribs reflected superiorly. This dissection exposes the contents of the thorax (the heart, great vessels, lungs, and diaphragm)

through the following structures: the bifurcation of the trachea, the superior border of the pericardium, the artificial division of the ascending and arch of the aortic artery, and the bifurcation of the pulmonary trunk into the pulmonary arteries.

The human heart assumes an oblique position in the thorax, with two-thirds to the left of midline (Figs. 5.2 and 5.3). The heart is roughly in a plane that runs from the right shoulder to the left nipple. The base is located below the 3rd rib as it approaches the sternum (note that the sternal angle occurs at the level of the 2nd rib). The base is directed superiorly, to the right of midline, and posterior. The pointed apex projects to the left of midline and anterior. Thus, the heartbeat can be easily palpated between the 5th and 6th ribs (just inferior to the left nipple) from the apex of the heart where it comes into close proximity of the thoracic wall. Importantly, the heart lies in such an oblique plane that it is often referred to as being horizontal. Thus, the anterior side may be imagined as the superior and the posterior side as inferior (for additional detail on attitudinally correct cardiac anatomy, see Chap. 2).

The heart is composed of four distinct chambers. There are two atria (left and right) responsible for collecting blood and two ventricles (left and right) responsible for pumping blood. The atria are positioned superior to (or posterior to) and somewhat to the right of their respective ventricles (Fig. 5.3). From superior to inferior down the anterior (or superior) surface of the heart runs the anterior interventricular sulcus ("a groove"). This sulcus separates the left and right ventricles. This groove continues around the apex as the posterior interventricular sulcus on the posterior (inferior) surface. Between these sulci, located within the heart, is the interventricular septum ("wall between the ventricles"). The base of the heart is defined by a plane that separates the atria from the ventricles also called the *atrioventricular groove* or *sulcus*. This groove appears like a belt cinched around the heart. Since this groove appears as though it might also be formed by placing a crown atop the heart, the groove is also called the *coronary* (*corona* = "crown") *sulcus*. The plane of this sulcus also contains the AV valves (and the semilunar valves) and a structure that surrounds the valves called the *cardiac skeleton*. The interatrial ("between the atria") septum is represented on the posterior surface of the heart as the atrial sulcus. Also on the posterior (inferior) side of the heart, the crux cordis ("cross of the heart") is formed from the atrial sulcus, posterior interventricular sulcus, and the relatively perpendicular coronary sulcus.

Note that the great arteries, aorta, and pulmonary trunk arise from the base of the heart and the inferior angle of the heart is referred to as the *apex*; this resembles an inverted pyramid. The right and left atrial appendages (or auricles, so named because they look like dog ears, *auricle* = "little ear") appear as extensions hanging off each atrium.

The anterior (superior) surface of the heart is formed primarily by the right ventricle. The right lateral border is formed by the right atrium, and the left lateral border by the left ventricle. The posterior surface is formed by the left ventricle and the left atrium which is centered equally upon the midline.

The acute angle found on the right anterior side of the heart is referred to as the *acute* margin of the heart and continues toward the diaphragmatic surface. The rounded left anterior side is referred to as the *obtuse* margin of the heart and continues posteriorly and anteriorly. Both right and left ventricles contribute equally to the diaphragmatic surface, lying in the plane of the diaphragm.

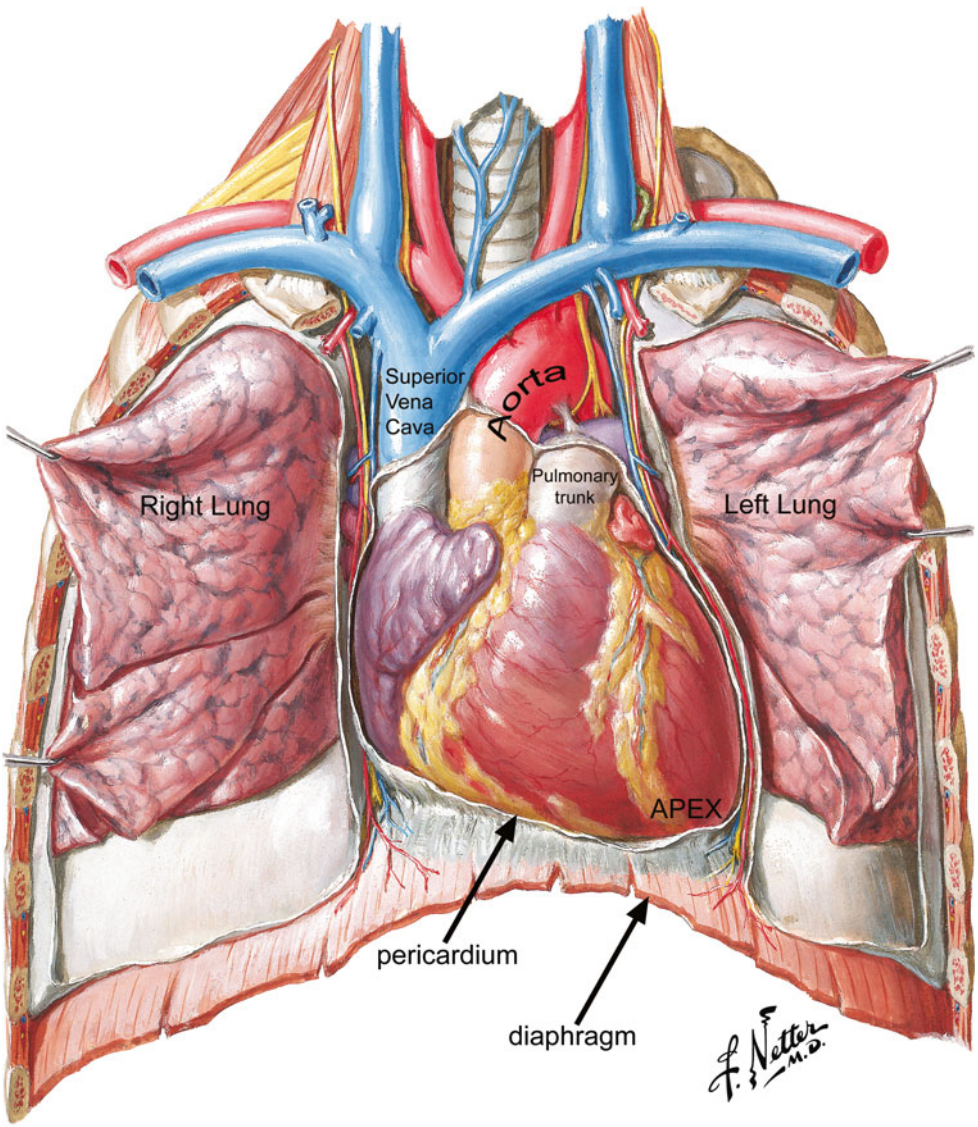

Fig. 5.3 The anterior surface of the heart. The atria are positioned superior to (posterior to) and to the right of their respective ventricles. From superior to inferior, down the anterior surface of the heart, runs the anterior interventricular sulcus ("a groove"). This sulcus separates the left and right ventricles. The base of the heart is defined by a plane that separates the atria from the ventricles called the atrioventricular groove or sulcus. Note that the great arteries, aorta, and pulmonary trunk arise from the base of the heart. The right and left atrial appendages appear as extensions hanging off each atrium. The anterior (superior) surface of the heart is formed primarily by the right ventricle. The right lateral border is formed by the right atrium, and the left lateral border by the left ventricle. The posterior surface is formed by the left ventricle and the left atrium which is centered equally upon the midline midline.

5.3 The Pericardium

The pericardium (peri = "around" + cardia = "heart") is the covering around the heart. It is a serous membrane, composed of two distinct but continuous layers that are separated from each other by a potential space containing a lubricating substance called serous fluid. During embryological development, the heart moves from a peripheral location into a space or cavity. This cavity has a serous fluid-secreting lining. As the heart migrates into the cavity, the serous lining wraps around the heart. This process can be described as being similar to a fist being pushed into a balloon (Fig. 5.4). Note that the fist is surrounded by balloon; however, it does not enter the balloon, and the balloon is still one continuous layer of material. These same properties are true for the pericardium. Furthermore, although it is one continuous layer, the pericardium is divided into two components. The part of the pericardium that is in contact with the heart is called the visceral pericardium (viscus = "internal organ") or epicardium (epi = "upon" + "heart"). The part of the pericardium forming the outer border is called the parietal pericardium (parietes = "walls"). The free or opposing surfaces of these serous membranes (epicardium and parietal pericardium) are covered by a single layer of flat-shaped epithelial cells called mesothelium. The mesothelial cells secrete a small amount of serous fluid to lubricate the movement of the epicardium against the parietal pericardium. The serous surfaces of the epicardium and parietal pericardium are often referred to as the serous pericardium. The outer surface of these serous membranes is a thin layer of fibroelastic connective tissue which supports the mesothelium. The epicardium also

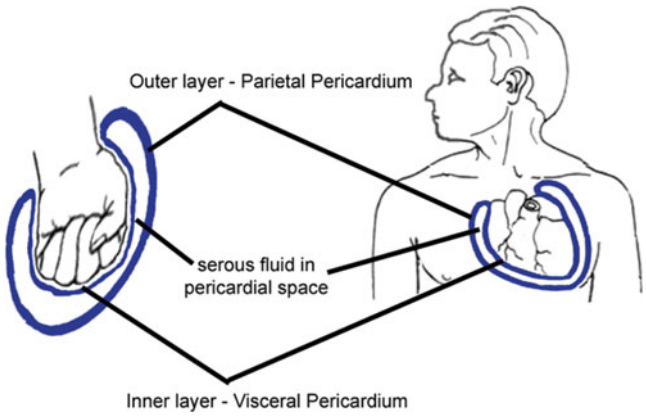

Fig. 5.4 The pericardium. The pericardium is the covering around the heart that is composed of two distinct but continuous layers that are separated from each other by a potential space containing a lubricating serous fluid. During embryological development, the heart migrates into the celomic cavity and a serous lining wraps around it, a process similar to a fist being pushed into a balloon (the balloon and pericardium is one continuous layer of material). The pericardium can be divided into the visceral pericardium (epicardium) and the parietal pericardium. A small amount of serous fluid is secreted into the pericardial space to lubricate the movement of the epicardium on the parietal pericardium. The parietal pericardium contains an epipericardial layer called the fibrous pericardium

contains a broad layer of adipose tissue between the fibroelastic layer and the heart muscle or myocardium. The parietal pericardium contains an additional layer referred to as the fibrous pericardium. This layer contains collagen and elastin fibers to provide strength to the parietal pericardium. It is important to note, however, that there is no potential space between the parietal and fibrous pericardium. The parietal pericardium, together with the fibrous pericardium, is often referred to as the fibrous pericardium.

Inferiorly, the parietal pericardium is attached to the diaphragm. Anteriorly, the superior and inferior pericardiosternal ligaments secure the parietal pericardium to the manubrium and the xiphoid process, respectively. Laterally, the parietal pericardium (specifically, the fibrous pericardium) is in contact with the parietal pleura (the covering of the lungs). Trapped between the fibrous pericardium and the parietal pleura are the phrenic nerves (motor innervation to the diaphragm). Accompanying these nerves are the pericardiacophrenic arteries and veins (supplying the nerve, pericardium, and diaphragm).

Under normal circumstances, only serous fluid exists between the visceral and parietal layers in the pericardial space or cavity. However, the accumulation of fluid (blood from trauma, inflammatory exudate following infection) in the pericardial space leads to the compression of the heart. This condition, called *cardiac tamponade* ("heart" + *tampon* = "plug"), occurs when the excess fluid limits the expansion of the heart (the fibrous pericardium resists stretching) between beats and reduces the ability to pump blood, leading to hypoxia (*hypo* = "low" + "oxygen").

Superiorly, the parietal pericardium surrounds the aorta and pulmonary trunk (about 3 cm above their departure from the heart) and is referred to as the *arterial reflections* or *arterial mesocardium*; the superior vena cava, inferior vena cava, and pulmonary veins are surrounded by the venous reflections or venous mesocardium. The outer fibrous (epipericardial) layer merges with the outer adventitial layer of the great vessels, which is continuous with the visceral pericardium. The result of this reflection is that the heart hangs "suspended" within the pericardial cavity. For more details on the Pericardium, see Chap. 9.

Within the parietal pericardium, a blind-ended saclike recess called the *oblique pericardial sinus* is formed from the venous reflections of the inferior vena cava and pulmonary veins (Fig. 5.5). A space called the *transverse pericardial sinus* is formed between the arterial reflections above and the venous reflections of the superior vena cava and pulmonary veins below. This sinus is important to cardiac surgeons in various procedures when it is important to stop or divert the circulation of blood from the aorta and pulmonary trunk. By passing a surgical clamp or ligature through the transverse sinus and around the great vessels, the tubes of a circulatory bypass machine can be inserted. For more details on cardiopulmonary bypass, see Chap. 33.

5.4 Internal Anatomy of the Heart

A cross-section cut through the heart reveals a number of layers (Fig. 5.6). From superficial to deep, these are (1) the parietal pericardium with its dense fibrous layer, the fibrous pericardium; (2) the pericardial cavity (containing only serous fluid); (3) a superficial visceral pericardium or epicardium (*epi* = "upon" + "heart"); (4) a middle myocardium (*myo* = "muscle" + "heart"); and (5) a deep lining called the endocardium (*endo* = "within"). The endocardium is the internal lining of the atrial and ventricular chambers and is continuous with the endothelium (lining) of the incoming veins and outgoing arteries. It also covers the surfaces of the AV valves, pulmonary and aortic valves, as well as the chordae tendineae and papillary muscles. The endocardium is a sheet of epithelium called *endothelium* that rests on a dense connective tissue layer consisting of elastic and collagen fibers. These fibers also extend into the core of the previously mentioned valves.

The myocardium is the tissue of the heart wall, the layer that actually contracts. The myocardium consists of cardiac muscles which are circularly and spirally arranged networks of muscle cells that squeeze blood through the heart in the proper directions (inferiorly through the atria and superiorly through the ventricles). Unlike all other types of muscle cells, (1) cardiac muscle cells branch; (2) cardiac muscles join together at complex junctions called *intercalated disks*, so that they form cellular networks; and (3) each cell contains

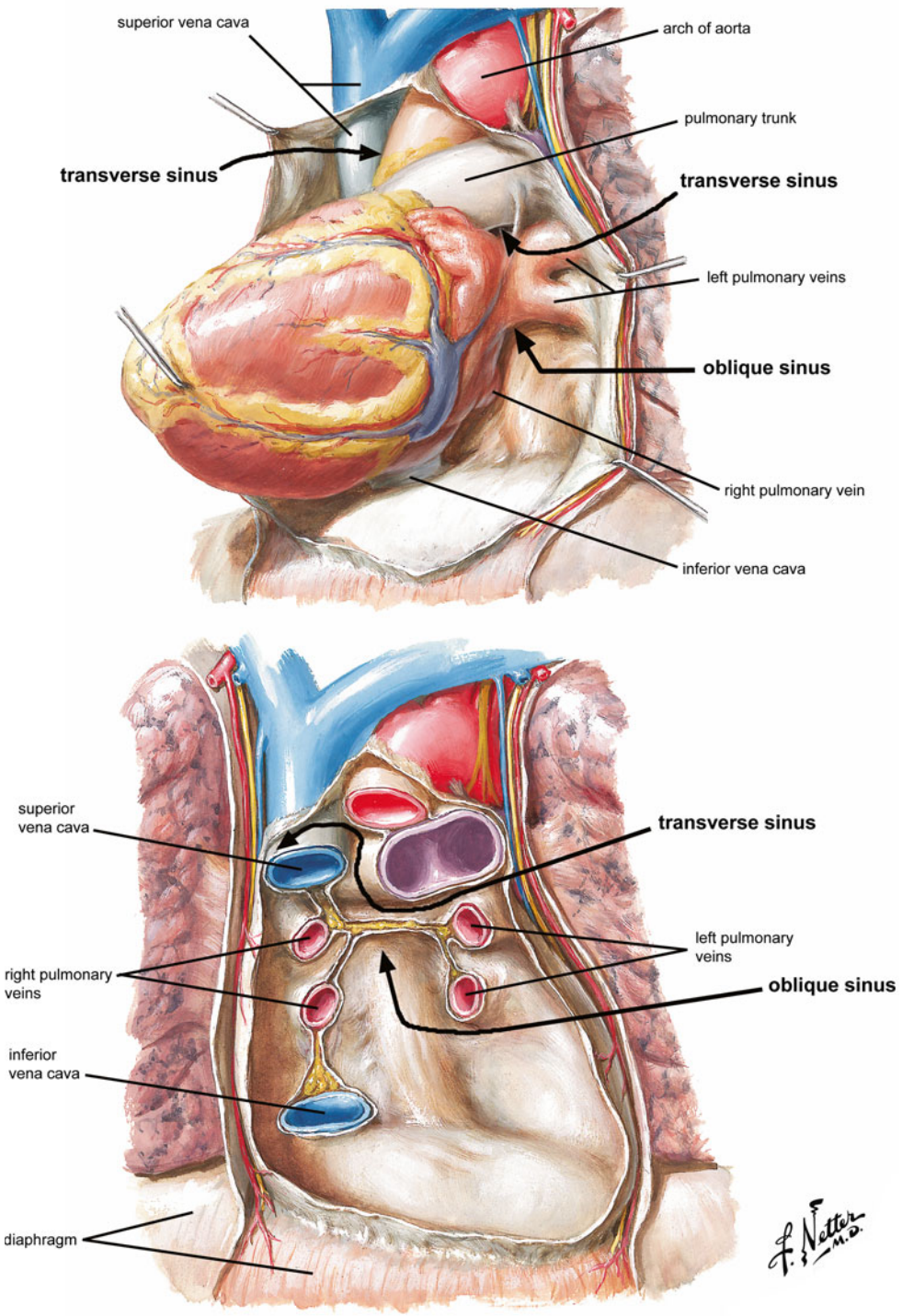

Fig. 5.5 Pericardial sinuses. (**a**) A blind-ended sac called the oblique pericardial sinus is formed from the venous reflections of the inferior vena cava and pulmonary veins. (**b**) Another sac, the transverse pericardial sinus, is formed between the arterial reflections above and the venous reflections of the superior vena cava and pulmonary veins below below. © 2006 Elsevier Inc. All rights reserved. www.netterimages.com, Frank Netter

single centrally located nuclei. A cardiac muscle cell is not called a fiber. The term cardiac muscle fiber, when used, refers to a long row of joined cardiac muscle cells.

Like skeletal muscle, cardiac muscle cells are triggered to contract by Ca^{2+} ions flowing into the cell. Cardiac muscle cells are joined by complex junctions called *intercalated disks*. The disks contain adherens to hold the cells together, and there are gap junctions to allow ions to pass easily between the cells. The free movement of ions between cells allows for the direct transmission of an electrical impulse through an entire network of cardiac muscle cells. This impulse, in turn, signals all the muscle cells to contract at the same time. For more details on the electrical properties of the heart, the reader is referred to Chap. 13.

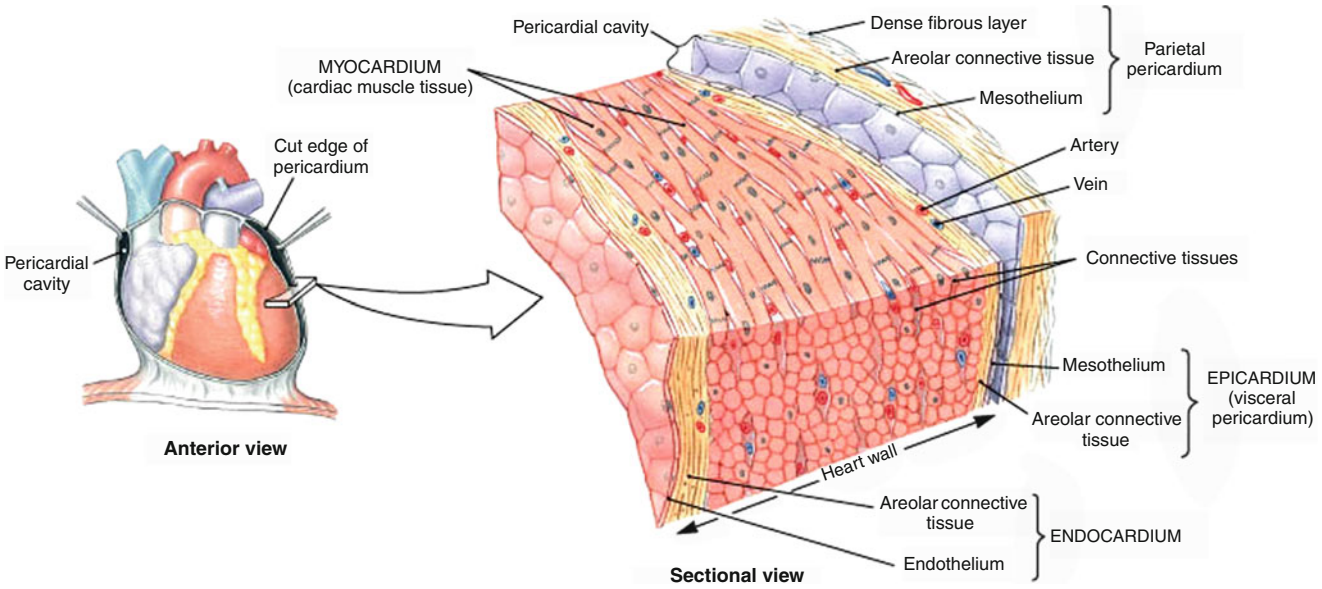

Fig. 5.6 Internal anatomy of the heart. The walls of the heart contain three layers—the superficial epicardium, the middle myocardium composed of cardiac muscle, and the inner endocardium. Note that cardiac muscle cells contain intercalated disks which enable the cells to communicate and allow direct transmission of electrical impulses from one cell to another. Martini, Frederic H.; Timmons, Michael J.; Tallitsch, Robert B., Human Anatomy, 4th, © 2003. Printed and electronically reproduced by permission of Pearson Education, Inc., New York, New York

5.4.1 Cardiopulmonary Circulation

In order to best understand the internal anatomy of the heart, it is desirable to first understand its general function. The heart has two primary functions—collect oxygen-poor blood and pump it to the lungs for the release of carbon dioxide in exchange for oxygen and collect oxygen-rich blood from the lungs and pump it to all tissues in the body to provide oxygen in exchange for carbon dioxide.

The four chambers in the heart can be segregated into the left and the right side, each containing an atrium and a ventricle. The right side is responsible for collecting oxygen-poor blood and pumping it to the lungs. The left side is responsible for collecting oxygen-rich blood from the lungs and pumping it to all tissues in the body. Within each side, the atria are the sites where blood collects and passes through to the ventricles and then they contract to eject the final volumes of blood into the ventricles. The ventricle is much stronger, and it is a site for the pumping of blood out and away from the heart (Figs. 5.7 and 5.8).

The right ventricle is the site for the collection of ALL oxygen-poor blood. The large superior and inferior venae cavae, among other veins, carry oxygen-poor blood from the upper and lower parts of the body to the right atrium. The right ventricle pumps the blood out of the heart and through the pulmonary trunk. The term *trunk*, when referring to a vessel, is a convention that indicates an artery that bifurcates. The pulmonary trunk bifurcates into the left and right pulmonary arteries that enter the lungs. It is important to note that the term "artery" is always used for a vessel that carries blood AWAY from the heart. This is irrespective of the oxygen content of the blood that flows through the vessel.

Once oxygenated, the oxygen-rich blood returns to the heart from the right and left lung through the right and left pulmonary vein, respectively ("vein"—a vessel carrying blood *toward* the heart). Each pulmonary vein bifurcates before reaching the heart. Thus, there are typically four pulmonary veins entering the left atrium. Oxygen-rich blood is pumped out of the heart by the left ventricle and into the aortic artery.

Observing the heart from a superior vantage point, the pulmonary trunk assumes a leftmost anterior location projecting upward from the base of the heart, the aorta is located in a central location, and the superior vena cava has the rightmost posterior location.

5.4.2 The Right Atrium

The interior of the right atrium has three anatomically distinct regions, each a remnant of embryologic development. The posterior portion of the right atrium has a smooth wall and is referred to as the *sinus venarum* (embryologically derived from the right horn of the sinus venosus). The wall of the anterior portion of the right atrium is lined by horizontal, parallel ridges of muscle bundles that resemble the teeth of a comb, hence the name *pectinate* muscle (*pectin* = "a comb," embryologically derived from the primitive right atrium).

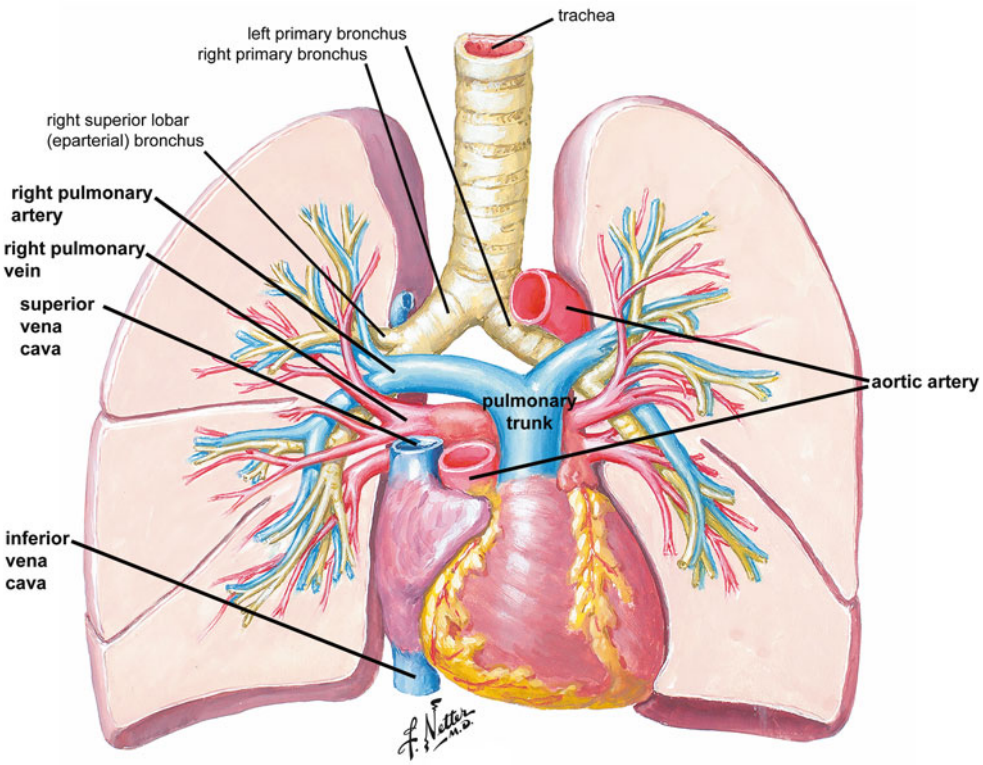

Fig. 5.7 Cardiopulmonary circulation. The four chambers in the heart can be segregated into the left and the right side, each containing an atrium and a ventricle. The *right side* is responsible for collecting oxygen-poor blood and pumping it to the lungs. The *left side* is responsible for collecting oxygen-rich blood from the lungs and pumping it to the body. An artery is a vessel that carries blood away from the heart, while a vein is a vessel that carries blood toward the heart. The pulmonary trunk and arteries carry blood to the lungs. Exchange of carbon dioxide for oxygen occurs in the lung through the smallest of vessels, the capillaries. Oxygenated blood is returned to the heart through the pulmonary veins and collected in the left atrium atrium. www.netterimages.com, Frank Netter

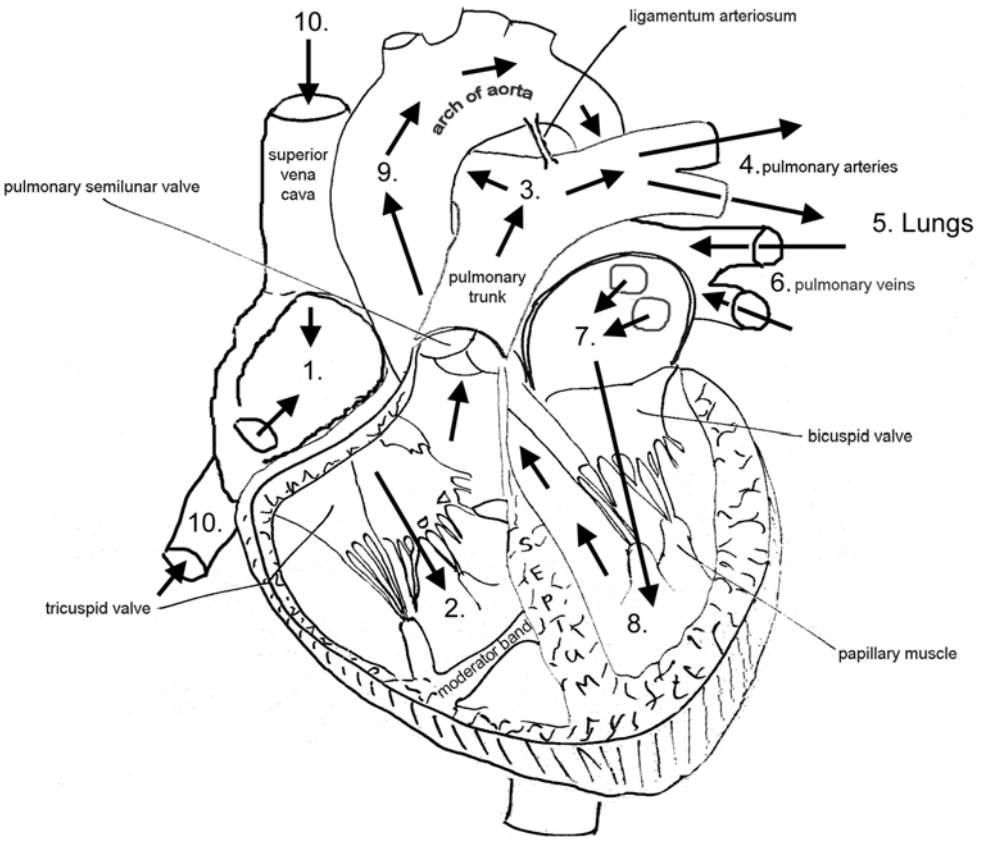

Fig. 5.8 Cardiac circulation. Blood collected in the right atrium is pumped into the right ventricle. Upon contraction of the right ventricle, blood passes through the pulmonary trunk and arteries to the lungs. Oxygenated blood returns to the left atrium via pulmonary veins. The left atrium pumps the blood into the left ventricle. Contraction of the left ventricle sends the blood through the aortic artery to all tissues in the body. The release of oxygen in exchange for carbon dioxide occurs through capillaries in the tissues. Return of oxygen-poor blood is through the superior and inferior vena cavae which empty into the right atrium. Note that a unidirectional flow of blood through the heart is accomplished by valves

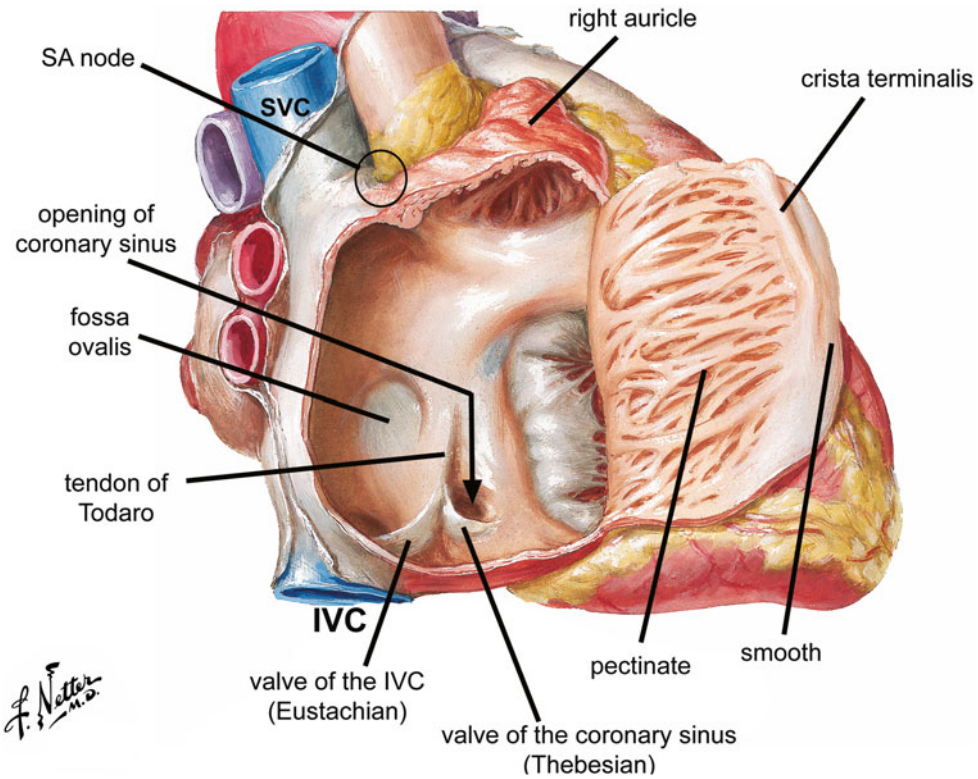

Fig. 5.9 Internal anatomy of the right atrium. The interior of the right atrium has three anatomically distinct regions: (1) the posterior portion (sinus venarum) which has a smooth wall; (2) the wall of the anterior portion which is lined by horizontal, parallel ridges of muscle referred to as pectinate; and (3) the atrial septum septum. © 2006 Elsevier Inc. All rights reserved. www.netterimages.com, Frank Netter

Finally, the interatrial septum is primarily derived from the embryonic septum primum and septum secundum. For more details on the embryology of the heart, refer to Chap. 3.

The smooth posterior wall of the right atrium holds the majority of the named structures of the right atrium. It receives both the superior and inferior vena cavae and the coronary sinus. It also contains the fossa ovalis, the sinoatrial (SA) node, and the AV node.

The inferior border of the right atrium contains the opening or ostium of the inferior vena cava and the os or ostium of the coronary sinus (Fig. 5.9). The coronary sinus is located on the posterior (inferior) side of the heart and receives almost all of the deoxygenated blood from the vasculature of the heart. The os of the coronary sinus opens into the right atrium anteriorly/inferiorly to the orifice of the inferior vena cava. A valve of the inferior vena cava (Eustachian valve, a fetal remnant) guards the orifice of the inferior vena cava (Bartolommeo E. Eustachio, Italian Anatomist, 1520–1574). The valve of the coronary sinus (Thebesian valve) covers the opening of the coronary sinus (fetal remnant to prevent backflow, Adam C. Thebesius, German physician, 1686–1732). Both of these valves vary in size and presence. These two venous valves insert into a prominent ridge, the Eustachian ridge (sinus septum), that runs medial–lateral across the inferior border of the atrium and separates the os of the coronary sinus and inferior vena cava. For more details on the valves of the heart, refer to Chap. 34.

On the medial side of the right atrium, the interatrial septum (atrial septum) has an interatrial and an atrioventricular part. The fossa ovalis (a fetal remnant) is found in the interatrial part of the atrial septum. It appears as a central depression surrounded by a muscular ridge or limbus. The fossa ovalis is positioned anterior and superior to the ostia of both the inferior vena cava and the coronary sinus. A tendinous structure, the tendon of Todaro, crosses the floor of the right atrium. It connects the valve of the inferior vena cava to a portion of the interventricular septum (between ventricles). More specifically, the tendon connects to the central fibrous body (the right fibrous trigone) as a fibrous extension of the membranous portion of the interventricular septum. It courses obliquely within the Eustachian ridge and separates the fossa ovalis above from the coronary sinus below. This tendon likely has a structural role to support the inferior vena cava via the Eustachian valve and is a useful landmark in approximating the location of the AV node (conduction system).

To approximate the location of the AV node, found in the floor of the right atrium and the atrial septum, it is necessary to form a triangle (triangle of Koch; Walter Koch, German surgeon, unknown–1880) using the following structures: (1) the os of the coronary sinus, posteriorly; (2) the right AV opening, anteriorly; and (3) the tendon of Todaro, posteriorly (Fig. 5.10).

In the lateral wall and the septum of the smooth portion of the right atrium are numerous small openings in the endocardial surface. These openings are the ostia of the smallest cardiac (Thebesian) veins. These veins function to drain deoxygenated blood from the myocardium to

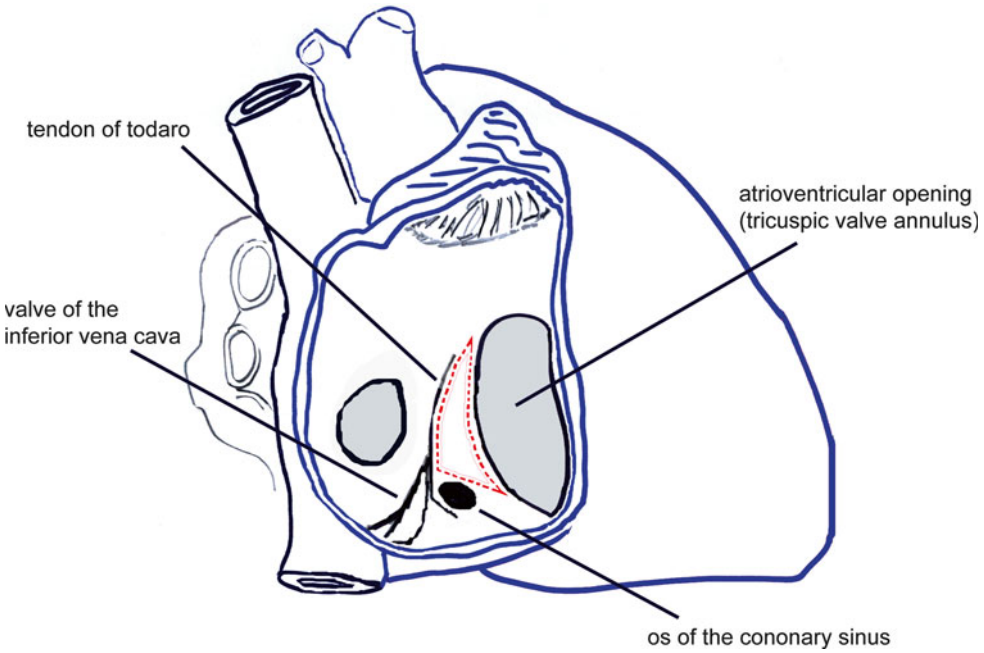

Fig. 5.10 Koch's triangle. Three landmarks are used to triangulate (*dotted red lines*) the location of the atrioventricular node (Taware's node) of the conduction system: (1) coronary sinus, (2) atrioventricular opening, and (3) tendon of Todaro

empty into the right atrium which is the collecting site for all deoxygenated blood (for more details on cardiac vasculature, see Chap. 8).

In the anterior–superior portion of the right atrium, the smooth wall of the interior becomes the pectinate portion of the right atrium. The smooth and pectinate regions are separated by a ridge, the *crista terminalis* (*crista* = "crest" + "terminal"). The ridge represents the end of the smooth wall and the beginning of the pectinate wall. It begins at the junction of the right auricle with the atrium and passes inferiorly over the "roof" of the atrium. The crista runs inferiorly and parallel to the openings of the superior and inferior vena cavae. As early as the developing embryo, the crista terminalis separates the sinus venosus and the primitive atrium and remains to separate the smooth and the pectinate portion of the right atrium in the definitive heart. The crista terminalis on the internal side results in a groove on the external side of the atrium called the sulcus terminalis.

The SA node is the "pacemaker" of the conduction system. The SA node is located between the myocardium and epicardium in the superior portion of the right atrium. The intersection of three lines indicates the location of the SA node: (1) the sulcus terminalis, (2) the lateral border of the superior vena cava, and (3) the superior border of the right auricle (Fig. 5.11). The name of the SA node is derived from its location between the sinus venarum and primitive atrium. The crista terminalis is the division between these two components in the fetus and adult. It seems logical that the sulcus terminalis is a useful landmark for the approximation of the location of the SA node.

5.4.3 The Right Ventricle

The right ventricle receives blood from the right atrium and pumps it to the lungs through the pulmonary trunk and arteries. Most of the anterior surface of the heart is formed by the right ventricle (Fig. 5.12). Abundant, coarse trabeculae carneae ("beams of meat") characterize the walls of the right ventricle. Trabeculae carneae are analogous to pectinate muscle of the right atrium and are found in both the right and left ventricles. The outflow tract, conus arteriosus ("arterial cone"), and infundibulum ("funnel") carry blood out of the ventricle in an anterior–superior direction and can be quite variable in structure—smooth walled or highly trabeculated. A component of the conus arteriosus forms part of the interventricular septum. This small septum, the infundibular (conal) septum, separates the left and right ventricular outflow tracts and is located just inferior to both semilunar valves. Four distinct muscle bundles, collectively known as the *semicircular arch*, separate the outflow tract from the rest of the right atrium. These muscle bundles are also known as the *supraventricular* crest and the *septomarginal trabeculae*.

5.4.3.1 Tricuspid Valve

Blood is pumped from the right atrium through the AV orifice into the right ventricle. When the right ventricle contracts, blood is prevented from flowing back into the atrium by the right AV valve or *tricuspid* ("three cusps") valve. The valve consists of the annulus, three valvular leaflets, three papillary muscles, and three sets of chordae tendineae (Figs. 5.12 and 5.13). The AV orifice is reinforced by the annulus fibro-

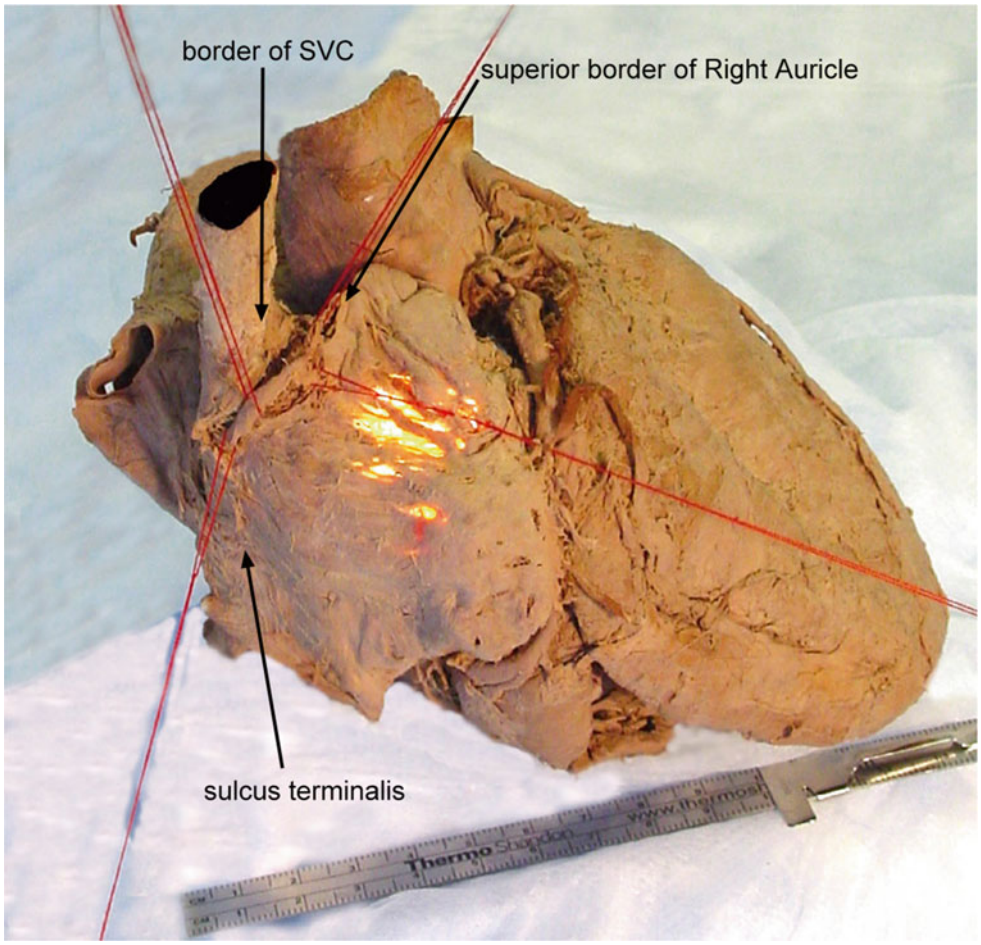

Fig. 5.11 Location of the sinoatrial node. Human cadaver heart demonstrating that the intersection of three lines indicates the position of the sinoatrial node (pacemaker of the conduction system) in the smooth muscle portion of the right atrium: (1) the sulcus terminalis, (2) the lateral border of the superior vena cava, and (3) the superior border of the right auricle. Note the muscle fiber bundles in the wall of the pectinate portion of right atrium. *IVC* inferior vena cava, *SVC* superior vena cava

sus of the cardiac skeleton (dense connective tissue). Medially, the annulus is attached to the membranous interventricular septum.

The tricuspid valve has three leaflets—anterior (superior), posterior (inferior), and septal. The anterior leaflet is typically the largest and extends from the medial border of the ventricular septum to the anterior free wall. This, in effect, forms a partial separation between the inflow and outflow tracts of the right ventricle. The posterior leaflet extends from the lateral free wall to the posterior portion of the ventricular septum. The septal leaflet tends to be somewhat oval in shape and extends from the annulus of the orifice to the medial side of the interventricular septum (on the inflow side), often including the membranous part of the septum (see also Chaps. 2 and 7 for other nomenclature describing these leaflets).

Papillary ("nipple") muscles contract and "tug" down on chordae tendineae ("tendinous cords") that are attached to the leaflets, in order to secure them in place in preparation for the contraction of the ventricle. This is done to prevent the prolapse of the leaflets up into the atrium. This is somewhat analogous to the tightening of the sails on a yacht, in preparation for a big wind. Note that the total surface area of the cusps of the AV valve is approximately twice that of the respective orifice, so that considerable overlap of the leaflets occurs when the valves are in the closed position. The leaflets remain relatively close together even during ventricular filling. The partial approximation of the valve surfaces is caused by eddy currents that prevail behind the leaflets and by tension that is exerted by the chordae tendineae and papillary muscle. As the filling of the ventricle reduces, the valve leaflets float toward each other, but the valve does not close. The valve is closed by ventricular contractions, and the valve leaflets, which bulge toward the atrium but do not prolapse, stay pressed together throughout ventricular contraction. The junction between two leaflets is called a *commissure* and is named by the two adjoining leaflets (anteroseptal, anteroposterior, and posteroseptal). Each commissure contains a relatively smooth arc of valvular tissue that is delineated by the insertion of the chordae tendineae.

There are three papillary muscles, just as there are three leaflets or cusps. The anterior papillary muscle is located in the apex of the right ventricle. This is the largest of the papillary muscles in the right ventricle, and it may have one, two, or more heads. When this papillary muscle contracts, it pulls on chordae tendineae that are attached to the margins of the anterior and posterior leaflets. The posterior papillary

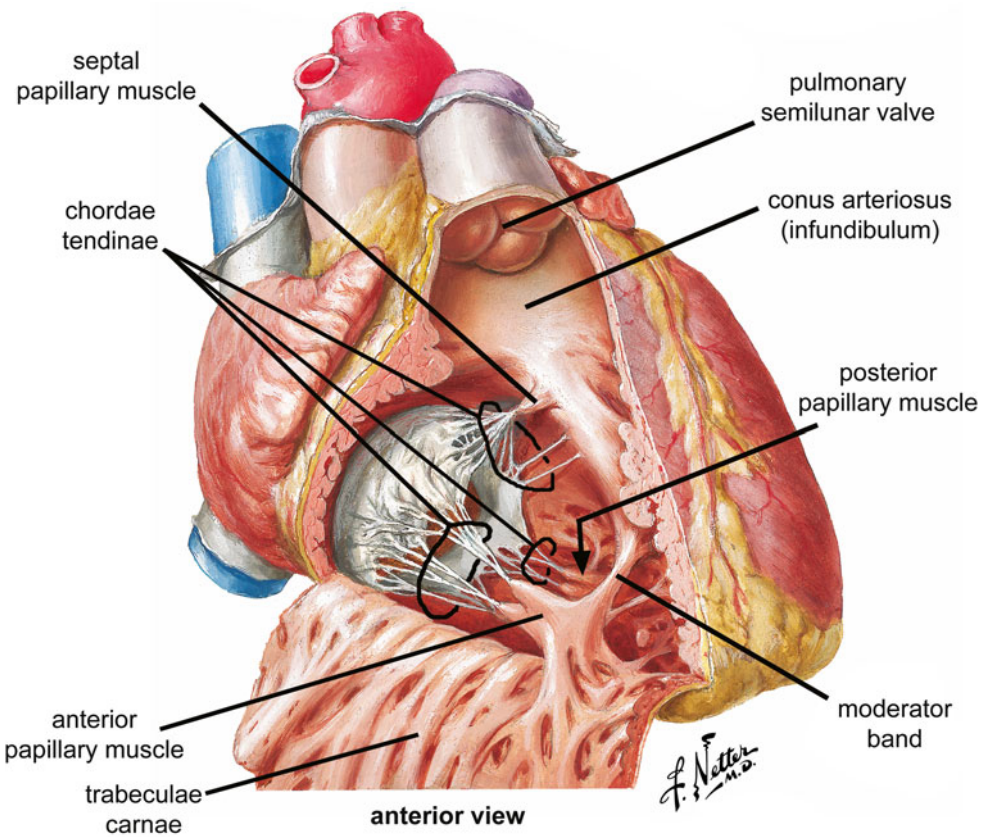

Fig. 5.12 Internal anatomy of the right ventricle. Coarse trabeculae carneae characterize the walls of the right ventricle. The conus arteriosus makes up most of the outflow tract. The right atrioventricular or tricuspid valve is made up of three sets of cusps, chordae tendineae, and papillary muscles.

muscle is small and located in the posterior lateral free wall. When this papillary muscle contracts, it pulls on chordae tendineae that are attached to posterior and septal leaflets. The septal papillary muscle (including the variable papillary of the conus) arises from the muscular interventricular septum near the outflow tract (conus arteriosus). This papillary muscle may consist of a collection of small muscles in close proximity and has attachments to the anterior and septal valve leaflets. In addition, chordae tendineae in this region may extend simply from the myocardium and attach to the valve leaflets directly without a papillary muscle. The most affected is the septal leaflet which has restricted mobility due to extensive chordae tendineae attachment directly to the myocardium. In addition, there is a variable set of papillary muscles that should be considered. The medial papillary muscle complex is a collection of small papillary muscles with chordae attachments to septal and anterior cusps. This complex is located in the uppermost posterior edge of the septomarginal trabeculae, just inferior to the junction of the septal and anterior leaflets of the tricuspid valve, and is superior and distinct from the septal papillary muscles. An important feature of this complex is that it serves as an important landmark for identification of the right bundle branch as it runs posterior to it, deep to the endocardium [1].

Near the anterior free wall of the right ventricle is a muscle bundle of variable size, the *moderator band*, which is occasionally absent. This muscle bundle extends from the interventricular septum to the anterior papillary muscle and contains a primary portion of the right bundle branch of the conduction system. It seems logical that the anterior papillary muscle, with its remote location away from the septum, would need special conduction fibers in order for it to contract with the other papillary muscles and convey control of the valve leaflets equal to the other valve leaflets. The moderator band is a continuation of another muscle bundle, the septal band (septal trabeculae). Together they are called *septomarginal trabeculae* and are components of the semicircular arch (delineation of the outflow tract).

5.4.3.2 Pulmonary Semilunar Valve

During ventricular systole, blood is pumped from the right ventricle into the pulmonary trunk and arteries toward the lungs. When the right ventricle relaxes, in diastole, blood is prevented from flowing back into the ventricle by the pulmonary semilunar valve (Figs. 5.12 and 5.13). The semilunar valve is composed of three symmetric semilunar-shaped cusps. Each cusp looks like a cup composed of a thin membrane. Each cusp acts like an upside-down parachute facing into the pulmonary trunk, opening as it

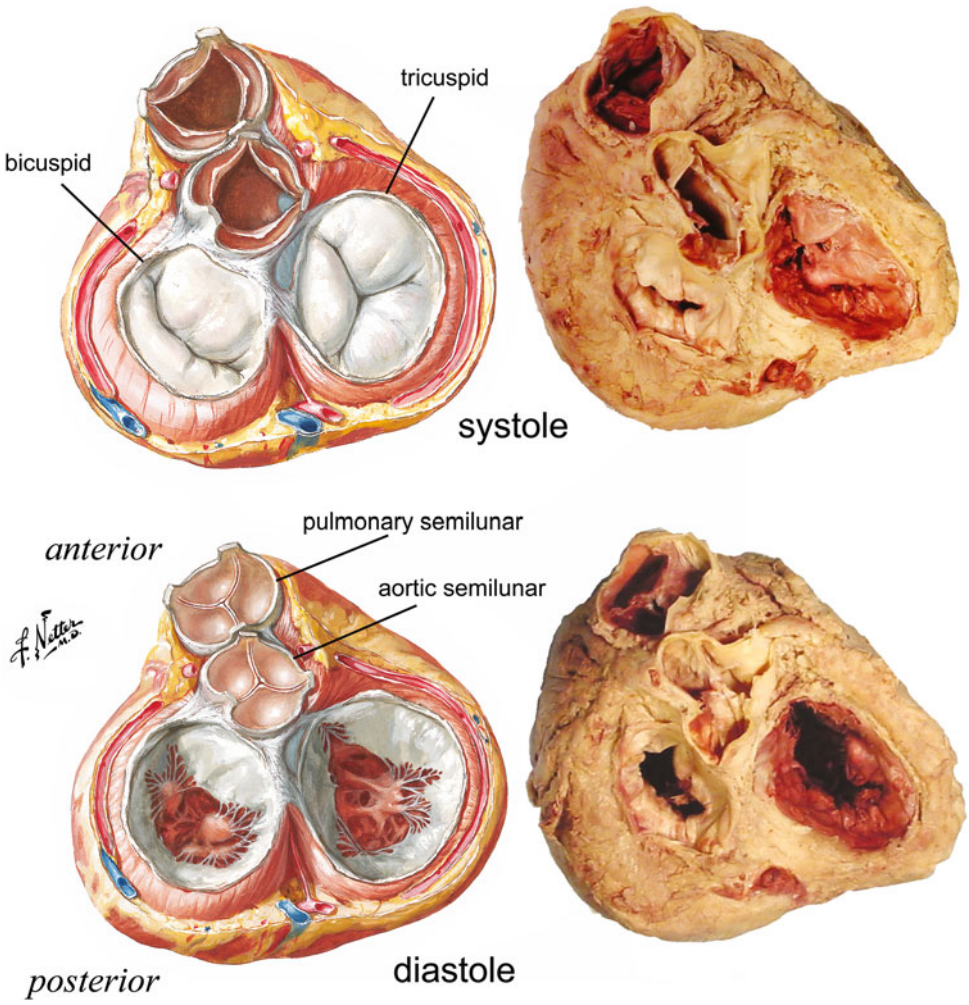

Fig. 5.13 Valves of the heart. During ventricular systole, atrioventricular (AV) valves close in order to prevent the regurgitation of blood from the ventricles into the atria. The right AV valve is the tricuspid valve; the left is the bicuspid valve. During ventricular diastole, the AV valves open as the ventricles relax, and the semilunar valves close. The semilunar valves prevent the backflow of blood from the great arteries into the resting ventricles. The valve of the pulmonary trunk is the pulmonary semilunar valve, and the aortic artery has the aortic semilunar valve. To the right of each figure are human cadaveric hearts.

fills with blood. This filled space or recess of each cusp is called the *sinus of Valsalva*. Upon complete filling, the three cusps contact each other and block the flow of blood. Each of the three cusps is attached to an annulus ("ring") such that the cusp opens into the lumen, forming a U shape. The annulus is anchored to both the right ventricular infundibulum and the pulmonary trunk. The cusps are named according to their orientation in the body—anterior, left (septal), and right.

During ventricular systole, as the right ventricle contracts, the cusps collapse against the arterial wall as blood is flowing past them. When the ventricle rests (diastole), the cusps meet in the luminal center. There is a small thickening on the center of the free edge of each cusp, at the point where the cusps meet. This nodule (of Arantius or Morgagni) ensures central valve closure (Giulio C. (Aranzi) Arantius, Italian anatomist and physician, 1530–1589; Giovanni B. Morgagni, Italian anatomist and pathologist, 1682–1771). Radiating from this nodule around the free edge of the cusp is a ridge, the *linea alba* ("line" + "white").

5.4.4 The Left Atrium

The left atrium (Fig. 5.14) receives oxygenated blood from the lungs via the left and right pulmonary veins. The pulmonary veins typically enter the heart as two pairs of veins inserting posteriorly and laterally into the left atrium (individuals with 3 or 5 pulmonary veins have also been identified).

The left atrium is found midline, posterior to the right atrium and superior to the left ventricle. Anteriorly, a left atrial appendage (auricle) extends over the atrioventricular (coronary) sulcus. The walls of the atrial appendage are pectinate, and the walls of the left atrium are smooth, reflecting their embryological origin. The atrial appendage is derived from the primitive right atrium (which was pectinate). The left atrium is derived from the fetal pulmonary vein as a connection with the embryonic pulmonary venous plexus. These venous structures are absorbed into the left atrium, resulting in the posterolateral connections of the right and left pulmonary veins.

The portion of the interatrial septum on the left atrial side is derived from the embryonic septum primum. In the left

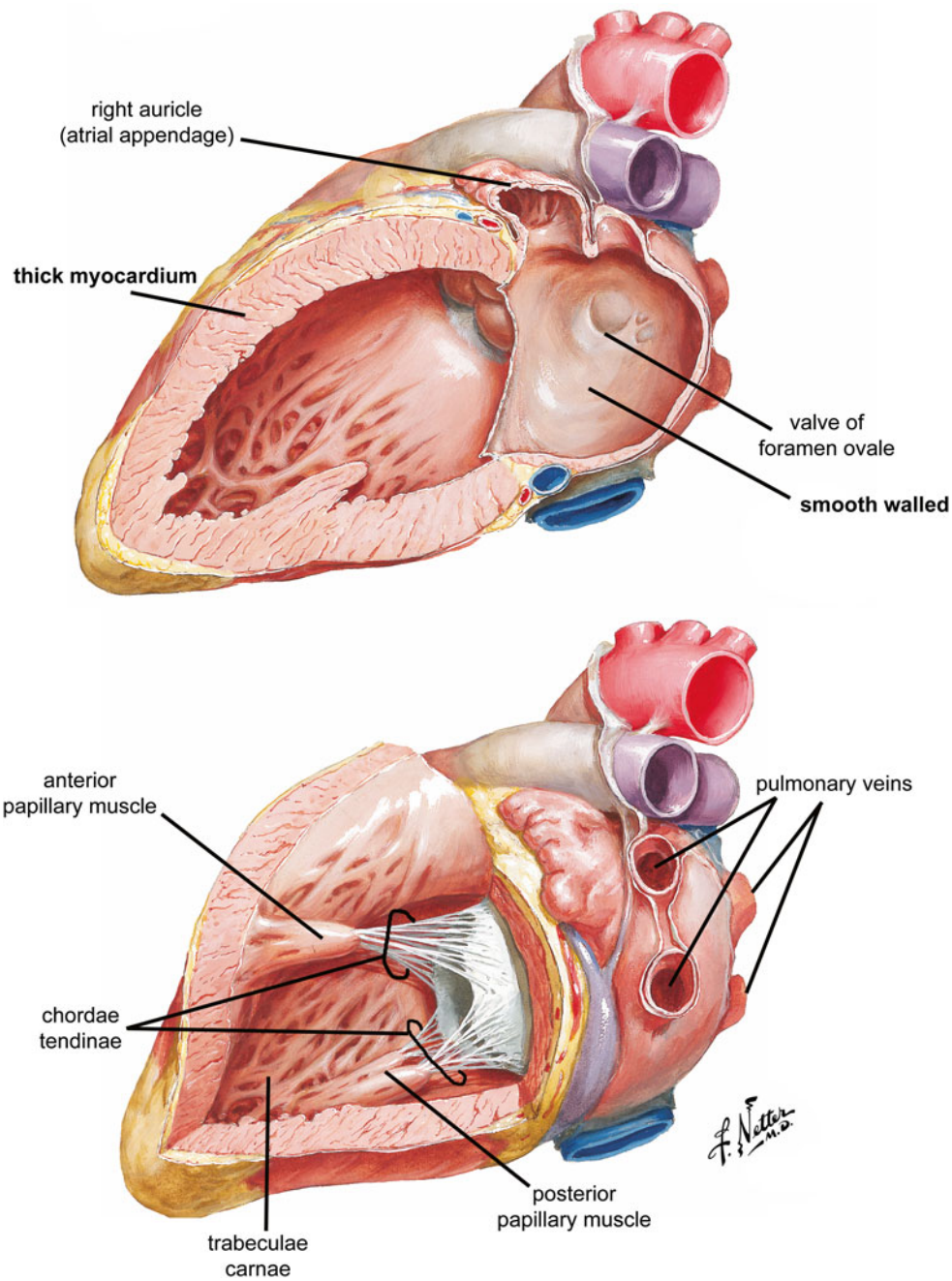

Fig. 5.14 Internal anatomy of the left atrium and ventricle. The left atrium receives oxygenated blood from the lungs via the left and right pulmonary veins. The pulmonary veins enter the heart as two pairs of veins inserting posteriorly and laterally. Anteriorly, the pectinate left auricle extends over the smooth-walled atrium. Most of the left lateral surface of the heart is formed by the left ventricle. Trabeculae carneae characterize the walls and the myocardium is much thicker than the left ventricle. The interventricular septum bulges into the right ventricle, creating a barrel-shaped left ventricle. © 2006 Elsevier Inc. All rights reserved. www.netterimages.com, Frank Netter

atrium, the resulting structure in the adult is called the *valve of the foramen ovale* (a sealed valve flap).

5.4.5 The Left Ventricle

The left ventricle receives blood from the left atrium and pumps it through the aortic artery to all the tissues of the body (Fig. 5.14). Most of the left lateral surface of the heart is formed by the left ventricle, also forming part of the inferior and posterior surfaces. As with the right ventricle, abundant trabeculae carneae ("beams of meat") characterize the walls of the left. However, in contrast to the right ventricle, the muscular ridges tend to be relatively finer. Also in contrast to the right ventricle, the myocardium in the wall of the left ventricle is much thicker. The interventricular septum appears from within the left ventricle to bulge into the right ventricle. This creates a barrel-shaped left ventricle.

5.4.5.1 Bicuspid (Mitral) Valve

Blood is pumped from the left atrium through the left AV orifice into the left ventricle. When the left ventricle contracts, blood

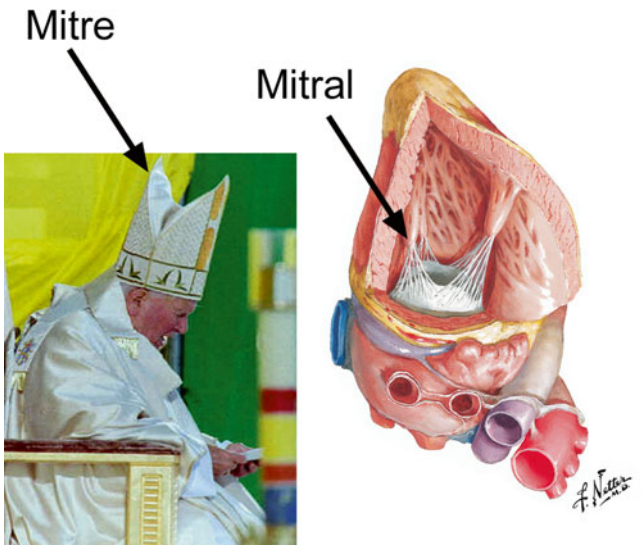

Fig. 5.15 The mitral valve. The mitral (left atrioventricular or bicuspid) valve is so named because of its resemblance to a cardinal's hat, known as a miter. *Left*: Photo of Pope John Paul II from the Vatican web site; *Right*: © 2006 Elsevier Inc. All rights reserved. www.netterimages.com, Frank Netter

is prevented from flowing back into the atrium by the left AV valve or bicuspid ("two cusps") valve (Figs. 5.13 and 5.14). The valve consists of the annulus, two leaflets, two papillary muscles, and two sets of chordae tendineae.

The atrioventricular orifice is partly reinforced by the annulus fibrosus of the cardiac skeleton. The annulus fibrosus supports the posterior and lateral two-thirds of the annulus. The remaining medial third is supported by attachment to the left atrium and by fibrous support to the aortic semilunar valve.

The bicuspid valve typically has two leaflets—anterior (medial or aortic) and posterior (inferior or mural, "wall"). The two opposing leaflets of the valve resemble a bishop's hat or miter. Thus, the bicuspid valve is often referred to as the *mitral valve* (Fig. 5.15).

The anterior leaflet is trapezoidal-shaped. The distance from its attachment on the annulus to its free edge is longer than the length of attachment across the annulus. In contrast, the posterior leaflet is relatively narrow, with a very long attachment distance across the annulus. The distance from annulus to free edge in the anterior cusp is twice as long as the posterior cusp. The posterior cusp is so long and narrow that the free edge is often subdivided into the anterior, central, and posterior crescent shapes. Note that each of these two leaflets may also have numerous scallops within them (see also Chap. 7).

Papillary muscles, in conjunction with chordae tendineae, attach to the leaflets in order to secure them in place. This is done in preparation for the contraction of the ventricle to prevent the prolapse of the leaflets up into the atrium. As with the other AV valve, the total surface area of the two cusps of the valve is significantly greater than the area described by the orifice. There is considerable overlap of the leaflets when the valves are in the closed position (Fig. 5.13).

As with the tricuspid valve, the leaflets remain relatively close together even when the atrium is contracting and the ventricle is filling. The partial approximation of the valve surfaces is caused by eddy currents that prevail behind the leaflets and by tension that is exerted by the chordae tendineae and papillary muscle. In the open position, the leaflets and commissures are in an oblique plane of orientation that is roughly parallel to the ventricular septum. The valve is closed by ventricular contractions. The valve leaflets, which bulge toward the atrium, stay pressed together throughout the contraction and do not prolapse. The junctions of the two leaflets are called the *anterolateral* and the *posteromedial* commissures. The line of apposition of the leaflets during valvular closure is indicated by a fibrous ridge.

There are commonly two papillary muscles of the left ventricle that extend from the ventricular free wall toward and perpendicular to the atrioventricular orifice. The anterior papillary muscle is slightly larger than the posterior, and each papillary muscle consists of a major trunk that often may elicit multiple heads from which extend the chordae tendineae. The chordae tendineae of each papillary muscle extend to the two valvular commissures and to the multiple crescent shapes of the posterior cusp. Thus, each papillary muscle pulls on chordae from both leaflets. In addition, the posterior leaflet occasionally has chordae that extend simply from the ventricular myocardium without a papillary muscle.

5.4.5.2 Aortic Semilunar Valve

During ventricular systole, blood is pumped from the left ventricle into the aortic artery to all of the tissues of the body. When the left ventricle relaxes in diastole, blood is prevented from flowing back into the ventricle by the aortic semilunar valve (Figs. 5.13 and 5.14). Like the pulmonary semilunar valve, the aortic valve is composed of three symmetric semilunar-shaped cusps, and each cusp acts like an upside-down parachute facing into the aortic artery, opening as it fills with blood. The filled space or recess of each cusp is called the *sinus of Valsalva* (Antonio M. Valsalva, 1666–1723). Upon complete filling, the three cusps contact each other and block the flow of blood. Each of the three cusps is attached to an annulus ("ring") such that the cusp opens into the lumen forming a U shape. The cusps are firmly anchored to the fibrous skeleton within the root of the aorta (Fig. 5.16). A circular ridge on the innermost aspect of the aortic wall, at the upper margin of each sinus, is the sinotubular ridge—the junction of the sinuses and the aorta.

At the sinotubular ridge, the wall of the aorta is thin, bulges slightly, and is the narrowest portion of the aortic artery. The cusps are named according to their orientation in the body—left and right (both facing the pulmonary valve) and posterior. Within the sinuses of Valsalva, there are open-

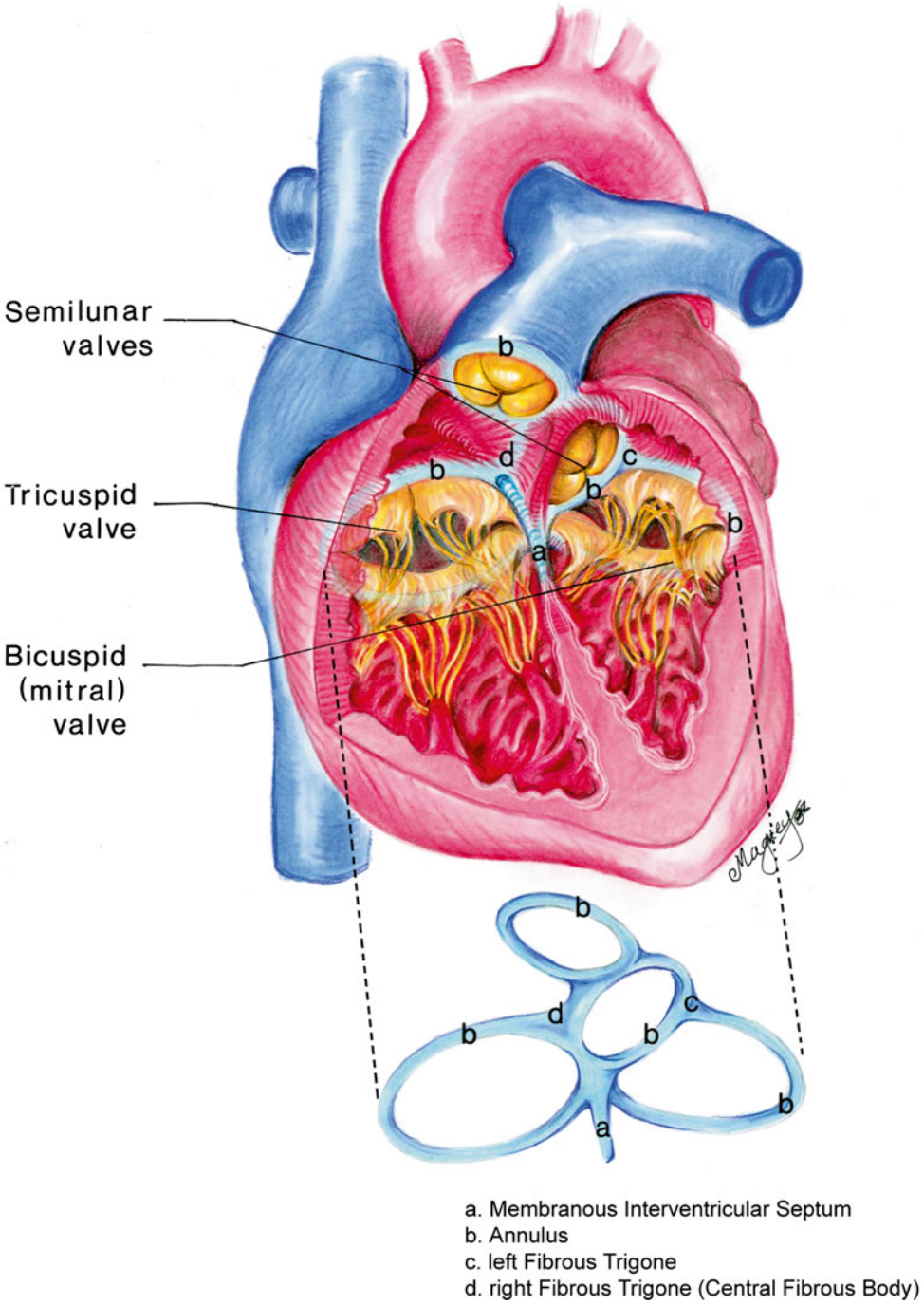

Fig. 5.16 The cardiac skeleton. The cardiac skeleton consists of a dense connective tissue that functions to attach the atrial and ventricular myocardium, support and reinforce the openings of the four valves of the heart, and electrically separate the ventricles from the atria. Courtesy of Jean Magney, University of Minnesota

ings or ostia (*ostium* = "door or mouth") into the blood supply of the heart called *coronary arteries*. These ostia are positioned below the sinotubular junction near the center of the sinuses. Only the two sinuses facing the pulmonary valve (left and right) have ostia that open into the left and right coronary arteries, respectively. Coronary arteries carry oxygenated blood to the myocardium of the heart. During ventricular diastole, the aortic valve snaps shut as pressure in the aorta increases. Under such pressure, the walls of the great artery distend, the sinuses fill, and blood is sent under great pressure through the coronary ostia into the coronary arteries. The posterior (noncoronary) sinus is in a position that it abuts the fibrous skeleton and the annuli of both AV valves (Fig. 5.13).

When the left ventricle contracts, the cusps collapse against the arterial wall as blood flows past them. When the ventricle rests (diastole), the cusps meet in the luminal center. As with the pulmonary valve, there is a small thickening

on the center of the free edge of each cusp, at the point where the cusps meet. This nodule (of Arantius or Morgagni) ensures central valve closure. Radiating from this nodule around the free edge of the cusp is a ridge, the *linea alba* ("line" + "white"). This valve is exposed to a greater degree of hemodynamic stress than the pulmonary valve. The aortic cusps can thicken and the linea alba can become more pronounced. For this and other reasons, the aortic pulmonary valve is the most likely valve to be surgically repaired or replaced.

5.5 The Cardiac Skeleton

Passing transversely through the base of the heart is a fibrous framework or "skeleton" made of dense connective tissue, not bone as the name might suggest. The purpose of this tough, immobile scaffold is to (1) provide an attachment for the atrial and ventricular myocardium, (2) anchor the four valves of the heart, and (3) electrically insulate the myocardium of the ventricles from the atria (see also Chap. 13).

The supporting framework of the cardiac skeleton (Figs. 5.13 and 5.16) provides immobile support for the AV openings during atrial and ventricular contractions and support for the semilunar valves against the high pressures generated during and after ventricular contractions. The skeleton is a formation of four attached rings with the opening for the aortic semilunar valve in the central position and the other valve rings attached to it.

The triangular formation between the aortic semilunar valve and the medial parts of the tricuspid and bicuspid valve openings is the right *fibrous trigone* ("triangle") or the central fibrous body, the strongest portion of the cardiac skeleton. The smaller left fibrous trigone is formed between the aortic semilunar valve and the anterior cusp of the mitral valve. Continuations of fibroelastic tissue from the right and left fibrous trigone partially encircle the AV openings to form the tricuspid and bicuspid annulus or annulus fibrosus. The annuli serve as attachment sites for the AV valves as well as atrial and ventricular myocardium. Strong collagenous tissue passes anteriorly from the right and left fibrous trigones to encircle and support the aortic and pulmonary semilunar valve annuli. The membranous interventricular septum is an inferior extension of the central fibrous body that attaches to the muscular interventricular septum. The membranous septum provides support for the medial (right and posterior) cusps of the aortic semilunar valve and continues superiorly to form part of the atrial septum. The tendon of Todaro is a fibrous extension of the membranous septum that is continuous with the valve (Eustachian) of the inferior vena cava. The AV bundle of conduction fibers from the AV node penetrates the central fibrous body, passes through the membranous septum, and splits into left and right bundle branches at the apex of the muscular septum (or the junction of the right and posterior cusps of the aortic semilunar valve).

5.6 The Fetal Heart

By the third month of fetal development, the heart and all major blood vessels are basically formed, and the blood flow is generally in the same direction as the adult. However, there are some major differences between fetal and postnatal circulation (Fig. 5.17). First, oxygenated blood flows toward the fetus and into the heart in umbilical veins, and deoxygenated blood flows away from the fetus in umbilical arteries. Second, the fetus obtains oxygen from the uterus through the placenta, and the fetal lungs are essentially nonfunctional. Therefore, fetal circulation has a number of features to direct most of the blood away from the lungs.

In fetal circulation, oxygenated blood from the placenta flows through the umbilical cord as the umbilical vein. The vein passes through the anterior abdominal wall (umbilicus) and then through the abdomen, into the thorax, and into the heart. As the umbilical vein travels through the abdomen, most of the blood is diverted away from entering the liver (through the ductus venosus) and into the inferior vena cava. Thus, unlike the adult heart, oxygenated blood mixes with deoxygenated blood and collects in the right atrium. Because very little of this blood is required in the lungs, the fetus has three unique features to ensure that the blood is shunted from the right (pulmonary) side of the heart to the left (systemic) side. The first is an oval hole in the interatrial septum called the foramen ovale (the foramen ovale is not really a hole but rather a valve composed of two flaps that prevent the regurgitation of blood). For more information on this topic, the reader is referred to Chap. 3.

Before birth, pressure is higher in the right atrium than in the left because of the large vasculature from the placenta. The foramen ovale is a passage for blood to flow from the right atrium into the left.

A second feature of the fetal heart is the ligament of the inferior vena cava. This ligament is located inferior to the opening of the vena cava and extends medially to the atrial septum, passing inferior to the foramen ovale. It is much more prominent in the fetus than in the adult. It functions in fetal circulation to direct, in a laminar flow, the blood coming into the right ventricle toward the foramen ovale of the interatrial septum, so blood can pass into the left atrium.

The third feature of fetal circulation is a way for oxygenated blood that has been pumped from the right atrium to the right ventricle to be diverted from the pulmonary circulation into the systemic circulation. Despite the shunt from the right atrium to the left, much of the oxygenated blood that enters the right atrium gets pumped into the right ventricle. The ductus arteriosus

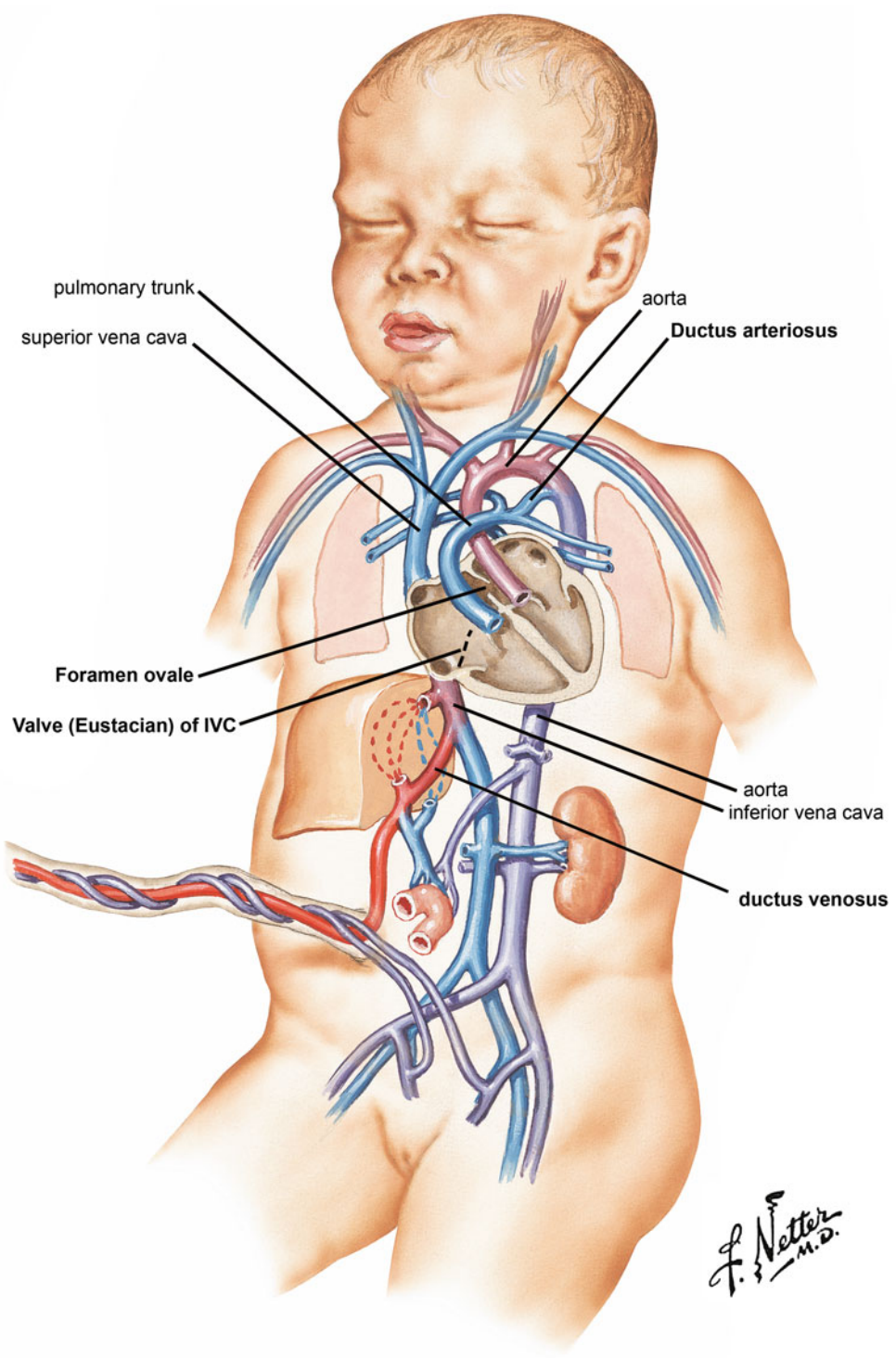

Fig. 5.17 Fetal circulation. The fetal heart has unique features to shunt blood away from the relatively nonfunctional lungs: (1) foramen ovale, (2) ductus arteriosus, and (3) valve (Eustachian) of the inferior vena cava. © 2006 Elsevier Inc. All rights reserved. www.netterimages.com, Frank Netter

("duct of the artery") is a connection between the left pulmonary artery and the aortic artery. Blood is diverted from the pulmonary artery to the aorta so that very little blood reaches the immature lungs. Because the pulmonary vascular resistance of the fetus is large, only one-tenth of right ventricular output passes through the lungs. The remainder passes from the pulmonary artery through the ductus arteriosus to the aorta. In the fetus, the diameter of the ductus arteriosus can be as large as the aorta.

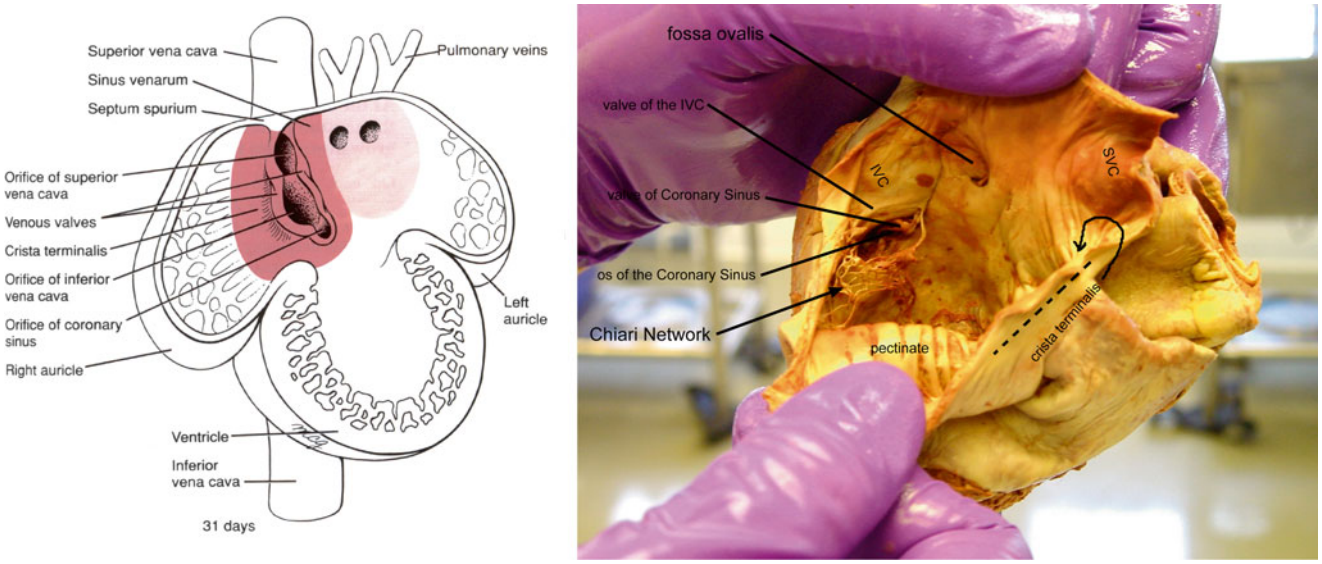

Fig. 5.18 Chiari network. *Left*: The sinus venosus incorporates into the posterior wall of the primitive right atrium. This becomes the sinus venarum (smooth) portion of the right atrium. A pair of tissue flaps, the left and right venous valves, develops on either side of connection between the sinus venarum and the right atrium. The left valve eventually gives rise to the septum secundum (definitive interatrial septum); the right valve gives rise to the valve of the inferior vena cava (Eustachian), the valve of the coronary sinus (Thebesian), and the crista terminalis. Incomplete resorption of the right valve of the embryonic sinus venarum leads to the presence of a meshwork of fibrous strands attached to the edges of the Eustachian valve or the Thebesian valve inferiorly and the crista terminalis superiorly. *Right*: human cadaveric heart. *IVC* inferior vena cava, *SVC* superior vena cava

Shortly after birth, the umbilical cord is cut and the newborn takes its first breath. Rising concentrations of the hormone prostaglandin are believed to result in the closure of the ductus arteriosus (ligamentum arteriosum), and the lungs receive much more blood. The increase in pressure is translated to the left atrium. This pressure pushes together the two valve flaps of the interatrial septum. One of the flaps covers the foramen ovale, thus closing it to form the fossa ovalis. This prevents the flow of blood from the right to the left atrium.

5.7 Other Fetal Remnants: Chiari Network

Around 4–5 weeks of fetal development, the sinus venosus incorporates into the posterior wall of the primitive right atrium. This becomes the sinus venarum (smooth) portion of the right atrium. A pair of tissue flaps, the left and right venous valves, develops on either side of connection between the sinus venarum and the right atrium.

The left valve eventually becomes part of the septum secundum (which becomes a portion of the definitive interatrial septum). The right valve remains intact and forms the valve of the inferior vena cava (Eustachian), the crista terminalis, and the valve of the coronary sinus (Thebesian) (Fig. 5.18).

Infrequently, incomplete resorption of the right valve of the sinus venarum may lead to the presence of a meshwork of fibrous strands attached to the edges of the Eustachian valve or Thebesian valve inferiorly and the crista terminalis superiorly. This is called a "Chiari net or network" (Fig. 5.18). Remnants of the other valve, the left sinus venarum valve, may be found adherent to the superior portion of the atrial septum or the fossa ovalis. For more information on this topic, see Chap. 3.

5.8 Other Fetal Remnants: Atrial Septal Defect

The first step in the separation of the systemic and pulmonary circulation in the fetal heart is the separation of the definitive atrium. The adult interatrial septum is formed by the fusion of two embryonic septa. Note that this embryonic septum always contains a hole such that right-to-left shunting of oxygenated blood remains.

Between 3 and 4 weeks of development, the roof of the atrium becomes depressed and produces a wedge of tissue called the *septum primum* ("first partition") that extends inferiorly. During the fifth week, this septum reaches the "floor" of the atrium, thus separating the right and left atria. Note that a crescent shape forms along its leading edge. This forms an "arch way" under the septum to function as an opening for the flow of blood called the ostium primum ("first mouth opening"). At the end of the sixth week, the growing edge of the septum primum reduces the ostium primum to nothing. At the same time, the septum primum grows perforations near the superior end of the septum that

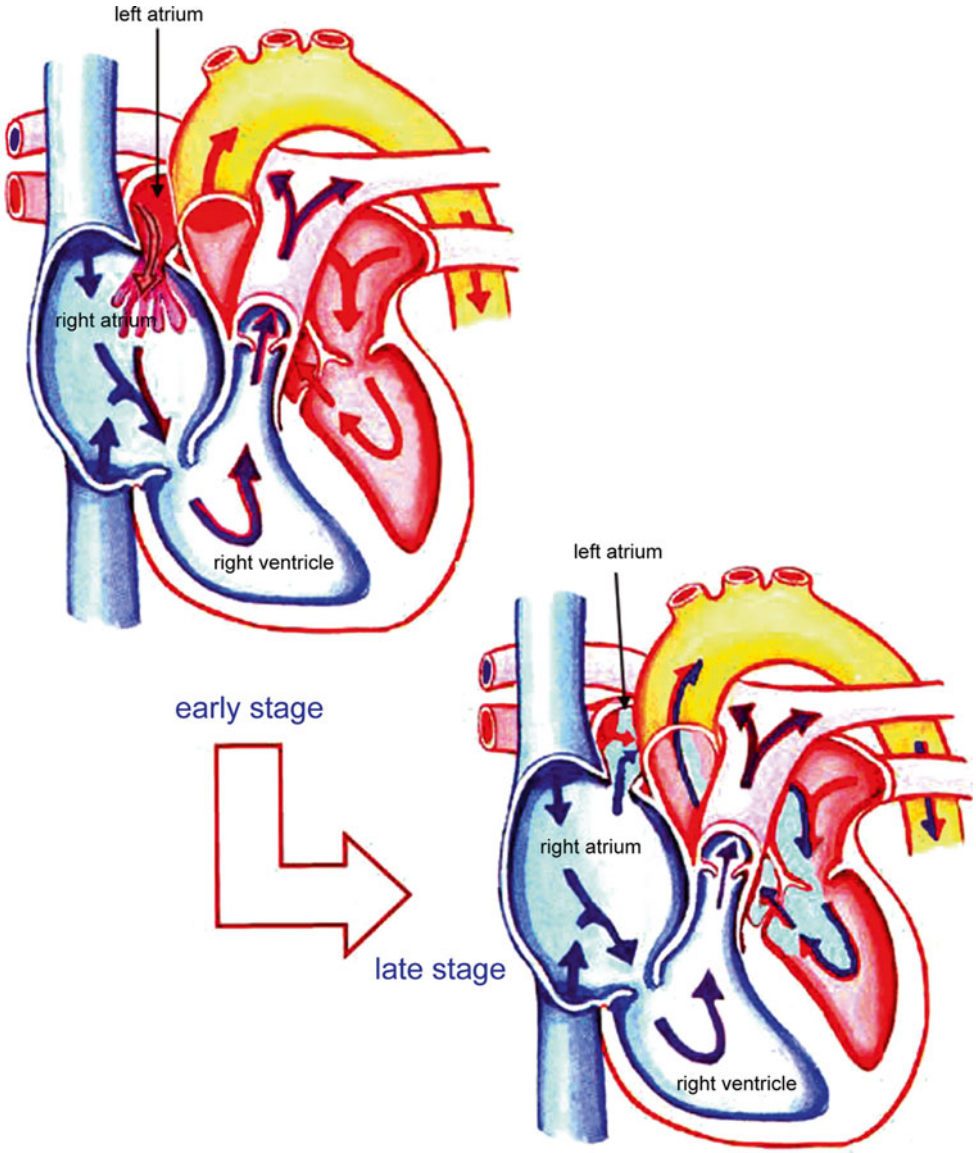

Fig. 5.19 Atrial septal defect (ASD). Incomplete formation of the interatrial septum results in a persistent opening or defect. After birth, the pressure in the left atrium is greater than the right, and there is modest left-to-right shunting of blood. The right atrium will frequently respond to the continuous increases in volume. The result is increased pressure generated by the right atrium and a reverse in the flow from the right to the left atrium. This results in oxygen-poor blood in the left atrium, ventricle, and aortic artery leading to symptoms of hypoxia. Modified from VanDeGraaf KM (ed) (1995) Human anatomy. Wm. C. Brown Publishers, Dubuque, p. 557

coalesce to form a new foramen, the ostium secundum ("second opening"). Thus, a new channel for right-to-left blood flow opens before the old one closes. At the same time, a second crescent-shaped wedge of tissue, the septum secundum ("second partition"), grows from the roof of the atrium. It is located adjacent to the septum primum on the side of the right atrium. Unlike the septum primum, the secundum is thick and muscular as it grows posteroinferiorly. It completely extends to the floor of the right atrium. The crescent shape at the leading edge leaves a hole in the inferior portion called the *foramen ovale* ("oval hole"); this might be considered the third hole. Throughout the rest of fetal development, blood shunts from the right to the left atrium. This shunt closes at birth due to the abrupt dilation of the pulmonary vasculature, combined with the loss of flow through the umbilical vein. The increase in pressure in the left atrium and the loss of pressure in the right pushes the flexible septum primum against the septum secundum. The septum primum covers the foramen ovale as the valve of the foramen ovale.

There are various mechanisms by which an opening can persist in the interventricular septum postnatally. This is referred to as an *atrial septal defect* (Fig. 5.19; see also Chap. 37). This abnormality is generally asymptomatic during infancy. However, the persistent increase in flow of blood into the right atrium can lead to hypertrophy of the right atrium, right ventricle, and the pulmonary trunk. In some cases, the left-to-right flow of blood between the atria con-

verts to right-to-left shunt. This causes oxygen-poor blood to mix with the oxygen-rich blood returning to the left atrium from the lungs. Oxygen-poor blood is then pumped out of the heart through the aortic artery and the symptoms of hypoxia ("low oxygen") result. Approximately 30 % of normal hearts have a small potency with a valve-competent foramen ovale.

5.9 Other Fetal Remnants: Ventricular Atrial Septal Defect

The developmental formation of the interventricular septum is extremely complex. Simply, the septum forms as the growing walls of the right and left ventricles become more closely apposed to one another. The growth of the muscular septum commences at the inferior end and proceeds superiorly. Septation of the ventricles and formation of the ventricular outflow tracts must occur in tight coordination. Ventricular septal defects can occur because of errors in this complex process. Failure of complete fusion of the membranous septum growing inferiorly from the superior portion of the ventricles and the muscular septum results in one type of ventricular septal defect (Fig. 5.20). Ventricular septal defects are the most common congenital heart defect.

Whatever the origin of a ventricular septal defect, the result is a massive left-to-right shunting of blood due to the ability of the left ventricle to generate higher pressures than the right. This is associated with postnatal pulmonary hypertension and deficient closure of AV valves. This type of condition is often referred to, in lay terms, as "baby being born with a hole in the heart." Because of extreme hypoxia and

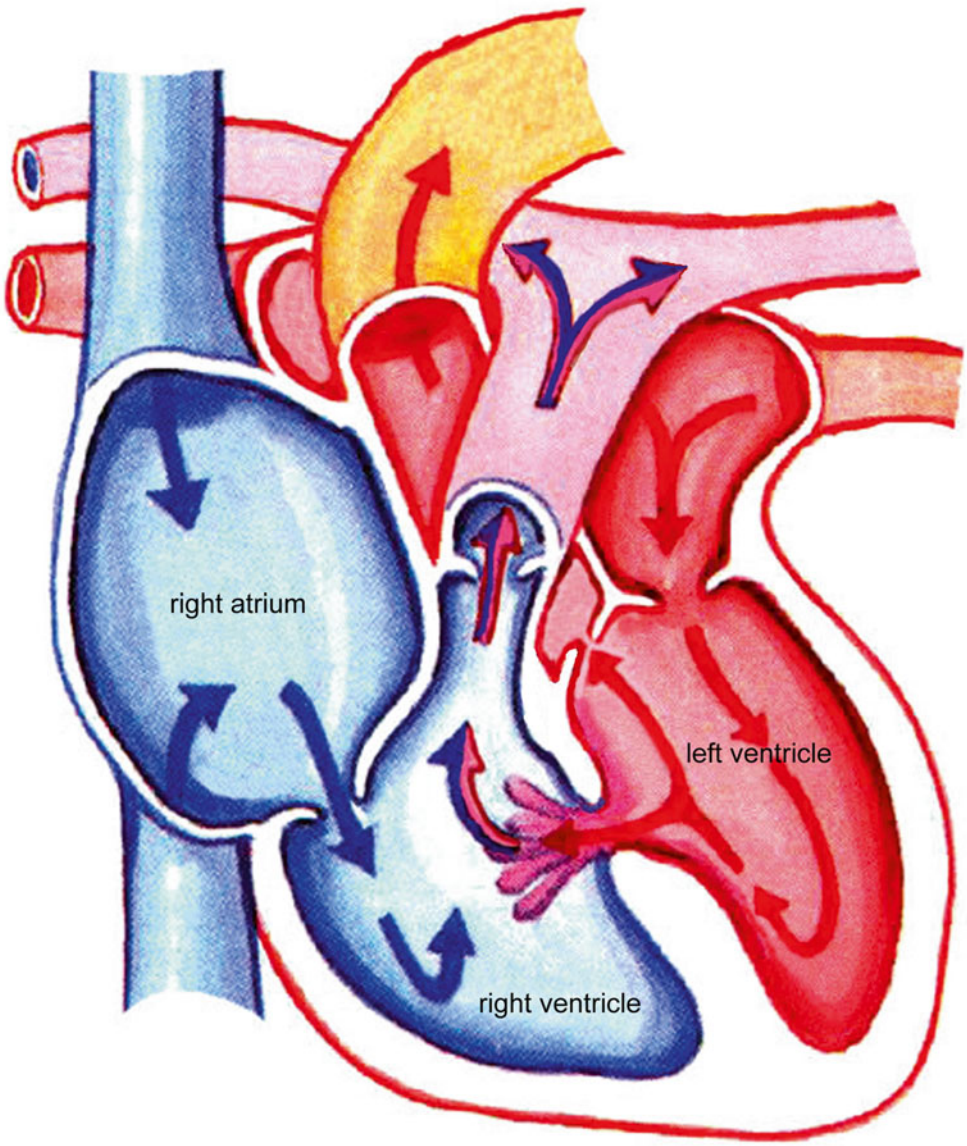

Fig. 5.20 Ventricular septal defect. Caused by abnormal development of the interventricular septum. This condition results in massive left-to-right shunting of blood. This is associated with pulmonary hypertension and deficient closure of atrioventricular valves after birth. Emergent surgical repair of this hole is indicated. Modified from VanDeGraaf KM (ed) (1995) Human anatomy. Wm. C. Brown Publishers, Dubuque

pulmonary hypertension, there is usually immediate surgical repair of the defect. For additional information on ventricular septal defects and their repair, refer to Chap. 37.

5.10 Vasculature of the Heart

The arterial supply to the heart arises from the base of the aorta as the right and left coronary arteries (running in the coronary sulcus). The venous drainage is via cardiac veins that return deoxygenated blood to the right atrium. The coronary arteries arise from the ostia in the left and right sinuses of the aortic semilunar valve, course within the epicardium, and encircle the heart in the AV (coronary) and interventricular sulci (Fig. 5.21).

5.10.1 Right Coronary Artery

The right coronary artery emerges from the aorta into the AV groove. It descends through the groove, then curves posteriorly, and makes a bend at the crux of the heart and continues downward in the posterior interventricular sulcus. Within millimeters after emerging from the aorta, the right coronary artery gives off two branches (Figs. 5.21 and 5.22). The conus (arteriosus) artery runs to the conus arteriosus (right ventricular outflow tract), and the atrial branch to the right atrium. This atrial branch gives off the SA nodal artery (in 50–73 % of hearts, according to various reports), which runs along the anterior right atrium to the superior vena cava, encircling it in a clockwise or counterclockwise direction before reaching the SA node. The SA nodal artery supplies the SA node, Bachman's bundle, crista terminalis, and the left and right atrial free walls. The right coronary artery continues in the AV groove and gives off a variable number of branches to the right atrium and right ventricle. The most prominent of these is the right marginal branch which runs down the right margin of the heart supplying this part of the right ventricle. As the right coronary curves posteriorly and descends downward on the posterior surface of the heart, it gives off two to three branches. One is the posterior interventricular (posterior descending) artery that runs in the posterior interventricular sulcus. It is directed toward the apex of the heart to supply the posterior free wall of the right ventricle. In 85–90 % of hearts, branches of this artery (posterior septal arteries) supply the posterior one-third of the interventricular septum (Fig. 5.23). The second artery is the AV nodal artery which branches from the right coronary artery at the crux of the heart and passes anteriorly along the base of the atrial septum to supply the AV node (in 50–60 % of hearts), proximal parts of the bundles (branches) of His, and the parts of the posterior interventricular septum that surround the

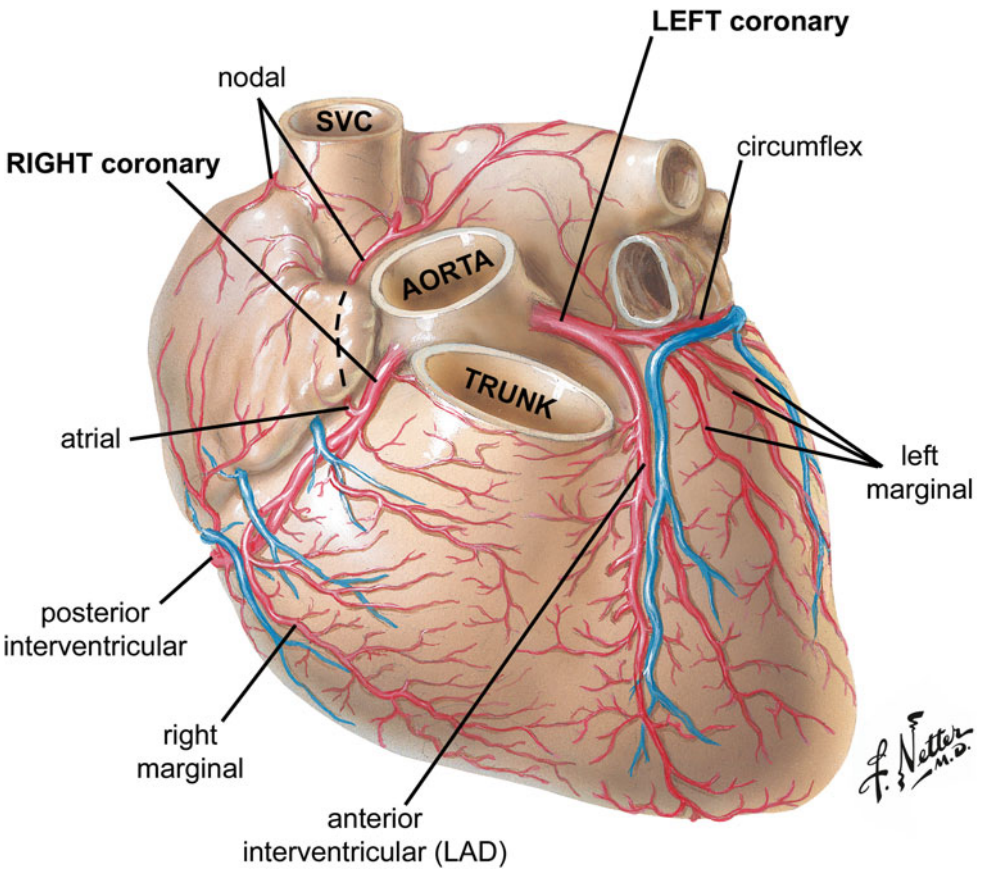

Fig. 5.21 Vascular supply to the heart. Arterial supply to the heart occurs via the right and left coronary arteries and their branches. Venous drainage occurs via cardiac veins. © 2006 Elsevier Inc. All rights reserved. www.netterimages.com, Frank Netter

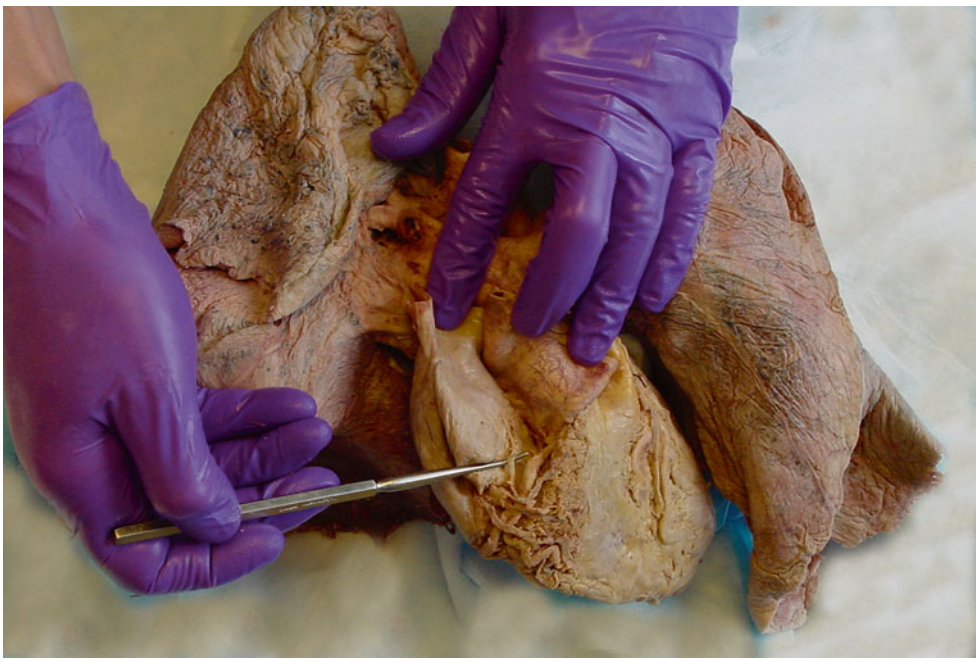

Fig. 5.22 Atrial branch of right coronary artery. This atrial branch gives off the sinoatrial (SA) nodal artery which runs along the anterior right atrium to the superior vena cava and encircles it in a clockwise, or sometimes counterclockwise, direction before reaching the SA node. The nodal artery can also pass intramurally through the right atrium to the SA node. The SA nodal artery supplies the SA node, Bachman's bundle, crista terminalis, and the left and right atrial free walls

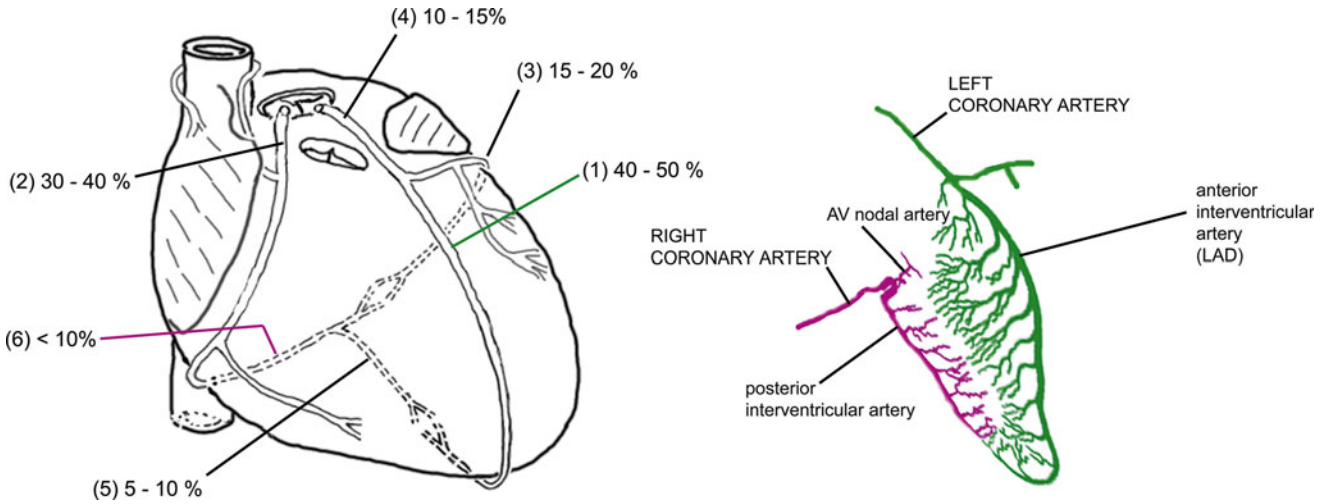

Fig. 5.23 Arterial supply to the interventricular septum. *Left*: Sites of coronary artery occlusion, in order of frequency and percentage of occlusions involving each artery. *Right*: The right coronary artery supplies the posterior one-third of the interventricular septum, and the left coronary supplies the anterior two-thirds. The artery to the atrioventricular node commonly branches off of the posterior interventricular artery. Occlusions occur most frequently in the anterior interventricular artery, which is the primary blood supply to the interventricular septum (and bundle branches within). *AV* atrioventricular

bundle branches. Another artery crosses the crux into the left AV groove to supply the diaphragmatic surface of the left ventricle and the posterior papillary muscle of the bicuspid valve. The right coronary artery also serves as an important collateral supply to the anterior side of the heart, left ventricle, and anterior two-thirds of the interventricular septum via the conus artery and communicating arteries in the interventricular septum (Fig. 5.23). Kugel's artery, which originates from either the right or left coronary artery, runs from anterior to posterior through the atrial septum. This artery serves as an important collateral connection from anterior arteries to the AV node and posterior arteries.

5.10.2 Left Coronary Artery

The left coronary artery (left main coronary artery) emerges from the aorta through the ostia of the left aortic cusp within the sinus of Valsalva (Fig. 5.21). The plane of the semilunar valve is tilted so that the ostium of the left coronary artery is superior

and posterior to the right coronary ostium. The left coronary artery travels from the aorta and passes between the pulmonary trunk and the left atrial appendage. Under the appendage, the artery divides (and is thus a very short vessel) into the anterior interventricular (left anterior descending artery) and the left circumflex artery. The left coronary artery may be completely absent, i.e., the anterior interventricular and circumflex arteries arise independently from the left aortic sinus.

The anterior interventricular artery appears to be a direct continuation of the left coronary artery which descends into the anterior interventricular groove. Branches of this artery, anterior septal perforating arteries, enter the septal myocardium to supply the anterior two-thirds of the interventricular septum (in about 90 % of hearts) (Fig. 5.23). The first branch, the first septal perforator, supplies a major portion of the AV conduction system. In about 80 % of hearts, the second or third perforator is the longest and strongest of the septal arteries and is often called the *main septal artery*. This artery supplies the middle portion of the interventricular septum. This artery also sends a branch to the moderator band and the anterior papillary muscle of the tricuspid valve (right ventricle), which is reasonable considering that the moderator band is part of the septomarginal trabeculae of the interventricular septum. This artery is often called the *moderator artery*. Other branches of the anterior interventricular artery extend laterally through the epicardium to supply adjacent right and left ventricular free walls. The anterior interventricular artery also sends a branch to meet the conus artery from the right coronary to form an important collateral anastomosis called the *circle of Vieussens* as well as branches to the anterior free wall of the left ventricle called *diagonal arteries*. These are numbered according to their sequence of origin as first, second, etc. diagonal arteries. The most distal continuation of the anterior interventricular artery curves around the apex and travels superiorly in the posterior interventricular sulcus to anastomose with the posterior descending from the right coronary artery. In summary, the anterior interventricular artery and its branches supply most of the interventricular septum—the anterior, lateral, and apical wall of the left ventricle; most of the right and left bundle branches; and the anterior papillary muscle of the bicuspid valve (left ventricle). It also provides collateral circulation to the anterior right ventricle, the posterior part of the interventricular septum, and the posterior descending artery.

The circumflex artery branches off of the left coronary artery and supplies most of the left atrium—the posterior and lateral free walls of the left ventricle and (with the anterior interventricular artery) the anterior papillary muscle of the bicuspid valve. The circumflex artery may give off a variable number of left marginal branches to supply the left ventricle. The terminal branch is usually the largest of these branches. More likely, the circumflex artery may continue through the AV sulcus to supply the posterior wall of the left ventricle and (with the right coronary artery) the posterior papillary muscle of the bicuspid valve. In 40–50 % of hearts, the circumflex artery supplies the artery to the SA node.

In 30–60 % of hearts, the left coronary artery may give off one or more intermediate branches that originate *between* the anterior interventricular and circumflex arteries. These extend diagonally over the left ventricle toward the apex of the heart and are thus named diagonal or intermediate arteries.

The anterior interventricular artery is the most commonly occluded of the coronary arteries (Fig. 5.23). It is the major blood supply to the interventricular septum and the bundle branches of the conducting system. It is easy to see why coronary artery disease can lead to impairment or death (infarction) of the conducting system. The result is a "block" of impulse conduction between the atria and the ventricles known as "right/left bundle branch block." Furthermore, branches of the right coronary artery supply both the SA and AV nodes in at least 50 % of hearts. An occlusion in this artery could result in necrosis of the SA or AV nodes, thus preventing or interrupting the conduction of electrical activity across the heart. For more details on the coronary arteries, see Chaps. 6 and 8.

5.10.3 Cardiac Veins

An extensive network of intercommunicating veins provides venous drainage from the heart. The venous drainage of deoxygenated blood from the rest of the body is returned to the right atrium, as is the venous drainage of the heart. Venous drainage of the heart is accomplished through three separate systems: (1) the cardiac venous tributaries which converge to form the coronary sinus, (2) the anterior cardiac (anterior right ventricular) veins, and (3) the smallest cardiac (Thebesian) venous system (Fig. 5.24).

Most of the myocardium is drained by the cardiac veins that course parallel to the coronary arteries. These three large veins (the great, middle, and small cardiac veins) converge to form the coronary sinus.

On the anterior side of the heart, the anterior interventricular vein lies within the anterior interventricular sulcus and runs from inferior to superior beside the anterior interventricular artery (Figs. 5.24 and 5.25). At the base of the heart, near the bifurcation of the left coronary artery, it turns and runs within the AV groove as the great cardiac vein around the left side of the heart to the posterior. In the AV groove on the posterior side of the heart, the great cardiac vein *becomes* the coronary sinus, which then empties into the right atrium. From the inside of the right atrium, it can be seen that the coronary sinus opens into the right atrium forming an opening or *os* that is located anteriorly and inferiorly to the orifice of the inferior vena cava. There is a valve (Thebesian valve) that covers the opening of the coronary sinus to prevent backflow. The great cardiac vein is formed

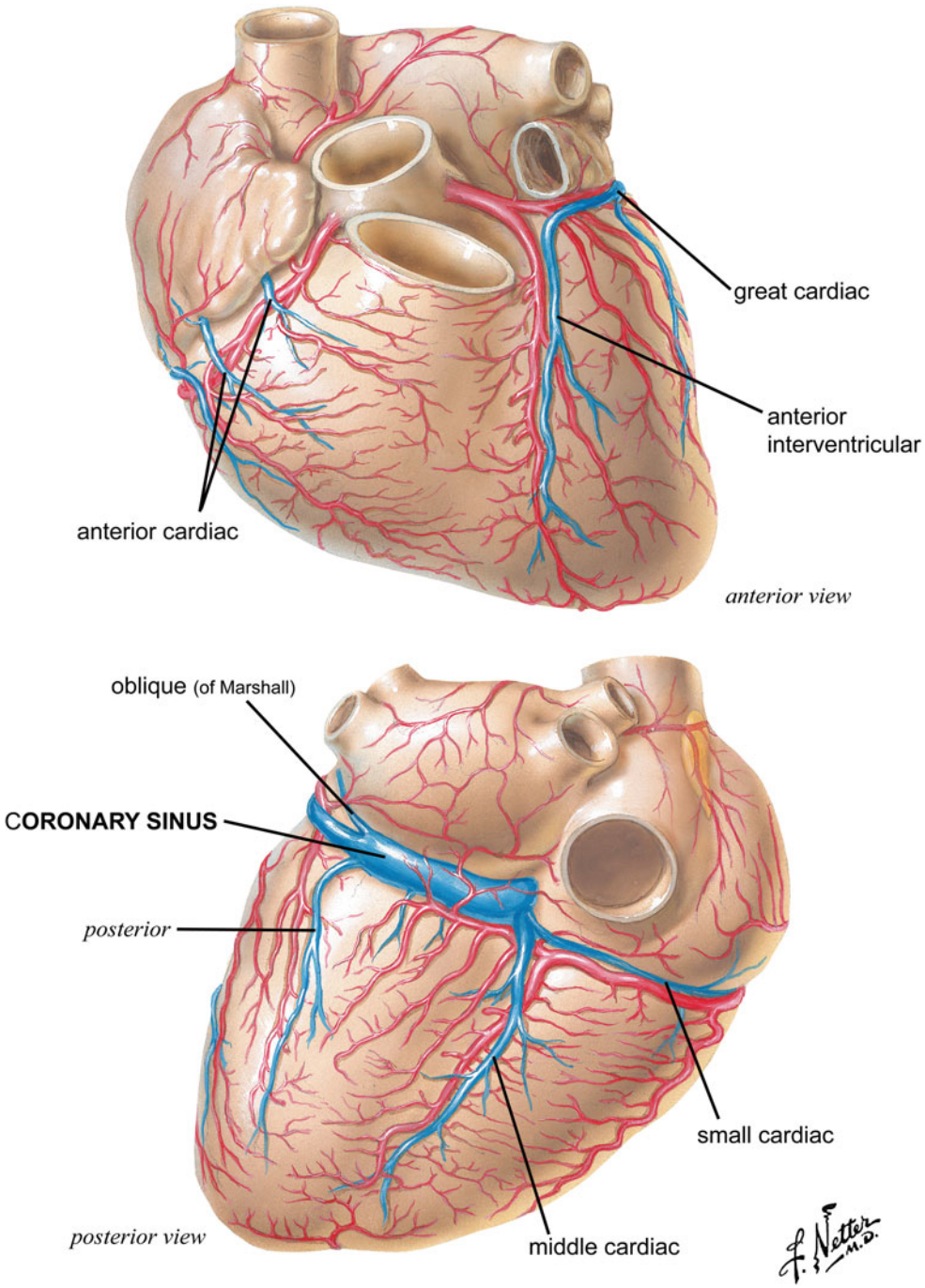

Fig. 5.24 Venous drainage of the heart. Three separate venous systems carry blood to the right atrium—the coronary sinus and its tributaries, the great, middle and small cardiac veins; the anterior cardiac veins; and the smallest (Thebesian) cardiac veins. © 2006 Elsevier Inc. All rights reserved. www.netterimages.com, Frank Netter

by the confluence of small venous tributaries from the left and right ventricles and anterior portion of the interventricular septum. As it ascends toward the coronary sinus, it receives small venous tributaries from the left atrium and left ventricle. It also receives a large left marginal vein, which runs parallel to the left marginal artery.

There are two structures that serve as the boundary between the termination of the great cardiac vein and the beginning of the coronary sinus. The first is the valve of Vieussens, which has the appearance of a typical venous valve and functions to prevent the backflow of blood from the coronary sinus into the great cardiac vein (Raymond Vieussens, French anatomist, 1641–1715). The second is the space between the entry points of the oblique vein of the left atrium (of Marshall) and the posterior (posteriolateral) vein of the left ventricle (John Marshall, English anatomist, 1818–1891). The oblique vein of Marshall runs superior to inferior along the posterior side of the left atrium, providing venous drainage of the area. The posterior vein ascends to the coronary sinus from the inferior portion of the left ventricle and provides drainage of the area.

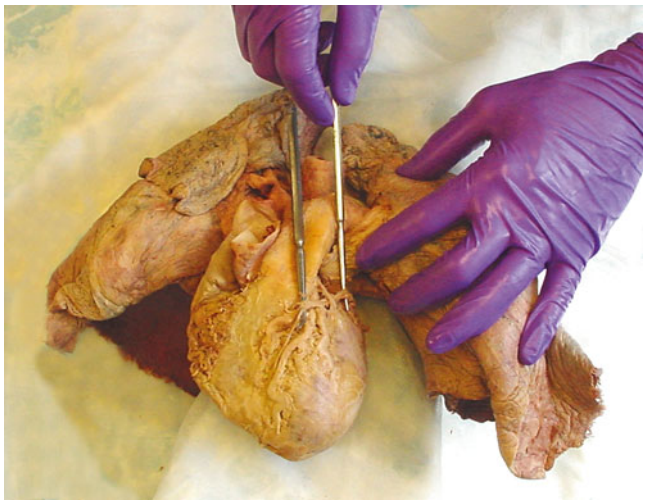

Fig. 5.25 The great cardiac vein. On the anterior side of the heart, the anterior interventricular vein lies within the anterior interventricular sulcus and runs from inferior to superior beside the anterior interventricular artery. At the base of the heart, it changes to the great cardiac vein as it runs within the atrioventricular groove around the left side of the heart to the posterior. In the atrioventricular groove on the posterior side of the heart, the great cardiac vein becomes the coronary sinus and empties into the right atrium

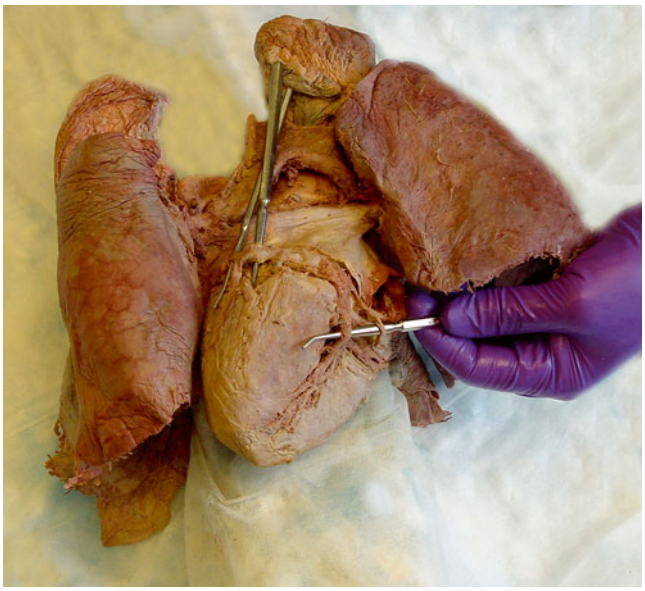

Fig. 5.26 The middle cardiac vein. The middle cardiac vein, located on the posterior surface of the heart, arises near the posterior aspect of the apex of the heart and runs from inferior to superior through the posterior interventricular sulcus before entering the coronary sinus. The middle cardiac vein is formed from venous confluence of tributaries that drain the posterior left and right ventricles and the interventricular septum

In addition to the great cardiac vein, the coronary sinus receives the posterior interventricular (or middle cardiac) vein (Figs. 5.24 and 5.26). Located on the posterior surface of the heart, it arises near the posterior aspect of the apex of the heart and runs from inferior to superior through the posterior interventricular sulcus. It then joins the coronary sinus within millimeters of the sinus entering into the right atrium. The middle cardiac vein is formed from venous confluence of tributaries that drain the posterior left and right ventricles and the interventricular septum.

The coronary sinus also receives the highly variable small cardiac vein. The small cardiac vein arises from the anterior/lateral/inferior portion of the right ventricle. It ascends and runs inferior to and roughly parallel with the marginal branch of the right coronary artery until it reaches the right AV sulcus. At this point, it turns and runs horizontally around to the posterior side of the heart and enters the coronary sinus with the middle cardiac vein. The small cardiac vein is extremely small or absent in 60 % of hearts. In about 50 % of hearts, the small cardiac vein enters the right atrium directly, and it infrequently drains into the middle cardiac vein.

Typically, about 85 % of the venous drainage of the heart occurs through the great, middle, and small cardiac veins through the coronary sinus to the right atrium. This elaborate system of veins drains the left ventricle, some of the right ventricle, both atria, and the anterior portion of the interventricular septum.

The second system of venous drainage of the heart involves the variable and delicate anterior cardiac veins (Figs. 5.24 and 5.27). This system is distinguished from the other cardiac venous system because the anterior cardiac veins do not drain into the coronary sinus. The two to four anterior cardiac veins originate and drain the anterior right ventricular wall, travel superiorly to cross the right AV sulcus, and enter the right atrium *directly*. The sulcus is usually packed with adipose tissue. Through this adipose tissue run the anterior cardiac veins, the right coronary artery, and a branch of the coronary artery, the right atrial or nodal artery. The anterior cardiac veins pass over the right coronary artery in close proximity and in a perpendicular angle. A right marginal vein (when present) runs parallel with the right marginal artery before entering the right atrium directly and is usually considered part of the anterior cardiac venous system.

The third system of venous drainage of the heart is the smallest cardiac venous system (Fig. 5.27). This system is composed of a multitude of small intramural ("within the walls") intramyocardial veins also called Thebesian veins (Adam C. Thebesius, German physician, 1686–1732). These are minute vessels that begin in the capillary beds of the myocardium and open directly into the chambers of the heart. Although called veins, they are valveless communications between myocardial capillaries and a chamber of the heart. Interestingly, ostia of Thebesian veins may be found in all chambers of the heart, but are most prevalent in the atrial and ventricular septa. They are more prevalent on the right side than the left. As much as 17 % of myocardial drainage occurs through these smallest cardiac veins, with 49 % through the cardiac veins and coronary sinus and 24 % through anterior

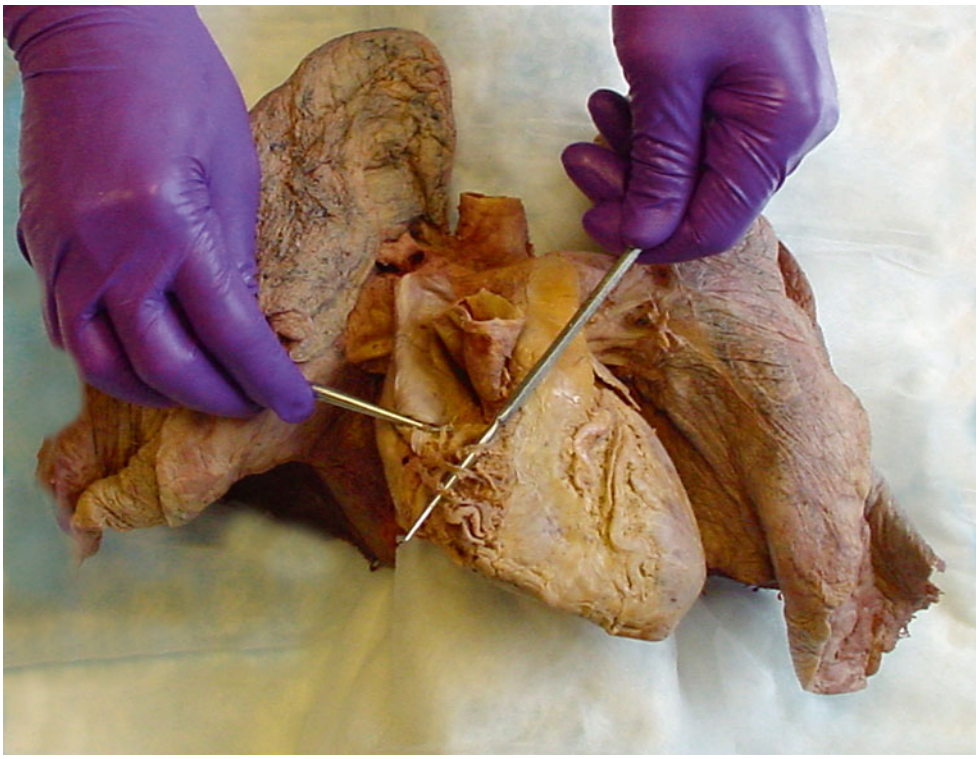

Fig. 5.27 Anterior cardiac veins. Two to four anterior cardiac veins originate and drain the anterior right ventricular wall. These veins travel superiorly to cross the right atrioventricular sulcus and enter into the right atrium. These veins are part of the smallest cardiac venous system which empties oxygen-poor blood directly into the right atrium without communication with the coronary sinus

cardiac veins. For additional details on the cardiac venous system, see Chap. 8.

5.10.4 Myocardial Bridges

The coronary arteries typically course upon the myocardium or under/within the epicardium of the heart. Frequently, a portion of an artery deviates from its usual subepicardial position to follow an intramyocardial (intramural) course, either by traveling a significant length within the myocardium or beneath an arrangement of muscular slips ("myocardial bridges"). Myocardial bridging is most common in the middle segment of the anterior interventricular artery [2]. The myocardial fibers that cover or "bridge over" the anterior interventricular artery are direct extensions of the myocardium of the conus arteriosus of the right ventricle and cross the artery in a perpendicular direction. Myocardial bridges over the right coronary and the circumflex arteries are much less common. When present, these bridges are extensions of the respective atrial myocardium [3]. The prevalence of myocardial bridges from various sources is reported to occur in 5–85 % of hearts when measured from the cadaver [4–6] and 0.5–16 % when measured from angiography in catheterization labs [4, 5, 7].

Coronary arteries have a tortuous pattern as they run across the heart. Interestingly, studies employing angiography followed by detailed microdissection show that a coronary artery with a typical tortuous shape takes on a perfectly straight pattern when it follows an intramyocardial course [8].

Angiography has also shown that myocardial bridges are associated with narrowing of the lumen of the coronary artery. The narrowing appears during systole and disappears during diastole [2]. The appearance of straight running or systolic narrowing patterns appears to be an important diagnostic technique during angiography to discover intramyocardial segments of coronary arteries [2].

Myocardial bridging is usually a benign condition. Although there is contrasting evidence, atherosclerosis is uncommon within a myocardial bridge [4]; bridging might provide some protection against plaque formation [2].

5.11 Autonomic Innervation of the Heart

The SA node spontaneously produces an impulse for contraction of the atrial myocardium, depolarizes the AV node, and sends an impulse through the bundle fibers to the ventricular myocardium. In addition to the pacemaker activity of the SA node, the heart is also under autonomic, or involuntary, control.

The autonomic nervous system is separated into the *sympathetic* and *parasympathetic* nervous systems. These two systems send neurons to the same target, but convey opposite effects. In emergency situations, sympathetic nerves travel to the heart and innervate the SA and AV nodes in order to increase the rate and force of contraction. In resting

situations, parasympathetic nerves that innervate the SA and AV nodes to slow down the heart rate reduce the force of contraction, thus saving energy.

Both the sympathetic and parasympathetic nerves are composed of a two-neuron pathway. These two neurons meet or synapse somewhere in the middle and form a structure called a *ganglion* ("swelling"). Neurons of the sympathetic nervous system emerge from the spinal cord. They emerge from all eight of the cervical segments and the first five of the thoracic spinal cord segments. These neurons travel laterally just centimeters from the spinal cord before they synapse. All of the neurons to the heart are believed to synapse in only two places—the middle cervical ganglion and the cervicothoracic (fused inferior cervical/1st thoracic or stellate "star-shaped") ganglion. Multitudes of fibers then emanate from these ganglia and run to the heart as sympathetic cardiac nerves.

Parasympathetic neurons emerge directly from the brain as part of the vagus nerve or cranial nerve X. The vagus nerve and its branches form the parasympathetic part of the cardiac nerves running toward the heart.

Sympathetic and parasympathetic cardiac nerves interconnect. In addition, nerves of the right and left side have connections. All together, this huge group of connections forms the cardiac plexuses. The dorsal cardiac plexus is located posterior to the arch of the aorta near the bifurcation of the trachea. The ventral plexus is located anterior to the aorta. Nerves from the cardiac plexuses extend to the atria and ventricles, SA node, AV node, coronary arteries, and the great vessels. It is generally believed that there is sympathetic and parasympathetic innervation of the myocardium that forms a network from the atria to the ventricles. For more details about the role of the autonomic nervous system in the physiological control of the heart, refer to Chap. 14.

5.12 Summary

This chapter covered the general internal and external anatomy of the human heart, its positioning within the thorax, and its basic function. It is important to note that this anatomy can be quite varied and also progressively modified by pathophysiologic conditions.

References

1. Wenink ACG (1977) The medial papillary complex. Br Heart J 39:1012–1018
2. Kalaria VG, Koradia N, Breall JA (2002) Myocardial bridge: a clinical review. Catheter Cardiovasc Interv 57:552–556
3. Garg S, Brodison A, Chauhan A (2000) Occlusive systolic bridging of circumflex artery. Cathet Cardiovasc Diagn 51: 477–478
4. Polacek P (1961) Relation of myocardial bridge and loops on the coronary arteries to coronary occlusions. Am Heart J 61:44–52
5. Irvin RG (1982) The angiographic prevalence of myocardial bridging. Chest 81:198–202
6. Noble J, Bourassa MG, Petitclerc R, Dyrda I (1976) Myocardial bridging and milking effect of left anterior descending artery: normal variant or obstruction. Am J Cardiol 37:993–999
7. Greenspan M, Iskandrin AS, Catherwood E, Kimbiris D, Bemis CE, Segal BL (1980) Myocardial bridging of the left anterior descending artery: evaluation using exercise thallium-201 myocardial scintigraphy. Cathet Cardiovasc Diagn 6:173–180
8. Lachman N, Satyapal KS, Vanker EA (2002) Angiographic manifestation and anatomical presence of the intra-mural LAD: surgical significance. Clin Anat 15:426

Further Reading

Berne RM, Levy MN, Koeppen BM, Stanton BA (eds) (2004) Physiology, 5th edn. Mosby, St. Louis
Garson A (ed) (1997) The science and practice of pediatric cardiology, 2nd edn. Williams and Wilkins, Baltimore
Goss CM (ed) (1949) Anatomy of the human body: Gray's anatomy. Lea and Febiger, Philadelphia
Hurst JW (ed) (1990) Hurst's the heart. McGraw-Hill, New York
Kumar V, Cotran RS, Robbins SL (eds) (2003) Robbins basic pathology, 7th edn. Saunders, Philadelphia
Larson WJ (ed) (1997) Human embryology, 2nd edn. Churchill Livingstone, New York
Moore KL, Dalley AF (eds) (2006) Clinically oriented anatomy, 5th edn. Lippincott Williams and Williams, Philadelphia
Netter FH (ed) (2003) Atlas of human anatomy, 3rd edn. ICON Learning Systems, Teterboro
Stedman TL (ed) (1972) Stedman's medical dictionary. Williams and Wilkins, Baltimore

Comparative Cardiac Anatomy

6

Alexander J. Hill and Paul A. Iaizzo

Abstract

The need for appropriate animal models to conduct translational research is vital for advancements in the diagnosis and treatment of heart disease. The choice of animal model to be employed must be critically evaluated. In this chapter, we present the comparative cardiac anatomies of several of the commonly employed animal models for preclinical research (dog, pig, and sheep). General comparisons focus on several specific anatomical features: the atria, ventricles, valves, coronary system, lymphatics, and the conduction system. Finally, we present novel qualitative and quantitative data obtained from perfusion-fixed specimens of these commonly used animal models.

Keywords

Comparative anatomy • Human • Sheep • Dog • Pig • Heart • Cardiac

6.1 Historical Perspective of Anatomy and Animal Research

Anatomy is one of the oldest branches of medicine, with historical records dating back at least as far as the third century BC; animal research dates back equally as far. More specifically, Aristotle (384–322 BC) studied comparative animal anatomy and physiology, and Erasistratus of Ceos (304–258 BC) studied live animal anatomy and physiology [1]. Galen of Pergamum (129–199 AD) is probably the most notable early anatomist who used animals in research in which he attempted to understand the normal structure and function of the body [2]. He continuously stressed the centrality of anatomy and made an attempt to dissect every day, as he felt it was critical to learning [3]. His most notable work was *De Anatomicis Administrationibus* (On Anatomical Procedures) which, when rediscovered in the sixteenth century, renewed interest in anatomy and scientific methods [2].

The Renaissance was a period of great scientific discovery and included important advances in our understanding of human and animal anatomy. Andreas Vesalius (1514–1564 AD) was arguably the greatest anatomist of the era [4]. To teach anatomy, he performed public nonhuman dissections at the University of Padua and is credited with creating the field of modern anatomy [2]. His immediate successors at Padua were Matteo Realdo Colombo (1510–1559 AD) and Gabriele Falloppio (1523–1562 AD). It was Colombo who, in great detail, described the pulmonary circulation and both the atrial and ventricular cavities; Falloppio is credited with the discovery of the Fallopian tubes among other things [4]. Animal research flourished during this period due to a number of popular ideas launched by both the Christian Church and one of the prominent scientific leaders at that time, Rene Descartes. The Church asserted that animals were under the dominion of man and, although worthy of respect, could be used to obtain information if it was for a "higher" purpose [2]. Descartes described humans and other animals as complex

A.J. Hill, PhD
Department of Surgery, University of Minnesota,
420 Delaware St. SE, B 172 Mayo, MMC 107,
Minneapolis, MN 55455, USA

Medtronic, 8200 Coral Sea Street NE, Mounds View,
MN 55112, USA

P.A. Iaizzo, PhD (✉)
Department of Surgery, University of Minnesota,
420 Delaware St. SE, B 172 Mayo, MMC 107,
Minneapolis, MN 55455, USA
e-mail: iaizz001@umn.edu

P.A. Iaizzo (ed.), *Handbook of Cardiac Anatomy, Physiology, and Devices*, DOI 10.1007/978-3-319-19464-6_6

machines, with the human soul distinguishing man from all other animals. This beast-machine concept was important for early animal researchers because if animals had no souls, it was thought that they could not suffer pain. Interestingly, it was believed that the reactions of animals were responses of automata and not pain [2].

The concept of functional biomedical studies can probably be attributed to another great scientist and anatomist, William Harvey (1578–1657 AD). He is credited with one of the most outstanding achievements in science and medicine—a demonstration of the circulation of blood which was documented in his publication *Exercitatio Anatomica De Motu Cordis et Sanguinis in Animalibus (De Motu Cordis)* in 1628. Very importantly, his work ushered in a new era in science, where a hypothesis was formulated and then tested through experimentation [4]. Many great anatomists emerged during this period and made innumerable discoveries; many of these discoveries were named after the individuals who described them and include several researchers who studied cardiac anatomy such as the Eustachian valve (Bartolomeo Eustachio), the Thebesian valve and Thebesian veins (Thebesius), and the sinus of Valsalva (Antonio Maria Valsalva). It should be noted that during this time period, in addition to animal research, dissections on deceased human bodies were performed, but not to the degree that they are today. In fact, it is written that, in general, during the post-Renaissance era, there was a serious lack of human bodies available for dissection. Oftentimes, bodies were obtained in a clandestine manner, by grave robbing or using bodies of executed criminals for dissection. In spite of the lack of bodies, most structures in the human body, including microscopic ones, were described by various anatomists and surgeons between the fifteenth and early nineteenth centuries.

Early in the nineteenth century, the first organized opposition to animal research occurred. In 1876, the Cruelty to Animals Act was passed in Britain. It was followed in the United States by the Laboratory Animal Welfare Act of 1966, which was amended in 1970, 1976, and 1985. These two acts began a new era in how laboratory animals were treated and utilized in experimental medicine. Importantly, the necessity of animal research is still great, and therefore animals continue to be used for a variety of purposes including cardiovascular device research.

6.2 Importance of Anatomy and Preclinical Animal Research

Anatomy remains as quite possibly one of the most important branches of medicine. In order to diagnose and treat medical conditions, normal structure and function must be known, as it is the basis for defining what is abnormal. Furthermore, structure typically has a great impact on the function of an organ, such as with the heart. For instance, a stenotic aortic valve will usually cause functional impairment of the left ventricle and lead to further pathologic conditions (e.g., ventricular hypertrophy). Thus, knowledge of anatomy and pathology is fundamental in understanding not only how the body is organized but also how the body works and how disease processes can affect it.

Likewise, preclinical animal research has been at the core of much of the progress made in medicine. Most, if not all, of what we know about the human body and biology, in general, has been initially made possible through animal research. A publication by the American Medical Association in 1989 listed medical advances emanating from animal research, including studies on AIDS, anesthesia, cardiovascular disease, diabetes, hepatitis, and Parkinson's disease, to name only a few [2]. More recently, in the field of transcatheter-delivered cardiac valves (see Chap. 36), the use of various animal models for preclinical research has been essential not only to optimize the device designs but also to ensure relative safety prior to their use in man. Furthermore, it has been through animal research that nearly all advances in veterinary medicine have also been established.

Animal research is still fundamental in developing new therapies aimed at improving the quality of life for patients with cardiovascular disease. Specifically, early cardiac device prototype testing is commonly performed utilizing animal models, both with and without cardiovascular disease. More specifically, before any invasively used device (a class III medical device) can be tested in humans, the Food and Drug Administration (FDA) requires that sufficient data be obtained from animal research indicating that the device functions in the desired and appropriate manner. It is also critical to subsequently extrapolate that a given device will be safe when used in humans, that is, it will behave in humans in a manner similar to its function in the chosen animal models in which it was tested. More specifically, this extrapolation of animal testing data to the human condition requires that the animal model(s) chosen for testing possesses similar anatomy and physiology as that of humans (normal and/or diseased). Unfortunately, detailed information relating human cardiac anatomy to that of the most common large mammalian animal models has been relatively lacking.

The following historical example illustrates how such a lack of knowledge can have a dramatic effect on the outcomes of cardiovascular research. During the 1970s and 1980s, dogs were employed as the primary animal model in numerous studies to identify potential pharmacological therapies for reducing infarct size. However, a detailed understanding of the coronary arterial anatomy was lacking or overlooked at the time; subsequently, it was shown that dogs have a much more extensive coronary collateral circulation relative to humans (Fig. 6.1). Thus, even when major coronary arteries were occluded, reliable and consistent

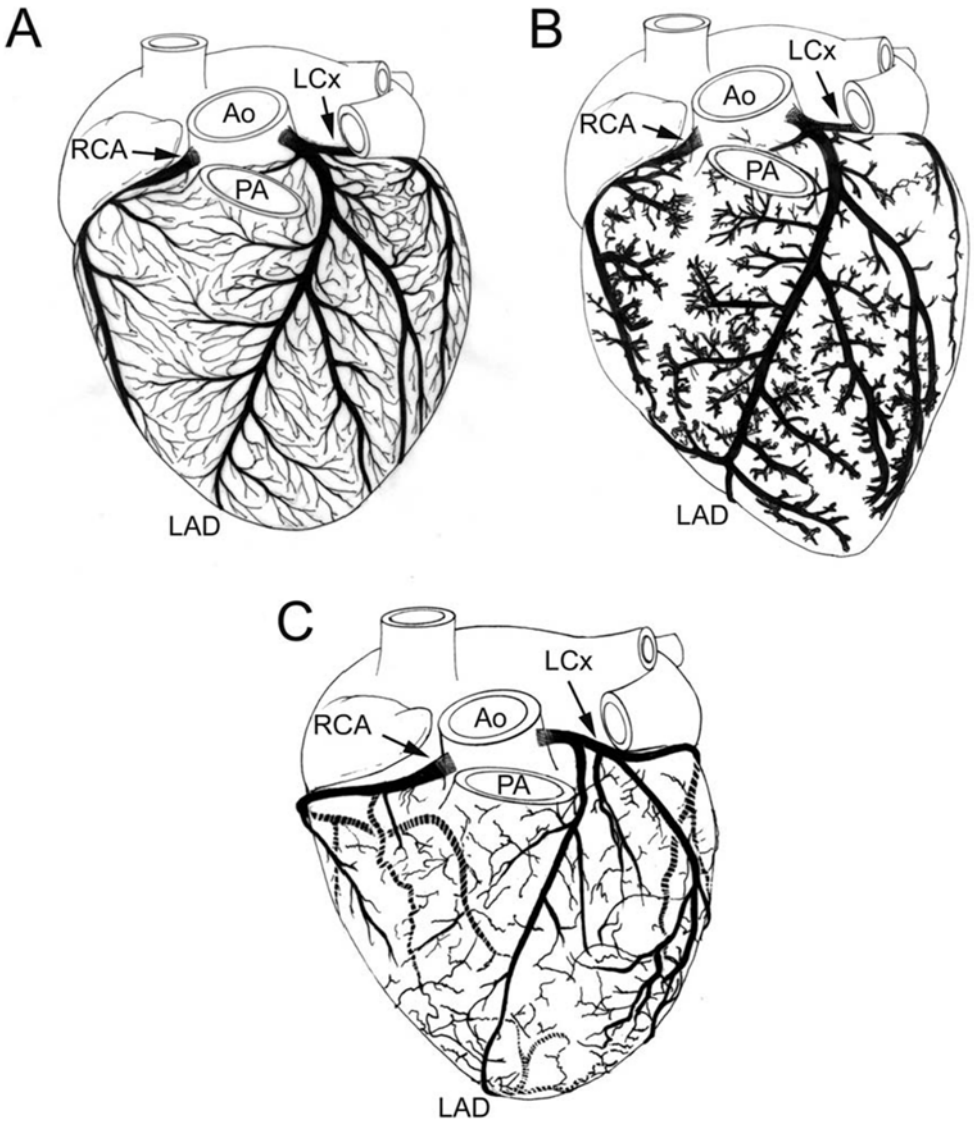

Fig. 6.1 Drawing of the coronary arterial circulation in the: (**A**) dog, (**B**) pig, and (**C**) human. Notice the extensive network of coronary collateralization in the dog heart, including many arterial anastomoses. The normal pig and human hearts have significantly less collateralization; each area of myocardium is usually supplied by a single coronary artery. *Ao* aorta, *LAD* left anterior descending artery, *LCx* left circumflex artery, *PA* pulmonary artery, *RCA* right coronary artery

myocardial infarcts were difficult to create. This led to false claims about the efficacy of many drugs in reducing infarct size which, when subsequently tested in humans, usually did not produce the same results as those observed in the canine experiments [5]. Therefore, ischemia studies with human-sized hearts have shifted to alternative species such as swine, which are considered to resemble the coronary collateral circulation of humans more precisely [6–9].

6.3 Literature Review of Large Mammalian Comparative Cardiac Anatomy

In general, the hearts of large mammals share many similarities, and yet the size, shape, and position of the hearts in the thoracic cavities can vary considerably between species [10]. Typically, the heart is located in the lower ventral part of the mediastinum in large mammals [11]. Most quadruped mammals tend to have a less pronounced left-sided orientation and a more ventrally tilted long axis of the heart when compared to humans [11] (Fig. 6.2). Additionally, hearts of most quadruped mammals tend to be elongated and have a pointed apex, with the exception of: (1) dogs which tend to have an ovoid heart with a blunt apex [11], (2) sheep which may have a somewhat blunt apex [12], and (3) pigs which have a blunt apex that is oriented medially [12]. Comparatively, human hearts typically have a trapezoidal shape [13] with a blunt apex. However, the apices of normal dog, pig, sheep, and human hearts are all formed entirely by the left ventricles [12–15] (Fig. 6.3).

It is important to note that differences exist in the heart weight to body weight ratios reported for large mammals. It is generally accepted that adult sheep and adult pigs have

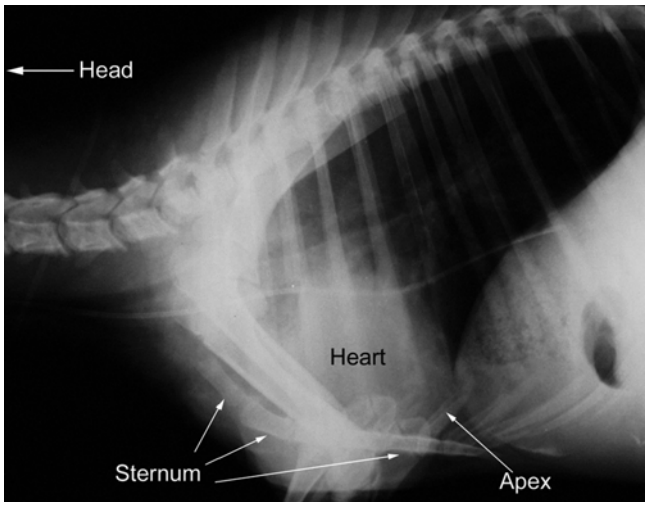

Fig. 6.2 Lateral radiograph of sheep thorax showing orientation of the heart while the animal is standing. The cranial direction is to the left and ventral to the bottom. The apex of the heart is more ventrally tilted (down toward the sternum) than is seen in humans, due to the posture of quadruped mammals. It should be noted, however, that this tilting is limited due to extensive attachments of the pericardium to the sternum and diaphragm

smaller heart weight to body weight ratios than those of adult dogs. More specifically, the adult dog may have as much as twice the heart weight to body weight ratio (6.9 to 7 g/kg) as pigs (2.9 to 2.5 g/kg) or sheep (3.0 to 3.1 g/kg) [16, 17], yet such findings will also likely be breed specific. The normal adult human heart weight to body weight ratio has been reported to be 5 g/kg which, on a comparative note, is similar to that of young pigs (25–30 kg animals) [7].

All large mammalian hearts are enclosed by the pericardium, which creates the pericardial cavity surrounding the heart. The pericardium is fixed to the great arteries at the base of the heart and is attached to the sternum and diaphragm in all mammals, although the degree of these attachments to the diaphragm varies between species [10, 11]. Specifically, the attachment to the central tendinous aponeurosis of the diaphragm is firm and broad in humans and pigs, the phrenopericardial ligament is the only pericardial attachment in dogs, and the caudal portion of the pericardium is attached via the strong sternopericardial ligament in sheep [10, 11].

The pericardium consists of three layers—the serous visceral pericardium (epicardium), the serous parietal pericar-

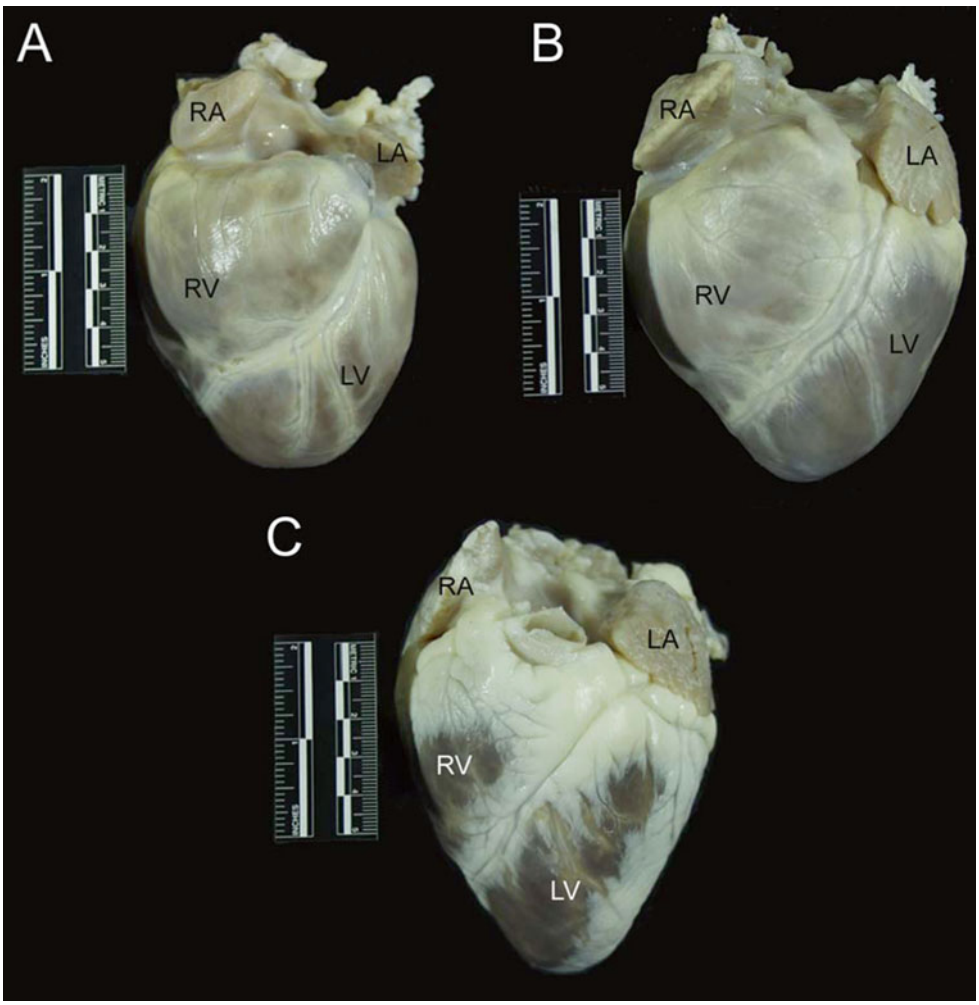

Fig. 6.3 The anterior aspect of the dog (**A**), pig (**B**), and sheep (**C**) hearts. The apex is formed entirely by the left ventricle in these hearts. Also notice the differences in overall morphology of the hearts. The dog heart is much more rounded than the pig and sheep hearts and has a blunt apex. The pig heart has more of a *valentine* shape with a somewhat blunt apex compared to the sheep heart. The sheep heart is much more conical in shape and has a much more pronounced apex than dog or pig hearts. Also noteworthy is the presence of significant amounts of epicardial fat on the sheep heart, compared with dog and pig hearts. *LA* left atrium, *LV* left ventricle, *RA* right atrium, *RV* right ventricle

dium, and the fibrous pericardium. The serous parietal pericardium lines the inner surface of the fibrous pericardium, and the serous visceral pericardium lines the outer surface of the heart. The pericardial cavity is found between the serous layers and contains the pericardial fluid. The pericardium is considered to serve many functions including: (1) preventing dilatation of the heart, (2) protecting the heart from infection and adhesion to surrounding tissues, (3) maintaining the heart in a fixed position in the thorax, and (4) regulating the interrelations between the stroke volumes of the two ventricles [18–20]. However, it should be noted that the pericardium is not essential for survival, since humans with congenital absence of the pericardium and pericardiectomized animals or humans can survive with minimal consequences for many years [18, 21].

Although the basic structure of the pericardium is the same, there are important differences between species [18, 19, 22]. For instance, pericardial wall thickness increases with increasing heart size [18]. Humans are the notable exception to this rule, having a much thicker pericardium than animals with similar heart sizes [18]. Specifically, the pericardium of the human heart varies in thickness between 1 and 3.5 mm [20], while the average thickness of the pericardium of various animal species was found to be considerably thinner (sheep hearts, 0.32 ± 0.01 mm; pig hearts, 0.20 ± 0.01 mm; dog hearts, 0.19 ± 0.01 mm) [19]. Differences in the amount of pericardial fluid are considered to exist as well. Holt reported that most dogs have 0.5–2.5 mL of pericardial fluid with some dogs having up to 15 mL, compared to 20–60 mL in adult human cadaver hearts [18]. For additional information on the pericardium, see Chap. 9.

The normally formed hearts of large mammals consist of four chambers—two thin-walled atria and two thicker walled ventricles. From both anatomical and functional perspectives, the heart is divided into separate right and left halves, with each half containing one atrium and one ventricle. In the fully developed heart with no associated pathologies, deoxygenated blood is contained in the right side of the heart and kept separate from oxygenated blood, which is on the left side of the heart. The normal path of blood flow is similar among all large mammals. Specifically, systemic deoxygenated blood returns to the right atrium via the caudal (inferior in humans) vena cava and the cranial (superior in humans) vena cava, subsequently passing into the right ventricle through the open tricuspid valve. At the same time, oxygenated blood returns from the lungs via the pulmonary veins to the left atrium and then through the open mitral valve to fill the left ventricle. After atrial contraction forces the last of the blood into the ventricles, ventricular contraction ejects blood through the major arteries arising from each ventricle, specifically the pulmonary trunk from the right ventricle and the aorta from the left ventricle. Via the pulmonary arteries, blood travels to the lungs to be oxygenated, whereas aortic blood travels through both the coronary arterial system (to feed the heart) and to the systemic circulation (to oxygenate bodily tissue). For additional discussions of flow patterns and function, see Chaps. 1 and 20.

6.3.1 The Atria

The right and left atria of the adult mammalian heart are separated by the interatrial septum. They are located at what is termed "the base" of the heart. The base receives all of the great vessels and is generally oriented cranially or superiorly, although there are reported differences in orientation among species, which are mostly dependent on the posture of the animal [13, 14, 23]. During fetal development, blood is able to pass directly from the right atrium to the left atrium, effectively bypassing the pulmonary circulation through a hole in the interatrial wall termed the *foramen ovale*. The foramen ovale has a valve-like flap located on the left atrial side of the interatrial septum, which prevents backflow into the right atrium during left atrial contraction [24]. At the time of birth or soon thereafter, the foramen ovale closes and is marked in the adult heart by a slight depression on the right atrial side of the interatrial wall termed the *fossa ovalis* [14, 24, 25]; it should be noted that it can remain patent in some individuals, and the rate of patent foramen ovale is comparable in adult humans and domestic swine at approximately 10–30 %. As compared to humans, the fossa ovalis is more posteriorly (caudally) positioned in dogs and sheep [11], but more deep-set and superior in the pig heart [13].

The sinus venosus, a common separate structure in non-mammalian hearts, is incorporated into the right atrium and is marked by the sinoatrial node in large mammals [24, 25]. According to Michaëlsson and Ho [11], all the mammals studied (including dogs, pigs, and sheep) have principally the same atrial architecture including: the sinus venosus, crista terminalis, fossa ovalis, Eustachian valve (valve of the inferior vena cava), and Thebesian valve (valve of the coronary sinus). All large mammalian atria also have an earlike flap called the auricle or appendage [13, 14, 25], although the size and shape of the auricles vary considerably between species [11, 13] (Fig. 6.4). In general, the junction between the right atrium and the right appendage is wide, whereas the junction on the left side is much more narrow [13]. Multiple pectinate muscles are found in both the right and left atrial appendages and on the lateral wall of the right atrium [11, 13, 14] (Figs. 6.5 and 6.6). Commonly, there is one posterior (caudal or inferior) and one anterior (cranial or superior) vena cava, although in some mammals there are two anterior venae cavae [24], and the location of the ostia of the venae cavae entering into the atrium varies [11, 13]. Specifically, the ostia of the inferior and superior vena cavae enter at right (or nearly right) angles in large mammalian animal models while entering the atrium nearly in line in humans [13].

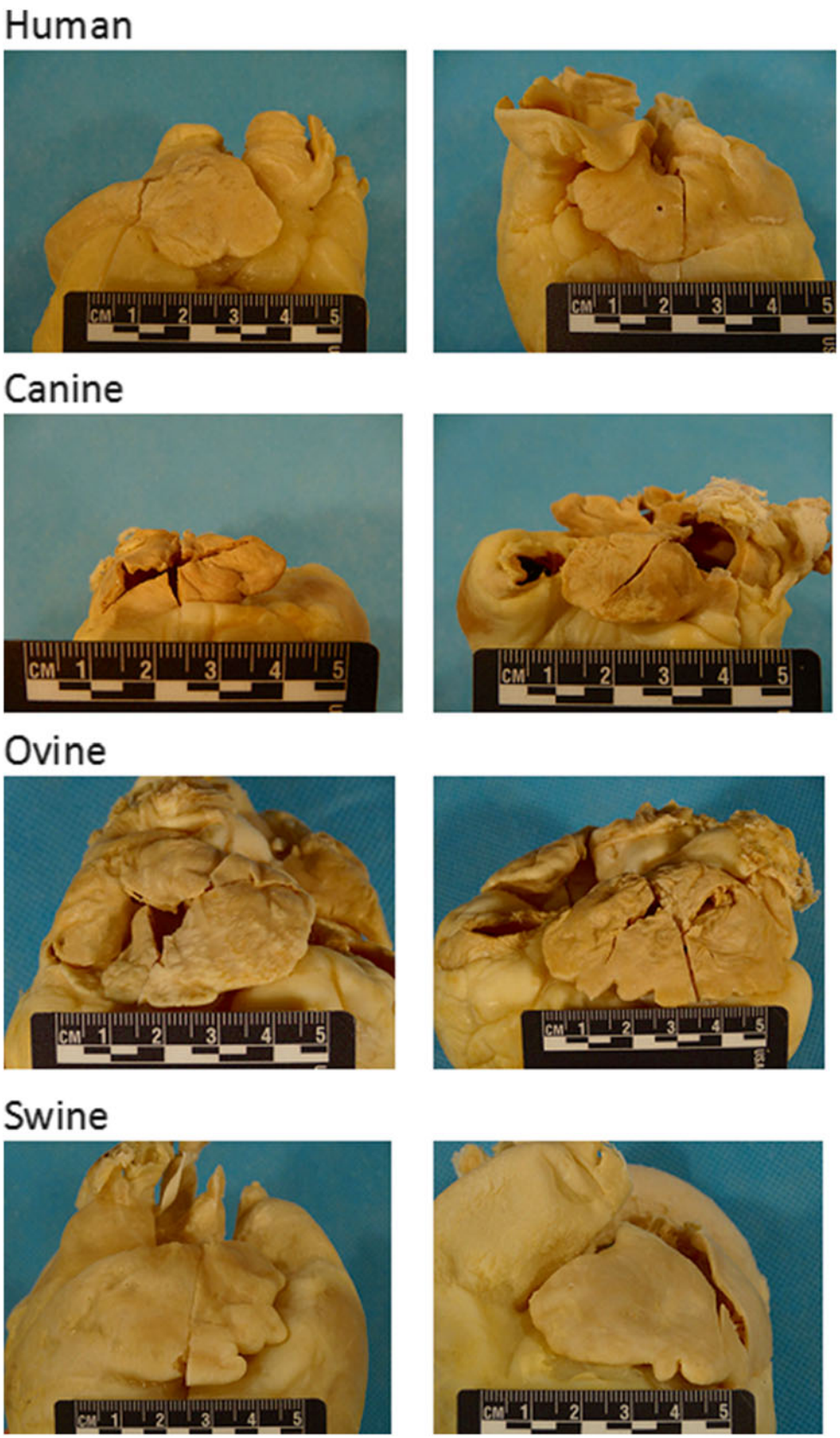

Fig. 6.4 Differences in large mammalian atria. Human: (*left*) Right atrial appendage is generally triangular in shape and may be larger or smaller than the left atrial appendage; (*right*) Left atrial appendage is generally tubular in shape. Canine: (*left*) Right atrial appendage is generally tubular and is larger than or similar in size to the left atrial appendage; (*right*) left atrial appendage is usually tubular. Ovine: (*left*) Right atrial appendage is generally half-moon in shape and is larger than the left atrial appendage; (*right*) left atrial appendage is generally triangular in shape. Swine: (*left*) Right atrial appendage is usually half-moon in shape and is generally smaller than the left atrial appendage; (*right*) left atrial appendage is generally triangular in shape. *Source*: www.vhlab.umn.edu/atlas, Comparative Anatomy Tutorial

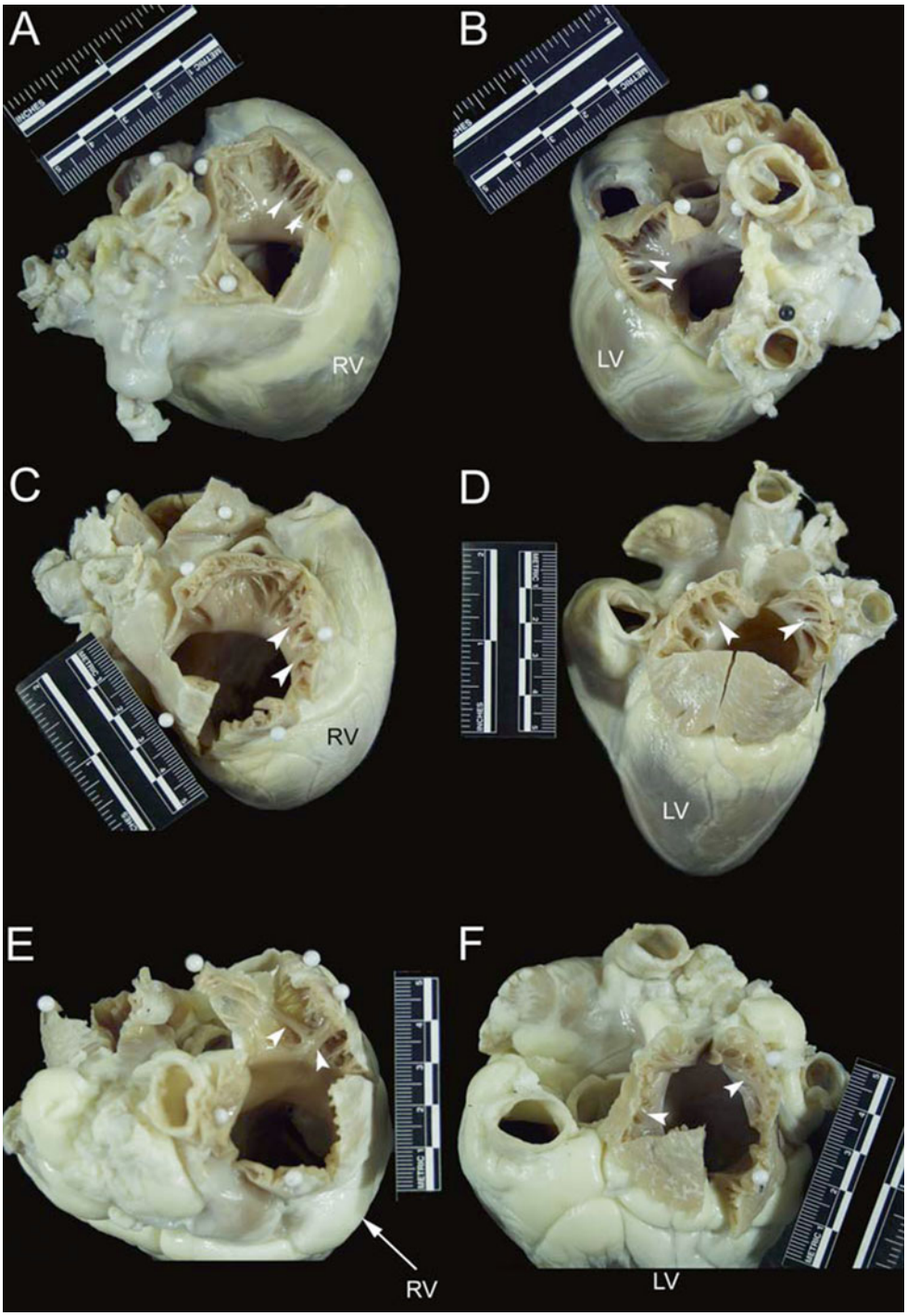

Fig. 6.5 The cranial (superior) aspect of dog (**A** and **B**), pig (**C** and **D**), and sheep (**E** and **F**) hearts. Images on the *left* of the figure (**A**, **C**, and **E**) show opened right atrial appendages, while images on the *right* (**B**, **D**, and **F**) show opened left atrial appendages. *White arrows* point to pectinate muscles that line the right and left atrial appendages. Notice that the *right* and *left* atrial appendages of the dog heart are tubular in nature. In contrast, the right and left atrial appendages of the pig and sheep heart are more triangular in morphology. *LV* left ventricle, *RV* right ventricle

Typically, the extent of the inferior vena cava between the heart and liver is long in domestic animals (>5 cm) and short in humans (1–3 cm) [11]. The coronary sinus ostium is normally located in the posterior wall of the right atrium, but its location can differ slightly between species. Interestingly, the number of pulmonary veins entering the left atrium also varies considerably between species; human hearts typically have four [13] or occasionally five [15], dog hearts have five or six [14], and pig hearts have two primary pulmonary veins [13]. In all large mammalian hearts, the atria are separated from the ventricles by a layer of fibrous tissue called the *cardiac skeleton*, which serves as an important support for the valves as well as to electrically isolate the atrial myocardium from the ventricular myocardium [23].

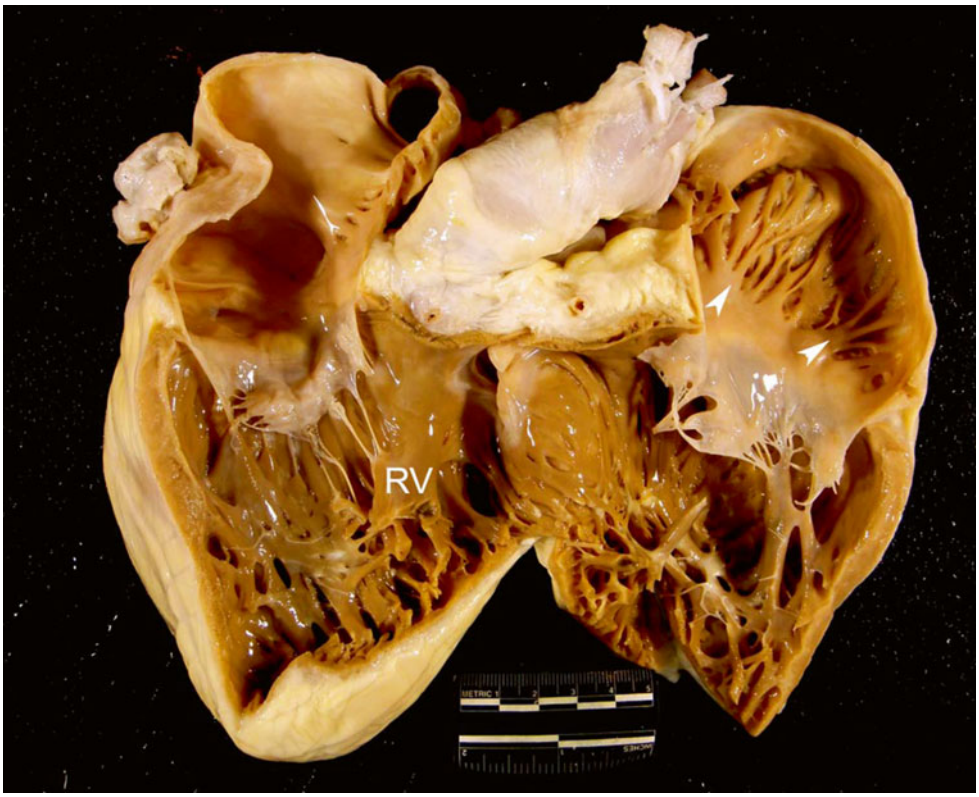

Fig. 6.6 A human heart opened on the inferior and superior aspects of the right ventricle, to show the anterior and posterior walls. *White arrows* point to pectinate muscles in the right atrial appendage on the anterior aspect. *RV* right ventricle

6.3.2 The Ventricles

The left and right ventricles of the large mammals used for cardiovascular research essentially contain the same components which are also structurally very similar to those in humans, including: an inlet (inflow) region, an apical region, and an outlet (outflow) region. The ventricles can be considered the major ejection/pumping chambers of the heart, and, as expected, their walls are significantly more muscular in nature than those of the atria. It should also be noted that the left ventricular walls are notably more muscular than those of the right ventricle, due to the fact that the left ventricle must generate enough pressure to overcome the resistance of the systemic circulation, which is much greater than the resistance of the pulmonary circulation (normally more than 4 times greater). The walls of both ventricles near the apex have interanastomosing muscular ridges and columns termed the *trabeculae carneae* which serve to strengthen the walls and increase the force exerted during contraction [11, 14, 24, 25]. However, large mammalian hearts reportedly do not have the same degree of trabeculation located in the ventricles as normal adult human hearts, and the trabeculations in animal hearts are commonly more coarse than those of human hearts [11, 13] (Figs. 6.7 and 6.8). One can also compare these relative anatomies by carefully studying various prepared plastinated cardiac specimens of large mammalian hearts, including humans. Papillary muscles supporting the atrioventricular valves are found attached to the walls of the ventricles. Similar to human anatomy, in the majority of large mammalian animal hearts, the right ventricle has three papillary muscles, and the left ventricle has two, although variations in individuals and species do occur [11]. It should be noted that, in general, each papillary muscle supplies chordae tendineae to at least 2 leaflets, ensuring redundancy. Both ventricles typically have cross-chamber fibrous or muscular bands, which usually contain Purkinje fibers. Within the right ventricle of most dogs, pigs, and ruminants, a prominent band termed the *moderator band* is typically present [11]. However, the origin and insertion of the band, as well as the composition of the band, differ notably between species. For example, in the pig heart, the band originates much higher on the septal wall compared to the analogous structure in the human heart [13], and the sheep heart has a similar moderator band as the pig heart (Figs. 6.6, 6.7, 6.8, and 6.9). In the dog heart, a branched or single muscular strand extends across the lumen from the septal wall near, or from the base of, the anterior papillary muscle [14] (Figs. 6.7, 6.8, 6.10, and 6.11). However, Truex and Warshaw [26] did not find any moderator bands in the dog hearts they examined ($n = 12$), but did observe them in all sheep hearts ($n = 12$) and all pig hearts ($n = 12$), compared to 56.8 % of the human hearts they examined ($n = 500$). Furthermore, they described three subtypes of moderator bands: a free arching band, a partially free arching band, and a completely adherent band.

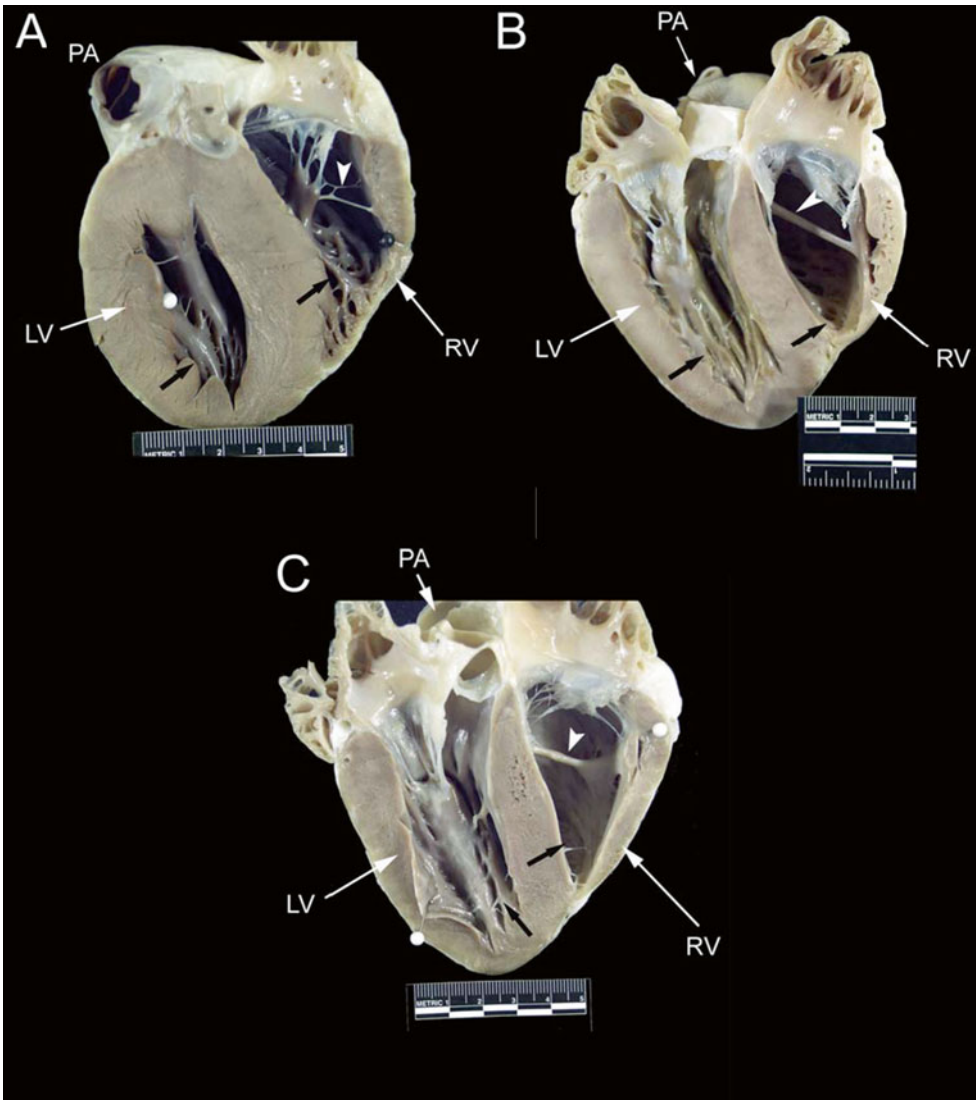

Fig. 6.7 Images showing dog (**A**), pig (**B**), and sheep (**C**) hearts that have been opened along the long axis to show both ventricular cavities. The anterior half of the heart is shown (left ventricle on the left and right ventricle on the right). *Black arrows* point to ventricular trabeculations which are large and coarse. *White arrows* point to the moderator band. Notice that a fibrous, branched moderator band extends from the anterior papillary muscle to the free wall in the canine heart. In contrast, a muscular, nonbranched moderator band extends from the septal wall to the anterior papillary muscle in pig and sheep hearts. Additionally, notice the presence of fibrous bands in the left ventricle. *LV* left ventricle, *PA* pulmonary artery, *RV* right ventricle

Nevertheless, one must also consider the potential for breed differences in animals and ethnic variability in humans. It is interesting to note that while, in general, anatomical textbooks state there is no specific structure named the moderator band in the left ventricle, left ventricular bands similar to the moderator band of the right ventricle have been described in the literature. For example, Gerlis et al. found left ventricular bands in 48 % of the hearts of children and in 52 % of the adult human hearts studied [27] (Fig. 6.8). They also reported that left ventricular bands were highly prevalent in sheep, dog, and pig hearts [27] (Fig. 6.7).

6.3.3 The Cardiac Valves

Large mammalian hearts have four cardiac valves with principally similar structures and locations. Two atrioventricular valves are located between each atrium and ventricle on both the right and left sides of the heart, and two semilunar valves lie between the ventricles and the major arteries arising from their outflow tracts (the pulmonary artery and aorta). Chordae tendineae connect the fibrous leaflets of both atrioventricular valves to the papillary muscles in each ventricle and serve to keep the valves from prolapsing into the atria during ventricular contraction, thereby preventing backflow of blood into the atria. The semilunar valves—the aortic and pulmonic—do not have attached chordae tendineae and close due to pressure gradients developed across them. See Chap. 34 for more details on valvular structures, function, and defects.

The valve separating the right atrium from the right ventricle is termed the *tricuspid valve* because it has three major cusps—the anterosuperior (anterior), inferior (posterior), and septal cusps. Typically, there are also three associated papillary muscles in the right ventricle. Interestingly, the commissures between the anterosuperior leaflet and the

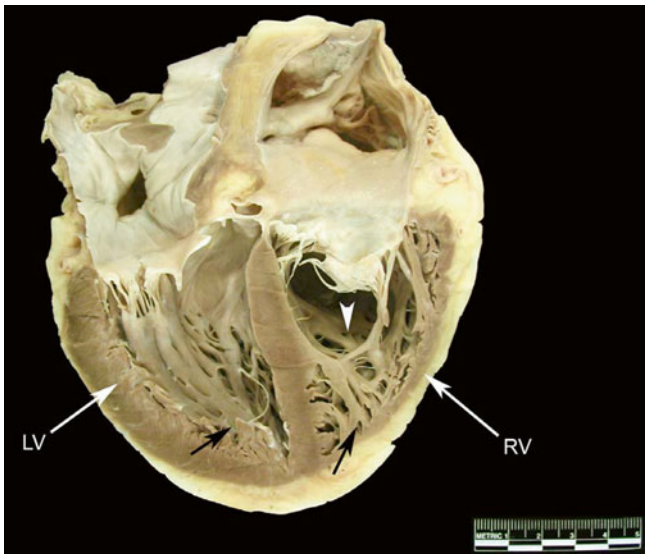

Fig. 6.8 Image of a human heart opened on the long axis to show both ventricular cavities. The left ventricle is on the left and the right ventricle on the right. *Black arrows* point to ventricular trabeculations, which are fine and numerous. The *white arrow* points to the moderator band, which is thick and muscular. It is different in size, shape, and location from the animal hearts shown in Fig. 6.7. *LV* left ventricle, *RV* right ventricle

inferior leaflets can be fused in dog hearts [14], giving the appearance of only two leaflets. Interindividual and interspecies variations in the number of papillary muscles have also been reported [11]. The valve separating the left atrium from the left ventricle is termed the *mitral or bicuspid valve* because it typically has two cusps, the anterior (aortic) and the posterior (mural). However, according to Netter [15], the human mitral valve actually can be considered to have four cusps, including the two major cusps listed above and two small commissural cusps or scallops; further publications on the mitral valve describe large variations in the number of scallops present in human hearts. Quill et al. studied the relative frequency of such variations in 38 human hearts and showed that the commonly described clefts on the posterior leaflet separating that leaflet into three regions (P1, P2, P3) were present in the majority of hearts; deviant clefts were also present in unexpected locations, such as the anterior leaflet, in some hearts [28]. In large mammalian hearts, two primary leaflets of the mitral valve are always present, but variations in the number of scallops exist and can be quite marked, giving the impression of extra leaflets [11]. A fibrous continuity between the mitral valve and the aortic valve is present in humans and most large mammals, extending from the central fibrous body to the left fibrous trigone [11] (Fig. 6.12). The length of this fibrous continuity, termed the *intervalvar septum or membranous septum*, varies considerably in length in different animals but notably is completely

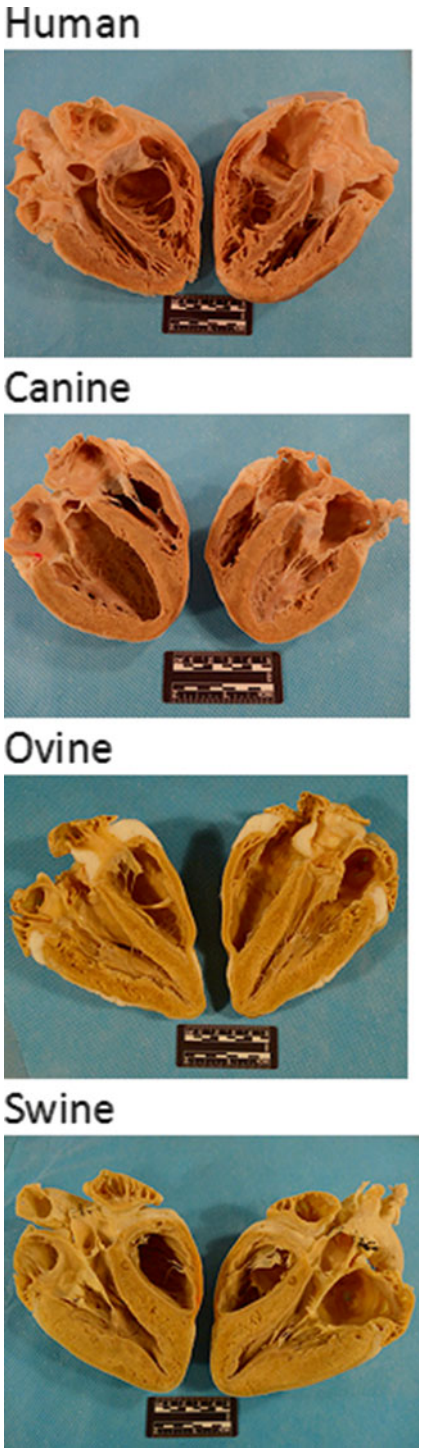

Fig. 6.9 Plastinated hearts of various species. *Human:* Trabeculae carneae in the apex are notably more numerous and finer than in the hearts of swine, canines, or sheep. *Canine:* Trabeculae carneae are coarser than those of humans; compared to swine and sheep hearts, the right ventricle has greater trabeculation though the left has similar trabeculation compared to these other animals. *Ovine:* Trabeculae carneae are noticeably fewer and coarser compared to those in human hearts. *Swine:* Trabeculae carneae are noticeably fewer and coarser compared to humans. *Source*: www.vhlab.umn.edu/atlas, Comparative Anatomy Tutorial

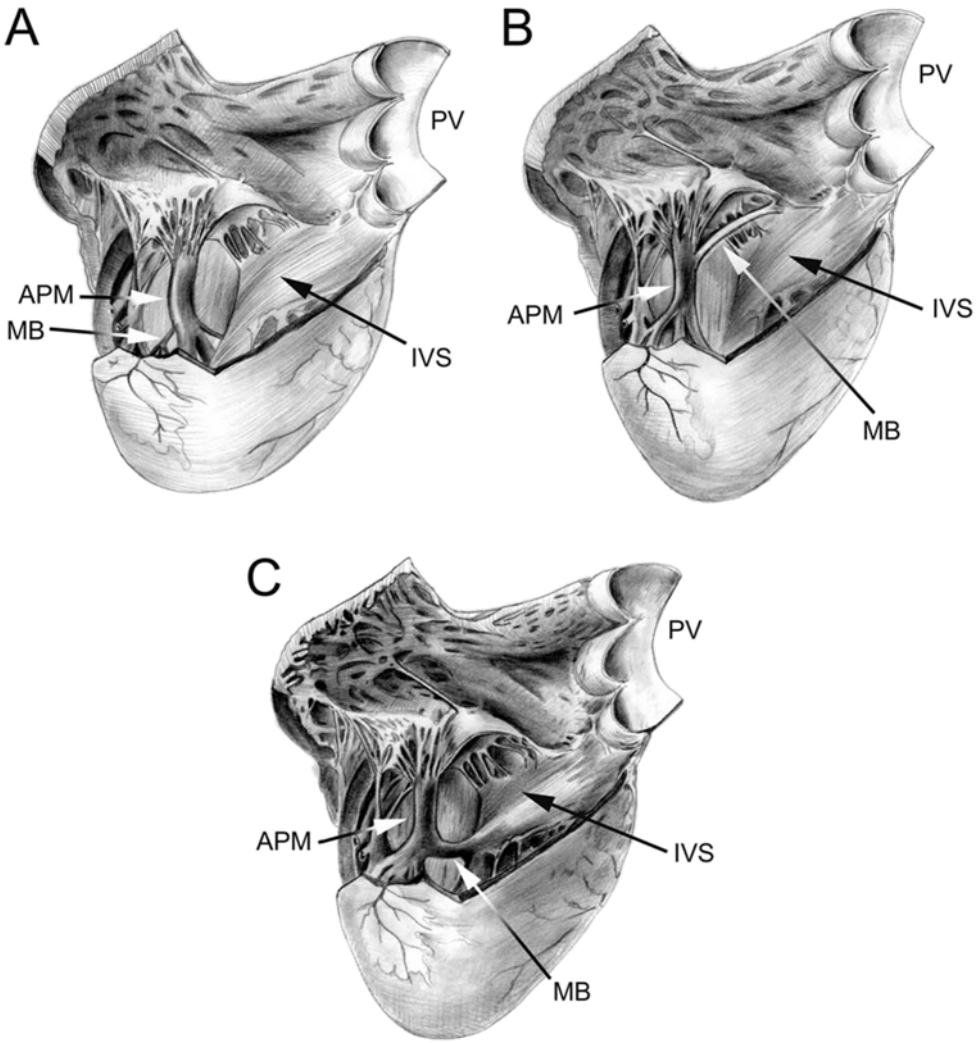

Fig. 6.10 Drawing of an opened right ventricular cavity in dog (**A**), pig and sheep (**B**), and human (**C**) hearts. The structure of the moderator band differs greatly between these hearts. In the dog heart, there is a branching fibrous band that runs from the anterior papillary muscle to the free wall of the right ventricle. In the human heart, the moderator band is typically located near the apex and is thick and muscular. In the pig and sheep hearts, the moderator band originates much higher on the interventricular septum and travels to the anterior papillary muscle. It is not as thick as in the human heart but is still muscular in nature. Also, note that the anterior papillary muscle in the dog heart originates on the septal wall, as opposed to originating on the free wall of the human, pig, and sheep hearts. *APM* anterior papillary muscle, *IVS* interventricular septum, *MB* moderator band, *PV* pulmonary valve

absent in sheep [29]. There are also differences in the fibrous ring supporting the mitral valve and in the composition of the leaflets of the mitral valve between species. For instance, according to Walmsley, a segment of the ring at the base of the mural cusp is always present in the human heart, but is difficult to distinguish in certain breeds of dogs and is inconspicuous in the sheep heart [29].

Differences in aortic valve anatomy have also been reported in the literature. For example, Sands et al. compared aortic valves of human, pig, calf, and sheep hearts [30], and they reported that interspecies differences in leaflet shape exist, but that all species examined had fairly evenly spaced commissures. Additionally, they found that variations in leaflet thickness existed; in particular, sheep aortic valves were described as especially thin and fragile. They also noted that there was a substantially greater amount of myocardial tissue supporting the right and left coronary leaflet bases in the animal hearts relative to humans [30].

6.3.4 The Coronary System

Mammalian hearts have an intrinsic circulatory system that originates with two main coronary arteries [11] whose ostia are located directly behind the aortic valve cusps. Deoxygenated coronary blood flow returns to the right atrium via the coronary sinus (into which the coronary veins drain) and also to the right atrium, the right and left ventricles [24, 31], and the left atrium [32, 33] by Thebesian veins. According to Michaëlsson and Ho [11], differences in perfusion areas exist between large mammalian species as well as within species (e.g., between breeds); these differences have also been described in humans. Dogs and sheep typically have a left coronary type of supply, such that the majority of the myocardium is supplied via branches arising from the left coronary artery. In contrast, pigs typically have a balanced supply where the myocardium is supplied equally from both right and left coronary arteries [11]. Yet, Crick et al. [13] reported that most of the pig hearts they examined

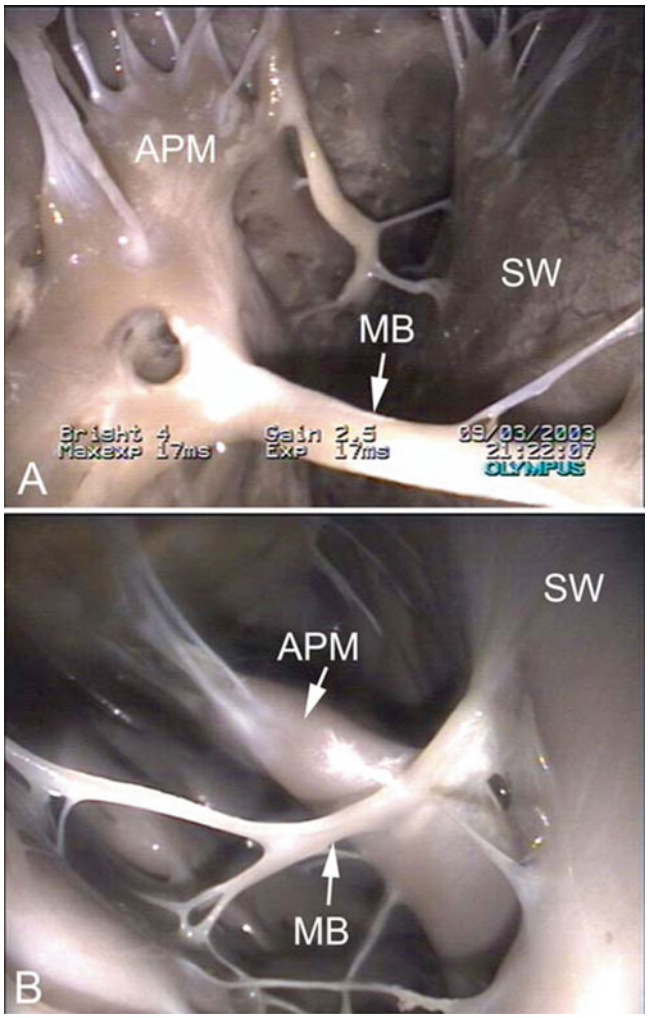

Fig. 6.11 Images showing the moderator band in the right ventricle of an ovine heart (**A**) and canine heart (**B**). The moderator band in the sheep is muscular, originating on the septal wall and running to the anterior papillary muscle. In contrast, the moderator band in the canine heart appears fibrous. It originates on the septal wall, runs to the anterior papillary muscle, and continues to the free wall of the right ventricle. *APM* anterior papillary muscle, *MB* moderator band, *SW* septal wall

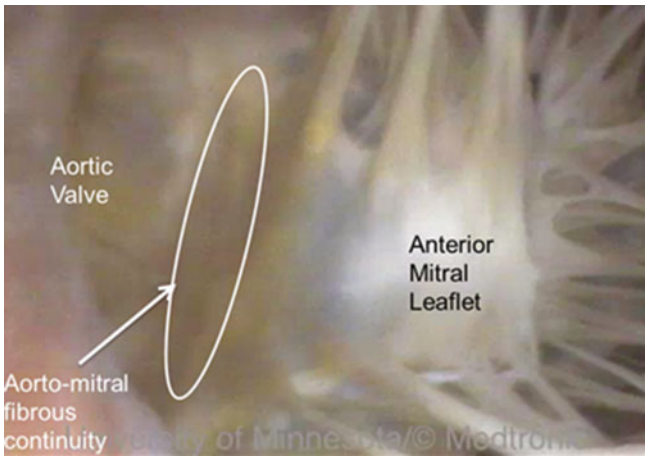

Fig. 6.12 Fibrous continuity between the mitral valve and aortic valve in a human heart. *Source*: www.vhlab.umn.edu/atlas, Left ventricle/Aortic valve/Visible Heart (functional)/Heart0284-2

(80 %) possessed right coronary dominance. Additionally, Weaver et al. [34] found that the right coronary artery was dominant in 78 % of the pigs they studied. Most human hearts (approximately 90 %) also display right coronary arterial dominance [35].

Another important aspect of the coronary arterial circulation, one that is of great importance in myocardial ischemia research, is the presence or absence of significant collateralization of the coronary circulation. Normal human hearts tend to have sparse coronary collateral development, which is very similar to that seen in normal pig hearts [34]. In contrast, it is now widely known that extensive coronary collateral networks can be seen in normal dog hearts [5, 36–39]. Furthermore, Schaper et al. [40] found that the coronary collateral network of dogs was almost exclusively located at the epicardial surface, while that of pig hearts, when present, was located subendocardially. They were unable to detect a significant collateral network in the hearts of sheep (Fig. 6.1).

There are three major venous pathways that drain the heart—the coronary sinus, anterior cardiac veins, and Thebesian veins [33, 41]. Drainage from each of these venous systems is present in human hearts as well as in dog, pig, and sheep hearts [13, 14, 24, 33]. While the overall structure of the coronary venous system is similar across species, interindividual variations are common. Nevertheless, there is one notable difference in the coronary venous system between species that warrants mention, that is, the presence of the left azygos vein draining the left thoracic cavity directly into the coronary sinus; a left azygos vein is typically present in both pig [13] and sheep [11] hearts (Fig. 6.13).

6.3.5 The Lymphatic System

In addition to an intrinsic circulatory system, large mammalian hearts have an inherent and substantial lymphatic system which serves the same general function of the lymphatic system in the rest of the body. More specifically, the mammalian lymphatic system has been described as follows. Hearts have subepicardial lymphatic capillaries that form continuous plexuses covering the whole of each ventricle [42]. Furthermore, the lymphatic channels are divided into five orders, with the first order draining the capillaries and joining to become the second order and so on, until the lymph is drained from the heart via one large collecting duct of the fifth order. In general, it has been described that dogs, pigs, and humans have extensive subepicardial and subendocardial networks with collecting channels directed toward large ducts in the atrioventricular sulcus that are continuous with

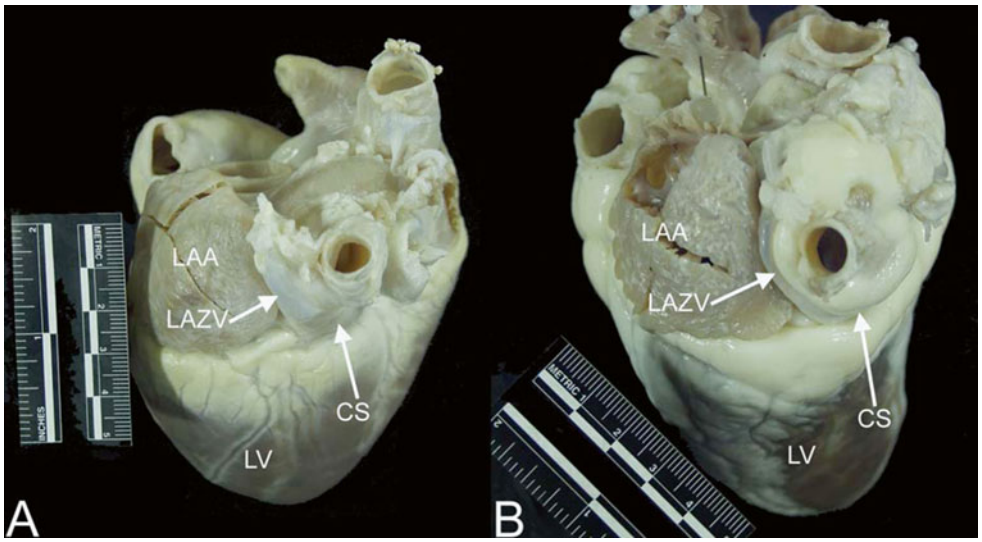

Fig. 6.13 Images showing the left azygos (hemiazygos) vein entering the coronary sinus in the pig (**A**) and sheep (**B**) hearts. The left azygos vein drains the thoracic cavity directly into the coronary sinus in these animals, rather than emptying into the superior vena cava via the azygos as seen in dog and human hearts. Notice that it travels between the left atrial appendage and the pulmonary veins; the oblique vein of Marshall (oblique vein of the left atrium) travels this path in human and dog hearts. *CS* coronary sinus, *LAA* left atrial appendage, *LAZV* left azygos vein, *LV* left ventricle

the main cardiac lymph duct [43]. Furthermore, it was found that the lymphatic vessels of the normal heart are distributed in the same manner as the coronary arteries and follow them as two main trunks to the base of the heart [44].

6.3.6 The Conduction System

All large mammalian hearts have a very similar conduction system whose main components are the sinoatrial node, atrioventricular node, bundle of His, right and left main bundle branches, and Purkinje fibers. Yet, interspecies variations are well recognized, especially with regard to the finer details of the arrangement of the transitional and compact components of the atrioventricular node [11]. In the mammalian heart, the sinoatrial node is the normal pacemaker [11, 24, 25] and is situated in roughly the same location in all hearts: high on the right atrial wall near the junction of the superior vena cava and the right atrium. Conduction spreads through the atria to the atrioventricular node (which interestingly is unique to both birds and mammals) [25] and then to the bundle of His, which is the normal conducting pathway from the atria to the ventricles, penetrating through the central fibrous body. The right and left main bundle branches emanate from the bundle of His and branch further into the Purkinje fibers which then rapidly spread conduction to the ventricles [11]. The atrioventricular node and bundle of His are typically located subendocardially in the right atrium within a region known as the *triangle of Koch*, which is delineated by the coronary sinus ostium, the membranous septum, and the septal/posterior commissure of the tricuspid valve (Fig. 6.14). The presence of the *os cordis* has been noted to be present in the sheep heart, but not in dog, pig, or human hearts. Specifically, it is a small, fully formed bone that lies deep in the atrial septum which, in turn, influences the location and course of the bundle of His in sheep hearts. Other known differences in the atrioventricular conduction system between human, pig, dog, and sheep hearts are illustrated in Table 6.1. For more details on the conduction system, see Chap. 13.

6.4 Qualitative and Quantitative Comparisons of Cardiac Anatomy in Commonly Used Large Mammalian Cardiovascular Research Models

The following section describes original research conducted at the University of Minnesota by the authors of this chapter.

6.4.1 Importance for Comparing the Anatomy of Various Animal Models

Selection of the proper experimental model for use in cardiovascular research depends on many factors including: (1) cost, (2) quality and quantity of data, (3) familiarity with the model, and/or (4) relevance to the human condition [49]. Typically, a balance as to the relative importance of these factors is determined when optimizing any experimental protocol. Yet, one important parameter that is often overlooked in such a design is the comparative cardiac anatomy of the model in question relative to that of humans.

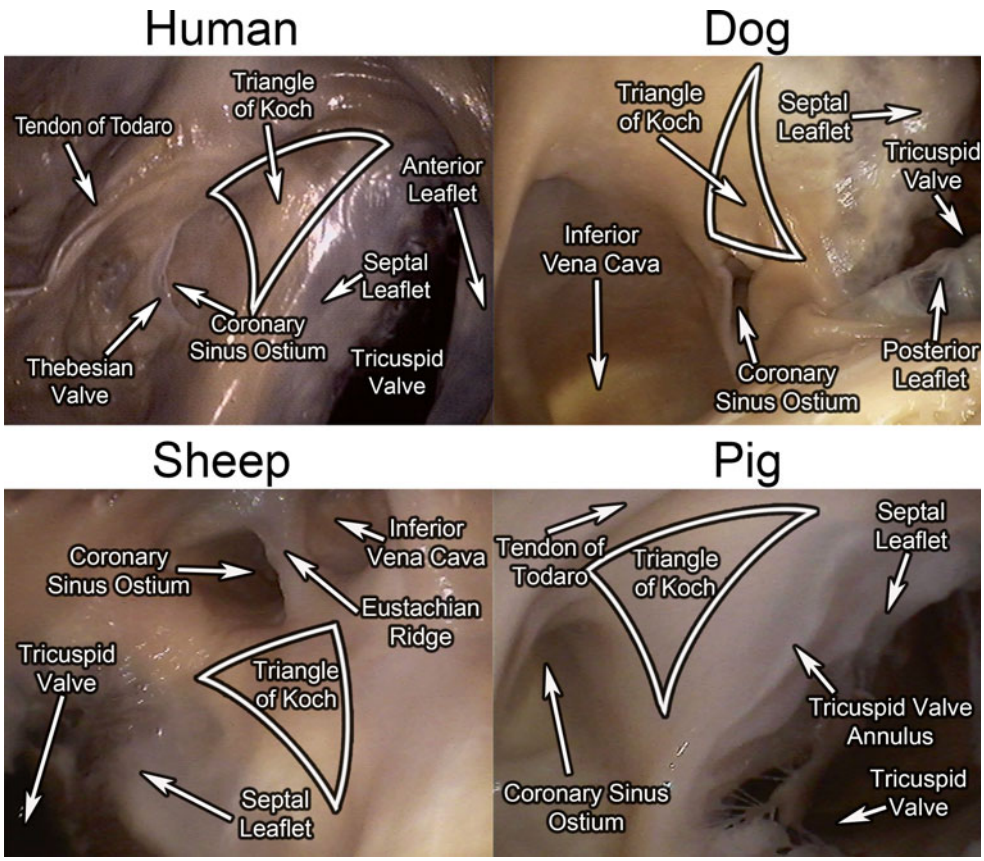

Fig. 6.14 The *triangle of Koch* in human, dog, sheep, and pig hearts

Even today, there is often considerable debate over which cardiovascular research model most closely resembles the human heart anatomically. Surprisingly, in spite of this debate, the comparative cardiac anatomy of such models as a specific topic is largely unexplored. Nevertheless, this question is especially important for biomedical device design and testing in which the goal is to test a product that directly interacts with specific anatomical structures. Furthermore, such comparisons often become even more complicated due to: (1) the relative orientation and/or position of each species' heart and (2) the various terminologies used to describe heart anatomy and position (attitudinally correct anatomy) which can vary between various animal models and in comparison to humans. In addition, one hopes to match the cardiac dimensions across species, but this can be further complicated by both gender and age. For example, a 6–7-month-old Yorkshire swine has a typical cardiac mass between 300 and 400 g, which is similar to that of the healthy adult human. Finally, genetic heritage influences expressed cardiac anatomy, and specific descriptors are often missing in previous reports (i.e., specific breeds of animals studied).

Thus, the following studies were designed to elucidate the major similarities and differences between the hearts of several major large mammalian cardiovascular research models and then relate these findings to humans. Specifically, qualitative and quantitative techniques were employed on post-mortem, formalin-fixed porcine, ovine, canine, and human hearts.

6.4.2 Methods and Materials

For this study, we obtained fresh hearts of humans (*Homo sapiens*; man), pigs (*Sus domestica*; swine, porcine), dogs (*Canis lupus familiaris*; canine), and sheep (*Ovis aries*; ovine). Human hearts ($n=8$) were obtained from the Anatomy Bequest Program at the University of Minnesota. All human hearts were previously unfixed and devoid of clinically diagnosed heart disease or defect. Swine (Yorkshire cross), canine (hound cross), and ovine (Polypay cross) ($n=10$ each) hearts were obtained from either Research Animal Resources at the University of Minnesota or the Physiological Research Laboratories at Medtronic, Inc. These animals were used for prior research studies that did not alter their anatomy. In other words, in all cases, care was taken to insure that hearts were only obtained from individuals and animals in which cardiac anatomy was not considered to be altered by disease processes or any prior experimental protocols.

6.4.2.1 Heart Preservation

To preserve the hearts and prepare them for comparative anatomical study, specimens were all similarly *pressure*

Table 6.1 Similarities and differences in the atrioventricular conduction systems of dog, pig, sheep, and human hearts [45–48]

	Location of AV node	AV node and bundle of His junction	Length of bundle of His	Route of bundle of His
Human	Located at the base of the atrial septum, anterior to the coronary sinus, and just above the tricuspid valve	End of the AV node and the beginning of bundle of His are nearly impossible to distinguish	Total length of the unbranched portion is 2–3 mm. Penetrating bundle is 0.25–0.75 mm in length. Bundle bifurcates just after emerging from the central fibrous body	Bundle lies just beneath the membranous septum at the crest of the interventricular septum
Pig	Lies on the right side of the crest of the ventricular septum and is lower on the septum than in humans	No explicit information found	Penetrating bundle is very short in comparison to humans	Climbs to the right side of the summit of the ventricular septum, where it enters the central fibrous body. The bifurcation occurs more proximally than in humans
Dog	Same as in humans	Consists of internodal tracts of myocardial fibers	Penetrating bundle is 1–1.5 mm long, significantly longer than the human penetrating bundle	His bundle runs forward and downward through the fibrous base of the heart, just beneath the endocardium. There are at least three discrete bundle of His branches of myocardium that join the atrial end of the AV node via a proximal His bundle branch
Sheep	Located at the base of the atrial septum, anterior to the coronary sinus, just above the tricuspid valve, and at the junction of the middle and posterior one-third of the os cordis	Junction is characterized by fingerlike projections, where the two types of tissue overlap; size and staining qualities of the initial Purkinje cells of the bundle of His make it easy to distinguish between the end of the AV node and the beginning of the bundle of His	Portion of the bundle passing through the central fibrous body is ~1 mm. Bundle extends 4–6 mm beyond the central fibrous body before it bifurcates	Unbranched bundle must pass beneath the os cordis to reach the right side of the ventricular septum. The bundle of His then remains relatively deep within the confines of the ventricular myocardium. Branching occurs more anteriorly in sheep than in humans

AV atrioventricular

perfusion fixed. Briefly, this consisted of suspending each heart in a large container of 10 % buffered formalin from cannulae tied into the following major vessels: the superior caval vein, the pulmonary trunk, the aorta, and one pulmonary vein. All remaining vessels were sealed, with the exception of small vents positioned in both the inferior caval vein and in one of the pulmonary veins. Formalin was gravity fed down the cannulae from a reservoir chamber positioned 35–40 cm above the fluid level in the suspension chamber. This system generated a reproducible perfusion pressure between 45 and 50 mmHg. The hearts were allowed to fix under these conditions for a minimum of 24 h in order to allow for adequate penetration of fixative. This method of fixation was quite reproducible to ensure that the hearts maintained a similar anatomical configuration.

6.4.2.2 Qualitative Anatomical Assessment of Perfusion-Fixed Hearts

Several observational assessments, similar to those conducted and previously described by Crick et al. [13], were completed on each heart. In addition to these assessments, a 6 mm endoscopic camera (Olympus Optical, Tokyo, Japan) was inserted into each chamber of each heart, with care taken not to distort any structure to be observed. This allowed for direct visualization of the internal chambers of the heart without dissection, hence allowing the anatomical structures to be examined in a more realistic state. Specific anatomical features assessed included:

- Overall shape of entire heart (conical, valentine, trapezoidal, elliptical, or rounded with blunt apex; Fig. 6.3)
- Overall shape and size of atria and free portions of the appendages (triangular, half-moon, or tubular)
- Ventricular formation of the apex (right, left, or both ventricles)
- Number of pulmonary veins (best estimates were made as some pulmonary veins were dissected close to the atrium)
- Presence or absence of noncardiac coronary sinus tributaries (left azygos vein)
- General shape of:
  - Inferior caval vein ostium
  - Superior caval vein ostium
  - Pulmonic valve

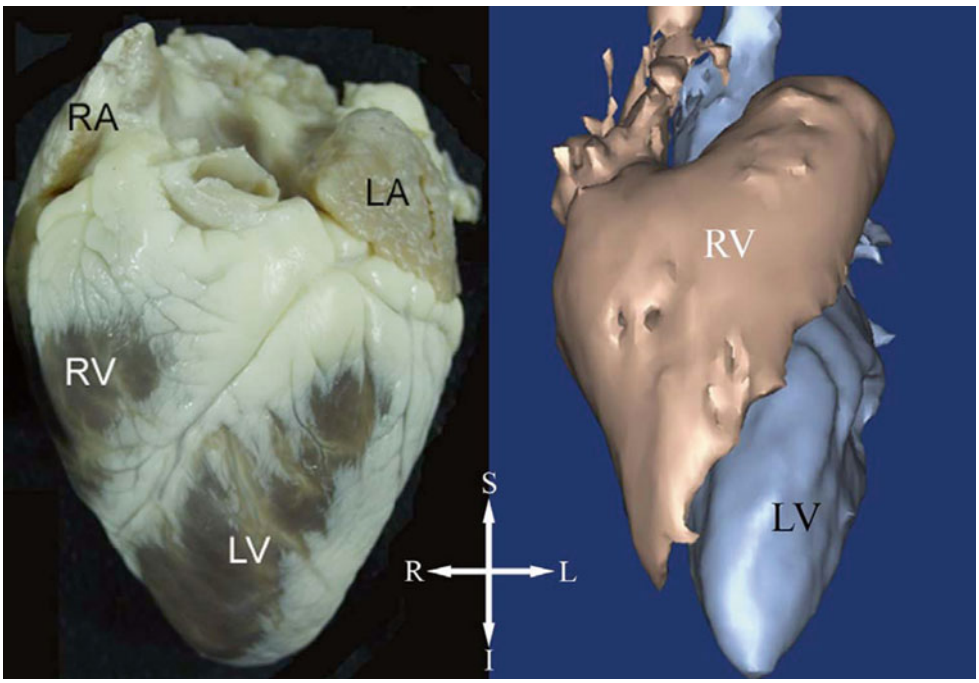

Fig. 6.15 Anterior surface of a fixed sheep heart and end-diastolic volumetric reconstruction of a sheep heart from magnetic resonance images. Note that the apex of the sheep heart is pointed inferiorly and slightly anteriorly. *LA* left atrium, *LV* left ventricle, *RA* right atrium, *RV* right ventricle

  - Tricuspid valve
  - Aortic valve
  - Mitral valve
  - Coronary sinus ostium
- Presence or absence of the valve of the coronary sinus ostium (Thebesian valve)
- Presence or absence of the moderator bands of the right ventricles (if present, the locations of attachment points were noted)
- Number of papillary muscles found in the right and left ventricles
- Degree of trabeculation of right and left ventricular endocardium (1–5; 1 = no trabeculations, 5 = highly trabeculated)
- Presence or absence of any left ventricular bands (i.e., similar structures to the moderator bands of the right ventricle).

6.4.2.3 Quantitative Anatomical Assessments of Perfusion-Fixed Hearts

The following quantitative measurements were performed on each heart by employing a novel 3D technique. Briefly, a MicroScribe® 3D digitizing arm (3DX, Immersion Corp., San Jose, CA, USA), consisting of a touch probe with six degrees of freedom, was used to gather the 3D data points. First, each heart was suspended and stabilized within a rectangular metal frame via sutures placed into the aorta, the right and left lateral ventricular walls, and the apex. More specifically, the heart was suspended in the classic *valentine heart* position, with the apex pointing toward the bottom of the frame and base toward the top, for easy comparison between hearts. In all cases, attitudinally correct nomenclature was used to describe structures in a more meaningful manner (Figs. 6.15 and 6.16; see also Chap. 2). To allow for the generation of a consistent coordinate axis system, three small holes for touch probe placement were drilled into a right angle scribe that was affixed to a corner of the support structure. This setup allowed for a consistent reference frame for all subsequent digitizations; each heart was maintained within the same 3D space, allowing for precise measurement between all digitized locations. Furthermore, this overall setup and experimental design allowed for free movement of the 3DX probe as the reference frame could be regenerated following each movement, allowing for complete probe access to all desired aspects of the heart.

For probe initialization, the coordinate axes were set up using the acquisition software (Inscribe, Immersion Corp.) on the right angle scribe by digitizing the location of the three holes that were set up as the origin, a point on the *x*-axis, and a point on the *y*-axis; the software then automatically generated the *z*-axis. Prior to dissection, eight external locations were digitized in each heart (Table 6.2) such that comparisons of the major external dimensions could be performed (Table 6.3). Then, small incisions were made in the right and left atrial appendages to allow for internal access in each heart. With the simultaneous use of endoscopic cameras, the touch probe was navigated to specific locations in each heart such that comparisons of valve dimension, ventricular chamber dimension, and those of the coronary sinus ostium could be subsequently calculated (Tables 6.2 and 6.3). It should be noted that all orientational terms are in rela-

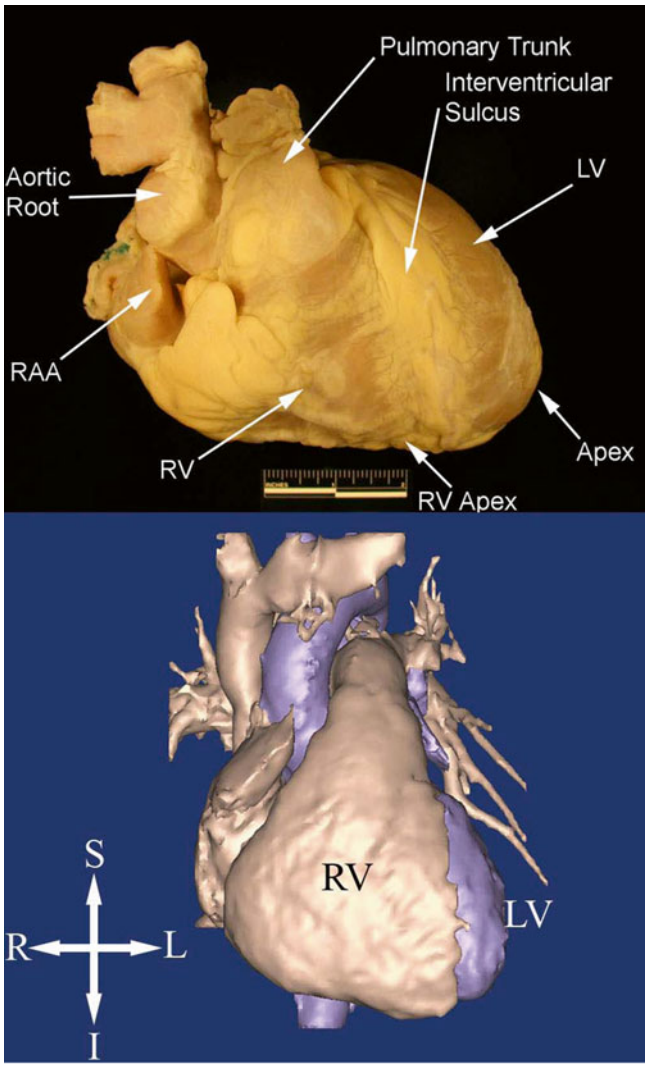

Fig. 6.16 Anterior surface of a fixed human heart and end-diastolic volumetric reconstruction of a human heart from magnetic resonance images. Note that the apex of the human heart is pointed to the left and slightly anteriorly. *LV* left ventricle, *RAA* free portion of right atrial appendage, *RV* right ventricle

tion to the reference frame, which closely mimics the orientation of the animal hearts in vivo. However, these terms do not necessarily describe the exact positions of the human hearts in vivo. In total, only three measurements from porcine heart number 1 needed to be removed due to improper coordinate axis regeneration. These were (1) posterior base to whole heart apex, (2) aortic valve mid-left coronary cusp to left ventricular apex, and (3) aortic valve center to left ventricular apex.

All calculations were analyzed both as raw data and as normalized data (divided by the given heart weight). Statistical significance tests were performed using one-way ANOVA and Bonferroni post analyses; significance was set at $\alpha = 0.05$. All values are presented as means ± standard deviation.

6.4.3 Results

The average heart weights were 367.3 ± 65.8 g for humans, 274.6 ± 50.4 g for pigs, 258.1 ± 36.2 g for dogs, and 353.1 ± 120.7 g for sheep. Human heart weights were significantly larger than dog heart weights ($p < 0.05$). The average age of the human donors was 63.8 ± 19.5 years. Although the exact age of the animals was not known, all porcine hearts were from younger rapidly growing animals (<1 years old); all canine (1–2 years old) and ovine hearts (1–3 years old) were from mature animals. Six of the human hearts were obtained from females and 2 were from males. All porcine and canine hearts were from male animals, while all ovine hearts were from female animals.

6.4.3.1 Qualitative Comparisons

The human hearts had the largest variation in overall shape compared to the animal hearts. Three human hearts were classified as having an elliptical shape, 2 were conical, 2 were rounded with a blunt apex, and 1 was valentine shaped. The overall defined shapes of the animal hearts were as follows: 6 ovine hearts were considered conical and 4 were valentine; 8 porcine hearts were valentine and 2 were trapezoidal; and all 10 canine hearts were elliptical. Nevertheless, the apexes of the hearts were formed entirely by the left ventricles in all animal hearts and in 5 of the 8 human hearts. In the other 3 human hearts, the apexes were mostly left but were considered slightly shifted toward a "joint apex."

Generally, the free portions of the right atrial appendages of the human hearts were defined as either triangular (7 of 8) or tubular on the left (8 of 8). The size of the free portion of the appendages was variable in the human hearts with 3 having larger right appendages, 3 having larger left appendages, and 2 having similar sized appendages. The free portions of the right atrial appendages of the ovine hearts were in the shape of a half-moon (9 of 10) and typically characterized as triangular on the left (8 of 10). The free portions of the right atrial appendages were larger than the left in 7 hearts and the same size as the left in the remaining 3 hearts. The free portions of the right atrial appendages of the porcine hearts were generally in the shape of a half-moon (9 of 10) and typically triangular on the left (6 of 10). The left atrial appendage was larger than the right in 9 hearts and the same size in the remaining heart. In the canine hearts, the free portions of both atrial appendages were considered to be tubular in 9 hearts and triangular in 1 heart. The free portions of the right atrial appendages were larger than the left in 5 hearts and the same

Table 6.2 Digitized locations

External locations	*Description*
Base	Anterior (anterosuperior) at the origin of the pulmonary trunk Posterior (posteroinferior) at the junction of the coronary sulcus and the interventricular sulcus Right lateral at the right atrial/right ventricular junction Left lateral at the left atrial/left ventricular junction
Apex coronary sinus	At the true apex of the heart (LV) The entry of the coronary sinus into the right atrium on the posterior aspect of the heart and three evenly spaced points to the end of the coronary sinus, defined as the junction of the great cardiac vein and the oblique vein of the left atrium (Marshall)
Internal locations	*Description*
Tricuspid valve	Anterior (superior) Posterior (inferior) Septal (posterior) Lateral (anterior) Center—best approximation
Coronary sinus	Superior (posterolateral) Inferior (anteroseptal) Lateral (superior) Septal (inferior) Thebesian valve leading edge (when present) Center—best approximation
Pulmonic valve	Midpoint on anterior cusp Midpoint of right cusp Midpoint of left cusp Center—best approximation
RV apex mitral valve	Deepest point in the RV apex Anterior (superior) Posterior (inferior) Septal (posterior) Lateral (anterior) Center—best approximation
Aortic valve	Midpoint of right coronary cusp Midpoint of left coronary cusp Midpoint of non-coronary cusp Right coronary/left coronary commissure tip Right coronary/non-coronary commissure tip Left coronary/non-coronary commissure tip Center—best approximation
LV apex	Deepest point in the LV apex

size as the left in the other 5 hearts. The left azygos (hemiazygos) vein was present as a tributary to the coronary sinus in all ovine and porcine hearts examined; it was not present in any of the canine hearts or human hearts. Thebesian valves covering some aspect of the coronary sinus ostium were present in all human hearts, but absent in all animal hearts examined.

Moderator bands were present in the right ventricles of all hearts examined (Figs. 6.7, 6.8, 6.10, and 6.11). However, the origin and attachment of these bands, as well as their appearance, were varied among species. In the human hearts, the moderator band typically arose more apically on the septal wall and attached to the base of the anterior papillary muscle (APM). Interestingly, the band was a free arc in 6 of the hearts and a ridge in 2 hearts. In both sheep and pigs, the moderator bands presented as muscular structures that originated on or near the septal papillary muscle (SPM), inserted at the body or head of the APM, and were free arcs in all. In contrast, the moderator bands of the canine hearts presented as fibrous networks that originated on the APM or septal wall and inserted on the free walls of the right ventricles (usually at multiple sites). Similar to all pig and sheep hearts and 75 % of the human hearts, the canine moderator band was a free arching structure across the ventricular cavity. There were left ventricular bands, similar to the moderator band (composed of or containing what are considered to be conduction fibers), identified in all but 1 porcine heart and 1 human heart.

All human, ovine, and porcine hearts had one well-defined APM in the right ventricle. In contrast, 6 canine hearts had 2 APMs and 4 hearts had a single APM. Nine ovine hearts had a single posterior papillary muscle (PPM) in the right ventricle and 1 heart had 2 PPMs. Six porcine hearts had a single PPM, 3 hearts had 2 PPMs, and 1 heart had 3 PPMs. Only 1 canine heart had a single PPM, 5 hearts had 2 PPMs, and 4 hearts had 3 PPMs. Three human hearts had a single PPM, 1

Table 6.3 Calculated measurements

External measurements	*Description*
Base to apex length	Anterior (anterosuperior) to apex Posterior (posteroinferior) to apex Right lateral to apex Left lateral to apex
Coronary sinus	Length of the coronary sinus
Internal measurements	*Description*
Coronary sinus ostium	Superior (posterolateral) to inferior (anteroseptal) diameter Lateral (inferior) to septal (superior) diameter Functional ostium—Thebesian valve to septal (superior) diameter
Tricuspid valve	Anterior (superior) to posterior (inferior) diameter Septal (posterior) to lateral (anterior) diameter
Right ventricular inflow	Anterior (superior) tricuspid valve to apex distance Posterior (inferior) tricuspid valve to apex distance Septal (posterior) tricuspid valve to apex distance Lateral (anterior) tricuspid valve to apex distance Center tricuspid valve to apex distance
Pulmonic valve	Sinotubular junction diameter Basal annular diameter
Right ventricular outflow	Mid-anterior cusp pulmonic valve to apex distance Mid-right cusp pulmonic valve to apex distance Mid-left cusp pulmonic valve to apex distance Center pulmonic valve to apex distance
Mitral valve	Anterior (superior) to posterior (inferior) diameter Septal (posterior) to lateral (anterior) diameter
Left ventricular inflow	Anterior (superior) mitral valve to apex distance Posterior (inferior) mitral valve to apex distance Septal (posterior) mitral valve to apex distance Lateral (anterior) mitral valve to apex distance Center mitral valve to apex distance
Aortic valve	Sinotubular junction diameter Basal annular diameter
Left ventricular outflow	Mid-right coronary cusp aortic valve to apex distance Mid-left coronary cusp aortic valve to apex distance Mid-non-coronary cusp aortic valve to apex distance Center aortic valve to apex distance

heart had 2 PPMs, and 4 hearts had 3 PPMs. Eight ovine hearts had a single SPM and 2 hearts had 2 SPMs. In contrast, 4 canine hearts had a single SPM and 6 hearts had 3 or more SPMs. Additionally, only 2 porcine hearts had a single SPM, 4 hearts had 2 SPMs, and 4 hearts had 3 or more SPMs. Three human hearts had a single SPM, 3 hearts had 2 SPMs, and 2 hearts had 3 SPMs. All hearts from all species had other small papillary muscles on the septal wall which were not fully formed and projected into the right ventricle, as well as chordae appearing to attach directly to the septal wall.

In the left ventricle, all animal hearts from all species had a single APM with varying numbers of heads. In contrast, 5 human hearts had a single APM, 1 heart had 2 APMs, and 2 hearts had 3 APMs. All porcine and canine hearts had a single PPM in the left ventricle, while 8 ovine hearts had a single PPM and 2 hearts had 2 PPMs. Four human hearts had a single PPM in the left ventricle, and 4 hearts had 2 PPMs.

Generally, the right ventricle and left ventricle apexes of human hearts were far more trabeculated as compared to each species of animal hearts. In the right ventricle, the canine hearts were more trabeculated than those of porcine and ovine hearts. In contrast, the degree of trabeculation in the left ventricular apexes was similar across animal hearts. It was also noted that the epicardia of the ovine hearts were typically covered in greater amounts of fatty tissue relative to the canine and porcine hearts.

The shape of the ostia of the superior vena cavae and the inferior vena cavae was circular in all hearts examined, with the exception of 1 human heart in which the inferior vena cava ostium was removed during heart removal. The shape of the tricuspid valves and mitral valves ranged within species and

included elliptical, circular, nearly circular, and half-moon. Similarly, the aortic and pulmonary valves were circular in all hearts examined. The coronary sinus ostia were elliptical in the majority of hearts.

Due to cannulation of the hearts for perfusion and dissection of the pulmonary veins near the left atrium, the number of pulmonary veins could not be reliably determined in all hearts. Typically, major ostia were seen within each heart, but bifurcation patterns were different within and between species. Oftentimes, the myocardium traveled deep into the "vein" which was defined by a major ostium, yet the veins could be bifurcated almost directly at the myocardial/venous tissue junction into 2 to 4 veins. The canine hearts were the only exception to this generalization, in which 7 hearts had greater than 5 pulmonary veins (range 5–8).

6.4.3.2 Quantitative Comparisons

In general, calculated dimensions and heart weights were not well correlated, with the highest correlations found in ovine hearts. Therefore, statistical analyses were performed on both raw measurements and on those normalized to heart weight values. Statistically significant differences between the species were found for both raw and normalized data. Although some overlap of statistically significant differences existed between the raw and normalized values, oftentimes statistical significance was not conserved between the two methods. Therefore, only raw data is presented throughout the remaining portion of this chapter and in Tables 6.4 and 6.5, with statistically significant differences noted.

Externally, the average anterior (anterosuperior) base to apex distance was significantly longer in sheep hearts than canine hearts. The average base to apex distance on the posterior (posteroinferior) and left lateral aspects was significantly longer in the human hearts than swine, canine, and ovine hearts. The average right lateral base to apex distance was significantly longer in human hearts compared to swine and canine hearts, and the ovine hearts were also significantly longer than the swine hearts. The average external length of the coronary sinus was significantly longer in the human hearts compared to the swine, canine, and ovine hearts (Table 6.4).

Internally, the average superior (posterolateral) to inferior (anteroseptal) coronary sinus ostium diameter was significantly larger in human hearts compared to swine, canine, and ovine hearts. The average lateral (inferior) to septal (superior) diameter was significantly smaller in canine hearts compared to human, swine, and ovine hearts. As stated earlier, Thebesian valves were present in all human hearts. Due to this valve, the functional ostium of the coronary sinus (i.e., that which was not covered by a Thebesian valve) was reduced in the superior/inferior dimension in these hearts as the attachment of the valve was typically in the posterolateral/anteroseptal direction. When taking into account the Thebesian valve, the average diameter of the functional ostium of the human hearts was significantly smaller than that of the swine and ovine hearts (Table 6.5).

The average tricuspid valve diameters were all of similar size, with the exception of the anterior (superior) to posterior (inferior) dimension, which was significantly larger in human hearts than pig hearts. The average right ventricular inflow tract length was significantly longer in human hearts compared to the animal hearts in all dimensions analyzed. No significant differences were seen in the average length of the outflow tracts of the right ventricles, with the exception of the mid-left cusp to apex dimension, which was significantly shorter in canine hearts than human hearts. The average diameter of the sinotubular junction of the pulmonic trunk was significantly greater in the human hearts as compared to the animal hearts. No significant differences were observed in the average diameters of the basal annular ring of the pulmonic valve (Table 6.5).

No significant differences were observed in the average diameter of mitral valve in the anterior (superior) to posterior (inferior) dimension. However, the average diameter of the mitral valve in the septal (posterior) to lateral (anterior) dimension was significantly larger in the human hearts as compared to the animal hearts. The average dimensions of the inflow tracts of the left ventricle were significantly shorter in the canine hearts compared to human, swine, and ovine hearts in all dimensions analyzed. The average diameter of the left ventricular outflow tract was generally longer in the human hearts than the animal hearts. The average

Table 6.4 External dimensions (mean ± std. dev)

Measurement	Human	Swine	Canine	Ovine
Anterior (anterosuperior) base to apex distance (mm)	98.7 ± 14.6	101.2 ± 6.8	93.5 ± 4.1	111.1 ± 16.8 **ζ**
Posterior (posteroinferior) base to apex distance (mm)	87.7 ± 12.4	65.6 ± 4.2	71.3 ± 2.9	72.6 ± 7.6 **αβθ**
Right lateral base to apex distance (mm)	106.4 ± 10.9	88.4 ± 4.8	94.3 ± 5.8	103.8 ± 12.7 **αβε**
Left lateral base to apex distance (mm)	99.7 ± 9.5	80.8 ± 5.3	78.6 ± 3.5	87.4 ± 10.2 **αβθ**
Coronary sinus length	46.5 ± 5.2	25.1 ± 2.7	29.8 ± 6.7	29.9 ± 8.6 **αβθ**

Significant differences are noted by the following symbols: α—human, swine; β—human, canine; θ—human, ovine; δ—swine, canine; ε—swine, ovine; ζ—canine, ovine

Table 6.5 Internal dimensions (mean ± std. dev)

Measurement	Human	Swine	Canine	Ovine
Coronary sinus ostium				
CS Os superior (posterolateral) to inferior (anteroseptal) diameter (mm)	12.3 ± 4.2	7.7 ± 1.4	5.0 ± 1.0	8.1 ± 3.2 **αβθ**
CS Os lateral (inferior) to septal (superior) diameter (mm)	15.7 ± 2.4	16.4 ± 2.9	9.8 ± 2.2	18.3 ± 5.0 **βδζ**
CS Os functional ostium—Thebesian valve to opposite edge diameter (mm)	8.1 ± 2.9	NA	NA	NA **αθδζ**
Tricuspid valve				
Tricuspid valve anterior (superior) to posterior (inferior) diameter (mm)	43.0 ± 3.1	37.2 ± 4.2	38.8 ± 3.0	39.9 ± 3.8 **α**
Tricuspid valve septal (posterior) to lateral (anterior) diameter	37.7 ± 7.2	30.3 ± 5.5	29.5 ± 4.6	36.0 ± 9.4
RV inflow tract				
Tricuspid valve anterior (superior) to RV apex distance (mm)	86.9 ± 12.9	72.0 ± 4.7	65.3 ± 4.1	66.1 ± 15.9 **αβθ**
Tricuspid valve posterior (inferior) to RV apex distance (mm)	78.9 ± 19.9	55.5 ± 3.3	49.3 ± 3.6	51.9 ± 11.1 **αβθ**
Tricuspid valve septal (posterior) to RV apex distance (mm)	77.4 ± 14.0	61.8 ± 4.3	55.5 ± 4.8	59.5 ± 10.1 **αβθ**
Tricuspid valve lateral (anterior) to RV apex distance (mm)	83.7 ± 21.0	61.6 ± 4.9	55.7 ± 3.8	58.7 ± 16.7 **αβθ**
Tricuspid valve center to RV apex distance (mm)	73.1 ± 19.2	51.8 ± 2.7	45.7 ± 4.5	50.4 ± 9.8 **αβθ**
Pulmonic valve				
Pulmonic valve sinotubular junction diameter (mm)	28.1 ± 3.8	18.7 ± 1.6	18.3 ± 3.3	22.8 ± 5.7 **αβθ**
Pulmonic valve basal annular diameter (mm)	31.1 ± 3.2	25.6 ± 2.0	25.5 ± 2.9	29.8 ± 6.8
RV outflow tract				
Pulmonic valve mid-anterior cusp pulmonic valve to apex distance (mm)	86.9 ± 14.7	93.3 ± 6.2	84.8 ± 5.0	90.4 ± 16.0
Pulmonic valve mid-right cusp pulmonic valve to apex distance (mm)	93.9 ± 15.0	85.4 ± 5.9	76.7 ± 4.1	82.4 ± 21.1
Pulmonic valve mid-left cusp pulmonic valve to apex distance (mm)	87.9 ± 13.6	79.0 ± 4.7	69.4 ± 4.3	79.2 ± 9.7 **β**
Pulmonic valve center pulmonic valve to apex distance (mm)	90.4 ± 16.7	85.6 ± 6.5	77.9 ± 4.3	81.4 ± 11.3
Mitral valve				
Mitral valve anterior (superior) to posterior (inferior) diameter (mm)	37.9 ± 4.6	31.0 ± 3.9	31.3 ± 4.6	36.9 ± 7.4
Mitral valve septal (posterior) to lateral (anterior) diameter (mm)	32.5 ± 5.6	23.7 ± 2.7	22.0 ± 4.9	25.8 ± 6.3 **αβθ**
LV inflow tract				
Mitral valve anterior (superior) to LV apex distance (mm)	83.7 ± 18.0	76.8 ± 6.3	63.1 ± 6.0	75.7 ± 13.5 **β**
Mitral valve posterior (inferior) to LV apex distance (mm)	78.2 ± 18.2	68.2 ± 5.5	60.0 ± 5.8	67.4 ± 11.6 **β**
Mitral valve septal (posterior) to LV apex distance (mm)	80.7 ± 15.7	70.6 ± 6.1	65.2 ± 5.8	70.2 ± 13.4 **β**
Mitral valve lateral (anterior) to LV apex distance (mm)	77.4 ± 17.3	72.1 ± 5.3	59.4 ± 4.8	72.1 ± 13.2 **β**
Mitral valve center to LV apex distance (mm)	69.5 ± 16.2	62.0 ± 5.9	52.1 ± 4.9	62.3 ± 11.3 **β**
Aortic valve				
Aortic valve sinotubular junction diameter (mm)	26.4 ± 3.0	21.4 ± 2.3	16.8 ± 2.7	20.4 ± 3.8 **αβθδ**
Aortic valve basal annular diameter (mm)	30.0 ± 2.6	25.1 ± 3.2	23.2 ± 4.1	28.9 ± 5.4 **βζ**
LV outflow tract				
Aortic valve mid-right coronary cusp to LV apex distance (mm)	89.9 ± 18.6	72.5 ± 6.2	65.2 ± 5.8	76.2 ± 13.3 **αβ**
Aortic valve mid-left coronary cusp to LV apex distance (mm)	89.7 ± 18.6	77.1 ± 5.5	67.1 ± 6.1	77.3 ± 14.5 **β**
Aortic valve mid-non-coronary cusp to LV apex distance (mm)	92.7 ± 20.1	73.8 ± 6.2	67.1 ± 7.1	73.0 ± 11.9 **αβθ**
Aortic valve center to LV apex distance (mm)	90.8 ± 18.3	75.9 ± 5.8	63.7 ± 6.6	75.2 ± 12.8 **βθ**

Significant differences are noted by the following symbols: α—human, swine; β—human, canine; θ—human, ovine; δ—swine, canine; ε—swine, ovine; ζ—canine, ovine

human dimensions were significantly longer than the swine and canine hearts in the mid-right cusp dimension, significantly longer than the canine hearts in the mid-left dimension, significantly longer than all hearts in the non-coronary dimension, and significantly longer than the canine and ovine hearts from the center of the aortic valve. The average diameter of the sinotubular junction of the aorta was significantly larger in the human hearts than all animal hearts. Additionally, the average diameter of the swine hearts was significantly longer than the canine hearts at this location. Finally, the average diameter of the basal annulus of the aortic valve was significantly larger in human and ovine hearts than canine hearts (Table 6.5).

6.4.4 Discussion and Consideration of Previous Studies on Comparative Anatomy

In the present study, we examined the gross morphology of the hearts of humans, pigs, dogs, and sheep and compared them both qualitatively and quantitatively. To the authors' knowledge, this is the first study specifically aimed at elucidating both qualitative and quantitative similarities and/or differences in the cardiac anatomy of these commonly employed species for cardiovascular research. These presented findings should be seen as a unique initial database on the overall shape of hearts, appendages, and valves, the presence or absence of specific anatomical features, and quantitative dimensions, which were measured in nondissected pressure-fixed, end-diastolic volume hearts. These comparisons demonstrate that important anatomical differences exist between hearts isolated from humans, pigs, dogs, and sheep. Hopefully, these results can be used by future investigators as an aid in making critical choices as to which animal model would be best for their specific biomedical/cardiovascular research.

A sizeable quantity of literature has been published on many qualitative aspects of large mammalian cardiac anatomy. However, much of this research is very general (i.e., all mammalian hearts have a right and left atrial appendage) [11, 13, 14, 25] or very specific (i.e., comparative cardiac anatomy of the cardiac foramen ovale) [50], and, importantly, most research is not done in a truly comparative fashion. Furthermore, much of this literature does not provide information useful for those specifically performing cardiovascular research with the hope of translating such results to relevant human research.

There are specific examples of anatomical structure that we studied in these comparative analyses that have been described somewhat differently in the previous literature. Crick et al. [13] reported that the shape of the porcine heart was valentine; we observed this shape in 8 of 10 hearts. They also reported a trapezoidal shape of the human hearts they examined. Greater variability was seen in the observed shape of our human hearts with no general trend seen. The formation of the apex of the heart entirely by the left ventricle has also been previously reported for all animals examined in this study [12–14]; this is also the case for most of the human hearts in this study and is widely reported in literature and textbooks. The presence of a moderator band in the right ventricle in all hearts examined has also been previously noted [11, 13, 51]. However, Truex and Warshaw [26], while finding a moderator band in the right ventricle of all sheep and pigs studied, failed to find such a band in the canine hearts they examined and only found a band in 56.8 % of human hearts. This discrepancy was likely due to definition and to the different morphology presented by the band in these animals. Interestingly, we observed left ventricular bands in nearly all of the hearts examined (7 human, 9 swine, 10 canine, and 10 ovine). Gerlis et al. [27] reported that they found left ventricular bands in 100 % of ovine hearts ($n=42$), 100 % of canine hearts ($n=12$), and 86 % of porcine hearts they examined ($n=36$), but only in 52 % of adult hearts examined ($n=50$). Joudinaud and colleagues [51] cataloged the papillary muscles of the swine heart in 2006, classifying them based on the leaflets they supported. They defined them as anteroposterior (APM in this study), anteroseptal (SPM in this study), and posteroseptal (PPM in this study). They found, on average, 1.1 anteroposterior papillary muscles, 2.4 posteroseptal papillary muscles, and 1.8 anteroseptal papillary muscles. These findings are similar to our observations of an average of 1 APMs, 1.9 PPMs, and 2.1 SPMs, with a slightly different weighting toward more SPMs than PPMs in our study compared to their research. While a specific report on the number of papillary muscles in the ventricles of other hearts could not be found, it has been reported that human, canine, porcine, and ovine hearts typically have three papillary muscles (APM, PPM, and SPM) in the right ventricle and two (APM and PPM) in the left ventricle [11]. While our findings are similar for the left ventricle, we found a much greater variability in the number of papillary muscles in the right ventricle of all species examined, with some canine hearts having as many as 6 right ventricular papillary muscles.

Relative to recent interest in the development of access and closure devices for the atrium or means for occluding the left atrial appendage in patients with atrial fibrillation, it should be noted that some of our qualitative findings were different from what has been previously reported. For example, Crick et al. [13] reported that the right atrial appendages of the swine hearts typically had a tubular shape, while we found that the right atrial appendages were shaped more like a half-moon. Also, they reported that the right and left atrial appendages of swine hearts were of similar size; we found that the left atrial appendages were larger in 90 % of the hearts examined. This discrepancy could be related to the breed differences; Crick et al. did not provide the specific

breed of the animals used in their study. Interestingly, they reported that the right atrial appendages of the human hearts were "appreciably" larger than the left, a finding which is similar to our findings in 3 of the 8 hearts examined. It should be noted that we believe the authors of that study were referring to the free portion of the right appendage for comparison, as it is believed that the atrial appendage of the right atrium technically includes all pectinate portions of the atrium arising from the terminal crest [52]. However, the authors reference that the appendage on the right side consists of pectinate muscles and that these pectinate muscles "surround entirely the parietal margin of the vestibule of the tricuspid valve." If the definition is used to describe the right atrial appendage, one would find that only in rare cases (most likely pathological) would the left atrial appendage be larger than the right as the pectinate muscles of the left atrium are nearly always contained within the free portion.

As mentioned previously, there has been a lack of published information comparing canine, porcine, and ovine hearts quantitatively. Yet, Lev et al. [53] eloquently described methods to study the congenitally malformed heart quantitatively in 2D in 1961 and followed with an excellent paper on the anatomy of the normal human child heart in 1963 [54]. These methods were applied to the swine heart in a publication by Eckner et al. [55]. More specifically, they measured the inflow and outflow tracts of the swine right and left ventricle using methods as described by Lev et al. in 1961. From 27 porcine hearts weighing in the range of 200–300 g, they found the length of the right ventricular inflow tract to be 5.4 ± 0.4 cm, the length of the right ventricular outflow tract to be 8.6 ± 0.5 cm, the length of the left ventricular inflow tract to be 7.6 ± 0.4 cm, and the length of the left ventricular outflow tract to be 7.4 ± 0.4. In the present study, we found the length of the right ventricular inflow tract to be 5.6 ± 0.3 cm, the right ventricular outflow tract to be 7.9 ± 0.5 cm, the length of the left ventricular inflow tract to be 6.8 ± 0.6 cm, and the length of the left ventricular outflow tract to be 7.3 ± 0.6 cm. Overall, the measurements from the two studies are similar; however, the right ventricular outflow tract and left ventricular inflow tract were noticeably shorter in the hearts examined in this study compared to those of Eckner et al. It should be noted that the methods described by Lev et al. and used by Eckner et al. were slightly ambiguous regarding their definitions of the measurement end points. For instance, the right ventricular inflow tract measurement was described as "the length of the inflow tract of the right ventricle is measured from a point at the tricuspid annulus in the center of the posterior wall to the apex" [53]. Thus, depending on one's interpretation of the location of this point, significantly varied measurements could be obtained. In spite of this, the measurement locations in the present study were selected so that they were as close as possible to as those measured by Eckner et al. Similarly, another group of investigators, Alvarez et al. [56], applied similar assessment methods to the right ventricles of 75 porcine hearts. They found the length of the right ventricular inflow tract was on average 5.9 ± 0.8 cm, and the outflow tract was 8.4 ± 1.0 cm. Interestingly, the outflow tract length was again longer than that measured in the current study, while the inflow tract length was similar among all three studies. While the breed of swine used by Eckner et al. was not reported, Alvarez et al. used hearts obtained from the Europa breed. The hearts used in the present study were from Yorkshire cross animals; this variation in breed may explain the differences in measured dimensions.

In contrast to the lack of publications examining the gross dimensions of the hearts, there have been publications concerned with the dimensions of the cardiac valves, mostly focused on the aortic and mitral valves. The sheep is the most common model used in experimental models of mitral regurgitation, and, due to this, there are numerous studies examining both the normal and pathological anatomy of the mitral valve (see also Chap. 27). Yet, many of these studies do not provide comparable measurements. However, in 1997, Gorman et al. published a study of 6 sheep, demonstrating that the end-diastolic anterior–posterior dimension was 26.6 mm and the end-diastolic commissure–commissure dimension was 35.4 mm [57]. In 2002, Timek et al. reported, in a study of 6 sheep instrumented with radiopaque markers, that the end-diastolic anterior–posterior dimension of the mitral valve was 2.6 ± 0.3 cm and the end-diastolic commissure–commissure dimension was 3.6 ± 0.4 cm [58]. While the nomenclature used between these studies and the data we presented is slightly different, these reported measurements are very similar overall: our measurements were 25.8 ± 6.3 mm septal–lateral (anterior–posterior) and 36.9 ± 7.4 mm anterior–posterior (superior–inferior or commissure–commissure). Tsakiris et al. [59] reported that the average early diastolic anterior–posterior dimension of 5 canine hearts was 2.1 ± 0.2 cm, similar to our findings of 22.0 ± 4.9 mm. Chandraratna and Aronow [60] reported a mean maximal diastolic anterior–posterior diameter of 2.2 ± 0.2 cm and end-systolic anterior–posterior diameter of 1.8 ± 0.2 cm from 23 normal human subjects studied with echocardiography. Nordblom and Bech-Hanssen [61] reported a mean end-diastolic anterior–posterior dimension of 2.9 ± 0.4, mean end-systolic anterior–posterior dimension of 3.3 ± 0.3 cm, and mean end-diastolic commissure–commissure dimension of 3.7 ± 0.4 cm in 38 normal human subjects. These two publications show the wide variation of reported results in the literature. Reporting on all of the mitral publications is beyond the scope of this paper; however, it should be noted that our results were more similar to the publication by Nordblom than that of Chandraratna. Added considerations in comparing anatomical studies that one needs to keep in mind are that differing methodologies may slightly

skew data or that newer methodologies may provide more accurate measurements. For example, this could be due to changes in the definition of the dimensions measured and also to higher resolution offered by newer ultrasound technology which provides important in vivo measurements.

Regarding the aortic valve, Sands et al. published the only available quantitative study examining the aortic valves of multiple hearts, including 10 swine, 9 ovine, 9 bovine, and 7 humans [30]. Interestingly, in their investigations, aortic valve diameters were measured via passing an obturator through fresh hearts until a snug fit was determined. They reported the average annulus diameters of 26.4 ± 3.2 mm in human hearts, 26.6 ± 1.8 mm in pig hearts, and 25.8 ± 0.3 mm in sheep hearts. It may be assumed that, by annulus, they were actually referring to the basal portion of the annulus. For the in vitro data on perfusion-fixed hearts we provided above, larger average basal annular diameters in human hearts (30.0 ± 2.6 mm) and in sheep hearts (28.9 ± 5.4 mm) were observed, and slightly smaller average diameters in pig hearts (25.1 ± 3.2 mm) were found. More recently, Lansac and colleagues published a sonometric study of 8 ovine aortic valves and ascending aortas, in which they reported average basal annular diameters of 20.7 ± 0.4 mm and commissure diameters of 14.1 ± 0.2 mm, which are both smaller than our reported diameters [62]. Sim and colleagues [63] published a comparison of 12 human and 12 swine aortic valves in which they reported mean diameters of 2.6 ± 0.1 cm for human hearts ($n = 12$) and 2.2 ± 0.3 cm for swine hearts, both which are smaller than that observed in our studies. Interestingly, Swanson and Clark [64] published a study of 5 normal human aortic valves in 1974, using silicone casts of aortic valves prepared at various pressures (0–120 mmHg). Regardless of the pressure used, on average, the basal annulus in their study was smaller than that observed in this study. Finally, in support of the fact that sheep are the most commonly used animal model for aortic valve studies, we found that the average basal annulus diameters were most similar between sheep and human hearts. However, we noted that the sinotubular junction diameters were significantly smaller in all animals studied as compared to the human hearts. This could have implications for selection of an animal model for newer technologies such as transcatheter-delivered aortic valves, as some technology engages the sinotubular junction for fixation of the device.

Publications on the valves on the right side of the heart are scarce, especially the pulmonic valve, and none were found with comparable measurements. The tricuspid valve has been quantitatively studied in sheep, canines, and humans, although like mitral valve studies, similar measurements to this study are not evident in many publications. Jouan and colleagues [65] studied the tricuspid annulus of 7 sheep and showed that during the cardiac cycle the minimum diameter (approximately perpendicular to the septum) changed from 17.8 ± 1.9 to 21.2 ± 2.0 mm and maximum diameter (approximately parallel to the septum) changed from 36.4 ± 2.4 to 40.1 ± 2.6 mm. While this report does not specifically give orientational references for these numbers, the minimum diameter is described as perpendicular to the septum and therefore is much smaller than that observed in this study. The maximum diameter, however, is similar to the anterior–posterior (superior–inferior) diameter of this study. In 2007, Anwar and colleagues reported the average tricuspid annular diameter of 100 normal patients to be 4.0 ± 0.7 cm [66]. Again, no orientational references were given to this diameter, but rather it appears to be the maximal diameter, which most likely correlates to the anterior–posterior (superior–inferior) diameter of this study with similar values observed.

The dimensions analyzed in the perfusion-fixed hearts we provided above can also be used to illustrate some differences in gross morphology. Interestingly, the average right ventricular inflow tract of the human hearts examined in this study was significantly longer than that of the other hearts examined, although the outflow tracts of the right ventricles were relatively the same length among all hearts. This has direct applicability to right ventricular apical pacemaker lead design, in which the designs intended ultimately for human hearts are studied in any of the animal species examined in this study—the lead length to reach the right ventricular apex from the tricuspid valve in the animal species is on average 1–2 cm shorter than in human hearts. The rest of the implant anatomy would also need to be considered for complete analysis. Another interesting finding was the significantly smaller diameter of the coronary sinus ostia in canine hearts compared to the other hearts examined. Coupled with the external measured length of the coronary sinus, which was significantly longer in human hearts than other hearts, implications for animal model selection in biomedical device research become obvious. Similar to the right ventricular apical lead length mentioned above, coronary venous-delivered left ventricular pacing lead lengths may need to be shortened for animal work. Furthermore, when choosing an animal model to simulate coronary sinus access similar to humans with Thebesian valves, the canine model becomes an obvious choice due to the similarity in size. Maric et al. [67] examined the diameter of the coronary sinus ostium in humans and dogs; they found the diameter to be 8.4 ± 2.6 mm in humans and 6.5 ± 1.3 mm in dogs. Unfortunately, Maric does not mention which diameter was measured (superior/inferior or lateral/septal).

6.5 Summary

Cardiac research is an important field that will continue to thrive for many years. It is critical that the appropriate animal models are employed to perform well-designed translational research prior to human clinical trials. In this chapter, we

presented a unique set of comparative information relative to cardiac anatomy of several large mammalian models commonly used for such laboratory testing: the pig, dog, and sheep. Important difference and similarities exist that may impact research results relative to either device testing or pharmacological therapeutic trials. The novel research data presented here from our laboratory were specifically designed to systematically compare the anatomical features of these animal models to humans, both qualitatively and quantitatively. The techniques employed were unique in that they allowed study of nondissected hearts, providing measurements from realistic geometric configurations. We observed that specific differences in the cardiac anatomy exist between the species, for hearts isolated and pressure perfusion fixed with similar weights, and that these differences may be useful in choosing an animal model for certain types of biomedical research. It is likely as CT and MRI methodologies continue to advance that more specific structural comparisons can be performed on functioning hearts, yet details about animal age, weight, health status, and/or breed will need to be well described in order to make such data sets of higher value.

References

1. Paul EF, Paul J (2001) Why animal experimentation matters: the use of animals in medical research. Social Philosophy and Policy Foundation: Transaction, New Brunswick
2. Monamy V (ed) (2000) Animal experimentation: a guide to the issues. Cambridge University Press, Cambridge/New York
3. Nutton V (2002) Portraits of science. Logic, learning, and experimental medicine. Science 295:800–801
4. Persaud TVN (ed) (1997) A history of anatomy: the post-Vesalian era. Charles C Thomas Publisher, Springfield
5. Hearse DJ (2000) The elusive coypu: the importance of collateral flow and the search for an alternative to the dog. Cardiovasc Res 45:215–219
6. Christensen GC, Campeti FL (1959) Anatomic and functional studies of the coronary circulation in the dog and pig. Am J Vet Res 20:18–26
7. Hughes HC (1986) Swine in cardiovascular research. Lab Anim Sci 36:348–350
8. Kong Y, Chen JT, Zeft HJ et al (1969) Natural history of experimental coronary occlusion in pigs: a serial cineangiographic study. Am Heart J 77:45–54
9. Verdouw PD, van den Doel MA, de Zeeuw S et al (1998) Animal models in the study of myocardial ischaemia and ischaemic syndromes. Cardiovasc Res 39:121–135
10. Getty R (1975) General heart and blood vessels. In: Getty R (ed) Sisson and Grossman's the anatomy of the domestic animals, 5th edn. Saunders, Philadelphia, pp 164–175
11. Michaëlsson M, Ho SY (eds) (2000) Congenital heart malformations in mammals: an illustrated text. Imperial College Press, London/River Edge
12. Ghoshal NG (1975) Ruminant, carnivore, porcine: heart and arteries. In: Sisson S, Grossman JD, Getty R (eds) Sisson and Grossman's: the anatomy of the domestic animals, 5th edn. Saunders, Philadelphia, pp 960–1023, 1594–1651, 1306–1342
13. Crick SJ, Sheppard MN, Ho SY et al (1998) Anatomy of the pig heart: comparisons with normal human cardiac structure. J Anat 193:105–119
14. Evans HE (1993) The heart and arteries. In: Miller ME, Evans HE (eds) Miller's anatomy of the dog, 3rd edn. Saunders, Philadelphia, pp 586–602
15. Netter FH (ed) (1979) Heart. Ciba Pharmaceutical Company. Medical Education Division. The Division, West Caldwell
16. Holt JP, Rhode EA, Kines H (1968) Ventricular volumes and body weight in mammals. Am J Physiol 215:704–715
17. Lee JC, Taylor FN, Downing SE (1975) A comparison of ventricular weights and geometry in newborn, young, and adult mammals. J Appl Physiol 38:147–150
18. Holt JP (1970) The normal pericardium. Am J Cardiol 26:455–465
19. Naimark WA, Lee JM, Limeback H et al (1992) Correlation of structure and viscoelastic properties in the pericardia of four mammalian species. Am J Physiol 263:H1095–H1106
20. Spodick DH (ed) (1997) The pericardium: a comprehensive textbook. M. Dekker, New York
21. Moore T, Shumacker HJ (1953) Congenital and experimentally produced pericardial defects. Angiology 4:1–11
22. Elias H, Boyd L (1960) Notes on the anatomy, embryology and histology of the pericardium. J N Y Med Coll 2:50–75
23. Hurst JW (ed) (1988) Atlas of the heart. McGraw-Hill: Gower Medical Pub, New York
24. Montagna W (ed) (1959) Comparative anatomy. Wiley, New York
25. Kent GC, Carr RK (eds) (2001) Comparative anatomy of the vertebrates, 9th edn. McGraw Hill, Boston
26. Truex RC, Warshaw LJ (1942) The incidence and size of the moderator band in man and mammals. Anat Rec 82:361–372
27. Gerlis LM, Wright HM, Wilson N et al (1984) Left ventricular bands. A normal anatomical feature. Br Heart J 52:641–647
28. Quill JL, Hill AJ, Laske TG, Alfieri O, Iaizzo PA (2009) Mitral leaflet anatomy revisited. J Thorac Cardiovasc Surg 137:1077–1081
29. Walmsley R (1978) Anatomy of human mitral valve in adult cadaver and comparative anatomy of the valve. Br Heart J 40:351–366
30. Sands MP, Rittenhouse EA, Mohri H et al (1969) An anatomical comparison of human pig, calf, and sheep aortic valves. Ann Thorac Surg 8:407–414
31. Ansari A (2001) Anatomy and clinical significance of ventricular Thebesian veins. Clin Anat 14:102–110
32. Pina JAE, Correia M, O'Neill JG (1975) Morphological study on the Thebesian veins of the right cavities of the heart in the dog. Acta Anat 92:310–320
33. Ruengsakulrach P, Buxton BF (2001) Anatomic and hemodynamic considerations influencing the efficiency of retrograde cardioplegia. Ann Thorac Surg 71:1389–1395
34. Weaver ME, Pantely GA, Bristow JD et al (1968) A quantitative study of the anatomy and distribution of coronary arteries in swine in comparison with other animals and man. Cardiovasc Res 20:907–917
35. Anderson RH, Becker AE (eds) (1992) The heart: structure in health and disease. Gower Medical Pub, London/New York
36. Kloner RA, Ganote CE, Reimer KA et al (1975) Distribution of coronary arterial flow in acute myocardial ischemia. Arch Pathol 99:86–94
37. Koke JR, Bittar N (1978) Functional role of collateral flow in the ischaemic dog heart. Cardiovasc Res 12:309–315
38. Redding VJ, Rees JR (1968) Early changes in collateral flow following coronary artery ligation: the role of the sympathetic nervous system. Cardiovasc Res 2:219–225
39. Weisse AB, Kearney K, Narang RM et al (1976) Comparison of the coronary collateral circulation in dogs and baboons after coronary occlusion. Am Heart J 92:193–200

40. Schaper W, Flameng W, De Brabander M (1972) Comparative aspects of coronary collateral circulation. Adv Exp Med Biol 22:267–276
41. Gregg D, Shipley R (1947) Studies of the venous drainage of the heart. Am J Physiol 151:13–25
42. Patek PP (1939) The morphology of the lymphatics of the mammalian heart. Am J Anat 64:203–249
43. Johnson RA, Blake TM (1966) Lymphatics of the heart. Circulation 33:137–142
44. Symbas PN, Cooper T, Gantner GEJ et al (1963) Lymphatic drainage of the heart: effect of experimental interruption of lymphatics. Surg Forum 14:254–256
45. Anderson RH, Becker AE, Brechenmacher C et al (1975) The human atrioventricular junctional area. A morphological study of the A-V node and bundle. Eur J Cardiol 3:11–25
46. Bharati S, Levine M, Huang SK et al (1991) The conduction system of the swine heart. Chest 100:207–212
47. Frink RJ, Merrick B (1974) The sheep heart: coronary and conduction system anatomy with special reference to the presence of an os cordis. Anat Rec 179:189–200
48. Ho SY, Kilpatrick L, Kanai T et al (1995) The architecture of the atrioventricular conduction axis in dog compared to man: its significance to ablation of the atrioventricular nodal approaches. J Cardiovasc Electrophysiol 6:26–39
49. Hearse DJ, Sutherland FJ (2000) Experimental models for the study of cardiovascular function and disease. Pharmacol Res 41:597–603
50. Macdonald AA, Johnstone M (1995) Comparative anatomy of the cardiac foramen ovale in cats (Felidae), dogs (Canidae), bears (Ursidae) and hyaenas (Hyaenidae). J Anat 186:235–243
51. Joudinaud TM, Flecher EM, Duran CM (2006) Functional terminology for the tricuspid valve. J Heart Valve Dis 15:382–388
52. Anderson RH, Cook AC (2007) The structure and components of the atrial chambers. Europace 9:vi3–vi9
53. Lev M, Rowlatt UF, Rimoldi HJ (1961) Pathologic methods for the study of the congenitally malformed heart. AMA Arch Pathol 72:493–511
54. Rowlatt UF, Rimoldi HJ, Lev M (1963) The quantitative anatomy of the normal child's heart. Pediatr Clin N Am 10:499–588
55. Eckner FA, Brown BW, Overll E et al (1969) Alteration of the gross dimensions of the heart and its structures by formalin fixation. A quantitative study. Virchows Arch A Pathol Pathol Anat 346:318–329
56. Alvarez L, Rodriquez JE, Saucedo R et al (1995) Swine hearts: quantitative anatomy of the right ventricle. Anat Histol Embryol 24:25–27
57. Gorman JH 3rd, Gorman RC, Jackson BM et al (1997) Distortions of the mitral valve in acute ischemic mitral regurgitation. Ann Thorac Surg 64:1026–1031
58. Timek TA, Lai DT, Tibayan F et al (2002) Atrial contraction and mitral annular dynamics during acute left atrial and ventricular ischemia in sheep. Am J Physiol Heart Circ Physiol 283:H1929–H1935
59. Tsakiris AG, Padiyar R, Gordon DA et al (1977) Left atrial size and geometry in the intact dog. Am J Physiol 232:H167–H172
60. Chandraratna PA, Aronow WS (1981) Mitral valve ring in normal vs dilated left ventricle. Cross-sectional echocardiographic study. Chest 79:151–154
61. Nordblom P, Bech-Hanssen O (2007) Reference values describing the normal mitral valve and the position of the papillary muscles. Echocardiography 24:665–672
62. Lansac E, Lim HS, Shomura Y et al (2002) A four-dimensional study of the aortic root dynamics. Eur J Cardiothorac Surg 22:497–503
63. Sim EK, Muskawad S, Lim CS et al (2003) Comparison of human and porcine aortic valves. Clin Anat 16:193–196
64. Swanson M, Clark RE (1974) Dimensions and geometric relationships of the human aortic valve as a function of pressure. Circ Res 35:871–882
65. Jouan J, Pagel MR, Hiro ME et al (2007) Further information from a sonometric study of the normal tricuspid valve annulus in sheep: geometric changes during the cardiac cycle. J Heart Valve Dis 16:511–518
66. Anwar AM, Geleijnse ML, Soliman OI et al (2007) Assessment of normal tricuspid valve anatomy in adults by real-time three-dimensional echocardiography. Int J Cardiovasc Imaging 23:717–724
67. Maric I, Bobinac D, Ostojic L et al (1996) Tributaries of the human and canine coronary sinus. Acta Anat (Basel) 156:61–69

Detailed Anatomical and Functional Features of the Cardiac Valves

7

Michael G. Bateman, Jason L. Quill, Alexander J. Hill, and Paul A. Iaizzo

Abstract

The use of high-resolution noninvasive imaging in modern cardiac clinics to collect detailed images of valve function has dramatically accelerated the understanding of functional human heart anatomy. In the healthy human, the cardiac valves determine the passage of blood through the heart. The atrioventricular valves open during diastole to allow the filling of the ventricles and close during systole (ventricular contraction), directing blood through the semilunar valves to the body; these valves, in turn, close during diastole to prevent the flow of blood back into the ventricle. By presenting a comprehensive review of the histology, functional anatomy, and morphology of the cardiac valves, this chapter promotes an understanding of the valve features that is required for valvar repair or replacement via either surgical or minimally invasive (transcatheter) means.

Keywords

Atrioventricular valve • Semilunar valve • Mitral valve • Tricuspid valve • Aortic valve • Pulmonary valve • Imaging

Abbreviations

APM	Anterior papillary muscle complex (superoposterior)
PPM	Posterior papillary muscle complex (inferoanterior)

7.1 Introduction

A critical understanding of cardiac anatomy is essential for design engineers and clinicians with the intent of developing and/or employing improved or novel technologies or therapies for treating an impaired cardiac valve. Likewise, such knowledge is required for directing translational research, including initiating preclinical investigations, assessing the feasibility of clinical trials, and performing first-in-man procedures. There are two atrioventricular valves in the human heart, namely, the *tricuspid and mitral valves*. Likewise, there are two arterial valves in the human heart, specifically the *pulmonary and aortic valves.* All valves are complex structures whose normal anatomical structure can vary greatly among individuals and/or also become modified by disease processes. In this review, we discuss the anatomy, pathology, and issues related to transcatheter and surgical repairs of the atrioventricular and arterial valves in a translational manner.

The high prevalence of aortic valvar pathologies in the burgeoning elderly population, coupled with poor clinical outcomes for patients who go untreated, has resulted in prolific spending in the research and development of more effective and less traumatic therapies. The accelerated development of therapies designed to treat the arterial valves has been guided by anatomical information gathered from high-resolution imaging technologies, which in turn have focused attention on the need for complete understanding of arterial valvar clinical anatomies.

M.G. Bateman, PhD (✉) • J.L. Quill, PhD • A.J. Hill, PhD
Medtronic, Inc., 8200 Coral Sea St. NE, Mounds View, Minneapolis, MN 55112, USA
e-mail: michael.g.bateman@medtronic.com

P.A. Iaizzo, PhD
Department of Surgery, University of Minnesota, Minneapolis, MN 55455, USA

P.A. Iaizzo (ed.), *Handbook of Cardiac Anatomy, Physiology, and Devices*, DOI 10.1007/978-3-319-19464-6_7

7.2 The Cardiac Skeleton

Before describing the specific anatomies of the cardiac valves, it is important to understand the anatomical framework that holds these valves in position and thus consequently the relationships of each valve to one another [1]. Figure 7.1 shows an anatomical plate of a human heart with the atria and great arteries removed, highlighting the close proximity of all four cardiac valves to each other. Traditionally, the four valves of the heart have been described as being supported by a fibrous framework or *cardiac skeleton* made of dense connective tissue passing transversely through the base of the heart between the atria and the ventricles. As described by Wilcox, Cooke, and Anderson [1] and by Bateman et al. [2], the strongest part of the skeleton is the area of fibrous continuity between the leaflets of the mitral and aortic valves. This fibrous strap, thickened at both its ends by the fibrous trigones, anchors the aortic-mitral valvar unit within the base of the left ventricle (Fig. 7.2). The coronet-like support of the aortic valvar leaflets extends antero-cranially from the region of fibrous continuity and is often considered to represent an aortic valvar annulus, but there are no anatomical structures supporting the semilunar hinges of the aortic valvar leaflets (Fig. 7.3) [2]. The right fibrous trigone is itself continuous with the membranous part of the ventricular septum and is an integral part of the aortic coronet (Fig. 7.2). The trigone and membranous septum together are usually described as the central fibrous body. The smaller left fibrous trigone is formed at the leftward end of this zone of fibrous continuity [4]. Inconstant cords of fibrous tissue then extend from the margins of the fibrous continuity between the aortic and mitral valve to support the mural (anterior) leaflet of the mitral valve.

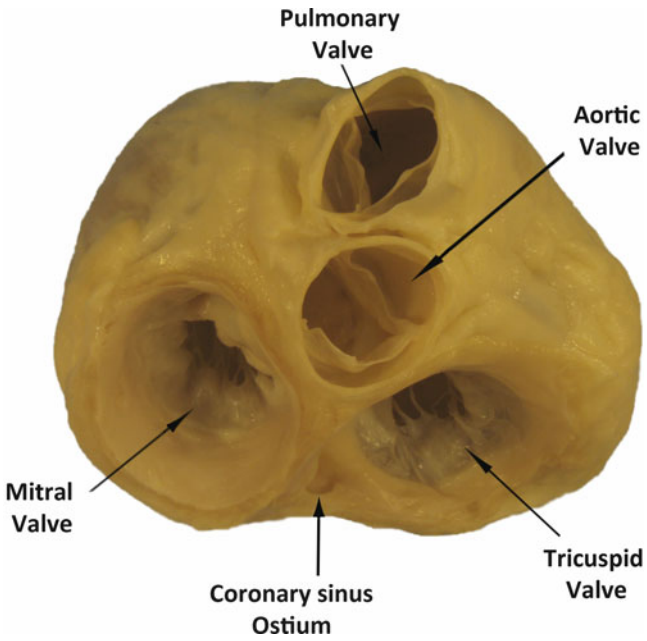

Fig. 7.1 An anatomical plate of a human heart with the atria and great arteries removed showing the relationship between the four valves at the base of the heart. Note the fibrous connection between the leaflets of the mitral valve creating a double orifice valve

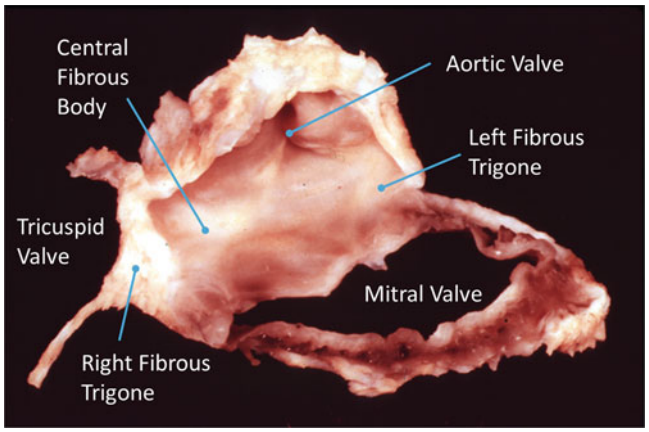

Fig. 7.2 Dissection of the cardiac skeleton showing the aortic valve (*center*), the mitral valve annulus (*below right*), and the fibrous sections of the tricuspid valve (to the *left*). The original image for this figure was kindly provided by Professor Robert H. Anderson. It was initially published in "Cardiac Anatomy" [3] and has been modified for this review. Professor Anderson retains the copyright of the initial image

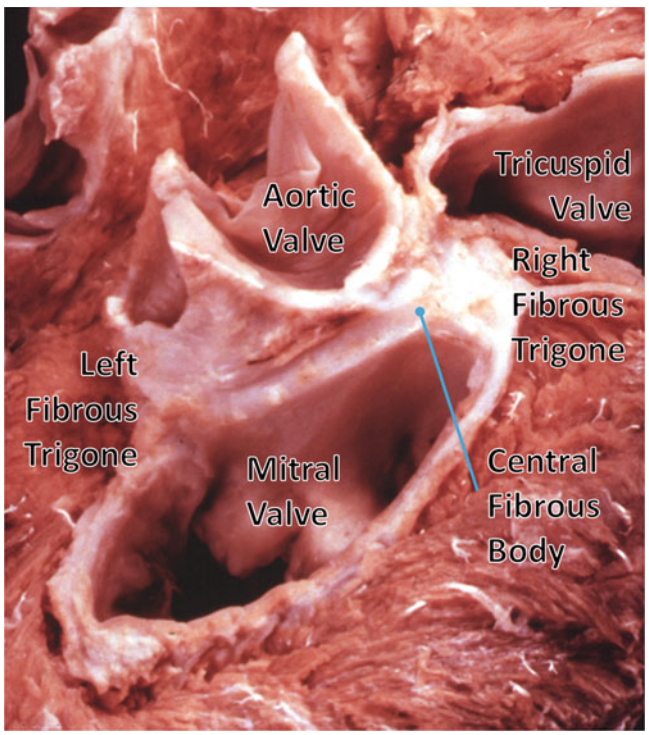

Fig. 7.3 Dissection of the cardiac skeleton with the atria and great vessels removed showing the coronet shape of the aortic annulus and the mitral valve. The original image for this figure was kindly provided by Professor Robert H. Anderson. It was initially published in "Cardiac Anatomy" [3] and has been modified for this review. Professor Anderson retains the copyright of the initial image

However, the extent of the skeleton is often greatly exaggerated. The so-called annular components of the atrioventricular valves then extend inferiorly and posteriorly from the central fibrous body and the left fibrous trigone, respectively (Fig. 7.3) [2]. It is the exception rather than the rule, however, for these fibrous cords to extend throughout the full circumference of the left and right atrioventricular junctions. The annuluses of the atrioventricular valves, as such, are better formed in the mitral as opposed to the tricuspid junction. In the mitral junction, it is normal to find segments of the valvar leaflets hinged from the fibroadipose tissue of the atrioventricular junction, rather than from a firm fibrous annulus [5]. In the tricuspid junction, the valvar leaflets are normally hinged from fibroadipose tissue [6]. The annuluses, as part of the atrioventricular junctions and rarely being complete fibrous rings, are highly dynamic and change dramatically in shape and size throughout the cardiac cycle from systole to diastole [1, 2]. It is also the fibroadipose tissue of the junctions that provides the greatest part of the insulation between the atrial and ventricular muscular masses, with the atrioventricular bundle of the conduction system being the only structure in the normal heart that crosses the insulating plane. The bundle penetrates through the atrioventricular component of the membranous septum.

The leaflets of the pulmonary valve have no direct fibrous support other than that provided by the valvar sinuses. The basal components of each leaflet are supported by the right ventricular infundibulum. It is this unique positioning of the pulmonary root away from the other valvar structures that makes possible its surgical removal during the Ross procedure, while the presence of the supporting skirt of infundibular musculature facilitates its use as an autograft to replace the aortic valve [7].

7.3 The Atrioventricular Valves

In the most basic anatomical sense, the atrioventricular valves are made up of three main components:

- Valve leaflets attached to the respective annulus
- Tendinous cords attaching the leaflets to the ventricular myocardium
- Papillary muscles providing the anchoring points for the tendinous cords to the ventricular wall

The leaflets of the atrioventricular valves can be thought as forming a *skirt* that hangs from the annulus; leaflets are divided into a series of sections that constitute the distinct leaflets of each valve. Due to the extent of variations between individuals with regard to leaflet morphologies, there has been much debate relative to nomenclature on the number of leaflets of both the mitral and tricuspid valves [8–10]. Traditionally, the division of the leaflets has been determined by the presence of commissures which can be described as the peripheral attachment of a break in the skirt [1].

The leaflets themselves are attached to the ventricles via the sub-valvar apparatus of each valve. In general, each apparatus consists of the tendinous cords and the papillary muscle complexes of each valve. The tendinous cords are usually categorized by (1) those that support the free edges of the valves, (2) those that support the rough zones (the region between the free edge and each annulus), and/or (3) those that attach to the leaflets near to the annulus. Typically, the cords supporting the free edges of the leaflets are known as *fan cords* due to the presence of multiple fenestrations. Those that attach to the rough zone of the leaflets are distinguished by their larger size and are commonly defined as *strut cords*. Finally, those that attach near the annulus are known as *basal cords*. The strut cords are of specific importance, as they bear the highest mechanical loads during systole [11]. Furthermore, the number and distribution of the tendinous cords across a given valve are critical to its function; it is well documented that dysfunction of these structures can lead to prolapse of the valves [12–14]. In general, the cords attach to the heads of the papillary muscles, which themselves play an important role in the function of each valve by contracting during systole to cushion the valve closure and help prevent the valve from prolapsing into the atrium.

7.3.1 Atrioventricular Valve Function

During systole, when the ventricles are contracting, the subvalvar apparatus of each valve prevents the leaflets from prolapsing into the atria and additionally aids in ventricular ejection by effectively drawing the apex of the ventricle toward the basal ring. Additionally, it has also been shown that the sub-valvar apparatus plays a crucial role during diastole, while the ventricle is filling, by moderating wall tensions and improving the efficiency of the ventricular myocardium [15, 16]. During systole in normal/healthy cardiac function, the valve leaflets, which bulge toward the atrium, can be considered to stay pressed together throughout the contraction and therefore do not prolapse. During diastole, when the ventricles are relaxing and the chambers are filling through the open atrioventricular valves, eddy currents that form behind the leaflets and tension in the subvalvar apparatus keep the leaflets close together.

Figures 7.4 and 7.5 show image sequences obtained employing Visible Heart® methodologies, as described in Chap. 41. These sequences display the normal cardiac function of the mitral and tricuspid valves, respectively [17, 18]; the images were obtained from the atria (above the valve) and from the ventricular apexes (below the valve).

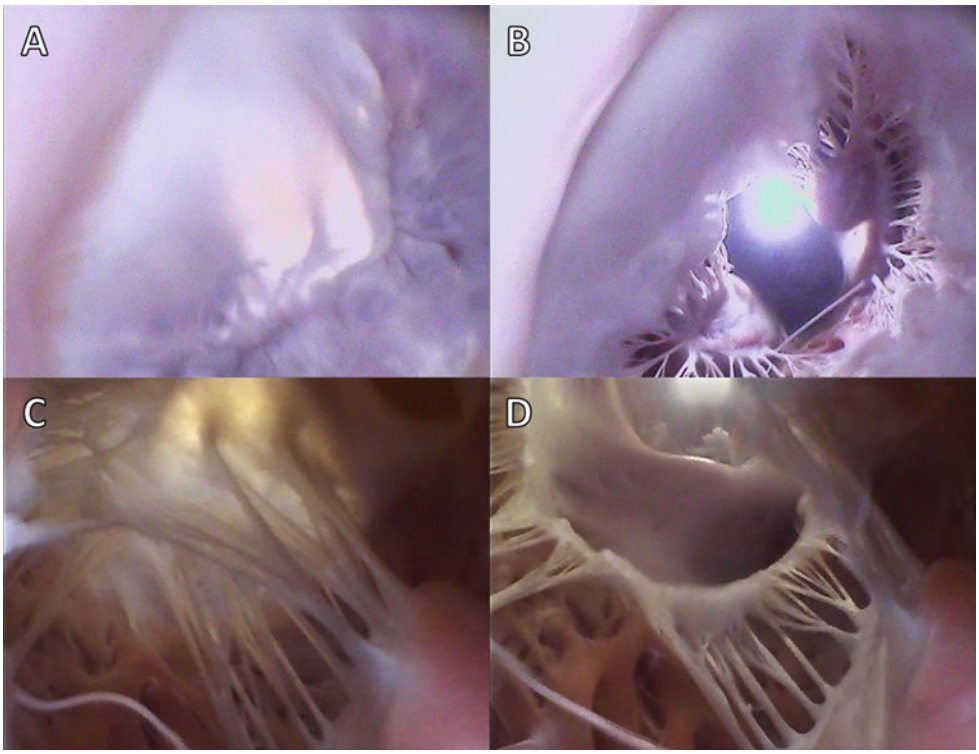

Fig. 7.4 Internal videoscopic images of the mitral valve from above (**a**, **b**) and below (**c**, **d**) during systole (**a**, **c**) and diastole (**b**, **d**) obtained employing Visible Heart® methodologies

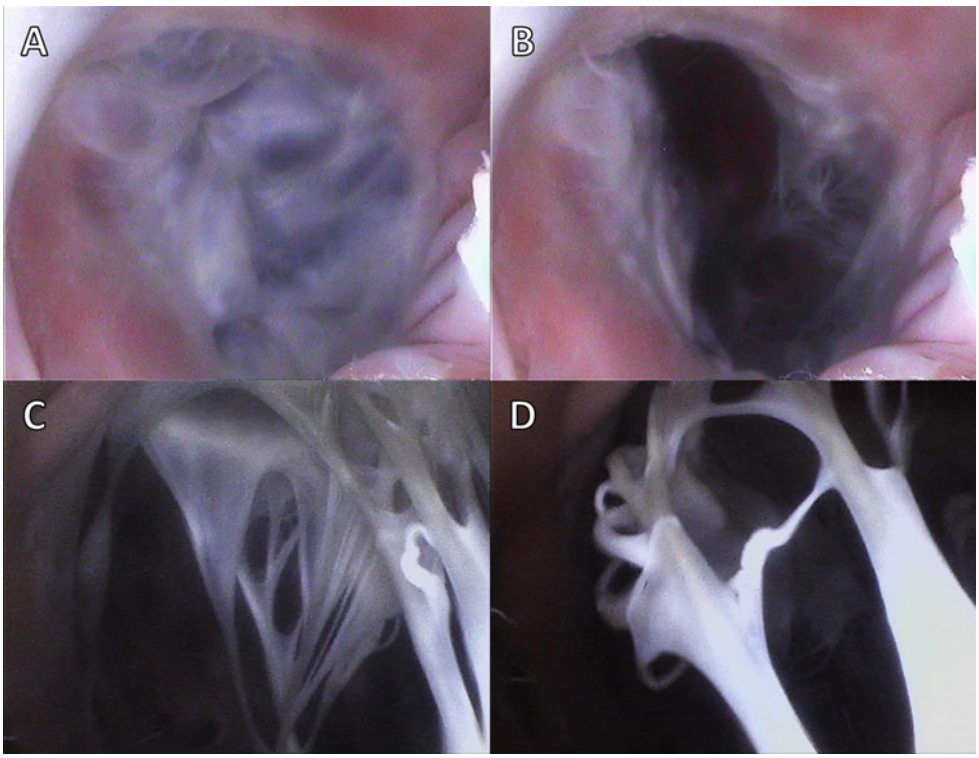

Fig. 7.5 Internal videoscopic images of the tricuspid valve from above (**a**, **b**) and below (**c**, **d**) during systole (**a**, **c**) and diastole (**b**, **d**) obtained employing Visible Heart® methodologies

Dysfunction of the atrioventricular valves is usually characterized by one of two symptoms: (1) failure of a valve to successfully close or (2) failure of a valve to successfully open. Dysfunction of the valves during systole (i.e., failure of the valve to successfully close) is known as valvar *incompetence* and results in the *regurgitation* of blood back in a retrograde direction though the atrioventricular junction. Such dysfunction results in a decrease in cardiac output and also increases the pressure within the atria during systole (potentially causing atrial dilation and/or eventually atrial

fibrillation). Dysfunction of the valves in diastole (failure of the valve to fully open and allow blood to fill the expanding ventricles) is termed *stenosis*. This decrease in effective orifice area of the open valve is often due to stiffening or calcification of the valve leaflets.

7.4 The Semilunar Valves

A healthy semilunar valve is composed of three valve leaflets, each attached to its respective sinus. These valves lie between the ventricular outflow tracts and the arterial trunks, the main arteries carrying blood away from the heart. This elegant structure is much simpler than that of the atrioventricular valves described previously, in that the semilunar valve leaflets do not require a tension apparatus to maintain competency. When closed, the three leaflets of each valve coapt along zones of apposition, or *commissures,* which are fibrous zones some distance from the free edge of the leaflets. At the center of the valve where all three leaflets coapt, a distinct fibrous nodule can be found. The valve leaflet margins are attached to the arterial wall in the shape of a half-moon, hence the *semilunar* moniker. Normally, the regions of the valves where the commissures meet the arterial wall are considerably higher than the seats of the leaflets, thereby giving the valve a crown-like shape. These three points, particularly in the aortic valve, are used to define the sinotubular junctions (Fig. 7.6). Although we have discussed the positioning of the valves in the heart by referring to their respective annuluses, many anatomists contest the idea that there are single defined annuluses for both the pulmonary and aortic valves [19]. Interestingly, there is a defined annulus where the respective arteries are attached to the ventricular outflow tract; however, due to the crown-like structure of the valve, the hemodynamic junction of the valves spans this annulus. This structural shape results in part of the arterial wall being considered a ventricular structure (in a hemodynamic sense) and, in turn, part of the ventricular wall an arterial structure. Just distal to the valves are the *arterial sinuses* that are represented by dilations of the artery positioned above each leaflet and additionally house the coronary artery ostium. The sinus also provides a recess for the valve leaflets to retract into, allowing for unrestricted flow from the ventricle to the artery. Finally, the virtual ring, upon which many annular measurements are based and which defines the basal plane of aortic valve, is defined by the three anatomical anchors at the nadir of each aortic leaflet [20]. These features are illustrated by the diagram in Fig. 7.6. The position and definition of the valve annulus is often contested by different medical specialists, and a recent questionnaire highlighted the current lack of consensus between physicians regarding the optimal means of describing the semilunar valve anatomy [21]. As such, it is important to be precise in the definition of exactly what is being measured when documenting the size and shape of the semilunar valve annuluses.

7.4.1 The Functioning of the Semilunar Valves

When a semilunar valve is functioning correctly, the leaflets are pushed into the sinus during myocardial contraction (systole) to allow blood to leave the ventricles. As the myocardium relaxes and the pressure within the ventricle drops below the pressure distal to the valve in the arterial system (the aorta or pulmonary artery), the valve snaps shut. This usually happens soon after ventricular systole but before the heart has completely relaxed, so that during diastole, when the chambers are filling through the atrioventricular valves, the leaflets of the semilunar valves remain tightly closed. A positive pressure difference between the aorta and the coronary sinus, which lies within the right atrium, allows for the flow of blood through the coronary vasculature. Thus, it should be noted that the heart muscle is perfused with blood when the semilunar valves are closed and the cardiac myocytes are relaxing.

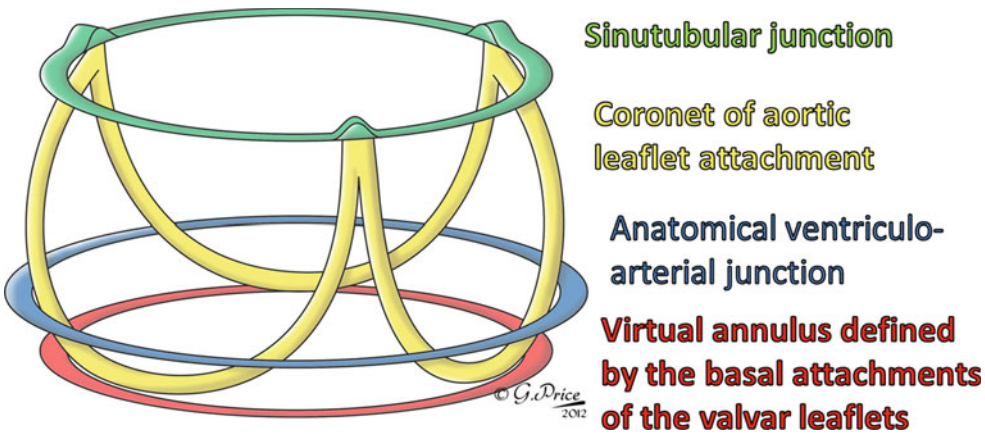

Fig. 7.6 Idealized three-dimensional arrangement of the semilunar valve (this diagram represents an aortic root). The model contains three circular rings with the leaflets suspended within the root in crown-like fashion. The cartoon is reproduced with kind permission of Professor Robert H. Anderson who retains the intellectual copyright in the original image. Special acknowledgment goes to Gemma Price as the artist [7]

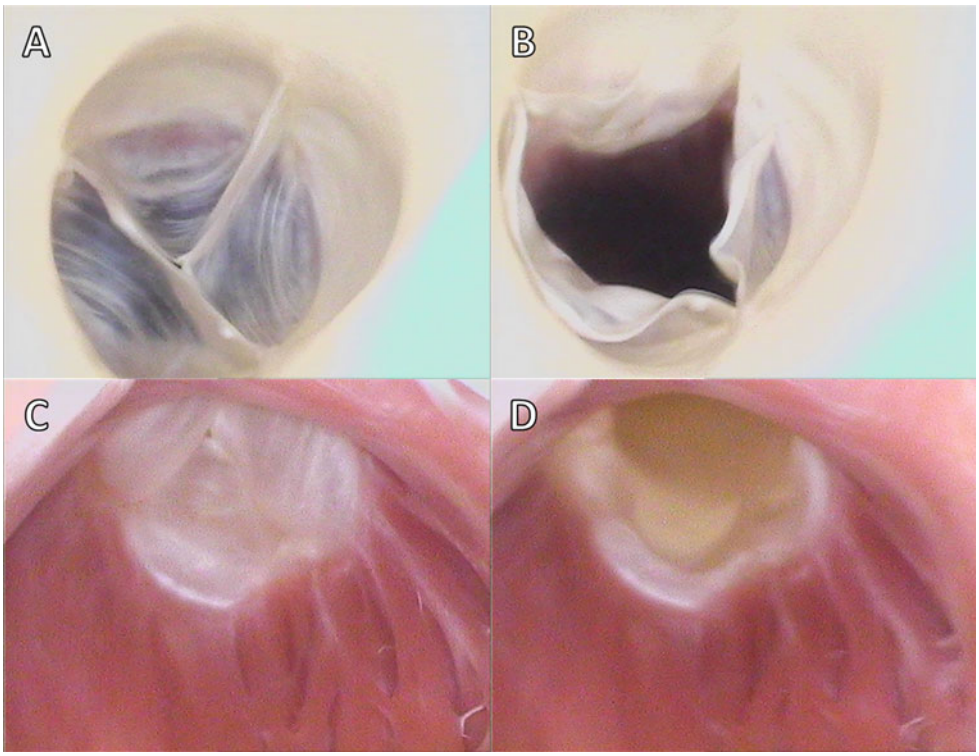

Fig. 7.7 Internal videoscopic images of the pulmonary valve from above (**a**, **b**) and below (**c**, **d**) during systole (**a**, **c**) and diastole (**b**, **d**) obtained employing Visible Heart® methodologies

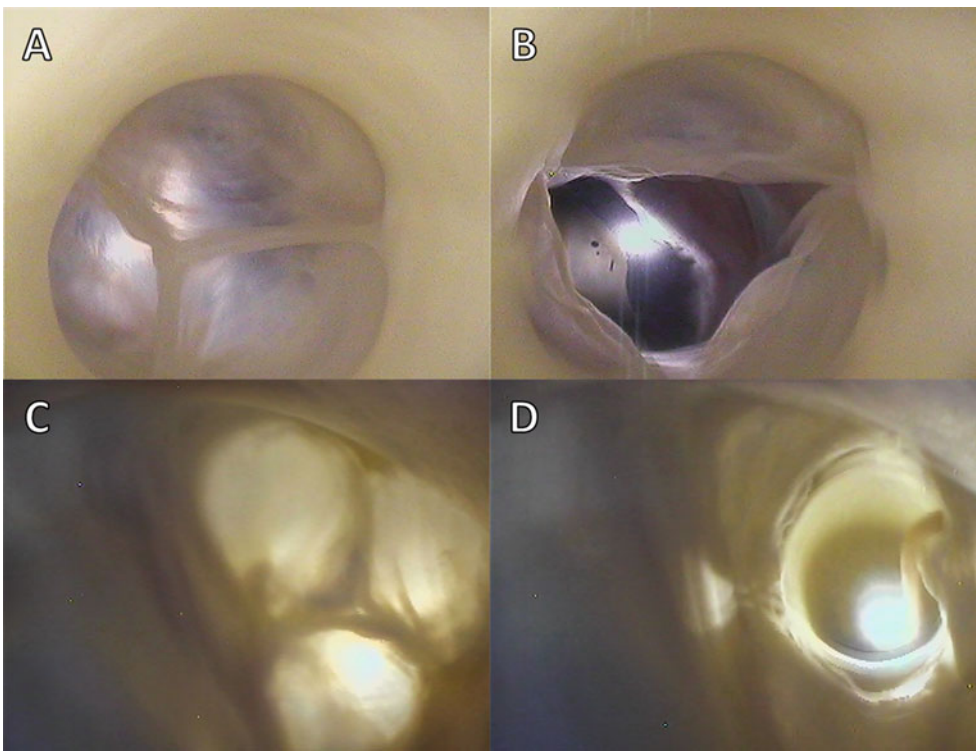

Fig. 7.8 Internal videoscopic images of the aortic valve from above (**a**, **b**) and below (**c**, **d**) during systole (**a**, **c**) and diastole (**b**, **d**) obtained employing Visible Heart® methodologies

Figures 7.7 and 7.8 show image sequences of the functional movements of the pulmonary and aortic valves, respectively; these images were obtained from reanimated human hearts employing Visible Heart® methodologies [17, 18]. The images include views of semilunar valves from above (i.e., from videoscopes within the pulmonary artery and the aorta) and from below (with videoscopes within the right and left ventricular outflow tracts).

In general, dysfunction of the semilunar valves is usually characterized by one of two symptoms: failure of the valves to successfully close or failure of the valves to successfully open. Dysfunction of the valves during systole, i.e., failure of the valve to successfully open, is defined as *stenosis* of the valve. This pathology is characterized by reduction in the effective orifice area of the valve (the size of the opening that allows blood to pass), which in turn forces the ventricles to work harder to move blood to the body or lungs. Dysfunction of the semilunar valves during diastole, when the ventricles are relaxing, results in *regurgitation*; this occurs when blood is allowed back into the ventricle from the arterial system, overloading the ventricles and potentially causing chronic heart failure.

7.5 Valve Histologies

Interestingly, the atrioventricular valves share very similar leaflet histology. The atrial sides of the leaflets consist of spongy tissue (lamina spongiosa) comprised of fibrocytes, histiocytes, and collagen fibers [22]. It is these collagen fibers that are considered to supply the mechanical strength required of the atrioventricular valves. The ventricular sides consist of fibrous tissue (lamina fibrosa), and both these layers are surrounded by endothelial cells. Additionally, the valve leaflets have been shown to incorporate both primary sensory and autonomic innervation. In general, it is considered that the anterior leaflet of the mitral valve has twice the innervation of the posterior leaflet [23]. These nerves are typically situated in the lamina spongiosa and extend over the proximal and medial portions of the leaflet [22]. Fibroblasts [24], smooth muscle cells [25, 26], and myocardial cells [27] are also commonly located within the leaflet tissue.

Cells within the leaflets have been shown to elicit two types of contractile activity: (1) a brief contraction or twitch at the beginning of each heartbeat (reflecting contraction of myocytes in the leaflet in communication with, and excited by, atrial muscle) which has relaxed by mid-systole and whose contractile activity is eliminated with β-receptor blockade, and (2) sustained tonic contractions (or tone) during isovolumic relaxation, which has been shown to be insensitive to β-blockade, but doubled by stimulation of the neurally rich region of aortic-mitral continuity [28]. These contractile activities within the leaflets are hypothesized to aid in the maintenance of anterior leaflet shape. This, in turn, could help prevent mechanical shock to the leaflets upon valve closure and also aid in optimizing the leaflet shape for funneling blood into the left ventricular outflow tract [28].

The tendinous cords are composed of a collagen core, surrounded by elastin fibers interwoven in layers of loose collagen. Similar to the valve leaflets, they also have an outer layer of endothelial cells, but it is the collagen cores that support the greatest degree of mechanical load during systole and allow for the wavy configuration during diastole. The elastin fibers are normally arranged in parallel fashion relative to the collagen fibers, and as the cords are stretched during systole, the elastin fibers are also stretched, straightening the collagen. It is hypothesized that it is this composite configuration of elastin and collagen that provides a smooth mechanism for the transmission of cordal forces from the leaflets to the papillary muscles. Additionally, during diastole, the stretched elastin fibers likely help to restore the wavy configuration of the primary collagen cores. The relative amount of collagen and elastin within the given chordae varies according to their relative types, as does the relative amount of contained DNA and their degree of vascularization. Normally the vascularization of the tendinous cords is located between their collagen cores and the elastin fibers and is further considered to supply nutrients to the leaflets. It has been reported that a higher DNA content within both the anterior and posterior marginal chordae relates to inherently higher rates of collagen syntheses in order to prevent mechanical deterioration compared with other types of chordae [13].

The papillary muscles can be considered part of the ventricular myocardium and hence are composed of aggregated myocytes. The cells exhibit complex junctions, called *intercalated discs*, allowing multiple cells to form long cellular networks. Within the papillary muscles, these muscle fibers run parallel to each other along the length of the muscle to increase contractile force and efficiency. The papillary muscles are extensively innervated and have complex vascular systems in order to maintain coordinated contractions with the continuum of the ventricular myocardium [29].

It was Gross who first drew attention to the specific histological structures of the arterial valves, his account then being endorsed by others such as Misfeld and colleagues [22, 30]. Each leaflet of the semilunar valve was described to have a fibrous core, or *fibrosa*, with an endothelial lining containing delicate sheets of elastin on its arterial and ventricular aspects. This so-called fibrous "backbone" is represented by a dense collagenous layer, which gives way to a much looser structure, or *spongiosa*, toward the ventricular aspects of the leaflet cusps. The zone of apposition of the leaflets consists of an abrupt thickening of the fibrous layer made up of closely packed vertically directed fibers and builds at the central portion of the free edge, creating a node termed the *nodulus Arantii* [22, 30]. Figure 7.9 displays a cross section of an aortic valve leaflet displaying the varying tissue types [31].

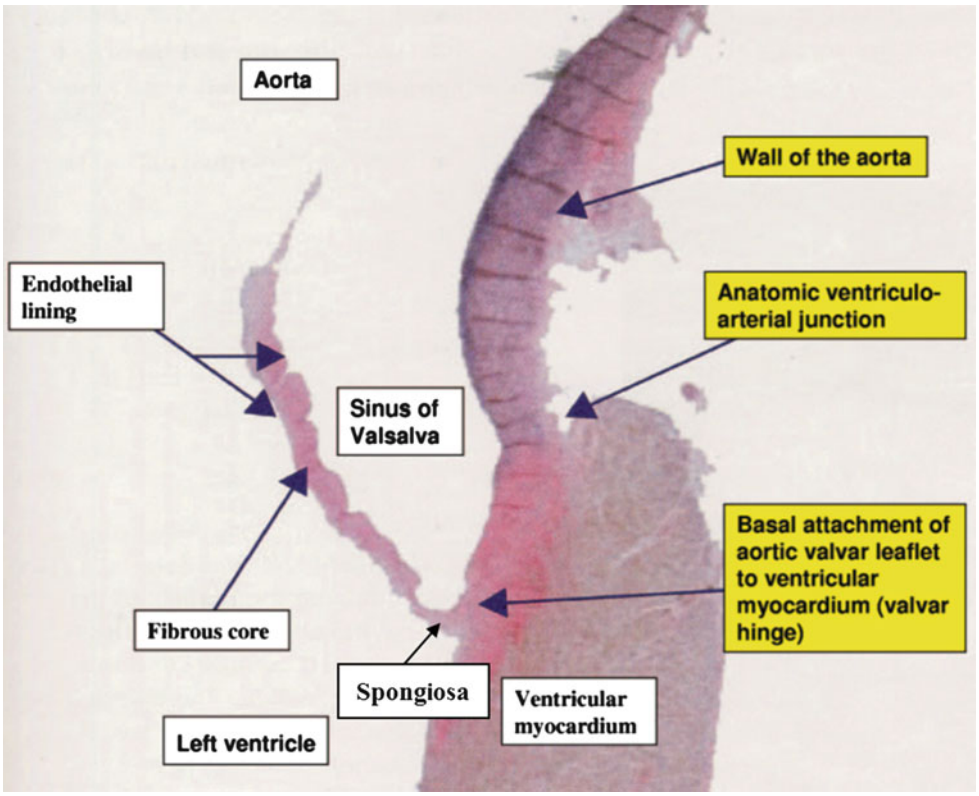

Fig. 7.9 Histologic features of the aortic valvar complex showing the anatomic ventriculoarterial junction. Also note that the basal attachment of the aortic valvar leaflets to the ventricular myocardium is proximal relative to the anatomic junction. Image is reproduced with permission from Piazza N et al. (2008) [31]

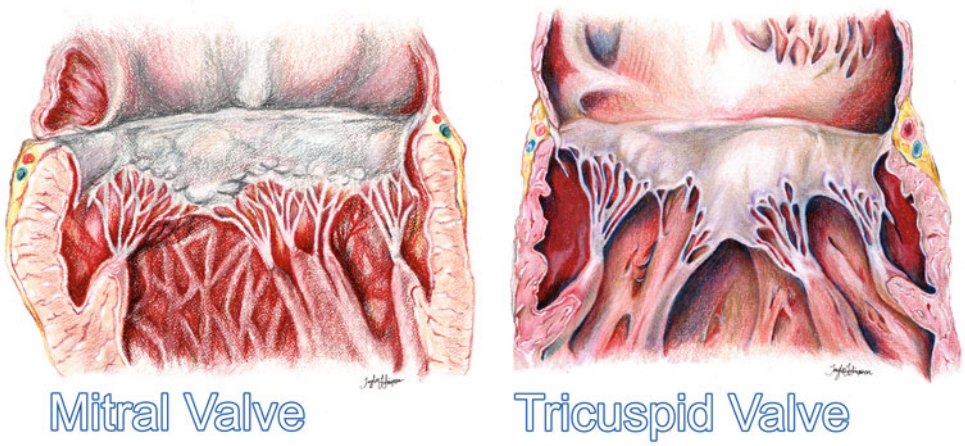

Fig. 7.10 An artist's rendition of the healthy mitral and tricuspid valves clearly showing the annuluses, leaflets, tendinous cords, and papillary muscles

7.6 The Mitral Valve

The left atrioventricular valve, or mitral valve, named by Andreas Vesalius due to its structural resemblance to the cardinal's mitre, is situated in the left atrioventricular junction and modulates the flow of blood between the left atrium and ventricle. Commonly, the valve consists of an annulus, two leaflets, two papillary muscle complexes, and two sets of tendinous cords, as seen in Fig. 7.10.

In 1976 Carpentier described the mitral valve as consisting of two apposing leaflets—a posterior leaflet with three scallops and an anterior leaflet with one scallop. Each region of the leaflets is designated an alphanumerical label to distinguish it from the rest of the valve (Fig. 7.11) [32]. However, when one considers these structures relative to the landmarks of the body (i.e., in an attitudinally correct nomenclature), the leaflets are located in posteroinferior and anterosuperior positions. Confusion regarding positional nomenclature can be avoided when adopting the more traditional approach suggested by Vesalius for distinguishing between the leaflets and recognizing that they are aortic and mural in their locations [33]; in this chapter, we will use such nomenclature. The

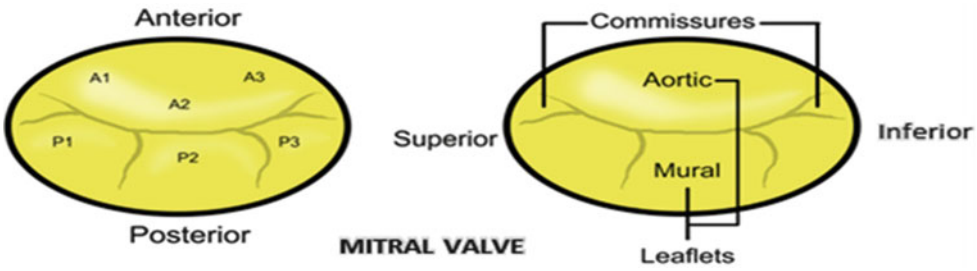

Fig. 7.11 Nomenclature of the mitral valve leaflets. The *left* diagram shows Carpentier's 1976 nomenclature, while the *right* depicts the modern attitudinally correct nomenclatures

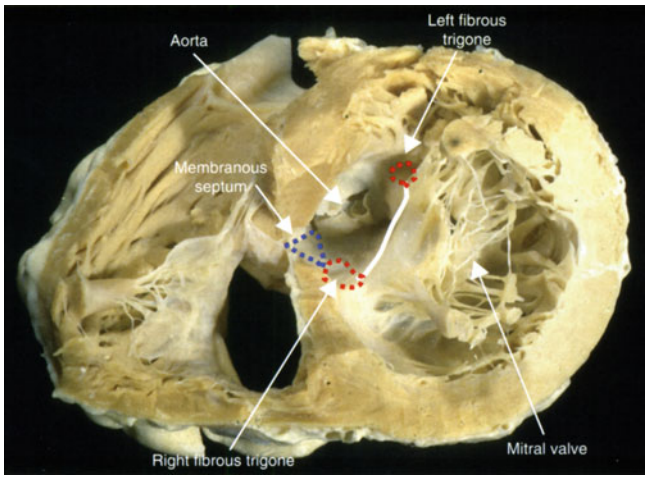

Fig. 7.12 Trigones and the aorto-mitral fibrous continuity within a sectioned human heart. In this case, the cardiac skeleton is being viewed from the apex of the heart. The anterior cardiac surface appears in the upper part of this image, whereas the posterior surface is below. Image is reproduced with permission from Anderson RH et al. (2006) [33]

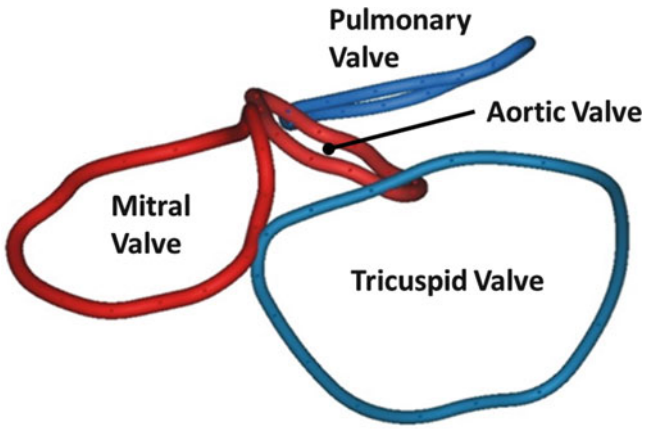

Fig. 7.13 3D reconstruction of the annuluses of the mitral (*red*) and tricuspid (*blue*) valves in Mimics® (Materialise, Leuven, Belgium) from CT scans of a human heart in vivo. The image also shows the location of the virtual rings formed by joining together the basal attachments of the leaflets of the aortic and pulmonary valves

junctions of the two leaflets are commonly referred to as the *anterolateral* and the *posteromedial* commissures; however, they are more accurately described as superior and inferior. The line of apposition of the leaflets during valve closure is known as the *fibrous ridge*. The simplicity and practicality of Carpentier's anatomic description of the mitral leaflets led to its widespread use after being introduced in 1976 [32]; yet, while this description depicts a majority of mitral valve anatomies, there can be wide variability in the number of scallops within each leaflet and their relative positions [34].

In general, the aortic leaflet is found to be attached to approximately one-third of the annulus circumference and is supported by the aorto-mitral fibrous continuity, which terminates in the left and right fibrous trigones (Fig. 7.12). The mural leaflet is attached to the remaining two-thirds of the annulus and also to the fibrous extensions that continue from the trigones around the mitral valve. However, the lengths of these extensions can be highly variable. Furthermore, a fibrous-fatty tissue surrounds the valve in areas where the cardiac skeleton is not present. The mitral annulus is a highly dynamic feature of the heart, changing dramatically in shape and size throughout the cardiac cycle. It is often described as being saddle-shaped with the highest point of the saddle, the *saddlehorn*, being found at the midpoint of the area of aortic-to-mitral valvar continuity [35] (Figs. 7.4 and 7.13). Both Delgado and Veronisi and their colleagues reported a series of annular dimensions that were recorded using echocardiography in healthy patients; these data are summarized in Table 7.1 [36–38].

Table 7.1 Data on the mitral valve annulus measured via CT [36] and 3D echocardiography [37, 38]

Measured anatomical feature	Data	Sample size
Systolic annular area [36, 37]	9.12 ± 1.71 cm^2 9.49 ± 1.25 cm^2	$n = 84$ $n = 13$
Septal-lateral (A2-P2) diameter [36, 37] (considered the short axis of the valve)	2.38 ± 0.40 cm 3.00 ± 0.45 cm	$n = 84$ $n = 13$
Commissure-commissure diameter [36, 37] (considered the long axis of the valve)	4.10 ± 0.48 cm 3.42 ± 0.40 cm	$n = 84$ $n = 13$
Annulus height during systole [38]	8.1 ± 1.7 mm	$n = 24$

In general, the sub-valvar apparatus of the mitral valve consists of two adjacent papillary muscle complexes—the superoposterior (anterior or APM) and the inferoanterior

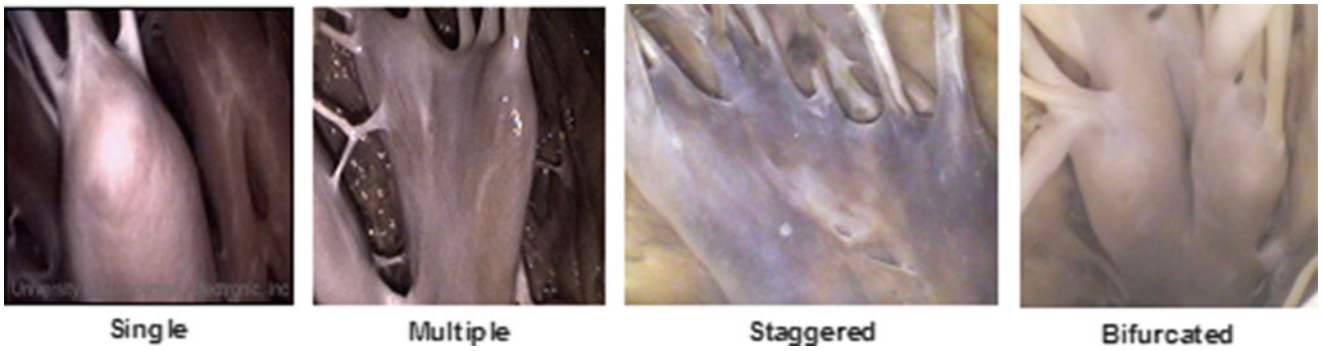

Fig. 7.14 Several representative examples of the enormous variation in anatomy with regard to the papillary muscle heads associated with the mitral sub-valvar apparatus from four different human hearts taken using Visible Heart® methodologies [40]

Table 7.2 Data on the chordal lengths of the mitral sub-valvar apparatus measured in vivo via 3D echocardiography [41] and post mortem [42, 43]

Measured anatomical feature	Data	Sample size
APM tethering length in systole [41]	3.54 ± 0.82 cm	n = 120
PPM tethering length in systole [41]	3.76 ± 0.78 cm	*n* = 120
Anterior leaflet insertion length [42]	1.81 ± 0.49 cm	*n* = 50
Posterior leaflet insertion length [42]	1.18 ± 0.26 cm	*n* = 50
Ratio of chordal origins to insertions [43]	1:5	*n* = 18

APM superoposterior (anterior) papillary muscle

PPM inferoanterior (posterior) papillary muscle

(posterior or PPM)—with their attached tendinous cords which, in turn, insert onto the ventricular surfaces of each of the two valve leaflets [33]. In other words, the superoposterior papillary muscle complex is not solely associated with the aortic leaflet, but rather both the leaflets; likewise, the inferoanterior papillary muscle complex is not solely associated with the mural leaflet. It is important to note that the morphologies of the papillary muscle complexes are highly variable [36]. Some have proposed a complicated alphanumeric classification to account for the number of heads within each muscle and the number of attachments with the ventricular walls [39]. Even this complex code can be deemed as an oversimplification, as both papillary complexes can exhibit enormous anatomic variation [40]. For example, Fig. 7.14 displays images of the sub-valvar apparatus of the mitral valve taken from human hearts in the Visible Heart® library [40].

The tendinous cords are typically classified by their number and length and quantified by one of two measurement techniques—tethering length and insertion length. *Tethering length* is defined as the distance from the papillary head to the saddlehorn of the mitral annulus. *Insertion length* is defined as the length of the cords from their origin at the papillary head to their insertion into the leaflet tissue. Anatomical dimensions obtained from patients with no reported mitral regurgitation or other valvar pathologies were reported by Sonne et al. and Lam et al. and are summarized in Table 7.2 [41, 42]. Yet, it should be emphasized that, as with other anatomical studies, these data do not account for all anatomical variations. For example, it has also been reported that the cordal attachments to the mural leaflet may extend simply from the ventricular myocardium to the leaflet without a papillary muscle attachment. Furthermore, it is well known that the tendinous cords themselves may elicit highly variably anatomies, and various subpopulations of chordae have been classified by both function [43] and type [44]. Figure 7.15 shows examples of these identified variations in the types of chordae, including posterior marginal chordae, commissural chordae, anterior strut chordae, anterior marginal chordae, basal posterior chordae, and posterior intermediate chordae.

7.7 The Tricuspid Valve

The right atrioventricular valve, or tricuspid valve, is situated within the right atrioventricular junction and modulates the flow of blood between the right atrium and right ventricle. This valve is typically defined by three leaflets suspended from the muscular atrioventricular junction and connected to the ventricular wall via three distinct papillary muscle complexes (as seen in Fig. 7.10). When defined using attitudinally correct nomenclature, these leaflets are located in septal, anterosuperior (traditionally anterior), and inferior (traditionally posterior) positions (Figs. 7.16 and 7.17) [45].

The anterosuperior leaflet is the largest of the three and extends from the medial border of the ventricular septum to the acute margin of the atrioventricular junction (Fig. 7.15). The leaflet is hinged from the undersurface of the supraventricular crest and provides a curtain between the inflow and outflow tracts of the right ventricle. The inferior leaflet is hinged from the diaphragmatic aspect of the atrioventricular junction. The septal leaflet is then hinged from the ventricular border of the triangle of Koch, with the hinge crossing the right-sided aspect of the membranous septum, dividing it into atrioventricular and ventriculoarterial components [46]. The septal leaflet is often cleft as it crosses the membranous

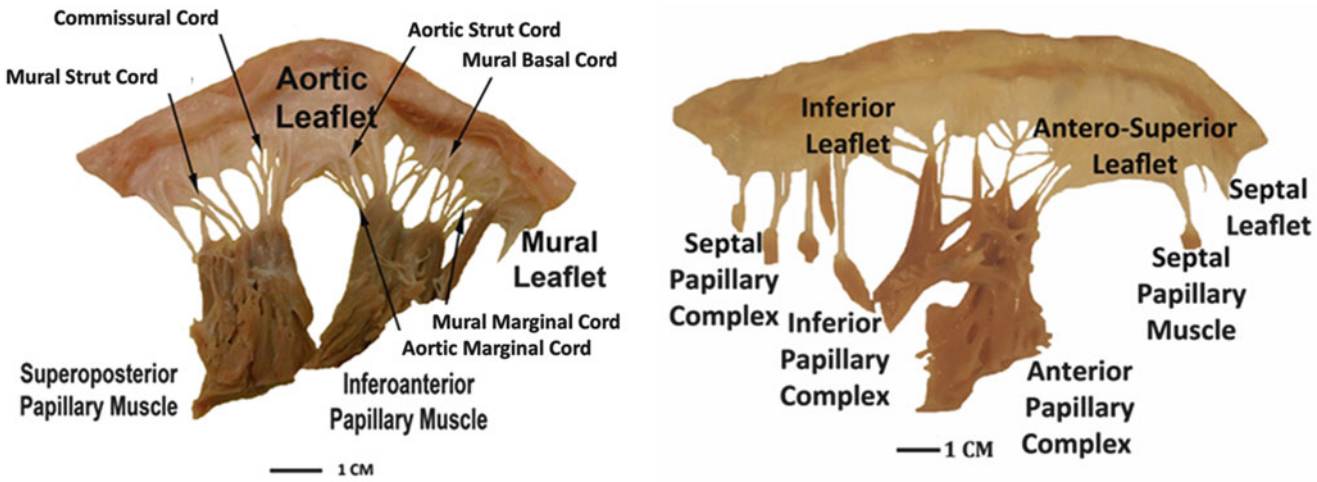

Fig 7.15 Dissections of a human mitral valve (*left*) and tricuspid valve (*right*), each labeled with attitudinally correct nomenclature. Note the dramatic differences between the two valves, including their respective sub-valvar apparatuses

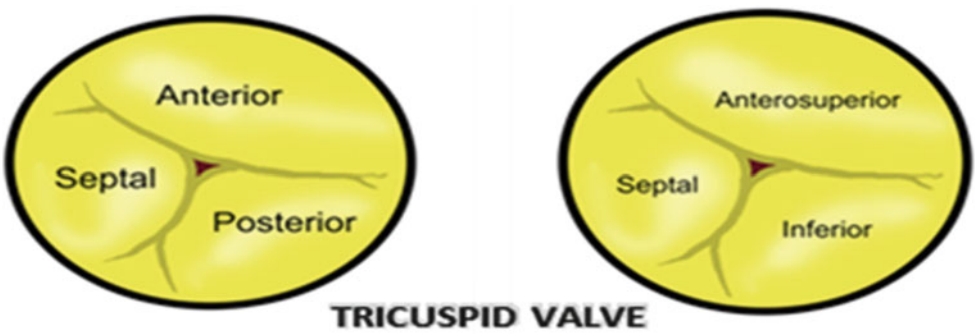

Fig. 7.16 Nomenclature of the tricuspid valve leaflets. The *left* diagram shows Carpentier's 1976 nomenclature, the *right* depicts the modern attitudinally correct nomenclatures

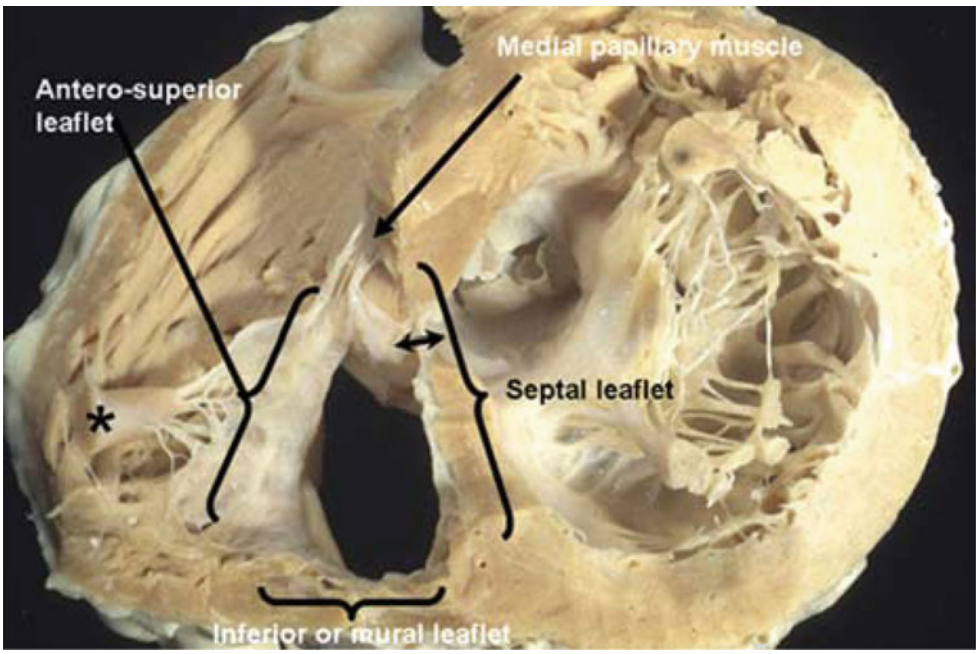

Fig. 7.17 Relative positions of the three leaflets of the tricuspid valve positioned septally, anterosuperiorly, and inferior or murally. Note the location of the membranous septum as indicated by the *double-headed arrow*. In this human heart, the anterior papillary muscle (*asterisk*) is attached to the midpoint of the anterosuperior leaflet. Image is reproduced with permission from Martinez RM et al. (2006) [45]

septum. When viewed in closed position, the trifoliate zones of apposition between the leaflets extend to their peripheral ends. It is these ends that are typically considered to represent the valvar commissures, which can be named as being anteroseptal, anteroinferior, and infero-septal [2].

To date, the morphology of the tricuspid valve has received less attention than the mitral valve; hence, thorough anatomical studies are limited. The tricuspid annulus is known to have a non-planar three-dimensional shape, similar to the mitral valve annulus (Fig. 7.13). Further, it has been described as changing its shape dramatically throughout the course of the cardiac cycle. These changes in annular geometry during systole, from a more circular shape to an elliptical shape, result in overall reduction of annular sizes by up to 40 % [47]. As the heart contracts, the annulus reaches its minimum size during isovolumetric relaxation and its maximum during isovolumetric contraction [35]. Data relating to the tricuspid annulus can be seen in Table 7.3 [37, 48–50].

As with the mitral valve, the leaflets of the tricuspid valve are complimented by a sub-valvar apparatus consisting of papillary muscle complexes that work to tether the valve leaflets via tendinous cords to prevent valve prolapse during ventricular contraction (systole). The three main papillary muscle complexes have grossly dissimilar morphology, albeit very characteristic (Fig. 7.18). The zone of apposition between the septal and anterosuperior leaflets is supported by the medial papillary muscle complex, also known as the papillary muscle of the conus, or the muscle of Lancisi [45, 51]. It arises from the posteroinferior limb of the septal band, or septomarginal trabeculation, although in some individuals the muscle is replaced by a series of smaller muscles or even by cords arising directly from the septal band. The anterior is typically the largest papillary muscle complex and supports the zone of apposition between the anterosuperior and inferior leaflets, but often inserts into the midportion of the anterosuperior leaflet. The muscle itself is usually in direct continuity with the moderator band [46]. This latter structure is one of a series of septoparietal trabeculations that arise from the anterior margin of the septal band. The smaller inferior muscle complex supports the zone of apposition between the inferior and septal leaflets. The septal leaflet is then supported in addition by multiple cords arising directly from the septum itself. This is a differentiating feature between the tricuspid and mitral valves, the leaflets of the latter valve lacking any septal attachments.

Figure 7.18 displays videoscopic images of the sub-valvar apparatus of the tricuspid valve taken from reanimated human hearts utilizing Visible Heart® methodologies, as described in Chap. 41. Such images emphasize the large anatomical variations that can exist from heart to heart (unpublished data).

Previously, Silver et al. reported the common insertion length of the tendinous cords of the tricuspid valve for healthy human hearts, which was defined as the distance from the origin of the papillary muscles to their corresponding insertion points on the valve leaflets (Table 7.4) [49]. These measurements were completed on 50 formalin-fixed human hearts; it should be noted that these data may have

Table 7.3 Data on the mitral valve annulus measured in vivo via 3D echocardiography [37] and post mortem [48–50]

Measured anatomical feature	Data	Sample size
Systolic annular area [37]	10.75 ± 1.81 cm^2	$n = 13$
Post mortem orifice area [48]	10.60 ± 3.40 cm	$n = 160$
Systolic septo-medial dimension [37]	3.31 ± 0.32 cm	$n = 13$
Systolic anterior-posterior dimension [37]	3.79 ± 0.43 cm	$n = 13$
Postmortem annular circumference [49, 50]	11.10 ± 1.10 cm 11.30 ± 0.50 cm	$n = 50$ $n = 24$

Table 7.4 Data on the chordal lengths of the tricuspid sub-valvar apparatus measured post mortem [49]

Measured anatomical feature	Data (cm)	Sample size
Septal leaflet insertion length [49]	1.50 ± 0.87	$n = 50$
Anterior leaflet insertion length [49]	1.53 ± 0.69	$n = 50$
Posterior leaflet insertion length [49]	1.37 ± 0.64	$n = 50$

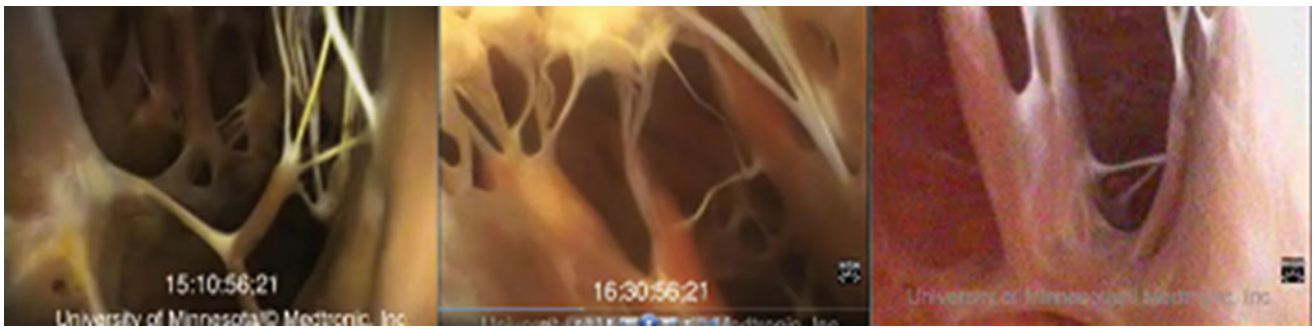

Fig. 7.18 Several representative examples of the septal (*left*), inferior (*center*), and anterior (*right*) papillary muscle complexes associated with the tricuspid sub-valvar apparatus taken using Visible Heart® methodologies (unpublished data)

specific limitations when compared to the modern imaging techniques, e.g., those used to measure the tethering length of the mitral cords mentioned earlier in the chapter. As such, we suggest that future detailed assessments of the tricuspid sub-valvar apparatus employing modern imaging techniques could greatly benefit the field.

7.8 The Aortic Valve

As previously mentioned, due to its location in the center of the heart between the mitral valve and the tricuspid valve, the aortic valve is considered as the "centerpiece" of the heart and is often the most important cardiac valve with respect to normal cardiac function [31]. An artist's rendition of the opened aortic root showing the features of the aortic valve can be seen in Fig. 7.20.

7.8.1 The Aortic Root

The aortic root contains three circular rings and one crown-like ring (Fig. 7.6) [19]. The connection of the leaflets to the arterial wall mimics the shape of a crown, whose base forms a virtual ring known as the basal plane of the valve. This plane represents the inlet from the left ventricular outflow tract into the aortic root. The top of the crown can be considered as a true ring, the sinotubular junction, defined by the sinus ridge and the related sites of attachment of the peripheral zones of apposition, between the aortic valve leaflets [31]. Hence the sinotubular junction dictates the transition from the aortic root into the ascending aorta. The semilunar hinges then cross another defined "ring" known as the anatomic *ventriculoarterial* junction. This overall anatomic arrangement was illustrated previously in Fig. 7.6, but can be readily observed when the aortic root is opened linearly as seen in Fig. 7.19.

The normal aortic root elicits a relatively consistent shape between patients, but can vary dramatically in size (Table 7.5) [29, 52]. Kunzelman et al. demonstrated a definable mathematical relationship between root diameter and clinically

Table 7.5 Data on the aortic valve annulus, sinus of Valsalva, and sinotubular junction measured using multislice computed tomography

Measured anatomical feature	Data (mm)	Sample size
Maximum aortic annular diameter [52, 29]	26.9 ± 2.8 26.4 ± 2.8	$n = 25$ $n = 150$
Minimum aortic annular diameter [52, 29]	21.4 ± 2.8 24.0 ± 2.6	$n = 25$ $n = 150$
Sinus of Valsalva mean diameter [29]	32.3 ± 3.9	$n = 150$
Sinus of Valsalva height above the basal plane [29]	17.2 ± 2.7	$n = 150$
Sinotubular junction mean diameter [29]	28.1 ± 3.1	$n = 150$
Sinotubular junction height above basal plane [29]	20.3 ± 3.1	$n = 150$

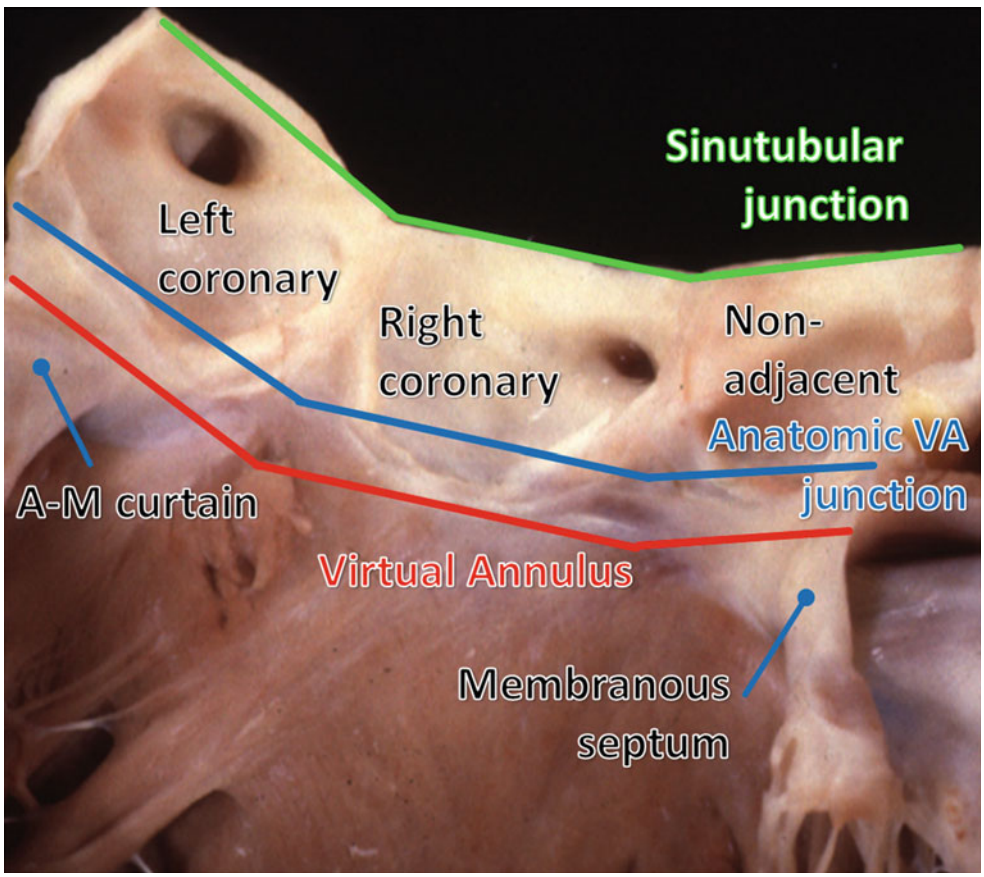

Fig. 7.19 The aortic leaflets have been removed from this human aortic root specimen. One can then observe the locations of the three defined aortic rings, i.e., relative to the crown-like hinges of the leaflets. *A-M* aortic-mitral, *VA* ventriculoarterial [7]. Image was modified from an original figure provided by Professor Robert H. Anderson; Professor Anderson retains the intellectual copyright of the original image

measurable leaflet dimensions [53]. In general, the diameter at the level of the sinotubular junction typically exceeds that at the level of the basal plane by a factor of 1:1.6 [53, 54]. The valvar complex is a dynamic structure with its geometric parameters changing continuously throughout the phases of the cardiac cycle and relative to the associated changes in pressure that will occur within the aortic root [55]. For example, from diastole to systole, the relative change in diameter at the level of the sinotubular junction and at the *ventriculo-arterial* junction has been noted to increase by ~12 % and decrease by ~16 %, respectively [56–58]. Additionally, the orientation of the left ventricular outflow tract and the aortic root (i.e., the angle between the two) is known to vary from patient to patient. It is also understood that this angle becomes more acute with age. Middelhof et al. reported that hearts from individuals aged >60 years exhibited angles between 90° and 120°, whereas individuals aged <20 years presented with angles between 135° and 180° [59].

It is important to note that one of the most critical functions of the aortic root is to facilitate coronary artery perfusion during ventricular diastole. This is achieved by directing 3–5 % of the circulating blood through both the left and right coronary arteries while the aortic valve itself is closed. In general, the orifices of the coronary arteries arise within the two anterior sinuses of Valsalva, usually positioned just below the sinotubular junctions [54, 60, 61]. However, it is not unusual to find these arteries positioned superior relative to the sinotubular junction. Cavalcanti et al. reported the mean distance measured from the orifice of the left coronary artery to the basal attachments of the corresponding leaflets was 12.6 ± 2.61 mm, and for the right coronary artery, it was 13.2 ± 2.64 mm in 51 normal postmortem hearts [62]. Variations in coronary arterial origin, nonetheless, can occur with some of these configurations posing as risk factors in sudden cardiac death [63, 64]. It should also be recalled that it is the location of these coronary arteries that dictates the naming of the aortic valve leaflets/cusps—the left coronary, the right coronary, and the nonadjacent (or non-coronary).

7.8.2 The Aortic Leaflets

As noted above, the leaflets of the aortic valve are named for the branching coronary arteries that feed the left and right sides of the heart (Fig. 7.20). More specifically, both the right and left leaflets attach to the aortic root in the predominantly muscular region of the left ventricular outflow tract, whereas the nonadjacent leaflet is chiefly attached to the fibrous region above the membranous septum (Fig. 7.19). This fibrous continuity connects the aortic valve to the anterior (aortic) leaflet of the mitral valve, forming the aortic-mitral curtain. The zone of apposition of the right leaflet to the nonadjacent leaflet is positioned above the membranous part of the ventricular septum. The zone of apposition of the nonadjacent leaflet with the left coronary aortic leaflet is adjacent to the anterior wall of the left atrium. The left leaflet

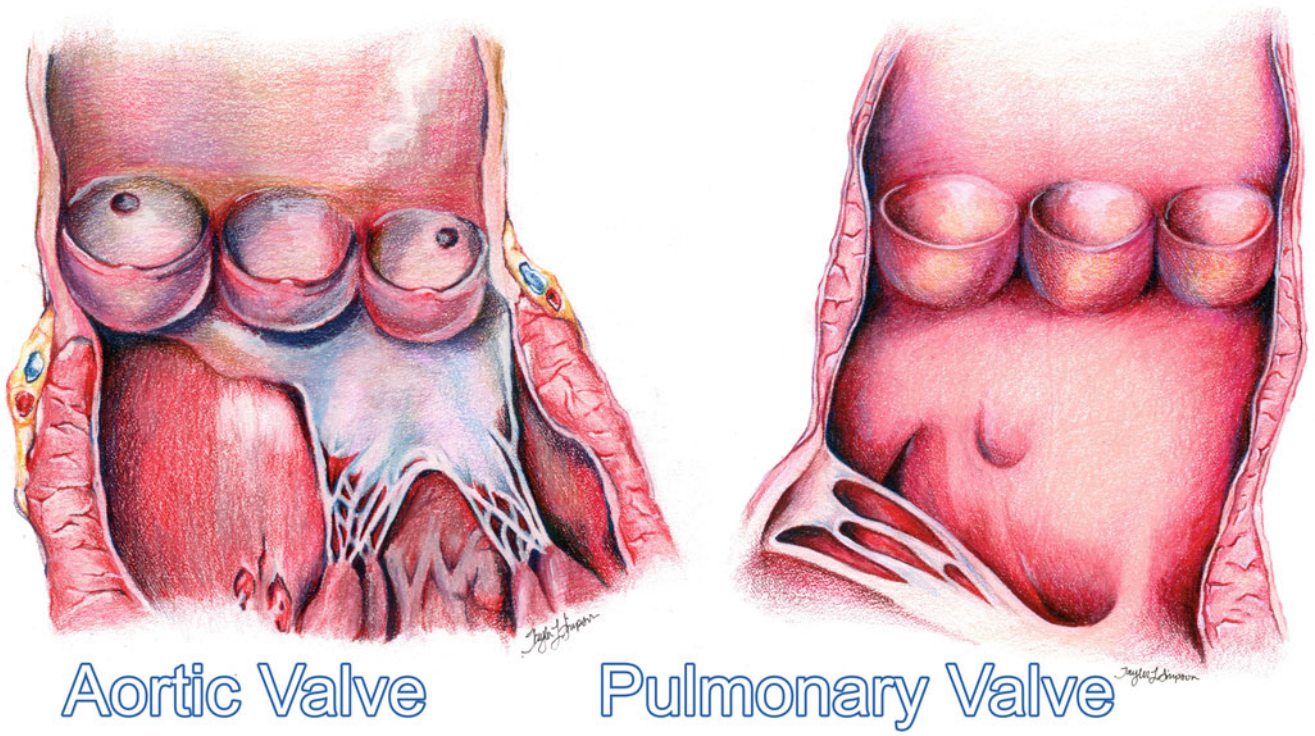

Fig. 7.20 Artist's rendition of the healthy aortic and pulmonary valves clearly showing the leaflets, sinuses, outflow tracts, and arterial trunks

then continues toward the right leaflet, again achieving support from the muscular part of the ventricular septum. As previously mentioned, the zones of apposition themselves ascend as they extend to be attached peripherally at the sinotubular junction; below each peripheral attachment, there is a fibrous interleaflet triangle that forms part of the ventricular outflow tract [65].

It should be noted that variations may exist in all dimensions of individual leaflets, including: (1) height, (2) width, (3) surface area, and (4) volume of their supporting sinuses of Valsalva [31]. Vollebergh et al. reported that the average widths (measured between the peripheral zones of attachment along the sinus ridge) for the right, the nonadjacent, and the left coronary leaflets were 25.9, 25.5, and 25.0 mm respectively, in an investigation of 200 normal hearts [66]. It was also described that the average heights (measured from the base of the center of the leaflet to their free edges) for the right coronary, nonadjacent, and left coronary cusps were 14.1, 14.1, and 14.2 mm, respectively. Such variations in the leaflet dimensions of healthy valves highlight the need to focus on the anatomy and function of each leaflet when developing prosthesis for either the surgical or transcatheter treatment of aortic valve pathologies.

7.9 The Pulmonary Valve

Due to its relative location within the infundibular musculature (at the distal portion of the right ventricular outflow tract), the pulmonary valve is considered, in an anatomical sense, a more simple valvar structure than the aortic valve (Fig. 7.20). The left and the right leaflets of the aortic valve face lie adjacent to the pulmonary trunk, and this relative anatomic orientation has been used to name the pulmonary valve leaflets: the right and left facing leaflets and the nonfacing leaflet (Fig 7.21) [1]. Anatomically, the commissure of both the right and left leaflets is supported by the supraventricular crest of the right ventricle, which separates the pulmonary valve from the tricuspid valve. Further, the opposite edge of the valve (i.e., the nonfacing leaflet is supported by the anterior wall of the infundibulum) is, in general, the most anterior part of the heart [1].

Pulmonary valve replacement is considered to be less challenging than aortic valve replacement due to the lower pressure gradient across the valve and the relative ease of access to the valve annulus. The ease of complete valve removal from the cardiac base has led to the use of an autograft replacement for the aortic valve in some congenital heart patients. Even so, information on the valve is less abundant and reports on variations in valve dimensions are less comprehensive. Capps et al. report the mean diameter of the valve as 25.4 ± 3.2 mm in a study comparing the size of the aortic and pulmonary valve to the overall body surface area (Table 7.6) [67]. It should be noted that these measurements were taken on valves removed postmortem using a Hegar dilator without annular dilation. By the authors' admission,

Table 7.6 Postmortem mean pulmonary and aortic diameters

Measured anatomical feature	Data (mm)	Sample size
Mean annular diameter [28]	25.4 ± 3.2	$n = 3997$
Mean aortic annular diameter [28]	22.4 ± 2.7	$n = 3370$

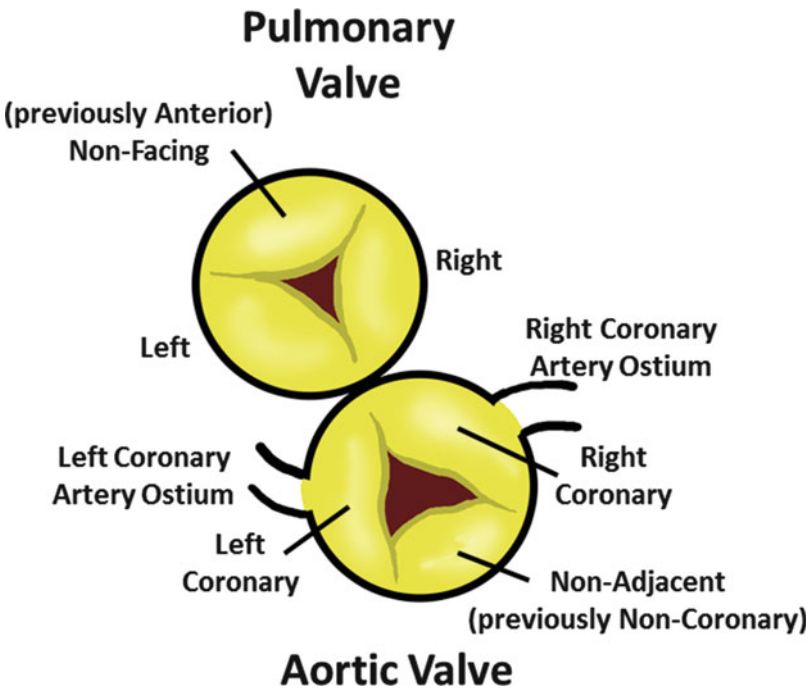

Fig. 7.21 Nomenclature for the individual leaflets of the aortic and pulmonary valves. The traditional naming system is displayed to the *left* and the updated attitudinally correct nomenclature to the *right*

this sizing presents limitations regarding the material properties of the pulmonary annulus differing significantly from the aortic [67]. As such, these measurements should be used as a rough guideline. The alternate methodology explains the difference in aortic measurements reported here from those measured at end systole in vivo by Schultz et al. and Tops et al. [20, 68], as shown in Table 7.5.

7.10 Valve Co-location with Other Cardiac Structures

When performing cardiac valve surgeries and/or contemplating novel percutaneous approaches to valvar repairs, it is vital to have a strong anatomical appreciation of the associated structures, i.e., those cardiac structures that surround the valves. The anatomical features surrounding the mitral and tricuspid valves are displayed in Figs 7.22 and 7.23. The position and course of the coronary vasculature is key to the clinical anatomy of both the mitral and tricuspid valves. The great coronary vein, continuing as the coronary sinus, circles the mural leaflet of the mitral valve [35, 69]. The circumflex artery, having branched from the main stem of the left coronary artery, courses in concert with the venous channel, usually running much closer to the hinge of the mural leaflet. In the majority of individuals with dominance of the right coronary artery, the circumflex artery does not extend through the full length of the left side of the inferior atrioventricular groove [35]. In the minority of individuals with left coronary arterial dominance, in contrast, the artery is directly related to the entirety of the mural leaflet, usually continuing into the floor of the triangle of Koch, where it gives rise to the artery supplying the atrioventricular node. In many individuals, the circumflex artery crosses underneath the coronary sinus at variable distances [33, 35, 69–71]. Both arterial and venous structures, therefore, are at risk when surgical procedures are performed on the mural leaflet of the mitral valve. Such considerations are particularly relevant when employing complex reconstructive techniques [35]. The proximity of the aortic valve is of importance when considering surgical procedures to the aortic leaflet of the mitral valve (Fig. 7.22). The interleaflet triangle between the left coronary and non-coronary (non-adjacent) aortic leaflets is directly related to the saddlehorn of the mitral valvar annulus. This feature should be remembered if sutures are to be placed to either side of the saddlehorn to prevent damage to the aortic valvar leaflets [35]. The tricuspid valve is bordered within the atrioventricular junction by the right coronary artery, but is less related to venous structures, the small cardiac vein being a relatively insignificant structure [7].

The atrioventricular node and its zones of transitional cells are closely related to the septal hinge of the tricuspid valve, with the slow pathway into the node being a constituent part of the vestibular atrial myocardium in this region. At the apex of the triangle of Koch [7, 35], the spe-

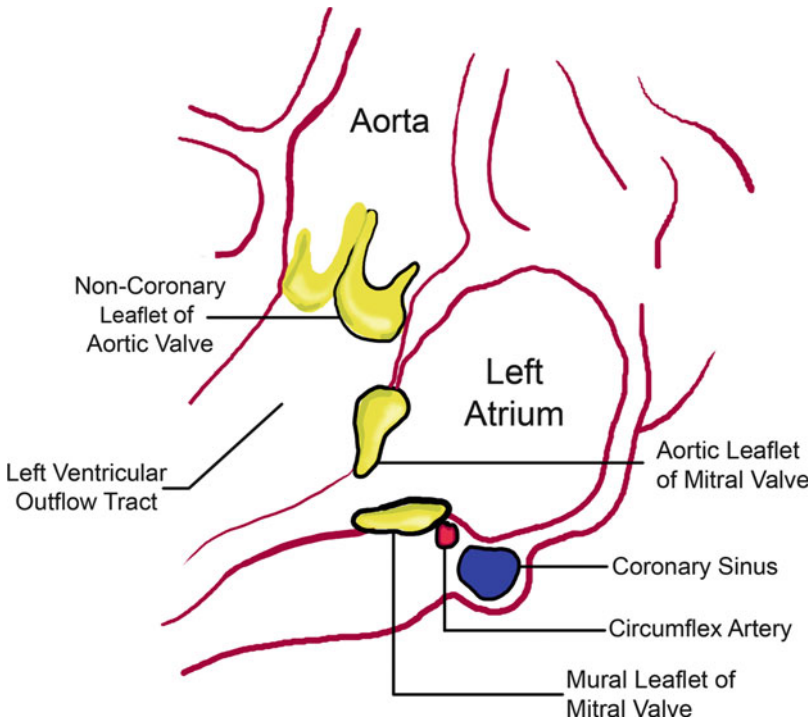

Fig. 7.22 Graphic representation of the co-location of the mitral valve to the coronary sinus, the left circumflex artery, and the aortic valve

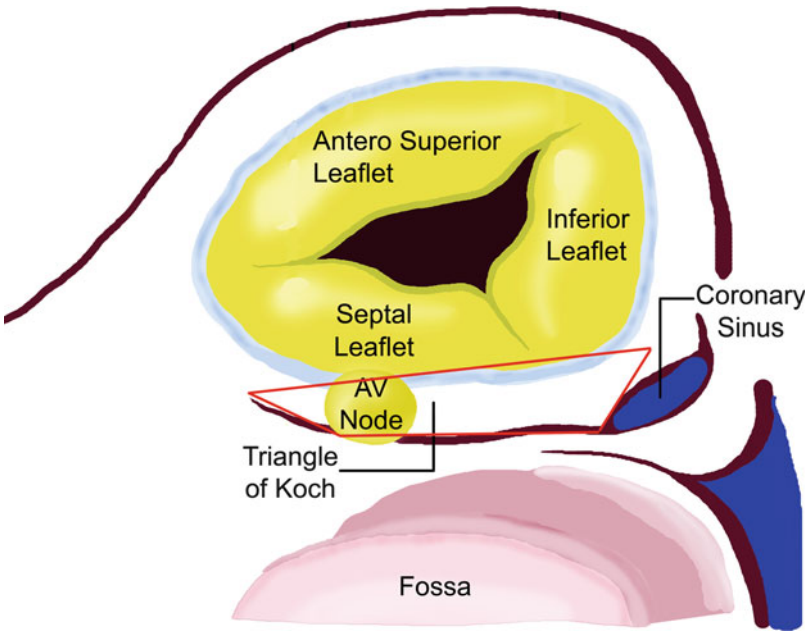

Fig. 7.23 Graphic representation of the relationship between the cardiac conduction system (i.e., the location of the atrioventricular node within the triangle of Koch) and the tricuspid valve when viewed from the right atrium

cialized cardiomyocytes of the atrioventricular node bundle themselves together and pierce the central fibrous body to become the penetrating atrioventricular bundle, or the bundle of His (Fig. 7.23). Although closely related again to the hinge of the septal leaflet of the tricuspid valve, and at potential risk whenever surgery is performed within the right atrium or through the tricuspid valve, the atrioventricular node should be sufficiently distant not to pose a threat to those operating on the mitral valve. The bundle of His, having passed through the membranous septum, divides on the crest of the muscular ventricular septum into the left and right bundle branches. These components are at greater risk during procedures on the aortic rather than the atrioventricular valves.

The most important anatomical structure related to the pulmonary root is the first perforating branch of the anterior interventricular artery; this artery is avoided during the Ross procedure. Note should also be taken of anomalous coronary arteries either coursing between the arterial roots or extending across the right ventricular infundibulum. Being located in the most anterior aspect of the heart, the pulmonary root is also directly adjacent to the sternum; thus, sternal compression may alter the performance of any prosthesis placed in the pulmonary annulus [4].

The anatomical orientation of the aortic valve is considered much more challenging; thus, the remainder of this section will focus on this valve. One of the most important and complex structures in proximity to the aortic valve is the *cardiac conduction system*. As mentioned previously, the atrioventricular node is located within the *triangle of Koch*, situating the atrioventricular node in close proximity to the subaortic region of the left ventricular outflow tract, helping to explain why the treatment of pathologies involving the aortic valve may lead to either a complete heart block or to an intraventricular conduction abnormality [31]. Further, as the atrioventricular conduction axis reaches the crest of the muscular ventricular septum, it then branches, with the left bundle branch cascading down the left ventricular septal surface, as illustrated so elegantly by Tawara over a century ago [72] (Fig 7.24).Thus, it is important that this anatomical relationship be considered when planning the repair and/or replacement of the aortic valve, as the interaction of a specific percutaneous prosthesis or the errant placement of sutures during surgical valve implantation can induce adverse effects on the conduction system and result in the patient requiring cardiac rhythm management.

In addition to the conduction system, an intimate knowledge of the aortic valve's proximity to both the coronary arteries and the mitral valve helps to minimize procedural complications.

In particular, the main stem of the left coronary artery can be remarkably short, bifurcating into the left anterior descending and circumflex arteries in close proximity to the root [4]. In the instance of transcatheter valve deployment, the prosthesis typically will crush the leaflets of the native valve against the aortic wall. Consequently, the combination of a relatively low-lying coronary artery ostium and a large, heavily calcified native aortic leaflet can lead to obstruction of the flow into the coronary arteries [31].

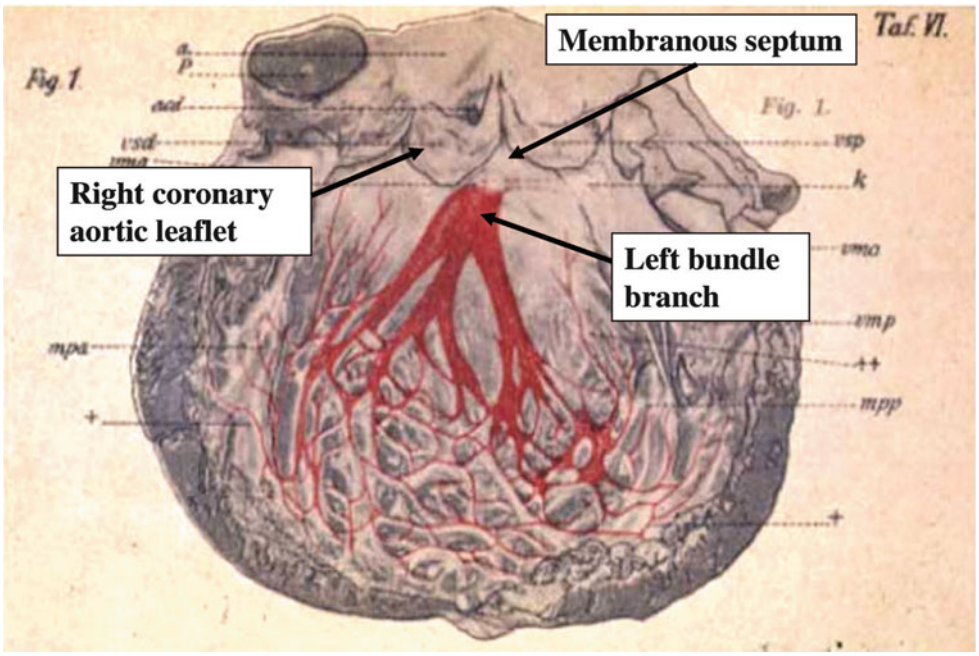

Fig. 7.24 Tawara's anatomical diagram of the left bundle branch showing the conduction system exiting from the base of the aortic valve between the nonadjacent and right coronary leaflets. It then branches out and descends along the septal endocardial surfaces of the left ventricular myocardium [9, 25]

7.11 Common Clinical Imaging of the Cardiac Valves

Due to its relatively high availability, ease of use, and minimal side effects to the patient, the standard 2D cross-sectional Doppler echocardiogram is considered as the most common imaging modality applied to assess the relative function and anatomical position of the cardiac valves [43, 73]. Clinically, both the mitral and tricuspid valves are commonly imaged via the parasternal long-axis view, allowing the echocardiographer to assess the following valve criteria [73]:

- Size and shape of the annulus
- Mobility of the leaflets, in particular, whether they prolapse or show flail or restricted motion (assessment will also include exclusion of thickening calcification, myxomatous degeneration, clefts, fusions along zones of apposition, perforations, vegetations, or abnormal shelves or membranes)
- Length and thickness of the tendinous cords and whether they are fused or ruptured
- Number, structure, and function of the papillary muscles
- Whether the function of the left ventricle is normal, is globally deranged, or shows evidence of regional abnormalities of motion of the walls

Examples of standard 2D cross-sectional Doppler echocardiograms of the mitral and tricuspid valve can be seen in Fig. 7.25.

The aortic valve can be readily viewed with echo from the apical, parasternal long-axis, and suprasternal views, whereas the pulmonary valve is usually imaged from the parasternal long-axis view (Fig. 7.26), allowing the echocardiographer to assess the following valve criteria [73]:

- Relative size and shape of the annulus.
- Number and mobility of the leaflets, in particular whether they show restricted motions. This assessment will also include exclusion of thickening calcification, fusions along zones of appositions, and/or leaflet damage.

For a comprehensive description of the echocardiographic techniques used to image and assess both healthy and diseased atrioventricular valves, the readers are referred to the *Textbook of Clinical Echocardiography* by Otto [74] and recommendations for clinical evaluation of stenosis by Baumgartner et al. [75] and regurgitation by Zoghbi et al. [76].

7.12 Summary

The atrioventricular and semilunar valves are highly complex anatomical structures. Their overall function and/or subsequent dysfunction can be due to abnormalities or failures within any of their respective subcomponents. Today, the detailed assessment of their anatomy and function, to determine optimal treatments approaches, provides critical information required by cardiologists, internationalists, and/or cardiac

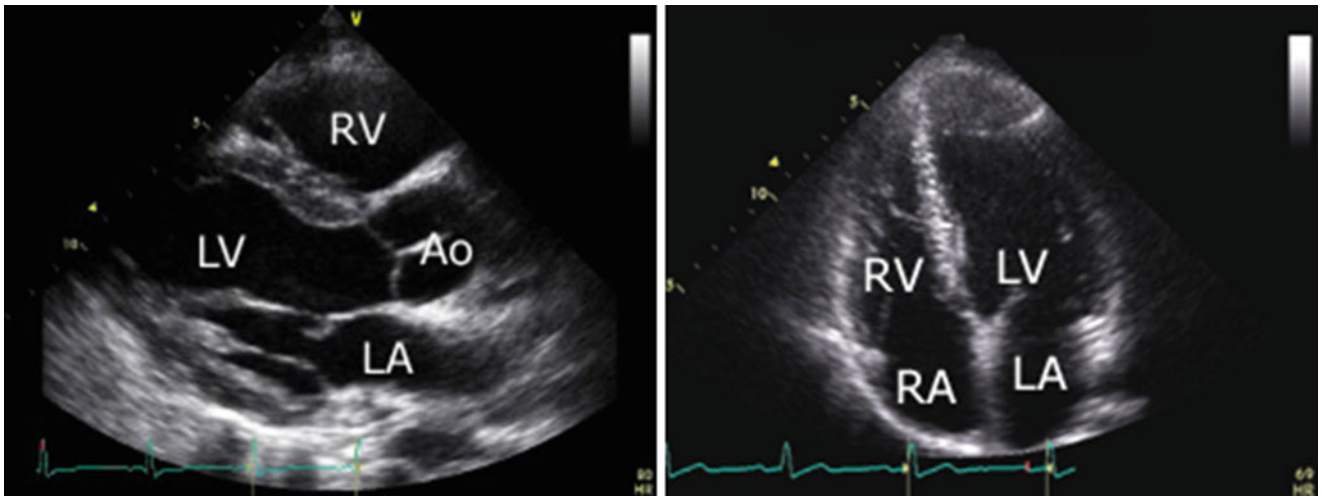

Fig. 7.25 Common echocardiographic parasternal long-axis and apical sections which show the leaflets of the mitral and tricuspid valves. The sub-valvar apparatus can clearly be seen tethering the leaflets to the ventricular free wall. *AO* aorta, *LA* left atrium, *LV* left ventricle, *RA* right atrium, *RV* right ventricle

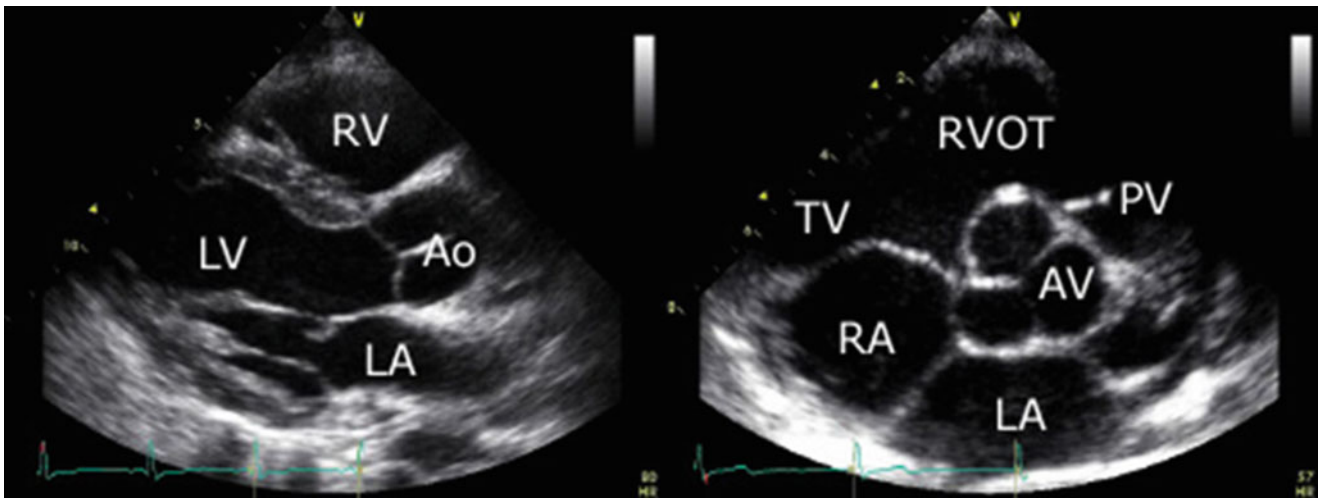

Fig. 7.26 Parasternal long-axis section through the aortic root (*left panel*) shows the closed aortic valve, while the short-axis section shows all three leaflets of the valve. *AO* aorta, *LA* left atrium, *LV* left ventricle, *RA* right atrium, *RV* right ventricle, *RVOT* right ventricular outflow tract, *PV* pulmonary valve, *TV* tricuspid valve

surgeons. Further, it is the detailed understanding of the valve features that will aid in the development and deployment of future clinical therapies, e.g., valvar repairs or replacement via either surgical or minimally invasive (transcatheter) means.

Although the anatomies of each valve type are similar, it should be noted that unique pathological changes can affect each valve resulting in differing approaches to disease assessment and treatment. Ultimately, a detailed understanding of the atrioventricular and semilunar valve anatomy will aid physicians and engineers alike in the development and deployment of future clinical therapies for the treatment of congenital and degenerative diseases affecting these valves. Furthermore, the use of common anatomical descriptions of these anatomical structures (defined as attitudinally correct anatomy) by anatomists, clinicians, and medical device designers is recommended for the successful and expedient communication of ideas and information in the modern world of medicine.

References

1. Wilcox BR, Cook AC, Anderson RH (2005) Surgical anatomy of the valves of the heart. In: Wilcox BR, Cook AC, Anderson RH (eds) Surgical anatomy of the heart. Cambridge University Press, Cambridge, pp 45–82
2. Bateman MG, Quill JL, Hill AJ et al (2013) The clinical anatomy and pathology of the human atrioventricular valves: implications for repair or replacement. J Cardiovasc Transl Res 6:155–165

3. Anderson RH, Becker AE, Allwork SP (1980) Cardiac anatomy: an integrated text and colour atlas. Gower Medical Publishing, Edinburgh/Churchill Livingstone, London
4. Bateman MG, Hill AJ, Quill JL, Iaizzo PA (2013) The clinical anatomy and pathology of the human arterial valves: implications for repair or replacement. J Cardiovasc Transl Res 6:166–175
5. Angelini A, Ho SY, Anderson RH et al (1988) A histological study of the atrioventricular junction in hearts with normal and prolapsed leaflets of the mitral valve. Br Heart J 59:712–716
6. Messer S, Moseley E, Marinescu M et al (2012) Histologic analysis of the right atrioventricular junction in the adult human heart. J Heart Valve Dis 21:368–373
7. Cook AC, Anderson RH (2002) Attitudinally correct nomenclature. Heart 87:503–506
8. Victor S, Nayak VM (1994) The tricuspid valve is bicuspid. J Heart Valve Dis 3:27–36
9. Yacoub M (1976) Anatomy of the mitral valve chordae and cusps. In: Kalmason D (ed) The mitral valve. A pluridisciplinary approach. Edward Arnold Publishers, London, pp 15–20
10. Kumar N, Kumar M, Duran CM (1995) A revised terminology for recording surgical findings of the mitral valve. J Heart Valve Dis 4:76–77
11. Ritchie J, Jimenez J, He Z et al (2006) The material properties of the native porcine mitral valve chordae tendineae: an in vitro investigation. J Biomech 39:1129–1135
12. Perloff JK, Roberts WC (1972) The mitral apparatus. Functional anatomy of mitral regurgitation. Circulation 46:227–239
13. Becker AE, de Wit APM (1979) Mitral valve apparatus. A spectrum of normality relevant to mitral prolapse. Br Heart J 42:680–689
14. Van der Bel-Kahn J, Duren DR, Becker AE (1985) Isolated mitral valve prolapse: chordal architecture as an anatomic basis in older patients. J Am Coll Cardiol 5:1335–1340
15. Gams E, Hagl S, Schad H et al (1992) Importance of the mitral apparatus for left ventricular function: an experimental approach. Eur J Cardiothorac Surg 6(Suppl 1):S17–23. Discussion S24
16. Gams E, Schad H, Heimisch W et al (1993) Importance of the left ventricular subvalvular apparatus for cardiac performance. J Heart Valve Dis 2:642–645
17. Hill AJ, Laske TG, Coles JA Jr et al (2005) In vitro studies of human hearts. Ann Thorac Surg 79:168–177
18. www.vhlab.umn.edu/atlas/index. Accessed November 20, 2014
19. Anderson RH, Devine WA, Ho SY et al (1991) The myth of the aortic annulus: the anatomy of the subaortic outflow tract. Ann Thorac Surg 52:640–646
20. Schultz CJ, Moelker A, Piazza N et al (2010) Three dimensional evaluation of the aortic annulus using multislice computer tomography: are manufacturer's guidelines for sizing percutaneous aortic valve replacement helpful? Eur Heart J 31:849–856
21. Sievers HH, Hemmer W, Beversdorf F et al (2012) The everyday used nomenclature of the aortic root components: the tower of Babel? Eur J Cardiothorac Surg 41:478–482
22. Misfeld M, Sievers HH (2007) Heart valve macro- and microstructure. Philos Trans R Soc Lond B Biol Sci 362:1421–1436
23. Marron K, Yacoub MH, Polak JM et al (1996) Innervation of human atrioventricular and arterial valves. Circulation 94:368–375
24. Filip DA, Radu A, Simionescu M (1986) Interstitial cells of the heart valves possess characteristics similar to smooth muscle cells. Circ Res 59:310–320
25. Icardo JM, Colvee E (1995) Atrioventricular valves of the mouse: III. Collagenous skeleton and myotendinous junction. Anat Rec 243:367–375
26. Icardo JM, Colvee E (1995) Atrioventricular valves of the mouse: II. Light and transmission electron microscopy. Anat Rec 241:391–400
27. Fenoglio JJ Jr, Tuan Duc P, Wit AL et al (1972) Canine mitral complex. Ultrastructure and electromechanical properties. Circ Res 31:417–430
28. Itoh A, Krishnamurthy G, Swanson JC et al (2009) Active stiffening of mitral valve leaflets in the beating heart. Am J Physiol Heart Circ Physiol 296:H1766–H1773
29. Laske TG, Shrivastav M, Iaizzo PA (2009) The cardiac conduction system. In: Iaizzo PA (ed) The handbook of cardiac anatomy, physiology, and devices, 2nd edn. Humana Press, Totowa, pp 15–21
30. Gross L, Kugel MA (1931) Topographic anatomy and histology of the valves in the human heart. Am J Pathol 7:445–473
31. Piazza N, de Jaegere P, Schulz C et al (2008) Anatomy of the aortic valvar complex and its implications for transcatheter implantation of the aortic valve. Circ Cardiovasc Interv 1:74–81
32. Carpentier A, Branchini B, Cour JC et al (1976) Congenital malformations of the mitral valve in children. Pathology and surgical treatment. J Thorac Cardiovasc Surg 72:854–866
33. Anderson RH, Razavi R, Taylor AM (2004) Cardiac anatomy revisited. J Anat 205:159–177
34. Quill JL, Hill AJ, Laske TG et al (2009) Mitral leaflet anatomy revisited. J Thorac Cardiovasc Surg 137:1077–1081
35. Barker TA, Wilson IC (2011) Surgical anatomy of the mitral and tricuspid valve. In: Bonser RS, Pagano D, Haverich A (eds) Mitral valve surgery. Springer-Verlag, London, pp 3–19
36. Delgado V, Tops LF, Schuijf JD et al (2009) Assessment of mitral valve anatomy and geometry with multislice computed tomography. JACC Cardiovasc Imaging 2:556–565
37. Kwan J, Kim G, Jeon M et al (2007) 3D geometry of a normal tricuspid annulus during systole: a comparison study with the mitral annulus using real-time 3D echocardiography. Eur J Echocardiogr 8:375–383
38. Veronesi F, Corsi C, Sugeng L et al (2009) A study of functional anatomy of aortic-mitral valve coupling using 3D matrix transesophageal echocardiography. Circ Cardiovasc Imaging 2:24–31
39. Berdajs D, Lajos P, Turina MI (2005) A new classification of the mitral papillary muscle. Med Sci Monit 11:BR18–BR21
40. Bateman MG, Russel C, Chan B et al (2010) A detailed anatomical study of the papillary muscles and chordae tendineae of the left ventricle in perfusion fixed human hearts. FASEB J. 24(Meeting Abstract Supplement):446.4
41. Sonne C, Sugeng L, Watanabe N et al (2009) Age and body surface area dependency of mitral valve and papillary apparatus parameters: assessment by real-time three-dimensional echocardiography. Eur J Echocardiogr 10:287–294
42. Lam JH, Ranganathan N, Wigle ED et al (1970) Morphology of the human mitral valve. I. Chordae tendineae: a new classification. Circulation 41:449–458
43. Kunzelman KS, Cochran RP, Verrier ED et al (1994) Anatomic basis for mitral valve modelling. J Heart Valve Dis 3:491–496
44. Ritchie J, Warnock JN, Yoganathan AP (2005) Structural characterization of the chordae tendineae in native porcine mitral valves. Ann Thorac Surg 80:189–197
45. Martinez RM, O'Leary PW, Anderson RH (2006) Anatomy and echocardiography of the normal and abnormal tricuspid valve. Cardiol Young 16(Suppl 3):4–11
46. Weinhaus AJ, Roberts KP (2009) Anatomy of the human heart. In: Iaizzo PA (ed) The handbook of cardiac anatomy, physiology, and devices, 2nd edn. Humana Press, Totowa, pp 59–85
47. Tsakiris AG, Mair DD, Seki S et al (1975) Motion of the tricuspid valve annulus in anesthetized intact dogs. Circ Res 36:43–48
48. Westaby S, Karp RB, Blackstone EH et al (1984) Adult human valve dimensions and their surgical significance. Am J Cardiol 53:552–556
49. Silver MD, Lam JH, Ranganathan N et al (1971) Morphology of the human tricuspid valve. Circulation 43:333–348
50. Seccombe JF, Cahill DR, Edwards WD (1993) Quantitative morphology of the normal human tricuspid valve: autopsy study of 24 cases. Clin Anat 6:203–212
51. Wenink AC (1977) The medial papillary complex. Br Heart J 39:1012–1018

52. Hill AJ (2009) Attitudinally correct cardiac anatomy. In: Iaizzo PA (ed) The handbook of cardiac anatomy, physiology, and devices, 2nd edn. Humana Press, Totowa, pp 15–21
53. Kunzelman KS, Grande KJ, David TE et al (1994) Aortic root and valve relationships: impact on surgical repair. J Thorac Cardiovasc Surg 107:162–170
54. Reid K (1970) The anatomy of the sinus of Valsalva. Thorax 25:79–85
55. Swanson M, Clark RE (1974) Dimensions and geometric relationships of the human aortic valve as a function of pressure. Circ Res 35:871–882
56. Brewer RJ, Deck JD, Capati B et al (1976) The dynamic aortic root: its role in aortic valve function. J Thorac Cardiovasc Surg 72:413–417
57. Thubrikar MPW, Shaner TW, Nolan SP (1981) The design of the normal aortic valve. Am J Physiol 10:H795–H801
58. Hamdan A, Guetta V, Konen E et al (2012) Deformation dynamics and mechanical properties of the aortic annulus by 4-dimensional computed tomography: insights into the functional anatomy of the aortic valve complex and implications for transcatheter aortic valve therapy. J Am Coll Cardiol 59:119–127
59. Middelhof CJFM, Becker AE (1981) Ventricular septal geometry: a spectrum with clinical relevance. In: Wenink ACG et al (eds) The ventricular septum of the heart. Martinus Nijhoff Publishers, The Hague
60. Turner K, Navartnam V (1996) The positions of coronary arterial ostia. Clin Anat 9:376–380
61. Muriago M, Sheppard MN, Ho SY et al (1997) Location of the coronary arterial orifices in the normal heart. Clin Anat 10:297–302
62. Cavalcanti JS, de Melo MN, de Vasconcelos RS (2003) Morphometric and topographic study of coronary ostia. Arq Bras Cardiol 81:359–362
63. Jo Y, Uranaka Y, Iwaki H et al (2011) Sudden cardiac arrest: associated with anomalous origin of the right coronary artery from the left main coronary artery. Tex Heart Inst J 38:539–543
64. Roynard JL, Cattan S, Artigou JY et al (1994) Anomalous course of the left anterior descending coronary artery between the aorta and pulmonary trunk: a rare cause of myocardial ischaemia at rest. Br Heart J 72:397–399
65. Sutton JP, Ho SY, Anderson RH (1995) The forgotten interleaflet triangles: a review of the surgical anatomy of the aortic valve. Ann Thorac Surg 59:419–427
66. Vollebergh FE, Becker AE (1977) Minor congenital variations of cusp size in tricuspid aortic valves: possible link with isolated aortic stenosis. Br Heart J 39:1006–1011
67. Capps SB, Elkins RC, Fronk DM (2000) Body surface area as a predictor of aortic and pulmonary valve diameter. J Thorac Cardiovasc Surg 119:975–982
68. Tops LF, Wood DA, Delgado V et al (2008) Noninvasive evaluation of the aortic root with multi-slice computed tomography: implications for transcatheter aortic valve replacement. J Am Coll Cardiol Img 1:321–330
69. Van Miegham NM, Piazza N, Anderson RH et al (2010) Anatomy of the mitral valvular complex and its implications for transcatheter interventions for mitral regurgitation. J Am Coll Cardiol 56:617–626
70. Choure AJ, Garcia MJ, Hesse B et al (2006) In vivo analysis of the anatomical relationship of coronary sinus to mitral annulus and left circumflex coronary artery using cardiac multidetector computed tomography: implications for percutaneous coronary sinus mitral annuloplasty. J Am Coll Cardiol 48:1938–1945
71. Tops LF, Van de Veire NR, Schuijf JD et al (2007) Noninvasive evaluation of coronary sinus anatomy and its relation to the mitral valve annulus: implications for percutaneous mitral annuloplasty. Circulation 115:1426–1432
72. Tawara S (1906) Das reizleitungssystem de saugetierherzens: eine anatomichhisologische studie uber das atrioventricularbundel und die Purkinjeschen faden. Verlag von Gustav Fischer, Jena
73. Asante-Korang A, O'Leary PW, Anderson RH (2006) Anatomy and echocardiography of the normal and abnormal mitral valve. Cardiol Young 16(Suppl 3):27–34
74. Otto CM (2009) Textbook of clinical echocardiography: expert consult, 4th edn. Saunders, Philadelphia
75. Baumgartner H, Hung J, Bermejo J et al (2009) Echocardiographic assessment of valve stenosis: EAE/ASE recommendations for clinical practice. J Am Soc Echocardiogr 22:1–23
76. Zoghbi WA, Enriquez-Sarano M, Foster E et al (2003) Recommendations for evaluation of the severity of native valvar regurgitation with two-dimensional and Doppler echocardiography. J Am Soc Echocardiogr 16:777–802

The Coronary Vascular System and Associated Medical Devices

8

Julianne H. Spencer, Sara E. Anderson, Ryan Lahm, and Paul A. Iaizzo

Abstract

Even as recent as several hundred years ago, the general function of the coronary vascular system was largely unknown. Today, it is well established that the coronary system is a highly variable network of both arteries supplying and veins draining the myocardium of oxygenated and deoxygenated blood, respectively. Due to recent advances in therapeutic technologies, the coronary vascular system has been utilized as a conduit in a variety of biomedical applications, e.g., cardiac resynchronization therapy. Additionally, symptomatic diseases such as coronary artery disease can be alleviated with stenting or coronary artery bypass grafts. It is well accepted that a comprehensive understanding of the geometric anatomical characteristics of the coronary system will allow for future medical devices to be engineered to more successfully deliver novel therapies to a greater variety of cardiac patients.

Keywords

Coronary arteries • Coronary veins • Venous valves • Stents • Transvenous pacing leads

Electronic supplementary material: The online version of this chapter (doi:10.1007/978-3-319-19464-6_8) contains supplementary material, which is available to authorized users. Videos can also be accessed at http://link.springer.com/book/10.1007/978-3-319-19464-6_8.

J.H. Spencer, PhD (✉)
Department of Biomedical Engineering, University of Minnesota, Minneapolis, MN 55455, USA

Department of Surgery, University of Minnesota, B172 Mayo, MMC 195, 420 Delaware Street SE, Minneapolis, MN 55455, USA

Medtronic, Inc., 8200 Coral Sea Street NE, Mounds View, MN 55112, USA
e-mail: eggu0008@umn.edu; julianne.spencer@medtronic.com

S.E. Anderson, PhD • P.A. Iaizzo, PhD
Department of Biomedical Engineering, University of Minnesota, Minneapolis, MN 55455, USA

Department of Surgery, University of Minnesota, B172 Mayo, MMC 195, 420 Delaware Street SE, Minneapolis, MN 55455, USA

R. Lahm, MS
Medtronic, Inc., 8200 Coral Sea Street NE, Mounds View, MN 55112, USA

8.1 Introduction

While anatomical studies of the heart began centuries ago, Herophilus (c. 335–c. 280 BC) was the first to observe and record differences between coronary arteries and veins, including the discovery that arteries were much thicker than veins; veins, in contrast to arteries, collapsed when emptied of blood [1]. More than a thousand years later, in 1628 AD, William Harvey, court physician to King James I and King Charles I, published "On the motion of the heart and blood in animals," the first accurate description of the circulatory system [2]. Subsequently, in 1689, Scaramucci conjectured that the contraction of the heart displaced blood from deeper coronary vessels into coronary veins [3]. However, the exact details of coronary blood flows were not well understood until the technology capable of measuring arterial and venous flows was more recently developed [3].

Today, it is known that the coronary system is comprised of arteries, arterioles, capillaries, and cardiac venules and veins. The coronary arteries originate with right and left

P.A. Iaizzo (ed.), *Handbook of Cardiac Anatomy, Physiology, and Devices*, DOI 10.1007/978-3-319-19464-6_8

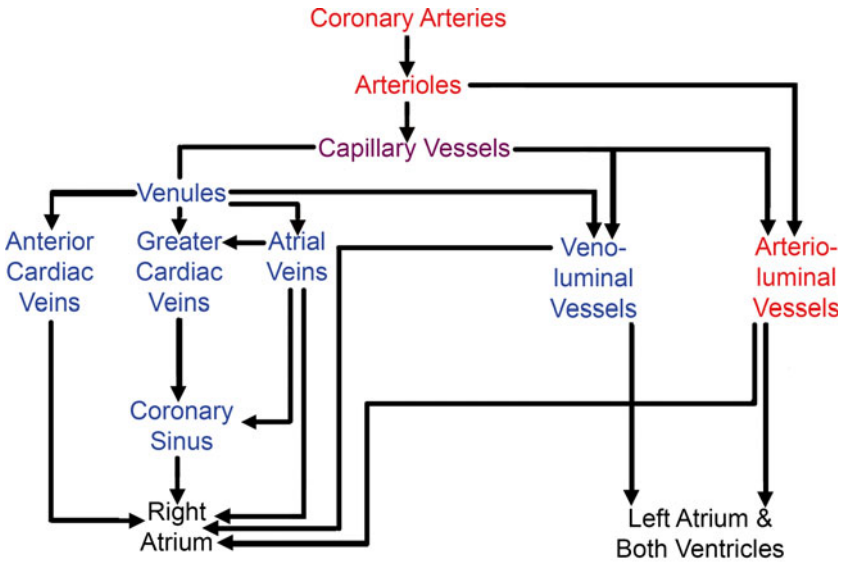

Fig. 8.1 The supply and drainage configuration of the coronary arterial and venous systems [28]. Reproduced with permission of Springer in the format Educational/ Instructional Program via Copyright Clearance Center

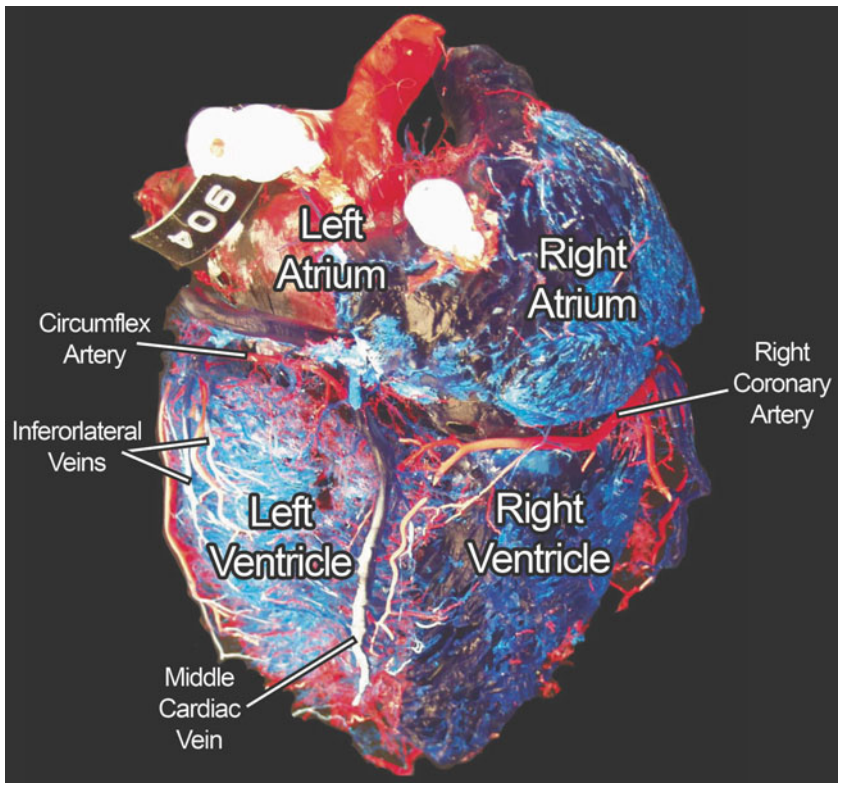

Fig. 8.2 *Red* and *blue* plastics were injected into the arterial and venous systems of this heart, respectively. The rest of the myocardial tissue was "corroded" away with digestive enzymes, thus only the extensive coronary system remains. The heart is viewed from the diaphragmatic surface. Figure courtesy of Alexander Hill (Medtronic, Inc.)

main coronary arteries which exit the ascending aorta just above the aortic valve. These two branches subdivide and course over the surface of the heart (epicardium) as they traverse away from the aorta. These arteries arborize into progressively smaller branches that progress inward to penetrate the epicardium and supply blood to the transmural myocardium. These coronary arteries branch into arterioles, which then branch into innumerable capillaries that ultimately deliver oxygenated blood to all of the heart's cells. Blood continues through these capillary beds to begin the return back into the cardiac chambers via various drainage routes illustrated in Fig. 8.1. The majority of capillaries drain into venules, which then empty into the coronary venous system. The coronary veins can be categorized into two subgroups: the greater and smaller cardiac venous system. A corrosion cast of a human heart reveals the complexity and extensiveness of the coronary vascular system in Fig. 8.2.

Coronary blood flow is critical in supporting cardiac function. If disease states or acute events occur that obstruct coronary flow, consequences are commonly detrimental and sometimes fatal. For example, changes in electrocardiograms can be recorded within beats when there is inadequate blood flow delivered to a given region of the heart. Whenever coronary blood flow falls below what is required to meet metabolic needs, the myocardium is considered ischemic; the pumping capability of the heart is impaired, and there are associated changes in electrical activity (e.g., increased risk of fibrillation). Prolonged ischemia can lead to myocardial infarction, commonly called a *heart attack*, which can cause irreversible myocardial cell death. Coronary artery disease, which is associated with obstruction of arterial blood flow, is the most common type of heart disease and currently the leading cause of death in the USA in both males and females [4]. For more details on cardiac oxygen and nutrient delivery and its association with ischemia, refer to Chap. 21.

8.2 Coronary Arteries

8.2.1 Coronary Arteries: Anatomical Description

Oxygenated blood is pumped into the aorta from the left ventricle. Located just above the aortic valve are the ostia of the left and right coronary arteries, which are situated in the left and right sinuses of Valsalva, respectively. In general, coronary arteries traverse the surface of the heart and are encased in varying amounts of epicardial fat. However, some branch arteries course directly into the myocardium [4]. Figure 8.3 shows the anatomy and nomenclature of the coronary artery system. Note that there is a high degree of variability in the human heart. (See Coronary Tutorial on the Atlas of Human Cardiac Anatomy; www.vhlab.umn.edu/atlas.)

Traditionally, some of the coronary arterial names were based on the heart oriented in the valentine position. This chapter refers to nomenclatures based on the heart's orientation in the chest cavity. See Chap. 2 for details on the clinical importance of using attitudinally correct descriptions.

8.2.2 The *Left Coronary Artery* and Its Branches

The *left coronary artery* and its branches supply the majority of oxygenated blood to the ventricular myocardium and additionally to the left atrium, left atrial appendage, pulmonary artery, and aortic root [5, 6]. The *left coronary artery main*, also called the *left main* for short, typically originates at the left sinus of Valsalva and courses in the left anterior direction. After approximately 1–2 cm, the left main bifurcates into the *left anterior descending artery* and the *circumflex artery*, at a location between the left atrial appendage and the pulmonary trunk [7]. Some individuals possess a third artery that

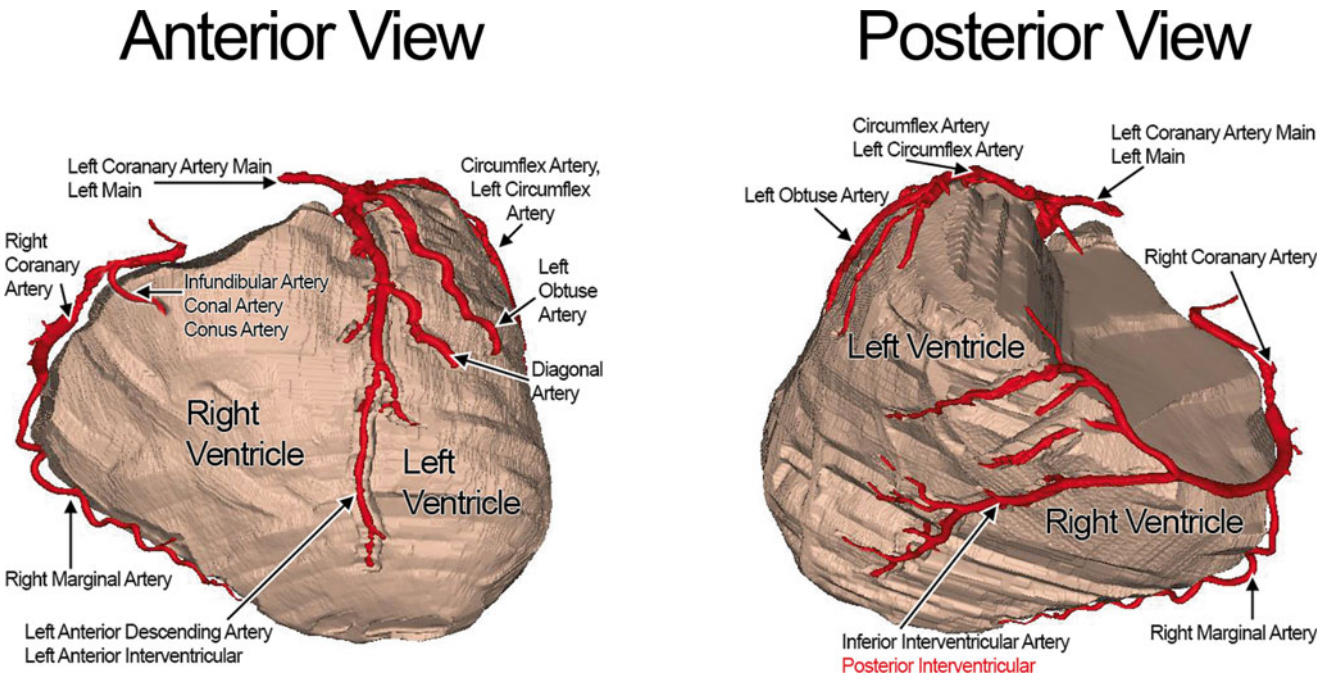

Fig. 8.3 Anterior (*left*) and posterior (*right*) views of the 3D reconstructed coronary arteries and ventricular tissue of a perfusion-fixed human heart generated from a contrast-CT scan. The atria have been removed for better visualization of the coronary arteries. Some of the arteries have varying nomenclatures present in the literature. The names highlighted in *red* are common in the literature, but are considered to be attitudinally incorrect

branches off the left main called the *intermediate artery*. This vessel usually supplies the left margin of the heart [7, 8].

8.2.2.1 Left Anterior Descending Artery and Its Branches

The left anterior descending artery, also known as the anterior interventricular artery, originates at the end of the left main at an angle close to 180°. The vessel curves around the pulmonary artery trunk and continues anteriorly down the interventricular septum to the apex of the heart. The left anterior descending artery typically branches into the diagonal arteries, deep septal perforators, and the left descending septal artery. Although there is a high amount of variation in the course of the diagonal arteries, they typically branch off at an angle and supply the free wall of the left ventricle. The deep septal perforators commonly branch at 90° angles into the interventricular septum. These arteries characteristically supply the anterior two-thirds of the septum, and can also have high degrees of variation. Finally, the left descending septal artery is an important vessel that supplies blood to the moderator band and anterior papillary muscle [7].

8.2.2.2 Circumflex Artery and Its Branches

The circumflex artery, also referred to as the *left circumflex artery*, stems from the left main and courses along the left atrioventricular groove. The circumflex artery gives rise to small arterial branches that supply the aortic root and myocardium near the atrioventricular groove. In patients who are right dominant, the circumflex artery terminates into the left obtuse artery. The left obtuse artery courses down the left margin of the heart towards the apex. In patients who are left dominant (approximately one-tenth of individuals), the circumflex continues along the atrioventricular groove until it terminates at the cardiac crux, where it branches into the artery that supplies the atrioventricular node [9, 10] and the inferior interventricular artery, traditionally known as the *posterior interventricular artery* [7].

8.2.3 The Right Coronary Artery and Its Branches

The *right coronary artery* originates in the right sinus of Valsalva and courses along the atrioventricular groove along the epicardial surface adjacent to the tricuspid valve annulus. The infundibular artery, also known as the conal artery, conus artery, and third coronary artery, can also originate directly from the right sinus of Valsalva or as a branch of the right coronary artery. In three-fifths of the population, the next branch of the right coronary artery is the artery to the sinus node [7, 8]. This artery branches off the circumflex artery in the remaining two-fifths of the population [7, 8]. The right marginal artery is typically the largest branch of the right coronary artery. This major artery supplies the free wall of the right ventricle [7, 10]. In most individuals, the right coronary artery becomes the inferior interventricular artery when it reaches the diaphragmatic surface of the heart. Note that the right coronary artery does not typically taper in diameter until it gives rise to the inferior interventricular artery [4]. The inferior interventricular artery runs toward the apex of the left ventricle and supplies the diaphragmatic surface of the heart.

8.2.4 Abnormal Coronary Artery Anatomy

Many anomalies of the coronary artery system are associated with the origin of the major arteries. The most common ostium abnormality happens when the left and/or right coronary artery originates at an opposite sinus, which has been found in 0.03–0.1 % of patients [7, 11]. There have also been reports of the presence of a single coronary artery that supplies the entire heart [7, 12, 13]. There is evidence that both of these abnormalities may increase the risk of sudden death [7, 12–14]. The right coronary artery has also been reported to originate outside of the sinuses of Valsalva including branching from the brachiocephalic artery, the aorta, or the pulmonary trunk [7]. The risk of these anomalies is dependent on the subsequent course of the artery. For example, an artery that courses between the aortic and pulmonary roots has a higher chance of compression [7, 15, 16]. A left coronary artery originating at the pulmonary trunk, also known as Bland-White-Garland Syndrome, is a more rare (1 in 300,000) and more dangerous anomaly [7, 17] that can cause decreased blood flow and typically requires surgical treatment [7, 18, 19]. Figure 8.4 summarizes examples of coronary ostia abnormalities.

Another known anatomical abnormality relative to this vasculature is the presence of coronary arterial fistulas. These are defined as a direct connection between a coronary artery and a cardiac chamber, superior vena cava, coronary sinus, pulmonary artery, or pulmonary vein [7, 19, 20]. The most common fistula sites are located in the right ventricle [7, 21]. It has been reported that these fistulas are benign for approximately half of the patients; the remaining half of patients have reported endocarditis, myocardial ischemia, ruptured aneurysm, and/or heart failure associated with their anomaly [7, 22].

There have also been reports of duplication of the major arteries. The anterior descending artery is the most commonly duplicated artery with an occurrence rate of approximately 1 % [7, 23]. Most coronary artery duplications do not cause clinical complications; however, it is important to be aware of such duplications during surgical interventions.

8.2.5 Coronary Arteries: Disease

Coronary arterial functional anatomy changes throughout a person's lifespan; in the elderly, coronary arteries typically become more tortuous, their inner diameters expand, and

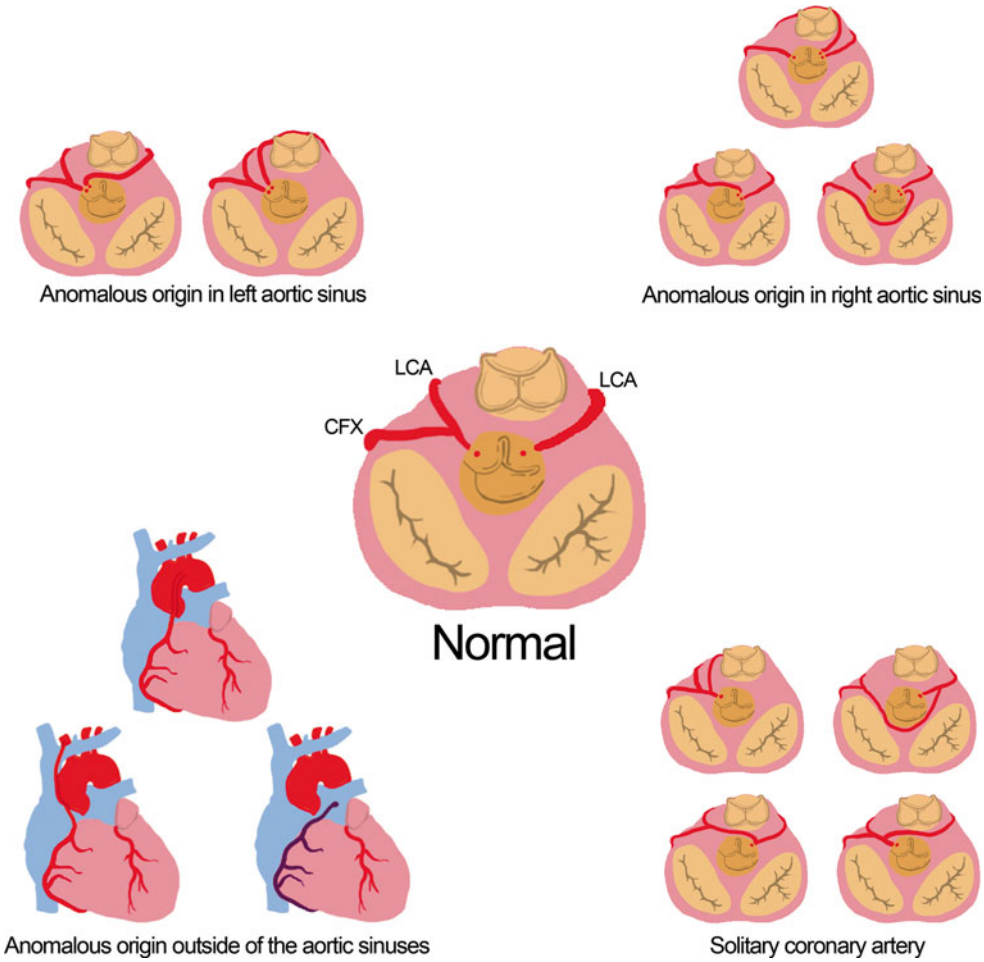

Fig. 8.4 Examples of abnormal coronary arterial origins. The anomalous origins outside the aortic sinuses include the brachiocephalic artery, the ascending aorta, and the pulmonary trunk. *LCA* left coronary artery, *RCA* right coronary artery, *CFX* circumflex artery

more calcific deposits can be observed [24]. While these changes are common with aging, certain disease states can significantly increase flow restrictions to the point of causing detrimental damage, myocardial ischemia, and/or death. More specifically, coronary artery disease is generally defined as the gradual narrowing of the lumen of the coronary arteries due to atherosclerosis. An example of an artery with calcifications is shown in Fig. 8.5. Atherosclerosis is a condition that involves thickening of the arterial walls via cholesterol and fat deposits that build up along the endoluminal surface of the arteries. With severe disease, these plaques may become calcified, increase in size, and eventually cause significant stenosis; a stenotic vessel has an increased vascular resistance relative to that of healthy vessels. A steady decrease in arterial cross-sectional area can eventually lead to complete blockage of the artery. As a result, oxygen and nutrient supply to the myocardium decreases below the level of demand, i.e., during exercise and during rest (when more extreme). As the disease progresses, the myocardium downstream from the occluded artery becomes ischemic. Eventually, myocardial infarction may occur if the coronary artery disease is not detected and treated in a timely manner. See Chap. 21 for additional descriptions of cardiac ischemia.

Myocardial ischemia not only impairs the electrical and mechanical function of the heart, but also commonly results in intense, debilitating chest pain known as *angina pectoris*. However, anginal pain can often be absent in individuals with coronary artery disease (or in individuals with early disease stages) at rest, but induced during physical exertion or with emotional excitement. Such situations are associated with an increase in sympathetic tone that increases myocardial oxygen consumption (and subsequently ischemia) when blood flow cannot keep up with myocardial metabolic needs. To date, typical treatment for angina resulting from coronary artery disease includes initial pharmacological approaches, such as the administration of: (1) coronary vasodilator drugs (e.g., nitroglycerin); (2) nitrates to reduce myocardial demand by dilating systemic veins, thus reducing preloads; or (3) β-blockers (e.g., propranolol).

8.3 Cardiac Capillaries

Capillaries are the smallest blood vessels in the human body and branch numerous times to ensure that every myocyte lies within a short distance (microns) of at least one of these

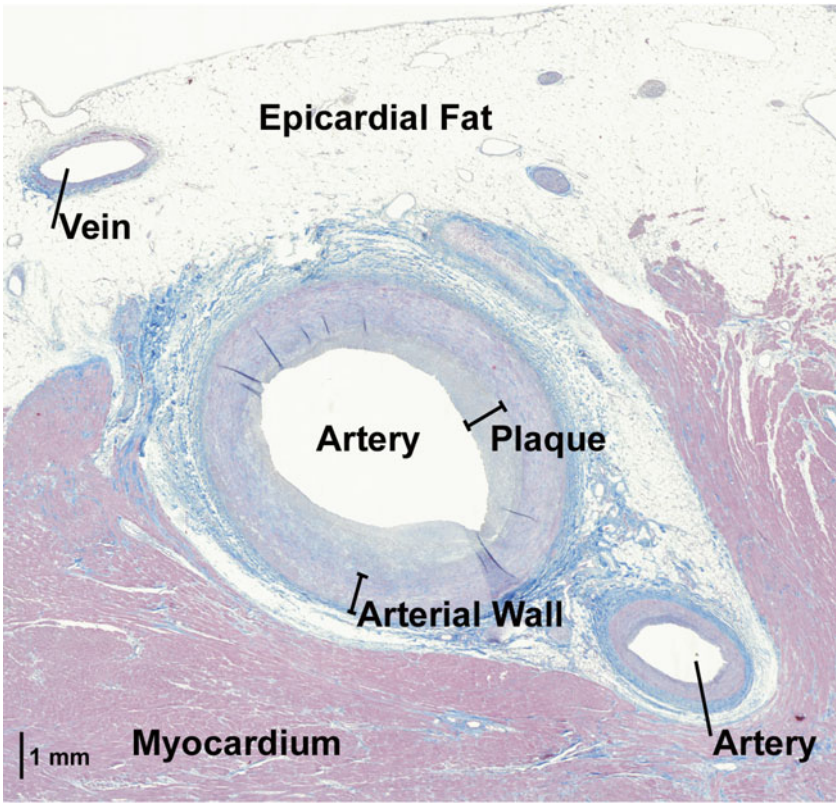

Fig. 8.5 This histologic view of an anterior arterial branch shows a layer of plaque that makes the interior lumen of the artery irregular. Additionally, this figure shows that this particular arterial branch was not completely encased by epicardial fat, but was partially surrounded by myocardium

branches. Via diffusion, nutrients and metabolic end products move between the capillary vessels and the surroundings of the myocytes through the interstitial fluid. Subsequent movement of these molecules into a cell is accomplished by both diffusion and mediated transport. Nevertheless, as with all organs, blood flow through the capillaries within the heart can be considered passive and occurs because coronary arterial pressure is higher than venous pressure. Although capillaries are a very important part of the coronary system, their current use for device therapies is relatively nonexistent due to their small diameters (i.e., size of a red blood cell).

8.4 Coronary Veins

Coronary venous flow occurs during diastole and systole, and the coronary venous system drains the myocardium of oxygen-depleted blood.

8.4.1 Coronary Veins: Anatomical Description

The relative size of the coronary venous system dominates the arterial system; there are at least twice as many veins as arteries in human myocardial tissue [25, 26]. In general, veins are considered to be *low-resistance conduits* to the heart and can alter their capacity to maintain venous pressure [27]. As previously mentioned, the coronary veins are considered to be primarily organized into two subgroups—the greater and smaller cardiac venous system. The greater cardiac venous system is comprised of the coronary sinus and its tributaries, as well as the anterior cardiac veins, atrial veins, and the veins of the ventricular septum [28, 29]. The smaller cardiac venous system, also known as the Thebesian vessels, is comprised of the arterioluminal vessels and venoluminal vessels [28–30].

8.4.1.1 The Greater Cardiac Venous System

The greater cardiac venous system, also referred to as the *major cardiac venous system*, delivers the majority of deoxygenated blood from the outer layers of the myocardium to the chambers of the heart. These veins are responsible for approximately three-quarters of the myocardial drainage [31]. Similar to some of the major coronary arteries, there are several nomenclatures present in the literature for many of the major veins in the greater cardiac venous system. This chapter refers to the attitudinally correct venous names, although some of these names are currently less common in the literature and in practice. (See Coronary Tutorial on the Atlas of Human Cardiac Anatomy; www.vhlab.umn.edu/atlas.)

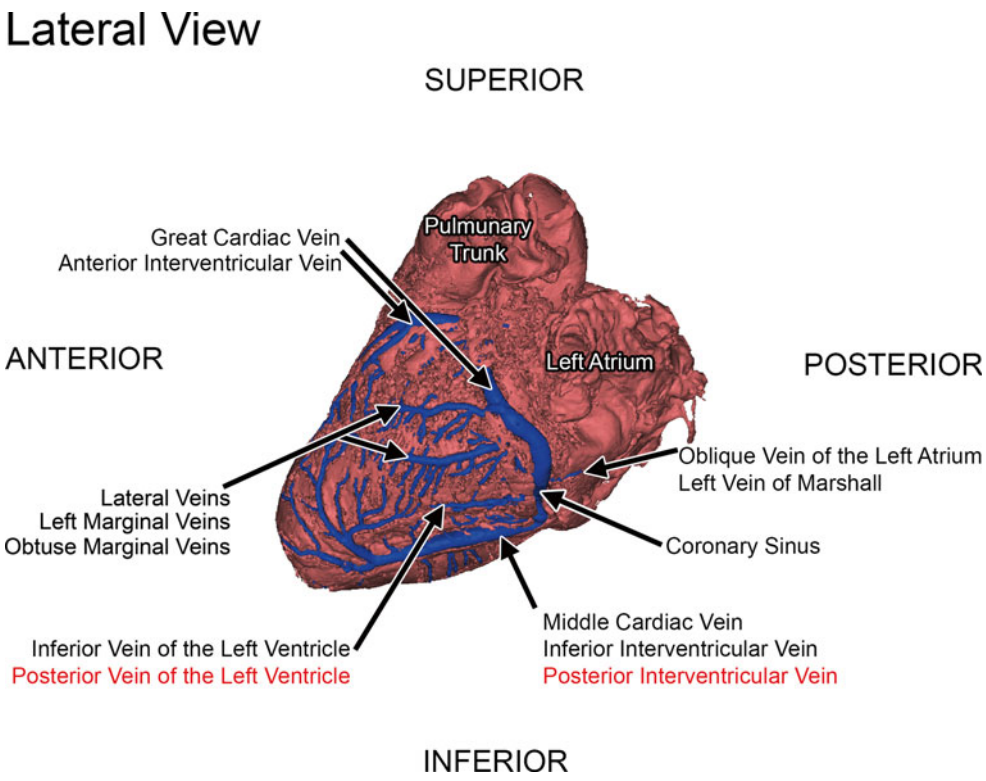

Fig. 8.6 3D reconstruction of the coronary veins and cardiac tissue from a contrast-CT of a perfusion-fixed human heart [28]. This is a left lateral view of the coronary sinus and its major tributaries. Some of these veins have varying nomenclatures present in the literature. The names highlighted in *red* are common in the literature, but are considered to be attitudinally incorrect. Reproduced with permission of Springer in the format Educational/ Instructional Program via Copyright Clearance Center

Coronary Sinus

The coronary sinus serves as the primary collector of cardiac venous blood [32–34], and is located in the atrioventricular groove on the diaphragmatic surface of the heart [6, 30, 31, 35–38]. Movie 8.1, found in the online supplemental material, shows a representative coronary sinus. The coronary sinus is the largest cardiac vein in terms of diameter. Many major cardiac veins, including the great cardiac vein, the inferior veins of the left ventricle, the oblique vein of the left atrium, the middle cardiac vein, and the small cardiac vein, generally feed into the coronary sinus [6, 28, 30–32, 35, 37, 39–42]. Figure 8.6 summarizes the anatomy and commonly used nomenclatures of the major coronary sinus tributaries. Various landmarks have been described as the location of the coronary sinus origin, including where the oblique vein of the left atrium meets the great cardiac vein and at the valve of Vieussens [28, 31, 32]. The coronary sinus empties directly into the right atrium near the juncture of the interventricular and coronary grooves (also known as the crux cordis area) [31, 39, 43], located on the inferior region of the right atrial septum between the inferior vena cava and tricuspid valve [6, 32, 35, 40, 44]. The atrial orifice can be partially covered by a Thebesian valve as demonstrated in Fig. 8.7, although the anatomy of this valve is highly variable [30–32, 34–36, 38, 39, 42–48].

Anterior Interventricular Vein and Great Cardiac Vein

The anterior interventricular vein courses between the left and right ventricle on the anterior side of the heart. It typically begins around the apex and ends as it reaches the atrioventricular groove. The great cardiac vein, the longest venous vessel of the heart, consists of the anterior interventricular vein and its continuation along the atrioventricular groove [28, 31, 46, 49, 50]. The great cardiac vein is commonly joined by numerous venous contributors from the interventricular septum, anterior aspects of both ventricles, and the apical region [6, 30–32, 37, 49, 51]. As the great cardiac vein courses around the inferior atrioventricular sulcus, it is also joined by venous drainage from the left atrium, including the oblique vein of the left atrium [30]. The lateral veins and left inferior veins from the left ventricle also flow into the great cardiac vein [30, 43]. As the great cardiac vein follows the left atrioventricular groove around the left side of the heart, the great cardiac vein is considered to be in close proximity to the anterolateral commissure of the mitral valve [38]. The great cardiac vein commonly continues until it merges with the coronary sinus described earlier [31, 43, 46, 50]. The great cardiac vein typically enters the coronary sinus at an approximate angle of 180° [49, 52].

Lateral Veins

The lateral veins, also known as the left marginal veins or the obtuse marginal veins, typically course along the left side of the heart and drain the left ventricular myocardium into the great cardiac vein or coronary sinus [31, 49]. They are commonly located in an inferior position at an obtuse angle of the heart [53] and parallel the course of the left marginal branch of the *left coronary artery* [49].

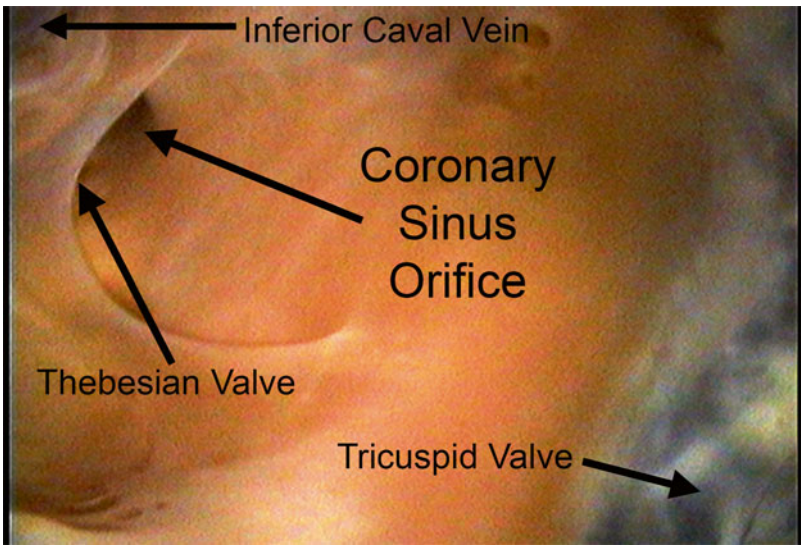

Fig. 8.7 Internal view of the coronary sinus orifice with a Thebesian valve and surrounding right atrial wall from within an isolated functioning human heart [28]. Reproduced with permission of Springer in the format Educational/ Instructional Program via Copyright Clearance Center

Inferior Veins

The inferior veins of the left ventricle, previously known as the posterior veins of the left ventricle, typically originate from the lateral and inferior aspects of the left ventricle and course between the great cardiac vein and middle cardiac vein [31, 41, 51, 52]. The vessels generally drain into the coronary sinus. Similar to the lateral veins, the anatomy of the inferior veins is also highly variable [28].

Middle Cardiac Vein

The middle cardiac vein, also referred to as the posterior interventricular vein or more correctly, the inferior interventricular vein, is a major coronary vein that typically originates near the apex and usually ascends in or very near to the posterior interventricular sulcus [6, 28, 30, 31, 41, 45, 51, 52, 54]. The middle cardiac vein drains into the coronary sinus or directly into the right atrium [28]. The middle cardiac vein is also one of the most consistently present coronary veins [28].

Small Cardiac Vein

The small cardiac vein, also known as the right cardiac vein [6], commonly drains the inferior and lateral wall of the right ventricle. A small vein in comparison to the previously mentioned veins, the small cardiac vein originates in the inferior part of the right coronary sulcus and courses the base of the right ventricle, paralleling the right coronary artery [31]. This vein typically empties into the coronary sinus, but sometimes drains into the middle cardiac vein or directly into the right atrium. The small cardiac vein is not always present in the human cardiac venous system [31, 55].

Oblique Vein of the Left Atrium

The oblique vein of the left atrium, also referred to as Marshall's vein since it was first reported by John Marshall, delivers deoxygenated blood from the lateral and inferior regions of the left atrium to the atrioventricular groove [28]. As mentioned earlier, the termination of this vein is an anatomical landmark for the origin of the coronary sinus and the end of the great cardiac vein.

Right Marginal Vein

The right marginal vein, also known as the vein of Galen, typically originates at or is superior to the cardiac apex and then courses along the free wall of the right ventricle towards the right atrium. The right marginal vein has highly variable anatomy [29]. The vessel has been cited to drain into the small cardiac vein, the middle cardiac vein, or the right atrium directly [28, 31, 56, 57].

Anterior Cardiac Veins

The anterior cardiac veins, also known as the minor cardiac veins, the accessory cardiac veins, and the unnamed veins of Vieussens [29, 56], return deoxygenated blood from the right ventricle directly to the right atrium. These vessels typically course along the right margin of the heart [31]. There are usually one to three major anterior cardiac veins present on the human heart [29, 56].

Atrial Veins

The atrial veins deliver deoxygenated blood from the atrial tissues back to the cavities of the atrial chambers. The left atrial veins consist of three categories based on the region of the atrium that they drain—the posterolateral veins, the posterosuperior veins, and the septal veins [29, 31]. The posterolateral veins, which include the oblique vein of the left atrium, course along the left atrial posteroinferior and lateral walls and then drain into the coronary sinus. The posterosuperior veins of the left atrium are present in approximately three-fourths of individuals. These vessels drain the posterosuperior region between the pulmonary veins and empty

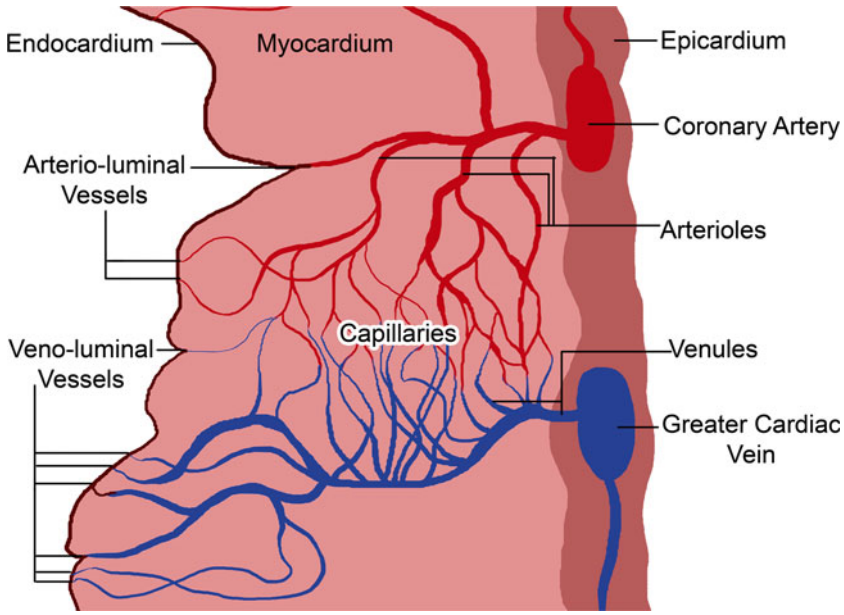

Fig. 8.8 Drawing of the relative coronary systems present within a section through a wall of the heart [28]. The arterio-luminal and veno-luminal vessels of the smaller cardiac system drain directly into the chambers of the heart, Reproduced with permission of Springer in the format Educational/ Instructional Program via Copyright Clearance Center

directly into the left atrium or pulmonary veins [31]. The left atrial septal veins, which can be further categorized into the anteroseptal veins and posteroseptal veins, typically drain directly into the right atrium. Anteroseptal veins have been found in almost all human hearts, while posteroseptal veins have been found in approximately one-third [31]. The right atrial veins are located in the intramural region of the right atrial wall and empty directly into the chamber [28, 29].

8.4.1.2 The Smaller Cardiac Venous System

The veins of the smaller cardiac venous system, also referred to as the Thebesian vessels, minor cardiac venous system, and lesser cardiac venous system, are typically smaller than 0.5 mm in diameter and originate from the endocardial layers of the myocardium [28, 29]. These vessels are responsible for draining approximately one-fourth of the deoxygenated blood used up by myocardium and drain directly into their respective heart chambers [31]. The majority of these small veins are present in the atria, although more Thebesian veins have been found in the right ventricle relative to the left ventricle [28, 58].

The main smaller cardiac veins consist of the arterio-luminal and veno-luminal vessels [31], as displayed in Fig. 8.8. The arterio-luminal vessels originate from coronary arterioles or capillaries and empty directly into their respective heart chamber. Similarly, the veno-luminal vessels originate in coronary capillaries and venules, and then empty into their respective heart chamber. The vessels that drain straight from the capillaries to the heart chamber are also referred to as Thebesian vessels [58, 59].

8.4.1.3 Coronary Veins: Valves

The role of venous valves, in general, is to prevent retrograde blood flow. Such valves in the heart are often present at the ostia to the coronary sinus [30–32, 34–36, 39–48], the lateral veins [46, 60], the inferior veins [31], and the middle cardiac vein [30, 31, 43, 61, 62]. A predominant valve can also be identified at the delineation between the coronary sinus and the great cardiac vein [43–49, 52]. Venous valves within the major left ventricular veins have been observed to be comparable in number of valves per vein except in the left marginal vein, which has fewer valves per vein [63]. These valves are most prevalent at the ostia to smaller contributor veins [63]. An example of a valve covering a venous contributor ostia is shown in Fig. 8.9 and in Movie 8.2 in the online supplemental material.

Abnormal Venous Anatomy

The human coronary venous anatomy is highly variable across patient populations. There have been reports of anatomic abnormalities associated with the cardiac veins. Fortunately, most abnormalities of the venous system do not cause clinical complications. The most common reported coronary venous abnormality is a persistent left superior caval vein, where the veins on the left superior side of the body drain into a left superior caval vein and then directly into the coronary sinus [28]. The persistent left superior caval vein on its own is a non-threatening anatomical variation, but it has been associated with other congenital cardiac malfunctions. Specifically, the abnormality is present in 0.3 % of patients with normal hearts and in 4.5 % of patients with congenital heart disease [64, 65].

Occlusion of the coronary sinus orifice is another reported anomaly of the coronary venous system. This abnormality is extremely rare, but is well reported [66–68]. In these patients, the major cardiac veins are instead drained through the superior vena cava. As a result, therapies requiring access to the coronary sinus ostium must be delivered into the superior vena cava [28].

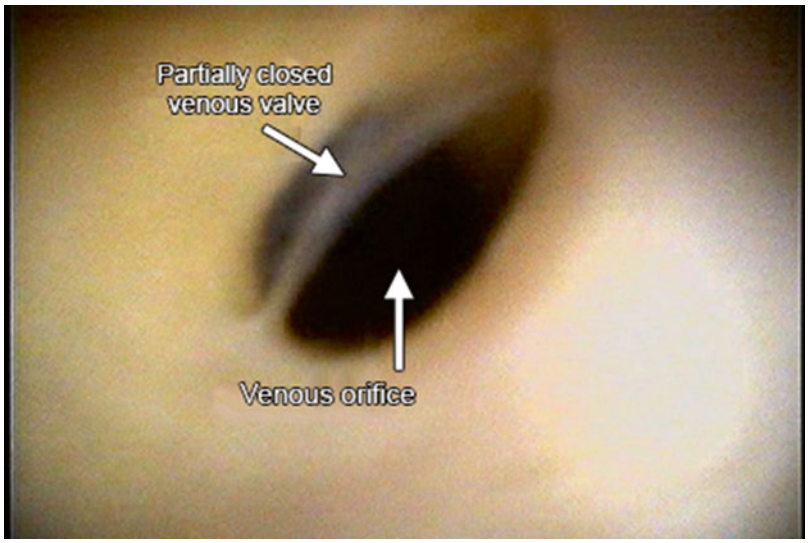

Fig. 8.9 A view of a venous valve located at the orifice of an inferior vein of the left ventricle. The image was obtained using a fiberscope in the coronary sinus of a reanimated human heart. Reproduced with permission of Springer in the format Educational/ Instructional Program via Copyright Clearance Center

Similar to the coronary arteries, some of the major cardiac veins have also been reported to be duplicated [29]. For example, the anterior interventricular vein has been observed to be duplicated in 3 % of patients. In these cases, two large veins run parallel ~1 mm apart along the anterior interventricular groove and merge to become one vessel at the atrioventricular groove [49]. The coronary sinus has also been reported to be duplicated with the one coronary sinus in its normal location and the other coronary sinus located intramurally [28, 69].

8.4.2 Coronary Veins: Disease

Cardiac veins are less likely to develop clinically significant disease states such as atherosclerosis. This is probably due to the inherently lower pressure within the venous portion of coronary circulation and the higher distensibility of the walls of the cardiac veins. When diseases such as heart failure induce myocardial remodeling, the venous system adapts to maintain both blood volume and venous pressure. However, it is generally accepted that the coronary venous system is not affected by atherosclerotic disease, and its "dense meshwork with numerous interconnections" allows blood to return to the heart via numerous pathways [70].

8.5 Microanatomy of Coronary Arteries and Veins

In general, vessels are composed of three layers, which vary in thickness depending on both vessel type and their relative size [71, 72]. These layers are the tunica intima, tunica media, and tunica adventitia, and can be seen in Fig. 8.10. The tunica intima is comprised of endothelium, subendothelial connective tissue, and an internal elastic lamina [29, 72]. The endothelium of vessels entering the heart is continuous with the heart's endothelium. In veins, the tunica intima and tunica media are less distinct than in arteries, e.g., the venous tunica intima is difficult to distinguish at low power magnification. Concentric layers of smooth muscle, along with collagenic and elastic fibers, make up the tunica media [71, 72]. The tunica media for a vein is much smaller than for an artery of similar size, as can be seen in Fig. 8.11 [72]. The tunica adventitia is composed of longitudinally arranged collagen fibers [72]. In contrast, the tunica adventitia is typically much larger in veins than in arteries.

8.6 Anastomoses and Collaterals

Connections between arteries that supply or veins that drain the same regions, known as *anastomoses*, provide alternate routes for blood to reach (via arteries) or leave (via veins) the same cardiac region. While numerous anastomoses have been observed on the epicardial surface of the heart, even more are considered present within the myocardium [5]. During fetal development, anastomoses are somewhat prominent; after birth, these channels decrease in both size and functionality [5].

In the general population, anterior interventricular and middle cardiac veins typically have the same origin and termination and follow the same course, while veins between the interventricular sulci are highly variable in number, size, course, and occurrence of anastomoses [31]. In addition, in general, coronary veins have a higher occurrence of anastomoses than coronary arteries [31], resulting in a highly interconnected venous network [6, 26, 70]. More specifically, the apical region of the heart will typically elicit the greatest density of venous anastomoses [66, 73].

Interestingly, in hearts with atherosclerotic damage, small anastomoses develop into larger, more efficient collaterals due to hypertrophic remodeling [5]. Such collaterals may

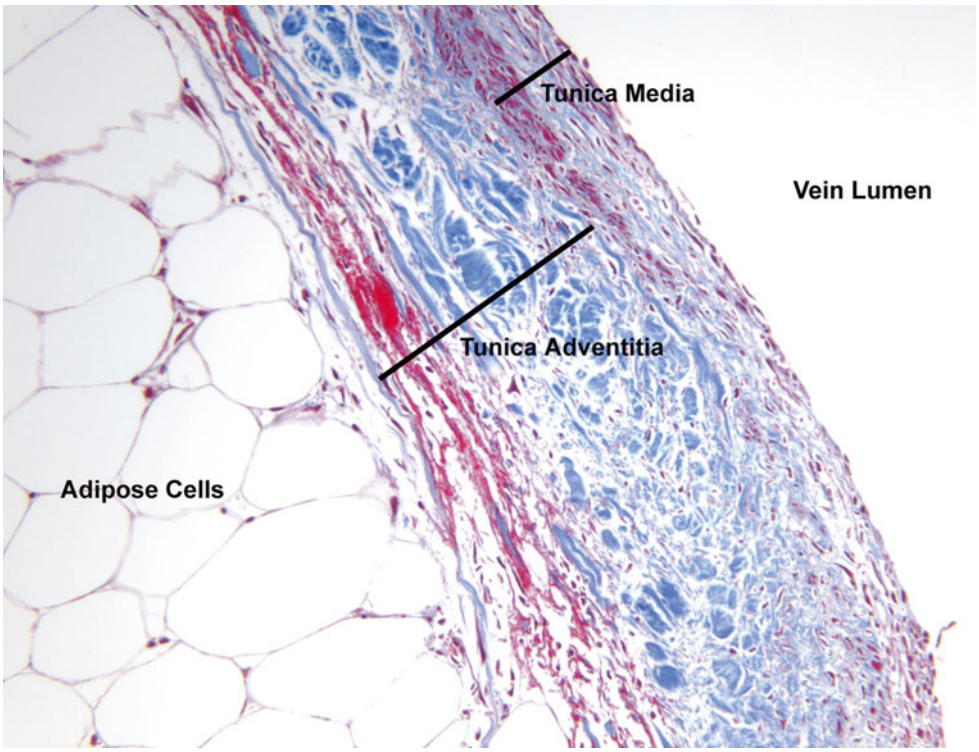

Fig. 8.10 View of coronary venous wall at 20× magnification. To the *left* are adipose cells and the far *right* is the vein lumen. The layers of the tunica adventitia and tunica media comprising the venous wall can be seen. The tunica intima cannot be observed at this magnification

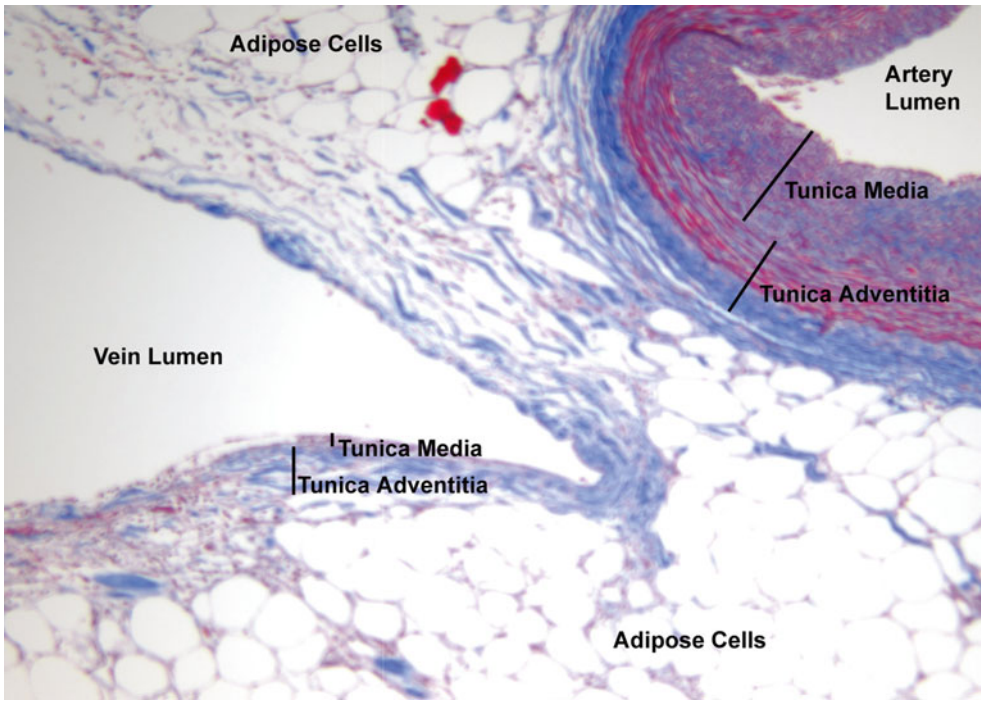

Fig. 8.11 This figure shows the relative differences between coronary arteries and veins. To the left is a coronary vein with a very thin venous wall. Both the tunica media and adventitia can be observed. The tunica intima cannot be observed at this magnification (10×). To the right, the coronary artery is significantly thicker in both the tunica media and adventitia layers. Epicardial fat encases both of these vessels

help to protect against ischemia by continuing to allow blood to flow to a given region of the heart when an original arterial route becomes obstructed [39, 73]. Collaterals protect against hypoxia and ischemia by continuing to supply oxygenated blood to a specific region of myocardium [5, 74]. While collaterals increase in size and number with age, whether this increase is related to atherosclerosis is considered unknown [74, 75]. Nevertheless, large and significant collaterals can often be observed near an infarcted area, which may indicate a slow remodeling process [39, 76]. However, in severe stages of coronary artery disease, even extensive collaterals will not allow certain regions of the myocardium to be ade-

quately perfused. To treat coronary artery disease patients, either the arterial branch can be reopened by coronary angioplasty and/or stenting, or a new pathway can be created via coronary artery bypass grafting. If such an obstruction is an acute event, collaterals will not have sufficient time to develop to adequately protect a given heart region from myocardial tissue damage.

8.7 Assessment and Visualization of the Coronary System

Catheterization of the heart is an invasive but commonly employed procedure for visualization of the heart's coronary arteries, chambers, valves, and/or great vessels. It can also be used to assess: (1) pressures in the heart and blood vessels; (2) function, cardiac output, and diastolic properties of the left ventricle; (3) relative flow of blood through the heart and coronary vessels; (4) regional oxygen content of the blood (e.g., aortic and within the coronary sinus); (5) status of the electrical conduction properties of the heart; and/or (6) septal or valvular defects.

Basic catheterization techniques involve inserting a long, flexible, radio-opaque catheter into a peripheral vein (for right heart catheterization) or a peripheral artery (for the left heart) under fluoroscopy (continuous X-ray observation). Commonly, during this invasive procedure, a radio-opaque contrast medium is injected into a cardiac vessel or chamber. The procedure may specifically be used to visualize the anatomical features of the coronary arteries, coronary veins, aorta, pulmonary blood vessels, and/or ventricles. Such investigations may provide pertinent clinical information about structural abnormalities in blood vessels that may be restricting flow (such as those caused by atherosclerotic plaque), abnormal ventricular blood volumes, inappropriate myocardial wall thickness, and/or altered wall motion. A sample venogram from an isolated heart preparation can be seen in Movie 8.3 in the online supplemental material; the catheter was inserted into the coronary sinus to block off antegrade flow, and then contrast was injected retrograde such that the coronary venous tree was more easily observable. Furthermore, this map of the coronary veins can be used as an aid in the placement of a pacing lead in the coronary veins.

To date, coronary angiography has been the primary visualization modality used clinically. However, multiple contrast injections can potentially be acutely deleterious to patients such as those with compromised cardiac output [77]. More recently, traditional coronary angiography methods have developed. Digital subtraction angiography has been observed to allow examination of venous occlusions and anatomical variants [78]. Rotational angiography has been shown to provide similar visualization of the coronary arteries as traditional methods, but with significantly less contrast volumes that need to be injected and less radiation exposure [79, 80].

Improving the quality of cardiac visualization allows for better planning of access to the coronary system during intervention and, therefore, decreased patient risk [81]. For example, in coronary artery bypass surgery, planning where sutures should be fixed is essential to avoid suturing to a rigid calcified arterial wall [7]. Several visualization modalities have recently been used and developed to enhance visualization of the coronary system. For instance, prior to lead implantation, tissue Doppler imaging can be utilized to identify the target implant region for a transvenous pacing lead [82, 83]. Additionally, noncontact electrical mapping (see Chap. 32) could be used to identify electrically viable target regions [84].

There have also been recent advances in intravascular imaging during interventions in the coronary system. Intravascular ultrasound (IVUS) is a catheterization method that utilizes ultrasound to identify plaques in vivo undetected by traditionally angiography and to guide coronary stent implantation [85, 86]. Also, IVUS has been used to assess coronary arterial wall elasticity, as this parameter has been associated with an increased risk for heart attack [87, 88]. Another current intravascular visualization method is optical coherence tomography (OCT). OCT generates infrared light and processes the reflections into in vivo images that can be used in the verification of implanted stents [87, 89]. Currently, OCT provides higher image resolution than IVUS, but it has more limited penetration in the vasculature [87, 89]. Photonic spectroscopy via catheterization, including near-infrared spectroscopy (NIRS) and Raman spectroscopy (RS) can also be applied within the vasculature to assess the chemical composition of plaque [87, 90, 91].

In addition to intravascular techniques, there are several noninvasive visualization methods available to assess the coronary system. With coronary artery disease being the highest cause of death, there is a benefit to screen asymptomatic patients at risk for heart attacks without requiring an invasive procedure [92]. Noninvasive imaging also prevents rare but reported adverse events associated with invasive catheterization [93]. The noninvasive methods also provide imaging of the surrounding structures and can identify clinically relevant anatomical anomalies that are not detectable with traditional coronary angiography methods [94]. Clinical computed tomography, both electron beam computed tomography (EBCT) and multidetector computed tomography (MDCT), can identify and quantify the atherosclerotic plaques in the coronary arteries, providing insight into the individual's risk for heart attack [92–94]. More recently, the use of prospective ECG gating has been incorporated with CT imaging to minimize radiation

dose [95, 96]. Coronary magnetic resonance angiography (MRA) is another method that can noninvasively image the coronary arteries without exposure to radiation [93]. Coronary MRA can also assess cardiac function when combined with other magnetic resonance imaging methods [93, 97]. However, coronary MRA has a lower temporal resolution when compared to CT and traditional angiography methods [93]. Positron emission tomography (PET) and single-photon emission computed tomography (SPECT) are additional noninvasive methods to visualize the coronary arteries, but are less common due to their relatively high costs [98, 99].

8.8 Medical Devices and the Coronary System

8.8.1 Devices and the Coronary Arteries

Intricate medical devices are required for performing interventional procedures with the coronary arteries. For example, percutaneous transluminal coronary angioplasty is a procedure during which a balloon catheter is introduced into the narrowed portion of the coronary artery lumen and inflated to reopen the artery to allow the return of normal blood flow. Recently, balloons coated with drugs have been developed for the unique delivery of agents during procedures. Relative to these procedures, oftentimes coronary stents are also placed such that restenosis of the artery is significantly delayed. A stent is a device comprised of wire mesh that provides scaffolding to support the wall of the artery and keep its lumen open and free from the buildup of plaque. A picture of a balloon angioplasty catheter and a coronary stent are shown in Fig. 8.12. Movie 8.4 demonstrates a stent deployment in the coronary arterial system of a reanimated human heart (see online supplementary material).

Balloon angioplasty and coronary stents have prevented numerous patients from having to undergo immediate coronary artery bypass graft surgery, which can be costly and painful. More recently, such stents have been produced with a variety of drug coatings in further attempts to minimize or eliminate the possibility of restenosis. Common drugs used to coat stents include sirolimus (also known as rapamycin), paclitaxel, zotarolimus, everolimus, and biolimus [86]. Drugs like sirolimus work by stopping cell growth; they also stop scar tissue from forming within arteries that have been opened. In addition, the use of biodegradable polymers and scaffolds for stents has been recently introduced to reduce stent thrombosis, improve imaging, and facilitate additional procedures in the same location [86, 100, 101].

While these drug-eluting stents have been a great improvement over angioplasty [102], it is generally considered that success rates could be further improved via new techniques. Several methods have been developed to successfully stent a coronary bifurcation [103], some of which are illustrated in Fig. 8.13. For example, the STAR (subintimal tracking and reentry) technique utilizes a small wire to dissect into the obstruction [104]. Additionally, several novel devices have recently been developed, e.g., radiofrequency signals can warn the user when the wire tip is too close to the vessel wall to prevent perforation, and can also be pulsed to facilitate passage through a coronary artery obstruction [105]. Another catheter design pulses the face of the obstruction to create a path into the obstruction [105]. Transmyocardial laser revascularization uses laser energy to create small conduits from oxygen-low areas of the heart directly to oxygen-rich blood in the left ventricular chamber to improve myocardial perfusion and angina symptoms [106, 107]. Additionally, techniques to open a stent to allow flow through a cover side branch are also becoming common practice, e.g., the *provisional technique* (see Device and Coronary Tutorials on the Atlas of Human Cardiac Anatomy; www.vhlab.umn.edu/atlas).

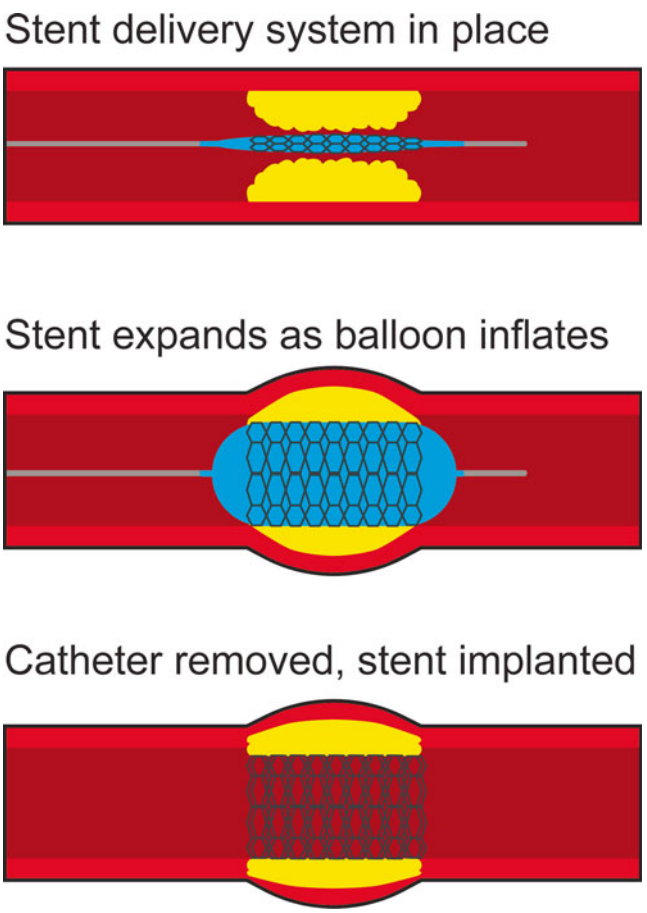

Fig. 8.12 An illustration of the stenting procedure. The balloon catheter with a mounted collapsed stent is placed in the artery at the target location. The balloon is inflated to open the artery and deploy the stent. Finally, the catheter is removed and the stent is left behind

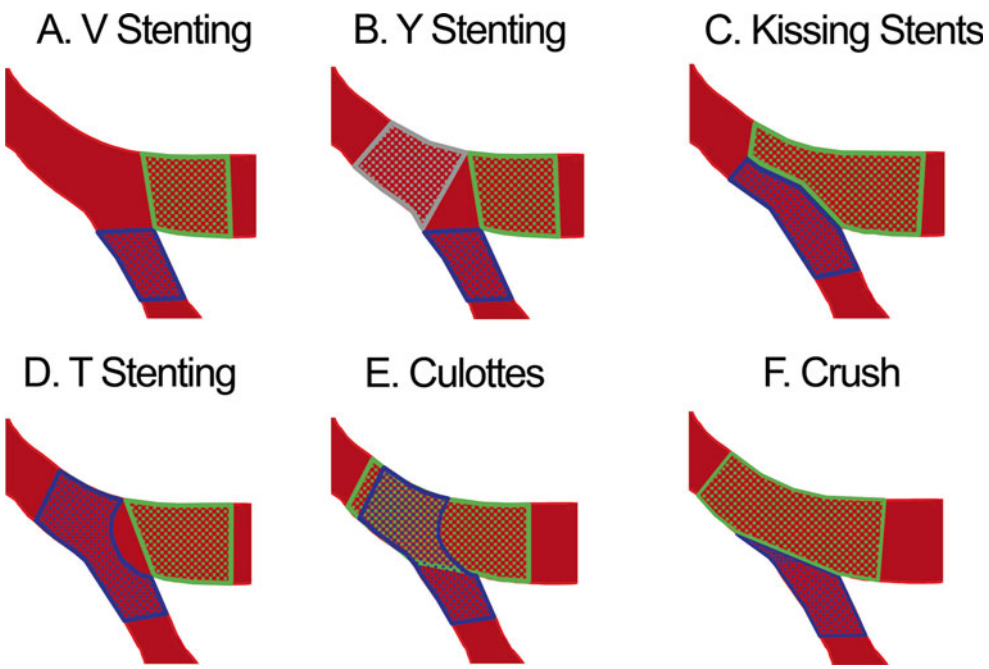

Fig. 8.13 Coronary bifurcation stenting techniques. (**A**) V stenting technique: a stent is deployed in each of the branching arteries. (**B**) Y stenting technique: a stent is deployed in each of the branching arteries. Next, a stent crimped over two balloons is deployed proximally in the parent branch. The balloons are inflated to deploy the proximal stent. The distal end of each balloon is positioned in each stented daughter branch during inflation. (**C**) Simultaneous kissing balloon technique: two stents are deployed by inflating both balloons simultaneously at the same pressure. (**D**) T stenting technique: the main branch is stented first. Next, angioplasty is performed on the side branch to create an opening in the first stent and a second stent is placed in the side branch. (**E**) Culottes technique: similar to the T stenting technique, except that the proximal end of the second stent is positioned in the main branch. (**F**) Crush technique: the first stent is deployed in the side branch. The main branch is then stented, which "crushes" the proximal end of the first stent against the wall of the main branch

8.8.2 Devices and the Coronary Veins

The coronary venous system has been utilized in a variety of ways to enhance cardiac therapies due to the venous system's "dense meshwork with numerous interconnections" and its relative immunity to atherosclerotic disease [63]. For example, local electrograms recorded from the coronary venous system can be recorded to indicate various arrhythmias and potential ablation target sites for left-sided accessory pathways [34, 108, 109]. Additionally, defibrillation coils implanted within the coronary venous system and, in particular, the middle cardiac or anterior interventricular veins can lower subsequent defibrillation thresholds significantly [110, 111]. These lower thresholds are likely attributable to more efficient transfer of the defibrillation current through the heart [110]. Furthermore, from the coronary venous system, the coronary flow reserve can be determined [34] and coronary perfusion during percutaneous transluminal angioplasty of coronary arteries can be monitored [112]. (See Coronary Tutorial on the Atlas of Human Cardiac Anatomy; www.vhlab.umn.edu/atlas.)

Because the coronary venous system is not prone to the effects of atherosclerotic disease, it is considered that it may also serve as an effective conduit for drug delivery or even as a potential avenue for coronary artery bypass. For example, for decades, the distribution of cardioplegia through the coronary sinus has been proven to be safe and effective in myocardial protection, and even superior to the traditional method of antegrade cardioplegia, especially in patients with coronary artery disease [34, 113]. More recently, restoration of coronary blood flow prior to an acute myocardial infarction can significantly reduce infarct size and improve myocardial function. Additionally, the administration of recombinant tissue-type plasminogen through the coronary venous system was shown to result in both shorter recovery times and significant reduction in infarct size when compared to intravenous administration [114]. The coronary venous system also can be employed to deliver cell therapies directly to the myocardium as a potential treatment for heart failure [115]. In one case study, it was demonstrated that a catheter-based system allowed arterialization of a cardiac vein to bypass a totally occluded left anterior descending coronary artery [116].

In the past decade, the coronary venous system has also been used as a site for pacing lead implantation to allow for cardiac resynchronization therapy (CRT). CRT involves pacing at least two ventricular sites (typically one in the right and one in the left ventricle) in order to minimize the required

time for total ventricular activation and thus improve cardiac synchrony in certain patients with heart failure eliciting ventricular dyssynchrony [117, 118]. More specifically, implantation of pacing leads via the coronary venous system is currently the most popular approach for left ventricular pacing and is accomplished by a transvenous approach [119]. It should also be noted that several studies have reported the beneficial results of pacing from the lateral or inferolateral region of the left ventricle [83, 119–124]; either the lateral vein or inferior vein of the left ventricle are considered optimal implant sites [117, 125, 126]. It should be qualified that, to date, response rates to CRT in general are still considered suboptimal with a typical success rate of around two-thirds [127, 128]. An example of a pacing lead implant in the coronary venous system is shown in Movie 8.5 in the online supplemental material. Transvenously placing the pacing lead is considered less invasive and allows for greater patient comfort [129]. For additional information on cardiac pacing, see Chap. 30.

The coronary sinus and great cardiac vein have specifically been used for a number of cardiac therapies. For example, the coronary sinus has been used as a means to deliver ablation therapy [130–133]. For example, an ablation catheter can be placed within the coronary sinus to treat atrial fibrillation in the left atrium. In another therapy, it has been reported that a reducer stent can be deployed within the coronary sinus to relieve chronic angina symptoms [134]. The reducer stent decreases the diameter of the vein to increase pressure in the coronary arteries, which then can increase blood flow to ischemic areas of the heart. This can reduce the patient's angina, and is considered as a last resort when other approaches have failed. Finally, several groups have described the deployment of mitral valve annuloplasty devices within the coronary sinus and/or great cardiac vein which surrounds the mitral valve annulus, in attempts to reduce mitral regurgitation [135, 136].

Lead extraction from the coronary venous system, if required, can be particularly difficult due to thin venous walls [137], but may be necessary in the event of an infection, complication, phrenic nerve stimulation, high pacing threshold, and/or lead dislodgement [138]. Leads that are implanted in the coronary venous system also tend to be smaller in diameter and therefore have a higher risk of damage to the lead during extraction [139]. Unlike non-CS leads, the majority of these leads can be extracted with simple traction [139, 140]. Leads that have been implanted for a longer period of time are more likely to require more complex tools for extraction, such as locking stylets and/or laser sheaths [140]. Also, the extraction of active fixation leads from the coronary venous system have been reported to be more challenging regardless of implant duration [139, 141, 142]. For additional details on lead extraction, see Chap. 30.

8.9 Notable Engineering Parameters and Design Criteria Associated with the Coronary System

When designing and testing the devices used in the interventional procedures which utilize the coronary system (see Sect. 8.8), a thorough understanding of the geometric parameters of this vasculature is considered critical. The main purpose of the following text is to summarize, at a basic level, the important anatomical parameters that one needs to consider when designing interventional devices and/or associated delivery procedures related to the coronary system.

From an engineering perspective, the development of any medical device requires knowledge and application of several important parameters; this is especially true for coronary system devices due to the complexity and variations found in these vessels. As with any device placed in the human body, a solid understanding of the fundamental anatomical properties of the tissue with which the device interacts is vital to obtain acceptable results regarding: (1) delivery efficacy; (2) long-term device stability; and/or (3) overall performance. These parameters are important not only from a chronic perspective, but also for initial device delivery. Although biological reactions to materials placed inside the human body must be understood to guarantee long-term stability and performance of the devices, the following discussion focuses on the macroscopic physical properties of the coronary vessels.

To simplify the coronary system to its basic structure, each vessel branch can be defined in terms of a flexible cylinder or tube. A tube is a hollow cylindrical structure of a known but variable length, radius, and wall thickness. This means the coronary arterial and venous networks can be represented by a large number of interrelated tubes that supply blood to and receive blood from one another. The parameters described here are those that must be defined to understand fully the geometric and dynamic properties of this tube network so devices may be optimized to interact with them.

8.9.1 Diameter

The most basic parameter that must be known about arteries and veins is their diameter. However, neither artery nor vein diameters are constant along their lengths [7, 143–145]. Typically, coronary arteries decrease in diameter along their length [143–145]. Thus, the left main and right coronary arteries generally have the largest diameters of the entire coronary arterial network; these diameters range from 1.5 to 5.5 mm for both vessels, with means of 4.0 mm and 3.2 mm, respectively [9, 73]; note that disease state can greatly affect these diameters. The more bifurcations an artery undergoes, the smaller its diameter will generally become. In the case of the coronary arteries, the vessels located at the very end of

the network are the capillaries, which are typically on the order of 5–7 μm in diameter [146]. Hence these vessel diameters are approximately 600 times smaller than those of either the left main or right coronary arteries.

Conversely, veins increase in diameter as they move from their source to their termination. Thus, the largest diameter venous vessel in the heart is the coronary sinus, which serves as the primary collector of cardiac venous blood and has a diameter that ranges from 4.5 to 19 mm at its ostium; average diameters of the coronary sinus are 6–10 mm [44, 46, 147, 148]. The difference in diameter from one end of the venous system to the other is roughly a factor of 1200. However, in diseased states such as heart failure, it has been reported that the ostium tends to increase in diameter [147]. The coronary sinus, although often reported as having a diameter, is typically elliptical (or ovular) in cross section [43, 50] and, therefore is considered to elicit major and minor axis dimensions rather than a true diameter or circular cross section. In one study, the average major axis diameter of the coronary sinus was reported to be approximately 14.6 mm, while the minor axis diameter was reported to be 9.1 mm [149]. It is also important to recall that because arteries and veins are made up of compliant tissue their diameters change throughout the cardiac cycle because of pressure changes that occur during systole and diastole [150].

The design of coronary stents and balloon angioplasty catheters relies heavily on the diameter of the vessels in which they are meant to reside. If a stent or balloon is designed with too large a diameter, when it is deployed within the artery it may cause a wall strain so great that it could be damaging to the artery. On the other hand, if the design has a diameter that is too small, the device will be ineffective. In the case of the balloon catheter with a diameter that is too small, the lumen will not be opened up enough to cause any significant decrease in the degree of occlusion. Yet, an interventionalist performing such a procedure can also choose to use either a compliant or non-compliant balloon which, in turn, can be inflated to various pressures (atmospheres).

Another device that must be designed with vessel diameter in mind is the left ventricular pacing lead. Because this lead is designed for placement in an inferolateral tributary of the coronary sinus, it must have a small enough diameter to fit inside the vein, yet a large enough diameter to stay reliably in its intended location. If such criteria are not met, the leads may not be useful or safely placed.

8.9.2 Cross-Sectional Profile

Cross-sectional shape profile is another parameter that is closely related to vessel diameter. Cross-sectional shape profile is determined by the shape of the vessel that results after slicing it perpendicular to its centerline. In a hypothetical cylinder, this profile would be a perfect circle. When arteries are diseased and may contain significant amounts of atherosclerotic plaque, their cross-sectional profiles can change from roughly circular to a variety of different, and often quite complex, profiles depending on the amount and relative orientation of the plaque. To date, coronary venous shape profiles have not been well documented, but they can be considered in general as noncircular because of the lower pressures within the vessel as well as the more easily deformable vessel walls in relation to the arteries. In Fig. 8.11, an example of the differences between arterial and venous cross-sectional profiles can be observed.

The design of two devices in particular should be considered in relation to the cross-sectional shape of the coronary vessels—coronary stents and angioplasty catheter balloons. Because coronary arteries are typically circular in cross section, stents are designed also to be circular in their cross section. Yet, if a similar device was ever needed for placement in the relatively healthy coronary venous network, a different design would probably be initially considered because the cross-sectional profile of a coronary vein, especially the coronary sinus, is generally noncircular. Angioplasty balloons have also been designed with the consideration that coronary arteries are typically circular in cross section. When inflated, the balloon generates a shape that has a uniform diameter in cross section, which may be consistent with a healthy coronary artery; thus the therapy in part aims to return this shape.

8.9.3 Ostial Anatomy

Understanding the anatomy of the ostia of each of the three most prominent vessels in the coronary system (right coronary artery, left main coronary artery, and coronary sinus) is especially important when interventional procedures require cannulation of the ostia to perform a specific procedure within the associated lumen of the vessel. This is true of nearly all procedures done on coronary vessels because they are typically aimed at the lumen of the vessel but, on occasion, one may want to temporarily block off or place a flow-through catheter in the ostium.

The ostia of the coronary arteries are generally open with no obstructions except when, in extreme disease cases, coronary plaques form; in some reported cases, ostia can become partially or even fully occluded (with no ostia access). On the other hand, when occlusion is not present at the ostial origin of the coronary arteries, there are generally no naturally occurring anatomical structures to impede entrance to these vessels.

The coronary sinus ostium, as discussed in Sect. 8.4, often has some form of Thebesian valve covering its opening into the right atrium [43, 53]. This valve can take many different forms and morphologies, and can cover the coronary

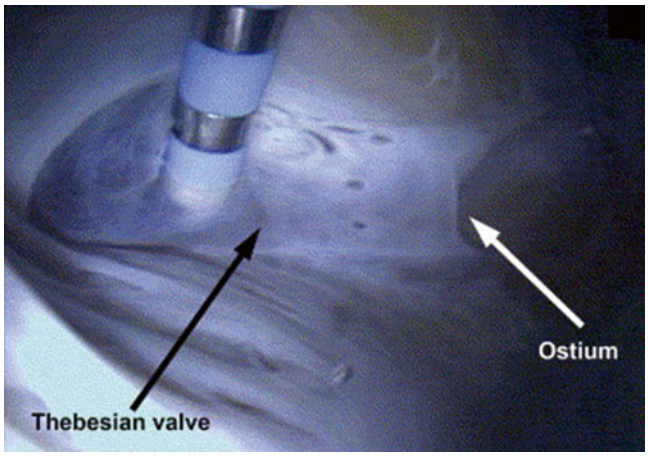

Fig. 8.14 An internal image of a Mariner catheter (Medtronic, Inc., Minneapolis, MN, USA) caught in the Thebesian valve of an isolated functioning human heart. Reproduced with permission of Springer in the format Educational/Instructional Program via Copyright Clearance Center

sinus ostium to varying degrees [34, 46, 151–155]. When the Thebesian valve is significantly prominent in the manner in which it covers the coronary sinus ostium, the relative cannulation of the sinus can be much more difficult than in other cases as illustrated in Fig. 8.14 [153, 154].

This consideration is important as it specifically applies to the implantation of pacing leads into the left ventricular coronary veins for CRT. In the process of delivering a lead to the coronary veins, coronary sinus cannulation is of paramount importance because it is currently considered the primary point of entry into the coronary venous network for pacemaker lead introduction for eventual pacing of the left ventricle. The relative ostial long and short axial ostial diameters for the major coronary veins are presented in Table 8.1 [156].

Additionally, venous valves are often present at the ostia and within the major left ventricular veins; an example can be seen in Fig. 8.9 [63, 157]. Coronary venous valves, such as the valve of Vieussens, could hinder or help advancement of guide wires, catheters, and pacing leads for a variety of cardiac interventional procedures, especially during subselection of venous branches where a large number of venous valves are observed [63]. To design the optimal catheter or lead delivery procedure, the presence of the Thebesian valve and other venous valves should be fully considered in addition to other anatomical features.

8.9.4 Vessel Length

Each tube that makes up a section of the coronary arterial or venous network is also a branch that arises from a parent vessel. Each of these vessel branches has starting and ending points. Typically, in early anatomical studies, vessel lengths were measured directly on a specimen after hearts were extracted. With the advent of 3D medical imaging technologies such as magnetic resonance imaging and computerized tomographic angiography, coronary vessel lengths can be measured in vivo by reconstructing them in space [158–160]. The length of the coronary sinus is often defined from its ostium at the right atrium to the location of the valve of Vieussens or the point where the vein of Marshall intersects it. Interestingly, the relative length of the coronary sinus in humans can vary from 15 to 65 mm [43]. Although there are published data on incidence and qualitative morphology of the tributaries of the coronary sinus [35, 40], length is generally not addressed.

Because coronary catheterization is both expensive and invasive, knowledge of coronary arterial lengths and relative disease state prior to implanting a stent will lead to better outcomes and reduced procedure times. When percutaneous transluminal coronary angioplasty procedures are performed, it is critical that the physician knows the exact location along the length of an artery where the occlusion occurs and the relative distance needed from catheter entry to that site. These parameters are often measured using contrast angiography. Thus contrast media is injected and fluoroscopic images are acquired, then the location of the occluded arterial region can be quickly identified.

A specific interventional application for which coronary venous length is an important consideration is implantation of left ventricular leads into the inferolateral branches of the coronary sinus. In other words, optimal lead designs (or selection for use) should take into account the average length along the coronary sinus of the normal and/or diseased human heart where a candidate inferolateral branch enters. Thus, prior knowledge of this parameter, either in a specific patient or across a population, might improve ease of implant and long-term efficacy of therapy. This information could also be useful in understanding the likelihood of a lead dislodging after initial implantation. Typical arc lengths for the major coronary veins are presented in Table 8.1 [156].

8.9.5 Tortuosity

Since the vessels in the coronary system course along a nonplanar epicardial surface, they are by nature tortuous. Therefore, they will elicit varying degrees of curvature along their lengths according to the topography of the epicardial surfaces on which they lie. If vessels were simply curvilinear entities such that they traversed in a single plane only, their tortuosity could be much more easily defined. In general, the vessels of the coronary system are not curvilinear, rather they are 3D curves that twist and turn in more than two dimensions. When the third dimension is added, the tortuosity becomes much more complex; both the curvature of each

Table 8.1 Mean and standard deviations of coronary venous anatomical parameters assessed for 121 human hearts using contrast-computed tomography

Vein	Distance to the coronary sinus ostium (mm)	Branching angle (°)	Arc length (mm)	Tortuosity	Number of branches	Ostial short axis diameter (mm)	Ostial long axis diameter (mm)
Small cardiac vein (SCV) $n=14$	18.5 ± 11.2	100.2 ± 21.8	33.0 ± 9.2	1.15 ± 0.06	0.2 ± 0.4	2.9 ± 1.4	4.5 ± 2.1
Middle cardiac vein (MCV) $n=121$	9.0 ± 5.4	87.8 ± 22.1	129.7 ± 23.4	1.37 ± 0.22	6.8 ± 4.4	4.1 ± 1.5	5.7 ± 1.9
Inferior vein (IV) $n=135$	21.3 ± 10.2	95.4 ± 19.4	79.4 ± 42.6	1.22 ± 0.17	4.0 ± 4.4	2.7 ± 0.9	4.0 ± 1.5
Inferolateral vein (ILV) $n=60$	42.4 ± 12.9	93.5 ± 17.0	67.2 ± 3 4.1	1.27 ± 0.39	3.7 ± 4.3	3.1 ± 1.3	4.0 ± 1.3
Left lateral vein (LLV) $n=153$	66.7 ± 12.9	103.0 ± 24.8	76.4 ± 35.6	1.24 ± 0.15	5.0 ± 4.6	3.3 ± 1.3	4.2 ± 1.5
Anterolateral vein (ALV) $n=70$	88.0 ± 17.8	95.7 ± 15.4	46.3 ± 23.2	1.18 ± 0.11	1.5 ± 2.3	2.4 ± 0.8	3.1 ± 1.1
Anterior interventricular vein (AIV) $n=121$	101.0 ± 15.0	164.8 ± 22.1	125.5 ± 31.3	1.35 ± 0.17	9.9 ± 5.6	4.5 ± 1.1	5.4 ± 1.3

segment element and the direction of curve orientation must be defined.

The levels of tortuosity encountered in the coronary vessels will significantly influence device delivery and chronic performance. When a device such as a catheter or lead must be passed through a tortuous anatomy such as that of the coronary vessels, the greater the curvature and change in curvature over the length of a vessel, the more difficult it will be to pass the device through it, due to friction generated at locations where a device contacts tissue. For vessels that more closely resemble a straight line, these devices should pass through more easily. To estimate tortuosity, the vessel length can be divided by the linear distance from the origin and end of a vessel. Typical tortuosity measurements for the major coronary veins are presented in Table 8.1 [156].

8.9.6 Wall Thickness

All coronary vessel walls have thickness related to their function as discussed earlier in this chapter. When a device is placed into the coronary system, there is always a danger of vessel perforation. In other words, perforation takes place when a device is inadvertently introduced into the vessel lumen with a level of force and angle of incidence to the vessel wall that causes the device to create a hole in the vessel wall. This situation, although not very common, is not only very dangerous but can be lethal if not dealt with appropriately. Perforation is more often fatal in arteries as opposed to veins for two reasons: (1) more blood is lost under high pressures in the arteries; and (2) loss of oxygenated blood to the body and the heart itself is more immediately detrimental than if deoxygenated blood were to exit the coronary veins.

Although it is clear that no device is meant to perforate the vessels of the coronary system, each should be developed with the worst-case scenario of perforation in mind, such that the deployed devices will not be problematic for either patients or physicians. It should be noted that the wall thickness of the larger coronary arteries is roughly 1 mm [161, 162]. To our knowledge, only one study has defined venous wall thickness [143]. In general, anterior and middle cardiac vein wall thickness (0.11–0.17 mm) was significantly larger when compared with the lateral veins and inferior vein of the left ventricle vein wall thickness (0.09–0.13 mm). Vein wall thickness in apical regions of all four major left ventricular veins was significantly smaller than those in basal regions; average vein wall thickness in apical regions ranged from 0.09 to 0.13 mm, in comparison to 0.11–0.17 mm in basal regions. Examples of relative wall thickness for arteries and veins can be observed in Fig. 8.11.

8.9.7 Relationship to Myocardium

The relationship between the coronary vessel and the myocardium is an important parameter to take into consideration when designing various cardiac devices. As noted above, both coronary arteries and veins exhibit significant tortuosity on the surface of the heart and sometimes course into the myocardium (see Sect. 8.2). Additionally, the hearts of "most adults in Western countries contain varying physiological amounts of fat, found mainly in the subepicardial region" [163]. Epicardial fat can represent a significant cardiac component [164–169] and may comprise up to half of the heart's weight, particularly in obese patients that have hypertension and atherosclerotic coronary artery disease [167]. In general, large epicardial fatty deposits are in the atrioventricular sulci and surround the anterior and inferior descending coronary arteries [167–170]; note that coronary vessels often are displaced off the epicardial surface of the heart and are surrounded by epicardial fat. As can be seen in Figs. 8.10 and 8.11, adipose cells can surround both epicardial arteries and veins.

The distance from a vessel to the myocardium added by epicardial fat could significantly affect cardiac device efficacy, particularly for transvenous pacing leads. Pacing thresholds for leads implanted in coronary veins have previously

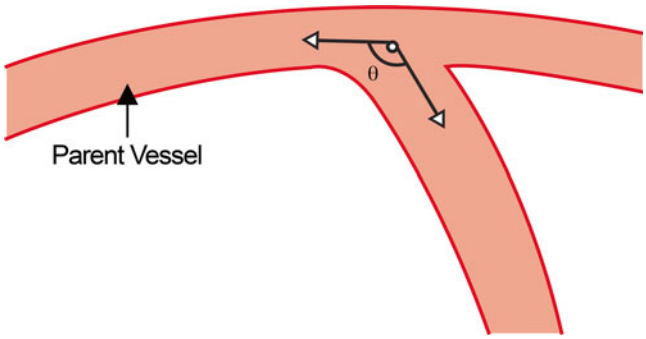

Fig. 8.15 Diagram of coronary vessel branching angle. Angle θ represents the branching angle generated between the parent and daughter vessels

been shown to be smaller at distal positions than at more proximal positions [3, 39, 171]. While increases in pacing thresholds towards the base of the heart could be due to larger vein circumferences, a larger amount of epicardial fat present at the base of the heart could also play a role. With increasing rates of obesity, particularly in the USA, epicardial fat must be taken into account when designing devices that depend on close proximity to myocardial tissue.

8.9.8 Branch Angle

As a vessel bifurcates, *daughter* branches are diverted in a different direction from the parent vessel. This creates a situation in which the smaller vessel has a certain branching angle in relation to the direction of the parent vessel. Branching angles can be measured by calculating the angle between the trajectory of the parent vessel and its daughter. In other words, the angle a catheter would have to make in order to access the daughter vessel. An example of this idea is illustrated in Fig. 8.15. Using EBCT, branching angles of coronary sinus tributaries are $117 \pm 25.3°$ for the middle cardiac vein, $88.9 \pm 24.0°$ for the inferior vein of the left ventricle, $85.3 \pm 30.0°$ for the left marginal vein, and $19.2 \pm 54.1°$ for the anterior interventricular vein [172]. These measurements are also presented in Table 8.1 for the major coronary veins [156].

The branch angle of a daughter vessel is important since it applies, for example, directly to the situation in which a transvenous pacing lead enters an inferior or lateral branch of the coronary sinus. Thus, the only way to optimize the design of this type of lead and its delivery system, such that it can easily make the turn into a branching vessel, is to know the general severity of the branching angle. In general, the more gradual the turn a lead has to take from a parent vessel to its daughter, the easier it is for an implanter to navigate.

8.9.9 Motion Characteristics

Since the vessels of the coronary system are located relative to the epicardium, it follows that they are not stationary due to the motion of the heart. Along with the simple 3D displacement that occurs over time because of motion, there are other mechanical parameters that are dynamic, such as curvature, stress, and torsion. Each of these fundamental mechanical parameters can have a significant effect on devices placed in the lumen of a deforming vessel. Thus, devices such as stents and leads must be designed to withstand all types of stress, curvature, and torsion changes that patients are expected to experience over their lifetimes within an arterial or venous vessel lumen. Additional necessary considerations include: (1) the relative changes in both the 3D path of each vessel and changes in lumen diameter during a given cardiac cycle; and (2) the relative influences associated with alterations in contractility states (e.g., the effects of exercise increasing cardiac output four- to sixfold).

8.9.10 Nearby Clinically Relevant Anatomy

An in-depth understanding of the anatomical surroundings of the coronary anatomy is essential for the prevention of injury to (or unwanted stimulation of) the adjacent anatomies during interventions delivered within these vessels. More specifically, it is important to understand the anatomical relationship between the coronary arteries and the coronary veins [173, 174]. For example, active-fix left-sided leads can be deployed in the coronary venous system for patients with lead dislodgement challenges [175, 176]. In these lead placement procedures, it is important to consider a patient's vein-to-artery distance because there is risk for arterial perforation if the lead is actively fixed in a vein in close proximity to a coronary artery. Another example is the use of the coronary veins for retrograde myocardial drug delivery via the coronary venous system [101, 177] or coronary venous arterialization [116, 178]. A coronary vein located near a major congested coronary artery may be an ideal target for this therapeutic approach.

The proximity of the circumflex artery relative to the coronary sinus also has clinical implications. For example, circumflex artery compression is a known concern for indirect mitral valve annuloplasty devices deployed in the coronary sinus if the circumflex courses between the valve and the coronary sinus [135, 149, 179–181]. Similarly, damage to the circumflex can occur as a result of ablation therapy delivered to the left atrium via the coronary sinus depending on the circumflex artery's course [182].

Another clinically relevant nearby structure one needs to consider when performing any cardiac procedure is the phrenic nerve, which stimulates the diaphragm. A current

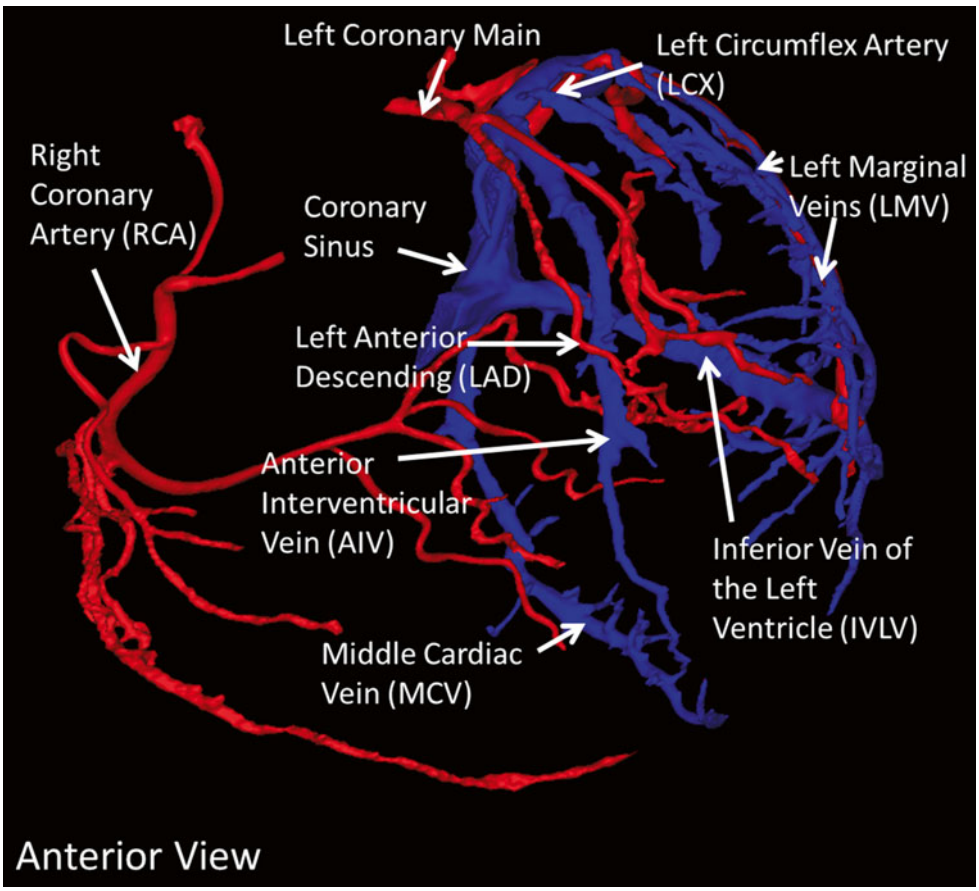

Fig. 8.16 3D reconstruction of contrast-computed tomography images for the coronary arterial and venous systems. Reproduced with permission of John/Wiley & Sons, Inc. in the format Educational/Instructional Program via Copyright Clearance Center

challenge associated with left ventricular lead implantation procedures is to avoid undesired stimulation of the left phrenic nerve. Note that phrenic nerve stimulation at implantation or follow-up has been reported, in one case series, to occur in over one-third of patients [183].

Finally, the anatomical relationship between the coronary sinus and the left atrial mitral isthmus is important to effectively treat atrial fibrillation when pulmonary vein isolation is inadequate [184–186]. However, ineffective ablation applications within this region have been reported to be pro-arrhythmic [187]. Thus, it is important to understand the anatomical proximity of the mitral isthmus to the coronary sinus in order to achieve optimal therapeutic outcomes.

8.9.11 Assessment of Anatomical Parameters

There are various methods that can be used to assess coronary arterial and venous parameters discussed here. Direct measurements on cadaveric heart specimens have been used to measure physical parameters [33, 34, 46, 171, 174]. However, there are limitations to these direct measurements including: (1) the presence of adipose tissue can hide the full anatomy of the vessels; and (2) the measurements are limited to two dimensions. Computed tomography [55, 156, 159, 172, 173, 188–191] and magnetic resonance imaging [149, 158, 160, 192, 193], both in vivo and in situ, have been used to analyze and quantify the coronary anatomy in three dimensions, as pictured in Fig. 8.16 and in Movie 8.6 in the online supplemental material.

8.10 Summary

Several hundred years ago, the function of the coronary system was unknown. Now, the coronary system is known to be a highly variable network of arteries and veins supplying and draining the myocardium of oxygenated and deoxygenated blood, respectively. Due to advances in biomedical technologies, the coronary system has been utilized in a variety of therapeutic applications, including CRT. Additionally, debilitating cardiac disorders such as coronary artery disease can be alleviated by surgical or interventional approaches, e.g., with coronary artery bypass grafts or with less invasive stenting. Nevertheless, a critical understanding of the structural and geometric anatomical characteristics of the coronary system is required to further optimize the development and delivery of future medical devices; devices need to be engineered to successfully deliver therapies to a variety of patients with unique coronary venous anatomies.

References

1. Harris CR (1973) The heart and the vascular system. In: Ancient Greek medicine; from Alcmeon to Galen. Clarendon Press, Oxford
2. Phillips R The heart and circulatory system. http://www.accessexcellenceorg/AE/AEC/CC/heart_backgroundphp. Accessed 05 May 2008
3. Kajiya F, Kimura A, Hiramatsu O, Ogasawara Y, Tsujioka K (1993) Coronary venous flow. In: Hirakawa, Rothe, Shoukas, Tyberg (eds) Veins, their functional role in the circulation. Springer-Verlag, Tokyo
4. Alexander R, Schlant R, Fuster V, O'Rourke R, Roberts R, Sonnenblick E (1999) Hurst's the heart. McGraw-Hill, New York
5. von Ludinghausen M (2003) The clinical anatomy of coronary arteries. Adv Anat Embryol Cell Biol 167:1–111
6. Williams P, Bannister L, Berry M (1995) Gray's anatomy. Churchill Livingston, London
7. Loukas M, Sharma A, Blaak C, Sorenson E, Mian A (2013) The clinical anatomy of the coronary arteries. J Cardiovasc Transl Res 6:197–207
8. Patel S (2008) Normal and anomalous anatomy of the coronary arteries. Semin Roentgenol 43:100–112
9. Angelini P (1989) Normal and anomalous coronary arteries, definitions and classification. Am Heart J 117:418–434
10. James T (1961) Anatomy of the coronary arteries. Paul B Hoeber, New York
11. Yamanaka O, Hobbs R (1990) Coronary artery anomalies in 126,595 patients undergoing coronary arteriography. Cathet Cardiovasc Diagn 21:28–40
12. Vlodaver Z, Neufeld H, Edwards J (1975) Coronary arterial variations in the normal heart and in congenital heart disease. Academic, New York
13. Koizumi M, Kawai K et al (2002) Anatomical study of the left single coronary artery with special reference to the various distribution patterns of bilateral coronary arteries. Ann Anat 182:549–557
14. Frescura C, Basso C, Thiene G et al (1998) Anomalous origin of coronary arteries and risk of sudden death, a study based on an autopsy population of congenital heart disease. Hum Pathol 29:689–695
15. Zimmermann E, Schnapauff D, Dewey M (2008) Cardiac and coronary anatomy in computed tomography. Semin Ultrasound CT MR 29:176–181
16. Pelliccia A (2001) Congenital coronary artery anomalies in young patients, new perspectives for timely identification. J Am Coll Cardiol 37:598–600
17. Manghat N, Morgan-Hughes G, Marshall A et al (2005) Multidetector row computed tomography, imaging congenital coronary artery anomalies in adults. Heart 91:1515–1522
18. Earls J (2006) Coronary artery anomalies. Tech Vasc Interv Radiol 9:210–217
19. Frommelt P, Frommelt M (2004) Congenital coronary artery anomalies. Pediatr Clin North Am 51:1273–1288
20. Koneru J, Sammual A, Joshi M, Hamden A, Shamoon F, Bikkina M (2011) Coronary anomaly and coronary artery fistula as cause of angina pectoris with literature review. Case Rep Vasc Med 2011:486187
21. Lowe J, Oldham H Jr, Sabiston D Jr (1981) Surgical management of congenital coronary artery fistulas. Ann Surg 194:373–380
22. Jung Y, Kim H, Yoon C (2012) Severe form of persistent Thebesian veins presenting as ischemic heart disease. Korean Circ J 42:714–717
23. Spindola-Franco H, Grose R, Solomon N (1983) Dual left anterior descending coronary artery, angiographic description of important variants and surgical implications. Am Heart J 105:445–455
24. Vlodaver Z, Edwards J (1971) Pathology of coronary atherosclerosis. Prog Cardiovasc Dis 14:256–274
25. Hutchins G, Moore G, Hatton E (1986) Arterial-venous relationships in the human left ventricular myocardium, anatomic basis for countercurrent regulation of blood flow. Circulation 74:1195–1202
26. Truex R, Angulo A (1952) Comparative study of the arterial and venous systems of the ventricular myocardium with special reference to the coronary sinus. Anat Rec 113:467–491
27. Widmaider E, Raff H, Strang K (2004) Vander, Sherman, Luciano's human physiology, the mechanisms of body function, 9th edn. McGraw-Hill, Boston
28. Spencer J, Anderson S, Iaizzo P (2013) Human coronary venous anatomy for interventions. J Cardiovasc Transl Res 6:208–217
29. Loukas M et al (2009) Cardiac veins, a review of the literature. Clin Anat 22:129–145
30. Ho S, Sanchez-Quintana D, Becker A (2004) A review of the coronary venous system, a road less travelled. Heart Rhythm 1:107–112
31. von Ludinghausen M (2003) The venous drainage of the human myocardium. Adv Anat Embryol Cell Biol 168:1–104
32. Giudici M, Winston S, Kappler J et al (2002) Mapping the coronary sinus and great cardiac vein. Pacing Clin Electrophysiol 25:414–419
33. Hood W Jr (1968) Regional venous drainage of the human heart. Br Heart J 30:105–109
34. Silver M, Rowley N (1988) The functional anatomy of the human coronary sinus. Am Heart J 115:1080–1084
35. Adatia I, Gittenberger-de A (1995) Unroofed coronary sinus and coronary sinus orifice atresia, implications for management of complex congenital heart disease. J Am Coll Cardiol 25:948–953
36. Malhotra V, Tewari S, Tewari P, Agarwal S (1980) Coronary sinus and its tributaries. Anat Anz 148:331–332
37. Ratajczyk-Pakalaska E (1990) The coronary venous anatomy. In: Myocardial perfusion, reperfusion, coronary venous retroperfusion. Springer, New York, pp 51–92
38. El-Maasarany S, Ferrett C, Firth A, Sheppard M, Henin M (2005) The coronary sinus conduit function, anatomical study (relationship to adjacent structures). Europace 7:475–481
39. Vlodaver D, Amplatz M, Burchell M, Edwards M (1976) Coronary heart disease, clinical angiographic, and pathologic profiles. Springer, New York
40. Roberts J (1958) Arteries, veins, and lymphatic vessels of the heart. In: Development and structure of the cardiovascular system. McGraw-Hill, New York, pp 85–118
41. Kawashima T, Sato K, Sato F, Sasaki H (2003) An anatomical study of the human cardiac veins with special reference to the drainage of the great cardiac vein. Ann Anat 185:535–542
42. Maros T, Racz L, Plugor S, Maros T (1983) Contributions to the morphology of the human coronary sinus. Anat Anz 154:133–144
43. Singh J, Houser S, Heist E, Ruskin J (2005) The coronary venous anatomy, a segmental approach to aid cardiac resynchronization therapy. J Am Coll Cardiol 46:68–74
44. Maric I, Bobinac D, Ostojic L, Petkovic M, Dujmovic M (1996) Tributaries of the human and canine coronary sinus. Acta Anat (Basel) 156:61–69
45. McAlpine W (1983) Heart and coronary arteries, an anatomical atlas for clinical diagnosis, radiological investigation, and surgical treatment. Springer, New York
46. Ortale J, Gabriel E, Iost C, Marquez C (2001) The anatomy of the coronary sinus and its tributaries. Surg Radiol Anat 23:15–21
47. Sun Y, Arruda M, Otomo K et al (2002) Coronary sinus-ventricular accessory connections producing posteroseptal and left posterior accessory pathways, incidence and electrophysiological identification. Circulation 106:1362–1367

48. von Ludinghausen M (1990) Microanatomy of the human coronary sinus and its major tributaries. In: Myocardial perfusion, reperfusion, coronary venous reperfusion. Steinkopff Verlag, Darmstadt, pp 93–122
49. Pejkovic B, Bogdanovic D (1992) The great cardiac vein. Surg Radiol Anat 14:23–28
50. Bales G (2004) Great cardiac vein variations. Clin Anat 17:436–443
51. Gerber T, Sheedy P, Bell M et al (2001) Evaluation of the coronary venous system using electron beam computed tomography. Int J Cardiovasc Imaging 17:65–75
52. Gilard M, Mansourati J, Etienne Y et al (1998) Angiographic anatomy of the coronary sinus and its tributaries. Pacing Clin Electrophysiol 21:2280–2284
53. Schaffler G, Groell R, Peichel K, Rienmuller R (2000) Imaging the coronary venous drainage system using electron-beam CT. Surg Radiol Anat 22:35–39
54. Schumacher B, Tebbenjohanns J, Pfieffer D, Omran H, Jung W, Luderitz B (1995) Prospective study of retrograde coronary venography in patients with posteroseptal and left-sided accessory atrioventricular pathways. Am Heart J 130:1031–1039
55. Jongbloed M et al (2005) Noninvasive visualization of the cardiac venous system using multislice computed tomography. J Am Coll Cardiol 45:749–753
56. Pina J (1975) Morphological study on the human anterior cardiac veins, venae cordis anteriores. Acta Anat 92:145–159
57. Mierzwa J (1975) Variations of the anterior cardiac veins and their orifices in the right atrium in man. Folia Morphol 34:125–132
58. Ansari A (2001) Anatomy and clinical significance of ventricular Thebesian veins. Clin Anat 14:102–110
59. Grant R (1929) Observations on the anatomy of the Thebesian vessels of the heart. Heart 15:103–123
60. Mochizuki S (1933) Vv cordis. In: Das venensystem der Japaner. Kenkyusha, Kioto, pp 41–64
61. Bergman R, Thompson S, Saadeh F (1988) Absence of the coronary sinus. Anat Anz 166:9–12
62. Parsonnet V (1953) The anatomy of the veins of the human heart with special reference to normal anastomotic channels. J Med Soc N J 50:446–452
63. Anderson S, Quill J, Iaizzo P (2008) Venous valves within left ventricular coronary veins. J Interv Card Electrophysiol 23:95–99
64. Buirski G et al (1986) Superior vena caval abnormalities, their occurrence rate, associated cardiac abnormalities and angiographic classification in a pediatric population with congenital heart disease. Clin Radiol 37:131–138
65. Pahwa R, Kumar A (2003) Persistent left superior vena cava, an intensivist's experience and review of the literature. South Med J 96:528–529
66. von Ludinghausen M (1987) Clinical anatomy of cardiac veins, Vv cardiacae. Surg Radiol Anat 9:159–168
67. Gerlis L et al (1984) Coronary sinus orifice atresia and persistent left superior vena cava: a report of two cases, one associated with atypical coronary artery thrombosis. Br Heart J 52:648–653
68. Harris W (1960) A case of bilateral superior venae cavae with a closed coronary sinus. Thorax 15:172–173
69. Sahinoglu K et al (1994) Human persistent left superior vena cava with doubled coronary sinus. Ann Anat 176:451–454
70. Mohl W (1994) Basic considerations and techniques in coronary sinus interventions. In: Coronary sinus interventions in cardiac surgery. R G Landes Company, Austin, pp 1–10
71. Junqueira LC, Kelley R (1998) Basic histology. Lange, Stamford Appleton
72. Kessel R (1998) Basic medical histology, the biology of cells, tissues, and organs. Oxford University Press, New York
73. Baroldi G, Mantero O, Scomazzoni G (1956) The collaterals of the coronary arteries in normal and pathologic hearts. Circ Res 4:223–229
74. Kitzman D, Edwards W (1990) Age-related changes in the anatomy of the normal human heart. J Gerontol 45:M33–M39
75. Moberg A (1967) Anatomical and functional aspects of extracardial anastomoses to the coronary arteries. Pathol Microbiol (Basel) 30:689–694
76. Waller B et al (1994) Anatomy of the heart. In: Hurst's the heart. McGraw-Hill, New York, pp 59–112
77. Leon A (2003) Cardiac resynchronization therapy devices, patient management and follow-up strategies. Rev Cardiovasc Med 4(Suppl 2):S38–S46
78. Oginosawa Y, Abe H, Nakashima Y (2005) Prevalence of venous anatomic variants and occlusion among patients undergoing implantation of transvenous leads. Pacing Clin Electrophysiol 28:425–428
79. Raman S, Morford R, Matthew N et al (2004) Rotational X-ray coronary angiography. Catheter Cardiovasc Interv 63:201–207
80. Maddux J, Wink O, Messenger J et al (2004) Randomized study of the safety and clinical utility of rotational angiography versus standard angiography in the diagnosis of coronary artery disease. Catheter Cardiovasc Interv 62:167–174
81. Coatrieux J, Hernandez A, Mabo P, Garreau M, Haigon, P (2005) Transvenous path finding in cardiac resynchronization therapy. In: Functional imaging and modeling of heart proceedings, pp 236–245
82. Ansalone G, Giannantoni P, Ricci R, Trambaiolo P, Fedele F, Santini M (2002) Doppler myocardial imaging to evaluate the effectiveness of pacing sites in patients receiving biventricular pacing. J Am Coll Cardiol 39:489–499
83. Cazeau S, Leclercq C, Lavergne T et al (2001) Effects of multisite biventricular pacing in patients with heart failure and intraventricular conduction delay. N Engl J Med 344:873–880
84. Lambiase P, Rinaldi A, Hauck J et al (2004) Non-contact left ventricular endocardial mapping in cardiac resynchronisation therapy. Heart 90:44–51
85. Minz G, Painte J, Pichard A et al (1995) Atherosclerosis in angiographically "normal" coronary artery reference segments, an intravascular ultrasound study with clinical correlations. J Am Coll Cardiol 25:1479–1485
86. Iqbal J, Gunn J, Serruys P (2013) Coronary stents, historical development, current status and future directions. Br Med Bull 106:193–211
87. Puri R, Worthley M, Nicholls S (2011) Intravascular imaging of vulnerable coronary plaque, current and future concepts. Nat Rev Cardiol 8:131–139
88. de Korte C, van der Steen A, Cespedes E, Pasterkamp G (1998) Intravascular ultrasound elastrography in human arteries, initial experience in vitro. Ultrasound Med Biol 24:401–408
89. Bezerra H, Costa M, Guagliumi G, Rollins A, Simon D (2009) Intracoronary optical coherence tomography, a comprehensive review clinical and research applications. JACC Cardiovasc Interv 2:1035–1046
90. Cassis L, Lodder R (1993) Near-IR imaging of atheromas in living arterial tissue. Anal Chem 65:1247–1256
91. Jaross W, Neumeister V, Lattke P, Schuh D (2008) Determination of cholesterol in atherosclerotic plaques using near infrared spectroscopy system. JACC Cardiovasc Imaging 147:327–337
92. Hoffmann U, Brady T, Muller J (2003) Use of new imaging techniques to screen for coronary artery disease. Circulation 108:e50–e53
93. Bluemke D, Achenbach S, Budoff M, Gerber TG et al (2008) Noninvasive coronary artery imaging: magnetic resonance angiography and multidetector computed tomography angiography. Circulation 118:1–21
94. Kantarci M, Karcaaltincaba SD, Karabulut M, Erol N, Yalcin M, Tatli A (2012) Clinical situation in which coronary CT angiography confers superior diagnostic information compared with coronary angiography. Diagn Interv Radiol 18:261–269

95. Earls J, Berman E, Urban B et al (2008) Prospectively gated transverse coronary CT angiography versus retrospectively gated helical technique, improved image quality and reduced radiation dose. Radiology 246:742–775
96. Wyler von Ballmoos M, Haring B, Juillerat R, Alkadhi H (2011) Meta-analysis, diagnostic performance of low-radiation-dose coronary computed tomography angiography. Ann Intern Med 154:413–420
97. Foo T, Ho V, Saranathan M et al (2005) Feasibility of integrating high-spatial-resolution 3D breath-hold coronary MR angiography with myocardial perfusion and viability examinations. Radiology 235:1025–1030
98. Al Moudi M, Sun Z, Lenzo N (2011) Diagnostic value of SPECT, PET and PET/CT in the diagnosis of coronary artery disease, a systematic review. Biomed Imaging Interv J 7, e9
99. Mc Ardle B, Dowsley T, deKemp R et al (2012) Does Rubidium-82 PET have superior accuracy to SPECT perfusion imaging for the diagnosis of obstructive coronary disease. J Am Coll Cardiol 60:1828–1837
100. Ormiston J, Serruys P (2009) Bioabsorbable coronary stents. Circ Cardiovasc Interv 2:255–260
101. Jain A, Smith E, Rothman M (2006) The coronary venous system, an alternative route of access to the myocardium. J Invasive Cardiol 18:563–568
102. Prasad A, Rihal C, Lennon R, Wiste H, Singh M, Holmes D Jr (2007) Trends in outcomes after percutaneous coronary intervention for chronic total occlusions, a 25-year experience from the Mayo Clinic. J Am Coll Cardiol 49:1611–1618
103. Iakovou I, Ge L, Colombo A (2005) Contemporary stent treatment of coronary bifurcations. J Am Coll Cardiol 46:1446–1455
104. Colomba A, Mikhail G, Michev I et al (2005) Treating chronic total occlusions using subintimal tracking and reentry, the STAR technique. Catheter Cardiovasc Interv 64:407–411
105. Weisz G, Moses J (2007) New percutaneous approaches for chronic total occlusion of coronary arteries. Expert Rev Cardiovasc Ther 5:231–241
106. Horvath K (2008) Transmyocardial laser revascularization. J Card Surg 23:266–276
107. Oskui PM et al (2014) Improved myocardial perfusion after transmyocardial laser revascularization in a patient with microvascular coronary artery disease. SAGE Open Medical Case Reports 2
108. Cappato R, Schluter M, Weiss C et al (2007) Mapping of the Coronary Sinus and Great Cardiac Vein Using a 2-French Electrode Catheter and a Right Femoral Approach. J Cardio Electrophys 8:371–376
109. Stellbrink C, Diem B et al (1997) Transcoronary venous radiofrequency catheter ablation of ventricular tachycardia. J Cardiovasc Electrophysiol 8:916–921
110. Dosdall D, Rothe D, Brandon T, Sweeney J (2004) Effect of rapid biphasic shock subpulse switching on ventricular defibrillation thresholds. J Cardiovasc Electrophysiol 15:802–808
111. Huang J, Walcott G, Killingsworth C, Smith W, Kenknight B, Ideker R (2002) Effect of rapid biphasic shock subpulse switching on ventricular defibrillation threshold. Pacing Clin Electrophysiol 25:42–48
112. Nitsch J (1989) Continuous monitoring of coronary perfusion during percutaneous transluminal coronary angioplasty of the left anterior descending artery. J Interv Cardiol 2:205–210
113. Gundry S (1982) A comparison of retrograde cardioplegia versus antegrade cardioplegia in the presence of coronary artery obstruction. Scientific Session of the American Heart Association, Dallas
114. Miyazaki A, Tadokoro H, Drury J et al (1991) Retrograde coronary venous administration of recombinant tissue-type plasminogen activator, a unique and effective approach to coronary artery thrombolysis. J Am Coll Cardiol 18:613–620
115. Thompson C, Nasseri B, Makower J et al (2003) Percutaneous transvenous cellular cardiomyoplasty: a novel nonsurgical approach for myocardial cell transplantation. J Am Coll Cardiol 41:1964–1971
116. Oesterle S, Reifart N, Hauptmann E et al (2001) Percutaneous in situ coronary venous arterialization, report of the first human catheter-based coronary artery bypass. Circulation 103:2539–2543
117. Barold S (2001) What is cardiac resynchronization therapy? Am J Med 111:224–232
118. Casey C, Knight B (2004) Cardiac resynchronization pacing therapy. Cardiology 101:72–78
119. Daubert J, Ritter P, Le Breton H et al (1998) Permanent left ventricular pacing with transvenous leads inserted into the coronary veins. Pacing Clin Electrophysiol 21:239–245
120. Walker S, Levy T, Rex D et al (2000) Initial United Kingdom experience with the use of permanent, biventricular pacemakers, implantation procedure and technical considerations. Europace 2:233–239
121. Gasparini M, Mantice M, Galimberti P et al (2003) Is the left ventricular lateral wall the best lead implantation site for cardiac resynchronization therapy? Pacing Clin Electrophysiol 26:162–168
122. Stevenson W, Sweeney M (2004) Single site left ventricular pacing for cardiac resynchronization. Circulation 109:1694–1696
123. Valls-Bertault V, Mansourati J, Gilard M, Etienne Y et al (2001) Adverse events with transvenous left ventricular pacing in patients with severe heart failure, early experience from a single centre. Europace 3:60–63
124. Abraham W et al (2004) Effects of cardiac resynchronization on disease progression in patients with left ventricular systolic dysfunction, an indication for an implantable cardioverter-defibrillator and mildly symptomatic chronic heart failure. Circulation 110:2864–2868
125. Alonso C, Leclercq C, d'Allonnes F et al (2001) Six year experience of transvenous left ventricular lead implantation for permanent biventricular pacing in patients with advanced heart failure, technical aspects. Heart 86:405–410
126. Rossillo A et al (2004) Impact of coronary sinus lead position on biventricular pacing, mortality and echocardiographic evaluation during long-term follow-up. J Cardiovasc Electrophysiol 15:1120–1125
127. Conti C (2006) Cardiac resynchronization therapy for chronic heart failure, why does it not always work? Clin Cardiol 29:335–336
128. Yu C, Wing-Hong F, Zhang Q, Sanderson J (2005) Understanding nonresponders of cardiac resynchronization therapy – current and future perspectives. J Cardiovasc Electrophysiol 16:1117–1124
129. Mair H, Sachweh J, Meuris B et al (2005) Surgical epicardial left ventricular lead versus coronary sinus lead placement in biventricular pacing. Eur J Cardiothorac Surg 27:235–242
130. Fisher J et al (1984) Attempted nonsurgical electrical ablation of accessory pathways via the coronary sinus in the Wolff-Parkinson-White syndrome. J Am Coll Cardiol 4:685–694
131. Haissaguerre M et al (1992) Radiofrequency catheter ablation of left lateral accessory pathways via the coronary sinus. Circulation 86:1464–1468
132. Gaita F, Riccard P, Ferraro A (2002) Cryothermic ablation within the coronary sinus of an epicardial posterolateral pathway. J Cardiovasc Electrophysiol 13:1160–1163
133. Haissaguerre M et al (2007) Impact of catheter ablation of the coronary sinus on paroxysmal or persistent atrial fibrillation. J Cardiovasc Electrophysiol 18:378–386
134. Banai S et al (2007) Coronary sinus reducer stent for the treatment of chronic refractory angina pectoris, a prospective, open label, multicenter, safety feasibility first-in-man study. J Am Coll Cardiol 49:1783–1789
135. Harnek J et al (2011) Transcatheter implantation of the MONARC coronary sinus device for mitral regurgitation, 1 year results from

the EVOLUTION phase I study. JACC Cardiovasc Interv 4:115–122
136. Choure A et al (2006) In vivo analysis of the anatomical relationship of coronary sinus to mitral annulus and left circumflex coronary artery using cardiac multidetector computed tomography. J Am Coll Cardiol 15:1938–1945
137. Tacker W, Vanvleet J, Schoenlein W, Janas W et al (1998) Postmortem changes after lead extraction from the ovine coronary sinus and great cardiac vein. Pacing Clin Electrophysiol 21:296–298
138. De Martino G, Orazi S, Bisignani G et al (2005) Safety and feasibility of coronary sinus left ventricular leads extraction, a preliminary report. J Interv Card Electrophysiol 13:35–38
139. Rickard J, Tarakji K, Cronin E et al (2012) Cardiac venous left ventricular lead removal and reimplantation following device infection. J Cardiovasc Electrophysiol 23:1213–1216
140. Sheldon S, Friedman P, Hayes D et al (2012) Outcomes and predictors of difficulty with coronary sinus lead removal. J Interv Card Electrophysiol 35:93–100
141. Cronin E, Ingelmo C, Rickard J et al (2012) Active fixation mechanism complicates coronary sinus lead extraction and limits subsequent reimplantation targets. J Interv Card Electrophysiol 36:81–86
142. Maytin M, Carillo R, Baltodano P (2012) Multicenter experience with transvenous lead extraction of active fixation coronary sinus leads. Pacing Clin Electrophysiol 35:641–647
143. Anderson S, Hill A, Iaizzo P (2009) Microanatomy of human left ventricular coronary veins. Anat Rec 292:23–28
144. Dodge J Jr, Brown B, Bolson E (1992) Lumen diameter of normal human coronary arteries: influence of age, sex, anatomic variation, and left ventricular hypertrophy or dilation. Circulation 86:232–246
145. Zubaid M, Buller C, Mancini G (2002) Normal angiographic tapering of the coronary arteries. Can J Cardiol 18:973–980
146. Ono T, Shimohara Y, Okada K, Irino S (1986) Scanning electron microscopic studies on microvascular architecture of human coronary vessels by corrosion casts, normal and focal necrosis. Scan Electron Microsc 263–270
147. Hellerstein H, Orbison J (1951) Anatomic variations of the orifice of the human coronary sinus. Circulation 3:514–523
148. Potkin B, Roberts W (1987) Size of coronary sinus at necropsy in subjects without cardiac disease and in patients with various cardiac conditions. Am J Cardiol 60:1418–1421
149. Spencer J, Prahl G, Iaizzo P (2014) The prevalence of coronary sinus and left circumflex artery overlap in relation to the mitral valve. J Interv Cardiol 27:308–316
150. Ge J, Erbel R, Gerger T et al (1994) Intravascular ultrasound imaging of angiographically normal coronary arteries: a prospective study in vivo. Br Heart J 71:572–578
151. Piffer C, Piffer M, Zoretto N (1990) Anatomic data of the human coronary sinus. Anat Anz 170:21–29
152. Felle P, Bannigan J (1994) Anatomy of the valve of the coronary sinus (Thebesian valve). Clin Anat 7:10–12
153. Hill A, Ahlberg S, Wilkoff B, Iaizzo P (2006) Dynamic obstruction to coronary sinus access, the Thebesian valve. Heart Rhythm 3:1240–1241
154. Hill A, Coles J Jr, Sigg D, Laske T, Iaizzo P (2003) Images of the human coronary sinus ostium obtained from isolated working hearts. Ann Thorac Surg 76:2108
155. Jatene M, Jatene F, Costa R et al (1991) Anatomical study of the coronary sinus valve – Thebesius valve. Chest 100(Suppl):90S
156. Spencer J, Larson A, Drake R, Iaizzo P (2014) A detailed assessment of the human coronary venous system using contrast computed tomography of perfusion-fixed specimens. Heart Rhythm 11:282–288
157. Andserson S, Hill A, Iaizzo P (2007) Venous valves, unseen obstructions to coronary access. J Interv Card Electrophysiol 19:165–166
158. Achenbach S, Kessler W, Moshage W et al (1997) Visualization of the coronary arteries in three-dimensional reconstructions using respiratory gated magnetic resonance imaging. Coron Artery Dis 8:441–448
159. Achenbach S, Ulzheimer S, Baum U et al (2000) Noninvasive coronary angiography by retrospectively ECG-gated multislice spiral CT. Circulation 102:2823–2828
160. Li D, Kaushikkar S, Haacke E et al (1996) Coronary arteries, three-dimensional MR imaging with retrospective respiratory gating. Radiology 201:857–863
161. Gradus-Pizlo I, Feigenbaum H (2002) Imaging of the left anterior descending coronary artery by high-frequency transthoracic and epicardial echocardiography. Am J Cardiol 90:28L–31L
162. Kim W, Stuber M, Bornert P, Kissinger K et al (2002) Three-dimensional black-blood cardiac magnetic resonance coronary vessel wall imaging detects positive arterial remodeling in patients with nonsignificant coronary artery disease. Circulation 299:296
163. Basso C, Thiene G (2005) Adipositas cordis, fatty infiltration of the right ventricle, and arrhythmogenic right ventricular cardiomyopathy. Cardiovasc Pathol 14:37–41
164. Corradi D, Maestri R, Callegari S et al (2004) The ventricular epicardial fat is related to the myocardial mass in normal, ischemic and hypertrophic hearts. Cardiovasc Pathol 13:313–316
165. Hangertner J, Marley N, Whitehead A, Thomas A, Davies M (1985) The assessment of cardiac hypertrophy at autopsy. Histopathology 9:1295–1306
166. Reiner L, Mazzoleni A, Rodriguez F, Freudenthal R (1959) The weight of the human heart. I. Normal cases. AMA Arch Pathol 68:58–73
167. Shirani J, Berezowski K, Roberts W (1995) Quantitative measurement of normal and excessive (cor adiposum) subepicardial adipose tissue, its clinical significance, and its effect on electrocardiographic QRS voltage. Am J Cardiol 76:414–418
168. Sons H, Hoffmann V (1986) Epicardial fat cell size, fat distribution and fat infiltration of the right and left ventricle of the heart. Anat Anz 161:355–373
169. Rokey R, Mulvagh S, Cheirif J, Mattox K, Johnston D (1989) Lipomatous encasement and compression of the heart, antemortem diagnosis by cardiac nuclear magnetic resonance imaging and catheterization. Am Heart J 117:952–953
170. Anderson S, Iaizzo P (2010) Effect of pacing lead positions and venous microanatomy on pacing parameters. J Electrocardiol 43:136–141
171. Mao S, Shinbane J, Girsky M et al (2005) Coronary venous imaging with electron beam computed tomographic angiography, three-dimensional mapping and relationship with coronary arteries. Am Heart J 150:315–322
172. Spencer J, Sundaram C, Iaizzo P (2014) The relative anatomy of the coronary arterial and venous systems: implications for coronary interventions. Clin Anat 27:1023–1029
173. Maselli D et al (2006) Percutaneous mitral annuloplasty, an anatomic study of human coronary sinus and its relation with mitral valve annulus and coronary arteries. Circulation 114:377–380
174. Hansky B et al (2007) Implantation of active fixation leads in coronary veins for left ventricular stimulation, report of five cases. Pacing Clin Electrophysiol 30:44–49
175. Nagele H et al (2007) First experience with a new active fixation coronary sinus lead. Europace 9:437–441
176. Bates R, Toscano M, Balderman S, Anagnostopoulos C (1977) The cardiac veins and retrograde coronary venous perfusion. Ann Thorac Surg 23:83–90
177. Oesterle S, Reifart N, Hayase M et al (2003) Catheter-based coronary bypass, a development update. Catheter Cardiovasc Interv 58:212–218
178. Schoger J et al (2009) Percutaneous mitral annuloplasty for functional mitral regurgitation, result of the CARILLON Mitral

Annuloplasty Device European Union Study. Circulation 120:326–333
179. Siminiak T et al (2012) Treatment of functional mitral regurgitation by percutaneous annuloplasty, results of the TITAN trial. Eur J Heart Fail 14(8):931–938
180. Machaalany J et al (2013) Treatment of functional mitral valve regurgitation with the permanent percutaneous transvenous mitral annuloplasty system. Am Heart J 165:761–769
181. Wong K, Lim C, Sadarim P (2011) High incidence of acute subclinical circumflex artery 'injury' following mitral isthmus ablation. Eur Heart J 32:1881–1890
182. Biffi M et al (2009) Phrenic stimulation, a challenge for cardiac resynchronization therapy. Circ Arrhythm Electrophysiol 2:402–410
183. Yokokawa M et al (2011) Impact of mitral isthmus anatomy on the likelihood of achieving linear block in patients undergoing catheter ablation of persistent atrial fibrillation. Heart Rhythm 8:1404–1410
184. Becker A (2004) Left atrial isthmus, anatomic aspects relevant for linear catheter ablation procedures in humans. J Cardiovasc Electrophysiol 15:809–812
185. Wong K et al (2011) Larger coronary sinus diameter predicts the need for epicardial delivery during mitral isthmus ablation. Europace 13:555–561
186. Wong K, Betts T (2012) A review of mitral isthmus ablation. Indian Pacing Electrophysiol J 12:152–170
187. Abbara S et al (2005) Noninvasive evaluation of cardiac veins with 16-MDCT angiography. AJR Am J Roentgenol 185:1001–1006
188. Muhlenbruch G et al (2005) Imaging of the cardiac venous system, comparison of MDCT and conventional angiography. AJR Am J Roentgenol 185:1252–1257
189. Tada H et al (2005) Three-dimensional visualization of the coronary venous system using multidetector row computed tomography. Circ J 69:165–170
190. Van de Veire N et al (2006) Non-invasive visualization of the cardiac venous system in coronary artery disease patients using 64-slice computed tomography. J Am Coll Cardiol 48:1832–1838
191. Manzke R et al (2011) Assessment of the coronary venous system in heart failure patients by blood pool agent enhanced whole-heart MRI. Eur Radiol 21:799–806
192. Ludinghausen M (2003) The clinical anatomy of coronary arteries. Springer, New York

The Pericardium

9

Eric S. Richardson, Alexander J. Hill,
Nicholas D. Skadsberg, Michael Ujhelyi,
Yong-Fu Xiao, and Paul A. Iaizzo

Abstract

The pericardium is a unique structure that surrounds the heart and serves several important physiological roles. The removal of the pericardium, certain pericardial disorders, or the buildup of fluids within this space will ultimately alter hemodynamic performance. Recent therapeutic approaches have been directed to exploit the space that exists between the pericardium and the epicardial surface of the heart. New devices and techniques are being developed to access this space with minimally invasive approaches. The pharmacokinetics of many drugs may be greatly enhanced if the drug is delivered into the pericardium. As more is learned about the pericardium, it may play a significant role in cardiac therapies.

Keywords

Pericardium • Pericardial fluid • Mechanical effects • Pericardial disorders • Comparative anatomy • Intrapericardial therapeutics

9.1 Introduction

The pericardium is a fibroserous conical sac structure encasing the heart and roots of the great cardiac vessels. In humans, it is located within the mediastinal cavity posterior to the sternum and cartilages of the 3rd through 7th ribs of the left thorax and is separated from the anterior wall of the thorax. It is encompassed from the posterior resting against the bronchi, the esophagus, the descending thoracic aorta, and the posterior regions of the mediastinal surface of each lung. Laterally, the pericardium is covered by the pleurae and lies along the mediastinal surfaces of the lung. It can come into direct contact with the chest wall near the ventricular apical region, but this varies with the dimensions of the long axis of the heart or with various disease states. Under normal circumstances, the pericardium separates and isolates the heart from contact by the surrounding tissues, allowing freedom of cardiac movement within the confines of the pericardial space (Fig. 9.1).

9.2 Anatomy

In humans, the 1–3 mm thick fibrous pericardium is commonly described as a *flask-shaped bag*. The neck of the pericardium (superior aspect) is closed by its extensions surrounding the great cardiac vessels, while the base is attached to the central tendon and to the muscular fibers of the left side of the diaphragm (Fig. 9.2). Much of the pericar-

Electronic supplementary material: The online version of this chapter (doi:10.1007/978-3-319-19464-6_9) contains supplementary material, which is available to authorized users.

E.S. Richardson, PhD (✉)
Department of Bioengineering, Rice University,
6500 Main Street, Suite 525, Houston, TX 77030, USA
e-mail: richardson@rice.edu

A.J. Hill, PhD • N.D. Skadsberg, PhD
M. Ujhelyi, PharmD, FCCP • Y.-F. Xiao, MD, PhD
Medtronic, Inc., Minneapolis, MN, USA

Y.-F. Xiao, MD, PhD
University of Medicine and Dentistry of New Jersey,
Newark, NJ, USA

P.A. Iaizzo, PhD
Department of Surgery, University of Minnesota,
Minneapolis, MN, USA

P.A. Iaizzo (ed.), *Handbook of Cardiac Anatomy, Physiology, and Devices*, DOI 10.1007/978-3-319-19464-6_9

dium's diaphragmatic attachment consists of loose fibrous tissue that can be readily separated and/or isolated, but there is a small area over the central tendon where the diaphragm and the pericardium are completely fused.

Examination of the pericardium reveals that it is composed of two interconnected structures: the serous pericardium and the fibrous pericardium. The serous pericardium is one continuous sac with a large infold that contains the heart (Fig. 9.3). An appropriate analogy would be a fist (representing the heart) pushed into the side of a deflated balloon (representing the serous pericardium), therefore enveloped by two individual layers of material. The interior surface of the pericardium is intimately connected to the surface of the heart and is known as the *visceral pericardium* or the *epicardium*. The exterior surface of the serous pericardium is known as the *parietal pericardium* and is fused with the thick lining of the fibrous pericardium. The pericardial space, where the pericardial fluid resides, is bounded on either side by the parietal and visceral pericardium. To the naked eye, however, the visceral pericardium cannot be distinguished from the surface of the heart, and the parietal pericardium cannot be distinguished from the fibrous pericardium. For this reason, the general use of the term *pericardium* refers to the composite of the parietal and fibrous pericardium, which appears to be a single sac that surrounds the heart. Yet, more accurately, the pericardium should be described as three total layers, with fluid lining between two of them (Fig. 9.3).

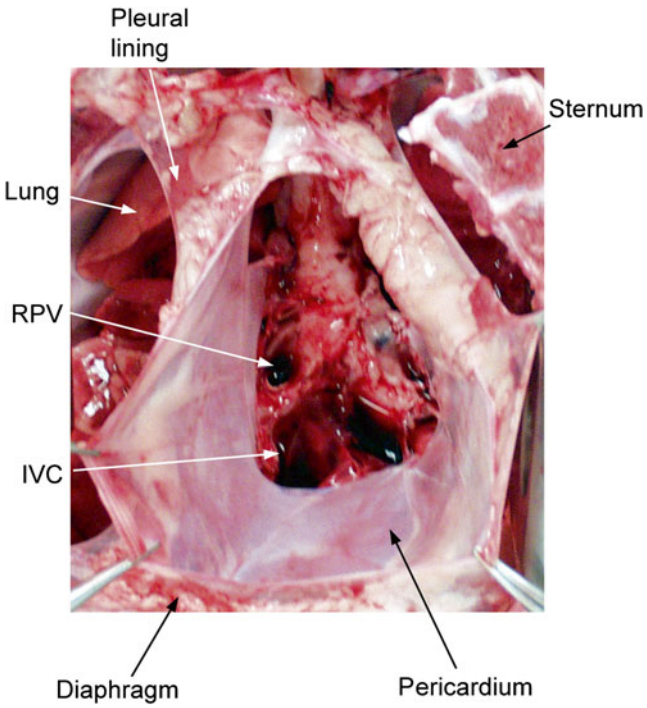

Fig. 9.1 Posterior view of the pericardial sac, with the anterior surface and heart cut away. One can see that the great vessels of the heart penetrate through the pericardium, which extends up these vessels for several centimeters

The inferior vena cava enters the pericardium through the central tendon of the diaphragm where there exists a small area of fusion between the pericardium and the central tendon, but it receives no covering from this fibrous layer. Between the left pulmonary artery and subjacent pulmonary vein is a triangular fold of the serous pericardium known as the *ligament of the left vena cava* (or vestigial fold of Marshall). It is formed by a serous layer over the remnant of the lower part of the left superior vena cava (duct of Cuvier) which regresses during fetal life but remains as a fibrous band stretching from the highest left intercostal vein to the left atrium, where it aligns with a small vein known as the *vein of the left atrium* (or oblique vein of Marshall), eventually opening into the coronary sinus. The pericardium is also attached to the posterior-sternal surface by superior and inferior sternopericardial

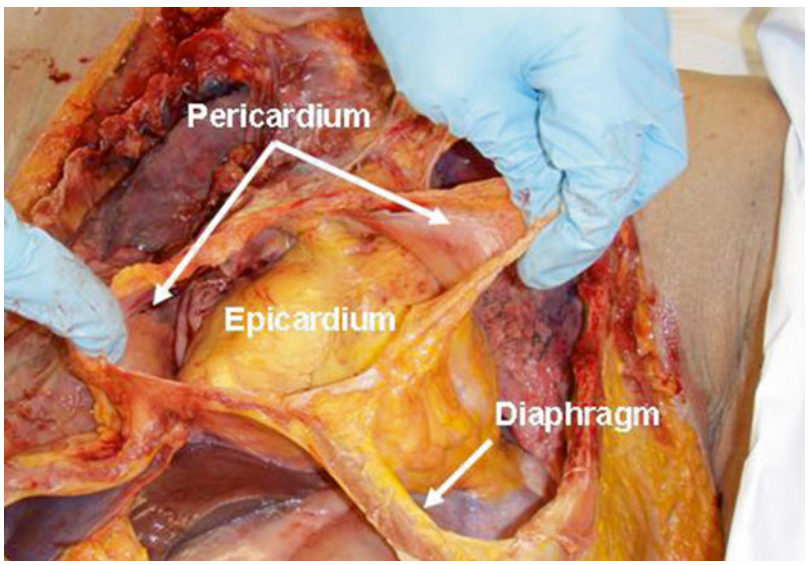

Fig. 9.2 The fibrous pericardium of a fresh human cadaver is opened to expose the epicardium of the heart. Note the attachment of the pericardium to the diaphragm

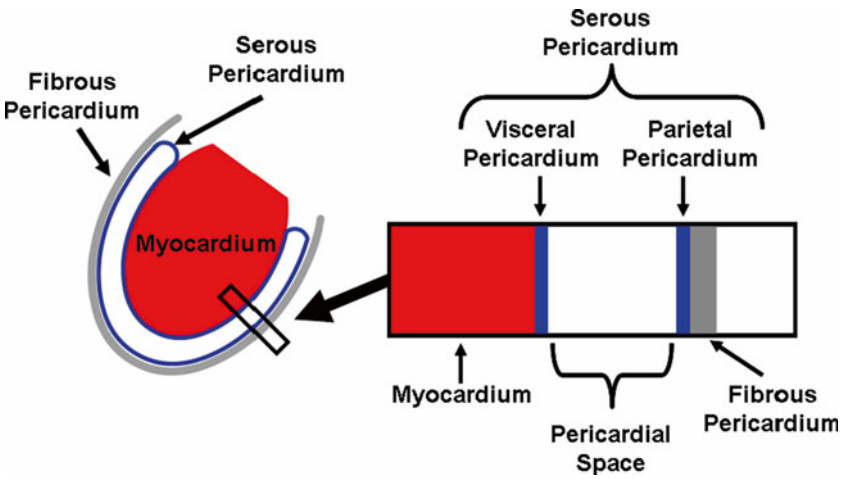

Fig. 9.3 *Left*: A schematic diagram of the serous and fibrous pericardium with respect to the heart. *Right*: An expanded cross-section view shows the attachment of two layers of the serous pericardium (visceral and parietal) to the myocardium and fibrous pericardium, respectively

ligaments that securely anchor the pericardium and also act to maintain the orientation of the heart inside the thorax.

As previously mentioned, the serous pericardium is a closed sac that lines the fibrous pericardium consisting of a visceral and a parietal portion. The visceral portion that covers the heart and great vessels is commonly referred to as the *epicardium* and is continuous with the parietal layer that lines the fibrous pericardium. The parietal portion covering the remaining vessels is arranged in the form of two tubes. The aorta and pulmonary artery are enclosed in one tube (the *arterial mesocardium*), while the superior and inferior venae cavae and the four pulmonary veins are enclosed in the second tube (the *venous mesocardium*) (see JPG 9.1 in the online supplemental material). There is an attachment to the parietal layer between the two branches, behind the left atrium, commonly referred to as the *oblique sinus*. There is also a passage between the venous and arterial mesocardia (i.e., between the aorta and pulmonary artery in front and the atria behind) that is termed the *transverse sinus*. The *superior sinus or superior aortic recess* extends upward along the right side of the ascending aorta to the origination point of the innominate artery. The superior sinus also joins the transverse sinus behind the aorta, and they are both continually fused until they reach the aortic root. For additional text describing this anatomy, also see Chap. 5.

The arteries of the pericardium are derived from the internal mammary and its musculophrenic branch and also from the descending thoracic aorta. The nerves innervating the pericardium are derived from the vagus and phrenic nerves, as well as the sympathetic trunks.

9.3 Physiology of the Normal Pericardium

9.3.1 Pericardial Fluid

In normal hearts, the pericardium should be considered as only a potential space. It contains 20–60 mL of pericardial fluid, most of which resides in the major pericardial sinuses and the atrioventricular grooves [1]. The fluid is an ultrafiltrate of plasma and therefore has many similarities to plasma in its electrolyte composition; pericardial fluid, however, contains about half the total protein concentration, one-third the triglyceride and cholesterol content, and one-fifth the amount of white blood cells [2]. A more complete comparison of plasma and pericardial fluid composition is shown in Table 9.1.

The details of the formation, clearance, and turnover of pericardial fluid have not yet been fully explained. Yet, it is generally agreed that pericardial fluid is derived from plasma leakage from myocardial capillaries [3], and this filtrate is eventually drained by the lymphatic system. During situations of high pericardial fluid pressure, such as in cardiac tamponade, investigators have found that fluid may pass through the pericardium and enter the pleural space [4]. The turnover time of pericardial fluid in humans has not been established, but in sheep it is observed to be every 5.4 h [5].

As mentioned previously, pericardial fluid distribution is not uniform. The majority of the fluid found in the major sinuses and grooves of the heart and makes up the pericardial reserve volume. The fluid is considered to be well mixed due to the motion of the heart, and agents injected into the pericardial space quickly and evenly disperse throughout [5]. Too much pericardial fluid, either due to disease or an intervention, may cause increased pericardial pressure and compromise cardiac performance, a syndrome called *cardiac tamponade*. As shown in Fig. 9.4, the pericardial reserve volume acts as a buffer against increasing pressure; once these groves and sinuses have filled, however, the pressure quickly increases with additional fluid volume.

9.3.2 Mechanical Effects of the Pericardium

The degree to which the pericardium alters heart wall movement(s) varies depending on the ratio of cardiac to pericardial size, loading conditions, and the degree of active and passive filling. Closure of the pericardial sac following open-heart

Table 9.1 Normal plasma composition compared to the pericardial fluid composition of 30 patients undergoing cardiac surgery

	Normal plasma range	Pericardial fluid mean value	Mean fluid/serum ratio
Total protein (g/dL)	6.5–8.2	3.3	0.6
Albumin (g/dL)	3.6–5.5	2.4	0.7
Glucose (mg/dL)	70–110	133	1.0
Urea (mg/dL)	15–45	33	1.0
Calcium (mg/dL)	8.1–10.4	7.3	0.9
LDH (IU/L)	100–260	398	2.4
Creatinine (mg/dL)	0.8–1.2	0.9	0.9
Cholesterol (mg/dL)	130–240	43	0.3
Triglycerides (mg/dL)	50–170	34	0.3
White blood cells (K/μL)	4.0–10.8	1.4	0.2

Data from Ben-Horin [2]

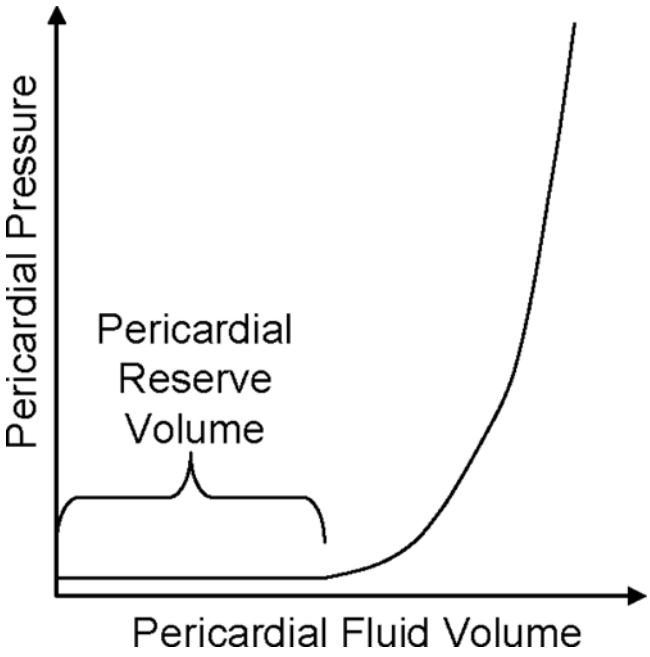

Fig. 9.4 As pericardial fluid volume increases, the pericardial reserve volume is filled. Once the reserve volume is full, pressure within the pericardium rapidly rises and cardiac performance may be compromised. Adapted from Spodick [1]

surgery has been proposed to (1): avoid possible postoperative complications, (2) reduce the frequency of ventricular hypertrophy, and/or (3) facilitate future potential reoperations by reducing fibrosis [6]. Furthermore, reported differences in ventricular performance, dependent on the presence of the pericardium, have been observed following cardiac surgery [7, 8].

In general, the presence of a pericardium physically constrains the heart, often resulting in a depressive hemodynamic influence limiting cardiac output by restraining diastolic ventricular filling [9, 10] (see Video 9.1 in the online supplemental material). The physical constraint by the pericardium is translated into direct external mechanical forces that can also alter patterns in myocardial and systemic blood flow [10, 11]. Direct primary and indirect secondary effects are observed as additional forces through the chamber free walls. Because both the left and right side atria and the left and right side ventricles are bound by a common septum, geometrical changes from chamber interaction(s) are dynamic, depending on the different filling rates and ejection rates of each of the four chambers [12, 13]. Thus, it is important to note that chamber-to-chamber interactions through the interventricular septum and by the pericardium further promote direct mechanical chamber interactions [14–16].

The effects of the pericardium on mechanical measures of cardiac performance are generally not evident until ventricular and atrial filling limitations are reached, changing geometrical and mechanical properties through factors such as maximum chamber volume and elasticity. These effects become more evident as the pericardial limitations become extended [17, 18]. With the known force-length dependence of cardiac muscle, variation of chamber volumes through removal of the pericardium will, in turn, alter isometric tensions and therefore directly impact systolic ejection. On the other hand, in specific cases where the restrictive role of the pericardium greatly increases, such as during cardiac tamponade, an increased intrapericardial fluid volume may result in critical restriction by the pericardium that then reduces cardiac performance (Fig. 9.5) [19, 20].

It should also be noted that increases in intrathoracic pressure will create an additional interaction between the ventricles, as well as between the heart and lungs in a closed chest. Thus, studying cardiac function in situ (with an opened chest) or in vitro allows for the elimination of these influences of intrathoracic pressure and for more direct identification and quantification of pericardial influences on cardiac performance and ejection [21]. Furthermore, such isolation of these pericardial effects from diastolic filling is an important consideration, since normal ventricular output is dependent on diastolic pressure and independent of the presence of the pericardium [22].

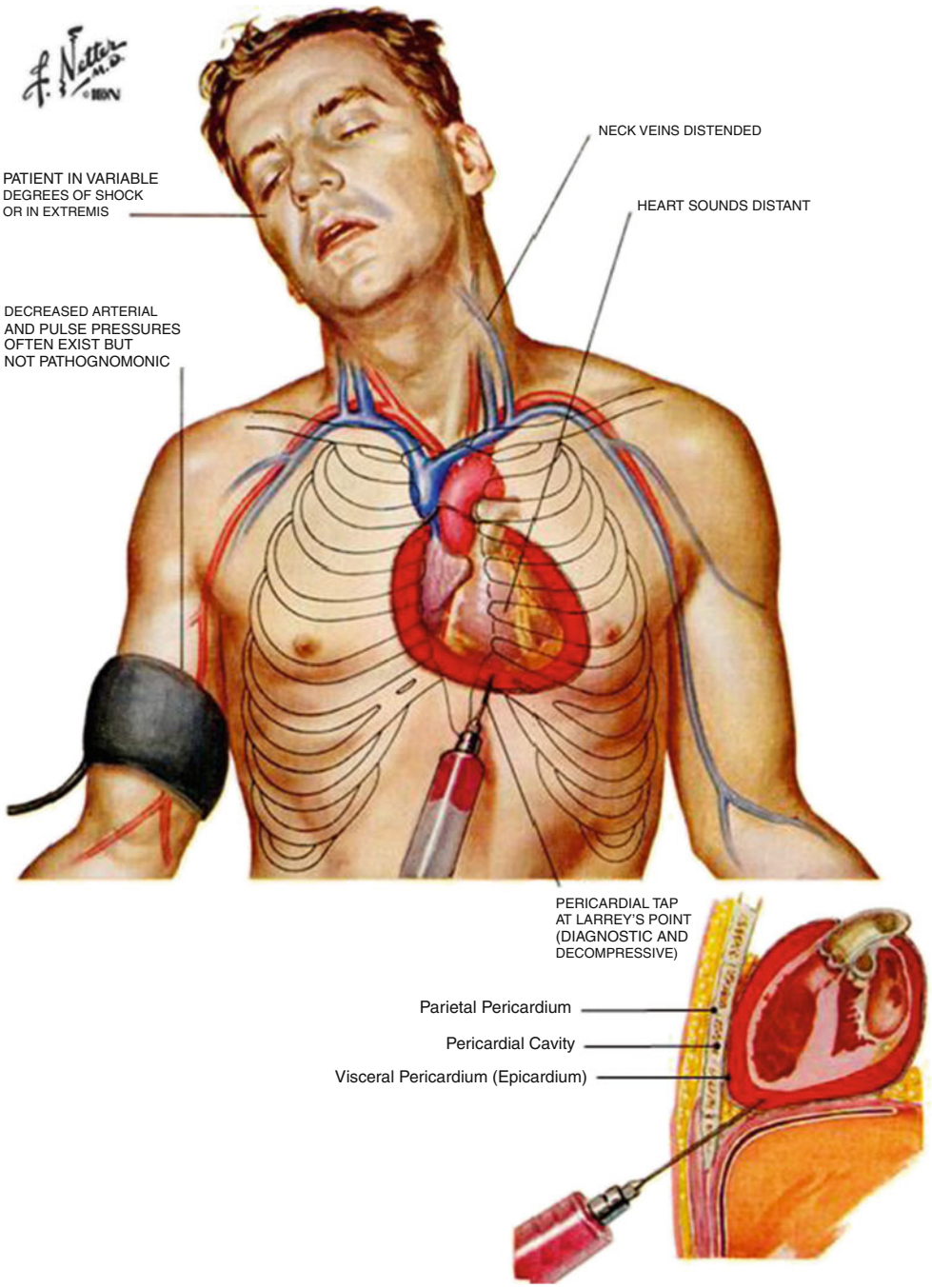

Fig. 9.5 Cardiac tamponade occurs when there is a large accumulation of fluid in the pericardium (*top*). During tamponade, hemodynamics may be seriously compromised. Distended neck veins, decreased blood pressure, various degrees of shock, and distant heart sounds may all be symptoms of tamponade. In most cases, tamponade is treated by pericardiocentesis or drainage of the sac with a long hypodermic needle (*bottom*). ©2006 Elsevier Inc. All rights reserved. www.netterimages.com, Frank Netter

9.4 Pericardial Disorders: Congenital, Pathological, and Iatrogenic

Sir William Osler referred to pericardial disease when he stated that "probably no serious disease is so frequently overlooked by the practitioner" [23]. Many pericardial disorders are asymptomatic and often go unnoticed throughout the patient's life, but some may be fatal (Fig. 9.6). Pericardial disorders may be classified as congenital, pathological, or iatrogenic.

Congenital abnormalities of the pericardium are extremely rare. Partial absence of the pericardium may occur, usually exposing the left side of the heart. Complete absence of the pericardium is even less frequent [23]. Cysts may also form during development in, on, or around the pericardium. These usually are not clinically significant and need to be treated only if they become symptomatic [1]. A list of these major congenital abnormalities is found in Table 9.2.

During disease or injury, the pericardium responds with the production of fluid, fibrin, cells, or a combination of the

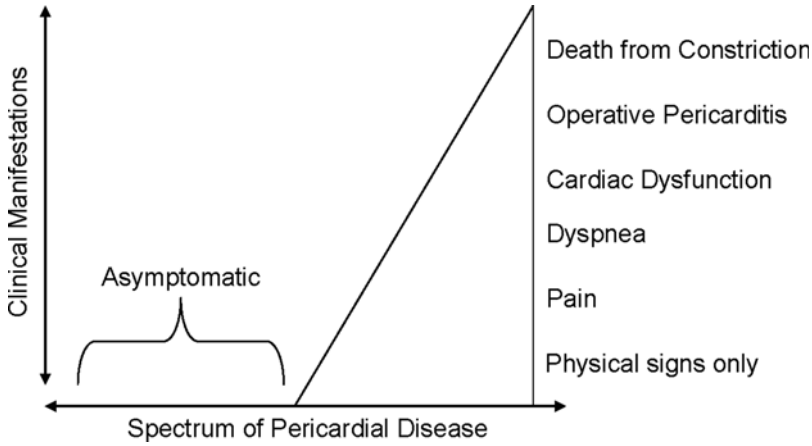

Fig. 9.6 Most pericardial diseases are discovered postmortem, implying that they were asymptomatic throughout the patient's life. Serious pericardial disease, however, may have many clinical manifestations, as shown in the figure. Adapted from Reddy [22]

Table 9.2 Major sources of pericardial disorders (congenital, pathological, or iatrogenic)

Congenital	Pathological	Iatrogenic
Primary	Idiopathic pericarditis	Surgical
Pericardial absence	Due to living agents—infectious, parasitic	Instrument trauma
Cysts	Vasculitis—connective tissue disease	Cardiac resuscitation
Teratoma	Immunopathies/hypersensitivity states	Iatrogenic pneumopericardium
Lymphangioma	Disease of contiguous structures	Drug reactions and complications
Diverticulum	Disorders of metabolism	Radiation
Pericardial bands	Trauma—indirect, direct	
Secondary	Neoplasms—primary, metastatic, multicentric	
Pericarditis due to maternal lupus	Uncertain pathogenesis	
Intrapericardial hernia of abdominal organs		

Adapted from Spodick [1]

three [23]. The amount of each depends upon the type of disease or injury. Numerous forms of pericarditis can initiate an inflammatory response, including fibrinous pericarditis, fibrous pericarditis, infective pericarditis, and cholesterol pericarditis. Diseases unrelated to the pericardium may also trigger a pericardial response, such as a nearby neoplasm or a myocardial infarction. After a transmural myocardial infarction, for example, patients almost always form adhesions between the necrotic area of the myocardium and the fibrous pericardium [23]. Pericardial effusions, or excess fluid in the pericardium, may occur with disease. Large volumes of lymph, chyle, or blood may accumulate in the pericardial sac. If the accumulation of fluid is significant, this may result in impaired cardiac function. This condition, cardiac tamponade, can be fatal if not treated. A list of several major pathologically induced pericardial disorders is also found in Table 9.2.

Finally, iatrogenic disorders often occur during the treatment of unrelated diseases. During cardiac surgery, the pericardium is often removed (partially or entirely) and is rarely repaired. There has been much debate as to whether closing the pericardium after surgery would be beneficial to the patient. Most surgeons believe that closing the pericardium may acutely compromise postoperative hemodynamics and increase the risk of tamponade. More recent research has shown that there are no clinical benefits, but there may be adverse effects resulting from closure of the pericardium after cardiac surgery [24]. Nevertheless, if the pericardium is left open, the exposed epicardium tends to become very fibrous, complicating future interventions. It should be noted that non-cardiac surgical procedures performed near the heart may also induce trauma to the pericardium and cause an inflammatory response. Furthermore, even nonsurgical interventions may damage the pericardium. For example, resuscitation from cardiac arrest (CPR) may cause a fibrous response. In some patients, irradiation may create an effusion and subsequent tamponade [23]. The pericardium may also adversely react to a number of commonly prescribed drugs such as procainamide, penicillin, doxorubicin, anticoagulants, and/or antithrombotics [1]. The reader is again referred to Table 9.2 for a list of major iatrogenic pericardial disorders.

In general, pericardial disorders can be diagnosed using ECG, echocardiography, radiography, and/or auscultation. Pericardial fluid samples and pericardial tissue biopsies may also aid in complicated diagnoses. Typically, once diagnosed, pericardial disorders are often treatable with a number of

drugs and/or interventions [25]. In situations of large pericardial effusions, pericardiocentesis is performed by draining the effusion with a hypodermic needle inserted near the xiphoid process (Fig. 9.5). This is usually done under guidance of echocardiography or fluoroscopy to prevent myocardial puncture, but in emergency situations (such as during acute cardiac tamponade), it may be done without guidance ("blindly"). Chronic effusions or other diseases may necessitate a partial or complete pericardiotomy. This is done by creating an opening into the mediastinum (called a pericardial window) to view and remove portions of the pericardium; visualization of the procedure can be enhanced by a laparoscope or thoracoscope. Balloon pericardiotomy is a recently developed minimally invasive technique that uses a balloon to enlarge a small hole in the pericardium [3].

9.5 Comparative Anatomy of the Pericardium

The pericardium is fixed to the great arteries at the base of the heart and is attached to the sternum and diaphragm in all mammals, although the degree of these attachments to the diaphragm varies between and within species [26, 27]. Specifically, the attachment to the central tendinous aponeurosis of the diaphragm is firm and broad in humans and pigs, the phrenopericardial ligament is the only attachment in dogs, and the caudal portion of the pericardium is attached via the strong sternopericardial ligament in sheep [26, 27] (see Video 9.2 in the online supplemental material).

Although the basic structure of the pericardium is the same, differences exist between various species with respect to both geometry and structure [28–30]. Generally, pericardial wall thickness usually increases with increasing heart and cavity size between the various species [28]. Humans are a notable exception to this rule, having a much thicker pericardium than animals with similar heart sizes [28]. Specifically, the pericardium of human hearts varies in thickness between 1 and 3.5 mm [1], while the average pericardial thickness of various animal species is considerably thinner (ovine hearts, 0.32 ± 0.01 mm; porcine hearts, 0.20 ± 0.01 mm; and canine hearts, 0.19 ± 0.01 mm) [29]). Differences in the relative volume of pericardial fluid also exist. Holt [28] reported that most dogs have between 0.5 and 2.5 mL of pericardial fluid (with some dogs having up to 15 mL), compared to 20–60 mL in adult human cadaver hearts. In the Visible Heart® Lab, we have found that 70–80 kg swine have about 7–8 mL of pericardial fluid. When selecting an appropriate animal model for pericardial access procedures or intrapericardial therapeutics, the significant differences of pericardial thickness, pericardial fluid volume, and pericardial attachments between humans and the various animal models must be considered.

9.6 Surgical Uses of the Pericardium

Due to the inherent mechanical properties of the fibrous pericardium, it has been used in various applications during surgery and has also been used in bioprosthetic heart valves. During cardiac surgery, fresh autografts, cryopreserved homografts, or glutaraldehyde-fixed xenografts can be used as patches during reconstructive repairs in both congenital and acquired heart diseases. For example, in congenitally malformed hearts, pericardial patches are used during surgical repairs of the right ventricular outflow tracts and/or during repair of torn aortic leaflets. Pericardial patches have also been used to repair the mitral and aortic valves as well as ventricular walls in acquired diseases [31].

Pericardial tissue has been used in heart valves for many years. The search for an alternative to mechanical valves has led people to investigate many types of bioprosthetic valves. These bioprostheses have consisted of homografts (preserved cadaveric valves), autografts (transplant of a patient's pulmonic valve to the aortic position—the Ross procedure), and xenografts. Xenograft valves have included preserved porcine aortic tissue as well as preserved bovine pericardium. More specifically, glutaraldehyde-fixed bovine or porcine pericardium has been used in the design of aortic and mitral bioprosthetic valves and has realized wide clinical success. Such pericardium is prepared and fixed using specific processes (which typically vary slightly between manufacturers) and then cut to resemble a tri-leaflet semilunar valve and assembled into a stent with a sewing cuff.

With ubiquitous use in heart valves, the biomechanics of glutaraldehyde-fixed pericardium have been carefully studied. Biomechanical properties have been shown to be dependent on species, anatomic orientation, and fixation process. For example, there are significant differences in uniaxial mechanical properties of bovine, porcine, and ostrich pericardium [32]. It has also been shown that collagen fiber orientation, and hence mechanical stiffness, is dependent on the location and orientation of the tissue within the pericardial sac [33]. Finally, uniaxial properties of glutaraldehyde-fixed bovine pericardium can be modulated depending on the stress applied during fixation [34].

9.7 Intrapericardial Therapeutics

9.7.1 Clinical Pericardial Access

Traditionally, pericardial access has been limited to patients with pericardial effusions. The effusion gives physician a buffer between the fibrous pericardium and the epicardium during pericardiocentesis or creating a pericardial window, thus preventing damage to the myocardium and coronary vessels. Recently, there has been an interest in accessing the

healthy pericardium for therapeutic procedures and the delivery of therapeutic agents. The challenge of accessing a healthy pericardium is to puncture and catheterize the pericardium with minimal risk to the heart. This is a difficult task considering the almost negligible layer of pericardial fluid in a healthy pericardial sac. The Tuohy needle, a hypodermic needle originally developed for insertion of an epidural catheter, is commonly used for pericardial access. This needle has an anti-coring curve at its tip to prevent puncture of the myocardium.

In an effort to improve the ease of access, several unique biomedical devices or tools have been (or are being) developed with novel catheter designs that allow controlled myocardial penetration during fluoroscopic visualization. For example, the PerDUCER® (Comedicus, Inc., Columbia Heights, MN, USA), which has now become PeriPort® (Cormedics Corp., Houston, TX, USA), uses a sheathed needle with a suction tip designed for grasping the pericardium and accessing the pericardial space while, at the same time, minimizing the risk of myocardial puncture. This device is placed following subxiphoid access into the mediastinum under fluoroscopic guidance from the apparatus positioned onto the anterior outer surface of the pericardial sac (Fig. 9.7). Under manual suction, the sac is retracted and a needle is inserted, allowing for the placement of a guidewire into the space via the needle lumen. The needle is then removed and a standard delivery catheter is placed into position. The Philipp University of Marburg has also developed a similar product called the Marburg Attacher (www.cardiorepair.com/attacher). Other percutaneous subxiphoid techniques have been proposed [35] but are not in current clinical use.

A novel transatrial technique has been developed by Verrier and colleagues [36] which has been successful in animal studies. In this procedure, a guide catheter is introduced into the right atrium from the femoral vein, and a needle catheter is advanced through the guide catheter to pierce the right atrial appendage. A guidewire is then passed through the needle catheter into the pericardial space. A soft delivery catheter can be passed over the guidewire and can reside in pericardial space for long-term drug delivery or for fluid sampling. Studies in swine have shown that catheters left in the pericardial space over long periods of time can remain patent and cause minimal fibrosis and inflammatory response at the epicardium [37, 38].

9.7.2 Intrapericardial Therapies

For quite some time, nonsurgical intrapericardial therapy has been employed in patients with sufficient fluid in the pericardial space allowing a needle to be safely placed within the space [1]. This methodology has been used for patients with clinical indications such as, but not limited to, malignancies, recurrent effusions, uremic pericarditis, and connective tissue disease. As mentioned above, instrumenting the pericardium has been made possible by numerous techniques that allow for the study of intrapericardial therapeutics and diagnostics by clinicians and investigators alike. In addition, with recent advances in minimally invasive cardiac surgical procedures, it is likely that the integrity of the pericardium will be preserved more often during cardiac surgery.

Intrapericardial access has become the foundation of many novel minimally invasive cardiac procedures. This includes epicardial mapping and ablation for both ventricular [39] and atrial [40] arrhythmias in patients where endocardial approaches are challenging or ineffective. Intrapericardial echocardiography, where an intracardiac ultrasound probe is introduced percutaneously into the pericardium, has been shown to aid in complex ablation procedures [41]. Epicardial lead placement can also be performed

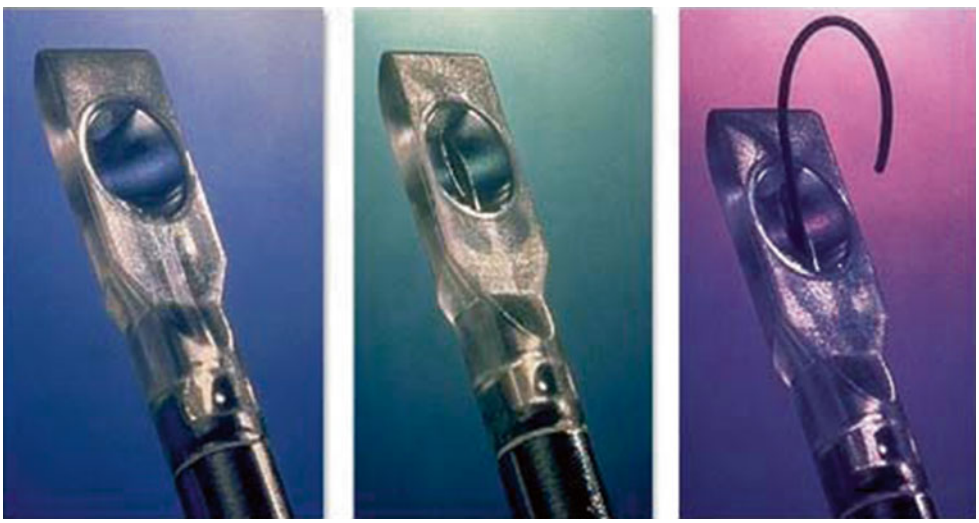

Fig. 9.7 The PerDUCER® instrument (Comedicus, Inc., Columbia Heights, MN, USA) uses a sheathed needle with a suction tip designed for grasping the pericardium to access the pericardial space using a transthoracic approach, thus minimizing the risk of myocardial puncture

through minimally invasive access to the pericardium in patients where traditional venous lead implantation has failed [42]. The LARIAT procedure and device (SentreHEART, Redwood City, CA, USA) is a novel approach to percutaneous ligation of the left atrial appendage that relies on both pericardial access and transseptal left atrial access. In this procedure, a device in the pericardium interacts magnetically with a device in the left atrium to position the system and perform the ligation. Initial clinical results of the procedure have shown promising results [43].

Beyond device-based interventions, intrapericardial access has been used to introduce therapeutic agents to treat cardiac disease. Specifically, the endoluminal delivery of various agents has been found to be clinically limited due to short residence time, highly variable deposited agent concentration, inconsistency in delivery concentrations, and relatively rapid washout of agents from the target vessel [44]. A desired example of targeted application includes infusion of concentrated nitric oxide donors, which could present undesirable effects if systemically delivered. Further, one is allowed increased site specificity and the delivery of label-specific therapeutic agents to target cells, receptors, and channels. A great deal of interest has been focused on delivery of angiogenic agents and various growth factors into the intrapericardial space [45–47]. In particular, research has concentrated on administration in patients with ischemic heart disease [48, 49]. Early results indicate several benefits associated with the delivery of angiogenic agents that include increased collateral vessel development, regional myocardial blood flow, myocardial function in the ischemic region, and myocardial vascularity.

In our lab, we have shown that intrapericardial delivery of omega-3 fatty acids can drastically reduce infarct size and lower the occurrence of ventricular arrhythmias. In one study [50], 23 swine were treated with an infusion of either omega-3 fatty acids or saline in the pericardial sac prior to occluding the left anterior descending artery. Prior to, during, and after the occlusion, hemodynamic and electrophysiological data were recorded. Upon sacrificing the animal, the heart was sectioned and stained to determine infarct size. We found that both infarct size and arrhythmia scores were reduced by half in animals treated with omega-3 fatty acids. Furthermore, the treatment had a minimal effect on hemodynamics, which is in contrast to many antiarrhythmic drugs. Current research is underway to determine if this therapy would be feasible in a clinical setting.

9.7.3 Pericardial Pharmacokinetics

As described previously, the pericardium in humans is generally believed to contain 20–60 mL of physiologic fluid (0.25 ± 15 mL/kg) situated within the cavity space [51]. Yet, dye studies suggest that pericardial fluid is not uniformly distributed over the myocardium, with the majority of pericardial fluid residing within the atrioventricular and interventricular grooves as well as the superior-transverse sinuses. Although the pericardial fluid is not uniformly distributed, pharmacokinetic studies suggest that there is complete mixing of the fluid so that pericardial fluid content is spatially uniform [52–54]. Hence, sampling pericardial fluid content should not vary functionally by sampling location [53].

Tissue distribution and drug clearance clearly affect all drug response. Because specific pericardial pharmacokinetic data remain unknown for the majority of compounds, pericardial drug disposition must be gleaned from physical chemical properties based upon a few select studies. Pericardial fluid is cleared via lymphatics and epicardial vasculature, with the former being a very slow process [55]. In addition to these passive clearance mechanisms, the epicardial tissues contain metabolic enzymes that may clear compounds via a biotransformation process. This is likely to occur with certain labile peptides and small molecules such as nitric oxide. Unfortunately, there is very little known today about pericardial drug metabolism. In general, it is considered that whether or not a compound residing in the pericardial space is cleared via lymphatic drainage, passive diffusion or biotransformation will depend on its molecular size, tissue affinity, water solubility, and enzymatic stability. Thus, compounds such as large proteins do not rapidly diffuse into the vascular space and are slowly cleared from the pericardial space perhaps via lymphatics unless, of course, they are biotransformed [53, 56]. Importantly, this yields a pericardial fluid clearance and residence time longer than the corresponding plasma half-life. For example, administering atrial naturetic peptide into the pericardial fluid space had a fivefold longer clearance and residence time within the pericardial fluid space, as compared to plasma clearance of an intravenous dose [56]. Similarly, small water-insoluble compounds may also have very prolonged pericardial fluid residual times.

One case report documented that the pericardial fluid half-life of 5-fluorouracil (sparingly soluble in water) was approximately tenfold longer than plasma half-life (168 versus 16 min); it should be noted that the patient in this investigation had metastatic breast carcinoma with pericardial involvement [52]. The patient had received a relatively large pericardial 5-fluorouracil dose (200 mg) to manage recurrent pericardial effusion. This large dose, however, was associated with nearly undetectable plasma levels, indicating minimal spillover from pericardial fluid into the systemic circulation. While it was expected that 5-fluorouracil would have a longer pericardial residual time because it is water insoluble, it is unknown if these findings would occur in a healthy pericardial fluid space.

On the other hand, small water-soluble compounds have up to five- to eightfold shorter pericardial fluid clearance and residence times as compared to plasma [52]. For example, procainamide is a water-soluble compound that has a pericardial fluid half-life ranging from 30 to 41±2.1 min as compared to the 180-min plasma half-life; it has been reported that the procainamide rapidly diffused out of the pericardial space with a terminal elimination half-life approximately 5–7 times shorter than plasma [57]. However, procainamide spillover from pericardial fluid into plasma was considered not to produce measurable plasma concentrations because of the relatively low pericardial doses (0.5–2 mg/kg). Similarly, it is not surprising that the converse was also true, that intravenously administered procainamide rapidly diffused into the pericardial space, across the plasma to pericardial fluid concentration gradient, such that pericardial fluid procainamide concentrations were similar to plasma approximately 20–30 min following an intravenous injection. The likely explanation for these findings is that the vast ventricular epicardial blood supply served as a clearing system (pericardial administration) or a delivery system (intravenous administration) according to drug concentration diffusion gradient. Importantly, the diffusion of pericardial-administered procainamide into the vascular space will likely prevent drug accumulation in ventricular tissue and a global pharmacologic response.

In addition to pericardial drug residence and clearance times, the determination of distribution volume may be of considerable importance, particularly to achieve desired peak drug concentrations. There is a direct and inverse relationship between peak drug concentrations and drug distribution volumes, such that a low drug distribution volume achieves higher peak concentrations. Perhaps of clinical importance, with the very small pericardial fluid volume, it is likely that pericardial drug doses can be substantially reduced to achieve therapeutic concentrations. This was evident whereby sequential pericardial procainamide doses of 0.5, 1, and 2 mg/kg produced peak pericardial fluid concentrations that ranged from 250 to 900 μg/mL; these concentrations were nearly 1000-fold greater than peak plasma concentrations of procainamide following the administration of a 2 mg/kg intravenous dose. In a follow-up study in which a single procainamide dose was employed, similar findings were documented; it was also reported that a pericardial fluid volume distribution of 1.6±0.16 mL/kg was observed, which is approximately 1000-fold smaller than the plasma procainamide volume distribution of 2000 mL/kg. While pericardial procainamide dosing produced very large pericardial fluid concentrations, procainamide could not be detected in the plasma given the very small doses. With such a powerful diffusion gradient, it is likely that pericardial procainamide delivery can achieve very high atrial tissue concentrations. Indirect evidence of tissue distribution is a procainamide distribution volume that is larger (40–50 mL) than the estimated pericardial fluid volume of 20–30 mL. Since the procainamide pericardial volume of distribution exceeded the expected pericardial volume, there was some tissue distribution. These pharmacodynamic data suggest that tissue distribution mainly occurs in the atrium, likely because the atrium is a very thin structure with a low blood supply. Thus, this tissue architecture is ideal for specialized therapeutic drug diffusion and therefore differs from that of the ventricle(s).

Unfortunately, most pericardial procainamide pharmacokinetic studies performed to date have not directly measured tissue concentrations following infusion. However, in one study which evaluated the pharmacodynamic effects of pericardial amiodarone delivery, the amiodarone tissue distribution was quantified at several myocardial locations [58]. Not surprisingly, it was reported that atrial and epicardial ventricular tissue had the highest amiodarone tissue concentration, while ventricular endocardial amiodarone tissue concentrations were approximately tenfold lower. Importantly, the amiodarone levels were likely still within a therapeutic range. This was supported by the fact that pericardial amiodarone delivery prolonged endocardial ventricular refractory periods by up to 13 %, which was equivalent to epicardial ventricular refractory period measurements and the magnitude of atrial refractory period prolongation. The similar refractory response between epicardial and endocardial measurements, with very large differences in amiodarone tissue concentrations, indicates that amiodarone effects are maximal at low tissue concentrations. Unlike pericardial amiodarone administration, pericardial procainamide had no effect on endocardial ventricular refractory periods [54]. It is likely that such a beneficial ventricular tissue distribution does not occur with more water-soluble compounds such as procainamide. On the other hand, it is not surprising that amiodarone, when administered into the pericardial space, could penetrate ventricular tissue and affect global ventricular electrophysiology because it is highly lipophilic and has a huge tissue distribution including the intracellular space [58]. A more recent study comparing intrapericardial and intravenous administration of amiodarone in goats [59] showed similar results; plasma drug concentrations were significantly lower when amiodarone was administered into the pericardium, yet the drug's antiarrhythmic effects were in many measures improved over intravenous administration. The study also confirmed a high gradient of amiodarone tissue concentration from epicardium to endocardium during intrapericardial administration. We have also shown similar beneficial effects in our lab when comparing intrapericardial and intravenous delivery of metoprolol in swine [60]. Intrapericardial delivery showed lower plasma concentrations, more sustained antitachycardic effects, and less negative effects on

contractility and mean arterial pressure when compared with intravenous delivery.

Lastly, perhaps it is possible to modify molecules to achieve an optimal pericardial fluid residence time and thus therapeutic outcomes. More specifically, for some agents, it may be desirable to have a short residence time. For example, pericardial drug delivery to cardiovert atrial fibrillation may require very high drug concentrations for only a brief duration, given the acute nature of the therapy. On the other hand, the ability to manage chronic conditions such as ischemic heart disease or heart failure may necessitate longer pericardial residual times. In this regard, Baek et al. recently showed that a derivatized nitric oxide donor molecule, diazeniumdiolate, with bovine serum albumin resulted in a fivefold increase in pericardial fluid clearance and residence time versus a small molecule nitric oxide donor (diethylenetriamine/NO) [61]. This group went on to show that it may be possible that a single pericardial dose of the nitric oxide donor could inhibit instent restenosis. Unlike patients with any type of effusion, the normal pericardium is a very thin layer, bringing it closer to the heart and subsequently increasing the risk of harm to the patient.

The ability to access the pericardial space has created new opportunities to further understand the pharmacokinetics of intrapericardial therapeutics, as well as the role of the pericardium under normal cardiac function and/or following cardiac disease. Despite the growing literature establishing the feasibility of intrapericardial therapeutics and diagnostics, the results of clinical trials employing pericardially delivered agents directed toward arrhythmias, angiogenesis, restenosis, and/or other coronary and myocardial indications are currently lacking.

9.8 Summary

The pericardium is a unique structure that surrounds the heart and serves several important physiological roles. The removal of the pericardium, certain pericardial disorders, or the buildup of fluids within this space will ultimately alter hemodynamic performance. Recent therapeutic approaches have been directed to exploit the space that exists between the pericardium and the epicardial surface of the heart. New devices and techniques are being developed to access this space in a minimally invasive fashion. An important consideration when utilizing animal models to study such devices is that the pericardium in humans is much thicker and there is more pericardial fluid than in commonly employed animal models. The pharmacokinetics of many drugs may be greatly enhanced if the drug is delivered into the pericardium. As more is learned about the pericardium, it may play a significant role in cardiac therapies.

References

1. Spodick DH (ed) (1997) The pericardium: a comprehensive textbook. Marcel Dekker, New York
2. Ben-horin S, Shinfeld A, Kachel E, Chetrit A, Livneh AR (2005) The composition of the normal pericardial fluid and its implications for diagnosing pericardial effusions. Am J Med 118:636–640
3. Shabetai R (ed) (2003) The pericardium. Kluwer Academic, Boston
4. Pegram BL, Bishop VS (1975) An evaluation of the pericardial sac as a safety factor during tamponade. Cardiovasc Res 9:715–721
5. Boulanger B, Yuan Z, Flessner M, Hay J, Johnston M (1999) Pericardial fluid absorption into lymphatic vessels in sheep. Microvasc Res 57:174–186
6. Angelini GD, Fraser AG, Koning MM et al (1990) Adverse hemodynamic effects and echocardiographic consequences of pericardial closure soon after sternotomy and pericardiotomy. Circulation 82:IV397–406
7. Reich DL, Konstadt SN, Thys DM (1990) The pericardium exerts constraint on the right ventricle during cardiac surgery. Acta Anaesthesiol Scand 34:530–533
8. Daughters GT, Frist WH, Alderman EL, Derby GC, Ingels NB Jr, Miller DC (1992) Effects of the pericardium on left ventricular diastolic filling and systolic performance early after cardiac operations. J Thorac Cardiovasc Surg 104:1084–1091
9. Hammond HK, White FC, Bhargava V, Shabetai R (1992) Heart size and maximal cardiac output are limited by the pericardium. Am J Physiol 263:H1675–1681
10. Abel FL, Mihailescu LS, Lader AS, Starr RG (1995) Effects of pericardial pressure on systemic and coronary hemodynamics in dogs. Am J Physiol 268:H1593–605
11. Allard JR, Gertz EW, Verrier ED, Bristow JD, Hoffman JI (1983) Role of the pericardium in the regulation of myocardial blood flow and its distribution in the normal and acutely failing left ventricle of the dog. Cardiovasc Res 17:595–603
12. Beloucif S, Takata M, Shimada M, Robotham JL (1992) Influence of pericardial constraint on atrioventricular interactions. Am J Physiol 263:H125–134
13. Calvin JE (1991) Optimal right ventricular filling pressures and the role of pericardial constraint in right ventricular infarction in dogs. Circulation 84:852–861
14. Hess OM, Bhargava V, Ross J Jr, Shabetai R (1983) The role of the pericardium in interactions between the cardiac chambers. Am Heart J 106:1377–1383
15. Janicki JS, Weber KT (1980) The pericardium and ventricular interaction, distensibility, and function. Am J Physiol 238:H494–503
16. Shabetai R, Mangiardi L, Bhargava V, Ross J Jr, Higgins CB (1979) The pericardium and cardiac function. Prog Cardiovasc Dis 22:107–134
17. Belenkie I, Dani R, Smith ER, Tyberg JV (1992) The importance of pericardial constraint in experimental pulmonary embolism and volume loading. Am Heart J 123:733–742
18. Watkins MW, LeWinter MM (1993) Physiologic role of the normal pericardium. Annu Rev Med 44:171–180
19. Janicki JS (1990) Influence of the pericardium and ventricular interdependence on left ventricular diastolic and systolic function in patients with heart failure. Circulation 81:III15–20
20. Netter FH (ed) (2003) Atlas of human anatomy, 3rd edn. ICON Learning Systems, Teterboro
21. Weber KT, Janicki JS, Shroff S, Fishman AP (1981) Contractile mechanics and interaction of the right and left ventricles. Am J Cardiol 47:686–695
22. Kingma I, Smiseth OA, Frais MA, Smith ER, Tyberg JV (1987) Left ventricular external constraint: relationship between pericardial, pleural and esophageal pressures during positive end-expiratory pressure and volume loading in dogs. Ann Biomed Eng 15:331–346

23. Reddy RS, Leon DF, Shaver JA (eds) (1982) Pericardial disease. Raven Press, New York
24. Bittar MN, Bernard JB, Khasati N, Richardson S (2005) Should the pericardium be closed in patients undergoing cardiac surgery? Interact Cardiovasc Thorac Surg 4:151–155
25. Fowler N (1985) The pericardium in health and disease. Futura Publishing Company, Inc., Mount Kisco
26. Getty R (1975) General heart and blood vessels. In: Getty R (ed) Sisson and Grossman's the anatomy of the domestic animals, 5th edn. Saunders, Philadelphia, pp 164–175
27. Michaëlsson M, Ho SY (eds) (2000) Congenital heart malformations in mammals: an illustrated text. Imperial College, River Edge
28. Holt JP (1970) The normal pericardium. Am J Cardiol 26:455–465
29. Naimark WA, Lee JM, Limeback H, Cheung DT (1992) Correlation of structure and viscoelastic properties in the pericardia of four mammalian species. Am J Physiol 263:H1095–1106
30. Elias H, Boyd L (1960) Notes on the anatomy, embryology and histology of the pericardium. N Y Med Coll News Notes 2:50–75
31. David TE (1998) The use of pericardium in acquired heart disease: a review article. J Heart Valve Dis 7:13–18
32. García Páez JM, Jorge Herrero E, Carrera Sanmartín A et al (2003) Comparison of the mechanical behaviors of biological tissues subjected to uniaxial tensile testing: pig, calf and ostrich pericardium sutured with Gore-Tex. Biomaterials 24:1671–1679
33. Sacks MS, Chuong CJ, More R (1994) Collagen fiber architecture of bovine pericardium. ASAIO J 40:M632–637
34. Lee JM, Corrente R, Haberer SA (1989) The bovine pericardial xenograft: II. Effect of tethering or pressurization during fixation on the tensile viscoelastic properties of bovine pericardium. J Biomed Mater Res 23:477–489
35. Laham RJ, Simons M, Hung D (1999) Subxyphoid access of the normal pericardium: a novel drug delivery technique. Catheter Cardiovasc Interv 47:109–111
36. Verrier RL, Waxman S, Lovett EG, Moreno R (1998) Transatrial access to the normal pericardial space. Circulation 98:2331–2333
37. Kolettis TM, Kazakos N, Katsouras CS et al (2005) Intrapericardial drug delivery: pharmacologic properties and long-term safety in swine. Int J Cardiol 99:415–421
38. Bartoli CR, Akiyama I, Godleski JJ, Verrier RL (2007) Long-term pericardial catheterization is associated with minimum foreign-body response. Catheter Cardiovasc Interv 70:221–227
39. Sosa E, Scanavacca M (2005) Epicardial mapping and ablation techniques to control ventricular tachycardia. J Cardiovasc Electrophysiol 16:449–452
40. Phillips KP, Natale A, Sterba R et al (2008) Percutaneous pericardial instrumentation for catheter ablation of focal atrial tachycardias arising from the left atrial appendage. J Cardiovasc Electrophysiol 19:430–433
41. Horowitz BN, Vaseghi M, Mahajan A et al (2006) Percutaneous intrapericardial echocardiography during catheter ablation: a feasibility study. Heart Rhythm 3:1275–1282
42. Costa R, Scanavacca M, da Silva KR, Martinelli Filho M, Carrillo R (2013) Novel approach to epicardial pacemaker implantation in patients with limited venous access. Heart Rhythm 10:1646–1652
43. Bartus K, Han FT, Bednarek J et al (2013) Percutaneous left atrial appendage suture ligation using the LARIAT device in patients with atrial fibrillation: initial clinical experience. J Am Coll Cardiol 62:108–118
44. March KL (1996) Methods of local gene delivery to vascular tissue. Semin Interv Cardiol 1:215–223
45. Laham RJ, Rezaee M, Post M et al (2003) Intrapericardial administration of basic fibroblast growth factor: myocardial and tissue distribution and comparison with intracoronary and intravenous administration. Catheter Cardiovasc Interv 58:375–381
46. Lazarous DF, Shou M, Stiber JA et al (1997) Pharmacodynamics of basic fibroblast growth factor: route of administration determines myocardial and systemic distribution. Cardiovasc Res 36:78–85
47. Tio RA, Grandjean G, Suurmeijer AJ et al (2002) Thoracoscopic monitoring for pericardial application of local drug or gene therapy. Int J Cardiol 82:117–121
48. Laham RJ, Hung D (1999) Therapeutic myocardial angiogenesis using percutaneous intrapericardial drug delivery. Clin Cardiol 22:I6–9
49. Landau C, Jacobs AK, Haudenschild CC (1995) Intrapericardial basic fibroblast growth factor induces myocardial angiogenesis in a rabbit model of chronic ischemia. Am Heart J 129:924–931
50. Xiao YF, Sigg DC, Ujhelyi MR, Wilhelm JJ, Richardson ES, Iaizzo PA (2008) Pericardial delivery of omega-3 fatty acid: a novel approach to reducing myocardial infarct sizes and arrhythmias. Am J Physiol Heart Circ Physiol 294:H2212–2218
51. Choe YH, Im JG, Park JH, Han MC, Kim CW (1987) The anatomy of the pericardial space: a study in cadavers and patients. AJR Am J Roentgenol 149:693–697
52. Lerner-Tung MB, Chang AY, Ong LS, Kreiser D (1997) Pharmacokinetics of intrapericardial administration of 5-fluorouracil. Cancer Chemother Pharmacol 40:318–320
53. Stoll HP, Carlson K, Keefer LK, Hrabie JA, March K (1999) Pharmacokinetics and consistency of pericardial delivery directed to coronary arteries: direct comparison with endoluminal delivery. Clin Cardiol 22:I10–16
54. Ujhelyi M, Hadsell K, Euler D, Mehra R (2002) Intrapericardial therapeutics: a pharmacodynamic and pharmacokinetic comparison between pericardial and intravenous procainamide. J Cardiovasc Electrophysiol 13:605–611
55. Hollenberg M, Dougherty J (1969) Lymph flow and 131-I-albumin resorption from pericardial effusions in man. Am J Cardiol 24:514–522
56. Szokodi I, Horkay F, Kiss P et al (1997) Characterization and stimuli for production of pericardial fluid atrial natriuretic peptide in dogs. Life Sci 61:1349–1359
57. Nolan PE (1997) Pharmacokinetics and pharmacodynamics of intravenous agents for ventricular arrhythmias. Pharmacotherapy 17:65–75S. Discussion 89–91S
58. Ayers GM, Rho TH, Ben-David J, Besch HR Jr, Zipes DP (1996) Amiodarone instilled into the canine pericardial sac migrates transmurally to produce electrophysiologic effects and suppress atrial fibrillation. J Cardiovasc Electrophysiol 7:713–721
59. Bolderman RW, Hermans JJ, Rademakers LM et al (2009) Intrapericardial delivery of amiodarone and sotalol: atrial transmural drug distribution and electrophysiological effects. J Cardiovasc Pharmacol 54:355–363
60. Richardson ES, Rolfes C, Woo OS, Elmquist WF, Benditt DG, Iaizzo PA (2012) Cardiac responses to the intrapericardial delivery of metoprolol: targeted delivery compared to intravenous administration. J Cardiovasc Transl Res 5:535–540
61. Baek SH, Hrabie JA, Keefer LK et al (2002) Augmentation of intrapericardial nitric oxide level by a prolonged-release nitric oxide donor reduces luminal narrowing after porcine coronary angioplasty. Circulation 105:2779–2784

Congenital Cardiac Anatomy and Operative Correction

10

Charles Shepard, Robroy McIver, and James D. St. Louis

Abstract

There are numerous congenital defects that may present with human hearts, and many typically require surgical intervention. The primary goal of this chapter is to briefly define such abnormalities and introduce the reader to the various classification schemes that have been used to describe their relative anatomical and functional features. The chapter will also highlight the more common surgical procedures utilized to treat congenital cardiac lesions.

Keywords

Septal defect • Aortopulmonary window defect • Coarctation of the aorta • Interrupted aortic arch • Tetralogy of Fallot • Atresia • Ebstein's anomaly • Transposition of the great vessels • Total anomalous pulmonary venous connection • Persistent truncus arteriosus • Cardiopulmonary bypass

10.1 Introduction

The spectrum of congenital heart disease is enormously diverse, yet affects a relatively small portion of the human population [1]. Disease severity ranges from benign to lethal, and many lesions require intervention to allow survival or enhance life expectancy. Several nomenclature classifications have evolved to describe abnormalities of the cardiovascular system, with the Van Praagh and Anderson/Edwards systems being the most prominent.

Richard Van Praagh presented a system based on the segmental anatomy of the developing heart. His generalized theory states that, by understanding the anatomical position of the cardiac segments, the majority of cardiac defects may be accurately described. The three segments which Van Praagh described consist of the atria, the ventricle, and the great vessels. These segments may be described by delineating their relative positional relationships. The *visceroatrial situs* is defined as the relative position of the right and left atria to the sidedness of the abdominal (visceral) organs; the term situs means position or location. The *bulb ventricular loop* is described as the orientation of the right and left ventricles to the great vessels (pulmonary artery and aorta). These segments are referenced in sequence, with each being designated by a letter. The connection of the visceral venous vessels (the superior and inferior vena cavae) and the atrial body is termed the visceroatrial situs and is described by the letters: S, *situs solitus*; I, *situs inversus*; and A, *situs ambiguous*. When the visceral situs is normal (*situs solitus*), the stomach and spleen lie to the left, the right lobe of the liver is larger than the left, and the appendix is right sided. In situs inversus, the position of the abdominal organs is reversed, with the stomach and spleen lying on the right and the dominant lobe of the liver to the left; the appendix and inferior vena cava are to the left, with the left lung being typically trilobed. Situs ambiguous describes a group of anomalies in

C. Shepard, MD
Division of Pediatric Cardiology, University of Minnesota
Children's Hospital, Minneapolis, MN, USA

R. McIver, MD
Division of Pediatric Cardiac Surgery, University of Minnesota
Children's Hospital, Minneapolis, MN, USA

J.D. St. Louis, MD (✉)
University of Missouri-Kansas City, School of Medicine,
Children's Mercy Hospital and Clinics, Kansas City, MO, USA
e-mail: jdstlouis@cmh.edu

P.A. Iaizzo (ed.), *Handbook of Cardiac Anatomy, Physiology, and Devices*, DOI 10.1007/978-3-319-19464-6_10

which the dominant characteristic is a lack of visceral sidedness. The abdominal organs may be positioned to the anatomical left or right, often with the liver lying in the midline. A unique characteristic of these individuals is the abnormal existence or a complete lack of a spleen. In general, polysplenic patients tend to have all atrial and pulmonary structures consistent with left-sided morphology, while asplenic patients tend to be right-side dominant.

The orientation of the right or left ventricular mass is described by how the embryonic cardiac tube loops during its development. In this system, the terms "right" and "left" are used to refer to the specific morphology of the ventricular mass rather than their spatial arrangement. The anatomical right ventricle has a very trabeculated endocardium, while the left ventricular endocardium is smoother, with finer trabeculations. The rightward (normal) orientation is given the term "D" for *D-loop*. This indicates that the morphologic right ventricle is oriented to the right and anterior to the morphologic left ventricle. If the cardiac tube undergoes looping in the leftward direction, the segment is given the reference letter "L" for *L-looping*. In this situation, the morphologic right ventricle lies posterior and to the left of the morphologic left ventricle. The final segmental orientation described by Van Praagh deals with the relationship of the great vessels and semilunar valves to the ventricles. The aorta is normally committed to the morphologic left ventricle with the aortic valve located leftward and posterior to the pulmonary valve. This normal relationship is given the reference letter "S." When the great vessels are transposed, with the aortic valve being rightward and anterior to the pulmonary valve, the convention used is "D." With *D-transposed* great vessels, the aorta is committed to the morphologic right ventricle and the pulmonary artery and valve to the morphologic left ventricle. When the orientation of these great vessels and semilunar valves is normal, but the aorta is committed to the right ventricle and the pulmonary artery to the left ventricle, the term *L-transposed* great vessels is used.

Efforts are underway to establish a common language in describing congenital cardiac defects, which will hopefully facilitate the tracking of outcomes and applications of procedures [2]. This chapter approaches the classification of these congenital heart lesions with a segmental anatomical method. Congenital heart abnormalities can also be categorized by whether or not they cause cyanosis (Table 10.1). Furthermore, cyanotic lesions refer to cardiac defects that typically result in systemic arterial desaturation. Finally, shunts refer to an anomalous pathway of blood flow resulting from anatomical defects and their relative resultant downstream pressures.

In the relative short history of surgical treatment for congenital heart defects, there has not been a more important technological breakthrough than the heart-lung bypass machine. Understanding of the various methods of its use is instrumental in understanding the logistics of surgical treatment of congenital heart disease.

Table 10.1 Anatomical lesions of the heart based on physiologic derangement

Acyanotic
• Left-to-right shunts Atrial septal defects Ventricular septal defects Atrioventricular septal defects Aortopulmonary window
• Left-sided obstructive lesions Aortic coarctation Congenital aortic stenosis Interrupted aortic arch
Cyanotic
• Right-to-left shunts Tetralogy of Fallot Pulmonary stenosis Pulmonary atresia – With intact ventricular septum – With ventricular septal defect Tricuspid atresia Ebstein's anomaly
• Complex mixing defects Transposition of the great vessels Total anomalous pulmonary venous connection Truncus arteriosus Hypoplastic left heart syndrome

10.2 Cardiopulmonary Bypass

Cardiac function is critical to the maintenance of ongoing hemostasis for any organism. Often, repair of congenital heart lesions requires interruption of this function for brief periods of time. The cardiopulmonary bypass circuit provides systemic support during these periods of cardiac arrest. A standard approach in cardiopulmonary bypass is draining blood from the right atrium and delivering it to the aorta past the aortic valve, with blood being oxygenated within the bypass machine. Blood not actively captured in the right atrium is sent through the lungs and out of the left ventricle when the heart is still beating. By directing the venous drains into the superior and inferior cavae and then snaring down on the cannulas, the right atrium can be safely entered as long as there is no communication with the left side of the heart (atrial septal defect, ventricular septal defect, etc.). Some lesions on the right side of the heart can therefore be fixed while the heart is still beating.

Alternatively, lesions that communicate with or are within the left side of the heart need an alternative strategy to prevent air being passed into the cranial vessels. To isolate the left heart, a clamp is placed between the aortic valve and the outflow of the cardiopulmonary bypass cannula. The heart is placed in a metabolically protected state by both physically cooling the heart and chemically inactivating it with a solution of cardioplegia. The length of time that the clamp can stay on depends on the solution used and the baseline function of the heart.

A third method in operating on the heart is to metabolically inactivate the entire body through cooling, therefore not needing any cardiopulmonary function for a short period of time. Cardioplegic arrest is used in procedures where maintaining the outflow of the bypass machine is not possible. In this method, the bypass machine is used to cool the entire body to a level where the period of decreased flow will not lead to permanent damage. The outflow of the bypass machine is turned off once the body has been sufficiently cooled and work is done expeditiously. Through these various bypass methods, the many varied congenital heart defects can be surgically treated. The remaining portions of the chapter will describe treatment methods used for specific lesions. For additional information, see Chap. 33.

10.3 Systemic Venous Anomalies

Persistence of the left-sided superior vena cava (LSVC) in isolation can be a variant of normal, when it drains to the coronary sinus, which is usually of no physiologic consequence. When an LSVC drains directly to the left atrium, or to an unroofed coronary sinus, systemic venous blood mixes with the pulmonary venous return, causing systemic desaturation. A persistent LSVC may herald additional anatomical issues or be part of a complex of lesions seen in heterotaxy syndromes. When an LSVC is paired with congenital heart lesions, this may alter the repair and must be identified and taken into consideration in preoperative planning [3].

The term interrupted inferior vena cava (IVC) describes the absence of the intrahepatic IVC, and the IVC blood is diverted to the superior vena cava (SVC) via the azygos vein. This finding is of physiologic significance in patients who need to undergo single ventricle palliative procedures in which the SVC blood is diverted to the pulmonary arteries (cavo-pulmonary or Glenn anastomosis), followed years later by diversion of the IVC blood to the pulmonary arteries (Fontan procedure). In this situation, the large majority of the systemic venous blood will be channeled to the pulmonary arteries with the Glenn anastomosis, which is not well tolerated at a young age, and different strategies must be employed. In the setting of an interrupted IVC, a full evaluation for other indicators of a heterotaxy syndrome must be performed [3].

10.4 Atrial Septal Defects

Fetal circulation requires the presence of a patent foramen ovale (PFO), or communication between the right and left atria, for the more highly saturated umbilical venous blood to bypass the lungs and be directed to the brain. After birth, pulmonary blood flow increases, closing the flap of the foramen ovale in approximately 75 % of all individuals, with the remainder maintaining at least probe patency of this communication [4]. This small communication is most commonly of no hemodynamic significance in early life.

Secundum-type atrial septal defects (ASDs) are due to deficiencies in the septum primum portion of the atrial septum, which allows a portion of the pulmonary venous return to cross the atrial septum into the right atrium, then into right ventricle, and finally recirculate to the lungs. When large enough, this leads to dilation of the right atrium and ventricle, and over time, this overcirculation of the lungs can lead to permanent damage of the pulmonary arterial vasculature and/or lung disease [5]. Primum type ASDs will be discussed in the atrioventricular septal defect section. Sinus venosus-type ASDs include defects in the septum separating the cavae from the pulmonary venous return. This allows for drainage of the associated pulmonary venous return to the right atrium, with the same hemodynamic consequences as a secundum-type ASD. This will be further discussed in the section on pulmonary venous anomalies.

Coronary sinus ASDs present variably, including as a partial or completely unroofed coronary sinus, i.e., allowing desaturated blood to drain to the left atrium and left atrial blood to cross the os of the coronary sinus into the right atrium. This can associated with a persistent LSVC (effectively draining directly to the left atrium), with additional atrial septal communications, or with atrioventricular valve abnormalities [6]. The physiologic consequences of this communication and shunting are similar to a secundum-type ASD (Fig. 10.1).

The correction of an ASD involves closing off the communication between the right and left atria. Correction is usually performed as a young child prior to long-term sequelae of a left-to-right shunt development. Surgical correction requires an arrested heart with a bicaval cannulation. As there are many types of ASDs, there are different surgical corrections. The most standard defect, the secundum defect, can be closed by simply closing the defect with suture or, if larger, using a patch material to close the defect. Traditionally the patient's own pericardial tissue has been used as patch material, although pericardium from animals or completely artificial materials such as GORE-TEX can be used. Closure of sinus venosus generally requires more extensive redirection of blood flow to allow proper drainage of the pulmonary veins to the left atrium. In these cases a patch must baffle the blood flow of the pulmonary veins to the left atrium. Pulmonary venous connection with the SVC requires disconnecting the portion of SVC communicating with the veins and using the right atrial appendage as a graft to the remaining SVC in a so-called *Warden procedure*.

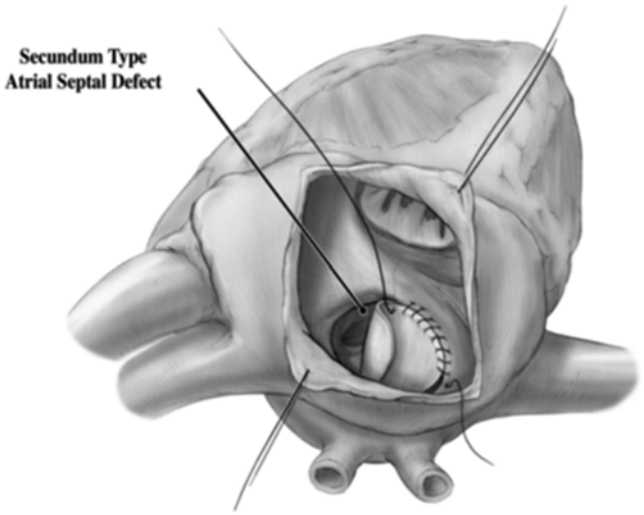

Fig. 10.1 Secundum-type atrial septal defect seen via an incision in the right atrial appendage

10.5 Anomalies of the Tricuspid Valve

Tricuspid atresia refers to a complete lack of communication between the right atrium and right ventricle and can present in multiple forms. The inlet portion of the right ventricle is underdeveloped, with the remainder of the ventricle dependent on the presence and size of a ventricular septal defect and the ventriculo-arterial connection. Table 10.2 describes the various subtypes of tricuspid atresia, organized by relationship of the great vessels, with type I referring to normally related great vessels, type II describing d-transposed great vessels, and type III as l-transposed great vessels; subtypes describe the amount of pulmonary stenosis (or atresia) [7].

Ebstein's anomaly is a spectrum of anomalies of both the tricuspid valve and right ventricle, with displacement of the tricuspid valve annulus toward the apex of the heart. The tricuspid valve is adherent to the right ventricle, prohibiting complete coaptation or closure of the tricuspid valve leaflets. This leads to regurgitation of the tricuspid valve and resultant dilation of the right atrium and ventricle. An ASD, pulmonary stenosis or atresia, and/or Wolf-Parkinson-White syndrome may often be associated with this anomaly [8]. In 1988, Carpentier and colleagues attempted to classify Ebstein's anomalies based on the relative volumes of the right ventricle. More specifically, these authors proposed four subtypes: (1) type A, the volume of the right ventricle is adequate; (2) type B, there is a large atrialized component of the right ventricle, but the anterior leaflet moves freely; (3) type C, the anterior leaflet is severely restrictive in its movement and may cause significant obstruction of the right ventricular outflow tract; and (4) type D in which there is almost complete atrialization of the ventricle, with the exception of a small infundibular component.

Table 10.2 Tricuspid atresia

Normally related great vessels
• Type I (a) pulmonary atresia
• Type I (b) pulmonary hypoplasia, small VSD
• Type I (c) no pulmonary hypoplasia, large VSD
D-transposed great vessels
• Type II (a) pulmonary atresia
• Type II (b) pulmonary or subpulmonary stenosis
• Type II (c) large pulmonary artery
L-transposed great vessels
• Type III (a) pulmonary or subpulmonary stenosis
• Type III (b) subaortic stenosis

VSD ventricular septal defect

Surgical repair of an Ebstein's anomaly is dependent on the degree and timing of presentation of tricuspid insufficiency. Neonates with severe tricuspid insufficiencies that inhibit forward flow through the right heart will need early interventions due to severe cyanosis; this approach typically leads neonates to a *Fontan circulation*. The first stage is performed as a neonate with an arrested heart. In addition to the creation of an aortopulmonary shunt, the tricuspid valve is patched closed, and the atrial septum is resected.

In patients that have less severe tricuspid regurgitation, repair is delayed until symptoms develop. Surgical goals are to form a well-functioning tricuspid valve and close any atrial septal communication. Many techniques have been developed, most of which involve plicating and/or resecting the atrialized portion of the right ventricle.

10.6 Ventricular Septal Defects

Ventricular septal defects (VSDs) are channels that permit interventricular shunting and can be found in isolation or in association with other congenital malformations. These channels may be described by their locations within the interventricular septum that is deficient, or by their anatomical nature [9], and also assigned a size relative to other anatomical structures of the heart (most often the aortic valve). The physiologic sequelae of VSDs depend on the size and location of the defects, with unrestricted VSDs leading to elevations of the right ventricular and pulmonary arterial pressures. Further, over time, the pulmonary vasculature develops muscular thickening which, if left unchecked, can lead to irreversibly high pulmonary vasculature resistance, or *Eisenmenger's syndrome*.

Redundant nomenclature exists for VSDs in the literature (Table 10.3). The intraventricular septum can be divided into four quadrants as seen in Fig. 10.2 [10] utilizing the *septomarginal trabecularis* as a landmark. For each region of the IVS, there are unique concerns and probabilities of spontaneous closure of a defect. Defects posterior to the posterior arm of the *septomarginal trabecularis*, inferior to

Table 10.3 Classification of ventricular septal defects

Type 1	Subarterial Supracristal Conal Infundibular
Type 2	Perimembranous Paramembranous Conoventricular
Type 3	Inlet Atrioventricular canal type
Type 4	Muscular • Anterior • Midventricular • Posterior • Apical

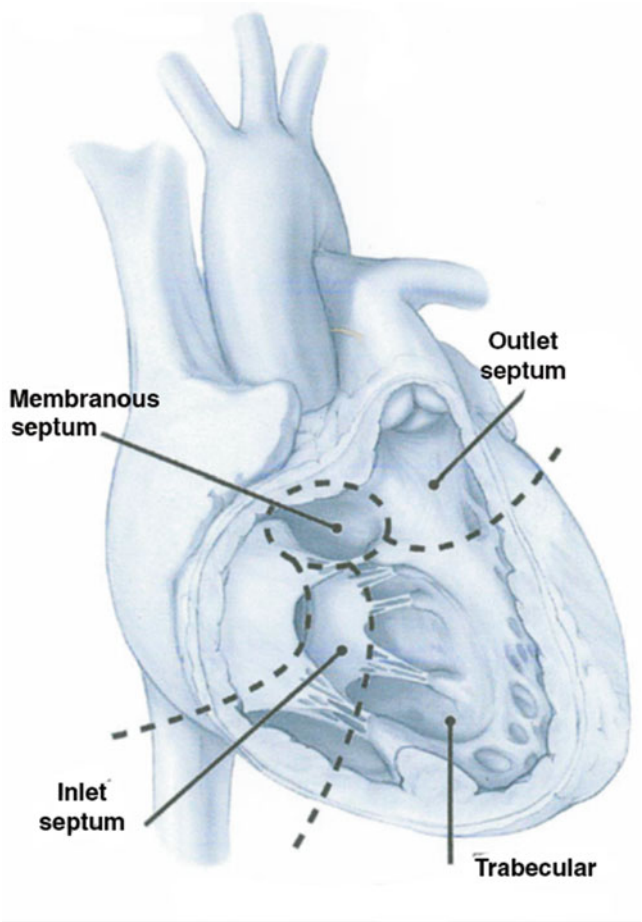

Fig. 10.2 Ventricular septum visualized through the right ventricular free wall. Note the three regions, including the inlet region supporting the tricuspid valve, the trabeculated muscular septum, and the outlet septum forming the pulmonary annulus

the atrioventricular valve, are termed inlet or atrioventricular canal-type VSDs and are further discussed in the atrioventricular septal defect section. Defects of the trabecular or muscular septum are the most likely to close spontaneously and can be subcategorized into anterior, posterior, mid-ventricular, or apical [10]. Those defects within or in close proximity to the membranous septum are termed perimembranous, paramembranous, or conoventricular VSDs. Defects in the outlet regions of the right ventricle (superior to the anterior portion of the septomarginal trabecularis) carry the names subarterial, supracristal, conal, or infundibular. These defects can lead to prolapse of the aortic valve and thus aortic regurgitation [11]. When closing these defects surgically or with a device, one must remain cognizant of the conductive tissues that pass in close proximity to many of these defects.

The correction of VSDs involves closing off the communications between the right and left ventricles. Corrections are usually performed in infants, as heart failure symptoms can develop that then, in turn, limit growth.

Surgical correction of VSDs typically requires an arrested heart with a bicaval cannulation. A correction almost always requires a patch, as the stresses on the repair site are much higher than that on an ASD (Fig. 10.3). The patch often will abut the conduction system which, if damaged, may lead to the lifelong need for an implanted pacemaker, i.e., secondary to third-degree heart block. The approach to a VSD repair depends on its specific location within the ventricular septum. Defects under the pulmonary valve can be approached through an incision in the right ventricular outflow tract. Muscular VSDs, although more likely to close on their own, can be more difficult to repair surgically due to their location within trabeculations of the heart. Surgical closure can often require a ventricular incision. Many muscular defects are now closed with an endovascular device either through a percutaneous or periventricular approach. The most commonly surgically closed VSD is a perimembranous defect and is approached through the right atrium.

10.7 Atrioventricular Septal Defect

Atrioventricular septal (canal type or endocardial cushion) defects (AVSDs) are a spectrum of defects that involve an ostium primum septal defect, the atrioventricular valves, and/or the inlet portions of the interventricular septum. Depending on the position of the atrioventricular valves, one ventricle may be favored over the other leading to an unbalanced size of the ventricles. The conduction system is often abnormal, with the usual pathways disturbed. A *complete* AVSD includes a large primum-type ASD, a common atrioventricular valve with varying number and distribution of leaflets, and an inlet (canal-type) VSD. A *transitional* AVSD has two separate atrioventricular valves, with an inlet VSD, and primum-type

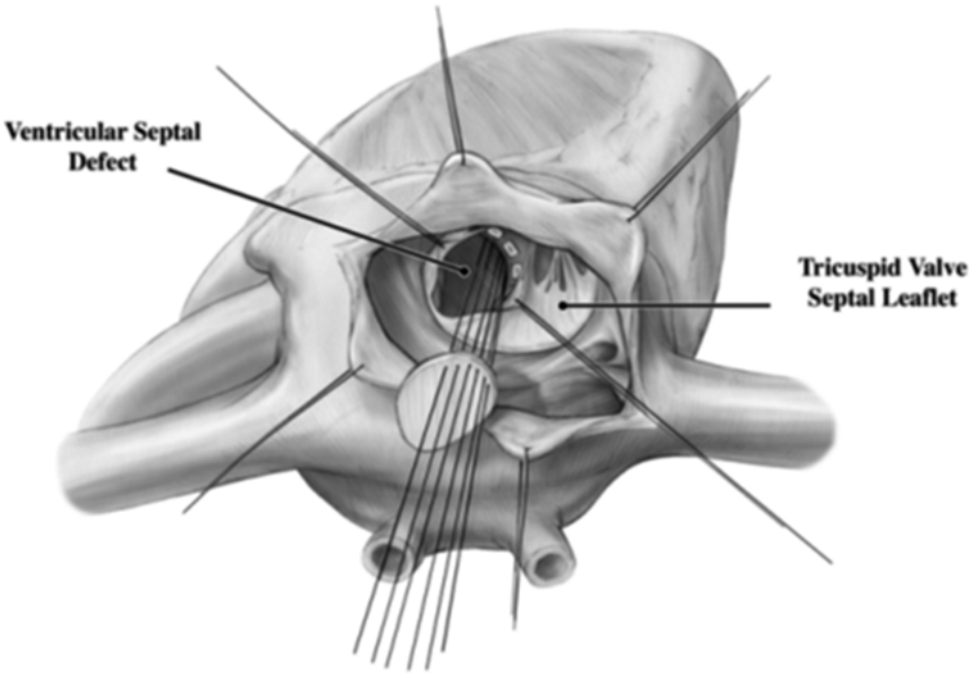

Fig. 10.3 Patch closure of a perimembranous septal defect working through the tricuspid valve

ASD. A *partial or incomplete* AVSD has a primum-type ASD and generally two separate atrioventricular valves, with a cleft in the anterior leaflet of the left-sided valve. An AVSD can be found in isolation, but there is a higher prevalence in trisomy 21, in heterotaxy syndrome with additional associated anomalies, or with variations including tetralogy of Fallot or double outlet right ventricle (DORV) [12].

Currently, repairs of these defects typically require bicaval cannulation and an arrested heart, and they are usually treated when the child is an infant. The goal of these repairs is to separate the ventricles and atrium into left and right sides; during this bipartition, the atrioventricular valves are reconstructed. There are many ways an atrioventricular canal can be repaired. In a traditional one patch repair, a single patch is first sewn to the crest of the VSD. The common atrioventricular valve is then divided into a left and right side. The two sides of the valve are then attached to the patch at its midpoint. The patch is brought up to the crest of the VSD completing the repair. Other groups have used two patches, one for the VSD and the atrioventricular valve and another for the ASD. Finally, a modified single patch technique uses a primary closure of the VSD with pledgeted suture; the sutures are then brought up through the atrioventricular valve and then through a patch which closes the ASD. Notably, the closure of the atrial and VSDs can lead to heart block requiring a permanent pacemaker.

10.8 Anomalies of the Great Arteries

10.8.1 Transposition of the Great Arteries

Transposition of the great arteries refers to the abnormal relationship and position of the great vessels at the base of the heart. Normally the pulmonary artery arises from the right ventricle, anterior to the aorta; the aorta arises from the left ventricle. In congenitally corrected transposition of the great arteries (cc-TGA), the aorta is anterior and leftward of the pulmonary artery and often arises from the morphologic right ventricle situated as the leftward ventricle (ventricular inversion). If there are no associated additional cardiac defects, this is often not found until later in life (if ever), as there are no physiologic embarrassments, outside of a right ventricle working as the systemic ventricle.

In dextro-transposition of the great arteries (d-TGA), the aorta arises from the right ventricle and is anterior and rightward to the pulmonary artery. The pulmonary artery arises from the left ventricle. Without additional cardiac defects, all of the desaturated systemic venous blood returns to the body without being refreshed in the lungs, and all of the fully oxygenated pulmonary venous blood returns to the lungs, acting as two parallel circuits and never intermixing. Newborns are able to survive initially with mixture from a patent ductus arteriosus (PDA) and a PFO, but as the PDA closes, the infant becomes progressively more cyanotic. Most frequently in

these children, in the first few days after birth, a balloon atrial septostomy (Rashkind) procedure is performed to tear open the atrial septum, followed within several days by an arterial switch operation, where the main pulmonary artery and ascending aorta are transected and the coronary arteries are excised from the aorta and transferred to the new aorta (native pulmonary artery) along with the ascending aorta. The branch pulmonary arteries are stretched over top of the newly reconstructed ascending aorta with the *LeCompte maneuver*, and the atrial septum is closed. This procedure restores the flow of desaturated blood to the lungs and the flow of fully saturated blood to the body and coronary arteries [13].

Transposition of the great arteries is now normally repaired shortly after birth. Repair is performed most often with an arrested heart and bicaval cannulation. Technically much of the repair depends on the location and insertion of the coronary arteries. Problems with the dissection and implantation of the coronaries lead to the majority of the mortalities associated with these procedures. In order to align the coronaries, often a LeCompte procedure is performed which involves bringing the pulmonary arteries anterior to the reconstructed aorta. Closure of the ASD finishes the repair.

10.8.2 Persistent Truncus Arteriosus

Persistent truncus arteriosus is the lack of separation of the pulmonary trunk and aorta, resulting in a common semilunar valve and artery arising from the ventricles, overriding an associated VSD. This common (truncal) artery supplies the coronary arteries, lungs, and aorta and was initially described by Collett and Edwards [14]; using the origin of the pulmonary blood supply, they differentiated subtypes (Fig. 10.4). In this categorization, type I refers to early bifurcation of the aorta and the pulmonary trunk from the arterial trunk. In type II, the branch pulmonary arteries arise in close proximity to each other but separately from the posterior aspect of the truncal artery. In type III, there is more separation of the origins of the branch pulmonary arteries. Type IV (also known as pseudotruncus) refers to the complete blood supply of the lungs from aortopulmonary collateral vessels, though such a defect can be argued to be pulmonary atresia with VSD. The Van Praagh classification system is also shown in Fig. 10.4 and varies slightly from the Collett/Edwards classification [15]. The anatomy of truncus arteriosus allows for the complete mixture of saturated and desaturated blood in the truncal artery and thus to the body; this will result in early heart failure, due to the often unprotected pulmonary circulation. The common surgical approach for the correction of these lesions varies depending on type but most often includes creation of an RV to pulmonary artery conduit and closure of the VSD.

In general, repair of truncus arteriosus involves separating the pulmonary artery or branches of the pulmonary arteries from the root of the aorta. Such surgical repair requires cardiopulmonary bypass with an arrested heart. The resulting aortic defect is normally patched. The VSD is normally closed through the pulmonary artery root or right ventricular

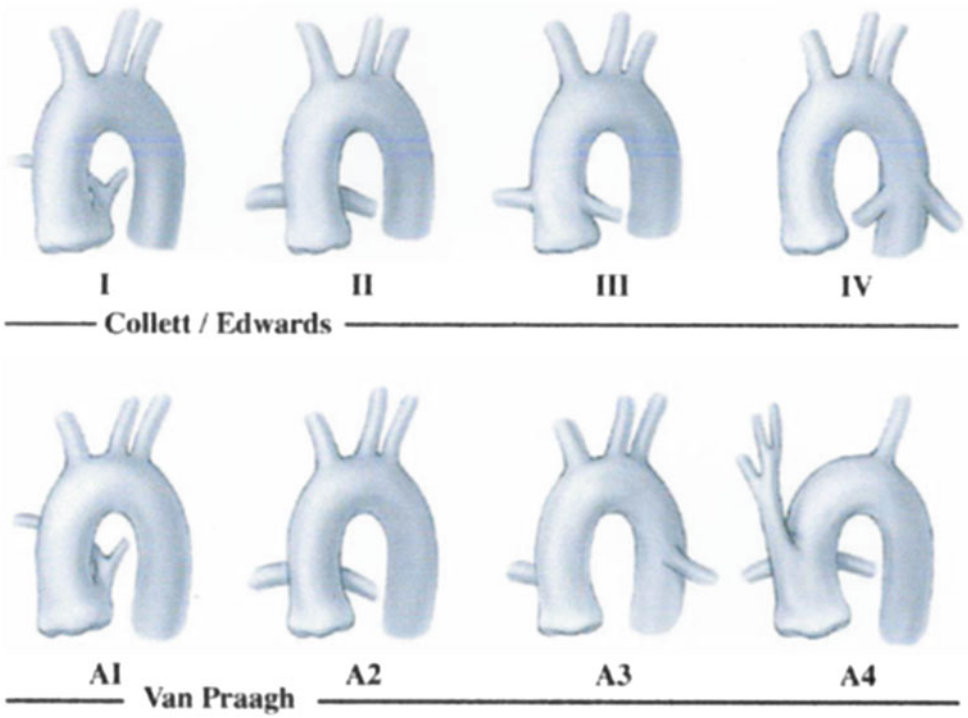

Fig. 10.4 Classification schemes for persistent truncus arteriosus

outflow; a valved conduit is used to create right ventricle to pulmonary artery continuity.

10.8.3 Aortopulmonary Window

An *aortopulmonary window* is the incomplete separation of the aorta and pulmonary trunk due to impaired or improper development of the truncal cushions during development (see also Chap. 3). In this case, there are two separate semilunar valves, and the communication can exist in the proximal portion of the aortopulmonary septum (type I), the distal septum (type II), or a combination of types I and II (also often noted as type III) [16, 17].

These defects are repaired again through the use of an arrested heart with either bicaval or single atrial cannulation. Isolation of the pulmonary arteries is important at the commencement of cardiopulmonary bypass so as not to create a circular circuit from the aortopulmonary-artery continuity. Once the pulmonary artery and aorta are separated, the resulting defects are closed usually with patches on both the pulmonary artery and aorta (Fig. 10.5).

10.8.4 Coarctation of Aorta

Coarctation of the aorta is a narrowing of the blood flow through the descending thoracic aorta in both varying degrees and locations. In the early 1990s, Amato and colleagues proposed a classification system based on the degree of aortic hypoplasia and the existences of associated cardiac lesions (Table 10.4). Type I describes obstruction in the juxta-ductal region, and type II is hypoplasia of the aortic isthmus in addition to type I narrowing. More specifically, type III includes severe (tubular) hypoplasia in much of the aortic arch, often including the distal transverse aorta [18]. During fetal life and immediately after birth, a PDA allows for blood to bypass the narrow areas and/or the right ventricle to supplement cardiac output to the lower half of the body. As the ductus arteriosus ampulla closes, the narrowing is worsened, and the infant will develop hypoperfusion of the lower body commensurate with the degree of narrowing.

Surgical repairs are normally performed on these patients as neonates, utilizing mild hypothermia without bypass. They are conducted through a posterolateral thoracotomy, which allows excellent exposure to the great vessels (Fig. 10.6). In older children, left heart bypass can be employed, diverting blood from the left atrium to the distal aorta, allowing continuous perfusion to the lower body. Most often the aortic lesion is isolated between two vascular clamps and then repaired expeditiously.

Table 10.4 Classification of coarctation of the aorta

Type I	Primary coarctation
Type II	Coarctation with isthmus hypoplasia
Type III	Coarctation with tubular hypoplasia of the distal arch • Coarctation associated with ventricular septal defects • Coarctation associated with other major cardiac defect

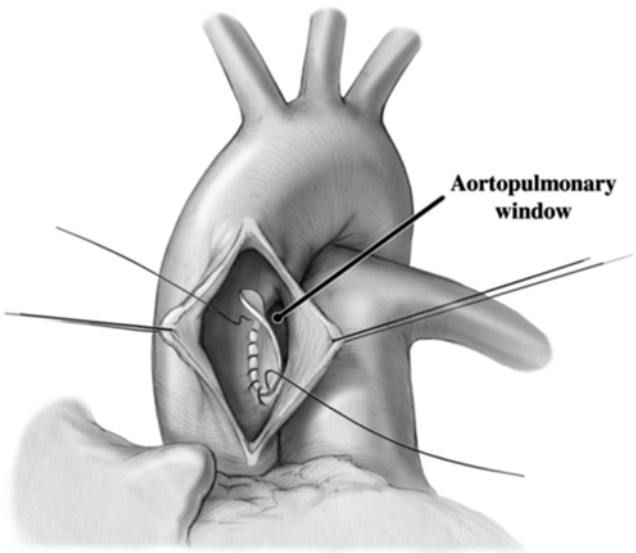

Fig. 10.5 An aortopulmonary window is created by a deficiency in the separation of the truncus. This defect is visualized through an incision in the ascending aorta and closed with a patch

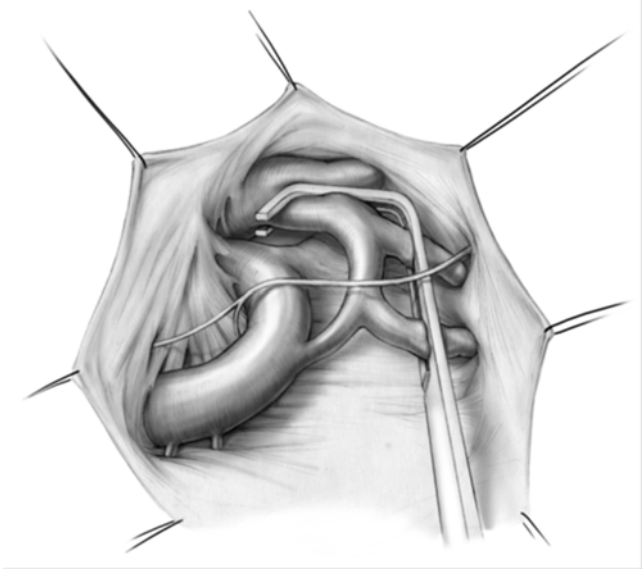

Fig. 10.6 Coarctation of the newborn is often associated with severe hypoplasia of the transverse aortic arch. A proximal vascular clamp has been placed in preparation for coarctation resection. Notice the recurrent laryngeal nerve rapping around the ductus arteriosus

Historically isolated lesions were opened by placing a patch of material across the narrowed segment. These defects now are most commonly repaired by resecting the narrowed sections and then performing end-to-end anastomoses. An alternative or additive option is using the subclavian artery as a patch of tissue to augment the narrowed section. Risks of these repairs include: damage to the recurrent laryngeal nerve, potential restenosis, scoliosis, and/or paralysis. Residual or recurrent narrowing of a coarcted site is normally treated by endovascular balloon arterioplasty.

10.8.5 Interrupted Aortic Arch

Interrupted aortic arch (IAA) is a congenital defect with a complete discontinuity in the transverse aortic arch, which may occur in the region of the aortic isthmus (type A), between the left common carotid artery and the left subclavian artery (type B, most common), or between the right innominate artery and the left common carotid artery (type C, least common), as described by Celoria and Patton [19]. Figure 10.7 demonstrates these different types, with a PDA supplying the vessels distal to the interruption, as well as the lower body. This defect is associated with a conoventricular septal defect with the conal septal tissue crowding the subaortic region. Surgical repair of this defect includes restoring continuity between the ascending and descending aorta and closure of the VSD.

Repair of IAA traditionally has been treated with the use of hypothermic arrest due to the inability to flow through an aortic cannula while working on the aortic reconstruction. A surgical alternative is to direct a lower volume of flow to the cranial circulation, through the innominate artery; some surgeons have included this low flow approach to the distal aorta as well. The interrupted segment can be reconstructed end to end, as in a coarctation repair or augmented with a patch. Occasionally an interposition graft is used to bridge the gap.

10.9 Pulmonary Atresia

Pulmonary atresia is the lack of blood flow across the pulmonic valve. This may happen in the setting of incomplete development of the pulmonic valve, or it may be functional atresia where the flow jet from a PDA holds the pulmonic valve shut. In such patients, the main and branch pulmonary arteries can be formed to varying degrees from normal size and branching pattern, to discontinuous pulmonary arteries with multiple collateral arteries supplying blood to the lungs [20]. Pulmonary atresia can also present either with a VSD or with an intact ventricular septum. When a large VSD is present, some argue it to be within the spectrum of a tetralogy of Fallot congenital abnormality (see below).

Patients with pulmonary atresia with an intact ventricular septum are associated with varying degrees of tricuspid valve hypoplasia, right ventricular hypoplasia, and/or fistulous ventriculocoronary connections. In this situation, there is often shunting of desaturated blood to the left side of the heart at the atrial level. Importantly, the relative extent of fistulous connections of the right ventricle to the coronary arteries must be understood prior to attempted repair or palliation, as the coronary blood flow may be dependent on the right ventricle.

10.10 Tetralogy of Fallot/Double Outlet Right Ventricle

Tetralogy of Fallot is a collection of lesions including: pulmonary stenosis (below, at, or above the level of the pulmonary valve), a large conoventricular VSD with anterior malalignment (override of the aorta), and right ventricular

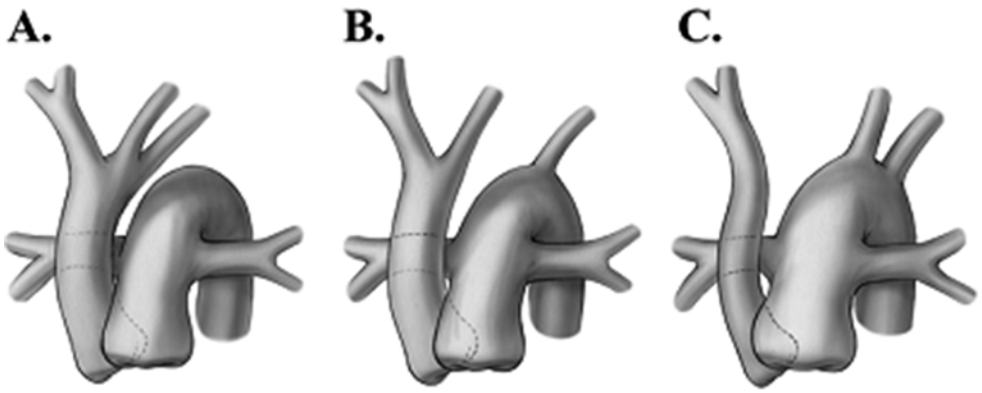

Fig. 10.7 Classification scheme for interrupted aortic arch. Type A occurs when all the arch vessels originate proximal to the interruption. Type B occurs when the left subclavian artery originates distal to the discontinuous segment

hypertrophy (Fig. 10.8). In DORV, both arterial trunks are dominantly associated with the right ventricular outflow tract [21]. The amount of right to left shunting of desaturated blood across the VSD depends on the degree of pulmonary outflow obstruction, which ranges from minimal stenosis to pulmonary atresia. Surgical repair includes closure of the VSD and relief of the pulmonary outflow obstruction. DORV can also be associated with malposition of the great arteries.

The timing of repair of tetralogy of Fallot is dependent on the severity of pulmonary arterial and/or infundibular narrowings. Severe narrowing as a neonate often requires augmentation of the pulmonary arterial flow with an aortopulmonary shunt. Most often the shunt is created with a GORE-TEX graft between the innominate artery and the pulmonary artery. Depending on pulmonary artery blood flow and hemodynamic stability, the procedure can be performed with or without cardiopulmonary bypass. Some groups are using a ductal stent to augment pulmonary arterial flow. Nevertheless, typically the full repair of tetralogy of Fallot requires an arrested heart with bicaval cannulation. The augmentation of the pulmonary arterial system can be either at the pulmonary valve or subvalvar level; repair of the VSD is performed with a patch.

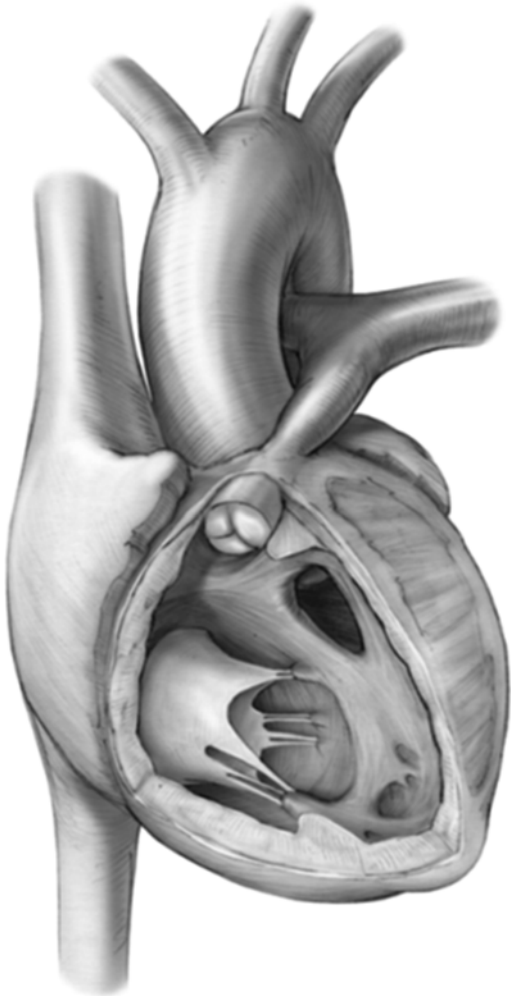

Fig. 10.8 Four components of tetralogy of Fallot include: pulmonary annular hypoplasia, a malaligned ventricular septal defect, right ventricular hypertrophy, and an overriding aortic annulus. The defect is viewed by removal of the right ventricular free wall

10.11 Pulmonary Venous Anomalies

Pulmonary venous anomalies are variable and include partial anomalous pulmonary venous connection (PAPVC) where some, but not all, of the pulmonary veins connect or drain to somewhere other than the left atrium. Total anomalous pulmonary venous connection (TAPVC) occurs when none of the pulmonary veins connect to the left atrium, or cor triatriatum, where the pulmonary venous return to the left atrium is separated by a wall of tissue (effectively forming three atria). TAPVC can connect to the right atrium or vessels above or below the heart or diaphragm, with the latter being more concerning for obstruction to blood flow. TAPVC can be classified into the following categories: (1) in type I, the pulmonary veins drain above the heart, to the SVC or innominate vein; (2) in type II, they connect directly to the heart in the right atrium or coronary sinus; (3) in type III, the connection is below the diaphragm; and (4) type IV is a mixture of several of the other types [22]. TAPVC is a mixing lesion and often presents with cyanosis reflective of the type and stability of the connections. Cor triatriatum can present with variable levels of obstructions of pulmonary venous return to the left atrium and additional connections to the heart and surrounding vessels. The physiologic consequences of these anomalies depend on the origin of the connections and any obstructions to blood flow. PAPVC is hemodynamically similar to an ASD and is often found later in life, if at all.

Repair of TAPVCs depends on the anatomical arrangement of either supracardiac-, intracardiac-, and/or infracardiac-type pulmonary venous connections. Infracardiac arrangements are most often associated with obstructions of pulmonary venous return; these can lead to pulmonary artery hypertension and cardiovascular collapse.

Repair of a TAPVC will necessitate cardiopulmonary bypass and an arrested heart. Adequate visualization often necessitates brief hypothermic arrest to allow precise anastomoses of the left atrium with the pulmonary venous confluences. Once anastomoses of the left atrium are complete, reconstruction of the atrial septum is performed, i.e., to enlarge the small left atrium.

10.12 Obstructive Left Heart Lesions

10.12.1 Mitral Valve Anomalies

Obstructive malformations of the mitral valve and its apparatus can include: (1) hypoplasia or atresia of the mitral valve, (2) abnormalities of the papillary muscles and chordae supporting the mitral valve leading to parachute or arcade mitral valve, and/or (3) left ventricular outflow tract obstructions [23]. As mitral obstruction worsens, left atrial pressure, and ultimately pulmonary arterial pressure, will increase.

10.12.2 Hypoplastic Left Ventricle

Hypoplastic left heart syndrome is characterized by varying degrees of underdevelopment of the left ventricle which can be due to a constellation of anomalies that lead to inadequate blood flow to the ascending aorta. For example, this abnormality may be secondary to mitral valve stenosis and/or atresia or aortic stenosis and/or atresia. In any case, these individuals are left with one functional ventricle (the right ventricle) and are dependent on a PDA and an atrial communication to supply saturated blood to the body. These patients typically require either cardiac transplantation or a series of palliative procedures to survive past early infancy [24].

10.12.3 Subaortic Ridge

A *subaortic ridge* is a defect with a fibromuscular ridge of tissue found below the aortic valve in the ventricular outflow tract, and it may restrict blood flow from the ventricle to the aorta. This can range from mild to severe and over time can lead to damage of the aortic valve from abnormally high turbulent blood flow. Further, in some cases, subaortic narrowing can be discrete or tunnellike and can be found in isolation or in association with other defects, primarily other left-sided obstructive lesions and VSDs [25].

10.12.4 Bicuspid Aortic Valve

A *bicuspid aortic valve* (BAV) is the most commonly presented congenital heart defect and generally consists of the lack of separation between two leaflets of the valve, effectively creating two leaflets rather than three. This leads to varying degrees of outflow obstruction and is often associated with regurgitation or leakage back across the valve back into the ventricle. Interestingly, mild cases may not be found until later in life, if ever, whereas severe cases need early intervention [26]. Note that a BAV may be found in isolation or in combination with other congenital cardiac malformations, especially coarctation of the aorta.

10.13 Coronary Artery Anomalies

Coronary artery anomalies may be found in isolation or in combination with other cardiac lesions. When the left coronary artery (LCA) arises, in part or in whole, from the right aortic sinus and travels between the aorta and pulmonary artery, there exists the potential for intermittent compression of the LCA, especially during exercise, thus resulting in inadequate blood supply to the myocardium. Multiple case series exist where this anatomy was thought to be the cause of sudden cardiac death [27]. Similarly, when the right coronary artery (RCA) originates from the left aortic sinus and courses between the aorta and pulmonary artery, a similar situation exists, especially in the setting of a right dominant coronary system; however, the actual risk to the individual remains debated in the literature.

In cases with an anomalous left coronary artery from the pulmonary artery (ALCAPA), the LCA arises from the pulmonary trunk, most often from the left sinus, or rarely from the pulmonary trunk or branch pulmonary arteries. In many patients, as the newborn pulmonary vascular resistance drops, the blood begins to flow from the coronary artery into the pulmonary artery causing a coronary steal phenomenon and resulting in underperfusion of the myocardium. These children may also present with: (1) depressed ventricular function and/or left ventricular dilation and (2) mitral valve regurgitation [28]. Surgical correction may include excision of the coronary arteries from the pulmonary artery (with a rim of surrounding tissue) and implantation onto the aorta or the creation of a tunnel to channel the blood away from the pulmonary artery.

10.14 Summary

There are numerous congenital defects that may present at birth within the human heart, and many typically require surgical intervention. In this chapter, we defined these abnormalities and introduced the reader to several classification schemes that have been used to describe their relative anatomical and functional features. This chapter also highlighted the more common surgical procedures utilized to treat congenital cardiac lesions. For additional technologies used to repair defects, the reader is referred to Chap. 37. Furthermore, Chap. 11 provides important information on mechanical circulatory support devices in the pediatric patient.

References

1. Marelli AJ, Mackie AS, Ionescu-Ittu R, Rahme E, Pilote L (2007) Congenital heart disease in the general population: changing prevalence and age distribution. Circulation 115:163–172
2. Jacobs JP, Jacobs LJ, Mavroudis C et al (2008) Nomenclature and databases for the surgical treatment of congenital cardiac disease – an updated primer and an analysis of opportunities for improvement. Cardiol Young 18:38–62
3. Uemura H, Ho SY, Devine WA, Kilpatrick LL, Anderson RH (1995) Atrial appendages and venoatrial connections in hearts from patients with visceral heterotaxy. Ann Thorac Surg 60:561–569
4. Hagen PT, Scholz DG, Edwards WD (1984) Incidence and size of patent foramen ovale during the first 10 decades of life: an autopsy study of 965 normal hearts. Mayo Clin Proc 59:17–20
5. Campbell M (1970) Natural history of atrial septal defect. Br Heart J 32:820–826
6. Raghib G, Ruttenberg HD, Anderson RC, Amplatz K, Edwards JE (1965) Termination of left superior vena cava in left atrium, atrial septal defect, and absence of coronary sinus: a developmental complex. Circulation 31:906–918
7. Rao PS (1890) Fundamentals of clinical cardiology: a unified classification for tricuspid atresia. Am Heart J 99:799–804
8. Celermajer DS, Bull C, Till JA et al (1994) Ebstein's anomaly: presentation and outcome from fetus to adult. J Am Coll Cardiol 23:170–176
9. Bailliard F, Spicer DE, Mohun TJ, Henry GW, Anderson RH (2014) The problems that exist when considering the anatomic variability between the channels that permit interventricular shunting. Cardiol Young 27:1–14 [Epub ahead of print]
10. Wilcox BR, Cook AC, Anderson RH (2005) Abnormal segmental connections. In: Wilcox BR, Cook AC, Anderson RH (eds) Surgical anatomy of the heart, 3rd edn. Cambridge University Press, United Kingdom, pp 157–170
11. Cho MS, Jang SJ, Sun BJ et al (2014) Prognostic implications of initial echocardiographic findings in adolescents and adults with supracristal ventricular septal defects. J Am Soc Echocardiogr 27:965–971
12. Smallhorn JF, Tommasini G, Anderson RH, Macartney FJ (1982) Assessment of atrioventricular septal defects by two dimensional echocardiography. Br Heart J 47:109–121
13. Villafane J, Lantin-Hermoso MR, Bhatt AB et al (2014) D-transposition of the great arteries; the current era of the arterial switch operation. J Am Coll Cardiol 64:498–511
14. Collett RW, Edwards JE (1949) Persistent Truncus arteriosus: a classification according to anatomic types. Surg Clin North Am 29:1245–1270
15. Van Praagh R, Van Praagh S (1965) The anatomy of common aorticopulmonary trunk (Truncus arteriosus communis) and its embryologic implications. A study of 57 necropsy cases. Am J Cardiol 16:406–425
16. Mori K, Ando M, Takao A, Ishikawa S, Imai Y (1978) Distal type of aortopulmonary window. Report of 4 cases. Br Heart J 40:681–689
17. Kutsche LM, Van Mierop LHS (1987) Anatomy and pathogenesis of aorticopulmonary septal defect. Am J Cardiol 59:443–447
18. Amato JJ, Douglas WI, James T, Desai U (2000) Coarctation of the aorta. Pediatr Card Surg 3:125–141
19. Celoria GC, Patton RB (1959) Congenital absence of the aortic arch. Am Heart J 58:407–413
20. Tchervenkov C, Roy N (2000) Congenital heart surgery nomenclature and database project: pulmonary atresia-ventricular septal defect. Ann Thorac Surg 69:S97–S105
21. Anderson RH, McCarthy K, Cook AC (2001) Double outlet right ventricle. Cardiol Young 11:329–344
22. Herlong JR, Jaggers JJ, Ungerleider RM (2000) Congenital heart surgery nomenclature and database project: pulmonary venous anomalies. Ann Thorac Surg 69:S56–S69
23. Wenink ACG, Gittenberger-de Groot AC, Brom AG (1986) Developmental considerations of mitral valve anomalies. Int J Cardiol 11:85–98
24. Barron DJ, Kilby MD, Davies B, Wright JGC, Jones TJ, Brawn WJ (2009) Hypoplastic left heart syndrome. Lancet 374:551–564
25. Lampros TD, Cobanoglu A (1998) Discrete subaortic stenosis: an acquired heart disease. Eur J Cardiothorac Surg 14:296–303
26. Fedak PWM, Verma S, David TE, Leask RL, Weisel RD, Butany J (2002) Clinical and pathophysiological implications of a bicuspid aortic valve. Circulation 106:900–904
27. Taylor AJ, Rogan KM, Virmani R (1992) Sudden cardiac death associated with isolated congenital coronary anomalies. J Am Coll Cardiol 20:640–647
28. Wesselhoeft H, Fawcett JS, Johnson AL (1968) Anomalous origin of the left coronary artery from the pulmonary trunk. Circulation 38:403–425

Mechanical Circulatory Support Devices in Pediatric Patients

11

Mark D. Plunkett and James D. St. Louis

Abstract

Acute heart failure can occur in children as a result of hemodynamic insults imposed on the heart by structural congenital defects or in anatomically normal hearts in which the myocardium is damaged by an inflammatory or infectious process (myocarditis, metabolic diseases leading to cardiomyopathy). Postcardiotomy heart failure following surgical repair of congenital heart defects can also lead to the need for postoperative support. Mechanical circulatory support devices have been used successfully as a bridge to recovery in children, especially in the management of acute myocarditis or postcardiotomy heart failure. The use of these devices as a bridge to transplantation has also been shown to decrease waiting list mortalities and improve the efficiency of donor organ utilizations in children. However, currently available mechanical circulatory support options for infants and children are still quite limited, especially with regard to size options for smaller patients and the long-term duration of support often required. Future devices are currently in development for clinical use on a broad scale and will greatly facilitate the successful support of children with heart failure as a bridge to myocardial recovery or heart transplantation.

Keywords

Pediatric ventricular assist device • Pediatric heart transplant • Cardiomyopathy • Myocarditis • Heart failure in children

11.1 Introduction

The development of devices designed for pediatric circulatory support has origins in the history of cardiopulmonary bypass (CPB) and the advent and development of adult ventricular assist devices (VADs). For many years, extracorporeal membrane oxygenation (ECMO) was the only reliable option for pediatric patients with heart failure, but this was only effective for short-term use. The recent miniaturization of existing technologies and the introduction of new technologies have produced potential new options and have advanced the field of pediatric mechanical circulatory support to the forefront of pediatric heart surgery. These recent advances are leading to a new and exciting world of future options for children with heart failure secondary to congenital or acquired heart disease.

M.D. Plunkett, MD (✉)
University of Illinois College of Medicine, Children's Hospital of Illinois, 420 N.E. Glen Oak Avenue, Peoria, IL 61603, USA
e-mail: mplunket@umn.edu; stlou012@umn.edu

J.D. St. Louis, MD
University of Missouri-Kansas City, School of Medicine, Children's Mercy Hospital and Clinics, Kansas City, MO, USA

11.2 Historical Notes

The history of pediatric mechanical support has its roots in the development of CPB and open-heart surgery and runs in parallel to the development of adult mechanical cardiac support. In May 1951, Dr. Gibbon used the Gibbon-IBM heart-lung

P.A. Iaizzo (ed.), *Handbook of Cardiac Anatomy, Physiology, and Devices*, DOI 10.1007/978-3-319-19464-6_11

machine successfully during closure of an atrial septal defect in an 18-year-old girl [1]. However, high mortality in the next several patients led Dr. Gibbon to abandon the use of his heart-lung machine. In response to the surgical need for heart-lung bypass, C. Walton Lillehei and his colleagues at the University of Minnesota began working in the laboratory with controlled cross circulation, and in April 1954, they began a successful series of operations for congenital heart disease using controlled cross circulation with the mother or father as the pump oxygenator [2]. By 1955, Dr. John Kirklin at the Mayo Clinic and Lillehei in Minnesota had refined the bubble oxygenator and the Mayo-Gibbon machine as well as heart-lung bypass techniques that allowed open-heart surgery [3]. Due to the growing use of CPB, the increase in procedures in open-heart surgery, and the advancement of heart transplantation, the need arose to develop a means of supporting patients with heart failure on both short- and long-term basis.

In 1966, DeBakey and Liotta implanted the paracorporeal Liotta-DeBakey left ventricular assist device (LVAD) in a patient suffering from postcardiotomy shock. The patient was supported for 10 days and ultimately survived to discharge [4]. Intensive research led to the first clinically usable systems in the late 1980s and culminated in FDA approval of an LVAD as a bridge to transplantation in 1994 [5]. Mechanical circulatory support has now evolved to a standard therapy for adults with progressive or medically refractory heart failure [6–10]. Various VAD options are readily available for adults as bridge to transplantation, bridge to myocardial recovery, or for destination therapy. For more details on this topic, see Chap. 39.

While VADs have been successfully used to support adult-sized patients to heart transplant or recovery for nearly two decades, ECMO has continued to be the main strategy to provide mechanical circulatory support for nearly all pediatric patients until recently. With advances in technology, more devices are now being used as a bridge to transplant for pediatric patients. At present, there are several devices available to pediatric patients and many others in various stages of development and investigation that are specifically designed for use in infants and smaller children for long-term mechanical support.

11.3 Heart Failure in Pediatric Patients

Acute heart failure can occur in children as a result of hemodynamic insults imposed on the heart by structural defects or in a structurally normal heart with myocarditis or metabolic disease of the myocardium. Following heart surgery for correction of structural defects, heart failure can also ensue due to myocardial ischemia or suboptimal myocardial protection referred to as *postcardiotomy failure*. Heart failure-related hospitalizations occur in 11,000–14,000 children annually in the United States, with an overall mortality of about 7 % [11]. While the number of pediatric patients with heart failure is steadily increasing, the number of annual pediatric heart transplants performed in the United States remains stable at about 300–350 annually and represents only 10–15 % of all heart transplants. Due to a relative shortage of donors and longer waiting times for these patients, an increasing experience with use of mechanical circulatory support has evolved and led to improved overall outcomes in this patient population. Approximately 25 % of all pediatric heart transplants currently involve ECMO or VAD support preoperatively, and this trend is increasing. Recent estimates of the number of children that might benefit from mechanical support with VADs range between 100 and 500 patients per year in the United States [12].

The overall strategy of mechanical support in a pediatric patient is developed based on the nature and etiology of the heart failure, the anticipated duration of support, the likelihood of myocardial recovery, the size of the patient, and the available technology at the institution. The use of mechanical circulatory support may be divided into one of four categories. *Bridge to recovery* is a term used when mechanical support is utilized temporarily until the native myocardium and cardiac function recovers from the acute pathological insult. The support options in this situation are either ECMO or temporary short-term VADs. *Bridge to transplant* is a term used when the heart dysfunction is considered permanent and the patient is supported until a donor heart is available for heart transplantation. In general, these patients often need to be supported with more long-term VADs. If it is unclear if the native cardiac dysfunction is reversible or if the patient is eligible for transplant due to evolving complicating factors or comorbidities, then support may be termed *bridge to decision*. Usually, a short-term device such as ECMO or a short-term VAD is used until recovery or until the patient is considered a candidate for transplant and then transitioned to a long-term device (*bridge to bridge*).

While the indications for VADs as *bridge to transplant* are well established, there is also an increasing role for mechanical circulatory support systems in the post-heart transplant patients. Overall, an estimate of 4.0 % of infants and younger children need mechanical circulatory assistance within the first year post-heart transplant, and children in the older age groups may also require this therapy [11]. In general, VADs are used to support the transplanted heart that is functioning poorly due to primary graft failure or acute rejection. If concomitant respiratory failure is present, then ECMO is indicated for most children.

11.4 Types of Circulatory Support Pumps

Several modalities exist for providing mechanical circulatory support to patients with heart failure. Although each device has its own unique characteristics, most of the available circulatory support pumps can be classified into one of

the following types: *counter-pulsation pumps*, *centrifugal pumps*, *axial-flow pumps*, *and volume-displacement pumps*.

Counter-pulsation pumps were among the first circulatory support devices developed, with the intra-aortic balloon pump becoming the most commonly used device for short-term support in the adult population. The cycling of the inflation and deflation of the intravascular balloon in the descending aorta in counter-pulsation with the diastolic and systolic phases of the heart produces forward flow in the arterial system and also increases coronary perfusion to the myocardium. These devices can be used in older children of adult size but have limited value in smaller children due to size limitations, potential for limb ischemia, and the increased compliance of the aortic wall in younger patients which dampens the counter-pulsation effect/benefit.

Centrifugal pumps have traditionally been used as short-term support as a means to provide either intraoperative CPB or of providing either right, left, or biventricular mechanical circulatory support. These pumps generate a vortex either through impellers (Sarns™ centrifugal pump, 3M, Ann Arbor, MI, USA; St. Jude Lifestream centrifugal pump, St. Jude Medical, Chelmsford, MA, USA) or through nested cones (Bio-Medicus Bio-Pump®, Medtronic Bio-Medicus, Inc., Eden Prairie, MN, USA) to drive non-pulsatile blood flow through a circuit. Blood is drawn in through the apex of the cone by the vortex and expelled through a port that is oriented tangential to the housing. Unlike positive displacement pumps, these pumps will not generate high forward drive pressures in the face of occlusions, but they are less prone to pump air because air in the pump leads to a loss of suction at the vortex. Today, they are widely available, easy to use, and relatively low cost. Yet, they require systemic anticoagulation, are not durable long term, and tend to create high levels of hemolysis with extended use.

Axial-flow pumps contain a rotating impeller with helical blades that curve around a central shaft. An external driveline provides electrical power to a motor that drives the rotation of the impeller by electromagnetic induction. The spinning impeller draws blood from the inflow cannula and sends it to the outflow cannula, and blood flow is essentially non-pulsatile. These pumps are typically quiet and use less power than the pulsatile devices. Further, due to the decreased number of moving parts and contact bearings, they offer the distinct advantage of enhanced durability. Miniaturization of these pumps has led to catheter-based axial-flow pumps that are now available for less invasive implantation and used as intracardiac devices.

Pulsatile volume-displacement pumps are generally pumps that consist of a chamber or sac that fills and empties cyclically. An external driveline provides electrical power to a motor within the device. The motor drives a pusher plate up and down repeatedly, expanding and compressing the volume-displacement chamber. Inflow and outflow valves maintain the direction of blood flow. These pumps produce a pulsatile flow and mimic the pumping action of the ventricles. Yet, with the current technologies, these pumps often generate considerable noise during their filling and emptying cycles.

In the current era, continuous-flow blood pumps (centrifugal pumps and axial-flow pumps) represent significant advances for mechanical circulatory support, particularly due to their enhanced mechanical longevity. Yet, questions remain regarding the long-term physiological effects of continuous non-pulsatile blood flow. One concern has been how this type of non-pulsatile support could alter the normal growth and development of a child. Despite this theoretical concern, clinical experience in adults to date has been encouraging, and recent evidence suggests that normal end-organ function can be maintained with continuous non-pulsatile blood flow with no adverse effects or increased morbidities or mortalities [13–16].

11.5 Short-Term Support

When the duration of a patient's mechanical support is anticipated to be short (2 or 3 weeks or less) or their candidacy for long-term mechanical support or transplant is unclear, centrifugal pumps can often provide effective support. With the same standard pump, the circuit can be customized to patients of various sizes by varying the tubing and cannula sizes. This strategy is useful for the short term only (as a *bridge to recovery or decision*), and patients must be transitioned to long-term VADs (*bridge to bridge*) if long-term support is necessary. Short-term support devices have the advantage of relative ease of implementation and provide either a bridge to recovery or a bridge to a more long-term ventricular support device. They are used primarily in clinical situations requiring support for several hours, days, or even up to 2–3 weeks.

Extracorporeal membrane oxygenation (*ECMO*) is a portable bedside CPB circuit, consisting of a pump head and oxygenator, with standard pressure and bubble monitoring alarms (Fig. 11.1). This system can provide circulatory support and respiratory support simultaneously. Unlike the CPB circuits, the ECMO circuit is a closed loop, without a venous reservoir to buffer any volume changes or to de-air the circulating blood. ECMO circuits have no arterial filter to prevent air or thrombotic debris from reaching the patient's systemic arterial system. Early ECMO circuits used roller head pumps, but more recently the newer centrifugal pumps have been favored due to less hemolysis and relative ease of use. Because ECMO systems include an oxygenator and a complex circuit, full anticoagulation is always required. Complications of bleeding, cerebral hemorrhage, infection, and/or thrombosis are common, and occurrences are increased with extended use [17].

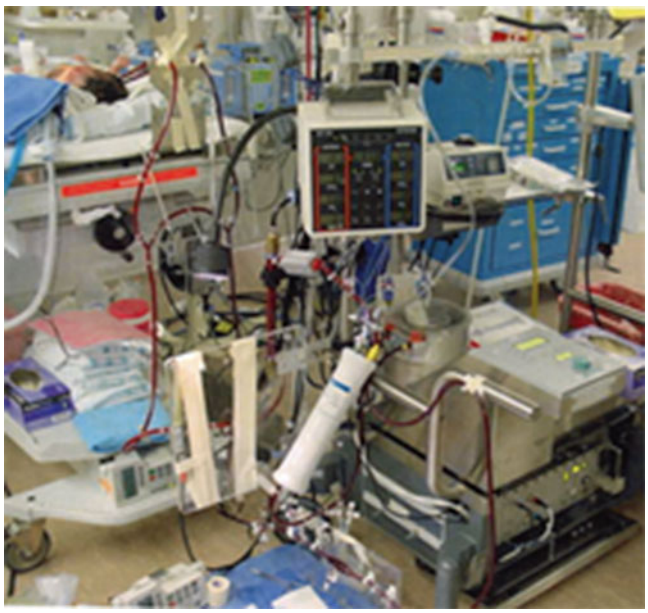

Fig. 11.1 Extracorporeal membrane oxygenation. This is a portable bedside cardiopulmonary bypass circuit, consisting of a pump head and oxygenator, with standard pressure and bubble monitoring alarms. The system provides circulatory support and respiratory support simultaneously

Fig. 11.2 Jostra Rotaflow® is an example of a new generation of centrifugal pumps that eliminates the central drive shaft/bearing

The use of ECMO continues to be a mainstay for short-term support of neonates, infants, and older children with acute hemodynamic compromise secondary to heart failure. It is frequently used to assist the pediatric patient with post-operative heart failure to support the circulation during recovery and has been invaluable in achieving improved surgical outcomes for the repair of complex congenital cardiac diseases [18, 19]. It can be rapidly deployed at the bedside or in the operating room and provides effective cardiopulmonary support for urgent and emergent conditions where either heart or lung support is needed. ECMO has been successfully used as a temporary support for 1–2 weeks for this population but is generally not considered suited for long-term support. In heart failure patients requiring heart transplantation, ECMO is still associated with a very high morbidity and mortality as a *bridge to transplant*, and survival to transplantation using long-term support with ECMO alone has been as low as 50 % [14]. Superior results have been achieved with long-term VADs [20].

Centrifugal pumps were among the earliest designs of successful pumps for pediatric cardiac support. These pumps utilize a spindle/bearing design to directly turn the spinning rotor. These early centrifugal pumps were frequently used for pediatric patient support for postcardiotomy failure and bridge to transplant when pulmonary oxygenation was adequate. In general, these pumps can be managed with lower anticoagulation requirements than an ECMO circuit. This *direct drive* method, however, has been implicated in a higher incidence of hemolysis and thrombus formation. A new generation of centrifugal pumps is now available that eliminates the central drive shaft/bearing. Each of these new generation pumps can generate in excess of 9 L/min of blood flow with very low priming volumes. Two of the most common examples of these pumps are the *Jostra Rotaflow*® (Maquet, Wayne, NJ, USA; Fig. 11.2) and the *CentriMag*® (Levitronix, Waltham, MA, USA). The *Jostra Rotaflow*® (32-mL prime) is a magnetically stabilized system on a mono-pivot with a sapphire bearing. The *CentriMag* utilizes a magnetically levitated (*maglev*) impeller to avoid the central drive shaft; currently there are two sizes available that can be utilized with the same pump console depending on the patient size—*adult CentriMag* (32 mL prime) and *pediatric CentriMag* (14-mL prime). Early clinical experiences have shown that these newer-generation pumps tend to be more durable and

Fig. 11.3 Berlin Heart Excor pediatric ventricular assist device. This was the first commercially available ventricular assist system designed specifically for the pediatric population (with miniaturized pumps and special cannula)

less prone to thrombus and hemolysis than the previous centrifugal pumps. A newer pump, the *PediMag* (Thoratec Corp., Pleasanton, CA, USA), is a 2.5 L/min centrifugal pump that is approved in the United States for 6-h use and is only designed for short-term support for up to 7 days.

Axial-flow pumps for short-term use are currently limited to the catheter-based devices. The *Abiomed Impella 2.5* (Abiomed Inc., Danvers, MA, USA) is a catheter-based micro-axial-flow device that is inserted intravascularly into the left ventricle in a retrograde manner across the aortic valve and can produce flows up to 2.5 L/min. It is currently approved for short-term support up to 7 days and has been used successfully in the older pediatric patients. These devices can be placed percutaneously using echocardiographic guidance.

11.6 Long-Term Support

When mechanical support is anticipated for longer than 2–3 weeks as bridge to recovery or (more often) as bridge to transplant, then devices capable of greater durability and low-risk long-term support are preferred. Short-term devices such as ECMO or centrifugal pumps may be used initially as a bridge to implantation of a longer-term device (*bridge to a bridge*).

A variety of options are available for long-term mechanical support of the pediatric patient. In contrast to adults, all currently available devices that are specifically designed for smaller children are paracorporeal, which does not allow patients to be discharged to home with the device. Newer and smaller devices currently under investigation are being designed for intracorporeal implantation with either an exiting driveline or possibly a transcutaneous energy transmission (TET) source. These devices would potentially allow pediatric patients to be discharged to their homes during long-term mechanical support, thus as a bridge to transplantation.

The *Berlin Heart Excor* pediatric VAD (Berlin Heart, Berlin, Germany) was the first commercially available ventricular assist system designed specifically for the pediatric population, i.e., with miniaturized pumps and special cannula. It is a paracorporeally placed, air-driven pump in a polyurethane, translucent, semirigid chamber that houses the blood-contacting membrane. The blood pumps come in 10-, 12-, 15-, 25-, or 30-mL stroke volumes and offer support options for pediatric patients as small as 2.5 kg (Fig. 11.3). These pumps are driven by a pulsatile electro-pneumonic system and can be used as a right, left, or using two as a biventricular system. The pumps can be easily exchanged for issues of thrombus formation or to increase the size of the pump in response to a growing child on long-term support. Today, the Berlin Heart Excor is the most commonly used pediatric mechanical support VAD and was approved by the FDA in December 2011. It has as high as a 90 % survival as bridge to transplant in pediatric patients and has proven more effective than ECMO for *bridge to transplant* support [21]. However, the incidence of neurologic dysfunction and complications from embolism has been reported to be as high as 29 %. To date, there have been over 1200 implants in pediatric patients in over 34 countries worldwide [22].

The *HeartMate II* (Thoratec Corp.) is an LVAD *axial-flow device* that can generate flows of up to 10 L/min, weighs 176 g, and measures 40 mm in diameter (Fig. 11.4). Early clinical trials show very effective hemodynamic support with improved patient functional status and quality of life. The HeartMate II was FDA approved in January 2010 for use as destination therapy in adults with heart failure. Today, over 4000 HeartMate II devices have been implanted in adults and children worldwide, making it the most frequently used and successful VAD in the current era [23, 24]. The pump was designed for patients greater than 1.1 m^2 BSA, but it has been used to support patients with BSAs less than this. Yet, because it is an implantable pump designed primarily for use in adults, it has limited use in smaller pediatric patients.

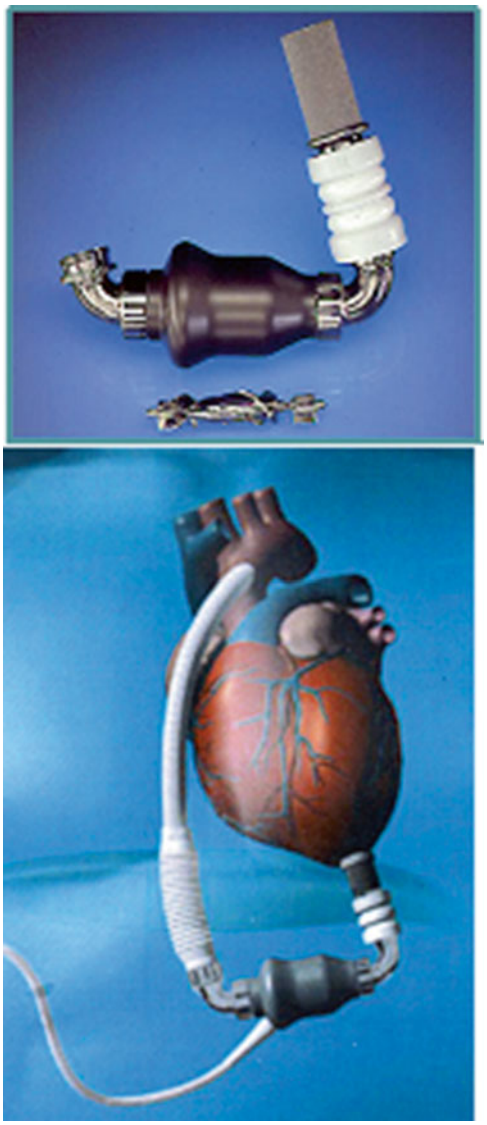

Fig. 11.4 HeartMate II left ventricular assist device. This axial-flow device can generate flows of up to 10 L/min and was FDA approved in January 2010 for use as destination therapy in adults with heart failure

The *Heartware HVAD*™ (HeartWare Ltd. Sydney, Australia) pump is an intracorporeal centrifugal maglev device that is implanted in the left ventricular apex and has been successfully used in smaller patients. At the core of the HVAD pump platform is a proprietary hybrid system for suspending the impeller (or rotor), the only moving part within the pump. Once power is applied to the device and the impeller begins to rotate, there are no points of mechanical contact within the HVAD pump, effectively ensuring a *contactless* system. The elimination of mechanical bearings is expected to lead to longer-term device reliability. The suspended impeller is designed to provide optimal blood flow paths through the system and to reduce red blood cell damage. The HVAD is accredited for patients with a BSA >1.2 cm^2; due to its small size, this pump has more recently been used in children. To date, over 160 implants have been reported worldwide in the pediatric age groups.

The *Medos HIA VAD* (Medos Medizintechnik GmbH, Stolberg, Germany) is similar to the Berlin Heart VAD. It is a pulsatile VAD, pneumatically driven with a pump chamber made of polyurethane that is available in various sizes from 10 to 80 mL so it can be used in pediatric patients as small as 3.0 kg. It can also be used in a right, left, or biventricular configuration. It still has limited availability in the United States and does not have FDA approval at this time.

Thoratec Corp. also offers both an intracorporeal (*Thoratec® IVAD*) and paracorporeal (*Thoratec® PVAD*) VAD system. They both allow the option of right, left, or biventricular support and are approved for use as a bridge to transplantation and for support in the setting of postcardiotomy shock. They provide pulsatile flow with a 65-mL blood chamber, and unidirectional flow is achieved with tilting disk mechanical valves. The paracorporeal placement of the PVAD allows use in patients with a BSA of <1.5 m^2 and has been used successfully in patients < 0.8 m^2.

The SynCardia Total Artificial Heart (*TAH*) (SynCardia, Inc., Phoenix, AZ, USA) is a pneumatically driven pulsatile device with two 70-mL polyurethane pumps that generate up to 9.0 L/min of flow and are designed for total biventricular support. It is FDA approved for *bridge to transplant* and has also received compassionate use approval as destination therapy. A portable driver was introduced in 2011 and has greatly facilitated the mobility of patients following device implant. Unlike other assist devices, the TAH actually replaces the failing ventricles and is implanted using the atrial chambers to fill the pumps through prosthetic valves. Long-term survival has been reported with the device. Recent use in single ventricle failing Fontan patients as bridge to transplant was reported [25]. While the 70-mL pump device is only used in adult-sized patients, a smaller 50-mL pump device for use in older children with a BSA as low as 1.22 m^2 is scheduled to be introduced in 2015.

11.7 Challenges of Designing Pediatric Ventricular Assist Devices

The challenge of designing pediatric VADs stems, in large part, from the issues of smaller-sized patients with limited chest capacity, rapid growth potential, and the fragility of the cardiovascular structures that may be involved with implantation. The challenge of miniaturization of devices to be used or implanted in the pediatric population has impeded the advancement and use of VADs in these patients until recently. In addition to the limited space in the thoracic cavity of smaller and younger children, there is also the issue of small caliber vasculature, small circulating blood volume, and

small cardiac chambers. Interfacing a VAD with the cardiovascular system of a child must allow for these factors. In addition, the fragility of the cerebral vasculature of neonates and younger children presents a concern that damage and hemorrhage may occur due to elevated systolic pressure generated by a device. Furthermore, the issues of growth in these patients and the sizing of devices for potentially rapidly growing children add yet another challenging dimension to these patients, not encountered in the adults.

Anticoagulation is also more difficult to manage in these young patients, and medications such as warfarin (Coumadin) can be difficult to maintain in a therapeutic range without significant fluctuations. In part this may be due to the less mature coagulation cascade systems present in younger children or variations in diet and better compliance in older age groups. It follows that the design of future pediatric devices needs to be associated with reduced risks of thromboembolism in the face of fluctuating levels of anticoagulation. The issues of mobility and ambulation are also concerns in this young patient population, with the possibility of kinking of drivelines and dislodgement of devices occurring if not securely implanted and anchored in an active and mobile child. Long-term support and the longevity of the pumps and materials over time are yet another challenge with pediatric devices. While totally implantable devices are desirable in some respects, issues like upsizing of pumps for growth and removal for thrombus, infection, or device failure make implantable devices more problematic for long-term support.

The variable anatomies of congenital heart defects (either before or after surgical intervention) and the interface of devices with abnormal anatomies can be surgically and technically challenging. More specifically, the presence of hypoplastic cardiac or vascular structures, residual shunts, insufficient valves, dextrocardia or heterotaxy, and abnormal venous return related to previous Glenn or Fontan cavopulmonary reconstructions all pose significant surgical challenges in this group of patients. Further, the presence of aortopulmonary shunts, either from previous palliative surgery or development related to the congenital defect, can create altered flow patterns during mechanical support by devices and result in pulmonary overcirculation.

It should be noted that the use of long-term devices in the single-ventricle patient population represents one of the greatest challenges in supporting patients with congenital heart disease. Given the anatomic complexities of the cavopulmonary connection and various modes of Fontan failure, any single configuration for mechanically supporting this circulation will probably not be effective for all patients. Research into the design and development of such devices and their interface with this Fontan circulation is increasing, to meet the growing population of patients with failing Fontans [26–28].

ECMO support for single-ventricle patients also poses particular challenges. Management of the systemic-to-pulmonary artery shunts must be determined based on the indication for ECMO support, systemic ventricular function, and flow characteristics of the ECMO circuit. In patients with an aortopulmonary shunt who are unable to handle any pulmonary overcirculation or cardiac volume overload, occlusion of a shunt may be indicated while on ECMO support [29]. The presence of a Glenn or Fontan reconstruction may also require a strategy of bi-caval cannulation for adequate venous decompression. Outcomes with ECMO and other devices in this patient population have been substantially lower than any other group [30]. A recent study from the ELSO registry on VAD use in pediatric patients showed only a 27 % survival in the single-ventricle cohort [31]. For more details relative to these congenital defects, the reader is referred to Chap. 10.

11.8 Future Pediatric Devices

The future development of pediatric devices will include the continued miniaturization of technologies, the development of alternate energy strategies, and the continued advancements in the designs, such as: (1) maglev technology, (2) the use of transcutaneous energy sources, and (3) laminar flow devices that are completely implantable without the need for an external driveline. Importantly, several devices are currently in clinical investigation or animal research trials that demonstrate many of these evolving trends in pediatric VADs.

HeartWare MVAD pump (MVAD, HeartWare®, Inc., Miramar, FL, USA) is a continuous axial-flow pump, approximately one-third the size of the HVAD® pump (Fig. 11.5). The MVAD pump is based on the same proprie-

Fig. 11.5 HeartWare MVAD pump. This continuous axial-flow pump utilizes proprietary *contactless* impeller suspension technology and was designed to support a wide range of flows that enable full and partial support capability. Its small size and wide range of flows will likely enable support of smaller patients and those with right ventricular failure

tary *contactless* impeller suspension technology used in the HVAD pump, with its single moving part held in place through a combination of passive-magnetic and hydrodynamic forces. The MVAD pump was designed to support a wide range of flows to enable both full and partial support capabilities. Additionally, it is expected that MVAD's small size and wide range of flows will enable support of smaller patients and those with right ventricular failure. A key focus is the development of a fully implantable system based on transcutaneous energy transfer technology. This technology enables a fully implanted battery pack to be periodically recharged using inductive coupling across the skin. This will allow implantation of the complete system, including batteries and controllers, and will eliminate the current need for a percutaneous driveline to a permanently connected controller. The HeartWare MVAD is scheduled to be available in the very near future.

Thoratec HM III (Thoratec Corp.) is a full-output centrifugal flow pump with a fully magnetically levitated rotor, which also allows the development of pulsatile flow. This near-physiological artificial pulse may have clinically important physiological benefits. Further, this pump has textured blood-contacting surfaces and a low shear stress rotor with large pump gaps, i.e., this may reduce the chances of thrombus formation and allow for reduction in anticoagulation requirements. The small pump size allows intrathoracic placement versus the typical large pump pocket required for the HeartMate II (Fig. 11.6). This system will also have lower power consumption and will include an improved modular driveline and pocket controller. This device has completed preclinical and animal testing and has been released for clinical trial use in the United States.

The *HeartMate X* (Thoratec Corp.) represents another versatile miniaturized platform technology, capable of providing either partial or full circulatory support. With a dramatic size reduction, this axial-flow pump will allow rapid, less invasive implantation techniques with versatile cannulation options. The high-efficiency motor and hydraulics will allow for lower power consumption and the potential for smaller external batteries and components. The rotor bearings are considered to have a projected lifespan of over 15 years. The design of HeartMate X is still being developed and finalized.

The *National Institutes of Health* (*NIH*) *PumpKIN trial* was initiated to promote the design and development of pediatric cardiac assist devices at several selected institutions. The National Heart, Lung, and Blood Institute solicited proposals to develop novel circulatory support systems for infants and children. The types of devices intended to be developed include left and right VADs, ECMO systems, and other novel bioengineered systems specifically for children ranging in weight from 2 to 25 kg. The goals set for the ideal pediatric device include: (1) routine deployment and functioning in less than 1 h after the decision to initiate support; (2) low priming volume; (3) flexible cannulation, suitable for abnormal anatomies; (4) minimal blood product exposure; (5) minimal risk of infection, bleeding, hemolysis, and/or thrombosis; and (6) suitable for long-term support (6 months) [12]. The following five projects were initially awarded contracts for development:

1. *PediaFlow VAD* is an implantable, magnetically suspended mixed-flow turbodynamic blood pump that is being designed and developed to provide chronic (6 months) circulatory support to patients from birth to 2 years of age (3–15-kg body weight) with congenital or acquired heart disease (Fig. 11.7). This device is based on rotary blood pump technology, has a single percutaneous lead crossing the skin for energy transmission, and may be used as a right, left, or biventricular device.

Fig. 11.6 Thoratec HeartMate III. This is a full-output centrifugal flow pump with a fully magnetically levitated rotor, which also allows the development of pulsatile flow. This near-physiological artificial pulse may have clinically important physiological benefits

Fig. 11.7 PediaFlow ventricular assist device. This is an implantable, magnetically suspended mixed-flow turbodynamic blood pump to provide chronic circulatory support to patients from birth to 2 years of age with congenital or acquired heart disease

2. *PediPump* is a magnetic bearing-supported, rotary dynamic circulatory support pump designed specifically for children. It is planned that there will be two configurations for deployment based on patient size, with intravascular implantation in larger children, and extravascular intracorporeal implantation for smaller children.
3. *Pediatric cardiopulmonary assist system* (*pCAS*) can deliver both continuous and pulsatile flows. The system is based around a compact, paracorporeal rotary flow device capable of the simultaneous pumping of blood and the delivery of oxygenation. The device rotor is fabricated from layers of microporous hollow fibers that include a custom coating to increase fiber life and minimize requirements for systemic anticoagulation.
4. *Penn State pediatric ventricular assist device* (*PVAD*) is a pulsatile, pneumatically actuated blood pump. It is intended primarily for paracorporeal placement, but it is also planned to be implantable for bridge to transplantation applications. It can be used for left, right, or biventricular support for up to 6 months. This device is not in clinical use at this time.
5. *Pediatric Jarvik 2000* is an axial-flow blood pump designed to support patients in all size ranges (3–25 kg; Fig. 11.8). These devices are designed to be implantable and provide chronic left, right, or biventricular support. The device features the implantation of the pump in the apex of the ventricular cavity as an intracardiac device.

Of the initial five devices described above, the *NIH PumpKin clinical trial 2014* is now initiated with the *Pediatric Jarvik 2000* and the *Berlin Heart Excor* VADs randomized for pediatric cardiac support in multiple centers in the United States.

Fig. 11.8 Pediatric Jarvik 2000. This is an axial-flow blood pump designed to support patients in all size ranges; additionally it is implantable and provides chronic left, right, or biventricular support

11.9 VAD Management and Complications

In general, the postoperative management issues and complications associated with the use of VADs and mechanical support in pediatric patients are similar to those encountered with the use of VADs in adults [32]. Yet, factors such as smaller circulating blood volume, difficult anticoagulation management, increased susceptibility to infections and sepsis, and rapid growth potential can make the management of postoperative issues and complications more challenging in these younger patients [33].

Mediastinal bleeding following device implantation has been reported to be relatively common in young populations. Predisposing factors include: (1) hepatic congestion and dysfunction related to heart failure, (2) compromised nutritional status, (3) the need for preoperative anticoagulation, (4) the need for extensive surgical dissection, (5) common preoperative procedures, (6) prolonged CPB and coagulopathy secondary to interactions between circulating blood elements, and/or (7) the artificial device surfaces used. Due to the requirement of systemic anticoagulation for many devices, as well as the possible use of aspirin as an anti-inflammatory agent, late bleeding and tamponade are common with all VAD implantations [34].

Infection remains a significant source of morbidity and mortality in young patients receiving mechanical circulatory support. Further, infections in VAD patients can affect different components of the device including: (1) infections at the driveline exit site, (2) device pocket infections, (3) device endocarditis, and/or (4) blood stream infections. Bacteria that are able to form a biofilm in such devices are common pathogens, including: staphylococcus, pseudomonas, enterococcus, and candida [35]. Other patient factors that may increase susceptibility to infection include nutritional compromise, renal failure, and immunologic derangement. Overall infection rates in adult patients receiving devices have been approximately 50 %, and up to 25 % of deaths in adult VAD patients are due to systemic sepsis [36]. As with adults, infections in pediatric patients may mandate removal or replacement of the assist device.

Thromboembolic events can lead to devastating neurologic and end-organ injury and remain a significant concern in pediatric patients undergoing mechanical device placement. Most device patients are maintained on anticoagulation with heparin and warfarin. In other words, the difficulty of managing these medications in a therapeutic range consistently in the pediatric patients often leads to an increased risk for thromboembolic events.

Of interest, right heart failure occurs in approximately 20 % of adult patients undergoing LVAD placement. The incidence of such failure is more variable and less defined in pediatric patients due to more variability in this population [37]. Yet, post-operation right ventricular failure can have

significant effects on clinical outcomes, leading to increased ICU stay, increased mortality following LVAD implantation, and/or a lower bridge-to-transplantation rate. It should also be noted that right heart failure can result from abnormalities in the right ventricle as well as the pulmonary vascular bed. Changes in ventricular interdependence and septal shifting secondary to mechanical unloading of the left ventricle can also contribute to impaired right-sided function [38]. In addition, pre-existing right ventricular defects or dysfunction may be unmasked secondarily to the augmented preload presented to the right side following LVAD implantation. On the other hand, evidence of right ventricular failure in the pediatric population may lead to the use of biventricular support options for mechanical support [39].

Device failure and durability are critical factors in establishing mechanical support as a feasible option for providing long-term use. Yet, device failure can occur in any of the components of such a system, including: (1) the inflow and outflow conduits, (2) the pumping chamber, or (3) the external components of the system, such as the driveline, power source, or controller unit. As clinical experience with individual devices continues to accumulate, modes of failure that are amenable to design changes become apparent, allowing for subsequent device modification and improvement. Newer-generation axial and centrifugal flow pumps attempt to address the shortcomings of the first-generation devices with smaller pumping chambers and drivelines, transcutaneous energy sources, and the use of magnetic levitation technologies to eliminate contact-bearing moving parts, offering the hope of enhanced durability and reduced risk of thrombus formation and/or embolism.

11.10 Summary

Continued advancements in both adult and pediatric mechanical circulatory support approaches have been remarkable over the last 50 years. This progress was initially the cornerstone of open-heart surgery (i.e., through use and refinement of heart-lung machines) and this paved the way for the development of VADs and the TAH. The quality and quantity of life for adult heart failure patients are now being improved by the use of cardiac assist devices as a bridge to heart transplant or myocardial recovery and more recently as a destination therapy. Miniaturization and refinement of these devices and recent incentives for the design of devices specifically made for smaller and younger pediatric patients now promise similar support for treatment of heart failure in the pediatric population [40].

Future trends in the development of newer pediatric devices will predictably include: (1) further miniaturization of pumps for increased implantability and biventricular support; (2) the use of less thrombogenic materials to reduce the need for anticoagulation; (3) improved pump durability by refinements in design, materials, and the use of newer technologies; (4) increased use of transcutaneous energy systems to avoid the need for drivelines exiting the body; (5) the use of improved and miniaturized energy sources to allow heart failure patients to live more "untethered" and unrestricted lives; and/or (6) ultimately the further development of a durable, reliable, and totally implantable devices for effective replacement of the human heart.

References

1. Ramaine-Davis A (1991) John Gibbon and his heart lung machine. University of Pennsylvania Press, Philadelphia
2. Lillehei CW, Cohen M, Warden HE et al (1955) Direct vision intracardiac correction of congenital anomalies by controlled cross circulation. Surgery 38:11
3. Kirklin JW (1989) The middle 1950s and C Walton Lillehei. J Thorac Cardiovasc Surg 98:822
4. DeBakey ME (2005) Development of mechanical heart devices. Ann Thorac Surg 79:S2228–S2231
5. Frazier OH, Rose EA, McCarthy P et al (1995) Improved mortality and rehabilitation of transplant candidates treated with a long-term implantable left ventricular assist system. Ann Surg 222:337–338
6. Gemmato CJ, Forrester MD, Myers TJ, Frazier OH, Cooley DA (2005) Thirty-five years of mechanical circulatory support at the Texas Heart Institute. Tex Heart Inst J 32:168–177
7. Dang NC, Topkara VK, Kim BT, Mercando ML, Kay J, Naka Y (2005) Clinical outcomes in patients with chronic congestive heart failure who undergo left ventricular assist device implantation. J Thorac Cardiovasc Surg 130:1302–1309
8. Bank AJ, Mir SH, Nguyen DQ et al (2000) Effects of left ventricular assist devices on outcomes in patients undergoing heart transplantation. Ann Thorac Surg 69:1369–1374
9. Rose EA, Gelijns AC, Moskowitz AJ et al (2001) Long-term mechanical left ventricular assist device for end-stage heart failure. N Engl J Med 345:1435–1443
10. Loforte A, Montallo A, Ranocchi F et al (2009) Long-term mechanical support with the HeartMate II LVAS. Transplant Proc 41:1357–1359
11. Rossano JW, Kim JJ, Decker JA et al (2012) Prevalence, morbidity, and mortality of heart failure-related hospitalizations in children in the United States: a population-based study. J Card Fail 18:459–470
12. Baldwin JT, Borovetz HS, Duncan BW et al (2006) The National Heart, Lung and Blood Institute Pediatric Circulatory Support Program. Circulation 113:147–155
13. Litwak KN, Kihara S, Kameneva MV et al (2003) Effects of continuous flow left ventricular assist device support on skin tissue microcirculation and aortic hemodynamics. ASAIO J 49:103–107
14. Ootaki Y, Kamohara K, Akiyama M et al (2005) Phasic coronary blood flow pattern during a continuous flow left ventricular assist support. Eur J Cardiothorac Surg 28:711–716
15. Letsou GV, Myers TJ, Gregoric ID et al (2003) Continuous axial-flow left ventricular assist device (Jarvik 2000) maintains kidney and liver perfusion for up to 6 months. Ann Thorac Surg 76:1167–1170
16. Saito S, Westaby S, Piggot D et al (2002) End-organ function during chronic nonpulsatile circulation. Ann Thorac Surg 74:1080–1085
17. Gupta P, McDonald R, Chipman CW et al (2012) 20-year experience of prolonged extracorporeal membrane oxygenation in critically ill children with cardiac or pulmonary failure. Ann Thorac Surg 93:1584–1590

18. del Nido PJ, Dalton HJ, Thompson AE, Siewers RD (1992) Extracorporeal membrane oxygenator rescue in children during cardiac arrest after cardiac surgery. Circulation 86:II300–II304
19. Kumar TKS, Zurakowski D, Dalton H et al (2010) Extracorporeal membrane oxygenation in postcardiotomy patients: factors influencing outcome. J Thorac Cardiovasc Surg 140:330–336
20. Imamura M, Dossey AM, Prodhan P et al (2009) Bridge to cardiac transplant in children: Berlin Heart versus extracorporeal membrane oxygenation. Ann Thorac Surg 87:1894–1901
21. Fraser CD Jr, Jaquiss RD, Rosenthal DN et al (2012) Prospective trial of a pediatric ventricular assist device. N Engl J Med 367:532–611
22. Sandica E, Knyphausen E, Blanz U, Rofe D, Morshuis M (2012) Safety of long-term mechanical support with Berlin Heart EXCOR in pediatric patients. World J Pediatr Congenit Heart Surg 3:72–76
23. Owens WR, Bryant R 3rd, Dreyer WJ et al (2010) Initial clinical experience with the HeartMate II ventricular assist system in a pediatric institution. Artif Organs 34:600–603
24. Reinhartz O, Hill JD, Al-Khaldi A et al (2005) Thoratec ventricular assist devices in pediatric patients: update on clinical results. ASAIO J 51:501–503
25. Rossano JW, Goldberg DJ, Fuller S, Ravishankar C, Montenegro LM, Gaynor JW (2014) Successful use of the total artificial heart in the failing Fontan circulation. Ann Thorac Surg 97:1438–1440
26. Rodefeld MD, Boyd JH, Myers CD et al (2003) Cavopulmonary assist: circulatory support for the univentricular Fontan circulation. Ann Thorac Surg 76:1911–1916
27. Throckmorton AL, Ballman KK, Myers CD et al (2007) Mechanical cavopulmonary assist for the univentricular Fontan circulation using a novel folding propeller blood pump. ASAIO J 53:734–741
28. Wang D, Plunkett M, Lynch J et al (2011) Dual lumen cannula leads to total cavopulmonary support in a failing Fontan sheep model. Ann Thorac Surg 91:1956–1960
29. Allan CK, Thiagarajan RR, del Nido PJ et al (2007) Indication for initiation of mechanical circulatory support impacts survival of infants with shunted single-ventricle circulation supported with extracorporeal membrane oxygenation. J Thorac Cardiovasc Surg 133:660–667
30. Rood KL, Teele SA, Barrett CS et al (2011) Extracorporeal membrane oxygenation support after the Fontan operation. J Thorac Cardiovasc Surg 142:504–510
31. Almond CS, Singh TP, Gauvreau K et al (2011) Extracorporeal membrane oxygenation for bridge to heart transplantation among children in the United States: analysis of data from the Organ Procurement and Transplant Network and Extracorporeal Life Support Organization Registry. Circulation 123:2975–2984
32. Stein ML, Robbins R, Sabati AA et al (2010) Interagency Registry for Mechanically Assisted Circulatory Support (INTERMACS)—defined morbidity and mortality associated with pediatric ventricular assist device support at a single US center/clinical perspective. Circ Heart Fail 3:682–688
33. Hehir DA, Niebler RA, Brabant CC et al (2012) Intensive care of the pediatric ventricular assist device patient. World J Pediatr Congenit Heart Surg 3:58–66
34. Spanier T, Oz M, Levin H, Weinberg A, Stamatis K, Stern D (1996) Activation of coagulation and fibrinolytic pathways in patients with left ventricular assist devices. J Thorac Cardiovasc Surg 112:1090–1097
35. Chinn R, Dembitsky W, Eaton L et al (2005) Multicenter experience: prevention and management of left ventricular assist device infections. ASAIO J 51:461–470
36. Holman WL, Rayburn BK, McGiffin DC et al (2003) Infection in ventricular assist devices: prevention and treatment. Ann Thorac Surg 75:48–57
37. Fukamachi K, McCarthy PM, Smedira NG et al (1999) Preoperative risk factors for right ventricular failure after implantable left ventricular assist device insertion. Ann Thorac Surg 68:2181–2184
38. Santamore WP, Gray LA (1996) Left ventricular contributions to right ventricular systolic function during LVAD support. Ann Thorac Surg 61:350–356
39. Gandhi SK, Huddleston CB, Balzer DT et al (2008) Biventricular assist devices as a bridge to heart transplantation in small children. Circulation 118:S89–S93
40. Morales DL, Zafar F, Rossano JW et al (2010) Use of ventricular assist devices in children across the United States: analysis of 7.5 million pediatric hospitalizations. Ann Thorac Surg 90:1313–1319

Part III

Physiology and Assessment

Cellular Myocytes

12

Vincent A. Barnett

Abstract

The function of the heart as a pump is ultimately dependent on the coordinated contractions of its chambers to move blood throughout the body. These contractions are produced by cardiac myocytes, the muscle cells of the heart. Understanding of the structure and function of these cells on an individual level provides insights into adaptations of the heart due to normal as well as pathophysiological changes over the course of a lifetime.

Keywords

Actin • Action potential • Adenosine triphosphate • Gap junctions • Intercalated disk • Membrane potential • Myofibril • Myosin • Sarcomere • Sarcoplasmic reticulum • Tropomyosin • Troponin • Transverse tubules

12.1 General Cellular Morphology

All human cells can be thought of as biological machines that are surrounded by a membrane bilayer (plasma membrane). The plasma membrane has a nominal thickness of ~5 nm (50 Å) and encloses the cellular machinery within the intracellular space whose environment is closely regulated for optimal performance. The average diameter of a non-muscle cell is approximately 10–20 μm. The encapsulating membrane is primarily composed of a bilayer of phospholipids, bipolar molecules with hydrophilic head groups, and hydrophobic lipid tails (Fig. 12.1). In addition, the plasma membrane is studded with receptors (Fig. 12.1) for various biochemical signaling molecules (hormones, neurotransmitters, etc.). Also resident in the plasma membrane are a number of ion-specific pumps and channels which function to regulate the ionic composition of the internal environment of the cell (endoplasm). The interior of each cell contains enzymes and organelles that are specialized to support a wide array of biological functions. Key organelles include: the nucleus (which contains the genetic blueprint for cellular function), mitochondria (which converts various energy sources to adenosine triphosphate, or ATP), the endoplasmic reticulum (protein and lipid synthesis as well as calcium storage), and the Golgi apparatus (which supports processing of newly synthesized proteins). The cells of each tissue anchor themselves together and to the surrounding connective tissues via membrane-bound anchoring proteins (Fig. 12.1).

12.2 Cardiac Muscle Cell Morphology

Muscle cells are similar in that they contain these common organelles but distinct in that they also include an elaborate protein scaffold within the cell that is anchored to the cell membrane and the extracellular matrix of connective tissue (Fig. 12.2). Force generation arising from protein–protein interactions within the internal protein lattice leads to the contraction of the cells and pumping of blood by the heart. Mammalian cardiac cells are roughly cylindrical but may also include short branch-like projections. The cells have an asymmetric profile with diameters in the range of 10–20 μm

V.A. Barnett, PhD (✉)
Department of Integrative Biology and Physiology,
University of Minnesota, 6-125 Jackson Hall,
321 Church St SE, Minneapolis, MN 55455, USA
e-mail: barne014@umn.edu

P.A. Iaizzo (ed.), *Handbook of Cardiac Anatomy, Physiology, and Devices*, DOI 10.1007/978-3-319-19464-6_12

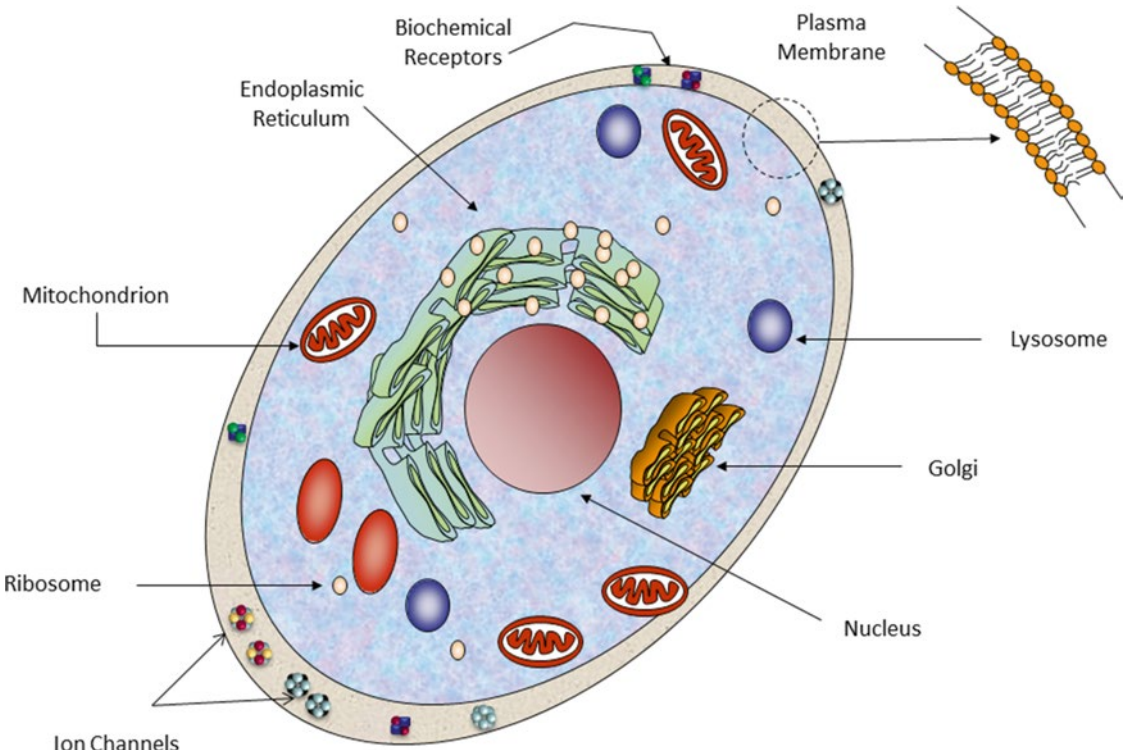

Fig. 12.1 A typical mammalian cell. The intracellular environment is separated from the extracellular environment by a lipid bilayer membrane (see area *encircled* in figure). Each cell contains a nucleus containing chromosomes and a collection of organelles to support biosynthetic and other "housekeeping" tasks. Shown here are the endoplasmic reticulum, ribosomes, mitochondria, Golgi apparatus, lysosomes, various ion channels, and biochemical receptors

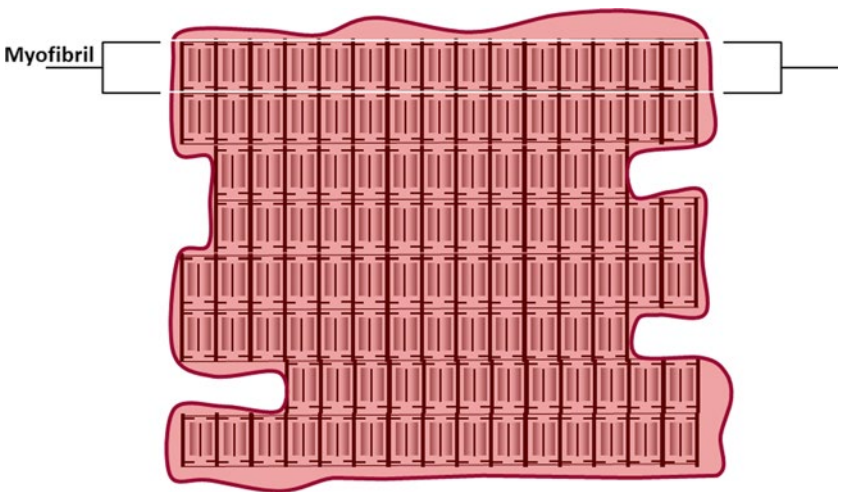

Fig. 12.2 A typical cardiac cell. The intracellular space is largely filled with contractile structures called myofibrils. The nucleus and other organelles that support cellular function are present but are often crowded to the periphery by the contractile apparatus

and lengths on the order of 50–100 μm. Force is produced primarily along the long axis of the cell. Most of the internal volume of myocytes is devoted to a cytoskeletal lattice of contractile proteins whose liquid crystalline order gives rise to a striated appearance under the microscope (Figs. 12.2 and 12.3). As with other cell types, the membrane bilayer contains a collection of ion channels and ion pumps and receptor proteins. In addition, the membranes of cardiac muscle cells contain some proteins which connect cardiac myocytes to one another as mechanical partners and other proteins which facilitate cell-to-cell electrical communications.

12.3 Cardiac Cell Membranes

The surface (or plasma) membranes of cardiac cells are punctuated by openings of membrane-lined channels, the *transverse tubules* (or T-tubules), that pass through the cell and are filled with extracellular fluid (Fig. 12.4). As they traverse the cell, individual T-tubule passages will branch and connect to other transverse tubule channels forming a reticular network that encircles the internal contractile structures known as myofibrils. Abutting the T-tubules, in the sarcoplasm

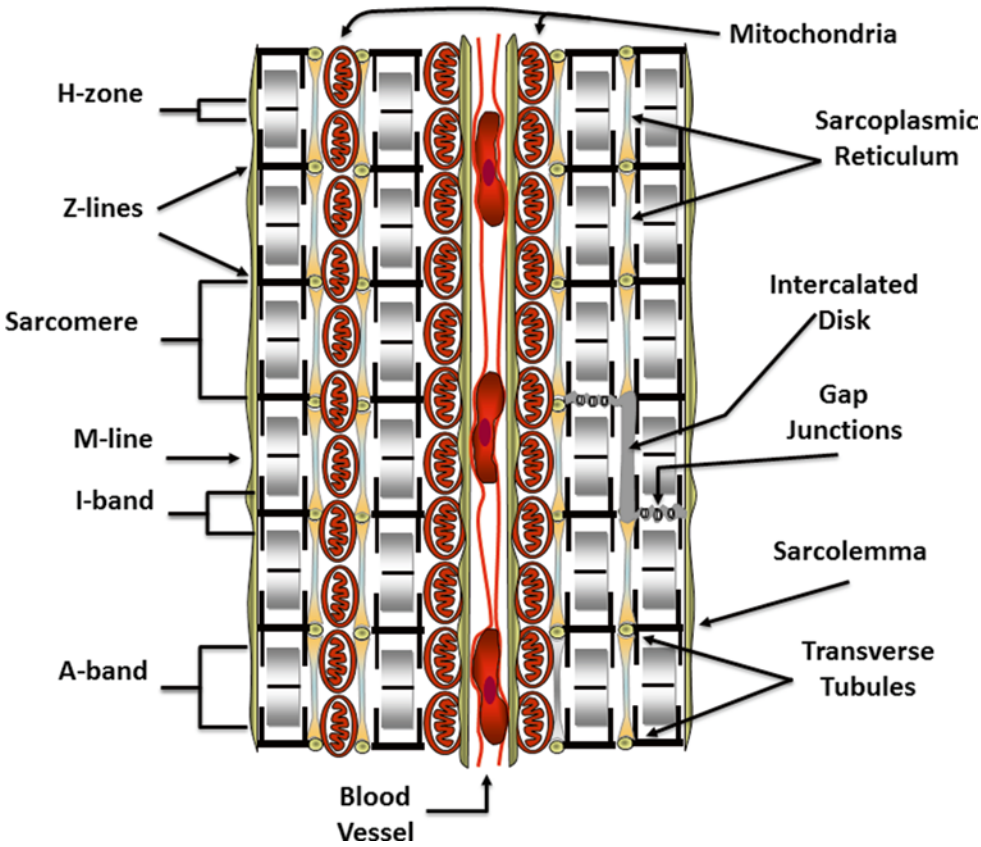

Fig. 12.3 A cross section of cardiac tissue showing two cells separated by a blood vessel containing red blood cells. The repeating sarcomeric structure of the myofibrils and the names of the sarcomeric landmarks are highlighted on the *left* of the figure. On the *right* of the figure, the legend points out the membrane specializations of the cell. These include the intercalated disks, gap junctions, the transverse tubules that punctuate the sarcolemma (plasma membrane), and the sarcoplasmic reticulum. Also shown are mitochondria compacted into a limited space because of the abundance of the myofibrils

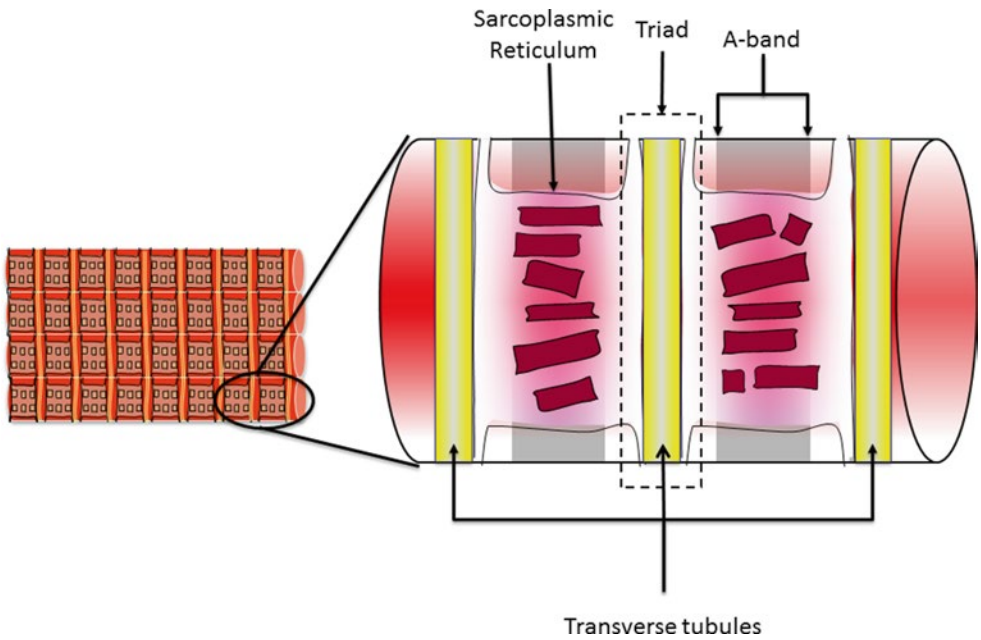

Fig. 12.4 A section of a cardiac cell showing the relationship of the sarcoplasmic reticulum and the transverse tubules (T-tubules). The sarcoplasmic reticulum surrounds each myofibril and lays adjacent to the T-tubules as they pass through a cardiac cell. The junction of the T-tubule with the adjacent sarcoplasmic reticulum is referred to as the *triad*. This close proximity allows the action potentials that pass through the T-tubular system to influence calcium release from the sarcoplasmic reticulum

(cytoplasm) of the myocytes, is the sarcoplasmic (endoplasmic) reticulum, a cytosolic organelle that is specialized to store calcium. The T-tubules provide a pathway for conduction of action potentials through the entire thickness of a cardiac myocyte. Their close association with the sarcoplasmic reticulum helps to couple cardiac action potentials to the release of calcium from internal stores. This arrangement of the T-tubules with the sarcoplasmic reticulum is also found in skeletal muscle, but not within smooth muscles.

12.4 Intercalated Disks

A structure referred to as the *intercalated disk* forms strong mechanical links between myocytes (Fig. 12.5). The intercalated disk structures are formed by the association of membrane-bound proteins projecting from the surfaces of the neighboring cardiomyocytes. The protein components of these membrane plaques include: N-cadherin, desmin,

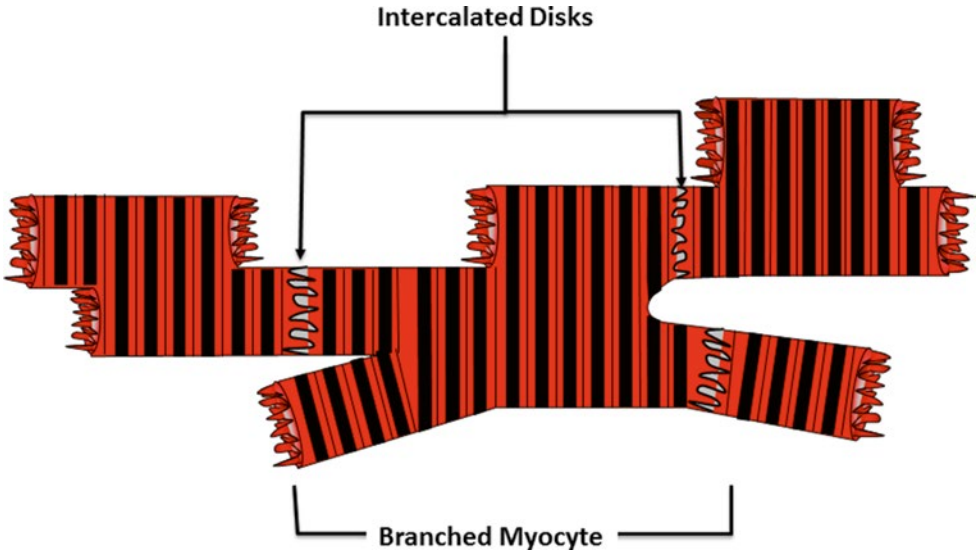

Fig. 12.5 A collection of interconnected cardiac muscle cells showing their characteristic branched structure. At the interface of adjoining cells, there is an interconnection of membrane-bound proteins known as the intercalated disk. This structure mechanically couples the cardiac cells so that the forces generated by each cell are communicated through the vessels of the heart

vinculin, α- and β-catenin, desmoplakin-1, desmocollin-2, and plakoglobin-2 [1, 2]. The tight cell-to-cell coupling of the intercalated disks contributes structural integrity to branches of myocardial cells. This connection of the cardiac myocytes facilitates some lateral shifting and the interdigitation of the cells. However, longitudinal shifting of cardiac myocytes relative to one another is practically impossible (Fig. 12.5). Importantly, it is the structural integrity of the intercalated disks between individual cells that allows force to be transmitted across the myocardium.

12.5 Gap Junctions

Gap junctions form electrical connections between cardiac cells [3]. Membrane proteins known as *connexins* form six-membered rings called *connexons* imbedded in the sarcolemma of cardiac cells (Fig. 12.6a). The connexons on the surface of one cell dock with connexons on the surface of a neighboring cell. A conformational change within the proteins of docked connexons results in openings of aqueous pores or *gap junctions* (Fig. 12.6b). When gap junctions are open, they provide for direct electrical and small molecule communication between the sarcoplasmic spaces of adjoining cells, creating a functional syncytium or network of synchronized cells. This connectivity allows activation signals to be passed from cell to cell in cardiac tissue. Electrical depolarizations can then pass from cell to cell through these gap junctions; this facilitates the seemingly simultaneous, coordinated contractions of cardiac muscle. For more details on movement of electrical signals through heart tissue, the reader is referred to Chap. 13.

12.6 Myofibrillar Structure

The arrangement of contractile proteins in cardiac muscle cells is similar to that found in skeletal muscle. Many contractile protein assemblies, known as *myofibrils*, run parallel to one another along the long axes of the myocardial cells (Fig. 12.2). Myofibrils fill most of the cytoplasmic space of each cardiac myocyte, with the remainder of these cells occupied by the normal intracellular machinery (Fig. 12.3). Each myofibril is composed of a serial array of contractile elements called *sarcomeres*, defined as the smallest functional units within muscle (Figs. 12.3 and 12.7). It is the arrangement of contractile proteins into the sarcomeres that gives cardiac and skeletal muscle the characteristic striated appearance under microscopic examination. At regular intervals along each myofibril, a transverse matrix composed primarily of the proteins α-actinin and actin forms boundaries known as *Z-disks* (or Z-lines; Fig. 12.7). A sarcomere is defined as the arrangement of contractile proteins that resides between two consecutive Z-disks along a myofibril. Actin filaments anchored on each face of a Z-disk extend for 1 μm toward the center of adjacent sarcomeres (thin filaments). Thick filaments of the protein myosin sit in the center of each sarcomere and extend toward the Z-disks at the ends of the sarcomere (thick filament length ~1.6 μm). The thick filaments are connected at their centers by a protein matrix referred to as the *M-line* (or M-disk) and tethered to the Z-disks by filaments of the protein titin. The region of the sarcomere in which the myosin filaments reside is known as the *A-band* (Figs. 12.3 and 12.7). The area between A-bands is known as the *I-band*; each I-band is bisected by a Z-line and is traversed by the actin thin filaments (Figs. 12.3 and 12.7).

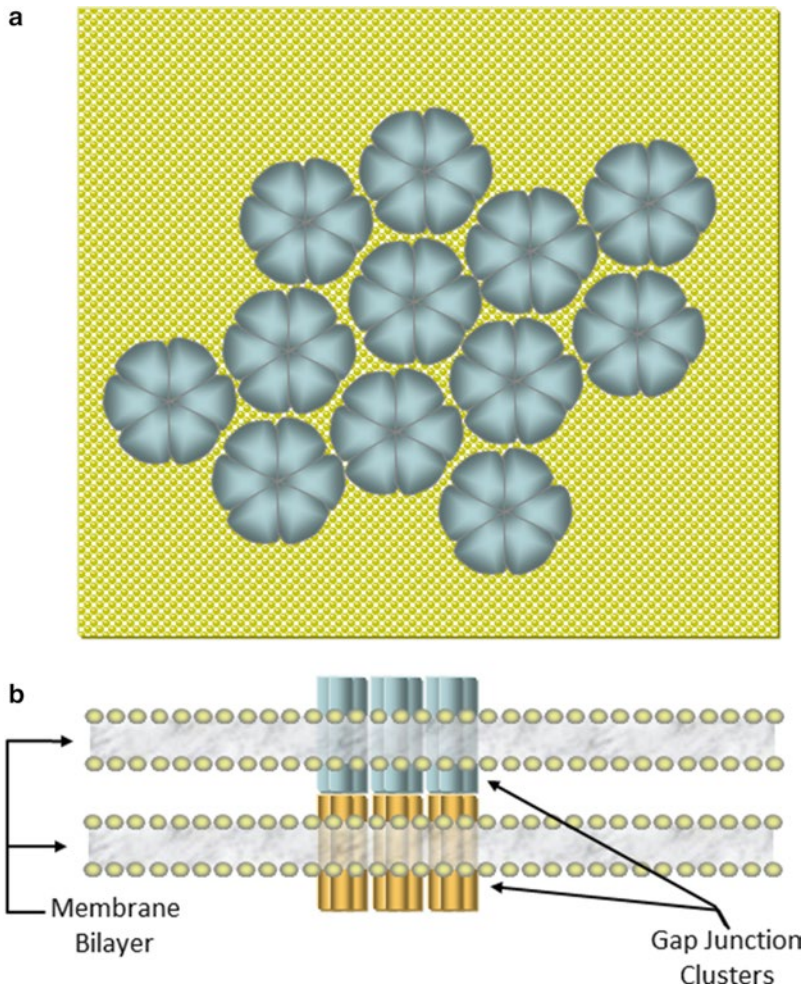

Fig. 12.6 (**a**) Overhead representation of a plaque of connexons on a cardiac membrane. Six connexins form each pore structure (connexons) on the membrane surface which cluster in the intercalated disk regions at cell–cell interfaces. (**b**) Side view of the interface between two cells showing the docking of connexons to form a gap junction between adjacent cells

12.7 Thin Filament

As noted above, the principle structural component of the thin filaments is a double-stranded filament of the globular protein actin (Fig. 12.7). The thin filaments also incorporate the regulatory proteins tropomyosin (Tm) and troponin (Tn). Tropomyosin is a double-stranded α-helical coiled-coil protein that spans seven actin monomers (~35 nm). Troponin is a globular protein complex with three subunits: TnC, a calcium-binding subunit; TnI, a subunit which facilitates inhibition of muscle contraction; and TnT, a subunit that connects the troponin complex to tropomyosin and actin. Tropomyosin molecules are aligned end to end around the helical coil of the thin filament with one Tn complex attached to each Tm molecule. In relaxed muscle, the track traced by tropomyosin as it binds to actin on the thin filament impedes the binding of the myosin crossbridge domains (see below) to actin-binding sites [4]. However, upon myocyte activation and the subsequent increase in myoplasmic calcium concentrations, free calcium binds to TnC inducing a conformational change of the entire troponin complex that is transmitted to tropomyosin. Tm then shifts its position on the actin thin filament, revealing the site on actin required for strong myosin binding. Myosin can then bind to the thin filament in a manner conducive to force production. This association of a tropomyosin-troponin complex over seven actin monomers represents a de facto regulatory subunit along the thin filament. The overlap of Tm molecules creates a mechanism for the communication of the activation signal along the thin filament, making the initiation of force generation via this mechanism highly cooperative [4].

This thin filament-based mechanism for the regulation of contraction is also used for the control of skeletal muscle. In contrast, in smooth muscle (e.g., the muscles of the vascular system, gut, and airways), while the regulation of contraction is also calcium dependent, the regulatory protein troponin is absent. The rise in calcium concentration is sensed by the cytosolic protein calmodulin, and activation occurs via a different thick filament-based mechanism.

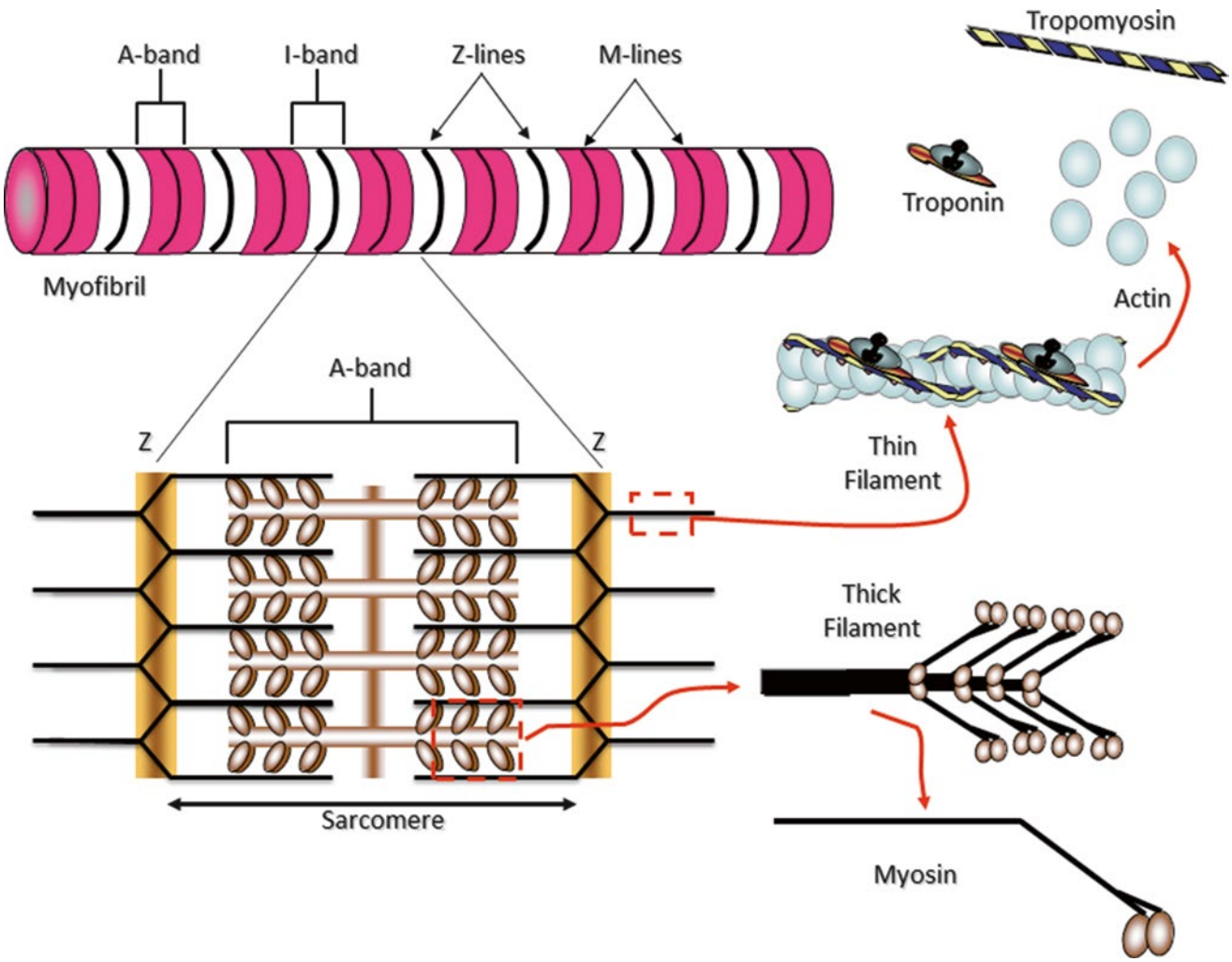

Fig. 12.7 Myofibrils are constructed of repeating sarcomeres within cardiac muscle cells. Each sarcomere is defined as the structures bounded on each end by Z-disks (Z-lines). Thin filaments of the protein actin are attached to the Z-line and reach toward the center of each sarcomere. Two regulatory proteins are found on the double-stranded actin thin filaments—tropomyosin and troponin. Tropomyosin is a double-stranded a-helical protein dimer that binds across seven actin monomers on the thin filament obscuring a binding site for myosin. Troponin is a three subunit globular protein that binds one per tropomyosin. Thick filaments of the protein myosin are found in the center of the sarcomere. The area that contains the thick filaments is also known as the A-band. The myosin molecules are asymmetrically shaped with a coiled-coil "tail" and two globular "head" domains. The head domains bind to actin to form cross-bridges between the filaments and generate contractile force

12.8 Thick Filament

Myosin is the molecular motor protein responsible for force production and movement of muscle cells. The functional protein is a hexamer (six-sub unit) composed of two protein *heavy chains* and four *light chains*. Each heavy chain is asymmetrically shaped with a long alpha-helical "tail" and two globular "head" domains (Fig. 12.7). Associated with each globular head domain are two smaller protein components, the "light chains" of myosin. The heavy chain tails form an alpha-helical coil which completes the assembly of the molecule. The coiled tails of myosin self-associate in an anti-parallel manner to form the backbone of the thick filament (Fig. 12.7). This results in a bipolar structure that has a bare zone in the center and the globular "head" domains of the myosin molecules projecting from each end. These head domains contain an actin-binding site and an ATP hydrolysis site. As will be discussed later, the cyclic interaction of these crossbridge forming head domains to the actin thin filaments forming crossbridges provides the underlying mechanism for myocyte contraction.

12.9 Energy Metabolism

ATP production in cardiac muscle is primarily accomplished via oxidative phosphorylation. Oxidative phosphorylation is a multistep enzymatic process that extracts energy from glucose, fatty acids, and other energy-rich compounds and

converts it to ATP. The energy extraction and ATP production occur in the mitochondria found in the cytoplasmic space of cardiac myocytes. Intracellular concentrations of ATP hover in the 4–5 millimolar (mM) range with additional energy stored in creatine phosphate which acts as a backup to the ATP supply. Creatine phosphate (~20 mM) can be used to regenerate ATP in a one-step enzymatic process catalyzed by the enzyme creatine kinase. There is an absolute requirement for oxygen in the ATP production mechanism, and it is the reason that blood flow to the myocardium is so critical. The amount of ATP and creatine phosphate normally present is insufficient to power the contractile activities and other uses of ATP in heart cells for more than a few beats. Therefore, continuous delivery of nutrients and oxygen and removal of waste products are crucial processes for the normal functioning of the myocardium. For a more detailed description, see Chap. 21.

12.10 Force Production: The Crossbridge Cycle

During diastole, myosin crossbridges bind ATP and hydrolyze it, but cannot use the energy released during hydrolysis to produce force (Fig. 12.8), because of the inhibitory influences of tropomyosin and troponin on the thin filament. The hydrolytic events (Fig. 12.8, step 1) induce conformational changes in myosin that allow it to hold on to the products of ATP hydrolysis (inorganic phosphate (Pi) and adenosine diphosphate (ADP)). The myosin heads then retain most of the energy released during the hydrolysis of the high-energy phosphate bond of ATP. During systole, calcium from the extracellular milieu and the sarcoplasmic reticulum floods the cytoplasm, raising the intracellular calcium concentration from micromolar to millimolar levels. As discussed above, the binding of calcium to TnC initiates conformational changes of the Tm–Tn complex that then moves these protein structures from their blocking position on the thin filament, thus removing inhibition. The energized myosin crossbridges can then bind to the actin-binding sites and thus to the thin filament (Fig. 12.8, step 2). This association with actin catalyzes the release of Pi and ADP and a concomitant force-generating conformational change of the myosin head occurs while it is bound to actin (Fig. 12.8, step 3). The conformational change pulls the thin filament past the thick filament. At the end of the force-generating transition, the vacant enzymatic active site of myosin can rebind ATP (Fig. 12.8, step 4), inducing a structural change which then reduces the affinity of the crossbridge for actin and thus causes crossbridge detachment. The subsequent hydrolysis of myosin-bound ATP, in turn, reenergizes the crossbridge and prepares it for the next force-generating cycle. The cycle continues as long as the intracellular calcium concentration is high enough to keep the Tm–Tn complexes from blocking the myosin-binding sites.

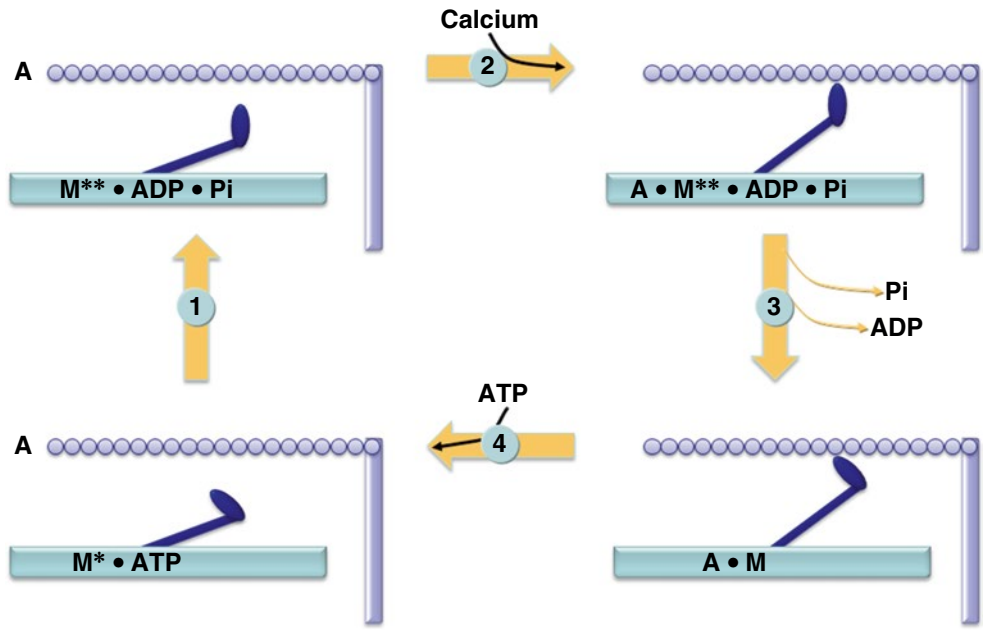

Fig. 12.8 Crossbridge cycle. Step 1: Myosin (M) binds ATP on its globular head domain and hydrolyzes it to ADP and phosphate (Pi); the energized myosin crossbridge (M**ADP-Pi) then waits for activation of the actin (A) thin filament. Step 2: After activation, the energized crossbridge binds to the actin thin filament. Step 3: The association with actin triggers the rapid release of ATP hydrolysis products ADP and Pi from the crossbridge; the release of ADP and Pi is coupled to a conformational change of the crossbridge domain which produces force, pulling the actin thin filament relative to the thick filament. Step 4: ATP binds to the crossbridge as it completes its power stroke causing the dissociation of myosin and actin; this forms the M*ATP state as the conformation of myosin changes again. The crossbridge cycle continues as long as the intracellular calcium concentration is high. At rest the system sits with myosin in an equilibrium between the M*ATP state and the M**ADP-Pi state

12.11 Length–Tension Relationship

The myofibrils of a cardiac myocyte are tethered to the membranes and intercalated disks at each end of the cell via connective protein linkages. Cell length is a dynamic variable with shortening of a cardiac cell occurring with each systolic contraction and stretch of the cell occurring during each diastole as the chambers refill with blood. This means that the myofibrils and sarcomeres also shorten and lengthen during the cardiac cycle. It is important then to realize that there is a direct connection between the overlap of the thick and thin filaments and the resultant force output developed by cardiac muscle cells.

Sarcomere length is defined as the distance from one Z-line to the next Z-line along a myofibril. When the sarcomere length in a cardiac myocyte is approximately 2 μm, this overlap of actin and myosin is optimal, and nearly all of the myosin crossbridge domains are in position to bind to the thin filaments. This configuration of the sarcomere leads to maximal isometric (isovolumic) force production (Fig. 12.9). If the myocyte is stretched, the potential force decreases because of the decrease in the overlap region of crossbridge, binding sites between the thick filaments with the thin filaments. Thus, the decreased force development is directly the result of the reduced potential for possible crossbridge formations as the cell is stretched (Fig. 12.9). If the myocyte is shortened from the full overlap position and then activated, the subsequent force generation also decreases but for a different reason. We have already stated that the arrangement of the thick and thin filaments in the sarcomere is semicrystalline. When the cells become over shortened, several types of filament misalignment are possible such as: (1) the thick filaments can run into the Z-disks and become disordered or (2) the thin filaments can cross the M-line and interact with each other or with myosin crossbridges from the other half-sarcomere. The disorder and/or interference that may occur in an overly shortened sarcomere is the cause for the decrease in myocyte tension. From the graph of the length–tension relationship (Fig. 12.9), you will notice a peak representing the noncompressed full overlap position.

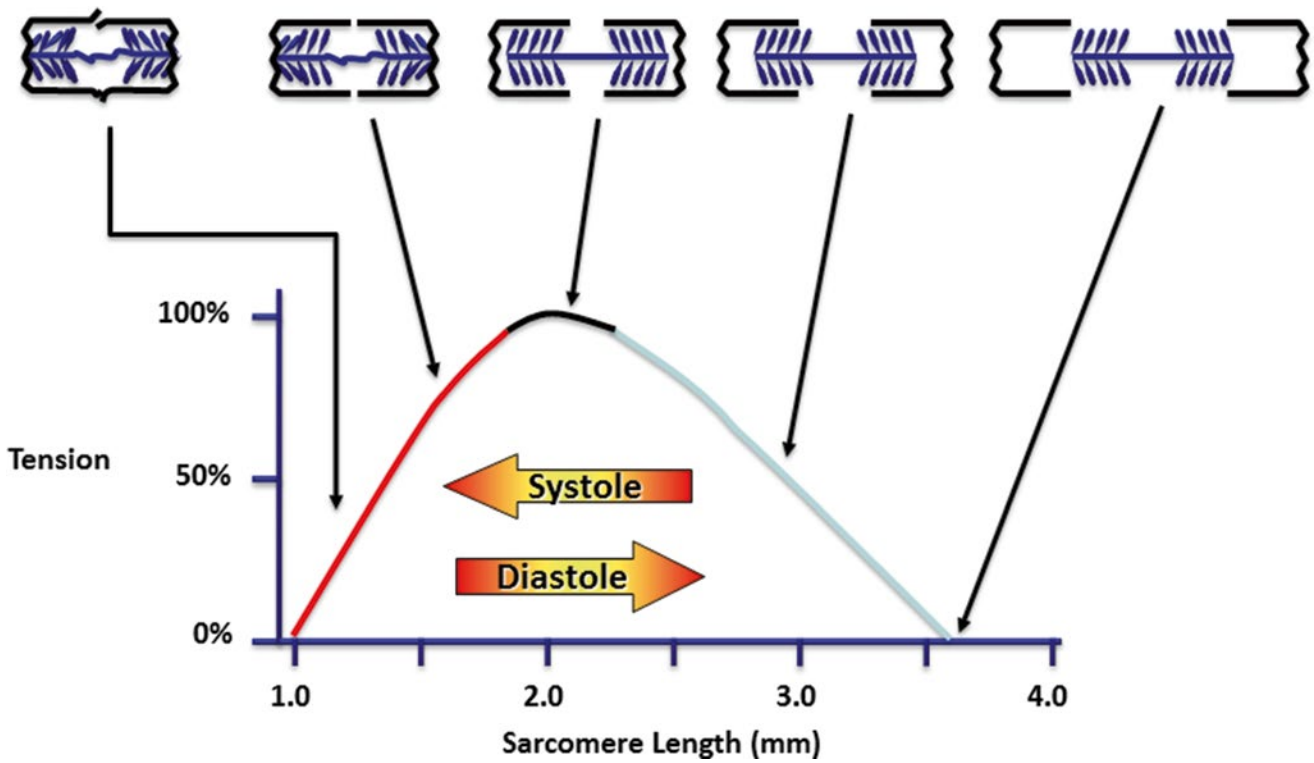

Fig. 12.9 Length–tension relationship. Mechanical coupling between the myofibrils and the membrane is such that a stretch or contraction of the cell alters the overlap of the thin and thick filaments of each sarcomere. At a sarcomere length of near 2.1 μm, there is complete overlap of the thick and thin filaments; if the length is unchanged, the cells have their maximal force production potential. At sarcomere lengths less than ~1.8 μm, the filaments become compressed in the sarcomere and interfere with one another, reducing the force that can be produced. As the sarcomere length is increased from the region that produces maximal force, the overlap of the crossbridge domains of the thick filament and the thin filament decreases with a near linear decline in force-generating potential

Shortening or lengthening the myocyte from this set point will decrease resultant muscle tension. In a normal cardiac cycle, the cell shortens during systole and has its length reset by stretching of the vessel wall during diastole. Since adjustment of the cell length changes the amount of force (or pressure) that can be generated, it is sometimes referred to as the preload of the cell.

12.11.1 Practical Applications of the Length–Tension Relationship

In general, the length of cardiac cells or myocytes is controlled in vivo through their shortening during systole and their being stretched during diastole (Fig. 12.9). That the set point of the length–tension relationship can be tuned in this manner is, in part, the mechanical underpinning for Starling's law of the heart (e.g., stroke volume increases as cardiac filling increases). Furthermore, if cardiac filling adjusts the sarcomere length to a point closer to the plateau of the length–tension relationship (Fig. 12.9), this length change produces an alignment of the contractile proteins that can then result in greater force production during the next systolic period. It then also follows that the increased force, which can occur during the isovolumic (isometric) phase of systole, will result in a greater stroke volume. However, in hypertrophic cardiomyopathies, filling pressures are less likely to stretch the myocytes and reset the length of the cells. In contrast, in dilated myopathies, myocytes may be overstretched during diastole, reducing the pressure building capacity of ventricular muscle.

12.12 Force and Velocity

The velocity of muscle cell shortening depends on the load that it works against. In cardiac muscle the load for the left ventricle is the systemic blood pressure, and it is referred to as the *afterload*. Importantly, as afterload increases the velocity of myocyte, shortening decreases. This relationship can impact ejection fraction as the ventricles are less effective in expelling blood against high systemic pressures.

12.13 Myocyte Hypertrophy

The structure of all muscle cells in the human body respond to the work they are required to do, and cardiac myocytes are no exception. The heart's continuous cycles of filling with blood, contraction, and ejection of blood throughout a person's lifetime maintain the healthy muscular tone of the myocytes. However, physiological and/or pathological conditions (exercise, pregnancy, hypertension, valvular insufficiency, etc.) place stresses on the heart that lead to remodeling. The remodeling of the myocardium, due to increased biomechanical stress, triggers activation of biochemical and neurohormonal signaling pathways that are dependent on the manner in which the stresses are applied to the heart.

Chronic high blood pressure forces the left ventricle to produce a higher internal pressure than normally required for the ejection of blood out of the heart into the aorta. Over time, this *pressure overload* will result in *left ventricular hypertrophy*. As more and more effort is required by the heart to compensate for the hypertension, myocardial protein synthesis is stimulated, and there is an increase in the production of sarcomeric proteins (myosin, actin, etc.). These myocardial proteins are then assembled to build additional myofibrils in myocytes. To accommodate the increase in the number of myofibrils, the cells also add phospholipids to the sarcolemma expanding their diameter and ultimately increasing the thickness of the overall myocardium. This adaptation to hypertension has been termed *concentric hypertrophy* [5, 6].

Alternatively, conditions such as valvular insufficiency, pregnancy, or an arteriovenous shunt can cause the ventricles to experience a *volume overload*; these stresses also result in a structural adaptation of cardiac myocytes. The stimulation of protein synthesis of sarcomeric proteins in these cases results in the addition of additional sarcomeres to existing myofibrils. The elongation of the myofibrils is also accommodated by incorporation of additional phospholipids the plasma membrane resulting in an expansion of cardiac myocytes along their long axes; this is referred to as *eccentric hypertrophy* [5, 6].

An interesting component of these changes in cellular morphology is that the concentric hypertrophy triggers an increase in protein synthesis during early phases of the hypertrophic adaptation, while eccentric hypertrophy first slows protein degradation, reducing myofibril turnover and then increases protein synthesis to extend myofibrillar lengths.

12.14 Cardiac Cell Action Potentials

The electrical activity of cardiac muscle cells is fundamental to normal function and takes advantage of the properties of the cell membrane to selectively pass charged species from inside to outside and vice versa. Most cells build a charge gradient through the action of ion pumps and ion selective channels. The charge difference across a membrane creates an electrical potential known as the resting membrane potential of the cell. In the resting state, the interior of the cell

Table 12.1 Major ionic species contributing to the resting potential of cardiac muscle cells

Ion	Inside (mM)	Outside (mM)	Ratio of inside/outside	$^{*}E_{ion}$ (mV)
Sodium	15	145	9.7	+60
Potassium	150	4	0.027	−94
Chloride	5	120	24	−83
Calcium	10^{-7}	2	2×10^{4}	+129

$^{*}E_{ion}$ is the equilibrium potential calculated from the Nernst equation

carries a negative charge relative to the exterior interstitial environment. The energy available through the discharging of this potential is commonly coupled with cellular functions. In excitable cells, transient changes in the electrical potential (action potentials) are used either to communicate or do work. Importantly, in the myocyte, action potentials are required to initiate the process known as *excitation-contraction coupling*.

The extracellular fluid has an ionic composition similar to that of blood serum. The total intracellular concentration of calcium is higher, but much of it is bound to proteins or sequestered in organelles (mitochondria, sarcoplasmic reticulum). Hence, free intracellular myoplasmic concentrations are very low and are in the micromolar range (Table 12.1).

ATP-dependent ion pumps, ion-specific channel proteins, and ion exchange proteins are all required to maintain the difference in ion concentrations. This separation of charged species across a resistive barrier (in this case, the cell membrane) generates the electrical potential (E_{ion}) mentioned above. For individual ions, the value of this potential can be calculated using the Nernst equation:

$$E_{ion} = -\frac{RT}{zF}\ln\frac{[\text{outside}]}{[\text{inside}]}$$

where R is the gas constant, T is the temperature (K), z is the valence of the ion (charge and magnitude), and F is the Faraday constant.

In Table 12.1, the concentrations of the ions (inside and outside the cell) that play a role in the resting membrane potential of cardiac muscle cells are shown with their respective calculated equilibrium potentials. The measured membrane potential of a cardiac muscle cell is in the range of −90 mV, suggesting that it is primarily determined by either the chloride or potassium distribution. However, measurements of ion movement have shown that chloride is distributed passively across the cell membrane (because of its negative charge, it follows positive ion movement) and can therefore be ignored in such a calculation; this leaves potassium as the dominant ion species in determining the resting potential of the cardiac myocyte.

The membrane potentials of living cells depend not just on their potassium distribution but also on several parameters including the concentrations of the other major ion species on both sides of the given cell membrane as well as their relative permeability. To determine the overall membrane potential (E_m), a modified Goldman–Hodgkin–Katz equation [7] is used to take into account the equilibrium potentials for individual ions and the permeability (conductance) of the membrane for each species such that:

$$E_m = \frac{g_{Na}}{g_{tot}}E_{Na} + \frac{g_K}{g_{tot}}E_K + \frac{g_{Ca}}{g_{tot}}E_{Ca}$$

where g_{Na} is the membrane conductance for sodium (Na), g_K is the membrane conductance for potassium (K), g_{Ca} is the membrane conductance for calcium (Ca), g_T is the total membrane conductance, E_{Na} is the equilibrium potential for sodium, E_K is the equilibrium potential for potassium, and E_{Ca} is the equilibrium potential for calcium. Evaluation of the Goldman-Hodgkin-Katz equation using the values in Table 12.1 and the conductance values for sodium, potassium, and calcium results in a membrane potential of −90 mV for a cardiac myocyte at rest.

As noted above, cells can have a variety of ion selective channels in their membranes. The term *gating* refers to the trigger required for opening a given channel. More specifically, voltage-gated ion channels respond to changes in the local membrane potential of the cell, and ligand-gated ion channels respond to specific circulating biochemical factors. Non-gated channels include: (1) spontaneously active ion channels that have a random frequency of opening and closing and (2) leak channels which seem to be constitutively open though at a low level. In addition to classification based on their control mechanisms, channels are also classified by their ion selectivity and/or the direction of ion passage that such a channel facilitates.

Cardiac action potentials occur because of transient changes in the cellular permeability to Na^+, Ca^{2+}, and K^+. An initial electrical depolarization initiated by current movement through the cell's gap junctions (threshold is ~40 mV above the resting potential) causes the transient opening of voltage-dependent Na^+ channels (Figs. 12.10, 12.11, and 12.12). Opening of these channels causes a transient increase in sodium permeability which further depolarizes the cell and drives the membrane potential toward the (positive) sodium equilibrium potential (Table 12.1; Figs. 12.10 and 12.12). Action potential initiation by the voltage-gated sodium channels in turn

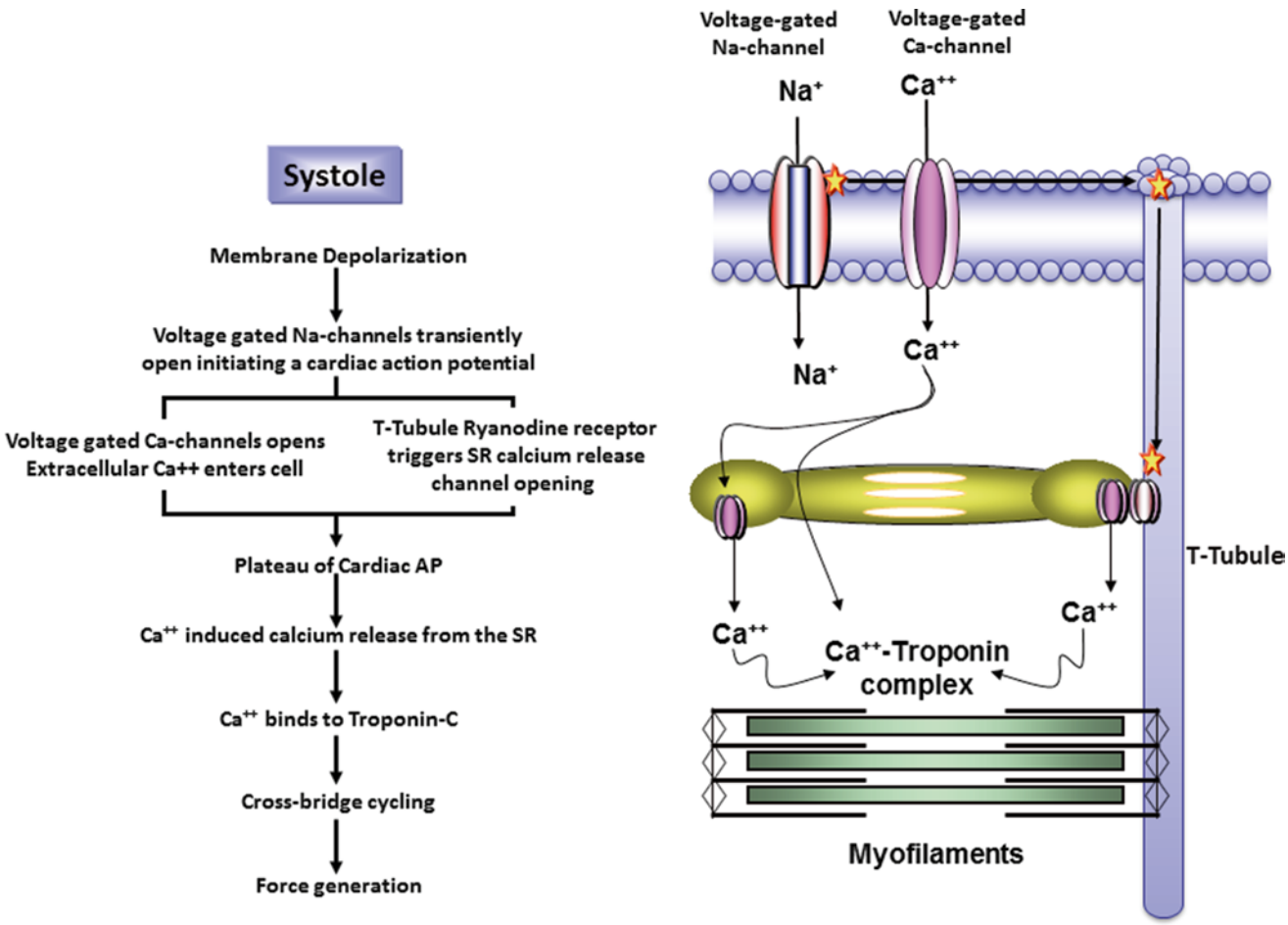

Fig. 12.10 Excitation-contraction coupling. In systole, an electrically depolarizing signal triggers the transient opening of voltage-gated Na channels; the influx of positively charged Na ions further depolarizes the cell. This further depolarization causes the opening of L-type Ca channels (long-duration opening), and calcium enters the cell. This also causes ryanodine receptors in the T-tubules to trigger the release of calcium from Ca channels in the sarcoplasmic reticulum. This initiates the plateau of the cardiac action potential. The rise in intracellular calcium concentration triggers additional calcium release from the sarcoplasmic reticulum via Ca channels. The calcium binds to troponin on the thin filaments, inducing the movement of tropomyosin. Crossbridge cycling begins generating tension in the cardiac myocytes

activates voltage-gated Ca^{2+} and K+ channels. The subsequent opening of the voltage-gated L-type (long opening duration) calcium channels allows calcium to enter the myocyte and sustains the depolarized state, despite the closing of the Na^+ channels. The opening of the voltage-gated K^+ channels is delayed in time and results in potassium efflux from the cell as the ion moves down its concentration gradient. This drives the membrane potential back toward the potassium equilibrium potential (more negative). The timing of these changes depends on the isoforms of the Ca^{2+} and K^+ channel proteins present in each cell with sinoatrial and atrioventricular action potentials lasting ~150 ms, ventricular myocytes ~250 ms, and Purkinje fibers ~300 ms (also see Chap. 13). The primary difference between these cell types is often the duration of the plateau phase (phase 2) which is primarily a response to changes in the isoforms of the Ca^{2+} channels (Figs. 12.12 and 12.13).

The various phases of the cardiac action potential are associated with changes in the flow of ionic currents across the cell membrane. Atrial and ventricular cardiac muscle cells have an extremely rapid initial transition from the resting membrane potential to depolarization (*phase 0*). In phase 0, the Na channels open, and there is a large amplitude, short duration inward Na current (Fig. 12.13). As the sodium channels begin to close, *phase 1* is defined as a small initial repolarization. The opening of the L-type calcium channels causes a calcium influx and is balanced by

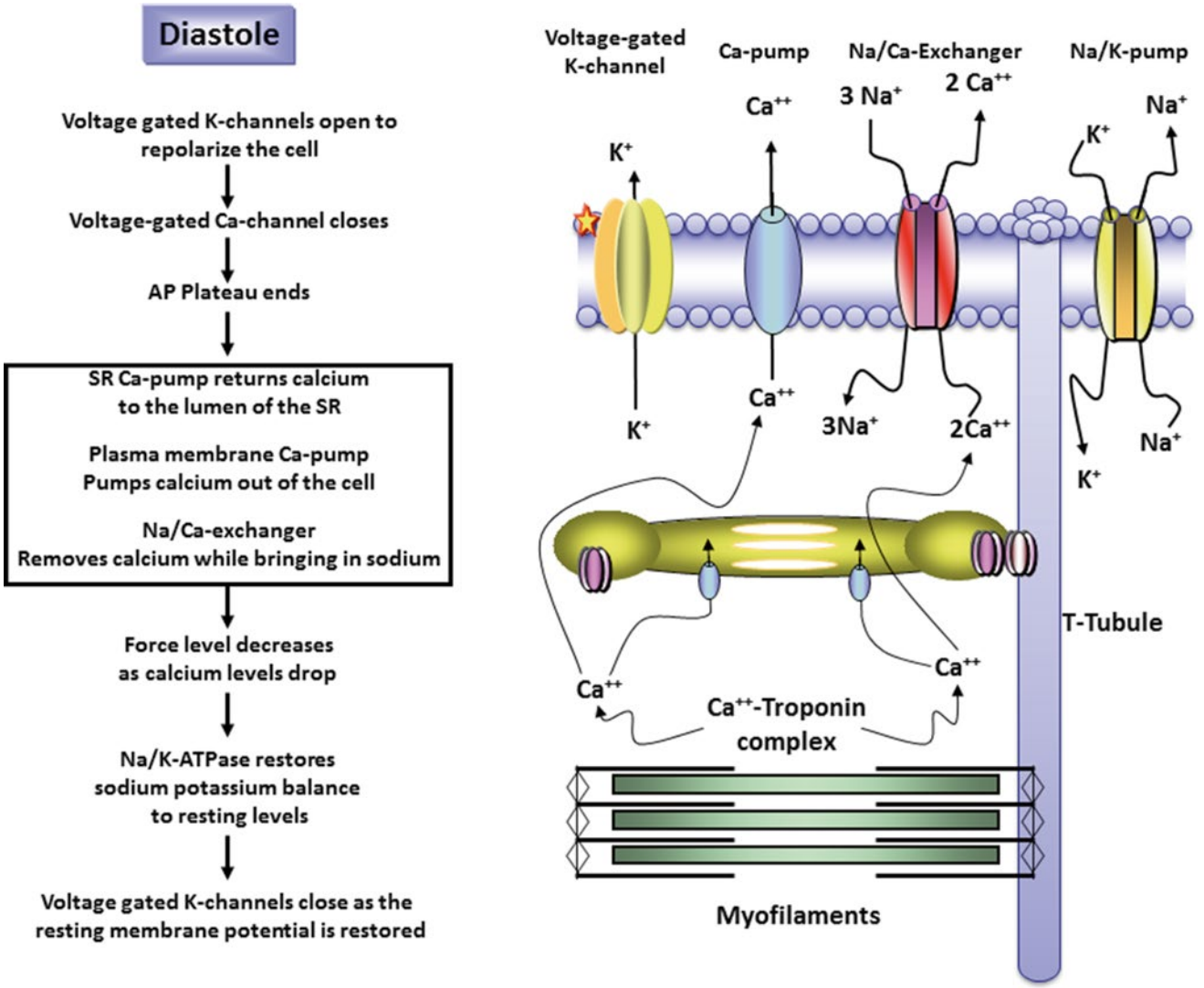

Fig. 12.11 Relaxation of cardiac muscle cells. The depolarization eventually opens voltage-gated K channels. K flows out of the cell, and, as the sarcolemmal Ca channels close, the cell begins to repolarize. Calcium is pumped out of the cytoplasm by ATP-driven pump proteins on the sarcoplasmic reticulum and sarcolemma. Calcium is also expelled from the cell via the Na/Ca exchange protein. To combat the rise in intracellular Na that this causes, the Na/K ATPase pumps K into the cell and Na out, helping to restore the resting potential and the ionic environment that existed before the cell was activated

the potassium efflux via the now open K^+ channels. This balance results in the electrically positive plateau (*phase 2*) of the cardiac action potential profile. As the Ca channels close, the flux of ions through the K^+ channels begins to dominate the membrane potential, and repolarization of the cells begins (*phase 3*). *Phase 4* is the restoration of the resting membrane potential and the closing of the K^+ channels. From the initiation of the action potential through approximately half of the repolarization, the cell is considered *refractory*, meaning that it could not respond to a new depolarization signal.

12.15 Pacemaker Cells

The sinoatrial (right atrium) and atrioventricular (interventricular septum) nodal cells have what are considered to be unstable resting potentials; a gradual rise in resting potential crosses the threshold for opening of T-type (transiently open) calcium channels. The movement of calcium into the cells (phase 0) initiates depolarization. No initial repolarization or plateau occurs, so phases 1 and 2 are said to be relatively absent. Repolarization (phase 3) is accomplished through

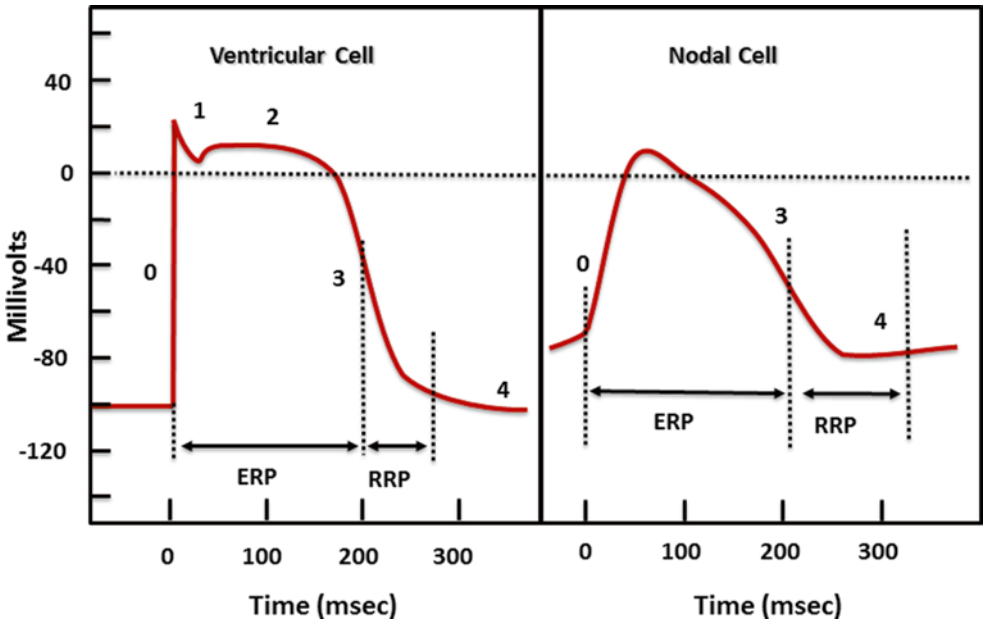

Fig. 12.12 Action potential profiles for ventricular and nodal cardiac cells. **Ventricular cell** (*left*). Before activation, the cell's membrane potential is negative (phase 0—*upstroke*). A small depolarizing event triggers the opening of voltage-gated Na channels (phase 1—*initial repolarization*). As the Na channels close, there is a small recovery in polarization; the voltage-gated Ca and K channels open followed by a *plateau* (phase 2) in the membrane potential. In phase 3, *repolarization*, as the Ca channels close, the K channels remain open, and the membrane potential grows more negative, eventually returning to *resting membrane potential* level (phase 4) where the K channels also close. From phase 0 through the middle of phase 3 is the effectively refractory period (ERP), meaning that another depolarization would not trigger the opening of the Na channels. The remainder of phase 3 is the relatively refractory period (RRP), during which a new depolarizing signal would cause some of the Na channels to reopen. **Nodal cell** (*right*). Pacemaker cells have a different electrical signature to their action potentials. The cells spontaneously rise to the threshold of T-type Ca channels whose opening is the cause of phase 0 upstroke that is not as rapid as that of the ventricular cells. There is no phase 1 or 2 as in ventricular cells. The opening of voltage-gated K channels causes repolarization, phase 3, ultimately reaching an unstable resting potential minimum from which the cells repeat the cycle. The spontaneous rise of the membrane potential has been attributed to leaky Na channels. The refractory periods of nodal cells reflect the potential for opening the T-type Ca channels

the opening of voltage-gated K^+ channels. Once the cell is repolarized (phase 4), leak channels (often attributed to slow Na^+ channels) contribute to instability of the resting potential and a gradual rise to the threshold value of the T-type Ca^{2+} channels (Fig. 12.12).

The sinoatrial node is a specialized collection of cardiac myocytes in the right atrium. These cells have unstable resting potentials that lead to spontaneous depolarizations of this cell cluster with a relatively rapid and regular repeat (i.e., more rapid than all other myocytes). Cardiac activation is governed by the principle of *overdrive suppression*. This principle states that the myocytes with the most rapid frequency of depolarization control the overall rhythm of the heart. Furthermore, the action potential of the sinoatrial node is referred to as a "slow response" because the upstroke of the depolarization is slower than that of the non-nodal cardiac cells that provide the contractile force during atrial or ventricular contraction. However, the rapid repeat of this "slow response" depolarization gives the sinoatrial node overall control of the heart rate. For additional details on this process, see Chap. 13.

12.16 Summary

The heart's function as a pump is dependent on coordinated contractions of its chambers to move blood throughout the body. These contractions are produced by cardiac myocytes, the muscle cells of the heart. This chapter describes the structure and function of these cells and provides insights into adaptations of the heart due to normal and pathophysiological changes over the course of a lifetime.

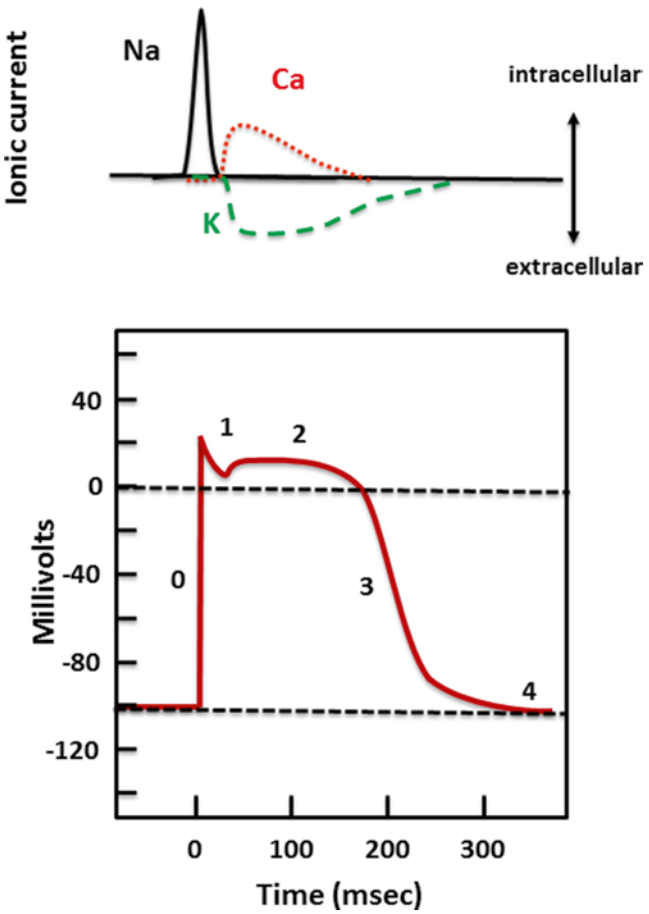

Fig. 12.13 Ionic currents corresponding to the phases of the ventricular action potential. The inward current associated with the opening of the voltage-gated Na channels is responsible for phase 0 of the cardiac action potential. The closing of the Na channels is reflected in the initial repolarization of phase 1. The depolarization of the cell by the Na current triggers the opening of the voltage-gated Ca channels and the voltage-gated K channels whose ionic currents are in balance during phase 2, the plateau. The closing of the Ca channels while the K channels are still passing an outward current causes the repolarization (phase 3) and return to the resting membrane potential (phase 4)

References

1. Colaco CALS, Evans WH (1981) A biochemical dissection of the cardiac intercalated disk: Isolation of subcellular fractions containing fascia adherentes and gap junctions. J Cell Sci 52:313–325
2. Kaplan SR, Gard JJ, Protonotarios N et al (2004) Remodeling of myocyte gap junctions in arrhythmogenic right ventricular cardiomyopathy due to a deletion in plakoglobin (Naxos disease). Heart Rhythm 1:3–11
3. Beauchamp P, Yamada KA, Baertschi AJ et al (2006) Relative contributions of connexins 40 and 43 to atrial impulse propagation in synthetic strands of neonatal and fetal murine cardiomyocytes. Circ Res 99:1216–1224
4. Boussouf SE, Geeves MA (2007) Tropomyosin and troponin cooperativity on the thin filament. Adv Exp Med Biol 592:99–109
5. Grossman W, Jones D, McLaurin LP (1975) Wall stress and patterns of hypertrophy in the human left ventricle. J Clin Invest 56:56–64
6. Carabello BA (2002) Concentric vs. eccentric remodeling. J Cardiac Fail 8:S258–S263
7. Sperelakis N (1979) Origin of the cardiac resting potential. In: Berne RM, Sperelakis N, Geiger SR (eds) The handbook of physiology Section 2, The cardiovascular system Section 1. American Physiological Society, Baltimore, pp 187–267

Other Resources

Berne RM, Levy MN (eds) (1979) Cardiovascular physiology, 7th edn. Mosby, St. Louis (Chapter 2, Electrical activity of the heart, pp 7–54; Chapter 3, The cardiac pump, pp 55–82)
Berne RM, Levy MN (eds) (1998) Physiology, 4th edn. Mosby, St. Louis (Chapter 23, The cardiac pump, pp 360–78)
Costanzo LS (1998) Physiology. Saunders, Philadelphia (Chapter 4, Cardiovascular physiology, pp 99–162)
Germann W, Stanfield C (eds) (2002) Principles of human physiology. Benjamin Cummings, San Francisco (Chapter 12, The cardiovascular system: Cardiac function, pp 369–402)
Mohrman DE, Heller LJ (eds) (2003) Cardiovascular physiology, 5th edn. McGraw-Hill, New York (Chapter 2, Characteristics of cardiac muscle cells, pp 19–46)
Rhoades RA, Tanner GA (eds) (1995) Medical physiology. Little, Brown, Boston (Chapter 10, Cardiac muscle, pp 193–206)
Vander A, Sherman J, Luciano D (eds) (2014) Human physiology: The mechanisms of body function, 13th edn. McGraw-Hill, Boston (Chapter 12, Cardiovascular physiology Section B: The heart, pp 368–376)

The Cardiac Conduction System

13

Timothy G. Laske, Maneesh Shrivastav, and Paul A. Iaizzo

Abstract

The intrinsic conduction system of the heart is comprised of several specialized subpopulations of cells that either spontaneously generate electrical activity (pacemaker cells) or preferentially conduct this activity throughout the chambers in a coordinated fashion. This chapter will discuss the details of this known anatomy as well as put such discoveries into a historical context. The cardiac action potential underlies signaling within the heart, and the various populations of myocytes will elicit signature waveforms. The recording or active sensing of these potentials is important in both research and clinical arenas. This chapter aims to present a basic understanding of the cardiac conduction system to provide the reader with a foundation for future research and reading on this topic. The information in this chapter is not comprehensive and should not be used to make decisions relating to patient care.

Keywords

Cardiac conduction • Sinoatrial node • Depolarization • Atrioventricular node • Electrophysiology • Cardiac action potential • Gap junction

Electronic supplementary material: The online version of this chapter (doi:10.1007/978-3-319-19464-6_13) contains supplementary material, which is available to authorized users. Videos can also be accessed at http://link.springer.com/book/10.1007/978-3-319-19464-6_13.

T.G. Laske, PhD (✉)
Department of Surgery, University of Minnesota, Minneapolis, MN, USA

Medtronic plc, 8200 Coral Sea Street NE, MVS 46, Minneapolis, MN 55112, USA
e-mail: tim.g.laske@medtronic.com

M. Shrivastav, PhD
Medtronic plc, 8200 Coral Sea Street NE, MVS 46, Minneapolis, MN 55112, USA

P.A. Iaizzo, PhD
Department of Surgery, University of Minnesota, Minneapolis, MN, USA

13.1 Introduction

Orderly contractions of the atria and ventricles are regulated by the transmission of electrical impulses that pass through an intricate network of modified cardiac muscle cells, the *cardiac conduction system*. These cells are interposed within the contractile myocardium. This intrinsic conduction system is comprised of several specialized subpopulations of cells that spontaneously generate electrical activity (pacemaker cells) and/or preferentially conduct this activity throughout the heart. Following an initiating activation (or depolarization) within the myocardium, this electrical excitation spreads throughout the heart in a rapid and highly coordinated fashion. This system of cells also functionally controls the timing

P.A. Iaizzo (ed.), *Handbook of Cardiac Anatomy, Physiology, and Devices*, DOI 10.1007/978-3-319-19464-6_13

of the transfer of activity between the atrial and ventricular chambers. Interestingly, a common global architecture is present in mammals, but significant interspecies differences exist at the histologic level [1, 2] (see also Chap. 6).

Discoveries relating to this intrinsic conduction system within the heart are relatively recent relative to cardiac function and anatomy. Johannes E. von Purkinje first described the ventricular conduction system in 1845 and Gaskell, an electrophysiologist, coined the phrase *heart block* in 1882. Importantly, Gaskell also related the presence of a slow ventricular rate to disassociation with the atria [3]. The discovery of the mammalian sinoatrial node was published by Sir Arthur Keith and Martin Flack in 1907 in the *Journal of Anatomy and Physiology*. Nevertheless, novel findings related to the functionality of this node are still being made today [4].

The elucidation of the bundle of His is attributed to its namesake, Wilhelm His Jr [5], who described the presence in the heart of a conduction pathway from the atrioventricular node through the cardiac skeleton that eventually connected to the ventricles. Tawara later verified the existence of the bundle of His in 1906 [6]. Due to the difficulty in distinguishing the atrioventricular nodal tissue from surrounding tissue, he defined the beginning of the bundle of His as the point at which these specialized atrioventricular nodal cells enter the central fibrous body (which delineates the atria from the ventricles). Tawara is also credited with being the first to clearly identify the specialized conduction tissues (modified myocytes) that span from the atrial septum to the ventricular apex, including the right and left bundle branches and Purkinje fibers.

Walter Karl Koch (1880–1962) was a distinguished German surgeon who discovered a triangular-shaped area in the right atrium of the heart that marks the atrioventricular node (known today as *Koch's triangle*). Among Koch's notable research findings was his hypothesis that the last part of the heart to lose activity when the whole organ died was the pacemaker region (*ultimum moriens*). Koch localized this last region of the heart to lose function through his detailed anatomical and histological studies of the hearts of animals and stillborn human fetuses. He postulated that the cardiac region near the opening of the wall of the coronary sinus was the true pacemaker of the heart [7, 8]; the atrioventricular node will elicit an escape rhythm when the sinoatrial node in the right atrium fails (see below).

Early discoveries by distinguished researchers such as Koch, Tawara, and Aschoff (to be discussed later in the text) have been immortalized in medical terminology (Koch's triangle, Tawara's node, and Aschoff's nodule). As history demonstrates, a thorough understanding of the anatomy and function of the cardiac conduction system is important for those designing cardiovascular devices and procedures. More specifically, surgical interventions (heart valve replacement/repair, repair of septal defects, coronary bypass grafting, congenital heart repair, etc.) are commonly associated with temporary or permanent heart block due to damage of the conduction system and/or disruption of its blood supply [9–13]. Hence, if one is designing corrective procedures and/or devices to be used, she/he needs to consider ways to avoid damage to cellular structures of the conduction system. For example, advances in surgical techniques for the repair of ventricular septal defects have reduced the incidence of complete atrioventricular block from 16 % in the 1950s to less than 1 % currently [14, 15]. Additionally, many rhythm control devices such as pacemakers and defibrillators aim to return the patient to a normal rhythm and contraction sequence [16–24]. Research has also continued relative to the repair or replacement of the intrinsic conduction system using gene and/or cell therapies [25].

A final example illustrating why an understanding of the heart's conduction system is critical to the design of devices and procedures is the therapeutic use of cardiac ablation. These methodologies purposely modify the heart to: (1) destroy portions of the conduction system (e.g., atrioventricular nodal ablation in patients with permanent atrial fibrillation), (2) eliminate aberrant pathways (e.g., accessory pathway ablation in Wolff–Parkinson–White syndrome), and/or (3) destroy inappropriate substrate behavior (e.g., ablation of ectopic foci or reentrant pathways in ventricular tachycardias, ablation for treatment of atrial fibrillation, etc.) [26–29].

13.2 Overview of Cardiac Conduction

The *sinoatrial node* is located in the right atrium in the healthy heart and serves as the natural pacemaker (Fig. 13.1). These pacemaker cells manifest spontaneous depolarizations and are thus responsible for generating the normal cardiac rhythm, also described as *intrinsic or automatic*. Importantly, the frequency of this earliest depolarization is modulated by both sympathetic and parasympathetic efferent innervation. In addition, the nodal rate can also be modulated by local changes associated with perfusion and/or the chemical environment (i.e., neurohormonal, nutritional, oxygenation, etc.). Although the atrial rhythms normally emanate from the sinoatrial node, variations in the initiation site of atrial depolarization have been documented outside of the histological nodal tissues, particularly when high atrial rates are elicited [30–33].

One of the most conspicuous features of sinoatrial nodal cells is that they possess poorly developed contractile apparati (a common feature to all myocytes specialized for conduction), comprising only about 50 % of the intracellular volume [34]. In general, although it cannot be seen grossly, the location of the sinoatrial node is on the "roof" of the right atrium at the approximate junction of the superior vena cava, the right atrial appendage, and the sulcus terminalis. In the adult human, the node is approximately 1 mm below the epicardium, 10–20 mm long and up to 5 mm thick [35]. For more details on cardiac anatomy, refer to Chaps. 5 and 6.

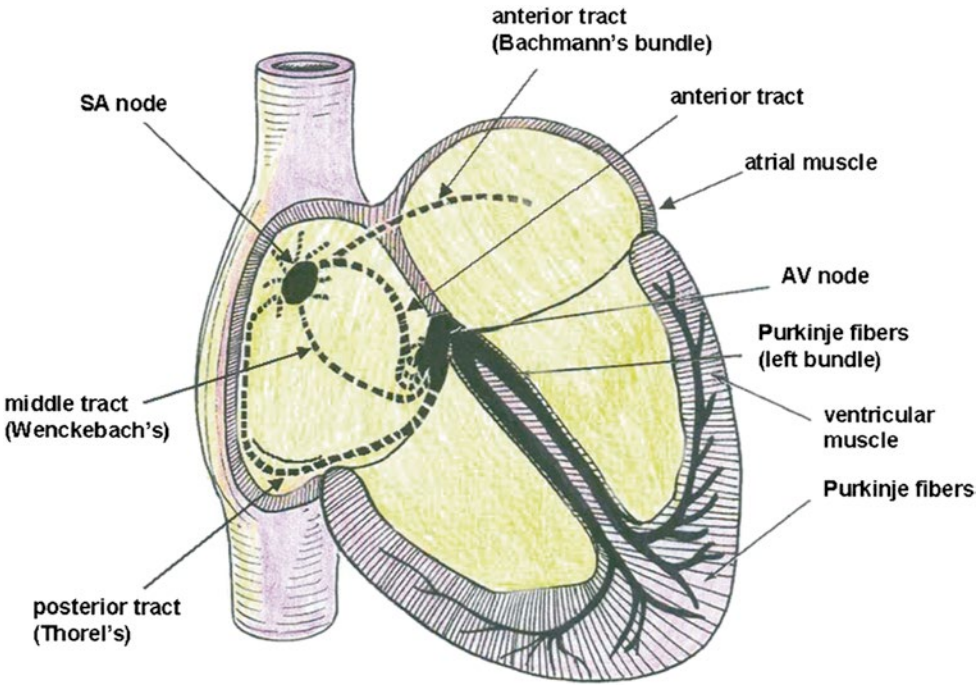

Fig. 13.1 Conduction system of the heart. Normal excitation originates in the sinoatrial node and then propagates through both atria (internodal tracts shown as *dashed lines*). The atrial depolarization spreads to the atrioventricular node and passes through the bundle of His (not labeled) and then to the Purkinje fibers which make up the left and right bundle branches; subsequently all ventricular muscle becomes activated. *AV* atrioventricular, *SA* sinoatrial

After initial sinoatrial nodal excitation, depolarization spreads throughout the atria. The exact mechanisms involved in the spread of impulses (excitation) from the sinoatrial node across the atria are somewhat controversial [36]. However, it is generally accepted that: (1) the spread of depolarizations from nodal cells can go directly to adjacent myocardial cells and (2) preferentially ordered myofibril pathways allow this excitation to rapidly transverse the right atrium to both the left atrium and the atrioventricular node. It is believed that there are three preferential anatomic conduction pathways from the sinoatrial node to the atrioventricular node (known as the node of Tawara) [37]. In general, these can be considered as the shortest electrical routes between the nodes. They are microscopically identifiable structures, appearing to be preferentially oriented fibers that provide a direct node-to-node pathway. In some hearts, pale staining Purkinje-like fibers have also been reported in these regions (tracts are shown as dashed lines in Fig. 13.1; also see Fig. 13.1 in the online supplemental material). More specifically, the anterior tract is described as extending from the anterior part of the sinoatrial node, bifurcating into the so-called Bachmann's bundle (delivering impulses to the left atrium) and a second tract that descends along the interatrial septum which connects to the anterior part of the atrioventricular node. The middle (or Wenckebach's pathway) extends from the superior part of the sinoatrial node, runs posteriorly to the superior vena cava, then descends within the atrial septum, and may join the anterior bundle as it enters the atrioventricular node. The third pathway is described as being posterior (Thorel's) which, in general, is considered to extend from the inferior part of the sinoatrial node, passing through the crista terminalis and the Eustachian valve past the coronary sinus to enter the posterior portion of the atrioventricular node. In addition to excitation along these preferential conduction pathways, general excitation spreads from cell to cell throughout the entire atrial myocardium via the specialized connections between cells, the *gap junctions*, which exist between all myocardial cell types (see below).

Toward the end of atrial depolarization, the excitatory signal reaches the atrioventricular node. This excitation reaches these cells via the aforementioned atrial routes, with the final excitation of the atrioventricular node generally described as occurring via the slow or fast pathways. The slow and fast pathways are functionally, and usually anatomically, distinct routes to the atrioventricular node. The slow pathway generally crosses the isthmus between the coronary sinus and the tricuspid annulus and has a longer conduction time but a shorter effective refractory period than the fast pathway. The fast pathway is commonly a superior route, emanating from the interatrial septum, and has a faster conduction rate but, in turn, a longer effective refractory period. Normal conduction during sinus rhythm occurs along the fast pathway, but higher heart rates and/or premature beats are often conducted through the slow pathway, since the fast pathway may be refractory at these rates.

Recent advances in the optical mapping of the human atrioventricular junction further elucidate the dual pathway electrophysiology [38]. More specifically, the dual characteristics of this function have been revealed using an S1–S2 pacing protocol; in this procedure, a stimulus (S1) of constant

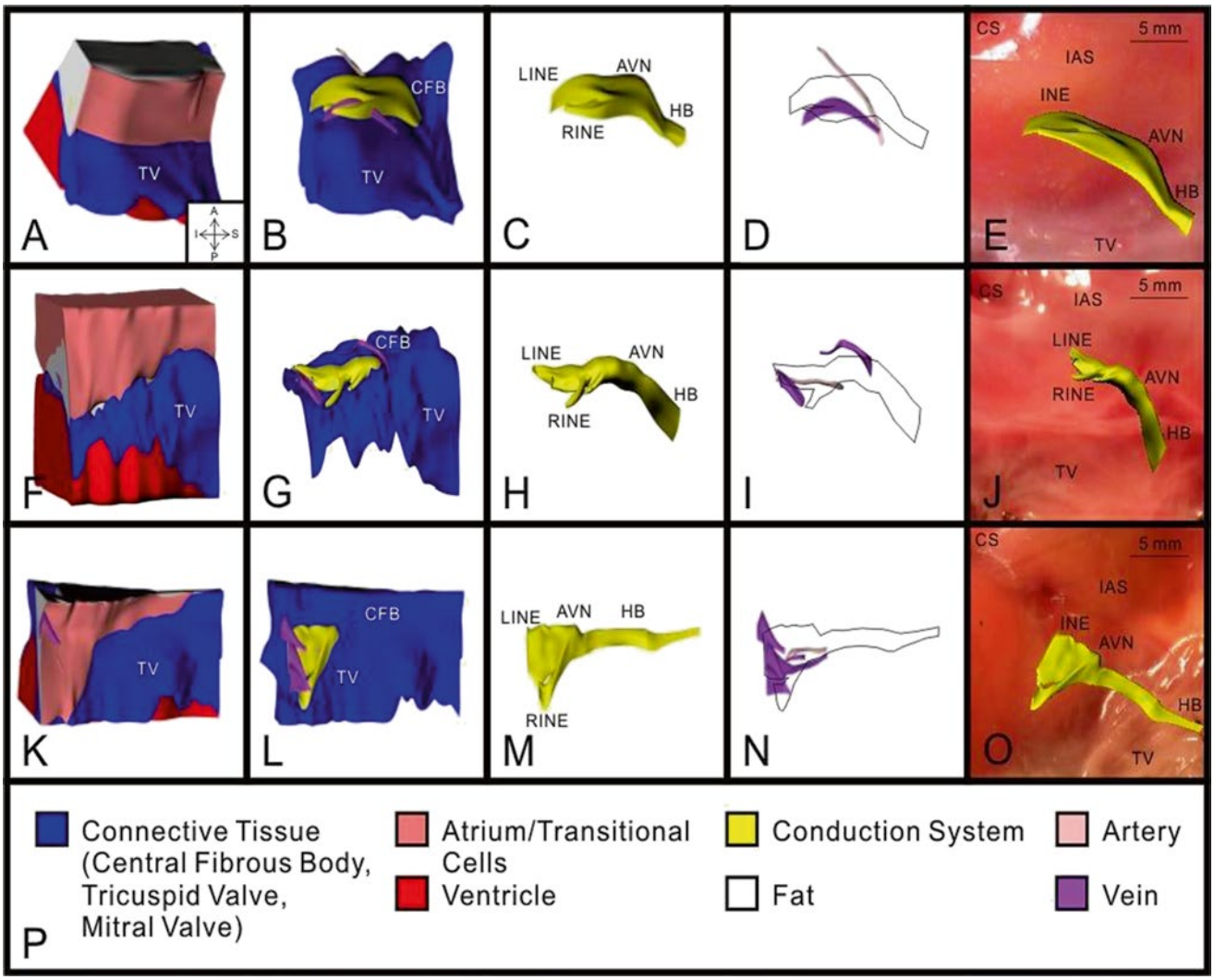

Fig. 13.2 3D reconstruction of atrioventricular (AV) junction from three human hearts: heart #1 (**A**–**E**), heart #2 (**F**–**J**), and heart #3 (**K**–**O**). **A**, **F**, and **K**: complete 3D reconstruction with all types of tissue visible. **B**, **G**, and **L**: 3D reconstruction with areas of atrium, ventricle, and fat removed. **C**, **H**, and **M**: 3D reconstruction of conduction system. **D**, **I**, and **N**: 3D reconstruction of major veins and arteries with conduction system outlined. **E**, **J**, and **O**: 3D reconstruction of conduction system superimposed on a photograph of the tissue used for its creation. **P**: key to the colors in **A**–**O**. *AVN* atrioventricular node, *CFB* central fibrous body, *HB* His bundle, *LINE* leftward inferior nodal extension, *RINE* rightward inferior nodal extension, *TV* tricuspid valve

duration and amplitude is applied followed by a second stimulus (S2) of varying duration and amplitude. The S1–S2 interval is iteratively reduced until conduction block in the fast pathway occurs due to the long refractory period [38].

Though the primary function of the atrioventricular node may seem simple, that is, to relay conduction between the atria and ventricles, its structure is very complex. As a means to describe these complexities, mathematical arrays and finite element analysis models have been constructed to elucidate the underlying structure–function relationship of the node [39]. Figure 13.2 shows a 3D reconstruction of the region using a model of the heart stained with the voltage sensitive dye di-4-ANEPPS. The reconstruction includes histological and immunolabeling of marker proteins to identify various tissue types. Figure 13.3 shows the nodal reconstruction of a normal human heart as well as one from a patient who had an implanted left ventricular assist device. For examples of these reconstructions, see Videos 13.1, 13.2, and 13.3 in the online supplemental material.

In general, the atrioventricular node is located in the so-called floor of the right atrium, over the muscular part of the interventricular septum and inferior to the membranous septum. Following atrioventricular nodal excitation, impulses are conducted to the His bundle (note that the bundle of His has also been referred to as the *common bundle* or *His bundle*). If conduction follows the slow pathway, a longer interval is present between atrial and His activation. As mentioned above, the anatomical region in which the His bundle and the

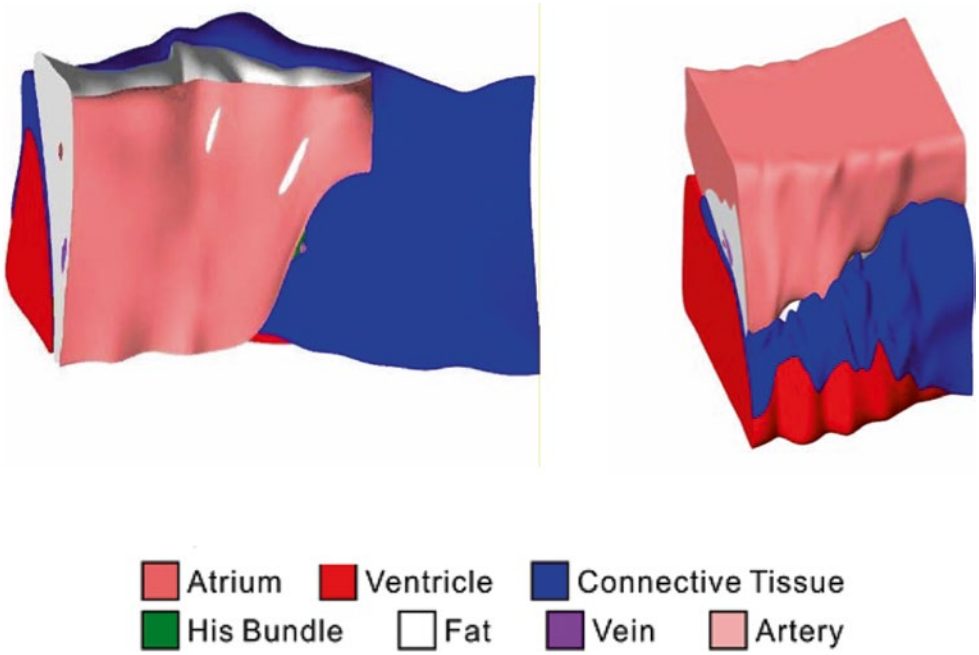

Fig. 13.3 Atrioventricular reconstruction with normal and pathologic human hearts. The normal human heart (*left*) and the heart of a left ventricular assist device patient (*right*) show different proportions of tissue type in the nodal region

atrioventricular node both reside has been termed the *triangle of Koch*. The triangle is bordered by the coronary sinus, the tricuspid valve annulus along the septal leaflet, and the tendon of Todaro.

After leaving the bundle of His, the normal wave of cardiac depolarization spreads to both the left and right bundle branches; these pathways carry depolarization to the left and right ventricles, respectively. Finally, the signal broadly travels through the remainder of the Purkinje fibers and ventricular myocardial depolarization spreads (see Video 13.4 in the online supplemental material).

In addition to the normal path of ventricular excitation, direct connections to the ventricular myocardium from the atrioventricular node and the penetrating portion of the bundle of His have been described in humans [40]. The function and prevalence of these connections, termed *Mahaim fibers*, is poorly understood. An additional aberrant pathway existing between the atria and ventricles has been termed the *bundle of Kent* (the clinical manifestation of ventricular tachycardia due to the presence of this pathway is termed *Wolff–Parkinson–White syndrome*); this pathway is commonly ablated.

Alternate representations of the cardiac conduction system are shown in Figs. 13.4 and 13.5. Details of the ventricular portion of the conduction system are shown in Fig. 13.6. More specifically, the left bundle branch splits into fascicles as it travels down the left side of the ventricular septum just below the endocardium (these can be visualized with proper staining). Its fascicles extend for a distance of 5–15 mm, fanning out over the left ventricle. Importantly, typically about midway to the apex of the left ventricle, the left bundle separates into two major divisions, the anterior and posterior branches (or fascicles). These divisions extend to the base of

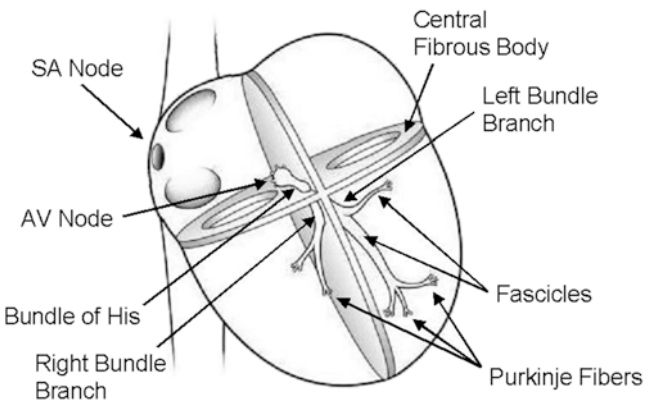

Fig. 13.4 Conduction system of the heart. Normal excitation originates in the sinoatrial node then propagates through both atria. The atrial depolarization spreads to the atrioventricular node and passes through the bundle of His to the bundle branches/Purkinje fibers. *AV* atrioventricular, *SA* sinoatrial

the two papillary muscles and the adjacent myocardium. In contrast, the right bundle branch continues inferiorly, as if it were a continuation of the bundle of His, traveling along the right side of the muscular interventricular septum. This bundle branch runs proximally just deep to the endocardium, and its course runs slightly inferior to the septal papillary muscle of the tricuspid valve before dividing into fibers that spread throughout the right ventricle. The complex network of conducting fibers that extends from either the right or left bundle branches is composed of the rapid conduction cells known as *Purkinje fibers*. The Purkinje fibers in both the right and left ventricles act as preferential conduction pathways to provide rapid activation and coordinate the excitation pattern within

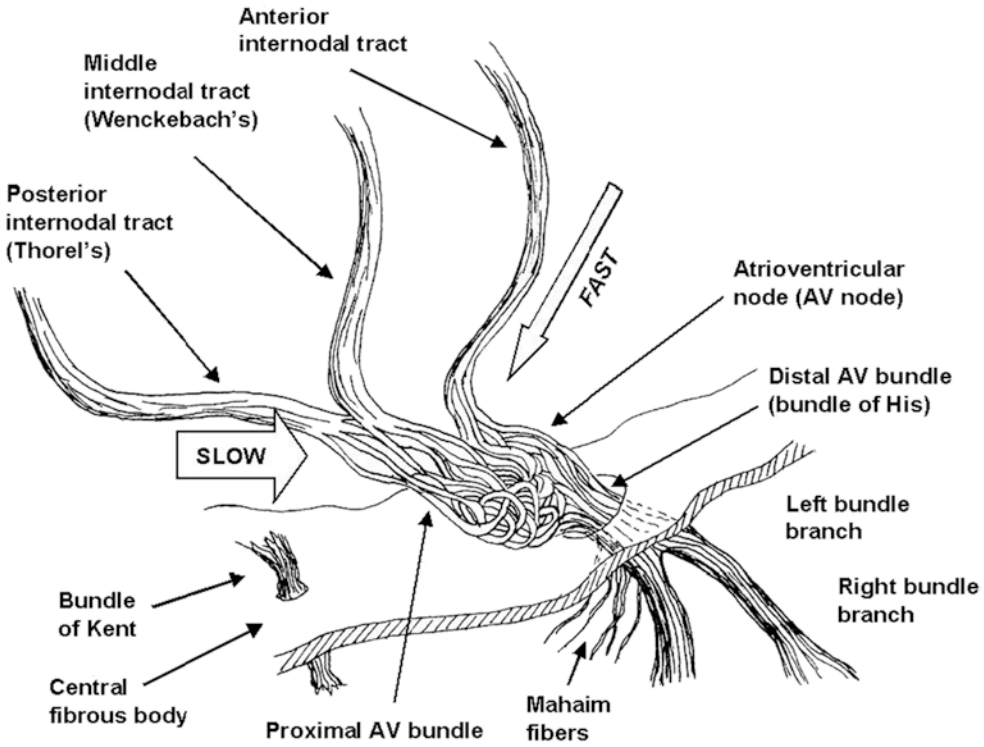

Fig. 13.5 Details of the atrioventricular nodal region. The so-called slow and fast conduction pathways are indicated by the *arrows*. To improve clarity in the visualization of the conduction anatomy, the fascicles of the atrioventricular node are not drawn to scale (their size was increased to allow the reader to visualize the tortuosity of the conduction pathway) and the central fibrous body has been thinned. *AV* atrioventricular

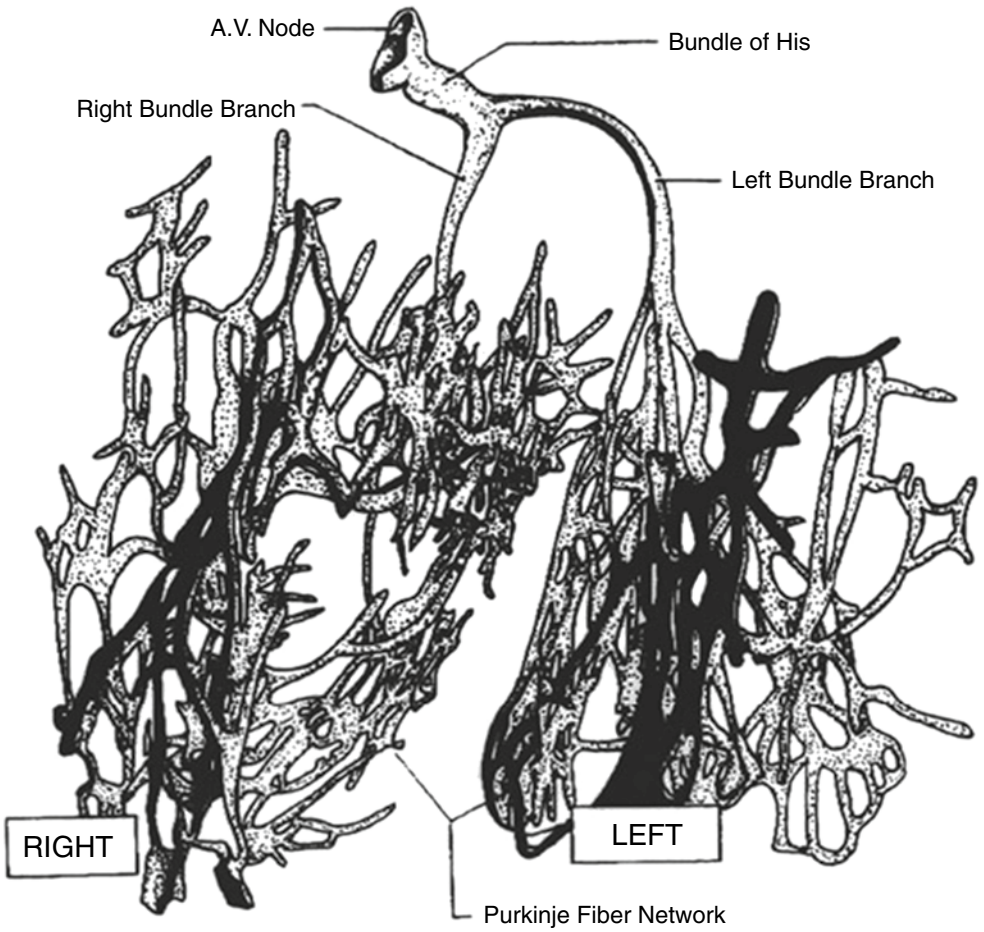

Fig. 13.6 Ventricular conduction system. The Purkinje network has a high interspecies and intraspecies variation, which likely results in variability in excitation and contractile patterns within the ventricles. This variability is evident in the dramatic differences seen in the degree and morphology of the cardiac trabeculations (which typically contain these fibers). Modified from DeHann DL, Circulation 1961; 24:458)

the various regions of the ventricular myocardium. As described by Tawara, these fibers travel within the trabeculations of the right and left ventricles, as well as within the myocardium. Due to the tremendous variability in the degree and morphology of trabeculations existing within and between species, it is likely that variations in the left ventricular conduction patterns also exist. It should be noted that one of the most easily recognized conduction pathways found in mammalian hearts is the moderator band, which contains Purkinje fibers from the right bundle branch (see also Chap. 6).

Three criteria for considering a myocardial cell as a *specialized conduction cell* were first proposed by Aschoff [41] and Monckeburg [42] in 1910, which include: (1) cells with the ability to histologically identify discrete features; (2) cells with the ability to track cells from section to section; and (3) these cells are insulated by fibrous sheaths from the nonspecialized contractile myocardium. It is noteworthy that only the cells within the bundle of His, the left and right bundle branches, and the Purkinje fibers satisfy all three criteria. No structure within the atria meets all three criteria, including Bachmann's bundle, the sinoatrial node, and the atrioventricular node (which are all uninsulated tissues).

13.3 Cardiac Rate Control

Under normal physiologic conditions, the dominant pacemaker of the heart is the sinoatrial node which, in adults, fires at rates between 60 and 100 beats per minute, faster than any other cardiac region. In an individual at rest, modulation by the parasympathetic nervous system dominates which slows the sinoatrial nodal rate to about 75 action potentials per minute (or beats per minute when contractions are elicited).

In addition to the cells of the sinoatrial node, other specialized conduction system cells are capable of developing spontaneous diastolic depolarization, specifically those found in the specialized fibers in the atrioventricular junction and His–Purkinje system. Rhythms generated by impulse formation within these cells range from 25 to 55 beats per minute in the human heart (Fig. 13.7). These lower-rate rhythms are commonly referred to as *ventricular escape rhythms* and are important for patient survival, since they maintain some degree of cardiac output in situations when the sinoatrial and/or atrioventricular nodes are nonfunctional or are functioning inappropriately. Note that the various populations of pacemaker myocytes (i.e., in the sinoatrial and atrioventricular nodes) elicit so-called slow-type action potentials (slow-response action potential; see below).

In addition to the normal sources of cardiac rhythm, myocardial tissue can also exhibit abnormal self-excitability; such a site is also called an *ectopic pacemaker* or *ectopic focus*. This pacemaker may operate only occasionally, producing extra beats, or it may induce a new cardiac rhythm for some period of time. Potentiators of ectopic activity include caffeine, nicotine, electrolyte imbalances, hypoxia, and/or toxic reactions to drugs such as digitalis. For more detail on rate control of the heart, refer to Chap. 14.

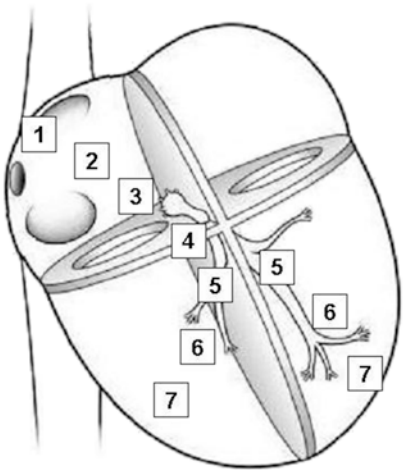

Normal Activation Sequence	Structure	Conduction velocity (m/sec)	Pacemaker rate (beats/min)
1	SA node	< 0.01	60 – 100
2	Atrial myocardium	1.0 – 1.2	None
3	AV node	0.02 – 0.05	40 – 55
4	Bundle of His	1.2 – 2.0	25 – 40
5	Bundle branches	2.0 – 4.0	25 – 40
6	Purkinje network	2.0 – 4.0	25 – 40
7	Ventricular myocardium	0.3 – 1.0	None

Fig. 13.7 Conduction velocities and intrinsic pacemaker rates of various structures within the cardiac conduction pathway. The structures are listed in the order of activation during a normal cardiac contraction, beginning with the sinoatrial node. Note that the intrinsic pacemaker rate is slower in structures further along the activation pathway. For example, the atrioventricular nodal rate is slower than the sinoatrial nodal rate. This prevents the atrioventricular node from generating a spontaneous rhythm under normal conditions, since it remains refractory at rates <55 beats per minute. If the sinoatrial node becomes inactive, the atrioventricular nodal rate will then determine the ventricular rate. Tabulation adapted from Katz AM (ed), Physiology of the Heart, 3rd edn., 2001)

13.4 Cardiac Action Potentials

Although cardiac myocytes branch and interconnect with each other (mechanically via the intercalated disk and electrically via the gap junctions), under normal conditions, the heart is thought to form two separate functional networks—the atria and the ventricles. The atrial and ventricular tissues are separated by the fibrous skeleton of the heart (the central fibrous body). This skeleton is comprised of dense connective tissue rings that surround the valves of the heart, fuse with one another, and merge with the interventricular septum. The skeleton can be considered to (1) form the foundation to which the valves attach, (2) prevent overstretching of the valves, (3) serve as a point of insertion for cardiac muscle bundles, and (4) act as an electrical insulator that prevents the direct spread of action potentials from the atria to the ventricles. See also Chap. 5 for further details on the cardiac skeleton.

A healthy myocardial cell has a resting membrane potential of approximately −90 mV. The resting potential is described by the Goldman–Hodgkin–Katz equation, which takes into account the permeabilities (Ps) as well as the intracellular and extracellular concentrations of ions [X], where X is the ion:

$$V_m = (2.3R*T/F)*\log_{10}\frac{P_K[K]_o + P_{Na}[Na]_o + P_{Cl}[Cl]_i + \ldots}{P_K[K]_i + P_{Na}[Na]_i + P_{Cl}[Cl]_o + \ldots}$$

In the cardiac myocyte, the membrane potential is dominated by the K^+ equilibrium potential. An action potential is initiated when this resting potential becomes shifted toward a more positive value of approximately −60 to −70 mV (Fig. 13.8). At this threshold potential, the cell's voltage-gated Na^+ channels open and begin a cascade of events involving other ion channels. In artificial electrical stimulation, this shift of the resting potential and subsequent depolarization is produced by the excitation delivered through the pacing system. The typical ion concentrations for a mammalian cardiac myocyte are summarized in Table 13.1 and graphically depicted in Fig. 13.9.

When a myocyte is brought to the threshold potential, normally via a neighboring cell, voltage-gated fast Na^+ channels actively open (activation gates); the permeability of the sarcolemma (plasma membrane) to sodium ions (P_{Na^+}) dramatically increases. Because the cytosol is electrically more negative than extracellular fluid, and the Na^+ concentration is higher in the extracellular fluid, Na^+ rapidly crosses the cell membrane. Importantly, within a few milliseconds, these fast Na^+ channels automatically inactivate (inactivation gates) and P_{Na^+} decreases.

The membrane depolarization due to the activation of the Na^+ induces the opening of the voltage-gated slow Ca^{2+} channels located within both the sarcolemma and sarcoplasmic reticulum (internal storage site for Ca^{2+}) membranes.

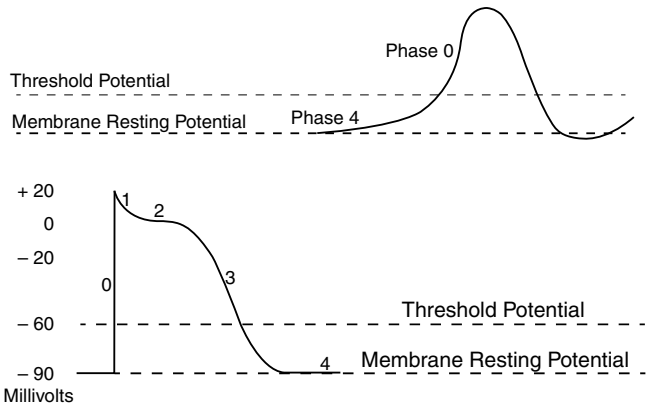

Fig. 13.8 Typical cardiac action potentials (slow on top and fast below). The resting membrane potential, the threshold potential, and the phases of depolarization (0–4) are shown

Table 13.1 Ion concentrations for mammalian myocytes

Ion	Intracellular concentration (mM)	Extracellular concentration (mM)
Sodium (Na)	5–34	140
Potassium (K)	104–180	5.4
Chloride (Cl)	4.2	117
Calcium (Ca)	–	3

Adapted from Katz AM (ed), Physiology of the Heart, 3rd edn., 2001

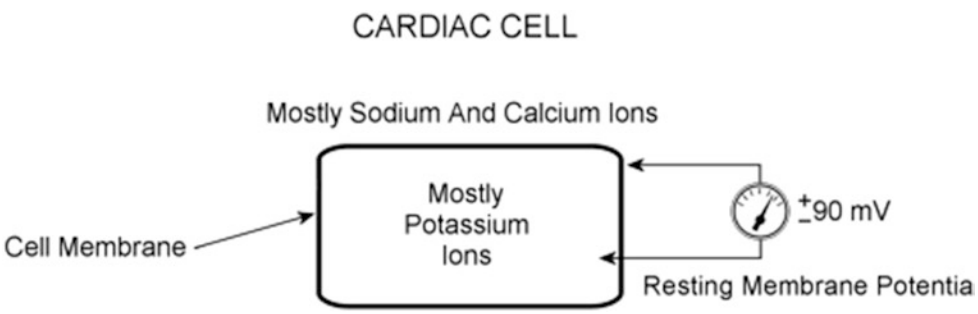

Fig. 13.9 Cardiac cell at rest. The intracellular space is dominated by potassium ions, while the extracellular space has a higher concentration of sodium and calcium ions

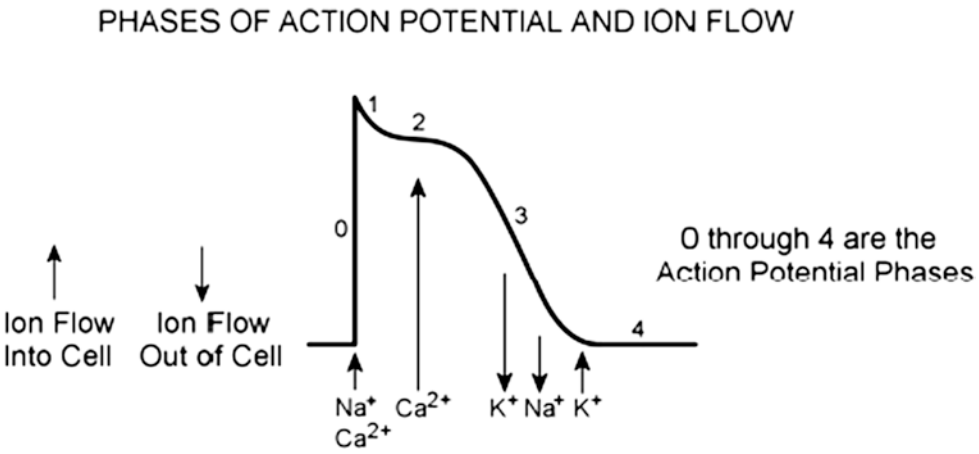

Fig. 13.10 Ion flow during the phases of a cardiac action potential

Thus, there is an increase in the permeability of Ca^{2+} ($P_{Ca^{2+}}$), which allows the concentration to dramatically increase intracellularly (Fig. 13.10). At the same time, the membrane permeability to K^+ ions decreases due to closing of K^+ channels. For approximately 200–250 ms, the membrane potential stays close to 0 mV, as a small outflow of K^+ just balances the inflow of Ca^{2+}. After this fairly long delay, voltage-gated K^+ channels open and active repolarization is initiated. The opening of these K^+ channels (increased membrane permeability) allows for K^+ to diffuse out of the cell due to its concentration gradient. At this same time, Ca^{2+} channels begin to close, and net charge movement is dominated by the outward flux of the positively charged K^+, restoring the negative resting membrane potential to approximately –90 mV (Figs. 13.10 and 13.11).

As mentioned above, not all action potentials that are elicited in the cardiac myocardium have the same time course; slow- and fast-response cells have differing shaped action potentials with different electrical properties in each phase. Recall that the pacemaker cells (slow-response type) have the ability to spontaneously depolarize until they reach threshold and thus elicit action potentials. Action potentials from such cells are also characterized by a slower initial depolarization phase, a lower amplitude overshoot, a shorter and less stable plateau phase, and repolarization to an unstable, slowly depolarizing resting potential (Fig. 13.12). In the pacemaker cells, at least three mechanisms are thought to underlie the slow depolarization that occurs during phase 4 (diastolic interval): (1) a progressive decrease in P_{K^+}, (2) a slight increase in P_{Na^+}, and (3) an increase in $P_{Ca^{2+}}$.

13.5 Gap Junctions (Cell-to-Cell Conduction)

In the heart, cardiac muscle cells (myocytes) are connected end to end by structures known as *intercalated disks*. These are irregular transverse thickenings of the sarcolemma, within which there are *desmosomes* that hold the cells together and to which the myofibrils are attached. Adjacent to the intercalated disks are the gap junctions, which allow action potentials to directly spread from one myocyte to the next. More specifically, the disks join the cells together by both mechanical attachment and protein channels. The firm mechanical connections are created between the adjacent cell membranes by proteins called adherins in the desmosomes. The electrical connections (low-resistance pathways, gap junctions) between the myocytes are via the channels formed by the protein connexin. These channels allow ion movements between cells (Fig. 13.13).

As noted above, not all cells elicit the same type of action potentials, even though excitation is propagated from cell to cell via their interconnections (gap junctions). The action potentials elicited in the sinoatrial nodal cells are of the slow-response type and those in the remainder of the atria have a more rapid depolarization rate (Fig. 13.14). Although a significant temporal displacement in the action potentials elicited by the myocytes of the two nodes (sinoatrial and atrioventricular) occurs, the action potential morphologies are similar.

It takes approximately 30 ms for excitation to spread between the sinoatrial and atrioventricular nodes, and atrial activation occurs over a period of approximately 70–90 ms (Fig. 13.14). The speed at which an action potential propagates through a region of cardiac tissue is called the *conduction velocity* (Fig. 13.7). The conduction velocity varies considerably in the heart and is directly dependent on the diameter of a given myocyte. For example, action potential conduction is greatly slowed as it passes through the atrioventricular node. This is due to the small diameter of these nodal cells, the tortuosity of the cellular pathway [2], and the slow rate of rise of their elicited action potentials. This delay is important to allow adequate time for ventricular filling.

Action potentials in the Purkinje fibers are of the fast-response type (Fig. 13.14), i.e., rapid depolarization rates that, in part, are due to their large diameters. This feature

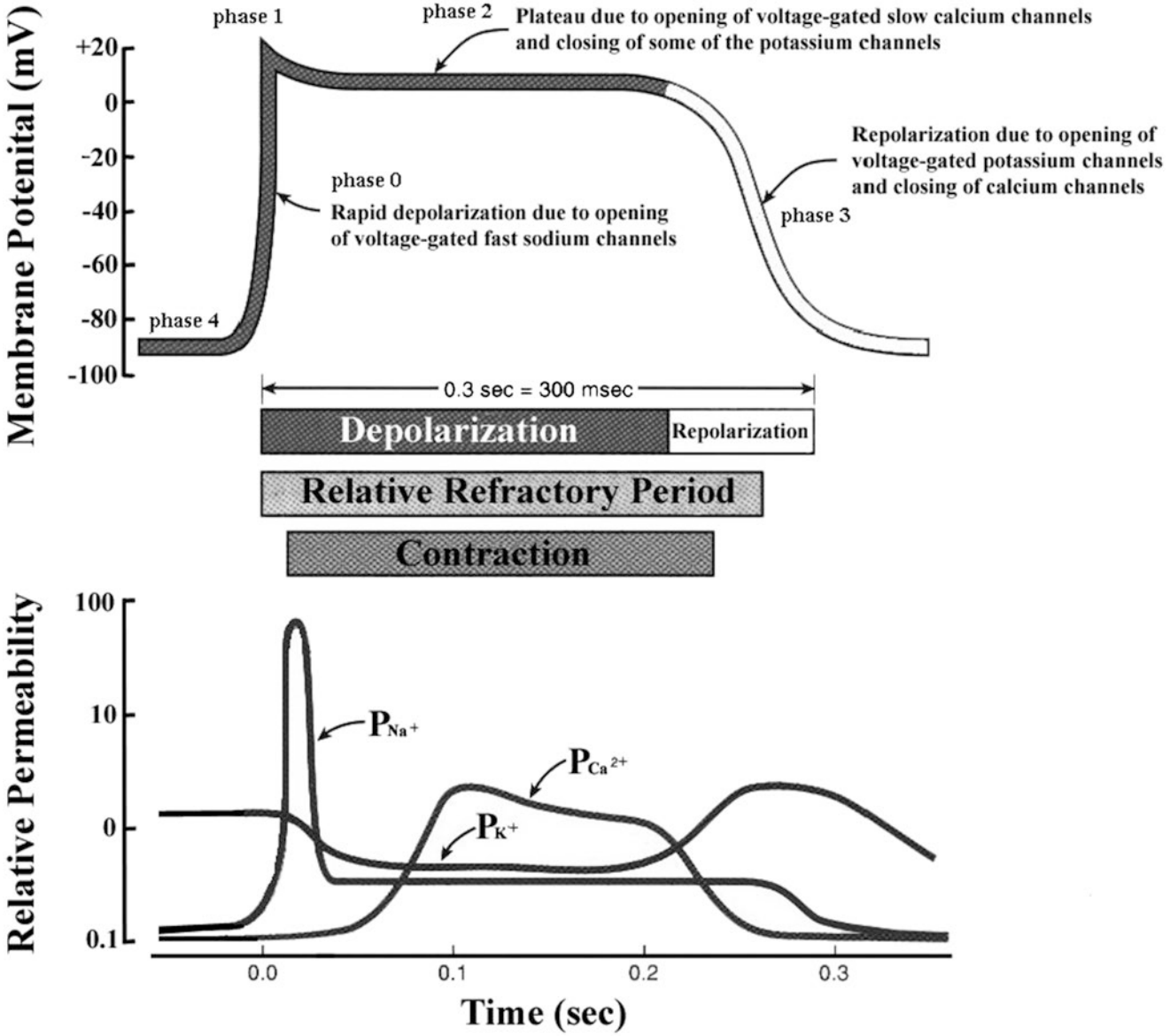

Fig. 13.11 A typical action potential of a ventricular myocyte and the underlying ion currents. The resting membrane potential is approximately −90 mV (phase 4). The rapid depolarization is primarily due to the voltage-gated Na^+ current (phase 0), which results in a relatively sharp peak (phase 1) and transitions into the plateau (phase 2) until repolarization (phase 3). Also indicated are the refractory period and timing of the ventricular contraction. Modified from Tortora GJ, Grabowski SR (eds), Principles of Anatomy and Physiology, 9th edn., 2000

allows the Purkinje system to transfer depolarization to the majority of cells in the ventricular myocardium nearly in unison. Because of the high conduction velocity in these cells which span the myocardium, there is a minimal delay in the cell's time of onset. It is important to note that the ventricular cells that are last to depolarize have shorter duration action potentials (shorter Ca^{2+} current) and thus are the first to repolarize. The ventricular myocardium repolarizes within the time period represented by the T-wave in the electrocardiogram.

13.6 The Atrioventricular Node and Bundle of His: Specific Features

The atrioventricular node and the bundle of His play critical roles in the maintenance and control of ventricular rhythms. As mentioned previously, the atrioventricular node is composed of heterogeneous gap junctions with electrical communication via the protein connexin. Specifically, there are four connexin proteins identified to date: Cx43, Cx40, Cx45, and Cx30.2/31.9. Cx43 and Cx40 are associated with the fast

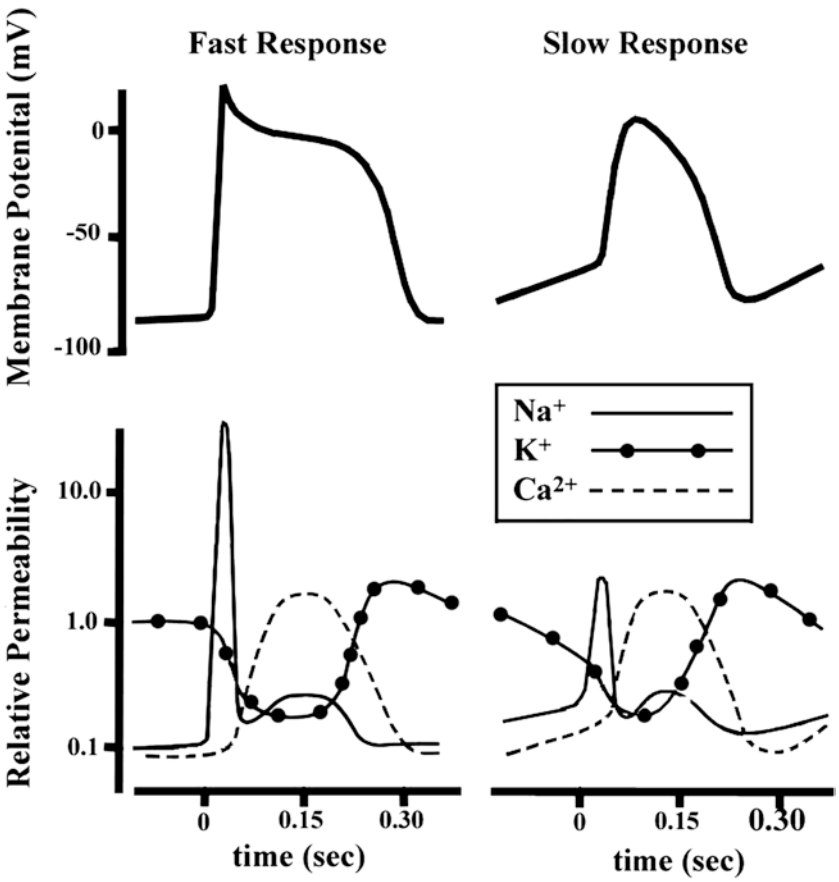

Fig. 13.12 The comparative time course of membrane potentials and ion permeabilities that would typically occur in a fast-response (*left*: ventricular myocyte) and a slow-response cell (*right*: nodal myocyte). Modified from Mohrman DE, Heller LJ (eds) Cardiovascular Physiology, 5th edn., 2003

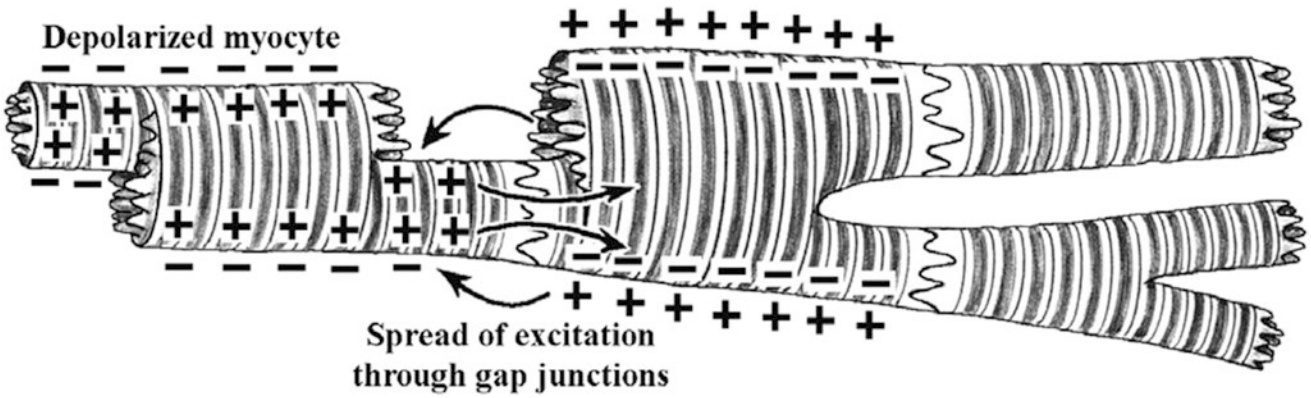

Fig. 13.13 Several cardiac myocytes in different states of excitation. The depolarization that occurred in the cell on the left causes depolarization of the adjacent cell through cell-to-cell conduction via the gap junctions (nexus). Eventually all adjoining cells will depolarize. An action potential initiated in any of these cells will be conducted from cell to cell in either direction

conduction pathway, whereas Cx45 and Cx30.2/31.9 are generally expressed in the slow conduction pathway [43]. The expression of these proteins is also species dependent; it should be noted that one study found Cx43, Cx40, and Cx45 are expressed in the human atrioventricular junction [44].

Additionally, both structures are frequently accessed during cardiac catheterization procedures: (1) as anatomic landmarks, (2) to allow insight into atrial–ventricular conduction behaviors, and/or (3) to ablate these structures or the surrounding tissues to terminate aberrant behaviors (e.g., reentrant tachycardias) or to prevent atrioventricular conduction in patients with chronic atrial fibrillation. Today, there is a strong interest by the medical device designer to understand the details of the structural and functional properties of the atrioventricular node and the bundle of His to develop new therapies and/or to avoid inducing complications.

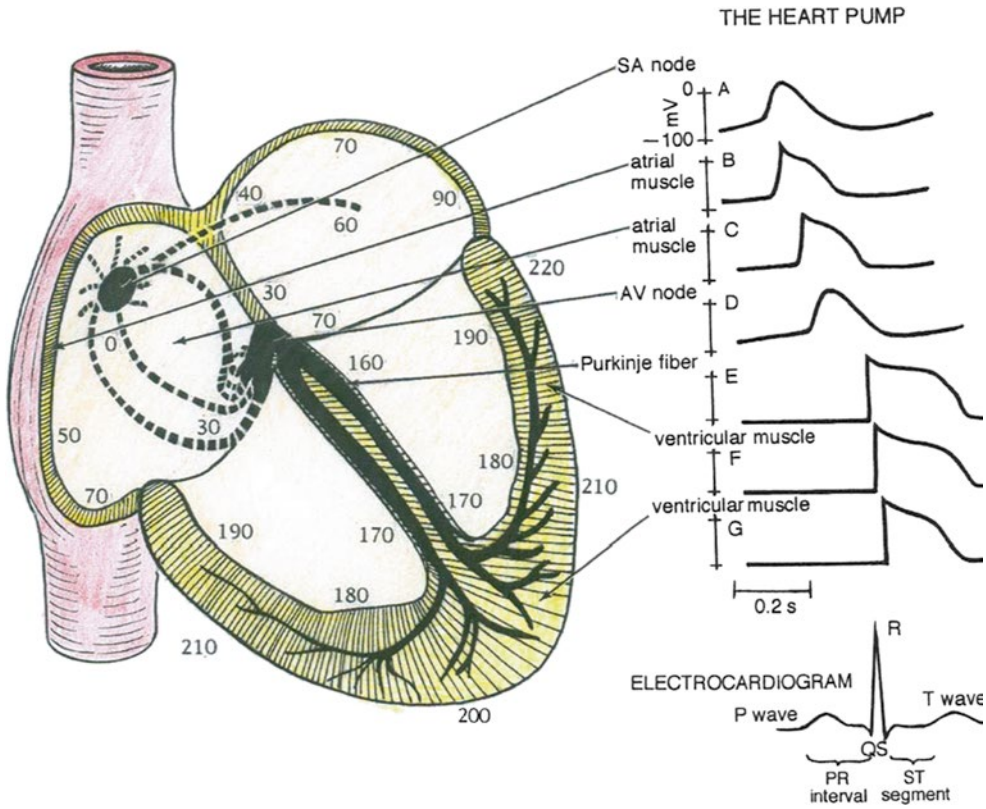

Fig. 13.14 Predominant conduction pathways in the heart and the relative time, in ms, that cells in these various regions become activated following an initial depolarization within the sinoatrial node. To the right are typical action potential waveforms that would be recorded from myocytes in these specific locations. The sinoatrial and atrioventricular nodal cells have similar shaped actions potentials. The non-pacemaker atrial cells elicit action potentials that have shapes somewhat between the slow-response (nodal) and fast-response cells (e.g., ventricular myocytes). The ventricular cells elicit fast-response-type action potentials; however, their durations vary in length. Due to the rapid excitation within the Purkinje fiber system, the initiation of depolarization of the ventricular myocytes occurs within 30–40 ms and is recorded as the QRS complex in the electrocardiogram

The myocytes located within the region of the atrioventricular node and the bundle of His have many unique characteristics. Specifically, both the atrioventricular node and His bundle are comprised primarily of "spiraled" myofibers that are then combined to form many collagen-encased fascicles. These fascicles are generally arranged in a parallel fashion in the proximal atrioventricular bundle (PAVB, the region of the atrioventricular node transitioning from the atrium into the body of the nodal tissues) and the distal atrioventricular bundle (DAVB, the penetrating portion of the bundle of His) and are interwoven within the atrioventricular node itself (the tortuosity of the cellular pathway within the atrioventricular node likely is a major contributor to the conduction delay in this region; Fig. 13.5). In general, the myocytes of the His are larger than those of the PAVB and the atrioventricular node, and the perinuclear regions of these myocytes are filled with glycogen. These cells uniquely utilize anaerobic metabolism instead of the normal aerobic metabolism used by the more abundant contractile myocardium. His myocytes have longer intercalated disks and, although all of the nodal tissues have thin end processes, they are less numerous in the His. His myocytes are innervated, but to a lesser extent than those in the atrioventricular node. Unlike the sinoatrial and atrioventricular nodes, the His bundle has no large blood vessels that supply it specifically. Table 13.2 provides a summary of histological characteristics of the His in comparison to the other nodal tissues.

It should be noted that the bundle of His can receive inputs from both the atrioventricular node and from transitional cells in the atrial septum. In general, the His bundle is located adjacent to the annulus of the tricuspid valve, distal to the atrioventricular node and slightly proximal to the right bundle branch and left bundle branch. The functional origin may be ill defined, but it is typically considered to anatomically begin at the point where the atrioventricular nodal tissue enters the central fibrous body. The bundle of His is described as having three regions—the penetrating bundle, nonbranching bundle, and branching bundle. The penetrating bundle is the region that enters the central fibrous body. At this point, the His fascicles are insulated but are surrounded by atrial

Table 13.2 Summary of the histological characteristics of nodal and perinodal tissues in canines

Feature	Atrioventricular bundle (DAVB, His bundle)	Atrioventricular node (AVN)	Proximal atrioventricular bundle (PAVB)
Nucleus	Clear perinuclear zone filled with glycogen	Clear perinuclear zone filled with glycogen	Clear perinuclear zone filled with glycogen
Metabolism	Anaerobic	Anaerobic	Anaerobic
Myofiber size	Largest	Mid	Smallest
Myofibers in fascicles?	Yes	Yes	Yes
Primary fascicles encased in collagen	Yes	Yes	Yes
Secondary fascicles present	Yes	Yes	Yes
Secondary fascicles encased in collagen	Yes	Yes	Yes
Fascicular arrangement	Parallel	Interwoven ("massive whorl")	Parallel
Myofiber arrangement within fascicles	Least spiraling	Spiraled	Most spiraling
Cross striations	Delicate	Delicate	Delicate
End processes present on the myocytes?	Yes. Short and delicate	Yes. Most numerous. Extend from proximal parallel myofibers to central whorled fibers	Yes
Intercalated disks	Broad	Form short stacks	Broadest
Fat vacuoles	Little or none	Little or none	Yes
Vascularization	No large vessels	No large vessels	Large vessels present
Innervation	Tendrils (sympathetic). No packets or fascicles of nerve endings present	Fascicles of boutons, tendrils (sympathetic), and varicosities (parasympathetic) present	Fascicles of boutons, tendrils (sympathetic), and varicosities (parasympathetic) present. Sheaves of nerve endings extend along the length of the myofibers

Compiled from Racker and Kadish [2]

tissue (superiorly and anteriorly), the ventricular septum (inferiorly), and the central fibrous body (posteriorly). Thus, the exact point where the atrioventricular nodal tissues end and the bundle begins is difficult to define, since it occurs over a transitional region. The penetrating bundle has been described as oval in shape and was found to be 1–1.5 mm long in young canines and 0.25–0.75 mm long in neonates [1]. The nonbranching bundle passes through the central fibrous body and is surrounded on all sides by the central fibrous body. In this cardiac region, the His bundle still has atrial tissue superior and anterior to it, the ventricular septum inferior to it, and now the aortic and mitral valves posterior to it. The branching bundle is described to begin as the His exits the central fibrous body. At this point, it is inferior to the membranous septum and superior to the ventricular septum. The bundle is also at its closest proximity to both the right and left ventricular chambers at this point. After leaving the central fibrous body, the bundle then bifurcates into the bundle branches; the right bundle branch passes into the myocardium of the interventricular septum and the left bundle branch travels subendocardially along the septum in the left ventricle. Figures 13.15 and 13.16 show canine histological sections of the bundle of His as they exit the central fibrous body (the branching bundle).

Electrophysiologic studies of the bundle of His commonly have been performed using catheters with polished electrodes and a short interelectrode spacing (i.e., those with diameters of 2 mm). Due to the small amplitude of the His potential, special high-pass filtering must be used (>30 Hz). This high-pass setting must be used in order to separate the His signal from the low-frequency shift in the isopotential line between the atrial depolarization and the atrial repolarization/ventricular depolarization. His potentials can commonly be mapped by deploying an electrode in one of three ways: (1) endocardially in the right atrium at a point on the tricuspid annulus near the membranous septum, (2) epicardially at the base of the aorta near the right atrial appendage, or (3) radially within the noncoronary cusp of the aortic valve [16–18, 20, 45].

Today, His potentials are commonly mapped to provide a landmark for ablation of the atrioventricular node as well as to assess A-to-V conduction timing. In addition to direct electrical mapping, much can be learned about the general anatomical and functional properties of the cells lying within the bundle via attempts to directly stimulate it. For example, direct stimulation of the His produces normal ventricular activation due to the initiation of depolarization into the intrinsic conduction pathway [16, 17, 19]. Thus, if one frequently

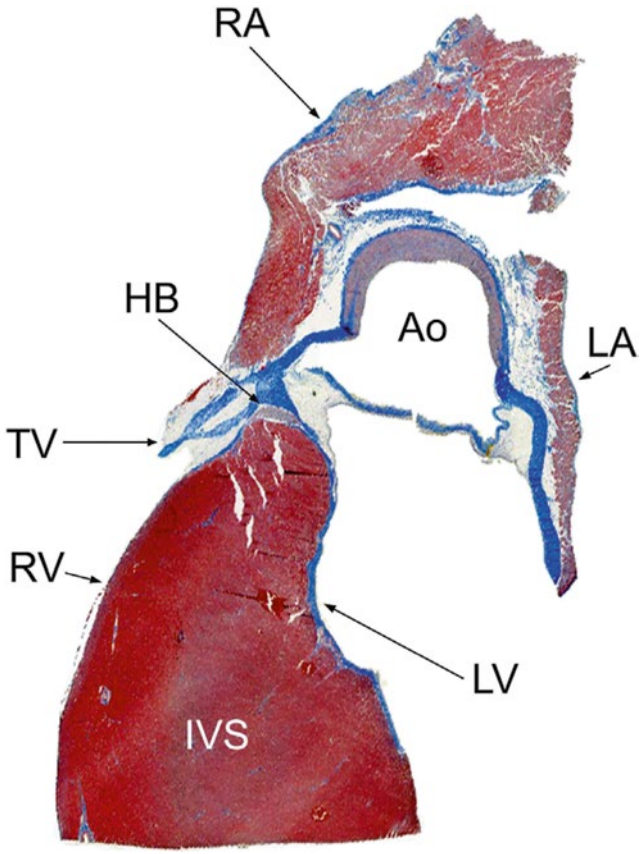

Fig. 13.15 Histologic section through the bundle of His in a canine heart. The section was prepared using a modified Masson's trichrome stain (collagen/nuclei stains *blue*, muscle/keratin/cytoplasm stains *red*). *Ao* aorta, *HB* His bundle, *IVS* interventricular septum, *LA* left atrium, *LV* left ventricular endocardium, *RA* right atrial endocardium, *RV* right ventricular endocardium, *TV* tricuspid valve

experiences failed attempts to selectively stimulate the His bundle, she/he may assume pathological changes [20].

The His bundle has historically been thought to act only as a conduit for transferring depolarization. Ventricular escape rhythms have been known to emanate from the His, but it was considered to be, in general, a relatively simple structure. To the contrary, recent evidence indicates that at least two general sources serve as inputs to the His and that it functions as at least two functionally distinct conduits. Using alternans (alternate beat variation in the direction, amplitude, and duration of any component of the ECG), the duality of its electrophysiology was recently demonstrated in isolated preparations from the region of the triangle of Koch in rabbit hearts [45].

13.7 Comparative Anatomy

All large mammalian hearts are considered to have a very similar conduction system with these main components: sinoatrial node, atrioventricular node, bundle of His, right and left main bundle branches, and Purkinje fibers. Yet, interspecies variations are well recognized [1, 46–48]. For a summary of the major differences in the atrioventricular conduction systems between human, pig, dog, and sheep hearts, refer to Chap. 6.

More specifically, Bharati et al. compared the electrophysiologic properties of the swine and human heart (Table 13.3) [46]. In addition to significant differences in atrial (HRA-LRA) and AV conduction times (much shorter in the swine), the authors also found significantly more autonomic innervation within the atrioventricular node and penetrating bundle of the swine heart (thought to be both adrenergic and cholinergic). They concluded that this indicates a more important neurogenic component to the swine conduction system, relative to the human heart. Due to this difference, they cautioned using swine as a model for assessing cardiac arrhythmias. Although the neurogenic differences between the human and swine are significant in vivo, isolation of such hearts results in denervation of the conduction system and thus reduces or eliminates the relevance of this finding.

The canine is another commonly used model in biomedical device research. Information on A-to-V timing in canines was published by Karpawich et al. [18]. These researchers placed tripolar electrodes on the right atrial epicardium near the noncoronary cusp of the aorta of canines; the resulting timing recorded was extracted from the paper and is tabulated in Table 13.4.

13.8 The Recording of Action Potentials and/or the Spread of Excitation Through the Myocardium

Action potential waveforms can be actively monitored from the epicardial, endocardial, or transmural surfaces of the heart. Several methods exist for the acquisition of such signals, including: (1) glass micropipette electrodes, (2) metal electrodes of various designs, (3) multielectrode arrays, (4) optical mapping, and (5) contact or noncontact endocardial mapping. Contact or noncontact endocardial mapping technologies measure primarily the intracardiac electrograms (endocardial, see also Chap. 32) rather than those from the epicardial surface or globally from the whole myocardium, as in a standard 12-lead ECG. It should be noted that for many ablative arrhythmia therapies, the measurement of intracardiac electrograms within a given cardiac chamber is more common than the recordings from the epicardium (see Chaps. 28 and 29) [49]. Furthermore, algorithms employed by implantable devices such as pacemakers and defibrillators typically use the intercardiac (transmural) electrogram (EGM) signal when detecting an arrhythmia. In this application it is common to use active fixation leads with distal electrodes screwed into the myocardium [50].

Typically, glass micropipettes are produced from small-diameter capillary tubing and then employed for intracellular recordings. These glass tubes are heated (with a burner or

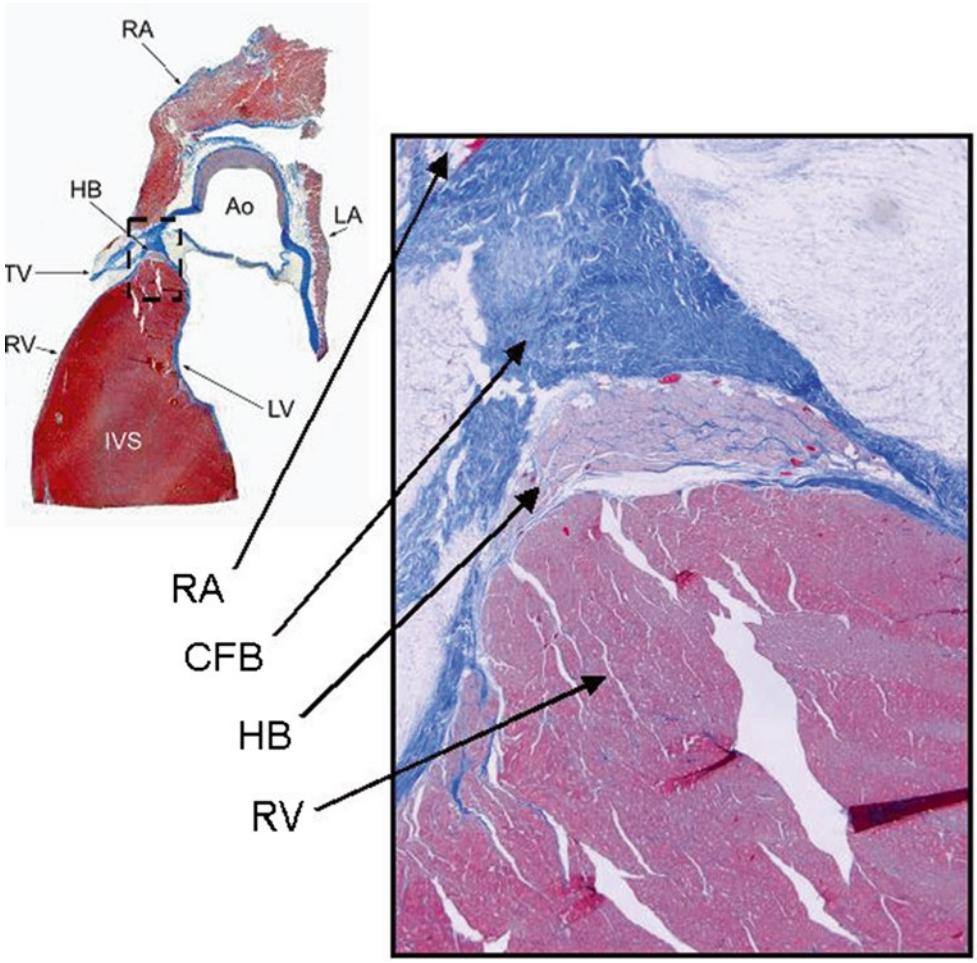

Fig. 13.16 Histologic section through the bundle of His in a canine heart. The region enlarged is noted by the *dashed lines* in the original histologic section. Both sections were prepared using a modified Masson's trichrome stain (collagen/nuclei stain *blue*, muscle/keratin/cytoplasm stain *red*). *Ao* aorta, *CFB* central fibrous body (provides structure and isolates the atrial from the ventricular tissues), *HB* His bundle, *IVS* interventricular septum, *LA* left atrium, *LV* left ventricular endocardium, *RA* right atrial endocardium, *RV* right ventricular endocardium, *TV* tricuspid valve

Table 13.3 Comparison of swine to human electrophysiology

Parameter	Swine (average ± std dev/range)	Normal human
Heart rate (beats per minute)	132 ± 32 (91–167)	60–100
PR interval (ms)	94 ± 27 (50–120)	3–5-year-old: 110–150 5–9-year-old: 120–160
QT interval (ms)	256 ± 69 (150–340)	HR = 150: 210–280 HR = 100: 260–350
HRA-LRA (ms)	10 ± 0 (10)	2–5-year-old: 6–38 6–10-year-old: 0–41
LRA-H (ms)	63 ± 2 (60–65)	2–5-year-old: 45–101 6–10-year-old: 40–124
H-V (ms)	25 ± 7 (20–35)	2–5-year-old: 27–59 6–10-year-old: 28–52

H His, *HR* heart rate, *HRA* high right atrium, *LRA* low right atrium, *V* ventricle

Adapted from Bharati et al. [46]

Table 13.4 Tabulation of activation timing

	P-wave to R-wave interval (ms)	Atrial activation to His bundle electrogram (ms)	His bundle electrogram to ventricular activation (ms)
Mean	92.1	77.5	29
Std Dev	18.4	11.5	8.9
Max	120	100	50
Min	70	60	20

Data compiled from Karpawich et al. [18]

heating element) and then, under tension, elongated (stretched) to produce a constriction that eventually breaks. Currently, this process is typically facilitated by a commercially available micropipette puller which reproducibly creates electrodes with tips of about 0.1 μm with resistances of 10–40 MΩ. The pipette is then filled with an electrolyte such as 3M KCl. A silver, platinum, or stainless steel wire is then positioned inside the pipette until it is in contact with the electrolytic solution [51]. The user must be careful manipulating the fragile electrode tip, especially when recording directly from a beating, moving cell. The ultimate goal of this recording approach is to impale the microelectrode through the cell membrane, so that the tip is into the myoplasm of a single cell while not inducing major damage to the cell; the membrane seals around the tip and the cell does not become depolarized.

There are various designs for metal recording electrodes which can be employed to monitor action potential wave-

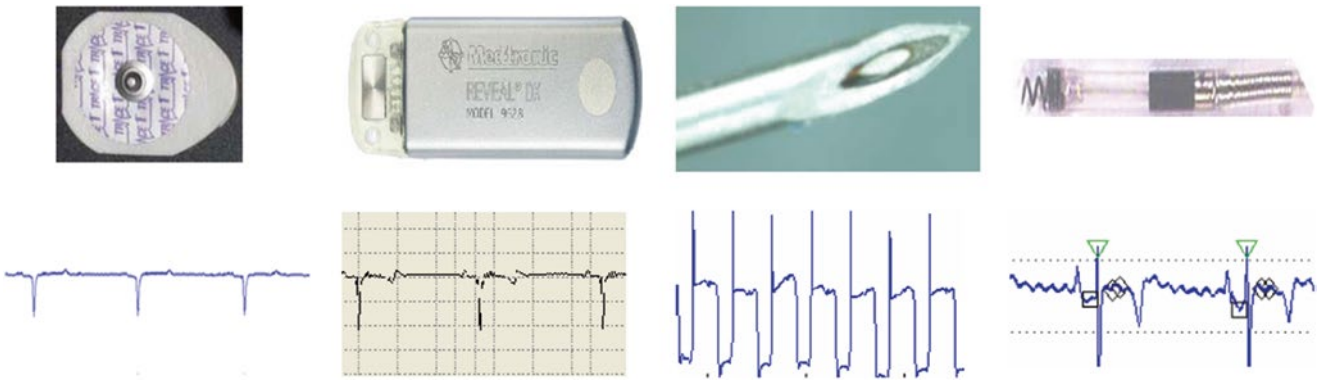

Fig. 13.17 Representative cardiac signals. The leftmost signal is from a standard Ag/AgCl surface electrode. The second signal was collected subcutaneously with a Medtronic Reveal® Dx insertable cardiac monitor (Medtronic, Inc, Minneapolis, MN, USA). The third signal was collected from a concentric bipolar needle electrode with 0.3 mm spacing between conductors. The last endocardial signal was obtained with a Medtronic 5076 screw-in electrode in the right ventricle; this electrogram has key fiducial points marked

forms extracellularly. One of the most common methods is to use a needle with two closely spaced embedded conductors. Yet, the relative spacing between the active and reference conductors can be manipulated to control the sensing area [52]. Another method is to use an internal conductor needle with the cannula of the needle as the reference electrode. In such cases, the internal conducting wire is electrically isolated from the cannula. In a monopolar configuration, the needle is a single shaft, and the reference is taken from the subject ground. Each of these designs can have needle tip diameters as small as 0.30 mm.

Various types of electrode designs and typical signals that can be recorded with each are shown in Fig. 13.17. Note that the morphology of a recorded signal will typically depend on: (1) the configuration of the electrode employed (monopolar/unipolar or bipolar), (2) the relative surface area that the electrode will monitor, (3) the anatomical placement (atrium or ventricle), and/or (4) the site-specific myocardial wall recording location (endocardial, epicardial, or transmural). Multiple ECG patches, for example, are used to cover a larger surface area on the skin and thus detect potential changes from a large transmural field, whereas a bipolar concentric needle placed epicardially records from a focal population of cells. In other words, the surface electrodes will provide a signal representative of a major portion of the whole heart, while the small bipolar needle electrode provides a much more localized signal.

Active and passive pacing leads can be used to detect action potential waveforms, commonly used today in either unipolar or bipolar configurations (i.e., with those leads that have both a distal-tip electrode and a distal-ring electrode). Such leads can be used for either sensing or pacing. Modern pacemaker lead diameters range from 4 to 10 French (1 French = one-third millimeter). Note, their relative dimensions will ultimately dictate the size of the field from which they are sensing electrical potentials. As with any active fixation lead or metal electrode which is engaged into the myocardium, an initial injury potential can be associated with its placement [53]. The current trend in the pacing lead industry is to continually decrease the diameter of both the body and tip dimensions (i.e., 2 Fr leads are currently in development and clinical trials).

One can consider that an extension of the single-electrode approach is the multielectrode array. As the name implies, such systems consist of an array of equally spaced electrodes supported by a base. Conducting wires are attached to the electrodes on the array. Depending on the design, one or more of the electrodes on the array can serve as the reference electrode, while the others become the active electrodes. These arrays allow for the mapping of electrical potentials within a given region of the heart [54]. The designer or eventual user must determine the appropriate electrode spacing for a given application while also considering the relative electrode configurations, employed sampling rates, and/or density of electrodes necessary to elucidate or monitor the nature of the desired local events.

Catheter-based cardiac mapping systems are primarily used to understand the underlying mechanisms of arrhythmias. In principle, electroanatomical mapping systems use low magnetic fields to reconstruct 3D maps and electrical activation sequences of the chamber of interest. Briefly, in sequential mapping systems, mapping catheters with radiofrequency capability are placed into the heart chamber with fluoroscopic guidance. Low magnetic fields are generated by pads located under the patient's bed. The sensor tip of the catheter attains data in order to compute information regarding magnetic field amplitude, frequency, and phase to reconstruct a spatial 3D position. After chamber reconstruction, sequential recording of electrical activation is recorded by dragging the catheter along the endocardial wall. The intercardiac electrogram is measured and typically the activation time is superimposed on the reconstructed 3D chamber,

resembling a contour map. The reconstruction process can be conducted in real time; however, the process is time consuming since it is a sequential process. Using these methods, one can gain insights on the relative spread of excitation through a given chamber or portions of the conduction system.

Contact mapping can also be conducted with basket catheters that typically contain 32–64 nickel or titanium electrodes that are 1–2 mm long and 1 mm in diameter with interelectrode distances from 3 to 10 mm. The endocardial surface is mapped at the basket's splines, making contact with the chamber wall. This technique has limitations, however, since a catheter that is too small or too large will result in poor-quality electrogram recordings. The technique is also susceptible to movement artifacts from the continuously beating heart [55, 56]. Nevertheless, one can track relative electrical activities through the heart with these methodologies.

Another approach to 3D chamber mapping is noncontact mapping technology. One such product is the EnSite® system manufactured by Endocardial Solutions (St. Jude Medical, St. Paul, MN, USA). This system includes a catheter with 64 laser-etched unipolar electrodes that lies within the chamber; one can track, on a beat-to-beat basis, the activation and repolarization patterns in a given chamber (see Chap. 32 for more details on these systems and new non-invasive mapping technologies). It is the continued development of cardiac mapping systems that helps physicians localize sites for catheter ablation for the treatment of complex cardiac arrhythmias such as tachycardia or atrial fibrillation [55, 57]. Catheters used for noncontact cardiac mapping of endocardial activation and repolarization processes are typically 9 Fr in diameter.

13.9 Future Research

Although much is already known, a great deal of supposition and controversy remains related to our understanding of the cardiac conduction system. Specifically, characterization of the anatomy and electrophysiology of the atrioventricular nodal region and the bundle of His continues to be an area of great scientific interest and debate [58–60]. For example, current clinical interest in the atrioventricular node and His bundle has focused research on their potential stimulation to ultimately improve hemodynamics in patients requiring pacing [16–21], as well as their use in treating atrioventricular nodal reentrant tachycardias [1, 2, 54, 61]. Also, there is increasing evidence about the critical role that cardiac innervation plays in the control and modulation of rhythms, including evidence of ganglia in the pulmonary vein sleeves modulating the rate of the sinus node [62]. A new cell type has also been discovered in the pulmonary vein sleeves, in the atrial tissue, and in the ventricular myocardium. These interstitial Cajal-like cells (*telocytes*) are leading to new hypotheses regarding the origins of rhythms, arrhythmias, and coordination of intercellular signaling [63–66]. In addition to a potential source of arrhythmias, these cells may prove to be an additional source of the ventricular rescue rhythms. Future scientific investigations will serve to improve our understanding of the fundamental physiology of the heart's conduction system and the mechanisms of cardiac activation in normal and diseased tissues. The findings from these studies will provide a better foundation for future therapies. For additional reviews on the human cardiac conduction system, the reader is referred to those by Iaizzo and Laske [67], Dobrzynski et al. [68], and Anderson et al. [69].

13.10 Summary

This chapter reviewed the basic architecture and function of the cardiac conduction system in order to provide the reader with a working knowledge and vocabulary related to this topic. While a great deal of literature exists regarding the cardiac conduction system, numerous questions remain related to the detailed histological anatomy and cellular physiology of these specialized conduction tissues and how they become modified in disease states. Future findings associated with the function and anatomy of the cardiac conduction system will likely lead to improvements in therapeutic approaches and medical devices.

Acknowledgments We would like to thank Medtronic Training and Education and Gorinka Shrivastav for graphical support; Rebecca Rose, DVM, Louanne Cheever, and Alexander Hill, PhD, of Medtronic for the histological sectioning and staining; Anthony Weinhaus, PhD, for additional details on atrial anatomy; and Igor Efimov, PhD, from George Washington University for 3D images of the human atrioventricular node.

References

1. Ho SY, Kilpatrick L, Kanai T et al (1995) The architecture of the atrioventricular conduction axis in dog compared to man–its significance to ablation of the atrioventricular nodal approaches. J Cardiovasc Electrophysiol 6:26–39
2. Racker DK, Kadish AH (2000) Proximal atrioventricular bundle, atrioventricular node, and distal atrioventricular bundle are distinct anatomic structures with unique histological characteristics and innervation. Circulation 101:1049–1059
3. Furman S (1995) A brief history of cardiac stimulation and electrophysiology – the past fifty years and the next century. NASPE Keynote Address
4. Boyett D, Dobrzynski H (2007) The sinoatrial node is still setting the pace 100 years after its discovery. Circ Res 100:1543–1545
5. His W Jr (1893) Die Tatigkeit des embryonalen herzens und deren bedcutung fur die lehre von der herzbewegung beim erwachsenen. Artbeiten aus der Medizinischen Klinik zu Leipzig 1:14–49
6. Tawara S (1906) Das Reizleitungssystem des Saugetierherzens: Eine anatomisch-histologische Studie uber das Atrioventrikularbundel und die Purkinjeschen Faden. Gustav Fischer, Jena, pp 9–70, 114–156

7. Conti AA, Giaccardi M, Yen Ho S, Padeletti L (2006) Koch and the "ultimum moriens" theory – the last part to die of the heart. J Interv Card Electrophysiol 15:69–70
8. Koch WK (1922) Der funktionelle bau des menschlichen herzen. Urban und Schwarzenberg, Berlin and Vienna
9. Sorensen ER, Manna D, McCourt K (1994) Use of epicardial pacing wires after coronary artery bypass surgery. Heart Lung 23:487–492
10. Villain E, Ouarda F, Beyler C, Sidi D, Abid F (2003) Predictive factors for late complete atrioventricular block after surgical treatment for congenital cardiopathy. Arch Mal Coeur Vaiss 96:495–498
11. Bae EJ, Lee JY, Noh CI, Kim WH, Kim YJ (2003) Sinus node dysfunction after Fontan modifications—influence of surgical method. Int J Cardiol 88:285–291
12. Hussain A, Malik A, Jalal A, Rehman M (2002) Abnormalities of conduction after total correction of Fallot's Tetralogy: a prospective study. J Pak Med Assoc 52:77–82
13. Bruckheimer E, Berul CI, Kopf GS et al (2002) Late recovery of surgically-induced atrioventricular block in patients with congenital heart disease. J Interv Card Electrophysiol 6:191–195
14. Ghosh PK, Singh H, Bidwai PS (1989) Complete A-V block and phrenic paralysis complicating surgical closure of ventricular septal defect-A case report. Indian Heart J 41:335–337
15. Hill SL, Berul CI, Patel HT, Rhodes J, Supran SE, Cao QL, Hijazi ZM (2000) Early ECG abnormalities associated with transcatheter closure of atrial septal defects using the Amplatzer Septal Occluder. J Interv Card Electrophysiol 4:469–474
16. Deshmukh P, Casavant DA, Romanyshyn M, Anderson K (2000) Permanent direct His-bundle pacing: a novel approach to cardiac pacing in patients with normal His-Purkinje activation. Circulation 101:869–877
17. Karpawich P, Gates J, Stokes K (1992) Septal His-Purkinje ventricular pacing in canines: a new endocardial electrode approach. Pacing Clin Electrophysiol 15:2011–2015
18. Karpawich PP, Gillette PC, Lewis RM, Zinner A, McNamera DG (1983) Chronic epicardial His bundle recordings in awake nonsedated dogs: a new method. Am Heart J 105:16–21
19. Scheinman MM, Saxon LA (2000) Long-term His-bundle pacing and cardiac function. Circulation 101:836–837
20. Williams DO, Sherlag BJ, Hope RR, El-Sherif N, Lazzara R, Samet P (1976) Selective versus non-selective His bundle pacing. Cardiovasc Res 10:91–100
21. Karpawich PP, Rabah R, Haas JE (1999) Altered cardiac histology following apical right ventricular pacing in patients with congenital atrioventricular block. Pacing Clin Electrophysiol 22:1372–1377
22. de Cock CC, Giudici MC, Twisk JW (2003) Comparison of the haemodynamic effects of right ventricular outflow-tract pacing with right ventricular apex pacing: a quantitative review. Europace 5:275–278
23. Cleland JG, Daubert JC, Erdmann E et al (2001) The CARE-HF study (CArdiac REsynchronisation in Heart Failure study): rationale, design and end-points. Eur J Heart Fail 3:481–489
24. Leclercq C, Daubert JC (2003) Cardiac resynchronization therapy is an important advance in the management of congestive heart failure. J Cardiovasc Electrophysiol 14:S27–S29
25. Rosen MR (2014) Gene therapy and biological pacing. N Engl J Med 371:1158–1159
26. Nattel S, Khairy P, Roy D et al (2002) New approaches to atrial fibrillation management: a critical review of a rapidly evolving field. Drugs 62:2377–2397
27. Takahashi Y, Yoshito I, Takahashi A et al (2003) AV nodal ablation and pacemaker implantation improves hemodynamic function in atrial fibrillation. Pacing Clin Electrophysiol 26:1212–1217
28. Bernat R, Pfeiffer D (2003) Long-term Rand learning curve for radio frequency ablation of accessory pathways. Coll Antropol 27:83–91
29. Gaita F, Riccardi R, Gallotti R (2002) Surgical approaches to atrial fibrillation. Card Electrophysiol Rev 6:401–405
30. Betts TR, Roberts PR, Ho SY, Morgan JM (2003) High density mapping of shifts in the site of earliest depolarization during sinus rhythm and sinus tachycardia. Pacing Clin Electrophysiol 26:874–882
31. Boineau JB, Schuessler RB, Hackel DB et al (1980) Widespread distribution and rate differentiation of the atrial pacemaker complex. Am J Physiol 239:H406–H415
32. Boineau JB, Schuessler RB, Mooney CR (1978) Multicentric origin of the atrial depolarization wave: the pacemaker complex. Relation to the dynamics of atrial conduction, P-wave changes and heart rate control. Circulation 58:1036–1048
33. Lee RJ, Kalman JM, Fitzpatrick AP et al (1995) Radiofrequency catheter modification of the sinus node for 'inappropriate' sinus tachycardia. Circulation 92:2919–2928
34. Tranum-Jensen J (1976) The fine structure of the atrial and atrioventricular (AV) junctional specialized tissues of the rabbit heart. In: Wellens HJJ, Lie KI, Janse MJ (eds) The conduction system of the heart: structure, function, and clinical implications. Lea & Febiger, Philadelphia, pp 55–81
35. Waller BF, Gering LE, Branyas NA, Slack JD (1993) Anatomy, histology, and pathology of the cardiac conduction system: Part I. Clin Cardiol 16:249–252
36. Boyett MR, Honjo H, Kodama I et al (2007) The sinoatrial node: cell size does matter. Circ Res 101:e81–e82
37. Garson AJ, Bricker JT, Fisher DJ, Neish SR (eds) (1998) The science and practice of pediatric cardiology, vol I. Williams & Williams, Baltimore, pp 141–143
38. Hucker WJ, Fedorov VV, Foyil KV, Moazami N, Efimov IR (2008) Optical mapping of the human atrioventricular junction. Circulation 117:1474–1477
39. Li JL, Greener ID, Inada S et al (2008) Computer three-dimensional reconstruction of the atrioventricular node. Circ Res 102:975–985
40. Becker AE, Anderson RH (1976) The morphology of the human atrioventricular junctional area. In: Wellens HJJ, Lie KI, Janse MJ (eds) The conduction system of the heart: structure, function, and clinical implications. Lea & Febiger, Philadelphia, pp 263–286
41. Aschoff L (1910) Referat uber die herzstorungen in ihren bezeihungen zu den spezifischen muskelsystem des herzens. Verh Dtsch Ges Pathol 14:3–35
42. Monckeberg JG (1910) Beitrage zur normalen und pathologischen anatomie des herzens. Verh Dtsch Ges Pathol 14:64–71
43. Hucker WJ, McCain ML, Laughner JI, Iaizzo PA, Efimov IR (2008) Connexin 43 expression delineates two discrete pathways in the human atrioventricular junction. Anat Rec 291:204–215
44. Davis LM, Rodefeld ME, Green K, Beyer EC, Saffitz JE (1995) Gap junction protein phenotypes of the human heart and conduction system. J Cardiovasc Electrophysiol 6:813–822
45. Zhang Y, Bharati S, Mowrey KA, Shaowei Z, Tchou PJ, Mazgalev TN (2001) His electrogram alternans reveal dual-wavefront inputs into and longitudinal dissociation within the bundle of His. Circulation 104:832–838
46. Bharati S, Levine M, Huang SK et al (1991) The conduction system of the swine heart. Chest 100:207–212
47. Anderson RH, Becker AE, Brechenmacher C, Davies MJ, Rossi L (1975) The human atrioventricular junctional area. A morphological study of the A-V node and bundle. Eur J Cardiol 3:11–25
48. Frink RJ, Merrick B (1974) The sheep heart: coronary and conduction system anatomy with special reference to the presence of an os cordis. Anat Rec 179:189–200
49. El-Sherif N, Lekieffre J (1997) Practical management of cardiac arrhythmias. Futura Publishing Co., Armonk, p 348
50. Shrivastav M, Iaizzo P (2007) Discrimination of ischemia and normal sinus rhythm for cardiac signals using a modified k means clustering algorithm. Conf Proc IEEE Eng Med Biol Soc, 3856–3859
51. Webster JG (2004) Bioinstrumentation. Wiley, Hoboken, p 383

52. Shrivastav M (1999) Methods of ambulatory detection and treatment of cardiac arrhythmias using implantable cardioverter-defibrillators. Biomed Instrum Technol 33:505–521
53. Webster JG (ed) (1995) Design of cardiac pacemakers. IEEE Press, Piscataway
54. Sahakian AV, Peterson MS, Shkurovich S et al (2001) A simultaneous multichannel monophasic action potential electrode array for in vivo epicardial repolarization mapping. IEEE Trans Biomed Eng 48:345–353
55. Shenasa M, Borggrefe M, Breithardt G (eds) (2003) Cardiac mapping, 2nd edn. Futura, New York, p 784
56. Shrivastav M, Iaizzo PA (2006) In vivo cardiac monophasic action potential recording using electromyogram needles. In: Proceedings of the IEEE biomedical circuits and systems conference, London
57. Schilling RJ, Kadish AH, Peters NS, Goldberger J, Davies DW (2000) Endocardial mapping of atrial fibrillation in the human right atrium using a non-contact catheter. Eur Heart J 21:550–564
58. Becker AE, Anderson RH (2001) Proximal atrioventricular bundle, atrioventricular node, and distal atrioventricular bundle are distinct anatomic structures with unique histological characteristics and innervation – response. Circulation 103:e30–e31
59. Bharati S (2001) Anatomy of the atrioventricular conduction system – response. Circulation 103:e63–e64
60. Magalev TN, Ho SY, Anderson RH (2001) Special Report: Anatomic-electrophysiological correlations concerning the pathways for atrioventricular conduction. Circulation 103:2660–2667
61. Kucera JP, Rudy Y (2001) Mechanistic insights into very slow conduction in branching cardiac tissue – a model study. Circulation Res 89:799–806
62. Zarzoso M, Rysevaite K, Milstein ML et al (2013) Nerves projecting from the intrinsic cardiac ganglia of the pulmonary veins modulate sinoatrial node pacemaker function. Cardiovasc Res 99:566–575
63. Hinescu ME, Popescu LM (2005) Interstitial Cajal-like cells (ICLC) in human atrial myocardium. J Cell Mol Med 9:972–975
64. Kostin S (2010) Myocardial telocytes: a specific new cellular entity. J Cell Mol Med 14:1917–1921
65. Gherghiceanu M, Popescu LM (2012) Cardiac telocytes – their junctions and functional implications. Cell Tissue Res 348:265–279
66. Cretoiu SM, Popescu LM (2014) Telocytes revisited. Biomol Concepts 5:353–369
67. Iaizzo PA, Laske TG (2010) Anatomy and physiology of the cardiac conduction system. In: Sigg DC, Iaizzo PA (eds) Cardiac electrophysiology methods and models. Springer, New York, pp 73–90
68. Dobrzynski H, Anderson RH, Atkinson A et al (2013) Structure, function and clinical relevance of the cardiac conduction system, including the atrioventricular ring and outflow tract tissues. Pharmacol Ther 139:260–288
69. Anderson RH, Boyett MR, Dobrzynski H, Moorman AF (2013) The anatomy of the conduction system: implications for the clinical cardiologist. J Cardiovasc Transl Res 6:187–196

Further Reading

Mohrman DE, Heller LJ (eds) (2003) Cardiovascular physiology, 5th edn. Langer Medical Books/McGraw-Hill, New York

Wellens HJJ, Lie KI, Janse MJ (eds) (1976) The conduction system of the heart: structure, function, and clinical implications. Lea & Febiger, Philadelphia

Alexander RW, Schlant RC, Fuster V (eds) (1998) Hurst's the heart: arteries and veins, 9th edn. McGraw-Hill, New York

Katz AM (ed) (2001) Physiology of the heart, 3rd edn. Lippincott, Williams, and Wilkins, Philadelphia

Tortora GJ, Grabowski SR (eds) (2000) Principles of anatomy and physiology, 9th edn. Wiley, New York

Autonomic Nervous System

14

Paul A. Iaizzo and Kevin Fitzgerald

Abstract

The autonomic nervous system and the role it plays in governing the behavior of the cardiovascular system are significant in both its complexity and importance for one's quality of life. The hypothalamus is the brain center which governs all essential "homeostatic" functions of the human body; these integrative functions include control over the autonomic nervous system, various somatic pathways, and the body's hormonal systems. The autonomic nervous system can be considered to have two subdivisions that are considered somewhat antagonistic but also function in a complementary nature; simultaneous changes within the parasympathetic and sympathetic branches of this system allow for rapid and essential changes in cardiac parameters such as heart rate, contractility, and/or stroke volume. Increased sympathetic outflow relative to normal resting conditions most often causes an excitatory response in physiologic parameters (such as increases in heart rate and/or smooth muscle contraction), whereas parasympathetic stimulation usually results in calming adjustments (lower heart rates, decreased contractility, and/or vasodilatation). Alterations of the cardiac and aortic baroreceptors, as well as the autonomic nerves that innervate the heart, are important to consider in many disease states.

Keywords

Sympathetic anatomy • Parasympathetic anatomy • Baroreceptors • Homeostasis • Hypothalamic control • Effector pathways • Heart rate • Stroke volume • Contractility • Arteriolar pressure • Cardiac denervation

14.1 Introduction

The autonomic nervous system coordinates the involuntary control of the viscera and other tissues throughout the body, with the primary exception of skeletal muscle. The hypothalamus is the brain center which governs all essential *homeostatic* functions of the human body; these integrative functions include control over the autonomic nervous system, various somatic pathways, and the body's hormonal systems. Briefly, h*omeostasis* can be defined as the control of the internal milieu, which in general is kept nearly constant within quite narrow limits, despite potential severe perturbations that human bodies can experience (e.g., extreme hot and cold temperatures). The hypothalamus is a small part of the brain considered as a neuronal continuum extending from the midbrain through to the basal regions of the telencephalon. Further, the lateral hypothalamus can be thought to be reciprocally connected with the upper brainstem and the limbic system (these are the brain centers which control emotions, learning, etc.). As such, it receives primary sensory inputs from afferents near the body surface and from internal structures via the ascending spinobulboreticular pathways.

P.A. Iaizzo, PhD (✉)
Department of Surgery, University of Minnesota,
420 Delaware St. SE, B172 Mayo, Minneapolis, MN 55455, USA
e-mail: iaizz001@umn.edu

K. Fitzgerald, MS
Medtronic, Inc., Minneapolis, MN, USA

P.A. Iaizzo (ed.), *Handbook of Cardiac Anatomy, Physiology, and Devices*, DOI 10.1007/978-3-319-19464-6_14

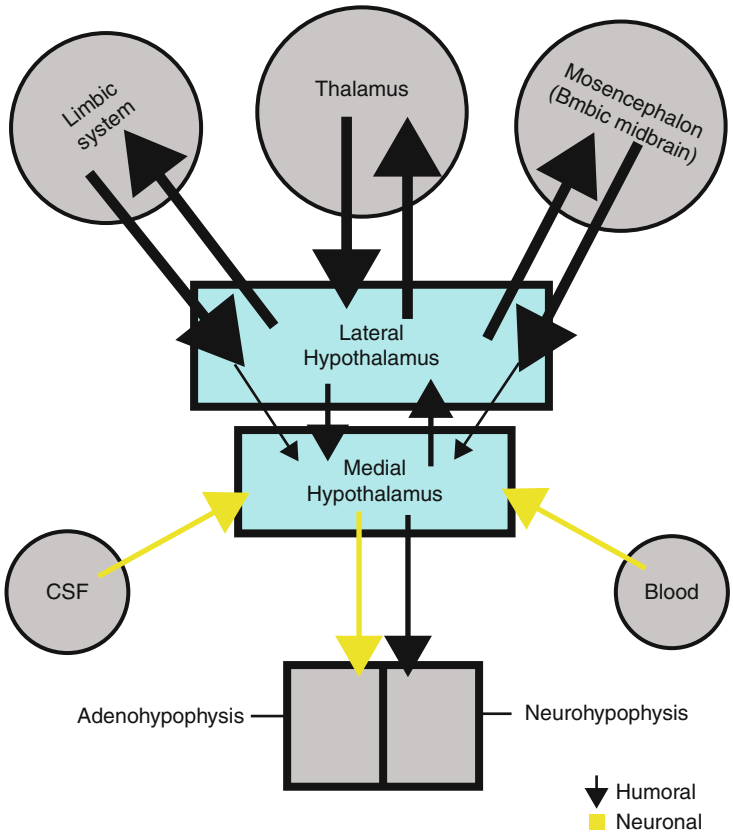

Fig. 14.1 General afferent and efferent pathways/ connections of the hypothalamus (medial and lateral), the pituitary gland (adeno- and neurohypophysis), the limbic system, the thalamus, and the mesencephalon. Note the medial hypothalamus, via the neuroendocrine interface, controls the primary functions of the pituitary gland

In contrast, the medial hypothalamus receives main inputs from the lateral hypothalamic regions. This brain region of the hypothalamus contains specialized neurons important for sensing the conditions of the blood and cerebrospinal fluid. In turn the medial hypothalamus makes numerous connections to the pituitary (hypophysis) and there are two main types: (1) neuronal connections to the neurohypophysis (axonal) and (2) hormonal releases affecting the adenohypophysis (anterior region). Thus, these multimodal connections are referred to as a *neuroendocrine interface* (Fig. 14.1). Also known as the hypothalamo-pituitary system, the activity of most endocrine glands is regulated by hormones from the adenohypophysis (anterior pituitary). The hypothalamus releases both stimulating and inhibitory-releasing hormones. It should be noted that there is a built-in, multilevel, negative feedback system (via blood concentrations).

The tight control of homeostatic functions that are modulated via the hormone system is accomplished by a multilevel, multi-hormone feedback mechanism. For example, the blood levels of releasing hormones and the released hormones can both be sensed within the medial hypothalamus (Fig. 14.2). Interestingly, electrical stimulation of nearly any region in the hypothalamus is likely to cause a cardiovascular response (change in activity). The hypothalamic effects on this system are mediated through both synergistic parasympathetic and sympathetic pathways. Additionally, afferent inputs for this control are many and include those from baro-, chemo-, and mechanoreceptors in the atria, ventricles, aorta, and elsewhere (see below).

In other words, the hypothalamus controls the autonomic nervous system which is organized into parasympathetic and sympathetic subdivisions and integrates efferent and afferent fibers that regulate the activities of the majority of organs (including the heart), glands, and smooth musculature found in the human body. The presynaptic cell bodies of these neurons originate in the gray matter of the spinal column but are classified by fundamental differences. Anatomically, the origin of the sympathetic (thoracolumbar) division of the central nervous system lies between the first thoracic (T1) and the second or third lumbar section (L2 or L3). In contrast, the exiting fibers of the parasympathetic division (craniosacral) originate from both the medulla oblongata and sacral portion of the spinal cord (S2–S4). The primary neurotransmitter released during depolarization is another means of characterizing these two subdivisions of the autonomic nervous system. In the sympathetic branch, norepinephrine is the principal postsynaptic neurotransmitter, whereas acetylcholine is the chief neurotransmitter found throughout the parasympathetic fibers. The primary physiological response induced by each respective neurotransmitter is also a useful way to categorize the divisions of the autonomic nervous system. Such

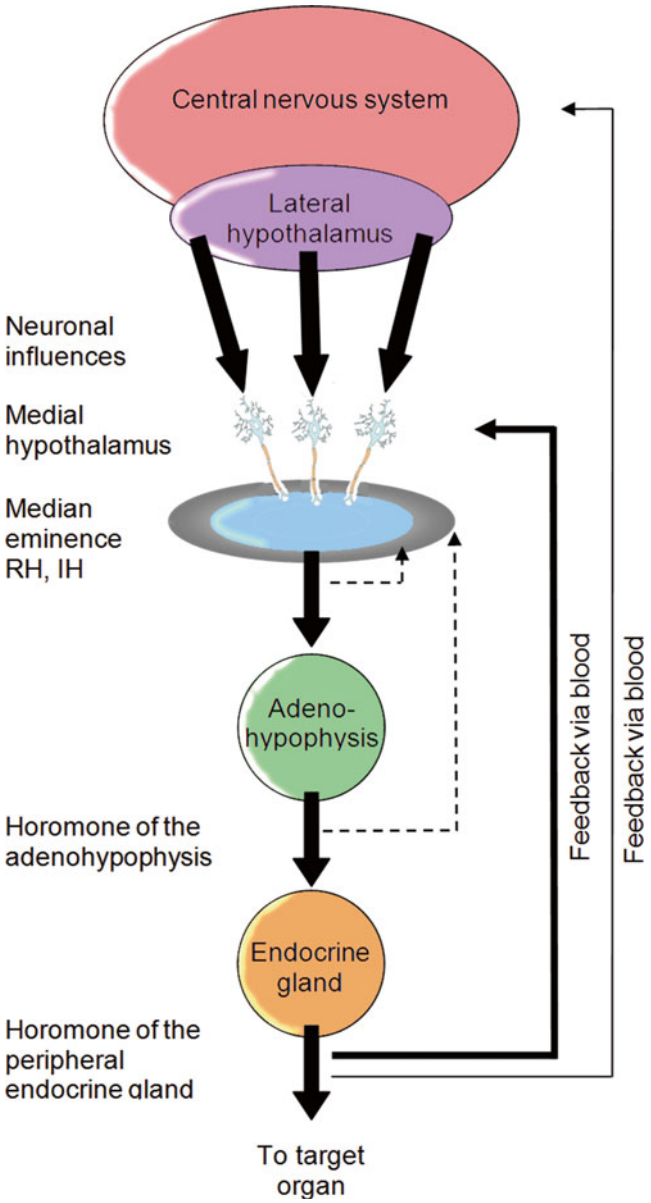

Fig. 14.2 Multilevel feedback loops are employed to regulate both hormone levels and neural responses. For example, the medial hypothalamus can sense blood levels of releasing hormones, the hormone levels released by the pituitary gland, and also those released by target endocrine glands

classifications are important considerations when investigating the autonomic nervous system regulation of the heart.

14.2 Sympathetic Anatomy

Cell bodies of presynaptic sympathetic efferent neurons are found in the paired lateral horns of the spinal cord, an area identifiable between the T1 and L2 or L3 vertebrae. The axons of these cells exit the interior of the spinal cord through ventral rootlets, which coalesce to form the larger ventral roots and eventually become ventral rami. Sympathetic fibers almost immediately divert into white rami communicantes (Fig. 14.3) branching from these spinal nerves, which connect them to paired columns of sympathetic ganglia located on either side of the spinal cord called the *sympathetic trunks*. Vertebrae from T1 to S5 have corresponding pairs of ganglia, each of which are interconnected with both ascending and descending nerve fibers, forming the complex column-like structures; these structures allow for rapid, coordinated, multi-segmental control of the cardiovascular system.

Preganglionic sympathetic neurons synapse within the ganglia of the sympathetic trunk. The 10–20 nm separation distance [1] between presynaptic and postsynaptic cells is called the synaptic cleft, where neurotransmitter is released from synaptic vesicles. Note that acetylcholine is the neurotransmitter released from preganglionic neurons in both the sympathetic and parasympathetic branches of the autonomic nervous system (Fig. 14.4). This compound binds to receptors on postsynaptic cell bodies, causing localized depolarization of cell membranes, which may subsequently initiate action potentials that propagate down the axons of postsynaptic cells. In the sympathetic nervous system, norepinephrine is the primary postsynaptic neurotransmitter released. Such junctions can also be activated by epinephrine, and both can often be found with cotransmitters such as dopamine [2] and/or histamine [3]. Both norepinephrine and epinephrine play important roles during sympathetic stimulation of the heart, as will be discussed in later portions of this chapter.

Three primary paths of travel are commonly identified for presynaptic (also referred to as *preganglionic*) nerve fibers upon reaching the sympathetic trunk. A preganglionic fiber can immediately synapse on the cell body of a postganglionic fiber at the level of the trunk upon which the fiber entered. Preganglionic fibers can also follow a route that traverses through the sympathetic trunk, either ascending or descending to synapse within a higher- or lower-level ganglion. A third but less common path of travel for presynaptic neurons involves passing through the sympathetic trunk completely, then synapsing within a prevertebral ganglion in close proximity to the viscera innervated. In general, presynaptic fibers traveling to the head, neck, thoracic cavity, and limbs will follow one of the first two courses. Innervation of organs and glands located in the abdominopelvic cavity follow the third path through prevertebral ganglia (Fig. 14.3).

A variation of the second path discussed above occurs primarily with innervation of sweat glands, hair follicles, and peripheral arteries. Presynaptic nerves that arrive at the paired sympathetic ganglion, as discussed previously, traverse through the white rami communicantes. Rather than immediately continuing to peripheral regions of the body after synapsing, the postsynaptic neurons next travel through gray (unmyelinated) rami (Fig. 14.3) and exit along large bundles of nerve fibers called *primary rami*. From the pri-

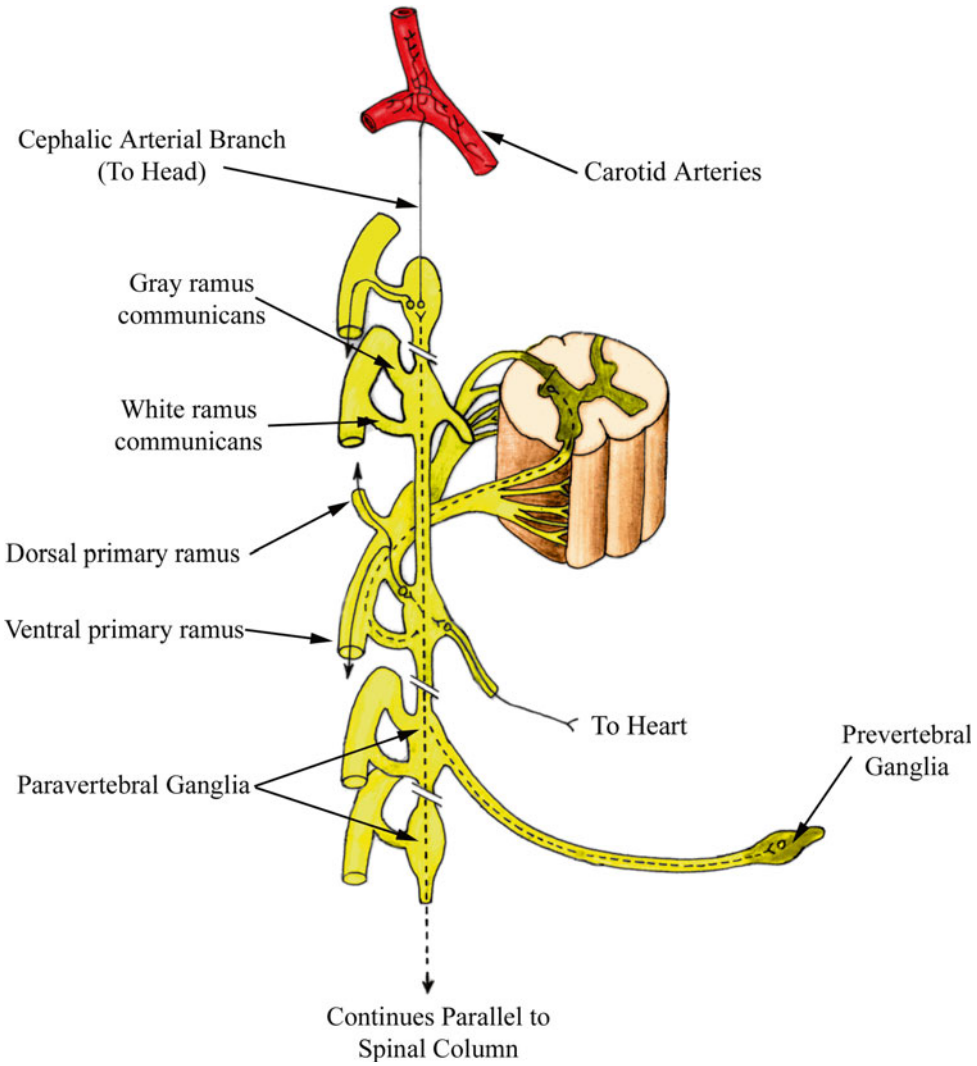

Fig. 14.3 Pathways of sympathetic motor fibers. The three potential paths of travel taken by presynaptic sympathetic motor fibers are shown. Preganglionic fibers traveling to the heart and other areas of the thoracic cavity synapse either immediately upon reaching the sympathetic trunk or traverse to other spinal levels to synapse. Complete passage through the paired trunks also occurs with prevertebral ganglia. Modified from Moore and Dalley [1]

mary rami, smaller nerve branches bifurcate and act to control the vasculature (either vasodilatation or vasoconstriction), hair follicle stimulation, and/or sweating. If the nerves are destined for the head, their cell bodies are located in the superior cervical ganglion and their axons follow the path of the carotid arteries to their respective destinations; the muscles of the eye are also innervated by this collection of sympathetic neurons.

Nerve fibers traveling from the central nervous system to a destination elsewhere in the body are termed *efferents*. In contrast, *afferents* carry sensory information from various locations in the body to the central nervous system. Frequently, these respective paths of travel occur in parallel but the flow of excitation is in the opposite direction; these fibers are typically bunched closely together to form larger nerve branches. The main nerve branches controlling the sympathetic behavior of the heart and lungs are the cardiopulmonary splanchnic nerves, which consist of both efferent and afferent fibers. Efferent nerves navigate a route originating from the ganglia in the upper cervical region (superior, middle, and inferior cervical ganglia) and the upper thoracic (T1–T5) levels of the sympathetic trunk. The inferior, middle, and superior cardiac nerves, in turn, originate from corresponding cervical ganglia and approach the base of the heart before splitting into smaller nerves and distributing themselves throughout much of the myocardium and vasculature. The cardiac plexus can be considered as groupings of the nerve bundles destined to and originating from the heart (Fig. 14.4); they are extremely difficult to visualize with the naked eye.

Incoming postsynaptic sympathetic neurons, which innervate the human heart, are highly concentrated around and near the aortic arch. Some of this innervation occurs throughout the aortic arch itself, as well as at the base of the ascending portion of this vessel. Many branches from these nerves continue down the aorta or under the arch to the pulmonary trunk, where they again diverge and track with the

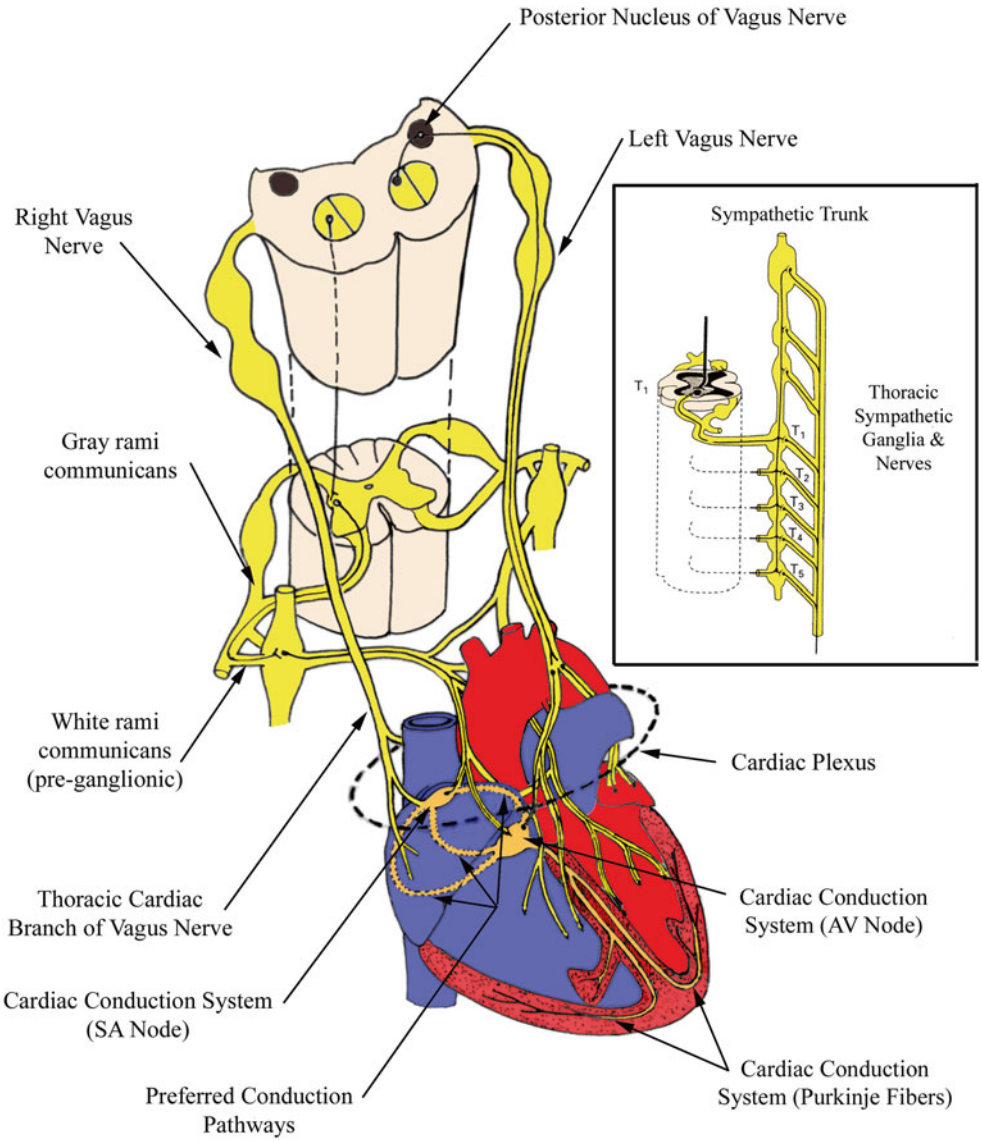

Fig. 14.4 Autonomic innervation of the heart. Vagal innervation of the right atrium can be observed. The area where many axons congregate just prior to innervation of the heart is depicted as the cardiac plexus. Sympathetic fibers branching from an arbitrary vertebral level of the paired sympathetic trunks is also illustrated. *AV* atrioventricular, *SA* sinoatrial. Modified from Martini [4]

pulmonary arteries. Still more neuronal bifurcations have been identified which extend to reach other areas of the heart, including both atria and the right and left ventricles. Sympathetic innervation of both the sinoatrial and atrioventricular nodes is important for control of heart rate, but has not been distinguished in greater concentration at these areas relative to elsewhere in the atria [5, 6]. Such nerves have been identified epicardially, often following the path of the coronary arteries and veins [5, 7]. In general, sympathetic innervation is more highly concentrated in the ventricles than in the atria [8]. Within the ventricles, a higher distribution is observed toward the base of the heart as opposed to the apex, with nerves in the epicardium at a slightly greater concentration than in the endocardium. This latter tendency is also evident in the atria [8].

14.3 Adrenal Medulla

The sympathetic nervous system also controls the hormonal secretions of the paired suprarenal (adrenal) glands lying within the abdomen, considered as components of the endocrine system. Specifically, preganglionic fibers, with their cell bodies located in the lower thoracic (T10–T12) segments of the spinal cord, travel to the adrenal medulla by means of the abdominopelvic splanchnic nerves. It is in the medulla, or central portions of these suprarenal glands, that both norepinephrine and epinephrine are released into the bloodstream [1]. The release of these *catecholamines* into the blood is considered a postsynaptic response initiated from this type of sympathetic

activation. Specifically, the cortex surrounding the medulla portions of the adrenal glands are responsible for producing multiple steroid hormones. As blood drains from the highly vascularized cortex to the medulla, the aforementioned hormones can be used to convert norepinephrine to epinephrine. The respective mechanisms of action for these two similarly structured catecholamines will be discussed later in this chapter.

14.4 Parasympathetic Anatomy

The parasympathetic (craniosacral) nervous system branches from four paired cranial nerves and the lower sacral segment of the spinal cord (S2–S4). The vagus nerve (cranial nerve X) is the main effector pathway for modulating cardiac function, i.e., controlled by input from the parasympathetic subdivision of the autonomic nervous system (Fig. 14.4). Efferent fibers of the vagus nerves originate in the medulla oblongata and weave through the neck alongside the carotid arteries to the thoracic and abdominopelvic cavities, bifurcating many times along the way to innervate an assortment of organs including the heart. More specifically, the efferent fibers of the cranial parasympathetic branch communicate with blood vessels of the head and other viscera; the sacral portion of the spinal cord innervates viscera of the lower abdominopelvic cavity like the urinary bladder and colon, as well as their respective blood vessels.

Unlike the short sympathetic preganglionic fibers, the parasympathetic division of the autonomic nervous system generally has very long preganglionic fibers and short postsynaptic fibers. Hence, the parasympathetic ganglia are often located very proximal to, or actually within, the target organ. As discussed previously, acetylcholine is this branch of the autonomic nervous system and is the primary neurotransmitter released at both preganglionic and postganglionic junctions.

Within the heart, the majority of the parasympathetic ganglia are located near the sinoatrial node and within the conduction tissue surrounding the atrioventricular node [5]. Consequently, the right and left vagus nerves envelope a large and overlapping portion of the atria, where short postsynaptic fibers from both branches act on the conduction centers of the heart (Fig. 14.4). However, the endings of the right vagus primarily innervate the sinoatrial nodal region, while a great number of projections from the left are typically observed innervating the atrioventricular node [5]. In fact, high concentrations of vagal innervation situated within a localized region of epicardial fat near the atrioventricular node have been described for the human heart, and it is hypothesized that nerves located within this "pad" have little effect on behavior of the sinoatrial node [9]. Thus, it is likely that each region is controlled independently of the other. Parasympathetic junctions are also observed in the ventricles, but only at one-half to one-sixth as frequently as sympathetic innervation [8]. Nevertheless, nerves of the parasympathetic division of the autonomic nervous system outnumber those of the sympathetic division in the atria by some 30–60 % [8]. Interestingly, while sympathetic innervation has been described to occur at approximately an equal distribution between the endocardial and epicardial surfaces of the heart, vagal nerve endings are reportedly located at almost twice the density (1.7–1) transmurally (within the myocardium) when compared with their epicardial distribution [8].

14.5 Baroreceptors

The autonomic nervous system plays a vital role in the overall regulation of blood pressure within the human body. Specialized receptors sensitive to changes in arterial diameter are located at various strategic locations within the upper thoracic cavity and neck; these nerve clusters are commonly known as *arterial baroreceptors*. Substantial groupings of such baroreceptors can be found at the arch of the aorta and on the internal carotid arteries (just distal to where the common carotid bifurcates). This focal density of carotid baroreceptors is also referred to as a *carotid sinus*. The majority of receptors are located at areas within these arteries where the walls decrease in thickness, enabling pressure changes to be somewhat magnified at these locations (Fig. 14.5). Under even minimal pressure increases, these large arteries will elicit detectable wall dilatations. In contrast, under decreased pressure, their internal diameters will decline, also resulting in changes of the firing frequencies of these receptors. The axons of these afferent neurons travel from baroreceptors along parasympathetic corridors to the medullary cardiovascular center in the brainstem. Under increases in the mean pressure detected by these arterial baroreceptors, efferent sympathetic stimulation will decrease, which is accompanied by an increase in parasympathetic outflow to the heart. This neural activity is intended to return the mean blood pressure to a normal state. The opposite autonomic response would commence if the mean arterial pressure at the baroreceptor locations decreased. The synergistic functioning, briefly noted here between both divisions of the autonomic nervous system, will be discussed in much greater detail in the following sections. It should be noted that the direct application of pressure to an individual's neck at the site of the carotid sinus can induce a reflex decrease in blood pressure, even to the point of causing unconsciousness, i.e., the so-called *sleeper hold*.

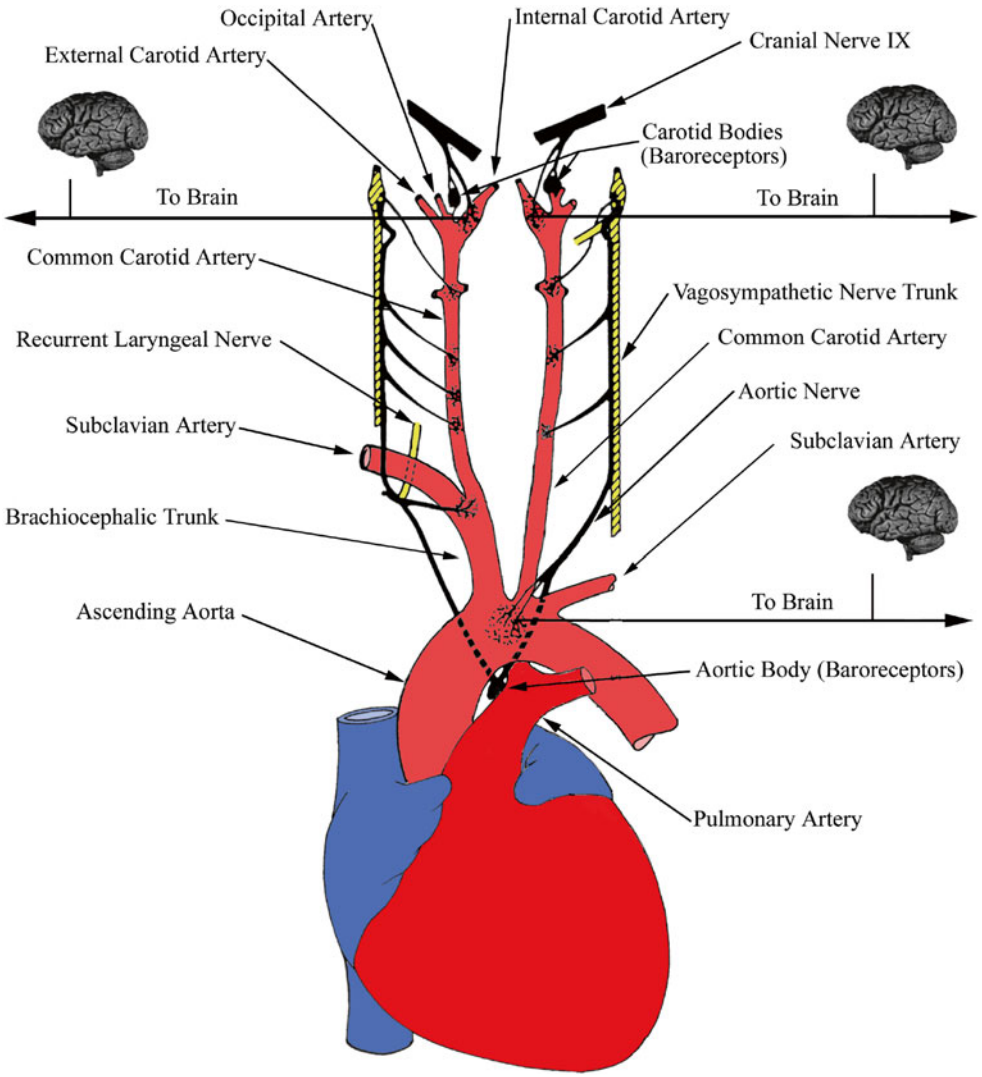

Fig. 14.5 Arterial baroreceptors. Receptors located at the bifurcations of the carotid arteries and aortic arch convey information to the brain and vasculature to help regulate pressure fluctuations. Modified from Mountcastle [10]

14.6 Homeostasis

The tendency to maintain the internal environment of the body at a relatively constant level is known as *homeostasis*. The heart itself exerts perhaps the greatest control on countless parameters involving the circulation of blood throughout the body. The heart communicates with the central nervous system via both branches of the autonomic nervous system. Both the sympathetic and parasympathetic divisions work together in synergistic control of their antagonistic influences, in order to prevent potentially harmful fluctuations in many vital bodily functions. While it is obvious that significant changes do occur, an array of physiologic responses involving the heart (homeostatic control mechanisms) mediated by the autonomic nervous system quickly reverses these changes to return within the reasonable ranges required to maintain overall health. In general, homeostatic control functions are the underlying determinants of the relative degrees of both parasympathetic and sympathetic activation.

14.7 Hypothalamic Control

More specifically, the autonomic control of the heart is greatly influenced by activity within the portion of the brain known as the *hypothalamus*. Afferent fibers from the brainstem (medulla oblongata) and spinal cord convey information via the autonomic afferent system to the hypothalamic nuclei within the central nervous system [11], whereas impulses that leave the hypothalamus travel along efferent fibers to the various sympathetic and parasympathetic ganglia as noted above. Most parasympathetic response signals have been determined to originate from the anterior portions of the hypothalamus, while sympathetic activity stems primarily from the posterior portions [6, 11]. Direct electrical stimulation of specific sites within the hypothalamus can initiate preprogrammed, simultaneous, patterned changes in heart rate, blood pressure, and peripheral resistance [5] (Fig. 14.6).

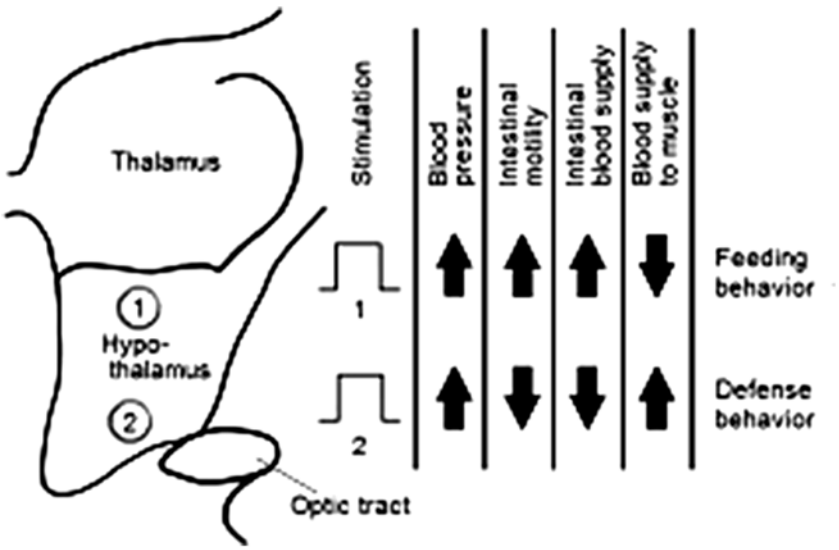

Fig. 14.6 The body's cardiovascular responses are more or less under involuntary control and are thus regulated by the autonomic nervous system (ANS). For example, stimulation of any region of the medial hypothalamus will induce characteristic changes in cardiovascular responses. These patterned responses are commonly associated with innate behavior responses that are also attributed to the hypothalamus, such as feeding or defensive behaviors, which in turn appropriately modulate other body systems under ANS control

As noted above, afferent axons from the aortic and carotid baroreceptors principally travel to the medullary cardiovascular centers, with neural pathways continuing onward to the hypothalamus [6]. Temperature regulation of the body is also centered within the hypothalamus. Thus, during exposure to cold, the hypothalamus initiates appropriate autonomic responses to maintain body temperature, such as vasoconstriction and shivering. The contraction of the peripheral vasculature motivates a redistribution of blood flow to vital organs like the heart and brain, in order to maintain their suitable function [2]. The shiver reflex induced by the hypothalamus increases heat production which, in turn, causes additional adjustments in blood flow and cardiac activity. The opposite outcome occurs during exposure to high degrees of heat, such that sweating is initiated via postganglionic sympathetic neurons and vasodilation of the vasculature supplying the skin is amplified. The regulation of bodily processes is an important responsibility of the hypothalamus, and it performs such tasks via the autonomic pathways, hence regulating countless systems within the body simultaneously. Keeping this relative state of constancy throughout the body regardless of extreme external changes is referred to as *homeostasis*; in nearly all cases, there are direct effects on cardiac performance.

In addition to the influence the hypothalamus has on autonomic pathways, emotional and hormonal changes are controlled in this region of the brain in order to promote homeostasis. The pituitary gland function is also mediated by the hypothalamus, initiating or suppressing hormonal release from this important part of the endocrine system to the rest of the body. Some of these hormones act as cotransmitters in the presence of acetylcholine or norepinephrine during synapses eliciting parasympathetic or sympathetic activity [2], dopamine being one example.

14.8 Effector Pathways to the Heart

Within the myocardium, parasympathetic nerve fibers release acetylcholine upon stimulation. Cardiac cells contain muscarinic receptors embedded within their lipid bilayer, which can activate G proteins found in their cytoplasm upon binding with acetylcholine. Activation occurs when a bound GDP (guanosine diphosphate) molecule is replaced by a GTP (guanosine triphosphate) structure. Subsequently, this response allows the altered protein to bind with potassium channels in the membrane and causes them to open, thus increasing potassium permeability (Fig. 14.7). As a result, heart rate will generally decrease due to an efflux of potassium ions (K^+) from cardiac cells, since the cellular membrane becomes more polarized as the potential moves closer to the K^+ equilibrium potential of −90 mV [6]. This hyperpolarization makes the spontaneous generation of action potentials more difficult and thus slows the rate of firing of the sinoatrial node. Activated G proteins will remain in such a state until GTP is hydrolyzed to form inactive GDP [2, 12].

The type of regulatory control in the case described above involves the direct opening of K^+ channels via G proteins within a cardiac muscle cell. It should also be noted that indirect opening of potassium channels may also occur after acetylcholine binds to the muscarinic receptors. Furthermore, activated G proteins may also cause some increase in the production of arachidonic acid, which acts as a secondary messenger that can result in increased K^+ permeability due to cleavage of membrane lipids [12].

Modulation of G proteins is also an important aspect of the underlying sympathetic effects on cardiac behavior. Sympathetic fibers release norepinephrine at postsynaptic terminals of cardiac muscle cells, and receptors located within the cellular membrane bind with the norepinephrine

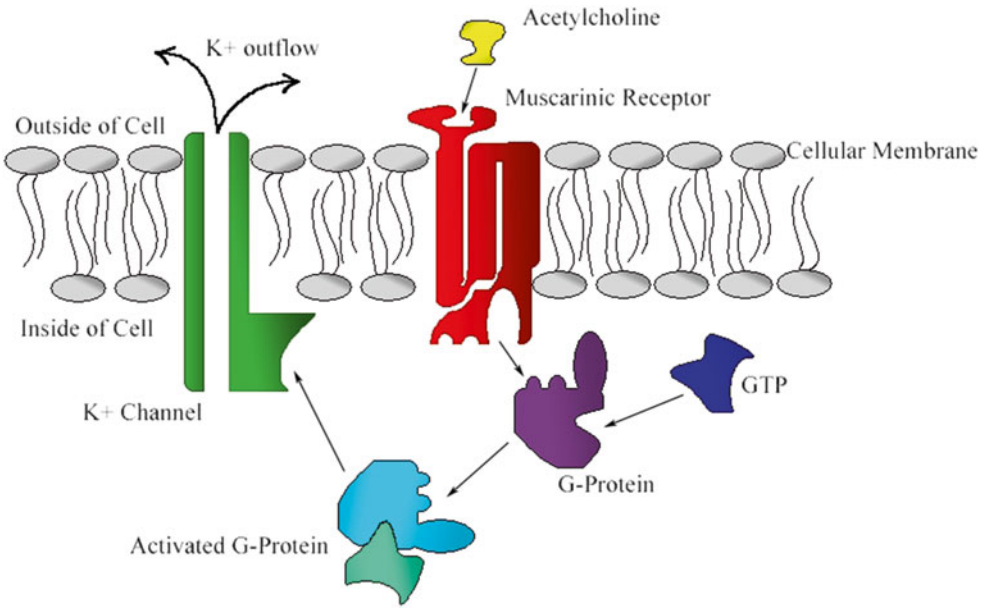

Fig. 14.7 The effect of acetylcholine on cardiac muscle cells. Potassium channels within a cellular membrane are opened as a result of binding an activated G protein. Acetylcholine released by parasympathetic neurons activates these G proteins by binding with muscarinic receptors within the membrane. The effect of norepinephrine on cardiac muscle cells is propagated in a similar manner, with differences as described in the text. *GTP* guanosine triphosphate

to stimulate β_1 adrenergic receptors. Next, G proteins replace GDP at their binding sites with GTP upon activation by the excited β_1 receptors, causing an increase in the production of cyclic AMP within the cardiac myocytes. The increased cAMP levels cause molecules of protein kinase A to phosphorylate large numbers of calcium channels within the cellular membrane. This addition of a phosphate group not only causes Ca^{2+} channels to remain open longer but also allows for a greater number of channels to open, thus contributing to the influx of calcium ions into each cell upon activation [6]. In other words, the threshold for depolarization will be more easily attained due to the greater number of available calcium channels, thus allowing greater calcium incursion during activation and resulting in higher contraction strength.

An advantage of the mechanisms of action involving G proteins is that autonomic modulation can be sustained without constant nerve fiber stimulation. That is, a burst of synaptic activity causing the release of either acetylcholine or norepinephrine can initiate the respective processes described above. For more details on cardiac receptors and intracellular signaling, refer to Chap. 15.

14.9 Specific Sympathetic and Parasympathetic Cardiac Controls

14.9.1 Heart Rate

The rate at which a normal adult heart completes cardiac cycles during rest is approximately 70 beats/min [6]. The heart rate is maintained at this relatively constant value via a continuous firing (resting-rate activation) of the vagus nerve, called *basal* (*or vagal*) *tone*. The heart rate will increase when vagal tone decreases and is further modulated by increased activity of sympathetic nerves to the heart, which releases norepinephrine and causes a rise in the sinoatrial nodal depolarization rate (Fig. 14.8). A rate increase of this nature is referred to as a *positive chronotropic effect*. As stated above, the fundamental cause of this increase in heart rate is due to an increase in activated calcium channels in myocardial cell membranes, increasing the speed at which depolarization occurs. This increased sympathetic outflow can be initiated by a large array of internal and external stimuli, including but not limited to: exercise, an increase in body temperature, trauma, and/or emotional stress. Additionally, a concurrent release of epinephrine from the adrenal medulla can further amplify these same effects on myocardial ion channels, although to elicit a significant rise in heart rate, the amount of the hormone liberated must be fairly substantial [6].

Parasympathetic discharge, in part, increases potassium ion permeability in cardiac myocytes, thus increasing the threshold for depolarization to occur spontaneously particularly within the sinoatrial node; as a result, the heart rate declines (Fig. 14.8). This autonomic neural input predominates during sleep and other sedentary states, eliciting an increase in cardiac cycle time and therefore enabling the heart to expend less energy [2]. In addition to decreasing the slope of the pacemaker potential, parasympathetic stimulation may also induce a so-called pacemaker shift [5]; true pacemaker cells can become more inhibited than the latent pacemakers, thus shifting the initiation of spontaneous depolarization from the true pacemakers to the latent ones [5].

Conduction velocity is the measure of the spread of action potentials through the heart. Parasympathetic stimulation above normal tonic activity also slows cardiac conduction velocity, and this response is termed *negative dromotropic*. It

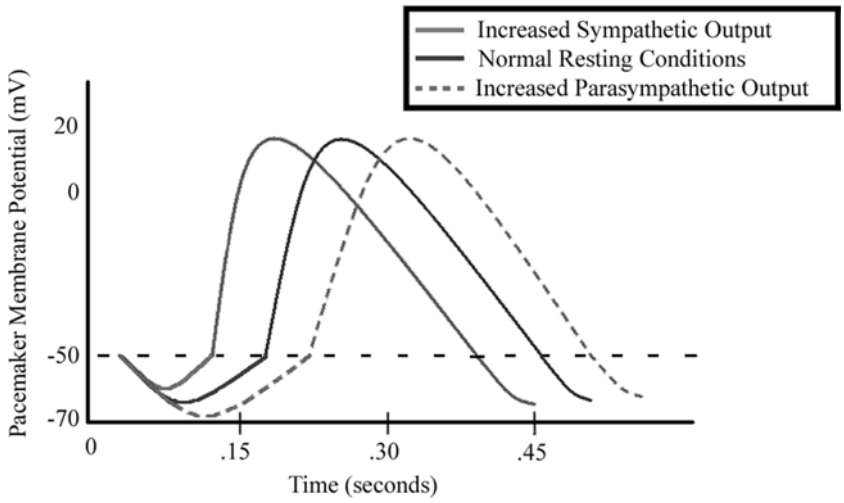

Fig. 14.8 The effects of changes in sympathetic and parasympathetic outflow to the heart. The heart will increase its rate of contraction during increased sympathetic neural stimulation. This decreases the time required for the cardiac pacemaker cells to reach threshold. In contrast, increased parasympathetic outflow will decrease the heart rate and increase the time to threshold

follows that an increase in conduction velocity, which commonly accompanies sympathetic stimulation, has a *positive dromotropic* effect. The atrioventricular node is the location within the heart where conduction speed variations are most notable. The reader is referred to Chap. 13 for more details on specific mechanisms of cardiac pacemaker mechanisms.

The control mechanisms of heart rate are also, in part, dependent on gender [13]. For example, women have been shown to exhibit higher-frequency parasympathetic input (using spectral analysis procedures) than men of similar age, possibly indicating a more dominant control of heart rate via vagal stimulation than their male counterparts [13].

14.9.2 Stroke Volume and Contractility

Like heart rate, the amount of blood ejected from the ventricles during systole is greater when the heart is modulated by an increased sympathetic input (Fig. 14.9). The underlying mechanism for this increased stroke volume is enhanced cardiac myocyte contractility, and the magnitude of this response is strongly affected by preload and afterload conditions, as predicted by the Frank–Starling Law [6]. Such an increase in contractility is characterized as a *positive inotropic* effect. By and large, myocytes increase in length in proportion to their preload, and since they become more elongated, they also have the capability to shorten over this greater distance. The increased amount of shortening leads to an enhanced strength of contraction of the heart by also increasing the number of available cross-bridge formations between the actin and myosin molecules (see also Chap. 12). As described previously, sympathetic excitation also facilitates a larger and more rapid Ca^{2+} influx into cardiac cells, which further augments the degree of overall contraction during systole [12].

Combined with a larger preload, the increased contractility due to calcium ion influx will raise the stroke volume of

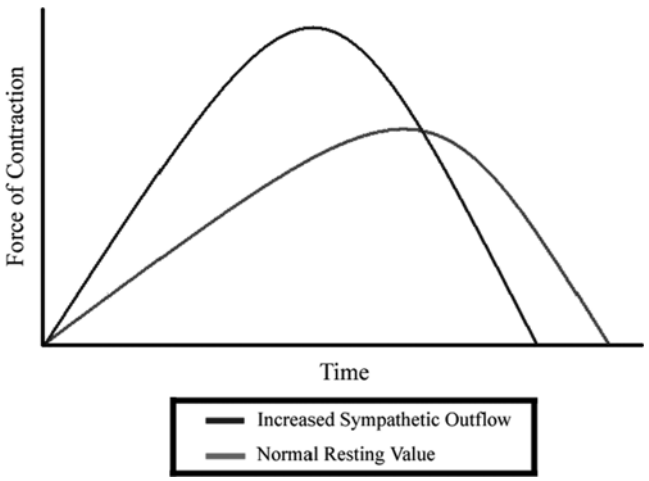

Fig. 14.9 Effect of increased sympathetic stimulation on contractility (see text for details)

the heart (Fig. 14.10). Likewise, the ejection fraction of blood from a given chamber of the heart also elevates accordingly [2]. However, stroke volume is also dependent on afterload created by the relative diameter of the peripheral arteries and will not increase as significantly under sympathetic stimulation if the afterload is elevated due to vasoconstriction. As expected from the often antagonistic nature of the autonomic nervous system, parasympathetic stimulation decreases contractility. However, the relative decrease in contractility is much less significant than the increase in this parameter that sympathetic input provides [2].

An important concept to note involves simultaneous increases in heart rate and stroke volume. Since cardiac output is the product of these two factors, its overall value typically increases with sympathetic stimulation. Conversely, cardiac output normally decreases with a higher rate of parasympathetic input. This happens when the body is in a seden-

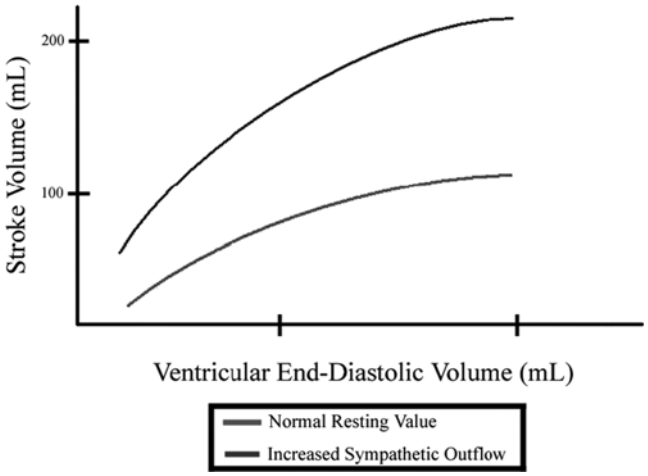

Fig. 14.10 The relative effects of increased sympathetic stimulation on altering stroke volumes (see text for details)

tary state; hence, tissue oxygen and metabolite requirements are not as high.

The time necessary for the heart to fully contract and relax decreases under sympathetic stimulation, due primarily to the larger proportion of the cardiac cycle that is made available for filling. While an increase in heart rate makes the total duration of the cardiac cycle shorter [2], the corresponding rise in contractility causes the muscular contractions to commence more rapidly and with greater force than under resting conditions. This translates to a decrease in the amount of time necessary for contraction of the heart during a complete cardiac cycle. Thus, the heart is relaxed for a greater portion of the cycle, enabling enhanced filling of the chambers to provide a greater volume of blood ejected for each contraction.

14.9.3 Baroreceptor Pressure Regulation

Arterial pressure, or afterload, is regulated in the short term by baroreceptors in the walls of the aorta and carotid arteries. In particular, baroreceptors sense both magnitude and the rate of stretch of arterial walls due to pressure fluctuations within the vessels [6]. The afferent fibers projecting from the baroreceptors convey this information concerning pressure shifts to the autonomic nervous system which, in turn, responds by either increasing or decreasing sympathetic and/or parasympathetic drive. A basal tonic activity can be identified from the receptors, which progresses to the higher cardiovascular centers. The frequency of impulses can be observed to increase or decrease in response to these pressure changes. Decreased arterial dilatation causes sympathetic nerves to increase their discharge rate and escalate the release of norepinephrine, thus increasing heart rate, stroke volume, and peripheral resistance [2]. The baroreceptor reflex functions as a negative feedback system [6], such that a decrease in arterial stretch will induce an increased sympathetic discharge, accordingly raising cardiac output (Fig. 14.11). This, in turn, will increase blood delivered to the vessels containing baroreceptors, increase pressure, and decrease the tonic activity of the receptors. Homeostatic control of arterial pressure is thus administered, since the decreased baroreceptor discharge rate will cause a lowered degree of sympathetic activity and revert the cardiac output back toward its basal value. In other words, the response of the baroreceptors ultimately removes the stimulus causing the initial response [6]. Carotid artery massage is sometimes suggested in an attempt to decrease overall sympathetic tone in the body, e.g., an individual eliciting an arrhythmia due to stress can sometimes convert back to a normal sinus rhythm with this maneuver.

Importantly, long-term pressure regulation is not accomplished via baroreceptor input, due to its adaptive nature (accommodation). That is, if pressure in the aorta and carotid arteries remains elevated for sustained periods, the tonic firing rates will eventually return toward resting values regardless of whether or not the pressures remain elevated. Long-term regulation of pressure involves numerous complex hormonal mechanisms, which are extensively influenced by the hypothalamic and medullary cardiovascular centers.

14.9.4 Arteriolar Pressure Regulation

Because the heart is responsible for delivery of blood to every part of the body, homeostatic control often involves changing the amount of blood provided by the circulatory system to a given tissue, organ, or organ system. For example, the gastrointestinal system normally receives approximately 20 % of the blood pumped by the heart during each cardiac cycle. However, during times of intense stress or exertion, the blood provided to this area may drastically decrease, while the proportion of blood provided to the heart and skeletal muscles may increase notably. Such changes in blood supply are commonly mediated by changes in resistance of the peripheral vasculature (see also Fig. 1.8 in Chap. 1).

At rest, the smooth muscle cells in the walls of arterioles throughout the body remain slightly contracted due to a combination of influences from the central nervous system, hormonal distributions within the vasculature, and/or localized organ effects. The relative degree of contraction within the arterioles is referred to as their basal tone. The stretching of the arterioles due to pulsatile blood pressure is thought to be the cause of the constant state of stress within such vessels [6]. Arterioles innervated by sympathetic fibers possess an increased contractile tone, termed the *neurogenic tone*, due to the sustained activation of these fibers. Control of the vascular

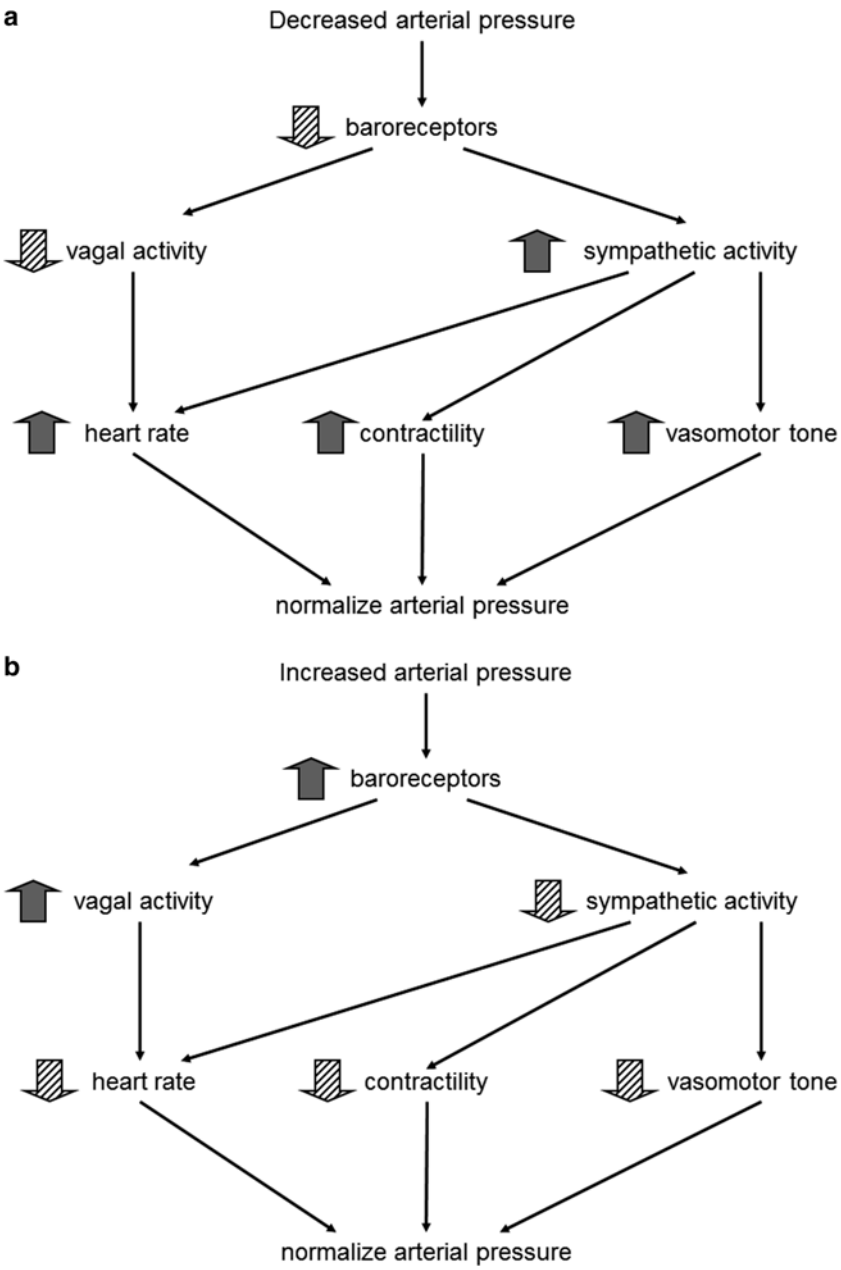

Fig. 14.11 The negative feedback control of blood pressure. In *Panel a*, there is decreased pressure detected by the baroreceptor, and in *Panel b* there is an elevated pressure. The relative responses that occur in order to maintain an overall normal systemic pressure are indicated

peripheral resistance is achieved by varying the firing frequency within these sympathetic fibers. More specifically, postganglionic fibers release the neurotransmitter norepinephrine, which binds to alpha (α_1) adrenergic receptors within the smooth muscle cells in arteriolar walls. Thus, an increase in the firing activity of these neurons produces an increase in norepinephrine levels which, in turn, binds with more α_1 receptors and causes an overall decrease in the diameters of arterioles. In contrast, a lowering of the basal tonic activity causes vasodilation, since less neurotransmitter is available for binding, causing the smooth muscle cells to relax.

The relative firing rates of arteriolar sympathetic neurons innervating a given tissue are also modulated by the need for blood elsewhere in the body. For example, if a hemorrhage occurs in the abdomen which results in significant bleeding, sympathetic activity to that area will increase, causing less blood to flow to these damaged tissues in an attempt to preserve adequate levels of flow to the heart and brain. It should be noted that other regulators exist for the control of vasomotion and the tonic activity of the sympathetic system. Local increases in extracellular cation concentrations, acetylcholine levels, and even norepinephrine itself can act to prevent extreme vasoconstriction. Adrenergic receptors that are pharmacologically different from those in smooth muscle cells [6] have been identified on postganglionic sympathetic neurons themselves and are given an α_2 designation. These

receptors bind with the neurotransmitter and inhibit its release if the amount previously liberated is excessive (negative feedback).

Blood flow through the coronary arterioles is primarily regulated by local metabolic controls that are highly coupled with oxygen consumption. That is, subtle increases in oxygen consumption by the heart will result in an increase in blood flow through the coronaries. Elevated sympathetic activity of the systemic vasculature typically induces a subsequent decrease in the diameter of the peripheral arteries. However, upon sympathetic excitation, vasodilatation predominates in the coronary arterioles instead of vasoconstriction, since oxygen consumption is raised significantly by concurrently inducing higher heart rates and levels of contractility. The factors motivating metabolic regulation therefore outweigh the vasoconstrictive effects of sympathetic innervation of the coronaries.

Blood flow to the skeletal muscle is controlled in a similar manner to that of the coronary arteries, in that local metabolic factors play a vital role in regulating vessel resistance. While increased sympathetic activity may decrease the blood flow to a resting skeletal muscle by a factor of four [6], a muscle undergoing exercise (and thus in the presence of elevated sympathetic activity) can elicit an increase in blood flow almost 20 times that of normal resting values [6]. However, this muscle response must occur in conjunction with a drastic decrease in the blood flow to other tissues or organs, such as those of the abdominal cavity or nonexercising muscles. This course of action allows the total peripheral resistance to remain at a functional level. Homeostatic control during exercise also exists at the skin. In order to cool the body from the increased metabolic heat production, sweat glands become active and cutaneous blood flow increases significantly over the normal resting value in order to dissipate excess body heat. The active vasodilatation is the result of metabolic activity overcoming the increased sympathetic outflow to skin arterioles.

During the digestion of food, remaining sympathetic activity predominates at the vasculature of skeletal muscles and there are increases in blood flow to the stomach and intestines. Parasympathetic discharge to the heart increases, while the sympathetic stimulus declines, lowering the heart rate. This concentration of blood to the abdominal organs facilitates the movement of nutrients to areas of the body in need; this is a good example of how both branches of the autonomic nervous system work together to sustain a level of balance throughout the entire body.

The suprarenal glands can also contribute to vasomotion. Since norepinephrine is released directly into the bloodstream from these endocrine glands, arteriolar constriction in the systemic organs can result. The *fight or flight* response in humans, elicited under stressful or exciting circumstances, originates from the hypothalamus via hormones that travel to the pituitary gland and later the adrenal cortex, where the agent cortisol is released into the bloodstream and adrenal medulla. It is in the medulla that cortisol activates the enzyme necessary to convert norepinephrine to epinephrine, which is released into the bloodstream to amplify increased sympathetic activity [2, 3]. Blood flow to the skin and other internal organs (like the stomach and intestines) is greatly decreased by increasing sympathetic (and decreasing parasympathetic) tonic activity, while flow to skeletal muscles and the heart increases considerably. This process can be thought of as simply delivering blood to the areas of the body most in need to deal with the demanding circumstances. The direct release of these agents into the bloodstream allows for their rapid circulation, which helps contract arterioles along with conventional sympathetic outflow. The "adrenaline rush" one experiences during periods of great tension or exhilaration comes from the adrenal glands.

Flow regulation through the veins and venules in the body is carried out by many of the same mechanisms as that for arterioles. While veins have smooth muscle in their walls, complete with α_1 receptors that respond to norepinephrine, their basal tonic activity is much lower than that observed in arterioles. Thus, venules at rest can be considered to be in a more dilated state. The wall thickness of veins is also significantly less than that found in arteries, which enables the consequences of physical effects to be more prominent in veins. That is, the overall blood volume associated with veins can be greatly affected by compressive forces. For example, in the skeletal muscle, the degree of muscle contraction around the vessel can push large amounts of blood back toward the heart, which enables quicker filling within the right atrium and enables sustained physical activity. If skeletal muscles surrounding veins are relaxed, the venous system can act as a blood reservoir (see also Fig. 1.4 in Chap. 1).

The vasculature within skeletal muscles and the liver can play a unique role relative to homeostasis, via noninnervated β_2 receptors located in their arteriolar walls. Increased blood levels of epinephrine can activate these receptors which, along with G proteins [6, 12], act to catalyze an intracellular chemical reaction resulting in decreased cytoplasmic levels of Ca^{2+} and a hyperpolarization of the cellular membranes. This in turn decreases the contractile machinery sensitivity to Ca^{2+}, thus causing vasodilatation [6]. Vasodilatation in the presence of epinephrine is in contrast to the decrease in vessel diameter caused by the chemically similar compound norepinephrine. β_2 receptors are more sensitive to epinephrine than α_1 receptors [6]. Thus, a small elevation in the concentration of epinephrine in the bloodstream (e.g., provided by the adrenal medulla) can cause vasodilatation. However, if the level of catecholamine increases, the more numerous α_1 receptors will be activated and cause vasoconstriction. It is important to note that there is no neural input to β_2 receptors; therefore, norepinephrine has no effect on their activation.

It can be seen that the parasympathetic and sympathetic effects of the heart and vasculature often elicit opposite physiologic responses yet work in conjunction to synergistically maintain homeostasis.

14.10 Cardiac Denervation

Denervation can be divided into two categories—preganglionic and postganglionic. Preganglionic denervation can be caused primarily by disease or injury of the vasomotor centers in the brain or spinal cord above T10; it leaves intact the postganglionic nerve fiber and many reflexes that occur at the ganglionic level. Preganglionic denervation results not only in loss of centrally mediated cardiac reflexes but also leads to abnormalities in the control of peripheral vascular tone as well as an inability to control blood pressure with changes in body position. Shy–Drager syndrome is a classic example of preganglionic denervation affecting the cardiovascular system [14].

Postganglionic denervation of the heart occurs as the result of several neurodegenerative processes, after certain types of cardiac surgery and/or after cardiac transplantation. Loss of the postganglionic nerve cell body results in Wallerian degeneration of the distal nerve, with loss of axonal integrity and neurotransmitters. Loss of neurotransmitters at the neural junction with the distal target (e.g., cardiac conduction tissue or cardiac myocytes) in turn leads to an increase in neurotransmitter receptor number and density. This, combined with a loss of neurotransmitter metabolism by the degenerated neurons, makes both the cardiac conduction system and muscle hypersensitive to circulating catecholamines (so-called denervation hypersensitivity). It should be noted that cardiac denervation is also considered as a potential means to alter the occurrence of arrhythmias in such patients [15].

Cardiac transplantation is the most complete form of cardiac denervation, resulting in loss of both sympathetic and parasympathetic innervation, with subsequent Wallerian degeneration of the intracardiac nerve fibers [16]. Diabetes is the most common cause of denervation in the general non-transplant population [17]. More specifically, a diabetic neuropathy can result in loss of both sympathetic and parasympathetic efferent and afferent pathways; hence, heart rate variability will diminish. As with other neurodegenerative diseases, neuronal loss is typically patchy and permanent. Infiltrative diseases such as amyloidosis may also lead to cardiac denervation.

14.10.1 Effects of Denervation on Basal Cardiac Function

Loss of tonic parasympathetic vagal inhibition of sinus node depolarization causes a rise in one's basal heart rate and loss of heart rate fluctuation with respiration, known as *respiratory sinus arrhythmia*. The resting heart rate of transplant patients typically is 95–100 beats/min. Further, the reflexes that are mediated primarily through the vagal nerves are absent, including carotid sinus slowing of heart rate, the pulmonary inflation reflex, and the Bezold–Jarisch reflex.

In contrast, resting inotropic state of the cardiac muscle and myocardial blood flow remain somewhat normal after denervation; basal ventricular function is changed minimally. Further, in such patients the measures of systolic contractility (such as dp/dt, ejection fraction, and cardiac output) are usually preserved. Preservation of pump function after denervation may be related in part to an upregulation of beta catecholamine receptors on both myocytes and the conduction system, leading to an amplification of the responses to blood-borne catecholamines [18].

Additionally, coronary blood flow is unchanged at rest and increases normally with exercise. Coronary flow reserve (a measure of maximal coronary blood flow) is normal, although in transplanted animals the responses to ischemia are blunted [19, 20].

Afferent sensation to pain (e.g., from ischemia), chemoreceptor stimulation (e.g., from ischemia, hyperosmolar contrast media), and stretch receptor stimulation (e.g., from pressure overload) are all initially absent. This aspect of denervation is important because coronary occlusion due to transplant-related coronary arteriopathy is common and the absence of anginal pain removes an important warning symptom.

14.10.2 Effects of Denervation on Exercise Hemodynamics

Cardiac denervation results in a blunting of the chronotropic response to exercise. With exercise, heart rate rises due to an increase in plasma catecholamines (released primarily from the adrenal glands) rather than from direct sympathetic stimulation of the sinus node. The heart rate increase is delayed; i.e., heart rate may peak well after the cessation of exertion and remains elevated until the circulating catecholamines can be metabolized (Fig. 14.12).

Exercise or stress also results in a delayed increase in inotropic state, similar to the changes in chronotropic response. Unlike resting ventricular function, peak inotropic state and ejection fraction are typically reduced.

14.10.3 Reinnervation

Sympathetic neural reinnervation of the heart has been observed in nearly all animals undergoing autotransplantation and in most patients undergoing orthotropic transplantation. Reinnervation typically occurs over the aortic and atrial suture lines (left more than right), extending from the base of the heart to the apex. Yet, the rate of reinnervation is typi-

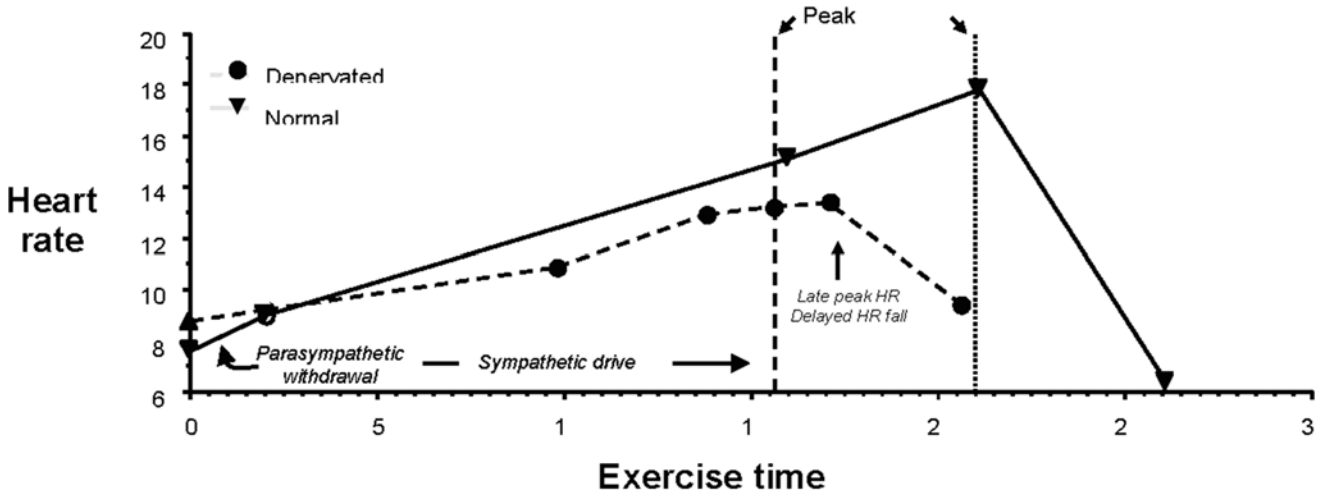

Fig. 14.12 The heart rate response to treadmill exercise is shown for normally innervated subjects (solid line) relative to patients with cardiac denervation after heart transplantation (dashed line). The denervated patients elicit higher resting heart rates, but heart rates rise more slowly with exercise because the induced increase in heart rate is dependent primarily on circulating catecholamines. After cessation of exercise, heart rates in the denervated patients continue to rise briefly and then fall slowly as circulating catecholamines are metabolized

cally slow (years), and in humans it is patchy and most often incomplete. Yet, it has been noted that the anterior wall typically reinnervates earlier and more densely than the rest of the left ventricle [21]. The sinus node reinnervates to some degree in over 75–80 % of patients.

Reinnervation results in partial normalization of the chronotropic and inotropic response to exercise [22, 23]. Reinnervated patients have been observed to exercise longer and have higher maximal oxygen consumption. Additionally, cardiac pain sensation (i.e., angina) also returns, although the regional nature of reinnervation results in reduced or patchy sensation to ischemia in most transplant recipients [24]. Parasympathetic reinnervation has been reported in a small number of transplant recipients; it is accompanied by return of respiratory mediated fluctuation in heart rate and carotid sinus slowing of heart rate.

It should be noted that in some transplant patients, the native sinus node is left intact, yet due to the suture line, these individuals require pacing therapy. There are known causes in which the activity in natively innervated nodes is sensed by a pacing system, which then rate adjusts the ventricular pacing accordingly, Hence, a more functional control of heart rate is maintained relative to the intrinsic activity within the autonomic nervous system.

14.11 Summary

The autonomic nervous system, and the role it plays in governing the behavior of the cardiovascular system, is intrinsically complex and important for sustaining life. The antagonistic nature of the parasympathetic and sympathetic branches of this system allows rapid and essential changes in cardiac parameters such as heart rate, contractility, and stroke volume in order to deliver metabolites and nutrients to tissues and organs that need them at any given time. Increased sympathetic outflow relative to normal resting conditions most often causes an excitatory response in physiologic parameters (such as heart rate and/or smooth muscle contraction), whereas parasympathetic stimulation usually results in calming adjustments (decreased heart rate, contractility, and/or vasodilatation).

References

1. Moore KL, Dalley AF II (eds) (1999) Clinically oriented anatomy, 4th edn. Lippincott Williams & Wilkins, Philadelphia
2. Vander A, Sherman J, Luciano D (eds) (2001) Human physiology, 8th edn. McGraw Hill, Boston
3. Hansen JT, Koeppen BM (eds) (2002) Netter's atlas of human physiology, 1st edn. Icon Learning Systems LLC, Teterboro
4. Martini FH (ed) (2001) Fundamentals of anatomy and physiology, 5th edn. Benjamin Cummings, New York
5. Berne RM, Levy MN (eds) (1977) Cardiovascular physiology, 3rd edn. C.V. Mosby Company, St. Louis
6. Mohrman DE, Heller LJ (eds) (2003) Cardiovascular physiology, 5th edn. Lange Medical Books/McGraw Hill, New York
7. Netter FH (ed) (1998) Atlas of human anatomy, 2nd edn. Novartis, East Hanover
8. Kawano H, Okada R, Yano K (2003) Histological study on the distribution of autonomic nerves in the human heart. Heart Vessels 18:32–39
9. Quan K, Lee JH, Van Hare G, Biblo L, Mackall J, Carlson M (2002) Identification and characterization of atrioventricular parasympathetic innervation in humans. J Cardiovas Electrophys 13:735–739

10. Mountcastle VB (ed) (1980) Medical physiology, 14th edn. C.V. Mosby Company, St. Louis
11. Nolte J (ed) (2002) The human brain: an introduction to its functional anatomy, 5th edn. Mosby, St. Louis
12. Matthews GG (ed) (1998) Cellular physiology of nerve and muscle, 3rd edn. Blackwell Science, Inc., Malden
13. Evans JM, Ziegler MG, Patwardhan AR et al (2001) Gender differences in autonomic cardiovascular regulation: spectral, hormonal and hemodynamic indexes. J Appl Physiol 91:2611–2618
14. Ziegler MG, Lake CR, Kopin IJ (1977) Sympathetic nervous system defect in primary orthostatic hypotension. N Engl J Med 296:293
15. DeSimone CV, Madhavan M, Venkatachalam KL, Knudson MB, Asirvatham SJ (2013) Percutaneous autonomic neural modulation: a novel technique to treat cardiac arrhythmia. Cardiovasc Revasc Med 14:144–148
16. Williams VL, Cooper T, Hanlon CR (1963) Neural responses following autotransplantation of the canine heart. Circulation 27:713
17. Watkins PJ, MacKay JD (1980) Cardiac denervation in diabetic neuropathy. Ann Intern Med 92:304–307
18. Vatner DE, Lavallee M, Amano J, Finizola A, Homcy CJ, Vatner SF (1985) Mechanisms of supersensitivity to sympathomimetic amines in the chronically denervated heart of the conscious dog. Circ Res 57:55–64
19. Lavallee M, Amano J, Vatner SF, Manders WT, Randall WC, Thomas JX (1985) Adverse effects of chronic denervation in conscious dogs with myocardial ischemia. Circ Res 57:383–392
20. McGinn AL, Wilson RF, Olivari MT, Homans DC, White CW (1988) Coronary vasodilator reserve after human orthotopic cardiac transplantation. Circulation 78:1200–1209
21. Schwaiger M, Hutchins GD, Kalff V et al (1991) Evidence for regional catecholamine uptake and storage sites in the transplanted human heart by positron emission tomography. J Clin Invest 87:1681–1690
22. Wilson RF, Johnson TH, Haidet GC, Kubo SH, Mianuelli M (2000) Sympathetic reinnervation of the sinus node and exercise hemodynamics after cardiac transplantation. Circulation 101:2727–2733
23. Bengel FM, Ueberfuhr P, Schlepel N, Reichart B, Schwaiger M (2001) Effect of sympathetic reinnervation on cardiac performance after heart transplantation. N Engl J Med 345:731–738
24. Stark RP, McGinn AL, Wilson RF (1991) Chest pain in cardiac transplant recipients: evidence for sensory reinnervation after cardiac transplantation. N Engl J Med 324:1791–1794

Cardiac and Vascular Receptors and Signal Transduction

15

Daniel C. Sigg and Ayala Hezi-Yamit

Abstract

Cellular physiological functions are regulated via signaling mechanisms in essentially any cell type of any organ within the human body. While myocardial cells are unique in that they are interconnected to each other via gap junctions and thus act as an electrical syncytium, a vast number of important cellular receptors and signal transduction pathways allow individual cells to receive and respond to various signals. These receptors and signal transduction pathways play important roles in normal cell/organ functions (their physiology), as well as in disease processes (pathophysiology). It is the aim of this chapter to review the major role and signaling mechanisms of selected physiologically and pathophysiologically important cardiac and vascular receptors, with emphasis on G protein-coupled receptors (e.g., beta-adrenergic receptors) and non-G protein-coupled receptor systems, such as guanylyl cyclase-related receptors (e.g., receptors for nitric oxide). Finally, we will discuss the importance and complexity of inflammation in the pathobiology of coronary artery disease and its treatment. Inflammation plays a very important role in cardiovascular disease. For example, device-based interventions such as coronary stenting may activate inflammation via a series of complex signaling processes. Importantly, inflammation pathways also play a central role in the elicitation of atherosclerosis, myocardial infarction, and/or heart failure.

Keywords

Coupling • G protein receptor • Beta-adrenergic receptor • Alpha-adrenergic receptor • Muscarinic receptor • Receptor cross talk

Abbreviations

AC	Adenylyl cyclase
ATP	Adenosine triphosphate
β-AR	Beta-adrenergic receptor
β-ARK	Beta-adrenergic receptor kinase
cAMP	Cyclic adenosine monophosphate
CDK	Cyclin-dependent kinase
cGMP	Cyclic guanosine monophosphate
DES	Drug-eluting stent
ERK	Extracellular signal-regulated kinase
GC	Guanylyl cyclase
GDP	Guanosine diphosphate
GTP	Guanosine triphosphate
IRAK	Interleukin-1 receptor-associated kinase
ISR	In-stent restenosis
JNK	JUN N-terminal kinase
MAPK	Mitogen-activated protein kinase
MCP	Monocyte chemoattractant protein

D.C. Sigg, MD, PhD (✉)
FocusStart LLC, 213 4th St. E., Suite 413, St. Paul, MN 55101, USA
e-mail: dcsigg@gmail.com

A. Hezi-Yamit, PhD
Avinger, Inc., 400 Chesapeake Drive, Redwood City, CA 94063, USA

P.A. Iaizzo (ed.), *Handbook of Cardiac Anatomy, Physiology, and Devices*, DOI 10.1007/978-3-319-19464-6_15

M-CSF	Macrophage colony-stimulating factor
NO	Nitric oxide
NOS	Nitric oxide synthase
pRB	Retinoblastoma gene product
PTCA	Percutaneous transluminal coronary angioplasty
SMC	Smooth muscle cell
TIR	Toll/interleukin-1 receptor
TLR	Toll-like receptor
TNF	Tumor necrosis factor
TNFR	Tumor necrosis factor receptor
TRAF	TNFR-associated factor

15.1 Introduction

Cellular physiological functions are regulated via signaling mechanisms in essentially any cell type of any organ. While myocardial cells are somewhat unique in that they are interconnected to each other with gap junctions and act as an electrical syncytium, a vast number of important cellular receptors allow the cells to receive and respond to various signals and transduce these signals within the cell. Many of these receptors are located on the cellular membrane. It would be beyond the scope of this review to discuss all the receptors of all the cell types in the cardiovascular system. Since our understanding of molecular cardiovascular biology is continuously growing, it is the general aim of this chapter to focus on selected physiologically and pathophysiologically important cardiac and vascular receptors. Nevertheless, many of the principles and mechanisms discussed in the following pages, using certain receptor subtypes as examples, are applicable to related receptor systems and should make it easier to study and understand a "new" or less well-studied/well-characterized receptor signaling system. Furthermore, a thorough review of the normal function of these receptors is important and very helpful in understanding the altered function of the same receptor systems and associated signaling mechanisms in disease states. For example, it will be reviewed how a β-receptor antagonist (beta-blocker; a drug that is known to depress cardiac contractility) may be beneficial in the treatment of heart failure, a state of depressed cardiac function. This chapter will also focus on the large and important family of G protein-coupled receptors, with particular emphasis on the β-adrenergic receptor (β-AR) signaling system; this system has very important functions in both normal cardiac physiology and associated pathophysiology. Other important G protein-coupled receptors will be reviewed, such as α-adrenergic receptors and muscarinic receptors. Non-G protein receptor systems, such as tyrosine kinase-linked receptors and guanylyl cyclase-related receptors, will be briefly discussed. Finally, an overview of the basic biology of coronary stenting is provided. Our goal is to depict the biological cascade that is triggered by coronary angioplasty and stenting, as well as the complexity of subsequent biological responses, and to explain how these responses are modulated by drug-eluting stents (DESs).

Table 15.1 Classification of cardiovascular receptors

By location	By receptor types
Cardiac receptors • Myocardial • Conduction system • Others	G protein-coupled receptors Tyrosine kinase-linked receptors Guanylyl cyclase-linked receptors
Vascular receptors • Endothelial • Vascular smooth muscle • Others	Other receptors (low-sensitivity lipoprotein receptor; nicotine acetylcholine receptor; peptidergic)

15.2 Definition

Cell receptors allow extracellular substances to bind for regulation of intracellular function or metabolism, typically without having to enter the cell. A number of types of cellular receptors can initiate a signal that ultimately modulates cellular function. Most of the "classic" receptors are cell surface receptors, spanning the whole cell membrane and thereby allowing mediation of signals from the extracellular site to the intracellular site. The largest, and possibly most important, group is the family of G protein-coupled receptors. A classification of cardiovascular receptors either by location or by receptor type is provided in Table 15.1.

15.3 G Protein-Coupled Receptor (Seven-Transmembrane-Spanning Receptors) and Signal Transduction

15.3.1 Overview

G protein-coupled receptors are functionally closely related to ion channels. The G protein-coupled receptors are part of a gene family being identified that binds agonists such as adenosine, catecholamines, acetylcholine, odorants, angiotensin, histamine, opioids, and many others.

15.3.2 Receptor Structure

There are several interesting structural similarities between ion channels and G protein-coupled receptors. Both are integral membrane proteins with seven-transmembrane domains, which form bundles with a central pocket. In G proteins, the pockets are the binding sites for the receptor ligands, and they are typically located on the extracellular site of the protein; the N-terminal tail is located extracellu-

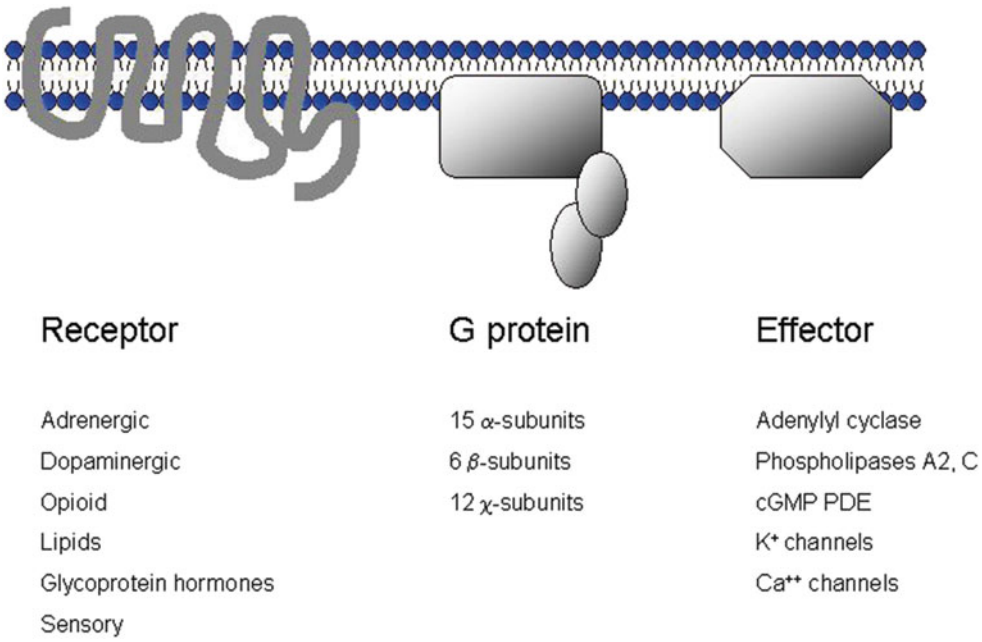

Fig. 15.1 G protein receptor-coupled signaling. The ubiquitous seven-transmembrane receptor systems are composed of a receptor, a heterotrimeric G protein, and an effector system. The complexity of this system can be appreciated by the number of receptor types and subtypes, G protein subtypes, and different effector systems

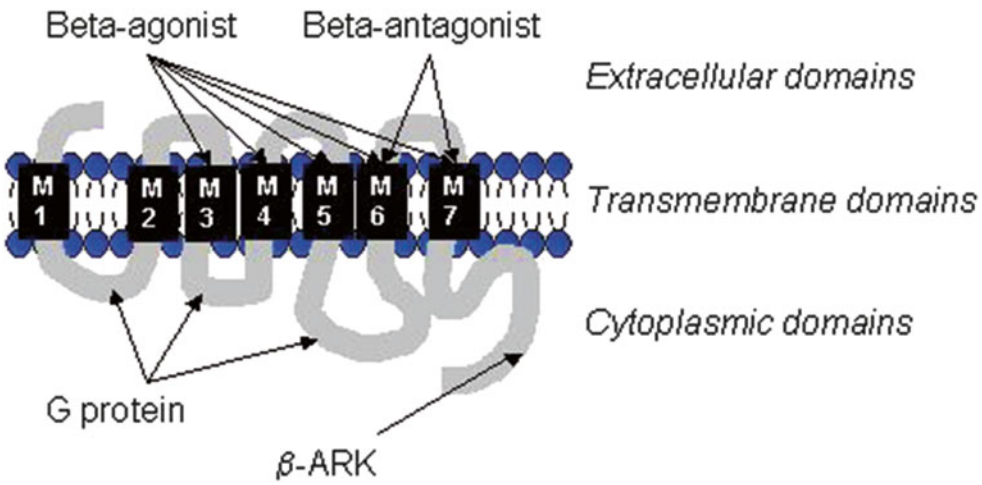

Fig. 15.2 The molecular schematic structure of a β-adrenergic receptor. Note the three main domains—extracellular, transmembrane, and cytoplasmic. The transmembrane domains are important for ligand binding. The transmembrane domain, M3-7, is important in agonist binding, whereas the domains M6 and M7 are involved in antagonist binding (β-receptor blockers). The cytoplasmic domains contain important binding sites for interactions with G proteins, as well as various kinases such as β-AR kinase (*β-ARK*)

larly as are three extracellular loops. Three loops connecting the transmembrane domains and the C-terminal domain are located intracellularly (Figs. 15.1 and 15.2). The exact function of the extracellular loops remains largely unknown. It is considered that the transmembrane domains are involved in receptor binding. The intracellular loops, particularly loop III and the C-terminal tail, are important for receptor coupling to the associated G protein. Finally, both loop III and C-terminal tail are important for regulation of receptor function and contain phosphorylation and other posttranslational modification sites.

15.3.3 Receptor Coupling

The G protein receptors interact intimately with G proteins. G proteins are complexes consisting of three subunits—α, β, and χ. There are different classes of G proteins, and attempts have been made to classify them as subtypes. For example, common α-subunits include: (1) α_s (stimulatory) which activates adenylyl cyclase, (2) α_i (inhibitory) which inhibits adenylyl cyclase, (3) α_0 which modulates calcium channels and phospholipase C, and (4) α_z which activates phospholipase C. In general, each α-subunit contains a region that interacts

with the receptor, a site that binds guanosine triphosphate (GTP), and a site interacting with the effector system.

15.3.4 Receptor Function and Regulation

The traditional concepts of G protein-coupled receptor function are best illustrated in Fig. 15.1. First, an agonist binds to a receptor molecule, and then the seven-transmembrane-spanning receptor molecule interacts with a specific G protein; this, in turn, modulates a specific effector. Examples of typical agonists, receptors, G proteins, and effectors are provided in Fig. 15.1. While this illustration provides a general summary of the individual components needed for proper G protein-coupled receptor function, a more thorough understanding of the G protein receptor-mediated signaling, as well as its regulation, is best accomplished by the more specific example of the well-characterized beta-adrenergic receptor (β-AR) system. Therefore, we will start our discussion with these physiologically, pathophysiologically, and clinically highly relevant seven-transmembrane-spanning β-ARs.

15.4 Beta-Adrenergic Receptors (β-ARs)

15.4.1 Classification of β-Adrenergic Receptors

Table 15.2 summarizes the general features of β-AR subtypes identified to date; note that there are three subtypes [1]. While all of the subtypes can be found in the heart, the predominant subtype in the vasculature is the β2-AR. Importantly, norepinephrine and epinephrine are the endogenous agonists (catecholamines) that bind specifically to all three β-AR subtypes.

Pharmacologically, β1- and β2-receptors are characterized by an equal affinity for the exogenous agonists isoproterenol and epinephrine, while norepinephrine (the neurotransmitter of the sympathetic nervous system) has a ten- to thirty-fold greater affinity for the β1-AR subtype. Also, β1-ARs are more closely located to synaptic nerve terminal than β2-ARs, thereby being exposed and activated by higher concentrations of released norepinephrine.

15.4.2 β-AR Activation and Cardiovascular Function

Cardiac β-ARs are likely one of the most important types of receptor systems. β-ARs regulate important cardiovascular functions and are integral to the body's *flight or fight* response. For example, during exercise, heart rate and contractility increase, cardiac conduction accelerates, and cardiac relaxation, an active process requiring adenosine triphosphate (ATP), is enhanced. Moreover, vascular relaxation (vasodilation) of many vascular beds can be observed during exercise (e.g., in skeletal muscles). All these effects are at least partially a direct consequence of β-AR activation and involve key elements of G protein receptor signaling: (1) receptor binding, (2) G protein activation, and (3) activation of an effector system. Importantly, most of these specific physiological cardiac effects are mediated via activation of β1-AR, while the vascular effects are mediated through the β2-receptor subtype. However, heart muscle also contains β2-receptors (as well as β3 receptors). Nevertheless, the β1-receptor subtype is the predominant cardiac isoform in healthy humans. More specifically, while there is a substantial population of β2-receptors in the atria, only around 20–30 % of the total β-AR population is β2-ARs in the left ventricle [2]. Not only is the activation of β-ARs and their associated signaling transduction critical in understanding the physiology of the cardiovascular system, but it has been recognized over the past decades that β-AR activations also play key roles in cardiac disease processes such as heart failure [3]. For example, an apparent paradox exists, namely, that β-adrenergic blockers (β-receptor antagonists) are beneficial in patients with heart failure; this will be discussed in more detail later in this chapter.

15.4.2.1 Effects of β-Receptor Activation on the Heart

β-Receptor activation on the heart regulates cardiac function on a beat-to-beat basis. Specifically, β-AR stimulation causes: (1) increases in heart rate (positive *chronotropic* effect), (2)

Table 15.2 Beta-adrenergic receptor subtypes: G proteins, tissue distributions, effectors, and signals

Receptor	β1	β2	β3
Primary G protein	Gs	Gs/Gi	Gs/Gi
Tissue distribution	Heart	Vessels, heart, lung, kidney	Adipose, heart
Primary effector in heart tissue	Adenylyl cyclase, L-type calcium channel	Adenylyl cyclase, L-type calcium channel	Adenylyl cyclase
Signals	cAMP/PKA	cAMP/PKA, MAPK	cAMP/PKA

cAMP cyclic adenosine 3′,5′-monophosphate (cyclic AMP), *Gi* inhibitory G protein, *Gs* stimulatory G protein, *MAPK* mitogen-activated protein kinase, *PKA* protein kinase A

increases in contractility (positive *inotropic* effect), (3) enhancements in cardiac relaxation (positive *lusitropic* effect), and/or (4) increases in conduction velocities (positive *dromotropic* effect). The molecular mechanisms leading to each of these specific effects will be discussed briefly. For further details, the reader is referred to the textbook by Opie [4]. Other important effects on cardiac myocytes that should be noted include those due to enhanced metabolism; the most significant effects on dilation in the coronary vasculature are mediated via metabolic waste products (CO_2, etc.). Also see Chap. 21 for a detailed discussion of energy metabolism and feedback mechanisms.

15.4.2.2 Positive Chronotropic Effect

When activated, β-ARs located on the cells that make up the sinoatrial node increase the firing rate of the sinoatrial node. While the mechanisms of these effects are not fully understood, they are known to involve activation of G proteins and formation of cyclic adenosine monophosphate (cAMP), called a *second messenger*. Cyclic AMP can then bind to ion channels that are, in part, responsible for the diastolic (phase 4) depolarization of sinoatrial nodal cells. These ion channels, referred to as hyperpolarization-activated cyclic nucleotide-gated channels, have several unique properties, as they: (1) activate during hyperpolarization (more negative membrane potentials), (2) are responsive to cAMP, (3) are conductive for both Na^+ and K^+ ions, and (4) can be blocked by cesium. Cyclic AMP binding to the intracellular domain of these ion channels shifts their activation curves to more positive potentials, which increases the rates of "spontaneous" depolarization of sinoatrial nodal cells and ultimately their firing rates. The chronotropic effects can also be mediated via norepinephrine released from sympathetic nerve endings in the sinoatrial node and/or from circulating catecholamines (epinephrine and norepinephrine). From an integrative physiology standpoint, an increasing heart rate is an adaptive response to an increased demand of oxygen and cardiac output in the periphery. Accelerating the heart rate will, in turn, increase cardiac output if stroke volume remains constant (cardiac output = heart rate × stroke volume).

15.4.2.3 Positive Inotropic Effects

As mentioned before, cardiac output needs to increase during exercise. One way to accomplish this is by increasing the heart rate; another is to increase stroke volume, e.g., by increasing cardiac filling (or increasing the preload). This can be accomplished by increasing the venous tone of the great veins that will increase filling of the heart chambers. It should be noted that this is an effect that is also mediated by adrenergic receptors but, in this particular case, by α-ARs causing venoconstriction (secondary to increased calcium influx). Such an increased preload then induces increased filling (and stretching) of the myocardial chambers, and via the Frank-Starling mechanism, stroke volume becomes augmented. However, stroke volume can also be efficiently improved by increasing the contractile force of the heart muscle at a given constant muscle length (i.e., independent of fiber length); this is called a positive inotropic effect and is mediated by activation of β-ARs, both β1-AR and β2-AR. The detailed molecular mechanisms involve the following processes (Fig. 15.3):

1. β-Agonist binds to either β1- or β2-receptor.
2. GTP binds to the stimulatory α-subunit of the G protein (Gαs) and activates it.
3. The G-subunits dissociate (the α-subunit dissociates from the β-subunit and χ-subunit).
4. The α-subunit (containing GTP) stimulates an effector protein called adenylyl cyclase (AC).
5. Cyclic 3′-5′ cAMP is formed and GTP is hydrolyzed to GDP (guanosine diphosphate) plus Pi (the α-subunit/GTP is a GTPase).
6. The α-subunit/GDP binds to the β- and χ-subunits, and the initial (inactive) resting state reforms.

15.4.2.4 The Second Messenger Concept

cAMP is one of the key effector molecules in many of the signaling processes involving β-ARs (but also in many other biologic receptor systems). This molecule is commonly referred to as a *second messenger* and is one of many such molecules identified that are involved in cellular signal transduction. Another highly relevant second messenger is cyclic guanosine monophosphate (cGMP); cGMP is typically formed in vascular cells after binding nitric oxide, but can also be formed in cardiac and other cells after binding natriuretic peptides. As the name implies, these molecules trigger additional signaling mechanisms. Importantly, cAMP is present in all cardiac myocytes; it is rapidly turned over, and there is a constant dynamic balance between cAMP generation and breakdown via phosphodiesterases (enzymes breaking down cAMP). While cAMP can increase in response to β-adrenergic activation, there are other pharmacologically active agents that can lead to increased cAMP levels via alternate mechanisms. For example, glucagon is known to stimulate AC via a non-β-AR mechanism; forskolin stimulates AC directly; phosphodiesterase inhibitors such as milrinone, amrinone, and others inhibit the breakdown of cAMP resulting in increased cAMP levels. The exact mechanism of how formation of cAMP leads to increased cardiac contractility in cardiac myocytes will be further discussed below.

It is known that cAMP enhances the activity of protein kinase A. Once activated, protein kinase A causes the subsequent phosphorylation of numerous proteins including voltage-dependent sarcolemmal calcium channels, phospholamban (located in the sarcoplasmic reticulum), troponin

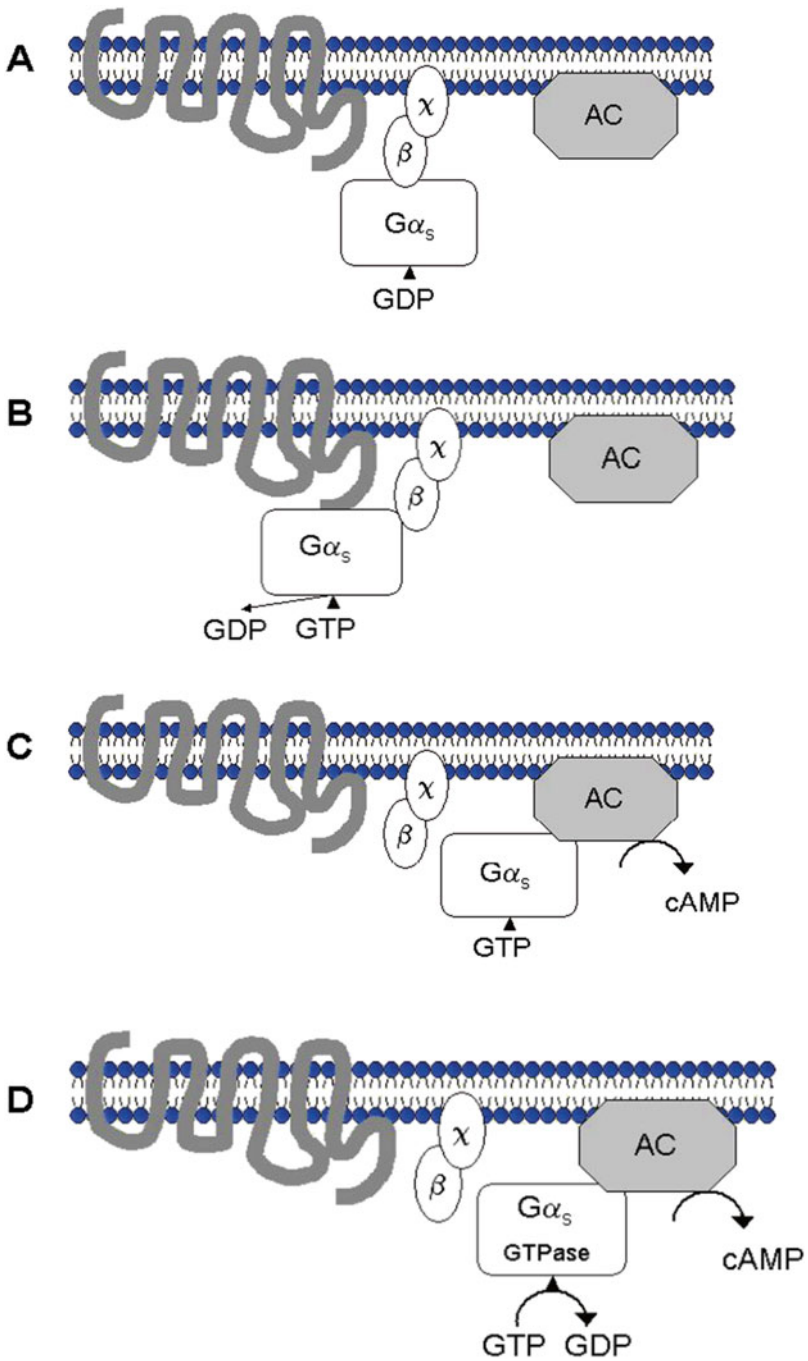

Fig. 15.3 G protein receptor activation and coupling with adenylyl cyclase (*AC*) during β-adrenergic receptor activation. *Panel A*: The receptor is inactive; GDP (guanosine diphosphate) is bound to α-subunit of stimulatory G protein. *Panel B*: The agonist binds to receptor which leads to receptor G protein interaction; GTP (guanosine triphosphate) binds to stimulatory G proteins (α-subunit, Gαs). *Panel C*: The G-subunits dissociate and Gαs stimulates adenylyl cyclase, with subsequent formation of cAMP (cyclic adenosine monophosphate). *Panel D*: Gαs GTPase becomes active, GDP reforms, and the activation cycle ends

I, and troponin C. The primary effect of phosphorylating the calcium channels and phospholamban is that this will increase calcium influx during a cardiac activation cycle and also increase calcium uptake by the sarcoplasmic reticulum. Working in concert, these effects will ultimately result in increased calcium transients during cardiac excitation-contraction coupling. Further, these increased intracellular calcium transients will result in increased ATP splitting by the myosin ATPase, which then increases the rate of development of contractile force (and also increases deinhibition of actin and myosin by the interaction of calcium with troponin C), ultimately causing an increase in total cardiac force development. If this stimulation is maintained, this effect or response often becomes attenuated over time. Also, cAMP levels may decrease, for example, due to activation of calmodulin that activates cAMP breakdown via phosphodiesterase activation and also via activation of β-AR kinase (β-ARK activation and downregulation).

It is important to recognize that the cellular and physiological responses to β-AR stimulation cannot simply be explained by overall increased tissue levels of cAMP. It has been speculated that cAMP may be compartmentalized in the heart, with

a specific compartment available to increase contractility [5]. In addition, it has been shown that β2-ARs and β1-ARs, which both mediate positive inotropic responses, are so largely independent on cAMP generation. This latter response may, in some cases, be one of the myopathic mechanisms in chronic heart failure by resulting in increased systolic and diastolic calcium levels [6]. The complexity of the β-AR stimulatory G protein adenylyl cyclase signaling system can be further illustrated by the fact that there are about 20 identified Gα-subtypes, about 5 β-subtypes, and about 11 χ-subtypes, in addition to about nine isoforms of AC [7]. In cardiac tissue, isoforms V and VI of AC are considered to predominate. It should also be noted that specific anchoring proteins enable the juxtaposition of protein kinase A with its specific target proteins (A-kinase anchoring proteins), which may account for the resulting compartmentalization (and complexity) of responses.

15.4.2.5 Positive Lusitropic Effects

Phospholamban can be activated by protein kinase A (via cAMP) or by increased calcium levels subsequent to voltage-gated calcium channel activation (secondary to protein kinase A phosphorylation). This typical phosphorylation of phospholamban leads to increased activity of this enzyme, which then results in enhanced calcium removal from the cytosol back into the sarcoplasmic reticulum. It is known that the activation of troponin I, via protein kinase A, increases the rate of cross-bridge detachment and thus relaxation. Importantly, both of these responses will increase the rate of relaxation, an active process to remove calcium from the cytosol. A basic summary of the mechanisms of β-adrenergic increase in cardiac contractility and relaxation is provided in Fig. 15.4.

15.4.2.6 Dromotropic Effects

Activation of the voltage-gated (L-type) calcium channels in the atrioventricular node may enhance conduction in these nodal cells, as well as those of the Purkinje fibers.

15.4.2.7 Metabolic Effects

In general, the metabolic effects mediated via the β-AR system include (1) increases in glycogen formation (via increased glycogenolysis as well as decreased formation of glycogen), (2) the stimulation of lipolysis, and/or (3) increases in ATP production (via glycolysis/citrate cycle). Some of these metabolic effects may be mediated via the β3-AR (e.g., control of lipolysis). The β3-AR is also considered to have some regulatory function in cardiac (and vascular) contractility (e.g., negative inotropic effects) [8].

15.4.2.8 Effects of β-Receptor Activation in the Vasculature

The main physiological function of β-AR activation in the vasculature is induced relaxation (vasodilation), which occurs via a reduction of cytosolic calcium levels in the smooth muscle cells (SMCs) composing these vessels, with relaxation having the greatest importance in arterioles. These relaxation responses are mediated via the β2-AR subtype and are antagonized by α-AR activation (α1-receptor subtype).

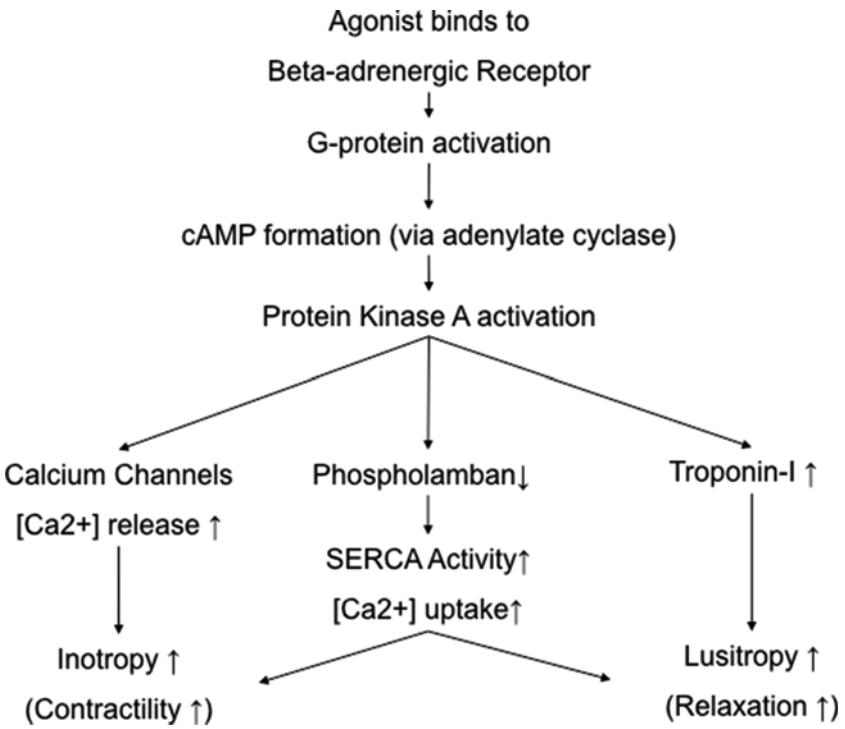

Fig. 15.4 The major intracellular signaling mechanisms involved in the regulation of cardiac contractility and relaxation following β-adrenergic receptor activation. It should be noted that there is also the possibility that L-type voltage-dependent calcium channels can be activated via a direct effect of a stimulatory G protein (Gαs) subsequent to β-adrenergic receptor (both β1- and β2-adrenergic receptors) activations. This overall signaling pathway is cAMP independent. The resulting increased systolic and diastolic calcium fluxes are considered to become a potentially myopathic mechanism in chronic heart failure

The effects of α-receptor signal transduction will be discussed further below.

15.4.3 β-AR Regulation

To best understand β-AR regulation, it is useful to review the molecular structure of this receptor. Basically, the receptor is composed of three types of domains: (1) the extracellular domain, (2) the transmembrane domains which are involved in the agonist and antagonist binding (ligand binding), and (3) the intracellular or cytoplasmic domains which are important for G protein interactions and interactions with kinases such as β-ARK (β-adrenergic receptor kinase) (Fig. 15.2).

15.4.3.1 β-Adrenergic Receptor Desensitization and Downregulation

Receptor *downregulation* can be defined as a reduced presence in functional numbers of receptors in the cell membrane. Downregulation can result from internalization (and destruction in lysosomes), decreased rates of receptor degradation (nonlysosomal), and/or decreased synthesis. *Desensitization* is typically defined as receptor refractoriness, a "state of decreased activity following continued stimulation." Yet, it should be noted that there is not always clear distinction between these two definitions in the literature. For example, the β-receptor can become desensitized during isoproterenol stimulation (a classic pharmacological β-adrenergic agonist). In contrast, during continuous β-AR stimulation, the enzyme β-ARK increases its activity; β-ARK phosphorylates the cytoplasmic domain sites of the β-AR (Fig. 15.2) and is able to uncouple the receptor from the Gαs (stimulatory G protein). This response acts as a block of the signal, and activation of adenylyl cyclase is decreased; in other words, adenylyl cyclase is uncoupled from the β-AR. Resensitization occurs once the receptor has been dephosphorylated; this mechanism is called *agonist-specific desensitization*. In contrast, *non-agonist-specific* desensitization can occur via second messenger cAMP (and also via diacylglycerol which activates protein kinases A and C) that phosphorylates the G protein-coupled receptors.

Specific examples of "physical" downregulation include internalization of receptors during continuous prolonged β-AR stimulation, which can be induced either pharmacologically (such as in an intensive care unit setting) or which is observed in heart failure (increased sympathetic tone and circulating catecholamines). This latter response may be a protective mechanism to minimize calcium overload of the cardiac myocytes secondary to β-adrenergic stimulation. Additional clinical examples of receptor regulation include "hypersensitivity" to β-AR agonists after propranolol (a β-AR blocker) withdrawal, following long-term use. This enhanced sensitivity is considered to be due to receptor externalization. Another example is drug tolerance to dobutamine (or other β-AR agonists); the molecular mechanisms underlying this clinical phenomenon may be desensitization.

While agonist-specific and unspecific desensitization can be viewed as one of the classical concepts of receptor regulation, G protein receptor kinases, such as β-ARK and associated proteins (β-arrestins), seem to function by other mechanisms. For example, β-arrestins are considered to interact with a G protein-coupled receptor and thus inhibit further G protein coupling after the receptor has been phosphorylated by β-ARK. While this more traditional role is now well established, β-arrestins have also been shown to be involved in receptor internalization as well as complex additional signaling mechanisms (e.g., mitogen-activated protein kinase pathways) [9, 10]. Internalization (also known as *sequestration* or *endocytosis*) is generally considered to serve various other functions including receptor resensitization (dephosphorylation) and recycling and/or altering signaling processes. Typically, the mechanisms of internalization involve the classical described clathrin-coated pit processes (caveolae) and also noncoated pit mechanisms. Another interesting role of β-arrestins is in ubiquitination; this is a means by which proteins are marked for subsequent degradation. For example, β-arrestin ubiquitination is important for β1-AR internalization, while receptor ubiquitination is necessary for lysosomal targeting and degradation of the receptors [11]. The gene regulation of the β-AR has been reviewed nicely elsewhere [7]).

15.5 The Association Between β-ARs and Cardiac Disease

The function of the β-AR signaling pathway is not only of great importance in the normal regulation of physiological cardiac vascular function but has critical, although different, roles in the development of chronic heart failure. In general, heart failure is a syndrome defined by an inability of the heart to pump adequate amounts of blood to the body organs. The normal physiological response to an inadequate blood (oxygen) supply is to increase the cardiac output (and thereby oxygen delivery) via activation of the adrenergic nervous system (sympathetic nervous system); this response is characterized by an increase in circulating catecholamines. While this sympathetic response would intuitively be seen as beneficial, and indeed is also initially adaptive, in reality, the sustained β-AR activation and increased norepinephrine tissue levels [12] are considered to be associated with negative biological effects. Therefore, a sustained β-AR response in the cardiac patient may be, in fact, considered both maladaptive and inappropriate. Consistent with this notion, adrenergic drive is increased in all chronically failing human hearts with systolic dysfunction, as well as in all animal models of hemodynamic overload. Thus, adrenergic drive can also be considered as a *servo-control* mechanism to maintain cardiac performance at an acceptable level [7]. For example, the proportion of β1- to

β2-adrenergic subreceptor population in normal human ventricles shifts from 70:30 in diseased human ventricles to about 50:50 in normal human ventricles [1]. Also on the molecular level, both receptor subtypes are typically desensitized, due to uncoupling of the receptors from their signaling pathways associated with both increased β-AR phosphorylation and upregulation of the inhibitory G protein, Gi.

To illustrate the maladaptive β-AR signaling response, it is important to consider that β-adrenergic agonists, given to patients with chronic heart failure, may actually increase mortality. In contrast, the administration of β-blockers has been shown to improve patient survival; β-AR blockers continue to be one of the cornerstones of medical/drug therapy for patients with chronic heart failure.

In certain patients with cardiac failure, there is a situation where increased adrenergic drive is required to maintain the circulatory needs of their bodies; the more the heart is activated adrenergically, the more profound are the effects of desensitization which, in turn, activates the adrenergic system even more, ultimately causing myocardial tissue damage. Based on the studies in which β-AR blocking agents were administered, it is generally believed that the β-AR system is central in this vicious pathological cycle (or positive feedback loop), which is commonly characterized by progressive remodeling and myocardial dysfunction.

15.5.1 Beta-Adrenergic Signaling and Heart Failure

One of the hallmarks of chronic heart failure is adrenergic overdrive leading to β-AR downregulation and desensitization. In particular, β1-ARs have been shown to be downregulated selectively, while the β2-ARs are relatively increased so that, as mentioned above, the population of β1 to β2 shifts from 75/25 to about 50/50. The marked uncoupling of the β-ARs from the G proteins is due to increased levels of β-ARK1, as well as an increased inhibitory G protein (Gi) [14]. This, in turn, results in not only attenuated β-AR signaling but also activation of additional pathways involved in ventricular remodeling.

The shift of the β1-/β2-AR subpopulation to an increased number of β2-receptors is only one of the phenomena associated with chronic heart failure. More specifically, β2-ARs couple to a number of signaling pathways, including a potential coupling to an inhibitory G protein (Gαi). Also, β2-ARs may modulate several G protein-independent pathways, including inhibition of sodium-hydrogen exchanges as well as a nonprotein kinase A-dependent interaction with L-type calcium channels [6, 15]. There are other G protein-independent pathways in which the β2-ARs have been implicated, such as those associated with phosphatidylinositol kinase, phospholipase C/protein kinase C, and/or arachidonic acid signaling. And while many details of these pathways remain poorly understood, it is becoming more clear that some of these pathways play important roles in the molecular pathobiology of heart failure.

One of the widely recognized mechanisms of β-AR desensitization is agonist-dependent β-ARK-mediated phosphorylation of the β-AR itself. Moreover, the beta-gamma subunits of the G proteins can act as signaling molecules themselves, with the potential of activating many downstream targets of pathways such as adenylyl cyclases, PLC, PLA2, PI3K, K^+ channels, and/or Src-Ras-Raf-MEK-MAPK (mitogen-activated protein kinase) [7].

The potentially toxic effects of long-term β1-AR activation are also illustrated by the fact that selective β1-AR agonist or receptor overexpression leads to increased cardiac *apoptosis* or programmed cell death [16–18]. The mechanisms by which such apoptosis is activated have been attributed, in part, to initial activation of calcineurin via increased intracellular calcium through L-type calcium channels [19]. Additionally, direct toxic effects of catecholamines on the myocytes have been described as a result of direct β-AR activation [12]. Other effects of chronic β-AR signaling include production of cytotoxicity via calcium overload, increased free radical formation, as well as stimulation of pathologic hypertrophy [7]. For example, the marked uncoupling of β1- and β2-receptors from their physiological signaling pathways not only results in attenuation of the β-AR signaling but also allows for the coupling of the receptors with other possible myopathic signaling pathways involved in ventricular remodeling (e.g., MAPK and PI(3)K cascades). As stated earlier, β-receptor antagonists may be a beneficial therapy in the chronic heart failure patient. Specifically, the β1-specific β-AR blocking drug metoprolol produces reverse remodeling similar to a combined α-β-blocker carvedilol, suggesting that β1-AR signaling is an important determinant of pathologic hypertrophy in human heart failure [20].

Lastly, genetic heterogeneity in expression of the β-AR in the general population has been identified which may be associated with disease susceptibility. For example, a substitution of threonine to isoleucine at amino acid 164 in the β2-AR has been linked with reduced survival and exercise tolerance in patients with heart failure [21, 22].

A summary of the known changes in β-AR signaling is provided in Table 15.3. Lastly, it should be mentioned that inves-

Table 15.3 β-Adrenergic receptor signaling pathways in heart failure

Molecule	Change
β1-AR	↓, uncoupled
β2-AR	NC, uncoupled
β-ARK1	↑
β-Arrestins 1 and 2	NC
Galpha1	↑

AR adrenergic receptor, *ARK* adrenergic receptor kinase
Modified from [1]

tigations using transgenic animal models have greatly helped to elucidate some of the important disease mechanisms associated with adrenergic receptor reception pathways; they have also served as tools in identifying and testing novel or evolving therapeutic targets for the treatment of heart failure [1].

15.6 Alpha-Adrenergic

15.6.1 Physiology

Two major α-AR subtypes have been identified—α1 and α2. The α1-type receptors have been described to be present in the heart, as well as in the vessels and smooth muscle. The primary response to their activation in cardiac cells is phospholipase C-β which leads to an increase in diacylglycerol and inositol triphosphate ($InsP_3$) and also activates both protein kinase C and MAPKs. Physiological receptor agonists include norepinephrine and epinephrine, and a Gq protein is the primary associated G protein [23]. In general, the primary physiological importance of α1-receptors is far greater in the vasculature, leading to calcium influx and vasoconstriction via the second messenger $InsP_3$. In cardiac muscle cells, α1-receptors have been shown to induce a positive inotropic effect; like β-receptors, this response is also associated with formation of $InsP_3$ [24]. Alpha-2-receptors have been identified on coronary vessels, as well as in the central nervous system (presynaptic); they reduce the activity of AC (and protein kinase A) via an inhibitory G protein.

In summary, the primary physiological role of α1-receptors is for the vasculature regulation of tone via vasoconstriction, which is secondary to calcium influx into the SMCs of the circulatory arterioles.

15.6.2 Role in Disease States

In general, in heart failure patients, the α1-AR system will elicit an increase in receptor density and is also characterized by changes in inotropic responses [25]. In addition, α1-AR activation has been shown to promote cardiomyocyte hypertrophy via activation of hypertrophic MAPK pathways).

15.7 Role of Adrenergic and Other Receptors in Myocardial Hypertrophy

Prolonged or repeated increased workloads on the heart lead to cardiac hypertrophy. Hypertrophy is typically characterized by increased contractile protein content (and muscle mass), myofilament reorganization, and reexpression of embryonic markers. As discussed earlier, myocyte cell growth by G protein-coupled receptors may involve not only Ras and MAPK pathways but also other signaling pathways (e.g., calcineurin, PI3K, and phosphatidylinositol-3-OH). Abnormal β-AR function with elicited hypertrophy is also characteristic; in particular, elevated myocardial levels of β-ARK1 can be detected [26]. As mentioned above, α1-receptor signaling also may be very important in the development of cardiac hypertrophy. Specifically, Gq-coupled receptors, such as angiotensin, α1-AR, and endothelin, can all activate hypertrophic MAPK pathways [27, 28]. To summarize, the cardiac hypertrophic response may not be compensatory to reduce wall stress but rather maladaptive and thus increase mortality. In particular, signaling pathways involving elevated catecholamine levels (norepinephrine and epinephrine) and activated Gq-coupled receptors seem to promote hypertrophic responses. Thus, targeting these specific signaling pathways may be a novel therapeutic approach for the potential treatment of "maladaptive" cardiac hypertrophy and ultimately heart failure. For further details on this topic, the reader is referred to the review by Rockman et al. [1].

15.8 Muscarinic Receptors

15.8.1 Physiology

The muscarinic receptor system in the heart is also an associated G protein-coupled receptor system, one fairly similar to the β-AR. The main cardiac receptor subtype (M2 receptor) is a cholinergic receptor and thus mediates primary parasympathetic (syn. nervus vagus, cholinergic, acetylcholine mediated) nervous system responses. For more details, refer to Chap. 14. Its general function is to simultaneously balance and antagonize the sympathetic effects of β-AR activation, with its most pronounced effects on the controls of the sinoatrial (heart rate, chronotropic effect) and atrioventricular nodes (conduction, dromotropic effect). There exist very few muscarinic M2 receptors in the ventricles, so activated negative inotropic (contractility) effects subsequent to M2 receptor activation are very small. The primary control signal mediated via the vagus nerve is that which leads to a local release of acetylcholine in the sinoatrial and atrioventricular nodes. Acetylcholine then binds to the M2 receptor, activates an inhibitory G protein (Gαi), and essentially decreases the activity of adenylyl cyclase, which directly leads to opening of K^+ channels. Thus, in the sinoatrial node, vagal stimulation tends to a flattening of the diastolic depolarization, which then induces a slowing of heart rate (bradycardia, negative chronotropic effect) possibly via the effects of reduced cAMP availability on I_f current (hyperpolarization-activated cyclic nucleotide-gated channel) but also via activation of a potassium outward current which in concert decreases the spontaneous firing rate of the sinoatrial node. In the atrioventricular nodal tissue, vagal stimulation also activates an inhibitory G

protein, which typically causes a slowing conduction velocity via a decreased calcium influx through L-type calcium channels. Clinically, the effects of vagal stimulation on the atrioventricular node are detected as increased atrioventricular nodal conduction times (e.g., prolonged PR interval).

The M3 muscarinic subtype is primarily found in vascular SMCs. Its activation leads to contraction of vascular smooth muscles via a Gq/11-PLC-InsP3-mediated calcium influx (as well as diacylglycerol/phospholipase C/protein kinase, cAMP elevation).

15.9 Other G Protein-Coupled Cardiovascular Receptors

There are other G protein-coupled cardiovascular receptor systems which have important roles in cardiac physiology and pathophysiology, yet it is beyond the scope of this chapter to review all these systems in detail. However, for some degree of comprehensiveness, a current list of important G protein-coupled receptor systems and their respective functions is provided in Table 15.4.

15.10 Receptor Cross Talk

Cross talk between receptors refers to a biological phenomenon whereby interactive regulatory (or modulatory) messages are sent from one receptor to another. Many of the aforementioned receptor pathways are engaged in some degree of cross talk, which is commonly via second messengers and/or protein kinases which, in turn, modulate G protein-mediated messages. While the current understanding of receptor cross talk is far from being complete, it is clear that receptor cross talk is integral for sustaining a coherent function of the cardiovascular system and has implications in both normal physiology and elicited cardiac disease states.

The following is an example of one such cardiovascular cross-talk interaction and its relevance to the pharmacological treatment of disease. Heart failure is generally characterized by dysfunction of the β-AR system (downregulation of β1-receptors, uncoupling of β-AR and AC) but also the renin-angiotensin system (downregulation of AT1 receptors); distinct signaling pathways have been identified which then characterizes both β-AR (e.g., via Gs and AC) and AT1 receptor signaling (e.g., via Gq/11 and PLCβ). In a recent study, it was shown that selective blockade of β-AR inhibited angiotensin-induced contractility, while selective blockade of AT1 receptors reduced catecholamine-induced reduction in heart rate [29]. These unusual transinhibitory effects were considered to be caused by underlying G protein receptor uncoupling. Furthermore, direct interactions of these receptor systems were demonstrated in vivo, and it is speculated that such interactions may have a profound role in determining the ultimate responses to drugs designed to block a given receptor subtype (e.g., β-AR blockers, AT1-receptor blockers). Note that cardiovascular receptor cross talk has been extensively reviewed by Dzimiri [30].

15.11 Guanylyl Cyclase-Linked Receptors

15.11.1 Soluble Guanylyl Cyclase (Receptor for Nitric Oxide)

Although structurally different, the general principles of receptor signaling as discussed for the β-AR apply also for nitric oxide/guanylyl cyclase signaling. Specifically, the ago-

Table 15.4 Other cardiovascular G protein-coupled receptor systems

Family	Type	Cardiovascular function	G protein	Signaling
Adenosine	A1	Bradycardia	Gi/o	AC inhibition; K^+ opening
	A2A	Vasodilation	Gs/G15	AC, PLCβ
	A2B	Vascular smooth muscle relaxation	Gq/11?	PLC/AC-mediated calcium activation
	A3	A1 modulation	Gi3	AC inhibition; PLC, InsP3-mediated calcium increase
Angiotensin	AT1	Vascular smooth muscle contraction; cell proliferation; cell hypertrophy; antinatriuresis	Gq/11	PLC/PKC-mediated calcium elevation
	AT2	Vasodilation; apoptosis; growth inhibition; natriuresis; nitric oxide production	Gia2/Gia3	MAPK activation; K^+ opening; PTPase activation leading to T-type calcium channel closure
Endothelin	ETA	Vasoconstriction	Gq/11	PLC/InsP3; cAMP
	ETB	Vasodilation/vasoconstriction (ETB2)	Gi; Gq/11	cAMP inhibition; PLC/InsP3 calcium increase
Opioid	OP1 (delta), OP3 (mu)	Central cardiovascular regulation (OP1, 3); cardioprotection (OP1)	Gialpha1/3; Go	IK conductance activation; reduction in neuronal Ica; AC inhibition; PKC and KATP channel activation (cardioprotection)

AC adenylyl cyclase, *cAMP* cyclic adenosine monophosphate, *MAPK* mitogen-activated protein kinase, *PKC* phospholipase C/protein kinase

nist nitric oxide (NO) is considered as a universal signaling molecule present in all tissues, and the role of NO signaling is similar to other signal transduction systems, not only important in normal cardiac function but also in disease processes. Physiologically, nitric oxide is produced by several isoforms of the enzyme nitric oxide synthase (NOS). To date, three isoforms have been described to function within the cardiovascular system—eNOS, iNOS, and nNOS. Nitric oxide is a small, lipid-soluble, gas molecule that readily crosses cell membranes. Inside the cell, it typically binds to a receptor, the soluble (cytoplasmic) guanylyl cyclase (GC, an enzyme which converts GTP to cyclic 3′-5′ GMP). Cyclic GMP is the second messenger in this signaling cascade and, in the cardiovascular system, can activate two major effector systems—cGMP-regulated phosphodiesterases and cGMP-dependent protein kinases (cGKs).

In the vascular SMCs, NO inhibits vascular smooth muscle constriction (causes vasodilation) via inhibition of cytoplasmic calcium release. However, the underlying mechanisms for the important vasodilatory effect of NO are complicated and minimally involve a cGMP-dependent protein kinase (cGKI); these pathways have been reviewed in detail elsewhere [31]. Nitric oxide has also been shown to reduce vascular smooth muscle proliferation (clinically important in in-stent restenosis) and migration. It is well established that NO release may reduce platelet adhesion and activation, as well as vascular inflammation [32]. Importantly, NO insufficiencies are considered to be an important factor in endothelial dysfunction, leading to the increased susceptibility for arterial thrombosis formations [33].

Nevertheless, the relevance of NO signaling is not limited to vascular biology or pathobiology; it has been demonstrated that NO has an important pathophysiological role in heart failure as well, i.e., in the modulation of cardiac function, cardiovascular protection, and/or in the regulation of apoptosis [34–36]).

15.11.2 Membrane Guanylyl Cyclase-A (Receptors for Natriuretic Peptides)

To date, at least seven membrane-bound enzymes synthesizing cyclic GMP (cGMP) have been identified. All seven of these membrane guanylyl cyclases (GCs) have a common structure (Fig. 15.5). For the purpose of this discussion, guanylyl cyclase-A has the greatest importance relative to the heart and will be discussed in detail.

15.11.3 Physiology

Currently, three natriuretic peptides have been identified—ANP, BNP, and CNP. Both ANP and BNP bind to GC-A and

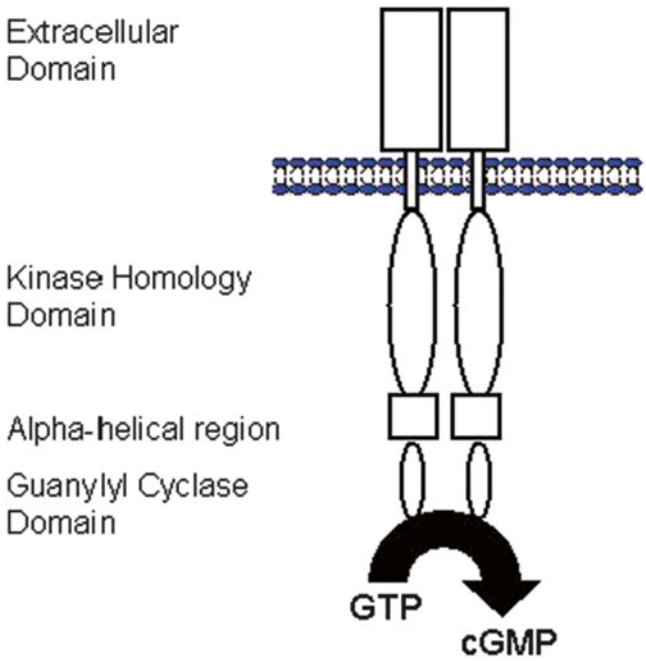

Fig. 15.5 Basic topology of membrane GC-A receptor. The membrane GC (guanylyl cyclase) form homodimers or higher-order structures (modified from [37]). *cGMP* cyclic guanosine monophosphate, *GTP* guanosine triphosphate

are released in the heart; they are considered as cardiac hormones. In general, CNP is mainly produced by the vascular endothelium and may be a regulator of vascular tone and cell growth through GC-B activation. This receptor consists of an extracellular domain, a kinase homology domain, an α-helical amphipathic region (hinge region), and a C-terminal guanylyl cyclase (catalytic) domain (Fig. 15.5). This receptor is considered to exist in dimers (two molecules coupled together).

The major effects of GC-A are via the formation of, and the activation by, cGMP. Since, in general, the agonists are circulating hormones (peptides), a variety of organ systems can be affected simultaneously following ANP/BNP release. ANP is mainly produced in the atrium, while BNP is produced primarily in the ventricles. The primary triggering factors for ANP/BNP release are wall stretch and/or pressure increases, but their release may also involve neurohumoral factors (glucocorticoids, catecholamines, angiotensin II, etc.). The primary effect of ANP/BNP release is modulation of blood pressure/volume; the half-lives of ANP/BNP are around 2–5 min. Interestingly, although both ANP and BNP bind to the same receptors, it has been shown that targeted genetic disruption of ANP or BNP in mice induces a unique phenotype; ANP-deficient mice show arterial hypertension, hypertrophy, and cardiac death. In contrast, the BNP-deficient mice phenotype is characterized by mostly cardiac fibrosis. More specifically, BNP has a lower affinity to GC-A than ANP and may act mostly as a local paracrine (antifibrotic) factor. Also, under physiological conditions, the ANP

levels are much higher than BNP levels in the circulating blood, and the potency for induced vasorelaxation is also less for BNP vs. ANP [37].

Nevertheless, the cardiovascular effects of ANP-GC-A are complex, but can generally be summarized as inducing hypovolemic and hypotensive effects, which are induced via hormonal, renal, vascular, central nervous system, and/or other mechanisms. The most important hypotensive effects also involve associated decreased sympathetic activity and complex renal responses which subsequently lead to increased diuresis [37].

15.11.4 Role in Cardiac Disease

During chronic hemodynamic overload, ANP and, to an even greater level, BNP expression in the cardiac ventricles is significantly increased. This response may not only be for the maintenance of arterial blood pressure and volume homeostasis but also as local antihypertrophic (ANP) and antifibrotic (BNP) factors. While ANP/BNP levels are increased in patients with cardiac hypertrophy and/or heart failure, the GC-A-mediated effects of these peptides are diminished. Mechanisms for these responses may be postreceptor defects such as dephosphorylation of GC-A, sequestration of natriuretic peptides by a clearance receptor, altered transcriptional regulation at the gene level, and/or others [30].

15.12 Vascular Response to Drug Eluting Stents (DES): Inflammation, Neointimal Formation, and Endothelial Function

15.12.1 The History of Angioplasty/Stenting

Percutaneous transluminal coronary angioplasty (PTCA) was introduced in 1977 as a novel device-based therapy for occlusive coronary artery disease and has been quickly accepted due to its established benefits [38, 39]. Basically, this technology enabled the physician to advance a balloon catheter to an occluded coronary artery via a minimally invasive image-guided catheter procedure. After identification of the culprit lesion, the physician would advance the catheters to that site and, using wire and catheter technology, inflate the balloon catheter to reopen the narrowed vessel and thus restore critically reduced blood flow. While this technique revolutionized the treatment of coronary artery disease, it was not without problems. Balloon angioplasty may, in itself, result in vessel injury, initiating negative vessel remodeling and neointimal proliferation, thus leading to a high incidence (30–50 %) of restenosis [37]. The introduction of bare metal stents in 1994 changed the face of interventional cardiology. Bare metal stents clearly demonstrated superiority over balloon angioplasty alone due to prevention of the elastic recoil and the negative remodeling effects [40–43]; nevertheless, neointimal proliferation continued to be a significant problem. In fact, bare metal stenting created a new disease—in-stent restenosis (ISR). The prevalence of ISR increased proportionally with use of stent implantation [44]. This was particularly true in patients with complex lesion subsets, such as diabetes, bifurcated lesions, long diffuse lesions, and/or in small vessels in which the restenosis rate remained as high as 30–60 % [45, 46]. DESs were introduced in 2003 to prevent or minimize ISR; they combined the mechanical benefits of bare metal stents with the controlled elution of a pharmacological agent that aimed to suppress neointimal proliferation [39, 47, 48]. Most DESs employed today consist of a metallic stent and a polymeric coating that controls a release of antiproliferative drugs [49]. By 2008, about 6 million people worldwide had been treated with DESs [50]. DESs have dramatically transformed the landscape of interventional cardiology, demonstrating substantial reduction in angiographic and clinical restenosis [51]. However, despite reduced restenosis rates, the frequency of in-stent thrombosis has not statistically decreased with DESs compared with bare metal stents [52, 53]. Stent thrombosis after percutaneous coronary intervention is an uncommon and potentially catastrophic event that might manifest as myocardial infarction and sudden death. Furthermore, recent data raise questions regarding the increased risk of late stent thrombosis; these events occur up to 3 years after implantation, and association with late stent thrombosis is often a more complex lesion in a higher-risk patient [54, 55]. There is still widespread controversy regarding the actual risks associated with DESs, as it relates to high morbidity and mortality [56].

15.12.2 The Vascular Biology of Restenosis

15.12.2.1 Overview

Restenosis can be defined as the arterial wall's healing response to mechanical injury, which results in neointimal hyperplasia and vessel wall remodeling [57, 58]. The cellular and molecular events and temporal sequence of events leading to restenosis have been described in animal models [59, 60] and include: (1) platelet aggregation, (2) inflammatory cell infiltration with release of inflammatory and growth factors, (3) medial SMC modulation and proliferation, and/or (4) proteoglycan deposition and extracellular matrix remodeling.

Interestingly, specific elastic wall remodeling is virtually absent after stent procedures, as observed by studies using volumetric intravascular ultrasound. Concerning ISR, the current paradigm is that injury, deendothelialization, and crush of the plaque due to stent deployment lead to immediate platelet activation and fibrin deposition [61]. The activated platelets, in turn, recruit circulating leukocytes from the blood stream to the injury site via surface expression of adhesion molecules, such as P-selectin. The leukocytes then

Table 15.5 Pathobiology of coronary angioplasty and stenting

PCI/stenting-related biology (post-PCI / stenting)	Effector cells (molecules)	Target cells	Therapeutically relevant agents
Endothelial denudation (min)	Endothelial cells	Smooth muscle cells Platelets	Nitric oxide inducers
Plaque rapture (min-days)	Macrophages (tissue factor, inflammatory cytokines)	Platelets	TF antagonists, platelet activation inhibitors PAR1 and PAR4 (protease-activated receptors) antagonists
Acute thrombosis (min-days)	Platelets (adhesion molecules)	Leukocytes/monocytes Neutrophils/T cells	Platelet activation inhibitors
Acute inflammation (hours-days)	Monocytes (growth factors and inflammatory mediators) Smooth muscle cells	Monocytes Smooth muscle cells Platelets	Anti-inflammatory agents
Neointimal formation	Smooth muscle cells Endothelial cells	Smooth muscle cells Endothelial cells	Inhibitors of cell cycle and proliferation Multiple MOA that modulate smooth muscle cell phenotype
Healing/reendothelialization (days-weeks)	Endothelial progenitor cells Platelets (SDF alpha, adhesion molecules, extracellular matrix)	Endothelial cells	Inducers of endothelial growth/function Cell- and gene-based therapy aimed at healing
Late stent thrombosis (30 days to years)	Endothelial cells Platelets Monocytes/macrophages	NA	

PAR1 protease-activated receptor 1, *PCI* percutaneous coronary intervention, *TF* tissue factor

bind tightly to the surface through these leukocyte integrin Mac-1 (CD11b/CD18) molecules. Driven by the chemical gradients of chemokines released from SMCs and resident macrophages, activated leukocytes then migrate into the tissue, and this is where they, in turn, release additional chemokines and growth factors. The growth factors that are subsequently released from platelets, leukocytes, and SMCs are believed to stimulate the migration of SMCs from the media into the neointima. The resultant neointima consists of SMCs, extracellular matrix, and macrophages recruited over several weeks. Cellular division takes place in this phase, which appears to be essential for the subsequent development of restenosis [61]. Subsequently, the artery enters the next phase of cell-driven remodeling involving both extracellular matrix protein degradation and resynthesis. Accompanying this period is a shift to fewer cellular elements and greater production of extracellular matrix protein, which is composed of various collagen subtypes and proteoglycans and constitutes the major component of the mature restenotic plaque. It should be noted that in the balloon-angioplastied artery, subsequent reorganization of the extracellular matrix protein (e.g., replacing hydrated molecules by collagen) may lead to shrinkage of the entire artery, thus negative remodeling [62]. In the stented artery, this phase has a reduced clinical impact because of negative remodeling, although constituents of extracellular matrix protein such as hyaluronan, fibronectin, osteopontin, and vitronectin also facilitate SMC migration [63]. In both balloon-angioplastied and stented arteries, reendothelialization of at least part of the injured vessel surface may occur. Continuous endothelial coverage, provided that the endothelium is properly functional, endows the stented vessel with a hemocompatible, antithrombotic, and anti-inflammatory lining [64]. Refer to Table 15.5 for a summary of the pathobiological events associated with coronary angioplasty and stenting.

Biology of Smooth Muscle Cells

In a normal vessel uninterrupted by turbulent flow, inflammation, or vascular disease, the SMCs are quiescent and thus elicit low levels of proliferative activity. In contrast, in response to mechanical injury following percutaneous coronary intervention and stenting, a biological cascade will be triggered that prompts SMCs to progress into an activated state [58]. More specifically, activated SMCs exhibit several phenotypic changes including switches in their differentiation phenotype (dedifferentiation), migration, proliferation, and/or increased protein syntheses [65]. In general, differentiated SMCs are spindle shaped, show contractile properties, and exhibit low frequency of proliferation, whereas dedifferentiated SMCs are rhomboid shaped and show a high degree of protein synthesis, proliferation, and migratory activity [65]. Platelet-derived growth factor-BB, produced by activated platelets, can modulate SMCs to evoke dedifferentiation phenotypes and has been shown to induce a suppression of the

SMC marker genes such as SM α-actin, SM-myosin heavy chain, and SM22α [66, 67].

The source of heterogeneous SMC populations that contributes to this vascular remodeling after vascular interventions is controversial and has been extensively studied by many researchers using various preclinical models. It is speculated that some of the potential sources of heterogeneous SMC are: (1) adventitia [68, 69], (2) in situ differentiation and expansion, and/or (3) distant sources such as the bone marrow [70].

Several signaling pathways have been described to be involved in SMC phenotype switching from differentiated to dedifferentiated SMCs. The most prominent pathway is the MAPK- MEKK1/2-extracellular signal-regulated kinase (ERK)1/2 pathway. The transposition of MAPK to the nucleus inhibits transcription of genes associated with the contractile phenotype and stimulates expression of genes associated with growth. The MAPK/ERK cascade is a well-known signal transduction pathway which governs migration, proliferation, survival, and apoptosis responses in SMC and various other cell types. MAPK/ERK is also considered to regulate the induction of growth factor secretion [70–72]. Upstream of the MAPK/ERK is a pertinent protein-tyrosine kinase receptor that is activated by a growth factor, resulting in receptor phosphorylation and binding of adaptor proteins such as Grb2 and Shc to the activated receptor. Adaptor protein binding leads to Ras activation of the GTP-binding protein family by the mammalian Son of Sevenless (mSOS; guanine nucleotide exchange factor), activating Raf MAPKK/MEK and the downstream molecules, p44 MAPK/p42 MAPK (ERK1/2). Next, phosphorylated MAPK enters the nucleus to form a complex with the transcriptional factors Elk-1 and Sap1 (an Ets family member), inducing transcription by binding to the SRE promoter of genes such as c-fos. This mechanism is thought to be critical in the regulation of gene expression for proliferation, migration, differentiation, and phenotypic switching [73–75].

It should be noted that Kawai and Owens recently reviewed several pathways that may be involved in SMC phenotype modulation. Some of these pathways include Krüppel-like factor 4, phosphorylated Elk-1, HERP1, FOXO4, YY1, FHL2, and several homeobox proteins [66, 76, 77].

Extracellular Matrix Accumulation

Irrespective of the origin of SMCs in vascular lesions, their interactions with the extracellular matrix are fundamental to initiate a proliferative response and to direct their migration [78]. These interactions are dependent upon specific cell surface integrins and can trigger intracellular signaling and cell cycle entry and also facilitate cell cycle progression induced by mitogens. In addition, extracellular matrix interactions may also control the availability and activity of growth factors such as heparin-binding mitogens which, in turn, can be sequestered by heparan sulfate containing extracellular matrix components and thus regulate SMC proliferation [78]. Extracellular matrix remodeling is the net result of the balance of matrix production and degradation; extracellular matrix synthesis is generally regulated primarily by the matrix metalloproteinases, whereas extracellular matrix degradation is regulated by matrix metalloproteinase inhibitors such as the tissue inhibitor of metalloproteinase. Conversely, the production and degradation of the extracellular matrix following vascular injury are required for SMC migration, proliferation, and thus the formation of the neointima [79]. Various mitogens, such as platelet-derived growth factor, angiotensin II, and TGF-β, have the ability to control extracellular matrix stability; this occurs primarily by changing the extracellular matrix components synthesized and secreted by SMCs [80].

SMC Cycle and Proliferation

The factors that stimulate SMC proliferation might include growth factors, inflammatory cytokines, coagulation, and prothrombotic factors. These factors are produced by SMCs and endothelial cells as a result of either vascular wall injury or by activation of platelets, leukocytes, monocytes, neutrophils, or macrophages. The resultant mitogenic stimuli these factors provide will then converge into final common signaling pathway regulating the cell cycle [81].

When quiescent SMCs enter more proliferative states, they first transit from the G0 to the G1 phase of the cell cycle and then enter the S phase in order to ultimately undergo replication [82]. Cell cycle progression is under the control of cyclins and cyclin-dependent kinases (CDKs), which phosphorylate the retinoblastoma gene product (pRB) [83, 84]. pRB phosphorylation represents the critical checkpoint of the phase transition, and increased pRB phosphorylation correlates with the induction of SMC proliferation in injured vessels; high levels of phosphorylated pRB are required for the development of intimal hyperplasia following PTCA and stenting [85] (Fig. 15.6). Upon pRB phosphorylation, sequestered E2F transcription factors are released to induce the transcription of genes involved in the regulation of S phase DNA synthesis. Through CDK inhibitors such as p27 (KIP1), the activity of cyclin/CDK complexes in quiescent SMCs is inhibited, providing an additional layer of regulation. In response to mitogens, p27 undergoes ubiquitination and degradation through the proteasome pathway allowing CDK/cyclin complexes to phosphorylate pRB [86–88].

Drugs for DES

The Limus Drugs: Rapamycin (sirolimus) was the first DES drug that was clinically shown to reduce or inhibit restenosis [89]. Rapamycin is a natural macrocyclic lactone that is

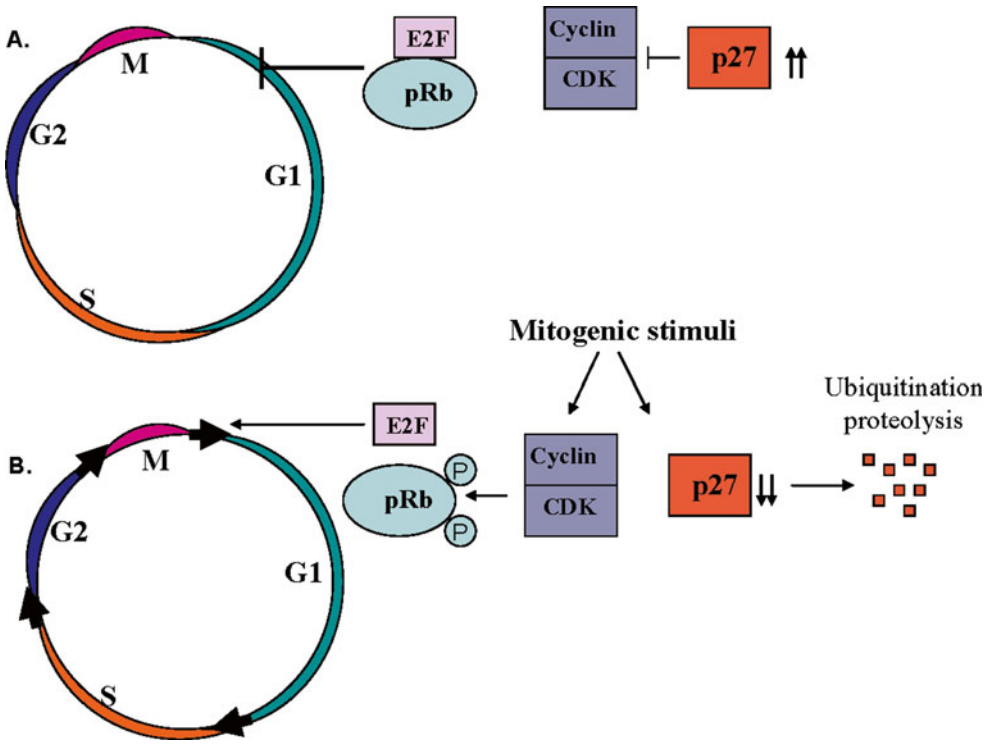

Fig. 15.6 Schematic representation of the smooth muscle cell (*SMC*) cycle. (**a**). The retinoblastoma gene product (*RB*) and the CDK inhibitor, p27, are the key regulators of the quiescent SMC cycle. (**b**). Initiation of a proliferative cell cycle in SMC, in response to mitogens, is controlled via the phosphorylation of Rb (*pRb*) by cyclins and cyclin-dependent kinases (*CDKs*) and by the removal of p27 through ubiquitination and degradation. The removal of the cell cycle inhibition allows the transcription factor E2F to induce activation of genes that are required for cell growth and proliferation

structurally related to the immunosuppressive agents, tacrolimus and cyclosporine A. Yet, the mechanism of action of rapamycin differs significantly from these latter agents, as it does not inhibit calcineurin and the subsequent T-cell activation pathway [90]. Rapamycin is a highly specific inhibitor of a multifunctional serine-threonine kinase, also known as the mammalian target of rapamycin. In essence, rapamycin gains function by binding to the immunophilin FK506-binding protein 12 (FKBP12), and the resultant complex inhibits the activity of the mammalian target of rapamycin. To date, the mammalian target of rapamycin is known to have two main functions: (1) activation of p70S6 kinase and (2) activation of the eukaryotic initiation factor 4E-BP1 (Fig. 15.7). The activation of p70S6 kinase leads to phosphorylation of 40S ribosomal protein that is phosphorylated on multiple sites after mitogen stimuli. These modifications are believed to favor the recruitment of the 40S subunit into actively translating polysomes, resulting in protein synthesis and mRNA translation. Furthermore, p70S6 kinase leads to an increase in the expression of proliferating nuclear antigen, thereby promoting DNA replication. Rapamycin blocks the activation of these downstream signaling elements, which results in G1 cell cycle arrest in various cells, including T and B cells, as well as nonimmune cells such as fibroblasts, endothelial cells, and SMCs [91]. Rapamycin is also thought to prevent cyclin-dependent kinase (CDK) activation by the induction of its inhibitor, p27, which inhibits pRb phosphorylation and thus accelerates the turnover of cyclin D1; this leads to a deficiency of active cdk4/cyclin D1 complexes, all of which potentially contribute to the prominent inhibitory effects of rapamycin at the G(1)/S phase transition.

The fact that rapamycin can block the cell cycle progression of SMCs and inhibit their proliferation was the primary finding that led to its incorporation into DESs [92]. Subsequently, rapamycin has been demonstrated to successfully control arterial renarrowing after percutaneous intervention and to abolish restenosis [93]. Currently, there are additional potent analogs of rapamycin which have been incorporated into DESs, including zotarolimus and everolimus, that exhibit similar mechanisms of action (i.e., the inhibition of mammalian target of rapamycin). Importantly, they have shown initial clinical efficacy in controlling ISR [89].

Paclitaxel: Paclitaxel is a microtubule-stabilizing agent belonging to the chemical class of taxanes, obtained originally from the yew tree. Paclitaxel promotes the assembly of microtubules from tubulin dimers and stabilizes microtubules by preventing depolymerization. This stability results in the inhibition of the normal dynamic reorganization of the microtubule network that is essential for vital interphase and mitotic cellular functions. Furthermore, paclitaxel induces abnormal arrays or "bundles" of microtubules throughout the cell cycle and multiple asters of microtubules during mitosis. Paclitaxel has also demonstrated potent antitumor activity and thus is an approved drug for the treatment of various types of cancers [94]. Paclitaxel inhibits both the migration and proliferation of SMCs. More recently, pacli-

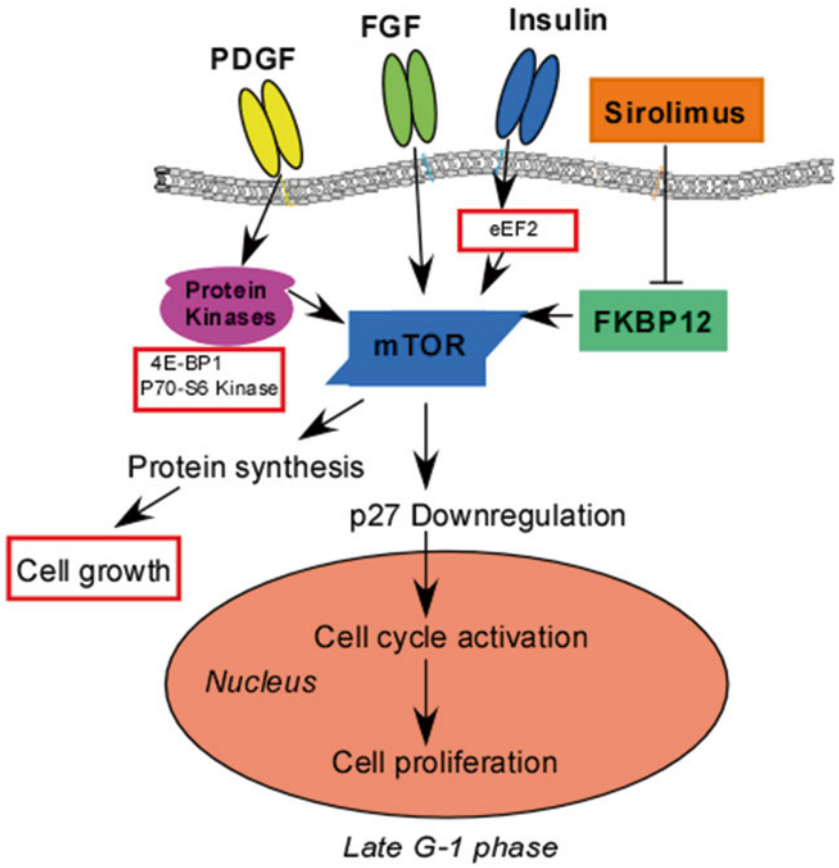

Fig. 15.7 Schematic representation of the mTOR signaling pathway and the mechanism of action of sirolimus (rapamycin). Sirolimus forms a complex with FKBP 12 which modulates downstream signaling events. *mTOR* mammalian target of rapamycin

taxel-eluting stents were shown to efficiently prevent angiographic and clinical restenosis [95].

Other Potential Drug Targets for DESs: Many candidate molecules that regulate vascular SMC growth have been studied in preclinical models using a variety of pharmacological and gene therapy approaches [96]. Results have suggested important roles in this process for: (1) the renin-angiotensin system, (2) catecholamines, (3) ET-1, (4) natriuretic peptides, (5) thrombin, (6) platelet-derived growth factor, (7) TGF and other activins [97, 98], (8) fibroblast growth factor, and (9) other stimuli including oxidative stress nitric oxide and the estrogen receptor [96, 99, 100].

Endothelial Cells

The healthy vascular endothelium is primarily a continuous single cell lining of the cardiovascular system that forms a critical interface between the blood and its components on one side and the tissues and organs on the other. Endothelial integrity is essential for maintaining vascular homeostasis [101]. Yet, the endothelium can also be considered as heterogeneous and has many synthetic and metabolic functions, i.e., it can synthesize several powerful vasodilators including NO, prostacyclin, and endothelium-derived relaxing factors which, in turn, control vascular tone. It also acts as a nonthrombogenic, noninflammatory, and selective permeable barrier. Importantly, endothelium-derived NO participates in the control of vascular healing by attenuating vascular inflammation and inhibiting SMC proliferation and migration [102]. Endothelial cells can also promote healing by close interaction with the extracellular matrix and with adjacent cells including pericytes and SMCs within the vessel wall [103]. In response to injury such as angioplasty or stenting, vascular endothelium has the ability to respond by modulating its microenvironment, e.g., activated endothelial cells can rapidly alter the interrelated processes of coagulation, fibrinolysis, growth, and inflammation by secreting prothrombotic molecules such as Willebrand factor and surface expression of adhesion molecules such as P-selectin. In addition, activated endothelial cells can induce plasminogen activator (tPA) that, in turn, inhibits clot lysis. The endothelium also loses its vasodilating ability, rendering the underlying vascular smooth muscle susceptible to the effects of vasoconstrictive and growth-promoting stimuli [104–106].

Importantly, endothelial denudation during PTCA has been postulated to be a fundamental incident contributing to development of restenosis. In addition, endothelial dysfunction has been associated with poor outcomes of coronary revascularization [107]. The term *endothelial dysfunction* most commonly refers to impairment of endothelium-dependent vasodilation and implies presence of widespread abnormalities in endothelial integrity and homeostasis.

In recent years, endothelial function and regeneration have been the focus of multiple preclinical and clinical studies aimed at establishing the mechanisms of action linking incomplete endothelial regeneration, as well as dysfunctional endothelium, with increased risk of vascular disease, including the increased risk for restenosis and late stent thrombosis [108]. Based on the established links, diverse strategies are currently being pursued to promote healing through restoration of proper endothelial growth and function. These include: (1) pharmacological modulation strategies to increase eNOS and NO production; (2) tissue engineering, gene and stem cell therapies, and procedural modifications (i.e., direct stenting); (3) vessel reconstruction with autologous endothelial cell/fibrin matrix; and (4) the use of estrogen-loaded stents and stents designed to capture progenitor endothelial cells [109, 110].

Effect of Shear Stress on Endothelial Cells and the Link to Restenosis

Biomechanical forces such as fluid shear stresses can activate the endothelium to stimulate the production of an array of biological mediators. Some of these mediators act by altering gene regulation and are analogous to endothelial activation by inflammatory cytokines [44, 111]. The endothelial cell is capable of responding not only to the magnitude of the applied forces but also to their temporal and spatial fluctuations (e.g., steady versus pulsatile flow, uniform laminar, disturbed laminar, or turbulent flow regions). In turn, this suggests the existence of primary flow sensors (receptors) that are coupled via distinct signaling pathways to nuclear events [112]. Endothelial cells have the capacity to discriminate among specific biomechanical forces and translate these input stimuli into distinctive phenotypes [113].

Endothelial cells subjected to weak shear stress exhibit increased proliferation, while strong shear stresses are associated with increased NO production and inhibition of endothelial cell proliferation [114]. In addition, in vitro modeling studies [115] have demonstrated focal areas within stents that have low shear stress values and may provide a milieu for endothelial cell activation and vascular proliferation. In vivo coronary stent implantation can change the three-dimensional geometry and shear stress distribution of the vessel [116].

15.12.2.2 The Role of Inflammation in Restenosis

Based on experimental and clinical data, the important role of inflammation in vascular healing and ISR has been suggested and increasingly emphasized [117, 118]. Endothelial injury, platelet and leukocyte interactions, and subcellular inflammatory mediators are pivotal in the development of the inflammatory response following PTCA and stenting.

The modulation of vascular repair by inflammatory cells is achieved via multiple mechanisms: (1) generation of injurious reactive oxygen intermediates, (2) release of growth and chemotactic factors, and (3) production of enzymes (e.g., matrix metalloproteinases, cathepsin S) capable of degrading extracellular constituents and thereby facilitating cell migration [119].

Leukocyte Recruitment

In animal models in which a stent is deployed to produce deep vessel wall trauma, it has been shown that a brisk early inflammatory response can be induced with abundant surface-adherent neutrophils and monocytes [120]. Days and weeks later, macrophages accumulate within the developing neointima and are observed clustering around stent struts. The number of vessel wall monocytes/macrophages is positively correlated with the neointimal area, suggesting a possible causal role for monocyte activity in restenosis [121]. The mechanisms that govern leukocytes recruitment and infiltration into these tissues following stent deployment are comprised of multistep adhesive and signaling events. More specifically, the initial adhesion tethering and rolling of leukocytes to the activated platelets at the site of stent deployment is mediated by the platelet adhesion molecule, P-selectin, which then accelerates fibrin formation and deposition. P-selectin also mediates the adherence of platelets to neutrophils via specific interaction with its endogenous ligand, P-selectin glycoprotein-1 (PSGL-1) [121]. Following initial rolling, the leukocytes adhere more firmly through the direct interaction of the surface integrin, Mac-1 (CD11b/ CD18) [122], with the platelet receptors such as GP Ib, and through cross-linking with fibrinogen to the GP IIb/IIIa receptor. Migration of leukocytes across the platelet-fibrin layer and diapedesis into the tissue is then driven by the chemical gradients of the chemokines produced by inflammatory cells, by inflammation deranged SMCs, and by the resident macrophages [123]. Finally, Mac-1 integrin also functions to amplify the inflammatory response by inducing neutrophil activation, upregulating the expression of cell adhesion molecules, and generating signals that promote integrin activation and chemokine synthesis.

Chemokines and Proinflammatory Cytokines

Chemokines are a group of chemoattractant cytokines produced by a number of somatic cells, including endothelial cells, SMCs, and leukocytes. Chemokines elicit a chemotactic stimulus to the adherent leukocytes, directing their migration into the intima [124]. Recent research has identified several candidate chemoattractant molecules responsible for leukocyte transmigration to areas of vascular injury, including monocyte chemoattractant protein (MCP-1) and proinflammatory cytokines such as TNF alpha and interleukin (IL)-1beta [125, 126]. In addition, T cells encounter signals that cause them to elaborate inflammatory cytokines such as

γ-interferon and lymphotoxin (tumor necrosis factor [TNF]-β) that, in turn, can stimulate macrophages as well as vascular endothelial cells and SMCs. These leukocytes, as well as resident vascular wall cells, will secrete cytokines and growth factors (such as platelet-derived growth factor, basic fibroblast growth factor, and epidermal growth factor) that will promote the migration and proliferation of SMCs [44].

MCP-1: MCP-1 belongs to the subfamily of CC (beta) chemokines and is considered responsible for the direct migration of monocytes into the intima at sites of lesion formation [119]. In addition to promoting the transmigration of circulating monocytes into tissues, MCP-1 exerts various other effects on monocytes including superoxide anion induction, cytokine production, and adhesion molecule expression. Inflammatory cytokines or peptide growth factors induce MCP-1 expression in endothelial cells or vascular SMCs. Since elevated levels of MCP-1 have been demonstrated in myocardial infarction, heart failure, and after angioplasty, this chemokine is considered as a probable key factor in initiating the inflammatory process and maintaining the proliferative response to vascular injury restenosis [127, 128]. Furthermore, following stent placement, MCP-1 levels in plasma increase after several days and are more likely to be elevated at follow-up 6 months later in patients who have restenosis.

M-CSF: In addition to MCP-1, macrophage colony-stimulating factor (M-CSF) contributes to the differentiation of the blood monocyte into the macrophage foam cell. Inflammatory mediators such as M-CSF augment expression of macrophage scavenger receptors, leading to the formation of lipid-laden macrophages. M-CSF promotes the replication of macrophages within the intima as well [129]. Moreover, elevated plasma levels of M-CSF were demonstrated in patients with restenosis after PTCA compared to patients without restenosis. Positive correlation was also observed with regard to elevated plasma levels of M-CSF and the extent of lumen loss by restenosis [130].

IL-1beta: Interleukin-1beta (IL-1beta) is the prototypical inflammatory cytokine and is believed to be a critical early mediator of inflammation [131]. Patients with coronary artery disease have markedly elevated levels of IL-1, with its levels being particularly elevated in unstable disease. IL-1beta is capable of inducing smooth muscle activation and leukocyte recruitment in restenosis and atherosclerosis. Recent experimental data reveal that various components of the IL-1 signaling pathway, namely, IL-1beta cytokine, IL-1 receptor antagonist (IL-1ra), and IL-1 receptors (IL-1RI and IL-1RII), exhibit differential but concomitant expression patterns following stenting [130] and likely play distinct roles in neointima formation. In addition, local release of IL-1beta cytokine occurs shortly after coronary stent placement, including DESs, which is possibly related to plaque rupture and/or endothelium trauma following the stenting procedure [132].

TNF-α: Tumor necrosis factor alpha (TNF alpha) is a multifunctional cytokine which is considered to play a key role in inflammation and immunity, as well as in apoptosis and cell survival [133]. TNF-α that is secreted from endothelial muscle cells, SMCs, and macrophages has been associated with coronary atheroma. It enhances monocyte recruitment into developing atherosclerotic lesions and is considered as a potential link between obesity and atherosclerosis. TNF-α was also shown to act locally at sites of tissue injury induced by vessel wall damage and may exert critical influence on the development of restenosis after percutaneous coronary intervention [134].

Systemic Markers of Inflammation and ISR

After balloon angioplasty and/or stenting procedures, there are several systemic markers of inflammation that appear to be predictive of restenosis. These markers are upregulated, transiently, or sustained following stent implantation and are also associated with an increased risk of clinical and angiographic restenosis. They include the C-reactive protein, the most common biomarker for inflammation and coronary disease. Formerly considered solely as a biomarker for inflammation, C-reactive protein is now viewed as a prominent component of the vascular inflammatory process [135]. It can activate the complement pathway, induce the secretion of inflammatory and procoagulant cytokines such as interleukin-6 and endothelin-1, and decrease the expression of endothelial NOS in endothelial cells. In addition, the C-reactive protein activates macrophages to express cytokine and tissue factors [136]. Several studies have indicated a positive association between elevated plasma levels of the C-reactive protein and stent restenosis [137].

Other markers of inflammation and coronary disease encompass key components of innate immunity, vascular injury, and disruption of the atherosclerotic plaque. These include elevated numbers of circulating leukocytes and monocytes in peripheral blood [138, 139], as well as increased levels of the integrin MAC-1 which marks their activation and adhesion [122]. Furthermore, levels of the proinflammatory and proatherothrombotic cytokines, IL-6, and soluble CD40L (sCD40L), each located in the culprit coronary arteries (measured in blood taken from the coronary artery ostium), have been found to increase early after coronary stenting and are associated with risk of restenosis of the revascularized coronary artery [140, 141]. Interleukin-6 is the principal procoagulant cytokine expressed by various cells, including macrophages, T cells, endothelial cells, and SMCs. It triggers an increase in plasma concentrations of fibrinogen, plasminogen activator inhibitor type 1, and the C-reactive protein [142]. Similarly, elevated levels of IL-6 are associated with increased risk of future myocardial

infarction in healthy men [143]. Furthermore, sCD40L was described to be released from activated platelets and interacts with CD40L expressed on vascular cells initiating inflammatory and proatherothrombotic cascade [144]. Importantly, elevated plasma levels of sCD40L can be used to identify patients with acute coronary syndromes at heightened risk of death and recurrent myocardial infarction, independent of other predictive variables [145].

The Cross Talk Between Inflammation and Thrombosis

Importantly, plaque rupture, whether spontaneous or as a result of stenting, promotes the activation of an inflammatory response. In turn, one of the primary consequences of increased proinflammatory cytokines in the vasculature is the elevated procoagulant state and an increase in thrombosis [146]. Proinflammatory cytokines such as IL-1β, IL-6, MCP-1, and TNF-αd will then increase the expression of a number of other specific proteins that serve to regulate coagulation. Foremost among these is the induction of *tissue factor* expression by endothelial cells, underlying SMCs, and monocytes [146]. Tissue factor (coagulation factor III or CD142) is a 46-kDa transmembrane glycoprotein that serves as one of the primary initiators of blood coagulation [147]. In this biochemical cascade, cell-anchored tissue factor interacts with soluble factor VIIa (FVIIa) to induce factor Xa (FXa) activation, leading to cleavage of prothrombin to thrombin, the proteolytically active protease. Thrombin, in turn, is responsible for conversion of plasma fibrinogen to fibrin, which envelopes and stabilizes developing thrombi (blood clots). Thrombin also cleaves and activates the platelet receptor protease-activated receptor 1 (also known as the thrombin receptor), which induces platelet aggregation and thrombus growth [148]. Activated platelets will release the contents of granules, which further promotes platelet recruitment, adhesion, aggregation, and activation. In addition to initiating coagulation, interaction of tissue factor with the adhesion molecule, P-selectin, has been demonstrated to accelerate the rate and extent of fibrin formation and deposition. P-selectin is expressed on activated platelets and endothelium and serves as the receptor for the endogenous ligand, P-selectin glycoprotein-1 (PSGL-1), expressed on various leukocytic cell types. In addition to mediating transient interactions between endothelial cells and leukocytes, P-selectin has been reported to mediate adherence of platelets to monocytes and neutrophils via specific interaction with PSGL-1. Finally, P-selectin is rapidly cleaved off the surface of the platelet membrane and appears in the circulation as a soluble form, which has been reported to be elevated in patients with acute coronary syndromes including unstable angina and non-Q-wave myocardial infarction [146].

The Molecular Signaling Leading to Inflammation due to Vascular Interventions

Inflammatory responses to vascular interventions are governed by the activation of signaling cascades central to

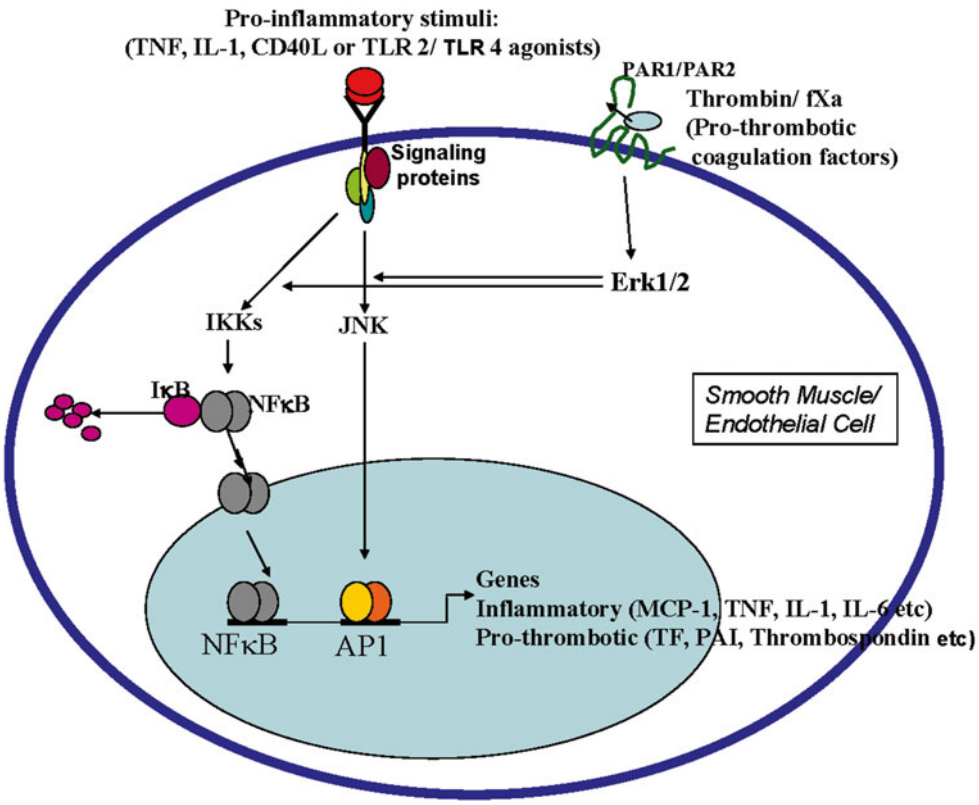

Fig. 15.8 Schematic representation of the cross talk between inflammatory and thrombotic signaling pathways, including the activation of the AP-1 and the NFκB transcription factors

inflammation and vascular disease and facilitated via thrombotic signaling (Fig. 15.8). These combine the classic and well-studied signal transduction pathways, triggered by the proinflammatory cytokines, such as TNF-α, IL-1β, and CD40L, with other signaling pathways which were recently elucidated, including toll-like receptor 2 (TLR2) and toll-like receptor 4 (TLR4). It should be noted that metabolic abnormalities such as high LDL, high glucose, and insulin resistance that are prevalent in diabetic and atherosclerotic patients undergoing PTCA can specifically impair or trigger undesired signaling pathways, which will further accelerate inflammation, coagulation, and/or thrombosis. These include impaired IGF-1 signaling, impaired PPAR signaling, and the activation of TLR4 signaling [149–153].

TNF-α Signaling: The interaction of TNF-αd with TNF receptor 1 and receptor 2 (TNFR-1, TNFR-2) activates several signal transduction pathways, leading to the diverse functions of TNF-αd. It has been recently shown that in the arterial wall, TNFR-1 mediates this signaling that will contribute to the pathogenesis of atherosclerosis; this response includes enhancing arterial wall chemokine and adhesion molecule expression, as well as augmenting medial SMC proliferation and migration [154]. The signaling molecules of TNFR-1 (collectively called the TNFR-1 signalosome) have been elucidated quite well, even though the regulation of the signaling still remains unclear. TNFR-1 signalosome consists of signaling proteins that mutual cross talk will trigger the activation of nuclear factor kappa B (NFκB) [155]. In addition, the TNFR-1 signalosome mediates the activation of the mitogen-activated protein kinases (MAPKs), including the MEK1 and MEK2 and their substrates extracellular-regulated kinases 1 and 2 (ERK1 and ERK2, ERK1/2) pathway and also the p38 MAPK and c-Jun N-terminal kinase (JNK) stress kinase pathways [154].

CD40-CD40L Signaling: Ligation of CD40 in circulating cells or in the vessel wall may promote mononuclear cell recruitment, participate in the weakening of the plaque, and contribute to thrombosis and neointimal formation [156]. CD40 belongs to the TNF receptor (TNFR) superfamily that also includes TNFR-1 and TNFR-2. CD40 has been shown to express in vascular cells, endothelial cells, and SMCs and in additional cells implicated in vascular disease, such as monocytes and macrophages. These cells commonly express the receptor constitutively in vitro and show basal expression in nondiseased tissue. Stimulation with inflammatory cytokines enhances expression of CD40 in vitro [157, 158]. CD40 ligand (recently renamed CD154) is a member of the TNF gene superfamily that also includes TNF-αd. Numerous cell types can express CD40L, particularly those implicated in atherogenesis, namely, endothelial cells, SMCs, macrophages, and platelets. The precise signaling mechanism by which the interaction between CD40L and its receptor CD40 mediates inflammatory secretion is not yet fully understood. The cytoplasmic region of CD40 consists of two major signaling domains that, through the association with binding proteins termed TNFR-associated factors (TRAFs), can trigger the activation of NFκB and MAPKs and ERK1/2, p38 MAPK, and JNK [159, 160]. It is notable that this signaling activation, resulting from CD40 ligation, appears to be cell specific and differs significantly within certain cell types and at various stages of activation and differentiation [160]. For example, within endothelial cells, CD40 ligation-induced activation of NFκB, interferon regulatory factor-1 (IRF-1), JNK and p38 MAPK signaling pathways, and CD40-mediated signaling events in SMCs include tyrosine phosphorylation as well as the activation of NFκB. In monocytes, ligation of CD40 triggers activation of MEK1/2 -ERK1/2, as well as the JNK pathway.

*IL-1β Signaling: I*ncreased levels of IL-1 enhance vascular adhesion, vascular permeability, macrophage activation, endothelial cell and SMC proliferation, and protease-induced plaque rupture—all key steps in the progression of vascular disease [161]. IL-1 activity is mediated by the formation of a complex involving the type 1 receptor, IL-1R [162]. This receptor is a member of a larger related family, most of which are involved in the mechanisms of host defense. IL-1R was the first receptor discovered in this superfamily, and the IL-1-mediated signaling pathway serves as a prototype for the other family members. This large superfamily is collectively called toll/interleukin-1 receptor (TIR) and encompasses the Ig domain family (IL-1 receptors, IL-18 receptors, and IL-1R-like receptors), the leucine-rich domain family (the toll-like receptors and similar receptors), and a series of TIR domain-containing intracellular adapter molecules. IL-1R mediates a complex pathway involving a cascade of kinases organized by multiple adapter molecules into signaling complexes, leading to activation of the transcription factors NFκB, p38 MAPK (activating the transcription factor ATF), and JNK pathways (activating the transcription complex AP-1, activator protein 1) [163].

Remarkably IL-1- and TNF-mediated signaling pathways also share several biological properties, particularly the inflammatory molecules they trigger (secretion of inflammatory cytokines and expression of surface adhesion molecules) and the downstream signaling activation such as NFκB and MAPK, p38, and JNK pathways. The prominent difference is that TNF receptor signaling induces programmed cell death, whereas IL-1 receptor signaling does not.

Initiation of IL-1R activation requires the assistance of the receptor accessory protein (IL-1RAcP) after which the death domain (containing protein MyD88) is recruited to the activated receptor complex. MyD88 functions as an adaptor to recruit the serine-threonine IL-1 receptor-associated kinase IRAK to the receptor through its death domain. IRAK then leaves the receptor complex and interacts with TRAF6, another adaptor signaling molecule that is required for the

activation of NFκB. To date, the TRAF family of adaptor proteins (a total of six) has been elucidated in several signaling pathways that lead to NFκB activation, such as TNF and CD40L. Finally, different TRAFs have been found to be used by the various NFκB-dependent pathways [164, 165].

Toll-Like Receptors and Vascular Pathogenesis: Members of the TLR subfamily (TLR1–9) will identify alarm indications incoming from microbial pathogens or the host itself and then, in response, mediate the initiation of the innate immunity [163]. Toll-like receptor ligation induces expression of a wide variety of genes such as genes encoding proteins involved in cytokine production (TLR4 in particular), leukocyte recruitment, and phagocytosis that all contribute to the inflammatory response. Toll-like receptors can form dimeric receptor complexes consisting of two different TLRs or homodimers in the case of TLR4. Recently, the expression of TLRs (TLR1, TLR2, and TLR4) was described in human atherosclerotic plaques [166, 167], and a significant amount of evidence is beginning to accumulate indicating that the TLRs are important in cardiovascular pathologies. Toll-like receptor expression has been shown to be elicited by both arterial and myocardial cells. The importance of TLR4 as well as TLR2 was recently considered to be verified through mouse knockout studies [168]. Among other data, it was demonstrated that the endothelium-dependent dilation in response to acetylcholine in vessels from TLR4(-/-) mice was greatly reduced, thus illustrating a novel role for TLR4 in the homeostatic control of a functional endothelium [169]. In addition, TLR2(-/-) mice exhibited marked suppression of neointimal hyperplasia. Endogenous TLR2 seems to play significant role in inflammatory responses and ROS production after vascular injury. Also, flow-dependent regulation of TLR2 was demonstrated in endothelial cells, both in vitro and in vivo; expression of endothelial TLR2 is induced under disturbed flow, but not laminar flow, which may explain how a TLR2 could be involved in atherogenesis with regional specificity of lesion development [170]. Similarly, human studies on polymorphisms also point to a role of TLR4 in neointima formation and atherosclerosis.

More specifically, TLRs are type I transmembrane receptors with extracellular leucine repeats and a carboxy-terminal intracellular tail containing a conserved region called TIR homology domain. The TIR domain is indispensable for signal transduction since it serves as a scaffold for a series of protein-protein interactions which result in the activation of a unique signaling module consisting of the adaptor protein myeloid differentiation factor 88 (MyD88), interleukin-1 receptor-associated kinase (IRAK) family members, and Tollip, which is used exclusively by TIR family members. Subsequently, several central signaling pathways are activated in parallel, the activation of NFκB being the most prominent event of the inflammatory response.

The extracellular domains of these receptors are involved in ligand binding, but are also necessary for dimerization; various ligands have been identified through in vitro systems or knockout mouse models. Most of these ligands can be classified as pathogen-associated molecular pattern molecules which are highly conserved. However, recent evidence suggests that TLR4 and TLR2 also respond to endogenous factors produced by stress or cell damaging, like heat shock proteins, extracellular matrix components of fibronectin and hyaluronan, and disturbed shear flow [163, 171].

NFκB: Among the various signal transduction pathways that are triggered by vascular inflammation, the activation of the transcription factor NFκB is considered today as the most prominent one. TNF-α, CD40L, IL-1β, and TLR vascular receptors use parallel proximal signaling components that distally converge into the activation of the transcriptional factor NFκB (Fig. 15.8). Once NFκB is fully activated, it participates in the regulation of various target genes in different vascular and immune cells to exert its biological functions. NFκB controls the expression of many inflammatory cytokines, chemokines, immune receptors, and cell surface adhesion molecules.

NFκB is also a collective term for a family of proteins that exist either as heterodimers or homodimers. In unstimulated cells, NFκB is sequestered in the cytoplasm because of its association with a member of the IκB family of inhibitory proteins [172]. IκB makes multiple contacts with NFκB, and these interactions mask the nuclear localization sequence of NFκB and can interfere with sequences important for DNA binding [173]. Inflammatory stimulation leads to the phosphorylation of IκBs by IκB kinases, which then targets the IκB for proteasomal degradation [174]. After IκB degradation, liberated NFκB translocates to the nucleus and triggers the transcription of its target genes. More recently, a second level of regulation of NFκB was demonstrated that relies on the phosphorylation of members of the second group of NFκB proteins (p65/RelA, RelB, and c-Rel), resulting in the activation of transcriptional activity of NFκB [175].

15.12.2.3 Late Stent Thrombosis

Although rare, stent thrombosis remains a severe complication after stent implantation owing to its associated high morbidity and mortality. Following stent implantation, patients are typically treated with antiplatelet agents such as clopidogrel and/or aspirin. Defined by the time of occurrence, thrombosis after stenting can be acute (<24 hours), subacute (<30 days), late (>30 days), or very late (>12 months) [54]. Recent data have associated the use of DESs with late and very late thrombosis, i.e., up to 3 years after implantation and predominantly after discontinuation of the antiplatelet therapy. Notable is a recent meta-analysis on 14

contemporary clinical trials that compared DESs (paclitaxel or sirolimus) with bare metal stents; the authors concluded that even though the overall incidence of late stent thrombosis (more than 1 year after coronary revascularization) was low (~0.5 %), DES appeared to increase the risk for late stent thrombosis [176]. However, this remains a topic of lively debate, as some data from large registries and meta-analyses of randomized trials have indicated a higher risk for DES thrombosis, whereas others suggest an absence of such a risk.

The factors that are associated with an increased risk of late stent thrombosis include: (1) the procedure itself (such as stent malapposition), (2) the patient and his/her general health, and (3) specifics of lesion characteristics (such as small vessels) [54, 177]. In addition, the drugs that are released from current DES exert their biological effects through inhibition of the cell cycle, aimed at preventing vascular SMC proliferation. Nevertheless, a combination of drug-induced inhibition of proliferation of endothelial cells, with denudation of endothelial cell layer caused by PTCA and stenting may, in fact, impair the reendothelialization and compromise arterial healing [178]. In addition, current DES drugs, such as sirolimus and paclitaxel, have been reported to induce tissue factor expression [179], which results in a prothrombogenic environment and might ultimately increase the risk of late thrombosis. For example, it has been reported previously that the nonerodible polymers of the Cypher and Taxus stents provoke chronic eosinophilic infiltration of the arterial wall, suggestive of hypersensitivity reactions in a small number of cases [180].

A recently developed network to perform meta-analyses investigated the relative safety and efficacy of bioabsorbable polymer-based biolimus-eluting stents, which were compared to durable polymer DES or bare metal stents. It was previously suggested that bioabsorbable polymer-based biolimus-eluting stents might reduce the risks of stent thrombosis and late adverse outcomes, compared with first-generation DES. Yet as of this date, the relative safety and efficacy of these bioabsorbable polymer-based biolimus-eluting stents versus newer-generation DESs coated with more biocompatible drug polymers have not been investigated in depth. However, analyses of 89 randomized controlled trials, including data from 85,490 patients, found that at 1-year follow-up, bioabsorbable polymer-based biolimus-eluting stents were associated with lower rates of cardiac death and myocardial infarction. Further, target vessel revascularization was better than for bare metal stents and also had lower rates of target vessel revascularization compared to fast-release zotarolimus-eluting stents. It was reported that these bioabsorbable polymer-based biolimus-eluting stents had similar rates of cardiac death, myocardial infarction, and target vessel revascularization compared with other second-generation durable polymer DESs, but elicited higher rates of 1-year stent thrombosis than cobalt-chromium everolimus-eluting stents. Interestingly, the bioabsorbable polymer-based biolimus-eluting stents were associated with improved late outcomes compared with bare metal stents, as well as paclitaxel-eluting stents (considering the latest follow-up data available, with nonsignificant outcomes compared with other durable polymer DESs, although higher rates of definite stent thromboses were noted compared with cobalt-chromium everolimus-eluting stents). In other words, bioabsorbable polymer-based biolimus-eluting stents were associated with superior clinical outcomes compared with bare metal stents and first-generation drug-eluting stents and elicited similar rates of cardiac death, myocardial infarction, and target vessel revascularization compared with second-generation durable polymer drug-eluting stents. Yet, higher rates of definite stent thrombosis were noted compared to the cobalt-chromium everolimus-eluting stents [181].

In general, overwhelming evidence suggests a pivotal role of inflammation in restenosis following stent placement. Inflammation plays a role during initial stent placement through progression of restenosis and most likely critically influences the pathobiology of stent-based thrombosis. It is unclear whether the striking similarities in the pathophysiology markers of atherosclerosis, restenosis, and the risk of cardiac events are due to underlying common pathologies or due to more direct, causal etiologies.

15.13 Summary

Cellular physiological functions are regulated via signaling mechanisms in essentially any cell type of any organ. While myocardial cells are unique in that they are interconnected to each other with gap junctions and act as an electrical syncytium, there are nevertheless an enormous number of important cellular receptors that allow the cells to receive and respond to various signals. Inflammation plays a very important role in cardiovascular disease. For example, device-based interventions such as coronary stenting may activate inflammation via a series of complex signaling processes. Importantly, inflammation also plays a central role in atherosclerosis, myocardial infarction, and heart failure. It was the general aim of this chapter to review the role and signaling mechanisms of selected physiologically and pathophysiologically important cardiac and vascular receptors with emphasis on G protein-coupled receptors (e.g., beta-adrenergic receptors) and non-G protein-coupled receptor systems, such as guanylyl cyclase-related receptors (e.g., receptors for nitric oxide), and, finally, to discuss the importance and complexity of inflammation in the pathobiology of coronary artery disease and stenting.

References

1. Rockman HA, Koch WJ, Lefkowitz RJ (2002) Seven-transmembrane-spanning receptors and heart function. Nature 415:206–212
2. del Monte F, Kaufmann AJ, Poole-Wilson PA et al (1993) Coexistence of functioning beta-1 and beta-2 adrenoreceptors in single myocytes from human ventricle. Circulation 88:854–863
3. Bristow MR, Hershberger RE, Port JD et al (1990) Beta-adrenergic pathways in non-failing and failing human ventricular myocardium. Circulation 82:112–125
4. Opie L (1998) Receptors and signal transduction. In: Opie L (ed) The heart: physiology, from cell to circulation, 3rd edn. Lippincott Williams & Wilkins, Philadelphia, pp 173–207
5. Hohl CM, Li Q (1991) Compartmentation of camp in adult canine ventricular myocytes. Relation to single cell free calcium transients. Circ Res 69:1369–1379
6. Lader AS, Xiao YF, Ishikawa Y et al (1998) Cardiac gsalpha overexpression enhances L-type calcium channels through an adenylyl cyclase independent pathway. Proc Natl Acad Sci U S A 95:9669–9674
7. Port JD, Bristow MR (2001) Altered beta-adrenergic receptor gene regulation and signaling in chronic heart failure. J Mol Cell Cardiol 33:887–905
8. Gauthier C, Langin D, Balligand JL (2000) Beta3-adrenoceptors in the cardiovascular system. Trends Pharmacol Sci 21:426–431
9. Laporte SA, Oakley RH, Holt JA, Barak LS, Caron MG (2000) The interaction of beta-arrestin with the AP-2 adaptor is required for the clustering of beta-2 adrenergic receptor into clathrin coated pits. J Biol Chem 275:23120–23126
10. Luttrell LM, Ferguson SS, Daakay Y et al (1999) Beta-arrestin-dependent formation of beta-2 adrenergic receptor-Src protein kinase complexes. Science 283:655–661
11. Shenoy SK, McDonald PH, Kohout TA, Lefkowitz RJ (2001) Regulation of receptor fate by ubiquitination of activated beta-2 adrenergic receptor and beta-arrestin. Science 294:1574–1577
12. Mann D, Kent R, Parsons B, Cooper IVG (1992) Adrenergic effects on the biology of the adult mammalian cardiocyte. Circulation 85:790–804
13. Bristow MR, Ginsburg R, Umans V et al (1986) Beta 1 and beta 2-adrenergic receptor subpopulations in nonfailing and failing human ventricular myocardium: coupling of both receptor subtypes to muscle contraction and selective beta 1-receptor down-regulation in heart failure. Circ Res 59:297–309
14. Ungerer M, Parruti G, Böhn M et al (1994) Expression of beta-arrestins and beta-adrenergic receptor kinases in the failing human heart. Circ Res 74:206–213
15. Steinberg SF (1999) The molecular basis for distinct beta-AR subtype action in cardiomyocytes. Circ Res 85:1101–1111
16. Communal C, Singh K, Sawyer DB, Colucci WS (1999) Opposing effects of beta-1 and beta-2 adrenergic receptor on cardiac myocyte apoptosis: role of a pertussis toxin sensitive G protein. Circulation 100:2210–2212
17. Zaugg M, Xu W, Lucchinetti E, Shafiq SA, Jamali NZ, Siddiqui MA (2000) Beta-adrenergic receptor subtypes differentially affect apoptosis in adult rat ventricular myocytes. Circulation 102: 344–350
18. Bisognano JD, Weinberger HD, Bohlmeyer TJ et al (2000) Myocardial-directed overexpression of the human beta-1-adrenergic receptor in transgenic mice. J Mol Cell Cardiol 32:817–830
19. Saito S, Hiroi Y, Zou Y et al (2000) Beta-adrenergic pathway induces apoptosis through calcineurin activation in cardiac myocytes. J Biol Chem 275:34528–34533
20. Lowes BD, Gill EA, Abraham WT et al (1999) Effects of carvedilol on left ventricular mass, chamber geometry, and mitral regurgitation in chronic heart failure. Am J Cardiol 83:1201–1205
21. Liggett SB, Wagoner LE, Craft LL et al (1998) The Ile164 Beta-2 AR polymorphism adversely affects the outcome of congestive heart failure. J Clin Invest 102:1534–1539
22. Wagoner LE, Craft LL, Singh B et al (2000) Polymorphisms of the beta-2 AR determine exercise capacity in patients with heart failure. Circ Res 86:834–840
23. Graham RM, Perez DM, Hwa J, Piascik MT (1996) Alpha-AR subtypes. Molecular structure, function and signaling. Circ Res 78:737–749
24. Otani H, Otani H, Das DK (1988) Alpha-1 adrenoceptor mediated phosphoinositide breakdown and inotropic response in rate left ventricular papillary muscles. Circ Res 62:8–17
25. Hwang KC, Grady CD, Sweet WE, Moravec CS (1996) Alpha-1 adrenergic receptor coupling with Gh in the failing human heart. Circulation 94:718–726
26. Choi DJ, Koch WJ, Hunter JJ, Rockman HA (1997) Mechanism of beta-adrenergic receptor desensitization in cardiac hypertrophy is increased beta-ARK. J Biol Chem 272:17223–17229
27. Knowlton KU, Michael MC, Itani M et al (1993) The alpha1A-adrenergic receptor subtype mediates biochemical, molecular, and morphologic features of cultured myocardial cell hypertrophy. J Biol Chem 268:15374–15380
28. Sugden PH (1999) Signaling in myocardial hypertrophy: life after calcineurin? Circ Res 84:633–646
29. Barki-Harrington L, Luttrell LM, Rockman HA (2003) Dual inhibition of beta-adrenergic and angiotensin II receptors by a single antagonist. Circulation 108:1611–1618
30. Dzimiri N (2002) Receptor crosstalk: implications for cardiovascular function, disease and therapy. Eur J Biochem 269:4713–4730
31. Münzel T, Feil R, Mülsch A, Lohmann SM, Hofmann F, Walter U (2003) Physiology and pathophysiology of vascular signaling controlled by cyclic guanosine 3′,5′-cyclic monophosphate–dependent protein kinase. Circulation 108:2172–2183
32. von der Leyen HE, Dzau VJ (2001) Therapeutic potential of nitric oxide synthase gene manipulation. Circulation 103:2760–2765
33. Loscalzo J (2001) Nitric oxide insufficiency, platelet activation, and arterial thrombosis. Circ Res 88:756–762
34. Champion HC, Skaf MW, Hare JM (2003) Role of nitric oxide in the pathophysiology of heart failure. Heart Fail Rev 8:35–46
35. Jugdutt BI (2003) Nitric oxide and cardiovascular protection. Heart Fail Rev 8:29–34
36. Young-Myeong K, Bombeck CA, Billiar TR (1999) Nitric oxide as a bifunctional regulator of apoptosis. Circ Res 84:253–256
37. Kuhn M (2003) Structure, regulation, and function of mammalian membrane guanylyl cyclase receptors, with a focus on guanylyl cyclase A. Circ Res 93:700–709
38. Nobuyoshi M, Kimura T, Nosaka H et al (1988) Restenosis after successful percutaneous transluminal coronary angioplasty: serial angiographic follow-up of 229 patients. J Am Coll Cardiol 12:616–623
39. Kipshidze NN, Tsapenko ML, Leon MB, Stone GW, Moses JW (2005) Update on drug-eluting coronary stents. Expert Rev Cardiovasc Ther 3:953–968
40. van den Brand MJ, Rensing BJ, Morel MA et al (2002) The effect of completeness of revascularization on event-free survival at one year in the ARTS trial. J Am Coll Cardiol 39:559–564
41. Topol EJ, Serruys PW (1998) Frontiers in interventional cardiology. Circulation 98:1802–1820
42. Serruys PW, Foley DP, Suttorp MJ (2002) A randomized comparison of the value of additional stenting after optimal balloon angioplasty for long coronary lesions: final results of the additional value of NIR stents for treatment of long coronary lesions (ADVANCE) study. J Am Coll Cardiol 39:393–399
43. Fischman DL, Leon MB, Baim DS et al (1994) A randomized comparison of coronary-stent placement and balloon angioplasty in the treatment of coronary artery disease. N Engl J Med 331:496–501

44. Scott NA (2006) Restenosis following implantation of bare metal coronary stents: pathophysiology and pathways involved in the vascular response to injury. Adv Drug Deliv Rev 58:358–376
45. Faries PL, Rohan DI, Takahara H (2001) Human vascular smooth muscle cells of diabetic origin exhibit increased proliferation, adhesion, and migration. J Vasc Surg 33:601–607
46. El-Omar MM, Dangas G, Iakovou I, Mehran R (2001) Update on in-stent restenosis. Curr Interv Cardiol Rep 3:296–305
47. Hill RA, Boland A, Dickson R et al (2007) Drug-eluting stents: a systematic review and economic evaluation. Health Technol Assess 11:iii, xi–221
48. Htay T, Liu MW (2005) Drug-eluting stent: a review and update. Vasc Health Risk Manag 1:263–276
49. Steffel J, Tanner FC (2007) Biological effects of drug-eluting stents in the coronary circulation. Herz 32:268–273
50. Mackman N (2008) Triggers, targets and treatments for thrombosis. Nature 451:914–918
51. Kaul S, Shah PK, Diamond GA (2007) As time goes by: current status and future directions in the controversy over stenting. J Am Coll Cardiol 50:128–137
52. Bavry AA, Kumbhani DJ, Helton TJ, Bhatt DL (2005) Risk of thrombosis with the use of sirolimus-eluting stents for percutaneous coronary intervention (from registry and clinical trial data). Am J Cardiol 95:1469–1472
53. Moreno R, Fernández C, Hernández R et al (2005) Drug-eluting stent thrombosis: results from a pooled analysis including 10 randomized studies. J Am Coll Cardiol 45:954–959
54. Luscher TF, Steffel J, Eberli FR et al (2007) Drug-eluting stent and coronary thrombosis: biological mechanisms and clinical implications. Circulation 115:1051–1058
55. Legrand V (2007) Therapy insight: diabetes and drug-eluting stents. Nat Clin Pract Cardiovasc Med 4:143–150
56. Kawaguchi R, Angiolillo DJ, Futamatsu H, Suzuki N, Bass TA, Costa MA (2007) Stent thrombosis in the era of drug-eluting stents. Minerva Cardioangiol 55:199–211
57. Forrester JS, Fishbein M, Helfant R, Fagin J (1991) A paradigm for restenosis based on cell biology: clues for the development of new preventive therapies. J Am Coll Cardiol 17:758–769
58. Costa MA, Simon DI (2005) Molecular basis of restenosis and drug-eluting stents. Circulation 111:2257–2273
59. Libby P (2006) Atherosclerosis: disease biology affecting the coronary vasculature. Am J Cardiol 98:3Q–9Q
60. Casscells W, Engler D, Willerson JT (1994) Mechanisms of restenosis. Tex Heart Inst J 21:68–77
61. Welt FG, Rogers C (2002) Inflammation and restenosis in the stent era. Arterioscler Thromb Vasc Biol 22:1769–1776
62. Mintz GS, Popma JJ, Hong MK et al (1996) Intravascular ultrasound findings after excimer laser coronary angioplasty. Cathet Cardiovasc Diagn 37:113–118
63. Lundmark K, Tran PK, Kinsella MG, Clowes AW, Wight TN, Hedin U (2001) Perlecan inhibits SMC adhesion to fibronectin: role of heparan sulfate. J Cell Physiol 188:67–74
64. Lerman A (2005) Restenosis: another "dysfunction" of the endothelium. Circulation 111:8–10
65. Muto A, Fitzgerald TN, Pimiento JM et al (2007) Smooth muscle cell signal transduction: implications of vascular biology for vascular surgeons. J Vasc Surg 45:A15–A24
66. Owens GK, Kumar MS, Wamhoff BR (2004) Molecular regulation of vascular smooth muscle cell differentiation in development and disease. Physiol Rev 84:767–801
67. Li X et al (1997) Suppression of smooth-muscle alpha-actin expression by platelet-derived growth factor in vascular smooth-muscle cells involves Ras and cytosolic phospholipase A2. Biochem J 327:709–716
68. Zalewski A, Shi Y, Johnson AG (2002) Diverse origin of intimal cells: smooth muscle cells, myofibroblasts, fibroblasts, and beyond? Circ Res 91:652–655
69. Powell DW, Mifflin RC, Valentich JD, Crowe SE, Saada JI, West AB (1999) Myofibroblasts. I. Paracrine cells important in health and disease. Am J Physiol 277:C1–C9
70. Yokote K, Take A, Nakaseko C et al (2003) Bone marrow-derived vascular cells in response to injury. J Atheroscler Thromb 10:205–210
71. Bornfeldt KE, Krebs EG (1999) Crosstalk between protein kinase A and growth factor receptor signaling pathways in arterial smooth muscle. Cell Signal 11:465–477
72. Seger R, Krebs EG (1995) The MAPK signaling cascade. FASEB J 9:726–735
73. Asada H, Paszkowiak J, Teso D et al (2005) Sustained orbital shear stress stimulates smooth muscle cell proliferation via the extracellular signal-regulated protein kinase 1/2 pathway. J Vasc Surg 42:772–780
74. Nishida E, Gotoh Y (1993) The MAP kinase cascade is essential for diverse signal transduction pathways. Trends Biochem Sci 18:128–131
75. Marshall CJ (1995) Specificity of receptor tyrosine kinase signaling: transient versus sustained extracellular signal-regulated kinase activation. Cell 80:179–185
76. Liu Y, McDonald OG, Shang Y, Hoofnagle MH, Owens GK (2005) Kruppel-like factor 4 abrogates myocardin-induced activation of smooth muscle gene expression. J Biol Chem 280:9719–9727
77. McDonald OG, Warnhoff BR, Hoofnagle MH, Owens GK (2006) Control of SRF binding to CArG box chromatin regulates smooth muscle gene expression in vivo. J Clin Invest 116:36–48
78. Hedin U, Roy J, Tran PK (2004) Control of smooth muscle cell proliferation in vascular disease. Curr Opin Lipidol 15:559–565
79. Geng YJ, Libby P (2002) Progression of atheroma: a struggle between death and procreation. Arterioscler Thromb Vasc Biol 22:1370–1380
80. Raines EW (2000) The extracellular matrix can regulate vascular cell migration, proliferation, and survival: relationships to vascular disease. Int J Exp Pathol 81:173–182
81. Dzau VJ, Braun-Dullaeus RC, Sedding DG (2002) Vascular proliferation and atherosclerosis: new perspectives and therapeutic strategies. Nat Med 8:1249–1256
82. Walworth NC (2000) Cell-cycle checkpoint kinases: checking in on the cell cycle. Curr Opin Cell Biol 12:697–704
83. Weinberg RA (1996) E2F and cell proliferation: a world turned upside down. Cell 85:457–459
84. Harbour JW, Dean DC (2000) Rb function in cell-cycle regulation and apoptosis. Nat Cell Biol 2:E65–E67
85. Tanner FC, Boehm M, Akyürek LM et al (2000) Differential effects of the cyclin-dependent kinase inhibitors p27(Kip1), p21(Cip1), and p16(Ink4) on vascular smooth muscle cell proliferation. Circulation 101:2022–2025
86. Gizard F, Bruemmer D (2008) Transcriptional control of vascular smooth muscle cell proliferation by peroxisome proliferator-activated receptor-gamma: therapeutic implications for cardiovascular diseases. PPAR Res 2008:429123
87. Sherr CJ, Roberts JM (1999) CDK inhibitors: positive and negative regulators of G1-phase progression. Genes Dev 13:1501–1512
88. Braun-Dullaeus RC, Mann MJ, Dzau VJ (1998) Cell cycle progression: new therapeutic target for vascular proliferative disease. Circulation 98:82–89
89. Quizhpe AR, Feres F, de Ribamar Costa J Jr et al (2007) Drug-eluting stents vs bare metal stents for the treatment of large coronary vessels. Am Heart J 154:373–378
90. Neuhaus P, Klupp J, Langrehr JM (2001) mTOR inhibitors: an overview. Liver Transpl 7:473–484
91. Sehgal SN (2003) Sirolimus: its discovery, biological properties, and mechanism of action. Transplant Proc 35:7S–14S
92. Ruygrok PN, Muller DW, Serruys PW (2003) Rapamycin in cardiovascular medicine. Intern Med J 33:103–109

93. Abizaid A (2007) Sirolimus-eluting coronary stents: a review. Vasc Health Risk Manag 3:191–201
94. Larkin JM, Kaye SB (2006) Epothilones in the treatment of cancer. Expert Opin Investig Drugs 15:691–702
95. Sheiban I, Moretti C, Oliaro E et al (2003) Evolving standard in the treatment of coronary artery disease. Drug-eluting stents. Minerva Cardioangiol 51:485–492
96. Kukreja N, Onuma Y, Daemen J, Serruys PW (2008) The future of drug-eluting stents. Pharmacol Res 57:171–180
97. Okamoto S, Inden M, Setsuda M, Konishi T, Nakano T (1992) Effects of trapidil (triazolopyrimidine), a platelet-derived growth factor antagonist, in preventing restenosis after percutaneous transluminal coronary angioplasty. Am Heart J 123:1439–1444
98. Powell JS, Clozel JP, Müller RK et al (1989) Inhibitors of angiotensin-converting enzyme prevent myointimal proliferation after vascular injury. Science 245:186–188
99. Garas SM, Huber P, Scott NA (2001) Overview of therapies for prevention of restenosis after coronary interventions. Pharmacol Ther 92:165–178
100. Reidy MA, Fingerle J, Lindner V (1992) Factors controlling the development of arterial lesions after injury. Circulation 86:III43–III46
101. Meredith IT, Anderson TJ, Uehata A, Yeung AC, Selwyn AP, Ganz P (1993) Role of endothelium in ischemic coronary syndromes. Am J Cardiol 72:27C–31C. discussion 31C–32C
102. Versari D, Lerman LO, Lerman A (2007) The importance of reendothelialization after arterial injury. Curr Pharm Des 13:1811–1824
103. Rao RM, Yang L, Garcia-Cardena G, Luscinskas FW (2007) Endothelial-dependent mechanisms of leukocyte recruitment to the vascular wall. Circ Res 101:234–247
104. Berk BC (2001) Vascular smooth muscle growth: autocrine growth mechanisms. Physiol Rev 81:999–1030
105. Langille BL, O'Donnell F (1986) Reductions in arterial diameter produced by chronic decreases in blood flow are endothelium-dependent. Science 231:405–407
106. Datta YH, Ewenstein BM (2001) Regulated secretion in endothelial cells: biology and clinical implications. Thromb Haemost 86:1148–1155
107. Celermajer DS (1997) Endothelial dysfunction: does it matter? Is it reversible? J Am Coll Cardiol 30:325–333
108. Leopold JA, Loscalzo J (2000) Clinical importance of understanding vascular biology. Cardiol Rev 8:115–123
109. Tanguay JF (2005) Vascular healing after stenting: the role of 17-beta-estradiol in improving re-endothelialization and reducing restenosis. Can J Cardiol 21:1025–1030
110. Adams B, Xiao Q, Xu Q (2007) Stem cell therapy for vascular disease. Trends Cardiovasc Med 17:246–251
111. Sprague EA, Luo J, Palmaz JC (2000) Endothelial cell migration onto metal stent surfaces under static and flow conditions. J Long Term Eff Med Implants 10:97–110
112. Davies PF (1995) Flow-mediated endothelial mechanotransduction. Physiol Rev 75:519–560
113. Garcia-Cardena G, Comander J, Anderson KR, Blackman BR, Gimbrone MA Jr (2001) Biomechanical activation of vascular endothelium as a determinant of its functional phenotype. Proc Natl Acad Sci U S A 98:4478–4485
114. Lin K, Hsu PP, Chen BP et al (2000) Molecular mechanism of endothelial growth arrest by laminar shear stress. Proc Natl Acad Sci U S A 97:9385–9389
115. Levesque MJ, Nerem RM, Sprague EA (1990) Vascular endothelial cell proliferation in culture and the influence of flow. Biomaterials 11:702–707
116. LaDisa JF Jr, Guler I, Olson LE et al (2003) Three-dimensional computational fluid dynamics modeling of alterations in coronary wall shear stress produced by stent implantation. Ann Biomed Eng 31:972–980
117. Colombo A, Sangiorgi G (2004) The monocyte: the key in the lock to reduce stent hyperplasia? J Am Coll Cardiol 43:24–26
118. Farb A, Sangiorgi G, Carter AJ et al (1999) Pathology of acute and chronic coronary stenting in humans. Circulation 99:44–52
119. Welt FG, Tso C, Edellman ER et al (2003) Leukocyte recruitment and expression of chemokines following different forms of vascular injury. Vasc Med 8:1–7
120. Tanaka H, Sukhova GK, Swanson SJ et al (1993) Sustained activation of vascular cells and leukocytes in the rabbit aorta after balloon injury. Circulation 88:1788–1803
121. Rogers C, Welt FG, Karnovsky MJ, Edelman ER (1996) Monocyte recruitment and neointimal hyperplasia in rabbits. Coupled inhibitory effects of heparin. Arterioscler Thromb Vasc Biol 16:1312–1318
122. Rogers C, Edelman ER, Simon DI (1998) A mAb to the beta2-leukocyte integrin Mac-1 (CD11b/CD18) reduces intimal thickening after angioplasty or stent implantation in rabbits. Proc Natl Acad Sci U S A 95:10134–10139
123. McEver RP, Cummings RD (1997) Role of PSGL-1 binding to selectins in leukocyte recruitment. J Clin Invest 100:S97–S103
124. Weber C (2005) Platelets and chemokines in atherosclerosis: partners in crime. Circ Res 96:612–616
125. Kitamoto S, Egashira K (2003) Anti-monocyte chemoattractant protein-1 gene therapy for cardiovascular diseases. Expert Rev Cardiovasc Ther 1:393–400
126. Wainwright CL, Miller AM, Wadsworth RM (2001) Inflammation as a key event in the development of neointima following vascular balloon injury. Clin Exp Pharmacol Physiol 28:891–895
127. Cipollone F, Marini M, Fazia M (2001) Elevated circulating levels of monocyte chemoattractant protein-1 in patients with restenosis after coronary angioplasty. Arterioscler Thromb Vasc Biol 21:327–334
128. Oshima S, Ogawa H, Hokimoto S et al (2001) Plasma monocyte chemoattractant protein-1 antigen levels and the risk of restenosis after coronary stent implantation. Jpn Circ J 65:261–264
129. Bursill CA, Channon KM, Greaves DR (2004) The role of chemokines in atherosclerosis: recent evidence from experimental models and population genetics. Curr Opin Lipidol 15:145–149
130. Tashiro H, Shimokawa H, Sadamatsu K, Aoki T, Yamamoto K (2001) Role of cytokines in the pathogenesis of restenosis after percutaneous transluminal coronary angioplasty. Coron Artery Dis 12:107–113
131. Arend WP, Guthridge CJ (2000) Biological role of interleukin 1 receptor antagonist isoforms. Ann Rheum Dis 59:i60–i64
132. Sardella G, Mariani P, D'Alessandro M et al (2006) Early elevation of interleukin-1beta and interleukin-6 levels after bare or drug-eluting stent implantation in patients with stable angina. Thromb Res 117:659–664
133. Odrowaz-Sypniewska G (2007) Markers of pro-inflammatory and pro-thrombotic state in the diagnosis of metabolic syndrome. Adv Med Sci 52:246–250
134. Monraats PS, Pires NM, Schepers A et al (2005) Tumor necrosis factor-alpha plays an important role in restenosis development. FASEB J 19:1998–2004
135. Kawamoto R, Hatakeyama K, Imamura T et al (2004) Relation of C-reactive protein to restenosis after coronary stent implantation and to restenosis after coronary atherectomy. Am J Cardiol 94:104–107
136. Mazer SP, Rabbani LE (2004) Evidence for C-reactive protein's role in (CRP) vascular disease: atherothrombosis, immunoregulation and CRP. J Thromb Thrombolysis 17:95–105
137. Gaspardone A, Versaci F, Tomai F et al (2006) C-Reactive protein, clinical outcome, and restenosis rates after implantation of different drug-eluting stents. Am J Cardiol 97:1311–1316
138. Moreno PR, Bernardi VH, López-Cuéllar J et al (1996) Macrophage infiltration predicts restenosis after coronary intervention in patients with unstable angina. Circulation 94:3098–3102
139. Stakos DA, Kotsianidis I, Tziakas DN et al (2007) Leukocyte activation after coronary stenting in patients during the subacute

phase of a previous ST-elevation myocardial infarction. Coron Artery Dis 18:105–110
140. Funayama H, Ishikawa SE, Kubo N, Yasu T, Saito M, Kawakami M (2006) Close association of regional interleukin-6 levels in the infarct-related culprit coronary artery with restenosis in acute myocardial infarction. Circ J 70:426–429
141. Cipollone F, Ferri C, Desideri G et al (2003) Preprocedural level of soluble CD40L is predictive of enhanced inflammatory response and restenosis after coronary angioplasty. Circulation 108:2776–2782
142. Lin ZQ, Kondo T, Ishida Y, Takayasu T, Mukaida N (2003) Essential involvement of IL-6 in the skin wound-healing process as evidenced by delayed wound healing in IL-6-deficient mice. J Leukoc Biol 73:713–721
143. Becker RC (2003) Complicated myocardial infarction. Crit Pathw Cardiol 2:125–152
144. Vishnevetsky D, Kiyanista VA, Gandhi PJ (2004) CD40 ligand: a novel target in the fight against cardiovascular disease. Ann Pharmacother 38:1500–1508
145. Yan JC, Ding S, Liang Y et al (2007) Relationship between upregulation of CD40 system and restenosis in patients after percutaneous coronary intervention. Acta Pharmacol Sin 28:339–343
146. Shebuski RJ, Kilgore KS (2002) Role of inflammatory mediators in thrombogenesis. J Pharmacol Exp Ther 300:729–735
147. Giesen PL, Fyfe BS, Fallon JT et al (2000) Intimal tissue factor activity is released from the arterial wall after injury. Thromb Haemost 83:622–628
148. Martorell L, Martinez-Gonzalez J, Rodriguez C, Gentile M, Calvayrac O, Badimon L (2008) Thrombin and protease-activated receptors (PARs) in atherothrombosis. Thromb Haemost 99: 305–315
149. Hideshima T, Rodar K, Chauhan D, Anderson KC (2005) Cytokines and signal transduction. Best Pract Res Clin Haematol 18:509–524
150. Barish GD, Atkins AR, Downes M et al (2008) PPARdelta regulates multiple proinflammatory pathways to suppress atherosclerosis. Proc Natl Acad Sci U S A 105:4271–4276
151. Baron AD (2002) Insulin resistance and vascular function. J Diabetes Complications 16:92–102
152. Kim F, Pham M, Luttrell I et al (2007) Toll-like receptor-4 mediates vascular inflammation and insulin resistance in diet-induced obesity. Circ Res 100:1589–1596
153. Nilsson J, Nilsson LM, Chen YM, Molkentin JD, Erlinge D, Gomez MF (2006) High glucose activates nuclear factor of activated T cells in native vascular smooth muscle. Arterioscler Thromb Vasc Biol 26:794–800
154. Zhang L, Peppel K, Sivashanmugam P et al (2007) Expression of tumor necrosis factor receptor-1 in arterial wall cells promotes atherosclerosis. Arterioscler Thromb Vasc Biol 27:1087–1094
155. Heyninck K, Beyaert R (2001) Crosstalk between NF-kappaB-activating and apoptosis-inducing proteins of the TNF-receptor complex. Mol Cell Biol Res Commun 4:259–265
156. Schonbeck U, Libby P (2001) CD40 signaling and plaque instability. Circ Res 89:1092–1103
157. Vanichakarn P, Blair P, Wu C, Freedman JE, Chakrabarti S (2008) Neutrophil CD40 enhances platelet-mediated inflammation. Thromb Res 122:346–358
158. Lutgens E, Lievens D, Beckers L, Donners M, Daemen M (2007) CD40 and its ligand in atherosclerosis. Trends Cardiovasc Med 17:118–123
159. Chakrabarti S, Blair P, Freedman JE (2007) CD40-40L signaling in vascular inflammation. J Biol Chem 282:18307–18317
160. Zirlik A, Bavendiek U, Libby P et al (2007) TRAF-1, -2, -3, -5, and -6 are induced in atherosclerotic plaques and differentially mediate proinflammatory functions of CD40L in endothelial cells. Arterioscler Thromb Vasc Biol 27:1101–1107
161. Hoge M, Amar S (2006) Role of interleukin-1 in bacterial atherogenesis. Drugs Today (Barc) 42:683–688
162. Fogal B, Hewett SJ (2008) Interleukin-1beta: a bridge between inflammation and excitotoxicity? J Neurochem 106:1–23
163. Li X, Qin J (2005) Modulation of Toll-interleukin 1 receptor mediated signaling. J Mol Med 83:258–266
164. Boraschi D, Tagliabue A (2006) The interleukin-1 receptor family. Vitam Horm 74:229–254
165. Gottipati S, Rao NL, Fung-Leung WP (2008) IRAK1: a critical signaling mediator of innate immunity. Cell Signal 20:269–276
166. Mullaly SC, Kubes P (2004) Toll gates and traffic arteries: from endothelial TLR2 to atherosclerosis. Circ Res 95:657–659
167. Schoneveld AH, Oude Nijhuis MM, van Middelaar B, Laman JD, de Kleijn DP, Pasterkamp G (2005) Toll-like receptor 2 stimulation induces intimal hyperplasia and atherosclerotic lesion development. Cardiovasc Res 66:162–169
168. Shishido T, Nozaki N, Takahashi H et al (2006) Central role of endogenous Toll-like receptor-2 activation in regulating inflammation, reactive oxygen species production, and subsequent neointimal formation after vascular injury. Biochem Biophys Res Commun 345:1446–1453
169. Harrington LS, Belcher E, Moreno L, Carrier MJ, Mitchell JA (2007) Homeostatic role of Toll-like receptor 4 in the endothelium and heart. J Cardiovasc Pharmacol Ther 12:322–326
170. de Kleijn MJ, Wilmink HW, Bots ML et al (2001) Hormone replacement therapy and endothelial function. Results of a randomized controlled trial in healthy postmenopausal women. Atherosclerosis 159:357–365
171. Martin MU, Wesche H (2011) Summary and comparison of the signaling mechanisms of the Toll/interleukin-1 receptor family. Biochim Biophys Acta 1592:265–280
172. Karin M, Ben-Neriah Y (2000) Phosphorylation meets ubiquitination: the control of NF-[kappa]B activity. Annu Rev Immunol 18:621–663
173. Chen FE, Huang DB, Chen YQ, Ghosh G (1998) Crystal structure of p50/p65 heterodimer of transcription factor NF-kappaB bound to DNA. Nature 391:410–413
174. Li ZW, Chu W, Hu Y et al (1999) The IKKbeta subunit of IkappaB kinase (IKK) is essential for nuclear factor kappaB activation and prevention of apoptosis. J Exp Med 189:1839–1845
175. Li X, Stark GR (2002) NFkappaB-dependent signaling pathways. Exp Hematol 30:285–296
176. Bavry AA, Kumbhani DJ, Helton TJ, Borek PP, Mood GR, Bhatt DL (2006) Late thrombosis of drug-eluting stents: a meta-analysis of randomized clinical trials. Am J Med 119:1056–1061
177. Iakovou I, Schmidt T, Bonizzoni E et al (2005) Incidence, predictors, and outcome of thrombosis after successful implantation of drug-eluting stents. JAMA 293:2126–2130
178. Waters RE, Kandzari DE, Phillips HR, Crawford LE, Sketch MH Jr (2005) Late thrombosis following treatment of in-stent restenosis with drug-eluting stents after discontinuation of antiplatelet therapy. Catheter Cardiovasc Interv 65:520–524
179. Eisenreich A, Celebi O, Goldin-Lang P, Schultheiss HP, Rauch U (2008) Upregulation of tissue factor expression and thrombogenic activity in human aortic smooth muscle cells by irradiation, rapamycin and paclitaxel. Int Immunopharmacol 8:307–311
180. Nakazawa G, Finn AV, Virmani R (2007) Vascular pathology of drug-eluting stents. Herz 32:274–280
181. Palmerini T, Biondi-Zoccai G, Della Riva D et al (2014) Clinical outcomes with bioabsorbable polymer-versus durable polymer-based drug-eluting and bare-metal stents: evidence from a comprehensive network meta-analysis. J Am Coll Cardiol 63:299–307

16 Reversible and Irreversible Damage of the Myocardium: Ischemia/Reperfusion Injury and Cardioprotection

Brian T. Howard, Tinen L. Iles, James A. Coles Jr., Daniel C. Sigg, and Paul A. Iaizzo

Abstract

Ischemia and reperfusion injuries can lead to major compromises in cardiac function. While the intent of many of the past cardioprotective therapies was to protect the myocardium from ischemic necrosis, it may be that reperfusion injury following ischemia may occur despite such preventative attempts. There are continued efforts to identify improvements in myocardial protective strategies (pre- and postconditioning), and their ultimate goals are to minimize the risk of cellular injuries to all types of patients undergoing cardiovascular therapies, treatments, or surgeries.

Keywords

Myocardial ischemia • Reperfusion injury • Cardioprotection • Myocardial stunning • Hibernating myocardium • Maimed myocardium • Ischemic preconditioning • Silent ischemia

16.1 Introduction

The goal of this chapter is to provide the reader with a general review of the physiology and pathophysiology of *myocardial ischemia*. In the past, it was thought that a lack of blood flow to the heart resulted in irreversible myocardial damage and necrosis (infarction). However, continued evidence has suggested that there are several identifiable clinical scenarios that present between these basic definitions of *ischemia* and *infarction*, and actually the heart may recover a variable degree of preischemic function, even when eliciting some degree of necrosis. Furthermore, with recent technological advances involving intentional cardiac arrest during cardiac surgery and noninvasive cardiac angioplasty (opening) of occluded coronary arteries, the phenomenon of reperfusion injury has also presented as a sometimes debilitating clinical syndrome. This chapter will explore these ischemic syndromes and present an up-to-date overview of several methods that can be employed to protect the heart from these conditions (cardioprotection).

B.T. Howard, PhD • T.L. Iles, MS (✉)
University of Minnesota, 420 Delaware St. SE, B172 Mayo, MMC 195, Minneapolis, MN 55455, USA
e-mail: thealy@umn.edu

J.A. Coles Jr., PhD
Medtronic, Inc., Minneapolis, MN, USA

D.C. Sigg, MD, PhD • P.A. Iaizzo, PhD
Department of Surgery, University of Minnesota, Minneapolis, MN, USA

16.2 Basic Cardiac Metabolism

The average healthy human heart weighs between 300 and 400 g and is approximately 0.5 % of the total body mass, yet the oxygen demand of the heart accounts for 7 % of the resting body oxygen consumption and, consequently, 5 % of the cardiac output. The normal myocardial oxygen consumption (MVO_2) is approximately 8 mL O_2/100 g/min, yet this varies widely in normal, diseased, and/or exercising states. The MVO_2 is primarily dependent on coronary blood flow (CBF) and the removal of oxygen from the coronary blood—arterial (CaO_2) minus venous (coronary sinus, CSO_2) contents—such that

P.A. Iaizzo (ed.), *Handbook of Cardiac Anatomy, Physiology, and Devices*, DOI 10.1007/978-3-319-19464-6_16

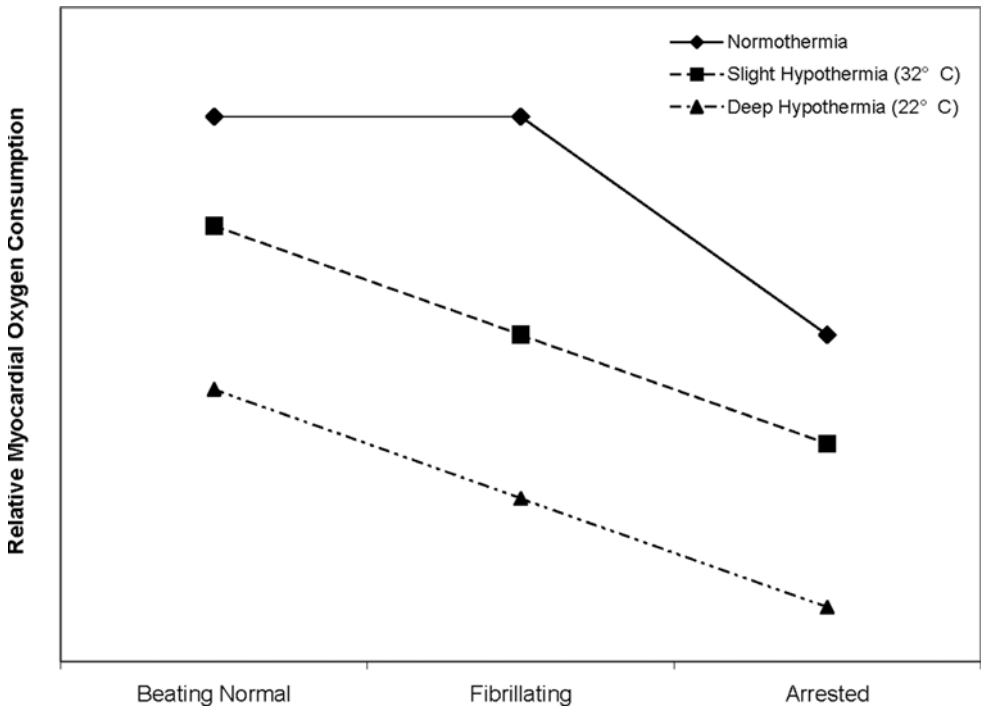

Fig. 16.1 Influence of temperature on myocardial metabolism. While it is expected that hypothermia decreases myocardial oxygen consumption in the beating and fibrillating heart, there also exists a significant difference between the normothermic and hypothermic arrested heart. This indicates that the heart still has a measurable oxygen demand while arrested. Also notable is the difference in myocardial oxygen consumption between the fibrillating and arrested heart at either temperature

$$MVO_2 = CBF \times \left(CaO_2 - CSO_2\right).$$

Secondary determinants influencing MVO_2 include (1) the relative heart rate, (2) myocardial stroke work, (3) imposed afterloads, and/or (4) the inotropic state of the myocardium.

Importantly, associated with cardiac surgery, MVO_2 can vary extensively, with the greatest MVO_2 occurring immediately after bypass; replenishing energy stores requires a high oxygen demand (i.e., repaying oxygen debt). In contrast, cardiac arrest combined with myocardial hypothermia dramatically reduces MVO_2 (Fig. 16.1). It should be noted that hypothermic and normothermic modes of cardiac arrest differ in their degrees of MVO_2 reduction. However, in all cases, the arrested heart still elicits an oxygen demand; hence, there will always be some degree of imbalance between oxygen demand and delivery, with ischemia resulting. See Chap. 33 for additional information about cardioprotection during surgery.

16.3 Myocardial Ischemia

The basic definition of *myocardial ischemia* is a greater myocardial tissue oxygen demand than supply. During short-term ischemic episodes, the heart's defense mechanism seeks to remedy this imbalance by downregulating myocardial contractile function and, concomitantly, increasing the rate of glycolysis (anaerobic energy production) from preferred lipid metabolism. Consequently, sarcolemmal glucose transport increases, and intracellular acidosis resulting from a buildup of the glycolytic breakdown products causes further inhibition of the contractile apparatus. Even though energy production continues in the absence of oxygen, the glycolytic pathway is an inefficient means for producing ATP. As an ischemic episode becomes more severe or prolonged, the heart becomes unable to produce enough energy via glycolysis and cellular necrosis ensues. For example, 10 min of ischemia generally results in about 50 % depletion of ATP; after approximately 30 min of normothermic ischemia without significant collateral blood flow, irreversible damage or necrosis occurs [1]. Anatomically, the most vulnerable layer of the heart is the subendocardium, due to the higher systolic wall stress in this layer compared to the mid- and epicardial layers; there exists a relatively greater metabolic demand. For additional discussion on myocardial energetics, see Chaps. 15 and 21.

16.4 Ischemic Syndromes

In the past, it was generally believed that extending the periods of myocardial ischemia would, in turn, lead to irreversible damage of the myocardial or infarcted (necrotic) tissue. However, between the clinical conditions of transient ischemia (angina pectoris) and myocardial infarction, five additional ischemic syndromes have been described (Figs. 16.2 and 16.3) [2, 3]. The *stunned myocardium* is characterized by postischemic impairment of myocardial function, but it is considered acute and completely reversible. The *hibernating myocardium* is also characterized by depressed myocardial

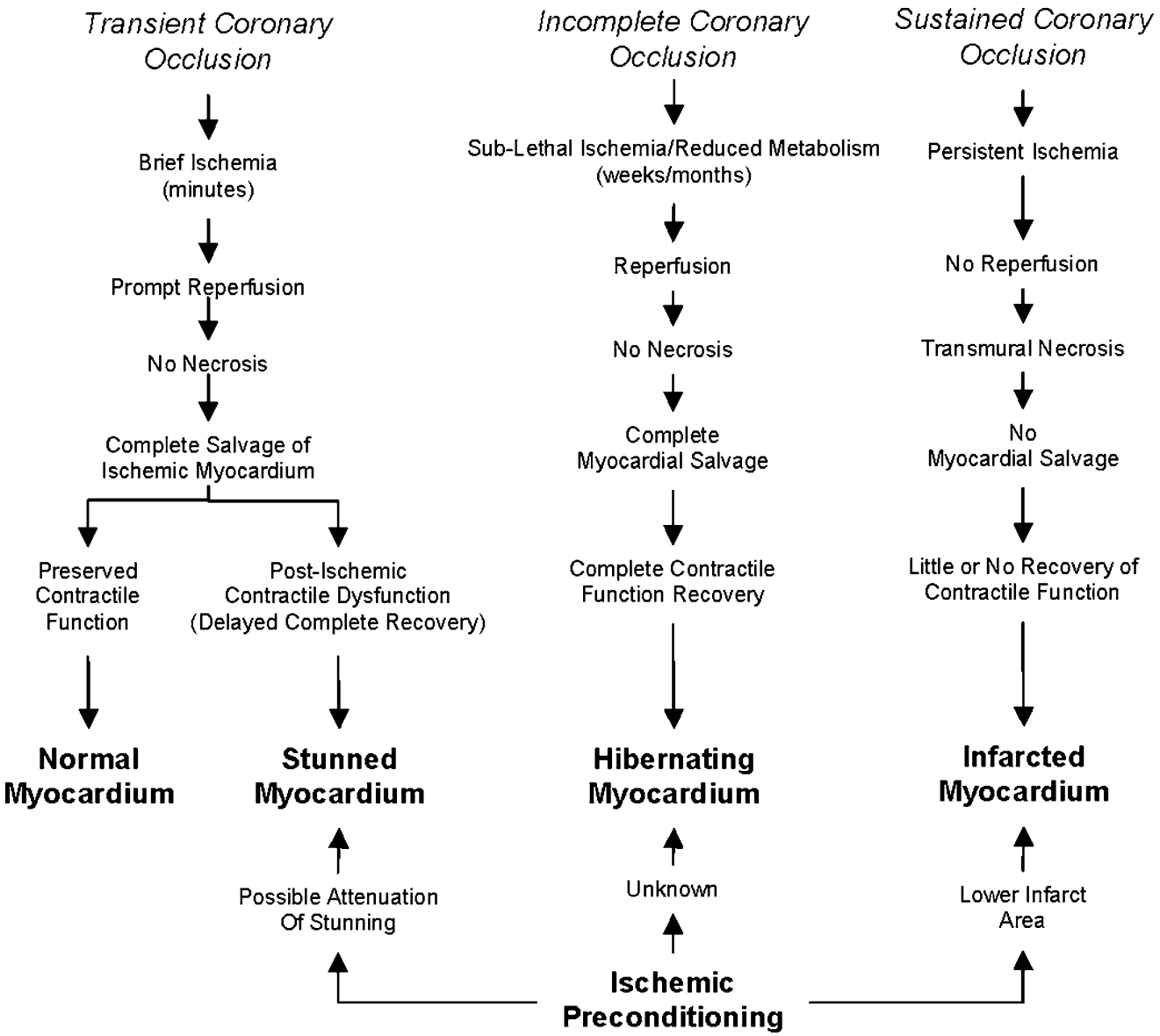

Fig. 16.2 Consequences of myocardial ischemia. The stunned myocardium usually results from a transient coronary occlusion followed by prompt reperfusion; however, it may also occur after prolonged ischemia in the preconditioned heart. Preconditioning lessens the infarct area following a sustained coronary occlusion, but only the area is reperfused. The relationship between preconditioning and the maimed myocardium is unknown. Modified from Boden et al. [17]

function of variable duration, primarily caused by impaired oxygen delivery through an occluded vessel, and, importantly, recovery of function occurs upon reflow to the ischemic region. Note that the hibernating myocardium is similar to the stunned myocardium, with the main difference being that reperfusion is not the cause of myocardial hibernation, as is the case with myocardial stunning. On the other hand, hibernation can be considered as a state of chronic stunning, yet the exact mechanism of hibernation remains largely unknown [4]. The *maimed myocardium* is considered the most severe of such syndromes and is characterized by irreversible myocardial damage that follows ischemia and reperfusion and in which there is a delayed recovery to only partial preischemic function. *Ischemic preconditioning* is the condition where multiple brief ischemic episodes (<5 min) followed by reperfusion subsequently enhance the myocardial tolerances to a longer (<45 min) ischemic event (Figs. 16.3 and 16.4). Finally, patients with ECG changes of ischemia and contractile failure who lack chest pain may be experiencing *silent ischemia*. It has been proposed that these patients are either less sensitive to painful stimuli or the ischemia is somewhat milder [3].

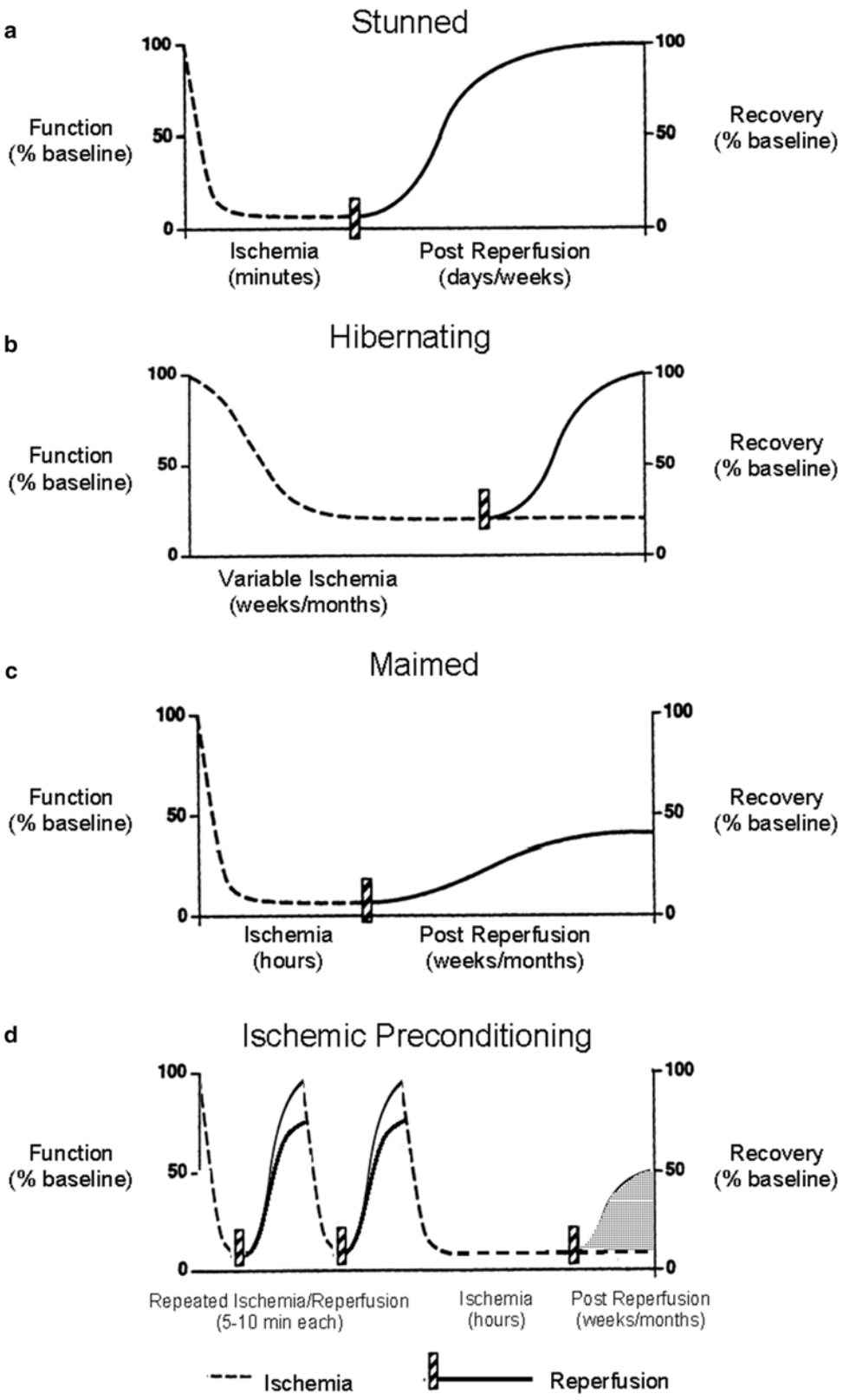

Fig. 16.3 New ischemic syndromes. New ischemic syndromes that do not fall within the realm of classic acute reversible and irreversible myocardial ischemia. (**a**) The stunned myocardium is characterized by a decrease in function following an ischemic event in which there is a complete absence of necrosis from ischemia or reperfusion and a complete functional recovery hours to days later. (**b**) The hibernating myocardium is characterized by chronic depressed myocardial function due to sublethal ischemia lasting for weeks to months, and revascularization may result in complete recovery of function. (**c**) The maimed myocardium has permanent damage resulting from a prolonged ischemic episode and has some functional recovery that does not return to preischemic levels. (**d**) Ischemic preconditioning exists when short ischemic episodes followed by reperfusion confer myocardial protection during a subsequent prolonged ischemic event. However, two areas of uncertainty exist in the preconditioning phenomenon: (1) functional recovery following the preceding short ischemic events may not return to preischemic levels; and (2) while it is known that ischemic preconditioning lessens infarct size, it is uncertain whether long-term functional recovery following the prolonged ischemic episode is significantly improved (via decreased myocardial stunning). Only delayed ischemic preconditioning has been shown to attenuate myocardial stunning. Modified from Boden et al. [17]

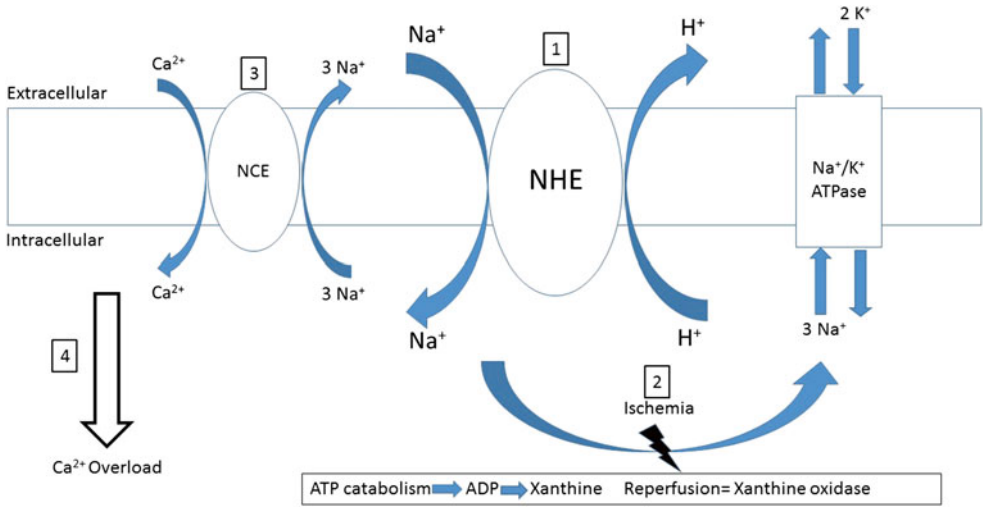

Fig. 16.4 Reperfusion injury via the Na^+–H^+ exchanger. Reperfusion injury-induced calcium overload can be explained, in part, by activation of the Na^+–H^+ exchanger (NHE). (*1*) Intracellular acidosis from a prior ischemic episode activates the NHE upon reperfusion, thereby decreasing intracellular acidosis and increasing Na^+ influx. (*2*) Intracellular sodium is primarily removed from the cell via the Na^+–K^+ATPase during normal myocardial function. However, after ischemia (i.e., during the early stages of reperfusion), the lack of abundance of ATP does not allow for normal operation of the pump and intracellular Na^+ increase. (*3*) Consequently, the Na^+–Ca^{2+} exchanger (NCE), which normally operates by extruding Ca^{2+} from the cytoplasm, is the primary mechanism for intracellular Na^+ removal operating in a reverse mode. (*4*) Intracellular Ca^{2+} overload results from NCE activation, possibly causing arrhythmias, stunning, and necrosis

16.4.1 Myocardial Stunning

There are two general theories for explaining the pathomechanisms underlying myocardial stunning, and they are generally not considered to be mutually exclusive. Episodes of ischemia are caused by: (1) the formation of free radical reactive species and/or (2) alterations in intracellular calcium regulation [5]. Furthermore, in such cases, intracellular acidosis occurring during ischemia can potentially generate intracellular calcium oscillations and calcium overload upon reperfusion via activation of the sarcolemmal Na^+/H^+ exchanger (NHE) (Fig. 16.4) [6].

Experimental studies have shown that the calcium sensitivity of the contractile apparatus is decreased in the stunned myocardium, thereby resulting in lower maximal force generation even at higher than normal transient calcium levels [7, 8]. Furthermore, decreased myofilament sensitivity to calcium is considered primarily responsible for systolic dysfunction; for example, the stunned myocardium is still responsive to inotropic stimulation. Of additional interest is the finding that troponin I (cTnI) degradation products were discovered in the human myocardium during aortic cross-clamping with bypass and that serum levels of cTnI increased during reperfusion, peaking approximately 24 h following cross-clamp removal [9]. This preliminary evidence further suggests that cTnI degradation products may potentially be utilized as biomarkers for occurrence of myocardial stunning.

During the early stage of stunning, it is considered beneficial to prevent calcium oscillations and thus attenuate significant injury caused by reperfusion. This has been accomplished experimentally by utilizing Ca^{2+} antagonists, inorganic blockers, ryanodine, low-calcium reperfusion buffers, and/or NHE blockers [10]. Conversely, when contractility is suppressed, as in the late stage of stunning, therapies should include those that increase the amplitudes of intracellular calcium transients, inducing inotropic responses. Included in this subset of therapeutics are high calcium buffers, Ca^{2+} agonists, catecholamines, and/or phosphodiesterase inhibitors. Importantly, many of these therapies are specific to the stage or degree of stunning, and hence, the timing of their use is critical, so as not to become a detrimental therapy. For instance, hypocalcemia during and following cardiopulmonary bypass is a common occurrence mainly attributed to the utilization of priming fluids, citrated blood, and large doses of heparin during bypass [11]. Normally, hypocalcemia is successfully corrected with the administration of calcium chloride; however, calcium levels may return to preoperative levels prior to removal from cardiopulmonary bypass without supplemental calcium [12]. Therefore, the risk of stunning and myocardial damage may actually be increased with generalized calcium chloride administration. While it may be used for post-bypass cardiac resuscitation, current Advanced Cardiac Life Support (ACLS) guidelines do not indicate calcium chloride for general resuscitation purposes, and administration if done at all is on an "as necessary" basis [13].

16.4.2 Hibernating Myocardium

As previously discussed, myocardial stunning and hibernation are related in that a depressed state of contractility exists and, yet importantly, there is the potential to reversibly return the dysfunctional myocardium back to normal. However, it must again be restated that while stunning can be attributed to the reperfusion following a brief bout of ischemia, the hibernating myocardium is in a chronic hypocontractile state, due to a decreased oxygen supply and thus may only recover full function with revascularization therapy. In other words, this reduction in oxygen delivery is attributable to reductions in local perfusion, and the corresponding reduction in contractility has been shown to be a proportional response of the myocardium, termed *perfusion-contraction matching* and elucidated by John Ross [14]. It may be beneficial to consider the hibernating myocardium as a viable tissue which is simply eliciting necessary physiological compromises in response to locally limited blood flow. Additionally, many of the underlying mechanisms of stunning are considered directly related to the detrimental effects of reperfusion injury (to be discussed later) [15]. While there is a general absence of necrosis with myocardial hibernation, morphological changes to the myocardial architecture, such as loss of myofibrils and increased interstitial fibrosis, may occur if this state persists [16].

16.4.3 Maimed Myocardium

The maimed myocardium closely resembles that of a heart with a classic myocardial infarction in that ischemia-induced necrosis leads to loss of contractile performance. In these cases, unlike in myocardial stunning, the duration of ischemia is long enough to result in necrosis. Importantly there can be partial recovery of function in this ischemic region, i.e., following timely reperfusion [17]. An example of the maimed myocardium syndrome would be a patient that exhibits an incomplete recovery of myocardial function following drug-induced or mechanical (angioplasty) reperfusion of an occluded coronary artery and then subsequently demonstrates regions of viable myocardium in the original ischemic area.

16.4.4 Ischemic Preconditioning

Ischemic preconditioning is a biological phenomenon whereby brief ischemic episodes followed by adequate reperfusion protect tissue from a subsequent *prolonged ischemic event* [18]. In general, cardiac protection from ischemic preconditioning has been characterized as biphasic. The first window of protection occurs immediately following the ischemic event for approximately 3 h mediated by effectors. The second window of protection occurs some 24 h after the ischemic event and can last for up to 3 days and is mediated by an upregulation of cardioprotective proteins. There are several signaling pathways that are involved in these mechanisms of ischemic preconditioning, including the activation of potassium channels that are located in the inner membrane of the mitochondria of the cardiac myocytes [19]. These pathways can be utilized as drug delivery targets for the therapeutic treatment of prevention for ischemic injury, by mimicking the natural progression of limited ischemic preconditioning. In the myocardium, ischemic preconditioning has been shown to be potentially infarct limiting [18] as well as antiarrhythmic [20], although the latter of these effects can be agent specific. It is also well established that endogenous opioid receptor activation participates in myocardial ischemic preconditioning [21] and that preischemic administration of synthetic opioid agonists can mimic the benefits of ischemic preconditioning [22]. While ischemic and opioid preconditioning have both been convincingly shown to delay cell death in various experimental animal models, the clinical applicability of these therapies in humans may be limited to situations where the ischemic event can be anticipated (e.g., on- or off-bypass cardiac surgery, percutaneous transluminal coronary angioplasty, or stenting procedures) [23]. For a more comprehensive review of ischemic and opioid preconditioning, see articles by Yellon and Downey [24] (*ischemic preconditioning)* and Gross [25] (*opioid preconditioning*).

16.4.5 Silent Ischemia

Silent ischemia refers to single or multiple asymptomatic episodes of transient ischemia. In some cases, silent ischemia can occur in the week(s) following an acute myocardial infarction in patients with a history of coronary artery disease. In other scenarios, seemingly normal healthy individuals may experience episodes of silent ischemia that go relatively unnoticed. Detection of silent ischemia primarily relies on electrocardiographic monitoring, either in the form of 24-h Holter monitoring (ambulatory) or exercise- and/or stress-induced assessment. In both cases, ischemia is typically detected by asymptomatic ST-segment elevations in an ECG tracing [26]; see also Chap. 19. Silent ischemia is postulated to be related to a lack of oxygen supply rather than an increase in oxygen demand; however, controversy remains regarding the mechanisms whereby silent ischemia can proceed unnoticed.

16.4.6 How Can the Heart Be Protected from Ischemia?

As shown in Fig. 16.1, there are several means of decreasing myocardial oxygen demand when the oxygen supply is compromised. These include hypothermia, pharmacologically decreasing the heart rate, and/or controlled cardiac arrest. Additionally, as mentioned above, ischemic and pharmacological

preconditioning of the heart are other ways to protect the myocardium from an ischemic episode and, hence, induce cardioprotection. However, these therapies require the anticipation of the ischemic event, such that treatment can be administered prior to or early during the ischemia. In situations where anticipation of ischemia is not possible, for example, in acute myocardial infarction, interventions which reestablish blood flow and oxygen to the ischemic zone (reperfusion) are the primary therapies. Nevertheless, it should be noted that dietary supplements such as omega-3 fatty acids have been considered as a potential means for prevention [27, 28].

16.5 Reperfusion Injury

While immediate restoration of blood flow and oxygen to ischemic tissue is ultimately a beneficial and important therapy, it should be noted that additional myocardial damage can occur with such myocardial reperfusion itself. In what has been termed the *oxygen paradox*, the resupply of oxygen to a hypoxic cell simultaneously activates two intracellular processes of particular interest—the membrane-bound calcium pumps and the contractile apparatus. Resumption of contractile activity in the presence of oscillating and increasing intracellular Ca^{2+} levels can force the heart into a state of hypercontracture and thus cause intracellular edema.

Another proposed mechanism of injury during reperfusion can result from xanthine oxidase. During periods of ischemia, ATP is catabolized and ATP is reduced to ADP, AMP, adenosine, and inosine and further reduced to xanthine. Xanthine alone is not cytotoxic, but when oxygen is reintroduced, the product is xanthine oxidase. This in turn releases free radicals into the myocardial tissue via super oxide dismutase, hydrogen peroxide, and uric acid [29]. Hence, the administration of xanthine oxidase inhibitors can diminish the effects of free radical production when a procedure is planned. For example, a patient could be given prophylactic xanthine oxidase inhibitors prior to a coronary artery bypass graft when reperfusion injury is anticipated. Collectively, these etiologies may ultimately result in membrane disruption and even cell death.

Reperfusion injury can present in (or is associated with) one or more of the following pathologies: (1) reperfusion arrhythmias, (2) microvascular damage and no-reflow, (3) accelerated cell death, (4) myocardial stunning, and/or (5) post-pump syndrome in procedures requiring cardiopulmonary bypass (Fig. 16.5). Further, reperfusion injury may

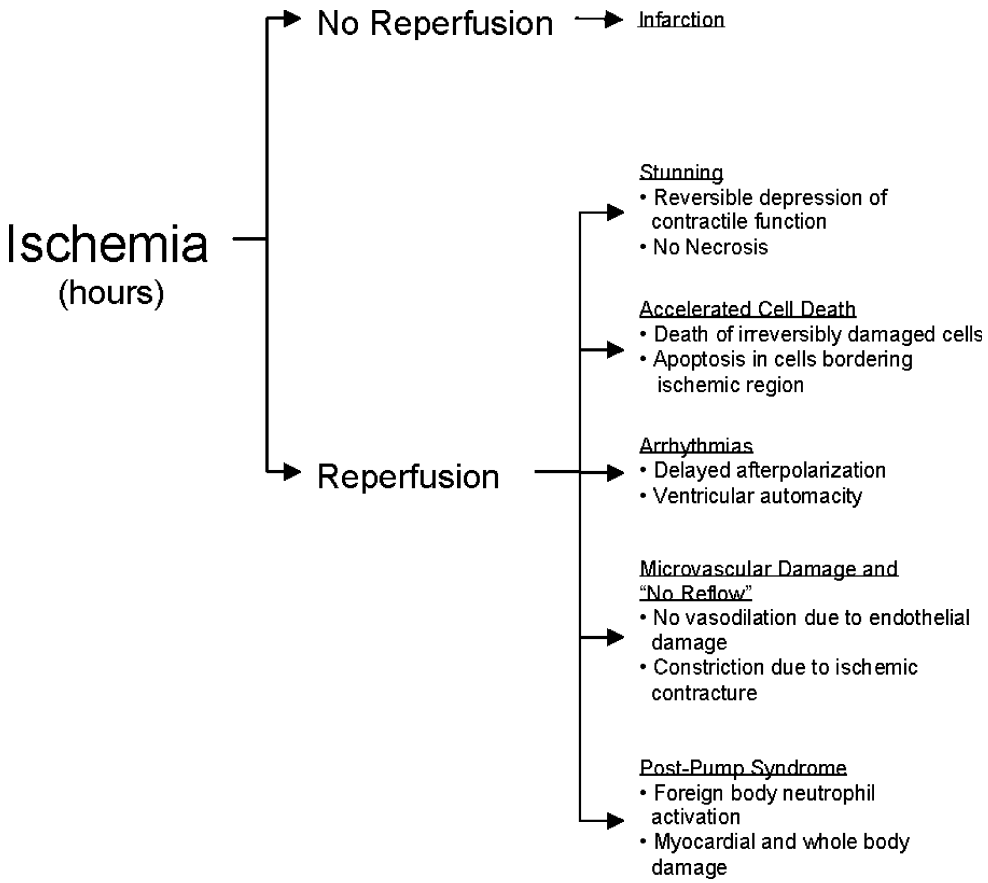

Fig. 16.5 Aspects of reperfusion injury. While reperfusion remains the most beneficial therapy for ischemia, any combination of stunning, accelerated cell death, arrhythmias, microvascular damage, or post-pump syndrome could occur, thus leading to postischemic dysfunction or necrosis

cause immediate myocardial necrosis in severely damaged cells and delayed necrosis in cells adjacent to the ischemic region; conversely, complete recovery of myocardial function may occur despite an ischemic episode. Of importance, necrosis occurring during the ischemic episode must be differentiated from that which may occur following reperfusion, especially when discussing clinical therapies targeted at attenuating reperfusion injury.

Assessment of reperfusion injury following ischemia is often difficult, especially in postsurgical patients. Yet, the determination of reperfusion injury and the relative extent of injury can be indirectly accomplished by hemodynamic monitoring (pressures, cardiac outputs, and echocardiography) and examination of blood levels of cardiac enzymes (CK-MB, troponin I, LDH, and AST). Ideally, left ventricular end-diastolic pressure volume measurements will provide both functional and quantitative information relative to the degree of reperfusion injury; yet, such data are difficult and rarely feasible to obtain clinically. With recent advances in echocardiography, relative changes in cardiac function and regional wall motion can be assessed more readily in such patients (see Chap. 22). Furthermore, improvements in cardiac magnetic resonance imaging have allowed for the functional mapping of ischemic myocardial zones (see Chap. 24).

Myocardial viability can be fairly easily assessed with inotropic stimulation, as the postischemic stunned (or the potentially reversibly injured) myocardium will display an increased heart rate and contractility. In contrast, the irreversibly injured (necrotic) myocardium exhibits little to no response to the inotrope (e.g., by dopamine stress echocardiography). Note that, by definition, myocardial stunning is reversible; therefore, within days, a depressed cardiac function due to stunning should recover (Figs. 16.2 and 16.3). This phenomenon is commonly observed clinically when patients following coronary artery bypass grafting require 24–48 h of inotropic support.

16.5.1 Aspects of Reperfusion Injury

16.5.1.1 Myocardial Stunning

The presence of intracellular oxygen free radicals and increased intracellular calcium during reperfusion leads to a reversible hypocontractile state of variability, yet this is relatively brief in duration.

16.5.1.2 Accelerated Cell Death

Typically, accelerated cell death upon reperfusion refers to cells that have been irreversibly damaged during the prior ischemic episode and are destined to die despite reperfusion. However, irreversible damage is not a prerequisite for cell death; upon reperfusion, detrimental ischemia-induced intracellular alterations may also occur in viable cells. More specifically, during reperfusion, the development of increased sarcolemmal permeability due to ischemia allows for the uncontrolled influx of calcium resulting in hypercontracture, decreased energy production, and/or cell death. Additionally, it should be noted that there is the paradoxical finding that apoptosis-related cell death in postischemic viable myocardium is reduced by early reperfusion and is accelerated in irreversibly ischemic-damaged cells [30].

16.5.1.3 Arrhythmias

Similar to myocardial stunning, increased episodes of arrhythmia upon reperfusion may be due, in part, to the presence of free radicals during ischemia and/or intracellular calcium oscillations at reflow. The restoration of flow enables the cell to resynthesize ATP. This abundance of energy and increased intracellular calcium at reperfusion may lead to excess cycling which, in turn, may cause delayed afterdepolarizations and ventricular automaticity [31]. Interestingly, a bell-shaped relationship has been described between duration of ischemia and severity of reperfusion arrhythmias, with the peak occurring with reperfusion after 5–20 min of ischemia [3]. This is presumably due to the finding that, in severe ischemic episodes, the production of ATP during reperfusion is limited due to increased cellular necrosis, and consequently energy-dependent calcium oscillations are reduced [32].

The timing and speed of the myocardial reperfusion are also considered to influence the occurrence and severity of induced arrhythmias. It has been speculated that sudden reperfusion is associated with a higher incidence of arrhythmias compared with a gradual reperfusion. Whether this phenomenon occurs in humans is unclear; for example, in one study comparing revascularization of patients diagnosed with acute myocardial infarction with either thrombolysis (a relatively slow reperfusion) or percutaneous transluminal coronary angioplasty (rapid reperfusion), researchers revealed no differences in the occurrence of arrhythmias upon reperfusion [33]. Yet, in a study from our laboratory, the pericardial administration of omega-3 fatty acids as a preconditioning agent significantly reduced elicited arrhythmias during induced ischemia (coronary artery clamping) and also somewhat during subsequent reperfusion [28].

16.5.1.4 Microvascular Damage and No-Reflow

The *no-reflow* phenomenon is defined to occur when an attempt to reperfuse an ischemic area, by removing an occlusion regionally or reestablishing coronary flow globally, does not result in reflow to the area at risk. In fact, a recent study in patients diagnosed with acute myocardial infarction and treated with thrombolytic therapy revealed that approximately one-third of this study group showed impaired regional coronary flow 5 days after treatment [34]. There are several proposed mechanisms to explain this immediate or delayed no-reflow, including the following: (1) endothelial

damage due to free radicals causes edema development and inhibits the release of vasodilatory agents into the coronary circulation; (2) ischemic contractures of the myocardium mechanically constrict flow through the coronary system [3]; (3) the accumulation of leukocytes causes vascular plugging; and/or (4) there exists cellular damage from mechanical compression (edema) [35]. Additionally, activated neutrophils reintroduced upon reperfusion can adhere to damaged endothelium and, in severe cases, cause platelet aggregation and thus restenosis [36]. It is important to note that, in some cases, cardioplegia-induced global myocardial ischemia itself can cause regional no-flow and regional infarctions which will develop as a consequence of this phenomenon.

16.5.1.5 Post-pump Syndrome

When blood comes in contact with foreign non-tissue surfaces, such as during cardiopulmonary bypass, a circulatory inflammatory response may be triggered. A large number of cells are typically activated during such a foreign body response, including monocytes, macrophages, endothelial cells, T cells, and eventually neutrophils. In a process collectively referred to as *neutrophil trafficking*, these cells accumulate and adhere to the damaged endothelial layer [3]. They then migrate into the vascular interstitial space, the latter of which results in liberation of free radicals and leukotrienes [3]. This phenomenon may promote not only postsurgical myocardial damage but also widespread systemic damage and/or even multiorgan dysfunction [37]. For example, it has been reported that cases of cerebral edema can develop after cardiopulmonary bypass which is considered to be mediated by bypass-related inflammation and endothelial cell activation [38]. For an additional discussion on the syndrome, see also Chap. 33.

16.6 Examples of Current Pharmacological Cardioprotective Therapies

Listed below are current examples of pharmacological therapies targeted at protecting the myocardium from damage due to ischemia and reperfusion injury. As noted above, our laboratory has investigated the pericardial delivery of omega-3 fatty acids, and we have observed significantly reduced infarct sizes in a swine model of ischemia/reperfusion injury by 50 % [28]. We are currently evaluating other potential agents (see below).

16.6.1 Na^+/H^+ Exchange Blockers

While activation of the exchanger in response to acidosis is a feedback mechanism that enables the myocardial cell to maintain a fairly stable pH range, it should be noted that NHE activation may not always be beneficial. During ischemia, there is often a buildup of metabolic products due to the anaerobic breakdown of ATP; the production of lactate and high CO_2 levels drive the intracellular pH below a tolerable level. However, a comparable decrease in the extracellular pH occurs during low-flow and no-flow ischemia, and, importantly, NHE activity is inhibited. When blood flow is reestablished to the ischemic region, this inhibition is removed, and both the NHE and the Na-HCO_3^- symport are simultaneously activated in an attempt to rapidly restore the internal pH [39]. With the normalization of intracellular pH via NHE, there is an associated increase in internal Na^+. Under normal conditions, cells primarily extrude Na^+ via the Na^+–K^+ ATPase exchanger; however, due to depleted energy reserves of such hearts, the postischemic cell relies on the Na^+–Ca^{2+} exchanger for Na^+ normalization. Importantly, this results in increased intracellular Ca^{2+} levels which, as mentioned previously, significantly contribute to the pathology of reperfusion injury (Fig. 16.4), e.g., the initiation of Ca^{2+} activated proteolytic enzymes.

In experimental animals, various NHE inhibitors have been shown to be beneficial when administered either prior to ischemia or prior to reperfusion. Specifically, cariporide (NHE-1 specific) has been reported to reduce postischemic edema, arrhythmias, apoptosis, infarct size, contracture, enzyme efflux, and hypertrophy, while also minimizing free radical damage, preserving ATP, and enhancing myocardial preservation following prolonged storage [40–47]. Notably, in the GUARDIAN (GUARd During Ischemia Against Necrosis) clinical trial, cariporide pretreatment prior to coronary artery bypass grafting resulted in a 25 % reduction in mortality or myocardial infarction following surgery [48]. Thus, further supporting its use during routine cardiac surgery, Myers et al. found that hypothermia potentiated the benefits of cariporide, specifically when cariporide was administered during reperfusion [49]. However, in a follow-up clinical trial (the ESCAMI trial) where eniporide (another NHE-1 inhibitor) was administered upon reperfusion to patients undergoing percutaneous transluminal coronary angioplasty or thrombolysis for acute myocardial infarction, eniporide failed to show any significant reductions in either infarct size or the occurrence of clinical events following treatment [50]. Furthermore, cariporide administration during reperfusion following global hypothermic ischemia failed to show any beneficial hemodynamic effects relative to control hearts (unpublished data from our laboratory). Nevertheless, while the use of NHE blockers is still considered experimental, its future use in cardiac surgery and ischemia/reperfusion remains promising. Interestingly, the prospect of using NHE blockers as a combined therapy with other cardioprotective therapies, such as ischemic preconditioning, is being addressed, and initial results have suggested that the combined therapies produce additive benefit [51].

16.6.2 Antioxidants

Antioxidants, or more specifically xanthine oxidase inhibitors, are speculated to attenuate or prevent reperfusion injury by acting as: (1) free radical scavengers; (2) inhibitors of free radical generation; (3) metal chelators, thereby removing the free radical generating catalyst; (4) promoters of endogenous antioxidant production; and/or (5) specific inhibitors of apoptosis via the upregulation of Bcl-2 (a gene involved in the apoptosis signaling pathway) [52]. However to date, experimental animal models and human clinical trials have provided conflicting results relative to the therapeutic benefits of antioxidants to attenuate reperfusion injury. Interestingly, many typical thiol-containing drugs commonly used for treating coronary artery disease and heart failure have also been shown to exhibit antioxidant-like effects within the myocardium; these include β-adrenergic antagonists propranolol [53], metoprolol [54], and carvedilol [55] as well as angiotensin-converting enzyme inhibitors, iron chelating agents, and Ca^{2+} channel blockers [56]. Our laboratory is currently investigating the focal delivery of such agents into the pericardial space as a potential means to allow for higher therapeutic concentrations, but with lower systemic effects (Fig. 16.6.)

16.6.3 Calcium Channel Antagonists

Experimentally, the administration of calcium channel antagonists was believed to help preserve myocardial function and metabolism in case studies utilizing normothermic ischemia, crystalloid cardioplegia, or blood cardioplegia [1]. More specifically, their use was reported to prevent ATP hydrolysis and calcium influx during ischemia and also improve cardioplegia delivery by eliciting coronary vasodilation. However, the potential use of calcium channel blockers for myocardial protection is considered to be limited, due to negative inotropic and dromotropic effects which could be problematic in patients with preoperative poor ventricular function. Hence, further studies are needed to determine the potential utility of newer calcium channel antagonists such as amlodipine and felodipine, agents, which may elicit fewer side effects in very ill patients. Nevertheless, calcium channel antagonists are typically administered in patients with normal preoperative function, but who are at risk for postoperative hypertension, tachycardia, coronary spasm, and/or ischemia [1].

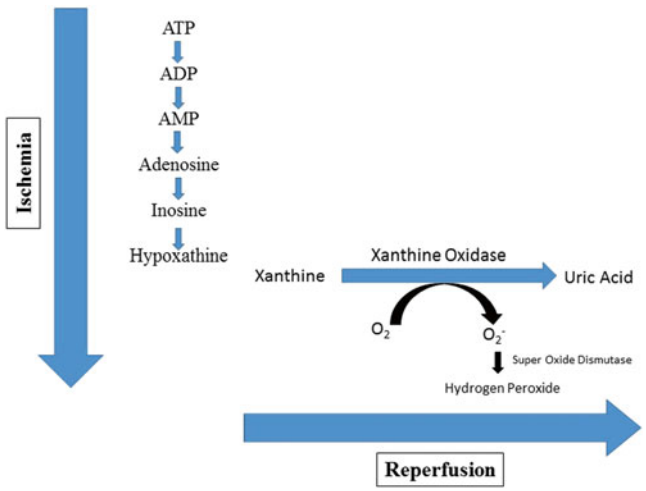

Fig. 16.6 A proposed mechanism for ischemia–reperfusion injury. During the time of ischemia, ATP is catabolized to hypoxanthine that accumulates in the ischemic tissue and cells. During the period of reoxygenation, xanthine produces xanthine oxidase, and the by-products are free radical production of super oxide dismutase, hydrogen peroxide, and uric acid

16.6.4 Glucose–Insulin–Potassium

Perioperative depletion of myocardial glycogen stores has been correlated with higher incidences of arrhythmias, low output syndrome, and/or infarction [56]. In one study, Iyengar et al. preoperatively dosed patients with a glucose–insulin–potassium solution and a bolus of exogenous glucose; subsequently, the researchers observed zero incidences of perioperative ischemic complications, compared to a 44 % occurrence in patients not receiving the solutions [56]. This beneficial effect was attributed to increased preoperative glycogen stores, enhanced perioperative aerobic metabolism, and reduced free fatty acid circulation in the hypoxic hearts, all of which are mediated by glucose and insulin. Nevertheless, future studies are needed to validate such a therapeutic approach.

16.6.5 Growth Factors

The administration of growth factors for cardioprotection has been conducted in attempts to minimize or prevent apoptosis, which is known to occur in addition to necrosis during (prolonged) myocardial ischemia and reperfusion. In general, it is thought that reperfusion injury accelerates apoptosis in viable postischemic cells, adding to the overall necrosis [57]. More specifically, a link was described between apoptosis and reperfusion in humans following acute myocardial infarction where apoptosis was significant in cells within and bordering infarcted regions [58]. Similarly, experimental preclinical studies have provided evidence of the infarct-reducing benefits of several growth factor proteins when given during ischemia and/or during reperfusion, including transforming growth factor-β1 (TGF-β1) [59], insulin [60], insulin-like growth factor

(IGF-1) [61], fibroblast growth factor (FGF-1) [62], and/or cardiotrophin-1 (CT-1) [63].

16.6.6 Glutamate/Aspartate

The specific amino acids, glutamate and aspartate, when added to the cardiopulmonary bypass circuit, have been shown to reduce lipid peroxidation and preserve myocardial function following tissue oxygenation [64]. Similarly, the addition of these amino acids to cardioplegia solutions has yielded similar positive results [65]. It has also been suggested that a combination of these amino acids could be administered via the pericardial space, thus as a target delivery during open heart surgery. In one preclinical study, a decrease in ischemic–hypoxic cardiac injury was observed via this approach, after extended cross-clamp in a rat model [66]. While most of the benefits were attributed to the ability of the amino acids to anaerobically produce ATP via substrate phosphorylation, subsequent evidence has further linked their potential benefits to inhibition of free radical production and also the better retention of endogenous antioxidants [64].

16.6.7 Nitric Oxide (NO)

In addition to being a potent vasodilator, nitric oxide has also been shown to: (1) reduce platelet aggregation, (2) reduce neutrophil adherence, and (3) act as a free radical scavenger. Nitric oxide is primarily synthesized from the amino acid L-arginine by nitric oxide synthase. It is thought that L-ARGININE levels decline during ischemia leading to lower nitric oxide production and thus a greater injury potential [1]. Furthermore, the addition of nitric oxide donors to cardioplegia solutions has been shown to beneficially increase ischemic nitric oxide levels [67]. Nevertheless, still today there are conflicting opinions regarding the benefits of nitric oxide due to its negative inotropic effects; hence, future investigation is required.

16.6.8 Hibernation-Specific Proteins

Many mammals will go into a hibernating state during the winter months, e.g., in locations in which food is scarce and/or environmental temperatures are suboptimal. Yet, their physiological conditions vary depending on the given species. For instance, the American black bear will stay relatively normothermic, while the core temperature of the hibernating ground squirrel will decrease dramatically to near that of the environment. These behaviors are considered to be a unique protective adaptation that may even have applications to human medicine. Such insights could possibly be used for the treatment or prevention of various clinical conditions, such as myocardial insult. For decades, numerous researchers have been studying these animals to determine what specific enzymes or hormones play essential roles in cardioprotection during hibernation. For example, the enzyme that induces hibernation in American black bears, defined as *hibernation induction trigger (HIT)*, has been studied for its cardioprotective properties. Data has suggested that HIT minimizes reperfusion injury when added to cardioplegia to arrest the heart and hence could be beneficial in various treatment strategies for cardioprotection [68–70]. Further, other mammals such as the ground squirrel have also shown interesting mechanisms for cardioprotection; during the winter months, ground squirrels upregulate chaperones and heat shock proteins (HSPA4, HSPB6, HSP90AB1) that protect against perfusion injury [19, 71].

16.6.9 Assessment of Pharmaceutical Agents via Target Pericardial Delivery

All of the aforementioned pharmaceutical agents (and others) noted for their potential for cardioprotection can also be assessed for their potential utility for target delivery in the pericardial space. In preclinical trials, the administration of such pharmaceutical agents into the pericardial space can be achieved by direct injection or by creating a pericardial cradle (Fig. 16.7). Further, the formation of pericardial cradles is a common surgical technique that provides a field for surgical manipulation while stabilizing heart motion. In addition to being a more localized application, it has been shown that even higher concentrations of agents than those recommended for intravenous administration can be used in this target approach. Our laboratory has employed this approach to study the prevention of reperfusion injury and/or generalized cardioprotection; such approaches could have translational application relative to bypass procedures or during organ recovery prior to transplantation. Further, such a targeted delivery approach may be optimal for clinical applications when intravenous treatments may result in: (1) systemic drops in blood pressure, (2) renal dysfunction, (3) anesthesia management issues, and/or (4) other long-term side effects. For example, it has been reported that hemolysis can occur from the intravenous administration of high levels of therapeutic fatty acids.

As noted above, these studies are ongoing in our laboratory and, in one set of preclinical studies, we have been utilizing Visible Heart® methodologies [3]. We consider that this preclinical treatment strategy allows for the observation of potential effects of various pharmacological agents administered alone or in combinations, to determine if they decrease the incidence of cardiac arrhythmias and/or ischemic damage that may occur during and after open heart surgery or transplantation [72] (Fig. 16.8).

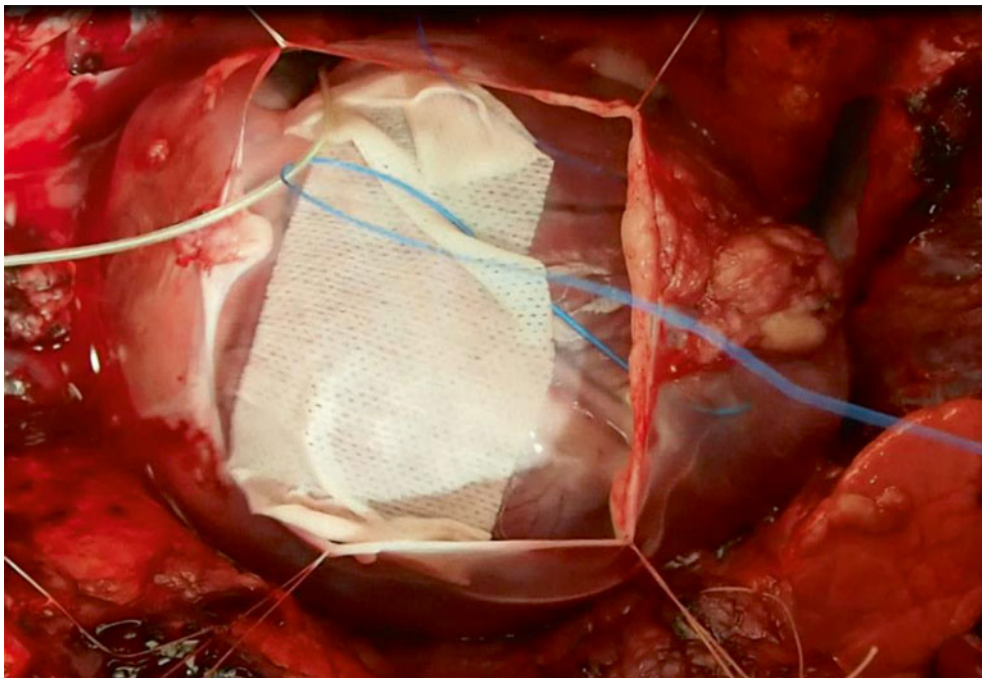

Fig. 16.7 A pericardial cradle is formed for in situ testing in the swine. An epicardial (unipolar) pacing lead is placed in the left atrial appendage, and a bipolar temporary pacing lead is placed in the ventricle; additional endocardial pacing leads and pressure catheters are also placed. A piece of gauze is placed over the heart to act as a wick over the anterior myocardial surface

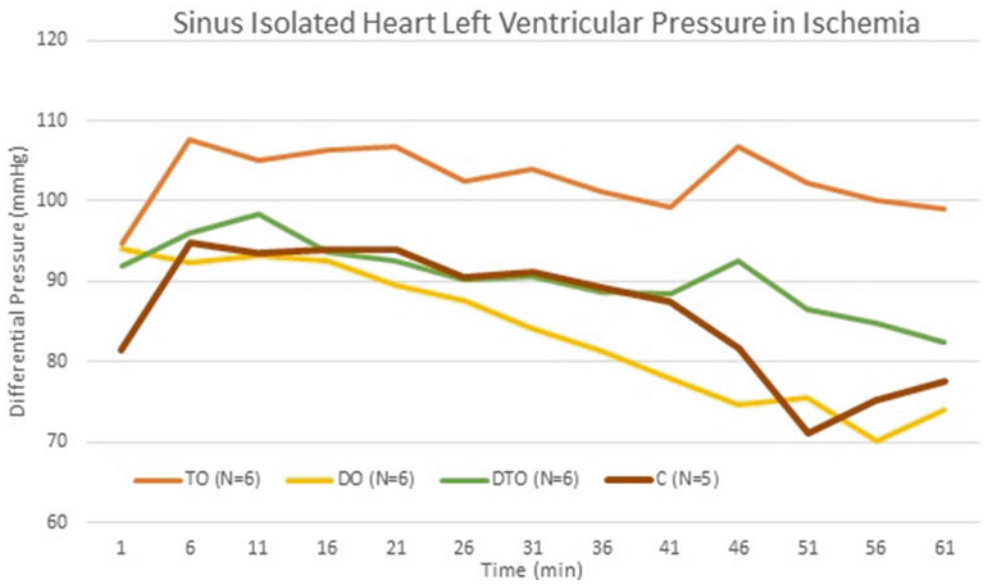

Fig. 16.8 Some results of a preconditioning experiment for monitoring hemodynamics in a swine model tracked over the course of an hour for an ischemic heart preparation treated with combinations of tauroursodeoxycholic acid (TO), docosahexaenoic acid (DO), Omegaven® (DTO), and saline controls (C). All combinations here demonstrate an initial benefit immediately following cardiac reanimation; the combination of Omegaven® and tauroursodeoxycholic acid demonstrates the best sustained performance over control at the end of the specified hour of monitoring ($p = 0.011$). This is only one such metric of global heart performance that can be used in assessing the benefits of various agents

16.6.10 Acute and Global Assessments of the Potential Benefits of Protective Agents Administered to In Vitro to Isolated Large Mammalian Hearts

In addition to assessing the local mitigation of injury such as with direct measurements of infarct size, it can be beneficial to take a more global perspective for minimizing injury and/or preserving function of the heart. It should be noted that the use of an isolated heart model for such studies inherently possesses the risk of ischemic and reperfusion injuries. On the other hand, these attributes may actually make these investigations an ideal platform for the assessment of such damage (and thus the potential therapeutic benefits) of these preventative therapies. Consequently, numerous studies have utilized mammalian heart preparations for such ischemic–reperfusion injury investigations [73]. Our laboratory has uniquely performed large mammalian isolated heart investigations (using Visible Heart® methodologies) to assess the potential therapeutic benefits of administering such agents and/or the delivery of combinations of agents (Fig. 16.8). This approach has allowed for complete hemodynamic monitoring including the use of 3D echocardiography. To date, we have employed this approach to demonstrate the relative effectiveness of preventative (preconditioning agents) and corrective (postconditioning agents, those administered following explant and reanimation) therapies. Again, we consider that these investigations of global cardiac treatment may be particularly relevant for the clinical presentation of acute surgical insults, such as open heart surgery, cardiopulmonary bypass, or transplant.

16.7 Conclusions

The intent of this chapter was to outline the principle consequences of ischemia and reperfusion injury and introduce the reader to the concepts of cardioprotective treatments. While the intent of many past cardioprotective therapies was to protect the myocardium from ischemic necrosis, it may be that reperfusion injury following ischemia in the forms of stunning, arrhythmias, and/or additional cellular necrosis may occur despite such cardioprotective efforts. Therefore, as the new era of hybrid catheterization/operating rooms designed to treat critically ill patients (considered too sick to survive open heart procedures) with novel interventions, it is imperative that myocardial protective strategies be enhanced to account for the potential increased risks of ischemia and reperfusion injury in such populations.

References

1. Edmunds LH (ed) (1997) Cardiac surgery in the adult. McGraw-Hill, New York, pp 295–318
2. Yellon DM, Rahimtoola SH, Opie LH et al (eds) (1997) New ischemic syndromes: beyond angina and infarction. Lippincott-Raven Publishers, New York, pp 10–20, 106–114
3. Opie LH (ed) (1998) The heart: physiology, from cell to circulation. Lippincott-Raven, Philadelphia, pp 515–589
4. Shen YT, Vatner SF (1995) Mechanism of impaired myocardial function during progressive coronary stenosis in conscious pigs. Hibernation versus stunning? Circ Res 76:479–488
5. Bolli R, Marban E (1999) Molecular and cellular mechanisms of myocardial stunning. Physiol Rev 79:609–634
6. Karmazyn M, Moffat MP (1993) Role of Na^+/H^+ exchange in cardiac physiology and pathophysiology: mediation of myocardial reperfusion injury by the pH paradox. Cardiovasc Res 27:915–924
7. Miller WP, McDonald KS, Moss RL (1996) Onset of reduced Ca^{2+} sensitivity of tension during stunning in porcine myocardium. J Mol Cell Cardiol 28:689–697
8. Kusuoka H, Koretsune Y, Chacko VP et al (1990) Excitation-contraction coupling in postischemic myocardium. Does failure of activator Ca^{2+} transients underlie stunning? Circ Res 66: 1268–1276
9. McDonough JL, Labugger R, Pickett W et al (2001) Cardiac troponin I is modified in the myocardium of bypass patients. Circulation 103:58–64
10. Opie LH, du Toit EF (1992) Postischemic stunning: the two-phase model for the role of calcium as pathogen. J Cardiovasc Pharmacol 20:S1–S4
11. Aguilera IM, Vaughan RS (2000) Calcium and the anaesthetist. Anaesthesia 55:779–790
12. Robertie PG, Butterworth JF, Royster RL et al (1991) Normal parathyroid hormone responses to hypocalcemia during cardiopulmonary bypass. Anesthesiology 75:43–48
13. Chair N, Otto CW, Link MS et al (2010) 2010 American Heart Association guidelines for cardiopulmonary resuscitation and emergency cardiovascular care science. Circulation 122:S729–S767
14. Heusch G (2013) The regional myocardial flow-function relationship: a framework for an understanding of acute ischemia, hibernation, stunning and coronary microembolization. Circ Res 112: 1535–1537
15. Bolli R, Patel BS, Jeroudi MO et al (1988) Demonstration of free radical generation in "stunned" myocardium of intact dogs with the use of the spin trap alpha-phenyl N-tert-butyl nitrone. J Clin Invest 82:476–485
16. Heusch G, Schulz R (2002) Myocardial hibernation. Ital Heart J 3:282–284
17. Boden WE, Brooks WW, Conrad CH et al (1995) Incomplete, delayed functional recovery late after reperfusion following acute myocardial infarction: "maimed myocardium.". Am Heart J 130: 922–932
18. Murry CE, Jennings RB, Reimer KA (1986) Preconditioning with ischemia: a delay of lethal cell injury in ischemic myocardium. Circulation 74:1124–1136
19. Nelson BT, Ding X, Boney-Montoya J et al (2013) Metabolic hormone FGF21 Is induced in ground squirrels during hibernation but its overexpression is not sufficient to cause torpor. PLoS One 8:e53574
20. Lawson CS, Coltart DJ, Hearse DJ (1993) "Dose"-dependency and temporal characteristics of protection by ischaemic preconditioning against ischaemia-induced arrhythmias in rat hearts. J Mol Cell Cardiol 25:1391–1402

21. Schultz JE, Rose E, Yao Z et al (1995) Evidence for involvement of opioid receptors in ischemic preconditioning in rat hearts. Am J Physiol 268:H2157–H2161
22. Coles JA Jr, Sigg DC, Iaizzo PA (2003) Role of kappa-opioid receptor activation in pharmacological preconditioning in swine. Am J Physiol Heart Circ Physiol 284:2091–2099
23. Sigg DC, Coles JA Jr, Gallagher WJ et al (2001) Opioid cardioprotection: myocardial function and energy metabolism. Ann Thorac Surg 72:1576–1582
24. Yellon DM, Downey JM (2003) Preconditioning the myocardium: from cellular physiology to clinical cardiology. Physiol Rev 83:1113–1151
25. Gross GJ (2003) Role of opioids in acute and delayed preconditioning. J Mol Cell Cardiol 35:709–718
26. Cohn PF, Fox KM (2003) Silent myocardial ischemia. Circulation 108:1263–1277
27. Leaf A, Kang JX, Xiao YF (2008) Fish oil fatty acids as cardiovascular drugs. Curr Vasc Pharmacol 6:1–12
28. Xiao YF, Sigg DC, Ujhelyi MR, Wilhelm JJ, Richardson ES, Iaizzo PA (2008) Pericardial delivery of Omega-3 fatty acid: a novel approach to reduce myocardial infarct sizes and arrhythmias. Am J Physiol Heart Circ Physiol 294:H2212–H2218
29. Pacher P, Nivorozhkin A, Szabo C (2006) Therapeutic effects of xanthine oxidase inhibitors: renaissance half a century after the discovery of allopurinol. Pharmacol Rev 58:87–114
30. Fliss H, Gattinger D (1996) Apoptosis in ischemic and reperfused rat myocardium. Circ Res 79:949–956
31. Opie LH, Coetzee WA (1988) Role of calcium ions in reperfusion arrhythmias: relevance to pharmacologic intervention. Cardiovasc Drugs Ther 2:623–636
32. Manning AS, Hearse DJ (1984) Reperfusion-induced arrhythmias: mechanisms and prevention. J Mol Cell Cardiol 16:497–518
33. Wehrens XH, Doevendans PA, Ophuis TJ et al (2000) A comparison of electrocardiographic changes during reperfusion of acute myocardial infarction by thrombolysis or percutaneous transluminal coronary angioplasty. Am Heart J 139:430–436
34. Maes A, Van de Werf F, Nuyts J et al (1995) Impaired myocardial tissue perfusion early after successful thrombolysis. Impact on myocardial flow, metabolism, and function at late follow-up. Circulation 92:2072–2078
35. Reffelmann T, Kloner R (2006) The no-reflow phenomenon: a basic mechanism of myocardial ischemia and reperfusion. Basic Res Cardiol 101:359–372
36. Forde RC, Fitzgerald DJ (1997) Reactive oxygen species and platelet activation in reperfusion injury. Circulation 95:787–789
37. Menasche P, Peynet J, Haeffner-Cavaillon N et al (1995) Influence of temperature on neutrophil trafficking during clinical cardiopulmonary bypass. Circulation 92:II334–II340
38. Anderson RE, Li TQ, Hindmarsh T et al (1999) Increased extracellular brain water after coronary artery bypass grafting is avoided by off-pump surgery. J Cardiothorac Vasc Anesth 13:698–702
39. Karmazyn M (1998) The myocardial sodium-hydrogen exchanger (NHE) and its role in mediating ischemic and reperfusion injury. Keio J Med 47:65–72
40. Inserte J, Garcia-Dorado D, Ruiz-Meana M et al (1997) The role of the Na^+-H^+ exchange occurring during hypoxia in the genesis of reoxygenation-induced myocardial oedema. J Mol Cell Cardiol 29:1167–1175
41. Garcia-Dorado D, Gonzalez MA, Barrabes JA et al (1997) Prevention of ischemic rigor contracture during coronary occlusion by inhibition of Na(+)-H(+) exchange. Cardiovasc Res 35:80–89
42. Klein HH, Bohle RM, Pich S et al (1997) Time delay of cell death by Na^+/H^+ exchange inhibition in regionally ischemic, reperfused porcine hearts. J Cardiovasc Pharmacol 30:235–240
43. Shipolini AR, Yokoyama H, Galinanes M et al (1997) Na^+/H^+ exchanger activity does not contribute to protection by ischemic preconditioning in the isolated rat heart. Circulation 96:3617–3625
44. Yoshida H, Karmazyn M (2000) Na(+)/H(+) exchange inhibition attenuates hypertrophy and heart failure in 1-wk postinfarction rat myocardium. Am J Physiol Heart Circ Physiol 278:H300–H304
45. Myers ML, Farhangkhoee P, Karmazyn M (1998) Hydrogen peroxide induced impairment of post-ischemic ventricular function is prevented by the sodium-hydrogen exchange inhibitor HOE 642 (cariporide). Cardiovasc Res 40:290–296
46. Mathur S, Karmazyn M (1997) Interaction between anesthetics and the sodium-hydrogen exchange inhibitor HOE 642 (cariporide) in ischemic and reperfused rat hearts. Anesthesiology 87:1460–1469
47. Hartmann M, Decking UK (1999) Blocking Na(+)-H(+) exchange by cariporide reduces Na(+)-overload in ischemia and is cardioprotective. J Mol Cell Cardiol 31:1985–1995
48. Theroux P, Chaitman BR, Danchin N et al (2000) Inhibition of the sodium-hydrogen exchanger with cariporide to prevent myocardial infarction in high-risk ischemic situations. Main results of the GUARDIAN trial. Guard during ischemia against necrosis (GUARDIAN) Investigators. Circulation 102:3032–3038
49. Myers ML, Karmazyn M (1996) Improved cardiac function after prolonged hypothermic ischemia with the Na^+/H^+ exchange inhibitor HOE 694. Ann Thorac Surg 61:1400–1406
50. Zeymer U, Suryapranata H, Monassier JP et al (2001) The Na^+/H^+ exchange inhibitor eniporide as an adjunct to early reperfusion therapy for acute myocardial infarction. J Am Coll Cardiol 38: 1644–1650
51. Bugge E, Yterhus K (1995) Inhibition of sodium-hydrogen exchange reduces infarct size in the isolated rat heart-a protective additive to ischaemic preconditioning. Cardiovasc Res 29:269–274
52. Dhalla NS, Elmoselhi AB, Hata T et al (2000) Status of myocardial antioxidants in ischemia-reperfusion injury. Cardiovasc Res 47: 446–456
53. Khaper N, Rigatto C, Seneviratne C et al (1997) Chronic treatment with propranolol induces antioxidant changes and protects against ischemia-reperfusion injury. J Mol Cell Cardiol 29:3335–3344
54. Kalaycioglu S, Sinci V, Imren Y et al (1999) Metoprolol prevents ischemia-reperfusion injury by reducing lipid peroxidation. Jpn Circ J 63:718–721
55. Feuerstein GZ, Yue TL, Cheng HY et al (1993) Myocardial protection by the novel vasodilating beta-blocker, carvedilol: potential relevance of anti-oxidant activity. J Hypertens 11:S41–S48
56. Iyengar SR, Charrette EJ, Iyengar CK et al (1976) Myocardial glycogen in prevention of perioperative ischemic injury of the heart: a preliminary report. Can J Surg 19:246–251
57. Yellon DM, Baxter GF (1999) Reperfusion injury revisited: is there a role for growth factor signaling in limiting lethal reperfusion injury? Trends Cardiovasc Med 9:245–249
58. Saraste A, Pulkki K, Kallajoki M et al (1997) Apoptosis in human acute myocardial infarction. Circulation 95:320–323
59. Baxter GFM, Brar BK, Latchman DS, Yellon DM (1998) Infarct-limiting action of transforming growth factor beta-1 in isolated rat heart is abolished. Circulation 100:1–9
60. Baines CP, Wang L, Cohen MV et al (1999) Myocardial protection by insulin is dependent on phosphatidylinositol 3- kinase but not protein kinase C or KATP channels in the isolated rabbit heart. Basic Res Cardiol 94:188–198
61. Buerke M, Murohara T, Skurk C et al (1995) Cardioprotective effect of insulin-like growth factor I in myocardial ischemia followed by reperfusion. Proc Natl Acad Sci U S A 92:8031–8035
62. Cuevas P, Carceller F, Martinez-Coso V et al (1999) Cardioprotection from ischemia by fibroblast growth factor: Role of inducible nitric oxide synthase. Eur J Med Res 4:517–524

63. Stephanou A, Brar B, Heads R et al (1998) Cardiotrophin-1 induces heat shock protein accumulation in cultured cardiac cells and protects them from stressful stimuli. J Mol Cell Cardiol 30:849–855
64. Morita K, Ihnken K, Buckberg GD et al (1995) Studies of hypoxemic/reoxygenation injury without aortic clamping. VIII. Counteraction of oxidant damage by exogenous glutamate and aspartate. J Thorac Cardiovasc Surg 110:1228–1234
65. Drinkwater DC Jr, Cushen CK, Laks H et al (1992) The use of combined antegrade-retrograde infusion of blood cardioplegic solution in pediatric patients undergoing heart operations. J Thorac Cardiovasc Surg 104:1349–1355
66. Us MH, Ozkan S, Oğuş T et al (2001) Efficacy of topically applied glutamate-aspartate and pentoxifylline solutions in decreasing myocardial damage during open-heart surgery in rats. J Int Med Res 29:497–502
67. Nakanishi K, Zhao ZQ, Vinten-Johansen J et al (1995) Blood cardioplegia enhanced with nitric oxide donor SPM-5185 counteracts postischemic endothelial and ventricular dysfunction. J Thorac Cardiovasc Surg 109:1146–1154
68. Bolling SF, Benedict MB, Tramontini NL et al (1998) Hibernation triggers and myocardial protection. Circulation 98:II220–II223 (discussion II223–II224)
69. Bolling SF, Tramontini NL, Kilgore KS, Su TP, Oeltgen PR, Harlow HH (1997) Use of "natural" hibernation induction triggers for myocardial protection. Ann Thorac Surg 64:623–627
70. Hong J, Sigg DC, Coles JA Jr et al (2005) Hibernation induction trigger reduces hypoxic damage of swine skeletal muscle. Muscle Nerve 32:200–207
71. Grabek KR, Karimpour-Fard A, Epperson LE et al (2011) Multistate proteomics analysis reveals novel strategies used by a hibernator to precondition the heart and conserve ATP for winter heterothermy. Physiol Genomics 43:1263–1275
72. Iles TL, Howard B, Howard SA et al (2015) Testing the efficacy of pharmacological agents in a pericardial target delivery model in the swine. JoVE (in press)
73. Skrzypiec-Spring M, Grotthus B, Szelag A, Schulz R (2007) Appraisal of state-of-the-art: isolated heart perfusion according to Langendorff–still viable in the new millennium. J Pharmacol Toxicol Methods 55:113–126

The Effects of Anesthetic Agents on Cardiac Function

17

Jason S. Johnson and Michael K. Loushin

Abstract

The perioperative management of patients with complex medical conditions, while providing cardiovascular stability, continues to offer both challenges and new developments. Furthermore, patients with cardiovascular disease or associated comorbidities such as obesity, diabetes, or pulmonary disease may require special attention during general anesthesia. Advancements in the field of anesthesiology include new anesthesia medications, medical equipment and/or surgical technology, and anesthetic and surgical techniques. The goal of this chapter is to familiarize the reader with commonly employed clinical methodologies and anesthetics, with particular attention to the potential influences on the cardiovascular system.

Keywords

Anesthesia • Inhalational anesthetics • Intravenous anesthetics • Anesthesia induction • Cardiac function • Hemodynamics • Cardioprotection • Myocardial preconditioning

17.1 Introduction

Anesthesia is considered necessary for many types of surgeries and procedures. Typically, anesthesia provides analgesia, amnesia, hypnosis, and/or muscle relaxation. The depth of anesthesia varies from minimal sedation to general anesthesia (Table 17.1). Importantly, medications used for general anesthesia can cause significant alterations in hemodynamics, especially during induction of anesthesia. Importantly, a critical understanding of the anesthetic impact on cardiovascular physiology can allow for both induction and maintenance of anesthesia with minimal alterations from normal cardiovascular function. Both inhalational and intravenous anesthetics can affect cardiovascular performance; this includes effects on cardiac output, heart rate, systemic vascular resistance, the cardiac conduction system, myocardial contractility, coronary blood flow, and/or blood pressure. The choice of inhalational and intravenous anesthetics is typically associated with the patient's underlying cardiovascular status such as heart failure, cardiac disease, and/or hypovolemia. The goal of this chapter is to familiarize the reader with commonly employed clinical methodologies and anesthetics, with particular attention to potential influences on the cardiovascular system.

17.2 Anesthesia Induction Sequence

A focused patient history and physical is necessary and required prior to anesthesia, to determine the most appropriate anesthetic management for that individual. Any changes to health condition since previous medical examination or anesthesia should be documented. Past history of any complications or reactions to anesthetics must also be considered. For example, patients with a family history of malignant hyperthermia are at risk of eliciting an episode of malignant hyperthermia when triggering agents such as succinylcholine or volatile anesthetics are administered. All patients undergoing elective surgery should follow the preoperative

J.S. Johnson, MD • M.K. Loushin, MD (✉)
Department of Anesthesiology, University of Minnesota,
420 Delaware St. SE, MMC 294, Minneapolis, MN 55455, USA
e-mail: loush001@umn.edu

P.A. Iaizzo (ed.), *Handbook of Cardiac Anatomy, Physiology, and Devices*, DOI 10.1007/978-3-319-19464-6_17

Table 17.1 Continuum of depth of sedation, definition of general anesthesia, and levels of sedation/analgesia

	Minimal sedation (anxiolysis)	Moderate sedation/analgesia ("conscious sedation")	Deep sedation/analgesia	General anesthesia
Responsiveness	Normal response to verbal stimulation	Purposeful response to verbal or tactile stimulation	Purposeful response following repeated or painful stimulation	Unarousable even with painful stimulus
Airway	Unaffected	No intervention required	Intervention may be required	Intervention often required
Spontaneous ventilation	Unaffected	Adequate	May be inadequate	Frequently inadequate
Cardiovascular function	Unaffected	Usually maintained	Usually maintained	May be impaired

ASA Standards, Guidelines and Statements. American Society of Anesthesiologists, October 2001 [2]

fasting guidelines established by the American Society of Anesthesiologists (ASAs) [1]. The ASA guideline recommends the minimum fasting duration for solid foods is six hours, breast milk for four hours, and clear fluids such as water for two hours. The NPO guidelines are useful to minimize the risks of gastric regurgitation and thus aspirations of stomach contents into the lungs during the induction of anesthesia. The need for laboratory or diagnostic studies is guided by the preexisting medical condition of each individual patient and type of surgery. Other cardiovascular studies such as electrocardiograms (ECGs), cardiac echocardiography, and/or cardiac stress tests may be considered depending on the given patient's risk factors.

Common anesthesia techniques include sedation (also known as monitored anesthesia care or *MAC*) and general anesthesia. Note that the choice of anesthesia technique is again dependent on the patient and/or proposed surgery or procedure. A typical general anesthesia induction sequence for an adult is as follows. After establishing intravenous access and placement of standard ASA [2] monitors, a patient is preoxygenated with 100 % oxygen by a face mask. An induction dose of intravenous medication such as propofol, an opioid such as fentanyl, and a muscle relaxant such as vecuronium are administered to facilitate the subsequent smooth induction of general anesthesia. Once the patient is rendered unconscious and anesthetized, direct laryngoscopy is performed with a laryngoscope and the trachea is intubated with an endotracheal tube. After confirmation of endotracheal intubation by auscultation of lungs and presence of end-tidal carbon dioxide by monitoring, the patient is placed on an anesthesia ventilator and ventilated with a combination of anesthetic gases, oxygen, and/or air. Note that if a total intravenous anesthetic (TIVA) technique with propofol and fentanyl is chosen, anesthetic gases are not administered. A TIVA technique may be chosen for patients who have reactions to volatile anesthetics, such as patients with malignant hyperthermia; the TIVA technique may also be utilized in patients with significant history of postoperative nausea and vomiting following an inhalational anesthetic. The cardiovascular depressant effects of most anesthetics typically become evident during and immediately following induction of anesthesia. Maintaining cardiovascular stability requires (1) careful titration of medications, (2) knowledge of both clinical and basic science in physiology and pharmacology, and (3) diligent monitoring of patients and their vital signs.

For the induction of general anesthesia in young children, a mask induction technique is often utilized. Since placement of an intravenous catheter preinduction may be traumatic to the child and/or difficult due to noncooperation, mask induction with sevoflurane and/or nitrous oxide is frequently employed. Sevoflurane is well tolerated and has a low risk of causing either laryngospasm or bronchospasm and therefore is commonly utilized for mask induction of anesthesia. After placement of ASA monitors, a high concentration of sevoflurane along with oxygen is administered via a face mask until the patient is determined to be anesthetized and unconscious. A peripheral intravenous catheter is then placed to administer additional medication, and a general anesthesia and airway management sequence subsequently follows, similar to the adult patient. Mask induction of anesthesia with sevoflurane is also possible for adults.

It is important to note that direct laryngoscopy and endotracheal intubation can often stimulate the upper and lower airways which, in turn, may cause significant changes in both blood pressure and heart rate, i.e., if airway responses are not blunted. In other words, tachycardia or hypertension can occur during laryngoscopy. Commonly, titration of anesthetics and opioids is administered to blunt these airways and associated sympathetic responses. In some patients (or during specific surgical procedures), it may be required to add invasive monitoring along with the standard ASA monitors. Specifically, such monitors may include (1) invasive arterial lines, (2) central venous catheters, (3) pulmonary artery catheters, and/or (4) transesophageal echocardiography.

17.3 Inhalational Anesthetics

Commonly used inhalational anesthetics include nitrous oxide, isoflurane, desflurane, and sevoflurane (Fig. 17.1). Each of these inhalational anesthetics has an identified specific minimum alveolar concentration (MAC) at which general

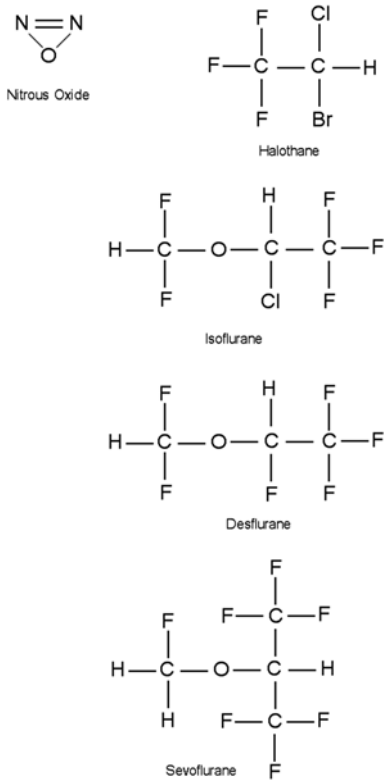

Fig. 17.1 Chemical structure of commonly administered inhalational anesthetics

Table 17.2 Minimal alveolar concentration (MAC) of inhalational anesthetics

Agent	MAC (% of 1 atmosphere)	Vapor pressure (at 20 °C)
Desflurane	6.0	680
Halothane	0.75	243
Isoflurane	1.2	240
Sevoflurane	2.0	160
Nitrous oxide	105	
Xenon	70	

anesthesia is induced (Table 17.2). MAC is defined as the MAC of an inhaled anesthetic required to prevent movement in 50 % of patients in response to a painful stimulus such as a surgical incision. It is important to note that both infants and children will tend to have a higher MAC requirement than adults, while pregnant women and elderly patients have lower MAC requirements. MAC is additive, that is, 0.5 MAC of nitrous oxide and 0.5 MAC of isoflurane result in 1 MAC total anesthesia. More specifically, the brain anesthetic partial pressure is dependent upon factors such as inspired (F_I) and alveolar (F_A) concentrations of a given anesthetic gas. Brain (F_B) concentration of an anesthetic is dependent upon F_A and F_I:

$$F_I \leftrightarrow F_A \leftrightarrow F_B$$

In general, anesthetic uptake is determined by (1) the relative blood solubility, (2) a patient's instantaneous cardiac output, and (3) the difference between alveolar and venous partial pressures [3]. Note that the greater the uptake of an anesthetic gas into the blood, the slower the rate of induction. Inhalational anesthetics with lower blood to gas solubility (i.e., desflurane and sevoflurane) will cause a more rapid induction and emergence from general anesthesia, yet higher concentrations of these agents are needed for the MAC requirements.

17.3.1 Blood Pressure and Systemic Vascular Resistance

All volatile anesthetics such as isoflurane, desflurane, sevoflurane, and halothane will cause dose-dependent effects on cardiovascular function. For example, these agents typically cause a dose-dependent decrease in mean arterial blood pressure [4–7]. The relative decrease in mean arterial blood pressure is considered due to decreases in systemic vascular resistance, myocardial contractility, sympathetic output, and/or a combination of the above. In particular, isoflurane, desflurane, and sevoflurane will induce greater decreases in systemic vascular resistance when compared to halothane (Table 17.3). Further, increasing doses of halothane result in small changes in systemic vascular resistance [8] and decreases in mean arterial pressure, yet halothane administration is associated with decreases in cardiac output. In general, volatile anesthetics decrease systemic vascular resistance by causing peripheral vasodilation and thus increasing blood flow to cutaneous and skeletal muscle tissues [4]. It should be noted that nitrous oxide causes minimal alteration of systemic vascular resistance when administered alone. Typically, an initial drop in blood pressure following induction of anesthesia is associated with a decrease in systemic vascular resistance and the associated preload. Lowered blood pressure can be increased by administration of intravenous fluids, placing the patient in a Trendelenburg position, and/or by giving peripheral vasoconstrictors such as phenylephrine or ephedrine.

17.3.2 The Cardiac Conduction System and the Control of Heart Rate

Baroreceptors located near the aortic root, carotid arteries, and other sites detect changes in arterial blood pressure and will automatically affect cardiovascular function. A typical baroreceptor reflex from the carotid artery includes the afferent (cranial nerve IX) and efferent (cranial nerve X) nerves. An increase in arterial blood pressure is detected by the baroreceptor, causing a reflex and nearly instantaneous decrease

Table 17.3 Cardiovascular effects of inhalational anesthetics

	Heart rate	Blood pressure	Systemic vascular resistance	Cardiac output	Sensitize to epinephrine	Coronary dilation
Desflurane	+	–	–	0/–	0/+	+
Halothane	0	–	0/–	–	+++	+
Isoflurane	+	–	–	–	0/+	++
Sevoflurane	0	–	–	0/–	0/+	0
Nitrous oxide	+	0	0	0	0	0

in the heart rate. A decrease in arterial blood pressure then causes a reflex increase in heart rate, to maintain cardiac output and organ perfusion. Importantly, volatile anesthetics will cause dose-dependent decreases in baroreceptor reflex activity [9]; hence, hemodynamic compensatory responses are attenuated by volatile anesthetics [10, 11]. It is common that alterations in hemodynamics due to volatile anesthetics may require administration of other pressor medications to offset the attenuation of these normal physiologic functions.

Volatile anesthetics may also cause specific cardiac dysrhythmias. Specifically, volatile anesthetics have been reported to slow the rate of sinoatrial node discharge and also increase ventricular and His bundle conduction times [12], which may increase the development of nodal rhythms. Further, volatile anesthetics may increase ventricular automaticity by altering potassium and calcium ion channels [12]. It has been reported that halothane increases the incidence of ventricular dysrhythmia, especially when coadministered with epinephrine; in contrast, the coadministration of epinephrine with isoflurane, desflurane, or sevoflurane has minimal effect on increasing the incidence of ventricular dysrhythmia [13–15]. Furthermore, halothane may blunt the reflex increases in heart rate which typically accompany decreases in blood pressure; it may also slow conduction from the sinoatrial node, resulting in junctional ventricular rhythms. Sevoflurane and desflurane are also known to partially blunt sympathetic baroreflex sensitivity. Importantly, isoflurane is well known to cause significant decreases in systemic vascular resistance and thus blood pressure. Yet, the baroreceptor response remains partially intact, and thus, cardiac output is maintained relatively stable, with isoflurane by associated increases in heart rate.

In patient populations such as young children and the elderly, it is not uncommon to see decreases in heart rate following induction of anesthesia. An anticholinergic agent such as atropine or glycopyrrolate is frequently administered to prevent and/or treat such bradycardia.

17.3.3 Coronary Blood Flow

In general, volatile anesthetics cause a dose-dependent coronary vasodilation, i.e., with isoflurane having a greater effect than halothane [16, 17]. Increasing the concentration of isoflurane increases coronary blood flow, and this also has the potential to cause *coronary steal* syndrome [18, 19]. Coronary steal is caused by vasodilation of healthy coronary arteries and shunting of blood from myocardium at risk for ischemia to areas not at risk. More specifically, in coronary artery disease, cardiac areas at risk for myocardial ischemia have coronary arteries that are already maximally vasodilated. Desflurane and sevoflurane have not been specifically associated with coronary steal syndrome [20, 21]. Nevertheless, the exact clinical significance of coronary steal in humans remains somewhat unresolved.

17.3.4 Contractility and Cardiac Output

Volatile anesthetics depress myocardial contractility by inducing alterations of calcium ion flux [22]. The mechanism of the negative inotropic effect of volatile anesthetics includes (1) decreased free Ca^{2+}, (2) decreased Ca^{2+} release from sarcoplasmic reticulum, and/or (3) altered contractile protein response to Ca^{2+} [22, 23]. Halothane diminishes myocardial contractility more than isoflurane, desflurane, and nitrous oxide. More specifically, isoflurane and sevoflurane cause minimal change in contractility and thus allow for better maintained systemic cardiac output [23]. Due to better cardiovascular stability following either isoflurane or sevoflurane administration compared to halothane, the former agents are typically utilized in patients with congenital heart defects and/or depressed myocardial function.

Due to the simultaneous stimulation of the sympathetic nervous system by volatile agents, the additive myocardial depressant effects of nitrous oxide are usually not evident in healthy individuals. Yet in a compromised and failing myocardium, its depressant effects on contractility become much more evident. More specifically, nitrous oxide has been associated with sympathomimetic effects, as it (1) increases plasma catecholamines, (2) causes mydriasis, and/or (3) induces vasoconstriction of systemic and pulmonary circulations [24]. When nitrous oxide is administered with opioids such as fentanyl, the sympathomimetic effects are minimized or abolished. Therefore, the combined administration of nitrous oxide and opioids may result in a significant decrease in mean arterial pressure and cardiac output.

It is important to note that an abrupt increase in a patient's desflurane concentrations has been associated with a significant increase in sympathetic output, resulting in increased heart rate and mean arterial pressure. A proposed mechanism for this sympathetic stimulation is that it is due to airway and lung irritations that occur with the administration of high concentrations of desflurane [25]. A smaller increase in sympathetic output is commonly associated with isoflurane administration, whereas sevoflurane (due to lack of airway irritation with its administration) is not associated with any increase in sympathetic output, even with a very rapid increase in concentration. Due to favorable airway properties, sevoflurane is used frequently for inhalational induction of anesthesia in children. High concentrations of sevoflurane (4–8 %) are needed for rapid mask induction and are well tolerated in children. Mask induction of anesthesia can also be used for adults.

17.3.5 Pulmonary Blood Flow

Volatile anesthetics are potent bronchodilators and, in some cases, have been used for the treatment of status asthmaticus [26]. In general, it is considered that volatile anesthetics may cause mild decreases in pulmonary vascular resistance, whereas nitrous oxide administration can cause an increase in pulmonary vascular resistance. Thus, the administration of nitrous oxide in patients with preexisting pulmonary artery hypertension may exacerbate the strain on the right heart by increasing their pulmonary vascular resistance. This elevated pulmonary vascular resistance may also result in right-to-left intracardiac shunting in susceptible patients (i.e., those with specific ventriculoseptal defects). In general, volatile anesthetics also diminish the degree of hypoxic pulmonary vasoconstriction, which may result in hypoxia. It is important that in patients with congenital heart defects (i.e., intracardiac shunts, single ventricle, transposition of great arteries, tetralogy of Fallot; see Chap. 10), the properties of select volatile anesthetics may be critical as they offer better cardiovascular stability.

17.3.6 Cardioprotection/Preconditioning

The potential for myocardial preconditioning with volatile anesthetics has been extensively studied. Importantly, halogenated volatile anesthetics have been shown to provide some degree of cardioprotection against injury associated with ischemia and reperfusion [27–30]. The mechanism of cardioprotection seems to be similar to ischemic preconditioning first described by Murray et al. [31] and thus likely ultimately involves the mitochondrial potassium (K_{ATP}) channels [32].

17.3.7 Future Inhalational Anesthetics

Xenon was first used as an anesthetic gas in humans by Cullen and Gross in 1951 [33]. Xenon, an inert gas, has many properties that make it an ideal anesthetic gas; it has very low toxicity and is nonexplosive and nonflammable. The MAC of xenon is approximately 70 %. Its very low blood to gas solubility partition coefficient (0.115) provides fast onset and emergence from anesthesia [34]. Preliminary clinical studies with xenon have shown minimal adverse effects on the cardiovascular system and general hemodynamic parameters [34–36]. More specifically, xenon has been shown to induce minimal effects on alterations in heart rate, coronary blood flow, left ventricular pressure, and atrioventricular conduction time [37]. However, factors that may limit the use of xenon as an anesthetic gas are its cost and requirements for a unique delivery system; xenon must be extracted from the atmosphere, and this process is expensive. Nevertheless, special breathing and delivery systems are in development [38].

It should be specifically noted that all commonly employed volatile anesthetics (i.e., isoflurane, desflurane, sevoflurane, halothane) trigger malignant hyperthermia in susceptible patients. Malignant hyperthermia is an inherited pharmacogenetic disorder that affects skeletal muscle and is characterized by a hypermetabolic response when exposed to a triggering agent such as these volatile anesthetics and/or succinylcholine. Dysregulation of the ryanodine receptor, the calcium release channel of sarcoplasmic reticulum, is typically involved in the induced/unregulated release of calcium from this storage site. Signs and symptoms of malignant hyperthermia include sympathetic hyperactivity, elevated carbon dioxide production, muscle rigidity, hyperthermia, metabolic acidosis, dysrhythmia, and hyperkalemia. Treatment of malignant hyperthermia requires immediate removal of the triggering agent, intravenous administration of dantrolene, and management of the associated symptoms. For more details on malignant hyperthermia, see http://www.mhaus.org/.

17.4 Intravenous Anesthetics

17.4.1 Barbiturates

In general, barbiturates cause central nervous system inhibition (depression) by enhancing the effects of g-aminobutyric acid (GABA) [39]. Barbiturates bind to the GABA receptor complexes which, in turn, increase chloride channel activities and cause subsequent inhibition of the central nervous system. More specifically, the GABA receptor complex has binding affinities for GABA, barbiturates, benzodiazepines, propofol, and/or alcohol [24].

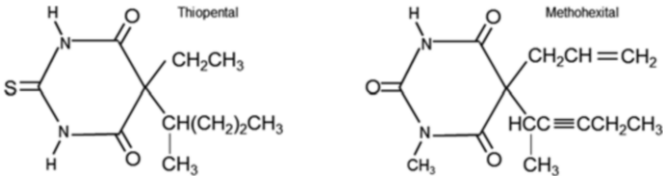

Fig. 17.2 Chemical structure of thiopental and methohexital

Table 17.4 Cardiovascular effects of intravenous anesthetics

	Heart rate	Blood pressure	Systemic vascular resistance	Cardiac output
Thiopental	+	–	–	+
Ketamine	++	++	+	++
Propofol	0/–	–	–	–
Etomidate	0	0/–	0	0
Fentanyl	0/–	0	0	0
Morphine	0/–	0/–	0/–	0
Midazolam	0	0	0	0
Methohexital	++	–	–	0/–
Meperidine	++	0/–	0/–	0/+

Thiopental (3–5 mg/kg) and methohexital (1.5–2 mg/kg) are common barbiturates used for induction of general anesthesia (Fig. 17.2). After the intravenous injection of thiopental or methohexital, anesthesia is induced rapidly, often within seconds. Yet, the duration of induced anesthesia after a single bolus dose of intravenous barbiturate is short (approximately 5 min), due to rapid redistribution from the brain to other tissues such as muscle and adipose. Importantly, intraarterial injection of thiopental can result in severe vasospasm which may lead to thrombosis, tissue injury, and/or even gangrene. If intraarterial injections do occur, counteractive measures such as sympathetic nerve blocks or administration of papaverine, phenoxybenzamine, or lidocaine may be initiated to decrease induced arterial vasospasm.

The administration of barbiturates is typically associated with decreases in mean arterial pressure which result from both induced vasodilation and decreased myocardial contractility (Table 17.4). Barbiturates have been also shown to cause dose-related myocardial depressions, which are typically not as pronounced as those associated with volatile anesthetics. Yet, barbiturates may cause a small depression of the carotid and aortic baroreceptors and therefore an induced decrease in mean arterial pressure leading to a reflex tachycardia. If intravenous barbiturates are administered slowly, relative hemodynamic stability can be maintained [40], especially in patients with normal intravascular volume status. In contrast, a rapid infusion of barbiturates, especially in hypovolemic patients, may result in significant hypotension. Subsequently, typical increases in heart rate upon barbiturate administration are not present if the baroreceptor reflex is not intact, as in heart transplant patients or in isolated heart preparations. Importantly, barbiturates do not generally sensitize the myocardium to the potential arrhythmic effects of administered catecholamines.

17.4.2 Benzodiazepines

Benzodiazepines are considered to produce central nervous system depression by binding to the GABA receptor complex and ultimately increasing chloride channel activities. Benzodiazepines, such as midazolam and diazepam, are often administered as adjuncts to anesthesia for sedation, amnesia, and anxiolysis. Benzodiazepines themselves do not have analgesic properties. Noteworthy, benzodiazepines possess anticonvulsant properties and hence can be utilized in acute management of seizures. Interestingly, the acute administration of benzodiazepines has not been associated with significant changes in hemodynamic parameters, i.e., blood pressure, heart rate, and systemic vascular resistance are fairly well maintained. However, it has been shown that with benzodiazepines, systemic vascular resistance decreases in a dose-related fashion [41]. In general, when administered alone, a typical clinical dose of benzodiazepine for preoperative sedation or anxiolysis in adults usually is not associated with any significant hemodynamic alteration.

More specifically, induction of anesthesia with midazolam (0.2–0.3 mg/kg intravenous) is associated with a decrease in systemic vascular resistance, but with minimal effects on cardiac output. Typically, the baroreceptor reflex is considered to remain intact, and thus, a relative decrease in mean arterial pressure will result in a responsive increase in heart rate. It has been reported that diazepam elicits even fewer cardiovascular effects than midazolam, i.e., a typical dose required for sedation and anxiolysis in adults usually is not associated with any significant hemodynamic alterations. At most, diazepam administration may cause minimal changes in both blood pressure and systemic vascular resistance. Therefore, the coadministration

of diazepam and nitrous oxide has not been observed to be associated with significant decreases in cardiovascular function [42].

17.4.3 Opioids

In general, opioids are analgesics that are commonly administered as adjuncts to anesthesia. Such agents currently used in clinical practice include fentanyl, morphine, meperidine, alfentanil, sufentanil, and remifentanil (Table 17.5). All opioids exert their effect by interacting with opioid receptors (mu_1, mu_2, kappa, or delta; Table 17.6); they are used as adjuncts to help blunt sympathetic responses to noxious stimuli. Overall, the clinical use of opioids causes minimal changes in either cardiac output or blood pressure, yet opioids may generally cause bradycardia due to increased vagal tones. At very high doses, opioids may have the following effects on a patient's hemodynamics: inhibition of autonomic nervous system, direct myocardial depression, and/or histamine release. More specifically, one in vitro study of human atrial myocardium found that fentanyl, remifentanil, and sufentanil did not modify inotropic effects, while alfentanil caused negative inotropy by affecting calcium regulation [43]. Yet, it has also been reported that opioids such as fentanyl may depress rat myocardial contractility by affecting calcium regulation [44]. Finally, it is considered that morphine may cause a decrease in mean arterial pressure by inducing histamine release and bradycardia. It should be noted that high doses of an intravenous opioid such as fentanyl may cause chest wall rigidity, making manual ventilation of nonparalyzed patients difficult.

17.4.4 Ketamine

Ketamine is a phencyclidine derivative (Fig. 17.3) that induces intense analgesia and dissociative anesthesia. Patients who receive ketamine can obtain a cataleptic state with open eyes and/or ocular nystagmus; intense hallucinations may also be experienced by patients receiving ketamine. The typical routes for ketamine administration include intravenous (1–2 mg/kg), intramuscular (3–6 mg/kg), or oral (5–6 mg/kg). In general, ketamine's effects on the central nervous system are considered due to interactions with multiple receptor pathways including N-methyl-D-aspartate (NMDA), monoaminergic, opioid, and/or muscarinic receptors. Due to interactions with pain receptors, ketamine possesses intense analgesic properties.

Potential side effects of ketamine administration include the stimulation of the central sympathetic nervous system

Table 17.5 Opioid agonists commonly used in clinical practice

	Heart rate	Blood pressure	System vascular resistance	Contractility	Histamine
Meperidine	++	–	–	+/–	++
Morphine	0/–	–	–	–	++
Fentanyl	0/–	0	0	0	0
Alfentanil	–	0/–	–	0/–	0
Sufentanil	–	0/–	0/–	0/–	0
Remifentanil	–	0	0	0	0

Table 17.6 Opioid and opioid receptors

Drug	Mu receptor	Delta receptor	Kappa receptor
Morphine	+++	+?	+
Fentanyl	+++	?	
Sufentanil	+++	+	+
Buprenorphine	+		–
Naloxone	–	–	–
Naltrexone	–	–	–
Nalbuphine	–		++
DPDPE		++	
DADLE	+	+++	+?
NorBNI	–	–	–
DSLET	+	++	
Naltrindole	–	–	–

Modified from Goodman and Gilman's The Pharmacological Basis of Therapeutics, 10th edition (Hardman, J.G., Limbird, L.E., eds., McGraw-Hill, New York, NY, 2001)

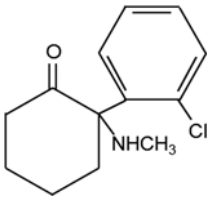

Fig. 17.3 Chemical structure of ketamine

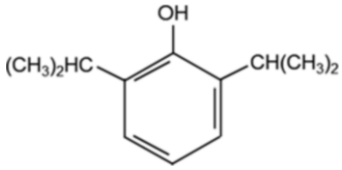

Fig. 17.4 Chemical structure of propofol

and associated increases in circulating epinephrine and norepinephrine. In patients where maintenance of myocardial contractility and systemic vascular resistance is vital (i.e., hypovolemia, trauma, and shock), ketamine may better stimulate the cardiovascular system to maintain cardiac output and blood pressure. More specifically, ketamine has been reported to cause an increase in heart rate, blood pressure, cardiac output, and myocardial oxygen consumption. Due to stimulation of cardiovascular function, ketamine may not be appropriate in patients with aortic stenosis, coronary artery disease, and/or hypertrophic left ventricle. It should be noted that pulmonary arterial pressure may also increase following administration of ketamine. Another important side effect attributed to ketamine administration is its bronchodilating effects; thus, patients with, or at risk for, bronchospasm may benefit from ketamine induction. In contrast, in patients with depleted catecholamine stores, ketamine may cause a serious depression of myocardial function [45]. In other words, the maintenance or elevation of cardiovascular function may not be observed following administration of ketamine in patients with depleted catecholamine stores such as those with sepsis. Furthermore, ketamine may also increase cerebral perfusion and intracranial pressure and thus should be used carefully in patients with neurovascular disease. Low dose of ketamine may be utilized for analgesia in the perioperative setting.

17.4.5 Propofol

Propofol (1 % solution) is a 2,6-diisopropylphenol (Fig. 17.4) that is typically administered intravenously for sedation or induction and maintenance of general anesthesia. Importantly, intravenous injections of propofol (1.5–2 mg/kg) are associated with rapid loss of consciousness (30–60 s) and onset of general anesthesia. Furthermore, a general anesthesia maintenance infusion of propofol is typically achieved with 150–200 mcg/kg/min intravenous. Additional advantages of propofol include clearer awakening, small cumulative effects, and/or decreased incidence of nausea and vomiting.

Propofol is considered to also interact with GABA receptors and activate them in a similar fashion as barbiturates. Likewise, activation of GABA receptors by propofol increases the conductance of chloride channels, resulting in inhibition of postsynaptic neurons.

Of clinical significance, the administration of propofol commonly causes a decrease in both systemic vascular resistance and cardiac contractility, hence resulting in decreased cardiac output. This reduction in systemic vascular resistance (and vasodilation) is considered due to decreased sympathetic vasoconstrictor activation of vascular smooth muscle [46]. The inhibition of sympathetic tone by propofol is reported to be greater than inhibition of parasympathetic activity; in some patients, this may result in significant bradycardia and even asystole [47–49]. The induced decrease in cardiac contractility is likely due to decreases in calcium uptake into the sarcoplasmic reticulum; decreased reuptake of calcium results in less calcium available for the next activation sequence [50].

Importantly, in patients with decreased left ventricular function, the administration of propofol may result in severe hypotension and suppressed myocardial contractility. Therefore, careful titration of propofol and adequate intravascular hydration is important in these types of patients.

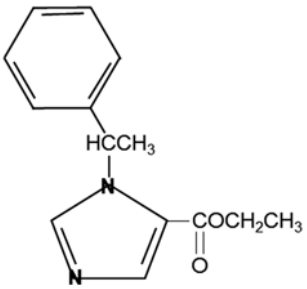

Fig. 17.5 Chemical structure of etomidate

17.4.6 Etomidate

Etomidate (Fig. 17.5) is an imidazole compound which is water soluble at lower pH and lipid soluble at physiologic pH. Rapid loss of consciousness is accomplished after intravenous injection of etomidate (0.2–0.4 mg/kg). Clinically, etomidate is utilized in patients with known conditions of decreased cardiac function, hypotension, and/or allergy to propofol. It is important to recognize that etomidate lacks analgesic properties and does not blunt sympathetic responses to direct laryngoscopy and endotracheal intubation.

Generally, etomidate provides cardiovascular and pulmonary stability; typical induction doses of etomidate result in minimal changes in either heart rate or cardiac output. Myocardial contractility is well maintained at doses needed to induce general anesthesia [24] and is considered to produce less myocardial depression when compared to thiopental [51]. Etomidate does not induce significant histamine release, but it does depress adrenocortical function by inhibiting the conversion of cholesterol to cortisol [52]. Specifically, a single induction dose of etomidate can cause adrenal suppression for 5–8 h [53], and a continuous infusion of etomidate will cause further adrenocortical suppression. Typically, there is minimal clinical effect to adrenal suppression following a single induction dose of etomidate.

17.4.7 Nondepolarizing Muscle Relaxants

In general, the majority of nondepolarizing muscle relaxants have minimal effects on either cardiovascular or hemodynamic stabilities. Yet when induced, nondepolarizing muscle relaxants are believed to elicit cardiovascular effects by stimulating the release of histamine and affecting muscarinic and nicotinic receptors (Table 17.7). For example, pancuronium may cause vagal blockade (antimuscarinic effect) at the sinoatrial node, resulting in elevation of heart rate. The administration of pancuronium is also associated with activation of the sympathetic nervous system [54, 55]. Large doses of atracurium and mivacurium are associated with histamine release which may result in tachycardia or hypotension; such patients may display facial flushing as a result of histamine release. Interestingly, cisatracurium (a stereoisomer of atracurium) is not associated with clinically significant histamine release. Finally, it is of interest to note that vecuronium and rocuronium are agents that are considered devoid of significant cardiovascular effects [56, 57].

17.4.8 Depolarizing Muscle Relaxant

Succinylcholine is a depolarizing muscle relaxant. It has a similar structure to and mimics acetylcholine by binding to nicotinic cholinergic receptors. The duration of action of succinylcholine is short (minutes) and is broken down by the abundant pseudocholinesterase enzyme in the plasma. Importantly, the administration of succinylcholine may be associated with cardiac dysrhythmias (i.e., junctional rhythm and sinus bradycardia) by its muscarinic action at the sinoatrial node. Administration of succinylcholine is associated with hyperkalemia in susceptible patients such as those with malignant hyperthermia, muscular dystrophy, spinal cord injury, and/or burn injury. More specifically, in boys with Duchenne muscular dystrophy, the administration of succinylcholine has been linked to episodes of sudden cardiac arrest.

Table 17.7 Nondepolarizing muscle relaxants

	Histamine release	Vagal blockade
Atracurium	+	0
Cisatracurium	0	0
Mivacurium	+	0
Pancuronium	0	++
Rocuronium	0	0/+
Vecuronium	0	0
Tubocurarine	+++	0
Succinylcholine	0	–

17.4.9 Dexmedetomidine

Dexmedetomidine is an alpha-2 adrenergic agonist which provides sedation, anxiolysis, and analgesia without depressing respiratory drive. It is similar to clonidine except that it has a significantly greater affinity to alpha-2 receptors than alpha-1 receptors. Dexmedetomidine is commonly used in the perioperative and intensive care unit settings as an adjunct to sedation and analgesia medications. Due to its effect on the centrally mediated alpha-2 adrenergic receptor, infusion of dexmedetomidine can cause bradycardia and hypotension [58]. During the administration of a rapid bolus or loading dose of intravenous dexmedetomidine, transient hypertension caused by peripheral vasoconstriction may occur.

17.4.10 Acupuncture

Acupuncture involves stimulation of specific anatomical locations on the skin to alter "energy flow patterns" throughout the body. The skin can be stimulated by manual or electrical stimulation, or the more typical placement of small metallic needles. Acupuncture has been used in China for thousands of years, and, more recently, there has been a surge of interest in these nontraditional methodologies within the United States. Acupuncture has been utilized for treatment and prevention of multiple health conditions such as chronic pain, nausea and vomiting, obesity, substance abuse, and/or asthma. Stress responses and cardiovascular effects of pain have reportedly been attenuated by nonpharmacologic techniques such as acupuncture, i.e., it is considered to modulate the body's pain/nociceptive system, increasing the release of endogenous opioids [59] and decreasing postoperative pain [60]. Interestingly, in one study using a feline cardiovascular

model, the utilization of electroacupuncture induced improvements in regional cardiac wall motion activity during myocardial ischemia [61]. Furthermore, it was reported that acupressure applied to females undergoing elective cesarean section with spinal anesthesia will elicit reductions in nausea and vomiting [62].

The potential advantages of acupuncture for the treatment of medical conditions continue to be investigated. Importantly, with initial studies indicating some promising benefits of acupuncture for treatment of multiple medical conditions, the National Institutes of Health Consensus Conference has recommended that acupuncture be included in comprehensive management and may be useful as an adjunct treatment or an acceptable alternative [63]. Finally, limitations in the validation of acupuncture may stem from difficulties in creating appropriate randomized, blinded, placebo-controlled clinical studies.

17.4.11 Anesthesia and Temperature Regulation

General and regional anesthesia is often associated with dysregulation of a patient's body thermoregulatory responses, which can ultimately be elicited as decreases in core body temperature. More specifically, during the first hour of general anesthesia, it is common for core body temperature to decrease 0.5–1 °C. Most of the body heat lost during anesthesia is via convection and radiation, with some losses due to conduction and evaporation. Principally, anesthetics cause the core body heat to redistribute to the periphery, resulting in a drop in core body temperature [64]. In general, one can consider that, under anesthesia, patients become poikilotherms (minimal ability to thermoregulate). Therefore, multiple modalities to maintain normothermia during surgery have been developed, including (1) forced air warming devices, (2) fluid warmers, (3) ventilator humidifiers, (4) water mattresses and vests, (5) radiant heat lamps, and (6) warming blankets or mattresses. Other modalities for warming patients include altering ambient room temperatures and/or the temperatures of irrigation solutions.

Importantly, postoperative hypothermia may be associated with (1) delayed awakening from general anesthesia, (2) slowed drug metabolism, (3) coagulopathy, (4) vasoconstriction and poor tissue perfusion, (5) increases in blood viscosity, (6) induced shivering, and/or (7) increased risk of surgical site infections [65]. More specifically, postoperative shivering may be detrimental in patients with coronary artery disease or other cardiovascular complications, as shivering causes increases in oxygen consumption and tachycardia. Currently, meperidine is clinically approved for the treatment of excessive shivering in postoperative situations.

17.4.12 Myocardial Preconditioning with Inhalational and Intravenous Anesthetics

Since the initial report by Murray et al. [31] on ischemic preconditioning of dog myocardium, there has been great interest in myocardial preconditioning with pharmacologic agents. This includes myocardial preconditioning with volatile anesthetics such as desflurane [66], isoflurane [67, 68], and sevoflurane [69] as well as intravenous opioid agonists [70, 71]. Pharmacologic preconditioning is not only limited to cardiac tissue; other tissues such as the lung, brain, and skeletal muscle [72] may benefit from preconditioning. In summary, preconditioning with anesthetics may offer life-extending benefits in the cardiac, vascular, and/or organ transplantation surgical patients.

17.4.13 Heart Transplant

With the increasing numbers of individuals surviving heart transplants, the anesthetic management of these patients after a heart transplant procedure requires special considerations. A transplanted heart is initially totally denervated and usually will elicit higher basal heart rates (90–110 beats per min), i.e., initial direct autonomic nervous system effects are absent. Thus, agents such as atropine and glycopyrrolate will not cause increases in heart rate. Vagal stimulation maneuvers such as carotid massage and oculocardiac reflex are also absent. However, the administration of acetylcholinesterase inhibitors, such as neostigmine, has been associated with severe bradycardia and even sinus arrest [73]. If bradycardia develops, administration of direct acting cardiac agents such as isoproterenol or epinephrine may be required to increase the intrinsic heart rate. In other words, the transplanted heart continues to respond to circulating catecholamines, and thus, maintenance of cardiac output is aided by increased stroke volume (Frank-Starling relationship); maintaining adequate preload is considered essential in heart transplant patients postoperatively.

17.5 Summary

The perioperative management of patients with complex medical conditions, while providing cardiovascular stability, continues to put forward both challenges and new developments. Patients with cardiovascular disease or associated comorbidities such as obesity, diabetes, or pulmonary disease

may require special attention during general anesthesia. Advancements in the field of anesthesiology have continued and include (1) new anesthesia medications, (2) improved medical equipment for enhanced anesthetic delivery and monitoring, and (3) less invasive surgical technologies that may not require general anesthetic techniques. Nevertheless, with our growing understanding of inhalational and intravenous anesthetics, the maintenance of stable, physiologic cardiovascular function is a common component of today's clinical practice.

References

1. American Society of Anesthesiologists Task Force (2011) Practice guidelines for preoperative fasting and the use of pharmacologic agents to reduce the risk of pulmonary aspiration: application to healthy patients undergoing elective procedures. Anesthesiology 114:495–511
2. Continuum of Depth of Sedation: Definition of General Anesthesia and Levels of Sedation/Analgesia. ASA Standards, Guidelines and Statements. American Society of Anesthesiologists. (2014)
3. Eger EI II (1974) Uptake of inhaled anesthetics: the alveolar to impaired anesthetic difference. In: Eger EI II (ed) Anesthetic uptake and action. Williams & Wilkins, Baltimore, p 77
4. Stevens W, Cromwell T, Halsey M et al (1971) The cardiovascular effects of a new inhalation anesthetic, forane, in human volunteers at constant arterial carbon dioxide tension. Anesthesiology 35:8–16
5. Eger EI II, Smith N, Stoelting R (1970) Cardiovascular effects of halothane in man. Anesthesiology 32:396–409
6. Weiskopf R, Cahalan M, Eger EI II et al (1991) Cardiovascular actions of desflurane in normocarbic volunteers. Anesth Analg 73:143–156
7. Holaday D, Smith F (1981) Clinical characteristics and biotransformation of sevoflurane in healthy human volunteers. Anesthesiology 54:100–106
8. Pavlin EG, Su JY (1994) Cardiopulmonary pharmacology. In: Miller RD (ed) Anesthesia. Churchill Livingstone, Philadelphia, p 145
9. Muzi M, Ebert TJ (1995) A comparison of baroreflex sensitivity during isoflurane and desflurane anesthesia in humans. Anesthesiology 82:919–925
10. Duke PC, Townes D, Wade JG (1977) Halothane depresses baroreflex control of heart rate in man. Anesthesiology 46:184–187
11. Korly KJ, Ebert TJ, Vucins E et al (1984) Baroreceptor reflex control of heart rate during isoflurane anesthesia in humans. Anesthesiology 60:173–179
12. Atlee JL, Bosnjak ZJ (1990) Mechanisms for cardiac dysrhythmias during anesthesia. Anesthesiology 72:347–374
13. Navarro R, Weiskopf RB, Moore MA et al (1994) Humans anesthetized with sevoflurane or isoflurane have similar arrhythmic response to epinephrine. Anesthesiology 80:545–549
14. Moore MA, Weiskopf RB, Eger EI et al (1994) Arrhythmogenic doses of epinephrine are similar during desflurane or isoflurane anesthesia in humans. Anesthesiology 79:943–947
15. Johnston PR, Eger EI, Wilson C (1976) A comparative interaction of epinephrine with enflurane, isoflurane, and halothane in man. Anesth Analg 55:709–712
16. Crystal GJ, Khoury E, Gurevicius J, Salem MR (1995) Direct effects of halothane on coronary blood flow, myocardial oxygen consumption, and myocardial segmental shortening in in situ canine hearts. Anesth Analg 80:256–262
17. Crystal GJ, Salem MR (2003) Isoflurane causes vasodilation in the coronary circulation. Anesthesiology 98:1030
18. Priebe H, Foex P (1987) Isoflurane causes regional myocardial dysfunction in dogs with critical coronary artery stenoses. Anesthesiology 66:293–300
19. Cason BA, Verrier ED, London MJ et al (1987) Effects of isoflurane and halothane on coronary vascular resistance and collateral myocardial blood flow: their capacity to induce coronary steal. Anesthesiology 67:665–675
20. Kersten JR, Brayer AP, Pagel PS et al (1994) Perfusion of ischemic myocardium during anesthesia with sevoflurane. Anesthesiology 81:995–1004
21. Eger E (1994) New inhaled anesthetics. Anesthesiology 80:906–922
22. Pagel PS, Kersten JR, Farber NE, Warltier DC (2005) Cardiovascular Pharmacology. In: Miller RD (ed) Miller's Anesthesia. Churchill Livingstone, Philadelphia, p 194
23. Rivenes SM, Lewin MB, Stayer SA et al (2001) Cardiovascular effects of sevoflurane, isoflurane, halothane, and fentanyl-midazolam in children with congenital heart disease. Anesthesiology 94:223–229
24. Stoelting RK (ed) (1999) Pharmacology and physiology in anesthetic practice, 3rd edn. Lippincott Williams & Wilkins, Philadelphia
25. Muzi M, Ebert TJ, Hope WG et al (1996) Site(s) mediating sympathetic activation with desflurane. Anesthesiology 85:737–747
26. Shankar V, Churchwell KB, Deshpande JK (2006) Isoflurane therapy for severe refractory status asthmaticus in children. Intensive Care Med 32:927–933
27. Warltier DC, Wathiqui MH, Kampine JP et al (1988) Recovery of contractile function of stunned myocardium in chronically instrumented dogs is enhanced by halothane or isoflurane. Anesthesiology 69:552–565
28. Marijic J, Stowe DF, Turner LA et al (1990) Differential protective effects of halothane and isoflurane against hypoxic and reoxygenation injury in the isolated guinea pig heart. Anesthesiology 73:976–983
29. Novalija E, Fujita S, Kampine JP et al (1999) Sevoflurane mimics ischemic preconditioning effects on coronary flow and nitric oxide release in isolated hearts. Anesthesiology 91:701–712
30. Conzen PF, Fischer S, Detter C et al (2003) Sevoflurane provides greater protection of myocardium than propofol in patients undergoing off-pump coronary artery bypass surgery. Anesthesiology 99:826–833
31. Murray CE, Jennings RB, Reimer KA (1986) Preconditioning with ischemia: a delay of lethal cell injury in ischemic myocardium. Circulation 74:1124–1136
32. Zaugg M, Lucchinetti E, Spahn DR et al (2002) Volatile anesthetics mimic cardiac preconditioning by priming the activation of mitochondrial K_{ATP} channels via multiple signaling pathways. Anesthesiology 97:4–14
33. Cullen SC, Gross EG (1951) The anesthetic properties of xenon in animals and human beings with additional observation on krypton. Science 1113:580–582
34. Rossaint R, Reyle-Hahn R, Schulte J et al (2003) Multicenter randomized comparison of the efficacy and safety of xenon and isoflurane in patients undergoing elective surgery. Anesthesiology 98:6–13
35. Lachmann B, Armbruster S, Schairer W et al (1990) Safety and efficacy of xenon in routine use as an inhalational anesthetic. Lancet 335:1413–1415
36. Luttrop HH, Romner B, Perhag L et al (1993) Left ventricular performance and cerebral hemodynamics during xenon anesthesia: a transesophageal echocardiography and transcranial Doppler sonography study. Anesthesia 48:1045–1049

37. Stowe DF, Rehmert GC, Wai-Meng K et al (2000) Xenon does not alter cardiac function or major cation currents in isolated guinea pig hearts of myocytes. Anesthesiology 92:516–522
38. Dingley J, Findlay GP, Bernard AF et al (2001) A closed xenon anesthesia delivery system. Anesthesiology 94:173–176
39. Franks NP, Lieb WR (1994) Molecular and cellular mechanisms of general anaesthesia. Nature 367:607–614
40. Seltzer JL, Gerson JI, Allen FB (1980) Comparison of the cardiovascular effects of bolus vs. incremental administration of thiopentone. Br J Anaesth 52:527–529
41. Sunzel M, Paalzow L, Berggren L et al (1988) Respiratory and cardiovascular effects in relation to plasma levels of midazolam and diazepam. Br J Clin Pharmacol 25:561–569
42. McCammon RL, Hilgenberg JC, Stoelting RK (1980) Hemodynamic effects of diazepam-nitrous oxide in patients with coronary artery disease. Anesth Analg 59:438–441
43. Hanouz J, Yvon A, Guesne G et al (2001) The in vitro effects of remifentanil, sufentanil, fentanyl, and alfentanil on isolated human right atria. Anesth Analg 93:543–549
44. Kanaya N, Kahary DR, Murray PA, Damron DS (1998) Differential effects of fentanyl and morphine on intracellular calcium transients and contraction in rate ventricular myocytes. Anesthesiology 89:1532–1542
45. Waxman K, Shoemaker WC, Lippmann M (1980) Cardiovascular effects of anesthetic induction with ketamine. Anesth Analg 58:355–358
46. Robinson JF, Ebert TJ, O'Brien TJ et al (1997) Mechanisms whereby propofol mediates peripheral vasodilation in humans. Sympathoinhibition or direct vascular relaxation? Anesthesiology 86:64–72
47. Bray RJ (1995) Fatal myocardial failure associated with a propofol infusion in a child. Anaesthesia 50:94
48. Tramer MR, Moore RA, McQuay HJ (1997) Propofol and bradycardia: causation, frequency and severity. Br J Anaesth 78:642–651
49. James MFM, Reyneke CJ, Whiffler K (1989) Heart block following propofol: a case report. Br J Anaesth 62:213–215
50. Sprun J, Lgletree-Hughes ML, McConnell BK et al (2001) The effects of propofol on the contractility of failing and nonfailing human heart muscles. Anesth Analg 93:550–559
51. Kissin I, Motomura S, Aultman DF et al (1983) Inotropic and anesthetic potencies of etomidate and thiopental in dogs. Anesth Analg 62:961–965
52. Fragen RJ, Shanks CA, Molteni A et al (1984) Effects of etomidate on hormonal responses to surgical stress. Anesthesiology 61:652–656
53. Wagner RL, White PF, Kan PB et al (1984) Inhibition of adrenal steroidogenesis by anesthetic etomidate. N Engl J Med 310:1415–1421
54. Ivankovich AD, Miletich DJ, Albrecht RF et al (1975) The effect of pancuronium on myocardial contraction and catecholamine metabolism. J Pharm Pharmacol 27:837–841
55. Domenech JS, Garcia RC, Sastain JMR et al (1976) Pancuronium bromide: an indirect sympathomimetic agent. Br J Anaesth 48:1143–1148
56. Morris RB, Cahalan MK, Miller RD et al (1983) The cardiovascular effects of vecuronium (ORG NC45) and pancuronium in patients undergoing coronary artery bypass grafting. Anesthesiology 58:438–440
57. Hudson ME, Rothfield KP, Tullock WC, Firestone LL (1998) Haemodynamic effects of rocuronium bromide in adult cardiac surgical patients. Can J Anaesth 45:139–143
58. Bloor BC, Ward DS, Belleville JP, Maze M (1992) Effects of intravenous dexmedetomidine in humans. Anesthesiology 77:1134–1142
59. Han JS (1986) Physiologic and neurochemical basis of acupuncture analgesia. In: Cheng TO (ed) The international textbook of cardiology. Pergamon, New York, pp 1124–1126
60. Felhendler DPT, Lisander B (1996) Pressure on acupoints decreases postoperative pain. Clin J Pain 12:326–329
61. Li P, Pitsillides KF, Rendig SV et al (1998) Reversal of reflex-induced myocardial ischemia by median nerve stimulation: a feline model of electroacupuncture. Circulation 97:1186–1194
62. Stein DJ, Birnbach DJ, Danzer BI et al (1997) Acupressure versus intravenous metoclopramide to prevent nausea and vomiting during spinal anesthesia for cesarean section. Anesth Analg 84:342–345
63. Acupunture. NIH Consensus Development Panel on Acupuncture JAMA. 1998;280(17):1518–1524
64. Sessler DI (1997) Mild perioperative hypothermia. N Engl J Med 336:1630–1637
65. Mauermann WJ, Nemergut EC (2006) The anesthesiologist's role in the prevention of surgical site infections. Anesthesiology 105:413–421
66. Hanouz J, Yvon A, Massetti M et al (2002) Mechanisms of desflurane-induced preconditioning in isolated human right atria in vitro. Anesthesiology 97:33–41
67. Kersten JR, Schmeling TJ, Hettrick DA et al (1996) Mechanism of myocardial protection by isoflurane: role of adenosine triphosphate-regulated potassium (KATP) channels. Anesthesiology 85:794–807
68. Belhomme D, Peynet J, Louzy M et al (1999) Evidence for preconditioning by isoflurane in coronary artery bypass graft surgery. Circulation 100:II340–II344
69. De Hert S, ten Broeck P, Mertens E et al (2002) Sevoflurane but not propofol preserves myocardial function in coronary surgery patients. Anesthesiology 97:42–49
70. Sigg DC, Coles JA Jr, Gallagher WJ, Oeltgen PR, Iaizzo PA (2001) Opioid preconditioning: myocardial function and energy metabolism. Ann Thorac Surg 72:1576–1582
71. Sigg DC, Coles JA Jr, Oeltgen PR, Iaizzo PA (2002) Role of delta-opioid receptors in infarct size reduction in swine. Am J Physiol Heart Circ Physiol 282:H1953–H1960
72. Hong J, Sigg DC, Upson K, Iaizzo PA (2002) Role of ∂-opioid receptors in preventing ischemic damage of isolated porcine skeletal muscle. Biophys J 82:610a (Abstract 2982)
73. Beebe DS, Shumway SJ, Maddock R (1994) Sinus arrest after intravenous neostigmine in two heart transplant recipients. Anesth Analg 78:779–782

Blood Pressure, Heart Tones, and Diagnoses

18

Jacob Hutchins

Abstract

The primary purpose of this chapter is to familiarize the reader with the basic concepts of blood pressure, heart tones, and some commonly associated diagnoses. Furthermore, it is important to reinforce the need for a deep understanding of basic physiological principles when interpreting physical examination findings. Commonly employed invasive and non-invasive methods for assessing blood pressure are discussed, as well as some of the newer technologies on the horizon. It remains the general consensus that even the most sophisticated electronic monitors cannot fully reduce the need for sound clinical skills such as: proper patient inspection, palpation, percussion, and/or auscultation.

Keywords

Blood pressure measurement • Palpation • Doppler effect • Auscultation • Oscillometry • Plethysmography • Arterial tonometry • Arterial cannulation • Heart tones

18.1 Blood Pressure

Fundamental to providing comprehensive care to patients is the ability to perform a physical examination. The optimal selection of further tests and treatments depends on a well-developed patient history and one's physical examination skills. Two key elements of a physical examination are: (1) properly measuring a patient's blood pressure and (2) careful auscultation of their heart sounds. These assessments provide important information about the patient's hemodynamics and aid in diagnosing anatomical or physiological pathologies.

Naive ideas concerning human circulation and blood pressure date as far back as ancient Greece. It took until the eighteenth century before the first official report describing an attempt to measure blood pressure was written, when Stephen Hales published a monograph on "Haemastatics" in 1733. He conducted a series of experiments involving invasive cannulation of arteries in horses, in which he directly monitored blood pressure. Unfortunately, such a method was not applicable for humans. During the subsequent two centuries, there were many contributions to medical science associated with blood pressure control and its assessment. One of the greatest of these contributions was a publication in Gazetta medica di Torino in 1896, called "A New Sphygmomanometer" by Dr. Riva-Rocci; this publication is still recognized as the single most important advancement in the field of practical noninvasive methods for blood pressure estimation.

In 1916, French physician Rene Laennec invented the first stethoscope, which was constructed from stacked paper rolled into a solid cylinder. Prior to his invention, physicians around the world would place an ear directly over the patient's chest to hear the heart and/or lung sounds. After Dr. Laennec's initial success, several new models were produced, primarily made of wood; this stethoscope was called a *monaural stethoscope*. The *binaural stethoscope* was invented in 1829 by a doctor from Dublin and later gained widespread acceptance. In the 1960s, the Camman binaural stethoscope was considered the standard because of its

J. Hutchins, MD (✉)
Department of Anesthesiology, University of Minnesota,
MMC 294, 420 Delaware St. SE, Minneapolis, MN 55455, USA
e-mail: hutc0079@umn.edu

P.A. Iaizzo (ed.), *Handbook of Cardiac Anatomy, Physiology, and Devices*, DOI 10.1007/978-3-319-19464-6_18

superior auscultation capabilities. Today, there continue to be advances relative to stethoscope technologies, e.g., there are electronic stethoscopes that can send signals to "smartphones." It is essential for healthcare professionals and bioengineers to understand how blood pressure and heart tones are obtained, the advantages and disadvantages of the different methods used to obtain them, and how to interpret the information.

18.1.1 Physiology of Blood Pressure

Blood pressure is the force applied on arterial walls as the heart pumps blood through the circulatory system. The rhythmic contractions of the left ventricle result in cyclic changes in arterial blood pressure. During ventricular systole, the heart pumps blood into the circulatory system, and the pressure within the arteries reaches its highest level—a point known as *systolic blood pressure*. During diastole, the pressure within the arterial system falls to its lowest level, a point called *diastolic blood pressure*.

Mean blood pressure, often used clinically, represents the time-weighted average of the arterial pressures recorded during one cardiac cycle. The alternating systolic and diastolic pressures create outward and inward movement of the arterial walls, perceived as arterial pulsation or arterial pulse. *Pulse pressure* is another clinical term which represents the difference between the systolic and diastolic blood pressures.

It is accepted convention that blood pressure is measured in millimeters of mercury (mmHg). A normal systolic blood pressure is less than 140 mmHg, and a normal diastolic blood pressure is less than 90 mmHg. Blood pressure higher than normal signifies *hypertension,* and one lower than normal is called *hypotension*. Normal mean arterial pressure is between 60 and 90 mmHg. The mean arterial pressure has significance in that it will drive tissue perfusion and can be measured directly using an automated blood pressure cuff or calculated using the following formulas:

$$\mathrm{MAP} = \mathrm{DBP} + \mathrm{PP}/3 \,\text{or}\, \mathrm{MAP} = \left[\mathrm{SBP} + \left(2 \times \mathrm{DBP}\right)\right]/3$$

where PP = SBP − DBP, MAP = mean arterial pressure, DBP = diastolic blood pressure, PP = pulse pressure, and SBP = systolic blood pressure.

Blood flow throughout the circulatory system follows pressure gradients. By the time blood reaches the right atrium, representing the end point of the venous system, pressure will decrease to approx. 0 mmHg. The two major determinants of the arterial blood pressure are: (1) cardiac output, representing the volume of blood pumped by the heart (left ventricle) per minute, and (2) systemic vascular resistance, which is the impediment to blood flow created by the vascular bed. Cardiac output depends on a complexity of numerous factors including: preload, contractility, afterload, heart rate, and/or the heart's relative rhythm. Systemic vascular resistance is equally complex and controlled by many additional factors including vasomotor tone of arterioles, terminal arterioles, and/or precapillary sphincters. Blood pressure as a function of the cardiac output and systemic vascular resistance can be expressed with the following abstract formula:

$$\mathrm{BP} = \mathrm{CO} \times \mathrm{SVR}$$

where BP = blood pressure, CO = cardiac output, and SVR = systemic vascular resistance.

Cardiac output is expressed by the formula: CO = HR × SV where HR = heart rate and SV = stroke volume. SVR is expressed by the formula: SVR = {(MAP − RAP) × 80}/CO where RAP is right atrial pressure.

Blood pressure decreases by 3–5 mmHg in arteries 3 mm in diameter and then reaches approx. 85 mmHg when entering arterioles; this accounts for approx. 50 % of the resistance of the entire systemic circulation. Blood pressure is further reduced to around 30–40 mmHg at the point of entry into capillaries and then becomes approx. 10 mmHg at the venous end of the capillaries.

The speed of the advancing pressure wave during each cardiac cycle far exceeds the actual blood flow velocity. In the aorta, the pressure wave speed may be 15 times faster than the flow of blood. In an end artery, the pressure wave velocity may be as much as 100 times the speed of the forward blood flow.

As the pressure wave moves peripherally through the arterial tree, wave reflection, refraction, and interference distort the pressure waveform, causing an exaggeration of systolic and pulse pressures. This enhancement of the peripheral pulse pressure can cause the systolic blood pressure in the radial artery to be 20–30 % higher than the aortic systolic blood pressure and the diastolic blood pressure to be approx. 10–15 % lower than the aortic diastolic blood pressure. Importantly, the mean blood pressure in the radial artery will closely correspond to the mean aortic arterial pressure.

18.2 Methods of Measuring Blood Pressure

Arterial blood pressure can be measured both noninvasively and invasively, as described in the following sections.

18.2.1 Noninvasive Methods

18.2.1.1 Palpation

Palpation is a relatively simple and easy method for assessing systolic blood pressure. For example, a blood pressure cuff containing an inflatable bladder is applied to the arm and inflated until the arterial pulse felt distal to the cuff disappears. Pressure in the cuff is then released at a speed of approx. 3 mmHg per heartbeat until an arterial pulse is felt again. The pressure at which the arterial pulsation can be detected is the systolic blood pressure; diastolic blood pressure and mean arterial pressure cannot be readily estimated using this method. Furthermore, the systolic blood pressure measured using the palpation method is typically an underestimation of the true arterial systolic blood pressure, i.e., because of insensitivity of one's sense of touch and the relative delay between blood flow below the cuff and the appearance of arterial pulsations distal to the cuff.

18.2.1.2 Doppler Method

The Doppler method for blood pressure measurement is a modification and improvement of the palpation method. It uses a sensor Doppler probe to determine blood flow distal to the blood pressure cuff. The *Doppler effect* represents a shift in the frequency of a sound wave when a transmitted sound is reflected back from a moving object. Such a sound wave shift (e.g., caused by blood movement in an artery) is detected by a Doppler monitor and presented as a specific swishing sound. The pressure in the cuff, at which blood flow is detected by the Doppler probe, is the systolic arterial blood pressure. Doppler-assisted blood pressure measurement is more accurate and less subjective in estimating systolic blood pressure, compared to the palpation method. Using Doppler for blood pressure assessment is quite useful for patients in shock and patients in low-flow states, as well as obese and pediatric (very young) patients. Disadvantages of the Doppler method include: (1) an inability to detect the diastolic blood pressure, (2) a necessity for sound-conducting gel between the skin and the probe (air is a poor conductor of ultrasound), (3) the likelihood of a poor signal if the probe is not applied directly over an artery, and/or (4) the potential for motion and electrocautery artifacts.

18.2.1.3 Auscultation (Riva-Rocci Method)

The auscultation method uses a blood pressure cuff placed around an extremity (usually an upper extremity) and a stethoscope placed above a major artery just distal to the blood pressure cuff (e.g., the brachial artery if using the cuff on the upper extremity). Inflation of the blood pressure cuff above the patient's systolic blood pressure flattens the artery and stops blood flow distal to the cuff. As the pressure in the cuff is released, the artery becomes only partially compressed, which creates conditions for turbulent blood flow within the artery and produces the so-called *Korotkoff* sounds, named after the individual who first described them. Dr. Nikolai Korotkoff first described these sounds which are caused by the vibrations created when blood flow in the partially flattened artery transforms from laminar into turbulent, and this state persists as long as there is a turbulent flow within the vessel. Systolic blood pressure is determined as the pressure of the inflated cuff at which Korotkoff sounds are first detected. Diastolic blood pressure is determined as the cuff pressure at which Korotkoff sounds become muffled or disappear.

Sometimes, in patients with chronic hypertension, there can be an auscultatory gap that represents disappearance of the normal Korotkoff sounds in a wide pressure range between the systolic and diastolic blood pressures. This condition will lead to an inaccurately low blood pressure assessment. Korotkoff sounds can also be difficult to detect in patients who are in shock, low cardiac output states, or in those with marked peripheral vasoconstriction. Increased systemic vascular resistance decreases vibration and decreases sound formation. Low systemic vascular resistance also leads to inaccurate readings as there is intermittent blood flow in the vessel. The use of microphones and electronic sound amplification can greatly increase the sensitivity of this method. Yet, considerations for systematic errors include motion artifact and electrocautery interference.

18.2.1.4 Oscillometry

Oscillometry is a noted method for blood pressure measurement which employs an automated blood pressure cuff. Arterial pulsations cause pressure oscillations in a cuff placed over an extremity. These oscillations are at their maximum when the cuff pressure equals the mean arterial pressure and decrease significantly when the cuff pressure is above the systolic blood pressure or below the diastolic blood pressure. Advantages of this approach include the ease and reliability of use; some of the potential technical problems include motion artifacts, electrocautery interference, and inability to measure accurate blood pressure when patients experience arrhythmias.

When selecting a blood pressure cuff for noninvasive blood pressure measurement, it is important to select the cuff in accordance with the given patient's size; blood pressure cuffs for adult and pediatric patients come in variable sizes. An appropriate size means that the cuff's bladder length is at least 80 % and the cuff width is at least 40 % of the patient's arm circumference. If the cuff is too small, it will need to be inflated to a greater pressure to completely occlude the arterial blood flow, and the measured pressure can be falsely elevated. On the other hand, if the cuff is too large, the pressure inside the cuff needed for complete occlusion of the arterial blood flow will be less, and the measured pressure will likely be falsely low.

Blood pressure is most commonly taken while the patient is seated with the arm resting on a table and slightly bent, which will typically position the patient's arm at the level of his/her heart. This same principle should be applied if the patient is in a supine position; the blood pressure cuff should be level with the patient's heart. If the location of the blood pressure cuff during blood pressure measurement is above or below the patient's heart level, measured blood pressure will be either falsely lower or higher than the actual pressure. This difference can be represented as the height of a column of water interposed between the level of the blood pressure cuff and the level of the patient's heart. To convert centimeters of water (cm H_2O) to millimeters of mercury, the measured height of the water column should be multiplied by a conversion factor of 0.74 (1 cm $H_2O = 0.74$ mmHg).

All of the aforementioned methods for assessing blood pressure do so indirectly, by registering blood flow below a blood pressure cuff. Other noninvasive methods include plethysmography and arterial tonometry.

18.2.1.5 Plethysmography

The plethysmographic method for blood pressure assessment employs the fact that arterial pulsations cause a transient increase in the blood volume of an extremity and thus in the volume of the whole extremity. A finger plethysmograph determines the minimum pressure needed by a finger cuff to maintain constant finger blood volume. A light-emitting diode and a photoelectric cell are used to detect changes in the relative finger volume; this information is, in turn, used to rapidly adjust the cuff pressure. Data can be displayed as a beat-to-beat tracing. Thus, in healthy patients and those who are vasodilated, the blood pressure measured on a finger will correspond to the aortic blood pressure. This method allows for continuous noninvasive blood pressure measurement and, in addition, can provide information regarding pulse pressure and stroke volume variations (SVVs). Importantly, this relationship does not hold true for patients with low peripheral perfusion, such as those with peripheral artery disease, hypothermia, and/or patients in low-flow states.

18.2.1.6 Arterial Tonometry

Tonometry devices can be used to determine beat-to-beat arterial blood pressure by adjusting the pressure required to partially flatten a superficial artery located between a tonometer and a bony surface (e.g., radial artery). These devices commonly consist of an electronic unit and a pressure-sensing head. The system includes an adjustable air chamber and an array of independent pressure sensors that, when placed directly over the artery, assess intraluminal arterial pressures. The resultant pressure records resemble invasive arterial blood pressure waveforms. Yet, limitations to this method include motion artifacts and the need for frequent calibration.

18.2.2 Invasive Methods of Blood Pressure Measurement

18.2.2.1 Indications

Indications for using direct blood pressure monitoring (arterial cannulation) include consistent hemodynamic instability, intraoperative monitoring in selected patients, and use of vasoactive drugs such as dopamine, epinephrine, and norepinephrine. Invasive arterial blood pressure allows for beat-to-beat measurement of blood pressure as well as a method to access arterial blood supply.

18.2.2.2 Cannulation Sites

Arteries most often selected for direct cannulation are the radial, ulnar, brachial, femoral, dorsalis pedis, or axillary. Cannulation of an artery should be avoided if there is: (1) a considered lack of appropriate collateral circulation, (2) a skin infection on or near the site of cannulation, and/or (3) a known preexisting vascular deficiency (e.g., Raynaud's disease). The radial artery is the most often selected artery for invasive blood pressure monitoring because of easy access, superficial location, and good collateral flow to the anatomic region it supplies.

18.2.2.3 Techniques

There are three techniques for arterial cannulation: (1) a catheter over a needle, (2) the *Seldinger's* technique, and (3) real-time ultrasound guidance. When using the catheter over a needle technique, the operator enters a selected artery with a needle over which a catheter has been placed. After free blood flow through the needle, the catheter is advanced over the needle and into the artery, after which the needle is withdrawn. The catheter is then connected to a pressure-transducing system. When using the Seldinger's technique, the operator first enters the artery with a needle. After confirmation of free blood flow through the needle, the operator places a steel wire into the artery and withdraws the needle. A plastic catheter is then advanced into the artery over the wire, and then the wire is removed and the catheter is connected to a transducer system. Real-time ultrasound guidance requires the use of a high-frequency transducer to visualize the artery and needle. One can use either the catheter over needle or Seldinger's technique with the ultrasound to aid in the placement of the catheter. All three methods require sterile techniques and skilled operators.

18.2.2.4 Considerations

Invasive arterial pressure monitoring systems include a catheter (20 gauge for adults and 20–24 gauge for pediatric patients), tubing, a transducer, and an electronic monitor for signal amplification, filtering, and analysis. Such pressure transducers are commonly based on the strain gauge principle—stretching a wire of silicone crystal changes its

electrical resistance. The catheter, the connective tubing, and the transducer are prefilled with saline, and the use of a pressure bag provides continuous saline flush of the system at a typical rate of 3–5 mL/h. These systems should also allow for intermittent bolus flushes.

Quality of information gathered using an invasive blood pressure monitoring depends on the dynamic characteristics of the whole system. For example, the complex waveform obtained from the arterial pulse can be expressed as a summation of simple sine and cosine waves using Fourier analysis. Most invasive blood pressure monitoring systems are designed to have natural frequencies of approx. 16–24 Hz, slightly exceeding the frequency of the arterial pulse waveform in order to reproduce it correctly. This natural frequency is described as that at which the system oscillates when disturbed. Another property of the catheter-tubing-transducer system is its dumping coefficient, characterizing how quickly oscillations in the system will spontaneously decay.

In a given case, both the natural frequency and the dumping coefficient are primarily determined by the length, size, and compliance of the catheter and tubing employed, as well as by the presence of any air bubbles or blood clots that may be trapped in the tubing. This chapter is not intended to go into details about how to determine and change the system characteristics but briefly describe how artifacts can be induced (e.g., underdamping the system will exaggerate artifacts). Further, a catheter whip can result in a significant overestimation of the systolic blood pressure. Likewise, overdamping will blunt the response of the catheter-tubing-transducer system and lead to an underestimation of the systolic blood pressure. In addition, systems with a low natural frequency will show amplifications of the pressure curves, thus causing overestimation of the systolic blood pressure. Diastolic blood pressure will also be affected by altering the abovementioned factors but to a lesser degree. Note that system response characteristics can be optimized by using short, low-compliance tubing and by avoiding air trapping by using a flushing system.

When an invasive blood pressure system is connected to a patient, it should be zero referenced and calibrated. Zero referencing is performed by placing the transducer at the level of the midaxillary line, which corresponds to the level of the patient's heart when the patient is supine. The system is then opened to air, closed to the patient, and adjusted to a 0 mmHg baseline. Note that for proper zero referencing, it is not necessary for the transducer to be at the level of the patient's heart as long as the stopcock, which is opened to air during zero referencing, is at that level. The system is then directed to record from the patient and thus is ready for use.

System calibration is a separate procedure and involves connecting the invasive blood pressure system to a mercury manometer, closing the system to the patient, and pressurizing it to certain predetermined pressures. The gain of the monitor amplifier is then adjusted until displayed pressure equals the pressure in the mercury manometer. Recommendations are to perform zero referencing at least once on every clinical shift and this type of calibration at least once daily. It should be noted that some of the more contemporary transducer designs rarely require external calibration.

When connected to a patient, today's invasive blood pressure monitoring systems provide digital readings of systolic, diastolic, and mean blood pressures and pressure waveforms. Watching the trend of a waveform and its shape can provide other important information as well. More specifically, the top of the waveform represents the peak systolic blood pressure, and the bottom is the diastolic blood pressure. The dicrotic notch is caused by the closure of the aortic valve and backsplash of blood against the closed valve. The anacrotic notch is rarely seen distal to aortic root cannulation and thus is not useful in invasive blood pressure management. The rate of the upstroke of the arterial blood pressure wave depends on the myocardial contractility, whereas the rate of the downstroke is affected by the systemic vascular resistance. As the arterial waveform progresses down the arterial system, a steeper upstroke and decreased diastolic blood pressure are observed. This is due to the loss of kinetic energy as the wave travels down the arterial system as well as the change in elasticity in the arterial walls.

Importantly, exaggerated variation in the size of the waves with respiration typically suggests hypovolemia. Thus, the trained eye can gain insight about a patient's cardiovascular status by evaluating aspects of this signal. Integrating the area under the waveform can be used for calculating the mean arterial pressure. Various invasive arterial line systems now perform arterial pressure waveform analysis in addition to calculating the mean arterial pressure. These systems allow for continuous cardiac output monitoring and also measurement of SVV, pulse pressure variation (PPV), and systolic pressure variation. Both SVV and PPV are excellent indicators of volume responsiveness. These systems use different methods of analyses which include: pressure recording analytical method, pulse power analysis, and pulse contour analysis. Despite these advances in arterial pressure waveform analyses, there are disadvantages to using such a system in that: (1) some require calibration or a central venous cannula to be placed; (2) some are inaccurate in patients with arrhythmias, hemodynamic instability, and/or the presence of ventricular assist devices and balloon pumps; and (3) some rely on an accurate arterial waveform to produce accurate information.

18.2.2.5 Complications

Potential complications associated with arterial cannulation include bleeding, hematoma, infection, thrombosis, ischemia distal to the cannulation site, vasospasm, embolization with air bubbles or blood clots, nerve damage, pseudoaneurysm formation, atheroma, and/or inadvertent intra-arterial drug injection.

18.3 Diagnoses

18.3.1 Pulsus Paradoxus

Normally, the arterial and venous blood pressures fluctuate throughout the respiratory cycle, decreasing with inspiration and rising with expiration. Yet, this fluctuation in the blood pressure under normal conditions is less than 10 mmHg. Inspiration increases venous return, therefore increasing the right heart output transiently, according to the Frank–Starling law. As the blood is sequestered in the pulmonary circulation during inspiration, the left heart output is reduced and is expressed as a lower systolic blood pressure. The right ventricle contracts more vigorously and mechanically bulges the interventricular septum toward the left ventricle, reducing its size and accounting for even lower systolic blood pressure. *Pulsus paradoxus* is defined as an inspiratory decrease of systolic blood pressure by more than 10 mmHg.

Certain conditions drastically reduce the transmural or distending (filling) pressure of the heart and interfere with the diastolic filling of the ventricles. In such cases, there is typically an exaggeration of the inspiratory fall in the systolic blood pressure, which results from reduced left ventricular stroke volume and the transmission of the negative intrathoracic pressure to the aorta. Common causes for such reduction include pericardial effusion, adhesive pericarditis, cardiac tamponade, pulmonary emphysema, severe asthma, paramediastinal effusion, endocardial fibrosis, myocardial amyloidosis, scleroderma, mitral stenosis with right heart failure, tricuspid stenosis, hypovolemia, and/or pulmonary embolism. Associated clinical signs include a palpable decrease in pulse with inspiration and decrease in the inspiratory systolic blood pressure of more than 10 mmHg compared to the expiratory pressure. On clinical examination, one can detect extra beats on cardiac auscultation during inspiration, when compared to a peripheral pulse. This may also be observed on an invasive arterial waveform.

18.3.2 Pulsus Alternans

Pulsus alternans is an alternating weak and strong peripheral pulse, caused by alternating weak and strong heart contractions. A weak contraction will decrease the ejection fraction, hence increasing the end-diastolic volume (the volume of blood remaining in the ventricle after a weak heart contraction). As a result, in the next cardiac cycle, the heart will be stretched more; according to the Frank–Starling mechanism, this will then generate higher pressures and a stronger perceived pulse. Pulsus alternans may be found in patients with severe heart failure, various degrees of heart block, alterations in calcium, and/or arrhythmias. Pulsus alternans is characterized by a regular rhythm and must be distinguished from pulsus bigeminus, which is an irregular heart rate (see below). One may observe an alteration in the amplitude of the peak systolic pressure on the invasive arterial waveform.

18.3.3 Bigeminal Pulse

A *bigeminal pulse* is caused by occurrences of premature contractions (usually ventricular) after every other heartbeat, resulting in an alternation in the relative pulse strength. Bigeminal pulse can often be confused with pulsus alternans. However, in contrast to the latter in which the rhythm is regular, in pulsus bigeminus the weak beat always follows a shorter pulse interval; thus there is an arrhythmia.

18.3.4 Pulse Deficit

Pulse deficit is the inability to detect some arterial pulsations when the heart beats, as can be observed in patients with atrial fibrillation, in states of shock, or with premature ventricular complexes. The easiest way to detect pulse deficit is to place a finger over an artery while monitoring the QRS complexes on an electrocardiogram monitor. A QRS complex without a detected corresponding pulse represents a pulse deficit. In the presence of atrioventricular dissociation, when atrial activity is irregularly transmitted to the ventricles, the strength of the peripheral arterial pulse depends on the relative timing of the atrial and ventricular contractions. In a patient with rapid heartbeats, the presence of such variations suggests ventricular tachycardia. With an equally rapid rate, an absence of variation of pulse strength suggests a supraventricular mechanism. See Chaps. 13 and 28 for an additional description of arrhythmias.

18.3.5 Wide Pulse Pressure

Wide pulse pressure, often called *water hammer pulse*, is observed in cases of severe aortic regurgitation and consists of an abrupt upstroke (percussion wave) because the left ventricle receives increased blood volume and then is followed by a rapid collapse later in systole with no dicrotic notch.

18.3.6 Pulsus Parvus Et Tardus

The phenomenon of *pulsus parvus (small) et tardus (late)* is observed in cases of aortic stenosis and is caused by reduction in stroke volume and prolonged ejection phase, producing reductions and delays in the volume increments inside the aorta. “Tardus” refers to delayed or prolonged early systolic acceleration, while “parvus” refers to diminished amplitude and rounding of the systolic peak.

18.3.7 Bisferiens Pulse

A *bisferiens (biphasic) pulse* is characterized by two systolic peaks—the percussion and tidal waves—separated by a distinct midsystolic dip. The peaks are often equal, or one may be larger. Bisferiens pulse occurs in conditions in which a large stroke volume is ejected rapidly from the left ventricle and is observed most commonly in patients with either pure aortic regurgitation or with a combination of aortic regurgitation and stenosis. A bisferiens pulse can also be elicited by patients with hypertrophic obstructive cardiomyopathy. In these patients, the initial prominent percussion wave is associated with rapid ejection of blood into the aorta during early systole, followed by a rapid decline as the obstruction becomes prominent in midsystole, followed by a tidal wave. Very rarely, bisferiens pulse occurs in individuals with a normal heart.

18.3.8 Dicrotic Pulse

Not to be confused with a bisferiens pulse, in which both peaks occur in systole, the *dicrotic pulse* is characterized by a second peak positioned in diastole immediately after the second heart sound. The normally small wave that follows aortic valve closure (dicrotic notch) is exaggerated and measures more than 50 % of the pulse pressure on direct pressure recordings. A dicrotic pulse usually occurs in conditions such as cardiac tamponade, severe heart failure, and hypovolemic shock, in which a low stroke volume is ejected into a soft elastic aorta. Rarely, a dicrotic pulse can be noted in healthy adolescents or young adults.

18.4 Heart Tones

18.4.1 Physiology and Normal Heart Sounds

The primary heart tones are caused by vibrations created by pressure differentials during closure of the heart valves. Normal valve opening is relatively slow and makes little or no audible sound. In general, heart tones are brief and characterized by varying intensities (loudness), frequencies (pitch), and qualities (timbre). To understand heart tones better, let us briefly review the physiology of the cardiac cycle. The electric impulse for cardiac contraction starts from the sinus node located in the right atrium, thus causing the right atrium to contract first. Contraction of the ventricles begins with the left ventricle, resulting in mitral valve closure slightly before closure of the tricuspid valve. Ejection, on the other hand, starts in the right ventricle, because the right ventricular ejection normally occurs at a much lower pressure than the left ventricular ejection. Yet ejection ends first in the left ventricle, causing the aortic valve to close slightly before the pulmonic valve.

The first heart sound (S1) arises from closure of the mitral valve (M1) and shortly thereafter by closure of the tricuspid valve (T1). There is some evidence that the first heart sound (S1) is due to the movement of blood in early systole and is due to the peak rate of rise of left ventricular systolic pressure. The initial component of the first heart sound (M1) is most prominent at the cardiac apex and occurs just before the upstroke of the carotid pulse. The second component (T1), when detected, normally presents at the left lower sternal border; it is less commonly heard at the apex and is seldom heard at the base. When the first heart sound noticeably splits, like in Ebstein's anomaly (often associated with delayed right ventricular activation), its first component is normally louder.

As mentioned previously, the intensity of heart sounds will increase with increases in pressure gradients across a particular valve. With an increasing pressure gradient, the blood velocity and the resultant force causing valve closure will increase, producing louder and more easily detectable sounds. Another factor affecting the intensity of the sound produced by an atrioventricular valve is the valvular position at the onset of systole. Note that when ventricular contraction occurs against a wide open valve, the leaflets will achieve higher velocity, and thus the heart sound will be louder compared to a sound produced by a valve with partially closed leaflets at the beginning of systole.

The second heart sound (S2) is caused by closure of the aortic and the pulmonic valves. Normally the first component of this second heart sound is caused by the aortic valve closure (A2), followed shortly thereafter by the pulmonic valve closure (P2).

The physiological third heart sound (S3) (Fig. 18.1) occurs shortly after A2 and is a low-pitched vibration caused by rapid ventricular filling during diastole. Physiological S3

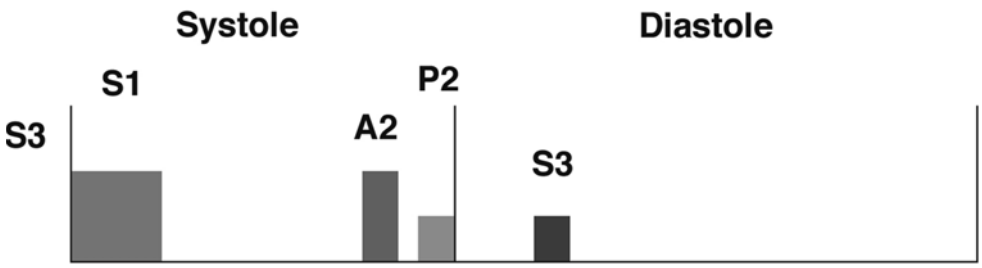

Fig. 18.1 Third heart sound (see text for details). *A2* aortic valve closure, *P2* pulmonic valve closure, *S1* first heart sound, *S3* third heart sound

sounds can commonly be heard in children, adolescents, and young adults. When detected after 30 years of age, S3 is referred to as *ventricular gallop* and is considered a sign of possible cardiac pathology. In most of the S3 ventricular gallop cases, there is diastolic dysfunction associated with ventricular failure. Normal third heart sounds sometimes persist beyond 40 years of age and are more commonly found in women.

The physiological fourth heart sound (S4) (Fig. 18.2) is typically soft and low pitched and best heard in late diastole just before S1. S4 is generated by rapid ventricular filling during atrial systole, causing vibrations of the left ventricular wall and the mitral apparatus. Normally, S4 is primarily heard in infants, small children, and adults over the age of 50 years. A loud S4, which can be associated with shock, is considered as a pathological sign and is referred to as a *S4 gallop*.

18.4.2 Auscultatory Areas

Heart sounds generated by different valves are best heard over certain auscultatory areas, which bear the valve names of (but do not specifically correspond to) the exact anatomical locations of the valves.

The aortic auscultation area is located over the second intercostal space at the right sternal border (Fig. 18.3). The pulmonic auscultation area is located in the second intercostal space at the left sternal border. The mitral auscultation area is just over the heart's apex, located in the fifth intercostal space, left of the sternum; this area is also called a left ventricular or apical area. The tricuspid auscultation area is located at the left lower sternal border. For patients with a left thoracic heart position (normal situs), auscultation should begin at the cardiac apex and continue with the left

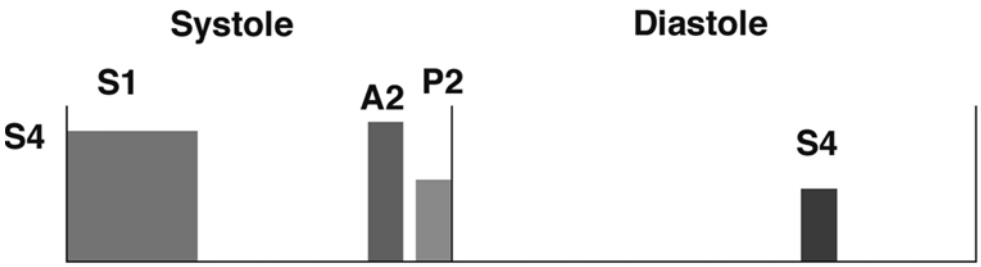

Fig. 18.2 Fourth heart sound (see text for details). *A2* aortic valve closure, *P2* pulmonic valve closure, *S1* first heart sound, *S4* fourth heart sound

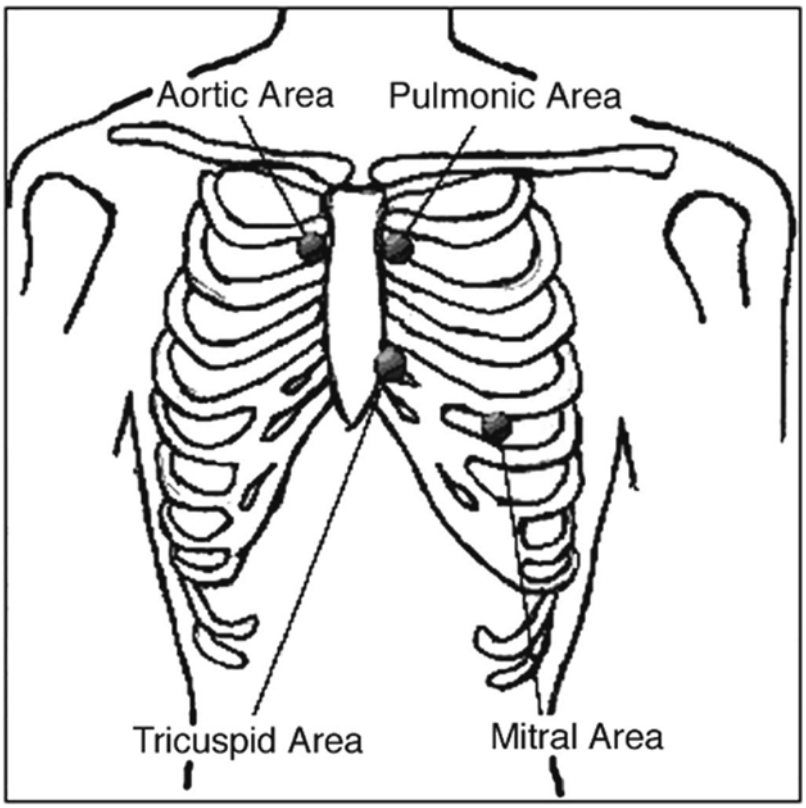

Fig. 18.3 Auscultatory areas, including the aortic, pulmonic, mitral, and tricuspid auscultation areas

lower sternal border (following the inflow), and then the session should proceed interspace after interspace, up the left sternal border, up to the left myocardial base, and then move to the right base (outflow). This type of examination permits clinicians to think physiologically, i.e., following the inflow–outflow direction of the blood flow.

To most easily distinguish between the first and second heart sounds, one should take into account that there is a longer pause between S2 and S1 than between S1 and S2, caused by the fact that systole is shorter than diastole. S1 is also of longer duration and lower pitch, compared to the shorter duration and higher pitch of S2. In general, S1 is best heard at the heart's apex, and S2 is best auscultated over the aortic and pulmonic areas.

The normal heart sounds represent naturally occurring phenomena in a healthy heart, whereas cardiac pathologies can change the intensity and/or the timing of the occurrence of sounds and/or even create new ones, often called *murmurs*.

18.4.3 Abnormal Heart Sounds

Conditions that accentuate S1 sounds include mitral stenosis (most often), left-to-right shunts, hyperkinetic circulatory states, accelerated atrioventricular conduction, and/or tricuspid stenosis. A diminished S1 can be caused by mitral and tricuspid stenosis, moderate or severe aortic regurgitation, slow atrioventricular conduction, and/or hypocontractility states. A diminished S1 sound can also be observed in patients with thick chest walls, such as in individuals with excessively developed body musculature, obese patients, or in patients with emphysema.

Variability in the S1 sound can be observed in states causing variation in the velocity of atrioventricular valve closure, such as ventricular tachycardia, atrioventricular block, ventricular pacemakers, atrial fibrillation, and so on. An accentuated S2 is commonly detected in patients with: (1) diastolic or systolic hypertension, (2) aortic coarctation, (3) aortic dilation, (4) atherosclerosis of the aorta, and/or (5) pulmonary hypertension which is characterized by a loud pulmonary component of the second heart sound. A diminished S2 sound is detected most often in aortic valvular stenosis, pulmonic stenosis, and/or pulmonary emphysema.

Some degree of the splitting of the S2 sound can be normally heard during inspiration. Yet, abnormal or persistent S2 splitting is clinically associated with: (1) delayed activation of the right ventricle; (2) prolonged right ventricular ejection time relative to left ventricular ejection time, like in pulmonic stenosis, mitral regurgitation, or ventricular septal defect; or (3) increased impedance of the pulmonary vasculature, as in massive pulmonary embolism or pulmonary hypertension. Persistent S2 splitting may also be observed in cases in which the aortic and pulmonic components of the second heart sound remain audible during both inspiration and expiration. This type of persistent splitting is often caused by a delay in the pulmonary component, such as that occurring in complete right bundle branch block, but it can also be caused by an early timing of the aortic component often associated with mitral insufficiency. Changes in the duration of the split interval (greater with inspiration, lesser with exhalation) in the presence of both components define the split as persistent and not fixed.

Fixed splitting of S2 is commonly found in patients with atrial septal defect, severe pulmonic stenosis, or right ventricular failure. S2 fixed splitting is characterized by wide and persistent intervals between the aortic and pulmonary components, remaining unchanged during the respiratory cycle.

Paradoxical splitting refers to a reversed sequence of the semilunar valve (aortic and pulmonic) closures, with the pulmonary component (P2) preceding the aortic component (A2). Paradoxical splitting of S2 is caused by a delay in the A2, varying with the inspiratory cycle and can be caused by: (1) a complete left bundle branch block, (2) premature right ventricle contractions, (3) ventricular tachycardia, (4) severe aortic stenosis, (5) left ventricular outflow obstruction, (6) hypertrophic cardiomyopathy, (7) coronary artery disease, (8) myocarditis, and/or (9) congestive cardiomyopathy.

Normally, blood flow in the heart is laminar and does not produce vibrations. *Murmurs* are created whenever there is a pathology causing increased turbulent flow, often associated with abnormal shunts, obstructions, or even the reversing of flow. In other words, turbulent flow within the heart creates vibrations that can be heard as murmurs. The various murmurs are described both on the basis of appearance in relation to the cardiac cycle and on the basis of changes in features such as intensity (loudness), frequency (pitch), configuration (shape), quality, duration, and/or direction of radiation. For example, intensity or loudness can be graded from 1 to 6. Based on time of existence relative to the cardiac cycle, murmurs are classified as systolic, diastolic, or continuous. Depending on their life cycle during systole or diastole, they are further subclassified into early-, mid-, and late-systolic or diastolic murmurs such that:

- Early systolic murmur begins with S1 and ends before the midsystole.
- Midsystolic murmur starts after S1 and ends before S2.
- Late systolic murmur begins in the middle of systole and ends at S2.
- Holosystolic murmur starts with S1 and continues for the duration of the whole systole.
- Early diastolic murmur begins with S2.
- Middiastolic murmur begins after S2.
- Late diastolic murmur begins just before S1.
- Continuous murmur continues during both systole and diastole.

Based on changes in intensity, murmurs are commonly described as: (1) crescendo, increasing in intensity; (2)

decrescendo, decreasing in intensity; (3) crescendo–decrescendo, when the intensity of the murmur first increases and then decreases; or (4) plateau, the intensity of the murmur remains constant.

18.4.4 Dynamic Auscultation

The term dynamic auscultation refers to a technique of adjusting circulatory dynamics by means of respiration or various other planned physiological or pharmacological maneuvers and then determining their effects on the dynamics of the heart sounds and murmurs. Commonly altered variables that can affect sound and murmurs include: (1) changes in venous return affecting cardiac preloads, (2) changes in systemic vascular resistance, (3) changes in contractility, (4) changes in heart rate or rhythm, and/or (5) maneuvers affecting pressure gradients within the heart. To date, diagnostic maneuvers frequently used for altering heart sounds include inspiration, expiration, exercise level, or body position (e.g., recumbent position, left semilateral position, standing up, sitting up, or leaning forward).

In general, spontaneous inspiration causes decreased intrathoracic pressure, increased venous return, increased right ventricular preload, and decreased pulmonary vascular resistance. Thus, modifying inspiration is used to increase the intensity of S3 and S4 gallops, tricuspid and pulmonic stenoses or regurgitation murmurs, or mitral and tricuspid clicks. Inspiration also causes some degree of splitting of S2, caused by prolonged right ventricular ejection. In contrast, expiration causes just the opposite—decreased venous returns (preloads) and decreased right-sided flows. Note that sounds and murmurs originating on the left side of the heart tend to be accentuated during expiration.

In addition, changes in a patient's positioning can affect heart sound intensity; this is caused by relative changes of ventricular preload, ventricular size, and movement of the heart closer to or farther from the chest wall. A recumbent position typically accentuates murmurs of mitral and tricuspid stenoses. Similarly, a left semilateral position accentuates left-sided S3 and S4, mitral opening snaps, and mitral regurgitation murmurs. Standing will affect general hemodynamics by pooling blood in the lower extremities and decreasing heart filling pressure and ventricular size. Thus, standing up is clinically used to accentuate mitral and tricuspid clicks. Sitting up accentuates tricuspid valve opening snaps, and sitting up and leaning forward are the best maneuvers for enhancing murmurs due to aortic and pulmonic regurgitation or aortic stenoses. Exercise causes increases in heart rate, shortens diastole, elevates left atrial pressure, and shortens the time for closure of the heart valves. Hence, physiological changes during exercise increase amplitude of S1, S2, S3, and S4, mitral opening snap, existing mitral regurgitation or stenosis, and/or patent ductus arteriosus murmur.

Two other pathological sounds, heard when auscultating the heart, are *clicks* and *opening snaps*. Clicks are caused by the rapid movement of valvular structures. Systolic clicks are referred to as ejection or nonejection clicks, depending on their timing relative to systole. Ejection clicks, occurring early in systole, commonly indicate semilunar valve anomalies and, in rare conditions, great vessel lesions. Nonejection clicks are heard in mid- to late systole and represent mitral (more often) or tricuspid valve prolapses. In contrast, a tricuspid valve opening snap is often heard when there is tricuspid valve stenosis and in conditions associated with increased blood flow across the tricuspid valve (e.g., presence of large atrial septal defect). Similarly, a mitral valve opening snap is caused by elevated left atrial pressure, resulting in rapid valve opening to the point of maximum excursion. Mitral valve opening snap is often associated with mitral stenosis and less often with a ventricular septal defect, second- or third-degree atrioventricular block, patent ductus arteriosus, and hyperthyroidism. The mitral valve opening snap is similar in quality to normal heart sound and is often clinically confused with a splitting of S2.

18.4.5 Specific Murmurs

The murmur caused by aortic stenosis (Fig. 18.4) is characterized as a holosystolic crescendo–decrescendo murmur which is best heard at the aortic auscultation area. The high-velocity jet within the aortic root results in radiation of the murmur upward, to the right second intercostal space, and further into the neck. Although this murmur when heard in the second right intercos-

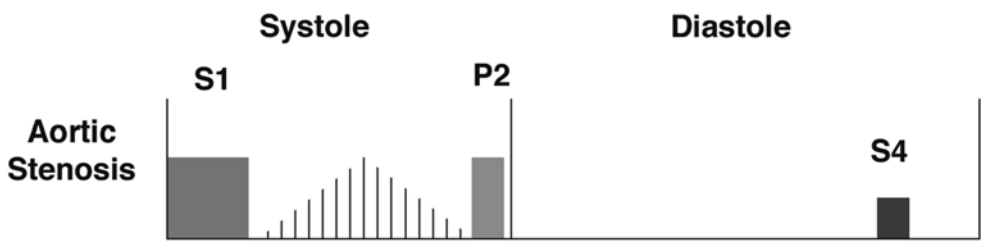

Fig. 18.4 Aortic stenosis murmur caused by stenotic aortic valve. Normally a holosystolic crescendo–decrescendo murmur is best heard at the aortic auscultatory area. *P2* pulmonic valve closure, *S1* first heart sound, *S4* fourth heart sound

tal space is typically harsh, noisy, and impure, the same murmur heard when auscultating over the left apical area can be pure and often considered musical. The harsh *basal murmur* is believed to be caused by vibrations created when high-velocity blood jets are ejected through the aortic root. The musical second component of the aortic stenosis murmur originates from periodic high-frequency vibrations of the fibrocalcific aortic cusps and can be quite loud and heard even from a distance without an auditory aid. Murmurs of aortic stenosis are accentuated by expiration, sitting up, and/or leaning forward. The high-frequency apical midsystolic murmur of aortic stenosis should be distinguished from the high-frequency apical murmur of mitral regurgitation, a distinction that may be difficult or even impossible to detect, especially if the aortic component of the second heart sound is soft or absent. In such patients, echocardiography will likely be required to determine the relative cardiac pathophysiology. See Chap. 22 for more information on echocardiographic methods.

A murmur caused by pulmonary valve stenosis is a characteristic midsystolic murmur originating in the right side of the heart and best auscultated over the pulmonic auscultation area. This murmur begins after the first heart sound, rises to a peak in crescendo, and then decreases in slow decrescendo, finishing before a delayed or soft pulmonary component of the second heart sound. In general, the length and the profile of this murmur depend on the severity of the pulmonary valve obstruction.

The murmur caused by aortic insufficiency (Fig. 18.5) is an early decrescendo diastolic murmur originating in the left side of the heart and best heard over the aortic and pulmonic auscultation areas. This murmur begins with the aortic component of the second heart sound (S2). The intensity and configuration of such a murmur tend to reflect the volume and rate of regurgitant flow. Radiation of this murmur to the right sternal border can signify aortic root dilation, often associated with Marfan's syndrome. In chronic aortic regurgitation, the aortic diastolic pressure always significantly exceeds the left ventricular diastolic pressure, so the decrescendo is subtle, and yet the murmur is well heard throughout diastole. The diastolic murmur of acute severe aortic regurgitation differs from the chronic aortic regurgitation murmur primarily in that the diastolic murmur is relatively short. The short duration of the acute severe aortic regurgitation murmur is due to the fact that aortic diastolic pressure rapidly equilibrates with the rapidly rising diastolic pressure in the nondilated left ventricle. The aortic insufficiency murmur is accentuated during expiration, sitting up, or leaning forward.

A pulmonary regurgitation murmur is an early diastolic murmur originating from the right side of the heart. In this case, the second heart sound is often split with the murmur proceeding from its latter part; it is loud because of relatively high transvalvular pressure. The high pulmonary diastolic pressure generates high-velocity regurgitant flows resulting in a high-frequency blowing murmur that may last throughout diastole. Because of the persistent and significant differences between the pulmonary arterial and right ventricular diastolic pressures, the amplitude of this murmur is relatively uniform throughout most of the diastole.

Mitral stenosis murmur (Fig. 18.6) is caused by a stenotic mitral valve and is crescendo–decrescendo holodiastolic by

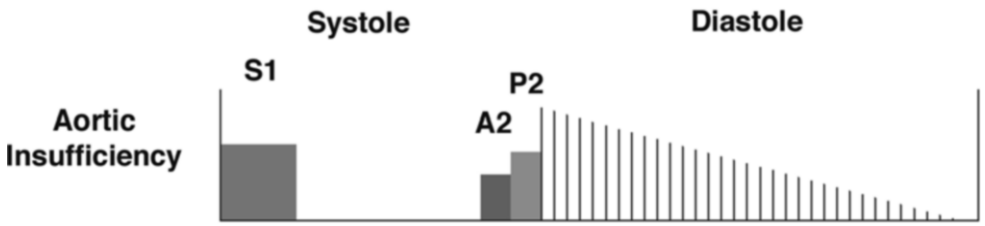

Fig. 18.5 Aortic insufficiency murmur. Early decrescendo diastolic murmur originating in the left side of the heart and best heard over the aortic and pulmonic auscultation areas. *A2* aortic valve closure, *P2* pulmonic valve closure, *S1* first heart sound

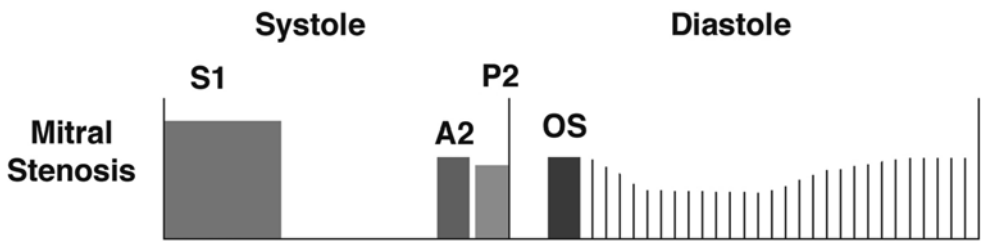

Fig. 18.6 Mitral stenosis murmur. Crescendo–decrescendo holodiastolic murmur, caused by a stenotic mitral valve. Best heard at the mitral auscultation area, this murmur is accentuated by exercise and by assuming a recumbent position. *A2* aortic valve closure, *OS* opening snap, *P2* pulmonic valve closure, *S1* first heart sound

nature. It is heard best at the mitral auscultation area and is typically accentuated both by exercise and assuming a recumbent position. A mitral stenosis murmur that lasts up to the first heart sound, even after long cardiac cycle, indicates that the stenosis is severe enough to generate a persistent gradient even at the end of long diastole.

The murmur caused by tricuspid stenosis is relatively middiastolic in origin and differs from the mitral stenosis middiastolic murmur in two important aspects: (1) the tricuspid stenosis murmur becomes increasingly louder with inspiration; and (2) to best hear this murmur, one auscultates over a relatively localized area along the left lower sternal border. Detectable inspiratory increases in loudness occur because of augmentation of the right ventricular volume, decreases in right ventricular diastolic pressure, and increases of the gradient and flow across the stenotic tricuspid valve. This murmur is best detected over the left lower sternal border, as it originates within the inflow portion of the right ventricle and is then transmitted to the overlying chest wall.

Mitral regurgitation murmurs (Fig. 18.7) are considered to be caused by insufficiencies of the mitral valve and are systolic murmurs best heard at the mitral auscultation area. These murmurs are accentuated by exercise and left semilateral position. Acute severe mitral regurgitation is often accompanied by an early systolic murmur or holosystolic murmur that has a decrescendo pattern, which diminishes or ends before the second heart sound. The physiological mechanism responsible for this early systolic decrescendo murmur is acute severe regurgitation into a relatively normal size left atrium with limited distensibility. In such patients, the regurgitant flow is typically maximal early in systole and reaches minimum by late systole.

Another early systolic murmur is the *tricuspid regurgitation murmur* (Fig. 18.8), which is often associated with infective "endocarditis." The mechanisms responsible for the timing and configuration of this murmur are analogous to those described for mitral regurgitation. It is also a systolic murmur best heard over the tricuspid area and accentuated by inspiration.

The typical murmur associated with an atrial septal defect (Fig. 18.9) is also a systolic murmur which is caused by increased blood flow through the pulmonary valve and thus is best heard over the pulmonic auscultation area. Most often, the atrial septal defect involves the fossa ovalis, which is midseptal in location and is of the ostium secundum type (for more details, see Chaps. 3 and 10). This type of defect is a true deficiency of the atrial septum and should not be confused with a patent foramen ovale. The magnitude of the left-to-right shunt through an atrial septal defect depends on the size of the defect and also the relative compliance of the ventricles, as well as the relative resistances in both the pulmonary and systemic circulations. The increased pulmonary valve flow causes a delay (splitting) of the pulmonic component of the second heart sound.

The murmur associated with a patent ductus arteriosus (Fig. 18.10) is caused by an abnormal continuous turbulent flow through a patent ductus connecting the aorta with the main pulmonary artery. It is also considered a continuous "machinery murmur," heard during both systole and diastole, because aortic pressure is higher than the pressure in the pulmonary artery throughout the cardiac cycle. Other associated clinical findings in patients with patent ductus arteriosus include: bounding peripheral pulse, wide pulse pressure, infraclavicular and interscapular systolic murmurs, precordial hyperactivity, hepatomegaly, bradycardia, episodes of apnea, and/or respiratory insufficiency.

The resultant murmur associated with a ventricular septal defect (Fig. 18.11) is systolic, with its intensity depending on the relative size of the defect. A ventricular septal defect murmur is caused by abnormal blood flow from the left to the right ventricle or from the right to the left ventricle, as in Eisenmenger's syndrome. This latter syndrome is the reversing of the left-to-right shunt in patients with atrial septal defects, ventricular septal defects, or a patent ductus arteriosus; all are caused by increased pulmonary and right-sided pressure, secondary to increased pulmonary blood flow. This murmur is best heard over the mitral auscultation area located over the myocardial apex. Septal defects are commonly treated, sometimes noninvasively, thus eliminating these murmurs. See also Chap. 37.

18.5 Recent Developments

The clinical applications of cardiac auscultation remained the same for centuries until recently, when some companies took auscultation to a whole new level by developing portable electronic stethoscopes. The central idea behind the electronic stethoscope is that human hearing is imperfect and can only detect a small fraction of the vast frequency ranges produced by the human heart. Therefore, recording the entire sound spectrum would provide novel information and thus increase our ability to diagnose pathologies. More specifically, using electronic auscultation, heart sounds can be recorded for: (1) storage, (2) later direct or remote playback, or (3) post-processing (i.e., sending via email, digital amplification, filtering for noise reduction, and/or electronic manipulation for accentuating particular sounds or eliminating noise). They allow the user to listen at various frequencies to better hear specific heart sounds and filter out ambient noise such as lung sounds. Today, electronic stethoscopes can easily record a phonocardiogram, providing visual sound representation. Furthermore, they can be viewed equally well by everyone, thus eliminating errors associated with different hearing levels and/or clinical skills.

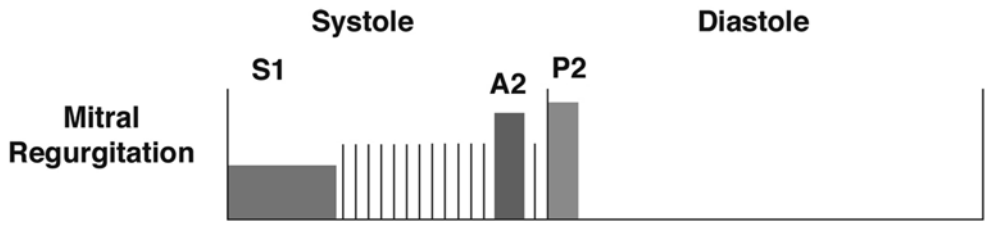

Fig. 18.7 Caused by an insufficiency of the mitral valve, the mitral regurgitation murmur is a systolic murmur best heard over the mitral auscultation area. *A2* aortic valve closure, *P2* pulmonic valve closure, *S1* first heart sound

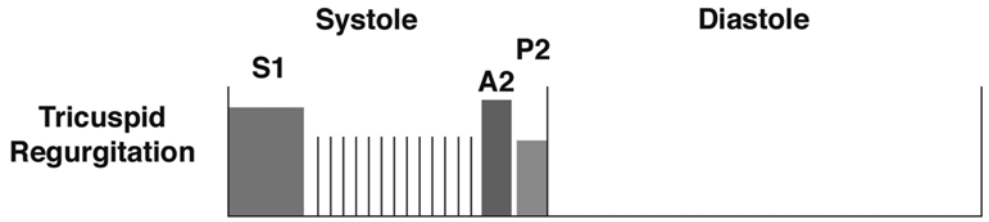

Fig. 18.8 The tricuspid regurgitation murmur is a systolic murmur best heard over the tricuspid area and is accentuated by inspiration. *A2* aortic valve closure, *P2* pulmonic valve closure, *S1* first heart sound

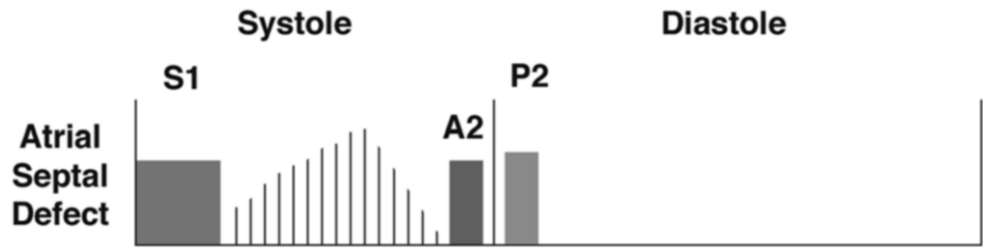

Fig. 18.9 The murmur associated with atrial septal defect is systolic and caused by increased blood flows through the pulmonic valve. Atrial sepal defect murmur is best heard over the pulmonic auscultation area. *A2* aortic valve closure, *P2* pulmonic valve closure, *S1* first heart sound

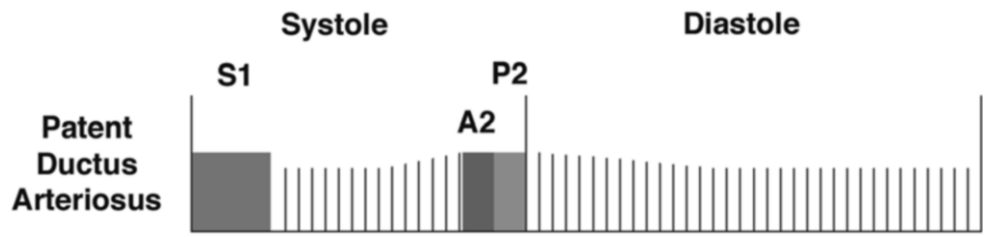

Fig. 18.10 Commonly associated with patent ductus arteriosus, this murmur is caused by a turbulent continuous flow through the ductus connecting the aorta with the main pulmonary artery. *A2* aortic valve closure, *P2* pulmonic valve closure, *S1* first heart sound

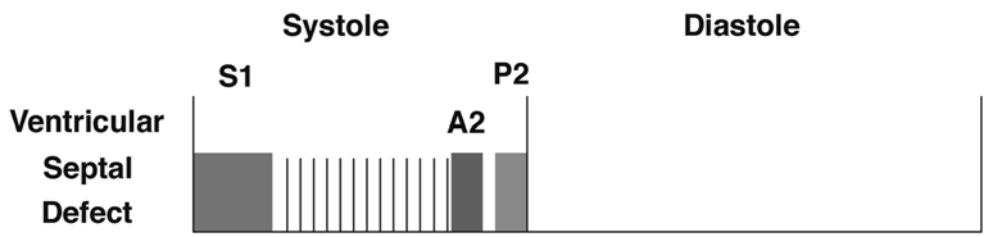

Fig. 18.11 Murmur associated with ventricular septal defect is systolic, caused by blood flow from the left to the right ventricle (or the right to the left ventricle in Eisenmenger's syndrome). *A2* aortic valve closure, *P2* pulmonic valve closure, *S1* first heart sound

Many companies typically employ proprietary technology and software and therefore offer: (1) different filtering capabilities, (2) various modes for presenting information, (3) varied sizes and weights, and/or (4) varied ease of use with some basic diagnostic capabilities. There are several signal processing techniques employed, each providing slight advantages or disadvantages in obtaining different parts of the sound spectrum. For example, Fourier transform, short-time Fourier transform, wavelet transform, and discrete wavelet transform are incorporated sound-processing techniques used in digital stethoscopes. These stethoscopes have also evolved to: (1) be pocket sized, (2) work with any pair of headphones, (3) have the capability to transmit the sound to any tablet or smartphone (for replays), and/or (4) be displayed within a visual waveform format. Nevertheless, the main limitation of digital stethoscopes is the somewhat subjective nature of sound interpretation. Despite the unique quality of heart tones and murmurs, the sounds obtained with digital stethoscopes must still be interpreted by physicians, similar to acoustic stethoscopes. One way to deal with this limitation is to run the digitally obtained and processed sound through an algorithm to identify key parameters and yield relative diagnoses. In the near future, promising technology for achieving this diagnostic approach may be made available through the use of the artificial neural network, i.e., so that input data can be compared against learned data. The potential advantage is that the network is adaptive and able to learn based on information fed to the system during a learning phase. However, this technology is still in development stages.

18.6 Summary

It remains the general consensus that even the most sophisticated electronic monitors cannot fully reduce the need for sound clinical skills like proper patient inspection, palpation, percussion, and/or auscultation. Furthermore, it is important to reinforce the need for a deep understanding of basic physiological principles when interpreting physical examination findings. In general, the application of technologies in this area is viewed as helpful and can speed up decision making, but it cannot replace one's knowledge of basic pathophysiologic mechanisms.

The primary purpose of this chapter was to familiarize the reader with the basic concepts of blood pressure, heart tones, and some common associated diagnoses. It should be noted that many descriptions of the general scientific and clinical principles used in the chapter are simplified for clarity; this is also true for many of the described underlying physiology and pathology mechanisms. By no means is this chapter a complete review of the presented topics. There are many medical books dedicated to each topic, and readers are strongly encouraged to further research sources and review in-depth information of interest.

References

1. Faulconer A, Keys TE (eds) (1993) Foundations of anesthesiology, vol I and II. The Wood Library–Museum of Anesthesiology, Park Ridge
2. McVicker JT (2001) Blood pressure measurement—does anyone do it right?: an assessment of the reliability of equipment in use and the measurement techniques of clinicians. J Fam Plann Reprod Health Care 27:163–164
3. O'Brien E, Pickering T, Asmar R et al (2002) Working group on blood pressure monitoring of the European Society of Hypertension, international protocol for validation of blood pressure measuring devices in adults. Blood Press Monit 7:3–17
4. Kim SH, Lilot M, Sidhu KS et al (2014) Accuracy and precision of continuous noninvasive arterial pressure monitoring compared to invasive arterial pressure. Anesthesiology 120:1080–1097
5. Marik PE (2013) Noninvasive cardiac output monitors: a state of the art review. J Cardiothorac Vasc Anesth 27:121–134
6. Miller RD, Eriksson LI, Fleisher L, Wiener-Kronish JP (eds) (2009) Anesthesia, vol I and II, 7th edn. Churchill Livingstone, New York
7. Barash RG, Cullen BF, Stoelting RK (eds) (2013) Clinical anesthesia, 7th edn. Lippincott Williams & Wilkins, Philadelphia
8. Stoelting RK, Hillier SC (eds) (2005) Pharmacology and physiology in anesthetic practice, 4th edn. Lippincott–Raven, Philadelphia
9. Kaplan JA, Reich DL, Savino J (eds) (2011) Kaplan's cardiac anesthesia: the echo era, 6th edn. W.B. Saunders, Philadelphia
10. Braunwald E (ed) (2011) Heart disease: a textbook of cardiovascular medicine, 9th edn. W.B. Saunders, Philadelphia
11. Mohrman DE, Heller LJ (eds) (2013) Cardiovascular physiology, 8th edn. McGraw–Hill, New York

Basic ECG Theory, 12-Lead Recordings, and Their Interpretation

19

Sarah Vieau and Paul A. Iaizzo

Abstract

The recorded electrocardiogram (ECG) remains as one of the most vital monitors of a patient's cardiovascular status and is used today in nearly every clinical setting. This chapter discusses the ECG as a measure of how the electrical activity of the heart changes over time, as action potentials within each myocyte propagate throughout the heart during each cardiac cycle. By utilizing the resultant electrical fields present in the body, electrodes can be placed around the heart to measure potential differences as the heart depolarizes and repolarizes. Furthermore, various techniques for obtaining ECG data are presented.

Electrocardiography has progressed rapidly since it was first employed back in the early 1900s. New instruments that are smaller and more sophisticated, as well as innovative analysis techniques, are continually being developed. The trend has been toward developing smaller, easier-to-use devices that can gather and remotely send a wealth of information to aid patient diagnosis and treatment.

Keywords

Electrocardiogram • ECG waveform • 12-Lead ECG • ECG placement • ECG recording devices • Holter monitor • Loop recorder

19.1 The Electrocardiogram

An *electrocardiogram* (ECG) is a measure of how the electrical activity of the heart changes over time, as action potentials within each myocyte propagate throughout the heart as a whole during each cardiac cycle. In other words, the ECG is not a direct measure of the cellular depolarization and repolarization, but rather the recording of the cumulative signals produced by populations of cells eliciting changes in their membrane potentials at a given point in time. The ECG provides specific waveforms of electrical differences when the atria and ventricles depolarize and repolarize.

The human body can be considered, for the purposes of an ECG, as a large volume conductor. It is filled with tissues surrounded by a conductive medium, in which the heart is suspended. During the cardiac cycle, the heart contracts in response to action potentials moving through the chambers of the heart in a coordinated fashion. As this normally occurs, one part of the cardiac tissue is depolarized and another part is at rest or polarized. This results in a charge separation, or dipole, which is illustrated in Fig. 19.1. The moving dipole causes current flow in the surrounding body fluids between the ends of the heart, resulting in fluctuating electric fields throughout the body. This is much like the electric field that would result, for example, if a common battery was suspended in a saltwater solution (an electrically conductive medium). The opposite poles of the battery would cause current flow in the surrounding fluid, creating an electric field that could be detected by electrodes placed in the solution. A

S. Vieau, MS (✉)
Medtronic, Inc.,
8200 Coral Sea Street NE, MVN61, Minneapolis, MN 55112, USA
e-mail: sarah.a.vieau@medtronic.com

P.A. Iaizzo, PhD
Department of Surgery, University of Minnesota, Minneapolis, MN, USA

P.A. Iaizzo (ed.), *Handbook of Cardiac Anatomy, Physiology, and Devices*, DOI 10.1007/978-3-319-19464-6_19

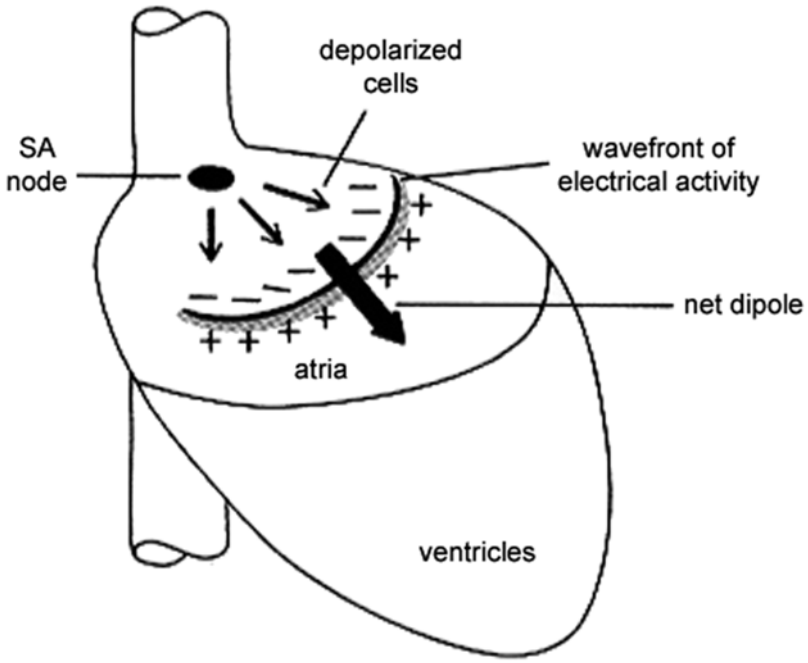

Fig. 19.1 After conduction begins at the sinoatrial node, cells in the atria begin to depolarize. This creates an electrical wavefront that moves down toward the ventricles, with polarized cells at the front, followed by depolarized cells behind. The separation of charge results in a dipole across the heart (with the large *black arrow* showing its direction). Modified from Mohrman and Heller (2003). *SA* = sinoatrial

similar electrical field around the heart can be detected using electrodes attached to the skin. The intensity of the voltages detected depends on the orientation of the electrodes with respect to that of the dipole ends. The amplitudes of the signals are proportional to the masses of tissue involved in creating that dipole at any given time. Typically one employs electrodes on the surface of the skin to detect the voltages of these electrical fields, which is what gives rise to the ECG.

It is important to note that, because the surface ECG is measured from the skin, any potential differences within the body will have an effect on the resultant electrical fields that are being detected. This is why it is important, for diagnostic purposes, that patients remain as still as possible while recording an ECG. Movements from skeletal muscle activation (electromyograms, EMGs) will contribute to the changes in voltage detected using electrodes on the surface of the body. A *resting ECG* is recorded when the patient is essentially motionless; this type of ECG signal is discussed in the majority of this chapter).

19.2 ECG Devices

The invention of electrocardiography had an immeasurable impact on the field of cardiology. It has provided insights into the structure and function of healthy and diseased hearts. Thus, the ECG has evolved into a powerful diagnostic tool for heart disease, including the detection of arrhythmias, myocardial infarction, and/or hypertrophy, among others. The use of ECG has become a standard of care in cardiology, and new technological advances are continually being made.

19.3 History of the ECG

The discovery of intrinsic electrical activity within the heart can be traced back to as early as the 1840s. In 1842, the Italian physicist Carlo Matteucci first reported that an electrical current accompanies each heartbeat. Soon after, the German physiologist, Emil DuBois-Reymond, described the first action potential that accompanies muscle contraction. Rudolph von Koelliker and Heinrich Miller recorded the first cardiac action potential using a galvanometer in 1856. Subsequently, the invention of the capillary electrometer in the early 1870s by Gabriel Lippmann led to the first recording of a human ECG by Augustus D. Waller.

The capillary electrometer is a thin glass tube containing a column of mercury that sits above sulfuric acid. With varying electrical potentials, the mercury meniscus moves and this can be observed through a microscope. Using this capillary electrometer, Waller was the first to show that the electrical activity precedes the mechanical contraction of the heart. He was also the first to show that the electrical activity of the heart can be seen by applying electrodes to both hands or to one hand and one foot. Waller's work was the first description of "limb leads." Interestingly, Waller would often publicly demonstrate his experiments with his dog, Jimmy, who would stand in jars of saline during the recording of the ECG.

A major breakthrough in cardiac electrocardiography came with the invention of the string galvanometer by Willem Einthoven in 1901. He reported the first ECG using his string galvanometer the following year. Einthoven's string galvanometer consisted of a massive electromagnet

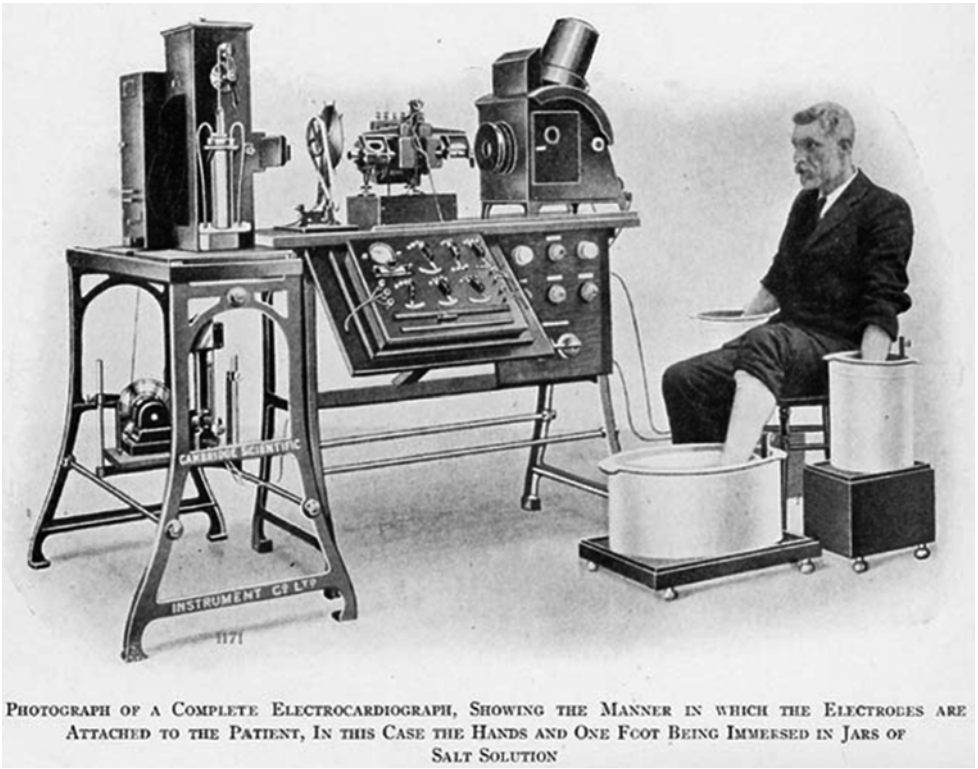

PHOTOGRAPH OF A COMPLETE ELECTROCARDIOGRAPH, SHOWING THE MANNER IN WHICH THE ELECTRODES ARE ATTACHED TO THE PATIENT, IN THIS CASE THE HANDS AND ONE FOOT BEING IMMERSED IN JARS OF SALT SOLUTION

Fig. 19.2 Willem Einthoven's string galvanometer consisted of a massive electromagnet with a thin silver-coated string stretched across it. Electric currents passing through the string caused it to move from side to side in the magnetic field generated by the electromagnet. The oscillations in the string provided information on the strength and direction of the electrical current. The deflections of the string were then magnified using a projecting microscope and recorded on a moving photographic plate. Reprinted with permission from NASPE-Heart Rhythm Society History Project

with a thin silver-coated string stretched across it; electric currents that passed through the string would cause it to move from side to side in the magnetic field generated by the electromagnet. The oscillations in the string would provide information regarding the strength and direction of the electrical current. The deflections of the string were then magnified using a projecting microscope and were recorded on a moving photographic plate (Fig. 19.2). Years earlier, utilizing recordings from a capillary electrometer, Einthoven was also the first to label the deflections of the heart's electrical activity as P, Q, R, S, and T waveforms.

In 1912, Einthoven made another major contribution to the field of cardiac electrophysiology by deriving a mathematical relationship between the direction and size of the deflections recorded by the three limb leads. This hypothesis became known as *Einthoven's triangle*. The standard three limb leads were used for three decades before Frank Wilson described unipolar leads and the precordial lead configuration. The 12-lead ECG configuration used today consists of the standard limb leads of Einthoven and the precordial and unipolar limb leads based on Wilson's work (see the following discussion for details on these recordings).

Following Einthoven's invention of the string galvanometer, electrocardiography quickly became a research tool for both physiologists and cardiologists. Much of the current knowledge involving arrhythmias was obtained through recording ECGs. In 1906, Einthoven published the first results of ECG tracings of atrial fibrillation, atrial flutter, ventricular premature contractions, ventricular bigeminy, atrial enlargement, and induced heart block within a dog. Einthoven was awarded the Nobel Prize for his body of work and inventions in 1924.

During this same era, Thomas Lewis was one of the pioneering cardiologists who utilized the capabilities of the ECG to further scientific knowledge of arrhythmias. His findings were summarized in his books *The Mechanism of the Heart Beat* and *Clinical Disorders of the Heart Beat* published in 1911 and 1912, respectively. He also published over 100 research papers describing his work. Importantly, Lewis was also the first to use the terms: sinoatrial node, pacemaker, premature contractions, paroxysmal tachycardia, and atrial fibrillation.

Myocardial infarction and angina pectoris were also extensively studied with ECG, using the early string galvanometer device. Numerous clinical investigators further studied the changes within ECG signals that were associated with the onset of myocardial infarction in both animals and humans. By the 1930s, characteristic features of the ECG for the diagnostic indications of myocardial infarction had been identified, and later on, the connection between angina pectoris and coronary occlusion was made. Further, while studying electrocardiographic changes accompanying angina pectoris, Francis Wood and Charles Wolferth performed the first exercise electrocardiographic stress test. Their use of exercise during ECG analyses stemmed from the observation that many of their patients experienced angina only during physical exertion. During this period, this technique was not routinely used, since it was thought to be very dangerous.

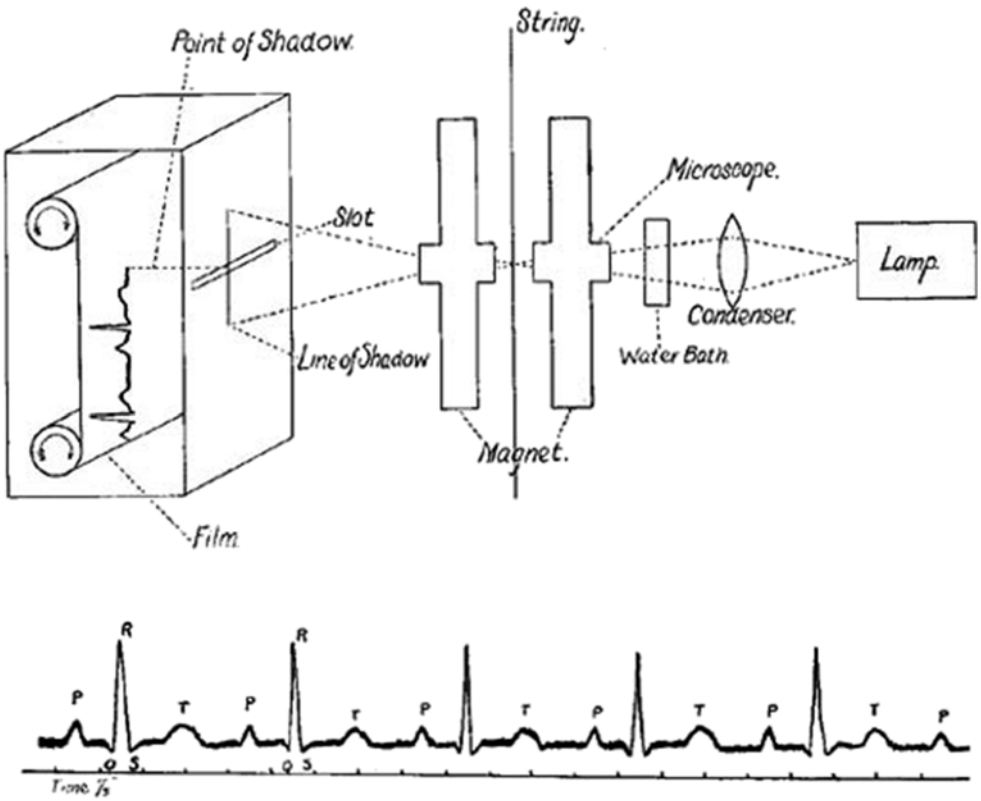

Fig. 19.3 A diagram of Cambridge Scientific Instrument Company's smaller version of the string galvanometer. Reprinted with permission from NASPE-Heart Rhythm Society History Project

Nevertheless, with advances in protocols and technologies, the ECG emerged as an important and commonly employed diagnostic tool for physicians.

ECG equipment has come a long way since Einthoven's string galvanometer. Of interest, the Cambridge Scientific Instrument Company in London was the first to manufacture this instrument back in 1905; it was massive, weighing in at 600 pounds. A telephone cable was used to transmit electrical signals from a hospital over a mile away to Einthoven's laboratory. A few years later, Max Edelman of Cambridge Scientific Instrument Company manufactured a smaller version of the instrument (Fig. 19.3). However, it wasn't until the 1920s that bedside machines became available. A few years later, a "portable" version was manufactured in which the instrument was contained in two wooden cases, each weighing close to 50 pounds. In 1935, the Sanborn Company manufactured an even smaller version of the unit that only weighed about 25 pounds.

Interestingly, the use of ECG in a nonclinical setting became possible in 1949, with Norman Jeff Holter's invention of the *Holter monitor*. The first version of this instrument was a 75-pound backpack that could continuously record the ECG and transmit these signals via radio. Subsequent versions of such systems have been dramatically reduced in size and now use a digital recording of the signal. Today, miniaturized systems (Fig. 19.4) allow patients to be monitored over longer periods of time (usually 24 h) to help diagnose any problems with rhythm or ischemic heart disease.

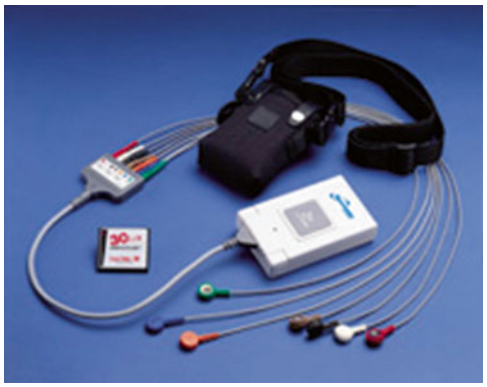

Fig. 19.4 A version of the Holter monitor that is used currently. The one seen here is manufactured by Medical Solutions, Inc. (Maple Grove, MN, USA)

19.4 The ECG Waveform

As an ECG is recorded, signals of voltage versus time are produced, which are normally displayed in millivolts (mV) versus seconds. A typical Lead II ECG waveform is shown in Fig. 19.5. For this recording, the negative electrode was placed on the right wrist and the positive electrode placed on the left ankle, a standard Lead II ECG. As such, one can observe a series of peaks and waves that correspond to ventricular or atrial depolarization and repolarization, with each segment of the signal representing a different event within the cardiac cycle.

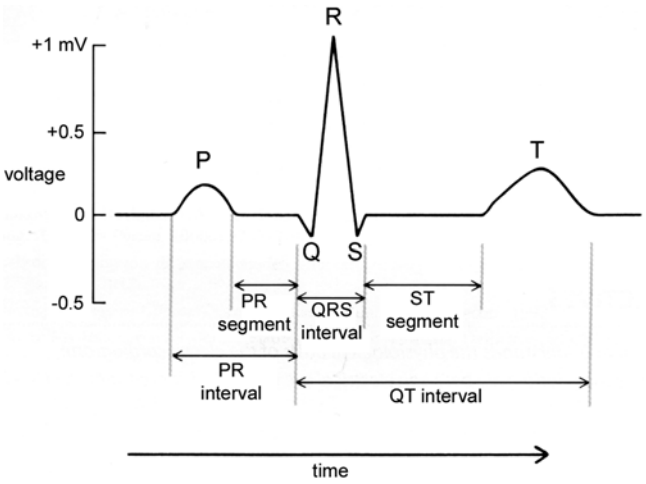

Fig. 19.5 A typical ECG waveform for one cardiac cycle, measured from the Lead II position. The P-wave denotes atrial depolarization and the QRS ventricular depolarization, and the T-wave denotes ventricular repolarization. The events on the waveform occur on a scale of hundreds of milliseconds. Modified from Mohrman and Heller (2003)

The normal cardiac cycle begins with the firing of the sinoatrial node, located within the right atrium. This initial firing is not detected by a typical ECG, because the sinoatrial node is not composed of an adequately large quantity of cells to create a detectable electrical potential, i.e., a signal with an amplitude high enough to be recorded with distal electrodes. The depolarization of the sinoatrial node is then conducted rapidly throughout the right and left atria, giving rise to the P-wave; this represents the depolarization of both atria and the onset of atrial contraction, and the P-wave is normally around 80–100 milliseconds (ms) in duration. As the P-wave ends, the atria are thus depolarized and this relates to their contraction. The signal then returns to baseline while action potentials (not large enough to be detected) spread through the atrioventricular node and bundle of His. Then, roughly 200 ms after the beginning of the P-wave, the right and left ventricles begin to depolarize resulting in the recordable QRS complex, which is approximately 100 ms in duration. The first negative deflection (if present) is the Q-wave, the large positive deflection is the R-wave, and if there is a negative deflection after the R-wave, it is called the S-wave. As the QRS complex ends, the ventricles are completely depolarized and are contracting. Importantly, the exact shape of the QRS complex depends on the placement of electrodes from which the signals are recorded.

Simultaneous with the QRS complex, atrial contractions have ended and the atria are repolarizing. However, it is important to note that the effects of this global atrial repolarization are sufficiently masked by the much larger amount of tissue involved in ventricular depolarization, and thus, it is not normally detected in the ECG. Toward the end of ventricular contraction, the ECG signal returns to baseline. The ventricles repolarize after contraction, giving rise to the T-wave. The T-wave is normally the last detected potential in the cardiac cycle; thus, it is followed by the P-wave of the next cycle, repeating the process.

It is clear that the QRS complex has a much higher and shorter duration peak than either the P- or T-waves. This is due to the fact that ventricular depolarization simultaneously occurs over a greater mass of cardiac tissue (i.e., a greater number of myocytes depolarizing at nearly the same time). Ventricular depolarization is much more synchronized than either atrial depolarization or ventricular repolarization. For additional details relative to the types of action potential that occur in various regions of the heart, the reader is referred to Chap. 13. It is important to note that deflections in the ECG waveforms represent the changes only in electrical activity and have different time courses of generalized cardiac contraction or relaxation which take place on a slightly longer time scale. Figure 19.6 details certain points on the ECG waveform and how they relate to other events in the heart during the cardiac cycle.

Lastly, the recorded ECG waveforms in some individuals may elicit a potential referred to as the U-wave. Its presence is not fully understood, but is considered by some to be caused by late repolarizations within the vast Purkinje system. If detected, the U-wave will be toward the end of the T-wave and have the same polarity (positive deflection). However, it typically has a much shorter amplitude and ascends more rapidly than it descends (which is the opposite of the T-wave).

19.5 Measuring an ECG

The ECG is typically measured from electrodes placed on the surface of the skin; this can be done by placing a pair of electrodes directly on the skin and then monitoring the potential difference between them, as these electrical signals are transmitted throughout the body. The detected waveform features depend not only on the amount of cardiac tissue involved but also the relative orientation of the electrodes, i.e., with respect to the major dipoles in the heart. Recall that ECG waveforms will look different when measured from different electrode positions, and typically an ECG investigation is obtained using a number of different electrode locations (e.g., limb leads or precordial) or configurations (unipolar, bipolar, modified bipolar) which have been standardized by universal applications of certain conventions.

19.5.1 Bipolar Limb Leads

Today, the three most commonly employed lead positions are referred to as Leads I, II, and III. Imagine the torso of the body as an equilateral triangle as illustrated in Fig. 19.7. This forms what is known as *Einthoven's triangle* (named for the

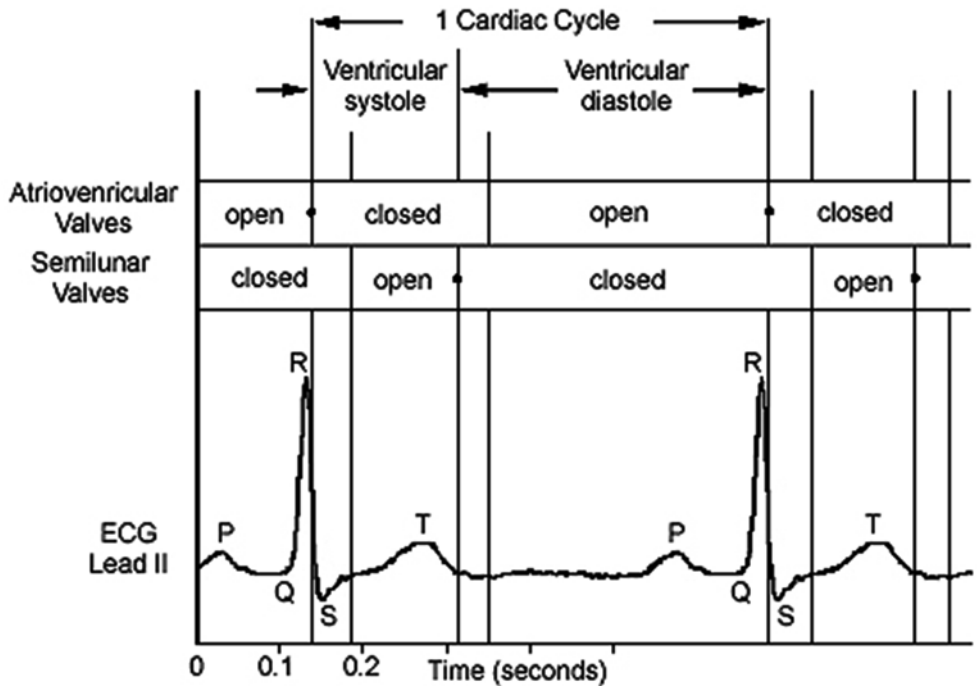

Fig. 19.6 A typical Lead II ECG waveform is compared to the timing of atrioventricular and semilunar valve activity, along with which segments of the cardiac cycle the ventricles are in systole/diastole. *ECG* = electrocardiogram

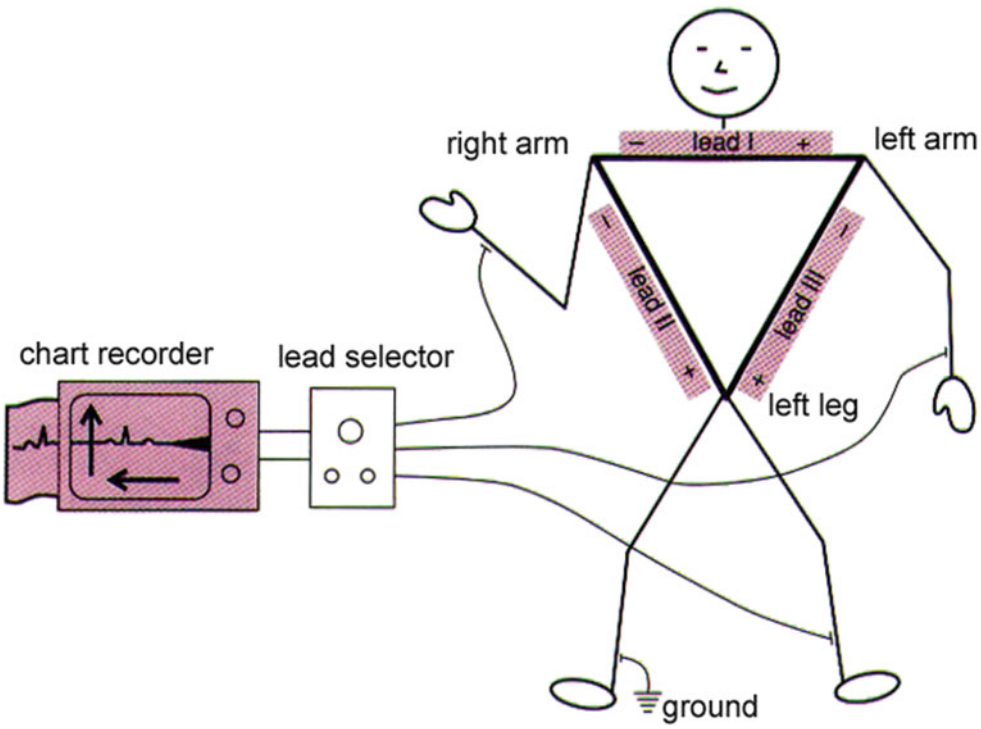

Fig. 19.7 The limb leads are attached to the corners of Einthoven's triangle on the body. Each lead uses two of these locations for a positive and negative lead. The "+" and "−" signs indicate the orientation of the polarity conventions. Modified from Mohrman and Heller (2003)

Dutch scientist who first described it). Electrodes are placed at each of the vertices of the triangle, and three ECG traces (either Lead I, II, or III) are measured along the corresponding sides of this triangle using the electrodes at each end. Because each lead uses one electrode on either side of the heart, Leads I, II, and III are also referred as the bipolar leads. The positive and negative signs shown in Fig. 19.7 indicate the polarity of each lead measurement, which are viewed as the universal convention. The vertices of the triangle can be considered to be at the wrists and left ankle for electrode placement, as well as the shoulders and lower torso.

As an example, if the Lead II ECG trace shows an upward deflection, it would mean that the voltage measured at the left leg (or bottom apex of the triangle) is more positive than the voltage measured at the right arm (or upper right apex of the triangle). One time point where this happens is during the P-wave. Imagine the orientation of the heart as shown in Fig. 19.8, with the action potential propagating across the

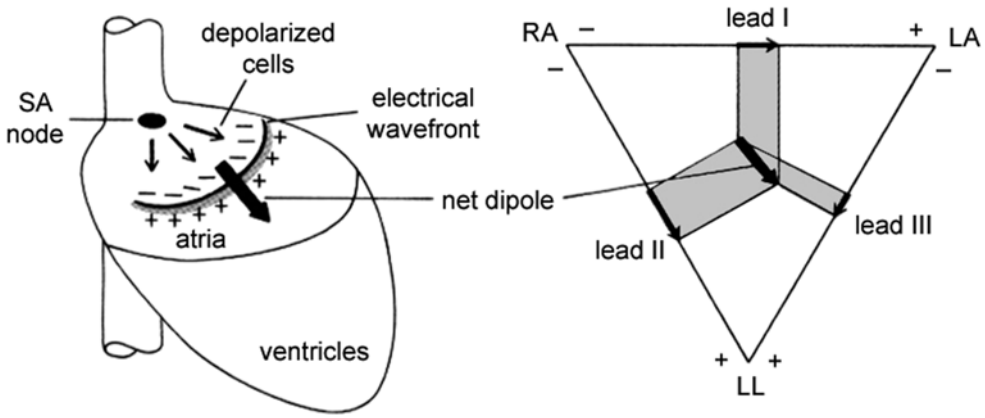

Fig. 19.8 The net dipole occurring in the heart at any one point in time is detected by each lead (I, II, and III) in a different way, due to the different orientations of each lead set relative to the dipole in the heart. In this example, the projection of the dipole on all three leads is positive (the *arrow* is pointing toward the positive end of the lead), which gives a positive deflection on the ECG during the P-wave. Furthermore, Lead II detects a larger amplitude signal than Lead III does from the same net dipole (i.e., the net dipole projects a larger arrow on the Lead II side of the triangle than on the Lead III side). ©2003, Cardiovascular Physiology, 5th ed., Mohrman D and Heller L, with permission of McGraw-Hill Education. *LA* = left arm, *LL* = left leg, *RA* = right arm, *SA* = sinoatrial

atria, creating a dipole pointed downward and to the left side of the body. This can be represented as an arrow (Fig. 19.8) showing the magnitude and direction of the dipole in the heart. This dipole would, overall, create a more positive voltage reading at the left ankle electrode than at the right wrist electrode, thus eliciting the positive deflection of the P-wave on the Lead II ECG.

Now, imagine how that same action potential propagations would appear on the other lead placements, Leads I and III, if placed at the center of Einthoven's triangle (Fig. 19.8, right side). One can think of each of these lead placements as viewing the electrical dipole from three different directions—Lead I from the top, Lead II from the lower right side of the body, and Lead III from the lower left side—all looking at the heart along the frontal plane. In this example, the atrial depolarization creates a dipole that gives a positive deflection for all three leads, because the arrow's projection onto each lead (in other words, measuring the cardiac dipole from each lead) results in the positive end of the dipole pointed more toward the positive end of the lead than the negative end. This is why atrial depolarization (P-waves) always appears as a *positive deflection*, but with different wave *magnitudes*, for Leads I, II, and III. Ventricular depolarization, however, is a bit more complicated and results in various directions of the Q- and S-wave potentials depending on which lead trace is being utilized for recording.

19.5.2 The Electrical Axis of the Heart

The direction and magnitude of the overall dipoles of the heart at any instant are also known as the heart's *electrical axis*, which can be plotted as a vector originating in the center of Einthoven's triangle such that the direction of the dipole is typically assessed in degrees. The convention for this is to use a horizontal line across the top of Einthoven's triangle as 0° and move clockwise downward (pivoting on the negative end of Lead I) as the positive direction. Note that the electrical axis changes direction throughout the cardiac cycle, as different parts of the heart depolarize and repolarize in different directions. The top row of panels in Fig. 19.9 shows the dipoles spreading across the heart during a typical cardiac cycle, beginning with atrial depolarization. The bottom row shows the corresponding deflections on each ECG lead (I, II, and III). Note that, at certain points, the electrical axis of the heart may give opposite deflections on the different ECG leads.

As can be observed in Fig. 19.9, depolarization begins at the sinoatrial node in the right atrium and then spreads through the atria forming the P-wave. The atria depolarize downward and to the left, toward the ventricles, followed by a slight delay at the atrioventricular node before the ventricles depolarize. The initial depolarization in the ventricles normally occurs on the left side of the septum, creating a dipole pointed slightly down and to the right. This gives a negative deflection of the Q-wave for Leads I and II; however, it is positive in Lead III. Depolarization then continues to spread down the ventricles toward the apex, which is when the most tissue mass is simultaneously depolarizing with the same relative orientation. This gives the large positive deflection of the R-wave for all three leads. Ventricular depolarization then continues to spread through the cardiac wall and finally finishes in the left ventricular wall. This results in a positive deflection for Leads I and II; however, Lead III shows a lower R-wave amplitude along with a negative S-wave deflection. After a sustained depolarized period

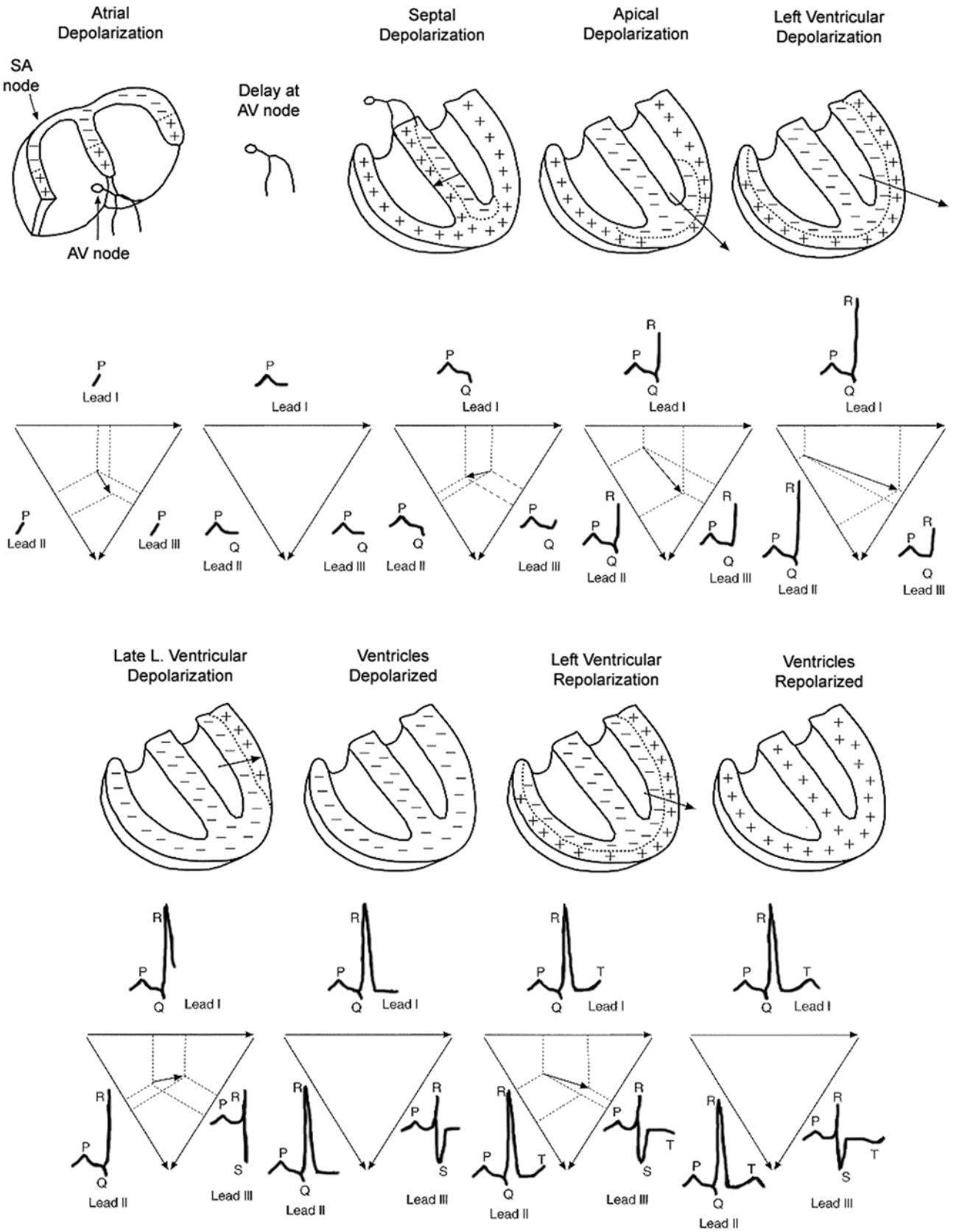

Fig. 19.9 The net dipole of the heart (indicated by the *arrow*) as it progresses through one cardiac cycle, beginning with firing of the sino-atrial node and finishing with the complete repolarization of the ventricular walls. The bottom row of panels displays how the net dipole is detected by each of the three bipolar limb Leads I, II, and III. Notice the change in direction and magnitude of the dipole during one complete cardiac cycle. Modified from Johnson (2003)

(the S–T segment), the myocytes within the ventricles then repolarize. However, this occurs in the opposite anatomical direction of depolarization, i.e., from base back toward the apex. The arrow in Fig. 19.9 represents the electrical axis of the heart (or the dipole) and does not necessarily show the direction that the repolarization wave is moving. Thus, even though the wave is moving from the epicardium to endocardium, the dipole (and therefore the electrical axis) remains in the same orientation as during depolarization. Therefore, the T-wave is also a positive deflection on Leads I and II and negative (if present) on Lead III. At the end of this waveform, the ventricles are then repolarized, returning the signal to its baseline potential.

During the cardiac cycle, the relative electrical axes of the heart are always changing in both magnitude and direction. The average of all instantaneous electrical axis vectors gives rise to the *mean electrical axis* of the heart. Most commonly this is studied as the average dipole direction during the QRS complex, being it is the highest and most synchronized signal of the overall ECG waveform. Typically, to find the mean electrical axis, area calculations from under the QRS complex from at least two leads are needed. However, it is easier and more commonly determined by an estimate using the deflection (positive or negative) and height of the R-wave. Figure 19.10 shows a simple example of using Leads I and II to find the relative electrical axis of the heart. It should be noted that, in the normal human heart, the electrical axis of the heart corresponds to the anatomical (axis) orientation of the heart (from base to apex). Also see Chap. 2 for more details on the heart orientation.

19.5.3 The 12-Lead ECG

Three of the twelve ECG leads are Leads I, II, and III; the bipolar limb leads that have been discussed thus far. Of the twelve, there are three other leads that use the limb electrodes, called the *unipolar limb leads*. Each of these leads uses an electrode pair that consists of one limb electrode and a "neutral reference lead" that is created by hooking up the

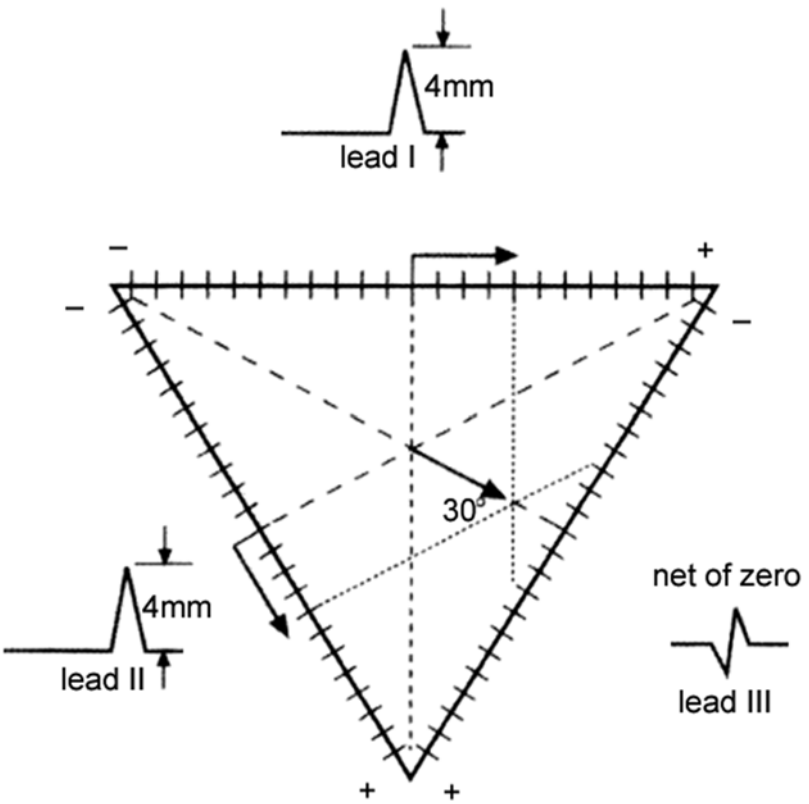

Fig. 19.10 The amplitude of the Lead I and II R-waves are plotted along the corresponding leg of Einthoven's triangle starting at the midpoint and drawn with a length equal to the height of the R-wave (units used to measure the amplitude can be arbitrary, since the direction, not the magnitude, of the axis is important). The direction of the plot is toward the positive end of the lead if the R-wave has a positive deflection and negative if it has a negative deflection. Perpendiculars from each point are then drawn into the triangle and they meet at a point. A line drawn from the center of the triangle to this point gives the angle of the mean electrical axis. Since the normal activation sequence in the heart generally goes down and left, this is also the direction of the mean electrical axis in most people. The normal range is anywhere from 0° to +90°. Modified from Johnson (2003)

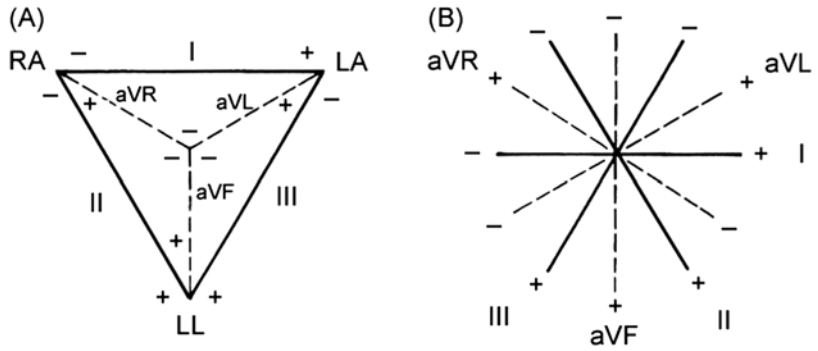

Fig. 19.11 (**A**) The augmented leads are shown on Einthoven's triangle along with the other three frontal plane leads (I, II, and III). (**B**) A hex-axial reference system for all six limb leads is shown, with *solid* and *dashed lines* representing the bipolar and unipolar leads, respectively. Modified from Mohrman and Heller (2003). *aVF* = voltage recorded between left leg lead and neutral reference lead, *aVL*= voltage recorded between left arm limb lead and neutral reference lead, *aVR* = voltage recorded between right arm limb lead and neutral reference lead, *LA* = left arm, *LL* = left leg, *RA* = right arm

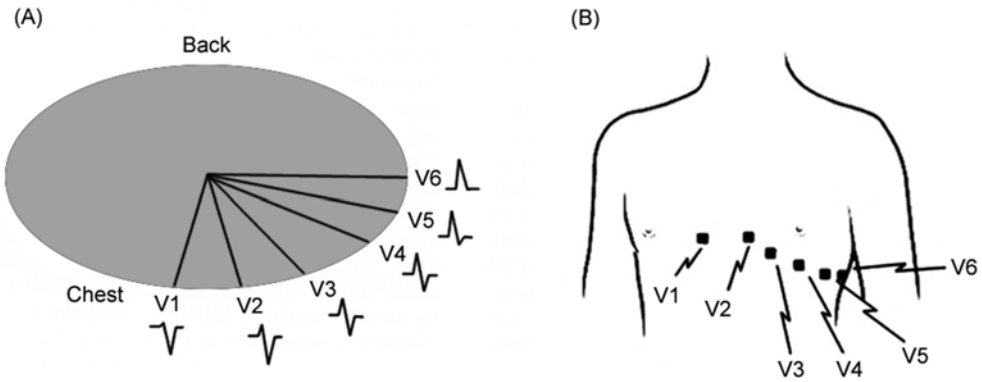

Fig. 19.12 (**A**) A cross section of the chest shows the relative position of the six precordial leads in the traverse plane, along with a typical waveform detected for ventricular depolarization. (**B**) An anterior view of the chest shows common placement of each precordial lead, V1 through V6

other two limb locations to the negative lead of the ECG amplifier. In other words, each lead has its positive end at the corresponding limb lead and runs toward the heart where its "negative" end is located, directly between the other two limb leads. These are referred to as the *augmented unipolar limb leads*. The voltage recorded between the left arm limb lead and the neutral reference lead is called Lead aVL; similarly, the right arm limb lead is aVR and the left leg lead is aVF (Fig. 19.11).

The remaining six of the twelve lead recordings are the chest leads. These leads are also obtained as unipolar; however, they uniquely measure electrical activity in the patient's traverse plane instead of the frontal plane. Similar to the unipolar limb leads, a neutral reference lead is created, but this time using all three limb leads connected as the negative ECG lead, which basically puts it in the center of the chest. The six positive, or "exploring," electrodes are placed as shown in Fig. 19.12 (around the chest) and are labeled V1 through V6 (V designates voltage). These chest leads are also known as the *precordial* leads. Figure 19.12a shows a simple cross section (looking superior to inferior) of the chest, depicting the relative position of each electrode in the traverse plane. Figure 19.12a also shows typical waveforms obtained from each of these leads. In summary, three bipolar limb leads, three unipolar limb leads, and six chest leads make up the 12-lead ECG.

The 12-lead ECG is widely used to evaluate overall cardiac electrical activity since it provides multiple views of how electrical conduction moves through a given patient's heart. For example, it can be used to help determine the location of many cardiac abnormalities, including (1) conduction disturbances (such as bundle branch block), (2) myocardial infarction or ischemia, (3) atrial or ventricular hypertrophy, and/or (4) electrolyte disturbances and drug effects.

19.6 Some Basic Interpretation of the ECG Trace

Analyses of the ECG waveforms and mean electrical axes are quite useful in the clinical setting. The ECG is considered to be one of the most important monitors of a patient's cardiovascular status but also can be used for basic measurements such as heart rate. Most monitoring devices used today include automated systems that detect changes in duration between subsequent QRS complexes.

Of clinical importance in the ECG waveform are several parameters (regions) which include the P–R interval, QRS interval, S–T segment, and Q–T interval (Fig. 19.5). The P–R interval is measured from the beginning of the P-wave to the beginning of the QRS complex and is normally 120–200 ms long. This is a measure of the time it takes for an impulse to travel from sinoatrial excitation through both the atria and atrioventricular node and induce the general onset of ventricular depolarization. The QRS interval measures how long the process of overall ventricular depolarization takes and is typically 60–100 ms. The S–T segment is the period of time when the ventricles are completely depolarized and contracting and is measured from the S-wave to the beginning of the T-wave. The Q–T interval is measured from the beginning of the QRS complex to the end of the T-wave; this is the time segment from when the ventricles begin their depolarization to the time when they have repolarized to their resting potential and is normally about 400 ms in duration.

Determination of the P–R interval provides useful information as to whether a patient may be eliciting some degree of heart block. Elongated P–R intervals (longer than ~200 ms) serve as a good indication that conduction through the atrioventricular node is slowed to some degree (first-degree heart block). Conduction in the atrioventricular node may even intermittently fail, which would elicit a P-wave without a subsequent QRS complex before the next P-wave (second-degree heart block). An ECG trace showing P-waves and QRS complexes beating independently of each other indicates the atrioventricular node has ceased to transmit impulses at all (third-degree heart block). For additional information on atrioventricular blocks, see Chap. 13.

A wide QRS complex (greater than 100 ms) may indicate conduction block or delays in electrical propagation through the bundle branches or Purkinje fibers that run through the ventricle. Delays or alterations in the conduction pathway through the ventricles can impact ventricular contraction and possibly cause dyssynchrony between the right and left ventricles. This, in turn, will negatively impact overall cardiac function and ultimately hemodynamics.

Prolonged Q–T intervals (which are usually no more that 40 % of the cardiac cycle length) are normally an indication of delayed repolarization of the cardiomyocytes, possibly caused by irregular opening or closing of sodium or potassium channels. Importantly, a long Q–T interval may indicate that a patient is at risk of developing a ventricular tachyarrhythmia (see Chap. 13 for more details).

Another clinically important interval is the S–T segment. Depression of the S–T segment (below the baseline) can indicate a regional ventricular ischemia. S–T segment elevation or depression can also be used as an indication of many other abnormalities including myocardial infarction, coronary artery disease, and/or pericarditis. For patients with established coronary artery disease, it is important to compare current ECG recordings to historical ones, to establish if any new regions of ischemia or infarction exist.

Estimation of the electrical axis is also a helpful diagnostic measure. In the case of left ventricular hypertrophy, the left side of the heart is enlarged with greater tissue mass. This could cause the dipole during ventricular contraction to shift to the left. Much more can be said about specific interpretations of the intervals and segments that make up the ECG waveform. For more details on changes in ECG patterns associated with various clinical situations, the reader is referred to Chap. 13 and Chap. 28.

19.7 Lead Placement in the Clinical Setting

In a clinical setting, all 12 leads may not be displayed at the same time and, most often, not all leads are being measured simultaneously. A common setup used is a five-wire system consisting of the two arm leads (placed on the shoulder areas), two leg leads (placed low where the legs join the torso), and one chest lead. This arrangement allows one to display any of the limb leads (I, II, III, aVR, aVL, and aVF) and one of the precordial leads, depending on where the chest electrode is placed. Figure 19.13 shows the positioning of these five electrodes on the patient's body.

It should be noted that the exact anatomical placement of the leads is very important to obtain accurate ECG traces for clinical evaluations; moving an electrode even slightly away from its correct position could cause dramatic variation in the parameters of a trace and possibly lead to misdiagnosis. A slight exception to this rule is the limb leads, which do not necessarily need to be placed at the distal portion of the limb as described earlier. Note that the limb leads need to be, for the most part, equidistant from each other relative to the heart for determination of the electrical axis to be accurate.

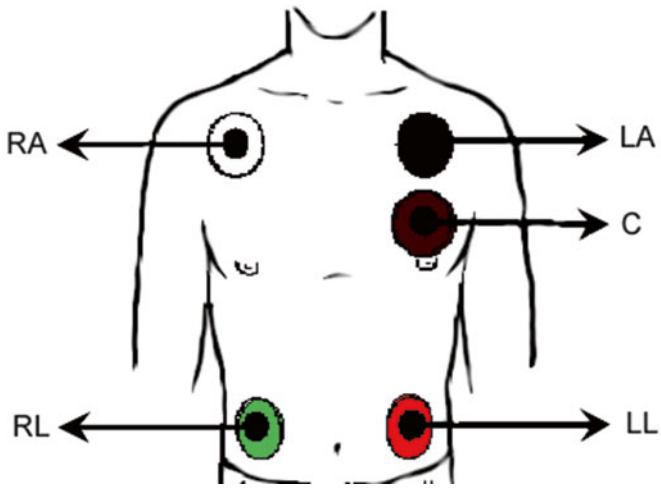

Fig. 19.13 Placement of the common five-wire ECG electrode system leads on the shoulders, chest, and torso. The chest electrode is placed according to the desired precordial lead position. *C* = chest, *LA* = left arm, *LL* = left leg, *RA* = right arm, *RL* = right leg

19.8 Computer Analyses

The use of computers for the analyses of ECG began in the 1960s. In 1961, Hubert Pipberger described the first computer analysis of ECG signals, an analysis which recognized basic abnormal activity. Computer-assisted ECG analyses were introduced into the general clinical setting in the 1970s. Subsequently, the use of computers, microcomputers, and microelectronic circuits has had a huge impact on field of electrocardiography. The size of such equipment has been drastically reduced to pocket-size or even smaller for some applications. This has allowed broader deployment of continuous monitoring of patients over much longer time periods, which has greatly helped in the diagnoses of patients with infrequent symptoms (paroxysmal).

Computer programs can also provide summaries of information recorded from the ECG including heart rate, multiple types of arrhythmias, and specific variations in QRS, S–T, Q–T, or T patterns. Additionally, there are several computer techniques that have been developed to further identify patients with cardiac dysfunction and previous myocardial infarctions that may be at risk for sudden death, e.g., signal-averaged ECGs, microvolt T-wave alternans, and/or heart rate variability. Signal-averaged ECG is a technique that uses computer analysis to identify late potentials appearing at the end of the QRS complex; these late potentials have been associated with an increased risk of ventricular arrhythmias. Microvolt T-wave alternans is another method that may be used to identify patients at risk for ventricular arrhythmias. This technique measures the presence of small changes in T-wave amplitudes that occur on an alternating beat-to-beat basis. Similarly, heart rate variability analysis measures subtle variations in ventricular rate to assess a patient's autonomic status (modulation of heart rate due to the influence of the autonomic nervous system). It is noteworthy that patients with low heart rate variability following a myocardial infarction may be at higher risk for sudden death. Studies have shown these techniques have high negative predictive value. They have been proposed as screening techniques but are not widely used in the clinical setting today due, in part, to their relatively low positive predictive value.

19.9 Long-Term ECG Recording Devices

Currently, there are four general types of devices that are utilized in the collection of long-term electrocardiographic recordings: continuous recorders, event recorders, real-time monitoring systems, and implantable recorders.

Continuous recorders, like the Holter monitor described above, are attached to the surface of the body and continuously record signals for a predetermined duration (usually 24–48 h). Such systems record from at least three different ECG leads. When using this method, patients must also record their daily activities and the time of any onset of symptoms (e.g., were they beginning to exercise?).

Event recorders are another type of instrument used for ECG collection. There are two basic types of event recorders—a symptom event recorder and a loop memory recorder. A symptom event recorder is activated by the patient to store a recording when their symptoms appear and therefore contains a post-event ECG recording. This type of recorder can be worn continuously or can be a handheld device which records the rhythm when the unit is activated and placed on the precordium. Pre-event or loop recorders are similar to post-event recorders, but a memory loop is used to enable the recording of information several minutes before and after the onset of symptoms. Today there are many different event

recorder devices including those connected to traditional ECG wires or devices consisting of a wireless patch electrode which adheres to the skin and can store and transmit data. A patient activator to prompt recording of the ECG during symptoms can be included on the event recorder itself or as a separate device, worn like a wristwatch, for example.

Fig. 19.14 A loop recorder with pacemaker and detection capabilities is shown. This model is manufactured by LifeWatch, Inc. (Rosemont, IL, USA)

Data from event recorders can also be transmitted wirelessly for viewing of the data by the physician electronically. The trend has been toward decreasing size, maximizing information, and improving data review by physicians and perhaps patients. Examples of loop recorders are shown in Figs. 19.14 and 19.15.

The third type of ECG instrument in clinical use today is a real-time monitoring system. Data are not recorded within the device, but rather are transmitted trans-telephonically to a distal recording station. Such instruments are commonly used for monitoring of patients that have a potentially dangerous condition, so the technician can quickly identify the rhythm abnormality and make arrangements for proper management of the condition.

Finally, implantable recorders are miniaturized loop recording devices that can be implanted subcutaneously. These implantable devices can be programmed to automatically store data when fast or slow heart rhythms are detected. Additionally, the patient can also self-trigger the device to store data when symptoms are felt. The latest implantable loop recorders can be placed for up to 3 years, during which time they can be used as a diagnostic tool to help manage the medical treatment of arrhythmias. Implantable recorders have typically been used for patients that elicit infrequent symptoms (hence they remain undiagnosed) and for those in

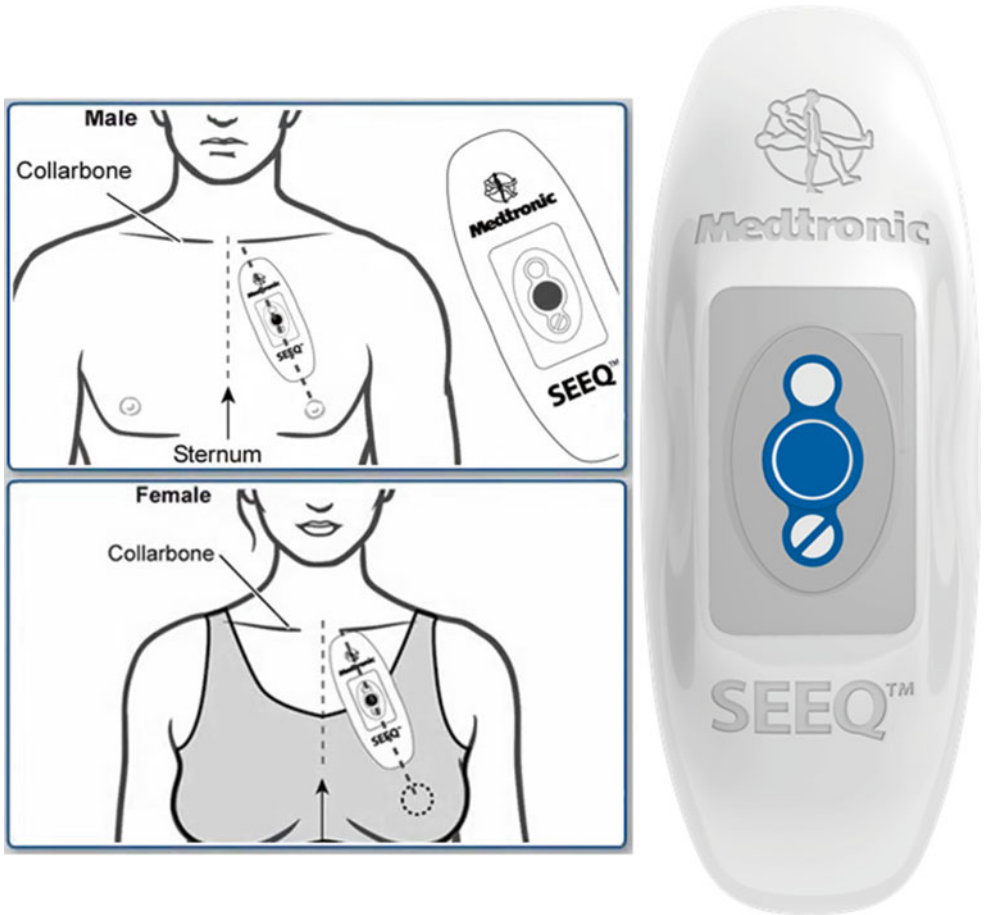

Fig. 19.15 The SEEQ™ Mobile Cardiac Telemetry System, manufactured by Medtronic, Inc. (Minneapolis, MN), is an external, wire-free adhesive loop recorder that can be worn for up to 30 days to help detect and diagnose arrhythmias. Data from this device can be transmitted via Bluetooth and cellular connections for physician review and analysis. Reproduced with permission of Medtronic, Inc.

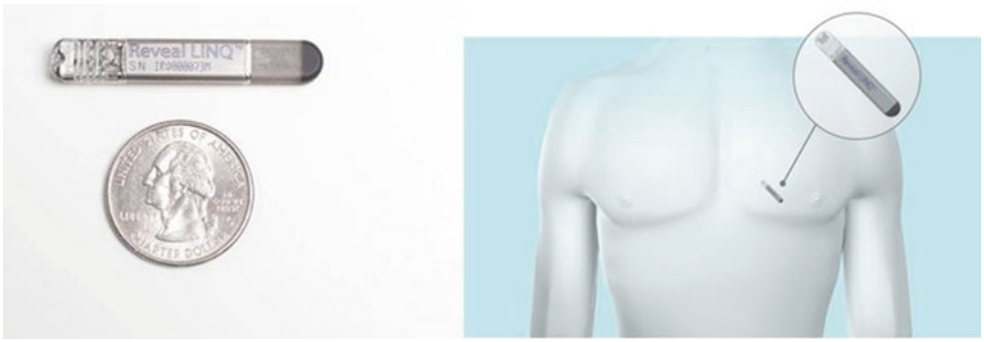

Fig. 19.16 The Reveal LINQ™, an implantable ECG loop recorder, is manufactured by Medtronic, Inc. (Minneapolis, MN, USA). This device can be inserted subcutaneously using an insertion tool with an incision of less than 1 cm. Reproduced with permission of Medtronic, Inc.

whom external recorders are considered impractical. Recent advances in technology have made these devices much smaller, with improved arrhythmia detection capabilities and wireless technology to facilitate transmission and viewing of the data by physicians for improved patient management. One of these devices, the Reveal LINQ™, is shown in Fig. 19.16 (Medtronic, Inc., Minneapolis, MN, USA).

19.10 Summary

As cardiomyocytes depolarize and propagate action potentials throughout the heart, an electrical dipole is created. By utilizing the resultant electrical field present in the body, electrodes can be placed around the heart to measure potential differences as the heart depolarizes and repolarizes. This measurement gives rise to the ECG, normally consisting of the P-wave via atrial depolarization, the QRS complex for ventricular depolarization, and the T-wave associated with ventricular repolarization.

To date, there are twelve standard lead positions which are clinically employed to detect the ECG. Most commonly, a 5-wire system is used clinically and can be used for the three bipolar limb leads (which make up Einthoven's triangle), the three unipolar limb leads, and one precordial (chest) lead at a time. At least two lead traces are needed to calculate the heart's electrical axis, which gives the general direction of the heart's dipole at any given instant. The heart's mean electrical axis is commonly defined as the average dipole direction recorded during ventricular depolarization (in the healthy heart this is same as the anatomical axis).

The recorded ECG remains as one of the most vital monitors of a patient's cardiovascular status and is used today in nearly every clinical setting. Yet, systems to monitor the electrocardiograph have come a long way since they were first developed in the early 1900s. New instruments that are smaller and more sophisticated as well as provide for innovative analysis techniques are continually being developed. ECG has also been used in combination with other implantable devices such as pacemakers and defibrillators. The trend has been toward developing smaller, easier-to-use devices that can gather and remotely send a wealth of information to use in both patient diagnosis and treatment (telemedicine).

Additional Resources

Alexander RW, Schlant RC, Fuster V (eds) (1998) Hurst's: the heart, arteries and veins, 9th edn. McGraw-Hill, New York

Bloomfield D, Steinman RC, Namerow PB et al (2004) Microvolt T-wave alternans distinguishes between patients likely and patients not likely to benefit from implanted cardiac defibrillator therapy: a solution to the Multicenter Automatic Defibrillator Implantation Trial (MADIT) II Conundrum. Circulation 110:1885–1889

Burchell HB (1987) A centennial note on Waller and the first human electrocardiogram. Am J Cardiol 59:979–983

Drew BJ (1993) Bedside electrocardiogram monitoring. AACN Clin Issues 4:25–33

Fye BW (1994) A history of the origin, evolution, and impact of electrocardiography. Am J Cardiol 73:937–949

Garcia TB, Holtz NE (eds) (2001) 12-Lead ECG: the art of interpretation. Jones and Bartlett Publishers, Sudbury

Hurst JW (1998) Naming of the waves in the ECG, with a brief account of their genesis. Circulation 98:1937–1942

Jacobson C (2000) Optimum bedside cardiac monitoring. Prog Cardiovasc Nurs 15:134–137

Johnson LR (ed) (2003) Essential medical physiology, 3rd edn. Elsevier Academic Press, San Diego

Katz A, Liberty IF, Porath A, Ovsyshcher I, Prystowsky EN (1999) A simple bedside test of 1-minute heart rate variability during deep breathing as a prognostic index after myocardial infarction. Am Heart J 138:32–38

Kossmann CE (1985) Unipolar electrocardiography of Wilson: a half century later. Am Heart J 110:901–904

Krikler DM (1987) Historical aspects of electrocardiography. Cardiol Clin 5:349–355

Mohrman DE, Heller LJ (eds) (2003) Cardiovascular physiology, 5th edn. McGraw-Hill, New York

Rautaharju PM (1987) A hundred years of progress in electrocardiography: early contributions from Waller to Wilson. Can J Cardiol 3:362–374

Scher AM (1995) Studies of the electrical activity of the ventricles and the origin of the QRS complex. Acta Cardiol 50:429–465

Wellens HJJ (1986) The electrocardiogram 80 years after Einthoven. J Am Coll Cardiol 3:484–491

Mechanical Aspects of Cardiac Performance

20

Michael K. Loushin, Jason L. Quill, and Paul A. Iaizzo

Abstract

This chapter is a review of commonly utilized monitoring techniques to assess the function of the general cardiovascular system. Specifically, means to assess arterial blood pressure, central venous pressure, pulmonary artery pressure, mixed venous oxygen saturation, cardiac output, pressure-volume loops, and Frank-Starling curves are described. Basic physiological principles underlying cardiac function are also briefly discussed.

Keywords

Cardiac pressure-volume loops • Blood pressure monitoring • Central venous pressure monitoring • Pulmonary artery pressure monitoring • Cardiac output • Cardiac index monitoring • Mixed venous saturation monitoring • Flow monitoring • Implantable monitoring

20.1 Introduction

This chapter is a review of commonly utilized monitoring techniques to assess the function of the general cardiovascular system. Specifically, means to assess arterial blood pressure, central venous pressure, pulmonary artery pressure, mixed venous oxygen saturation, cardiac output, pressure-volume loops, and Frank-Starling curves are described. Basic physiological principles underlying cardiac function are also briefly discussed.

Under normal physiologic conditions, the human heart functions as two separate pumps working in series; the right heart pumps blood through the pulmonary circulation and the left heart pumps blood through the systemic circulation. Each contraction of the heart and subsequent ejection of blood creates pressures that can be monitored clinically to assess the function of the heart and its work against resistance. In general, the mechanical function of the heart is described by the changes in pressure, volume, and flow that occur within each phase of the cardiac cycle, which is one complete sequence of myocardial contractions and relaxations.

20.2 Cardiac Cycle

The normal electrical and mechanical events of a single cardiac cycle of the left heart are correlated in Fig. 20.1. The mechanical events of the left ventricular pressure-volume curve are displayed in Fig. 20.2. During a single cardiac cycle, the atria and ventricles do not beat simultaneously; rather the atrial contraction occurs prior to ventricular contraction. This timing delay allows for proper filling of all four chambers of the heart. Recall that the left and right heart pumps function in series but contract simultaneously. The diastolic phase of the cardiac cycle begins with the opening

Electronic supplementary material: The online version of this chapter (doi:10.1007/978-3-319-19464-6_20) contains supplementary material, which is available to authorized users.

M.K. Loushin, MD (✉)
Department of Anesthesiology, University of Minnesota, MMC 294, 420 Delaware Street SE, Minneapolis, MN 55455, USA
e-mail: loush001@umn.edu

J.L. Quill, PhD
Medtronic, Inc., Minneapolis, MN, USA

P.A. Iaizzo, PhD
Department of Surgery, University of Minnesota, Minneapolis, MN, USA

P.A. Iaizzo (ed.), *Handbook of Cardiac Anatomy, Physiology, and Devices*, DOI 10.1007/978-3-319-19464-6_20

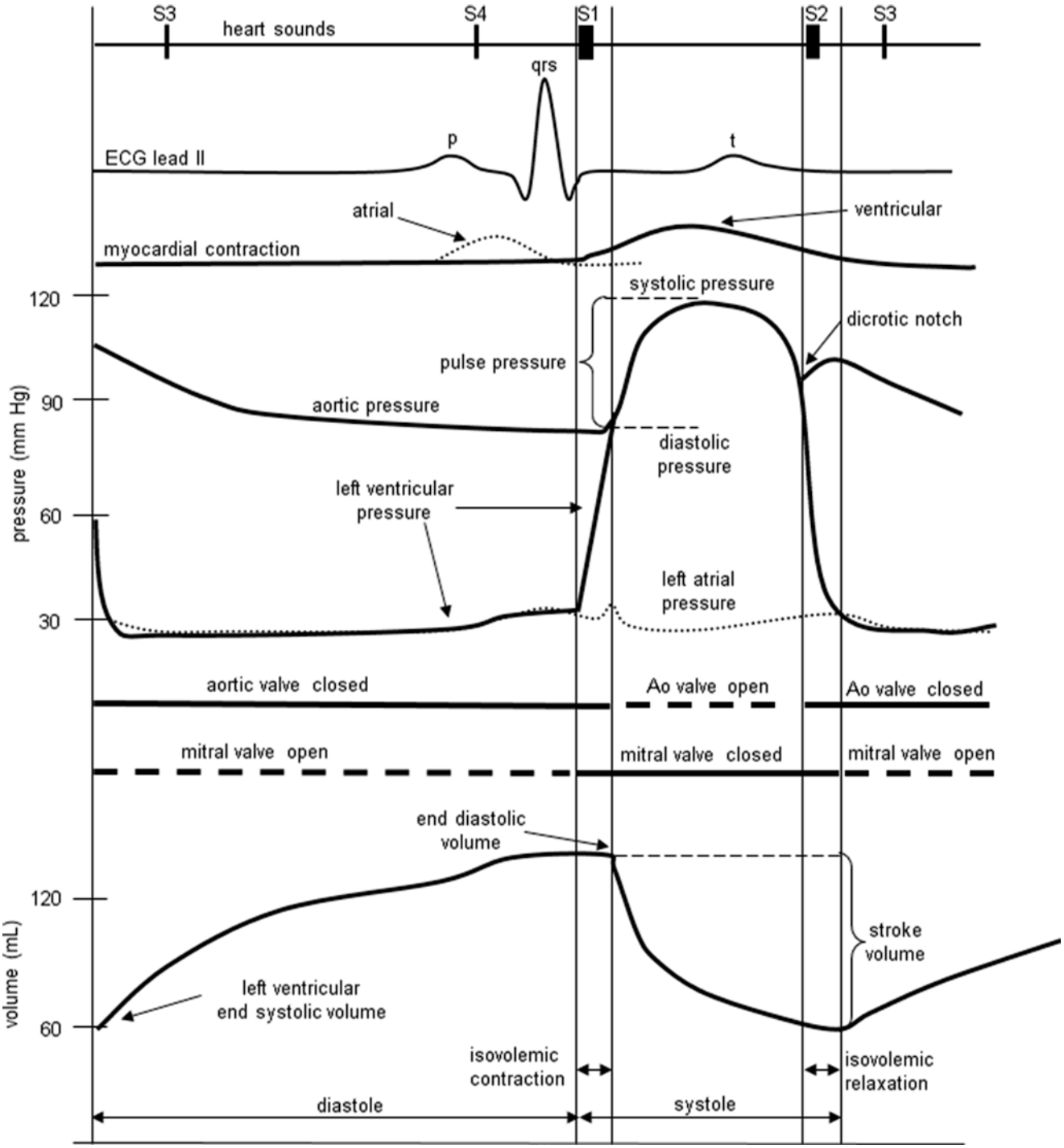

Fig. 20.1 Electrical and mechanical events of a single cardiac cycle within the left heart (see text for details)

of the tricuspid and mitral valves (atrioventricular valves). The atrioventricular valves open when the pressure in the ventricles falls below that in the atria. This can be observed in Fig. 20.1 for the left heart, in which the mitral valve opens when the left ventricular pressure falls below the left atrial pressure. At this moment, passive filling of the ventricle begins. In other words, blood that has accumulated in the atria behind the closed atrioventricular valves passes rapidly into the ventricles, and this causes an initial drop in atrial pressure. Later, pressure in all four chambers rises together as the atria and ventricles continue to passively fill in unison with blood returning to the heart through the veins (pulmonary veins to the left atrium and the superior and inferior vena cavae to the right atrium).

Contractions of the atria begin near the end of ventricular diastole, which is initiated by depolarization of the atrial

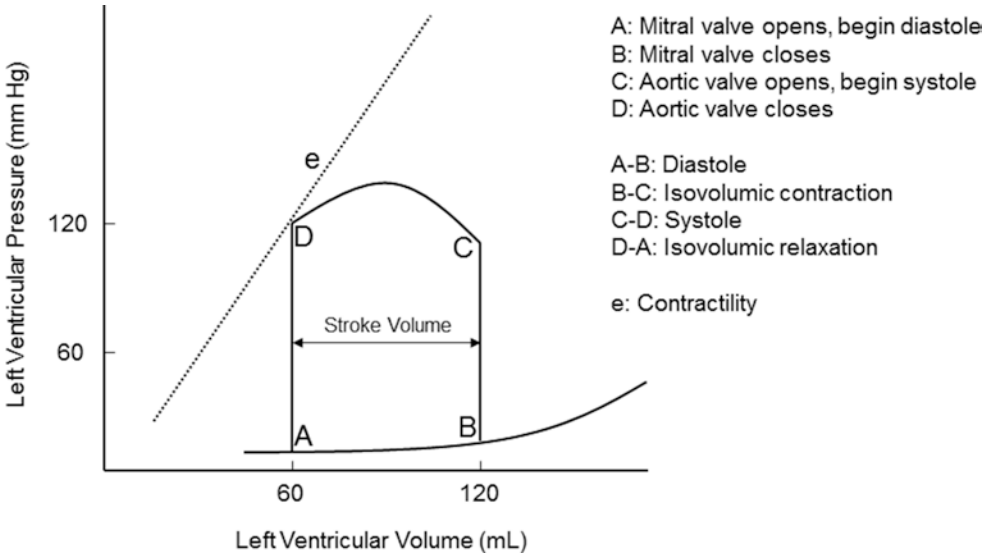

Fig. 20.2 Pressure-volume diagram of a single cardiac cycle (see text for details)

myocardial cells (sinoatrial node). Atrial depolarization is elicited at the P-wave of the electrocardiogram (Fig. 20.1, ECG lead II). The excitation and subsequent development of tension and shortening of atrial cells cause atrial pressures to rise. Active atrial contraction forces additional volumes of blood into the ventricles (often referred to as *atrial kick*). The atrial kick can contribute a significant volume of blood toward ventricular preload (approximately 20 %). At normal heart rates, the atrial contractions are considered essential for adequate ventricular filling. As the heart rate increases, atrial filling becomes increasingly important for ventricular filling because the time interval between contractions for passive filling becomes progressively shorter. Atrial fibrillation and/or asynchronized atrioventricular contractions can result in minimal contribution to preload, via the lack of a functional atrial contraction. Throughout diastole, atrial and ventricular pressures are nearly identical due to the open atrioventricular values which offer little or no resistance to blood flow. It should also be noted that contraction and movement of blood out of the atrial appendage (auricle) can be an additional source for increased blood volume.

Ventricular systole begins when the excitation passes from the right atrium, through the atrioventricular node, and through the remainder of the conduction system (His bundle and left and right bundle branches) to cause ventricular myocardial activation. This depolarization of ventricular cells underlies the QRS complex within the ECG (Fig. 20.1). As the ventricular cells contract, intraventricular pressures increase above those in the atria, and the atrioventricular valves abruptly close. Closure of the atrioventricular valves results in the first heart sound, S1 (Fig. 20.1). As pressures in the ventricles continue to rise together in a normally functioning heart, they eventually reach a critical threshold pressure at which the semilunar valves (pulmonary valve and aortic valve) open. The mechanical events of a single cardiac cycle and its pressure-volume relationship are displayed in Fig. 20.2. The normal time period between semilunar valve closures and atrioventricular valve openings is referred to as the *isovolumic contraction phase*. During this interval, the ventricles can be considered as closed chambers. Ventricular wall tension is greatest just prior to opening of the semilunar valves. Ventricular ejection begins when the semilunar valves open. In early left heart ejection, blood enters the aorta rapidly and causes the pressure within it to rise. Importantly, pressure builds simultaneously in both the left ventricle and the aorta as the ventricular myocardium continues to contract. This period is often referred to as the *rapid ejection phase*. A similar phenomenon occurs in the right heart; however, the pressures developed and those required to open the pulmonary valve are considerably lower, due to lower resistance within the pulmonary vascular system.

Pressures in the ventricles and outflow vessels (the aorta and pulmonary arteries) ultimately reach maximum peak systolic pressures. Under normal physiologic conditions, the contractile forces in the ventricles diminish after achieving peak systolic pressures. Throughout ejection, there are minimal pressure gradients across the semilunar valves due to their normally large annular diameters. Eventually the ventricular myocardium elicits minimal contraction to a point where intraventricular pressures fall below those in the outflow vessels. This fall in pressures causes the semilunar valves to close rapidly and is associated with the second heart sound, S2 (Fig. 20.1). A quick reversal in both aortic and pulmonary artery pressures is observed at this point, due to back pressure filling the semilunar valve leaflets. The back pressure on the valves causes the *incisura* or *dicrotic notch*, which can be detected by local pressure recording (e.g., with a locally placed Millar catheter). After complete closure of these valves, the intraventricular pressure falls rapidly and the ventricular myocardium relaxes. For a brief period, all four

cardiac valves are closed, which is commonly referred to as the *isovolumetric relaxation phase*. Eventually, intraventricular pressure falls below the rising atrial pressures, the atrioventricular valve opens, and a new cardiac cycle is initiated.

20.3 Cardiac Pressure-Volume Curves

Ventricular function can be analyzed and graphically displayed with a pressure-volume diagram. Both systolic and diastolic pressure-volume relationships during a single cardiac cycle are displayed in Fig. 20.2. Pressure-volume assessment of myocardial function on intact myocardium involves multiple factors such as preload, afterload, heart rate, and contractility. The area inside the pressure-volume loop is an estimate of the myocardial energy (work = pressure × volume) utilized for each stroke volume (stroke volume = end-diastolic volume − end-systolic volume). The shape of the normal pressure-volume loop changes with alterations in myocardial compliance, contractility, and valvular or myocardial disease.

Pressure-volume loops are displayed by plotting ventricular pressure (*y* axis) against ventricular volume (*x* axis) during a single cardiac cycle (Fig. 20.2). Points and segments along the pressure-volume loop correlate with specific mechanical events of the ventricle. The width of the pressure-volume loop is the stroke volume. Myocardial contractility is represented by the slope of the end-systolic pressure-volume relationship; this relationship defines the maximal pressure generated over time with a given myocardial contractility state. Contractility is proportional to change in pressure over time (dP/dt). The passive ventricular filling during diastole is defined by the end-diastolic pressure-volume relationship, and ventricular compliance is inversely proportional to the slope of the end-diastolic pressure-volume relationship. The effect of heart rate on the pressure-volume relationship cannot be assessed with a single pressure-volume loop. Instead, multiple pressure-volume loops must be obtained to assess effects of heart rate on the pressure-volume loop. By altering variables such as afterload, contractility, and/or preload, the mechanical events and pressure-volume relationship are displayed.

The pressure-volume diagram shows events of a single cardiac cycle (Fig. 20.2):

A: mitral valve opens; diastole begins.
B: mitral valve closes; diastole ends.
C: aortic valve opens; systole begins.
D: aortic valve closes; systole ends.
A-B: diastole, ventricular filling.
B-C: isovolumic contraction.
C-D: systole, ventricular ejection.
D-A: isovolumic relaxation.
e: contractility slope.

20.3.1 Preload

Preload is determined by the end-diastolic ventricular volume; it results from passive and active emptying of the atrium into the ventricle. Factors that affect this relationship, such as mitral stenosis and/or ventricular hypertrophy, will affect preload. The Frank-Starling curve also defines the relationship between preload and stroke volume; as end-diastolic volume increases, the stroke volume increases until the end-diastolic volume gets too excessive to allow proper ventricular contraction (Fig. 20.3). A pressure-volume loop is an alternative way to display the relationship between preload and stroke volume (Fig. 20.4); preload is the volume of blood in the ventricle at the end of diastole (point B in Fig. 20.4). An increase in preload is displayed by a right shift of the end-diastolic volume curve (A-B* in Fig. 20.4). In a normally functioning ventricle, an increase in preload while maintaining normal contractility and afterload results in increased stroke volume (SV* in Fig. 20.4). Excessive preload will not always result in increased stroke volume; excessive overdistention of the ventricle may result in heart failure (Fig. 20.5).

20.3.2 Contractility

Contractility is the relative ability of the myocardium to pump blood without changes in preload or afterload; it is influenced by intracellular calcium concentrations, the autonomic nervous system, humoral changes, and/or pharmacologic agents. A sudden increase in contractility with unchanged preload and afterload will result in increased stroke volume by ejecting more volume out of the ventricle (Fig. 20.6). The aortic valve opens at the same pressure and the ventricle ejects blood forward. Increased myocardial

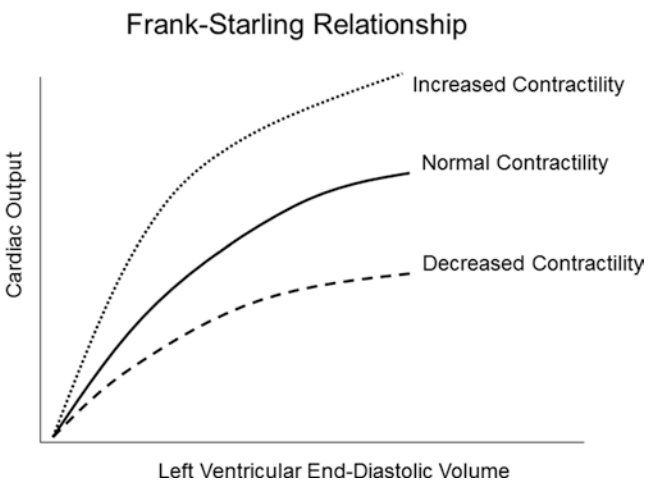

Fig. 20.3 The Frank-Starling relationship. As the end-diastolic volume increases, the cardiac output also increases. Excessive preload may eventually result in decreased cardiac output

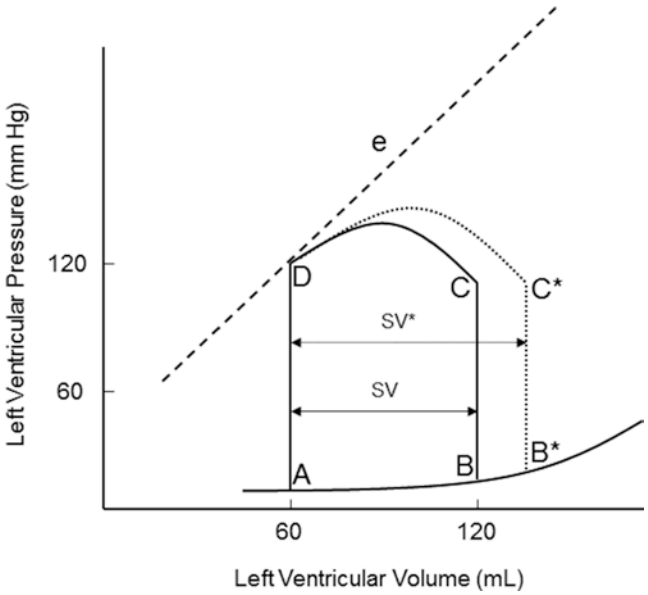

Fig. 20.4 Effect of acutely increased preload on the pressure-volume loop. Increasing preload while maintaining normal afterload and contractility results in increased stroke volume (*SV**). *e* contractility line, *SV* stroke volume

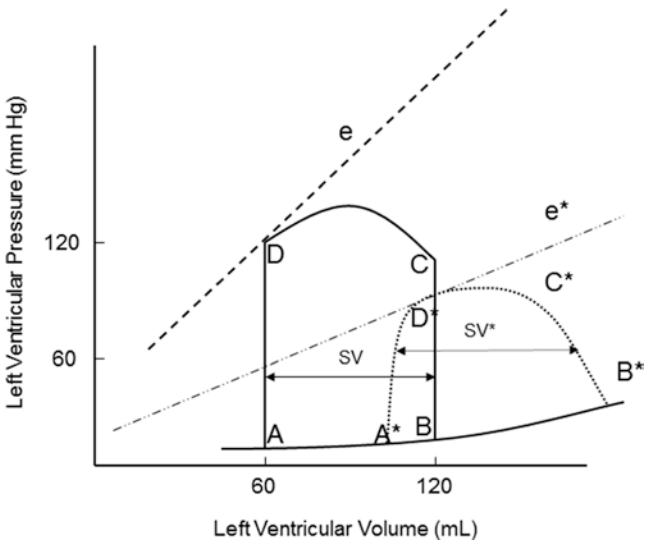

Fig. 20.5 Effect of ventricular failure on the pressure-volume loop. In heart failure, the myocardium compensates its inability to contract by increasing preload in an attempt to maintain stroke volume. Excessive preload eventually leads to worsening of heart failure. *e* and *e** contractility lines, *SV* stroke volume

contractility forces more blood out of the ventricle during systole, which is displayed by a lower end-systolic volume. Note the change in SV* (Fig. 20.6) with increased contractility; the end-systolic volume is lower due to increased contractility resulting in increased stroke volume. With increased myocardial contractility and unchanged preload, the resulting pressure-volume loop shifts to the left, maintaining normal

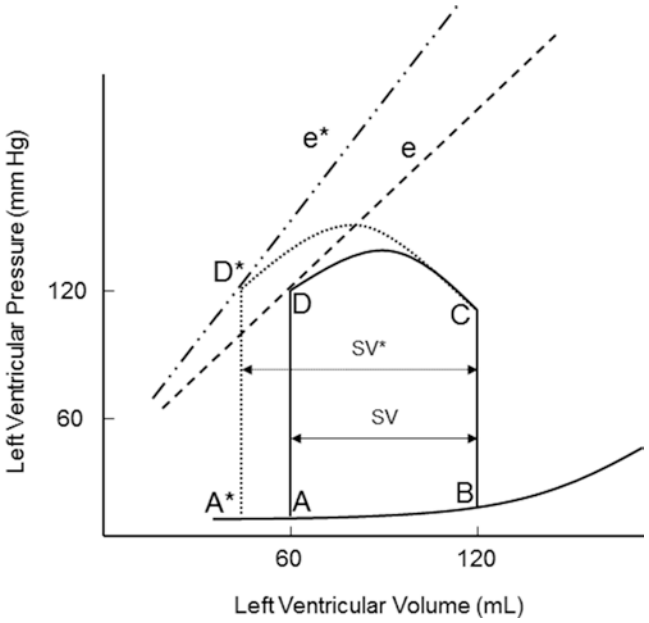

Fig. 20.6 Effects of acutely increasing contractility on the pressure-volume loop. Increasing contractility while maintaining normal preload and afterload results in increased stroke volume (*SV**). Note the increased slope of the contractility line (*e**). The area of loop D* is larger, indicating greater myocardial work per stroke volume. *e* and *e** contractility lines, *SV* stroke volume

stroke volume**.** An increase in contractility is graphically displayed by the increase in the slope of line e* in Fig. 20.6. During ejection, the myocardium contracts from C to D* (Fig. 20.6). During conditions of lower end-diastolic volume, a normal stroke volume may be maintained by increasing contractility. Inotropes such as dopamine and epinephrine will increase contractility, which assists in maintaining adequate stroke volume during low contractility states such as heart failure and/or cardiogenic shock.

In heart failure, the myocardium has decreased capacity to pump blood and maintain normal cardiac output. Heart failure may be acute (e.g., acute myocardial infarction, acute cardiogenic shock, or fluid overload) or it may be chronic (e.g., chronic congestive heart failure). In progressive heart failure, the myocardium often compensates its inability to contract by increasing preload and decreasing afterload in an attempt to maintain stroke volume (Fig. 20.5).

The increase in preload moves the myocardium up the Frank-Starling curve such that, by increasing end-diastolic volume, normal stroke volume may be maintained. The increase in preload and worsening heart failure eventually leads to ventricular dilatation and venous congestion. During heart failure, sympathetic tone increases as levels of circulating norepinephrine and epinephrine attempt to maintain normal cardiac output by increasing contractility and heart rate. The body's compensatory mechanism for heart failure may eventually become counterproductive and thus even worsen the situation.

20.3.3 Afterload

Afterload is another vital factor relative to stroke volume and therefore blood pressure. Afterload is most often equated with ventricular wall tension, which is also considered as the pressure the ventricle must overcome to eject a volume of blood past the aortic valve. In most normal clinical situations, afterload is assumed to be proportional to systemic vascular resistance. Wall tension is greatest at the moment just before opening of the aortic valve and can be described by LaPlace's law:

$$\text{Circumferential stress} = \text{Pr}/\,2H$$

where circumferential stress = wall tension, P = intraventricular pressure, r = ventricular radius, and H = wall thickness.

An increase in afterload requires ventricular pressure to increase during isovolumic contraction before the aortic valve opens (Fig. 20.7). Due to the increase in afterload, the ability of the ventricle to eject blood is decreased. This results in decreased stroke volume (SV* in Fig. 20.7a) and increased end-systolic volume (B* in Fig. 20.7b). If afterload remains increased, the myocardium establishes a new steady state that is shifted to the right and stroke volume is restored. A patient with severe aortic stenosis will likely elicit a pressure-volume loop as in Fig. 20.7. The myocardium usually compensates by increasing contractility to maintain adequate stroke volume. Thus, patients with hemodynamically significant aortic stenosis often develop left ventricular hypertrophy.

Afterload may be inversely related to cardiac output. In a dysfunctional myocardium, such as congestive heart failure, stroke volume decreases with increases in afterload. Importantly, increase in afterload also requires the myocardium to expend more energy to eject blood during systole. Conditions such as supravalvular or infravalvular stenoses or obstructions can also impact afterload or wall tension. A clinical example is idiopathic hypertrophic subaortic stenosis (IHSS), a heart condition characterized by significant hypertrophy of the left ventricle and interventricular septum. In turn, the hypertrophied muscle can then obstruct left ventricular outflow of blood during systole, increasing afterload and wall tension.

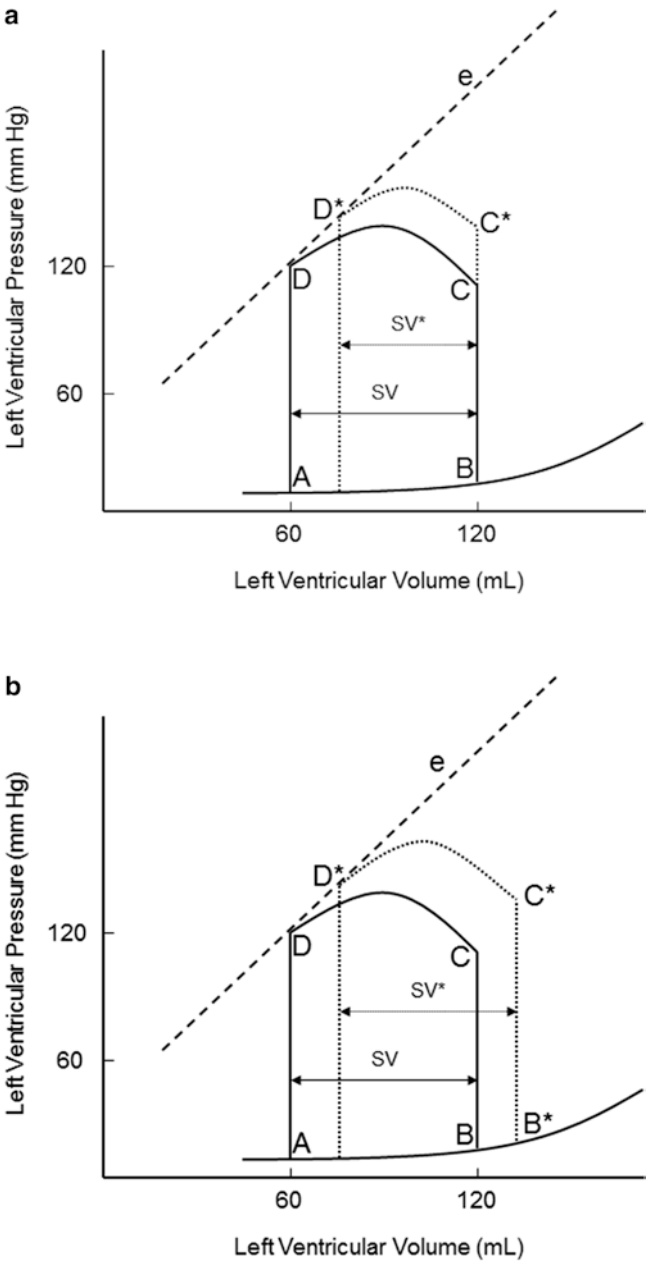

Fig. 20.7 (**a**) Effects of acutely increasing afterload on the pressure-volume loop. An increase in afterload, while maintaining normal contractility and preload, results in decreased stroke volume (*SV**). A higher pressure is also required before the aortic valve opens (*C**). (**b**) Restoration of stroke volume after increasing afterload. An increase in afterload, while maintaining normal contractility and preload, results in decreased stroke volume (*SV**). A higher pressure is also required before the aortic valve opens (*C**). *e* contractility line, *SV* stroke volume

20.3.4 Sonomicrometry Crystals

A common method for obtaining pressure-volume loops, and the changes observed by varying preload, afterload, or contractility, is to use sonomicrometry crystals for volume measurements in combination with a pressure-sensing catheter placed in the left ventricle. Sonomicrometry consists of piezoelectric crystals that transmit ultrasound signals through tissue to other crystals, where the signal is received; a distance measurement between two given crystals can be determined based upon the travel time of the ultrasound signal and the fiber orientation of the tissue. The piezoelectric (sonomicrometry) crystals function omnidirectionally and act as both receiver and transmitter with as many as 32 peers (in most commonly available systems). Complex, moving

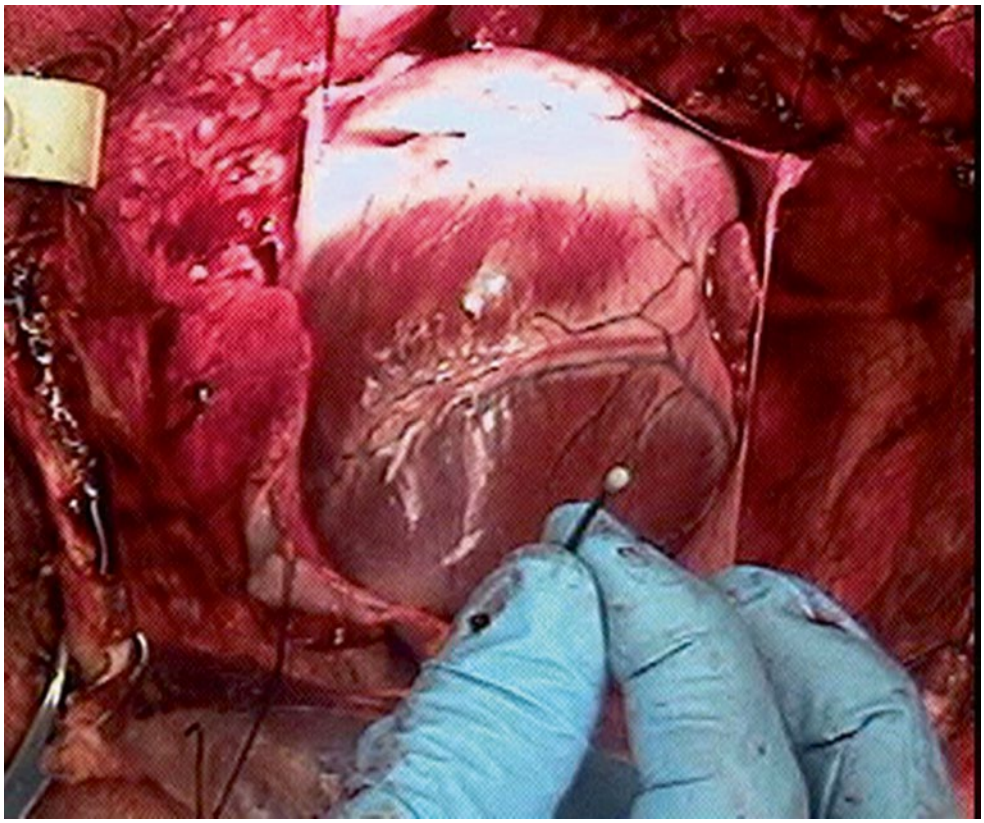

Fig. 20.8 A common sonomicrometry crystal placement. The crystal is shown prior to transmural implantation in a swine heart

3D geometries can then be modeled using techniques like sonomicrometry array localization. A sonomicrometry crystal can be seen in Fig. 20.8, where it is held in preparation for insertion through the epicardium.

Placement of four sonomicrometry crystals transmurally within the left ventricle, as well as the resulting pressure-volume loops, can be viewed online (Online Videos 20.1 and 20.2). The method shown in these supplemental videos places four sonomicrometry crystals—one on the anterior surface, the second on the posterior surface, a third crystal at the base of the left ventricle (superior), and a final crystal at the left ventricular apex (inferior). The placement of the crystals in this pattern creates two distance measurements (anterior-posterior and base-apex) that are measured continuously through the cardiac cycle. By assuming the left ventricle is the shape of an ellipsoid, changes in volume can be continuously estimated.

Traditionally, sonomicrometry has been used to determine cardiac function relative to large research animals (dogs, pigs, sheep, etc.). Both in vivo and in vitro studies can be performed which elucidate global cardiac function under a variety of conditions. Understanding the velocity of ultrasound through tissue is critical to acquiring accurate dimensions in a sonomicrometry system. The velocity of ultrasound is affected by a variety of factors including muscle fiber direction and composition, as well as the contractile state. In most biological tissues, the velocity of sound is approximately 1540 m/s.

A sonomicrometry system can use as few as two transducers but typically employs between six and thirty-two transducers. Transducers are the piezoelectric crystals which are attached to electronics consisting of a pulse generator and a receiver. Distance is measured by energizing the transmitter with a train of high-voltage spikes or square waves (both less than a microsecond in duration) to produce ultrasound. This excites the piezoelectric crystal to begin oscillating at its resonant frequency. This vibratory energy propagates through the medium and eventually comes in contact with piezoelectric crystals acting as receivers. These crystals begin vibrating and generate signals on the order of one millivolt. The piezoelectric signals are amplified and the distances between pairs of crystals are calculated. By monitoring the difference in time from transmission to reception of such signals and knowing the speed of sound through the particular medium, the intercrystal distances can be calculated. With current systems, these computations take less than 1 ms.

In addition to sonomicrometry crystals being used in the manner described, several other types of studies have found sonomicrometry measurements to be helpful. Regional studies have been performed that focus on specific areas of the heart, investigating regional timing and left ventricular shortening [1]. The advent of three-dimensional sonomicrometry,

or *sonomicrometry array localization*, has made possible the detailed study of discrete anatomical points throughout the cardiac cycle [2, 3]. A volume of data now exists describing the motion of valves, papillary muscles, ventricles, and atria. Another application involves tracking mobile components through the heart such as cardiac catheters [4]. We believe that these applications of sonomicrometry are important enough to be described in detail below.

In sonomicrometry array localization, the 3D position of each crystal is calculated from multiple intertransducer distances. This is done using a statistical technique called *multidimensional scaling*; such assessment gives the experimenter the ability to take the scalar sonomicrometer measurements and generate 3D geometry. Multidimensional scaling generates 3D coordinates for each crystal from a group of chord lengths in the array. By starting with an initial coordinate estimate and applying the Pythagorean theorem, a matrix of estimated distances is generated which corresponds to the actual measured distances. Using an iterative approach, multidimensional scaling then optimizes the value for the distance calculation by minimizing what is called the *stress function*. If the distances measured between crystals are exact (no measurement error), then one solution with zero stress exists, which represents the intercrystal distances exactly. As measurement error increases, a zero solution to the stress function becomes impossible and the iterations begin seeking a minimum value. The globally minimum stress point defines the optimum 3D configuration. A similar style is used to generate an estimate of the error associated with each distance. The result of this analysis is a 3D moving model with an average error of approximately 2 mm. The advent and description of the feasibility assessment of this technique is described in detail by Ratcliffe et al. [2] and Gorman et al. [3].

The first reported application of this technology described the 3D modeling of the ovine left ventricle and mitral valve. The study involved a 16-transducer array in which three transducers were sutured to the chest wall and the remaining thirteen were placed both epicardially and endocardially on the ventricular wall, the papillary muscles, and the mitral valve. The three crystals attached to the chest wall provided a fixed coordinate system from which whole-body motion could be differentiated from cardiac motion. This study produced 3D depictions of the shape of the mitral annulus throughout the cardiac cycle, as well as quantitative images of ventricular torsion. Such applications open up many possibilities relative to chronic studies focusing on ventricular remodeling following trauma like myocardial infarction.

Another interesting application of sonomicrometry, available due to the development of sonomicrometry array localization, is the cardiac catheter tracking described by Meyer et al. [4]. The system involves placing seven sonomicrometric crystals in the epicardium of an ovine heart and tracking the position of a catheter anywhere from one to five attached crystals. In this system, average distance errors on the order of 1.0 mm were demonstrated by Meyer et al. The clinically relevant endpoint for this tool would be to replace the epicardial transceivers with transceivers mounted in catheters and deployed endocardially in a minimally invasive manner.

20.3.5 Conductance Catheter

Conductance catheters offer an alternative method for obtaining pressure-volume loops. In this method, a catheter is typically equipped with eight electrodes and a pressure lumen. The conductance catheter is placed retrograde across the aortic valve, so that the first electrode is positioned in the left ventricular apex and the eighth electrode is positioned across the aortic valve (Fig. 20.9). The pressure lumen is located within the left ventricle, usually at the distal tip of the conductance catheter.

The outermost electrodes of the conductance catheter produce an electric field, with the remaining electrodes sensing differentials in voltage potential. The use of conductance to measure volume arises from the fact that blood is a good conductor relative to the surrounding myocardium (160 vs.

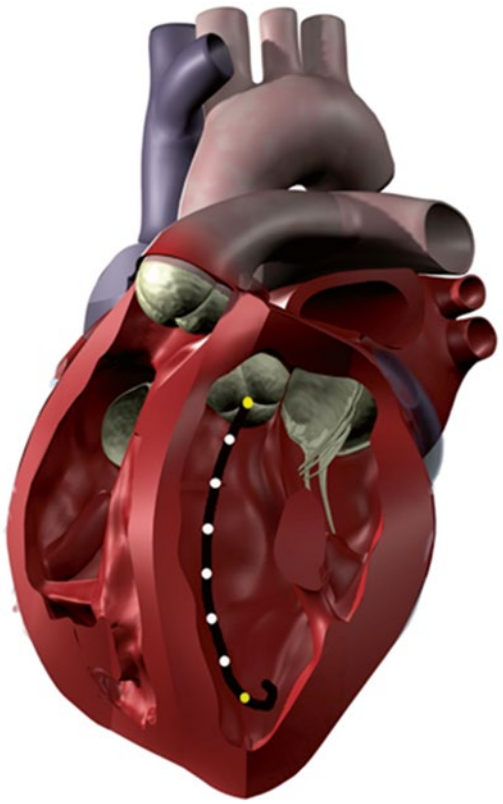

Fig. 20.9 When properly placed within the left ventricle, a conductance catheter spans from the apex to the aortic valve. The outermost electrodes (*yellow*) produce an electric field, and the inner electrodes (*white*) measure voltage differences that are related to volume changes within the chamber. A pressure sensor is typically incorporated into the distal tip of the catheter

400 Ω cm) [5]. When the ventricle is in diastole and filled with blood, the conductivity of the chamber will be much higher than during systole. The volume of the heart chamber is then analyzed as a series of conductive cylinders stacked upon each other, with a height predetermined as the distance between the electrodes. A change in the cross-sectional area of one of these cylinders is synonymous with a decrease in blood volume and a change in resistance, which is measured by the sensing electrodes.

The left ventricular volume can then be calculated as a voltage varying with time ($V(t)$), based upon the distance between the electrodes (L), the specific conductivity of blood (σ), the sum of the conductances that vary with time ($G(t)$), a dimensionless constant (α), and a correction term (C) [6]:

$$V(t) = \frac{L^2}{\alpha\sigma} G(t) - C$$

The conductance catheter was developed in the early 1980s by Baan et al. [6]. This method has shown reliable left ventricular segmental volumes when compared to cine-CT scans [7] and sonomicrometry crystals. Additionally, the conductance methods could be optimally suited for right ventricular pressure-volume curves [8]. Sonomicrometry methods and angiography require the assumption of an ellipsoid shape for left ventricular measurements; the complex geometric shape of the right ventricle makes these methods ill suited for volume measurements on the right side of the heart.

Both sonomicrometry crystals and conductance catheters are proven techniques for the measurement of left ventricular and aortic root volumes [9]. These technologies are applicable to many different study designs, yet care should be taken to choose the best method based upon the needs of the study. For studies involving complex geometric shapes, a conductance catheter may be the easiest method to obtain absolute volume changes, but a technique such as sonomicrometry array localization may be advantageous if the relative motion of geometric components is of interest.

20.4 Blood Pressure Monitoring

The cardiovascular system is most commonly assessed by monitoring arterial blood pressure. Blood pressure is proportional to the product of cardiac output and systemic vascular resistance:

$$\mathrm{BP} = \mathrm{CO} \times \mathrm{SVR}$$

$$\mathrm{CO} = \mathrm{HR} \times \mathrm{SV}$$

$$\mathrm{MAP} = 1/3\,\mathrm{SBP} + 2/3\,\mathrm{DBP}$$

where BP = blood pressure, CO = cardiac output, SVR = systemic vascular resistance, HR = heart rate, SV = stroke volume, MAP = mean arterial pressure, SBP = systolic blood pressure, and DBP = diastolic blood pressure. Stroke volume is dependent upon preload, afterload, and contractility (Fig. 20.10).

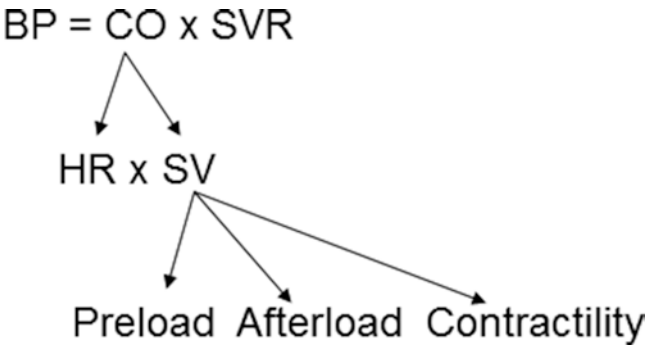

Fig. 20.10 Blood pressure monitoring which is proportional to the product of cardiac output and systemic vascular resistance. *BP* blood pressure, *CO* cardiac output, *HR* heart rate, *SV* stroke volume, *SVR* systemic vascular resistance

Blood pressure can be defined to consist of three components: systolic blood pressure, mean arterial pressure, and diastolic blood pressure. Systolic blood pressure is the peak pressure during ventricular systole, mean arterial pressure is a crucial determinant for adequate perfusion of other major organs, and diastolic blood pressure is the main determinant for myocardial perfusion. Recall that the majority of coronary blood flow occurs during diastole.

Commonly, arterial blood pressure monitoring involves two primary techniques—noninvasive (indirect) and invasive (direct) methods. The decision to utilize either blood pressure monitoring method depends on multiple factors such as: (1) level of a patient's cardiovascular stability, (2) perceived need for frequent arterial blood samples, (3) relative frequency of blood pressure recordings, and/or (4) type of major surgery or trauma the patient will undergo. One of the advantages of an invasive blood pressure monitor is that it provides continuous, beat-to-beat blood pressures (Online JPG 20.1). Typically, direct arterial blood pressure monitoring is considered to be required when a cardiopulmonary bypass machine is utilized during cardiac surgery. Since there is no pulsatile flow during such surgery, the noninvasive methods to monitor blood pressure cannot be employed. Also, patients with a ventricular assist device may require an invasive arterial monitor, as the noninvasive technique may not provide accurate systemic blood pressures (for more information on ventricular assist devices, see Chap. 39).

20.4.1 Noninvasive Arterial Blood Pressure Monitoring

Noninvasive blood pressure assessment is the most utilized and simplest technique to monitor arterial blood pressure. This technique utilizes a blood pressure cuff and the principle

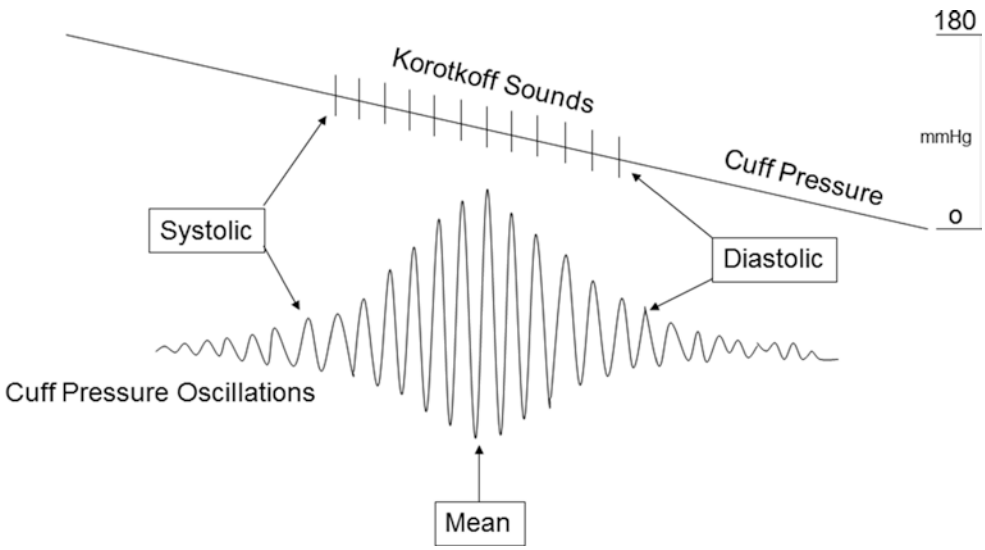

Fig. 20.11 An example of noninvasive blood pressure monitoring. As blood flow is restored with release of the blood pressure cuff, the arterial wave oscillations increase. The increase in oscillation amplitudes is associated with systolic blood pressure and presence of Korotkoff sounds. The peak of oscillations is associated with mean arterial pressure. Return of oscillations to baseline is diastolic blood pressure and end of Korotkoff sounds

of pulsatile flow. A blood pressure cuff is applied to a limb such as forearm or leg and is inflated to a pressure greater than systolic blood pressure, which stops blood flow distal to the inflated cuff. As the pressure in the cuff is gradually decreased, blood flow through the artery is restored. The change in arterial pressure and blood flow creates oscillations which can be detected by auscultation of Korotkoff sounds and oscillometric methods. For accurate blood pressure measurement, the width of the cuff should be approximately one-third the circumference of the limb. A small, improperly sized cuff will overestimate systolic blood pressure, while a large cuff will underestimate the pressure. The rate of cuff deflation should be slow enough to hear Korotkoff sounds or detect oscillations. Noninvasive blood pressure monitors do not work if there is no pulsatile flow.

The automated method of noninvasive blood pressure monitoring is the *oscillometric* technique. Most oscillometric blood pressure monitors have oscillotonometers and a microprocessor. The blood pressure cuff is inflated until no oscillation is detected. As the cuff pressure is decreased, flow in the distal blood vessel is restored and amplitude of oscillations increases. A large increase in arterial wave oscillation amplitude is recorded as systolic blood pressure, the peak oscillation as mean arterial pressure, and the sudden decrease in amplitude as diastolic blood pressure (Fig. 20.11). Due to the sensitivity of the monitoring system, the mean arterial pressure is usually the most accurate and reproducible. For more details on such monitoring, refer to Chap. 18.

20.4.2 Invasive Arterial Blood Pressure Monitoring

Continuous blood pressure monitoring is best accomplished by direct intra-arterial blood pressure monitoring. Direct pressure monitoring allows for continuous beat-to-beat monitoring of arterial pressure, and the recorded arterial waveform provides temporal information relative to cardiovascular function. Direct pressure monitoring is often employed in clinical settings such as: (1) during major trauma and vascular surgery, (2) in patients with sepsis, (3) during cardiopulmonary bypass where there is no pulsatile flow, (4) in patients with significant cardiovascular instability or fluctuations, and (5) in patients requiring tight blood pressure control, such as hypotension. Further, patients with significant cardiopulmonary disease (i.e., those in an intensive care unit) may require invasive arterial blood pressure monitoring (Table 20.1).

Table 20.1 Accepted indications for direct arterial blood pressure monitor

Major surgery
Major trauma
Major vascular (i.e., carotid endarterectomy, aortic aneurysm)
Cardiopulmonary bypass surgery
Myocardial dysfunction (i.e., myocardial ischemia/infarct, heart failure, dysrhythmias)
Uncontrolled/labile blood pressure (i.e., hypertension, hypotension)
Inaccurate noninvasive monitor (i.e., morbid obesity)
Sepsis/shock
Pulmonary dysfunction

Besides providing blood pressure assessment, the arterial waveform also presents information about cardiovascular function. For example, the upstroke of an arterial waveform correlates with myocardial contractility (dP/dT), while the downstroke gives information relative to peripheral vascular resistance. The position of the dicrotic notch gives insights as to the systemic vascular resistance; a low dicrotic notch position on the arterial waveform may infer low vascular resistance, while a high dicrotic notch usually relates to higher systemic vascular resistance. Furthermore, by integrating the area under the curve of the arterial waveform, the stroke volume may also be estimated.

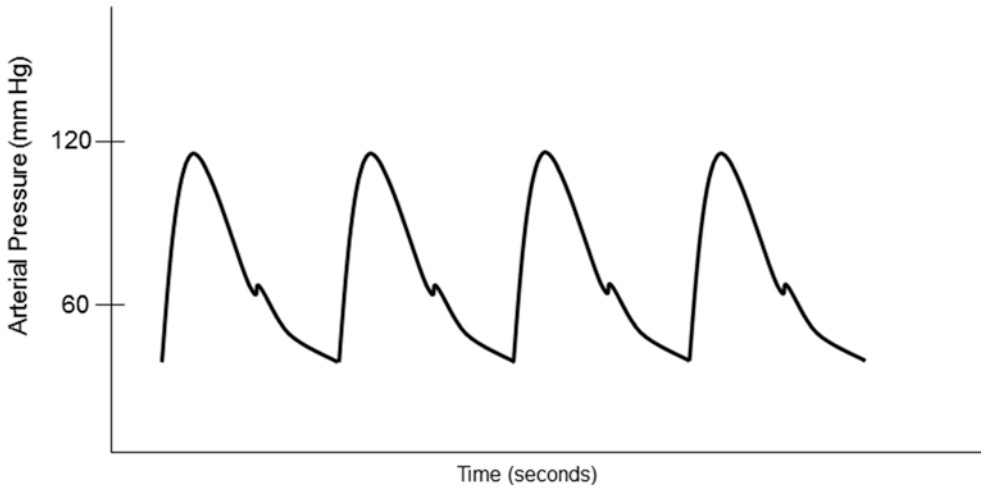

Fig. 20.12 An example of an arterial blood pressure wave from a typical optimally damped arterial blood pressure waveform. The peak portion of the waveform corresponds to the systolic blood pressure and the trough corresponds with the diastolic blood pressure. The dicrotic notch is associated with closing of the aortic valve. Information about cardiovascular function can be estimated from the waveform. The upstroke correlates with myocardial contractility. The downstroke and position of the dicrotic notch give information about systemic vascular resistance. The stroke volume is estimated by integrating the area under the curve

Direct arterial blood pressure monitoring typically involves cannulation of a peripheral artery and transducing the pressure (Online JPGs 20.2 and 20.3). An indwelling arterial catheter is connected to pressure tubing containing saline, which is then connected to a pressure transducer and monitoring system. Typical transducers contain strain gauges (stretch wires or silicon crystals) that distort with changes in blood pressure. The strain gauges contain a variable resistance transducer and a diaphragm which links the fluid wave to electrical signals. When the transducer diaphragm is distorted, there is a change in voltage across resistors of a Wheatstone bridge circuit (Online JPG 20.4). The transducer is constructed using a circuit so that voltage output can be calibrated proportional to the blood pressure. Standard pressure transducers are calibrated to 5 μV per volt excitation per mmHg [10]. Commonly, the electrical signals from such pressure monitoring systems are filtered, amplified, and displayed on a monitor, thus providing a typical arterial pressure waveform. It is important that the arterial pressure transducer be positioned and calibrated accurately at the level of the heart. Improper transducer height will result in inaccurate blood pressures; if the pressure transducer is positioned too high, the blood pressure is underestimated, while a lower positioned transducer will overestimate the actual blood pressure.

Common sites for intra-arterial cannulation for arterial pressure monitoring are the radial, brachial, axillary, or femoral arteries. Although the ascending aorta is the ideal place to monitor central arterial pressure waveforms, this is not practical in most clinical settings. However, it should be noted that pressure measurements in the more peripheral arteries become distorted when compared to central aortic pressure waveform (Fig. 20.12). Peripherally, the systolic blood pressure may be higher and diastolic blood pressure lower, while the mean

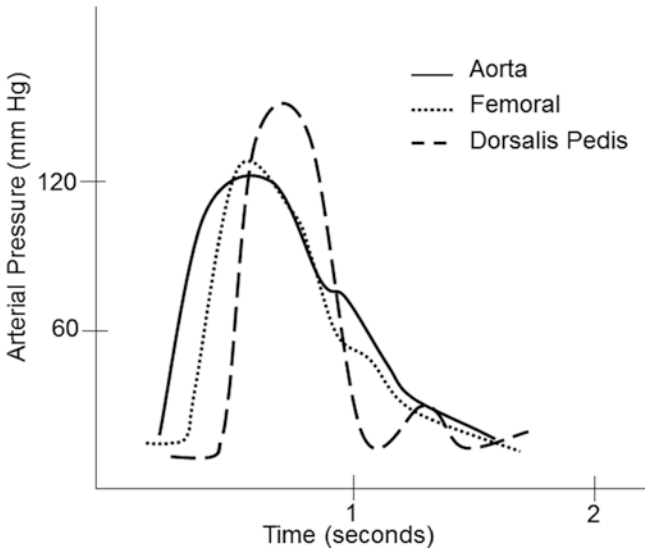

Fig. 20.13 A typical example of an arterial pressure waveform recorded from the ascending aorta. As the pressure monitoring site is moved more peripherally, the morphology of the waveform changes due to changes in arterial wall compliance as well as oscillation and reflection of the arterial pressure wave. Notice in the dorsalis pedis arterial waveform the absence of the dicrotic notch, overestimation of systolic blood pressure, and underestimation of diastolic pressure. Also note the presence of a small reflection wave

arterial pressure is usually similar to central aortic pressure. The pressure waveform becomes more distorted as pressure is measured farther away from the aorta. This distortion is due to a decrease in arterial compliance and reflection and oscillation of the blood pressure waves. For example, an arterial pressure wave monitored from the dorsalis pedis will be significantly different from a central aortic wave when it is graphically displayed (Fig. 20.13). There is also a loss in

amplitude or absence of the dicrotic notch, an increase in systolic blood pressure, and a decrease in diastolic blood pressure. One should also be aware of the possible appearance of a reflection wave as the blood pressure is monitored from a peripheral site. Importantly, risks associated with indwelling intra-arterial pressure catheter include thrombosis, emboli, infection, nerve injury, and hematoma.

20.4.3 Pressure Transducer System

In clinical settings, arterial and venous blood pressures and waveforms are displayed by utilization of a pressure transducer monitoring system. A typical system includes: (1) an indwelling intravascular catheter, (2) pressure tubing, (3) a pressure transducer, (4) stopcock and flush valve, (5) a high-pressure fluid bag, and (6) a graphical display monitor and microprocessor (Figs. 20.14a, b).

The pressure wave derived from the transducer system is a summation of sine waves at different frequencies and amplitudes. The fundamental frequency (first harmonic) is equal to the heart rate. Therefore, at a heart rate of 120 beats per minute, the fundamental frequency is 2 Hz. Since the first ten harmonics of the fundamental frequency make significant contributions to the arterial waveform [11], frequencies up to 20 Hz make major contributions to the pressure waveform. It is generally considered for most recording systems that the maximum significant frequency in the arterial blood pressure signal is approximately 20 Hz [12].

All materials have a natural frequency, also known as *resonant frequency*. The natural frequency of the monitoring system is the frequency at which the pressure monitoring system resonates and amplifies the actual blood pressure signal [12, 13]. If the natural frequency of the system is near the fundamental frequency, the blood pressure waveform will be amplified, giving an inaccurate pressure recording. The natural frequency is defined by the following equation [14]:

$$\mathrm{fn} = \left(d / 8\right) * \left(3 / \pi L \rho V_{\mathrm{d}}\right)^{1/2}$$

$$\varsigma = \left(16n / d^{3}\right) * \left(3LV_{\mathrm{d}} / \pi\rho\right)^{1/2} \left(\text{damping coefficient}\right)$$

where fn = natural frequency, d = tubing diameter, n = viscosity of fluid, L = tubing length, ρ = density of fluid, and V_{d} = transducer fluid volume displacement

In order to increase accuracy of the blood pressure waveform, the natural frequency needs to be increased while the amount of distortion is reduced. The optimal natural frequency should be at least 10 times the fundamental frequency, which is then greater than the tenth harmonic of the fundamental frequency [11, 12]. Therefore, the natural frequency should be greater than 20 Hz. In clinical settings, the input frequency is usually close to the monitoring system's natural frequency, which ranges from 10–20 Hz. When the input frequency is close to the natural frequency, the system amplifies the actual pressure signal. Ideally, the natural frequency should exceed the maximum significant frequency in a blood pressure signal which is about 20 Hz [12]. An amplified system typically requires damping to minimize distortion; an underdamped system will result in amplification, while an overdamped system will result in reduced amplification.

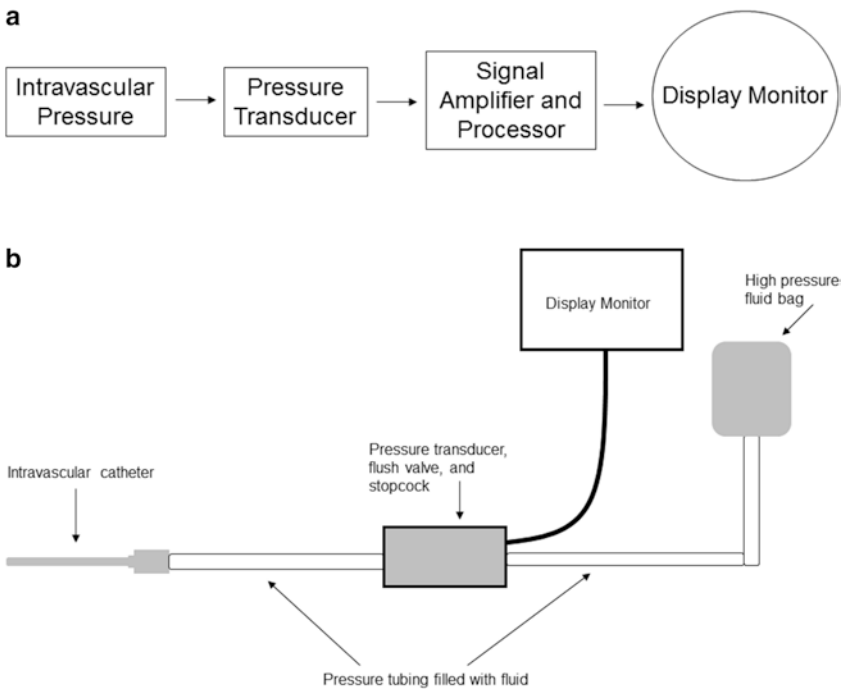

Fig. 20.14 Schematics of a pressure transducer monitoring system (see text for details)

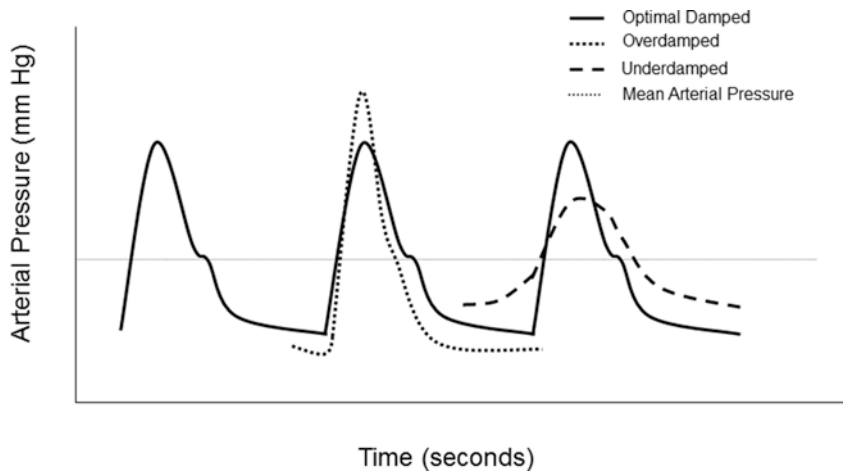

Fig. 20.15 Effects of damping on the arterial pressure waveform. In an underdamped pressure monitoring system, the pressure wave overestimates the systolic blood pressure and underestimates the diastolic blood pressure. In an overdamped system, the pressure wave underestimates the systolic blood pressure and overestimates the diastolic blood pressure. The mean arterial pressure remains essentially unchanged

The ability of the system to extinguish oscillations through viscous and frictional forces is the damping coefficient (ς) [15]. Some degree of damping may be required to prevent overamplification of blood pressure waveforms. It is considered that more damping is required especially in patients with higher heart rates, such as neonates. At higher heart rates, the tenth harmonic of the fundamental frequency will approach the natural frequency and the waveform is amplified. Overamplification, or ringing, can be adjusted by increasing the damping coefficient. Specifically, in an overamplified system, a connector with an air bubble can intentionally be placed in line with the pressure transducer; the air bubble damps the system to diminish ringing.

The accuracy of pressure transducers is considered optimal in the following situations: low compliance of the pressure catheter and tubing, low density of fluid in the pressure tubing, and short tubing with a minimal number of connectors. Note that a suboptimal pressure system may produce an underdamped or overdamped pressure waveform; an underdamped waveform will overestimate systolic blood pressure, while an overdamped waveform will underestimate systolic blood pressure. Damping occurs when factors such as compliance of tubing, air bubbles, and blood clots decrease the peaks and troughs of the pressure sine waves by absorbing energy and diminishing the waveform. In an underdamped system, the pressure waves generate additive harmonics, which may also lead to an overestimated blood pressure. In an overdamped system, a pressure wave may be impeded from adequately propagating forward. Overdamping may occur due to air bubbles in the pressure lines, kinks, blood clots, low-flush bag pressures, and multiple stopcocks or injection ports. This often results in underestimation of systolic blood pressure and overestimation of diastolic blood pressure. Fortunately, the mean arterial pressure is minimally affected by dampening (Fig. 20.15).

Optimal pressure waveforms can be obtained when there is balance between the degree of damping and distortion from the pressure tubing system. A simple way to assess damping is to observe the results from a high-pressure fluid flush. In the flush test, the pressure transducer system is flushed and the resulting oscillations (ringing) are observed. In an optimally damped system, a baseline results after one oscillation (Fig. 20.16). In an overdamped system, the baseline is reached without oscillations and the waveform is blunted. In an underdamped system, the flush test results in multiple oscillations before the waveform reaches baseline.

20.4.4 Transducer Catheters

Common clinical methods to monitor arterial and venous pressures utilize a pressure transducer system that requires a fluid-filled system. Transducer catheters such as Millar catheters (Online JPG 20.5) monitor pressures directly from a sensor incorporated within the tip of the catheter. A sensor (Online JPG 20.6) placed directly at the end of the catheter allows direct and constant measurement of pressures, thus eliminating the intrinsic inaccuracies of a fluid-filled system.

In general, transducer catheters are more accurate than conventional fluid-filled systems. Motion artifact is nearly eliminated and the issues of overdamped and underdamped systems are not present. Accurate pressure readings can be obtained with the catheter at any height; readings are not affected by the height of the pressure transducer as in the conventional system. With transducer catheters, there is no time delay since pressure is monitored directly at the source. Compared to the conventional fluid system, transducer catheters have high inherent fidelity (>10 MHz).

20.5 Central Venous Pressure Monitoring

An estimate of intravascular volume status and right heart function can be assessed with a central venous pressure catheter. Central venous pressure is ideally considered as the mean venous blood pressure at the junction of the right

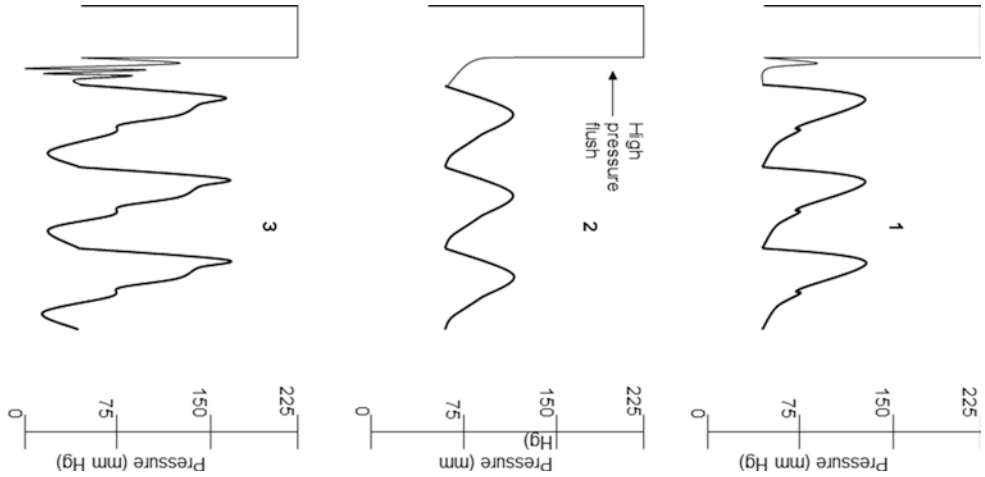

Fig. 20.16 An example of a high-pressure flush test. (*1*) In an optimally damped pressure monitoring system, the pressure wave returns to baseline after one oscillation. (*2*) In an overdamped system, the wave returns to baseline without any oscillations. The systolic blood pressure is underestimated and diastolic pressure overestimated. (*3*) In an underdamped system, the wave oscillates multiple times before returning to baseline. The arterial wave is amplified. The systolic pressure is overestimated and diastolic pressure underestimated. The mean arterial pressure usually is not significantly affected by overdamping or underdamping

Table 20.2 Relative intracardiac pressures in the healthy heart

Pressures	Mean	Range
Left atrium	8	4–12
Left ventricle systolic	125	90–140
Left ventricle end diastolic	8	4–12
Right atrium	5	2–12
Right ventricle systolic	25	15–30
Right ventricle end diastolic	5	0–10
Pulmonary artery systolic	23	15–30
Pulmonary artery diastolic	10	5–15
Pulmonary capillary wedge	10	5–15
Mean pulmonary artery	15	10–20

Table 20.3 Cardiac hemodynamic parameters (normal ranges)

Hemodynamic parameter	Derived formula	Range
CO	HR × SV	4–6 L/min
CI	CO/BSA	2.6–4.3 L/min/m^2
SV	CO × 1000/HR	50–120 mL/beat
SI	SV/BSA	30–65 mL/beat/m^2
SVR	(MAP − CVP) × 80/CO	800–1400 dyne s cm^{-5}
SVRI	(MAP − CVP) × 80/CI	1500–2300 dyne s cm^{-5} m^2
PVR	(PAP − PCWP) 80/CO	140–250 dyne s cm^{-5}
PVRI	(PAP − PCWP) 80/CI	240–450 dyne s cm^{-5} m^2
LVSWI	1.36 (MAP − PCWP) SI/100	45–60 g m/m^2
RVSWI	1.36 (PAP − CVP) SI/100	5–10 g m/m^2

BSA body surface area, *CI* cardiac index, *CO* cardiac output, *CVP* central venous pressure, *HR* heart rate, *LVSWI* left ventricular stroke work index, *MAP* mean arterial pressure, *PAP* pulmonary artery pressure, *PCWP* pulmonary capillary wedge pressure, *PVR* pulmonary vascular resistance, *PVRI* pulmonary vascular resistance index, *RVSWI* right ventricular stroke work index, *SI* stroke index, *SV* stroke volume, *SVR* systemic vascular resistance, *SVRI* systemic vascular resistance index

atrium and the inferior and superior vena cavae. The central venous pressure (Tables 20.2 and 20.3) is an estimate of right heart filling pressures and may be used to assess right heart function and circulating blood volume. The central venous pressure is dependent upon multiple factors such as intravascular volume, functional capacitance of veins, and status of the right heart. A limitation of central venous pressure monitoring is that it does not give direct information about the left heart function. Indications for central venous catheter placement may include monitoring of cardiac filling pressures, administration of drugs, and/or rapid infusion of large amounts of fluids (Table 20.4). A typical central venous pressure kit is shown in JPG 20.7 (online). It is critical to properly calibrate and position the pressure transducer system at the level of the right atrium. Since the numeric value of central venous pressure is small (2–12 mmHg), minor changes in transducer height will cause significant inaccuracies in central venous pressure assessment.

There are multiple sites for placement of central venous catheters. Common sites used in clinical practice are the internal jugular and subclavian veins (Online JPG 20.8). Central venous access can also be accomplished by placement of a long catheter via the antecubital, external jugular, and femoral veins. Complications of central venous catheter placement may include inadvertent arterial puncture (i.e., carotid and subclavian arteries), venous air embolism, pneumothorax, chylothorax, loss of guide wire, nerve injury,

Table 20.4 Relative indications for using a central venous pressure catheter

Large fluid shifts
Vascular access
Infusion of medication
Venous blood sampling
Major trauma and surgery
Monitoring of intravascular volume status
Aspiration of venous air embolus

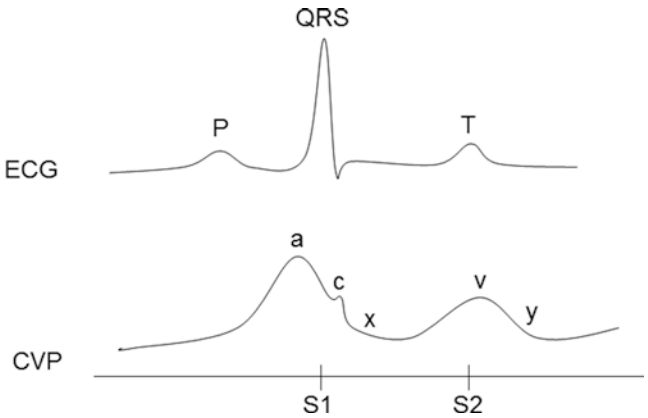

Fig. 20.17 A typical example of a central venous pressure waveform consisting of ***a***, ***c***, and ***v*** waves and ***x*** and ***y*** descents. The ***a*** wave is associated with atrial contraction. The ***c*** wave occurs as the tricuspid valve bulges up toward the right atrium during early ventricular systole. The ***v*** wave is associated with passive filling of the right atrium with closed valve. The ***x*** descent corresponds to the tricuspid valve being pulled down toward the right ventricle during late systole. The ***y*** descent corresponds with opening of the tricuspid valve as the right atrium begins to empty. *CVP* central venous pressure, *ECG* electrocardiogram

cardiac dysrhythmias, and/or line infections. There are multiple types of central venous catheters ranging from a single lumen to multiple lumen (double, triple, quad) catheters. Typically, multilumen catheters have slower flow rates due to the smaller radii of these lumens; recall that resistance to flow is proportional to the fourth power of the radius. After placement of a central venous pressure catheter, all ports must be aspirated and flushed to confirm proper intravascular placement of the catheter and eliminate any potential air in the line. The use of ultrasound for placement of a central venous line is currently common practice and has reduced the incidence of inadvertent arterial punctures. In clinical practice, a chest X-ray is often obtained to confirm proper positioning of the catheter. If a pneumothorax develops after accidental puncture of a lung, it will also be evident on chest X-ray.

The central venous pressure waveform can provide important information about the mechanical events occurring during a cardiac cycle (Fig. 20.17). An ***a*** wave is caused by atrial contraction which occurs after the P-wave on the

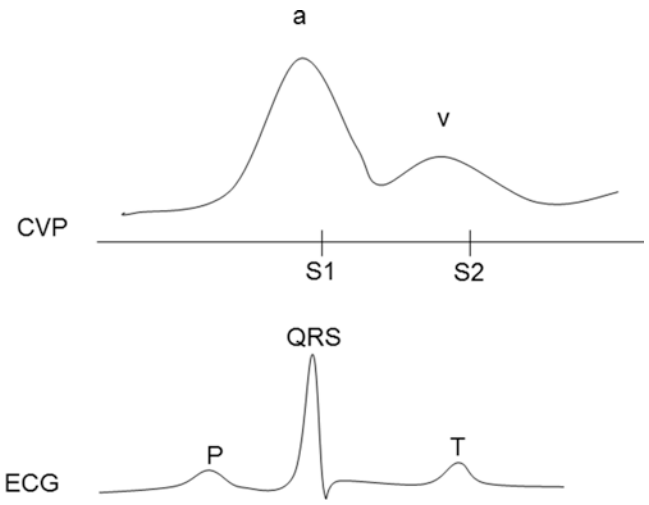

Fig. 20.18 An example of cannon ***a*** waves. A severely stenotic tricuspid valve or a junctional rhythm (atrium contracting against a close tricuspid valve) causes a large *a* wave. The mechanical events of the waveform must be correlated with the electrical events of the ECG

ECG. The ***c*** wave occurs during the start of ventricular systole as the tricuspid valve is pushed up toward the right atrium. The next portion of the waveform is the ***x*** descent, which represents the tricuspid valve being pulled down toward the right ventricle in late systole. The ***v*** wave correlates with passive filling of the right atrium while the tricuspid valve is closed. The ***y*** descent completes the waveform and represents the opening of the tricuspid valve, passive emptying of the right atrium, and filling of the right ventricle during diastole. Again it should be noted that the central venous pressure waveform provides information primarily concerning the right heart. Yet, the same waveform can be observed for the left heart by recording the pulmonary capillary wedge pressure from a pulmonary artery catheter (discussed later in this chapter). The central venous pressure waveform is affected by respirations; thus it should be read at end expiration. There will be central venous pressure variation with each respiratory cycle. Central venous pressure value is typically defined as the mean venous pressure at the end of exhalation during spontaneous or controlled ventilation. At end expiration, the intrathoracic pressure is closest to atmospheric pressure.

There are multiple clinical conditions that will affect the recorded central venous pressure waveform. For example, tricuspid stenosis may result in large (*cannon*) ***a*** waves (Fig. 20.18) as the right atrium contracts and pushes blood past a stenotic valve. Abnormal cardiac nodal rhythms, ventricular arrhythmias, or heart block will result in cannon ***a*** waves, as the atrium and ventricle are not synchronized and the atrium may be contracting against a closed tricuspid valve. Large ***a*** waves may also occur during situations where the resistance to right atrium emptying is significantly

increased, as in tricuspid and pulmonary valve stenosis, right ventricular hypertrophy, and/or pulmonary artery hypertension. Regurgitant valve disorders such as tricuspid regurgitation will result in large ***v*** waves (Fig. 20.19), representing overfilling of the atrium. Specifically, the large ***v*** wave occurs as blood volume from the right ventricle back flows into the right atrium past the incompetent tricuspid valve during systole. A noncompliant right ventricle, as in ischemia and heart failure, may also result in large ***v*** waves. During atrial fibrillation, ***a*** waves are absent due to ineffective atrial contractions. Again, similar waveforms for the left heart are seen from a pulmonary capillary wedge pressure waveform. Diagrams of cannon ***a*** and ***v*** waves are displayed in Figs. 20.18 and 20.19.

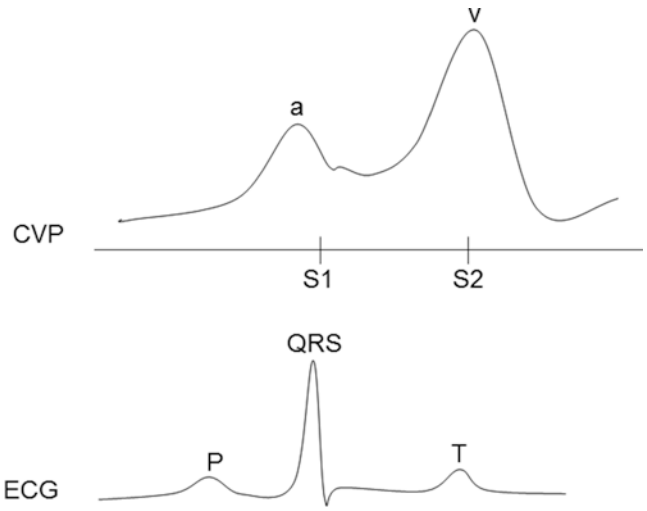

Fig. 20.19 An example of cannon ***v*** waves. An incompetent tricuspid valve (tricuspid regurgitation) abolishes the ***x*** descent and causes cannon ***v*** waves, as volume from the right ventricle back flows into the right atrium during ventricular systole. *CVP* central venous pressure, *ECG* electrocardiogram

20.6 Pulmonary Artery Pressure Monitoring

The pulmonary artery catheter was first introduced into clinical practice by Swan and Ganz [16]. Since its introduction, the pulmonary artery catheter has often been used in the management of critically ill patients and in those undergoing major cardiac surgery (Table 20.5) or solid organ transplantation surgeries. The effectiveness of pulmonary artery catheter monitors and their effect on patient morbidity and mortality continues to be debated and researched [17]. Current modifications also allow for continuous monitoring of pulmonary artery pressure, cardiac output, central venous pressure, mixed venous oxygen saturation (S_VO_2), and pulmonary capillary wedge pressure (Fig. 20.20, Online JPG 20.9).

Table 20.5 Relative indications for using a pulmonary artery catheter

Major organ transplant (liver, heart, lung)
Cardiopulmonary bypass surgery
Pulmonary hypertension
Sepsis/shock
Aortic aneurysm surgery
Heart failure (right and/or left heart)
Pulmonary embolus

See ASA Guidelines for more detailed indications and contraindications [35]

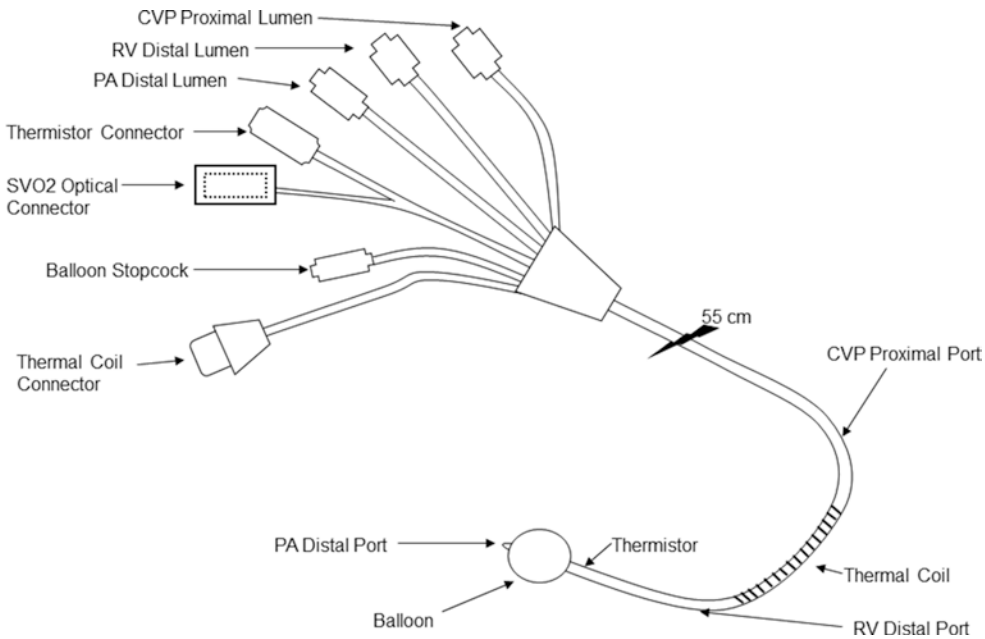

Fig. 20.20 A diagram of a typical pulmonary artery catheter with continuous cardiac output and mean venous oxygen saturation monitoring capabilities. Notice the addition of the thermal coils, thermistors, and optical components to the catheter. Diagram courtesy of Sock Lake Group, LLC. *CVP* central venous pressure, *PA* pulmonary artery, *RV* right ventricle, *SVO2* venous oxygen saturation

One of the advantages of the pulmonary artery catheter is that blood pressure information associated with the left heart may also be obtained via the pulmonary capillary wedge pressure. Under conditions of normal pulmonary physiology and left ventricular function and compliance, the pulmonary capillary wedge pressure is proportional to the left ventricular end-diastolic pressure, which is proportional to left ventricular end-diastolic volume. Left ventricular preload is best measured by left ventricular end-diastolic volume:

$$\text{CVP} \sim \text{PAD} \sim \text{PCWP} \sim \text{LAP} \sim \text{LVEDP} \sim \text{LVEDV}$$

where CVP = central venous pressure, PAD = pulmonary artery diastolic pressure, PCWP = pulmonary capillary wedge pressure, LAP = left atrial pressure, LVEDP = left ventricular end-diastolic pressure, and LVEDV = left ventricular end-diastolic volume.

Typically, after establishing central venous access, a pulmonary artery catheter is floated into the pulmonary artery with the catheter balloon inflated (Online Video 20.1). The location of the pulmonary artery catheter balloon is monitored by analysis of the waveform as the catheter is floated from the vena cava to the right atrium, to the right ventricle, and ultimately into the pulmonary artery (Fig. 20.21). Once the catheter is in the pulmonary artery, it is advanced further until the balloon wedges into a distal arterial branch (smaller diameter) of the pulmonary artery (Fig. 20.22). The resultant mean pressure and waveform is the pulmonary capillary wedge pressure. Under normal physiologic conditions, this pressure correlates well with the left atrial pressure. However, the pulmonary artery catheter balloon should not be kept inflated for a long duration or kept in a wedged position due to the possibility of causing pulmonary artery rupture. Note that whenever the catheter is advanced, the balloon (Online JPG 20.10) should be inflated, and when it is pulled back, the balloon should be deflated. The balloon on most pulmonary artery catheters holds a specific volume of air (1.5 mL). Exceeding this volume may result in balloon rupture and/or catastrophic pulmonary artery rupture. Most currently available catheter systems come with a balloon inflation syringe (built-in limiter) which minimizes the risk of such an error.

As with all pressure transducers, the pulmonary artery catheter pressure transducer must be accurately calibrated and zeroed prior to obtaining pressure readings. The pressure transducer should be zeroed at the level midway between the anterior and posterior chest at the level of the sternum; this is usually near the level of the right atrium. The pulmonary artery pressure should be obtained at end expiration (either during spontaneous or mechanical ventilations).

Proper positioning of the pulmonary artery catheter in the lung region is important in obtaining accurate pressure measurements. Since a greater portion of blood flow goes to the right lung (approximately 55 %), the balloon of the pulmonary artery catheter most often floats to the right pulmonary artery. West et al. categorized three lung zones (I, II, III) based on the correlation between pulmonary arterial pressure, alveolar pressure, and venous pressure [18]. Ideal placement of the pulmonary artery catheter requires the catheter tip to be in zone III. This is the area in the lung where blood flow is uninterrupted and therefore capable of transmitting the most accurate blood pressure; it is also the zone least affected by airway pressures. In order for the pulmonary capillary wedge pressure to best correlate with left atrial pressure, the distal tip of the catheter should be in a patent vascular bed. If the catheter tip is in the area of the lung where alveolar pressure is greater than perfusion pressure, the pulmonary capillary wedge pressure will reflect the alveolar pressure and not left atrial pressure. Controlled mechanical ventilation utilizing positive end-expiratory pressure decreases the size of west zone III and may affect correlation of pulmonary capillary wedge pressure and left atrial pressure [13]. Other clinical settings in which pulmonary capillary wedge pressure may not accurately reflect left atrial pressure include patients with pulmonary vascular disease, mitral valve disease, and chronic obstructive pulmonary disease and/or those being administered with positive end-expiratory pressure [19]. It is possible to convert zone III into

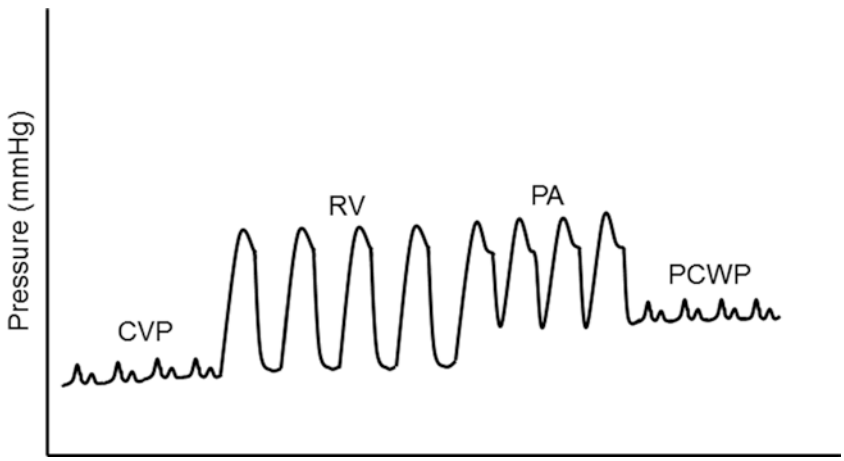

Fig. 20.21 A typical example of right heart blood pressure waveforms. As the pulmonary artery catheter is floated into the distal pulmonary artery, the morphology of the pressure wave changes as it goes through the chambers of the heart. *CVP* central venous pressure, *PA* pulmonary artery pressure, *PCWP* pulmonary capillary wedge pressure, *RV* right ventricle pressure

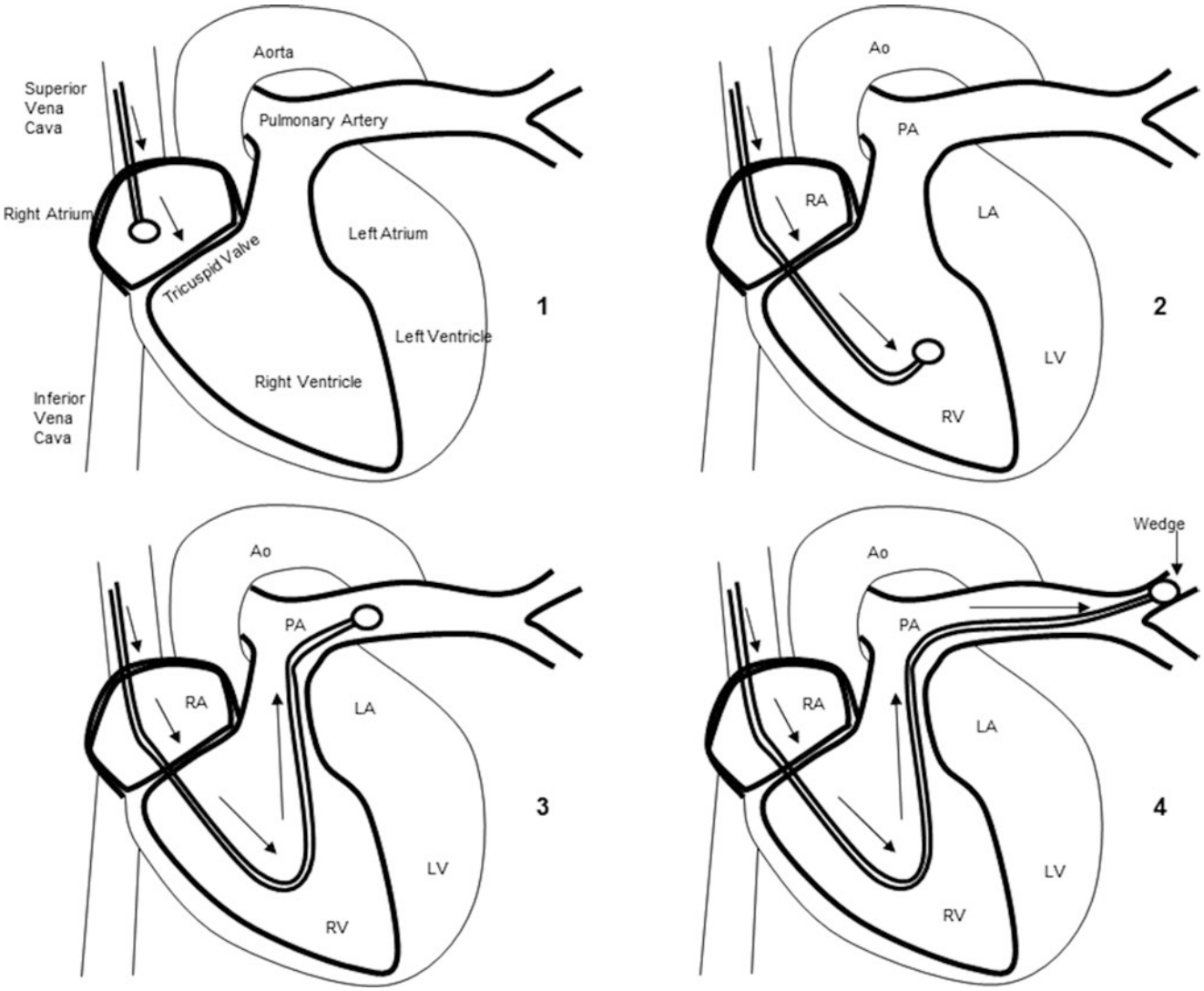

Fig. 20.22 Floating a pulmonary artery catheter through chambers of a heart until the balloon wedges in the distal pulmonary artery. Diagram courtesy of Sock Lake Group, LLC. *Ao* aorta, *LA* left atrium, *LV* left ventricle, *PA* pulmonary artery, *RA* right atrium, *RV* right ventricle

zone II and even zone I, with major increases in pulmonary alveolar pressure, such as positive pressure ventilation and positive end-expiratory pressure [20]. Again, conditions such as positive pressure ventilation, obstructive and restrictive lung disease, and cardiac diseases (i.e., valvular and altered ventricular compliance, tachycardia, and pneumonectomy) are situations where pulmonary capillary wedge pressure does not accurately correlate with left ventricular end-diastolic pressure [21, 22] and hence left ventricular end-diastolic volume.

The pulmonary capillary wedge pressure waveform is similar to the central venous pressure waveform and occurs at a similar time point within the cardiac cycle. Myocardial changes (i.e., myocardial ischemia), which commonly occur in compliance, and valvular disease will affect the waveform. Large ***v*** waves occur with mitral regurgitation, myocardial ischemia, papillary muscle dysfunction, and infarction (Fig. 20.19). Large ***v*** waves may look similar to the pulmonary artery waveform. To prevent errors in interpreting pulmonary capillary wedge pressure and pulmonary artery pressure, the waveform must be viewed and correlated with the ECG tracing. The ***v*** wave will always occur after the QRS complex and peak systemic arterial waveform and will not have a dicrotic notch. The pulmonary artery waveform has a dicrotic notch. A large ***a*** wave typically occurs in patients with mitral stenosis and/or left ventricular hypertrophy.

Pulmonary artery catheters may be contraindicated in patients with known abnormal anatomy of the right heart, such as tricuspid and pulmonic valve stenosis or masses in the right heart. Such catheters may also be contraindicated in patients with left bundle branch block of the myocardial con-

duction system; floating the pulmonary artery catheter through the right heart may cause right bundle branch block and increase the risk of developing complete heart block. The existence of cardiac pacer leads is not a contraindication but may make placement of a pulmonary artery catheter difficult (Online Video 20.2). Care also must be taken when removing such a catheter. Reported complications associated with pulmonary artery catheters include: cardiac arrhythmias, heart block, pulmonary artery rupture, infection, and/or pulmonary infarction [23]. During cardiac surgery such as lung and heart transplant, it is possible to have the pulmonary artery catheter inadvertently sutured in the surgical field. Note that any resistance to catheter removal must alert the clinician to the above possibility.

20.7 Cardiac Output/Cardiac Index Monitoring

Determining cardiac output is now considered vital when managing any critically ill patient, in particular those with severe cardiac disease, pulmonary disease, and/or multiorgan failure. Cardiac output is the total blood flow by the heart measured in liters per minute (L/min); in an average adult, cardiac output is approximately 5–6 L/min. Cardiac output is often equated with global ventricular systolic function. Any increase in demand for oxygen delivery is usually accomplished with an increase in cardiac output. Furthermore, increasing cardiac output is an important factor in oxygen delivery. Cardiac output is dependent upon heart rate and stroke volume. In a normal heart, stroke volume is dependent upon preload, afterload, and contractility. Note that myocardial wall motion abnormalities and/or valvular dysfunction will also affect stroke volume.

Starling's law describes the relationship between cardiac output and left ventricular end-diastolic volume (Fig. 20.3). As preload is increased, the cardiac output increases in direct proportion to the left ventricular end-diastolic volume until an excessive preload is reached. At this point, increases in left ventricular end-diastolic volume do not result in increased cardiac output and may actually decrease it.

Due to variations in body size and weight, cardiac output is frequently expressed as a cardiac index. Cardiac index is equal to cardiac output divided by body surface area and has a normal range of 2.5–4.3 L/min/m^2:

$$\mathrm{CO} = \mathrm{HR} \times \mathrm{SV}$$

$$\mathrm{CI} = \mathrm{CO} / \mathrm{BSA}$$

where CO = cardiac output, HR = heart rate, SV = stroke volume, CI = cardiac index, and BSA = body surface area.

The equation for cardiac output can also be derived by rearranging the oxygen extraction equation. Oxygen extraction is the product of cardiac output and the difference between arteriovenous oxygen content:

$$\mathrm{VO}_2 = \mathrm{CO} \times \left(\mathrm{CaO}_2 - \mathrm{CvO}_2\right)$$

where VO_2 = oxygen extraction, CO = cardiac output, CaO_2 = arterial oxygen content, and CvO_2 = venous oxygen content.

Rearranging the oxygen extraction equation allows calculation of cardiac output:

$$\mathrm{CO} = \mathrm{VO}_2 / \left(\mathrm{CaO}_2 - \mathrm{CvO}_2\right)$$

A limitation of the Fick method is that frequent blood samples from the arterial and venous circulation are required. Expiratory gas must also be analyzed to measure oxygen consumption.

Cardiac output can also be measured by utilizing an indicator (dye) dilution technique or a thermodilution technique. In the indicator dilution technique, a nontoxic dye (e.g., methylene blue or indocyanine green) is injected into the right heart. The dye mixes with blood and goes out the pulmonary artery to the systemic circulation. A circulating arterial blood sample with diluted indicator dye is collected and measured using spectrophotometric analysis. Repeat cardiac output measurements utilizing the indicator dilution technique are limited due to increasing concentrations of dye with each subsequent measurement.

The thermodilution method to measure cardiac output is a modification of the indicator dilution technique initially described by Fegler [24] in 1954. Thermodilution techniques are not considered to be affected by recirculation, as are the indicator dilution techniques. Typically, the distal tips of the pulmonary artery catheters contain thermistors that detect temperatures of circulating blood. The more proximal portion of the pulmonary artery catheter contains an opening that allows for injection of fluid such as normal saline or D_5W. The injected solution may be at an ambient temperature or iced. An iced solution increases the temperature difference and therefore the signal-to-noise ratio [25]; thus, it is considered better than an injectate at room temperature. A computer program within the monitoring system commonly calculates the cardiac output utilizing the thermodilution cardiac output equation. Components of the equation include the following: specific heat of blood, specific gravity of blood and injectate, volume of injectate, and area of blood temperature curve. A modified Stewart-Hamilton equation [26] can also be used to calculate cardiac output using this approach:

$$\mathrm{CO} = \mathrm{V}\left(\mathrm{Tb} - \mathrm{Ti}\right) \times K1 \times K2 / \int \mathrm{Tb}(t)\,dt$$

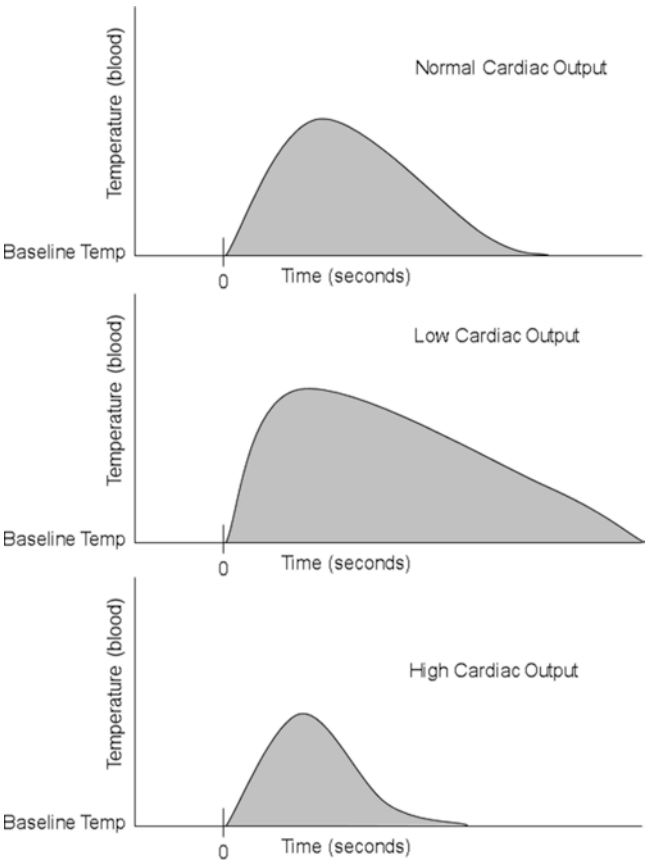

Fig. 20.23 An example of cardiac output monitoring. In this case, cardiac output is inversely proportional to the area under the thermodilution curve

where CO = cardiac output in L/min, V = volume of injectate (mL), Tb = initial blood temperature (°C), Ti = initial injectate temperature, $K1$ = density factor, $K2$ = computation constant, and $\int \Delta \mathrm{Tb}(t)dt$ = integral of blood temperature change over time.

Cardiac output is inversely proportional to the area under the curve (Fig. 20.23).

Nevertheless, an accurate calculation of cardiac output requires both proper position of the pulmonary artery catheter and a consistent volume of injectate. Note that conditions such as tricuspid and pulmonic value regurgitation and intracardiac shunts will cause recirculation of blood and thus result in the false elevation of cardiac output. The errors of intermittent bolus thermodilution techniques include valuable volumes and temperatures of injectate, technique of injection, and timing of injection with the respiratory cycle [27]. Cardiac output measurements are also affected by clinical conditions such as tricuspid insufficiency, intracardiac shunts, and/or atrial fibrillation [19].

More recently, continuous cardiac output monitoring has been made possible with advanced pulmonary artery catheters (Online JPG 20.11). Typically, continuous cardiac output monitors utilize a thermal coil which is positioned in the right ventricle; this coil intermittently heats the blood. Once the continuous cardiac output catheter and system reaches a steady state with its surroundings, the thermal coil intermittently heats blood. The temperature change of the surrounding blood is detected by a thermistor located at the distal tip of the pulmonary artery catheter; the recorded blood temperature varies inversely with cardiac output.

The accuracy of the system depends on the measurement of temperature differences from the injection port to the distal measurement thermistor. In the thermodilution technique, the volume of injectate must be constant (10 mL). Smaller amounts of cold solution reaching the thermistor will result in a higher cardiac output. Such detected differences may be caused by actual increased cardiac output, small amounts of injectate, warm indicator and/or injectate, a clot on the thermistor, or a wedged catheter. A calculated small cardiac output will result when the solution reaching the thermistor is too cold; this may occur if there is too large an amount of injectate, if the solution is too cold, if there is an actual decrease in cardiac output, and/or if the patient has an intracardiac shunt. A major limitation of continuous cardiac output method is its slow response time to acute changes in cardiac output [27, 28]. Although the response time may be slow, it is still faster in detecting cardiac output changes than the traditional intermittent thermodilution technique. Furthermore, continuous cardiac output monitoring is generally considered to be more accurate than the intermittent thermodilution technique [29, 30].

Noninvasive methods to measure cardiac output include Doppler modalities, the transpulmonary dilution technique [31, 32], gas rebreathing technology [32, 33], and/or a bioimpedance [32, 34, 35] technique. Briefly, the noninvasive Doppler method to measure cardiac output is an esophageal Doppler monitor. As such, an esophageal Doppler probe is placed and an ultrasound beam is directed at the descending aorta. By knowing the cross-sectional area of the aorta and blood velocity, the stroke volume is calculated [32].

The transpulmonary dilution method for measuring cardiac output requires injections of an indicator (lithium or thermodilution) in the venous circulation (central or peripheral) and subsequent assessment of the indicator level of the systemic arterial circulation; a typical example is the lithium chloride solution technique [36–38]. Lithium chloride indicator is injected through a central or peripheral vein, and the plasma concentration of this indicator is measured via a lithium-specific electrode connected to the arterial line [39]. A concentration-time curve is generated and cardiac output is calculated from the area under the curve associated with the lithium ion concentrations [40].

The thoracic bioimpedance method measures cardiac output by detecting the change in flow of electricity with alteration in blood flow [31]. For thoracic bioimpedance, a low-amplitude and high-frequency current is transmitted and

then sensed by sets of electrodes placed on both sides of the thorax and neck. The cardiac alterations in impedance (resistance to current flow) are analyzed and calculated as the blood volume changes for each heart beat (stroke volume). The thoracic bioimpedance method of measuring cardiac output may be useful in clinical situations such as major trauma [41, 42] and cardiac disease [43].

Gas technology utilizing the measurement of carbon dioxide [32, 44] applies the Fick principle of oxygen consumption and cardiac output but substitutes carbon dioxide production for oxygen consumption. By determining the change in CO_2 production and end-tidal CO_2, modification of the Fick equation can be applied to calculate cardiac output [45]:

$$CO = \quad VCO_2 / \quad EtCO_2$$

where CO = cardiac output, ΔVCO_2 = change in CO_2 production, and $\Delta EtCO_2$ = end-tidal CO_2.

It should be noted that the accuracy of the carbon dioxide rebreathing method to measure cardiac output is, at present time, inconclusive [45–48].

20.8 Mixed Venous Saturation Monitoring (SvO_2)

Mixed venous oxygen saturation monitoring (SvO_2) typically utilizes reflective spectrophotometric technology to measure the amount of oxygen in mixed venous blood. Yet, a true mixed venous blood sample is measured in the pulmonary artery. Systemic venous blood with different oxygen extraction ratios returns to the right atrium via the superior vena cava and inferior vena cava, mixes and equilibrates in the right ventricle, and flows out past the pulmonic valve to the pulmonary artery. As blood travels past the SvO_2, catheter light emitted from the catheter tip is reflected off the red blood cells and is detected by a photodetector. The difference in wavelengths of emitted and reflected light is processed to estimate SvO_2 (Fig. 20.24). Continuous venous saturation (SvO_2) monitoring has been made possible with the adaptation of a pulmonary artery catheter with fiber-optic technology (Online JPG 20.11). Such monitoring utilizes the principle of reflectance spectrophotometry, which uses multiple wavelengths of transmitted light at specific intensities that is then reflected from red blood cells. For example, oxygenated hemoglobin absorbs most infrared light (940 nm) and reflects or transmits most red light (660 nm); this is the reason that oxyhemoglobin looks red and deoxyhemoglobin appears blue. The tip of the SvO_2 catheter emits light with specific wavelengths which measure both oxyhemoglobin and deoxyhemoglobin, as red blood cells flow past the tip of the catheter. The difference between absorption of light between saturated and desaturated hemoglobin results in the calculated SvO_2 value.

The SvO_2 equation is a modification of the Fick equation; SvO_2 is derived by rearranging the Fick equation as follows:

$$VO_2 = C(a-v)O_2 \times CO \times 10$$

$$SvO_2 = SaO_2 - VO_2 / DO_2$$

$$DO_2 = \text{volume of } O_2 \text{ delivered per minute} = CO \times CaO_2 \times 10$$

$$VO_2 = \text{oxygen consumption per minute} = C(a-v)O_2 \times CO \times 10$$

$$SaO_2 = \text{arterial } O_2 \text{ saturation}(1.0)$$

$$CaO_2 = 1.39 \times Hgb \times SpO_2 + 0.003 \times PaO_2$$

where VO_2 = oxygen consumption, CaO_2 = arterial oxygen content, CvO_2 = venous oxygen content, CO = cardiac output, DO_2 = oxygen delivery, SaO_2 = arterial oxygen saturation, Hgb = hemoglobin, SpO_2 = oxygen saturation, and PaO_2 = partial pressure of arterial oxygen.

Accurate measurement of SvO_2 requires that vasoregulation be intact [49], and there must be a continuous flow of

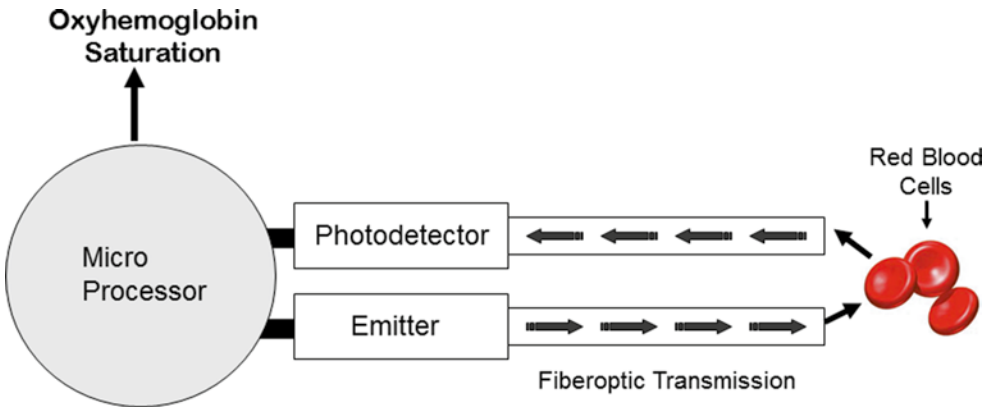

Fig. 20.24 An example of mixed venous saturation monitoring (*SvO2*). Spectrophotometric technology such as pulse oximeter and mixed venous oxygen saturation monitors are utilized to measure the amount of oxygenated hemoglobin in circulating blood. A specific wavelength (infrared) is emitted and the reflected wavelength off the red blood cells is detected and processed

blood past the tip of the catheter. SvO_2 values may be incorrect if the tip of the pulmonary artery catheter migrates into the distal pulmonary artery and/or comes in contact with the arterial wall. Other causes of incorrect SvO_2 values include miscalibration of the microprocessor or light intensity that is too low (some sensor systems have incorporated intensity monitors). Note that the tip of the catheter must be in the pulmonary artery in order to have true mixed venous oxygen.

Mixed venous oxygen saturation (SvO_2) monitoring provides information about the balance between total body oxygen consumption and delivery. SvO_2 (0.65–0.75) measures the amount of oxygen not taken up by organs and tissues. Therefore, the lower the SvO_2, the higher the fraction extraction of oxygen by the tissues and a possible imbalance between oxygen consumption and oxygen delivery. SvO_2 is dependent upon arterial oxygen saturation, oxygen consumption, concentration of hemoglobin, and cardiac output. A significant change in SvO_2 may be caused by decreased oxygen delivery (decreased cardiac output and hemoglobin), increased oxygen consumption, or decreased arterial oxygen saturation. Continuous SvO_2 monitoring is useful in conditions where there is significant oxygen transport imbalance including: severe cardiac and respiratory disease, sepsis, and/or dysfunctional oxygen transport [50]. During stable arterial oxygen content and consumption, SvO_2 reflects the relative cardiac output [51, 52]. Furthermore, monitoring of SvO_2 may provide vital information in the medical management of critically ill [53, 54] and/or cardiac surgery patients [55]. If SvO_2 drops during a period of increased oxygen demand, it may indicate inadequate tissue perfusion and oxygen delivery; this information would not be available with monitoring cardiac output only.

It is considered that SvO_2 may be a better measurement of myocardial performance than cardiac output alone. Acute decrease in SvO_2 below 0.65 indicates a disparity between oxygen delivery and oxygen consumption. A change in SvO_2 greater than ±0.1 is considered significant. Medical management of critically ill patients by implementing measures to keep SvO_2 normal is considered important for decreasing morbidity and mortality [39, 56]. Conditions where SvO_2 is greater than 0.75 include increased oxygen delivery and low oxygen consumption. SvO_2 may be elevated during septic shock, hyperoxygenation, and cyanide toxicity and in patients with arterial venous shunts [49, 50]. The increase in SvO_2 during sepsis is considered, in part, due to the loss of vasoregulation and yet does not mean that organ tissues are being adequately oxygenated. It should be noted that, under general anesthesia, the SvO_2 value is increased due to the decreased metabolic requirement for oxygen by tissues.

In clinical settings where a pulmonary artery SvO_2 catheter is not possible (i.e., pediatric patients), a central venous oxygen saturation ($ScvO_2$) monitor may be used. The advantage of $ScvO_2$ is that a pulmonary artery catheter is not required; only central venous access is needed. The $ScvO_2$ obtains venous oxygen saturation readings from the superior vena cava or right atrium. During normal physiological and hemodynamic conditions, $ScvO_2$ correlates well with SvO_2 [57–59]. However, in critical illness and shock, the $ScvO_2$ does not accurately reflect the true SvO_2 [60–62] and, therefore, true SvO_2 can only be measured in the pulmonary artery in such cases [63]. Resuscitation and medical management of critically ill patients with a $ScvO_2$ monitor may provide benefits over conventional monitors such as vital signs and/or central venous pressure [60].

20.9 Flow Monitoring

While cardiac output is similar regardless of where it is measured within the heart, the flow profiles can change dramatically within different anatomical structures and disease states. Given a constant cardiac output, flow velocity increases with a smaller diameter vessel, with larger velocities seen at the center of the flow profile and with zero velocity at the vessel wall.

For example, flow through the cardiac valves is important for diagnoses of stenosis and regurgitation. Stenosis is defined as a narrowing of the orifice area of the valve. This can be caused by a variety of factors including sclerosis formation on leaflets and is characterized by abnormally high flow velocities through the valve. Regurgitation is defined as flow reversal through a valve and can be caused by annular dilatation, leaflet prolapse, and/or changes in chamber dimensions affecting the valve performance. While a small amount of regurgitation is normal (caused by valve closing called the *closing volume*), patients with pathologic regurgitation have abnormally high flows traveling retrograde across the valve orifice.

Clinical diagnoses of regurgitation and stenosis are typically done using echocardiography (see Chap. 22). Pulsed wave Doppler measures a frequency shift in the ultrasound waves to calculate a flow velocity. Color flow mapping allows for visualization of the flow through the valve. By standards, areas flowing toward the transducer head appear red, areas flowing away from the transducer head appear blue, and areas of regurgitation or turbulent flow appear in a third color, typically yellow or green. Flow rates, pressure gradients, and orifice area measurements are available in Table 20.6 for the varying degrees of stenosis for each of the cardiac valves, as reported by the American College of Cardiology (ACC)/American Heart Association (AHA) guidelines [64]. Consult the ACC/AHA guidelines for diagnosing the severity of regurgitation.

In a research setting, several other methods are available for flow monitoring across the cardiac valves in an in vivo setting. Doppler sensors, using the same principles as echocardiography, are available in a number of forms, a c-ring transducer (transonic) being common. This flow probe takes frequency

Table 20.6 Indications for diagnosing stenosis of the cardiac valves

	Jet velocity (m/s)	Pressure gradient (mm Hg)	Orifice area (cm^2)
Aortic stenosis			
Mild	<3.0	<25.0	>1.5
Moderate	3.0–4.0	25.0–40.0	1.0–1.5
Severe	>4.0	>40.0	<1.0
Mitral stenosis			
Mild	<5.0	<30.0	>1.5
Moderate	5.0–10.0	30.0–50.0	1.0–1.5
Severe	>10.0	>50.0	<1.0
Tricuspid stenosis			
Severe	NA	NA	<1.0
Pulmonic stenosis			
Severe	>4.0	>60.0	NA

measurements, calculates a velocity from the measurement, and then multiplies the velocity by the area of the c-ring to determine the flow through the vessel. This type of sensor is useful for flows downstream of the aortic or pulmonary valves but cannot be attached in the atrioventricular positions.

Electromagnetic sensors take advantage of Faraday's law of inductance to measure velocity of a conducting fluid, such as blood. A rapidly reversing magnetic field is produced and, as the fluid moves through this field, a voltage is generated. This voltage is measured and translated into a frequency signal which is proportional to flow rate. Sensors are capable of measuring the instantaneous velocity of a small area with high temporal resolution and can be attached to a catheter. The disadvantage of electromagnetic sensors is that the measurements are affected by catheter placement, the exact location of which can be difficult to determine through fluoroscopy.

Cardiac magnetic resonance can be utilized in both a clinical and research role to investigate flow through valves and major vessels. Phase-contrast cardiac magnetic resonance enables the measurement of blood flow velocity across the cardiac valves and the great vessels with a high temporal and spatial resolution. As blood flows through the static magnetic field, the precession frequency changes in the hydrogen atoms of the tissue. This frequency change results in a dephasing effect on the magnetization of the atoms. The net dephasing of the atomic spins is a function of the velocity of the blood flow as well as the direction. This technique is used for clinical diagnoses of valvular regurgitation and aortic stenosis and to investigate coronary flow. For more information on these methods, the reader is referred to Chap. 24.

Angiograms are utilized to observe acute flow through the coronary system. While this is a qualitative technique for flow monitoring, it is of clinical importance, particularly for the assessment of coronary blockages. In an angiogram, the patient is typically cannulated via a femoral artery and the catheter is fed into or near the coronary ostia. Contrast is then injected through the catheter and into the bloodstream. By imaging via fluoroscopy (continuous X-rays), the contrast can be observed traveling through the coronary system. Flow is considered interrupted anywhere that contrast cannot traverse, indicating a blockage or reduced flow in the coronary system. An arterial dissection of the left anterior descending coronary artery is shown in Online JPG 20.12. The dissection is a tear in the tunica intima of the blood vessel, which allows blood into the space between the inner and outer layers of the vessel wall, resulting in vessel stenosis and possible occlusion. The area of the dissection is circled on the left of the image and the reduction in flow is visible downstream of the dissection. The image on the right shows the same artery after the vessel has healed.

Classification of blood flow using engineering terms is not a simple task. Blood flow through vessels is typically laminar, but partial occlusions can lead to turbulence downstream of the occlusion. This phenomenon is utilized in blood pressure measurements (i.e., Korotkoff sounds). Flow through or near a cardiac valve becomes quite a bit more complicated, as it is neither laminar nor turbulent. Yoganathan et al. classify the pulsatile flow of blood through cardiac valves as *borderline turbulent flow*, characterized by regions of flow reversal, 3D separation, and vortex formation, with borderline turbulent flow being defined as unsteady laminar flow with more than one temporal frequency excited. Yet, they further describe the flow to transition into a fully turbulent state during peak systole [65].

20.10 Implantable Monitoring

In both research and clinical settings, the ability to more optimally and continuously monitor hemodynamic properties is being realized. Furthermore, devices are being developed for researchers who work with small animals, for clinical researchers, and for physicians to monitor their patients without clinical visits. These devices may consist of sensors that transmit data to an implantable loop recorder, where the information is stored until it is collected by the researcher or physician by telemetry or other means.

An implantable loop recorder is a valuable tool for researchers conducting chronic studies and for clinicians. For example, data can be collected continuously when investigating properties that occur only rarely or change slowly over time. Clinically, implantable loop recorders that gather ECG data are used for diagnosis of patients with unexplained syncope, near syncope, episodic or recurrent palpitations, and seizure-like events. The use of an implantable loop recorder has diagnosed patients in which standard tilt-table testing has failed to induce syncope [66–68] and is now advised for management of patients with syncope [69, 70]. Two examples of implantable loop recorders are the Sleuth (Transoma Medical, Inc., Arden Hills, MN, USA) and the Reveal Plus (Medtronic, Inc., Minneapolis, MN, USA).

Perhaps the most advanced implantable hemodynamic monitoring system to date is the investigational device called Chronicle (Medtronic, Inc.). It is a pressure sensor-equipped lead that is implanted in the right ventricle to provide continuous hemodynamic monitoring of heart rate, right ventricular systolic pressure, right ventricular diastolic pressure, right ventricular pulse pressure, maximum right ventricular dP/dt, and/or estimated pulmonary artery diastolic pressure [71, 72]. The data storage period of this device can be adjusted with the desired sampling rate but can also be reprogrammed as desired.

Another application of implantable sensors is the monitoring of patients with congestive heart failure. Signs and symptoms of congestive heart failure are not well correlated with the disease status [73, 74]. Investigational devices combining pacing capabilities with monitoring capabilities have been implanted in ambulatory patients with congestive heart failure to monitor parameters such as the mixed venous oxygen saturation and right ventricular pressures. The feasibility of these devices has been shown [75], but clinical validation studies are ongoing.

Implantable monitors are only as valuable as the information they collect and the manner and ease in which that information is transferred to those interpreting it. Collection of the data is less of an issue in a research setting, where the researcher can personally ensure the data is retrieved at the proper time and in the desired format. Clinicians, on the other hand, could have a large number of patients with implantable monitors who reside in a large geographic area. In addition, numerous home telemonitoring units are in use to gather data from patients with implantable devices and send the data to a location where it can be processed and interpreted by their physicians. Examples of telemonitoring systems include the LATITUDE® Patient Management system (Boston Scientific, Inc., Natick, MA, USA) and the CareLink® network (Medtronic, Inc.). The field of implantable cardiac monitoring is growing rapidly and with the advent of printed flexible electronics it will continue to accelerate.

20.11 Summary

Advanced methods and technology continue to develop for the assessment of cardiac hemodynamics. Such monitoring can be used acutely; however, many new technologies are being developed for chronic monitoring of the cardiac patient (e.g., employing miniaturized implantable sensors and noninvasive hemodynamic monitors). In this chapter, we provided a general overview of several devices and/or systems that can be used either clinically or experimentally to monitor cardiac performance. However, it should be reiterated that to best understand how the output of such devices can be used for the assessment of cardiac function, one needs to first possess an in-depth understanding of underlying basic cardiac physiology.

References

1. Sengupta PP, Khandheria BK, Korinek J et al (2006) Apex-to-base dispersion in regional timing of left ventricular shortening and lengthening. J Am Coll Cardiol 47:163–172
2. Ratcliffe MB, Gupta KB, Streicher JT et al (1995) Use of sonomicrometry and multidimensional scaling to determine the three-dimensional coordinates of multiple cardiac locations: feasibility and initial implementation. IEEE Trans Biomed Eng 42:587–597
3. Gorman JH III, Gupta KB, Streicher JT et al (1996) Dynamic three-dimensional imaging of the mitral valve and left ventricle by rapid sonomicrometry array localization. J Thorac Cardiovasc Surg 112:712–725
4. Meyer SA, Wolf PD (1997) Application of sonomicrometry and multidimensional scaling to cardiac catheter tracking. IEEE Trans Biomed Eng 44:1061–1067
5. Geddes LA, Baker LE (1967) The specific resistance of biological material–a compendium of data for the biomedical engineer and physiologist. Med Biol Eng 5:271–293
6. Baan J, van der Velde ET, de Bruin HG et al (1984) Continuous measurement of left ventricular volume in animals and humans by conductance catheter. Circulation 70:812–823
7. van der Velde ET, van Dijk AD, Steendijk P et al (1992) Left ventricular segmental volume by conductance catheter and cine-CT. Eur Heart J 13 Suppl E:15–21
8. White PA, Redington AN (2000) Right ventricular volume measurement: can conductance do it better? Physiol Meas 21:R23–R41
9. Hettrick DA, Battocletti J, Ackmann J, Linehan J, Warltier DC (1998) In vivo measurement of real-time aortic segmental volume using the conductance catheter. Ann Biomed Eng 26:431–440
10. Gardner RM (1996) Accuracy and reliability of disposable pressure transducers coupled with modern monitors. Crit Care Med 24:879–882
11. Skeehan TM, Thys DM (1995) Monitoring of the cardiac surgical patient. In: Hensley FA, Martin DE (eds) A practical approach to cardiac anesthesia, 2nd edn. Little, Brown and Company, Boston, p 102
12. Gorback MS (1988) Considerations in the interpretation of systemic pressure monitoring. In: Lumb PD, Bryan-Brown CW (eds) Complications in critical care medicine. Year Book, Chicago, p 296
13. Shasby DM, Dauber IM, Pfister S et al (1980) Swan-Ganz catheter location and left atrial pressure determine the accuracy of wedge pressure when positive end expiratory pressure is used. Chest 80:666–670
14. Snyder JV, Carroll GC (1982) Tissue oxygenation: a physiologic approach to a clinical problem. Curr Probl Surg 19:650
15. Stanley TE, Reves JG (1994) Cardiovascular monitoring. In: Miller RD (ed) Anesthesia, 4th edn. Churchill Livingstone, Boston, p 1167
16. Swan HJC, Ganz W, Forrester J, Marcus H, Diamon G, Chonette D (1970) Catheterization of the heart in man with use of a flow-directed balloon-tipped catheter. N Engl J Med 283:447–451
17. Practice Guidelines for Pulmonary Artery Catheterization: An Updated Report by the American Society of Anesthesiologists Task Force on Pulmonary Artery Catheterization. Anesthesiology 2003;99:988–1014
18. West JB, Dollery CT, Naimark A (1964) Distribution of blood flow in isolated lung; relation to vascular and alveolar pressures. J Appl Physiol 19:713–724
19. Wesseling KH (1996) Finger arterial pressure measurement with Finapres. Z Kardiol 3:38–44
20. Brandstetter RD, Grant GR, Estilo M, Rahim R, Sing K, Gitler B (1998) Swan-Ganz catheter: misconceptions, pitfalls, and incomplete user knowledge-an identified trilogy in need of correction. Heart Lung 27:218–222

21. Wittnich C, Trudel J, Zidulka A, Chiu RC (1986) Misleading "pulmonary wedge pressure" after pneumonectomy: its importance in postoperative fluid therapy. Ann Thorac Surg 42:192–196
22. Van Aken H, Vandermeersch E (1988) Reliability of PCWP as an index for left ventricular preload. Br J Anaesth 60:85S–89S
23. Stanley TE, Reves JG (1994) Cardiovascular monitoring. In: Miller RD (ed) Anesthesia, 4th edn. Churchill Livingstone, Boston, pp 1184–1185
24. Fegler G (1954) Measurement of cardiac output in anesthetized animals by thermodilution method. Q J Exp Physiol 39:153
25. Pearl RGB, Rosenthal MH, Mielson L et al (1986) Effect of injectate volume and temperature on thermodilution cardiac output determination. Anesthesiology 64:798
26. Reich DL, Moskowitz DM, Kaplan JA (1999) Hemodynamic monitoring. In: Kaplan JA, Reich DL, Konstaelt SN (eds) Cardiac anesthesia, 4th edn. WB Saunders Co, Philadelphia
27. Burchell SA, Yu M, Takiguchi SA, Ohta RM, Myers SA (1997) Evaluation of a continuous cardiac output and mixed venous oxygen saturation catheter in critically ill surgical patients. Crit Care Med 25:388–391
28. de Figueiredo LFP, Malbouisson LMS, Varicoda EY et al (1999) Thermal filament continuous thermodilution cardiac output delayed response limits its value during acute hemodynamic instability. J Trauma 47:288–293
29. Mihaljevi T, vonSegesser LK, Tonz M et al (1995) Continuous versus bolus thermodilution cardiac output measurements: a comparative study. Crit Care Med 23:944–949
30. Mihm FG, Gettinger A, Hanson CW et al (1998) A multicenter evaluation of a new continuous cardiac output pulmonary artery catheter system. Crit Care Med 26:1346–1350
31. Della RG, Costa MG, Pompei L et al (2002) Continuous and intermittent cardiac output measurement: pulmonary artery catheter versus aortic transpulmonary technique. Br J Anaesth 88:350–356
32. Pamley CL, Pousman RM (2002) Noninvasive cardiac output monitoring. Curr Opin Anaesthesiol 15:675–680
33. Christensen P, Clemensen P, Andersen PK et al (2000) Thermodilution versus inert gas rebreathing for estimation of effective pulmonary blood flow. Crit Care Med 28:51–56
34. Imhoff M, Lehner JH, Lohlein D (2000) Noninvasive whole-body electrical bioimpedance cardiac output and invasive thermodilution cardiac output in high-risk surgical patients. Crit Care Med 28:2812–2818
35. Shoemaker WC, Wo CC, Bishop MH et al (1994) Multicenter trial of a new thoracic electrical bioimpedance device for cardiac output estimation. Crit Care Med 22:1907–1912
36. Linton RA, Band DM, Haire KM (1994) A new method of measuring cardiac output in main using lithium dilution. Br J Anaesth 71:262–266
37. Linton R, Band D, O'Brian T et al (1997) Lithium dilution cardiac output measurement: a comparison with thermodilution. Crit Care Med 25:1767–1768
38. Kurita T, Morita K, Kato S et al (1997) Comparison of the accuracy of the lithium dilution technique with the thermodilution technique for measurement of cardiac output. Br J Anaesth 79:770–775
39. Rivers E, Nguyen B, Havstad S et al (2001) Early goal-directed therapy in the treatment of severe sepsis and septic shock. N Engl J Med 345:1368–1377
40. Band DM, Linton RA, Jonas MM et al (1997) The shape of indicator dilution curves used for cardiac output measurement in man. J Physiol 498:225–229
41. Shoemaker WC (2002) New approaches to trauma management using severity of illness and outcome prediction based on noninvasive hemodynamic monitoring. Surg Clin North Am 82:245–255
42. Shoemaker WC, Wo CC, Chan L et al (2001) Outcome prediction of emergency patients by noninvasive hemodynamic monitoring. Chest 120:528–537
43. Drazner MH, Thompson B, Rosenberg PB et al (2002) Comparisons of impedance cardiography with invasive hemodynamic measurements in patients with heart failure secondary to ischemic or nonischemic cardiomyopathy. Am J Cardiol 89:993–995
44. Binder JC, Parkin WG (2001) Non-invasive cardiac output determination: comparison of a new partial-rebreathing technique with thermodilution. Anaesth Intensive Care 28:427–430
45. Maxwell RA, Gibson JB, Slade JB et al (2001) Noninvasive cardiac output by partial CO_2 rebreathing after severe chest trauma. J Trauma 51:849–853
46. Tachibana K, Imanaka H, Miyano H et al (2002) Effect of ventilatory settings on accuracy of cardiac output measurement using partial CO_2 rebreathing. Anesthesiology 96:96–102
47. Botero M, Lobato EB (2001) Advances in noninvasive cardiac output monitoring: an update. J Cardiothorac Vasc Anesth 15:631–640
48. Kotake Y, Moriyama K, Innami Y et al (2003) Performance of noninvasive partial CO_2 rebreathing cardiac output and continuous thermodilution cardiac output in patients undergoing aortic reconstruction surgery. Anesthesiology 99:283–288
49. Keech J, Reed RL II (2003) Reliability of mixed venous oxygen saturation as an indicator of the oxygen extraction ratio demonstrated by a large patient data set. J Trauma 54:236–241
50. Snyder JV, Carroll GC (1982) Tissue oxygenation: a physiologic approach to a clinical problem. Curr Probl Surg 19:650
51. Jain A, Shroff SG, Jnicki JS et al (1991) Relation between venous oxygen saturation and cardiac index. Nonlinearity and normalization for oxygen uptake and hemoglobin. Chest 99:1403–1409
52. Inomata S, Nishikawa T, Taguchi M (1994) Continuous monitoring of mixed venous oxygen saturation for detecting alterations in cardiac output after discontinuation of cardiopulmonary bypass. Br J Anaesth 72:11–16
53. Rivers E, Nguyen B, Vastad S et al (2001) Early goal-directed therapy in the treatment of severe sepsis and septic shock. N Engl J Med 345:1368–1377
54. Kraft P, Steltzer H, Hiesmayr M et al (1993) Mixed venous oxygen saturation in critically ill septic shock patients: the role of defined events. Chest 103:900–906
55. Waller JL, Kaplan JA, Bauman LI et al (1982) Clinical evaluation of a new fiberoptic catheter oximeter during cardiac surgery. Anesth Analg 61:676–679
56. Vedrinne C, Bastien O, De Varax R et al (1997) Predictive factors for usefulness of fiberoptic pulmonary artery catheter for continuous oxygen saturation in mixed venous blood monitoring in cardiac surgery. Anesth Analg 85:2–10
57. Goldman RH, Klughaupt M, Metcalf T et al (1968) Measured central venous oxygen saturation in patients with myocardial infarction. Circulation 38:941–946
58. Berridye JC (1992) Influence of cardiac output on correlation between mixed venous and central venous oxygen saturation. Br J Anaesth 89:409–410
59. Davies GG, Mendehall J, Symrey T (1988) Measurement of right atrial oxygen saturation by fiberoptic oximetry accurately reflects mixed venous oxygen saturation in swine. J Clin Monit 4:99–102
60. Rivers EP, Ander DS, Powell D (2001) Central venous oxygen saturation monitoring in the critically ill patient. Curr Opin Crit Care 7:204–211
61. Lee J, Wright F, Barber R et al (1972) Central venous oxygen saturation in shock: a study in man. Anesthesiology 36:472–478
62. Scheinman MM, Brown MA, Rapaport E (1969) Critical assessment of use of central venous oxygen saturation as a mirror of mixed venous oxygen in severely ill cardiac patients. Circulation 40:165–172
63. Edwards JD, Mayall RM (1998) Importance of the sampling site for measurement of mixed venous oxygen saturation in shock. Crit Care Med 26:1356–1360

64. Bonow RO, Carabello B, de Leon AC et al (1998) ACC/AHA guidelines for the management of patients with valvular heart disease. J Heart Valve Dis 7:672–707
65. Yoganathan AP, Chandran KB, Sotiropoulos F (2005) Flow in prosthetic heart valves: state-of-the-art and future directions. Ann Biomed Eng 33:1689–1694
66. Brignole M, Sutton R, Menozzi C et al (2006) Lack of correlation between the responses to tilt testing and adenosine triphosphate test and the mechanism of spontaneous neurally mediated syncope. Eur Heart J 27:2232–2239
67. Deharo JC, Jego C, Lanteaume A, Djiane P (2006) An implantable loop recorder study of highly symptomatic vasovagal patients: the heart rhythm observed during a spontaneous syncope is identical to the recurrent syncope but not correlated with the head-up tilt test or adenosine triphosphate test. J Am Coll Cardiol 47:587–593
68. Moya A, Brignole M, Menozzi C et al (2001) Mechanism of syncope in patients with isolated syncope and in patients with tilt-positive syncope. Circulation 104:1261–1267
69. Strickberger SA, Benson DW, Biaggioni I et al (2006) AHA/ACCF scientific statement on the evaluation of syncope. Circulation 113:316–327
70. Brignole M, Alboni P, Benditt DG et al (2004) Guidelines on management (diagnosis and treatment) of syncope-update 2004. Eur Heart J 25:2054–2072
71. Adamson PB, Magalski A, Braunschweig F et al (2003) Ongoing right ventricular hemodynamics in heart failure: clinical value of measurements derived from an implantable monitoring system. J Am Coll Cardiol 41:565–571
72. Reynolds DW, Bartelt N, Taepke R, Bennett TD (1995) Measurement of pulmonary artery diastolic pressure from the right ventricle. J Am Coll Cardiol 25:1176–1182
73. Stevenson LW, Perloff JK (1989) The limited reliability of physical signs for estimating hemodynamics in chronic heart failure. JAMA 261:884–888
74. Wilson JR, Hanamanthu S, Chomsky DB, Davis SF (1999) Relationship between exertional symptoms and functional capacity in patients with heart failure. J Am Coll Cardiol 33: 1943–1947
75. Bennett T, Kjellstrom B, Taepke R, Ryden L (2005) Development of implantable devices for continuous ambulatory monitoring of central hemodynamic values in heart failure patients. Pacing Clin Electrophysiol 28:573–584

Fueling Normal and Diseased Hearts: Myocardial Bioenergetics

21

Arthur H.L. From and Robert J. Bache

Abstract

Cardiac contractile performance depends upon: (1) the delivery of carbon substrates and oxygen present in the blood to the cardiac extracellular space (via the coronary circulation), (2) the ability of the cardiomyocytes to efficiently extract these substrates from the extracellular space, and (3) the pathways via which the chemical energy stored within the carbon substrates is transferred to adenosine triphosphate (ATP), an energy storage molecule that can be directly utilized by most chemical energy driven processes. Importantly, ATP synthetic capacity must be sufficient to support a wide range of energy demands with high rates of ATP generation and must not be associated with destabilization of cytosolic and intraorganelle chemical milieus. The latter characteristic is crucial if the performance of the contractile apparatus and intracellular organelles is to remain optimal over the broad range of cardiac work states required by a physically active organism. Hence, even a high rate of myocardial energy expenditure must not induce the fatigue that is known to develop in heavily working skeletal muscle. This chapter describes the ways in which the chemical energy stored in ingested carbon substrates (glucose, fatty acids, and, to a modest extent, proteins) is transferred to ATP and reviews some of the regulatory systems which integrate the function of these pathways and make them responsive to changes in ATP demand without destabilizing the intracellular chemical milieu. The generation of toxic by-products of the metabolic processes and mechanisms that limit their adverse effects are also reviewed. Last of all, the effects of several physiological states and diseases on these processes are briefly discussed, and the concept that the diseased heart may be energy limited is presented.

Keywords

Adenosine triphosphate • Myocardial blood flow • Glucose metabolism • Fatty acid metabolism • Electron transport • Oxidative phosphorylation • Regulatory processes • Stable intracellular chemical milieu reactive oxygen species

Abbreviations

ADP	Adenosine diphosphate
AMP	Adenosine monophosphate
AMPK	Adenosine monophosphate-activated kinase
ATP	Adenosine triphosphate
$FADH_2$	Flavin adenine dinucleotide
LDH	Lactic acid dehydrogenase
NADH	Nicotinamide adenine dinucleotide
NEFA	Nonesterified free fatty acids

A.H.L. From, MD (✉) • R.J. Bache, MD
Department of Medicine (Cardiovascular Division), Lillihei Heart Institute and Center for Magnetic Resonance Research, University of Minnesota, 2021 6th St. SE, Minneapolis, MN 55455, USA
e-mail: fromx001@umn.edu

P.A. Iaizzo (ed.), *Handbook of Cardiac Anatomy, Physiology, and Devices*, DOI 10.1007/978-3-319-19464-6_21

PDH	Pyruvate dehydrogenase
ROS	Reactive oxygen species
TCA	Tricarboxylic acid
VLCAD	Very long-chain acyl-CoA dehydrogenase

21.1 Introduction

In the interest of putting the subject of *myocardial metabolism* into a broader perspective, it should be understood that the heart is ultimately a *solar-powered organ* (as are all other organs). Virtually, all energy-driven biological processes in our biosphere are ultimately dependent upon energy radiated by the sun (in the form of photons). Photons are captured by plants, and their energy is used to synthesize energy-rich carbon molecules that are then used to fuel many biological processes. In green plants, a portion of the solar photon energy is first trapped by chlorophyll and then stored in the form of highly energetic chemical bonds resident in adenosine triphosphate (ATP) and NADPH (Fig. 21.1); the equation for this process is as follows:

$$2H_2O + 2NADP^+ + 3ADP + 3P_i + \text{light} \rightarrow 2NADPH + 2H^+ + 3ATP + O_2$$

The distal phosphate bonds of ATP store high levels of chemical energy. In plants, the energy released by breakdown of the terminal high-energy phosphate bond of ATP and the reduction of NADPH is used to drive the synthesis of simple carbohydrates and ultimately glucose. The chemical energy stored in glucose can be released in a controlled fashion by enzyme-catalyzed reactions and drives the synthesis of all other species of biomolecules including fatty acids (another convenient storage molecule for chemical energy) and amino acids, as well as for resynthesis of ATP. Hence, because animals are unable to directly convert solar photon energy to a storage form of chemical energy, simple and complex animal life is ultimately powered by plants that carry out photosynthesis. The ingestion of plants and (other) animals containing energy-rich molecules supplies animals with carbohydrates, fatty acids, and amino acids that can be metabolized to support the generation of ATP.

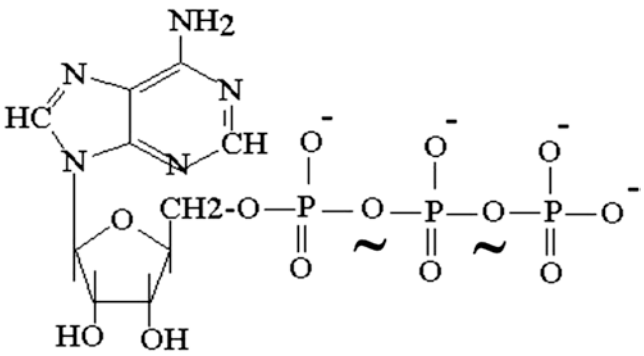

ATP

Fig. 21.1 Adenosine triphosphate (*ATP*). ATP is the major source of chemical energy used to power the reactions that support contractile and other processes in myocardium and all other living tissues. The ~ symbol is used to designate a phosphate bond which has a very high level of stored chemical energy. Although ATP contains two ~ phosphate bonds, it is the hydrolysis of the terminal phosphate bond that releases the energy that directly powers cellular processes

In the myocardium, as in other biologic tissues, most energy-driven processes use ATP as the immediate source of energy. Hydrolysis of the terminal phosphate bond of ATP releases energy that can be captured and used to drive (energy-dependent) processes such as protein synthesis, muscle contraction, ion transport, etc. Therefore, the ability of the heart to pump blood to the pulmonary and systemic circulations is dependent on the presence of adequate concentrations of ATP. Unfortunately, myocardial stores of ATP are modest in relation to the rate of expenditure, and continuous ATP synthesis is required to support energy-requiring processes. Importantly, most of the energy required for ATP synthesis is derived from the controlled breakdown of the chemical bonds in carbohydrates (glucose) and fatty acids; body protein-derived amino acids are used to fuel ATP generation only when supplies of the major fuels are compromised, as would be the case during a period of starvation.

To summarize, this chapter will describe: (1) how carbon substrates and oxygen are delivered to the heart, (2) the biochemical pathways within the heart (most of the same pathways are present in all tissue types) that transfer the chemical bond energy stored in carbon substrates to ATP, (3) some of the ways that these pathways are regulated such that they are capable of responding to the increased ATP demand associated with increased cardiac work states, and (4) some of the alterations in these processes that occur under changing physiological states in normal and diseased hearts. The reader should understand that this relatively brief summary of myocardial metabolism is, by necessity, an extremely superficial overview of the individual topics. For those readers wishing to review some of the major topics in greater detail, a list of recent references—primarily current topical reviews, research reports, and a standard biochemistry textbook—is provided at the end of the chapter.

21.2 Myocardial Blood Flow: Carbon Substrate and Oxygen Delivery to the Heart

Blood containing carbon substrates and oxygen is delivered into human and animal hearts (see Chap. 6) by coronary arteries that originate from the proximal aorta. These arteries then subdivide to form progressively smaller branches that arborize inward throughout the ventricular wall and

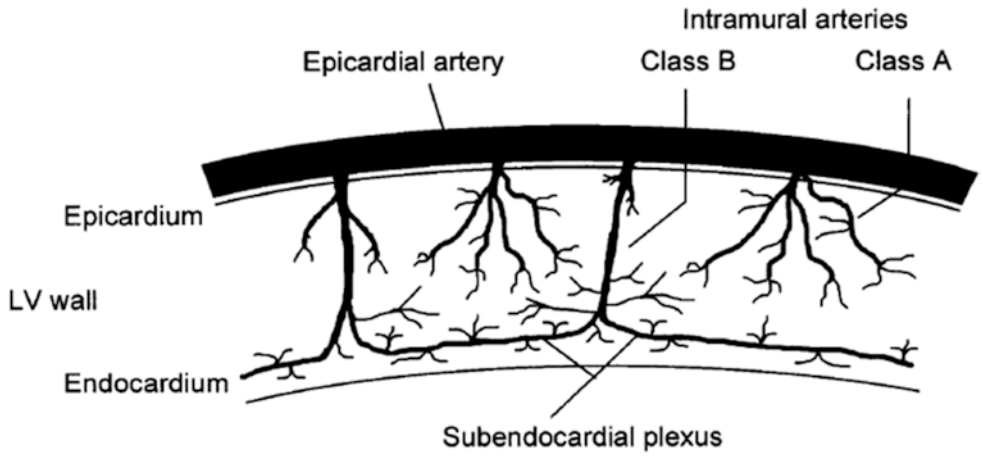

Fig. 21.2 Transmural distribution of the coronary arterial system. The large epicardial conductance arteries supply shallow and deep branches to the subepicardium and subepicardium, respectively. These perforating vessels arborize to create the arteriolar network that supplies the myocardial capillary bed. *LV* left ventricle. Reprinted from Duncker DJ and Bache RJ, Regulation of coronary vasomotor tone under normal conditions and during acute myocardial hypoperfusion, Pharmacol Ther, Vol. 86, 87–110, 2000. Pharmacology and Therapeutics (by International Union of Pharmacology). Reproduced with permission of Elsevier Inc., in the format Book via Copyright Clearance Center

supply blood to the myocardium (Fig. 21.2). The left ventricular wall (for descriptive purposes) is arbitrarily subdivided into transmural layers termed the subepicardium (outermost layer), the midmyocardium, and the subendocardium (innermost layer). The coronary arterial tree terminates in muscular vessels 60–150 mm in diameter termed *arterioles*. The arterioles are the major locus of resistance to blood flow, and contraction or relaxation of the smooth muscle in the walls of the arterioles (vasomotion) provides the mechanism for control of the rate of blood flow into the myocardium. Each arteriole supplies an array of capillaries, thin-walled tubes comprised of a single layer of endothelial cells, across which most of the exchange of nutrients, oxygen, and metabolic waste products occurs. As their terminal end capillaries coalesce into venules, the initial component of the cardiac venous system then conducts most postcapillary blood back into the cardiac chambers, primarily through the coronary sinus that drains into the right atrium. For more details on the coronary circulation, see Chap. 8.

21.2.1 Regulation of Myocardial Blood Flow

Coronary blood flow is highly regulated and falls or rises appropriately in response to subtle or large changes in the rate of myocardial energy expenditure. The principal purpose of the heart is to generate the pressure that forces blood from the ventricles into the pulmonary and systemic circulations. Elevation of the cardiac rate of ATP expenditure during exercise or other stresses increases myocardial demand for oxygen and carbon substrates. In clinical practice, there is often a need to assess the effects of changes of the rate of myocardial energy expenditure on cardiac performance (e.g., during exercise stress testing). Since routine direct measurement of myocardial oxygen consumption is not practical, a rough estimate of the change in the energy demands of the heart is afforded by the product of systolic blood pressure multiplied by the times per minute that pressure generation occurs (heart rate); this is termed the *rate-pressure product*. This measurement provides a simple estimate of changes in the metabolic requirement of the heart resulting from different cardiac work states in animals and humans.

The coronary circulation operates on the principle of "just-in-time" delivery of oxygen and carbon substrates. In other words, coronary blood flow is regulated to be only minimally greater than required to meet the instantaneous metabolic demands of the heart. Furthermore, the heart extracts 70–80 % of the O_2 from the blood as it flows through the coronary capillaries. Because of this high level of basal oxygen extraction, there is little ability to increase oxygen uptake by means of increased extraction of oxygen from the blood. As a result, increases in myocardial energy requirement during exercise or other stresses must be satisfied by concomitant increases of coronary blood flow. As noted, ATP and oxygen stores in the myocardium are relatively small. Therefore, the response time for the increase in coronary flow following an increase in cardiac work must be rapid (i.e., a few seconds). From these considerations, it is clear that highly responsive signaling systems exist which link the rate of myocardial energy expenditure to vasomotor activity in the resistance vessels that control coronary blood flow. Interestingly, these signaling systems are not fully understood despite intense study over the last 100 years.

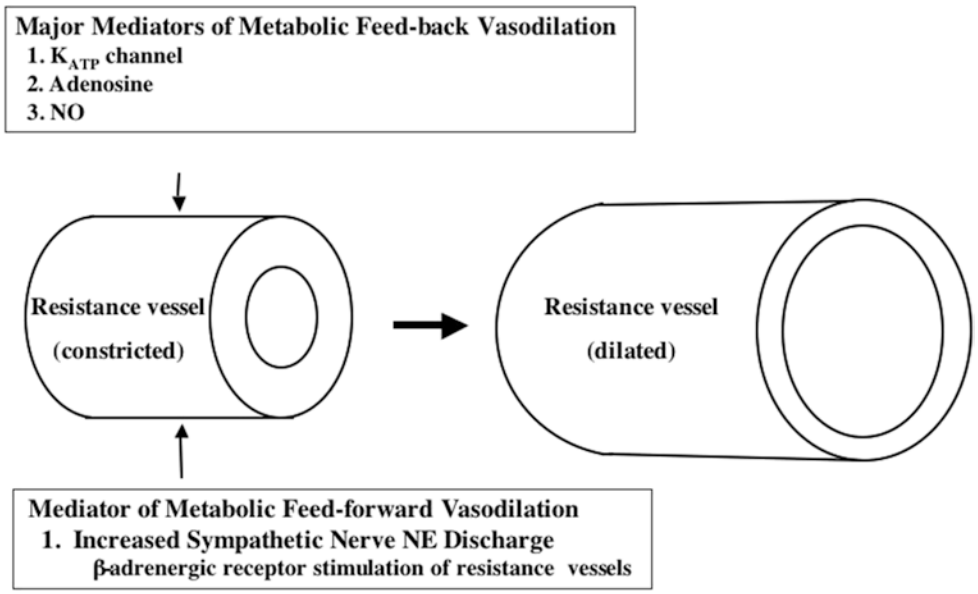

Fig. 21.3 Major feedback and feed-forward mechanisms underlying metabolic vasodilatation of resistance vessels are depicted (see text for discussion). *K_{ATP} channel* ATP-inhibited potassium channel, *NO* nitric oxide

21.2.2 Signaling Pathways Regulating the Coronary Circulation

The regulatory signals that increase blood flow in response to increases/decreases of cardiac work can be classified as having feedback or feed-forward characteristics; the final common response to these signals is relaxation/contraction of vascular smooth muscle cells within the arteriolar resistance vessels that control coronary blood flow (Fig. 21.3). Several major feedback mechanisms resulting from increased cardiomyocyte metabolism (including adenosine, nitric oxide, ATP, H_2O_2, and others) cause opening of ATP-sensitive potassium channels (K_{ATP}) located within the sarcolemma of arteriolar smooth muscle cells. Opening of these channels allows potassium to escape from the cytosol of the smooth muscle cells, resulting in hyperpolarization (increased negativity) of the arteriolar smooth muscle cell membrane. The increased negativity of the membrane causes sarcolemmal voltage-dependent calcium channels to close; as a result, calcium entry into the smooth muscle is reduced, the vessel relaxes (i.e., dilates), and coronary blood flow increases. In addition to effects on the K_{ATP} channels, adenosine (a product of ATP utilization in the cardiomyocyte) also has potent, direct dilator effects on arteriolar smooth muscle. Another metabolic feedback signal is nitric oxide generated by the vascular endothelium. Mechano-transduction of flow-induced shear forces exerted on the endothelial cells augments nitric oxide synthesis. In addition to causing potassium channel opening, nitric oxide also initiates direct relaxation processes in vascular smooth muscle. It is important to note that this brief discussion does not include many of the known feedback mechanisms involved in regulation of coronary blood flow.

Notably, increased cardiac sympathetic nerve activity (i.e., during exercise) activates a feed-forward mechanism for control of coronary blood flow which augments the local metabolic vasodilator influences. The sympathetic neurotransmitter norepinephrine activates α- and β-adrenergic receptors located within the sarcolemma of arteriolar smooth muscle cells. Activation of similarly located α-adrenergic receptors causes modest constriction of the large coronary arteries; since these arteries function as conduit vessels that offer little resistance to blood flow, this has little effect on coronary flow. However, activation of arteriolar β-adrenergic receptors results in relaxation (vasodilation) of these small resistance vessels; the resultant decrease of coronary resistance causes a feed-forward increase in blood flow that is independent of local metabolic mechanisms and augments the increase of coronary blood flow during exercise.

Pharmacologic studies have shown that simultaneous blockade of the coronary K_{ATP} channels, adenosine, and nitric oxide pathways significantly decreases myocardial blood flow in the resting animal. Moreover, the increase of coronary flow that normally occurs during exercise is severely blunted, resulting in a perfusion-metabolism mismatch that is accompanied by evidence of ischemia even in the normal heart. Hence, activation of these three pathways appears to be the primary means by which metabolic vasodilatation is achieved in the heart. However, in the healthy heart, blockade of any one of these mechanisms for smooth muscle relaxation will elicit compensatory (i.e., increased) activation of the other pathways to minimize changes in coronary blood flow. Lastly, other (not discussed) circulatory regulatory mechanisms may also be of biological significance.

21.2.3 Blood Flow in the Diseased Heart

Coronary blood flow in the diseased heart can be limited by: (1) partial or complete obstruction of the large coronary arteries (e.g., atherosclerotic disease), (2) decreased responsiveness of the signaling systems relating blood flow to energy requirements, and/or (3) increases in extravascular mechanical forces acting to compress the small vessels in the wall of the left ventricle. In the case of obstructive (generally atherosclerotic) disease of the epicardial coronary arteries, a moderately narrowed vessel may only restrict blood flow during periods of increased blood flow demand (i.e., it reduces vasodilator reserve), while a severely narrowed vessel may limit blood flow even when the subject is at rest. In the presence of a moderate coronary obstruction, the arteriolar bed can maintain adequate blood flow by metabolic signaling-based arteriolar vasodilatation. That is, a decrease in small vessel resistance can compensate for the increased resistance caused by a proximal coronary artery stenosis. However, when the capacity for vasodilation of the arterioles has been exhausted, any further increase in cardiac work cannot induce an increase of blood flow, and the myocardium supplied by the narrowed epicardial vessel will become ischemic. There is also considerable evidence that malfunction of metabolic signaling pathways in the arteriolar resistance vessels (e.g., in the absence of obstructed large coronary arteries) can cause myocardial ischemia in certain patients.

In the normal heart, blood flow to the inner layers of the left ventricle occurs principally during diastole. This is because tissue pressures in the wall of the left ventricle during systole are so great that inner layer arterioles are squeezed shut by the extravascular compressive forces produced by cardiac contraction. Diastolic left ventricular tissue pressures are also greatest in the subendocardium. When the heart fails and/or becomes hypertrophied, these extravascular compressive forces increase as left ventricular filling pressure increases. In the hypertrophied or failing heart, slowing of myocyte relaxation also shortens the duration of the diastolic interval and thus limits coronary flow reserve in the inner cardiac layers. In the normal heart, autoregulatory (i.e., metabolic vasodilatation) processes cause enough arteriolar vasodilation in the subendocardium to compensate for systolic underperfusion. However, increased left ventricular diastolic pressure (and myocardial tissue pressure) in the failing heart may compress the arteriolar bed in the inner myocardial layers sufficiently to overwhelm autoregulatory mechanisms, particularly those that normally maintain adequate subendocardial blood flow. Since subendocardial blood flow occurs almost exclusively during diastole, tachycardia also acts to impede blood flow in the subendocardium by shortening of the diastolic interval. Thus, even in the absence of obstructive coronary artery disease or intrinsic arteriolar abnormalities, increased arteriolar compression can limit blood flow to the inner myocardial layers of the diseased heart. Importantly, if these abnormalities limit substrate delivery to the inner myocardial layers, they will disrupt the balance between ATP synthetic capacity and ATP utilization in this region of the ventricular wall. Thus, the extravascular forces cause the subendocardium to be the region of the ventricular wall that is most vulnerable to hypoperfusion and ischemia.

21.3 Intermediary Metabolism and Bioenergetics in the Normal Heart

Glucose and fatty acids are the main substrates consumed by the heart, with fatty acid consumption predominating under most circumstances (Fig. 21.4). Exceptions to this statement will be discussed later.

21.3.1 Glucose Metabolism

Figure 21.5 shows a flowchart for glucose metabolism. Glucose enters the cardiomyocyte via the sarcolemmal glucose transport proteins, GLUT 1 (that is insulin independent) and GLUT 4 (that is insulin dependent). Once in the cell, glucose is phosphorylated to glucose-6-phosphate by the enzyme hexokinase. Since glucose-6-phosphate is membrane impermeable, this effectively traps glucose within the cell. Glucose-6-phosphate can enter the glycogen synthesis pathway (glycogen is a macromolecular polymeric storage form of glucose), the pentose monophosphate shunt (that generates NADPH and ribose, moieties utilized in many important cellular processes), or it can undergo molecular rearrangement via the enzyme phosphohexose isomerase to form fructose-6-phosphate and continue on through the glycolytic series of reactions. A second phosphorylation of fructose-6-phosphate via phosphofructokinase generates fructose-1,6-bisphosphate. Each of these phosphorylations consumes one molecule of ATP. Fructose-1-6-bisphosphate is next split into glyceraldehyde-3-phosphate and dihydroxyacetone phosphate by the enzyme aldolase. These two molecules are in constant exchange with each other via the enzyme phosphotriose isomerase. Glyceraldehyde-3-phosphate is then phosphorylated to form 1,3-bisdiphosphoglycerate by the enzyme glyceraldehyde-3-phosphate dehydrogenase. The phosphate bond in the 1 position is a high-energy-containing bond (signified by the ~P symbol); this reaction also simultaneously reduces NAD^+ to NADH. Cytosolic oxidation of NADH and transport of the two removed electrons and H^+ into the mitochondrial matrix then occur in cardiac muscle via the malate-aspartate shuttle (not shown in Fig. 21.5). In the mitochondrial matrix, NAD^+ is then reduced back to NADH which can be utilized by the mitochondria to generate ATP (to be discussed later). In the next cytosolic reaction, the high-energy phos-

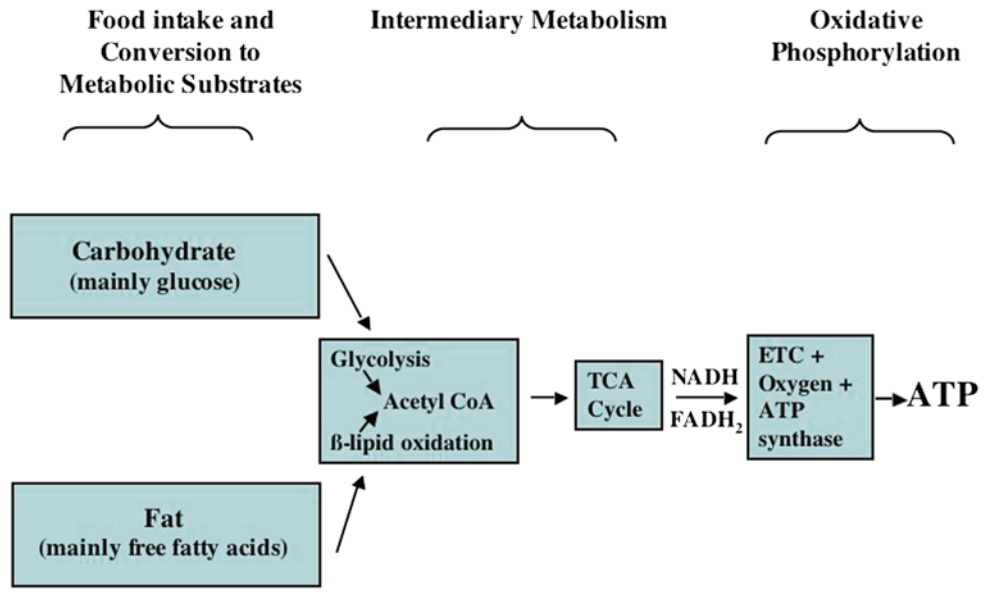

Fig. 21.4 A general overview of carbon substrate metabolism in the heart. First, ingested food is broken down into usable carbon substrates, primarily amino acids (not major contributors to ATP synthesis), glucose, and fatty acids. The pathways which convert amino acids and other molecules to glucose are not shown. Glucose and fatty acids are processed (via intermediary metabolic processes) to yield the reducing equivalents, NADH and $FADH_2$, which supply the energy necessary to power oxidative phosphorylation. The latter process, which occurs within the mitochondria in the presence of oxygen, supplies almost all of the ATP synthesized and utilized in the heart. *ATP* adenosine triphosphate, *ETC* electron transport chain, *$FADH_2$* flavin adenine dinucleotide, *NADH* nicotinamide adenine dinucleotide, *TCA* tricarboxylic acid

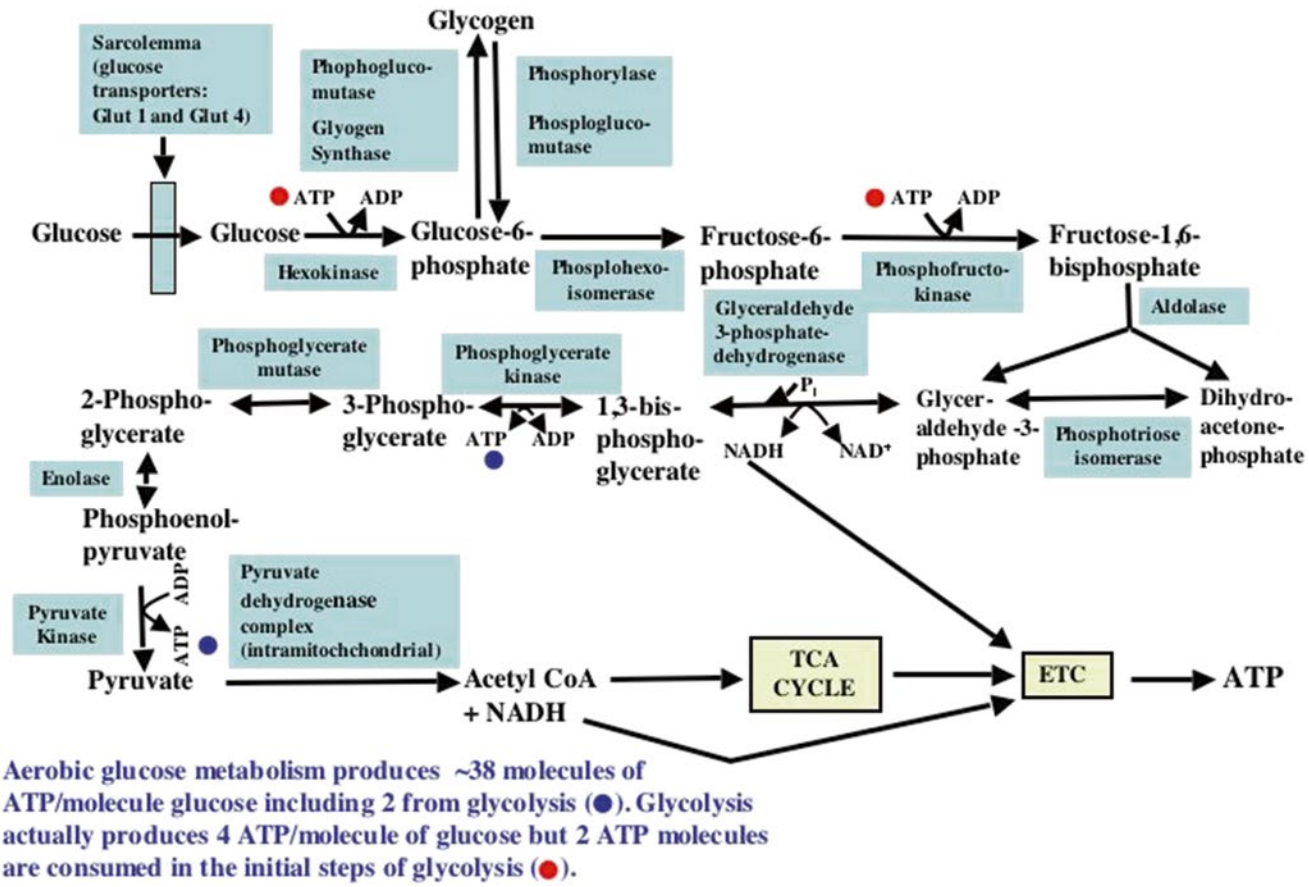

Fig. 21.5 Flowchart of cellular uptake of glucose and the pathways through which glucose metabolism proceeds. See text for discussion. *ADP* adenosine diphosphate, *ATP* adenosine triphosphate, *ETC* electron transport chain, *NADH* nicotinamide adenine dinucleotide, *TCA* tricarboxylic acid

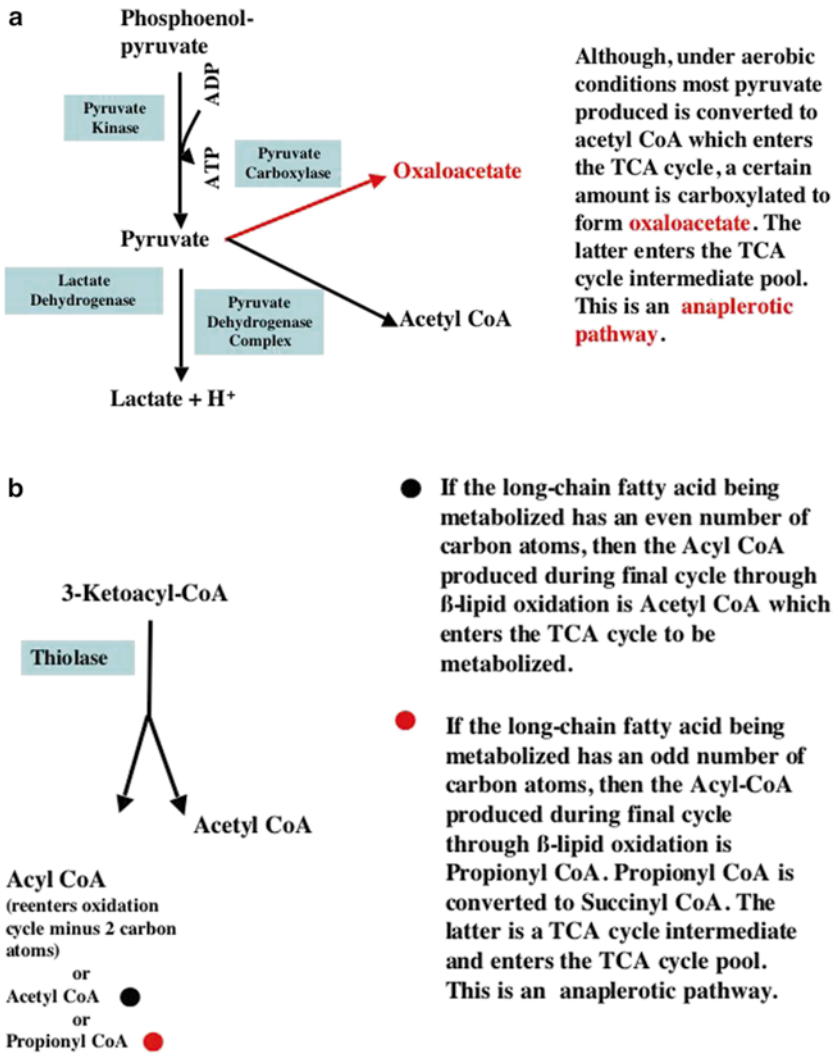

Fig. 21.6 Anaplerotic and cataplerotic processes. Anaplerotic processes are those which supply substrate used to maintain the TCA cycle intermediate pool size. In contrast, cataplerotic processes remove substrates from the TCA cycle intermediate pool and decrease its size. The balance between these two processes determines the TCA cycle pool size. (**a**) Shows how glucose (via its metabolic product, pyruvate) contributes to anaplerosis. (**b**) Shows how the β-oxidation of odd-numbered carbon chain fatty acids contributes to anaplerosis. (Note that readers may want to review Fig. 21.13, a flowchart for β-lipid oxidation, before examining (b) which depicts the terminal reaction of β-lipid oxidation.) *ADP* adenosine diphosphate, *ATP* adenosine triphosphate, *TCA* tricarboxylic acid

phate bond in 1,3-bisdiphosphoglycerate is transferred to adenosine diphosphate (ADP) to form ATP and 3-phosphoglycerate via the enzyme phosphoglycerate kinase. The latter molecule is converted to 2-phosphoglycerate by the enzyme phosphoglycerate mutase. Enolase, another cytosolic enzyme, then converts 2-phosphoglycerate to the ~P-containing molecule phosphoenolpyruvate. The latter is converted to pyruvate by the enzyme pyruvate kinase. During this reaction, the ~P in phosphoenolpyruvate is transferred to ADP to form a second ATP molecule. Pyruvate can then enter the mitochondria to be further metabolized by the pyruvate dehydrogenase (PDH) complex of enzymes. Both the pyruvate dehydrogenase complex that converts pyruvate to acetyl-CoA (and NAD^+ to NADH), and the tricarboxylic acid (TCA) cycle that metabolizes acetyl-CoA are located within the mitochondria (Figs. 21.5, 21.6a, and 21.7). Within the mitochondria another metabolic pathway for pyruvate metabolism also exists. The enzyme, pyruvate carboxylase, converts pyruvate to oxaloacetate, which is a TCA cycle intermediate (Figs. 21.6a and 21.8). The significance of the latter reaction will be discussed later.

Within the cytosol, pyruvate can be converted to lactic acid by lactic acid dehydrogenase (LDH). Lactate and a hydrogen ion are then exported from the cell via the monocarboxylic acid transporter (Figs. 21.5, 21.6a, and 21.9). This pyruvate to lactic acid reaction is associated with the oxidation of NADH to NAD^+ and, as will be shown, is critical to maintaining glycolysis when the availability of oxygen to the cardiomyocyte is limited. Conversely, under aerobic conditions, lactate in the blood can be transported into the cardiomyocyte by the monocarboxylic acid transporter, to be converted to pyruvate by LDH. The LDH-catalyzed reaction also reduces NAD^+ to NADH, and the reducing equivalents from NADH can be transferred into the mitochondrial matrix by the malate-aspartate shuttle, and the pyruvate generated is available for processing by PDH.

During glycolysis of one glucose molecule, two pyruvate molecules, four ATP molecules, and two NADH molecules are produced. However, because two ATP molecules are consumed early in the glycolytic pathway, the net production of ATP in the cytosol is two molecules/glucose molecule. As previously indicated, pyruvate and NADH are utilized in the

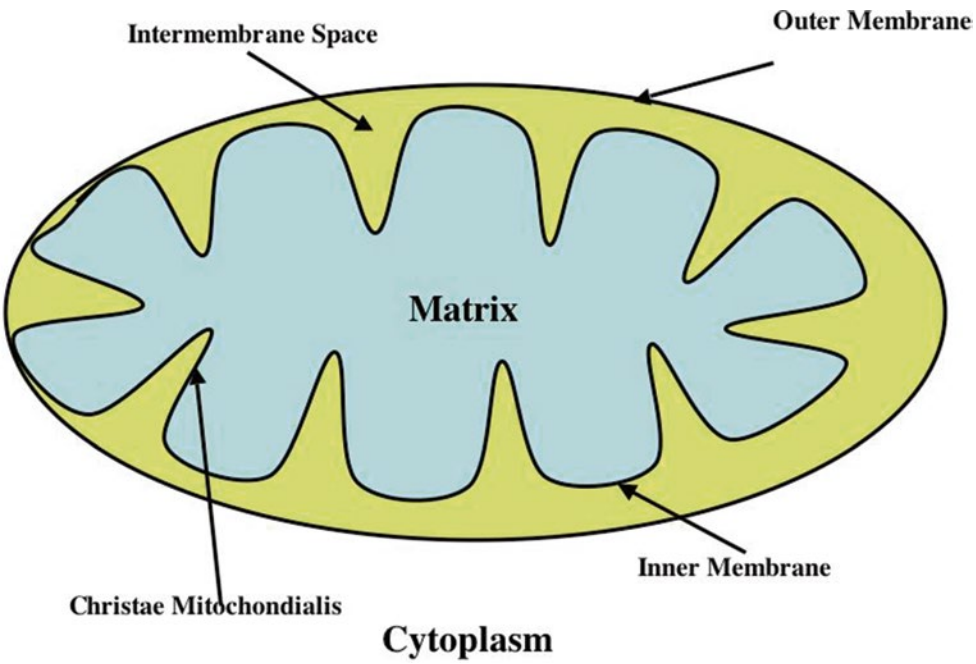

Fig. 21.7 Major features of mitochondrial morphology. See text for discussion

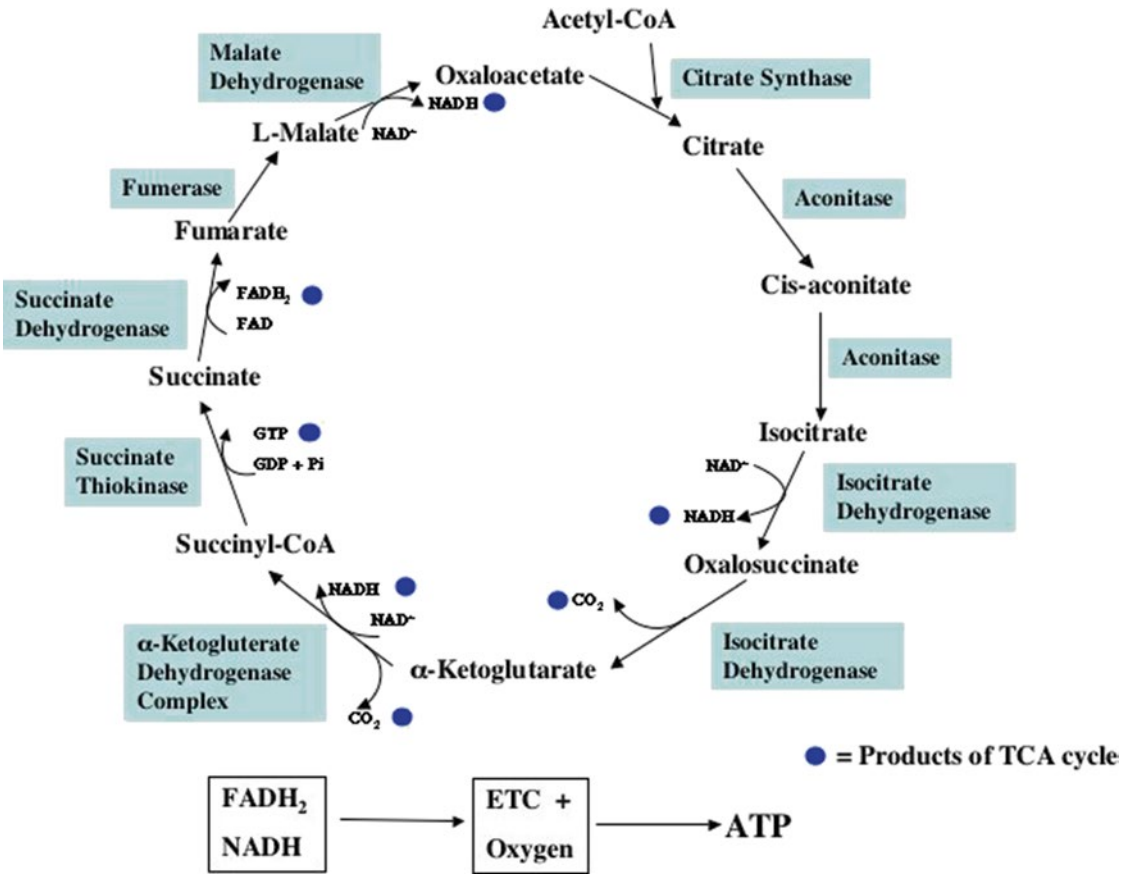

Fig. 21.8 Tricarboxylic acid (*TCA*) cycle. The filled blue circles are the products resulting from one turn of the TCA cycle. See text for discussion. *ATP* adenosine triphosphate, *ETC* electron transport chain, *$FADH_2$* flavin adenine dinucleotide, *NADH* nicotinamide adenine dinucleotide, *TCA* tricarboxylic acid

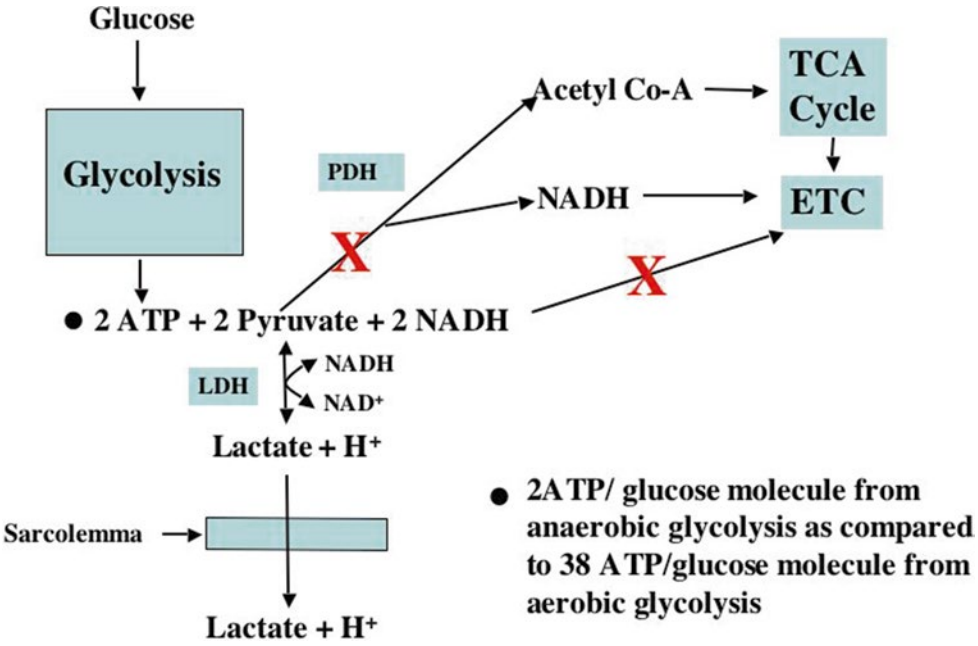

Fig. 21.9 Flowchart for anaerobic glucose metabolism. A *large red X* indicates metabolic pathways blocked during ischemia. See text for discussion. *ATP* adenosine triphosphate, *ETC* electron transport chain, *LDH* lactic acid dehydrogenase, *NADH* nicotinamide adenine dinucleotide, *PDH* pyruvate dehydrogenase, *TCA* tricarboxylic acid

mitochondria for oxidative generation of ATP. Complete metabolism of one glucose molecule (i.e., including oxidation of the products of glycolysis in mitochondria) results in the formation of many additional ATP molecules (30–36, depending on the literature cited) than does glycolysis alone. However, under conditions when mitochondrial function is severely oxygen limited, the oxidative contribution to ATP synthesis is lost, and only two ATP molecules can be formed from each glucose molecule.

21.3.2 The Mitochondrion

Mitochondria, which are the primary site of ATP synthesis in most mammalian cells, contain the β-lipid oxidation pathway enzymes, the TCA cycle enzymes, the electron transport chain, and the F_1F_0-H^+-ATPase (also called F_1F_0-ATP synthase or ATP synthase). To better understand the location of these systems, mitochondrial structure will be briefly reviewed (Fig. 21.7). The inner mitochondrial membrane contains the electron transport chain, F_1F_0-H^+-ATPase, the adenine nucleotide translocase, and other transporters. The mitochondrial matrix contains the TCA cycle enzymes, β-lipid oxidation enzymes, and many other enzymes and reactants. The cristae are invaginations that markedly expand the surface area of the inner membrane and, thereby, the quantity of energy generation-associated proteins that can be contained within the inner membrane. The inner membrane-bound components of the metabolic pathways are positioned to optimize the flow of substrates through their reaction sequences. The mitochondrial outer membrane forms a boundary between the cellular cytoplasm and the mitochondrial intermembrane space. The intermembrane space contains creatine kinase which is important for high-energy phosphate transport out of mitochondria (Figs. 21.7, 21.10, and 21.11) and cytochrome c, a component of the electron transport chain. The importance of the intermembrane space to oxidative ATP synthesis will be discussed subsequently. The outer mitochondrial membrane also contains voltage dependent anion channels (VDAC) through which ATP and other moieties exit the intermembrane space and through which ADP and many other molecules enter the intermembrane space.

21.3.3 Fatty Acid Metabolism

Figure 21.12 presents a flowchart for the β-lipid oxidation pathway. Dietary long-chain, nonesterified, free fatty acids (NEFAs) are generally the predominant carbon substrate in normal myocardium. They are transported in the blood bound to plasma albumin, lipoprotein moieties, or in the form of triacylglycerol which is also bound to albumin. The latter can be broken down to release NEFAs by an enzyme present in the plasma and at the surface of the capillary and cardiomyocyte. After dissociating from albumin, NEFAs are transported accross capillary walls and into cardiomyocytes by fatty acid transport proteins. Within the cell, NEFAs are bound to fatty acid-binding proteins which provide solubility and intracellular transport. Once in the cell, NEFAs are either reesterified and stored as triglycerides or activated by acyl-CoA synthetase (which requires the presence of free CoA and ATP) to form a long-chain acyl-CoA. Because long-chain acyl-CoA cannot readily diffuse through the mitochondrial inner membrane, it is converted to long-chain acyl carnitine by carnitine palmitoyltransferase 1 at the outer surface of the inner mitochondrial

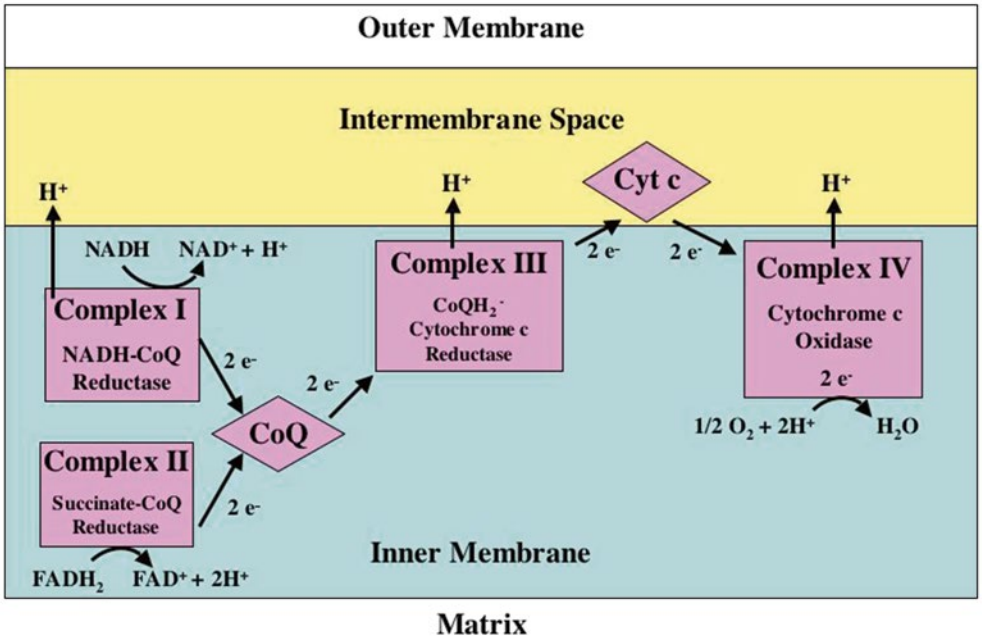

Fig. 21.10 Electron transport chain (*ETC*). See text for discussion. *$FADH_2$* flavin adenine dinucleotide, *NADH* nicotinamide adenine dinucleotide

membrane and then transported across the inner membrane by carnitine-acylcarnitine translocase (which also transports free carnitine liberated by carnitine palmitoyltransferase 2 back into the intermembrane space; see below). The long-chain acyl carnitine is next converted back to acyl-CoA at the inner surface of the mitochondrial inner membrane by carnitine palmitoyltransferase 2. Long-chain acyl-CoA is then processed by a sequence of enzyme-catalyzed reactions that comprise the β-lipid oxidation pathway. If the long-chain acyl-CoA has an even number of carbon atoms, then the final products of the last cycle (i.e., the metabolism of a four-carbon acyl-CoA molecule) through the β-oxidation sequence are two acetyl-CoA molecules (Fig. 21.6b). However, if the last long-chain acyl-CoA has an odd number of carbon atoms (i.e., 5), then the products of the last cycle through β-oxidation are one acetyl-CoA and one propionyl CoA. Unlike acetyl-CoA, propionyl-CoA cannot enter the TCA cycle. However, propionyl-CoA is readily converted to succinyl-CoA, a TCA cycle intermediate (Fig. 21.6b). Hence, this is another pathway that contributes to the maintenance of the TCA cycle intermediate pool size. Both pyruvate molecules produced from glucose and odd-numbered fatty acid molecules that undergo complete β-oxidation contribute to maintenance of the TCA intermediate pool. Processes that add molecules to the TCA intermediate pool are termed *anaplerotic* (Fig. 21.6a, b), and those that remove intermediates from the pool are called *cataplerotic*. The importance of these processes to TCA cycle function will be illustrated in a clinical example of an inborn metabolic abnormality to be presented later.

The products of complete β-oxidation of a fatty acid are acetyl-CoA (and propionyl-CoA if the chain has an odd number of carbons), NADH, and flavin adenine dinucleotide ($FADH_2$). However, consumption of these products by the TCA cycle and the electron transport chain cannot occur in the absence of oxygen. Thus, β-oxidation cannot occur under anoxic or ischemic conditions, and markedly ischemic myocardium does not support either pyruvate- or fatty acid-derived ATP synthesis. Hence, during ischemia, the only source of ATP synthesis is anaerobic glycolysis.

21.3.4 Regulation of Carbon Substrate Metabolic Pathways

Myocardial glycolysis is regulated at several levels (some of which are shown in Fig. 21.13a); the first is entry of glucose into the cell. In the heart and skeletal muscle, this process is largely dependent on the activity of the GLUT 4 glucose transporter. The quantity of the GLUT 4 transporter in the plasma membrane is determined by the action of insulin on the sarcolemmal insulin receptor, the activation of which begins a sequence of biochemical events that ultimately triggers migration of GLUT 4 molecules to the plasma membrane from cytoplasmic storage sites. Increased levels of fatty acid metabolites in cardiomyocytes inhibit insulin receptor activation and the consequent transport of GLUT 4 to the plasma membrane. Blood glucose levels are generally well defended by an organism, so glucose availability is not usually limiting to transport. Rather, the number of GLUT 4 molecules present in the plasma membrane usually determines the rate of glucose transport. In addition to insulin-associated increases, plasma membrane GLUT 4 levels are also enhanced during

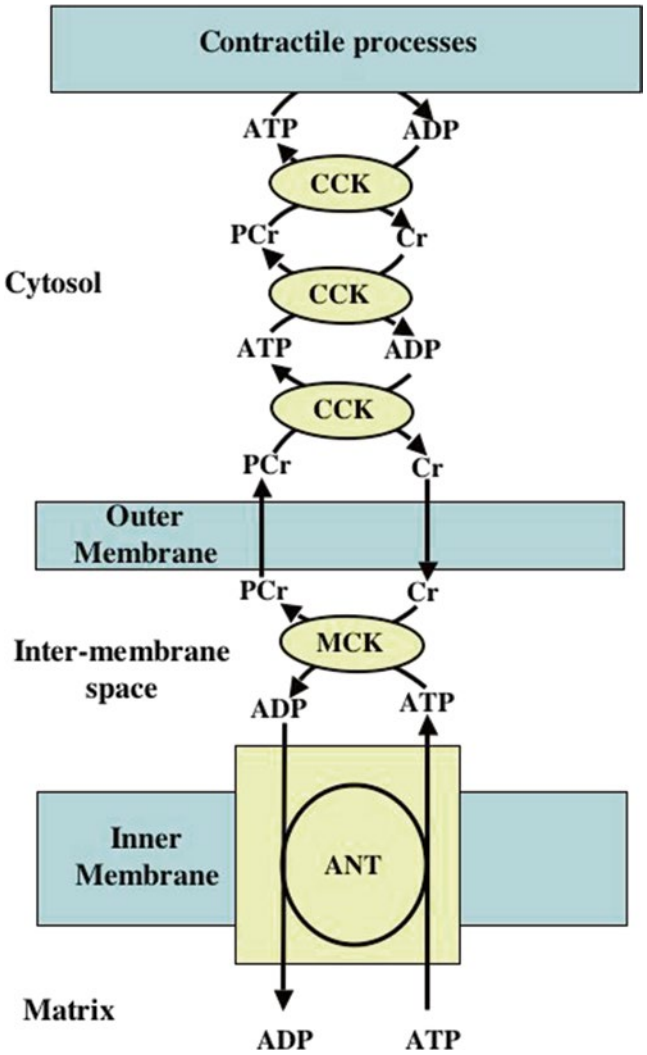

Fig. 21.11 Creatine kinase shuttle hypothesis. The diffusion rates of ATP out of the intermembrane space and through the cytosol and ADP through the cytosol and into the intermembrane space are considered to be relatively slow compared to those of creatine and creatine phosphate. The creatine kinase shuttle is thought to facilitate the transfer of ADP from sites of ATP utilizing reactions to the mitochondrial intermembrane space and also to facilitate the transfer of ATP to the sites of utilization. The way the shuttle is proposed to function is described below. The adenine nucleotide transporter (*ANT*), which is not rate limiting, transports ADP from the mitochondrial intermembrane space to the mitochondrial matrix where it is rephosphorylated back to ATP. The ANT simultaneously transports newly synthesized ATP from the matrix to the intermembrane space. Within the intermembrane space, the mitochondrial isozyme of creatine kinase (*MCK*) transfers the terminal high-energy phosphate of ATP to creatine to form phosphocreatine. Phosphocreatine then diffuses into the cytosol, and the ADP produced by this reaction in the intermembrane space is returned to the mitochondrial matrix by ANT, where it is rephosphorylated. The phosphocreatine which has diffused into the cytosol is then used as a high-energy phosphate donor for the rephosphorylation of cytosolic ADP by the cytosolic isozyme of creatine kinase. Because the isozymes of creatine kinase have extremely rapid turnover rates, they can facilitate transport of ATP (by, in effect, shuttling the terminal high energy phosphate bonds) from the mitochondria to the sites of ATP hydrolysis and of ADP from ATP hydrolysis sites back to the mitochondrial outer membrane. There, phosphocreatine leaving the mitochondria is used to rephosphorylate ADP, and the creatine liberated from phosphocreatine diffuses into the mitochondrial intermembrane space to be rephosphorylated. Obviously, ATP and ADP also pass through the VDAC, but at slower rates than creatine and phosphocreatine. As a result, cytosolic ADP levels (including those in proximity to the points of ATP utilization) are kept at low levels even if the rate of ATP utilization increases. The stability of ADP levels in the face of increasing ATP utilization permits ATP to maintain a high level of free energy that can be transferred to energy-requiring cellular processes. *ADP* adenosine diphosphate, *ANT* adenine nucleotide transporter, *ATP* adenosine triphosphate, *CCK* cytosolic creatine kinase, *Cr* creatine, *MCK* mitochondrial creatine kinase, *PCr* phosphocreatine

increased myocardial work states via the associated elevation of cytosolic adenosine monophosphate (AMP) and ADP. Increased AMP levels activate AMP-activated protein kinase (AMPK), which causes increased GLUT 4 trafficking to the plasma membrane. The subsequent reactions of the glycolytic sequence (and glycogen breakdown) are also activated by a number of factors including increased cytosolic Ca^{++}, AMPK, protein kinases A and C, PI3K, and fructose 2,6-bisphosphate, as well as AMP and ADP. These reactions are inhibited by increased levels of ATP and increased cytosolic levels of H^+ and/or citrate and other factors as well. For example, increased free fatty acid metabolism increases mitochondrial citrate synthesis, and increased citrate exiting the mitochondria inhibits glycolysis. The first step of oxidative glucose metabolism (the decarboxylation of pyruvate to form acetyl-CoA) by PDH is also highly regulated by PDH kinases and phosphatases, and a high level of β-lipid oxidation causes inactivation of PDH by stimulating its phosphorylation by specific kinases. The regulatory pathways are complex and discussed in more detail in several references cited at the end of the chapter.

Fatty acid metabolism has two major regulatory sites (Fig. 21.13b). The first is at the level of fatty acid transport through the plasma membrane; transport occurs by means of specific proteins located within the membrane (major path) and via free diffusion through the plasma membrane (minor path). This process is mainly regulated by the blood concentrations of fatty acids, i.e., fatty acid uptake is blood level dependent. This means that if the rate of fatty acid utilization is slower than the uptake rate, cardiomyocytes will accumulate fatty acids. The latter are mainly stored as triglycerides. Excess lipid accumulation can be damaging to cardiomyocytes (and other cells as well). A second regulatory site is at the level of long-chain fatty acid transport into mitochondria. As discussed above, long-chain acyl-CoA must be converted to long-chain acylcarnitine at the outer mitochondrial membrane by the enzyme carnitine palmitoyltransferase 1. This enzyme is inhibited by malonyl-CoA, a molecule produced by cytosolic acetyl-CoA carboxylase in response to increased cytosolic levels of acetyl-CoA. The latter occurs as a result of increased fatty acid or pyruvate oxidation by the mitochondria; this overall signaling pathway is complex. Hence, in nonischemic myocardium, increased fatty acid

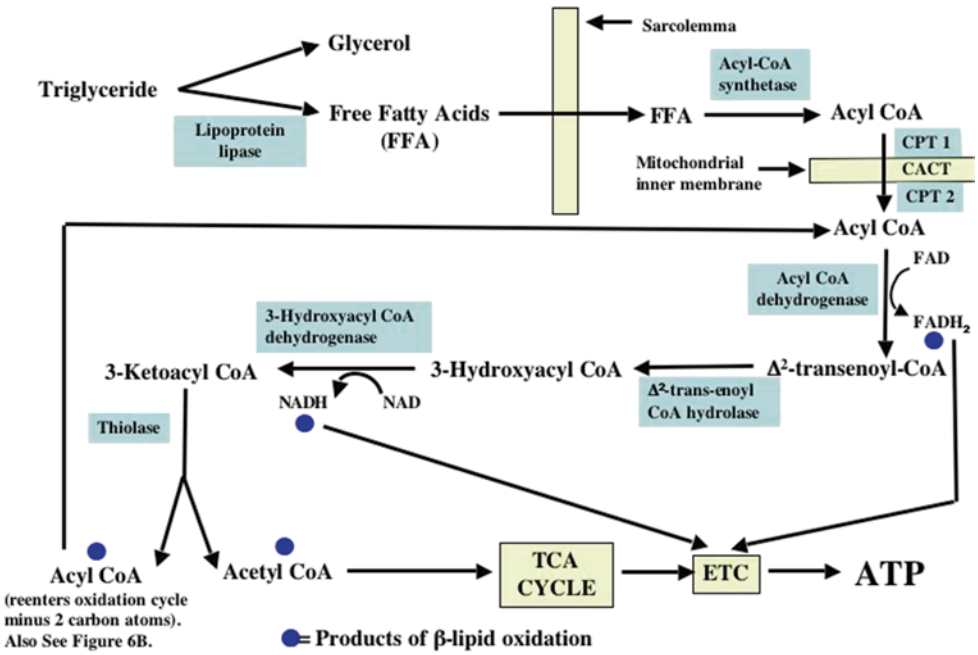

Fig. 21.12 Flowchart depicting the cellular uptake of free fatty acids and the pathways through which their metabolism proceeds. See text for discussion. *ATP* adenosine triphosphate, *CPT 1* carnitine palmitoyltransferase 1, *CPT 2* carnitine palmitoyltransferase 2, *ETC* electron transport chain, $FADH_2$ flavin adenine dinucleotide, *FFA* free fatty acids, *NADH* nicotinamide adenine dinucleotide, *TCA* tricarboxylic acid

oxidation or high blood concentrations of lactate (the latter, by virtue of increasing cytosolic pyruvate levels) will increase cytoplasmic citrate levels, and this increases malonyl-CoA synthesis and thereby limits fatty acid uptake and utilization by mitochondria. This explains why lactate (and exogenously supplied pyruvate; see below) is able to compete successfully with fatty acids for oxidation by mitochondria. Activation of AMPK by an increased cardiac work state can directly inhibit acetyl-CoA carboxylase and thereby reduce malonyl-CoA levels. This will relieve inhibition of carnitine palmitoyltransferase 1 and facilitate fatty acid entry into mitochondria. The rate of mitochondrial fatty acid or pyruvate oxidation (assuming no limitation of transport into mitochondria) is, of course, ultimately controlled by the rate of consumption of the products of these metabolic pathways. The latter is determined by the rate at which the cell utilizes ATP (see below for discussion of this point). A more detailed discussion of the regulation of fatty acid metabolic pathways and of how malonyl-CoA levels are controlled is available in references cited at the end of this chapter.

21.3.5 Myocardial Carbon Substrate Selection

Although the primary carbon substrates (Fig. 21.4) taken up and metabolized by the myocardium are free fatty acids and glucose, the heart also readily takes up and metabolizes pyruvate, lactate, ketone bodies, and amino acids (that are converted to pyruvate if availabilities of glucose and fatty acids are limited). However, the relatively low blood concentrations of the latter substrates and the normal availability of glucose and fatty acids limit their utilization. In contrast, during intense exercise that is associated with marked elevation of blood lactate content or during periods when blood levels of ketone bodies are elevated, the utilization of these substrates increases markedly, and glucose and fatty acid utilization is decreased. A more detailed discussion of the regulation of blood levels of these substrates exceeds the scope of this chapter, yet a few orienting comments are appropriate with regard to glucose and fatty acid utilization patterns. Blood glucose levels are maintained within a narrow range (~4–5 mM) in nondiabetic subjects. Glucose homeostasis reflects a balance between the alimentary uptake of glucose, glucose release from the liver (which can synthesize glucose or release glucose from the glycogen storage pool), and removal of glucose from the blood by various organs. As noted, glucose uptake in both cardiac and skeletal muscle is stimulated by insulin, a hormone secreted by specialized cells in the pancreas in response to increased blood glucose levels.

The heart has often been called an *omnivore* because of its capacity to consume virtually any available carbon substrate (either directly or following processing). As already noted, glucose is transported into the cardiomyocyte by a family of sarcolemmal glucose transport proteins and the predominant transporter (GLUT 4) is insulin dependent. Fatty acids enter myocytes via sarcolemmal fatty acid transport proteins, while lactate and pyruvate are taken up by the sarcolemmal monocarboxylic acid transporter. Utilization of glucose by

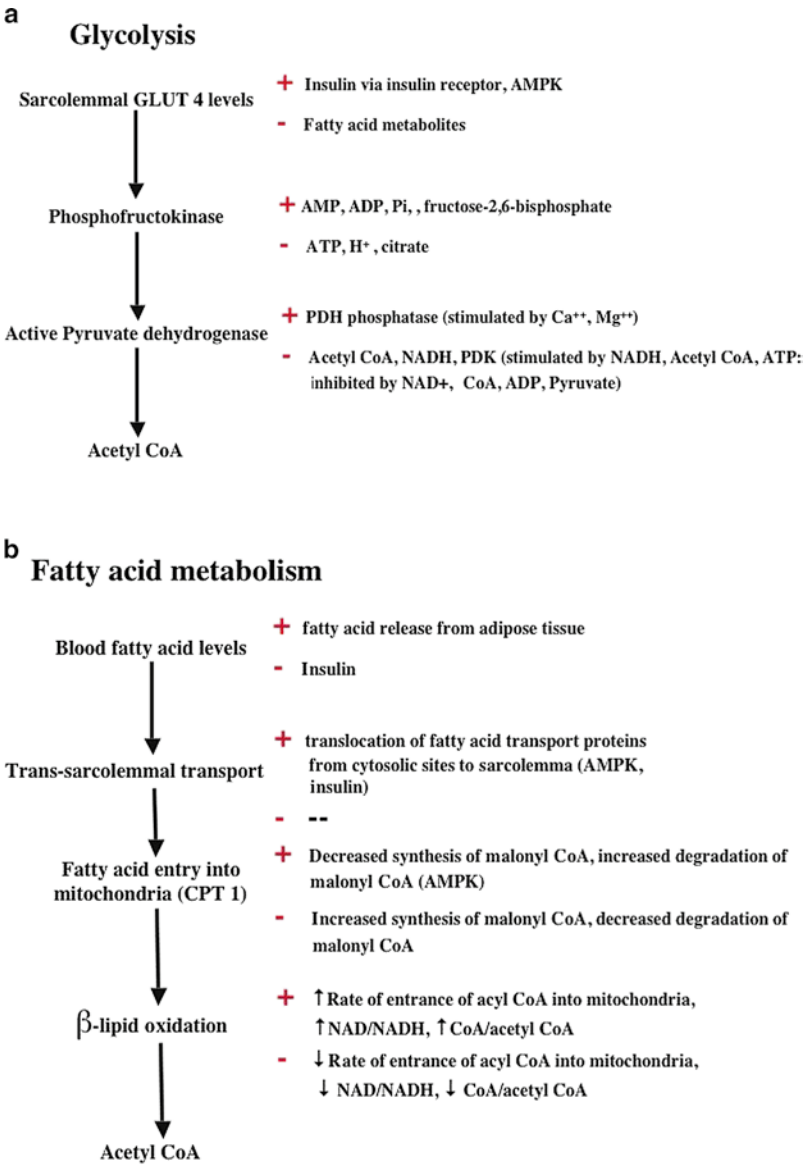

Fig. 21.13 (**a**) Major regulatory sites in the glycolytic pathway (including pyruvate dehydrogenase which is immediately distal to the glycolytic sequence). (**b**) Major regulatory sites in the fatty acid metabolic pathway (including β-lipid oxidation). *ADP* adenosine diphosphate, *AMP* adenosine monophosphate, *AMPK* adenosine monophosphate-activated kinase, *ATP* adenosine triphosphate, *CPT 1* carnitine palmitoyltransferase 1, *NADH* nicotinamide adenine dinucleotide, *PDH* pyruvate dehydrogenase

the heart is largely regulated by the availability of fatty acids, glucose, and insulin in the blood. In the fasted state, glucose levels are generally normal, but insulin secretion is modest, and blood fatty acid levels (released from the liver and adipose tissue) are high. Hence, fatty acids are the predominant cardiac substrate despite normal blood glucose levels. In contrast, during vigorous exercise, blood lactate levels can rise markedly (remember, they are a by-product of skeletal muscle glycolysis which is markedly enhanced by exercise). Lactate competes favorably with the myocardial metabolism of fatty acids, and glucose despite the presence of substantial blood levels of the latter substrates and much more lactate is consumed by the heart.

In contrast, after a high-carbohydrate meal, blood glucose levels rise, and this elicits insulin secretion. Increased insulin levels stimulate glucose uptake by the heart, skeletal muscle, and certain other tissues and also cause blood fatty acid levels to decrease by stimulating their uptake by the liver and adipose tissue. As a result, myocardial glucose consumption increases, and fatty acid consumption decreases. Of interest, lactate (and pyruvate) are the most favored substrates when the relative blood concentrations of all of the substrates are experimentally equalized. Of major importance, under physiological conditions, the switching of carbon substrates *does not* affect myocardial performance.

21.3.6 The TCA Cycle

Acetyl-CoA is the carbon substrate consumed by the (tricarboxylic acid) TCA cycle. As already discussed, when oxygen is available, acetyl-CoA is produced (within mitochondria)

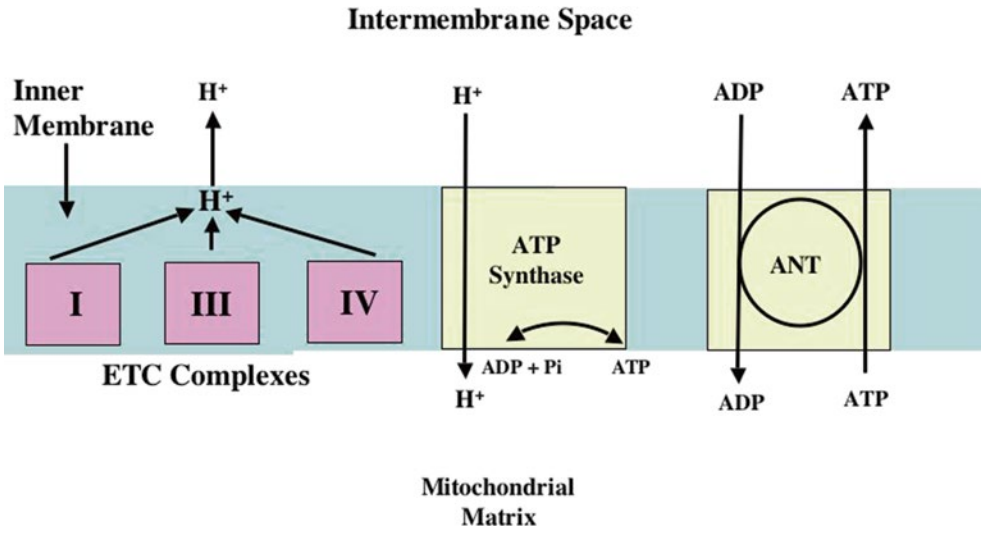

Fig. 21.14 Mechanism of oxidative phosphorylation and the transport of ATP from the mitochondrial matrix to the intermembrane space. See text for discussion. *ADP* adenosine diphosphate, *ANT* adenine nucleotide transporter, *ATP* adenosine triphosphate, *ETC* electron transport chain

from glycolysis derived pyruvate and by β-oxidation of fatty acids. Figure 21.8 shows the individual reactions of the TCA cycle. In the first step of the cycle, acetyl-CoA is combined with oxaloacetate to form citrate and free CoA; this reaction is catalyzed by the enzyme citrate synthase. Citrate then enters a sequence of reactions that ultimately generate two molecules of CO_2 and four reducing equivalents in the form of NADH (3) and $FADH_2$ (1). One high-energy phosphate molecule (GTP) is also produced, which can be directly utilized or converted to ATP. During this process, citrate (a six-carbon molecule) is stepwise decarboxylated and ultimately converted back to oxaloacetate, the four-carbon molecule which, when condensed with a new acetyl-CoA, reinitiates the sequence of reactions just described. The reducing equivalents generated (NADH and $FADH_2$) deliver electrons to the electron transport chain. Rate-limiting enzymes of the TCA cycle are the pyruvate dehydrogenase complex (which precedes, but is not really a component of the TCA cycle), isocitrate dehydrogenase, and α-ketoglutarate; these enzymes are highly regulated as will be discussed later. For elucidating the TCA cycle (also known as the Krebs cycle), Sir Hans Krebs was awarded the Nobel Prize in Medicine or Physiology in 1953.

21.3.7 The Electron Transport Chain and Oxidative Phosphorylation

The two substrates of the electron transport chain are NADH and $FADH_2$. These molecules are produced by glycolysis, β-lipid oxidation, and the TCA cycle as previously discussed; in this context, they transfer electrons to the electron transport chain. The electron transport chain (Fig. 21.10) is comprised of: (1) two freely diffusible compounds, ubiquinone (also known as coenzyme Q) which is confined to the mitochondrial inner membrane and cytochrome c which is located in the intermembrane space, and (2) four multi-protein functional complexes (I, II, III, and IV) that are contained within the mitochondrial inner membrane. NADH interacts with the electron transport chain by transferring electrons to (and thereby reducing) complex I; this, in turn, reduces coenzyme Q (ubiquinone). $FADH_2$ interacts with the electron transport chain by transferring electrons to complex II that, like complex I, also transfers its electrons to coenzyme Q. It should be noted that complex II is also a component of the TCA cycle (it is succinate dehydrogenase) and, thereby, directly links the TCA cycle to the electron transport chain by virtue of its coidentity as complex II. Reduced coenzyme Q then diffuses to complex III and transfers its electrons. Next, complex III reduces cytochrome c, and this molecule diffuses to complex IV and transfers electrons to this complex. The latter, when reduced by four electrons, reduces O_2 to two O^{-2} ions. Each O^{-2} ion combines with two H^+ ions to form H_2O in an irreversible reaction. In recent years, it has become apparent that the individual complexes of the electron transport chain (many of which contain multiple proteins) are organized to form "super-complexes" (see references for additional information if desired). These super-complexes appear to increase the efficiency of oxidative phosphorylation and to reduce the generation of toxic by-products of the oxidative phosphorylation process such as reactive oxygen species (ROS), etc. Toxic metabolites generated by metabolic processes such as ROS and the cellular defenses against them will be discussed later.

During the process of electron transport, energy is released as electrons pass sequentially through the complexes of the electron transport chain. The purpose of electron transport chain complexes I, III, and IV is to capture this released energy and use it to pump H^+ from the mitochondrial matrix across the inner mitochondrial membrane into the intermembrane space (Fig. 21.10). These pumps create an electrochemical gradient ($\Delta\mu H^+$) comprised of an electrical potential and a chemical potential (the latter reflected by

ΔpH) across the inner mitochondrial membrane. As a consequence of proton transport, the mitochondrial matrix is more negative than the intermembrane space. The F_1-F_0-ATPase, which is also located in the inner mitochondrial membrane (Fig. 21.14), is the major pathway of H^+ return from the intermembrane space into the matrix. The energy released by the passage of H^+ down this electrochemical potential gradient is captured by the F_1F_0-ATPase and used to drive the next reaction [**inorganic phosphate (Pi) + ADP → ATP**]. In this way, much of energy released by the metabolism of glucose and fatty acids is transferred to the terminal high-energy phosphate bond of ATP. The concept of proton pumping into the intermembrane space, and the use of the electrochemical gradient thus formed to synthesize ATP, is known as the chemiosmotic theory. In recognition of his insight into how these processes function (ideas initially considered to be quite controversial), Sir Peter Mitchell was awarded the Nobel Prize in Chemistry in 1978. The production of ATP by mitochondria is termed oxidative phosphorylation; in virtually every human tissue (heart, brain, kidney, but not red blood cells), oxidative phosphorylation is the primary source of ATP generation.

To date, the precise mechanism by which the F_1F_0-H^+-ATPase generates ATP from its substrates (ADP and Pi) remains under investigation. However, a number of characteristics of the process are well established. For example, the F_1F_0-H^+-ATPase has been shown to be a near-equilibrium enzyme. In other words, the reaction can occur in both directions. However, it has also been shown, both in isolated mitochondria (which generate ATP under conditions of carbon substrate, ADP, and oxygen excesses) and in the perfused rat heart that the F_1F_0-H^+-ATPase operates far out of equilibrium so that virtually all fluxes are in the ADP + Pi -> ATP direction. In the presence of abundant oxygen, the F_1F_0-H^+-ATPase is kinetically controlled by the concentrations of its immediate substrates (ADP and Pi) and the magnitude of the proton electrochemical potential gradient. Hence, in principle, ADP and Pi levels can regulate the rate of ATP synthesis *as long as oxygen and carbon substrates are not limiting and the proton gradient is large*. However, in vivo regulatory mechanisms are far more complicated than those described by this relatively simple scheme first presented by B. Chance and G.R. Williams in 1955.

21.3.8 Regulation of the TCA Cycle, Electron Transport Chain, and Oxidative Phosphorylation

As pointed out by Chance and Williams, a simple kinetic regulatory scheme for oxidative phosphorylation with ADP (and Pi) availability controlling the ATP synthetic rates is valid when both oxygen and reducing equivalents are in excess. Under these conditions, the high proton electrochemical gradient will drive ATP synthesis until ADP and/or Pi fall to levels that are rate limiting to ATP synthesis. From this point on, ADP availability (i.e., the rate of ADP production) determines the steady-state rate of ATP synthesis. Therefore, because ADP is a product of ATP hydrolysis, the rate of ATP synthesis is determined by the rate of ATP hydrolysis (i.e., the rate of ATP utilization). This simple feedback regulation of ATP synthesis can be demonstrated in the perfused rat heart by providing a perfusate containing unphysiologically high concentrations of pyruvate or octanoate. Under these experimental conditions, mitochondrial NADH levels are very high, and it appears that extramitochondrial ADP and/or Pi levels become low enough to kinetically regulate oxygen consumption. In this case, increased ATP utilization will cause ADP and Pi levels to rise and the rate of ATP synthesis to speed up, in association with an increase in the rate of oxygen consumption. In this construct, the increased rate of delivery of ADP and Pi to the F_1F_0-ATPase increases the rate of ATP synthesis. In other words, ADP levels *must increase concordantly* with the increased rate of ATP synthesis.

In the in vivo mammalian heart (e.g., rat, dog, swine, human, etc.), however, free ADP levels in the cytosol (as estimated by means of ^{31}P magnetic resonance spectroscopy) are higher than those in the isolated perfused rat heart and are well above the usual kinetic regulatory range described in studies of isolated mitochondria or perfused rat hearts. Further, in the in vivo animal heart, ADP levels actually remain fairly constant even when increased rates of ATP utilization (increased cardiac work) drive substantial increases of myocardial oxygen consumption. However, this does not mean that ADP availability is not crucial to the rate of ATP synthesis. When the rate of ATP expenditure is increased in normal myocardium, there is an obligatory identical increase in the rate of ADP delivery to mitochondria (once a new steady state is reached). To emphasize this point, the increase in the *rate of ADP delivery* to the ATP synthase (e.g., as myocardial work increases) is obligatory, despite the fact that a change in *steady-state ADP levels* is not.

The observation that ADP levels did not increase in the in vivo myocardium as the rates of ATP utilization and synthesis increase led to the recognition that additional regulatory systems are required to explain the data obtained in the in vivo heart. Further, these overall regulatory processes must have very rapid response times with regard to facilitation of ATP synthesis. The latter is required because myocardial contents of ATP and creatine phosphate (another high-energy phosphate bond storage molecule which serves to buffer ATP levels) are only sufficient to support a few seconds of ATP expenditure in the absence of continuing ATP synthesis. The reaction converting cytosolic ATP to phosphocreatine is rapid and near equilibrium via the enzyme creatine kinase as discussed earlier. See Fig. 21.11 provides a brief overview of the ~P shuttle function of phosphocreatine.

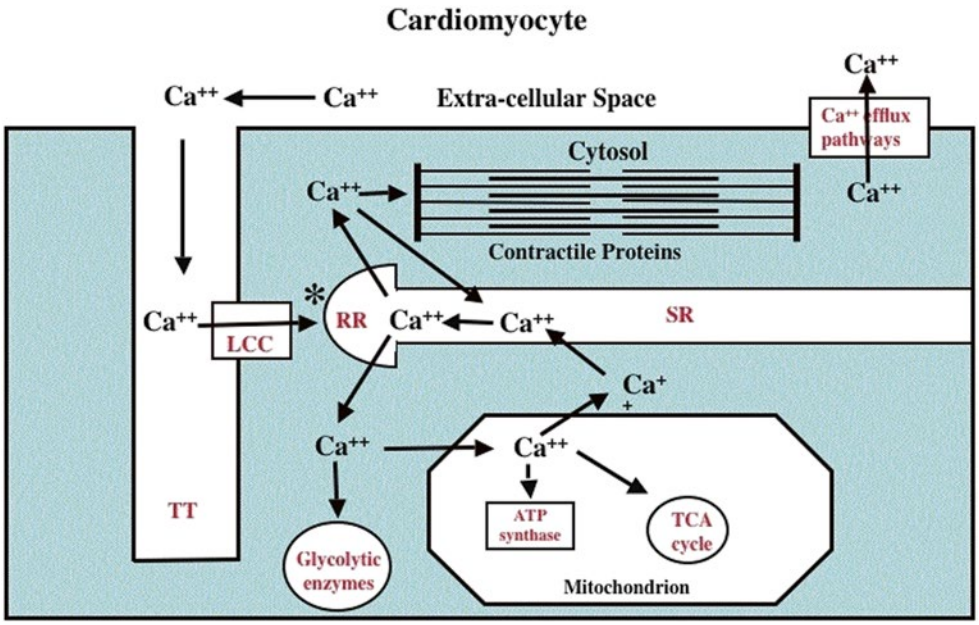

Fig. 21.15 Pathways of Ca^{++} entry and exit in the cardiomyocyte and several intracellular organelles relevant to excitation-contraction coupling and energy metabolism. The strong linkage between the stimulatory effects of intracellular [Ca^{++}] on contraction and ATP generation is also shown. See text for discussion. *ATP* adenosine triphosphate, *LCC* l-type voltage-activated Ca^{++} channel, *RR* ryanodine receptor, *SR* sarcoplasmic reticulum, *TCA* tricarboxylic acid, *TT* t-tubule

It is now known the overall regulation of metabolism in cardiomyocytes is a complex process that is quite far from being fully understood. It is comprised of a large number of parallel, sequential, and massively interacting feedback and feed-forward regulatory pathways, the effects of which combine to allow the cell to alter ATP synthetic rates sufficiently to meet changing demands without destabilizing the cellular chemical milieu and inducing fatigue. In contrast, ATP demand can exceed synthetic capacity in tissues such as skeletal muscle, and destabilization of the cellular chemical milieu and fatigue develop under these circumstances. To offer the reader a feel for such regulatory processes, a discussion of several (but far from all) Ca^{++}-based mechanisms for regulation of oxidative phosphorylation will be presented next. Readers can review the discussion of Ca^{++}-based contraction and relaxation mechanisms presented elsewhere in this book and also briefly in Fig. 21.15 to refresh their understanding of cardiomyocyte Ca^{++} dynamics.

During exercise, increased norepinephrine release from sympathetic nerve fibers and increased epinephrine from the adrenal glands activate β-adrenergic receptors in cardiomyocytes. This receptor activation causes an increase of Ca^{++} entry into the cytosol (per beat) via sarcolemmal voltage-dependent Ca^{++} channels. Cytosolic Ca^{++} levels are further augmented by the increased heart rate (which reflects an increased number of Ca^{++} channel openings/min). The increased Ca^{++} entering the cytosol, together with β-adrenergic receptor-mediated activation of sarcoplasmic reticulum Ca^{++} sequestration, increases the sarcoplasmic reticulum Ca^{++} store. The more fully loaded sarcoplasmic reticulum (which is the predominant source of "contraction activation" Ca^{++}) can then release more Ca^{++} per beat (via its Ca^{++} release site, the ryanodine receptor) into the cytosol. The larger systolic cytosolic Ca^{++} transient present following adrenergic stimulation and/or heart rate increase then generates increased force and shortening. The ryanodine receptor is also activated by β-adrenergic receptor stimulation and other factors. Concomitantly, the increased frequency of Ca^{++} transients (heart rate) and their larger size increase the "average" Ca^{++} level in the cytosol. Mitochondria normally transport Ca^{++} both in and out of their matrix and maintain a "steady-state" matrix Ca^{++} level that is related to average cytosolic Ca^{++}. In response to higher average cytosolic Ca^{++} levels, mitochondrial Ca^{++} uptake increases, resulting in an increase in the steady-state level of matrix Ca^{++}. It is important to note that increased mitochondrial matrix Ca^{++} has multiple effects on oxidative phosphorylation. First, as already mentioned, the TCA cycle has three rate-limiting enzymes (PDH, isocitrate dehydrogenase, and α-ketoglutarate dehydrogenase), and the activities of these enzymes are regulated, in part, by mitochondrial matrix Ca^{++} levels. Specifically, when these enzymes interact with Ca^{++}, their sensitivity to respective substrates is increased. This accelerates their reaction rates and increases the rate of acetyl-CoA entry into and flux through the TCA cycle without requiring pyruvate, acetyl-CoA levels, or immediate substrate levels of the TCA cycle pool to rise, provided that the rates of delivery of acetyl-CoA to the TCA cycle (and anaplerotic processes) are increased sufficiently to support the increased TCA cycle flux rate. Therefore, glucose uptake and glycolysis-mediated delivery of pyruvate to (and its rate of metabolism by) PDH must increase, and/or the rates of fatty acid uptake and β-oxidative delivery of acetyl-CoA to the TCA cycle must increase to support the increased rate of TCA cycle flux.

As noted above, the rates of cellular substrate uptake, glycolytic flux, and β-oxidation also respond to metabolic signaling to produce the required increases in the rate of acetyl-CoA production.

A major consequence of an increased TCA cycle flux is the more rapid generation of both mitochondrial NADH and $FADH_2$; this results in maintenance or increases in their steady-state levels despite the increased rate of electron transfer to the electron transport chain. Hence, stimulation of the electron transport chain fluxes is facilitated by an increased rate of reducing equivalent generation and also by direct stimulation of electron transport chain complex activities by other metabolic signals which are present during periods of increased ATP demand. Increased rates of electron transport chain fluxes will then result in an increased rate of H^+ pumping by the electron transport chain, which serves to maintain the electrochemical gradient across the inner mitochondrial membrane at a level adequate to support the increased rate of ATP synthesis despite the fact that the rate of H^+ passage (through the ATP synthase) is markedly increased to support the increased ATP synthesis rate. Additionally, the F_1F_0-ATPase is also regulated in that the fraction of this enzyme that is in an active state is increased by elevations of mitochondrial matrix Ca^{++}. An increased fraction of this enzyme in the active state is beneficial during periods of increased ATP synthesis, because an increased amount of active enzyme increases the rate of ATP synthesis without requiring ADP levels to rise. Hence, so long as the rate of ADP delivery to mitochondria increases appropriately (which it does when the rate of ATP utilization increases), ADP levels can remain reasonably stable. This is crucial because elevated ADP levels have direct effects on the contractile protein interactions and also decrease the amount of energy that hydrolysis of the terminal phosphate bond of ATP can release to drive energy-dependent processes. Nevertheless, it should be realized that although coordinated activation of carbon substrate metabolic pathways, the TCA cycle, the electron transport chain, and ATP synthase are all crucial to meeting work increase-associated ATP synthetic requirements, control of respiration is equally linked *to the rate of ATP utilization and the resulting rate of delivery of ADP* to the mitochondrial matrix. Hence, the newer, more complex model of respiratory regulation still includes aspects of the simpler Chance and Williams model.

To summarize, these observations support the concept that increases of average cardiomyocyte cytosolic Ca^{++} levels (e.g., that occur during exercise) act as an important feedforward signal for oxidative phosphorylation. This signal stimulates, in a parallel manner, ATP utilization by the contractile processes and ATP synthesis by the F_1F_0-ATPase as well as many preceding reactions in the energy-generating scheme (Fig. 21.15). The net effects of these regulatory mechanisms (and additional feedback regulatory mechanisms which are not discussed) are to facilitate fluxes of basic food-derived carbon substrates through the metabolic sequences without requiring the cytosolic concentrations of the initial and intermediate substrates (including ADP) to increase. The rapid response time of this entire system also allows ATP levels to remain relatively constant despite wide and rapid fluctuations in the rate of ATP utilization. Since these mechanisms allow both ADP and ATP levels and the ATP/ADP ratio to remain stable during increased ATP synthetic rates, the free energy (ΔG ATP) that can be released by hydrolysis of the terminal high-energy phosphate bond of ATP (and transferred to the reactions it drives) is maintained constant despite the increased rate of ATP expenditure. Metabolic control theory as applied to the regulation of oxidative phosphorylation, glycolysis, β-lipid oxidation, and the TCA cycle has been the subject of detailed study; for further discussion of this topic, refer to the references listed at the end of this chapter.

21.3.9 Toxic By-Products Generated by Mitochondria and Other Cellular Moieties that Impact Energy Generation and Contraction-Associated Processes

Carbon substrate metabolism, oxidative phosphorylation, and a number of other cellular processes produce potentially toxic by-products (Fig. 21.16). The descriptor "potentially" is employed because a number of these by-products (when generated at low levels) can exert useful influences on intracellular signaling pathways; in contrast, when generated at high levels, they are highly toxic. As a generalization, these moieties can induce modifications of proteins, lipids, and carbohydrates which can alter the performance of these molecules in diverse ways including the stimulation and/or disruption of their normal function. Some examples of the "toxic by-products" included in this category are highly reactive oxygen and highly reactive nitrogen species (ROS and RNS), hydrogen sulfide (H_2S), carbon monoxide (CO), nitric oxide (NO), and others. Consequently, the heart and all other tissues have evolved strong defense systems at sites of generation of these reactive species (i.e., in the cytosol, mitochondria, and other organelles). These systems are capable of maintaining the concentration of reactive molecules below levels that can adversely affect cardiomyocyte structure and function while preserving their physiological signaling roles. Discussion of all of these systems is far beyond the scope of this survey chapter, but several reactive species generation and degradation systems will be briefly described to convey the concept.

The most often cited ROS species produced by the mitochondrial electron transport chain (complexes 1, 2, and 3)

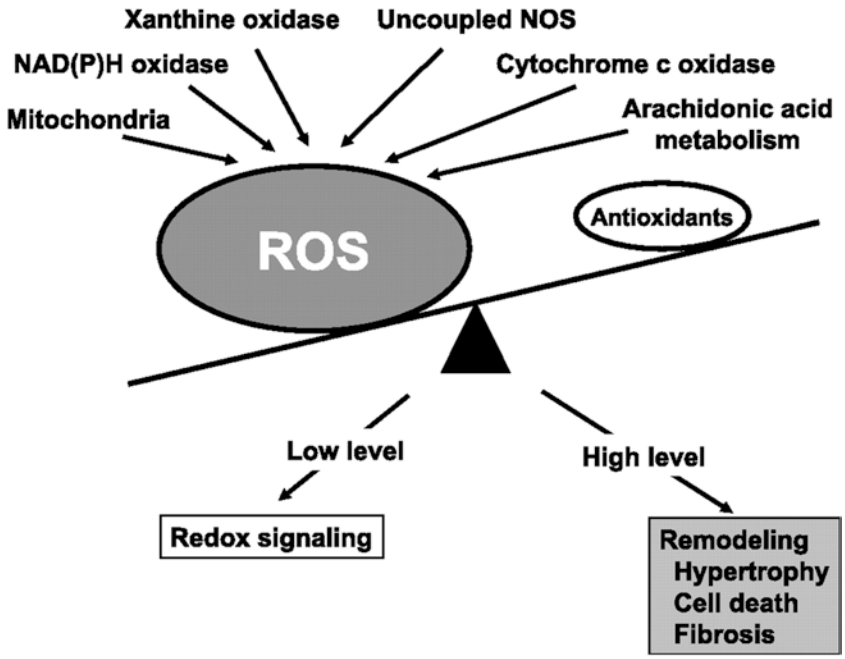

Fig. 21.16 Sources of reactive species in myocardium. These sources are located in various cellular compartments including the plasma membrane, cytosol, and subcellular organelles. Low levels of ROS generation stemming from physiological activation of these mechanisms serve as intracellular signals, while high levels of ROS activate adverse signaling pathways that induce pathological remodeling of the myocardium. Antioxidant defenses limit accumulation of ROS from the various sources shown. *ROS* reactive oxygen species, *NOS* nitric oxide synthase. Reprinted from Tsutsui H, Kinugewa S, and Matsusima S, Oxidative stress and heart failure, Am J Physiol Heart Circ Physiol, Vol. 301, H2181-H2190, 2011. Reprinted from American Journal of Physiology Heart and Circulatory Physiology (by American Physiological Society). Reproduced with permission of American Physiological Society, in the format of Republish in a book via Copyright Clearance Center

and by NADPH oxidases located in the plasma membrane, sarcoplasmic reticulum, and peroxisomes (as well as other intracellular sources) is the superoxide radical ($^{-}O_2$). $^{-}O_2$ in itself is not highly toxic, and its mobility (i.e., diffusivity) is limited. However, $^{-}O_2$ is readily converted to a more diffusible ROS such as hydrogen peroxide (H_2O_2). The latter can then be rapidly converted the hydroxyl radical, a highly toxic entity. Additionally, $^{-}O_2$, by interacting with NO, forms peroxynitrite, another highly toxic molecule. Somewhat paradoxically, low concentrations of H_2O_2 (and other reactive molecules) can act to modulate a number of intracellular molecular signaling pathways. However, at high concentrations, these reactive species are quite toxic and interfere with many important processes required for cellular homeostasis. For example, in the heart ROS are generated in huge quantities during the postischemic reperfusion period and adds substantially to the injury accrued during the ischemic period (see later discussion of effects of ischemia on myocardium). ROS are also produced in normal working myocardium at low non-toxic levels that have signaling functions. Somewhat surprisingly, recent experimental work suggests that in *normal* working cardiac and skeletal muscle, reactive species originate mainly from non-mitochondrial sources. In the heart, the levels reached during endurance exercise do not significantly decrease myocardial contractile performance. In contrast, in working skeletal muscle, exercise-induced ROS generation has been considered to be one of the many contributing causes of the fatigue associated with substantial levels of work.

Fortunately, cardiomyocytes and skeletal muscle cells (and most other cell types) have a number of defenses against accumulation of excessive levels of $^{-}O_2$ and its toxic derivatives. The enzyme superoxide dismutase, isoforms of which are located in the interstitial space, cytoplasm, and within mitochondria, converts $^{-}O_2$ into H_2O_2. H_2O_2, in turn, is converted to water by catalase, another protective enzyme that is widely distributed within cells. The destruction of H_2O_2 limits the formation of the highly reactive (and thereby toxic) hydroxyl radical. In experimental models, augmenting ROS defenses by transgenic techniques or by administration of small molecule scavengers of ROS has been shown to protect against ROS-induced damage occurring during the postischemic reperfusion period. However, it should be noted that large clinical trials involving ingestion of substantial doses of antioxidants (e.g., vitamin E) in an attempt to prevent age-associated degenerative processes have been negative, possibly because the antioxidant molecules do not reach the intracellular site of ROS generation and/or because they may ablate the effects of beneficial signaling induced by low levels of ROS generation. There are also small molecules present in the cytosol and mitochondria which can nonenzymatically scavenge the reactive species.

Another defense against the deleterious effects of reactive species (in addition to their destruction) is the reversal of the chemical "damage" they induce. There are a number of coupled enzyme/substrate systems that do this, and the interested reader can review a reference listed at the end of the chapter for more insight. One cogent example of ROS-induced damage is the sequential oxidation of the sulfur atoms contained in some of the amino acids that form a protein. Oxidation of these sulfur atoms can disrupt the functional properties of the protein. Under these circumstances, another enzyme, glutaredoxin, uses glutathione, an SH group-containing molecule that is abundant in cardiomyocytes (and many other cell types), as a cofactor and reduces the oxidized sulfur atoms on the protein at the cost of the oxidation of glutathione molecules. The oxidized glutathione is then reduced back to its native form by another enzyme, glutathione reductase. Notably, if the sulfur atom undergoes multistage oxidation as a result of the interaction with ROS, the process may then not be reversible by antioxidative defenses.

Within limits, irreversibly modified proteins and other molecules can be replaced by cellular synthetic processes. However, if large numbers of these molecules are damaged by an oxidative insult, then repair capacity will be exceeded, and the cell will die. Taken together, the oxidant defenses of the *normal* cardiomyocyte are extremely effective and are highly protective over a wide range of myocardial work states. However, they are clearly inadequate to protect diseased myocardium which is often subjected to quite severe oxidant stresses induced by various types of pathological processes.

21.4 Metabolism in Diseased Myocardium

21.4.1 Ischemic Myocardium

The most common cause of inadequate myocardial ATP synthesis is ischemia, and the most frequent cause of myocardial ischemia is occlusive disease of the major coronary arteries. *Demand ischemia* occurs when: (1) a narrowed coronary artery can conduct sufficient blood to sustain aerobic metabolism in the portion of myocardium that it supplies during basal levels of physical activity and (2) the degree of narrowing is sufficient to limit increases of blood flow that normally (and seamlessly) occur during the increased demands for ATP production that are present during exercise or other stress. This phenomenon is the basis of exercise- or stress-induced angina pectoris (i.e., heart-associated chest pain). Patients with this pathophysiology are asymptomatic at rest or during mild exertion, but when the work of the heart exceeds the ability of a narrowed coronary artery to meet the increased blood flow required to support the increased rate of ATP demand, ischemia ensues, and the patient experiences chest pain. In response to the symptom of chest pain, the patient will typically discontinue exercise, and during the rest period, the cardiac work and ATP synthetic needs fall to levels where the narrowed coronary artery can meet the blood flow demand; hence, ischemia is relieved.

In contrast, *supply ischemia* occurs when the coronary artery narrowing is so severe that it limits blood flow in the absence of increased ATP demand, i.e., ischemia occurs even when the patient is at rest. Supply ischemia is generally caused by an acute narrowing or abrupt complete closure of coronary vessels and may cause myocardial infarction. Less commonly, supply ischemia can occur as the result of coronary artery spasm, in which inappropriate (pathologic) vasoconstriction of a major coronary artery causes transient total (or near total) occlusion of blood flow. Although the nature of the myocardial ischemia is qualitatively similar in supply and demand ischemia, supply ischemia is generally more clinically severe. Because of the greater vulnerability of the inner myocardial layers of the left ventricle to blood flow reduction, mild ischemia is usually confined to the subendocardium. However, as the coronary obstruction becomes more severe, ischemia proceeds as a wave front from subendocardium to subepicardium until the full myocardial wall is involved.

When myocardial blood flow is inadequate, the limited availability of both oxygen and carbon substrate may limit the ATP synthetic rate, but it is usually the oxygen deficiency that is most critical. This is because the myocyte has substantial glucose reserves (i.e., in the form of glycogen that can be converted to glucose); the glucose released from glycogen can then undergo anaerobic glycolysis and generate modest amounts of ATP. In contrast, myocardial oxygen stores are very small and can only support a short period of oxidative metabolism. Consequently, when coronary blood flow is limited, the severity of the induced oxygen deficit determines the extent of limitation of oxidative phosphorylation and secondarily enhances the rate of glycogen breakdown and glycolysis. As indicated, the early effects of oxygen limitation are confined to pathways supporting oxidative phosphorylation (Figs. 21.5 and 21.17). During hypoxia or anoxia (i.e., when blood oxygen content is moderately or markedly reduced, but blood flow is maintained) or during ischemia (where blood flow is restricted), electron transport within the electron transport chain slows or stops depending on the severity of the oxygen deficit. This is because electrons cannot be transferred from cytochrome oxidase to molecular oxygen (the terminal electron acceptor). In consequence, the pumping of H^+ from the mitochondrial matrix into the intermembrane space stops because it depends on energy liberated as electrons pass through the electron transport chain on their way to interacting with oxygen within cytochrome oxidase. As a result, the proton-motive force across the inner

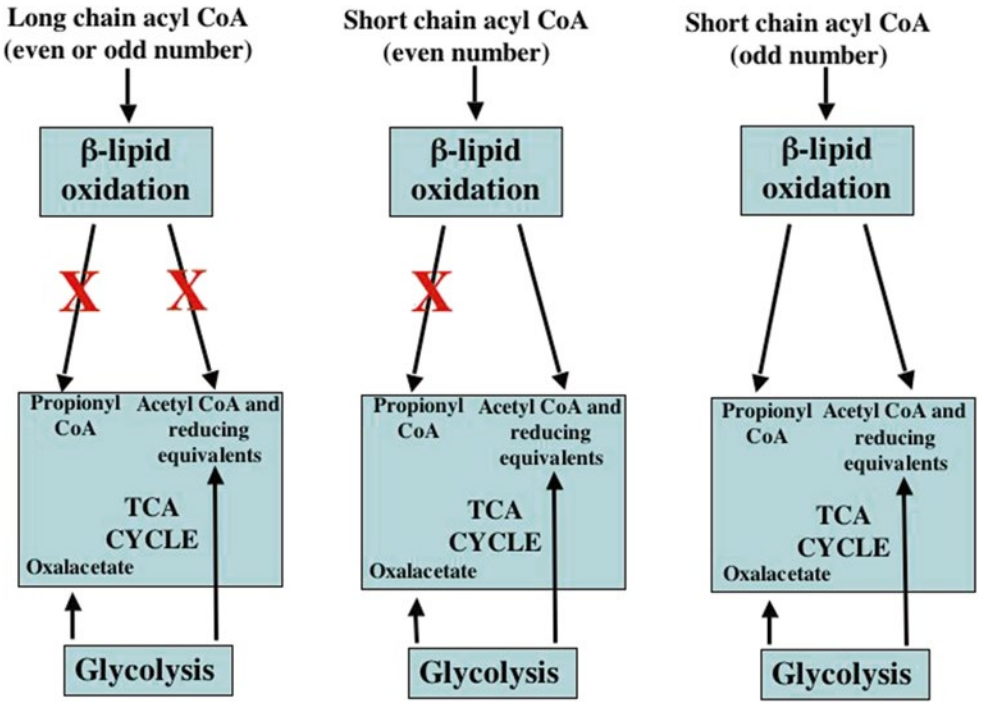

Fig. 21.17 Effects of very long-chain acyl-dehydrogenase deficiency on the metabolism of long-chain fatty acids (even and odd numbered), short-chain fatty acids (even numbered), and short-chain fatty acids (odd numbered). Only the last one can also supply anaplerotic substrate to the TCA cycle. A *large red X* indicates metabolic pathways which cannot be used by a specific type of free fatty acid. See discussion in text. *TCA* tricarboxylic acid

mitochondrial membrane begins to dissipate, and mitochondrial ATP synthesis fails. If the oxygen deficiency is severe, the dissipation of the H^+ gradient is marked, and the F_1F_0-H^+-ATPase begins to operate in the reverse direction, i.e., it converts ATP to ADP and uses energy liberated by ATP hydrolysis to pump H^+ back into the intermembrane space. Because the H^+ electrochemical potential is also used to energize other mitochondrial functions in addition to supporting ATP synthesis, mitochondrial degradation of ATP during periods of oxygen limitation may serve to preserve nonoxidative mitochondrial function and prolong the time when mitochondrial oxidative function can respond to resumption of blood flow. However, this mechanism of mitochondrial preservation occurs at the expense of hastening the fall in cytoplasmic ATP levels, and the latter limits all other cardiomyocyte functions that are ATP dependent.

Glycolysis can, in principle, proceed normally in the absence of oxygen, but it is also limited when blood flow is reduced or stops. Oxygen limitation causes cessation of forward electron transport chain function and, thereby, stops the mitochondrial oxidation of NADH generated by the TCA cycle and/or transferred from cytosolic NADH into mitochondria. Cytosolic NAD^+ is a substrate of glyceraldehyde phosphate dehydrogenase, a key enzyme of the glycolytic sequence, and if the NADH generated by that reaction is not oxidized back to NAD^+ by the transfer of reducing equivalents into the mitochondria by the malate-aspartate shuttle or into cytosolic lactate by LDH (see below), the lack of NAD^+ will then inhibit glyceraldehyde phosphate dehydrogenase. Other factors limiting the rates of glycolytic ATP synthesis during ischemia are cytosolic accumulations of lactate and hydrogen ions (Figs. 21.5 and 21.9). Under conditions of normal coronary flow, the myocardium can rapidly export both of these ions even when the glycolytic rate is augmented. Thus, in a model in which low oxygen content of coronary arterial blood is associated with preserved blood flow, lactate and H^+ export are not inhibited. But, when the myocardium is ischemic, the capacity to export lactate and protons decreases in proportion to the severity of the blood flow reduction. Furthermore, the increase in cytosolic lactate concentration during ischemia can inhibit the conversion of pyruvate to lactate via LDH, so that pyruvate generated by glycolysis may have limited exit possibilities, since pyruvate oxidation is also inhibited. Because the conversion of pyruvate to lactate results in the oxidation of cytosolic NADH, the availability of NAD^+ to glyceraldehyde phosphate dehydrogenase is further reduced when rising cytosolic levels of lactate slow this reaction (Figs. 21.5, 21.9, and 21.13a). In contrast, during hypoxia, if coronary flow is not restricted, glycolysis proceeds at a rapid rate because metabolic signaling activates the rate-limiting glycolytic reactions, the transport of glucose into the myocyte and lactate export. During moderate ischemia, when both glucose and oxygen deliveries are impaired, myocyte glycogen stores are the main source of glucose for glycolysis. When glycogen stores are exhausted, the limited rates of glucose delivery to (and lactate clearance from) the ischemic myocyte control the rate of glycolysis.

These concepts have specific importance in patients with coronary artery disease, because they typically define the

temporal boundary for viability of the ischemic myocardium. For example, in the moderately ischemic myocardium, contractile function rapidly decreases in response to: (1) decreased ATP availability, (2) accumulation of H^+ ions, and (3) many other factors. However, if residual coronary blood flow during ischemia is sufficient to permit some glycolysis (by allowing the export of some lactate and H^+ and the import of some glucose), then modest (glycolytic) ATP production may preserve tissue viability for some time. In contrast, following acute total coronary occlusion, glycolysis is rapidly inhibited, and myocyte death will occur much more rapidly. In other words, a level of coronary blood flow that is insufficient to maintain oxidative phosphorylation and contractile function may support glycolytic ATP production at a rate sufficient to sustain myocardial viability until appropriate medical or surgical treatment can restore blood flow to the ischemic myocardium.

Another adverse biochemical event that occurs during the ischemic period, and especially during a subsequent period of reperfusion, is a markedly enhanced rate of generation of highly chemically reactive species (ROS and others) by mitochondria and extramitochondrial enzymes. The interaction of these species with myocardial lipids, proteins, and carbohydrates further damages the structural and functional capabilities of cardiomyocytes. Cardiomyocyte endogenous protective mechanisms (see earlier discussion) offer a partial defense against the effects of the high levels of reactive species generated during and following a relatively short period of ischemia, but they are inadequate to forestall the injury consequent to a long period of ischemia. Reactive species-induced damage contributes to both ischemic and post-ischemic cardiomyocyte loss. In experimental models of cardiac ischemia/reperfusion, augmentation of defenses against reactive species has been shown to decrease cardiomyocyte loss.

21.4.2 Metabolism in Hypertrophied and Failing Hearts

During fetal life, the myocardium primarily metabolizes glucose and not fatty acids. This pattern of metabolism is well suited to the low oxygen levels in fetal arterial blood; glucose metabolism requires less oxygen than fatty acid metabolism. Additionally, the lower cardiac work levels (lower blood pressure) in the fetus are adequately supported by ATP production through glycolysis and pyruvate oxidation. However, after birth substrate preference of the heart (now in a higher oxygen environment and operating at a higher work load) rapidly shifts to the adult metabolic pattern, which is predominantly dependent on fatty acid oxidation. This change of substrate preference is the result of upregulated expression of genes controlling the transport of fatty acids into the myocyte and their subsequent metabolism in the cytosol and mitochondria. This upregulation in the expression of genes involved in fatty acid metabolism and oxidative phosphorylation is commonly referred to as the shift from a fetal to an adult gene expression pattern.

A chronic mechanical overload produced by hypertension, heart valve abnormalities, and/or ischemic destruction of a portion of the left ventricle can result in left ventricular dilation as well as cellular hypertrophy. The severity of the dilation is dependent on the excess stress placed upon the viable myocardium. In general, left ventricular wall tension (systolic and diastolic) increases as ventricular dimensions increase; this is a consequence of the law of LaPlace that relates the internal chamber pressure and chamber radius (and wall thickness) to the level of chamber wall tension. The increased left ventricular wall tension (this principle applies to all cardiac chambers) can activate changes in the expression patterns of a number of genes involved in control of myocyte growth (hypertrophy), energy metabolism, and many of the processes that support cardiomyocyte contraction. It does this, in part by directly activating sarcolemmal receptors (e.g., angiotensin type 2 receptors) that are responsive to stretch. Among the adverse consequences of activation of these receptors is the stimulation of ROS generation and increased levels of reactive species that may overwhelm antioxidant capacity and cause oxidant damage to many important structural and functional molecules. This damage then limits a variety of cardiomyocyte functions (i.e., metabolism, ion pumping, and contraction).

Initially, the stress-activated growth stimulation pathways stimulate cardiomyocytes to grow (i.e., hypertrophy), and this can increase chamber wall thickness. Because the increased wall thickness can reduce systolic wall stress toward normal (via the LaPlace relationship), this may result in a prolonged period of stable compensated myocardial hypertrophy. However, chronic (*pathological*, *not exercise induced*) myocardial hypertrophy is usually associated with important changes in energy metabolism, including reductions of ATP and creatine phosphate levels. This shift in the myocardial gene expression is often referred to as a reversion to the fetal gene expression pattern. Subsequently, reductions also occur in the level of molecules participating in energetic processes such as oxidative phosphorylation. Although the increased glucose metabolism and decreased fatty acid metabolism associated with this reversion (to a fetal gene expression pattern) may have short-term energetic benefits (perhaps by modestly decreasing the oxygen cost of ATP synthesis), the overall ATP synthetic capacity of severely hypertrophied and failing myocardium is significantly reduced. The period of compensated hypertrophy in the chronically overloaded heart is often followed by a significant contractile dysfunction of the ventricular myocytes with ultimate progressive left heart dilation and dysfunction and

mild to severe symptoms such as marked fatigue and shortness of breath. At this point, the clinical syndrome known as *heart failure* is present.

The question arises as to whether the decreased ATP synthetic capacity observed in hypertrophied and/or failing cardiomyocytes *induces* the decompensated state. It has been shown that all of the operational subsystems in the failing cardiomyocyte (i.e., energetic, contractile, and electrical) are severely dysfunctional and that this dysfunction occurs in a parallel manner. However, whether contractile dysfunction in the failing heart is caused primarily by a limited ability of the abnormal contractile apparatus *to consume ATP* or whether the reduced ability *to produce ATP* (i.e., the concept of the energy-starved heart) is also causal is still unclear.

In animal models, molecular and other interventions that have been specifically directed toward improving *either* disordered energetic functions or contractile processes have often attenuated the development of *both* contractile and energetic dysfunctions. Hence development of malfunctions in both systems appear to be inter-dependent. As discussed elsewhere in this book, interventions that block the adverse effects of the neurohumoral activation present in patients and animals with heart failure are also beneficial. This is because neurohumoral activation is associated with stimulation of many of adverse intracellular signaling pathways.

Lastly, significant abnormalities of left ventricular chamber function can add an ischemic component to the intrinsic metabolic abnormalities of hypertrophied and failing myocardium, even when occlusive coronary artery disease is not present. Increased ventricular filling pressures, impaired diastolic relaxation, and tachycardia present in the abnormal heart can limit the ability of myocardial blood flow (especially in the subendocardium) to increase normally in response to an increased metabolic rate. Hence, in the chronically overloaded heart, acquired intrinsic abnormalities of the cardiomyocytes and superimposed limitations of blood flow can act together to compromise cardiomyocyte ATP synthetic capacity and thus further impair overall cardiac function.

21.4.3 Primary (Genetic) Myocardial Metabolic Abnormalities

As described above, changes in gene expression in the hypertrophied or failing cardiomyocyte can cause various abnormalities of myocardial metabolism that, in turn, can act to constrain contractile function. However, "primary" (genetically determined) abnormalities of carbon substrate metabolism or oxidative phosphorylation can also cause myocyte hypertrophy and/or failure. Interested readers can refer to the references at the end of this chapter for more information on such defects. A dramatic example of one abnormality and a successful therapeutic approach to treat this metabolic defect will be discussed below.

An inherited deficiency of the enzyme very long-chain acyl-CoA dehydrogenase (VLCAD) is known to be associated with cardiomyopathy and skeletal muscle myopathy (Fig. 21.17). This enzyme is the first component of the β-lipid oxidation sequence. Because most dietary fatty acids are of the long-chain type, the deficiency of VLCAD results in a markedly increased cardiac dependence on glucose for ATP generation. The fact that even upregulated glucose metabolism cannot adequately support cardiac function is indicated by the development of progressive myopathy (although the cytosolic accumulation of long-chain fatty acids, which cannot be fully metabolized, also contributes to the myopathy). The classical treatment for this condition has been to replace the long-chain fatty acids in an individual's diet with even-numbered short- or medium-chain length fatty acids such as octanoate or decanoate. Importantly, the short-chain fatty acids bypass the metabolic roadblock, because the medium- and short-chain acyl-CoA dehydrogenases are normal in these patients. This therapeutic strategy induces increased fatty acid utilization and causes clinical improvement, but unfortunately cardiac and skeletal muscle myopathies may persist in many patients treated in this manner.

The question arose as to why feeding even-numbered short-chain length fatty acids did not fully correct the muscle defects in these patients despite the augmentation of acetyl-CoA delivery to the TCA cycle. The answer was that VLCAD deficiency caused limitation of metabolism of both even- and odd-numbered long-chain fatty acids; hence, both acetyl-CoA and propionyl-CoA deliveries (i.e., from beta oxidation of fatty acids) to the TCA cycle were limited by this inherited defect. Although the metabolism of even-numbered short-chain fatty acids supplied acetyl-CoA, it did not supply the anaplerotic substrate propionyl-CoA. Consequently, even-numbered short-chain fatty acids could not correct the defect in the anaplerotic delivery of substrate to the TCA cycle and, therefore, were unable to correct a possible decrease in TCA intermediate pool size resulting from propionyl-CoA deficiency (Fig. 21.6b). Following this logic, dietary supplementation with an odd-numbered short-chain fatty acid would be expected to permit β-lipid oxidation to supply both acetyl-CoA and propionyl-CoA. In fact, when patients were treated with heptanoate, a seven-carbon fatty acid, they showed marked improvement in both skeletal muscle and cardiac abnormalities. Hence, this disorder was effectively managed by defining all of the biochemical defects and prescribing a biochemical treatment strategy that compensated for these defects. Unfortunately, most inborn abnormalities of energy-generating systems in the heart and other organs are not amenable to such a simple dietary manipulation. Over the long term, work in the molecular biology of genetic manipulation shows promise in remedying these diseases.

21.5 Summary

This chapter summarized how chemical energy stored in ingested carbon substrates is transferred to ATP, as well as some of the regulatory systems which integrate the function of these pathways and make them responsive to changes in ATP demand without destabilizing the intracellular chemical milieu. Also reviewed were the generation of toxic by-products of the metabolic processes and mechanisms that limit their adverse effects and the effects of several physiological states and diseases on these processes.

Acknowledgment Supported by NIH (NIBIB) P41 EB015894

References

References for Regulation of Myocardial Blood Flow

1. Ishibashi Y, Duncker DJ, Zhang J, Bache RJ (1998) ATP-sensitive K+ channels, adenosine, and nitric oxide-mediated mechanisms account for coronary vasodilation during exercise. Circ Res 82: 346–359
2. Gorman MW, Tune JD, Richmond KN, Feigl EO (2000) Feedforward sympathetic coronary vasodilation in exercising dogs. J Appl Physiol 89:1892–1902
3. Duncker DJ, Bache RJ (2000) Regulation of coronary vasomotor tone under normal conditions and during acute myocardial hypoperfusion. Pharmacol Ther 86:87–110
4. Duncker DJ, Bache RJ (2008) Regulation of coronary blood flow during exercise. Physiol Rev 88:1009–1086

General Biochemistry Text

5. Berg JM, Tymoczko JL, Stryer L (eds) (2010) Biochemistry, 7th edn. W.H. Freeman & Co., New York

References for Glucose and Fatty Acid Metabolism and Regulation of Glycolysis and Fatty Acid Metabolism

6. Coven DL, Hu X, Cong L et al (2003) Physiological role of AMP-activated protein kinase in the heart: graded activation during exercise. Am J Physiol Endocrinol Metab 285:E629–E636
7. Nickerson JG, Momken I, Benton CR et al (2007) Protein-mediated fatty acid uptake: regulation by contraction, AMP-activated protein kinase, and endocrine signals. Appl Physiol Nutr Metab 32:865–873
8. Roden M (2004) How free fatty acids inhibit glucose utilization in human skeletal muscle. News Physiol Sci 19:92–96
9. Stanley WC, Recchia FA, Lopaschuk GD (2005) Myocardial substrate metabolism in the normal and failing heart. Physiol Rev 85:1093–1129

References for Myocardial Substrate Selection

10. Lehman JJ, Kelly DP (2002) Transcriptional activation of energy metabolic switches in the developing and hypertrophied heart. Clin Exp Pharmacol Physiol 29:339–345
11. Drake AJ, Haines JR, Noble M (1980) Preferential uptake of lactate by the normal myocardium in dogs. Cardiovasc Res 14:65–72
12. Drake-Holland AJ, Van der Vusse GJ, Roemen TH et al (2001) Chronic catecholamine depletion switches myocardium from carbohydrate to lipid utilisation. Cardiovasc Drugs Ther 15:111–117
13. Hardie DG, Ashford ML (2014) AMPK: regulating energy balance at the cellular and whole body levels. Physiology (Bethesda) 29:99–107

References for the TCA Cycle, Electron Transport Chain, and Oxidative Phosphorylation and Their Regulation

14. From AH, Zimmer SD, Michurski SP et al (1990) Regulation of the oxidative phosphorylation rate in the intact cell. Biochemistry 29:3731–3743
15. Ludwig B, Bender E, Arnold S, Huttemann M, Lee I, Kadenbach B (2001) Cytochrome C oxidase and the regulation of oxidative phosphorylation. Chembiochem 2:392–403
16. Brand MD, Curtis RK (2002) Simplifying metabolic complexity. Biochem Soc Trans 30:25–30
17. Kushmerick MJ, Conley KE (2002) Energetics of muscle contraction: the whole is less than the sum of its parts. Biochem Soc Trans 30:227–231
18. Zhang J, Murakami Y, Zhang Y et al (1999) Oxygen delivery does not limit cardiac performance during high work states. Am J Physiol 277:H50–H57
19. Territo PR, Mootha VK, French SA, Balaban RS (2000) Ca(2+) activation of heart mitochondrial oxidative phosphorylation: role of the F(0)/F(1)-ATPase. Am J Physiol Cell Physiol 278:C423–C435
20. Hochachka PW (2003) Intracellular convection, homeostasis and metabolic regulation. J Exp Biol 206:2001–2009
21. Das AM (2003) Regulation of the mitochondrial ATP-synthase in health and disease. Mol Genet Metab 79:71–82
22. Levy C, Ter Keurs HE, Yaniv Y, Landesberg A (2005) The sarcomeric control of energy conversion. Ann N Y Acad Sci 1047: 219–231
23. Maack C, O'Rourke B (2007) Excitation-contraction coupling and mitochondrial energetics. Basic Res Cardiol 102:369–392
24. Glancy B, Balaban RS (2012) Role of mitochondrial Ca2+ in the regulation of cellular energetics. Biochemistry 51:2959–2973
25. Genova ML, Lenaz G (2014) Functional role of mitochondrial respiratory supercomplexes. Biochim Biophys Acta 1837:427–443
26. Guzun R, Kaambre T, Bagur R et al (2014) Modular organization of cardiac energy metabolism: energy conversion, transfer and feedback regulation. Acta Physiol (Oxf). doi: 10.1111/apha.12287 [Epub ahead of print]

References for Toxic Metabolic By-products; Reactive Species

27. Powers SK, Ji LL, Kavazis AN, Jackson MJ (2010) Reactive oxygen species: impact on skeletal muscle. Compr Physiol 1:941–969
28. Radak Z, Zhao Z, Koltai E, Ohno H, Atalay M (2013) Oxygen consumption and usage during physical exercise: the balance between

oxidative stress and ROS-dependent adaptive signaling. Antioxid Redox Signal 18:1–37
29. Ward CW, Prosser BL, Lederer WJ (2014) Mechanical stretch-induced activation of ROS/RNS signaling in striated muscle. Antioxid Redox Signal 20:929–935
30. Kohlhaas M, Liu T, Knopp A, Zeller T, Ong MF, Böhm M, O'Rourke B, Maack C (2010) Elevated cytosolic Na+ increases mitochondrial formation of reactive oxygen species in failing cardiac myocytes. Circulation 121:1606–1613
31. Reily C, Mitchell T, Chacko BK, Benavides G, Murphy MP, Darley-Usmar V (2013) Mitochondrially targeted compounds and their impact on cellular bioenergetics. Redox Biol 1:86–93

References for Modeling of Energetic Function

32. Cortassa S, Aon MA, O'Rourke B et al (2006) A computational model integrating electrophysiology, contraction, and mitochondrial bioenergetics in the ventricular myocyte. Biophys J 91:1564–1589
33. Saks VA, Kuznetsov AV, Vendelin M, Guerrero K, Kay L, Seppet EK (2004) Functional coupling as a basic mechanism of feedback regulation of cardiac energy metabolism. Mol Cell Biochem 256–257:185–199
34. Saks V, Dzeja P, Schlattner U, Vendelin M, Terzic A, Wallimann T (2006) Cardiac system bioenergetics: metabolic basis of the Frank-Starling law. J Physiol 571:253–273
35. Korzeniewski B (2002) Parallel activation in the ATP supply–demand system lessens the impact of inborn enzyme deficiencies, inhibitors, poisons or substrate shortage on oxidative phosphorylation in vivo. Biophys Chem 96:21–31
36. Korzeniewski B (2001) Theoretical studies on the regulation of oxidative phosphorylation in intact tissues. Biochem Biophys Acta 1504:31–45
37. Aimar-Beurton M, Korzeniewski B, Letellier T, Ludinard S, Mazat JP, Nazaret C (2002) Virtual mitochondria: metabolic modelling and control. Mol Biol Rep 29:227–232

Reference for High-Energy Phosphate Shuttles

38. Dzeja PP, Terzic A (2003) Phosphotransfer networks and cellular energetics. J Exp Biol 206:2039–2047

References for Metabolism During Ischemia

39. Stanley WC, Recchia FA, Lopaschuk GD (2005) Myocardial substrate metabolism in the normal and failing heart. Physiol Rev 85:1093–1129
40. Sambandam N, Lopaschuk GD (2003) AMP-activated protein kinase (AMPK) control of fatty acid and glucose metabolism in the ischemic heart. Prog Lipid Res 42:238–256

References for Metabolism in Hypertrophied and Failing Myocardium

41. Ning XH, Zhang J, Liu J et al (2000) Signaling and expression for mitochondrial membrane proteins during left ventricular remodeling and contractile failure after myocardial infarction. J Am Coll Cardiol 36:282–287
42. Lehman JJ, Kelly DP (2002) Transcriptional activation of energy metabolic switches in the developing and hypertrophied heart. Clin Exp Pharmacol Physiol 29:339–345
43. Young ME, Laws FA, Goodwin GW, Taegtmeyer H (2001) Reactivation of peroxisome proliferator-activated receptor alpha is associated with contractile dysfunction in hypertrophied rat heart. J Biol Chem 276:44390–44395
44. Liao R, Jain M, Cui L et al (2002) Cardiac-specific overexpression of GLUT1 prevents the development of heart failure attributable to pressure overload in mice. Circulation 106:2125–2131
45. Stanley WC, Recchia FA, Lopaschuk GD (2005) Myocardial substrate metabolism in the normal and failing heart. Physiol Rev 85:1093–1129
46. Ashrafian H, Frenneaux MP, Opie LH (2007) Metabolic mechanisms in heart failure. Circulation 116:434–448
47. Gauthier LD, Greenstein JL, O'Rourke B, Winslow RL (2013) An integrated mitochondrial ROS production and scavenging model: implications for heart failure. Biophys J 105:2832–2842
48. Maack C, Cortassa S, Aon MA, Ganesan AN, Liu T, O'Rourke B (2006) Elevated cytosolic Na+ decreases mitochondrial Ca2+ uptake during excitation-contraction coupling and impairs energetic adaptation in cardiac myocytes. Circ Res 99:172–182
49. Kohlhaas M, Liu T, Knopp A, Zeller T, Ong MF, Böhm M, O'Rourke B, Maack C (2010) Elevated cytosolic Na+ increases mitochondrial formation of reactive oxygen species in failing cardiac myocytes. Circulation 121:1606–1613

References for Inherited Defects in Myocardial Metabolism

50. Mochel F, DeLonlay P, Touati G et al (2005) Pyruvate carboxylase deficiency: clinical and biochemical response to anaplerotic diet therapy. Mol Genet Metab 84:305–312
51. Roe CR, Mochel F (2006) Anaplerotic diet therapy in inherited metabolic disease: therapeutic potential. J Inherit Metab Dis 29:332–340

Introduction to Echocardiography

22

Jamie L. Lohr and Shanthi Sivanandam

Abstract

Advances in ultrasound technology in the last 30 years have allowed transthoracic echocardiography to become the primary technique for noninvasive assessment of cardiac structure and function in patients with congenital and acquired heart disease. Advanced ultrasound techniques, including transesophageal echocardiography and intravascular ultrasound, are widely used and can refine imaging and improve outcomes during invasive cardiac procedures. Better resolution and advanced Doppler techniques have allowed more accurate diagnoses and improved monitoring of pathologic conditions, and provide tools to study embryonic and fetal cardiac development. Finally, ultrasound technologies play an important role in cardiovascular research as well and are currently applied to research in physiology, molecular biology, vascular and cardiac regeneration, and stem cell therapies.

Keywords

Echocardiography • Cardiac ultrasound • Cardiac development • Fetal echocardiography • Doppler • Ejection fraction • Cardiac function

22.1 Introduction

The use of ultrasound to provide noninvasive evaluation of cardiac structure and function was a revolutionary advancement in cardiac care in the late twentieth century [1]. Development of the field of echocardiography has allowed detailed serial examinations of the development, structure, and function of the human heart both in normal physiologic states and in pathologic conditions Echocardiography has increased the diagnostic accuracy of noninvasive cardiac evaluation and provides a tool for the monitoring of diagnostic and therapeutic procedures. The goals of this chapter are to: (1) provide the reader with a brief overview of the types of echocardiography in clinical use today; (2) review the physical principles that underlie this clinical tool; and (3) demonstrate how echocardiography can be used to assess cardiac structure and function.

Prior to the 1970s, diagnosis of congenital and acquired heart disease was achieved by the combination of physical examination, electrocardiography (ECG), and invasive cardiac catheterization. Unfortunately, clinical examination and ECG are often not very specific diagnostic tools. Cardiac catheterization can augment clinical information, but can be a stressful and risky procedure, particularly in the young or very ill patient. Noninvasive imaging, including echocardiography, CT, and MRI, has become the mainstay of cardiac anatomic and functional diagnoses in congenital heart disease.

J.L. Lohr, MD (✉)
Department of Pediatrics, Division of Pediatric Cardiology, University of Minnesota, 2450 Riverside Avenue, MB 560, Minneapolis, MN 55454, USA

Pediatric Cardiology, University of Minnesota Children's Hospital, East Building MB560, 2450 Riverside Avenue, Minneapolis, MN 55454, USA
e-mail: lohrx003@umn.edu

S. Sivanandam, MD
Department of Pediatrics, Division of Pediatric Cardiology, University of Minnesota, 2450 Riverside Avenue, MB 560, Minneapolis, MN 55454, USA

P.A. Iaizzo (ed.), *Handbook of Cardiac Anatomy, Physiology, and Devices*, DOI 10.1007/978-3-319-19464-6_22

Currently, cardiac catheterization is reserved primarily for focused hemodynamic information that compliments noninvasive methods or intervention.

Initial attempts at imaging the heart using reflected sound waves were made in the 1950s, with improvement in the experimental technology and its initial clinical application in the 1960s [1]. During the 1970s, simple motion-mode (M-mode) or linear images were available to define cardiac structures, but these were not adequate for providing great diagnostic detail in complex congenital heart disease. During the 1980s, the technology to provide two-dimensional real-time imaging of the heart was developed, and this subsequently revolutionized noninvasive evaluation of cardiac structure and function. In the late 1980s, techniques of Doppler ultrasound, including color mapping, were developed to extend the analyses of cardiac function and hemodynamics [1]. By the late 1980s, many cardiac defects could be diagnosed accurately and repaired completely without invasive testing. Currently, techniques of echocardiography are being refined to provide more accurate noninvasive assessments of cardiac function in normal and disease states.

22.2 Physical Principles of Echocardiography

22.2.1 Ultrasound Imaging of Tissues

Echocardiography uses the properties of sound waves to differentiate tissues of varied density in the human body. Sound travels in mechanical waves with a speed dependent on the density and the elastic properties of the medium in which they are traveling [2]. This property of tissue is termed its *acoustic density*. Ultrasound waves, which are used in medical applications, have frequencies that are higher than those audible to the human ear. Ultrasound frequencies are generally over 20,000 cycles/s or Hertz, and most cardiac applications are performed using frequencies of two million to ten million Hertz or 2–10 mega Hertz (MHz). When a sound wave, which is generated by electrical stimulation of a piezoelectric crystal, travels through an interface between two tissues of varied acoustic density, such as myocardium and blood, a portion of the energy is reflected backward (the reflected wave) and the rest travels forward through the next tissue (the refracted wave). The reflected wave is received by the transducer, turned back into electrical energy, amplified, and displayed [1]. If there is too much variance between the acoustic density of the tissues being imaged (as in air-filled lung and myocardium or bone and myocardium), the entire ultrasound wave is reflected and the cardiac structures cannot be imaged [1]. The amount of reflected wave detected during ultrasound imaging depends not only on the acoustic characteristics of the interface but also on the angle of incidence or interrogation. An ultrasound beam that encounters a flat surface that is perpendicular to the beam will reflect a wave in the direction of the transmitted sound. In contrast, a beam that is parallel to a structure or that encounters an irregularly shaped structure, as is common in tissue imaging, will be reflected with a degree of scatter that is proportional to the angle of incidence [2].

22.2.2 Resolution of Structures

The ability of cardiac ultrasound to provide anatomical resolution depends on the wavelength of the sound used. The speed of transmission, the frequency, and the wavelength are related by the equation $c = f \times \lambda$ or $\lambda = c/f$, where c = the speed of sound in the medium, f = the frequency of the wave (in Hertz or cycles per second), and λ = the wavelength. Thus, a higher frequency transducer will produce a smaller wavelength and improved resolution along the path of the beam, also termed *axial resolution* [1]. Axial resolution is generally two times the wavelength used, so that a 3.5 MHz transducer has a wavelength of 0.43 mm and an axial resolution of 0.86 mm, while a 7.5 mHz transducer (appropriate for use in pediatric imaging) has a wavelength of 0.2 mm and axial resolution of approximately 0.4 mm [1]. Unfortunately, the use of high-frequency transducers is limited because the smaller wavelengths cannot penetrate as deeply into tissue, and they are therefore less useful for cardiac imaging in adults. Lateral resolution in echocardiography is impacted by the diameter of the beam width, which is a function of the transducer size, shape, and focal plane, as well as the frequency [1].

22.3 Imaging Modalities

22.3.1 M-Mode Echocardiography

M-mode, or motion-mode, echocardiography was the first type of ultrasound used for clinical cardiovascular imaging. Its use today is primarily limited to assessment of valve motion and reliable reproducible measurements of chamber sizes and function [1, 3]. In M-mode echocardiography, a narrow ultrasound beam is pulsed rapidly in a single plane through the heart, and the movements of the structures in that single plane are plotted against time with very high temporal and axial resolution. M-mode echocardiography can be used to assess cardiac wall thickness, aortic root size, chamber sizes, and ventricular function. In general, left ventricular function is quantitated using M-mode by determining the percent of fractional shortening of the left ventricle, which is calculated using the following equation:

$$\mathrm{SF}(\%) = (\mathrm{LVEDD} - \mathrm{LVESD}) / \mathrm{LVEDD} \times 100$$

where SF = shortening fraction, LVEDD = left ventricular end-diastolic dimension, and LVESD = left ventricular

end-systolic dimension. Normal values vary with age and range from 35–45 % in infants to 28–44 % in adolescents and adults [4, 5].

22.3.2 Two-Dimensional Imaging

Two-dimensional imaging provides an arc of imaging planes by employing multiple ultrasound beams to provide cross-sectional views of the heart. Currently, two-dimensional imaging provides the majority of information about cardiac structure and function in routine clinical studies. Two-dimensional imaging requires the presence of multiple beams of ultrasound interrogation in a single transducer, and several types of transducers are available to achieve this. Transducers available for two-dimensional imaging include mechanical (a sweeping or rotating ultrasound beam), phased array (multiple independently controlled sources), and linear array (a line of crystals simultaneously generating a beam of ultrasound). Today, phased array transducers are most commonly used due to their: (1) small size, (2) ability to provide simultaneous two-dimensional and M-mode or Doppler imaging, and (3) improved control of focal length for more uniform images throughout the field of view [6]. In addition to using two-dimensional imaging for viewing anatomic detail, left ventricular function can be quantitated using this mode by estimating left ventricular ejection fractions. This method, which has been shown to correlate well with angiographic estimates of ventricular function, takes advantage of the conical shape of the left ventricle to estimate end-diastolic and end-systolic ventricular volumes from tracings of two-dimensional images using Simpson's biplane rule [3]. The ejection fraction is calculated as follows:

$$\mathrm{EF}(\%) = (\mathrm{LVEDV} - \mathrm{LVESV}) / \mathrm{LVEDV} \times 100$$

where EF = ejection fraction, LVEDV = left ventricular end-diastolic volume, and LVESV = left ventricular end-systolic volume.

Normal values for ejection fractions are approximately 55–65%, and cardiac outputs can be estimated by multiplying the volume ejected with each beat (stroke volume) by the heart rate, using the equation:

$$\mathrm{CO} = \mathrm{HR} \times \mathrm{SV}$$

where CO = cardiac output, HR = heart rate, and SV = stroke volume.

22.3.3 Doppler Ultrasound

The *Doppler Principle*, described by Christian Johann Doppler in 1843, states that the frequency of transmitted sound is altered when the source of the sound is moving [2]. The classic example is the change in pitch of a train whistle as it moves, getting higher as it approaches the receiver and lower as it moves away from it. This change in frequency, or Doppler shift, also occurs when the source of sound is stationary and the waves are reflected off a moving target, including red blood cells in the vasculature. The shift in frequency is related to the velocity of the moving target, as well as the angle of incidence, and is described by the equation:

$$F_{\mathrm{d}} = (2(f_0)(V)\cos\ \phi\ ) / C$$

where F_{d} = observed Doppler frequency shift, f_0 = transmitted frequency, C = velocity of sound in human tissue at 37°C (approximately 1560 m/s), V = blood flow velocity, and ϕ = the intercept angle between the ultrasound beam and the blood flow. Using this principle, Doppler ultrasound can be used to noninvasively estimate the velocity of blood flow in the human heart and vasculature. Using a modified Bernoulli equation where pressure drop is equal to four times the velocity squared (4 V^2), Doppler ultrasound can also be used to estimate chamber pressures and gradients and to provide significant noninvasive hemodynamic data.

22.3.4 Continuous Wave Doppler

Continuous wave Doppler is performed by using a single transducer with two separate elements for transmission and reception of sound waves, so that there is continuous monitoring of the Doppler shift. This technique enables detection of very high-velocity blood flow, but does not allow localization of the site of velocity shift along the line of interrogation [1].

22.3.5 Pulse Wave Doppler

Pulse wave Doppler uses bursts of ultrasound alternating with pauses to detect Doppler shift in a localized region. The timing between the generation of the ultrasound wave and detection of the reflected wave determines the depth of interrogation. Pulse wave Doppler is useful to measure velocity changes in a region defined by two-dimensional echocardiography, however, the spatial resolution limits the velocity shifts detected. In general, the maximal velocity shift detectable is one half of the Doppler sampling rate (pulse repetition frequency or PRF) and is designated the *Nyquist limit* [1]. The maximal sampling rate is determined by the distance of the sampling site from the transducer and the transducer frequency, so that sampling from a transducer position nearer to the region to be interrogated and using a lower frequency transducer will improve the detection and localization of higher velocity flow [1].

22.3.6 Color Doppler Flow Mapping

Color Doppler flow mapping uses the principles of pulsed Doppler to examine multiple points along the scan lines. The mean velocity and direction of these signals are calculated and then displayed and superimposed upon a two-dimensional image. By convention, flow directed toward the transducer is red, and flow directed away from the transducer is blue. Accelerated or turbulent flow is given a different color, typically yellow and green. Color flow mapping is valuable because of the large amount of information that can be obtained in a single image. It can also aid in the: (1) localization of flow accelerations, (2) quantitation of valvar regurgitation, (3) visualization of intracardiac shunting, and/or (4) assessment of arterial connections. Information obtained from color Doppler can be further refined by pulse wave Doppler and continuous wave Doppler interrogation.

22.3.7 Quantification of Pressure Gradients Using Doppler Shift Measurements

Today, quantification of pressure gradients using Doppler echocardiography can provide hemodynamic information that could previously be obtained only by invasive cardiac catheterization. Specifically, the Bernoulli equation [3, 7] defines the relationship between velocity shifts across an obstruction and the pressure gradients caused by the obstruction. For practical purposes, the proximal velocity is neglected and the simplified equation becomes: pressure difference = distal velocity squared × 4. This is a valuable way to estimate pressure drops across obstructive valves and/or pressure differences between chambers (based on the velocities of valvar regurgitation or intracardiac shunting).

22.3.8 Myocardial Performance Index

The *myocardial performance index* (MPI) is a noninvasive Doppler measurement of global) ventricular function that incorporates both systolic and diastolic function and may be applied to the right ventricle (RV) or left ventricle (LV) [8]. The MPI (or Tei index) is defined as a ratio of the sum of the isovolumic contraction time (IVCT) and isovolumic relaxation time (IVRT) divided by the systolic ejection time (ET) (Fig. 22.1). The index is easily measured with high reproducibility and is important in the assessment of global performance, as the active energy cycles of contraction and relaxation occur during IVCT and IVRT. The Tei index is independent of heart rate and blood pressure and can be a useful tool to evaluate myocardial function in different clinical situations [8].

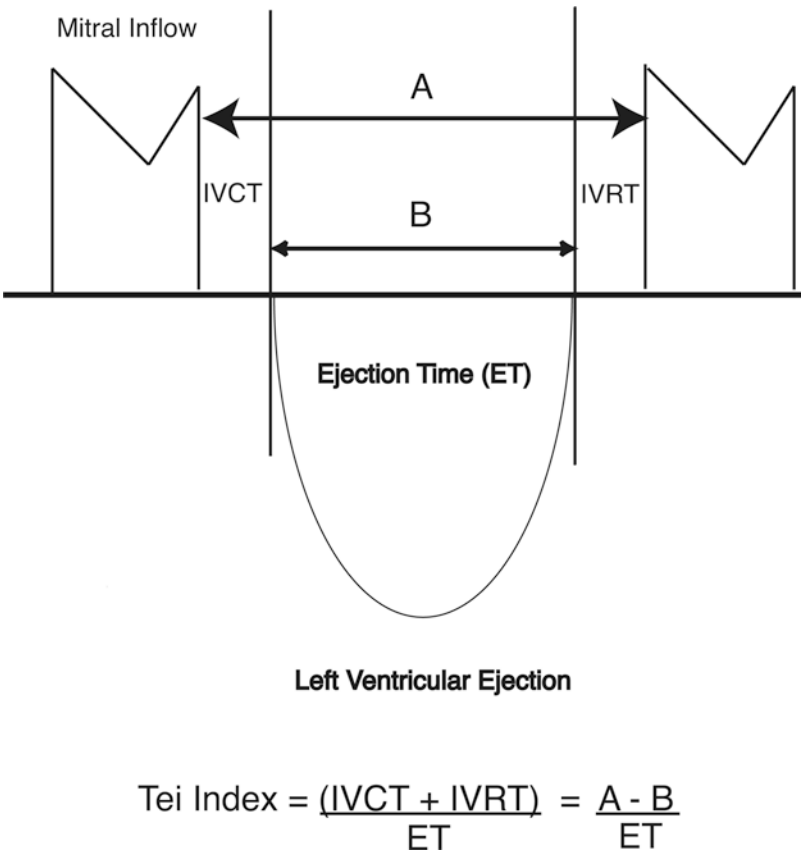

$$\text{Tei Index} = \frac{(\text{IVCT} + \text{IVRT})}{\text{ET}} = \frac{\text{A} - \text{B}}{\text{ET}}$$

Fig. 22.1 Diagrammatic representation of the myocardial performance index or Tei index. The Tei index is the sum of the isovolumetric contraction time (IVCT) and isovolumetric relaxation time (IVRT) divided by the ejection time (ET). Adapted from Pellet et al. [8]

22.3.9 Tricuspid Annular Plane Systolic Excursion

The *tricuspid annular plane systolic excursion* (TAPSE) can be used to estimate the right) ventricular global systolic function. TAPSE is an easily obtainable, simple, and generally reliable measure of right ventricular ejection fraction, which allows it to be used routinely in clinical studies. TAPSE is defined as the distance traveled by the tricuspid annulus along the direction of the line joining the tricuspid annulus and right ventricular apex at end-diastole. TAPSE assumes that the displacement of the basal and adjacent segments of the RV are representative of the longitudinal function of the entire right ventricle and that longitudinal myocardial shortening is a significant contributor to overall right ventricular function. TAPSE is assessed with M-mode echocardiography oriented on a two-dimensional image in an apical four-chamber view, placing the M-mode cursor on the lateral tricuspid annulus (Fig. 22.2). The annular plane is identified as the first continuous line immediately below the RV cavity (which appears "above" the RV cavity on apical images). Maximum systolic excursion of the lateral annulus is measured and compared to normal values (Fig. 22.2).

22.3.10 Tissue Doppler Imaging

Tissue Doppler imaging (TDI) is an extension of conventional Doppler flow echocardiography that measures myocardial motion and velocity [9] (Fig. 22.3A). Myocardial velocity information can be displayed as a pulse tissue Doppler signal and data color-coded and displayed in real time. Color Doppler allows for visual semi-quantitation of myocardial motion superimposed on conventional M-mode and two-dimensional images. Velocity data from a region of interest can be arranged to obtain spectral displays of tissue velocities. The graphic display includes one positive systolic (S) deflection and two negative diastolic waveforms. The systolic waveform is preceded by regional isovolumic contraction time (RIVCT), and the diastolic waves are preceded by regional isovolumic relaxation time (RIVRT). The first diastolic deflection represents the early rapid filling phase of diastole (E), which is followed by a period of diastasis, and a second late active filling phase of diastole (A) due to atrial contraction (Fig. 22.3B).

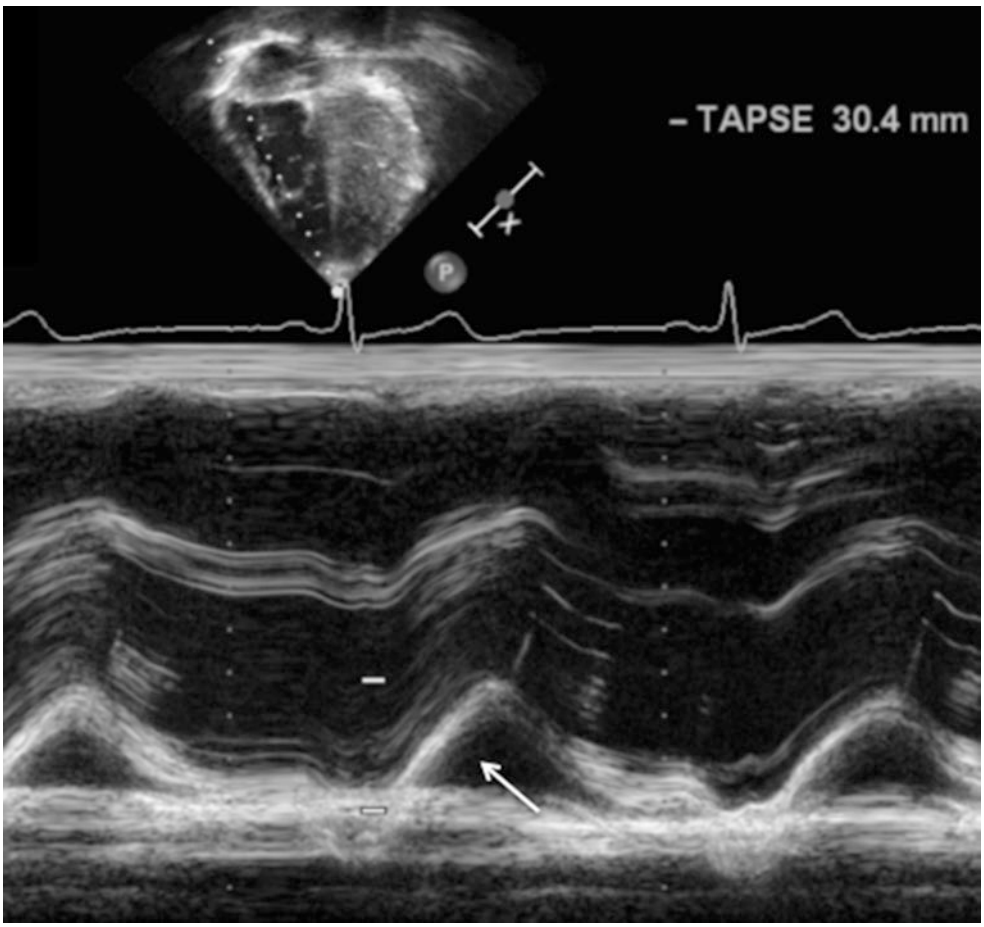

Fig. 22.2 Measurement of the tricuspid annular plane systolic excursion (TAPSE). TAPSE measures the motion of the lateral tricuspid valve annulus (*white arrow*) as it moves toward the RV apex during systole. Normal values are greater than 16 mm and reflect longitudinal shortening as a measure of global RV function

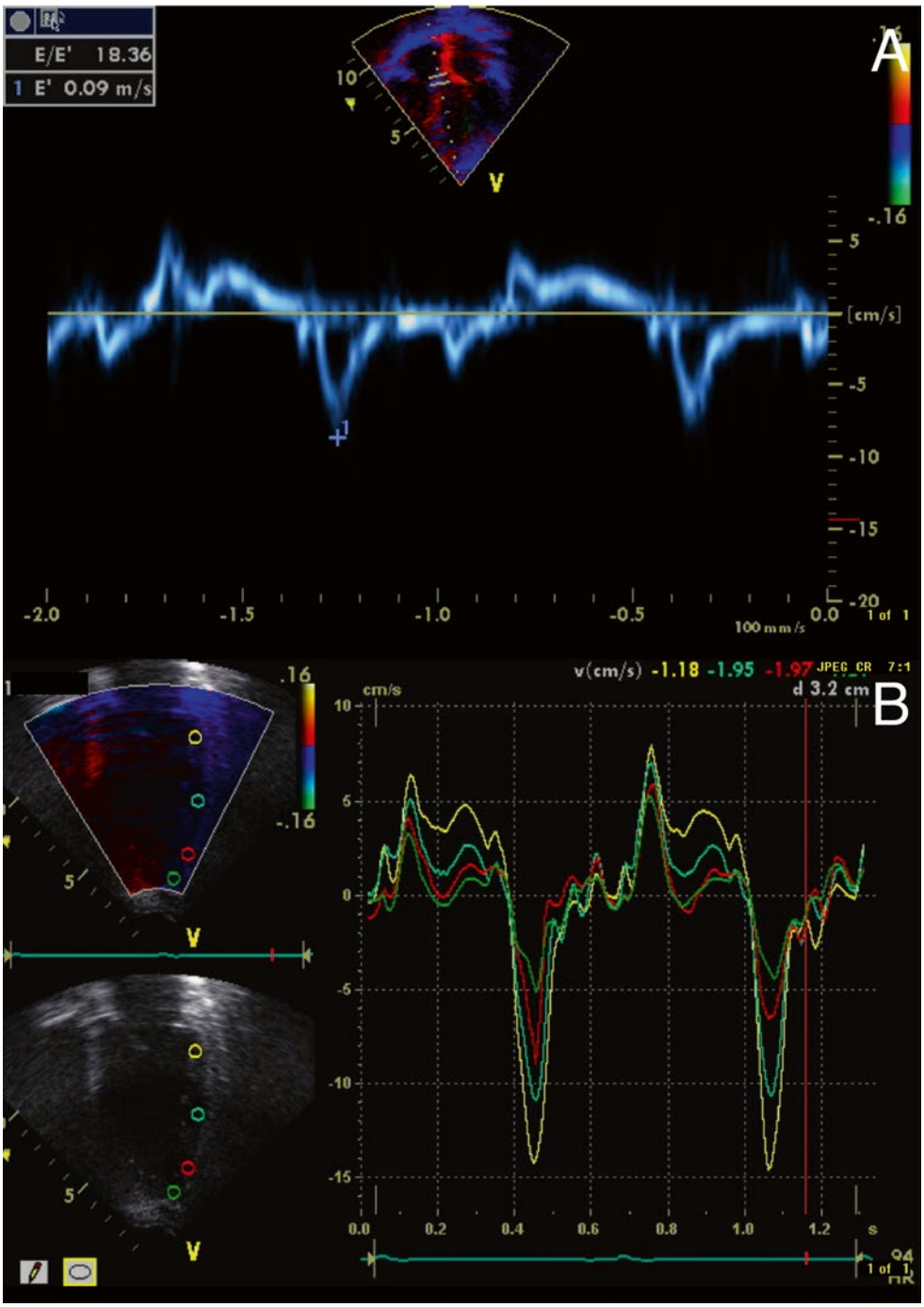

Fig. 22.3 Tissue Doppler imaging. (A) Pulse wave tissue Doppler provides a spectral display of peak tissue velocity. (B) Tissue Doppler velocity data for the quantification of asynchrony from apical four-chamber view. Sample volumes are in the lateral septal segment

22.4 Clinical Applications of Cardiac Ultrasound

22.4.1 Transvaginal and Transabdominal Fetal Echocardiography

The human fetal heart is fully developed and functional by 11 weeks after conception. Using transvaginal ultrasound, the structure and functional characteristics of the fetal heart can be observed as early as 9 weeks of gestational age [10]. This technique remains the most useful type of fetal cardiac imaging until approximately 16 weeks of gestation. At that time, transabdominal imaging becomes the preferred method (Fig. 22.4). Fetal imaging is routinely performed at 16–20 weeks of gestational age, and image quality improves until about 24–28 weeks of gestational age [10]. The quality of fetal images can be reduced by loss of amniotic fluid, maternal body habitus, fetal bone density, and/or the fetal position. M-mode, two-dimensional, and Doppler ultra-

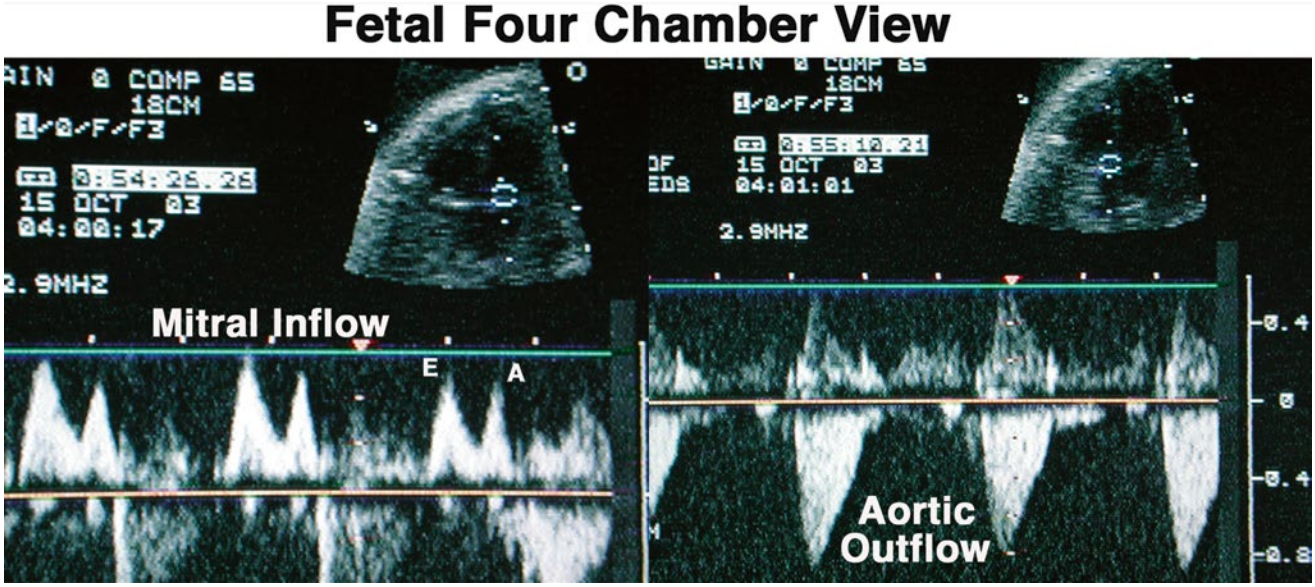

Fig. 22.4 Fetal echocardiogram at approximately 24 weeks gestation. Four-chamber views are shown with pulse wave Doppler analysis of mitral inflow and aortic outflow. Mitral inflow is characterized by two waves, an E wave representing passive filling of the left ventricle in diastole and an A wave representing active filling of the ventricle with atrial systole. Doppler flows are less than 1 m/s (indicating unobstructed blood flow), and the interval between aortic outflow signals is approximately 0.5 s (indicating a fetal heart rate of 120 beats/min)

sound techniques are useful for analyses of the anatomy and function of the fetal heart, the diagnoses and monitoring of fetal arrhythmias, and the guidance of fetal interventional procedures. In general, fetal echocardiography has contributed to: (1) improved understanding of the natural history of many forms of congenital heart disease; (2) improved monitoring and obstetric care of fetuses with structural heart diseases and arrhythmias; and (3) attempts at in utero correction of vascular, valvular, and structural cardiac abnormalities [11, 12].

22.4.2 Transesophageal Echocardiography

Transesophageal echocardiography allows imaging of the heart from the esophagus or stomach, which improves image resolution by eliminating much of the acoustic interference from the lungs and chest wall while, at the same time, allowing for reduced distance of the ultrasound source to the heart. Transesophageal imaging is performed using either a biplane probe (two single plane arrays set at perpendicular planes) or a rotating single array probe that provides multiple planes of view (an omniplane probe). Today, transesophageal probes come in sizes appropriate for use in adults, children, and infants. Transesophageal echocardiography is used when improved resolution is required or when transthoracic windows are unavailable, as is typical in the operating room or cardiac catheterization laboratory [3]. It also has become a routine form of intraoperative monitoring for open-heart surgery and is specifically useful to detect incomplete repairs prior to separation from cardiopulmonary bypass [13]. It is also a useful adjunct to interventional cardiac catheterization procedures. Transesophageal echocardiography typically requires sedation or anesthesia and thus adequate patient monitoring. Note that it is significantly more invasive than standard transthoracic echocardiography and can be complicated by airway compromise, dysphagia, or esophageal perforation [3, 14, 15].

22.4.3 Transthoracic Echocardiography

Today, *transthoracic echocardiography* remains as the most common method for cardiac imaging. It is noninvasive, can be performed in any cooperative patient, and only rarely requires sedation. Yet, images obtained are limited by patient size and can be complicated by interference from soft tissues, bone, or lung. The transthoracic echocardiogram is performed from standard windows on the chest (Fig. 22.5) and requires the use of multiple transducers at varied ultrasound frequencies to maximize the two-dimensional image resolution and Doppler ultrasound information obtained. Most commonly, images are obtained by trained and licensed cardiac sonographers and then interpreted by a cardiologist.

22.4.4 Standard Transthoracic Examination

Currently, the *standard transthoracic cardiac echo* includes images from parasternal, apical, suprasternal notch, and subcostal imaging windows (Fig. 22.5). Two-dimensional sec-

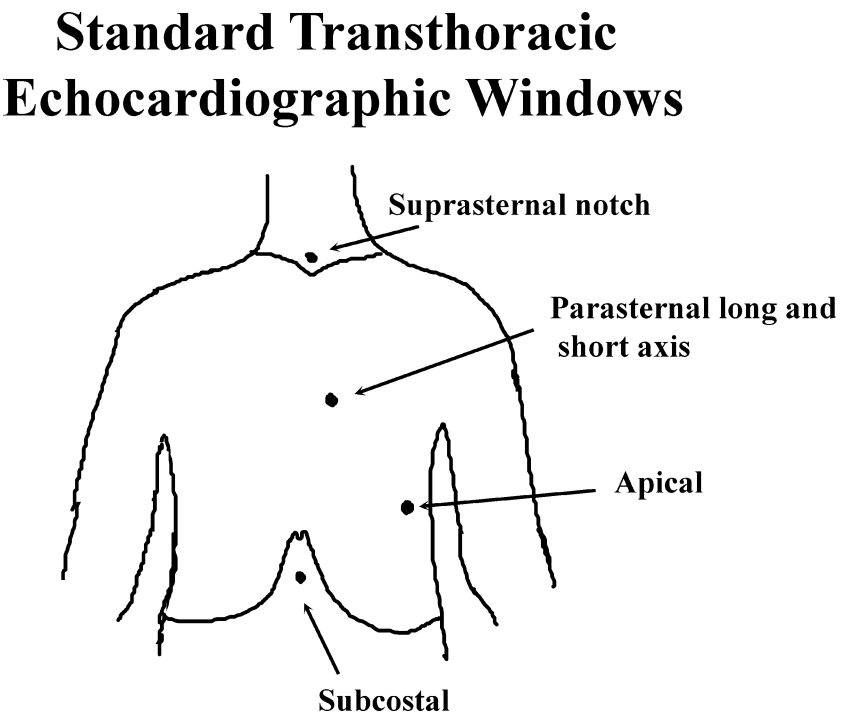

Fig. 22.5 Diagram of the chest showing transducer position for standard transthoracic echocardiographic windows. A typical examination in a cooperative patient is performed in a standard order: parasternal, apical, subcostal, and then suprasternal notch views. Perpendicular imaging planes can be obtained from each position by rotating the transducer 90°

tors are imaged in each window to provide anatomic details and functional analyses. The highest frequency transducer set at the lowest depth possible is used to maximize image resolution while scanning for anatomical detail. Two-dimensional images are then used to guide Doppler ultrasound interrogations, often with a lower frequency transducer that will optimize Doppler information. Two-dimensional images are also used to guide M-mode measurements of chamber size and function, and Doppler gradients are calculated across valves and shunts to maximize the hemodynamic information obtained.

The standardized transthoracic echocardiograms are obtained by scanning at four regions on the chest wall: the parasternal window, apical window, subcostal region, and suprasternal notch (Fig. 22.5). Parasternal long-axis views are used to obtain *long-axis* images of the left side of the heart, including the left atrium, left ventricle, and aorta (Fig. 22.6). A subtle tilt of the transducer inferiorly from this position gives views of the right atrium, tricuspid valve, and right ventricle, and tilting leftward brings the pulmonary valve and main pulmonary artery into view. Turning the transducer and scan plane by 90° results in short-axis views of the heart in planes from the base of the heart (region of the aorta, tricuspid, and pulmonary valves) to the apex (Fig. 22.7A–D). M-mode measurements of the left-sided chambers are obtained from parasternal short-axis windows and can be used to assess chamber size and function (Fig. 22.7E, F). Apical windows reveal standard four-chamber views of the left atrium, mitral valve, left ventricle, right atrium, tricuspid valve, and right ventricle (Fig. 22.8A, B). This view sends the ultrasound beam parallel to the septal structures, so is not adequate to assess the integrity of the atrial or ventricular septums. Tilting the transducer anteriorly results in a five-chamber view that allows excellent visualization of the left ventricular outflow tract and aorta. Doppler gradients across the mitral, tricuspid, and aortic valves can also be obtained from this view (Fig. 22.8C), and the velocity of tricuspid valve regurgitations can be used to estimate right ventricular and pulmonary artery systolic pressures.

Subcostal views are particularly useful in patients with lung disease or in those who have had recent open-heart surgery. From subcostal images, the orientation of the heart in the chest and the major vascular connections can be established. Subcostal views also provide excellent visualization of the intra-atrial septum (Fig. 22.9A) and four-chamber views in patients with poor apical windows. Suprasternal notch views are most useful for visualization of the aortic arch, its branching vessels, and the descending thoracic aorta (Fig. 22.9C), as well as for determining the Doppler shifts across the aortic valve. This view is also important to exclude vascular abnormalities, including coarctation of the aorta.

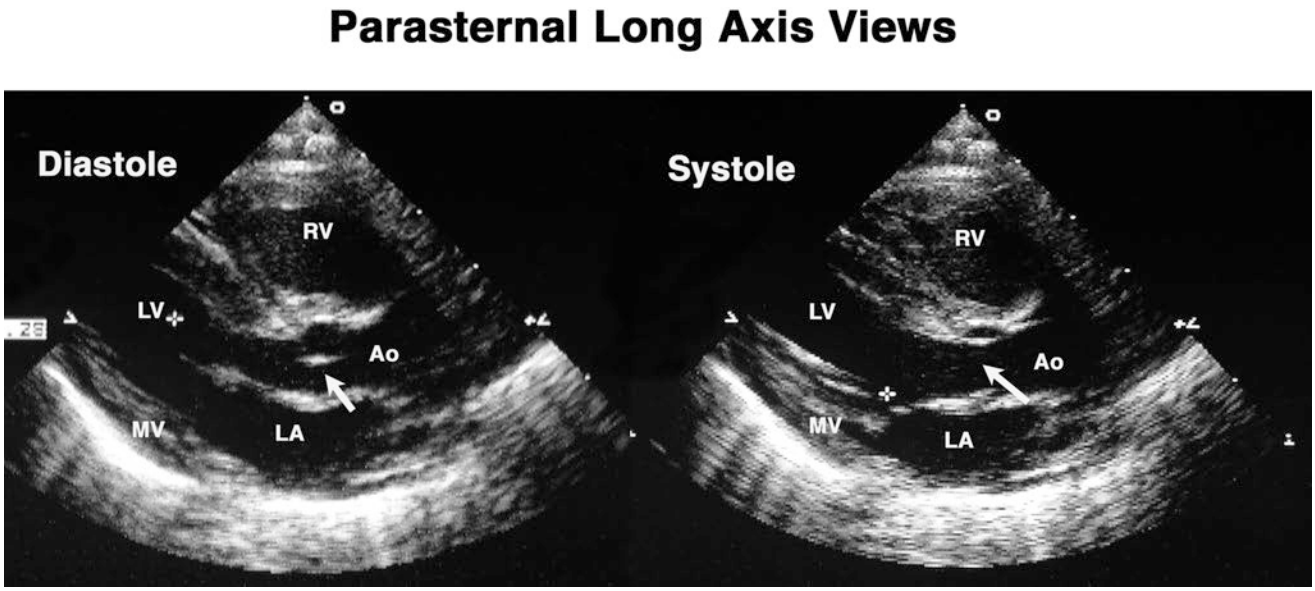

Fig. 22.6 Transthoracic parasternal long-axis views in a newborn infant. These views demonstrate the long axis of the left side of the heart. Frame 1 is in diastole with an open mitral valve to accommodate left ventricular filling and a closed aortic valve (*arrow*). Frame 2 is in systole with an open aortic valve (*arrow*) and closed mitral valve (*asterisk*). *White dots* on the sector border represent centimeter marks. *Ao* aorta, *LA* left atrium, *LV* left ventricle, *RV* right ventricle, *MV* mitral valve

22.5 Other Techniques in Cardiac Ultrasound

The use of ultrasound for cardiac imaging and investigation of hemodynamics has been revolutionary in the diagnoses and treatment of heart disease. Currently, ultrasound techniques available for use on a limited clinical basis include intravascular ultrasound (IVUS) and three- and four-dimensional imaging. Research applications of cardiac ultrasound include embryonic and small animal cardiac imaging. IVUS uses catheters with ultrasound transducers mounted on the tips. These transducers are capable of cross-sectional imaging or true sector imaging using phased array ultrasound transducers mounted on their tips [3, 16]. As technology has improved, relatively small catheters (5 and 6 French) and high-frequency transducers (40–45 MHz) are available for the imaging of the aorta and pulmonary arteries, aortic and pulmonary valves, and/or coronary arteries [17]. Coronary artery imaging has been particularly useful in heart transplant patients as a means to detect intimal thickening associated with chronic rejection [18] and in patients with Kawasaki syndrome who commonly develop coronary artery aneurysms [3]. IVUS has also been used for intracardiac monitoring of interventional procedures [16] and has recently been shown to reduce rates of stent thrombosis and adverse cardiac events in drug-eluting stents [17, 19]. Lead extraction procedures are also aided by the use of IVUS.

Three-dimensional imaging technology has recently been improved so that cardiac images can be displayed in real time (four-dimensional imaging). Three- and four-dimensional images are useful for the re-creation of a movable three-dimensional image to assist with surgical planning [1]. Unfortunately, currently large transducer sizes and slow image processing capabilities make three- and four-dimensional imaging less desirable for routine cardiac ultrasound examinations [7]. Ultrasound imaging technology has been improved so that the heart can be studied during embryonic development. For example, pregnant mice can be anesthetized and undergo fetal cardiac imaging as early as 8–9 days after conception, so that the anatomy and blood flow patterns can be observed during both normal and abnormal cardiac development [2, 20, 21]. Additionally, ultrasound techniques can be applied to vertebrate and nonmammalian model systems to study physiology, cardiac regeneration, and cell therapies [22–25].

22.6 Summary

The development and application of clinical echocardiography has enabled thorough, accurate, and noninvasive evaluations of both cardiac structure and function. Today, transthoracic echocardiography remains as the mainstay of cardiac diagnosis and monitoring in both adult and pediatric

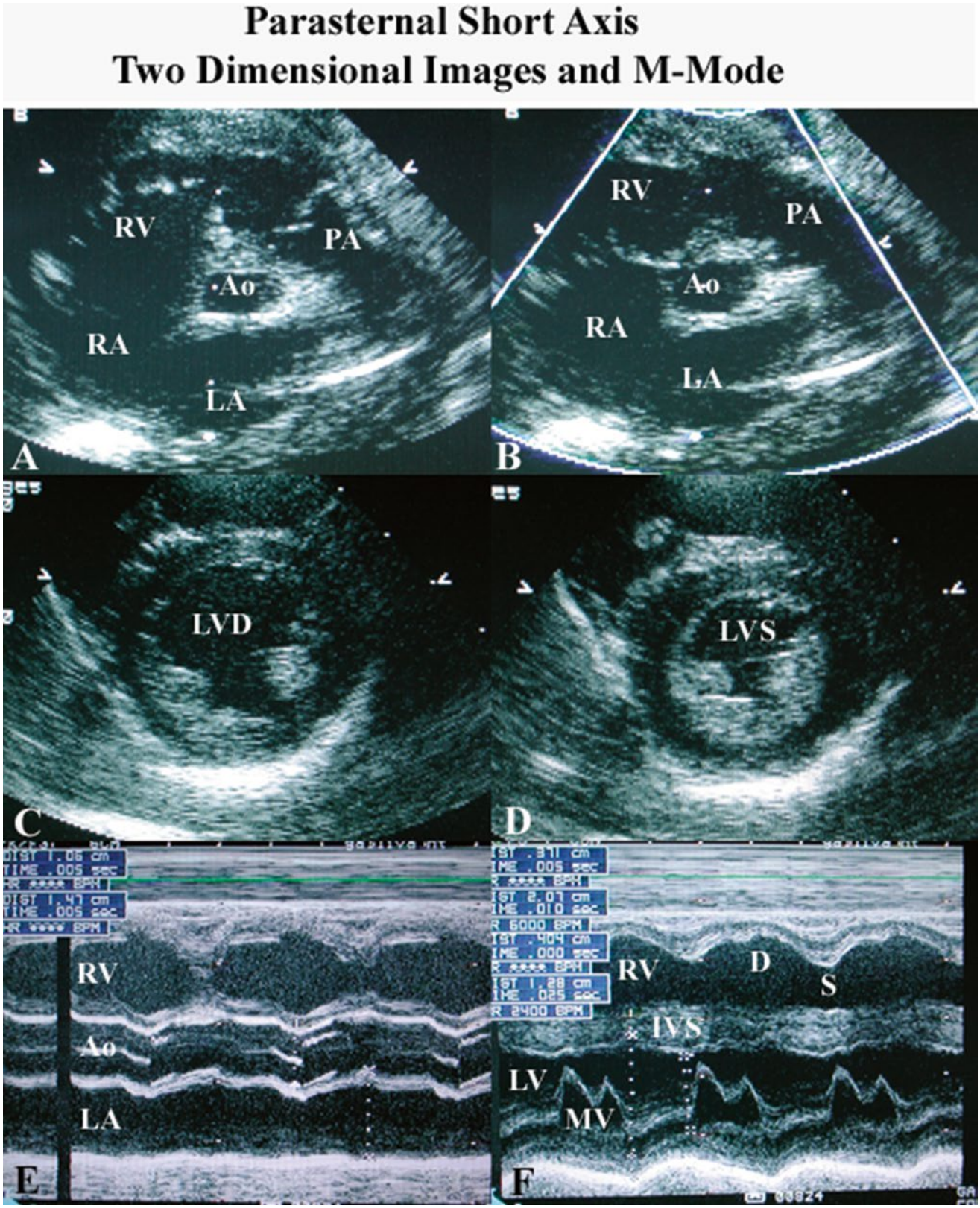

Fig. 22.7 Two-dimensional and M-mode images obtained from parasternal short-axis views. Panel A shows a view through the base of the heart in diastole. Panel B shows the same imaging plane in systole, with the pulmonary valve open. M-mode measurements of the right ventricle, aorta, and left atrium (Panel E) are obtained in this plane. Panel C demonstrates a cross-sectional or short-axis view of the left ventricle at the level of the papillary muscles in diastole, and Panel D is at the same plane in systole. This is the appropriate level for quantification of left ventricular function by shortening fraction. Panel F shows an M-mode recording at the level of the mitral valve, a plane just above that seen in Panels C and D. Abnormalities of mitral valve motion can be demonstrated in this plane. *LA* left atrium, *RA* right atrium, *RV* right ventricle, *Ao* aorta, *PA* main pulmonary artery, *LVD* left ventricle, diastole, *LVS* left ventricle, systole, *D* diastole, *S* systole, *IVS* interventricular septum

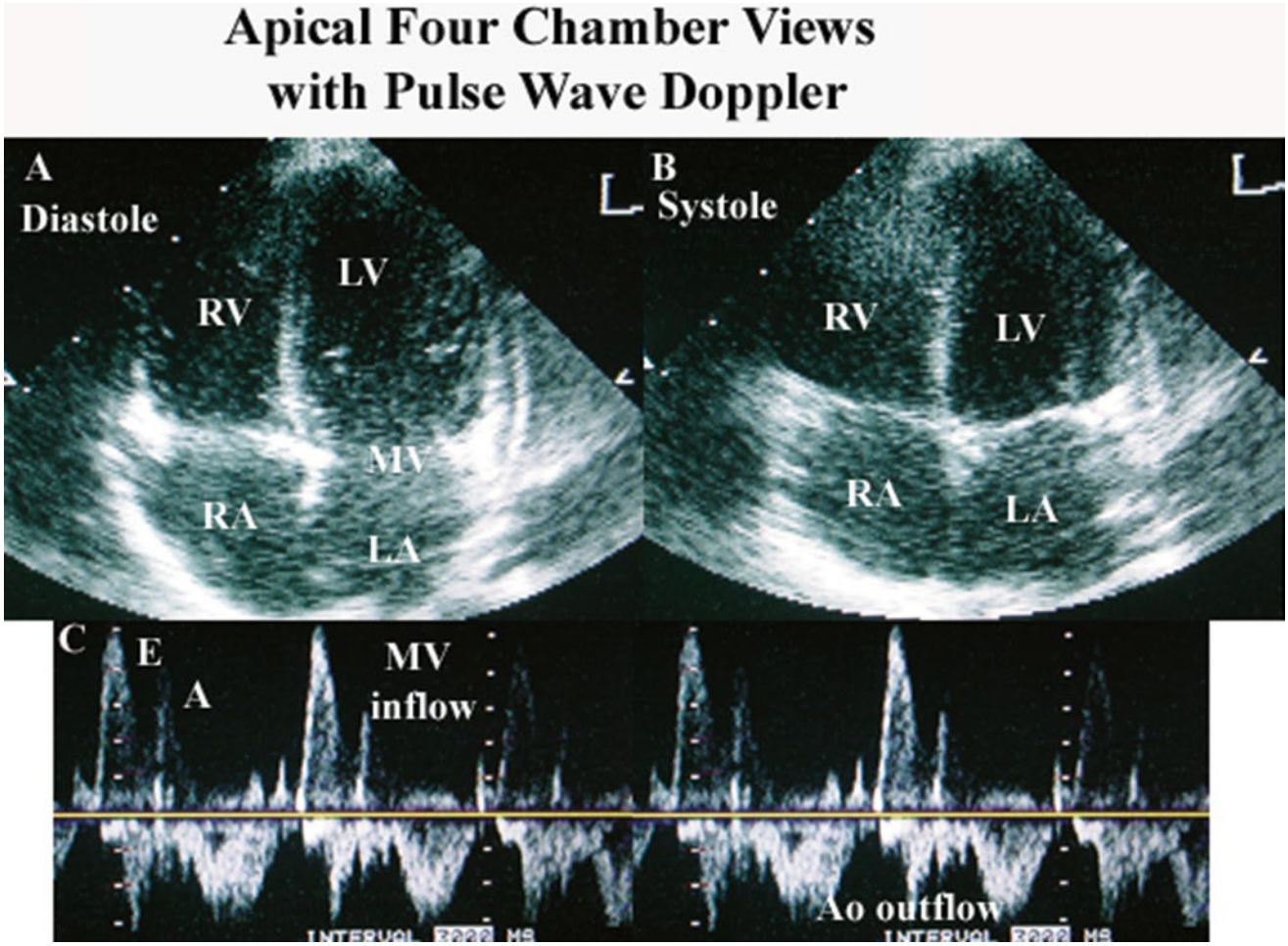

Fig. 22.8 Panel A is a two-dimensional apical four-chamber views of the heart in diastole (open mitral valve), and Panel B shows the same imaging plane in systole (closed atrioventricular valves). The pulsed wave Doppler tracing shown in Panel C demonstrates mitral inflow toward the transducer (above the baseline) and aortic outflow away from the transducer (below the baseline). The mitral valve inflow tracing shows passive filling of the left ventricle during early diastole (E) followed by active filling of the left ventricle in late diastole with the onset of atrial contraction (A). Aortic outflow occurs in systole. *LA* left atrium, *RA* right atrium, *RV* right ventricle, *LV* left ventricle, *MV* mitral valve

patients. Advances in two-dimensional imaging allow significant anatomic detail to be visualized, especially in smaller patients, and Doppler ultrasound allows for direct visualization of altered flow patterns and noninvasive investigations of hemodynamics. New Doppler methods have improved the quantification of regional and diastolic myocardial function. The use of transesophageal echocardiography, although slightly more invasive, has also become routine when improved resolutions and/or intraprocedural monitoring are required. Future directions in echocardiography include: (1) increased utilization of IVUS for diagnoses and monitoring of interventional procedures; (2) improvements in three-dimensional ultrasound techniques that will make them appropriate for routine imaging; and (3) the use of embryonic imaging to study normal and abnormal heart development.

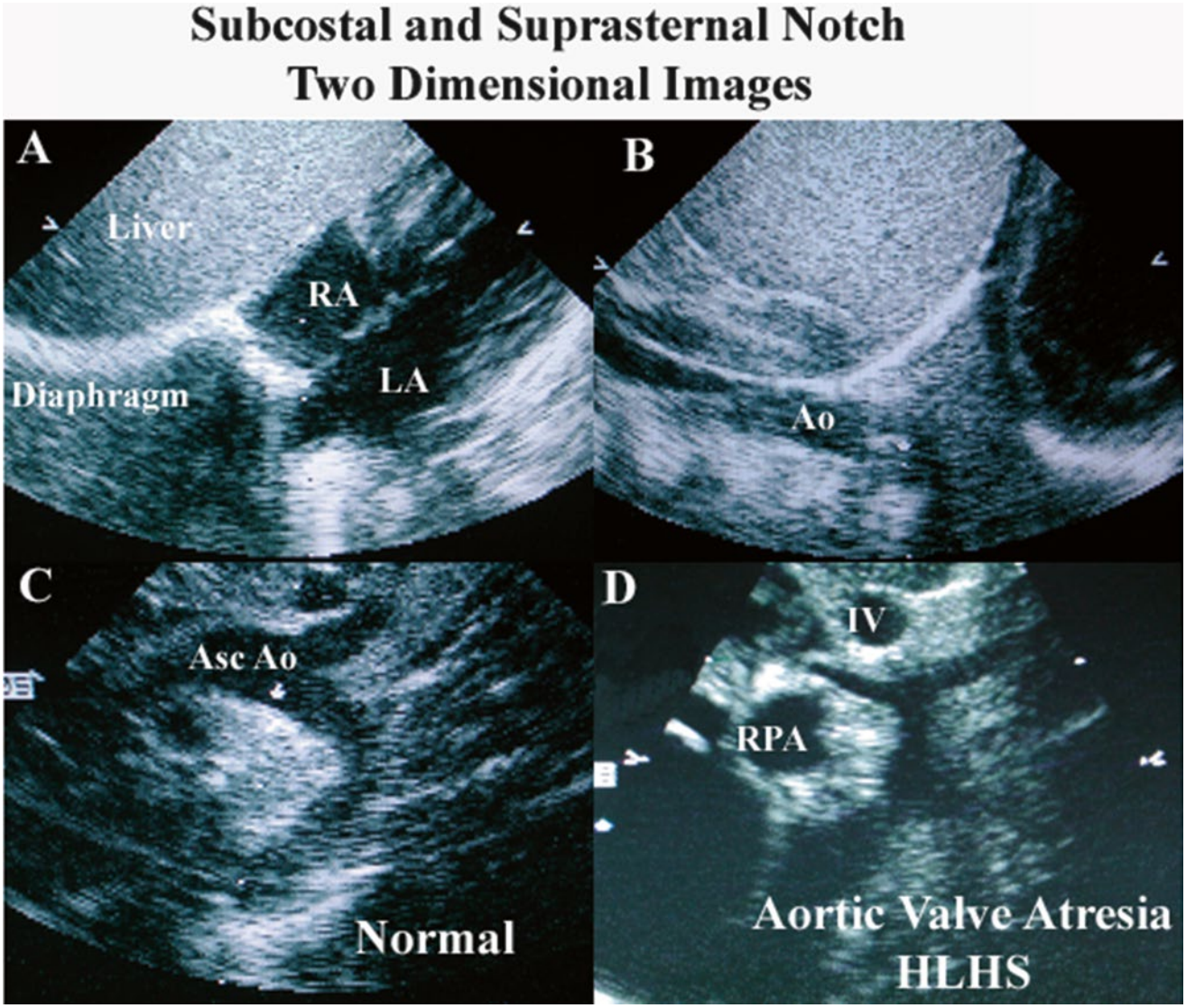

Fig. 22.9 Two-dimensional images from subcostal windows (A, B) and suprasternal notch windows (C, D). Subcostal views provide orientation of the heart relative to the abdominal organs as in Panel A, which shows a rightward liver and leftward cardiac apex. Subcostal windows also provide excellent four-chamber views as well as short-axis views of the interatrial septum in smaller individuals, as shown in Panel A. Panel B is a subcostal view showing the descending thoracic aorta at the level of the diaphragm. Panel C is a suprasternal notch view of a normal aortic arch. Panel D shows the severe hypoplasia of the ascending aorta seen in a patient with hypoplastic left heart syndrome (HLHS) caused by aortic atresia. *LA* left atrium, *RA* right atrium, *Ao* aorta, *AscAo* ascending aorta, *RPA* right pulmonary artery, *IV* innominate vein

Acknowledgments The author would like to thank Jim Berry, Kim Berry, and Jay Hall for providing the images shown in this chapter and Kim Berry and Jay Hall for the review of this manuscript.

References

1. Geva T (1998) Echocardiography and Doppler ultrasound. In: Garson A Jr (ed) The science and practice of pediatric cardiology. Williams and Wilkins, Philadelphia, pp 789–843
2. Vermilion RP (1997) Basic physical principles. In: Snider R (ed) Echocardiography in pediatric heart disease. Mosby-Year Book, St. Louis, pp 1–10
3. Snider R, Serwer G, Ritter S (eds) (1997) Echocardiography in pediatric heart disease. Mosby-Year Book, St. Louis
4. Colan SD, Parness IA, Spevak PJ (1992) Developmental modulation of myocardial mechanics: age and growth related alterations in afterload and contractility. J Am Coll Cardiol 19:619–629
5. Gutgessel HP, Paquet M, Duff DF, McNamara DG (1977) Evaluation of left ventricular size and function by echocardiography: results in normal children. Circulation 56:457–462
6. Vermilion RP (1997) Technology and instrumentation. In: Snider R (ed) Echocardiography in pediatric heart disease. Mosby-Year Book, St. Louis, pp 11–21
7. Danford DA, Murphy DJ Jr (1998) Basic foundations of echocardiography and Doppler ultrasound. In: Garson A Jr (ed) The science and practice of pediatric cardiology. Williams and Wilkins, Philadelphia, pp 539–558

8. Pellet AA, Tolar WG, Merwin DG, Kerut EK (2004) The Tei index: methodology and disease state values. Echocardiography 21:669–672
9. Knebel F, Reibis RK, Bondke HJ et al (2004) Tissue Doppler echocardiography and biventricular pacing in heart failure: patient selection, procedural guidance, follow-up, quantification of success. Cardiovasc Ultrasound 2:17
10. Allan L (2000) The normal fetal heart. In: Allan L (ed) Textbook of fetal cardiology. Greenwich Medical Media Limited, London, pp 55–91
11. Freud LR, McElhinney DB, Marshall AC et al (2014) Fetal aortic valvuloplasty for evolving hypoplastic left heart syndrome: postnatal outcomes of the first 100 patients. Circulation 130:638–645
12. Allan LD (2012) Rationale for and current status of prenatal cardiac intervention. Early Hum Dev 88:287–290
13. Randolph GR, Hagler DJ, Connolly HM et al (2002) Intraoperative transesophageal echocardiography during surgery for congenital heart defects. J Thorac Cardiovasc Surg 124:1176–1182
14. Stevenson JG (1999) Incidence of complications in pediatric transesophageal echocardiography: experience in 1650 cases. J Am Soc Echocardiogr 12:527–532
15. Rousou JA, Tighe DA, Garb JL et al (2000) Risk of dysphagia after transesophageal echocardiography during cardiac operations. Ann Thorac Surg 69:486–489
16. Ziada KM, Tuzcu EM, Nissen SE (1999) Application of intravascular ultrasound imaging in understanding and guiding percutaneous therapy for atherosclerotic coronary disease. Cardiol Rev 7:289–300
17. McDaniel MC, Eshtehardi P, Sawaya FJ et al (2011) Contemporary clinical applications of coronary intravascular ultrasound. JACC Cardiovasc Interv 4:115511–115567
18. Costello JM, Wax D, Binns HJ et al (2003) A comparison of intravascular ultrasound with coronary angiography for evaluation of transplant coronary artery disease in pediatric heart transplant recipients. J Heart Lung Transplant 22:44–49
19. Witzenbichler B, Maehara A, Weisz G et al (2014) Relationship between intravascular ultrasound and clinical outcomes after drug-eluting stents: the assessment of dual-antiplatelet therapy with drug-eluting stents (ADAPT-DES) study. Circulation 129:463–470
20. Srinivasan S, Baldwin HS, Aristizabal O, Kwee L, Labow M, Turnbull DH (1998) Noninvasive, in utero imaging of mouse embryonic heart development with 40-MHz echocardiography. Circulation 98:912–918
21. Zhou YQ, Foster FS, Qu DW, Zhang M, Harasiewic KA, Adamson SL (2002) Applications for multifrequency ultrasound biomicroscopy in mice from implantation to adulthood. Physiol Genomics 10:113–126
22. Insight through In Vivo Imaging, Vevo 660 System Product Information, Visualsonics (Canada). www.visualsonics.com. Accessed 21 Nov 2014
23. Bartlett HL, Escalera RB 2nd, Patel SS et al (2010) Echocardiographic assessment of cardiac morphology and function in Xenopus. Comp Med 60:107–113
24. Porello ER, Mahmoud AI, Simpson E et al (2011) Transient regenerative potential of the neonatal mouse heart. Science 331:1078–1080
25. Silva GV, Litovsky S, Assad JAR et al (2005) Mesenchymal stem cells differentiated into an endothelial phenotype, enhance vascular density, and improve heart function in a canine chronic ischemia model. Circulation 111:150–156

Monitoring and Managing the Critically Ill Patient in the Intensive Care Unit

23

Fahd O. Arafat and Gregory J. Beilman

Abstract

The need for better acquisition and monitoring of patient physiological information within and outside of healthcare settings is especially important, as our healthcare system prepares to care for an aging population of more critically ill patients. Monitors serve several purposes, including: identification of shock and abnormal cardiac physiology, evaluation of cardiovascular function, and/or to allow for optimizing titration of therapy. An important function of an effective monitoring device is the reliable detection of abnormal physiology. Despite much research on the use of monitoring techniques in critical care, there is little evidence to support improved outcome related to routine use of monitors. Mainstays of invasive monitoring in the ICU include central venous pressure monitoring and arterial pressure monitoring, with pulmonary arterial monitoring reserved for occasional patients with multisystem disease. Recent trends in monitoring have included development of less invasive monitoring techniques that yield a number of cardiovascular parameters potentially useful to clinicians. New noninvasive measures of tissue perfusion (e.g., StO_2) have significant potential for identification and treatment of pathophysiologic states resulting in inadequate tissue perfusion. Developers of new monitors, despite facing regulatory requirements that are less stringent than those of drug manufacturers, will increasingly be expected to demonstrate clinical efficacy of new devices. In the final analysis, the most important "monitor" is a caring healthcare provider at the patient bedside carefully evaluating the patient's response to intervention and therapy.

Keywords

ICU monitoring • Near-infrared spectroscopy • Pulse waveform contour analysis • Sublingual capnometry • Pulmonary artery catheter

All exact science is dominated by the idea of approximation (Bertrand Russell, 1870–1972)

23.1 History

The treatment of shock is closely related to healthcare workers' experience during times of war. Ambroise Pare, a French military surgeon practicing during the sixteenth century, first described ligature to control bleeding in 1545. Experiences during World War I resulted in a clear understanding of the need for operative interventions for bowel perforation, with this operative intervention available due to the accessibility of general anesthetics. The discovery of blood types by Karl Landsteiner in 1901 (for which he received the Nobel Prize in 1930) enabled the safe and practical use of blood transfusions by medical providers during World War II, thus allowing resuscitation of combat-injured casualties. Advances utilized in the Korean War included new surgical techniques such as vascular anastomosis and new medical therapies including renal dialysis.

F.O. Arafat, MD • G.J. Beilman, MD (✉)
Department of Surgery, University of Minnesota,
MMC 11, 420 Delaware Street SE, Minneapolis, MN 55455, USA
e-mail: beilman@umn.edu

P.A. Iaizzo (ed.), *Handbook of Cardiac Anatomy, Physiology, and Devices*, DOI 10.1007/978-3-319-19464-6_23

The use of positive pressure ventilation and renal dialysis was broadened during the Vietnam War due to the development of complications of resuscitation in patients with previously nonsurvivable injury, including acute respiratory distress syndrome and/or renal failure.

The first described use of an intensive care unit (ICU) as a separate area to care for patients was in the early 1950s, as a result of a poliomyelitis epidemic in Denmark. The first coronary care unit was established in Kansas City, KS, in the early 1960s with the observation that new techniques of cardiopulmonary resuscitation could reduce mortality in patients suffering myocardial infarction. Their use expanded to postsurgical patients during the mid-1960s, as more complicated surgery mandated a closer observation of patients and more aggressive interventions in the ICU. More specifically, physiological monitoring displays were introduced in the ICU in the 1970s, and, unfortunately, they have not changed substantially since then. In contrast, the last four decades have seen significant efforts and resources expended toward improving data display design in high-risk fields, such as aviation and power plant control. These efforts have yielded marked improvement in the safety and efficiency of air travel and nuclear power plant operations.

Our ability to care for sicker patients has also improved. The first "monitors" were the five senses of the physician. Lanneac described the first stethoscope as an extension of the sense of hearing in the late eighteenth century. The development of neurosurgery as a specialty in the early twentieth century and the need to monitor blood pressure during these operations led to development of the sphygmomanometer. The need to monitor the physiology of astronauts in space led to the capability of continuous EKG and other types of monitors. EKG was one of the very first technical approaches to monitor patient physiology and was clinically developed by the British cardiologist, Sir Thomas Lewis, in 1908. Some of today's most innovative monitors still employ elements of Lewis' original strip chart (for a more complete history of the EKG, see Chap. 19). ICU monitoring techniques developed over the last four decades have resulted in a significant improvement in our overall understanding of cardiac physiology and pathophysiology. The last three decades have seen a plethora of invasive and noninvasive monitoring tools developed for critical care use. Despite these tools, the most important tool available to the clinician remains his/her five senses, mandating a careful examination of patients on a daily routine basis.

23.2 Goals of Monitoring

23.2.1 Diagnosis of Shock

Many monitoring strategies relate to identification of shock; therefore, an important issue is the clinical definition of shock. In the final analysis, shock can be simply defined as inadequate oxygen delivery to a tissue bed, resulting in decreased adenosine triphosphate (ATP) production and flux at the mitochondrial level related to decreased oxidative phosphorylation. Therefore, the ideal monitor for diagnosis of shock would be able to identify the rate of ATP production and turnover. Unfortunately to date, such a monitor does not exist for routine clinical use; hence, clinicians use common clinical end points to identify shock and other associated abnormalities in patients. A list of commonly used clinical monitoring end points is listed in Table 23.1. It requires an astute clinician to balance the sometimes contradictory findings identified during evaluation of the patient and to develop an appropriate treatment strategy. An important component of this process is frequent reevaluation of the patient to assess results of the initial intervention. Importantly, a response to intervention contradictory to initial evaluation should prompt reconsideration of the initial diagnosis.

Table 23.1 Commonly used clinical end points of resuscitation

Heart rate
Blood pressure
Mentation
Skin perfusion
Urine output 50 cm^3/h
Normal lactate/acid base status
Appropriate response to therapeutic interventions

23.2.2 Evaluation of Cardiac Function

Another reason for consideration of advanced monitoring is for frequent evaluation of cardiac function. In particular, serious illness in patients with underlying cardiac disease (e.g., cardiomyopathy, congestive heart failure, congenital heart disease, etc.) may require a careful titration of therapy to prevent decompensation. Situations that commonly result in invasive monitoring of patients include serious infectious episodes, planned major operations, and/or decompensation of the underlying disease.

23.2.3 Titration of Vasoactive Therapy

Many patients receive advanced monitoring due to hemodynamic instability (i.e., hypotension or severe hypotension) or due to the need to titrate vasoactive therapy for other therapeutic purposes (e.g., optimization of cerebral perfusion in patients with neurologic insult). Most vasoactive agents have short half-lives, requiring frequent titration of therapy to achieve monitoring targets. This need mandates accurate, continuous monitoring of blood pressure (or other end point), typically via an invasive route.

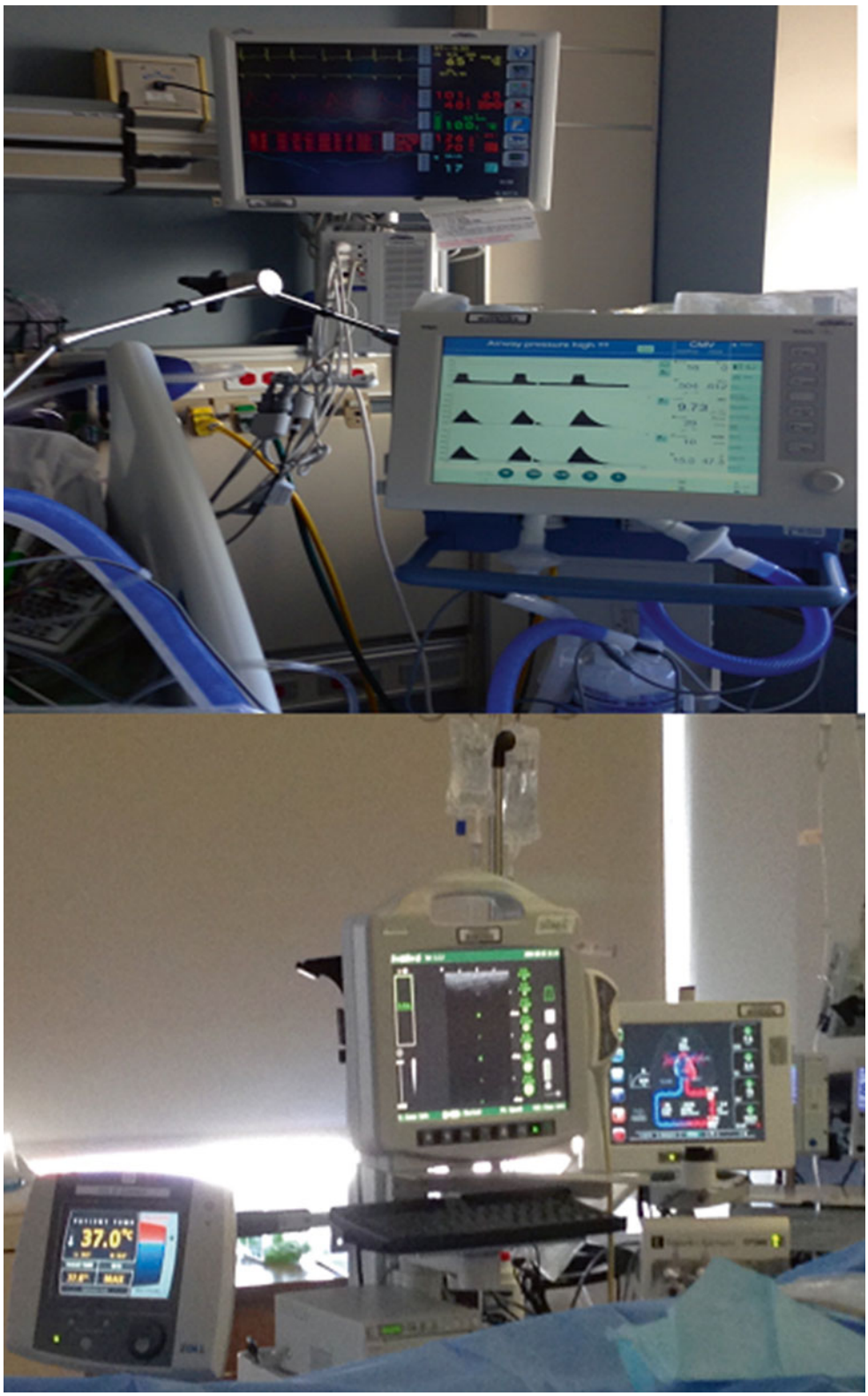

Fig. 23.1 Different monitors used in the ICU. Heart rate, arterial blood pressure, and mechanical ventilation settings (*top*). Intravascular temperature manager, ECHO, and perfusion monitors (*below*)

An important, but frequently unstated, reason for invasive monitoring in the critically ill patient is to allow a more definitive diagnosis and/or end point for treatment. This more definitive observation after initial evaluation may allow ongoing management of the patient's issues with the clinician away from the bedside, allowing the clinician to perform other duties (Fig. 23.1).

23.3 Monitors: Do They Help?

Despite the common reliance on monitors in the modern ICU, a number of monitoring end points commonly used have not demonstrated consistent benefit with respect to patient outcome, including continuous EKG monitoring, pulse oximetry, pulmonary artery catheters, and/or intracranial pressure monitoring. For example, with regard to pulse oximetry, Pedersen et al. in the Cochrane database systems review of 2003 [1] noted that "the conflicting subjective and objective results of the studies, despite an intense methodological collection of data from a relatively large population (>20,000 patients) indicates that the value of perioperative monitoring with pulse oximetry is questionable in relation to improved quality outcomes effectiveness and efficacy."

Another randomized nonblinded study was performed in 2006 [2] which was designed to compare the effects of continuous and standard monitoring of pulse oximetry on patient outcomes in 1219 subjects. Ochroch and colleagues observed that there was no difference in the rate of ICU readmission from postcardiothoracic surgery care floor, mortality, or overall estimation of costs of hospitalization between the CPOX and standard monitor groups. The same can be said regarding pulmonary artery catheters. Shah et al. [3] noted that "despite almost 20 years of randomized controlled trials, a clear strategy leading to improved survival with a pulmonary artery catheter has not been devised." This has led to the near abandonment of the use of pulmonary artery catheters in many institutions.

One nuance with regard to monitors is that the use of such devices will not change the outcome for a fatal disease if there is no treatment available for the disease [4]. For instance, while you can monitor the progression of end-stage organ function in a patient with metastatic cancer, it is unlikely that utilizing a monitor to guide therapy in such a patient will affect the ultimate survival outcome of the patient.

On the other hand, one positive bit of evidence demonstrating beneficial effects for physiologic monitoring relates to the significant decrease in anesthesia-related deaths over the last two decades. Anesthesia care is currently highly dependent on multiple physiologic monitors. As monitors have become increasingly utilized during anesthesia, the anesthesia-related mortality rate of 1 per 20,000 anesthetics reported in the late 1970s has decreased to a rate of 1 in 300,000 anesthetics at the turn of the century. Most knowledgeable clinicians in this area would agree that much of this decrease in mortality is related to both better understanding of pathophysiology and more widespread use of continuous monitoring.

23.3.1 What About Telemedicine?

Telemedicine applied to the ICU is an innovative approach to providing critical care services and to treating critical ill patients, especially those residing in broad or remote geographic areas (Fig. 23.2). Rosenfeld et al. published, in 2000 [5], the first feasibility study of telemedicine. Their study

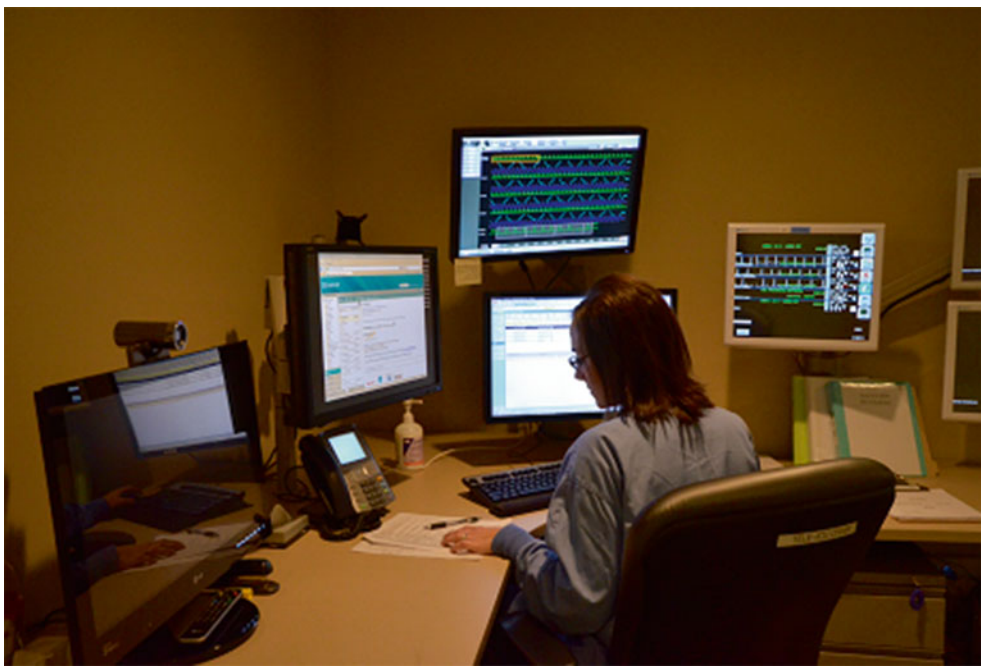

Fig. 23.2 Tele-ICU. The workstation arrangement in the tele-ICU may vary, but usually there are between 5 and 7 monitor screens displaying real-time patient data, including vital signs, medications, lab results, and the patient's entire medical history

looked at a single open model surgical ICU that, for a 16-week period, was provided with 24-h off-site monitoring. Compared with the baseline periods prior to the intervention, the mortality rate, length of stay, and costs were all reduced. In another study, one from a large university medical center, administrators retrospectively reviewed their data from 2011 to 2012, which showed a reduction in mortality rates from 6.5 % before to 4.9 % after the implantation of an enhanced monitoring system [6]. Subsequently, other larger trials have also identified similar improvements in mortality [7, 8]. Finally, it was also suggested that if the hospital is able to provide the initial capital and financing for the ongoing operation, a tele-ICU may positively benefit the hospital's profit margin [9].

23.4 Invasive Monitoring Techniques in the ICU

23.4.1 Central Venous Pressure (CVP) Monitoring

Pressure monitoring in a central venous location, using a large-bore catheter, is likely the most frequently utilized invasive monitoring technique in current ICUs. Central venous catheters allow an estimate of "cardiac preload" and are typically placed via the internal jugular or subclavian venous route (Fig. 23.3). These monitors are very accurate for the identification of situations in which cardiac output is affected by a low preload. However, the assumption is made when monitoring CVPs that this value is proportional to pulmonary artery pressure, which is proportional to left atrial pressure, which is proportional to left ventricular end-diastolic volumes. Unfortunately, there are many common conditions in ICU patients which may elevate CVP that do not relate to increased filling of the left ventricle. These include: pneumonia, positive pressure ventilation, acute respiratory distress syndrome, pulmonary emboli, and others. Thus, one should have a strong concern for the situation in which a high CVP does not correlate with the clinical condition of the patient.

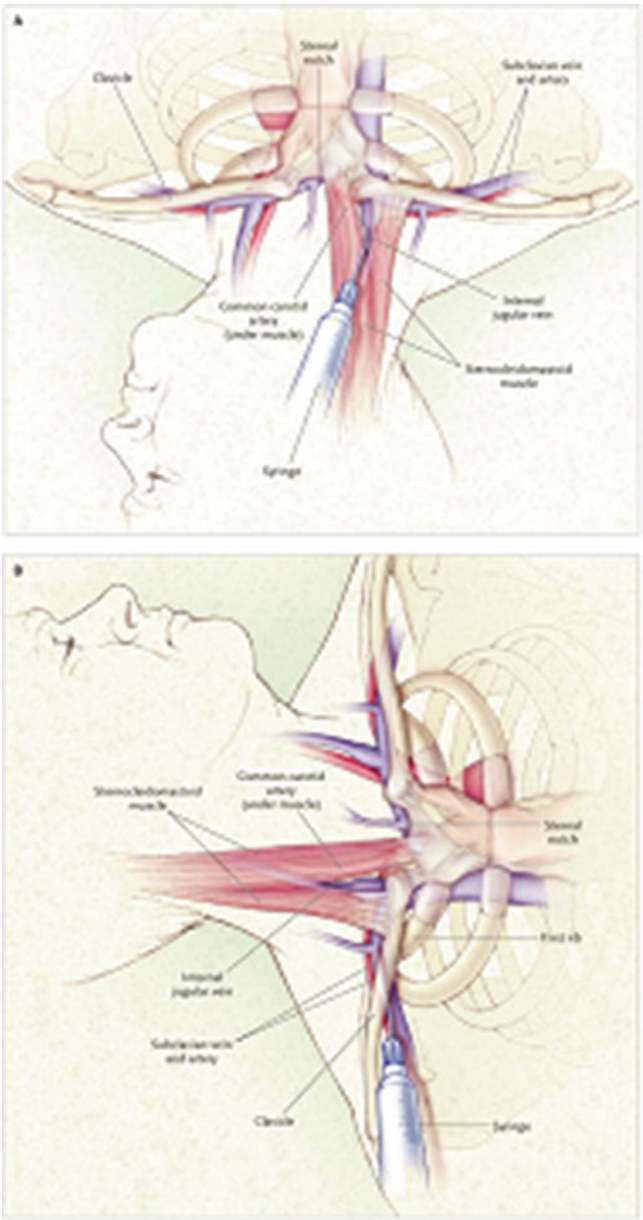

Fig. 23.3 Venous anatomy of subclavian (*top*) and internal jugular veins. Veins are in blue. Outline of clavicle and manubrium are in black (*upper panel*). Sternocleidomastoid muscle (*lower panel*) is in red

23.4.2 Arterial Blood Pressure Monitoring

Arterial blood pressure monitoring can be performed using both noninvasive and invasive techniques. Noninvasive monitors have progressed significantly over the years and currently allow a hands-off approach to intermittent measurement of blood pressure. Unfortunately, it is difficult to noninvasively measure blood pressure more frequently than every 5 min due to patient comfort and potential for inducing pressure sores. In situations where more frequent measures are necessary, invasive catheters placed percutaneously into a peripheral artery are utilized (Fig. 23.4). Typically, continuous beat-to-beat blood pressure is measured using an arterial catheter placed in one of several positions (most commonly radial or femoral arteries). However, this can be associated with injury, greater expense, and the need for required skills to acquire the data [10].

Recently, a continuous noninvasive arterial pressure (CNAP) measurement was made possible by using a finger cuff technology (Fig. 23.5). It has been shown to be superior to intermittent oscillometric measurements in detecting rapid changes in arterial pressure [11]. Such an approach employs

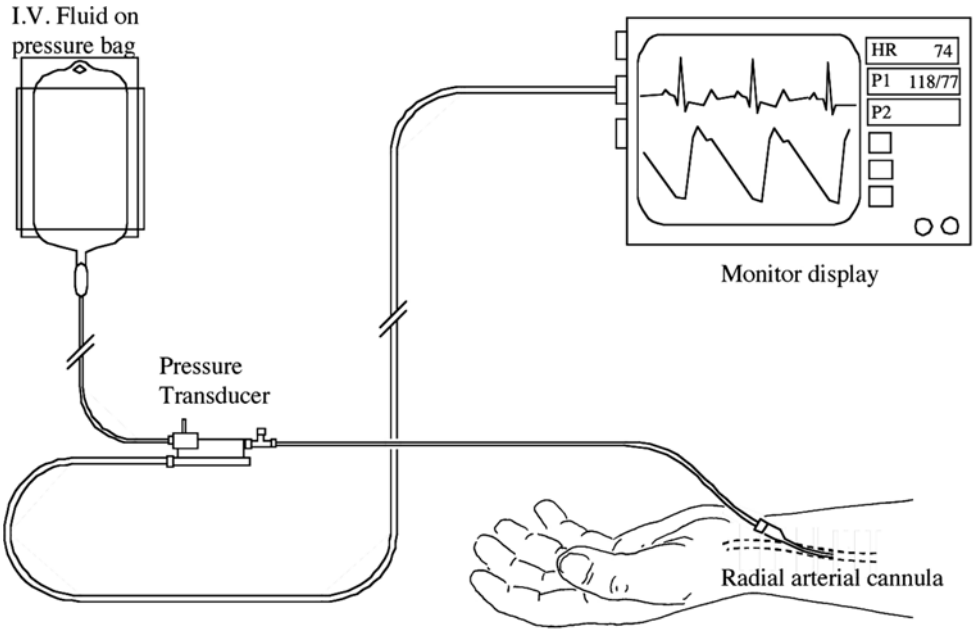

Fig. 23.4 Arterial line placed into radial artery. The line is attached to a pressure transducer which measures blood pressure and allows slow flush of intravenous fluid though the line. This line can also be utilized for sampling of arterial blood

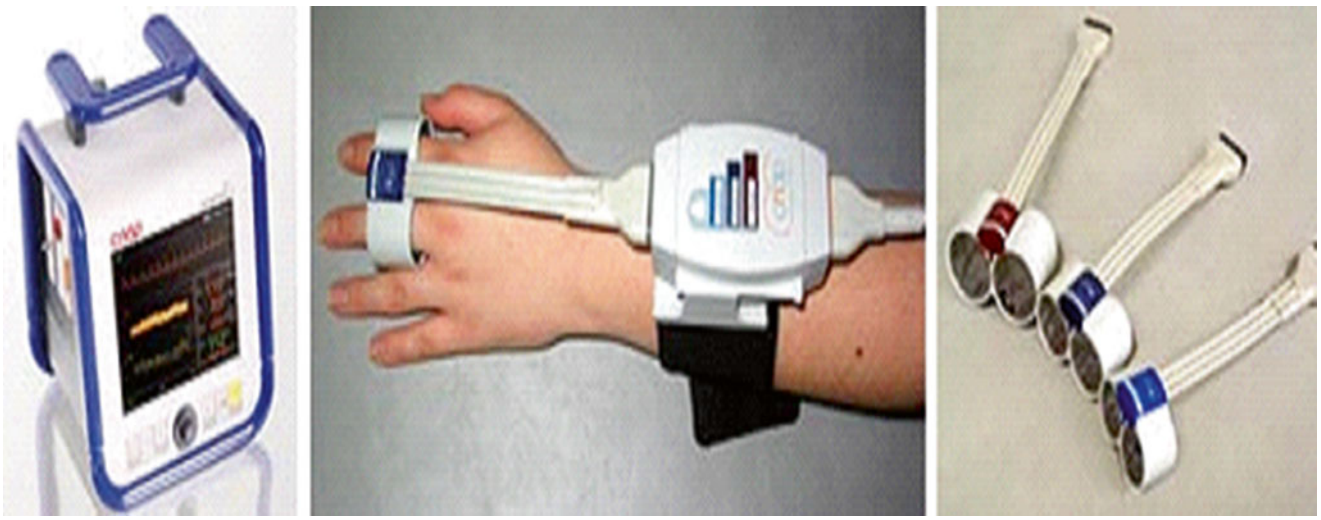

Fig. 23.5 Continuous noninvasive arterial blood pressure (CNAP) provides a continuous, beat-to-beat, blood pressure signal recorded from the fingers of a subject. The monitoring system uses a double finger cuff in three cuff sizes to accommodate small children through large adults. The system outputs a continuous blood pressure waveform that is similar to a direct arterial pressure waveform. Adopted from biopac.com

a double finger cuff that is easy to place on the patients' hand, a pressure transducer mounted on the forearm, and an upper arm oscillometric cuff for calibration. The system outputs a continuous noninvasive blood pressure waveform that is similar to a direct arterial blood pressure waveform and also displays values for systolic, diastolic, and mean blood pressures as well as heart rate.

CNAP is obtained by applying pressure via the finger cuffs such that the blood volume flowing through the finger arteries is held constant (i.e., volume clamping). The diameter of a finger artery under a cuff is "clamped," i.e., kept at a constant diameter in the presence of the changes in arterial pressure during each heart beat. The finger diameters are measured by means of an infrared photo-plethysmograph built into the finger cuff. The finger diameter is held constant by dynamically applying a counter pressure throughout the cardiac cycle. The pressure in the cuff that is needed to keep the volume constant during arterial pulsation corresponds to the relative arterial pressure. Recent studies have demonstrated comparable results to continuous invasive arterial blood pressure measurements [12]. For additional information on blood pressure monitoring, see Chap. 18.

Like CVP monitoring, there are assumptions built into blood pressure monitoring that are occasionally incorrect.

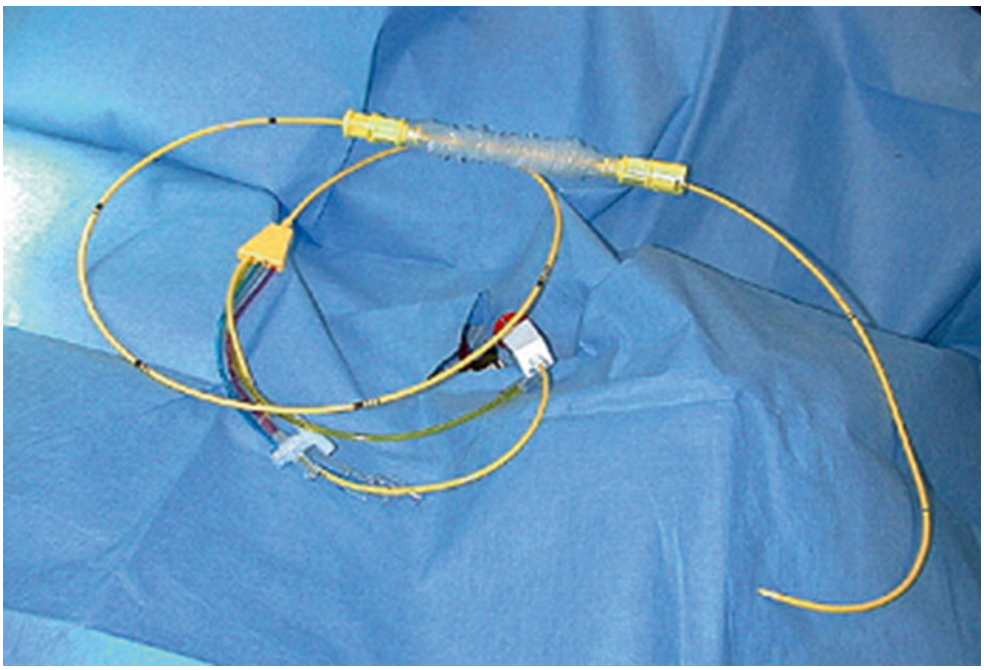

Fig. 23.6 Pulmonary artery catheter. This catheter has an inflatable balloon at the tip, allowing the catheter to be carried through the right heart and into the pulmonary artery during insertion

Table 23.2 Calculations for invasive hemodynamic measurements

Hemodynamic formula	Normal
CI = CO/BSA	2.8–4.2 l/min/m^2
SV = CO/HR	60–90 ml/beat
MAP = DBP + 1/3 (SBP − DBP)	80–120 mmHg
SVR = [(MAP − CVP)/CO] × 80	900–1400 dynes cm s^3
SVRI = [(MAP − CVP)/CI]	1900–2400 dynes cm m^3
PVR = [(MPAP − PAOP)/CO] × 80	100–250 dynes cm s^3
Arterial oxygen content: $CaO_2 = (SaO_2)$ (Hb × 1.34) + PaO_2 (0.0031)	21 ml/100 ml
Venous oxygen content: $CvO_2 = (SvO_2)$ (Hb × 1.34) + PvO_2 (0.0031)	15 ml/100 ml
Oxygen consumption: $VO_2 = CO\ (CaO_2 - CvO_2) \times 10$ (VO_2 not indexed, indexed by weight, BSA)	225–275 ml/min, 3.5 ml/kg/min; 110 ml/min/m^2
Oxygen delivery: $DO_2 = CO(CaO_2) \times 10$	1000 ml/min
Oxygen extraction ratio: $O_2ER = VO_2/DO_2$	22–30 %

BSA body surface area, *CI* cardiac index, *CO* cardiac output, *CVP* central venous pressure, *DBP* diastolic blood pressure, *Hb* hemoglobin, *HR* heart rate, *MAP* mean arterial pressure, *MPAP* mean pulmonary artery pressure, *PAOP* pulmonary artery occlusion, *PVR* peripheral vascular resistance, pressure, *SBP* systolic blood pressure, *SV* stroke volume, *SVR* systemic vascular resistance, *SVRI* systemic vascular resistance index

Importantly, the assumption that a normal arterial blood pressure has excluded the presence of shock may be false, since afterload may be increased due to low cardiac output. This results in a normal blood pressure but inadequate oxygen delivery to tissues.

23.4.3 Pulmonary Artery Catheter

Since pulmonary artery catheterization was first described in 1970 by Drs. Swan and Ganz [13], it has been widely used as a diagnostic tool and to understand the physiology of the cardiovascular system during critical illness. The pulmonary artery catheter is inserted via central venous access through the femoral, subclavian, or internal jugular route. A balloon at the tip of the catheter allows the catheter to be "floated" to the right side of the heart and into the pulmonary artery, where it wedges into a smaller branch of the pulmonary artery (Fig. 23.6). It allows the measurement of stroke volume, cardiac output, mixed venous saturation, and pressures on the right side of the heart (Table 23.2). This catheter allows for a more accurate measure of intravascular volume than CVP because it bypasses the situations that can falsely elevate CVP; additionally, the information it provides can be utilized to distinguish among the various types of shock (Table 23.3). Since the pulmonary artery system is a high

Table 23.3 Changes in cardiac preload (PAOP), systemic vascular resistance, and cardiac output in various causes of shock

Type of shock	PAOP	SVR	CO	Prime mover
Hemorrhagic	Decreased	Increased	Decreased	Decreased preload
Septic	Unchanged	Decreased	Increased	Decreased SVR
Cardiogenic	Increased	Increased	Decreased	Decreased CO
Neurogenic	Unchanged	Decreased	Increased	Decreased SVR

CO cardiac output, *PAOP* pulmonary capillary wedge pressure, *SVR* systemic vascular resistance, *prime mover* variable primarily responsible for shock in clinical syndrome

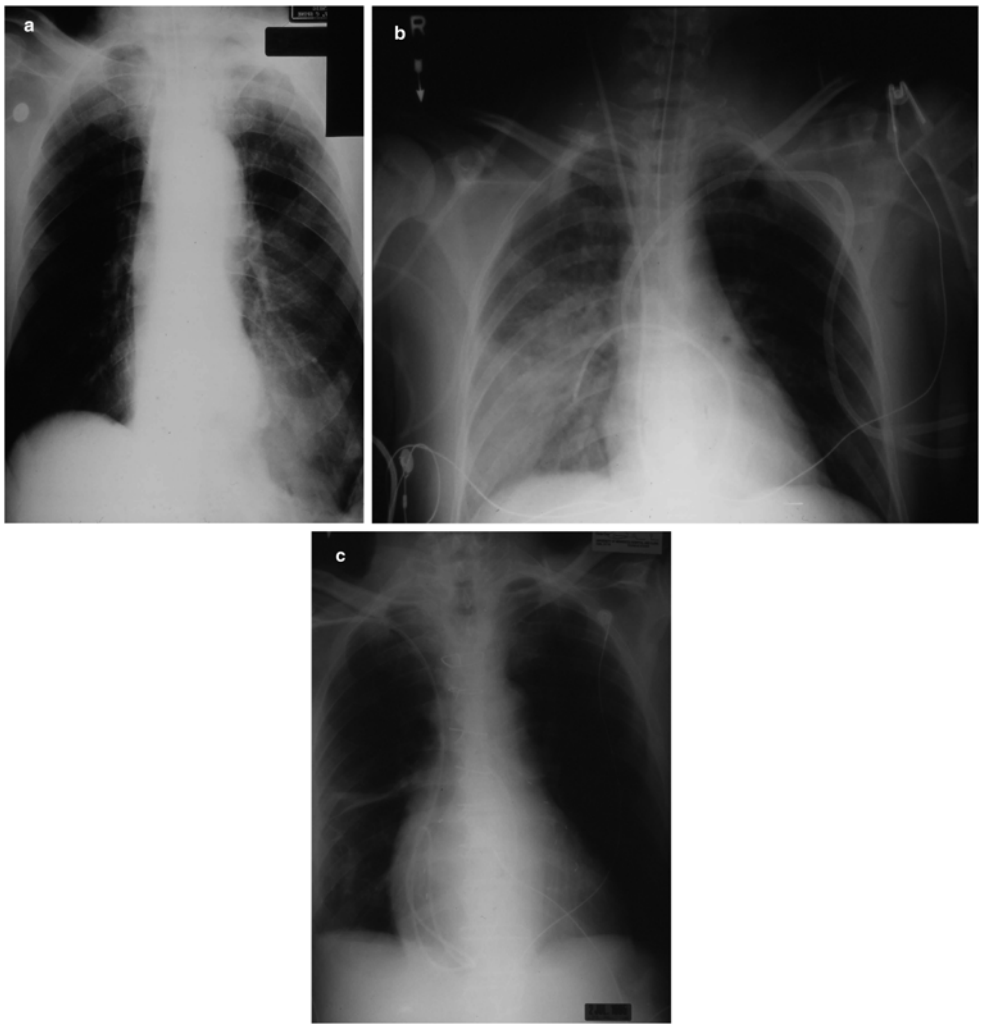

Fig. 23.7 Complications associated with insertion of central access and pulmonary artery catheter including: (**a**) right pneumothorax, (**b**) pulmonary hemorrhage due to distal migration of pulmonary artery catheter, and (**c**) knotting of pulmonary artery catheter in right ventricle

flow, low resistance system, those conditions which falsely elevate pulmonary artery pressure do not affect pulmonary artery wedge pressure. As noted previously, the use of this catheter has significantly declined in the last decade due to paucity of data supporting improved mortality, general ICU or hospital length of stay, or cost for adult patients in intensive care [14, 15]. Despite the decreased use, the pulmonary artery catheter can still be indispensable to assist in the evaluation and titration of therapy of the patient with multisystem disease.

23.4.4 Complications of Invasive Monitors

A major issue with all invasive monitors involves complications such as those related to insertion, infectious complications, and/or problems associated with an indwelling catheter. Insertion complications can result when the catheter: (1) is placed in the wrong vessel, (2) creates a pneumothorax, or (3) causes bleeding related to coagulopathy or inappropriate dilation of a vessel (Fig. 23.7). Furthermore, centrally placed catheters can allow air within the central circulation,

occasionally resulting in stroke [16]. Unfortunately, catheter-associated central line infections are common and represent a major and expensive source of hospital morbidity. Typical infection rates for central venous catheters are in the range of 3–5 infections per 1000 patient catheter days. Thus, it is important to remove central venous catheters at the point where they are no longer necessary. Since indwelling catheters are made of a foreign material, there is risk of thrombosis and embolus [17]. Both of these risks are well described in the literature, and attempts to decrease these risks with heparin bonding or using other coatings are prevalent.

23.5 Less Invasive Monitoring Techniques

There are many new monitors making their way into daily clinical use. The utility of these monitors varies widely depending on clinician experience and understanding of monitoring end points, patient populations chosen for study of these monitors, and the clinical relevance of these monitors. The two questions clinicians should ask themselves when evaluating any new monitoring strategy are as follows: (1) Does this monitoring system provide the information needed to make a decision about the patient's status that is clinically relevant? (2) How should the clinician intervene related to the results of the monitor? If results from the monitoring system are not clinically relevant or do not allow decisions to be made with respect to intervention, then the monitor is likely not useful for patient care.

23.5.1 Cardiac Hemodynamics

There are several new measurements available allowing less invasive measurement of cardiac hemodynamics.

23.5.1.1 Pulse Contour Wave Processing

Recently, several investigations have validated the benefits of employing less invasive measures of hemodynamics, including pulse contour wave processing and the ability to predict whether a patient is going to respond to fluid boluses as the initial step of the hemodynamic resuscitation. Some of these commonly used methods (e.g., PiCCO, LiDCO, FloTrac) are based on assessing changes in left ventricular output during positive pressure ventilation, e.g., pulse pressure variation (PPV) and stroke volume variation (SVV). Underlying these measures, intrathoracic pressure increases during respiration, causing right arterial pressure to increase as a consequence; cardiac preload will decrease, leading to a decrease in right ventricular output and thus left ventricular output after few beats. The PiCCO monitor utilizes intermittent arterial thermodilution with beat-to-beat analyses of the arterial pulse waveforms to provide several hemodynamic parameters. This monitoring approach requires both a central arterial line (femoral or axillary) and a central venous line [18]. The LiDCO monitor also uses pulse contour analysis and is calibrated using a dye dilution technique employing lithium chloride as an indicator. This approach requires only a peripheral venous line and arterial catheter [19]. The aforementioned techniques also allow evaluation of preload using different calculated measures including SVV, PPV, and others. Importantly, these measures of preload have been demonstrated to be well correlated with fluid responsiveness in a number of clinical settings [20].

It should be noted that the previous measures have some general and specific limitations, one being that the results become inaccurate in the setting of atrial fibrillation, frequent premature ventricular contractions, and/or intra-aortic balloon central pulsation. They also require the patient to be heavily sedated and to be receiving mechanical ventilation with a tidal volume of >6 ml/kg for obtaining accurate PPV and SVV values. Therefore, their use becomes more challenging during periods of hemodynamic instability, requiring frequent recalibration of the system. An additional limitation of the LiDCO monitor approach is that some nondepolarizing muscle relaxants (e.g., vecuronium) will interfere with the sensor [21].

A new pulse contour method, the FloTrac/Vigileo™ system (Edwards LifeSciences, Irvine, CA, USA), has been recently introduced. It uses intra-arterial pressure waveform-based pulse contour analyses to measure cardiac output and SVVs, without the need for continual calibration. For estimation of the cardiac output, the standard deviation of pulse pressure sampled in 20 s is related to normal stroke volume based on the patient's demographic data (height, weight, age, and gender). Unlike PiCCO which requires femoral or brachial arterial cannulation to estimate SVV, the FloTrac/Vigileo system uses only a peripheral arterial pressure waveform without any other invasive monitoring. SVV measured by the FloTrac/Vigileo™ system (SVV-FloTrac) has been reported to have acceptable sensitivity and specificity for the prediction of fluid responsiveness [22].

23.5.1.2 Ultrasonography/Echocardiography

Ultrasonography and echocardiography have been used to measure flow volume and diameter of the aorta and left ventricular function as a noninvasive hemodynamic evaluation (Fig. 23.8). The described methods include transthoracic or transesophageal echocardiograms (TEE). Transthoracic methods are less invasive but significantly less accurate, while transesophageal techniques require a sedated and/or mechanically ventilated patient. Subramaniam and co-authors suggest a method of rapid echocardiographic assessment using a standardized algorithm [23]. This approach uses transesophageal echocardiography for assessment but requires an experienced operator to prevent misinterpretation

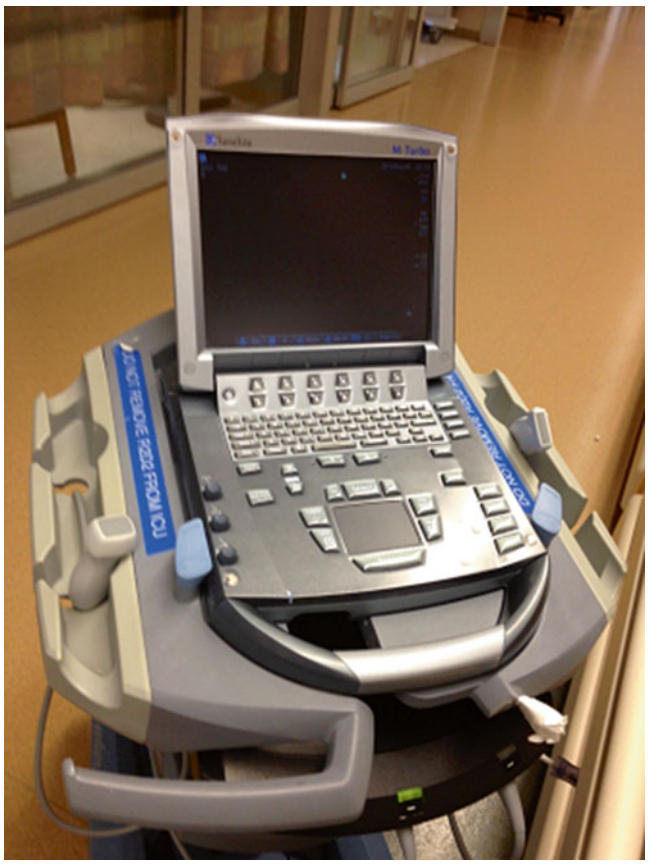

Fig. 23.8 Bedside ultrasound machine commonly used in the ICU setting and easy to move and handle (three different probe sizes)

of findings. Over the last few years, several studies within different ICU and critical care settings have demonstrated the feasibility of utilizing TEE in the management of hemodynamic instability. It is now clear that this semi-invasive tool can provide critical information about the heart. Further, even when invasive continuous monitoring by a pulmonary artery catheter is used, TEE can further help define a patient's diagnosis by acquiring morphological and functional information that can be integrated with the pulmonary artery catheter data. Several recent reports have demonstrated the potential utility of this semi-invasive approach in the ICU patient [24–26].

Preload can also be evaluated by measuring left ventricular end-diastolic area (which correlates well with end-diastolic volume) and also by evaluating respiratory variation in the diameter of the inferior vena cava or the collapsibility of the superior vena cava and then sampling the velocity time integral of the aortic valve flow during inspiration. To date, this technique is finding limited, but increasing, use in ICUs in the United States, in part due to lack of training and experience with this technique for many ICU physicians.

23.5.1.3 CO_2 Partial Rebreathing Technique

The CO_2 partial rebreathing technique can be used via a modified Fick technique in mechanically ventilated patients. The NiCO device (Respironics, Murrysville, PA, USA) allows measurement of cardiac output using this method. The technique involves measurement of end-tidal CO_2 obtained before and during rebreathing periods. The ratio of the change in end-tidal CO_2 allows a noninvasive estimate of cardiac output [27]. To achieve optimal results with the NiCO monitor, the patient should be maintained under fully controlled mechanical ventilation. This technique is limited by the fact that the calculation includes blood flow perfusing ventilated portions of the lung and bypassing any blood flow bypassing ventilated alveoli. Therefore, these results can be a significant underestimation of cardiac output, corrected by making an estimate of shunt fraction (the amount of blood flow bypassing ventilated alveoli). Compared with conventional cardiac output methods, the partial CO_2 rebreathing technique is noninvasive, can easily be automated, and can provide real-time and continuous cardiac output monitoring [28, 29].

23.5.2 Perfusion Monitors

There are a number of recently developed noninvasive measures of regional tissue perfusion including near-infrared spectroscopic measurement of StO_2, sublingual and other capnometry methods, and the use of the $ScvO_2$ catheter.

23.5.2.1 Reflectance Near-Infrared Spectroscopy

Tissue hemoglobin saturation (StO_2) is derived from near-infrared spectroscopy and is a potentially useful, noninvasive adjunct for monitoring critically ill patients. StO_2 reflects changes in microcirculatory tissue perfusion. Unlike pulse oximetry signal (SpO_2), which measures oxygen contents in large, pulsatile vessels, StO_2 measures the oxygen content in vessels less than 1 mm in diameter (i.e., arterioles, capillaries, and venules) and describes the oxygen content at the tissue level; thus, it alerts the clinician that peripheral blood flow is being redistributed to vital organs, as the normal balance between the proportion of oxyhemoglobin and deoxyhemoglobin in the peripheral tissues undergoes adverse changes. There are several studies that have showed correlations between StO_2 and multiple organ failure, ICU admission, ICU outcome, and mortality [30, 31]. In patients with septic shock, StO_2 has been shown to correlate with higher mortality [32]. Additionally, one study conducted on 158 emergent cancer patients who presented to the emergency department with hypotension and/or systemic inflammatory response syndrome found that a SpO_2 less than 70 % significantly increased the risk of ICU admission [31]. Iyegha et al. [33] concluded, in a study of 620 ICU patients, that low StO_2 (<70 %) is common and associated with poor outcomes in SICU patients. However, no studies to date have utilized a randomized sampling or established a cause-and-effect relationship between a specific intervention that aimed toward normalization of StO_2 and specific patient outcomes.

23.5.2.2 Capnometry

In shock states, it is common to see redistribution of flow away from the gastrointestinal tract, resulting in increased gastrointestinal mucosal pCO_2. Many investigators have demonstrated this effect in both septic and hemorrhagic shock [34, 35]. Unfortunately, techniques to measure pCO_2 in the gastrointestinal tract have been limited by the efforts involved in appropriate placement of catheters within that area. This has led to the development of sublingual capnometry, capitalizing on the fact that the oral tissues are embryologically continuous with the gastrointestinal tract. This technique has the potential to allow rapid information regarding adequacy of tissue perfusion in critically ill patients; however, clinical studies utilizing this technology are lacking at this time.

23.5.2.3 Central Venous O_2 Saturation Monitors

The measurement of mixed venous oxygen saturation in either the pulmonary artery (SvO_2) or in the right atrium ($ScvO_2$) has been studied as a reflection of resuscitation of patients in a variety of settings [36–38]. It has also been used to guide the treatment of shock [39]. This technique has the potential advantage of yielding both an end point for resuscitative efforts and intravenous access. Since a decreased cardiac output and a resultant decrease in oxygen delivery to tissues will result in increased peripheral tissue extraction of oxygen from circulating blood, a low $ScvO_2$ in a critically ill patient has typically carried the implication that the patient is suffering from inadequate cardiac output. One potential shortcoming of this technique is the lack of sensitivity related to mixing of venous blood returning from organs with high and low metabolic needs, resulting in a falsely high reading. Despite these theoretic concerns, a recent study by Rivers and colleagues [36] used $ScvO_2$ as an end point of resuscitation in a group of septic patients presenting to an emergency department and demonstrated improved survival in patients who received interventions designed to improve $ScvO_2$ levels to greater than 70 % (defined as early goal-directed therapy). These findings have resulted in incorporation of early goal-directed therapy into protocols for treatment of patients with severe sepsis or septic shock.

23.5.3 Subcutaneous Continuous Glucose Monitoring

Hyperglycemia is common in acutely ill patients, especially within the ICU population [40]. Tight glucose control has been proposed to be crucial in these critically ill patients, especially for reduction in morbidity and mortality in the SICU populations. However, recent studies showed no evidence that intensive insulin therapy and tight glycemic control in ICU patients has led to decreased 28-day mortality; on the other hand, it can be associated with a high incidence of hypoglycemia and death [41, 42].

23.5.4 Conclusions

The need for monitoring of the critically ill patient has grown as the healthcare system has developed the ability to care for progressively more compromised and elderly patients. Monitors serve several purposes including: (1) the identification of shock and abnormal cardiac physiology, (2) the evaluation of cardiovascular function, and (3) to allow titration of therapy. An important function of an effective monitoring device is reliable detection of abnormal physiology. Despite much research on the use of monitoring techniques in critical care, there is little evidence of improved outcome related to routine use of monitors. To date, the mainstays of invasive monitoring in the ICU include CVP monitoring and arterial pressure monitoring, with pulmonary arterial monitoring reserved for occasional patients with multisystem disease. Recent trends in monitoring have included development of less invasive monitoring techniques that yield a number of cardiovascular parameters potentially useful to clinicians. New noninvasive measures of tissue perfusion (StO_2, sublingual capnometry) and semi-invasive techniques (TEE) have significant potential in identification and treatment of pathophysiologic states resulting in inadequate tissue perfusion. Tele-ICU is a new trend that has so far proven to reduced mortality and morbidity. Developers of new monitors (despite facing regulatory requirements that are considered less stringent than those of drug manufacturers) will increasingly be expected to demonstrate clinical efficacy of new devices. In the final analysis, the most important "monitor" is a caring healthcare provider at the patient bedside evaluating the patient's response to intervention and therapy.

References

1. Pedersen T, Dyrlund Pedersen B, Møller AM (2003) Pulse oximetry for perioperative monitoring. Cochrane Database Syst Rev 3, CD002013
2. Ochroch EA, Russell MW, Hanson WC 3rd et al (2006) The impact of continuous pulse oximetry monitoring on intensive care unit admissions from a postsurgical care floor. Anesth Analg 102:868–875
3. Shah MR, Hasselblad V, Stevenson LW et al (2005) Impact of the pulmonary artery catheter in critically ill patients: meta-analysis of randomized clinical trials. JAMA 294:1664–1670
4. Berthelsen PG (2006) Double jeopardy. Acta Anaesthesiol Scand 50:391–392
5. Rosenfeld BA, Dorman T, Breslow MJ et al (2000) Intensive care unit telemedicine: alternate paradigm for providing continuous intensivist care. Crit Care Med 28:3925–3931
6. Fortis S, Weinert C, Bushinski R, Koehler AG, Beilman G (2014) A health system-based critical care program with a novel tele-ICU:

implementation, cost, and structure details. J Am Coll Surg 219:676–683
7. Lilly CM, Cody S, Zhao H et al (2011) Hospital mortality, length of stay, and preventable complications among critically ill patients before and after tele-ICU reengineering of critical care processes. JAMA 305:2175–2183
8. McCambridge M, Jones K, Paxton H et al (2010) Association of health information technology and teleintensivist coverage with decreased mortality and ventilator use in critically ill patients. Arch Intern Med 170:648–653
9. Kruklitis RJ, Tracy JA, McCambridge MM (2014) Clinical and financial considerations for implementing an ICU telemedicine program. Chest 145:1392–1396
10. Mandel MA, Dauchot PJ (1977) Radial artery cannulation in 1000 patients: precautions and complications. J Hand Surg 2:482–485
11. Wagner JY, Prantner JS, Meidert AS, Hapfelmeier A, Schmid RM, Saugel B (2014) Noninvasive continuous versus intermittent arterial pressure monitoring: evaluation of the vascular unloading technique (CNAP device) in the emergency department. Scand J Trauma Resusc Emerg Med 22:8
12. Ilies C, Grudev G, Hedderich J et al (2014) Comparison of a continuous noninvasive arterial pressure device with invasive measurements in cardiovascular postsurgical intensive care patients: a prospective observational study. Eur J Anaesthesiol Aug 7 [Epub ahead of print]
13. Swan HJ, Ganz W, Forrester J, Marcus H, Diamond G, Chonette D (1970) Catheterization of the heart in man with use of a flow-directed balloon-tipped catheter. N Engl J Med 283:447–451
14. Harvey S, Young D, Brampton W et al (2006) Pulmonary artery catheters for adult patients in intensive care. Cochrane Database Syst Rev 3, CD003408
15. Rajaram SS, Desai NK, Kalra A et al (2013) Pulmonary artery catheters for adult patients in intensive care. Cochrane Database Syst Rev 2, CD003408
16. Brouns R, De Surgeloose D, Neetens I, De Deyn PP (2006) Fatal venous cerebral air embolism secondary to a disconnected central venous catheter. Cerebrovasc Dis 21:212–214
17. Kirkpatrick A, Rathbun S, Whitsett T, Raskob G (2007) Prevention of central venous catheter-associated thrombosis: a meta-analysis. Am J Med 120:901.e1–901.e13
18. Hamzaoui O, Monnet X, Richard C, Osman D, Chemla D, Teboul JL (2008) Effects of changes in vascular tone on the agreement between pulse contour and transpulmonary thermodilution cardiac output measurements within an up to 6-hour calibration-free period. Crit Care Med 36:434–440
19. Costa MG, Della Rocca G, Chiarandini P et al (2008) Continuous and intermittent cardiac output measurement in hyperdynamic conditions: pulmonary artery catheter vs. lithium dilution technique. Intensive Care Med 34:257–263
20. Belloni L, Pisano A, Natale A et al (2008) Assessment of fluid-responsiveness parameters for off-pump coronary artery bypass surgery: a comparison among LiDCO, transesophageal echocardiography, and pulmonary artery catheter. J Cardiothorac Vasc Anesth 22:243–248
21. Connors AF Jr, Speroff T, Dawson NV et al (1996) The effectiveness of right heart catheterization in the initial care of critically ill patients. SUPPORT Investigators. JAMA 276:889–897
22. Suehiro K, Tanaka K, Matsuura T et al (2014) The Vigileo-FloTrac™ system: arterial waveform analysis for measuring cardiac output and predicting fluid responsiveness: a clinical review. J Cardiothorac Vasc Anesth 28:1361–1374
23. Subramaniam B, Talmor D (2007) Echocardiography for management of hypotension in the intensive care unit. Crit Care Med 35:S401–S407
24. Slama MA, Novara A, Van de Putte P et al (1996) Diagnostic and therapeutic implications of transesophageal echocardiography in medical ICU patients with unexplained shock, hypoxemia, or suspected endocarditis. Intensive Care Med 22:916–922
25. Charron C, Caille V, Jardin F, Vieillard-Baron A (2006) Echocardiographic measurement of fluid responsiveness. Curr Opin Crit Care 12:249–254
26. Slama M, Maizel J (2006) Echocardiographic measurement of ventricular function. Curr Opin Crit Care 12:241–248
27. Jaffe MB (1999) Partial CO_2 rebreathing cardiac output operating principles of the NICO system. J Clin Monit Comput 15:387–401
28. Heigenhauser GJ, Jones NL (1989) Measurement of cardiac output by carbon dioxide rebreathing methods. Clin Chest Med 10: 255–264
29. Haryadi DG, Orr JA, Kuck K et al (2000) Partial CO2 rebreathing indirect Fick technique for non-invasive measurement of cardiac output. J Clin Monit Comput 16:361–374
30. Cohn SM, Nathens AB, Moore FA et al (2007) Tissue oxygen saturation predicts the development of organ dysfunction during traumatic shock resuscitation. J Trauma 62:44–54
31. Bazerbashi H, Merriman KW, Toale KM et al (2014) Low tissue oxygen saturation at emergency center triage is predictive of intensive care unit admission. J Crit Care 29:775–779
32. Leichtle SW, Kaoutzanis C, Brandt MM, Welch KB, Purtill MA (2013) Tissue oxygen saturation for the risk stratification of septic patients. J Crit Care 28:1111.e1–1111.e5
33. Iyegha UP, Conway T, Pokorney K, Mulier KE, Nelson TR, Beilman GJ (2014) Low StO_2 measurements in surgical intensive care unit patients is associated with poor outcomes. J Trauma Acute Care Surg 76:809–816
34. Creteur J, De Backer D, Sakr Y et al (2006) Sublingual capnometry tracks microcirculatory changes in septic patients. Intensive Care Med 32:516–523
35. Marik PE (2006) Sublingual capnometry: a non-invasive measure of microcirculatory dysfunction and tissue dysoxia. Physiol Meas 27:R37–R47
36. Rivers E, Nguyen B, Havstad S et al (2001) Early goal-directed therapy in the treatment of severe sepsis and septic shock. N Engl J Med 345:1368–1372
37. Collaborative Study Group on Perioperative $ScvO_2$ Monitoring (2006) Multicentre study on peri- and postoperative central venous oxygen saturation in high-risk surgical patients. Crit Care 10:R158
38. Vedrinne C, Bastien O, De Varax R et al (1997) Predictive factors for usefulness of fiberoptic pulmonary artery catheter for continuous oxygen saturation in mixed venous blood monitoring in cardiac surgery. Anesth Analg 85:2–10
39. Vallée F, Vallet B, Mathe O et al (2013) Central venous-to-arterial carbon dioxide difference: an additional target for goal-directed therapy in septic shock? J Crit Care 28:1110.e1–1110.e5
40. Inzucchi SE (2006) Management of hyperglycemia in the hospital setting. N Engl J Med 355:1903–1911
41. van den Berghe G, Wouters P, Weekers F et al (2001) Intensive insulin therapy in critically ill patients. N Engl J Med 345: 1359–1367
42. Marik PE, Preiser JC (2010) Toward understanding tight glycemic control in the ICU: a systematic review and metaanalysis. Chest 137:544–551

Cardiovascular Magnetic Resonance Imaging and MR-Conditional Cardiac Devices

24

Michael D. Eggen and Cory M. Swingen

Abstract

This chapter provides a condensed review of the basic principles of magnetic resonance imaging (MRI) and introduces the reader to some of the concepts and terminology necessary to understand the use of MRI to study the heart. We then proceed to describe a wide range of MRI cardiac applications, both in vivo and ex vivo, which should interest the biomedical engineer. While the capabilities of cardiac MRI are quite extensive, our choice of topics for this chapter is rather judicious, as cardiac MRI has evolved to the point where entire books are published on the subject.

Keywords

MRI • CMRI • Magnetic resonance imaging • Myocardial viability • Myocardial perfusion • Myocardial function • Morphology • Blood flow velocity • Fiber structure • Interventional MRI • Wall motion • Wall thickening • Myocardial strain • MR-Conditional pacemaker • MR-Conditional ICD

24.1 Introduction

"Magnetic resonance imaging" (MRI) of the heart has rapidly become very popular worldwide, because of its clinical versatility and flexibility, i.e., since it allows one to acquire information on anatomical structure and function simultaneously. An additional benefit of MRI is that patients are not subjected to any ionizing radiation or invasive procedures (e.g., catheterization). Recently, many specialized MR techniques have become available for cardiovascular imaging and thus may potentially replace other types of imaging modalities. As such, cardiac MR may become the "one-stop shop" for imaging, as it is able to: (1) measure myocardial blood flow; (2) differentiate viable from nonviable myocardial tissue; (3) depict the structure of peripheral and coronary vessels (magnetic resonance angiography); (4) measure blood flow velocities (MR velocity mapping); (5) examine metabolic energetics (MR spectroscopy); (6) assess myocardial contractile properties (multislice, multiphase cine imaging, MR tagging); and/or (7) guide interventional procedures with real-time imaging (interventional MRI). The capabilities of MRI as a tomographic imaging modality to capture, with high spatial resolution, the anatomy of 3D structures were already well appreciated before the first attempts were made to apply MRI to the heart. Yet cardiac motion, compounded by respiratory motion and turbulent blood flow in the ventricular cavities and large vessels, initially imposed formidable barriers to the acquisition of artifact-free images that could depict cardiac anatomy with sufficient detail. It has taken well over a decade for cardiac MRI to mature to the point where it is currently being applied in routine fashion in the clinical setting. Therefore, in future medical centers of

Electronic supplementary material: The online version of this chapter (doi:10.1007/978-3-319-19464-6_24) contains supplementary material, which is available to authorized users. Videos can also be accessed at http://link.springer.com/book/10.1007/978-3-319-19464-6_24.

M.D. Eggen, PhD (✉)
Medtronic, 8200 Coral Sea Street NE, Mounds View, Minneapolis, MN 55112, USA
e-mail: michael.d.eggen@medtronic.com

C.M. Swingen, PhD
Department of Medicine, University of Minnesota, Minneapolis, MN, USA

P.A. Iaizzo (ed.), *Handbook of Cardiac Anatomy, Physiology, and Devices*, DOI 10.1007/978-3-319-19464-6_24

excellence, other cardiac imaging modalities such as ultrasound imaging and nuclear imaging may be partially eclipsed by MRI for selected applications.

This chapter provides a condensed review of the basic principles of MRI and introduces the reader to some of the concepts and terminology necessary to understand the application of MRI to the heart. We then proceed to describe a wide range of cardiac applications of MRI, both in vivo and ex vivo, which should interest the biomedical engineer. While the capabilities of cardiac MRI are quite extensive, our choice of topics for this chapter is rather judicious, as cardiac MRI has evolved to the point where entire books are published on the subject.

24.2 Overview of MRI

MRI works using the principle of nuclear magnetic resonance. That is, in the presence of a strong magnetic field (typically 1.5–3 Tesla range for clinical systems), protons in the body are stimulated to emit radio waves. These radio waves are detected by an antenna, or coil, placed around the body region of interest and the signals are decomposed to reconstruct an image. We present a short summary of the basic concepts here and refer the reader to the overall literature for an in-depth examination.

24.2.1 Resonance

Inside the MRI scanner protons in the body align with the magnetic fields, similar to what happens to a compass needle placed in a magnetic field. These magnetic dipoles, if tipped away from the direction of the magnetic field, will precess about the direction of the static magnetic field (Fig. 24.1). This precession has a rotation frequency, ν_L, that is directly proportional to the magnetic field strength B_0. For hydrogen nuclei, the precession frequency varies with field strength as:

$$\nu_L = 42.6\left(\text{MHz / Tesla}\right)\cdot B_0\left(\text{Tesla}\right).$$

The precession frequency is also known as the *Larmor frequency*. Tipping a nuclear magnetic moment away from the direction of the z axis (B_0 direction) can be accomplished by applying an oscillating magnetic field, denoted by B_1, in a direction perpendicular to B_0. The radiofrequency transmitter should be tuned to a frequency close to the Larmor frequency to elicit a resonant excitation. After a radiofrequency excitation pulse, the static magnetic field, B_0, causes precession of the transverse magnetization component, which can be detected with an external coil as shown in Fig. 24.2. It is customary to refer to the magnetic fields which are oscillating at radiofrequencies and turned on for brief durations as *radiofrequency pulses*. A pulse that tips the magnetic moment from the z axis into the x–y plane is referred to as a *90° radiofrequency pulse*; a pulse that inverts the orientation of the magnetic moment is called a *180° or inversion pulse*. In general, the degree to which the spins are tipped into the transverse (x–y) plane is referred to the *flip angle*.

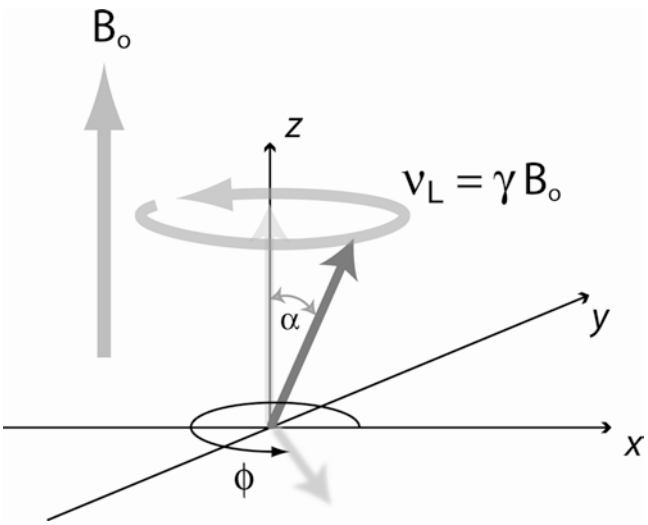

Fig. 24.1 A single magnetic dipole moment in a static magnetic field of strength, B_0. It is customary to align the z axis of a rectangular coordinate system with the direction of the externally applied static magnetic field, B_0. In this example, the magnetic moment, initially aligned with the applied magnetic field, was tipped away from the z direction by an angle α through application of an oscillating magnetic field (not shown). The oscillating magnetic field is kept on only for the time necessary to tip the magnetic dipole moment by a certain angle, α in this example. After turning the oscillating magnetic field off, the magnetic dipole moment precesses about the B_0 direction at a frequency, $\nu_L = \gamma B_0$, where γ is a constant, the gyromagnetic ratio, and represents a property of the nucleus. For ^{1}H nuclei, γ equals 42.6 MHz/Tesla. The angle ϕ denotes the phase angle of the magnetization component in the x–y plane, orthogonal to the direction of B_0

Immediately after a radiofrequency excitation, individual magnetic moments that were tipped into the transverse plane become in-phase, i.e., they have the same phase angle. If all magnetic moments were to precess at exactly the same Larmor frequency, this phase coherence would persist. Residual magnetic field inhomogeneities, magnetic dipole interactions between neighboring nuclei, molecule-specific shifts of the precession frequency, and other factors produce a distribution of Larmor frequencies. The frequency shifts relative to a reference frequency can be tissue-specific, as in the case of ^{1}H nuclei in fatty tissue. The spread of Larmor frequencies results in a slow loss of phase coherence of the transverse magnetization, i.e., the sum of all transverse magnetization components decays with time. The decay following a radiofrequency excitation is called *free induction decay*, and often has the shape of an exponential function with an exponential time constant denoted as T_2, roughly on the order of ~0.1 to ~10^2 ms for ^{1}H nuclei in biological systems. In the presence of field inhomogeneities and other

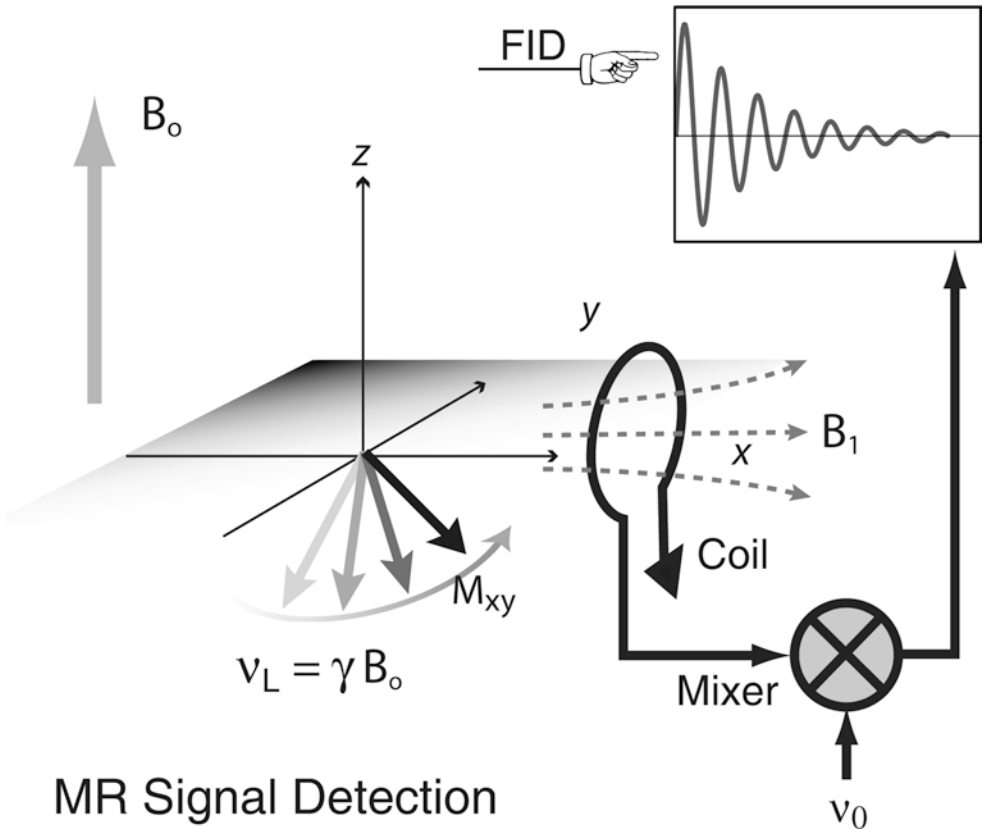

Fig. 24.2 The transverse magnetization component of a nuclear dipole precesses at the Larmor frequency, and produces an oscillating magnetic flux density that can be detected with a wire loop that is part of a resonant circuit. The induced voltage is amplified and mixed with the signal of an oscillator. The low frequency component from the mixer is a free induction decay with frequency, $\nu_L - \nu_o$. Often two coils, oriented perpendicular to each other, are used to detect the signal from the *Mx* and *My* components of the transverse magnetization, which are in quadrature, i.e., they have a relative phase difference of 90°. By detection of the quadrature components, it is possible to determine the sign of the difference $\nu_L - \nu_o$, and by combination of the two signals, after phase shifting one by 90°, one improves the signal-to-noise by a factor of $\sqrt{2}$. *FID* free induction decay, *MR* magnetic resonance

factors that cause a spread of Larmor frequencies, the transverse magnetization decay is further shortened. To distinguish this latter situation, one introduces a time constant, T_2^*, that is characteristic of the exponential decay of the transverse magnetization in "heterogenous" environments. It follows that T_2^* is always shorter than T_2.

After any radiofrequency excitation that tips the magnetization vectors away from the direction of the applied static magnetic field, B_0, the nuclear spins will, over time, realign themselves with the magnetic field to reach the same alignment as before the radiofrequency excitation. This time constant is denoted as T_1.

24.2.2 The Echo

A loss of phase coherence due to any spread in Larmor frequencies, for example, due to magnetic field inhomogeneities, can be (at least partially) reversed by applying a 180° pulse that flips the magnetization in the *x*–*y* plane such that the faster precessing spins now lag behind and the more slowly precessing spins are ahead, compared to spins precessing at the mean Larmor frequency. Once the echo amplitude peaks, the spread of Larmor frequencies again causes a loss of phase coherence. Multiple 180° pulses can be applied to repeatedly reverse the loss of phase coherence and thereby produce a train of spin echoes, referred to as *fast spin echo imaging*. The decay of the spin echo amplitudes is governed by the decay constant T_2, while a free induction decays with a characteristic time constant T_2^*, with $T_2^* < T_2$. Importantly, for cardiac imaging applications, it is useful to note that the spin echo (and spin echo trains in particular) provides a method to attenuate the signal from flowing blood, while obtaining "normal" spin echoes from stationary or slow moving tissue.

Spin echoes provide an effective means of refocusing the transverse magnetization for optimal MR signal detection. A similar, but nevertheless different, type of echo-like effect can be achieved by applying two magnetic field gradient pulses of opposite polarity instead of a 180° radiofrequency pulse. The first gradient pulse causes a rapid dephasing of the transverse magnetization; the second gradient pulse, of opposite polarity, can reverse this effect. An echo-type signal is observed, and peaks at the point where the phase wrap produced by the first pulse is . This type of echo is called a *gradient echo*.

A train of gradient echoes can be created by consecutive pairs of dephasing and rephasing gradient waveforms. The acquisition of multiple phase-encoded gradient echoes after a single radiofrequency excitation is useful for very rapid image acquisition, but is limited by the T_2^* decay of the signal.

A variation of the gradient echo technique that reestablishes phase coherence to the best possible degree before application of the next radiofrequency excitation (i.e., the next phase encoding step) can be used to produce a steady state. This allows the application of radiofrequency pulses with fairly large flip angles. Instead of relying on T_1 relaxation to return the magnetization from the transverse plane to the B_0 direction, the magnetization is toggled back and forth by the radiofrequency pulses between the z axis and the transverse plane. The attainable signal-to-noise ratio with this approach is significantly higher than with "conventional" gradient echo imaging. This type of gradient echo imaging is referred to in the literature by various acronyms—*steady-state free precession imaging*, *true FISP*, or *balanced fast field echo imaging*. In particular, for cardiac cine studies, this technique has led to a marked improvement of image quality. Steady-state free precession (SSFP) works best with very short repetition times which, in turn, impose high demands on the gradient system of the MR scanner in terms of ramping gradients up and down.

24.2.3 Image Contrast

Biological tissues and blood have approximately the same density of ^{1}H nuclei, and spin-density images show poor contrast to differentiate (e.g., tissue from blood or fat from muscle). One of the most appealing aspects of MRI is the ability to manipulate the image contrast, based on differences in the T_1 or T_2 relaxation times. For a gradient echo sequence, the T_1 weighting is determined by the combination of flip angle and repetition time. Reducing repetition time or increasing the flip angle increases the T_1 weighting in the image.

The T_2^* weighting of a gradient echo image is controlled by the time delay between the radiofrequency pulse and the center of the readout window, i.e., the echo time TE. The T_2 weighting the spin echo signal is similarly determined by the echo time. In a fast spin echo sequence, one can use multiple echoes to read out the signal with different phase encodings for each echo. Controlling the T_1 weighting through adjustment of repetition time and the flip angle imposes some limits that can be circumvented by applying an inversion pulse before the image acquisition and performing the image acquisition as rapidly as possible. The time between the inversion pulse and the start of the image acquisition controls the T_1 contrast in this case. The image acquisition after the magnetization inversion is typically performed with a gradient echo sequence that uses small flip angles, i.e., the T_1 contrast is controlled by the prepulse and the delay after the prepulse, instead of the repetition time and the flip angle, α, of the gradient echo image acquisition. Gradient echo imaging with a magnetization preparation in the form of a 180° or 90° radiofrequency pulse is often the method of choice to acquire rapidly T_1-weighted images of the heart.

MR contrast agents, such as gadolinium, provide a further means for controlling the image contrast by injecting a compound with paramagnetic ions that reduce the T_1 of blood and tissue permeated by the agent. The local T_1 reduction depends on: (1) delivery of contrast agent to the tissue region through the blood vessels; (2) the degree to which the contrast agent molecules can cross barriers such as the capillary barrier; and (3) the distribution volume of the contrast agent within the tissue. The contrast seen after the injection of such an agent can be used to determine pathology, such as the breakdown of the cardiac cell membranes and/or an above normal concentration of contrast agent in infarcted myocardium.

24.3 Cardiac MR Techniques and Applications

24.3.1 Cardiac Morphology

The accurate depiction of cardiac morphology is important in most imaging applications. Numerous MR techniques have been developed and they are generally categorized based on the appearance of the intracardiac blood in the image, as either *black-blood* or *bright-blood* techniques.

Spin-echo (SE) was the first sequence used for the evaluation of cardiac morphology, however it was not until the advent of ECG-gating that SE imaging became substantially more important by reducing motion artifacts associated with the beating heart. SE images are called *black-blood* images due to the signal void created by flowing blood, which provides very good contrast between the myocardium and the blood. Slower moving blood, particularly adjacent to the ventricular walls, however, can cause the blood signal to appear brighter, effectively reducing the quality of the image. So, presaturating with a radiofrequency pulse and reducing the echo time (TE) is used to minimize the blood signal and increase the contrast in the image [1]. Although widely available, SE imaging is limited due to its poor temporal resolution and susceptibility to respiratory and other motion artifacts. Nevertheless, these problems have been overcome through the development of sequences with shorter acquisition times, so-called fast (or turbo) SE pulse sequences. Although soft tissue contrast is not as optimal, these sequences have become the frontline sequence for depiction of cardiac morphology (Fig. 24.3).

24.3.2 Global Cardiac Function

Global and regional assessments of ventricular function with MRI are very well established and have been shown to be accurate and reproducible compared with other imaging modalities for the calculation of volume, mass, and derived

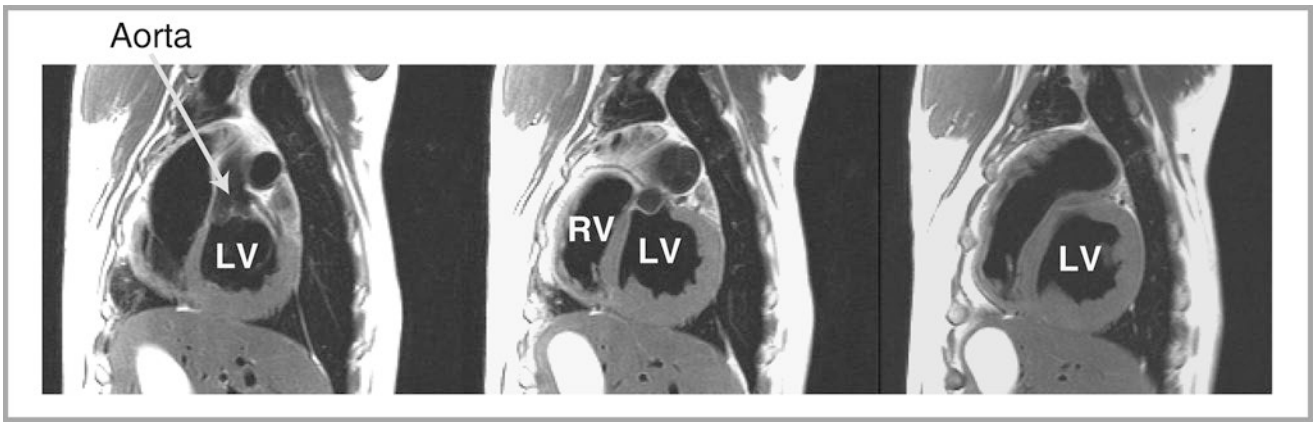

Fig. 24.3 Cardiac anatomy of a canine heart imaged with a *T2-weighted* fast spin echo sequence and in-plane resolution of 1.2 mm. Cardiac structures such as the left ventricle (*LV*), right ventricle (*RV*), and aorta are labeled. The signal from blood in the ventricular cavities was nulled by a magnetization preparation consisting of radiofrequency inversion pulses. Furthermore, the use of an echo train (with seven spin echoes in this case) and a long effective echo time also causes attenuation of the signal from moving blood. These so-called *black-blood* imaging techniques are very useful for anatomical imaging to avoid image artifacts from flowing blood

parameters such as stroke volume and ejection fraction [2, 3]. Thus, it is now considered the gold standard for the evaluation of cardiac function and mass in numerous studies comparing different imaging modalities [4].

Cine loops are acquired to follow the changes in ventricular dimensions over the entire cardiac cycle and thus to assess cardiac function. The acquisition of each image in the cine loop is broken up into several "segments," and the image segments are acquired over consecutive heart beats, as shown in Fig. 24.4. The acquisition of such image segments for each cardiac phase is subsequently synchronized with the heart cycle by gating of the encoding steps with the patient's electrocardiogram. This technique works well as long as the subject has a regular heart beat. The final result of the segmented acquisition is a series of images, one for each phase of the cardiac cycle. These images can be played as a cine loop, e.g., to assess ventricular function. To increase the sharpness of the quality of images, clinicians ask patients to hold their breath during image acquisition. The segmented data acquisition approach always involves a tradeoff between temporal resolution (i.e., number of frames covering one R-to-R interval) and spatial resolution, as the image acquisition needs to be performed within a time short enough to allow for suspended breathing.

Typically, for the measurement of global cardiac function, *bright-blood cine MRI* is performed in multiple short-axis views, covering the heart from base to apex, using a multiphase, segmented *k*-space, *gradient echo* (GRE) sequence [5–7]. Yet to date, GRE studies have suffered due to saturation effects in areas of low blood velocity, causing reduced contrast between blood and myocardium within the ventricular cavity [8]. In general, this problem causes difficulties in detection of the endocardial border, most dramatically in long-axis views of the heart where there is very minimal motion of blood through the imaging plane, as the majority of blood is moving within the image plane in these views as shown in Fig. 24.5A. Such problems associated with GRE cine imaging have recently been minimized with the advent of SSFP sequences (Fig. 24.5).

Although the concept of SSFP imaging has been described in the literature for many years, only recently has MR hardware developed to the point that these techniques have become practical and available on clinical scanners (e.g., those from multiple vendors) [9, 10]. SSFP sequences have dramatically improved contrast-to-noise, shortened acquisition times, and increased both spatial and temporal resolution in comparison with previous GRE techniques [2, 11, 12]. These improvements have enhanced the detection of the epicardial and endocardial surfaces (delineation of trabeculation and papillary muscle), both manually and with automated detection schemes, resulting in improved accuracy and reproducibility for the quantification of cardiac mass and volumes [13, 14]. Scan times have been reduced as well, such that SSFP sequences for an entire 3D data set covering the heart can be acquired within a single breath-hold.

SSFP techniques are also employed in the emerging area of real-time MR imaging. Recently, real-time imaging techniques have been developed and improved such that they will be employed in future cardiac function studies, as well as in the emerging field of interventional imaging with MRI. These real-time sequences continuously acquire images of the heart with sufficiently high temporal resolution similar to fluoroscopy [15] without the need for ECG triggering or breath-holding, therefore making it possible to image patients with severe arrhythmias or heart disease. In the past, these were difficult requirements to fulfill with segmented *k*-space GRE or SSFP sequences. Furthermore, newly developed sequences implementing image reconstruction techniques with sensitivity encoding (SENSE) and simultaneous acquisition of spatial harmonics (SMASH) have reported imaging temporal resolutions down to 13 ms with a spatial resolution of 4.1 mm [16].

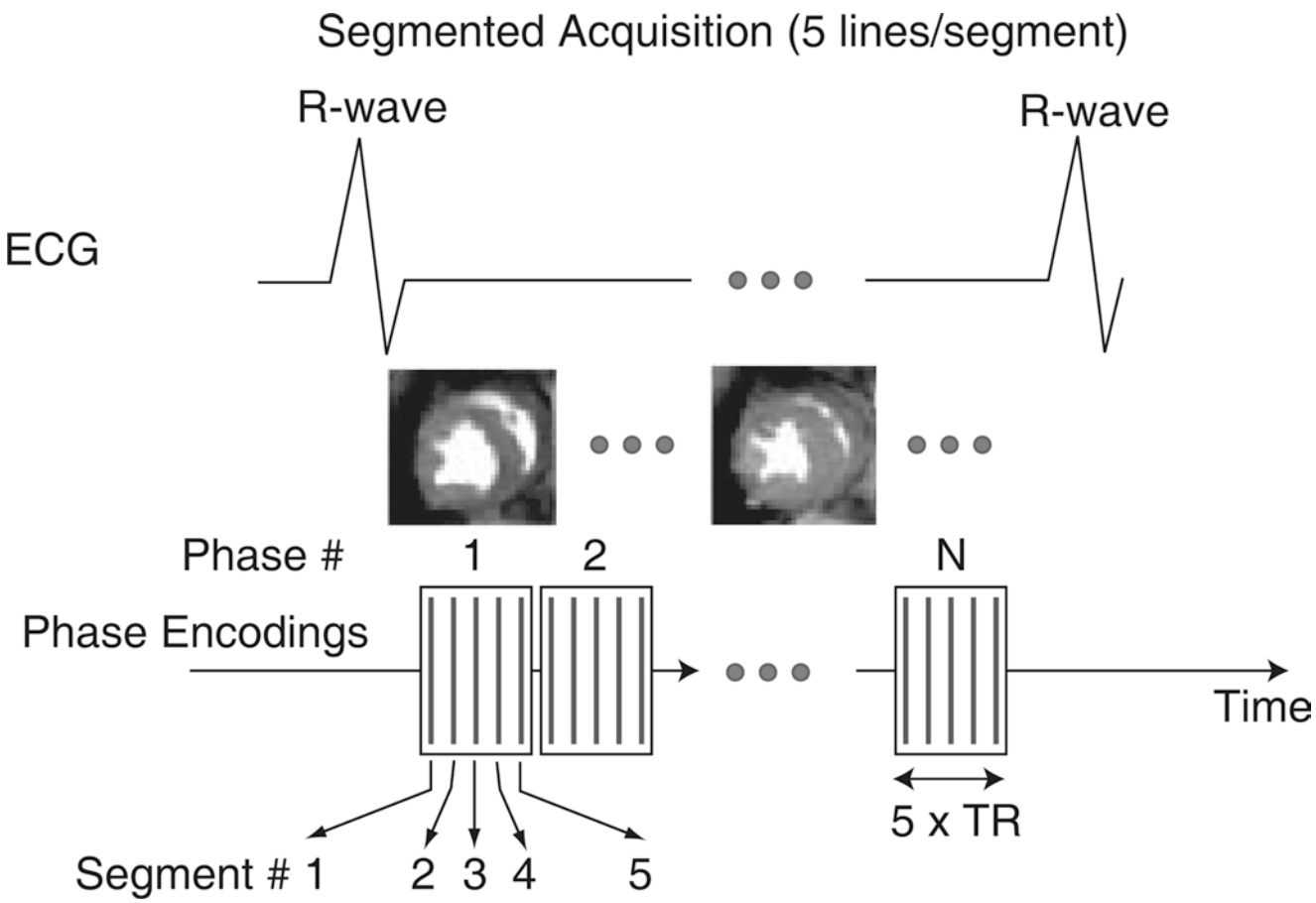

Fig. 24.4 Illustration of the principle of segmented acquisition of data, as that used for imaging multiple phases of the cardiac cycle in ventricular function studies. The image acquisition is synchronized to the cardiac cycle by triggering of the pulse sequence with the R-wave on the ECG. The total number of phase encodings is split into five groups or segments in this example. The same five phase encodings are performed during each phase of one cardiac cycle. During the next R-to-R interval, five other phase encodings are performed for each cardiac phase. The R-wave-triggered acquisition of phase encodings is repeated k number of times to obtain a total of $k \cdot 5$ phase encodings. The temporal extent of each cardiac phase is shown in the diagram by the *boxes* that contain the symbolic representations of the phase-encoded lines as *vertical lines*. The temporal resolution (TR) of the resulting cine loop is determined by the number of lines per segment (five in this example) and the repetition time for each phase encoding step. Typical resolutions are on the order of 40–50 ms for resting heart rates, and higher during inotropic stimulation of the patient's heart. The image acquisition is performed while the patient holds his/her breath. In this example the required duration of the breath-hold would be k heart beats, with k typically on the order of 10–20, depending on the heart rate

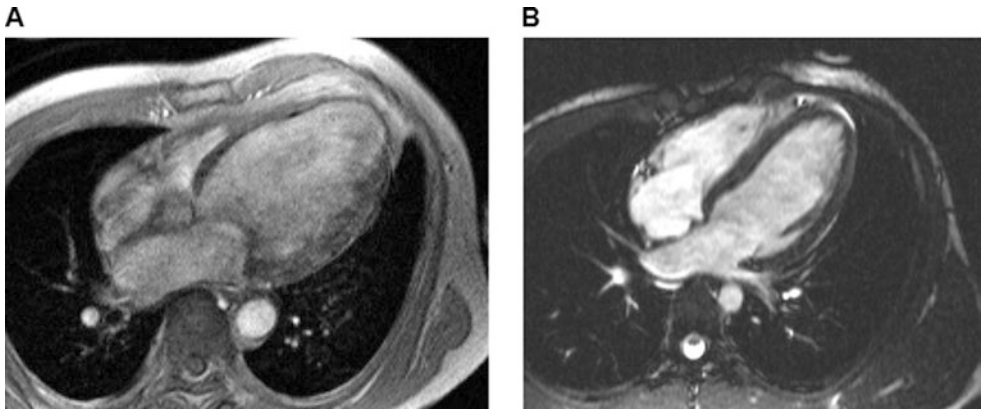

Fig. 24.5 Comparison of end-diastolic long-axis views acquired with a segmented gradient echo sequence (*left*) and a steady-state free precession (*SSFP*) sequence (*right*). The SSFP technique provides significantly higher contrast to noise between intraventricular blood and myocardium, resulting in improved endocardial border definition throughout the cardiac cycle, as compared with the older gradient echo sequence

24.3.3 Regional Myocardial Function

Ventricular volumes and derived parameters such as stroke volume and ejection fraction are the most commonly used variables for the assessment of systolic function in the clinical setting, however they have associated limitations related to the measurement of contractile properties of the heart. Furthermore, these descriptors of cardiac performance do not take into consideration the importance of regional contractile dysfunction, the degree and extent of which are important prognostic factors with ischemic heart disease, and/or following myocardial infarction [17–19]. It is generally accepted that quantitative estimates of wall motion and relative changes in wall thickening (expressed as % of end-diastolic wall thickness) are useful for measuring regional function and are also more precise than the subjective visual wall motion scoring system which is commonly used in the clinic today [20, 21]. Wall motion changes and thickening are usually measured along the length of a center line between the segmented endocardial and epicardial borders of the heart. They are further divided into myocardial segments of equal circumferential extent which are positioned relative to the location of an anatomical landmark such as the anterior-septal junction of the left ventricle and right ventricle. Dynamic changes in wall thickening can be considered as the radial component of myocardial strain, defined as the percent change in dimension from a resting state. Such strain analyses have proven very useful for the assessment of regional contractile function in both animals and human patients [22–24].

Circumferential shortening and radial thickening are two components of myocardial strain typically assessed by MRI tagging [25–29]. This approach has a higher sensitivity to the identification of noncontracting regions of the myocardium compared to "conventional" cine MRI. As such, cine imaging of the heart can be combined with a series of magnetization preparation pulses that null the longitudinal magnetization along thin parallel stripes in the slice plane. The stripes or tags appear as black lines on the MR images and can be applied in two directions in a single slice, forming a grid pattern. This grid pattern is created immediately after the R-wave of the EKG and before acquisition of the segmented phase encodings (Fig. 24.4). The grid tags visible in the resulting images are "imbedded" in the tissue and are therefore distorted if any myocardial motion occurs. Thus, intramyocardial displacements and myocardial strain can be tracked through monitoring visible motion and deformation of the tag lines, respectively. Figure 24.6 shows an example of a myocardial grid pattern laid down at end-diastole and, in a second frame, the same pattern is recorded at end-systole with evident distortion of the tag lines due to myocardial contraction. The tag lines, created right after the R-wave, tend to fade during the cardiac cycle due to T_1 relaxation, but for normal resting heart rates (e.g., 60–70 beats/min) the tag lines can persist long enough to allow visualization of cardiac motion over nearly the entire R-to-R interval. Importantly, tag lines in the ventricular blood pool disappear very quickly because of the rapid motion and mixing of blood in the ventricle; this effect is then useful for clearly defining the endocardial borders.

24.3.4 Myocardial Perfusion

Myocardial blood flow is assessed using very rapid MR imaging of the heart during the first passage of an administered contrast agent through the heart. T_1 changes in the myocardium are directly proportional to the contrast agent concentration in the blood or tissue [30, 31], so that through the use of T_1-weighted imaging techniques, myocardial territories affected by a coronary artery lesion can be both qualitatively and quantitatively evaluated. Furthermore, the myocardial territory affected by a coronary artery lesion may or may not show a perfusion deficit under resting conditions; however, during an imposed pharmacological stress, a stenotic vessel cannot respond (dilate) like a healthy vessel resulting in *vascular steal*, a phenomenon in which increased blood flow to the myocardium is supplied by nonstenotic vessels [32]. Consequently, the relative blood flow is reduced through stenotic vessels resulting in a detectable perfusion deficit in the images; as such, both areas of reversible and nonreversible (scar) defects can be represented [33].

First pass perfusion imaging in typically performed using multislice fast gradient-echo imaging with saturation-recovery magnetization preparation obtained during the rapid administration (7 ml/s) of a small contrast agent dose (approximately 0.04 mmol/kg for the extracellular gadolinium agent Gd-DTPA). A saturation-recovery magnetization preparation consists of a nonslice selective 90° radiofrequency pulse, followed by a gradient crusher pulse designed to dephase the transverse component of the magnetization [34]. This preparation drives the magnetization into a well-defined state, permitting the acquisition of a T_1-weighted GRE signal that is independent of the properties of any previous relaxation delay, thus preventing fluctuations in the image signal intensities due to variations in the heart rate or ECG trace. Nevertheless, imaging is typically performed throughout the duration of 40–50 heart beats to adequately capture the first pass of the injected contrast agent through the heart. With currently employed clinical 1.5 Tesla MRI scanners (with state-of-the-art gradient coils and amplifiers producing gradient field amplitudes of 20–40 mT/m with slew rates up to 150 mT/m/s), this imaging can be done in approximately 3–4 slices for every heart beat, with an in-plane image resolution of 2 mm or better.

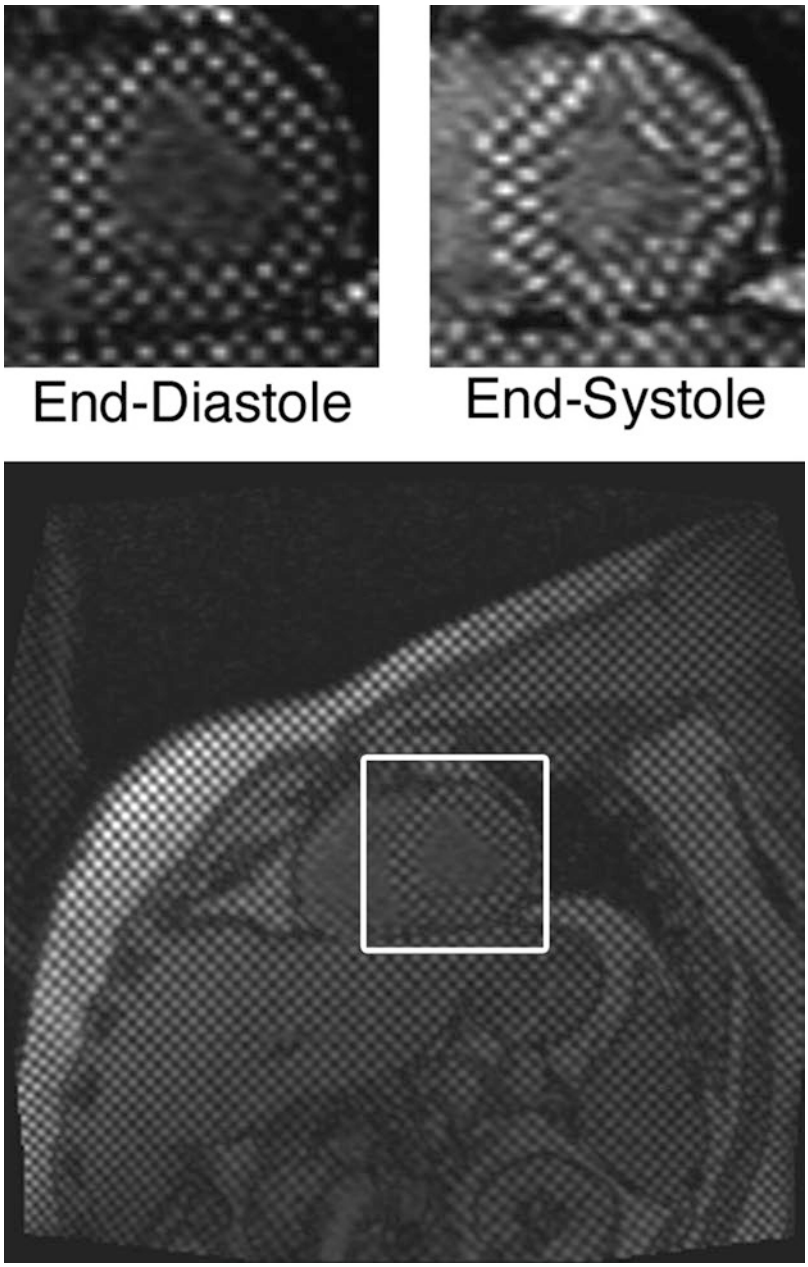

Fig. 24.6 Images with spatial modulation of magnetization in the form of vertical and horizontal stripes in a human volunteer. The grid-tag lines spaced 6 mm apart were created immediately after the R-wave of the ECG. The *upper left panel* shows a magnified view of the heart during this initial phase. A second image is shown on the *upper right* for an end-systolic phase, with the distortion of the tag lines due to cardiac contraction clearly apparent. The tagging technique is equivalent to the implantation of intramyocardial markers. Tracking of the tag lines over the cardiac cycle allows determination of myocardial strains, and has been shown to provide a sensitive method for assessing regional wall motion abnormalities

Qualitative analyses of perfusion studies can be made by viewing the sequence of images as a movie loop, and then visually grading the rate of contrast enhancement in myocardial segments. However, qualitative assessments are highly observer-dependent and thus are also subjective to misinterpretation based on image artifacts or variations in the image brightness due to the inhomogeneous detection of the MR signal by the surface coils. Therefore, in the future, a more quantitative technique based on the time course of signal intensity in the different myocardial segments of interest can provide an objective and robust method of analysis (Fig. 24.7).

24.3.5 Myocardial Viability

The ability to distinguish nonviable myocardium is of critical importance in the management of patients with both acute and chronic coronary artery disease syndromes, yet this is complicated by the presence of reversibly damaged and infarcted myocardium. Until very recently, thalium single proton emission computed tomography (SPECT) and positron emission tomography (PET) were the primary tools for evaluation of myocardial viability. However, with the development of delayed contrast-enhanced MRI (ce-MRI), the cardiac MRI method has quite dramatically and rapidly

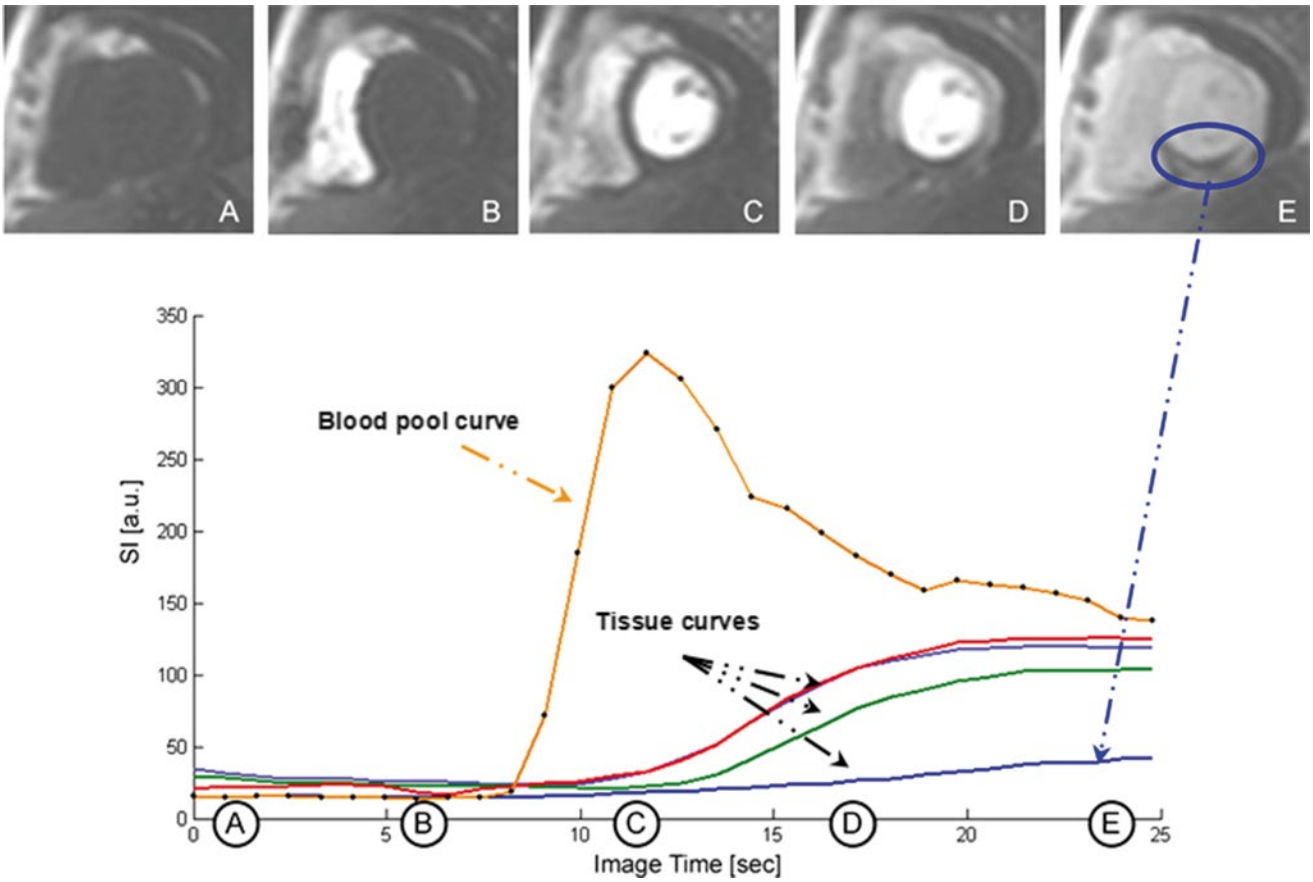

Fig. 24.7 A sample of images acquired using a fast T_1-weighted gradient echo sequence during a bolus injection of 0.04 mmol/kg of the extracellular contrast agent Gd-DTPA is shown, with the resulting signal intensity curves for the left ventricular blood pool and several myocardial segments below. The first image in the series (*A*) shows a short-axis image of the heart prior to injection of the contrast agent. Following injection, the contrast agent quickly enters the right ventricle (*B*) and left ventricle (*C*) and then passes through the coronary and microcirculation (*D*, *E*) causing signal enhancement throughout the myocardium. This example shows a clear perfusion defect in the inferior wall of the left ventricle which can be seen in images *D* and *E* (*circled*) and also the corresponding tissue curve immediately following the first pass of the contrast through the left ventricle

ascended into the forefront of viability imaging [35, 36]. In general, this technique has been shown to identify irreversibly damaged myocardium in both acute and chronic settings following a myocardial infarction and, in tandem with cine imaging, can be used to consistently predict reversibly damaged tissue that may benefit from revascularization and/or other therapies [37, 38]. Furthermore, with the availability of substantially higher spatial resolution than nuclear techniques, ce-MRI can detail the transmural extent of irreversibly damaged tissue and detect both small and large subendocardial defects not identified by either SPECT or PET [39, 40].

So-called *delayed ce-MRI* is performed following the intravenous administration of a gadolinium-chelate contrast agent; typical dosages for imaging viability are on the order of 0.1–0.2 mmol/kg. The contrast agents more readily cross the cell membrane due to the severe myocardial injury and loss of viability [33, 35, 41, 42]. After an appropriate delay (approximately 10–15 min), the contrast agent achieves approximate distribution equilibrium, and loss of functional viability and subsequent leakage of contrast agent result in T_1-weighted signal enhancement because the distribution volume of the contrast agent is larger in the injured tissue compared to normal. Such imaging is typically performed under resting conditions using a breath-hold "inversion recovery" prepared and T_1-weighted segmented GRE sequence. The appropriate inversion delay time following the inversion pulse (approximately 250 ms or less) results in signal nulling of viable myocardium. Note that, for the best results, appropriate inversion delay times are iteratively chosen for each patient. This results in images where the normal viable myocardium is dark, nonviable, fibrotic, or scarred tissue has dramatically increased (hyperenhanced) signal intensity (Fig. 24.8). Typically, one or two signal averages are

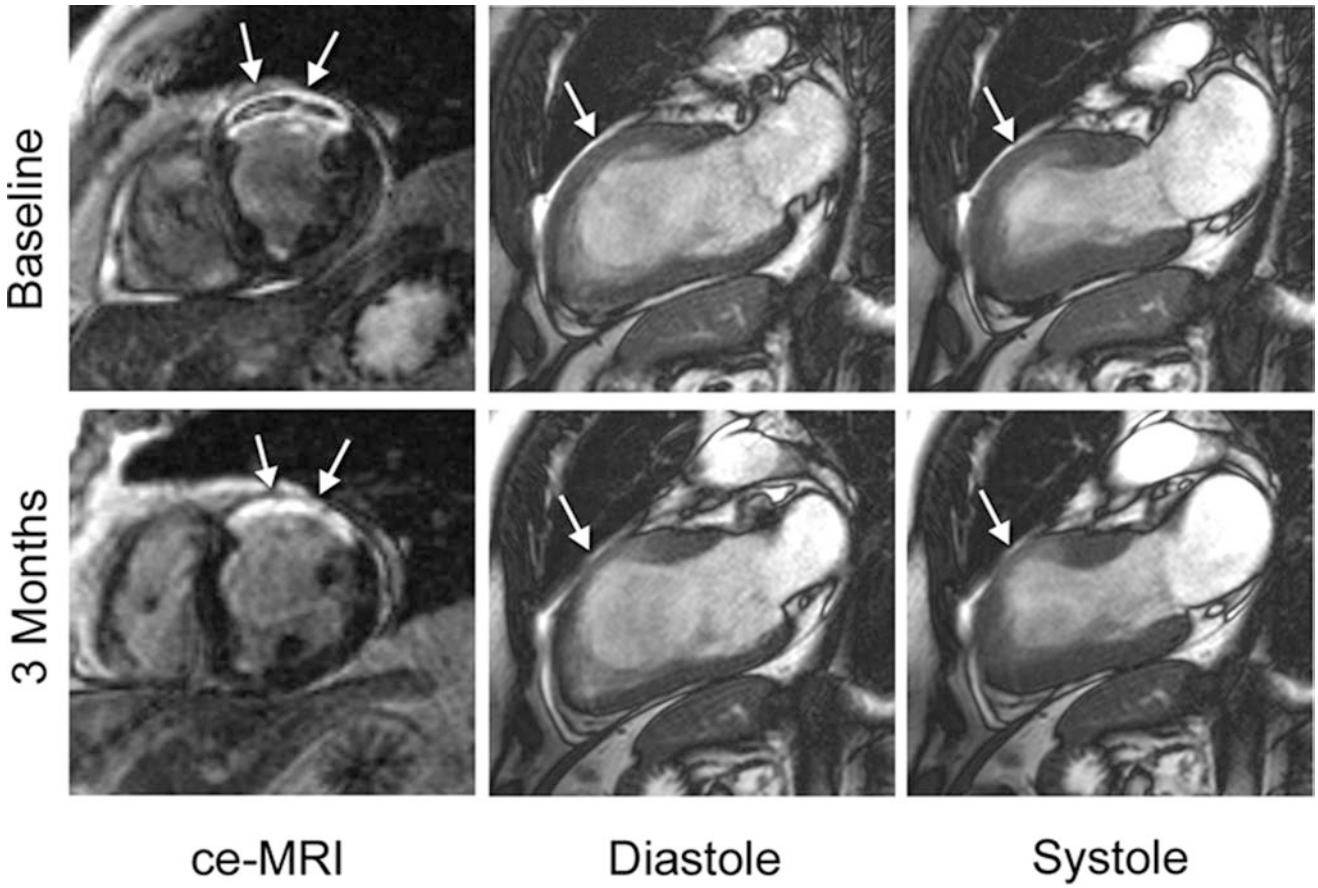

Fig. 24.8 Example of an initial and follow-up MRI exam comparing the region of infarction (*arrows*) with wall thickness and contractility. The acute study at 2 days (*top*) shows evidence of microvascular obstruction within the infarct and reduced wall thickening in the anterior region, shown here by long-axis cine images. During the 3-month study (*bottom*), there is no longer a sign of microvascular obstruction within the infarct territory, diastolic wall thickness has decreased, and contractility has improved in regions adjacent to the infarcted territory

used with an in-plane image resolution of approximately 1.5 mm; this approach as a 2D sequence requires multiple breath-holds to encompass the left ventricle and can be typically accomplished in less than 10 min. In addition, 3D approaches can also be used which cover the entire ventricle in a single, yet longer breath-hold with comparable, but not as good, image quality.

While the delayed ce-MRI sequence is the most widely accepted approach for viability imaging with MRI, there are other less popular techniques that should be mentioned (e.g., imaging with the use of a manganese-based contrast agent). Manganese is a Ca^{++} analog which is actively taken up by viable cells, thus in obtaining T_1-weighted images, viable tissue is enhanced (bright) while nonviable tissue remains dark [43]. Manganese contrast agents are not currently being used in clinical cardiac imaging; however, this may provide an effective alternative method in the near future. MRI of sodium or potassium are also effective methods with potential for imaging viability, but their use remains strictly a research tool due to the very limited availability of multifrequency MRI scanners for clinical use [44].

24.3.6 Blood Flow Velocity

A recorded MR signal can be represented in terms of a magnitude and a phase component. As such, MRI images can be analyzed to elicit the spatial variations of the signal magnitude, but it is also possible to create maps showing the spatial variations of the signal phases. Furthermore, it has been shown that the phase of the signal is sensitive to the velocity of tissue or blood. The so-called phase *contrast MRI technique* uses the phases of the signals to measure relative velocities. For an in-depth discussion of these methodologies, we refer the reader to the literature. Yet, an example of a phase contrast flow velocity measurement in an aorta is shown in Fig. 24.9, which has been used to calculate pulse wave velocities for measuring vessel stiffness [45].

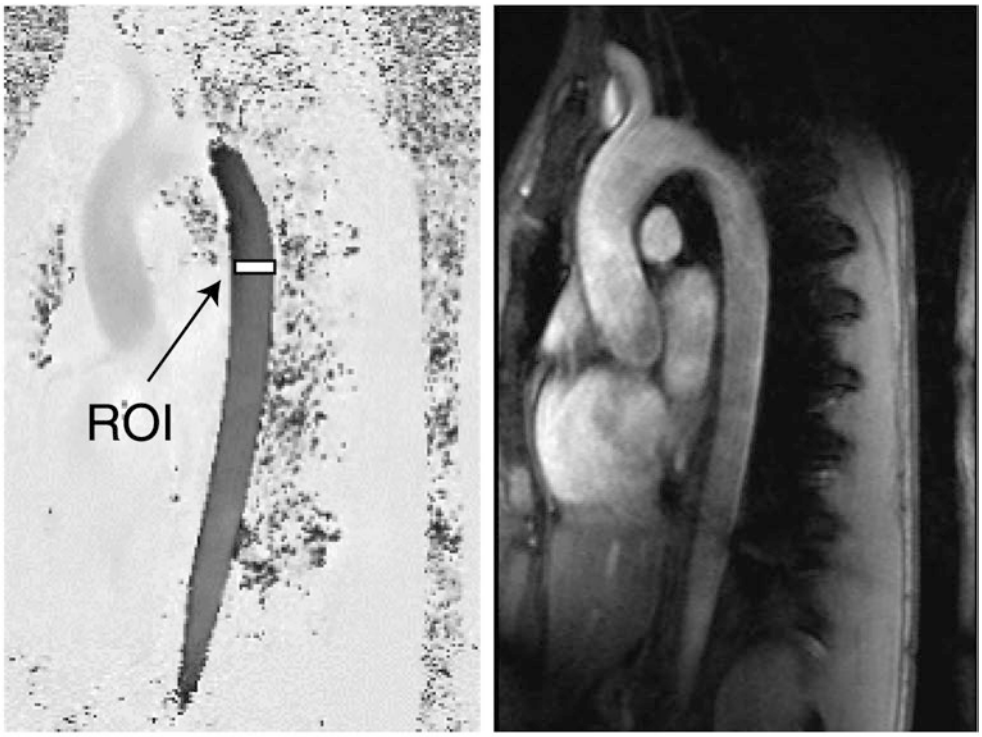

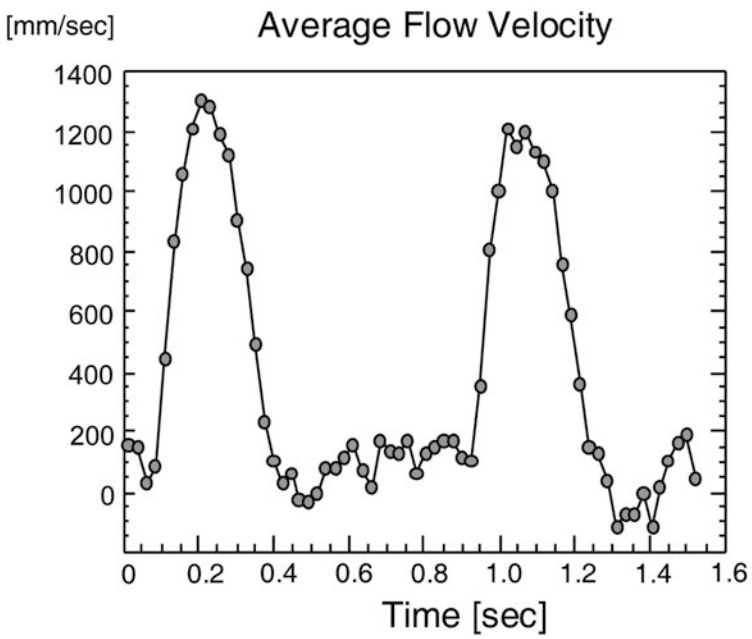

Fig. 24.9 Phase contrast imaging of the aorta in a human volunteer. Both the magnitude and phase images are shown. Images were acquired for X cardiac phases, covering approximately 2.5 heart beats. A region of interest (*white box*) was placed on the phase images in the thoracic aorta to determine the variation of flow velocity in the vertical direction of the image plane. The variation of the velocity is shown in the graph. *ROI* region of interest

24.3.7 Fiber Structure

24.3.7.1 Importance of Myofiber Orientation

The analysis of myocardial microstructure continues to be considered an important factor in better understanding underlying pathologies and/or associated arrhythmias. This is due to the fact that structural fiber arrangement is modified over the time course of various cardiomyopathies. In the healthy heart, it is generally accepted that cardiac muscle fibers or myofibers are arranged as counter-wound helices encircling the ventricular cavities and where fiber orientation is a function of their transmural location [46–48]. Further, myofibers are predominantly organized in the base–apex direction at the epicardial and endocardial surfaces, and rotate to a circumferential direction in the mid-wall. This counter-wound helical structure is considered to be respon-

sible for the torsional or wringing motion of the left ventricle which serves three main mechanical functions: (1) equalizing myofiber strain and workload; (2) optimizing the volume of blood ejected during systole (stroke volume); and (3) storing torsional energy in the intracellular and extracellular matrix, and when released, increasing ventricular filling during diastole [49–56]. Therefore, cardiac fiber orientation can also be considered as one of the primary determinants of ventricular pump function.

24.3.7.2 Quantifying Fiber Structure with Diffusion Tensor MRI

More recently, *diffusion tensor MRI* (DTMRI) has been developed and employed as a nondestructive means to quantify 3D ventricular fiber orientation [46, 57–60]. The underlying principle in determining cardiac fiber orientation by DTMRI is that the fastest direction of water diffusion corresponds to the local myofiber orientation. Therefore, by obtaining a series of diffusion-weighted images, the effective diffusion tensor of water in the myocardium can be estimated using a relationship between the measured echo attenuation in each imaging voxel and the applied diffusion sensitizing gradient [61]. As such, diffusion-weighted pulse sequences are designed such that molecular displacements in the direction of the applied diffusion sensitizing gradients will attenuate the echo signal, thus enabling the estimation of water diffusivity in a given direction. The strength of the diffusion weighting or *b*-value usually ranges from 500 to 1500 s/mm^2 in cardiac DTMRI. The diffusion tensor, which is a symmetric 3×3 second rank tensor, is determined for each imaging voxel and represents the net 3D diffusion in the tissue. In order to determine the required six independent parameters of the diffusion tensor, at least seven images must be obtained for a given slice—six diffusion-weighted images applied in six noncolinear directions and one diffusion-independent image. However, it is also common to estimate the diffusion tensor by obtaining many diffusion-weighted images varying in direction (12–16 directions) and *b*-value, where the best fit for the diffusion tensor can be determined using multilinear regression. Nevertheless, ventricular fiber orientation can be obtained with DTMRI due to the anisotropic nature of water diffusion in the myocardium [62]. The fastest direction of diffusion or primary eigenvector of diffusion has been validated to coincide with the local longitudinal myofiber orientation, as water diffusion in the cross fiber directions is restricted by the cellular borders and laminar sheets in the myocardium [63, 64]. Note that the secondary and tertiary eigenvectors of diffusion correlate with the laminar sheet direction and sheet normal, respectively [58, 65, 66].

From a research perspective, it is also interesting to note that DTMRI can be used to obtain fiber orientation both in vivo or ex vivo [67, 68]. In addition, it has been shown that DTMRI can successfully be performed on isolated human hearts if collected within 3 days postmortem from the donor [69]. Currently, cardiac DTMRI is primarily used as a research tool, and is not a routinely employed cardiac MR protocol in a clinical setting. Today, this imaging technique does not contribute to the diagnosis of cardiomyopathies, or provide information that can be used to determine patient treatment options. However, in concert with myocardial tagging, in vivo DTMRI does provide valuable insights into the myofiber structure–function relationship in the ventricles in both normal and diseased states as discussed in Sect. 24.3.7.3. In general, the spatial resolution of diffusion imaging is dependent on the diffusion sensitizing pulse sequence and magnetic strength of the scanner. For example, for in vivo diffusion imaging of large mammalian hearts in a 1.5 Tesla magnetic field, a spatial resolution of approximately $3\times3\times3$ mm can be expected [70]. For ex vivo diffusion imaging with high field MRI scanners (3–9.4 Tesla), a spatial resolution less than $1\times1\times1$ mm can easily be obtained. An example of ex vivo DTMRI of a freshly cardiopleged and isolated human heart is shown in Fig. 24.10. The raw diffusion images are shown along with the fiber orientation projected into the imaging plane as determined by the primary eigenvector of diffusion for a mid-ventricular slice. Furthermore, Fig. 24.11 shows a 2D contour plot of the fiber inclination angle α of a healthy human heart fixed directly postmortem using the methodologies described in Eggen et al. [69].

24.3.7.3 Pathological Changes in Fiber Structure

It was reported that by using cardiac DTMRI in conjunction with phase contrast strain-rate imaging, Tseng et al. were able to determine that a state of fiber disarray exists in hypertrophic cardiomyopathy which results in a disordered pattern of principle myocardial shortening. In the same study, these investigators observed that a positive correlation exists between fiber disarray and myocardial hypokinesis [70]. Additionally, several studies have attempted to quantify cardiac fiber architectural remodeling after the occurrence of myocardial infarction [71, 72]. In these reports, fiber disarrays and increases in diffusivity were evident in the infarcted regions; this was considered to be consistent with abnormal wall motion and/or cell death. More recently cardiac DTMRI has played a key role in developing computational approaches to investigating the electromechanics of healthy and diseased hearts, which are becoming necessary for the comprehensive understanding of cardiac function [73]. Such sophisticated models have provided important insights into arrhythmia induction in peri-infarct zones surrounding necrotic scar in chronically infarcted canine hearts [74].

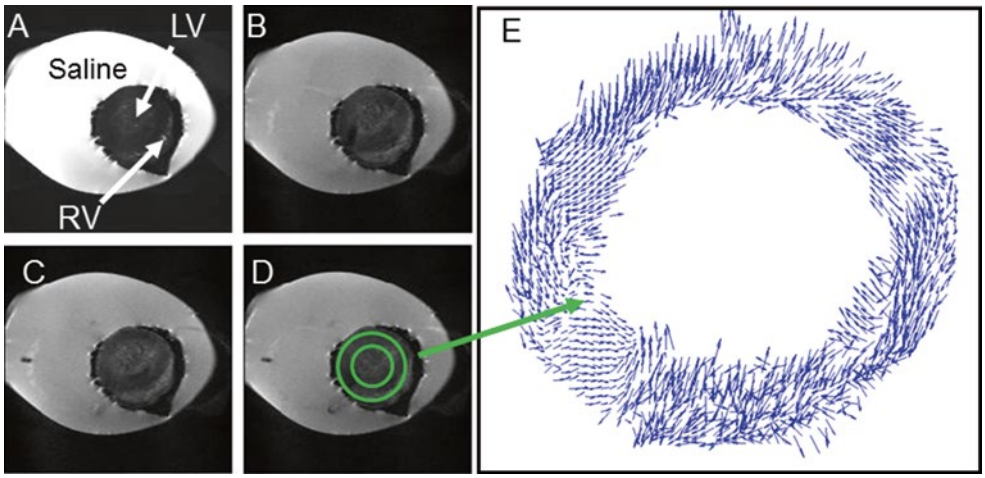

Fig. 24.10 Diffusion tensor MRI imaging of a freshly excised normal human heart. The unfixed heart was submerged in saline and all air was removed prior to imaging. For the determination of cardiac fiber orientation, six diffusion-weighted images were acquired with one nondiffusion-weighted image (**A**) at the mid-ventricular level. Three diffusion-weighted images are shown (**B**–**D**) acquired with diffusion gradients applied in three orthogonal directions. The left ventricular fiber orientation is projected onto the imaging plane (**E**) as determined by the primary eigenvector of diffusion or direction of fastest diffusion. Imaging parameters were as follows: field of view = 180 × 180 mm, matrix = 196 × 196, and in-plane spatial resolution = 0.9 × 0.9 mm, *b*-value = 1000 s/mm^2; the slice thickness was 3 mm. *LV* left ventricle, *RV* right ventricle

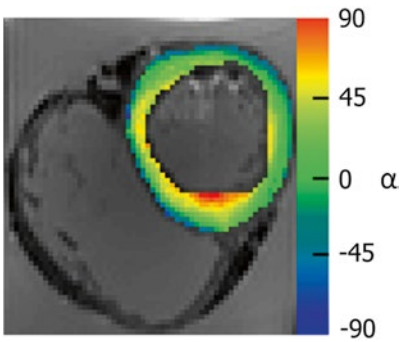

Fig. 24.11 2D contour plot of the fiber inclination angle α in a healthy human heart fixed directly postmortem. The short-axis image was obtained from the mid-level of the left ventricle

24.4 MRI and Biomedical Devices

24.4.1 Real-Time Imaging and Cardiovascular Interventions

To date, X-ray-based fluoroscopic techniques have been the gold standard for most invasive diagnostic and/or therapeutic applications relative to the heart. However, with the advent of ultrafast MRI and the development of MRI-compatible catheters and guide wires, the goal of achieving real-time guidance by MRI for cardiovascular interventions is emerging as a new alternative [75]. More specifically, the use of MRI for guided interventions would minimize or even eliminate reliance on ionizing radiation and iodinated contrast agents, an advantage particularly for pediatric patients. To date, continuous improvements of MRI techniques and MRI scanner hardware have rendered it feasible to achieve the relative clinical fluoroscopic image rates of 5–15 images/s [76]. Thus, it is considered highly probable to use MRI for guiding interventional cardiovascular procedures, such as coronary catheterization [77] and cell or gene therapy delivery [15], with close to real-time image refresh rates. Initial interventional studies with MRI guidance have demonstrated the advantages of MRI, including: (1) the ability to image arbitrarily oriented cross-sections; (2) interactive steering of the image plane; and (3) excellent soft tissue contrast for the detection and visualization of lesions [78].

Several other technical advances have also been considered as crucial for advancing the possibility of performing interventional procedures under MRI guidance, including: (1) development of 1.5 Tesla magnets with short bores that allow access to the groin area for catheter-based procedures; (2) LCD monitors that can be exposed to high magnetic fields to allow the operator to perform an intervention and control MRI scan parameters from a position right next to the magnet; and (3) development of catheter-based MRI antennae for localized intravascular signal reception and high-resolution imaging [79].

For MRI-guided cardiac interventions, one of the basic requirements is to visualize and track the catheters and devices used in the therapies while they are manipulated through the heart and vascular spaces [80]. In general, catheter tracking techniques can be divided into two categories—active and passive. Active tracking of catheters and devices requires the instrument to receive or send a signal in order to

identify its relative location. For example, a receiving coil can be incorporated into the device and thus connected to the scanner such that the position can be located based on the frequency of the received signal from the body coil. MRI-guided active catheter tracking used for real-time 3D intracardiac navigation, mapping, and ablation has been successfully demonstrated in work by Gaspar et al. [81]. Passive tracking of catheters involves creating a signal void without interfering with the image quality of the tissue being imaged. This latter method can be achieved through the choice of materials incorporated into the catheter or device. For example, small amounts of titanium, gold, or copper can be deposited into the catheter tip in order to introduce a susceptibility artifact such that the tip of the catheter can be continuously tracked. The details of one passive design of a deflectable guiding catheter constructed from nitinol and Kevlar is further described in Bell et al. [82].

A recent development in the emerging field of MRI-guided cardiac interventions is the real-time delivery of transcatheter valves. Recently, McVeigh et al. demonstrated that a transcatheter bioprosthetic aortic valve could be delivered via a direct approach through the left ventricular apex in approximately 90 s with real-time interactive MRI guidance [83]. Importantly, immediately after the procedure, myocardial perfusion, blood flow through the valve, and ventricular function were assessed with MRI in order to verify proper placement of the valve. It is considered that this minimally invasive MRI-guided aortic valve replacement technique may prove to be a less morbid approach than conventional valve replacement surgeries, and thus may have added benefits for the very ill and/or elderly patient population. Research in swine has also proven the feasibility of a transarterial aortic valve implantation using a commercially released valve (CoreValve®, Medtronic, Minneapolis, MN, USA) and a modified delivery system [84].

To date, other reported MRI-guided cardiac interventions and applications include, but are not limited to [80, 85]: (1) diagnostic cardiac catheterization; (2) electrophysiological recording/radiofrequency ablation [81, 86]; (3) balloon dilation and stent placement [87]; and (4) atrial septal defect closure. For an in-depth discussion of the advantages and difficulties associated with these MRI-guided cardiac interventions, we refer the reader to the growing body of related literature (see also Chaps. 32 and 36).

24.4.2 MR-Conditional Implantable Devices and Nomenclature

Today, most implantable cardiac devices contain metallic parts that can interfere with MR cardiac imaging and/or pose potential safety risks for the patient. Such potential interactions can include mechanical effects from the static magnetic field that could cause movement or dislodgement of an implanted device, or device heating due to the RF field and gradient magnetic field. For example, when scanning patients with cardiovascular implantable electronic devices (CIEDs) such as pacemakers or implantable cardioverter-defibrillators (ICDs), there is a potential risk of increasing the pacing threshold because of lead tip heating, due to the RF and gradient magnetic field. Even though there are potential risks of scanning patients with such devices, it can still be permissible to conduct an MRI scan under certain conditions. Importantly, implantable devices with demonstrated safety in the MR environment within defined conditions are referred to as *MR-conditional*, whereas devices that pose no known hazards resulting from exposure to any MR environment are termed *MR-safe* [88]. An MR-safe item is typically composed entirely of electrically nonconductive, nonmetallic, and nonmagnetic materials; most cardiac implantable devices do not fall into this category. Lastly, devices which pose unacceptable risks to the patient, medical staff, or other persons within the MR environment are termed *MR-unsafe*.

Until recently, CIEDs such as pacemakers or ICDs were a strict contraindication to MRI. The potential interactions of a CIED with the MR environment include, but are not limited to [89]

- Mechanical movement of the device or lead dislodgment (static magnetic field interaction)
- Lead tip heating (RF and gradient magnetic field interaction)
- Current induction leading to rapid pacing (RF and gradient magnetic field interaction)
- Over-sensing and under-sensing the cardiac EGM (RF and gradient magnetic field interaction)
- Reed switch interference (static magnetic field interaction)
- Electrical reset or permanent device damage (static, RF, and gradient magnetic field interaction).

Recently, the risks of these potential hazards have been minimized by specially engineering CEIDs to be MR-conditional. In a randomized, prospective, controlled worldwide clinical trial, patients ($n=464$) were randomized to undergo an MRI scan between 9 and 12 weeks postimplant (MRI group, $n=258$) or not to undergo MRI (control group, $n=206$) after successful implantation of a specially engineered dual-chamber pacemaker and leads. MR imaging was performed under the following conditions: static magnetic field strength of 1.5 T, maximum SAR value of 2 W/kg for each sequence, and a maximum gradient slew rate of 200 T/m/s. In addition, only head and lumbar sequences were performed such that the isocenter of the RF transmitter coil was above the C1 vertebra and below T_{12}. The results of the study demonstrated that no MRI-related complications occurred during or after MRI, including sustained ventricular arrhythmias, changes in pacing thresholds or sensed EGMs, pacemaker inhibition or output failures, electrical

resets, or other pacemaker malfunctions [90]. This pacemaker (EnRhythm MRI system, renamed RevoMRI™ SureScan® system, Medtronic) received Conformité Européenne (CE) mark in 2008, and was approved for use in the USA in 2011. Although CIEDs have been specially engineered to be MR-conditional, the problem remains to be very complex. For example, the potential hazard of lead tip heating, which can lead to an increase in pacing threshold, is dependent on many parameters including [91]:

- Patient size
- Anatomy
- Body composition
- Position in the bore
- Scan sequence
- Lead routing
- Lead design.

Because of these complexities, computer-aided modeling has been used as a practical and efficient method for exploring millions of variable combinations in a holistic manner [91].

It should be noted that a device may be MR-conditional, but that does not necessarily mean it is "MR-compatible." MR-compatibility is used to describe the interaction of the device with the diagnostic quality of the MR image. In the example of the MR-conditional pacemaker, researchers have found that high-quality CMR images for the assessment of cardiac anatomy and function can be obtained in most patients with an implantable pacing system [92]. Furthermore, new scan sequences have been proven effective at reducing artifacts in patients scanned with ICDs [93].

It is foreseen that a new set of MRI safety concerns may arise when such imaging is performed using intravascular coils [94, 95]. Such intravascular coils may, for example, be used to examine vulnerable plaque on vessel walls; localized heating in the vicinity of the coil could disrupt the plaque, thus causing catastrophic consequences. Note that heating strongly depends on the wavelength (MRI frequency), geometry of the body and the device, and placement of the body and device with respect to each other and within the MR system. On the other hand, one could also foresee potentially using this heating phenomenon to induce therapy itself (e.g., tumor ablation to lesion formation). For further information on MR-conditional and/or MR-compatible biomedical devices and additional contraindications for cardiac MRI exams, we refer the reader to the growing body of literature on this topic.

24.4.3 Assessment of Biomedical Device Performance

Cardiac MRI also provides a unique opportunity to test, in vivo, the performance of implanted devices such as prosthetic heart valves and heart pacing devices (those that would be considered both MRI-compatible and safe). For example, in patients with artificial aortic valves, the flow downstream from the implanted valve may be severely altered. These changes have been associated with an increased risk of thrombus formation and mechanical hemolysis. Therefore the capabilities of MRI velocity mapping would be considered very useful for the noninvasive evaluation of the flow profiles in patients with a mechanical valve prosthesis [96, 97]. For example, in one report, Botnar et al. found that peak flow velocity in the aorta was significantly higher in patients with valvular prosthesis than in normal patients [98]. In that same study, the investigators also reported that diastolic mean flow was negative in patients after valve replacement, but not in controls. Furthermore, in instances where real-time MRI is used to guide the placement of a stented artificial valve, an assessment of the flow profile can be obtained immediately to determine the relative success of the implant procedure.

The usefulness of MRI for assessing the function of cardiac pacing devices has already been proven in experimental animal studies [99], with early feasibility data obtained in humans using MR-conditional pacemakers [92]. For example, in our laboratory, we have quantified pacing-induced left ventricular dyssynchrony in swine paced from the right ventricular apex, a standard pacing lead implant site, using MR tissue tagging. Figure 24.12 demonstrates that right ventricular apex pacing alters the mechanical activation pattern of the left ventricle, resulting in circumferential stretch in the lateral and posterior walls and regional variations in circumferential shortening in end-systole (see also online Video 24.1). Our lab has also demonstrated intraventricular dyssynchrony during right ventricular apical pacing in an isolated human heart [100]. Furthermore, the myocardial strain in a normal swine heart and healthy human volunteer can be viewed in real time in online Videos 24.2 and 24.3.

24.5 Quantitative Analyses of Cardiac MR

It is important to note that post-processing of cardiac MRI studies represents the stage at which the full potential of the cardiac MRI examination may be best realized. Post-processing is comprised of two major steps, namely image post-processing and data post-processing. The first step largely involves segmentation algorithms to delineate and extract features and structures of interest from the collected images. The second step consists mainly of applying mathematical and statistical methods to aid in diagnosis.

For many cardiac investigative protocols, the myocardium is the area of interest for analysis, so one needs to segment the myocardium from the rest of the image to extract further information, e.g., utilize contrast enhancement in a perfusion study or monitor systolic thickening of the wall for a MR cine study.

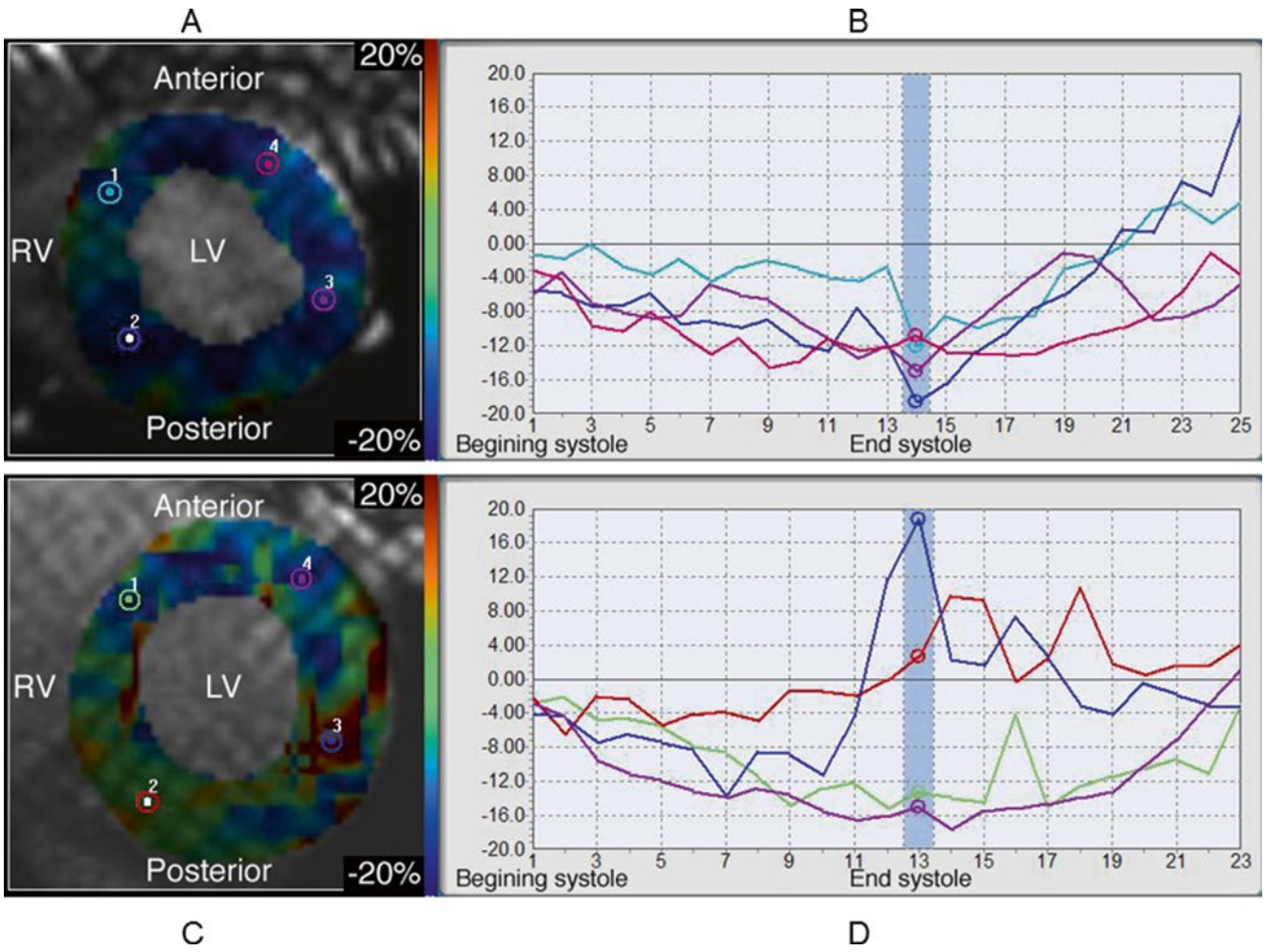

Fig. 24.12 Circumferential strain quantified by MR tissue tagging in a normal porcine heart (**A**–**B**) and after 6 weeks of cardiac pacing from the right ventricular apex in the same heart (**C**–**D**). Graphs (**B**) and (**D**) plot the circumferential strain values throughout the cardiac cycle prior to pacing and after 6 weeks of pacing at the specified probe locations in (**A**) and (**C**) respectively. Pacing from the right ventricular apex caused regional disarray in cardiac strain in the left ventricle at end-systole (**C**) and throughout the cardiac cycle (**D**), in comparison to the same heart 6 weeks prior to the onset of pacing (**A**–**B**). Right ventricular apex pacing induces left ventricular dyssynchrony and results in poor left ventricular pump function. *LV* left ventricle, *RV* right ventricle

24.5.1 Ventricular Function

Quantitative analyses of relative ventricular function are also based on the segmentation of the myocardium. In general, this is achieved by drawing contours on the endocardial and epicardial borders of the myocardium (Fig. 24.13). In general, the ventricular volumes of interest are the end-diastolic and end-systolic volumes, as well as derived parameters such as the stroke volume and ejection fraction. Although ventricular volumes have been computed from differently orientated views of the heart, analyses of the short-axis views are most widely used in cardiac MRI due to their proven accuracy [101–104]. In the simplest case, myocardial segmentation is performed only for the images corresponding to the end-diastolic and end-systolic phases. The end-diastolic phase is defined as the phase containing the largest blood pool area in the left ventricle, whereas the end-systolic phase is identified as the image containing the smallest blood pool area (Fig. 24.14).

Once the end-diastolic and end-systolic phases are fixed, the contours are drawn in the images for the end-diastolic and end-systolic phases for all slices containing left ventricle. In images for a basal slice of the left ventricle, parts of the aorta and aortic valve may be visible. It should be noted that inclusion of contours above the mitral valve plane will significantly overestimate the values for myocardial mass and ventricular volume. Thus, the careful inclusion or exclusion of slices near the base of the heart for determination of the volumes at end-diastole and end-systole is of considerable importance for an accurate determination of the relative ventricular volumes. Once all contours are drawn and verified, the ventricular volume can be computed by simple slice

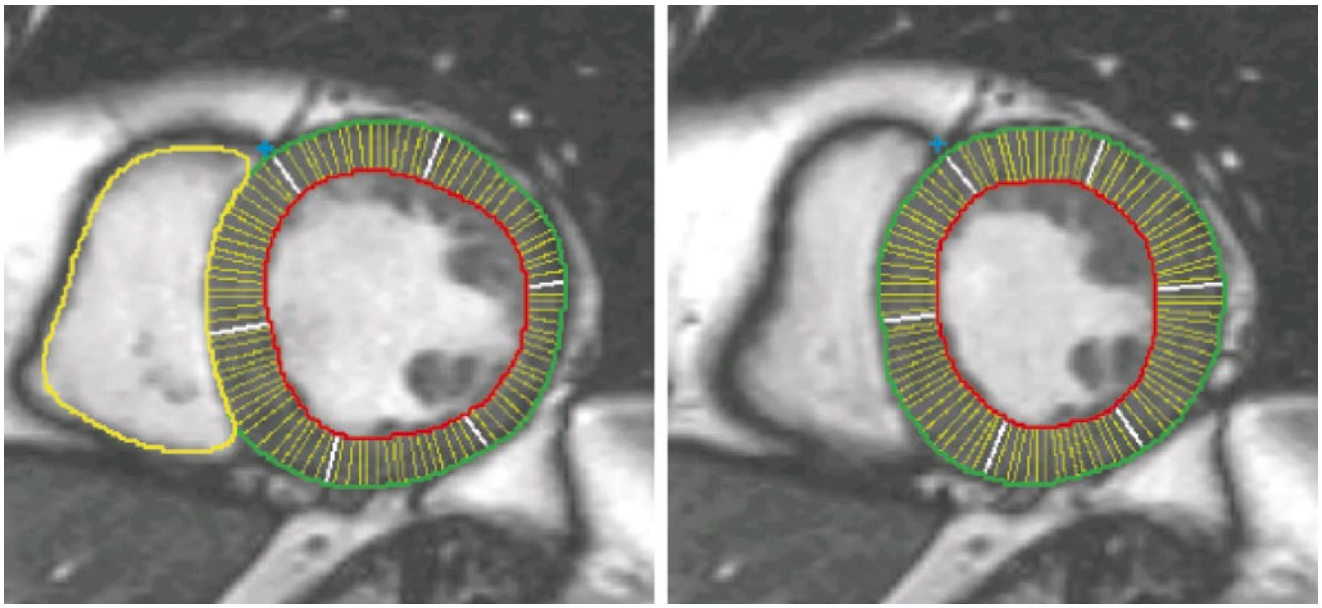

Fig. 24.13 Example of myocardial segmentation for two images corresponding to the end-diastolic (*left*) and end-systolic (*right*) phases in a patient with poor cardiac function. Contours are drawn around the blood pool demarking the endocardium and the epicardium. A contour is also drawn around the right ventricular blood pool. For this particular patient, the cross-section of ventricular cavity with the short-axis view changed significantly less than in a healthy normal. Also shown are chords connecting the endocardial and epicardial borders. The chords are orthogonal to a center line between the two contours. The chords measure the true thickness of the myocardium as opposed to radial chords that emanate from the center of the left ventricle

summation using Simpson's rule with the slice thickness as the increment.

Recently, Young et al. [104] proposed an optimization method for speeding up the process of contour drawing by placing guide points on the endocardial and epicardial borders, instead of drawing continuous contours for both borders. The algorithm then automatically detects the myocardial borders by interpolation between the guide points. This user-friendly method reduces the burden of generating contours compared to the conventional tracing of the contours. Subsequently, Swingen et al. [105] modified the guide point technique by including feedback from continuously updated 3D models of the heart, to evaluate both the placement of guide points and the accuracy of the computed volumes. They showed that the combined use of short- and long-axis views results in more accurate estimates of the ventricular volume and myocardial mass, compared to exclusive reliance on short-axis views [106] (Fig. 24.15).

Common parameters of interest for volumetric analyses are:

- *Left ventricular mass*: The myocardial mass is obtained by multiplying the myocardial volume by the myocardial specific gravity (1.05). Myocardial volume is calculated as the difference between the epicardial and endocardial volumes. The normal mean for left ventricular mass is 92 ± 16 g/m^2 of body surface area.
- *Stroke volume*: The stroke volume is calculated as the difference between end-diastolic and end-systolic blood or chamber volumes, and it represents the volume of blood ejected by a ventricle per heart beat (in the absence of aortic regurgitation). Unless shunts and valvular regurgitation are present, the calculated stroke volumes of the two ventricles should be nearly equal. This is a rule of thumb for verification of the volume computation.
- *Ejection fraction*: This is the ratio of the ventricular stroke volume to the end-diastolic volume. The normal range is between 55 and 65 %. An ejection fraction of less than 40 % is considered to indicate impaired ventricular function.
- *Cardiac output*: This is the product of stroke volume and heart rate. It is a measure of the volume of blood ejected by the heart per beat. For an average adult, cardiac output is 4–8 l/min. Cardiac output is often corrected by normalization with respect to the body surface area.

24.5.2 Analyses of Wall Motions and Regional Myocardial Strains

24.5.2.1 Analyses of Relative Wall Motions

MRI wall motion analyses are typically performed to measure the changes in thickness of the left ventricular wall, from diastole to systole [107–112]. Wall motion abnormali-

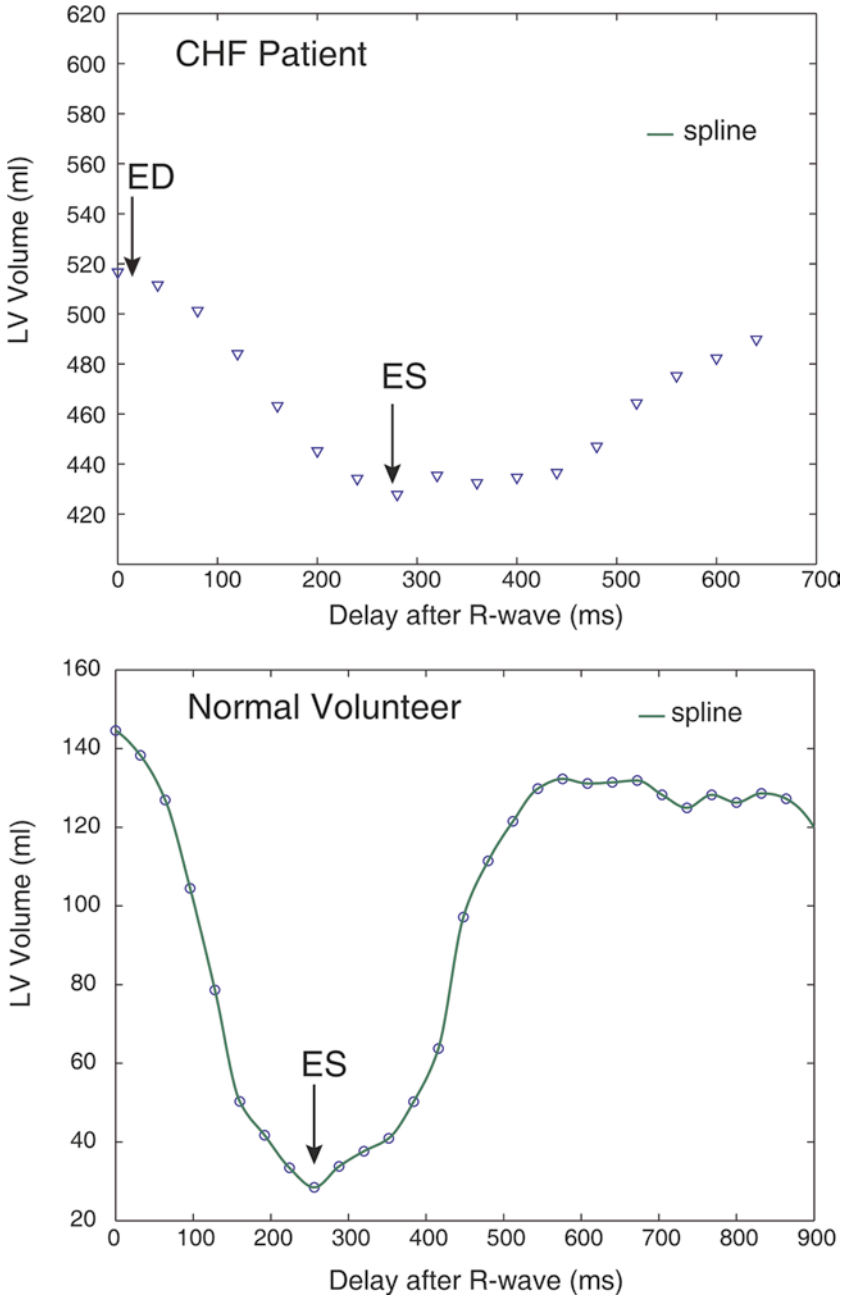

Fig. 24.14 Volume-time graph with the end-diastolic (*ED*) and end-systolic (*ES*) phases. The *upper graph* shows the variation of left ventricular (*LV*) volume over the cardiac cycle for a patient with congestive heart failure (*CHF*), and the *lower graph* is the same type of graph for a healthy volunteer. The CHF patient had an enlarged ventricle (i.e., large volume) and a very low ejection fraction. Because of the low ejection fraction, the curve in the CHF patient is relatively flat. Ventricular volumes were calculated by Simpson's rule from a set of short-axis images. The endocardial border had been traced on each cine frame to obtain a complete left ventricular volume versus time curve

ties are commonly associated with many cardiac diseases, including dilated cardiomyopathy, end-stage valvular disease, and ischemic heart disease.

The assessment of relative myocardial wall thickness, thickening, and wall motion abnormalities proceeds from the MRI segmentation along the endocardial and epicardial borders. For example, a center line can be drawn between the myocardial contours [113]; approximately 100 chords are then drawn orthogonal to the center line at equal intervals to intersect the two myocardial contours (Fig. 24.13). With the center line technique, the chords are optimally placed to measure the exact thickness of the transmural myocardium [113].

Parameters of interest for wall motion analyses include:

- *Myocardial thickness*: The length of the orthogonal chords, from the endocardial to the epicardial borders, measuring myocardial thicknesses.
- *Myocardial thickening*: Differences in end-diastolic and end-systolic thickness, as a percentage of end-diastolic thickness; these are measures of relative wall thickening and can be considered as the radial component of myocardial strain.

24.5.2.2 Analyses of Regional Myocardial Strains with Tagged MR Images

Although the time-consuming analysis of tagged MR images has been a limiting factor for the widespread quantitative analyses of myocardial strains, a recently developed *harmonic phase* (HARP) MR technique permits fast and accurate analyses of strains from MRI-tagging protocols [114–116]. The resultant analyses based on this technique are very fast, accurate, and observer-independent since the myocardial strains are computed from information contained in the images, not the manual operator task of tracking the tag line intersections [117]. Figure 24.16 demonstrates a typical analysis of cardiac circumferential strain in three phases of the cardiac cycle using the HARP technique from data obtained from a human volunteer (HARP, Diagnosoft, Inc., Palo Alto, CA, USA). The circumferential strain values peak at ~20 % in the mid-wall where myofibers are predominately oriented in the plane of the cardiac short axis, consistent with the maximal amount of shortening permissible in a cardiac myocyte.

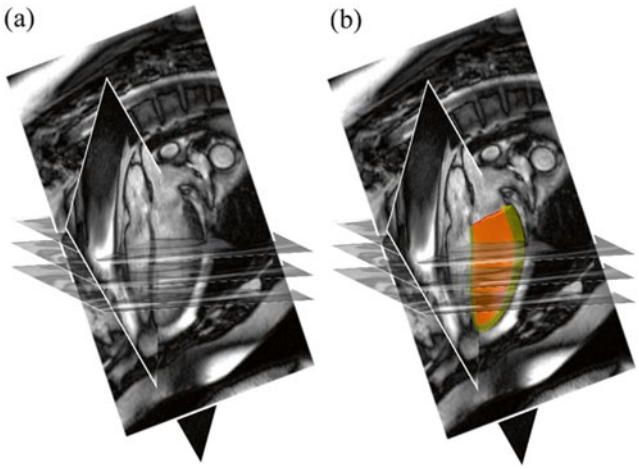

Fig. 24.15 A typical set of TrueFISP slices using a 3D analysis protocol (**a**) with co-registered long- and short-axis images (three of six short-axis images shown for clarity). Image set with 3D model of the left ventricle (**b**)

24.5.3 Perfusion Analyses

Myocardial perfusion is a measure of blood flow (e.g., ml/min) per unit mass of myocardial tissue. Myocardial perfusion should ideally match the demand for oxygen in the myocardium. Commonly, perfusion is assessed at both rest and during stress to evaluate the capacity of the coronary circulation to increase blood flow above its baseline level, and thus match increases in oxygen demand. A ratio of the perfusion parameters, measured at stress and divided by the value for rest, will give a so-called *perfusion reserve*. In healthy individuals, myocardial blood flow increases approximately three to fourfold above its baseline level with maximal vasodilation; with disease, the perfusion reserve decreases, and a flow reserve on the order of 2.5:1 is often used as the cutoff for deciding whether or not cardiovascular disease is present.

Analyses of myocardial perfusion can be carried to different levels of study, depending on the diagnostic needs and clinical resources available. One type of qualitative analysis associated with nuclear imaging is performed by visual comparison of the peak contrast enhancement in different myocardial segments during the first pass of the contrast medium through the left ventricle. The images are often viewed for this purpose in cine mode; delays in contrast enhancement and/or a reduced peak contrast enhancement relative to other myocardial sectors are then interpreted as signatures of locally reduced myocardial blood flow. However, to do this accurately, the absence of image artifacts is important if the analysis is purely qualitative and visual; if this is the case, then no image post-processing is necessary. Nevertheless, a qualitative analysis does have limited capabilities to detect global reductions of myocardial perfusion, especially in patients with multiple vessel coronary artery disease.

Quantitative analyses of MRI perfusion studies commonly start with image segmentation, similar to the procedure used for the analysis of cine studies. First, a technician typically segments one image with good contrast enhancement along the endocardial and epicardial borders of the left ventricle. These contours are then either copied to the remaining images

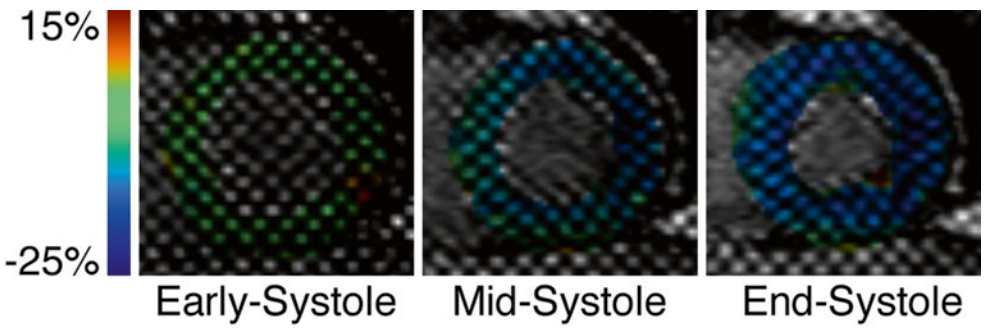

Fig. 24.16 Analysis of cardiac circumferential strain in a human volunteer for three phases of the cardiac cycle using the HARP technique for MR tissue tagging analysis (HARP, Diagnosoft, Inc., Palo Alto, CA, USA). Circumferential strain in the images is indicated by the *color palette*. The grid-tag spacing used in this analysis was 6 mm

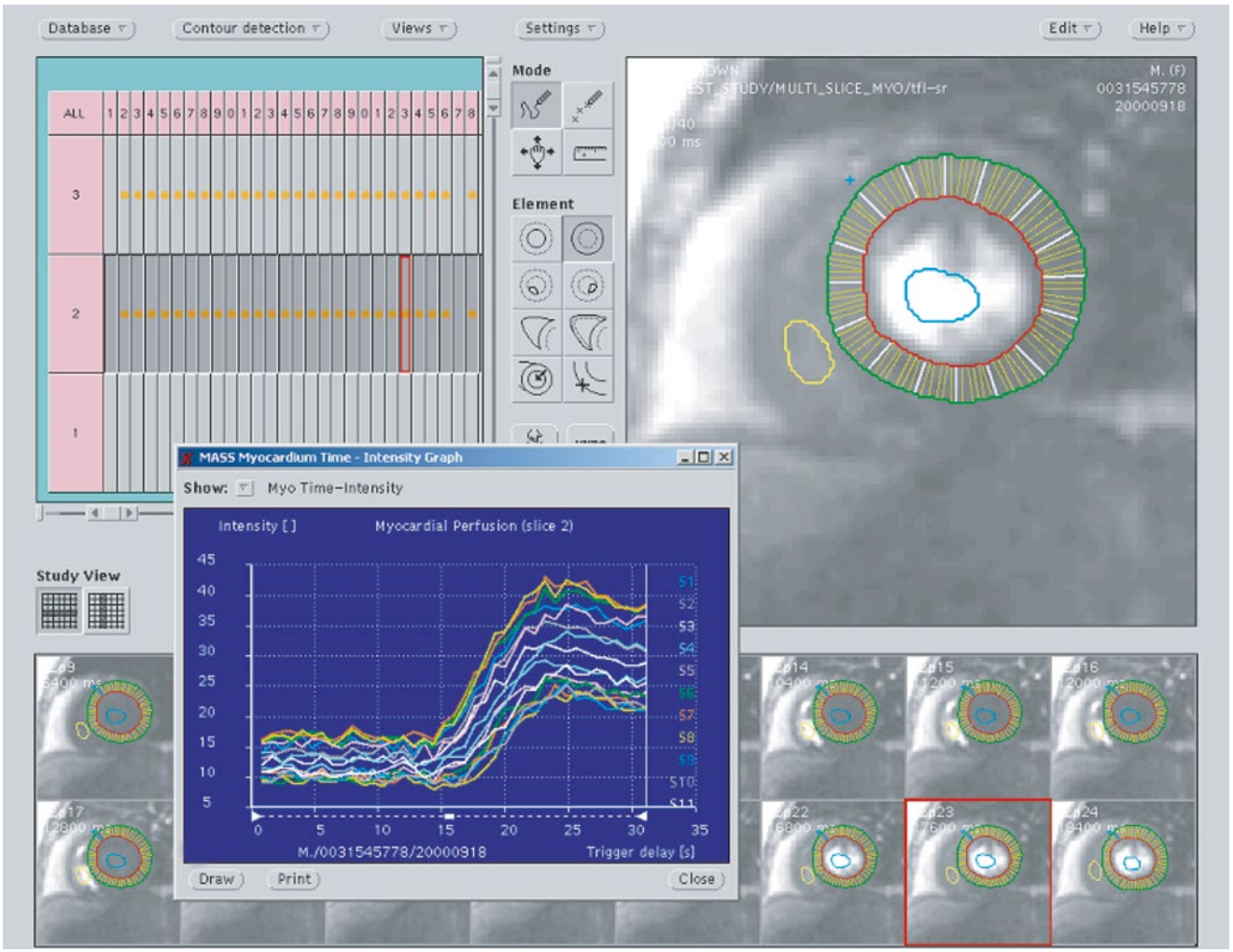

Fig. 24.17 Example of a typical graphical user interface software for analysis of perfusion studies. Segmentation contours are drawn by the user to define the endocardial and epicardial borders. Similar to the approach used for cine analysis, the analysis is carried out on a sector basis; in this case, 16 sectors have been defined. The drawn contours can be copied to other images for the same slice position in the perfusion study. After adjustment of the contours in each image, the software calculated the mean signal intensity in each myocardial sector. As a result, one can obtain graphs depicting the change in signal intensity in each myocardial sector as a function of image number or time (see *inset panel*)

in the data set, or an automated algorithm is employed to identify the borders of the myocardium and this self-adjusts the contour positions. The latter approach is extremely useful (or even essential), as the number of images in a perfusion data set can be very large compared to a cine data set. In other words, the task of simply copying the contours to all other images would require extensive manual editing of the contour by the user. Unlike cine images, the myocardial boundaries can be slightly blurred in perfusion images due to the reduced spatial resolution and cardiac motion. Segmentation of myocardial perfusion images is therefore considered typically more challenging than for cine MR studies.

Once the myocardium is extracted by image segmentation, it is divided into smaller segments or sectors similar to those defined in cine wall motion analyses and corresponding to the individual coronary supplied territories [118]. The signal intensity averages can be plotted versus the image number or versus the time from the beginning of the perfusion scan. Various parameters that will characterize the contrast enhancement kinetics are computed from these signal intensity curves for assessing perfusion (see below). A typical interface with the software tool that can be used for analysis of MR perfusion studies is shown in Fig. 24.17.

As the perfusion images are acquired quite rapidly (<250 ms per image), there is often significant noise in the embedded images. Thus, to extract perfusion parameters, it is useful to perform some curve fitting, to smooth out these signal intensity curves. One widely used method for this purpose is the gamma variate function [119] which approximates the first pass portion of the measured curves quite well. A gamma variate curve fitted to a signal intensity curve obtained from an MR perfusion study in a patient study is

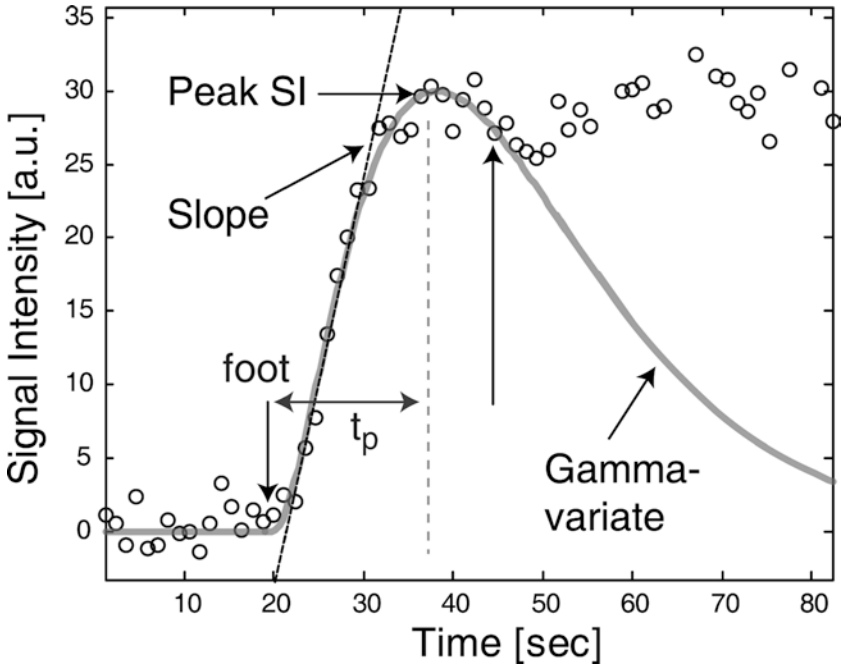

Fig. 24.18 Signal intensity curve for a myocardial sector in the lateral wall. Each of the data points (*round circles*) represents the mean signal intensity measured in the images for the user-defined myocardial sector. The images were acquired with a fast T_1-weighted gradient echo sequence during injection of a 0.075 mmol/kg bolus of Gd-DTPA, an extracellular MR contrast agent. The gamma variate function can only be used to fit the portion of the tissue curve corresponding to the first pass of the contrast agent. The *gray curve* represents the best fit of gamma variate function to be part of the experimental data, covering the range indicated by the *vertical arrows*. The gamma variate fit was extrapolated to the end of the measurement range. In many cases, the end of the first pass and the appearance of the recirculation component can be best ascertained from the signal intensity changes observed in the left ventricular blood pool. Also shown are semi-quantitative perfusion parameters such as the slope, peak signal intensity, and the time from the foot to the peak (t_p)

shown in Fig. 24.18. Nevertheless, there are certain constraints for gamma variate analysis, e.g., it is best optimized only when the first pass portion of the curve is used (from the foot to the peak of the curve).

To date, a number of parameters have been proposed for a semi-quantitative assessment of perfusion. Commonly used parameters are:

- *Percent peak enhancement*: The peak signal normalized by the derived average baseline signal, i.e., signal before arrival of contrast agent expressed as a percentage.
- *Upslope*: The slope of the first pass segment primarily from the start of appearance of the contrast (foot) in the myocardium to the peak.
- *Time to peak*: The time from the foot to the peak of the curve.
- *Mean transit time*: The average time required for a unit volume of blood to transit through the region of interest. It can be determined as the ratio of blood volume in the region of interest to the blood flow through the region of interest. This value can be estimated from the gamma variate fit to the tissue curve.
- *Dynamic distribution volume*: The area under the signal intensity curve, often normalized by the area under the corresponding curve for the left ventricle.

More recently, the upslope parameter has become the most widely used parameter for a semi-quantitative evaluation of myocardial perfusion. The upslopes of the tissue curves are generally normalized by the upslope of the signal intensity curve for a region of interest in the center of the left ventricle, with the latter being considered as an arterial input in such analyses. A ratio, defined as the normalized upslope of the tissue curve measured for maximal vasodilation, divided by the corresponding upslope value at rest, has been proposed as a perfusion reserve index [120–123]. Yet, the perfusion reserve derived from the upslopes generally underestimates the actual ratio of blood flow for maximal vasodilation and rest by approximately 40 % [124].

Our research group has shown that accurate myocardial blood flow estimates can be obtained by MRI methodologies, in comparison to invasive studies employing radio isotope labeled microspheres [125–128]; note that the latter are acknowledged as gold standards for the measurement of blood flow in tissues. MRI perfusion imaging may therefore play a pivotal future role in assessing novel therapeutic approaches for treating coronary artery disease, and automated quantitative analyses of MR perfusion measurements would play an essential role in this task.

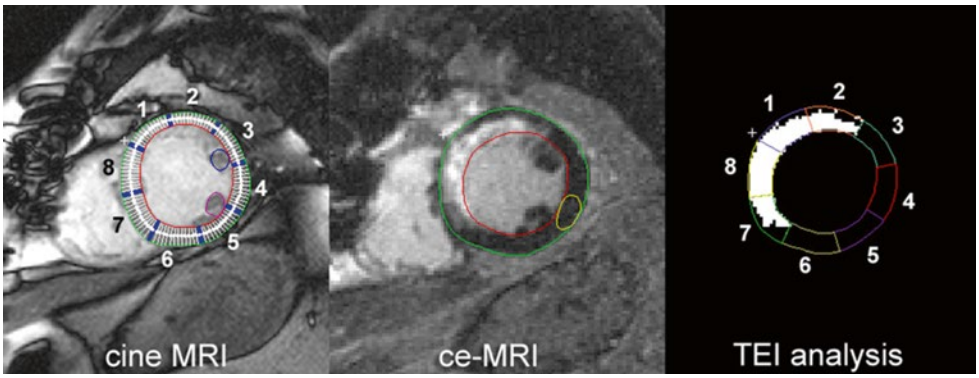

Fig. 24.19 Relative correspondence between the cine (*left*) image showing the 100 chords calculated using the center line method (grouped into eight segments per slice), contrast-enhanced MRI (ce-MRI) (*middle*) showing hyperenhanced scar region with the transmural extent of infarction (*TEI*) calculated in the eight segments (*right*)

24.5.4 Myocardial Scar Size

Myocardial infarct scar sizing and the identification of dysfunctional but potentially viable myocardium are the major prognostic indicators for the recovery of function after a myocardial infarction and have important clinical implications [129–132]. As such, myocardial infarct sizes measured using delayed ce-MRI has been shown to correlate well with histological measurements in both acute and chronic settings [35, 133]. Furthermore, ce-MRI offers distinct advantages over other imaging modalities that either rely on the functional recovery of wall motion abnormalities to identify viability [17] or which are not able to accurately depict smaller subendocardial infarctions [40]. Because of these advantages, ce-MRI is increasingly being used to quantify scar sizes in the acute and chronic setting and to predict the recovery of regional myocardial function using measurements of the segmental "transmural extent of infarction" (TEI) [37, 38, 134, 135]. Importantly, the exact measurement of given infarct size with ce-MRI is of particular interest because both early revascularization and lytic therapy have been shown to lead to a reduced incidence of transmural infarctions, and also myocardial infarcts tend to be patchy [136, 137].

For the ce-MRI images, pixels containing nonviable myocardium have signal intensities statistically greater (hyperenhanced) than a baseline sample from a remote normal region. Typically, hyperenhanced pixels have been classified as those with signal intensities greater than the mean ± standard deviations of a remote normal region [138, 139]. This threshold, whether manually or statistically defined, is highly subjective and highly dependent on the image quality and the noise present. Regions of signal hypoenhancement, associated with microvascular obstruction [33, 134] in the acute infarct case are typically manually segmented and included as scar. The TEI can also be computed for each segment as the ratio (%) of scar to nonscar pixels (Fig. 24.19). Overall scar size is computed by summing the myocardial scar volume in each slice throughout the heart. Finally, infarct extent can be calculated as the scar volume divided by the myocardial volume.

24.6 Summary

For the biomedical engineer, cardiac MRI represents an opportunity to study the function of the heart and use these insights to design better biomedical devices. Due to the increasing relevance of cardiac MRI in the clinical arena, it will become even more important to address the challenges inherent in the use of cardiac MRI in patients with implanted devices, although recent advancements have been made. It should be noted that numerous topics such as MR coronary angiography and plaque imaging, although of great interest, have been left out of this overview of cardiac MRI.

References

1. Pettigrew RI (1989) Dynamic cardiac MR imaging. Techniques and applications. Radiol Clin North Am 27:1183–1203
2. Bloomgarden DC et al (1997) Global cardiac function using fast breath-hold MRI: validation of new acquisition and analysis techniques. Magn Reson Med 37:683–692
3. Sakuma H et al (1993) Evaluation of left ventricular volume and mass with breath-hold cine MR imaging. Radiology 188:377–380
4. Anand IS et al (2002) Noninvasive assessment of left ventricular remodeling: concepts, techniques, and implications for clinical trials. J Card Fail 8(6 Suppl):S452–S464
5. Atkinson DJ, Edelman RR (1991) Cineangiography of the heart in a single breath hold with a segmented turboFLASH sequence. Radiology 178:357–360
6. Bluemke DA et al (1997) Segmented K-space cine breath-hold cardiovascular MR imaging: Part 1. Principles and technique. AJR Am J Roentgenol 169:395–400
7. Bluemke DA et al (1997) Segmented K-space cine breath-hold cardiovascular MR imaging: Part 2. Evaluation of aortic vasculopathy. AJR Am J Roentgenol 169:401–407
8. Chien D, Edelman RR (1991) Ultrafast imaging using gradient echoes. Magn Reson Q 7:31–56
9. Oppelt A et al (1986) FISP: a new fast MRI sequence. Electromedica 54:15–18
10. Zur Y, Wood ML, Neuringer LJ (1990) Motion-insensitive, steady-state free precession imaging. Magn Reson Med 16:444–459
11. Pereles FS et al (2001) Usefulness of segmented trueFISP cardiac pulse sequence in evaluation of congenital and acquired adult cardiac abnormalities. AJR Am J Roentgenol 177:1155–1160

12. Plein S et al (2001) Steady-state free precession magnetic resonance imaging of the heart: comparison with segmented k-space gradient-echo imaging. J Magn Reson Imaging 14:230–236
13. Francois CJ et al (2004) Left ventricular mass: manual and automatic segmentation of true FISP and FLASH cine MR images in dogs and pigs. Radiology 230:389–395
14. Shors SM et al (2004) Accurate quantification of right ventricular mass at MR imaging by using cine true fast imaging with steady-state precession: study in dogs. Radiology 230:383–388
15. Yang X et al (2001) Magnetic resonance imaging permits in vivo monitoring of catheter-based vascular gene delivery. Circulation 104:1588–1590
16. Weiger M, Pruessmann KP, Boesiger P (2000) Cardiac real-time imaging using SENSE. SENSitivity Encoding scheme. Magn Reson Med 43:177–184
17. Penicka M et al (2004) Tissue Doppler imaging predicts recovery of left ventricular function after recanalization of an occluded coronary artery. J Am Coll Cardiol 43:85–91
18. Sanz G et al (1982) Determinants of prognosis in survivors of myocardial infarction: a prospective clinical angiographic study. N Engl J Med 306:1065–1070
19. Weiss JL, Marino PN, Shapiro EP (1991) Myocardial infarct expansion: recognition, significance and pathology. Am J Cardiol 68:35D–40D
20. Lieberman AN et al (1981) Two-dimensional echocardiography and infarct size: relationship of regional wall motion and thickening to the extent of myocardial infarction in the dog. Circulation 63:739–746
21. Sasayama S et al (1976) Dynamic changes in left ventricular wall thickness and their use in analyzing cardiac function in the conscious dog. Am J Cardiol 38:870–879
22. Azhari H et al (1995) A noninvasive comparative study of myocardial strains in ischemic canine hearts using tagged MRI in 3-D. Am J Physiol 268:H1918–H1926
23. Gotte MJ et al (2001) Quantification of regional contractile function after infarction: strain analysis superior to wall thickening analysis in discriminating infarct from remote myocardium. J Am Coll Cardiol 37:808–817
24. Rickers C et al (2004) Applications of magnetic resonance imaging for cardiac stem cell therapy. J Interv Cardiol 17:37–46
25. Axel L, Goncalves RC, Bloomgarden D (1992) Regional heart wall motion: two-dimensional analysis and functional imaging with MR imaging. Radiology 183:745–750
26. Clark NR et al (1991) Circumferential myocardial shortening in the normal human left ventricle. Assessment by magnetic resonance imaging using spatial modulation of magnetization. Circulation 84:67–74
27. McVeigh ER (1996) MRI of myocardial function: motion tracking techniques. Magn Reson Imaging 14:137–150
28. McVeigh ER, Atalar E (1992) Cardiac tagging with breath-hold cine MRI. Magn Reson Med 28:318–327
29. McVeigh ER, Zerhouni EA (1991) Noninvasive measurement of transmural gradients in myocardial strain with MR imaging. Radiology 180:677–683
30. Koenig SH et al (1986) Relaxation of water protons in the intra- and extracellular regions of blood containing Gd(DTPA). Magn Reson Med 3:791–795
31. Strich G et al (1985) Tissue distribution and magnetic resonance spin lattice relaxation effects of gadolinium-DTPA. Radiology 154:723–726
32. Braunwald E (ed) (1997) Heart disease: a textbook of cardiovascular medicine. W.B. Saunders Company, Philadelphia
33. Lima JA et al (1995) Regional heterogeneity of human myocardial infarcts demonstrated by contrast-enhanced MRI. Potential mechanisms. Circulation 92:1117–1125
34. Tsekos NV et al (1995) Fast anatomical imaging of the heart and assessment of myocardial perfusion with arrhythmia insensitive magnetization preparation. Magn Reson Med 34:530–536
35. Kim RJ et al (1999) Relationship of MRI delayed contrast enhancement to irreversible injury, infarct age, and contractile function. Circulation 100:1992–2002
36. Simonetti OP et al (2001) An improved MR imaging technique for the visualization of myocardial infarction. Radiology 218:215–223
37. Bello D et al (2003) Gadolinium cardiovascular magnetic resonance predicts reversible myocardial dysfunction and remodeling in patients with heart failure undergoing beta-blocker therapy. Circulation 108:1945–1953
38. Kim RJ et al (2000) The use of contrast-enhanced magnetic resonance imaging to identify reversible myocardial dysfunction. N Engl J Med 343:1445–1453
39. Klein C et al (2002) Assessment of myocardial viability with contrast-enhanced magnetic resonance imaging: comparison with positron emission tomography. Circulation 105:162–167
40. Wagner A et al (2003) Contrast-enhanced MRI and routine single photon emission computed tomography (SPECT) perfusion imaging for detection of subendocardial myocardial infarcts: an imaging study. Lancet 361:374–379
41. Lekx KS et al (2004) The partition coefficient of Gd-DTPA reflects maintained tissue viability in a canine model of chronic significant coronary stenosis. J Cardiovasc Magn Reson 6:33–42
42. Tong CY et al (1993) Measurement of the extraction efficiency and distribution volume for Gd-DTPA in normal and diseased canine myocardium. Magn Reson Med 30:337–346
43. Wendland MF et al (2002) Thallium-like test for myocardial viability with MnDPDP-enhanced MRI. Acad Radiol 9(Suppl 1):S82–S83
44. Kim RJ et al (1999) Relationship of elevated 23Na magnetic resonance image intensity to infarct size after acute reperfused myocardial infarction. Circulation 100:185–192
45. Duprez DA et al (2007) Heterogeneous remodelling of the ascending and descending aorta with age. J Hum Hypertens 21:689–691
46. Hsu EW et al (1998) Magnetic resonance myocardial fiber-orientation mapping with direct histological correlation. Am J Physiol 274:H1627–H1634
47. LeGrice IJ et al (1995) Laminar structure of the heart: ventricular myocyte arrangement and connective tissue architecture in the dog. Am J Physiol 269:H571–H582
48. Streeter DD Jr et al (1969) Fiber orientation in the canine left ventricle during diastole and systole. Circ Res 24:339–347
49. Ingels NB Jr (1997) Myocardial fiber architecture and left ventricular function. Technol Health Care 5:45–52
50. Rijcken J et al (1997) Optimization of cardiac fiber orientation for homogeneous fiber strain at beginning of ejection. J Biomech 30:1041–1049
51. Rijcken J et al (1999) Optimization of cardiac fiber orientation for homogeneous fiber strain during ejection. Ann Biomed Eng 27:289–297
52. Sallin EA (1969) Fiber orientation and ejection fraction in the human left ventricle. Biophys J 9:954–964
53. Tomioka H et al (2006) The effect of ventricular sequential contraction on helical heart during pacing: high septal pacing versus biventricular pacing. Eur J Cardiothorac Surg 29(Supp 1):S198–S206
54. Tseng WY et al (2000) Myocardial fiber shortening in humans: initial results of MR imaging. Radiology 216:128–139
55. Van Der Toorn A et al (2002) Transmural gradients of cardiac myofiber shortening in aortic valve stenosis patients using MRI tagging. Am J Physiol Heart Circ Physiol 283:H1609–H1615
56. Shapiro EP, Rademakers FE (1997) Importance of oblique fiber orientation for left ventricular wall deformation. Technol Health Care 5:21–28

57. Tseng WY et al (2003) Diffusion tensor MRI of myocardial fibers and sheets: correspondence with visible cut-face texture. J Magn Reson Imaging 17:31–42
58. Helm PA et al (2005) Ex vivo 3D diffusion tensor imaging and quantification of cardiac laminar structure. Magn Reson Med 54:850–859
59. Scollan DF et al (2000) Reconstruction of cardiac ventricular geometry and fiber orientation using magnetic resonance imaging. Ann Biomed Eng 28:934–944
60. Geerts L et al (2002) Characterization of the normal cardiac myofiber field in goat measured with MR-diffusion tensor imaging. Am J Physiol Heart Circ Physiol 283:H139–H145
61. Basser PJ, Mattiello J, LeBihan D (1994) Estimation of the effective self-diffusion tensor from the NMR spin echo. J Magn Reson B 103:247–254
62. Garrido L et al (1994) Anisotropy of water diffusion in the myocardium of the rat. Circ Res 74:789–793
63. Holmes AA, Scollan DF, Winslow RL (2000) Direct histological validation of diffusion tensor MRI in formaldehyde-fixed myocardium. Magn Reson Med 44:157–161
64. Scollan DF et al (1998) Histological validation of myocardial microstructure obtained from diffusion tensor magnetic resonance imaging. Am J Physiol 275:H2308–H2318
65. Helm P et al (2005) Measuring and mapping cardiac fiber and laminar architecture using diffusion tensor MR imaging. Ann N Y Acad Sci 1047:296–307
66. Dou J et al (2003) Combined diffusion and strain MRI reveals structure and function of human myocardial laminar sheets in vivo. Magn Reson Med 50:107–113
67. Reese TG et al (1995) Imaging myocardial fiber architecture in vivo with magnetic resonance. Magn Reson Med 34:786–791
68. Rohmer D, Sitek A, Gullberg GT (2007) Reconstruction and visualization of fiber and laminar structure in the normal human heart from ex vivo diffusion tensor magnetic resonance imaging (DTMRI) data. Invest Radiol 42:777–789
69. Eggen MD, Swingen CM, Iaizzo PA (2012) Ex vivo diffusion tensor MRI of human hearts: relative effects of specimen decomposition. Magn Reson Med 67:1703–1709
70. Tseng WY et al (2006) Imaging myocardial fiber disarray and intramural strain hypokinesis in hypertrophic cardiomyopathy with MRI. J Magn Reson Imaging 23:1–8
71. Chen J et al (2003) Remodeling of cardiac fiber structure after infarction in rats quantified with diffusion tensor MRI. Am J Physiol Heart Circ Physiol 285:H946–H954
72. Wu MT et al (2006) Diffusion tensor magnetic resonance imaging mapping the fiber architecture remodeling in human myocardium after infarction: correlation with viability and wall motion. Circulation 114:1036–1045
73. Vadakkumpadan F et al (2010) Image-based models of cardiac structure in health and disease. Wiley Interdiscip Rev Syst Biol Med 2:489–506
74. Arevalo H et al (2013) Tachycardia in post-infarction hearts: insights from 3D image-based ventricular models. PLoS One 8, e68872
75. Lardo AC (2000) Real-time magnetic resonance imaging: diagnostic and interventional applications. Pediatr Cardiol 21:80–98
76. Kerr AB et al (1997) Real-time interactive MRI on a conventional scanner. Magn Reson Med 38:355–367
77. Serfaty JM et al (2003) MRI-guided coronary catheterization and PTCA: a feasibility study on a dog model. Magn Reson Med 49:258–263
78. Lardo AC et al (2000) Visualization and temporal/spatial characterization of cardiac radiofrequency ablation lesions using magnetic resonance imaging. Circulation 102:698–705
79. Atalar E et al (1996) High resolution intravascular MRI and MRS by using a catheter receiver coil. Magn Reson Med 36:596–605
80. Moore P (2005) MRI-guided congenital cardiac catheterization and intervention: the future? Catheter Cardiovasc Interv 66:1–8
81. Gaspar T et al (2014) Three-dimensional real-time MRI-guided intracardiac catheter navigation. Eur Heart J 35:589
82. Bell JA et al (2012) A deflectable guiding catheter for real-time MRI-guided interventions. J Magn Reson Imaging 35:908–915
83. McVeigh ER et al (2006) Real-time interactive MRI-guided cardiac surgery: aortic valve replacement using a direct apical approach. Magn Reson Med 56:958–964
84. Kahlert P et al (2012) Towards real-time cardiovascular magnetic resonance guided transarterial CoreValve implantation: in vivo evaluation in swine. J Cardiovasc Magn Reson 14:21
85. Saikus CE, Lederman RJ (2009) Interventional cardiovascular magnetic resonance imaging: a new opportunity for image-guided interventions. JACC Cardiovasc Imaging 2:1321–1331
86. Eitel C et al (2014) Catheter ablation guided by real-time MRI. Curr Cardiol Rep 16:511
87. Saeed M et al (2012) MR fluoroscopy in vascular and cardiac interventions (review). Int J Cardiovasc Imaging 28:117–137
88. ASTM F2503-13 (2013) Standard practice for marking medical devices and other items for safety in the magnetic resonance environment. ASTM International, West Conshohocken, PA
89. Cronin EM, Mahon N, Wilkoff BL (2012) MRI in patients with cardiac implantable electronic devices. Expert Rev Med Devices 9:139–146
90. Wilkoff BL et al (2011) Magnetic resonance imaging in patients with a pacemaker system designed for the magnetic resonance environment. Heart Rhythm 8:65–73
91. Wilkoff BL et al (2013) Safe magnetic resonance imaging scanning of patients with cardiac rhythm devices: a role for computer modeling. Heart Rhythm 10:1815–1821
92. Schwitter J et al (2013) Impact of the Advisa MRI pacing system on the diagnostic quality of cardiac MR images and contraction patterns of cardiac muscle during scans: Advisa MRI randomized clinical multicenter study results. Heart Rhythm 10:864–872
93. Stevens SM et al (2014) Device artifact reduction for magnetic resonance imaging of patients with implantable cardioverter-defibrillators and ventricular tachycardia: late gadolinium enhancement correlation with electroanatomic mapping. Heart Rhythm 11:289–298
94. Nitz WR et al (2001) On the heating of linear conductive structures as guide wires and catheters in interventional MRI. J Magn Reson Imaging 13:105–114
95. Yeung CJ, Susil RC, Atalar E (2002) RF safety of wires in interventional MRI: using a safety index. Magn Reson Med 47:187–193
96. Houlind K et al (1996) Magnetic resonance imaging of blood velocity distribution around St. Jude medical aortic valves in patients. J Heart Valve Dis 5:511–517
97. Walker PG et al (1995) Magnetic resonance velocity imaging: a new method for prosthetic heart valve study. J Heart Valve Dis 4:296–307
98. Botnar R et al (2000) Assessment of prosthetic aortic valve performance by magnetic resonance velocity imaging. MAGMA 10:18–26
99. Wyman BT et al (2002) Effects of single- and biventricular pacing on temporal and spatial dynamics of ventricular contraction. Am J Physiol Heart Circ Physiol 282:H372–H379
100. Eggen MD et al (2010) MRI assessment of pacing induced ventricular dyssynchrony in an isolated human heart. J Magn Reson Imaging 31:466–469
101. van der Geest RJ et al (1997) Quantitative analysis of cardiovascular MR images. Int J Card Imaging 13:247–258
102. van der Geest RJ, Lelieveldt BP, Reiber JH (2000) Quantification of global and regional ventricular function in cardiac magnetic resonance imaging. Top Magn Reson Imaging 11:348–358

103. van der Geest RJ, Reiber JH (1999) Quantification in cardiac MRI. J Magn Reson Imaging 10:602–608
104. Young AA et al (2000) Left ventricular mass and volume: fast calculation with guide-point modeling on MR images. Radiology 216:597–602
105. Swingen CM, Seethamraju RT, Jerosch-Herold M (2003) Feedback-assisted three-dimensional reconstruction of the left ventricle with MRI. J Magn Reson Imaging 17:528–537
106. Swingen C, Wang X, Jerosch-Herold M (2004) Evaluation of myocardial volume heterogeneity during end-diastole and end-systole using cine MRI. J Cardiovasc Magn Reson 6:829–835
107. Baer FM et al (1995) Comparison of low-dose dobutamine-gradient-echo magnetic resonance imaging and positron emission tomography with [18F]fluorodeoxyglucose in patients with chronic coronary artery disease. A functional and morphological approach to the detection of residual myocardial viability. Circulation 91:1006–1015
108. Baer FM et al (1996) Comparison of dobutamine transesophageal echocardiography and dobutamine magnetic resonance imaging for detection of residual myocardial viability. Am J Cardiol 78:415–419
109. Nagel E et al (1999) Noninvasive diagnosis of ischemia-induced wall motion abnormalities with the use of high-dose dobutamine stress MRI: comparison with dobutamine stress echocardiography. Circulation 99:763–770
110. Matheijssen NA et al (1993) Left ventricular wall motion analysis in patients with acute myocardial infarction using magnetic resonance imaging. Magn Reson Imaging 11:485–492
111. Holman ER et al (1995) Quantitative analysis of regional left ventricular function after myocardial infarction in the pig assessed with cine magnetic resonance imaging. Magn Reson Med 34:161–169
112. Nagel E, Fleck E (1999) Functional MRI in ischemic heart disease based on detection of contraction abnormalities. J Magn Reson Imaging 10:411–417
113. Sheehan FH et al (1986) Advantages and applications of the centerline method for characterizing regional ventricular function. Circulation 74:293–305
114. Osman NF et al (1999) Cardiac motion tracking using CINE harmonic phase (HARP) magnetic resonance imaging. Magn Reson Med 42:1048–1060
115. Osman NF, McVeigh ER, Prince JL (2000) Imaging heart motion using harmonic phase MRI. IEEE Trans Med Imaging 19:186–202
116. Osman NF, Prince JL (2000) Visualizing myocardial function using HARP MRI. Phys Med Biol 45:1665–1682
117. Kraitchman D et al (2001) Detecting the onset of ischemia using real-time HARP. Proceedings of the International Society of Magnetic Resonance in Medicine
118. Cerqueira MD et al (2002) Standardized myocardial segmentation and nomenclature for tomographic imaging of the heart: a statement for healthcare professionals from the Cardiac Imaging Committee of the Council on Clinical Cardiology of the American Heart Association. Circulation 105:539–542
119. Thompson HK Jr et al (1964) Indicator transit time considered as a gamma variate. Circ Res 14:502–515
120. Al-Saadi N et al (2000) Noninvasive detection of myocardial ischemia from perfusion reserve based on cardiovascular magnetic resonance. Circulation 101:1379–1383
121. Al-Saadi N et al (2000) Improvement of myocardial perfusion reserve early after coronary intervention: assessment with cardiac magnetic resonance imaging. J Am Coll Cardiol 36:1557–1564
122. Panting JR et al (2002) Abnormal subendocardial perfusion in cardiac syndrome X detected by cardiovascular magnetic resonance imaging. N Engl J Med 346:1948–1953
123. Schwitter J et al (2001) Assessment of myocardial perfusion in coronary artery disease by magnetic resonance: a comparison with positron emission tomography and coronary angiography. Circulation 103:2230–2235
124. Ibrahim T et al (2002) Assessment of coronary flow reserve: comparison between contrast-enhanced magnetic resonance imaging and positron emission tomography. J Am Coll Cardiol 39:864–870
125. Jerosch-Herold M et al (2003) Magnetic resonance imaging of myocardial contrast enhancement with MS-325 and its relation to myocardial blood flow and the perfusion reserve. J Magn Reson Imaging 18:544–545
126. Jerosch-Herold M et al (2004) Analysis of myocardial perfusion MRI. J Magn Reson Imaging 19:758–770
127. Jerosch-Herold M, Swingen C, Seethamraju RT (2002) Myocardial blood flow quantification with MRI by model-independent deconvolution. Med Phys 29:886–897
128. Jerosch-Herold M et al (1999) Direct comparison of an intravascular and an extracellular contrast agent for quantification of myocardial perfusion. Cardiac MRI Group. Int J Card Imaging 15:453–464
129. Baer FM et al (1999) MRI assessment of myocardial viability: comparison with other imaging techniques. Rays 24:96–108
130. Haas F et al (1997) Preoperative positron emission tomographic viability assessment and perioperative and postoperative risk in patients with advanced ischemic heart disease. J Am Coll Cardiol 30:1693–1700
131. Lee KS et al (1994) Prognosis of patients with left ventricular dysfunction, with and without viable myocardium after myocardial infarction. Relative efficacy of medical therapy and revascularization. Circulation 90:2687–2694
132. Pagley PR et al (1997) Improved outcome after coronary bypass surgery in patients with ischemic cardiomyopathy and residual myocardial viability. Circulation 96:793–800
133. Fieno DS et al (2000) Contrast-enhanced magnetic resonance imaging of myocardium at risk: distinction between reversible and irreversible injury throughout infarct healing. J Am Coll Cardiol 36:1985–1991
134. Beek AM et al (2003) Delayed contrast-enhanced magnetic resonance imaging for the prediction of regional functional improvement after acute myocardial infarction. J Am Coll Cardiol 42:895–901
135. Mahrholdt H et al (2003) Relationship of contractile function to transmural extent of infarction in patients with chronic coronary artery disease. J Am Coll Cardiol 42:505–512
136. Marino P, Zanolla L, Zardini P (1989) Effect of streptokinase on left ventricular modeling and function after myocardial infarction: the GISSI (Gruppo Italiano per lo Studio della Streptochinasi nell'Infarto Miocardico) Trial. J Am Coll Cardiol 14:1149–1158
137. Sheehan FH et al (1988) Early recovery of left ventricular function after thrombolytic therapy for acute myocardial infarction: an important determinant of survival. J Am Coll Cardiol 12:289–300
138. Gerber BL et al (2002) Accuracy of contrast-enhanced magnetic resonance imaging in predicting improvement of regional myocardial function in patients after acute myocardial infarction. Circulation 106:1083–1089
139. Kolipaka A et al (2005) Segmentation of non-viable myocardium in delayed enhancement magnetic resonance images. Int J Cardiovasc Imaging 21:303–311

Part IV

Devices and Therapies

Historical Perspective of Cardiovascular Devices and Techniques Associated with the University of Minnesota

25

Paul A. Iaizzo and Monica A. Mahre

Abstract

The University of Minnesota has a unique history relative to advances in cardiovascular research, surgery, and the development of medical devices. Interestingly, the writing of this textbook coincides with two important anniversaries in cardiovascular medicine at the University. Sixty years ago, in 1954, cross-circulation for intracardiac operations was first introduced, sparking a number of innovations in the area of open-heart surgery. Additionally, in 2014, the University of Minnesota celebrated the 800th heart transplant performed since 1978 and sustains one of the longest-running heart transplant centers in the world. In this chapter, we will review some of this history and how it has led to the creation of a dynamic medical device industry in the state of Minnesota and surrounding regions.

Keywords

Medical device development • Cross-circulation • Bubble oxygenator • Pacemaker • Heart valves

25.1 Introduction

The era from 1950 to 1967 was an incredible time of innovation at the University of Minnesota's Department of Surgery in the newly emerging fields of open-heart surgery and medical devices. There were many reasons for this, but most importantly (1) the university had excellent facilities, including a unique privately funded 80-bed heart hospital for pediatric and adult patients (this Variety Club Heart Hospital was the first dedicated heart hospital in the USA) (Fig. 25.1) and (2) the Department of Surgery was chaired by Owen H. Wangensteen, M.D., a leader who "created the milieu and the opportunities for great achievements by many of his pupils" and was considered the "mentor of a thousand surgeons" (Fig. 25.2 and Table 25.1) [1]. More specifically, Dr. Wangensteen encouraged his medical students, residents, and junior faculty to "step out of the box," innovate, and solve problems in different ways. In other words, take action and not assume that those who went before them had all the answers. He also believed strongly in collaborations with the basic science departments, specifically the Department of Physiology whose department head, Maurice Visscher, played an integral role in supporting both research and the clinical training of surgical residents. To that end, Wangensteen instituted a 2-year research program for all residents; this surgical Ph.D. program was the only one in the country at its inception, and students were required to take various advanced physiology courses offered through the Department of Physiology.

In the early 1950s, the innovative surge was credited to the fact that many surgical residents were returning from World War II, where they had experienced life and death situations when managing surgical field units. They had little or no fear of death and their generation was not afraid to "push the envelope" to help patients. By today's standards, these residents would be viewed as mavericks but, in fact, they had little to lose, not unlike situations they faced on the

P.A. Iaizzo, PhD • M.A. Mahre, BS (✉)
Department of Surgery, University of Minnesota,
B 172 Mayo, MMC 195 420 Delaware St. SE,
Minneapolis, MN 55455, USA
e-mail: mahre002@umn.edu

P.A. Iaizzo (ed.), *Handbook of Cardiac Anatomy, Physiology, and Devices*, DOI 10.1007/978-3-319-19464-6_25

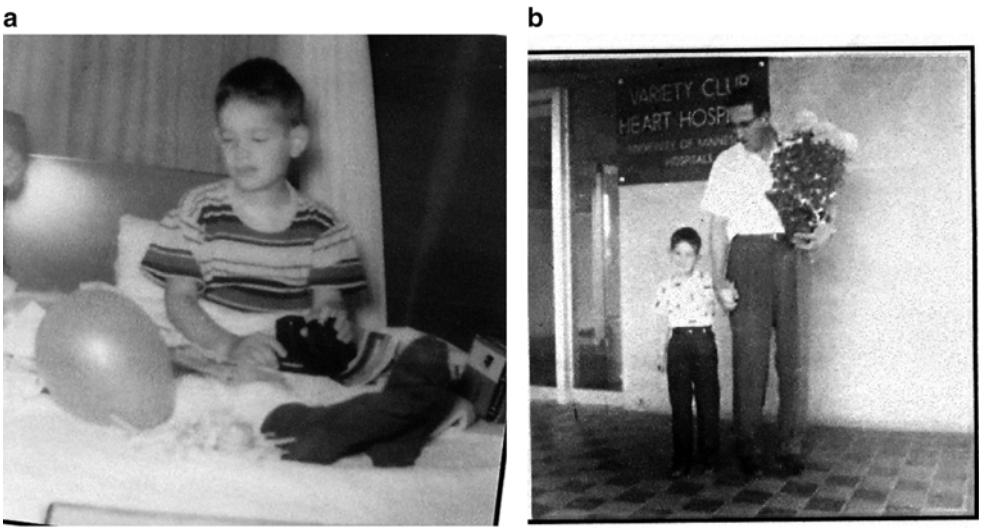

Fig. 25.1 John Dilorio (Dr. Iaizzo's cousin) was a young cardiac patient of Dr. Lillehei and his team, shown here in 1958 (**a**) in his hospital bed at the University Variety Club Hospital and then (**b**) leaving the hospital with his father

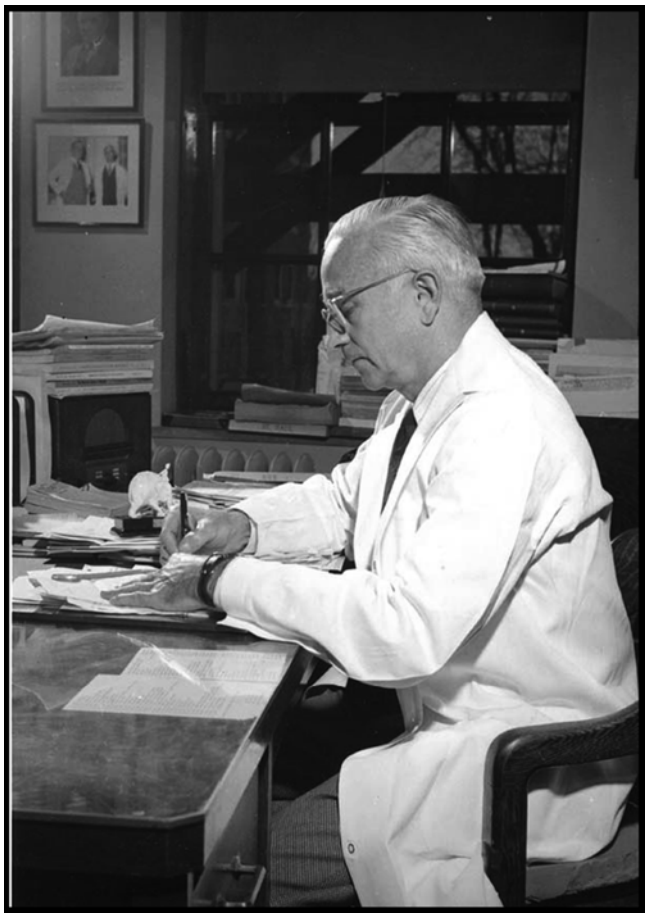

Fig. 25.2 "The Chief" Owen H. Wangensteen, the youngest Surgery Department Chairman at age 31, served as chairman of the department from 1930 to 1967

battlefield. Their heart patients were dying and/or had little chance of survival without the novel techniques that were successfully implemented in Minnesota.

One of these young war-experienced surgeons was C. Walton Lillehei, who returned to the University of Minnesota in 1950 to complete his surgical residency after leading an army surgical field unit in both North Africa and Italy (Fig. 25.3). Lillehei was very bright (he also completed M.S. and Ph.D. degrees during this time) and was known as an impulsive maverick, always pushing to the next level of care for his clinical patients for whom he had great empathy. Lillehei and his team launched many surgical innovations during this period, primarily due to their hands-on research experience in the experimental dog laboratories; one site for this research was located in the basement of the Mayo Hospital building, just three floors below the main operating rooms. Today, this lab space houses the Visible Heart® Laboratory under the direction of Dr. Paul Iaizzo (Figs. 25.4 and 25.5) [2].

Interestingly, prior to 1950, the heart was considered to be the core of human emotion, even the soul itself. For perspective, Table 25.2 depicts some highlights of a typical operating room in the 1950s. Relative to open-heart surgery in 1951, congenital heart defects were responsible for 1 % of all deaths in this age group; thus the prognosis was poor for a child with such a defect. There were no methods for conducting external heart surgery and no way to oxygenate the brain during surgery. In other words, attempts were made to repair a patient's heart while it remained beating, obscuring the view with blood; any stoppage of blood flow would result in damage of the brain. Therefore, only the simplest surgeries could be performed on the beating heart.

When the medical profession eventually began to view the heart more physiologically, as a pump or machine within the body, researchers and clinicians began to develop new ways to repair and replace worn-out parts of the heart. Innovations in the field of cardiac surgery then flourished (Table 25.3). Such innovation became prominent at the University of

Table 25.1 Department of Surgery at the University of Minnesota: chairs/interim heads

Surgery Department chair/interim head	Position	Years served
Arthur C. Strachauer	Department Chair	-1925, 1927–1929
Owen H. Wangensteen	Department Chair	1930–1967
John S. Najarian	Department Chair	1967–1993
Edward W. Humphrey	Interim Chair	1993–1994
Frank B. Cerra	Interim Chair	1994–1995
David L. Dunn	Department Chair	1995–2005
David A. Rothenberger	Interim Chair	2005–2006
Selwyn M. Vickers	Department Chair	2006–2013
David A. Rothenberger	Department Chair	2013–present

Fig. 25.3 Walt Lillehei in his army uniform

Minnesota. For example, Dr. Clarence Dennis designed one of the first heart–lung machines for total cardiopulmonary bypass, which was subsequently tested successfully on dogs (Figs. 25.4 and 25.6). However, when Dennis and his team used the heart–lung machine in the clinical area for the first time on April 5, 1951, the patient died due to complications; a second patient also died during surgery from a massive air embolism. Not long after, Dr. Dennis moved his machine and most of his team to New York City [1].

Worldwide, one of the next major milestones in cardiac surgery was the first open-heart surgery performed using hypothermia, a procedure first attempted on September 2, 1952, by Drs. F. John Lewis and Richard Varco and colleagues at the University of Minnesota (Figs. 25.4 and 25.7). This procedure, proposed by Dr. W.G. Bigelow of Toronto, lowered the body temperature of patients 12–15 °F to reduce their blood flow, thereby reducing the body's need for oxygen. Brain cells would die after 3–4 min at normal temperature without oxygen, but hypothermia allowed the University of Minnesota team (Drs. F. John Lewis, C. Walton Lillehei, Mansur Taufic, and Richard Varco) to successfully complete a 5½-min repair of the atrial septum of a 5-year-old patient. This was recognized as a significant landmark in the history of cardiac surgery; until this time, no surgeon had succeeded in opening the heart to perform intracardiac repair under direct vision. Hypothermia with inflow stasis proved to be excellent for some of the less complicated surgical repairs, but it was not a viable option for more extensive cardiac procedures. Major drawbacks of this approach at that time were the inability to rewarm a cold, nonbeating heart and the lack of clinical defibrillators [3].

From a historic perspective, another key milestone in cardiac surgery, though not accomplished at the University of Minnesota, occurred on May 6, 1953 when Dr. J. Gibbon closed an atrial septal defect using a pump oxygenator for an intracardiac operation. Although this first success with the pump oxygenator was well received, it aroused surprisingly little excitement or enthusiasm among cardiologists and cardiac surgeons at that time, likely because other centers had launched their own experiments with bubble oxygenators. Interestingly, Gibbon was never able to repeat his one clinical success; he ultimately became discouraged and did not use the pump oxygenator again.

During this era, "there was a common scenario, namely, good results with acceptable survival in the experimental animals but nearly universal failure when the same apparatus and techniques were applied to human beings [3]." Furthermore, it was written that "many of the most experienced investigators concluded with seemingly impeccable logic that the problems were not with the perfusion techniques or the heart lung machines [3]. Rather, they came to believe that the 'sick human heart' ravaged by failure, could not possibly be expected to tolerate the magnitude of the operation required and then recover with good output, as occurred when the same machines and techniques were applied to healthy dogs [3]." It is important to consider that these experimental animals were typically healthy dogs and that anatomical differences between canine and human hearts may have been a significant distinguishing factor (see Chap. 6).

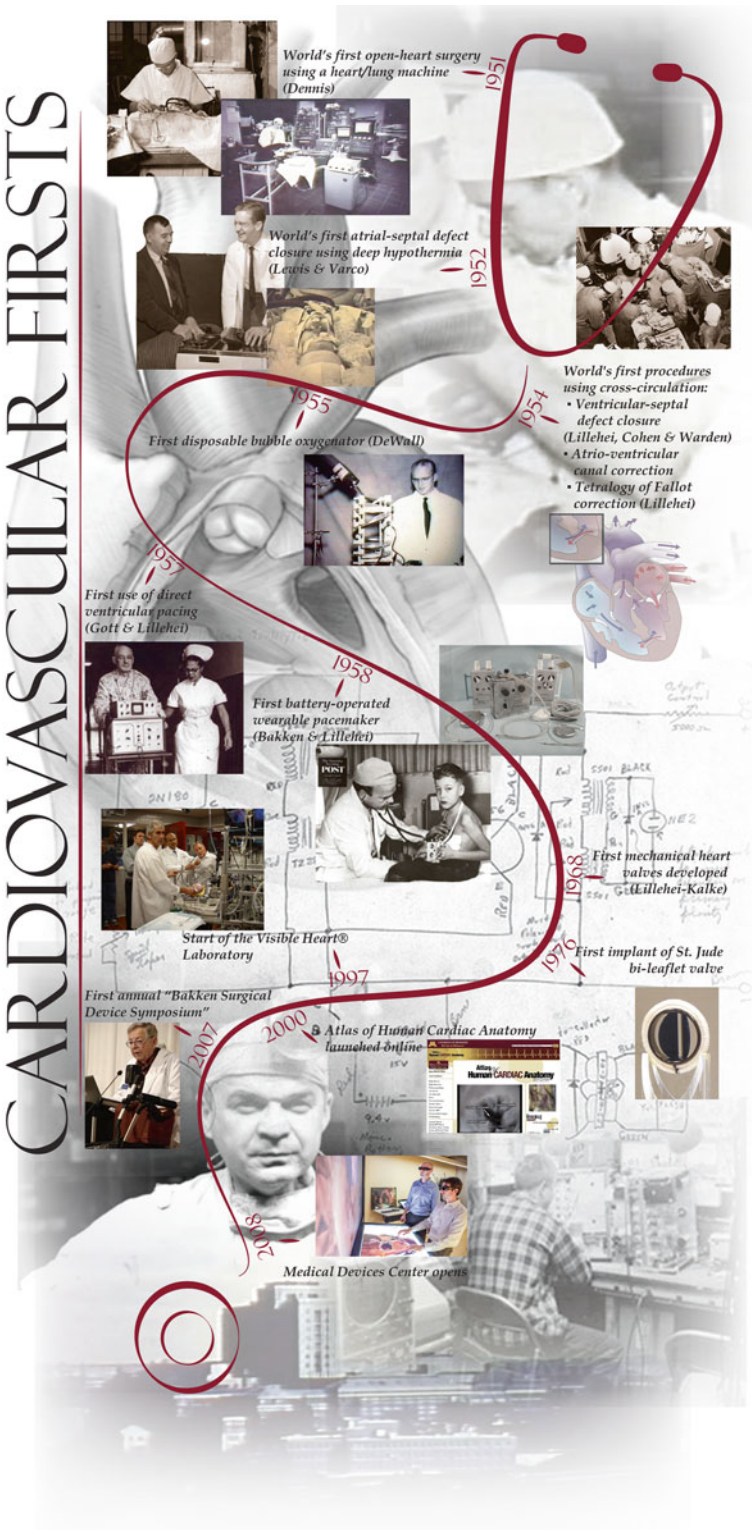

Fig. 25.4 Schematic of "cardiovascular firsts" at the University of Minnesota

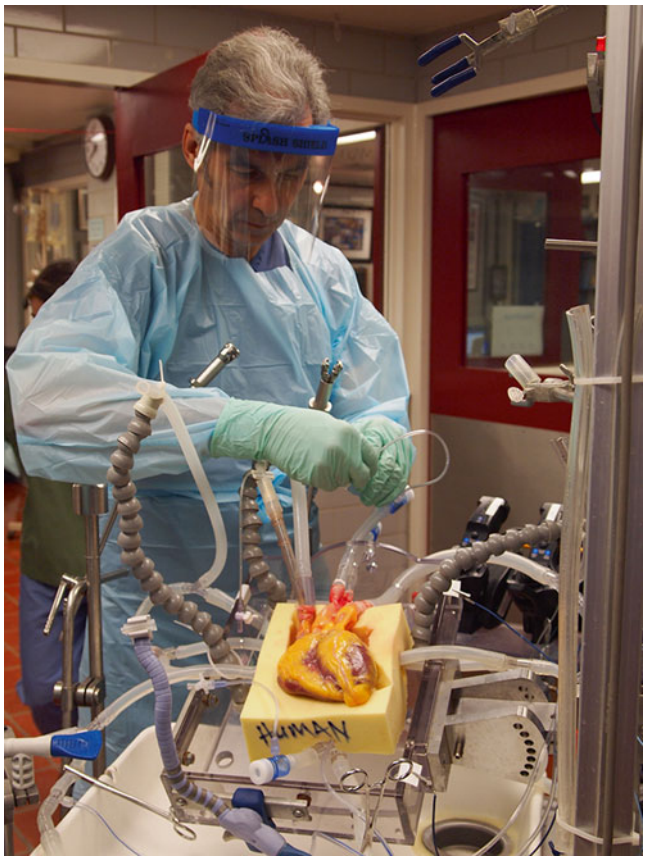

Fig. 25.5 Photo of Dr. Paul Iaizzo in the Visible Heart® Laboratory at the University of Minnesota

Table 25.2 1950s operating room environment

• No computers or digital equipment existed
• Glass thermometers, blood pressure cuffs, and a finger pressed against the wrist were used to obtain vital signs
• Anesthesia was supplied on a soaked rag and delivered by squeezing the black bag
• (Nonoperating room) X-rays were the only imaging equipment available
• Flammable gases could cause explosions in the operating room
• Head lamps lit the operative field
• The second hand on a wall clock was one of the most useful instruments to a surgeon
• No pulse oximeters, pacemakers, blood-gas analyzers, or specialized imaging existed

25.2 Cross-Circulation

Extracorporeal circulation by controlled cross-circulation was introduced clinically on March 26, 1954, after much animal experimentation (Figs. 25.4 and 25.8). The use of cross-circulation for intracardiac operations was an immense departure from established surgical practice at the time and was considered as a major breakthrough that motivated numerous innovations in the area of open-heart surgery [4]. The thought of taking a normal healthy human being into the operating room to provide donor circulation was considered "unacceptable and even immoral" by some critics. The risks to the donors included blood incompatibility, infection, air embolism (stroke), and/or blood volume imbalances.

From March 1955 onward, three additional bypass methods were introduced and successfully used, including (1) perfusion from a reservoir of arterialized blood, (2) heterologous (dog) lungs as an oxygenator, and (3) the Lillehei–DeWall disposable bubble oxygenator [3]. Yet, many believe that the single most important discovery that contributed to the success of clinical open-heart operations was the realization of the vast discrepancy between the total body flow rate *thought* necessary and what was *actually* necessary to maintain cerebral viability. Lillehei and his team are credited with applying the findings of two British surgeons (Andreasen and Watson) who identified the *azygos factor*—the ability of dogs to survive up to 40 min without brain damage when all blood flow was stopped except through the azygos vein. Specifically, Morley Cohen and Lillehei hypothesized that when blood flow was low, the blood vessels dilated to receive a larger share of the blood, while the tissues absorbed a much higher proportion of the oxygen as compared to normal circulation [3]. Previously, it was thought that basal or resting cardiac output at 100–160 ml/kg/min was safe maintenance during cardiopulmonary bypass. The azygos flow studies showed that 8–14 ml/kg/min maintained the physiological integrity of the vital centers, but Lillehei added a margin of safety and set his basic perfusion rate at 25–30 ml/kg/min. This approach reduced excessive complications of blood loss, excessive hemolysis, abnormal bleeding, and/or renal shutdown [3].

Altogether, 45 patients (aged 5 months to 10 years) underwent open-heart surgery with the cross-circulation approach at the University in 1954–1955; prior to these pioneering surgeries, such patients were considered to have lesions that were hopelessly unrepairable. Of this group, 22 (49 %) of the patients lived to be long-term survivors (greater than 30 years) and lead normal productive lives; 11 of the female long-term survivors subsequently gave birth to a total of 25 children who were free from any congenital heart defects. In addition, all 45 donors survived, with only one donor experiencing a major complication. At a more recent 53-year follow-up, 20 (44 %) of the original cross-circulation patients were living with no problems or significant limitations related to their original surgeries [5].

During this period of time, an intense competitive/collaborative relationship existed between the University of Minnesota and the Mayo Clinic (Rochester, MN, USA), the only other primary site where open-heart surgery was being performed. Lillehei recalled in his interview with G. Wayne Miller (author of *King of Hearts*) that the Mayo Clinic operated 7 days a week, so on Saturdays when Lillehei's team

Table 25.3 University of Minnesota milestones

1887	New standards requiring medical students to pass exams and gain medical examining board approval (led by Medical School Dean, Perry Millard)
1911	Minnesota became the first state to mandate hospital internships for medical students
1930s	Discovery of the link between cholesterol and heart disease (Ancel Keys)
1950	First adaptation of the mass spectrograph (Alfred Nier)
1951	First attempt to use a heart–lung machine (Clarence Dennis)
1952	First successful open-heart surgery using hypothermia (F. John Lewis)
1953	First jejunoileal bypass (Richard L. Varco)
1954	First open-heart procedure using cross-circulation (C. Walton Lillehei)
1954	First surgical correction of tetralogy of Fallot (C. Walton Lillehei)
1955	First successful use of the bubble oxygenator (Richard DeWall)
1958	First use of a small, portable battery-powered pacemaker (Earl Bakken)
1963	First human partial ileal bypass (Henry Buchwald)
1966	First clinical pancreas transplant (William D. Kelly and Richard C. Lillehei)
1966–1968	First prosthetic heart valves (Lillehei–Nakib toroidal disk in 1966, Lillehei–Kaster pivoting disk in 1967, Kalke–Lillehei rigid bileaflet prosthesis in 1968)
1967	Bretylium, a drug developed by Marvin Bacaner, saved the life of Dwight Eisenhower
1967	World's first heart transplant (Dr. Christiaan Barnard, trained by C. Walton Lillehei)
1968	First successful bone marrow transplant (Robert A. Good)
1969	Invention of implantable drug pump (Henry Buchwald, Richard Varco, Frank Dorman, Perry L. Blackshear, Perry J. Blackshear)
1976	Medical Device Amendment to FDA Cosmetic Act
1977	First implant of St. Jude mechanical heart valve at University Hospital
1978	Human heart transplantation was performed at University
1978	Pediatric human heart transplantation was performed at University Hospital (Ernesto Molina)
1988	HDI/Pulse Wave® profiler founded (Hypertension Diagnostics, Inc., Jay Cohn, Stanley Finkelstein)
1993	Angel Wings® transcatheter closure device invented (Gladwin Das)
1994	First successful simultaneous pancreas–kidney transplant using a living donor (David Sutherland)
1995	Amplatzer® Occlusion Devices founded (AGA Medical Corp., Kurt Amplatz)
1997	First kidney–bowel transplantation (Rainer Gruessner)
1999	CardioPump Device evaluated (Keith Lurie, et al.)
2000	University's Medical School has produced more family doctors than any other institution in the USA
2003	Robotic cardiac surgery performed at the University of Minnesota (Kenneth Liao)
2005	Launch of free-access website "Atlas of Human Cardiac Anatomy" (Visible Heart Laboratory; www.vhlab.umn.edu/atlas)
2006	Implant of left ventricular assist device using minimally invasive approach (Kenneth Liao)

was not scheduled for surgery, they would travel to the Mayo Clinic and watch Dr. John Kirklin and his colleagues (Miller, G.W., Transcriptions of audio tapes for *King of Hearts*, University of Minnesota Archives) [6]. Dr. Kirklin was successfully using a modification of the Gibbon heart–lung machine, and after observing his achievements, Lillehei began a slow transition away from cross-circulation and toward using a heart–lung machine of his own design (Figs. 25.4 and 25.9). In the beginning, Lillehei used the heart–lung machine for simpler, more straightforward cases and continued using cross-circulation for more complicated surgeries. Although its clinical use was short lived, cross-circulation is still considered today as one of the most important stepping stones in the development of the discipline of cardiac surgery.

25.3 Lillehei–DeWall Bubble Oxygenator

Importantly, John Gibbon, M.D., from Boston, invented the cardiopulmonary bypass procedure and performed the first intracardiac repair using extracorporeal perfusion in 1953. His bubble oxygenator, which looked surprisingly like a computer, was manufactured and financed by IBM. His reported achievements stimulated rapid development of the knowledge base and equipment necessary for both accurate diagnoses of cardiac disease and successful intracardiac operations. Yet at that time, it was recognized that the main problems with film oxygenators were (1) poor efficiency, (2) excessive hemolysis, (3) large priming volumes, and (4) development of bubbles and foam in the

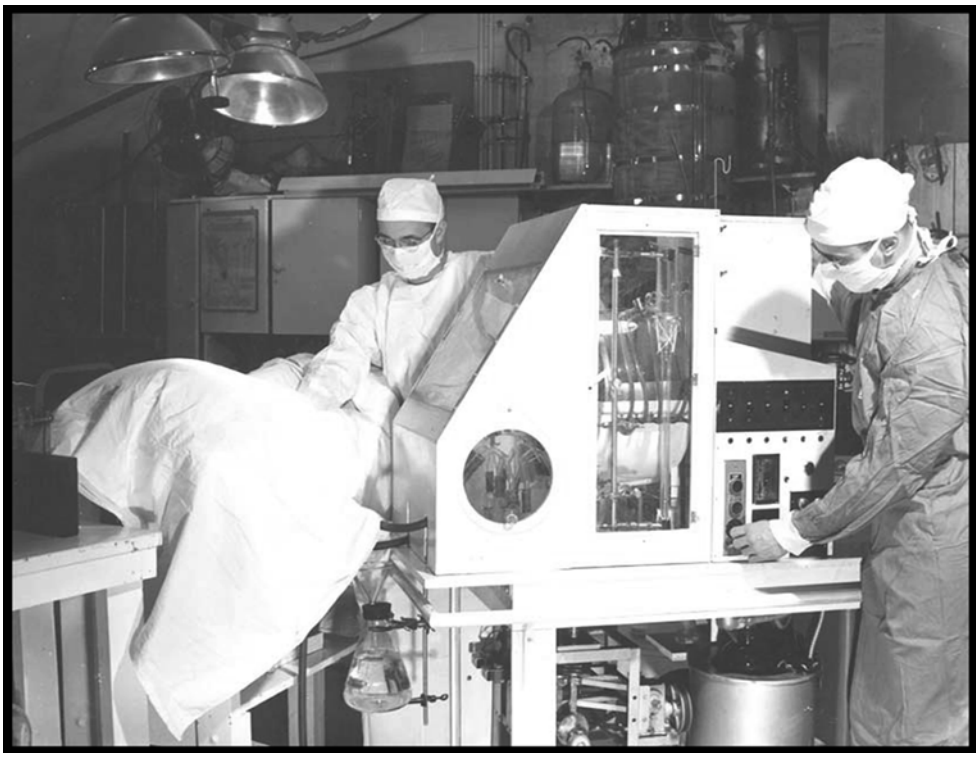

Fig. 25.6 Clarence Dennis with the first heart–lung machine at the University of Minnesota

Fig. 25.7 In this 1952 photo, Richard L. Varco (left) and F. John Lewis stand behind the hypothermia machine that they used during the world's first successful open-heart surgery

blood. All designs required blood flows of 2.2 l/m^2/min, usually three to four units of blood for priming and another two units for the remainder of the circuit. Furthermore, after each use, the machine needed to be broken down, washed, rinsed in hemolytic solution, reassembled, resterilized, and reconfigured.

During this era, Richard DeWall came to work at the University of Minnesota as an animal attendant in Lillehei's

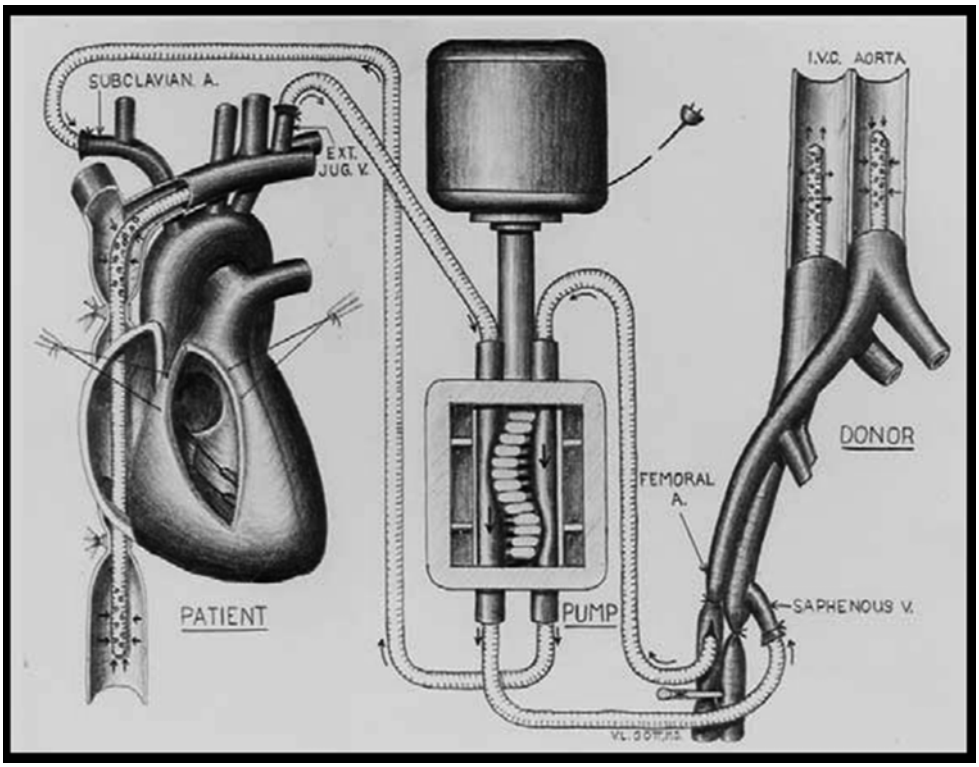

Fig. 25.8 Diagram of cross-circulation

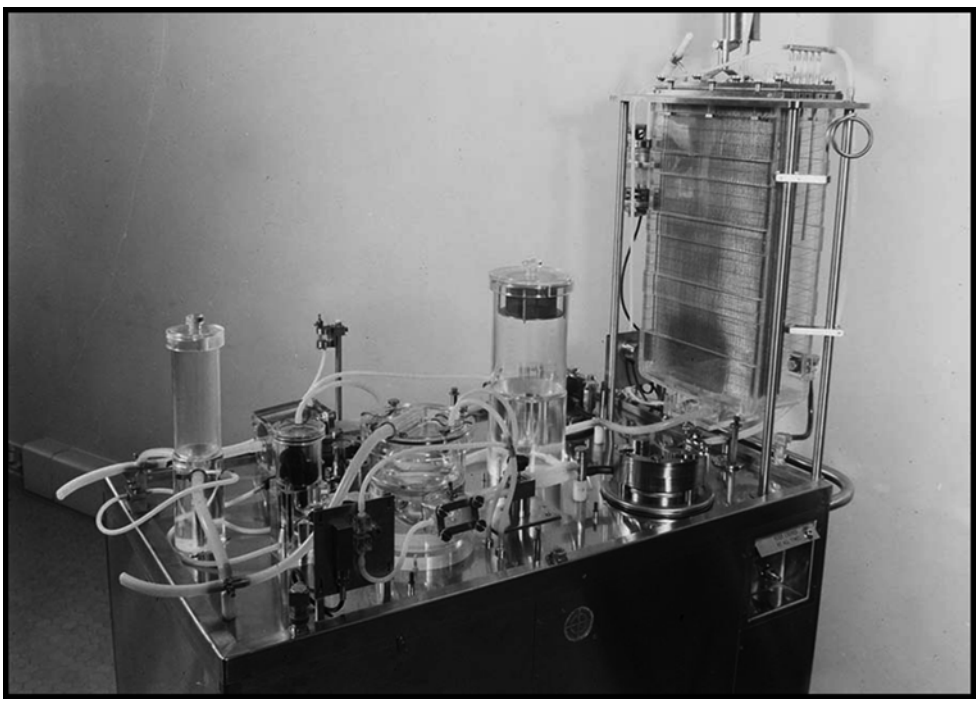

Fig. 25.9 Mayo Clinic's heart–lung machine was as big as a Wurlitzer organ; it cost thousands of dollars and required great skill to operate

research laboratory. It was noted that DeWall would manage the pump while the anesthesiologists would take breaks, and soon he began to take an interest in the problems associated with oxygenating blood. Eventually, Lillehei challenged DeWall to find a way to eliminate bubbles in the oxygenator procedure. Importantly, DeWall brought to fruition a dramatic technological breakthrough in 1955 by developing the first bubble oxygenator with a unique method for removing bubbles from the freshly oxygenated blood (Figs. 25.4 and 25.10). In DeWall's design, blood entered the bottom of a tall cylinder along with oxygen passed through sintered glass to create bubbles. As the bubbles and blood rose, gas exchange

Fig. 25.10 University of Minnesota's bubble oxygenator cost $15 and was easy to use. Richard DeWall is shown here with his model in 1955

occurred at the surface of each bubble. At the top of the cylinder, arterialized bubble-rich blood passed over stainless steel wool coated with silicone antifoam; it then traveled through a long helical settling coil to allow bubbles to slowly rise and exit the blood.

Two important components in the Lillehei–DeWall bubble oxygenator were the tubing and the silicon antifoam solution. The tubing was Mayon polyethylene tubing (typically used in the dairy and beer industries and specifically in the production of mayonnaise) available from Mayon Plastics, a company whose CEO was a classmate of Lillehei's and a graduate of the University's chemical engineering program. The silicone antifoam solution, Antifoam A, was used to coat the tubing to prevent foaming of the liquids being transported.

The oxygenator was wonderfully efficient; experimental animals (and later patients) did not show detectable effects of residual gas emboli. More importantly, this design eventually led to the development of a plastic, prepackaged, disposable, sterile oxygenator that replaced the expensive stainless steel, labor-intensive screen, and film devices. An economic and reliable oxygenator had arrived and the medical industry began to consider using disposable components for the heart–lung machine.

Two years after its introduction, the Lillehei–DeWall bubble oxygenator had been used in 350 open-heart operations at the University of Minnesota. DeWall steadily improved the device through three models, but it remained a very simple, disposable, heat-sterilizable device that could be built to accommodate only the amount of blood required for each patient and then discarded.

In 1956, another one of Lillehei's residents, Vincent Gott, invented a bubble oxygenator in which DeWall's helix design was flattened and enclosed between two heat-sealed plastic sheets (Fig. 25.11). This sheet bubble oxygenator proved to be the key to widespread acceptance of the device in open-heart surgery, because it could be easily manufactured and distributed in a sterile package and it was inexpensive enough to be disposable. The University of Minnesota eventually licensed the rights to manufacture and sell the device to Travenol, Inc. With the bubble oxygenator and techniques developed by Lillehei and his colleagues, the University of Minnesota had become even more prominent for making open-heart surgery possible and relatively safe [7].

By coincidence, Dr. Paul Iaizzo has a cousin, John Dilorio, who had a ventricular septal defect repaired by Dr. Lillehei in 1958, and a bubble oxygenation system was utilized during his surgery (Fig. 25.1). Interestingly, John's family journaled

Fig. 25.11 Richard DeWall and Vincent Gott look at the first commercially manufactured sterile bubble oxygenator in 1956

during his stay at the university's Variety Club Heart Hospital and noted the following events: (1) admitted to Variety Club Hospital on May 26, 1958; (2) surgery date of June 11, 1958, with a 6:45 start; (3) brought patient to the recovery room at 14:00; (4) treated postsurgically within an oxygen tent for 24 h and a cold room for 5 days; and (5) discharged on July 2, 1958. John is still alive today living in Texas, another testimony to the legacy of Dr. Lillehei.

25.4 Heart Block and the Development of the Pacemaker

An unexpected clinical consequence of the development of open-heart surgery was the discovery of a revolutionary new concept for treatment of complete heart block. Heart block is typically defined as the inability of electrical impulses that begin high in the right atrium to reach the ventricles. Deprived of their normal signal, the ventricles may beat slowly on their own (escape rhythm) or not at all; any prolonged decrease in heart rate that limits a patient's normal activity will typically result in heart failure. At that time, with the only existing treatment for complete block being positive chronotropic drugs or electrodes applied to the surface of the chest, there were no 30-day survivors.

Fortunately, in 1952, Paul Zoll, a cardiologist in Boston, invented the first pacemaker unit, which was a large tabletop external unit with a chest electrode. It was successfully used to resuscitate patients in the hospital, but required the transcutaneous delivery of 50–150 V, which was incredibly painful for children and typically left scarring blisters.

Complete heart block developed in 10–20 % of Dr. Lillehei's early patients undergoing closure of ventricular septal defects (e.g., due to induced injury of the heart's conduction system by stitches) and, unfortunately, hospital mortality was 100 % in this group of patients. Importantly, early fatality from heart block was completely eliminated with the use of a myocardially placed electrode in combination with an external plug-in electric stimulator [8]. This method of treatment, suggested by Dr. John A. Johnson, a professor of physiology at the University of Minnesota, required electrical stimuli of small magnitude (5–10 milliamps and 1–2 V) and provided very effective control of the heart rate. Such an approach was almost painless but, at that time, it required an AC electrical source, thus limiting the mobility of the patient to the length of the extension cord. It was first used by Dr. Lillehei on a patient on January 30, 1957; subsequently an 89 % survival rate for patients with prior heart block was reported (Fig. 25.4). More specifically, the pacemaker approach employed a multistrand, braided stainless steel wire in a Teflon sleeve that was directly implanted into the ventricular myocardium, with the other end brought through the surgical wound and attached to external stimulation. The first pacemaker (pulse generator) was a Grass physiological stimulator borrowed from the university's Physiology Department. This procedure was designed for short-term pacing, with removal of the wires 1–2 weeks after the heart regained a consistent rhythm.

The surgical operating rooms in the 1950s were equipped with EKG and pressure-monitoring devices, and the vacuum tubes required frequent monitoring and maintenance to keep them running and calibrated. Hence, the University Hospital

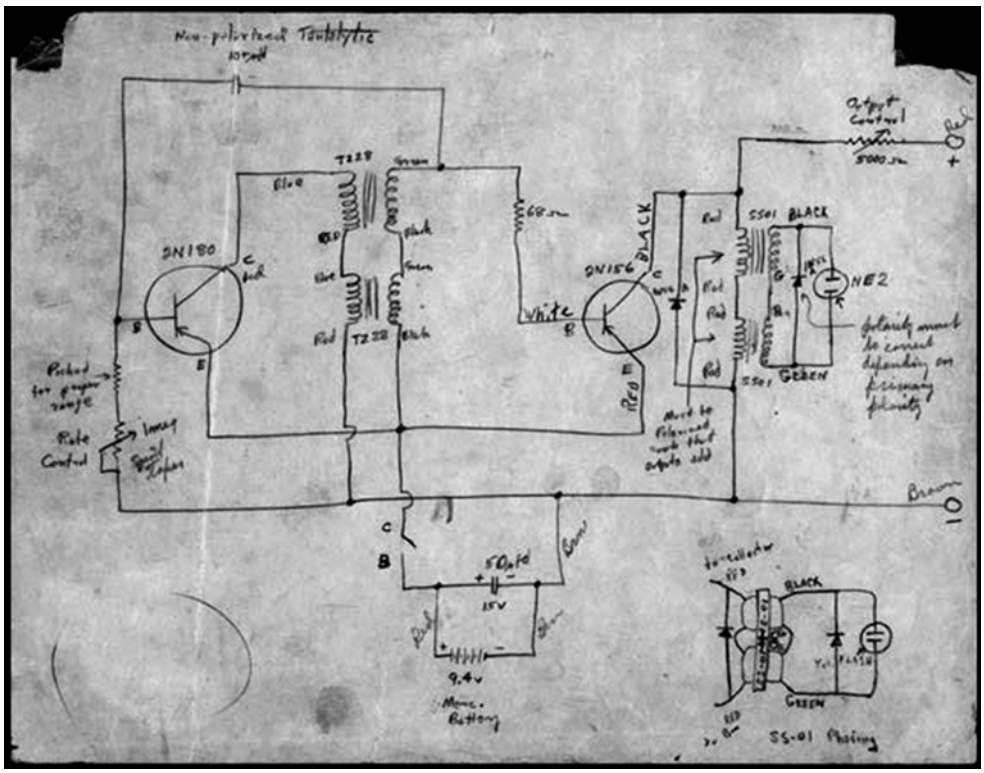

Fig. 25.12 Earl Bakken's original design for the battery-operated pacemaker

subcontracted with a local electric equipment repair company, Medtronic Inc., to perform these maintenance tasks. At that time, Medtronic was a two-person company—Earl Bakken and his brother-in-law Palmer Hermundslie. Earl was a trained electrical engineer who received his degree from the University of Minnesota; he was present during the surgical procedures in the University's operating rooms. It is reported that, following a disaster during which all electrical power service failed in the University Hospital due to a storm on October 31, 1957, Lillehei eventually asked Earl to design a battery backup for their pacemaker system, to avoid heart block due to power failures. Bakken began this work in 1957, using a circuit modified (in his words "plagiarized") from a circuit diagram for a transistorized metronome described in a *Popular Electronics* magazine (Fig. 25.12). During this period, Bakken spent numerous hours working in the operating rooms alongside Lillehei, and they became steadfast friends.

On April 14, 1958, the "battery-powered, wearable pacemaker" was first used clinically, even though this was somewhat unplanned. Bakken's transistor pulse generator made a miraculous "overnight" transition from preclinical animal testing to clinical use. Bakken brought his first prototype to the Surgery Department's research lab, where Dr. Vincent Gott used it on an animal with an imposed heart block and it functioned as planned. Excited by this progress, Bakken went home for the evening. That night, Lillehei worked late in the hospital and visited the laboratory where he observed the battery-powered pacemaker performing well; he immediately removed the pacemaker from the animal and brought it upstairs four floors to the ICU to use on a patient. The next day, when Bakken arrived back at the hospital, he was overwhelmed to see this device keeping a young child's heart beating (Fig. 25.4).

It was this wearable, battery-powered invention that set the stage for further development in the cardiac pacing industry. For the next decade or so, it would become common practice to put new devices or prototypes (even fully implantable ones) into clinical use immediately and then iron out the imperfections later based on accumulated clinical experience. This humanitarian practice developed because most of the early patients were close to death and no other treatments existed [9]. It should be noted that the Food and Drug Administration (FDA) was created by the US government in 1938, but it did not assume the role of regulating medical devices until 1976.

Eventually, Medtronic Inc., under Bakken's leadership, became the world's leading manufacturer of cardiac pacemakers beginning with the Model 5800. The first model of the 5800 pacemaker was black, but was quickly changed to white to look cleaner, more sanitary, and "hospital-like" (Fig. 25.13). Between 1959 and 1964, only a few hundred pacemakers were sold due to the reusability of the pacemaker and the short-term postsurgery focus. Orders soared once the

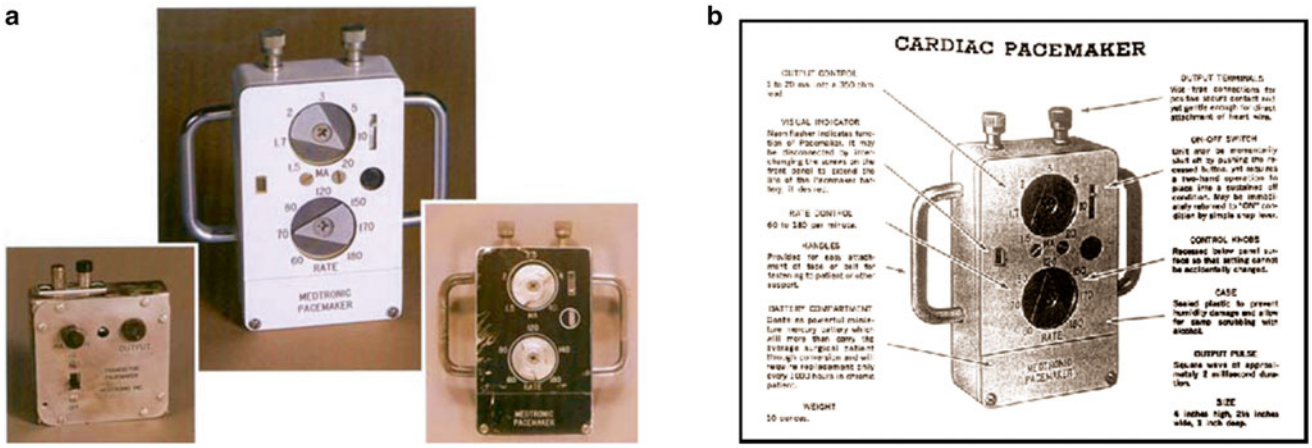

Fig. 25.13 (**a**) The first pacemaker prototype (*left*), the "black box" 5800 external pacemaker (the preliminary test model, *right*) and the "white box" 5800 production model (*center*). (**b**) A page from the Medtronic catalog advertising the 5800 pacemaker

pacemaker became implantable and redefined for long-term pacing use (Fig. 25.14). Nevertheless, the 5800 pacemaker became the symbol for Medtronic's shared belief in medical progress through technology; this was celebrated during an unveiling of a bronze statue of Earl Bakken holding the 5800 pacemaker at his retirement celebration in 1994. Years later, the 5800 was viewed by Lillehei as a technological watershed—it fostered interdisciplinary collaboration and exemplified the productive and successful marriage of medicine and technology.

Both Lillehei and Bakken have named professorships at the University of Minnesota. In addition, the Lillehei Heart Institute (LHI) was created in 2002 to honor the past with the C. Walton Lillehei Museum, while supporting the future through its unique research and educational programs. LHI is an interdisciplinary institute within the Academic Health Center and Medical School at the University of Minnesota, made possible by a generous gift from Kaye Lillehei, wife of C. Walton Lillehei. Dr. Daniel Garry, Chief of the Cardiovascular Division of Medicine, was named Director of the LHI in 2007. The LHI has flourished since its inception, and a new cardiovascular research building/facility opened in the University's Bioscience District in 2013; this facility is the home of numerous dedicated basic and applied scientists working on the next innovative breakthroughs in cardiovascular medicine.

More specifically, guided by a vision to sustain and enhance world leadership in the prevention, detection, and treatment of heart and vascular diseases, LHI supports these important efforts [10]:

1. Clinical and basic science research focused on cardiovascular genomics, heart development, heart regeneration, stem cell therapies, personalized medicine, heart failure, vascular biology, and device design to treat cardiovascular diseases. In recent years, LHI has established and recruited new research teams that work in their new state-of-the-art research facilities.
2. Participation as the Midwestern hub of the National Heart, Lung, and Blood Institute's (NHLBI) Progenitor Cell Biology Consortium, commissioned to lead new cardiovascular therapies.
3. LHI Lecture Series (established in 2003). In addition to showcasing leading edge research taking place at the University of Minnesota, the weekly lecture series invites scientists from institutions across the USA and abroad to share their research.
4. Summer Research Scholars Program. Annual summer research scholarships in basic science related to cardiovascular disease are awarded to highly qualified high school and undergraduate students. These highly competitive, prestigious scholarships are designed to expose students to several disciplines within cardiovascular disease research and its clinical applications.
5. Lillehei Endowed Scholars Program. This program provides cardiovascular and respiratory research fellowships and grants to University of Minnesota faculty and students, including undergraduates, medical students, and predoctoral and postdoctoral fellowships.
6. "A Heart to Learn" Youth Educational Program. Hosted by faculty, staff, and graduate/medical students from the Visible Heart Laboratory [2], this community outreach program is designed to teach concepts of cardiac anatomy, physiology, medical devices, and heart health to students in elementary, middle, and high schools.

In December 2007, at a celebration of the 50th anniversary of the wearable, battery-powered pacemaker, the University of Minnesota awarded Earl Bakken with an honorary M.D. degree (Fig. 25.15). In the same month, the University's Department of Surgery hosted the first annual Bakken Surgical Device Symposium to celebrate this legacy.

Fig. 25.14 Dr. Samuel Hunter (*inset*) and adult pacing patient Warren Mauston. Dr. Hunter and Medtronic engineer Norman Roth developed a bipolar electrode that represented a major advance in pacing technology. First implanted in 1959, the Hunter–Roth lead helped contribute 7 years of life to a Stokes–Adams disease patient, Warren Mauston in 1960

Fig. 25.15 Earl Bakken, the founder of Medtronic Inc., received an honorary M.D. degree from the University of Minnesota in 2007. He is shown here with his M.D. white coat and medical bag, presenting his historic prospective lecture at the first Bakken Surgical Device Symposium, hosted by the Department of Surgery at the University of Minnesota on December 13, 2007

Since its inception, this symposium has focused on various topics related to cutting-edge medical devices including:

- The Pacemaker: Past, Present, and Future (2007)
- Cardiac Valves: Past, Present, and Future (2008)
- Minimally Invasive Cardiac Surgery (2009)
- Heart Failure (2010)
- Recent Advances in Cardiac Devices and Procedures (2011)
- Innovations in Cardiovascular Therapy (2012)
- The Evaluation, Management and Long-Term Follow-up of Children with Congenital Heart Disease (2013)
- Advances in Congenital and Adult Heart and Lung Transplantations

25.5 Heart Valves

Initial development in the field of prosthetic heart valves involved the search for biologically compatible materials and hemologically tolerant designs; it is considered today that early successes could not have been achieved without the union of these two factors. At that time, as there was no satisfactory mechanism to scientifically achieve this goal, the trial and error method was used; it is important to note that much of this early work was also performed at the University of Minnesota. The development of prosthetic heart valves

became the purview of several cardiovascular surgeons who often collaborated with engineers. To distinguish one valve from the others, each prosthesis often became identified and named after its surgeon developer [11].

It is notable that Lillehei and his colleagues developed four different valves: (1) a non-tilting disk valve called the Lillehei–Nakib toroidal valve in 1967; (2) two tilting disk valves, the Lillehei–Cruz–Kaster in 1963 and the Lillehei–Kaster in 1970 (produced by Medical Inc. in 1970 and eventually distributed by Medtronic Inc. in 1974); and (3) a bileaflet valve, the Lillehei–Kalke in 1965 (manufactured by Surgitool in 1968 and used clinically by Dr. Lillehei at the New York Cornell Medical Center) (Figs. 25.4 and 25.16).

The St. Jude bileaflet valve was primarily designed by Chris Posis, an industrial engineer who approached Demetre Nicoloff, M.D., a cardiovascular surgeon at the University of Minnesota. This valve had floating hinges located near the central axis of the rigid housing as well as an opening to the outer edge of each leaflet, leaving a small central opening (Figs. 25.4 and 25.17) [12]. Nicoloff first implanted this valve in October 1977, and it provided the foundation for the beginning of St. Jude Medical as a significant biomedical device company. Dr. Nicoloff was asked to serve as the Medical Director of the new company; however, he declined due to the demands of his clinical practice. Rather, he suggested that Dr. C. W. Lillehei be named as the Medical Director, a post that Lillehei held until his death in 1999 [11].

It is important to note that most of these past valve designs, as well as current designs, were evaluated in animal trials at the University of Minnesota. More specifically, Richard Bianco, Director of Experimental Surgical Services, has been at the University for over 35 years working with a core of clinicians, scientists, and engineers on the design, evaluation, and redesign of their cardiac valves. For more details on such experimental trials, refer to Chap. 27.

More recently, Dr. Robert Wilson, the former Head of Interventional Cardiology at the University of Minnesota, continued this innovative legacy in the field of cardiac heart valves by developing a third-generation approach to a transcatheter aortic valve; he founded Heart Leaflet Technologies, a company that continues to commercialize these devices (www.heartleaflet.com/).

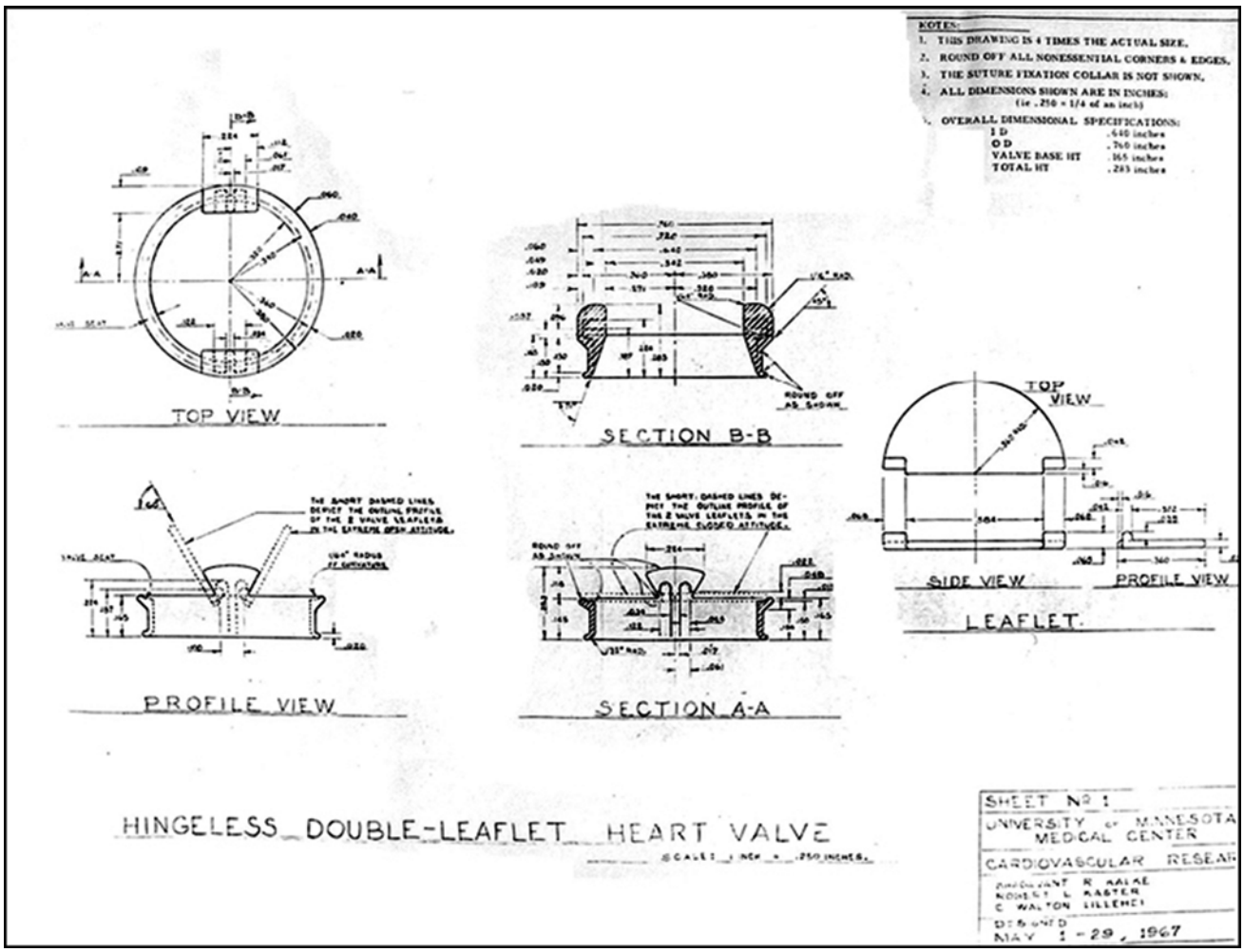

Fig. 25.16 The Lillehei–Kalke rigid bileaflet prosthesis (1968)

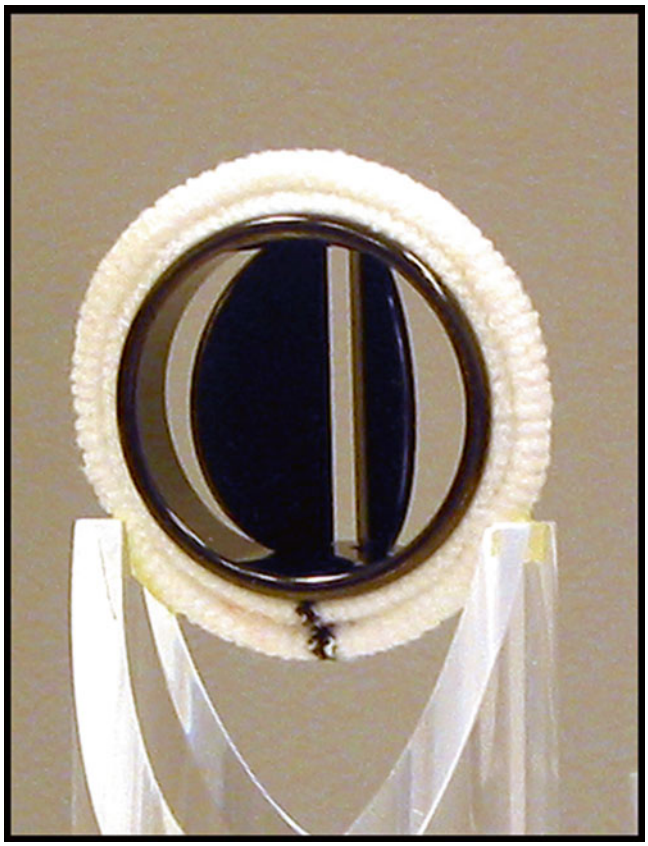

Fig. 25.17 St. Jude bileaflet prosthesis developed in 1976

25.6 Other University-Affiliated Medical Devices

Many of the major breakthroughs in cardiac device development at the University of Minnesota occurred via associated collaborations with the Surgery Department. In more recent times, several more cardiovascular medical devices have been invented in areas other than the Department of Surgery, specifically the Departments of Medicine and Radiology. Examples of such devices and technologies include compression/decompression cardiopulmonary resuscitation devices (Chap. 38) and transcatheter closure devices that are permanent cardiac implants designed to close defects between chambers of the heart (Chap. 37). The later devices are self-expanding, self-centering umbrella-like devices whose design and shape varies, as does the exact mode of their deployment. They are implanted in the heart through catheters inserted into either the artery or vein in a cardiac catheterization laboratory. Transcatheter closure devices are intended to provide a less invasive alternative to open-heart surgery, which has been the standard of care. These closure devices were the brainchild of Dr. Kurt Amplatz, who spent most of his 40-year career in radiology as the Chairman of Interventional Radiology at the University of Minnesota. In 1995, he founded AGA Medical, a publicly held medical technology company that is now a part of St. Jude Medical. Dr. Amplatz also developed many other catheters, guidewires, etc., and these designs remain as the foundation for numerous technologies still commonly employed today; he is an inventor on 45 US patents.

25.7 Medical Device Regulation

In the 1950s, Earl Bakken adopted the motto of his friend and colleague, Dr. Lillehei, for his initial method of device development—"Ready, Fire, Aim." In other words, devices were actually tested in humans; therefore, the transition from bench to bedside happened at an accelerated pace [10]. However, in 1976, the Medical Device Amendments to the Federal Food, Drug, and Cosmetic Act established three regulatory classes for medical devices, based upon the degree of control necessary to assure the safety and effectiveness of various types of devices. The most regulated devices are considered class III that, by definition, (1) are devices designed to support or sustain human life, (2) are of substantial importance in preventing impairment of human health, or (3) present a potential unreasonable risk of illness or injury. All devices placed into class III are subject to premarket approval requirements, including a scientific review to ensure their safety and effectiveness.

Under Medical Device Reporting in the FDA, all manufacturers, importers, and user facilities are required to report adverse events and correct them quickly. Although, since 1984, manufacturers and importers of medical devices have been required to report all device-related deaths, serious injuries, and certain malfunctions to the FDA, numerous reports show underreporting. Therefore, the Safe Medical Devices Act (SMDA) of 1990 was implemented; device user facilities must report device-related deaths to the FDA and the manufacturer. In addition, the SMDA requires that device user facilities submit reports to the FDA on an annual basis (FDA Modernization Act of 1998). In the past several years, recalls of defective pacing systems and leads have had a major impact on the medical device industry in the USA, resulting in dramatic shifts within vitally affiliated companies. For more details, refer to Chap. 42.

25.8 LifeScience Alley

Spurred by the flurry of innovations from Minnesota inventors such as the pacemaker, bubble oxygenator, and artificial heart valve, LifeScience Alley (formerly Medical Alley) was established in 1984 as a nonprofit trade association to support the region's growing healthcare industry [10]. LifeScience Alley was founded by Earl Bakken, founder of

Medtronic Inc.; Bakken, at the current age of 90, remains on the LifeScience Alley Board of Directors to this day as Chairman (Emeritus), and Shaye Mandle currently presides over the association.

In 2010, Dale Wahlstrom (then President and CEO of both LifeScience Alley and the BioBusiness Alliance of Minnesota) led the collaboration between these organizations. Focused on their shared mission to grow and secure Minnesota's position as a global leader in the life sciences, LifeScience Alley now serves nearly 700 member organizations from all sectors of the life science sector, including medical technology and equipment manufacturers, pharmaceutical and biopharmaceutical companies, healthcare providers and insurers, agricultural and industrial biotechnology organizations, academic institutions and government entities, and a broad range of service and consulting companies.

Furthermore, LifeScience Alley hosts a rigorous calendar of events designed to connect, educate, and strengthen the regional life science community including (1) informational programs on the latest industry trends, regulations, and standards; (2) networking events; (3) member updates on trends in employment, capital, and policy issues; and (4) leadership forums and luncheons. Additionally, they host two annual conferences:

1. LifeScience Alley Conference. An event that brings together life science leaders from their diverse member network to discuss trends, promote industry growth, and create valuable connections.
2. MedTech Investing Conference. An event for medical device investors, entrepreneurs, and corporate business development executives to discuss critical issues in the medical device sector and serve as an intimate networking venue to foster the development and financing of companies.

On behalf of its members, LifeScience Alley also develops and supports public policies that promote growth of the life science industry locally, nationally, and globally.

25.9 Design of Medical Device Conference

Since 2001, the University of Minnesota's Medical Device Center, the College of Science and Engineering, the Institute for Engineering in Medicine, and the Academic Health Center have hosted an annual Design of Medical Devices (DMD) Conference every April. This remains today as the largest medical device conference worldwide; its primary goal is to provide an international forum bringing together world-class medical device designers, researchers, manufacturers, and the public sector, to share perspectives and innovations related to medical device design. The conference further showcases the University of Minnesota as a leader in the medical device community and generates funds from corporate sponsorships to support medical device education at the University. In recent years, the conference has grown to over 1,100 participants annually from 17 different countries and multiple companies and academic institutions [13] (www.dmd.umn.edu).

25.10 The Institute for Engineering in Medicine

The Institute for Engineering in Medicine (IEM) is an interdisciplinary research organization that strives to strengthen collaborative efforts between the disciplines of engineering and biomedicine at the University of Minnesota. Five main themes dominate IEM's focus on research: cardiovascular engineering, neuroengineering, cellular and molecular bioengineering, medical and biological imaging, and medical devices. The IEM mission revolves around creating and applying innovative engineering solutions to medical and health problems, in addition to fostering collaborations with industry. To achieve these goals, IEM sponsors three endowed chairs and a fellowship program, as well as various seminars, workshops, and conferences (Neuromodulation Symposium, Design of Medical Devices Conference, IEM Conference & Retreat). IEM is currently directed by Professor Bin He [14].

25.11 Medical Devices Center

Under the direction of Professor Arthur Erdman, the Medical Devices Center (MDC) was established by the University of Minnesota in 2007 (Fig. 25.4). A primary goal of this center is to strengthen interdisciplinary medical device research among faculty in the Academic Health Center and the College of Science and Engineering. The MDC recently opened a new core facility, which includes (1) a computer-aided design (CAD)/precision instrumentation laboratory with 3D printing, (2) an electronic fabrication laboratory, (3) a mechanical prototyping facility, (4) a testing room–wet laboratory, (5) an anatomy–physiology SimPORTAL laboratory, and (6) a multipurpose room for modeling, assembly, demonstrations, or conferences [15]. The center supports an Innovation Fellows Program to recruit and hire individuals across the medical engineering and clinical disciplines to form cross-functional teams that aim to develop novel medical technologies.

The MDC, in collaboration with Professor Daniel Keefe from the Department of Computer Sciences and various corporate collaborators, has developed a Virtual Prototyping Lab with the goal of simulating the placement of existing or

novel device concept within virtual anatomies (www.mdc.umn.edu/mdc/vrlab). Further support is provided by the Minnesota Supercomputing Institute that provides access to high-performance advanced computational resources and user support to facilitate cutting-edge research in all disciplines, as well as promote technology transfer through the interchange of ideas in the field of supercomputing research. Researchers have ready access to informatics, visualization, and application development services (www.msi.umn.edu).

25.12 Cardiovascular Physiology at the University of Minnesota

The Department of Physiology at the University of Minnesota has a rich history of performing basic cardiovascular research and establishing clinical collaborations within the institution (see Sect. 25.1). Not only have these individuals published many important basic research papers, but they have also been integrally involved in the training of many generations of cardiac physiologists, surgeons, and biomedical engineers.

One of the more notable Chairmen of the Department of Physiology was Maurice Visscher, who was present during the Owen Wangensteen and C. Walton Lillehei eras. In 1936, Dr. Visscher returned to the University of Minnesota to succeed Dean Lyon as the Head of the Department of Physiology (Table 25.4). He first came to Minnesota in 1922 as a graduate student in physiology under the mentorship of Frederick Scott and satisfied the requirements for both Ph.D. and M.D. degrees in a 4-year period of time [16]. Interestingly, subsequent to his studies, Visscher served as a postdoctoral fellow in England at the University College London. While there, he worked under the advisement of the notable cardiac physiologist, Ernest Starling, who, at that time, was near the end of his brilliant career (e.g., Starling's Law of the Heart). Together in 1927, Starling and Visscher published a classic paper in which, using a heart–lung preparation (introduced by Starling in 1910), they reported that the oxygen consumption of the heart was correlated directly with its volume in diastole, without regard to the amount of work the heart was exerting in pumping blood [17, 18]. After Starling's death in 1927, Visscher continued research on this topic while serving as the Physiology Department Chairman in Minnesota; his research was considered to shed valuable light on the mechanisms underlying heart disease due to coronary occlusion, in general.

Table 25.4 Department of Physiology at the University of Minnesota: chairs/interim heads

Physiology Department chair/interim head	Position	Years served
Richard O. Beard	Department Chair	1889–1913
Elias P. Lyon	Department Chair	1913–1936
Dr. Maurice B. Visscher	Department Chair	1936–1968
Eugene Grim	Department Chair	1968–1986
Richard E. Poppele	Interim Head	1986–1988
Robert F. Miller	Department Chair	1988–1998
Joseph DiSalvo	Interim Head	1998–2002
Douglas Wangensteen	Interim Head	2002–2008
Joseph M. Metzger	Department Chair	2008–present

It has been described that Owen Wangensteen, having recognized how many of these findings were directly applicable to surgery, initiated collaborations with Visscher and the Physiology Department. To this extent, Wangensteen initiated and conducted a regular Physiology–Surgery Conference that was considered "invaluable in acquainting surgical residents with the techniques of experimental physiology" [18]. Many also credit Wangensteen's academic philosophies for enabling the pioneering advancements in open-heart surgery and subsequent pacemaker technologies at the University of Minnesota. For example, Earl Bakken asked C. Walton Lillehei in 1997, "How did you have the courage to go ahead with these pioneering-type experiments?" Lillehei replied, "As I think, when I look back, that was part of the Wangensteen training system" [19]. He further elaborated, "[Wangensteen] was a unique person in many regards. One [aspect of his] uniqueness was his training system. He had a great faith in research, animal or other types of laboratory research. He felt that the results of his research gave the young investigator the courage to challenge accepted beliefs and go forward, which you would not have had, as I look back, as a young surgical resident. That's why many of the great universities didn't produce much in the way of innovative research, because they were so steeped in tradition. Wangensteen had a wide open mind. If research showed some value, then you should pursue it."

Importantly, the past few years have brought a renewed interest in refocusing the Physiology Department to again be a leader in the cardiovascular field. In the spirit of Maurice Visscher, the new Department of Integrative Biology and Physiology emerged in recent years under the direction of Professor Joseph Metzger. Departmental research focuses on integrative systems biology of the heart and vasculature, including close linkages among cardiovascular diseases and obesity, diabetes, and metabolism, thus bridging the gap between basic science discovery and clinical application. The department offers a unique intense short course, Advanced Cardiac Physiology and Anatomy, for individuals in industry as well as postdoctoral and graduate students; this course consists of multiple lectures, delivered by clinicians and researchers, related to basic cardiac anatomy, physiology, cardiovascular disease, and clinical diagnosis and treatment, as well as hands-on gross anatomy labs. Further, as a tribute to Maurice Visscher, an annual Visscher Symposium is organized, featuring world-renowned keynote speakers and showcasing graduate student research [20].

Dr. Lillehei believed that "What mankind can dream, research and technology can achieve." And with the support of the Lillehei Heart Institute, in collaboration with the Institute for Engineering in Medicine and other organizations, the circle has been completed.

25.13 Summary

The University of Minnesota has a rich tradition of research and development in the fields of cardiovascular science and medical device design. Today, Minnesota has one of the highest densities of medical device companies in the world, and thus the university remains uniquely positioned to (1) educate the next generation of employees for this industry, (2) be a strong academic collaborator with industry by being an international leader in both basic and clinical cardiovascular research, and (3) serve the additional outreach mission of the university relative to cardiovascular sciences (e.g., partnering with LifeScience Alley and other organizations). The rich legacy of the early pioneers in cardiovascular research, medicine, and surgery lives on at the University of Minnesota.

References

1. Lillehei CW (1994) The birth of open heart surgery: then the golden years. Cardiovasc Surg 2:308–317
2. www.vhlab.umn.edu. Accessed 8/5/14
3. Lillehei CW et al (1986) The first open heart repairs of ventricular septal defect, atrioventricular communis, and Tetralogy of Fallot using extracorporeal circulation by cross-circulation. Ann Thorac Surg 41:4–21
4. Lillehei CW (1982) A personalized history of extracorporeal circulation. Trans Am Soc Artif Intern Organs 28:5–16
5. Moller JH, Shumway SJ, Gott VL (2009) The first open-heart repairs using extracorporeal circulation by cross-circulation: a 53-year follow-up. Ann Thorac Surg 88:1044–1046
6. Miller GW (ed) (2000) King of hearts. Crown Publishers, New York
7. Moore M (1992) The genesis of Minnesota's Medical Alley. UMN Medical Foundation Bulletin
8. Gott VL (2007) Critical role of physiologist John A. Johnson in the origins of Minnesota's billion dollar pacemaker industry. Ann Thorac Surg 83:349–353
9. Rhees D, Jeffrey K (2000) Earl Bakken's little white box: the complex meanings of the first transistorized pacemaker. In: Finn B (ed) Exposing electronics. Harwood Academic Publishers, Amsterdam
10. www.lhi.umn.edu. Accessed 8/5/14
11. DeWall R (2000) Evolution of mechanical heart valves. Ann Thorac Surg 69:1612–1621
12. Villafana M (1989) It will never work! The St. Jude valve. Ann Thorac Surg 48:S53–S54
13. www.dmd.umn.edu. Accessed 8/5/14
14. www.iem.umn.edu. Accessed 8/5/14
15. www.mdc.umn.edu. Accessed 8/5/14
16. Visscher MB (1969) A half century in science and society. Annu Rev Physiol 1017:1–18
17. Starling EH, Visscher MB (1927) The regulation of the energy output of the heart. J Physiol 62:243–261
18. Wilson LG (ed) (1989) Medical revolution in Minnesota: a history of the University of Minnesota medical school. Midewiwin Press, St. Paul
19. Minnesota Historical Society (2002) Pioneers of the medical device industry in Minnesota: an oral history project, Earl E. Bakken and Dr. C. Walton Lillehei. Minnesota Historical Society Oral History Office, David Rhees (Interviewer)
20. www.physiology.med.umn.edu. Accessed 8/5/14

Additional Resources

U.S. Food and Drug Administration, Center for Devices and Radiological Health, website: www.fda.gov/opacom/7org.html

Rigby M (1999) The era of transcatheter closure of atrial septal defects. Heart 81:227–228

Stephenson L (ed) (1999) State of the heart: the practical guide to your heart and heart surgery. Write Stuff Syndicate, Inc., Fort Lauderdale

Pharmacotherapy for Cardiac Diseases

26

Anna Legreid Dopp and Katie Willenborg

Abstract

Clinical trial design inclusion criteria typically require that patients be on optimal medical therapy prior to their enrollment or randomization, i.e., they are currently being managed by medical regimens proven to be safe and effective and considered standard in clinical practice for the particular disease state being studied. Only if this is the case can any trial's clinical or statistical significance be determined between study groups. This chapter outlines the current optimal medical management/therapy for patients eliciting: (1) hypertension, (2) acute coronary syndromes and myocardial infarction, (3) heart failure, and/or (4) arrhythmias.

Keywords

Diuretics • Beta-blockers • Angiotensin-converting enzyme inhibitors • Angiotensin receptor blockers • Calcium channel blockers • Antiplatelets • Anticoagulants • Aldosterone antagonists

26.1 Abbreviations

ACE	Angiotensin-converting enzyme
AF	Atrial fibrillation
ARB	Angiotensin receptor blocker
CHD	Coronary heart disease
CRT	Cardiac resynchronization therapy
CVD	Cardiovascular disease
HF	Heart failure
ICD	Implantable cardioverter defibrillator
NSTEMI	Non-ST segment elevation myocardial infarction
PCI	Percutaneous coronary intervention
STEMI	ST segment elevation myocardial infarction

A.L. Dopp, PharmD (✉)
Pharmacy Society of Wisconsin,
701 Heartland Trail, Madison, WI 53717, USA
e-mail: annad@pswi.org; amlegreid@yahoo.com

K. Willenborg, PharmD, BCPS
University of Wisconsin Hospital and Clinics, Madison, WI, USA

26.2 Introduction

Chronic disorders such as heart disease, diabetes, stroke, obesity, and cancer remain today as the leading causes of death and disability in the United States. Nearly half of all Americans have at least one chronic condition, and seven out of the top ten causes of death are due to chronic diseases [1]. Importantly, heart disease, or cardiovascular disease (CVD), is the chronic disorder that is the leading cause of death in the United States, accounting for 600,000 deaths annually or roughly 25 % of all deaths [2]. Yet this represents a 2 % rate of decline for deaths attributed to heart disease over the past few years. In addition, between 1999 and 2010, the prevalence of adults with at least one of the three following CVD risk factors: uncontrolled high blood pressure, uncontrolled high levels of low-density lipoproteins cholesterol, or current smoking, decreased from 58 to 47 % [3]. For a complete list of CVD risk factors, see (Table 26.1). While these morbidity and mortality improvements represent important successes, the medical management of patients living with CVD

P.A. Iaizzo (ed.), *Handbook of Cardiac Anatomy, Physiology, and Devices*, DOI 10.1007/978-3-319-19464-6_26

Table 26.1 Cardiovascular disease risk factors

• Tobacco use
• Dyslipidemia
• Overweight (body mass index ≥ 25 kg/m^2)
• Diabetes mellitus
• Age (>45 years for men; >55 years for women)
• Physical inactivity
• Family history of early cardiovascular disease or hypertension (men <55 years; women <65 years)

Table 26.2 American College of Cardiology Foundation/American Heart Association level of evidence designations

Level A	Data derived from multiple *randomized* clinical trials involving a large number of individuals
Level B	Data derived from a limited number of trials involving comparatively small numbers of patients or from well-designed data analysis of *nonrandomized* studies or *observational* data registries
Level C	Consensus of expert opinion is the primary source of recommendation

continues to require significant utilization of healthcare dollars and resources.

Cardiovascular disease is comprised of multiple disease states, the pathogeneses of which are often interrelated. Today, the most common form of CVD is coronary heart disease (CHD), which occurs in 17.6 million Americans [4]. This chapter will provide general pharmacotherapy treatment guidelines for the management of the following CVDs: hypertension, acute coronary syndrome and myocardial infarction, heart failure, and arrhythmias.

26.3 Evidence-Based Medicine

In order to describe the drug therapy regimens for the disease states listed above, first there needs to be a brief explanation of how general clinical guidelines are developed and implemented. As such, evidence-based medicine is the process of conscientious, explicit, and judicious use of current best evidence in making decisions about the care of an individual patient [5]. Several expert working groups and agencies have developed systems for grading recommendations and classifying evidence according to the scientific rigor of the study results available. The system used most often in medicine is GRADE, the Grading of Recommendations Assessment, Development, and Evaluation system. For the purposes of this chapter, which focuses on pharmacotherapy for the treatment of cardiac diseases, strength of recommendation and evidence levels developed by the American College of Cardiology Foundation (ACCF)/American Heart Association (AHA) clinical data standards will be utilized for the discussion that follows (Tables 26.2 and 26.3) [6]. Treatment recommendations will focus primarily on those that have a class I or IIa strength of recommendation.

26.4 Hypertension

Nearly one-third of people in the United States have high blood pressure [7, 8], defined as systolic blood pressure >140 mmHg or diastolic blood pressure >90 mmHg [8, 9], yet less than half (47 %) of these individuals have their blood pressure controlled. Unfortunately, this not only increases morbidity and mortality but ultimately impacts healthcare consumption and cost.

26.4.1 Goals of Therapy for Hypertension

Left untreated, hypertension can lead to target organ disease in the cardiovascular system and also within the cerebrovascular system, peripheral vascular system, kidneys, and/or eyes; it can eventually lead to consequences such as stroke, transient ischemic attacks, peripheral artery disease, chronic kidney disease, and retinopathy. Figure 26.1 illustrates the generally accepted continuum of hypertensive disease and, specifically, its effects on the myocardium. The primary goal of treatment for hypertension is to reduce the blood pressure to a level below that which was used to diagnose the condition; however, these thresholds have been recently debated in the literature. In addition, the role that an individual's race plays in the development of hypertension is rightfully gaining more research and clinical attention, e.g., African Americans develop hypertension earlier in life and have higher average blood pressures than Caucasians [10]. Recent guidelines account for this difference and contain specific recommendations for black and non-black patients [11].

The highly anticipated and debated Eighth Report of the Joint National Committee on Prevention, Detection, Evaluation, and Treatment of High Blood Pressure (JNC8) outlines nine recommendations for the management of

Table 26.3 American College of Cardiology Foundation/American Heart Association classification of recommendations

Class I	Conditions for which there is evidence and/or general agreement that a given procedure or treatment is beneficial, useful, and effective
Class II	Conditions for which there is conflicting evidence and/or a divergence of opinion about the usefulness or effectiveness of a procedure or treatment • Class IIa: Weight of evidence/opinion favor usefulness/efficacy • Class IIb: Usefulness/efficacy is less well established by evidence/opinion
Class III	Conditions for which there is evidence and/or general agreement that a procedure or treatment is not useful or effective and, in some cases, may be harmful

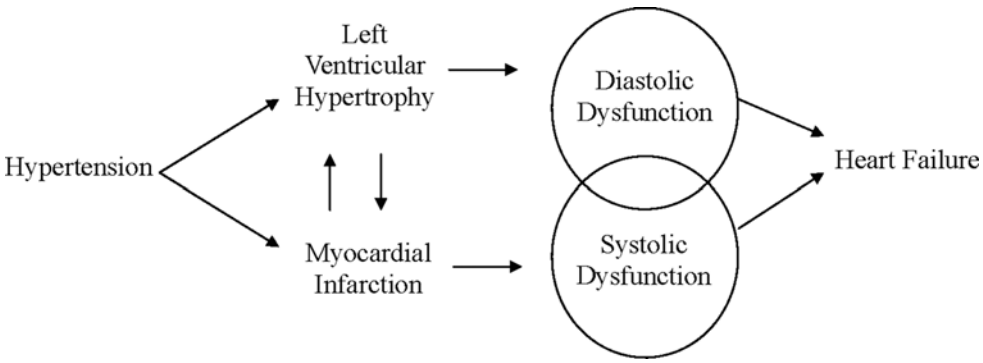

Fig. 26.1 Continuum of hypertensive disease and its effects on the myocardium

hypertension based on evidence published exclusively from randomized controlled trials [11]. While continuing to endorse a hypertension goal of <140/90 mmHg for patients less than 60 years old, the new recommendations relax to some extent the previously published goals if patients are ≥60 years old (new goal: <150/90 mmHg), have diabetes, or have chronic kidney disease (new goal: <140/90 mmHg for both) [9]. Since the release of these JNC8 guidelines, a number of other groups such as the American Society of Hypertension (ASH), European Society of Hypertension, and the National Institute for Health and Clinical Excellence have reaffirmed recommendations of a blood pressure goal of <140/90 mmHg for all patients, providing an exception that it may be appropriate to target a blood pressure of <150/90 in patients over 80 years old [12–14]. For example, ASH delineates staging of hypertension (e.g., prehypertension versus hypertension) and blood pressure goals based on age and comorbid conditions. They recommend that the general population and patients with diabetes, kidney disease, and coronary artery disease should attempt to achieve a blood pressure of <140/90 mmHg but recommend <150/90 mmHg for patients over 80 years old and a diastolic goal of <90 mmHg for patients less than 50 years old [12]. Despite this controversy and uncertainty in optimal blood pressure targets, the ultimate goal of hypertension prevention and management is to prevent disease progression and reduce overall morbidity and mortality.

26.4.2 Treatment Guidelines for Hypertension

Lifestyle modifications are considered as a key component in the treatment regimen for patients with hypertension. Modifications such as smoking cessation, weight loss, increased physical activity, and decreased sodium intake have all been shown to have profound effects on lowering blood pressure and improving overall health [9, 11–14]. Medications of choice for managing hypertension have also changed with the release of recent guidelines. The JNC8 guidelines indicate that an angiotensin-converting enzyme (ACE) inhibitor (or angiotensin receptor blocker [ARB]), a dihydropyridine calcium channel blocker, and thiazide-type diuretics are considered "first-line" therapy options for such patients [11]. Selection of an antihypertensive will also be determined by patient race (black or non-black) and/or whether the patient has a concomitant condition. In following JNC8 recommendations, additional considerations should be determined relative to patients with various races, diabetes mellitus, and/or chronic kidney disease; however, other organizations such as ASH consider the presence of other compelling indications for selection of medication or combination of medications (Table 26.4). Indeed, beta-blockers are no longer a preferred agent unless the patient has a compelling indication. For example, for those patients with hypertension and coronary artery disease, a beta-blocker plus an ACE inhibitor may be warranted. Lastly, if blood pressure therapeutic goals are not

Table 26.4 Agents with compelling indications for treatment of hypertension [12]

Compelling indication	Diuretic	Beta-blocker	ACE inhibitor	Angiotensin receptor blocker	Calcium channel blocker	Aldosterone antagonist
Heart failure	X	X	X	X	X[a]	X
Post-myocardial infarction		X	X			X
High coronary heart disease risk	X	X	X	X	X	
Diabetes	X	X	X	X	X	
Chronic kidney disease			X	X	X	
Recurrent stroke prevention	X		X	X	X	

[a]A dihydropyridine calcium channel blocker may be added if needed for blood pressure control

achieved with a single agent, a second or third antihypertensive may need to be added.

26.5 Acute Coronary Syndrome and Myocardial Infarction

Acute coronary syndrome is a condition used to describe any clinical symptoms associated with acute myocardial ischemia, including: unstable angina, ST segment elevation myocardial infarction (STEMI), or non-ST segment elevation myocardial infarction (NSTEMI). It is estimated that nearly 1.7 million hospital admissions associated with acute coronary syndrome occur annually in the United States; 500,000 of these are classified as STEMI [4, 15]. Typically, an imbalance between myocardial oxygen supply and demand occurs when a thrombus develops where an atherosclerotic plaque was disrupted, thereby blocking the arterial blood flow. Subsequently, the detection of biochemical cardiac markers such as troponin or the MB isoenzyme of creatine phosphokinase (CK-MB) indicates that myocardial cell death has occurred in STEMI or NSTEMI; however, these markers are not released in the setting of unstable angina [16]. Further, typically an electrocardiogram can be utilized to differentiate between STEMI and NSTEMI.

26.5.1 Goals of Therapy for Treating Acute Coronary Syndromes

The proper and immediate management for acute coronary syndrome is pivotal in preventing the progression of myocardial tissue damage. Aside from early recognition and response, goals of therapy are to remove the precipitating factor(s) causing the ischemia and to minimize irreversible damage from occurring to the myocardial tissue. Importantly, patients are at a higher risk of death or worsening myocardial infarction if they have prolonged ischemic symptoms, clinical and ECG findings, and/or elevated biochemical cardiac markers [17, 18].

26.5.2 Treatment Guidelines for Acute Coronary Syndromes

After an initial stratification of risks for the determination of the planned intervention (i.e., percutaneous coronary intervention, or PCI), patients with unstable angina/NSTEMI should undergo a medical therapy regimen that includes: (1) rapid vasodilation with nitroglycerin; (2) supplemental oxygen to achieve a goal arterial oxygen saturation >90 %; (3) morphine sulfate for pain and agitation control; (4) beta-blockade in patients without contraindications (e.g., bradycardia, lung disease, or hemodynamic decompensation); (5) correction of serum potassium and magnesium levels as indicated; (6) antihyperlipidemia treatment, (e.g., with a statin either initially or upon discharge for lipid management); (7) arrhythmia management, both atrial and ventricular; and (8) an ACE inhibitor for blood pressure control and prevention of myocardial injury progression [16]. In addition to this regimen, antiplatelet and anticoagulation therapy should be initiated immediately. Antiplatelets include aspirin and adenosine diphosphate $P2Y_{12}$ protein receptor blocker such as clopidogrel, prasugrel, or ticagrelor; these are drugs of choice, and a glycoprotein IIb/IIIa receptor antagonist can be considered if ischemia persists or if a patient is deemed at high risk for immediate death or severe complications. If revascularization with PCI is performed, dual antiplatelet therapy (e.g., aspirin and clopidogrel) is typically indicated for at least one year post-procedure. In some settings dual antiplatelet therapy may also be indicated for medical management in the absence of PCI. In other words, the decision to use an anticoagulant agent in the setting of unstable angina/NSTEMI depends on whether the patient undergoes reperfusion therapy with PCI. Currently, the common anticoagulation options include: heparin, unfractionated or low molecular weight (e.g., enoxaparin), direct thrombin inhibitors (e.g., bivalirudin), or factor Xa inhibitors (e.g., fondaparinux) [16, 18].

It is imperative to achieve myocardial reperfusion of STEMI patients in a timely manner, to salvage as much viable myocardium as possible. The preferred method of

myocardial reperfusion is PCI [19]. Fibrinolytic pharmacologic therapy (tissue plasminogen activator, streptokinase, or urokinase) is an alternative option for patients being first treated in a non-PCI-capable hospital, with expected transport delays exceeding 120 min [16, 17]. The timing of reperfusion therapy is essential in achieving the highest survival benefit; it has the most impact on infarct size and preservation of left ventricular function. For example, the goal of first medical contact (FMC) to PCI time is 90 min with initial presentation to a PCI-capable center and 120 min with initial presentation to a non-PCI-capable center necessitating transport to a PCI-capable center. In cases where PCI is not feasible, a goal time to initiation of fibrinolytic therapy is within 30 min after a diagnosis of STEMI. After reperfusion efforts, continued management is achieved through routine measures listed above, including oxygen, nitroglycerin, aspirin, analgesia, statin, beta-blocker, and an ACE inhibitor [17]. Aldosterone antagonists are also recommended after STEMI in patients who develop heart failure.

26.6 Heart Failure

Heart failure (HF) is considered a major public health problem; over five million people in the United States [4] have been diagnosed with HF, and data indicate that it affects both men and women in equal proportions. It is defined as a complex clinical syndrome that can result from any structural or functional cardiac disorder that impairs the ability of the ventricle to fill with or eject adequate blood volumes [20–22]. In general, the incidence of HF will increase to 10 in 1,000 after the age of 65, and nearly 75 % of all HF cases have hypertension as a previously diagnosed medical condition [4]. Other common risk factors for HF patients are CHD, hyperlipidemia, and/or diabetes. Heart failure has several types of classifications such as ischemic or non-ischemic, diastolic or systolic, acute or chronic, and preserved or reduced ejection fraction. Efforts have been made to designate the severity of HF by New York Heart Association (NYHA) classification and ACCF/AHA staging systems (Table 26.5). One ranking is based primarily on physical assessment of symptoms (NYHA), and the other (ACCF/AHA) is based on the origins of the underlying cardiac disease. Unfortunately, mortality remains between 50 and 70 % at 5 years for all classes of HF, and the cause of death is typically either sudden cardiac arrest or pump failure [23, 24].

26.6.1 Goals of Therapy for Heart Failure

Heart failure is a progressive disease in which initial compensatory mechanisms will eventually become themselves detrimental to the patient (Fig. 26.2). Therefore, pharmacologic treatment is aimed at those neurohormonal mechanisms, such as the renin-angiotensin-aldosterone system and sympathetic nervous system, which mediate the progression of the disease. Goals of therapy include: (1) improving quality of life, (2) reducing HF symptoms and hospitalizations, and (3) prolonging overall survival.

Table 26.5 New York Heart Association (NYHA) functional classification and American College of Cardiology Foundation/American Heart Association stages of heart failure

Functional classification	Definition	Stage	Definition
None		**A**	Patients with normal heart structure and function, no signs or symptoms of heart failure, and at increased risk for developing heart failure due to comorbid conditions (hypertension, coronary artery disease, diabetes) (**asymptomatic risk**)
I	Patients with cardiac disease but *without limitations* of physical activity	**B**	Asymptomatic patients with abnormal heart structure or function (left ventricular hypertrophy, enlarged, dilated ventricles, asymptomatic valve disease, previous myocardial infarction) (**asymptomatic damage**)
II	Patients with cardiac disease resulting in *slight limitations* of physical activity	C	Patients with abnormal structure or function and symptomatic heart failure (symptomatic damage)
III	Patients with cardiac disease resulting in *marked limitations* of physical activity	C	Patients with abnormal structure or function and symptomatic heart failure (symptomatic damage)
IV	Patients with cardiac disease resulting in inability to carry on any physical activity without discomfort. *Symptoms present at rest*	**D**	Patients with extremely abnormal and symptomatic heart failure despite optimal medical therapy and specialized interventions (**extreme symptomatic damage**)

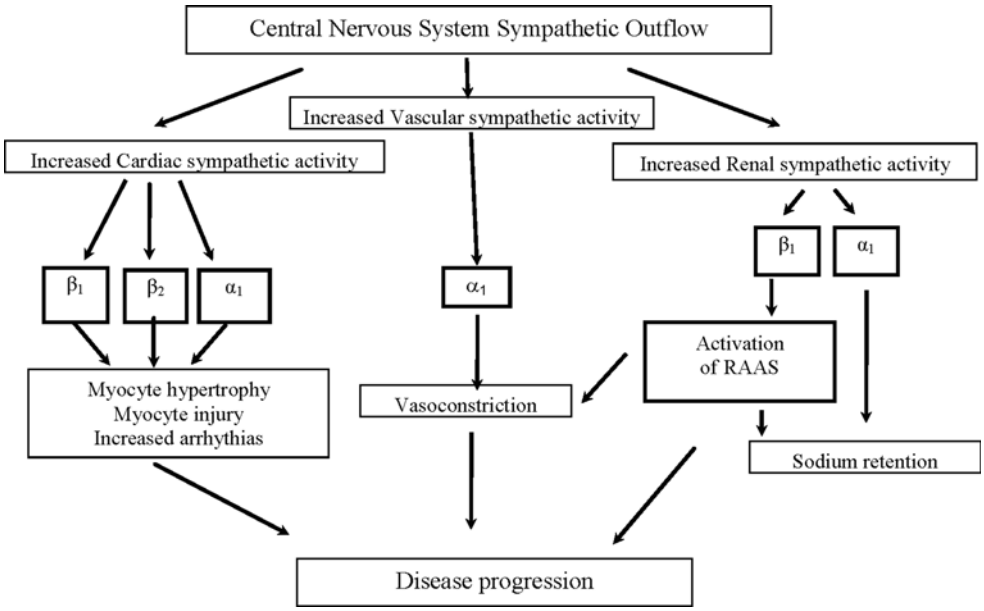

Fig. 26.2 Neurohormonal activation in heart failure. *RAAS* renin-angiotensin-aldosterone system

Table 26.6 Heart failure medication selection based on American College of Cardiology Foundation/American Heart Association staging

At risk for heart failure		Heart failure	
Stage A	Stage B	Stage C	Stage D
ACE inhibitor or ARB	ACE inhibitor or ARB; beta-blocker as indicated	Diuretics for fluid management; ACE inhibitor or ARB; beta-blocker as indicated; aldosterone antagonist In selected patients, consider hydralazine/isosorbide dinitrate or digoxin	Presser support; chronic inotropes; symptom management with diuretics and/or digoxin as indicated

ACE angiotensin-converting enzyme, *ARB* angiotensin receptor blocker

26.6.2 Treatment Guidelines for Heart Failure

In the past, treatment decisions were largely guided by NYHA classification; however, in recent years they are increasingly determined by ACCF/AHA disease staging (Table 26.6) [22]. Management of HF begins with correcting any factors (e.g., infection or nonsteroidal anti-inflammatory drugs) and addressing comorbid conditions (e.g., sleep-disordered breathing) that may be contributing to the progression of the disease. After underlying conditions have been improved or corrected, efforts are made to follow guideline-directed medical therapy (GDMT) in order to realize the mortality and morbidity benefits demonstrated in reported clinical trials. To date, ACE inhibitors and beta-blockers remain the cornerstones of GDMT and are proven to provide significant morbidity and mortality benefits [25–29]. Initial doses for each agent are very low and titrated as tolerated over 3–6 months, until goal doses are reached (Tables 26.7). In circumstances where a patient has a contraindication or experiences an adverse event with an ACE inhibitor, an ARB may be substituted as a means to retain mortality benefits [30]. Aldosterone antagonists have a role in decreasing mortality and hospitalization rates in patients with class III and IV heart failure [31]. The vasodilators hydralazine and isosorbide dinitrate, given in combination, are recommended for the management of black patients with NYHA III and IV on GDMT and for patients with contraindications to ACE inhibitors or ARBs [32]. Other agents such as diuretics and digoxin can also be given for symptom relief and to reduce subsequent hospitalizations. Currently, loop diuretics are the most potent class of clinically used diuretics and are the mainstay in volume control for HF pharmacotherapy. In all such patients, fluid status is an important monitoring parameter; for example, fluid retention can blunt the response of ACE inhibitors and increase beta-blocker adverse events, whereas fluid depletion can increase the risk of renal insufficiency. Importantly, both electrolyte levels and kidney function need to be monitored regularly when these agents are used in combination. Recently, cardiac resynchronization therapy (CRT) is a nonpharmacologic strategy that has been shown to reduce mortality and hospitalization rates in patients with class III or IV heart failure, who are already receiving optimal medical management [23]. Implantable cardioverter defibrillators (ICDs) may be used in selected

Table 26.7 Medications with indications for heart failure

Drug	Starting dose	Target dose or maximum dose
Angiotensin-converting enzyme inhibitors		
Captopril	6.25 mg three times daily	50 mg three times daily
Enalapril	2.5 mg twice daily	10–20 mg twice daily
Fosinopril	5–10 mg daily	40 mg daily
Lisinopril	2.5–5 mg daily	20–40 mg daily
Perindopril	2 mg daily	8–16 mg daily
Quinapril	5 mg twice daily	20 mg twice daily
Ramipril	1.25–2.5 mg daily	10 mg daily
Trandolapril	1 mg daily	4 mg daily
Angiotensin receptor blockers		
Candesartan	4–8 mg daily	32 mg daily
Losartan	25–50 mg daily	50–150 mg daily
Valsartan	20–40 mg twice daily	160 mg twice daily
Aldosterone antagonists		
Spironolactone	12.5–25 mg daily	25 mg once-twice daily
Eplerenone	25 mg daily	50 mg daily
Beta-blockers		
Bisoprolol	1.25 mg daily	10 mg daily
Carvedilol	3.125 mg twice daily	50 mg twice daily
Carvedilol controlled release	10 mg daily	80 mg daily
Metoprolol succinate extended release	12.5–25 mg daily	200 mg daily

Table 26.8 Definitions of atrial fibrillation and goals of therapy

Type of atrial fibrillation	Definition	Goals of therapy
Paroxysmal	Rhythm restores to normal sinus rhythm spontaneously or with interventions within 7 days of onset	1. Anticoagulation 2. Rate control 3. Rhythm control as indicated
Persistent	Rhythm is continuous and sustained for longer than 7 days	1. Anticoagulation 2. Rate control 3. Rhythm control as indicated
Permanent	Attempts to restore and/or maintain normal sinus rhythm are unsuccessful	1. Anticoagulation 2. Rate control

individuals for the primary prevention of sudden cardiac death [33]. For more information on these technologies, the reader is referred to Chap. 30.

26.7 Arrhythmias

Atrial fibrillation (AF) is defined as a supraventricular arrhythmia characterized by chaotic electrical activity in the atria. AF affects nearly two and a half million people in the United States alone [34], and its prevalence increases rapidly after the sixth decade of life [35]. Patients with AF often experience a lower quality of life and frustration with currently available pharmacotherapy options for treatment; to date, prescribed agents offer marginal safety and efficacy. Risk factors for AF include hypertension, CHD, valvular disease, cardiomyopathy, chronic obstructive pulmonary disease, thyroid disease, electrolyte disturbances, alcohol abuse, and/or vagal stimulation. Clinically, AF is classified as paroxysmal, persistent, or permanent (Table 26.8).

Types of ventricular arrhythmias include: (1) premature ventricular complexes, (2) nonsustained ventricular tachycardia, (3) sustained ventricular tachycardia, and (4) ventricular fibrillation. Each rhythm is complex and has a unique electrocardiography classification (see Chap. 28 for more details). Of late, *sudden cardiac arrest* and *sudden cardiac death* have gained more attention as they claim nearly 450,000 lives annually in the United States [35, 36]. Ventricular fibrillation is the primary mechanism of sudden cardiac arrest, but evidence also attributes the elicitation of bradyarrhythmia, ventricular tachycardia, and torsades de pointes as additional mechanisms [32, 36].

Table 26.9 $CHADS_2$ scoring for stroke risk assessment in atrial fibrillation

	Risk factor	Point(s)
C	Recent cardiac failure	1
H	Hypertension	1
A	Age ≥75 years	1
D	Diabetes	1
S	Stroke	2
Add points for total $CHADS_2$ score		Total

Table 26.10 CHA_2DS_2-VASc scoring for ischemic stroke risk in patients with atrial fibrillation

	Risk factor	Point(s)
C	Congestive heart failure	1
H	Hypertension	1
A	Age ≥75 years	2
D	Diabetes mellitus	1
S	Stroke, TIA, or TE	2
V	Vascular disease	1
A	Age 65–74 years	1
SC	Sex category[a]	1
Add points for total CHA_2DS_2-VASc score		Total

TIA transient ischemic attack, *TE* thromboembolism
[a]Female sex indicates higher risk

26.7.1 Goals of Therapy for Treating Arrhythmias

Atrial fibrillation has been linked with an increased risk of ischemic stroke; therefore, the primary goal of pharmacotherapy in such patients is to prevent embolic events through the use of oral anticoagulants [37]. The risk of ischemic stroke increases with age and risk factors such as heart failure, hypertension, diabetes, history of stroke or transient ischemic attack, gender, and/or vascular disease. The $CHADS_2$ and CHA_2DS_2VASc stroke risk assessment scores have been developed to determine the annual stroke risk and determine the need for anticoagulant therapy (Tables 26.9 and 26.10) [38, 39]. Significant advancements have been made in recent years for the treatment and prevention of thromboembolic diseases, beyond that of the traditionally used heparin and warfarin. Newer oral agents known as factor Xa inhibitors (e.g., rivaroxaban and apixaban) and direct thrombin inhibitors (e.g., dabigatran) act later and in a more targeted fashion in the clotting cascade than heparin or warfarin [40]. All of these agents, however, target thrombin, the final enzyme of the clotting cascade. It should be noted that several studies have evaluated the newer agents for safety and efficacy, using non-inferiority trial designs versus warfarin. While they have all proven non-inferior, careful consideration in patient selection is essential in determining which agent is best to use. Table 26.11 compares the differences between warfarin and the new agents, dabigatran, rivaroxaban, and apixaban.

Additional goals of therapy in such patients are to prevent tachycardia-induced cardiomyopathy, reduce symptoms of AF, and minimize adverse consequences of therapy [41]. Risk factor awareness and minimization are the main goals in the prevention of sudden cardiac arrest; risk factors are CHD, heart failure, or decreased left ventricular ejection fraction (≤30 %), previous sudden cardiac arrest event, prior episode of ventricular tachycardia, hypertrophic cardiomyopathy, and/or long QT syndrome [30]. To date, beta-blockers are the only antiarrhythmic drugs to have shown benefits in the primary prevention of sudden cardiac death; all other agents should be considered as adjuvant therapies to implantable cardioverter defibrillators [42–44].

26.7.2 Treatment Guidelines for Arrhythmias

All currently available antiarrhythmic drugs exert inhibitory activity on different phases of the cardiac action potential. In nodal tissue, type II and IV antiarrhythmic drugs control rate by decreasing calcium entry and therefore decreasing automaticity and associated conduction velocities in the depolarization phase. Type I and III antiarrhythmic drugs inhibit either sodium entry or potassium outflow, thereby decreasing automaticity and/or conduction velocities or increasing the refractory periods of the nodal action potential. For a summary of these primary mechanisms, see Table 26.12. In general, antiarrhythmic agents are used to either control ventricular rates or maintain normal sinus rhythm. Each strategy has

Table 26.11 Comparison of oral anticoagulants

	Vitamin K antagonists (e.g., warfarin)	Direct thrombin inhibitors (e.g., dabigatran)	Factor Xa inhibitors (e.g., rivaroxaban, apixaban)
Mechanism of action	Vitamin K inhibition prevents the hepatic synthesis of coagulation factors II, VII, IX, X, and protein C and protein S	Thrombin inhibition prevents thrombin-mediated effects such as factor activation and platelet aggregation	Inhibition of factor Xa prevents the conversion of prothrombin to thrombin; prevent clot formation and platelet aggregation
Indications	– Treatment and prevention of DVT and PE – Embolic risk from AF or cardiac valve replacement – Systemic embolic risk after myocardial infarction	– Treatment and prevention of DVT and PE – Prevention of stroke and embolism for nonvalvular AF	– Prevention of DVT in hip or knee replacement – Treatment of DVT (rivaroxaban only) – Prevention of stroke and embolism for nonvalvular AF
Dosing	Once daily	Twice daily	Once or twice daily
Monitoring requirements	International normalized ratio/ prothrombin time	None	None
Drug interactions	Multiple	Multiple	Multiple
Reversal agent	Vitamin K, fresh frozen plasma, prothrombin complex concentrates, or factor products	Not identified, prothrombin complex concentrates may be used or hemodialysis	Not identified, prothrombin complex concentrates may be used or hemodialysis
Dosing considerations/ alterations	Based on INR	Requires consideration in renal dysfunction	Requires consideration in renal dysfunction, elderly, obesity, or administration with food

DVT deep vein thrombosis, *PE* pulmonary embolism, *AF* atrial fibrillation

Table 26.12 Antiarrhythmic drug mechanism of action

Type	Drug	Channel activity	Automaticity	Conduction velocity	Refractory period
Ia	Quinidine	– Na + blocker – K+ blocker	↓	↓	↓
	Procainamide[a]		↓	↓	↓
	Disopyramide		↓	↓	↓
Ib	Lidocaine	–Na + blocker	↓	↓	__
	Mexiletine		↓	↓	__
Ic	Flecainide	– Na + blocker	↓	↓↓	__
	Propafenone		↓	↓↓	__
II	Beta-blockers	– Decreases Ca++ (nodal cells)	↓	↓	__
III	Amiodarone	– K+ blocker – Na + blocker – Ca ++ and beta-blocker (nodal cells)	↓	__	↑↑
	Dronedarone (Multaq)	– K+ blocker – Na + blocker – Ca ++ and beta-blocker (nodal cells)	↓	__	↑↑
	Dofetilide (Tikosyn)	– K+ blocker	__	__	↑↑
	Ibutilide (Corvert)	– K+ blocker	__	__	↑↑
	Sotalol (Betapace)	– K+ blocker – Beta-blocker (nodal cells)	↓	__	↑↑
IV	Diltiazem	– Ca++ blocker (nodal cells)	↓	↓	__
	Verapamil				

[a]Metabolized to *N*-acetylprocainamide (NAPA) which has class III activity

important considerations for minimizing consequences of AF and thus burdensome symptoms. Figure 26.3a, b outline commonly employed treatment algorithms for maintaining normal sinus rhythm in both paroxysmal and persistent AF in patients, with and without associated structural heart disease [41].

Type III antiarrhythmic agents are used more frequently than type I agents in the setting of ventricular tachycardia/ventricular fibrillation. Note that amiodarone, a type III agent, is often used to decrease the frequency of supraventricular or ventricular arrhythmias in patients with an implantable cardioverter defibrillator to minimize defibrillation shock delivery [44, 45].

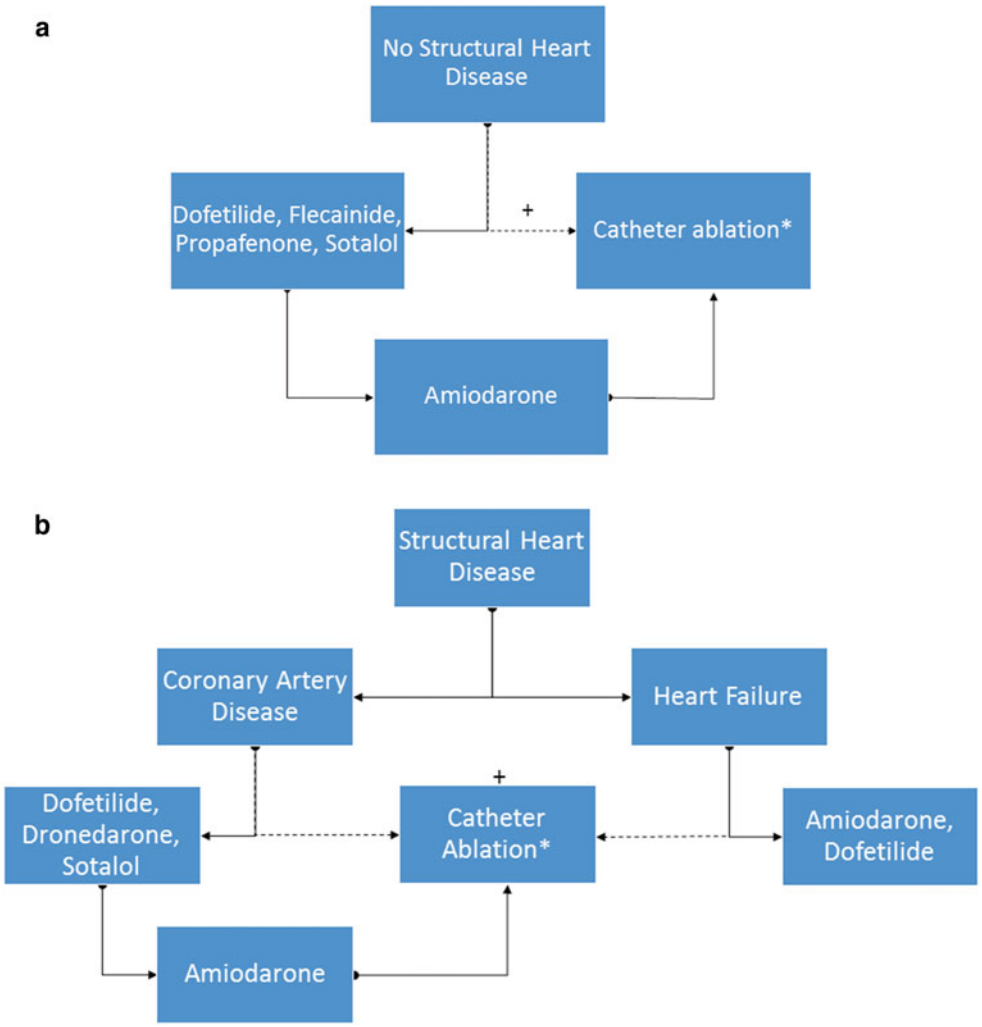

Fig. 26.3 (**a**, **b**) Commonly employed treatment algorithms maintaining normal sinus rhythm in patients with paroxysmal and persistent atrial fibrillation [41]. +Depends on patient preference; *Considered first-line for paroxysmal atrial fibrillation only

26.8 Local Drug Delivery

Local drug delivery allows for therapeutic concentration of a drug to be administered to a designated target without exposing the rest of the body to potential adverse effects or toxic concentrations. Several methods for local drug delivery are already used in clinical practice. Transdermal delivery systems allow for localized penetration of a drug into the skin through a patch. Intrathecal drug pumps, through intraspinal catheters, deliver drugs to treat chronic pain and spasticity disorders with smaller doses of agents that traditionally would have been less effective and more sedating [46, 47]. Further, drug-eluting stents release drugs with anti-inflammatory properties from a polymer to prevent restenosis after a PCI and need for target lesion revascularization [48]. For that reason, they are generally preferred over bare metal stents. Researchers have evaluated drug delivery into the pericardial space with antiarrhythmic agents and vasodilators and have found benefits such as enhanced efficacy, increased duration of action, lower doses, and less toxicity [49–51]. See Chap. 9 for an additional discussion of this topic.

26.8.1 Future Potential for Targeted Drug Delivery

Polymers being designed to allow for controlled, targeted release of drugs (i.e., technology used with drug-eluting stents) are successful in preventing vessel restenosis relative to that seen with bare metal stents. Similarly, drug-containing hydrogels placed next to a therapeutic target allow for controlled delivery [52]. As such, drug-eluting implants using these materials are intended to deliver a drug over a period of hours to months. In contrast, recent catheter technology has the potential for delivering a precise amount of drug to a very specific target while maintaining the efficiency of intravascular delivery but without obstructing blood flow [53]. It is predicted that these local drug delivery methodologies, and those being developed, will become more prevalent as biologics and personalized medicine, such as gene therapy, begin to play a larger role in the treatment of cardiovascular diseases.

26.9 Summary

This chapter has provided a very brief overview of the pharmacotherapy decisions that have shown to be most beneficial for the current treatments of hypertension, acute coronary syndrome, heart failure, and arrhythmias. Such guidelines and subsequent updates, developed by experts in each of these respective areas of specialty, should be routinely consulted to maintain one's awareness of the optimal medical therapies, including pharmacotherapy, for the treatment of cardiovascular disorders.

References

1. Ward BW, Schiller JS, Goodman RA (2014) Multiple chronic conditions among US adults: a 2012 update. Prev Chronic Dis 11:130389
2. Murphy SL, Xu JQ, Kochanek KD (2013) Deaths: final data for 2010. Natl Vital Stat Rep 61:1–117
3. Fryar CD, Chen T, Li X (2012) Prevalence of uncontrolled risk factors for cardiovascular disease: United States, 1999–2010. NCHS data brief, no 103. National Center for Health Statistics, Hyattsville, MD
4. Lloyd-Jones D, Adams RJ, Brown TM et al (2010) Heart disease and stroke statistics: 2010 update. Circulation 121:948–954
5. Sackett DL, Rosenberg WM, Gray JA et al (1996) Evidence based medicine: what it is and what it isn't. BMJ 312:71–72
6. Radford MJ, Heidenreich PA, Bailey SR et al (2007) ACC/AHA 2007 methodology for development of clinical data standards. Circulation 115:936–943
7. Egan BM, Zhao Y, Axon RN (2010) US trends in prevalence, awareness, treatment, and control of hypertension, 1988–2008. JAMA 303:2043–2050
8. Centers for Disease Control and Prevention (2012) Vital signs: awareness and treatment of uncontrolled hypertension among adults–United States, 2003–2010. Morb Mortal Wkly Rep 61:703–712
9. Chobanian AV, Bakris GL, Black HR et al (2003) The seventh report of the Joint National Committee on prevention, detection, evaluation, and treatment of high blood pressure. JAMA 289:2560–2572
10. Hertz RP, Unger AN, Cornell JA, Saunders E (2005) Racial disparities in hypertension prevalence, awareness, and management. Arch Intern Med 165:2098–2104
11. James PA, Oparil S, Carter BL et al (2014) 2014 evidence-based guideline for the management of high blood pressure in adults: report from the panel members appointed to the Eighth Joint National Committee (JNC 8). JAMA 311:507–520
12. Weber MA, Schiffrin EL, White WB et al (2014) Clinical practice guidelines for the management of hypertension in the community: a statement by the American Society of Hypertension and the International Society of Hypertension. J Clin Hypertens 16:14–26
13. Mancia G, Fagard R, Narkiewicz K et al (2013) 2013 ESH/ESC Guidelines for the management of arterial hypertension: the Task Force for the management of arterial hypertension of the European Society of Hypertension (ESH) and of the European Society of Cardiology (ESC). J Hypertens 31:1281–1357
14. National Institute for Health and Clinical Excellence (2011) Hypertension: clinical management of primary hypertension in adults. Clinical guidelines: methods, evidence and recommendations. National Institute for Health and Clinical Excellence, London
15. Go AS, Mozaffarian D, Roger VL et al (2013) Heart disease and stroke statistics—2013 update: a report from the American Heart Association. Circulation 127:e6–e245
16. Braunwald E, Antman EM, Beasley JW et al (2000) ACC/AHA guidelines for the management of patients with unstable angina and non-ST-segment elevation myocardial infarction. Circulation 102:1193–1209
17. O'Gara PT, Kushner FG, Ascheim DD et al (2013) 2013 ACCF/AHA guidelines for the management of patients with ST-elevation myocardial infarction: Report of the ACCF/AHA Task Force on Practice Guidelines. Circulation 127:e362–e425
18. Antman EM, Morrow DA, McCabe CH et al (2006) Enoxaparin versus unfractionated heparin with fibrinolysis for ST-elevation myocardial infarction. N Engl J Med 354:1477–1488
19. King SB 3rd, Smith SC, Hirshfield JW et al (2008) 2007 focused update of the ACC/AHA/SCAI 2005 guideline update for percutaneous coronary intervention. Circulation 117:261–295
20. Steinhubl SR, Berger PB, Mann JT 3rd et al (2002) Early and sustained oral antiplatelet therapy following percutaneous coronary intervention: a randomized controlled trial. JAMA 288:2411–2420
21. Hunt SA, Baker DW, Chin MH et al (2005) ACC/AHA 2005 guidelines for the diagnosis and management of chronic heart failure in the adult. Circulation 112:e154–e235
22. Yancy CW, Jessup M, Bozkurt B et al (2013) 2013 ACCF/AHA Guideline for the management of heart failure: a report of the ACCF/AHA Task Force on Practice Guidelines. Circulation 128:e240–e327
23. Pagley PR, Beller GA, Watson DD et al (1997) Improved outcome after coronary bypass surgery in patients with ischemic cardiomyopathy and residual myocardial viability. Circulation 96:793–800
24. Fowles RE, Mason JW (1982) Endomyocardial biopsy. Ann Intern Med 97:885–894
25. The SOLVD Investigators (1991) Effect of enalapril on survival in patients with reduced left ventricular ejection fractions and congestive heart failure. N Engl J Med 325:293–302.
26. The CONSENSUS Trial Study Group (1987) Effects of enalapril on mortality in severe congestive heart failure: results of the Cooperative North Scandinavian Enalapril Survival Study (CONSENSUS). N Engl J Med 316:1429–1435
27. MERIT–HF Study Group (1999) Effect of metoprolol CR/XL in chronic heart failure: metoprolol CR/XL randomized intervention trial in congestive heart failure (MERIT-HF). Lancet 253:2001–2007
28. Packer M, Coats AJ, Fowler MB et al (2001) Carvedilol Prospective Randomized Cumulative Survival Study Group: effect of carvedilol on survival in severe chronic heart failure. N Engl J Med 344:1651–1658
29. Granger CB, McMurray JJ, Yusef S et al (2003) Effects of candesartan in patients with chronic heart failure and reduced left-ventricular systolic function intolerant to angiotensin-converting-enzyme inhibitors: the CHARM-alternative trial. Lancet 362:772–776
30. The RALES Investigators (1996) Effectiveness of spironolactone added to angiotensin-converting enzyme inhibitor and a loop diuretic for severe chronic congestive heart failure (The Randomized Aldactone Evaluation Study [RALES]. Am J Cardiol 78:902–907
31. Franciosa JA, Taylor AL, Cohn JN et al (2002) African-American Heart Failure Trial (A-HeFT): Rationale, design, and methodology. J Card Fail 8:128–135
32. Luu M, Stevenson WG, Stevenson LW et al (1989) Diverse mechanisms of unexpected cardiac arrest in advanced heart failure. Circulation 80:1675–1680
33. Go AS, Hylek EM, Phillips KA et al (2001) Prevalence of diagnosed atrial fibrillation in adults: national implications for rhythm management and stroke prevention: the AnTicoagulation and Risk Factors in Atrial Fibrillation (ATRIA) Study. JAMA 285:2370–2375

34. Feinberg CD, Blackshear JL, Laupacis A et al (1995) Prevalence, age distribution, and gender of patients with atrial fibrillation: analysis and implications. Arch Intern Med 155:469–473
35. Zheng ZJ, Croft JB, Giles WH, Mensah GA (2001) Sudden cardiac death in the United States, 1989–1998. Circulation 104:2158–2163
36. Bayes de Luna A, Coumel P, Leclercq JF (1989) Ambulatory sudden cardiac death: mechanisms of production of fatal arrhythmias on the basis of data from 157 cases. Am Heart J 117:151–160
37. Holbrook A, Schulman S, Witt DM et al (2012) Evidence-based management of anticoagulant therapy and prevention of thrombosis, 9th edn: American College of Chest Physicians Evidence-Based Clinical Practice Guidelines. Chest 141(2_suppl):e152S–e184S
38. Gage BF, Waterman AD, Shannon W et al (2011) Validation of clinical classification schemes for predicting stroke – results from the national registry of atrial fibrillation. JAMA 285:2864–2870
39. Olesen JB, Torp-Pedersen C, Hansen ML, Lip GY (2012) The value of the CHA2DS2-VASc score for refining stroke risk stratification in patients with atrial fibrillation with a CHADS2 score 0–1: a nationwide cohort study. Thromb Haemost 107:1172–1179
40. Ageno W, Gallus AS, Wittkowsky A et al (2012) Oral anticoagulant therapy: antithrombotic prevention of thrombosis, 9th edn: American College of Chest Physicians Evidence-Based Clinical Practice Guidelines. Chest 141(2_suppl):e44S–e88S
41. January CT, Wann LS, Alpert JS et al (2014) 2014 AHA/ACC/HRS Guideline for the management of patients with atrial fibrillation. J Am Coll Cardiol 64:e1–76
42. Buxton AE, Lee KL, Hafley GE et al (1999) The Multicenter Unsustained Tachycardia Trial Investigators. A randomized study of the prevention of sudden death in patients with coronary artery disease. N Engl J Med 341:1882–1890
43. Bardy GH, Lee KL, Mark DB et al (2005) Amiodarone or an implantable cardioverter defibrillator for congestive heart failure. N Engl J Med 352:225–237
44. The Antiarrhythmics Versus Implantable Defibrillators (AVID) Investigators (1997) A comparison of antiarrhythmic-drug therapy with implantable defibrillators in patients resuscitated from near-fatal ventricular arrhythmias. N Engl J Med 337:1576–1583
45. Santini M, Pandozi C, Ricci R (2000) Combining antiarrhythmic drugs and implantable devices therapy: benefits and outcomes. J Interv Card Electrophysiol 4:65–89
46. Anderson VC, Burcheil K (1999) A prospective study of long-term intrathecal morphine in the management of chronic nonmalignant pain. Neurosurgery 44:289–300
47. Albright LA, Gilmartin R, Swift D et al (2003) Long-term intrathecal baclofen therapy for severe spasticity of cerebral origin. J Neurosurg 98:291–295
48. Sarno G, Lagerqvist B, Frobert O (2012) Lower risk of stent thrombosis and restenosis with unrestricted use of 'new-generation' drug-eluting stents: a report from the nationwide Swedish Coronary Angiography and Angioplasty Registry (SCAAR). Eur Heart J 33:606–613
49. Waxman S, Moreno R, Rowe KA, Verrier RL (1999) Persistent primary coronary dilation induced by transatrial delivery of nitroglycerin into the pericardial space: a novel approach for local cardiac drug delivery. J Am Coll Cardiol 33:2073–2077
50. Ujhelyi MR, Hadsall KZ, Eular DE, Mehra R (2002) Intrapericardial therapeutics: a pharmacodynamic and pharmacokinetic comparison between pericardial and intravenous procainamide delivery. J Cardiovasc Electrophysiol 13:605–611
51. van Brakel TJ, Hermans JJ, Janssen BJ et al (2004) Intrapericardial delivery enhances cardiac effects of sotalol and atenolol. J Cardiovasc Electrophysiol 44:50–56
52. Slepian MJ (1996) Polymeric endoluminal gel paving: therapeutic hydrogel barriers and sustained delivery depots for local arterial wall biomanipulation. Semin Interv Cardiol 1:103–116
53. Brieger D, Topal E (1997) Local delivery systems and prevention of stenosis. Cardiovasc Res 35:405–413

Animal Models for Cardiac Research

27

Nicholas Robinson, Laura Souslian, Robert P. Gallegos, Andrew L. Rivard, Agustin P. Dalmasso, and Richard W. Bianco

Abstract

The modern era of cardiac surgery is largely considered to have begun in the animal research laboratories. Today, animal models continue to be used for the study of cardiovascular diseases and are required for the preclinical assessment of pharmaceuticals, mechanical devices, therapeutic procedures, and/or continuation therapies. This chapter was written to provide readers and potential investigators with important background information necessary for the process of matching an experimental hypothesis to an animal species that will serve as an appropriate model for studying a specific cardiovascular disease or for testing a given medical device. A review of the current animal models used in cardiac research is provided and arranged by disease state. Critical factors to consider when choosing an appropriate animal model including costs, reproducibility, and degree of similarity of the model to human disease are discussed. Thus, this chapter can be utilized as a practical guide for planning of research protocols.

Keywords

Animal model • Isolated cardiomyocytes • Isolated perfused heart • Valve disease • Atrial fibrillation • Myocardial ischemia • Heart failure • Heart transplantation • Mechanical device testing • Cardiomyoplasty • Stem cell research

27.1 Protocol Development

Several scientific governing bodies have developed guidelines and periodic review processes to ensure that research animals are used in an ethical and scientifically appropriate manner. Investigators who plan to utilize animal subjects in their research should first familiarize themselves with the document entitled "Guide for the Care and Use of Laboratory Animals" prepared by the US National Academy of Sciences [1]. In addition, investigators should use these guidelines in conjunction with accepted scientific methods in order to develop a standardized protocol for each research project. It is a requirement that prior to commencing research, a detailed protocol undergoes review and is approved by the local governing body responsible for the safe and ethical use of animals in research. In most organizations in the USA where research using animals is performed, the standard governing body is known as the Institutional Animal Care and Use Committee, or IACUC (www.iacuc.umn.edu).

Both large and small animals have been extensively used in cardiovascular research. The choice of animal model should be primarily based on: (1) the scientific hypotheses; (2) the laboratory's capability to safely employ the model in the species chosen (i.e., expertise in the selected procedure, appropriate animal housing and care, equipment, laboratory resources); and (3) the degree of the species similarity to the human anatomy relative to the device or procedure to be tested. It is important to note that many of the best animal models can be expensive to establish and maintain and, as

N. Robinson, BVSc (Hons), PhD, DACVP • L. Souslian, MD
R.P. Gallegos, MD, PhD • A.L. Rivard, MD • A.P. Dalmasso, MD
R.W. Bianco (✉)
Department of Surgery, University of Minnesota,
MMC 195, 420 Delaware St. SE, Minneapolis, MN 55455, USA
e-mail: bianc001@umn.edu

P.A. Iaizzo (ed.), *Handbook of Cardiac Anatomy, Physiology, and Devices*, DOI 10.1007/978-3-319-19464-6_27

such, funding must be appropriate to complete the required number of animal experiments to satisfy a pre-calculated statistical power. Several obvious technical limitations for the use of small animals exist, for example in the case of implanting mechanical devices such as heart valves. The sheer size of the animal is not large enough to implant a valve fit for a human; the animal species must be chosen to fit the device to be studied. Great strides have been made in both imaging (ultrasound and MRI) and miniaturizing electronic equipment that can be used for monitoring physiological parameters, allowing for more intensive cardiac monitoring within small animal models. In choosing the animal species, the researcher should attempt to match physiological parameters (of the animal) as closely as possible to those of humans to obtain results that are the most clinically relevant. Note that many tables of physiological values are available for commonly used research animal species, and these should be used to assist in choosing the appropriate model [2–6]. For more details see Chap. 6.

27.2 Spontaneously Occurring Animal Models of Congenital Cardiac Disease

Naturally occurring animal models of cardiac disease arise infrequently; however when they do occur, there is marked variability in the observed phenotype and they also frequently occur with other congenital abnormalities that hinder breeding efforts. Furthermore, genetic manipulation of breeding stock for specific mutations has economical, ethical, and moral issues that preclude the development of such breeding lines. As a result, the commercial availability of animals for such specific research purposes continues to be quite limited, necessitating the development of contrived models in most cases. Yet, great strides have been made in the application of classical breeding techniques and, more recently, molecular engineering to develop breeding stocks of mice and, in some cases, rats. Specifically, the use of transgenic mice and mice with gene deletions or other induced genetic changes has been considered essential for investigating pathophysiologic mechanisms of disease, including those of the cardiovascular system. Moreover, these genetically modified animals, in some instances, are useful for the initial in vivo testing of pharmaceuticals and/or certain devices [7].

27.3 Alternatives to Whole Animal Models

In some cases, isolated cardiac cell lines in culture, segments of myocardium, or isolated heart models may provide an effective alternative to whole animal research. Isolated preparations have been particularly useful for the study of metabolic pathways, as the perfusate can be modified while the effluent can be easily collected for analysis. Additionally, functional measurements can be easily completed in this in vitro environment. Given the need to reduce cost and limit the number of animals used in research, the attraction of using alternatives to whole animal models is strong. However, regulations typically do not permit the direct extrapolation of the experimental findings from isolated in vitro models to subsequent clinical trials. For example, in vitro studies often demonstrate whether a pharmaceutical agent is potentially useful; however, the concentrations used may be either toxic or the agent may lack efficacy when pharmacokinetics and pharmacodynamics are investigated in the live animal. Nevertheless, these in vitro alternatives are essential for initial studies pertaining to myocardial ischemia, transplantation, and/or pharmaceutical development.

27.3.1 Isolated Cardiomyocytes

The use of isolated cardiomyocytes has allowed researchers to eliminate confounding interactions with surrounding tissue elements. It has also allowed for the measurement of intracellular changes at the single cell level. Yet, care must be taken to match the culture conditions to those of the intact organ to ensure both the viability of the cells used and the quality of the data collected [8, 9]. This simple model provides an important approach before the use of whole animals in early phase testing of experimental protocols, and is of particular interest for use in the testing of new pharmacological agents and/or gene therapies. Cardiac myocyte cultures can be obtained from freshly isolated tissue, differentiated embryonic stem cells or multipotent adult progenitor cells, or immortalized tumor cell lines such as HL-1 from the At-1 mouse [10]. Some functions of cardiac myocytes that can be examined include: (1) contractility, using optical or mechanical detectors; (2) RNA expression (e.g., using Q-PCR); and/or (3) membrane integrity, and measuring release of lactate dehydrogenase, creatine phosphokinase, or troponin [9, 11–15]. Nevertheless, one has to consider that cultured cells may respond differently to a given therapy than those within a living organism.

27.3.2 Isolated Perfused Hearts

An isolated heart perfusion system replicates the physiological conditions outside of the body, allowing for easy access for measurement of the perfused effluent. Isolated in vitro perfusion studies have been performed using the entire heart or a portion of the heart (e.g., intraventricular septum, papillary muscle). Commercially available setups for such in vitro studies are available for the mouse, rat, and guinea pig hearts (ADInstruments, Colorado Springs, CO, USA; Fig. 27.1).

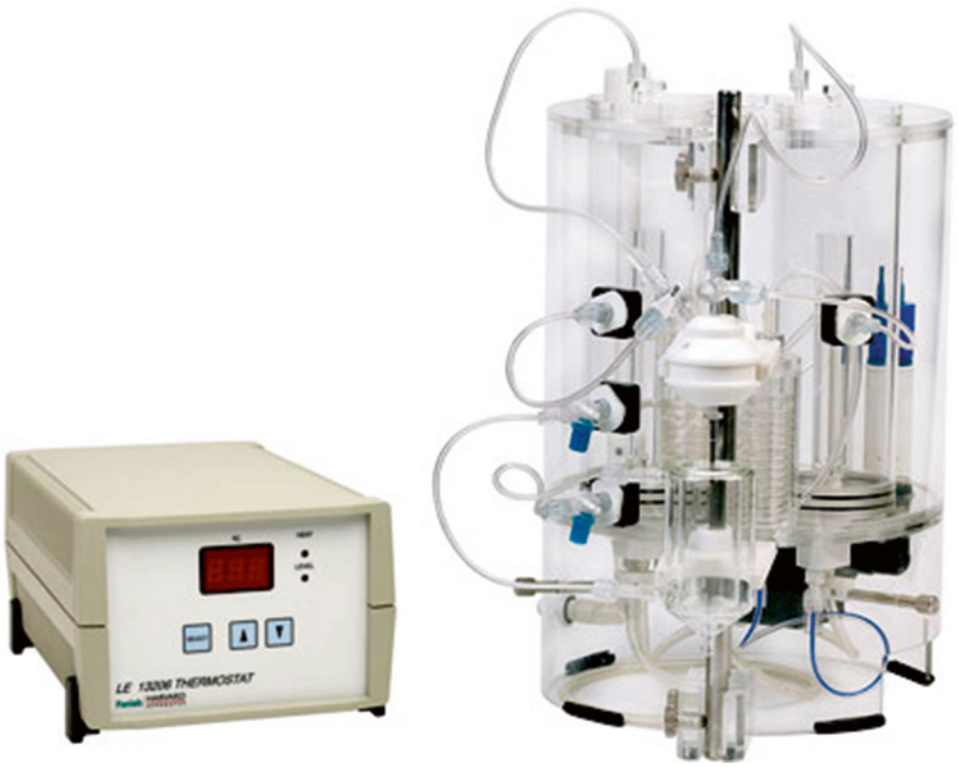

Fig. 27.1 ADInstruments Langendorff perfusion setup. Courtesy of ADInstruments

Larger setups have also been described to accommodate canine, porcine, ovine, and human hearts. An excellent example of an application of the isolated heart model can be seen on the Atlas of Human Cardiac Anatomy website (www.vhlab.umn.edu/atlas) and on The Visible Heart website (www.vhlab.umn.edu).

Several different methods for studying the isolated heart are possible, two of these methods are the Langendorff perfusion approach and the isolated working heart model [16, 17]. In the Langendorff system, constant pressure flow through an aortic cannula forces the aortic valve closed, and the perfusate passes through the coronary arteries without retrograde flow entering the left ventricle. This perfusion provides the myocardium with a physiologic solution, allowing the heart to beat without blood flowing through the four chambers. This method was named after Oscar Langendorff who, in 1895, was the first to describe an experimental model of an isolated mammalian heart as a technique to assess its required contractile activity. The advantage of the Langendorff perfusion method is that the measurement of EKG changes can be easily assessed, as well as measurement of metabolites that drain from the coronary sinus. Yet, the lack of flow in the left ventricle may limit its usefulness, i.e., minimal blood entering into the ventricle may promote clot formation, in turn, affecting the viability of the preparation. Additionally, the lack of flow in the ventricle may result in abnormal three-dimensional conformational changes in the heart that may cause coronary vascular compression. However, placement of a fluid balloon connected to a pressure transducer may allow for partial control of this problem, and may also be useful experimentally to assess changes in left ventricular function. Recent studies utilizing variations of the Langendorff working heart have adapted the setup for a range of different heart sizes. The classic hydrostatic afterload column is replaced with a centrifugal pump, allowing for easy adjustment and tight regulation of perfusion pressures, meaning the same setup can be used for various species or heart sizes [18].

The major disadvantage of the Langendorff preparation is that it does not eject the perfusate from the left ventricle and is therefore a non-work-producing model. This problem was initially overcome by Neely who used an isolated working heart which simulates physiological flow through the heart's four chambers [19]. In this model, the perfusate is supplied by a cannula inserted into the left atrium; outflow through the left ventricle is monitored, while left atrial pressure or aortic pressure is controlled. This setup is considered ideal for the study of pressure and flow in the aorta as well as the left and right ventricles.

27.3.3 Additional Problems with Isolated Perfused Heart Models

Both types of isolated heart preparations have problems in common that should be considered when attempting to

extrapolate results to the in vivo condition. First, the isolation process used for these models requires global myocardial ischemia (a period of no perfusion). Typically, once the organ is reperfused, baseline data (heart rate, left ventricular pressure, coronary blood flow) must be collected after a stabilization period to ensure relative viability of the preparation. Clearly, both the ischemic time and stabilization time may influence research outcomes. Therefore, any results obtained must be carefully analyzed with reference to the preparation's baseline state as well as to the normal in vivo values, to avoid falsely attributing changes in cardiac function to the experimental protocol.

The composition of the perfusate can greatly impact the function and viability of the preparation in both of the aforementioned models. Early studies utilizing isolated heart models have employed whole blood as a perfusate [20]. However, significant problems with clotting and hemolysis may limit the time that the preparation remains viable. Saline compounds, which lack the potential for clotting and hemolysis, are considered useful alternatives to whole blood. However, such buffers have a lower colloid osmotic pressure and, coupled with the lower coronary vascular resistance, will typically result in progressive and severe edema; this results in interstitial edema formation and nonuniform perfusion. To extend the usefulness of the preparation, one can add osmotically active substances to the medium used for bathing and perfusing the preparation in an attempt to limit edema [21, 22]. Nevertheless, despite the technical difficulties associated with these models, isolated hearts have been used in research ranging from ischemia to transplant studies. For more details on isolated heart experimentation, the reader is also referred to Chap. 41.

27.4 Animal Models Used to Test Devices for Treatment of Valvular Disease

The significant morbidity and mortality associated with heart valve disease has produced a highly competitive market for manufactured prosthetic valves. Efforts to develop the ideal replacement heart valve have focused on producing a device that functions like the native valve (Table 27.1). To this end, certain basic principles of physics are fundamental in the design of mechanical valves, as evidenced by the evolution of various designs. The dynamics of blood flow through a tube with its specific viscosity is such that the flow is greatest in the center of the tube. Thus, any structure in the center of the valve (i.e., mechanical valve leaflets) will reduce the velocity through that valve (Fig. 27.2).

Table 27.1 Qualities of the ideal device for heart valve replacement

• Durable
• Does not leak
• Biologically inert
• Nonthrombogenic
• Facilitates laminar flow
• Easily implanted by the surgeon
• Quiet

Guidelines for the design and testing of bio-artificial and/or mechanical heart valves have been established by the Center for Devices and Radiological Health of the Food and Drug Administration (FDA) and the International Organization for Standardization (ISO). The FDA has provided industry assistance in the form of guidance documents, advice, reporting, premarket approval, development of standards, and third-party reviews. Typically, prosthetic valve replacements are classified as either tissue (Fig. 27.3) or mechanical (Figs. 27.2 and 27.4), yet despite their common purpose, specific valve composition and function vary widely. Nevertheless, all valves must undergo performance-based testing to examine hydrodynamic performance (Table 27.2). For example, accelerated cyclic testing provides wear information, allowing for estimates of structural performance by providing data on fatigue, endurance limits, and damage tolerances of the valve.

Importantly, the FDA requires the demonstration of both efficacy and safety of prototype heart valve replacements prior to final approval for human implantation. This is based on the principle that additional technical and biological information can be gained by observing the valve in actual use. As a result, animal studies remain a crucial component in the overall evaluation of replacement heart valves [23]. To date, all investigational valves undergo a preclinical animal study with valve implantation in the orthotopic or anatomically normal position (with a required 20-week minimum period of evaluation). Specifically, the FDA looks for separate data from mechanical and biological valve studies. For example, mechanical valves generally place extreme shearing forces on the red blood cells and platelets, causing hemolysis and thrombosis that necessitate chronic anticoagulation after valve implantation. On the other hand, biologic valves place very low shear forces on the red blood cells and platelets, and thus there is no need for anticoagulation; however, they are sensitive to formation of calcium deposition, requiring the incorporation of some measures in their manufacturing that will attempt to prevent calcification after implantation. The lack of naturally occurring models of valve disease and the need for standardized models for FDA/ISO approval has led to the use of iatrogenic models of valve disease. To date, the ovine model has been used for producing a graded stenosis in the aortic and mitral valves by banding the aorta in young animals [24]. In contrast, aortic supravalvular stenosis, as well as aortic valvular stenosis, has been commonly induced in the canine model [25, 26]. Additionally, induction of mitral valve regurgitation in the

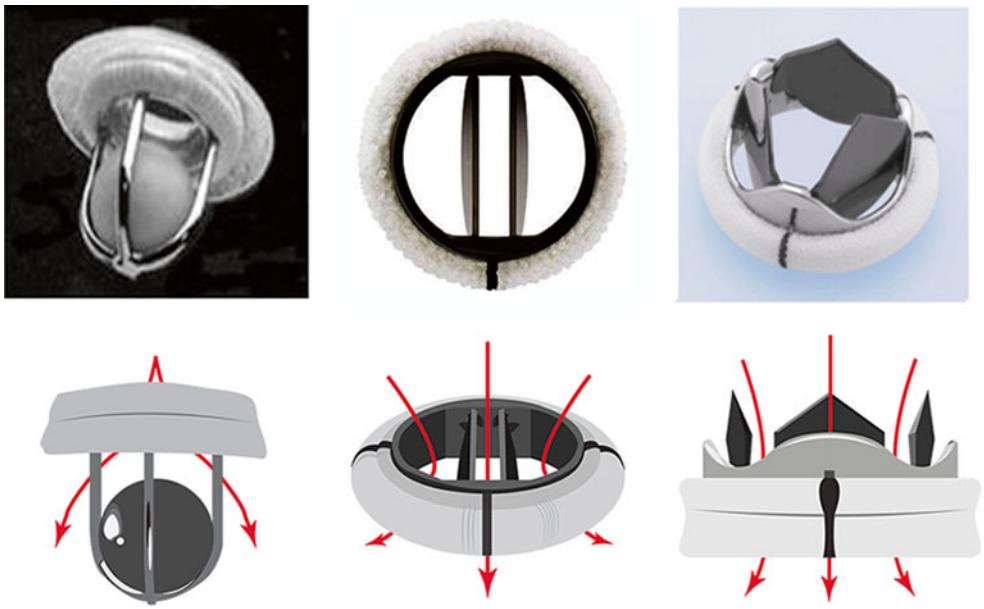

Fig. 27.2 Comparison of different mechanical valves with their flow characteristics. The evolution of the valve from the Starr-Edwards ball (*left*), the current standard bi-leaflet (*center*; St. Jude Medical, St. Paul, MN, USA), and a novel trileaflet design (*right*, Triflow Medical Inc.) currently in development. Below each valve is a stylized representation of the flow patterns reflecting the improvement in valve design

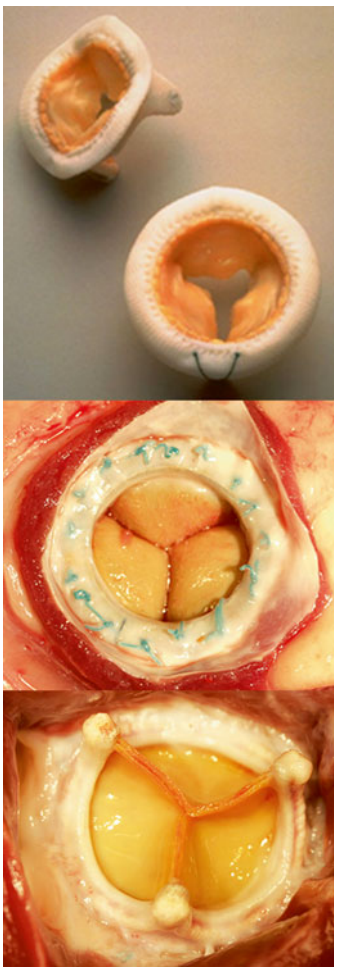

Fig. 27.3 (*Top*) The Medtronic Mosaic® stented tissue valve (Medtronic, Inc., Minneapolis, MN, USA). (*Middle*) Carpentier-Edwards Perimount Plus 6900P stented tissue valve, inflow aspect in the Mitral position in a sheep. (*Bottom*) Carpentier-Edwards Perimount Plus 6900P stented tissue valve, outflow aspect in the Mitral position in a sheep

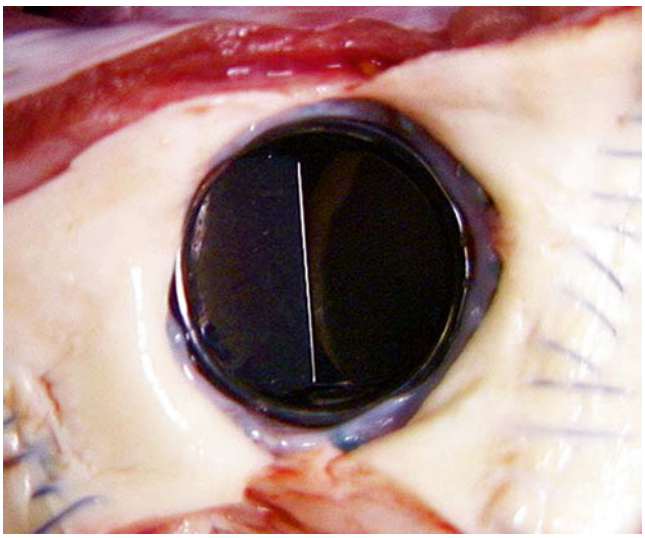

Fig. 27.4 Ovine model of a normal bileaflet mechanical valve implantation

canine is possible by placement of a shunt [27] or by transection of the chordae tendineae. Interestingly, experiments have also been performed to induce stenosis or regurgitation in the tricuspid and pulmonic valves [28]. However, most valve implantation studies approved for human use are completed in normal animals and their primary goals are to strictly examine valve performance (Fig. 27.4). A thorough understanding of the background and natural history of heart valve disease in standard laboratory animal species is needed to ensure that spontaneous valve lesions are not misinterpreted as treatment related [29].

A principal advantage of employing the canine model is the large amount of background information available in the cardiovascular surgical literature. Historically, the dog was

Table 27.2 Mechanical valve fluid dynamic testing

• Forward flow testing
• Backflow leakage testing
• Pulsatile flow pressure drop
• Pulsatile flow regurgitation
• Flow visualization
• Cavitation potential
• Verification of the Bernoulli relationship

Source: "Replacement Heart Valve Guidelines," formulated by the US Department of Health and Human Services, Food and Drug Administration, Center for Devices and Radiological Health

considered to be the gold standard for both acute and chronic models of valve replacement that was accepted by the FDA. Early success with the canine model in valve replacement identified the need for minimizing the risk of surgical infection at the time of prosthesis implantation. Specifically, the use of preoperative parenteral and postoperative topical antibiotics, strict sterile techniques, minimum numbers of operative arterial and venous lines, and short cardiopulmonary bypass times were all noted parameters to minimize the risk of bacterial valve implant seeding [30].

As described in Chap. 6, the anatomy of the porcine heart is most similar to that of the human heart in regards to the conduction system, coronary arteries, blood supply to the conduction system, and great vessels. In addition, the coagulation cascade of the swine is quite similar to that of humans. Despite these advantages, several problems have been identified in using this model for valvular research. First, the porcine heart is extremely sensitive to anesthesia, and surgical manipulation often results in postsurgical complications, arrhythmias, and/or death. Second, the growth of young swine is rapid, resulting in heart size and physiological flow that is not constant over required follow-up periods of several months; yet, if you want to investigate the effects of heart growth on a device, using the swine may be beneficial. Specifically, these alterations often result in fibrous sheathing and obstruction of the valve orifice, thrombus formation, or dehiscence (separation) of the sewing cuff from the native annulus. Finally, significant bleeding complications due to application of anticoagulation therapy and poor survival have limited the use of the pig in studying valve-related thrombosis [31]. A recent porcine model for aortic valve sclerosis was able to mimic early human aortic valve disease by feeding swine a high-fat/high-cholesterol diet. This study showed the efficacy of modifying certain factors in a study, allowing for animal models to mimic changes seen in humans [32].

The ovine model is currently accepted as the gold standard for valve replacement using defined survival surgeries that meet FDA requirements. Normal cardiovascular physiological parameters of sheep approximate those of humans in blood pressure, heart rate, cardiac output, and intracardiac pressure [33]. In addition, the anatomy of the adult heart provides valve orifice diameters that are similar to humans [34]. The use of animals of similar age and weight (8–12 months, 30–40 kg) allows for the testing of replacement valves using a single orifice size for comparison of valve performance to an appropriate standard. Although the heart and vessels are small in animals within this weight range, the sheep's relatively large left and right atria allow for straightforward surgical approaches to either the mitral or tricuspid valves.

In general, sheep as experimental animals allow for easy handing and long-term husbandry. Furthermore, juvenile sheep grow at a rate that does not cause excessive mitral or aortic stenosis during the postimplantation test periods, as compared to the porcine model [31]. However, specific attention to gastric decompression, perioperative antibiotics, sterile techniques, and minimally invasive interventions in the postoperative period will all increase the success of valve implantation studies in the ovine model [35].

27.4.1 Animal Models of Atrial Fibrillation for Preclinical Valve Testing

Given the increasing number of patients afflicted with atrial fibrillation worldwide, an animal model of the disorder is needed to predict valvular function and its effects on the natural course of the disease. For example, in one study, atrial fibrillation was associated with morbidity secondary to stroke (13 %) and congestive heart failure (24 %) despite anticoagulant treatment and independent of New York Heart Association (NYHA) functional classification, type of surgery, coronary artery disease, history of coronary artery bypass graft surgery, or other cardiac risk factors [10]. Previous research has uncovered a number of cardiovascular structural and electrophysiological alterations associated with atrial fibrillation [23–26]. More specifically, the fibrillating heart will have a shorter refractory period at the right atrial appendage, shorter action potential duration, electrophysiological remodeling, and changes in gene expression [24, 26]. Myocardial remodeling leading to atrial enlargement appears to be a direct result of atrial fibrillation. From a structural standpoint, the fibrillating left atrium is larger, has relative stasis of blood particularly in the atrial appendage, and fails to give the "atrial kick" which comprises approximately 20 % of ventricular filling. These characteristics also explain the increased thromboembolic risk and decreased cardiac output associated with atrial fibrillation.

27.4.2 Pacing-Induced Atrial Fibrillation

Control of the heart beat using electrical stimulation is usually achieved using an intracardiac or transesophageal

approach. Intracardiac pacing, subdivided into burst pacing and continuous pacing, is the most commonly used procedure for the induction of atrial fibrillation in the sheep model and in animal models overall. Rapid atrial pacing is the most common method of inducing atrial fibrillation for in vivo investigation. The transesophageal approach to pacing represents another possibility; however, it is used in humans and animal models primarily in the detection and assessment of irregular cardiac rhythms and coronary artery disease [36]. It should also be noted that implantable systems offer another alternative for the delivery of right atrial rapid pacing in order to induce atrial fibrillation in conscious animals [37].

27.4.3 Pharmacologic-Induced Atrial Fibrillation

Administration of catecholamines and acetylcholine perfused through the sinoatrial nodal artery can induce atrial fibrillation. Isoproterenol (nonselective beta-adrenergic agonist) and adrenaline (alpha-and beta-adrenergic agonist) induce atrial fibrillation in dogs [38]. Atropine treatment prevented catecholamine-mediated atrial fibrillation, indicating a critical role of cholinergic tone in these atrial fibrillation episodes. Acetylcholine-mediated atrial fibrillation is facilitated by isoproterenol, which decreases the threshold of acetylcholine concentration required for atrial fibrillation induction and increases the atrial fibrillation duration. The focal delivery of these agents into atrial tissues can also cause episodic fibrillation.

27.4.4 Other Potential Atrial Fibrillation Models

Given that many genes are associated with cardiac contractility, it is reasonable to postulate that genetic engineering may have a potential role in the development of an atrial fibrillation model. The first important advance in this direction has been the identification of a genetic locus for familial atrial fibrillation on chromosome 10q22-q24 [39]. The discovery that stem cell-derived cardiomyocytes have an intrinsic arrhythmic potential further leads to the question whether stem cell therapy could be the basis for a model of atrial fibrillation [40].

27.5 Animal Models in Myocardial Ischemia

Despite great advances in treatment options, atherosclerotic coronary vascular disease remains one of the leading causes of death worldwide. As a result, this disease continues to be an active area of cardiovascular research. Originally defined by the Greeks as a lack of blood flow, the modern definition of ischemia emphasizes both the imbalance between oxygen supply and demand as well as the inadequate removal of waste products. Impaired oxygen delivery causes a reduction in oxidative phosphorylation, resulting in myocardial dependence on anaerobic glycolysis for the production of high-energy phosphates. This shift in metabolism produces excess lactate which then accumulates in the myocardium. As impaired ATP production and local tissue acidosis prevails, there is a resultant decline in cardiac contractility. Ultimately, if ischemia is not reversed, myocardial infarction occurs with permanent cellular loss and impaired cardiac function. Multiple experimental techniques have been developed for the study of cardiac ischemia. Currently, scientists consistently use isolated myocytes to examine single cell responses, while isolated perfused hearts and whole animal models allow for a better understanding of the whole organ responses. Regardless of the model type, experimental animals remain a crucial tool in the area of research.

27.5.1 Experimental Methods for Creating Ischemia

The ideal model for investigations of ischemic myocardium would theoretically be the intact chronically instrumented awake animal, as acute surgical trauma and anesthetic agents both depress cardiac function [2]. The conscious animal model also has the advantage that it can be used in studies requiring physiological stress, e.g., stress produced by exercise. However, the high cost of the implanted transducers and probes as well as difficulties with measurement techniques often preclude the use of such an approach. To date, the majority of studies use anesthetized animal models for the study of ischemia in either closed or open chest models. Closed chest models have the advantage that tissue trauma is minimized, but in such models, direct access to the heart for metabolite measurement is a major limitation. In contrast, the open chest preparation has the advantage that regional function and metabolism can be studied in detail. The open chest models suffer from drawbacks that include a greater susceptibility to temperature variations and a potential for surgical trauma that may considerably alter cardiac function (Fig. 27.5).

Multiple techniques have been used to create models of myocardial ischemia for research purposes, depending on whether the desired occlusion is to be permanent, temporary, or progressive. Methods to produce complete permanent occlusions include surgical coronary artery ligation or radiological embolization with microparticles. Furthermore, permanent or temporary partial coronary occlusions are commonly induced by ligation, balloon occlusion, or clamping.

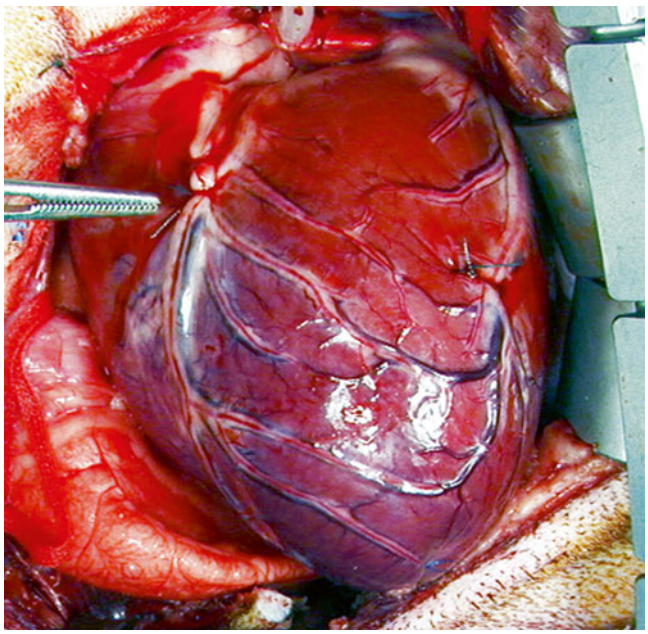

Fig. 27.5 Ligated left anterior descending coronary artery (adjacent to forceps) in an open chest canine model

Typically, models of progressive coronary artery occlusions use either balloon/catheter occlusion or ameroid constrictors (Fig. 27.6). Regardless of the method chosen, the researcher must be aware that the concentric experimental lesions that are created will differ from those of naturally occurring atherosclerotic coronary vascular disease which are typically eccentric. Normally, such eccentric stenoses remain vasoactive and are capable of altering coronary blood flow by changing their lumen diameter. It should be noted that no such vasoactivity remains in experimentally created concentric lesions which will prohibit humoral agents from altering regional coronary flow (Fig. 27.7).

Experience has shown that an induced occlusion of the left anterior descending coronary artery is favored over that in the left circumflex coronary artery for the production of regional myocardial ischemia. It is generally accepted that the occlusion of the left anterior descending coronary artery results in a larger area of myocardial ischemia, and therefore greater impairment of global left ventricular function. However, estimates of infarction size alone have not correlated well with ventricular function [41]. Thus, it has been demonstrated that for the same amount of ischemic myocardium, the compensatory increase by the nonischemic myocardium is different for the left anterior descending coronary artery and the left circumflex coronary arteries [42]. Therefore, in an ideal model, both infarct size and its location must be similar in order to achieve the same degree of impairment in left ventricular global function. If possible, one should also estimate the ischemic area at risk due to an imposed occlusion, e.g., with imaging or the use of dyes.

27.5.2 Localizing and Quantifying Myocardial Ischemia

Blood samples collected from the coronary sinus or from a regional coronary vein are commonly obtained and used for metabolic studies. Yet, such results must be interpreted with the knowledge that these samples include blood from adjacent noninjured myocardium. The use of coronary venous samples for studying metabolism is decreasing because of new approaches using microdialysis, MRI, nuclear magnetic resonance spectroscopy, and positron emission tomography [43–45].

The size and location of myocardial infarction can be determined by Triphenyltetrazolium chloride (TTC) staining, which has been the gold standard for quantifying the extent of myocardial infarction in pathological specimens [46] (Fig. 27.8). In addition, the assessment of localized tissue blood flow using microspheres (radioactive or colored) remains another important standard. However, newer noninvasive methods of determining blood flow in the live animal that allow for repeated follow-up determinations are being developed and improved upon, including spectroscopy and MRI.

27.5.3 Specific Animal Models for Ischemia Investigations

Both large and small animal models have been developed for the study of myocardial ischemia. Advantages of large animal models are their similarity in physiology to humans and ease of instrumentation, and disadvantages include significantly greater care and cost issues that may make small animal models more attractive, particularly when large numbers of animals are required to achieve significant statistical power [47].

The dog has been the most frequently utilized species for in vivo studies of chronic ischemia because dogs have a well-developed coronary collateral circulation, similar to humans with chronic ischemia (progressive heart failure). Furthermore, dogs are easy to handle and lack significant growth as adults, which allows long-term follow-up. However, the significant variability in coronary collateral circulation may hamper efforts to create consistent sizes of ischemic regions between animals, or may result in a minimized ischemic zone.

The pig heart is closer to the relatively healthy human heart with limited collateral blood flow; this makes the swine heart ideal for acute ischemia studies. However, long-term follow-up using the swine model, in general, is considered problematic; if juvenile animals are utilized, significant changes in animal weight will result in both increased difficulties with handling as well as alterations in basic cardiac

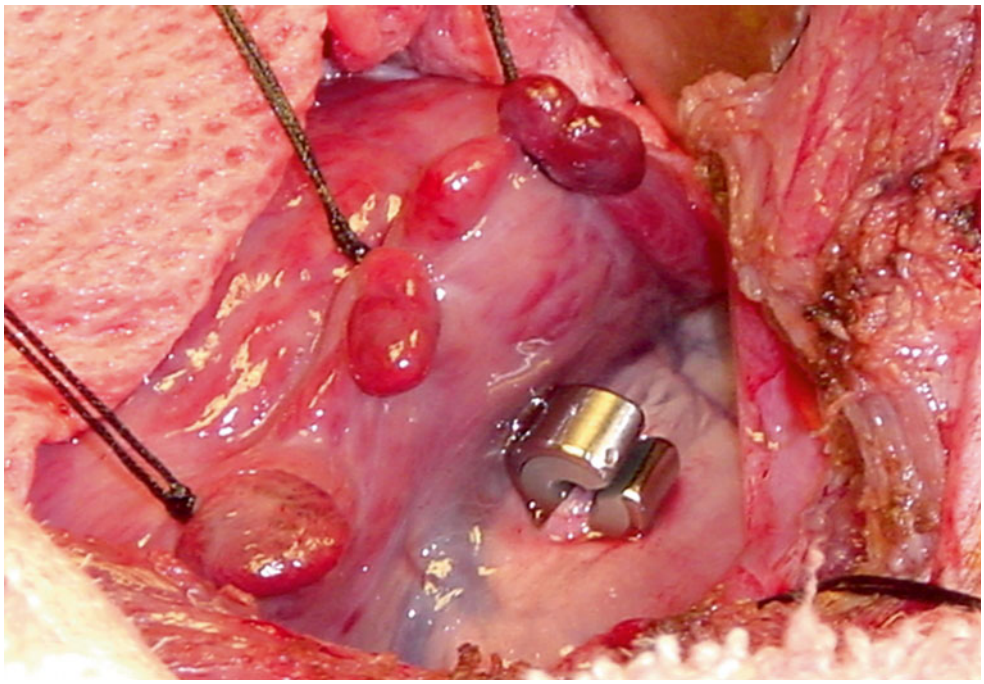

Fig. 27.6 Ameroid occluder in the canine model. Photo courtesy of Michael Jerosch-Herold and Cory Swingen

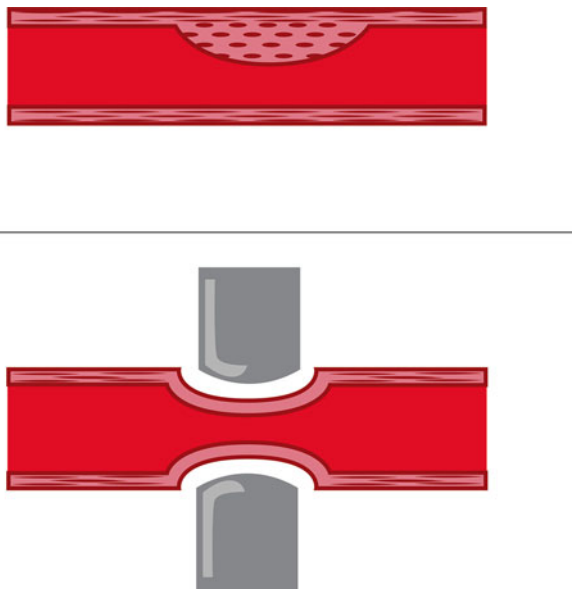

Fig. 27.7 (*Top*) Example of an eccentric vascular constriction as with coronary artery disease. (*Bottom*) Concentric lesion as created by experimental ligation or ameroid occlusion

physiology. More specifically, in consideration of heart to body weight ratios, in a healthy person the ratio is about 5 g/kg, for pigs weighing between 25 and 30 kg, the ratio is similar to that in humans, but for animals exceeding 100 kg, it is only half that value [42]. Importantly, such ratio changes must be considered when interpreting experimental results.

Small animals have also been used as models for investigations of regional myocardial ischemia. However, it has been established that the collateral circulation of the rat is sparse and that of the rabbit may show intraspecies differences [48]. In turn, the guinea pig has such an extensive collateral network that normal perfusion is maintained after a coronary artery occlusion and often infarction does not develop. Another problem with using these animals is that the small vessel diameters may delay or prevent instantaneous reperfusion following transient vessel occlusion, which is further complicated by the inability to make quantitative assessments of coronary blood flow in these small vessels to verify reperfusion. Nevertheless, the use of small animal models for studying myocardial ischemia remains important, including recent studies using stem cells for treatment. See also Chap. 6 for additional details on the comparative coronary circulations.

27.6 Animal Models in Heart Failure and Transplantation

Alexis Carrel reported the first heterotopic transplantation (Table 27.3) of a canine heart connected to the neck vessels of another dog in 1905, but the transplant succumbed to massive clotting and the animal survived for only 2 h. Many years later, Richard Lower and Norman Shumway perfected an orthotopic transplantation technique in the canine and achieved heart graft survivals of up to 21 days. Translation of this research to clinical practice was first performed by Christiaan Barnard in 1967, but acceptable graft survival required further studies in animal models to overcome rejection by the host immune system.

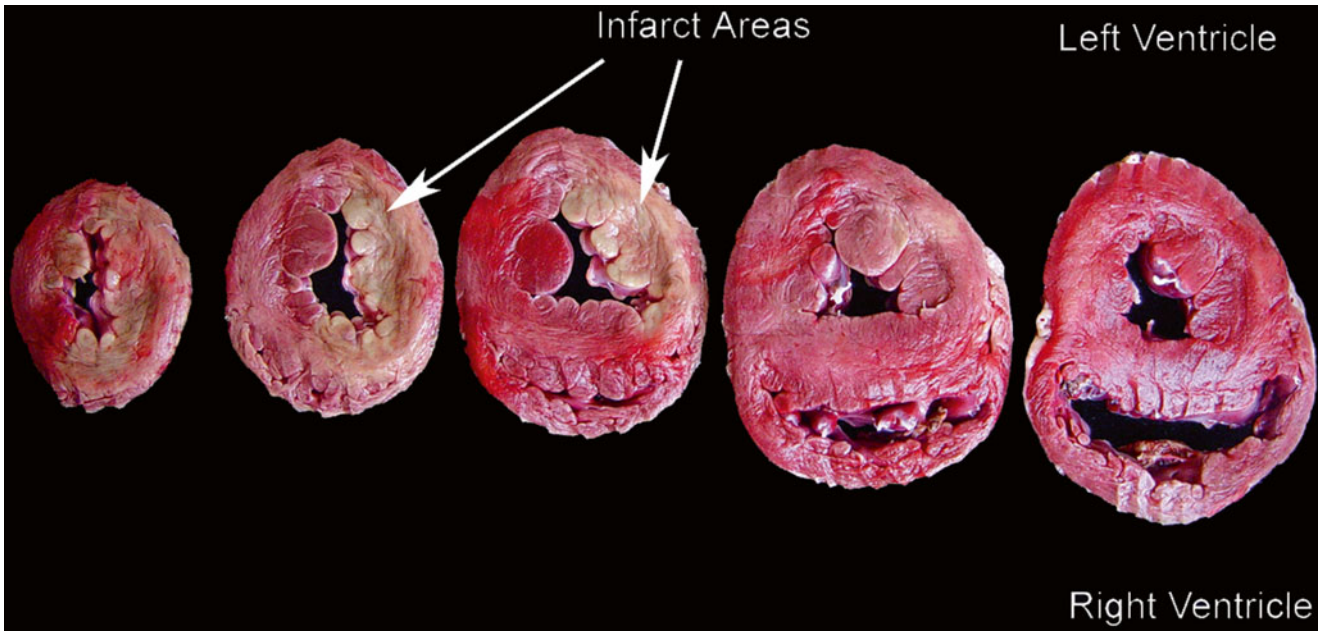

Fig. 27.8 Triphenyltetrazolium chloride (TTC) staining in canine infarct model showing pallor of myocardium (infarcts, *arrows*) in left anterior coronary artery distribution

Table 27.3 Definition of graft types

Graft Type	Definition
Autograft	Transplant from one site to another in the same individual
Isograft	Transplant from a donor to a genetically identical individual (monozygotic twin)
Syngraft	Transplant from a donor to a recipient with no detectable genetic difference (inbred strain)
Allograft (homograft)	Transplant from a donor to a genetically different individual of the same species
Xenograft (heterograft)	Transplant from a donor to a recipient of another species

Today, the successful treatment of end-stage cardiac failure is possible with organ transplantation. In addition, mechanical assist devices are employed for patients who may not initially qualify for transplantation. However, it is clear that too few suitable donor organs are available to meet the current needs (Fig. 27.9). This lack of a reliable and stable source of donor hearts serves as the main impetus for further research into: (1) stem cell therapy used before heart failure; (2) the means to expand cardiac donor pools (e.g., the use of Organ Care System, TransMedics, Boston, MA, USA); and (3) the use of mechanical assist devices and xenotransplantation.

27.6.1 Methods in Transplantation Research

Extensive research has been conducted in the field of cardiac transplantation (Fig. 27.10). *Orthotopic* heart transplantation (the placement of the donor heart in the anatomically correct position) was made possible only after the pioneering efforts of C. Walton Lillehei (refer to Heart Transplantation by Kirklen et al. [49] for a complete discussion of the surgical technique). Orthotopic transplantation is technically feasible using available cardiopulmonary bypass circuits in both the canine and porcine animal models and has often been chosen for the study of organ preservation, graft rejection immunology, immunosuppressive regimens, and/or ischemia/ reperfusion injury [50–53].

Heterotopic cardiac transplantation places the heart in an anatomical location other than the mediastinum. Clinically, a heart transplanted into the heterotopic position ("working" model) is performed by connecting the donor aorta to the recipient aorta, and the donor pulmonary artery to the recipient pulmonary artery while the donor and recipient right atria are anastomosed. Experimentally, a "non-working" model of heterotopic heart transplantation is achieved by connecting the donor aorta to the recipient aorta, and the donor pulmonary artery to the recipient vena cava [54]. As a result, blood

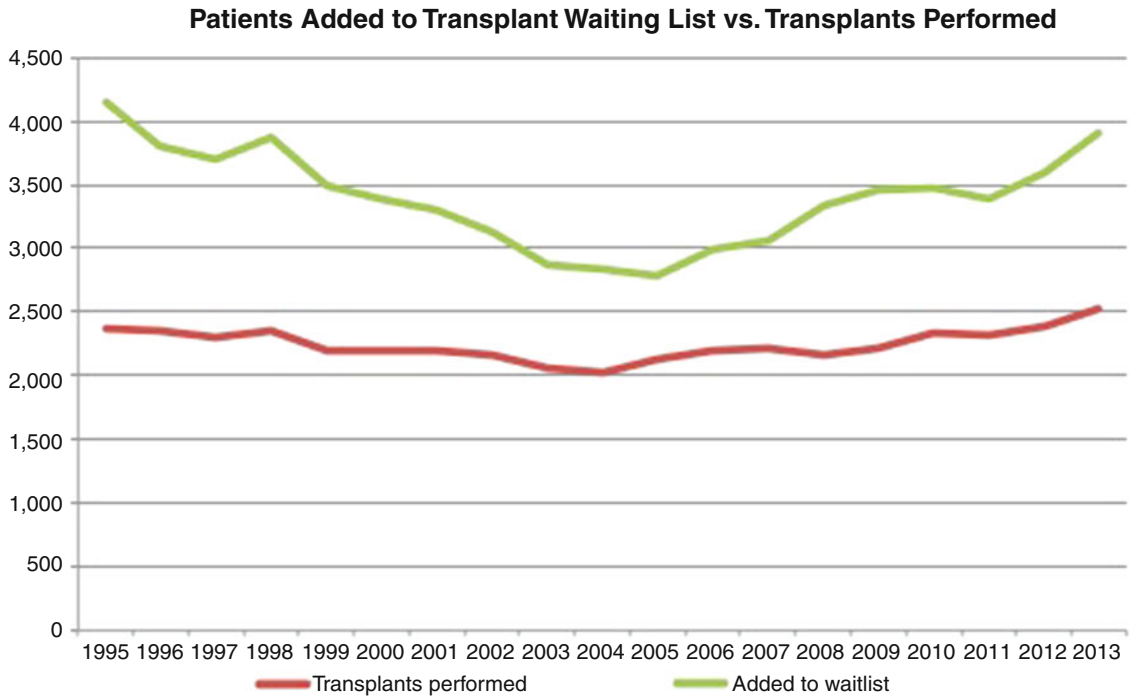

Fig. 27.9 Total number of United Network for Organ Sharing (UNOS) cardiac transplant waiting list registrants and donor hearts per year. Adapted from the UNOS database

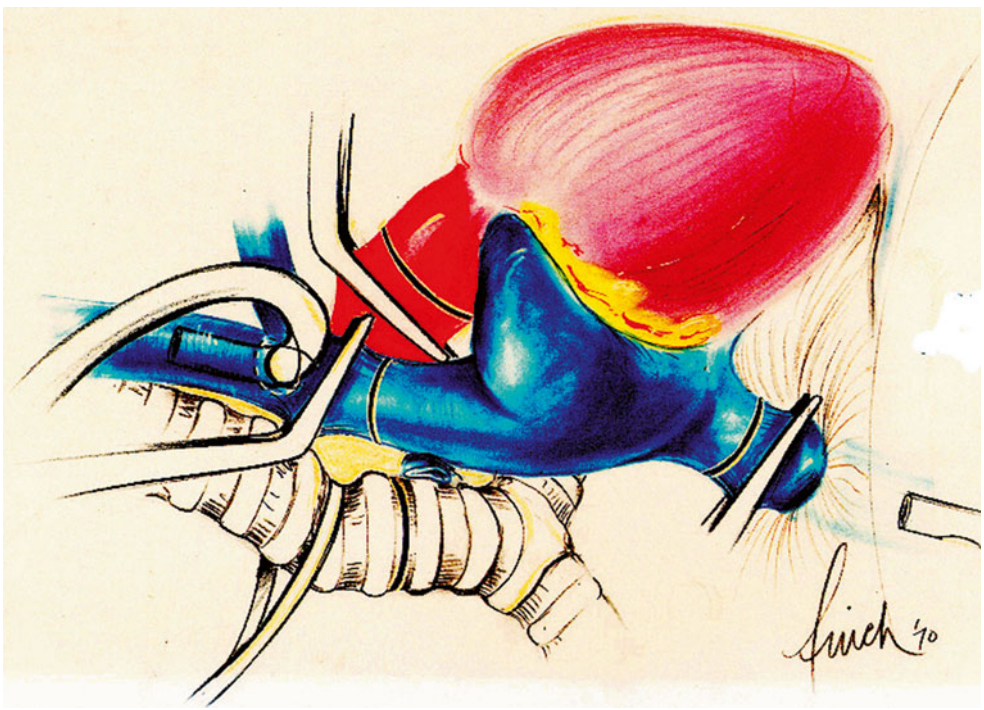

Fig. 27.10 Orthotopic heart transplant (original art by Martin E. Finch)

flow is typically non-physiologic; normal patterns are limited to the coronary arterial and venous system. Absence of significant flow in the ventricles, except for drainage of blood from the coronary sinus into its right ventricle, may promote clot formation and graft failure. Heterotopic transplantation is typically used for studies on ischemia/reperfusion injury [55], prevention of rejection and immunosuppression [56], xenotransplantation, and/or coronary vascular pathology [57]. Heterotopic heart transplantations are most commonly performed using small mammal models such as the mouse, rat, hamster, guinea pig, or rabbit; yet additional skills with microsurgical techniques are then

required. An advantage of this approach is that recipients may retain complete function of their native hearts whether or not the heterotopic donor hearts survive.

27.6.2 Specific Animal Models for Transplantation Research

The choice of an animal model for cardiac transplantation depends greatly upon the area of pathophysiological research. The following is a brief introduction to models that are currently used in this field.

27.6.2.1 The Rodent Transplantation Model

The development of microsurgical techniques has allowed the performance of heart transplantation in rodents. Importantly, the use of rodents in transplantation research can dramatically reduce the costs associated with larger animal models. Typically, Lewis rats have been used for transplantation experiments related to ischemia and reperfusion, prevention of rejection, immunosuppression, and coronary vascular pathology. Because of the small size of rodents, the technique of heterotopic heart transplantation to the abdominal aorta and inferior vena cava, as described by Ono and Lindsey, has been used extensively [58].

Anatomically, the coronary artery blood flow in rodents differs somewhat from higher order mammals in that the left and right coronary arteries traverse the lateral wall of the right ventricle rather than the atrioventricular sulcus. In addition, an extra vessel branching from the cardiomediastinal trunk supplies the sinoatrial node. Some further disadvantages of the rodent model are that hemodynamic measurement of the transplanted hearts can be difficult and transplantation requires microvascular surgical techniques and a surgical microscope. Yet an advantage of this model is its use for xenotransplantation experiments with grafts from mouse to rat, hamster to rat, guinea pig to rat, or hamster to guinea pig. In addition, preservation solutions can be fairly easily evaluated for the end points of survival, histology, and/or for high-energy phosphate analyses. Furthermore, the heterotopic rat transplant model has been extensively used in the pharmaceutical industry to evaluate the effectiveness of anti-rejection medications. More recently, the availability of transgenic or "knock-out" rodents continues to have a large impact in this area of research, i.e. animals with a gene deleted to induce a desired phenotype.

27.6.2.2 The Canine Transplantation Model

The anatomy of the canine heart is similar to that of the human heart (for more details see Chap. 6). As mentioned above, the dog heart has an extensive collateral circulation connecting the left and right coronary circulation. In contrast, nonathletic humans elicit few bridging collaterals. This collateral circulation in the dog is considered to be theoretically advantageous in heart transplantation experiments, as it may protect marginal areas of the heart from ischemia. From the perspective of an easy-to-employ model, dogs have a minimal amount of adipose tissue and their skin is loose, allowing tunneling of catheters if vascular access is needed postoperatively. Furthermore, the dog's relatively large thorax and mediastinum allow for clear visualization of the heart and great vessels. Thus, the canine model for heart transplantation is generally considered most easy to employ for animal studies on organ preservation, reperfusion injury, rejection studies, and/or post-transplant organ monitoring.

27.6.2.3 The Swine Transplantation Model

The porcine heart is often considered the most anatomically similar to the human heart. Specifically, as noted above, the porcine heart has few collateral vessels and an end artery coronary anatomy predominates. Yet, cannulation for cardiopulmonary bypass may be difficult, and the right atrial tissue has typically been described as fragile or friable [2]. In addition, a surgical cut-down for venous and arterial access may be required, secondary to the thick subcutaneous layer of adipose tissue. The pig transplantation model is also prone to postoperative wound infections, necessitating strict sterile techniques during cardiac surgery. Furthermore, juvenile pigs have a rapid rate of somatic growth, which can challenge long-term foreign body implantations. Physiologically, the porcine heart is considered to be prone to arrhythmias and is sensitive to physical manipulation. Bretylium tosylate can be given to limit such arrhythmias; however, ventricular fibrillation can be a recurrent problem following cardiopulmonary bypass [59]. The swine model is considered appropriate for heart transplantation; however, it is often described to be more suited to acute or short-term graft survival studies [60]. Ongoing projects to create a porcine heart with compatible tissue antigens to be used as a substitute for the human donor heart are exciting areas of research that will make the increased use of swine heart donors more likely. Thus, transgenic pigs that express human membrane-associated complement inhibitors in the vasculature have been used for studies of xenotransplantation in nonhuman primate recipients. Moreover, pigs with genetic deletions to prevent the expression of certain antigens that are involved in rejection are currently used as donors for nonhuman primates, making it possible to achieve significant prolongations of graft survival.

27.6.2.4 The Nonhuman Primate Transplantation Model

Researchers in the field of cardiac transplantation have used the nonhuman primate model extensively in developing both

the technique of transplantation and the scientific background necessary for the survival of the donor heart [61, 62]. Numerous programs have successfully used the nonhuman primate in small and large cardiac transplant studies [63–65]. Yet, particular problems with the use of primates have been associated with their veterinary care requirements during preoperative and postoperative times, and thus appropriate facilities are needed. Furthermore, nonhuman primates are extremely susceptible to mycobacterium tuberculosis and appropriate precautions must be taken to minimize the risk of infection. It should be noted that baboons are sensitive to stress and are prone to develop gastroenteritis and bacteremia after surgery, and handling of the baboon typically requires sedation. Nevertheless, the use of baboons and other nonhuman primates has many advantages as an experimental model in transplant research. First, the anatomy of baboons is similar to that of humans, except that the baboon heart has only two aortic arch vessels compared to the three found in humans. Second, the growth of the baboon can be controlled, and adult weights in the 20–30 kg range are maintained for 20–30 years. Additionally, physiologic characteristics of the baboon heart are similar to those of humans, allowing for the use of standard operative instrumentation. From a technical standpoint, the cardiac tissue of the nonhuman primate is not considered as friable or prone to serious arrhythmias as that of swine.

Adverse immunological responses in the primate are a main concern with xenotransplantation and also with antirejection treatments. Interestingly, the human ABO blood type system is applicable with simian tissue and saliva, but not with simian blood [66]. Tissue typing with the major histocompatibility system using primate tissue is also possible. Hyperacute rejection of a pig heart is inherent to xenotransplantation in this model because of the preexisting antibodies in the recipient. Specifically, the donor antigens on the surface of the endothelium of the donor's heart react with antibodies of the recipient, resulting in rejection upon subsequent activation of complement [67]. Inhibition of complement activation or depletion of complement factors was shown to abrogate cardiac xenotransplant rejection [68]. Heterotopic (nonanatomic and nonfunctional) heart transplantation in the nonhuman primate is an established surgical procedure appropriate for investigation of immunosuppressive drug therapies and study of immune reactions between the donor heart and recipient. Typical locations for heterotopic implantation of the donor heart include the neck or abdomen of the primate [69].

27.7 Animal Models for the Testing of Mechanical Devices

Maximizing surgical therapies in end-stage heart failure is a field of great interest. Recently, devices [i.e., ventricular assist devices (VADs)] have become increasingly important because of the large numbers of patients presenting with end-stage heart failure. Interestingly, mechanical VADs are filling a niche where they are both a "bridge to transplant" and a "destination therapy" at centers such as the University of Minnesota. Before such a device can be implanted into a human, the procedure requires years of high-level preclinical and animal testing.

27.7.1 Animal Model Selection for Device Testing

Animal models are necessary for research and development of mechanical devices such as the VAD and for training of the medical personnel involved in their use. The justification for use of a particular animal model is primarily based on: (1) the investigator's past and current success using a particular animal; (2) device size; and/or (3) the relative comparative anatomy. Careful selection of an appropriate model will decrease the difficulty of implanting such devices; devices designed for human use will require a comparably sized research animal for testing. For example, the size of in-line axial flow pumps (Fig. 27.11) has become relatively compact, and they have been implanted into the dog, sheep, and calf models [70, 71]. Larger pumps still require a larger animal [72] (Figs. 27.12 and 27.13). See Chap. 39 for more details.

27.7.2 Federal Guidelines for Device Testing

Although VAD technology is a rapidly advancing field, the FDA has not yet published official guidance documents for such devices. However, the FDA does have specific evalu-

Fig. 27.11 Example of an axial flow pump impeller

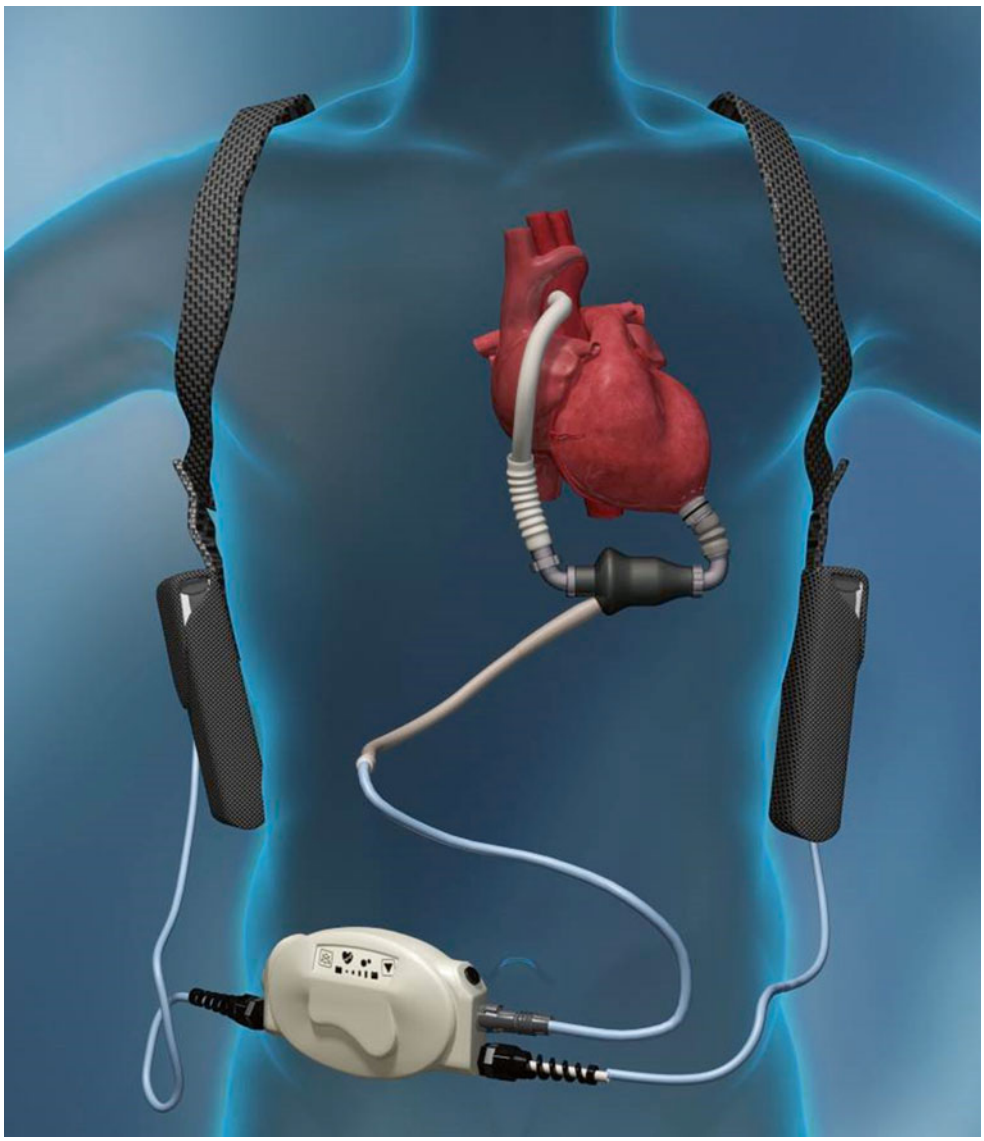

Fig. 27.12 Schematic of a left ventricular assist device (Heartmate II, Thoratec) in human use. Courtesy of Thoratec Corporation

ation criteria for VADs that are designed to identify possible hazards prior to clinical usage. Long-term reliability is a current issue of concern with such devices, as some patients waiting for a transplant survive longer, and destination therapy has become a reality for several device recipients. Consequently, long-term biocompatibility, thrombogenesis (long-term surface coating antithrombogenic integrity), bacterial infection, battery life, and hardware and software reliability have become important parameters for FDA evaluation of such devices. Ultimately, the ease of patient use related to VADs is also of central importance.

27.7.3 Explant Analysis

27.7.3.1 Background

The major types of prosthetic valves currently used in clinical practice are the mechanical valve and the bioprosthetic (or tissue) valve. Percutaneous delivery technology is just beginning to be applied to bioprosthetic valves within the last few years; there is a wave of clinical application in Europe which is gaining momentum in North America in certain select patients.

The role of pathology in the evaluation of cardiac devices is integral for the end results, which is to have data that is

Fig. 27.13 Left ventricular assist device (Heartmate II, Thoratec) in human use. Courtesy of Thoratec Corporation

acceptable for regulatory submission. This is not an exhaustive review of cardiovascular pathology in the context of cardiac devices, but an overview of how regulatory agencies use industry-derived standards to deliver guidance on pathology evaluation.

The use of pathology as the gold standard for explanted device analysis requires more than classical pathology analysis used in diagnostic settings. The integration of regulatory standards is critical to achieve an outcome from each study that will be acceptable for submission to the desired regulatory agency. There are numerous guidance documents from different regulatory bodies and organizations that contribute to the regulatory framework that exist for complete preclinical analysis of medical devices. The ISO 5840 series of documents are not prescriptive in the approach to certain areas of the device or surrounding anatomy, but do require that broad areas be investigated (e.g., calcification). The ISO 5840 document relies on approximately 25 other supporting ISO documents that include risk assessment, pathology evaluation, and marketing approaches. The most heavily involved companion document is ISO 10993, which currently is comprised of 18 different documents, the most important for heart valves being the one pertaining to biocompatibility. In addition to the ISO documents there are FDA guidance documents and, of course, relevant published literature. Interpreting these guidance documents often relies upon experience; researchers should keep themselves abreast of updates to these documents.

27.7.3.2 Pathology in Context of the Study

The two largest divisions of a study for a pathologist are the in-life and explant (i.e., postmortem) stages. These two stages are separated by timing; an animal that goes to the full study term is euthanized and is evaluated based on the study protocol (Fig. 27.14). The departure from this occurs when there is an early "unexpected" death. The unexpected death introduces a number of additional factors to the postmortem analysis, primarily the investigation of whether or not the death was device related. In a well-maintained animal colony, there should be few cases in which the death is not device related in some way (whether this is device failure or surgical error). Careful investigation of the device is often difficult, as an unexpected death precludes administration of heparin to the animal allowing large postmortem clots to surround the device.

The in-life stage involves the analyses of clinical pathology samples which can range from complete blood counts (CBC) and blood chemistries to blood cultures. Clinical pathology tests used can be separated into three categories: (1) hematology; (2) clinical chemistry; and (3) coagulation profiles. There are many natural disease entities that clinical pathology can screen for, but the device-induced changes are the areas of interest, particularly device-induced hemolysis and blood calcium levels. Hemolysis is analyzed by weighing multiple factors such as hematocrit, red cell morphology, haptoglobin, and free hemoglobin. Most often, the serum is macroscopically unremarkable but, in severe cases, there can

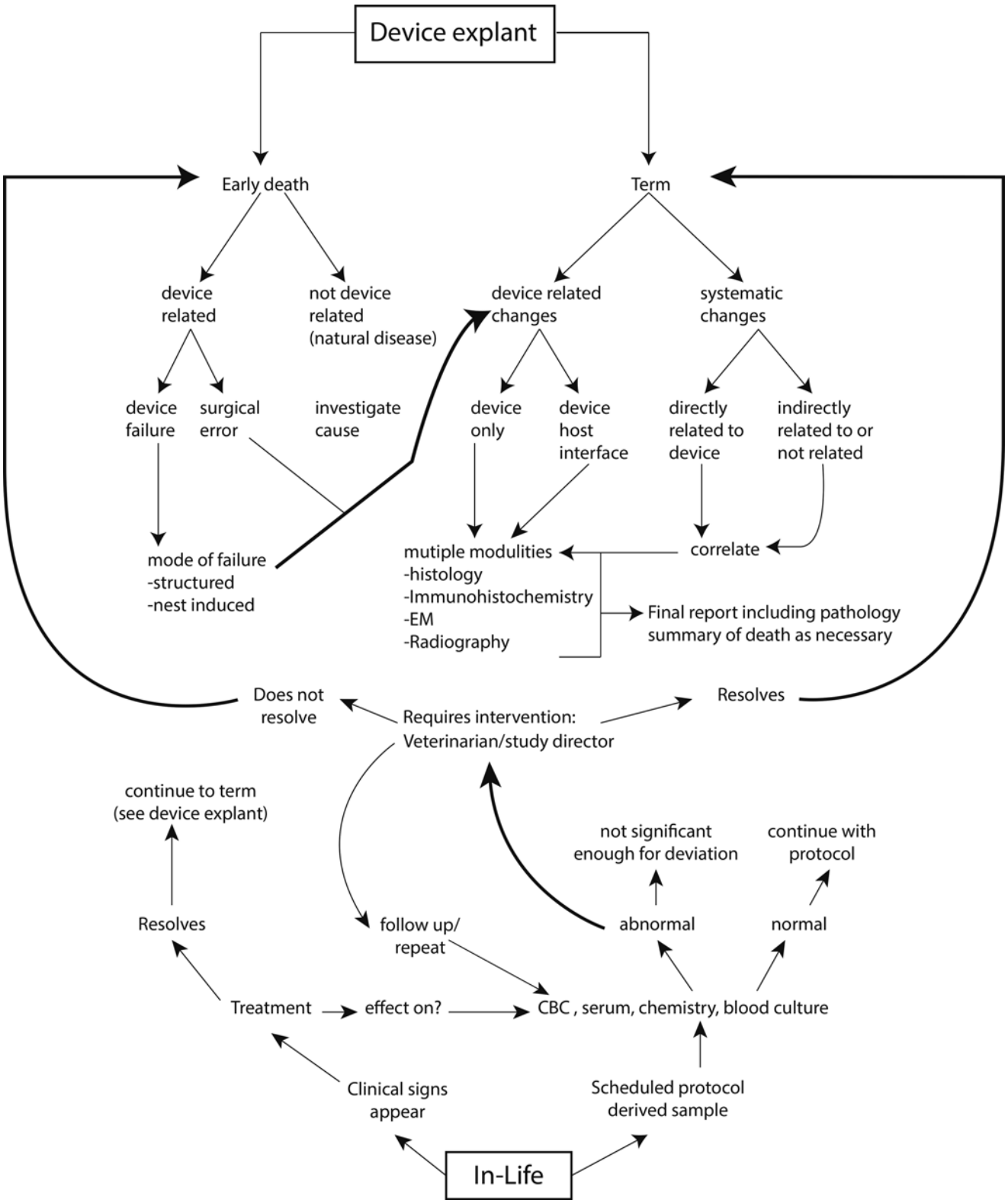

Fig. 27.14 The intricate relationship that pathology has to the in-life phase and the explant phase of a preclinical study

be overt reddening of the serum indicating intravascular hemolysis. Calcification is a particular problem in bioprosthetic (tissue) valves; while dystrophic calcification is found to be the cause in the overwhelming majority of cases, serum calcium must still be assessed to rule out metastatic calcification. This is particularly true if sheep are housed outside in regions of the world where calcinogenic plants are known to exist; such plants contain glycosides of the active metabolite of vitamin D.

27.7.3.3 Process of Using Pathology

The overall analyses of the post-implant device have gross, microscopic, and radiographic components. Yet, typically there are small differences in the way that 4-chambered mammalian hearts are analyzed when they contain devices. Depending on the objectives of the study, the analyses performed under non-Good Laboratory Practice (GLP) conditions can differ substantially from those performed under GLP conditions. On the other hand, while the depth of analyses can differ widely between GLP and non-GLP studies, most laboratories will employ similar techniques or approaches.

In general, there is a core set of methods that needs to be included. First, the radiographic analyses of devices allow the structural integrity (i.e., presence of metal fractures), presence of radio-opaque material, and orientation within the ventricular outflow tract (particularly with TAVI devices) to be assessed. Second, the gross necropsy represents the first time the pathologist is able to lay hands on the test system. This procedure can be conducted in a number of different ways, and standard approaches to necropsy have been covered in other texts [73]. Prior to the necropsy of each animal, terminal procedures are often performed such as echocardiography and angiography, after which heparin is delivered and the animal is euthanized. Necropsy procedures can vary widely depending on the location of the device and whether sterile collection is to be attempted. For cardiac devices that are not collected in a sterile manner, the animal is presented in either left lateral or dorsal recumbency and the abdomen is opened; all organs are evaluated in situ and removed for further evaluation. Following the abdominal cavity evisceration, half the thoracic cage is removed to expose the thoracic viscera. This allows close evaluation of the thoracotomy site and the relationship that the heart and lungs have to the mediastinum and parietal pleura. The tongue, esophagus, and trachea are removed "en bloc" with the heart and lungs (often called the "pluck"). The lungs can then be carefully dissected from the heart to allow detailed external evaluation. At this time, the heart can either be further dissected to reveal the internal device or it can be perfusion fixed (in formalin). More often, dissection of the heart and device is performed at the time of necropsy, and photographs are taken of the inflow and outflow aspects. It is important to note that some of the photographs should be taken directly over the sewing ring to evenly include all features of the device. Third, as part of the regulatory guidance documents, a gross evaluation is performed. It is imperative that a thorough gross examination of each organ is performed, as this is the only opportunity for adverse events to be identified. The most important distant (or end) organs to be examined depends on which side of the heart the device is located. For devices on the left side (aortic and mitral valve devices), the aorta (full length to the iliac bifurcation) should be examined. Kidneys, brain, and eyes should be investigated for embolic debris of various types, and the lungs should be investigated for evidence of left-sided heart failure (pulmonary edema). For the right side (right AV valve, pulmonic valve), the lungs and liver are the major organs of interest. Due to the systemic nature of right-sided heart failure, body cavities and other organs must be thoroughly investigated. It should be noted that bioprosthetic valves delivered to the aortic position via a transcatheter approach (transcatheter aortic valve implantation, or TAVI) have an additional set of analytical criteria that need attention such as device migration. In addition, the approach to device analyses must include considerations relative to the delivery of the device into the vascular site; these include biofilms, host reparative response to surgery, and materials used to implant the device compared with the device itself (i.e., suture material).

Histologic analyses of the device are accomplished primarily by the use of formalin-fixed paraffin-embedded sections of the device stained with hematoxylin and eosin (HE). Additional stains that can be used for paraffin sections can include: Von Kossa, alizarin red (mineralization/ calcification), Mason's trichrome, and Movat's pentachrome (fibrosis/smooth muscle hypertrophy/hyperplasia). For plastic sections (embedded in resin), HE, toluidine basic fuschin, or elastin trichrome can be used as a starting point. For immunohistochemistry, smooth muscle actin (Table 27.4) and a wide range of CD markers can be used for inflammation classification.

For assessing biocompatibility, in particular, it is highly desirable for the device to be visible while it is in contact with the host tissue. This often necessitates the use of other embedding modalities such as plastic embedding. Plastic embedding allows hard materials such as hardened plastics and metals to be analyzed in situ (in close contact with the host tissue), rather than the hard structures removed for paraffin processing. Similar stains can be used between plastic and paraffin (Table 27.4); however, there are some minor issues with tinctorial properties in tissues embedded in plastic. The major drawback with plastic embedding is cost and the length of time to complete the preparation.

The written pathology report is the final document that, once signed, represents the pathology data that has been col-

Table 27.4 Histology stains[a]

Technique	Stain/method	Use
Histochemistry (paraffin)	Hematoxylin and Eosin (HE)	General stain used for initial survey of the tissue. Many changes can be identified with this stain
	Movat's pentachrome (MP)/Masson's trichrome	Identifies (smooth) muscle, collagen fibers and with MP elastic fibers, mucin and fibrin
	Alizarin red (AR)/ Von Kossa (VK)	Highlights calcification (AR) and mineralization (VK)
	Toluidine blue-Basic Fuschin or elastin	Demonstrates mucopolysaccharides and other metachromatic substances in tissue sections
	Periodic Acid Schiff (PAS)	Highlights glycoproteins present extracellularly as well as in chondroid matrix
Immunohistochemistry (paraffin)	Factor VIII, CD31	Identifying endothelial cells
	Alpha smooth muscle actin	Identifies smooth muscle presence within
Plastic embedding	HE, Toluidine blue-Basic Fuchsin or elastin, PAS	See above for use

[a]This list is not exhaustive, but highlights some of the major methods and stains used in histologic valve analysis

lected throughout the study and is now used as a major piece for the regulatory authorities to decide whether the device can move to human clinical trials. There are many different versions of the pathology report that can be created; the authors prefer to have a complete pathology report with all findings included in chronological order of the study. In general, these parts include: (1) clinical pathology; (2) gross pathology including photographs (animal and device); (3) digital radiographs of the device; and (4) microscopic analyses of the device and organs of interest. This allows the report reader to have the complete analyses of each animal/device interaction in one document. The second document one should typically prepare is the pathology summary which should combine all findings from each animal in the study and provide conclusions based on the study protocol and any other regulatory document related items.

27.8 Cellular Cardiomyoplasty

Cellular cardiomyoplasty, the process by which the injured myocardium is repaired by cell transplantation, has significant clinical potential [74, 75]. Much of the excitement about cell-based therapy lies on the premise that repairing the injured heart will overcome inherent limitations for the broad application of organ transplantation and mechanical assist devices. Validation of such therapies needs to be performed in appropriate animal models. A thorough review of the literature for stem cell-mediated cardiac therapy has been provided in Chap. 40, and thus will only be reviewed briefly in this section.

27.8.1 The Ideal Cell Population for Cardiomyoplasty

While advances in the field of cardiomyoplasty have recently been achieved with the advent of stem cell technology, the "ideal" population of cells that is able to effectively engraft damaged myocardium and restore cardiac function without improper differentiation to other contaminating cell types is still an issue of debate. Many cell types with the potential to repair the injured heart have been considered, including differentiated cells (fetal myocytes or satellite muscle cells) and undifferentiated cells (embryonic or adult stem cells). While pluripotent embryonic stem cells offer the promise of functional plasticity and the ability to differentiate into any cell type in vitro, extensive experimentation in vivo is still necessary to properly direct the formation of integrated, functional cardiac tissue at the site of injury without improper differentiation to form teratomas (tumors) or other noncardiac cell types. Multipotent tissue-specific cells that have already committed to a distinct lineage, such as hematopoietic stem cells, mesenchymal stem cells, and endothelial progenitor cells, have also produced encouraging results [76]. However, to date, the use of these cells often results in incomplete engraftment and a failure to restore cardiac function over time [77]. Regardless of the cell type used in cardiomyoplasty, it is clear that animal models will again play a crucial role in the translational research that will be necessary to advance this theory into clinical practice. Hence, such cell preparations need to be appropriately prepared for each selected species of animal to be included within a given trial.

27.8.2 Animal Models for Stem Cell Research

Although multiple animal species have been used for the study of cellular cardiomyoplasty, most investigators have chosen acute ischemia as their experimental model of choice. However, while effective treatment options for acute ischemia do exist, only limited options are available for chronic myocardial ischemia. This observation strongly suggests that further development of the chronic ischemia models using cardiomyoplasty is warranted. As with most research, the experimental hypothesis will remain fundamental in choosing the correct animal model. However, the lack of appropriate stem cell lines in the desired species will add more limitations in selection. Fully characterizing cell lines are important and advantageous so that functional changes of the therapy are correctly attributed to the appropriate precursor cell.

The multiple types of stem cells available for the rodent, specifically the rat and mouse, have made small animal models effective for investigations of stem cell engraftments. However, the differences in myocardial perfusion and ventricular thickness may confer differences in nutrient supplies that would support engraftment in small animal models, but the results obtained may not be translatable to either large mammalian models or humans.

Ultimately, large animal models that better approximate the diseased human heart will be required to fully assess stem cell engraftment, differentiation, and/or functional improvement. Furthermore, large animal models, in general, are considered better suited for assessment of myocardial function via angiography, echocardiography, or MRI; however, to date, the limited availability of appropriate stem cell lines for use in these models has prevented the widespread use of large animal models. Nevertheless, stem cell lines are currently being developed for the pig, dog, and monkey at a number of institutions. More specifically, one lab has developed a canine model of cardiomyoplasty for chronic ischemia in which bone marrow-derived stem cells are used (Fig. 27.15). Two of this chapter's authors, (RPG, RWB), have demonstrated successful engraftment and statistically significant, sustained long-term improvement in regional myocardial function by MRI follow-up. Though successful, this first effort has resulted in additional questions that need resolution: (1) How and when should we deliver the cells? (2) How many cells should be implanted? (3) How often do cells need to be delivered? Much work has yet to be completed before one can be certain that stem cell therapies can be considered a viable treatment for various forms of myocardial disease.

27.8.3 Stem Cell Delivery Methods

Multiple methods of stem cell delivery have been investigated including: (1) direct myocardial injection; (2) peripheral transfusion; and/or (3) stem cell mobilization [78]. Direct epicardial-myocardial injection can be fairly consistently completed intraoperatively during procedures such as coronary arterial bypass or valve operations. Endocardial injection will likely be completed by using commercially available, radiographically guided stem cell injection catheters (Fig. 27.16). Both transfusion and mobilization of resident stem cells offer the least invasive means of stem cell delivery, but require the availability of effective cellular homing signals to direct the correct location for engraftment. This latter hurdle could possibly be overcome by using guided direct myocardial injections, either surgically or via interventional catheter techniques. Available information suggests that multiple stem cell injections may be required to achieve full myocardial regeneration for therapeutic repair. As a result, the use of stem cell injection catheters may become the standard of practice. In addition, advanced imaging techniques such as MRI could be used to localize the injured myocardium and direct, in real-time, stem cell injection catheters to the damaged area.

27.8.4 Stem Cell Engraftment Issues

The ability to track the implanted cell is critical not only to assess the potential of engraftment but also for later determination of differentiation and incorporation into the native tissue. Multiple techniques of cell labeling are currently under investigation including the use of viral gene transduction (e.g., DAPI, Green Fluorescent Gene, Lac Z), incorporation of dyes, and the use of metallic microparticles [79, 80]. For example, gene insertion can be fairly easily accomplished, i.e., allowing for fluorescence microscopy or Q-PCR identification of the stem cell. However, the exact insertion site into the DNA of the cell cannot currently be well controlled, introducing the possibility for nonexpression of the gene or potential disruption of normal cellular transcription and translation processes. The use of dyes incorporated into the cells by pinocytosis has been reported. The primary disadvantage of this technique has been the potential for dye incorporation into native cells in vivo. The use of metallic microparticles has received recent attention, since such particles may allow for real-time identification of cells by MRI imaging and later pathologically by staining. However, information about the potential disruption of cellular function and possible uptake in vivo by native cells has yet to be fully elucidated.

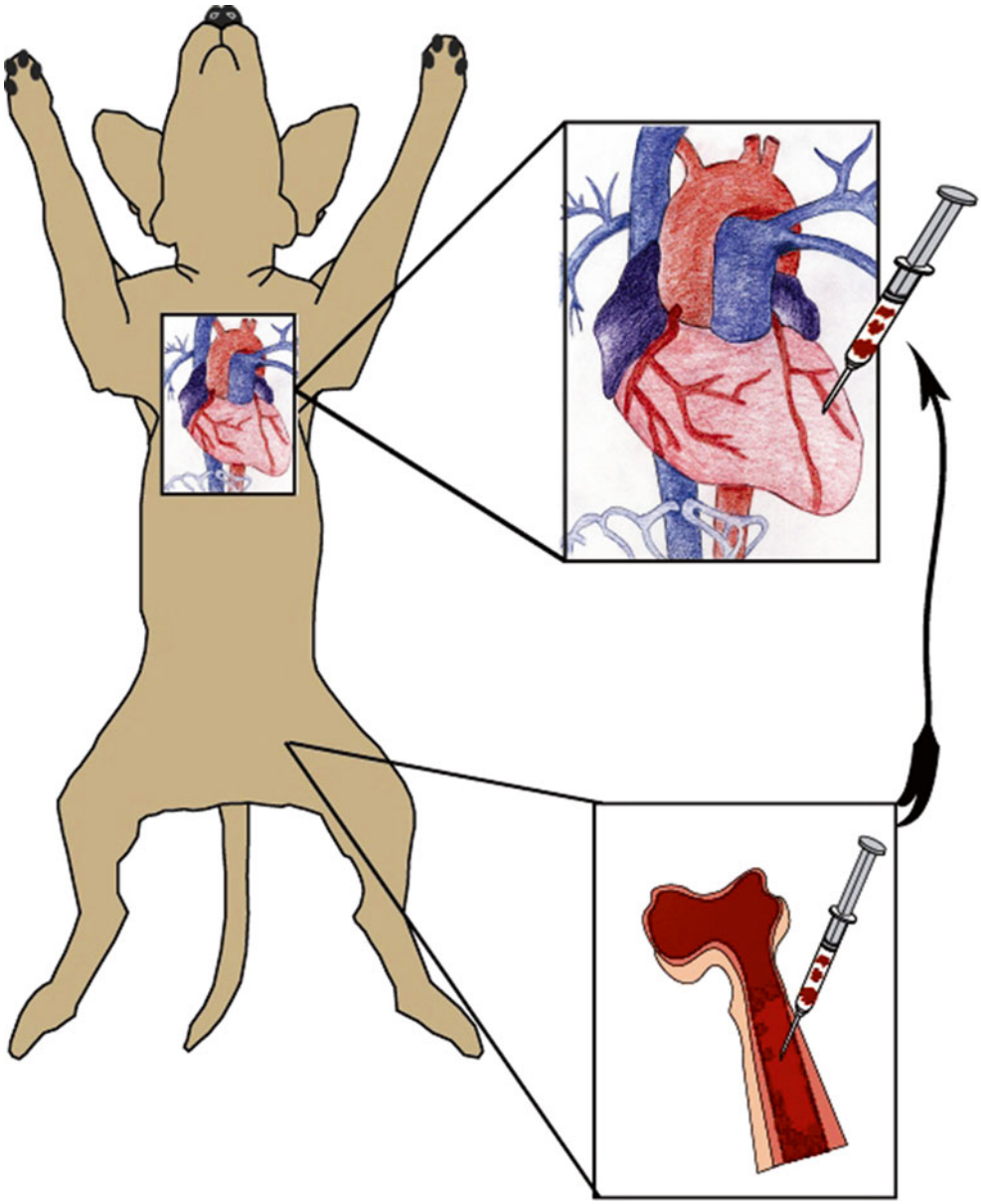

Fig. 27.15 Canine model for bone marrow-derived multipotent stem cell cardiomyoplasty (Illustration courtesy of Kathy B. Nichols)

27.8.5 Functional Assessment of Stem Cell Therapies

Many efforts to demonstrate improvement in cardiac function following cellular cardiomyoplasty have been undertaken. Methods include pressure measurements, ultrasonic microcrystal placement, echocardiography, and/or MRI. Regardless of the specific method used by the investigators, to date, there are only a few significant long-term follow-up studies that exist in the literature. Thus, we conclude that much more research is required before this approach can be applied to humans.

27.9 Summary

In preparing to embark on a preclinical study of a new cardiovascular device, procedure, drug, and/or therapy, it is important to carefully select the animal model. Once the model has been selected, the study design to be followed carries immense importance, particularly with regard to the rigor of the scientific method, regulatory intricacies and, last but not least, the ethical considerations involved with animal use. Attention to all these details is essential and will allow a successful preclinical study outcome. New cardiovascular technologies will continue to be introduced into an ever-

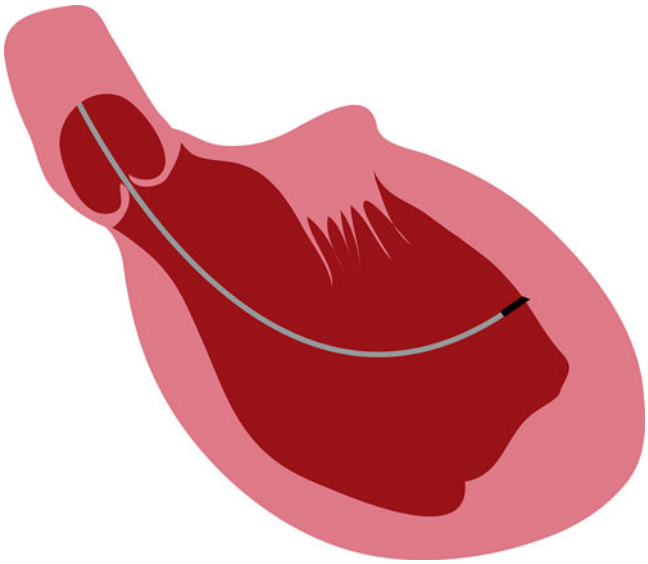

Fig. 27.16 Example of catheter-guided stem cell therapy for myocardial infarction

increasing environment of tighter regulations for animal use and human safety. At some stage of a device's evolution, consultation with experienced centers of experimental research is recommended, as they can provide additional assistance for preparing research protocols and completing the research necessary for well-performed preclinical studies. The progression of a device from design to clinical use is the end goal of these studies and, as such, preclinical research will remain a necessary step for the foreseeable future.

References

1. National Research Council (US) Committee for the Update of the Guide for the Care and Use of Laboratory Animals (2011) Guide for the Care and Use of Laboratory Animals, 8th edition Washington (DC): National Academies Press (US)
2. Gross DR (ed) (1994) Animal models in cardiovascular research, 2nd edn. Kluwer Academic Press, Dordrecht, p 494
3. Ettinger SJ (2000) Congenital heart diseases. In: Ettinger SJ, Feldman EC (eds) Textbook of veterinary internal medicine: diseases of the dog and cat. WB Saunders, Philadelphia, pp 737–787
4. Turk JR, Root CR (1983) Necropsy of the canine heart: a simple technique for quantifying ventricular hypertrophy and valvular alterations. Comp Cont Ed Pract Vet 5:905–906
5. Swindle MM, Makin A, Herron AJ, Clubb FJ Jr, Frazier KS (2012) Swine as models in biomedical research and toxicology testing. Vet Pathol 49:344–356
6. Ahlberg SE, Bateman MG, Eggen MD et al (2013) Animal models for cardiac valve research. In: Iaizzo PA, Bianco RW, Hill AJ, St. Louis JD (eds) Heart valves: from design to clinical implantation. Springer, New York
7. Breckenridge R (2010) Heart failure and mouse models. Dis Model Mech 3:138–143
8. Haworth RA, Hunter DR, Berkoff HA, Moss RL (1983) Metabolic cost of the stimulated beating of isolated adult rat heart cells in suspension. Circ Res 52:342–351
9. Spieckermann PG, Piper HM (1985) Oxygen demand of calcium-tolerant adult cardiac myocytes. Basic Res Cardiol 80:71–74
10. Claycomb WC, Lanson NA Jr, Stallworth BS et al (1998) HL-1 cells: a cardiac muscle cell line that contracts and retains phenotypic characteristics of the adult cardiomyocyte. Proc Natl Acad Sci U S A 95:2979–2984
11. Niggli E (1988) A laser diffraction system with improved sensitivity for long-time measurements of sarcomere dynamics in isolated cardiac myocytes. Pflugers Arch 411:462–468
12. Roos KP, Brady AJ, Tan ST (1982) Direct measurement of sarcomere length from isolated cardiac cells. Am J Physiol 242:H68–H78
13. Roos KP, Brady AJ (1982) Individual sarcomere length determination from isolated cardiac cells using high-resolution optical microscopy and digital image processing. Biophys J 40:233–244
14. Murphy MP, Hohl C, Brierley GP, Altschuld RA (1982) Release of enzymes from adult rat heart myocytes. Circ Res 51:560–568
15. Tung L (1986) An ultrasensitive transducer for measurement of isometric contractile force from single heart cells. Pflugers Arch 407:109–115
16. Chinchoy E, Soule CL, Houlton AJ et al (2000) Isolated four-chamber working swine heart model. Ann Thorac Surg 70:1607–1614
17. Hill AJ, Coles JA, Sigg DC, Laske TG, Iaizzo PA (2003) Images of the human coronary sinus ostium obtained from isolated working hearts. Ann Thorac Surg 76:2108
18. Schechter MA, Southerland KW, Feger BJ et al (2014) An isolated working heart system for large animal models. J Vis Exp 11:88
19. Neely JR, Liebermeister H, Morgan HE (1967) Effect of pressure development on membrane transport of glucose in isolated rat heart. Am J Physiol 212:815–822
20. Wicomb WN, Cooper DK, Barnard CN (1982) Twenty-four-hour preservation of the pig heart by a portable hypothermic perfusion system. Transplantation 34:246–250
21. Dunphy G, Richter HW, Azodi M et al (1999) The effects of mannitol, albumin, and cardioplegia enhancers on 24-h rat heart preservation. Am J Physiol 276:H1591–H1598
22. Menasche P, Hricak B, Pradier F et al (1993) Efficacy of lactobionate-enriched cardioplegic solution in preserving compliance of cold-stored heart transplants. J Heart Lung Transplant 12:1053–1061
23. Gallegos RP, Nockel PJ, Rivard AL, Bianco RW (2005) The current state of in-vivo pre-clinical animal models for heart valve evaluation. J Heart Valve Dis 14:423–432
24. Taylor DE, Whamond JS (1975) A method of producing graded stenosis of the aortic and mitral valves in sheep for fluid dynamic studies. J Physiol 244:16P–17P
25. Su-Fan Q, Brum JM, Kaye MP, Bove AA (1984) A new technique for producing pure aortic stenosis in animals. Am J Physiol 246:H296–H301
26. Rogers WA, Bishop SP, Hamlin RL (1971) Experimental production of supravalvular aortic stenosis in the dog. J Appl Physiol 30:917–920
27. Spratt JA, Olsen CO, Tyson GS Jr, Glower DD Jr, Davis JW, Rankin JS (1983) Experimental mitral regurgitation. Physiological effects of correction on left ventricular dynamics. J Thorac Cardiovasc Surg 86:479–489
28. Swindle MM, Adams RJ (eds) (1988) Experimental surgery and physiology: induced animals models of human disease. Williams & Wilkins, Philadelphia

29. Donnelly KB (2008) Cardiac valvular pathology: comparative pathology and animal models of acquired cardiac valvular diseases. Toxicol Pathol 36:204–217
30. Bianco RW, St Cyr JA, Schneider JR et al (1986) Canine model for long-term evaluation of prosthetic mitral valves. J Surg Res 41:134–140
31. Grehan JF, Hilbert SL, Ferrans VJ, Droel JS, Salerno CT, Bianco RW (2000) Development and evaluation of a swine model to assess the preclinical safety of mechanical heart valves. J Heart Valve Dis 9:710–719, discussion 719–720
32. Sider KL, Blaser MC, Simmons CA (2011) Animal models of calcific aortic valve disease. Int J Inflam 2011:364310
33. Barnhart GR, Jones M, Ishihara T, Chavez AM, Rose DM, Ferrans VJ (1982) Bioprosthetic valvular failure. Clinical and pathological observations in an experimental animal model. J Thorac Cardiovasc Surg 83:618–631
34. Sands MP, Rittenhouse EA, Mohri H, Merendino KA (1969) An anatomical comparison of human pig, calf, and sheep aortic valves. Ann Thorac Surg 8:407–414
35. Salerno CT, Droel J, Bianco RW (1998) Current state of in vivo preclinical heart valve evaluation. J Heart Valve Dis 7:158–162
36. Yu WC, Chen SA, Lee SH et al (1998) Tachycardia-induced change of atrial refractory period in humans: rate dependency and effects of antiarrhythmic drugs. Circulation 97:2331–2337
37. Au-Yeung K, Johnson CR, Wolf PD (2004) A novel implantable cardiac telemetry system for studying atrial fibrillation. Physiol Meas 25:1223–1238
38. Sharifov OF, Fedorov VV, Beloshapko GG, Glukhov AV, Yushmanova AV, Rosenshtraukh LV (2004) Roles of adrenergic and cholinergic stimulation in spontaneous atrial fibrillation in dogs. J Am Coll Cardiol 43:483–490
39. Brugada R, Roberts R (1999) Molecular biology and atrial fibrillation. Curr Opin Cardiol 14:269–273
40. Rivard AL, Suwan PT, Imaninaini K, Gallegos RP, Bianco RW (2007) Development of a sheep model of atrial fibrillation for preclinical prosthetic valve testing. J Heart Valve Dis 16:314–323
41. Gallegos RP, Wang X, Clarkson C, Jerosch-Herold M, Bolman RM (2003) Serum troponin level predicts infarct size. In: American Heart Association. American Heart Association, San Antonio
42. Verdouw PD, van den Doel MA, de Zeeuw S, Duncker DJ (1998) Animal models in the study of myocardial ischaemia and ischaemic syndromes. Cardiovasc Res 39:121–135
43. McFalls EO, Baldwin D, Palmer B, Marx D, Jaimes D, Ward HB (1997) Regional glucose uptake within hypoperfused swine myocardium as measured by positron emission tomography. Am J Physiol 272:H343–H349
44. Headrick JP, Emerson CS, Berr SS, Berne RM, Matherne GP (1996) Interstitial adenosine and cellular metabolism during beta-adrenergic stimulation of the in situ rabbit heart. Cardiovasc Res 31:699–710
45. Massie BM, Schwartz GG, Garcia J, Wisneski JA, Weiner MW, Owens T (1994) Myocardial metabolism during increased work states in the porcine left ventricle in vivo. Circ Res 74:64–73
46. Lie JT, Holley KE, Kampa WR, Titus JL (1971) New histochemical method for morphologic diagnosis of early stages of myocardial ischemia. Mayo Clin Proc 46:319–327
47. Zaragoza C, Gomez-Guerrero C, Martin-Ventura JL et al (2011) Animal models of cardiovascular diseases. J Biomed Biotechnol 2011:497841
48. Winkler B, Binz K, Schaper W (1984) Myocardial blood flow and infarction in rats, guinea pigs, and rabbits. J Mol Cell Cardiol 16:48
49. Kirklin JK, Young JB, McGiffin D (eds) (2002) Heart transplantation. Churchill Livingstone, New York, p 883
50. Wicomb W, Cooper DK, Hassoulas J, Rose AG, Barnard CN (1982) Orthotopic transplantation of the baboon heart after 20 to 24 hours' preservation by continuous hypothermic perfusion with an oxygenated hyperosmolar solution. J Thorac Cardiovasc Surg 83:133–140
51. Tsutsumi H, Oshima K, Mohara J et al (2001) Cardiac transplantation following a 24-h preservation using a perfusion apparatus. J Surg Res 96:260–267
52. Fischel RJ, Matas AJ, Platt JL et al (1992) Cardiac xenografting in the pig-to-rhesus monkey model: manipulation of antiendothelial antibody prolongs survival. J Heart Lung Transplant 11:965–973, discussion 973–974
53. Hunt SA, Haddad F (2008) The changing face of heart transplantation. J Am Coll Cardiol 52:587–598
54. Newcomb AE, Esmore DS, Rosenfeldt FL, Richardson M, Marasco SF (2004) Heterotopic heart transplantation: an expanding role in the twenty-first century? Ann Thorac Surg 78:1345–1350, discussion 1350–1351
55. Langman LJ, Nakakura H, Thliveris JA, LeGatt DF, Yatscoff RW (1997) Pharmacodynamic monitoring of mycophenolic acid in rabbit heterotopic heart transplant model. Ther Drug Monit 19:146–152
56. Beschorner WE, Sudan DL, Radio SJ et al (2003) Heart xenograft survival with chimeric pig donors and modest immune suppression. Ann Surg 237:265–272
57. Perrault LP, Bidouard JP, Desjardins N, Villeneuve N, Vilaine JP, Vanhoutte PM (2002) Comparison of coronary endothelial dysfunction in the working and nonworking graft in porcine heterotopic heart transplantation. Transplantation 74:764–772
58. Ono K, Lindsey ES (1969) Improved technique of heart transplantation in rats. J Thorac Cardiovasc Surg 57:225–229
59. Swindle MM, Horneffer PJ, Gardner TJ et al (1986) Anatomic and anesthetic considerations in experimental cardiopulmonary surgery in swine. Lab Anim Sci 36:357–361
60. Kozlowski T, Shimizu A, Lambrigts D et al (1999) Porcine kidney and heart transplantation in baboons undergoing a tolerance induction regimen and antibody adsorption. Transplantation 67:18–30
61. Goddard MJ, Dunning J, Horsley J, Atkinson C, Pino-Chavez G, Wallwork J (2002) Histopathology of cardiac xenograft rejection in the pig-to-baboon model. J Heart Lung Transplant 21:474–484
62. DeBault L, Ye Y, Rolf LL et al (1992) Ultrastructural features in hyperacutely rejected baboon cardiac allografts and pig cardiac xenografts. Transplant Proc 24:612–613
63. Brenner P, Schmoeckel M, Reichenspurner H et al (2000) Technique of immunoapheresis in heterotopic and orthotopic xenotransplantation of pig hearts into cynomolgus and rhesus monkeys. Transplant Proc 32:1087–1088
64. Kurlansky PA, Sadeghi AM, Michler RE et al (1987) Comparable survival of intra-species and cross-species primate cardiac transplants. Transplant Proc 19:1067–1071
65. Lambrigts D, Sachs DH, Cooper DK (1998) Discordant organ xenotransplantation in primates: world experience and current status. Transplantation 66:547–561
66. Wiener AS, Socha WW, Moor-Jankowski J (1974) Homologous of the human A-B-O blood groups in apes and monkeys. Haematologia (Budap) 8:195–216
67. Kroshus TJ, Rollins SA, Dalmasso AP et al (1995) Complement inhibition with an anti-C5 monoclonal antibody prevents acute cardiac tissue injury in an ex vivo model of pig-to-human xenotransplantation. Transplantation 60:1194–1202
68. Salerno CT, Kulick DM, Yeh CG et al (2002) A soluble chimeric inhibitor of C3 and C5 convertases, complement activation blocker-2, prolongs graft survival in pig-to-rhesus monkey heart transplantation. Xenotransplantation 9:125–134
69. Cramer DV, Podesta L, Makowka L (eds) (1994) Handbook of animal models in transplantation research. CRC, Boca Raton, p 352
70. Li X, Bai J, He P (2002) Simulation study of the Hemopump as a cardiac assist device. Med Biol Eng Comput 40:344–353

71. Snyder TA, Watach MJ, Litwak KN, Wagner WR (2002) Platelet activation, aggregation, and life span in calves implanted with axial flow ventricular assist devices. Ann Thorac Surg 73:1933–1938
72. Mussivand T, Fujimoto L, Butler K et al (1989) In vitro and in vivo performance evaluation of a totally implantable electrohydraulic left ventricular assist system. ASAIO Trans 35:433–435
73. King JM, Dodd DC, Roth L (eds) (2006) The necropsy book, 5th edn. Cornell University, New York
74. Reffelmann T, Leor J, Muller-Ehmsen J, Kedes L, Kloner RA (2003) Cardiomyocyte transplantation into the failing heart-new therapeutic approach for heart failure? Heart Fail Rev 8:201–211
75. Reffelmann T, Kloner RA (2003) Cellular cardiomyoplasty–cardiomyocytes, skeletal myoblasts, or stem cells for regenerating myocardium and treatment of heart failure? Cardiovasc Res 58:358–368
76. Reffelmann T, Dow JS, Dai W, Hale SL, Simkhovich BZ, Kloner RA (2003) Transplantation of neonatal cardiomyocytes after permanent coronary artery occlusion increases regional blood flow of infarcted myocardium. J Mol Cell Cardiol 35:607–613
77. Sakai T, Ling Y, Payne TR, Huard J (2002) The use of ex vivo gene transfer based on muscle-derived stem cells for cardiovascular medicine. Trends Cardiovasc Med 12:115–120
78. Hill JM, Dick AJ, Raman VK et al (2003) Serial cardiac magnetic resonance imaging of injected mesenchymal stem cells. Circulation 108:1009–1014
79. Kraitchman DL, Heldman AW, Atalar E et al (2003) In vivo magnetic resonance imaging of mesenchymal stem cells in myocardial infarction. Circulation 107:2290–2293
80. Kraitchman DL, Sampath S, Castillo E et al (2003) Quantitative ischemia detection during cardiac magnetic resonance stress testing by use of FastHARP. Circulation 107:2025–2030

Catheter Ablation of Cardiac Arrhythmias

28

Henri Roukoz, Fei Lü, and Scott Sakaguchi

Abstract

In humans, the typical range of the resting sinus heart rate is 50–90 beats per minute (bpm); most average healthy individuals have resting rates in the 60–70 bpm range. *Bradycardia* (slow heart beat) is a term used to refer to any heart rate <60 bpm, and *tachycardia* (fast heart beat) indicates rates >100 bpm. Disturbances of cardiac impulse formation and/or transmission comprise the principal mechanisms causing abnormalities of heart rhythm. In basic terms, these are classified as being either brady- or tachy-arrhythmias. The primary goals for treatment of arrhythmias are: (1) to alleviate symptoms and thus improve an individual's quality of life; and (2) to prolong patient survival. Pharmacologic treatment has been the mainstay for management of most cardiac arrhythmias, although in recent years, implantable devices and ablations have become increasingly important. Therefore, non-pharmacologic therapies have begun to play an increasingly important role in curing many arrhythmias (catheter ablation), and preventing their life-threatening consequences [implantable cardioverter defibrillator (ICD) therapy for both primary and secondary prevention of sudden cardiac death (SCD)].

Keywords

Arrhythmias • Tachycardia • Bradycardia • Cardiac ablation • Defibrillator therapy

Abbreviations

AFib	Atrial fibrillation
AT	Atrial tachycardia
AV	Atrioventricular
AVNRT	Atrioventricular nodal reentry tachycardia
AVRT	Atrioventricular reentry tachycardia
Bpm	Beats per minute
CFAE	Complex fractionated atrial electrogram
DC	Direct current
ECG	Electrocardiography
EPS	Electrophysiologic study
ICD	Implantable cardioverter defibrillator
IST	Inappropriate sinus tachycardia
LV	Left ventricular
PAC	Premature atrial complex
PSVT	Paroxysmal supraventricular tachycardia
PVC	Premature ventricular complex
RF	Radiofrequency
RV	Right ventricular
SCD	Sudden cardiac death
SND	Sinus node dysfunction
SVT	Supraventricular tachycardia
TdP	Torsades de Pointes
VT	Ventricular tachycardia
WPW	Wolff–Parkinson–White syndrome

H. Roukoz, MD, FACC, FHRS (✉) • F. Lü, MD, PhD
S. Sakaguchi, MD
Department of Medicine, Cardiovascular Division and Electrophysiology, University of Minnesota,
420 Delaware Street SE, MMC 508, Minneapolis,
MN 55455, USA
e-mail: rouko001@umn.edu

P.A. Iaizzo (ed.), *Handbook of Cardiac Anatomy, Physiology, and Devices*, DOI 10.1007/978-3-319-19464-6_28

28.1 Introduction

Since it is fundamentally important to understand the mechanisms underlying each individual cardiac arrhythmia that may be treated by catheter ablation therapy, the basics of cardiac electrophysiology and individual arrhythmias are first described in this chapter. The normal heartbeat is initiated by pacemaker cells in the sinus node located in the right atrium, adjacent to its junction with the superior vena cava. These cells comprise a specialized, albeit somewhat diffuse, region of the right atrium called the sinus node. The rate and regularity of sinus node activity is determined by the intrinsic firing rate (automaticity) of the cells within the node and the influence of extrinsic factors on these cells, including autonomic neural tone, electrolytes, and drugs. The usual range of the resting sinus rate is 50–90 beats per minute (bpm), although rates as low as 35–40 bpm can be common in fit athletic individuals. The average healthy adult's resting rates are in the 60–70 bpm range. *Bradycardia* (slow heart beat) is a term used to refer to any heart rate <60 bpm, and *tachycardia* (fast heart beat) indicates rates >100 bpm. These definition boundaries are somewhat arbitrary relative to a given individual.

Once generated by the sinus node cells, the cardiac electrical impulse traverses the atria by means of preferential conduction routes (determined by intra-atrial muscle band pathways) to the atrioventricular (AV) node, which is the beginning of the true anatomic specialized conduction system in the ventricle (i.e., the His bundle, bundle branches, and penetrating Purkinje fiber network). Normally, impulse transit through the AV node is relatively slow (the delay that occurs accounts for the majority of the PR interval recorded on the surface electrocardiogram), thereby offering the opportunity for optimized transfer of blood from the atria to the ventricles prior to initiation of ventricular activation (see Chap. 13).

28.2 Mechanism of Cardiac Arrhythmias

The term *arrhythmia* is typically used to refer to disturbances of the normal heart rhythm. An exception to this rule is *sinus arrhythmia* which refers to the normal variations in sinus rhythm associated with physiologic alterations (neural influences) on the sinus node, or cellular pacemaker automaticity. The most important cause of such variations is the influence of the respiratory cycle, but other factors such as beat-to-beat changes in cardiac output (i.e., ventriculophasic feedback) may also contribute.

Disturbances of cardiac impulse formation and/or propagation comprise the principal mechanisms causing abnormalities of heart rhythm. In basic terms, these are classified as being either brady- or tachy-arrhythmias. Bradycardia may be *physiologic* in some individuals, or it may be the result of either: (1) *sinus node dysfunction* (SND; the older term *sick sinus syndrome* is still used by some); or (2) AV conduction block (i.e., intermittent or permanent block of impulse transmission from the site of normal pacemaker activity in the atria through the specialized cardiac conduction system to the ventricles). Either of these conditions can be caused by intrinsic disease within the pacemaker cell or conduction system or by extrinsic factors such as medications or autonomic system disturbances or disease.

The mechanisms underlying tachycardia are multiple and more complex than those causing bradycardia. Nevertheless, tachycardia can be classified as being due to either abnormally rapid impulse initiation (i.e., *abnormal automaticity* from the sinus node region or other subsidiary or abnormal pacemaker sites) or *abnormal impulse conduction*, or both (see Table 28.1).

Table 28.1 Mechanisms of tachycardias

Abnormal impulse initiation
• Automaticity
– Enhanced normal automaticity: as seen in inappropriate sinus tachycardia.
– Abnormal automaticity: as in ectopic atrial tachycardia, accelerated junctional rhythm, and idiopathic ventricular tachycardias.
• Triggered activity
– Early after-depolarization: implicated in *Torsades de pointes* in long QT syndromes.
– Delayed after-depolarization: seen in digitalis-induced arrhythmias and paroxysmal catecholaminergic ventricular tachycardia (CPVT).
Abnormal impulse conduction
• Anatomical reentry:
– Related to normal anatomic boundaries: typical atrial flutter.
– Related to acquired boundaries: ventricular tachycardia late after myocardial infarction or surgical ventricular incisions, atrial tachycardias related to surgical atrial incisions.
– Random reentry and rotors: as seen in atrial fibrillation.
• Other concepts (reflection, functional reentry, and anisotropic reentry).

28.3 Clinical Presentation and Diagnosis

Arrhythmias can and often do occur in an apparently normal heart [e.g., premature atrial or ventricular beats, paroxysmal supraventricular tachycardias (PSVTs)]. However, other clinically important rhythm disturbances are more commonly associated with genetic or structural heart disease. Today, myocardial ischemia is the most important substrate for serious arrhythmias in the Western world, but other forms of nonischemic cardiomyopathy, valvular heart disease, and genetically determined disorders (e.g., long QT syndrome, Brugada syndrome) are also culprits. In Western countries,

viral and rare bacterial infections such as Lyme disease can cause myocarditis, and can be sources of serious arrhythmias. In other parts of the world, infections such as rheumatic heart disease in Africa and Asia, or Chagas disease in South America, remain as important underlying causes of heart rhythm disturbances.

Importantly, the clinical presentation of cardiac arrhythmias may range widely from being completely asymptomatic or mildly symptomatic (palpitations and anxiety) to syncope and even sudden cardiac death (SCD); the clinical impact is largely dependent on arrhythmia-induced hemodynamic changes. The electrophysiologic and hemodynamic consequences of a particular arrhythmia are primarily determined by the: (1) ventricular rate and duration; (2) site of origin; (3) underlying cardiovascular status (i.e., severity of associated heart and vascular disease); and/or (4) promptness and completeness of autonomic nervous system responses to the arrhythmia-induced "stress."

Some arrhythmias can be readily diagnosed by standard 12-lead electrocardiography (ECG), but in other patients its use is often too brief to detect transient rhythm problems. Consequently, other techniques are frequently required to establish an accurate diagnosis including: (1) prolonged ambulatory ECG monitoring (e.g., event monitors, Holter monitors, or mobile outpatient cardiac telemetry); (2) implantable loop recorders; and/or (3) clinical electrophysiologic testing. In selected cases, additional exercise stress testing and signal-averaged ECG recordings may also be used to assess the general susceptibility of a given patient to arrhythmias. Other techniques have provided useful research information, but their value in daily practice remains to be fully defined at this time, such as: (1) analyses of heart rate variability; (2) relative baroreflex sensitivity; (3) assessment of QT dispersion or T-wave alternans; and/or (4) body surface potential mapping.

28.4 Treatment Considerations

The primary goals of the treatment for arrhythmias are twofold: (1) to alleviate symptoms and thus improve the given patient's quality of life; and (2) to prolong survival. Still today, pharmacologic treatments are the initial choice for management of most cardiac arrhythmias, although, in recent years, implantable devices and ablation have become increasingly important, and in several cases the "first line" therapy. The principal pharmacologic effects of antiarrhythmic drugs can be found within the *Vaughn-Williams classification* (Table 28.2). A more comprehensive classification, termed *the Sicilian Gambit*, was introduced in 1991 [1]; this was based on a more comprehensive consideration of the cellular basis of drug actions. In general, neither scheme is fully useful in the treatment of specific arrhythmias. Selection of antiarrhythmic drugs for a given patient should be individualized based on the arrhythmia being treated, the underlying heart disease and comorbidities, individualized responses, and potential side effects.

Table 28.2 Vaughn-Williams classification[a]

Class I: **Sodium channel blockers**
• Class Ia: drugs that reduce Vmax (phase 0 upstroke of action potential) and prolong action potential duration, such as quinidine, procainamide, and disopyramide. • Class Ib: drugs that do not reduce Vmax and shorten action potential duration, such as lidocaine, mexiletine, and phenytoin. • Class Ic: drugs that predominantly slow conduction, moderately reduce Vmax, and minimally prolong refractoriness, such as flecainide, propafenone, and moricizine.
Class II: **β-adrenergic receptor blockers**
• β-blockers may be cardio- or β1-selective such as atenolol, esmolol, and metoprolol or noncardioselective such as carvedilol, pindolol, and propranolol. • Some exert intrinsic sympathomimetic activity (acebutolol, bucindolol, and pindolol) • Some have quinidine-like membrane stabilizing activity (acebutolol, carvedilol, and propranolol). • D-sotalol has strong Class III effect and has been regarded as a Class III agent in many conditions.
Class III: **Potassium channel blockers that prolong refractoriness, such as amiodarone, bretylium, dofetilide, ibutilide, and sotalol. Amiodarone has all the four class effects.**
Class IV: **Calcium channel blockers**
• Dihydropyridine (almodipine and nifedipine) • Nondihydropyridine drugs (diltiazem and verapamil).

[a]As discussed in the text, the utility of this classification in terms of selection of therapy is limited, but the grouping permits important toxicity issues to be more readily kept in mind, an important factor when choosing drugs for individual patients

In patients with ischemia associated with left ventricular dysfunction, Class I antiarrhythmic agents should be avoided due to their proarrhythmic risks (as well as the tendency of this class to exhibit marked negative inotropic effects). Class III drugs, on the other hand (i.e., amiodarone, sotalol, and dofetilide), appear to elicit neutral effects on survival in these patients and have lesser negative inotropic concerns. Beta-blockers (Class II agents) have been shown to prolong survival in patients with structural heart disease. In terms of their use for suppression of symptomatic arrhythmias, beta-blockers are mainly useful for prevention of AV node-dependent reentrant supraventricular tachycardias (SVT) and for rate control of atrial fibrillation (AFib). Nevertheless, nonpharmacologic interventions, such as catheter ablation and implantable cardioverter defibrillator (ICD) therapy for primary and secondary prevention of SCD, are considered the treatment of choice in some clinical scenarios. For more details on pharmacologic effects on the heart, see Chaps. 26 and 30.

28.5 Tachyarrhythmias

28.5.1 Premature Complexes

Ectopic premature beats may originate from the atria, the AV junction, and/or the ventricles. Treatment of premature complexes is generally not necessary. In the symptomatic patient, precipitating factors (such as alcohol, tobacco, and caffeine) should be identified and eliminated. Although anxiolytic agents and beta-blockers may be tried, their efficacy is limited. Antiarrhythmic drugs may be used depending on the severity of symptoms and associated underlying cardiac disease, but avoidance of these drugs is the preferred strategy when possible.

28.5.1.1 Premature Atrial Complexes

Premature atrial complexes (PACs) are typically recognized on the ECG as early P-waves, with a P-wave morphology different from that of the sinus P-wave (Fig. 28.1a). Since the premature P-wave is often superimposed in the preceding T-wave, the T-wave preceding a premature beat should be carefully compared to other T-waves to identify any *buried P-waves*. PACs can conduct to the ventricles with a normal PR interval when the AV junction is not refractory, or with a prolonged PR interval when the AV junction is in its relative refractory period, or they can be blocked when the AV junction is in its *effective refractory period*. PACs almost always enter the sinus node and reset the sinus cycle length, resulting in an *incomplete compensatory pause* (the sum of pre- and post-PAC intervals is thus less than that of two normal sinus PP intervals). They are frequently found in normal subjects and are usually asymptomatic. Treatment is usually not necessary.

28.5.1.2 Multifocal Atrial Tachycardias

Multifocal atrial tachycardia is a relatively uncommon arrhythmia characterized by atrial rates between 100 and 130 bpm with marked variations in P-wave morphology, arbitrarily defined as at least three different P-wave contours (Fig. 28.1d). Typically, multifocal atrial tachycardias occur in older patients with moderate to severe cardiopulmonary disease; they may be especially elicited during an exacerbation. Treatment in such cases is often difficult, and should be primarily directed toward the underlying lung disorder; typically calcium channel blockers are the treatment of choice. Beta-blockers and amiodarone can also be effective, but they are usually avoided due to underlying lung disease.

28.5.1.3 AV Junctional Premature Complexes

AV junctional premature complexes are typically recognized on the ECG as normal QRS complexes without a preceding P-wave (Fig. 28.1b). Further, *retrograde P-waves* (inverted in II, III, and aVF) may be seen after the QRS complexes. AV junctional complexes are less common than PACs and are often associated with drug intoxication and cardiac disease. Most junctional beats have an incomplete compensatory pause (like PACs) because they generate a retrograde atrial activation that resets the sinus node. On rare occasions, a

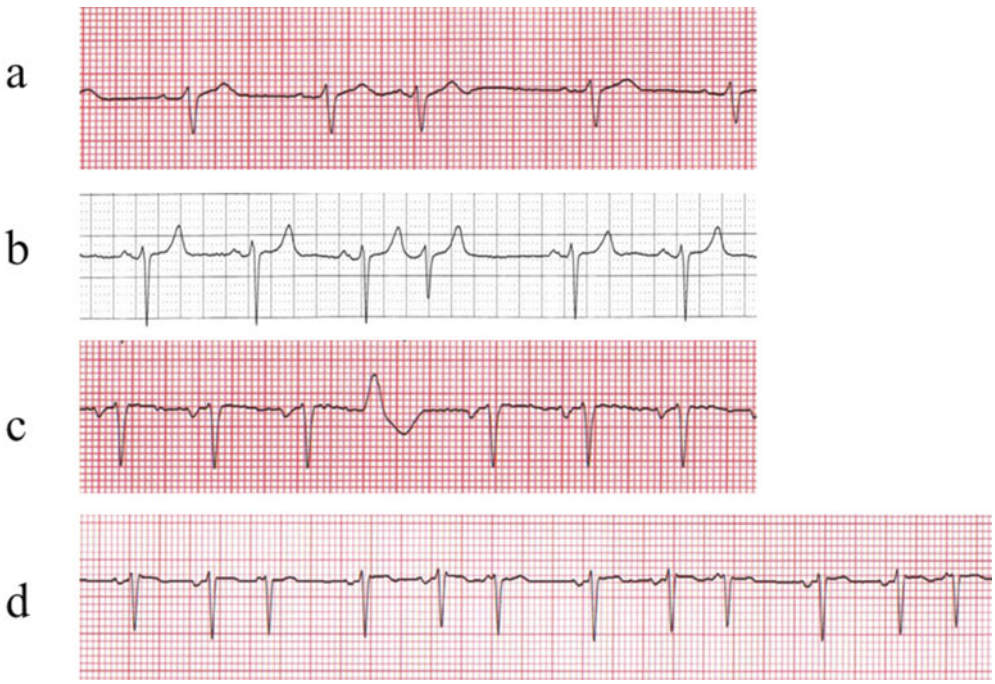

Fig. 28.1 Atrial (**a**), junctional (**b**), and ventricular (**c**) premature complexes, as well as multifocal atrial tachycardia (**d**)

junctional premature beat may fail to conduct to either the atria or ventricles (*concealed junctional beats*), but results in refractoriness in the AV junction and intermittent AV block.

28.5.1.4 Premature Ventricular Complexes

Premature ventricular complexes (PVCs) are recognized as wide QRS complexes of ventricular origin that are not preceded by P-waves (Fig. 28.1c). In addition, because they are premature they often fail to conduct retrograde to the atria. Thus, PVCs do not typically reset the sinus node, but they typically render the AV junction refractory to the subsequent sinus beat. The result is a *full compensatory pause* (the sum of pre- and post-PVC intervals equals that of two normal sinus PP intervals). On rare occasions, a PVC occurs between two consecutive normal sinus beats (*interpolated PVC*). In this case, the PVC neither resets the sinus node nor renders the AV node refractory, so the second sinus beat is conducted to the ventricle. PVCs may occur as a single event, but they also occur in patterns of *bigeminy* (sinus beat and PVC alternating) and *trigeminy* (two sinus beats followed by a PVC). *Couplets* or *pairs* (two consecutive PVCs) and *nonsustained ventricular tachycardia* (arbitrarily defined as 3 or more consecutive PVCs at a rate of >100 bpm) are also relatively common observations during the monitoring of patients with associated heart disease.

PVCs often bear a fixed *coupling interval* (between the onset of PVC and the onset of its preceding sinus QRS complex). When there is a protected ventricular ectopic focus, it is constantly firing without being reset by the preceding sinus beats; this is called *ventricular parasystole* which is characterized by varying coupling intervals. These intervals between the PVCs can be fixed or a multiplier of a common factor.

The relationship of PVCs to SCD is poorly defined. Frequent PVCs (>5–10 per minute) have been shown to be associated with increased risk of SCD. Recent data suggest that a high PVC burden could also be the etiology of left ventricular (LV) dysfunction. The challenge is to make sure to assess ejection fractions during the sinus rhythm beat in patients with very high burden. It should be noted that suppression of PVCs using antiarrhythmic drugs does not reduce, and may actually increase, the risk of SCD in patients following myocardial infarction [2, 3]. This indicates that mortality is primarily determined by the severity of underlying disease, and that the ectopy is an associated finding but not an independent determinant. Alternatively, any benefit derived from PVC suppression by conventional antiarrhythmic drugs may be counterbalanced by a drug-induced increment in mortality due to their negative inotropic and proarrhythmic effects.

Currently, intervention is indicated if the PVC: (1) becomes symptomatic; (2) is thought to be the source of LV dysfunction; or (3) is a trigger for more serious arrhythmias like ventricular tachycardia or ventricular fibrillation. In such cases, ablation therapy is often the preferred treatment since it has a relatively high success rate and can avoid prolonged medical therapies and their potential side effects.

28.5.2 Sinus Tachycardias

28.5.2.1 Physiological Sinus Tachycardias

Physiological sinus tachycardia represents a normal response to a variety of physiological (anxiety and exercise) and pathological stresses (fever, hypotension, thyrotoxicosis, hypoxemia, and congestive heart failure). Sinus tachycardia rarely exceeds 200 bpm. It should not be treated for itself, but its causes must be explored and some of these may require therapy (e.g., treatments of fever, anemia, or hyperthyroidism).

28.5.2.2 Inappropriate Sinus Tachycardias

Inappropriate sinus tachycardia (IST) is characterized by an increased resting heart rate (often >100 bpm) and an exaggerated heart rate response to minimal stress. Such a tachycardia is usually associated with distressing symptoms (palpitations, fatigue, anxiety, and/or shortness of breath). Unfortunately, their etiology and underlying mechanisms are often unclear.

Care must be taken in making a diagnosis of IST. Bona fide ISTs are rare, but it may be observed after previous cardiac arrhythmia ablation procedures or in the setting of symptoms suggestive of postural orthostatic tachycardia syndrome. When considering IST as a diagnosis, it is crucial to exclude secondary sinus tachycardias and to correlate symptoms with an elicited tachycardia. Electrophysiologic studies can be used to exclude atrial tachycardias originating close to the sinus node. Further, beta-blockers and calcium channel blockers can be used to treat IST, although typically with imperfect results. Radiofrequency (RF) modification of the sinus node may be considered if drug therapy fails, but currently this treatment has limited efficacy and high recurrence rates.

28.5.3 Paroxysmal Supraventricular Tachycardias

PSVTs are a group of SVTs associated with sudden onset and termination. They are usually recurrent and often occur in otherwise seemingly healthy individuals. As a group, PSVTs are among the arrhythmias most amenable to catheter ablation.

28.5.3.1 Sinus Nodal Reentry Tachycardias

Sinus nodal reentry tachycardias are relatively rare (i.e., accounting for approximately 3 % of all PSVTs), and tend to occur mainly in older individuals with other manifestations

of sinus node disease. The average rate of sinus node reentry tachycardia is 130–140 bpm, yet these rates can be quite labile, suggesting that autonomic influences may be at play. By definition, the P-wave morphology is identical or very similar to the sinus P-wave. Vagal maneuvers can slow or terminate these tachycardias, since they reenter within a region of the sinus node that is heavily influenced by vagal (parasympathetic) nerve endings. Further, a sinus nodal reentry tachycardia should be suspected in "anxiety-related sinus tachycardia." Beta-blockers and calcium channel blockers (e.g., verapamil, diltiazem), as well as ablation, all remain as viable treatment options.

28.5.3.2 Atrial Tachycardias (ATs)

Atrial tachycardias (ATs) refer to those tachyarrhythmias that arise in atrial tissues and which are due to abnormal automaticity or reentry. They are classified separately from sinus node reentry or AV nodal reentry because, although these latter tachyarrhythmias also arise within or utilize the atria, the sinus node and AV node are critical components of their respective re-entrant tachycardias. A typical AT has an atrial rate of 150–200 bpm with a P-wave morphology that is usually different from that of sinus P-wave; ATs account for 5–10 % of all PSVTs.

Since ATs arise within and are sustained by atrial tissues alone, AV block may develop without interrupting the tachycardia. The later is, in fact, one of the most valuable ways to distinguish ATs from other SVTs, in that they are AVN-dependent such as AV nodal reentry. ATs may be due to automaticity or triggered activities as well as reentry. A typical automatic AT has the following features: (1) it cannot be initiated or terminated by atrial stimulation; (2) the first P-wave of the tachycardia is the same as the subsequent P-waves of the tachycardia; (3) its rate often accelerates after initiation until it stabilizes (at 100–175 bpm), the so-called *warm-up phenomenon*; (4) a premature atrial stimulation can reset automatic AT with a full or incomplete compensatory pause, usually accompanied by a constant return cycle; and/or (5) overdrive suppression is a hallmark of automaticity. Currently, both reentrant and automatic ATs are treated with ablation as a first line therapy.

28.5.3.3 AV Nodal Reentry Tachycardias (AVNRTs)

An AV nodal reentry tachycardia (AVNRT) is the most common of PSVTs (representing 50–65 % of all such arrhythmias) and usually presents as a narrow QRS complex with regular rates between 120 and 250 bpm. In the absence of ventricular preexcitation (i.e., Wolff–Parkinson–White or WPW syndrome and related disorders), AVNRTs and AV reentry tachycardias (see below) typically utilize a concealed bypass tract in >90 % of all PSVTs cases.

A schematic of a typical AV nodal reentry circuit is shown in Fig. 28.2. The AV node has two functional pathways with

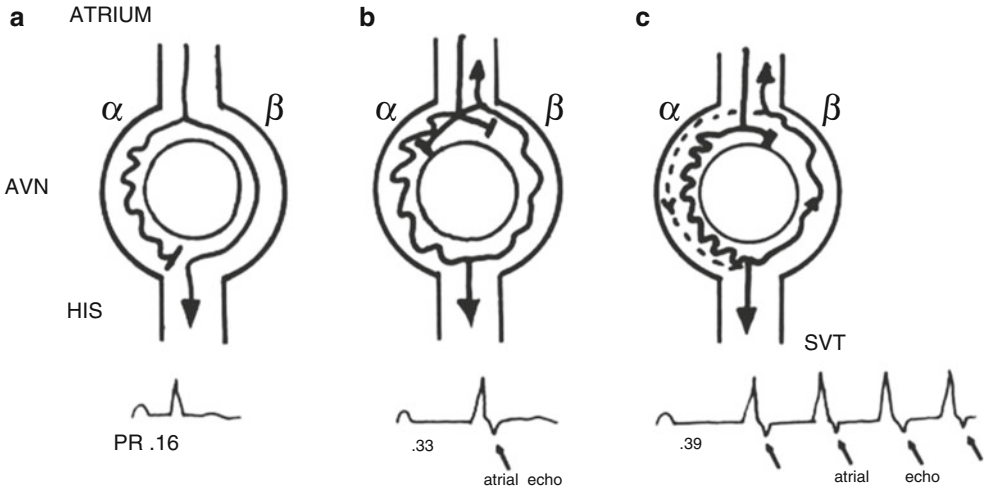

Fig. 28.2 Schema of the typical atrioventricular nodal reentry tachycardia (AVNRT). The atrioventricular node (AVN) has a slow pathway with short refractoriness and a fast pathway with long refractoriness. (**a**) During sinus rhythm, the impulse conducts to the ventricles through the fast pathway, yielding a normal PR interval. The impulse simultaneously goes down the slow pathway, but cannot conduct to the His bundle antegradely or retrogradely to the fast pathway since they are rendered refractory by the prior beat. (**b**) An atrial premature complex reaches the effective refractory period of the fast pathway and is blocked in the fast pathway. This atrial premature complex is able to conduct slowly down to the slow pathway, yielding a prolonged PR interval. The delay in conduction over the slow pathway allows enough time for the fast pathway to recover and enables the impulse conducted from the slow pathway to continue over the fast pathway retrogradely to the atria, producing an atrial echo beat. At the same time, the returned impulse tries to conduct down over the slow pathway and fails due to unrecovered refractoriness of the slow pathway. (**c**) A sufficient early atrial premature complex occurs, producing a similar echo beat as in (**b**). However, the returned impulse is able to conduct down over the slow pathway, repeatedly producing another ventricular beat and atrial echo, i.e., supraventricular tachycardia (SVT). Reproduced from reference [4] with permission. ©1993, Clinical cardiac electrophysiology: techniques and interpretations, 2nd edition. Reproduced with permission by Wolters Kluwer

different conduction velocities and refractory periods. In normal sinus rhythm, conduction is usually over the faster of the two pathways. During the tachycardia, retrograde P-waves may not be apparent because their signals are buried in the QRS complexes or they appear as subtle distortions at the terminal parts of the QRS complex. In general, AVNRTs can be reproducibly initiated and terminated by appropriately timed atrial extra stimuli; this is routinely done as part of the diagnostic electrophysiologic study (EPS) in patients. Spontaneous PACs that initiate an AVNRT are usually associated with a significantly prolonged PR interval due to prolonged conduction within the AV node. In intracardiac recordings during EPS, this is demonstrated by a prolonged "AH" interval, the conduction time between the local atrial tissue adjacent to the AV node and the activation of the His bundle. This PR (or AH) prolongation represents refractoriness of the faster AV nodal pathway with resultant conduction on the so-called slow AV nodal pathway. If the conduction delay in the slow AV nodal pathway (Fig. 28.2) is sufficient to allow recovery of the fast pathway and permit the fast pathway to conduct retrogradely back toward the atrium, the reentry circuit is completed and tachycardia may ensue. Commonly, a critical balance between conduction delay and recovery of refractoriness in these two pathways is required to sustain the tachycardia. Simultaneous antegrade conduction to the ventricles and retrograde conduction to the atria often lead to the "retrograde" P-waves being hidden within the QRS complex, as noted earlier. Furthermore, as a consequence of this physiology, in typical "slow-fast" AVNRT the RP interval is short (i.e., <80–100 ms) in AVNRT (Fig. 28.3). In contrast, in AVRT (i.e., a PSVT using an accessory AV connection such as in WPW syndrome), the ventricles and atria are activated sequentially and the RP interval is expected to be longer than 80 ms (Fig. 28.4).

Acute treatment to terminate AVNRT includes vagal maneuvers (e.g., carotid sinus massage, Valsalva maneuver), adenosine injections, administration of verapamil or diltiazem or beta-blocker, or electrical cardioversion. The majority of these interventions are designed to interrupt AV nodal conduction transiently, thereby "breaking" the fragile reentry circuit. Drugs used for long-term prevention of AVNRT recurrence include digitalis (not recommended currently due

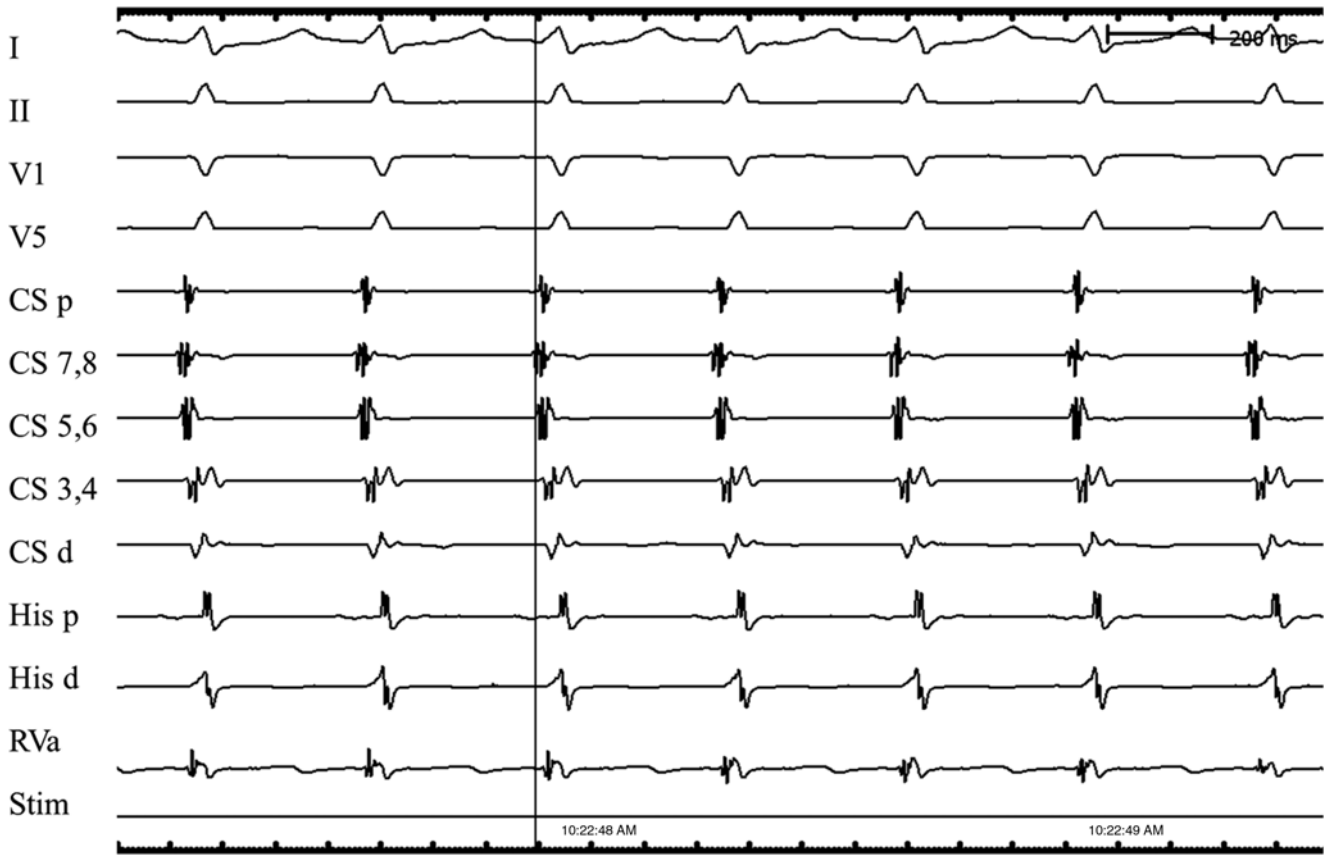

Fig. 28.3 Typical atrioventricular (AV) nodal reentry tachycardia. Since the tachycardia circuit is within the AV node, and it conducts simultaneously antegrade to the ventricles and retrograde to the atria, the time difference between ventricular and atrial activation is relatively short. The retrograde P-wave is often buried in QRS complex (RP interval is 0 ms), as shown in this case. *I* surface ECG lead I, *II* surface ECG lead II, *V1* surface ECG lead V1, *V5* surface ECG lead V5, *CS* coronary sinus, *d* distal, *His* His bundle, *p* proximal, *RVa* right ventricular apex, *stim* stimulation

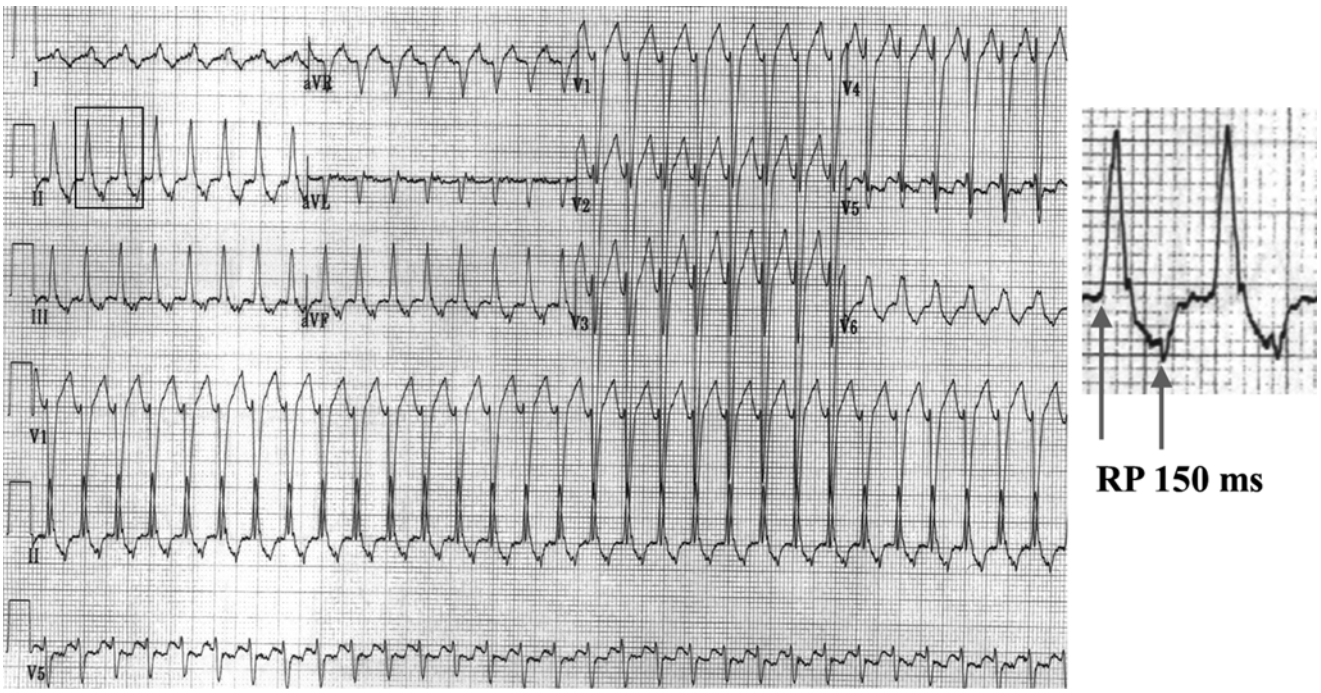

Fig. 28.4 Typical atrioventricular reentry tachycardia. Note that the retrograde P-wave is 150 ms after the onset of QRS complex (RP interval is 150 ms)

to low efficacy), beta-blockers, calcium channel blockers, and Class Ia and Ic antiarrhythmic drugs. However, catheter ablation (principally of the "slow" pathway region) is currently the first line therapy, as it has a success rate of more than 95 % with relatively low risk.

28.5.3.4 AV Reentry Tachycardias (AVRTs) using an Accessory Pathway

AV reentry tachycardia (AVRT) which uses an accessory pathway is another common form of PSVT. In these patients, accessory conduction tissue remaining from embryonic development of the heart can create the substrate for reentry PSVT. The most common form of an accessory pathway is one connecting the atria to the ventricles (i.e., an accessory AV connection). Such a connection is typically composed of working muscle tissue that is so small that it is usually undetectable during open-heart surgery. When these connections conduct in the antegrade direction (i.e., from atrium to ventricle), they modify the first part of the QRS configuration, usually by virtue of earlier than expected activation of the connected part of the ventricular muscle (i.e., preexcitation). The classic case is the "delta" wave observed at the onset of the QRS in WPW syndrome (see below).

In many patients, accessory connections only conduct in the retrograde direction (from ventricle to atrium) and are known as *concealed* accessory connections. In these cases, there is no apparent ECG footprint, since ventricular preexcitation does not occur. Nevertheless, since retrograde conduction can occur, a reentry tachycardia is possible. This form of accessory pathway most often occurs on the left side of the heart, and accounts for approximately 30 % of all PSVTs. In general, the electrical impulses in this type of PSVT circulate in an antegrade direction through the AV node and retrograde through the concealed accessory pathway (Fig. 28.5). In other words, both the atria and ventricles are parts of the reentry circuit. Since atrial activation always follows ventricular activation, the P-wave usually occurs after the QRS complex and the RP interval is relatively long (RP interval >80 ms, but usually in the range of 120 ms).

An AVRT can be initiated and terminated by either an atrial or ventricular extra stimuli. Even when the His bundle is refractory, a PVC may be able to reset the atria by virtue of being transmitted to the atria through the accessory pathway(s). In contrast to the concentric atrial activation sequence in AVNRT, the atrial activation sequences in AVRT are eccentric when the accessory pathways are located at a distance from the AV node. On occasion, however, the connection may be close to the AV node, making the distinction between the two arrhythmias clinically more challenging.

Medical treatment of an AVRT is similar to that of AVNRT. However, transcatheter ablation is highly effective (>95 %) for eliminating accessory AV connections and has become the preferred approach, especially in younger individuals.

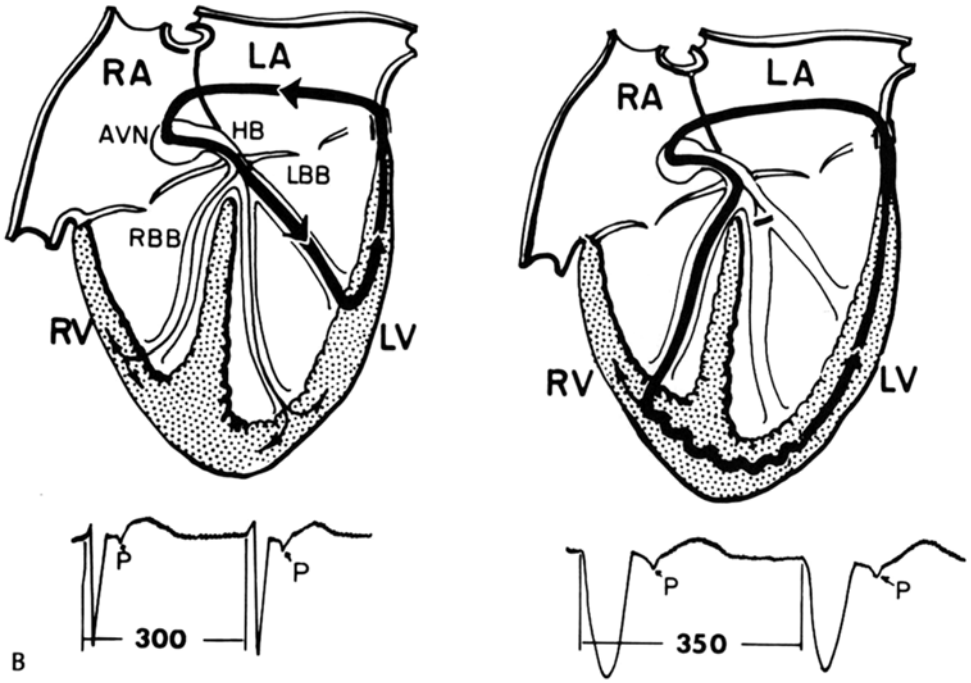

Fig. 28.5 Atrioventricular reentry tachycardia using a left-sided concealed accessory pathway (*left*). Left bundle branch block prolongs the tachycardia cycle length by 50 ms due to the conduction delay of the tachycardia circuit in the left ventricle (*right*). Reproduced from reference [4] with permission. *AVN* atrioventricular node, *HB* His bundle, *LA* left atrium, *LBB* left bundle branch, *LV* left ventricle, *RA* right atrium, *RBB* right bundle branch, *RV* right ventricle. ©1993, Clinical cardiac electrophysiology: techniques and interpretations, 2nd edition. Reproduced with permission by Wolters Kluwer

28.5.3.5 Wolff–Parkinson–White (WPW) Syndrome and Related Preexcitation Syndromes

When there are one or more accessory AV pathways or connections that conduct in the antegrade direction, the ventricles may become overtly preexcited to a varying degree, as discussed earlier. The term *WPW syndrome* is applied when palpitations/tachyarrhythmias occur in patients with overt preexcitation during sinus rhythm. Tachycardias associated with WPW syndrome include: (1) *orthodromic reciprocating or reentry tachycardia*, in which the conduction path is antegrade through the normal AV conduction system and retrograde through the AV accessory pathways; (2) *antidromic reciprocating or reentry tachycardia*, in which the conduction path is antegrade through the AV accessory pathways and retrograde through the normal AV conduction system or another accessory connection; and (3) separate *pre-excited tachycardia* (AFib or flutter, atrial tachycardia, or AVNRT), in which the activation of the ventricles occurs antegrade through both the normal AV conduction system and AV accessory pathways. In these last cases, the accessory pathways typically do not play a critical role in sustaining the tachycardia and thus are not part of the circuit. The ECG features of a typical AV connection in WPW syndrome (Fig. 28.6) are: (1) shortened PR intervals, <120 ms during sinus rhythm; (2) widened QRS durations; and (3) presence of delta waves (a slurred, slowly rising onset of the QRS). Note that the terminal QRS portion is usually normal in appearance, yet sometimes it is associated with secondary ST-T changes.

In addition to typical AV accessory pathways, where the accessory connection is between the atrium and the ventricle, other variants may exist, including: (1) atriofascicular (also called *Mahaim fibers*), in which there is a connection between the atrium and one of the bundles of the conduction system; (2) fasciculoventricular, where there is a connection between one of the bundles and the ventricle outside the normal Purkinje fibers; and (3) the very rare nodofascicular and nodoventricular fibers. Fasciculoventricular fibers typically cause subtle pre-excitation but do not cause tachycardia.

The majority of the atriofascicular connections are long right-sided pathways, commonly at the lateral and anterolateral tricuspid annulus and connecting the right atrium to the right bundle branch or the right ventricular free wall. These fibers almost represent a duplication of the AV nodal pathway and are typically capable of only decremental antegrade conduction [5], therefore, they can only cause *preexcited tachycardia*. In such a patient, often preexcitation is not initially apparent, but can be exposed via right atrial stimulation. Importantly, the associated ECG tends to exhibit a left bundle branch block type of morphology, with a leftward frontal axis similar to that associated with right ventricular apical pacing.

An incessant form of SVT has been described that is usually associated with a slow conducting posteroseptal atrioventricular accessory pathway as its retrograde limb (the so-called *permanent junctional reciprocating tachycardia*). This tachycardia tends to be more often observed in children than in adults. Importantly, its sustained nature can result in deterioration of left ventricular function over time. Hence, an

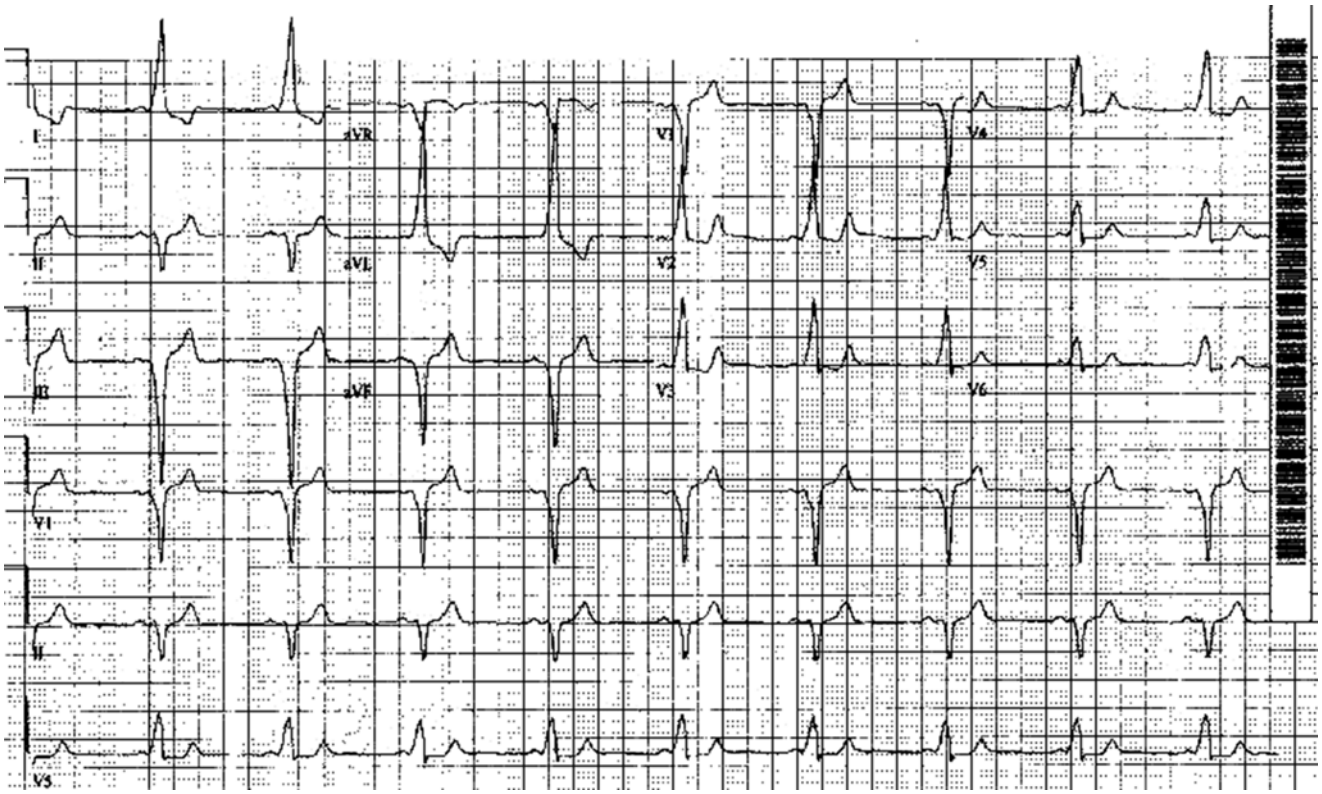

Fig. 28.6 Wolff–Parkinson–White syndrome using a right posterior septal accessory pathway. See text for discussion

early diagnosis is crucial to prevent subsequent heart failure, and ablation therapy in such patients is currently the treatment of choice.

It is important to note that the mere presence of an accessory pathway does not necessarily mean that it is involved in the underlying mechanism of presented tachycardia in a given patient. Not infrequently, these pathways behave as innocent bystanders, yet during the elicitation of AFib they create additional stress on the heart by permitting conduction of very rapid rates to the ventricles. Therefore, one needs to consider that multiple tachycardia mechanisms may reside in a patient simultaneously. For example, AV nodal echoes or AVNRT may be present in 15–20 % of patients after successful ablation of accessory pathways; moreover, up to 10 % of patients with AVRT have multiple accessory connections.

It is estimated that 10–35 % of patients with preexcitation will experience an AFib episode at some point in time. In fact, AFib and atrial flutter may be the presenting arrhythmia in up to 20 % of patients with accessory AV pathways. In patients with WPW syndrome, atrial tachyarrhythmias, such as AFib, may conduct to the ventricles via the accessory pathway and produce an extremely rapid ventricular response that then may degenerate into ventricular fibrillation. Importantly, a grossly irregular RR interval with widened QRS complexes and extremely rapid ventricular rates should immediately suggest the presence of antegrade accessory AV pathway conduction that is associated with AFib (Fig. 28.7). It is considered that patients with preexcited AFib are at increased risk of developing ventricular fibrillation if the shortest preexcited RR interval during AFib is less than 250 ms. Intravenous procainamide is the acute treatment of choice for hemodynamically stable *preexcited AFib* (but it must be administered slowly to avoid hypotension). Note, intravenous *AV nodal blocking agents*, such as digoxin and verapamil, are contraindicated in these patients because they may paradoxically enhance antegrade AV conduction via the accessory pathway, resulting in hypotension or even cardiac arrest. Patients who are hemodynamically unstable may benefit from immediate cardioversion. Among patients with WPW, many episodes of AFib may result from degeneration of orthodromic AV tachycardia (*tachycardia-induced tachycardia*). In general, a successful ablation of the accessory AV pathway often eliminates AFib in these patients. Furthermore, RF ablation of the accessory pathway is the treatment of choice for symptomatic patients with WPW syndrome. It is safe and effective in more than 95 % of patients. For more details on the technological methods for ablation, see Chap. 29.

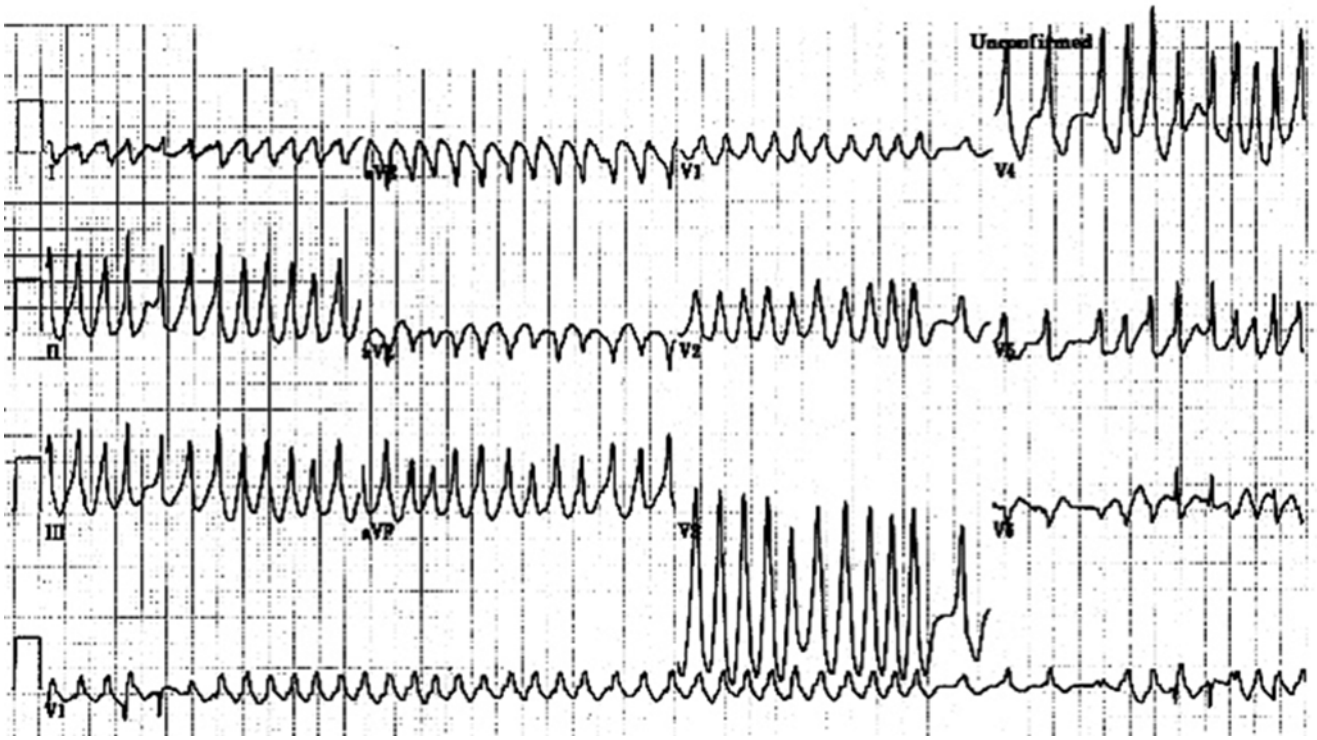

Fig. 28.7 Preexcited atrial fibrillation. See text for discussion

28.5.4 Atrial Flutter and Fibrillation

28.5.4.1 Atrial Flutter

In general, atrial flutter is characterized by an atrial electrical rate between 250 and 350 bpm usually accompanied by 2:1 AV conduction, and thus resulting in ventricular rates of approximately 150 bpm. Classical flutter waves (*F-waves*) are regular sawtooth-like deflections within the ECG, most prominent in the inferior leads and sometimes V1 (Fig. 28.8). A typical *F*-wave may appear to be similar to one generated by other atrial tachycardias with rates between 200 and 300 bpm. Yet, the flutter rates can be as low as 200 bpm in some patients, particularly in the presence of antiarrhythmic drug therapy. Although antiarrhythmic drugs may be useful to prevent recurrence of atrial flutter, they are not very effective for conversion back to sinus rhythm. To date, DC electrical cardioversion (i.e., utilizing 50–100 joules) has been the most effective means for termination of atrial flutter.

Typically, atrial flutter is a macroreentrant rhythm confined to the right atrium. In most cases, the tachycardia circulates around the tricuspid annulus but passes through a relatively narrow isthmus of tissue between the inferior vena cava and the tricuspid valve annulus (cavotricuspid isthmus). Therefore, creating conduction block with ablation within this isthmus is a highly effective means for terminating the tachycardia and also avoiding recurrence. Therefore, ablation in such cases remains the treatment of choice. Although systemic embolization is less common in atrial flutter than in AFib, anticoagulation for patient with atrial flutter should also follow the recommended guidelines for the management of AFib (see below) [6, 7].

28.5.4.2 Atrial Fibrillation

In general, AFib is an uncoordinated atrial tachyarrhythmia characterized by ECG recording as an absence of distinct P-waves before each QRS complex, the presence of rapid atrial oscillations, and variable RR intervals (Fig. 28.9). *Paroxysmal* AFib is arbitrarily defined as AFib that terminates spontaneously or with intervention within 7 days of onset. *Persistent* AFib is defined as AFib lasting longer than 7 days. If a number of attempts of termination by cardioversion have failed, or if the patient and physician have decided to cease further attempts to restore and/or maintain sinus rhythm, AFib is regarded as *permanent*. When no prior history of AFib is available, the term *recent or new onset* is often employed.

Importantly, the relative incidence of AFib is strongly age-dependent, with a substantial increase after the age of 50–60 years (6.2 % in men and 4.8 % in women of 65 years or older). In addition to age, other common cardiac precursors include history of: (1) congestive heart failure; (2) valvular heart disease; (3) hypertension; and/or (4) coronary artery disease. Nevertheless, rheumatic valvular disease, together with overt heart failure, to date have been the most

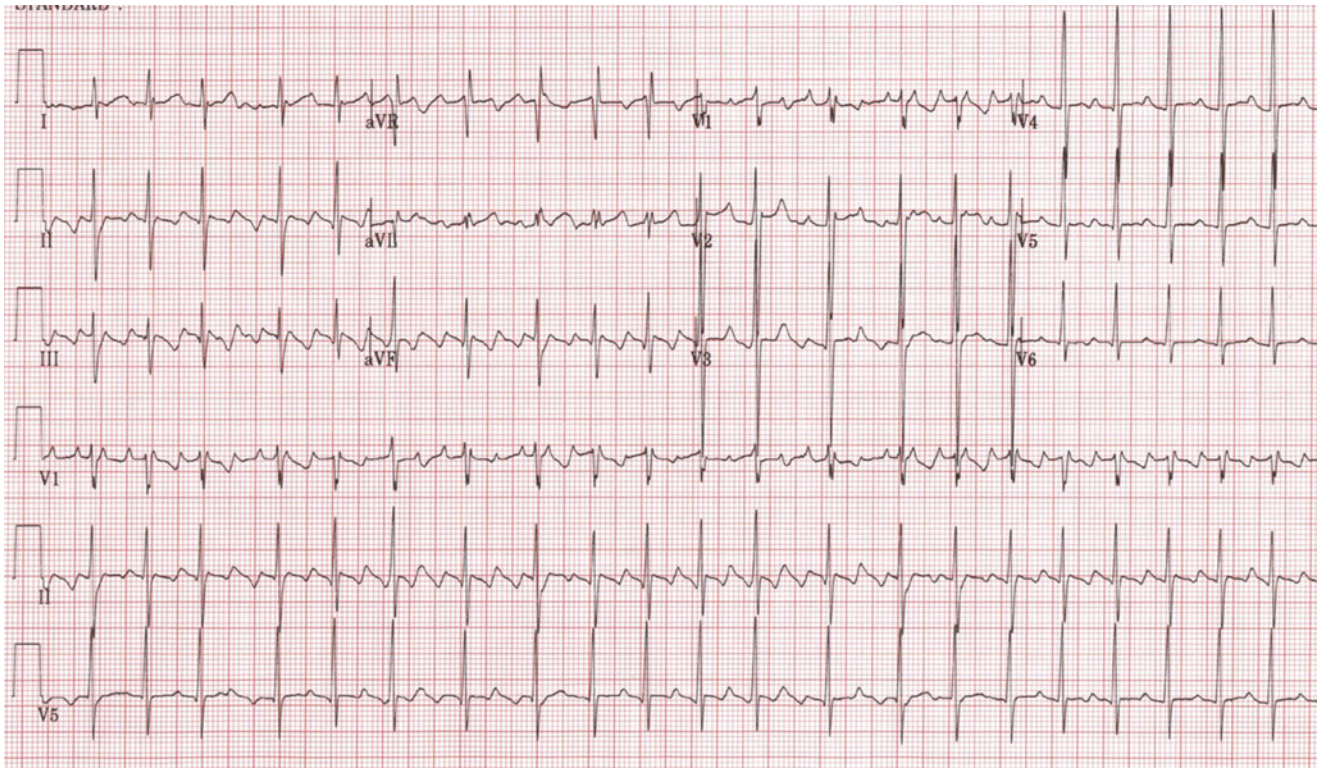

Fig. 28.8 Atrial flutter. See text for discussion

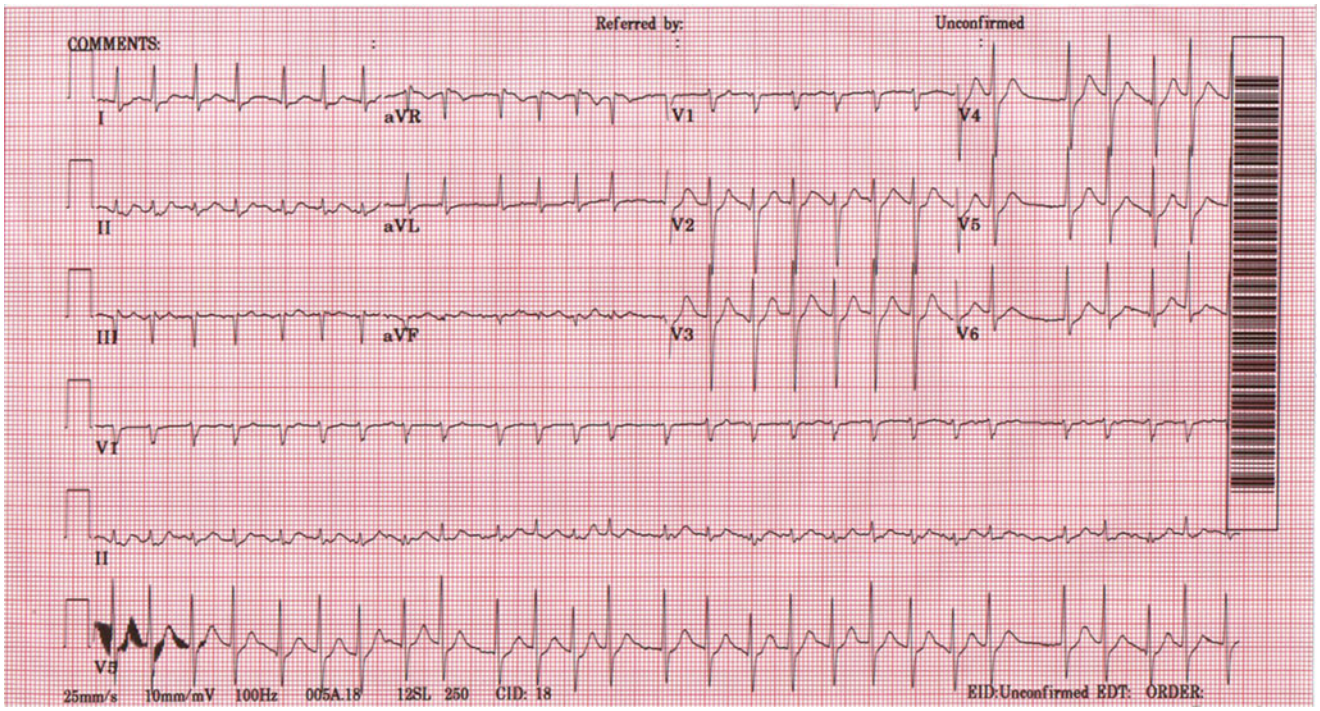

Fig. 28.9 Atrial fibrillation. See text for discussion

powerful predictors for AFib. As rheumatic heart disease has become less common in Western countries, heart failure alone has become the most important predisposing factor. The occurrence of AFib is notably common following either acute myocardial infarction (10 %) or cardiac surgery (~35 %); it is rare after heart transplantation. Usually, postoperative AFib is self-limited, but often its occurrence will prolong hospital stay. Noncardiac precursors associated with AFib, include: thyrotoxicosis, anemia, and/or pulmonary pathology (e.g., infections, embolism) leading to hypoxemia. *Lone AFib* is said to be present when such a tachyarrhythmia occurs in the absence of underlying structural heart disease or transient precipitating factors.

The underlying mechanisms for AFib have been described to include multiple wavelet reentry and/or focal enhanced automaticity. Importantly, the atrial "rate" during AFib can range from 350 to 600 bpm, hence physiologically they are nonfunctional. In general, due to *concealed AV nodal penetration* as well as subsequent variable degrees of AV block, the characteristic *irregularly irregular* ventricular activation rates are commonly between 100 and 160 bpm in untreated patients (those with normal AV conduction properties). *Aberrant conduction* may occur when a long ventricular cycle is followed by a short cycle (*Ashman phenomenon*). Importantly, AFib itself modifies atrial electrical properties in a way that promotes the occurrence and maintenance of the arrhythmia, a process termed *atrial electrical remodeling and also described as AFib begets AFib*.

Both branches of the autonomic nervous system may be involved in the initiation, maintenance, and termination of AFib in some patients. *Vagally mediated AFib* (parasympathetic) is relatively common and is characterized by its onset during rest, especially in the middle of the night. *Adrenergically mediated AFib* (sympathetic) is associated with elevated catecholamine states. For more details on the autonomic nervous system, the reader is referred to Chap. 14.

The major adverse clinical consequences of AFib include palpitations, impaired cardiac function, and/or increased risk of thromboembolism. Typical physical findings in such patients include: (1) an irregularly irregular ventricular rhythm; (2) variations in the intensity of the first heart sounds; and (3) the absence of "*a*" waves in the jugular venous pulse. A peripheral *pulse deficit* (pulse rate less than heart rate) is often noted during a fast ventricular response due to insufficient time for ventricular filling. Importantly, patients with continuous rapid ventricular rates for a prolonged period are at risk of developing a *tachycardia-induced cardiomyopathy*, in a manner similar to that seen among patients with the permanent form of junctional reciprocating tachycardia.

The primary goals for treating patients with AFib are improvement of symptoms and reduction of AFib-associated morbidity. The three basic tenets of therapy for AFib are: (1) control of ventricular rate responses, or *rate control*; (2) restoration and maintenance of a sinus rhythm, or *rhythm control*; and (3) prevention of thromboembolism and thus more particularly *stroke prevention*.

A resting ventricular rate under 90 bpm and ventricular rates between 90 and 115 bpm during moderate exercise are considered acceptable. Commonly used medications for rate control include beta-blockers, calcium channel blockers, and less often digoxin when hypotension is a concern. Ablation of the AV node and the use of a pacemaker may be necessary in some cases to achieve adequate rate control. See Chaps. 29–31 for more therapeutic details.

Approximately 50 % of patients with recent onset of AFib will convert spontaneously to sinus rhythm within <48 h. Potential precipitating factors should be sought and treated. Sinus rhythm can be restored pharmacologically or electrically. Class Ia, Ic, and III antiarrhythmic drugs all have the potential to restore sinus rhythm. Both ibutilide and flecainide have been shown to be effective and commonly used in pharmacological cardioversion of AFib and atrial flutter. Flecainide (class Ic) should be avoided in patients with coronary artery disease or left ventricular dysfunction. For long-term prevention of recurrence, approximately 40–60 % of patients remain in sinus rhythm when treated with various Class I and III drugs (6 months to 3 years of follow-up), with amiodarone being the most effective but with the highest side effect profile.

Catheter ablation may be superior to medical therapy alone in maintaining sinus rhythm, especially in patients with the paroxysmal form of AFib. It is currently recommended as a second line therapy in patients who are refractory or intolerant to medical therapy due to side effects. The *Maze procedure* is also a surgical intervention that has been shown to be effective in decreasing the recurrence of AFib. It has several variations and is most frequently considered in patients undergoing cardiac surgery for other reasons.

Anticoagulation for AFib can be achieved with warfarin or with a new anticoagulant class that includes dabigatran, rivaroxaban, and apixaban. Patients with AFib and high risk factors for stroke should be on chronic anticoagulation. Patients with thyrotoxicosis, rheumatic valvular disease (especially mitral stenosis), and prosthetic valves should receive anticoagulation. Patients with *nonvalvular AFib* are risk stratified based on the $CHADS_2$ and CHA_2DS_2VASc scores. The $CHADS_2$ score has been widely used in the USA and assigns one point each for hypertension, diabetes, heart failure, age above 75 years, and 2 points for previous stroke. Patients with a $CHADS_2$ score of 2 and above require chronic anticoagulation. In 2014, the American Heart Association, American College of Cardiology, and the Heart Rhythm Society jointly recommended adoption of the CHA_2DS_2VASc score. This system is similar to the $CHADS_2$ score but assigns 2 points for age >75 years and adds one point for age

65–74, vascular disease (such as previous myocardial infarction or peripheral vascular disease), and female gender. It also recommends that patients who undergo electrical cardioversion be on anticoagulation for 4 weeks. A complete guideline for management of AFib was recently published in 2014 [6]. In addition, the American College of Cardiology/American Heart Association physician consortium on clinical performance measures for adults with nonvalvular AFib or atrial flutter was published in 2008 [7].

28.5.5 Ventricular Tachyarrhythmias

28.5.5.1 Ventricular Tachycardias (VTs)

Although ventricular tachycardia (VT) can occur in a clinically normal heart, it generally accompanies some form of structural heart disease. VTs associated with a structurally normal heart include idiopathic VT, fascicular VT, and VT related to channelopathies. VTs associated with structural heart disease are most frequently due to previous myocardial infarction, but also nonischemic cardiomyopathy, arrhythmogenic right ventricular cardiomyopathy, hypertrophic cardiomyopathy, and congenital heart disease.

VT is typically characterized on an ECG by a wide QRS complex tachycardia at a rate of >100 bpm (Fig. 28.10). Like PVCs, VTs can be monomorphic (Fig. 28.10a) or polymorphic. *Sustained VT* is defined as a VT that persists for >30 s or requires termination due to hemodynamic compromise. *Nonsustained VT* is defined as VT lasting >3 consecutive beats but less than 30 s. Key markers of VT on an ECG, if present, include ventriculo-atrial dissociation, capture, and fusion beats. The presentation, prognosis, and management of VT largely depend on the underlying cardiovascular state.

Antiarrhythmic medical therapy includes amiodarone, sotalol, mexiletine, and sometimes dofetilide. Class I antiarrhythmics can be used in the absence of structural heart disease. Amiodarone is the most commonly used drug for termination of hemodynamically stable and sustained VT. If the VT is hemodynamically unstable, immediate synchronized electrical cardioversion should be performed.

Therapy also includes implantable cardiac defibrillators (ICD) for prevention of SCD among patients with underlying structural heart disease and catheter ablation. Ablation can provide a cure for idiopathic VT in an otherwise normal heart. However, in patients with diminished LV function, it is frequently appropriate to place an ICD even after successful ablation. A complete guideline for management of ventricular arrhythmias was recently published in 2006 [8].

28.5.5.2 Ventricular Flutter and Ventricular Fibrillation

Electrocardiographically, *ventricular flutter* (Fig. 28.10b) usually appears as a sine wave with a rate between 150 and 300 bpm. It is essentially impossible to assign a specific morphology for these oscillations. In contrast, *ventricular fibrillation* (Fig. 28.10c) is recognized by grossly irregular

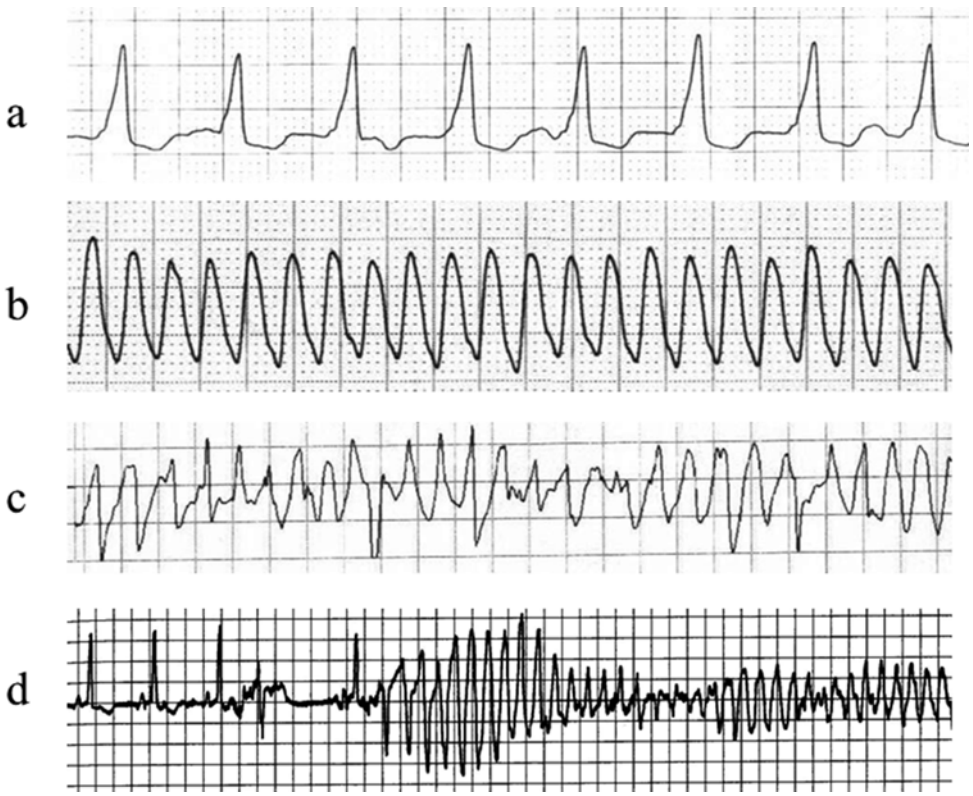

Fig. 28.10 Ventricular tachycardia (**a**), ventricular flutter (**b**), ventricular fibrillation (**c**), and Torsades de pointes (**d**). See text for discussion

undulations of varying amplitudes, contours, and rates. The spontaneous conversion of ventricular fibrillation to sinus rhythm is rare, and thus prompt electrical defibrillation is essential. Longer-term prevention of SCD in these patients predominately depends on ICDs.

28.5.5.3 Accelerated Idioventricular Rhythm

Accelerated idioventricular rhythm can be regarded as a type of slow VT with a rate between 60 and 110 bpm. This rhythm usually occurs in patients with acute myocardial infarction, particularly during reperfusion. Since the rhythm is usually transient without significant hemodynamic compromise, treatment is rarely required.

28.5.5.4 Torsades de Pointes

In the presence of prolonged QT intervals (congenital or acquired), a unique form of polymorphic VT, termed *Torsades de Pointes* (TdP), may occur. A *long-short sequence* of QRS complexes (e.g., produced by AFib or PVCs) will typically initiate this arrhythmia (Fig. 28.10d). TdP often presents with multiple nonsustained episodes causing recurrent syncope, but it also has a predilection to degenerate into ventricular fibrillation leading to SCD. Identification of TdP has important therapeutic implications because its treatment is different from that of common polymorphic VT. Magnesium, overdrive pacing, and isoproterenol can be used in the acute management of TdP. An ICD is recommended for TdP that does not have a reversible cause. Left cervicothoracic sympathectomy may reduce the incidence of TdP and may be used as adjunctive therapy (after ICD implant) in patients with congenital long QT syndrome. In selected cases, ablation of the PVCs preceding the onset of TdP may reduce TdP recurrences (Fig. 28.11).

28.5.5.5 Nonparoxysmal Junctional Tachycardias

Nonparoxysmal junctional tachycardia, also called *accelerated junctional rhythm*, is recognized by a narrow QRS complex without a consistent P-wave preceding each QRS complex, and has a typical rate between 70 and 130 bpm usually associated with a warm-up period at its onset. Nonparoxysmal junctional tachycardia frequently results from conditions that produce enhanced automaticity or triggered activity in the AV junction, such as inferior acute myocardial infarction, digitalis intoxication, and post valve surgery. Treatment should be primarily directed toward the underlying diseases.

28.6 Bradyarrhythmias

As discussed in the introduction, bradycardia may be caused by either an SND, *sick sinus syndrome*, or an AV conduction block. Acute treatment options for symptomatic bradycardia include atropine, isoproterenol, or temporary pacing. When the underlying cause is reversible, such as in the case of drug toxicity (e.g., excess digitalis or beta-blocker), temporary pacing and elimination of the offending agent is usually a sufficient therapy. However, if the cause is irreversible, the implantation of a permanent pacemaker is usually warranted.

28.6.1 Sinus Node Dysfunction

Often sinus node performance deteriorates as we age and/or is associated with age-related disease states, thus the clinical syndrome of SND emerges. In such cases, the clinical manifestations may be: (1) excessive sinus bradycardia; (2) alternating periods of bradycardia and atrial tachycardia; and/or (3) AFib. Additionally, the sinus node may simply become less responsive to physical exertion over time, in terms of generating an appropriate heart rate; this is a special form of SND called *chronotropic incompetence*.

Sinus bradycardia is defined as a sinus rate of <60 bpm. As mentioned above, sinus rates between 50 and 60 bpm may not be pathological in many subjects, e.g., the highly trained athlete. Yet, SND may manifest as either significant sinus bradycardia or abrupt and prolonged sinus pauses due to sinus arrest (spontaneous halting of the intrinsic automatic of the sinus node) or sinus exit block (failure of impulses to exit the sinus node). The typical resultant symptoms include: fatigue, dizziness, confusion, exertional intolerance, diminished mental acuity, syncope, and/or congestive heart failure. Atrial tachyarrhythmias are particularly frequent in SND, and often alternate with periods of excessive bradycardia (*bradycardia-tachycardia syndrome*). SND may present certain stereotypical forms of sinoatrial exit block. On the surface ECG, only second-degree sinoatrial block (Wenckebach type conduction from sinus node to atrium) can be diagnosed by observing progressive PP interval shortening prior to a pause in the P-waves that results from a sinus impulse being blocked from activating the atrium. In general, first- and third-degree sinoatrial blocks cannot be easily recognized (i.e., in the absence of specialized intracardiac recording techniques). It should be noted that Holter monitors or implantable event monitors are useful for confirming a suspected diagnosis of SND, particularly when bradycardia is associated with symptoms.

Carotid sinus massage is frequently performed when evaluating for SND; although carotid sinus syndrome is not the same as SND, the two often coexist in the same patient. A sinus pause >3 seconds induced by a 5-second unilateral carotid sinus massage is usually considered clinically significant.

Because one's sinus rate can be slowed by vagal tone, the resultant *intrinsic heart rate* after complete autonomic blockage is often used to assess the relative integrity of the patient's

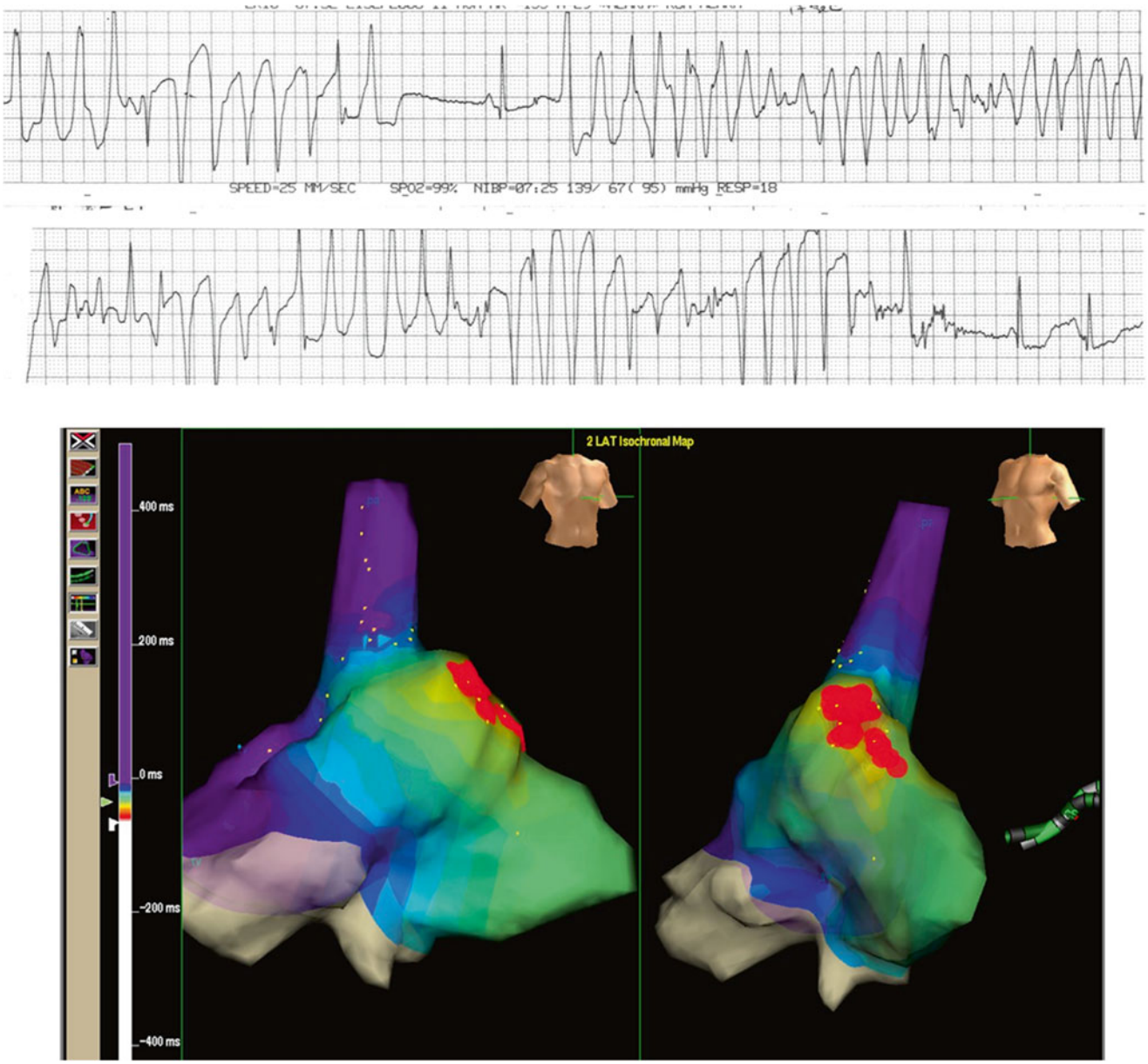

Fig. 28.11 Torsades de pointes. Successful catheter ablation of premature ventricular ectopics in the anteroseptal wall of the right ventricular outflow tract eliminates frequent episodes of Torsades de pointes (*top*) that are refractory to medical management. The *bottom* shows an activation map using the Ensite NavX system. The *red dots* indicate the ablation lesions

sinus nodal function. As such, complete autonomic blockade can be achieved after intravenous propranolol (0.2 mg/kg) and atropine (0.04 mg/kg). A patient's normal intrinsic heart rate can be estimated by the following equation: $118-(0.57\times\text{age})$. An intrinsic heart rate <80 bpm in the elderly is usually suggestive of sick sinus syndrome. Furthermore, determining the sinus node recovery times (normal value <1500 ms), corrected sinus node recovery times (normal value <550 ms), and, less frequently, the sinoatrial conduction times (normal value <125 ms) can be used by an electrophysiologic assessment to evaluate sinus nodal function when the initial clinical diagnosis remains uncertain.

Pacemakers are the mainstay of therapy for treating symptomatic bradyarrhythmias in patients with SND. However, it is not uncommon that antiarrhythmic drugs are also needed to suppress the tachycardic component of the condition. Yet in the latter cases, drug therapies may aggravate any tendency towards bradycardia, thereby further necessitating pacemaker therapy.

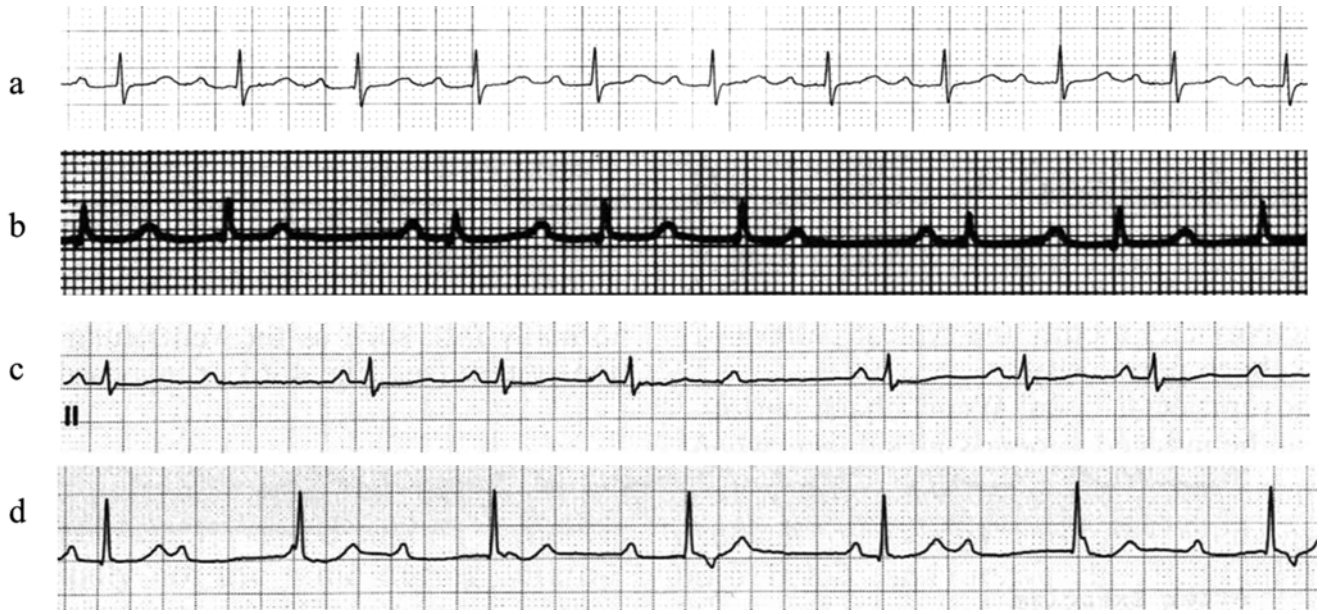

Fig. 28.12 Atrioventricular (AV) block. The figures show first degree (**a**), Mobitz type I second degree (**b**), Mobitz type II second degree (**c**), and third degree AV block (**d**). See text for discussion

28.6.2 Atrioventricular (AV) Block

The clinical significance of AV block depends on: (1) the site of block; (2) the risk of a progression to complete block; and (3) the patient's subsidiary escape rate. When complete AV block occurs above the His bundle, the ventricular escape rhythm is believed to originate from the His bundle (40–60 bpm); this is usually called a *junctional escape rhythm* and the patient has an associated narrow QRS complex. Note that a bundle branch block appearance may occur if the given patient has preexisting conduction system disease. When AV block occurs below the His bundle, the escape is generated in the distal His-Purkinje fibers and thus is much slower and less reliable (25–45 bpm); this is usually called *ventricular escape rhythm* with associated wide QRS complex. The *first degree AV block* is characterized by a PR interval >0.20 s without drop of QRS complex following each P-wave (Fig. 28.12a). For additional information on the intrinsic properties of the conduction system, see Chap. 13.

AV conduction delays can also occur within the right atrium, the AV node, or the His-Purkinje system. A *first degree AV block* is characterized by a PR interval >0.20 s, without a drop of QRS complex following each P-wave (Fig. 28.12a). The *second degree AV block* is considered present when some atrial impulses fail to conduct to the ventricles. In its classically defined form, *Mobitz type I* second degree AV block (Fig. 28.12b) is characterized by progressive PR interval prolongations until an atrial impulse is blocked (*Wenckebach phenomenon*). Furthermore, after an incomplete compensatory pause, the Wenckebach cycle starts again with a shorter PR interval, compared with the PR interval prior to block. In some patients, the Wenckebach periodicity may be very long (greater than 6:5) and the progressive PR prolongations of the typical Mobitz I block becomes less apparent. The relative site of a Mobitz type I block is almost always located near the AV node, and the general risks of progressing to a complete AV block are low. In *Mobitz type II* second-degree AV block (Fig. 28.12c), AV conduction fails suddenly without a change preceding the PR interval. This type of block is usually due to His-Purkinje disease and is associated with higher risks for developing complete AV block; the escape rates are generally slow and unreliable. When two or more consecutive atrial impulses fail to conduct, a *high degree AV block* is considered to be present and pacemaker implantation is mandatory. The *third degree AV block* (Fig. 28.12d) is defined as a complete AV block, and thus no atrial impulses conduct to the ventricles. A permanent pacemaker is usually required in the third degree AV block, i.e., whether congenital or acquired in origin. In this regard, dual-chamber pacing (i.e., pacing both the atrium and ventricle) has become widely accepted as the approach of choice for such patients. See Chap. 30 for more details on these devices.

28.7 Electrophysiological Studies and Catheter Ablations

The clinical electrophysiological study (EPS) is important for evaluating a broad spectrum of cardiac arrhythmias. More specifically, it can help to: (1) assess the relative function of the sinus and AV nodes, as well as the His-Purkinje system;

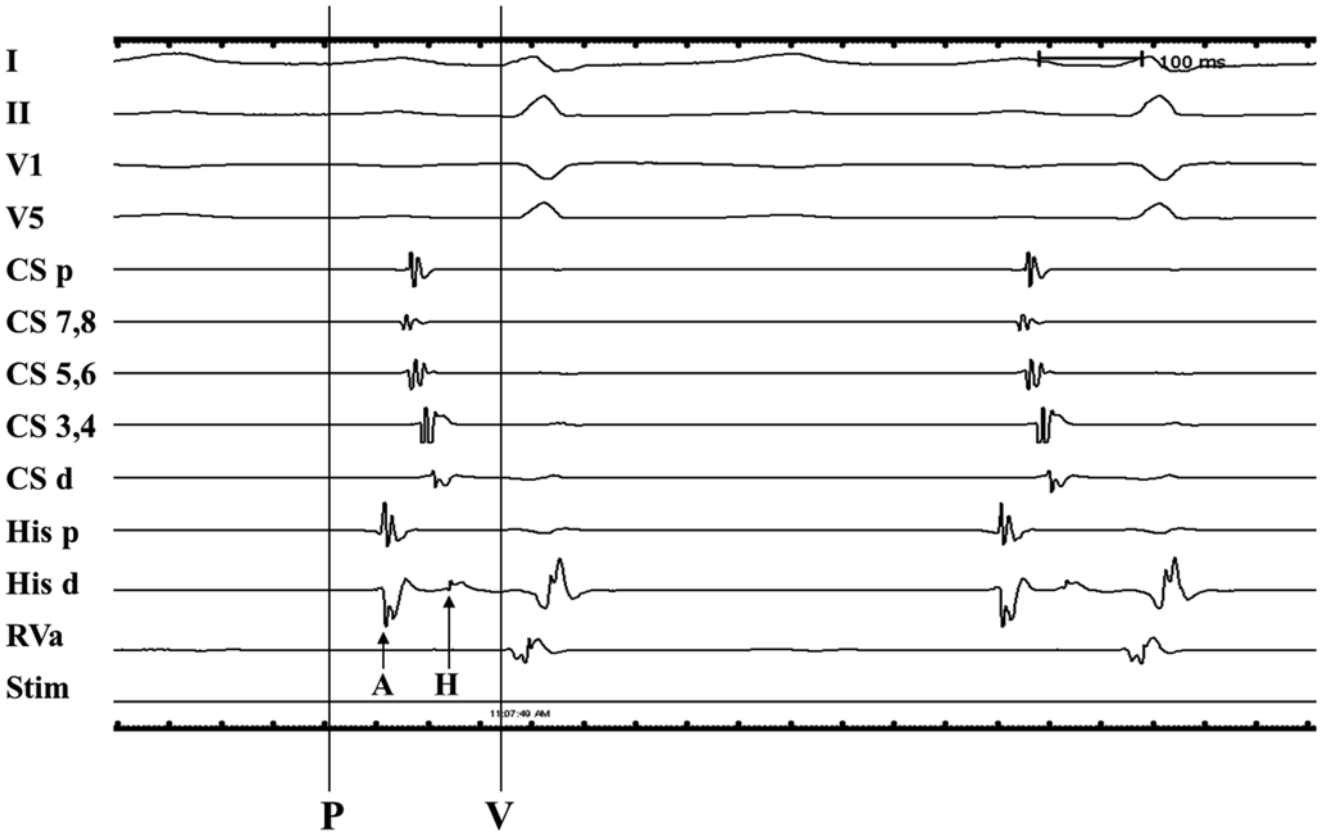

Fig. 28.13 Measurements in the His bundle electrogram. These measurements are important for evaluation of atrioventricular conduction. The AH interval, measured from the earliest reproducible rapid deflection of the atrial electrogram in the His recording to the onset of the His deflection, represents conduction time from the low right atrium at the interatrial septum through the atrioventricular node to the His bundle (atrioventricular node function). The HV interval, measured from the beginning of the His deflection to the earliest onset of ventricular activation (surface leads or intracardiac recordings), represents conduction time from the proximal His bundle to the ventricular myocardium (infra-His conduction function). *I* surface ECG lead I, *II* surface ECG lead II, *V1* surface ECG lead V1, *V5* surface ECG lead V5, *A* onset of atrial activation, *CS* coronary sinus, *d* distal, *H* onset of His activation, *His* His bundle, *p* proximal, *P* onset of the P-wave, *RVa* right ventricular apex, *stim* stimulation, *V* onset of ventricular activation

(2) determine the characteristics of reentry tachycardias; (3) map the relative locations of arrhythmogenic foci; and/or (4) ultimately define proper locations to apply ablative therapy. The EPS is typically performed in an *electrophysiology catheterization laboratory* which is, in many respects, similar to a conventional heart catheterization suite. The minimum equipment requirements for a comprehensive EPS include: (1) a radiographic table; (2) a fluoroscopy unit (biplane is preferred); (3) a physiologic recording and analysis system; (4) a programmable stimulator; (5) an RF generator and variety of electrode catheters and introducers; (6) a sterile working environment; (7) monitoring and resuscitation equipment; and (8) for the most complex arrhythmias, a 3D mapping system. Nevertheless, it is essential that a well-trained team, experienced in dealing with a range of cardiac emergencies, should be in place before such studies are considered.

EPS is usually performed on the patient in both fasting and antiarrhythmic drug-free states and in a sterilized fashion, using various degrees of conscious sedation (such as fentanyl and midazolam), depending on the specific procedure. Typically, vascular access is obtained percutaneously through the femoral, subclavian, and/or internal jugular veins under local anesthesia, i.e., using 1 % lidocaine. Next, multiple electrode catheters are placed at key locations within the heart such as the high right atrium close to the sinus node, the coronary sinus (for recording and stimulating the left atrium), the His bundle region, and/or the right ventricular apex. Generally, AH and HV intervals are routine baseline measurements of EPS (Fig. 28.13). A mapping and ablation catheter is also inserted when ablation is performed. For example, we often have employed an ablation catheter with a varying deflectable distal segment (1.5–3 in.), with distal electrodes of 2.2–2.8 mm in diameter (7–8.5 French) and either 3.5, 4, or 8 mm tip electrode lengths. Physiological signals are usually digitized at 1000 Hz and filtered between 30 and 500 Hz; pharmacological provocations, such as isoproterenol, are often required to facilitate induction of the underlying tachycardias.

The purpose of ablation is to destroy the myocardial tissue by delivering electrical energy (or, in some cases, cryoablation or other forms of energies) over a distal electrode of a catheter placed usually on the endomyocardium at the arrhythmia substrate; i.e., the tissue integrally related to the initiation or maintenance of the given tachycardia.

For a historic perspective, the first successful ablation using DC shock in a human was performed in 1982. Yet, due to potential vast and untargeted damage to the heart that can be induced by DC shocks, this approach has now been replaced by other energy forms (i.e., with RF energy in the range of 100 kHz to 1.5 MHz commonly used). More recently, cryoablation has been introduced in clinical practice. Laser and microwave energy sources have been investigated and these methods continue to be of interest. For a more detailed discussion on ablation technologies and related biophysics, read Chap. 29.

Diagnostic EPS and ablative procedures are usually accomplished in a single combined session. Ablation of arrhythmias is usually indicated as a first or second line therapy, based on the type of arrhythmia and a patient's refractoriness to drug therapy. Other technologies such as intracardiac echocardiography, nonfluoroscopic electroanatomical mapping, and noncontact endocardial activation mapping have significantly contributed to advancements in interventional cardiac electrophysiology (see Chap. 32).

The general indications for recommending an ablation procedure are summarized in Table 28.3. Note that both polymorphic VT and ventricular fibrillation are usually not amenable to ablation therapy with the current technologies available, unless a trigger can be targeted like a PVC. In general, an ablation procedure is now considered as first-line therapy for typical atrial flutter, AVNRT, and AVRT. AV junctional ablation, plus pacemaker implantation, is generally accepted as a means to control symptoms due to AFib which is refractory to both medical and focal ablation therapy. Commonly today, catheter-based ablative approaches specifically designed to isolate the pulmonary veins, together with other ablative strategies (e.g., isthmus and roof-line ablations), are indicated for drug-refractory AFib. In experienced hands, catheter ablation can also be employed to eliminate spontaneous episodes of VT in up to two-thirds of patients after myocardial infarction [9]. At present, catheter ablation of VT is largely adjunctive to amiodarone administration and the implantation of an ICD. It should be noted that the more recent advent of epicardial ablation permits access to epicardial arrhythmic targets otherwise unreachable from the endocardium.

Complications of intracardiac ablation treatments, in general, can be related to: (1) the catheterization procedure itself, e.g., vasovagal reactions, perforation of the heart and vessels leading to tamponade, or extended radiation exposure; (2) difficult vascular access, including pneumothorax, hemothorax, subclavian artery injury, branchial nerve injury, subclavian arteriovenous fistula in subclavian and jugular vein access, and/or hematomas and retroperitoneal bleeding in common femoral vein and artery access; (3) thromboembolic events, including embolic strokes and myocardial infarction; and/or (4) those associated with ablation energy delivery, including postablation pain, esophageal damage, phrenic nerve injury, AV block requiring a pacemaker, cardiac vascular injury, and perforation. It is important to note that the risks for complications are significantly dependent on the experience and skill of the operator, as well as the type of ablation procedure being employed.

Table 28.3 Indications for ablation of arrhythmias

• Atrial tachycardias:
– Inappropriate sinus tachycardia (controversial)
– Focal atrial tachycardia
– Typical atrial flutter
– Atypical atrial flutter
• Atrial fibrillation:
– Atrioventricular nodal ablation for rate control
– Pulmonary vein isolation
– Hybrid ablation techniques
• Atrioventricular nodal reentry tachycardia.
• Atrioventricular reentry tachycardia using concealed bypass tracts.
• Wolff–Parkinson–White syndrome.
• Ventricular tachycardia:
– Ischemic ventricular tachycardia (monomorphic, stable or unstable)
– Nonischemic ventricular tachycardia (stable monomorphic)
– Polymorphic ventricular tachycardia and fibrillation: ablation of triggers.
– Idiopathic ventricular tachycardia (including symptomatic ventricular premature complexes)
– Bundle branch reentry tachycardia

28.7.1 Ablations of ISTs

Ablation of drug-refractory IST can be performed as a potential means to eliminate the portion of the sinus node that generates the fast heart rate along the superior aspect of the crista terminalis. Yet, today many do not consider ablation as the preferred approach due to its documented low long-term efficacy. Further, due to the anatomical structure of the sinus node, multiple lesions over 3–4 cm along the crista terminalis are often required. In other words, it is difficult to ablate or *modify* the sinus node because it is largely an epicardial structure, especially in its superior portion. Nevertheless, during sinus rhythm, the site of earliest activation of the atrium is targeted as the presumed site of the sinus node. Additionally, 3D cardiac mapping and intracardiac echocardiography can be useful for the identification of the earliest activation sites and the crista terminalis, respectively.

The primary ablation goal is to achieve ~30 % reduction in maximal heart rate during infusion of isoproterenol and atropine or to decrease the patient's baseline heart rate to normal ranges. Unfortunately, less than half of these patients have sustained improvement of symptoms. Therefore, many patients will require multiple ablation sessions in order to obtain more sustained heart rate slowing. Note that care must be taken to avoid ablations nearby the phrenic nerve, as this may result in paralysis of the diaphragm. To avoid this, the phrenic nerve may be identified and mapped by using high output pacing to stimulate the nerve and physically monitor for diaphragmatic stimulation.

28.7.2 Ablations of Focal Atrial Tachycardias

Right atrial tachycardias often originate along the length of the crista terminalis from the sinus node to the coronary sinus (*cristal tachycardia*), and they account for 83 % of all ATs. Other sites of AT clustering include the pulmonary vein ostia, coronary sinus ostia, and/or the mitral and tricuspid valve rings. Appropriate identification of the earliest onset of the P-wave is critical for mapping. Mapping in the right atrium and finding the earliest activation in the midseptum (particularly when the presystolic activity is not significantly early) or observing multiple sites that have similar early activation time may suggest an origin of tachycardia in the left atrium. AT arising in the anteroseptal region or near the His bundle is an infrequent diagnosis that is challenging to ablate because it is associated with a high risk of AV block during an RF ablation procedure. Yet, such risks may be reduced by either using RF just superior to the focus on the anterior tricuspid valve or by using a different ablation technology (e.g., cryo-ablation from the noncoronary cusp of the aortic valve). Early data has suggested that the average success rate for AT ablation is approximately 91 %, with a complication rate of 3 % and recurrence rate of only 9 %. Complications associated with these procedures include: SND, AV block, phrenic nerve damage, and/or other common complications associated with catheter ablations. It should be noted that the outcomes of AT ablation have been significantly improved by employing 3D electro-anatomic mapping strategies.

28.7.3 Ablations of Atrial Flutter

28.7.3.1 Ablations of Typical Atrial Flutter

Endocardial mapping in patients with typical atrial flutter has confirmed that macroreentry commonly occurs in the right atrium. Most often, atrial flutter rotates in a counterclockwise direction in a frontal plane, although clockwise rotation has also been observed. On 12-lead ECG (see Chap. 19), counterclockwise atrial flutter presents a stereotypical *sawtooth* pattern, an upright flutter wave in V1 and inverted flutter waves in the inferior leads and V6. In contrast, during clockwise rotation, flutter waves in V1 are inverted, while those in the inferior leads and V6 are upright. Further, these macroreentrant circuits pass through a critical isthmus, bounded by the inferior aspect of the tricuspid annulus, the ostium of the inferior vena cava, and the ostium of coronary sinus (*cavotricuspid isthmus*). During endocardial detection of these circuits, a multielectrode catheter is typically placed around the macroreentrant circuit adjacent to the tricuspid valve to evaluate the relative rotation around the tricuspid annulus and through the isthmus. Therapeutically, linear lesions that transect this isthmus will typically block the reentry circuit and essentially cure these typical atrial flutters. However, some atrial flutter circuits may not travel through the isthmus; consequently, it is important to confirm that the isthmus is critical to the maintenance of the flutter circuit by using pacing maneuvers to demonstrate *concealed entrainment*. Employing a 3D mapping system, although not always necessary, may help to better identify these types of underlying tachycardia circuits and also provide a more precise and effective way to complete a linear ablative lesion.

Currently, the success rates for typical atrial flutter ablation procedures are >90 %, with recurrence rates <10 %. It is important to note that the confirmation of bidirectional (both clockwise and counterclockwise) isthmus blocks significantly reduces recurrence rates [10]. Typically, the trans-isthmus conduction times are measured during proximal coronary sinus pacing, at rates just below the sinus rhythm (from the pacing spike to the lateral edge of the cavotricuspid isthmus at approximately 7 o'clock at the left anterior oblique view, and then in the opposite way by pacing from the lateral cavotricuspid isthmus). There is >50 % increased conduction time compared to before ablation, corresponding to a minimum trans-isthmus time of roughly 140 ms; this was noted to be a very good predictor of complete block [11].

28.7.3.2 Ablations of Atypical Atrial Flutter

From an ablative viewpoint, the term *atypical atrial flutter* is sometimes used to describe any macroreentrant atrial tachycardia that does not utilize the cavotricuspid isthmus as a critical component of the tachycardia circuit. Therefore, atypical atrial flutter consists of a heterogeneous group of arrhythmias presenting with a stable, flutter wave-like morphology on a standard 12-lead ECG recording. Nevertheless, the key for the successful ablation of an atypical flutter is to identify and ablate the critical isthmus of the macroreentry flutter circuit arising from either the right or left atrium. Yet, identifying this critical myocardial tissue is often challenging; currently, both 3D mapping systems and pacing maneuvers are used in concert to find these critical targets.

More specifically, a proximal-to-distal coronary sinus activation sequence does not necessarily mean that the

tachycardia is located within the right atrium, such as in perimitral annular reentry or periseptal reentry. The following data can be used to identify a left atrial origin:

1. Failure to demonstrate concealed entrainment at multiple right atrial sites.
2. Less than 50 % of tachycardia cycle length can be mapped within the right atrium.
3. Passive conduction to the right atrium from the left atrium, with early septal activation in the right atrium, typically in the Bachmann's bundle or the coronary sinus ostium.
4. Possible left-right atrial dissociation or conduction delays evidenced by a relatively fixed cycle length in the left atrium versus significant cycle length variations in the right atrium.

Special forms of atypical atrial flutter include: (1) upper loop reentry; (2) right atrial free wall flutter; (3) dual loop right atrial reentry; (4) left atrial macroreentry; or (5) left septal flutter.

28.7.3.3 Ablations of Incisional Atrial Tachycardia

Macro-reentrant incisional atrial tachycardias frequently occur following surgeries performed for congenital repairs or for other heart diseases. Importantly, the presence of multiple anatomic barriers (surgical incisions, patches, conduits, cannulas, the coronary sinus ostium, and the pulmonary venous ostia) as well as atrial tissue damage (hypoxemia, ischemia, surgical scars, and fibrosis) will all provide potential substrates for reentry tachycardias. Furthermore, either partially successful Maze surgeries or RF ablative procedures for AFib may also leave substrates for intraatrial reentries. Subsequently, the locations for successful ablation will vary from patient to patient, but can typically be identified by entrainment maneuvers. Yet, in such patients, 3D mapping has been shown to be quite useful for identifying and then ablating the reentrant circuits.

28.7.4 Ablations of AFib

In addition to ablation of the AV node for rate control, current guidelines recommend catheter ablation in patients with symptomatic paroxysmal (class I) or persistent (class IIa) AFib, specifically those resistant or intolerant to at least one antiarrhythmic medication [6]. In its early days of procedural development, catheter ablation of AFib aimed to imitate the surgical Maze approach, i.e., aiming to compartmentalize the atrium. Yet, this approach has proven problematic due to long procedure times and associated unacceptably high thromboembolic complications. More recently, AFib ablation has evolved to primarily ablation of triggers versus the ablation of the total underlying substrates. Several catheter-based ablative approaches are currently utilized to provide symptomatic improvements in patients with drug-refractory AFib. For example, an Expert Consensus Statement on catheter and surgical ablation of AFib was published in 2012 [12].

28.7.4.1 AV Nodal Ablations for Rate Control

Catheter ablations of the AV junction and the concomitant insertion of a permanent pacemaker have been shown to be effective in achieving ventricular rate control in patients with drug and ablation refractory AFib. In general, this approach can also be used for rate control in patients with drug-refractory multifocal AT. Yet, pacing from the conventional right ventricular apex could have detrimental effects on cardiac function. Recent data suggest that *cardiac resynchronization* (simultaneously pacing the right ventricle and lateral wall of the left ventricle) might be more favorable than conventional right ventricular (RV) pacing after AV nodal ablation for AFib [13].

28.7.4.2 Catheter-Based Maze Procedure

Surgical treatment of AFib by compartmentalizing the atrium from an electrical transmission perspective is designed to preclude coexistence of multiple micro-reentry loops or fibrillatory waves. To date, surgical approaches have included: (1) the modified Cox Maze procedure; (2) a left atrial isolation procedure; and (3) various iterations of the Maze procedure. Still today in some centers, the Maze procedure is used for patients with AFib who require a cardiac surgical procedure for other reasons. The reported overall success rates in eliminating AFib are high (over 90 %), with mortality rates of 2–3 %. A catheter-based replication of the Maze procedure has been previously employed. More recently, technical difficulties in achieving stable linear conduction blocks have been improved by employing both intracardiac echocardiography and 3D mapping. In patients with paroxysmal AFib, success rates with and without drug therapy at 11 months follow-up were approximately 33 % and 13 % for linear ablation limited to the right atrium, and 85 % and 60 % for the biatrial approach, respectively. Again it should be noted that, due to long procedure times and high thromboembolic risks, catheter ablation-based replication of the MAZE procedure has been abandoned in favor of more targeted approaches.

28.7.4.3 Evolution of AFib Ablations

Focal AFib Ablation

One of the most significant advancements in transcatheter ablation of cardiac arrhythmias was the identification of patients with *focal* AFib [14, 15]. In some patients with paroxysmal AFib, focal sources of automaticity may serve as

either the main abnormality (focal drivers) or as the dominant trigger to induce repetitive episodes of AFib (focal triggers). A single rapidly discharging focus leads to fibrillatory conduction, mimicking the surface ECG features of AFib. Very early techniques of catheter ablation of AFib attempted to identify and ablate individual focal sites of spontaneous firing in the atria.

Subsequently, numerous EPS have demonstrated that the pulmonary veins are the predominant source of AFib triggers for many patients. Specifically, the left superior pulmonary vein is the most common focal source, followed in order by the right superior, left inferior, and right inferior pulmonary veins. Although the technique of ablating individual foci produced fairly high acute success rates, the recurrence of AFib was unacceptably common. Of significance, when investigators repeated the ablation procedure in these patients, triggers were often found in other areas of the vein initially targeted and/or in remote veins. Because it appeared that often in such patients, either new triggers could arise in nonablated areas of veins or that these areas were arrhythmogenic but not realized during initial ablation, the technique of complete isolation of the pulmonary veins has been utilized.

Segmental Ostial Isolations of Pulmonary Veins

To perform a segmental ostial isolation of pulmonary veins procedure, typically a circular mapping catheter is placed at the funnel-shaped opening of each vein to map electrical exit sites of the veins into the atrium [16]. Ablations are then performed in the ostium of each pulmonary vein until the veins are completely isolated from the left atrium (i.e., segmental ostial isolation). It has been shown that electrical isolation of the pulmonary veins results in marked reduction or the elimination of AFib. More recently, the use of saline-irrigated RF lesions has facilitated ablation procedures by successfully creating deeper lesions and decreasing the risk of char formation and thromboembolic events. The main concern with this isolation technique employing RF energy delivery within the pulmonary vein ostia is its association with a small but significant (2 %) risk of pulmonary vein stenosis.

Circumferential Isolations of Pulmonary Veins

Concurrent with the development of segmental ostial isolations of the pulmonary veins, the circumferential approach has been developed which also employs electroanatomical mapping [17]. More specifically, RF ablation is performed circumferentially around each vein within the left atrium outside the ostia, with the end point being the absence or marked reduction (80 %) in the amplitude of electrical signals within the encircling lesions.

Early attempts at electrical isolations of the pulmonary veins at their ostia occasionally caused pulmonary vein stenosis, which necessitated angioplasty or stenting of the veins in some patients. This phenomenon has caused investigators to isolate the veins by using much larger circles with far greater diameters along the posterior left atrium—usually two larger circles encircling the left- and right-sided veins, respectively (Fig. 28.14). These wide circumferential isolation techniques have significantly improved the success rates for AFib ablation in such patients. It is important to note that macroreentry left atrial flutters are relatively common complications following such isolations (Fig. 28.15), so many investigators add additional ablation lines along the roof of

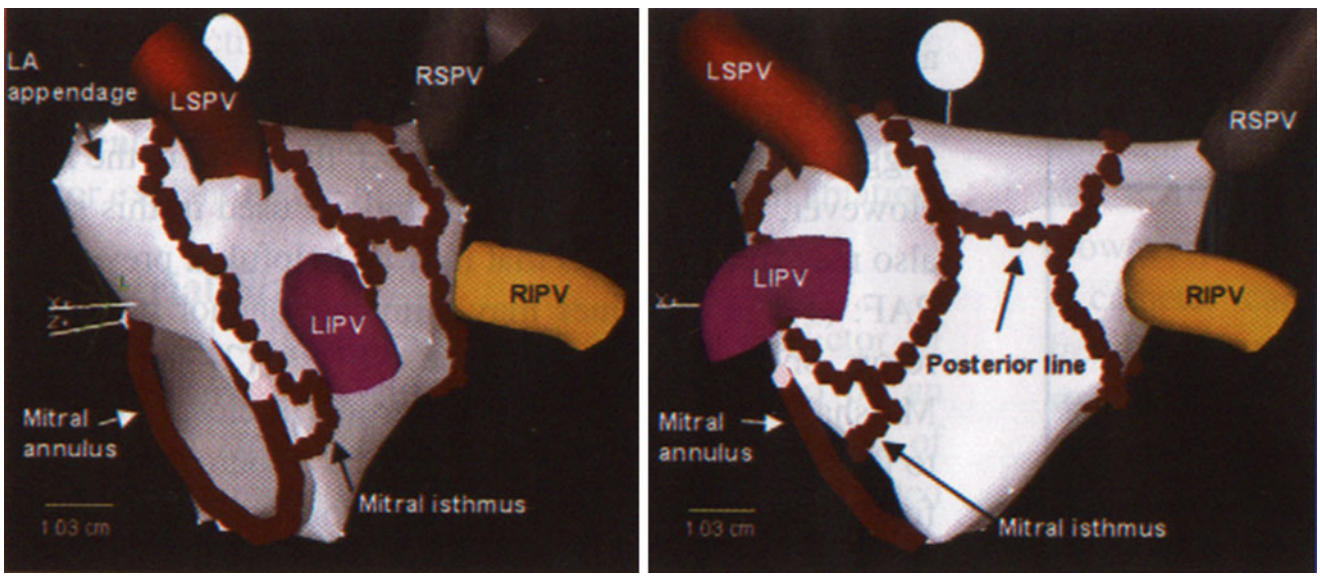

Fig. 28.14 Circumferential isolation of pulmonary veins for ablation of atrial fibrillation. Reproduced from reference [18] with permission. *LA* left atrial, *LIPV* left inferior pulmonary vein, *LSPV* left superior pulmonary vein, *RIPV* right inferior pulmonary vein, *RSPV* right superior pulmonary vein. Circulation by American Heart Association. Reproduced with permission of American Heart Association in the format reuse in book/textbook via Copyright Clearance Center

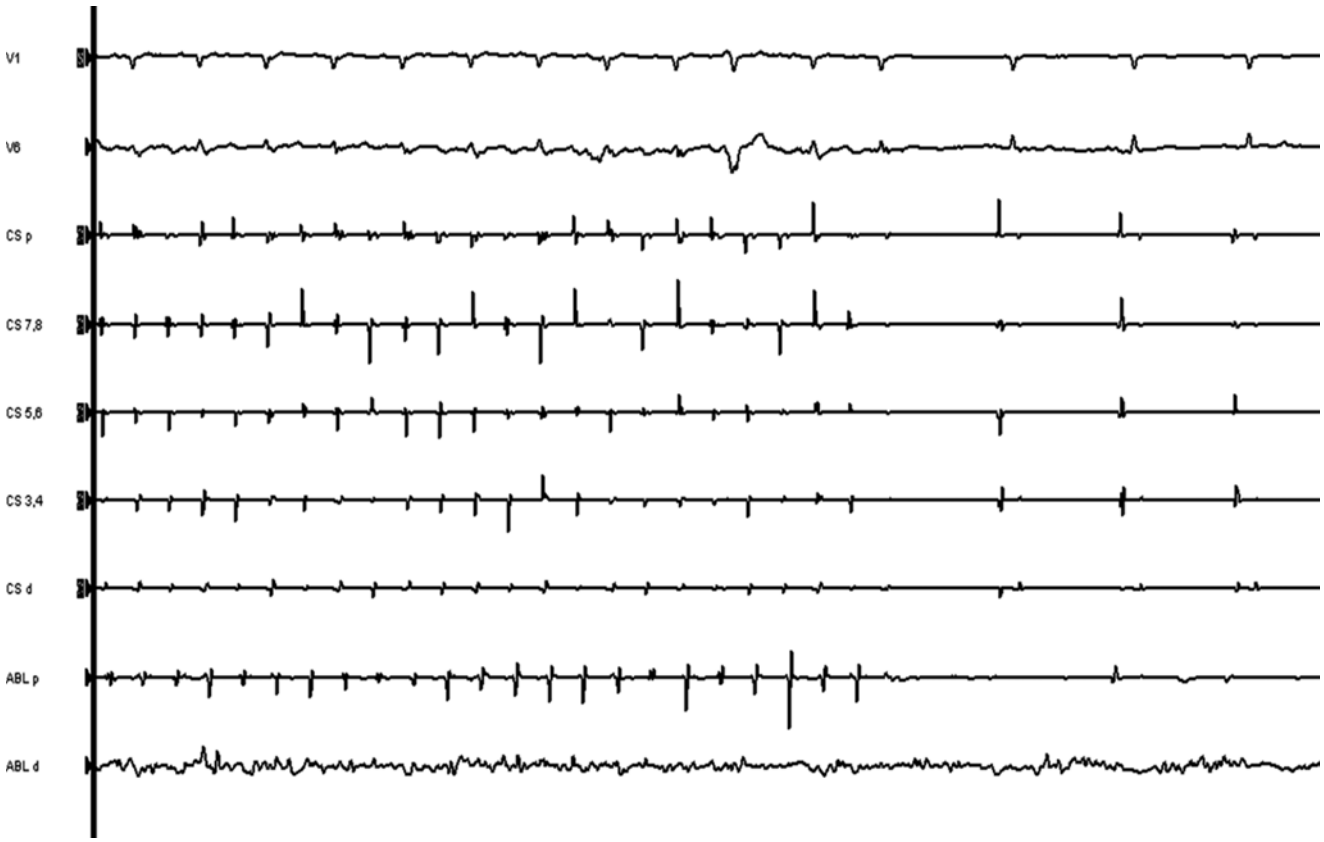

Fig. 28.15 Termination of atrial fibrillation during ablation. Atrial fibrillation is converted to left atrial flutter after circumferential isolation of all pulmonary veins. The flutter is terminated during the linear ablation in the roof of the left atrium. *V1* surface ECG lead V1, *V6* surface ECG lead V6, *ABL* ablation, *CS* coronary sinus, *d* distal, *p* proximal

the left atrium as well as down to the mitral valve annulus from the lesions encircling the left pulmonary veins [19]. Furthermore, some investigators also isolate the ostium of superior vena cava and the coronary sinus, and add ablation lines connecting the superior and inferior vena cava. Such techniques may isolate triggers as well as prevent arrhythmia propagation, analogous to the surgical Maze procedure. However, if extensive ablations are performed, particularly on the posterior wall of left atrium, a fistula between the left atrium and esophagus may occur, but this is rare; this complication often presents with subacute infection and embolization or deadly upper gastrointestinal bleeding usually weeks to months after the given procedure. Hence, it is recommended to use low power ablation on the posterior wall.

Substrate Ablations

A substrate ablation technique is based on the assumption that AFib is more dependent on perpetuation of the arrhythmia in the diseased atria, rather than being initiated from within the pulmonary veins [20, 21]. In such cases, complex fractionated atrial electrograms (CFAEs) are sought and, if they occur, they are targeted for ablation. It is controversial whether adding CFAE ablations to wide circumferential ablations will decrease long-term recurrence rates of AFib. Note that both spot and linear ablation lesions have been successfully used to ablate the myocardial regions eliciting CFAEs.

Ablations of Autonomic Targets

It is well known that the autonomic nervous system plays a critical role in pathogenesis of AFib. It has been reported that ablation of ganglions in the atria may be associated with higher likelihood of successful ablation of AFib [22]. The location of vagal innervation/ganglions is identified using stimulation/ablation-induced vagal effects such as bradycardia or long pauses.

Cryoballoon Ablations of AFib

More recently, a new technique for pulmonary vein isolation emerged using a balloon inflated at the ostia of the pulmonary veins and applying cryoablation in a circumferential fashion [23]. It appears to have similar success and complication rates

as those reported for RF ablation, but can only be useful for pulmonary vein isolation without the capacity to perform lines of focal ablations. Randomized studies are underway comparing both techniques.

The overall complication rate from AFib ablation is steadily decreasing with more experience and newer technology (2.5 % overall complication rate compared to 4–5 % about 5 years ago). Complications include embolic stroke, cardiac effusion and tamponade, esophageal fistula, pulmonary vein stenosis, and vascular access complications. For more details on these systems, see Chap. 29.

Ablations of AVNRT

The abnormal conduction circuits of most AVNRTs proceed antegrade through the slow pathways and then retrogradely through the fast pathways (these are typical AVNRTs). In a small number of patients (4 %), the tachycardia circuits may run in the opposite direction (atypical AVNRT). The common characteristic of most AVNRTs is *dual pathways* or *dual physiology*, which is demonstrated as sudden increases of at least 50 ms in AH intervals, with 10 ms decreases in coupling intervals from an atrial stimulus (Fig. 28.16). Dual pathway conduction can be detected in the majority (85 %)

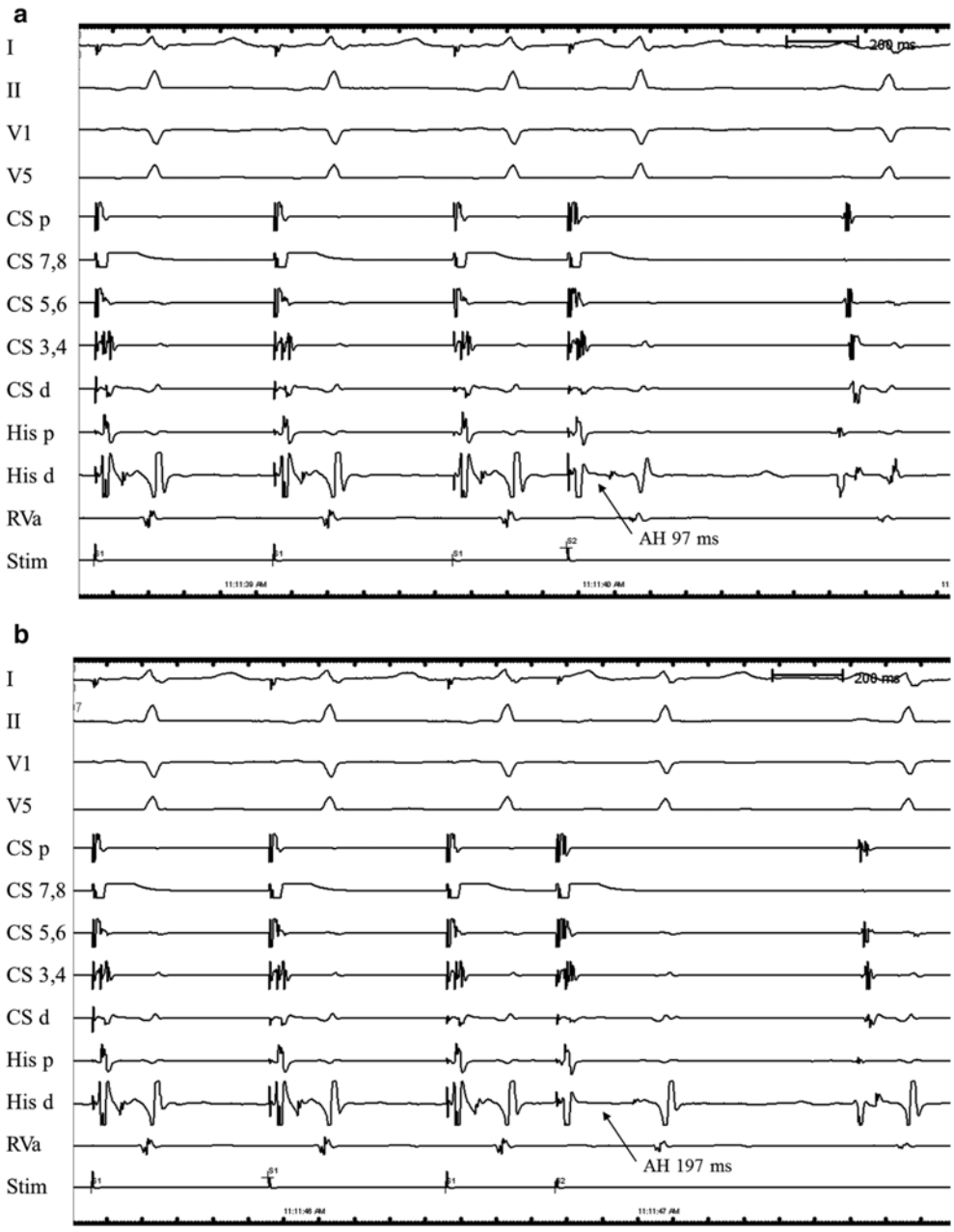

Fig. 28.16 Dual physiology (jump). An extra stimulus is delivered at different coupling intervals after 8-beat pacing at 500 ms from proximal coronary sinus. (**a**) AH interval is 97 ms following an extra stimulus with coupling interval of 320 ms. (**b**) AH is suddenly increased (jumped) by 100–197 ms at coupling interval of 310 ms. The sudden increase of >50 ms in AH interval associated with a 10 ms decrease in coupling interval is called a jump, indicating the presence of dual physiology of the atrioventricular node. *I* surface ECG lead I, *II* surface ECG lead II, *V1* surface ECG lead V1, *V5* surface ECG lead V5, *CS* coronary sinus, *d* distal, *His* His bundle, *p* proximal, *RVa* right ventricular apex, *stim* stimulation

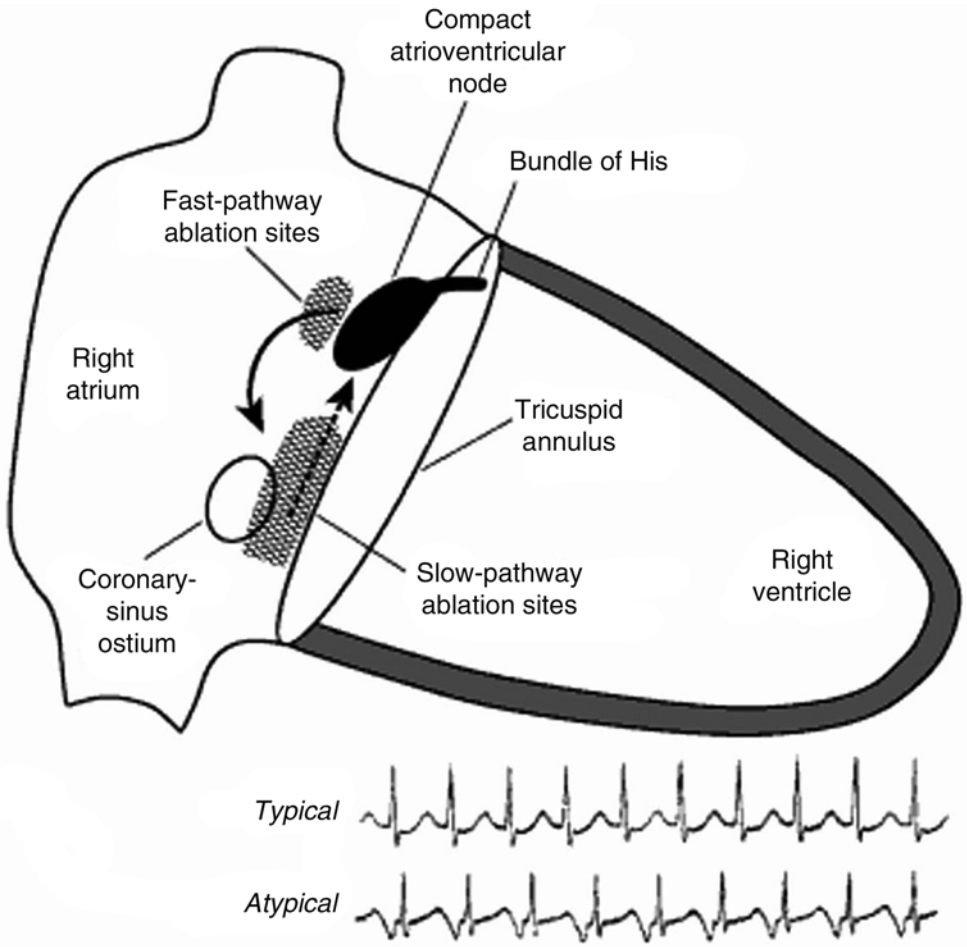

Fig. 28.17 The slow pathway (posterior) and fast pathway (anterior) ablation sites for atrioventricular nodal reentry tachycardia. Reproduced from reference [24] with permission. See text for discussion. The New England Journal of Medicine by Massachusetts Medical Society. Reproduced with permission of Massachusetts Medical Society, in the format reuse in a standard/custom book (basic rights) via Copyright Clearance Center

of patients with an AVNRT, whereas dual physiology exists in 25 % of patients without SVTs.

Ablation of AVNRT is commonly aimed at ablating first the slow pathways in the posteroinferior areas of the *Koch's triangle*, those between the coronary sinus ostium and the tricuspid annulus (*posterior approach*; Fig. 28.17). The A/V ratios for slow pathway ablations from the distal electrode pairs in sinus rhythm should be less or equal to 1:3. Ablations of the fast pathways in the anterosuperior areas of the Koch's triangle are rarely attempted due to the increased risk of damaging normal AV conduction (*anterior approach*). For example, the reported risk of AV block is 1.0 % with the posterior approach and 5.1 % with the anterior approach. Nevertheless, in experienced clinical hands, the success rate of these procedures is almost 100 %, with recurrence rates of <5 % and the risk of complete AV block being <1 %. Subsequently, an accelerated junctional rhythm can be typically observed following the successful ablation of the slow pathway conduction (i.e., 100 % of the time in successful ablations versus 65 % in unsuccessful ablations). Yet, residual slow pathway conductions or AV nodal echo beats may be detectable after a successful AVNRT ablation, but these are not associated with increased recurrence during follow-up.

It is important to note that AVNRT ablations can be performed using cryoablation, with the risks of complete AV block approaching zero. Further, patients eliciting a transient AV block during cryothermia ablations usually recover within minutes if ablation is terminated promptly when prolongation of PR interval or AV block is noted. However, cryoablation is considered as more time-consuming, given that each application requires a freeze–thaw–freeze sequence with each freeze lasting as long as 4 min.

Ablations of Accessory Pathways (WPW syndrome)

Accessory pathways are most frequently found in the left-sided cardiac chambers. The approximate locations of such accessory pathways can be typically determined from a surface ECG, i.e., if preexcitation is present (Fig. 28.18). In these clinical cases, a preablation EPS is performed to determine the precise locations of the accessory pathways and their role in inducing arrhythmias. Note that accessory AV

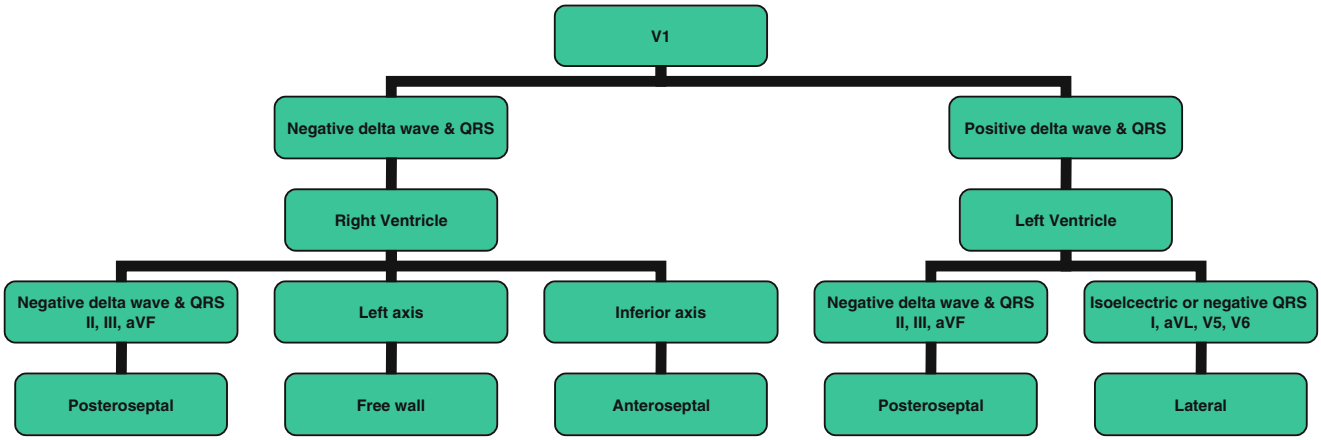

Fig. 28.18 Determination of the location of accessory pathways based on the delta wave and the QRS complex on surface 12-lead ECG. Reproduced from reference [25] with permission

pathways can exist at almost any site around the tricuspid and mitral annulus (with exception of where the mitral and aortic valve annuli coincide)—in the free wall (anterolateral, lateral, and posterolateral) and septum (anteroseptal, midseptal, and posteroseptal) locations. To date, the elicitation of multiple accessory pathways has been reported in 5–18 % of ablation cases.

In the transcatheter ablation procedures of left-sided accessory AV pathways, either a *retrograde transaortic approach* or *transseptal approach* can be employed in conjunction with anticoagulation therapy (e.g., heparin and targeted Activated Clotting Time, between 250 and 350 s). Further, therapeutic ablation can be performed at atrial sites (during orthodromic AVRT or relatively fast ventricular pacing) or ventricular sites (during sinus rhythm or atrial pacing), with either targeting the sites of earliest atrial or ventricular activation, respectively. Accessory AV pathways often cross the left AV groove obliquely, with the atrial insertion closer to the coronary sinus ostium.

In contrast to the virtually invisible left-sided accessory pathways, right-sided accessory AV pathways are often considered as more common in nature. Note, in general the optimal ablation site is best identified when accessory pathway potentials can be detected and these signals and the recording catheter positions are stable.

The success rate for ablations of left free wall accessory pathways is >95 %, with recurrence rates of 2–5 % and complication rates of <4 %; major complications include tamponade (1.2 %), AV block (0.5 %), and systemic embolization (0.08 %). Ablations of right-sided accessory pathways are typically associated with a lower success rate (~88 %) and higher recurrence rates (up to 17 % in earlier studies). On the other hand, the annual risk of natural SCD in WPW syndrome with symptomatic tachycardia is estimated to be 0.05–0.5 % [26].

28.7.5 Ablations of VTs

28.7.5.1 Ablations of VTs in Otherwise Clinically Normal Hearts

There are two main substrates for VTs in the otherwise clinically normal heart: focal and reentrant. Focal VTs are commonly seen in patients without underlying organic heart disease and are denoted as *idiopathic VT*; they account for 10–15 % of all diagnosed sustained VTs. Approximately 70 % of idiopathic VTs exhibit a left bundle branch block pattern, suggesting an origin in the right ventricle or septum. These VTs almost uniformly elicit an inferior frontal plane axis, indicating an origin within the outflow tract, mostly on the right. In such patients, *arrhythmogenic right ventricular dysplasia cardiomyopathy* should be suspected when other morphologies exist. The origin of idiopathic left VTs is usually at the inferior left ventricular midseptum, in the regions of the posterior fascicles or in the left ventricular outflow tract. Fortunately, ablations of these idiopathic VTs are curative in >90 % of patients.

28.7.5.2 Ablations of VT Associated with Ischemic Heart Disease

Reentrant VTs can be elicited in the presence of underlying organic heart disease, particularly in the patient with a prior myocardial infarction. Unfortunately, while mapping of these tachycardias is increasingly feasible with modern technology, the ability to undertake ablation of ischemic heart disease VTs remains limited due to the hemodynamic instability of these patients. Hence, there are three general ways to approach a VT ablation in these patients: (1) entrainment and activation mapping of stable VT; (2) substrate mapping and then modification; and/or (3) the careful mapping of the underlying triggers.

Entrainment is a very useful technique for assessing a reentry tachycardia. This refers to the continuous resetting of reentry tachycardia circuits by pacing at a slightly faster rate than the elicited tachycardia, with the intrinsic rate of tachycardia resuming when the pacing is stopped. More specifically, each pacing stimulus creates a wavefront that travels in an antegrade direction and thus resets the tachycardia to the pacing rate; a wavefront propagating retrogradely in the opposite direction collides with the wavefront of the previous beat. Criteria for entrainment mapping were developed to help define, locate, and target the critical isthmus of a tachycardia in such patients. However, this procedure requires that the VT is sustained and the patient is hemodynamically stable enough to allow one to perform activation mapping with 3D mapping systems and perform entrainment maneuvers. Yet, this group of patients accounts for only 5–10 % of all elicited ischemic VTs, or 20 % of all ventricular tachyarrhythmias requiring clinical assessment. In some cases, hemodynamic support can be provided during presentation of the VT, again to stabilize the patient while performing activation mapping and entrainment. More specifically, this can be accomplished with cardiac bypass or the use of a Tandem heart (CardiacAssist, Inc., Pittsburgh, PA, USA), Impella pump (Abiomed, Danver, MA, USA), or an intra-aortic balloon pump. Nevertheless, hemodynamic support is associated with its own potential vascular complications and their short- and long-term outcomes are still controversial.

Substrate mapping and modifications are useful approaches for hemodynamically unstable VTs, which make up the majority of clinical VTs. This approach typically consists of defining the scar borders by applying voltage mapping and pacing within and at the edges of a scar area to locate potential exit sites for the VT. Subsequently, ablation procedures are performed at these locations while the patient is in sinus rhythm. This methodology is less accurate in targeting a clinical VT; however, it has the advantage of avoiding the complications of hemodynamic support and, if performed extensively around the scar, can decrease the recurrence of VTs other than the clinical VT that the patient presented with.

Trigger mapping is used mainly for required ablations of polymorphic VTs and VFs, i.e., if there are consistent triggers for the arrhythmias (typically a PVC). Since polymorphic VTs and VFs cannot be mapped with current technologies, this approach can be quite useful to decrease ICD shocks and ventricular arrhythmia burden in patients requiring such devices.

The relative success of VT ablations is difficult to assess due to the current variability in procedure endpoints, e.g., the defined long-term outcomes and relative length of follow-ups. Nevertheless, reported success rates of RF catheter ablations of VTs in patients after myocardial infarctions (those acutely eliminated spontaneous episodes of VTs) can be as high as 60 % of treated patients in experienced centers [9]. Furthermore, if one or two clinically documented VTs are targeted, successful ablations may be achieved in 71–76 % [27] with serious complications occurring in <2 % of cases [24]. However, the reported risk of recurrences in multiple series may range from 30 to 46 %, mainly due to the high risk of developing new VTs. At present, catheter ablation of VT in patients following myocardial infarction is used primarily as an adjunctive to amiodarone and ICD therapy.

28.7.5.3 Ablations of Bundle Branch Reentry Tachycardias

A somewhat rare form of VT that can be cured by ablations is the bundle branch reentry tachycardia, in which the bundle branches of the His-Purkinje system form the reentrant circuit. In patients with the substrate resulting from a dilated cardiomyopathy and/or from significant conduction system disease, it is usually necessary to maintain reentry within the bundle branches. In these cases, commonly the normal His-Purkinje system does not support sustained reentry because the rapid conduction times around the bundle branches are normally shorter than the refractory periods of the bundle branches. Although cure of bundle branch reentry tachycardia can be easily accomplished by ablating the right bundle branch, long-term survival after ablations, to date, has been limited, with such patients eliciting the uniform presence of severe LV dysfunction. Therefore, in such cases, ICD therapy is usually recommended. For additional technological descriptions of ablation, mapping, and pacing systems, the reader is referred to Chaps. 29–32.

28.8 Summary

Cardiac arrhythmias encompass a wide spectrum of abnormalities in electrical generation and conduction at all levels within the human heart. These arrhythmias can be manifested as either tachycardia or bradycardia. The clinical significance of these cardiac arrhythmias is predominantly related to their associated hemodynamic consequences and their impact on mortality and the risk for SCD. Both clinical and basic laboratory research have offered important insights into the mechanisms underlying various arrhythmias and have also provided valuable tools for their identification and treatment.

Pharmacological therapies continue to be widely used in the management of arrhythmias. However, nonpharmacologic therapies have an increasingly important role and have become first-line therapy for a wide range of arrhythmias. The advent of 3D mapping systems, intracardiac echocardiography, and new sources of energy for ablation have

increased the accuracy, efficacy, and safety of ablation therapies. Continued advances in clinical research and innovation in biomedical engineering will achieve a more thorough understanding of the underlying mechanisms of many clinically elicited arrhythmias, leading to overall better patient care.

References

1. Task Force of the Working Group on Arrhythmias of the European Society of Cardiology (1991) The Sicilian Gambit. A new approach to the classification of antiarrhythmic drugs based on their actions on arrhythmogenic mechanisms. Circulation 84:1831–1851
2. The Cardiac Arrhythmia Suppression Trial (CAST) Investigators (1989) Preliminary report: effect of encainide and flecainide on mortality in a randomized trial of arrhythmia suppression after myocardial infarction. N Engl J Med 321:406–412
3. The Cardiac Arrhythmia Suppression Trial II Investigators (1992) Effect of the antiarrhythmic agent moricizine on survival after myocardial infarction. N Engl J Med 327:227–233
4. Josephson ME (ed) (1993) Clinical cardiac electrophysiology. Techniques and interpretations, 2nd edn. Lea & Febiger, Malvern, PA
5. Benditt DG, Lu F (2006) Atriofascicular pathways: fuzzy nomenclature or merely wishful thinking? J Cardiovasc Electrophysiol 17:261–265
6. January CT, Wann LS, Alpert JS et al (2014) 2014 AHA/ACC/HRS guideline for the management of patients with atrial fibrillation: executive summary. J Am Coll Cardiol 64:2246–2280
7. Estes NA 3rd, Halperin JL, Calkins H et al (2008) 2008 clinical performance measures for adults with nonvalvular atrial fibrillation or atrial flutter: a report of the American College of Cardiology/American Heart Association Task Force on Performance Measures and the Physician Consortium for Performance Improvement. J Am Coll Cardiol 51:865–884
8. Zipes DP, Camm AJ, Borggrefe M et al (2006) 2006 guidelines for management of patients with ventricular arrhythmias and the prevention of sudden cardiac death: a report of the American College of Cardiology/American Heart Association Task Force and the European Society of Cardiology Committee for Practice Guidelines. J Am Coll Cardiol 48:e247–e346
9. Stevenson WG, Friedman PL, Kocovic D, Sager PT, Saxon LA, Pavri B (1998) Radiofrequency catheter ablation of ventricular tachycardia after myocardial infarction. Circulation 98:308–314
10. Nabar A, Rodriguez LM, Timmermans C, Smeets JL, Wellens HJ (1999) Isoproterenol to evaluate resumption of conduction after right atrial isthmus ablation in type I atrial flutter. Circulation 99: 3286–3291
11. Oral H, Sticherling C, Tada H et al (2001) Role of transisthmus intervals in predicting bidirectional block after ablation of typical atrial flutter. J Cardiovasc Electrophysiol 12:169–217
12. Calkins H, Kuck KH, Cappato R et al (2012) 2012 HRS/EHRA/ECAS expert consensus statement on catheter and surgical ablation of atrial fibrillation: recommendations for patient selection, procedural techniques, patient management and follow-up, definitions, endpoints, and research trial design: a report of the Heart Rhythm Society (HRS) Task Force on Catheter and Surgical Ablation of Atrial Fibrillation. Heart Rhythm 9:632–696
13. Stavrakis S, Garabelli P, Reynolds DW (2012) Cardiac resynchronization therapy after atrioventricular junction ablation for symptomatic atrial fibrillation: a meta-analysis. Europace 14: 1490–1497
14. Haissaguerre M, Jais P, Shah DC et al (1998) Spontaneous initiation of atrial fibrillation by ectopic beats originating in the pulmonary veins. N Engl J Med 339:659–666
15. Chen SA, Tai CT, Tsai CF, Hsieh MH, Ding YA, Chang MS (2000) Radiofrequency catheter ablation of atrial fibrillation initiated by pulmonary vein ectopic beats. J Cardiovasc Electrophysiol 11:218–227
16. Haissaguerre M, Shah DC, Jais P et al (2000) Electrophysiological breakthroughs from the left atrium to the pulmonary veins. Circulation 102:2463–2465
17. Pappone C, Rosanio S, Oreto G et al (2000) Circumferential radiofrequency ablation of pulmonary vein ostia: a new anatomic approach for curing atrial fibrillation. Circulation 102:2619–2628
18. Oral H, Scharf C, Chugh A et al (2003) Catheter ablation for paroxysmal atrial fibrillation: segmental pulmonary vein ostial ablation versus left atrial ablation. Circulation 108:2355–2360
19. Pappone C, Manguso F, Vicedomini G et al (2004) Prevention of iatrogenic atrial tachycardia after ablation of atrial fibrillation: a prospective randomized study comparing circumferential pulmonary vein ablation with a modified approach. Circulation 110:3036–3042
20. Nademanee K, McKenzie J, Kosar E et al (2004) A new approach for catheter ablation of atrial fibrillation: mapping of the electrophysiologic substrate. J Am Coll Cardiol 43:2044–2053
21. Nademanee K, Schwab M, Porath J, Abbo A (2006) How to perform electrogram-guided atrial fibrillation ablation. Heart Rhythm 3:981–984
22. Pappone C, Santinelli V, Manguso F et al (2004) Pulmonary vein denervation enhances long-term benefit after circumferential ablation for paroxysmal atrial fibrillation. Circulation 109:327–334
23. Packer DL, Kowal RC, Wheelan KR et al (2013) Cryoballoon ablation of pulmonary veins for paroxysmal atrial fibrillation: first results of the North American Arctic Front (STOP AF) pivotal trial. J Am Coll Cardiol 61:1713–1723
24. Morady F (1999) Radio-frequency ablation as treatment for cardiac arrhythmias. N Engl J Med 340:534–544
25. Zipes DP (1997) Specific arrhythmias: diagnosis and treatment. In: Braunwald E (ed) Heart disease: a text book of cardiovascular medicine, 5th edn. W.B. Saunders Company, Philadelphia, pp 640–704
26. Triedman J, Perry J, Van Hare G (2005) Risk stratification for prophylactic ablation in asymptomatic Wolff–Parkinson–White syndrome. N Engl J Med 352:92–93
27. Stevenson WG, Friedman PL (2000) Catheter ablation of ventricular tachycardia. In: Zipes DP, Jalife J (eds) Cardiac electrophysiology from cell to bedside, 3rd edn. W.B. Saunders Company, Philadelphia, pp 1049–1056

Cardiac Ablative Technologies

29

Boaz Avitall and Arthur Kalinski

Abstract

Device technologies to treat cardiac arrhythmia continue to advance at a rapid pace; this is a highly competitive field with numerous corporate powerhouses playing significant roles. The primary goals for treatment of arrhythmia are to: (1) alleviate symptoms and improve an individual's quality of life; (2) prolong the patient's life by preventing complications such as ventricular tachycardia/fibrillation, syncope, and/or stroke; and (3) reduce an individual's dependency on pharmacologic therapies that often carry significant side effects. Pharmacologic treatment has been the mainstay for management of most cardiac arrhythmias, although in recent years implantable devices and ablation have become increasingly more important. In this chapter we review several ablation technologies that are in current use as well as others that are being developed. This review contains descriptions of: (1) various energy sources; (2) the mechanisms of action for lesion formation; (3) required power sources; (4) the variety of catheters that can be used to apply these therapies; (5) potential treatment complications; and (6) the recent sensor technologies that are being developed to improve therapeutic efficacy and/or minimize complications.

Keywords

Radiofrequency • Microwave • Cryotherapy • Cryoablation • Laser ablation • Ultrasound ablation • Thermal therapy • Arrhythmia • Atrial fibrillation • Electrophysiology

29.1 Introduction

As technology for percutaneous catheter interventions evolved, the result has been the design of specialized catheters for cardiac ablative therapies. These specialized catheters and their required energy sources have employed a variety of approaches, each with its advantages and disadvantages. Importantly, this variety of catheters and approaches has broadened the types of arrhythmia that can be treated by interventional approaches and improved their efficiency and efficacy. In this chapter, we will review the underlying ablative mechanisms for current leading technologies in catheter ablation; we will also highlight the current applications of these technologies in the clinical setting.

The range of the normal human resting sinus heart rate is 50–90 beats per minute (bpm); most average healthy individuals have resting rates in the 60–70 bpm range. Disturbances of cardiac impulse formation and/or transmission comprise the principal mechanisms, causing abnormalities of heart rhythm. In basic terms, these abnormalities are classified as being either brady- or tachy-arrhythmias. Today, in North America alone, it is estimated that there are over five million individuals who require treatment for some form of arrhythmia. Arrhythmias can occur at any age, but they become increasingly more prevalent as a function of age. Therefore, as our current population of senior citizens grows, so will the prevalence of arrhythmias.

B. Avitall, MD, PhD, FACC, FHRS (✉) • A. Kalinski, BS
Division of Cardiology, Department of Medicine,
University of Illinois at Chicago, 840 S. Wood St., MC 15,
Chicago, IL 60612, USA
e-mail: bavitall@uic.edu

P.A. Iaizzo (ed.), *Handbook of Cardiac Anatomy, Physiology, and Devices*, DOI 10.1007/978-3-319-19464-6_29

The classic line of therapy for treating arrhythmia has been the utilization of pharmaceuticals, but as with any medication, there are complications and/or side effects that have in part sparked the innovation of nondrug-based interventional procedures. The first cardiac catheter ablative procedure in a human was conducted in 1981 by Dr. Melvin Scheinman, who used direct current (DC) high-energy shocks to ablate myocardial tissues. Subsequently, DC ablation utilized a defibrillator output to deliver high-voltage discharge via a catheter to the tissues to elicit an ablation, usually of the atrioventricular node. The electrical discharge caused a spark between the catheter electrode and the tissue, and the resultant high temperature caused tissue ablation. However this approach did not allow for a fine control of the amount of energy to be delivered, and was associated with complications and/or tissue recovery. Thus, DC ablation was replaced by a more controllable radiofrequency (RF) energy source, which remains today as the mainstay of cardiac arrhythmia ablation in adult patients; note that cryoablation is currently more prevalently employed in pediatric patients. Nevertheless, as obstacles and complications associated with these technologies were discovered, a host of new catheter/modality types were created. For example, extensive research and clinical trials have been undertaken for microwave, laser, and ultrasound ablative technologies. Over the last decade, there has been incredible growth in the cardiac ablation industry as a whole; even during times of recession, this market has reported positive growth. This market is backed by corporate giants who stay competitive through a plethora of smaller start-up and privately owned ventures. The global cardiac catheter market is expected to grow to $2.1 billion in the USA alone by 2015; furthermore, Canada and the USA make up the North American segment which accounts for 35 % of the world's global value.

The primary clinical goals for treatment of arrhythmias are to: (1) alleviate symptoms and improve a patient's quality of life; (2) prolong a patient's life; (3) prevent associated complications such as ventricular arrhythmias, syncope, and/or stroke; and (4) reduce an individual's dependency on pharmacologic therapies that often carry significant side effects.

In this chapter, we review the foundation of several ablation technologies that are in current use and discuss others that are being developed. This review includes discussions of: (1) employed energy sources; (2) the mechanisms of action of these technologies; (3) the basis for lesion formation; (4) the variety of catheters developed to utilize various energy sources; (5) associated therapeutic complications; and (6) the developed sensor technologies aimed to improve treatment efficacy and minimize complications.

29.2 Radiofrequency (RF) Ablation: Utility

RF energy is the most commonly used energy form to treat cardiac arrhythmia. As with all catheter treatments aimed at treating arrhythmia, the goal is the removal of problematic regions of tissue (in case of automatic foci) or part of the circuit that maintains the arrhythmia. The method by which this tissue is electrically silenced is by induction of necrosis by the application of heat. The created region of tissue necrosis, in time, yields to fibrosis and scar formation which in turn maintains the structural integrity of the heart, but is electrically silent.

29.2.1 Mechanism of Tissue Ablation

RF lesion formation (Fig. 29.1) is the primary result of tissue heating. Once tissue exceeds temperatures above 45–50 °C, this results in denaturing of proteins and changes in cellular integrity and structures, and induces dehydration of tissues, thus causing permanent damage [1–3]. Tissue heating with RF energy is a result of resistive heating at the interface between the catheter and the tissue in contact with the ablation electrode. This heating is a direct function of the current density at the catheter ablation electrode onto the myocardium interface extending a few millimeters into the tissue [4]. The depth and width of lesion formation depends on the location of ablation in the heart (thin atrial tissues versus thick ventricular tissues as noted in Fig. 29.2), and is a result of conductive heating through the tissues [4–7]. Furthermore, the size and degree of tissue heating is a function of RF power, duration, impedance, catheter tip orientation, tip metal composition, irrigation, degree of contact with tissue, and/or the relative size of electrode [1–3, 5, 6, 8–10]. Currently, there are a variety of ablation catheters available for clinical use or in clinical trials.

The majority of RF ablation catheters are unipolar, that is, where RF energy is delivered at the ablation electrode and then sent to a dispersive pad located on the thigh or back of the patient. A bipolar mechanism consists of energy passing between electrodes of the catheter itself, but the use of this kind of mechanism is not commonly practiced.

29.2.2 The RF Generator

Typically, clinically used RF generators produce frequencies from 100 to 3000 kHz (the range of electrosurgery), with an ablation range of 300–1000 kHz (550 kHz is the FDA-suggested optimal frequency). It is important to note that the

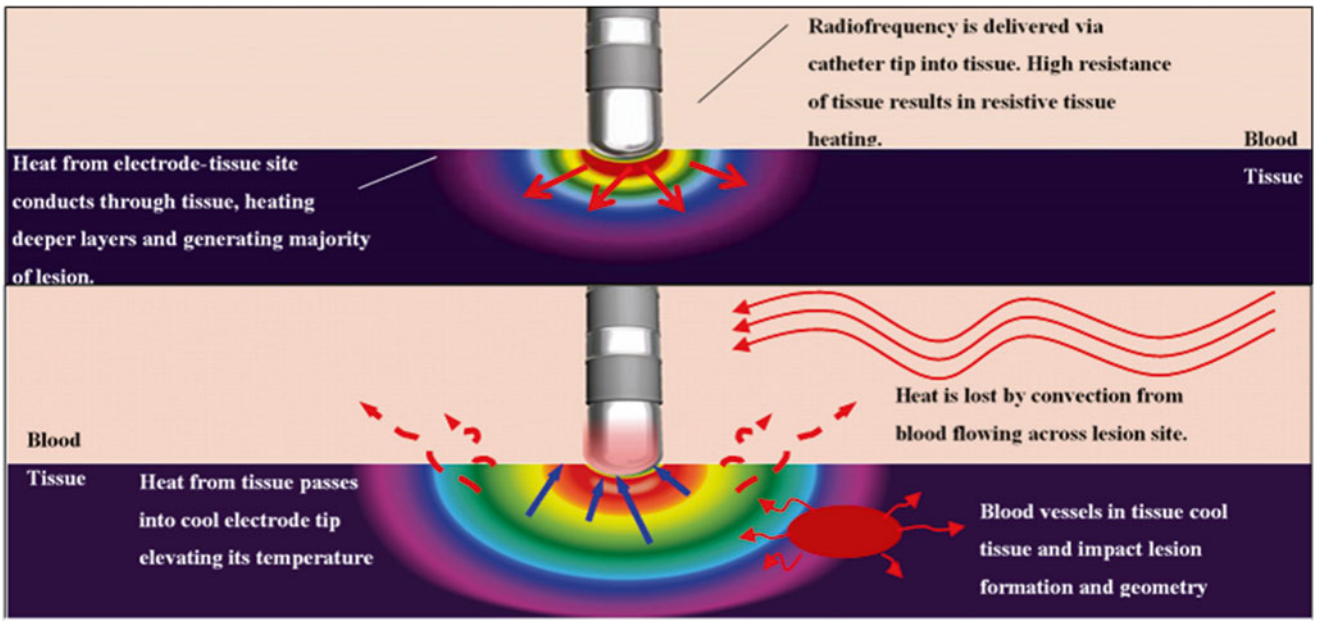

Fig. 29.1 Schematic of radiofrequency lesion formation

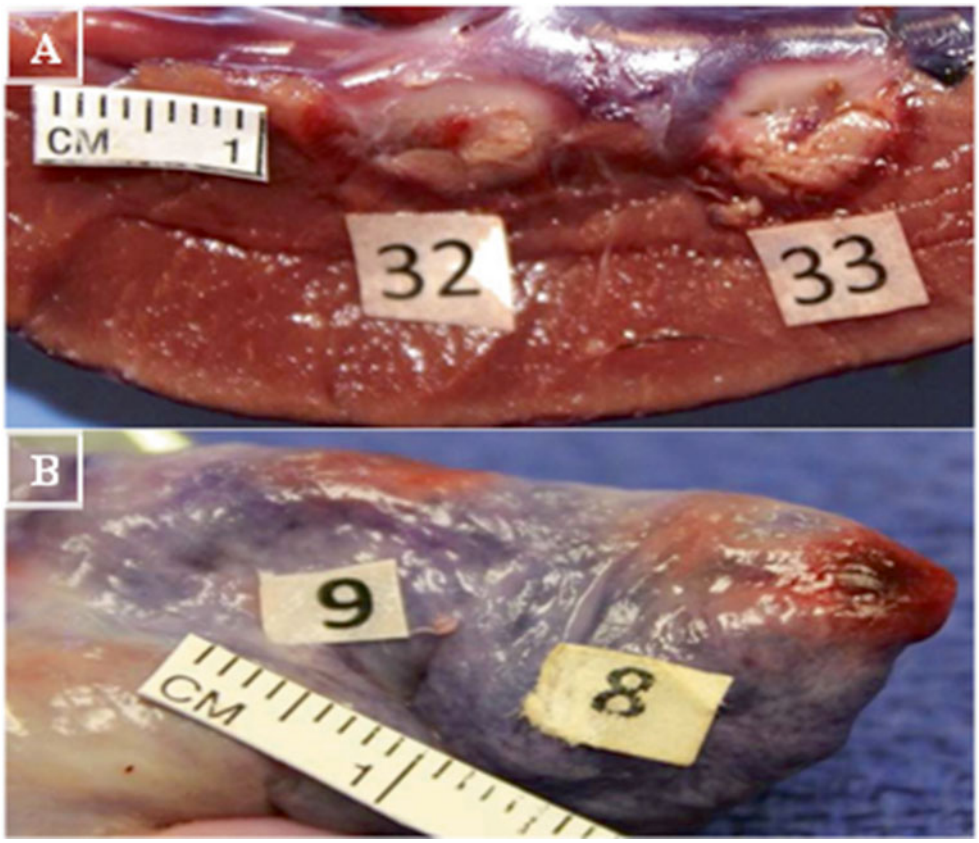

Fig. 29.2 Illustration of depth and width of lesion formation. (**A**) Left ventricle (8 mm catheter tip; *32:* 9.2 mm wide, 10 mm long, 7 mm deep, 16w, 64c, 44 s; *33*: 8 mm wide, 11.7 mm long, 7.7 mm deep, 30w, 65c, 42 s). (**B**) Right atrium (8 mm catheter tip; *8*: 6.8 mm wide, 7.2 mm long, 2.2 mm deep 18 W, 63c, 60 s; *9:* 5.5 mm wide, 8.2 mm long, 3.7 mm deep 10 W, 65c, 60 s). Pictures from Avitall Lab 2014

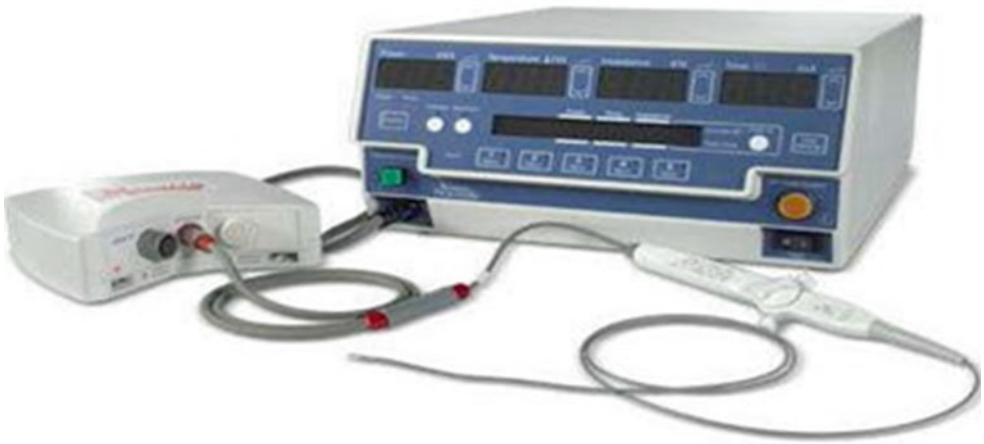

Fig. 29.3 Radiofrequency (RF) generator from Boston Scientific (EPT-1000X). Along with the basic functionality of RF generators, it also provides memory tabs to preset specific values for each variable. This particular system is specifically designed for use with catheters designed from Boston Scientific (Blazer series) and connects to catheter via the Maestro 3000 system. *Source*: Boston Scientific webpage

high frequency of RF does not depolarize the cardiac tissues, and thus lacks the possibility of triggering deadly arrhythmia (ventricular fibrillation) [1, 11].

In general, an RF generator controls power, temperature, and duration of the applied ablation, while also measuring impedance and temperature during the procedure. Both power and temperature may be set as a maximal control with the latter being typically set as control in clinical procedures, allowing for power delivery to be modulated and thus maintaining a given temperature. Power settings range from 10 to 100 W with temperature ranges dependent on specific models. For instance, the EPT-1000X generator from Boston Scientific (Marlborough, MA, USA) has a temperature range of 30–120 °C (Fig. 29.3). The RF generator allows ablation duration to be set (maximal duration is preset at 120 s; 60 s is commonly used), but ablation can be manually terminated at any time during an application.

29.2.3 Additional RF Clinical Generator Information

It is important for users to understand and verify that maximal power applications via a generator are dependent on a per-catheter basis. For instance, the 4 mm ablation catheter tip electrode's maximal power is limited to 50 W, while the 8 mm is limited at 65 W [12]. The power limitations were established to minimize the potential of tissue overheating leading to boiling, char, and gas formation within the tissues; in turn, this can cause pressure buildup leading to a burst known as a *steam pop* and tissue shredding. The RF power supply is also set to a maximal temperature limit which also depends on the catheter being used. For an 8 mm standard tip catheter, a typical maximal temperature of 65 °C is used [12]. It should also be noted that, in general, RF power cannot be applied (or terminates) if the impedance is too high prior to an ablation or rises during an ablation, as this may be an indication of coagulum formation at the tip [5, 6, 13]. The usual catheter-to-tissue impedance is 80–240 Ω [5]. A lower impedance may indicate a system short or failure, whereas a high impedance cutoff is to prevent char formation and ensure that the reference patch electrodes are properly attached to the patient's skin. If the size, or the contact of the reference electrodes with the skin, is poor, it may lead to severe skin burns (Fig. 29.4a).

More specifically, since tissue and blood heating results in denaturation of proteins, blood products can adhere to the catheter thus increasing the impedance (Fig. 29.5a). Importantly, the early detection of impedance rises and automatic terminations of the RF powers can potentially prevent a stroke.

Of interest to note, an atypical generator that is currently awaiting FDA approval—the GENius RF Generator (Medtronic, Inc., Minneapolis, MN, USA)—uses a unique duty-cycle energy delivery system to power a multielectrode catheter called a pulmonary vein ablation catheter (PVAC; Fig. 29.6). The GENius generator is capable of simultaneously delivering power up to 12 electrodes in a temperature-controlled and power-limited manner. The generator is capable of delivering energy in a bipolar, unipolar, or mixed fashion (bipolar:unipolar) 4:1, 2:1, and 1:1 [14, 15].

29.2.4 RF Catheter: Standard Features

The baseline design for RF catheters features a simple metal electrode tip (usually platinum) which delivers the radiofrequency energy. A recent study showed that tip metal composition influences lesion formation, with gold-tipped catheters leading to lesions with greater depth which the researchers

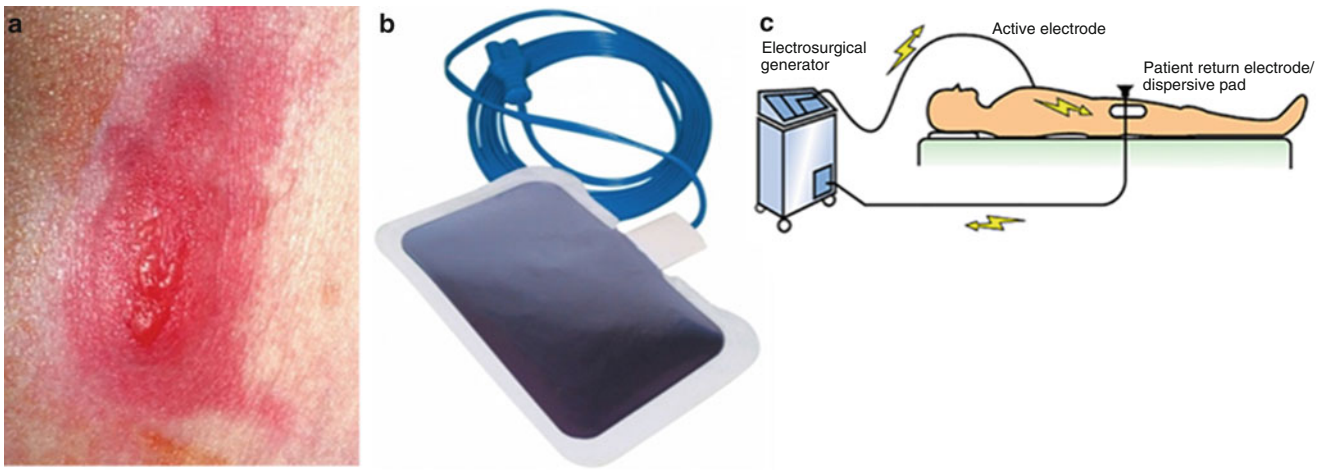

Fig. 29.4 (**a**) Second degree burn from improper patch use. (**b**) Typical dispersive patch. (**c**) Sketch of circuit that dispersive pad is used to complete

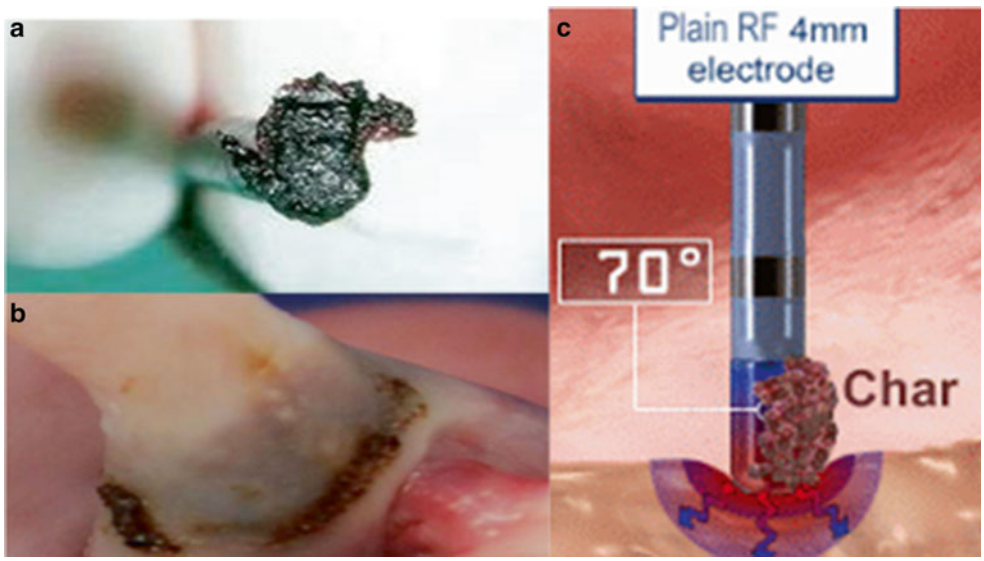

Fig. 29.5 (**a**) Char formation on a catheter tip. *Source*: http://drwes.blogspot.com/2007/08/remote-magnetic-catheter-ablation-of.html). (**b**) Char formation on a lesion on a pulmonary vein with a nonirrigated 8 mm tip. (Picture from Avitall Lab 2014). (**c**) Depiction of char formation during a catheter ablation. Note the high temperature (70 °C) at tissue–electrode interface. *Source*: http://wesleytodd.blogspot.com/2013/09/rf-ablation.html

attributed to the increased conductance of gold compared to platinum [9]. Typically, such catheters are 7–8 F in diameter with the tip size typically ranging between 4 mm and 10 mm in length. Larger tips have greater surface area for circulating blood to cool the ablation electrode. These factors allow for higher power and create larger and deeper lesions [1, 3, 8]. On the other hand, ablation tips that are too large may ultimately create uneven heating which can result in the occurrence of char and/or *crater* (focal tissue deformations with hyper-contraction zones) formation [3].

In most currently available RF ablation catheters, metal rings are embedded proximally to the ablation tip for the purpose of obtaining focal electrophysiological recordings. Additional electrodes can be placed along the distal portion of the catheter. Importantly, electrophysiological information such as electrogram amplitudes and pacing data can be used to better elucidate type of contact, identify tissues for ablation (or to define tissues that have been ablated or scarred), and give insight related to lesion maturation (Fig. 29.7).

The handle of most catheters offers bidirectional deflections with specific models providing varying degrees of deflection (Fig. 29.8). Depending on the catheter model, there are various dilators and introducer sheaths available to aid in the insertion of the catheters into the vascular space and the ensuing procedure. The proximal end of the catheter has the electrical umbilical cord that attaches the catheter to the RF generator and to the monitoring/mapping systems simultaneously (Fig. 29.3).

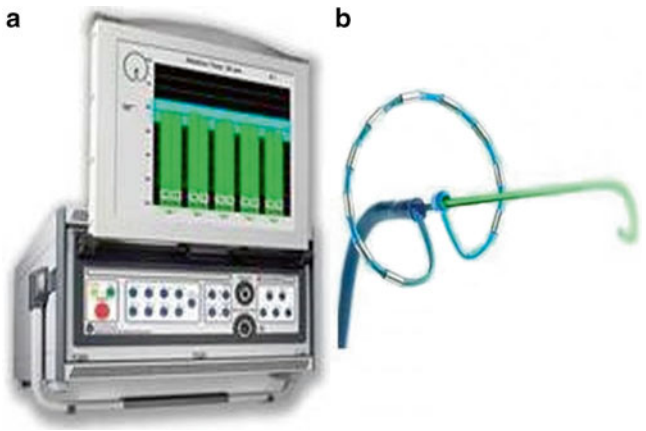

Fig. 29.6 (**a**) GENius Radiofrequency Generator from Medtronic, Inc. (Minneapolis, MN, USA). The system uses software to control a user-defined temperature, and delivers power to individual electrodes. To maintain the temperature, the power delivery is limited to 10 W at all settings except the 4:1, in which it is limited to 8 W. Power delivery limitation is necessary due to the small surface area of electrodes on the PVAC (3 mm long, 1.5 mm diameter). A display screen shows individual readouts of temperature, power delivery, and time within optimal temperature range for up to 12 individual electrodes [14, 15]. *Source*: http://www.whichmedicaldevice.com/by-manufacturer/49/151/genius-multi-channel-rf-generator. (**b**) Pulmonary vein ablation catheter. A multielectrode circumferential ablation catheter anatomically designed for pulmonary vein isolation, powered exclusively by the GENius RF Generator Source. *Source*: http://www.mprodserver.com/meddevices/pvac

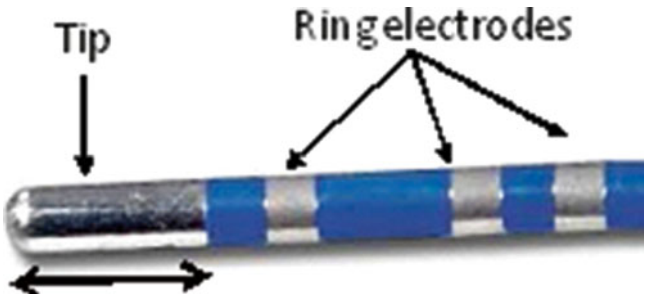

Fig. 29.7 Radiofrequency catheter: 8 mm Dual-8 Therapy Catheter (St. Jude Medical, St. Paul, MN, USA). Picture from Avitall Lab 2014

29.2.5 Multielectrode Catheter

One specific type of a multielectrode catheter—the PVAC—was anatomically designed for pulmonary vein isolation (PVI; Fig. 29.6b). It features ten platinum electrodes that are 3 mm long with a diameter of 1.5 mm, and are spaced apart 3 mm. The diameter of the distal loop is 25 mm; the catheter is a 9 F ablation catheter and can also be used as a mapping catheter. It has bidirectional deflection and distal and proximal retraction that is controlled by two switches located at the handle. The catheter is operated in conjunction with GENius RF Generator. PVAC uses less power (10 W) than most RF catheters with standard metal tips, but due to the small electrode sizes, the current densities are quite comparable [14–16].

29.2.6 Irrigated Tip RF Catheters

The irrigated catheter tip uses a circulating fluid to cool the tip during RF ablation. Open irrigation passes heparinized saline through the tip and discreet irrigation ports, typically 6–12 ports; these fluids then enter into the patient's blood stream. Porous open irrigation utilizes a similar method to open irrigation, but the fluid "sweats" through a multitude of small pores [8] (Fig. 29.9).

The concept of the irrigated tip catheter is that focal cooling at the tip–tissue interface helps to prevent char formation at the interface, i.e., by lowering surface temperature while allowing a large and deep lesion to mature as conductive heating continues unabated into deeper layers. It has been shown that deep tissue exhibits will be subjected to higher temperatures than the tip–tissue interface, with temperatures differences ≥10 °C when ablating with irrigated catheters [6].

With surface tissue temperatures being kept relatively low, greater power and durations can be applied before coagulum formation begins [2]. There is reported evidence that the risk of thrombus, char, and crater formation is reduced when using irrigation [2, 8]. However, irrigation at high power levels (>50 W) has a higher risk of creating a steam pop. As noted above, steam pops can be created by either entrapment of gas at the tip–tissue interface or gas forming just under tissue surface, which then ruptures as the pressure builds within the tissues. This occurs as a result of reaching temperatures that cause boiling [2]. Steam pops can result in shredding of cardiac tissue or perforation, and thus result in severe clinical complications.

In general, irrigated catheters use a specialized irrigation system to control fluid flow rates. While placed within the heart, passive flow rates (≤5 CC/min) are used to keep blood from entering the irrigation pores, thus minimizing clot formation which would stop the irrigation flow. Higher irrigation rates are typically used during the ablation procedure itself. These rates can range from 15 to 30 CC/min, with 30 CC/min being the traditionally recommended value. It is important to note that irrigation flow rates can impact lesion maturation, with high irrigation rates (≥20 CC/min) being shown to reduce lesion diameter but not effecting lesion depth [17]. Additionally the solution used for irrigation can have an effect on lesion formation. Research by Shake et al. has shown that lesion depth is inversely proportional to increasing electrolyte content of irrigation solution; they also showed that the use of non-electrolyte solutions can result in tissue destruction [18]. Further, some applied irrigation solutions like dextrose are electrically insulating and negatively affect lesion formation [19]. To date, an irrigation solution of 0.9 % sodium chloride saline is recommended for RF irrigation.

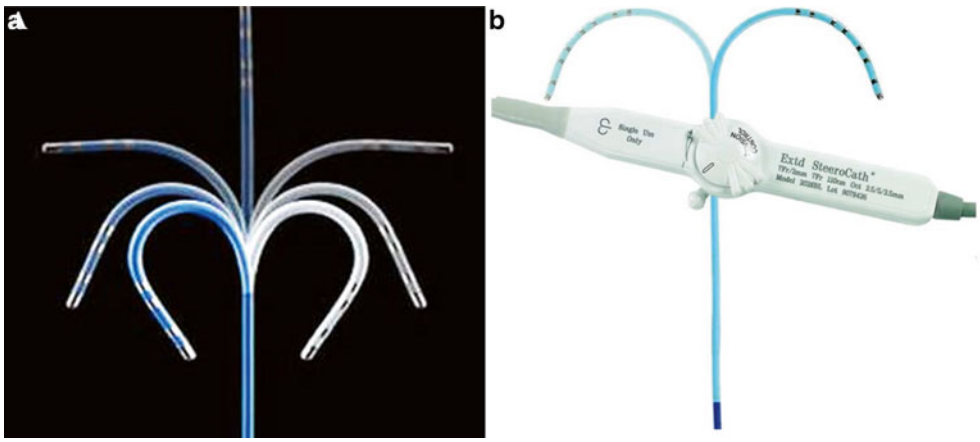

Fig. 29.8 (**a**) Range of bidirectional deflection seen in a typical radiofrequency catheters. *Source*: http://www.medicalexpo.com/prod/st-jude-medical/ablation-catheters-bidirectional-irrigated-70886-446600.html. (**b**) Simple deflection and the handle control for a electrophysiology recording catheter. *Source*: http://www.eplabdigest.com/articles/Use-a-Steerable-Bi-directional-Coronary-Sinus-Octapolar-Catheter-During-Atrial-Fibrillation

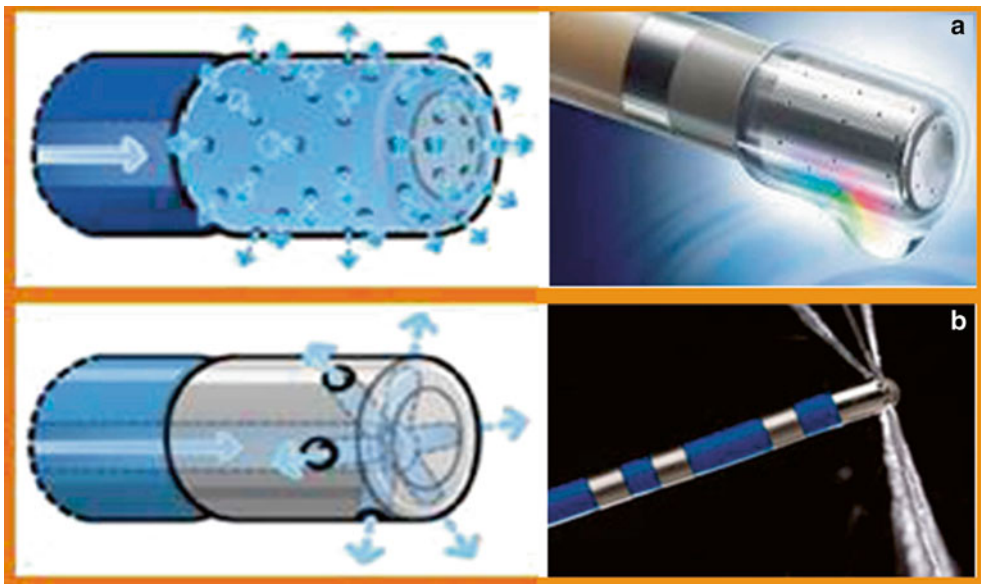

Fig. 29.9 (**a**) Porous irrigation which "weeps" out. Multiple channel ports evenly disperse fluid. (**b**) Traditional irrigation with six ports that spray fluid over an area. *Both catheters are from the Thermocool line from Biosense Webster (Diamond Bar, CA, USA). *Source*: http://www.biosensewebster.com/thermocoolsf.php

29.2.7 Additional Sensors and Modifications of RF Catheters and Technologies: MicroFidelity Technologies

An ablation/mapping product currently available from Boston Scientific, called MicroFidelity (MiFi) Sensor Technology, uniquely utilizes especially sensitive mini electrodes spaced circumferentially around the catheter (Fig. 29.10). The mini electrodes are closely spaced to provide localized readings of tissue while minimizing far field recording. The circumferential placement of these mini electrodes ensures that at least one pair is in direct tissue contact. The MiFi technology is intended to: (1) improve recognition of gaps in linear lesion sequences; (2) help map previously ablated tissues; and (3) provide insights as to the relative maturation of a lesion. Recent research has suggested that electrogram amplitude reductions from mini electrodes can be used to determine the timing of lesion maturation [12]. The nonirrigated MiFi catheter is currently available in 8 mm, while a 4.5 mm irrigated version is currently awaiting FDA approval.

29.2.8 Contact Force

An important aspect of any ablation procedure is understanding the relative amount and type of contact between the electrode and tissue. For example, a poor or partial contact with tissue can result in incomplete lesions and extend procedure times. It was previously reported that good contact ablation has a clear decrease in impedance (10–15 Ω), and results in significantly higher temperatures at the tissue–electrode

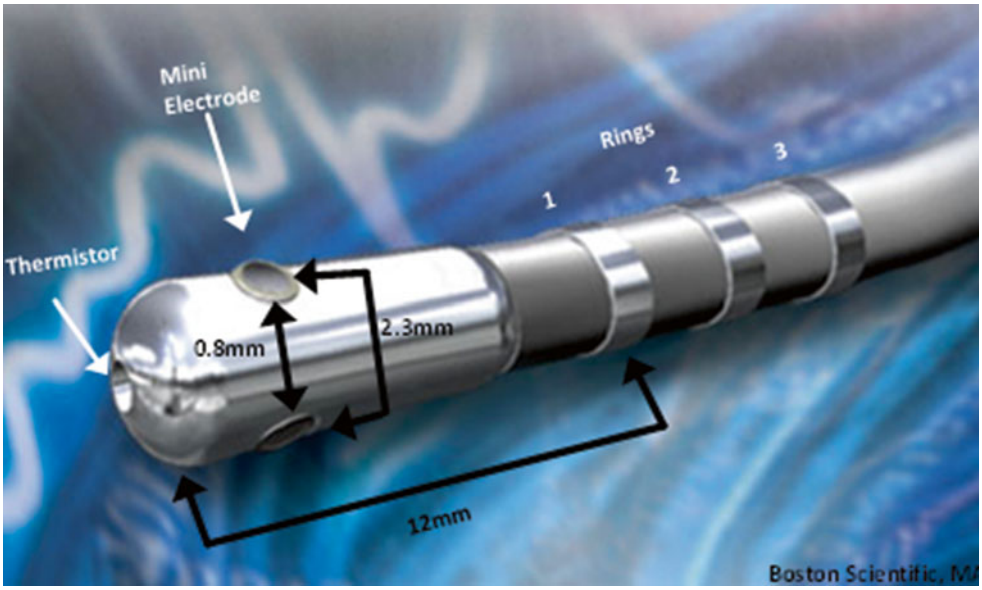

Fig. 29.10 8 mm IntellaTip Mifi XP Temperature: Pictured is a graphical sketch of the locations of various components and spacing between them. Space between mini electrodes is 0.8 mm, space from center of mini electrode to the next is 2.3 mm, and the distance from tip to ring is 12 mm. *Source*: http://www.bostonscientific.com/redefining-ep/IntellaTip.html

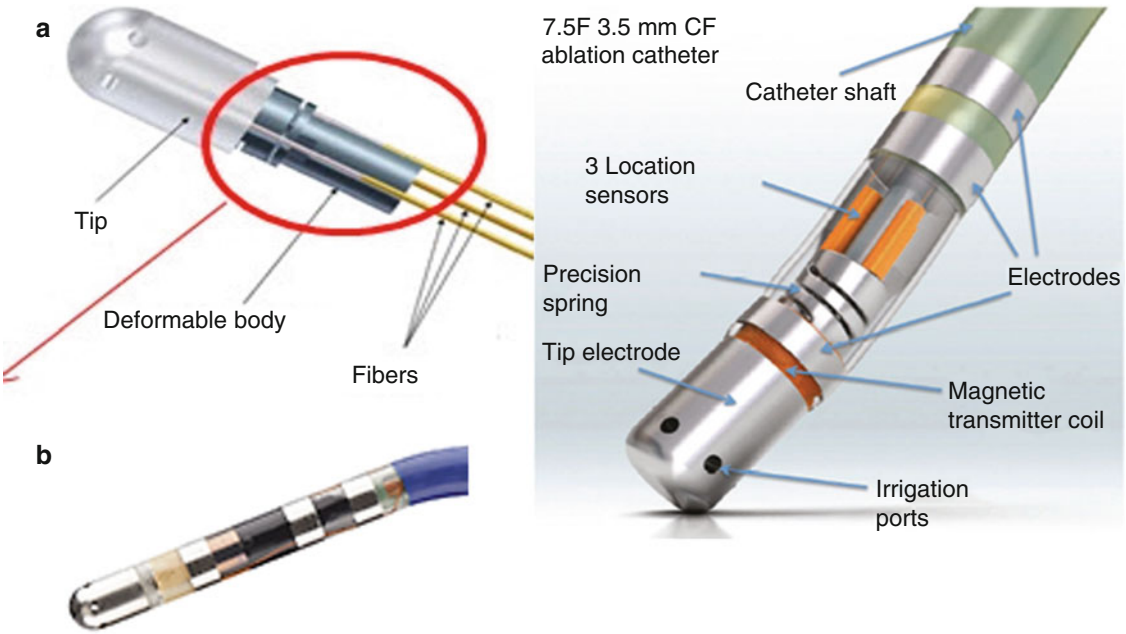

Fig. 29.11 (**a**) Tacticath quartz contact force catheter (St. Jude Medical, St. Paul, MN, USA). *Source*: http://professional-intl.sjm.com/products/ep/therapy/advanced-ablation/tactisys-quartz#technology. (**b**) Thermocool Smart touch Catheter from Webster Biosense (Diamond Bar, CA, USA). *Source*: http://www.radcliffecardiology.com/articles/thermocool-smarttouch-catheter-evidence-so-far-contact-force-technology-and-role-visitag

interface than incomplete or poor contact [5]. The study also showed that better contact with tissue correlated closely with both temperature increases and impedance decreases within the first 5 seconds of an ablation [5]. However, good tissue contact is difficult to assess. Operators have currently employed the use of fluoroscopy, ultrasound, mapping technologies, and electrophysiological readings such as pacing threshold to guide catheters to ablation sites and establish tissue contact. These measures add a level of accuracy, but cannot ascertain the direct degree of contact with target tissue. As a result, contact force sensors have been developed and are being assessed in clinical trials. Today, the two primary contact force sensors being studied are the Thermocool Smart touch (Webster Biosense, Diamond Bar, CA, USA) and the Tacticath Quartz Contact Force catheter (St. Jude Medical, St. Paul, MN, USA) (Fig. 29.11). More specifically, the Tacticath Quartz Contact Force catheter has three built-in optical fibers that will deliver light to tip; a central cavity within the cathe-

ter measures micro deformation via a deformable body as contact is made (Fig. 29.11a) [20]. The Thermocool Smart touch utilizes a precision spring and three magnetic sensors built into the tip of a standard RF catheter, to calculate contact force based on micro-deformations of the spring (Fig. 29.11b) [20].

Generally, sensed contact forces are measured as grams; in one study, these forces ranged from 2 to 60 g and correlated with decreases in impedance of 9.7–41.7 Ω (respectively) within the first 5 seconds of ablation [21]. In another report, it was shown that when titrating power to achieve an impedance drop of 15 Ω, less power was required with increasing contact force [21]. Also, the utilization of contact force sensors has been described to better predict the occurrence of deeper lesions as well as steam pop and/or thrombus formation [22]. In general, it is considered that information on contact force will allow operators to realize if catheter contact is too great, thus allowing them to ease off and reduce the chance of charring and thrombus. On the other hand, the use of such sensors will allow operators to identify if contact is poor and then move the catheter closer to tissue for proper ablation [21–23].

Related to catheter contact forces for proper lesion formation is catheter tip orientation. Catheter tip orientation has also been shown to impact lesion genesis, with one study showing that smaller catheter tips produce larger lesions in the perpendicular orientation, but larger tips generate larger lesions in parallel orientation [3, 7]. It should be noted that steam pops are more common in the perpendicular orientation [2].

29.3 Cryothermal Ablation

Cryothermal clinical techniques have been used in medicine for several decades, but the cryothermal ablation approach using percutaneous catheters is a more recent development. Cryothermal energy has gained traction as an alternative method for ablating cardiac tissue with RF, but one needs to understand that it relies on a significantly different mode of lesion formation, that is, extracting heat from tissues to induce freezing [24]. Currently, in most procedures where cryoablation has been used, individuals utilize either 9F 8 mm metallic tipped catheters or the 23 and 28 mm diameter cryoballoons; these have been employed to treat atrial fibrillation, atrial flutter, and atrial-ventricular nodal reentrant tachycardia, along with other forms of tachycardia [25–28].

29.3.1 Mechanism of Cryoablation

Cryoablative technologies commonly utilize the circulation of a refrigerant in a closed, pressurized system to rapidly cool the target tissues. These circuits capitalize on the Joules–Thomson effect to deliver full cooling of the refrigerant, such as liquid nitrous oxide (−88.6 °C), to the distal catheter tips. The Joules–Thomson effect is the phenomena where liquid enters an expansion chamber, where it then rapidly cools upon expansion and transitions from a liquid to a gas.

As cardiac tissue cools, it becomes less excitable, electrical conductance slows, and cellular metabolic processes shut down (i.e., when tissue temperature reaches <20 °C). It is important to note that from 0 to −5 °C, the loss of function in most excitable tissues can be restored by allowing the tissue to thaw, but from −5 to −15 °C there is a delay between thaw and restoration of function. This return to function after freezing is known as *reversible suppression*. Cardiac tissues held at −20 °C for ≥4 min sustain permanent damage and electrical silence [29]. Furthermore, prolonged freezing between temperatures of −10 and −25 °C will typically result in permanent damage, but extreme cold temperatures of ≤−50 °C will result in permanent damage regardless of the therapeutic durations [29, 30]. Cryothermal injury is characterized by three distinct stages: (1) a freeze/thaw cycle; (2) a hemorrhage and inflammation phase; and (3) a fibrosis replacement phase [31, 32]. More specifically, ice crystal formation that occurs within cells causes irreversible damage to subcellular organelles, the most important of which are mitochondria; the electron transport chain of mitochondria is particularly susceptible to ice formation. Once mitochondria are compromised, the cell loses its ability to generate energy and, along with damage to other key organelles, dies. Additionally, coagulative necrosis results shortly after ablation and dead tissue is gradually replaced with fibrosis. The ablation of myocardium by cryothermal energy is considered to help maintain the ultrastructure (due to resistivity of fibroblasts and collagen to freezing), and therapeutic borders are sharply demarcated [30, 33]. Furthermore, it has been reported that a significant decrease in thrombus formation has been associated with the clinical use of cryoablation (Fig. 29.12) [25, 28, 29, 34].

From a therapeutic delivery standpoint, as refrigerant cools the tissue, ice forms at the tissue contact site. Unlike radiofrequency, the cryo-catheter or cryoballoon outer surfaces will adhere to the applied tissues stabilizing them in place, an important factor for tissue contact during ablation. It should be noted that, depending on the extent of the tissue contact and blood flow, cryotherapy may require 2–5 min to reach temperatures low enough to induce permanent tissue damage [33].

As described above, a unique phenomenon of cryotherapy is the ability to reversibly silence tissues through gentle freezing (0 to −15 °C). By electrically silencing certain tissues an operator performs what is called cryomapping, which aids one to determine which tissues are problematic and require ablation without causing widespread damage [31, 34]. This technique has been shown to be particularly effective with treatment aimed at AV nodal reentrant tachycardias [37].

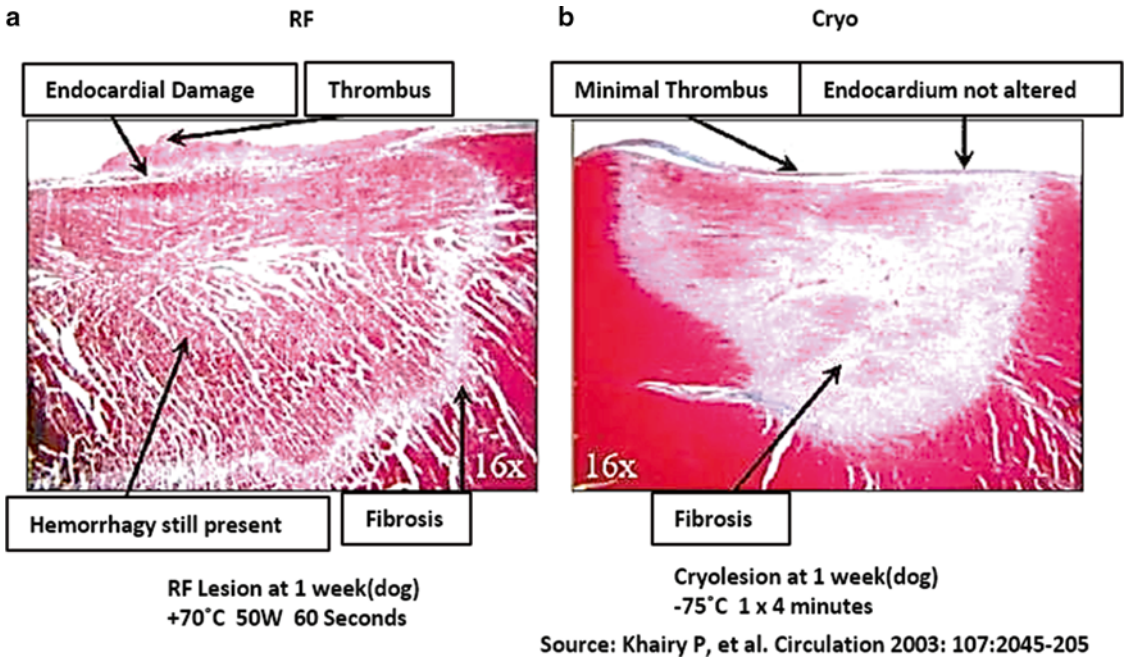

Fig. 29.12 (**a**) Radiofrequency lesion; note hemorrhaged tissue and nonhomogenous fibrosis. (**b**) Lesion derived from cryothermal treatment, showing well-demarcated lesion with homogenous fibrosis and no remaining hemorrhage [29]

29.3.2 Available Tools for the Application of Cryotherapies

The delivery of cryotherapy via catheters requires a cryoconsole for operation. Typically, the cryoconsole is connected to catheters via an electrical umbilical cord and liquid gas line. The console performs several critical functions, specifically it: (1) houses the refrigerant (nitrous oxide); (2) creates a vacuum for return of the gas from the catheter; (3) monitors internal temperatures and pressures; and (4) controls the flow of refrigerant to the catheter. If the circuit for the refrigerant is in anyway compromised, the console automatically shuts down the system, deflates the balloon (in the case of balloon catheters), and alerts operators to the issues detected. Currently, such consoles utilize a touchscreen to give readouts of pressure and internal temperature, and also control the functions of the catheter (Fig. 29.13). Refrigerant (nitrous oxide gas) is recycled through the console and then passed to the hospital's disposal system.

Currently, clinically available cryo-catheters come in two distinct types—traditional tip ablation catheters and balloon. For example, the Freezor Max from Medtronic, Inc. (Fig. 29.14) has an 8 mm tip with electrodes at the tip and on three subsequent rings, allowing for electrophysiological recordings/mapping. This particular catheter utilizes unidirectional deflections; it fits into a 10 F introducer and comes equipped with a thermocouple that allows for

Fig. 29.13 Cryocath console from Medtronic, Inc. (Minneapolis, MN, USA). *Source*: http://www.medicalexpo.com/prod/medtronic/mobile-cryosurgery-units-70691-441874.html

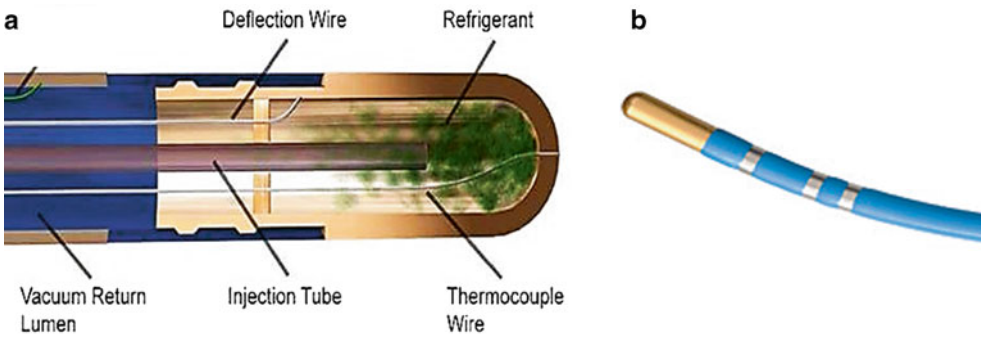

Fig. 29.14 (**a**) General schematic of the inner components of a tip-based cryo-catheter. (**b**) Freezor Max 3 from Medtronic, Inc. (Minneapolis, MN, USA). *Source*: http://www.medtronic.com/

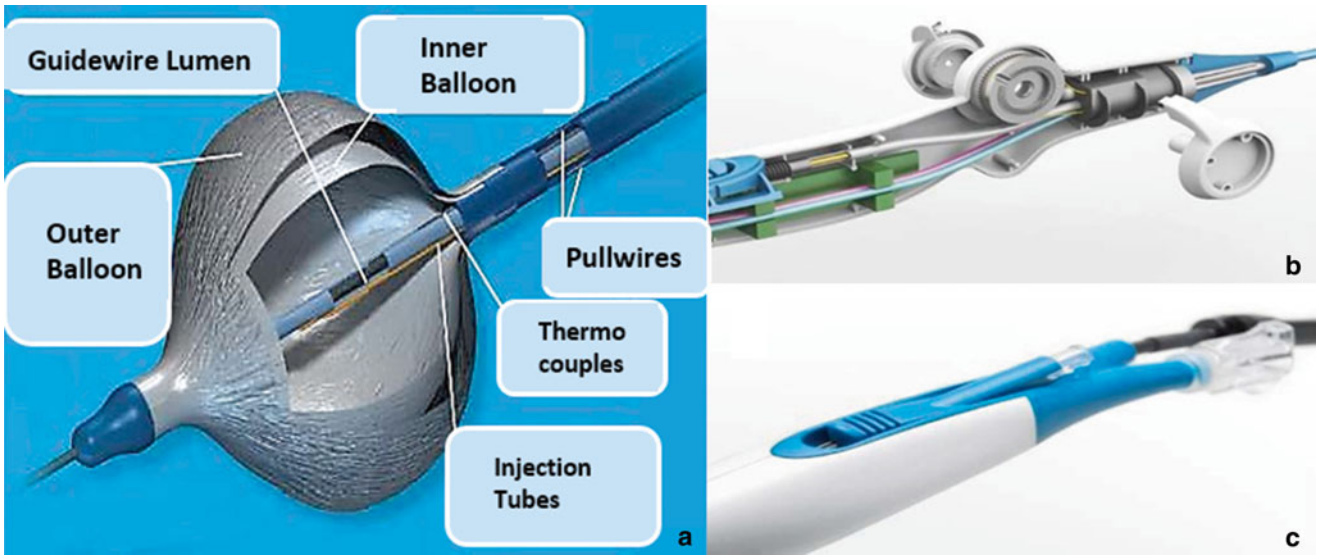

Fig. 29.15 (**a**) Inner components of a balloon catheter. *Source*: http://www.medgadget.com/cardiac_surgery/page/34. (**b**) Inner components of the handle of a balloon catheter. *Source*: http://www.farmpd.com/medical-equipment-product-development/cryocath-technologies-6/. (**c**) Gas lead, electrical umbilical cord, and guidewire/catheter lumen at bottom of handle. *Source*: http://www.farmpd.com/medical-equipment-product-development/cryocath-technologies-4/

monitoring temperature at the catheter tip. There are two models currently available, one 55 mm and the other 66 mm (handle to tip length). These cryo-catheters feature a central lumen for the passage of refrigerant, which then terminates at the tip of the catheter. A larger lumen is kept under vacuum which returns the refrigerant to the delivery system for disposal. Also, pending model variability, there are typically deflection wires, thermocouple wires, and electrical leads extending to the handle. Handles will feature an electrical umbilical cord, deflection controls, and a gas connector (these are terminated onto the cryoconsole). The tip-based catheters are commonly used to treat pediatric arrhythmia. Additionally, these catheters are also used to treat paroxysmal atrial fibrillation by ablating focal triggers, and are used in conjunction with cryoballoon catheters as spot treatment to complete left atrial PVI procedures.

The cryoballoon catheters were anatomically designed for use in PVI. They utilize the same functional mechanism as the tip-based cryo-catheters (i.e., with a central lumen supplying refrigerant and a larger lumen acting as a vacuum return). Uniquely, the cryoballoon catheters feature an inflatable balloon that is designed to generate a circumferential lesion around the balloon and thus treat pulmonary veins. There are currently two sizes of balloons available clinically, 23 and 28 mm. These balloons are made of a compliant material that can withstand the high pressures. Additionally, an outer balloon is employed as a safety feature, in the event of an internal balloon rupture or leak. Importantly, the space between the two balloons is under constant vacuum and any change in pressure immediately results in termination of the refrigerant delivery and suction of gas from the balloon. An internal thermocouple monitors balloon internal temperature. Current models do not feature any electrodes for electrophysiological readings, but they do feature a central lumen where an Achieve mapping catheter (3.3F lasso type catheter) can be maneuvered to the distal end to provide the ability to monitor pulmonary vein electrical activities (Fig. 29.15). To date, due to the size and stiffness of the cryoballoon,

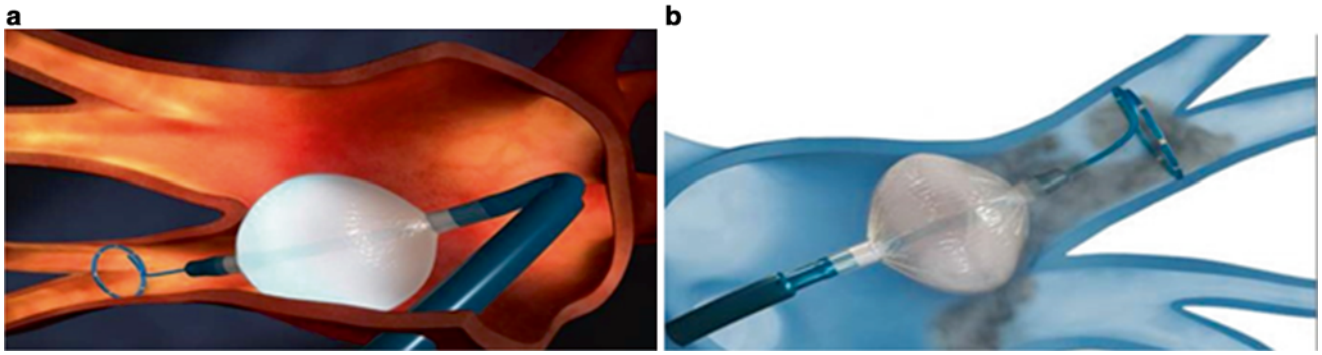

Fig. 29.16 (**a**) Cryoballoon with lasso catheter in position to take pulmonary vein isolation electrophysiological readings. (**b**) Dye is injected through central lumen to determine if the pulmonary vein is occluded. A leak is present indicating partial occlusion

catheters have deflections that are very limited. Furthermore, the deployment of the balloon catheter in the left atrium at the os of the pulmonary veins require the use of a 12F sheath, which is introduced into the femoral vein and transseptally into the left atrium; currently, this sheath has unidirectional deflection which helps to facilitate the proper positioning of the balloon catheter.

For ablation procedures performed with these technologies, the cryoballoon is introduced into a patient in a percutaneous manner and is positioned in the antrum portion of the pulmonary veins (Fig. 29.16a). When the balloon obstructs the flow from the pulmonary vein, a required circumferential lesion and PVI can be achieved. Operators typically will utilize a contrast medium (such as iodine) that is injected through the central lumen of the catheter. The dye is used to determine if occlusion is achieved or if leaks are present (Fig. 29.16b).

29.3.3 Complications and Clinical Outcomes with Cryotherapies

For procedures performed with the standard tip cooling cryocatheter (e.g., Freezor 3), success rates have been reported to be very high and comparable to RF, with rates ≥84 %. Total cryoprocedure times range from mean time of 126–152 min [24–26]. The most common complication from these standard tip cryo-catheters is the potential for thrombus formation; however, it should be noted that in an in vitro study, it was determined that the rates of thrombus formation associated with cryothermal ablation compared to radiofrequency were significantly less [29].

To date, cryoballoon ablation results have been observed for acute success of PVI to range from 84 to 97 % [35–37]. The long-term success rate is comparable to RF and other balloon technologies, ranging from 60 to 75 % [35–37]. It is important to note that the most frequent complication associated with this therapeutic approach is phrenic nerve palsy (i.e., when specifically ablating the right superior pulmonary vein ostia) [36, 37].

29.4 Utility of Ultrasound Technology

The ultrasound ablation catheter was initially developed to generate transmural myocardial lesions within the ventricles [38], and later was adopted for the isolation of the pulmonary veins. Ultrasound technology may offer benefits over RF for the isolation of pulmonary vein triggers responsible for the initiation of atrial fibrillation; it has been shown to generate well-demarcated lesions with minimal collateral damage to surrounding tissues [38–40]. Additionally, due to the underlying mechanisms of ultrasound ablation, this technology has been shown to be effective regardless of tissue contact, thereby increasing the likelihood of proper lesion formation and PVI [40–42].

29.4.1 Mechanisms of Ultrasound Ablation

Ultrasound waves are created mechanical pressure waves with frequencies used in the medical field, ranging from 20 kHz to 200 MHz, in order to generate thermal heating in a variety of tissues. Commonly, the frequencies used for cardiac ablative procedures range from 1 to 10 MHz, with a frequency of 9 MHz being most commonly used [38, 43, 44]. Two primary mechanisms lead to tissue destruction: (1) the propagation of waves and ensuing oscillation of molecules within cells; and (2) induced acoustic cavitation. The oscillations produce heat and form lesions through coagulative necrosis [43]. Acoustic cavitation is the process in which sound waves elicit intracellular water to briefly enter a gaseous phase, thus forming bubbles within the cell. These bubbles will, in turn, burst and cause pressure waves that mechanically destroy surrounding tissue [38, 39]. It is considered that these two events occur simultaneously and are

histologically indistinguishable; ultrasound lesion formation is most likely caused by composite of both processes [38].

In such therapies, ultrasound waves are focused to concentrate the energy and localize the injury as desired; research has shown that lower frequency unfocused ultrasound does not significantly affect tissues [38]. In cardiac ultrasound treatments, tissue heating ranges from 56 to 80 °C within the sharply demarcated zone of necrosis, while adjacent tissues outside the focal area are nearly unaffected by ultrasound waves [38, 39]. Ultrasound waves are unimpeded by intervening medium and are therefore capable of delivering energy without requiring a need to assess tissue contact [42, 44, 45]. Lesion depth is directly correlated with delivered power as increasing power generates larger lesions [45] (Fig. 29.17).

29.4.2 High-Intensity Focused Ultrasound Balloon Catheter Systems

There are various ultrasound devices intended to focus ultrasound waves for ablation, but currently the most widely used is the high-intensity focused ultrasound balloon catheter (HIFU BC) from ProRhythm (Ronkonkoma, NY, USA; Fig. 29.18) [38, 41, 42, 44, 46]. This catheter has a 9.0 MHz transducing crystal surrounded by a distal balloon that is filled with a 6:1 mixture of water and dye (respectively). This water mixture is circulated around the transducer in a closed circuit to maintain its temperature below 42 °C. The distal balloon is kept inflated by a pressure of 8 PSI. A more proximal balloon is inflated at 1.5 PSI and filled with carbon

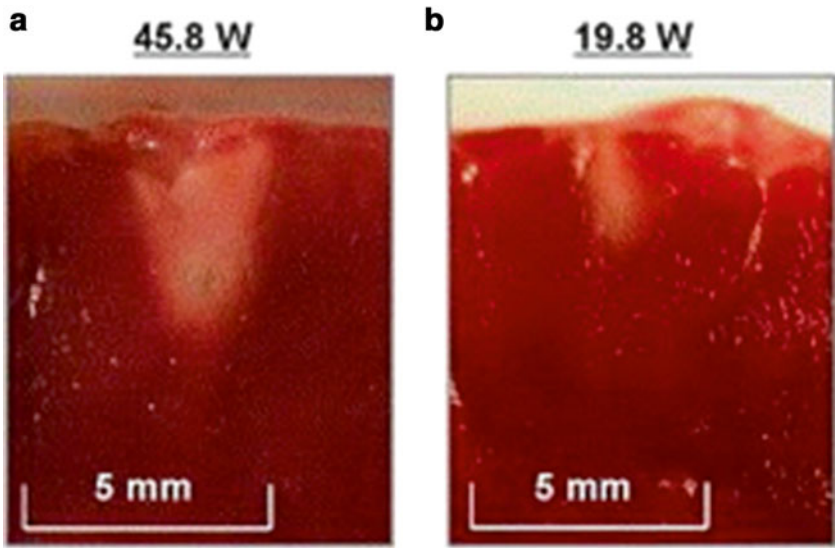

Fig. 29.17 After a fixed duration of ablation, lesion dimensions were strongly impacted by variance of delivered power. Ablations were conducted on prepared muscle sections [45]

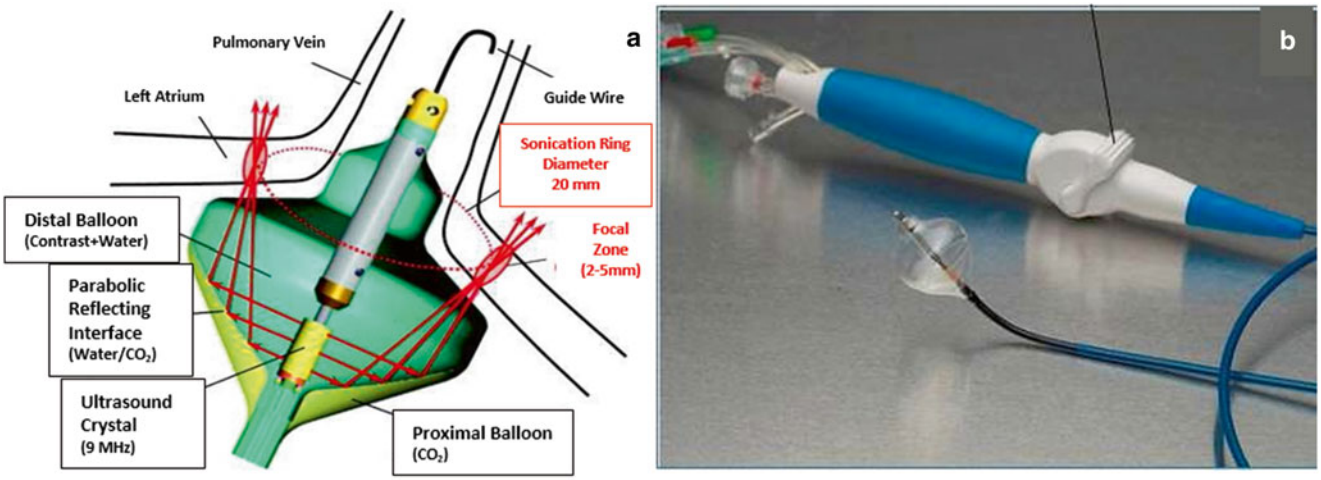

Fig. 29.18 (**a**) Schematic of the catheter tip displaying both balloons, sonicating ring, and relative placement in pulmonary vein ostium [44]. (**b**) Picture of balloon along with catheter handle [38]

dioxide, which acts as a reflector to direct and focus the ultrasound forward. This catheter has a central lumen which allows for guidewire placement to aid in positioning the balloon at the pulmonary vein, and also allows for placement of a recording catheter to ascertain pulmonary vein isolation. The more recent models also feature pull-wires to provide a limited bidirectional deflection. To date, the distal balloon comes in three sizes—24, 27, and 32 mm (diameter)—with a sonicating ring size of 20, 25, and 30 mm (respectively) for each model [38].

Clinical cardiac ablations with HIFU BC are typically conducted between 35 and 45 W using a 9.0 MHz transducer with a standard application of 40 s per ablation [38, 41, 42, 44, 46]. Recent studies have shown that successful pulmonary vein isolation can be achieved with one application, but typically 2–4 applications per pulmonary vein are considered necessary [38, 42]. It is interesting to note that for this approach, mean procedure times range from 127 to 164 min [38, 42].

29.4.3 Complications and Clinical Outcomes Employing HIFU Ablations

There is limited clinical data concerning HIFU BC ablation; however, there have been no reported incidents of thromboembolic events during any previous clinical procedure. The most common procedure-related complication has been induced phrenic nerve palsy, a common issue for balloon catheters when ablating at the right superior pulmonary vein [38, 41, 42, 47]. Nevertheless, it is important to note that an atrial-esophageal fistula occurred in one study [41]. Further, in an independent study assessing the likelihood of esophageal injury from ultrasound technology, investigators found that ablations at the right superior pulmonary vein could potentially result in esophageal fistula if tissue temperatures were allowed to reach ≥50 °C. It has been suggested that this issue could be remedied with careful temperature monitoring of the esophagus and by positioning the transducer further away from the ablation site to reduce penetrance of ultrasound waves to the esophagus [44]. Finally, other complications observed during clinical trials of this technology were hemorrhaging of tissues as a result of the mechanical manipulation of the catheter [42, 46] and an incidence of thrombus formation in one study [38].

The overall success rates for pulmonary vein isolation with HIFU were ≥80 %, with the highest reported percentage of 89 %. Note that the higher percentages were achieved when using the steerable HIFU BC [38, 42, 46, 47]. Successful treatment of atrial fibrillation by ultrasound technology is between 45 and 75 %, with a median value of 60 % [38, 42, 46, 47]. According to statistics, the ultrasound catheter has favorable outcomes for the treatment of atrial fibrillation through pulmonary vein isolation when compared to RF, but it still suffers from a relatively high rate of phrenic nerve palsy and does not completely eliminate the potential for esophageal fistula. Additional trials and continued innovations and refinements of such catheter technologies are ongoing and necessary.

29.4.4 Low-Intensity Collimated Ultrasound System

Recently, the novel robotically controlled low-intensity collimated ultrasound ablation system (LICU®, VytronUS Inc., Sunnyvale CA, USA) has been described. This system is comprised of the following major components: (1) a deflectable transseptal sheath; (2) a robotic tip open-irrigated catheter with an additional manually deflectable section (Fig. 29.19a–c); and (3) an electronic control console (Fig. 29.19d). The deflectable sheath is 13F ID and capable of 135° of deflection. The distal tip of the catheter contains a proprietary LICU® ultrasound transducer that emits a collimated ultrasound beam with well-characterized spatial intensities. Furthermore, the system produces two- and three-dimensional chamber endocardial therapeutic geometries, by robotically scanning the left atrium and pulmonary veins with the ultrasound-equipped catheter tip and spatially registering the ultrasound echo data to the catheter's position without contact between the catheter and the target tissue (Fig. 29.19d, e). On this mapped atrial anatomy, the user determines the desired free-form lesion trajectories that are then automatically ablated under robotic control, i.e., without need for continuous operator manipulations (Fig. 29.19e). It is considered that because the maps and lesion trajectories are all self-referencing and nearly real-time, they are insensitive to external spatial error introduced by normal cardiac motion, fluid intake, etc. Further, a constant ultrasound beam speed at the endocardial surface has been achieved by first scanning the target tissue along the desired trajectory to map the endocardial topography, and then using this data to robotically control the catheter's tip velocity. The highly directional ultrasound beam generates thermal injury by absorption and dissipation of ultrasound energy, as sound waves propagate through the target myocardial tissue. Because of the negligible dissipation of ultrasound energy by blood, lesion formation is insensitive to the distance from the catheter tip to the target tissue.

To date, the catheter has been cooled by saline irrigation during creation of the lesion (Fig. 29.19c). The maximum therapeutic and imaging distances of the LICU® beam are described to be 17 and 40 mm, respectively. An example of a pulmonary vein isolating lesion generated by this system is shown in Fig. 29.19f. Currently, this catheter is in the preclinical stage of testing and therefore there has been no clinical data to report.

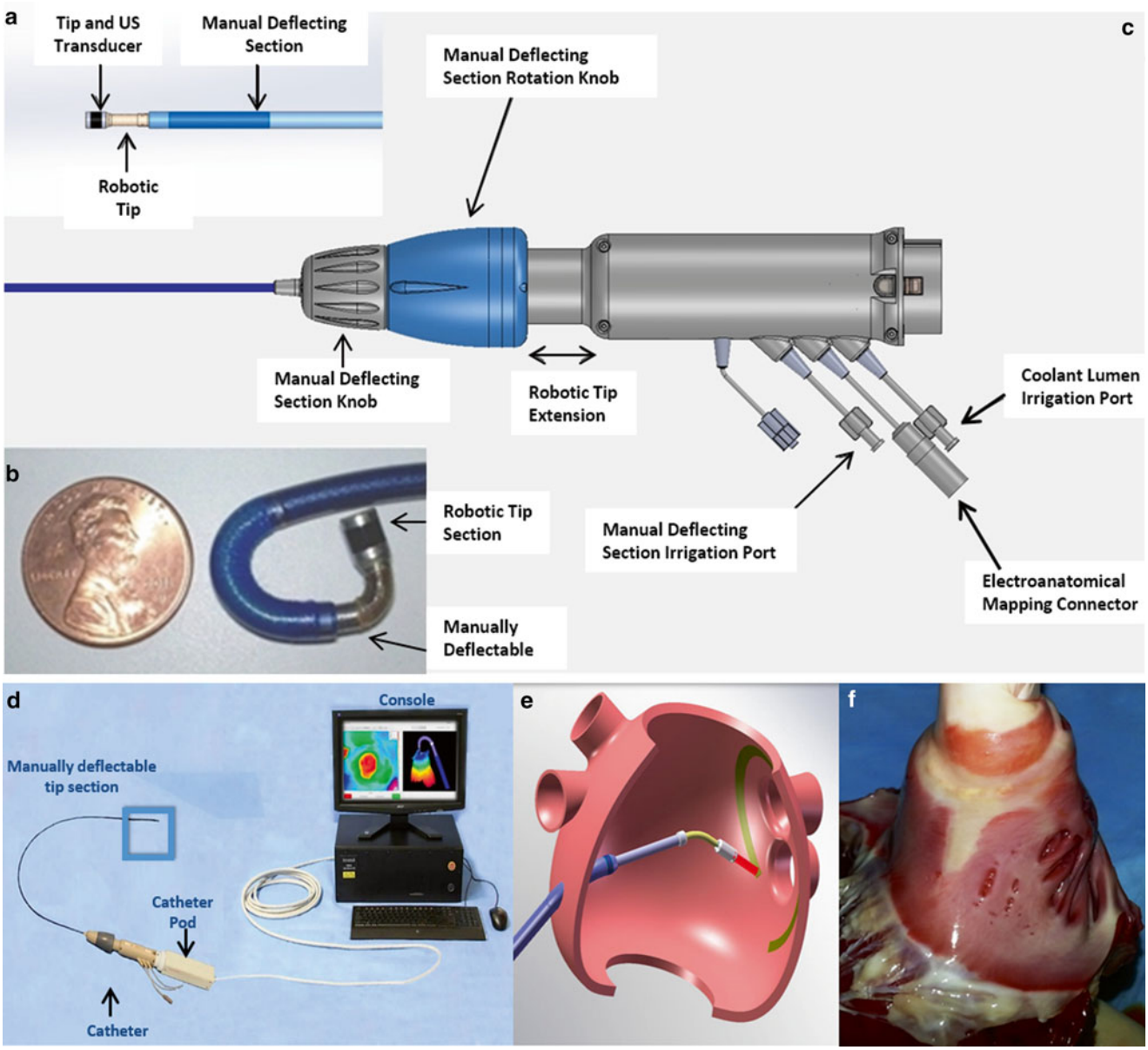

Fig. 29.19 (**a–c**) Components of ultrasound mapping and ablation system. (**d**) Schematic of LICU catheter inside the left atrium demonstrating the robotically controlled ablation. (**e**) Example of post-pulmonary vein isolation lesion. (**f**) Example of a pulmonary vein isolating lesion. *Source*: Avitall lecture, "Redefining Ablation," VytronUS, Chicago, IL, January 2014

29.5 Microwave Energy

Another technology that has been described as a potential alternative to RF for cardiac ablation is microwave. One potential advantage of microwave technology is the ability of this energy source to create larger and deeper lesions without the need for tissue contact. Furthermore, it is not limited by concerns of coagulum formation, since it does not operate as a circuit (it does not require a grounding pad) and is not significantly affected by intervening medium (blood, fat) [48, 49]. Microwave ablation relative to the heart was initially intended for ablations of ventricular tachycardia; however, more recently atrial tissues have been ablated as well [49–53].

29.5.1 Mechanisms of Cardiac Microwave Ablation

The mechanism of heat generation associated microwave technology is referred to as *dielectric hysteresis*. Electromagnetic waves produced through microwave appli-

cations induce polar inversions at rapid speeds, i.e., billions of inversions per second (30–3,000 MHz) in polar molecules such as water. As ions and other polar molecules oscillate with the electromagnetic field kinetic energy is increased and, as a consequence, tissue temperatures rapidly increase [5, 54]. Yet, the mechanism of heat generation is dependent on the applied: (1) electric field frequency; (2) dielectric constant; and (3) conductivity of material absorbing the electromagnetic waves (Fig. 29.20a). Note that the water content of biological tissues (~70 % of cellular mass, on average) provides both high dielectric current and good conductivity. The result is high absorption of energy from microwaves.

Microwave lesions have been shown to be well demarcated with more uniform tissue heating (Fig. 29.20b). Further, tissue ablations utilizing microwave energy have been noted, when temperature is kept constant, to have a greater volumetric penetrance than RF lesions [48, 55]. However, it has also been reported that as microwave frequencies increase, lesion depths will in turn decrease. Nevertheless, when considering cardiac ablation, the increased volumetric heating of microwave technologies should, in theory, result in fewer applications and reduced procedure times. One notable and important consequence of the increased volumetric heating is an increased risk of thrombus formation as a result of boiling blood. The functioning of microwave catheters is not affected by the formation of coagulum, so care must be taken to prevent char formation and the potential embolism [48].

29.5.2 Current Microwave Generators

There are two types of generators that have been employed to date to power microwave technologies. The most commonly used generator is known as a magnetron; this system generates energy by rapidly accelerating electrons within a resonant cavity using magnetic fields. More specifically, the geometry of the resonant cavity determines the power output capabilities; magnetrons are capable of outputting power levels ≥10 kW (Fig. 29.21a). This system has reported a 70 % efficiency rate, but can be expensive to produce and maintain [54]. A second type of generator is a steady-state amplifier that generates power through a series of steps, with each step amplifying power. This kind of generator is less

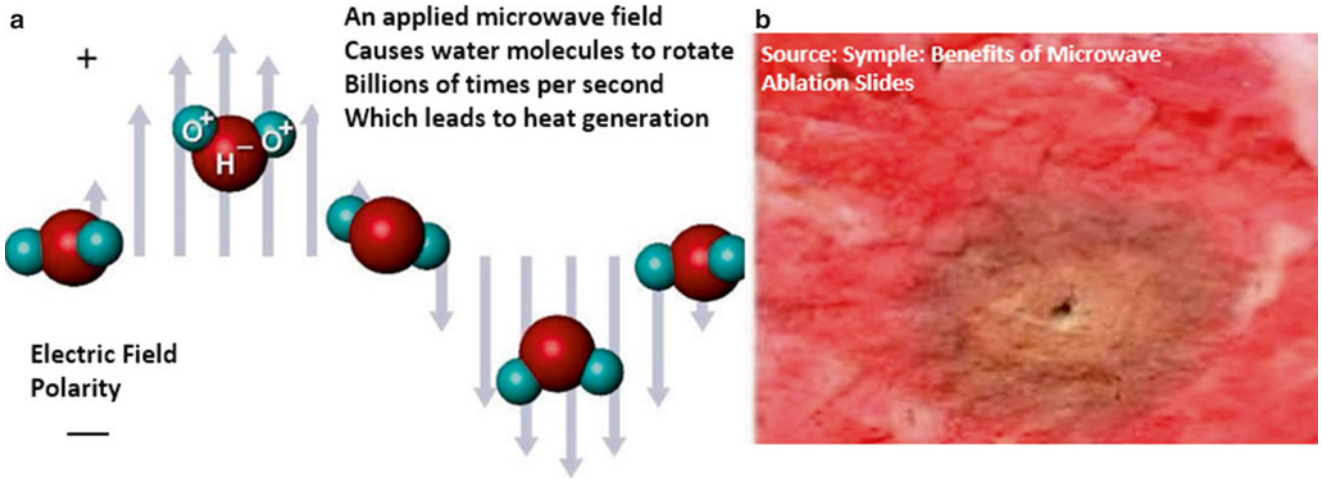

Fig. 29.20 (**a**) Mechanism of tissue heating from electromagnetic waves [54]. (**b**) Microwave lesion on porcine lung. *Source*: Symple, Benefits of Microwave Ablation Slides

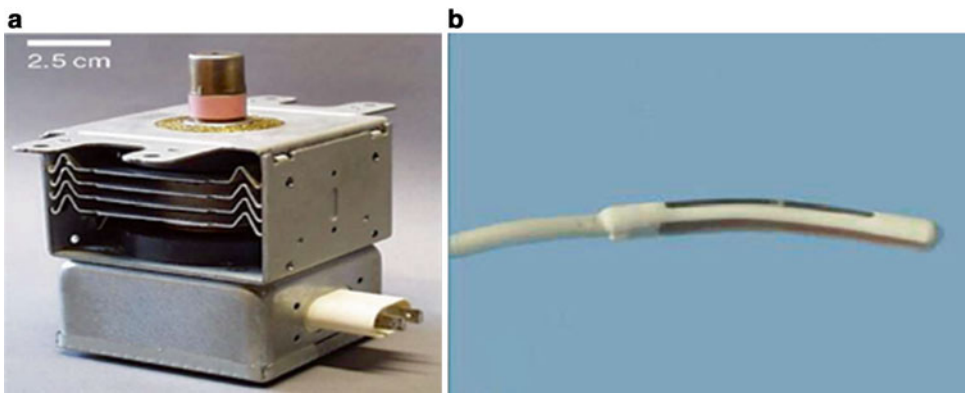

Fig. 29.21 (**a**) Magnetron generator for microwave ablation [54]. (**b**) Flex 4 Microwave Catheter from AFx Inc. (Fremont, CA, USA). *Source*: http://www.revespcardiol.org/en/ablation-of-permanent-atrial-fibrillation/articulo/13066579/

efficient and, as a result, suffers from overheating and lower power outputs (150 W); yet, the system's power outputs are lower and easier to manipulate [54].

29.5.3 Microwave Ablation Catheters

The primary components of a microwave catheter are the antenna and coaxial capable. The coaxial cable is composed of an inner and outer conductor separated by a dielectric material and wrapped in an insulating jacket [54]. An issue seen in early models was leakage of electromagnetic waves that resulted in hotspot radiation along the cable, such as the percutaneous entry or at the catheter lead plug-in. Radiation leakage can cause heating in areas that are removed from the microwave antenna. The use of more durable and insulating materials such as Teflon is proposed to fix this issue [56]. The diameter ultimately controls the level of power delivery possible with larger diameters, allowing greater power outputs [54]; a typical diameter of 2.44 mm is seen [56].

The microwave antenna acts as the catheter tip (Fig. 29.21b). The antenna has a range of sizes that have been employed in clinical testing, ranging from 5 mm to 4 cm, and is typically composed of copper [48–53, 55, 56]. The geometry of the antenna controls how power distribution is focused, the frequency at which waves propagate, and how much power reflects back onto the catheter.

Electromagnetic waves rebound to varying degrees back onto the antenna which can cause heating of the antenna and cable. Heating of the cable and antenna can lead to unanticipated burns to the patient and may damage the system. While antenna geometry varies, the most common variation is a helical loop which has been shown to allow better energy focus, be less invasive, and mitigate power reflection to ≤10 W [48, 50, 55]. Greater power has been shown to lead to deeper lesion formation; however, increasing power output must be done cautiously as increasing power results in greater reflected power and incidental heating as mentioned above [51].

One of the important factors for lesion formation by a microwave antenna is that lesion formation is independent of contact and minimally impacted by orientation [48]. Ablations are conducted in a power range of 20–75 W, with a preferred operating power around 50 W and frequency ranges from 1 to 3 GHz, with an operating frequency of 2.45 GHz being most common. Ablations are conducted from 60 to 120 s [49–51]. A study found that lesion formation is progressive and consecutive ablations at the same site result in increases in lesion size [51]. A clinical study determined that 25 s of ablation at a frequency of 2.45 GHz and 45 W power was sufficient to produce 3–5 mm deep lesions during open-heart surgery [53].

29.5.4 Complications and Clinical Applications

With this therapeutic approach, the risk of charring and coagulum formation during ablation is considered to be minimal and, while thrombus formation may be a concern, there have been no reported incidents [48, 53, 55, 57]. One needs to be aware that reflected power heating of the antenna is another issue, but careful temperature monitoring at the probe can alleviate this concern [51]. Additionally, leakage of electromagnetic waves along the coaxial delivery system, e.g., from insufficient insulation, can result in unintentional heating to both the system and the patient affected anatomy [51, 54].

To date, published research has focused on microwave technologies for the treatment of atrial fibrillation. An overall success rate of conversion and retention to normal sinus rhythm was reported to be within the range of 65.6–88 %, with the most common values ≥80 % [52, 53, 57, 58]. In one reported single randomized study (for treatment of paroxysmal atrial fibrillation), researchers compared RF to microwave therapeutic technologies and noted that the RF approach elicited superior outcomes, with 81.3 % of patients returning to sinus rhythm compared to 65.6 % for microwave ablation. Yet, is should be noted that a commonality among all such described studies was the distinct lack of procedural complications associated with the use of the microwave catheter systems and, importantly, there were no reported deaths [52, 53, 57, 58]. In other words, while the apparent safety of the microwave ablation system is very high, the overall effectiveness is comparable but may be a bit less than RF ablation.

29.6 Balloon Laser Catheter: Endoscopic Ablation System

The endoscopic ablation system (EAS) utilizes a balloon catheter that uses laser energy for the elicitation of ablation therapy. Typically, it has been used to treat paroxysmal atrial fibrillation by ablating the pulmonary vein tissues which are considered capable of inducing atrial fibrillation. The novelty of this approach versus technologies like cryoballoon therapy is that an endoscope built into the balloon catheter system also allows for direct visualization of the pulmonary ostium during treatment; in theory, this provides some visual assessment of the ablation process and may insure lesion contiguity, resulting in more effective pulmonary vein isolations.

The current rendition of this catheter is nonsteerable and requires the use of a 12F deflectable sheath for proper positioning. Importantly, the therapeutic power is titratable, thus

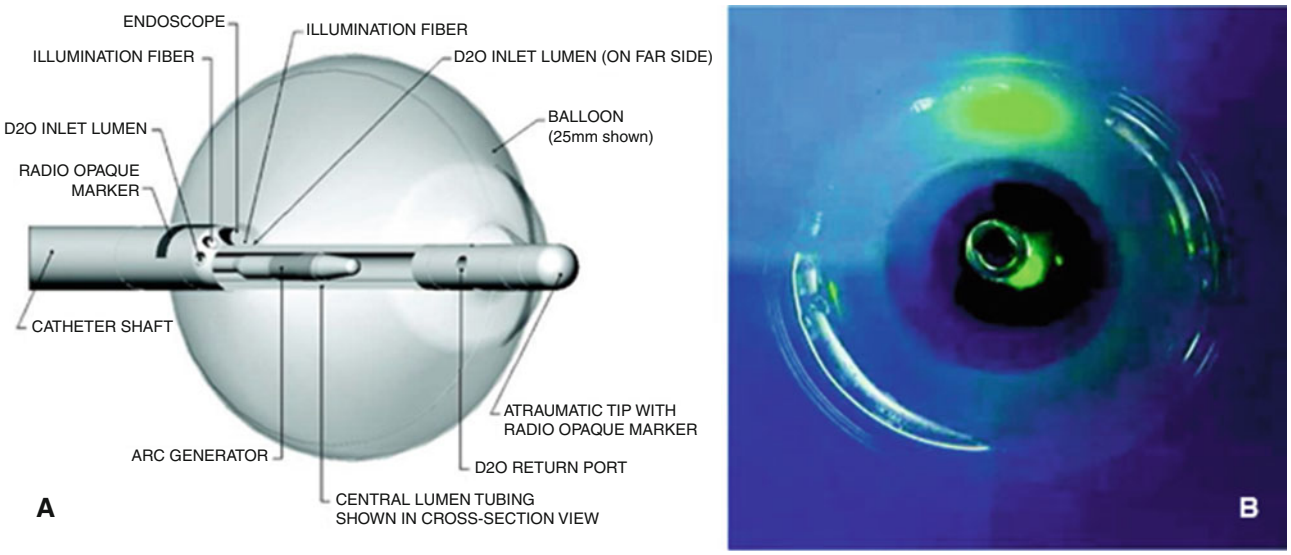

Fig. 29.22 (**A**) Balloon laser catheter and components [50]. (**B**) Head on view of distal end of catheter [50]

allowing for the potential to control lesion formation. To date, compliant balloons with a variety of sizes are available, providing additional flexibility for treating the known variable pulmonary vein anatomies seen in atrial fibrillation patients. It should be noted that, as of this writing, the EAS system has been tested at the clinical level, but has yet to be approved for clinical use.

29.6.1 The Endoscopic Laser Ablation System

The current design of the cardiac laser ablation system employs: (1) a 12F catheter which houses a central lumen that circulates, in a closed loop, deuterium oxide (heavy water); (2) a 2F endoscope, an illumination fiber (for the endoscope); and (3) an arc generator with a 980 nm diode that creates the laser energy (Fig. 29.22). More specifically, the distal end has a balloon made of compliant material that can increase, in nine inflation steps, from a base of 9–35 mm (approximately 3 mm per step). Balloon inflation and the final shape are maintained via fluid pressure from the delivered deuterium oxide. The current system has an atraumatic tip with a radiopaque marker for orientation purposes; this forms the distal most end of the catheter. It should be noted that the tip designs and radiopaque markers were integrated from user key opinion leaders' feedback relative to the previous tips causing mechanical damage and difficult orientation issues with the blind spot created by the catheter shaft [59, 60].

This system's catheter handle design provides controls for the orientation of the arc generator. More specifically, the arc generator can be moved both distally and proximally and can be rotated, allowing laser energy to create a completely circumferential lesion. This system utilizes a work station that: (1) connects to the catheter; (2) houses the deuterium supply; (3) contains the laser power generator; and (4) contains a white light source (for illumination fiber). All controls and endoscopic displays are run through the work station, at which they are manipulated using a touchscreen with a two panel display (Fig. 29.23). One panel provides a live feed from the endoscope, while the other panel displays a frozen reference image of the last ablation site. This setup was created from feedback about noted difficulties in producing linear lesions with the use of the live endoscopic view only. Further, on the current system, touch controls are available to adjust: (1) the output power (wattage from 5.5 to 12 W); (2) time intervals (typical ablations lasting 20 or 30 s); and (3) balloon inflation parameters (minimum 9 mm, maximum 35 mm). To aid the user, snapshots of previous lesions are stored in the system and can be accessed at any time during an ongoing procedure [59].

29.6.2 Laser Energy and Cardiac Ablations

In general, laser energy is considered to provide a volumetric heating of tissue. As the ablation proceeds, laser energy passes through the arc generator in a direction perpendicular to the catheter in a 30° arc. In theory, laser energy passes unabsorbed through the deuterium oxide, but is absorbed by water in tissues and blood. As this energy hits tissues, it will penetrate beyond the endothelial strata, and ultimately most of the delivered energy will be absorbed by the endocardium. Note that water molecules absorbing laser energy lead to vaporization and incidental heating; coagulation necrosis occurs at these contact sites. Conductive heating allows heat to penetrate the deeper layers and can lead to lesions as deep as 12 mm, as

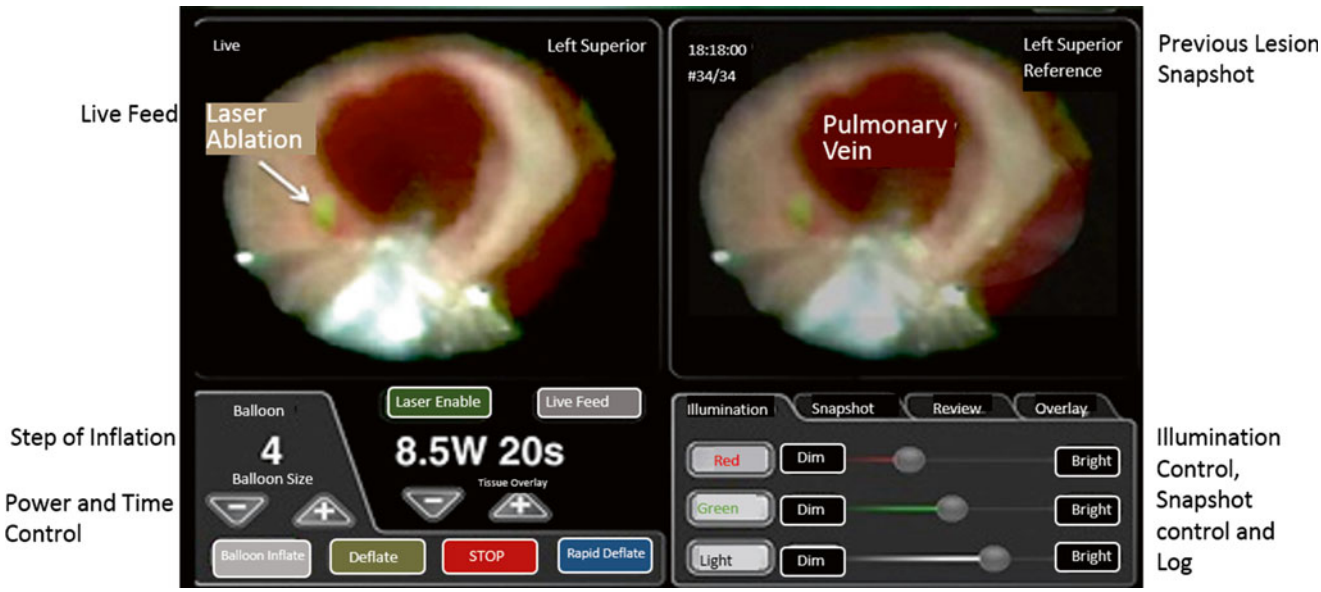

Fig. 29.23 Touchscreen display of the endoscopic ablation system for a laser balloon catheter [59]

were previously observed within canine model studies by Reddy et al. [61]. With this therapeutic approach, the titration of energy delivery is possible by varying wattage at the EAS console (5.5–12 W). Importantly, because the endocardium absorbs most of the laser energy and the endothelium rests in contact with a deuterium-filled balloon, the probability of charring and thrombus is reduced; canine studies by Reddy et al. revealed no left atria lesions with char [61].

Laser energy can be delivered in an arc of 30° and, for proper therapeutic application, will require manipulation of the arc generator throughout rotations to create a circumferential lesion. As such, using the console's dual display capabilities, the user will overlap lesions by rotating the laser arc. The radiopaque materials built into the catheter tip have been noted to help the user orient the laser arc in relation to the blind spot produced by the catheter shaft. Nevertheless, with this current technology, in order to account for the blind spot, the balloon needs to be rotated at least 90° to finish creating a full circumferential lesion [62, 63]. Lesions produced by the EAS system have been shown to be homogenous, well-demarcated, and occur with minimal disruption of tissues and charring.

An additional benefit observed from the procedural use of the EAS system has been the ability to visualize the ablation site and determine if arc will primarily hit tissues or blood. More specifically, light coming from the fiber optics cable is reflected back by tissues. In other words, the wavelengths of reflected light differ within tissue and blood; both reflect red light, but tissue also reflects green light. Thus, when focused on blood only, red light is seen; when focused on tissue wavelengths, red and green cancel and the yellow spectrum can be detected. Therefore, this allows the operators to distinguish if the ablation tip is too distant to the tissue, as only red light will be reflected. Using this method, a distinct area and distance from tissue can be determined prior to ablation [61].

29.6.3 Clinical Use and Safety Aspects of Laser Cardiac Ablation

Early clinical trials have suggested that the therapeutic use of EAS has efficacy and safety levels comparable to other currently employed AF ablation systems [61, 64]. Furthermore, with this approach, chronic pulmonary vein isolation occurs with high percentage in single procedure ablations, with rates ≥90 % [60, 61, 65, 66]. Many of these PVIs can be done solely using the EAS system, but it should be noted that certain pulmonary veins may require additional mapping and ablations using RF catheters [63]. Success rates for treating paroxysmal atrial fibrillation with laser ablation were noted to range from 60 to 70 %, a rate comparable to treatment with RF technologies [61]. Despite current successes, there was a rather high incidence of cardiac tamponade and phrenic nerve palsy associated with such laser procedures [60–63]. It was considered that the implementation of redesigned atraumatic catheter tips, in response to the high incidence of tamponade, should reduce these problems; clinical trials have yet to determine if this was a sufficient modification to prevent complications. Additionally, the current laser ablation system does not feature mapping electrodes, so there is no real-time electrophysiological monitoring of pulmonary vein isolation. Thus, operators rely on visualization of tissue to create full circumferential lesions. Therefore, in current clinical applications, after completing an ablation for PVI,

one needs to determine therapeutic results using additional multielectrode recording catheters.

To date, procedure times using this technological approach have been long, ranging from an average of 250–278 min [60, 61]. Additionally, during the application of laser ablation, temperature monitoring of the esophagus is considered to be necessary to prevent extracardiac damage [60]. It has been suggested that pacing of the phrenic nerve is of value, to prevent the elicitation of phrenic nerve palsy. It has also been noted that extra caution is needed when ablating near mapping catheters. More specifically, there have been reported incidents where the balloon of the EAS overheats and is, in turn, damaged when ablation was performed in close proximity to mapping catheters [62].

29.7 Summary

Technologies for the treatment of cardiac arrhythmias continue to develop at a rapid pace, with some system approaches employing automation (robotics) and others that have greatly improved the usability by clinicians. These technologies are highly variable and provide unique advantages and disadvantages that make them each more suitable in specific therapeutic circumstances. The evolution of these ablative technologies is driven by the variety of obstacles clinicians encounter which include (but are not limited to): (1) the potential to induce stroke and/or extracardiac damage; (2) lesion efficiency issues; (3) anatomical obstruction or accessibility limitations; (4) the relative lack of accurate localization and/detection of the underlying mechanisms of the dysrhythmic source; and (5) current limited mapping and navigation capabilities. An additional factor that is becoming increasingly important is the cost of the therapy versus the anticipated likelihood of successful procedural outcome. In this chapter, we reviewed the current application of RF and cryothermal ablation technologies, and we also discussed various ultrasound, microwave, and laser balloon ablation technologies that are being developed.

References

1. Avitall B, Khan M, Krum D et al (1993) Physics and engineering of transcatheter cardiac tissue ablation. J Am Coll Cardiol 22:921–932
2. Aliot EM, Stevenson WG, Almendral-Garrote JM et al (2009) EHRA/HRS expert consensus on catheter ablation of ventricular arrhythmias. Heart Rhythm 6:886–933
3. Eick OJ (2003) Factors influencing lesion formation during radiofrequency catheter ablation. Indian Pacing Electrophysiol J 3:117–128
4. Haines DE (1993) The biophysics of radiofrequency catheter ablation in the heart: the importance of temperature monitoring. Pacing Clin Electrophysiol 16:586–591
5. Avitall B, Mughal K, Hare J, Helms R, Krum D (1997) The effects of electrode-tissue contact on radiofrequency lesion generation. Pacing Clin Electrophysiol 20:2899–2910
6. Nakagawa H, Yamanashi WS, Pitha JV et al (1995) Comparison of in vitro tissue temperature profile and lesion geometry for radiofrequency ablation with a saline-irrigated electrode versus temperature control in a canine thigh muscle preparation. Circulation 91:2264–2273
7. Chan RC, Johnson SB, Seward JB et al (2002) The effect of ablation electrode length and catheter tip to endocardial orientation on radiofrequency lesion size in the canine right atrium. Pacing Clin Electrophysiol 25:4–13
8. Dorwarth U, Fiek M, Remp T et al (2003) Radiofrequency catheter ablation: different cooled and noncooled electrode systems induce specific lesion geometries and adverse effects profiles. Pacing Clin Electrophysiol 26:1438–1445
9. Akca F, Hubay M, Zima E et al (2014) High-volume lesions using a new second-generation open irrigation radiofrequency catheter are associated with the development of inhomogeneous lesions. Pacing Clin Electrophysiol 37:864–873
10. Martinek M, Lemes C, Sigmund E et al (2012) Clinical impact of an open-irrigated radiofrequency catheter with direct force measurement on atrial fibrillation ablation. Pacing Clin Electrophysiol 35:1312–1318
11. Issa Z, Miller JM, Zipes DP (2009). In: Issa Z (ed) Clinical arrhythmology and electrophysiology: a companion to Braunwald's heart disease. Philadelphia, Elsevier, p 487
12. Avitall B, Singh I, Arora P et al (2012) Novel ablation catheter technology that improves mapping resolution and monitoring of lesion maturation. J Innov Cardiac Rhythm Manag 3:599–609
13. Watanabe I, Masaki R, Min N et al (2002) Cooled-tip ablation results in increased radiofrequency power delivery and lesion size in the canine heart: importance of catheter tip temperature monitoring for prevention of popping and impedance rise. J Interv Card Electrophysiol 6:9–16
14. Wijffels MC, Van Oosterhout M, Boersma LV et al (2009) Characterization of in vitro and in vivo lesions made by a novel multichannel ablation generator and a circumlinear decapolar ablation catheter. J Cardiovasc Electrophysiol 20:1142–1148
15. Boersma LV, Wijffels MC, Oral H, Wever EF, Morady F (2008) Pulmonary vein isolation by duty-cycled bipolar and unipolar radiofrequency energy with a multielectrode ablation catheter. Heart Rhythm 5:1635–1642
16. Gaita F, Leclercq JF, Schumacher B et al (2011) Incidence of silent cerebral thromboembolic lesions after atrial fibrillation ablation may change according to technology used: comparison of irrigated radiofrequency, multipolar nonirrigated catheter and cryoballoon. J Cardiovasc Electrophysiol 22:961–968
17. Weiss C, Antz M, Eick O, Eshagzaiy K, Meinertz T, Willems S (2002) Radiofrequency catheter ablation using cooled electrodes: impact of irrigation flow rate and catheter contact pressure on lesion dimensions. Pacing Clin Electrophysiol 25:463–469
18. Shake JG, Larson DW, Salerno CT, Bianco RW, Bolman RM III (1997) The role of electrolyte in lesion size using an irrigated radio frequency electrode. J Invest Surg 10:339–348
19. Demazumder D, Mirotznik MS, Schwartzman D (2001) Biophysics of radiofrequency ablation using an irrigated electrode. J Interv Card Electrophysiol 5:377–389
20. Nakagawa H, Kautzner J, Natale A et al (2013) Locations of high contact force during left atrial mapping in atrial fibrillation patients: electrogram amplitude and impedance are poor predictors of electrode-tissue contact force for ablation of atrial fibrillation. Circ Arrhythm Electrophysiol 6:746–753
21. Thiagalingam A, D'Avila A, Foley L et al (2010) Importance of catheter contact force during irrigated radiofrequency ablation:

evaluation in a porcine ex vivo model using a force-sensing catheter. J Cardiovasc Electrophysiol 21:806–811
22. Yokoyama K, Nakagawa H, Shah DC et al (2008) Novel contact force sensor incorporated in irrigated radiofrequency ablation catheter predicts lesion size and incidence of steam pop and thrombus. Circ Arrhythm Electrophysiol 1:354–362
23. Kuck KH, Reddy VY, Schmidt et al (2011) A novel radiofrequency ablation catheter using contact force sensing: Toccata study. Heart Rhythm 9:18–23
24. Jensen-Urstad M, Tabrizi F, Kennebäck G, Wredlert C, Klang C, Insulander P (2006) High success rate with cryomapping and cryoablation of atrioventricular nodal reentry tachycardia. Pacing Clin Electrophysiol 29:487–489
25. Schwagten B, Knops P, Janse P et al (2011) Long-term follow-up after catheter ablation for atrioventricular nodal reentrant tachycardia: a comparison of cryothermal and radiofrequency energy in a large series of patients. J Interv Card Electrophysiol 30:55–61
26. Bastani H, Drca N, Insulander P et al (2013) Cryothermal vs. radiofrequency ablation as atrial flutter therapy: a randomized comparison. Europace 15:420–428
27. Wadhwa MK, Rahme MM, Dobak J et al (2000) Transcatheter cryoablation of ventricular myocardium in dogs. J Interv Card Electrophysiol 4:537–546
28. Collins NJ, Barlow M, Varghese P, Leitch J (2006) Cryoablation versus radiofrequency ablation in the treatment of atrial flutter trial (CRAAFT). J Interv Card Electrophysiol 16:1–5
29. Khairy P, Chauvet P, Lehmann J et al (2003) Lower incidence of thrombus formation with cryoenergy versus radiofrequency catheter ablation. Circulation 107:2045–2050
30. Shepherd JP, Dawber RP (1984) Wound healing and scarring after cryosurgery. Cryobiology 21:157–169
31. Gage AA, Guest K, Montes M, Caruana JA, Whalen DA Jr (1985) Effect of varying freezing and thawing rates in experimental cryosurgery. Cryobiology 22:175–182
32. Lustgarten DL, Keane D, Ruskin J (1999) Cryothermal ablation: mechanism of tissue injury and current experience in the treatment of tachyarrhythmias. Prog Cardiovasc Dis 41:481–498
33. Andrade JG, Khairy P, Dubuc M (2013) Advances in arrhythmia and electrophysiology. Circulation 6:218–227
34. Weimar T, Lee AM, Ray S, Schuessler RB, Damiano RJ (2012) Evaluation of a novel cryoablation system: in-vitro testing of heat capacity and freezing temperatures. Innovations 7:403–409
35. Sarabanda AV, Bunch TJ, Johnson SB et al (2005) Efficacy and safety of circumferential pulmonary vein isolation using a novel cryothermal balloon ablation system. J Am Coll Cardiol 46:1902–1912
36. Neumann T, Vogt J, Schumacher B et al (2008) Circumferential pulmonary vein isolation with the cryoballoon technique: results from a prospective 3-Center study. J Am Coll Cardiol 52:273–278
37. Van Belle Y, Janse P, Rivero-Ayerza MJ et al (2007) Pulmonary vein isolation using an occluding cryoballoon for circumferential ablation: feasibility, complications, and short-term outcome. Eur Heart J 28:2231–2237
38. Schmidt B, Chun KR, Kuck KH, Antz M (2007) Pulmonary vein isolation by high-intensity focused ultrasound. Indian Pacing Electrophysiol J 7:126–133
39. Chen L, Rivens I, ter Haar G, Riddler S, Hill CR, Bensted JP (1993) Histological changes in rat liver tumours treated with high-intensity focused ultrasound. Ultrasound Med Biol 19:67–74
40. Fujikura K, Otsuka R, Kalisz A et al (2006) Effects of ultrasonic exposure parameters on myocardial lesions induced by high-intensity focused ultrasound. J Ultrasound Med 25:1375–1386
41. Neven K, Schmidt B, Metzner A et al (2010) Fatal end of a safety algorithm for pulmonary vein isolation with use of high-intensity focused ultrasound. Circ Arrhythm Electrophysiol 3:260–265
42. Schmidt B, Chun KR, Metzner A, Fuernkranz A, Ouyang F, Kuck KH (2009) Pulmonary vein isolation with high-intensity focused ultrasound: results from the HIFU 12F study. Europace 11:1281–1288
43. He DS, Zimmer JE, Hynynen K et al (1994) Preliminary results using ultrasound energy for ablation of the ventricular myocardium in dogs. Am J Cardiol 73:1029–1031
44. Yokoyama K, Nakagawa H, Seres KA et al (2009) Canine model of esophageal injury and atrial-esophageal fistula after applications of forward-firing high-intensity focused ultrasound and side-firing unfocused ultrasound in the left atrium and inside the pulmonary vein. Circ Arrhythm Electrophysiol 2:41–49
45. Engel DJ, Muratore R, Hirata K et al (2006) Myocardial lesion formation using high-intensity focused ultrasound. J Am Soc Echocardiogr 19:932–937
46. Nakagawa H, Antz M, Wong T et al (2007) Initial experience using a forward directed, high intensity focused ultrasound balloon catheter for pulmonary vein antrum isolation in patients with atrial fibrillation. J Cardiovasc Electrophysiol 18:136–144
47. Natale A, Pisano E, Shewchik J et al (2000) First human experience with pulmonary vein isolation using a through-the-balloon circumferential ultrasound ablation system for recurrent atrial fibrillation. Circulation 102:1879–1882
48. Langberg JJ, Wonnel TL, Chin MC, Finkbeiner W, Scheinnman MM, Stauffer PR (1991) Catheter ablation of the atrioventricular junction using a helical microwave antenna: a novel means of coupling energy to the endocardium. Pacing Clin Electrophysiol 14:2105–2113
49. Liem LB, Mead RH (1998) Microwave linear ablation of the isthmus between the inferior vena cava and tricuspid annulus. Pacing Clin Electrophysiol 21:2079–2086
50. Iwasa A, Storey J, Yao B, Liem LB, Feld GK (2004) Efficacy of a microwave antenna for ablation of the tricuspid valve – inferior vena cava isthmus in dogs as a treatment for Type 1 atrial flutter. J Cardiovasc Electrophysiol 10:191–198
51. Liem LB, Mead RH, Shenasa M et al (1996) In vitro and in vivo results of transcatheter microwave ablation using forward firing tip antenna design. Pacing Clin Electrophysiol 19:2004–2008
52. Lin Z, Shan ZG, Liao CX, Chen LW (2011) The effect of microwave and bipolar radio-frequency ablation in the surgical treatment of permanent atrial fibrillation during valve surgery. Thorac Cardiovasc Surg 59:460–464
53. Schuetz A, Schulze CJ, Sarvanakis KK et al (2003) Surgical treatment of permanent atrial fibrillation using microwave energy ablation: a prospective randomized clinical trial. Eur J Cardiothorac Surg 24:475–480
54. Brace CL (2009) Microwave ablation technology: what every user should know. Curr Probl Diagn Radiol 38:61–67
55. Wonnell TL, Stauffer PR, Langberg JJ (1992) Evaluation of microwave and radiofrequency catheter ablation in a myocardium-equivalent phantom model. IEEE Trans Biomed Eng 39:1086–1095
56. Nevels RD, Arndt GD, Raffoul GW, Carl JR, Pacifico A (1998) Microwave catheter design. IEEE Trans Biomed Eng 45:885–890
57. Wisser W, Khazen C, Deviatko E et al (2004) Microwave and radiofrequency ablation yield similar success rates for treatment of chronic atrial fibrillation. Eur J Cardiothorac Surg 25:1011–1017
58. Knaut M, Tugtekin SM, Jung F, Matschke K (2004) Microwave ablation for the surgical treatment of permanent atrial fibrillation—a single centre experience. Eur J Cardiothorac Surg 26:742–746
59. Bordignon S, Chun KR, Gunawardene M et al (2013) Endoscopic ablation systems. Expert Rev Med Devices 10:177–183
60. Schmidt B, Metzner A, Chun KR et al (2010) Feasibility of circumferential pulmonary vein isolation using a novel endoscopic ablation system. Circ Arrhythm Electrophysiol 3:481–488
61. Reddy VY, Neuzil P, Themistoclakes S et al (2009) Visually-guided balloon catheter ablation of atrial fibrillation: experimental feasibility and first in-human multicenter clinical outcome. Circulation 120:12–20

62. Schade A, Krug J, Szollosi A, El Tarahony M, Deneke T (2012) Pulmonary vein isolation with a novel endoscopic ablation system using laser energy. Expert Rev Cardiovasc Ther 10:995–1000
63. Reddy VY, Houghtaling C, Fallon J et al (2004) Use of a diode laser balloon ablation catheter to generate circumferential pulmonary venous lesions in an open-thoracotomy caprine model. Pacing Clin Electrophysiol 27:52–57
64. Phillips KP, Schweikert RA, Saliba WI et al (2008) Anatomic location of pulmonary vein electrical disconnection with balloon-based catheter ablation. J Cardiovasc Electrophysiol 9:14–18
65. Themistoclakis S, Wazni OM, Saliba W et al (2006) Endoscopic fiberoptic assessment of the balloon occlusion of the pulmonary vein ostium in humans: comparison with phased-array intracardiac echocardiography. Heart Rhythm 3:44–49
66. Reddy VY, Neuzil P, d'Avila A et al (2008) Balloon catheter ablation to treat paroxysmal atrial fibrillation: what is the level of pulmonary venous isolation? Heart Rhythm 5:353–360

Pacing and Defibrillation

30

Timothy G. Laske, Anna Legreid Dopp,
Michael D. Eggen, and Paul A. Iaizzo

Abstract

Pacing and defibrillation systems monitor and treat inappropriate cardiac rhythms. In general, these inappropriate rhythms result in cardiac outputs that are inadequate to meet metabolic demands, and thus can be life-threatening. In order to best understand the function of such pacing and defibrillation systems, the underlying physiologic situations indicated for their use must also be defined and understood. Furthermore, as with the design of any biomedical device or system, a *first principles* understanding of the appropriate physiologic behavior is a prerequisite to the definition of the performance characteristics of the device. This chapter primarily aims to provide a basic understanding of the physiologic conditions that require intervention with pacing and/or defibrillation systems, as well as introduce technical information about these systems to provide the reader with a foundation for future research and reading on this topic.

Keywords

Cardiac pacing • Defibrillation • Cardiac arrhythmia • Electrical stimulation • Antiarrhythmic drugs • Drug interactions • Implantable pulse generator • Implantable cardioverter defibrillator • Leadless pacemaker

Electronic supplementary material The online version of this chapter (doi:10.1007/978-3-319-19464-6_30) contains supplementary material, which is available to authorized users.

T.G. Laske, PhD (✉)
Department of Surgery, University of Minnesota, Minneapolis, MN, USA

Medtronic plc, 8200 Coral Sea Street NE, MVS 46, Minneapolis, MN 55112, USA

Pharmacy Society of Wisconsin, Madison, WI, USA
e-mail: tim.g.laske@medtronic.com

A.L. Dopp, PharmD
Pharmacy Society of Wisconsin, Madison, WI, USA

M.D. Eggen, PhD
Department of Surgery, University of Minnesota, Minneapolis, MN, USA

Medtronic plc, 8200 Coral Sea Street NE, MVS 46, Minneapolis, MN 55112, USA

P.A. Iaizzo, PhD
Department of Surgery, University of Minnesota, Minneapolis, MN, USA

30.1 Introduction

Pacing and defibrillation systems both monitor and treat inappropriate cardiac rhythms. In general, these inappropriate rhythms result in cardiac outputs that are inadequate to meet metabolic demands, and thus can be life-threatening. Currently, over 600,000 Americans have pacemakers and 150,000 have implantable cardioverter defibrillators (ICDs) [1].

In order to best understand the function of such pacing and defibrillation systems, the underlying physiologic situations indicated for their use must also be defined and understood. Furthermore, as with the design of any biomedical device or system, a *first principles* understanding of the appropriate physiologic behavior is a prerequisite to the definition of the performance characteristics of the device. This chapter primarily aims to provide a basic understanding of the physiologic conditions that require intervention with

P.A. Iaizzo (ed.), *Handbook of Cardiac Anatomy, Physiology, and Devices*, DOI 10.1007/978-3-319-19464-6_30

pacing and/or defibrillation systems, as well as introduce technical information on these systems to provide the reader with a foundation for future research and reading on this topic. The information provided in this chapter is by no means comprehensive and thus should not be used to make decisions relating to patient care.

30.2 Cardiac Rhythms and Arrhythmias

30.2.1 Cardiac Function and Rhythm

Cardiac output (CO) is defined as the heart rate (HR, beats per minute) multiplied by the stroke volume (SV, liters), or CO = HR × SV (L/min). Normally, the heart rate is determined by the rate at which the sinoatrial node (the *biologic pacemaker*) depolarizes. In healthy individuals, the sinoatrial node maintains the appropriate heart rate to meet variable metabolic demands (e.g., increasing with exercise). More specifically, the sinoatrial nodal rate is modulated by: (1) sympathetic and parasympathetic innervation; (2) local tissue metabolites and other molecules; (3) neurohormonal factors; and/or (4) the perfusion of the nodal tissues. Stroke volume is the quantity of blood ejected from the heart during each ventricular contraction. The instantaneous stroke volume is governed by a number of factors including: heart rate, degree of ventricular filling/atrial performance, atrial-ventricular synchrony, and/or myocardial contractility.

It is important to note that multiple physiologic and pathologic conditions exist that may result in an inappropriate cardiac output. These conditions need to be defined to understand the functional requirements of pacing and defibrillation systems, and to motivate the logic behind the system features and performance characteristics (Tables 30.1, 30.2, and 30.3) [2, 3].

30.2.2 Conditions of the Sinoatrial Node

Normal sinus rhythm	Sinoatrial nodal rate is appropriate for the current metabolic demand (see online Video 30.1).
Sinus bradycardia	A slow sinoatrial nodal rate, resulting in a slow heart rate which may or may not be functionally appropriate. HR↓ → CO↓
Sinus tachycardia	A fast sinoatrial nodal rate, resulting in a higher heart rate which may or may not be functionally appropriate. HR↑ → CO↑ (for excessive heart rates, CO↓ due to reduced filling time).
Sick sinus syndrome	Unpredictable sinoatrial nodal rate. The rate is not appropriately coordinated with physiologic demand. CO↑ or CO↓
Chronotropic incompetence	Inappropriate response of the sinoatrial node to exercise. CO is too low for metabolic demands.
Block	No sinoatrial nodal rhythm. The patient will have either no heart rate (asystole) or a rate defined by other regions within the heart. A rescue rhythm from the atrioventricular node normally occurs (40–60 beats per minute, a so-called *junctional rhythm*). HR = 0 → CO = 0 or HR↓ → CO↓

30.2.3 Conditions of the Atrioventricular Node

1st degree heart block	An atrioventricular interval >200 ms (normal atrioventricular interval is ~120 ms). SV↓ → CO↓
2nd degree heart block	Atrial and ventricular activity is not 1:1. Two types of 2nd degree block are defined: Mobitz types I and II.
	Mobitz type I: *Wenckebach phenomenon*. A ventricular beat is dropped after a progressive elongation of the atrioventricular interval. HR↓ (missed beat) → CO↓
	Mobitz type II: A ventricular beat is dropped without a progressive elongation of the atrioventricular interval. This is often an early indication of progressive disease of the conduction system. HR↓ (missed beat) → CO↓
3rd degree heart block	No atrioventricular nodal conduction (conduction from the atrium to the ventricles). The atria contract at the sinoatrial nodal rate, and the ventricles are either asystolic or contract at a ventricular rescue rate (40–60 beats per minute). HR↓ and SV↓ → CO↓

30.2.4 Arrhythmias

Atrial tachycardia/flutter	High atrial rate of non-sinoatrial nodal origin. Not a physiologic rate, therefore decoupled from metabolic demand (see online Video 30.2). HR↑ SV↓ → CO↑ or CO↓
Atrial fibrillation	Chaotic depolarization of the atrium. No atrial hemodynamic input to the ventricles and a nonphysiologic rate is conducted through the atrioventricular node to the ventricles. Ventricular output is decoupled from metabolic demand. Stasis of blood in the atria can result in clot formation and stroke (see online Video 30.3). HR↑ SV↓ → CO↑ or CO↓
Ventricular tachycardia	High ventricular rate decoupled from sinoatrial nodal and atrial activity. This commonly results from a reentrant conduction loop or an ectopic foci (spontaneously beating region of myocardium). Ventricular rate is nonphysiologic, therefore decoupled from metabolic demand (see online Video 30.4). HR↑ SV↓ → CO↑ or CO↓
Ventricular fibrillation	Chaotic depolarization of the ventricles. No organized heart rate (see online Video 30.5). CO = 0

Table 30.1 Recommendation for permanent pacing in acquired atrioventricular block in adults

Class I	Permanent pacemaker implantation is indicated for: 1. third-degree and advanced second-degree AV block at any anatomic level associated with bradycardia with symptoms (including heart failure) or ventricular arrhythmias presumed to be due to AV block (Level of Evidence: C) 2. third-degree and advanced second-degree AV block at any anatomic level associated with arrhythmias and other medical conditions that require drug therapy that results in symptomatic bradycardia (Level of Evidence: C) 3. third-degree and advanced second-degree AV block at any anatomic level in awake, symptom-free patients in sinus rhythm, with documented periods of asystole greater than or equal to 3.0 s or any escape rate less than 40 bpm, or with an escape rhythm that is below the AV node (Level of Evidence: C) 4. third-degree and advanced second-degree AV block at any anatomic level in awake, symptom-free patients with AF and bradycardia with 1 or more pauses of at least 5 s or longer (Level of Evidence: C) 5. third-degree and advanced second-degree AV block at any anatomic level after catheter ablation of the AV junction (Level of Evidence: C) 6. third-degree and advanced second-degree AV block at any anatomic level associated with postoperative AV block that is not expected to resolve after cardiac surgery (Level of Evidence: C) 7. third-degree and advanced second-degree AV block at any anatomic level associated with neuromuscular diseases with AV block, such as myotonic muscular dystrophy, Kearns-Sayre syndrome, Erb dystrophy (limb-girdle muscular dystrophy), and peroneal muscular atrophy, with or without symptoms (Level of Evidence: B) 8. second-degree AV block with associated symptomatic bradycardia regardless of type or site of block (Level of Evidence: B) 9. asymptomatic persistent third-degree AV block at any anatomic site with average awake ventricular rates of 40 bpm or faster if cardiomegaly or LV dysfunction is present or if the site of block is below the AV node (Level of Evidence: B) 10. second- or third-degree AV block during exercise in the absence of myocardial ischemia (Level of Evidence: C)
Class IIa	Permanent pacemaker implantation is reasonable for: 1. persistent third-degree AV block with an escape rate greater than 40 bpm in asymptomatic adult patients without cardiomegaly (Level of Evidence: C) 2. asymptomatic second-degree AV block at intra- or infra-His levels found at electrophysiological study (Level of Evidence: B) 3. first- or second-degree AV block with symptoms similar to those of pacemaker syndrome or hemodynamic compromise (Level of Evidence: B) 4. asymptomatic type II second-degree AV block with a narrow QRS. When type II second-degree AV block occurs with a wide QRS, including isolated right bundle branch block, pacing becomes a Class I recommendation (Level of Evidence: B)
Class IIb	Permanent pacemaker implantation may be considered for: 1. neuromuscular diseases such as myotonic muscular dystrophy, Erb dystrophy (limb-girdle muscular dystrophy), and peroneal muscular atrophy with any degree of AV block (including first-degree AV block), with or without symptoms, because there may be unpredictable progression of AV conduction disease (Level of Evidence: B) 2. AV block in the setting of drug use and/or drug toxicity when the block is expected to recur even after the drug is withdrawn (Level of Evidence: B)
Class III	Permanent pacemaker implantation is not indicated for: 1. asymptomatic first-degree AV block (Level of Evidence: B) 2. asymptomatic type I second-degree AV block at the supra-His (AV node) level or that which is not known to be intra- or infra-Hisian (Level of Evidence: C) 3. AV block that is expected to resolve and is unlikely to recur (e.g., drug toxicity, Lyme disease, or transient increases in vagal tone or during hypoxia in sleep apnea syndrome in the absence of symptoms) (Level of Evidence: B)

AV atrioventricular, *AF* atrial fibrillation, *LV* left ventricle
Adapted from ACCF/AHA/HRS Guidelines [2]

Table 30.2 NASPE/BPEG classifications for pacing and defibrillation systems

I	II	III	IV
Chamber(s) paced	Chamber(s) sensed	Response to sensing	Programmability/rate modulation
O = none	O = none	O = none	O = none
A = atrium	A = atrium	T = triggered	P = simple programmability
V = ventricle	V = ventricle	I = inhibited	M = multiparameter programmability
D = dual (A + V)	D = dual (A + V)	D = dual (T + I)	C = communication with programmer R = rate modulation

Roman numerals I–IV indicate the position in the coding
NASPE North American Society of Pacing and Electrophysiology, *BPEG* British Pacing and Electrophysiology Group
Adapted from Bernstein et al. [3]

Table 30.3 Pacing and timing abbreviations

AP = Atrial pace
VP = Ventricular pace
AS = Atrial sense
VS = Ventricular sense
AR = Atrial refractory event
VR = Ventricular refractory event
AEI = Atrial escape interval—longest allowable interval between ventricular and atrial event (also called VA interval)
ARP = Atrial refractory period
AV = Atrioventricular
AV interval = Longest allowable interval between atrial and ventricular event
LR = Lower rate—slowest pacing rate allowed
LR interval = Longest period of time allowed before delivery of a pacing stimulus
MS = Mode switch
PAV = Paced atrioventricular interval—longest allowable interval between paced atrial beat and paced or sensed ventricular beat
PMT = Pacemaker-mediated tachycardia
PVAB = Postventricular atrial blanking period
PVARP = Postventricular atrial refractory period
SAV = Sensed atrioventricular interval—longest allowable interval between sensed atrial beat and paced or sensed ventricular beat
TARP = Total atrial refractory period (AV + PVARP)
UAR = Upper activity rate (also called maximum sensor-indicated rate)
UR = Upper rate—fastest pacing rate allowed
UR interval = Shortest allowable interval between paced beats or a sensed and paced beat
UTR = Upper tracking rate—fastest rate the ventricles may be paced in 1:1 synchrony with the sensed atrial rate (also called maximum tracking rate)
VA interval = Time between ventricular and atrial event
VRP = Ventricular refractory period
VSP = Ventricular safety pacing

30.3 Introduction to Implantable Pacing and Defibrillation Systems

For proper function and programming, implantable pacing and defibrillation systems require multiple components as well as external instruments. The implantable portion of the system is typically comprised of the implantable pulse generator (IPG, or pacemaker) or an implantable cardioverter defibrillator (ICD, or defibrillator) and the pacing and/or defibrillation leads. The IPG or ICD is most commonly implanted in a subcutaneous location in the left pectoral region. Depending on handedness, the condition of the upper venous system, the presence of other devices, and/or physician/patient preference, the device may also be placed in the right pectoral region. The device may be placed in a submuscular location in situations where the physician is concerned about either erosion of the IPG or ICD through the skin (most common in thin, elderly, or very young patients) or for cosmetic reasons (to reduce the obvious nature of the device). Another variation is to place the device in an abdominal location. This is commonly done in small children to avoid discomfort and/or interference with the motion of the arm and is of course dependent upon device size. This may also be a more practical device location in association with epicardial leads.

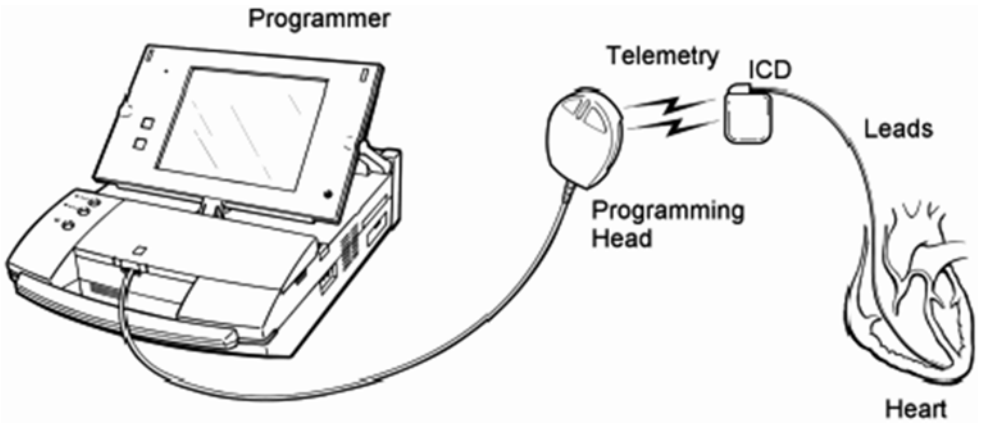

Fig. 30.1 Schematic of a typical implantable defibrillation system and the associated programmer. *ICD* implantable defibrillation device

In support of the implanted hardware, an external programmer is used to noninvasively telemeter information to and from the programmable IPG. This allows the physician to set/reset parameters within the device and download information relating to the status of the patient and the device. A complete defibrillation system is shown schematically in Fig. 30.1 (pacing systems use a similar configuration).

Pacing and defibrillation systems can be implanted using several methods. Early systems used leads attached to the epicardial surface of the heart, with the IPG or ICD placed in the abdomen of the patient (due to their larger sizes). Although this technique is still used in certain clinical situations (i.e., neonates), a transvenous approach for attaching the leads to the heart and a pectoral placement of the IPG or ICD is far more common. The implantation technique for implantable pacing and defibrillation will be described to provide a more thorough understanding of the system requirements.

Following anesthesia and a sterile preparation of the incision site, typically one of two techniques is used to access the venous system for the implantation of transvenous leads. Accordingly, venous access is achieved through either a surgical *cutdown* to the cephalic vein (the jugular vein is also used, but this is rare) or a transcutaneous needle puncture into the subclavian vein. The cutdown involves a careful surgical dissection down to the vessel, placement of a cut through the vessel wall, and direct insertion of the lead into the vessel lumen. The subclavian puncture uses a needle to puncture the vessel, followed by passage of a guidewire through the needle. Subsequently, an introduction catheter (percutaneous lead introducer) with an internal dilator is forced over the wire and into the vein. The dilator is removed, leaving the catheter behind. The lead is then inserted through the catheter (this *Seldinger Technique* can be viewed in online Video 30.6).

Following insertion into the vein, the lead(s) are advanced through the superior vena cava and into the right atrium for final placement in the right atrium, right ventricle, and/or the coronary sinus/cardiac veins (providing access to the left atrium and ventricle). Once positioned properly, the leads are secured in the desired location within the heart using either a passive or active means of fixation (see the section on leads). Next, an anchoring sleeve is used at the venous entry site to secure the lead into the vein and the surrounding tissue. This isolates the lead from mechanical forces outside of the vein, ensuring that adequate lead length remains within the heart to accommodate motion due to activity, respiration, and/or heart motion. Following lead implantation, the proximal terminal ends are connected to the IPG or ICD, which is then placed in a subcutaneous or submuscular pocket formed in the tissue. The implant site is then sutured closed, thus completing the implantation. Chest X-rays of a dual-chamber endocardial pacing system are shown in Fig. 30.2, and additional radiographic images of several pacing configurations are found in online JPGs 30.7–30.12.

30.4 Cardiac Pacing

30.4.1 History

Discoveries relating to the identification of the electrophysiological properties of the heart and the ability to induce cardiac depolarization through artificial electrical stimulation are relatively recent. Gaskell, an electrophysiologist, coined the phrase *heart block* in 1882 and Purkinje first described the ventricular conduction system in 1845. Importantly, Gaskell also related the presence of a slow ventricular rate to disassociation with the atria [4]. The discovery of the bundle of His is attributed to its namesake, Wilhelm His Jr. [5]. He described the presence in the heart of a conduction pathway from the atrioventricular node through the cardiac skeleton that eventually connected to the ventricles. Tawara later verified the existence of the bundle of His in 1906 [6]. He is also credited with being the first to clearly identify the specialized conduction tissues (modified myocytes) that span from the

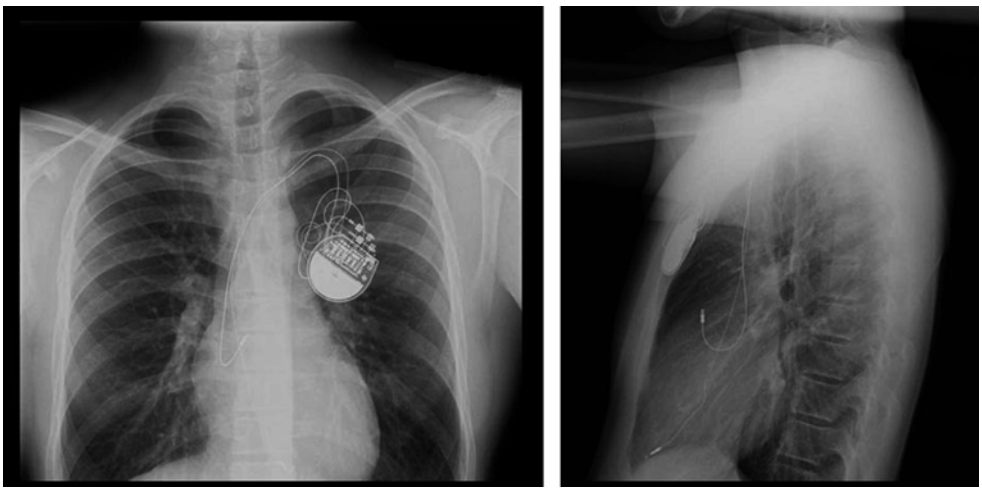

Fig. 30.2 Chest X-rays of an endocardial, dual-chamber pacing system in a young patient (anterior view on the *left*; lateral view on the *right*; Sainte-Justine Hospital, Montreal, QC, Canada used with permission). The implantable pulse generator (IPG or pacemaker) is implanted in the left pectoral region. The superior lead is implanted in the right atrial appendage and the inferior lead is in the right ventricular apex

Fig. 30.3 Dr. C. Walton Lillehei with the first battery-powered, wearable pacemaker

atrial septum to the ventricular apex, including the right and left bundle branches and Purkinje fibers.

The first known instance of electrical resuscitation of the heart was by Lidwell in 1929. Further, Hyman produced the first device for emergency treatment of the heart in 1932. Paul Zoll performed the first clinical transcutaneous pacing in 1952. Importantly for the pacing industry, the first battery-powered pacemaker was developed by Earl Bakken and used in postsurgical pediatric patients by C. Walton Lillehei in 1957 at the University of Minnesota (Fig. 30.3) [4, 7, 8]. Also see Chap. 25.

30.4.2 Artificial Electrical Stimulation

In addition to the spontaneous contraction that occurs within the heart, artificial electrical stimulus (cardiac pacing) can be used to initiate myocardial contraction. This stimulation, in the form of cardiac pacing, is routinely performed as a means to manage patients with cardiac arrhythmias and conduction abnormalities [9, 10]. Pacing induces myocardial contraction through the delivery of an electrical pulse to the patient's heart using an IPG and a cardiac pacing lead. The cardiac pacing lead acts as the electrical conduit for both stimulation and sensing, thus interfacing with the myocardial tissue. The electrical pulse is delivered either in a bipolar mode (involving cathodal and anodal electrodes on the lead) or in a unipolar mode (with a cathode on the lead and the metallic housing of the IPG serving as the anode).

To initiate depolarization, an action potential must be created on a given volume of myocardium. As was described in previous chapters, a normal myocardial cell has a resting membrane potential of approximately –90 mV. The resting membrane potential is dominated by the concentration of potassium (K). A cellular action potential occurs when the resting membrane potential is shifted towards a more positive value (i.e., less negative value) to approximately –60 to –70 mV. At this threshold potential, the cell's voltage-gated Na channels open and begin a cascade of events. In artificial electrical stimulation (pacing), this shift in the resting potential and subsequent depolarization is produced by the pacing system.

Two theories describe the mechanism by which artificial electrical stimulation initiates myocardial depolarization. The *Current Density Theory* states that a minimum current density (amps/cm^3) is required for stimulation of an excitable tissue. The *Electric Field Theory* requires that a minimum voltage gradient (volts/cm) be produced within the myocardium to initiate depolarization [11]. These two theories can, in part, be considered related, since the passage of current through the tissue (Current Density Theory) will induce a potential difference across the cell membranes due to the limited conductivity of the tissue. Similarly, the creation of a potential within the tissue (Electric Field Theory) will also induce a current. Regardless of the theoretical position taken

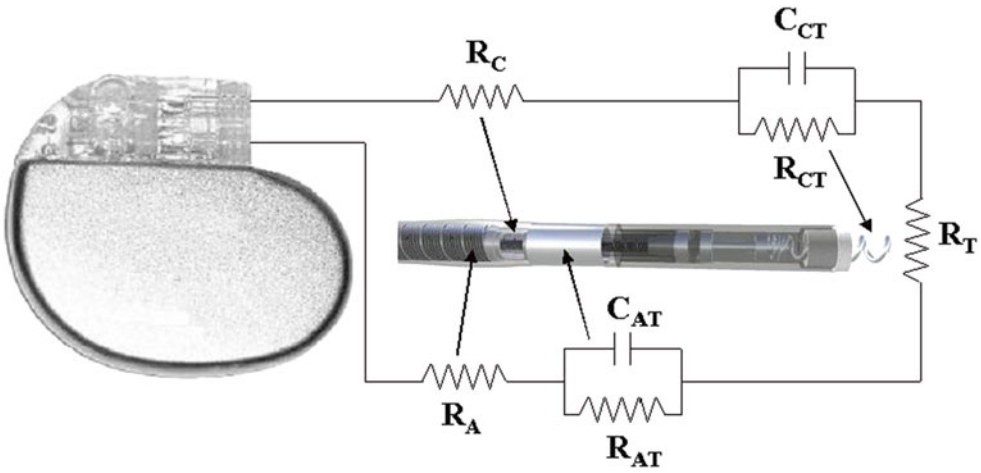

Fig. 30.4 Bipolar pacing circuit, including an implantable pulse generator and a pacing lead. Resistances: *RC* cathodic lead conductor, *RCT* cathode–tissue interface, *RT* tissue, *RAT* anode–tissue interface, *RA* anodic lead conductor. Capacitances: *CCT* cathode–tissue interface, *CAT* anode–tissue interface

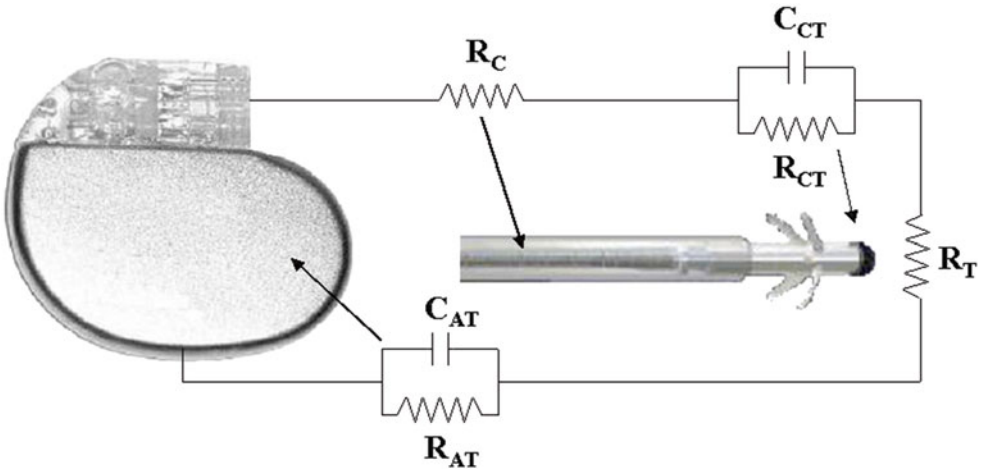

Fig. 30.5 A pacing circuit (unipolar type) which includes an implantable pulse generator and a pacing lead. Resistances: *RC* cathodic lead conductor, *RCT* cathode–tissue interface, *RT* tissue, *RAT* anode–tissue interface. Capacitances: *CCT* cathode–tissue interface, *CAT* anode–tissue interface

regarding stimulation, the requirement for artificial stimulation is the shifting of the resting membrane potential from its normal value (typically –90 mV) towards a more positive value, until the depolarization threshold is reached.

The impedance associated with charge transfer from an IPG to the cardiac tissue is comprised of resistive (R) and reactive components (X_C = capacitive; X_L = inductive):

$$Z^2 = R^2 + \left(X_C + X_L\right)^2$$

The resistive term (R) includes the DC resistance associated with the conductors internal to the lead (R_C = cathodic conductor; R_A = anodic conductor), the cathode–tissue interface (R_{CT}), the anode–tissue interface (R_{AT}), and the tissue itself (R_T):

$$R = R_C + R_{CT} + R_T + R_{AT}$$

The capacitive term (X_C) is the sum of the capacitance of the cathode–tissue interface (C_{CT}) and the anode–tissue interface (C_{AT}).

$$X_C = C_{CT} + C_{AT}$$

The inductance within the conductors and circuit is extremely small and this term is typically neglected. Ignoring inductance, the resulting equation for lead impedance is:

$$Z^2 = R^2 + X^2\mathrm{C}$$

Schematic representations of the circuitry for bipolar and unipolar pacing systems are shown in Figs. 30.4 and 30.5. In these figures, the electric circuit for the delivery of energy to the myocardium is described as a simple RC circuit in which the IPG acts as the voltage/charge source and the lead conductors, electrodes, and cardiac tissue act as the load. Figure 30.4 depicts a bipolar pacing circuit in which the cathode and anode both reside on the pacing lead. Figure 30.5 represents the circuitry associated with a unipolar pacing system. In this case, the circuit is still bipolar but the anode is the metallic housing of the IPG; the term *unipolar* refers to the polarity of the lead.

Typical pacing circuit impedances range from 400 to 1500 Ω. Approximately 80 % of the total impedance is at the tissue interface; as an example, this will result in a 0.8 V drop at the tissue interface when a 1.0 V pacing pulse amplitude is used. Using the aforementioned impedances (400–1500 Ω),

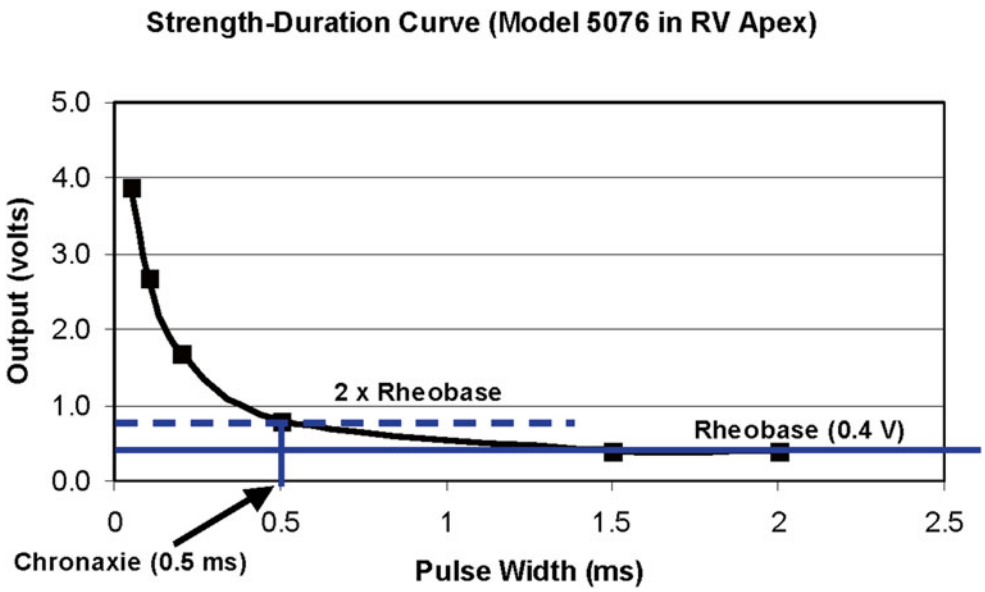

Fig. 30.6 A typical strength-duration curve for cardiac pacing. This particular curve was obtained using a Medtronic model 5076 bipolar pacing lead positioned in the right ventricular (*RV*) apex of a canine. In this plot, chronaxie and rheobase were 0.5 ms and 0.4 V, respectively

a pacing output of 1.0 V produces currents of 2.5 mA and 0.67 mA, respectively.

To date, the most common pacing stimulation waveform used to electrically activate the myocardial tissue is an exponentially decaying square wave. An active recharge is also commonly included at the trailing edge of the stimulation pulse to reduce the post-pace polarization on the electrodes by balancing the charge delivered. The stimulating portion of the waveform is characterized by its amplitude (volts) and width (milliseconds). A relationship exists between the amplitude and pulse width that will be required for depolarization (*pacing*) of the tissue. This relationship, termed a *strength-duration curve* is most commonly plotted as shown in Fig. 30.6.

Terminology relating to the strength-duration curve includes the rheobase and chronaxie values. Rheobase is the threshold voltage at an infinitely long pulse width, and chronaxie is the threshold pulse width at two times the rheobase voltage. The output of a clinical IPG is commonly set at twice the voltage threshold corresponding at the chronaxie pulse width, thus insuring a safety margin [11].

30.4.3 Indications for Pacing

Pacing and defibrillation systems are designed to maintain appropriate cardiac rhythms to maximize the patient's safety and quality of life. With the exception of cases of sudden cardiac death where an external defibrillator is clearly required, the determination of when to use a pacing or implantable defibrillation system can be complex. This section will describe the current classification of indications for pacing and provide a few practical examples of these indications and the decision process associated with choosing the appropriate system for a given patient's condition.

The indications for either pacing or defibrillation therapies are commonly classified in the standard ACCF/AHA/HRS (American College of Cardiology Foundation/American Heart Association/Heart Rhythm Society) format as follows [2]:

Class I	Benefit >>> Risk. Procedure/treatment should be performed/administered.
Class II	Conditions for which there is conflicting evidence and/or a divergence of opinion about the usefulness/efficacy of a procedure or treatment.
Class IIa	Benefit >> Risk. Additional studies with focused objectives needed. It is reasonable to perform procedure/administer treatment.
Class IIb	Benefit ≥ Risk. Additional studies with broad objectives needed; additional registry data would be helpful. Procedure/treatment may be considered.
Class III	Classified as "No benefit" (Procedure/test is not helpful with no proven treatment benefit) or "Harm" (Procedure/test is associated with excessive cost without benefit or is harmful and the treatment is harmful to the patient).

For each classification listed above, a Level of Evidence is also referenced: Level A—multiple populations evaluated with data derived from multiple randomized clinical trials or meta-analyses; Level B—limited populations evaluated with data derived from a single randomized trial or nonrandomized studies; and Level C—very limited populations evaluated and only consensus opinions of experts, case studies, or standards of care.

Cardiac pacing can be used for both temporary and permanent management of heart rhythm and function. Although the permanent pacing systems are the most well known, there are numerous indications for temporary pacing. The most common

Table 30.4 Recommendations for permanent pacing in sinus node dysfunction

Class I	Permanent pacemaker implantation is indicated for: 1. SND with documented symptomatic bradycardia, including frequent sinus pauses that produce symptoms (Level of Evidence: C) 2. symptomatic chronotropic incompetence (Level of Evidence: C) 3. symptomatic sinus bradycardia that results from required drug therapy for medical conditions (Level of Evidence: C)
Class IIa	Permanent pacemaker implantation is reasonable for: 1. SND with heart rate less than 40 bpm when a clear association between significant symptoms consistent with bradycardia and the actual presence of bradycardia has not been documented (Level of Evidence: C) 2. syncope of unexplained origin when clinically significant abnormalities of sinus node function are discovered or provoked in electrophysiological studies (Level of Evidence: C)
Class IIb	Permanent pacemaker implantation may be considered in minimally symptomatic patients with chronic heart rate less than 40 bpm while awake (Level of Evidence: C)
Class III	Permanent pacemaker implantation is not indicated for: 1. SND in asymptomatic patients (Level of Evidence: C) 2. SND in patients for whom the symptoms suggestive of bradycardia have been clearly documented to occur in the absence of bradycardia (Level of Evidence: C) 3. SND with symptomatic bradycardia due to nonessential drug therapy (Level of Evidence: C)

SND sinus node dysfunction
Adapted from ACCF/AHA/HRS Guidelines [2]

temporary pacing systems utilize transcutaneous wires that are stitched directly into the myocardium and connected to an external stimulator. The stimulator is usually a small portable unit, but it can be a console. Common indications for temporary pacing include: postsurgical heart block, heart block following an acute myocardial infarction, pacing for post- or intra-operative cardiac support, pacing prior to implantation of a permanent pacemaker, and/or pacing during a pulse generator exchange.

The primary indication for the implantation of a permanent pacing system (pacemaker and leads) is to chronically eliminate the symptoms associated with the inadequate cardiac output due to bradyarrhythmias. Typical causes of these bradyarrhythmia are: (1) sinus node dysfunction; (2) acquired permanent or temporary atrioventricular block; (3) chronic bifascicular or trifascicular block; (4) hypersensitive carotid sinus syndrome; (5) neurocardiogenic in origin; and/or (6) a side effect due to a drug therapy. The type of pacing system to be employed is dependent on the nature and location of the arrhythmia, the patient's age, previous medical/surgical history, as well as additional medical conditions.

For conditions related to dysfunction of the sinoatrial node, an IPG with atrial features is commonly used in combination with a lead placed in (or on) the atrium. When management of the ventricular rate is required, a device with ventricular functionality and a ventricular lead are used. When management of the rhythms of both the upper and lower chambers of the heart is required, a dual-chamber system is implanted.

Two clinical situations are outlined below to illustrate common indications for pacing, as well as the decision tree that is often used to determine the type of pacing system for the particular indication. The indications for pacing in a patient with sinus node dysfunction are found in Table 30.4 [2] and the decision tree in Fig. 30.7 [12]. The indications for pacing in an adult with acquired atrioventricular block are found in Table 30.1 and the decision tree in Fig. 30.8 [2]. As an example, a patient with symptomatic chronotropic incompetence would have a Class I indication for pacing (Table 30.4). Since this is related to dysfunction of the sinus node, Fig. 30.7 would then be used to determine the type of pacing system required. In this situation, a rate response system (a pacing system that responds to patient activity/exercise) would clearly be desired. If atrioventricular synchrony were also required, a rate-responsive ventricular pacemaker would be implanted (mostly commonly a DDDR system; see the next section on the standard coding system and Table 30.2).

30.4.4 NASPE/BPEG Codes

In order to describe the function of a pacing system in a standardized manner, the North American Society of Pacing and Electrophysiology (NASPE) and British Pacing and Electrophysiology Group (BPEG) had developed a standard coding system [3]. This code describes the pacing system's functionality using a multi-letter designation. The first four letters are typically used, although this practice is evolving as new pacing features and indications are being developed. In the four letter code system, the first letter indicates the pacing activity (A = atrial pacing, V = ventricular pacing, D = dual-chamber pacing, O = no pacing), the second letter

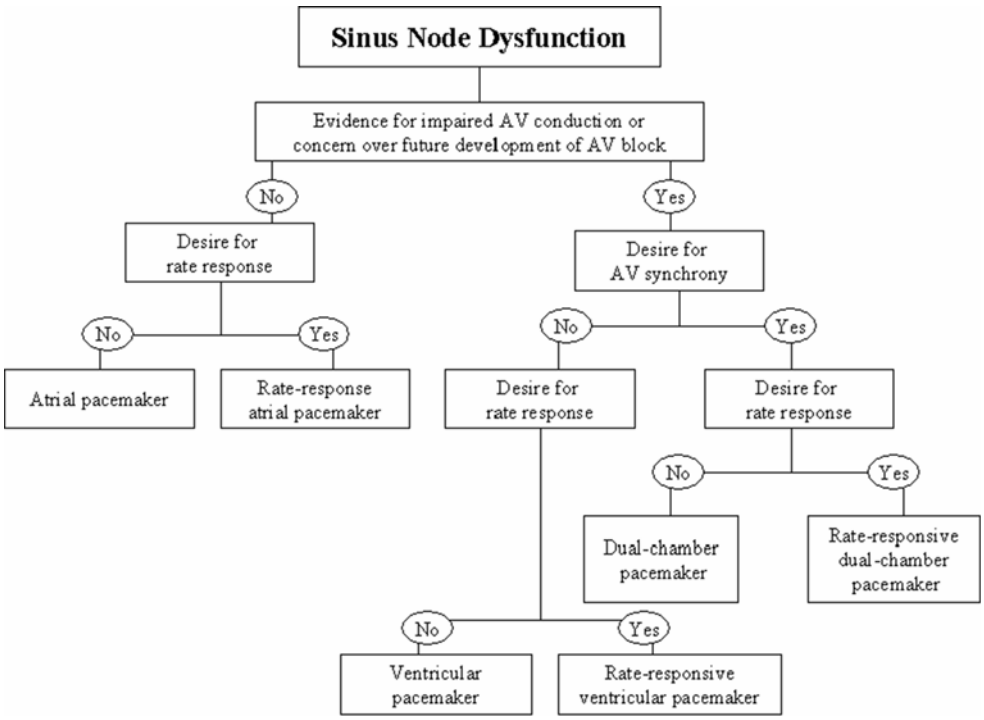

Fig. 30.7 A typical decision tree employed for determining proper therapy when the implantation of a pacemaker for sinus node dysfunction is being considered. *AV* atrioventricular. Adapted from ACC/AHA/HRS Guidelines [12]

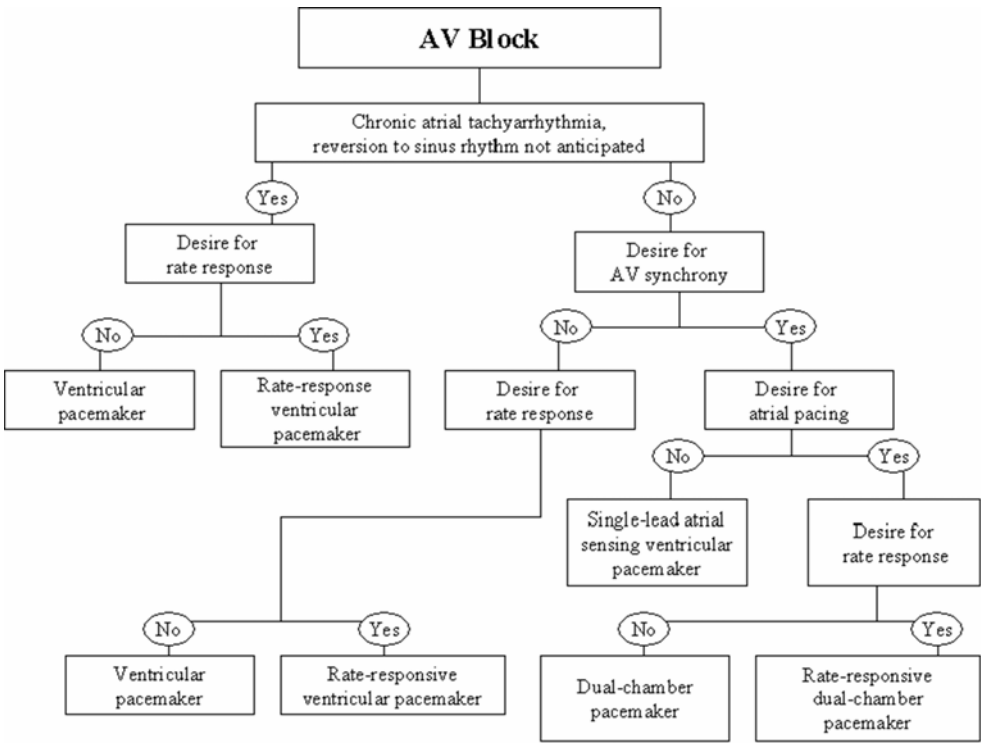

Fig. 30.8 A typical decision tree employed for determining proper therapy when the implantation of a pacemaker for atrioventricular (*AV*) block is being considered. Adapted from ACC/AHA/HRS Guidelines [12]

indicates sensing (A = atrial sensing, V = ventricular sensing, D = dual-chamber sensing, O = no sensing), the third letter indicates the reaction to a sensed event (I = inhibit pacing, T = trigger pacing, D = inhibit and trigger, O = no reaction to sensing), and the fourth letter is used to describe unique device functionality (R = rate responsive, for example). Thus, a VVIR system would pace the ventricles (V---), sense ventricular activity (-V--), inhibit or withhold pacing upon detection of a sensed event in the ventricle (--I-), and provide rate response to manage chronotropic incompetence (---R). See Table 30.2 for a more complete explanation of the coding system.

30.4.5 Implantable Pulse Generators

The IPG is an implantable computer with an integral pulse generator and battery. The componentry is typically encased within a hermetically sealed stamped titanium housing with the battery taking up approximately half of the device volume. The most common battery chemistry used in modern pacemakers is lithium iodide. Device longevity is typically 8–10 years, but may vary significantly depending on system utilization (Fig. 30.9). Electrically insulated feedthroughs connect the internal circuitry to an external connector block, which acts as the interface between the internal circuitry of the IPG and the leads. Typically today, the connector block consists of a molded polyurethane superstructure which houses metallic contacts. The contacts may be simple machined blocks or "spring-type" metallic beams. Most connector blocks employ set screws to ensure permanent retention of the leads and these may also enhance electrical contact. A cutaway view of an IPG can be found in Fig. 30.10, and the scheme for connection between the IPG and the leads is shown in Fig. 30.11 and online Video 30.13. In addition to the standard IS-1 and DF-1 connectors shown in Fig. 30.11, a new standard connection scheme is now available. The so-called *DF-4* connector is an in-line quadripolar connector that includes electrical connections for both the pacing and defibrillation electrode circuits. The new connector is documented in ISO 30186:2010 (Active implantable medical devices—Four-pole connector system for implantable cardiac rhythm management devices—Dimensional and test requirements).

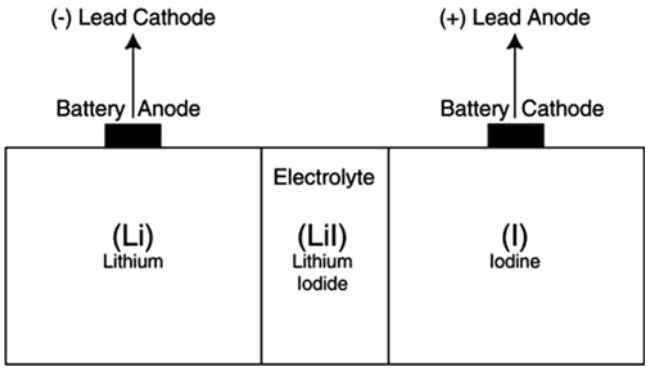

Fig. 30.9 Schematic of a lithium iodide battery. This is the most common chemistry used in modern pacemakers

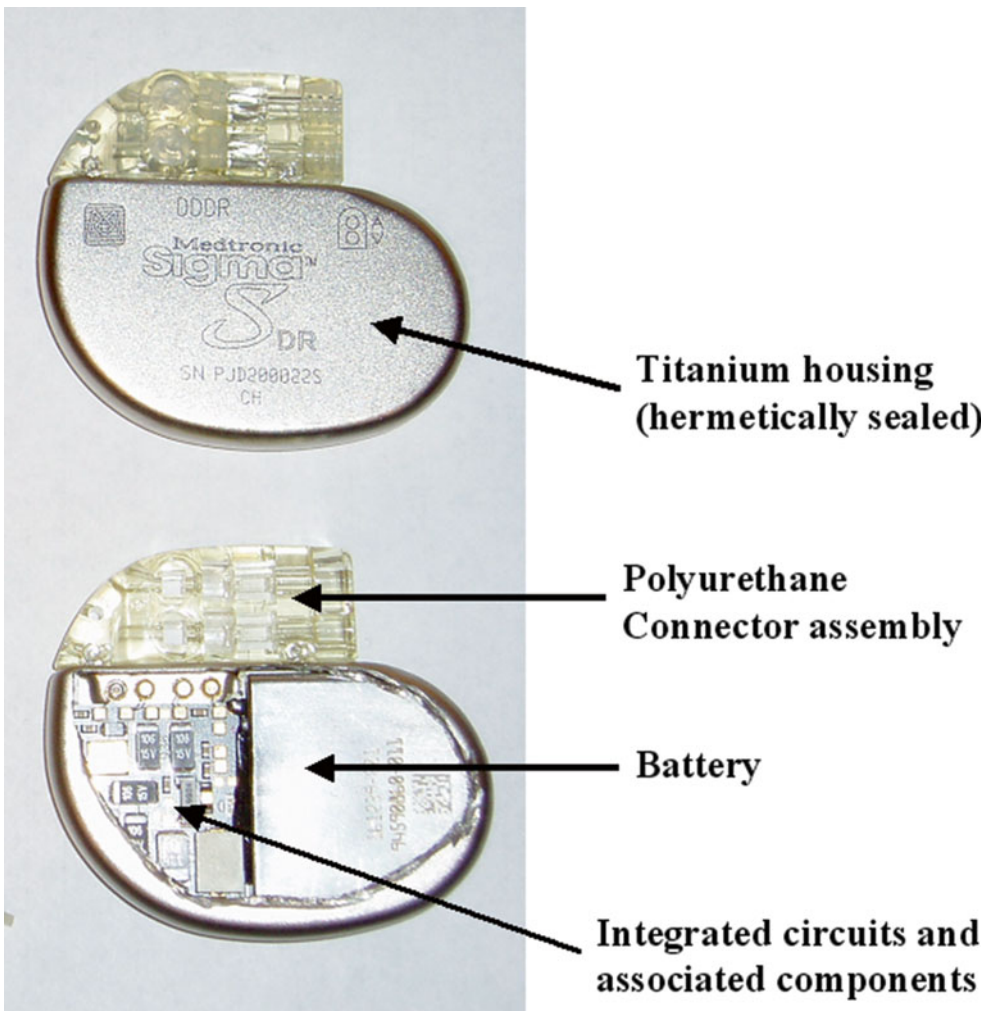

Fig. 30.10 Cutaway view of an implantable pulse generator (IPG or "pacemaker")

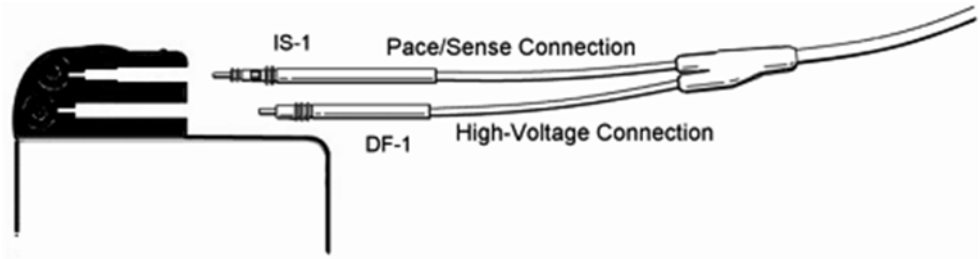

Fig. 30.11 Schematic of the implantable pulse generator-to-lead interface. The IS-1 connector is the standard configuration for pacing. The DF-1 connector is the standard configuration for high-voltage defibrillation (see Video 30.13)

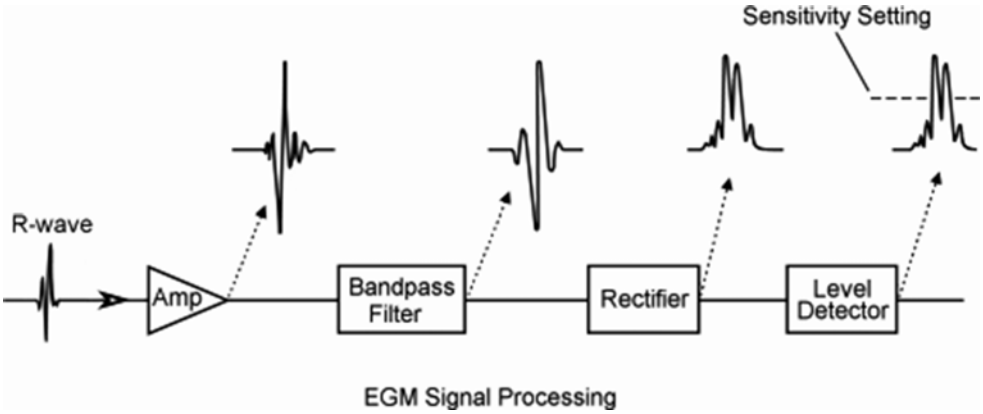

Fig. 30.12 The electrogram amplification and rectification scheme that is used in most modern implantable pacing and defibrillation systems. *EGM* electrogram

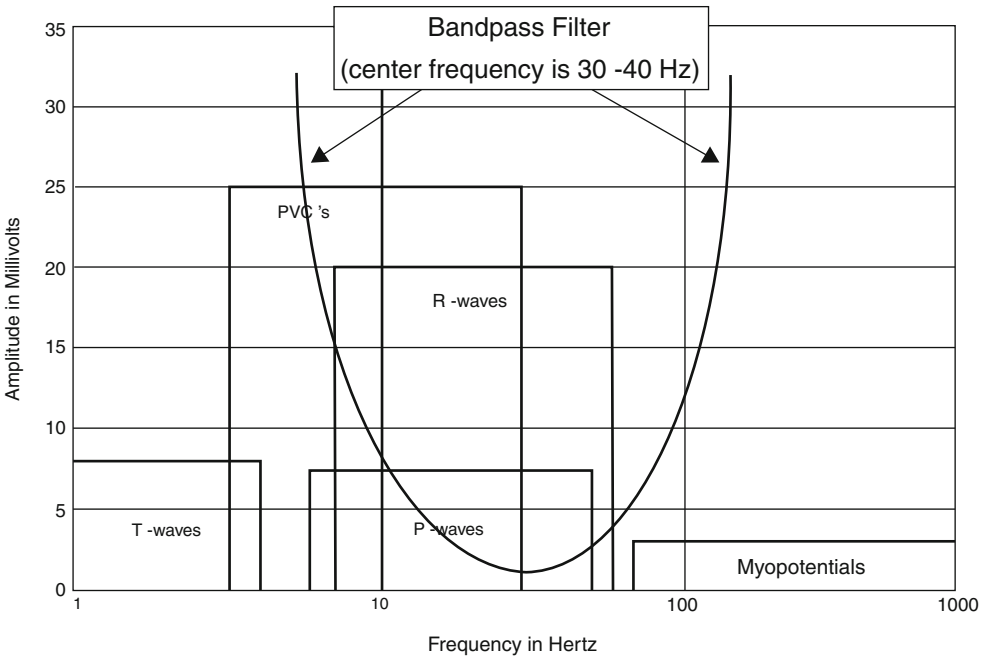

Fig. 30.13 Plot of electrical signals (amplitude and frequency) frequently encountered by pacing and defibrillation sensing algorithms. A bandpass filter for preferential detection of P-waves and R-waves is shown (*parabolic line*). This filter is designed to "reject" myopotentials and T-waves

30.4.6 Sensing Algorithms

In order to assess the need for therapeutic intervention, the pacing system must be able to accurately detect and interpret the various electrical activities of the heart. The instantaneous electrical activity of the heart, or electrogram (EGM), is recorded as a differential voltage measured between the bipolar electrode pair on the lead (bipolar lead) or between the cathode on the lead and the housing of the IPG (unipolar lead). This signal is then processed within the IPG and analyzed by the sensing algorithms. Typically, such signals are amplified, filtered, and rectified prior to undergoing analyses by the device (Figs. 30.12 and 30.13). The resulting signals are then passed through a level detector to determine if they exceed the minimum threshold for detection that was preprogrammed into the device by the clinician. The sensitivity

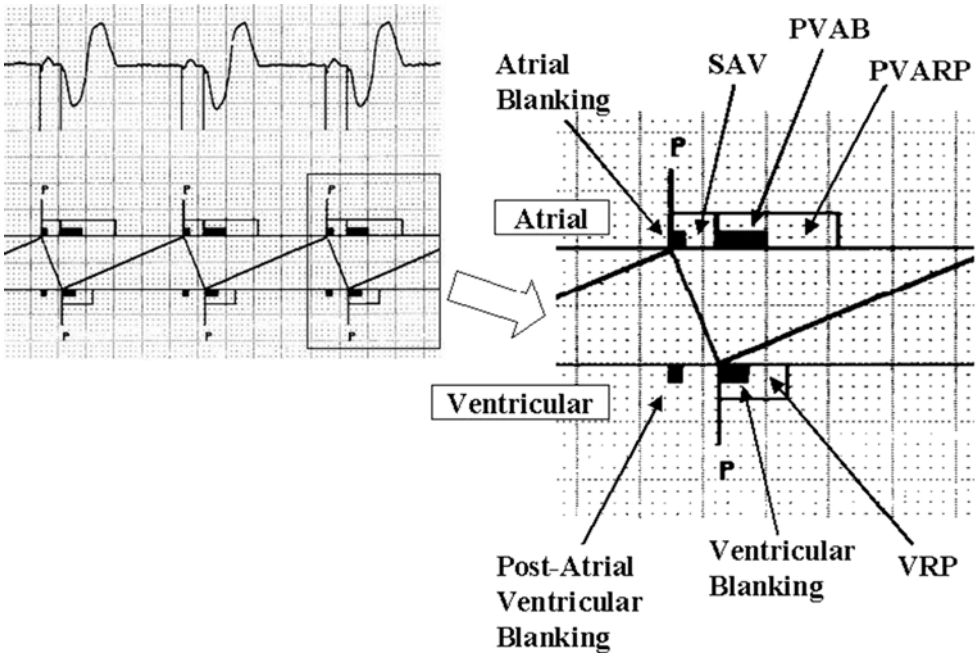

Fig. 30.14 A typical dual-chamber timing diagram, including subdiagrams for the atrial and ventricular channels. The sequence of events begins with a paced atrial beat (P). This paced beat occurs when the maximum allowable interval between sensed atrial events is exceeded. For example, if the minimum rate is programmed to 60 beats per minute, an atrial pace will occur when a 1000 ms interval between sensed events is exceeded. Immediately following this pacing pulse, both the atrial and ventricular sensing algorithms are blanked. This means that the threshold detector ignores all sensed activity. The system is blanked to avoid sensing the resultant atrial depolarization on the atrial channel, and the atrial pacing spike and the atrial depolarization on the ventricular channel. Concurrently in the atrium, a sensed atrioventricular (SAV) interval occurs. This is the longest interval that will be allowed by the device without a paced ventricular beat. The SAV is commonly programmed to 150 ms, and is set to optimize filling of the ventricle due to the atrial contraction. During a cardiac cycle, if the SAV value is reached (meaning an intrinsic ventricular beat does not occur within the programmed interval following the intrinsic or paced atrial beat), a ventricular pacing pulse is then delivered. This pacing pulse is again accompanied by blanking in both channels to avoid oversensing of the pacing pulse and the resultant ventricular depolarization. This interval is referred to as the postventricular atrial blanking (*PVAB*) period on the atrial channel. Concurrently, the postventricular atrial refractory period (*PVARP*) occurs on the atrial channel in which the device attempts to avoid sensing of retrograde P-waves (i.e., atrial contractions conducted through the atrioventricular node in a retrograde manner) and the ventricular refractory period (*VRP*) occurs on the ventricular channel to avoid oversensing of T-waves. Following these intervals, the timing is repeated. If the atrial rate stays above the minimum programmed rate (the lower rate) and the SAV is never reached, the device will never pace unless inappropriate sensing occurs

setting (in mV) determines what is discarded as noise by the algorithm and which signals will be detected. An ideal sensitivity setting is one that will reliably detect the depolarization spike of the chamber (P-wave in the atrium; R-wave in the ventricle) while ignoring repolarization and other physiologic and nonphysiologic signals.

Most rhythm management decisions are based on the heart rate detected. The modern IPG continuously measures the time from one sensed event to the next, and compares the interval to the rates and intervals programmed by the clinician. For example, if two atrial events occur with a separation of 1500 ms (1.5 s), the heart rate is 40 beats per minute (HR = 60/measured beat-to-beat interval; 60/1.5 = 40 beats per minute). In order to understand the logic behind sensing algorithms and pacing timing diagrams, the terminology needs to be introduced. Table 30.3 includes the most commonly used terms and abbreviations. These terms will be freely used in further discussions of the logic behind pacing and defibrillation sensing and therapies without further explanation. This table will also provide the reader with the vocabulary required for interpreting and understanding current literature and publications on the topic.

The decision processes and behaviors of the typical pacing algorithm are usually described using a timing diagram (Fig. 30.14). An understanding of this diagram will provide the basis for analysis of the behavior of pacing systems and will communicate the various parameters that the clinician and device manufacturer must be concerned with. The concepts associated with pacemaker timing are shown in Fig. 30.14; the information is presented in an alternate form in Fig. 30.15.

The actual behaviors of pacing systems can deviate from the ideal for a number of reasons. For example, the pacing pulse can be of an inadequate energy to pace the chamber, losing capture on one or more beats (Fig. 30.16). Another undesired situation that commonly arises is oversensing. In this case, the device inappropriately identifies electrical activities as an atrial or ventricular event (Fig. 30.17). Clinically, oversensing is resolved by reprogramming the

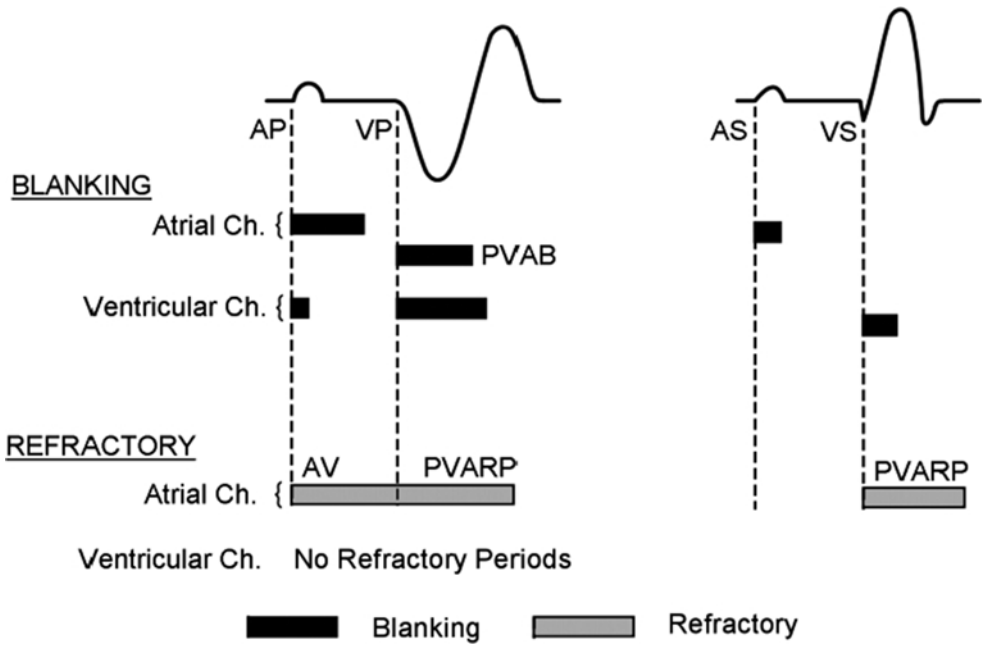

Fig. 30.15 Blanking and refractory periods. The *top trace* represents the electrocardiogram. The portion of the diagram on the left is a situation in which both the atrial and ventricular leads are pacing. The portion on the right is a situation where the system is sensing intrinsic atrial and ventricular activity (i.e., no pacing is occurring). *AP* atrial pace, *AS* atrial sense, *AV* atrioventricular, *PVAB* postventricular atrial blanking period, *PVARP* postventricular atrial refractory period, *VP* ventricular pace, *VS* ventricular sense

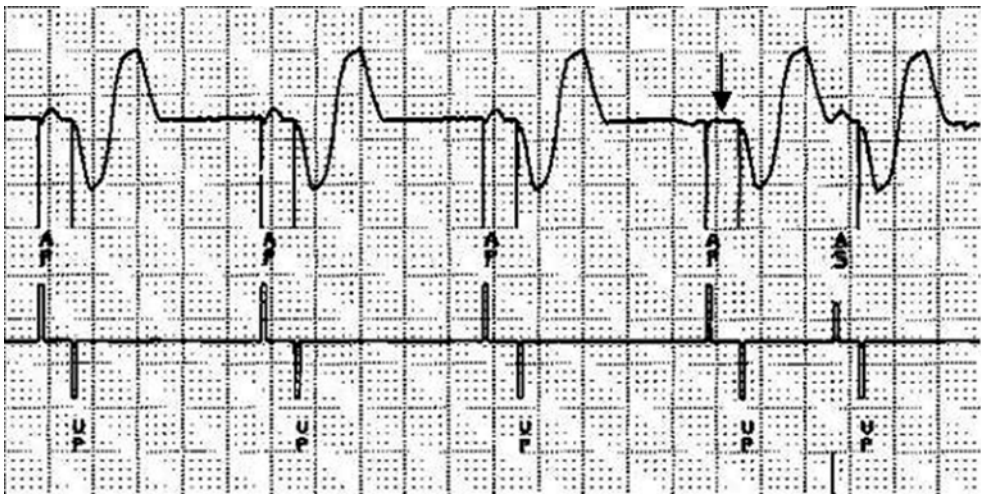

Fig. 30.16 An electrocardiogram (*above*) and pacemaker marker channel (*below*) printed from a programmer. Note the loss of capture on the atrial channel (indicated by the *arrow*); notice that no P-wave follows the pacing pulse

device to a lower sensitivity. Conversely, if a system is undersensing, the sensitivity is increased. Assessment of the behavior of the pacing system is vastly simplified through the use of marker channels. These are shown below the electrograms in both Figs. 30.16 and 30.17. The marker channel is used to report the overall behavior of the pacing system (i.e., documenting how the pacing system interprets the signals transmitted by the device and/or is sensed), allowing a quick assessment of the performance of the algorithms and device output levels.

30.4.7 Drug Interactions with Pacing Systems

It is important to note that certain drug therapies have been reported to impact pacing system performance. Although it is rare for antiarrhythmic drugs to significantly affect pacing thresholds, they have been found to alter stimulation thresholds by inducing changes in the lead-myocardial interfacial conductivity and excitability. Additionally, they can slow the intrinsic sinus rate or atrioventricular rate, which then necessitates pacing of the resultant bradycardia or heart block, respectively. In general, Class Ia antiarrhythmic drugs can increase pacing thresholds at toxic dosages and sotalol and amiodarone, Class III antiarrhythmic drugs can increase pacing thresholds while at therapeutic levels; however, due to the advent of steroid-coated leads and efficient pacing systems, these potential interactions are rarely clinically significant [13, 14]. Rate controlling agents such as beta-blockers, calcium channel blockers, and digoxin decrease the sinoatrial node and atrioventricular rates thereby decreasing heart rate and increasing the PR interval, respectively, which may increase the need for pacing. A summary of the more commonly administered drugs and their impact on

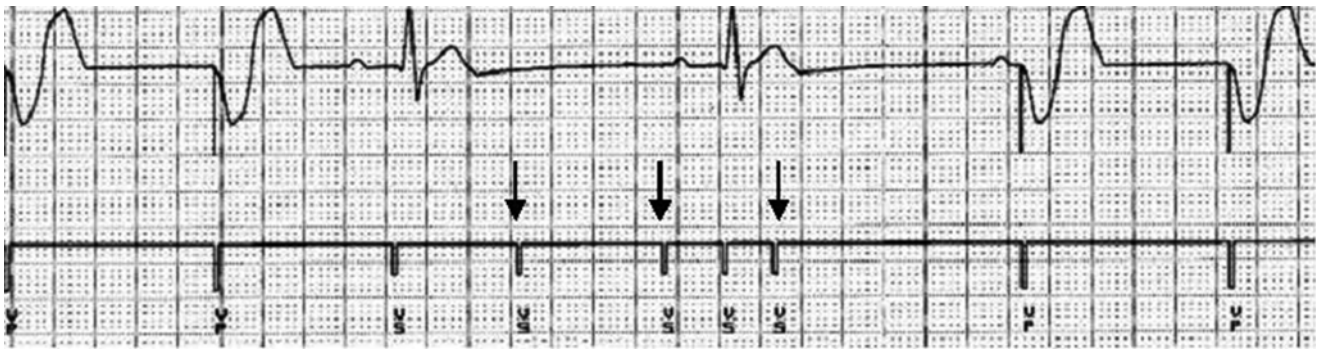

Fig. 30.17 An electrocardiogram (*above*) and pacemaker marker channel (*below*) printed from a programmer. Note the ventricular oversensing (indicated by the *arrow*); notice that no QRS complex is associated with the detected event

Table 30.5 Effect of antiarrhythmic drugs on pacing thresholds

Increase at normal drug levels	Increase at toxic drug levels	No increase
Flecainide	Quinidine	Lidocaine
Propafenone	Procainamide[a]	
Amiodarone	Disopyramide	
Sotalol		

[a]Procainamide, a Class Ia antiarrhythmic drug, is metabolized to *N*-aceyl-procainamide (NAPA) which has Class III activity

pacing thresholds, action potentials, and the physiologic consequences of their action is found in Tables 30.5 and 30.6.

30.4.8 New Indications/Recent Clinical Trials

Today, single- and dual-chamber pacing systems have become the standard method of treating many bradyarrhythmias. Recent clinical evidence has raised interest in the selection of the frequency at which patients are paced and the optimal site of stimulation [15]. It has long been known that pacing produces a nonphysiologic contraction pattern, but recent research has also indicated that potentially detrimental effects may result from long-term pacing [16–19]. Currently, alternate choices in ventricular stimulation sites are of particular interest due to the presumed physiologic and hemodynamic benefits. For example, pacing of the bundle of His is thought to produce a more physiologic contraction pattern, while additional evidence exists that there may also be hemodynamic benefits associated with right ventricular septal and outflow tract pacing [16, 20–25]. In patients with heart failure and associated wide QRS complexes, biventricular pacing has been adopted [26, 27] (see online Video 30.14). Finally, research in atrial pacing has focused on reducing atrial fibrillation, improving methods of pace terminating atrial tachycardias, and/or improving ventricular filling and atrial hemodynamics [28–30]. Recent research is even investigating the possibility of genetically engineering a biologic pacemaker [31].

30.5 Cardiac Defibrillation

Today, sudden cardiac arrest is one of the most common causes of death in developed countries. During 2013, the incidence of in-hospital and out-of-hospital cardiac arrest in the USA was 209,000 and 359,400, respectively. Sudden cardiac arrest claims more lives in the USA each year than the combination of deaths from Alzheimer's disease, assault with firearms, breast cancer, cervical cancer, colorectal cancer, diabetes, HIV, house fires, motor vehicle accidents, prostate cancer, and suicides [32].

Several studies have identified multiple risk factors for sudden cardiac arrest, which include: (1) coronary artery disease; (2) heart failure and/or decreased left ventricular ejection fraction; (3) previous events of sudden cardiac arrest; (4) prior episodes of ventricular tachycardia; (5) hypertrophic cardiomyopathies; and/or (6) long QT syndrome [33]. The combination of any three of these factors significantly increases the risk for sudden cardiac arrest. Ninety percent of sudden deaths occur in patients with two or more occlusions in their major coronary arteries [34].

30.5.1 History

The first documentation of ventricular fibrillation was noted in 1850 [35]. A little over a century later, in 1962, the first direct current defibrillator was developed. Ventricular fibrillation began to be recognized as a possible cause of sudden death in the 1970s and the first transvenous ICD was implanted in the 1990s. Since then, the medical device industry has provided dramatic reductions in ICD size, while

Table 30.6 Antiarrhythmic drugs, action potential phases, and physiologic consequences

Class	Drug	Action potential phase	Physiologic consequence
Ia	Quinidine Procainamide Disopyramide	0	Decreases automaticity of the sodium channel Slows conduction velocity Prolongs refractory period
Ib	Lidocaine Mexiletine Tocainide Phenytoin	0	Decreases automaticity of the sodium channel May or may not slow conduction velocity Decreases refractory period
Ic	Flecainide Propafenone Encainide Moricizine	0	Decreases automaticity of the sodium channel Slows conduction velocity No effect on refractory period
II	Propranolol Atenolol Metoprolol	SA node	Decreases automaticity of nodal tissue Decreases conduction velocity Increases refractory period
III	Bretylium Sotalol Amiodarone Ibutilide Dofetilide Dronedarone	3	Increases refractory period No effect on conduction velocity No effect on automaticity
IV	Verapamil Diltiazem	SA node	Decreases automaticity of nodal tissue Decreases conduction velocity Increases refractory period

SA sinoatrial

simultaneously increasing safety, efficacy, battery longevity, diagnostics, and memory capability. Figure 30.18 shows the evolution in the size of one manufacturer's ICD model.

30.5.2 Tachyarrhythmias

The commonly recognized mechanisms that lead to tachyarrhythmias (tachycardias and fibrillation) include reentry circuits, triggered activities, and automaticity. Reentry is considered as the most common tachyarrhythmia mechanism. It can be described as an electrical loop within the myocardium that has a circular, continuous series of depolarizations and repolarizations (Fig. 30.19). In general, there are three requirements for reentry to occur: (1) the presence of a substrate, for example, an area of ischemia or scar tissue; (2) two parallel pathways which encircle the substrate; and (3) one pathway that conducts slowly and one that exhibits unidirectional block. An impulse reaching the substrate is slowed by the unidirectional block and is allowed to slowly conduct down the slow pathway. As the impulse continues to move around the substrate, it conducts in a retrograde manner up the fast pathway and the impulse continues to conduct in a circular fashion.

Inappropriate atrial or ventricular tachycardias can be further classified as either hemodynamically stable or unstable. The level of hemodynamic compromise that occurs is typically considered to depend on both the rate and the pathway of the arrhythmia. In general, atrial tachycardias usually result in higher ventricular rates due to conduction through the atrioventricular node. As atrial rates increase, the rate conducted to the ventricles may or may not be 1:1, since the atrioventricular node has inherent limitations in its ability to conduct depolarizations. If, however, an abnormal pathway exists from the atria to the ventricles, then 1:1 conduction may be possible even at very high rates. Nevertheless, a patient's clinical risks are related to the level of hemodynamic compromise, with the most extreme case being ventricular fibrillation which, if not immediately reversed, most often results in death.

Triggered activity, or hyperautomaticity, is typically not consistently spontaneous and is a less common mechanism. Early and delayed after depolarizations seen in phase 3 and 4 of the action potential are associated with triggered activity. Automaticity is defined as the ability of the cell to depolarize spontaneously at regular intervals. However, in a diseased heart, often cells will exhibit abnormal automaticity that causes them to depolarize at rates faster than the intrinsic nodal rates.

Common symptoms observed in patients with tachyarrhythmias may include syncopal episodes, palpitations, fatigue, and/or dyspnea. Both invasive and noninvasive diagnostic tools are available for diagnosing tachyarrhythmias. The typical noninvasive procedures include: (1) a thorough patient interview; (2) blood work; (3) a 12-lead ECG; (4) tilt table testing; (5) holter monitoring; (6) exercise stress

Fig. 30.18 The evolution of the implantable cardioverter defibrillator (*ICD*). Dramatic reductions in size have occurred, with simultaneous improvements in longevity, diagnostics, functionality, and memory

Fig. 30.19 Reentrant circuits. *Panel A* = unidirectional block, *Panel B* = slow conduction, *Panel C* = reentry circuit

test; (7) echocardiography; (8) signal average ECG; and/or (9) SPECT/MuGA. Currently, an electrophysiological study using cardiac catheterization and/or insertable cardiac monitors is the most commonly used invasive diagnostic procedure.

Therapeutic interventions to manage tachyarrhythmias have a common objective of affecting the behavior of myocardial cells or the conduction of the electrical impulse in the diseased tissue. They include attempts to correct the underlying complication such as coronary reperfusion in the presence of a myocardial infarction, restoration and maintenance of normal sinus rhythm with antiarrhythmic drugs, use of electrical therapies such as antitachycardia pacing, cardioversion, defibrillation, and lastly, ablation performed surgically or with the assistance of a catheter. The role of medical devices in the management of these arrhythmias will become clear as device function is described in subsequent text.

30.5.3 ICD Indications

As was the case for the pacing indications previously discussed, the indications for an ICD are also complex. The indications by class are shown in Table 30.7 [2].

Table 30.7 Recommendations for implantable cardioverter defibrillators

Class I	ICD therapy is indicated in: 1. patients who are survivors of cardiac arrest due to VF or hemodynamically unstable sustained VT after evaluation to define the cause of the event and to exclude any completely reversible causes (Level of Evidence: A) 2. patients with structural heart disease and spontaneous sustained VT, whether hemodynamically stable or unstable (Level of Evidence: B) 3. patients with syncope of undetermined origin with clinically relevant, hemodynamically significant sustained VT or VF induced at electrophysiological study (Level of Evidence: B) 4. patients with LVEF less than 35 % due to prior MI who are at least 40 days post-MI and are in NYHA functional Class II or III (Level of Evidence: A) 5. patients with nonischemic DCM who have an LVEF less than or equal to 35 % and who are in NYHA functional Class II or III (Level of Evidence: B) 6. patients with LV dysfunction due to prior MI who are at least 40 days post-MI, have an LVEF less than 30 %, and are in NYHA functional Class I (Level of Evidence: A) 7. patients with nonsustained VT due to prior MI, LVEF less than 40 %, and inducible VF or sustained VT at electrophysiological study (Level of Evidence: B)
Class IIa	ICD implantation is reasonable for: 1. patients with unexplained syncope, significant LV dysfunction, and nonischemic DCM (Level of Evidence: C) 2. patients with sustained VT and normal or near-normal ventricular function (Level of Evidence: C) 3. patients with HCM who have one or more major risk factors for SCD (Level of Evidence: C) 4. the prevention of SCD in patients with ARVD/C who have one or more risk factors for SCD (Level of Evidence: C) 5. reducing SCD in patients with long-QT syndrome who are experiencing syncope and/or VT while receiving beta-blockers (Level of Evidence: B) 6. nonhospitalized patients awaiting transplantation (Level of Evidence: C) 7. patients with Brugada syndrome who have had syncope (Level of Evidence: C) 8. patients with Brugada syndrome who have documented VT that has not resulted in cardiac arrest (Level of Evidence: C) 9. patients with catecholaminergic polymorphic VT who have syncope and/or documented sustained VT while receiving beta-blockers (Level of Evidence: C) 10. patients with cardiac sarcoidosis, giant cell myocarditis, or Chagas disease (Level of Evidence: C)
Class IIb	ICD therapy may be considered in patients with: 1. nonischemic heart disease who have an LVEF of less than or equal to 35 % and who are in NYHA functional Class I (Level of Evidence: C) 2. long-QT syndrome and risk factors for SCD (Level of Evidence: B) 3. syncope and advanced structural heart disease in whom thorough invasive and noninvasive investigations have failed to define a cause (Level of Evidence: C) 4. a familial cardiomyopathy associated with sudden death (Level of Evidence: C) 5. LV noncompaction (Level of Evidence: C)
Class III	ICD therapy is not indicated: 1. for patients who do not have a reasonable expectation of survival with an acceptable functional status for at least 1 year, even if they meet ICD implantation criteria specified in the Class I, IIa, and IIb recommendations above (Level of Evidence: C) 2. for patients with incessant VT or VF (Level of Evidence: C) 3. in patients with significant psychiatric illnesses that may be aggravated by device implantation or that may preclude systematic follow-up (Level of Evidence: C) 4. for NYHA Class IV patients with drug-refractory congestive heart failure who are not candidates for cardiac transplantation or CRT-D (Level of Evidence: C) 5. for syncope of undetermined cause in a patient without inducible ventricular tachyarrhythmias and without structural heart disease (Level of Evidence: C) 6. when VF or VT is amenable to surgical or catheter ablation (e.g., atrial arrhythmias associated with the Wolff-Parkinson-White syndrome, RV or LV outflow tract VT, idiopathic VT, or fascicular VT in the absence of structural heart disease) (Level of Evidence: C) 7. for patients with ventricular tachyarrhythmias due to a completely reversible disorder in the absence of structural heart disease (e.g., electrolyte imbalance, drugs, or trauma) (Level of Evidence: B)

ARVD/C arrhythmogenic right ventricular dysplasia/cardiopathy, *CRT-D* cardiac resynchronization therapy device and defibrillator, *DCM* dilated cardiomyopathy, *HCM* hypertrophic cardiomyopathy, *ICD* implantable cardioverter defibrillator, *LV* left ventricle, *LVEF* left ventricular ejection fraction, *MI* myocardial infarction, *RV* right ventricle, *SCD* sudden cardiac death, *VF* ventricular fibrillation, *VT* ventricular tachycardia

Adapted from Adapted from ACCF/AHA/HRS Guidelines [2]

30.5.4 External Cardiac Defibrillators

External defibrillators have become ubiquitous in most countries worldwide. In addition to traditional use in hospitals and by paramedics, these systems are now commonly found in many schools, public buildings, airplanes, and even in homes. As with ICDs, these systems are used to treat sudden cardiac death. These systems deliver high-voltage shocks (up to 360 joules) directly to the chest of the patient, using either patches or paddles. One electrode is typically placed in the right pectoral region and the second in the left axilla for delivery of this energy (Fig. 30.20).

30.5.5 Implantable Cardioverter Defibrillators

Similar to a pacemaker, an ICD is a self-contained, implantable computer with an integral pulse generator and battery. In addition to providing pacing therapies for bradyarrhythmia and tachyarrhythmia, ICDs also deliver high-energy discharges. The major components of an ICD include: (1) a battery; (2) electronic circuitry and associated components; (3) high-voltage capacitors; (4) high-voltage transformers; (5) a telemetry antenna; (6) a reed switch triggered upon application of a magnetic field; and (7) a connector block. To date, this componentry is most commonly housed within a hermetically sealed stamped titanium case. Feedthroughs connect the internal circuitry to an external connector block, which acts as the interface between the internal circuitry of the ICD and the leads. The connector block is commonly fabricated from a molded polyurethane superstructure, which houses metallic contacts for interconnection with the leads. The contacts may be simple machined blocks or "spring-type" metallic beams. Most connector blocks used today have set screws to ensure permanent retention of the leads. A cutaway view of an ICD can be found in Fig. 30.21.

Fig. 30.20 An external cardiac defibrillator (LIFEPAK® 1000, Medtronic, Inc.)

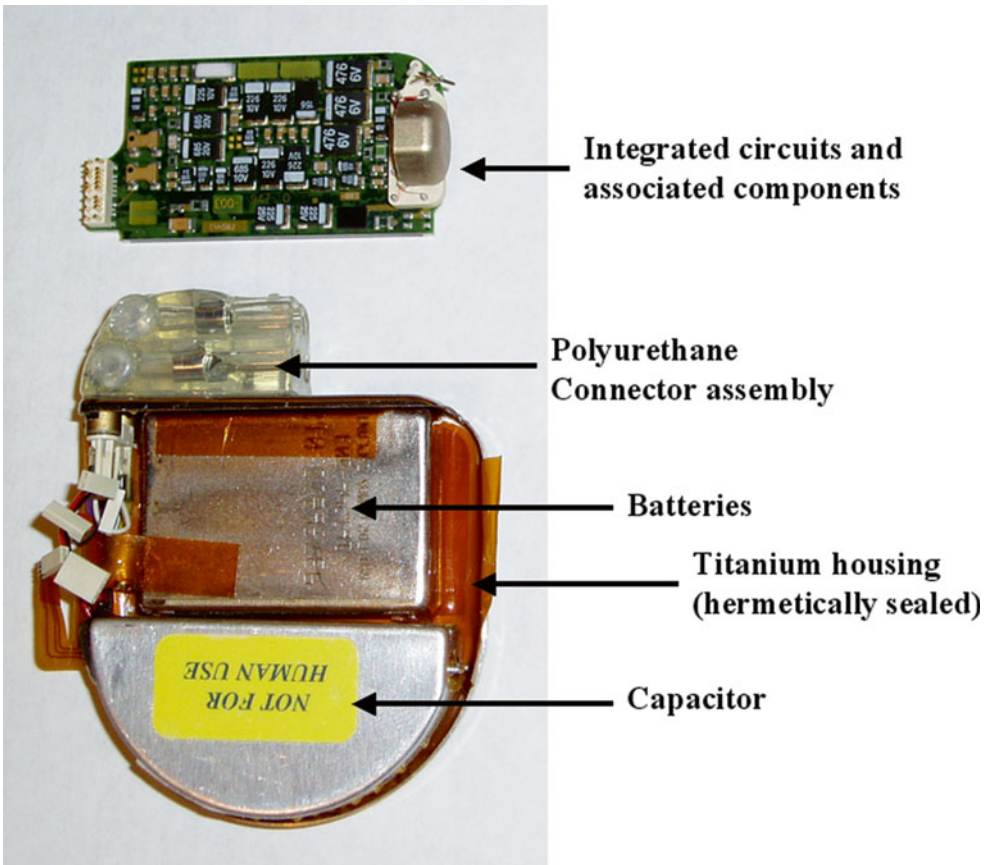

Fig. 30.21 The inner workings of a modern implantable cardioverter defibrillator (*ICD*). A portion of the titanium housing has been removed to expose the typical internal components

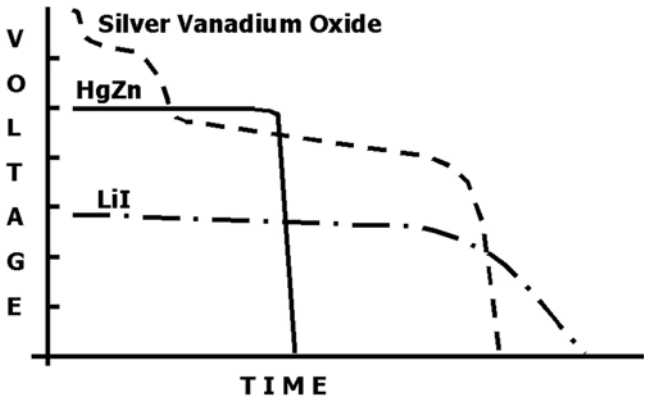

Fig. 30.22 A typical example of an implantable cardioverter defibrillator (*ICD*) depletion curve for a silver vanadium oxide battery. Lithium iodide and mercury zinc batteries included for comparative purposes

Today, most ICDs will use one or two batteries with silver lithium vanadium oxide chemistry. A typical full charge of this type of battery is 3.2 V. As the ICD battery energy starts to deplete, the voltage will follow the path shown in Fig. 30.22, where there are two characteristic plateaus. The voltage is provided to the clinician upon device interrogation to determine if the battery is at the beginning of life, middle of life, elective replacement indicator, or end of life [36]. Each manufacturer and each device will have its own elective replacement indicator voltage. This value is representative of the voltage and current drain from the circuitry, and is also related to the characteristics of the capacitor used. All devices should be replaced before end of life is reached. The longevity of such devices depends on the number of therapies delivered, but is typically between 6 and 8 years.

The primary function of the ICD's capacitor is the accumulation and storage of an adequate amount of energy to shock-terminate a fibrillating heart. As previously mentioned, a typical voltage of an ICD battery is 3.2 V, whereas the capacitor can store up to 800 V (delivering energy of 30–35 joules). Periodic conditioning of each capacitor is required to maintain charge efficiency and therefore guarantee short charge times to allow rapid conversion of the arrhythmia [37]. The materials currently used in the capacitors slowly lose efficiency, especially when they are not used for a period of time due to a chemical decay process. This process (termed *deformation*) is mitigated by conditioning the capacitors (termed *reformation*). Reforming of the capacitor should be performed regularly by charging the capacitor to its maximum capacity and leaving the charge on it until it gradually discharges the energy. Fortunately, reformation can be easily programmed at regular intervals in most modern devices (e.g., every 6 months) without affecting the patient.

30.5.6 Sensing and Detection

It is desirable for an ICD to be able to accurately sense ventricular rhythms that vary in amplitude, rate, and/or regularity, in order to distinguish between normal sinus rhythm, ventricular tachycardia, ventricular flutter, ventricular fibrillation, and/or supraventricular (atrial) arrhythmias (see examples in Fig. 30.23). Current devices adjust their sensitivity on a beat-to-beat basis in order to sense fine waves of ventricular fibrillation and to avoid oversensing of intrinsic T-waves. If an ICD undersenses (misses cardiac activity that it was intended to detect), the device may fail to treat a ventricular tachycardia, which subsequently may accelerate into ventricular fibrillation. If an ICD oversenses, overestimating the cardiac rate, it may deliver inappropriate therapy which will lead to patient discomfort or, more seriously, it may even induce a tachyarrhythmia.

The steps involved in sensing and detection are similar to those discussed previously for the pacemakers. In fact, almost all ICDs on the market today include the pacing algorithms described previously, with additional functionality/logic for detection and management of tachyarrhythmias. Arrhythmia detection typically occurs via the following steps: (1) sense the R-wave or P-waves; (2) measure the interval or cycle length between consecutive beats; and (3) compare the cycle length to prescribed detection zone intervals to classify the arrhythmia (Fig. 30.24). For the sake of simplicity, this chapter will focus on only two detection zones—the ventricular fibrillation and ventricular tachycardia zones. A fibrillation zone is commonly programmed to detect any interval faster than the interval prescribed by the clinician (e.g., 320 ms = 187.5 beats per minute). If a minimum number/percentage of beats is sensed within this interval, the rhythm will be detected as ventricular fibrillation and the device will treat the rhythm using the high-energy shock amplitudes preprogrammed by the clinician.

During the process of arrhythmia detection, the device counts the number of events in each of the detection zones and compares them to prescribed rules in order to classify the arrhythmia. Most ICD designs employ two different counters when classifying whether an arrhythmia is ventricular fibrillation or a ventricular tachycardia. The ventricular fibrillation counter uses a probabilistic approach. Since ventricular fibrillation waves are chaotic and vary in amplitude and cycle length, the device will look for a programmed percentage of cycle lengths to fall within the fibrillation detection zone (e.g., 75 %, Fig. 30.25); if that criterion is met, the device will detect a ventricular fibrillation and deliver the appropriate therapy. Ventricular tachycardias, on the other hand, usually have regular cycle lengths. A consecutive event counter is used which states that a programmed number of

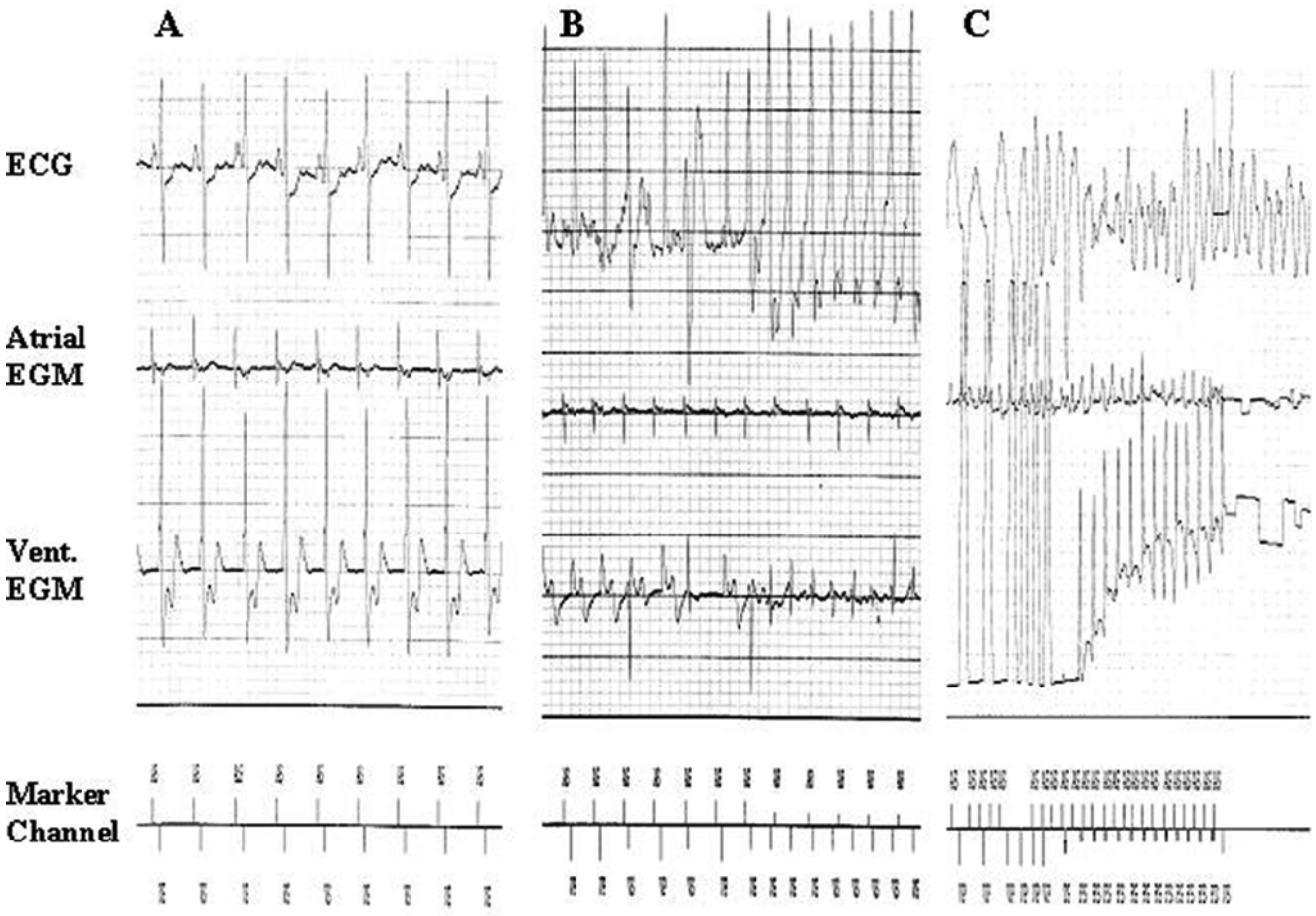

Fig. 30.23 Examples of recorded tachyarrhythmias and the associated device response (refer to the marker channel). *Panel A* = sinus rhythm; *Panel B* = spontaneous ventricular tachycardia; *Panel C* = atrial fibrillation resulting in ventricular fibrillation. *ECG* electrocardiogram, *EGM* electrogram

cycle lengths (e.g., 18 out of 18) needs to be within the tachycardia detection zone in order to classify the rhythm as a ventricular tachycardia. If one cycle length falls out of the tachycardia detection zone, the consecutive counter is reset to zero and the count begins again. Each ICD has the capability to redetect the same arrhythmia if the initial therapy was not successful. Redetection criteria will often be more aggressive (fewer number of beats sampled) than the initial detection criteria to ensure that subsequent therapies can be delivered quickly. An example of when the redetection criteria may not be as aggressive is in cases where the patient has a long QT interval and is prone to developing Torsades de Points which may spontaneously terminate.

Typical devices available today have the option of programming an additional detection zone, which is referred to as a *fast ventricular tachycardia* zone. This is a zone that can be programmed for those patients with a fast ventricular tachycardia who may benefit from antitachycardia pacing. Treating a fast ventricular tachycardia with antitachycardia pacing may decrease the number of high-voltage shocks delivered, increase the patient's quality of life, and prolong device longevity [38]. Evidence of the benefit of this therapeutic approach was seen in the PainFREE Rx trial which concluded that fast ventricular tachycardias with ventricular cycle length less than 320 ms could be terminated by antitachycardia pacing 3 out of 4 times with a low incidence of acceleration into ventricular fibrillation and syncopal episodes [38]. If a fast ventricular tachycardia zone is programmed, the device will always ensure that the most aggressive therapy is being delivered. For example, if a fast ventricular tachycardia is detected, the device will verify that no ventricular fibrillation intervals falls within that fast ventricular tachycardia zone before delivering antitachycardia pacing.

When targeting treatment of ventricular arrhythmias, it is important to verify that the arrhythmia is of a ventricular origin. Therefore, it is common that each manufacturer will have a unique algorithm for distinguishing a supraventricular tachycardia from a ventricular tachycardia. This is very important in order to avoid inappropriate shocking of a

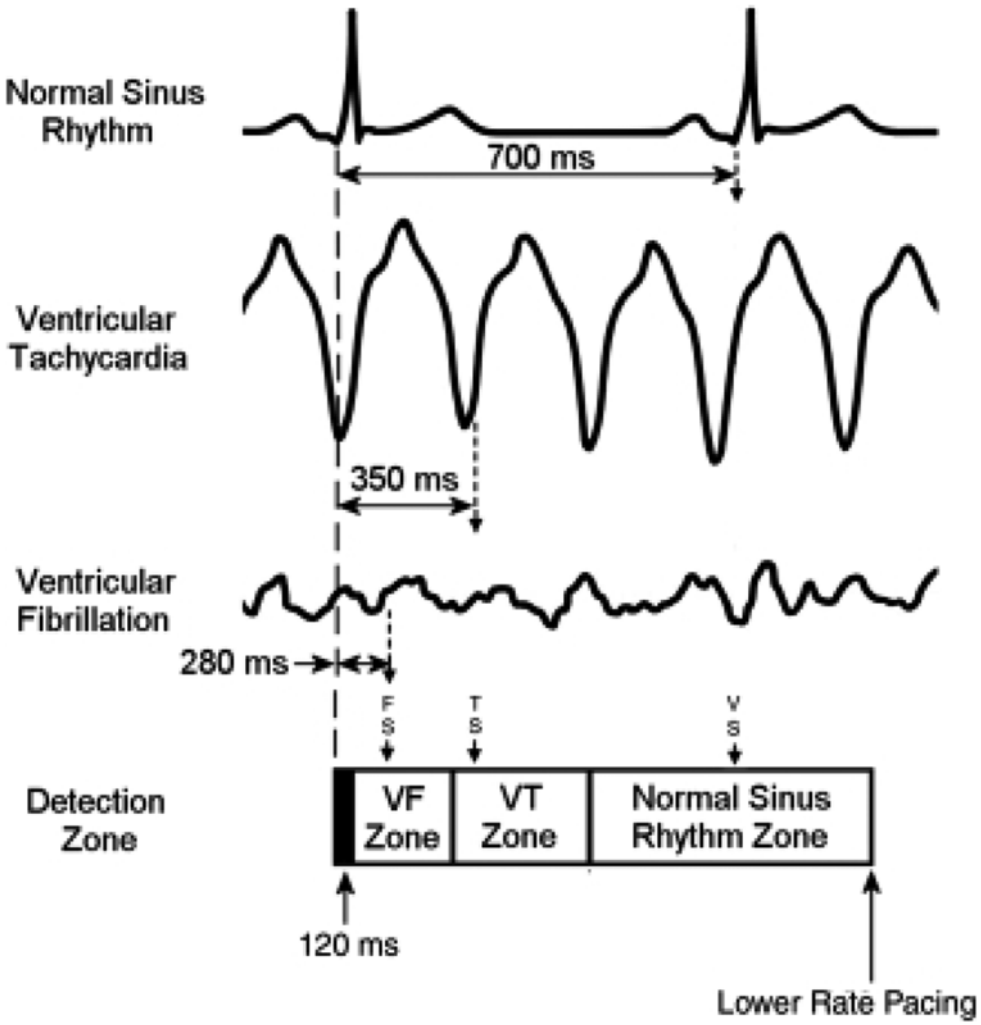

Fig. 30.24 Tachyarrhythmia detection intervals. The *top three traces* represent typical electrocardiograms that might be encountered by the device. The detection zones for ventricular fibrillation, ventricular tachycardia, and sinus rhythm are shown at the *bottom*. Note that an event with a cycle length of 700 ms is categorized as sinus rhythm, 350 ms as a ventricular tachycardia, and 280 ms as ventricular fibrillation. *VF* ventricular fibrillation, *VT* ventricular tachycardia

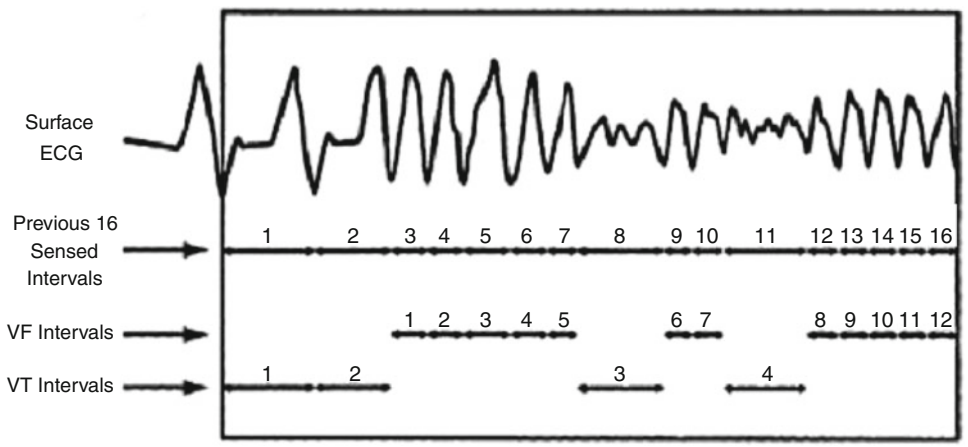

Fig. 30.25 An example of an implantable cardioverter defibrillator (*ICD*) device record including 16 consecutive beats and their classification. Since 12 of 16 events (75 %) were within the ventricular fibrillation detection zone, the arrhythmia would be classified as ventricular fibrillation and high-voltage shocks would be delivered. *ECG* electrocardiogram, *VF* ventricular fibrillation, *VT* ventricular tachycardia

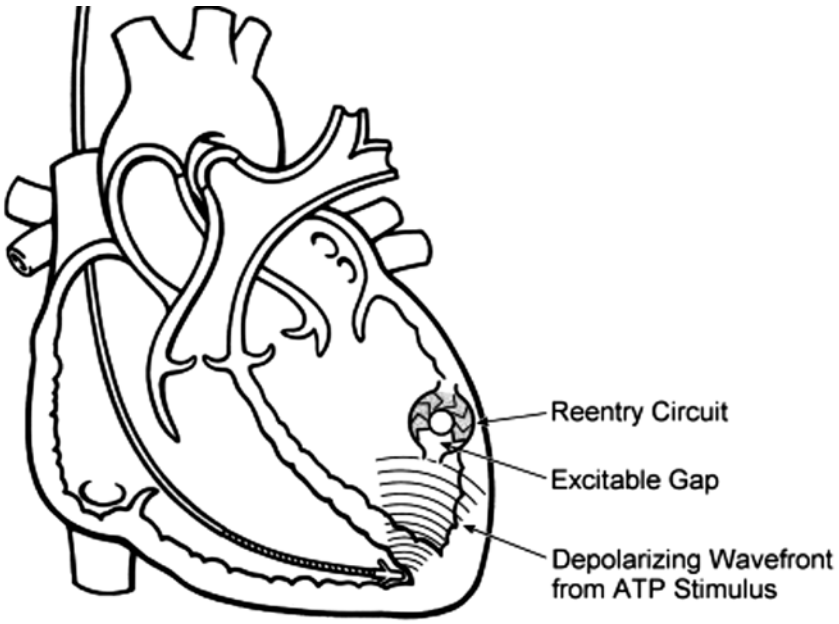

Fig. 30.26 Antitachycardia pacing therapy. A pacing stimulus is applied to entrain an excitable gap in the reentrant circuit. This disrupts the reentrant circuit and terminates the tachycardia. *ATP* antitachycardia pacing

patient with sinus tachycardia due to exercise or an atrial arrhythmia (atrial fibrillation or atrial flutter).

30.5.7 ICD Therapies

ICD therapies are programmed to ensure maximum patient safety, while attempting to deliver the lowest energy therapies (least painful and least impact on device longevity) that will terminate the arrhythmia. ICD therapies can be tiered, such that the device initially delivers low energy which is subsequently increased until the desired treatment is obtained. A typical delivery order is as follows: antitachycardia pacing (delivering the least amount of energy), followed by cardioversion, and finally defibrillation. Nevertheless, each of these therapies can be programmed to the physician's preference.

Antitachycardia pacing is typically used in a clinical situation where one reentrant circuit is repeatedly activating the ventricles and causing a rapid, but regular, ventricular tachycardia. The goal of the antitachycardia pacing therapy is to deliver, via a pacing stimulus, a depolarization wave into the area of the excitable gap (an area of repolarized tissue) of the reentry circuit. Recall that a reentrant circuit causes the majority of tachyarrhythmias. Thus, if a pacing pulse reaches the excitable gap before a new wavefront of the reentrant circuit, the reentrant activity is terminated (Fig. 30.26).

Cardioversion and defibrillation shocks are high-energy shocks that are delivered between two or three high-voltage electrodes, one of which is typically the ICD itself (i.e., the titanium housing acts as an electrode). The goal of these shocks is to defibrillate a critical mass of the myocardial cells

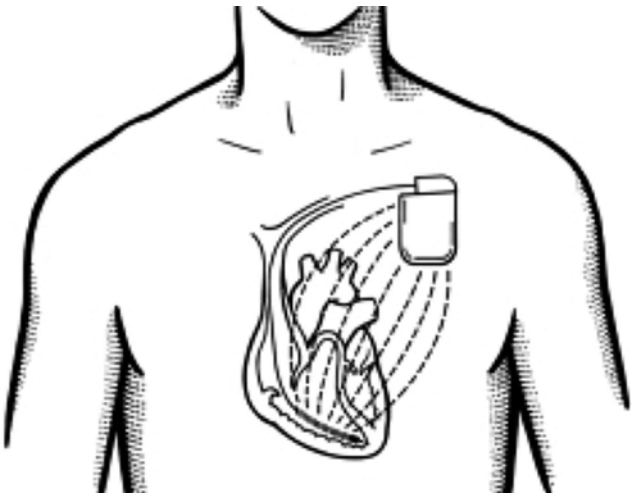

Fig. 30.27 Electric field between high-voltage electrodes during a shock; note that the implantable cardioverter defibrillator (*ICD*) is functioning as one of the electrodes

that are depolarizing at a rapid and irregular rate (Figs. 30.27 and 30.28), thus returning the heart to a normal rhythm.

Cardioversion can be described as a synchronized high-voltage shock because the shock needs to be synchronized to an R-wave or the shock will not be delivered. Cardioversion shocks are used to treat ventricular tachycardias or regular fast ventricular tachycardias. Therefore, the shock is delivered on an R-wave that has been detected in the tachycardia detection zone. If the shock would happen to be delivered on a T-wave, the underlying arrhythmia could be dangerously accelerated into ventricular fibrillation, which is why a cardioversion shock will be aborted if it is not synchronized

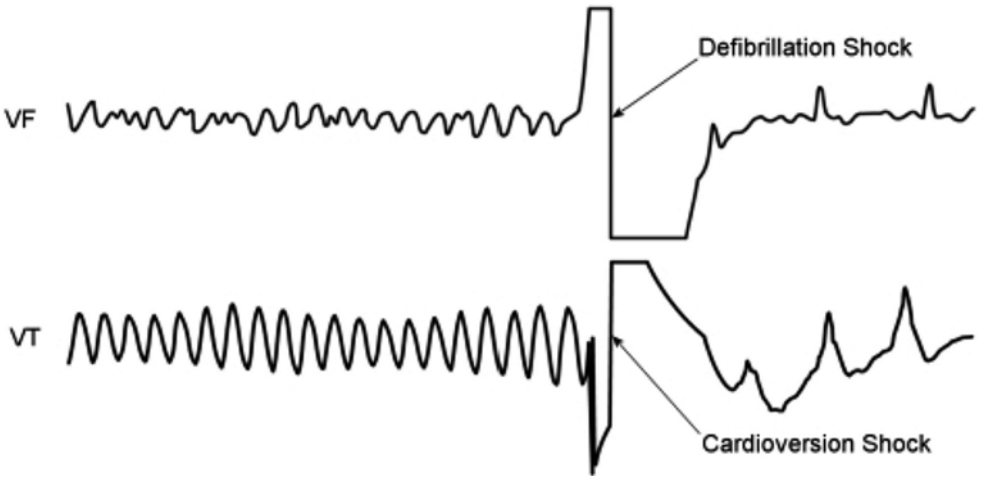

Fig. 30.28 Examples of successful defibrillation (*top electrogram*) and cardioversion (*lower electrogram*) therapies. *VF* ventricular fibrillation, *VT* ventricular tachycardia

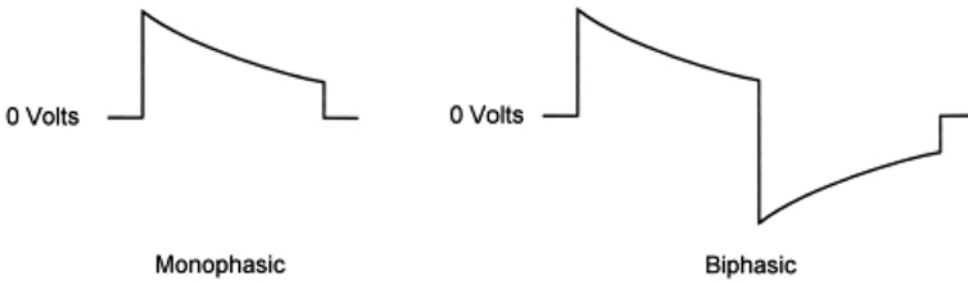

Fig. 30.29 Monophasic and biphasic shock waveforms

to an R-wave. The chaotic nature of ventricular fibrillation is treated by delivering an asynchronous shock. Both cardioversion and defibrillation gain their energy from the discharge of the ICD's high-voltage capacitor.

Depending on the manufacturer, each device will offer a number of programmable therapies per detection zone, again all of which can be programmed to physician preferences. Yet, the programming of the defibrillation therapy is typically based on a specific patient's defibrillation threshold. This threshold is defined as the minimum amount of energy needed to rescue the heart from the fibrillating state (various algorithms exist for determining this energy). The physician commonly will set the first defibrillation therapy at an energy output that is greater than the defibrillation threshold, to provide a margin of safety for the patient. A safety margin of at least 10 joules greater than the defibrillation threshold is common. For example, if a patient's defibrillation threshold has been determined to be 15 joules, the device will be programmed to deliver its first therapy at 25 joules. Therefore, the maximum output of the device needs to be considered when assessing an appropriate safety margin. If a device has a maximum output of 35 joules and the patient's defibrillation threshold is 30 joules, there would only be an 5-joule safety margin.

The relative shape of shock waveforms delivered by the ICD has evolved over time. Early systems used a monophasic waveform delivered between a dedicated set of electrodes (i.e., delivered with a constant direction of current flow or polarity). Later, sequential monophasic shocks between selected pairs of electrodes were employed, since they were found to produce lower defibrillation thresholds in certain patients. Modern devices typically use a biphasic shock that reverses polarity during the discharge of the capacitors (Fig. 30.29).

The development of biphasic waveforms was considered as a significant improvement in ICD technology, and they have been almost exclusively used since the mid-1980s [39]. The percentage of the drop in voltage, prior to termination of the waveform, is the current polarity, also known as *tilt.* Tilt is measured from the instant the current starts to flow in one direction (leading edge) to the time that it ends its flow in that same direction (trailing edge). A tilt value can be measured for each direction that the current is flowing; typical tilts are between 50 and 65 % (Fig. 30.30).

As mentioned previously, most modern ICDs also include pacemaker functionality. As a final summary of the similarities and differences between IPGs and ICDs, Table 30.8 is provided.

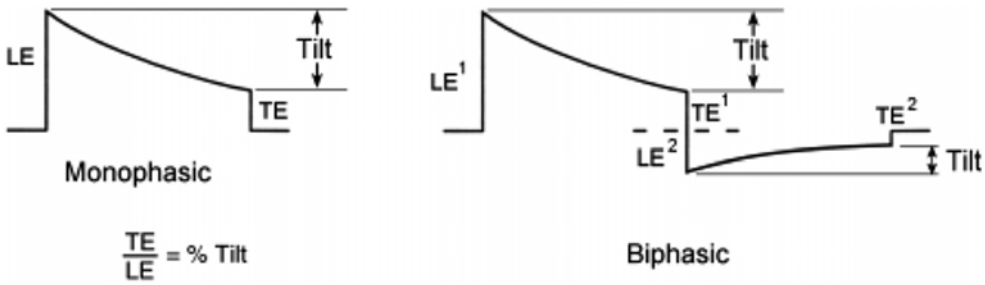

Fig. 30.30 Determination of the percent tilt of a defibrillation waveform. *LE* leading edge, *TE* trailing edge

Table 30.8 Comparison of the principal differences between implantable pulse generator (IPG) and implantable cardioverter defibrillator (ICD)

ICD	IPG
Senses intrinsic rhythms, ventricular tachycardia/ ventricular fibrillation, and prefers to oversense	Senses intrinsic rhythms, and prefers to undersense
Paces and shocks when appropriate	Paces when appropriate
Saves episode data	Rejects signals that occur at high rates
Battery requires high current capability for shocking	Battery optimized for long-term, low current use

30.5.8 Pharmacologic Considerations in the Management of Tachyarrhythmias

In contrast to the relatively small effect that antiarrhythmic drugs typically have on pacing thresholds, the defibrillator threshold of an ICD may be significantly altered when used in conjunction with antiarrhythmic drug therapies. Nevertheless, there are several positive benefits that have been considered useful in the concomitant use of ICDs and antiarrhythmic drugs. For example, antiarrhythmic drugs may act to decrease the frequency and duration of sustained and nonsustained ventricular tachycardia events that would otherwise require a shock from an ICD. In addition, they may also slow the rate of the ventricular tachycardia to increase the efficacy of antitachycardia pacing, decreasing the need for shock therapy. Lastly and importantly, antiarrhythmic agents may lower defibrillation thresholds. Therefore, the use of antiarrhythmic drugs with ICDs can decrease the frequency and/or amplitude of therapeutic shocks, thereby improving patient comfort and prolonging battery longevity [40].

As opposed to the benefits explained earlier, there are also potentially undesired consequences associated with the concurrent use of ICDs and antiarrhythmic drugs [13]. Specifically, antiarrhythmic drugs may: (1) alter the detection of the arrhythmia leading to an increase in the duration of a tachyarrhythmia; (2) increase defibrillation thresholds, making it more difficult to successfully defibrillate the heart; (3) slow the rate of the tachyarrhythmia so much that it no longer falls within the detection zone for both antitachycardia pacing and shock; and/or (4) increase the width of the QRS complex on the EKG, thus causing double counting and inappropriate shocks. The typical antiarrhythmic drugs that may affect defibrillation thresholds are: (1) Type I agents, those with sodium channel blocking activities and the membrane stabilization effects; (2) beta-blockers and calcium channel antagonists due to their effect on the nodal tissues; and (3) Type III agents which may either increase or decrease defibrillation thresholds after long-term therapy (Table 30.9) [14]. Studies have also revealed that the use of illicit drugs, such as cocaine, may increase defibrillation thresholds.

Table 30.9 Impact of select antiarrhythmic drugs on defibrillation thresholds

Increase	Mixed effect	Decrease
Flecainide	Quinidine	Sotalol
Propafenone	Procainamide[a]	Bretylium
Lidocaine	Amiodarone[b]	Dofetilide

[a]Procainamide, a Class Ia antiarrhythmic drug, is metabolized to *N*-aceylprocainamide (NAPA) which has Class III activity
[b]Amiodarone decreases defibrillation thresholds initially but increases defibrillation thresholds with chronic utilization

Antiarrhythmic agents can also be proarrhythmic, which may even lead to an increased requirement for ICD therapies. Predisposing factors to proarrhythmias are: (1) prolonged ventricular repolarization (i.e., prolonged QT wave); (2) electrolyte imbalances such as hypomagnesemia or hypokalemia; (3) underlying ventricular arrhythmias; (4) ischemic heart disease; and/or (5) poor left ventricular function. One of the most dangerous forms of proarrhythmia is considered to be Torsades de Pointes or "twisting of the points." Specifically, Torsades is a rapid form of polymorphic ventricular tachycardia that is associated with delayed ventricular repolarization. It should be noted that both inherited conditions such as long QT syndrome and exposure to Type Ia or Type III

antiarrhythmic drugs that prolong the refractory period on the cardiac action potential put patients at an increased risk of Torsades de Pointes.

30.5.9 New Indications/Recent Clinical Trials

This section will focus on some of the recent clinic trials assessing the value of ICD therapy. Clinical trials serve the important role of assessing therapeutic safety and efficacy for: (1) determining the validity of current clinical indications; (2) discovering new indications for use; and/or (3) driving reimbursement through identification of clinical value. Properly run clinical studies continue to play an important role in continuous improvement of patient outcomes. Yet, an important distinction to make here is that there are major differences between primary and secondary studies. Specifically, primary studies seek to find morbidity and mortality benefit in those patients who have not experienced an event. These studies identify a patient population that is considered "at risk" and attempt to determine means to treat such patients before they experience an event such as myocardial infarction or sudden cardiac arrest. In contrast, secondary studies evaluate post-treatment morbidity and mortality benefits to patient populations that have already suffered from an event (e.g., postmyocardial infarction patients or patients who have survived sudden cardiac arrest).

An example of an important clinical trial associated with the identification of the indications for ICD therapy is the Multicenter Automatic Defibrillator Implantation Trial (MADIT). This trial was instrumental in providing clinical evidence for identifying patients who would benefit from an ICD therapy. The clinical hypothesis stated "in patients with previous myocardial infarction and left ventricular dysfunction, prophylactic therapy with an ICD improves survival versus treatment with conventional medical therapy" [41]. The primary end point of the study was a reduction in total patient mortality, and the secondary end points evaluated mortality-associated with arrhythmias as well as cost-effectiveness. Of 196 patients included in the study, there were 39 deaths in the conventional therapy arm and 15 deaths in the ICD group. The stated conclusions were that, in postmyocardial infarction patients at a high risk for ventricular tachycardia, prophylactic therapy with an ICD reduced overall mortality by 54 % and arrhythmic mortality by 75 % when compared with conventional therapy.

A follow-up to MADIT was the Multicenter Automatic Defibrillator Implantation Trial-II (MADIT-II). The purpose of this study was to investigate the effects of prophylactic implantation of an ICD on the survival of patients postinfarction who presented with significant left ventricular dysfunction (left ventricular ejection fraction $\leq$30 %). The primary conclusion of this study was that prophylactic implantation of an ICD in such patients resulted in improved survival and decreased mortality by 28 % after 3 years. Importantly, the noted benefits of this study have changed practice in that physicians now routinely implant an ICD in postmyocardial infarction patients with left ventricular dysfunction [42].

30.5.10 Pacing and Defibrillation Leads

Cardiac pacing and defibrillation leads are the electrical conduit between the IPG or ICD and the heart. Specifically, they transmit therapeutic energy to the cardiac tissue and return sensed information to the IPG or ICD for diagnostic and monitoring purposes. It is noteworthy that such leads must: (1) withstand the extremely harsh environment of the internal human body and its intense foreign body responses; (2) permanently span multiple anatomic and physiologic features, e.g., the moving body and heart (Fig. 30.31); and (3) undergo approximately 400 million heartbeat-induced deformations over each 10-year period within the heart (see online Video 30.15).

Leads can be placed either endocardially or epicardially, depending on the patient's indication, physician preference, and/or anatomic considerations. In the case of the endocardial pacing systems (those implanted through the venous system to the endocardial surface of the cardiac chambers), the lead travels from subcutaneous tissue including muscle and fat into the blood stream. These leads then pass through the upper vasculature and finally are permanently placed within the beating heart. Today, the vast majority of pacing and defibrillation systems utilize endocardial leads (this lead placement technique can be viewed in online Video 30.6). In contrast, epicardial leads are attached directly to the surface of the heart and are routed through the subcutaneous tissue to the ICD or IPG. Epicardial leads are most commonly used in pediatric patients and in adults with compromised venous accesses to their hearts. Typical implanted configurations for endocardial single- and dual-chamber pacing systems are shown in Fig. 30.32, endocardial defibrillation systems in Fig. 30.33 and online Video 30.16, and an epicardial defibrillation system with epicardial pacing leads in Fig. 30.34.

Modern leads are generally constructed of highly biostable and biocompatible polymers and metals. Configurations for the body of the leads (i.e., the portion traveling from the IPG or ICD to the distal electrodes) are chosen based on the number of circuits required, as well as considerations relating to size, handling, and manufacturer preferences (Fig. 30.35). The electrodes for stimulation and sensing are designed to provide stable electrical performance acutely and chronically.

In order to provide stability at the cardiac–tissue interface, leads often use a mechanism for fixation to cardiac tissue and structures. Passive mechanisms for fixation include

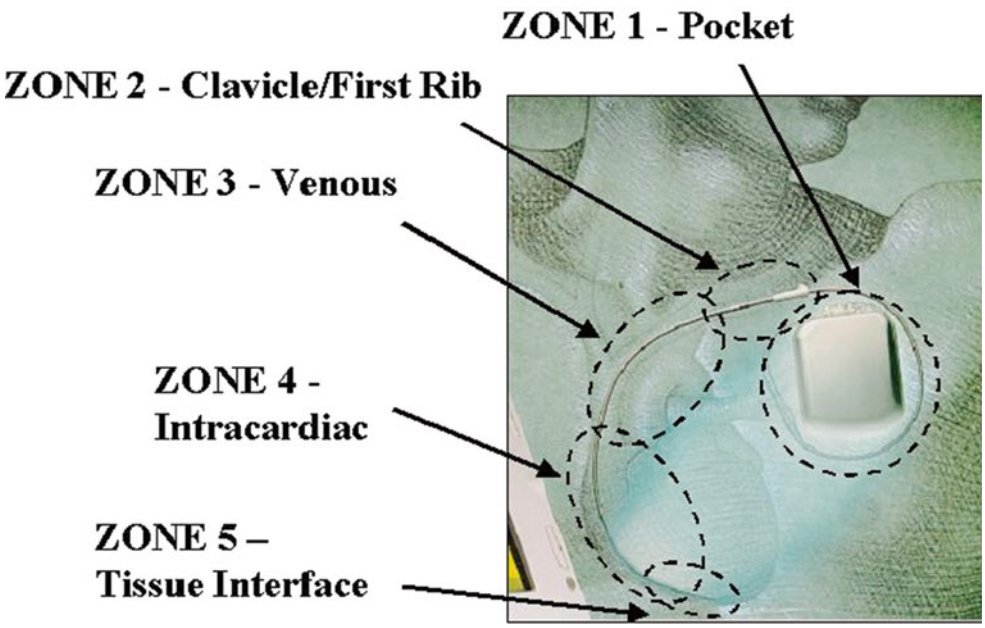

Fig. 30.31 The anatomic regions commonly spanned by transvenous endocardial pacing leads

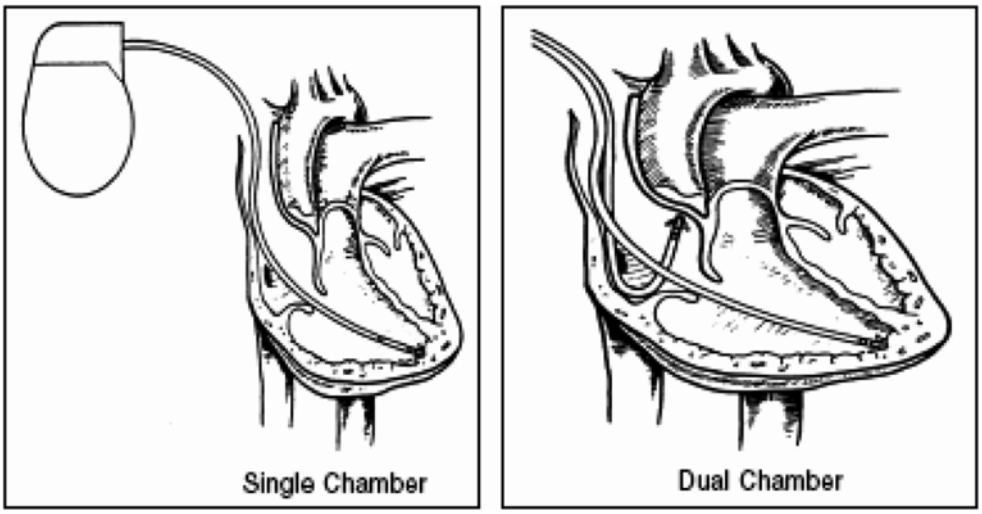

Fig. 30.32 Examples of single- and dual-chamber endocardial lead configurations

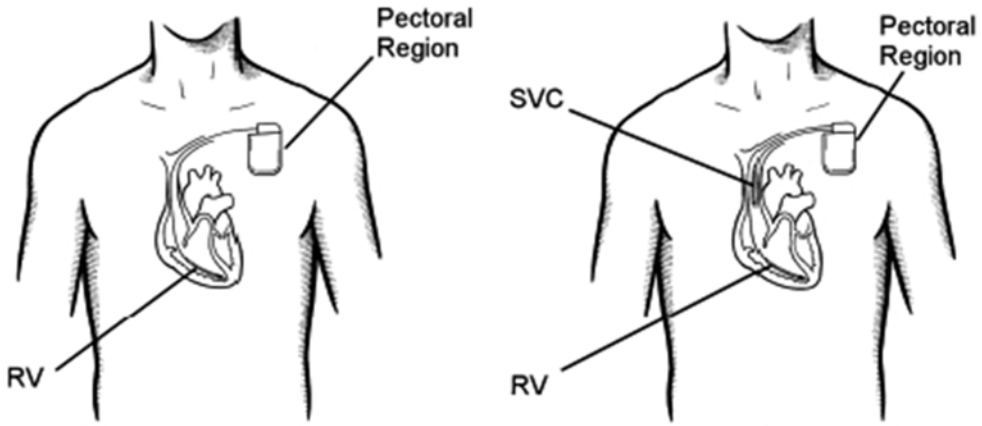

Fig. 30.33 Implanted configurations for two endocardial defibrillation systems with pectoral ICD placements. The single coil system (*left*) delivers the shock energy from the right ventricular coil to the ICD. The dual coil system (*right*) can deliver the energy from right ventricular coil to the ICD, or from the right ventricular coil to a superior vena cava coil and/or the ICD (see Video 30.16). *RV* right ventricle, *SVC* superior vena cava

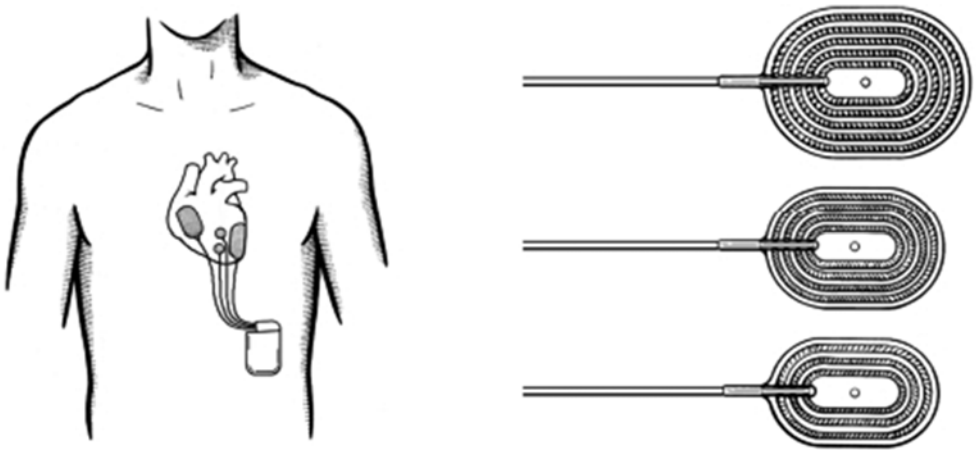

Fig. 30.34 Implanted configuration of an epicardial defibrillation system with an abdominal ICD placement. The system shown includes two unipolar epicardial pacing leads for stimulation and sensing as well as a pair of epicardial defibrillation patches

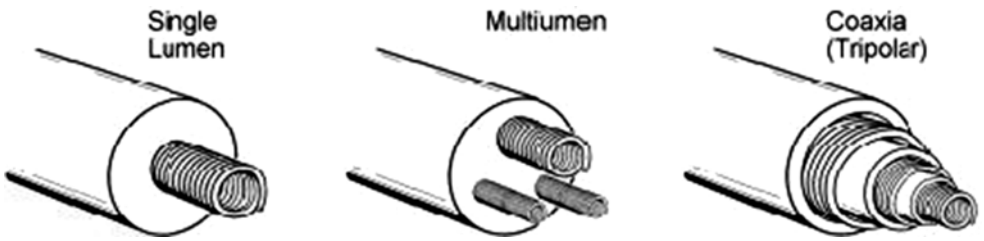

Fig. 30.35 Typical constructions used for cardiac pacing and defibrillation leads: (1) the single lumen design (*left*) has a central conductor surrounded by a polymeric insulation; (2) the multilumen design (*center*) uses an extruded polymer to insulate the conductors from one another and from the implanted environment; and (3) the coaxial design has conductors embedded within concentric layers of insulation. Today, the most commonly used insulation materials are silicones and polyurethanes and the conductors are usually coiled or cabled wires. Modern lead body diameters range from approximately 4–10 French (one French = 1/3 of a millimeter)

polymeric tines and shaped segments along the length of the lead. They are termed *passive* because they do not require an active deployment by the clinician. Common active means of fixation include helices, hooks, or barbs. Additionally, some epicardial leads require sutures to maintain a stable position. Finally, some leads have no fixation means whatsoever and count solely on lead stiffness to maintain locational stability (Figs. 30.36, 30.37, 30.38, and 30.39). To view examples of leads placed within the Visible Heart® preparation, see the following online material: Video 30.17, Video 30.18, Video 30.19, Video 30.20, and Video 30.21.

Various electrode configurations have been utilized on a variety of commercially available leads. As described previously, unipolar pacing circuits use a lead with a single cathodal electrode, with the IPG serving as the anode. Bipolar pacing systems use electrodes placed distally on the lead as both the cathode and anode. Pacing leads commonly use a cylindrical electrode placed along the lead body (ring electrode) as the anode, while defibrillation leads may use a dedicated ring (the so-called *true bipolar* leads) or a defibrillation coil as the anode (an *integrated bipolar* lead). Defibrillation leads utilize electrodes with large surface areas, which allow for the delivery of high-energy shocks within and around the heart. Defibrillation leads may be unipolar (defibrillation electrode only) or they may have a combination of defibrillation electrodes and pacing electrodes. The most common defibrillation lead configurations used today

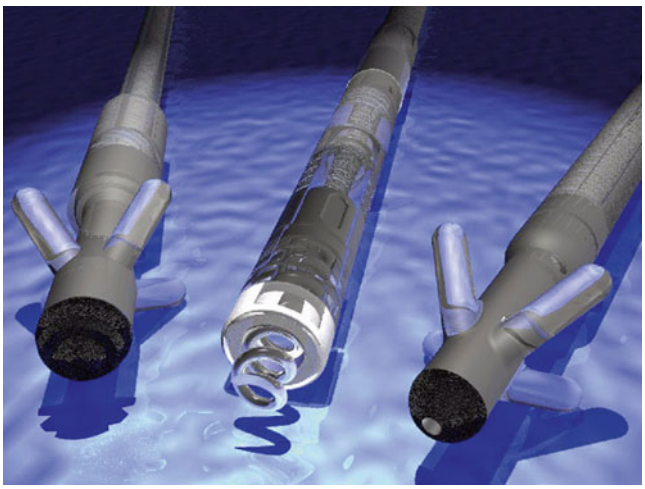

Fig. 30.36 Endocardial pacing leads: passive fixation leads (tined) are shown on the *left* and *right*. An active fixation lead (extendable, retractable helix) is shown in the *center*

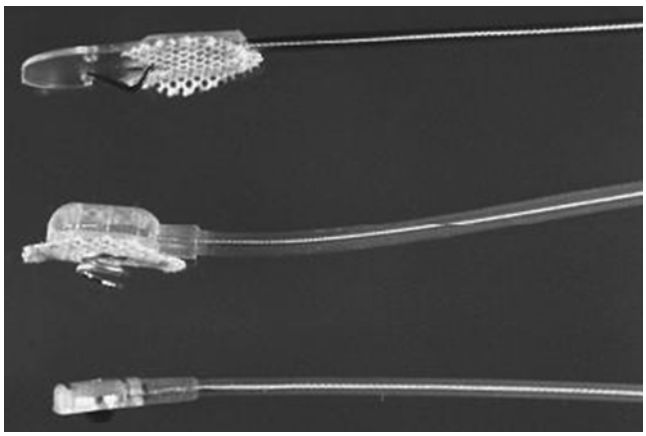

Fig. 30.37 Epicardial pacing leads: stab-in active fixation lead (*top*), active fixation lead with helical fixation (*middle*), and a hemispherical electrode secured by sutures (*bottom*)

are shown in Figs. 30.38, 30.39, and 30.40. For examples of leads placed within the Visible Heart® preparation, see the following online material: Video 30.22 and Video 30.23.

Typically, the portion of the lead that interfaces with the cardiac tissue has been designed to: (1) minimize inflammatory responses; (2) provide low polarizations; (3) provide high capacitances and impedances; and/or (4) act as a fixation mechanism. This distal electrode is most commonly used as the cathode but, in some cases, a similar electrode is used as the anode on a separate unipolar lead. To suppress inflammation, most modern electrodes incorporate a system for the elution of an anti-inflammatory agent (e.g., dexamethasone sodium phosphate); this helps to manage acute changes in the local tissue which will then aid in stabilizing pacing and sensing performance. Coatings are also applied to many pacing electrodes to produce a large surface area that is

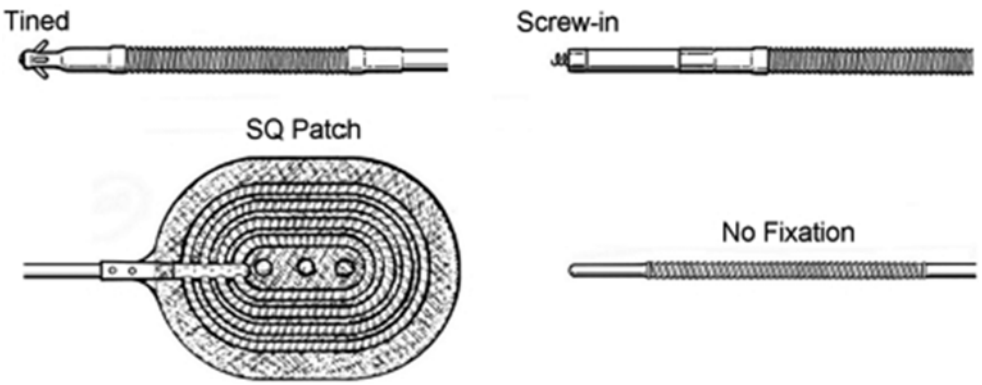

Fig. 30.38 Cardiac defibrillation leads. Clockwise from upper left: a passive fixation endocardial lead ("integrated bipolar"), an active fixation endocardial lead ("true bipolar"), an endocardial lead with no fixation, and an epicardial patch (commonly sewn to the pericardium)

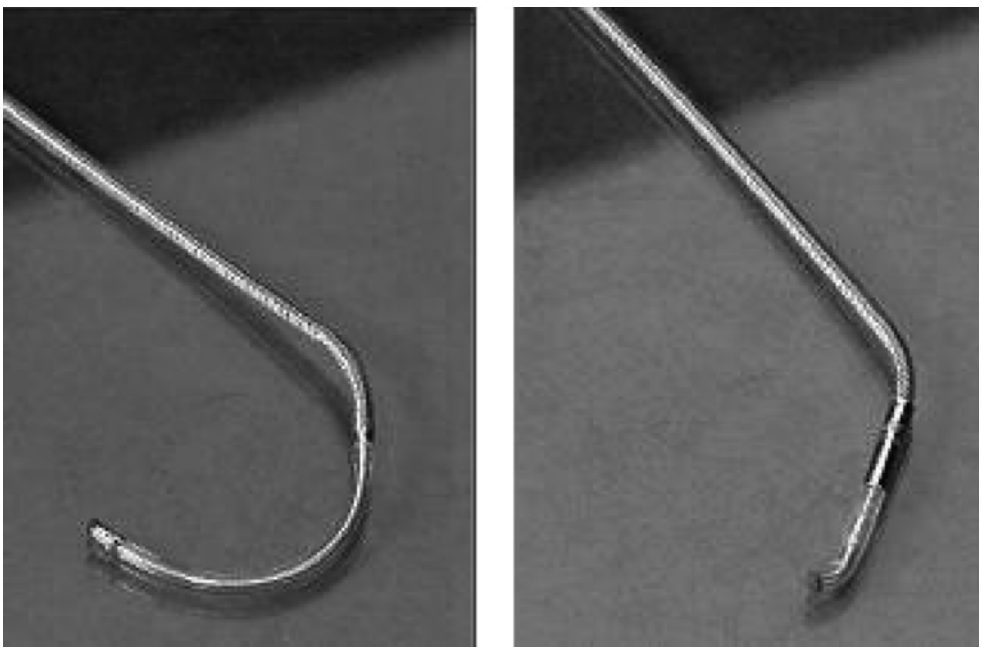

Fig. 30.39 Pacing leads designed for placement in the cardiac veins; they are shaped to enhance stability. The leads shown are primarily used in biventricular pacing systems for the management of heart failure patients with the appropriate clinical indications

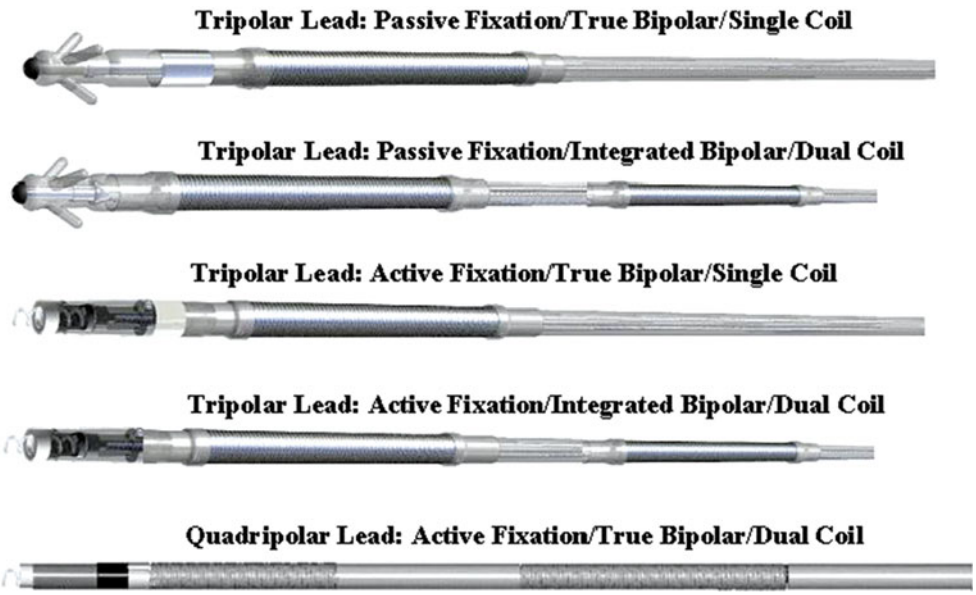

Fig. 30.40 Endocardial defibrillation leads. Various configurations are shown, including leads with active and passive fixation mechanisms, true and integrated bipolar pace/sense circuits, and/or single and dual defibrillation electrodes. The designs shown are typically placed in the right ventricle with the distal defibrillation coil within the right ventricular chamber and the proximal coil located in the superior vena cava

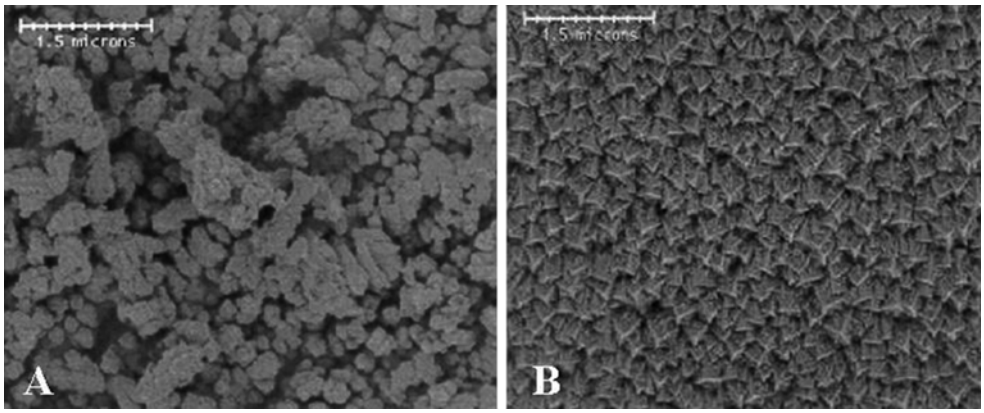

Fig. 30.41 Common electrode coatings for high capacitance and low polarization. The left panel (**A**) shows a platinized surface at 20,000× and the right panel (**B**) a titanium nitride (TiN) surface at 20,000×

highly capacitive (i.e., to reduce battery drain), and have a low level of polarization following a pacing pulse (to avoid undersensing; Fig. 30.41). Interestingly, the size of the pacing cathode has decreased over time, as a means to increase the cathode-tissue impedance and increase system efficiency by reducing current drain (Figs. 30.42 and 30.43) [43].

30.5.11 Leadless Pacing

Although pacing systems with leads have been utilized since the inception of cardiac pacing, recent advances in miniaturization technology and battery chemistry have made it possible to develop a self-contained pacemaker small enough to be implanted entirely within the heart, i.e., while still aiming to provide similar battery longevity as in conventional pacemakers. In general, leadless pacemakers (or transcatheter-delivered pacemakers) are self-contained devices designed to be implanted within the chambers of the heart directly at the site of desired pacing. Further, by eliminating the need for a subcutaneous device pocket and insertion of permanent leads within the vasculature, some of the complications associated with traditional pacing systems can be avoided, including pocket infection/erosion/hematoma and lead dislodgement/fracture/infection.

To date, leadless pacemakers have been developed for both bradycardia and CRT patients. For example, the Micra™ Transcatheter Pacing System (Medtronic, Inc., Minneapolis, MN, USA; not available for sale, but currently under clinical investigation) is a self-contained, percutaneously delivered transcatheter pacemaker (VVIR) that is designed to be implanted in the right ventricle via femoral vein access [44, 45]. The pacemaker is 0.8 cc, 1.76 g, 25.9 mm long, and 6.7 mm in diameter and contains a 3-axis accelerometer used for rate response pacing (Fig. 30.44). In addition, the fixation mechanism consists of four self-expanding nitinol tines which are used to anchor the system within the right ventricle and to stabilize the pacing electrode

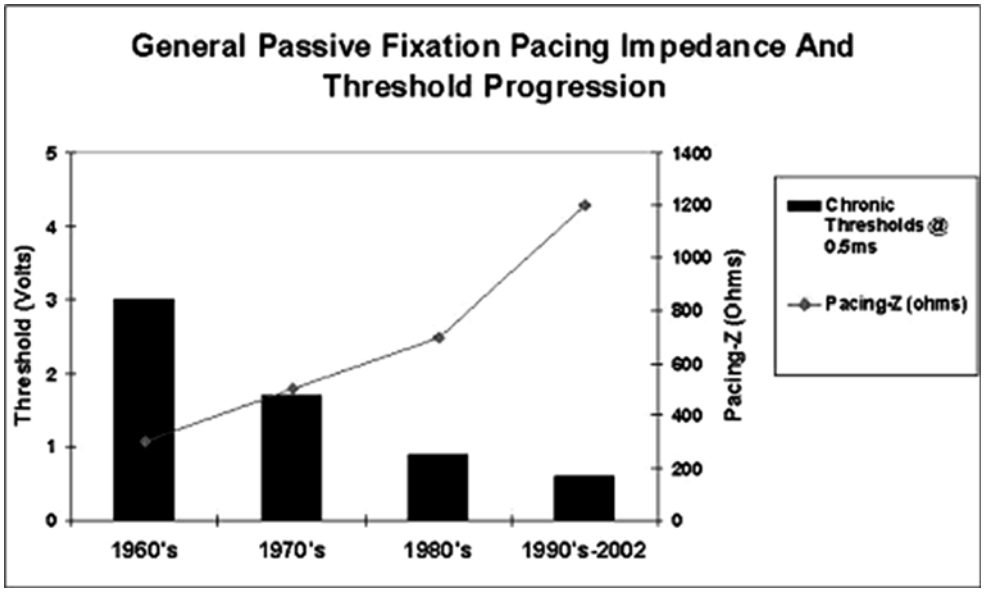

Fig. 30.42 Evolution of pacing lead impedances and pacing thresholds. Modified from Brabec and Laske [43]

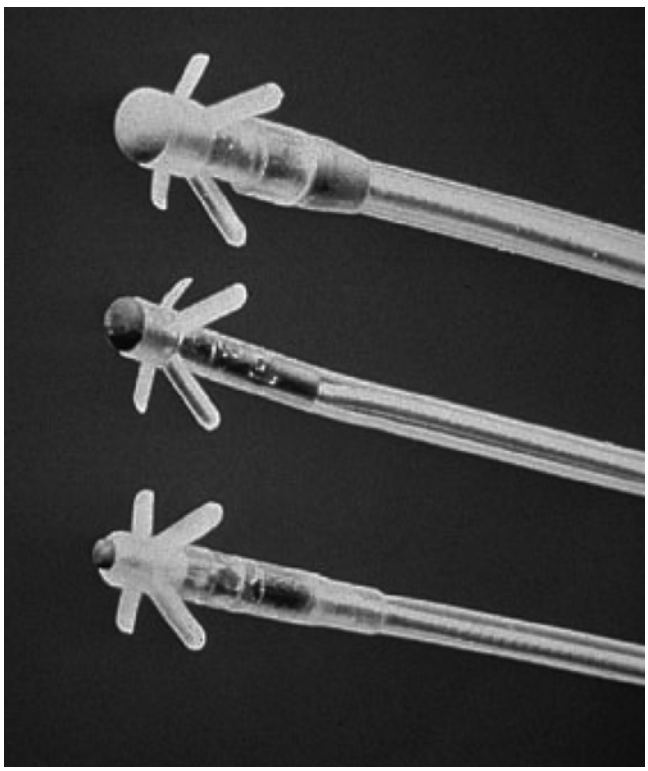

Fig. 30.43 Passive fixation leads with low (*top*; ~400–600 Ω), medium (*middle*; ~600–800 Ω), and high (*bottom*; ~800–1200 Ω) impedance pacing cathodes

Fig. 30.44 Micra™ Transcatheter Pacing System (Medtronic, Inc., Minneapolis, MN, USA; not available for sale, but currently under clinical investigation)

against viable myocardium. This system can be seen implanted in an isolated human heart using direct visualization in online Video 30.24, as published in Eggen et al. [44]. In another recent example, a VVIR leadless pacemaker is implanted in the right ventricle and attached to the myocardium using a helix mechanism (Nanostim, St. Jude Medical, St. Paul, MN, USA); this device has shown promise in the LEADLESS clinical trial [46] and in animal studies [47]. These leadless pacemakers are currently restricted to clinical investigation in the USA. Lastly, a leadless ultrasound-based endocardial left ventricular resynchronization system (WiCSw-LV system, EBR Systems Inc., Sunnyvale, CA, USA) has been developed for heart failure patients [48].

The WiCSw-LV system is a hybrid system which consists of a traditional lead system that stimulates the right atrial and right ventricular chambers, and a transmitter/receiver combination that stimulates the left ventricular endocardium. As such, after activation of the right ventricle by the traditional system, an ultrasound wave is emitted by a subcutaneous transmitter, and the ultrasound energy is converted into pacing energy by a receiver (containing a pacing electrode) implanted in the left ventricle which results in left ventricular stimulation. With these recent developments in pacemaker technology, we can expect the leadless pacemaker to partially eclipse the use of the traditional pacing systems in the near future.

30.6 Summary

This chapter has reviewed the basic methodologies and devices employed to provide pacing and/or defibrillation therapy to the patient with specific needs. A brief history was provided on the use of external electricity to deliver lifesaving therapy to the heart. Although significant progress has been made, future developments in materials, electronics, and communication systems (e.g., wireless) will allow ever-increasing utility and patient value.

Acknowledgements We would like to thank Mike Leners for the development of procedural animations, Medtronic Training and Education for the use of various graphics, the Visible Heart® team for support in capturing the intracardiac footage, Monica Mahre for editorial support, LifeSource, and Drs. Anne Fournier and Suzanne Vobecky of Sainte-Justine Hospital, Montreal, Quebec, Canada for the radiographic images.

References

1. Maisel WH, Sweeney MO, Stevenson WG, Ellison KE, Epstein LM (2001) Recalls and safety alerts involving pacemakers and implantable cardioverter-defibrillator generators. JAMA 286:793–799
2. Epstein AE, Darbar D, DiMarco JP et al (2012) ACCF/AHA/HRS focused update incorporated into the ACCF/AHA/HRS 2008 guidelines for device-based therapy of cardiac rhythm abnormalities: a report of the American College of Cardiology Foundation/American Heart Association Task Force on Practice Guide. Circulation 127:e283–e352
3. Bernstein AD, Daubert JC, Fletcher RD et al (2002) The revised NAPSE/BPEG generic code for antibradycardia, adaptive-rate, and multisite pacing. Pacing Clin Electrophysiol 25:260–264
4. Furman S (1995) A brief history of cardiac stimulation and electrophysiology—the past fifty years and the next century. NASPE Keynote Address
5. His W Jr (1893) Die Tatigkeit des embryonalen Herzens und deren Bedcutung fur die Lehre von der Herzbewegung beim Erwachsenen. Artbeiten aus der Medizinischen Klinik zu Leipzig 1:14–49
6. Tawara S (1906) Das reizleitungssystem des saugetierherzens, Eine anatomisch-histologische studie uber das atrioventrikularbundel und die purkinjeschen faden, Jean, Germany: Gustav Fischer 9–70, 114–156
7. Lillehei CW, Gott VL, Hodges PC, Long DM, Bakken EE (1960) Transistor pacemaker for treatment of complete atrioventricular dissociation. JAMA 172:2006–2010
8. Furman SC. Walton Lillehei http://www.naspe.org/ep-history/notable_figures/walton_lillehei. Accessed 25 Nov 2003
9. Winters SL, Packer DL, Marchlinski FE et al (2001) Consensus statement on indications, guidelines for use, and recommendations for follow-up of implantable cardioverter defibrillators. Pacing Clin Electrophysiol 24:262–269
10. Parsonnet V (1984) Indications for dual-chamber pacing. NASPE Position Statement, June 1, 1984
11. Stokes KB, Kay GN (1995) Artificial electrical stimulation. In: Ellenbogen KA, Kay GN, Wilkoff BL (eds) Clinical cardiac pacing. W.B. Saunders, Philadelphia
12. Epstein AE, DiMarcok JP, Ellenbogen KA et al (2008) ACC/AHA/HRS 2008 Guidelines for device-based therapy of cardiac rhythm abnormalities. Circulation 117:e350–e408
13. Fogoros RN (1997) Antiarrhythmic drugs: a practical guide. Blackwell Science, Boston, p 112
14. Legreid Dopp A, Miller JM, Tisdale JE (2008) Effect of drugs on defibrillation capacity. Drugs 68:607–630
15. Wilkoff BL, Cook JR, Epstein AE et al (2002) Dual-chamber pacing or ventricular backup pacing in patients with an implantable defibrillator: the Dual-chamber and VVI Implantable Defibrillator (DAVID) Trial. JAMA 288:3115–3123
16. Karpawich PP, Rabah R, Haas JE (1999) Altered cardiac histology following apical right ventricular pacing in patients with congenital atrioventricular block. Pacing Clin Electrophysiol 22:1372–1377
17. Andersen HR, Nielsen JC, Thomsen PE et al (1997) Long-term follow-up of patients from a randomised trial of atrial versus ventricular pacing for sick-sinus syndrome. Lancet 350:1210–1216
18. Lamas GA, Orav EJ, Stambler BS et al (1998) Quality of life and clinical outcomes in elderly patients treated with ventricular pacing as compared with dual-chamber pacing. Pacemaker Selection in the Elderly Investigators. N Engl J Med 338:1097–1104
19. Lamas GA, Lee K, Sweeney M et al (2000) The mode selection trial (MOST) in sinus node dysfunction: design, rationale, and baseline characteristics of the first 1000 patients. Am Heart J 140:541–551
20. Deshmukh P, Casavant DA, Romanyshyn M, Anderson K (2000) Permanent direct His bundle pacing: a novel approach to cardiac pacing in patients with normal His-Purkinje activation. Circulation 101:869–877
21. Karpawich P, Gates J, Stokes K (1992) Septal His-Purkinje ventricular pacing in canines: a new endocardial electrode approach. Pacing Clin Electrophysiol 15:2011–2015
22. Karpawich PP, Gillette PC, Lewis RM, Zinner A, McNamera DG (1983) Chronic epicardial His bundle recordings in awake nonsedated dogs: a new method. Am Heart J 105:16–21
23. Scheinman MM, Saxon LA (2000) Long-term His-bundle pacing and cardiac function. Circulation 101:836–837
24. Williams DO, Sherlag BJ, Hope RR, El-Sherif N, Lazzara R, Samet P (1976) Selective versus non-selective His bundle pacing. Cardiovasc Res 10:91–100
25. de Cock CC, Giudici MC, Twisk JW (2003) Comparison of the haemodynamic effects of right ventricular outflow-tract pacing with right ventricular apex pacing: a quantitative review. Europace 5:305–308
26. Cleland JG, Daubert JC, Erdmann E et al (2001) The CARE-HF study (CArdiac REsynchronisation in Heart Failure study): rationale, design and end-points. Eur J Heart Fail 3:481–489
27. Leclercq C, Daubert JC (2003) Cardiac resynchronization therapy is an important advance in the management of congestive heart failure. J Cardiovasc Electrophysiol 14:S30–S39
28. Saksena S (2003) The role of multisite atrial pacing in rhythm control in AF: insights from sub-analyses of the dual-site atrial pacing for prevention of atrial fibrillation study. Pacing Clin Electrophysiol 26:1565

29. Leclercq JF, De Sisti A, Fiorello P, Halimi F, Manot S, Attuel P (2000) Is dual-site better than single site atrial pacing in the prevention of atrial fibrillation? Pacing Clin Electrophysiol 23:2101–2107
30. Kindermann M, Schwaab B, Berg M, Frohlig G (2000) The influence of right atrial septal pacing on the interatrial contraction sequence. Pacing Clin Electrophysiol 23:1752–1757
31. Miake J, Marban H, Nuss B (2002) Biological pacemaker created by gene transfer. Nature 419:132–133
32. Go AS, Mozaffarian D, Roger VL et al (2014) Heart disease and stroke statistics—2014 update: a report from the American Heart Association. Circulation 129:e28–e292
33. Myerburg RJ (ed) (1997) Heart disease: a textbook of cardiovascular medicine (Chapter 24), 5th edn. W.B. Saunders, Philadelphia
34. Coronary artery disease overview. http://imaginis.com/heart-disease/cad_ov.asp?mode=1. Accessed 1 Dec 2014
35. Electricity and the heart: a historical perspective. http://www.naspe.org/ep-history/timeline. Accessed 25 Nov 2003
36. Hayes DL, Lloyd MA, Friedman PA (eds) (2000) Cardiac pacing and defibrillation: a clinical approach. Blackwell Publishing, Inc., New York, pp 1–599
37. Cummins RO (1989) From concept to standard-of-care? Review of the clinical experience with automated external defibrillators. Ann Emerg Med 18:1269–1275
38. Wathen MS, Sweeney MO, DeGroot PJ et al (2001) Shock reduction using antitachycardia pacing for spontaneous rapid ventricular tachycardia in patients with coronary artery disease. Circulation 104:796–801
39. Electricity and the heart: a historical perspective. http://www.naspe.org/ep-history/timeline/1980s. Accessed 26 Nov 2003
40. Carnes CA, Mehdirad AA, Nelson SD (1998) Drug and defibrillator interactions. Pharmacotherapy 18:516–525
41. Moss AJ, Hall WJ, Cannom DS et al (1996) Improved survival with an implanted defibrillator in patients with coronary disease at high risk for ventricular arrhythmia. Multicenter Automatic Defibrillator Implantation Trial Investigators. N Engl J Med 335:1933–1940
42. Kloner RA, Birnbaum Y (eds) (2002) Cardiovascular trials review, 7th edn. Le Jacq Communications Inc., Shelton, CT, pp 1065–1066
43. Brabec S, Laske TG (2003) The evolution of bradycardia pacing electrodes. XII World Congress on Cardiac Pacing & Electrophysiology (Hong Kong)
44. Eggen MD, Bonner MD, Williams ER, Iaizzo PA (2014) Multimodal imaging of a transcatheter pacemaker implantation within a reanimated human heart. Heart Rhythm 11:2331–2332. doi: 10.1016/j.hrthm.2014.03.052
45. *Micra Transcatheter Pacing Study* [cited 2014 November 13]; Available from: http://clinicaltrials.gov/show/NCT02004873
46. Reddy VY, Knops RE, Sperzel J et al (2014) Permanent leadless cardiac pacing: results of the LEADLESS trial. Circulation 129: 1466–1471
47. Koruth JS, Rippy MK, Khairkhahan A et al (2015) Feasibility and efficacy of percutaneously delivered leadless cardiac pacing in an in vivo ovine model. J Cardiovasc Electrophysiol 26:322–328. doi:10.1111/jce.12579
48. Auricchio A, Delnoy PP, Butter C et al (2014) Feasibility, safety, and short-term outcome of leadless ultrasound-based endocardial left ventricular resynchronization in heart failure patients: results of the Wireless Stimulation Endocardially for CRT (WiSE-CRT) study. Europace 16:681–688

Additional Text Sources

Furman S, Hayes DL, Holmes DR (eds) (1993) A practice of cardiac pacing. Futura Publishing Company, Inc., New York, pp 1–753

Ellenbogen KA, Kay GN, Wilkoff BL (eds) (1995) Clinical cardiac pacing. W.B. Saunders, Philadelphia

Cardiac Resynchronization Therapy

31

Nathan A. Grenz and Zhongping Yang

Abstract

Congestive heart failure (CHF) continues to be a major source of morbidity, mortality, and health-care spending in today's society. In the past 20 years, device-based therapies such as implantable cardioverter defibrillators (ICDs), cardiac resynchronization therapy (CRT), and left ventricular assist devices have been developed and demonstrated to improve outcomes in patients with CHF and systolic dysfunction. These therapies treat two of the major causes of death associated with CHF, namely sudden cardiac death and pump failure. This chapter focuses on the application of CRT for treatment of CHF, with a focus on the therapeutic mechanisms, historical development, evolution of the technologies, implant techniques and patient follow-ups, clinical trials, evolving indications, approaches for optimizing therapies, and future directions.

Keywords

Cardiac resynchronization therapy • Physiologic pacing • Cardiac function • Implantable cardioverter defibrillator • Congestive heart failure • Biventricular pacing • Mechanical remodeling

Abbreviations

6MWD	6-minute hall walk distance
AF	Atrial fibrillation
AV	Atrioventricular
BiV	Biventricular
CCS	Clinical composite score
CHF	Congestive heart failure
CRT	Cardiac resynchronization therapy
CS	Coronary sinus
EP	Electrophysiology
ESV	End-systolic volume
ICD	Implantable cardioverter defibrillator
ICM	Ischemic cardiomyopathy
IPG	Implantable pulse generator
IVCD	Interventricular conduction delay
LBBB	Left bundle branch block
LGE	Late gadolinium enhancement
LV	Left ventricular
LVEF	Left ventricular ejection fraction
LVLED	Left ventricular lead electrical delay
MRI	Magnetic resonance imaging
NCM	Noncontact mapping
NICM	Nonischemic cardiomyopathy
NYHA	New York Heart Association
PEA	Peak Endocardial Acceleration
PNS	Phrenic nerve stimulation
QoL	Quality of life
RA	Right atrial
RBBB	Right bundle branch block
RV	Right ventricular
SPECT	Single-photon emission computed tomography
TDI	Tissue Doppler imaging

N.A. Grenz, BSEE, CCDS, CEPS (✉) • Z. Yang, PhD
Therapy Delivery Systems Research, Cardiac Rhythm and Heart Failure, Medtronic plc, 8200 Coral Sea St NE, MVN 41, Mounds View, MN 55126, USA
e-mail: nathan.a.grenz@medtronic.com

P.A. Iaizzo (ed.), *Handbook of Cardiac Anatomy, Physiology, and Devices*, DOI 10.1007/978-3-319-19464-6_31

31.1 Introduction

Congestive heart failure (CHF) is a cardiovascular syndrome associated with high morbidity, mortality, and major healthcare expenditures. In general, it can be characterized by pump dysfunction, reduced functional capacity, neurohumoral imbalance, and/or myocardial remodeling [1]. The prevalence of CHF continues to grow, estimated in 2013, at approximately five million people in the USA alone [2]. As the number of patients with CHF grows, expenditures have also continued to climb, with estimated associated costs of $31 billion in the USA in 2012 [2]. Pharmacological treatments with beta-blockers, angiotensin-converting enzyme inhibitors, and/or angiotensin receptor blockers revolutionized therapeutic options in the 1980s and 1990s [3–7]. Also in the 1990s, interest in device-based therapies gained ground and led to the application of implantable cardioverter defibrillators (ICDs) and cardiac resynchronization therapy (CRT), which helped to reduce mortality and morbidity associated with CHF [8–12]. It should be noted that the development of new pacing leads that were able to reliably stimulate the left ventricle and new stimulator technologies enabled multisite pacemakers that could resynchronize the contractions of both ventricles and improve outcomes for CHF patients.

31.2 Development of CRT

By the early 1990s, in the decades preceding the development of CRT, advances in lead and pacing generator technologies led to reliable dual-chamber pacing systems. More specifically, the development of polyurethane leads with smaller and more lubricious lead bodies made it easier to implant two leads for both right atrial (RA) and right ventricular (RV) pacing [13]. Advances in tined lead design reduced the rate of atrial lead dislodgement from 14 % to less than 2 % [14]. Also noteworthy, lead tips with steroid elution reduced the foreign body response at the implant site, reducing chronic thresholds and the incidence of exit block [15]. Similarly, advances in integrated circuit technologies and microprocessor-based pacemakers led to the development of implantable pulse generators (IPG) with more sophisticated algorithms for novel treatments and monitoring, and the development of rate responsive pacemakers improved the quality of life and exercise capacity for patients with chronotropic incompetence [16].

Prior to development of CRT, multisite stimulation in the form of biatrial pacing had been proposed as a therapy to suppress atrial tachyarrhythmias (AT), by pacing the left atrium through the coronary sinus (CS) [17]. The Model 2188 CS lead (Medtronic plc, Minneapolis, MN, USA) was developed specifically for this purpose in collaboration with French investigators. In 1994, a patient with dilated cardiomyopathy, New York Heart Association (NYHA) class 4, QRS durations >150 ms, and left ventricular ejection fractions (LVEF) <35 % was implanted with a 4-chamber pacing system and subsequently experienced incredible improvement in symptoms [18]. The work of this group, as well as others, led to the adaptation of technologies for left ventricular (LV) stimulation, with associated intense research and development to establish CRT as a viable CHF therapy.

31.3 Mechanisms of CRT

31.3.1 Impact of Left Bundle Branch Block and CHF on Ventricular Electrical and Mechanical Functions

The native conduction system consists of the sinoatrial node, specialized atrial conduction fibers, atrioventricular (AV) node, His bundle, and right and left bundle branches which terminate in Purkinje fibers. This system provides rapid, orderly depolarization and contraction of the heart. The presence of *left bundle branch block* (LBBB) is associated with: (1) delayed contraction of the left ventricle; (2) reduced ventricular performance; and (3) widening of the QRS complex. LBBB typically leads to both interventricular and intraventricular dyssynchrony, with early depolarizations and contractions of the septum followed by delayed contractions of the LV free wall via slow cell-to-cell conductions. Overall mechanical pump function becomes reduced due to prolongations of isovolumic contractions and relaxations with shortening of the diastolic filling periods [19]. These changes in systolic and diastolic performance result in reduced LVEF. It should be noted that even the mild dyssynchronous contraction, illustrated by ventricular pacing within normal hearts, leads to differences in regional workload and oxygen consumption, with reduced workload near the septum due to early contractions against low pressures and stretching of remote, inactivated regions [20, 21]. Strain and regional work both increase the delayed segments which must contract against a higher afterload (i.e., pressure). Thus asynchronous contractions between ventricular segments with differing workload may lead to asymmetric remodeling, with thinning of the myocardial wall near early contracting segments and hypertrophy at the lateral wall [22].

The prevalence of LBBB has been reported as high as 25 % in patients with CHF [23]. LV depolarizations in LBBB are heterogeneous and may differ between patients with ischemic cardiomyopathy (ICM) and nonischemic cardiomyopathy (NICM). Endocardial mapping in patients with LBBB and normal hearts, NICM, or coronary artery disease all demonstrated that LV activation occurs after RV activation

via transseptal conduction [24]. All patients had at least one septal breakthrough site, with approximately one-third of patients having an additional site of early activation. LV activation times were significantly longer in patients with ischemic heart disease, possibly due to the impact of scar or slow-conducting tissues. Noncontact mapping (NCM) has provided further insights into LV conduction variations in patients with CHF. For example, Rodriguez et al. described two patterns of LV endocardial activation originating from the septum in LBBB and CHF: either slow conduction through a portion of the left bundle branch with mid-septal or apical breakthrough, or breakthrough at the high septum due to slow cell-to-cell conduction [25]. The former pattern tended to generate an apical and basal wavefront which met in the basal posterior lateral wall, while high septal breakthrough generated only one wavefront which spread toward the apex. These authors speculated these two patterns may also have different hemodynamic implications for the application of CRT. Aurrichio et al. also reported these differences in transseptal activation, but additionally described U-shaped conduction patterns caused by functional conduction blocks (e.g., not anatomical due to scar) in almost all CHF patients with LBBB [26]. Functional blocks were confirmed by demonstrating that the location of blocks (lateral, inferior, or anterior) could be altered by pacing from different sites. Patients with QRS durations ≤150 ms had shorter transseptal conduction times and more homogenous LV activations with a site of lateral block, while patients with longer QRS durations tended to have an anterior line of block.

NCM has also provided evidence that simultaneous biventricular (BiV) pacing can have dramatically different effects on LV conduction patterns depending on the individual. In the study by Pratola et al., LV endocardial conduction in one patient was almost completely dominated by the RV-paced wavefront during BiV pacing, i.e., due to a long delay between LV epicardial-paced activations and LV endocardial depolarizations [27]. In contrast, LV conduction in another patient was almost entirely due to the LV pacing, the result of long transseptal conduction times. In yet another patient, only BiV pacing eliminated the identified U-shaped activations and created homogenous LV depolarizations. This technique has also been used to demonstrate that LV pacing in areas of slow conduction, which are often present in patients with ICM, is associated with suboptimal hemodynamic responses [28]. Pacing in an area of normal conduction or preactivating the LV via VV delay can improve hemodynamic responses to CRT and reduce total LV activation times.

31.3.2 Improvement of Cardiac Function with CRT

In its simplest conception, CRT can improve cardiac performance by restoring coordinated contractions between the ventricular septum and LV lateral wall. This is most commonly achieved by stimulating the RV with a standard endocardial pacing lead and the LV via a transvenous lead placed in a coronary vein (Fig. 31.1). The addition of an RA lead allows control of ventricular stimulation prior to intrinsic, delayed conduction during atrial sensing and pacing. The immediate hemodynamic impact of CRT can be reflected in significant increases in maximum rate of LV pressure rise (LV dP/dt_{max}) and systolic blood pressure [29, 30]. These changes are accompanied by improvements in systolic and diastolic time intervals. In one study, AV optimization with a

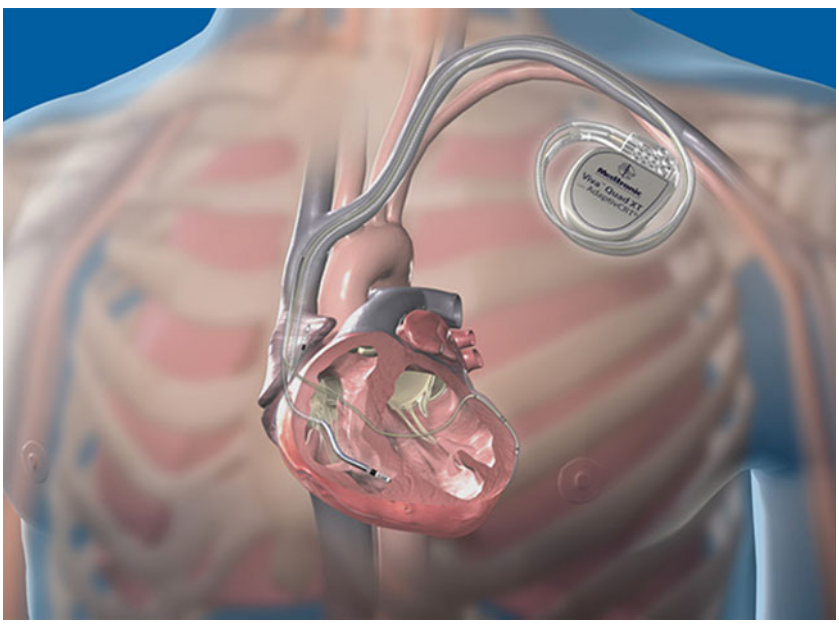

Fig. 31.1 Illustration of an implanted CRT system with right atrial, right ventricular, and left ventricular leads. Courtesy of Medtronic plc

mitral inflow method and simultaneous BiV pacing was shown to significantly increase normalized LV filling time ($p<0.001$), shorten interventricular mechanical delay ($p<0.001$), and shorten isovolumic contraction ($p<0.05$) in patients with CRT compared to controls [31]. Reduction in severity of mitral regurgitation may also occur with CRT due to improved coordination of the papillary muscle contractions, LV synchrony, and hemodynamic closing forces [32–35]. The beneficial effects of CRT have also been noted to be accompanied by a reduction in sympathetic nerve activity, which is frequently elevated in CHF patients. Reduction in sympathetic activity after CRT has, in turn, been associated with improved peak oxygen consumption (peak VO_2), LVEF, LV end-systolic volume index (ESVi), and NYHA class [36, 37]. Acute improvements are maintained chronically and further promote improvements in LV structure and volumes, termed *reverse remodeling*. In the MIRACLE study, it was shown that CRT reduced LV volumes, improved LVEF, and reduced severity of mitral regurgitation up to 12 months postimplant [38]. These changes were accompanied by reduced dyssynchrony, reflected by increased diastolic filling time, and reduced interventricular mechanical delay.

31.4 Implantation of CRT

Implantation of a CRT system typically involves delivery of an RA lead, an RV lead, and an LV lead. The RV lead is typically positioned first to allow backup pacing if the AV node is temporarily blocked during CS cannulation and delivery of the LV lead. To date, the RV apex has been the most common implant site, but other locations such as the RV septum are also used. The first step for implanting the LV lead is cannulation of the CS. A combination of an outer sheath with or without a guidewire may be used, as well as an electrophysiology (EP) catheter. An EP catheter may also be used with recording of EGMs for guidance. Once CS access is obtained, an occlusive coronary venous angiography may be performed by introducing a balloon catheter through the delivery sheath, to determine coronary veins suitable for LV lead delivery. Venography is often recorded with cine fluoroscopy in one or two views (Fig. 31.2). Some implanters may only "puff" contrast through the sheath, or not introduce contrast at all out of concern for toxicity in patients with poor kidney function or to reduce the number of steps in the procedure [39]. The LV lead can then be delivered via stylet or guidewire to the target vein. Telescoping catheter systems consisting of an inner and outer sheath can also be used to aid in the delivery of the LV lead with greater support (Fig. 31.3). These systems may reduce the number of failed implants, improve LV lead implant location, and shorten LV positioning time [40]. A lateral or posterolateral vein is often

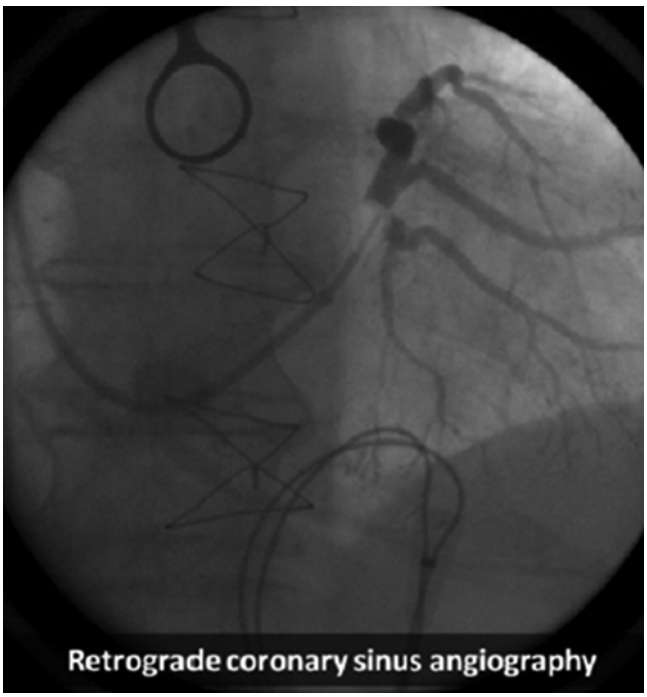

Fig. 31.2 Retrograde coronary sinus venography showing multiple coronary venous branches. Modified from Merkely et al. [166], available under a Creative Commons Attribution license. http://creativecommons.org/license/by/3.0

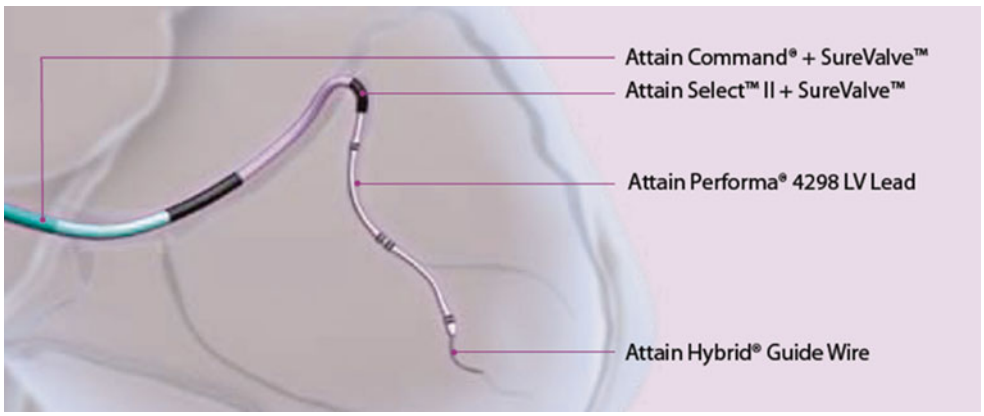

Fig. 31.3 Illustration of Attain Command® coronary sinus cannulation catheter, Attain Select™ II subselection catheter and Attain Performa® LV lead with guidewire. Courtesy of Medtronic plc

preferred for implant, based on studies that suggest these branches are more likely to be beneficial for CRT therapy than anterior positions [41, 42]. Implanters also prefer to avoid the apex for permanent LV pacing, as this location has been associated with inferior outcomes in studies such as MADIT-CRT [43]. Once a stable position is attained, electrical testing for acceptable pacing capture thresholds and phrenic nerve stimulation (PNS) is performed. An LV pacing capture threshold $\leq$2.5 V, and a difference (i.e., margin) between PNS threshold and LV capture threshold of at least 3 V, is preferred to avoid complications [44]. Note that the potential for PNS is often tested by pacing at maximum outputs (e.g., 10 V). Multiple vectors may be tested to find an acceptable configuration before resorting to repositioning the lead, i.e., when such leads have multiple pacing electrodes (see below). The delivery catheter(s) are removed after the lead position is deemed acceptable. Removal requires slitting the length of the sheath using a slitting tool or separating the sheath by hand in the case of peelable catheters. The LV lead thresholds are often retested prior to insertion into the pacing device to ensure that electrical performance has not deteriorated during removal of the implant tools. If an LV lead cannot be implanted via the transvenous approach, a common alternative is to place an epicardial lead surgically, if the procedure can be tolerated by the patient.

31.4.1 Left Ventricular Leads

Currently, a variety of lead body shapes and electrode configurations are available for LV leads. The majority of LV leads employ passive fixation, meaning the lead body shape primarily holds the lead in place. Typical shapes include compound cants, sigmoidal S-shapes, spirals, and straight leads with tines. Since dislodgement remains a concern for all lead systems, LV leads with active fixation components have also been developed. For example, the Attain Starfix® (Model 4195, Medtronic plc) lead was developed specifically to address dislodgement by incorporating deployable lobes on the lead body (Fig. 31.4) [45]. The lobes are deployed by using a tool to push the outer lead body tubing distally and forcing the lobes to expand. More recently, the Attain Stability® (Model 20066, Medtronic plc) lead has been developed with a side helix for fixation, and it has demonstrated acceptable performance through 12 months in humans (Fig. 31.5) [46]. This lead was designed to be positioned in a

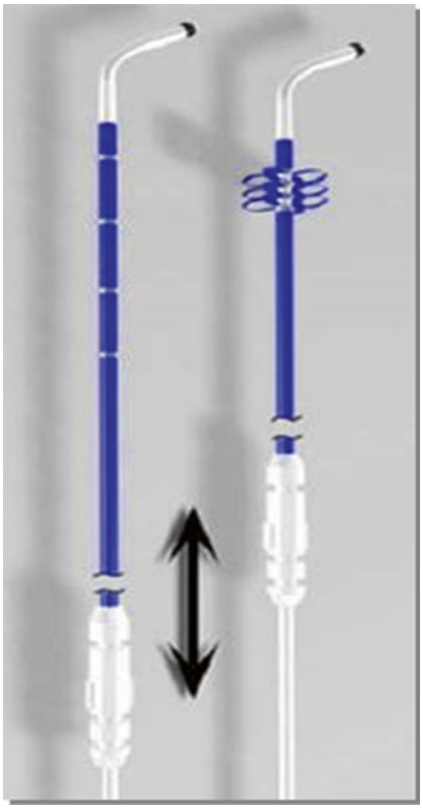

Fig. 31.4 Illustration of Attain StarFix® Model 4195 lead design with deployable lobes for fixation. Courtesy of Medtronic plc

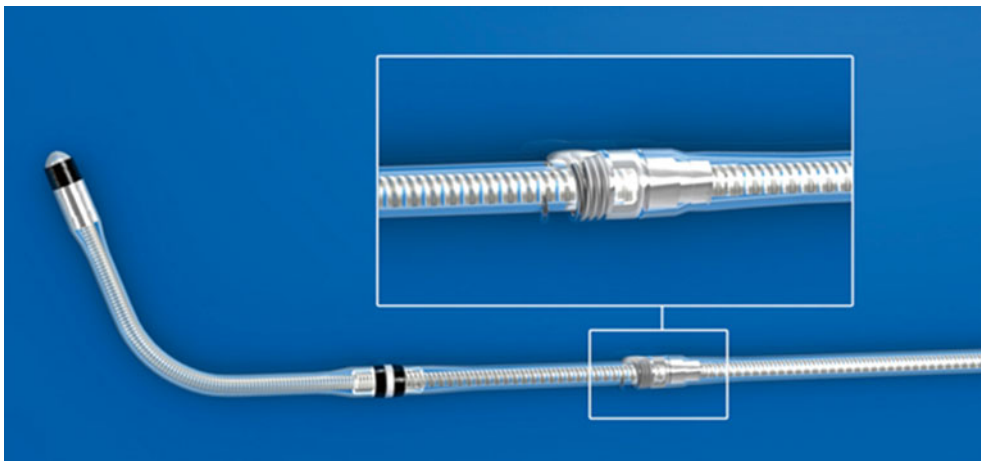

Fig. 31.5 Illustration of Attain Stability® Model 20066 lead design with co-radial helix for fixation. Courtesy of Medtronic plc

wider range of vein sizes with enhanced extractability if required.

A key characteristic of LV leads is the polarity or number of electrodes. Options include unipolar, bipolar, and quadripolar leads (Fig. 31.6). Unipolar leads are still commercially available but are less attractive due to limited options for programming LV stimulation. Bipolar leads are more common and allow three to six stimulation vectors, depending on the capabilities of the pulse generator. More recently, quadripolar LV leads have been developed to further increase the number of pacing vectors, to help manage problems such as high pacing thresholds, PNS, and/or dislodgement [47]. In contrast to unipolar and bipolar leads, quadripolar leads have a newer connector pin which conforms to the ISO 27186:2010 (E) four-pole connector standard (Fig. 31.7). This standard was developed to ensure interchangeability of leads and devices between manufacturers.

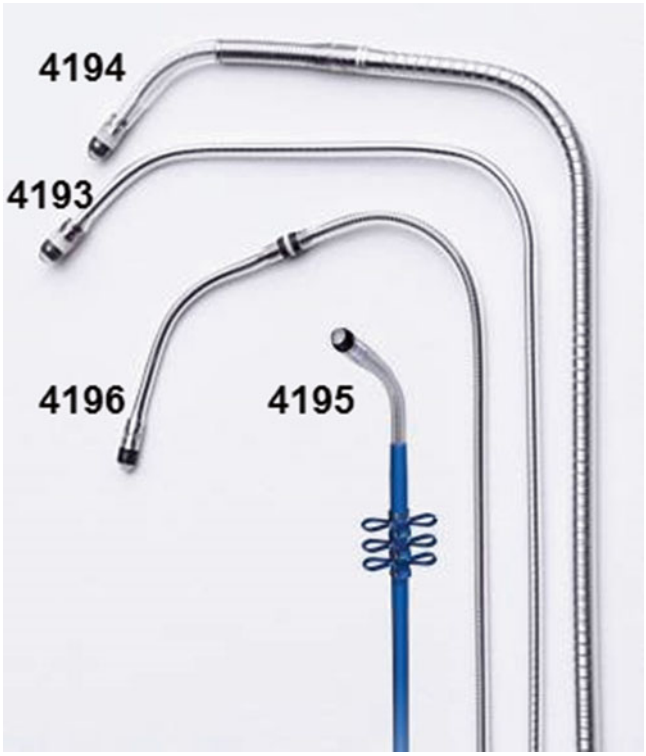

Fig. 31.6 Example of unipolar (4193 & 4195) and bipolar (4194 & 4196) LV leads. Courtesy of Medtronic Inc.

31.4.2 Complications Associated with CRT

Complications related to CRT can be divided into either acute or chronic events. Acute complications during implant include: (1) CS dissection; (2) high pacing thresholds; (3) dislodgement; and (4) stimulation of the phrenic nerve. Coronary sinus dissection occurs when the venous wall is damaged, and this is often visualized after injection of contrast. Common causes for this include the advancement of the cannulation catheter, guidewire, lead, or other implant tools into difficult anatomies. Though dissection rarely requires additional treatment intervention, the trauma may be extensive enough to prevent LV lead implantation or it may be severe enough to require pericardiocentesis to prevent tamponade. Left ventricular lead dislodgement may occur during removal of implant tools or it may be due to unstable implant positions. PNS may sometimes occur along the entire length of the target vein. Therefore, dislodgement, high thresholds or inability to capture, and PNS may cause implant failure in some cases.

Complications related to CRT have declined considerably since the therapy was introduced. For example, in one report, implant success rates by French investigators improved from 60 % without dedicated tools in the early years to 98 % by the end of the 1990s; this was accompanied by a reduction in LV lead dislodgements from 30 to 12 % during the same time period [48]. Other studies have demonstrated a learning

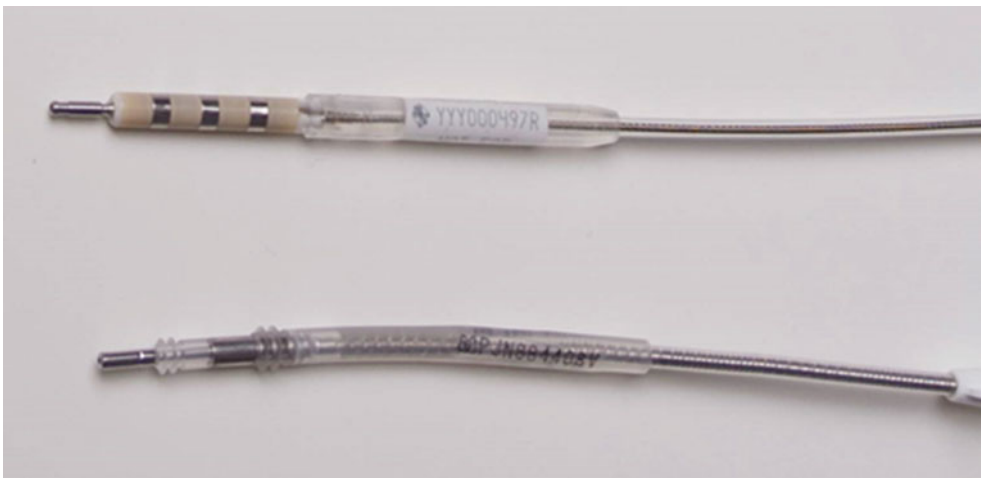

Fig. 31.7 Examples of an IS4 lead connector (*top*) and IS1 connector (*bottom*). Courtesy of Medtronic Inc.

curve for CRT, with greater implant success and lower complication rates occurring as implanting center and operator experience increases [48, 49]. Today, implant success rates of greater than 95 % are not uncommon with transvenous CRT systems, especially when repeated implant attempts are considered [50–52]. Yet, it should be noted that the etiology of CHF may also impact LV lead implant success. For example, Macias et al. found that ICM was the only independent predictor of a failed LV lead implant at a preferred empirical lateral site [52]. This may be due to lack of veins secondary to scar formation in ICM, since 50 % of ICM patients with a failed lateral implant had no target vein in this region; note that the inability to deliver the lead to the target vein was the most common reason for failed implants in NICM patients. Procedure-related complication rates have reduced over time, from 24 % of patients in the MIRACLE, MIRACLE ICD, and Insync III studies [49] to approximately 16 % in the CARE-HF study [50]. The need for LV lead reintervention after implant varies from 5 to 10 % in studies with up to 1-year follow-up [49, 51, 53]. The most frequent cause of reintervention is dislodgement in approximately 7–10 % of patients; however intractable PNS, high capture thresholds, and infections have also been noted. To date, data on coronary vein thrombosis and implant success rates after LV lead revision are relatively limited. Yet, Borleffs et al. reported an 86 % first success LV lead revision rate at a median of 85 days, and the same branch as the original implant could be used in 57 % of the cases [51]. Additionally, Biffi et al. reported that the original branch could only be used in 33 % of patients with the majority of LV lead revisions occurring less than 6 months post-implant [53].

Clinically relevant PNS is observed in approximately 20 % of patients when the LV lead is placed in a lateral or posterolateral position [54, 55]. The rate of PNS varies considerably by anatomical zone of the LV lead implant. A retrospective analysis of over 1000 patients found that a lateral lead position was associated with greater than four times the risk of PNS than an anterior position, and the apical position was associated with greater than six times the risk [53]. Pacing systems with multiple programmable cathode and anode combinations provide an effective means to avoid high pacing threshold and PNS [54, 55]. Bipolar pacing from a closely spaced electrode, recently incorporated into a quadripolar lead design (Fig. 31.8), has also been demonstrated to avoid PNS by reducing the size of the stimulating electrical fields. The resulting increases in PNS thresholds with minimal change in LV pacing thresholds thus increases the safety margin, and has been demonstrated in both preclinical and human studies [56, 57]. For more specific information about cardiac venous anatomy, see Chap. 8.

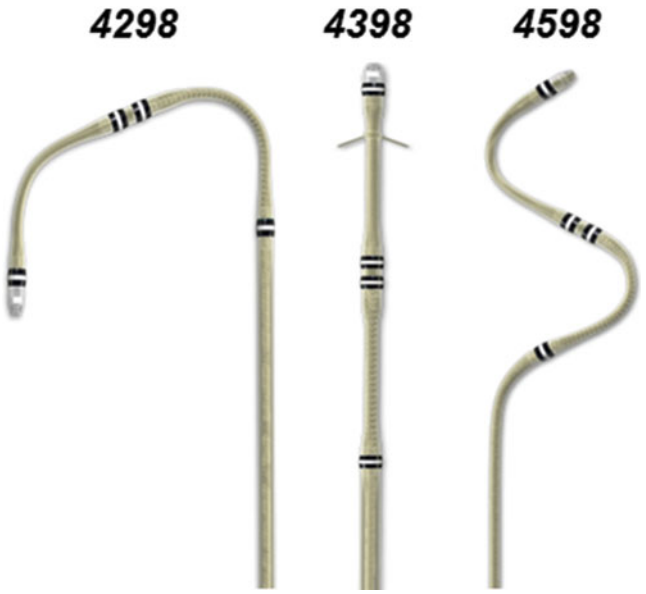

Fig. 31.8 Attain Performa® quadripolar LV lead family. Courtesy of Medtronic plc

31.5 Clinical Trials in CRT

31.5.1 Moderate-to-Severe CHF

Multicenter clinical studies of CRT began in the latter half of the 1990s. MUSTIC was a multicenter study which enrolled 67 patients with QRS durations ≥150 ms, LVEFs <35 %, and NYHA class III while receiving optimal medical therapy for at least 1 month [58]. The primary endpoint of this single-blinded, randomized, crossover study was a 6-minute hall walk distance (6MWD). Secondary endpoints included quality of life (QoL), peak oxygen consumption, CHF hospitalization, and mortality. Patients underwent a period of inactive and active pacing for 3 months each. Distance walked during the active phase was 23 % longer than during the inactive phase ($p<0.001$). Quality of life and peak oxygen consumption significantly improved during pacing, and CHF hospitalizations were reduced. PATH-CHF was a single-blinded, randomized, crossover study that enrolled 42 patients. Patients were in NYHA classes III or IV, with QRS durations >120 ms and sinus rhythms; the use of chronic univentricular or BiV pacing configuration was determined by invasive hemodynamic optimization, using aortic pulse pressure and LV dP/dt_{max} [30]. Notably, in patients with BiV therapy, LV end-systolic and end-diastolic volumes decreased, NYHA class improved, and LVEF increased from 22±7 % to 26±9 % ($p=0.03$) [59]. Around the same time period, larger randomized, double-blinded studies were initiated to definitively

demonstrate the effectiveness of CRT. The Multicenter InSync Randomized Clinical Evaluation (MIRACLE) study enrolled patients with LVEF ≤35 %, QRS duration ≥130 ms, and individuals with moderate-to-severe CHF (NYHA class III or IV) [8]. Patients were randomized to CRT or control (no pacing therapy) for 6 months. Patients receiving CRT had significantly improved 6MWD, QoL, time during treadmill exercise, and LVEF. CRT also reduced LV end-diastolic dimensions and mitral regurgitation. More patients were classified as improved (67 % vs. 39 %) by Packer's clinical composite score (CCS) and fewer patients were worsened (16 % vs. 27 %) than in the control group ($p<0.001$). Further, CHF-related hospitalizations, as well as a combined endpoint of death or CHF hospitalizations, were also reduced in the CRT group. This study led to FDA approval of CRT pacemaker (CRT-P) therapy in August 2001.

The next progression in the use of this therapy was the initiation of trials with combined CRT and defibrillator therapy (CRT-D); these were initiated to determine the additional potential benefits of CRT in patients indicated for ICD. The double-blinded CONTACT CD approval study randomized 490 patients in NYHA classes II–IV, with LVEF ≤35 % and QRS duration ≥120 ms, to either CRT-D or ICD therapy alone for up to 6 months [60]. The primary endpoint was a composite of all-cause mortality, CHF hospitalization, and occurrence of VT/VF requiring ICD therapy. Secondary endpoints included peak levels of VO_2, 6MWD, relative NYHA class, QoL, and echocardiographic changes. There was a nonsignificant 15 % reduction in the primary endpoint of the CRT group ($p=0.35$). In some patients the NYHA class improved prior to CRT because optimal medical therapy was instituted for 1 month prior to randomization. In the group with NYHA class I–II, there were no significant improvements in any secondary endpoint. In contrast, there were significant improvements in peak VO_2, 6MWD, NYHA class, and QoL in patients in NYHA classes III–IV. Based on this study, CRT-D therapy was approved by the FDA in February 2002 for patients with moderate-to-severe CHF (NYHA classes III–IV), LVEF ≤35 %, and QRS duration ≥120 ms.

Subsequently, clinical trials with longer study durations demonstrated the benefits of CRT on mortality. The Comparison of Medical Therapy, Pacing, and Defibrillation in CHF (COMPANION) trial randomized 1520 patients in NYHA classes III–IV, LVEF ≤35 % and QRS duration ≥120 ms into three groups: optimal medical therapy, CRT-P, or CRT-D [10]. The primary endpoint was time to all-cause death or hospitalization, with a secondary endpoint of all-cause death. The primary endpoint was reduced in both the CRT-P (HR = 0.81, $p=0.014$) and the CRT-D groups (HR = 0.80, $p=0.01$) with 12 months follow-up. The risk of death or hospitalization due to CHF was reduced by 34 % with CRT-P ($p<0.002$) and 40 % with CRT-D ($p<0.001$). CRT-D reduced the risk of all-cause mortality by 36 % ($p=0.003$), although the 24 % reduction with CRT-P did not reach significance ($p=0.06$). Next, the Cardiac Resynchronization-Heart Failure (CARE-HF) study demonstrated that CRT alone (CRT-P) reduced the risk of death beyond the benefits of optimal medical therapy [11]. In this trial, 813 patients in NYHA classes III–IV, LVEF ≤35 %, and with QRS duration ≥120 ms were randomized into optimal medical therapy or CRT-P. Patients with QRS intervals between 120 and 149 ms were required to meet 2 of 3 mechanical dyssynchrony criteria for inclusion. The primary endpoints were time to all-cause death or unplanned hospitalization associated with a major cardiovascular event. With a mean follow-up of 29.4 months, 39 % of patients with CRT reached the primary endpoint vs. 55 % of patients receiving only optimal medical therapy (HR = 0.63, $p<0.001$). For the principal secondary endpoint of death from any cause, the rates were 20 % in the CRT group vs. 30 % for those patients receiving optimal medical therapy (HR = 0.64, $p<0.002$). It was also noted in this trial that CRT improved interventricular mechanical delay, LV ESV, mitral regurgitation, LVEF, and QoL, which was in agreement with previous studies.

31.5.2 Mild CHF

The next major focus of clinical trials and the expansion for indications for CRT was the treatment of patients with milder CHF. The Resynchronization Reverses Remodeling in Systolic Left Ventricular Dysfunction (REVERSE) trial was a double-blinded, randomized study of patients in NYHA classes I–II, QRS ≥120 ms, and LVEF ≤40 % [61]. In this trial, 610 patients were implanted and randomized to CRT, on or off. The primary endpoint was a CHF CCS, and the prospectively powered secondary endpoint was LV ESVi. There were no significant differences in the percentage of patients categorized as "worsened" between CRT on and off over 12 months of follow-up (16 % worsened with CRT on vs. 21 % with CRT off, $p=0.10$). However, patients programmed to CRT elicited significant improvements in LV ESVi and had longer time to first CHF hospitalization (HR = 0.47, $p=0.03$). The larger Multicenter Automatic Defibrillator Implantation Trial with Cardiac Resynchronization Therapy (MADIT-CRT) trial randomized 1820 patients in NYHA classes I–II, with QRS duration ≥130 ms and LVEF ≤30 % in a 3:2 ratio to CRT-D or ICD alone [62]. The primary endpoint was a composite of all-cause death or nonfatal CHF events. This primary endpoint was reached in 17.2 % of patients implanted with CRT-D vs. 25.3 % in the ICD group, with an average follow-up of 2.4 years (HR = 0.66, $p=0.001$). This was primarily driven by a 41 % reduction in risk of CHF events with CRT, which was greater

in a prespecified group of patients with QRS ≥150 ms. The annual mortality rates in each group were similar at approximately 3 %. Improvements in LV volumes and LVEF, from baseline to 1 year, were also significantly greater in the CRT group.

The double-blinded, Resynchronization–Defibrillation for Ambulatory Heart Failure Trial (RAFT) extended these results to patients in sinus rhythm or with rate-controlled permanent atrial fibrillation (AF) or atrial flutter [63]. Altogether, 1798 patients in NYHA classes II–III, QRS duration ≥120 ms, and LVEF ≤30 % were randomized to either CRT-D or ICD. The original protocol was later revised to enroll only patients in NYHA class II, resulting in a total of 20 % of patients in NYHA class III. The primary endpoint of all-cause death or CHF hospitalization was lower in the CRT-D group (33.2 %) than in the ICD group (40.3 %). Time to first primary endpoint was significantly prolonged with CRT-D (HR = 0.75, $p < 0.001$). Both death and CHF hospitalizations were significantly lower in the CRT-D group, though this was associated with approximately twice the number of adverse events at 30 days postimplant.

31.5.3 Mechanical Dyssynchrony, Narrow QRS Duration, and AV Block

The role of mechanical dyssynchrony for improving patient selection for CRT remains controversial. The multicenter, nonrandomized Predictors of Response to CRT (PROSPECT) study evaluated the ability of 12 echocardiographic indices of dyssynchrony to predict CRT responses at 6 months [64]. A positive response was defined as an improved CCS, with at least a 15 % reduction in LV ESV. These indices provided only modest sensitivity and specificity, and the investigators reported large variability in quantification of dyssynchrony. Mechanical dyssynchrony has also been used to select CRT candidates with a narrow QRS duration ≤120 ms, with limited success in randomized multicenter studies. The earliest of these studies, the Cardiac Resynchronization Therapy in Patients with Heart Failure and Narrow QRS (RethinQ) study, was a double-blinded, randomized study of patients in NYHA class III, LVEF ≤35 %, and QRS duration ≤120 ms with evidence of mechanical dyssynchrony [65]. Tissue Doppler imaging (TDI) or M-mode delay between opposite cardiac wall segments were used to determine the presence of dyssynchrony. The primary endpoint of improved peak VO_2 at 6 months was not significantly improved with CRT. There were no significant differences in QoL, 6MWD, or cardiac structure and function between CRT-on and CRT-off, although more patients experienced significant improvement in NYHA class with CRT (54 % vs. 26 %, $p = 0.006$). It should be noted that these findings were in contrast to smaller, single center studies reporting benefits in patients with narrow QRS duration [66–68]. The largest study in this population, the Echocardiography Guided Cardiac Resynchronization Therapy (EchoCRT) study, randomized 809 patients implanted with CRT-D to CRT-D or ICD therapies only [69]. Patients in NYHA classes III–IV, LVEF ≤35 %, and QRS duration ≤130 ms with evidence of mechanical dyssynchrony (defined by TDI or speckle tracking radial strain) were enrolled. The primary efficacy endpoint was all-cause death or CHF hospitalization. This study was stopped for futility, with a potential for harm based on recommendations from the data and safety monitoring board in 2013. The differences in the primary endpoint were not different between the CRT and ICD groups (28.7 % vs. 25.2 %, HR = 1.2, $p = 0.15$). Yet, there was a significantly higher rate of death in the CRT group (11.1 % vs. 6.4 %, HR = 1.81, $p = 0.02$), with more deaths due to cardiovascular causes, and there were no differences at 6 months in NYHA class or QoL. This study further reinforced the importance of QRS duration over mechanical dyssynchrony as the more important determinant of CRT responses.

One potential group of patients with CHF and narrow QRS durations that may benefit from CRT are those with AV block who then require a high percentage of ventricular pacing. The prospective, double-blinded, randomized Biventricular versus Right Ventricular Pacing in CHF Patients with AV Block (BLOCK HF) study enrolled patients in NYHA classes I–III, LVEF ≤50 %, and a standard class I or IIa indication for pacing due to high-degree AV block [70]. In this trial, 691 patients were implanted with CRT-D or CRT-P, randomized to CRT or RV pacing, and followed for an average of 37 months. The primary endpoint was time to event, which included death from any cause, urgent care visits for CHF requiring IV therapy, or ≥15 % increase in LV ESV index. It was shown that 55.6 % of patients in the RV pacing group met the primary endpoint, significantly more than the 45.8 % patients in the CRT group (HR = 0.74). The secondary endpoints of death from any cause or urgent care CHF visits, death or CHF hospitalization, and CHF hospitalization were also significantly reduced with CRT. This trial led to an expanded indication in April 2014 for use of CRT devices in patients in NYHA classes I–III with AV block and LVEF ≤50 % who are expected to require a high percentage of ventricular pacing. The Biventricular Pacing for AV Block to Prevent Cardiac Desynchronization (BioPace) study is an ongoing trial in a similar patient cohort. Approximately 1900 patients with a class I indications for permanent ventricular pacing and high likelihood of ventricular pacing ≥66 %, without restriction on LVEF, were randomized and implanted with a CRT or RV pacing systems [71]. The primary endpoints include all-cause mortality and time to first CHF hospitalization.

31.6 Factors Influencing CRT Responses

31.6.1 QRS Duration, Morphology, and QRS to LV EGM Onset (QLV)

The relative QRS duration provides powerful prognostic value for patients with CHF and is a primary indicator of eligibility for CRT. A cut-off of 120 ms for QRS duration was established in the initial guidelines, based on randomized trials of CRT, although smaller studies suggested that patients with a QRS duration <150 ms had limited benefit from CRT [30]. Evidence obtained from REVERSE, MADIT-CRT, and RAFT trials, as well as recent meta-analyses, has concluded that patients with QRS durations of at least 150 ms derive greater benefit from CRT. Patients with QRS durations <140 ms did not experience significant reverse remodeling in the REVERSE trial [72]. Analysis of the prespecified subgroup of patients with QRS durations <150 ms did not elicit significant reductions in death or CHF in the MADIT-CRT [62] or RAFT [63] trials. Similarly, meta-analyses of COMPANION, CARE-HF, RAFT, MADIT-CRT, and REVERSE concluded that CRT did not reduce clinical events in patients with QRS durations <150 ms [73]. Analysis of almost 15,000 patients in the Medicare ICD registry, implanted between 2005 and 2006, identified that patients with QRS durations >150 ms had significantly lower mortality and combined mortality or CHF hospitalizations at both 1 and 3 years after CRT [74]. A prospective 10-year observational registry study demonstrated that mortality after CRT benefits were similar between patients with QRS durations of 120–149 ms and those of 150–199 ms, with significantly increased mortality in patients with QRS durations of 200 ms and greater [75]. This finding is not inconsistent with studies concluding that patients with QRS durations of 150 ms and greater benefit more with CRT, since CRT may offset the greater mortality rate associated with increasing QRS durations.

Recent studies have also concluded that patients with LBBB are more likely to respond to CRT than those with right bundle branch block (RBBB) or nonspecific interventricular conduction delays (IVCDs). This is somewhat intuitive, since correction of delayed lateral wall contraction with early activation of the septum in LBBB is the hallmark of CRT. An LBBB morphology was the only baseline ECG characteristic that was significantly associated with improved clinical composite score (CCS) and reverse remodeling in a sub-study of PROSPECT [76]. CRT reduced the risk of CHF hospitalization or death by 53 %, relative to ICD in patients with LBBB in MADIT-CRT, with no significant reduction in patients with non-LBBB morphology [77]. It should be noted that similar findings were found in the RAFT trial [63]. Meta-analyses of COMPANION, CARE-HF, MADIT-CRT, and RAFT data have demonstrated greater benefits in reduction of mortality and morbidity in patients with LBBB vs. IVCD or RBBB [78]. Analyses of the Medicare ICD registry also revealed that patients with RBBB had significantly greater mortality than those with LBBB after adjusting for baseline covariates [74]. Recently, Adelstein et al. also reported that patients with RBBB elicited less reverse remodeling, lower improvement in NYHA at 6 months, and had lower survival and fewer transplants or LVADs than patients with LBBB [79].

Left ventricular lead placement at a site of latest electrical delay, measured by local EGM, is also associated with an increased probability of a positive response to CRT (Fig. 31.9). Some of the earliest evidence supporting this concept was demonstrated in the PATH-CHF-II study, where the difference in LV conduction delay between the free wall and anterior coronary veins was correlated with the difference in

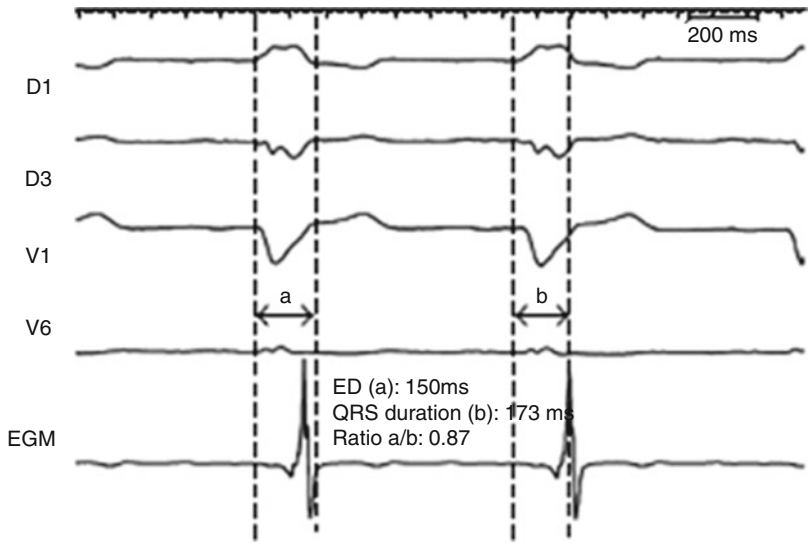

Fig. 31.9 QLV electrical delay (*a*) and QRS duration measurement. Modified from Fatemi et al. [167], available under a Creative Commons Attribution license. http://creativecommons.org/license/by/2.0

improved LV dP/dt_{max} while pacing within each vein [41]. Another study found that both RV to LV conduction and QLV (i.e., QRS onset to LV EGM) correlated with improved LV dP/dt_{max} during optimized BiV pacing; yet no clear cut-off was identified to predict acute hemodynamic response [80]. Normalizing the QLV by QRS duration, termed LV lead electrical delay (LVLED), was also shown to correlate with Doppler-derived dP/dt values, and an LVLED greater than or equal to 50 % was associated with significantly greater reductions in all-cause death or CHF hospitalization at 12 months follow-up in patients with ICM or NICM [81]. The same group of investigators later showed that LVLED was similarly associated with improved outcomes in patients with apically placed LV leads. An LVLED of at least 50 % with an apical LV lead placement was associated with greater freedom of all-cause deaths, CHF hospitalizations, and need for transplant at 2 years (81 % vs. 30 %, $p=0.007$), as well as greater reductions in LV ESV and increased LVEF [82]. Similarly, Gold et al. also found that longer QLVs were associated with improvements in reverse remodeling and QoL in a subanalysis of SMART-AV [83]. A QLV of 120–195 ms was associated with 3.2 times greater odds of reverse remodeling compared to a QLV <70 ms, via multivariate analysis. However, the ability of QLV-guided LV lead placement to improve outcomes after CRT remains to be tested in prospective, randomized studies.

31.6.2 LV Lead Position, Scar, and Mechanical Dyssynchrony

Left ventricular lead position has been recognized as an important determinant for response to CRT since the initial development of this therapy. Initially, acute studies demonstrated greater improvements in hemodynamics during LV free wall pacing than during anterior stimulation, thus providing the basis of empirical targeting of lateral or posterolateral veins [41]. In this series of studies, pacing anterior locations actually decreased LV dP/dt_{max} and pulse pressures below baseline levels in approximately one-third of patients. However, a lateral position cannot be assumed to provide the maximal benefit for all patients. For example, Dekker et al. demonstrated that even though pacing the mid-lateral or basal LV segments corresponded to the best hemodynamic function during surgical epicardial mapping in the majority of patients, these regions corresponded to the worst function in other patients [42]. Expanding on these findings, Gold et al. tested multiple pacing locations within a lateral or anterior vein to determine the impact of activating different sites within a vein [84]. They observed large individual variations in the hemodynamic responses between apical and basal regions, with no significant differences between both regions on average. Additional acute studies investigating the benefits of LV endocardial pacing have confirmed that the location of the optimal pacing site varies significantly between patients, supporting a strategy of individualized LV lead placement to maximize the benefit of CRT [85, 86].

Retrospective analyses of large clinical studies have provided additional insights as to the role of anatomical LV lead positions on chronic outcomes after CRT. Multiple studies have concluded that a more apical LV lead position carries a negative prognosis, while the role of circumferential lead position is less certain. An apical lead position was associated with significantly increased risk for CHF hospitalizations or death after adjusting for clinical covariates in MADIT-CRT [43]. Similar impacts of apical LV lead positions on CHF hospitalization and death were demonstrated in other retrospective single center and multicenter studies [87–89]. Apical lead placement has also been associated with lower levels of subsequent reverse remodeling and a smaller improvement in the patient's assessed NYHA class [87, 88]. Anterior LV lead positions have traditionally been avoided, but data on the impact of circumferential position on chronic outcomes after CRT are conflicting. For example, in one assessment there were no significant differences in outcome between lateral, anterior, and posterior lead positions in MADIT-CRT [43]. Changes in 6MWD, QoL, and percentage of patients with improved NYHA class were similar between lead positions in COMPANION [90]. Similarly, there were no differences in all-cause mortality or CHF hospitalizations, though risk of all-cause mortality or all-cause hospitalizations was not significantly reduced in patients with posterior leads. In contrast, two retrospective analyses found that lateral lead positions were associated with lower incidence of death or first hospitalizations [87] and two to three times less risk for a non-response, death, or necessary transplant [91].

31.6.2.1 Role of Baseline Mechanical Dyssynchrony, Scar, and Implications for LV Lead Position

Corrections of AV, interventricular, and intraventricular dyssynchrony are believed to be the major mechanisms of action for improved cardiac function with CRT. Numerous studies have concluded that the presence of baseline dyssynchrony improves the likelihood of a patient's CRT response. For example, an interventricular mechanical delay of at least 40 ms was an independent predictor of response in a subanalysis of the CARE-HF trial [92]. Though the PROSPECT study reported a relatively weak ability of echocardiographic measures of dyssynchrony to predict outcomes after CRT, subsequent analyses concluded that patients who experienced improvement in both CCS and reverse remodeling had greater baseline dyssynchrony [93]. Furthermore, a recent study utilizing speckle tracking radial strain showed that a lack of baseline radial strain was associated with worse freedom from death, transplant, or LVAD [94]. Cardiac magnetic

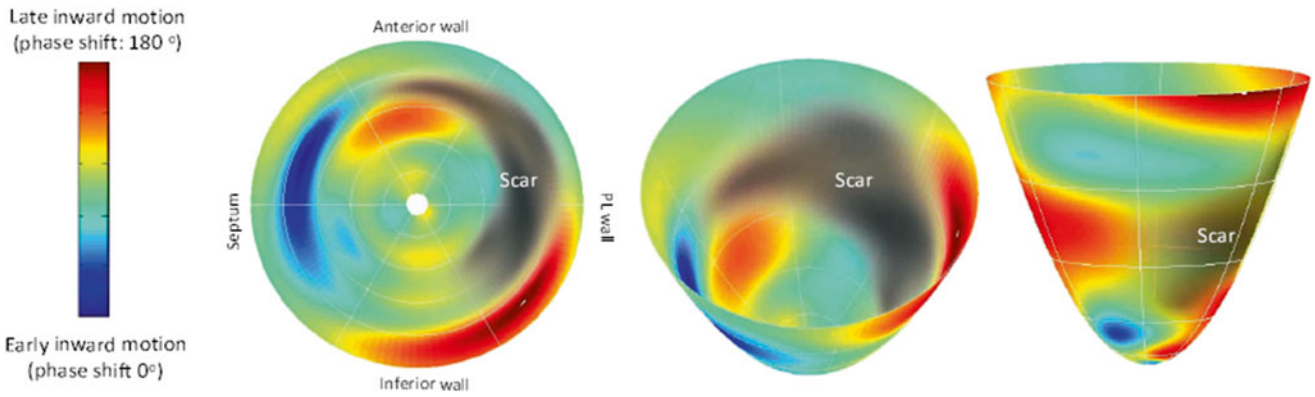

Fig. 31.10 Inward radial motion timing fused with myocardial scar from late gadolinium enhancement on cardiac magnetic resonance imaging. Modified from Foley et al. [168], available under a Creative Commons Attribution license. http://creativecommons.org/license/by/2.0

resonance imaging (MRI) and single-photon emission computed tomography (SPECT) are also useful for the quantification of mechanical dyssynchrony, tissue viability and scar (Fig. 31.10) [95, 96].

CHF etiology and scar size also impact the probability and extent of a positive CRT response. Though patients with NICM and ICM may receive benefits from CRT, the magnitude of response tends to be reduced in the ICM patients. After 6 months of CRT in the MIRACLE study, LV volumes were significantly reduced in both groups, but magnitudes were almost twice as large in the NICM group [38]. These differences remained significant after adjusting for covariates. Reverse remodeling was also lower in patients with ICM in the MADIT-CRT and REVERSE studies [72, 97]. However, the primary endpoint of all-cause death or nonfatal CHF events was not significantly different between patients with ICM and NICM in MADIT-CRT [62]. A longitudinal database study, as well as analyses of the Medicare ICD registry identified that ICM patients had significantly higher mortality than NICM patients after receiving CRT-D [74, 98]. This apparent difference in survival may reflect the worsening prognoses for ICM observed in studies of patients without CRT [99–101]. The presence of scar in patients with ICM may limit the effectiveness of CRT, especially if the LV lead is placed in the scar or if there is a limited amount of myocardium recruitable by pacing. The location of a myocardial scar also appears to be a critical factor. A transmural scar, defined as scar >50 % of the LV wall thickness on late gadolinium enhancement (LGE) MRI, is associated with reduced efficacy of CRT. A posterolateral transmural scar was associated with nonresponse and a lack of improvement in mechanical dyssynchrony after CRT [102]. In one report, Chalil et al. observed that a posterolateral scar measured by LGE MRI was the strongest predictor of CV death or CHF hospitalizations after CRT (HR = 3.06, $p < 0.0001$) [103]. A lack of anteroseptal or posterolateral scars accompanied by septal-to-lateral dyssynchrony on MRI was significantly associated with improved CCS in another study [104]. Similarly, patients with LV leads positioned at transmural scars experienced no improvement in LVEF, ESV, QoL, and 6MWD after CRT [105], and pacing on scar was associated with higher mortality and morbidity [103]. In contrast, patients with LV leads positioned outside of scarred regions by MRI guidance had reduced risk of death and CHF hospitalization compared to leads positioned inside scar [106]. High scar burden (i.e., the percentage of LV mass comprised of scar) is also associated with reduced CRT response. Numerous studies have demonstrated that increased scar burden measured by LGE MRI or by low amplitude echocardiographic speckle tracking strain is associated with less reverse remodeling after CRT [95, 107–109]. A scar burden of 15 % or less by LGE MRI was reported to predict clinical response with an 85 % sensitivity and 90 % specificity [110]. Adelstein et al. found that patients with ICM and low scar burden had survival free of death, transplant, or LVAD similar to patients with NICM [111]. Patients with ICM and high scar burden in that study had significantly reduced survival and lack of improvements as assessed by echocardiographic function.

While mechanical dyssynchrony, scar burden, and LV lead position appear to influence the effectiveness of CRT therapy separately, additional studies have further highlighted their relative importance by considering these factors simultaneously. An acute hemodynamic study in an animal model of LBBB demonstrated that the maximal improvement in pump function was similar in ICM and NICM at the optimal LV site and AV delay, although the optimal LV pacing site varied depending on scar location in the ICM animals and hemodynamics were more sensitive to AV delay than in animals with NICM. [112]. Wong et al. found that dyssynchrony at the LV pacing site was not predictive of reduction in LV ESV, while LGE-MRI scar at the LV and RV lead sites was associated with volumetric nonresponse [113]. Another study concluded that LV lead placement

at a late contracting segment with normal amplitude identified by speckle tracking echo, but not baseline dyssynchrony, predicted a reduction in LV ESV of at least 15 % [114]. Retrospective analysis of 389 patients with ICM and speckle tracking radial strain revealed that LV lead placement remote from the latest contracting segments (HR = 2.086, $p = 0.001$) or scar (HR = 2.913, $p < 0.001$) was associated with higher all-cause mortality on multivariate analysis with a small but statistically significant benefit of baseline dyssynchrony (HR = 0.995, $p = 0.001$) [115]. The prospective, randomized, double-blinded, controlled TARGET and STARTER studies investigated the impact of echocardiographic speckle tracking radial strain guided LV lead placement on CRT outcomes [116, 117]. LV lead placement in the echo-guided arm was targeted to a delayed contracting segment with either explicit or implicit avoidance of low amplitude or abnormal strain, while standard of care implant was performed in the control group. The echo-guided group in TARGET had superior volumetric responses (70 % vs. 50 %, $p = 0.031$). Higher proportions of patients improved at least 1 NYHA class (83 % vs. 65 %, $p = 0.003$), and they demonstrated lower rates of all-cause mortality and CHF hospitalizations. Similarly, the echo-guided group in STARTER had higher freedom from first CHF hospitalizations or death (HR = 0.48, $p = 0.0006$), and elicited greater reverse remodeling. Placement of the LV leads on or adjacent to the latest contracting segments, regardless of randomization, was associated with improved event-free survival (HR = 0.40, $p = 0.002$). In summary, these studies suggest avoidance of scar tissue at the LV pacing site while targeting a latest contracting site is a viable strategy to improve the probability of benefit after CRT (Fig. 31.11).

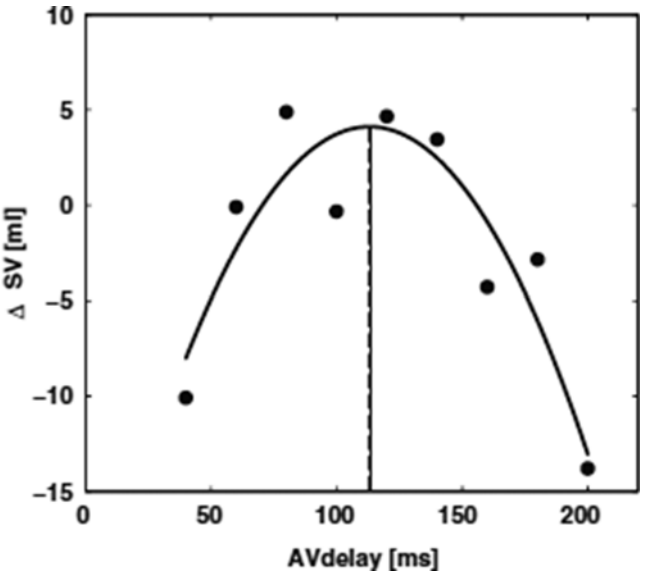

Fig. 31.11 Changes in stroke volume with AV delay. The optimal setting is indicated by the peak of the curve. Modified from Molenaar et al. [169], available under a Creative Commons Attribution license. http://creativecommons.org/license/by/2.0

31.6.3 AV and VV Optimization

Individualized programming of the AV and VV intervals is not typically performed in most patients in normal clinical practice, and it has been primarily reserved for nonresponders [118]. A survey of investigators in the FREEDOM trial found that echocardiography was the most common method used for optimization, yet almost 20 % of respondents never performed optimization. Mullens et al. described a multidisciplinary approach to managing non-responders to CRT at the Cleveland Clinic [119]. The most common factor contributing to suboptimal CRT was impaired filling due to inappropriate AV delay settings in 47 % of patients. In contrast to general clinical practice, the majority of major clinical CRT trials required AV optimization, often using the Doppler mitral inflow technique to maximize filling [8, 11]. The value of individualized tailoring of the AV and VV intervals is somewhat difficult to ascertain, due to the different methods used for verifying optimization and also variable criteria used to characterize CRT response [120–125]. Single point-in-time device optimization algorithms based on analyses of conduction properties from EGMs have demonstrated limited value over fixed programming or standard of care in the general population of patients receiving CRT. The FREEDOM trial randomized 1647 patients to empiric programming, which could have included one-time optimization, or the QuickOpt™ algorithm (St. Jude Medical, St. Paul, MN, USA), a programmer-based feature which provides recommended AV and VV delays based on EGM measurements [126]. Patients were followed for 12 months, with repeated optimizations in the QuickOpt™ group every 3 months. There were no significant differences between groups in the primary endpoint of the number of patients with improved CCS. Only 32 % of the patients in the empiric programming group were echo-optimized, highlighting the lack of AV and VV optimizations in clinical practice. The SMART-AV trial randomized 980 patients to echo-optimized AV delay, a fixed delay of 120 ms, or an AV optimization with the EGM-based SmartDelay® feature (Boston Scientific, Natick, MA, USA) [127]. After 6 months of pacing, there was no significant difference in the primary endpoint of reduction in ESV between groups. Additionally, changes in NYHA class, QoL, 6MWD, LV EDV, and LVEF were also not significantly different. The investigators concluded that while the routine use of AV optimization techniques studied in the trial did not translate to improved outcomes, optimization may still provide benefit to individual non-responders. In contrast to EGM-based methods, an optimization algorithm based on the Peak Endocardial Acceleration (PEA)

sensor (SonR®, Sorin CRM SAS, Clamart, France) contained in the RV or RA lead has been developed. The PEA sensor measures mechanical vibrations associated with cardiac contraction [128]. This algorithm provides manual AV and VV intervals via the programmer with weekly automatic AV interval optimizations. The randomized, single-blinded CLEAR pilot study randomized 238 patients to SonR® or standard of care optimization [129]. The primary endpoint at 1 year—the percentage of patients defined as improved by a composite of all-cause death, CHF hospitalizations, NYHA class change, and QoL—were all significantly higher in the PEA group (76 % vs. 62 %, $p=0.0285$). This difference was mainly driven by an unblinded assessment of the given patient's NYHA class. The results of this study are being confirmed in the randomized, double-blinded RESPOND-CRT study [130]. AdaptivCRT™ (aCRT), a fully automated and ambulatory AV and VV optimization algorithm based on EGM conduction measurements, has recently been developed (Medtronic plc). This algorithm measures AV conduction every minute and provides LV-only pacing synchronized to RV conduction when AV conduction is normal. In cases of long AV conduction, the algorithm provides AV and VV optimized BiV pacing. The double-blinded Adaptive CRT study randomized 522 patients to the aCRT algorithm or mandatory AV and VV echo optimization in 2:1 ratio [131]. Noninferiority of AdaptivCRT™ to echo at 6 months was achieved for the three primary endpoints, which included the number of patients with improved CCS. Further analyses of this trial data demonstrated an absolute 12 % improvement in CCS in the AdaptivCRT™ study arm over historical controls by propensity score analysis [132]. Another retrospective analysis of this same study found that AdaptivCRT™ in patients with normal AV conduction was associated with lower risk of death or CHF hospitalizations than in the echo-optimized control group (HR = 0.52, $p=0.044$) [133]. The percentage of patients with improved CCS was also higher in the AdaptivCRT™ group at 6 months (81 % vs. 69 %, $p=0.041$). The potential superiority of the aCRT algorithm over standard of care CRT in patients with normal AV conduction and LBBB is being prospectively studied in the AdaptResponse trial.

31.6.4 Atrial Arrhythmias, AF, and Percentage of Biventricular Pacing

Atrial fibrillation (AF) can eliminate some of the benefits of improved filling with CRT by eliminating AV synchrony, as well as by reducing the ability to provide consistent BiV capture and effective CRT due to fast rates and irregular AV nodal conduction. The prevalence of AF increases with NYHA class, with rates <10 % in NYHA class I and increasing to approximately 50 % in NYHA class IV [134]. In the 2009 European CRT survey, 23 % of patients receiving CRT were reported to be in AF [135].

Patients with AF have been underrepresented in trials of CRT, prompting interest in how the benefits of CRT in AF may differ from patients in sinus rhythm. A meta-analysis by Upadhyay et al. of 1164 patients from 5 studies concluded that patients in both AF and sinus rhythm benefited from CRT, though patients in AF seemed to benefit less [136]. Importantly, there were no significant differences between groups in mortality or change in NYHA classes at 1 year. However, patients in sinus rhythm elicited significantly greater improvements in both 6MWD and QoL. A larger, more recent meta-analyses of 7495 patients from 33 observational trials included 25.5 % patients with AF [137]; patients with AF had higher all-cause mortality (10.8 %/year vs. 7.1 %/year, $p=0.015$) and higher risk of nonresponse (34.5 % vs. 26.7 %, $p=0.001$). Similar to the analysis by Upadhyay et al., AF was associated with smaller improvements in 6MWD, QoL, and ESV but with no differences in LVEF. These analyses also identified that AV junctional ablations were associated with lower risk of non-response (RR = 0.40, $p<0.001$). Two studies also found a mortality benefit of AV junctional ablation, likely due to increased delivery of BiV pacing in patients with competing intrinsic conduction during AF [138, 139].

Ensuring a high percentage of BiV pacing is a main determinant of improved mortality and CHF hospitalization with CRT. Koplan et al. found that the greatest benefits in terms of mortality and CHF hospitalization were associated with BiV pacing more than 92 % of the time [140]. They also found a significant interaction between history of atrial arrhythmias and percent BiV pacing. An analysis of almost 37,000 patients from the LATITUDE Patient Management System (Boston Scientific) found that the greatest benefit of reduced mortality was found in patients with greater than 98 % pacing, emphasizing that the goal for BiV pacing should be as close to 100 % as possible [141]. Recognition and resolution of low percent BiV pacing remains challenging. A holter monitoring study of 19 patients with permanent AF found that only 47 % had effective BiV pacing, defined as greater than 90 % fully paced beats [142]. In the remaining 10 patients, 16 % ± 5 % beats were fusion and 24 ± 9 % were pseudo-fusion (i.e., pacing with no evidence of capture). Additionally, device diagnostics may be useful in determining reasons for loss of BiV pacing. In an analysis of almost 81,000 patients enrolled in the CareLink Network (Medtronic plc), device-diagnosed AT/AF was the most frequent identifiable cause of reduced BiV pacing [143]. The contribution of AT/AF was more pronounced in patients with BiV pacing <90 %. Management of patients with permanent or persistent AF and intact AV conductions to ensure a high percentage BiV pacing remains challenging. Patients with permanent, persistent, and paroxysmal AF defined by device diagnostics

had a prevalence of 8 % each in a remote monitored group of almost 55,000 patients [144]. In terms of percent BiV pacing, 69 % of patients diagnosed with permanent AF and 62 % with persistent AF had BiV pacing <98 %. Using multivariate analysis, patients with AF had higher mortality than patients with little or no AF after adjusting for factors including BiV pacing (HR = 1.28, $p < 0.001$ for permanent AF; HR = 1.51, $p < 0.001$ for persistent). Similarly, mortality was higher in patients with BiV pacing 90–98 % (HR = 1.20, $p < 0.001$) and <90 % (HR = 1.32, $p < 0.001$) compared to patients with BiV pacing >98 %.

These findings highlight the potential benefits of improving the overall percentage of BiV pacing in patients with frequent AT/AF. In patients whose AV conduction cannot be pharmacologically controlled and have a low percentage of BiV pacing, the 2013 ESC guidelines recommend that AV junctional ablation should be performed [145]. The largest comparison of CRT in patients with AF and AV junctional blocks ($n = 443$), AF with rate-slowing drugs ($n = 895$) and patients in sinus rhythm ($n = 6046$) was reported from the prospective, multicenter, observational CERTRIFY registry [146]. In this study, there was no significant difference in all-cause or cardiac mortality between patients in sinus rhythm and those with AF and AV junctional block. In contrast, mortality was significantly higher in patients receiving rate-slowing drugs with AF, both before and after these multivariate analysis (HR = 1.52, $p < 0.001$ for total mortality; HR = 1.57, $p < 0.001$ for cardiac mortality). These findings were in agreement with the meta-analysis of 768 patients from 7 trials that evaluated differences in CRT outcomes between AV junctional block and rate control [147]. AV junctional block was associated with significantly reduced all-cause mortality (RR = 0.42), cardiovascular mortality (RR = 0.44), and NYHA class reduction (RR = −0.52).

31.7 Future Directions

Future developments in CRT technology will likely focus on improved systems for delivering CRT pacing and new implant techniques. Advances in pacing multiple LV sites, LV endocardial pacing, leadless technologies, and image guidance for lead placement (e.g. fusion of functional imaging and anatomy) will likely play roles for improving the benefits of CRT and reducing complications. Early data on multisite LV pacing suggested that pacing two LV sites in different veins could improve acute hemodynamics more than pacing either site alone [148]. Only a handful of studies have investigated the chronic benefits of CRT with two LV pacing leads (i.e. "TriV pacing"), in part due to the technical complexity of implanting two LV leads and adapting the leads to IPGs which are not designed for the additional LV lead. A small, nonrandomized single center study demonstrated that such systems could be implanted with an approximately 87 % success rate and reported a 96 % response rate in 27 patients at 3 months [149]. The results from the prospective, randomized, single-blinded, crossover TRIP-HF study in 26 patients did not meet the primary endpoint after 3 months of pacing, but reduction in LV ESV was significantly greater with TriV pacing [150]. This approach is being further studied in the prospective, randomized, single center, single-blinded TRUST-CRT study [151]. The development of quadripolar LV leads has opened the possibility of pacing more than one LV site via a single lead. At present, it is unclear if pacing two LV sites along a quadripolar LV lead is superior to an optimized, single LV site [152, 153]. A study in patients with TriV pacing concluded that pacing multiple LV sites significantly improved hemodynamics more than the best single site, but not when pacing the best single LV site at an optimized AV interval [154]. Currently, the relative safety and efficacy of multisite LV pacing with a quadripolar LV lead is being studied in the MPP IDE study.

LV endocardial pacing has been suggested as an alternative implant approach in CRT nonresponders or patients with failed coronary sinus implants. Various implant techniques have been described to introduce a lead inside the LV including (1) an atrial transseptal puncture [155], (2) a ventricular transseptal puncture [156], and (3) a transapical puncture [157]. Acute preclinical and clinical studies of ICM and NICM suggest that LV endocardial pacing improves hemodynamics more than epicardial pacing [85, 86, 158, 159]. These superior hemodynamic responses may be due to a more physiological endocardial to epicardial conduction activation, as well as greater access to LV pacing sites and faster endocardial conduction with a smaller path length [160]. Anticoagulation is considered mandatory for LV endocardial pacing since the major risk associated with this lead placement technique is the risk of thromboembolism due to the presence of a lead in the systemic circulation. Further, required lead extractions and potential interactions of the lead with cardiac structures (such as the mitral valve apparatus) are additional concerns. Recently, the safety and efficacy of a totally superior atrial transseptal approach using a deflectable catheter system and RF puncture wire was reported [161]. Future advancements in pacing technology miniaturization and leadless pacing devices may help overcome some of these issues. For example, a small 0.05 cc ultrasound powered leadless electrode and pacing system (WiCS®-LV, EBR Systems Inc., Sunnyvale, CA, USA) is currently undergoing clinical study in the SELECT-LV trial. The receiver electrode is designed to endothelialize and minimize the risk of thromboembolism.

New techniques of integrating functional and anatomic imaging during CRT implantation are also being explored. Preprocedural targeting and implantation at the latest contracting regions, identified from 3D transesophageal

echocardiography with fusion of rotational CS anatomy, was highly successful (>90 %) and associated with a 90 % clinical response and an 80 % echocardiographic response [162]. This approach has also been used to guide implantation of two LV leads to separate late activated regions with associated improvements in clinical symptoms and reduced dyssynchrony [163]. Intraoperative technologies using fluoroscopy or electroanatomical mapping systems combined with preprocedural imaging are also being explored. Feasibility of delivering an LV lead to a site free from scar, determined by LGE-MRI, while navigating on a virtual venogram from electroanatomical mapping has been described [164]. Fusion of preprocedural anatomy from CT or MRI with live fluoroscopy has also been developed to improve targeted LV lead placement, including in those patients with previously failed implants [165].

31.8 Summary

This chapter discussed the application of CRT for the treatment of CHF, highlighting various technologies and implant techniques along with clinical trial findings. Furthermore, future directions were proposed in the arena of CRT.

References

1. Braunwald E (2013) Heart failure. JACC Heart Fail 1:1–20
2. Go AS, Mozaffarian D, Roger VL et al (2014) Executive summary: heart disease and stroke statistics–2014 update: a report from the American Heart Association. Circulation 129:399–410
3. The CONSENSUS Trial Study Group (1987) Effects of enalapril on mortality in severe congestive heart failure. Results of the Cooperative North Scandinavian Enalapril Survival Study (CONSENSUS). N Engl J Med 316:1429–1435
4. MERIT-HF Study Group (1999) Effect of metoprolol CR/XL in chronic heart failure: Metoprolol CR/XL Randomised Intervention Trial in Congestive Heart Failure (MERIT-HF). Lancet 353:2001–2007
5. Packer M, Coats AJ, Fowler MB et al (2001) Effect of carvedilol on survival in severe chronic heart failure. N Engl J Med 344:1651–1658
6. Young JB, Dunlap ME, Pfeffer MA et al (2004) Mortality and morbidity reduction with Candesartan in patients with chronic heart failure and left ventricular systolic dysfunction: results of the CHARM low-left ventricular ejection fraction trials. Circulation 110:2618–2626
7. The SOLVD Investigators (1991) Effect of enalapril on survival in patients with reduced left ventricular ejection fractions and congestive heart failure. N Engl J Med 325:293–302
8. Abraham WT, Fisher WG, Smith AL et al (2002) Cardiac resynchronization in chronic heart failure. N Engl J Med 346:1845–1853
9. Bardy GH, Lee KL, Mark DB (2005) Amiodarone or an implantable cardioverter-defibrillator for congestive heart failure. N Engl J Med 352:225–237
10. Bristow MR, Saxon LA, Boehmer J et al (2004) Cardiac-resynchronization therapy with or without an implantable defibrillator in advanced chronic heart failure. N Engl J Med 350:2140–2150
11. Cleland JG, Daubert JC, Erdmann E et al (2005) The effect of cardiac resynchronization on morbidity and mortality in heart failure. N Engl J Med 352:1539–1549
12. Moss AJ, Zareba W, Hall WJ et al (2002) Prophylactic implantation of a defibrillator in patients with myocardial infarction and reduced ejection fraction. N Engl J Med 346:877–883
13. Pande GS (1983) Thermoplastic polyurethanes as insulating materials for long-life cardiac pacing leads. Pacing Clin Electrophysiol 6:858–867
14. Mond H, Sloman G (1980) The small-tined pacemaker lead—absence of dislodgement. Pacing Clin Electrophysiol 3:171–177
15. Mond HG, Helland JR, Stokes K, Bornzin GA, McVenes R (2014) The electrode-tissue interface: the revolutionary role of steroid-elution. Pacing Clin Electrophysiol 37:1232–1249
16. Strobel JS, Kay GN (2000) Programming of sensor driven pacemakers. Cardiol Clin 18:157–176
17. D'Allonnes GR, Pavin D, Leclercq C et al (2000) Long-term effects of biatrial synchronous pacing to prevent drug-refractory atrial tachyarrhythmia: a nine-year experience. J Cardiovasc Electrophysiol 11:1081–1091
18. Cazeau S, Ritter P, Bakdach S et al (1994) Four chamber pacing in dilated cardiomyopathy. Pacing Clin Electrophysiol 17:1974–1979
19. Grines CL, Bashore TM, Boudoulas H, Olson S, Shafer P, Wooley CF (1989) Functional abnormalities in isolated left bundle branch block. The effect of interventricular asynchrony. Circulation 79:845–853
20. Prinzen FW, Augustijn CH, Arts T, Allessie MA, Reneman RS (14990) Redistribution of myocardial fiber strain and blood flow by asynchronous activation. Am J Physiol 259:H300–308
21. Prinzen FW, Hunter WC, Wyman BT, McVeigh ER (1999) Mapping of regional myocardial strain and work during ventricular pacing: experimental study using magnetic resonance imaging tagging. J Am Coll Cardiol 33:1735–1742
22. Prinzen FW, Cheriex EC, Delhaas T et al (14995) Asymmetric thickness of the left ventricular wall resulting from asynchronous electric activation: a study in dogs with ventricular pacing and in patients with left bundle branch block. Am Heart J 130:1045–1053
23. Baldasseroni S, Opasich C, Gorini M et al (2002) Left bundle-branch block is associated with increased 1-year sudden and total mortality rate in 5517 outpatients with congestive heart failure: a report from the Italian network on congestive heart failure. Am Heart J 143:398–405
24. Vassallo JA, Cassidy DM, Marchlinski FE et al (1984) Endocardial activation of left bundle branch block. Circulation 69:914–923
25. Rodriguez LM, Timmermans C, Nabar A, Beatty G, Wellens HJ (2003) Variable patterns of septal activation in patients with left bundle branch block and heart failure. J Cardiovasc Electrophysiol 14:135–141
26. Auricchio A, Fantoni C, Regoli F et al (2004) Characterization of left ventricular activation in patients with heart failure and left bundle-branch block. Circulation 109:1133–1139
27. Pratola C, Notarstefano P, Toselli T et al (2010) Noncontact mapping of left ventricle during CRT implant. Pacing Clin Electrophysiol 33:74–84
28. Lambiase PD, Rinaldi A, Hauck J et al (2004) Non-contact left ventricular endocardial mapping in cardiac resynchronisation therapy. Heart 90:44–51
29. Kass DA, Chen CH, Curry C et al (1999) Improved left ventricular mechanics from acute VDD pacing in patients with dilated cardiomyopathy and ventricular conduction delay. Circulation 99:1567–1573
30. Auricchio A, Stellbrink C, Block M, Sack S, Vogt J, Bakker P, Klein H, Kramer A, Ding J, Salo R, Tockman B, Pochet T, Spinelli

J (1999) Effect of pacing chamber and atrioventricular delay on acute systolic function of paced patients with congestive heart failure. Circulation 99:2993–3001
31. St John Sutton MG, Plappert T, Abraham WT et al (2003) Effect of cardiac resynchronization therapy on left ventricular size and function in chronic heart failure. Circulation 107:1985–1990
32. Breithardt OA, Sinha AM, Schwammenthal E et al (2003) Acute effects of cardiac resynchronization therapy on functional mitral regurgitation in advanced systolic heart failure. J Am Coll Cardiol 41:765–770
33. Ypenburg C, Lancellotti P, Tops LF et al (2007) Acute effects of initiation and withdrawal of cardiac resynchronization therapy on papillary muscle dyssynchrony and mitral regurgitation. J Am Coll Cardiol 50:2071–2077
34. Porciani MC, Macioce R, Demarchi G et al (2006) Effects of cardiac resynchronization therapy on the mechanisms underlying functional mitral regurgitation in congestive heart failure. Eur J Echocardiogr 7:31–39
35. Kanzaki H, Bazaz R, Schwartzman D, Dohi K, Sade LE, Gorcsan J III (2004) A mechanism for immediate reduction in mitral regurgitation after cardiac resynchronization therapy: insights from mechanical activation strain mapping. J Am Coll Cardiol 44:1619–1625
36. Cha YM, Oh J, Miyazaki C et al (2008) Cardiac resynchronization therapy upregulates cardiac autonomic control. J Cardiovasc Electrophysiol 19:1045–1052
37. Cha YM, Chareonthaitawee P, Dong YX et al (2011) Cardiac sympathetic reserve and response to cardiac resynchronization therapy. Circ Heart Fail 4:339–344
38. St John Sutton MG, Plappert T, Hilpisch KE, Abraham WT, Hayes DL, Chinchoy E (2006) Sustained reverse left ventricular structural remodeling with cardiac resynchronization at one year is a function of etiology: quantitative Doppler echocardiographic evidence from the Multicenter InSync Randomized Clinical Evaluation (MIRACLE). Circulation 113:266–272
39. Cowburn PJ, Patel H, Pipes RR, Parker JD (2005) Contrast nephropathy post cardiac resynchronization therapy: an underrecognized complication with important morbidity. Eur J Heart Fail 7:899–903
40. Jackson KP, Hegland DD, Frazier-Mills C et al (2013) Impact of using a telescoping-support catheter system for left ventricular lead placement on implant success and procedure time of cardiac resynchronization therapy. Pacing Clin Electrophysiol 36:553–558
41. Butter C, Auricchio A, Stellbrink C et al (2001) Effect of resynchronization therapy stimulation site on the systolic function of heart failure patients. Circulation 104:3026–3029
42. Dekker AL, Phelps B, Dijkman B et al (2004) Epicardial left ventricular lead placement for cardiac resynchronization therapy: optimal pace site selection with pressure-volume loops. J Thorac Cardiovasc Surg 127:1641–1647
43. Singh JP, Klein HU, Huang DT et al (2011) Left ventricular lead position and clinical outcome in the Multicenter Automatic Defibrillator Implantation Trial-Cardiac Resynchronization Therapy (MADIT-CRT) Trial. Circulation 123:159–166
44. Biffi M, Boriani G (2010) Phrenic stimulation management in CRT patients: are we there yet? Curr Opin Cardiol 26:12–16
45. Crossley GH, Exner D, Mead RH et al (2010) Chronic performance of an active fixation coronary sinus lead. Heart Rhythm 7:472–478
46. Yee R, Gadler F, Hussin A et al (2014) Novel active fixation mechanism permits precise placement of a left ventricular lead: early results from a multicenter clinical study. Heart Rhythm 11:1150–1155
47. Tomassoni G, Baker J, Corbisiero R et al (2013) Postoperative performance of the Quartet(R) left ventricular heart lead. J Cardiovasc Electrophysiol 24:449–456
48. Alonso C, Leclercq C, d'Allonnes FR et al (2001) Six year experience of transvenous left ventricular lead implantation for permanent biventricular pacing in patients with advanced heart failure: technical aspects. Heart 86:405–410
49. Leon AR, Abraham WT, Curtis AB et al (2005) Safety of transvenous cardiac resynchronization system implantation in patients with chronic heart failure: combined results of over 2,000 patients from a multicenter study program. J Am Coll Cardiol 46:2348–2356
50. Gras D, Bocker D, Lunati M et al (2007) Implantation of cardiac resynchronization therapy systems in the CARE-HF trial: procedural success rate and safety. Europace 9:516–522
51. Borleffs CJ, van Bommel RJ, Molhoek SG, de Leeuw JG, Schalij MJ, van Erven L (2009) Requirement for coronary sinus lead interventions and effectiveness of endovascular replacement during long-term follow-up after implantation of a resynchronization device. Europace 11:607–611
52. Macias A, Gavira JJ, Castano S, Alegria E, Garcia-Bolao I (2008) Left ventricular pacing site in cardiac resynchronization therapy: clinical follow-up and predictors of failed lateral implant. Eur J Heart Fail 10:421–427
53. Biffi M, Bertini M, Ziacchi M, Diemberger I, Martignani C, Boriani G (2014) Left ventricular lead stabilization to retain cardiac resynchronization therapy at long term: when is it advisable? Europace 16:533–540
54. Gurevitz O, Nof E, Carasso S et al (2005) Programmable multiple pacing configurations help to overcome high left ventricular pacing thresholds and avoid phrenic nerve stimulation. Pacing Clin Electrophysiol 28:1255–1259
55. Biffi M, Moschini C, Bertini M et al (2009) Phrenic stimulation: a challenge for cardiac resynchronization therapy. Circ Arrhythm Electrophysiol 2:402–410
56. Biffi M, Foerster L, Eastman W et al (2012) Effect of bipolar electrode spacing on phrenic nerve stimulation and left ventricular pacing thresholds: an acute canine study. Circ Arrhythm Electrophysiol 5:815–820
57. Biffi M, Zanon F, Bertaglia E et al (2013) Short-spaced dipole for managing phrenic nerve stimulation in patients with CRT: the "phrenic nerve mapping and stimulation EP" catheter study. Heart Rhythm 10:39–45
58. Cazeau S, Leclercq C, Lavergne T et al (2001) Effects of multisite biventricular pacing in patients with heart failure and intraventricular conduction delay. N Engl J Med 344:873–880
59. Stellbrink C, Breithardt OA, Franke A et al (2001) Impact of cardiac resynchronization therapy using hemodynamically optimized pacing on left ventricular remodeling in patients with congestive heart failure and ventricular conduction disturbances. J Am Coll Cardiol 38:1957–1965
60. Higgins SL, Hummel JD, Niazi IK et al (2003) Cardiac resynchronization therapy for the treatment of heart failure in patients with intraventricular conduction delay and malignant ventricular tachyarrhythmias. J Am Coll Cardiol 42:1454–1459
61. Linde C, Abraham WT, Gold MR, St John SM, Ghio S, Daubert C (2008) Randomized trial of cardiac resynchronization in mildly symptomatic heart failure patients and in asymptomatic patients with left ventricular dysfunction and previous heart failure symptoms. J Am Coll Cardiol 52:1834–1843
62. Moss AJ, Hall WJ, Cannom DS et al (2009) Cardiac-resynchronization therapy for the prevention of heart-failure events. N Engl J Med 361:1329–1338
63. Tang AS, Wells GA, Talajic M et al (2010) Cardiac-resynchronization therapy for mild-to-moderate heart failure. N Engl J Med 363:2385–2395
64. Chung ES, Leon AR, Tavazzi L et al (2008) Results of the Predictors of Response to CRT (PROSPECT) trial. Circulation 117:2608–2616

65. Beshai JF, Grimm RA, Nagueh SF et al (2007) Cardiac-resynchronization therapy in heart failure with narrow QRS complexes. N Engl J Med 357:2461–2471
66. Foley PW, Patel K, Irwin N et al (2011) Cardiac resynchronisation therapy in patients with heart failure and a normal QRS duration: the RESPOND study. Heart 97:1041–1047
67. Achilli A, Sassara M, Ficili S et al (2003) Long-term effectiveness of cardiac resynchronization therapy in patients with refractory heart failure and "narrow" QRS. J Am Coll Cardiol 42:2117–2124
68. Bleeker GB, Holman ER, Steendijk P et al (2006) Cardiac resynchronization therapy in patients with a narrow QRS complex. J Am Coll Cardiol 48:2243–2250
69. Ruschitzka F, Abraham WT, Singh JP et al (2013) Cardiac-resynchronization therapy in heart failure with a narrow QRS complex. N Engl J Med 369:1395–1405
70. Curtis AB, Worley SJ, Adamson PB et al (2013) Biventricular pacing for atrioventricular block and systolic dysfunction. N Engl J Med 368:1585–1593
71. Funck RC, Mueller HH, Lunati M et al (2014) Characteristics of a large sample of candidates for permanent ventricular pacing included in the Biventricular Pacing for Atrio-ventricular Block to Prevent Cardiac Desynchronization Study (BioPace). Europace 16:354–362
72. Sutton MS, Ghio S, Plappert T et al (2009) Cardiac resynchronization induces major structural and functional reverse remodeling in patients with New York Heart Association class I/II heart failure. Circulation 120:1858–1865
73. Sipahi I, Carrigan TP, Rowland DY, Stambler BS, Fang JC (2011) Impact of QRS duration on clinical event reduction with cardiac resynchronization therapy: meta-analysis of randomized controlled trials. Arch Intern Med 171:1454–1462
74. Bilchick KC, Kamath S, DiMarco JP, Stukenborg GJ (2010) Bundle-branch block morphology and other predictors of outcome after cardiac resynchronization therapy in Medicare patients. Circulation 122:2022–2030
75. Gasparini M, Leclercq C, Yu CM et al (2014) Absolute survival after cardiac resynchronization therapy according to baseline QRS duration: a multinational 10-year experience: data from the Multicenter International CRT Study. Am Heart J 167:203–209
76. Hsing JM, Selzman KA, Leclercq C et al (2011) Paced left ventricular QRS width and ECG parameters predict outcomes after cardiac resynchronization therapy: PROSPECT-ECG substudy. Circ Arrhythm Electrophysiol 4:851–857
77. Zareba W, Klein H, Cygankiewicz I et al (2011) Effectiveness of cardiac resynchronization therapy by QRS morphology in the Multicenter Automatic Defibrillator Implantation Trial-Cardiac Resynchronization Therapy (MADIT-CRT). Circulation 123:1061–1072
78. Sipahi I, Chou JC, Hyden M, Rowland DY, Simon DI, Fang JC (2012) Effect of QRS morphology on clinical event reduction with cardiac resynchronization therapy: meta-analysis of randomized controlled trials. Am Heart J 163:260–267
79. Adelstein EC, Saba S (2009) Usefulness of baseline electrocardiographic QRS complex pattern to predict response to cardiac resynchronization. Am J Cardiol 103:238–242
80. van Gelder BM, Meijer A, Bracke FA (2009) Timing of the left ventricular electrogram and acute hemodynamic changes during implant of cardiac resynchronization therapy devices. Pacing Clin Electrophysiol 32:S94–S97
81. Singh JP, Fan D, Heist EK et al (2006) Left ventricular lead electrical delay predicts response to cardiac resynchronization therapy. Heart Rhythm 3:1285–1292
82. Kandala J, Upadhyay GA, Altman RK et al (2012) Electrical delay in apically positioned left ventricular leads and clinical outcome after cardiac resynchronization therapy. J Cardiovasc Electrophysiol 24:182–187
83. Gold MR, Birgersdotter-Green U, Singh JP et al (2011) The relationship between ventricular electrical delay and left ventricular remodelling with cardiac resynchronization therapy. Eur Heart J 32:2516–2524
84. Gold MR, Auricchio A, Hummel JD et al (2005) Comparison of stimulation sites within left ventricular veins on the acute hemodynamic effects of cardiac resynchronization therapy. Heart Rhythm 2:376–381
85. Spragg DD, Dong J, Fetics BJ et al (2010) Optimal left ventricular endocardial pacing sites for cardiac resynchronization therapy in patients with ischemic cardiomyopathy. J Am Coll Cardiol 56:774–781
86. Derval N, Steendijk P, Gula LJ et al (2010) Optimizing hemodynamics in heart failure patients by systematic screening of left ventricular pacing sites: the lateral left ventricular wall and the coronary sinus are rarely the best sites. J Am Coll Cardiol 55:566–575
87. Thebault C, Donal E, Meunier C et al (2012) Sites of left and right ventricular lead implantation and response to cardiac resynchronization therapy observations from the REVERSE trial. Eur Heart J 33:2662–2671
88. Merchant FM, Heist EK, McCarty D et al (2010) Impact of segmental left ventricle lead position on cardiac resynchronization therapy outcomes. Heart Rhythm 7:639–644
89. Jastrzebski M, Wilinski J, Fijorek K, Sondej T, Czarnecka D (2013) Mortality and morbidity in cardiac resynchronization patients: impact of lead position, paced left ventricular QRS morphology and other characteristics on long-term outcome. Europace 15:258–265
90. Saxon LA, Olshansky B, Volosin K et al (2009) Influence of left ventricular lead location on outcomes in the COMPANION study. J Cardiovasc Electrophysiol 20:764–768
91. Wilton SB, Shibata MA, Sondergaard R, Cowan K, Semeniuk L, Exner DV (2008) Relationship between left ventricular lead position using a simple radiographic classification scheme and long-term outcome with resynchronization therapy. J Interv Card Electrophysiol 23:219–227
92. Richardson M, Freemantle N, Calvert MJ, Cleland JG, Tavazzi L (2007) Predictors and treatment response with cardiac resynchronization therapy in patients with heart failure characterized by dyssynchrony: a pre-defined analysis from the CARE-HF trial. Eur Heart J 28:1827–1834
93. van Bommel RJ, Bax JJ, Abraham WT et al (2009) Characteristics of heart failure patients associated with good and poor response to cardiac resynchronization therapy: a PROSPECT (Predictors of Response to CRT) sub-analysis. Eur Heart J 30:2470–2477
94. Gorcsan J III, Oyenuga O, Habib PJ et al (2010) Relationship of echocardiographic dyssynchrony to long-term survival after cardiac resynchronization therapy. Circulation 122:1910–1918
95. Marsan NA, Westenberg JJ, Ypenburg C et al (2009) Magnetic resonance imaging and response to cardiac resynchronization therapy: relative merits of left ventricular dyssynchrony and scar tissue. Eur Heart J 30:2360–2367
96. Friehling M, Chen J, Saba S et al (2011) A prospective pilot study to evaluate the relationship between acute change in left ventricular synchrony after cardiac resynchronization therapy and patient outcome using a single-injection gated SPECT protocol. Circ Cardiovasc Imaging 4:532–539
97. Barsheshet A, Goldenberg I, Moss AJ et al (2011) Response to preventive cardiac resynchronization therapy in patients with isch-

aemic and nonischaemic cardiomyopathy in MADIT-CRT. Eur Heart J 32:1622–1630
98. McLeod CJ, Shen WK, Rea RF et al (2011) Differential outcome of cardiac resynchronization therapy in ischemic cardiomyopathy and idiopathic dilated cardiomyopathy. Heart Rhythm 8:377–382
99. Ng AC, Sindone AP, Wong HS, Freedman SB (2008) Differences in management and outcome of ischemic and non-ischemic cardiomyopathy. Int J Cardiol 129:198–204
100. Bart BA, Shaw LK, McCants CB Jr et al (1997) Clinical determinants of mortality in patients with angiographically diagnosed ischemic or nonischemic cardiomyopathy. J Am Coll Cardiol 30:1002–1008
101. Likoff MJ, Chandler SL, Kay HR (1987) Clinical determinants of mortality in chronic congestive heart failure secondary to idiopathic dilated or to ischemic cardiomyopathy. Am J Cardiol 59:634–638
102. Bleeker GB, Kaandorp TA, Lamb HJ et al (2006) Effect of posterolateral scar tissue on clinical and echocardiographic improvement after cardiac resynchronization therapy. Circulation 113:969–976
103. Chalil S, Stegemann B, Muhyaldeen SA et al (2007) Effect of posterolateral left ventricular scar on mortality and morbidity following cardiac resynchronization therapy. Pacing Clin Electrophysiol 30:1201–1209
104. Taylor AJ, Elsik M, Broughton A et al (2010) Combined dyssynchrony and scar imaging with cardiac magnetic resonance imaging predicts clinical response and long-term prognosis following cardiac resynchronization therapy. Europace 12:708–713
105. Ypenburg C, Schalij MJ, Bleeker GB et al (2007) Impact of viability and scar tissue on response to cardiac resynchronization therapy in ischaemic heart failure patients. Eur Heart J 28:33–41
106. Leyva F, Foley PW, Chalil S et al (2011) Cardiac resynchronization therapy guided by late gadolinium-enhancement cardiovascular magnetic resonance. J Cardiovasc Magn Reson 13:29
107. Ypenburg C, Roes SD, Bleeker GB et al (2007) Effect of total scar burden on contrast-enhanced magnetic resonance imaging on response to cardiac resynchronization therapy. Am J Cardiol 99:657–660
108. Mele D, Agricola E, Monte AD et al (2013) Pacing transmural scar tissue reduces left ventricle reverse remodeling after cardiac resynchronization therapy. Int J Cardiol 167:94–101
109. Ascione L, Muto C, Iengo R et al (2008) End-diastolic wall thickness as a predictor of reverse remodelling after cardiac resynchronization therapy: a two-dimensional echocardiographic study. J Am Soc Echocardiogr 21:1055–1061
110. White JA, Yee R, Yuan X et al (2006) Delayed enhancement magnetic resonance imaging predicts response to cardiac resynchronization therapy in patients with intraventricular dyssynchrony. J Am Coll Cardiol 48:1953–1960
111. Adelstein EC, Tanaka H, Soman P et al (2011) Impact of scar burden by single-photon emission computed tomography myocardial perfusion imaging on patient outcomes following cardiac resynchronization therapy. Eur Heart J 32:93–103
112. Rademakers LM, van Kerckhoven R, van Deursen CJ et al (2010) Myocardial infarction does not preclude electrical and hemodynamic benefits of cardiac resynchronization therapy in dyssynchronous canine hearts. Circ Arrhythm Electrophysiol 3:361–368
113. Wong JA, Yee R, Stirrat J et al (2013) Influence of pacing site characteristics on response to cardiac resynchronization therapy. Circ Cardiovasc Imaging 6:542–550
114. Khan FZ, Virdee MS, Read PA et al (2010) Effect of low-amplitude two-dimensional radial strain at left ventricular pacing sites on response to cardiac resynchronization therapy. J Am Soc Echocardiogr 23:168–176
115. Delgado V, van Bommel RJ, Bertini M et al (2011) Relative merits of left ventricular dyssynchrony, left ventricular lead position, and myocardial scar to predict long-term survival of ischemic heart failure patients undergoing cardiac resynchronization therapy. Circulation 123:70–78
116. Khan FZ, Virdee MS, Palmer CR et al (2012) Targeted left ventricular lead placement to guide cardiac resynchronization therapy: the TARGET study: a randomized, controlled trial. J Am Coll Cardiol 59:1509–1518
117. Saba S, Marek J, Schwartzman D et al (2013) Echocardiography-guided left ventricular lead placement for cardiac resynchronization therapy: results of the Speckle Tracking Assisted Resynchronization Therapy for Electrode Region trial. Circ Heart Fail 6:427–434
118. Gras D, Gupta MS, Boulogne E, Guzzo L, Abraham WT (2009) Optimization of AV and VV delays in the real-world CRT patient population: an international survey on current clinical practice. Pacing Clin Electrophysiol 32:S236–S239
119. Mullens W, Grimm RA, Verga T et al (2009) Insights from a cardiac resynchronization optimization clinic as part of a heart failure disease management program. J Am Coll Cardiol 53:765–773
120. Boriani G, Biffi M, Muller CP et al (2009) A prospective randomized evaluation of VV delay optimization in CRT-D recipients: echocardiographic observations from the RHYTHM II ICD study. Pacing Clin Electrophysiol 32:S120–S125
121. van Gelder BM, Bracke FA, Meijer A, Lakerveld LJ, Pijls NH (2004) Effect of optimizing the VV interval on left ventricular contractility in cardiac resynchronization therapy. Am J Cardiol 93:1500–1503
122. Sawhney NS, Waggoner AD, Garhwal S, Chawla MK, Osborn J, Faddis MN (2004) Randomized prospective trial of atrioventricular delay programming for cardiac resynchronization therapy. Heart Rhythm 1:562–567
123. Morales MA, Startari U, Panchetti L, Rossi A, Piacenti M (2006) Atrioventricular delay optimization by doppler-derived left ventricular dP/dt improves 6-month outcome of resynchronized patients. Pacing Clin Electrophysiol 29:564–568
124. Auricchio A, Ding J, Spinelli JC et al (2002) Cardiac resynchronization therapy restores optimal atrioventricular mechanical timing in heart failure patients with ventricular conduction delay. J Am Coll Cardiol 39:1163–1169
125. Abraham WT, Leon AR, St John Sutton MG et al (2012) Randomized controlled trial comparing simultaneous versus optimized sequential interventricular stimulation during cardiac resynchronization therapy. Am Heart J 164:735–741
126. Abraham WT, Gras D, Yu CM et al (2010) Randomized clinical trial to assess the safety and efficacy of Frequent Optimization of Cardiac Resynchronization Therapy Using the QuickOpt Method (FREEDOM) trial results. Am Heart J 159(6):944–948.e1
127. Ellenbogen KA, Gold MR, Meyer TE et al (2010) Primary results from the SmartDelay determined AV optimization: a comparison to other AV delay methods used in cardiac resynchronization therapy (SMART-AV) trial: a randomized trial comparing empirical, echocardiography-guided, and algorithmic atrioventricular delay programming in cardiac resynchronization therapy. Circulation 122:2660–2668
128. Delnoy PP, Marcelli E, Oudeluttikhuis H et al (2008) Validation of a peak endocardial acceleration-based algorithm to optimize cardiac resynchronization: early clinical results. Europace 10:801–808
129. Ritter P, Delnoy PP, Padeletti L et al (2012) A randomized pilot study of optimization of cardiac resynchronization therapy in sinus rhythm patients using a peak endocardial acceleration sensor vs. standard methods. Europace 14:1324–1333

130. Brugada J, Brachmann J, Delnoy PP et al (2014) Automatic optimization of cardiac resynchronization therapy using SonR-rationale and design of the clinical trial of the SonRtip lead and automatic AV-VV optimization algorithm in the paradym RF SonR CRT-D (RESPOND CRT) trial. Am Heart J 167:429–436
131. Martin DO, Lemke B, Birnie D et al (2012) Investigation of a novel algorithm for synchronized left-ventricular pacing and ambulatory optimization of cardiac resynchronization therapy: results of the adaptive CRT trial. Heart Rhythm 9:1807–1814
132. Singh JP, Abraham WT, Chung ES et al (2013) Clinical response with adaptive CRT algorithm compared with CRT with echocardiography-optimized atrioventricular delay: a retrospective analysis of multicentre trials. Europace 15:1622–1628
133. Birnie D, Lemke B, Aonuma K et al (2013) Clinical outcomes with synchronized left ventricular pacing: analysis of the adaptive CRT trial. Heart Rhythm 10:1368–1374
134. Maisel WH, Stevenson LW (2003) Atrial fibrillation in heart failure: epidemiology, pathophysiology, and rationale for therapy. Am J Cardiol 91:2D–8D
135. Dickstein K, Bogale N, Priori S et al (2009) The European cardiac resynchronization therapy survey. Eur Heart J 30:2450–2460
136. Upadhyay GA, Choudhry NK, Auricchio A, Ruskin J, Singh JP (2008) Cardiac resynchronization in patients with atrial fibrillation: a meta-analysis of prospective cohort studies. J Am Coll Cardiol 52:1239–1246
137. Wilton SB, Leung AA, Ghali WA, Faris P, Exner DV (2011) Outcomes of cardiac resynchronization therapy in patients with versus those without atrial fibrillation: a systematic review and meta-analysis. Heart Rhythm 8:1088–1094
138. Gasparini M, Auricchio A, Metra M et al (2008) Long-term survival in patients undergoing cardiac resynchronization therapy: the importance of performing atrio-ventricular junction ablation in patients with permanent atrial fibrillation. Eur Heart J 29:1644–1652
139. Ferreira AM, Adragao P, Cavaco DM et al (2008) Benefit of cardiac resynchronization therapy in atrial fibrillation patients vs. patients in sinus rhythm: the role of atrioventricular junction ablation. Europace 10:809–815
140. Koplan BA, Kaplan AJ, Weiner S, Jones PW, Seth M, Christman SA (2009) Heart failure decompensation and all-cause mortality in relation to percent biventricular pacing in patients with heart failure: is a goal of 100% biventricular pacing necessary? J Am Coll Cardiol 53:355–360
141. Hayes DL, Boehmer JP, Day JD et al (2011) Cardiac resynchronization therapy and the relationship of percent biventricular pacing to symptoms and survival. Heart Rhythm 8:1469–1475
142. Kamath GS, Cotiga D, Koneru JN et al (2009) The utility of 12-lead Holter monitoring in patients with permanent atrial fibrillation for the identification of nonresponders after cardiac resynchronization therapy. J Am Coll Cardiol 53:1050–1055
143. Cheng A, Landman SR, Stadler RW (2012) Reasons for loss of cardiac resynchronization therapy pacing: insights from 32 844 patients. Circ Arrhythm Electrophysiol 5:884–888
144. Ousdigian KT, Borek PP, Koehler JL, Heywood JT, Ziegler PD, Wilkoff BL (2014) The epidemic of inadequate biventricular pacing in patients with persistent or permanent atrial fibrillation and its association with mortality. Circ Arrhythm Electrophysiol 7:370–376
145. Brignole M, Auricchio A, Baron-Esquivias G et al (2013) 2013 ESC guidelines on cardiac pacing and cardiac resynchronization therapy: the Task Force on cardiac pacing and resynchronization therapy of the European Society of Cardiology (ESC). Eur Heart J 34:2281–2329
146. Gasparini M, Regoli F (2009) Cardiac resynchronisation therapy in patients with atrial fibrillation. Heart 95:83–84
147. Ganesan AN, Brooks AG, Roberts-Thomson KC, Lau DH, Kalman JM, Sanders P (2012) Role of AV nodal ablation in cardiac resynchronization in patients with coexistent atrial fibrillation and heart failure a systematic review. J Am Coll Cardiol 59:719–726
148. Pappone C, Rosanio S, Oreto G et al (2000) Cardiac pacing in heart failure patients with left bundle branch block: impact of pacing site for optimizing left ventricular resynchronization. Ital Heart J 1:464–469
149. Lenarczyk R, Kowalski O, Kukulski T et al (2009) Mid-term outcomes of triple-site vs. conventional cardiac resynchronization therapy: a preliminary study. Int J Cardiol 133:87–94
150. Leclercq C, Gadler F, Kranig W et al (2008) A randomized comparison of triple-site versus dual-site ventricular stimulation in patients with congestive heart failure. J Am Coll Cardiol 51:1455–1462
151. Lenarczyk R, Kowalski O, Sredniawa B et al (2009) Triple-site versus standard cardiac resynchronization therapy study (TRUST CRT): clinical rationale, design, and implementation. J Cardiovasc Electrophysiol 20:658–662
152. Thibault B, Dubuc M, Khairy P et al (2013) Acute haemodynamic comparison of multisite and biventricular pacing with a quadripolar left ventricular lead. Europace 15:984–991
153. Pappone C, Calovic Z, Vicedomini G et al (2014) Multipoint left ventricular pacing improves acute hemodynamic response assessed with pressure-volume loops in cardiac resynchronization therapy patients. Heart Rhythm 11:394–401
154. Padeletti L, Colella A, Michelucci A et al (2008) Dual-site left ventricular cardiac resynchronization therapy. Am J Cardiol 102:1687–1692
155. Leclercq F, Hager FX, Macia JC, Mariottini CJ, Pasquie JL, Grolleau R (1999) Left ventricular lead insertion using a modified transseptal catheterization technique: a totally endocardial approach for permanent biventricular pacing in end-stage heart failure. Pacing Clin Electrophysiol 22:1570–1575
156. Betts TR, Gamble JH, Khiani R, Bashir Y, Rajappan K (2014) Development of a technique for left ventricular endocardial pacing via puncture of the interventricular septum. Circ Arrhythm Electrophysiol 7:17–22
157. Kassai I, Mihalcz A, Foldesi C, Kardos A, Szili-Torok T (2009) A novel approach for endocardial resynchronization therapy: initial experience with transapical implantation of the left ventricular lead. Heart Surg Forum 12:E137–E140
158. van Deursen C, van Geldorp IE, Rademakers LM et al (2009) Left ventricular endocardial pacing improves resynchronization therapy in canine left bundle-branch hearts. Circ Arrhythm Electrophysiol 2:580–587
159. Bordachar P, Grenz N, Jais P et al (2012) Left ventricular endocardial or triventricular pacing to optimize cardiac resynchronization therapy in a chronic canine model of ischemic heart failure. Am J Physiol Heart Circ Physiol 303:H207–H215
160. Strik M, Rademakers LM, van Deursen CJ et al (2011) Endocardial left ventricular pacing improves cardiac resynchronization therapy in chronic asynchronous infarction and heart failure models. Circ Arrhythm Electrophysiol 5:191–200
161. Morgan JM, Biffi M, Geller LA et al (2014) Safety and efficacy of left ventricular endocardial lead pacing for cardiac resynchronization therapy: primary results of the Alternate Site Cardiac Resynchronization (ALSYNC) Study. Heart Rhythm LBCT02 Session: Late-Breaking Clinical Trials II, 3-4. 5-9-2014
162. Doring M, Braunschweig F, Eitel C et al (2013) Individually tailored left ventricular lead placement: lessons from multimodality integration between three-dimensional echocardiography and coronary sinus angiogram. Europace 15:718–727

163. Eitel C, Doring M, Gaspar T et al (2010) Cardiac resynchronization therapy with individualized placement of two left ventricular leads at the sites of latest mechanical left ventricular contraction: guided by 3D-echocardiography and coronary sinus rotation angiography. Eur J Heart Fail 12:411–414
164. Schwartzman D, Schelbert E, Adelstein E, Gorcsan J, Soman P, Saba S (2010) Image-guided cardiac resynchronization. Europace 12:877–880
165. Duckett SG, Ginks MR, Knowles BR et al (2011) Advanced image fusion to overlay coronary sinus anatomy with real-time fluoroscopy to facilitate left ventricular lead implantation in CRT. Pacing Clin Electrophysiol 34:226–234
166. Merkely B, Molnar L, Roka A (2012) Interventional and minimally invasive surgical techniques facilitating cardiac resynchronization therapy. In: Roka A (ed) Current issues and recent advances in pacemaker therapy. InTech Books
167. Fatemi M, Le GG, Blanc JJ, Mansourati J, Etienne Y (2011) The use of epicardial electrogram as a simple guide to select the optimal site of left ventricular pacing in cardiac resynchronization therapy. Cardiol Res Pract 2011:956062
168. Foley PW, Khadjooi K, Ward JA et al (2009) Radial dyssynchrony assessed by cardiovascular magnetic resonance in relation to left ventricular function, myocardial scarring and QRS duration in patients with heart failure. J Cardiovasc Magn Reson 11:50
169. Molenaar MM, Oude VB, Scholten MF, Stevenhagen JY, Wesselink WA, van Opstal JM (2013) Optimisation of cardiac resynchronization therapy in clinical practice during exercise. Neth Heart J 21:458–463

Cardiac Mapping Technology

32

Nicholas D. Skadsberg, Bin He, Timothy G. Laske, Charu Ramanathan, and Paul A. Iaizzo

Abstract

In general, the methodologies for cardiac electrical mapping entail registration of the electrical activation sequences of the heart by recording extracellular electrograms. The initial use of cardiac mapping was primarily to better understand the normal electrical excitations of the heart. However, the focus in mapping over time has shifted to the study of mechanisms and substrates underlying various arrhythmias; these techniques have been employed to aid in the guidance of curative surgical and/or catheter ablation procedures. More recently, the advent and continued development of high-resolution mapping technologies have considerably enhanced our understanding of rapid, complex, and/or transient arrhythmias that typically cannot be sufficiently characterized with more conventional methodologies. For example, the ability to visualize endocardial structures during electrophysiology procedures has greatly advanced the understanding of complex cardiac arrhythmias in relation to their underlying anatomy. In addition, such technologies provide powerful tools in the subsequent treatment of cardiac patients, particularly with the promise of accurately pinpointing the source of arrhythmias and thereby providing possible curative treatments. This chapter will summarize the most recent developments in catheter navigation and three-dimensional arrhythmia mapping technologies including both intracardiac and noninvasive approaches.

Keywords

Activation maps • Body surface potential mapping • Cardiac mapping • Continuous mapping • Electroanatomic mapping • Endocardial mapping • Epicardial mapping • Isopotential maps • Noninvasive mapping • Sequential mapping

N.D. Skadsberg, PhD (✉) • T.G. Laske, PhD
Medtronic, Inc.,
8200 Coral Sea St. NE, Mailstop MVS46, Mounds View,
Minneapolis, MN 55112, USA

Department of Surgery, University of Minnesota,
Minneapolis, MN USA
e-mail: nick.skadsberg@medtronic.com

B. He, PhD
Department of Biomedical Engineering, University of Minnesota,
Minneapolis, MN USA

C. Ramanathan, PhD
CardioInsight, Inc., Cleveland, OH, USA

P.A. Iaizzo, PhD
Department of Surgery, University of Minnesota,
Minneapolis, MN USA

32.1 Introduction and Background

The first recorded electrocardiogram (ECG) detailing the structure of atrioventricular conduction was made by Tawara nearly a hundred years ago [1]. Soon thereafter, Mayer was the first to observe rhythmical pulsations in ring-like preparations of the muscular tissue of a jellyfish (Scyphomedusa Cassiopeia) [2, 3]. In similar ring-like preparations of the tortoise heart, Mines was able to initiate circulating excitation by employing electrical stimulation [4]. Shortly thereafter, Lewis and Rothschild described the excitatory process in a canine heart [5], and after a delay due to the events of World War I, Lewis next reported the first real *mapping*

P.A. Iaizzo (ed.), *Handbook of Cardiac Anatomy, Physiology, and Devices*, DOI 10.1007/978-3-319-19464-6_32

experiment in 1920 [6]. These groundbreaking studies were the first attempts to illustrate and document electrical reentry in an intact heart, and these results have greatly influenced those who have continued to perform mapping studies. Hence, the field of *cardiac electrical mapping* was established. Soon afterwards, the idea of mapping arrhythmic activation encompassed an ever larger number of studies, including the early pioneering work of Barker et al., who performed mapping of the first intact human heart in 1930 [7]. Many research groups have continued along this line of investigation, leading to several major discoveries in cardiac function as well as in the development of numerous systems to record such electrical activities in detail. One representative approach is the so-called body surface potential mapping [8], in which an array of electrodes is used to record and visualize the electrical potentials over the body surface. Much of the research performed to date has focused primarily on the mechanisms and substrates underlying various arrhythmias, and cardiac mapping has been employed to aid in the guidance of curative surgical and catheter ablation procedures [9–14]. More recently, the advent and continued development of high-resolution mapping technology has considerably enhanced our understanding of rapid, complex, and/or transient arrhythmias that cannot be sufficiently characterized with more conventional methodologies.

32.2 Conventional Methodologies

Currently, approximately ten million Americans annually are afflicted with cardiac arrhythmias (both ventricular and atrial), yet only a small percentage of these patients are expected to have electrophysiological (EP) mapping procedures. It is generally accepted that cardiac electrical mapping is critical in understanding the pathophysiological mechanisms that underlie arrhythmias, as well as the mechanisms that control their initiation and sustenance. Furthermore, cardiac mapping is commonly used for evaluating the effect of pharmacological therapies and directing surgical and/or catheter ablation procedures in the clinical EP laboratory.

Mapping of the depolarization and repolarization electrical processes is considered critical for the selection of optimal therapeutic procedures. In particular, mapping of potential distribution and its evolution in time is required for precisely determining activation patterns, locating specific arrhythmogenic sites, and identifying anatomical areas of abnormal activity and/or slow conduction.

In short, the purpose of such advanced clinical cardiac mapping techniques is to better characterize and localize arrhythmogenic structures, and this can be accomplished by a variety of different methods. Thus, *cardiac mapping* is a broad term that encompasses many applications such as body surface potential maps (BSPMs), epicardial mapping, or endocardial mapping, as well as approaches including activation maps and/or isopotential maps. Such applications can be clinically applied via either invasive or noninvasive approaches. Nevertheless, there are many fundamental similarities in all of these techniques.

Currently, the gold standard is the clinical EP study, which is primarily used to: (1) determine the source of cardiac arrhythmias; (2) support the management of treatment through pharmacological means; and/or (3) support nonpharmacologic interventions such as implantable pacemakers, defibrillators, and/or ablation therapies (see also Chap. 28). More specifically, these methods are also used to assess the timing and propagation of cardiac electrical activities involving the 12-lead ECG and/or recordings of electrical activation sequences termed *extracellular electrograms*. These signals are obtained by using multiple intravascular electrode catheters positioned at various locations within the heart. The technique of catheter-based mapping not only permits a better understanding of the underlying mechanisms of various arrhythmias, but also serves as the basis for most of the emerging concepts for treatment, namely ablative techniques. Subsequently, the need for more invasive arrhythmia surgery (e.g., maze procedures) has significantly decreased as a result of advances in (and increased use of) these particular catheter-based endocardial mapping and ablation methodologies [15].

Nevertheless, the EP study is not without limitations. The electrophysiologist can only record electrical activity from electrodes located on the surface of the catheter, which must be in contact with the chamber wall. Such electrode areas (mm in diameter) are relatively small in comparison to the heart's total surface area. Thus, to adequately obtain complete global electrical activation patterns, it often dictates the placement of one or more catheters at multiple locations within the chamber of interest. As a consequence, this process requires a considerable amount of time, thus leading to extensive use of fluoroscopy and exposing the medical staff and patients to undesirable levels of ionizing radiation [16].

Secondly, and perhaps more importantly, fluoroscopy does not sufficiently provide for the visualization of the complex 3D cardiac anatomy and soft tissue characteristics of a heart's chambers (Fig. 32.1). As a direct result, the expedient and reproducible localization of sites of interest is often poor. More specifically, this inability to precisely relate EP information to a specific spatial location in the heart limits conventional techniques for employing ablation catheters for treatment of complex cardiac arrhythmias. Lastly, such techniques for mapping electrical potential activities from multiple sites do so sequentially over several cardiac cycles, without accounting for likely beat-to-beat variability in activation patterns. Despite these known limitations, electrophysiologists still use these conventional techniques as the "gold standard" for validation purposes.

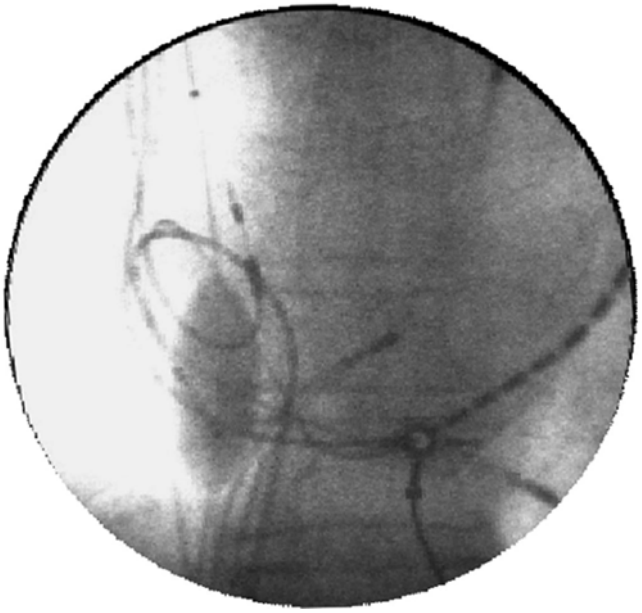

Fig. 32.1 Image illustrating fluoroscopy's poor soft tissue contrast

32.3 Recent Developments

In an effort to overcome the limitations associated with conventional EP mapping techniques, considerable advances have been made with both invasive and noninvasive imaging of cardiac electrical activity. More specifically, several high-resolution mapping technologies have been developed that can function in a complementary role to conventional mapping techniques, or they can be used independently. Moreover, it is now possible to integrate these techniques with imaging modalities such as magnetic resonance imaging, computed tomography, and real-time 3D ultrasound. These techniques can broadly be categorized into two primary technologies, each possessing unique advantages and disadvantages: *sequential mapping* and *continuous mapping*.

There are two distinct technologies that primarily comprise the first category (sequential mapping systems) including electroanatomical mapping systems such as the CARTO3® System (Biosense Webster, Diamond Bar, CA, USA), the EnSite Velocity™ System (St. Jude Medical, St. Paul, MN, USA), and the LocaLisa® system (Medtronic, Inc., Minneapolis, MN, USA). Common to each system is the capability to collect 3D locations as well as their respective electrogram recordings in the target cardiac chamber, to create an accurate picture of the heart's electrical sequence. A third mapping system that is ultrasound-based (Real-Time Position Management System, Boston Scientific Corporation, Natick, MA, USA) was previously marketed but is not readily available, and will therefore not be described in this review.

Continuous mapping systems represent the second major mapping technology category, and typically consist of either basket or noncontact catheter mapping (NCM). Such systems allow for the recording of global data so that the rhythm can be characterized with a minimal number of cardiac beats. In general, basket catheter mapping technologies necessitate electrode contact with the chamber's walls in order to obtain sufficiently accurate reconstructed electrograms, whereas NCM simply needs to be placed in the blood pool of the chamber of interest. Yet, both methodologies overcome some of the limitations of fluoroscopy by allowing for the creation of accurate 3D intracardiac maps, hence providing new and unique insights on the specific diagnosis and treatment of complex arrhythmias. Examples of this technology category include the EnSite™ Array™ noncontact mapping catheter and system (St. Jude Medical) and the Rhythmia mapping system (Boston Scientific Corporation).

Recently, exciting advancements have been made in the field of noninvasive imaging such that cardiac electrical activities are spatially represented over the 3D space of the heart. He and coworkers have pioneered the development of 3D cardiac electrical activity from bioelectric recordings [17–19]. The goal of such cardiac electrical imaging, also known as the *inverse problem* of electrocardiography, is to noninvasively image and visualize the electrical activity of the heart from BSPMs. Due to the high temporal resolution inherent in these bioelectric measurements, the availability of bioelectric source imaging modalities provides much needed high temporal resolution in mapping functional status of the heart and, in turn, aids clinical diagnosis and treatment. In a series of studies, He and colleagues have developed data-driven 3D cardiac electrical imaging techniques that are based upon the fundamental biophysics of cardiac activation, to image activation sequences throughout the heart [20]; they further validated such an imaging approach in animal models using intracardiac mapping [21–24]. These rigorously conducted experiments demonstrate the ability to map transmural cardiac activation throughout the entire heart from noninvasive BSPMs. CardioInsight, Inc. has developed a revolutionary noninvasive electrocardiographic mapping platform (ECVUE™, Cleveland, OH, USA) that gathers information about the heart using a proprietary, multi-sensor electrode "vest" placed upon the patient's body. The system combines this electrical information with images from the patient's CT scan, to provide 3D maps of the electrical activity of the heart. Unlike conventional catheter-based mapping methods, the ECVUE system is noninvasive and provides a view of the entire heart's electrical activity during a single beat.

Fig. 32.2 CARTO® sequential mapping system (Biosense Webster, Inc.). Image from www.biosensewebster.com

32.3.1 Sequential Mapping Systems

32.3.1.1 Electroanatomical Mapping Technologies

Principally, electroanatomical mapping (EAM) refers to the integration of spatial data and temporal electrical data collected by catheters in contact with either the endocardial or epicardial surfaces of the heart. One such technology utilizes ultra-low magnetic field technology in order to localize the relative positions of mapping catheters in space and then to reconstruct 3D maps and activation sequences of the chamber of interest [25–27]. In short, the CARTO3® system uses one reference catheter (RefStar™), one mapping catheter (NaviStar™), and a pad that transmits three ultra-low magnetic fields (Fig. 32.2). Further, the amplifiers for the system are separate pieces of equipment that extract the information from the catheters and location pad, and then these data are sent to the workstation.

More specifically, three ultra-low magnetic fields are generated by coils in the locator pad positioned under the patient's bed. These ultra-low fields are detected by sensors in the distal tips of the mapping catheters, which are then positioned into the heart chamber(s) to be mapped under fluoroscopic guidance. Information within the magnetic fields such as amplitude, frequency, and phase of the field is subsequently used to determine the instantaneous spatial 3D position (x, y, and z axes) and temporal characteristics (pitch, yaw, and roll) of the catheter's distal tip location within a chamber. Catheters are then strategically placed at major anatomical landmarks (i.e., superior and inferior vena cava, tricuspid valve annulus, coronary sinus ostium, crista terminalis, and His bundle for a right atrium map) to serve as reference points for the subsequently derived electroanatomic map. Recordings of the 3D locations of the catheter tips (via a triangulation calculation) and correlating local electrical information from a multitude of points within the chamber are then sequentially recorded and used to reconstruct a 3D representation of the chamber.

After completion of the 3D reconstruction of the chamber's endocardial geometry, the timing of unipolar and bipolar electrogram signals, related to the fiducial point of the reference electrogram, allows for collection and display of activation times on the map in relation to the location of the catheter in the heart. To create the activation map, reconstructed locations on the map are typically color-coded, with red and purple representing the regions of earliest and latest electrical activation, respectively, and yellow and green showing the intermediate activated areas. Local activation times are then represented on a normal color scale sequence, where red is the earliest signal and purple is the latest recorded signal in reference to the chosen fiducial point. As a result, the sequential recording of different points by dragging the catheter along the endocardial walls of the chamber provides real-time, color-coded 3D activation maps.

A relative voltage map displaying the peak-to-peak amplitude of the electrogram sampled at each site may also be produced and superimposed on the reconstructed chamber. Using custom software, all maps can be shown in single or multiple views concurrently, with the capability to be rotated in virtually any direction. As described, a second catheter equipped with a sensor in its distal tip is also positioned in the chamber of interest, and is used to identify small changes in the mapping catheter's relative position that may have been caused by respiration and/or patient movement. Movement of the patient relative to the coils is continuously monitored by the system and the operator is notified to the need for repositioning, if the system detects relative motions beyond a set threshold. The most recent version (CARTO-3) allows the position of non-proprietary diagnostic catheters to be displayed on the system. For each specific magnetic location in space, the CARTO-3 system®registers the corresponding electrical current pattern emitted by the magnetic sensor-equipped mapping catheter. The position of conventional catheters can then be determined based on the detection of the current pattern emitted from each intracardiac electrode on the diagnostic catheter. However, it is still not

possible to process electrical information from these catheters for display on the virtual geometry.

Such EAM has experienced relatively widespread clinical use, and has also been utilized for the study of a variety of cardiac arrhythmias including: atrial fibrillation [28], atrial flutter [29–32], ventricular tachycardia [33, 34], and atrial tachycardia [35, 36]. One of the primary reasons for the success of this method lies in its capability to return an ablation catheter to any endocardial location on a previous map of the chamber without relying on fluoroscopy, i.e., with in vivo validation studies demonstrating that the location of the catheter can be determined with a high degree of accuracy using the system with mean distance error <1 mm. In most cases, the ablation catheter and mapping catheter are one and the same. This enables potential ablation target sites to be analyzed and treated in a single procedure, and provides the ability to precisely register the location of individual and/or linear lesions.

The reconstruction process using such a system can be generated in real time; however, due to the fact that this approach must sequentially acquire points, the process can be somewhat time-consuming [36, 37]; timing is governed by the number of points collected. Nevertheless, in practical use, the amount of the time required to reconstruct a chamber's geometry relies on the comfort level of the physician manipulating the catheter and the knowledge of the individual participating at the workstation. It should be noted that other potential limitations associated with EAM include the inability to simultaneously acquire maps of different heart rhythms [37], as well as the potential for inaccurate mapping due to movement of the patient and/or catheter. As a direct result, an unstable rhythm may prove too complicated to delineate and, therefore, may not be a primary indication for this technology.

32.3.1.2 LocaLisa® Technologies

Although no longer commercially available, the first technology developed for real-time 3D localization of intracardiac catheter electrodes within the chambers of the heart worked on the principle that when an electrical current is externally applied through the thorax, a voltage drop occurs across the internal organs, including the heart. This particular voltage drop can then be recorded via standard catheter electrodes and subsequently used to determine electrode positions within a given 3D space.

Using similar physical properties, the LocaLisa® system (Fig. 32.3) delivers an external electrical field that is detected via standard catheter electrodes. This is achieved by sensing impedance changes between the catheter and reference points. Analogous to the Frank lead system, the electric field is applied in three orthogonal directions (x, y, and z) with different frequencies (~30 kHz) via three applied skin electrode pairs. This system then records the voltage potentials

Fig. 32.3 The LocaLisa® mapping system (Medtronic, Inc.). Image courtesy of Medtronic, Inc.

detected by the catheter's electrodes within the three electric fields, thus allowing for a defined coordinate system to be created.

These voltage potentials are next translated into a measure of distance relative to a fixed reference catheter, giving the user a 3D representation of the catheter location within the heart's chamber. Important catheter locations are subsequently recorded and represented as color-coded spots on a 3D grid, a process that requires a skilled operator's interpretation (Fig. 32.4). Individual catheter locations can be saved, annotated, and revisited later in the procedure.

Due to the fact that the system displays real-time electrode movements, catheter movements due to cardiac and respiratory cycles are similar to those observed with fluoroscopy. In initial human validation studies, the LocaLisa® system was described to provide clinically feasible and accurate catheter locations within the heart [38]. Developers of the system reported successful use in over 250 complex ablation procedures for both ventricular and supraventricular tachyarrhythmias. The novel capabilities of this system included: (1) its ability to use any general catheter to collect data; (2) relative improvements in the visualization of catheters in 3D

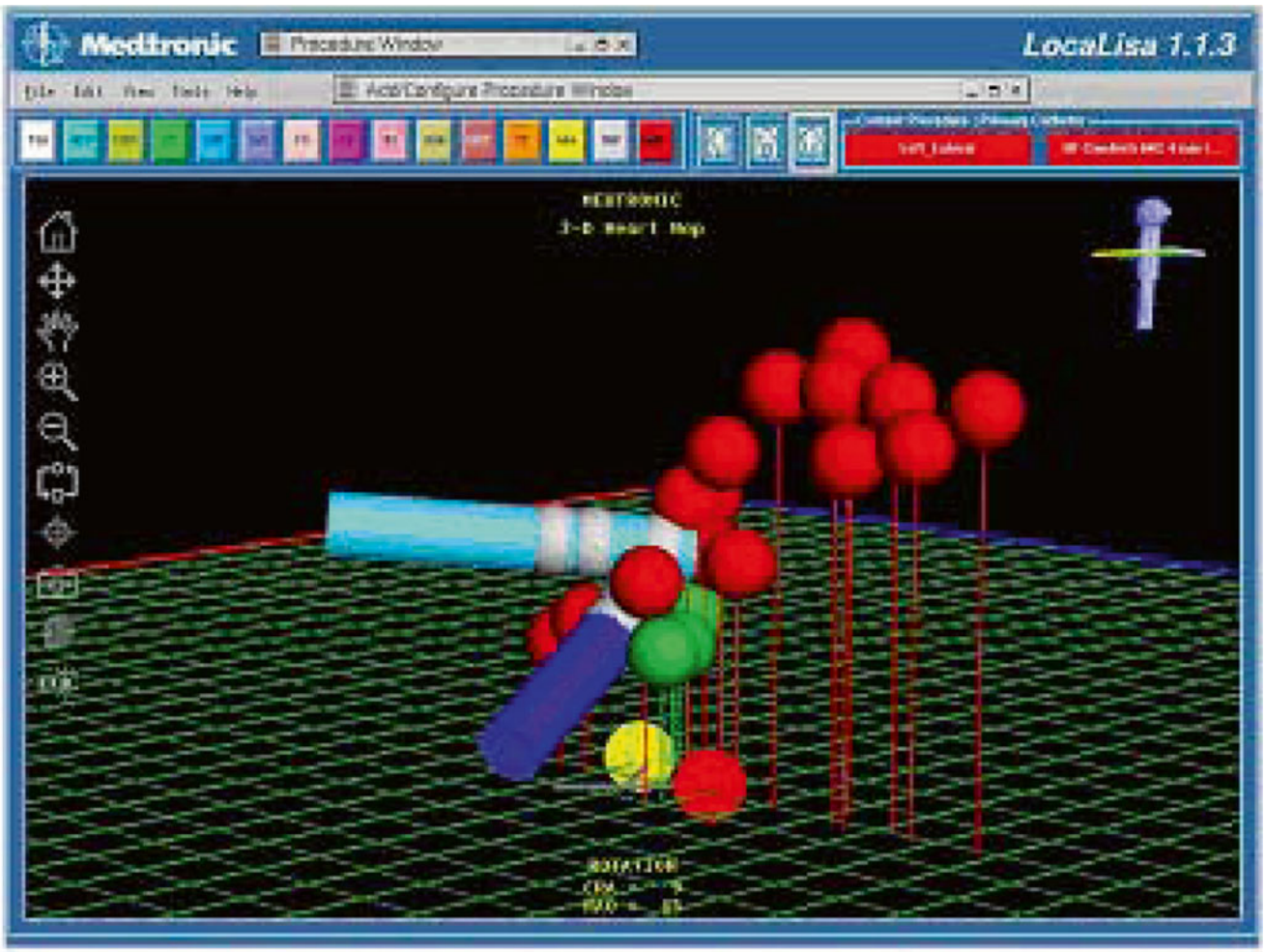

Fig. 32.4 Screen shot of LocaLisa®'s mapping software (Medtronic, Inc.). Image courtesy of Medtronic, Inc.

Fig. 32.5 Constellation® multielectrode basket catheter (Boston Scientific, Inc.)

space; and (3) a broad clinical applicability. Finally, this methodology could be applied with complex catheter designs such as multielectrode catheters, irrigated electrode catheters, and/or basket catheters [39–41].

32.3.2 Continuous Mapping Systems

32.3.2.1 Basket Catheter Mapping Technologies

In general, the limited mapping resolution of conventional catheters may be greatly overcome via the use of a multielectrode basket catheter. Initial efforts to place multiple electrodes on a single mapping catheter were limited by electrode size. As such, basket catheter mapping was developed in the 1990s, and typical catheters contain 32–64 nickel, titanium, or platinum electrodes that are 1–2 mm long and 1 mm in diameter (Fig. 32.5) [41, 42]. Depending on the basket catheter shape and radius, the interelectrode distance can vary between 3 and 10 mm. Regardless, the accuracy in reconstruction of the chamber's geometry and electrical activity created by the basket system relies on: (1) the number of splines on the basket; (2) the number of electrodes on each spline; and (3) the percentage of those electrodes which achieve adequate contact with the endocardial surface. These multielectrode mapping catheters facilitate the creation of high-density maps, i.e., through the simultaneous collection

of data from closely spaced electrodes. It should be noted that, due to specific anatomic features of the chambers that do not allow complete endocardial coverage by the basket catheter electrodes, the quality of contact of all the electrodes with the endocardium cannot be ensured, and thus it is common that some anatomic regions cannot be adequately mapped.

The initial use of basket catheters was reported in a number of animal studies which were aimed at characterizing either atrial [41] and/or ventricular arrhythmias [42]. More specifically, Triedman et al. [43] reported studies in which they utilized a Webster-Jenkins catheter (Cordis Webster, Inc., Baldwin Park, CA, USA) and a 5-spoke flexible ellipsoid with 25 bipolar electrode pairs for the mapping of right ventricular activation patterns. Data were obtained from catheters placed into the right atria and ventricles of juvenile sheep which were eliciting either normal sinus rhythm or acute and chronic pathological sequelae [43]. They concluded that employing a basket catheter had the potential to provide rapid, nearly real-time, activation sequence maps which improved their understanding of the mechanisms of complex reentrant tachyarrhythmias. Subsequently, Schalij et al., [44] reported on the first application of a basket catheter and resultant animation programs in 20 human patients with ventricular tachycardia. They reported that percutaneous endocardial mapping with basket catheters was feasible, of clinical value, and reasonably safe. Since then, basket catheter mapping has been employed in the study of numerous cardiac arrhythmias in various human populations [45–47].

Most recently, a novel multielectrode catheter and its integrated mapping system (Rhythmia mapping system, Boston Scientific) have been commercialized. The multielectrode mapping catheter (IntellaMap Orion™) has an 8 Fr profile and is equipped with a mechanism for bidirectional tip deflection. At the tip, there are 64 electrodes distributed on eight splines with an interelectrode spacing of 2.5 mm (Fig. 32.6). Electrodes can be used in either bipolar or unipolar configurations. The catheter is part of an integrated EAM system, which also includes an electronic patient interface unit and a computer workstation that is used to run the mapping software. Advanced front-end technology filters and collects high quality signals with low noise, and its open architecture allows the operator the freedom to choose and visualize most ablation or diagnostic tools. Further, the system's dynamic review capabilities allow the user to quickly review and edit data points; it also offers automated annotation to help minimize the time required to manually annotate data collected. The position of the multielectrode array is tracked utilizing a combination of magnetic and electrical field information. Initial preclinical feasibility was reported, demonstrating that the multielectrode catheter was capable of producing high-resolution electroanatomical maps of the right atrium and the left ventricle in animal models [48, 49]. Average map acquisition times for the catheter (with continuous data collection) ranged from 5.2 to 9.5 min and these maps contained an average of 2753–3566 points.

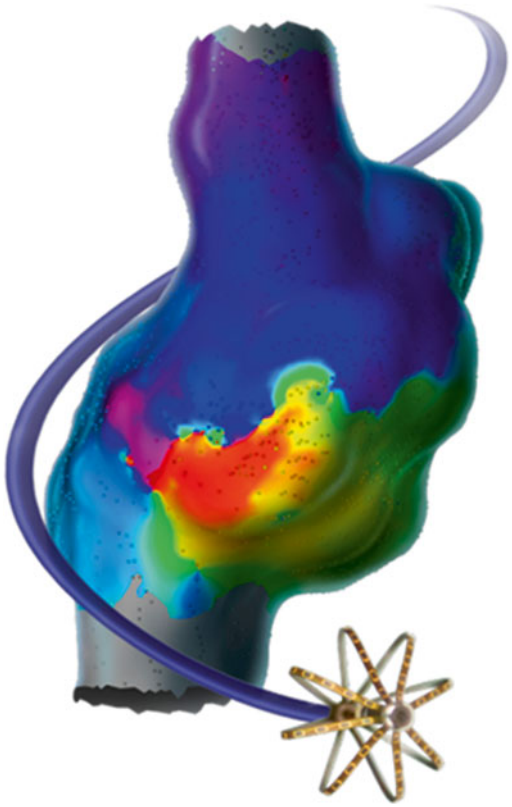

Fig. 32.6 Rhythmia mapping system's IntellaMap Orion™ high resolution mapping catheter (Boston Scientific, Inc.). Image from http://www.bostonscientific.com/en-US/products/capital-equipment--mapping-and-navigation/rhythmia-mapping-system/redefined.html

Yet another technology has been commercialized that includes a 64 electrode basket (Topera, Inc., Menlo Park, CA, USA). The Topera 3D mapping system consists of the FDA cleared and CE marked RhythmView™ workstation and FIRMap™ panoramic contact-mapping tool, which are used in combination for the identification and localization of the sustaining mechanisms of cardiac arrhythmias such as atrial fibrillation, atrial flutter, atrial tachycardia, and/or ventricular tachycardia. The RhythmView workstation provides a graphical display of the right and left atrial electrical activities to assist in the diagnoses of arrhythmias and also to facilitate patient-specific atrial fibrillation treatment decisions. The FIRMap panoramic contact-mapping tool has been used to capture electrical potentials from the endocardium, which can then be used in conjunction with RhythmView to create activation maps to aid in the diagnosis of complex cardiac arrhythmias. The diagnostic tool ("basket") consists of 64 evenly spaced electrodes distributed among 8 splines. Images of both the RhythmView workstation and the FIRMap cath-

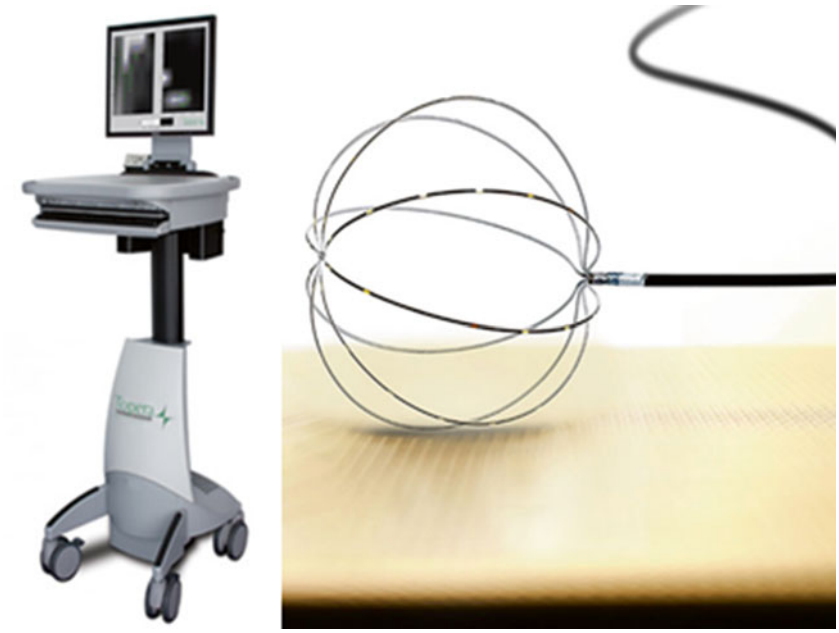

Fig. 32.7 RhythmView™ workstation and the FIRMap™ catheter. Image from http://www.toperamedical.com/patients/solution/

eter are shown in Fig. 32.7. To date, several reports have been recently published highlighting the clinical utility of this system [50–54].

It should be noted that there are limitations associated with basket catheter mapping. First, the use of a basket catheter that is too large or small compared with the relative dimensions of the chamber of interest will result in poor quality of electrograms in terms of morphology, stability, and relation with the given anatomic structures. Second, it has been cited that the relative movement between the beating heart and the electrodes can be detrimental to the electrical reconstruction process or may even cause irritation of the myocardium. Lastly, due to product size constraints, the basket catheter approach does not have the ability to map areas of the atrial appendage or pulmonary veins, which play major roles in the sustenance of atrial fibrillation.

32.3.2.2 Noncontact Mapping Technologies

Recently, NCM approaches have been more widely used in the clinical diagnosis and ablative treatment of complex cardiac arrhythmias, as described by Schilling et al. [12, 55, 56]. More specifically, the EnSite™ Array™ noncontact mapping catheter, used in combination with EnSite™ Velocity system (St. Jude Medical) introduced by Taccardi et al. [57], is comprised of a catheter-mounted, inflatable multielectrode array, a reference patch electrode, amplifiers, and a workstation (Fig. 32.8). The EnSite NavX technology is an open platform that is compatible with catheters from most manufacturers and can simultaneously display up to 12 catheters and 64 electrodes.

Specifically, this system's EnGuide® locator technology utilizes a single-use 9 Fr, 110 cm transvenous multielectrode array catheter (Fig. 32.9) consisting primarily of: (1) a polyamide insulated wire braid with 64 laser-etched unipolar electrodes; (2) a 7.5 mL inflatable polyurethane balloon; and (3) distal and proximal E1 and E2 ring electrodes. Additionally positioned on the proximal end of the catheter is a handle and cable connector that allows the physician to deploy a balloon in the chamber of interest, providing the electrical connection from the array to the patient interface unit of the system.

Typically, the multielectrode array is inserted transvenously into the patient's chamber of interest over a standard 0.032″ guidewire. Once positioned within a given chamber, the multielectrode array wire braid is mechanically expanded and the balloon is inflated using a 50/50 contrast-saline solution. Next, a second catheter, termed the *roving* catheter, is introduced into the same chamber of interest. Following connection to the breakout box, the system's EnGuide® technology emits a low 5.68 kHz signal via the tip of the roving catheter that is detected by the E1 and E2 ring electrodes on the multielectrode array catheter. Subsequently, by determination of the locator signal angles and strengths, the system is able to compute the 3D relationship of the tip of the roving catheter to that of the multielectrode array catheter ring electrodes. In order to reconstruct the 3D *virtual* endocardium of the chamber, the roving catheter continues to emit the 5.68 kHz signal as it is moved around the chamber by dragging the tip around the endocardial wall's contour.

A convex-hull algorithm is then utilized to omit the previously collected points that are inferior to the facets created during the collection process, so that the system essentially stores only the most distant points visited by the roving catheter (i.e., those from the endocardial surface during diastole).

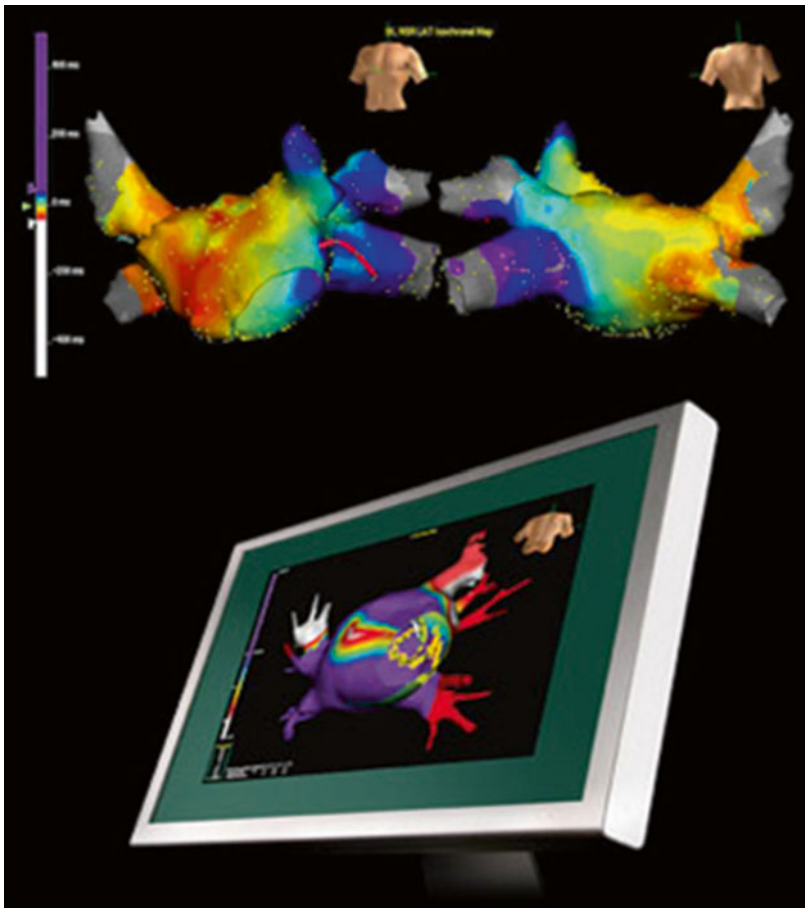

Fig. 32.8 EnSite™ NavX™ navigation and visualization technology (St. Jude Medical, Inc.)

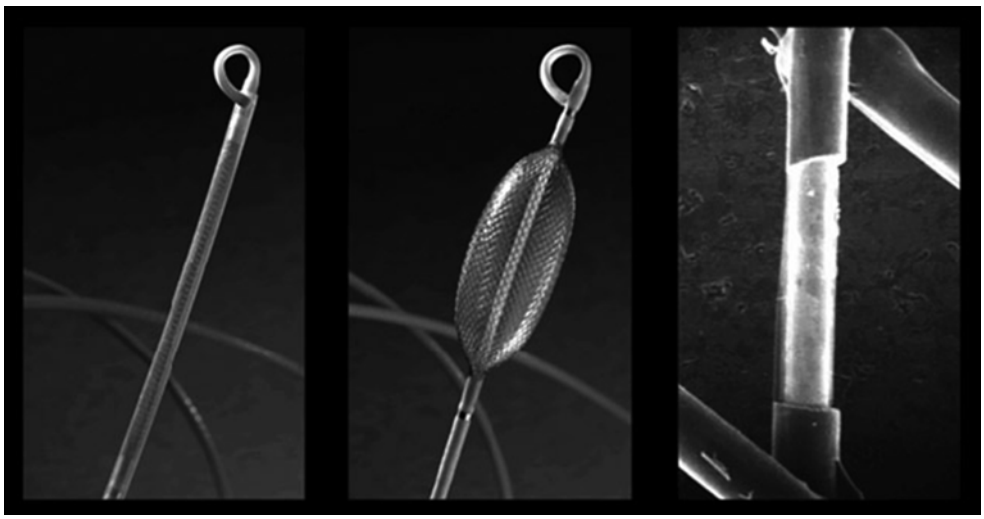

Fig. 32.9 Multielectrode array catheter (St. Jude Medical, Inc.)

The roving catheter is used to locate the major anatomical locations associated with fluoroscopic imaging, and these anatomical landmarks are subsequently labeled on the reconstructed geometry to provide a frame of reference for the physician.

Once the geometry reconstruction is complete, the multielectrode array is used to detect and record the far-field intracavitary electrical potentials from the surrounding myocardium by employing an approximation method based on algorithms developed for inverse problems [58]. To further explain, the potentials in this field are typically lower in amplitude and frequency than the source potentials of the endocardium itself. Therefore, to improve accuracy and stability in reconstruction, a technique is used based on an

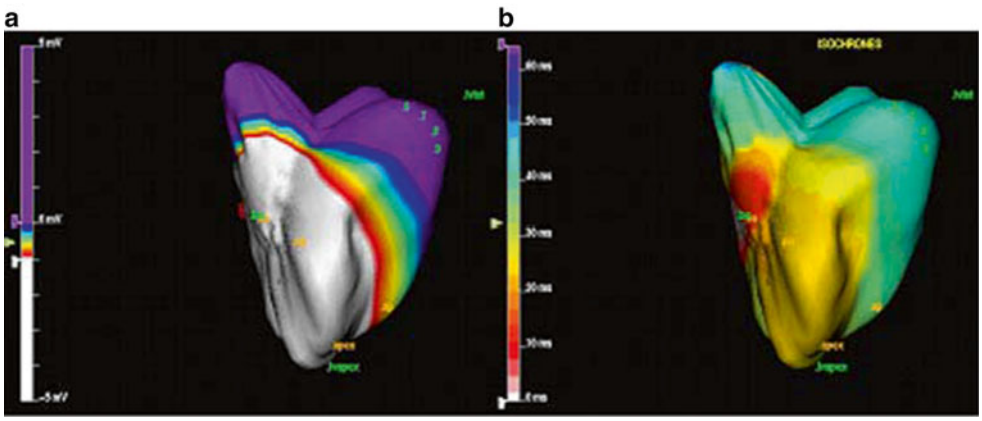

Fig. 32.10 Swine left ventricular (**a**) isopotential activation map and (**b**) isochronal activation map

inverse solution to Laplace's equation by use of a boundary element method so that the resulting signals are used to reconstruct and display >3300 *virtual* electrograms.

After establishment of the chamber's voltage field, cardiac activation can be displayed as computed *virtual* electrograms or as *isopotential maps*. More specifically, these resulting isopotential maps are dynamic representations of the propagation of the electrical wavefront. As such, the electrophysiological information is visually represented by color coding that describes voltage, ranging from red (representing regions of depolarized myocardium) to purple (representing regions electrically neutral) (Fig. 32.10a). Additionally, the system allows for the creation of a static representation of the electrical propagations via *isochronal maps* (Fig. 32.10b). Consequently, the color-coded EP information is representative of the time required to activate different regions of the chamber. In cases where ablation is employed, the EnGuide® technology aids in navigating RF catheters to the appropriate site with an accuracy of ±1 mm.

The EnSite™ NavX™ EAM system is functionally very similar to the CARTO EAM but utilizes externally applied high frequency electric fields from cutaneous patches to determine catheter locations rather than magnetic sensors within the catheter tip. It requires three pairs of skin patches, one for each of *x*, *y*, and *z*-axes, thus creating a 3D coordinate system. Therefore, the NavX™ system can, in theory, be used to perform EP studies and catheter ablation procedures with a very low amount of fluoroscopy, which has been recently demonstrated with the introduction of the MediGuide™ system (St. Jude Medical) [59]. The MediGuide system is a visualization and navigation system that can display the relative positions and orientations of MediGuide Enabled™ devices (equipped with a MediGuide sensor) on both live and prerecorded fluoroscopy in real time. With the NavX™ software system, it is also possible to import a 3D reconstruction of anatomy taken from a high-resolution computed tomographic scan performed prior to the procedure; this is then synchronized to the images so that 3D images and maps can be manipulated simultaneously [60].

NCM has been utilized and validated in several clinical settings such as the evaluation and treatment of atrial flutter, atrial fibrillation [61–63], and/or ventricular tachycardia [64]. In such cases, this system has been used to aid in the identification of critical regions of slow conduction, to identify and then precisely return catheters to areas of interest in the chamber, and to subsequently visualize ablation lesion lines that have been created. Therefore, this system permits for the detailed reconstruction of global and local cardiac electrical events in a timely fashion within the EP lab. Most importantly, the system allows for a great deal of data to be recorded within the short duration of only one to two heartbeats, thus allowing the physician to adequately evaluate the origination, maintenance, and termination of nonsustained complex cardiac arrhythmias, pathways of reentrant activity, and/or electrical changes that may occur on a beat-to-beat basis.

Despite the vast number of advantages associated with NCM mapping, there are several current limitations worth noting. The NavX system has the disadvantage of not being able to specifically define the positions of given electrode (*x*, *y,* and *z* coordinates). Yet, the orientation of the catheter tip (pitch, roll and yaw) is not directly measured but can be partially inferred by determining the location of multiple electrodes along the path of a catheter. Background noise can greatly affect the quality of the recordings; this commonly originates from the surrounding environment or from the amplifier circuitry due to electrical fluctuations. In order to obtain optimally reconstructed electrograms, it has been documented that the distance from the area mapped to the multielectrode array should be less than 40 mm [55, 56, 65]; beyond this distance, there is an overall decrease in accuracy of the reconstructed electrograms. Additionally, the accuracy of the NavX system is adversely affected by heterogeneity in the electrical fields within the chest (i.e., different structures within the thoracic cavity have different electrical properties), which will reduce the accuracy of 3D localizations. NCM is only able to reconstruct the electrical activity on the endocardial surface of a given chamber, thus it is unable to

identify subendocardial activation characteristics which may play a critical role in the successful identification of various arrhythmias and, hence, the subsequent therapy employed. The dimensions of the multielectrode array when in full profile are 1.8×4.6 cm^2, which can restrict mapping catheter manipulation when placed in particular areas of the heart, such as right and left atrial appendages. Lastly, despite several software updates, the system is still complex and quite expensive.

32.4 Noninvasive Cardiac Mapping

Significant and innovative advancements have been made in the noninvasive imaging of cardiac electrical activity. Ongoing research in this area is aimed at improving our overall understanding of the mechanisms of cardiac function and dysfunction, in turn, aiding clinical diagnosis and management of cardiac diseases. Employing such an approach allows clinicians the opportunity to precisely localize the arrhythmic substrate and study mechanisms prior to the intervention by solving the so-called *inverse problem*. As a result, one can quickly focus therapy at the primary source of the arrhythmia and subsequently decrease the need for a lengthy EP procedure and, importantly, minimize fluoroscopy exposure to the patient and clinical staff.

The investigation of the epicardial potential inverse solution has garnered interest since the 1970s [66]. Recently the epicardial potential inverse solution has demonstrated the ability to reconstruct epicardial potentials in in vivo humans [67]. In addition, heart surface activation mapping, where activation maps over both the epicardial and endocardial surfaces are estimated from BSPMs, has been investigated [68].

Quite recently, He and coworkers proposed and developed the 3D cardiac electrical imaging (3DCEI) approach for noninvasively imaging 3D cardiac electrical activity employing BSPMs [17–20, 69]. In this 3D approach, cardiac electrical activity is estimated and visualized over the 3D myocardium by solving a linear or nonlinear inverse problem. This 3DCEI approach has been rigorously validated using 3D intracardiac mapping in rabbit [21, 70], swine [71], and canine models [22, 24].

The validation study of the 3DCEI in the swine model [71] is reviewed below, as the swine represents perhaps the most similar model to humans. In brief, a heart-excitation model and heart-torso volume conductor model were constructed based on preoperative MRI scans and prior physiological knowledge of the swine heart. The MR images were segmented to obtain detailed cardiac geometry and the cellular-automaton heart model. The entire heart excitation process could be simulated and the corresponding BSPMs were calculated by employing a boundary element method. A preliminary classification system was also employed to initialize the parameters of the heart-excitation model, and then model parameters were iteratively adjusted in an attempt to minimize any dissimilarity between the measured and heart-model-generated BSPMs until the convergent criteria were satisfied. In this swine validation study, we employed site-specific pacing and, for each pacing site, both the 3D location of the initiation site for electrical activation and the corresponding activation sequence throughout the ventricles were noninvasively estimated using the above procedure. In total, data from 5 right ventricular and 5 left ventricular pacing sites from control and heart failure animals were collected and, subsequently, sequences of 100 paced beats were analyzed. It was demonstrated that the averaged localized error of the right and left ventricular sites was 7.3 ± 1.8 mm ($n = 50$) and 7.0 ± 2.2 mm ($n = 50$), respectively. The global 3D activation sequences throughout the ventricular myocardium were also derived. The endocardial activation sequences as a subset of the estimated 3D activation sequences were first compared with those reconstructed from simultaneously obtained data collected using an NCM system in order to validate the procedure. Figure 32.11 shows an example of the 3D activation sequence estimated from acquired BSPMs which were induced by ventricular pacing in a healthy animal. In addition to the heart-excitation-model-based approach [18, 19, 71], He and co-workers recently developed a data-driven imaging approach [20] and validated it in a series of animal studies [21–24], including pacing and ventricular tachycardia in healthy animals and animals with heart failure. These promising results suggest that the 3DCEI approach may, in the near future, provide a useful tool for both basic cardiovascular research and the clinical diagnosis and management of arrhythmias.

The ECVUE system (CardioInsight) is another noninvasive electrocardiographic mapping system under evaluation. The ECVUE system is built on the foundation of the Electrocardiographic Imaging (ECGI) technology. The ECGI approach was developed to reconstruct potentials of the epicardial cardiac surface to provide proximity to the heart's electrical sources and therefore have much improved resolution than the body surface potentials they are derived from (Fig. 32.12). ECVUE is considered as the first mapping system to combine electrical data from the body surface with heart-torso anatomy from a CT scan, to then calculate the 3D images of the electrical activity of a patient's heart. Importantly, due to the noninvasive nature of the system, it enables advanced cardiac mapping to be utilized outside the existing confines of the EP lab.

The physics of ECGI technology is based on a property that the electric fields generated by the beating heart within the passively conducting torso volume can be represented by the relationship: $\varphi_T = A\varphi_E$, where epicardial potentials (φ_E)

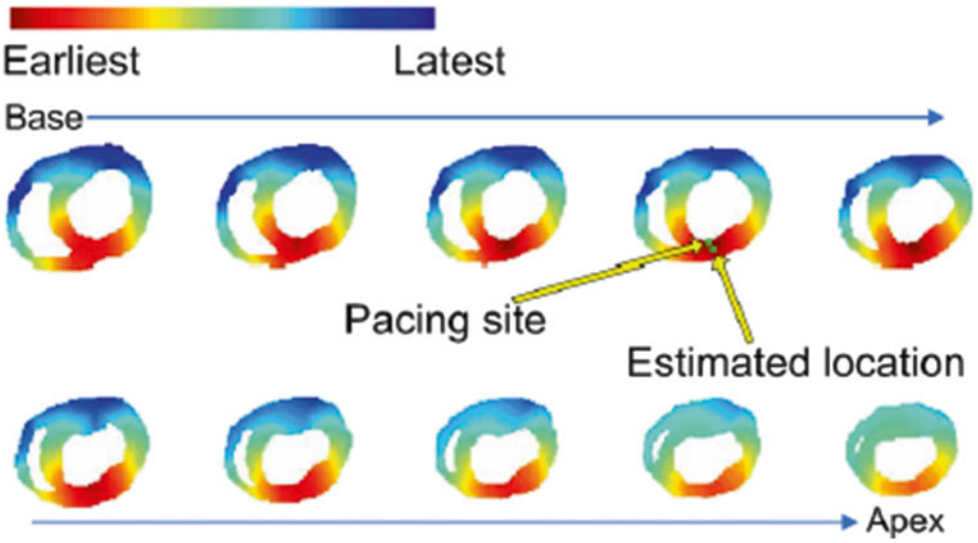

Fig. 32.11 Example of a 3D activation sequence imaged from noninvasive body surface potential maps in a control swine, following left ventricular pacing. Modified from [71]

must be calculated from body surface potentials (φ_T) via a matrix (A) that approximates the electrical relationship between the surface of the body and the epicardial surface of the heart. A detailed description of these methodologies, as well as validation and practical considerations are included in various sources [72–78].

The ECVUE system is comprised of a single-use disposable 252 electrode vest, an amplifier system, and a workstation for advanced data analyses and visualizations (Fig. 32.13). The vest was designed to accommodate a variety of torso shapes and sizes [79]. The system received its CE mark in 2011 and has been used in over 1000 clinical cases for mapping either atrial tachycardia or fibrillation and thus in support of patients undergoing cardiac resynchronization procedures. To date, the system has been used particularly in patients with intermittent, unstable, transient, and polymorphic arrhythmias, and also in cases where the attributes of the system in providing single beat, dual chamber (bi-atrial or biventricular) global mapping information was perceived as a distinct clinical advantage. The aggregate clinical success or performance use of the ECVUE (compared to an EP study) approach ranged from 85 to 100 % for a given chamber or region of interest within the cardiac chamber. Further, it is considered that use of the ECVUE system has specific advantages in patients with: (1) complex arrhythmias, including polymorphic arrhythmias; (2) complicated congenital cardiac anatomies; and/or (3) fibrillatory arrhythmias. It has been reported that the noninvasive mapping information provided by the ECVUE system was especially useful in facilitating EP diagnoses with lower amounts of catheter manipulation; recent literature relating to the use of the system is included in other sources [80, 81].

32.5 Future Directions

The mapping technologies developed and employed to date have revolutionized the clinical EP laboratory, and their use has led to numerous novel insights into the mechanisms underlying all types of arrhythmias. Relative to the multicatheter approach, such technologies have improved resolution, 3D spatial localization, and/or rapid acquisition of the detailed characteristics of cardiac activation in both normal and diseased hearts. In general, these technologies employ novel computational approaches to accurately determine the 3D location of mapping catheters and anatomic-specific local electrograms. Acquired data of the relative intracardiac catheter position and recorded intracardiac electrograms are commonly used by such technologies to reconstruct, in real time, a representation of the 3D geometry of the cardiac chamber of interest.

Nevertheless, to date, such mapping systems are relatively expensive and generally not required for the diagnosis of more common clinical arrhythmias such as atrioventricular nodal reentry, accessory pathway mediated tachycardia (Wolff–Parkinson–White syndrome and concealed pathways), or typical atrial flutter. Furthermore, it should be noted that other emerging technologies, such as intracardiac echocardiography, and the incorporation of high-resolution imaging modality datasets (such as CT or MRI) are considered useful adjuncts for more precise and rapid catheter positioning, perhaps even providing more reproducible catheter positioning towards specific intracardiac structures that are more difficult to identify for mapping or ablation. Yet, the mechanistic contribution of the newer cardiac mapping systems to treat various arrhythmias is likely to be well substantiated. Despite the theoretical clinical advantages highlighted by the technologies discussed in this chapter, further

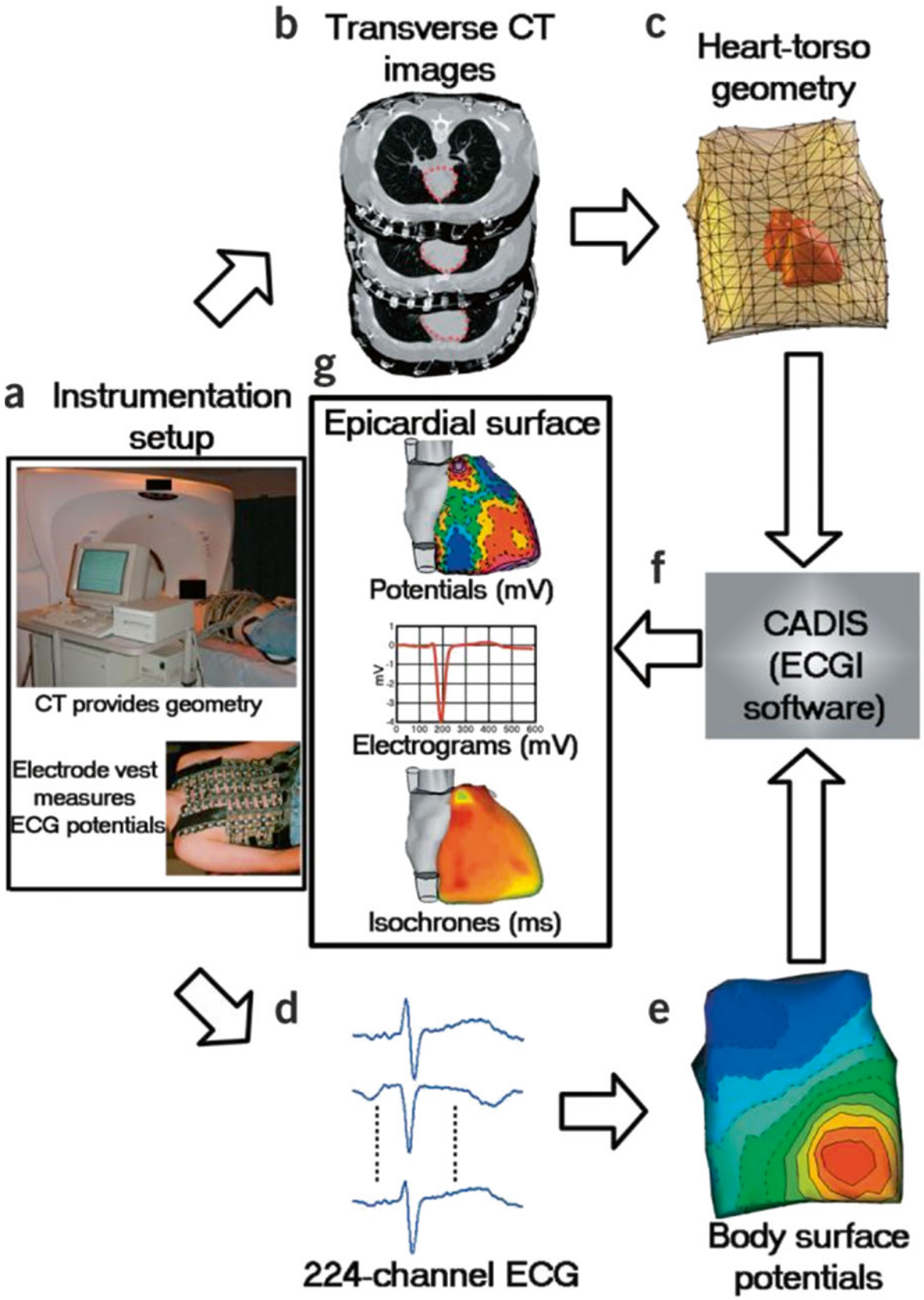

Fig. 32.12 Block diagram of the ECGI procedure. (**a**) Instrumentation setup, (**b**) Computed tomography slices showing heart contours (*red*) and body-surface electrodes (*shiny dots*), (**c**) Meshed heart-torso geometry, (**d**) Sample ECG signals obtained from mapping system, (**e**) Spatial representation of body surface potentials, (**f**) ECGI software package (CADIS), (**g**) Examples of non-invasive ECGI images, including epicardial potentials, electrograms, and isochrones

Fig. 32.13 ECVUE system and non-invasive vest. Image from http://www.cardioinsight.com/product/the-ecvue-vest-at-work/

prospective human clinical trials will ultimately need to be performed to provide validation of optimal clinical utility.

References

1. Tawara S (1906) Das Reizleitungssystem des Säugetierherzens. Eine anatomisch-histologische studie über das atrioventrikularbündel und die Purkinjeschen fäden.
2. Mayer AG (1906) Rhythmical pulsation in scyphomedusae. Carnegie Institute of Washington, Washington, DC
3. Mayer AG (1908) Rhythmical pulsation in scyphomedusae. In: II. Papers from the marine biological laboratory at Tortugas. Carnegie Institution, Washington DC, pp 115–131
4. Mines GR (1916) On dynamic equilibrium in the heart. J Physiol (Lond) 46:349–382
5. Lewis T, Rothschild MA (1915) The excitatory process in the dog's heart, II: the ventricles. Philos Trans R Soc Lond B Biol Sci 206:181–266
6. Lewis T, Feil S, Stroud WD (1920) Observations upon flutter and fibrillation. II The nature of auricular flutter. Heart 7:191–346
7. Barker PS, McLeod AG, Alexander J (1930) The excitatory process observed in the exposed human heart. Am Heart J 5:720–742
8. Taccardi B (1962) Distribution of heart potentials on dog's thoracic surface. Circ Res 11:862–869
9. Jackman WM, Wang XZ, Friday KJ et al (1991) Catheter ablation of accessory atrioventricular pathways (Wolff–Parkinson–White syndrome) by radiofrequency current. N Engl J Med 324:1605–1611
10. Gasparini M, Coltorti F, Mantica M, Galimberti P, Ceriotti C, Beatty G (2000) Noncontact system-guided simplified right atrial linear lesions using radiofrequency transcatheter ablation for treatment of refractory atrial fibrillation. Pacing Clin Electrophysiol 23:1843–1847
11. Schmitt H, Weber S, Tillmanns H, Waldecker B (2000) Diagnosis and ablation of atrial flutter using a high resolution, noncontact mapping system. Pacing Clin Electrophysiol 23:2057–2064
12. Schilling RJ, Davies DW, Peters NS (1998) Characteristics of sinus rhythm electrograms at sites of ablation of ventricular tachycardia relative to all other sites: a noncontact mapping study of the entire left ventricle. J Cardiovasc Electrophysiol 9:921–933
13. Sra J, Thomas JM (2001) New techniques for mapping cardiac arrhythmias. Indian Heart J 53:423–444
14. Schumacher B, Jung W, Lewalter T, Wolpert C, Luderitz B (1999) Verification of linear lesions using a noncontact multielectrode array catheter versus conventional contact mapping techniques. J Cardiovasc Electrophysiol 10:791–798
15. Calkins H, Langberg J, Sousa J et al (1992) Radiofrequency catheter ablation of accessory atrioventricular connections in 250 patients. Abbreviated therapeutic approach to Wolff–Parkinson–White syndrome. Circulation 85:1337–1346
16. Wittkampf FH, Wever EF, Vos K et al (2000) Reduction of radiation exposure in the cardiac electrophysiology laboratory. Pacing Clin Electrophysiol 23:1638–1644
17. He B, Wu D (2001) Imaging and visualization of 3D cardiac electric activity. IEEE Trans Inf Tech Biomed 5:181–186
18. Li G, He B (2001) Localization of the site of origin of cardiac activation by means of a heart-model-based electrocardiographic imaging approach. IEEE Trans Biomed Eng 48:660–669
19. He B, Li G, Zhang X (2002) Noninvasive three-dimensional activation time imaging of ventricular excitation by means of a heart-excitation model. Phys Med Biol 47:4063–4078
20. Liu Z, Liu C, He B (2006) Noninvasive reconstruction of three-dimensional ventricular activation sequence from the inverse solution of distributed equivalent current density. IEEE Trans Med Imaging 25:1307–1318
21. Han C, Pogwizd S, Killingsworth C, He B (2011) Noninvasive imaging of three-dimensional cardiac activation sequence in hearts with pacing and ventricular tachycardia: a quantitative comparison to intra-cardiac mapping on a rabbit model. Heart Rhythm 8:1266–1272
22. Han C, Pogwizd S, Killingsworth C, He B (2012) Noninvasive reconstruction of three-dimensional ventricular activation sequence during pacing and ventricular tachycardia in the canine heart. Am J Physiol Heart Circ Physiol 302:H244–H252
23. Han C, Pogwizd S, Killingsworth C, Zhou Z, He B (2013) Noninvasive cardiac activation imaging of ventricular arrhythmias during drug-induced QT prolongation in the rabbit heart. Heart Rhythm 10:1509–1515
24. Han C, Pogwizd SM, Yu L, Zhou Z, Killingsworth C, He B (2015) Imaging cardiac activation sequence during ventricular tachycardia in a canine model of nonischemic heart failure. Am J Physiol Heart Circ Physiol 308:H108–H114. doi:10.1152/ajpheart.00196.201
25. Ben-Haim SA, Osadchy D, Schuster I (1996) Nonfluoroscopic, in vivo navigation and mapping technology. Nat Med 2:1393–1395
26. Gepstein L, Hayam G, Ben-Haim SA (1997) A novel method for nonfluoroscopic catheter-based electroanatomical mapping of the

heart. In vitro and in vivo accuracy results. Circulation 95:1611–1622
27. Shpun S, Gepstein L, Hayam G, Ben-Haim SA (1997) Guidance of radiofrequency endocardial ablation with real-time three-dimensional magnetic navigation system. Circulation 96:2016–2021
28. Pappone C, Oreto G, Lamberti F et al (1999) Catheter ablation of paroxysmal atrial fibrillation using a 3D mapping system. Circulation 100:1203–1208
29. Poty H, Saoudi N, Abdel Aziz A, Nair M, Letac B (1995) Radiofrequency catheter ablation of type 1 atrial flutter. Prediction of late success by electrophysiological criteria. Circulation 92:1389–1392
30. Sra J, Bhatia A, Dhala A et al (2000) Electroanatomic mapping to identify breakthrough sites in recurrent typical human flutter. Pacing Clin Electrophysiol 23:1479–1492
31. Willems S, Weiss C, Ventura R et al (2000) Catheter ablation of atrial flutter guided by electroanatomic mapping (CARTO): a randomized comparison to the conventional approach. J Cardiovasc Electrophysiol 11:1223–1230
32. Shah DC, Jais P, Haissaguerre M et al (1997) Three-dimensional mapping of the common atrial flutter circuit in the right atrium. Circulation 96:3904–3912
33. Stevenson WG, Delacretaz E, Friedman PL, Ellison KE (1998) Identification and ablation of macroreentrant ventricular tachycardia with the CARTO electroanatomical mapping system. Pacing Clin Electrophysiol 21:1448–1456
34. Tomassoni G, Stanton M, Richey M, Leonelli FM, Beheiry S, Natale A (1999) Epicardial mapping and radiofrequency catheter ablation of ischemic ventricular tachycardia using a three-dimensional nonfluoroscopic mapping system. J Cardiovasc Electrophysiol 10:1643–1648
35. Kottkamp H, Hindricks G, Breithardt G, Borggrefe M (1997) Three-dimensional electromagnetic catheter technology: electroanatomic mapping of the right atrium and ablation of ectopic atrial tachycardia. J Cardiovasc Electrophysiol 8:1332–1337
36. Marchlinski F, Callans D, Gottlieb C, Rodriguez E, Coyne R, Kleinman D (1998) Magnetic electroanatomical mapping for ablation of focal atrial tachycardias. Pacing Clin Electrophysiol 21:1621–1635
37. Varanasi S, Dhala A, Blanck Z, Deshpande S, Akhtar M, Sra J (1999) Electroanatomic mapping for radiofrequency ablation of cardiac arrhythmias. J Cardiovasc Electrophysiol 10:538–544
38. Wittkampf FH, Wever EF, Derksen R et al (1999) LocaLisa: new technique for real-time 3Dimensional localization of regular intracardiac electrodes. Circulation 99:1312–1317
39. Avitall B, Helms RW, Kotov AV, Sieben W, Anderson J (1996) The use of temperature versus local depolarization amplitude to monitor atrial lesion maturation during the creation of linear lesions in both atria. Circulation 94:I-558
40. Borggrefe M, Budde T, Podczeck A, Breithardt G (1987) High frequency alternating current ablation of an accessory pathway in humans. J Am Coll Cardiol 10:576–582
41. Jenkins KJ, Walsh EP, Colan SD, Bergau DM, Saul JP, Lock JE (1993) Multipolar endocardial mapping of the right atrium during cardiac catheterization: description of a new technique. J Am Coll Cardiol 22:1105–1110
42. Eldar M, Ohad DG, Goldberger JJ et al (1997) Transcutaneous multielectrode basket catheter for endocardial mapping and ablation of ventricular tachycardia in the pig. Circulation 96:2430–2437
43. Triedman JK, Jenkins KJ, Colan SD, Van Praagh R, Lock JE, Walsh EP (1997) Multipolar endocardial mapping of the right heart using a basket catheter: acute and chronic animal studies. Pacing Clin Electrophysiol 20:51–59
44. Schalij MJ, van Rugge FP, Siezenga M, van der Velde ET (1998) Endocardial activation mapping of ventricular tachycardia in patients: first application of a 32-site bipolar mapping catheter electrode. Circulation 98:2168–2179
45. Triedman JK, Jenkins KJ, Colan SD, Saul JP, Walsh EP (1997) Intra-atrial reentrant tachycardia after palliation of congenital heart disease: characterization of multiple macroreentrant circuits using fluoroscopically based three-dimensional endocardial mapping. J Cardiovasc Electrophysiol 8:259–270
46. Greenspon AJ, Hsu SS, Datorre S (1997) Successful radiofrequency catheter ablation of sustained ventricular tachycardia post-myocardial infarction in man guided by a multielectrode "basket" catheter. J Cardiovasc Electrophysiol 8:565–570
47. Schmitt C, Zrenner B, Schneider M et al (1999) Clinical experience with a novel multielectrode basket catheter in right atrial tachycardias. Circulation 99:2414–2422
48. Nakagawa H, Ikeda A, Sharma T, Lazzara R, Jackman W (2012) Rapid high resolution electroanatomic mapping. Circ Arrhythm Electrophysiol 5:417–424
49. Ptaszek LM, Chalhoub F, Perna F et al (2013) Rapid acquisition of high-resolution electroanatomical maps using a novel multielectrode mapping system. J Interv Card Electrophysiol 36:233–242
50. Arshad A, Mittal S, Musat D et al (2013) Long-term success from FIRM ablation is maintained even if acute endpoint is not achieved. Heart Rhythm 10(P004-133)
51. Baykaner T, Clopton P, Lalani GG et al (2013) Targeted ablation at stable atrial fibrillation sources improves success over conventional ablation in high-risk patients: a substudy of the CONFIRM trial. Can J Cardiol 29:1218–1226
52. Miller JM, Krummen DE, Narayan SM et al (2013) Multicenter validation of focal impulse and rotor modulation (FIRM) ablation for atrial fibrillation (CONFIRM-Multicenter Validation). AHA Scientific Sessions, November 2013, Oral presentation
53. Narayan SM, Krummen DE, Shivkumar K, Clopton P, Rappel WJ, Miller J (2012) Treatment of atrial fibrillation by the ablation of localized sources: the conventional ablation for atrial fibrillation with or without focal impulse and rotor modulation: CONFIRM trial. J Am Coll Cardiol 60:628–636
54. Narayan SM, Krummen DE, Clopton P, Shivkumar K, Miller JM (2013) Direct ablation of coincidental elimination of stable rotors or focal sources may explain successful atrial fibrillation ablation: on-treatment analysis of the CONFIRM trial. J Am Coll Cardiol 60:138–147
55. Schilling RJ, Peters NS, Davies DW (1998) Simultaneous endocardial mapping in the human left ventricle using a noncontact catheter: comparison of contact and reconstructed electrograms during sinus rhythm. Circulation 98:887–898
56. Schilling RJ, Peters NS, Davies DW (1999) Feasibility of a noncontact catheter for endocardial mapping of human ventricular tachycardia. Circulation 99:2543–2552
57. Taccardi B, Arisi G, Macchi E, Baruffi S, Spaggiari S (1987) A new intracavitary probe for detecting the site of origin of ectopic ventricular beats during one cardiac cycle. Circulation 75:272–281
58. Khoury DS, Taccardi B, Lux RL, Ershler PR, Rudy Y (1995) Reconstruction of endocardial potentials and activation sequences from intracavitary probe measurements. Localization of pacing sites and effects of myocardial structure. Circulation 91:845–863
59. Tuzcu V (2007) A nonfluoroscopic approach for electrophysiology and catheter ablation procedures using a three-dimensional navigation system. Pacing Clin Electrophysiol 30:519–525
60. Novak P, Macle L, Thibault B, Guerra P (2004) Enhanced left atrial mapping using digitally synchronized NavX three-dimensional nonfluoroscopic mapping and high-resolution computed tomographic imaging for catheter ablation of atrial fibrillation. Heart Rhythm 4:521–522
61. Schilling RJ, Kadish AH, Peters NS, Goldberger J, Davies DW (2000) Endocardial mapping of atrial fibrillation in the human right atrium using a noncontact catheter. Eur Heart J 21:550–564

62. Schneider MA, Ndrepepa G, Zrenner B et al (2000) Noncontact mapping-guided catheter ablation of atrial fibrillation associated with left atrial ectopy. J Cardiovasc Electrophysiol 11:475–479
63. Liu TY, Tai CT, Chen SA (2002) Treatment of atrial fibrillation by catheter ablation of conduction gaps in the crista terminalis and cavotricuspid isthmus of the right atrium. J Cardiovasc Electrophysiol 13:1044–1046
64. Strickberger SA, Knight BP, Michaud GF, Pelosi F, Morady F (2000) Mapping and ablation of ventricular tachycardia guided by virtual electrograms using a noncontact, computerized mapping system. J Am Coll Cardiol 35:414–421
65. Kadish A, Hauck J, Pederson B, Beatty G, Gornick C (1999) Mapping of atrial activation with a noncontact, multielectrode catheter in dogs. Circulation 99:1906–1913
66. Barr RC, Spach MS (1978) Inverse calculation of QRS-T epicardial potentials from normal and ectopic beats in the dog. Circ Res 42:661–675
67. Ramanathan C, Raja NG, Jia P, Ryu K, Rudy Y (2004) Noninvasive electrocardiographic imaging for cardiac electrophysiology and arrhythmia. Nat Med 10:422–428
68. Tilg B, Fischer G, Modre R et al (2002) Model-based imaging of cardiac electrical excitation in humans. IEEE Trans Med Imaging 21:1031–1039
69. He B, Li G, Zhang X (2003) Noninvasive imaging of ventricular transmembrane potentials within three-dimensional myocardium by means of a realistic geometry anisotropic heart model. IEEE Trans Biomed Eng 50:1190–1202
70. Zhang X, Ramachandra I, Liu Z, Muneer B, Pogwizd SM, He B (2005) Noninvasive three-dimensional electrocardiographic imaging of ventricular activation sequence. Am J Physiol Heart Circ Physiol 289:H2724–H2732
71. Liu C, Skadsberg N, Ahlberg S, Swingen C, Iaizzo P, He B (2008) Estimation of global ventricular activation sequences by noninvasive 3Dimensional electrical imaging: validation studies in a swine model during pacing. J Cardiovasc Electrophysiol 19:535–540
72. Tikhonov AN, Arsenin VY (1977) The regularization method. In: Tikhonov AN, Arsenis VY (eds) Solutions of ill-posed problems. V.H. Winston & Sons, Washington, DC, pp 45–94
73. Rudy Y, Messinger-Rapport BJ (1988) The inverse problem in electrocardiography: solutions in terms of epicardial potentials. Crit Rev Biomed Eng 16:215–268
74. Rudy Y, Oster HS (1992) The electrocardiographic inverse problem. Crit Rev Biomed Eng 20:25–45
75. Rudy Y, Burnes JE (1999) Noninvasive electrocardiographic imaging. Ann Noninvasive Electrocardiol 4:340–358
76. Ramanathan C, Rudy Y (2001) Electrocardiogaphic imaging. I. Effect of torso inhomogeneities on body surface electrocardiographic potentials. J Cardiovasc Electrophysiol 12:229–240
77. Ramanathan C, Rudy Y (2001) Electrocardiographic imaging. II. Effect of torso inhomogeneities on noninvasive reconstruction of epicardial potentials, electrograms, and isochrones. J Cardiovasc Electrophysiol 12:241–252
78. Ramanathan C, Jia P, Ghanem RN, Calvettie D, Rudy Y (2003) Noninvasive electrocardiographic imaging (ECGI): application of the generalized minimal residual method (GMRes). Ann Biomed Eng 31:981–994
79. http://www.cardioinsight.com/. Accessed 30 Dec 2014
80. Haissaguerre M, Hocini M, Shah AJ et al (2013) Noninvasive panoramic mapping of human atrial fibrillation mechanism: a feasibility report. J Cardiovasc Electrophysiol 24:711–717
81. Haissaguerre M, Hocini M, Denis A et al (2014) Driver domains in persistent atrial fibrillation. Circulation 130:530–538

Cardiopulmonary Bypass and Cardioplegia

33

Gabriel Loor and J. Ernesto Molina

Abstract

This chapter describes the history and techniques of cardiopulmonary bypass, a process that effectually excludes the heart from the general circulation and leaves it empty so that it can accommodate open cardiac surgical intervention. Since its first implementation, cardiopulmonary bypass has improved significantly to become a very highly sophisticated, but reliably performed procedure. The near future promises even more improvements because research and innovations continue to make cardiac operations safer and more efficient.

With the advent of coronary bypass in the late 1960s and early 1970s, surgeons became increasingly interested in finding ways to protect the heart during the period of global ischemia via infusion of cold perfusates into the coronary circulation (i.e., cardioplegia). Therefore, this chapter further details the advantages and disadvantages of various cardioplegia solutions which have been developed at several separate institutions, including extracellular- and intracellular-type solutions.

Keywords

Cardiopulmonary bypass • Cross-circulation • Anticoagulation • Heart–lung machine • Cardioplegia

33.1 Cardiopulmonary Bypass

Extracorporeal circulation and *cardiopulmonary bypass* are synonymous terms denoting a method by which the blood that usually returns directly to the heart is temporarily drained from superior and inferior vena cavae. The blood is diverted into a reservoir where it is oxygenated and subsequently returned to the patient's arterial circulation. This process effectually excludes the heart from the general circulation and leaves it empty so that it can accommodate surgical intervention (Fig. 33.1).

The breakthrough technologies that first allowed this type of *open-heart* operation were developed by two separate centers in the USA in the early 1950s. Importantly, Lillehei and Varco [1] at the University of Minnesota developed a cross-circulation technique. This technique utilized a human donor (usually the parents of a child undergoing cardiac surgery) who, in essence, functioned as an extracorporeal pump for the patient's circulatory system. This type of extracorporeal circulation also allowed the blood to be drained from the child's vena cava so that the surgical procedure could be performed within the empty heart. The subsequent development of the heart–lung machine by Gibbon [2] was considered revolutionary in that it eliminated the need for a support donor (a second patient). Gibbon's system has been improved since the mid-1950s and has gradually evolved into the standardized, but very complex and sophisticated machine it is today. The bubble oxygenator developed by DeWald and Lillehei in 1955 was additive technology that also aided in the advancement of this field (see also Chap. 25).

G. Loor, MD (✉) • J.E. Molina, MD, PhD
Division of Cardiothoracic Surgery, University of Minnesota,
420 Delaware St. SE, MMC 207, Minneapolis, MN 55455, USA
e-mail: gloor@umn.edu

P.A. Iaizzo (ed.), *Handbook of Cardiac Anatomy, Physiology, and Devices*, DOI 10.1007/978-3-319-19464-6_33

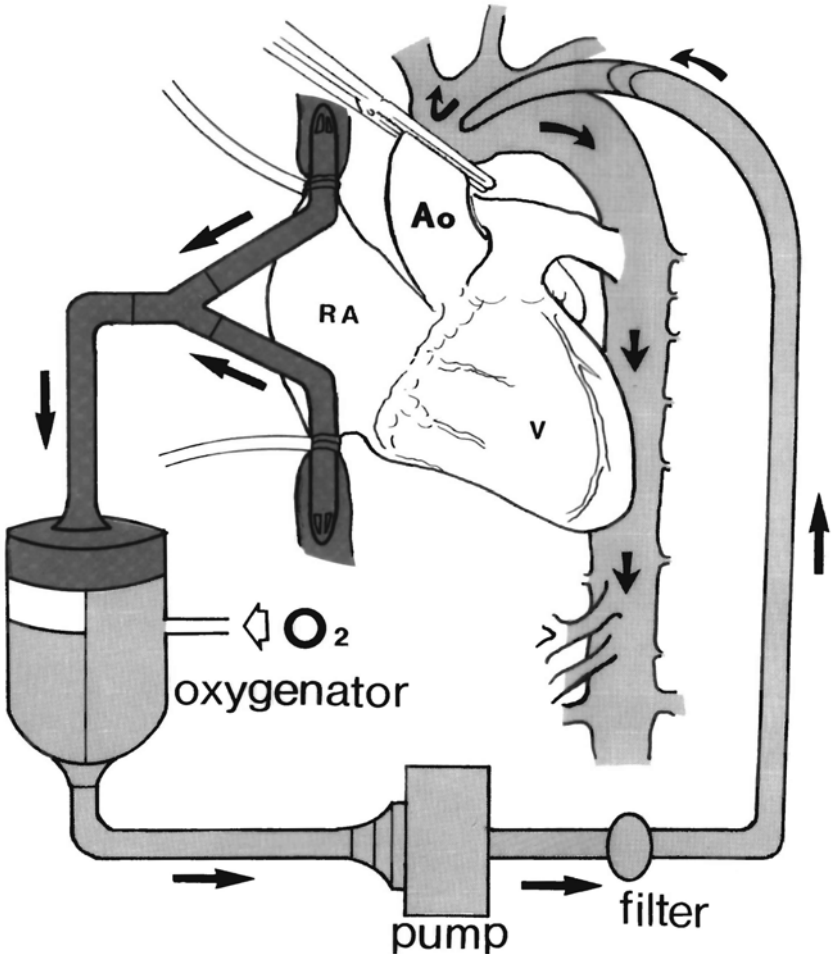

Fig. 33.1 Total cardiopulmonary bypass showing the venous cannulas in the superior and inferior vena cavae with constrictions placed around the respective veins. The venous blood is draining to the oxygenator and is propelled by the pump into the distal ascending aorta to maintain perfusion of the entire body. A cross-clamp is applied to the ascending aorta, and all chambers of the heart therefore are excluded from the perfusion system. Note that modern day systems often place the pump ahead of the oxygenator such that blood from the reservoir is actively pumped through the oxygenator. *Ao* aorta, *RA* right atrium, *V* ventricle

The basic components of an extracorporeal circuit include: (1) a reservoir into which the patient's blood is diverted; (2) an oxygenator that replaces the function of the lungs; and (3) a pump that propels the oxygenated blood back into the patient's arterial circulation. In this manner, the machine bypasses both the heart and the lungs while maintaining the function of other organs during surgical interventions within the heart.

A solid understanding of cardiopulmonary bypass and ways to control the patient's physiology is just as important as efficient and meticulous techniques to achieve the best outcomes in cardiac surgery. Today, dedicated perfusionists work closely with the surgical team to ensure that bypass runs properly; they rely on detailed communication from the operative field. This chapter details the components of cardiopulmonary bypass.

33.1.1 Venous Drainage

The venous blood that is normally delivered to the right atrium is commonly diverted to the heart–lung machine, either by cannulating the veins themselves or by cannulating the right atrial chamber. Surgery performed in or through the right atrial chamber requires that both the right atrium and right ventricle be empty. To do so, cannulas are typically placed directly into the superior and inferior vena cavae. Constricting tourniquets are then placed around the vein over the cannulas, and thus blood is diverted into the heart–lung machine (Fig. 33.1). This constitutes *total cardiopulmonary bypass*.

Cannulation of the superior vena cava (SVC) is normally performed by placing a purse string suture either directly in the SVC or in the right atrium. The cannula is advanced either directly into the SVC or indirectly through the right atrium. It should be noted that direct cannulation of the SVC generally provides more room for any work that may need to be done inside the right atrium. Conversely, for large ascending aortic aneurysms it may be necessary to advance the cannula indirectly through the atrium.

Cannulation of the inferior vena proceeds through purse strings placed on the inferior portion of the right atrium. By placing tourniquets around both cannulas and snaring down on them, the surgeon establishes total cardiopulmonary

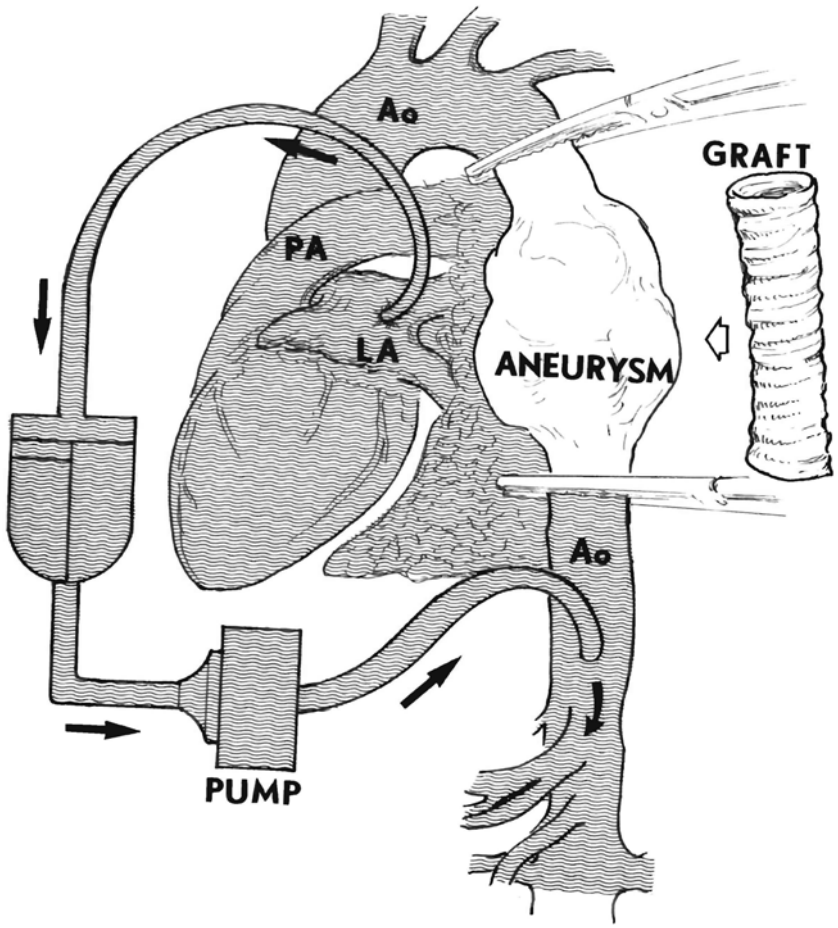

Fig. 33.2 Left heart bypass showing a cannula inserted in the left atrium draining approximately half of the cardiac output into the oxygenator through the pump, and reinfusing it in the distal aorta for perfusion of the abdominal organs. The excluded portion is only the descending thoracic aorta (between clamps). The left heart continues to beat and pumps half of the cardiac output to the head and upper organs. The graft is shown in the position in which it will be implanted after the aneurysm is resected. *Ao* aorta, *LA* left atrium, *PA* pulmonary artery

bypass. The only flow that enters the right atrium is that from the coronary sinus, i.e., until the aorta is clamped. With the aorta cross-clamped and no flow entering the aortic root and coronary arteries, the surgeon can work inside the atrium in a completely bloodless field. Typically, access to the left atrium is obtained by opening the fossa ovalis. A bloodless field here allows insertion of the retrograde coronary artery catheter directly into the coronary sinus for direct cardioplegia, as discussed later.

A modification of this type of bypass can be used when the cardiac chambers are not surgically entered, such as in coronary bypass operations involving procedures on the surface of the heart. In such cases, a double-staged cannula is placed with the tip of the cannula in the inferior vena cava and the side drainage holes positioned at the level of the right atrium. Coronary bypass surgery does not involve direct vision of the inside of the cardiac chambers so there is no need to constrict the superior or inferior vena cava. This configuration is often referred to as *full cardiopulmonary bypass* rather than total cardiopulmonary bypass. When coronary bypass operations are undertaken simultaneously with cardiac valve repairs or replacements, total cardiopulmonary bypass is typically implemented.

If venous drainage is not optimal, then two critical issues may result: (1) the heart may become distended with warm systemic blood, resulting in persistent myocardial activity or undue strain on the myocardium leading to injury; and (2) venous congestion may result in hepatic impairment. Thus, adequate venous drainage must be ensured prior to proceeding with these types of operations.

33.1.2 Arterial Return

Once the blood has been oxygenated in the heart–lung machine, it is returned to the patient's general circulation via cannulas placed directly in the arterial system (Fig. 33.1). The most common method involves the placement of a cannula in the highest portion of the ascending aorta below or at the origin of the innominate artery. This is typically the first cannula that is inserted. The aorta must be free of calcific disease in order to cannulate it without increased risk of

stroke. The axillary artery is the next best alternative in the setting of calcific aortic disease and/or for cases requiring circulatory arrest for replacement of all or parts of the aortic arch [3].

Depending on the type of surgery, other sites are also used, including cannulation of the femoral artery in the groin and infusion of the arterial system in a retrograde manner. This is useful for minimally invasive heart surgery in younger patients without calcific disease in whom the thoracic incision does not allow exposure to the ascending aorta. Yet, if calcific disease is present the retrograde flow can shower plaque up toward the carotids with increased risk of stroke.

Once the arterial cannula is secured and both the forward flow and venous drainage are adequate, the ascending aorta is cross-clamped. At this point no systemic blood enters the coronary artery circulation. The heart is, therefore, totally excluded from the circulation. Thus the heart needs to be protected by using one of a number of methods to infuse cardioplegic solutions (see Sect. 33.2). Any blood remaining in the operative field is removed via cardiotomy suction lines which are used to aspirate it back to the heart–lung machine, where it reenters the bypass circulation with the rest of the removed blood.

In some operations involving the descending thoracic aorta, total cardiopulmonary bypass is not necessary. For example, if the portion of the aorta that needs to be isolated lies between the left carotid artery and the diaphragm, only part of the total blood volume needs to be removed, and partial bypass can be implemented (Fig. 33.2). The blood is removed by the heart–lung machine via a cannula inserted into either the left atrium or left superior pulmonary vein. Then, the blood is infused back into the descending thoracic aorta beyond the level of distal aortic cross-clamp. Doing so allows the heart to continue to beat normally and helps maintain the viability of the proximal organs (head, neck, and arms), while the rest of the lower body is perfused and thus maintained by the pump. This technique is called *left heart bypass* because it involves only removal of blood and decompression of the left-side cardiac chambers. As shown in Fig. 33.2, after a descending thoracic aorta aneurysm operation is completed, the bypass is discontinued. The clamps which were placed to occlude the aorta in the arch and the descending portion are removed. The normal physiological perfusion of the body (which was interrupted during surgery without ever stopping the heartbeat) is thus reestablished.

After an operation applying full or total cardiopulmonary bypass and cardiac arrest, the aortic clamp is released, allowing the general circulation to reperfuse the coronary arteries and to rewarm the heart. After the air is expelled from the cardiac chambers, the heart often elicits ventricular fibrillation. Such fibrillation normally requires cardioversion with an electric shock administered directly to the heart by employing paddles that deliver currents that vary from 20 to 30 W/s. The patient is then ventilated using the endotracheal tube connected to the anesthesia machine, which reinflates the lungs. After the normal sinus rhythm of the heart is reestablished, the patient is gradually weaned off the extracorporeal circulation until the heart takes over full function. At this point the heart–lung machine is stopped, and all cannulas are removed and access areas closed

In some complex surgical cases involving the aortic arch, separate independent perfusion of the arch vessels may require implementation, that is, in addition to the perfusion of the lower part of the body through the cannula inserted in the femoral artery. This is most commonly seen in situations where the arch and descending aorta are bypassed simultaneously. The perfusionist must monitor two separate infusions to regulate pressures and make certain that a balance and sufficient perfusion is achieved in both the upper and the lower areas of the patient's body. With the advent of staged aortic procedures such as the "elephant trunk procedure" and hybrid stent grafting, it is less common to deal with such an extensive amount of aortic replacement in a single setting [4].

Another specialized bypass method that needs description is the *deep hypothermia and total circulatory arrest* technique. This type of total cardiopulmonary bypass requires decreasing body temperature to very low levels (15°–25 °C); this is typically accomplished using heat exchangers installed in the heart–lung machine circuits. Circulation is stopped altogether when the proper temperature is reached, and the heart is emptied for several minutes with the entire volume of the patient's blood remaining in the reservoir of the heart–lung machine. The pump is then stopped and the arterial perfusion ceases. The venous return line, however, is left open to continue emptying the patient's blood volume completely into the reservoir of the heart–lung machine.

This technique is used in special cases to allow repair of very complicated conditions. The period of total circulatory arrest induced during deep hypothermia is usually less than 45 min [5, 6]. This time restriction is to insure that the patient does not suffer neurological deterioration or central nervous system damage during such global ischemia. In general, cooling alone is sufficient for circulatory arrest times less than 20 min. However, since the time required to perform the aortic arch repair can be unpredictable, most surgeons will utilize some sort of brain perfusion strategy. Retrograde brain perfusion is commonly used for periods of 30–45 min. It requires the arterial outflow from the pump to be connected to the SVC cannula either directly or through a separate circuit. By snaring the SVC, oxygenated blood is delivered up the vena cava to perfuse the brain in a retrograde fashion. The flow rates are typically 300–500 mL/min and the central venous pressure is kept no higher than 35 mmHg.

Antegrade brain perfusion is more typically used for planned circulatory arrest periods ranging 45–90 min. In this mode of

perfusion, the axillary artery graft is used to deliver oxygenated blood up the carotids once the innominate artery is snared; typical flow rates vary between 500 and 1000 mL/min. The patient should have some evaluation of the brain vessels beforehand to ensure a complete *Circle of Willis*, an anastomotic system of arteries that sits at the base of the brain.

As soon as the repair is completed, normal cardiopulmonary bypass is reestablished. The patient is gradually rewarmed to a normal core temperature of 37 °C prior to removal from extracorporeal circulation. The use of deep hypothermia always requires careful evaluation by the surgical team. In such clinical cases, the danger of inducing neurological damage must be weighed against the benefits of correcting a major cardiac anomaly. Conversely, the long-term quality of the arch repair should not be compromised by concerns over circulatory arrest, especially with proper usage of selective brain perfusion techniques.

It is important to note that aortic cannulation can have important consequences (pitfalls) associated with it. The patient must be completely anticoagulated before instituting flow through the cannula. If there is calcific disease, cannulating or clamping the aorta has been associated with increased incidences of stroke or distal embolic events. Finally, during aortic cannulation, there is commonly a 1–2 % incidence of aortic dissection related to a tear caused by the cannula. If such a condition is suspected due to high line pressures or enlargement of the ascending aorta, the flow through the cannula should be immediately stopped; a transesophageal echo can be used to confirm the diagnosis, and then an alternative cannulation strategy should be identified. This situation often requires circulatory arrest to repair the tear.

33.1.3 Anticoagulation

To prevent the formation of clots during cardiopulmonary procedures, both within the body and within the extracorporeal heart–lung machine, it is necessary to anticoagulate the patient's blood. The most common agent used for such anticoagulation is heparin. It is commonly administered intravenously before cannulation at a dose of 300 units/kg. There are two types of heparin: (1) the lung beef type which is extracted from a bovine source; and (2) the porcine mucosal type which is from a swine source. Since the mid-1980s, the porcine mucosal heparin has been preferred because it is less likely to lead to thrombocytopenia and/or the production of heparin antibodies in the patient, a condition known as HIT syndrome [7].

A small percentage of patients have experienced heparin-induced thrombocytopenia (HIT) from prior heparin exposure. They have antibodies to heparin molecules which attack heparin-platelet aggregates and this, in turn, depletes their platelet pool to dangerously low levels.

The effectiveness of anticoagulation therapy requires testing, usually by measuring the activated clotting time (ACT) of the patient's blood. These test results are expressed in seconds, with normal values ranging between 100 and 120 s. Heparinization is deemed adequate for cardiopulmonary bypass when the ACT runs above 400 s. Typically, the anticoagulant effects induced during such surgeries must be reversed postoperatively. Still today, porotamine sulfate is the drug of choice to neutralize the effects of the heparin and allow the patient to elicit normal clotting values. Yet, this drug is a macromolecule compound that may produce pulmonary vasoconstriction and severe hypotension [8, 9], particularly in diabetic patients. Nevertheless, such side effects are rare and, in most patients, this drug can be used safely, as it neutralizes the effects of heparin. Naturally, the amount of protamine necessary to achieve neutralization depends on the amount and timing of therapeutic heparin administered. Initially, a test dose is given; if no reaction occurs, protamine is then administered in the appropriate amounts. Its effects are monitored by measuring ACTs until they return to a normal range. It should be noted that if any reaction or side-effects occur, additional treatments are commonly employed, such as the administration of epinephrine, calcium, steroids, or fluids [9].

Occasionally patients cannot be given heparin because they have developed heparin antibodies from previous exposure. Other anticoagulant agents are studied and occasionally used in such cases, including hirudin (Lepirudin) [10], a potent anticoagulant that is extracted from leaches and lampreys. Other drugs include the heparinoids [11] like Orgaran (Org10172, Organon Company, West Orange, NJ, USA), for which a different monitoring protocol is implemented. Unfortunately, to date, no drug has been identified that can reverse the effects of Orgaran, thus it must be metabolized by the human body. For such patients bleeding is a constant, and often very difficult, postoperative complication. Bivalrudin (Angiomax) is currently the most commonly used agent for cardiac surgery in patients with HIT [12].

If the cardiopulmonary bypass takes an extended time, coagulopathies often pose complications. In such cases, the body, primarily the liver, is unable to produce the appropriate clotting factors to reverse the anticoagulation status. Other factors that can contribute to coagulopathies include ischemia of the abdominal organs, particularly if necrosis occurs in the liver cells and/or in the intestine. Bleeding, therefore, can be a very serious and difficult complication to treat; in such patients, the administration of multiple coagulation factors, platelets, and cryoprecipitates may be required.

33.1.4 Temperatures of Perfusion

Since their inception, cardiopulmonary bypass and extracorporeal circulation have been implemented using some degree

of hypothermia. Lowering core body temperature decreases the overall oxygen demands of body tissues, and a more desirable protective state during pulseless circulation is provided by the heart–lung machine.

Several degrees of clinical hypothermia are commonly identifiable relative to extracorporeal circulation interventions. *Normothermia* indicates that core body temperature is between 35.5° and 37 °C [13], *mild hypothermia* is between 32° and 35 °C, and *moderate hypothermia* is between 24° and 32 °C. An important distinction must be made between mild and moderate hypothermia. If the heart is perfused at mild levels (above 31 °C), the heart will continue to beat although at slower rates. Therefore, this mild level of hypothermia allows surgical correction of some congenital anomalies without arresting the heart. An additional level of hypothermia used occasionally is *deep or profound hypothermia*, which usually brings the body temperature below 20 °C.

Currently, most open-cardiac operative procedures are conducted under conditions somewhere between moderate and mild hypothermia. Some centers routinely use moderate hypothermia, while others employ normothermia [14, 15]. One reason to maintain normothermic perfusion is to avoid coagulopathies that may develop when body temperature is lowered to the moderate levels, and thus allow for normal function of the body's enzyme systems. Normothermic temperatures also enable the kidneys to respond better to diuretics.

Several reports have indicated the relative safety of normothermic perfusion [13–19], but an equal number have suggested complications with this modality [20, 21]. As a result, the spontaneous drifting to mild hypothermic levels is generally preferred. Deep or profound hypothermia is associated with the implementation of total circulatory arrest as mentioned before. With this level of hypothermia, body temperature is lowered to between 15° and 18 °C. Such operations are usually prolonged given the time it takes to cool the body to those levels before surgery and also by the required time to rewarm it afterwards. The goal of systemic cooling is not so much to decrease metabolic demands in the peripheral organs, but rather to drop the temperature of collateral arterial flow that reaches the heart such as the bronchial arteries. If one stays normothermic and has difficulty maintaining cardiac arrest, it is likely that the warm bronchial artery flow is making its way through the pulmonary arteries or veins and warming the inside of the heart.

33.1.5 Perfusion Pressures

Under normal physiological conditions, the heart provides a pulsatile pressure and flow. The systolic pressure depends on the ventricular function. The diastolic pressure in normal states is primarily regulated by the blood volume and the vascular tonus (the degree of constriction experienced by venous vessels relative to their maximally dilated states). During cardiopulmonary bypass, the heart–lung machine facilitates pulseless perfusion; there is no systolic or diastolic pressure, but rather one steady mean pressure throughout the arterial circulatory system. Therefore, this pressure should be high enough to provide adequate blood oxygen to all organs of the body, particularly the brain and kidneys. Since the patient is typically hypothermic, the oxygen requirements are lower; the perfusion pressure is usually maintained around 70 mm of mercury Hg. Occasionally, specifically in patients with severe obstructive carotid disease, a higher perfusion pressure is recommended to ensure proper perfusion of the brain. Nevertheless, this recommendation is somewhat debated because the brain is known to have its own regulatory system to maintain low resistance near obstructed areas [15, 17]. A useful rule of thumb is to keep the mean arterial pressure close to the patient's decade of life (i.e., 74 years old = 70 mmHg, 86 years old = 80 mmHg).

During cardiopulmonary bypass, if the patient shows decreased vascular tonus (despite adequate volume of fluid), vasoconstrictors are routinely used; a typical therapy is a bolus or drips of neosynephrine [13]. A decreased vascular tonus is common in septic patients with bacterial endocarditis, for whom an emergency operation sometimes is necessary to replace the affected valve and reverse the profound heart failure. Remember that the perfusion pressure is a product of the cardiopulmonary flow and resistance. If the flow has been optimized (ideal flow = 2.4 × body surface area) then the resistance needs to be increased to meet the desired perfusion pressure. Markers of end organ perfusion during bypass include: urine output, mixed venous saturation, lactic acid, and base deficit.

33.1.6 Hemodilution

Up to a certain level, hemodilution can be a desirable side effect of cardiopulmonary bypass. Lowering the hematocrit prevents *clumping* of the red cells or *sludging*, thereby providing better circulation at the capillary level; viscosity of the circulating blood is decreased, on the other hand, to also ensure that oxygen is adequately delivered to the body's tissues during cardiopulmonary bypass. Hematocrit levels are monitored and maintained at a minimum between 22 and 26 %. Toward the end of the bypass operation, typically the perfusionist deliberately removes some of the fluid from the patient's circulation to hemoconcentrate the blood toward more normal hematocrit levels [22, 23]; this rises to above 30 % by the time the patient is removed from cardiopulmonary bypass. Subsequent diuresis and/or removal of red blood cells (RBC) will further aid in reestablishing the hematocrit to normal levels.

Transfusion of RBC is sometimes necessary if the hematocrit cannot be maintained above 22 %. Risk factors for a low hematocrit on bypass include: (1) the female gender; (2) older age; (3) lower body mass index; (4) a high New York Heart Association class and combined valve and coronary bypass procedures; and/or (5) anemia, the strongest risk factor [24].

It is important to note that there are multiple problems associated with RBC transfusion including: (1) increased renal dysfunction; (2) arrhythmias and infections; and, (3) increased long-term mortality [24]. Interestingly, anemia and RBC transfusions for the bypass patient have additive adverse effects [25]. Therefore, every effort should be made to prevent severe anemia without transfusion, including: (1) use of smaller bypass circuits and less priming volumes; (2) proper preoperative hemoglobin optimization; (3) increasing RBC transfusion thresholds; (4) retrograde autologous priming; and (5) meticulous hemostasis [26].

Pulseless perfusion, as provided by the heart–lung machine, and hemodilution will both invariably lead to a transfer of fluid across the capillary walls into the third space (interstitial). Therefore, all patients develop, to some degree, peripheral third spacing or edema, which often develops within the first 24–72 h after bypass. This usually manifests as pulmonary edema, pleural effusions, atrial fibrillation, and lower extremity edema. This is why patients often require diuresis on day 2–4 following bypass. In an attempt to avoid edema, plasma expanders (such as albumin, hetastarch, dextran, and mannitol) are usually added to the priming solution of the heart–lung machine.

33.1.7 Heart–Lung Machine Basics

The basic components and sequence of modern day heart–lung machines are as follows: venous drainage (vacuum assist) → reservoir → perfusion pump → oxygenator (with heat exchanger) → arterial line filters → aorta. The reservoir of the cardiopulmonary bypass machine is important for proper drainage and emptying of the heart. Without the reservoir, the blood in the human body and the blood in the machine would be in a constant equilibrium of roughly 1:1. With the reservoir, approximately 100 mL to 2 L of volume can be housed outside of the body during perfusion. This negative volume balance drains the human venous capacitance system and leaves the heart flat and empty. An empty heart does little work and consumes minimal oxygen. This is different than the modern day extracorporeal membrane oxygenator circuits which do not have a reservoir and do not allow decompression of the ailing heart.

Although the classic heart–lung machine used gravity to drain the venous blood into the reservoir, modern machines like the Performer CPB (Medtronic, Inc., Minneapolis, MN, USA) (Fig. 33.3) employ an active vacuum in a very small system that reduces the need for large volumes in the reservoir [27, 28]. The Performer CPB is smaller in size and can be placed closer to the operating table, saving tubing length, and it accommodates to any position. In addition, the tubing used for the heart–lung machine where the blood circulates has undergone significant improvement with the use of Carmeda [29, 30], which is a bioactive surface with which the inner side of the tubing is coated. Carmeda is bonded to the wall tubing, mimicking the human endovascular endothelium to reduce coagulation and inflammatory responses of the patient's body, due to the blood-material surface interaction. The Performer CPB machine displayed in Fig. 33.3 incorporates multiple safety features consisting of alarm sensors for air bubbles, debris, pressure changes, and temperatures, making its use practically fool proof for protection of the patient.

In addition, the newer centrifugal pumps (Fig. 33.3), like the Bio-Medicus and the Performance CPB (both from Medtronic, Inc.), offer a distinct advantage over the older roller-type pumps such as the standard DeBakey type. More specifically, the roller pumps use occlusive pressure to propel the blood within the tubing, and can cause damage to the RBC and dislodge debris from the tubing material. In contrast, the newer centrifugal pumps minimize trauma to the RBC because the motion required to move the blood does not constrict the tubing. Although the bubble oxygenator has been used for many years, it has been largely supplanted by the membrane oxygenator. The membrane oxygenator is associated with less trauma to RBC and is less likely to produce micro-bubbles that might pass into the patient's arterial system and cause air embolism.

As the blood is oxygenated, it passes through heat exchangers that cool or rewarm it as necessary for a given stage of the operation. Typically, one heat exchanger provides temperature control for systemic perfusion to the patient's body, whereas a second exchanger controls the temperature within the cardioplegia line. In most current systems, the temperature within each circuit is separately controlled by a central regulatory unit. The blood is then filtered which helps prevent microembolization when it is returned to the patient's arterial system. In addition, two suction lines are employed to aspirate any blood from the operative field, thus recovering and returning the blood to the reservoir where it is oxygenated before being pumped back into the patient's arterial system.

Importantly, the perfusionist needs to monitor the general circulation flow, electrolyte parameters, anticoagulation parameters, and the ultrafiltration system (which extracts fluids from the patient's arterial system to avoid over hydration). The perfusionist is also responsible for maintaining the proper pressures within each circuit and monitoring the temperature of the cardioplegic solution that will be used to protect

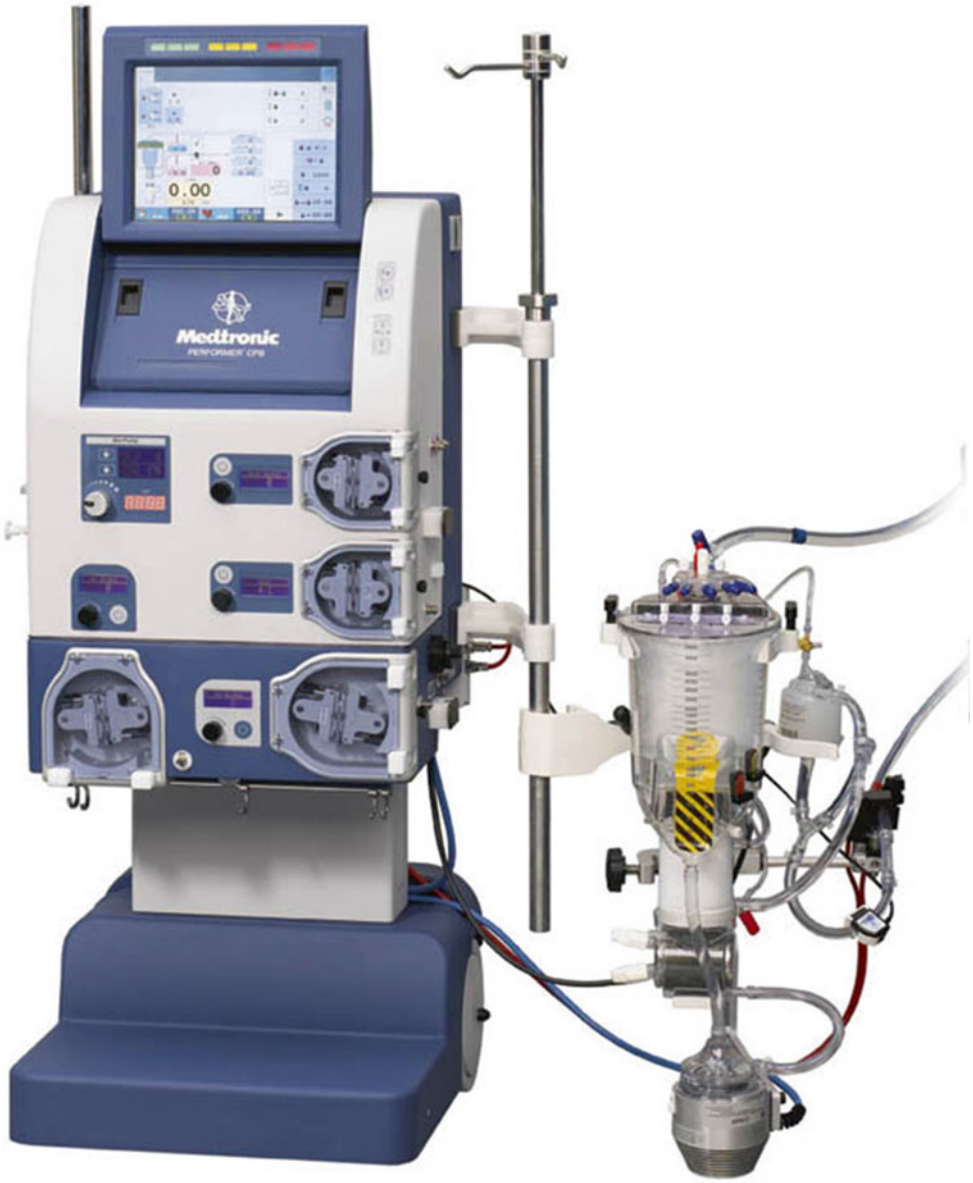

Fig. 33.3 Performer CPB cardiopulmonary bypass machine manufactured by Medtronic, Inc. (Minneapolis, MN, USA) shows a smaller size adjustable to any position. Attached to the machine is the Resting Heart Device which eliminates most of the large size reservoirs. It contains the filters and monitoring devices. All tubing is coated with Carmeda (see description in the text)

the heart during the period of its exclusion from general circulation. Normally, at 15- to 20-min intervals, the perfusionist apprises the surgeon of the elapsed time of perfusion and reinfuses the heart as necessary to maintain a temperature within the appropriate range (below 15 °C). The perfusionist also remains in direct communication with the anesthesiologist to coordinate administration of any drugs or any other action necessary to maintain the balance of the patient's other organ systems. Finally, at the end of cardiopulmonary bypass, the perfusionist administers protamine in an amount sufficient to neutralize the effects of the heparin, thus returning the patient's coagulation system to normal function.

At the conclusion of the surgery, cardiopulmonary bypass is discontinued and the patient's heart resumes systemic blood circulation. A small volume of blood often remains in the pump and needs to be reinfused into the patient. This remaining blood is sometimes reinfused directly from the reservoir or it may be concentrated and reinfused later.

33.1.8 Heart–Lung Machine Priming

Before cardiopulmonary bypass is undertaken, the heart–lung machine needs to be primed. For an adult patient, a typi-

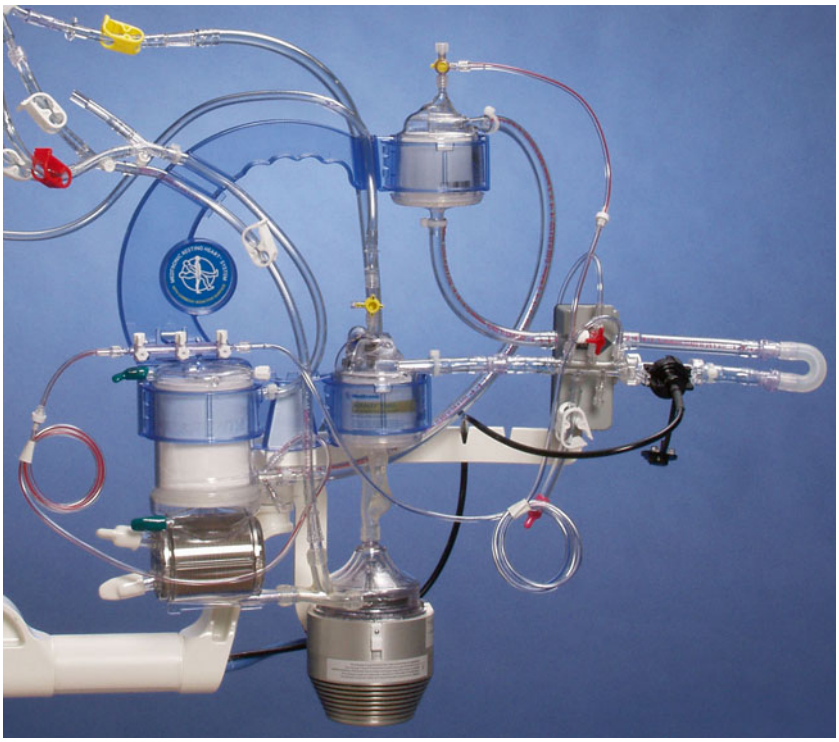

Fig. 33.4 Close-up image of the Resting Heart System showing the small reservoir in the center. The centrifugal pump is shown at the bottom. The rest are filters provided with alarm systems for air venting

cal 1500 mL of priming fluid is primarily a basic crystalloid solution. Plasmalite is the preferred crystalloid solution to which albumin or hetastarch (about 500 mL for a normal sized patient) is typically added. Doing so helps maintain osmolality and volume in the intravascular space, and helps prevent peripheral third spacing and edema. Red cell sludging usually is prevented within the system by the addition of extra heparin, however with the new systems like the Performer CPB, this is no longer required. In the pediatric patient, ideally one should have much less volume than what is required in adults. In such cases, the so-called Resting Heart System provided by Medtronic, Inc. (Fig. 33.4) can be integrated into the regular Performer CPB system to significantly reduce the entire volume needed for priming the pump. This integrated unit also provides for an automatic venous air removal and integrated air removal from the cardioplegic system. As mentioned before, at the end of the perfusion the blood is hemoconcentrated to normal levels by eliminating the extra fluid from the circulation; all the air is eliminated as well.

33.1.9 Hemodynamics

As cardiopulmonary bypass is implemented, the patient's blood pressure usually drops briefly as the blood is diverted from the heart to the heart–lung machine. This drop is precipitated by the cold (ambient) temperature of the fluid, that was used to prime the machine and which the heart–lung machine has now introduced into the patient's aorta. It also results from the emptying of blood from the heart. This drop should last no more than a minute or two, i.e., before the proper pressure and flow is reestablished. The surgeon should not continue with the procedure unless s/he is confident that forward flow and drainage are optimized. In general, it is preferable to maintain a systemic pressure of approximately 70 mmHg and flows between 1500 and 2500 mL-m^2 of body surface area throughout the entire surgical procedure (ideally 2.4 × body surface area). If the systemic pressure tends to sag, which can happen because of the various factors (e.g., loss of vascular tonus), the anesthesiologist and perfusionist must coordinate administration of vasoconstrictor agents (such as neosynepherine). If the pressure is too high, vasodilators are administered and/or the rate of perfusion is decreased to restore safe pressures.

Importantly, venous pressure and oxygen saturations should be monitored very carefully throughout any bypass procedure. An altered venous pressure is one of the most important indicators that a potential obstruction in the venous return has occurred, either at the level of the venous cannula or within the superior or inferior vena cava. Such obstructions will often lead to major procedural complications if they are not monitored and immediately corrected. Typically the perfusionist reports any concern to the surgeon so that s/he can check whether any obstruction may exist. During cardiopulmonary bypass, the venous pressure should usually be near zero and saturation above 70 % because all the blood is completely diverted into the heart–lung machine. Once the

pressures are equilibrated, the temperatures must be maintained at the level of hypothermia that the surgeon has chosen.

Elevated central venous pressures and pulmonary artery pressures suggest poor drainage, as does a heart that is distending. Markers of end organ perfusion during bypass include: urine output, mixed venous saturation, lactic acid, and/or base deficit. Acidosis, low urine output, and decreased mixed venous saturation suggest poor oxygen delivery to the tissues.

The written records for the cardiopulmonary bypass are normally called *pump records*. They must contain all pertinent information including: (1) pressures; (2) flows; (3) temperatures; (4) medications; (5) periods of ischemia; and (6) beginning and end times. These records provide important information and trends that add to our understanding of cardiopulmonary bypass. Precise monitoring during cardiopulmonary bypass is extremely important especially in patients with compromised renal function (i.e., those who cannot produce urine to remove extra fluid from their own systems). In such patients, the most important electrolyte to monitor is potassium which, after any major operation, usually rises above the normal level of 4.0–4.5 mEq/L. Potassium must be very strictly monitored to prevent associated severe bradycardia and/or cardiac arrest. A dialysis system can be used during cardiopulmonary bypass, if necessary, to prevent such serious complications. Even in large medical centers, patients who are normally on dialysis rarely receive potassium during cardiopulmonary bypass.

In general, after weaning from cardiopulmonary bypass, most patients will display various degrees of bradycardia, usually due to the persistent effect of large amounts of β-blockers administered preoperatively or because of large amounts of cardioplegia solution. Few patients will elicit heart beats greater than 80 beats/min when taken off cardiopulmonary bypass. Most patients are commonly provided with a temporary pacemaker system postoperatively. This consists of wires placed on the surface of the heart (external leads) and connected to an external pacemaker unit (much like the first wearable pacemaker developed by Earl Bakken in 1958, see Chap. 25). Based on many years of research and experience, the optimal post cardiopulmonary heart rate has been determined as 70–90 beats/min in an adult; atrial pacing is set at that rate, with appropriate ventricular sensing. Such pacing is usually necessary for only 24–48 h which, in general, provides higher cardiac output and significantly improved hemodynamics, and allows the patient to eliminate the extra water that is usually third spaced during such an operation. Ventricular leads are routinely implanted in all patients as a very simple and safe prophylactic lifesaving measure [31]. This practice is highly advisable during the postoperative period because serious problems such as complete heart block are frequently unpredictable regardless of the patient's age or general health. If serious problems occur, there is no substitute for the ability to pace the ventricle immediately. Once the acute recovery period is over and the patient is stable (typically 5 days after surgery), the temporary pacemaker wires can usually be removed. In rare cases when heart block or severe bradycardia occurs, a permanent pacemaker system may be necessary to implant. See Chap. 30 for more details.

33.1.10 Weaning from Cardiopulmonary Bypass

In order to discontinue cardiopulmonary bypass the patient needs to be warm (37 °C) with a perfusing heart rhythm and good ventilation. These are the most important elements for weaning from bypass. However, there are several other important details that can be summed up in a simple pneumonic suggested by Lars Svensson from Cleveland Clinic [32]. The pneumonic is as follows:

A—Anastomosis (check all surgical bleeding sites)
B—Beat of the heart, Breathing (defibrillate if needed, place pacing wires, suction out the pleural spaces to allow proper ventilation, slowly ventilate the heart watching for any tethered bypass grafts)
C—Circulation (forward flow and drainage; fill up the heart with volume and allow it to eject)
D—Degrees (normothermia 37 °C); Deair (have the root vent on and check the echo to ensure that the heart has been adequately deaired)
E—Electrolytes (potassium is the main factor; some add calcium to optimize contraction); Echo (confirm function, valves, air)
F—Flows (start coming down on the bypass flows toward about 2 L/min and reassess blood pressure, heart distention, and contractility)
G—Gasses (ensure that blood gasses are normalizing)
H—Hypertension/Hypotension (treat any swings in blood pressure with the appropriate agents)
I—Ionotropes (select appropriate ionotropes, i.e., epinephrine for longer pump runs or sluggish heart, vasopressors for systemic vasoplegia)—ideal pressure for coming off bypass is 70 mmHg.
J—Juices (ensure adequate urine output and potassium. If urine is sluggish and K^+ is high, then you may need to dialyze the patient to wean from bypass)

33.2 Cardioplegia

In the 1950s, the consensus among cardiac surgeons was that the results of the surgical methods were satisfactory [33]. Yet, numerous reports described low cardiac output syndromes occurring after surgical correction of congenital anomalies [34]. Unfortunately, at that time no definite connection was provided between the lack of proper myocardial protection during surgery and the potential for postoperative cardiac dysfunction and/or high mortality rates. Not until the advent of coronary bypass in the late 1960s and early 1970s were intraoperative myocardial infarctions or deaths clearly attributed to poor protection of the myocardium [35, 36]. At that time, several reports also noted that the levels of cardiac enzymes after surgery were significantly elevated, indicating that additional myocardial damage had occurred even during the operation [36]. As a result, surgeons of that era showed an increasing interest in attempting to protect the heart during the period of global ischemia (aortic cross-clamping) via infusion of cold perfusates into the coronary circulation. Cold infusion of any solution into the heart separate from the total body perfusion is one of the methods known collectively as *cardioplegia*. After continued demonstration of its effectiveness, the use of hypothermic cardioplegia became quite widespread. In order to implement the use of cardioplegia, the general circulation to the coronary arteries must be interrupted. This is achieved by placing a vascular clamp across the aorta just above the coronary arteries; in this manner, as the heart is excluded from the general circulation, the infusion of cardioplegic solution is done in the aortic root entering in the coronary circulation to achieve a rapid and complete stoppage of the cardiac activity. Other modes of inducing cessation of cardiac activity employ chemical additions to perfusates or shocking the heart with electrical stimuli.

Yet, today many issues still need to be investigated concerning optimizing cardioplegic methodologies, such as: (1) what type of solution to use; (2) how much solution to inject; (3) how often to reinfuse these solutions; (4) how long to extend global ischemia safely using cardioplegia approaches; (5) how well a specific solution protects the energy reserves of the myocardium; and/or (6) the optimal route of delivery to ensure proper distribution to the right and left ventricles. As mentioned above, operative settings requiring the injection of cardioplegia involve aortic cross-clamping and coronary infusion (Fig. 33.5) of usually a cold chemical solution [37–41]. Some cardiac surgeons prefer to inject warm [42, 43] or tepid [44] solutions that have been mixed with chemical components (e.g., high potassium concentrations). However, normal warm myocardial cells require uninterrupted coronary perfusion. The principles of applying cardioplegia are aimed at: (1) conserving energy through the rapid induction of diastolic arrest; (2) slowing the metabolic demands and degenerative processes that inevitably follow global myocardial ischemia; (3) preventing unfavorable ischemic changes; and (4) preventing myocardial edema through adequate venting, drainage, and osmolality of the protective solutions. Extensive research over the past 30+ years has provided several formulations of chemical components, with or without cooling, to obtain these goals. Interestingly, the relative use of these solutions still varies widely, likely because they have been independently developed at several separate institutions.

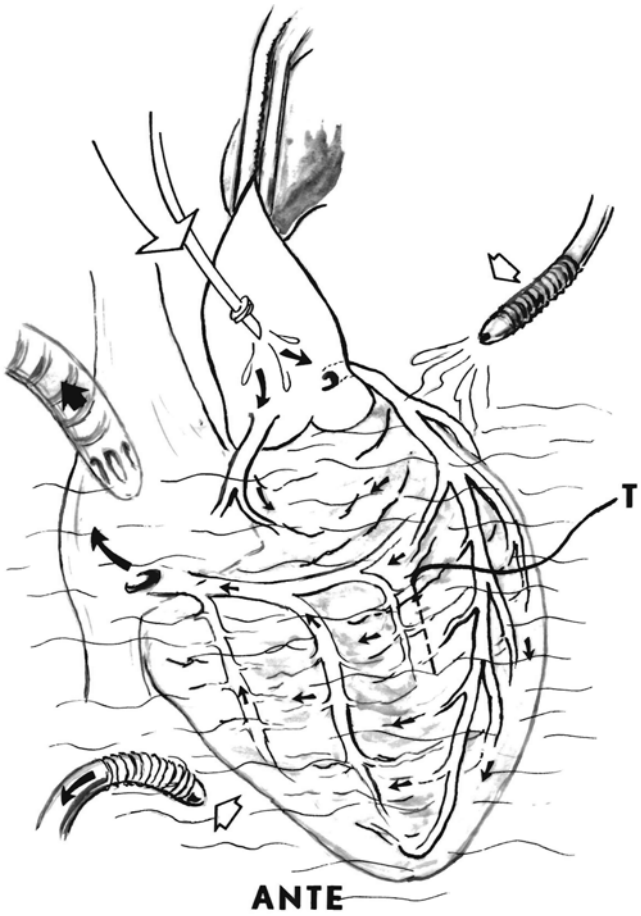

Fig. 33.5 Antegrade cardioplegia (*ANTE*). The ascending aorta is cross-clamped and cardioplegia is infused into the root of the aorta. The solution runs through the coronary arterial system and leaves the heart via the coronary sinus in the right atrium. At the upper right corner is an irrigating catheter that provides continuous topical hypothermia. This solution is removed by the suction line at the lower left (*clear arrows*). *T* temperature probe positioned in interventricular septum for monitoring purposes

33.2.1 Types of Solutions

Crystalloid solutions generally can be divided into two categories based on their approximate formulation—extracellular or intracellular. Extracellular solutions contain calcium and sodium, the primary determinants for transcellular calcium exchange. Cardioplegic cardiac arrest can still be

achieved by extracellular solutions containing only moderate amounts of potassium or magnesium. Cold blood cardioplegia solution [39–45], the most commonly used throughout North America, is considered an extracellular ionic formula. The principle advantage to extracellular-type solutions is that they make it simpler to control equilibration characteristics within the ischemic myocardial tissue. Because no calcium or sodium variant exists in the extracellular fluid, subsequent replacement is easily achieved without any major reequilibration with the intracellular fluid. The disadvantage of extracellular solutions is that they are more easily washed out by noncoronary flow, but this effect can be counteracted by adding calcium channel blockers or procaine. Cardioplegic solutions that mimic intracellular ionic concentrations usually contain no sodium or calcium. Their advantage, at least in theory, is that their lack of sodium or calcium generates a large osmolar space which is available for other potentially protective components. In turn, this allows the solution to contain a high concentration of glucose, dextrose, mannitol, or histidine without eliciting excessive hyper-osmolarity. Another advantage of intercellular-type solutions is that their minimal or reduced levels of extracellular calcium will limit contraction or restrict ischemia-induced calcium entry. The primary disadvantage of such solutions is that the lack of sodium and calcium may, under extreme conditions, predispose the heart to elicit the so-called *calcium paradox*. Another disadvantage is the potentially complex pattern of subsequent reequilibration then required. As Hearse et al. [46] pointed out, low-volume infusion of intracellular solutions offers good protection, intermediate volumes offer only marginal protection, and high volumes may actually exacerbate injury to the myocardium.

Each of the described crystalloid cardioplegic solutions is considered to contain several components that have been "proven" by various researchers to provide enhanced protection. For example, in one study published by Hearse et al. [37], the effects of changing the composition of the simple cardioplegic solution when used during a 30-min period of ischemia were compared. It was shown that, at the end of a period of ischemia when no cardioplegia was used, the percentage of ventricular function recovery was practically nil, only about 3 %. However, if potassium was added, the recovery increased to about 30 %. Furthermore, if both potassium and magnesium were added, the recovery was even better (up to 68 %). And if potassium, magnesium, and adenosine triphosphate were used in combination, the recovery reached 86 %. Finally, if a combination of potassium, magnesium, adenosine triphosphate, creatine phosphate, and procaine was used, the recovery peaked at a dramatic 93 %.

After using crystalloid cardioplegia alone for several years, it was considered whether mixing cold blood with the crystalloid solution would offer better protection than the crystalloid alone; it was suggested that the ability of the blood to carry oxygen to the tissues and its buffering capacity particularly if the period of ischemia was more than 90 min and, in such cases, the ventricular function was less than normal. Although the idea of protecting the heart with blood cardioplegia originated in the early 1950s with Ebert et al. [47], it was not until 20 years later when it was reintroduced by Buckberg and associates [39, 43, 45, 48, 49] that it became popular among most surgeons in the USA and throughout the world to use cold blood cardioplegia. Nevertheless, controversy persists regarding the "optimal" formulation to protect and prevent damage to the heart. The following solutions are some of the most commonly used for such procedures today.

33.2.2 St. Thomas II Solution

The formulation for the St. Thomas II solution (Plegisol: Abbott Laboratories, Abbott Park, IL, USA) originated with the published research of Hearse, Braimbridge, Stuart, and Jynge [37, 46, 50, 51] from the St. Thomas Hospital in London. The basic vehicle was Ringers solution to which potassium chloride, procaine, and magnesium were added (Table 33.1).

St. Thomas II solution is an extracellular-type formulation. It is used extensively as an isolated clear cardioplegic solution and also as the base mix for the cold blood cardioplegic solution proposed by Buckberg et al. It is usually injected into the root of the aorta at temperatures between 4° and 6 °C (Fig. 33.5), depending on the surgeon's preference with an initial volume of about 1000 mL for a 70 kg adult, followed by 100 mL infusions intermittently every 15–20 min. This method has long been combined with or without topical hypothermia to maintain the heart's temperature below 15 °C. The size of the catheter used for its infusion and the pressure for injection are discussed in Sect. 33.2.8.

Table 33.1 Composition of St. Thomas II solution

Sodium chloride	120 mmol/L
Potassium	16 mmol/L
Sodium bicarbonate	10 mmol/L
Calcium	1.2 mmol/L
Magnesium	16 mmol/L
Procaine	1 mmol/L
Osmolality	280 mOsm/kg H_2O
Oncotic pressure	0.4
pH	7.8

Table 33.2 Composition of Birmingham solution

Sodium	100 mmol/L
Potassium	30 mmol/L
Calcium	0.7 mmol/L
Glucose	5 g/L
Chloride	84 mmol/L
Albumin	50 g/L
Mannitol	5 g/L
Osmolality	300–335 mOsm/L

Table 33.3 Composition of Bretschneider (Custodiol) solution

Sodium	15 mM
Potassium	9 mM
Magnesium	4 mM
α-Histidine	180 mM
α-Histidine Hcl	18 mM
Calcium chloride	0.015 mM
Mannitol	30 mM
Tryptophane	2 mM
Ketoglutarate	1 mM
pH	7.1–7.2
Osmolality	295–325 mOsm/kg H_20

33.2.3 Birmingham Solution

Various extracellular solutions were also developed in the USA. Most solutions sought to attain relatively high extracellular concentrations of potassium as an arrest-inducing agent. More specifically, Birmingham solution was developed by Conti et al. [52]; its effectiveness was primarily demonstrated by the publications of Kirklin et al. [53]. The importance of the Birmingham solution is that glucose was included as a substrate for the myocardium (Table 33.2). The development of this solution gave origin to many other formulations that use the basic additions of glucose, potassium, and insulin.

33.2.4 Bretschneider Solution (Custodiol)

During the early 1960s and 1970s, Bretschneider in Goettingen, Germany published his studies introducing HTK (Histidine-Tryptophane-Ketoglutarate) also known as Custodiol crystalloid cardioplegic solution (Dr. F. Köhler Chemie GmbHD-6146 Alsbach-Hähnlein, Germany) [54, 55] (Table 33.3). This intracellular-type solution has also been shown to be very effective in protecting the heart during surgery. It has been used extensively in Germany since its introduction and has also been used widely throughout Asia, North Africa, and Latin America. It is used not only as a protective solution for the heart during periods of surgical ischemia, but also as a preservation solution for hearts [56–58], livers, and kidneys [59] prior to transplantation. According to Preusse et al. [55], this solution must be provided in large amounts, between 3000 and 4000 mL per organ. Therefore, double cannulation of the right atrium with exclusion of this chamber must be implemented during surgery in order to allow opening of the atrium and to eliminate the large volume of solution from the coronary sinus orifice to prevent the fluid from reaching the general circulation (Fig. 33.6). For Custodiol solution to be most effective, the period of equilibration is crucial [54, 55]; that is, it takes about 7 min of infusion to equilibrate the extracellular and intracellular spaces before the patient's operation should proceed. This solution has also been used for both antegrade and retrograde (through the coronary sinus) perfusions. One of the considered significant advantages of this solution is its buffering capacity, which even surpasses the buffering properties of blood. Importantly, Custodiol solution needs to be stored at a specific temperature (12°–16 °C) to prevent denaturation of the components.

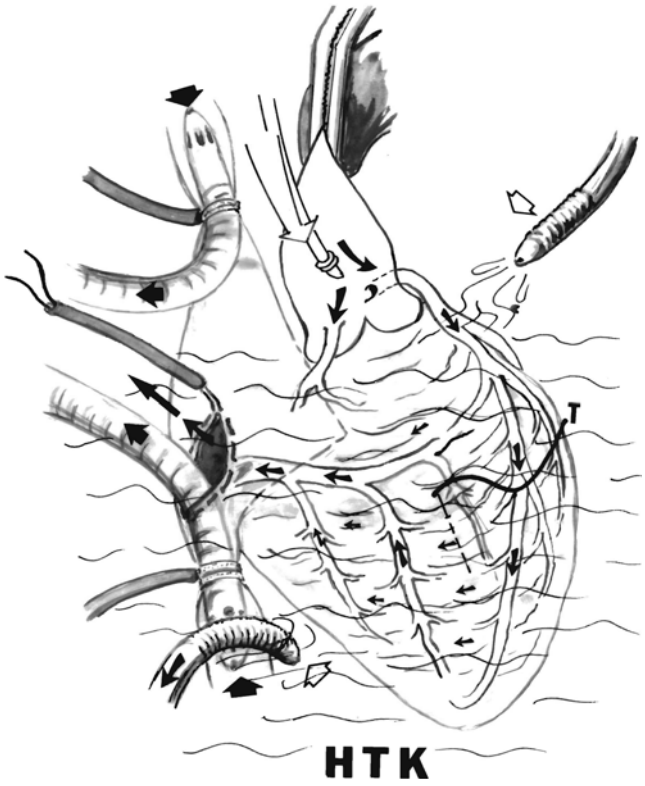

Fig. 33.6 Antegrade infusion of the Bretschneider (HTK, "Custodiol" solution containing Histidin-Tryptophane-Ketoglutarate). The solution is infused in an antegrade manner into the aortic root while the aorta is cross-clamped. Because this method requires a large volume of solution, the right atrium is open and the solution exiting in the coronary sinus is aspirated and discarded. The superior and inferior vena cavae are individually cannulated to allow the right atrium to remain empty so that the HTK solution can be evacuated. Topical continuous hypothermia is shown with the irrigating cannula at the upper right and the suction catheter at the lower left. *T* temperature probe

Table 33.4 Composition of Crystalloid Potassium Insulin (University of Minnesota) solution

Dextrose	50 g/1000 mL
Sodium	3.5 mEq/L
Potassium	30 mEq/L
Chloride	30 mEq/L
Sodium bicarbonate	3.5 mEq/L
Regular insulin	10 units
Mannitol	12.5 g
Albumin	12.5 g
Osmolality	364 mOsm/L
pH	7.8
Oncotic pressure	3

33.2.5 Glucose–Insulin–Potassium Solutions

Most of the research performed on glucose–insulin–potassium (GIK) solutions was done in the USA. Multiple formulations with these components have been widely used for the past 30 years. Studies by Hewitt et al. [60] and later by Lolley et al. [61] demonstrated that continuous infusion of a solution containing 278 mmol/L of glucose, 20 mmol/L of potassium, and 20 U insulin with 69 mmol/L of mannitol dramatically improved myocardial protection. Those studies illustrated that the combination of glucose, insulin, and potassium improved anaerobic glycolysis and the washout of toxic substances. A slight modification of this basic solution, which included albumin to increase osmolality, was used extensively for many years at the University of Minnesota (Minneapolis, MN, USA) [62–64] (Table 33.4). The only concern with the use of GIK solution is the inevitable degradation of its constituent insulin over time. Therefore GIK solutions must be prepared fresh for each use and cannot be stored for prolonged periods of time.

Many investigators contributed to the formulation of GIK solutions, among them Follete et al. [45] and Todd and Tyers [65]. We consider here that Roe et al.'s classical solution [41] also belongs in this category. The common denominator among these formulations is the use of dextrose as the basic vehicle. Multiple publications have shown protective effects. However when used alone, GIK solutions often provide insufficient protection during long periods of ischemia (i.e., beyond 120 min) or when the left ventricular function is marginal initially.

Several crystalloid solutions have been formulated without dextrose. The main difference among these is the basic vehicle which could be formulated with Ringers or Krebs-Henseleit. Potassium is commonly added at doses between 15 and 125 mmol/L. Some solutions in this group are the University of Wisconsin [57, 66] and Celsior [67] solutions which are also used to preserve organs for transplantation. Several agents are considered available to help increase the osmolality of cardioplegic solutions (Table 33.5); for example, mannitol has been included in such solutions to stabilize osmolality and to act as a potential scavenger for oxygen radicals.

Table 33.5 Components used to raise osmolality

Component	Oncotic pressure (mmHg)	Osmolality (mOsm)
Hespan (hetastarch) (6 % in 0.9 % saline solution)	18.4	311
Mannitol 25 % (12.5 g/50 mL)	0.1	–
Albumin 25 %	>200	239
Dextran (10 % in dextrose)	130.2	319
Plasmanate (5 % albumin)	16.86	239
Tris hydroxymethyl aminomethane (THAM)	–	370

Table 33.6 Composition of Buckberg's Cold Blood cardioplegic solution

5 % dextrose with ¼ normal saline	422 mL
Potassium chloride	2 mEq/mL
Tris hydroxymethyl aminomethane (THAM)	72 mL CPD 6
Diluent volume	500 mL
Blood hematocrit	22 % = 500 mL
Osmolality	360 mOsm/kg
Potassium	22 mEq/L
pH	7.8
Calcium	0.3 mEq/L
Hematocrit	10 %

33.2.6 Additional Components

Other components have been added to crystalloid cardioplegic solutions by various investigators based on their own research. These include aspartate as the substrate to generate adenosine triphosphate [48]; glutamate as a substrate [49]; 1.5 % hetastarch as an additive [68]; procaine as a membrane stabilizer [46, 51]; nifedipine to prevent calcium paradox [69]; phosphates as a base for adenosine triphosphate regeneration [70–72]; and/or steroids (methylprednisolone) as a cellular wall stabilizer [73–75]. Other elements found to help maintain an alkaline pH include Tris hydroxymethyl amimomethane (THAM), as advocated by Buckberg [39], and histidine as in the HTK solution.

Del Nido cardioplegia uses lidocaine to prolong the period of myocardial arrest. It uses a 1:4 blood to crystalloid mixture, and is commonly employed for pediatric surgery. This is particularly useful in minimally invasive surgery where the retrograde access is not always reliable and avoids stopping for antegrade at multiple points throughout the procedure. Use of Del Nido requires a normal coronary circulation without obstructions. Microplegia is another form of cardioplegia that is being investigated; it contains much smaller volumes than standard solutions and presumably causes less myocardial edema.

Fig. 33.7 Roller pumps of cardioplegia infusion system. The upper pump utilizes ¼ inch tubing to move the blood, and the lower pump runs crystalloid cardioplegic solution using 1/16 inch tubing. The blood and cardioplegic solution are automatically mixed in a 4:1 proportion in the outflow line before entering the ascending aorta

33.2.7 Cold Blood Cardioplegia

The mixture of blood with crystalloid cardioplegia has become the most favored formulation for cardioplegia among cardiac surgeons both in the USA and throughout the world. It is considered superior to any other cardioplegic solution alone. The standard proportion of blood to crystalloid solution has remained fairly constant at 4:1 (4 parts of blood to 1 part of crystalloid cardioplegia), although some surgeons prefer a proportion of 8:1 in special circumstances. Nevertheless, as mentioned before, the actual formulation of the crystalloid portion varies across institutions [76].

Administration of cold blood cardioplegia in the proportions proposed by Buckberg (Table 33.6) can be easily accomplished using the appropriate equipment available as a kit. This contains the necessary caliber of tubing which is placed in a roller pump that automatically mixes the blood with the clear solution before injection into the root of the aorta (Fig. 33.7). As an example, the Performer CPB machine can accommodate any mixing proportion desired (4:1, 4:6, 4:8). The kit includes a heat exchanger which maintains the temperature of the solution between 4° and 6 °C and allows the myocardial temperature to decrease even below 15 °C. The significant advantage of cold blood cardioplegia is that it is considered to provide oxygen and nutrients to the ischemic myocardium and offer optimal buffering capacity. This mixture can be injected antegrade (in the root of the aorta) or retrograde (by coronary sinus cannulation using a self-inflating balloon to perfuse the entire heart) [77] (Fig. 33.8). Cold blood cardioplegia has endured many years of testing, both in its initial form of providing cardioplegia at cold temperatures and in its more recent adaptation to warm cardioplegia as promoted by Lichtenstein et al. [78]. The cold blood method is widely used in the pediatric population as well for surgeries to correct all types of congenital anomalies.

33.2.8 Cardioplegia Administration

Our previous clinical work showed that cardioplegic solutions should be administered at a rapid rate and under moderate pressure. Doing so shortens the prearrest period, provides better flow distribution, and accelerates the decreasing myocardial temperature. In addition, rapid injection results in postoperative isoenzyme levels that are lower than those in patients who undergo slower cardioplegic injections [62].

Experimental studies on animals with normal coronary arteries have shown that low infusion pressures (less than 30 mmHg) and peak flow rates less than 125 mL/min result in a higher incidence of cellular ischemia, focal necrosis, and uneven flow distribution [64]. Consequently, patients with obstructive coronary disease who undergo low-pressure or low-volume cardioplegic injections will inevitably experience an increase in flow distribution problems.

Conversely pressures higher than 110 mmHg and peak flow rates greater than 1500 mL/min may result in a higher incidence of mechanical and physical trauma to the vascular endothelium [64]. These higher levels, however, greatly enhance cellular protection. It should be noted that the use of

Fig. 33.8 Cold blood cardioplegia. This may be administered by antegrade infusion into the root of the aorta below the cross-clamp. It may also be accomplished in a retrograde manner through a catheter inserted in the coronary sinus provided with a balloon which is inflated to prevent reflux into the right atrium. Continuous topical hypothermia is used in conjunction with cold blood cardioplegia to potentiate the hypothermic protection of the heart. *P* pressure monitoring line of the coronary sinus, *T* temperature probe

high pressures in the aortic root of patients with coronary obstructions does not necessarily raise a concern. Rapid administration of cardioplegic solutions causes the temperature of the myocardium to fall rapidly within seconds to the protective range below 15 °C and induces immediate cardiac arrest. This is important because one would prefer not to have the heart beating against the clamp for more than a few seconds, as it wastes myocardial energy and can lead to edema and injury.

Cardioplegic solutions are most commonly administered via cannulas placed into the aortic root below the level of the aortic cross-clamp (Fig. 33.5). This site provides a normal antegrade flow to all areas of the heart. Several aortic valve procedures, however, require the aortic root to remain open for long periods of time. Therefore, infusion of cardioplegia can be done by direct injection into the coronary ostia by handheld cannulas or, alternatively, cardioplegic solution may be administered retrograde through the coronary sinus. This gives the added advantage of not having to stop the procedure to administer cardioplegia and allows the surgeon to flush out the coronary system of air and debris. This option may be used to slow and continuously protect the heart (Fig. 33.9). Yet, this approach has some limitations that are dependent on the degree of hypertrophy of the myocardium due to the preexisting condition. The delivery pressures in the coronary sinus must be intentionally kept between 20 and 50 mmHg. Too low suggests a lack of occlusion by the catheter balloon in the coronary sinus with inadequate perfusion and too high may lead to vessel ruptures. Decompression of the left ventricular chamber is helpful to facilitate the perfusion of all areas of the heart [79].

The perfusion to the right heart is one of the most challenging issues that surgeons face. Antegrade and retrograde very reliably provide good flow to the left ventricle, unless there is a significant coronary blockage that needs to be considered. As mentioned, hypertrophy may limit perfusion to the left ventricle and cooling systemically and topically is a useful adjunct. However, perfusion of the right coronary system is not always as predictable. Retrograde catheters often miss the middle cardiac vein which is required to perfuse the right ventricle (see Chap. 8). Direct retrograde insertion prevents this error but relies on opening the right atrium. This is an important technique to be able to perform. A saphenous vein graft to a distal right coronary artery or branch also allows reliable right ventricular perfusion but is only used if a blockage is present in the right system. A temperature probe in the right ventricle can reveal the degree of right ventricular cooling.

General conduct of cardioplegia at our institution using the Buckberg's cold blood cardioplegia protocols is as follows:

1. 500–1000 mL cold antegrade induction dose with high potassium, followed by 500 mL retrograde
2. 300 mL maintenance doses through the retrograde route and down vein grafts with high potassium and higher glucose concentrations every 15–20 min
3. Final "hot shot" dose with a high glucose, substrate replete solution and low potassium
4. Once the hot shot is complete and the root is deaired, the cross-clamp is removed

Over the past 30 years, to increase the safety of such operations, the use of cardioplegic solutions has been noted as one of the most significant advances in cardiac surgery. Continued research will search for optimal systems and methods to provide even better protection of the heart during cardiac surgery.

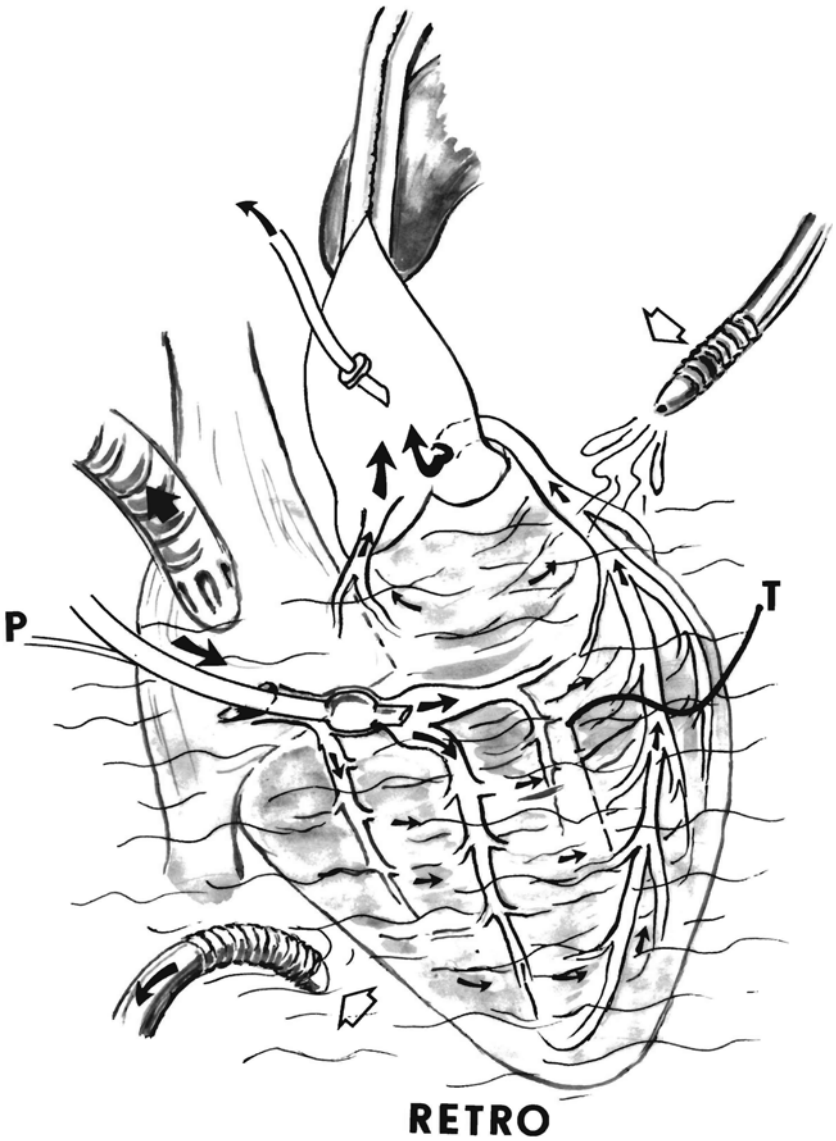

Fig. 33.9 Retrograde (*RETRO*) administration of crystalloid cardioplegia. This is accomplished via the coronary sinus with a catheter provided with a balloon that is inflated to prevent reflux into the atrium. The solution eventually reaches the aortic root from where it is aspirated. It may also be allowed to drain into the left ventricle which is vented to the pump. Continuous topical hypothermia is again shown using cold saline over the heart. *P* pressure line monitoring, *T* temperature probe

33.2.9 Adjunct Topical Hypothermia

The use of cardiac hypothermia has been one of the most important tools for increasing the safety of cardiac operations. The application of topical hypothermia in the form of ice slush was first introduced in the 1960s by Shumway, Lower, and Stofer [80, 81], and was used exclusively through the 1970s until the introduction of crystalloid cardioplegia. Still today, topical hypothermia is considered to potentiate the use of all methods of cardioplegic perfusion, keeping the temperature of the heart in the safe range to tolerate global ischemia. This is particularly important for hypertrophied ventricles where uniform distribution of the cardioplegia to the microvascular subendocardium is unpredictable. The heart can be effectively cooled externally by a continual flow of cold (6 °C) saline or Ringers solution over the heart, eliminating the overflow solution using wall suction (Figs. 33.5 and 33.9). This technique is preferred to the older method of applying slush ice over the heart; the latter method has been blamed for causing frostbite lesions to the muscle and damage to the phrenic nerve which runs along the pericardial sac. To avoid these problems, insulated pads have been designed to be placed around the heart to protect the phrenic nerves. Several types of plastic jackets were proposed and designed in the past, through which cold water was pumped continuously, while the jacket wrapped the heart entailing both ventricles. They are currently rarely used due to cumbersome application and crowding of the operative field. The topical cooling (whichever method is used), as well as the infusion of cold cardioplegia in the coronary circulation, is discontinued when the operation is completed and rewarming of the patient begins. The aortic clamp placed in the ascending portion isolating the heart from systemic circulation is removed, and the heart receives the systemic warm blood from the body into the coronaries, reestablishing the normal perfusion of the organ. Once the

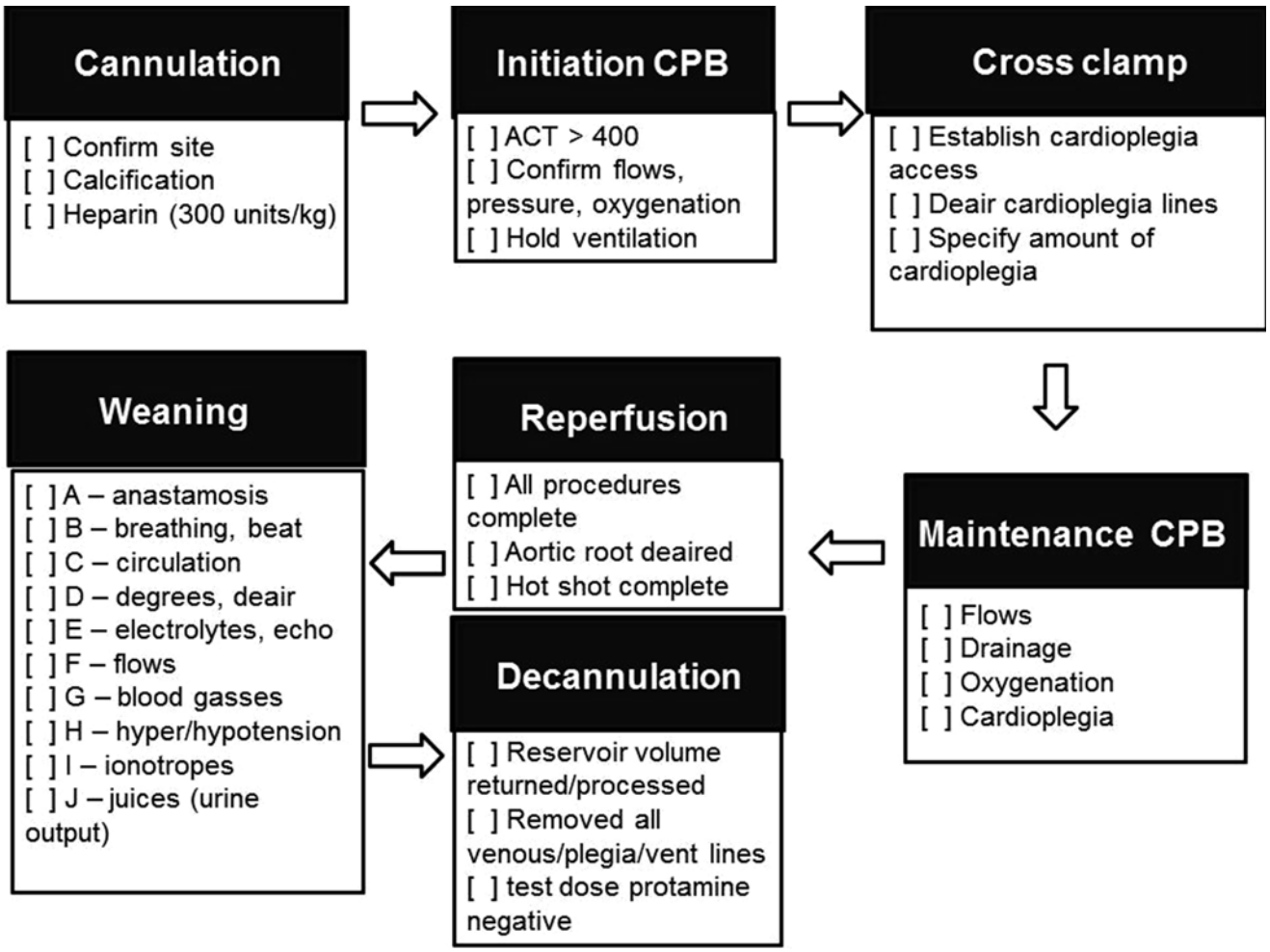

Fig. 33.10 Overview of critical events in cardiopulmonary bypass (*CPB*). Good communication between the operative field and perfusion is required at each step to ensure safety. There is no advancement along the algorithm unless the individual component has been clearly checked off by the team. The process begins with cannulation of the ascending aorta and atrium and continues with initiation of bypass. Cross clamp occurs next, followed by reperfusion and weaning. Aortic decannulation is the very last part of the process

heart temperature reaches 37 °C and its function is reestablished, cardiopulmonary bypass is terminated and all cannulas are removed. Sometimes the normal beating of the heart reappears spontaneously but, if not, electrical cardioversion is implemented using external paddles until a normal heart beat is reestablished.

33.3 Summary

Figure 33.10 summarizes the various parts of cardiopulmonary bypass and emphasizes critical events confirmed at each step. The process typically begins with cannulation of the ascending aorta and atrium and continues with initiation of bypass. Cross-clamp occurs next, followed by reperfusion and weaning. Once complete, aortic decannulation is the very last part of the process. Both cardiopulmonary bypass and the use of cardioplegia represent major medical breakthroughs that have extended the lives of millions of people worldwide. It is impossible to provide the level of surgical precision required for complex cardiac surgical procedures without a firm understanding of the components and steps involved in cardiopulmonary bypass.

References

1. Lillehei CW, Cohen M, Warden HE, Varco RL (1955) The direct-vision intracardiac correction of congenital anomalies by controlled cross circulation. Surgery 38:11–29
2. Gibbon JH (1954) Application of a mechanical heart and lung apparatus to cardiac surgery. Minn Med 37:171–180
3. Sabik JF, Nemeh H, Lytle BW et al (2004) Cannulation of the axillary artery with a side graft reduces morbidity. Ann Thorac Surg 77:1315–1320

4. Svensson LG, Kim KH, Blackstone EH et al (2004) Elephant trunk procedure: newer indications and uses. Ann Thorac Surg 78:109–116, discussion 109–116
5. Bjork VO, Hultquist G (1962) Contraindications to profound hypothermia in open-heart surgery. J Thorac Cardiovasc Surg 44:1–13
6. Brunberg JA, Reilly EL, Doty DB (1974) Central nervous system consequences in infants of cardiac surgery using deep hypothermia and circulatory arrest. Circulation 60:49–50
7. Bell WR, Royall RM (1980) Heparin-associated thrombocytopenia: a comparison of three heparin preparations. N Engl J Med 303:902–907
8. Fadali MA, Papacostas CA, Duke JJ et al (1976) Cardiovascular depressant effect of protamine sulfate: experimental study and clinical implications. Thorax 31:320–323
9. Goldman BS, Joison J, Austen WG (1969) Cardiovascular effects or protamine sulfate. Ann Thorac Surg 7:459–471
10. Greinacher A, Volpel H, Janssens U et al (1999) Recombinant hirudin (lepirudin) provides safe and effective anticoagulation in patients with heparin-induced thrombocytopenia: a prospective study. Circulation 99:73–80
11. Rowlings PA, Evans S, Mansberg R, Rozenberg MC, Evans S, Murray B (1991) The use of a low molecular weight heparinoid (Org 10172) for extracorporeal procedures in patients with heparin dependent thrombocytopenia and thrombosis. Aust N Z J Med 21:52–54
12. Warkentin TE, Greinacher A (2003) Heparin-induced thrombocytopenia and cardiac surgery. Ann Thorac Surg 76:2121–2131
13. Molina JE, Irmiter RJ, Vogelpohl DC, Nielsen KL, Callander D, Mueller R (1995) Normothermic cardiopulmonary bypass for all cardiac operations. Cor Europ 4:76–79
14. Sing AK, Bert AA, Feng WC, Rotenberg FA (1995) Stroke during coronary artery bypass grafting using hypothermic versus normothermic perfusion. Ann Thorac Surg 59:84–89
15. Lazenby WD, Ko W, Zelano JA et al (1992) Effects of temperature and flow rate in regional blood flow and metabolism during cardiopulmonary bypass. Ann Thorac Surg 53:957–964
16. Nomoto S, Shimahara Y, Kumada K, Ogino H, Okamoto Y, Band T (1992) Arterial ketone body ratio during and after cardiopulmonary bypass. J Thorac Cardiovasc Surg 103:1164–1167
17. Croughwell ND, Frasco P, Blumenthal JA, Leone BJ, White WD, Reves JG (1992) Warming during cardiopulmonary bypass is associated with jugular bulb desaturation. Ann Thorac Surg 53:827–832
18. Durandy Y, Hulin S, LeCompte Y (2002) Normothermic cardiopulmonary bypass in pediatric surgery. J Thorac Cardiovasc Surg 123:194
19. Swaminathan M, East C, Phillips-Bute B et al (2001) Report of a sub-study on warm versus cold cardiopulmonary bypass: changes in creatinine clearance. Ann Thorac Surg 72:1603–1609
20. Mora CT, Henson WB, Weintraub WS et al (1996) The effect of temperature management during cardiopulmonary bypass on neurologic and neuropsychologic outcomes in patients undergoing coronary revascularization. J Thorac Cardiovasc Surg 112:514–522
21. Craver JM, Bufkin BL, Weintraub WS, Guyton RA (1995) Neurologic events after coronary bypass grafting: further observations with warm cardioplegia. Ann Thorac Surg 59:1429–1433
22. Naik SK, Knight A, Elliot M (1991) A prospective randomized study of a modified technique of ultrafiltration during pediatric open-heart surgery. Circulation 84:422–431
23. Davies MJ, Nguyen K, Gaynor JW, Elliot MJ (1998) Modified ultrafiltration improves left ventricular systolic function in infants after cardiopulmonary bypass. J Thorac Cardiovasc Surg 115:361–370
24. Loor G, Li L, Sabik JF 3rd, Rajeswaran J, Blackstone EH, Koch CG (2012) Nadir hematocrit during cardiopulmonary bypass: end-organ dysfunction and mortality. J Thorac Cardiovasc Surg 144:654–662
25. Loor G, Rajeswaran J, Li L et al (2013) The least of three evils: exposure to red blood cell transfusion, anemia or both? J Thorac Cardiovasc Surg 146:1480–1487
26. Loor G, Koch CG, Sabik JF 3rd, Li L, Blackstone (2012) Implications and management of anemia in cardiac surgery: current state of knowledge. J Thorac Cardiovasc Surg 144:538–546
27. Mahoney CB, Donnelly JE (2000) Impact of closed versus open venous reservoirs on patient outcomes in isolated coronary artery bypass surgery. Perfusion 15:467–472
28. McCusker K, Vijay V, DeBois W et al (2001) MAST system: a new condensed cardiopulmonary bypass circuit for adult cardiac surgery. Perfusion 16:447–452
29. Aldea GS, Doursovnian M, O'Gara P et al (1996) Heparin-bonded circuits with a reduced anticoagulation protocol in primary CABG: a prospective randomized study. Ann Thorac Surg 62:410–417
30. Svenmarker S, Haggmark S, Jansson E et al (2002) Use of heparin-bonded circuits in cardiopulmonary bypass improves clinical outcome. Scand Cardiovasc J 35:241–246
31. Molina JE (1989) Temporary dual-chamber pacing after open cardiac procedures. Medtronic News 19:24–28
32. Svensson LG, Crawford ES (eds) (1997) Cardiovascular and vascular disease of the aorta. WB Saunders Co., Philadelphia
33. Melrose DG, Dreyer B, Bentall HH, Baker JB (1955) Elective cardiac arrest. Preliminary communication. Lancet 2:21–22
34. Helmsworth JA, Kaplan S, Clark LC Jr, McAdams AJ, Matthews EC, Edwards FK (1959) Myocardial injury associated with asytole induced with potassium citrate. Ann Surg 149:200–203
35. Brewer DL, Bilbro RH, Bartel AG (1973) Myocardial infarction as a complication of coronary bypass surgery. Circulation 47:58–64
36. Assad-Morell JL, Wallace RB, Elveback LR et al (1975) Serum enzyme data in diagnosis of myocardial infarction during or early after aorto-coronary saphenous vein bypass graft operations. J Thorac Cardiovasc Surg 69:851–857
37. Hearse DJ, Stewart DA, Braimbridge MV (1975) Hypothermic arrest and potassium arrest: metabolic and myocardial protection during elective cardiac arrest. Circ Res 36:481–489
38. Nelson RL, Goldstein SM, McConnell DH, Maloney JV, Buckberg GD (1976) Improved myocardial performance after aortic cross-clamping by combining pharmacologic arrest with topical hypothermia. Circulation 54:11–16
39. Buckberg GD, Olinger GN, Mulder DG, Maloney JV (1975) Depressed postoperative cardiac performance: prevention by adequate myocardial protection during cardiopulmonary bypass. J Thorac Cardiovasc Surg 70:974–994
40. Molina JE, Feiber W, Sisk A, Polen T, Collins B (1977) Cardioplegia without fibrillation or defibrillation in cardiac surgery. Surgery 81:619–626
41. Roe BB, Hutchinson JC, Fishman NH, Ullyot DJ, Smith DL (1977) Myocardial protection with cold ischemic potassium induced cardioplegia. J Thorac Cardiovasc Surg 73:366–374
42. Chocron S, Kaili D, Yan Y et al (2000) Intermediate lukewarm (20°C) antegrade intermittent blood cardioplegia compared with cold and warm blood cardioplegia. J Thorac Cardiovasc Surg 119:610–616
43. Rosenkranz ER, Vinten-Johansen J, Buckberg GD, Okamoto F, Edwards H, Bugyi H (1982) Benefits of normothermic induction of blood cardioplegia in energy-depleted hearts, with maintenance of arrest by multidose cold blood cardioplegic infusions. J Thorac Cardiovasc Surg 84:667–677
44. Hayashida N, Ikonomidis JS, Weisel RD et al (1994) The optimal cardioplegic temperature. Ann Thorac Surg 58:961–971
45. Follete DM, Fey K, Becker H et al (1979) Superiority of blood cardioplegia over asanguineous cardioplegia: an experimental and clinical study. Chir Forum Exp Klin Forsch 279–283
46. Hearse DJ, Stewart DA, Braimbridge MV (1976) Cellular protection during myocardial ischemia: the development and characterization of a procedure for the induction of reversible ischemic arrest. Circulation 54:193–202

47. Ebert PA, Greenfield LJ, Austen WG, Morrow AG (1962) Experimental comparison of methods for protecting the heart during aortic occlusion. Ann Surg 155:25–32
48. Rosenkranz ER, Buckberg GD, Laks H, Mulder DG (1983) Warm induction of cardioplegia with glutamate-enriched blood in coronary patients with cardiogenic shock who are dependent on inotropic drugs and intra-aortic balloon support. J Thorac Cardiovasc Surg 86:507–518
49. Beyersdorf F, Kirsh M, Buckberg GD, Allen BS (1992) Warm glutamate/aspartate-enriched blood cardioplegic solution for perioperative sudden death. J Thorac Cardiovasc Surg 104:1141–1147
50. Jynge P, Hearse DJ, Braimbridge MV (1977) Myocardial protection during ischemic cardiac arrest. A possible hazard with calcium-free cardioplegic infusates. J Thorac Cardiovasc Surg 73:848–855
51. Harlan BJ, Ross D, Macmanus Q, Knight R, Luber J, Starr A (1978) Cardioplegic solutions for myocardial preservation: analysis of hypothermic arrest, potassium arrest, and procaine arrest. Circulation 58:114–118
52. Conti VR, Bertranov EG, Blackstone EH, Kirklin JW, Digerness SB (1978) Cold cardioplegia versus hypothermia for myocardial protection: randomized clinical study. J Thorac Cardiovasc Surg 76:577–589
53. Kirklin JW, Conti VR, Blackstone EH (1979) Prevention of myocardial damage during cardiac operations. N Engl J Med 301:135–141
54. Bretschneider J, Hubner G, Knoll D, Lohr B, Nordbeck H, Spieckermann PG (1975) Myocardial resistance and tolerance to ischemia: physiological and biochemical basis. J Cardiovasc Surg (Torino) 16:241–260
55. Preusse CJ, Gebhard MM, Bretschneider HJ (1981) Myocardial "equilibration processes" and myocardial energy turnover during initiation of artificial cardiac arrest with cardioplegic solution-reasons for a sufficiently long cardioplegic perfusion. Thorac Cardiovasc Surg 29:71–76
56. Preusse CJ, Schulte HD, Birks W (1987) High volume cardioplegia. Ann Chirurg Gynaecol 76:39–45
57. Human PA, Holl J, Vosloo S et al (1993) Extended cardiopulmonary preservation: University of Wisconsin solution versus Bretschneider's cardioplegic solution. Ann Thorac Surg 55:1123–1130
58. Reichenspurner H, Russ C, Uberfuhr P et al (1992) Myocardial preservation using HTK-solution for heart transplantation. A multicenter study. Eur J Cardiothorac Surg 7:414–419
59. Groenewoud AF, Thorogood J (1992) A preliminary report of the HTK randomized multicenter study comparing kidney graft preservation with HTK and Eurocollins solutions. Transpl Int 5:429–432
60. Hewitt RL, Lolley DM, Adrouny GA, Drapanas T (1974) Protective effect of glycogen and glucose on the anoxic arrested heart. Surgery 75:1–10
61. Lolley DM, Ray JF III, Myers WO, Sheldon G, Sautter RD (1978) Reduction of intraoperative myocardial infarction by means of exogenous anaerobic substrate enhancement: prospective randomized study. Ann Thorac Surg 26:515–524
62. Molina JE, Gani KS, Voss DM (1982) How should clear cardioplegia be administered? A method of rapid arrest with high flow and pressure. J Thorac Cardiovasc Surg 84:762–772
63. Molina JE, Gani KS, Voss DM (1982) Pressurized rapid cardioplegia versus administration of exogenous substrate and topical hypothermia. Ann Thorac Surg 33:434–444
64. Molina JE, Galliani CA, Einzig S, Bianco R, Rasmussen T, Clack R (1989) Physical and mechanical effects of cardioplegic injection on flow distribution and myocardial damage in hearts with normal coronary arteries. J Thorac Cardiovasc Surg 97:870–877
65. Todd GJ, Tyers GF (1975) Amelioration of the effects of ischemic cardiac arrest by the intracoronary administration of cardioplegic solutions. Circulation 52:1111–1116
66. Fremes SE, Zhang J, Furukawa RD, Mickle DA, Weisel RD (1995) Cardiac storage with University of Wisconsin solution, calcium, and magnesium. J Heart Lung Transplant 14:916–925
67. Ackemann J, Gross W, Mory M, Schaefer M, Gebhard MD (2002) Celsior versus Custodiol: early postischemic recovery after cardioplegia and ischemia at 5°C. Ann Thorac Surg 74:522–529
68. Coles JA Jr, Sigg DC, Iaizzo PA (2005) The potential benefits of 1.5% hetastarch as a cardioplegia additive. Biochem Pharmacol 69:1553–1558
69. Nayler WG (1982) Protection of the myocardium against postischemic reperfusion damage. The combined effect of hypothermia and nifedipine. J Thorac Cardiovasc Surg 84:897–905
70. Bolling SF, Bies LE, Gallagher KP, Bove EL (1989) Enhanced myocardial protection with adenosine. Ann Thorac Surg 47:809–815
71. Sharov VG, Saks VA, Kupriyanov VV et al (1987) Protection of ischemic myocardium by exogenous phosphocreatine. J Thorac Cardiovasc Surg 94:749–761
72. Foker JE, Einzig S, Wang T (1980) Adenosine metabolism and myocardial preservation. J Thorac Cardiovasc Surg 80:506–516
73. Vejlsted H, Andersen K, Hansen BF et al (1983) Myocardial preservation during anoxic arrest. Scand J Thorac Cardiovasc Surg 17:269–276
74. Rao G, King J, Ford W, King G (1977) The effects of methylprednisolone on the complications of coronary artery surgery. Vasc Surg 11:1–7
75. Kirsh MM, Behrendt DM, Jochim KE (1979) Effects of methylprednisolone in cardioplegic solution during coronary bypass grafting. J Thorac Cardiovasc Surg 77:896–899
76. The Warm Heart Investigators (1994) Randomized trial of normothermic versus hypothermic coronary bypass surgery. Lancet 343:559–563
77. Menasche P, Kural S, Fauchet M et al (1982) Retrograde coronary sinus perfusion. A safe alternative for ensuring cardioplegic delivery in aortic valve surgery. Ann Thorac Surg 34:647–658
78. Lichtenstein SV, Ashe KA, El Dalati H, Cusimano RJ, Panos A, Slutsky AS (1991) Warm heart surgery. J Thorac Cardiovasc Surg 101:269–274
79. Wechsler AS (1982) Deficiencies of cardioplegia—the hypertrophied ventricle. In: Engelman RM, Levisky S (eds) A textbook of clinical cardioplegia. Futura, Mount Kisco, pp 381–439
80. Shumway NE, Lower RR, Stofer RC (1959) Selective hypothermia of the heart in anoxic cardiac arrest. Surg Gynecol Obstet 109:750–754
81. Shumway NE, Lower RR (1959) Topical cardiac hypothermia for extended periods of anoxic arrest. Surg Forum 10:563–566

Heart Valve Disease

34

Laura Harvey, Kenneth K. Liao, and Ranjit John

Abstract

This chapter was designed to provide the reader with a brief overview of the current treatment options for heart valve disease. Major topics of discussion are: (1) development of prosthetic valve replacements; (2) current issues with valve replacement; (3) major valvular diseases that affect humans in the Western world; and (4) recent advances in therapeutic options for valvular diseases.

Keywords

Mechanical prosthetic valve • Biologic prosthetic valve • Aortic stenosis • Aortic sclerosis • Aortic regurgitation • Mitral stenosis • Mitral regurgitation • Tricuspid valve disease

34.1 Introduction

The function of the heart is to circulate blood in closed circuit to the lungs where blood is oxygenated, and out to the body where oxygen provides fuel for cellular metabolism. To accomplish this task, blood is pumped by the right heart system from the body to the lungs. Once oxygenated in the lungs, blood is returned to the left heart where it is then pumped out to the body. Although described as a biologic pump, the heart is actually two biological pumps in series, composed of a right and left heart. Each unit of the heart is composed of an atrial and ventricular chamber, whose synchronized contractions result in the forward flow of blood out of the heart. Crucial to the appropriate function of the heart are four valves (the mitral, aortic, tricuspid, and pulmonic valves) that function in concert to maintain forward flow of blood across the heart (Fig. 34.1). Diseases affecting the heart valves result in either obstruction to forward flow (stenosis) or reversal of flow across an incompetent valve (regurgitation). In either case, significant morbidity and mortality will result if no treatment is offered to the patient. This chapter was designed to provide the reader with a brief overview of the current treatment options for heart valve disease. Major topics of discussion are: (1) development of prosthetic valve replacements; (2) current issues with valve replacement; (3) major valvular diseases that affect humans in the Western world; and (4) recent advances in therapeutic options for valvular diseases.

34.2 A New Frontier: Valve Replacement

Before 1950, the ability to safely and effectively operate on the human heart was considered an insurmountable goal. Attempts to operate to correct valvular diseases without stopping the heart resulted in severe, often fatal complications including uncontrollable bleeding and the introduction of air emboli [1]. The ability to maintain forward flow of blood while stopping the heart to allow the surgeon access to the valve would have to wait for the development of cross-circulation, and later for the perfection of the cardiopulmonary bypass procedure by Dr. C. Walton Lillehei, Richard L. Varco, and Dr. F. John Lewis at the University of Minnesota [2] (see also Chap. 25). With this new technology, a new frontier in surgical options for the treatment of heart valve

L. Harvey, MD • K.K. Liao, MD • R. John, MD (✉)
Division of Cardiovascular and Thoracic Surgery, Department of Surgery, University of Minnesota, 420 Delaware Street SE, MMC 207, Minneapolis, MN 55455, USA
e-mail: johnx008@umn.edu

P.A. Iaizzo (ed.), *Handbook of Cardiac Anatomy, Physiology, and Devices*, DOI 10.1007/978-3-319-19464-6_34

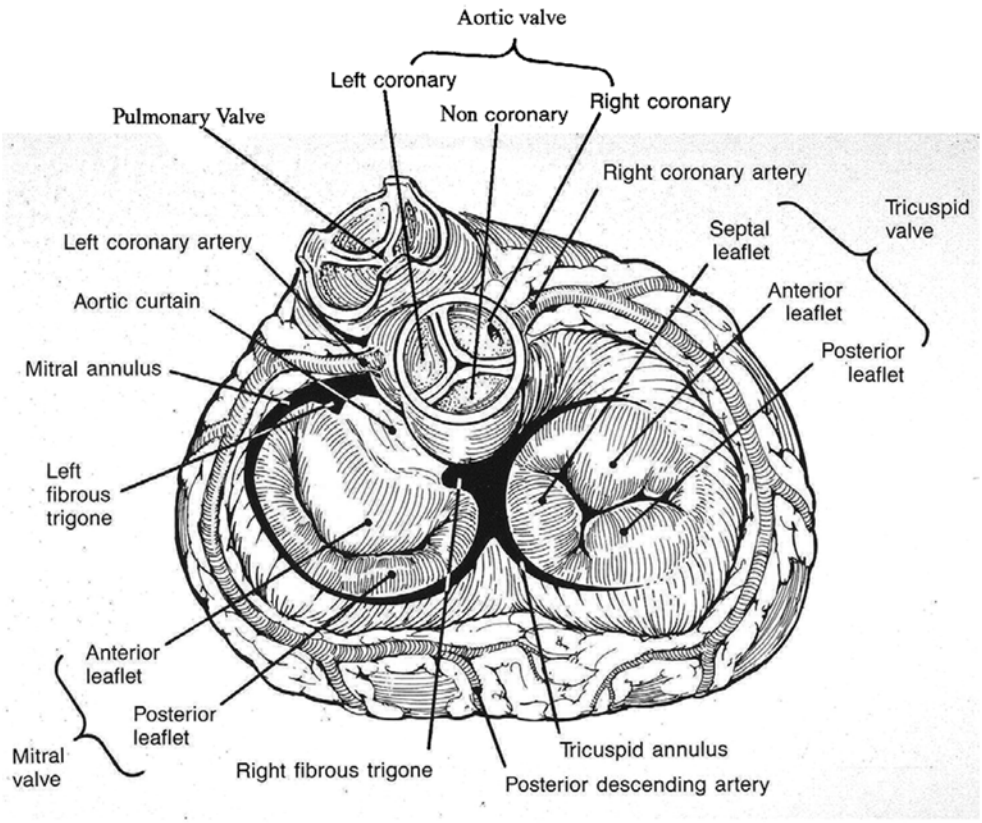

Fig. 34.1 Apical view of the four heart valves—aortic, mitral, pulmonic, and tricuspid

disease began to emerge. During the past several years, major advances have occurred in diagnostic techniques (i.e., imaging) and therapeutic interventions for valvular diseases, as well as improved understanding of the natural history of both treated and untreated valvular disease (for more detail, see Chaps. 35 and 36).

34.2.1 Mechanical Prosthetic Valves

By 1961, Dr. Albert Starr and Lowell Edwards had successfully implanted the world's first mechanical valve into a human to replace a mitral valve that had been deformed by rheumatic fever [3]. Initially, this steel ball and cage design was successful in approximately 50 % of implantations. Major complications were soon recognized, including: (1) clot formation resulting in embolic strokes; (2) significant noise; (3) red blood cell destruction; and/or (4) tissue ingrowth causing subsequent valve obstruction. A complete history of the development of currently used mechanical prostheses is beyond the scope of this text. However, it is important to mention two key aspects of any successful new valve design: (1) improved valve hemodynamics; and (2) reduced thrombogenic (or clot forming) potential. Efforts to optimize valve hemodynamic function date back to the development of the Lillehei/Kaster tilting disk valve which allowed blood to flow centrally through the valve. At that time, this new type of valve emphasized the requirement to design a valve that would reduce turbulent blood flow, reduce cell destruction, and minimize the transvalvular gradients [4]. A transvalvular gradient is defined as the pressure difference across the valve. Despite the advantages of a new steel tilting disk design, careful strict anticoagulation therapy was still required to reduce the risk of clot formation [5]. The next improvements of these valves came with the development of the pyrolytic carbon valve leaflets. The nonthrombogenic weight and strength properties were determined by Drs. Jack Bokros and Vincent Gott. Subsequently, pyrolytic carbon was used in the creation of a bileaflet valve inspired by Dr. Kalke. This valve, originally manufactured by St. Jude Medical (St. Paul, MN, USA), provided exceptional performance, and today this design remains the gold standard for mechanical valves [6]. To date, all patients with mechanical valves require anticoagulation, e.g., with oral warfarin therapy which reduces the risk of thromboembolism to 1–2 %/year (Table 34.1) [7]. It should be noted that numerous studies have demonstrated that the risk of thromboembolism is directly related to the valve implant position, i.e., in the

Table 34.1 Anticoagulation after prosthetic heart valves [8]

		Warfarin INR 2.5	Warfarin INR 3.0	Aspirin 75–100 mg
Mechanical prosthesis				
First 3 months post implantation		+		+
After initial 3 months	Aortic valve	+		
	Aortic valve + Risk factor		+	+
	Mitral valve		+	+
	Mitral valve + Risk factor		+	+
Biological prosthesis				
First 3 months post implantation		+		+
After initial 3 months	Aortic valve			+
	Aortic valve + Risk factor	+		+
	Mitral valve			+
	Mitral valve + Risk factor	+		+

descending order of risk, the tricuspid, mitral, and aortic valves. In addition, this risk of emboli appears to be greatest in the early post-implant period, and then becomes reduced as the valve sewing cuff becomes fully endothelialized.

In general, management of anticoagulation must be individualized to the patient to minimize risk of thromboembolism and, at the same time, prevent bleeding complications. In situations where a patient with a valve prosthesis requires noncardiac surgery, warfarin therapy should be stopped only for procedures where risk of bleeding is substantial. A complete discussion of anticoagulation therapy is beyond the scope of this chapter, however several excellent reviews are available on this subject [7, 8].

34.2.2 Biological Prosthetic Valves

Because of the problems related to anticoagulation, a majority of subsequent valve research focused on developing tissue alternatives that avoid the need for anticoagulation. From a historical perspective, Drs. Lower and Shumway performed the first pulmonary valve autotransplant in an animal model [9]. Later in 1967, Dr. Donald Ross completed the first successful replacement in a human. The *Ross Procedure* is a well-established method still used today to replace a diseased aortic valve with the patient's own pulmonary valve (Fig. 34.2); a donor tissue valve or homograft (Table 34.2) is then used as a prosthetic pulmonary valve. In general, tissue valves are significantly more biocompatible than their mechanical counterparts. These valves are naturally less thrombogenic, and thus the patient does not require aggressive anticoagulation. Specifically, a risk of <0.7 %/year of clinical thromboembolism has been reported in valve replacement patients eliciting sinus rhythm without warfarin therapy [7]. Therefore, this treatment option is advantageous in clinical situations where the use of anticoagulation would significantly increase morbidity and mortality. Yet, to date, a potential major disadvantage of tissue valve implantation is early valvular degeneration as a result of leaflet calcification. Thus, methods for tissue preservation to prevent such calcifications are currently a major focus of research in this field.

34.2.3 Biological Versus Mechanical Valves

The choice of a mechanical or biologic valve for implant will typically depend on various factors: (1) the patient's current disease status; (2) the specific native valve involved; and/or (3) the surgeon's preference and experience. If these factors are not limiting, the choice of valve type should be based on the maximization of benefits over risks for the individual patient. Unfortunately, the ideal prosthetic valve that combines excellent hemodynamic performance and long-term durability without increased thromboembolic risk or the need for lifelong anticoagulation remains elusive. In general, mechanical valves offer greater durability at the cost of requiring lifelong anticoagulation, as well as the risk of thromboembolism. In contrast, bioprosthetic valves have a much lower thromboembolic risk without the need for anticoagulation, but elicit a higher risk for structural degeneration and thus potential need for reoperation. As such, mechanical valves are perhaps most well suited for the younger patient who does not desire future reoperations. Currently, mechanical valve replacement in the USA is quite standardized and commonplace, i.e., yielding satisfactory valve function that is reproducible from patient to patient. Furthermore, the flow gradients with newer bileaflet mechanical valves have dramatically improved from the early ball valve type; currently, a trileaflet valve is in the preclinical stages of development and may eventually not require anticoagulation therapy. Nevertheless in the interim, bioprosthetic or tissue valves offer a safe alternative for patients in

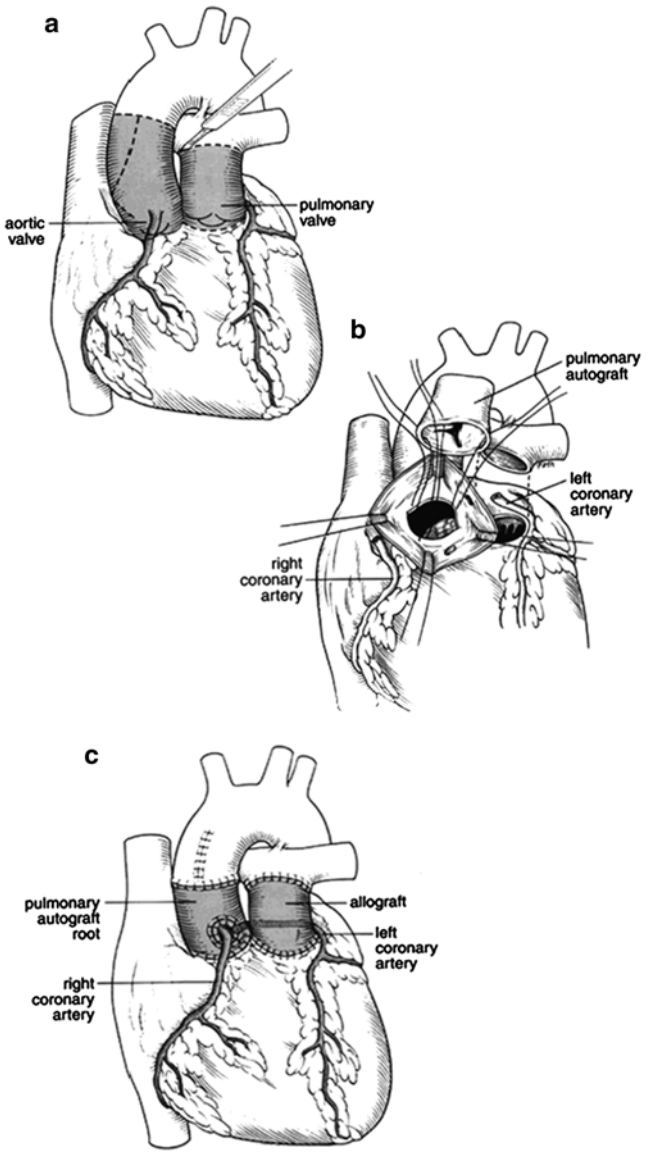

Fig. 34.2 Schematic drawing of the Ross Procedure. (**a**) Resection of the diseased aortic valve. (**b**) Harvesting of native pulmonary valve. (**c**) Implantation of the pulmonic valve in the aortic position and reimplantation of coronary arteries

whom the risk of anticoagulation is prohibitively high (e.g., elderly patients >70 years of age, women of child bearing years desiring pregnancy). Yet, the length of their durability remains a serious concern for tissue valves, and thus a patient whose life expectancy is greater than that of the prosthesis will likely encounter the risk of another surgery for a second valve replacement. Note that a transcatheter-delivered *valve in valve* procedure is a more recent option (Chap. 36).

It is important to note that two historic randomized clinical trials have compared outcomes between early generation tissue and mechanical valves—the Edinburgh Heart Valve trial and the Veteran Affairs Cooperative Study on Valvular Heart Disease [9–11]. Both trials showed increased bleeding associated with mechanical valves and increased reoperations with tissue valves. While the strength of these trials is a prospective randomized design, the disadvantages are that the valves used in these trials are currently obsolete. More recently, a large meta-analysis comparing mechanical versus bioprosthetic aortic valves found no difference in risk-corrected mortality regardless of patient age [12]. Based on this and other studies, the choice of valve should not be based on age alone. Clearly, there is a trend towards increasing use of bioprosthetic valves in younger patients; this is based on the fact that advances in tissue fixation and improved anti-calcification treatments have resulted in superior durability of the newer generation bioprosthetic valves. Specifically, third generation bioprosthetic valves have been shown to have a greater than 90 % freedom from structural generation at 12-year follow-up [13]. Furthermore, improvements in cardiac surgery including better techniques for myocardial preservation, less invasive procedures (i.e., robotic surgery), as well as strategies for cardiac reoperation have significantly reduced the risk for cardiac reoperation. This has further allowed an increasing application of bioprosthetic valves in patients younger than 55–60 years old. In conclusion, in the absence of current randomized trials, physicians must make a choice based on existing data and individualize that choice based on patient-related factors such as age, lifestyle, tolerance for anticoagulation, and/or position of the replacement valve [14].

Table 34.2 Tissue valve graft options: classification of bioprosthetic valves

Bioprosthetic valve	Description
Stented porcine valve (Xenograft)	A three leaflet valve supported by three artificial struts or stents to maintain leaflet structure and geometry.
Stentless porcine valve (Xenograft)	A length of porcine aorta including tissue below (proximal) and above (distal) to the valve, called the "root."
Bovine pericardial valve (Xenograft)	A three leaflet valve created from bovine pericardium attached to a stented frame.
Homograft	A human aortic valve and root.
Autograft	A pulmonary valve and root excised from the patient and reimplanted in the same patient.

Table 34.3 Reportable valve prosthesis complications [9]

Complication	Description
Structural valvular deterioration	Any change in function of an operated valve resulting from an intrinsic abnormality, causing stenosis or regurgitation.
Nonstructural dysfunction	Any stenosis or regurgitation of the operated valve that is not intrinsic to the valve itself, including inappropriate sizing, but excluding thrombosis and infection.
Valve thrombosis	Any thrombus, in the absence of infection, attached to or near an operated valve that occludes part of the blood flow path or interferes with function of the valve.
Embolism	Any embolic event that occurs in the absence of infection after the immediate perioperative period (new temporary or permanent, focal or global neurological deficit, and peripheral embolic event).
Bleeding event (anticoagulant hemorrhage)	Any episode of major internal or external bleeding that causes death, hospitalization, permanent injury, or requires transfusion.
Operated valvular endocarditis	Any infection involving an operated valve, resulting in valve thrombosis, thrombotic embolus, bleeding event, or paravalvular leak.

34.2.4 Prosthetic Heart Valve Endocarditis and Performance Tracking

All patients with prosthetic valves also need appropriate antibiotics for prophylaxis against infective endocarditis. Details of these therapies are beyond the scope of this chapter, but the reader is referred to guidelines published by a joint committee from the American Heart Association (AHA) and American College of Cardiology (ACC) for the applicable protocols. In addition, a registry has been established to track the long-term performance of all clinically approved implanted valve prostheses. Established standards were revised in 1996 and are briefly summarized in Table 34.3. As alluded to in Chap. 27, investigators seeking approval for all new valves must also report any complications that occur in the preclinical animal testing phase to the appropriate regulatory authority.

34.3 Specific Valvular Diseases: Etiologies and Treatments

The remainder of this chapter is devoted to a generalized summary of the most common valvular diseases affecting patients in the Western world. Of the four heart valves, significant clinical disease can primarily affect all but the pulmonary valve. Yet, compromised function of this valve is noted to occur in the adult congenital heart patient who previously underwent reparative surgeries. Indications for diagnostic, therapeutic, and follow-up intervention will be discussed for each disease. Note that a complete evidence-based summary of recommendations for intervention and level of physical activity for individuals with valvular disease is available from several excellent reviews [8, 15, 16].

34.3.1 Aortic Valve Disease

Anatomically, the normal aortic valve is composed of the annulus and the left, right, and noncoronary leaflets (sometimes referred to as *cusps*) (Fig. 34.3). Diseases affecting these structures can be subdivided into aortic stenosis or regurgitation, or some combination thereof. Overall, aortic stenosis is considered a surgical disease with aortic valve replacement considered to be the standard of care. Treatment of aortic regurgitation is also typically surgical, though the exact method chosen will vary widely based on the etiology of the disease.

34.3.1.1 Aortic Stenosis

Aortic stenosis causes varying degrees of left ventricular outflow tract obstruction [17, 18]. The various etiologies of aortic stenosis are subdivided into acquired versus congenital. Regardless of the etiology, the most common two causes of aortic stenosis in adults are calcification of a normal trileaflet or a congenital bicuspid aortic valve. Interestingly, among individuals under the age of 70, bicuspid aortic valve disease is the most common cause of aortic stenosis. These congenitally abnormal valves typically develop progressive fibrosis and calcification of the leaflets over several decades, and can present for surgery at any time during an individual's life, i.e., depending on the degree of deformity and rate of progression of the narrowing. Patients over the age of 70 more typically elicit the so-called *senile aortic stenosis*; these valves start out as normal valves, but develop thickening, calcification, and stenosis with aging. In a patient with any degree of aortic stenosis, careful clinical follow-up is mandatory to follow the progression of stenosis, and typically surgery is indicated at the onset of any symptoms (see below). Congenital malformation (typically presenting in bicuspid aortic valves) results in progressive fibrosis and calcification

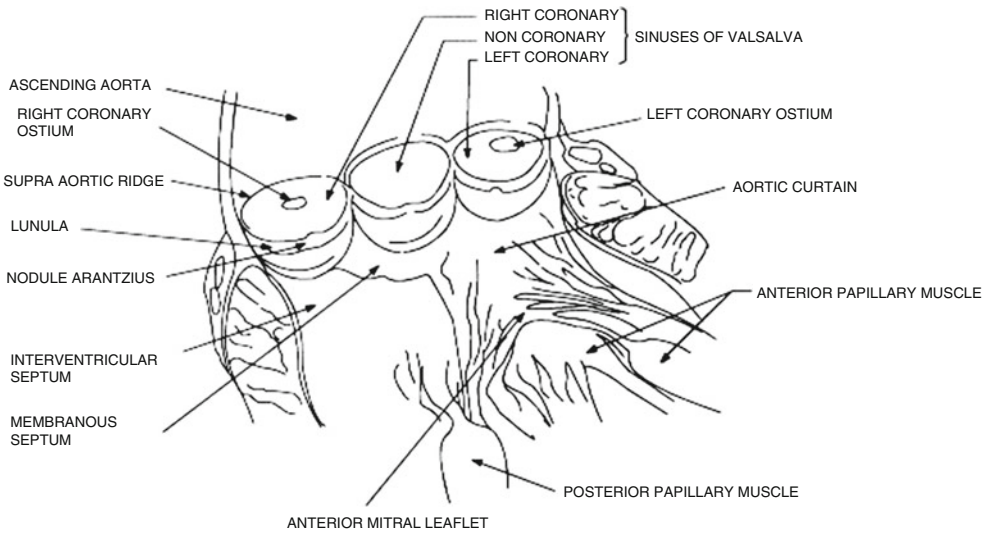

Fig. 34.3 Anatomy of the aortic valve. Adapted from Duran CMG (1994) Conservative valve surgery. In: Zaibag MA, Duran CMG (eds) Valvular heart disease. Marcel Dekker, New York, p 584

Table 34.4 Degree of aortic stenosis [83]

	Valve orifice area (cm^2)	Peak aortic velocity (m/s)
Mild	>1.5	<3.0
Moderate	>1.0 to 1.5	3.0–4.0
Severe	<1.0	>4.0

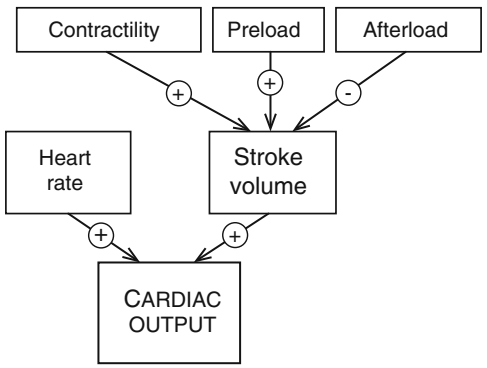

Fig. 34.4 Determinants of cardiac output include contributions from preload and afterload pressures, contractility, and heart rate. Adapted from Lilly LS (ed) (1993) Pathophysiology of heart disease. Lea & Febiger, Philadelphia, p 149

of the leaflets over several decades. The average rates of reduction in valve orifice area have been estimated to be ~0.12 cm^2/year, and valve orifice areas are typically used to grade the relative severity of valve stenosis (Table 34.4) [19]. Nevertheless, progression of aortic stenosis varies significantly and the appearance of symptoms may not correlate well with the given measured valve area. Therefore, careful clinical follow-up is mandatory, as it is difficult to predict an actual individual rate of stenotic progression. In general, aortic stenosis is graded into various categories of severity based on degrees of mean pressure gradient, aortic jet velocity, and/or valve area.

Valve stenosis may also be associated with progressive outflow tract obstruction, which can then cause additional increases in left ventricular pressure. As a result, concentric left ventricular hypertrophy is an early response, which assists initially in maintaining normal left ventricular systolic wall tension and ejection fraction [20]. However, once this response becomes functionally inadequate, afterload tends to increase which, in turn, results in a gradual reduction in overall ejection fraction (Fig. 34.4). In some patients, an initial ventricular hypertrophy itself may also be detrimental, producing subendocardial ischemia even in the absence of coronary artery disease [21, 22]. As such, this results in further systolic and diastolic left ventricular dysfunction and may predispose such patients to a potentially larger degree of myocardial ischemia and higher mortality [7, 8, 17, 18, 23].

Although aortic stenosis may not produce symptoms early in its clinical course, in time symptoms of angina, syncope, heart failure, and/or even sudden death will develop. Although the latter are the classic symptoms of aortic stenosis, more subtle symptoms such as reduced effort tolerance, fatigue, and exertional dyspnea can also occur. Once symptoms are present, average survival without intervention is less than 2–3 years [17, 18, 24–29]. Furthermore, the mortality of patients with aortic stenosis, in the absence of surgical treatment, present with: (1) angina, 50 % within 5 years; (2) syncope, 50 % mortality within 3 years; and (3) heart failure, 50 % mortality within 2 years. Therefore, a high degree of skepticism is necessary to make the diagnosis prior to the onset of symptoms to maximize a given patient's outcome. In general, aortic stenosis can be detected early based on: (1) the presence of a systolic outflow murmur; (2) the occurrence of delayed/diminished carotid upstrokes; (3) a sustained left ventricular impulse; (4) a reduced intensity of the aortic component of the second heart sound; and/or (5)

evidence of left ventricular hypertrophy on exam, chest X-ray, and/or EKG. Typically, results of echocardiography can be further used to confirm the diagnosis of aortic stenosis and also provide for the detailed assessment of: (1) mean transvalvular pressure gradient; (2) derived valve area; (3) relative left ventricle size (degree of hypertrophy) and function; and/or (4) presence of other associated valvular disease. For more details on the clinical use of echocardiography, the reader is referred to Chap. 22. It should also be noted that advances in magnetic resonance imaging may be applied in diagnosing such patients (Chap. 24).

Physicians who follow patients with known aortic stenosis commonly perform an annual history and physical examination, and urge these patients to promptly self-report the development of any new symptoms. Although changes in valve area alone are not totally predictive, annual echocardiography is also useful to assess progression of ventricular hypertrophy and alterations in function. In any case, the development of any new symptoms (e.g., exertional chest discomfort, shortness of breath, or fainting spells) warrants additional clinical assessment, given that aortic stenosis progresses rapidly once such symptoms are present.

In patients being considered for aortic valve replacement secondary to aortic stenosis, cardiac catheterization is generally indicated in individuals >40 years of age to assess for any degree of significant coronary artery disease. Additional indications include the assessment of: (1) hemodynamic severity of the aortic stenosis in situations where there is a discrepancy between clinical and echocardiographic findings; and (2) situations where there is evidence of pulmonary hypertension or other valvular or congenital disease. Complete diagnostic evaluation should include: (1) measurement of transvalvular flows (liters/min); (2) determination of the transvalvular pressure gradients (mmHg); and (3) calculation of the effective valve areas (cm^2) [30].

Stress testing is recommended in patients with equivocal symptoms, and should only be carried out under close monitoring by a physician. Positive findings suggestive of hemodynamically significant aortic stenosis include the development of symptoms, limited exercise tolerance, and a blunted blood pressure response to exercise. In all such cases, surgical replacement of the aortic valve is indicated.

Medical therapy for aortic stenosis is primarily relegated to the prevention of endocarditis and the control of arterial hypertension. As most asymptomatic patients lead a normal life, no interventions are typically considered. Yet, there are some studies that have shown slowing of disease progression with statins. While there are theoretical benefits for the use of ACE inhibitors, studies so far have not shown significant benefits on this disease progression [31, 32]. Nevertheless, once symptoms develop, prompt intervention should be offered to prevent morbidity and mortality. In some patients, interventional radiological therapy using balloon aortic valvotomy can effectively reduce the transvalvular pressure gradients. This procedure uses percutaneously inserted catheters advanced into the aortic valve, then a balloon is inflated to fracture calcific deposits and separate fused commissures [33, 34]. Though successful at providing clinical improvements, the post-procedure valve area rarely exceeds 1.0 cm^2, and aortic regurgitation is often created, thus increasing the burden on the left ventricle. To date, the rate of significant complications (10 %) and symptomatic restenosis (6–12 months) unfortunately makes balloon valvotomy an undesirable substitute for aortic valve replacement in adults with aortic stenosis [7]. Yet, percutaneous aortic balloon dilations may be considered as a bridge to surgical aortic valve replacement or transcatheter aortic valve replacement in patients with severe symptomatic aortic stenosis [8].

Aortic valve replacement is technically possible at any age, and is the treatment of choice for aortic stenosis in most adults [35]. Yet, the degree of stenosis mandating surgery in asymptomatic patients remains an issue of debate. Nevertheless, the degree of improvement following aortic valve replacement is directly related to preoperative left ventricular function; patients with depressed ejection fractions caused by excessive afterloads demonstrate significant improvement in left ventricular function after aortic valve replacement. Conversely, if depressed left ventricular function is caused by myocardial insufficiency, improvement in left ventricular function and resolution of symptoms may not be reversed after valve replacement. In general, survival is improved for patients undergoing aortic valve replacement, with the possible exception of a subset of patients with severe left ventricular dysfunction caused by coronary artery disease [36, 37]. In summary, in contrast to the dismal survival rates for patients with untreated severe aortic stenosis, the long-term survival of patients who have undergone aortic valve replacement approaches the rate in the normal population. Therefore, it is recommended that patients with severe aortic stenosis, with or without symptoms, who are undergoing coronary artery bypass surgery should also undergo aortic valve replacement at the time of the revascularization procedure. Similarly, patients with moderate-to-severe aortic stenosis undergoing surgery for the replacement of other heart valves or an aortic root repair should also undergo an aortic valve replacement as part of their overall surgical procedure. Hence, in the absence of contraindications, aortic valve replacement is indicated in virtually all symptomatic patients with severe aortic stenosis (Table 34.5).

In recent years, transcatheter aortic valve replacements have been increasing in use. According to ACC/AHA guidelines, transcatheter aortic valve replacement is a reasonable alternative to surgical aortic valve replacement in patients who meet an indication for replacement and/or who have a high surgical risk for surgical aortic valve replacement.

Table 34.5 Aortic valve replacement in aortic stenosis [8]

- Symptomatic patients with severe aortic stenosis alone or:
  - Undergoing coronary artery bypass surgery.
  - Undergoing surgery on the aorta or other heart valves.
- Patients with moderate aortic stenosis and:
  - Undergoing coronary artery bypass surgery.
  - Undergoing surgery on the aorta.
  - Undergoing surgery on other heart valves.
- Asymptomatic patients with severe aortic stenosis and left ventricular systolic dysfunction typified by:
  - Abnormal response to exercise (e.g., hypotension).
  - Ventricular tachycardia.
  - Marked or excessive left ventricular hypertrophy (>15 mm).
  - Valve area <0.6 cm2.
  - Prevention of sudden death without the findings listed.

However, transcatheter aortic valve replacement should only be performed in patients with an expected post-procedure survival longer than 12 months [8, 38, 39]. For a more detailed discussion of these valves, see Chap. 36.

Currently, there are two areas of major controversy in the management of aortic stenosis including: (1) the asymptomatic patient with a severe aortic stenosis; and (2) the patient with low ejection fraction with a reduced gradient aortic stenosis [17, 18]. There is low (1–2 %) risk of sudden death or rapid progression to symptoms in the asymptomatic patient with a severe aortic stenosis. Adverse clinical outcomes are more likely in the asymptomatic patient with severe aortic stenosis who demonstrates more rapid progression of hemodynamic parameters, such as: (1) an increase in aortic jet velocity greater than 0.3 m/s/year; or (2) a decreasing aortic valve area greater than 0.1 cm^2/year. Therefore, other than in a small selected group of patients, the risk of surgery may still exceed any potential benefits in this group of patients, i.e., those with a severe aortic stenosis with normal ventricular function who are truly asymptomatic. On the other hand, patients with low ejection fractions and reduced gradient aortic stenosis may present an even more challenging problem. These complexities partly lie in the difficulty to distinguish this entity from those patients with reduced ejection fractions and only mild-to-moderate aortic stenosis; this latter group will not benefit from aortic valve replacement. It should be noted that patients with severe aortic stenosis who present with reduced ejection fractions and reduced gradients will ultimately face increased operative mortality. The use of dobutamine stress echocardiography to measure the pressure gradients and the effective valve areas, both during baseline and at stress, can help determine the true severity of aortic stenosis [40]. It should be noted that, in general, patients with reduced ejection fractions with low transvalvar gradients who elicit no response to stress such as inotropes have poorer outcomes, even with surgery.

34.3.1.2 Aortic Sclerosis

Aortic sclerosis is a common finding in older patients, and is present in approximately 25 % of patients older than 65 years [16, 17]. The classic findings of aortic sclerosis include focal areas of valve thickening with otherwise relatively normal leaflet mobility. It is important to note that, by definition, valvular hemodynamics in these patients are within normal limits. In other words, other than the presence of a systolic murmur, these individuals elicit no clinical signs or associated symptoms. Histologic findings in aortic sclerosis include focal subendocardial plaque-like lesions with accumulations of lipoproteins. The similarity of these findings to atherosclerosis suggests that both are, in some way, an age-related process.

Despite the lack of valve-related symptoms with aortic sclerosis, it is generally associated with an increased risk of cardiovascular mortality. This may be related to the development of coronary artery disease and/or occasionally to a progression to severe aortic stenosis. Thus, while symptoms in the patient identified with aortic sclerosis may be initially benign, these individuals warrant close cardiovascular follow-ups.

34.3.1.3 Aortic Regurgitation

Aortic regurgitation results from a structural defect in the aortic valve that allows for blood flow to reverse direction across the valve during diastole (i.e., re-enter the ventricle). The etiologies of aortic regurgitation are best discussed if one subdivides this disease into acute or chronic regurgitation (Table 34.6). The majority of such lesions result in chronic aortic regurgitation, with insidious dilatation of the left ventricle. In contrast, lesions responsible for acute aortic regurgitation may result in sudden catastrophic elevation of

Table 34.6 Etiologies of aortic regurgitation (subdivided by presentation time)

Acute	Chronic
Infective endocarditis	Idiopathic aortic root dilatation
Aortic dissection	Congenital bicuspid valves
Trauma	Calcific degeneration
	Rheumatic disease
	Infective endocarditis
	Systemic hypertension
	Myxomatous proliferation
	Ascending aortic dissection
	Marfan syndrome
	Syphilitic aortitis
	Rheumatoid arthritis
	Osteogenesis imperfecta
	Giant cell aortitis
	Ehlers-Danlos syndrome
	Reiter's syndrome
	Discrete subaortic stenosis
	Ventricular septal defects with aortic cusp prolapse

left ventricular filling pressures, reduction in cardiac outputs, and/or sudden death.

Chronic Aortic Regurgitation

Valve damage that results in progressively larger retrograde flows across the aortic valve produces the condition of *chronic aortic regurgitation*. The patient's left ventricle responds to the volume load of aortic regurgitation with several compensatory mechanisms such as an increase in end-diastolic volumes and a combination of eccentric and concentric hypertrophy [41]. The increased diastolic volume allows the ventricle to eject a larger total stroke volume, thereby initially maintaining stroke volume within a relative normal range. As a result, the majority of such patients remain asymptomatic for prolonged periods of compensation, during which time they maintain forward stroke volume within the normal ranges. Yet, after a while, the compensatory mechanisms become inadequate, and further increases in afterload result in reduced ejection fractions. Once the left ventricle can no longer compensate, patients typically present with symptoms of: (1) dyspnea and exertional angina, reflecting declining systolic function; (2) elevated filling pressures; and/or (3) diminished coronary flow reserves of the hypertrophied myocardium [42]. Several natural history studies have identified age and left ventricular end-systolic pressures (or volumes) as predictive factors associated with higher risks of mortality in these clinical populations (Table 34.7) [7].

Importantly, although the progression of asymptomatic aortic regurgitation is slow, approximately one-fourth of patients will develop systolic dysfunction, or even die, before the onset of warning symptoms [7]. Therefore, quantitative evaluation of left ventricular function with echocardiography is necessary, as a serial history and physical exam alone are considered as insufficient, in general.

The clinical diagnosis of chronic severe aortic regurgitation by a trained physician can be made on: (1) the presence of a diastolic murmur (the third heart sound) and/or a rumble (Austin–Flint sign) on auscultation; and (2) the detection of a displaced left ventricular impulse and wide pulse pressure [43, 44]. Similar to aortic stenosis, the chest X-ray and ECG will typically reflect left ventricular enlargement/hypertrophy and may also elicit evidence of conduction disorders. Echocardiography is then indicated to: (1) confirm the diagnosis of aortic regurgitation; (2) assess valve morphology; (3) estimate the severity of regurgitation; (4) assess aortic root size; and (5) determine left ventricular dimensions, relative mass, and systolic function. If the patient has severe aortic regurgitation and is sedentary, or has equivocal symptoms, exercise testing is helpful to assess the following: functional capacity, symptomatic responses, and/or the hemodynamic effects of exercise.

In patients who are symptomatic on initial evaluation, cardiac catheterization and angiography is considered indicated for the subsequent evaluation of coronary artery disease for the possible need of revascularization therapy, i.e., if the echocardiogram is of insufficient quality to assess left ventricular function and the severity of aortic regurgitation. The ultimate aim of any serial evaluation of the asymptomatic patient with chronic aortic regurgitation is to detect the onset of symptoms and objectively assess changes in left ventricular size and function that may occur in the absence of physical symptoms (Fig. 34.3). Medical therapy for aortic regurgitation is primarily based on the use of vasodilating agents which are believed to improve forward stroke volumes and reduce regurgitant volumes; note, the use of such agents can often result in regression of both left ventricular dilatation and hypertrophy.

Initial left ventricular systolic dysfunction in chronic aortic regurgitation has been commonly associated with an increased afterload pressure, and is considered to be reversible following aortic valve replacement, i.e., with nearly full recovery of left ventricular size and function [7]. However, if depressed myocardial contractility (rather than volume overload) is responsible for the systolic dysfunction as the ventricle becomes more hypertrophic and dilatation progresses, the chamber becomes more spherical geometry. At this stage, neither return of normal left ventricular function nor improved long-term survival has been documented even after aortic valve replacement [7]. For patients with chronic aortic regurgitation, left ventricular systolic function and end-systolic size have been identified as the most important determinants of postoperative survival and/or normalization of left ventricular function following aortic valve replacement [7].

Medical therapy using vasodilating agents is generally indicated for chronic therapy in patients with severe aortic regurgitation who have symptoms of left ventricular dysfunction and for whom surgery is not recommended, i.e., because of either cardiac or noncardiac factors. The benefits of vasodilating agents are based on their potential ability to improve stroke volume and reduce regurgitant volume [45].

Table 34.7 Natural history of aortic regurgitation

Asymptomatic patients with normal left ventricular systolic function	• Progression to symptoms and/or left ventricular dysfunction	<6 %/year
	• Progression to asymptomatic left ventricular dysfunction	<3.5 %/year
	• Sudden death	<0.2 %/year
Asymptomatic patients with left ventricular systolic dysfunction	• Progression to cardiac symptoms	>25 %/year
Symptomatic patients	• Mortality rate	
	– with angina	>10 %/year
	– with heart failure	>20 %/year

In general, the acute administration of vasodilating agents such as sodium nitroprusside, hydralazine, and nifedipine reduces peripheral vascular resistance and results in immediate augmentation in forward cardiac outputs and decreases in regurgitant volumes. The ACC/AHA recommends three guidelines for the use of vasodilating agents in the patient with severe aortic regurgitation: (1) the long-term treatment of patients with severe aortic regurgitation who have symptoms and/or left ventricular dysfunction who are considered poor candidates for surgery; (2) improvements in the hemodynamic profile of patients with severe heart failure symptoms and severe left ventricular dysfunctions with short-term vasodilator therapy, before proceeding with aortic valve replacement; and (3) prolonged use during the compensated phase of asymptomatic patients who have volume overloads, but have normal systolic functions.

Acute Aortic Regurgitation

When damage to the aortic valve is acute and severe, subsequent and sudden large regurgitant volumes return into the left ventricle, and this will decrease the functional forward stroke volumes dramatically. In contrast to chronic aortic regurgitation, in such acute cases, there has been no time for compensatory ventricular hypertrophy and/or dilatations to develop. As a result, the considered typical exam findings of ventricular enlargement and diastolic murmur associated with chronic aortic regurgitation are absent. Instead, the patient with acute aortic regurgitation presents with pronounced tachycardia, pulmonary edema, and/or potentially life-threatening cardiogenic shock.

Echocardiography, which is considered crucial for the initial workup of the acute aortic regurgitation patient, will likely demonstrate a rapid equilibration of aortic and left ventricular diastolic pressures, and may provide some insights as to the etiologies of aortic regurgitations. Echocardiography also allows for a rapid assessment of the associated valve apparatus, the aorta, and/or the relative degree of pulmonary hypertension (if tricuspid regurgitation is present). Transesophageal echocardiography is indicated when aortic dissection is suspected [46, 47] (Chap. 22). Importantly, acute aortic regurgitation resulting from aortic dissection is a known surgical emergency requiring prompt identification and management. Cardiac catheterization, aortography, and coronary angiography are considered as important components of such an evaluation of aortic dissection with acute aortic regurgitation, and thus should be performed if these procedures do not unduly delay urgent surgery. Additionally, following trauma, computed tomographic imaging can be quite useful in obtaining the appropriate clinical status and underlying diagnoses.

Nevertheless, appropriate treatment of acute aortic regurgitation is dependent on the etiology and severity of the disease. For example, only antibiotic treatment may be required in a hemodynamically stable patient with mild acute aortic regurgitation, i.e., resulting from infective endocarditis. Conversely, severe acute aortic regurgitation is a surgical emergency, particularly if hypotension, pulmonary edema, and/or evidence of low cardiac outputs are present. In such cases, temporary preoperative management may include the use of agents such as nitroprusside (to reduce afterload) and inotropic agents such as dopamine or dobutamine (to augment forward flow and reduce left ventricular end-diastolic pressure). Note that intraaortic balloon counterpulsation is contraindicated in such patients, and beta-blockers should be used cautiously because of their potential to further reduce outputs by blocking the compensatory tachycardia. Typically, mortalities associated with acute aortic regurgitation are usually the result of pulmonary edema, ventricular arrhythmias, electromechanical dissociation, and/or circulatory collapse.

In general, aortic valve replacement is the treatment of choice in aortic regurgitation. In such cases of aortic disease, additional aneurysm repair (Fig. 34.5) or aortic root replacement (Figs. 34.6 and 34.7) needs to be considered. Aortic root replacement with a homograft or autograft should be offered to patients in whom anticoagulation is contraindicated (e.g., elderly with risk, women of child bearing years), as the tissue valve grafts do not require anticoagulation. In addition, patients with disease resulting from endocarditis also benefit, as a homograft appears to have more resistance to subsequent infection. Finally, although the use of mechanical valves is effective, the prosthesis may impose a clinically relevant degree of stenosis in certain patients due to unavoidable size mismatch. Naturally, homografts and autografts are superior as they can be tailored to provide a larger outflow tract. Nevertheless, in certain situations, repair of the aorta may involve the use of an artificial conduit using materials such as Dacron.

Careful post-aortic valve replacement follow-ups are necessary during both the early and long-term postoperative courses, to evaluate both prosthetic valve and left ventricular function. An accepted excellent predictor of long-term success of aortic valve replacement is the reduction in left ventricular end-diastolic volume, typically occurring within the first 14 days after the operation. It should be emphasized that, in most patients, as much as 80 % of the overall reduction in end-diastolic volume that will occur will happen within this time period. In addition, the degree of regression in left ventricular dilatation typically correlates well with the magnitude of functional increases in ejection fraction [44]. Nevertheless, long-term follow-ups should include an exam at 6 months post-aortic valve replacement, and then yearly examinations are recommended if the patient's clinical course is uncomplicated. Note that serial postoperative echocardiograms after the initial early postoperative study are usually not indicated. However, repeat echocardiography is warranted at any point when there is evidence of: (1) a new murmur; (2) questions of prosthetic valve integrity; and/or (3) concerns about adequate left ventricular function.

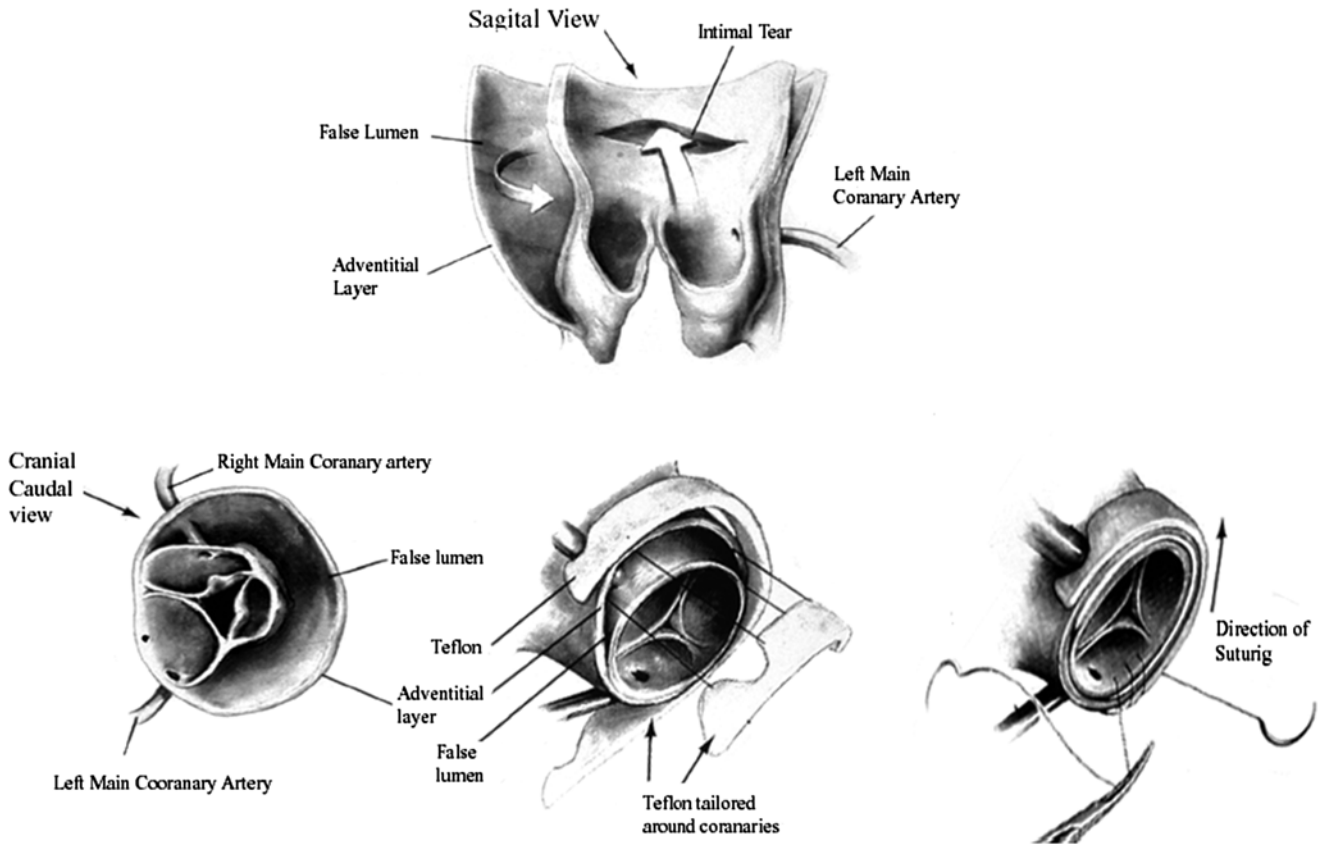

Fig. 34.5 Aortic aneurysm repair using a Teflon felt reinforcement technique preserving the aortic valve and coronary arteries. 81Operative Techniques in Cardiac and Thoracic Surgery: A Comparative Atlas by W.B. Saunders, Co. Reproduced with permission of W.B. Saunders, Co., in the format book via Copyright Clearance Center

Aortic Valve Disease Associated with Disease of the Ascending Aorta

Dilatation of the ascending aorta is a common cause of aortic regurgitation. It is well recognized that patients with bicuspid aortic valves will typically also have disorders of the vascular connective tissue system, which can result in dilatation of the ascending aorta and/or aortic root even in the absence of hemodynamically significant valvular disease. The dilatation of the aorta can be progressive over time, with an increased risk for aortic dissection. Currently, echocardiography is the primary diagnostic modality used for these patients. However, a more detailed anatomic study can be obtained with either computerized tomography or cardiac magnetic resonance imaging (Chap. 24).

Regardless of the etiology of the dilated ascending aorta, the recommended indications for operative intervention include an aortic diameter >5.5 cm or growth of the aorta >0.5 cm/year. In patients with bicuspid aortic valves undergoing aortic valve replacement, repair of the aortic root or replacement of the ascending aorta is commonly indicated if the diameter of the aorta is >4.5 cm [8]. Note that aortic valve-sparing operations are feasible in many patients with dilatation of the aorta who do not elicit significant aortic regurgitation or aortic valve calcification. The techniques for aortic valve-sparing surgery have been pioneered by Yacoub and David [48, 49]. In early stages of this disease, the use of beta-adrenergic blocking agents may slow the progression of aortic dilatations.

34.3.2 Diseases of the Mitral Valve

Diseases of the mitral valve can be subdivided in a similar fashion as those affecting the aortic valve—stenosis and regurgitation. The general anatomy of the mitral valve consists of a pair of leaflets attached to the left ventricle by chordae tendinae. Normal mitral valve area ranges between 4.0 and 5.0 cm^2. However, in the case of mitral stenosis, symptoms do not typically develop until the functional valve area is reduced to <2.5 cm^2 [50]. For more details on valve anatomy, the reader is referred to Chaps. 4, 5, 7 and the Atlas of Human Cardiac Anatomy (www.vhlab.umn.edu/atlas).

34.3.2.1 Mitral Stenosis

Stenosis of the mitral valve orifice typically produces a funnel-shaped mitral apparatus described to resemble a “fish mouth” which then hinders normal diastolic filling of the left ventricle. In the past, roughly 60 % of all patients with mitral

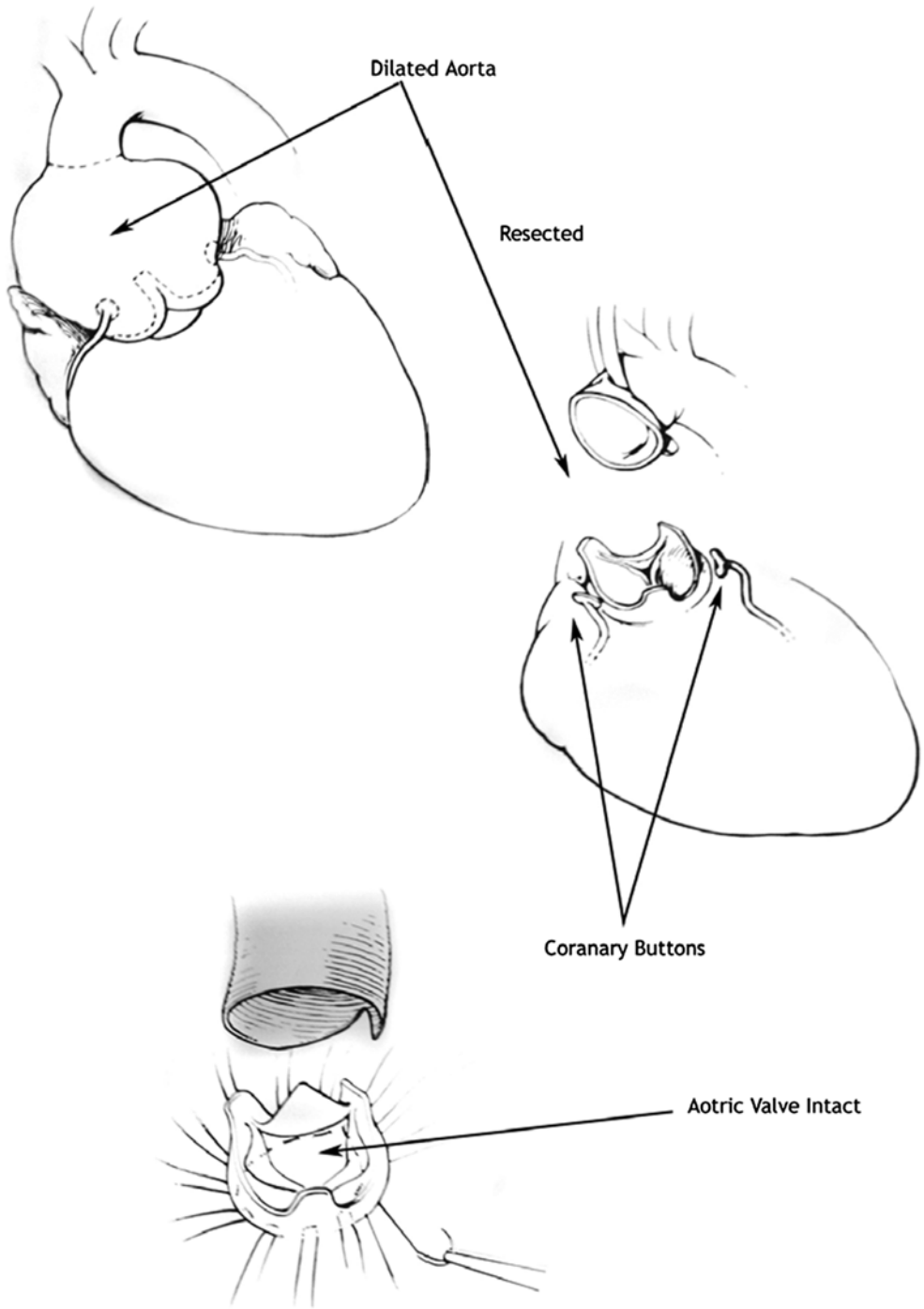

Fig. 34.6 David procedure for aortic root replacement. The dilated aorta is resected, sparing the aortic valve and coronary buttons. The repair is then completed with insertion of a graft with reimplantation of the coronary arteries. Adapted from Smedira NG (2003) Mitral valve replacement with a calcified annulus. In: Cox JL, Sundt TM III (eds) Operative techniques in cardiac and thoracic surgery. Saunders, Philadelphia, pp 2–13

stenosis presented with a history of rheumatic fever [51, 52]. Typical pathological processes observed in such patients include: (1) leaflet thickening and calcification; (2) commissural and chordal fusion; or (3) a combination of these processes [53, 54]. Yet, congenital malformations of the mitral valve, though rare, are usually responsible for mitral stenosis observed in infants and children [54] (see Chap. 10). Currently, women (2:1) account for the overall majority of mitral stenosis cases [51, 52, 55]. Other entities can also simulate the clinical features of rheumatic mitral stenosis, such as left atrial myxoma, infective endocarditis, or mitral annulus calcification in the elderly.

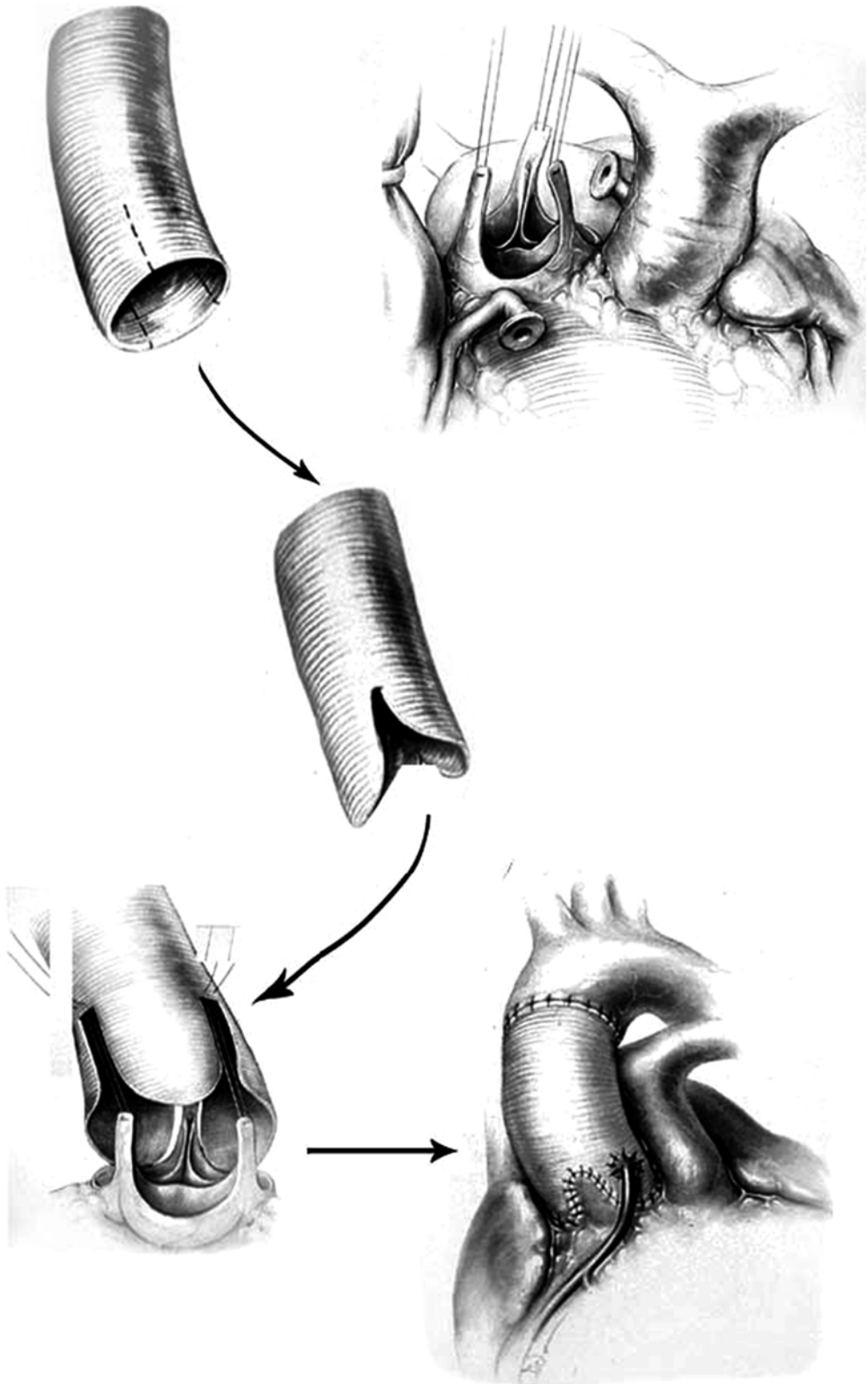

Fig. 34.7 Aortic root replacement using Dacron graft as the technique used for correct sizing, for suturing in place to yield the final graft implantation along with coronary re-implantation. Adapted from Yacoub M. Valve-conserving operation for aortic root aneurysm or dissection. In: Operative techniques in cardiac and thoracic surgery, pp 57–67

Mitral stenosis is normally a slowly progressive process with a typical mean age of presentation of symptoms in the fifth to sixth decade of life [56, 57], i.e., with narrowing of the valve to <2.5 cm^2 before the development of symptoms. As the severity of stenosis increases, cardiac output becomes reduced even at rest and will fail to be increased with exercise. The relative degree of pulmonary vascular resistance also influences the development of symptoms. The diagnosis of mitral stenosis may be made solely on the presence of abnormal physical exam findings, or may be suggested by symptoms of fatigue, dyspnea, frank pulmonary edema, atrial fibrillation, and/or embolus [52]. In the asymptomatic patient survival is 80 % at 10 years, with 60 % of these patients eliciting no progression of symptoms [7]. However, once symptoms related to pulmonary hypertension develop, to date, there remains a dismal 10-year survival rate of 0–15 % [7]. Common causes of death in these untreated patients with mitral stenosis are due to: (1) progressive heart failure (60–70 %); (2) systemic embolism (20–30 %); (3) pulmonary embolism (10 %); or (4) infection (1–5 %) [54, 55].

It should be noted that shortness of breath (dyspnea) precipitated by exercise, emotional stress, infection, pregnancy, or atrial fibrillation are typically the first symptoms which present in patients with underlying mild mitral stenosis [58]. Yet, as the obstructions across the mitral valve increase, there will typically be progressive symptoms of dyspnea, as the left atrial and pulmonary venous pressures increase [59]. Increased pulmonary artery pressures and distension of the pulmonary capillaries can lead to pulmonary edema, which occurs as pulmonary venous pressure exceeds that of plasma oncotic pressure. Subsequently, the pulmonary arterioles will elicit vasoconstriction, intimal hyperplasia, and medial hypertrophy, which then further exacerbate pulmonary arterial hypertension.

Commonly, the diagnosis of mitral stenosis can be made based on a given patient's history, physical examination, chest X-ray, and ECG. Nevertheless, at the initial examination, a patient may be asymptomatic although abnormal physical findings, including a diastolic murmur, may be present [56, 57]. In such patients, diagnostic imaging is recommended and currently the tool of choice is 2D and Doppler transthoracic echocardiography. Transesophageal echocardiography or cardiac catheterization is not required unless questions concerning diagnoses remain [7]. Yet, heart catheterization may be indicated to: (1) assess the potential for either coronary artery or aortic valve disease; (2) assess pulmonary artery pressures; (3) perform balloon valvotomy; and/or (4) evaluate the situations when the clinical status of a symptomatic patient is not consistent with the echocardiography findings.

Typically, echocardiography is capable of providing an appropriate assessment of: (1) the morphological appearance of the mitral valve apparatus; (2) ventricular chamber size/function; (3) the mean transmitral gradient [60, 61]; (4) the relative functional mitral valve area; and (5) the relative pulmonary artery pressures [62]. In addition, if deemed necessary, noninvasive dobutamine or exercise stress testing can be completed with either the patient supine (using a bicycle) or upright (on a treadmill) to assess changes in heart rate and blood pressure in response to their overall exercise tolerance. Patients who are symptomatic with a significant elevation of pulmonary artery pressure (>60 mmHg), mean transmitral gradient (>15 mmHg), or pulmonary artery wedge pressure (>25 mmHg) on exertion have, by definition, hemodynamically significant mitral stenosis that may require further intervention [7].

In mitral stenosis, medical treatment is typically indicated for the prevention of emboli (10–20 %), which is primarily associated with the onset of atrial fibrillation [51, 52, 63–65]. Atrial fibrillation ultimately develops in 30–40 % of patients with symptomatic mitral stenosis and, importantly, ~65 % of all embolic events occur within the first year after the onset of atrial fibrillation [51, 52]. The etiology behind atrial fibrillation is thought to be a disruption of the normal conduction pathways caused by structural changes in the myocardium resulting from a pressure/volume overloaded atrium; in fewer cases, it may also result from rheumatic fibrosis of the atrium [57]. The development of atrial fibrillation associated with mitral stenosis occurs more commonly in older patients and has been associated with a decreased 10-year survival rate (25 % versus 46 %) [52, 55]. In addition to the thromboembolic potential, acute onset of atrial fibrillation can herald sudden deterioration in patients with mitral stenosis. This is considered as secondary to an acute reduction in left ventricular ejection fractions and elevated pulmonary artery pressures, which will result from loss of the atrial contribution to left ventricular filling. The urgent treatment for an acute episode of atrial fibrillation with a rapid rate typically consists of: (1) anticoagulation with heparin; (2) heart rate control (digoxin, calcium channel blockers, beta-blockers, or amiodarone); and/or (3) electrical cardioversion. It should be noted that in patients with atrial fibrillation for more than 24–48 h without anticoagulation, cardioversion is then associated with an increased risk of embolism. Today, in chronic or recurrent atrial fibrillation that is resistant to prevention or cardioversion, heart rate control (digoxin, calcium channel blockers, beta-blockers, or amiodarone), and long-term anticoagulation are considered as the mainstay of therapy [65, 66]. Yet, use of anticoagulation for patients with mitral stenosis who have not had atrial fibrillation or embolic events is not indicated due to the risk of bleeding complications. For more details on this topic, the reader is referred to Chaps. 30 and 31.

The principle for treating symptomatic mitral stenosis rests on alleviation of the fixed left ventricular inflow obstruction, thereby reducing the transvalvular gradient. Methods of disrupting the fused valve apparatus (open or

closed mitral commissurotomy, or percutaneous mitral balloon valvotomy) or mitral valve replacement have both demonstrated significant post-procedural improvement in both symptoms and survival rates. The timing of intervention is commonly related to the identified severity of disease, while the method of intervention is chosen based on: (1) morphology of the mitral valve apparatus; (2) presence of other comorbid diseases; and/or (3) expertise at each specific clinical center. Significant calcification, fibrosis, and subvalvular fusion of the valve apparatus can make either commissurotomy or percutaneous balloon valvotomy less likely to be successful. It should also be noted that the presence of mitral regurgitation is a contraindication for valvotomy/commisurotomy, and it is considered best to treat such patients with a mitral valve replacement.

Closed commissurotomy is a surgical technique that uses finger fracture of the calcified valve (Fig. 34.8). This procedure has the advantage of not requiring cardiopulmonary bypass, however the operator is not afforded direct visual examination of the valve apparatus. In contrast, open commissurotomy, which commonly employs cardiopulmonary bypass, has gained favor in the United States because it allows inspection of the mitral valve apparatus under direct vision. During such a procedure, division of the commissures, splitting of fused chordae tendinae/ papillary muscles, debridement of calcium deposits [7], and/or mitral valve replacement can be completed to attain optimal functional results. The 5-year reoperation rate following open commissurotomy has been reported to be between 4 % and 7 %, and the 5-year complication-free survival rate ranges from 80 to 90 %.

More recently, both these operative techniques have given way to percutaneous balloon valvotomy. This is now the initial procedure of choice for the symptomatic patient with moderate-to-severe mitral stenosis, or those patients with favorable valve morphologies and non-significant mitral regurgitation and/or left atrial thrombus (Fig. 34.9). Immediate reduction in the transvalvular gradient (by at least 50–60 %) has been associated with gradual regression of pulmonary hypertension over several months [8]. If selected appropriately, 80–95 % of patients undergoing this procedure will achieve a functional mitral valve area >1.5 cm^2 and a resultant decrease in left atrial pressures without complications. Yet, potential acute complications include: subsequent mitral regurgitation (10 %), an induced atrial septal defect (5 %), left ventricle perforation (0.5–4.0 %), emboli formation (0.5–3 %), myocardial infarction (0.3–0.5 %), and/or increased mortality (<1 %) [67]. Currently, echocardiographic assessments of mitral valve morphology are the most important predictor of outcomes for percutaneous balloon valvotomy. Patients with valvular calcification, thickened fibrotic leaflets with decreased mobility, and/or subvalvular fusion have higher incidence of acute complications following balloon valvotomy and higher rates of recurrent stenosis on follow-up. Presence of left atrial thrombus, detected by transesophageal echocardiography, is a relative contraindication and, at a minimum, warrants 3 months of oral warfarin anticoagulation in an attempt to resolve the thrombus prior to any planned procedure. A post-procedure echocardiogram, typically within 72 h after the procedure, is useful to assess postoperative hemodynamics, as well as to exclude significant complications such as mitral regurgitation, left ventricular dysfunction, and/or an atrial septal defect. However, recurrent symptoms have been reported to occur in as many as 60 % of patients 9 years post-procedure [62, 68, 69]; it should be noted that recurrent stenoses account for such symptoms in <20 % of such patients [68]. In patients with an adequate initial result, progressive mitral regurgitation and development of other valvular or coronary problems are more frequently responsible for the subsequent presentation of symptoms [68]. Thus, in the patient presenting with symptoms late after commissurotomy, a comprehensive evaluation is required to look for other causes.

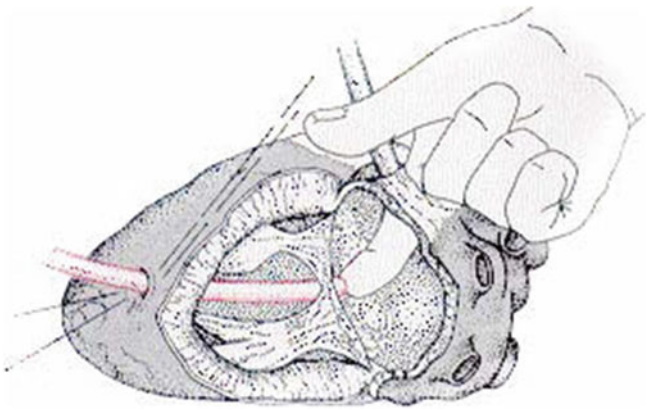

Fig. 34.8 Treatment of mitral stenosis using the finger fracture closed mitral commissurotomy technique. Adapted from Zipes DP (ed) (1992) Braunwald's heart disease: a textbook of cardiovascular medicine. W.B. Saunders Co., Philadelphia, p 1016

Mitral valve replacement is an accepted surgical procedure for patients with severe mitral stenosis who are not candidates for surgical commissurotomy or percutaneous mitral valvotomy (Table 34.8, Figs. 34.10 and 34.11). In addition, patients with recurrent severe symptoms, severe deformities of their mitral apparatus, severe mitral regurgitation, or a large atrial septal defect should be offered mitral valve replacement. The risks associated with mitral valve replacement are also highly dependent on patient age, left ventricular functional status, low cardiac outputs, presence of comorbid medical problems, and/or concomitant coronary artery disease. More specifically, morbidity and mortality associated with mitral valve replacements are directly correlated with age, with risks in a young healthy person of <5 %, increasing to as high as 10–20 % in the older patient with concomitant medical problems or pulmonary hypertension.

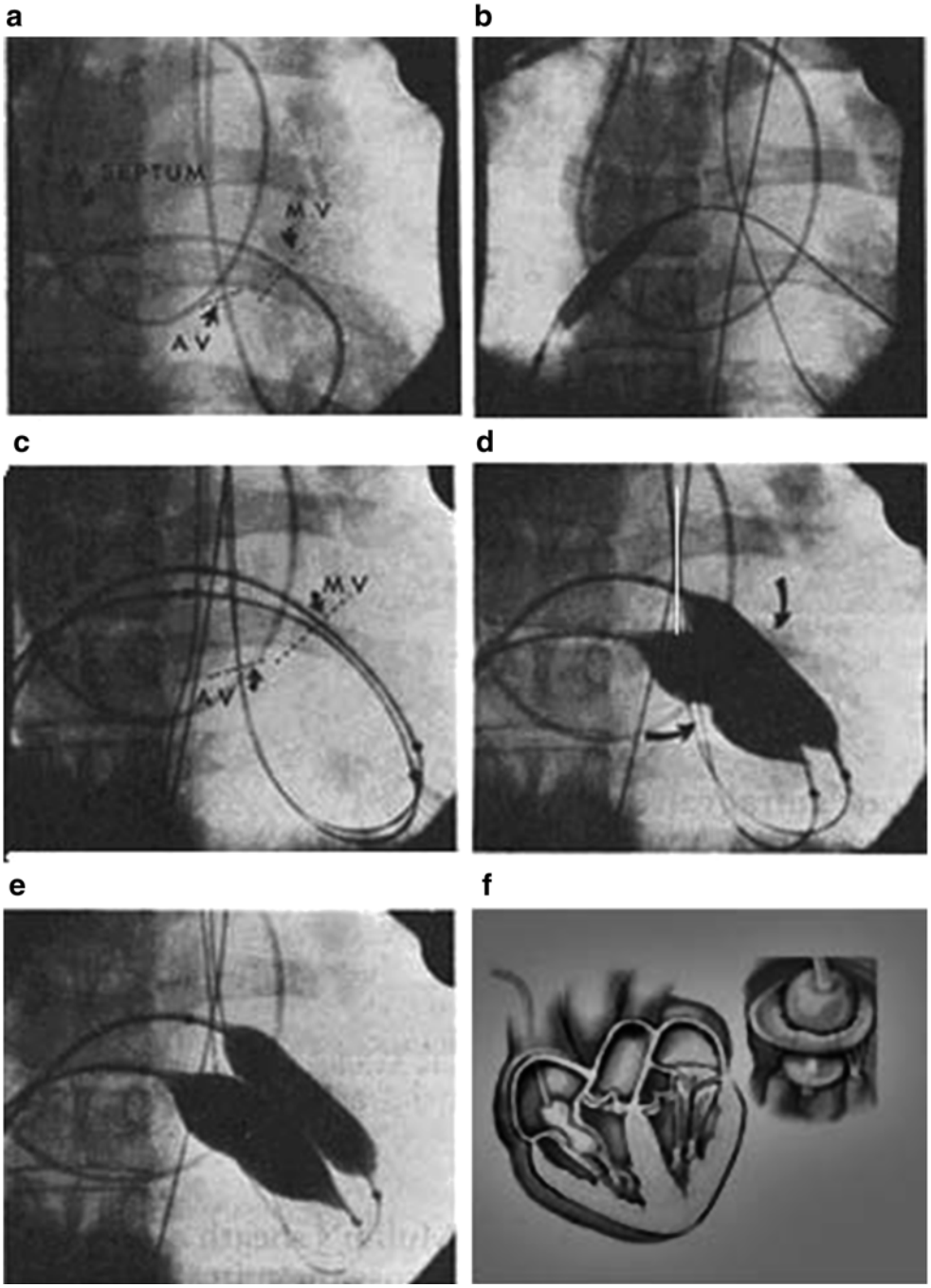

Fig. 34.9 Treatment of mitral stenosis using balloon valvotomy. Sequence of percutaneous mitral valvotomy: (**a**) floating balloon catheter in position across the atrial septum through the mitral and aortic valves. The tip is in the ascending aorta; (**b**) an 8 mm dilating balloon catheter enlarging the atrial septal puncture site; (**c**) two 20 mm dilating balloon catheters advanced into position across the stenotic mitral valve over two separate 0.038 in transfer guide wires; (**d**) partially inflated dilating balloon catheters across the mitral valve; note the "waist" produced by the stenotic valve (*arrows*); (**e**) fully inflated dilating balloon catheters in position across the mitral valve; (**f**) illustration of balloon commissurotomy technique. Adapted from www.rjmatthews.com and Zipes DP (ed) (2003) Braunwald's heart disease: a textbook of cardiovascular medicine. Saunders, Philadelphia

Table 34.8 Mitral valve replacement for mitral stenosis [8]

- Moderate to severe mitral stenosis (mitral valve area <1.5 cm^2):
  - With NYHA functional Class III–IV symptoms.
  - Who are not considered candidates for percutaneous balloon valvotomy or mitral valve repair.
- Patients with severe mitral stenosis (mitral valve area <1 cm^2):
  - With severe pulmonary hypertension (pulmonary artery systolic pressure >60-80 mmHg).
  - With NYHA functional Class I–II symptoms who are not considered candidates for percutaneous balloon valvotomy or mitral valve repair.

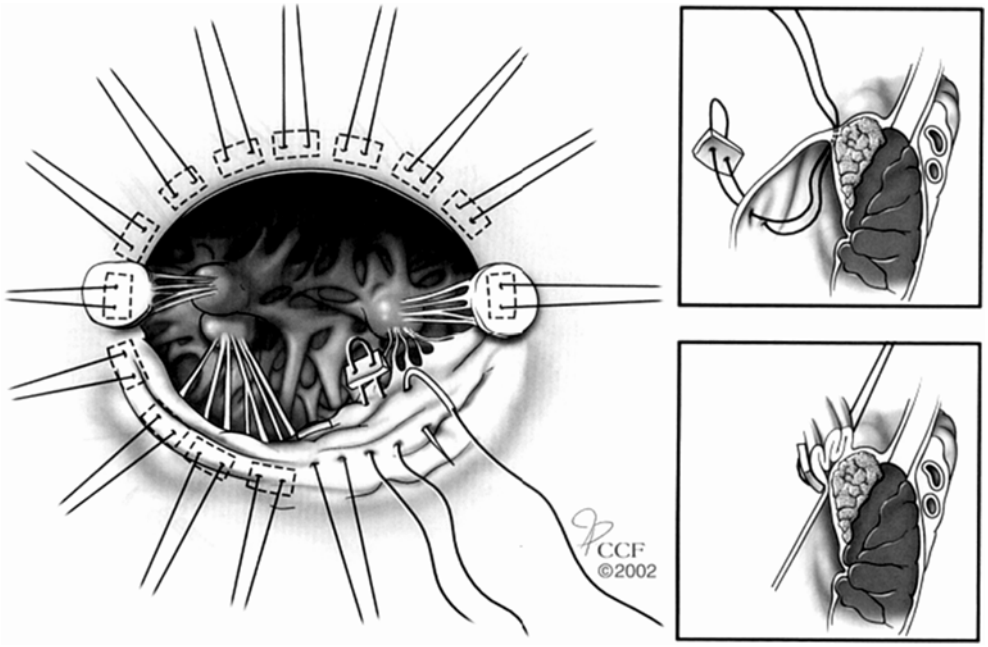

Fig. 34.10 Placement of circumferential sutures and plication of the anterior leaflet of the mitral valve. Adapted from Smedira NG (2003) Mitral valve replacement with a calcified annulus. In: Cox JL (ed) Operative techniques in thoracic and cardiovascular surgery. Saunders, Philadelphia, pp 2–13

Mitral valve replacement can be further complicated by the: (1) potential for embolic events; (2) need for (and risk of) long-term anticoagulation therapy; and/or (3) potential for valve thrombosis, dehiscence, infection, or malfunction.

34.3.2.2 Mitral Regurgitation

The common etiologies for mitral regurgitation include: (1) mitral valve prolapse secondary to myxomatou degeneration; (2) rheumatic heart disease; (3) coronary artery disease; (4) infective endocarditis; or (5) collagen vascular disease. As with aortic regurgitation, mitral regurgitation can be categorized as both acute and chronic presentations. In some cases, mitral regurgitation due to ruptured chordae tendinae or infective endocarditis may present as both acute and severe. Alternatively, mitral regurgitation may worsen gradually over a prolonged period of time. Yet, these very different presentations of mitral regurgitation are both treated with surgical intervention as dictated by the character of the symptoms presented.

Acute Severe Mitral Regurgitation

In acute severe mitral regurgitation, a sudden volume overload is imposed on the left atrium and the left ventricle is without time for typical compensatory hypertrophy. Thus, sudden drops in forward stroke volume and cardiac output occur (cardiogenic shock) in such a patient, with simultaneous pulmonary congestion. In severe mitral regurgitation, the hemodynamic overload often cannot be tolerated, and mitral valve repair or replacement must be performed urgently.

The acute nature of this form of mitral regurgitation results in patients who almost always present with symptoms upon physical exams; they are typically positive for a holosystolic murmur and a third heart sound (see Chap. 18). Transthoracic echocardiography is commonly used to confirm the diagnosis and also to assess the general degree of disruptions within the mitral valve apparatus. Furthermore, the use of transesophageal echocardiography is warranted if mitral valve morphology and regurgitation are still not clearly elucidated following transthoracic echocardiography. Note that it is the high level

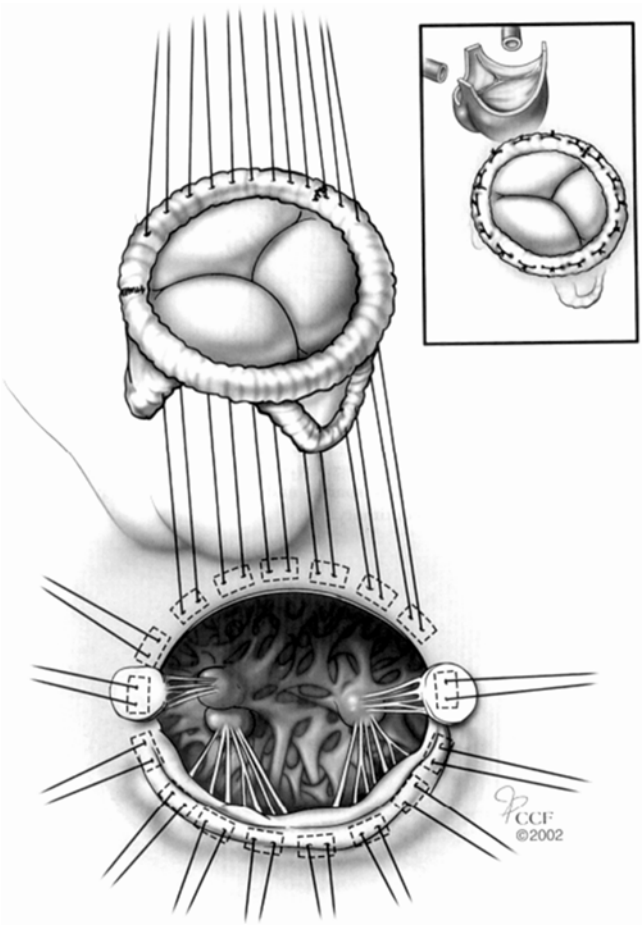

Fig. 34.11 Mitral valve positioning into the mitral oriface. Adapted from Smedira NG (2003) Mitral valve replacement with a calcified annulus. In: Cox JL (ed) Operative techniques in thoracic and cardiovascular surgery. Saunders, Philadelphia, pp 2–13

of details provided by transesophageal echocardiography that is also helpful in demonstrating the anatomic causes of mitral regurgitation and, subsequently, directing successful surgical repairs (see Chap. 22). Coronary arteriography is necessary before surgery in all such patients >40 years of age, unless hemodynamic stability is of concern. If necessary, myocardial revascularization should be performed during mitral valve surgery in those patients with concomitant coronary artery disease [70, 71].

If the patient is not a candidate for surgery or if preoperative stabilization is required, medical therapy can help to diminish the relative amount of mitral regurgitation, thus increasing forward output and reducing pulmonary congestion, yet this therapy should be initiated promptly. However, in cases of acute severe mitral regurgitation, medical therapy has a limited role and is primarily used to stabilize patients prior to surgery. In normotensive patients, nitroprusside has been used to increase forward outputs, not only by preferentially increasing aortic flows, but also by partially restoring mitral valve competence as the left ventricular size diminishes [72, 73]. In hypotensive patients with severe reductions in forward output, aortic balloon counterpulsation can be employed to increase forward output and mean arterial pressure while, at the same time, diminishing mitral valve regurgitant volume and left ventricular filling pressure. If infective endocarditis is the cause of acute mitral regurgitation, identification and treatment of the infectious organism is important to optimize successful clinical outcomes.

Chronic Asymptomatic Mitral Regurgitation

As with chronic aortic regurgitation, time for hypertrophy and chamber dilatation is typically present in the patient presenting with chronic severe mitral regurgitation [33, 74]. These dilatations, or increases in left ventricular end-diastolic volume, are a compensatory mechanism which permits an increased total stroke volume and allows for restoration of forward cardiac outputs [75]. At the same time, increases in left ventricular and left atrial sizes accommodate the regurgitant volume with lower filling pressure; consequentially, symptoms of pulmonary congestion abate. Such patients with mild-to-moderate mitral regurgitation may remain without symptoms for several years with very little hemodynamic compromise. This compensated phase of mitral regurgitation is variable and in many cases can last several years. However, the prolonged burden of volume overloads may eventually result in left ventricular dysfunction. At this time, contractile dysfunction impairs myocardial ejection and end-systolic volume increases; there may also be further left ventricular dilatations and increased left ventricular filling pressures. Therefore, correction of mitral regurgitation is generally recommended shortly following the diagnosis of severe mitral regurgitation, irrespective of the presence or absence of symptoms.

The initial diagnosis of chronic mitral regurgitation is commonly accomplished by physical examination which may demonstrate findings of left ventricular apical impulse displacement, indicating that the mitral regurgitation is severe and chronic and has likely caused cardiac enlargement. Typically, ECG and chest X-ray can be useful to evaluate rhythm changes and heart size, respectively. Nevertheless, an initial echocardiogram, including Doppler interrogation of the mitral valve, is considered indispensable for the subsequent management of the patient with mitral regurgitation. Such an echocardiogram typically provides a baseline estimation of left ventricular and left atrial volumes, an estimation of the left ventricular ejection fraction, and an approximation of the severity of regurgitation. Note that any presence of pulmonary hypertension is worrisome because it likely indicates advanced disease with a worsened prognosis [76]. Serial clinical follow-ups are used to assess changes in symptomatic status, left ventricular function, and/or exercise tolerance. Annual echocardiography is also recommended once patients elicit a moderate mitral regurgitation.

Left ventricular end-systolic dimensions (or volumes) can typically aid in the planned timing for mitral valve surgery. For example, an end-systolic dimension, which may be less load-dependent than ejection fraction, should be <45 mm preoperatively to ensure normal postoperative left ventricular function [75, 77]. If patients become symptomatic, they should undergo mitral valve surgery even if left ventricular function is considered appropriately normal. Similar to acute mitral regurgitation, cardiac catheterization is considered indicated if: (1) there is discrepancy between clinical and noninvasive findings; (2) there is a need for preoperative coronary assessment for potential revascularization at the time of mitral valve replacement; and/or (3) an absence of chamber enlargement raises the question of the accuracy of the diagnosis, which should then be assessed with ventriculography at cardiac catheterization.

To date, there is no generally accepted therapy for asymptomatic patients with chronic mitral regurgitation. In such patients who develop symptoms, but have preserved left ventricular function, surgery is considered as the most appropriate therapy. Atrial fibrillation is commonly associated with mitral regurgitation, and preoperative atrial fibrillation can be an independent predictor of reduced long-term survival after mitral valve surgery for chronic mitral regurgitation [78]. Atrial fibrillation should be treated with heart rate control (digitalis, calcium channel blockers, beta-blockers, or amiodarone) and anticoagulation to avoid embolism [79, 80]. Common predictors for the persistence of atrial fibrillation after successful valve surgery include the presence of atrial fibrillation for >1 year and/or a left atrial size >50 mm [81]. Although patients who develop atrial fibrillation also usually manifest other symptomatic or functional changes that would warrant mitral valve repair or replacement, today many clinicians would also consider the onset of episodic or chronic atrial fibrillation to be an indication, in and of itself, for valvular surgery [82, 83].

To date, three categories of surgical procedures are now in vogue for correction of mitral regurgitation: (1) mitral valve repair; (2) mitral valve replacement with preservation of part or all of the mitral apparatus; and (3) mitral valve replacement with prior removal of the mitral apparatus. Each procedure has its advantages and disadvantages, as well as separate indications. Still today, with the appropriate valve morphology and sufficient surgical expertise, mitral valve repair is the operation of choice. Yet, valve repair may require longer extracorporeal circulation time and may also occasionally fail, then again requiring mitral valve replacement. Valve calcification, rheumatic involvement, and anterior leaflet involvement all decrease the likelihood of an adequate repair, whereas uncalcified posterior leaflet disease is almost always repairable. The primary advantage of repair is the avoidance of anticoagulation and/or a rare prosthetic valve failure. In addition, postoperative left ventricular function and survival are improved with preservation of the mitral apparatus, as the mitral apparatus is considered essential for maintenance of normal left ventricular chamber shape, volume, and function [7]. Similar advantages are gleaned with the use of mitral valve replacement with preservation of the mitral chordal apparatus, except that it adds both the risk of deterioration inherent in tissue valves and the need for anticoagulation with mechanical valves. It is generally considered today that mitral valve replacement, in which the mitral valve apparatus is excised, should be performed only in circumstances when the native valve and apparatus are so distorted by the preoperative pathology (rheumatic disease, for example) that the mitral apparatus cannot be spared.

In an asymptomatic patient with normal left ventricular function, repair of a severely regurgitant valve may be offered as a means to: (1) preserve left ventricular size and function; and/or (2) prevent the sequelae of chronic mitral regurgitation (Fig. 34.12). Similarly, this approach has proven successful in the hemodynamically stable patient with newly acquired severe mitral regurgitation as the result of a ruptured chordae or recent onset of atrial fibrillation. The timing of surgery in asymptomatic patients is indicated by the appearance of echocardiographic indicators of left ventricular dysfunction (i.e., left ventricular ejection fraction <60 % or left ventricular end-systolic dimension >45 mm). Mitral valve repair or replacement at this stage will likely prevent further deterioration in left ventricular function and thus improve overall survival [78]. Patients with symptoms of congestive heart failure, despite normal left ventricular function, as determined by echocardiography (ejection fraction >60 %, end-systolic dimension <45 mm), will likely require surgery. In both situations, mitral repair is preferred when possible. Mitral valve surgery is recommended for severe symptomatic mitral regurgitation with evidence of left ventricular systolic dysfunction; it is likely to both improve symptoms and prevent further deterioration of left ventricular function [84].

Ischemic mitral regurgitation is, by common definition, caused by left ventricular myocardial infarction, resulting in an associated papillary muscle dysfunction. The prognosis for such a patient with ischemic mitral regurgitation is substantially worse when compared with other etiologies [71, 85]. Following an acute infarction with the development of severe mitral regurgitation, hypotension and pulmonary edema often also occur. Hemodynamic stabilization, usually with insertion of an intraaortic balloon pump, is completed preoperatively followed by coronary revascularization; note that this only rarely improves mitral valve function. Unlike the case with nonischemic mitral regurgitation, it is more difficult to demonstrate a benefit of repair over replacement with ischemic mitral regurgitation. In general, operative mortality increases and survival is reduced in patients >75 years of age with coronary artery disease, especially if mitral valve

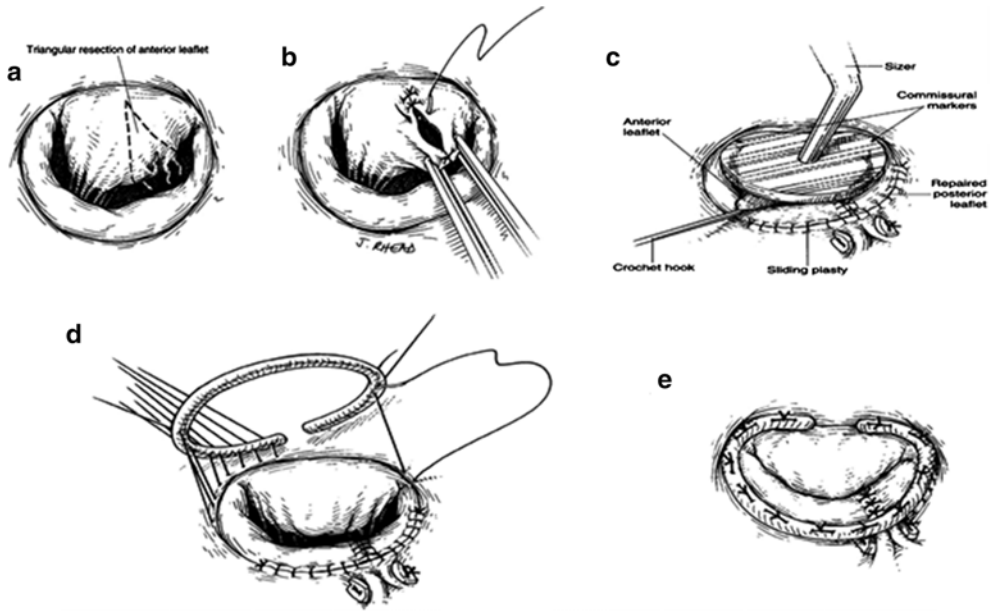

Fig. 34.12 Operative repair of the mitral valve using a technique developed by Carpentier. (**a**) Triangular resection of anterior leaflet; (**b**) Anterior leaflet repair; (**c**) Sizing of annulus; (**d**) Annuplasty ring suture technique; and (**e**) Completed repair. Adapted from Kirklin JW (2003) Cardiac surgery, 3rd edn. Churchill Livingstone, New York, pp 673–675

replacement must be performed [86]. In these patients, the goal of therapy is typically to improve the quality of life rather than prolong it, and medical therapy may be utilized to a greater extent to control cardiac symptoms.

34.3.3 Tricuspid Valve Disease

Tricuspid valve disease can be subclassified as regurgitation, stenosis, or a combination of both; it is most commonly the result of rheumatic fever, with rare cases attributed to infective endocarditis, congenital anomalies, carcinoid, Fabry's disease, Whipple's disease, or methysergide therapy [7]. Rheumatic tricuspid disease commonly presents as a combination of tricuspid stenosis and regurgitation. Furthermore, tricuspid disease commonly presents with concomitant mitral or aortic valve defects since acute rheumatic fever is also a common etiology for these disorders. It should be noted that right atrial myxomas or any type of large vegetations that produce an outflow tract obstruction will mimic tricuspid stenosis; however, regurgitation may also result, as it often causes associated damage to the leaflet apparatus. Pure tricuspid regurgitation may result from rheumatic fever, infective endocarditis, carcinoid syndrome, rheumatoid arthritis, radiation therapy, anorectic drugs, trauma, Marfan's syndrome, tricuspid valve prolapse, papillary muscle dysfunction, and/or congenital disorders [7]. In addition, pressure/volume overload conditions that do not cause direct damage to the leaflets themselves, such as those associated mitral stenosis and mitral regurgitation, typically cause ventricular enlargement, resultant tricuspid annular dilatation, and thus a sole tricuspid regurgitation [7].

The clinical features of tricuspid stenosis include auscultation of a tricuspid opening snap and a characteristic murmur. Auscultation may reveal a holosystolic murmur in the lower left parasternal region that may increase on inspiration (Carvallo's sign; see also Chap. 18). In rare instances, severe tricuspid regurgitation may produce systolic propulsion of the eyeballs, pulsatile varicose veins, or a venous systolic thrill and detectable murmur in the neck. Echocardiography is commonly used to: (1) assess tricuspid valve structure and function; (2) measure annular sizes; (3) evaluate right pressures; and (4) rule out other abnormalities influencing tricuspid valve function. Systolic pulmonary artery pressure estimations, combined with information about annular circumferences, further improve the accuracy of clinical assessments [7].

The etiology of tricuspid valve disease and the overall condition of the patient ultimately dictate the therapeutic approach. Tricuspid balloon valvotomy can be used to treat tricuspid stenosis, however one must be aware of the potential for subsequently inducing severe tricuspid regurgitation. It has been documented that a poor long-term outcome is associated with right ventricular dysfunction and/or systemic venous congestion associated with severe tricuspid regurgitation [7]. In the situation where pulmonary hypertension is the underlying cause of tricuspid annular dilatation, medical management alone may result in substantial improvement of the tricuspid regurgitation, and thus minimize the need for surgical intervention. Surgical options for treating tricuspid regurgitation include valve repair or valve replacement (Fig. 34.13).

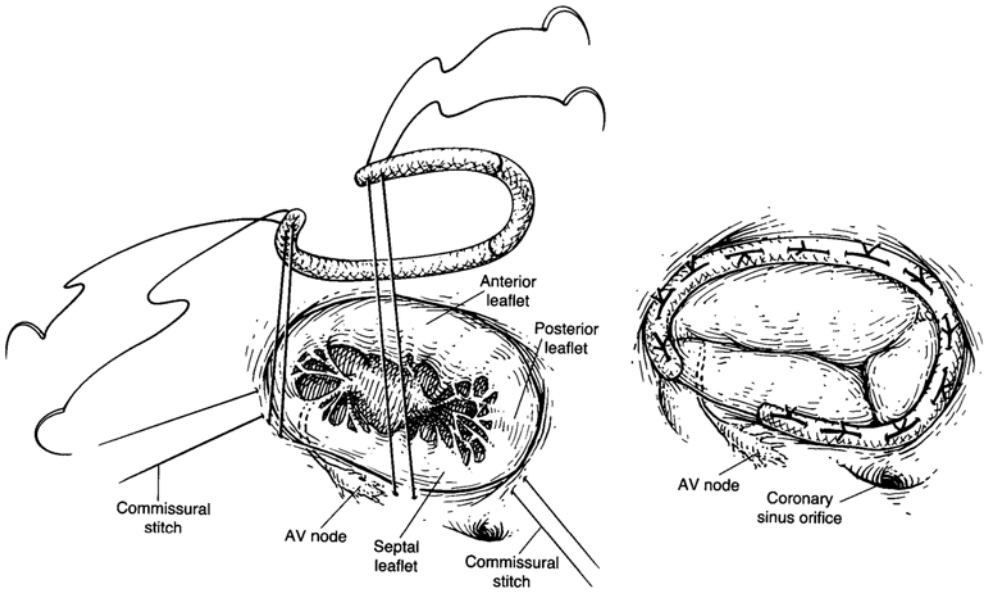

Fig. 34.13 Tricuspid annuloplasty procedure

Today in the United States, the vast majority of diseased tricuspid valves are repaired. The basic techniques for tricuspid valve repair include bicuspidization, annular placation, and various types of annuloplasty, commonly using artificial rings. Tricuspid regurgitation annuloplasty is effective and can be optimized using intraoperative transesophageal echocardiography. Valve replacement with a low profile mechanical valve or bioprosthesis is often necessary when the valve leaflets themselves are diseased, abnormal, or totally destroyed [87]. In both procedures, care must be taken to avoid causing damage to the heart's conduction system. In such cases, use of biological prostheses is preferred to avoid the high rate of thromboembolic complications known to occur with mechanical prostheses placed in the tricuspid position. Combined tricuspid and mitral valve procedures are often completed in the same interventions, as in the setting of rheumatic disease; however, to date, no long-term data regarding the value of such an approach exist. There is an increasing awareness of the importance of correcting tricuspid valve disease in the setting of associated cardiac diseases, most commonly mitral valve disease. In patients with associated conduction defects, insertion of a pacing system at the time of valve replacement is also suggested.

34.4 Summary

The use of cross-circulation followed by the development of the bubble oxygenator for cardiopulmonary bypass was the turning point in the history of cardiac surgery. However, cardiac valvular surgery may be considered to still be in its infancy, with most of the major developments occurring only in the last 50 years. Tremendous advances in the field of cardiac surgery are certain to result from the numerous ongoing efforts of researchers and clinicians alike. This chapter was designed to give the reader an introduction to the complex nature of valve diseases. Several excellent textbooks have been written that provide greater detail for each valve procedure discussed. Such reference texts are valuable for both the clinician and the engineer interested in understanding the underlying etiologies and the current treatment techniques for these diseases. In other words, this basis of understanding, along with the use of further animal and clinical research, will allow for the development of the next generation of treatment options for heart valve disease. The reader is also referred to Chaps. 35 and 37. These topics will have a dramatic impact in this field into the future.

References

1. Miller GW (ed) (2000) King of hearts. Times Books, New York
2. Bolman RM 3rd, Black SM (2003) Open cardiac repair under direct vision: F. John Lewis and the University of Minnesota. J Card Surg 18:328–332, discussion 333
3. Lewis RP, Herr RH, Starr A, Griswold HE (1966) Aortic valve replacement with the Starr-Edwards ball-valve prosthesis. Indications and results. Am Heart J 71:549–563
4. Lillehei CW, Kaster RL, Coleman M, Bloch JH (1974) Heart-valve replacement with Lillehei-Kaster pivoting disk prosthesis. N Y State J Med 74:1426–1438
5. Lillehei CW, Kaster RL, Bloch JH (1972) New central flow pivoting disk aortic and mitral prosthesis. Clinical experience. N Y State J Med 72:1738
6. Emery RW, Palmquist WE, Mettler E, Nicoloff DM (1978) A new cardiac valve prosthesis: in vitro results. Trans Am Soc Artif Intern Organs 24:550–556

7. Bonow RO, Carabello BA, Kanu C et al (2006) ACC/AHA guidelines for the management of patients with valvular heart disease. A report of the American College of Cardiology/American Heart Association Task Force on Practice Guidelines. Circulation 114: e84–e234
8. Nishimura RA, Otto CM, Bonow RO et al (2014) 2014 AHA/ACC guideline for the management of patients with valvular heart disease: executive summary: a report of the American College of Cardiology/American Heart Association Task Force on Practice Guidelines. J Am Coll Cardiol 63:2438–2488
9. El Oakley R, Kleine P, Bach DS (2008) Choice of prosthetic heart valve in today's practice. Circulation 117:253–256
10. Oxenham H, Bloomfield P, Wheatley DJ et al (2003) Twenty year comparison of a Bjork-Shiley mechanical heart valve with porcine bioprosthesis. Heart 89:715–721
11. Hammermeister K, Sethi GK, Henderson WG, Grover FL, Oprian C, Rahimtoola SH (2000) Outcomes 15 years after valve replacement with a mechanical versus a bioprosthetic valve: final report of the Veterans Affairs randomized trial. J Am Coll Cardiol 36: 1152–1158
12. Lund O, Bland M (2006) Risk-corrected impact of mechanical versus bioprosthetic valves on long-term mortality after aortic valve replacement. J Thorac Cardiovasc Surg 131:1267–1273
13. Bach DS, Metras J, Doty JR, Yun KL, Dumesnil JG, Kon ND (2008) Freedom from structural valve deterioration among patients 60 years of age and younger undergoing Freestyle aortic valve replacement. J Heart Valve Dis 16:649–655
14. Pibarot P, Dumesnil JG (2009) Prosthetic heart valves: selection of the optimal prosthesis and long-term management. Circulation 119:1034–1048
15. Edmunds LH Jr, Clark RE, Cohn LH, Grunkemeier GL, Miller DC, Weisel RD (1996) Guidelines for reporting morbidity and mortality after cardiac valvular operations. Thorac Cardiovasc Surg 112: 708–711
16. Cheitlin MD, Douglas PS, Parmley WW (1994) 26th Bethesda conference: recommendations for determining eligibility for competition in athletes with cardiovascular abnormalities. Task Force 2: Acquired valvular heart disease. J Am Coll Cardiol 24:874–880
17. Carabello BA (2002) Aortic stenosis. N Engl J Med 346:677–682
18. Freeman RV, Otto CM (2005) Spectrum of calcific aortic valve disease: pathogenesis, disease progression, and treatment strategies. Circulation 111:3316–3326
19. Otto CM, Pearlman AS, Kraft CD, Miyake-Hull CY, Burwash IG, Gardner CJ (1992) Physiologic changes with maximal exercise in asymptomatic valvular aortic stenosis assessed by Doppler echocardiography. J Am Coll Cardiol 20:1160–1167
20. Krayenbuehl HP, Hess OM, Ritter M, Monrad ES, Hoppeler H (1988) Left ventricular systolic function in aortic stenosis. Eur Heart J 9:E19–E23
21. Marcus ML, Doty DB, Hiratzka LF, Wright CB, Eastham CL (1982) Decreased coronary reserve: a mechanism for angina pectoris in patients with aortic stenosis and normal coronary arteries. N Engl J Med 307:1362–1366
22. Bache RJ, Vrobel TR, Ring WS, Emery RW, Andersen RW (1981) Regional myocardial blood flow during exercise in dogs with chronic left ventricular hypertrophy. Circ Res 48:76–87
23. Koyanagi S, Eastham C, Marcus ML (1982) Effects of chronic hypertension and left ventricular hypertrophy on the incidence of sudden cardiac death after coronary artery occlusion in conscious dogs. Circulation 65:1192–1197
24. Ross J Jr, Braunwald E (1968) Aortic stenosis. Circulation 38:61–67
25. Schwarz F, Baumann P, Manthey J et al (1982) The effect of aortic valve replacement on survival. Circulation 66:1105–1110
26. Sprigings DC, Forfar JC (1995) How should we manage symptomatic aortic stenosis in the patient who is 80 or older? Br Heart J 74:481–484
27. Horstkotte D, Loogen F (1988) The natural history of aortic valve stenosis. Eur Heart J 9:E57–E64
28. Iivanainen AM, Lindroos M, Tilvis R, Heikkila J, Kupari M (1996) Natural history of aortic valve stenosis of varying severity in the elderly. Am J Cardiol 78:97–101
29. Kelly TA, Rothbart RM, Cooper CM, Kaiser DL, Smucker ML, Gibson RS (1988) Comparison of outcome of asymptomatic to symptomatic patients older than 20 years of age with valvular aortic stenosis. Am J Cardiol 61:123–130
30. Cheitlin MD, Alpert JS, Armstrong WF et al (1997) ACC/AHA guidelines for the clinical application of echocardiography. A report of the American College of Cardiology/American Heart Association Task Force on Practice Guidelines (Committee on Clinical Application of Echocardiography). Circulation 95:1686–1744
31. Rosenhek R, Rader F, Loho N et al (2004) Statins but not angiotensin-converting enzyme inhibitors delay progression of aortic stenosis. Circulation 10:1291–1295
32. Rajamannan NM, Otto CM (2004) Targeted therapy to prevent progression of calcific aortic stenosis. Circulation 110:1180–1182
33. McKay RG, Safian RD, Lock JE et al (1986) Balloon dilatation of calcific aortic stenosis in elderly patients: postmortem, intraoperative, and percutaneous valvuloplasty studies. Circulation 74:119–125
34. Safian RD, Mandell VS, Thurer RE et al (1998) Postmortem and intraoperative balloon valvuloplasty of calcific aortic stenosis in elderly patients: mechanisms of successful dilation. J Am Coll Cardiol 9:655–660
35. Tsai TP, Denton TA, Chaux A et al (1994) Results of coronary artery bypass grafting and/or aortic or mitral valve operation in patients > or = 90 years of age. Am J Cardiol 74:960–962
36. Smith N, McAnulty JH, Rahimtoola SH (1978) Severe aortic stenosis with impaired left ventricular function and clinical heart failure: results of valve replacement. Circulation 58:255–264
37. Connolly HM, Oh JK, Orszulak TA et al (1997) Aortic valve replacement for aortic stenosis with severe left ventricular dysfunction. Prognostic indicators. Circulation 95:2395–2400
38. Makkar RR, Fontana GP, Jilaihawi H et al (2012) Transcatheter aortic-valve replacement for inoperable severe aortic stenosis. N Engl J Med 366:1696–1704
39. Smith CR, Leon MB, Mack MJ et al (2011) Transcatheter versus surgical aortic-valve replacement in high-risk patients. N Engl J Med 364:2187–2198
40. Monin JL, Monchi M, Gest V, Duval-Moulin AM, Dubois-Rande JL, Gueret P (2001) Aortic stenosis with severe left ventricular dysfunction and low transvalvular pressure gradients: risk stratification by low-dose dobutamine echocardiography. J Am Coll Cardiol 37:2101–2107
41. Grossman W, Jones D, McLaurin LP (1975) Wall stress and patterns of hypertrophy in the human left ventricle. J Clin Invest 56:56–64
42. Nitenberg A, Foult JM, Antony I, Blanchet F, Rahali M (1988) Coronary flow and resistance reserve in patients with chronic aortic regurgitation, angina pectoris and normal coronary arteries. J Am Coll Cardiol 11:478–486
43. Fortuin NJ, Craige E (1972) On the mechanism of the Austin Flint murmur. Circulation 45:558–570
44. Parker E, Craige E, Hood WP Jr (1971) The Austin Flint murmur and the A wave of the apexcardiogram in aortic regurgitation. Circulation 43:349–359
45. Miller RR, Vismara LA, DeMaria AN, Salel AF, Mason DT (1976) Afterload reduction therapy with nitroprusside in severe aortic regurgitation: improved cardiac performance and reduced regurgitant volume. Am J Cardiol 38:564–567

46. Smith MD, Cassidy JM, Souther S et al (1995) Transesophageal echocardiography in the diagnosis of traumatic rupture of the aorta. N Engl J Med 332:356–362
47. Cigarroa JE, Isselbacher EM, DeSanctis RW, Eagle KA (1993) Diagnostic imaging in the evaluation of suspected aortic dissection. Old standards and new directions. N Engl J Med 328:35–43
48. Yacoub MH et al (1983) Results of valve sparing operations for aortic regurgitation. Circulation 68:311–321
49. David TE (2001) Aortic valve-sparing operations for aortic root aneurysm. Semin Thorac Cardiovasc Surg 13:291–296
50. Gorlin R, Gorlin S (1951) Hydraulic formula for calculation of the area of stenotic mitral valve, other cardiac values and central circulatory shunts. Am Heart J 41:1–29
51. Rowe JC, Bland EF, Sprague HB, White PD (1960) The course of mitral stenosis without surgery: ten- and twenty-year perspectives. Ann Intern Med 52:741–749
52. Wood P (1954) An appreciation of mitral stenosis. I. Clinical features. Br Med J 4870:1051–1063
53. Edwards JE, Rusted IE, Scheifley CH (1956) Studies of the mitral valve. II. Certain anatomic features of the mitral valve and associated structures in mitral stenosis. Circulation 14:398–406
54. Roberts WC, Perloff JK (1972) Mitral valvular disease. A clinicopathologic survey of the conditions causing the mitral valve to function abnormally. Ann Intern Med 77:939–975
55. Olesen KH (1962) The natural history of 271 patients with mitral stenosis under medical treatment. Br Heart J 24:349–357
56. Carroll JD, Feldman T (1993) Percutaneous mitral balloon valvotomy and the new demographics of mitral stenosis. JAMA 270:1731–1736
57. Selzer A, Cohn KE (1972) Natural history of mitral stenosis: a review. Circulation 45:878–890
58. Hugenholtz PG, Ryan TJ, Stein SW, Abelmann WH (1962) The spectrum of pure mitral stenosis. Hemodynamic studies in relation to clinical disability. Am J Cardiol 10:773–784
59. Braunwald E, Moscovitz HL, Amram SS et al (1955) The hemodynamics of the left side of the heart as studied by simultaneous left atrial, left ventricular, and aortic pressures; particular reference to mitral stenosis. Circulation 12:69–81
60. Holen J, Aaslid R, Landmark K, Simonsen S (1976) Determination of pressure gradient in mitral stenosis with a non-invasive ultrasound Doppler technique. Acta Med Scand 199:455–460
61. Hatle L, Brubakk A, Tromsdal A, Angelsen B (1978) Noninvasive assessment of pressure drop in mitral stenosis by Doppler ultrasound. Br Heart J 40:131–140
62. Currie PJ, Seward JB, Chan KL et al (1985) Continuous wave Doppler determination of right ventricular pressure: a simultaneous Doppler-catheterization study in 127 patients. J Am Coll Cardiol 6:750–756
63. Coulshed N, Epstein EJ, McKendrick CS, Galloway RW, Walker E (1970) Systemic embolism in mitral valve disease. Br Heart J 32:26–34
64. Daley R, Mattingly TW, Holt CL, Bland EF, White PD (1951) Systemic arterial embolism in rheumatic heart disease. Am Heart J 42:566
65. Abernathy WS, Willis PW 3rd (1973) Thromboembolic complications of rheumatic heart disease. Cardiovasc Clin 5:131–175
66. Adams GF, Merrett JD, Hutchinson WM, Pollock AM (1974) Cerebral embolism and mitral stenosis: survival with and without anticoagulants. J Neurol Neurosurg Psychiatry 37:378–383
67. Orrange SE, Kawanishi DT, Lopez BM, Curry SM, Rahimtoola SH (1997) Actuarial outcome after catheter balloon commissurotomy in patients with mitral stenosis. Circulation 95:382–389
68. Higgs LM, Glancy DL, O'Brien KP, Epstein SE, Morrow AG (1970) Mitral restenosis: an uncommon cause of recurrent symptoms following mitral commissurotomy. Am J Cardiol 26:34–37
69. Dahl JC, Winchell P, Borden CW (1967) Mitral stenosis. A long term postoperative follow-up. Arch Intern Med 119:92–97
70. Cohn LH, Couper GS, Kinchla NM, Collins JJ Jr (1990) Decreased operative risk of surgical treatment of mitral regurgitation with or without coronary artery disease. J Am Coll Cardiol 16:1575–1578
71. Connolly MW, Gelbfish JS, Jacobowitz IJ et al (1986) Surgical results for mitral regurgitation from coronary artery disease. J Thorac Cardiovasc Surg 91:379–388
72. Chatterjee K, Parmley WW, Swan HJ, Berman G, Forrester J, Marcus HS (1973) Beneficial effects of vasodilator agents in severe mitral regurgitation due to dysfunction of subvalvar apparatus. Circulation 48:684–690
73. Yoran C, Yellin EL, Becker RM, Gabbay S, Frater RW, Sonnenblick EH (1979) Mechanism of reduction of mitral regurgitation with vasodilator therapy. Am J Cardiol 43:773–777
74. Carabello BA (1988) Mitral regurgitation: basic pathophysiologic principles. Part 1. Mod Concepts Cardiovasc Dis 57:53–58
75. Zile MR, Gaasch WH, Carroll JD, Levine HJ (1984) Chronic mitral regurgitation: predictive value of preoperative echocardiographic indexes of left ventricular function and wall stress. J Am Coll Cardiol 3:235–242
76. Crawford MH, Souchek J, Oprian CA et al (1990) Determinants of survival and left ventricular performance after mitral valve replacement. Department of Veterans Affairs Cooperative Study on Valvular Heart Disease. Circulation 81:1173–1181
77. Wisenbaugh T, Skudicky D, Sareli P (1994) Prediction of outcome after valve replacement for rheumatic mitral regurgitation in the era of chordal preservation. Circulation 89:191–197
78. Enriquez-Sarano M, Tajik AJ, Schaff HV, Orszulak TA, Bailey KR, Frye RL (1994) Echocardiographic prediction of survival after surgical correction of organic mitral regurgitation. Circulation 90:830–837
79. Blackshear JL, Pearce LA, Asinger RW et al (1993) Mitral regurgitation associated with reduced thromboembolic events in high-risk patients with nonrheumatic atrial fibrillation. Am J Cardiol 72: 840–843
80. Beppu S, Nimura Y, Sakakibara H, Nagata S, Park YD, Izumi S (1985) Smoke-like echo in the left atrial cavity in mitral valve disease: its features and significance. J Am Coll Cardiol 6:744–749
81. Betriu A, Chaitman BR (1982) Preoperative determinants of return to sinus rhythm after valve replacement. In: Cohn LH, Gallucci V (eds) Cardiac bioprosthesis. Yorke Medical Books, New York, pp 184–191
82. Chua YL, Schaff HV, Orszulak TA, Morris JJ (1994) Outcome of mitral valve repair in patients with preoperative atrial fibrillation. Should the maze procedure be combined with mitral valvuloplasty? J Thorac Cardiovasc Surg 107:408–415
83. Horskotte D, Schulte HD, Bircks W, Strauer BE (1993) The effect of chordal preservation on late outcome after mitral valve replacement: a randomized study. J Heart Valve Dis 2:150–158
84. Bonow RO, Nikas D, Elefteriades JA (1995) Valve replacement for regurgitant lesions of the aortic or mitral valve in advanced left ventricular dysfunction. Cardiol Clin 13(73-83):85
85. Akins CW, Hilgenberg AD, Buckley MJ et al (1994) Mitral valve reconstruction versus replacement for degenerative or ischemic mitral regurgitation. Ann Thorac Surg 58:668–675, discussion 675–676
86. Enriquez-Sarano M, Schaff HV, Orszulak TA, Tajik AJ, Bailey KR, Frye RL (1995) Valve repair improves the outcome of surgery for mitral regurgitation. A multivariate analysis. Circulation 91:1022–1028
87. Silverman N (1998) Tricuspid valve. In: Kaiser K (ed) Mastery of cardiac surgery. Lippincott-Raven, Philadelphia, pp 354–360

Less Invasive Cardiac Surgery

35

Kenneth K. Liao

Abstract

To date, more and more cardiac surgeons are moving toward smaller incisions and the use of specialized less invasive surgical methodologies. The use of (and advances in) less invasive approaches or minimally invasive cardiac surgery can minimize or eliminate complications that may occur in conventional cardiac surgery. For example, for some surgeons, partial sternotomy and minithoracotomy have supplanted standard sternotomy as their preferred route for aortic valve and mitral surgeries.

Keywords

Less invasive cardiac surgery • Cardiac robotic surgery • Minimally invasive cardiac surgery • Incision size • Laparoscopic surgery • Thoracoscope • Minithoracotomy • Partial sternotomy • Partial thoracotomy • Off-pump beating heart coronary artery bypass grafting surgery

35.1 Introduction

The history of cardiac surgery reflects a constant search by cardiac surgeons for safer and less invasive ways to treat their patients. Since Dr. F. John Lewis' pioneering operation in 1952, followed by Dr. C. Walton Lillehei's first successful series of intracardiac defect repairs in the mid-1950s, cardiac surgery as a surgical subspecialty has expanded dramatically. Notably, one of the most important technological innovations in cardiac surgery was the development and modification of a cardiopulmonary bypass machine. For years, this machine has been used extensively by cardiac surgeons. Its use has enabled cardiac surgery to become a safe and reproducible daily routine in many hospitals across the world. Nowadays, though most cardiac operations are considered somewhat standardized, the continued pursuit of less invasive surgical approaches, as well as recognition of the importance of quick postoperative recovery and quality of life, remains significant for patients and physicians.

In recent years, there have been continued efforts to provide and adapt "less invasive cardiac surgery" as standard care. All four of the major steps used in conventional cardiac surgery need to be considered when attempting to develop less invasive modifications: (1) gaining access to the heart through a full sternotomy; (2) supporting the vital organs through a cardiopulmonary bypass machine; (3) arresting the heart by administering cardioplegia; and/or (4) manipulating the ascending aorta during aortic cannulation, during cross-clamping and side-clamping, and during proximal anastomosis in coronary artery bypass grafting. Unfortunately, any of these steps can impose significant risks or adverse effects. More specifically, a large incision typically corresponds to greater pain, a more noticeable scar, more complications, and/or a longer recovery time. Similarly, cardiopulmonary bypass has been known to trigger adverse inflammatory reactions and/or subsequently cause multiple organ dysfunction. Finally, manipulating the aorta can lead to strokes

K.K. Liao, MD (✉)
Department of Surgery, University of Minnesota,
420 Delaware Street SE, MMC 207, Minneapolis,
MN 55455, USA
e-mail: liaox014@umn.edu

P.A. Iaizzo (ed.), *Handbook of Cardiac Anatomy, Physiology, and Devices*, DOI 10.1007/978-3-319-19464-6_35

(e.g., plaque dislodgement) and/or other neurologic deficits. Importantly, less invasive approaches or minimally invasive cardiac surgery can minimize or eliminate complications that may occur relative to each of the four steps commonly used in conventional cardiac surgery. This chapter focuses on less invasive methodologies commonly employed in adult cardiac surgical procedures.

35.2 Impact of Incision Size

For years, the physical and emotional impact of a large incision size on the individual patient has been ignored by most cardiac surgeons. Historically, adequate exposure of the target tissue or organ through large skin incisions took priority over concern about incision size; this mind-set remained unchallenged until the early 1990s. Subsequently, with novel specially designed instruments, experience with laparoscopic surgery demonstrated that those surgical procedures traditionally performed through large incisions could actually be accomplished with much smaller incisions. More recently, the patient benefits of small incisions have been clearly shown including less pain, quicker recovery, lower infection rate, shorter hospital stays, and/or better quality of life [1, 2]. In some studies, less immune function disturbance has also been reported [3]. Encouraged by positive results from the laparoscopic surgical community, cardiac surgeons began to modify their approaches to perform less invasive cardiac surgery. Currently, a variety of approaches have been used to replace full sternotomy: (1) thoracoscopy or minithoracotomy and/or (2) partial sternotomy. Nevertheless, cardiopulmonary bypass support, if required, is established through cannulation in the peripheral vessels such as the femoral arteries, femoral veins, and internal jugular veins. Various studies have reported advantages with smaller incisions or sternum-sparing incisions in terms of pain, blood loss, postoperative respiratory function, time to recovery, infection, cosmesis, and survival rate [4–7]. However, one must also consider that smaller incisions have certain drawbacks. In order to have the same access and visualization as with larger incisions, special instruments and specialized surgical skills are required, and only selected patients are eligible. For surgeons, the initial learning curve to be able to perform such procedures clinically can be very steep. Nevertheless, smaller incisions are certainly very appealing to both patients and referring physicians. To date, more and more surgeons are moving toward smaller incisions and the use of these specialized less invasive surgical methodologies. For some surgeons partial sternotomy and minithoracotomy have supplanted standard sternotomy as their preferred route for aortic and mitral valve surgeries.

35.3 Side Effects of Cardiopulmonary Bypass

Cardiopulmonary bypass procedures have become commonplace in cardiac surgical suites; however, capabilities to perform the same clinical procedure safely without its use would be desirable, for such bypass procedures are not performed without risk. More specifically, cardiopulmonary bypass has been associated with a complex systemic inflammatory reaction in the host patient. The hallmarks of this reaction are typically increased microvascular permeability in multiple organs, resulting in an increase in interstitial fluid and the activation of humoral amplification systems. The complement system, including the kallikrein-bradykinin cascade, the coagulation cascade, the fibrinolytic cascade, and the arachidonic acid cascade, is activated. Inflammatory mediators, such as cytokines and proteolytic enzymes, are released.

In most classic cardiac cases where cardiopulmonary bypass is utilized, the heart is stopped to provide for a motionless field. Cardiac arrest is initiated with infusion of cardioplegia to the myocardium. Unfortunately, subsequent reperfusion of the heart can cause ischemic reperfusion injury to the myocardium.

Clinical manifestations of this systemic inflammatory reaction and myocardial ischemic reperfusion injury can be subtle but also serious and even lethal in some patients. The incidence of this systemic reaction has been reported in 5–30 % of cardiac surgery patients after cardiopulmonary bypass [8–13]. Importantly, this inflammatory response can affect multiple organs. More specifically, examples of this systemic response can vary: (1) from transient subtle cognitive impairment to a permanent stroke, (2) from coagulopathy requiring transfusion of blood products to disseminated intravascular coagulation, (3) from pulmonary edema to adult respiratory distress syndrome requiring prolonged ventilation support, (4) from low cardiac output to acute heart failure requiring inotropic or mechanical circulatory support, and/or (5) from transient kidney insult with increased creatinine to permanent kidney failure requiring hemodialysis. Any of these, or a combination thereof, commonly result in prolonged intensive care unit stays requiring intense monitoring and often increased patient mortality. Importantly, the severity of these reactions tends to be related to cardiopulmonary bypass time, the patient's age, and/or comorbidities [11, 12].

To date, coronary artery disease remains as the leading cause of death for individuals living in developed countries. Despite widespread use of drug-eluting stents in treating coronary artery disease and sharply decreased patient volume for coronary artery bypass grafting (CABG) numbers,

CABG operations still remain the most commonly performed cardiac procedures in the United States. Compared to percutaneous coronary artery interventions such as stenting, CABG has shown advantages of improved patient event-free survival and lower re-intervention rate, especially in patients with multivessel coronary artery disease, diabetes, and decreased left ventricular function. These benefits are attributed mainly to the use of in situ left internal mammary artery bypass to the left anterior descending artery, in which the patency rate remains over 90 % even after 15 years of implantation. Furthermore the use of bilateral internal mammary arteries as bypass conduits has shown to offer a better patient survival rate and less reoperation rate, when compared with the use of only left internal mammary artery as a bypass conduit.

In the past 15 years, off-pump beating heart coronary artery bypass grafting surgery (OPCABG, a less invasive surgical approach) has entered the mainstream of clinical cardiac surgical practice, and the number of such procedures has been steady in the United States, making up ~10–20 % of all CABG surgeries performed annually. An increasing number of studies, including prospective randomized studies, have demonstrated that when compared to conventional CABG, OPCABG procedures result in: (1) a lower incidence of postoperative neurologic deficits, (2) fewer blood transfusions, (3) shorter intubation times, (4) less release of cardiac enzyme, (5) less renal insult, (6) shorter ICU stays, (7) less release of cytokines IL 8 and IL 10, and/or (8) lower mortality [13–17]. It should be noted that the difference in these parameters between OPCABG and CABG procedures mostly ranges from 2 to 10 %. In most OPCABG procedures, however, there has been the tendency to bypass fewer vessels; this may result in an incomplete revascularization. Moreover, certain anatomic locations and the nature of target coronary arteries may preclude safe and reliable anastomoses with OPCABG, e.g., arteries located in the posterolateral wall of hypertrophied hearts, intramyocardial arteries, and severely calcified arteries. Furthermore, with today's available methodologies, OPCABG is more challenging technically for most cardiac surgeons. It should also be noted that emergency conversion of OPCABG to conventional CABG because of hemodynamic instability carries a significantly higher morbidity and mortality rate than conventional CABG (about 6 times higher mortality) [18]; fortunately, the overall conversion is rare, with a rate of only 3.7 %.

Though OPCABG surgery took off rapidly in the earlier part of the last decade, the enthusiasm for OPCABG has faded in recent years due to the lack of highly anticipated "drastic" clinical benefits of this procedure over conventional CABG and the additional technical challenges faced by the surgeons. Currently OPCABG comprises 10–20 % of all CABG procedures performed in the United States, which has decreased compared to 10 years ago. Although isolated centers perform virtually all CABG procedures off-pump, in many centers, OPCABG is a seldom-used procedure. Such a large discrepancy appears due to the lack of effective education of practicing surgeons and a steep learning curve to master the tricks of performing OPCABG.

35.4 Effects of Manipulating the Aorta

Coronary artery disease is often considered as a component of systemic vascular disease. The same risk factors that contribute to coronary artery disease, such as smoking, diabetes, hypertension, and hyperlipidemia, also contribute to carotid artery disease and atherosclerotic changes in the aorta; this is especially true for the ascending aorta. Atheroma in the aorta can present with calcified plaques or with "cheese-like" soft plaques, which can be disrupted (dislodged) during: (1) cannulation of the ascending aorta for cardiopulmonary bypass, (2) cross-clamping in general, and/or (3) side-clamping of ascending aorta for attachment of proximal anastomoses of bypassed grafts. The mobilized plaques can then cause microembolization or macroembolization of brain vessels, resulting in neurologic deficits. Multiple episodes of microembolic events have been documented by transcranial Doppler studies during routine CABG surgery. The number of microembolic signals is reported to be related to the extent that the ascending aorta is manipulated [19]. Nevertheless, calcified areas of the aorta (or porcelain aorta) can be identified by palpation and thus avoided during surgery, whereas soft plaques are typically unnoticed until they are disrupted during surgical manipulation. The incidence of plaque formation in the ascending aorta can be as high as 30 % [20].

Recently, several methodologies have been described to avoid disrupting plaques when working in the region of the ascending aorta. For example, topical ultrasound devices have been used to identify hidden plaques, especially the soft types. In addition, a single aortic cross-clamp technique has been shown to reduce the risk of plaque disruption during conventional CABG surgery [21]. Similarly, aortic cross-clamping or side-clamping can be avoided by using proximal anastomotic devices during OPCABG. More recently, totally aortic *non-touch* techniques have been described that can be applied during OPCABG by using: (1) bilateral in situ internal mammary arteries; (2) sequential grafts; (3) in situ gastroepiploic arteries; (4) radial artery Y or T grafts from internal mammary arteries; (5) radial artery or vein grafts from innominate, subclavian, and axillary arteries; or (6) descending thoracic aorta. Currently, non-touch techniques during OPCABG are gaining popularity, especially in high-risk patients (Fig. 35.1). Nevertheless, given limited patient numbers and short follow-up times, the long-term graft patency rate for the latter procedures remains unknown.

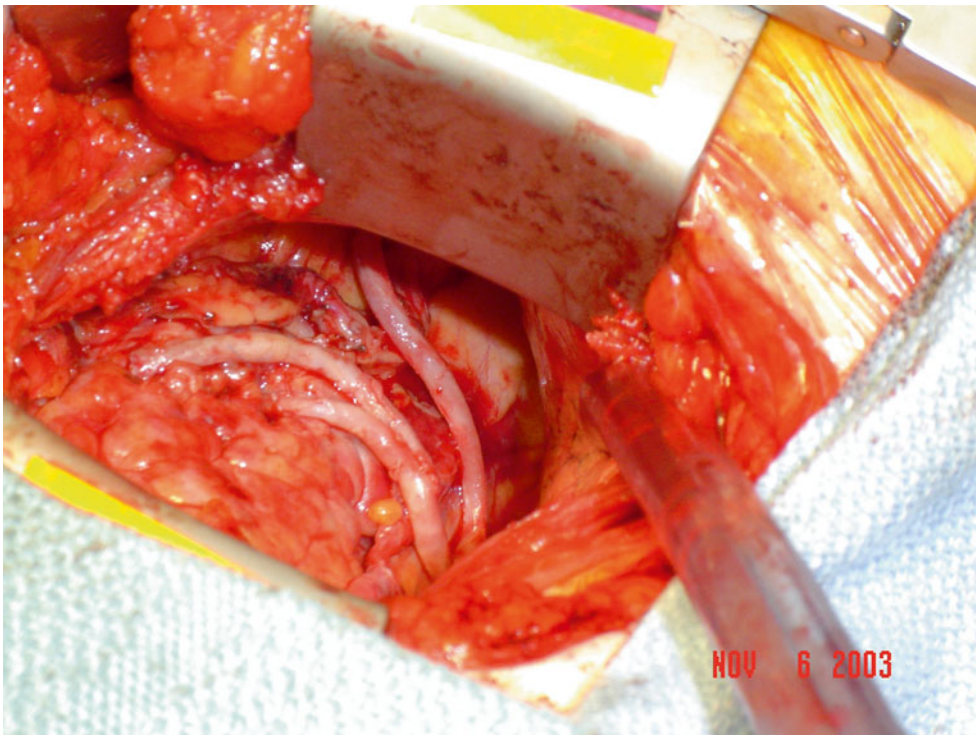

Fig. 35.1 Totally aortic "non-touch" technique in off-pump three-vessel coronary artery bypass grafting surgery via left minithoracotomy; the inflow vein grafts come from the distal left subclavian artery in addition to in situ left internal mammary artery graft

35.5 Technological Innovations

New technologies have played a crucial role in the evolution of less invasive cardiac surgery. Importantly, they have changed the perceptions of cardiac surgeons regarding how cardiac surgery can or should be performed. With the help of new instruments specifically designed to meet the surgeon's need, less invasive cardiac surgical procedures once deemed impossible or impractical have now become reality, or even common practice, in some medical centers. These technological innovations have typically involved the following aspects of cardiac surgery.

35.5.1 Sternum-Sparing Surgery: Partial Sternotomy, Minithoracotomy, and Thoracoscopy

Major advances in this area include the development of a cardiopulmonary bypass support system via peripheral access. The application of suction to the venous drainage has made possible aortic valve and mitral valve surgery via partial sternotomy and minithoracotomy. An earlier breakthrough device in this field was the HeartPort system (developed by Stanford University and New York University Hospital in 1994) which was composed of peripheral vessel-based cardiopulmonary bypass perfusion, an endo aortic balloon occlusion catheter, transvenously placed venting and cardioplegia cannulas, and extra-long operating instruments. Though its early use proved impractical in most cardiac operations, its potential to be less invasive has significantly changed cardiac surgeons' and medical engineers' perception of future technologies. Furthermore, the concept of the HeartPort system led to numerous other technological modifications and innovations in the field of less invasive cardiac surgery. Such innovations include: (1) the development of small caliber multistage peripheral venous cannula, (2) the safe application of vacuum-assisted venous drainage to ensure bloodless exposure inside heart, (3) the small thin blade minithoracotomy retractor and atrial retractor, (4) development of the Chitwood aortic cross-clamp, (5) thoracoscopy or endoscopic robotics to assist in the mitral valve repair or replacement, and (6) liberal use of transesophageal echocardiography to guide the insertion of various intracardiac cannulas.

35.5.1.1 Upper Partial Sternotomy or Minithoracotomy Approaches for Aortic Valve Replacement

Currently more and more aortic valve replacements are performed via upper partial sternotomy or minithoracotomy. In such procedures, a limited partial sternotomy is made and the splitting of sternum is terminated at the 3rd or 4th intercostal space with either a "J" or inverted "T" incision, or a 6 cm incision is made at the right 2nd intercostal space (Fig. 35.2). Even an aortic valve replacement surgery can be performed via such a small incision, by using a combination

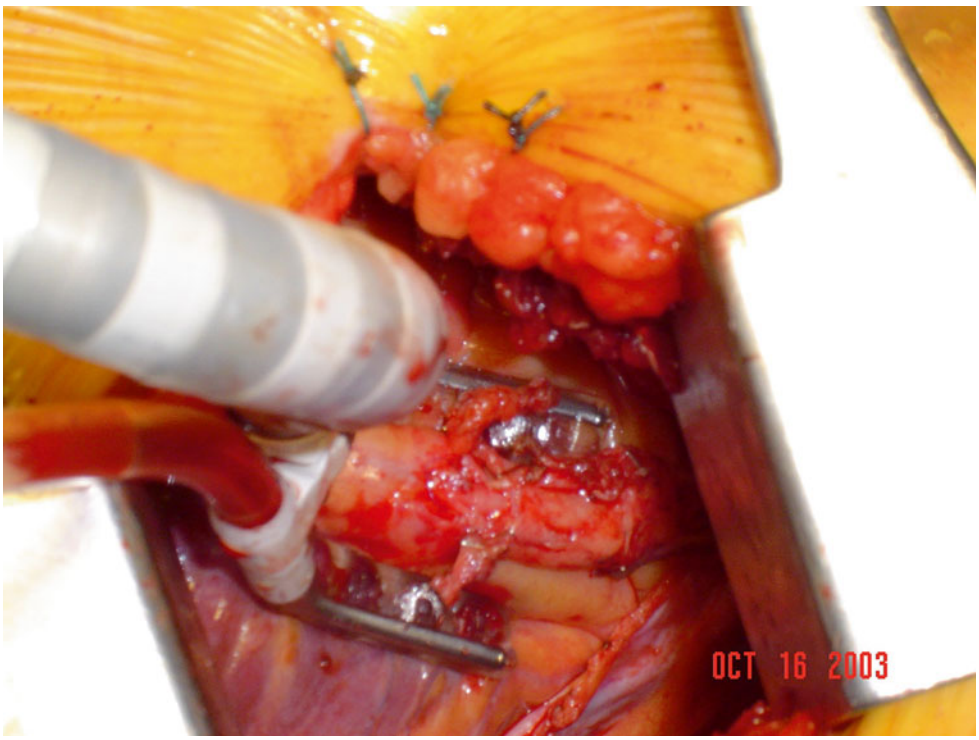

Fig. 35.2 Drawing of incisions used in minimally invasive aortic valve replacement. An upper sternotomy incision ends at the 3rd intercostal space at a "J" angle; a minithoracotomy incision is located at the right 2nd intercostal space

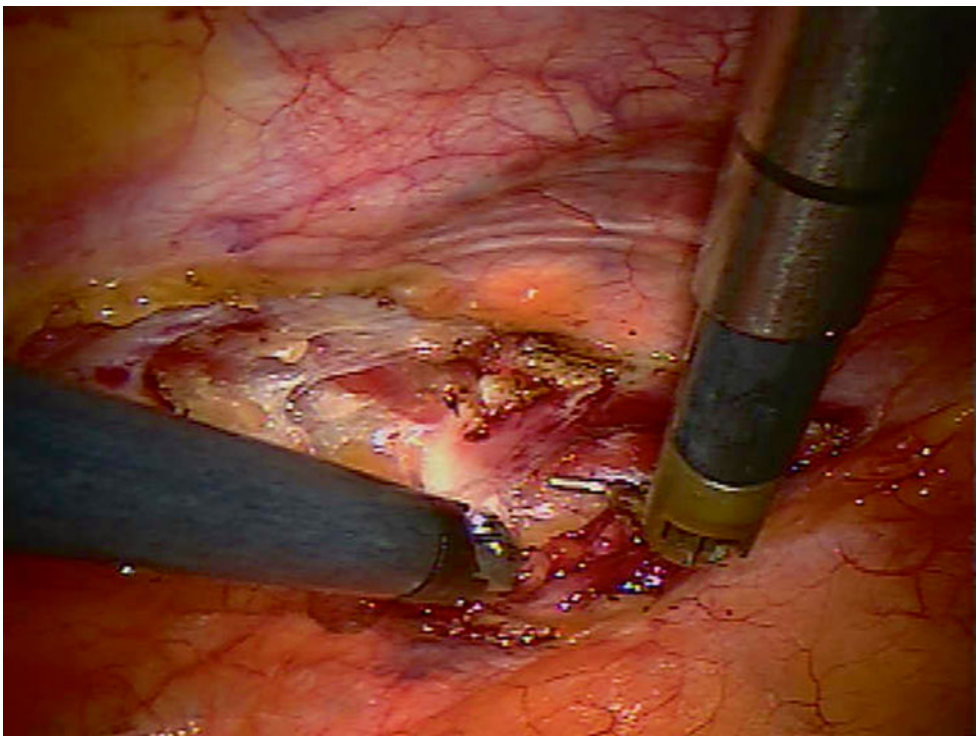

Fig. 35.3 The small incision allows for insertion of a combination of central and peripheral cannula for the establishment of cardiopulmonary bypass

of central and peripheral cardiopulmonary bypass circuits. Note that the aortic valve can be adequately exposed and replaced (Figs. 35.3 and 35.4).

A right minithoracotomy procedure is increasingly being used for minimally invasive mitral valve repair and/or replacement surgery. In these procedures, a 6 cm incision is typically made at the right 3rd intercostal space and a specially designed small retractor is inserted. A combination of central and peripheral cardiopulmonary bypass circuits is established, and intracardiac cannulas are inserted under the guidance of transesophageal echocardiography (Fig. 35.5). Currently, special instruments

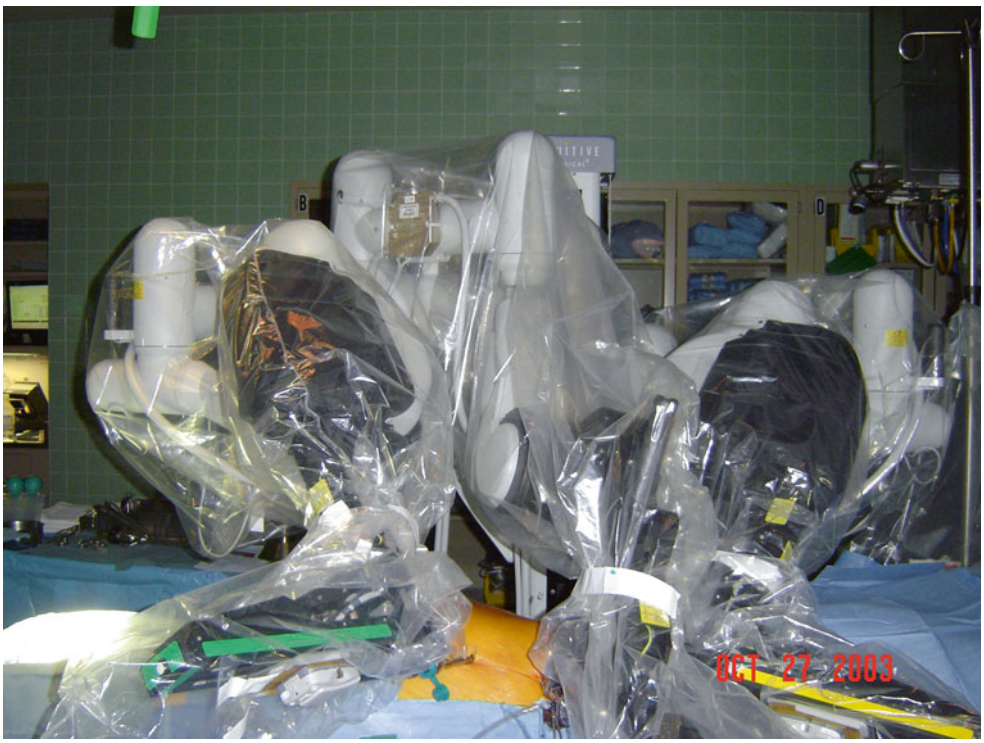

Fig. 35.4 The exposure is adequate for aortic valve replacement. A bioprosthetic valve is visible

Fig. 35.5 A right minithoracotomy incision at the 3rd intercostal space. A combination of central and peripheral cannula insertion is used for the establishment of cardiopulmonary bypass

including clamps, scissors, forceps, and a knot-tying device are used for these procedures (Fig. 35.6). In other words, both mitral valve repair and replacement procedures can be safely performed using this approach (Fig. 35.7). The main advantages of these procedures are decreased blood loss and the quick return of the patient to physical activities when compared to conventional sternotomy approach (Fig. 35.8).

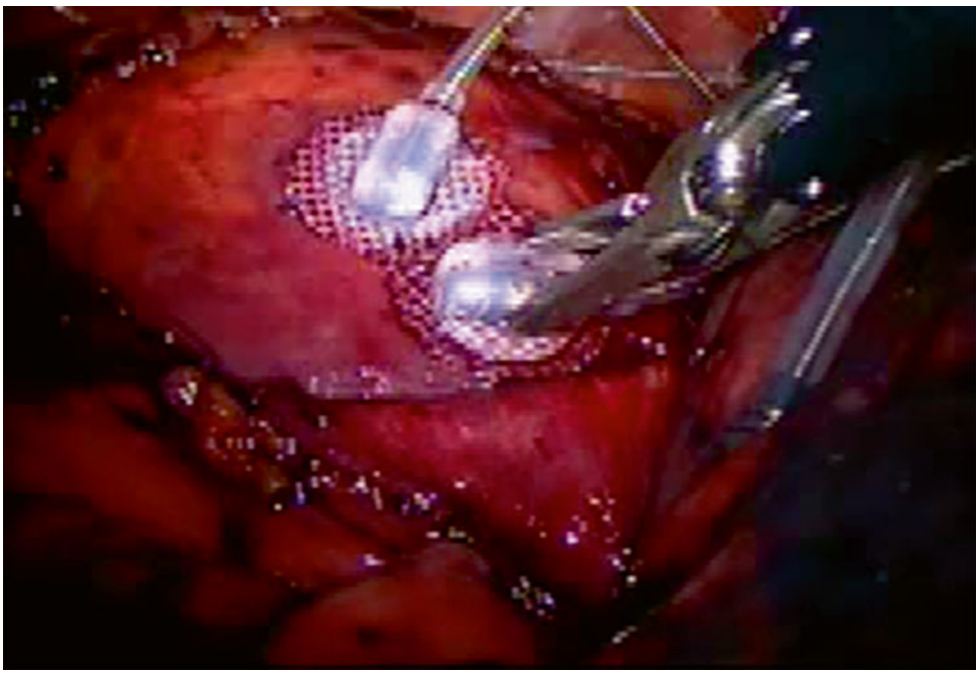

Fig. 35.6 Special instruments with extra-long handles and small tips are used for minimally invasive mitral valve surgery

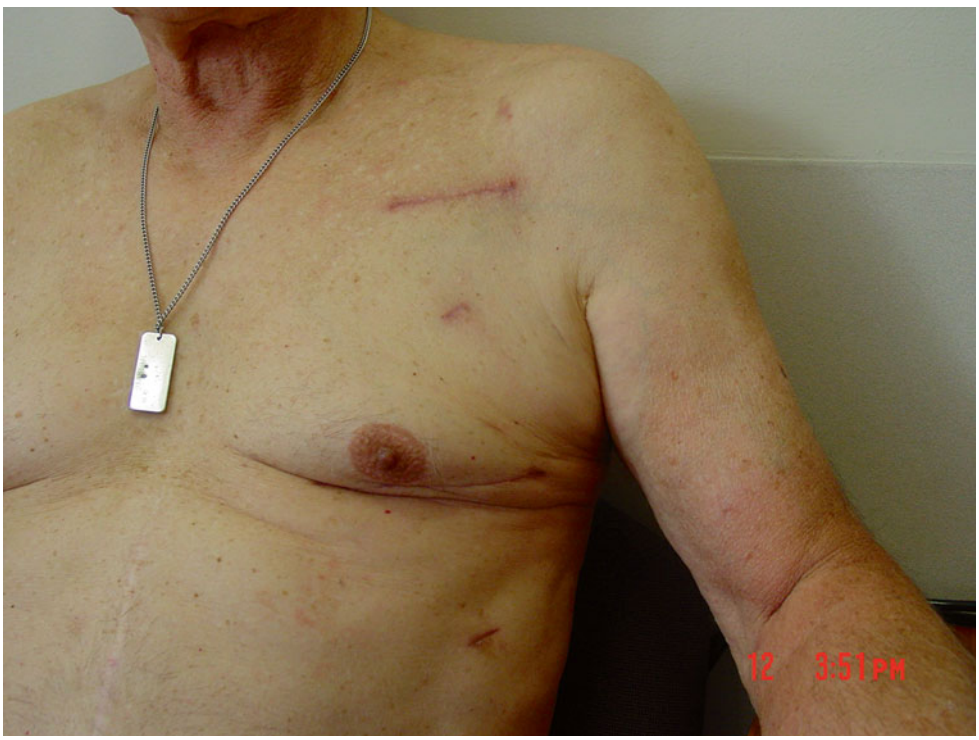

Fig. 35.7 Mitral valve repair with minithoracotomy can achieve good exposure

35.5.2 OPCABG Improvement

New instruments have also been developed to position the heart and to stabilize and improve the visualization of target arteries. For example, an available left ventricle suction device applies −400 mmHg suction to the left ventricular apex and can hold the heart up in different positions. Now widely used in OPCABG surgery, this device has less of an effect on the venous return as compared with the old "suture retraction" technique. Similarly, a focal myocardial stabilization device has been developed to stabilize segments of target arteries; it has both suction and compressing effects on the topical epicardial tissue and thus significantly decreases the motion of target arteries (Fig. 35.9). An additional note-

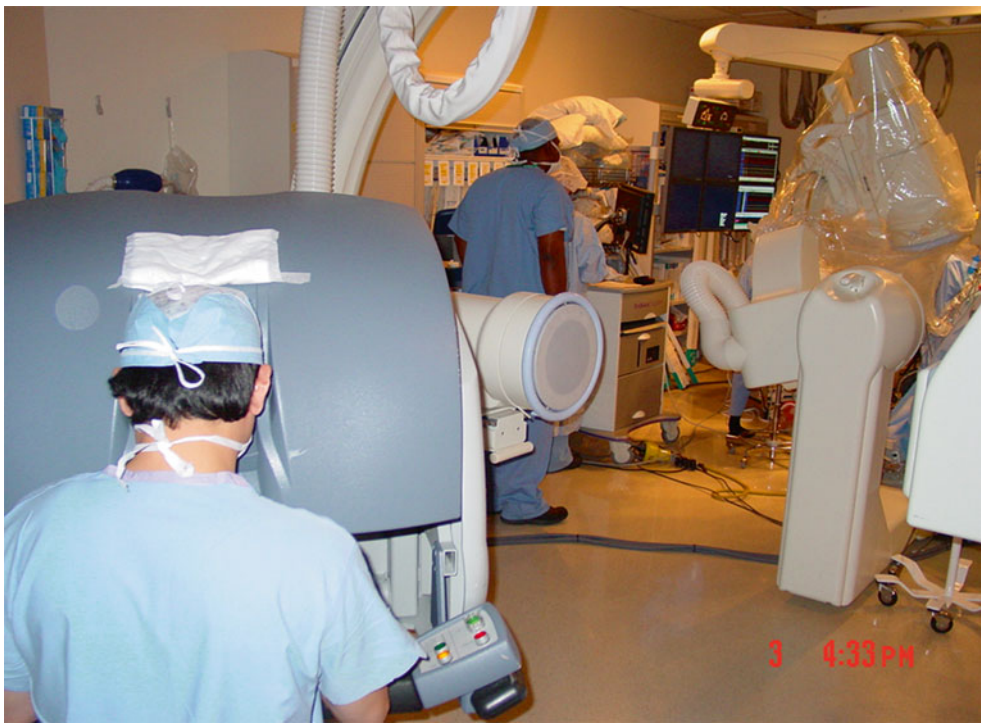

Fig. 35.8 Minithoracotomy results in less blood loss, quick return to work, and a better cosmetic outcome

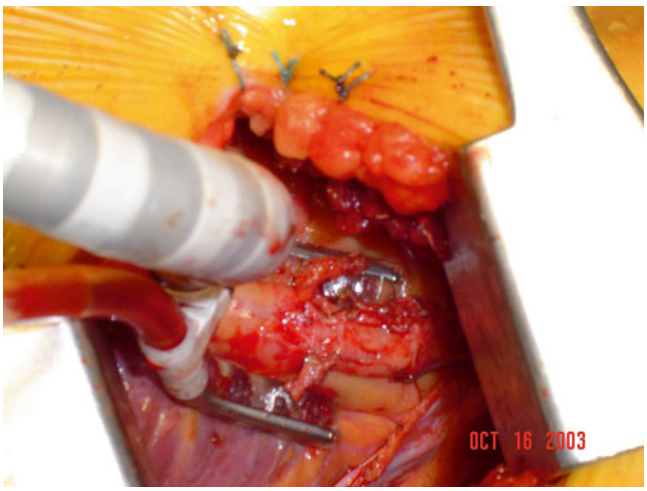

Fig. 35.9 An "octopus" myocardium-stabilizing device was used to steady the coronary artery during direct bypass grafting anastomosis

worthy device is the temporary intracoronary plastic shunt that can be inserted via arteriotomy to maintain blood flow to the distal myocardium during anastomosis, thus avoiding or minimizing ischemia time. Importantly, the use of such a shunt is considered to be crucial when the target artery supplies a large territory of myocardium. In order to facilitate the distal coronary anastomosis during OPCABG, especially in the anatomically difficult-to-reach areas, two innovative distal coronary artery anastomotic devices, C-PortxA (for the open sternotomy approach) and C-Port Flex A™ (for the minithoracotomy or endoscopic robotic approach) (Cardica Inc., Redwood City, CA, USA), were developed and recently approved for clinical use by the FDA. It should be noted that although the early clinical results of such devices are encouraging [22], their clinical adaption has been lackluster.

35.5.3 Aortic *Non-touch* Techniques

Different proximal anastomotic devices or hand-sewn facilitators have been developed and used to avoid clamping on the aorta during OPCABG surgery. Unfortunately, the clinical performance of most of these devices has been unsatisfactory, resulting in denial of FDA approval or termination of the products after FDA approval, i.e., the previously FDA-approved symmetry (St. Jude Medical, St. Paul, MN, USA) automated proximal connector being one example.

Currently the Heartstring proximal seal system (Boston Scientific, Inc., Marlborough, MA, USA) is the only clinically available facilitator for proximal hand-sewn suture anastomosis. It temporarily occludes aortotomy during direct suture anastomosis of the proximal vein graft to the aortotomy; yet, to date, one of the major drawbacks of its use is that the suture can catch the device, which requires that the anastomosis be redone.

35.5.4 Endoscopic Robotics

Someday soon will operating rooms be devoid of cardiac surgeons? Perhaps, with the addition of robotics as a forefront technology. For example, Intuitive Surgical's da Vinci robotic system (Sunnyvale, CA, USA) has improved significantly in the past 15 years and has made operating inside the chest cavity possible. As of today, they have developed three generations of this technology; its 3rd generation, which is smaller and more user-friendly and has a "third arm" (one more arm than the 1st generation) and dual operating consoles for training purposes, has been recently available for clinical use. Its three-dimensional visualization, seven degrees of wrist motion, and capability to eliminate human hand tremors facilitate fine cutting and suturing tasks. For an increasing number of surgeons that are currently using this sophisticated machine, it has made both internal mammary artery takedown and OPCABG surgery via thoracoscopy or minithoracotomy easier (Fig. 35.10). Further, it has been described to have been used to repair atrial septal defects and mitral valves without sternotomy or thoracotomy. Currently, the employment of such systems will lead the way in moving toward total endoscopic CABG surgery (Figs. 35.11 and 35.12).

Nevertheless, complementary innovations have been required to allow for robotic surgery on the heart. For example, to make OPCABG surgery easier when it is performed via minithoracotomy or total endoscopic robotic approaches, an *endo suction device* and an *endo myocardium stabilizer* (Medtronic, Inc., Minneapolis, MN, USA) have been developed to position the heart and stabilize the target artery through port accesses.

The endoscopic robotic has greatly enhanced surgeons' ability to perform OPCABG via thoracoscopy and minithoracotomy. Robotic-assisted OPCABG performed at our institution and others [23] has shown the advantages of less pain, less blood loss, shorter length of stay, and fewer complications when compared to conventional CABG, especially in elderly high-risk patients. Another robotic application in cardiac surgery is mitral valve repair and replacement via thoracoscopy and minithoracotomy. When comparing robotic mitral surgery with standard sternotomy, major reductions in blood product utilization and length of stay are observed, while equivalence in complexity and success of mitral repairs is preserved [24]. Recent use of robotics to

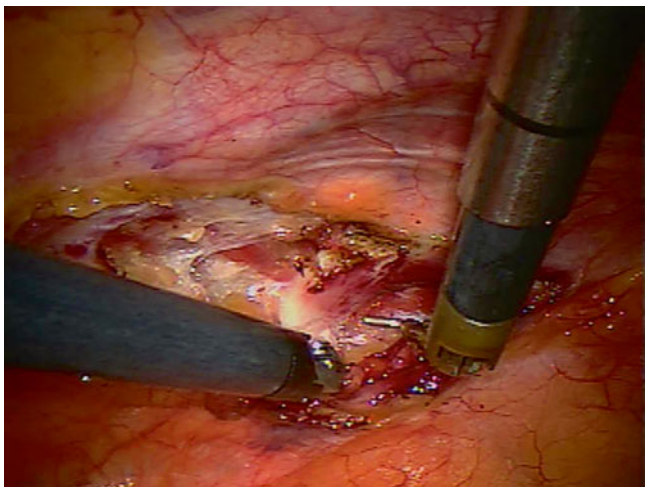

Fig. 35.10 Robotic arms operating inside the chest cavity to take down the left internal mammary artery

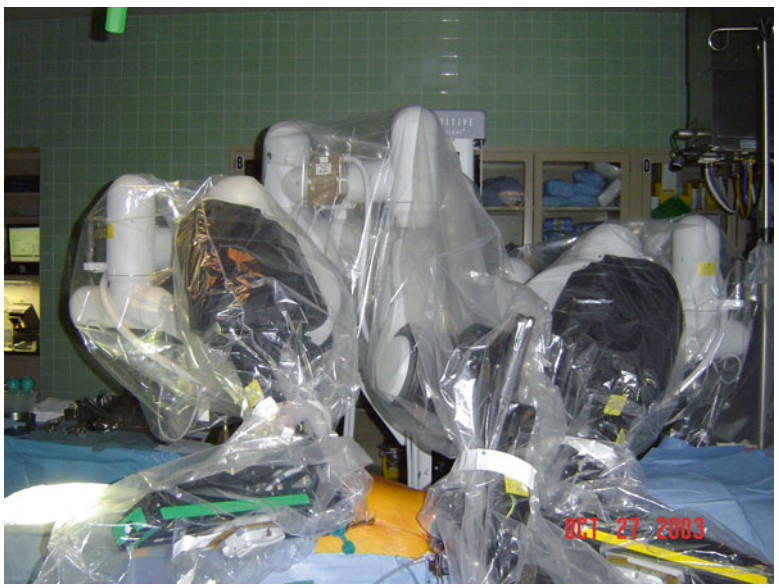

Fig. 35.11 Robotic arms in the operating room

Fig. 35.12 Surgeon is operating on the robotic console away from the patient

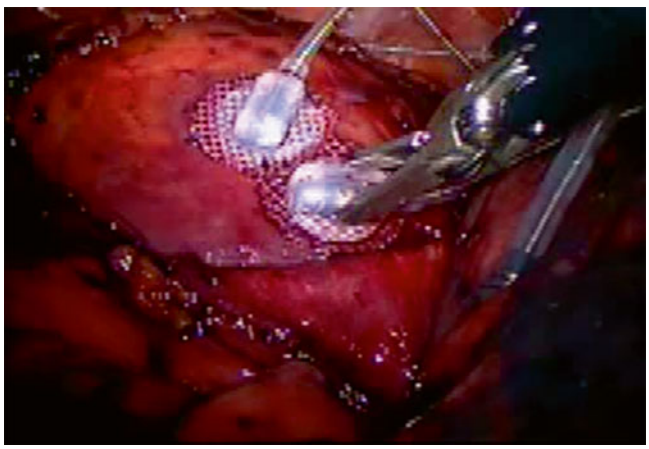

Fig. 35.13 Two left ventricular epicardial leads are placed by a robotic grasper in a patient who had previous coronary artery bypass grafting surgery

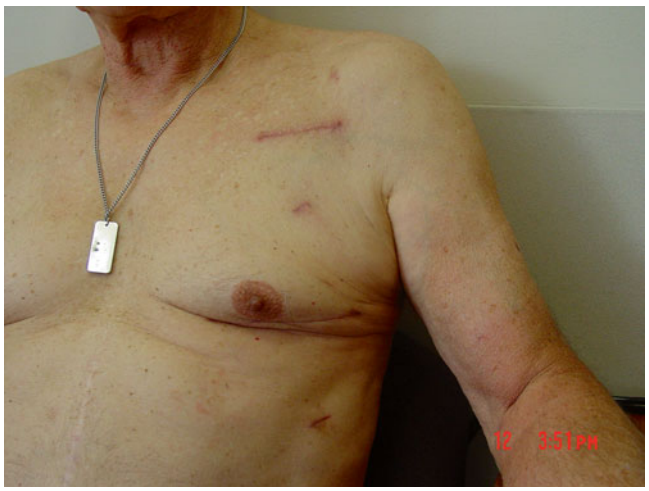

Fig. 35.14 Small incisions after multivessel off-pump sternum-sparing coronary artery bypass grafting surgery

implant left ventricular pacing leads as part of cardiac resynchronization therapy for congestive heart failure has shown the advantages of accuracy of locating the optimal pacing site and shorter procedure length compared to the cathlab percutaneous implantation (Fig. 35.13) [25].

35.6 Future Directions

The ultimate goal of less invasive cardiac surgery is to avoid cardiopulmonary bypass support and sternotomy and rather to perform surgery through tiny incisions. Various specially designed instruments are still being developed to make such procedures possible, including: (1) automated proximal and distal CABG anastomotic devices, (2) the endo myocardium stabilizer, (3) the endo suture device, and (4) the endo vascular clamp. The da Vinci surgical robotic system has enabled the use of such instruments inside the closed chest cavity. It is likely that in the very near future, cardiac surgery will be performed utilizing only three to four key holes in the chest wall (Fig. 35.14).

The following cardiac procedures will likely advance in the near future with regard to the less invasive approaches: (1) total endoscopic robotic OPCABG using single or bilateral in situ internal mammary artery, with the help of flexible distal coronary artery anastomotic devices; (2) hybrid robotic-assisted OPCABG and percutaneous stenting in the hybrid operating room or hybrid CathLab (Fig. 35.15);

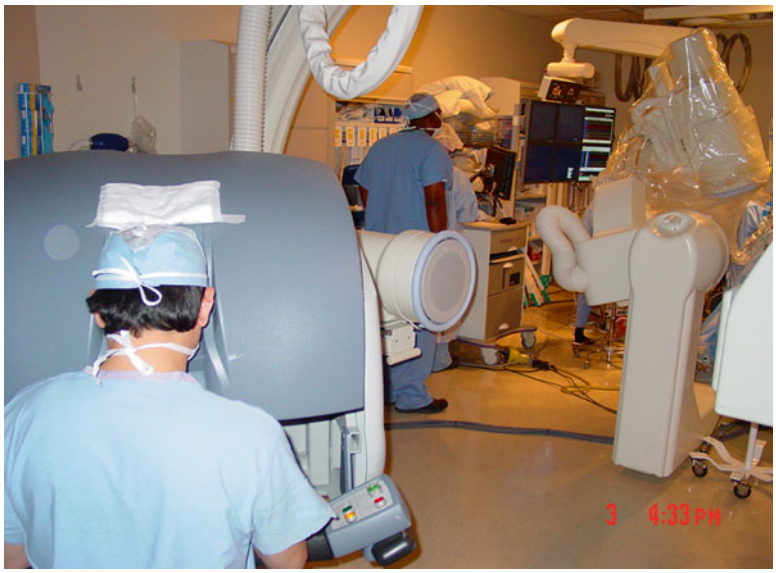

Fig. 35.15 Surgeon is performing robotic-assisted hybrid surgery in the CathLab

(3) total endoscopic robotic mitral valve repair; (4) increased the use of robotic-assisted left ventricular pacing lead implantation or hybrid electrophysiology ablation therapy; and (5) aortic valve replacement via percutaneous or transpical approaches in the hybrid operating room or CathLab.

References

1. Grace PA, Quereshi A, Coleman J et al (1991) Reduced postoperative hospitalization after laparoscopic cholecystectomy. Br J Surg 78:160–162
2. Southern Surgeons Club (1991) A prospective analysis of 1518 laparoscopic cholecystectomies. N Engl J Med 324:1073–1078
3. Bruce DM, Smith M, Walker CBJ et al (1999) Minimal access surgery for cholelithiasis induces an attenuated acute phase response. Am J Surg 178:232–234
4. Szwerc MF, Benchart DH, Wiechmann RJ et al (1999) Partial versus full sternotomy for aortic valve replacement. Ann Thorac Surg 68:2209–2214
5. Cosgrove DM, Sabik JF, Navia JL (1998) Minimally invasive valve operations. Ann Thorac Surg 65:1535–1539
6. Svensson LG (2007) Minimally invasive surgery with a partial sternotomy "J" approach. Semin Thorac Cardiovasc Surg 19:299–303
7. Bakir I, Casselman FP, Wellens F et al (2006) Minimally invasive versus standard approach aortic valve replacement: a study in 506 patients. Ann Thorac Surg 81:1599–1604
8. Zilla P, Fasol R, Groscurth P et al (1989) Blood platelets in cardiopulmonary bypass operations. J Thorac Cardiovasc Surg 97:379
9. Ko W, Hawes AS, Lazenby WD et al (1991) Myocardial reperfusion injury. J Thorac Cardiovasc Surg 102:297
10. Sladen RN, Berkowity DE (1993) Cardiopulmonary bypass and the lung. In: Graylee GP, David RF, Utley JR (eds) Cardiopulmonary bypass. William & Wilkins, Baltimore, p 468
11. Tuman KJ, McCarthy RJ, Najafi H et al (1992) Differential effects of advanced age on neurologic and cardiac risks of coronary artery operations. J Thorac Cardiovasc Surg 104:1510
12. Abel RM, Buckley MJ, Austen WG et al (1976) Etiology, incidence and prognosis of renal failure following cardiac operations: results of a prospective analysis of 500 consecutive patients. J Thorac Cardiovasc Surg 65:32
13. Castillo FC, Harringer W, Warshaw AL et al (1991) Risk factors for pancreatic cellular injury after cardiopulmonary bypass. N Engl J Med 325:382
14. Cleveland JC, Shroyer AJ, Chen AY et al (2001) Off-pump coronary artery bypass grafting decrease risk-adjusted mortality and morbidity. Ann Thorac Surg 72:1282–1289
15. Ascione R, Lloyd CT, Underwood MJ et al (2000) Inflammatory response after coronary revascularization with or without cardiopulmonary bypass. Ann Thorac Surg 69:1198–1204
16. Diegeler A, Doll N, Rauch T et al (2000) Humoral immune response during coronary artery bypass grafting: a comparison of limited approach, "off-pump" technique, and conventional cardiopulmonary bypass. Circulation 102:III95–III100
17. Reston JT, Tregear SJ, Turkelson CM (2003) Meta-analysis of short-term and mid-term outcomes following off-pump coronary artery bypass grafting. Ann Thorac Surg 76:1510–1515
18. Edgerton JR, Dewey TM, Magee MJ et al (2003) Conversion in off-pump coronary artery bypass grafting: an analysis of predictors and outcomes. Ann Thorac Surg 76:1138–1142
19. Stump DA, Newman SP (1996) Embolic detection during cardiopulmonary bypass. In: Tegler CH, Babikian VL, Gomez CR (eds) Neurosonology. Mosby, St. Louis, pp 252–255
20. Goto T, Baba T, Matsuyama K et al (2003) Aortic atherosclerosis and postoperative neurological dysfunction in elderly coronary surgical patients. Ann Thorac Surg 75:1912–1918
21. Tsang JC, Morin JF, Tchervenkov CI et al (2003) Single aortic clamp versus partial occluding clamp technique for cerebral protection during coronary artery bypass: a randomized prospective trial. J Card Surg 18:158–163
22. Matschke KE, Gummert JF, Demertzis S et al (2005) The Cardica C-Port System: clinical and angiographic evaluation of a new device for automated, compliant distal anastomoses in coronary artery bypass grafting surgery—a multicenter prospective clinical trial. J Thorac Cardiovasc Surg 130:1645–1652
23. Poston RS, Griffith B, Bartlett (2008) Superior financial and quality metrics with robotic-assisted coronary artery revascularization (abstract), presented at the 128th annual American Surgical Association, New York, 26 April 2008
24. Woo YJ, Nacke EA (2006) Robotic minimally invasive mitral valve reconstruction yields less blood product transfusion and short length of stay. Surgery 140:262–267
25. Liao K (2008) Surgical implantation of left ventricular epicardial pacing leads for cardiac resynchronization therapy. In: Lu F, Benditt D (eds) Cardiac pacing and defibrillation–principle and practice. People's Medical Publishing House, Beijing

Transcatheter Valve Repair and Replacement

36

Lars M. Mattison, Timothy G. Laske, and Paul A. Iaizzo

Abstract

Cardiac device technologies continue to advance at a rapid pace, with heart valve design and placement procedures continuing to be one of the major focus areas. Minimally or less invasive procedures to replace cardiac valves will enable an increasing number of individuals to receive this therapy, including the older and more frail individual, the adult patient with prior surgeries for repair of congenital defects, and/or an individual with previous valve replacement (valve-in-valve procedures). Transcatheter-delivered replacement valves for the four heart valves are either available on the market today or are in development. This chapter provides a brief introduction to this rapidly emerging device area, as well as general considerations related to delivering a device via catheter into the heart (e.g., percutaneous beating heart interventional procedures performed under fluoroscopic and/or echocardiographic guidance).

Keywords

Transcatheter valve repair • Transcatheter valve replacement • Transcatheter-delivered valve system • Pulmonic valve • Aortic valve • Mitral valve • Tricuspid valve

36.1 Introduction

Transcatheter valve repairs and replacements have the potential to reduce operative morbidity, expand the indications for valve replacements for nonsurgical candidates, and treat patients who have been declined for (or choose to decline) surgery. Worldwide, catheter-based valve therapies are rapidly expanding entry into the medical practitioner's arsenal.

L.M. Mattison, BS (✉) • P.A. Iaizzo, PhD
Department of Surgery, University of Minnesota,
420 Delaware Street SE, B172 Mayo, MMC 195, Minneapolis,
MN 55455, USA
e-mail: matti137@umn.edu

T.G. Laske, PhD
Department of Surgery, University of Minnesota,
420 Delaware Street SE, B172 Mayo, MMC 195, Minneapolis,
MN 55455, USA

Cardiovascular Division, Medtronic, Inc., Minneapolis, MN, USA

Balloon valvuloplasties for aortic and mitral stenoses were perhaps the earliest incarnations of this current, rapidly changing environment. In 1990, Cribier demonstrated the technique of balloon aortic valvuloplasty for patients with calcific degenerative aortic stenosis. Although temporarily very successful, these patients often experienced restenosis of the aortic valve and then even worsening of their symptoms. Balloon valvuloplasty was also a popular technique to treat post-rheumatic mitral stenosis but, with rheumatic fever essentially eliminated in most developed nations, this technique is currently not in widespread practice. Similarly, pulmonic stenting with bare metal stents has been utilized as a treatment for patients with recurrent pulmonary stenosis due to repaired congenital heart malformations over the past two decades or so. Both types of treatment were radically changed when Andersen demonstrated the feasibility of the first transcatheter valve replacement in 1992 in animals [1]. While this device was not suitable for use in humans at that time (device required a 41 Fr delivery system), it sparked the

P.A. Iaizzo (ed.), *Handbook of Cardiac Anatomy, Physiology, and Devices*, DOI 10.1007/978-3-319-19464-6_36

minds of other inventors who soon expanded on the idea of a transcatheter-delivered valved stent.

The first report of a transcatheter valve replacement was in 2000 by Professor Philipp Bonhoeffer and colleagues in France who successfully delivered and implanted a valved stent in a right ventricle to pulmonary artery conduit of a patient with a congenital heart malformation [2, 3]. Shortly thereafter, Cribier et al. reported on a transcatheter-delivered valve stent into the aortic position of a patient with degenerative calcific aortic stenosis [4]. Since that time, large and small medical device corporations, as well as individual inventors, have been developing techniques to treat valvular heart disease which can be delivered (or affected) via catheter. The focus of these developments has been to treat the pulmonic and aortic valves with valve replacement, with a recent shift to mitral valves as well. Currently, there are approved devices in the United States, Europe, and Canada for pulmonic and aortic valve replacement for select groups of patients. Additionally, there is a big push to develop transcatheter mitral valves; we noted 18 potential valves in development, from filing for intellectual property to *first in man* studies. In addition to market-released devices and formalized clinical trials, there are many devices which are currently being tested in preclinical animal and human cadaver feasibility trials around the world. These devices and trials will be discussed in greater detail in the following sections.

The development of transcatheter-delivered valve systems requires a combination of numerous technologies including access systems, delivery systems, a stent or support structure with a valve or repair system (i.e., a clip to capture native leaflets), closure systems, and imaging and/or navigation systems. Currently, transcatheter valve replacement stents can generally be classified as balloon-expandable or self-expanding. Balloon-expandable devices are typically made from materials such as cobalt chromium, stainless steel, or platinum iridium alloys, while self-expanding devices are usually made from nitinol (a temperature-dependent, shape memory material). Typically, the valves themselves employ either bovine jugular vein valves or bovine/porcine pericardial constructs. It should be noted that valvuloplasty is often recommended or employed prior to the placement of a transcatheter-delivered valve, but it is not necessarily required in many transcatheter repair procedures [5]. Additionally, if a minimally invasive surgical approach or procedure is employed, then additional specific technologies and/or devices are needed as well. Furthermore, depending on the valve design, a company may also be required to develop systems to load the valves within the delivery systems (e.g., crimping systems). Finally, many device developers are simultaneously creating training simulation systems for the delivery of each product type or procedural approach.

36.2 Pulmonic Valve

A transvenously delivered transcatheter pulmonic valve can be employed as a novel nonsurgical means to treat complications associated with congenital heart disease, such as pulmonary valve insufficiency [3]. A minimally invasive surgical approach is also an option if warranted, depending on individual patient history and/or other interventions that need to be performed. For example, Fig. 36.1 demonstrates that a transcatheter pulmonic valve could be delivered into position either transvenously (via the superior or inferior vena cava) through the tricuspid valve or via a transventricular puncture through the right ventricular wall.

The needs of congenital heart patients inspired the original creation of the transcatheter-delivered stented valve. As noted above, Philipp Bonhoeffer is the pioneer of this technology. One example of such a replacement system is the Melody® Transcatheter Pulmonary Valve (Medtronic, Inc., Minneapolis, MN, USA) [3]. The stent supporting the valve is composed of a platinum iridium alloy, which is expanded during delivery by balloons located within the delivery system. The valve is that of a native bovine jugular valve isolated from the vein, which is sewn to the stent. The Melody valve is delivered using the Ensemble® Transcatheter Delivery System (Medtronic, Inc.) through the cardiovascular system, eliminating the need to open the patient's chest

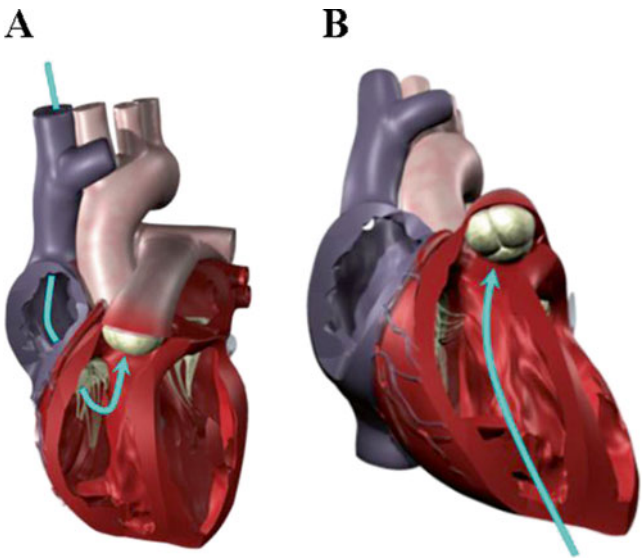

Fig. 36.1 Two potential approaches for the delivery of a transcatheter pulmonic valve: (**A**) transvenously into the right atrium, then through the tricuspid valve, or (**B**) transapically through the right ventricular wall. The later approach would require a minimally invasive surgery

Fig. 36.2 The Melody® Transcatheter Pulmonary Valve and Ensemble® Transcatheter Delivery System (Medtronic, Inc.) has received CE mark approval and is available for distribution in Europe. Additionally, a Medical Device License has been granted and the system is available for distribution in Canada. Products are available for sale in the United States for patients that have congenital heart disease. The system consists of a bovine jugular valve vein sewn inside a platinum iridium stent (**A**) and delivered via a sheathed balloon-in-balloon delivery catheter (**B**)

(Fig. 36.2). The overall procedure minimizes trauma and offers a quicker recovery than traditional surgical procedures. Furthermore, it is considered that such procedures: (1) could reduce the total number of surgeries required by these patients during their lifetimes (e.g., by postponing time to surgery while restoring pulmonic function), (2) would allow for earlier intervention and potentially better outcomes for patients while avoiding surgical complications, (3) avoid the risks of bleeding and infection associated with reoperation, and/or (4) reduce costs by avoiding postoperative intensive care [3, 6, 7].

Currently, there are two commercially available valves that have been used for transcatheter pulmonary valve replacements: the Melody (Medtronic, Inc.) and SAPIEN XT (Edwards Lifesciences, Irvine, CA, USA). To date, the Melody valve is FDA approved for patients with congential heart disease in the United States and CE marked in Europe, whereas the SAPIEN XT valve is CE marked in Europe. The largest difference between these two balloon-expandable valves is their sizing, with the Melody® valve being 18–22 mm in diameter and the Sapien XT being 23 or 26 mm. In a recent clinical assessment, both valves performed very comparably [8].

It is common that developers of these technologies partner with leading congenital interventional cardiologists and cardiac surgeons. Furthermore, managing these complex congenital heart disease patients requires a cohesive team approach. It is likely that such patients will be treated in the hybrid catheter lab/operating room by a "heart team," including an interventional cardiologist and cardiac surgeon.

36.3 Aortic Valve

Currently, transcatheter aortic valve replacement is considered for high- or extreme-risk patients with severe calcific aortic stenosis; these patients are not considered as appropriate candidates for conventional surgical valve replacements. In general, these procedures have similar benefits as those mentioned above, such as eliminating the need for cardiopulmonary bypass and allowing for shorter patient recovery times. It is conceivable that a transcatheter aortic valve could be delivered by one of four different approaches: (1) transarterially (e.g., via the femoral artery, subclavian artery, or the ascending aorta), (2) transseptally via the right heart, (3) transatrially through the left atrial wall or a port in the atrial appendage, or (4) transapically through the left ventricular wall (Fig. 36.3).

Currently, the *transfemoral* approach for the delivery of transcatheter aortic valves is the most common access route; this approach is used 69–91 % of the time [9, 10] and is the preferred access route. Primary alternate access routes are *transapical* (through the apex of the heart in the myocardium), *transaortic* (through the aorta), and *subclavian* (subclavian

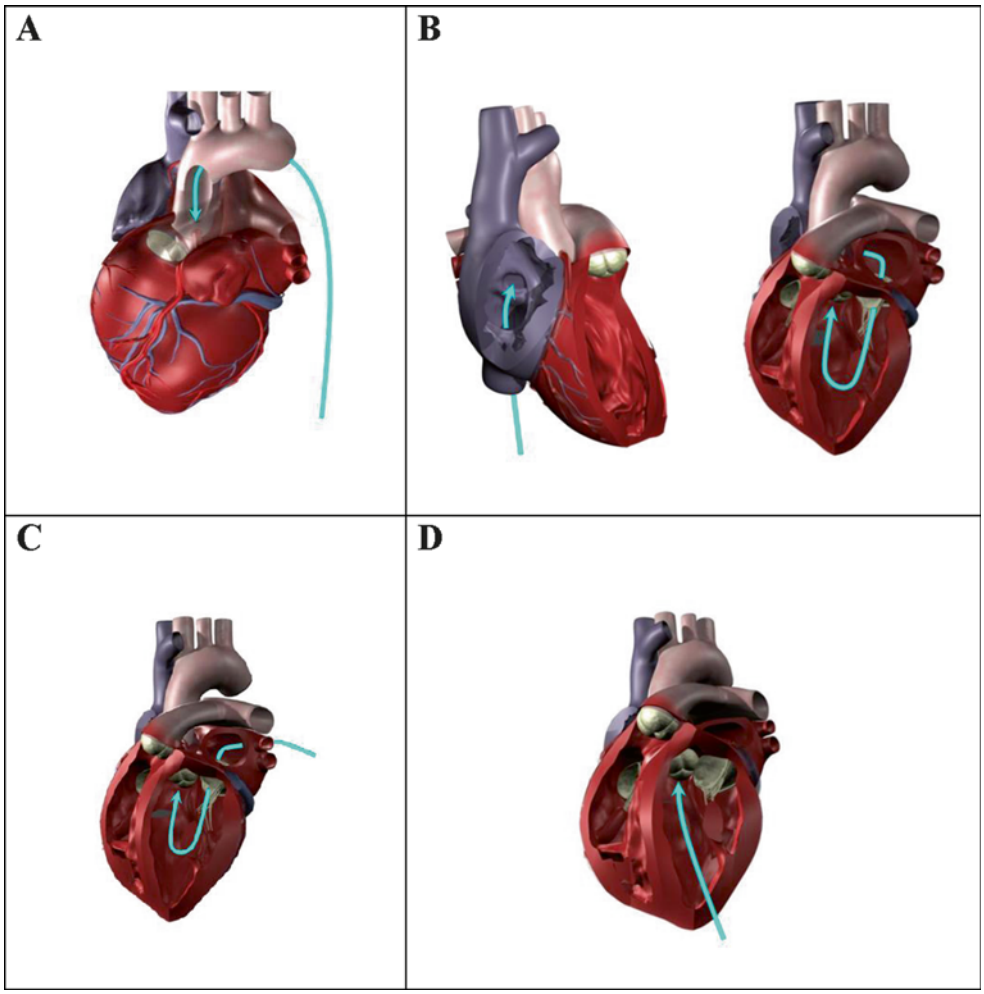

Fig. 36.3 Four potential approaches for the delivery of a transcatheter aortic valve or repair tool: (**A**) transarterially (e.g., via femoral artery access); (**B**) transseptally from the right heart (transvenous access) into the left atrium, then through the mitral valve; (**C**) transatrially through the left atrial wall or through a port in the left atrial appendage, then through the mitral valve; or (**D**) transapically through the left ventricular wall. The latter two approaches would currently require a minimally invasive surgical procedure

artery) routes. These alternate routes are typically used when the *transfemoral* approach is deemed not possible due to: (1) the size of the patient's arteries; (2) the tortuosity of the arteries and/or aorta; and/or (3) the degree of calcification within the aorta, some which could potentially be knocked free by the delivery system. Note that the transfemoral, transaortic, and subclavian routes all require retrograde delivery, while transapical requires an antegrade approach.

In current practice, both the *transapical* and *transaortic* approaches require a minimally invasive surgery (see Chap. 35), yet they provide the most direct anatomical approach. The *transapical* approach must go through the left ventricular wall (myocardium) which can be difficult to close if a large delivery system is used and/or if the myocardial tissue is abnormally frail. The *transaortic* approach also requires closure of a hole that is placed into the ascending aorta. This can be especially difficult if the aorta is extremely calcified, a condition known as a *porcelain aorta*. As technology advances, the need for minimally invasive surgery with these approaches may be eliminated. The *transseptal* approach, which has the advantage of employing transvenous access for the delivery system, has the potential drawback that if the system passing through the interatrial wall is large, the physician may create a septal defect which will require a subsequent repair (see Chap. 37). Additionally, the system must make a turn of approximately 180 degrees in the left ventricle, after passing through the complex structures of the mitral valve, to be positioned in the aortic valve, a maneuver that can be technically challenging. Anatomically, inferior access via a femoral vein is considered advantageous due to the proximity of the inferior vena caval ostium and the fossa ovalis, which is the preferred transseptal puncture location.

It has been reported that rapid ventricular burst pacing can be employed to facilitate transcatheter heart valve implantation. Pacing rates between 150 and 220 bpm with durations of 12 ± 3 s were relatively well tolerated ($n = 40$) when cautiously used. Rapid pacing was associated with a rapid and effective reduction in systemic blood pressure, pulse pressure, transvascular flow, as well as cardiac and catheter motion [11].

As can be observed in Fig. 36.3, the potential pathways/approaches to place a transcatheter-delivered valve in the aortic position are quite varied and have dramatic differences

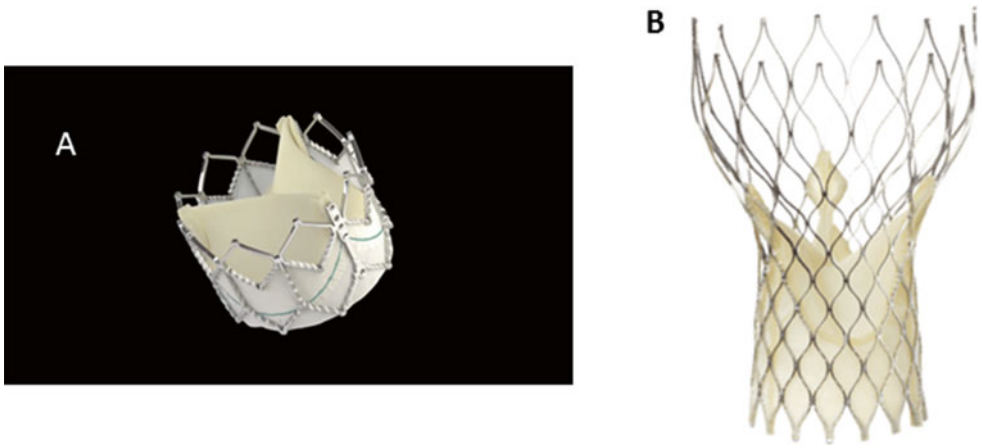

Fig. 36.4 (**A**) The Edwards Lifesciences SAPIEN XT transcatheter heart valve consists of a cobalt chromium balloon-expandable stent with an attached pericardial valve. It has been designed for transfemoral placement with the NovaFlex+ delivery system or for transapical placement with the Ascendra delivery system. It has been approved for high- and extreme-risk surgical patients in the United States and Europe. (**B**) The ReValving System by CoreValve, Inc. (Medtronic, Inc.), consists of a self-expandable nitinol stent with an attached pericardial valve. It is designed for transarterial delivery and is currently approved for high- and extreme-risk cases in the United States and Europe

in the angles and anatomical features that would be required to be navigated within or through, e.g., vessels, chamber walls, valves, or chordae tendineae. Due to this complexity, the flexibility of the delivery system (with the valve loaded inside) will be a major factor to consider when selecting a delivery approach; furthermore, the patient's cardiac anatomy is a major consideration. This is true for the delivery of the system and also for the positioning of the valve stent into the aortic position, as one must prevent obstruction to the ostia of the coronary arteries.

Currently, there are several transcatheter aortic valves available for clinical use, in clinical trials, or in animal testing. The CoreValve (Medtronic, Inc.) and the SAPIEN XT (Edwards Lifesciences) are FDA approved for high- and extreme-risk patients, and to date, several hundred thousand devices have been implanted in patients worldwide (Fig. 36.4). More specifically, for the transarterial placement of the SAPIEN XT transcatheter heart valve, the surgeon uses the NovaFlex+ delivery system (Edwards Lifesciences), whereas he/she uses the Ascendra+ delivery system (Edwards Lifesciences) for a transapical placement. The CoreValve system is also delivered via a transarterial approach in a specialized delivery catheter. In addition, several other companies that have developed (and continue to develop) competing technologies, including Boston Scientific (Marlborough, MA, USA) and St. Jude Medical (St. Paul, MN, USA) as well as smaller companies such as Direct Flow Medical, Inc. (Santa Rosa, CA, USA) and Heart Leaflet Technologies Inc. (Maple Grove, MN, USA). Nevertheless, nearly all the major players in cardiac valve replacement have a keen interest in these technologies and clinical approaches (Fig. 36.5) [12].

It is important to note that, currently, a percentage of patients that have received transcatheter-delivered aortic valves have elicited conduction abnormalities which may include heart block. Most of the self-expanding or balloon-expanded valve prostheses exert radial forces on the interventricular septal wall and surrounding structures which is required to maintain proper position and to minimize paravalvular leaks. This force, coupled with the close anatomic proximity of the atrioventricular node, the bundle of His, and/or the left bundle branch with the basal annulus of the aortic valve, is the likely explanation for this phenomenon (Fig. 36.6) (see Chap. 13).

36.4 Mitral Valve

Mitral valve dysfunction can be related to several factors including diseased leaflets [13], annular changes [14], abnormal or damaged chordae [15], and ventricular dilatation [16] causing displacement of the papillary muscles. Due to this large variability in disease process, a wide variety of transcatheter devices are being investigated for the mitral valve. These transcatheter devices can be subdivided into five general types: (1) devices for Alfieri-type edge-to-edge repair, (2) indirect annuloplasty devices deployed into the coronary sinus, (3) direct annuloplasty devices placed on or near the mitral annulus, (4) devices for dimensional control of the left ventricle or left atrium, and (5) devices for mitral valve replacement [17, 18].

The edge-to-edge technique involves placing a stitch to join the anterior and posterior leaflets at the location of regurgitation [19–21]. This technique is most commonly

Manufacturer	Edwards SAPIEN XT	Medtronic CoreValve	Direct Flow Medical	Boston Scientific Sadra Medical	St. Jude Medical Portico
Access	TF, TA, TAo	TF, SC, TAo	TF	TF	TF
Deployment	Balloon-expandable	Self-expandable	Inflatable	Self-expandable	Self-expandable
Support structure	Cobalt chromium	Nitinol	Inflatable	Nitinol	Nitinol
Leaflets	Bovine pericardium	Porcine pericardium	Bovine pericardium	Bovine pericardium	Bovine pericardium
Skirt	Polyethylene terephalate	Porcine pericardium	Polyester	Polyurethane	Porcine pericardium
Delivery catheter	18 Fr/19 Fr	18 Fr	18 Fr	18 Fr/20 Fr	18 Fr
R[3]	No	Partially	Yes	Yes	Yes

Fig. 36.5 This figure shows a variety of transcatheter aortic valves that are currently working through the regulatory process. It provides an insight into the design and delivery of the valve as well [12]. *SC* subclavian, *TA* transapical, *TAo* transaortic, *TF* transfemoral. ©2013 Heart Valves: From Design to Clinical Implantation, Transcatheter aortic valve implantation, Piazza N, Mylotte D, Martucci G. With kind permission of Springer Science+Business Media, New York

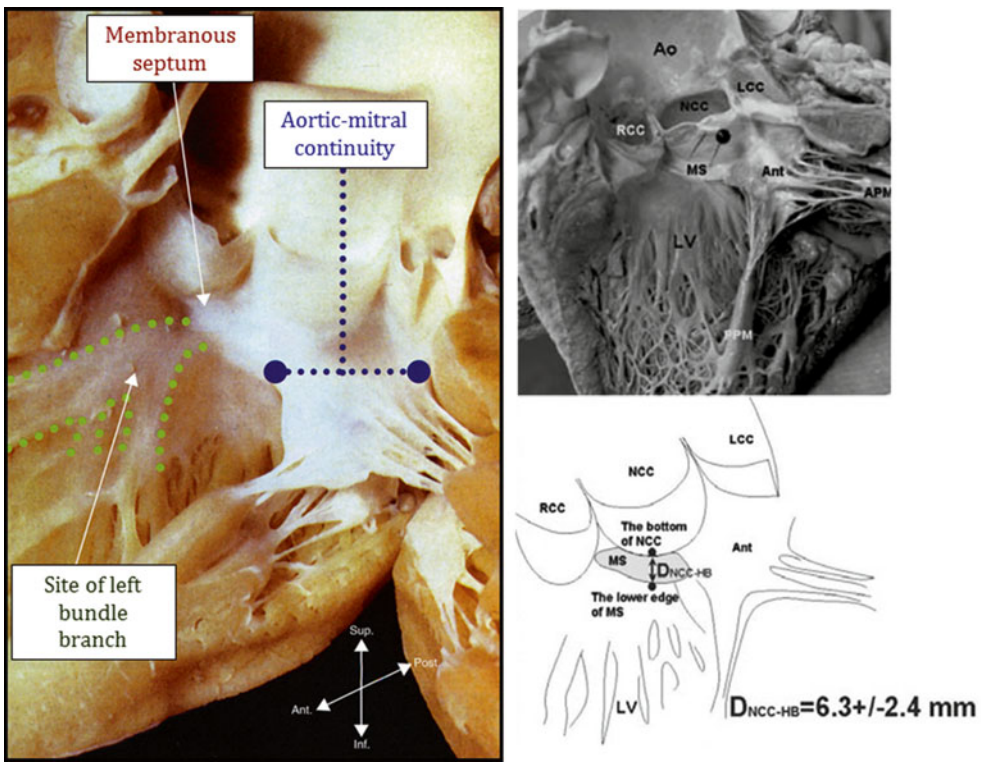

Fig. 36.6 A dissected human heart that shows the proximity of the aortic valve to the left bundle branch. The noncoronary cusp is 6.3 ± 2.4 mm from left bundle branch as depicted in the right picture. It is more common in self-expanding valves to experience issues with the conduction system in the heart [12], ©2013 Heart Valves: From Design to Clinical Implantation, Transcatheter aortic valve implantation, Piazza N, Mylotte D, Martucci G. With kind permission of Springer Science+Business Media, New York

used in patients with A2 or P2 prolapse, and the simplicity of the edge-to-edge technique has led to opportunities for percutaneous valve repair [22–24]. More recently, the MitraClip repair system was designed to use transcatheter clips to grasp the ventricular sides of the anterior and posterior mitral leaflets, leaving the clip in place upon deployment (Abbott Vascular, Bloomington, IN, USA). This technology was FDA approved in 2013.

For patients with annular dilatation, many devices are currently being developed to simulate a traditional annuloplasty procedure. These products are classified as either indirect, which typically involves a transvenous coronary sinus approach, or direct, which involves placing the device in direct contact with the mitral annulus. Percutaneous, transvenous mitral annuloplasty is a technology that implants a metal bar with flexible ends and a stiff midsection to reshape the posterior leaflet; it is a reversible procedure (Viacor, Inc., Wilmington, MA, USA). The Monarc system features two self-expanding stents tethered together which reshape the posterior region of the annulus in 2–3 weeks (Edwards Lifesciences). Similar to the Monarc, Carillon XE (Cardiac Dimensions, Inc., Kirkland, WA, USA) utilizes tethered stents in the coronary sinus to reshape the posterior annulus. These technologies rely on the proximity of the coronary sinus to the posterior aspect of the mitral annulus. Additionally, direct mitral annuloplasty is also being investigated; these devices are in direct contact with the mitral annulus either temporarily or permanently. MiCardia Corporation (Irvine, CA, USA) is developing adjustable annuloplasty devices which are currently implanted surgically but can be adjusted on the beating heart. The Mitralign device (Mitralign, Inc., Tewksbury, MA, USA) places implants around the annulus and then cinches them closer together, thereby reducing the orifice area of the valve. Nevertheless, the goal of these devices is to restore valve coaptation and thus eliminate mitral regurgitation.

Indirect approaches to mitral valve repair that influence left ventricular or left atrial dimensions are also under investigation. By changing left ventricular dimensions, products such as Coapsys and iCoapsys (Myocor® Inc., Maple Grove, MN, USA) are designed to improve mitral valve and left ventricular performance. The PS^3 system (Ample Medical, Inc., Foster City, CA, USA) shortens the left atrial dimension between the fossa ovalis and the great cardiac vein and consequently the septal-lateral dimension of the mitral annulus [25].

As described for the aortic valve, it is possible to deploy a transcatheter mitral valve or affect a transcatheter repair using four different approaches: (1) transarterial (e.g., via the femoral artery), (2) transseptal via the right heart, (3) transatrial through the left atrial wall or a port in the atrial appendage, or (4) transapical through the left ventricular wall (Fig. 36.7). The human mitral valve is a very complex, dynamic, and highly variable structure. Therefore, complications in the deployment of a replacement valve or repair device into this position will potentially interact with the (1) valve leaflets themselves, (2) the chordae tendineae, and/or (3) the papillary muscles. As mentioned earlier, the valvular and subvalvular anatomy can be quite variable, with some individuals eliciting bifurcated or trifurcated papillary muscles, distinct chordae tendineae patterns, and numerous scallops of each mitral valve leaflet. Due to the complexity of the mitral valve apparatus and underlying disease processes, it is likely that a combination of the aforementioned devices will be required to provide percutaneous solutions for mitral valve repair.

There is currently intense competition to develop the first reliable transcatheter-delivered mitral valve replacement. For example, we identified more than 18 transcatheter valves that are in production phases, ranging from filing intellectual property to first in man clinical studies (see Table 36.1) [26]. At present, most of these devices are further along the clinical trial process in Europe than the United States, due to different regulations (see Chap. 43). To date, the valves that are in first in man studies are the Fortis (Edwards Lifesciences), CardiAQ (Irvine, CA, USA), Tiara (Neovasc, Richmond, BC, Canada), and Tendyne/Lutter TMVR (Tendyne, Roseville, MN, USA). At least 18 additional devices have been developed to help treat mitral regurgitation. It will be exciting and interesting to see how these transcatheter mitral valve products continue to develop in the upcoming years.

36.5 Tricuspid Valve

As described for the mitral valve, the human tricuspid valve is a very complex, dynamic, and highly variable structure. The transcatheter approach to this valve structure is similar to those described for the pulmonic valve (Fig. 36.1). It is envisioned that a transcatheter mitral valve or repair tool could be delivered into position either transvenously (via the superior or inferior vena cava) or via a transapical puncture through the right ventricular wall. Furthermore, as described above for the repair and/or replacement of the mitral valve, nearly all options would hold true for the tricuspid valve, which many surgeons feel is often overlooked when treating heart failure patients (for a more detailed discussion, see Chap. 34). On the other hand, the potential complications of damaging or altering the conduction system would also be evident for procedures that involve the tricuspid septal annular structures, i.e., atrioventricular node, the bundle of His, and/or the right bundle branch of the conduction system (see Chap. 13).

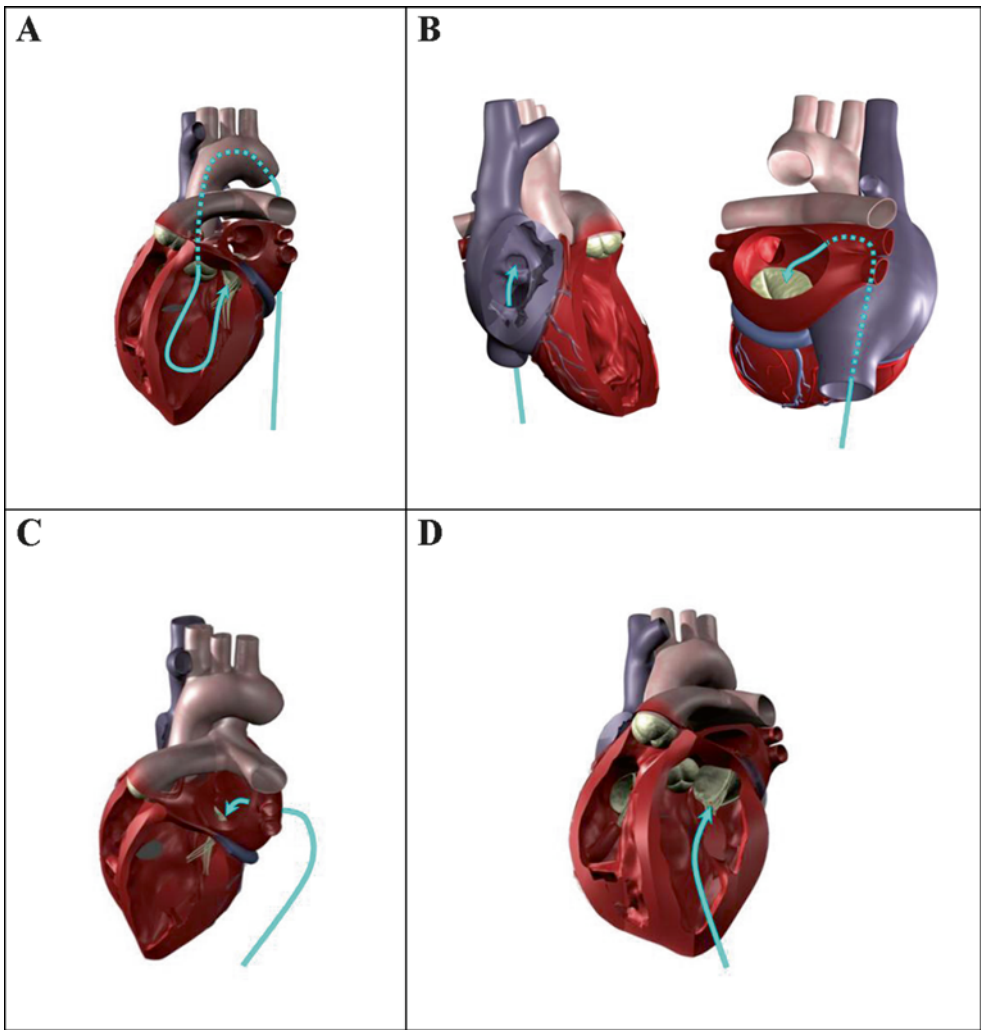

Fig. 36.7 Four potential approaches for the delivery of a transcatheter mitral valve or repair tool: (**A**) transarterially (e.g., via femoral artery access) retrograde through the aortic valve and up to the mitral valve via the left ventricular chamber; (**B**) transseptally from the right heart (transvenous access) into the left atrium, then to the mitral valve; (**C**) transatrially through the left atrial wall or through a port in the left atrial appendage, then to the mitral valve; or (**D**) transapically through the left ventricular wall. The latter two approaches currently require a minimally invasive surgical procedure

36.6 Imaging

The development and use of transcatheter-delivered cardiac valves has transformed (and will continue to transform) heart valve procedures for those requiring open-heart surgery and/or cardiopulmonary bypass (see Chap. 33) to a "percutaneous beating heart interventional procedure performed under image guidance" (fluoroscopy or echocardiography). Yet, these imaging modalities are considered to have advantages and disadvantages. For example, cardiac computed tomography (CT) imaging is considered extremely useful for identifying the relative degree of calcification that exists on a heart valve leaflet as well as the delivery anatomy, but is not useful as an intraoperative technique, and it exposes the patient to considerable radiation doses.

Importantly, advanced imaging modalities will be required for preplanning and intraoperative guidance of these interventions. More specifically, to date, there is no single imaging modality for intracardiac interventions without clinical limitations, which include low temporal or spatial resolution, excessive exposure to ionizing radiation, and interference with the clinical operator's freedom of movement. We believe that, in the near future, a combination of imaging modes will provide the information required to guide these complex interventions. Recently, our group set out to provide "a glimpse into the future" by demonstrating the unique direct visualization of transcatheter pulmonary valve implantation utilizing the Visible Heart® techniques (Figs. 36.7, 36.8 and 36.9) [27, 28]. See also Chap. 41.

Current pre-procedural imaging consists of a combination of CT scans and echocardiography. This is important for determining the sizes of the various valve annuli and the relative amounts of calcification that may exist along the given delivery route, as well as the position of the coronary artery ostia for aortic valve replacement. Utilization of these 3D renderings can be invaluable to aid the interventional cardiologist and/or cardiac surgeon to make informed decisions about the proper treatment for each given patient (Fig. 36.10).

Table 36.1 Current products that are being developed for transcatheter mitral valve repair

Company	Valve name	Status	
		International	United States
Edwards	Fortis	First in man	In development
Caisson	Caisson TMVR		Preclinicals
CardiAQ*	TMVI-TA		Preclinicals
CardiAQ*	TMVI-TF	First in man	Preclinicals
Emory University	MitraCath		In development
HighLife	HighLife mitral valve replacement	Preclinicals	
INVALVE	INVALVE device	IP	
Medtronic	Medtronic TMVR	Preclinicals	Preclinicals
Micro Interventional Devices	Endovalve-transapical		In development
MitrAssist	MitrAssist valve	Preclinicals	
Mitralix	MAESTRO	In development	
MITRICARES	MITRICARES device	IP	
NCSI	Navigate TMVR	Clinical implants	Preclinicals
Neovasc	Tiara	First in man	First in man
Tendyne	Tendyne/Lutter TMVR	First in man	Preclinicals
Twelve	TMVR		IP
Valtech	Cardiovalve	Preclinicals	

Note that there are several first in man studies in Europe, while most valves in the United States are only in the preclinical level. A few valves are only conceptual at the moment, as intellectual property has just been filed * CardiAQ was recently acquired by Edwards

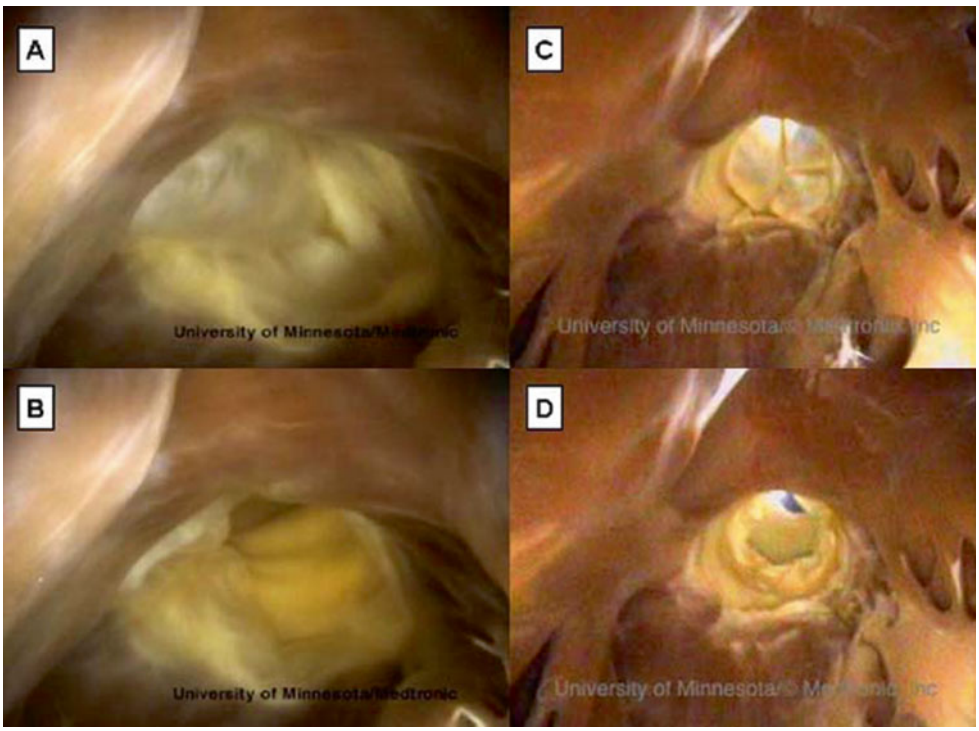

Fig. 36.8 Comparison of a human pulmonic valve (**A**) during diastole and (**B**) during systole to a transcatheter pulmonic valve placed in a human heart (**C**) during diastole and (**D**) during systole [28]. ©2008 Expert Review in Medical Devices, vol. 5, Cardiac device testing enhanced by simultaneous imaging modalities: the Visible Heart®, fluoroscopy, and echocardiography. Permission granted by Informa (http://informahealthcare.com/)

We also suggest that, as cardiac repair and device implantation procedures become less invasive, we will need to study the deployment of these systems or techniques within beating heart models. Utilization of Visible Heart® methodologies provides unique visualization of cardiac device technologies. The preparation and images obtained can be used by design engineers and physicians to develop implant methodologies as well as support clinical education and training. As more of these devices are implanted within the beating heart, unique means will be required to train individuals in the techniques to navigate and deploy them. For example, Fig. 36.9 shows simultaneously obtained images of a stent being placed in the aortic position, including endoscopic views and time-synchronized images from fluoroscopy and ultrasound (Fig. 36.11).

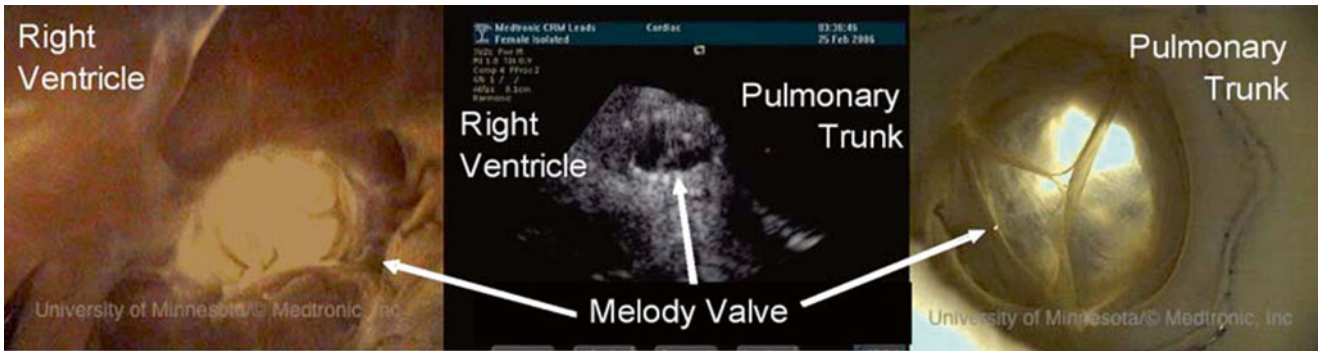

Fig. 36.9 Simultaneous endoscopic images on the left and right depict a deployed transcatheter pulmonary valve (Melody® Transcatheter Pulmonary Valve, Medtronic, Inc.) in the native right ventricular outflow tract, with the corresponding ultrasound image displayed in the center [28]. ©2008 Expert Review in Medical Devices, vol. 5, Cardiac device testing enhanced by simultaneous imaging modalities: the Visible Heart, fluoroscopy, and echocardiography. Permission granted by Informa (http://informahealthcare.com/)

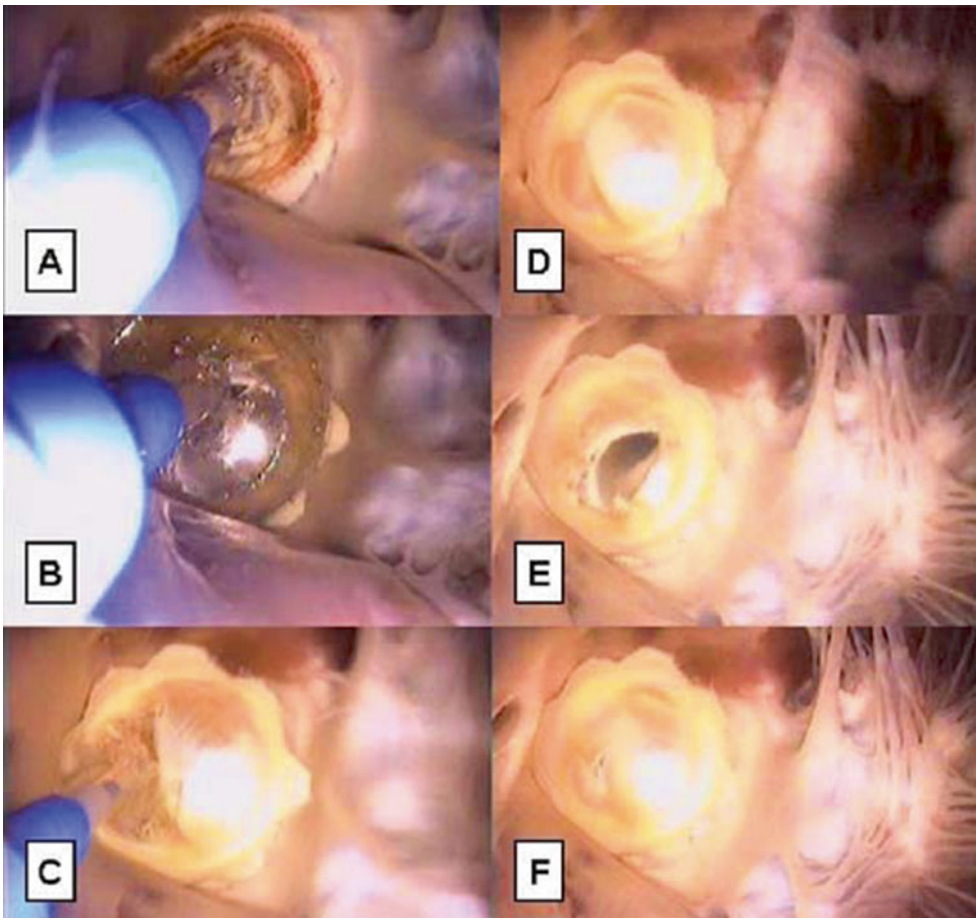

Fig. 36.10 Positioning (**A**), deployment (**B** and **C**), and function (Panels **D**–**F**) of a transcatheter aortic valve implanted into a surgically placed bioprosthetic aortic valve. It is interesting to note the lack of (or minimal) interactions between the implanted aortic valve and the native mitral valve [28]. ©2008 Expert Review in Medical Devices, vol. 5, Cardiac device testing enhanced by simultaneous imaging modalities: the Visible Heart®, fluoroscopy, and echocardiography. Permission granted by Informa (http://informahealthcare.com/)

36.7 Training Systems

The complexity of intracardiac interventions has increased with the advent of transcatheter valve replacement and is expected to further escalate as clinicians become more comfortable with complicated cardiac repairs within the beating heart and as engineers invent new product solutions. Simulators designed to demonstrate the technical aspects of transcatheter-delivered valves have already been developed. Many state-of-the-art patient simulators enable pseudo-visualization via various imaging modes. For instance, one can practice using fluoroscopy for the valve implant without any exposure to radiation. The delivery systems for these transcatheter valves are often complex and require guidewires, introducers, and/or dilators; hence, prior practice on handling such tools is essential.

Fig. 36.11 3D model of a patient's ascending aorta, aortic arch, and descending aorta. The vessel is modeled in the gold color, while the calcium deposits are white in color. It is also possible to see the coronary arteries that come off the root. Using this model the size of the aortic annulus can be measured, as well as the height of the coronaries from the annulus [29]

Furthermore, for those physicians not familiar with performing such catheter-delivered and/or minimally invasive surgical approaches, these training sessions can be invaluable and highly educational. If such procedures are performed in a newly instrumented hybrid catheter lab/operating room, then the dynamics of team interactions could also be developed in such training sessions. More specifically, studies employing virtual reality simulation of such procedures have indicated that there is a documented learning curve, and catheter handling errors significantly decrease as assessed with measurable dynamic metrics with high test-retest reliability [30] (Fig. 36.12).

36.8 Summary

The clinical application of transcatheter delivery systems to repair or replace cardiac valves is an area of intense growth, and there is also continued research development. The potential to treat patients with valvular disease without the use of open-heart surgery will ultimately affect millions of individuals worldwide, improving quality of life for these patients. The future of this field will likely see smaller delivery systems with greater intracardiac mobility, as well as replacement valves that better mimic healthy native valve function. Affecting the ultimate clinical success of these therapies will be adequate cardiac visual and function assessments prior to, during, and after these procedures. One can also foresee that simulation training will be employed even before such techniques are performed in preclinical animal studies, as many procedures will require numerous tool components (e.g., introducers, dilators, balloon catheters, delivery catheters, etc.). For additional detailed discussions on these topics, the reader is referred to manuscripts by Schoenhagen and To [31], Quill et al. [32], Scheivano et al. [3], and Piazza et al. [5].

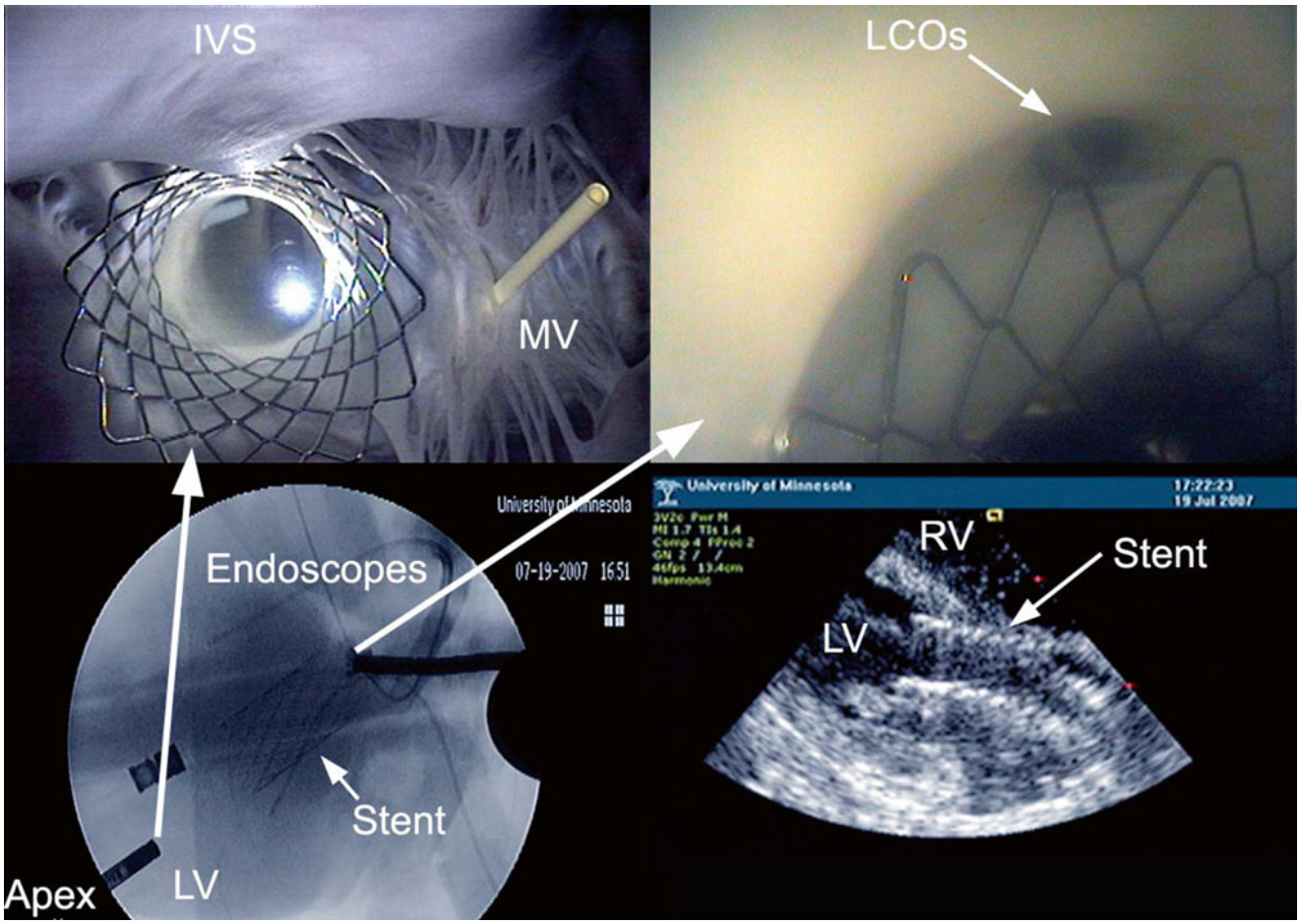

Fig. 36.12 *Top images* show endoscopic views of a prototype stent placed in the aortic position, and *bottom images* show time-synchronized images from fluoroscopy (*lower left*) and ultrasound (*lower right*). The *upper left image* shows the view from the ventricle; the interventricular septum (IVS) is at the top and the mitral valve (MV) is located on the right. The *upper right image* is a view from the aorta, specifically showing the interaction of the stent and left coronary artery ostium (LCO); in this case, there would be minimal obstruction of flow into the left coronary artery. The fluoroscopic image clearly shows the stent as well as the endoscopes in the left ventricle and aorta. The stent is also visible on the ultrasound image, projecting slightly into the left ventricle (LV). The right ventricle (RV) is located at the top of this image [23]. ©2008 Expert Review in Medical Devices, vol. 5, Cardiac device testing enhanced by simultaneous imaging modalities: the Visible Heart®, fluoroscopy, and echocardiography. Permission granted by Informa (http://informahealthcare.com/)

References

1. Andersen HR, Knudsen LL, Hasenkam JM (1992) Transluminal implantation of artificial heart valves. Description of a new expandable aortic valve and initial results with implantation by catheter technique in closed chest pigs. Eur Heart J 13:704–708
2. Bonhoeffer P, Boudjemline Y, Saliba Z et al (2000) Percutaneous replacement of pulmonary valve in a right-ventricle to pulmonary-artery prosthetic conduit with valve dysfunction. Lancet 356:1403–1405
3. Schievano S, Taylor AM, Bonhoeffer P (2013) Percutaneous pulmonary valve implantation: the first transcatheter valve. In: Iaizzo PA, Bianco RW, Hill AJ, St. Louis JD (eds) Heart valves: from design to clinical implantation. Springer, New York, pp 211–226
4. Cribier A, Eltchaninoff H, Bash A et al (2002) Percutaneous transcatheter implantation of an aortic valve prosthesis for calcific aortic stenosis: first human case description. Circulation 106:3006–3008
5. Piazza N, Mylotte D, Martucci G (2013) Transcatheter aortic valve implantation. In: Iaizzo PA, Bianco RW, Hill AJ, St. Louis JD (eds) Heart valves: from design to clinical implantation. Springer, New York, pp 227–260
6. Coats L, Tsang V, Khambadkone S et al (2005) The potential impact of percutaneous pulmonary valve stent implantation on right ventricular outflow tract re-intervention. Eur J Cardiothorac Surg 27:536–543
7. Khambadkone S, Bonhoeffer P (2004) Nonsurgical pulmonary valve replacement: why, when, and how? Catheter Cardiovasc Interv 62:401–408
8. Ghawi H, Kenny D, Hijazi ZM (2012) Transcatheter pulmonary valve replacement. Cardiol Ther 1:5
9. Moat NE, Ludman P, de Belder MA et al (2011) Long-term outcomes after transcatheter aortic valve implantation in high-risk patients with severe aortic stenosis: the U.K. TAVI (United Kingdom Transcatheter Aortic Valve Implantation) Registry. J Am Coll Cardiol 58:2130–2138
10. Hamm CW, Mollmann H, Holzhey D et al (2013) The German Aortic Valve Registry (GARY): in-hospital outcome. Eur Heart J 35:1588–1598

11. Webb JG, Pasupate S, Achtem L, Thompson CR (2006) Rapid pacing to facilitate transcatheter prosthetic heart valve implantation. Catheter Cardiovasc Interv 68:199–204
12. Iaizzo PA, Bianco RW, Hill AJ, St. Louis JD (eds) (2013) Heart valves: from design to clinical implantation. Springer, New York
13. Roberts WC (1983) Morphologic features of the normal and abnormal mitral valve. Am J Cardiol 51:1005–1028
14. Yiu SF, Enriquez-Sarano M, Tribouilloy C, Seward JB, Tajik AJ (2000) Determinants of the degree of functional mitral regurgitation in patients with systolic left ventricular dysfunction: a quantitative clinical study. Circulation 102:1400–1406
15. Hickey AJ, Wilcken DE, Wright JS, Warren BA (1985) Primary (spontaneous) chordal rupture: relation to myxomatous valve disease and mitral valve prolapse. J Am Coll Cardiol 5:1341–1346
16. Kono T, Sabbah HN, Rosman H, Alam M, Jafri S, Goldstein S (1992) Left ventricular shape is the primary determinant of functional mitral regurgitation in heart failure. J Am Coll Cardiol 20:1594–1598
17. Babaliaros V, Block P (2007) State of the art percutaneous intervention for the treatment of valvular heart disease: a review of the current technologies and ongoing research in the field of percutaneous valve replacement and repair. Cardiology 107:87–96
18. Feldman T, Leon MB (2007) Prospects for percutaneous valve therapies. Circulation 116:2866–2877
19. Nakanishi K, Raman J, Hata M, Buxton B (2001) Early outcome with the Alfieri mitral valve repair. J Cardiol 37:263–266
20. Alfieri O, Maisano F, De Bonis M et al (2001) The double-orifice technique in mitral valve repair: a simple solution for complex problems. J Thorac Cardiovasc Surg 122:674–681
21. Alfieri O, Maisano F (1999) An effective technique to correct anterior mitral leaflet prolapse. J Card Surg 14:468–470
22. Alfieri O, Maisano F, Colombo A (2004) Percutaneous mitral valve repair procedures. Eur J Cardiothorac Surg 26:S36–37; discussion S37–38
23. Alfieri O, De Bonis M, Lapenna E et al (2004) "Edge-to-edge" repair for anterior mitral leaflet prolapse. Semin Thorac Cardiovasc Surg 16:182–187
24. Alfieri O, Maisano F, Colombo A, Pappone C, La Canna G, Zangrillo A (2004) Percutaneous mitral valve repair: an attractive perspective and an opportunity for teamwork. Ital Heart J 5:723–726
25. Rogers JH, Macoviak JA, Rahdert DA, Takeda PA, Palacios IF, Low RI (2006) Percutaneous septal sinus shortening: a novel procedure for the treatment of functional mitral regurgitation. Circulation 113:2329–2334
26. Maisano, Francesco. "Transcatheter Mitral Valve Implantation." EuroPCR 2014. Paris, France. Lecture.
27. Quill JL, Laske TG, Hill AJ, Bonhoeffer P, Iaizzo PA (2007) Direct visualization of a transcatheter pulmonary valve implantation within the Visible Heart®—a glimpse into the future. Circulation 116, e548
28. Iaizzo PA, Hill AJ, Laske TG (2008) Cardiac device testing enhanced by simultaneous imaging modalities: The Visible Heart®, fluoroscopy, and echocardiography. Expert Rev Med Devices 5:51–58
29. Edwards Scientific. (2015 November). *A Less Invasive Treatment Option For Severe Aortic Stenosis*. Retrieved November 2015 from promotional CD
30. Patel AD, Gallagher AG, Nicholson WJ, Cates CU (2006) Learning curves and reliability measures for virtual reality simulation in the performance assessment of carotid angiography. J Am Coll Cardiol 47:1796–1802
31. Schoenhagen P, To ACY (2013) Advanced 3D imaging and transcatheter valve repair/implantation. In: Iaizzo PA, Bianco RW, Hill AJ, St. Louis JD (eds) Heart valves: from design to clinical implantation. Springer, New York, pp 159–186
32. Quill JL, Menk AR, Tang GHL (2013) Transcatheter mitral repair and replacement. In: Iaizzo PA, Bianco RW, Hill AJ, St. Louis JD (eds) Heart valves: from design to clinical implantation. Springer, New York, pp 187–210

Cardiac Septal Defects: Treatment via the Amplatzer® Family of Devices

37

John L. Bass

Abstract

The majority of patients with congenital heart disease present with defects resulting from vascular narrowing or absence (such as interruption or coarctation of the aorta or pulmonary arteries) or failure of structures to fuse or separate during development (total anomalous pulmonary venous connection, septal defects, fusion of valve cusps). Correction of these defects initially began with open-heart surgery, but now many of these repairs can be performed through catheter-delivered closure devices (e.g., Amplatzer closure devices). This chapter will present a brief history of defect repairs and provide information on the design, development, and preclinical animal testing of such systems.

Keywords

Interventional cardiac catheterization • Atrial septal defect • Transcatheter closure • Patent ductus arteriosus • Muscular ventricular septal defect • Perimembranous ventricular septal defect

37.1 Introduction

Congenital heart disease affects eight of every thousand live births. Correction of these defects initially began with open-heart surgery and was originally limited to repairs that could be performed without stopping the patient's circulation (patent ductus arteriosus or coarctation of the aorta). The subsequent development of cardiopulmonary bypass allowed the surgeon to safely visualize the inside of the heart, and more complex repairs were successful developed. This was the true beginning of caring for children with congenital heart disease, dramatically extending and improving the quality of their lives. However, with these advances, the art of diagnosis by physical examination was no longer sufficient to provide details of anatomy needed by the surgeon. Cardiac catheterization and X-ray visualization during the 1950s and 1960s also underwent a similar clinical explosion as the primary diagnostic tool. Still, surgeons had to be prepared to deal with the unique individual anatomies found during a given operation, i.e., as some details were unexpected. This surgical license to make plans "on the fly" is critical to a successful operation and explains the historical liberation of surgery from restrictions by the Food and Drug Administration (FDA) and Institutional Review Boards.

Next, echocardiography developed to the point where it began to replace cardiac catheterization as the primary diagnostic tool for congenital heart disease (see Chap. 22). Thus, the number of cardiac catheterizations diminished. On the other hand, interventional cardiac catheterization, pioneered by Dr. Gruntzig's coronary angioplasty, became an important clinical tool; these techniques were applied to relieve congenital narrowing of the pulmonary arteries and aorta. Experimental testing preceded the use of these techniques in children with congenital heart disease [1, 2]. Importantly, it was observed that no foreign materials were left behind while performing these angioplasty procedures. Interventional cardiac catheterization further expanded

J.L. Bass, MD (✉)
University of Minnesota Children's Hospital,
2450 Riverside Avenue, East Building Room MB547,
Minneapolis, MN 55454, USA
e-mail: bassx001@umn.edu

P.A. Iaizzo (ed.), *Handbook of Cardiac Anatomy, Physiology, and Devices*, DOI 10.1007/978-3-319-19464-6_37

with Dr. Porstmann's use of an Ivalon plug to close the persistent patent ductus arteriosus (PDA) [3], as well as Dr. King's [4] and Dr. Rashkind's [5] devices for closure of secundum *atrial septal defects* (ASDs). Nevertheless, technical difficulties (i.e., limited retrievability and large delivery systems) and residual shunts plagued the early development of these devices and their application remained limited.

Two companies in particular—NuMED, Inc. (Hopkinton, NY, USA) and the former AGA Medical Corporation (now St. Jude Medical, St. Paul, MN, USA)—focused their efforts on developing devices aimed at correcting congenital cardiac defects. In 2001, the Amplatzer Septal Occluder became the first device to receive FDA approval for closure of secundum ASDs, followed in 2003 by the Amplatzer Ductal Occluder. This, along with development of stents that could be applied to the larger vascular narrowings of congenital heart diseases, opened the floodgates for interventional cardiac catheterization in children. We consider that both Allen Tower (NuMED, Inc.) and Kurt Amplatz (AGA Medical Corporation) deserve special recognition for choosing to focus their innovative efforts on improving care for children with congenital heart disease, instead of the larger volume and remuneration of fixing adult problems with coronary artery stents or patent foramen ovale closure devices.

37.2 Amplatzer Devices

The Amplatzer devices designed to close congenital cardiac defects are all quite similar; basically, they all are self-expanding stents shaped to fit a specific anatomical defect. These devices are primarily composed of a closed nitinol wire frame fashioned with a waist containing polyester fabric baffles or stuffing to fill the defect, as well as retention discs. The shapes of the wire frames are tailored to fit the various abnormal vascular or intracardiac communications. In other words, the retention discs fix the device against vascular or cardiac walls. The central waist further holds the device in place by placing radial forces against the margins of the communications, i.e., providing stable fixation of the device. Most available devices are concentric and designed to fill defects that are centrally located and thus are surrounded by cardiac structures that will not be injured by the edges of these devices. In general, subsequent occlusion occurs through thrombosis within the polyester baffles or stuffing inside of the wire frame. Importantly, within approximately 3 months, these devices are considered to be covered with protein and cellular layers, reducing the potential for forming a surface thrombus and eliminating the risk of infective endocarditis [6].

Historically, the development of Amplatzer devices began when thin wire technologies reached a point that allowed for the unique construction of frames employing nontoxic nitinol wires. Like all stents, the collapsed device is required to be long and narrow to fit through the delivery sheath. Uniquely, nitinol metal has shape memory such that, as it exits the sheath, the device expands and assumes its original shape at body temperatures. Each device has a microscrew fixed to the proximal end allowing attachment to a delivery cable. Thus, these devices can be retrieved with the cable after deployment and then either removed or repositioned. Finally, the Amplatzer devices can be detached via unscrewing once an optimal, secure, and effective position is confirmed.

37.2.1 Safety

Nickel-containing alloys, such as stainless steel, have been employed in human medicine for over 100 years. They have been used in surgical instruments as well as implants such as pacemaker wires, vascular clips, mechanical cardiac valves, orthopedic prostheses, Harrington rods, and inferior vena cava filters. This demonstrates the relative lack of toxicity of nickel-containing metallic implants; no systemic effects were observed or have been reported. Local fibrotic reactions surrounding stainless steel implants were thought to be due to passivation of nickel ions into surrounding tissue, despite the absence of microscopically visible corrosion. Interestingly, the US Navy developed the new nickel-containing metal, nitinol, in the 1960s. This alloy of nickel and titanium displayed superior corrosion resistance, and it still carries the name of its heritage—NIckel TItanium-Naval Ordnance Laboratory.

Nitinol has numerous properties besides corrosion resistance that make it desirable for use in medical devices, including: (1) super elasticity (pseudo-elasticity), (2) thermal shape memory, (3) high resiliency, and (4) fatigue resistance. Originally, thin wire technology, more specifically the development of the *diamond-drawn* wire, provided a shape that could be used in endodontic appliances. The tendency for nitinol to return to its nominal shape when deformed was especially useful in this application. This property also made nitinol a valuable material in the production of endoluminal devices. Importantly, a nitinol device can be stretched for introduction through a small delivery catheter, and then it expands back to its original shape when deployed. This new alloy replaced most stainless steel devices, especially self-expanding stents. Furthermore, nitinol's fatigue resistance properties prevent wire fractures and extend device durability. The absence of ferromagnetic properties is compatible with magnetic resonance imaging.

To date, all Amplatzer devices have proven to be nontoxic [7]. In addition, such devices performed well in fatigue testing, and when immersed in a saline bath, they did not corrode. A patient's serum nickel levels may rise immediately after insertion of an Amplatzer device, but return to normal over 3 months. Furthermore, devices examined 18 months

post implantation in humans and animals have not revealed any detectable surface corrosion. It should be noted that the incidence of cutaneous nickel allergy is approximately 10 % in humans. Yet, with over 100,000 current implants of Amplatzer devices worldwide over the past 13 years, no definitive case of a reaction has been reported in the literature.

37.3 Animal Models Mimicking Congenital Defects

Originally, the diagnosis of an ASD was established solely by typical findings on physical examination, electrocardiogram, and chest roentgenogram [8]. Surgical repair of cardiac defects, such as those of the atrial or ventricular septa, specifically required the surgeon to evaluate the shape and surrounding structures on an individual basis. Associated abnormalities, such as anomalous pulmonary venous connection, could be identified and dealt with by the surgeon at the time of the operative repair.

Animal models created to test experimental devices may not always account for associated anatomic details encountered in human congenital defects. For most congenital heart defects, an exact animal model is not readily available. Nevertheless, devices can be tested for ease of use, reliability, and efficacy, i.e., by creating an experimental defect by dilating a thin septum, sewing in an artificial vascular connection, or removing a portion of the thicker muscular septum. It should be noted that the concept of these "defects" is chosen from imaging and/or examination of pathological specimens, but may not always mimic the actual defect in humans.

37.4 Atrial Septal Defects

37.4.1 History

Atrial septal defects are congenital deficiencies in the wall separating the systemic and pulmonary venous returns as they enter the heart. These ASDs allow blood from the lungs to flow through the defect and increase the volume of blood passing through the pulmonary arteries. In most patients, after 2 decades of life with this flow pattern, this defect can permanently damage the pulmonary vasculature. Therefore, to prevent this and other problems such as associated cardiac arrhythmias, closure of an ASD is recommended during the first few years of life [9].

The University of Minnesota performed the first surgical closure of an ASD in 1952 [10] (see Chap. 25). This successful operative approach for correction of a congenital intracardiac defect remains as one of the safest open-heart operations performed, with a mortality rate under 0.5 % [9]. Nevertheless, surgical closure may include morbidity from the median sternotomy (or a right thoracotomy), the risk of exposure to blood products, insertion of a chest tube, a 3–5-day hospitalization, convalescence of 4–6 weeks, and/or the chance of postpericardiotomy syndrome. Hence, the potential consequences of these procedures spurred attempts to develop a safe and less invasive method of transcatheter closure.

It is generally accepted that transcatheter closure to treat secundum ASDs is an ideal procedure. These types of ASDs are typically surrounded by rims of tissue that a device can clasp, with no borders formed by or thus impeding the valves or the walls of the heart. King and Mills reported the first attempted transcatheter closure of a secundum ASD in 1974 [4]. This was followed by development of the Clamshell/CardioSEAL (NMT Medical, Inc., Boston, MA, USA) [11], Sideris button (Custom Medical Devices, Inc., Gainesville, FL, USA) [12], ASDOS (Sulzer Osypka, Rheinfelden, Germany) [13], and Angel Wings (Das et al.) [14] devices. Each of these devices provided an alternative to surgical closure, but also resulted in a number of new challenges. For example, large devices were required with the central post design, yet most of these early designs were not self-centering, and the center post could move within the defect. Further, these early devices required large delivery systems, and, additionally, some were plagued by unwanted embolization (e.g., unbuttoning) [15]. It was also found that frame fatigue and arm fracture occurred in up to 10 % of some of these designs, with asymptomatic wire embolization observed in several patients. It was concluded that most of these designs were difficult or impossible to recapture or retrieve after deployment. Hence, surgical removal was required if they were deployed in an improper position, and residual shunt rates were significant [16].

37.5 Amplatzer Device Designs

An ideal septal closure device should be: (1) easily delivered and implanted, (2) self-centering, (3) able to pass through a small delivery system, (4) recapturable and redeployable, (5) highly resilient (without fracturing), and (6) highly effective (without significant residual shunts). The materials used in the construction of such devices should also be biocompatible and nontoxic. It should be emphasized that durability is important, for the majority of patients are children and there is a long device "lifetime" after implantation.

The Amplatzer ASD devices were designed to fulfill these requirements. For example, the Amplatzer Septal Occluder is a woven mesh of 72 nitinol wires 0.003–0.008 in. in diameter with shape memory. There are two retention discs with a central waist that is placed within the defect (Fig. 37.1); the

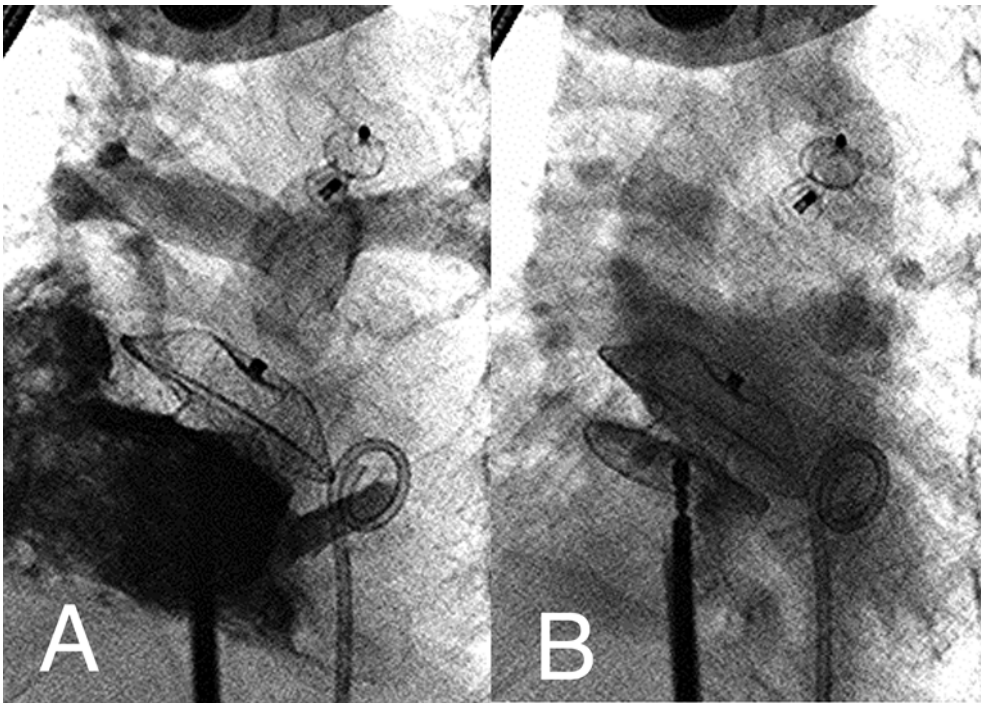

Fig. 37.1 Amplatzer Septal Occluder device. (**A**) Right atrial angiogram performed after deployment of the device in a secundum atrial septal defect, but before release. The right atrial disc is obscured by contrast with the waist within the atrial septal defect. (**B**) The levophase of the right atrial angiogram opacifying the left atrium. Contrast outlines the left atrial disc completely within the left atrium

left atrial disc is 12–14 mm larger than the waist. The stenting action of the waist and the retention discs clasps the atrial septum, thus holding the device stable and in place. Additionally, fabric baffles sewn inside the discs and waist promote thrombosis and thus the overall occlusive ability of the device. Importantly, the delivery systems are also relatively small (6–12 Fr delivery sheaths). In addition, these devices are recapturable and redeployable with microscrew/cable attachments. Available waist diameters range from 4 to 40 mm, thus allowing closure of relatively large defects [16].

37.5.1 Animal Testing of the Amplatzer Device Designs

The Amplatzer Septal Occluder device was originally designed for occlusion of a secundum ASD. Initial animal studies focused on reproducibly creating such atrial septal communications, as a natural model of a secundum ASD did not exist. To do so, nonsurgically the flap of the foramen ovale in the experimental animal was perforated and dilated with a balloon to induce an atrial communication [6]; subsequently, devices were implanted, and, in most cases, there were no complications or residual leaks. It was important to show that no thrombus formed on the devices. Afterwards, human clinical trials confirmed that no retroaortic rim was required for stable device position and complete closure. Importantly, patients could be discharged the morning after device placement, and they remained on low dose aspirin and endocarditis prophylaxis for 6 months after closure [16].

37.5.2 Required Testing for FDA Approval

An FDA-approved study to provide clinical evidence of the effectiveness of the Amplatzer Septal Occluder was originally initiated, based on the prior success of animal studies and European trials in humans. Yet, the clinical study design for this device was considered difficult. In general, patients and their families wanted to avoid surgery, despite the long history of safe surgical closure and the lack of long-term follow-up with this new device. Therefore, a blinded randomization was unsuccessful, as many patients and families that were chosen for the surgical group simply opted out of the trial, preferring to wait for final FDA approval. The overall study design was subsequently modified to allow device closure at some institutions with patients recruited to designated surgical centers. This is not true randomization, but is representative of the difficulty of study design in the real world.

Later, the results of Phase II of the FDA trial also showed that the Amplatzer Septal Occluder was an effective and safe therapy as compared to the surgical group. Importantly, at the end of 12 months, there was complete closure or a small (<2 mm) residual shunt in 98.5 % of device patients, compared to 100 % of surgically closed patients. Furthermore, there were no differences between groups in the incidence of major complications. Minor complications were more common in surgical patients (27/442, 6.1 % versus 29/154, 18.8 %); however, one needs to consider that all patients were not truly randomized. There were differences between groups, with the surgical patients being younger (18.1 ± 19.3

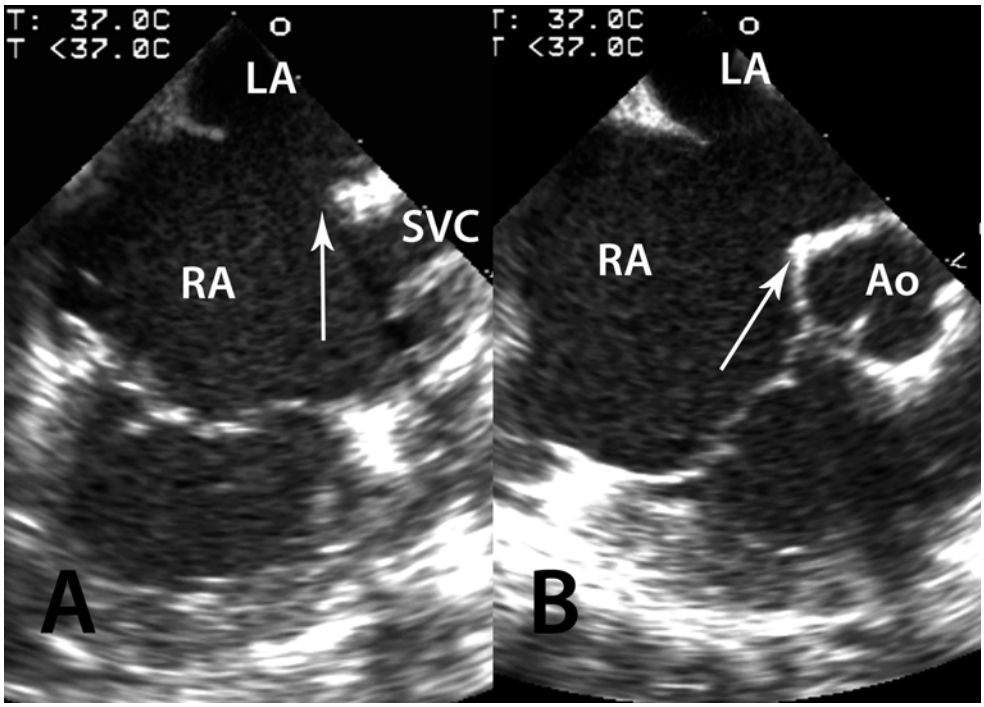

Fig. 37.2 Transesophageal images of an atrial septal defect with minimal superior and anterior (retroaortic) rims. (**A**) A bicaval view is recorded with almost no rim (*arrow*) by the superior vena cava (SVC). (**B**) A short axis view of the aorta (Ao) is recorded with minimal retroaortic rim (*arrow*). Atrial septal defects with minimal rims in these two areas are likely to bring the edges of right or left atrial retention discs in contact with the right or left atrial wall against the ascending aorta and may have a higher risk of cardiac perforation. *LA* left atrium, *RA* right atrium

versus 5.9 ± 6.2 years, $p < 0.001$) and smaller (42.3 ± 27.3 kg versus 20.6 ± 15.2 kg, $p < 0.001$) [16]. In December 2001, the FDA granted premarket approval of the Amplatzer Septal Occluder, the first ASD closure device with such an approval.

37.5.3 Continued Animal Research and Translation to Humans

After extensive successful clinical use, several reports of perforation of the heart by the device began to appear in a small number of patients with secundum ASDs [17]. Subsequently, a careful review of information from patients suffering from erosion after Amplatzer Septal Occluder placement suggested that individuals with "deficiency" of the superior and anterior rims of the atrial septum were at highest risk of this complication (Fig. 37.2). In fact, the majority of patients with secundum ASDs have very little retroaortic rims, so many patients with ASDs may be at increased risk of erosions of the Amplatzer Septal Occluder through the superior, anterior left, or right atrial walls. This anatomical relationship of the ascending aorta to the anterior rim of the secundum ASD was not fully appreciated until these complications of erosion were reported. It should also be noted that the original animal model studied did not truly mimic the anatomies of many patients with secundum ASDs. More recently, using stop flow to eliminate oversizing of the Amplatzer Septal Occluder device [17] has reduced the frequency of these complications (personal communications with Ken Lock, St. Jude Medical Corporation).

37.6 Patent Ductus Arteriosus

A *patent ductus arteriosus* is a failure of closure of a vascular channel present in the fetus that normally closes within the first few days after birth. When this vessel remains open, overcirculation of the lungs results. This, in turn, can damage the pulmonary vasculature, overwork the heart, and predispose these individuals to infective endocarditis. Closure of this channel is recommended to reduce the workload of the heart, when spontaneous closure is no longer likely (beyond 1–2 years of age) [18]. Much like operative closure of a secundum ASD, surgical closure of a PDA is a low risk procedure that has been used for decades [19]. Therefore, any attempt to employ transcatheter closure methods must carry a procedural risk at least as low as surgery. Furthermore, a PDA is similar to a secundum atrial defect in that the vascular communication is surrounded by normal vessels. It has been shown that concentric devices modified from the design of the Amplatzer Septal Occluder provided the opportunity for transcatheter closure procedures in patients with these defects.

Successful transcatheter closure of a small PDA was available before a specific closure device was developed. More specifically, coil occlusion of a PDA was first performed at the University of Minnesota in 1972. These early procedures included filling the aortic ampulla with stainless steel coils and their attached Dacron fibers, or "hanging" a coil across the narrowest part of a PDA; both procedures produced reliable closure. The first embolization coils were not attached to delivery wires, and the coils sometimes embolized

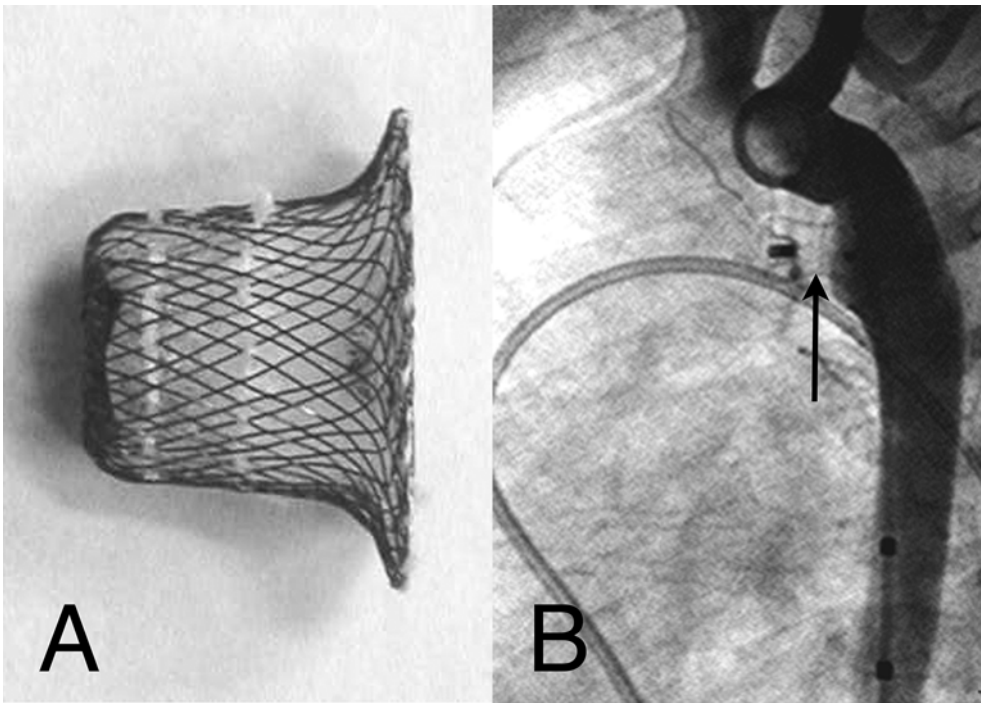

Fig. 37.3 Amplatzer Ductal Occluder device. (**A**) Photograph of the device with clearly visible suturing of the baffle and stuffing to the ductal plug. (**B**) Aortogram immediately after device placement. The aortic disc is flat against the aortic wall with the plug within the ductal lumen. There is no flow through the ductus and no obstruction of the aorta or left pulmonary artery

into the pulmonary circulation. These techniques were most effective when the narrowest diameter of the patent ductus was less than 3 mm [20]. During this period of time, a retrievable device that would occlude larger ductus defects was considered desirable.

The Amplatzer Ductal Occluder is shaped like a plug, sized to the aortic ampulla with an aortic retention disc designed to prevent embolization through the ductus (Fig. 37.3). This device is typically delivered via a venous route, and the delivery catheter is small (5–8 Fr) because of the small collapsed device diameter. This simple modification of a self-expanding stent was found to be extremely successful in producing complete occlusion of even larger PDAs. In the Phase II FDA trial, there was an observed complete closure of over 97 % of PDAs at 6 and 12 months. There was only a 2.3 % incidence of serious or major adverse events (including one embolization that required surgical removal and one death of a child, not device related, with a chromosomal trisomy) [21]. Premarket FDA approval of the Amplatzer Ductal Occluder device was received in January 2003.

37.6.1 Animal Testing of the Amplatzer Ductal Occluder and Translation to Human Use

A persistent PDA does not occur reliably in animals; therefore, a model needed to be created to test the efficacy of the Amplatzer Ductal Occluder. An asynthetic tube was sewn between the descending aorta and the pulmonary artery in animals [22]. The Amplatzer Ductal Occluder device worked well in these animals, completely occluding the surgically created PDA with endothelialization within 3 months. In animal trials, there were no complications, the device was retrievable, and there were no residual hemodynamic abnormalities.

Subsequent to the successful animal studies, clinical trials were undertaken with a high rate of success in occluding various sizes of PDAs in patients [23]. Yet with more extensive clinical use, a few case reports began to surface of partial obstruction of the descending thoracic aorta by the retention disc of the Amplatzer Ductal Occluder device. This was the result of the angle (approximately 65°) of insertion of the naturally occurring PDA with the descending aorta. In these cases, the superior portion of the retention disc was shown to be angled into the aorta by the plug within the PDA (Fig. 37.4), sometimes producing partial aortic obstruction in smaller patients with larger PDAs. It should be noted that the surgically created experimental PDA in the animal model was sewn at a 90° angle to the aorta, so this complication was not predicted by the anatomically inaccurate orientation.

37.6.2 Animal Trials Designed to Test Prototype Angled Amplatzer Ductal Occluder Devices

To reduce the complexity of manufacturing the Amplatzer Ductal Occluder device and, at the same time, address the issues of the angle of the descending aorta with the PDA, a new device was designed with an angled retention disc; the wire

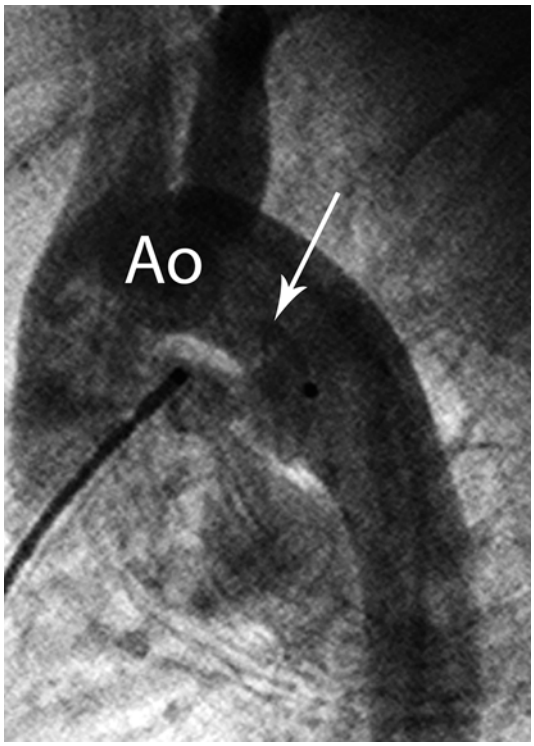

Fig. 37.4 An aortogram recorded in lateral projection after placement of an Amplatzer Ductal Occluder device, fully deployed before release. The aortic retention rim protrudes superiorly (*arrow*) into the aortic lumen (Ao). The angle of the human patent ductus arterosus is at an angle of approximately 65°, instead of 90° in the animal model. This device is oversized and can be retrieved using the delivery cable still attached to the device

count was also increased from 72 to 144 wires, thus eliminating the need for fabric in the device [24]. For animal testing of this new design in next stage trials, a synthetic tube was sewn between the pulmonary artery and aorta at the angle of the more naturally occurring human PDA. Subsequently, in all animals in this preclinical trial, the angled Amplatzer Ductal Occluder device was successful in occluding the created PDA (Fig. 37.5A); however, the initial human use of the device revealed shortcomings with these animal trials. Specifically, an angled Amplatzer Ductal Occluder was successfully placed in a young infant with initial success, which also avoided any protrusion of the device into the aorta; however, after 3 months, the device expanded the PDA resulting in "recanalization" (Fig. 37.5B) [25]. This complication was considered to result from two unanticipated design problems. First, the hoop strength of the angled Amplatzer Ductal Occluder was sufficient to dilate the PDA in a young infant. This, in turn, resulted in an increase in the distance between the radial "spokes" of the device, with less occlusive resistance. In retrospect, the animal model trial used a non-expandable PDA with small diameters that limited the distance between the wires of the device.

37.6.3 Redesign of a Device Without Fabric and Flexible Retention Disc Orientation

The latest iteration of the Amplatzer family of ductal occluder devices (Amplatzer Ductal Occluder device 2—ADO2) is longitudinally symmetrical with retention discs on each end and with flexibility at the connection of the retention discs to the occluding plug (Fig. 37.6). This allows the retention discs to angle and lie smoothly against the aortic or pulmonary wall. To create an animal model for testing this device, infant piglets had balloon dilation of the probe PDA so that an anatomically true defect was available [26]. Subsequently, the size of the discs was further reduced to allow implantation in smaller infants (ADO2-Additional Sizes, ADO2-AS). This device was tested after ductal dilation in newborn piglets weighing 1800–2200 g and implanted under echocardiography to mimic occlusion in a premature infant in the isolette, similar to surgical ligation in this population. The animal testing was successful [27], and there are early positive results in clinical trials of premature infants outside the United States [28].

37.7 Muscular Ventricular Septal Defect

Muscular ventricular septal defects can occur in the lower, thicker ventricular septum. Closure of such defects is clinically recommended for the same indications as ASDs and PDAs—eliminating overwork of the heart and overcirculation of the lungs. However, unlike for the other two defects, surgery to close a muscular ventricular septal defect is generally not a simple or low risk option. More specifically, the surgical closure of muscular ventricular septal defects can be difficult at best, e.g., the right ventricular aspect of the defect can be hidden from the surgeon's view by trabeculations within the right ventricular cavity. This, in turn, can result in a high incidence of residual leaks with a right ventricular approach. On the other hand, directly incising the left ventricle would allow clearer visualization of the defect margins, but left ventricular aneurysms or diminished left ventricular function has resulted in some cases [29]. These surgical difficulties make the transcatheter closure of such ventricular defects an attractive alternative.

In general, the Amplatzer Muscular Ventricular Septal Occluder is very similar to the Amplatzer Septal Occluder. Like a secundum ASD, muscular ventricular septal defects are separated from cardiac valves by myocardium; the obvious difference is the thickness of the ventricular myocardium. Therefore, these devices were designed with greater distances between the discs to accommodate for the differences in myocardial thickness (Fig. 37.7). Greater stability was found to be produced by the radial force applied against

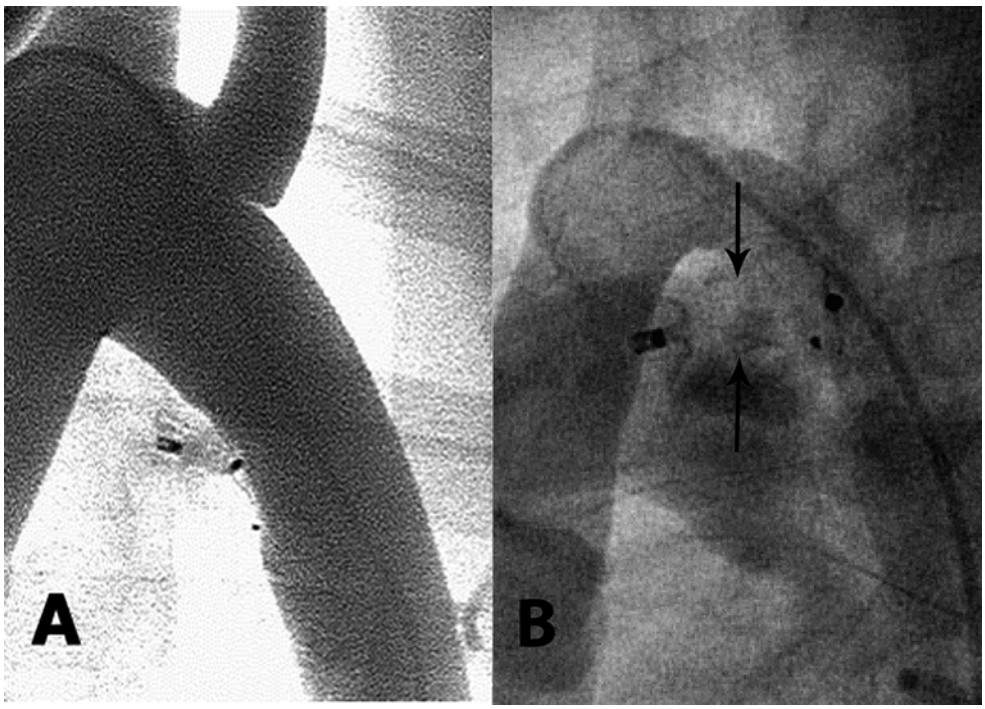

Fig. 37.5 (**A**) An aortogram is performed after placement and release of an angled ductal occluder device in a canine model with the artificial ductus sewn to mimic the natural angle of the human patent ductus arteriosus. The angled aortic retention disc lies flat against the aortic wall with no protrusion into the aortic lumen. The "plug" of the device is compressed with immediate complete occlusion. (**B**) A similar angled patent ductus arteriosus device has been placed in a human infant. The angiogram is recorded 3 months after implantation. The device plug was initially compressed with minimal flow through the middle. After 3 months, the device has expanded the ductus (*arrows*) with increased interwire distance and "recanalization"

the thicker muscular ventricular septum, thus the retention disc diameters were decreased to 6–8 mm larger than the waist. From a design standpoint, it should be noted that initial attempts of transcatheter closure of muscular ventricular septal defects, using the Clamshell/CardioSEAL device, produced a 40 % incidence of residual leaks [30]. These devices have a central post instead of a waist the size of the defect. Therefore, a ventricular "retention" disc had to be sized at least twice the diameter of the defect; residual leaks could result from migration of the central post within the defect. In contrast, the self-centering Amplatzer Muscular Ventricular Septal Occluder is fixed within the defect by its waist. Another advantage of the Amplatzer device is the smaller maximum device diameter required to close a muscular ventricular septal defect, compared with central post devices.

37.7.1 Animal Trials Designed to Test Ventricular Closure Devices

It was the successful animal trials to close surgically created muscular ventricular septal defects [31] that eventually led to human use [32], but once again the clinical use in humans subsequently demonstrated the shortcomings of these preclinical experimental models. In general, naturally occurring muscular ventricular septal defects in humans frequently are not circular (Fig. 37.8); at least 60 % are twice as wide as they are tall [33]. The typical method of sizing muscular ventricular septal defects is to look at the vertical dimension of the defect using either echocardiography or angiography. Angiography, in particular, demonstrates only the vertical dimension, and, because the shunt occurs primarily during systole, the defect is best outlined during contraction when the diameter of the muscular ventricular septal defect is smallest. Measuring the muscular ventricular septal defect from en face or 3D echocardiographic imaging accounts for the oval shape of the defect and can be timed in diastole; note the capability of these imaging modalities has advanced dramatically in the last 5–10 years. The frequency of residual shunts is reduced by using a device with the same circumference as the defect in diastole [33].

37.8 Perimembranous Ventricular Septal Defect

Amplatzer devices designed for closing secundum ASDs, PDAs, and muscular ventricular septal defects are concentrically symmetrical, as there are typically no valves near the edges of the defects they are designed to close. In contrast, in

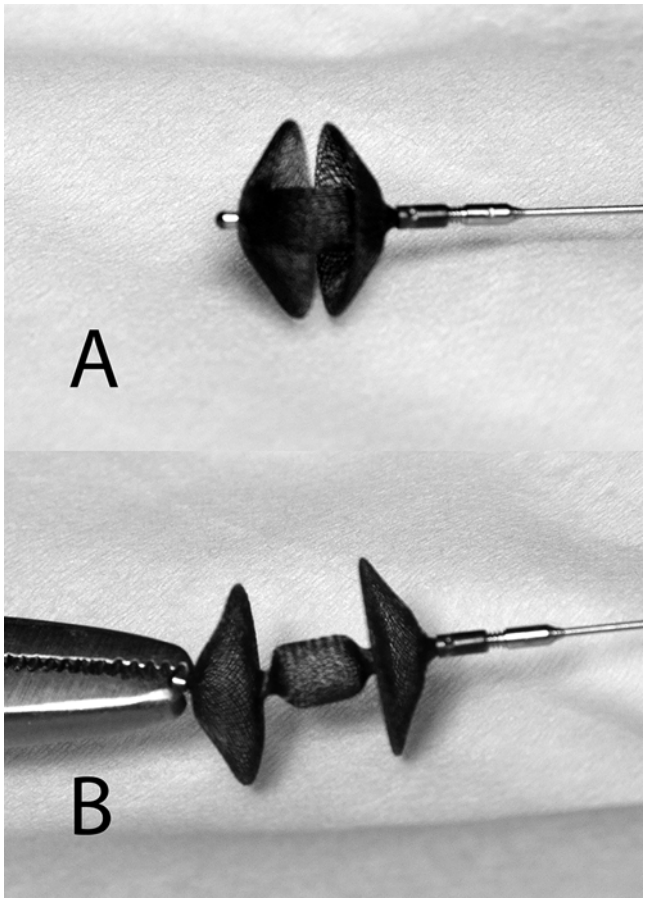

Fig. 37.6 Amplatzer Ductal Occluder II device. The device is longitudinally symmetrical allowing implantation from either the aortic or pulmonary approach. The constriction of the device between the central plug and the retention discs allows the discs to swivel and align against the vascular wall of the aorta and pulmonary artery

perimembranous ventricular septal defects, both the aortic and tricuspid valves can be close to the defect margins. From a historic perspective, early attempts were made to close perimembranous ventricular septal defects with the Clamshell and Sideris button devices. However, it was soon reported that distortions of the aortic valves resulted in aortic insufficiency and, in some cases, the devices were found to have embolized [34]. It was considered that the flexibility of shaping the basic Amplatzer device frames could be advantageous to produce an eccentric, asymmetric device. More specifically, an Amplatzer Perimembranous Ventricular Septal Occluder (Fig. 37.9) was designed with a minimal rim of the left ventricular disc (0.5 mm); to sit beneath the aortic valve, a longer (5.5 mm) inferior left ventricular disc and a short waist (1.5 mm) are needed to keep the right ventricular disc away from the tricuspid valve. In subsequent animal trials, it was shown that an eccentric design protected the aortic and tricuspid valves, yet closed perimembranous ventricular septal defects [35].

However, the difficulty with such systems was in the reliability of delivering the device in the proper orientation. Advancing a pigtail catheter from the pulmonary artery through a patent ductus often results in the curl of the catheter oriented along the lesser curvature of the aorta. Therefore, a sharply curved delivery sheath was designed to deliver these devices to the left ventricular apex, mimicking this property. In addition, simply advancing the asymmetric device through this sheath did not always result in proper device orientation. A sharply curved delivery catheter was designed that forced attachment of the device with the longer left ventricular disc along the lesser curvature of the catheter (Fig. 37.10). Yet, it was determined that when combined

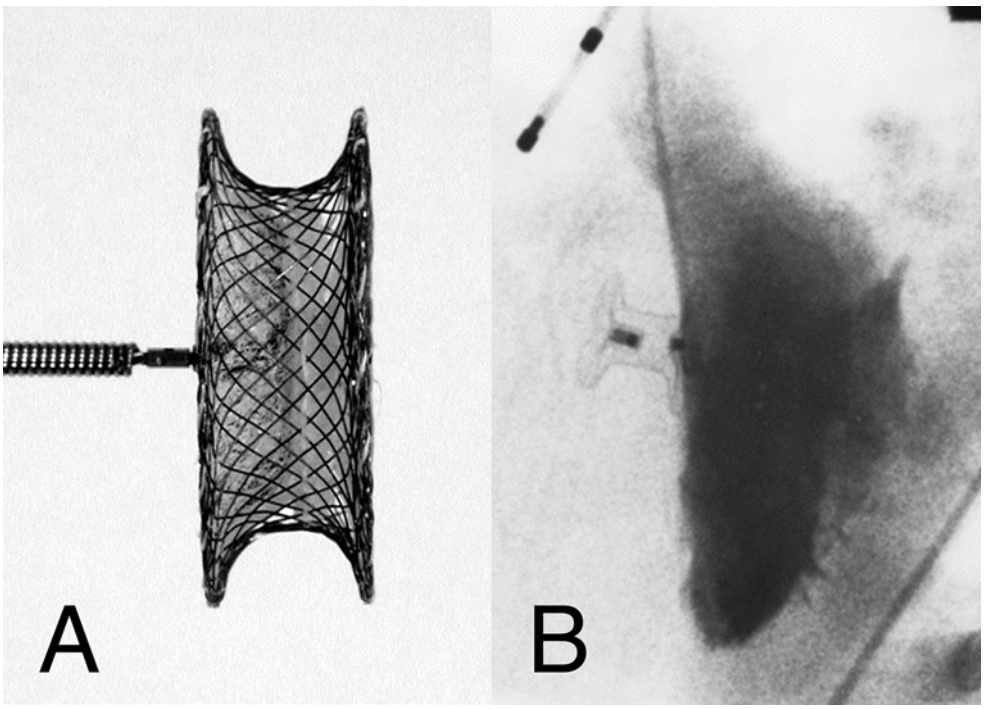

Fig. 37.7 Amplatzer Muscular Ventricular Septal Occluder. (**A**) Photograph of the device; the waist is wider than that of the Amplatzer Septal Occluder to allow for the thicker muscular ventricular septum. (**B**) Left ventricular angiogram 3 months after device placement showing complete occlusion of a mid-muscular ventricular septal defect

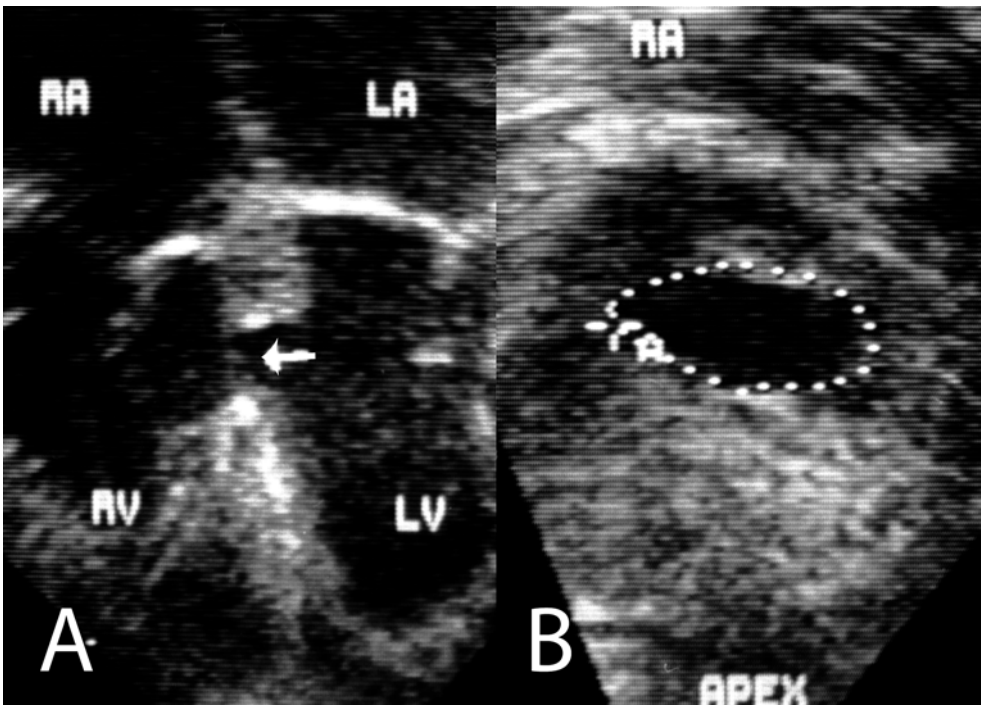

Fig. 37.8 Echocardiographic images of a mid-muscular ventricular septal defect. (**A**) An apical four-chamber view is recorded. There is "dropout" of echoes from the mid septum (*arrow*) with a short vertical dimension. (**B**) An en face view of the right ventricular surface of the ventricular septum is recorded in the same patient. The ventricular septal defect is outlined by the dotted line. The vertical dimension is significantly less than the horizontal one. If only the vertical dimension is considered in choosing the device size, there would be a significant residual shunt, or device embolization might be possible. *LA* left atrium, *LV* left ventricle, *RA* right atrium, *RV* right ventricle

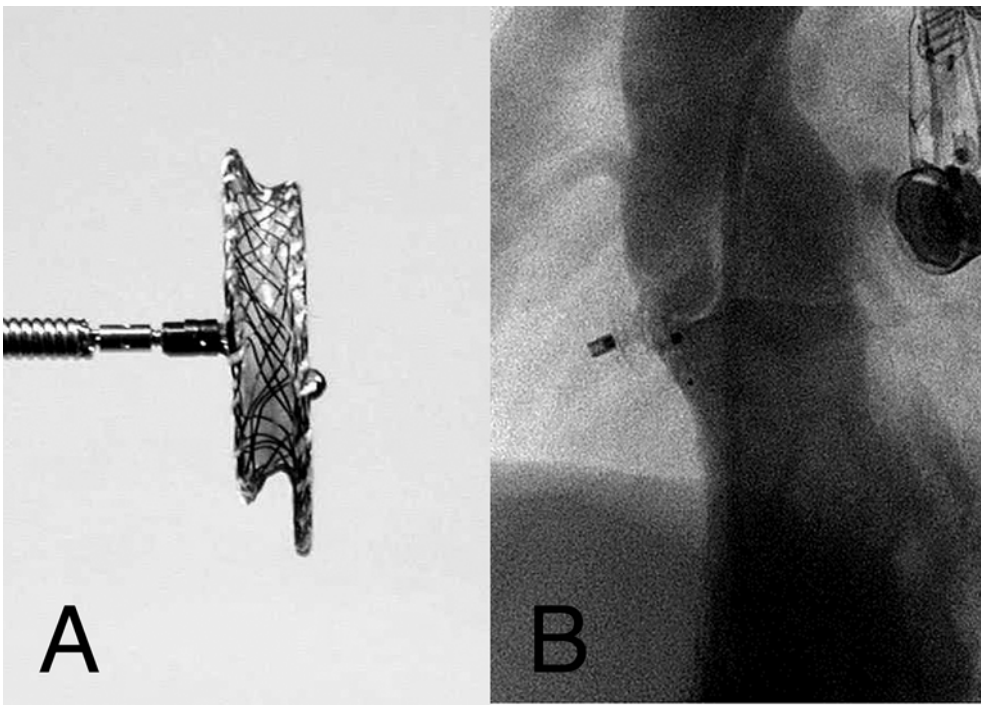

Fig. 37.9 Amplatzer Perimembranous Ventricular Septal Occluder device. (**A**) Photograph of the perimembranous device in which the delivery cable is attached to the right ventricular disc. The asymmetric left ventricular disc is positioned with the minimal rim of the subaortic portion at the top of the device. This prevents interference with the aortic valve. (**B**) Left ventriculogram after device placement. The asymmetric left ventricular disc avoids distortion of the aortic valve. There is no flow through the device immediately after deployment

with the sharply curved delivery sheath positioned in the left ventricular apex, a device advanced to the tip of the delivery sheath assumed proper orientation [35]. This was confirmed in human trials, and complete closures have subsequently been reported to occur in 96 % of patients. In these trials, there were also no serious complications, although the number of patients was notably small [32].

With expanded clinical experience, reports of complete heart block after transcatheter closure of perimembranous ventricular septal defects ranged from 2.1 to 22 % [36–38]. This compared to a contemporary review of surgical closure in patients the same age and size range with an incidence of complete heart block of only 0.8 % [39]. Interestingly, this complication did not occur in the preclinical animal trials or in the

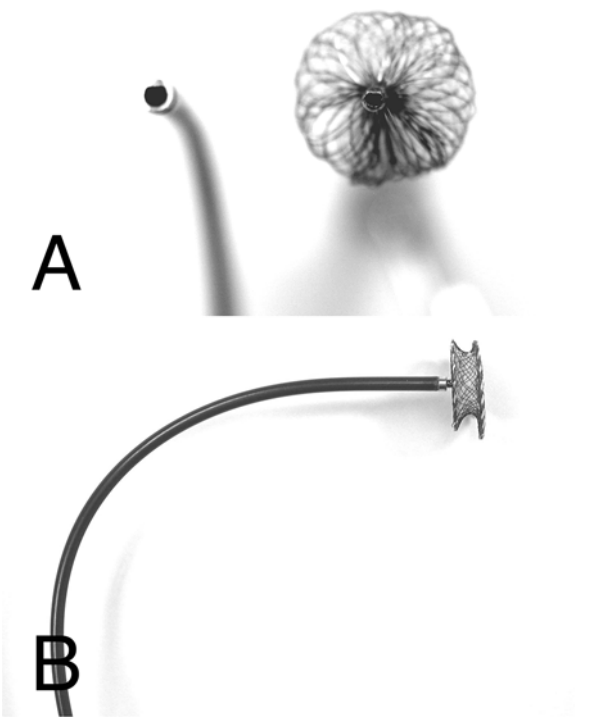

Fig. 37.10 Delivery system for an asymmetric device. (**A**) Photograph of the slot in the delivery catheter, flat at the upper margin. This matches a flattened area at the upper surface of the microscrew. The microscrew will only fit into the slot in the correct orientation. (**B**) The asymmetric perimembranous ventricular septal occluder is attached to the curved delivery catheter. The longer rim of the left ventricular disc is oriented along the lesser curvature of the delivery catheter

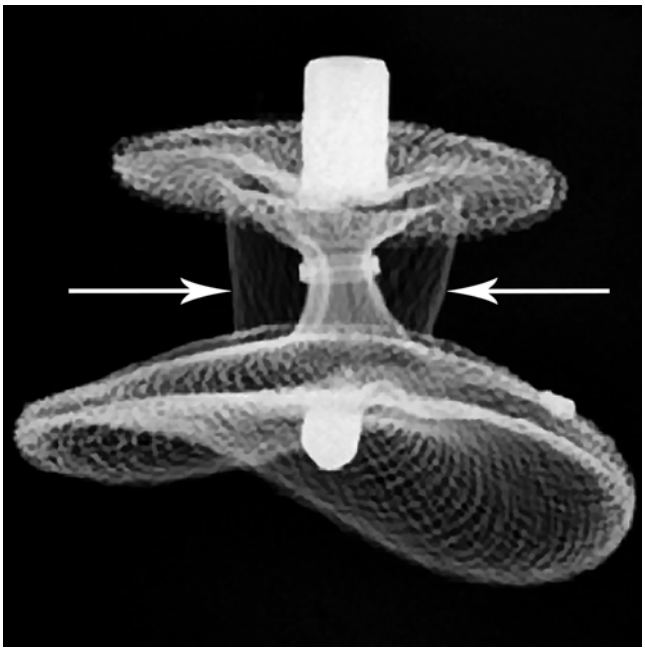

Fig. 37.11 Amplatzer Perimembranous Ventricular Occluder device 2 (pmVSO2). The central device with a narrow waist is made of heavier gauge wire with strength to maintain the device shape. A second softer device surrounding the stiff central device has a wider occluding waist (*arrows*). This significantly decreases the radial force against margins of the defect and the neighboring conduction system. The discs are also further apart than the original design decreasing the "clasping" force of the discs against the septum. The inferior edge of the left ventricular disc has been reduced to decrease possible trauma from contact with the left ventricular side of the septum, while side "wings" improve retention of the device in the defect

initial reported use in humans [32]. Although some investigators continued to implant the pmVSO1 device by avoiding oversizing and aggressive manipulation, they still detected an incidence of heart block around 1 %, thus this complication remained. Possible explanations for this included: (1) trauma to the conduction system from the radial force of the device (exacerbated by oversizing), (2) compression of the conduction system by the short distance between the discs, and (3) abrasion from the elongated inferior left ventricular disc. Accordingly, the device was redesigned with an innovative double-walled construction—a stiff inner layer that maintained device configuration and a softer outer layer with reduced radial force. The interdisc distances were increased slightly to minimize the clamping forces on both the septum and conduction tissue. More specifically, the long, inferior left ventricular disc was reduced to remove a possible source of trauma, while the sideways wings of the left ventricular disc were expanded to maintain stability (Fig. 37.11). Improved control over the orientation of the left ventricular disc was also achieved. Subsequent preclinical animal testing of the new design continued to demonstrate high closure rates, with no trauma to either the aortic or tricuspid valves. As with the original design, there was no occurrence of complete heart block in the animal model [40]. Importantly, initial human experience with 1-year follow-up demonstrated no AV conduction problems in 18 human implants [41]. Validation in humans awaits further clinical trials.

37.8.1 Animal Trials Designed to Test Perimembranous Ventricular Septal Occluders

Unlike all the previously described surgically created animal models of congenital cardiovascular defects, the perimembranous ventricular septal occluder device was tested in a naturally occurring defect animal model (Yucatan mini pig). Morphologically, the porcine defect closely resembles that in humans [42]. It was shown that the device and its unique delivery system were successful in occluding these congenital defects [35]. More specifically, subsequent examination of pathological specimens in this animal model did not show any evidence to explain this complication [43]. It was considered

that this could be a result of minor differences in the conduction system of these mini pigs as compared to humans, or perhaps a consequence of the extremely low incidence of complications associated with these devices. Therefore, caution must be taken when selecting an animal model that mimics a human defect; in this case, it did not foresee a complication when the device was taken to human trials (see also Chaps. 6 and 27). It should be noted that some of these reported problems may have resulted from implanting larger devices, as several European investigators continue to implant this device, minimizing the device size without suffering the complication of complete heart block. Nevertheless, redesigning these devices and carefully avoiding oversizing during implant may aid to further reduce the incidence of complete heart block to acceptable clinical levels.

37.9 Summary

The Amplatzer family of occluder devices has provided for unique minimally invasive methods for the transcatheter closure of congenital cardiovascular abnormalities. In general, the simple underlying device designs allow for easy modification, thus enabling numerous different types and sizes of devices for treating a variety of abnormal cardiac communications. The unique characteristics of these devices include ease of delivery, small delivery systems, retrievability, safety, and effectiveness.

Despite the clinical success of these devices, the transition from an animal trial to the human condition clearly demonstrated the failure of animal model designs to ideally mimic the intricacies of human cardiac anatomies (congenital and adult). Prior to the preclinical studies described here, many of these features had not been appreciated because surgical treatment was easily adjusted to account for them. For example, suture closure of a secundum ASD did not pin the atrial free wall between a stiff device rim and an aorta pulsating with systemic pressure. Likewise, suture ligation of the PDA is not affected by the angle between the PDA and aorta, or the ability of the PDA to expand when internal force is placed against it. Furthermore, surgical patches can be easily and precisely shaped to fit margins of an irregular muscular ventricular septal in a patient's defect. Complete heart block was a known complication of surgical repair of perimembranous ventricular septal defects, and this eventually led to the development of the cardiac pacemaker. The relative occurrence of complete heart block with device closure was not a total surprise due to the proximity of the penetrating bundle to ventricular septal defect margins, although it did not appear in preclinical trials. Therefore, one must consider that there may be minor variations in the relationship of the penetrating bundle and the ventricular septal defect in the porcine perimembranous ventricular septal defect (or even from patient to patient) that account for this variability. On the other hand, one should not consider this as a failure of the animal model design; ASD, muscular ventricular septal defect, and PDA devices are symmetrical, and a central defect was primarily created to test feasibility and efficacy of the device. Thus, these devices functioned perfectly in these designed preclinical models.

It is important to consider that various factors—proximity of a patient's ascending aorta to the anterior margin of a secundum ASD, angle of the PDA to the aorta, expansion of the PDA in younger patients, and frequent occurrence of oval muscular ventricular septal defects—all become significant only under certain treatment conditions. For example, the anatomic details of secundum ASDs and PDAs become more significant when interventional cardiologists tend to oversize devices, either in fear of embolization or due to a perceived lack of previous risk with oversized devices. This is likely also true with perimembranous ventricular septal occluder devices, where a small aortic rim may lead to the risk of embolization. Further, it is likely that an oversized ventricular septal occluder device will increase the pressures against the conduction system in perimembranous ventricular septal defects and thus increase the risk of complete heart block.

There are notable limitations in creating any preclinical animal model for studying therapies for congenital heart disease. For example, tearing the interatrial septum to create an ASD generally does not produce relatively large enough defects, and often there remains an anterior rim of atrial tissue. Furthermore, acutely creating larger communications between systemic and pulmonary circulations (a PDA or ventricular septal defect) is poorly tolerated in these animals, and acute congestive heart failure and pulmonary edema soon develop; long-term animal survival in control groups can be quite low. Likewise, testing the ability of these devices to close large defects in the animal models is also difficult, i.e., even the porcine congenital perimembranous ventricular septal defect is small or moderate in size when the animal is ultimately ready to be used for a closure procedure. Despite these limitations, preclinical testing of any such device is exceedingly valuable to better define device function prior to first use in human procedures.

We consider here that when translating from a given animal model to human use, great care should be taken in defining the specific anatomies of a congenital heart defect to which the devices are to be applied therapeutically. In particular, we suggest that careful review of pathological specimens should be supplemented by 3D imaging (echocardiographic, computed tomographic, or magnetic resonance imaging) to define the proximity of critically important anatomical structures and their relative relationships, such as between the inferior vena cava and interatrial septum or between the aorta and PDA. Critical knowledge of prior surgical experience can also lend important insights to the anatomies of congenital defects, although some surgeons may be a bit reluctant to participate in creating "competitive" treatments.

Finally, devices whose central cores expand to fill an abnormal communication should not be oversized. When possible, device edges should be smooth and rounded rather than sharp, as they may have unanticipated contact with critical cardiac structures. Nevertheless, device closures of congenital cardiovascular defects have revolutionized the care for children with congenital heart diseases. For many transcatheter closures, the Amplatzer devices have been the first successfully employed nonsurgical treatment. Finally, animal testing is an integral part of the process for developing new devices, and the translation to human use requires careful thought.

References

1. Lock JE, Niemi T, Einzig S, Amplatz K, Burke B, Bass JL (1981) Transvenous angioplasty of experimental branch pulmonary artery stenosis in newborn lambs. Circulation 64:886–893
2. Lock JE, Castaneda-Zuniga WR, Bass JL, Foker JE, Amplatz K, Anderson RW (1982) Balloon dilation of excised human coarctations. Radiology 143:689–691
3. Porstmann W, Wierny L, Warnke H (1968) Closure of ductus arteriosus persistens without thoracotomy. Fortschr Geb Rontgenstr Nuklearmed 109:133–148
4. King TD, Mills NL (1974) Nonoperative closure of atrial septal defects. Surgery 75:383–388
5. Rashkind WJ (1983) Transcatheter treatment of congenital heart disease. Circulation 67:711–716
6. Sharafuddin MJA, Gu X, Titus JL, Urness M, Cervera-Ceballos JJ, Amplatz K (1997) Transvenous closure of secundum atrial septal defects. Preliminary results with a new self-expanding nitinol prosthesis in a swine model. Circulation 95:2162–2168
7. Kong H, Wilkinson JL, Coe JY et al (2002) Corrosive behaviour of Amplatzer devices in experimental and biological environments. Cardiol Young 12:260–265
8. Neal WA, Moller JH, Varco RL, Anderson RC (1975) Operative repair of atrial septal defect without cardiac catheterization. J Pediatr 86:189–193
9. Latson LA (2000) Atrial septal defect. In: Moller JH, Hoffman JIE (eds) Pediatric cardiovascular medicine. Churchill Livingstone, New York, pp 311–321
10. Lewis FJ, Varco RL, Taufic M (1954) Repair of atrial septal defects in man under direct vision with the aid of hypothermia. Surgery 36: 538–556
11. Rome JJ, Keane JF, Perry SB, Spevak PJ, Lock JE (1990) Double-umbrella closure of atrial septal defects: initial clinical applications. Circulation 82:751–758
12. Sideris EB, Sideris SE, Thanopoulos BD, Ehly RL, Fowlkes JP (1990) Transvenous atrial septal defect occlusion by the buttoned device. Am J Cardiol 66:1524–1526
13. Hausdorf G, Schneider M, Granzbach B, Kampmann C, Kargus K, Goeldner B (1996) Transcatheter closure of secundum atrial septal defects with the atrial septal defect occlusion system: initial experience in children. Heart 75:83–88
14. Das GS, Voss G, Jarvis G, Wyche K, Gunther R, Wilson RF (1993) Experimental atrial septal defect closure with a new, transcatheter, self-centering device. Circulation 88:1754–1764
15. Agarwal SK, Ghosh PK, Mittal PK (1996) Failure of devices used for closure of atrial septal defects: mechanisms and management. J Thorac Cardiovasc Surg 112:21–26
16. Du ZD, Hijazi ZM, Kleinman CS, Silverman NH, Larntz L (2002) Comparison between transcatheter and surgical closure of secundum atrial septal defect in children and adults. J Am Coll Cardiol 39:1836–1844
17. Amin Z, Hijazi ZM, Bass JL, Cheatham JP, Hellenbrand WE, Kleinman CS (2004) Erosion of Amplatzer septal occluders after closure of secundum atrial septal defects: review of registry of complications and recommendations to minimize future risk. Catheter Cardiovasc Interv 63:496–502
18. Gersony WM, Apfel HD (2000) Patent ductus arteriosus and other aortopulmonary anomalies. In: Moller JH, Hoffman JIE (eds) Pediatric cardiovascular medicine. Churchill Livingstone, New York, pp 323–330
19. Kirklin JW, Barratt-Boyes BG (1993) Patent ductus arteriosus. In: Kirklin JW, Barratt-Boyes BG (eds) Cardiac surgery, 2nd edn. Churchill Livingstone, New York, p 854
20. Nykanen DG, Hayes AM, Benson LN, Freedom RM (1994) Transcatheter patent ductus arteriosus occlusion: application in the small child. J Am Coll Cardiol 23:1666–1670
21. Pass RH, Hijazi Z, Hsu DT, Lewis V, Hellenbrand WE (2004) Multicenter USA Amplatzer patent ductus arteriosus occlusion device trial: initial and one-year results. J Am Coll Cardiol 44:513–519
22. Sharafuddin MJA, Gu X, Titus JL et al (1996) Experimental evaluation of a new self-expanding patent ductus arteriosus occluder in a canine model. J Vasc Interv Radiol 7:877–887
23. Masura J, Walsh KP, Thanopoulous B et al (1998) Catheter closure of moderate- to large-sized patent ductus arteriosus using the new Amplatzer duct occluder: immediate and short-term results. J Am Coll Cardiol 31:878–882
24. Kong H, Gu X, Bass JL et al (2001) Experimental evaluation of a modified Amplatzer duct occluder. Catheter Cardiovasc Interv 53:571–576
25. Ewert P (2005) Challenges encountered during closure of patent ductus arteriosus. Pediatr Cardiol 26:224–229
26. Gruenstein DH, Bass JL (2009) Experimental evaluation of a new articulated Amplatzer ductal occlude device without fabric. Catheter Cardiovasc Interv 74:482–487
27. Bass JL, Wilson N (2014) Transcatheter occlusion of the patent ductus arteriosus in infants—experimental testing of a new Amplatzer device. Catheter Cardiovasc Interv 83:250–255
28. Kenny D, Morgan GJ, Bentham JR et al (2013) Early clinical experience with a modified Amplatzer ductal occlude for transcatheter arterial duct occlusion in infants and small children. Catheter Cardiovasc Interv 82:534–540
29. Kirklin JK, Castaneda AR, Keane JF, Fellows KE, Norwood WI (1680) Surgical management of multiple ventricular septal defects. J Thorac Cardiovasc Surg 80:485–493
30. Lock JE, Block PC, Mckay RG, Baim DS, Keane JF (1988) Transcatheter closure of ventricular septal defects. Circulation 78:361–368
31. Amin Z, Gu X, Berry JM et al (1999) New device for closure of muscular ventricular septal defects in a canine model. Circulation 100:320–328
32. Bass JL, Kalra GS, Arora R et al (2003) Initial human experience with the Amplatzer perimembranous ventricular septal occluder device. Catheter Cardiovasc Interv 58:238–245
33. Berry JM, Krabill KA, Pyles LA, Lohr J, Steinberger J, Bass JL (1999) Muscular ventricular septal defect geometry and Amplatzer device closure: a new en face view. Circulation 100(18):I–30 (Abstract)
34. Rigby ML, Redington AN (1994) Primary transcatheter closure of perimembranous ventricular septal defect. Br Heart J 72:368–371
35. Gu X, Han YM, Titus JL et al (2000) Transcatheter closure of membranous ventricular septal defects with a new nitinol prosthesis in a natural swine model. Catheter Cardiovasc Interv 50:502–509

36. Holzer R, de Giovanni J, Walsh KP et al (2006) Transcatheter closure of perimembranous ventricular septal defects using the Amplatzer membranous VSD occluder: immediate and midterm results of an international registry. Catheter Cardiovasc Interv 68:620–628
37. Butera G, Carminati M, Chessa M et al (2007) Transcatheter closure of perimembranous ventricular septal defects. J Am Coll Cardiol 50:1189–1195
38. Predescu D, Chaturvedi RR, Friedberg MK, Benson LN, Ozawa A, Lee KJ (2008) Complete heart block associated with device closure of perimembranous ventricular septal defects. J Thorac Cadiovasc Surg 136:1223–1228
39. Tucker EM, Pyles LA, Bass JL, Moller JH (2007) Permanent pacemaker for atrioventricular conduction block after operative repair of perimembranous ventricular septal defect. J Am Coll Cardiol 50:1196–1200
40. Bass JL, Gruenstein DH (2012) Transcatheter closure of the perimembranous ventricular septal defect—preclinical trial of a new Amplatzer device. Catheter Cardiovasc Interv 79:1153–1160
41. Tzikas A, Ibraham R, Belasco-Sanchez D et al (2014) Transcatheter closure of perimembranous ventricular septal defect with the Amplatzer membranous ventricular septal occluder 2: initial world experience and 1-year follow-up. Catheter Cardiovasc Interv 83: 571–580
42. Ho SY, Thompson RP, Gibbs SR, Swindle MM, Anderson RH (1991) Ventricular septal defects in a family of Yucatan miniature pigs. Int J Cardiol 33:419–425
43. Mackey-Bojack S, Urness M, Titus J, Bass J (2005) HIS bundle pathology after insertion of the Amplatzer® perimembranous ventricular septal defect occluder in an animal model. Circulation 112(17):II–547 (Abstract 2600)

Harnessing Cardiopulmonary Interactions to Improve Circulation and Outcomes After Cardiac Arrest and Other States of Low Blood Pressure

38

Anja Metzger and Keith Lurie

Abstract

This chapter reviews the traditional therapies used to treat sudden cardiac arrest and shock (cardiopulmonary resuscitation or CPR) and presents modifications of this standard technique to enhance the delivery of oxygenated blood to the heart and brain. In addition, the authors provide descriptions of novel noninvasive technologies that can be used to increase the chance for survival, in particular technologies that provide intrathoracic pressure regulation (IPR) therapy to improve perfusion in profound states of shock. Furthermore, impedance threshold devices and active compression-decompression (ACD) CPR treatment are described, and the results of numerous animal and clinical studies are presented.

Keywords

Cardiac arrest • Sudden cardiac death • Shock • Intrathoracic pressure regulation

Abbreviations

ACD	Active compression-decompression
ACD-CPR	Active compression-decompression cardiopulmonary resuscitation
BLS	Basic life support
CePP	Cerebral perfusion pressure
CPP	Coronary perfusion pressure
CPR	Cardiopulmonary resuscitation
DBP	Diastolic blood pressure
EMS	Emergency medical services
ETP	Endotracheal pressure
FDA	Food and Drug Administration
ICP	Intracranial pressure
IPR	Intrathoracic pressure regulation
ITD	Impedance threshold device
ITP	Intratracheal pressure
ITPR	Intrathoracic pressure regulator
LBNP	Lower body negative pressure
MAP	Mean arterial pressure
PEA	Pulseless electrical activity
RA	Right atrial
ROC	Resuscitation Outcomes Consortium
ROSC	Return of spontaneous circulation
SBP	Systolic blood pressure
VF	Ventricular fibrillation

A. Metzger, PhD (✉) • K. Lurie, MD
Zoll Minneapolis, 1905 County Road C West, Roseville, MN 55113, USA
e-mail: ametzger@zoll.com

38.1 Introduction

Cardiac arrest and life-threatening hypotension typically occur suddenly and without warning. This chapter will briefly review the traditional therapies used to treat sudden cardiac arrest and shock. In addition, we provide descriptions of novel noninvasive technologies that can be used to increase the chance for survival, in particular technologies that provide intrathoracic pressure regulation (IPR) therapy to improve perfusion in profound states of shock.

P.A. Iaizzo (ed.), *Handbook of Cardiac Anatomy, Physiology, and Devices*, DOI 10.1007/978-3-319-19464-6_38

38.2 Sudden Cardiac Arrest

Despite the widespread practice of basic and advanced life support, the vast majority of patients in cardiac arrest never survive to hospital discharge. The clinical toll is enormous—more than 1000 adults die each day in the United States alone from an out-of-hospital cardiac arrest, and a similar number of individuals die daily inside the hospital. Many of these patients have no prior warning signs and thus die in the prime of their lives. Sadly, little has changed in the practice of cardiopulmonary resuscitation (CPR) in the past 50 years; thus, it is not surprising that survival rates have remained relatively constant for decades at ~6 % nationwide for all patients with an out-of-hospital cardiac arrest. For patients who present with ventricular fibrillation (VF), survival rates range from 10 to 45 %, depending upon the city where they arrest. Since the frequency of VF is declining, and nearly 70 % of all patients currently present with either pulseless electrical activity (PEA) or asystole, new approaches are desperately needed to decrease mortality from this nation's #1 killer. While the differences in patient outcome between regions are due to many factors, the intrinsic mechanical inefficiency of conventional manual CPR limits the potential of even the most highly skilled rescuers. Moreover, the vast majority of the 300,000+ cardiac arrests that occur annually in the United States occur in the home, and delays to treatment severely limit the chances for patient survival. As a result, even with the most efficient emergency medical services (EMS), less than 20 % of all patients with an out-of-hospital cardiac arrests are discharged from the hospital with intact neurological function [1, 2].

The immediate application of CPR is critical when sudden cardiac arrest occurs. The primary purpose of manual standard CPR is to pump blood from the heart to vital organs during the compression phase and to enhance the return of blood back into the heart (preload) during the chest wall recoil (or decompression) phase. Compression and decompression are illustrated in Fig. 38.1. Devices that optimize this cardiovascular physiology are helpful adjuncts and have been shown to improve outcomes after cardiac arrest. Conversely, there have been several common mistakes identified in standard CPR techniques that result in suboptimal CPR quality, including: (1) not allowing full chest wall recoil, (2) inadequate compression forces, (3) incorrect compression rates, and/or (4) hyperventilation.

It is critical to understand that blood flow to the vital organs is severely reduced during standard CPR, even under the best of circumstances [3, 4]. During standard CPR, chest compression results in an elevation of intrathoracic pressure and indirect cardiac compression. Both of these mechanisms result in forward blood flow out of the chest to perfuse the brain and other vital organs. However, the effectiveness of standard CPR is largely determined by the amount of blood returned to the chest to refill the heart after each compression phase. This process is highly dependent on the degree of chest wall recoil. When the chest recoils, intrathoracic pressures fall relative to extrathoracic pressures, and venous blood returns to the right heart.

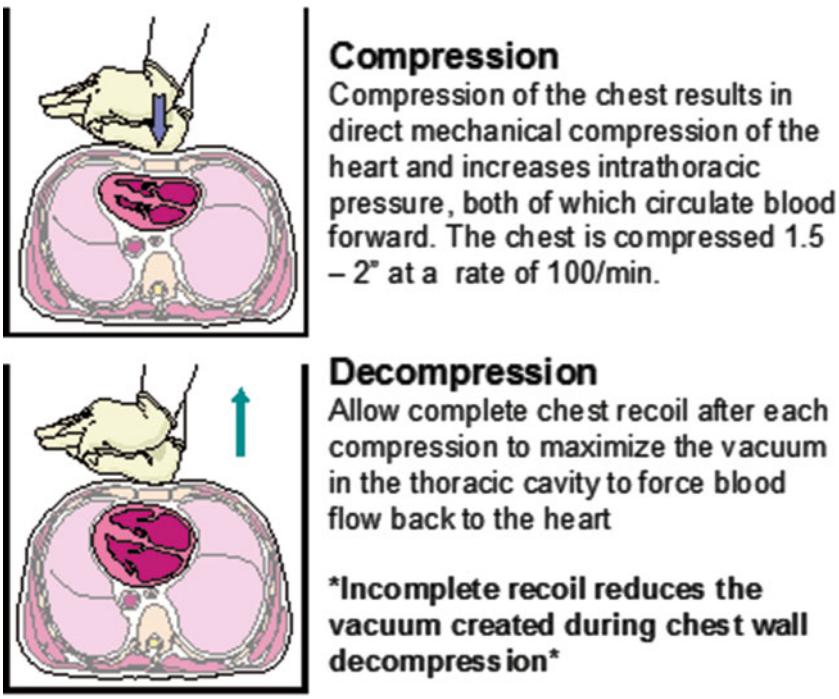

Fig. 38.1 Compression and decompression phases of cardiopulmonary resuscitation

38.3 The Impedance Threshold Device for Cardiac Arrest

Standard CPR by itself has been shown to be inherently inefficient, in large part due to the lack of adequate blood return to the thorax during the chest wall recoil phase [3, 4]. Moreover, the coronary perfusion pressure (CPP), a critical determinant of CPR efficacy, is only marginally adequate as the pressure gradient between the aorta, the right atrium, and left ventricle is far from optimal. During the decompression (or passive relaxation) phase of standard CPR, a small decrease in intrathoracic pressure (relative to atmospheric pressure) develops, which promotes blood flow back to the heart. Myocardial perfusion predominantly occurs during this decompression phase. Uniquely, the impedance threshold device (ITD) (ResQPOD®, Advanced Circulatory, Roseville, MN, USA) was designed to improve venous return to the heart during the decompression phase of CPR [3–9]. In so doing, the ITD increases the CPP during CPR, enhancing delivery of oxygenated blood to both the heart and brain. The ITD shown in Fig. 38.2 works effectively with both a face mask and an advanced airway (e.g., endotracheal tube, supraglottic airway).

The concept underlying the ITD was first discovered when measuring intrathoracic pressures in patients undergoing a new type of CPR, active compression-decompression (ACD) CPR [10]. It was found that if the endotracheal tube was transiently occluded during the active decompression phase, intrathoracic pressures became markedly more negative. This led to the idea of transiently blocking the airway or impeding inspiratory gas exchange during the chest wall decompression phase of CPR to create a greater pressure differential between the thorax and the rest of the body, thereby enhancing blood flow back into the thorax. As such, the ITD harnesses the kinetic energy of the chest wall recoil, thereby augmenting the "bellows-like" action of the chest with each compression-decompression cycle [8, 9]. The ITD contains pressure-sensitive valves that selectively impede the influx of inspiratory gas during chest wall decompression, thereby augmenting the amplitude and duration of the vacuum within the thorax. This vacuum draws more venous blood back into the heart, resulting in increased cardiac preload, followed by improved cardiac output and vital organ perfusion. During chest compression, the one-way valve is open and does not cause any resistance to exhalation. When the resuscitation bag is squeezed for active ventilation, the one-way valve remains open and does not cause any resistance to gas exchange. In this manner, the ITD functions to lower intrathoracic pressure only during the decompression phase of CPR without compromising patient ventilation. The ITD consists of a valve body, a one-way pressure-sensitive silicone valve, and a safety check valve [5]. When a spontaneous pulse returns, the ITD is removed from the respiratory circuit. The safety check valve serves as a precautionary measure to prevent negative pressure pulmonary edema and potential barotrauma and to enable the patient to breathe if there is a return of spontaneous ventilation and the ITD has not been removed.

Positive data from animal studies and clinical trials, described in detail below, formed the basis for the American Heart Association's Level IIb recommendations for the use of ITDs in the 2010 American Heart Association (AHA) guidelines. Today, the ResQPOD® is sold in the United States

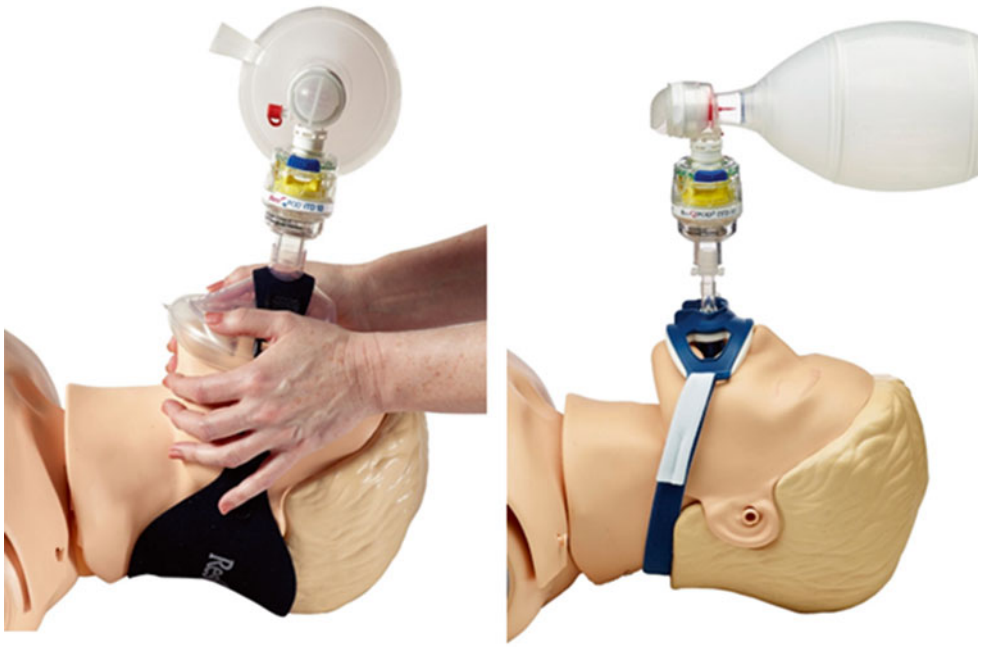

Fig. 38.2 ResQPOD® impedance threshold device on a face mask and endotracheal tube

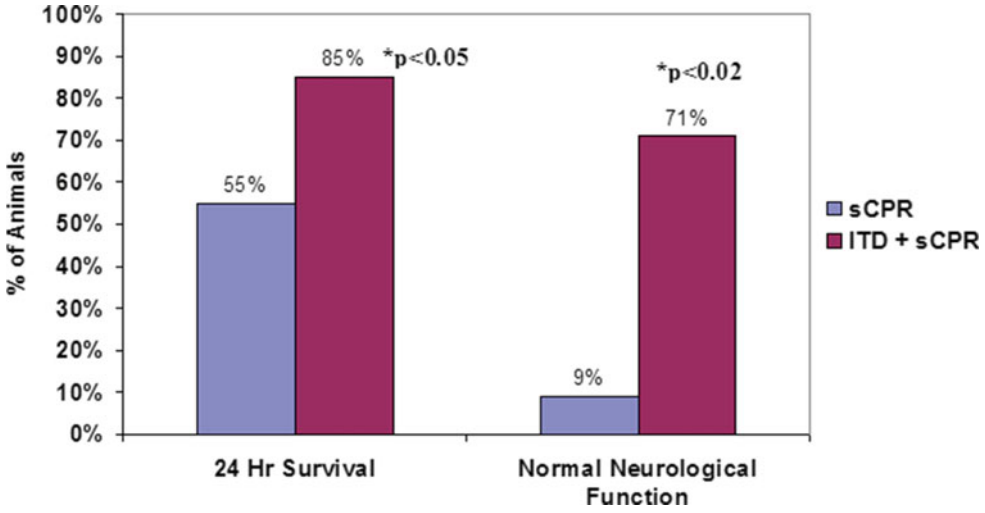

Fig. 38.3 Percentage of animals with 24-h survival and normal neurological function comparing standard CPR (*sCPR*) to impedance threshold device (*ITD*) + standard CPR after cardiac arrest in pigs

as a device that can be used to increase circulation in patients with low blood pressure, including patients in cardiac arrest. Further, Aufderheide et al. reported outcomes from the use of the ITD in seven EMS systems in the United States. They showed that the changes in CPR practice, which now emphasize more compressions and fewer ventilations, complete chest wall recoil, uninterrupted chest compressions during advanced airway management, and the use of the ITD during basic life support (BLS) and advanced life support resulted in a doubling of hospital discharge rates for all patients, regardless of presenting heart rhythm, i.e., from 8 to 16 % [11]. In addition, the neurological outcomes were similar between groups, and patients who had an initial rhythm of ventricular fibrillation had a hospital discharge rate of 28.1 % compared with 17.2 % in the historical control group.

One of the first animal studies performed with the ITD demonstrated that the use of the active ITD increased 24-h survival and preserved neurological function after cardiac arrest in swine [8]. There was a statistically significant increase in both of these key outcome parameters, as shown in Fig. 38.3. The improved neurological function was observed in the overall study group, as well as in the subset of animals that were resuscitated with defibrillation shock therapy and epinephrine. Blood gas data demonstrated that oxygenation was adequate in both groups and no differences were observed between groups on autopsy. The intrathoracic pressures were significantly lower in the ITD group. Subsequent studies have demonstrated that the use of the ITD also lowers intracranial pressures (ICPs) more rapidly than in animals treated with standard CPR alone. It is hypothesized that these observations help to explain the markedly improved neurological outcomes in this porcine survival study [8].

Importantly, the first randomized double-blinded prospective clinical trial showed that the use of the ITD during standard CPR resulted in an increase in systolic blood pressure. However, in that study nearly all of the patients also received excessively high ventilation rates. Follow-up animal studies demonstrated that excessive ventilation (termed *hyperventilation*) during cardiac arrest actually inhibited venous return, compromised hemodynamics, and resulted in increased mortality rates [12, 13]. In addition, frequent incomplete decompression of the chest was also witnessed and recorded in that study. Follow-up studies in animals demonstrated that incomplete chest wall recoil resulted in positive intrathoracic pressures, which in turn decreased venous return and caused markedly poorer cardiac and cerebral blood flows; incomplete decompression is thus a key component in the deficiency of standard CPR [14]. These observations also demonstrate how important the cardiopulmonary cerebral interactions are during CPR.

In the first US double-blinded randomized survival study of the ITD, there was nearly a threefold increase in 1-h and 24-h survival rates in patients with an initial rhythm of PEA when comparing treatment with a sham versus active ITD. Figure 38.4 shows the relative percent survival in all subjects initially presenting with PEA. It is important to emphasize that the results from this study were observed in the setting of real-world CPR, prior to the use of tools to help control ventilation frequency or the adequacy of compression rates, depths, and complete chest wall decompressions. Figure 38.5 shows the percent survival in all subjects presenting with various types of cardiac rhythms.

The benefits of the ITD in patients with PEA can be better understood by examining the hemodynamic tracings of one of the substudy group patients, as shown in Fig. 38.6. When CPR was discontinued, there was a persistent regular electrical activity, but the aortic pressures were inadequate to generate a palpable pulse. This example of PEA demonstrates that although there were small rises in the arterial pressure with each cardiac contraction, this was insufficient to cause a palpable pulse or effective vital organ blood flows. Importantly, without effective vital

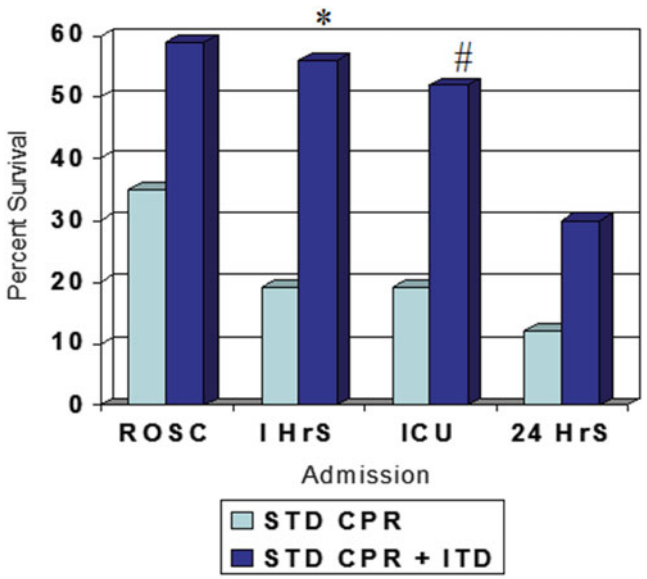

Fig. 38.4 Outcomes for all subjects initially presenting with pulseless electrical activity. *$p=0.01$, #$p=0.02$. *ROSC* return of spontaneous circulation, *1 HrS* 1-hour survival; *ICU* ICU admission rate, *24 HrS* 24-hour survival

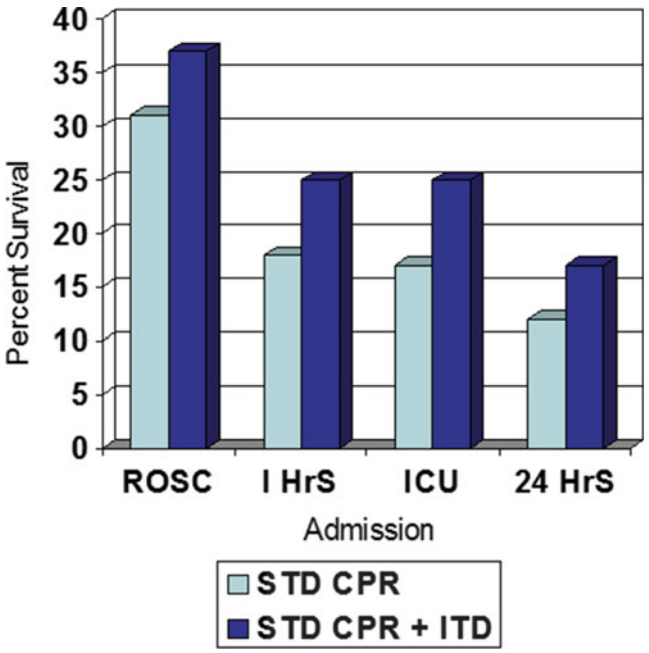

Fig. 38.5 Outcomes for all subjects presenting in all rhythms. *ROSC* return of spontaneous circulation, *1 HrS* 1-hour survival, *ICU* ICU admission rate, *24 HrS* 24-hour survival

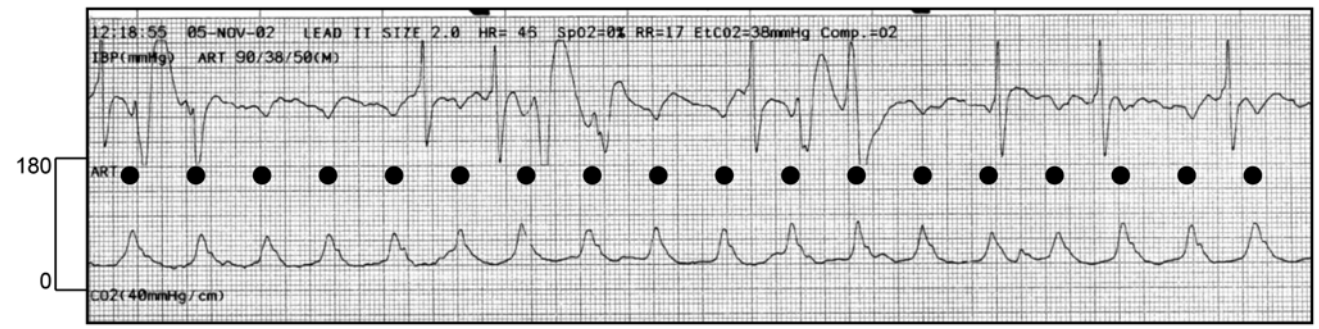

Top Tracing: Arterial pressures during CPR with initial rhythm of PEA. In both tracings, top channel is the ECG; bottom channel shows invasive arterial pressures; black dots denote chest compressions. ECG deflections are seen with each compression. In this example, BP is 90/38 mmHg during CPR.

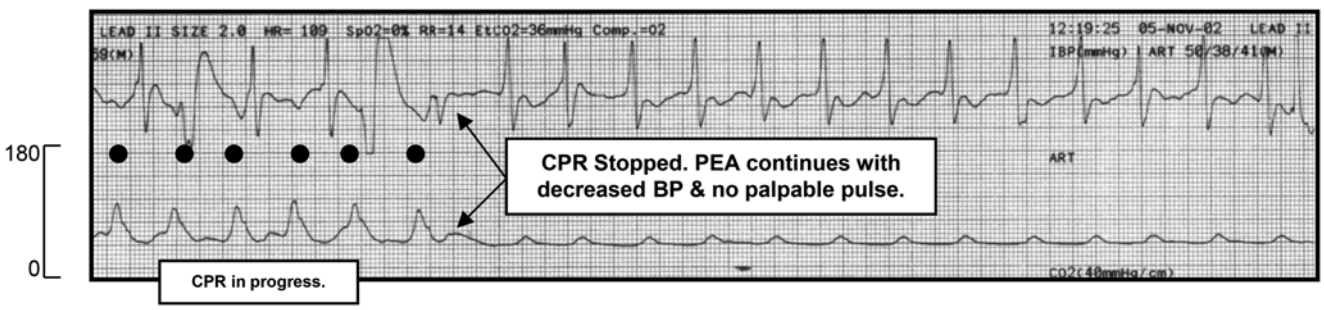

Bottom Tracing: Example of what happens to arterial pressures when CPR is stopped in PEA. In this example, BP is 95/40 during CPR, then decreases to 50/38 when CPR is discontinued.

Fig. 38.6 Hemodynamic tracing of a patient with pulseless electrical activity (*PEA*). *BP* blood pressure, *CPR* cardiopulmonary resuscitation

organ perfusion, return of spontaneous circulation (ROSC) is not possible. We speculate that the known increase in circulation and blood pressures associated with the use of the ITD, in both animals and humans, is enough to increase the aortic systolic and diastolic pressures to a sufficient level to allow for effective vital organ perfusion. It should be noted that the number of patients in VF treated with the ITD in that study was too low to definitively determine if the ITD would benefit this patient subgroup. Nonetheless, hospital discharge rates were 6 % in the control group and 14 % with the active ITD in that study.

One of the most important findings from the first clinical study when the ITD was used with standard CPR was that the overall quality of administered CPR was very poor. Based on the hemodynamic substudy data collected in this clinical trial, hyperventilation was recorded in 100 % of cases, and incomplete chest wall recoil was recorded in approximately 50 % of cases. These critical findings demonstrated the challenges of performing standard CPR with a pair of human hands alone, and this resulted in a change in the initial design of the ITD; a timing light was added that flashes at 10 times per minute to provide the rescuer with guidance on when to ventilate the patient and how to assure that compressions are performed 100 times per minute (compress 10 times per light flash). In the future, the use of the ITD will be even more effective once improved standard CPR is practiced and performed uniformly.

It is also important to emphasize that one of the very exciting recent advances in CPR research has been the rediscovered benefit of therapeutic hypothermia after successful resuscitation. Several studies have demonstrated a 50 % increase in long-term survival rate and improved neurological function in survivors of cardiac arrest with VF who received therapeutic hypothermia in the hospital shortly after resuscitation [15–17]. Therefore, when hypothermia is applied to patients resuscitated after PEA, there should be a similar increase in long-term survival rate with good neurological function. Fortunately, a growing number of patients are now routinely treated with therapeutic hypothermia after successful resuscitation.

38.4 Effects of Incomplete Chest Wall Recoil and Hyperventilation on the Quality of Standard CPR

The AHA recognized the inefficiencies of standard CPR in 2000, 2005, and 2010 when they issued new guidelines for performing CPR. The latest guideline reinforces the importance of the chest decompression phase in teaching CPR: *Rescuers should allow complete recoil of the chest after each compression, to allow the heart to fill completely before the next compression* [18].

As mentioned previously, Aufderheide et al. observed rescuers frequently leaning on the chest during the decompression phase, thereby maintaining some residual and continuous pressure on the chest wall during the decompression phase of CPR. This prevented complete chest wall recoil. More specifically, airway pressures were consistently measured as positive during the decompression phase (>0 mmHg) in 6/13 (46 %) of consecutive adults. This was caused by incomplete chest wall recoil alone or combined with prolonged, positive ventilations. With standard CPR and incomplete chest wall recoil, insufficient intrathoracic vacuum pressures are achieved. In contradistinction, when active compression and decompression are performed in conjunction with the use of an ITD, a significant intrathoracic vacuum results.

In 2005, Yannopoulos et al. conducted an animal study to address the question of the physiological impact of incomplete chest wall recoil [14]. Nine pigs in VF for 6 min were treated with an automated CPR device with compressions at 100/min, a compression depth of 25 % of the anteroposterior diameter, and a compression to ventilation ratio of 15:2. After complete (100 %) chest wall decompression for 3 min during standard CPR, the decompression depth was reduced to 75 % of complete decompression for one minute of CPR and then restored for another one min of CPR to 100 % decompression. CPP was calculated as the diastolic aortic—right atrial (RA) pressure. Cerebral perfusion pressure (CePP) was calculated by measuring the area between the aortic pressure curves and the ICP curves. Figure 38.7 sum-

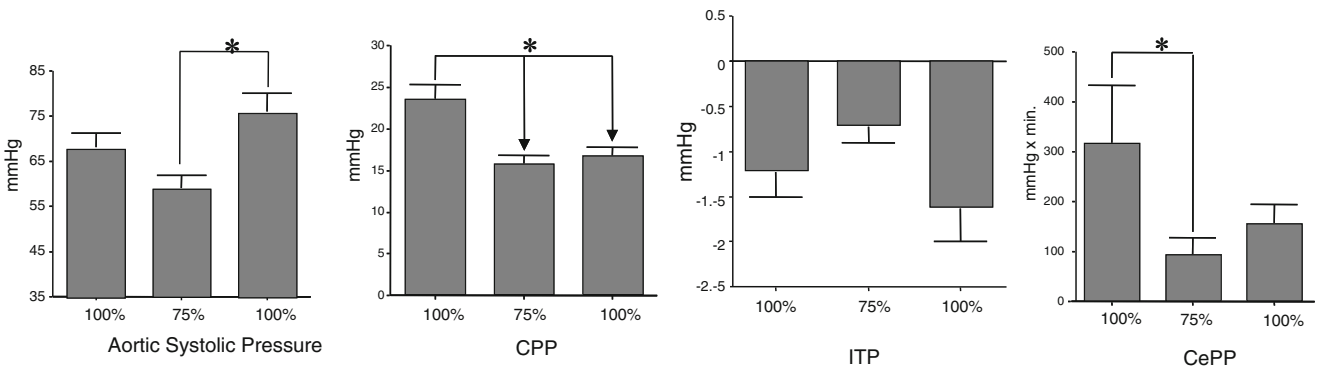

Fig. 38.7 Aortic pressures, coronary perfusion pressure (*CPP*), intrathoracic pressure (*ITP*), and cerebral perfusion pressure (*CePP*) decreases when complete decompression is not allowed (75 %). *$p < 0.05$

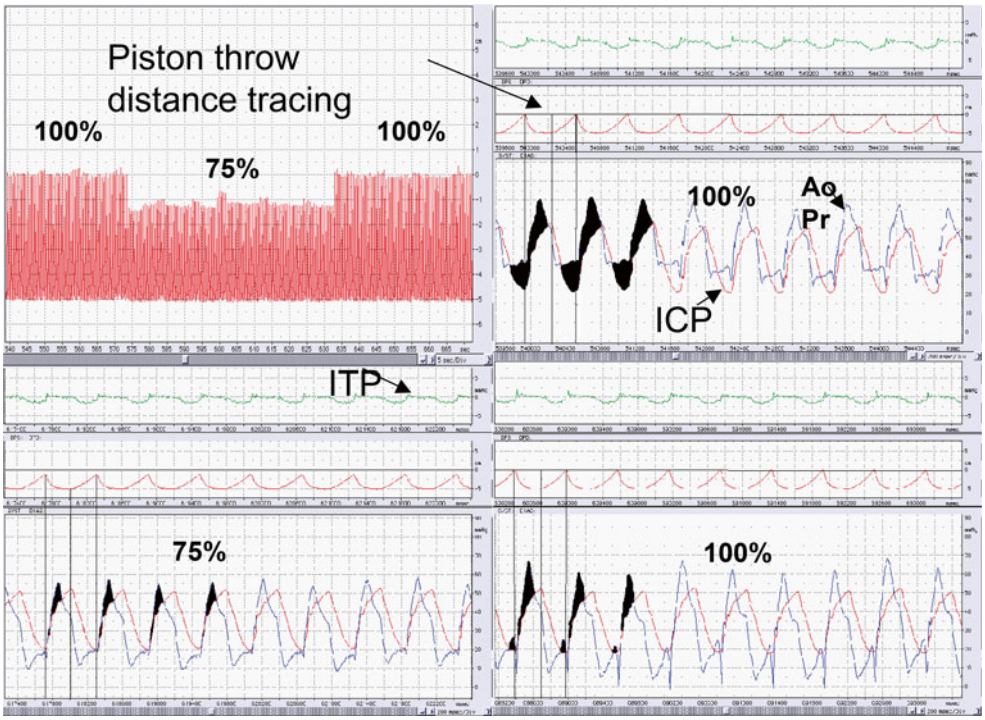

Fig. 38.8 Effect of incomplete chest wall recoil on reducing cerebral perfusion (see text for details). *AoPR* aortic pressure, *ICP* intracranial pressure, *ITP* intrathoracic pressure, *blue* tracings = aortic pressure, *pink* tracings = intracranial pressures

marizes the results of this study including the differences in aortic systolic pressure, CPP, intratracheal pressure (ITP), and CePP. With 100 %–75 %–100 % chest wall recoil, the CPP was 24.2 ± 2.0, 15.0 ± 1.2, and 15.6 ± 1.3 mmHg ($p < 0.05$); CePP was 320 ± 120, 95 ± 15, and 150 ± 30 mmHg min ($p < 0.05$); diastolic aortic pressure was 26.8 ± 2.8, 18.9 ± 2.3, and 18.2 ± 2.1 mmHg ($p < 0.05$); ICP during decompression was 18.1 ± 2.8, 21.6 ± 2.3, and 17.4 ± 2.6 mmHg ($p < 0.05$); RA diastolic pressure was 2.7 ± 1.9, 3.9 ± 1.9, and 2.7 ± 1.6 mmHg ($p < 0.05$); and mean arterial pressure (MAP) was 41.4 ± 2.8, 32.5 ± 2.2, and 36.6 ± 1.9 mmHg ($p < 0.05$). The CPP and CePP never fully recovered after treatment with the 75 % incomplete chest wall decompression. It is striking that a small reduction of chest wall recoil (1 cm), which is a common occurrence during the performance of CPR, resulted in such a marked reduction in cerebral and CPPs.

The effect of incomplete chest wall recoil on reducing cerebral perfusion can be seen graphically in Figs. 38.8 and 38.9 [14]. Figure 38.8a represents, condensed in time, the sequential 100 % chest recoil, 75 % chest wall recoil, and return to 100 % chest wall recoil. Tracings of ITP, aortic pressure (AoPr), and ICP with 200 ms per division are indicated with arrows. Piston throw (in cm) is also shown to sequentially demonstrate the complete (100 %) chest wall recoil (38.8b), 75 % chest wall recoil (38.8c), and return to complete chest wall recoil (38.8d). The positive area between the AoPr and ICP tracing represents cerebral perfusion (marked as black). Note how the area decreases, especially during decompression with incomplete chest wall recoil (75 %) and that it partially recovers when full recoil was restored. Figure 38.9 shows the effect of positive pressure ventilation on CePP. The first tracing shows the aortic and ICP waveforms with full chest wall recoil after a ventilation cycle, while the second tracing shows the aortic and ICP waveforms with incomplete chest wall recoil after a ventilation cycle. Positive pressure gradient (Ao-ICP) is colored black. Note the marked difference in total area during each compression-decompression cycle with and without a positive pressure breath. The bar graphic shows the mean 4-beat area of all animals during and after a ventilation cycle. The mean ± SEM values during 100 and 75 % decompression have been graphed. During positive pressure ventilation, ICP rises and the positive gradient disappears. There was effectively no blood flow to the brain (Fig. 38.9, second panel). This study demonstrated that incomplete decompression has significant deleterious effects on both CPP and CePP. The residual positive intrathoracic pressure during the decompression phase associated with incomplete chest wall recoil decreased forward blood flow, impeded venous return, increased ICP, and undermined the efficiency of CPR. These recent animal studies underscore the fundamental hemodynamic importance of complete chest wall decompression during CPR. Whether rescuers can be retrained to allow for complete chest wall decompression during standard CPR remains an important issue.

A change in CPR technique to allow for the palm of the compressing hand to lift off the chest at the end of decompression may be important to assure full chest wall recoil during standard CPR. Accordingly, Aufderheide et al.

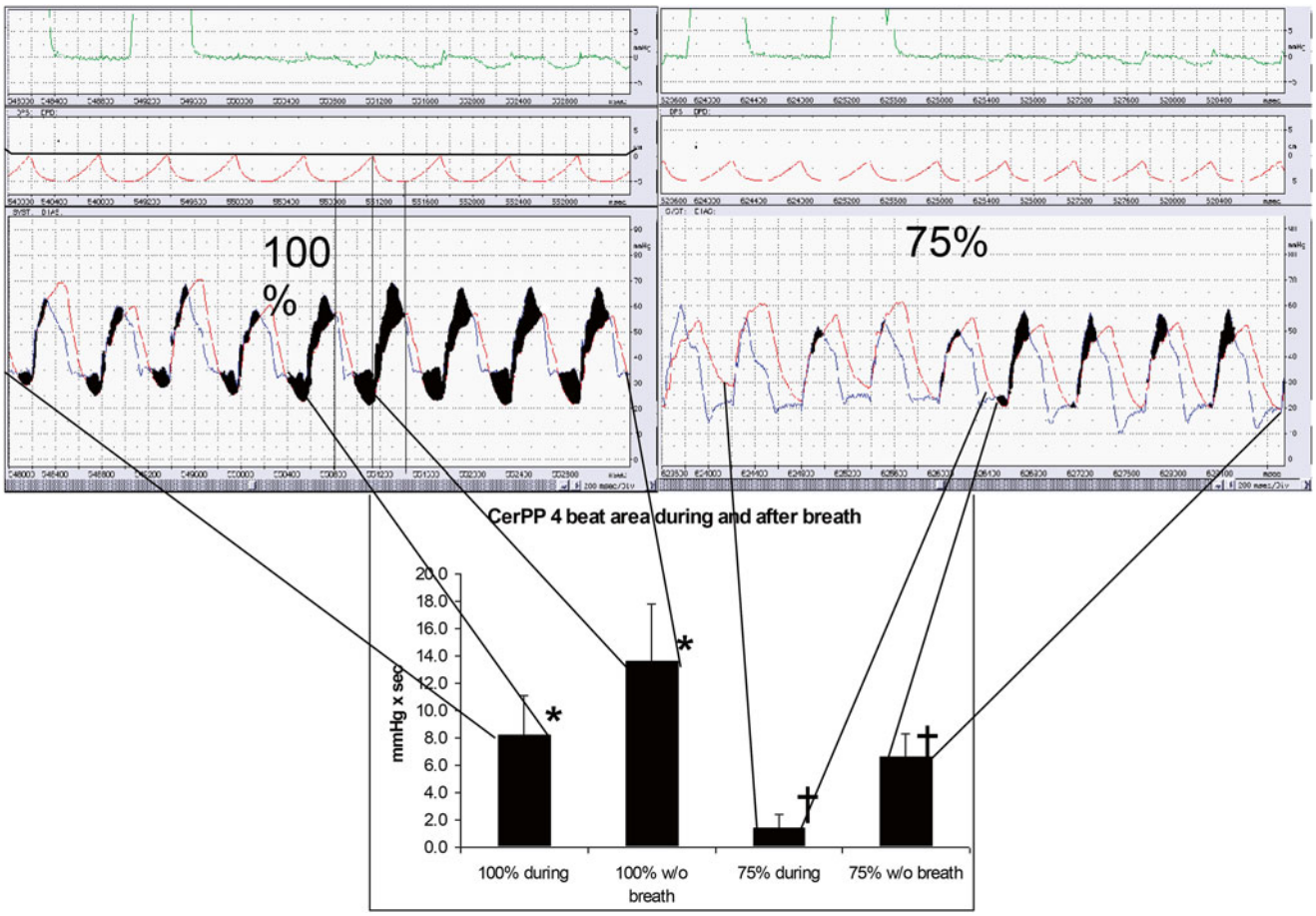

Fig. 38.9 Effect of incomplete chest wall recoil on reducing cerebral perfusion (see text for details). *CerPP* cerebral perfusion pressure

implemented a randomized prospective clinical trial using an independent group of 30 actively practicing and certified EMS providers, not aware of the ongoing trial, in a controlled setting using a recording CPR manikin. The purpose of the study was to evaluate three alternative CPR techniques to determine if they would improve complete chest wall recoil compared with standard CPR while maintaining adequate compression depth and proper hand position placement. The three alternative CPR techniques were: (1) two-finger fulcrum technique (lifting the heel of the hand slightly but completely off the chest during the decompression phase of CPR while using the thumb and little finger as a fulcrum), (2) five-finger fulcrum technique (lifting the heel of the hand slightly but completely off the chest during the decompression phase of CPR, using all five fingers as a fulcrum), and (3) hands-off technique (lifting the heel and all fingers of the hand slightly but completely off the chest during the decompression phase of CPR).

In this study, during standard CPR using the traditionally taught hand position (standard hand position), complete chest wall decompression was recorded in only 16.3 % of all compression-decompression cycles, adequate depth of compression in 48.5 %, and acceptable hand placement in 85.0% of compression-decompression cycles. When compared with standard CPR, the hands-off technique achieved the highest rate of complete chest wall recoil (95.0 % versus 16.3 %, $P<0.0001$) and was 129 times more likely to provide complete chest wall recoil (OR: 129.0; CI: 43.4–382.0) [19]. There were no significant differences in the accuracy of hand placement, depth of compression, or reported increase in fatigue or discomfort with its use compared with the standard hand position. The hands-off technique was easily learned and applied by participating EMTs, because it uses the same hand configuration as is currently recommended by the AHA.

38.5 Optimizing Outcomes with Standard CPR and the Impedance Threshold Device

Aufderheide and colleagues have recently analyzed and applied the combined lessons learned from the initial clinical trials of the ITD and standard CPR. They analyzed data from seven EMS systems that serve a population of more than 3 million patients and reported that, when CPR is performed

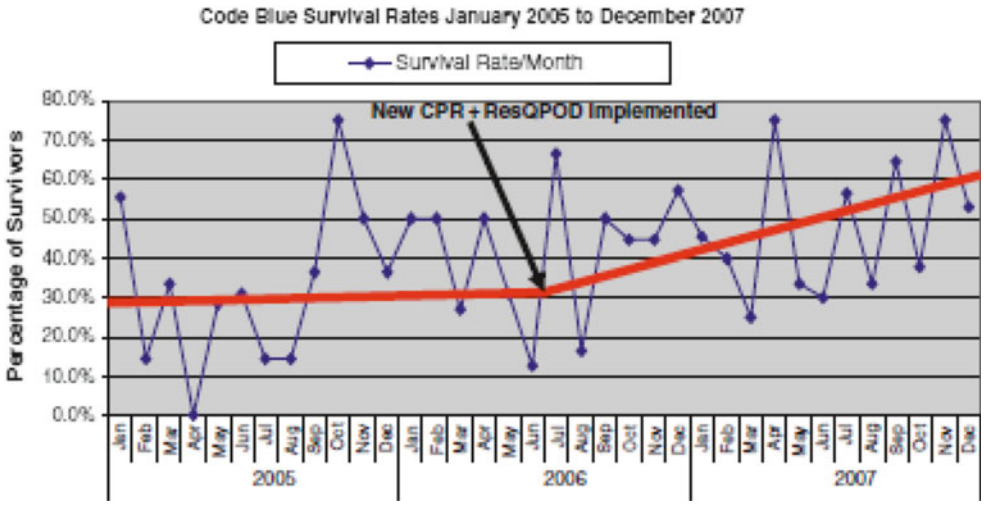

Fig. 38.10 Code blue survival rates in St. Cloud, Minnesota (January 2005 to December 2007). *CPR* cardiopulmonary resuscitation

correctly with the ITD and the mistakes described above are reduced or eliminated by rigorous training and correct ITD used, survival rates increased from 7.9 to 15.7 % for all patients who presented with cardiac arrest; survival rates for those with an initial rhythm of VF increased from 17 to 28 % [11]. Therapeutic hypothermia was not yet in use in these EMS systems and their associated hospitals when these data were obtained. Similar benefits from performing CPR according to the AHA 2005 and 2010 guidelines and the use of the ITD have also been reported for patients in in-hospital cardiac arrest. For example, Thigpen reported that hospital discharge rates in one large Mississippi hospital increased from 17 to 28 % with the administration of this new resuscitation approach [20, 21]. Similar data from St. Cloud Hospital in Minnesota are shown in Fig. 38.10; data from before the change in practice in July 2006 were compared to data after implementation of the new CPR techniques and the ITD. Importantly, the survival rates after an in-hospital cardiac arrest nearly doubled.

A study by Lick et al. investigated the effects of stricter adherence to the AHA guidelines for CPR which included the recommended use of the ITD. The *Take Heart America* initiative was started in an attempt to increase survival from cardiac arrest by focusing on the implementation of the 2005 and 2010 AHA guidelines. It is centered not on a single treatment but rather on a bundle of care approach including community-wide initiatives, including: (1) increased cardiac arrest awareness, (2) increased bystander CPR rates, (3) promoting the use of automated external defibrillator, and (4) the administration of immediate high-quality CPR with the use of the ITD throughout the duration of the code. Further, additional in-hospital treatments such as therapeutic hypothermia, revascularization, and implantable cardiac defibrillators were also emphasized. Survival and outcomes data for patients receiving the bundled interventions were compared to control data prior to implementation of the initiative. Importantly, survival to hospital discharge increased significantly from 8.5 to 19.0 %. These differences were especially striking in the subset of patients who had VF as the initial arrest rhythm; their numbers increased from 17.0 % versus 41.0 % [22]. These results show that when focus is applied to the AHA guidelines including recommended use of the ITD, cardiac arrest survival rates can be greatly improved. In summary, with greater attention to enhancing circulation, based on the newly discovered mechanisms underlying circulation during CPR, significant progress has been made by simply using a pair of hands and the ITD.

It should be noted that a large multicenter study conducted by the Resuscitation Outcomes Consortium (ROC) group looked at outcomes from cardiac arrest using an active ITD versus a sham ITD. The results, originally published in 2011, reported no statistical differences in survival with good neurological function in the active group and the sham group [23]. Additional analyses revealed that the chest compression rates varied widely throughout the study, ranging from 50 compressions/minute to 240 compressions/minute [24]. When the subset of patients received compressions at a rate of 100 ± 10 compressions/minute, the active device showed a marked benefit on survival with good neurological function compared to the sham device. There was also a significant benefit identified for subjects who suffered VF arrests. This second look at the ROC data shows that when CPR is performed correctly, per AHA guidelines, the ITD can increase the rate of survival to hospital discharge with improved neurological function.

Another analysis of the ROC data was independently performed by Yannopoulos et al. [25]. In addition to investigating compression rates as a surrogate for quality CPR, they also included only subjects receiving CPR at a depth of 4–6 cm (AHA recommends depth of 2 in or 5 cm) and a compression fraction (% of time performing chest compressions in a given minute) of >50 %. When these filters were

applied, 7.2 % of subjects receiving CPR with the active ITD survived to hospital discharge with good neurological function, while the rate was only 4.1 % for subjects receiving CPR with the sham ITD ($p = 0.006$). This represents a 43 % increase in survival rate with good neurological function with the active ITD, over the sham ITD. Again, when quality CPR is delivered according to guidelines, the use of an ITD provides benefits to patients.

38.6 Active Compression-Decompression CPR

It has been shown that despite training, it is difficult to perform standard manual CPR correctly, e.g., allowing for the chest to fully recoil following each compression. These problems result in significantly less blood flow back to the heart and reemphasize that perhaps another device is needed to correct this widespread problem. Correction of this basic flaw (incomplete chest wall recoil) through the use of a technique that ensures full chest wall recoil and user guidance has the potential to significantly improve the chance for survival after cardiac arrest. One such technique is ACD-CPR which is performed with an ACD-CPR device.

More specifically, ACD-CPR increases the naturally occurring negative intrathoracic pressure by physically lifting the chest wall and helping it to return to its resting decompressed position. During standard CPR, the chest wall's natural elasticity will partially recoil from compression. Several factors can contribute to less than optimal recoil: (1) patient age, (2) brittle or broken ribs, (3) a separated or broken sternum, (4) a barrel-shaped chest, (5) the presence of chest concavity, and/or (6) the tendency for rescue personnel to lean on the chest and thus cause incomplete chest wall recoil during performance of CPR. The use of an ACD-CPR helps ensure that the chest re-expands to generate the negative intrathoracic pressure needed to allow passive filling of the heart.

For example, ACD-CPR can be performed with a hand-held suction device (ResQPUMP®, Advanced Circulatory Systems) fixed on the anterior chest wall. During the compression phase, the chest is compressed, and blood is forced out of the heart to perfuse the vital organs, as with standard CPR. Next, when the chest is actively pulling up with the device, a vacuum is created within the thorax, drawing more blood back into the heart. This technique improves hemodynamics [26, 27] and, in some studies, long-term survival rates with patients in cardiac arrest, as compared with patients receiving standard CPR alone [28, 29]. The ACD-CPR device is currently being used in many countries throughout the world including France and Israel, as well as parts of China, Japan, and Germany (Fig. 38.11). ACD-CPR in combination with the ITD, known as the ResQCPR™ System, received regulatory clearance in May of 2015 from the Food and Drug Administration (FDA) with an indication for use as a CPR adjunct to improve the likelihood of survival in adult patients with non-traumatic cardiac arrest.

It should also be noted that ACD-CPR + ITD has been evaluated in multiple animal and clinical trials and is currently recommended in the AHA guidelines as an alternative to standard CPR. Importantly, the device combination has been shown to quadruple blood flow to both the heart and brain, compared with manual standard CPR alone.

Fig. 38.11 ResQPUMP®, the US version of the active compression-decompression cardiopulmonary resuscitation device. The force gauge and metronome are used to guide the rescuer in the proper performance

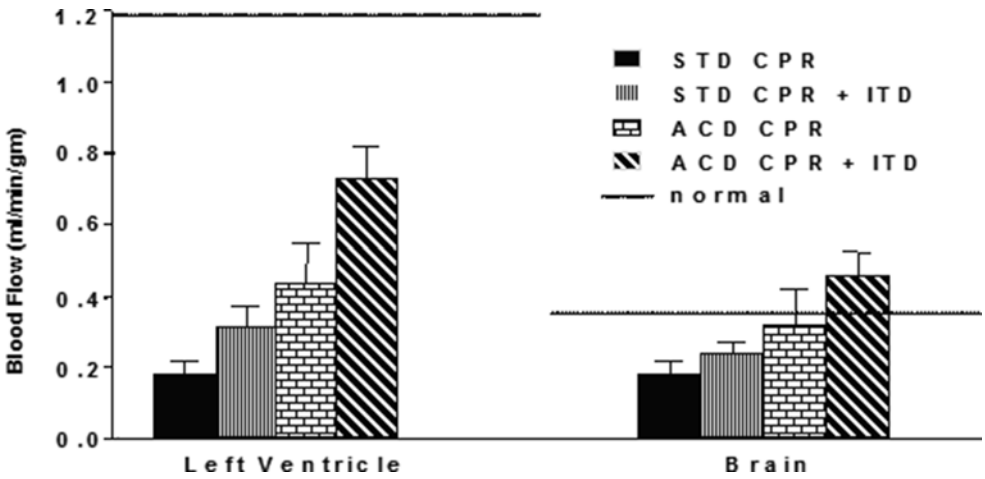

Fig. 38.12 Blood flow in a porcine model. The cumulative effect of ACD-CPR and ITD devices [9]. Solid horizontal line represents normal baseline values. *STD* standard, *ACD* active compression-decompression, *CPR* cardiopulmonary resuscitation, *ITD* impedance threshold device

This device combination also significantly increases blood pressures and survival rates [29–31].

Lurie et al. specifically studied the effects of ACD-CPR and an ITD on blood flow; the results are summarized in Fig. 38.12. Preclinical animal studies demonstrated that left ventricle and cerebral blood flows were markedly improved with ACD-CPR+ITD [10, 32]. In these studies, CPPs were >20 mmHg, the minimum CPP thresholds needed to optimize the chance for survival in both humans and in a porcine model of cardiac arrest [33, 34]. The device combination also optimized perfusion within the brain, which was found to be even greater than baseline levels after a prolonged arrest, when comparing standard CPR to the combination of ACD-CPR+ITD [10]. The investigators believe that one of the reasons that the clinical trials with ACD-CPR+ITD have been successful is secondary to the marked increases in cerebral perfusion that can be achieved with this new approach. These findings have been reproduced by several other investigators using both pediatric and adult pigs in cardiac arrest [4, 35]. Improved forward blood flow and vital organ perfusion with use of ACD-CPR+ITD also enhances drug efficacy during CPR [36]. For example, it was shown that the effects of exogenous vasopressin were significantly enhanced with ACD-CPR+ITD for hypothermic pigs, as reflected by higher coronary and CePPs and improved cerebral metabolic profiles.

In general, the use of the combination of ACD-CPR and the ITD can be considered to be synergistic. To date, four randomized clinical trials have been performed to evaluate the relative effectiveness and safety of the ACD-CPR+ITD in humans [30, 31, 37, 38]. The first blinded randomized clinical trial focused on resultant hemodynamics in patients with out-of-hospital cardiac arrest [37]. Eleven patients were treated with an active (functional) ITD and 10 with a sham (placebo) ITD. In that study, end-tidal carbon dioxide ($ETCO_2$) levels rose more rapidly and reached higher levels with the active ITD; systolic and diastolic blood pressures were nearly normal in the active ITD group (109/57 mmHg) versus the sham ITD group (89/35 mmHg, $P<0.01$). In addition, ROSC occurred more rapidly in the active ITD group compared with the sham ITD group. Based upon these data, the use of ACD-CPR+ITD was recommended as an alternative to standard CPR in the 2000 AHA guidelines [39].

Another study demonstrated that the ITD augments negative intrathoracic pressure when applied to a face mask [38]. This is important because it indicates that inspiratory impedance can be added during BLS airway management (by first responders and perhaps even lay rescuers prior to intubation). Patients with out-of-hospital cardiac arrest were randomized prior to endotracheal intubation to either a sham or active ITD, and intrathoracic pressure tracings were recorded. Addition of the active ITD to the face mask resulted in an immediate decrease in intrathoracic pressures during ACD-CPR. Each time the active ITD was used, there were significant reductions in the decompression phase intrathoracic pressures. These studies demonstrated, for the first time, the degree of negative intrathoracic pressures achieved with ACD-CPR+ITD in humans. The average maximum negative intrathoracic pressure was −7.3 mmHg with the active ITD on an endotracheal tube versus only −1.3 mmHg with the sham ITD. A second important finding was that it took up to 5 compression-decompression cycles to achieve the maximum negative intrathoracic pressures, as respiratory gases are expelled from the chest and prevented from reentry. This mechanism plays a key role in the function of the ITD. Each time an active, positive pressure, ventilation was delivered, the decompression phase intrathoracic vacuum was lost and required regeneration. Thus, the less frequently the ventilation rate was employed, the greater the blood flow back to the heart. A recent study using standard CPR with the ITD in pigs confirmed this important observation [12]. This has become an important theme for all types of CPR; ventilations interrupt CPP and should be reduced to the minimum required to maintain oxygenation and transpulmonary circulation.

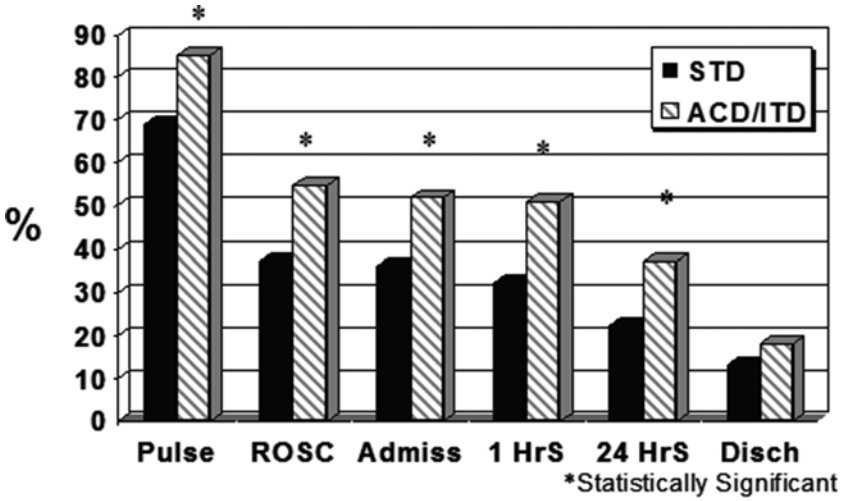

Fig. 38.13 Outcomes associated with comparison of standard cardiopulmonary resuscitation (STD) and ACD-CPR + ITD ($n = 210$) in Mainz, Germany. *1HrS* 1-hour survival, *24HrS* 24-hour survival, *ACD* active compression-decompression, *Admis* hospital admission, *CPR* cardiopulmonary resuscitation, *Disch* hospital discharge, *ITD* impedance threshold device, *ROSC* return of spontaneous circulation

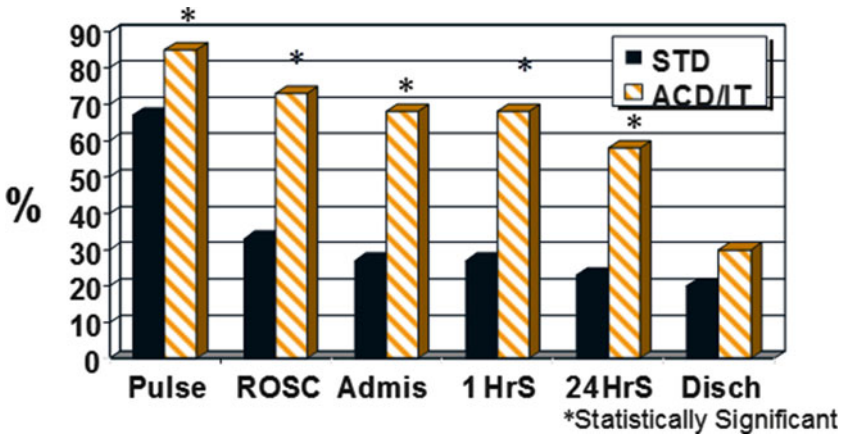

Fig. 38.14 Outcomes in patients randomized with either standard CPR (STD) or ACD-CPR + ITD with witnessed ventricular fibrillation in Mainz, Germany ($n = 70$). *1HrS* 1-hour survival, *24HrS* 24-hour survival, *ACD* active compression-decompression, *Admis* hospital admission, *CPR* cardiopulmonary resuscitation, *Disch* hospital discharge, *ITD* impedance threshold device, *ROSC* return of spontaneous circulation

It is generally accepted that ACD-CPR with an ITD improves short-term survival rates after cardiac arrest. A recent prospective controlled trial was performed in Mainz, Germany [37]; patients with out-of-hospital arrest of presumed cardiac etiology were sequentially randomized to ACD-CPR + ITD or standard CPR (control subjects) by the advanced life support team after intubation. Patients with an identified initial heart rhythm of VF (42 % of the total), who could not be resuscitated by BLS early defibrillation, were enrolled in this clinical trial, as well as patients with an initial rhythm of asystole or PEA. The primary endpoint was 1-h survival after a witnessed arrest. With ACD-CPR + ITD ($n = 103$), ROSC, 1-h and 24-h survival rates were 55 %, 51 %, and 37 % versus 37 %, 32 %, and 22 % for standard CPR alone ($n = 107$; $p = 0.016$, 0.006, and 0.033), respectively (shown in Fig. 38.13).

One-hour and twenty-four-hour survival rates in patients with a witnessed arrest were dramatically higher after ACD = CPR + ITD—68 and 55 %, respectively, versus 27 and 23 % with standard CPR ($p = 0.002$ and 0.009) (shown in Fig. 38.14).

Hospital discharge rates were 18 % after ACD-CPR + ITD versus 13 % in control subjects ($P = 0.41$). Overall neurological function trended higher with ACD-CPR + ITD versus control subjects ($P = 0.07$).

Importantly, patients randomized >10 min after the call for help to the ACD + ITD CPR group had a greater than three times higher 1-h survival rate (44 %) than control subjects (14 %) ($P = 0.002$). These time-related benefits were observed regardless of presenting rhythm. It should be noted that neurological outcomes in the survivors with delays to treatment with ACD-CPR + ITD were similar to those who were treated with ACD-CPR + ITD more rapidly.

Another prospective blinded study performed in France also demonstrated significantly increased 24-h survival rates with use of ACD-CPR + ITD [31]. In one arm of this study, 200 patients were treated by advanced life support personnel with ACD-CPR and an active ITD, and another 200 patients were randomized to the control group and received treatment with ACD-CPR and a sham ITD. As in other studies from France, most of the patients had an initial rhythm of asystole [28, 29]. The group treated with ACD-CPR and an active

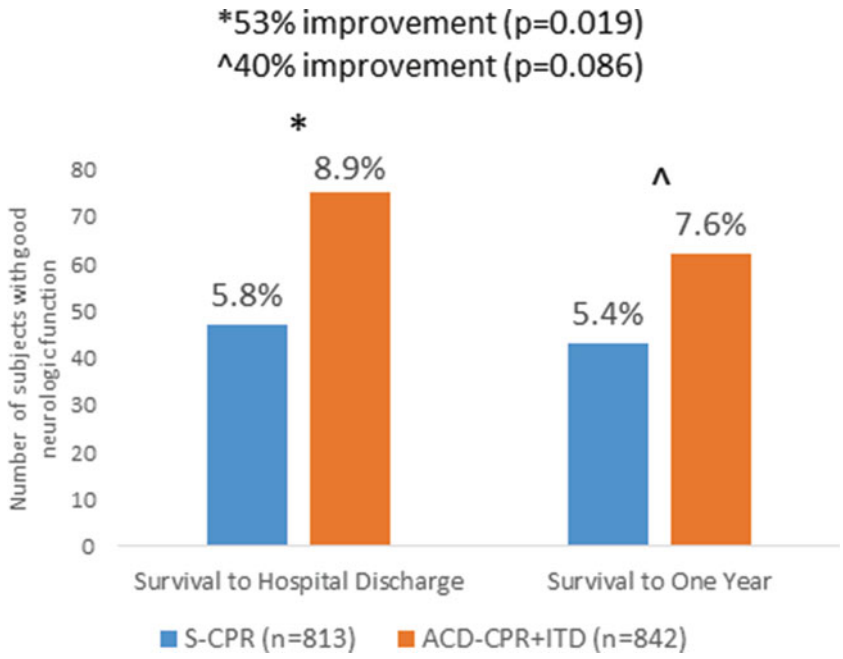

Fig. 38.15 Percentage survival to hospital discharge with favorable neurological outcome in patients randomized to either standard CPR (S-CPR) or ACD-CPR + ITD ($n = 1653$). *ACD-CPR* active compression-decompression cardiopulmonary resuscitation, *ITD* impedance threshold device

ITD had 24-h survival rates of 32 % compared with 24-h survival rates of 22 % in the control population ($P < 0.05$). Because of long EMS response times, survival rates in both groups were very low, but differences in neurological function in the survivors trended in favor of the ACD-CPR + ITD group. Only 1/8 (12 %) of survivors treated with the sham device had normal cerebral function at the time of hospital discharge, versus 6/10 (60 %) in the functional ITD group ($p < 0.07$).

Perhaps the most definitive proof of the effect of ACD-CPR + ITD on long-term survival was demonstrated in a large prospective, randomized clinical trial funded by the National Institutes of Health [40]. This out-of-hospital study compared ACD-CPR plus an ITD to manual standard CPR in adult, nontraumatic cardiac arrest patients. A total of 2470 subjects were randomized and received CPR with one of the two CPR methods, with 1653 subjects meeting final inclusion criteria: 813 in the control group (standard CPR) and 840 in the intervention (ACD-CPR + ITD) group. First, the results of the study demonstrated that the use of these devices was safe. The overall rate of major adverse events, including chest fractures, was not significantly different between groups, although there were more reports of pulmonary edema in the intervention group; this was coexistent with increased survival in this group. Neurological function was similar between groups at 90 days and one year after cardiac arrest. There were no increases in the number of patients with severe neurological impairments in the intervention group.

This study also demonstrated the efficacy of these employed devices. ACD-CPR with the augmentation of negative intrathoracic pressure using an ITD improved long-term survival (to hospital discharge) with favorable neurological function by 53 % ($p = 0.019$), and the survival benefits persisted to a 1-year time point following cardiac arrest, as shown in Fig. 38.15. In the patient population which typically resulted in poor neurological function at hospital discharge, the use of ACD-CPR with an ITD and therapeutic hypothermia resulted in a sixfold improvement in neurological function by 90 days, compared to standard CPR with therapeutic hypothermia [41]. In patients with out-of-hospital cardiac arrest from a variety of nontraumatic etiologies, ACD-CPR with an ITD resulted in a 38.5 % increase in survival to hospital discharge, with favorable neurological function ($p = 0.027$) and a 35.4 % increase in survival at 1 year with favorable neurological function (not significant), compared to patients receiving S-CPR [42]. In the absence of treatment with therapeutic hypothermia after cardiac arrest, survival rates with favorable neurological function at hospital discharge and 90 days after cardiac arrest were nearly twice as high with ACD-CPR plus an ITD compared to standard CPR, indicating that the combination therapy is neuroprotective, independent of in-hospital therapeutic hypothermia.

38.7 Treatment of Life-Threatening Hypotension with the ITD in Spontaneously Breathing Patients

Shock can be defined as life-threatening hypotension and results in inadequate tissue perfusion. Hypovolemia caused by uncontrolled hemorrhage in trauma is the most common form or cause of shock and is referred to as *hemorrhagic*

shock. Death following severe blood loss commonly develops secondary to profound hypotension and vital organ ischemia. In other words, in the absence of a critical central blood volume, both stroke volume and cardiac output are decreased and hypotension ensues.

Intravenous fluids and vasopressor agents have traditionally been the mainstay of therapy for patients with marked hypotension. Commonly, intravenous fluids and blood replacement, together with intravenous therapies such as epinephrine and other vasopressors, have been effective as short-term therapies, i.e., providing a bridge to more definitive repair of the primary injury. Yet, their use is also associated with significant clinical shortcomings such as the following: (1) they require intravenous or intraosseous access; (2) nonblood volume expanders can decrease the effectiveness of normal thrombus formation (by dilution of critical clotting factors); and (3) their use can ultimately reduce the oxygen carrying capacity of the blood. In addition, massive intravenous fluid replacement can in turn cause both pulmonary and peripheral edema (in some cases, cerebral edema), as well as hypothermia. Furthermore, vasopressors can also cause ischemia, especially to the gut. Vasopressors and fluids have been associated with "popping the clot" in the patient with significant blood loss secondary to sudden increases in blood pressure to normal or above normal values. Moreover, vasopressors like epinephrine can cause supraventricular or ventricular tachycardias, which can lead to a further compromise of the patient's already tenuous hemodynamic status. It should be noted that even the sinus tachycardia that is normally observed after epinephrine therapy can be detrimental in the setting of shock, as it results in a decreased amount of time for cardiac filling after each ventricular systole. This is an important issue since blood flow back to the heart is markedly decreased because of the low central venous pressures. In other words in this setting, one needs more time (and thus a slower heart rate) for effective refilling of the heart after each contraction.

As such, there is strong evidence that one of the primary mechanisms that contribute to reduced cardiac filling, decreased stroke volumes, and ultimately shock following an acute hemorrhage is the reduction in the circulating blood volume and a subsequent reduction in cardiac filling pressures (i.e., lower central venous pressures or cardiac preloads). Therefore, countermeasures designed to increase venous return and decrease cardiac filling without causing hemodilution and without "popping the clot" may be an effective therapy for the acute treatment of massive blood loss. It is important to recognize that the primary goal of any therapy used for the treatment of hemorrhagic shock is the restoration of sufficient vital organ perfusion to prevent death, even if the primary cause of the blood loss has not yet been established or repaired. Such therapies should act primarily to increase stroke volumes rather than to increase peripheral resistance, as the latter may cause more harm than good. Ideally, a new therapy designed to improve vital organ perfusion in the setting of hemorrhagic shock should act primarily to optimize stroke volumes, improve vital organ blood flow by a mechanism that is independent of increasing peripheral vascular resistance, and help to stabilize a permissive hypotensive state that provides adequate cerebral perfusion.

Fig. 38.16 ResQGARD® impedance threshold device on a face mask

Building upon the needs described above, two new technologies have been developed by Advanced Circulatory Systems to treat clinically significant hypotension. One is termed the ITD for spontaneously breathing patients (ResQGARD® ITD), and the other is called the intrathoracic pressure regulator (ITPR, CirQlator®). The ResQGARD, shown in Fig. 38.16, is designed for the spontaneously breathing patient and can be considered as a natural extension of a normal physiological process, i.e., the transformation of the normal respiratory muscle function from a primary gas exchange function to the dual functions of gas exchange and augmentation of venous return, as well as enhancement of cardiac stroke volume. The ITPR was designed for the mechanically ventilated patient where it actively provides a low level of negative pressure during the expiratory phase of ventilation, thereby increasing venous return and improving cardiac output, stroke volume, and blood pressure. To avoid confusion, the differences between the ITDs and the ITPR device are summarized in Fig. 38.17.

ResQGARD ITD	Intended Use: Used in spontaneously breathing patients to assist in enhancing circulation. Device can be used on a facemask.	
ResQPOD ITD	Intended Use: Used in non-spontaneously breathing patients in cardiac arrest where CPR is being performed to assist in enhancing circulation. Device can be used on a facemask or an endotracheal tube.	
ITPR	Intended Use: Used in non-spontaneously breathing patients who are hypotensive and intubated, including those in cardiac arrest undergoing CPR. Device is directly attached to an endotracheal tube or other airway adjunct.	

Fig. 38.17 Differences between an impedance threshold device (*ITD*) for spontaneously breathing patients and for those in cardiac arrest and the intrathoracic pressure regulator (*ITPR*)

The ITD works by lowering intrathoracic pressure in the thorax with each inspiration, thereby enhancing venous blood flow back to the heart and lowering ICPs. These mechanisms serve to enhance both cardiac output and blood pressure. There is also experimental data suggesting that the use of the ITD will reduce the amount of vasopressors needed, since it increases overall cardiac outputs and circulation [36]. In this manner, the ITD provides an indirect drug-enhancing effect, enabling the rescuers to use less of a vasopressor drug, and perhaps less fluid resuscitation, to obtain the same or greater hemodynamic effectiveness.

The spontaneously breathing version of the ITD is a small disposable plastic airflow regulator that can be attached to a face mask, mouthpiece, or tracheal tube. The device has a spring-loaded diaphragm that requires a certain threshold (*cracking pressure*) to be achieved before it opens to allow airflow, thus functioning like a partial Mueller maneuver (inhaling against a closed glottis) to augment negative intrathoracic pressure with each inspiration [9]. In this manner, the device harnesses the patient's own respiratory pump to enhance circulation. In 1947, Cournand was the first to show that *increases* in mean airway pressure result in decreased systemic venous return, decreased pulmonary blood flow, and a fall in cardiac output. Lower negative intrathoracic pressure during spontaneous inspiration, however, represents a natural mechanism for enhancing venous return and cardiac filling. Several natural physiological reflexes, such as gasping and the Mueller maneuver, augment negative intrathoracic pressure and increase cardiac output. Several authors have shown that artificially induced negative pressure ventilation can be used to increase cardiac output [43, 44]. The ITD has been evaluated in animals and humans for the treatment of: (1) cardiac arrest, (2) hemorrhagic and heat shock, and (3) orthostatic hypotension and (4) for enhancing blood donation.

In 2004, Lurie et al. demonstrated that spontaneous breathing through the ITD during hemorrhagic and heat shock in a porcine animal model resulted in an immediate sustained rise in systolic blood pressure in both conditions [45]. As shown in Fig. 38.18, addition of the ITD (set to open at a cracking pressure of −12 cmH_2O) after an acute hemorrhage resulted in immediate rises in systolic blood pressure that was sustained for 30 min. Upon removal of the ITD, the blood pressure decreased back to values identical with the controls. These studies showed a 30 % increase in cardiac output when the ITD was utilized for the pigs in shock. Subsequent studies showed that the use of the ITD in spontaneously breathing pigs after severe hemorrhage resulted in increased cardiac output, blood pressure, cardiac chamber dimensions, transvalvular blood flow, and survival rates [46]. These studies demonstrate how the ITD augments cardiac output, improves hemodynamics, and increases survival in spontaneously breathing pigs under conditions of hypovolemic hypotension [47].

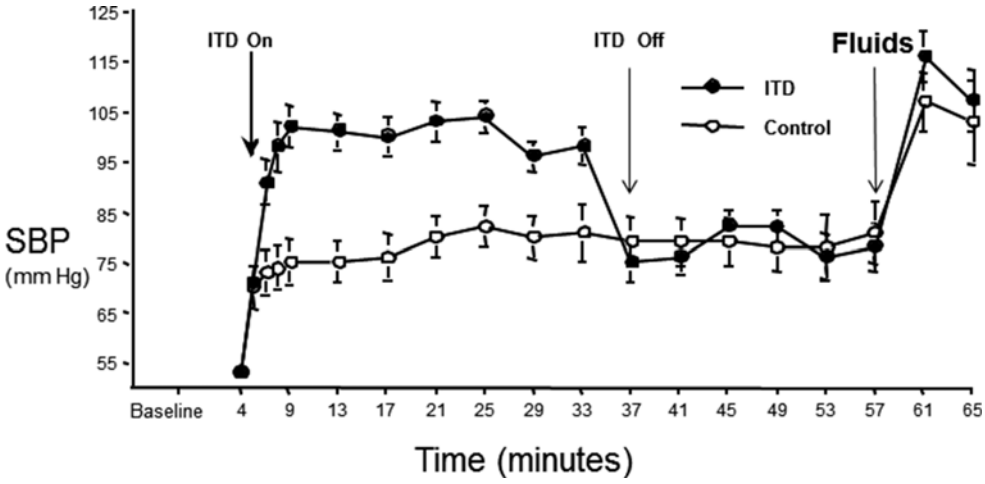

Fig. 38.18 Changes in systolic blood pressure (*SBP*) with and without impedance threshold device (*ITD*) breathing following controlled hemorrhage and shock in spontaneously breathing pigs

More recently, Metzger et al. studied the use of the ITD in a porcine hemorrhagic model to determine if the negative intrathoracic pressure therapy provided by the device could improve systolic blood pressure but still allow permissive hypotension, thereby avoiding "popping the clot" [48]. They compared the use of the ITD to the current standard of care, i.e., infusing normal saline to treat a 55 % hemorrhage. Maximum systolic blood pressure during 15 min of treatment was significantly higher in the normal saline group compared to the ITD and control groups, but at a level of 131 ± 7.6 mmHg, it was well above the threshold believed for the risk clot dislodging in animals (94 ± 3 mmHg). Conversely, pigs treated with the ITD had significant improvements in systolic blood pressure throughout the 30-min course of treatment compared to controls, but the levels were much more moderate and well within the levels of permissive hypotension. Another benefit to the ITD was that blood pressures were considered adequate for organ perfusion, but importantly the ICPs were not elevated. This allowed for improved perfusion to the brain, while increased ICP resulting from normal saline infusion would likely impede cerebral blood flow. These results show that the ITD can be effective in treating hypotension secondary to trauma or hemorrhage without the negative effects associated with excessive systolic blood pressure.

The ITD with a cracking pressure of −6 cmH_2O was first studied in normal volunteers by Convertino et al. at NASA, in studies related to post-flight orthostatic hypotension [49]. Inspiration through the ITD increased cardiac output by about 1.5 L/min in supine subjects and was well tolerated. The ITD increased stroke volume and was shown to maintain blood pressure in normal volunteers subjected to acute orthostatic stresses and later in patients with symptomatic orthostatic hypotension. The use of the ITD in normal volunteers resulted in: (1) an immediate increase in cardiac stroke volume, (2) increases in both systolic blood pressure and heart rate, and (3) improved cardiac output as shown in Fig. 38.19 [50]. It was also observed that total peripheral resistance was reduced by the ITD.

Also highly relevant is how the ITD affects the work of breathing. To assess the work of breathing associated with the use of the ITD, the power of breathing was measured in collaboration with NASA scientists in 9 female and 9 male subjects breathing through a face mask at two separate ITD conditions: (1) −6 cmH_2O and (2) control (0 cmH_2O). The results from this study demonstrated that breathing through the ITD was well tolerated by all subjects. For the sham and active ITD groups, respectively, peak inspiratory pressures were −1.13 ± 0.63 cmH_2O and −9.92 ± 6.2 cmH_2O ($p < 0.0001$); tidal volumes were 958 ± 396 mL and 986 ± 389 mL (not significant); and inspiratory times were 189 ± 81 ms and 296 ± 109 ms ($p = 0.002$). For the sham and active ITD groups, respectively, imposed work of breathing (WOBi) was 0.064 ± 0.04 J/L and 0.871 ± 0.117 J/L ($p < 0.0001$); power of breathing (POBi) was 0.88 ± 0.63 J/min and 7.56 ± 3.55 J/min ($p < 0.0001$); peak inspiratory pressures were −1.13 ± 0.63 cmH_2O and −9.92 ± 6.2 cmH_2O ($p < 0.0001$); tidal volumes were 958 ± 396 mL and 986 ± 389 mL (not significant); and inspiratory times were 189 ± 81 ms and 296 ± 109 ms ($p = 0.002$). Interestingly, there were no significant observable differences between men and women in terms of work of breathing [51].

To put these data into perspective, one must understand the power of breathing for a normal individual, where power is work per unit time ($W = W \times f$, where f is respiratory frequency). The maximal power output for normal young adults is 613 cal/min (range: 500–860) [52]. Thus, the amount of power output required during quiet breathing or the use of the ITD seems rather minimal, amounting to less than 1.0 % of maximum. Vigorous exercise requiring minute volume of 60–80 L requires ~80 J/min of power. The −6 cmH_2O ITD requires about 1–2 cal/min of respiratory power. For the ITD to be functional, the energy required for its operation should not exceed the energy available in the patient population in

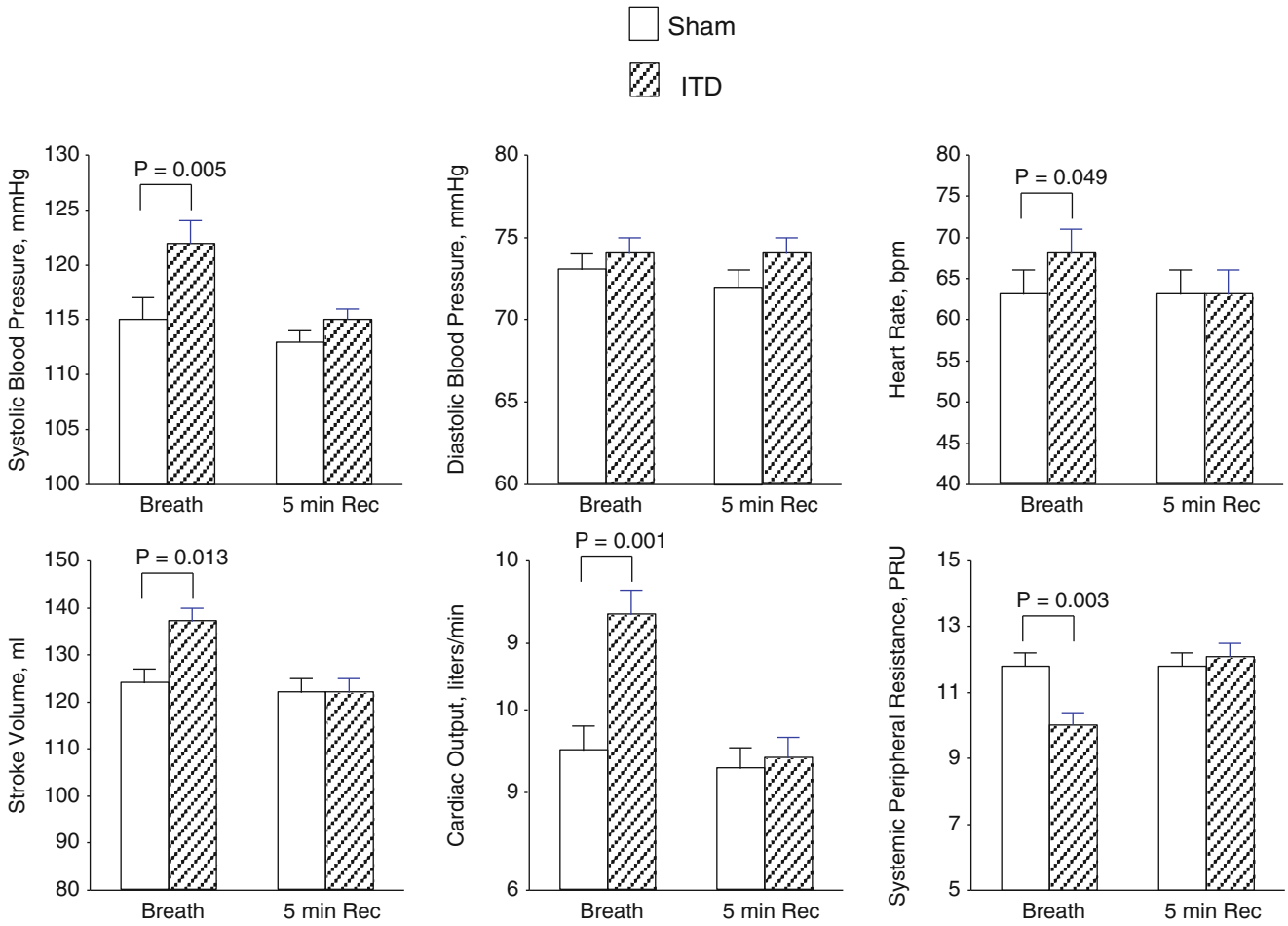

Fig. 38.19 Hemodynamic results. Systolic and diastolic blood pressures, heart rate, stroke volume, cardiac output, and total peripheral vascular resistance during (breath) and after (5-min recovery) spontaneous breathing on the impedance threshold device (*ITD*) at 0 cmH_2O resistance (sham control, *open bars*) and −6 cmH_2O resistance (*solid bars*) ($n = 20$)

which it is expected to be applied, for example, ill and injured patients with hypotension. It is known that ill patients who require mechanical ventilator support use about 1–2 cal/min for self-triggered ventilation and are generally able to sustain this level of effort for long periods (hours to days) [52]. Therefore, we expect that most patients will be able to tolerate the use of the ITD without excessive fatigue, given that it requires only a fraction of the respiratory power needed for a similarly ill group of patients to self-trigger a mechanical ventilator. Based on these measurements, we conclude that the vast majority of conscious but hypotensive patients will be able to inspire through the ITD with a resistance of −7 cmH_2O and should therefore benefit hemodynamically from the device.

Most recently, the ITD was studied by Convertino et al. at the US Army Institute of Surgical Research, using a lower body negative pressure chamber (LBNP) to lower central blood volume and thus induce a state of severe hypotension [53]. A photo of the LBNP chamber is shown in Fig. 38.20. The application of negative pressure to the lower body (below the iliac crest) results in a redistribution of blood away from the upper body (head and heart) to the lower extremities and abdomen. Thus, this model provides a unique method of investigating interventions such as the ITD under conditions of controlled, experimentally induced hypovolemic hypotension. Absolute equivalence between the magnitude of negative pressure applied and the magnitude of actual blood loss has recently been evaluated in a baboon model which demonstrated the absolute equivalence between the simulated bleed and the actual blood loss [54]. On the basis of the magnitude of central hypovolemia induced, Convertino et al. provide data to support that 10–20 mmHg negative pressure induces hemodynamic responses that are equivalent to those resulting from blood loss ranging from 400 to 550 mL, 20 to 40 mmHg negative pressure induces hemodynamic responses that are equivalent to those resulting from blood loss ranging from 550 to 1000 mL, and greater than 40 mmHg negative pressure induces hemodynamic responses that are equivalent to those resulting from blood loss approximating 1000 mL or more

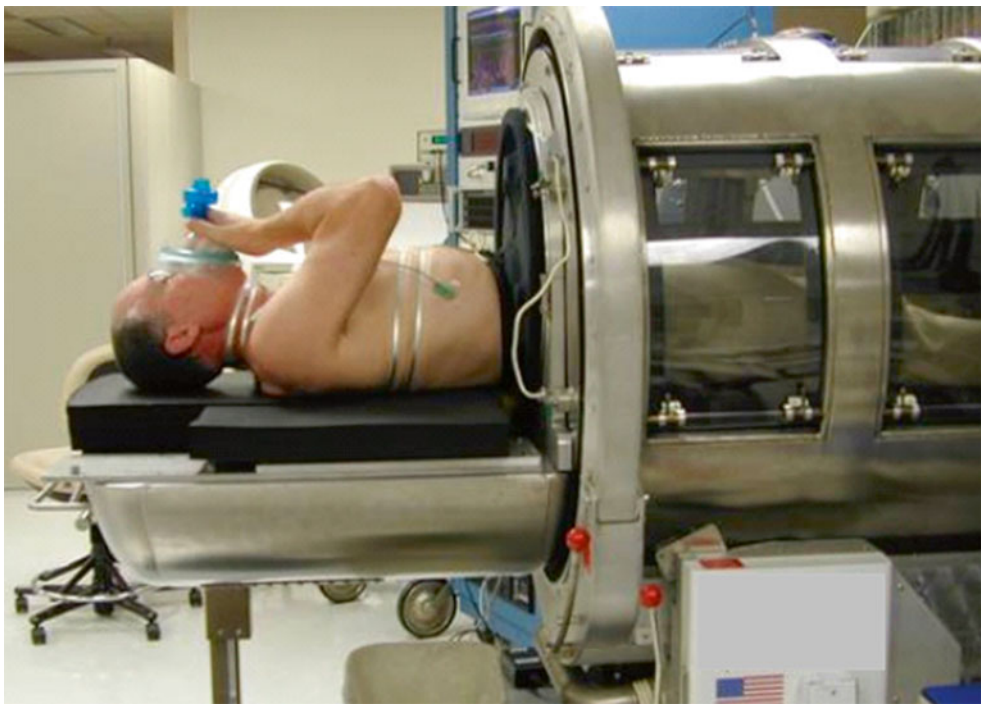

Fig. 38.20 Lower body negative pressure chamber used to simulate severe hypotension

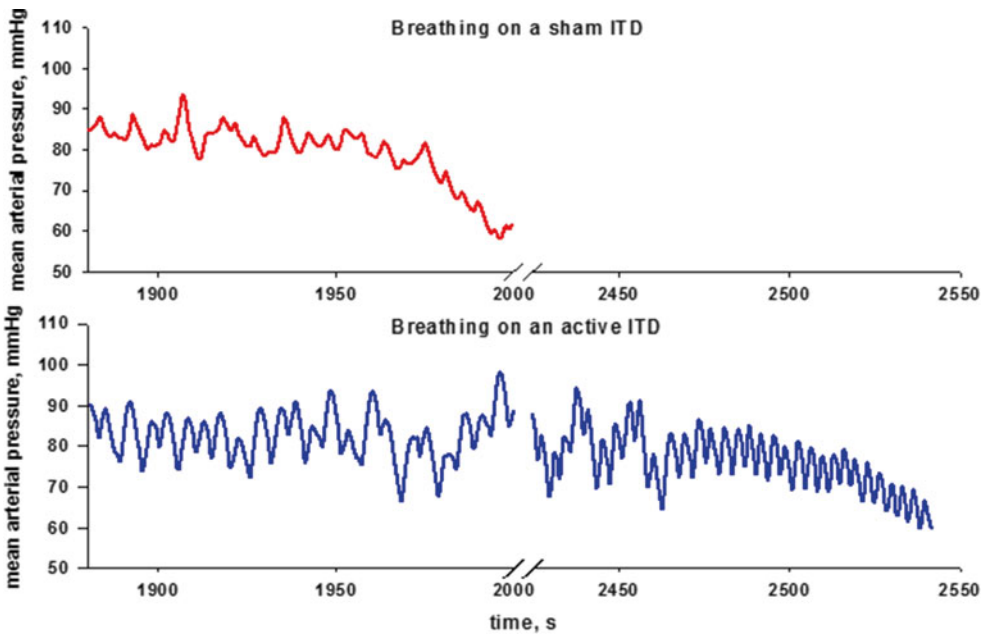

Fig. 38.21 Representative tracings of beat-to-beat mean arterial blood pressure obtained from the same subject while breathing on a sham impedance threshold device (ITD; *top panel*) and active ITD (*bottom panel*) during the final two minutes of lower body negative pressure chamber exposure prior to cardiovascular collapse

[53]. Nine healthy normotensive volunteers completed two counterbalanced protocols with (active) and without (sham) an ITD set to open at −6 cmH_2O pressure. Continuous non-invasive measures of systolic (SBP), diastolic (DBP), and mean (MAP) arterial blood pressures were obtained during a LBNP protocol consisting of a 5-min rest period (baseline) followed by 5 min of chamber decompression at −15, −30, −45, and −60 mmHg, as well as additional increments of −10 mmHg every 5 min until the onset of cardiovascular collapse. Overall, SBP (79 ± 5 mmHg), DBP (57 ± 3 mmHg), and MAP (65 ± 4 mmHg) at the time of cardiovascular collapse were lower ($P < 0.02$) when subjects breathed through the sham ITD than when they breathed through the active ITD at the same time points of LBNP (102 ± 3, 77 ± 3, 87 ± 3 mmHg, respectively). Elevated blood pressures were associated with a 23 % increase ($P = 0.02$) in LBNP tolerance using an active ITD (1639 ± 220 mmHg-min) compared with a sham ITD (1328 ± 144 mmHg-min). A representative tracing of data obtained in these studies is shown in Fig. 38.21.

These results are the first to demonstrate, in humans, that the time to cardiovascular collapse associated with progressive reduction in central blood volume and subsequent

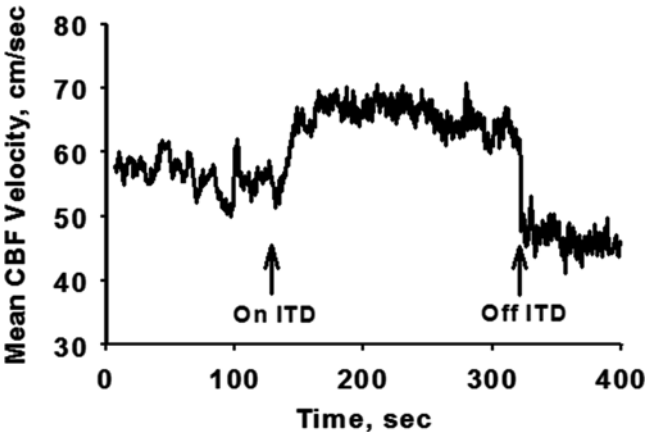

Fig. 38.22 Typical continuous recording of mean cerebral blood flow (*CBF*) velocity in a subject before, during (On ITD), and at the cessation (Off ITD) of spontaneous breathing on the impedance threshold device (*ITD*)

development of severe hypotension can be significantly improved by inspiratory resistance induced by spontaneous breathing through an ITD. The results from the present experiment demonstrated an average elevation in SBP of 23 mmHg when estimated central blood volume was reduced by more than 2 L [53].

Importantly, the use of an ITD also has striking effects on cerebral artery blood flow. With each inspiration through the ITD, ICPs are lowered, and simultaneously cardiac output is increased. Measurement of middle cerebral intracranial Doppler demonstrated that the use of the ITD increased middle cerebral artery blood flow in spontaneously breathing adult humans, as shown in Fig. 38.22 [55].

Our group recently performed another clinical trial which evaluated the use of the ITD to treat non-life-threatening hypotension (SBP<95 mmHg) in the emergency room setting. In this randomized double-blind clinical trial, patients received the current standard of care for hypotension, which consists of controlling the bleeding, reversing other potential causes of low blood pressure such as correcting hyperthermia, and administering fluids, oxygen, and/or blood products as appropriate. The use of the ITD did not interfere with standard therapy. Once it was determined that the subjects met enrollment criteria based upon the inclusion and exclusion criteria and informed consent was obtained, subjects were randomized to either a sham ITD or an active (functional) ITD; the sham and active ITDs appeared identical. The devices were kept in an opaque package, preventing anyone involved with the study from knowing whether any given device was a sham or active ITD based upon visual inspection. Baseline blood pressure, heart rate, respiratory rate, oxygen saturation, and clinical findings including quality of the pulse and quality of respirations were recorded immediately. The ITD was then placed, and hemodynamic parameters were assessed every 2 min, for a minimum of 6 min and up to 10 min. Standard therapies, including intravenous fluids, were administered as deemed clinically necessary, regardless of the effect of the ITD. The active device was found to be significantly more effective than the sham. Specifically, the mean rise in SBP for the active ITD group was 13.2 ± 7.8 mmHg ($n = 16$) versus 5.9 ± 5.5 mmHg for the sham ITD group ($n = 19$) ($p = 0.003$). Mean fluids given during the study were 92 ± 170 ml for the active ITD group and 192 ± 200 ml for the sham ITD group ($p = 0.13$). In a subgroup of patients that received no fluids during device use, the maximum rise in SBP (mean ± STD) was 12.8 ± 7.8 mmHg for the active ITD group and 5.6 ± 5.0 mmHg for the sham ITD group ($p = 0.04$). MAP was also statistically higher in the active ITD group (9.2 ± 7.8 versus 4.8 ± 3.3, $p = 0.03$) [56].

More recently, a study conducted by Wampler et al. looked at the use of the ITD in patients with hypotension, which was defined as a SBP less than 90 mmHg [57]. The primary endpoint was MAP before application of the ITD versus MAP after 2–4 min of ITD use. They found that average systolic and diastolic blood pressures and MAPs all increased by a statistically significant amount with ITD use in all patients (78 ± 13 mmHg versus 97 ± 19 mmHg, 51 ± 13 mmHg versus 63 ± 15 mmHg, and 60 ± 10 mmHg versus 70 ± 15 mmHg, respectively). Additionally, systolic and diastolic pressures were increased for the subset of patients who elicited hypotension due to trauma. These findings support the use of the ITD as a safe and tolerable means to treat hypotension from traumatic and nontraumatic causes.

It is now the general consensus that the ITD harnesses the patient's own thoracic pump to enhance circulation and offers a noninvasive means to treat some of these patients. However, the spontaneous breathing version of the ITD requires that patients be able to breathe on their own, and most patients in severe shock are usually intubated and require assisted ventilation. To fill this gap, the ITPR was developed. This technology was developed based on the concept of lowering intrathoracic pressures to enhance circulation for patients with life-threatening hypotension that are dependent upon assisted ventilation.

38.8 ITPR Therapy: A Potential Novel Treatment of Severe Hypotension in Severely Ill Patients

To date, the ITPR described below has been tested in animals and in limited clinical studies. It combines a way to generate a controlled intrathoracic vacuum with a method to provide controlled positive pressure ventilation. It can be used for the treatment of cardiac arrest, multiple forms of shock to buy time until more definitive therapy is available, or cerebral

injuries. The device can be used with a handheld resuscitator bag or it can be attached to a mechanical ventilator or anesthesia machine. While multiple designs are possible to embody this concept, the main function of the ITPR is to create a preset continuous and controlled expiratory phase negative intrathoracic pressure that is interrupted only when positive pressure ventilation is needed to maintain oxygenation and provide gas exchange. Today, the ITPR has been cleared for sale by the FDA with the approved indication of a device to "temporarily decrease intrathoracic pressure to increase blood circulation."

It was recognized from the start of device development that it would be important to develop a modification of the ITD for the use with nonbreathing and more critically ill hypotensive patients; this resulted in the concept of the ITPR. The ITPR employs an external vacuum source to lower intrathoracic pressures and thus enhance venous blood flow back to the heart in nonbreathing hypotensive patients. This refinement is based on the breakthrough in our clinical understanding of the basic physiological principles of blood flow in hypotensive states. By transforming the chest into an active bellows during CPR, the combination of a relatively low level expiratory phase intrathoracic vacuum and intermittent positive pressure ventilation results in a significant augmentation of venous blood flow to the right heart, thereby increasing both stroke volume and cardiac output.

Contemporaneously, the decrease in intrathoracic pressure results in decreases in ICP and thus provides an additional mechanism whereby the ITPR increases CePP; this is illustrated in Fig. 38.23. When the ITPR is turned on, the intrathoracic pressure between positive pressure breaths is lowered immediately, as is the ICP. Based on these findings, the ITPR may also ultimately have the potential for treatment of brain injury.

To date, the potential beneficial effects of the ITPR have been studied in pigs in VF during CPR. In this setting, the ITPR was used to lower intrathoracic pressure and thus enhance venous return to the heart and increase overall efficacy [58]. Vital organ perfusion pressures and end-tidal carbon dioxide levels were significantly improved with ITPR-CPR, and animal survival was 100 % (10/10) with ITPR-CPR versus 10 % (1/10) with standard CPR alone. The use of ITPR-CPR improved hemodynamics, vital organ perfusion pressure, and carotid blood flow in animals eliciting both VF and hypovolemic cardiac arrest. Figure 38.24 demonstrates the significant hemodynamic differences observed when using the ITPR during standard CPR in this animal model of cardiac arrest.

The physiological goals of the ITPR are to lower intrathoracic pressure during the expiratory phases of ventilation and provide positive pressure ventilation in patients requiring assisted ventilation. The first preclinical studies evaluating the effects of the ITPR on vital organ perfusion pressure were performed in both normovolemic and hypovolemic swine [59, 60]. Six anesthetized animals received 5-min interventions with endotracheal pressure (ETP) set to 0, −5, 0, −10, 0, −10, 0, −5, 0 mmHg during euvolemia and then after a fixed hemorrhage of 50 % of their total blood volumes. Hemodynamic parameters were continuously measured, and blood gases were obtained at the end of the first four 5-min intervals. Under both euvolemic and hypovolemic conditions, right atrial pressure and ICP decreased proportionally to the intrathoracic pressure, with the more marked changes observed with hypovolemic conditions. By contrast, the increases in MAP, coronary perfusion pressure, and CePPs

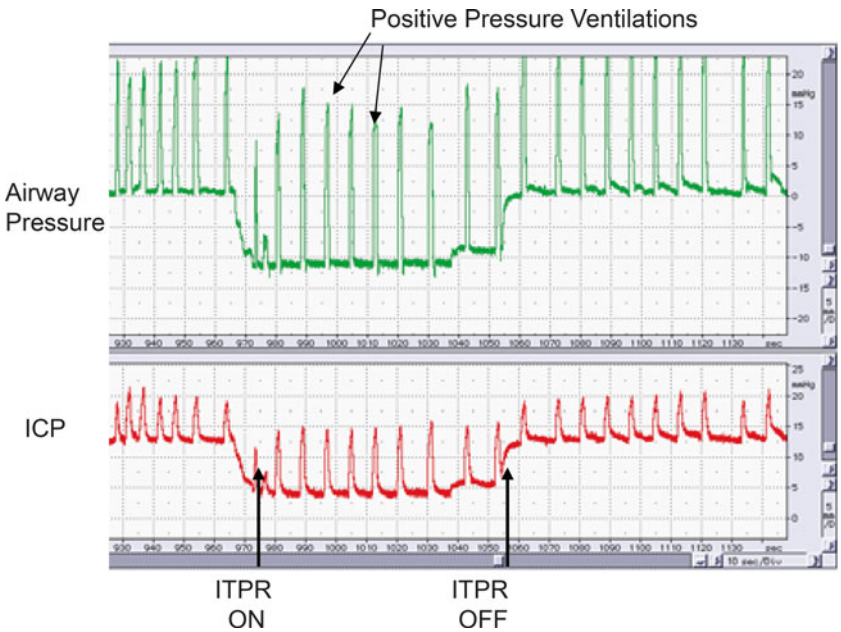

Fig. 38.23 Changes in airway pressure and intracranial pressure (*ICP*) when the intrathoracic pressure regulator (*ITPR*) is turned on and then off again

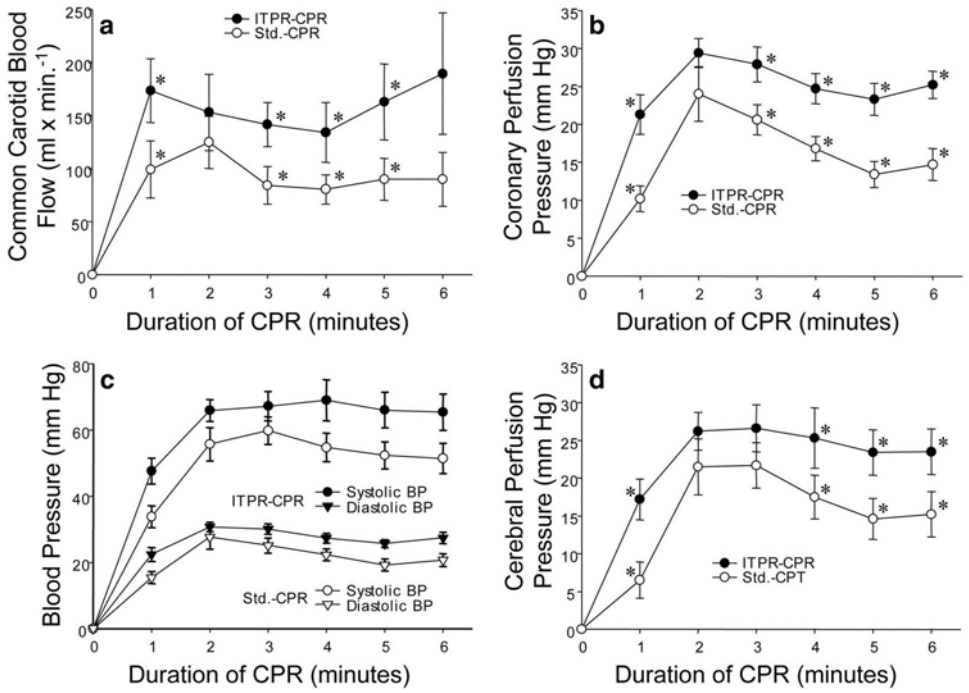

Fig. 38.24 Effect of intrathoracic pressure regulator (*ITPR*) CPR on carotid blood flow, coronary perfusion pressure, blood pressure, and cerebral perfusion pressure compared to standard CPR (*Std-CPR*). *BP* blood pressure, *CPR* cardiopulmonary resuscitation

Table 38.1 Basic hemodynamic parameters with endotracheal pressure set at 0, −5, and −10 mmHg with the ITPR for blood volumes after 0 and 50 % blood loss

Blood loss (%)	ETP	0	−5	−10
0	MAP	89.9 ± 4.5	104.3 ± 7.3*	108.5 ± 6.1*
	RAP	1.8 ± 0.4	−0.8 ± 0.6*	−4.8 ± 0.4†,*
	CPP	80 ± 3.9	94.2 ± 6.4*	103.3 ± 5.3*,†
	CerPP	74 ± 4.8	90.3 ± 7.4*	95.1 ± 6*
	ICP	15.6 ± 0.6	14 ± 0.7	13.5 ± 0.6*
50	MAP	28.8 ± 4.3	39.8 ± 5.9*	47.3 ± 7.3*,†
	RAP	−2 ± 0.9	−5.7 ± 0.6*	−9.3 ± 0.3*,†
	CPP	25.8 ± 5	38.5 ± 3.7*	48.3 ± 3.8*,†
	CerPP	18.1 ± 4.4	32.9 ± 5.8*	43.1 ± 7.2*,†
	ICP	10.7 ± 1.3	6.8 ± 1.4*	4.2 ± 1*,†

ETP endotracheal pressure, *MAP* mean arterial pressure, *RAP* right atrial pressure, *CPP* coronary perfusion pressure, *CerPP* cerebral perfusion pressure, *ICP* intracranial pressure

*Statistically significant difference ($0.05 > p > 0.001$) when compared to the values with ETP of 0 mmHg

†Statistically significant difference between values with −5 and −10 mmHg of ETP ($p < 0.05$)

were inversely proportional to the negative intrathoracic pressure both in the normovolemic pigs and after induced hemorrhage. These data are consistent with findings in spontaneously breathing adult and pediatric swine models of shock and the use of the ITD [45, 46]. The major hemodynamic parameters for 0, −5, −10 mmHg of ETP are shown in Table 38.1. Based on the data available to date, we believe that the generation of intrathoracic pressures greater than −15 mmHg may be excessive and not beneficial with long-term use.

Our initial studies demonstrated that the ITPR could reproducibly decrease ETP, intrathoracic pressure (as seen by the decreases in right atrial pressure), and ICP. The ITPR provided hemodynamic improvements with no acid-base changes during normovolemia. We have applied the ITPR in euvolemic anesthetized pigs for up to 6 h, with an intrathoracic vacuum set to −9 mmHg, without obvious adverse effects on gas exchange or the overall metabolic state of these animals. The long-term benefits of the ITPR after hemorrhage are considered to be much more dependent upon the degree of hypotension. During 50 % hypovolemia, there was more acidosis associated with the generation of negative ETP, as reflected by a lower pH and higher $PaCO_2$. However,

despite the lower pH values, which may be secondary to greater clearance of lactate, ITPR use increased blood pressure, pulse pressure, vital organ perfusion pressure, and $ETCO_2$ levels suggesting there was improved balance between the increase in circulation and the potential for induced metabolic acidosis with ITPR use. Oxygenation saturations remained at 100 % with ITPR use.

To date, the 510k cleared IPR device (CirQlator®) has been used by emergency medical personnel in Toledo, Ohio, during CPR administration [61]. In these cases, end-tidal CO_2 ($ETCO_2$) was assessed as an indirect surrogate for circulation. $ETCO_2$ values in 11 patients were compared pre- and during IPR therapy and then compared to 74 patients that were not treated with IPR therapy, but that were treated with an ITD. $ETCO_2$ levels increased from 21 ± 1 mmHg immediately prior to IPR application to an average of 32 ± 5 mmHg and a maximum of 45 ± 5 mmHg during IPR treatment ($p < 0.0001$). Note that $ETCO_2$ levels did not change significantly in the group not receiving active IPR therapy. More importantly, ROSC rates were 46 % in the standard CPR plus ITD group (34/74) and 74 % in the IPR-treated group (8/11) ($p < 0.001$). Huffmyer et al. reported that in 20 patients about to undergo coronary artery bypass graft surgery, thermodilution cardiac output increased significantly with the application of the ITPR (4.9 versus 5.5 L/min, $p = 0.017$); similarly, cardiac output measured by transesophageal echocardiography was 5.1 versus 5.7 L/min, respectively ($p = 0.001$). There were also significant increases in pulmonary artery systolic blood pressure (35 mmHg versus 38 mmHg, $p < 0.001$) and mean pulmonary artery pressure (24 mmHg versus 26 mmHg, $p = 0.008$) with this therapy [62].

Additional clinical experiences with the IPR device have further demonstrated the potential of this technology to treat brain insult. For example, Kiehna et al. recently reported the first use of the ITPR (10-min applications) in 10 patients with compromised cerebral perfusion, highlighting increases in CePP and decreases in ICP with use of this new technology [63].

To date, studies on the potential benefits of longer-term application of negative intrathoracic pressure have been initiated in a preliminary manner. For example, in pilot studies on spontaneously breathing swine, in collaboration with researchers at the US Army Institute of Surgical Research, we applied the ITD to spontaneously breathing animals in severe hemorrhagic shock, an uncontrolled model of severe blood loss [47, 64]. These splenectomized swine were subjected to a 60 % blood loss, followed by a 4 mm hole created in their abdominal aortas. Remarkably, the use of the ITD in pilot studies stabilized these animals for about 60 min after the hemorrhage and injury occurred. However, after 75 min, we observed the development of a significant metabolic acidosis, as reflected by a progressive negative base excess. At that point, the swine were hemodynamically stable, but shortly thereafter they became extremely agitated, hypotensive, and then died [47]. These pilot studies provided us with some fundamental insights related to the limitations of using the ITD, and by analogy the ITPR by itself, in the setting of severe blood loss. While these devices can be used to "buy time," ultimately some fluid resuscitation and correction of the underlying causes of the blood loss are essential. Although some fluids are ultimately needed, we hypothesize that the use of the ITD and ITPR can function by actually being fluid sparing and will extend the window of opportunity to provide lifesaving care in the setting of severe blood loss.

The ITPR was designed to provide a noninvasive means to increase MAP in the setting of cardiac arrest and significant hypotension in apneic patients. The effects are rapid and can be turned on or off by the flip of a switch, unlike more long-lasting and sometimes harmful effects of fluid and drug administration. This switch-like effect is shown in Fig. 38.23. In another study (shown in Fig. 38.25), the intrathoracic pressures were varied between 0, −5, and −10 mmHg; with each change, there were rapidly adjustments in key hemodynamic variables and ICPs. Based upon the combined effects of the ITPR shown in multiple preclinical studies, we believe

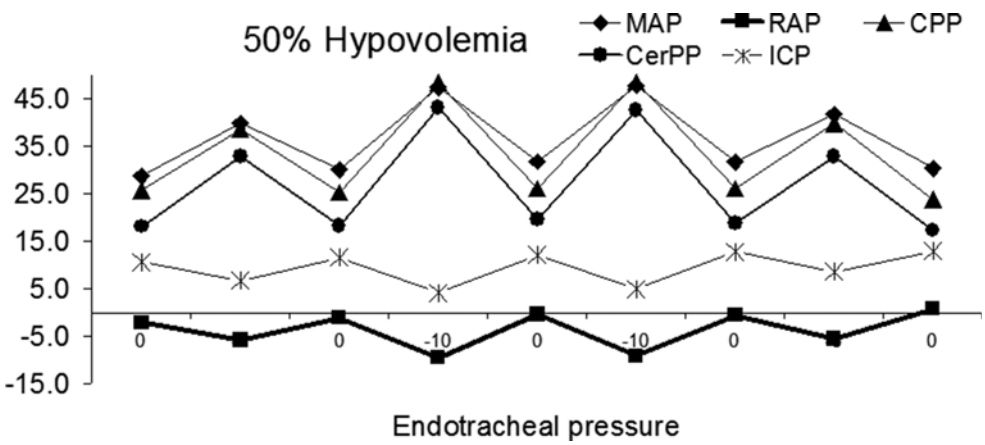

Fig. 38.25 Sequential changes in mean arterial pressure (*MAP*), coronary perfusion pressure (*CPP*), cerebral perfusion pressure (*CerPP*), right atrial pressure (*RAP*), and intracranial pressure (*ICP*) for sequential changes of endotracheal pressure (a surrogate for intrathoracic pressure) of 0, −5, 0, −10, 0, −10, 0, −5, 0 mmHg during 50 % hypovolemia. Differences between the values of all parameters are statistically significant with $p < 0.05$

that that ITPR has the potential to become a *first-line therapy* for all patients in cardiac arrest, as well as provide benefits for many individuals eliciting hypotension from a wide variety of causes. Importantly, the device can be applied quickly, often before intravenous access and intraosseous access, or fluids may be available, and it safely and quickly increases systemic, coronary, and CePPs. Based upon our experience in noncardiac preclinical arrest models, the use of the ITPR may be of significant benefit after traditional therapies have been provided, in that the ITPR application may reduce: (1) the amount of fluid volume needed for resuscitation from multiple etiologies, (2) secondary brain injury, and/or (3) the amount of vasopressors needed to maintain "permissive hypotension." The clinical use of ITPR may thereby become a commonplace therapy in both operating rooms and intensive care units, to help maintain vital organ perfusion. To date, the ITPR has been used in patients with acute hypotension intraoperatively; it has been well tolerated and resulted in significant increases in MAP, pulse pressure, and systolic blood pressure in the absence of fluid administration or vasopressor therapy [65].

Studies to date have also shown that the application of ITPR therapy in cardiac arrest cases results in marked improvements in hemodynamics in both human and animal models. Application of the device in hypovolemic pigs was shown to enhance circulation, stroke volume, MAP, CPP, and CePP and decrease ICP. Studies in a porcine model of peritonitis (septic shock) have indicated an augmentation in cardiac index and MAP while simultaneously lowering pulmonary artery pressure during ITPR use [66, 67]. Yet, it should be noted that the longer-term potential consequences of the ITPR remain unknown. One known limitation is that, in order for this technology to be of clinical benefit, the thorax must be intact; otherwise, it is not possible to generate expiratory phase negative intrathoracic pressure with the ITPR. Furthermore, it is not possible to lower the expiratory phase intrathoracic pressure and use positive end expiratory pressure concurrently, unless the ITPR is used as a pulsed therapy (currently under evaluation). Thus, the benefit of circulatory enhancement with the ITPR must be balanced clinically with the need to concurrently maintain at least minimally adequate ventilator support. Animal studies to date have suggested the ITPR can provide both circulatory and ventilatory support for up to 24 h in duration, without negative pulmonary consequences.

38.9 Summary

Clinicians and researchers continue to investigate methods for enhancing standard CPR techniques and design various novel devices to treat sudden cardiac arrest and shock. The limitations of standard CPR are discussed, as well as methods to improve this technique to enhance the delivery of oxygenated blood to the heart and brain. A recent advance in CPR research has been the rediscovered benefit of therapeutic hypothermia after successful resuscitation, a therapy that has shown increased long-term survival rates and improved neurological function. Further, we described some novel noninvasive technologies that can be used to increase the patient's chance for survival, such as IPR therapy to improve perfusion in profound states of shock, impedance threshold devices, and ACD-CRP treatment.

References

1. Niemann JT (1990) Cardiopulmonary resuscitation. N Engl J Med 327:1075–1080
2. Eisenberg MS, Horwood BT, Cummins RO, Reynolds-Haertle R, Hearne TR (1990) Cardiac arrest and resuscitation: a tale of 29 cities. Ann Emerg Med 19:179–186
3. Lurie KG, Voelckel WG, Zielinski T et al (2001) Improving standard cardiopulmonary resuscitation with an inspiratory impedance threshold valve in a porcine model of cardiac arrest. Anesth Analg 93:649–655
4. Voelckel WG, Lurie KG, Sweeney M et al (2002) Effects of active compression-decompression cardiopulmonary resuscitation with the inspiratory threshold valve in a young porcine model of cardiac arrest. Pediatr Res 51:523–527
5. Lurie K, Voelckel W, Plaisance P et al (2000) Use of an inspiratory impedance threshold valve during cardiopulmonary resuscitation: a progress report. Resuscitation 44:219–230
6. Lurie KG, Lindner KH (1997) Recent advances in cardiopulmonary resuscitation. J Cardiovasc Electrophysiol 8:584–600
7. Lurie KG, Mulligan KA, McKnite S, Detloff B, Lindstrom P, Lindner KH (1998) Optimizing standard cardiopulmonary resuscitation with an inspiratory impedance threshold valve. Chest 113:1084–1090
8. Lurie KG, Zielinski T, McKnite S, Aufderheide T, Voelckel W (2002) Use of an inspiratory impedance valve improves neurologically intact survival in a porcine model of ventricular fibrillation. Circulation 105:124–129
9. Lurie KG, Zielinski T, Voelckel W, McKnite S, Plaisance P (2002) Augmentation of ventricular preload during treatment of cardiovascular collapse and cardiac arrest. Crit Care Med 30:S162–S165
10. Lurie KG, Coffeen P, Shultz J, McKnite S, Detloff B, Mulligan K (1995) Improving active compression-decompression cardiopulmonary resuscitation with an inspiratory impedance valve. Circulation 91:1629–1632
11. Aufderheide T (2007) A tale of seven EMS systems: an impedance threshold device and improved CPR techniques double survival rates after out-of-hospital cardiac arrest. Circulation 116:II-936
12. Aufderheide TP, Sigurdsson G, Pirrallo RG et al (2004) Hyperventilation-induced hypotension during cardiopulmonary resuscitation. Circulation 109:1960–1965
13. Aufderheide TP, Lurie KG (2004) Death by hyperventilation: a common and life-threatening problem during cardiopulmonary resuscitation. Crit Care Med 32:S345–S351
14. Yannopoulos D, McKnite S, Aufderheide TP et al (2005) Effects of incomplete chest wall decompression during cardiopulmonary resuscitation on coronary and cerebral perfusion pressures in a porcine model of cardiac arrest. Resuscitation 64:363–372
15. Holzer M, Sterz F (2003) Therapeutic hypothermia after cardiopulmonary resuscitation. Expert Rev Cardiovasc Ther 1:317–325
16. Holzer M, Bernard SA, Hachimi-Idrissi S, Roine RO, Sterz F, Mullner M (2005) Hypothermia for neuroprotection after cardiac

arrest: systematic review and individual patient data meta-analysis. Crit Care Med 33:414–418
17. Holzer M, Behringer W, Schorkhuber W et al (1997) Mild hypothermia and outcome after CPR. Acta Anaesthesiol Scand Suppl 111:55–58
18. Berg RA, Hemphill R, Abella BS et al (2010) Part 5: adult basic life support: 2010 American Heart Association guidelines for cardiopulmonary resuscitation and emergency cardiovascular care. Circulation 122:S685–S705
19. Aufderheide TP, Pirrallo RG, Yannopoulos D et al (2005) Incomplete chest wall decompression: a clinical evaluation of CPR performance by EMS personnel and assessment of alternative manual chest compression-decompression techniques. Resuscitation 64:353–362
20. Thigpen K, Davis SP, Basol R et al (2010) Implementing the 2005 American Heart Association guidelines, including use of the impedance threshold device, improves hospital discharge rate after in-hospital cardiac arrest. Respir Care 55:1014–1019
21. Davis S, Thigpen K, Basol R, Aufderheide T (2008) Implementation of the 2005 American Heart Association guidelines together with the impedance threshold device improves hospital discharge rates after in-hospital cardiac arrest. Circulation 118S:S765
22. Lick CJ, Aufderheide TP, Niskanen RA et al (2011) Take heart America: a comprehensive, community-wide, systems-based approach to the treatment of cardiac arrest. Crit Care Med 39:26–33
23. Aufderheide TP, Nichol G, Rea TD et al (2011) A trial of an impedance threshold device in out-of-hospital cardiac arrest. N Engl J Med 365:798–806
24. Idris A, Guffey D, Pepe PE et al (2011) Compression rate and survival during out-of-hospital cardiopulmonary resuscitation at resuscitation outcomes consortium (roc) regional sites. Circulation 124:A289
25. Yannopoulos D, Abella BS, Duval S, Aufderheide T (2014) The effect of CPR quality: a potential confounder of CPR clinical trials. Circulation 130:A9
26. Cohen TJ, Tucker KJ, Lurie KG et al (1992) Active compression-decompression. A new method of cardiopulmonary resuscitation. JAMA 267:2916–2923
27. Lindner KH, Pfenninger EG, Lurie KG, Schurmann W, Lindner IM, Ahnefeld FW (1993) Effects of active compression-decompression resuscitation on myocardial and cerebral blood flow in pigs. Circulation 88:1254–1263
28. Plaisance P, Adnet F, Vicaut E et al (1997) Benefit of active compression-decompression cardiopulmonary resuscitation as a prehospital advanced cardiac life support. A randomized multicenter study. Circulation 95:955–961
29. Plaisance P, Lurie KG, Vicaut E et al (1999) A comparison of standard cardiopulmonary resuscitation and active compression-decompression resuscitation for out-of-hospital cardiac arrest. N Engl J Med 341:569–575
30. Plaisance P, Lurie KG, Vicaut E et al (2004) Evaluation of an impedance threshold device in patients receiving active compression-decompression cardiopulmonary resuscitation for out of hospital cardiac arrest. Resuscitation 61:265–271
31. Plaisance P, Lurie KG, Payen D (2000) Inspiratory impedance during active compression-decompression cardiopulmonary resuscitation: a randomized evaluation in patients in cardiac arrest. Circulation 101:989–994
32. Lurie KG (1997) Recent advances in mechanical methods of cardiopulmonary resuscitation. Acta Anaesthesiol Scand Suppl 111:49–52
33. Goetting MG, Paradis NA, Appleton TJ, Rivers EP, Martin GB, Nowak RM (1991) Aortic-carotid artery pressure differences and cephalic perfusion pressure during cardiopulmonary resuscitation in humans. Crit Care Med 19:1012–1017
34. Paradis NA, Martin GB, Rosenberg J et al (1991) The effect of standard- and high-dose epinephrine on coronary perfusion pressure during prolonged cardiopulmonary resuscitation. JAMA 265:1139–1144
35. Bahlmann L, Klaus S, Baumeier W et al (2003) Brain metabolism during cardiopulmonary resuscitation assessed with microdialysis. Resuscitation 59:255–260
36. Raedler C, Voelckel WG, Wenzel V et al (2002) Vasopressor response in a porcine model of hypothermic cardiac arrest is improved with active compression-decompression cardiopulmonary resuscitation using the inspiratory impedance threshold valve. Anesth Analg 95:1496–1502
37. Wolcke BB, Mauer DK, Schoefmann MF et al (2003) Comparison of standard cardiopulmonary resuscitation versus the combination of active compression-decompression cardiopulmonary resuscitation and an inspiratory impedance threshold device for out-of-hospital cardiac arrest. Circulation 108:2201–2205
38. Plaisance P, Soleil C, Lurie KG, Vicaut E, Ducros L, Payen D (2005) Use of an inspiratory impedance threshold device on a face-mask and endotracheal tube to reduce intrathoracic pressures during the decompression phase of active compression-decompression cardiopulmonary resuscitation. Crit Care Med 33:990–994
39. (2000) Guidelines for cardiopulmonary resuscitation and emergency cardiovascular care. Part 2: ethical aspects of CPR and ECC. Circulation 102:I12-21
40. Aufderheide TP, Frascone RJ, Wayne MA et al (2011) Standard cardiopulmonary resuscitation versus active compression-decompression cardiopulmonary resuscitation with augmentation of negative intrathoracic pressure for out-of-hospital cardiac arrest: a randomised trial. Lancet 377:301–311
41. Wayne M, Tupper D, Swor R, Frascone R, Mahoney B, Lurie KG (2012) Improvement of long-term neurological function after sudden cardiac death and resuscitation: impact of CPR method and post-resuscitation care. Prehosp Emerg Care 16:152–153
42. Frascone RJ, Wayne MA, Swor RA et al (2013) Treatment of non-traumatic out-of-hospital cardiac arrest with active compression decompression cardiopulmonary resuscitation plus an impedance threshold device. Resuscitation 84:1214–1222
43. Fritsch-Yelle JM, Convertino VA, Schlegel TT (1999) Acute manipulations of plasma volume alter arterial pressure responses during Valsalva maneuvers. J Appl Physiol 86:1852–1857
44. Shekerdemian LS, Bush A, Shore DF, Lincoln C, Redington AN (1997) Cardiopulmonary interactions after Fontan operations: augmentation of cardiac output using negative pressure ventilation. Circulation 96:3934–3942
45. Lurie KG, Zielinski TM, McKnite SH et al (2004) Treatment of hypotension in pigs with an inspiratory impedance threshold device: a feasibility study. Crit Care Med 32:1555–1562
46. Marino BS, Yannopoulos D, Sigurdsson G et al (2004) Spontaneous breathing through an inspiratory impedance threshold device augments cardiac index and stroke volume index in a pediatric porcine model of hemorrhagic hypovolemia. Crit Care Med 32:S398–S405
47. Sigurdsson G, Yannopoulos D, McKnite SH, Sondeen JL, Benditt DG, Lurie KG (2006) Effects of an inspiratory impedance threshold device on blood pressure and short term survival in spontaneously breathing hypovolemic pigs. Resuscitation 68:399–404
48. Metzger A, Rees J, Segal N et al (2013) "Fluidless" resuscitation with permissive hypotension via impedance threshold device therapy compared with normal saline resuscitation in a porcine model of severe hemorrhage. J Trauma Acute Care Surg 75:S203–S209
49. Convertino VA, Ratliff DA, Crissey J, Doerr DF, Idris AH, Lurie KG (2005) Effects of inspiratory impedance on hemodynamic responses to a squat-stand test in human volunteers: implications for treatment of orthostatic hypotension. Eur J Appl Physiol 94:392–399

50. Convertino VA, Ratliff DA, Ryan KL et al (2004) Hemodynamics associated with breathing through an inspiratory impedance threshold device in human volunteers. Crit Care Med 32:S381–S386
51. Idris A, Convertino VA, Ratliff MS et al (2007) Imposed power of breathing associated with use of an impedance threshold device. Respir Care 52:177–183
52. Milic-Emili J (1991) The lung: scientific foundations. Raven Press, New York
53. Cooke WH, Ryan KL, Convertino VA (2004) Lower body negative pressure as a model to study progression to acute hemorrhagic shock in humans. J Appl Physiol 96:1249–1261
54. Hinojosa-Laborde C, Shade RE, Muniz GW et al (2014) Validation of lower body negative pressure as an experimental model of hemorrhage. J Appl Physiol 116:406–415
55. Convertino VA, Cooke WH, Lurie KG (2005) Inspiratory resistance as a potential treatment for orthostatic intolerance and hemorrhagic shock. Aviat Space Environ Med 76:319–325
56. Smith SW, Parquette B, Lindstrom D, Metzger AK, Kopitzke J, Clinton J (2010) An impedance threshold device increases blood pressure in hypotensive patients. J Emerg Med 41:549–558
57. Wampler D, Convertino VA, Weeks S, Hernandez M, Larrumbide J, Manifold C (2014) Use of an impedance threshold device in spontaneously breathing patients with hypotension secondary to trauma: an observational cohort feasibility study. J Trauma Acute Care Surg 77:S140–S145
58. Yannopoulos D, Nadkarni VM, McKnite SH et al (2005) Intrathoracic pressure regulator during continuous-chest-compression advanced cardiac resuscitation improves vital organ perfusion pressures in a porcine model of cardiac arrest. Circulation 112:803–811
59. Yannopoulos D, Metzger A, McKnite S et al (2006) Intrathoracic pressure regulation improves vital organ perfusion pressures in normovolemic and hypovolemic pigs. Resuscitation 70:445–453
60. Yannopoulos D, McKnite S, Metzger A, Lurie KG (2007) Intrathoracic pressure regulation improves 24-hour survival in a porcine model of hypovolemic shock. Anesth Analg 104:157–162
61. Segal N, Parquette B, Ziehr J, Yannopoulos D, Lindstrom D (2013) Intrathoracic pressure regulation during cardiopulmonary resuscitation: a feasibility case-series. Resuscitation 84:450–453
62. Huffmyer JL, Groves DS, Desouza DG, Littlewood KE, Thiele RH, Nemergut EC (2011) The effect of the intrathoracic pressure regulator on hemodynamics and cardiac output. Shock 35:114–116
63. Kiehna E, Huffmyer J, Thiele R, Scalzo D, Nemergut E (2013) Utilizing the intrathoracic pressure regulator to lower intracranial pressure in patients with altered intracranial elastance: a pilot study. J Neurosurg 119:756–759
64. Sigurdsson G, McKnite SH, Sondeen JL, Benditt DB (2005) Extending the golden hour of hemorrhagic shock in pigs with an inspiratory impedance threshold valve. Paper presented at Critical Care in Medicine, 2005
65. Birch M, Beebe D, Kwon Y et al (2010) A novel intrathoracic pressure regulator improves hemodynamics in hypotensive patients during surgery. Circulation 122:A27
66. Cinel I, Goldfarb R, Carcasses P et al (2008) Intrathoracic pressure regulation augments cardiac index in porcine peritonitis. Crit Care Med 36:A6
67. Cinel I, Goldfarb RD, Metzger A et al (2014) Biphasic intrathoracic pressure regulation augments cardiac index during porcine peritonitis: a feasibility study. J Med Eng Technol 38:49–54

End-Stage Congestive Heart Failure in the Adult Population: Ventricular Assist Devices

39

Kenneth K. Liao and Ranjit John

Abstract

Congestive heart failure (CHF) is a major cause of morbidity and mortality within the adult population. If these patients progress to the end stages of this disease, then heart transplantation or ventricular support devices are required. However, due to a shortage of donor hearts, the use of ventricular assist devices (VADs) as either a *bridge to transplant* or *destination support* has grown dramatically as a therapy. Furthermore, with the increased use of these devices, there have been major efforts to develop these technologies as well.

Keywords

Congestive heart failure • Ventricular assist device

39.1 Introduction

Approximately five million Americans have congestive heart failure (CHF), and approximately 50,000 new cases are diagnosed every year. Furthermore, CHF is the most frequent cause of hospital admissions in patients older than 65 years, and it is the largest single expense for Medicare [1]. To date, with current medical management the 5-year mortality rate of CHF can be as high as 50 %. Fortunately, advances in medical therapy such as biventricular pacing, defibrillator implantation, and the ability to successfully perform surgery in high-risk patients have revolutionized the management of patients with CHF and greatly delayed the progression of CHF to end stage. Note that once a patient develops end-stage CHF, the treatment options are limited and typically ineffective, and thus subsequent mortality is high. In such patients, heart transplant becomes the last resort. Yet, in general, it is a very effective therapy which offers an excellent short-term and long-term survival benefits (over 90 and 50 % survival rates at one year and 10 years, respectively); most patients enjoy a near-normal lifestyle after heart transplant [2]. However, the donor hearts available for transplantation are limited to an average of 2200 per year, compared to over 35,000 people per year who could benefit from such a therapy [1].

Besides the scarcity of donor hearts, many patients die each year while waiting for an acceptably matched donor heart. Importantly in the past fifteen years, ventricular assist devices (VADs), especially left ventricular assist devices (LVADs), have been increasingly used to support such patients as a *bridge to transplant* [3]. After the landmark REMATCH trial, the LVAD has been used more and more as the *destination therapy* for end-stage CHF [4, 5]. In addition to the increased use of these devices, newer generations of VADs with better mechanics, smaller size, and longer durability have been developed in recent years [6–11]. Nevertheless, the ultimate goal of future VAD development is to produce a small, totally implantable, biocompatible, and durable heart pump that can physiologically function like a human heart. Clinically effective VADs should be judged by a variety of mechanical and physiological performance parameters; specifically, they should: (1) provide sufficient cardiac output to allow patients to perform their usual daily activities, (2) have a low risk of thromboembolism and pump or driveline infections, (3) have a low incidence of device malfunction, (4) be easily implantable and removable, and (5) be small in size.

K.K. Liao, MD (✉) • R. John, MD
Division of Cardiothoracic Surgery, University of Minnesota, 420 Delaware Street, SE, Minneapolis, MN 55455, USA
e-mail: liaox014@umn.edu

P.A. Iaizzo (ed.), *Handbook of Cardiac Anatomy, Physiology, and Devices*, DOI 10.1007/978-3-319-19464-6_39

39.2 Classification of VADs

In general, VADs can be classified based on: (1) their internal mechanics (volume displacement, axial flow, or centrifugal), (2) therapeutic purposes (temporary, bridge to decision, bridge to recovery, bridge to transplant, and destination), (3) sites of support (LVAD, right VAD, or BiVAD), (4) location of the pump (implantable, paracorporeal, or extracorporeal), and/or (5) implanting approaches (sternotomy, thoracotomy, laparotomy, subcostal, or percutaneous).

39.3 VADs Defined by Mechanics and Clinical Applications

39.3.1 Volume Displacement Pumps (Pulsatile Pumps)

The functioning human left and right ventricles are physiologic volume displacement pumps. During each cardiac cycle, they generate over 60 cc of stroke volume, and each ventricle has a pair of inflow and outflow valves to maintain a unidirectional blood flow. The end result is that a human heart generates a pulsatile blood pressure and yet a steady cardiac output. The mitral and tricuspid valves function as the inflow valves, while the aortic and pulmonary valves function as outflow valves. A volume displacement VAD functions exactly like human ventricles; it has a pump chamber that generates a stroke volume between 40 and 80 cc during each cardiac cycle, and it has two artificial valves—either bioprostheses or mechanical valves.

The valves used inside VADs (i.e., bioprosthetic versus mechanical) are considered to ultimately determine the durability of the VAD and the need for anticoagulation. More specifically, bioprostheses may have the advantage of not requiring anticoagulation therapy, thus reducing the patient's risk for thromboembolism. However, the valve's limited life span inside the VAD may result in premature VAD failures, thus requiring VAD replacement. On the other hand, mechanical valves have the advantage of being durable, but then the patient will require adequate anticoagulation therapy to prevent clotting. Under- or over-anticoagulation treatment can increase the risk of thromboembolism or bleeding which can subsequently affect the patient's outcome.

Typically one of the two mechanisms is used to eject blood in this type of VAD: (1) compressed air is employed to squeeze the blood-filled sac or to displace a flexible diaphragm within a hard shell to generate stroke volume, or (2) a slow torque electrical motor is used to displace a flexible diaphragm inside the implantable unit within a hard shell to generate stroke volume. In general, the compressed air approach seems to provide a simple and reliable way of either moving the diaphragm or compressing the sac, with a pressure more comparable to a physiologically acceptable waveform. However to date, this design has required a bulky driving console, compromising the patient's mobility. In addition such driving consoles typically will make loud noises. If the diaphragm is propulsed by an electrical motor within a noncompressible metal chamber, the early systolic pressure generated by this pump is much higher than the pump driven by the compressed air. It has been found that such unphysiologically high pressures can speed the calcification process in the inflow bioprostheses and/or even cause early valve failures [12].

The blood to pump contact surface interaction plays an important role in determining the relative degree of resultant thrombogenicity of the pump and therefore the required needs for anticoagulation. This is particularly important for volume displacement pumps, because of their relatively large contact surface areas with blood, as compared to an axial flow pump. Historically, first the smooth surface was pursued during VAD design and then manufactured to avoid thrombosis, but later it turned out that an evenly distributed textured surface actually generated less thrombosis. More specifically, such textured surfaces promote early platelet and fibrin depositions during initial contact with blood, which in turn results in formation of stable pseudointima which subsequently prevents the formation of thrombosis [13].

Common volume displacement pumps include: (1) HeartMate® XVE LVAD (Figs. 39.1 and 39.2) and (2) Thoratec VAD (Fig. 39.2) (Thoratec Corp., Pleasanton, CA, USA). The HeartMate XVE was once the mostly implanted and most studied pulsatile LVAD worldwide until axial flow pumps, the second-generation LVAD such as HeartMate II, demonstrated the superiority in durability, easy to implant, and pump-related complications. It was approved by the FDA for use as both a bridge to heart transplant and as destination therapy for end-stage CHF. This system is driven by an electrical motor, but it can also be driven by compressed air if and when the electrical motor wears out. It is implantable and powered through the driveline which exits from the abdominal wall; common implant locations are in the abdomen or in the preperitoneal space. The inflow cannula is inserted into the left ventricle via an opening in the left ventricular apex, and the outflow graft is connected in the proximal ascending aorta. It has textured interface surfaces and thus has a very low risk of thromboembolism (Fig. 39.3). Therefore, patients with these implanted systems do not need to be anticoagulated with coumadin or Plavix, yet it is recommended that they take aspirin once a day.

The HeartMate XVE LVAD is no longer used in the adult clinical setting, yet it played a very significant historical role in demonstrating that end-stage CHF patients could be successfully supported with an LVAD. When compared to maximal medical management including home inotropic therapy, the use of the HeartMate XVE LVAD significantly improved the quality of life and survival of end-stage CHF patients [5].

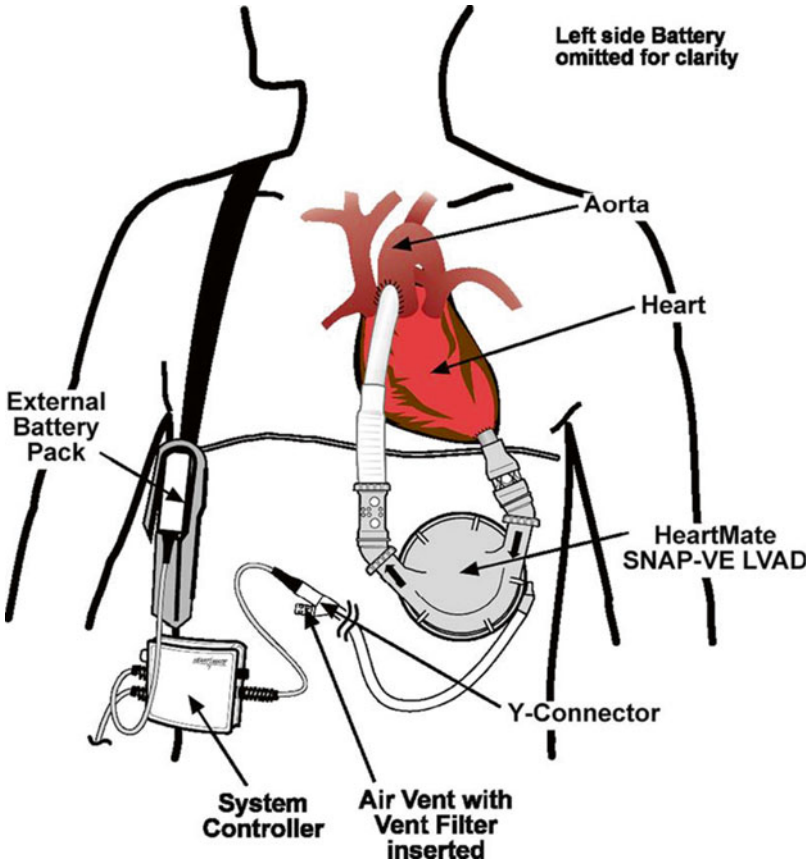

Fig. 39.1 Schematic of a HeartMate SNAP-VE ventricular assist device system. One can see the internal connections at the apex of the left ventricle where there is inflow into the device and outflow connected directly to the aorta. This system utilizes an external battery pack and controller system. *LVAD* left ventricular assist device

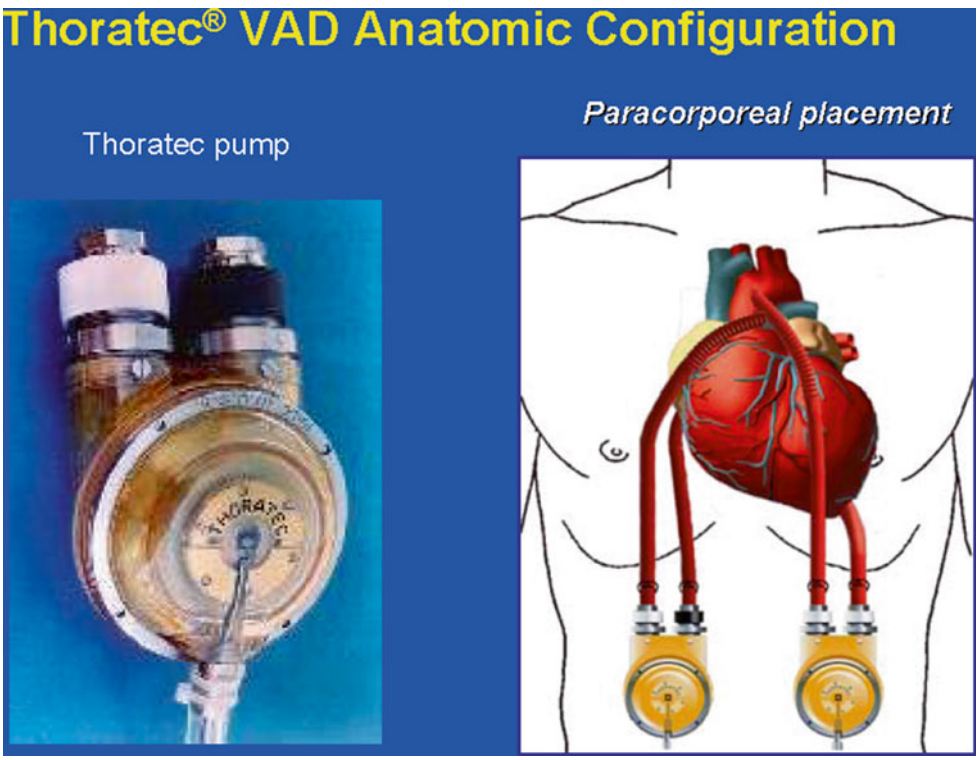

Fig. 39.2 Thoratec ventricular assist device (*VAD*). *Left*: pump with both inflow and outflow valve housing connectors pointing upward and the compressed air driveline pointing downward. *Right*: cannulas and grafts are implanted inside the body cavity, while the pumps are connected outside the body cavity

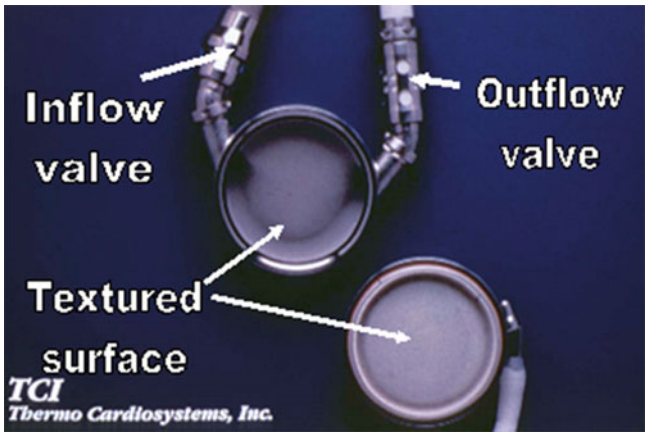

Fig. 39.3 Textured inner surface of HeartMate XVE left ventricular assist device. The textured surface promotes formation of pseudointima which subsequently prevents thrombosis formation

It is the first implantable LVAD that was approved as the destination therapy for end-stage heart failure in the USA. However, the disadvantages of this system include (1) its overall heavy weight, (2) its bulky size, and (3) frequent inflow valve and/or electrical motor failures, after an average of 12 months of implantation [3–5, 14, 15].

The Thoratec VAD [16] can be used as an LVAD, RVAD, or BiVAD. It is commonly described as an implanted paracorporeal pump, with the inflow cannula inserted in the left ventricle via the left ventricular apex and the outflow graft sewed to the ascending aorta when used as an LVAD (or the inflow cannula inserted in the right atrium and the outflow graft sewed to the pulmonary artery as an RVAD). This system allows for numerous cannulation options. Its pump is made of a flexible sac housed in a plastic ball-shaped container. Currently, the sac material is composed of Thoralon which has a smooth surface to reduce the risk of thrombosis. This sac is squeezed by the compressed air via an air-driven console, and it has two mechanical valves, one as an inflow and the other an outflow valve. Importantly, these units can be implanted in small- or large-size patients (weight between 17 and 144 kg) and can be readily employed for short-term as well as long-term support. To date, this device is approved by the FDA to be used as a bridge to heart transplant and as postcardiotomy support to recovery. The disadvantages of this system include the paracorporeal pump being attached outside the body, which can be inconvenient to patients, and patients require anticoagulation with coumadin to maintain an INR between 2.5 and 3.0 to prevent thromboembolism.

39.3.2 Continuous Flow Pumps: Axial Design

The axial flow pumps are typically regarded as second-generation VADs, as compared to the first generation of volume displacement pumps. Such pumps incorporate both

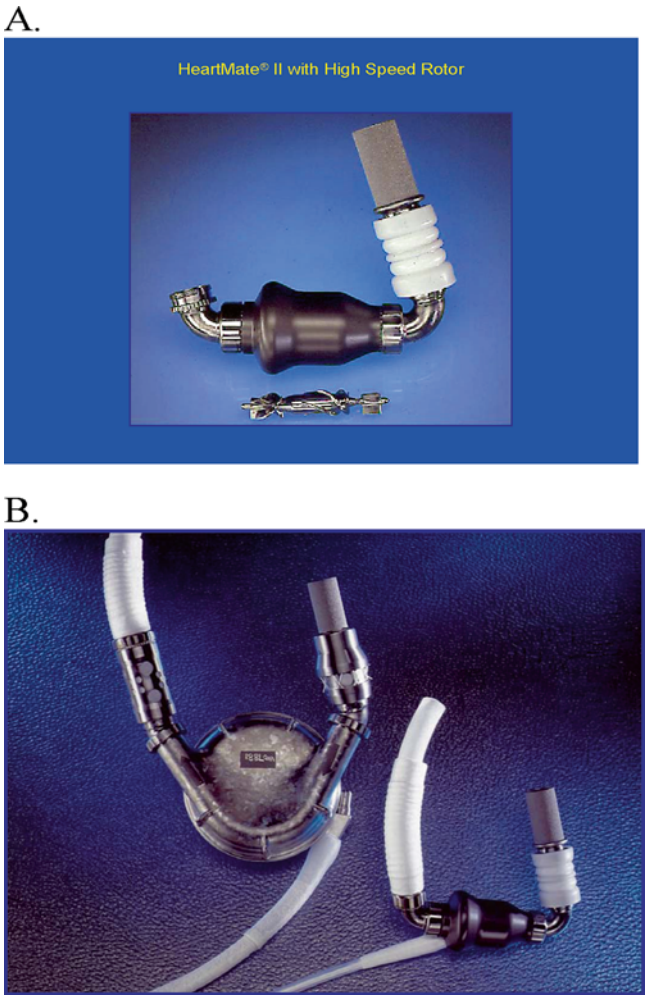

Fig. 39.4 HeartMate II left ventricular assist device. (**A**) HeartMate II pump and the high-speed rotor. The inflow cannula is connected to the pump. (**B**) Size comparison between the HeartMate VE and HeartMate II pumps. The inflow cannulas of both pumps are the same

continuous flow and rotary pump technologies as the foundation of their design and construction. They have an impeller inside the pump that can generate high-speed rotations in a blood system (Fig. 39.4). Depending on the motor capacity and rotational speed, an axial flow pump can function either as a partial-flow or full-flow support VAD. The speed of a rotor can reach an RPM of 9000, and it can generate up to 10 L/min of flow with a mean pressure of 100 mmHg.

Initially, serious doubts about the utility of such pumps were raised due to the concerns of red blood cell destruction and heat generated by the high-speed motor inside the blood system. But (starting with conjunction) such theoretical concerns were discarded when a Hemopump was successfully used in a clinical setting without significant hemolysis [17]. The Hemopump thus set the stage for evaluation of other types of axial flow pumps that could be used to pump blood in the human body [6, 7, 9–11].

The common features of axial flow pumps include the following: (1) the simpler design of continuous flow rotary

pump technology promises increased long-term mechanical reliability; (2) they do not require valves to create a unidirectional flow nor do they require an external vent or a compliance chamber, thus making them more likely to be used as the platform for future development of a totally implantable VAD; (3) the inflow cannulas are inserted into the left ventricular apexes or totally inside the left ventricle, and the outflow grafts can be connected to either the ascending or descending thoracic aorta (i.e., which is important if abnormalities in the ascending aorta exist); (4) the size of such pumps is relatively small, one-fifth to one-seventh the size of the volume displacement pumps, thereby extending therapy to underserved patient populations including women and even some children; and/or (5) these pumps are associated with minimal noise generation and overall greater patient comfort [6, 7, 9–11, 14, 15].

The HeartMate II LVAD (Thoratec Corp.), the DeBakey MicroMed LVAD (MicroMed Cardiovascular, Inc., Houston, TX, USA), and Jarvik 2000 (Jarvik Heart, Inc., Manhattan, NY, USA) are currently available representatives of this group of VADs. Among them the HeartMate II and the DeBakey MicroMed LVAD have many similarities: (1) they are about the same size, (2) both devices consist of an internal blood pump with a percutaneous lead that connects the pump to an external system driver and power source, and (3) both pumps can generate up to 10 L/min of flow. The initial results appeared to be encouraging, with data supporting effective circulatory support and durability [6, 7, 9–11, 14, 15]. Of particular interest is that the diminished pulse pressures that are associated with utilizing an axial flow pump seemed to be tolerated well in patients, at least for the short term. Importantly, the long-term consequences of using axial flow pumps have yet to be evaluated. Additionally, hemolysis associated with the use of axial flow pumps has been detectable, yet the level has been considered clinically insignificant. Nevertheless, these pumps seem to activate platelets because of the physical strain on blood cells; such activation could be an important source of intravascular thrombosis and/or embolic complications. It should be noted that the incidence of thromboembolism seems to be particularly high for the MicroMed LVAD. Therefore, intense anticoagulation regimens targeting platelet activation and clotting cascade have been employed to deal with these potential problems. A combination of coumadin and Plavix has been recommended for patients who have been provided with a MicroMed LVAD.

The HeartMate II LVAD has shown improved clinical outcomes both as bridge to transplant and destination therapy, with markedly better functional status and quality of life. An actuarial survival of 89 % at 1 month and 75 % at 6 months was reported [14]. The HeartMate II LVAD has proven to be safe and effective as bridge to transplantation. Furthermore, compared to HeartMate XVE, the HeartMate II significantly reduced the device- and surgery-related complications. It is considered that the lower incidence of postoperative bleeding and device-related infection may be due to its smaller size and the lack of need for a large pocket to house its pump and smaller driveline. The absence of a large preperitoneal pocket (which was required with the larger pulsatile devices) has reduced: (1) the need for extensive dissection, (2) postoperative bleeding, and (3) LVAD pocket hematomas and the development of pocket infection. Based on multiple clinical trial outcomes [14, 15, 18], the FDA approved the HeartMate II LVAD to be used as bridge to transplant as well as destination therapy for end-stage CHF patients in 2008 and 2010, respectively. To date, the clinical use of the HeartMate II LVAD has increased rapidly since FDA approval, and thus far over 17,000 patients have received implantation of the HeartMate II LVAD worldwide.

39.3.3 Continuous Flow Pumps: Centrifugal Design

The continuous flow pumps with centrifugal designs are considered the third-generation VADs. The technology used in these pumps includes noncontact bearings and hydrodynamic levitation that offer the advantages of (1) minimizing the friction of blood flow, (2) reducing platelet damage, and (3) reducing wear of the rotor (Fig. 39.5). The HeartWare pump (HeartWare, Framingham, MA, USA) is representative of this type of LVAD.

Compared to the HeartMate II system, the HeartWare pump is smaller and can fit inside the pericardial space; anatomically, it can fit into smaller adults as well as congenital patients. The pump can be inserted via a minimally invasive procedure, and this, in turn, potentially minimizes blood transfusions. Today, this is the only pump that can be readily used as an implantable RVAD and thus can be used for BiVAD support in those patients requiring such therapy.

Initial clinical trials of the HeartWare LVAD as bridge to heart transplant showed that patients' 30-day and 1-year survival rates were 99 and 86 %, respectively [19]. The pump received FDA approval for implantation as bridge to heart transplantation in 2012 and currently is in clinical trials to assess its use as destination therapy for end-stage CHF patients. So far over 6000 thousand patients have received HeartWare LVAD implantation worldwide.

39.4 VAD Implantation Techniques

In general, the implantation techniques currently employed for these three types of VADs are not very different from each other. The implantation for the latter two VADs is

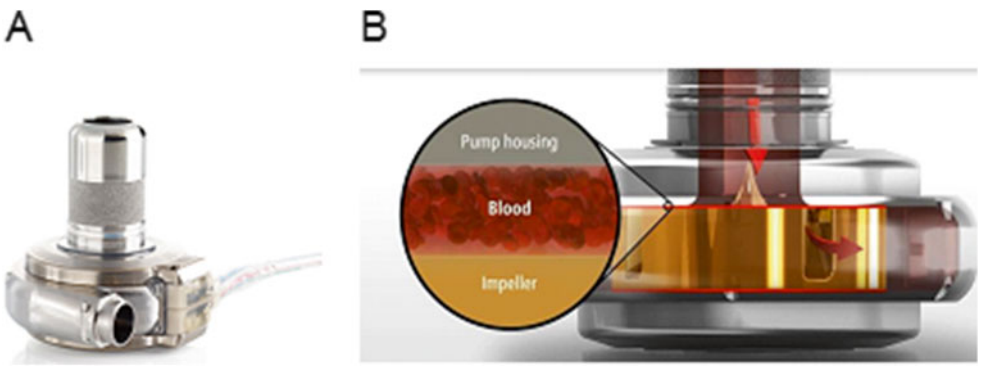

Fig. 39.5 HeartWare left ventricular assist device pump. (**A**) HeartWare pump. (**B**) Cross section of the inside structure of the pump showing the contactless design as well as magnetic and hydrodynamic bearings

probably easier because the need for tissue dissection is less for the smaller pumps and subsequently there is less bleeding. Typically a median sternotomy is made, and the patient is placed on cardiopulmonary bypass. The HeartMate II pump is inserted in the pre-created preperitoneal pocket, below the posterior rectus sheath. The HeartWare LVAD is inserted inside the pericardial space. The inflow cannula is inserted through a cored out portion of the apex of the left ventricle. The outflow graft is sewn to a longitudinal aortotomy in the proximal ascending aorta. Following appropriate connections, the patient is weaned off cardiopulmonary bypass, and the pump is started. Optimizing pump speed is performed under echocardiographic guidance, as well as by continuously monitoring the patient's hemodynamic status. Adequate flow is achieved by adjusting pump speed and by ensuring adequate preload and appropriate inotropic support for right ventricular function. After meticulous hemostasis is achieved, the chest is closed with appropriately placed chest tubes. The HeartWare LVAD can be inserted via a combination of left mini-thoracotomy and upper sternotomy or right mini-thoracotomy.

39.5 Device Management

It is imperative that standard postoperative care is used in the management of these patients. First, device settings can be monitored and adjusted based on patient hemodynamics as well as echocardiographic findings. Additionally, a combination of aspirin and warfarin is typically used as part of the anticoagulation protocol to maintain an INR between 2.5 and 3.5 for all the devices, except for patients with the HeartMate XVE for which only aspirin is needed. The VAD flow is generally maintained above 4 L/min, and the mean blood pressure is maintained over 60 mmHg. After LVAD placement, typically a patient does not change defibrillator and/or biventricular pacing settings if s/he had such a device implanted prior to VAD implantation. Finally, all patients undergo a standard postoperative rehabilitation program.

39.6 University of Minnesota VAD Experience

The University of Minnesota VAD and heart transplant program is one of the largest programs in the world. We have been among the participating centers and leaders in multiple NIH-sponsored clinical trials. Ten different types of VADs had been tried or used at our center. Since 1995, we have implanted 700 VADs, including over 250 continuous flow VADs for bridge to heart transplantation, bridge to bridge, bridge to recovery, and/or for destination therapy. We developed an effective VAD implantation algorithm to successfully treat patients with refractory acute cardiogenic shock and multiorgan failure who would typically die (Fig. 39.6) [20]. We also pioneered a minimally invasive LVAD exchange technique to avoid sternotomy (Figs. 39.7 and 39.8) [21].

39.7 Summary

Over the last 15 years, VADs (especially continuous flow LVADs) have been increasingly used in the clinical management of the chronic heart failure patient, as either a bridge to transplant or as the destination therapy. Abundant and important knowledge and experience has been obtained from the early clinical use of VADs. We believe that the future of VADs is very promising. The ideal design of any future VAD should embody, at a minimum, the following features:

1. It can provide adequate blood flow to meet the various physiological requirements.
2. It must be reliable and durable. For a VAD to be used as a destination therapy, 5–7 years has been suggested as an acceptable length of time for durability.
3. It must be biocompatible with the host patient and also require no, or minimal, anticoagulation therapy.

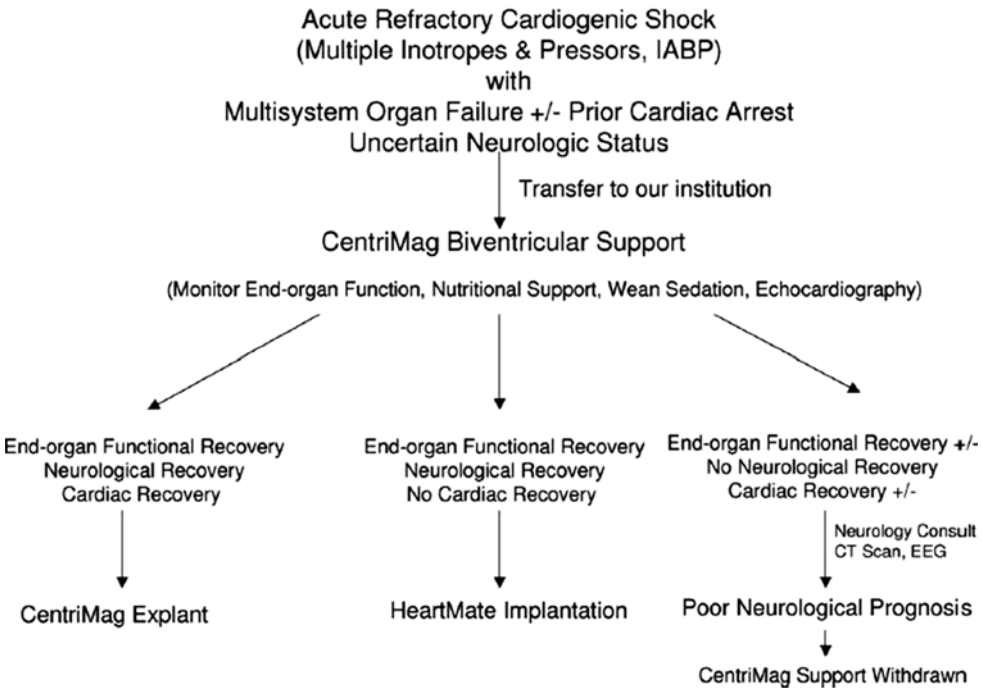

Fig. 39.6 Algorithm depicting the management of patients with refractory acute cardiogenic shock with multiorgan failure

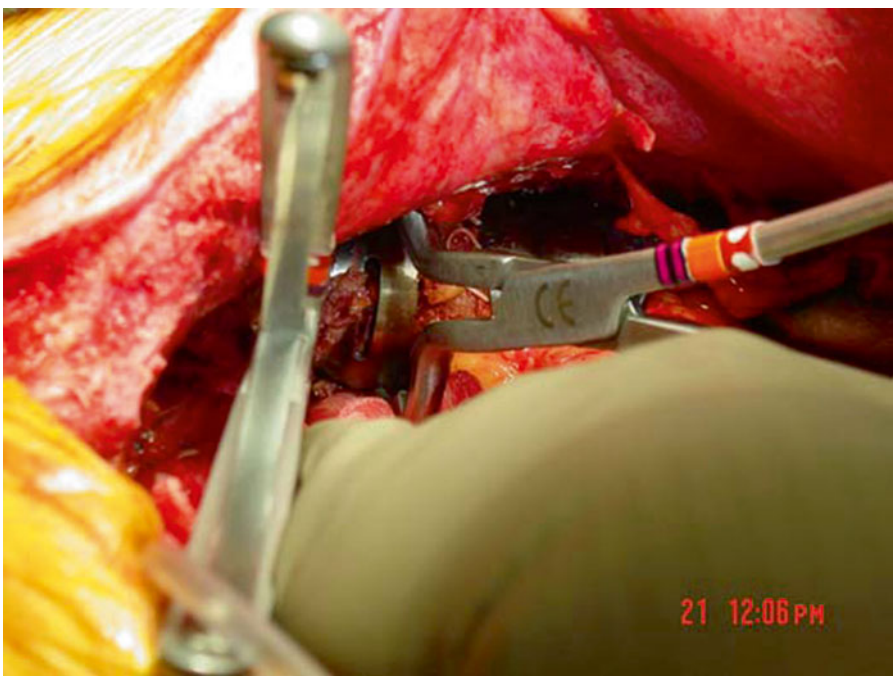

Fig. 39.7 Left ventricular assist device exchange is performed via laparotomy only; sternotomy is avoided

4. It must be small in size to minimize patient discomfort and ensure an improved quality of life.
5. It should be easy to implant, preferably through developing minimally invasive approaches.

It is considered that within the next ten years, we will see the birth of the "dream" VAD that meets these criteria. Perhaps one day implanting a VAD will be similar to implanting a prosthetic valve. Ultimately, the future of treating end-stage CHF lies in the cell therapy which can either reverse myocardium remodeling or regrow new myocardium, yet such a therapy may require VAD support of the patient during administration. For additional information on LVADs and their use in congenital populations, the reader is referred to Chap. 11.

Fig. 39.8 Patient who received the fifth left ventricular assist device (*LVAD*) exchange. Photo was taken together with the author/surgeon 3 weeks after his fifth LVAD exchange surgery

References

1. Franco KL (2001) New devices for chronic ventricular support. J Card Surg 16:178–192
2. Hosenpud JD, Bennett LE, Keck BM, Boucek MM, Novick RJ (2001) The Registry of the International Society for Heart and Lung Transplantation: eighteenth official report. J Heart Lung Transplant 20:805–815
3. Frazier OH, Rose EA, Oz MC et al (2001) Multicenter clinical evaluation of the HeartMate vented electric left ventricular assist system in patients awaiting heart transplantation. J Thorac Cardiovasc Surg 122:1186–1195
4. Rose EA, Moskowitz AJ, Packer M et al (1999) The REMATCH trial: rationale, design, and end points. Randomized evaluation of mechanical assistance for the treatment of congestive heart failure. Ann Thorac Surg 67:723–730
5. Rose EA, Gelijns AC, Moskowitz AJ et al (2001) Long-term use of a left ventricular assist device for end-stage heart failure. N Engl J Med 345:1435–1443
6. Griffith BP, Kormos RL, Borovetz HS et al (2001) HeartMate II left ventricular assist system: from concept to first clinical use. Ann Thorac Surg 71:116–120
7. Frazier OH, Myers TJ, Westaby S et al (2004) Clinical experience with an implantable, intracardiac, continuous flow circulatory support device: physiologic implications and their relationship to patient selection. Ann Thorac Surg 77:133–142
8. Esmore D, Kaye D, Spratt P et al (2008) A prospective, multicenter trial of the VentrAssist left ventricular assist device for bridge to transplant: safety and efficacy. J Heart Lung Transplant 27:579–588
9. Goldstein DJ (2003) Worldwide experience with the MicroMed DeBakey ventricular assist device as a bridge to transplantation. Circulation 108:II272–II277
10. Westaby S, Banning AP, Jarvik R et al (2000) First permanent implant of the Jarvik 2000 Heart. Lancet 356:900–903
11. Wieselthaler GM, Schima H, Hiesmayr M et al (2000) First clinical experience with the DeBakey ventricular assist device continuous-axial-flow pump for bridge to transplantation. Circulation 101: 356–359
12. Liao K, Li X, John R et al (2008) Mechanical stress: an independent determinant of early bioprosthetic calcification in human. Ann Thorac Surg 86:491–495
13. Rose EA, Levin HR, Oz MC et al (1994) Artificial circulatory support with textured interior surfaces. A counterintuitive approach to minimizing thromboembolism. Circulation 90:II87–II91
14. Miller LW, Pagani FD, Russell SD et al (2007) Use of a continuous-flow device in patients awaiting heart transplantation. N Engl J Med 357:885–896
15. Feller ED, Sorensen EN, Haddad M et al (2007) Clinical outcomes are similar in pulsatile and nonpulsatile left ventricular assist device recipients. Ann Thorac Surg 83:1082–1088
16. Farrar DJ (2000) The Thoratec ventricular assist device: a paracorporeal pump for treating acute and chronic heart failure. Semin Thorac Cardiovasc Surg 12:243–250
17. Wampler RK, Baker BA, Wright WM (1994) Circulatory support of cardiac interventional procedures with the Hemopump cardiac assist system. Cardiology 84:194–201
18. Slaughter S, Rogers JG, Milano C et al (2009) Advanced heart failure treated with continuous-flow left ventricular assist device. N Engl J Med 361:2241–2251
19. Aaronson KD, Slaughter MS, Miller LW et al (2012) Use of an intrapericardial, continuous-flow, centrifugal pump in patients awaiting heart transplantation. Circulation 125:3191–3200
20. John R, Liao K, Lietz K et al (2007) Experience with the Levitronix CentriMag Circulatory support system as a bridge to decision in patients with refractory acute cardiogenic shock and multisystem organ failure. J Thorac Cardiovasc Surg 134:351–358
21. Liao K, Barksdale A, Park S et al (2007) Non-sternotomy approach for left ventricular assist device implantation, exchange or explantation. J Heart Lung Transplant 26:S199

Cell Transplantation for Ischemic Heart Disease

40

Jianyi Zhang and Daniel J. Garry

Abstract

Recent studies support the notion that cardiomyocyte regeneration may occur during physiological and pathological states in the adult heart. These data highlight the possibilities that myocardial regeneration may occur via cardiomyocyte proliferation and/or differentiation of putative cardiac stem cells. To date, various cell types have been used for cardiac repair, including skeletal myoblasts, bone marrow-derived cells, mesenchymal stem cells (MSCs), endothelial progenitor cells (EPCs), umbilical cord blood (UCB) stem cells, cardiac stem cells, and embryonic stem cells (ESCs). This chapter will review each of these different stem cell populations in regards to the potential treatment of heart disease. We will examine the in vitro and in vivo animal studies, and then briefly discuss the cell therapy clinical trials that are currently underway for the treatment of ischemic heart disease.

Keywords

Embryonic stem cells • Adult stem cells • Skeletal myoblasts • Bone marrow-derived stem cells • Mesenchymal stem cells • Endothelial progenitor cells • Umbilical cord blood stem cells • Cardiac stem cells

Abbreviations

CPCs	Cardiac progenitor cells
EPCs	Endothelial progenitor cells
ESCs	Embryonic stem cells
HGF	Hepatocyte growth factor
hiPSCs	Human induced pluripotent stem cells
IGF-1	Insulin-like growth factor
LV	Left ventricular
MI	Myocardial infarction
MSCs	Mesenchymal stem cells
Sca-1	Stem cell antigen-1
SDF-1	Stromal cell-derived factor-1
SP	Side population
UCB	Umbilical cord blood
VEGF	Vascular endothelial growth factor

J. Zhang, MD, PhD (✉) • D.J. Garry, MD, PhD
Lillehei Heart Institute, Minneapolis, MN, USA

University of Minnesota, 268 Variety Club Research Center, 401 East River Road, Minneapolis, MN 55455, USA
e-mail: zhang047@umn.edu

40.1 Introduction

Although coronary interventions and associated medical therapies have improved postinfarction cardiac function in patients with coronary artery disease, approximately half of the patients will still progress to end-stage or advanced heart failure [1]. To date, cardiac transplantation remains the only definitive therapy for replacing the lost muscle, but it is a widespread approach limited by the inadequate supply of donor hearts (approximately 2000 donor hearts are available each year in the USA). An alternative potential therapy for limiting postinfarction left ventricular (LV) remodeling, and thus the development of congestive heart failure, is the directed replacement of infarcted myocardium with the new myocardium being generated from transplanted stem cells.

P.A. Iaizzo (ed.), *Handbook of Cardiac Anatomy, Physiology, and Devices*, DOI 10.1007/978-3-319-19464-6_40

Recent studies have provided evidence to support the notion that cardiomyocyte regeneration may occur during physiological and pathological states in the adult heart. These data highlight the possibility that myocardial regeneration may occur via cardiomyocyte proliferation and/or differentiation of putative cardiac stem cells [2]. To date, various cell types have been used for cardiac repair including skeletal myoblasts, bone marrow-derived cells, mesenchymal stem cells (MSCs), endothelial progenitor cells (EPCs), umbilical cord blood (UCB) stem cells, cardiac stem cells, and embryonic stem cells (ESCs). This chapter will review each of these different stem cell populations with regard to their potential treatment of heart disease. We will begin by examining the in vitro and in vivo animal studies, and then briefly discuss the cell therapy clinical trials that are currently underway for treating ischemic heart disease. We will conclude by summarizing selected techniques that have been used to enhance the beneficial effects of stem cell transplantation.

40.2 Cells for Myocardial Repair in Ischemic Heart Disease

40.2.1 Embryonic Stem Cells

ESCs can differentiate into all three developmental germ layers (including the mesoderm, which is the source of the cardiac lineage) and can proliferate with self-renewal in an unlimited fashion. Thus, ESCs have the potential of producing a limitless number of cells and cell types for regenerative therapy. However, ESCs must be differentiated into specific cell lineages before transplantation as the ESCs themselves are tumorigenic [3], and the cells derived from ESCs must be administered with immunosuppressive therapy [4] because ESCs can only be obtained from an allogenic source. Yet, the use of human ESCs (hESCs) is limited due to ethical concerns regarding the need to destroy human embryos in order to produce hESCs.

40.2.1.1 Mouse ESCs

The cardiogenic potential of mouse ESCs was first demonstrated in 1985 when these cells were cultured in suspension and formed 3D cystic bodies, termed *embryoid bodies*, which differentiated into cell types of the visceral yolk sac, blood islands, and myocardium [5]. Currently, such cells are separated from their feeder layer and then resuspended in leukemia inhibitory factor-free culture medium at a low density [6]. Mouse ESCs are then cultured in small drops which are formed on the lid of tissue culture dishes. When kept in this hanging droplet setting for 2 days, the cells aggregate and form differentiating embryoid bodies [6]. Embryoid bodies are then transferred into ultralow attachment dishes where they further differentiate. Spontaneous contracting cells (cardiomyocytes) can be observed between 7 and 8 days of differentiation [6]. This process of cardiac differentiation can be further enhanced by the use of selective growth factors and inhibitors of signaling pathways.

Importantly, mouse ESCs have been shown to engraft and regenerate myocardium after an experimentally induced myocardial infarction (MI) [7–9]. These cells can form cardiomyocytes that electrically couple with the host myocardium, endothelial cells, and blood vessels [7–9]. More recently, multipotent cardiac progenitor cells (CPCs) derived from mouse ESCs have been characterized from three independent laboratories [10–12]; Brachyury+/Flk+ and Isl1+ CPC cell lines were shown to differentiate into cardiomyocytes, endothelial cells, and smooth muscle cells, while Nkx2-5/c-kit CPCs could differentiate into cardiomyocytes and smooth muscle cells.

40.2.1.2 Human ESCs

Human ESCs were first isolated from the human blastocyst in 1998 [3], and later it was shown that they could differentiate into cardiomyocytes [13]. Human ESCs also form embryoid bodies when cultured in suspension form; these are positive for cardiomyocyte markers such as myosin heavy chain, α-actinin, desmin, and troponin I [13]. Electrophysiological studies showed that most of the human ESC-derived cardiomyocytes resemble human fetal ventricular myocytes that can propagate action potentials [14]. Human ESCs can also differentiate into endothelial and smooth muscle cell lineages.

Initial in vivo studies have demonstrated that human ESC-derived cardiomyocytes can form new myocardium in the uninjured heart of athymic rats [15] or immunosuppressed pigs [14]. It was shown that the size of the graft could be increased fourfold by prior heat shock treatment of the cells [15]. When human ESCs are implanted in animal models that have a slow heart rate (such as in pigs or guinea pigs), they can form pacemakers when the native pacemaker (node) is dysfunctional, implying electrical integration with surrounding cardiomyocytes [14, 16]. However, when these cells are transplanted in the setting of MI, only 18 % form myocardial grafts and these grafts also contain substantial noncardiac elements [17]. To enhance the yield and purity of cardiomyocytes from human ESCs, Laflamme et al. developed a new technique to direct the differentiation of human ESCs into cardiomyocytes using sequential treatment of high-density undifferentiated monolayer cultures with activin A and bone marrow morphogenic protein 4 [17]. This protocol has yielded greater than 30 % cardiomyocytes, as compared to less than 1 % with the embryoid body-based system which used serum to induce differentiation [17]. Furthermore, Percoll gradient centrifugation, which allows specific enrichment of human ESC-derived cardiomyocytes, resulted in cultures containing 82.6 ± 6.6 % cardiomyocytes

[17]. Moreover, this laboratory used a prosurvival engraftment cocktail to improve graft survival in infarcted hearts. This cocktail included Matrigel to prevent anikis, a cell-permeant peptide from Bcl-XL to block mitochondrial death pathways, cyclosporine A to attenuate cyclophilin D-dependent mitochondrial pathways, a compound that opens ATP-dependent K+ channels (pinacidil) to mimic ischemic preconditioning, insulin-like growth factor (IGF-1) to activate Akt pathways, and the caspase inhibitor ZVAD-fmk [17]. Importantly, transplantation of human ESC-derived cardiomyocytes, in combination with this prosurvival cocktail into infarcted hearts, resulted in myocardial grafts with improved ventricular function [17]. The other intriguing aspect of this study was that almost all noncardiac human ESC-derived cells died by the 4-week period [17].

40.2.2 Human Induced Pluripotent Stem Cells

The immunogenicity and ethical concerns associated with hESCs have led to the development of human induced pluripotent stem cells (hiPSCs), which possess an ESC-like capacity for differentiation and self-replication but can be generated from an individual patient's own somatic cells. The somatic cells are reprogrammed with pluripotency factors such as Oct3/4, Sox2, Klf4, and c-Myc; however, hiPSCs (like hESCs) can be tumorigenic and must be differentiated into specific cell types before administration. Effective protocols for differentiating hiPSCs into smooth-muscle cells (hiPSC-SMCs) have been available for several years [18, 19], while methods for obtaining sufficiently large, pure, and stable populations of hiPSC-derived endothelial cells (hiPSC-ECs) [20] and cardiomyocytes (hiPSC-CMs) [21, 22] have recently been established. Studies in pigs with experimentally induced ischemia-reperfusion injury indicate that all three hiPSC-derived cell lineages are retained at the site of administration for at least 4 weeks after injection, and that the combined treatment can lead to improvements in contractile performance, myocardial wall stress, and cellular metabolism [22]; furthermore, treatment with hiPSC-CMs alone was not associated with arrhythmogenic complications such as those reported when hESC-derived cardiomyocytes (hESC-CMs) were administered to monkeys [23], perhaps because the number of cells administered was much smaller (i.e., 10 million hiPSC-CMs versus 1 billion hESC-CMs).

Although hiPSCs can in principle be used to generate cells of any lineage, the efficiency of the differentiation protocol and function of the hiPSC-derived cells after transplantation may be influenced by epigenetic factors that the hiPSCs retain from their tissues of origin [24, 25]. Thus, hiPSC-derived cells may be more effective for regenerative myocardial therapy if the hiPSCs were reprogrammed from cardiac lineage cells rather than from other organ-specific lineages. Notably, Zhang et al. [26] have successfully generated hiPSCs from cardiac fibroblasts which were obtained from the hearts of patients who were undergoing open-chest surgery. When these cardiac lineage hiPSCs (hciPSCs) were used to generate sheets of cardiomyocytes, the efficiency of the differentiation protocol exceeded 92 %, compared to 60–85 % when dermal- or cord blood lineage hiPSCs have been used [21]. Approximately 30 % of the hciPSC-derived cardiomyocytes were retained for at least 28 days after administration to the infarcted hearts of immunodeficient mice.

40.2.3 Adult Stem Cells

40.2.3.1 Skeletal Myoblasts

Skeletal myoblasts can be derived from myogenic stem cells also known as satellite cells. These myogenic stem cells are quiescent and located in a niche; they are sublaminar and sandwiched between the basal lamina and the plasmalemma of the skeletal muscle fibers. In response to injury, the myogenic stem cells become activated, they proliferate and differentiate, and typically completely restore the skeletal muscle architecture [27]. Previous studies have demonstrated that skeletal myoblasts form viable, long-term skeletal myotube grafts following transplantation into adult hearts [28]. In one study, it was shown that transplantation of autologous skeletal myoblasts in cryoinfarcted rabbit myocardium leads to myoblast engraftment by 3 weeks with subsequent improvement in systolic performance [27]. Importantly, as these cells are specified and committed to the skeletal muscle lineage, they do not differentiate into cardiomyocytes [29], and thus they are also not electromechanically coupled to each other or to the surrounding cardiomyocytes of the host [30, 31].

40.2.3.2 Bone Marrow-Derived Stem Cells

The bone marrow contains many adult stem cells which have been used to treat hematological disorders for decades. It has recently been shown that bone marrow-derived stems can traverse cell lineage boundaries and, upon appropriate stimulation, transdifferentiate into hepatocytes, endothelial cells, skeletal muscle, and/or neurons [32–34]. Yet, the ability of bone marrow-derived cells to differentiate into cardiomyocytes remains controversial. For example, Bittner et al. were the first researchers to suggest that cardiac muscle cells may be derived from bone marrow cells [35]. Goodel et al. demonstrated that transplantation of murine bone marrow side population (SP) cells (c-kit+, Sca-1+, CD34−/low) resulted in donor-derived cells with cardiomyocyte morphologies, as well as smooth muscle and endothelial cells which were

found in the heart following left anterior descending coronary artery ligation [36]. Orlic et al. [37] demonstrated that transplantation of GFP-labeled $Lin^{-}c\text{-}kit^{+}$ cells (presumably containing both hematopoietic stem cells and MSCs) into the ventricular wall after left anterior descending coronary artery ligation resulted in improved function of the ventricle, and they also detected a large number of GFP^{+} cells that coexpressed myocardial proteins in the myocardium. In contrast to these findings, other laboratories using genetic mouse models to label cell populations (and their derivatives) have shown that lineage negative, c-kit-positive cells were not able to differentiate into cardiomyocytes [38, 39]. Alternatively, Anversa and colleagues have shown, using similar genetic techniques, that c-kit+ bone marrow cells can engraft in the injured myocardium and differentiate into cells of the cardiogenic lineage, forming functionally competent cardiomyocytes and vascular structures [40].

40.2.3.3 Mesenchymal Stem Cells

Phenotype and Differentiation Potential

In the late 1980s and through the 1990s, Caplan's laboratory identified a subset of cells within the bone marrow which gave rise to osteoblasts and adipocytes. These cells were termed MSCs [41]. MSCs are present in many different organs of the body including muscle, skin, adipose tissue, and bone marrow. They can be isolated from the bone marrow by a simple process involving Ficoll centrifugation and adhering cell culture in a defined serum-containing medium. In the early studies, MSCs were shown to be expanded for 4–20 population doublings only [42], with preservation of the karyotype, telomerase activity, and telomere length [43, 44]. Phenotypically, these cells were negative for CD31, CD34, and CD45, unlike hematopoietic progenitors from bone marrow, and were positive for CD29, CD44, CD71, CD90, CD105, CD106, CD120a, CD124, SH2, SH3, and SH4 [45, 46]. In the bone marrow, only 0.001–0.01 % of the initial unfractionated bone marrow mononuclear cell population consists of MSCs [33, 36]. However, in a number of rodent studies, the adherent fibroblastic cells obtained from the unfractionated mononuclear class of the bone marrow are termed MSCs [47, 48].

MSCs were reported to have the potential to differentiate into any tissue of mesenchymal origin [41]. MSCs derived from rodent marrow aspiration have been shown to differentiate into cardiomyocyte-like cells in the presence of 5-azacytidine [49, 50]. The cellular morphology changes from spindle-shaped to ball-shaped, and finally a rod-shaped form; thereafter, these cells fuse together to form a syncitium which resembles a myotube [51]. In addition, these cells exhibit markers of fetal cardiomyocytes [50]; specific transcription factors of the myocyte and cardiac lineage including GATA4, Nkx2.5, and HAND 1/2 can be detected [49]. Yet compared to native cardiomyocytes, there are noteworthy differences in those which are derived from MSCs. First, the β-isoform of cardiac myosin heavy chain is more abundant than the α-isoform in these cells. Second, there is increased α-skeletal actin relative to α-cardiac actinin; myosin light chain 2v is also present. Third, both MEF2A and MEF2D isoforms replace MEF2C from early to late passages. Additionally, it was reported that these cells will beat spontaneously and synchronously, which is most likely due to the formation of intercalated discs, as has been shown when they are co-cultured with neonatal myocytes [52]. Finally, the differentiated cells will express competent α- and β-adrenergic and muscarinic receptors, as indicated by increased rates of contraction in response to isoproterenol and by decreased rates of contraction induced by β-adrenergic blockers [53]. Yet, it should be noted that other studies suggest that bone marrow stem cells cannot differentiate to cardiac myocytes [38, 39]. Whether or not MSCs can differentiate into functional cells of the other three lineages will require further investigation.

MSCs for Myocardial Repair

MSCs have several unique features that make them attractive candidates for cell transplantation. First, as they are easily accessible and expandable, MSCs could potentially become a so-called "off the shelf" allogeneic product, one which would be more cost-effective, easier to administer, and allow a greater number of cells to be transplanted. Additionally, they may also permit transplantation at the time of urgent interventions, e.g., to relieve ischemia and injury such as percutaneous or surgical revascularization procedures. Importantly, these cells appear to be hypoimmunogenic [54–56]. Additionally, these cells lack MHC-II and B-7 costimulatory molecule expression and thus limit T-cell responses [57, 58]. Yet, they are considered to directly inhibit inflammatory responses via paracrine mechanisms including production of transforming growth factor beta 1 and hepatocyte growth factor (HGF) [59, 60]. Importantly, all the above properties taken together make them attractive candidates for cell transplantation.

It should be noted that MSC transplantation was tested in a study in which isogenic adult rats were used as donors and recipients to simulate autologous transplantation clinically. MSC intracoronary delivery in these rat hearts following an experimentally induced MI showed that there was a milieu-dependent differentiation of these cells, a fibroblastic phenotype within the scar, and cardiomyocyte phenotype outside the infarction area [61]. However, direct intramyocardial injection of autologous MSCs into the region of the scar resulted in the focal differentiation of these cells into "cardiac-like" muscle cells within the scar tissue. There was also noted increased angiogenesis and improved myocardial function [62]. In a different approach, the delivery of MSCs

via direct left ventricular cavity infusion in a rat MI model resulted in the preferential migration and colonization of these cells in the ischemic myocardium (i.e., at 1 week) [63]. This MSC infusion also resulted in both increased vascularity and improved cardiac function 2 months following delivery in a canine model of chronic ischemic disease [64]. However, it should be noted that Kloner's laboratory, using a rat model of postinfarction LV remodeling, found that the beneficial effects on left ventricular function were short term and were absent after 6 months [65].

Importantly, MSC transplantation has been reported to result in functional improvement in large animal ischemic models. For example, the direct intramyocardial injection of 5-azacytidine-treated autologous MSCs was performed 4 weeks after MI in a swine model; these injected cells formed islands of cardiac-like tissue, induced angiogenesis, prevented thinning and dilatation of the infarct region, and ultimately improved regional and global contractile functions [66]. Similarly, allogeneic intramyocardial transplantation of MSCs in a porcine model of MI resulted in profound improvements in border zone energetics and regional contractile function [67]. These latter findings were hypothesized to be related to a paracrine mechanism, as evidenced by increased vascularity in the border zone and spared native cardiomyocytes in the infarct zone [67]. Finally, the percutaneous delivery of allogenic MSCs 3 days after MI in a porcine model resulted in long-term engraftments (detected at 8 weeks), profound reductions in scar sizes, and near normalization of cardiac function [68].

40.2.3.4 Endothelial Progenitor Cells

EPCs were first isolated from blood in 1997 [69]. They originate from a common hemangioblast precursor in the bone marrow [70]. However, many other cells including myeloid/monocyte (CD14+) cells and stem cells from adult organs can also differentiate into cells with EPC characteristics. Thus, circulating EPCs are a heterogeneous group of cells originating from multiple precursors within the bone marrow and can be isolated in different stages of endothelial differentiation within peripheral blood. Therefore, the characterization of these cells can be challenging because they share certain surface markers of hematopoietic cells and adult endothelial cells. Typically, they express CD34 (a hematopoietic cell characteristic), CD-133 (a more specific marker of EPCs), and KDR (kinase insert domain-containing receptor), which is the receptor for vascular endothelial growth factor (VEGF). Interestingly, in a study of sex-mismatched bone marrow transplant patients by Hebbel and coworkers, 95 % of circulating endothelial cells in the peripheral blood of transplant patients had the recipient genotype, but 5 % had the donor genotype [71]. It was found that the endothelial cells with the donor phenotype had delayed growth in culture, but had a high proliferative capacity with more than a 1000-fold expansion within 1 month; these were termed *endothelial outgrowth cells*. It was concluded that the endothelial outgrowth cells were of bone marrow origin [71]. In contrast, the cells with the recipient phenotype only had a 17-fold expansion within the same time period; these circulating endothelial cells most likely originated from the vessel wall [71].

EPCs have been used for treatment in different animal models of cardiovascular disease. For example, the intravenous delivery of CD34+ cells into athymic nude rats following MI was shown to promote angiogenesis in the peri-infarct region, leading to decreased myocyte apoptosis, reduced interstitial fibrosis, and improvement of left ventricular function [72]. Similarly, intramyocardial implantation of CD34+ selected human peripheral blood mononuclear cells into nude rats after MI resulted in neovascularization and improved LV function [73].

40.2.3.5 UCB Stem Cells

Human UCB is rich in stem and progenitor cells, which have high proliferative capacities [74–76]. Human UCB also contains fibroblast-like cells termed *unrestricted somatic stem cells*, which adhere to culture dishes, are negative for c-kit, CD34, and CD45, and differentiate both in vitro and in vivo into a variety of tissue types, including cardiomyocytes [77]. Direct intramyocardial injection of these human unrestricted somatic cells into the infarcted hearts of immunosuppressed pigs resulted in: (1) improved perfusion and wall motion; (2) reduced infarct size; and (3) enhanced cardiac function [78]. Further, intravenous injection of human mononuclear UCB cells, a small fraction of which were CD34+, into NOD/SCID mice led to enhanced neovascularization with capillary endothelial cells of both human and mouse origin and reduced infarct sizes [79]. However, no myocytes of human origin were found, thus arguing against cardiomyogenic differentiation and regeneration of cardiomyocytes from donor cells. Finally, the direct intramyocardial injection of UCB CD34+ cells into the peri-infarct rim in a rat model resulted in improved cardiac function [80]. To date, there have been no reported clinical studies of UCB transplantation for cardiac repair.

40.2.3.6 Cardiac Progenitor Cells

The innate ability of the cardiomyocytes to replicate has been a highly controversial issue for a long time. Previous studies have established that increases in cardiac mass in mammals during fetal life occur mainly due to cardiomyocyte proliferation. However, during the perinatal period, mammalian cardiomyocytes withdraw from the cell cycle, thus limiting their ability to divide and increase in number [81–83]. Thus, normal postnatal growth and adaptive increases in cardiac mass in adults, as a result of hemodynamic burden, are achieved mainly through the increases in

cell sizes, known as *hypertrophy* [81–83]. This belief was supported by the inability to identify mitotic figures in myocytes, as well as the observation that regions of transmural infarction evolved into essentially avascular, thin collagenous scar. This paradigm of heart growth had been dominant over the past 50 years, i.e., the heart is a postmitotic organ, consisting of a predetermined number of parenchymal cells, that is defined at birth and preserved throughout life until the death of the organ and/or organism. However, recent studies have challenged this concept of the heart being a postmitotic organ, one being incapable of regeneration. For example, it has been shown that the human heart contains cycling myocytes undergoing mitosis and cytokinesis under normal and pathological conditions [84–87]. The occurrence of these mitotic events is considered to support the hypothesis that CPC populations reside in the adult heart and can contribute to limited growth, turnover, and/or regeneration. This notion further supports that the adult heart belongs to the group of renewable adult tissues, and that this capacity for renewal is provided by a population of stem cells (i.e., CPCs) that reside in the myocardium [88, 89].

Origins of CPCs

To date, the primary origins of CPCs remain unclear. It is feasible that the cycling cardiomyocytes might be derived from uncommitted stem-like population cells that reside in the heart which expand and differentiate into cardiomyocytes in response to signals and cues in response to growth and/or injury. Alternatively, these stem-like cells may reside in extracardiac tissues such as the bone marrow, and are capable of being recruited into the circulation and induced to home to the heart by signals emanating from the injured heart.

For example, Mouquet et al. demonstrated that cardiac SP cells are maintained by local progenitor cell proliferation under physiological conditions [90]. After MI, this cardiac SP is decreased by as much as 60 % in the infarct and to a lesser degree in the noninfarct regions within 1 day. Cardiac SP pools are subsequently reconstituted to baseline levels within 7 days after MI, through both proliferation of resident cardiac SP cells and by homing of bone marrow-derived stem cells to specific areas of myocardial injury. These cells then undergo immunophenotypic conversions and adopt a cardiac SP phenotype (CD45+ to CD45−) [90]. Interestingly, bone marrow-derived stem cells accounted for approximately 25 % of the SP cells in the heart under pathological conditions, as compared to <1 % under physiological conditions [90]. In addition to these CD45+ cells that Mouquet et al. reported, bone marrow also contains CD45−, CXCR4+, and Sca-1+ cells within the nonadherent, nonhematopoietic mononuclear fraction, which will express early cardiac markers such as Nkx2.5 and GATA-4 [91]. These cells can also mobilize into the blood after MI and eventually home to the infarcted myocardium in mice. Cerisoli et al. [92] also demonstrated that (at least in pathological conditions) a subpopulation of the c-kit+ CPC population may derive from cells that originate in the bone marrow which are capable of contributing to myocardial regeneration in a similar fashion as the CPCs that are resident in the adult heart.

Number of CPCs

In 2005, Anversa and coworkers proposed that CPCs are undifferentiated multipotent cells that express the stem cell-related antigens, c-kit, MDR-1 (another ABC transporter), and Sca-1, in variable combinations [93]. Quantitative data from mouse, rat, dog, and human hearts were provided that demonstrated there is approximately one CPC for every 30,000–40,000 myocardial cells. Interestingly, ~65 % of all CPCs possess the three stem cell antigens, ~20 % express two stem cell antigens, and ~15 % express only one; roughly 5 % each of these CPCs exclusively express c-kit, MDR1, or Sca-1 [93].

Importantly, none of the above-mentioned reports demonstrated a signature CPC phenotype; this cell population also has significant overlap in the expression of other surface markers. It remains to be determined whether these CPCs are actually the same stem cell type and that differing surface markers reflect differing developmental phases or qualitatively separate subpopulations. Nevertheless, it is believed that these CPCs may participate in myocyte turnover, the rate of which remains to be determined.

Isolation of CPCs

CPCs have been isolated based on their expression (or absence) of specific cell surface markers, proteins, and/or tissue culture methods using the following strategies:

1. Isolation based on expression of the cell surface stem cell marker c-kit;
2. Isolation based on expression of the cell surface stem cell marker Sca-1;
3. Isolation based on the ability to efflux Hoechst 33342 dye (SP cells);
4. Isolation based on the expression of the islet-1 transcription factor;
5. Tissue culture of cardiac explants resulting in the spontaneous shedding of CPCs in vitro.

Isolation Based on Expression of the Cell Surface Stem Cell Marker c-kit

Belrami et al. [94] isolated cells expressing the tyrosine kinase receptor for stem cell factor (also referred to as steel factor; c-kit) from the interstitial regions of the adult rat heart. The highest density of these lineage negative (lin-), c-kit+ stem cells was in the atria and ventricular apex.

These cells were identified to be self-renewing, clonogenic, and multipotent. Further, they had the ability to differentiate into cardiomyocytes, endothelial cells, and smooth muscle cells. Moreover, the delivery of these c-kit-expressing clonogenic stem cells following myocardial injury resulted in both improved functional recovery and evidence of myocardial regeneration. Recently, the same laboratory expanded their analyses to include preclinical studies using large animal models. They have demonstrated that the canine model also harbors a c-kit-expressing stem cell population in the adult heart that is clonogenic, multipotent, and capable of activation following injury. In response to myocardial injury, these c-kit-expressing stem cells are activated by cytokines (including HGF and insulin-like growth factor 1), and also home to areas of injury to participate in repair and regeneration. These preclinical studies have been further extended to the study of the human heart. A similar c-kit-expressing stem cell population (c-kit-positive but negative for the expression of the hematopoietic and endothelial antigens including CD45, CD31, and CD34) has been isolated from the adult human heart that was identified to be multipotent (capable of forming myocyte, smooth muscle cell, and endothelial cell lineages) in vivo and in vitro [95, 96]. Moreover, studies have established that these human c-kit-expressing cardiac stem cells undergo both symmetrical and asymmetrical cell divisions [96]. Importantly, these studies are also currently being validated by other cardiac stem cell laboratories. For example, van Berlo et al., utilizing genetic labeling strategies, demonstrated that c-kit-expressing stem cells were able to daughter cardiomyocytes, yet this was an infrequent event [97]. Rather, these investigators showed that c-kit-expressing stem/progenitors give rise largely to the endothelial cell population within the adult mouse heart. These studies underscore the ongoing controversies associated with many therapeutic approaches being developed within this field [98].

Isolation Based on the Expression of the Cell Surface Stem Cell Marker Sca-1

Resident murine CPCs have also been isolated on the basis of stem cell antigen-1 (Sca-1) expression [98]. These Sca-1-expressing CPCs were small interstitial cells that lacked hematopoietic lineage markers such as CD45, B220, TER119, or Flk-1, and they lacked c-kit expression, supporting the notion that they are distinct from the c-kit stem cell population. Using RT-PCR analyses, the Sca-1-expressing CPC population expressed the vascular marker CD31 and the cardiogenic transcription factors including Gata4, Mef2c, and TEF-1 (but lacked expression of Nkx2-5). A small percentage of these Sca-1-expressing CPCs activated cardiac genes, but did not exhibit spontaneous contractile properties in response to DNA demethylation with 5-azacytidine [98]. This laboratory further examined the abilities of the Sca-1 CPCs to form cardiomyocytes independent of fusion to the differentiated host cardiomyocytes, using genetic mouse models (Cre/Lox and the R26R genetic mouse models) for cellular labeling. Genetically tagged Sca-1 CPCs isolated from the αMHC-Cre transgenic mouse model and delivered into the R26R (all host cells are labeled with LacZ) injured these hearts. Two weeks following injury, the animals were sacrificed and hearts were examined for Cre and LacZ expression. Interestingly, approximately half of the cells expressing αMHC-Cre did not express LacZ, suggesting that the Sca-1-expressing cells are capable of myocardial differentiation independent of fusion to existing (host) cardiomyocytes [98]. Additional studies from another laboratory (Matsura and coworkers) have also isolated Sca-1+ cells from adult murine hearts, and have demonstrated that they are capable of differentiation into beating cardiomyocytes in the presence of oxytocin but not 5-azacytidine [99]. These Sca-1 CPCs are heterogeneous, but a subpopulation is capable of effluxing Hoechst 33342 dye.

Isolation Based on the Ability to Efflux Hoechst 33342 Dye (SP Cells)

Other laboratories have utilized flow cytometry to identify an adult stem cell population that is capable of effluxing Hoechst 33342 dye. Due to their ability to efflux Hoechst 33342 dye, these cells were located as a side population using flow cytometry and were termed SP cells. Subsequently, these SP cells have been isolated from a number of lineages including: adult bone marrow, skeletal muscle, lung, brain, liver, and mouse ESCs. These respective SP cell populations are multipotent when placed in a permissive environment. The ability of the SP cells to efflux the Hoechst dye is due to the presence of multidrug resistance proteins. Studies have demonstrated that Abcg2 is a member of the ATP [100] binding cassette (ABC) transporters (also known as multidrug resistance proteins), and is the molecular determinant for the SP cell phenotype. Both specific (FTC) and nonspecific (calcium channel blockers such as verapamil) blockers of Abcg2 prevent Hoechst 33342 dye exclusion. Abcg2-expressing SP cells participate in cardiac development and reside in the adult mouse heart. Following injury, these Abcg2-expressing cardiac SP cells increase in number and form fetal cardiomyocytes. In addition to serving as a marker for the SP cell population, Abcg2 has a cytoprotective function in response to oxidative stress. Moreover, previous studies have demonstrated that Hif2α is a direct upstream regulator of the Abcg2 gene. These results support the notion that CPCs in the adult heart likely play a protective role that promotes survival following injury.

To date, whole genome analyses using microarray platforms have examined the molecular signature of adult cardiac SP cells, adult bone marrow SP cells, adult skeletal muscle SP cells, and SP cells isolated from ESCs. As expected, cardiac

SP cells express Abcg2, Sca-1, and c-kit. They also have induction of signaling pathways including the notch signaling pathway and the Wnt signaling pathway, which are characteristic of a number of other stem cell populations. Yet, the cardiac SP cells largely lack expression of hematopoietic markers (CD45 and TER119). Importantly, the cardiac SP cells appear to be a subpopulation of the Sca-1-expressing CPCs. Other groups have isolated the so-called SP cells from mouse hearts based on their ability to exclude Hoechst 33342 dye [100, 101]. These cells express Abcg2, an ATP-binding cassette (ABC) transporter, and they are Sca-1+ and c-kit low, and differentiate into cardiomyocytes after co-culture with rat cardiomyocytes.

Isolation Based on *Islet-1 Gene* Expression

Recent studies by Laugwitz et al. have identified Isl-1-expressing cells as an important stem cell population during cardiac development [102]. The heart is derived from a primary heart field and a secondary heart field which segregate from a common progenitor during gastrulation. The primary heart field (which gives rise to the cardiac crescent) contributes to the left ventricle and atria, while the secondary heart field (which is derived from the pharyngeal mesoderm) gives rise to the right ventricle and the outflow tract. Utilizing a gene disruption strategy, embryos lacking Isl-1 are lethal and lack a secondary heart field (i.e., right ventricle and outflow tract), supporting the notion that Isl-1 is a critical regulator for cardiac development. Additional studies have further uncovered an Isl-1-expressing multipotent cardiac stem cell population that expresses Nkx2-5 and Flk-1 and gives rise to all the cardiac lineages (cardiomyocyte, smooth muscle, and endothelial cells) during heart development. While Isl-1-expressing cells are resident in the neonatal heart, there is no evidence of an Isl-1-expressing CPC population in the unperturbed or injured adult heart. Future studies will be necessary to define distinct and common molecular pathways that govern stem cell populations during cardiac development and regeneration of the adult injured heart. For more information on cardiac development, refer to Chap. 3.

Tissue Culture of Cardiac Explants with Spontaneous Shedding of CPCs In Vitro

In 2004, Messina et al. isolated undifferentiated cells that grew as self-adherent clusters (termed *cardiospheres*) from subcultures of postnatal atrial or ventricular human biopsy specimens and also from murine hearts [103]. These cardiospheres varied in size (20–150 μm) and were observed to beat spontaneously in culture. The cardiosphere-forming cells had the properties of adult cardiac stem cells as they were clonogenic, they expressed stem and EPC antigens/markers (c-kit, Sca-1, CD31, and Flk-1), were capable of long-term self-renewal, and could differentiate in vitro and in vivo into myocytes and endothelial cells [103]. Importantly, the expansion of the cardiosphere-forming cells resulted in more than one million human cardiospheres within a 1-month period. These studies were confirmed and expanded as Marban's laboratory obtained ventricular tissue from percutaneous endomyocardial biopsies from both humans and pigs. These ventricular biopsy specimens were cultured to form cardiospheres, which were further plated to yield cardiosphere-derived cells [104]. Cardiospheres and cardiosphere-derived cells expressed antigenic characteristics of stem cells at each stage of processing, as well as proteins vital for cardiac contractile and electrical function [104]. Human and porcine cardiosphere-derived cells co-cultured with neonatal rat ventricular myocytes exhibited biophysical signatures characteristic of myocytes, including calcium transients synchronous with those of neighboring myocytes [104]. Moreover, the delivery of cardiosphere-derived cells following myocardial injury resulted in improved myocardial function compared to their respective controls.

Myocardial Regeneration from CPCs

Anversa and coworkers demonstrated that the direct intramyocardial injection of c-kit+ cells into an ischemic rat heart reconstituted well-differentiated myocardium, comprised of new blood-carrying vessels and cardiomyocytes with the characteristics of fetal cells; these cells were present in approximately 70 % of the ventricle [95]. Later, it was also shown that intracoronary delivery of these cardiac stem cells in an ischemia/reperfusion rat model resulted in myocardial regeneration, infarct size reduction of 29 %, and improvement of LV function [105]. Given intravenously after ischemia/reperfusion, Sca-1 cells also homed to injured myocardium and differentiated into cardiomyocytes [98]. The relative contributions of regenerated cardiomyocytes and preservation of injured native cardiomyocytes in these studies requires clarification.

Wang et al. recently reported that heart-derived Sca-1$^+$/CD31$^-$ cells possess stem cell characteristics and play an important role in cardiac repair [106]. In that study, immunofluorescent staining and fluorescence-activated cell sorter analysis indicated that endogenous Sca-1$^+$/CD31$^-$ cells significantly increased in the infarct and peri-infarct areas at 3 and 7 days after MI. Western blot analyses confirmed elevated Sca-1 protein expression 7 days after MI. Sca-1$^+$/CD31$^-$ cells cultured in vitro were induced to express both endothelial cell and cardiomyocyte markers. Transplantation of Sca-1$^+$/CD31$^-$cells into a murine model of MI led to functional preservation and decreased remodeling after MI [106]. Immunohistochemical data indicated a significant increase of neovascularization, but a low level of cardiomyocyte regeneration at the infarct border zone. Despite the absence of significant cardiomyocyte regeneration, cell transplantation

remarkably improved myocardial bioenergetics [106]. These findings provide evidence that Sca-1^{+}/CD31^{-} cells possess both endothelial cell and cardiomyocyte progenitor cell characteristics. However, this study also reported that the regeneration rates of cardiomyocytes and/or endothelial cells from the engrafted stem cells were very low. Hence, trophic effects associated with the transplanted cells were most likely the primary basis of the beneficial effects of these cells [106]. Nevertheless, the expansion of these progenitor cells may have therapeutic applicability for the treatment of MI.

CPCs and early committed cells have been shown to: (1) express c-Met and IGF-1 receptors; and (2) synthesize and secrete the corresponding ligands, such as HGF and IGF-1 [107]. HGF mobilizes cardiac stem cells-early committed cells, and IGF-1 promotes both their survival and proliferation [107]. Therefore, in a separate study, HGF and IGF-1 were injected in mice following MI and a growth factor gradient was introduced between the site of storage of primitive cells in the atria and the region bordering the infarct to facilitate homing. Importantly, the newly formed myocardium contained arterioles, capillaries, and functionally competent myocytes that increased in size over time. This regenerative response was associated with improved ventricular performance and overall increased survival. Surprisingly, this intervention rescued animals with infarcts that comprised as much as 86 % of ventricular mass, which implied the elicited low ejection fractions. Subsequently, the above findings were replicated in a dog model, where HGF and IGF-1 were also used to stimulate resident cardiac stem cells after MI; noteworthy growth factor therapy again resulted in improvement of myocardial function [108].

Before they can be used therapeutically, CPCs have to be isolated from fragments of the myocardium and subsequently expanded in vitro. This was achieved in a pig model [109] where c-kit+ cells were isolated and each cell was propagated to form approximately 400,000 cells. Another group performed autologous transplantation of CPCs in an ischemia/reperfusion swine model [110]. To accomplish this, each pig had an initial biopsy from the right ventricular septum at the time of injury. The biopsies weighed approximately 92 mg, and yielded mean cell counts of 14.2×10^{6} cells after isolation and expansion (after 2.8 cell passages over 23 days). Intracoronary delivery was then performed 4 weeks after injury; engraftment primarily occurred in the MI border zone and islands of engrafted cells were present within the scar 8 weeks after coronary delivery [110].

Human CPCs have also been isolated from the myocardium, expanded in vitro, and then used for transplantation in animal models of ischemic myocardium. For example, Hosoda et al. isolated human CPCs from surgical samples [111], then these c-kit+ human CPCs were injected into the hearts of immunodeficient mice and rats. Foci of myocardial regeneration were identified at 2–3 weeks which consisted of myocytes, resistance arterioles, and capillaries [111]. The presence of connexin 43 and N-cadherin in the developing human myocytes strongly suggested that the engrafted human cells were functionally competent. Two-photon microscopy was used to further demonstrate the functional integration of enhanced green fluorescent protein-positive human myocytes with the surrounding myocardium [111]. More recently, Torella et al. [112] also isolated human CPCs from myocardial samples from all four chambers of the human heart; these were c-kit+, MDR-1+, and CD133+. In these studies, one clone was shown to generate over 5×10^{9} cells and form functional myocardium after injection into infarcted rat hearts [112].

Altogether, these studies provide early evidence of the rationale for the use of human CPCs in patients with ischemic heart disease. These cells appear to be excellent candidates for exogenous stem cell therapy, yet they must be harvested from patients and expanded ex vivo to generate numbers sufficient for transplantation. To date, there have been no reported clinical trials of human CPC therapy.

40.3 Update of Clinical Trials of Stem Cell Treatment in Heart Disease

Skeletal myoblasts were the first cell type to be used in therapeutic clinical trials. These cells can be transplanted in an autologous fashion without immunosuppression, and have several advantages including a high proliferative potential that allows an initial biopsy to be easily expanded in vitro. They are also terminally differentiated, thus decreasing the chances of tumorigenesis, and are known to be resistant to ischemia, allowing them to survive in scar or peri-scar areas where there is minimal perfusion. To date, there have been six phase I safety and feasibility studies of skeletal myoblast transplantation in patients with severe LV dysfunction caused by MI. Four of these studies [113–116] were surgical and entailed myoblast implantation at the time of coronary artery bypass grafting or left ventricular assist device implantation, and two were catheter-based trials [117, 118] using an endoventricular or coronary sinus transvenous approach. Although not the primary outcome of these studies, modest left ventricular functional improvement was noted following transplantation. Engraftment of myoblasts has been documented in pathological specimens up to 18 months after transplantation [115, 119]. Yet, some concerns regarding the development of ventricular tachycardia have prompted the use of intracardiac defibrillators in protocols for skeletal myoblast transplantation. Future studies may utilize the use of skeletal muscle stem cells (i.e., satellite cells) as opposed to well-differentiated myoblasts.

Bone marrow cells have also received intense interest as a cell therapy for patients with cardiovascular disease.

Importantly, the Transplantation of Progenitor Cells and Regeneration Enhancement in Acute Myocardial Infarction (TOPCARE-AMI) trial revealed significant improvement in LV ejection fraction as well as significantly enhanced myocardial viability and regional wall motion in the infarct regions following transplantation of bone marrow mononuclear cells or blood-derived progenitor cells [120, 121]. The BOOST (bone marrow cell transfer to enhance ST-elevation infarct regeneration) study [122] also resulted in an increase in LV ejection fraction at 6 months following cell transplantation, but surprisingly there was no statistical difference between the treated and placebo groups at 18 months. The Reinfusion of Enriched Progenitor Cells and Infarct Remodeling in Acute Myocardial Infarction (REPAIR-AMI) trial [123] randomized 204 patients with acute MI to receive either an intracoronary infusion of progenitor cells derived from bone marrow or a placebo medium into the infarct artery 3–7 days after successful reperfusion therapy. It was reported that the absolute increase in LV ejection fraction was significantly greater (2.5 %) in the bone marrow cell group than in the placebo group at 4 months, although this represents a modest improvement. However, other trials (i.e., ASTAMI—Autologous Stem Cell Transplantation in Acute Myocardial Infarction and STEMI—ST-elevation Acute Myocardial Infarction) [124, 125] have shown negative results with no improvement in ejection fraction with cell transplantation; differences in cell preparation [126] and numbers have been proposed as possible causes for these conflicting results. Bone marrow cells have also been used in the chronic heart failure setting. For example, in the Transplantation of Progenitor Cells and Recovery of LV Function in Patients with Chronic Ischemic Heart Disease (TOPCARE-CHD) trial [127], 75 patients with stable ischemic heart disease who had a MI at least 3 months previously were assigned to receive: (1) no cell infusion; (2) infusion of circulating progenitor cells; or (3) bone marrow cell into the patent coronary artery supplying the most dyskinetic LV area. It was reported that the transplantation of bone marrow cells was associated with a moderate (2.9 percentage points), but significant improvement in LV function 3 months post-transplantation.

MSC transplantation has been used therapeutically in patients with acute MI 18 days after primary percutaneous intervention, and this resulted in significant improvement in LV ejection fraction up to 6 months following delivery [128, 129]. Furthermore, this was associated with a significant reduction in the size of the perfusion defect measured by positron emission tomography at 3 months following delivery [127, 129]. More recently, it has been demonstrated in a randomized double-blind placebo controlled trial that intravenous delivery of allogenic human MSCs led to improved ventricular function after MI [130]. Yet, the degree of response to intravenous therapy occurred early after MI, and compared favorably with previous studies using intracoronary infusions of bone marrow cells [130].

The clinical application of EPCs is limited by the fact that it is difficult to expand them into sufficient numbers without either inducing a change in their phenotype or the development of cell senescence. Recently, Erb et al. randomized patients with chronically occluded coronary arteries to receive intracoronary progenitor cells or a placebo; they mobilized bone marrow cells using GCSF, harvested them from peripheral blood, and expanded them ex vivo. Subsequently, the intracoronary delivery of these cells led to improvement in coronary flow reserve and cardiac function at 3 months post-transplant [131]. Currently, clinical trials using CD34+ cells from bone marrow that are enriched in EPC content are underway.

Phase I clinical studies that deliver cardiosphere-derived cells (CADUCEUS or CArdiosphere-Derived aUtologous stem CELLs to reverse ventricular dysfunction) following MI have been evaluated at 6 months and 1 year postdelivery. As these were Phase I safety studies and were not associated with major complications, they also supported the notion that cell therapy was associated with reduced scar size and improved regional function of injured myocardium. Future studies will require larger patient numbers which will have the statistical power to determine functional improvement [132].

Similarly, Phase I clinical studies to assess the safety of autologous c-kit+ cells isolated from the patient's heart and delivered at the time of surgical revascularization supported the notion that this cell population also was safe, reduced scar formation and was associated with increased left ventricular viable mass compared to controls [133]. These studies will warrant further analysis to determine their impact as a putative therapeutic approach.

40.4 Cardiac Patches

Stem cells, and more frequently, fully differentiated cardiac cells can be used to engineer a patch of myocardial tissue by either (1) culturing the cells in a monolayer until confluence [26, 134] or (2) seeding the cells into a scaffold of biomaterial, and the biomaterial can be modified to contain factors that enhance neovascularization and cell survival. For example, when gelatin microspheres containing thymosin β4 (Tβ4), which promotes angiogenesis while impeding inflammation and apoptosis, were incorporated into an MSC-containing fibrin patch, the engraftment and survival of the transplanted cells increased, and more endogenous CPCs were recruited to the site of injury [135]. More mature and structurally aligned patches can be created by constructing a ring of cardiac-cell-containing fibrin and then rhythmically stretching the ring for several days before implantation over the injury site; when

tested in a rat model of myocardial injury, this approach was associated with a remarkable (>77 %) decline in infarct size and complete functional recovery. Note that this was only when the cells seeded into the rings included a population of cardiomyocytes [136]. A recent, and much more extensive, review of the various materials and methods used to create myocardial patches has been published elsewhere [137].

40.5 Mechanisms of Beneficial Effects of Stem Cell Treatment

Several studies using animal models have established that stem cell treatment leads to a functional benefit after MI. The initial results from the human clinical trials are also promising; however, the mechanisms underlying the beneficial effects of stem cell transplantation remain somewhat unclear. The proposed mechanisms are discussed below.

40.5.1 Primary Remuscularization

First, the replacement of infarcted tissue by new myocardium generated by the transplanted cells is one explanation for the beneficial effects. This was observed in the case of human cardiac stem cells, which are able to form functional myocardium after transplantation into mice with MI; the transplanted cardiomyocytes were structurally integrated with the host myocardium and led to improvement in ventricular function [96]. This was also observed after the delivery of cardiomyocytes derived from human ESCs which were transplanted into mice with induced MIs [17]. To date, the ability of bone marrow cells to transdifferentiate into cardiomyocytes remains controversial with some reports suggesting that these cells can transdifferentiate into cardiomyocytes [40], while other reports refute this claim [38]. Other adult stem cells such as skeletal myoblasts and EPCs are not able to form cardiomyocytes, but have been found to still exert a beneficial effect, thus suggesting other mechanisms for improvement in LV function.

40.5.2 Attenuation of Adverse Remodeling

The structural changes that occur after myocardial injury, such as ventricular dilatation, wall thinning, increased chamber volume, and hypertrophy of the surrounding myocardium [138], are accompanied by substantial hypoxia-induced changes in cellular ATP metabolism [139]. After the heart recovers from the initial infarction, these metabolic changes can persist and are believed to contribute to progressive declines in cardiac function that eventually lead to heart failure [140, 141]. The transplantation of stem cells, or especially a patch of hiPSC-derived cells [142], can reduce adverse structural changes and partially restore a more native-like metabolic profile in the myocardium, thereby preserving or perhaps improving myocardial performance during the chronic phase of heart disease. For more details on cardiac bioenergetics, the reader is referred to Chap. 21.

40.5.3 Improved Perfusion

Enhanced blood flow, as measured by microspheres, has been shown to increase after stem cell transplantation in a rat model following MI [143]. Increased blood flow can be due to new vessel formation (angiogenesis) or enlargement of preexisting collaterals (arteriogenesis). A number of the stem cell populations discussed in this chapter have been shown to promote or contribute to neovascularization after transplantation in the setting of MI. Yet, some groups have challenged this concept and have shown that stem cells home to the region of developing vascular collateralization, but do not anatomically incorporate into the vessel as either endothelial or smooth muscle cells [144]; however, the delivery of these cell populations still improve collateral flow.

40.5.4 Paracrine Effects

Stem cells may secrete factors that act through totally different repair pathways to ultimately promote cardioprotection. Evidence supporting such a hypothesis recently emerged from Dzau's laboratory; they showed that the injection of the conditioned medium from Akt-overexpressing MSCs alone can decrease the infarct size and lead to functional improvement in an animal model of MI [145, 146]. Hypoxic Akt-transduced MSCs showed increased release of VEGF, FGF-2, IGF-1, HGF, and thymosin β4. It is likely that various factors acting in concert will ultimately exert numerous beneficial effect, as anti-VEGF and anti-FGF antibodies only partially decrease the conditioned medium-induced proliferation of endothelial and smooth muscle cells [147, 148].

40.5.5 Immunomodulation of the Infarct Environment

The inflammatory response after a MI has been recognized as a potential target for improving functional outcome after acute MI. Some stem cells may act, in part, by modulating the immune environment within the recently infarcted heart. For example, MSCs have been shown to directly inhibit the

inflammatory responses via paracrine mechanisms including the production of transforming growth factor beta 1 and HGF [60, 61].

40.5.6 Modulation of Extracellular Matrix Homeostasis

Remodeling of the ventricle is also known to involve modifications in the extracellular matrix which are thought to contribute to myocardial dysfunction. As such, MSC implantation in a rat model of MI significantly attenuated the increased expression of collagen types I and III, TIMP-1, and TGF-β, but had no effects on MMP-1 levels [149, 150]. This was associated with reduced LV dilatation and improved global ventricular function.

40.5.7 Stimulation of Endogenous Cardiac Progenitors Cells

Stem cell treatment could also lead to increased mobilization, differentiation, survival, and function of endogenous CPCs that are associated with the paracrine effects. This possibility is receiving intense interest as cell therapy has uniformly been shown to improve cardiac function but has variable contributions to newly regenerated myocardium.

40.6 Techniques of Enhancing Efficacy of Stem Cell Therapy

Although stem cell transplantation improves LV function after MI, to date, the observed stem cell engraftment is still found to be minimal. Furthermore, the majority of transplanted cells that do engraft remain as spindle-shaped stem cells and do not fully differentiate into the host cardiac cell phenotypes. Therefore, other techniques are considered necessary to enhance the efficacy of stem cell transplantation.

40.6.1 Mobilization

Granulocyte colony stimulating factor, VEGF, stromal cell-derived factor-1 (SDF-1), angiopoietin-1, placental growth factor, and erythropoietin are several factors that may be utilized as therapies to mobilize stem cells from the bone marrow to the systemic circulation. Once these stem cells are mobilized, they may participate in endogenous repair or alternatively be collected and expanded in vitro for future cell therapy uses. As an example, intracoronary infusion of peripheral blood stem cells mobilized by granulocyte colony stimulating factor resulted in the improvement of LV function in patients with MI [151].

40.6.2 Homing

An important goal is to enhance the homing of stem cells to the injured region of the heart. It is known that factors that contribute to the homing of stem cells include stromal-derived growth factor (SDF-1) [152, 153], high mobility group box protein 1 [154], and integrins. It is also known that the microenvironment after acute MI is more favorable to cell homing as compared to the chronically infarcted myocardium. For example, Lu et al. [155] examined the local conditions requisite for cell homing and migration using a rat model of permanent coronary artery ligation, and concluded that the optimal time period for cell homing and migration is within the 2-week period following an MI.

40.6.3 Function and Survival

Assuming that the number of transplanted cells that survive is critical to therapeutic benefit, multiple research groups are exploring new methods to increase the survival of transplanted cells As such, apoptosis can be decreased by the constitutive expression of Akt (a serine threonine kinase with potent prosurvival activity) or by heat shock prior to transplantation [156]. Furthermore, rat MSCs transduced to overexpress Akt1 (encoding the Akt protein) transplanted into ischemic myocardium were found to inhibit cardiac remodeling by reducing inflammation, collagen deposition, and myocyte hypertrophy in a dose-dependent fashion [157]. Similarly, MSCs transduced to express Akt were also studied in an ischemic porcine model, which showed an improvement in ejection fraction as compared to nontransduced MSCs. Recently, in order to determine the exact mechanisms of these beneficial effects, the effects of the apoptotic stimulus, H_2O_2, on MSCs transduced with Akt was studied in vitro. Specifically, Akt-MSCs were found to be more resistant to apoptosis and were related to higher levels of extracellular signal-regulated protein kinase activation and VEGF expression [158]. Yet, a significant concern also exists regarding the potential tumorigenicity of Akt-transduced cells, particularly when Akt is constitutively expressed because Akt has been shown to be sufficient to induce oncogenic transformation of cells and tumor formation; therapeutic efforts are underway to target the Akt pathway for the treatment of malignancies [159]. Additional strategies that have been widely tested involve those which increase vasculogenesis with VEGF; transfection with VEGF and IGF-1 improved survival of transplanted bone marrow cells in a rat model of MI [160]. Furthermore, it was observed that the delivery of cells which had undergone adenoviral transduction and overexpressed VEGF also resulted in improved LV function and neovascularization [161], but the addition of VEGF protein alone to cells did not show any benefit in a rat model of fetal cardiomyocyte transplantation [162].

Enhanced expression of other gene products has also been examined and found to be effective, including cardiotrophin-1, heme oxygenase-1, an IL-1 inhibitor, and CuZn-superoxide dismutase. It was also shown that MSCs transfected with a hypoxia-regulated heme oxygenase-1 vector were found to be more tolerant to hypoxia-reoxygen injury in vitro and result in improved viability in ischemic hearts [163]. Likewise, treatment with CuZn-superoxide dismutase has been shown to attenuate the initial rapid cell death following transplantation, leaving a twofold increase in the total number of engrafted cells at 72 h compared with controls [164].

To date, the use of viruses for gene expression cannot be translated into clinical studies due to the risk of mutagenesis, carcinogenesis, and induction of an immune response. Yet recently, Jo et al. [165] developed a nonviral carrier of cationized polysaccharide for the genetic engineering of MSCs. When genetically engineered by a spermine-dextran complex with plasmid DNA of adrenomedullin, MSCs secreted a large amount of adrenomedullin, an anti-apoptotic and angiogenic peptide. Transplantation of these adrenomedullin gene-engineered MSCs improved cardiac function after MI significantly more than did nontransduced MSCs. Thus, this genetic engineering technology using the nonviral spermine-dextran (and other promising new methods) is an emerging strategy to improve MSC therapy for ischemic heart disease.

40.6.4 Use of Biomaterials to Design Microenvironment

The microenvironment in which the cells are injected is of extreme importance for their survival and subsequent beneficial effects. It has been shown that biomaterials can be designed to regulate quantitative timed release of factors, which direct cellular differentiation pathways such as angiogenesis and vascular maturation. Moreover, it is believed that smart biomaterials are capable of responding to the local environment, such as protease activity or mechanical forces, with controlled release or activation [166]. Recently, Davis et al. [167] designed self-assembling peptide nanofibers for the prolonged delivery of IGF-1, a cardiomyocyte growth and differentiation factor, to the myocardium using a "biotin sandwich" strategy. Specifically, biotinylated IGF-1 was complexed with tetravalent streptavidin and then bound to biotinylated self-assembling peptides. After injection into rat myocardium, biotinylated nanofibers provided sustained IGF-1 delivery for 28 days, and targeted delivery of IGF-1 in vivo increased the activation of Akt in the myocardium. Therefore, cell therapeutic strategies using IGF-1 delivery by biotinylated nanofibers improved systolic function after experimental MI, demonstrating the importance of engineering the local cellular microenvironment and the impact of these and future interventions to improve the outcomes of cell therapy.

Importantly, many of these new biomaterials provide improved flexibility for regenerating tissues ex vivo, but emerging technologies such as self-assembling nanofibers can now establish intramyocardial cellular microenvironments following injection. This may allow percutaneous cardiac regeneration and repair approaches, i.e., injectable tissue engineering. It has been shown that materials can be made to multifunction by providing sequential signals with the custom design of differential release kinetics for individual factors. Thus, new rationally designed biomaterials no longer simply coexist with tissues, but can provide precision bioactive control of the microenvironment that may be required for cardiac regeneration and repair.

40.7 Summary

Recent studies continue to support the notion that cardiomyocyte regeneration may occur both during normal physiological adaptation and during the expression of pathological states in the adult human heart. Such findings may indicate the possibility for myocardial regeneration to occur via cardiomyocyte proliferation and/or differentiation of putative cardiac stem cells. To date, various cell types have been used for cardiac repair, including: skeletal myoblasts, bone marrow-derived cells, MSCs, EPCs, UCB stem cells, cardiac stem cells, and ESCs. This chapter has reviewed the current knowledge relative to these different stem cell populations being utilized for the potential treatment of heart disease. Findings to date continue to be promising, but much work remains before these therapeutic approaches become commonplace. Furthermore, specific cardiac devices/technologies for the clinical delivery of such cellular therapies will be required and are being currently being developed.

References

1. Weir RA, McMurray JJ (2006) Epidemiology of heart failure and left ventricular dysfunction after acute MI. Curr Heart Fail Rep 3:175–180
2. Anversa P, Nadal-Ginard B (2002) Myocyte renewal and ventricular remodelling. Nature 415:240–243
3. Thomson JA, Itskovitz-Eldor J, Shapiro SS et al (1998) Embryonic stem cell lines derived from human blastocysts. Science 282:1145–1147
4. Nussbaum J, Minami E, Laflamme MA et al (2007) Transplantation of undifferentiated murine embryonic stem cells in the heart: teratoma formation and immune response. FASEB J 21:1345–1357
5. Doetschman TC, Eistetter H, Katz M et al (1985) The in vitro development of blastocyst-derived embryonic stem cell lines: formation of visceral yolk sac, blood islands and myocardium. J Embryol Exp Morphol 87:27–45

6. Wobus AM, Guan K, Yang HT et al (2002) Embryonic stem cells as a model to study cardiac, skeletal muscle, and vascular smooth muscle cell differentiation. Methods Mol Biol 185:127–156
7. Kolossov E, Bostani T, Roell W et al (2006) Engraftment of engineered ES cell-derived cardiomyocytes but not BM cells restores contractile function to the infarcted myocardium. J Exp Med 203:2315–2327
8. Min JY, Yang Y, Converso KL et al (2002) Transplantation of embryonic stem cells improves cardiac function in postinfarcted rats. J Appl Physiol 92:288–296
9. Singla DK, Hacker TA, Ma L et al (2006) Transplantation of embryonic stem cells into the infarcted mouse heart: formation of multiple cell types. J Mol Cell Cardiol 40:195–200
10. Kattman SJ, Huber TL, Keller GM (2006) Multipotent flk-1+ cardiovascular progenitor cells give rise to the cardiomyocyte, endothelial, and vascular smooth muscle lineages. Dev Cell 11:723–732
11. Moretti A, Caron L, Nakano A et al (2006) Multipotent embryonic isl1+ progenitor cells lead to cardiac, smooth muscle, and endothelial cell diversification. Cell 127:1151–1165
12. Wu SM, Fujiwara Y, Cibulsky SM et al (2006) Developmental origin of a bipotential myocardial and smooth muscle cell precursor in the mammalian heart. Cell 127:1137–1150
13. Kehat I, Kenyagin-Karsenti D, Snir M et al (2001) Human embryonic stem cells can differentiate into myocytes with structural and functional properties of cardiomyocytes. J Clin Invest 108: 407–414
14. Kehat I, Khimovich L, Caspi O et al (2004) Electromechanical integration of cardiomyocytes derived from human embryonic stem cells. Nat Biotechnol 22:1282–1289
15. Laflamme MA, Gold J, Xu C et al (2005) Formation of human myocardium in the rat heart from human embryonic stem cells. Am J Pathol 167:663–671
16. Xue T, Cho HC, Akar FG et al (2005) Functional integration of electrically active cardiac derivatives from genetically engineered human embryonic stem cells with quiescent recipient ventricular cardiomyocytes: insights into the development of cell-based pacemakers. Circulation 111:11–20
17. Laflamme MA, Chen KY, Naumova AV et al (2007) Cardiomyocytes derived from human embryonic stem cells in pro-survival factors enhance function of infarcted rat hearts. Nat Biotechnol 25:1015–1024
18. Woll PS, Morris JK, Painschab MS et al (2008) Wnt signaling promotes hematoendothelial cell development from human embryonic stem cells. Blood 111:122–131
19. Hill KL, Obrtlikova P, Alvarez DF et al (2010) Human embryonic stem cell-derived vascular progenitor cells capable of endothelial and smooth muscle cell function. Exp Hematol 38:246–257.e1.
20. Zhang S, Dutton JR, Su L et al (2014) The influence of a spatiotemporal 3D environment on endothelial cell differentiation of human induced pluripotent stem cells. Biomaterials 35: 3786–3793
21. Ye L, Zhang S, Greder L et al (2013) Effective cardiac myocyte differentiation of human induced pluripotent stem cells requires VEGF. PLoS One 8, e53764
22. Ye L, Chang YH, Xiong Q et al (2014) Cardiac repair in a porcine model of acute myocardial infarction with human induced pluripotent stem cell-derived cardiovascular cells. Cell Stem Cell 15:750–761.
23. Chong JJ, Yang X, Don CW et al (2014) Human embryonic-stem-cell-derived cardiomyocytes regenerate non-human primate hearts. Nature 510:273–277
24. Kim K, Doi A, Wen B et al (2010) Epigenetic memory in induced pluripotent stem cells. Nature 467:285–290
25. Bar-Nur O, Russ HA, Efrat S et al (2011) Epigenetic memory and preferential lineage-specific differentiation in induced pluripotent stem cells derived from human pancreatic islet beta cells. Cell Stem Cell 9:17–23
26. Zhang L, Guo J, Zhang P et al (2015) Derivation and high engraftment of patient-specific cardiomyocyte-sheet using induced pluripotent stem cells generated from adult cardiac fibroblast. Circ Heart Fail 8:156–166
27. Taylor DA, Atkins BZ, Hungspreugs P et al (1998) Regenerating functional myocardium: improved performance after skeletal myoblast transplantation. Nat Med 4:929–933
28. Koh GY, Klug MG, Soonpaa MH et al (1993) Differentiation and long-term survival of C2C12 myoblast grafts in heart. J Clin Invest 92:1548–1554
29. Dowell JD, Rubart M, Pasumarthi KB et al (2003) Myocyte and myogenic stem cell transplantation in the heart. Cardiovasc Res 58:336–350
30. Murry CE, Wiseman RW, Schwartz SM et al (1996) Skeletal myoblast transplantation for repair of myocardial necrosis. J Clin Invest 98:2512–2523
31. Leobon B, Garcin I, Menasche P et al (2003) Myoblasts transplanted into rat infarcted myocardium are functionally isolated from their host. Proc Natl Acad Sci U S A 100:7808–7811
32. Ferrari G, Cusella-De Angelis G, Coletta M et al (1998) Muscle regeneration by bone marrow-derived myogenic progenitors. Science 279:1528–1530
33. Krause DS, Theise ND, Collector MI et al (2001) Multi-organ, multi-lineage engraftment by a single bone marrow-derived stem cell. Cell 105:369–377
34. Mezey E, Chandross KJ, Harta G et al (2000) Turning blood into brain: cells bearing neuronal antigens generated in vivo from bone marrow. Science 290:1779–1782
35. Bittner RE, Schofer C, Weipoltshammer K et al (1999) Recruitment of bone-marrow-derived cells by skeletal and cardiac muscle in adult dystrophic mdx mice. Anat Embryol 199:391–396
36. Jackson KA, Majka SM, Wang H et al (2001) Regeneration of ischemic cardiac muscle and vascular endothelium by adult stem cells. J Clin Invest 107:1395–1402
37. Orlic D, Kajstura J, Chimenti S et al (2001) Bone marrow cells regenerate infarcted myocardium. Nature 410:701–705
38. Murry CE, Soonpaa MH, Reinecke H et al (2004) Haematopoietic stem cells do not transdifferentiate into cardiac myocytes in myocardial infarcts. Nature 428:664–668
39. Balsam LB, Wagers AJ, Christensen JL et al (2004) Haematopoietic stem cells adopt mature haematopoietic fates in ischaemic myocardium. Nature 428:668–673
40. Rota M, Kajstura J, Hosoda T et al (2007) Bone marrow cells adopt the cardiomyogenic fate in vivo. Proc Natl Acad Sci U S A 104:17783–17788
41. Caplan AI (1991) Mesenchymal stem cells. J Orthop Res 9:641–650
42. Prockop DJ (1997) Marrow stromal cells as stem cells for nonhematopoietic tissues. Science 276:71–74
43. Phinney DG, Kopen G, Righter W et al (1999) Donor variation in the growth properties and osteogenic potential of human marrow stromal cells. J Cell Biochem 75:424–436
44. Pittenger MF, Mackay AM, Beck SC et al (1999) Multilineage potential of adult human mesenchymal stem cells. Science 284:143–147
45. Pittenger MF, Martin BJ (2004) Mesenchymal stem cells and their potential as cardiac therapeutics. Circ Res 95:9–20
46. Haynesworth SE, Baber MA, Caplan AI (1992) Cell surface antigens on human marrow-derived mesenchymal cells are detected by monoclonal antibodies. Bone 13:69–80
47. Alhadlaq A, Mao JJ (2004) Mesenchymal stem cells: isolation and therapeutics. Stem Cells Dev 13:436–448
48. Minguell JJ, Erices A, Conget P (2001) Mesenchymal stem cells. Exp Biol Med 226:507–520

49. Fukuda K (2002) Molecular characterization of regenerated cardiomyocytes derived from adult mesenchymal stem cells. Congenit Anom 42:1–9
50. Makino S, Fukuda K, Miyoshi S et al (1999) Cardiomyocytes can be generated from marrow stromal cells in vitro. J Clin Invest 103:697–705
51. Fukuda K (2003) Use of adult marrow mesenchymal stem cells for regeneration of cardiomyocytes. Bone Marrow Transplant 32:S25–S27
52. Tomita S, Nakatani T, Fukuhara S et al (2002) Bone marrow stromal cells contract synchronously with cardiomyocytes in a coculture system. Jpn J Thorac Cardiovasc Surg 50:321–324
53. Hakuno D, Fukuda K, Makino S et al (2002) Bone marrow-derived regenerated cardiomyocytes (CMG Cells) express functional adrenergic and muscarinic receptors. Circulation 105:380–386
54. Bartholomew A, Sturgeon C, Siatskas M et al (2002) Mesenchymal stem cells suppress lymphocyte proliferation in vitro and prolong skin graft survival in vivo. Exp Hematol 30:42–48
55. Le Blanc K, Tammik L, Sundberg B et al (2003) Mesenchymal stem cells inhibit and stimulate mixed lymphocyte cultures and mitogenic responses independently of the major histocompatibility complex. Scand J Immunol 57:11–20
56. Tse WT, Pendleton JD, Beyer WM et al (2003) Suppression of allogeneic T-cell proliferation by human marrow stromal cells: implications in transplantation. Transplantation 75:389–397
57. Zimmet JM, Hare JM (2005) Emerging role for bone marrow derived mesenchymal stem cells in myocardial regenerative therapy. Basic Res Cardiol 100:471–481
58. Ryan JM, Barry FP, Murphy JM et al (2005) Mesenchymal stem cells avoid allogeneic rejection. J Inflamm 2:8
59. Le Blanc K, Tammik C, Rosendahl K et al (2003) HLA expression and immunologic properties of differentiated and undifferentiated mesenchymal stem cells. Exp Hematol 31:890–896
60. Di Nicola M, Carlo-Stella C, Magni M et al (2002) Human bone marrow stromal cells suppress T-lymphocyte proliferation induced by cellular or nonspecific mitogenic stimuli. Blood 99:3838–3843
61. Wang JS, Shum-Tim D, Chedrawy E et al (2001) The coronary delivery of marrow stromal cells for myocardial regeneration: pathophysiologic and therapeutic implications. J Thorac Cardiovasc Surg 122:699–705
62. Tomita S, Li RK, Weisel RD et al (1999) Autologous transplantation of bone marrow cells improves damaged heart function. Circulation 100:II247–II256
63. Barbash IM, Chouraqui P, Baron J et al (2003) Systemic delivery of bone marrow-derived mesenchymal stem cells to the infarcted myocardium: feasibility, cell migration, and body distribution. Circulation 108:863–868
64. Silva GV, Litovsky S, Assad JA et al (2005) Mesenchymal stem cells differentiate into an endothelial phenotype, enhance vascular density, and improve heart function in a canine chronic ischemia model. Circulation 111:150–156
65. Dai W, Hale SL, Martin BJ et al (2005) Allogeneic mesenchymal stem cell transplantation in postinfarcted rat myocardium: short- and long-term effects. Circulation 112:214–223
66. Tomita S, Mickle DA, Weisel RD et al (2002) Improved heart function with myogenesis and angiogenesis after autologous porcine bone marrow stromal cell transplantation. J Thorac Cardiovasc Surg 123:1132–1140
67. Zeng L, Hu Q, Wang X et al (2007) Bioenergetic and functional consequences of bone marrow-derived multipotent progenitor cell transplantation in hearts with postinfarction left ventricular remodeling. Circulation 115:1866–1875
68. Amado LC, Saliaris AP, Schuleri KH et al (2005) Cardiac repair with intramyocardial injection of allogeneic mesenchymal stem cells after MI. Proc Natl Acad Sci U S A 102:11474–11479
69. Asahara T, Murohara T, Sullivan A et al (1997) Isolation of putative progenitor endothelial cells for angiogenesis. Science 275:964–967
70. Masuda H, Asahara T (2003) Post-natal endothelial progenitor cells for neovascularization in tissue regeneration. Cardiovasc Res 58:390–398
71. Lin Y, Weisdorf DJ, Solovey A et al (2000) Origins of circulating endothelial cells and endothelial outgrowth from blood. J Clin Invest 105:71–77
72. Kocher AA, Schuster MD, Szabolcs MJ et al (2001) Neovascularization of ischemic myocardium by human bone-marrow-derived angioblasts prevents cardiomyocyte apoptosis, reduces remodeling and improves cardiac function. Nat Med 7:430–436
73. Kawamoto A, Tkebuchava T, Yamaguchi J et al (2003) Intramyocardial transplantation of autologous endothelial progenitor cells for therapeutic neovascularization of myocardial ischemia. Circulation 107:461–468
74. Lewis ID, Verfaillie CM (2000) Multi-lineage expansion potential of primitive hematopoietic progenitors: superiority of umbilical cord blood compared to mobilized peripheral blood. Exp Hematol 28:1087–1095
75. Murohara T, Ikeda H, Duan J et al (2000) Transplanted cord blood-derived endothelial precursor cells augment postnatal neovascularization. J Clin Invest 105:1527–1536
76. Mayani H, Lansdorp PM (1998) Biology of human umbilical cord blood-derived hematopoietic stem/progenitor cells. Stem Cells 16:153–165
77. Kogler G, Sensken S, Airey JA et al (2004) A new human somatic stem cell from placental cord blood with intrinsic pluripotent differentiation potential. J Exp Med 200:123–135
78. Kim BO, Tian H, Prasongsukarn K et al (2005) Cell transplantation improves ventricular function after a MI: a preclinical study of human unrestricted somatic stem cells in a porcine model. Circulation 112:I96–I104
79. Ma N, Stamm C, Kaminski A et al (2005) Human cord blood cells induce angiogenesis following MI in NOD/scid-mice. Cardiovasc Res 66:45–54
80. Hirata Y, Sata M, Motomura N et al (2005) Human umbilical cord blood cells improve cardiac function after MI. Biochem Biophys Res Commun 327:609–614
81. MacLellan WR, Schneider MD (2000) Genetic dissection of cardiac growth control pathways. Annu Rev Physiol 62:289–319
82. Rubart M, Field LJ (2006) Cardiac regeneration: repopulating the heart. Annu Rev Physiol 68:29–49
83. Soonpaa MH, Field LJ (1998) Survey of studies examining mammalian cardiomyocyte DNA synthesis. Circ Res 83:15–26
84. Beltrami AP, Urbanek K, Kajstura J et al (2001) Evidence that human cardiac myocytes divide after MI. N Engl J Med 344:1750–1757
85. Quaini F, Urbanek K, Beltrami AP et al (2002) Chimerism of the transplanted heart. N Engl J Med 346:5–15
86. Anversa P, Kajstura J (1998) Ventricular myocytes are not terminally differentiated in the adult mammalian heart. Circ Res 83:1–14
87. Nadal-Ginard B, Kajstura J, Leri A et al (2003) Myocyte death, growth, and regeneration in cardiac hypertrophy and failure. Circ Res 92:139–150
88. Anversa P, Sussman MA, Bolli R (2004) Molecular genetic advances in cardiovascular medicine: focus on the myocyte. Circulation 109:2832–2838
89. Sussman MA, Anversa P (2004) Myocardial aging and senescence: where have the stem cells gone? Annu Rev Physiol 66:29–48
90. Mouquet F, Pfister O, Jain M et al (2005) Restoration of cardiac progenitor cells after MI by self-proliferation and selective homing of bone marrow-derived stem cells. Circ Res 97:1090–1092

91. Kucia M, Dawn B, Hunt G et al (2004) Cells expressing early cardiac markers reside in the bone marrow and are mobilized into the peripheral blood after MI. Circ Res 95:1191–1199
92. Cerisoli F, Chimenti I, Gaetani R et al (2006) Kit-Positive Cardiac Stem Cells (CSCs) can be generated in damaged heart from bone marrow-derived cells. Circulation 114:II-164
93. Leri A, Kajstura J, Anversa P (2005) Cardiac stem cells and mechanisms of myocardial regeneration. Physiol Rev 85:1373–1416
94. Beltrami AP, Barlucchi L, Torella D et al (2003) Adult cardiac stem cells are multipotent and support myocardial regeneration. Cell 114:763–776
95. Wang X, Hu Q, Nakamura Y, Lee J, Zhang G, From AH, Zhang J. The Role of Sca-1+/CD31- Cardiac Progenitor Cell Population in Postinfarction LV Remodeling. Stem Cells. 2006;24(7): 1779–88
96. Bearzi C, Rota M, Hosoda T et al (2007) Human cardiac stem cells. Proc Natl Acad Sci U S A 104:14068–14073
97. van Berlo JH, Kanisicak O, Maillet M et al (2014) C-Kit+ cells minimally contribute cardiomyocytes to the heart. Nature 509:337–341
98. Oh H, Bradfute SB, Gallardo TD et al (2003) Cardiac progenitor cells from adult myocardium: homing, differentiation, and fusion after infarction. Proc Natl Acad Sci U S A 100:12313–12318
99. Matsuura K, Nagai T, Nishigaki N et al (2004) Adult cardiac Sca-1-positive cells differentiate into beating cardiomyocytes. J Biol Chem 279:11384–11391
100. Martin CM, Meeson AP, Robertson SM et al (2004) Persistent expression of the ATP-binding cassette transporter, Abcg2, identifies cardiac SP cells in the developing and adult heart. Dev Biol 265:262–275
101. Pfister O, Mouquet F, Jain M et al (2005) CD31- but Not CD31+ cardiac side population cells exhibit functional cardiomyogenic differentiation. Circ Res 97:52–61
102. Laugwitz KL, Moretti A, Lam J et al (2005) Postnatal isl1+ cardioblasts enter fully differentiated cardiomyocyte lineages. Nature 433:647–653
103. Messina E, De Angelis L, Frati G et al (2004) Isolation and expansion of adult cardiac stem cells from human and murine heart. Circ Res 95:911–921
104. Smith RR, Barile L, Cho HC et al (2007) Regenerative potential of cardiosphere-derived cells expanded from percutaneous endomyocardial biopsy specimens. Circulation 115:896–908
105. Dawn B, Stein AB, Urbanek K et al (2005) Cardiac stem cells delivered intravascularly traverse the vessel barrier, regenerate infarcted myocardium, and improve cardiac function. Proc Natl Acad Sci U S A 102:3766–3771
106. Wang X, Hu Q, Nakamura Y et al (2006) The role of the sca-1+/CD31- cardiac progenitor cell population in postinfarction left ventricular remodeling. Stem Cells 24:1779–1788
107. Urbanek K, Rota M, Cascapera S et al (2005) Cardiac stem cells possess growth factor-receptor systems that after activation regenerate the infarcted myocardium, improving ventricular function and long-term survival. Circ Res 97:663–673
108. Linke A, Muller P, Nurzynska D et al (2005) Stem cells in the dog heart are self-renewing, clonogenic, and multipotent and regenerate infarcted myocardium, improving cardiac function. Proc Natl Acad Sci U S A 102:8966–8971
109. Bearzi C, Muller P, Amano K et al (2006) Identification and characterization of cardiac stem cells in the pig heart. Circulation 114:II-125
110. Johnston P, Sasano T, Mills K et al (2006) Isolation, expansion and delivery of cardiac derived stem cells in a porcine model of MI. Circulation 114:II-125
111. Hosoda T, Bearzi C, Amano S et al (2006) Human cardiac progenitor cells regenerate cardiomyocytes and coronary vessels repairing the infarcted myocardium. Circulation 114:II-51
112. Torella D, Elliso GM, Karakikes I et al (2006) Biological properties and regenerative potential, in vitro and in vivo, of human cardiac stem cells isolated from each of the four chambers of the adult human heart. Circulation 114:II-87
113. Menasche P, Hagege AA, Vilquin JT et al (2003) Autologous skeletal myoblast transplantation for severe postinfarction left ventricular dysfunction. J Am Coll Cardiol 41:1078–1083
114. Herreros J, Prosper F, Perez A et al (2003) Autologous intramyocardial injection of cultured skeletal muscle-derived stem cells in patients with non-acute MI. Eur Heart J 24:2012–2020
115. Pagani FD, DerSimonian H, Zawadzka A et al (2003) Autologous skeletal myoblasts transplanted to ischemia-damaged myocardium in humans. Histological analysis of cell survival and differentiation. J Am Coll Cardiol 41:879–888
116. Siminiak T, Kalawski R, Fiszer D et al (2004) Autologous skeletal myoblast transplantation for the treatment of postinfarction myocardial injury: phase I clinical study with 12 months of follow-up. Am Heart J 148:531–537
117. Smits PC, van Geuns RJ, Poldermans D et al (2003) Catheter-based intramyocardial injection of autologous skeletal myoblasts as a primary treatment of ischemic heart failure: clinical experience with six-month follow-up. J Am Coll Cardiol 42:2063–2069
118. Siminiak T, Fiszer D, Jerzykowska O et al (2005) Percutaneous trans-coronary-venous transplantation of autologous skeletal myoblasts in the treatment of post-infarction myocardial contractility impairment: the POZNAN trial. Eur Heart J 26:1188–1195
119. Hagege AA, Carrion C, Menasche P et al (2003) Viability and differentiation of autologous skeletal myoblast grafts in ischaemic cardiomyopathy. Lancet 361:491–492
120. Assmus B, Schachinger V, Teupe C et al (2002) Transplantation of progenitor cells and regeneration enhancement in acute myocardial infarction (TOPCARE-AMI). Circulation 106:3009–3017
121. Schachinger V, Assmus B, Britten MB et al (2004) Transplantation of progenitor cells and regeneration enhancement in acute MI: final one-year results of the TOPCARE-AMI Trial. J Am Coll Cardiol 44:1690–1699
122. Wollert KC, Meyer GP, Lotz J et al (2004) Intracoronary autologous bone-marrow cell transfer after MI: the BOOST randomised controlled clinical trial. Lancet 364:141–148
123. Schachinger V, Erbs S, Elsasser A et al (2006) Intracoronary bone marrow-derived progenitor cells in acute MI. N Engl J Med 355:1210–1221
124. Lunde K, Solheim S, Aakhus S et al (2006) Intracoronary injection of mononuclear bone marrow cells in acute MI. N Engl J Med 355:1199–1209
125. Janssens S, Dubois C, Bogaert J et al (2006) Autologous bone marrow-derived stem-cell transfer in patients with ST-segment elevation MI: double-blind, randomised controlled trial. Lancet 367:113–121
126. Seeger F, Tonn T, Krzossok N et al (2006) Cell isolation procedures matter: a comparison of different isolation protocols of bone marrow mononuclear cells used for cell therapy in patients with acute MI. Circulation 114:II-51
127. Assmus B, Honold J, Schachinger V et al (2006) Transcoronary transplantation of progenitor cells after MI. N Engl J Med 355:1222–1232
128. Chen SL, Fang WW, Qian J et al (2004) Improvement of cardiac function after transplantation of autologous bone marrow mesenchymal stem cells in patients with acute MI. Chin Med J (Engl) 117:1443–1448
129. Chen SL, Fang WW, Ye F et al (2004) Effect on left ventricular function of intracoronary transplantation of autologous bone marrow mesenchymal stem cell in patients with acute MI. Am J Cardiol 94:92–95
130. Zambrano J, Traverse JH, Henry T et al (2007) Abstract 1014: The impact of intravenous allogeneic human mesenchymal stem cells

(ProvacelTM) on ejection fraction in patients with myocardial infarction. II_202
131. Erbs S, Linke A, Adams V et al (2005) Transplantation of blood-derived progenitor cells after recanalization of chronic coronary artery occlusion: first randomized and placebo-controlled study. Circ Res 97:756–762
132. Malliaras K, Makkar RR, Smith RR et al (2014) Intracoronary cardiosphere-derived cells after myocardial infarction: evidence of therapeutic regeneration in the final 1-year results of the CADUCEUS trial (CArdiosphere-Derived aUtologous stem Cells to reverse ventricular dysfunction). J Am Coll Cardiol 63:110–122
133. Chugh AR, Beache GM, Loughran JH et al (2012) Administration of cardiac stem cells in patients with ischemic cardiomyopathy: the SCIPIO trial: surgical aspects and interim analysis of myocardial function and viability by magnetic resonance. Circulation 126:S54–S64
134. Miyahara Y, Nagaya N, Kataoka M et al (2006) Monolayered mesenchymal stem cells repair scarred myocardium after MI. Nat Med 12:459–465
135. Ye L, Zhang P, Duval S et al (2013) Thymosin β4 increases the potency of transplanted mesenchymal stem cells for myocardial repair. Circulation 128:S32–S41
136. Wendel JS, Ye L, Zhang P et al (2014) Functional consequences of a tissue-engineered myocardial patch for cardiac repair in a rat infarct model. Tissue Eng Part A 20:1325–1335
137. Ye L, Zimmermann WH, Garry DJ et al (2013) Patching the heart: cardiac repair from within and outside. Circ Res 113:922–932
138. Pfeffer MA, Braunwald E (1990) Ventricular remodeling after MI. Experimental observations and clinical implications. Circulation 81:1161–1172
139. Jameel NM, Hu Q, Zhang J (2014) Myocytes oxygenation and high energy phosphate levels during hypoxia. PLoS One 9, e101317
140. Ingwall JS, Weiss RG (2004) Is the failing heart energy starved? On using chemical energy to support cardiac function. Circ Res 95:135–145
141. Katz AM (1998) Is the failing heart energy depleted? Cardiol Clin 16:633–644
142. Xiong Q, Ye L, Zhang P et al (2013) Functional consequences of human induced pluripotent stem cell therapy: myocardial ATP turnover rate in the in vivo swine heart with postinfarction remodeling. Circulation 127:997–1008
143. Reffelmann T, Dow JS, Dai W et al (2003) Transplantation of neonatal cardiomyocytes after permanent coronary artery occlusion increases regional blood flow of infarcted myocardium. J Mol Cell Cardiol 35:607–613
144. Ziegelhoeffer T, Fernandez B, Kostin S et al (2004) Bone marrow-derived cells do not incorporate into the adult growing vasculature. Circ Res 94:230–238
145. Gnecchi M, He H, Liang OD et al (2005) Paracrine action accounts for marked protection of ischemic heart by Akt-modified mesenchymal stem cells. Nat Med 11:367–368
146. Gnecchi M, He H, Noiseux N et al (2006) Evidence supporting paracrine hypothesis for Akt-modified mesenchymal stem cell-mediated cardiac protection and functional improvement. FASEB J 20:661–669
147. Kinnaird T, Stabile E, Burnett MS et al (2004) Marrow-derived stromal cells express genes encoding a broad spectrum of arteriogenic cytokines and promote in vitro and in vivo arteriogenesis through paracrine mechanisms. Circ Res 94:678–685
148. Kinnaird T, Stabile E, Burnett MS et al (2004) Local delivery of marrow-derived stromal cells augments collateral perfusion through paracrine mechanisms. Circulation 109:1543–1549
149. Xu X, Xu Z, Xu Y et al (2005) Effects of mesenchymal stem cell transplantation on extracellular matrix after MI in rats. Coron Artery Dis 16:245–255
150. Xu X, Xu Z, Xu Y et al (2005) Selective down-regulation of extracellular matrix gene expression by bone marrow derived stem cell transplantation into infarcted myocardium. Circ J 69:1275–1283
151. Kang HJ, Lee HY, Na SH et al (2006) Differential effect of intracoronary infusion of mobilized peripheral blood stem cells by granulocyte colony-stimulating factor on left ventricular function and remodeling in patients with acute MI versus old MI: the MAGIC Cell-3-DES randomized, controlled trial. Circulation 114:I145–I151
152. Ceradini DJ, Kulkarni AR, Callaghan MJ et al (2004) Progenitor cell trafficking is regulated by hypoxic gradients through HIF-1 induction of SDF-1. Nat Med 10:858–864
153. Askari AT, Unzek S, Popovic ZB et al (2003) Effect of stromal-cell-derived factor 1 on stem-cell homing and tissue regeneration in ischaemic cardiomyopathy. Lancet 362:697–703
154. Limana F, Germani A, Zacheo A et al (2005) Exogenous high-mobility group box 1 protein induces myocardial regeneration after infarction via enhanced cardiac C-kit+ cell proliferation and differentiation. Circ Res 97:e73–e83
155. Lu L, Zhang JQ, Ramires FJ et al (2004) Molecular and cellular events at the site of MI: from the perspective of rebuilding myocardial tissue. Biochem Biophys Res Commun 320:907–913
156. Zhang M, Methot D, Poppa V et al (2001) Cardiomyocyte grafting for cardiac repair: graft cell death and anti-death strategies. J Mol Cell Cardiol 33:907–921
157. Mangi AA, Noiseux N, Kong D et al (2003) Mesenchymal stem cells modified with Akt prevent remodeling and restore performance of infarcted hearts. Nat Med 9:1195–1201
158. Lim SY, Kim YS, Ahn Y et al (2006) The effects of mesenchymal stem cells transduced with Akt in a porcine MI model. Cardiovasc Res 70:530–542
159. Cheng JQ, Lindsley CW, Cheng GZ et al (2005) The Akt/PKB pathway: molecular target for cancer drug discovery. Oncogene 24:7482–7492
160. Yau TM, Kim C, Li G et al (2005) Maximizing ventricular function with multimodal cell-based gene therapy. Circulation 112:I123–I128
161. Askari A, Unzek S, Goldman CK et al (2004) Cellular, but not direct, adenoviral delivery of vascular endothelial growth factor results in improved left ventricular function and neovascularization in dilated ischemic cardiomyopathy. J Am Coll Cardiol 43:1908–1914
162. Schuh A, Breuer S, Al Dashti R et al (2005) Administration of vascular endothelial growth factor adjunctive to fetal cardiomyocyte transplantation and improvement of cardiac function in the rat model. J Cardiovasc Pharmacol Ther 10:55–66
163. Tang YL, Tang Y, Zhang YC et al (2005) Improved graft mesenchymal stem cell survival in ischemic heart with a hypoxia-regulated heme oxygenase-1 vector. J Am Coll Cardiol 46:1339–1350
164. Suzuki K, Murtuza B, Beauchamp JR et al (2004) Dynamics and mediators of acute graft attrition after myoblast transplantation to the heart. FASEB J 18:1153–1155
165. Jo JI, Nagaya N, Miyahara Y et al (2007) Transplantation of genetically engineered mesenchymal stem cells improves cardiac function in rats with MI: benefit of a novel nonviral vector, Cationized Dextran. Tissue Eng 13:313–322
166. Davis ME, Hsieh PC, Grodzinsky AJ et al (2005) Custom design of the cardiac microenvironment with biomaterials. Circ Res 97:8–15
167. Davis ME, Hsieh PC, Takahashi T et al (2006) Local myocardial insulin-like growth factor 1 (IGF-1) delivery with biotinylated peptide nanofibers improves cell therapy for MI. Proc Natl Acad Sci U S A 103:8155–8160

The Use of Isolated Heart Models and Anatomical Specimens as Means to Enhance the Design and Testing of Cardiac Devices

41

Michael G. Bateman, Michael D. Eggen, Julianne H. Spencer, Tinen L. Iles, and Paul A. Iaizzo

Abstract

In recent years, the use of perfusion-fixed cadaveric specimens and isolated heart models has helped to develop an improved understanding of the device-tissue interface and has also contributed to the rapid evolution of surgically and percutaneously delivered cardiac therapies. This chapter describes a novel series of techniques utilized within the Visible Heart® laboratory by engineers, scientists, and anatomists to visualize and analyze the heart and assess potential repair or replacement therapies. The study of reanimated large mammalian hearts (including human hearts) and specially prepared anatomical specimens, using various clinical and nonclinical imaging modalities, has provided feedback for design engineers and clinicians that seek to develop and/or employ cardiac therapies for patients with acquired or congenital heart disease.

Keywords

Isolated heart model • Cardiac device design and development • Human cardiac anatomy • Reanimated heart

41.1 Introduction

A detailed and comprehensive understanding of human cardiac anatomy remains a crucial component of cardiovascular medical practice, research, and cardiac device design and development [1, 2]. The successful deployment and performance of a particular cardiac device is continually impacted by the ability of the device to conform and adapt to the changing anatomical landscape of the heart, as well as to anatomical variations that may exist in a given patient. In other words, successful device design and development requires a well-developed understanding of the relevant cardiovascular anatomies (in relation to both vascular approaches and within the heart itself) at every stage of the process [3–5].

The study of fixed and reanimated human hearts, using the various methodologies described here, has provided for novel insights as to the details of human cardiac anatomy. For almost two decades, the Visible Heart® methodologies have provided a unique perspective on functional cardiac anatomy. By reanimating human hearts not deemed viable for transplant, we have been able to visualize the beating heart using a variety of imaging modalities, including: (1) endoscopes placed directly within the various heart chambers and/or within the large diameter vessels, (2) echocardiography, (3) fluoroscopy, (4) magnetic resonance imaging (MRI), (5) infrared thermography, and/or (6) high-speed cameras. This database of images and videos exemplifies the large degree of variability that exists in human cardiac anatomy (from both a static and functional perspective) [6]. Additionally, such imaging techniques allow for visualization of the anatomical changes that occur as a result of various

M.G. Bateman, PhD (✉) • M.D. Eggen, PhD • J.H. Spencer, PhD
Medtronic, Inc., 8200 Coral Sea Street NE, Mounds View, MN 55112, USA
e-mail: michael.g.bateman@medtronic.com

T.L. Iles, BS • P.A. Iaizzo, PhD
Department of Surgery, University of Minnesota, Minneapolis, MN, USA

P.A. Iaizzo (ed.), *Handbook of Cardiac Anatomy, Physiology, and Devices*, DOI 10.1007/978-3-319-19464-6_41

pathologies and/or those that may occur following the deployment of devices within the heart.

Recent advances in intracardiac interventions have increased the need for a greater understanding of the anatomical complexities of the heart prior to the respective procedure. Further, as clinicians become more comfortable with the delivery of novel devices within beating hearts, the already widespread utilization of percutaneous technologies such as coronary stenting and transcatheter valve replacement will continue to intensify. This is highlighted today by the highly competitive field of transcatheter aortic valve implants, where competing designs attempt to provide the most effective treatment for the patient in a package that enables physicians to comfortably and reliably administer the therapy. Consequently, it has become more critical than ever for device developers to have a thorough understanding of: (1) the variations of cardiac anatomy that will present in the patient populations they treat and (2) the results they obtain from in vitro and in vivo testing of potential therapies.

This chapter will discuss the use of anatomical specimens and isolated heart preparations as important methodologies to provide the required educational foundation needed for the fields of cardiac device design, development, and deployment.

41.2 Anatomical Specimens and Static Imaging

Throughout history, anatomists such as Galen, Vesalius, da Vinci, and more recently Hunter, Gray, and Netter have recreated their knowledge gained from the dissection of animal and human cadavers in elegant treatises. However, with the advent of high-resolution noninvasive imaging in the past century, our understanding of the functional internal anatomy of the body has progressed even more rapidly. This accelerated growth of knowledge has led to the proposed utilization of attitudinally correct nomenclature, in an attempt to ensure that anatomists, surgeons, radiologists, cardiologists, echocardiographers, and biomedical engineers are able to communicate using common anatomical terms (see Chap. 2) [7].

Combined with these advances in our understanding of cardiac anatomy, there has also been progress in the preparation of anatomical specimens for research. The ancient Egyptians, as part of the ritual preparation of their deceased kings for burial, preserved bodies through the technique of embalming. However, until the discovery of glutaraldehyde and formaldehyde in the mid-nineteenth century, human cadavers used for medical dissections were not typically preserved in embalming solutions with anatomists relying on the cooler temperatures of winter to extend their dissection times. The introduction of powerful chemical preservation techniques extended the period of time anatomists could study a particular specimen and also increased the integration of anatomical classes in medical teaching. However, the fixation of the heart within the body as prepared for an anatomical study preserves the myocardium in a state of rigor, usually with the various heart chambers collapsed and potentially full of clotted materials (blood). In 1978, researchers at the Mayo Clinic (Rochester, MN, USA) adapted a formalin pressure perfusion system used in the study of pulmonary disorders to prepare the heart for anatomical investigations [8, 9]. However, the technique was time consuming and did not become more commonly used until Thomas and Davies reported the use of a simple apparatus to allow for the perfusion fixation of fresh cardiac specimens [10]. This technique has since been used extensively for the preparation of cardiac specimens by cardiac morphologists such as Robert Anderson [11] and has been adopted by the Visible Heart® laboratory as the preferred method of preparation for the cardiac specimens within the Visible Heart® library [5].

41.3 The Visible Heart® Library

Our laboratory has the privilege to obtain fresh human heart specimens for educational and research purposes from: (1) organ donors whose hearts are not deemed viable for transplantation and are donated for research (via LifeSource, the Upper Midwest Organ Procurement Organization, St. Paul, MN, USA) and (2) bodies donated to the University of Minnesota's Anatomy Bequest Program. After excision, these fresh, unfixed specimens are subsequently cleaned and perfusion fixed in 10 % buffered formalin, by attaching the cannulated great vessels of each heart to a pressure head of approximately 50 mmHg. This technique, modified from Thomas and Davies [10] and described by Anderson et al. [5], fixes the hearts in an approximation of the end-diastolic state, providing a unique insight into the anatomical dimensions of a given specimen. Figure 41.1 demonstrates various images that can be acquired from these specimens and shows some of the cardiac pathologies (those depicted here are diseases of the cardiac valves) that can be subsequently visualized [12].

To date, our library of more than 350 hearts of various disease states continues to provide researchers with the ability to investigate how the cardiac anatomy may change/remodel under specific pathologies. In addition to anatomical investigations, these specimens can be employed to provide information as to how a specific device will fit the cardiac anatomies of the intended patient population, or how a delivery system will navigate through the chambers and

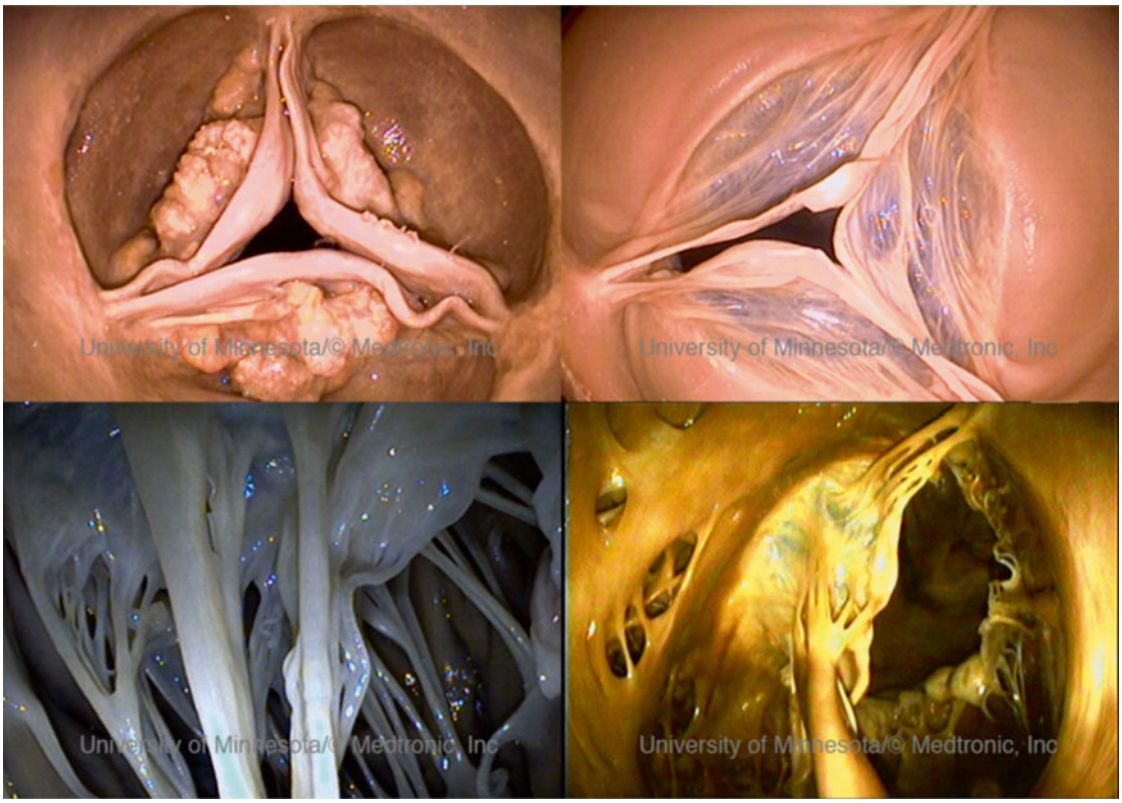

Fig. 41.1 Images from perfusion-fixed hearts from the Visible Heart® laboratory's library: (1) calcified aortic valve (*upper left panel*), (2) pulmonary valve (*upper right panel*), (3) subvalvular apparatus of the mitral valve (*lower left panel*), and (4) tricuspid valve from the right ventricle (*lower right panel*). Modified from The Atlas of Human Cardiac Anatomy [12]

vasculature of the heart. Such resources have allowed for the placement of multiple prototype devices and rapid comparison of how specific devices interact with the surrounding cardiac anatomies in a variety of human specimens [13, 14]. This information is critical in the development process, as it allows for engineers to highlight challenges regarding implantation of the device or the navigation of the delivery system that may have been overlooked in bench top testing.

Fresh cadaver hearts received by the Visible Heart® laboratory are documented at each stage of the acquisition process to record global anatomical changes during the fixation process, such as tissue weight and overall dimensions. Images of the fresh preparation, the resulting fixed specimen, and the nondestructive imaging of a sample specimen from the library (adapted from the Atlas of Human Cardiac Anatomy [12]) can be seen in Fig. 41.2.

Recent advances in high-resolution noninvasive cardiac imaging have fostered extensive work in the in vivo analyses of anatomical variations from patient to patient using a variety of imaging modalities:

1. Cardiac ultrasound (e.g., transthoracic, transesophageal, intracardiac, 2D, 3D, and/or 4D) [15]
2. Computed tomography (CT) [16]
3. Multi-slice computed tomography [17]
4. Magnetic resonance imaging (MRI, e.g., 1.5 T, 3 T, or greater) [18]

Nondestructive imaging of specimens from the Visible Heart® library via ultrasound, CT, and MRI has been used to collate a digital database of these hearts for educational and research purposes. The perfusion-fixed specimens are prepared by suspending them in a gel medium, allowing for a full complement of multimodal imaging to be performed on the hearts without changing the orientation [19]. Obtaining high-resolution images has allowed for detailed analyses of cardiac anatomies for a variety of normal and pathologic specimens; this spectrum of imaging is considered not possible with available clinical imaging protocols. For example, the analysis of fiber orientations of specimens obtained from patients in end-stage heart failure, using diffusion tensor MRI [20], provided critical insight into the remodeling of the ventricular tissue in patients with chronic heart failure. In addition, it has been possible to compare the ability of different imaging modalities to assess the anatomical characteristics of specific cardiac pathologies such as aortic stenosis, thus building on the work of other researchers [21, 22]. For additional imaging of such specimens, see Chaps. 6, 7, and 8.

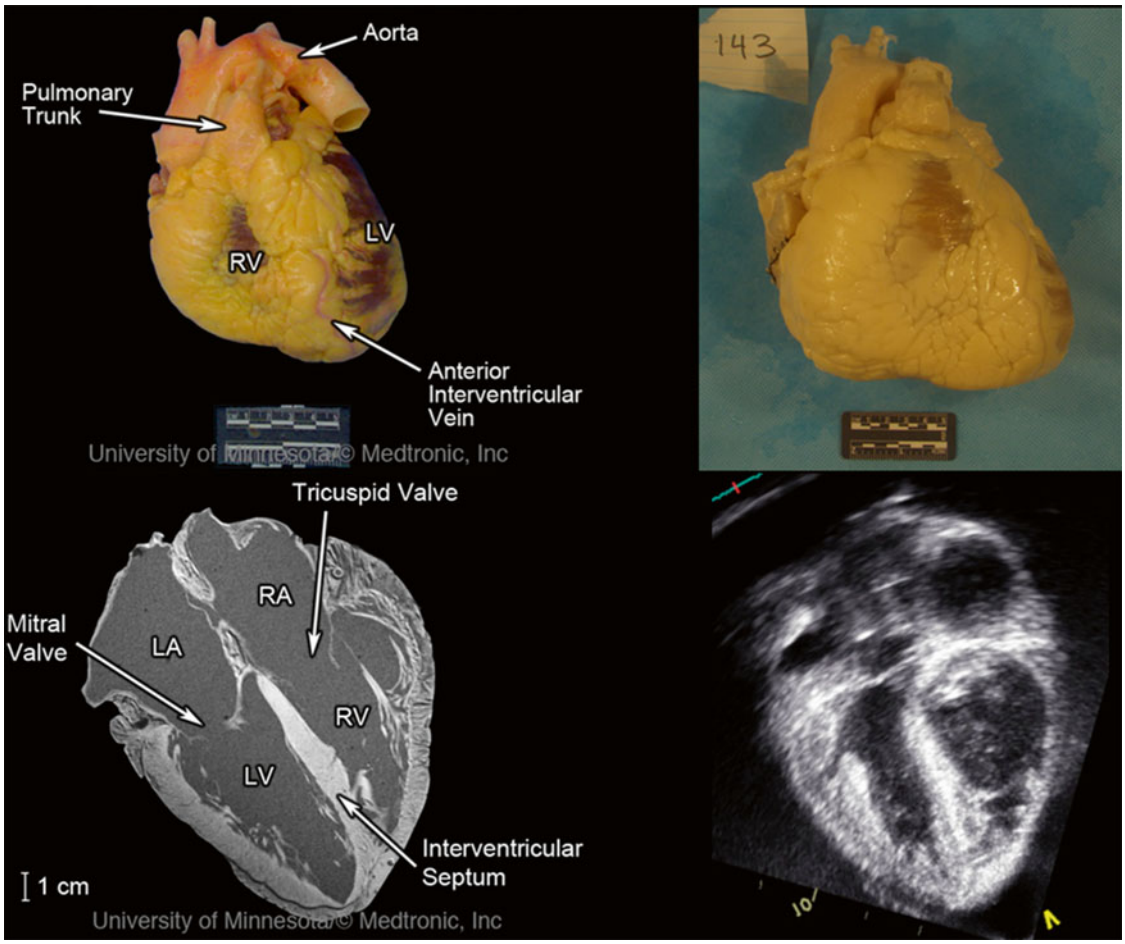

Fig. 41.2 Images of a heart received by the Visible Heart® library and imaged fresh (*upper left panel*), after perfusion fixation (*upper right panel*), and scanned in a 3 T Siemens MRI scanner (*bottom left panel*) and GE Vivid I ultrasound (*lower right panel*) in the four-chamber long-axis view. Modified from The Atlas of Human Cardiac Anatomy [12]

41.4 In Vitro Isolated Heart Models

A comprehensive understanding of the cardiac anatomy provides device designers with fundamental information regarding the anatomical dimensions and variations of the environment into which the device or therapy will be delivered. However, these static human heart specimens do not address the complications surrounding the delivery and function of a device or therapy in a beating heart. Before embarking upon complex and expensive chronic animal testing protocols which are required to prove the efficacy of novel cardiac devices, there is exceptional value in testing in reanimated beating heart models. Our laboratory at the University of Minnesota has reanimated over 1500 large mammalian hearts (canine, ovine, swine, mini-pigs, and human) for such studies in the last 15 years. There have been several other academic institutions and private companies that have developed in vitro large mammalian heart models, with many groups effectively developing systems based upon the mechanical reanimation of cadaveric large mammalian hearts. For example, Richards et al. were able to consistently and reliably quantify mitral regurgitation across a range of severity in explanted porcine hearts and investigate the efficacy of various repair techniques [23]. Further, two other groups have succeeded in studying the electrophysiology of explanted human hearts by sustaining the heart with a pressurized coronary flow of oxygen saturated salt solution via Langendorff perfusion [24, 25]. However, it should be noted that the true *reanimation* of large mammalian hearts (whereby the heart functions independently of any mechanical or electrical assistance) has only been achieved by a small number of research groups. Araki et al. (Nagoya University, Japan) reported that they were able to complete optical and hemodynamic analyses of cardiac valves in reanimated swine hearts [26]. Most recently, Weger et al. at the Leiden University Medical Center, Netherlands, have monitored transcatheter valve implantations in reanimated swine hearts

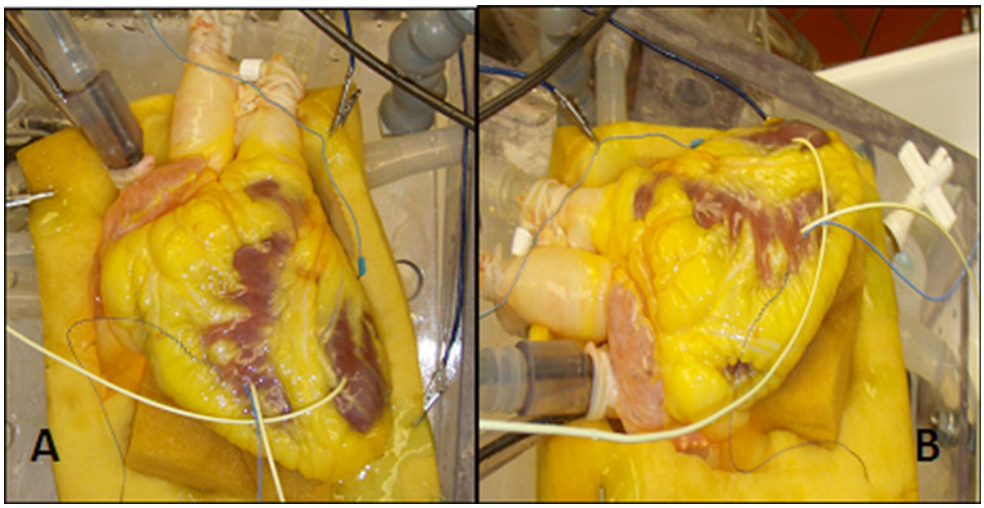

Fig. 41.3 Images of a human heart connected to the Visible Heart® apparatus from an approximation of the anterior-posterior aspect (A) and from the left anterior oblique aspect (B)

using their described PhysioHeart system [27]. However, it should be noted that in these preparations, the researchers were limited by the amount of time the heart remained viable, a factor considered key to the accessibility of the heart for device testing.

The Visible Heart® laboratory partnered with Medtronic, Inc. in 1997 to develop the Visible Heart® methodologies, which consist of a large mammalian isolated heart model that can be controlled to function in either Langendorff [25], right-side working, or four-chamber working modes [28]. Over this time and continuing today, we have been developing/optimizing this apparatus for reanimation whereby isolated large mammalian hearts are perfused and then actively pump a clear crystalloid perfusate in the place of blood. Images of a human heart connected to the Visible Heart® apparatus can be seen in Fig. 41.3. This approach has allowed our group to visualize what occurs inside the heart during device deployment procedures and subsequently to determine how such devices interact with the specific anatomies of the heart throughout all the phases of the cardiac cycle.

Briefly, our approach includes the initial step of removing hearts from humans or animals using standard cardioplegia procedures [28, 29]. Once isolated, cannulae are inserted into the great vessels allowing the placement of endoscopes or devices into all four working chambers. Following reanimation, cardiac and systemic pressures and outputs can be monitored and preloads and afterloads adjusted accordingly to simulate systemic vascular pathologies such as hypertension. Additionally, the isolated heart apparatus allows researchers to quickly switch the perfusion system to operate in Langendorff, right-side working, or four-chamber working modes. During the Langendorff mode, the left-side afterload is held constant with a coronary perfusion pressure of approximately 60 mmHg [28]; thus, the flow through the coronaries is determined by dilation or constriction of the coronary arteries. Right-side working mode combines Langendorff retrograde aortic perfusion with antegrade, or physiologic, flow through the right atrium and right ventricle (adjustable between ~3–5 L/min). During four-chamber working mode, the flow through a heart is normally determined by its intrinsic heart rate, preloads, afterloads, and the relative contractility of the various heart chambers. By controlling the orientation of the heart in our apparatus and determining the preload and afterload pressures exerted on the specimen, we can recreate specific cardiac states. Interestingly, the intrinsic heart rate and hemodynamic performance can be modified by altering the temperature of the buffer or by adding pharmacological agents (e.g., catecholamines or anesthetics), which are discussed later in this chapter. Although no model can perfectly mimic in vivo conditions, to date our apparatus has allowed researchers to simulate a broad range of particular physiological environments that are observed in various clinical settings.

41.5 How Can an Isolated Heart Prep Augment and Complement Bench Top Testing?

The combination of a "live" functional anatomy within a controlled "bench top" experimental setting provides a unique stepping stone between in vitro device testing and in vivo implantation required for implantable medical devices. Figure 41.4 shows how the typical stages of device testing and development compare in terms of the relevance of the testing environment to the intended functional environment, the quantity of data one can reasonably expect to collect, and the cost of performing such investigations. It can easily be observed that as the relevance of a particular testing methodology increases, the relative costs will dramatically

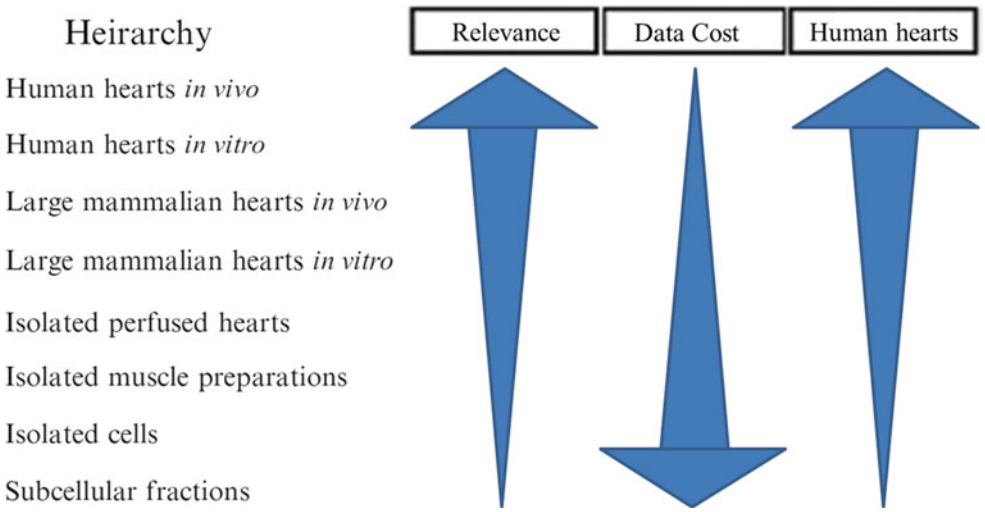

Fig. 41.4 Proposed hierarchy between the relevance of various experimental approaches, the amount of data one can obtain, and the relative costs. For example, if you wish to perform medical device design research in the field of prosthetic valves, ideally you would like to perform human trials in vivo, but this not only raises medical ethical issues but is highly costly and may provide useful data for one specific valve design and procedure. Whereas if you move the research approach downward (i.e., employ an isolated large mammalian heart model in vitro), you can obtain more data at a lower cost, but then you must justify the appropriateness of the chosen model. Yet, in one given study, it may be possible to perform multiple procedures for comparison or at least multiple implants in multiple hearts with fairly consistent anatomies

increase; thus, the likely number of possible iterations decreases. Consequently, any possible augmentations to device testing prior to chronic animal implants (e.g., via isolated beating heart preps) can, in turn, greatly reduce the overall product development costs and speed clinical use of novel valve repair, implant, and their associated delivery systems.

Due to the large number of cycles seen in the lifetime of a cardiac device, accelerated wear and fatigue testing are required gold standards for the assessment of durability. In accelerated wear testing for bioprosthetic valves, the hydrodynamic conditions are tightly controlled and easily varied allowing the durability of the valve leaflets to be assessed under a variety of predetermined conditions. Similarly, the boundary conditions imposed on the valve frame or commissure posts during fatigue testing can assess frame durability. Isolated heart preparations, including the Visible Heart® methodologies, will never replace these forms of testing, but unique information regarding the device-tissue interactions in the later can be observed. It should be noted that since the hydrodynamics of isolated heart preparations are typically less aggressive environments than what is experienced during accelerated wear testing, the boundary conditions observed for a device in such studies are not directly transferable to accelerated wear test methodologies. Yet on the other hand, they can serve as means to obtain additional information to ascertain the validity of any boundary conditions within the accelerated testing protocol, ensuring that all forms of boundary conditions have been taken into account, i.e., the change in curvature throughout the cardiac cycle of a left-sided pacing lead within the coronary vasculature. Most importantly, such experimentation has provided us with a so-called physiological link between bench top testing of devices and animal testing. Acute phenomena observed during accelerated wear testing and the insights gained with both invasive and noninvasive imaging techniques in animal studies may be directly observed during a device implant study in vitro. For example, a procedural issue observed under fluoroscopy during an in vivo animal implant could be recreated by employing the Visible Heart® approach (under direct visualization) with simultaneous fluoroscopy, thus gaining a better understanding of potential adverse issues. We consider that having the Visible Heart® apparatus as a tool for device design has allowed us to obtain a more rapid understanding of phenomena observed in both bench top and preclinical settings; as such, it is an invaluable tool for a device designer, especially at the early stages of development. See other chapters for addition descriptions and images of cardiac devices that have been implanted in reanimated human hearts [30].

41.6 The Importance of Species Selection in In Vitro Cardiac Device Research

The ultimate utility of studies performed with Visible Heart® methodologies, such as transcatheter valve development, is in part determined by the heart chosen for reanimation.

We suggest that the criteria for species selection for acute in vitro studies are slightly different from those for chronic valve assessments, due to the elimination of all systemic factors that may contribute to device performance. In other words, the species of the donor can be chosen specifically for its relative cardiac anatomy rather than for factors such as thrombogenesis, immune response, and/or growth rates.

For years, the canine heart has been used for such experimentation and has provided useful information. Yet it should be recognized that canine hearts have an unusually large amount of collateral coronary circulation (similar to humans in end-stage chronic heart failure), and this in turn results in the inconsistent creation of ischemic (infarct) regions. Sheep have been historically employed for chronic valve implantation studies, as valve function and valve orifice sizes observed in sheep are very similar to those of a human heart. Additionally, the relatively large atria of the sheep's heart allow for straightforward surgical approaches to the atrioventricular valves. However, it has recently been proposed that swine are an excellent model for acute cardiac device testing, as porcine hearts have very similar anatomy to that of humans with respect to the cardiac valves, conduction system, coronary arteries, and great vessels. Importantly the relationship between the cardiac conduction system and surrounding anatomical features is comparable between swine and human anatomies. Nevertheless, it is important to note that there are some specific variations in animal anatomy that should be known; such interindividual and interspecies variations have been extensively researched [28, 29, 31] and are described in greater detail in Chaps. 6 and 27.

Due to their specific anatomical similarity with human hearts and the relative ease of procurement (excision and reanimation), the mainstay of cardiac research done in the Visible Heart® laboratory is completed using swine hearts. Nevertheless, as previously mentioned, our laboratory has also had the privilege to obtain fresh human heart specimens for reanimation, for both educational and research purposes. Such hearts, if received in a timely manner and with complete anatomies including the great vessels, have been reanimated using the same methodologies as previously described for swine hearts. By reanimating these hearts using a clear perfusate, visualization of the internal cardiac anatomy has provided novel insights into the relative variations of human cardiac anatomy (in healthy individuals) and has highlighted the alterations that occur with various pathologies. Finally, this approach provides the unique opportunity to deliver existing or novel devices within functional human anatomies without the concerns and considerations required in clinical trials; thus, it has allowed researchers to garner invaluable knowledge about their device designs that otherwise could not be generated using animal models.

41.7 Understanding and Controlling Heart Function In Vitro

The performance of the reanimated heart can be influenced by several additional mechanisms. For example, subsequent cardiac function will be compromised by the amount of cell injury that occurs, governed in part by the amount of time between heart explant and reanimation. It is considered that if this period exceeds 6 h, performance will be compromised, even if the heart is stored under ideal conditions. To reduce such time-associated myocardial injury due to global ischemia, we have investigated the use of cardioprotective agents delivered before explanting the heart [32]. Most recently, we have been investigating the effect of omega-3 polyunsaturated fatty acids administered before explant on the acute function upon reanimation; for additional discussion of these topics, see Chap. 16.

Because of the isolation process, the reanimated heart has no direct parasympathetic or sympathetic innervation and thus is not affected by any signals from the autonomic nervous system. However, pharmaceuticals/hormones such as dobutamine and epinephrine can be administered to the circulating perfusate. These catecholamines work by stimulating the β1 receptor on the myocytes, acting as chronotropes and inotropes, increasing heart rate and contractility and, thus, overall cardiac output. Furthermore, the ionic balance of the circulating buffer can have very dramatic effects; e.g., increasing the calcium Ca^{2+} concentration in the buffer will act as a potent inotrope by increasing the Ca^{2+} inside the cell during the action potential. We will often utilize such inotropic agents shortly after deploying a prosthetic valve within an isolated heart to increase cardiac output and ejection fraction and therefore optimize function of the device.

Understanding the electrophysiology of the reanimated specimen is important during the assessment of cardiac devices and therapies designed to monitor and/or treat cardiac rhythm disease. It should be noted that by utilizing our Visible Heart® methodologies, the reanimated heart tissue is alive on the apparatus, and the heart rate is driven by the sinoatrial node. However, occasionally the heart will display an anomalous intrinsic rhythm, such as 2 to 1 block, and will consequently require pacing to ensure a consistent heart rate. This is of less concern when testing the ability of cardiac rhythm devices such as pacemakers or defibrillators to pace, as these will override any native signal to control the heart rate. However, such heart rate irregularities must be monitored and understood when testing the sensing capabilities of a particular device. For such studies, the electrophysiology can be monitored either on a gross scale using a 3-lead electrocardiogram or in detail using intracardiac electrical mapping techniques such as noncontact mapping systems. These systems are described at length in Chap. 32,

and the clinical setup can be adapted to record an accurate endocardial activation map of the heart in reanimated hearts on the Visible Heart® apparatus. Such detailed assessment of the cardiac electrophysiology is of particular interest when researching cardiac ablation therapies, as electrical mapping can provide information about the size and efficacy of ablation sites. Additionally, the use of the noncontact mapping system in the Visible Heart® apparatus has augmented the assessment of acute post-procedural conduction complications during transcatheter aortic valve implantations. See also Chaps. 29 and 36 for additional discussion of these devices.

41.8 Comparative Imaging in the Visible Heart® Apparatus

The ability to reanimate, control, and optically visualize human hearts has allowed for the collection of unique videoscopic footage of the functional human heart [28, 29]. By utilizing endoscopic video systems in conjunction with clinically relevant imaging modalities, such as fluoroscopy (continuous X-ray) and cardiac ultrasound (echocardiography), we have been able to create novel comparative anatomy footage. This has provided a direct visualization of what the physician would see in the clinical setting and has also offered valuable insights into device and delivery system performance. Examples of the imaging capabilities of the Visible Heart® methodology within a human specimen can be seen in Fig. 41.5. In addition to video images of the functional anatomies, extensive footage of device implantations has been obtained utilizing Visible Heart® methodologies, including transcatheter-delivered valve prostheses to the pulmonary and aortic positions as seen in Figs. 41.6 and 41.7 [33, 34]. Such visualization of the delivery of a transcatheter pulmonic valve has provided new information to assist designers in the adaptation of the valve leaflets in the pulmonary position to accommodate the low pressure gradients that may be encountered in this anatomic location [33]. Furthermore, the implantation of transcatheter aortic valve replacements into the native aortic root of human hearts has highlighted the interaction of the frame with the native leaflets of the mitral valve and the interventricular septum, thus illustrating the importance of precise frame sizing and positioning in order to avoid interaction with the anterior leaflet of the mitral valve and excessive pressure on the cardiac conduction system [34]. Such simultaneous imaging in the Visible Heart® can be used

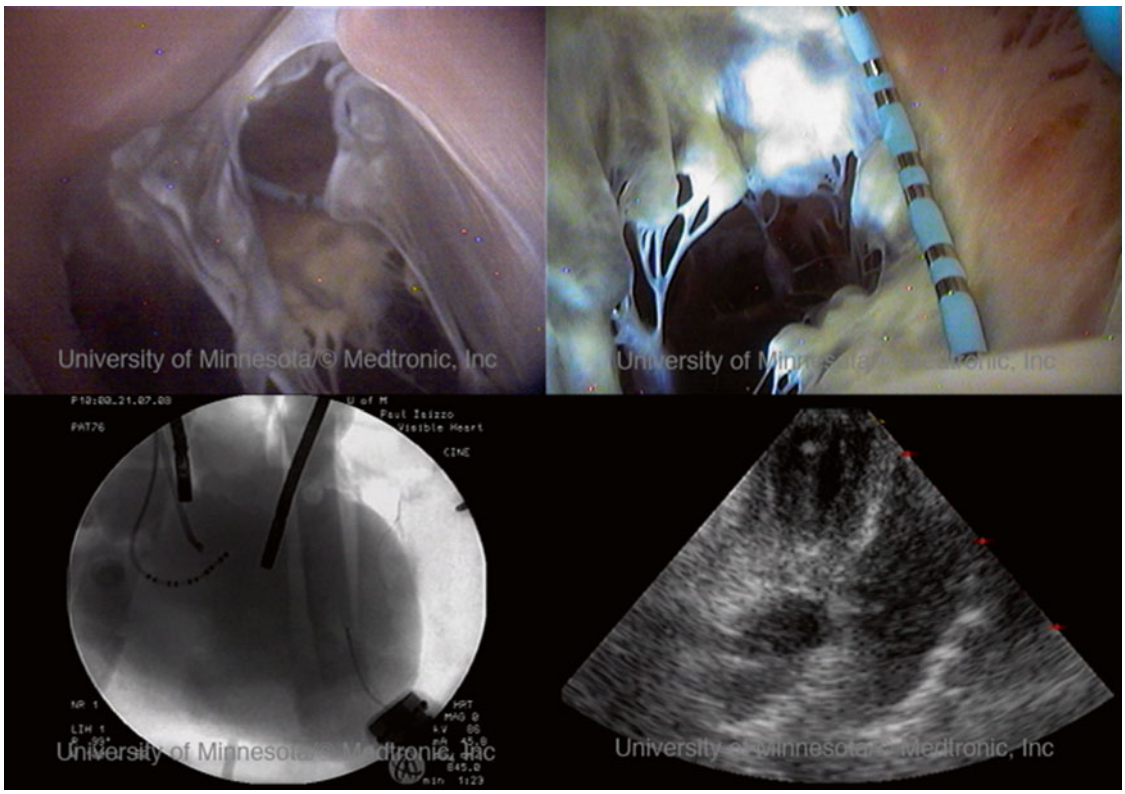

Fig. 41.5 Unique views of the tricuspid valve within a reanimated human heart imaged using (1) an endoscope placed within the right ventricle (*upper left panel*), (2) an endoscope placed within the right atrium (*upper right panel*), (3) fluoroscopy with an anterior-posterior orientation (*lower left panel*), and (4) ultrasound (*lower right panel*). Modified from The Atlas of Human Cardiac Anatomy [29]

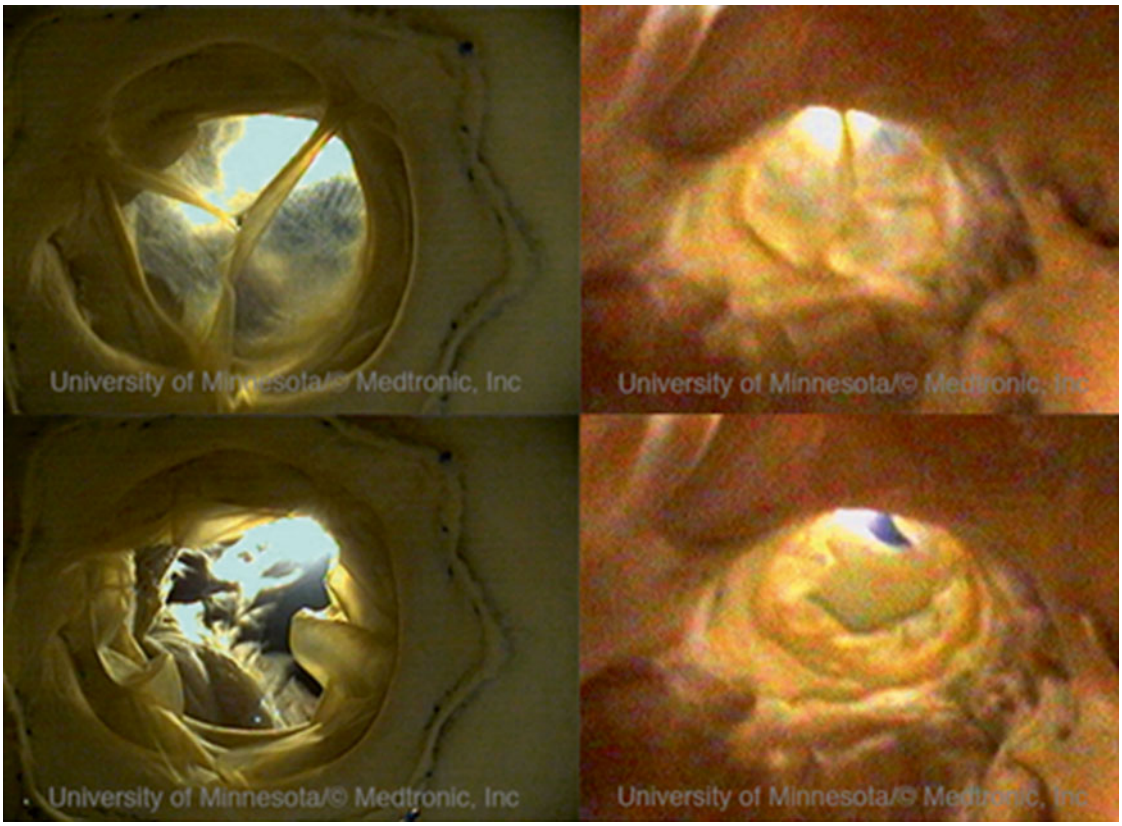

Fig. 41.6 Images of a transcatheter-delivered pulmonary valve which was imaged with endoscopes placed within (1) the pulmonary trunk during diastole (*upper left panel*), (2) the right ventricle during diastole (*upper right panel*), (3) the pulmonary trunk during systole (*lower left panel*), and (4) the right ventricle during systole (*lower right panel*). Modified from Quill et al. [33]

to capture unique internal and/or external images of device implantations during near normal hemodynamic conditions (left ventricular systolic pressures of 70–90 mmHg).

41.9 The Portable Visible Heart®

Due to the inherent advantages of MRI and CT for assessment of cardiac function and anatomy in vivo, it was considered desirable for our group to develop a portable Visible Heart® system which would allow MR or CT imaging of an isolated beating heart. A portable system would enable physiologic perfusion of an isolated large mammalian heart during simultaneous MR or CT imaging. Full details of the development of a portable apparatus and associated methodologies for isolated heart imaging in the CT and MRI environment were described by Eggen et al. [35]. Briefly, one needs to first consider the strong magnetic field in the MR environment that poses specific design challenges; we considered that this required the construction of a two-unit system to remove all ferromagnetic materials from the proximity of the MR scanner. The apparatus contains the necessary preload and afterload chambers required for physiological cardiac function (i.e., Langendorff or four-chamber working modes) and allows for independent control of the chambers in order to augment the pressure gradients across the valves. This novel system allows for the isolated heart to be placed safely on the patient bed of the scanner (Fig. 41.8).

To date, this system has been successfully used to obtain MR and CT images in both swine and human hearts (Figs. 41.9 and 41.10) [35, 36]. We consider that some of the advantages of isolating and reanimating a heart within the MRI/CT environment for device testing with such a portable system include the following:

- High-resolution studies of use conditions or device-tissue interactions with precise controls over physiological conditions. Without the need for breath holds, as is required for the intact animal or human scan sessions, image averaging and sequence times can be increased, thereby increasing the ultimate signal-to-noise ratios.
- The function and efficacy of MRI-safe devices can be tested in a dynamic beating heart environment without the costs incurred during intact animal testing.
- Comparative imaging. Direct imaging methods (i.e., endoscope) can be subsequently compared to MRI/CT imaging

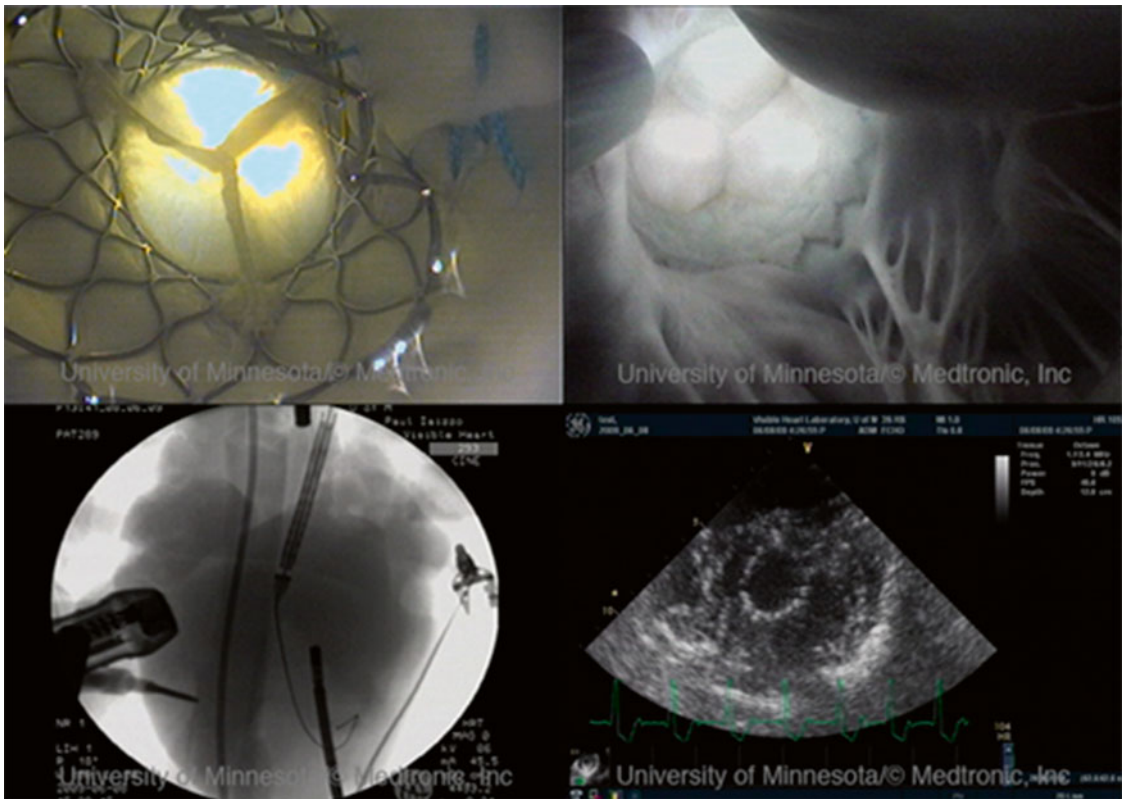

Fig. 41.7 Images of a transcatheter-delivered aortic valve imaged using (1) an endoscope placed within the ascending aorta (*upper left panel*), (2) an endoscope placed within the left ventricle (*upper right panel*), (3) fluoroscopy with an anterior-posterior orientation (*lower left panel*), and (4) ultrasound (*lower right panel*). Modified from Iaizzo et al. [34]

of cardiac function and anatomy or interaction with devices as a means to evaluate the best clinical imaging modalities for the desired target variable/interaction of interest.

- Multiple device implantation studies can be conducted under endoscopic visualization before analyzing the implantations using MRI/CT imaging, without requiring an XRM suite or combination CT-X-ray surgical suite.

41.10 Limitations of Visible Heart® Methodologies

The Visible Heart® methodologies are not without known limitations. For example, ischemic time prior to reanimation can compromise cardiac function, specifically contractility and thus pressure generation. Additionally, the lack of a pericardium may contribute to overexpansion of the atrial chambers, slightly different respective anatomical orientations of the great vessels and chambers, and/or differences in contractility compared to in vivo performance. However, it should also be noted that one can isolate these large mammalian hearts for the use with the pericardium primarily intact [37]. Additionally, the relative positioning of a given heart on the apparatus may also affect its overall performance. Furthermore, the use of a clear perfusate, without a specific oxygen carrier (i.e., a hemoglobin substitute like a perfluorocarbon), will lead to progressive global ischemia and the development of tissue edema which has effects on the long-term viability of these reanimated hearts.

The altered hydrodynamic state of the heart and progressive edema that occurs during reanimation on the Visible Heart® apparatus limits use of the apparatus for certain types of device testing. For example, deterioration of the tissue does not allow for chronic valve testing and limits most investigations related to the acute consequences of device implantations. Additionally, bench top tests such as accelerated wear testing have established guidelines for testing valves, which cannot be reliably reproduced on the Visible Heart® apparatus. Valve testing conducted in animals typically includes an artificially induced "challenge" state, which produces hemodynamic profiles that are unattainable on the isolated heart preparation. In other words, while the Visible Heart® apparatus in its current form does not replicate or replace bench top or preclinical testing, it can provide unique comparative imaging of functional anatomy and device-tissue interface which is not available in bench top or preclinical animal testing.

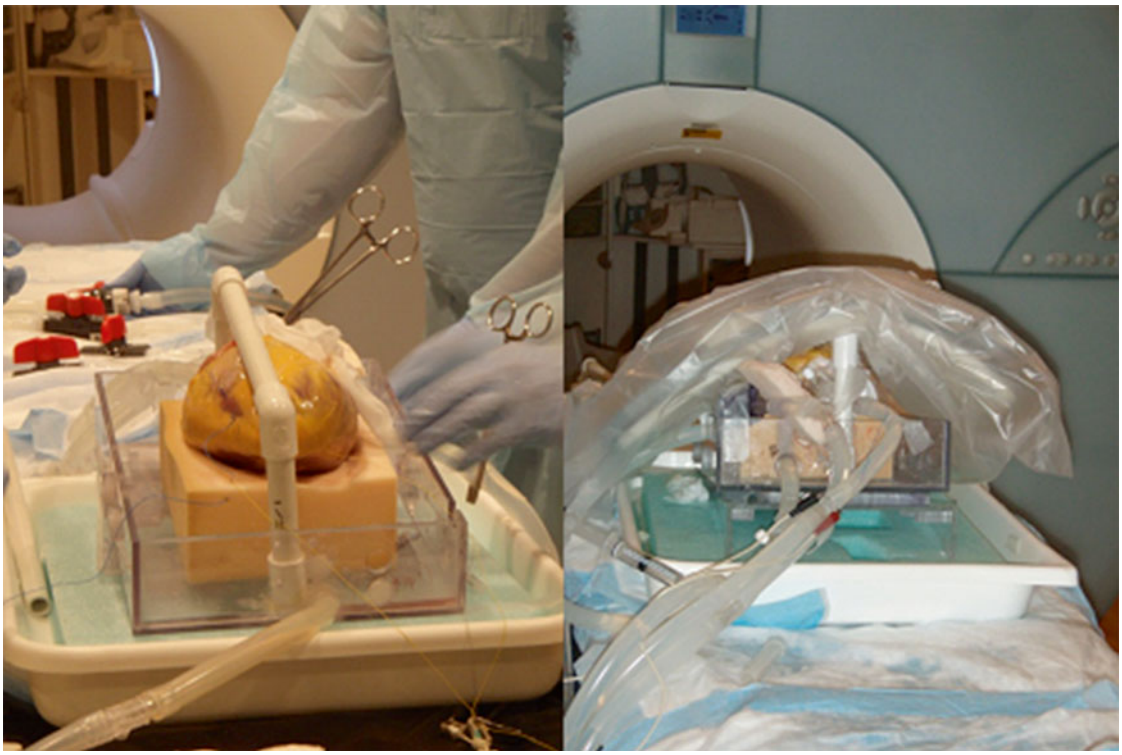

Fig. 41.8 Portable Visible Heart® apparatus. The isolated heart support system enables the heart to be positioned in the anatomically correct position during imaging in a magnetic resonance scanner (*left panel*; human heart shown). The isolated heart system with receiver coil positioned on the patient bed prior to MR imaging (*right panel*)

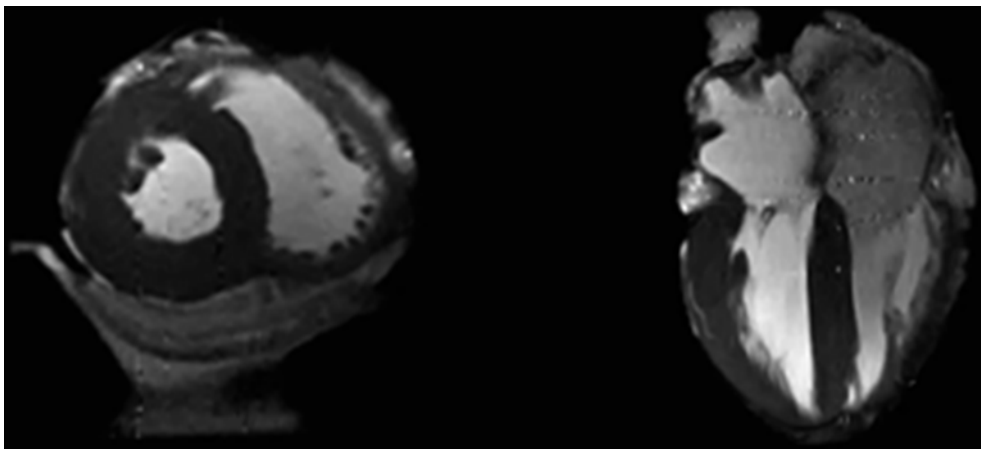

Fig. 41.9 MRI images obtained from a reanimated human heart placed in a 1.5 T MRI scanner: short-axis view (*left*) and long-axis view (*right*)

41.11 Acute Testing of Pathological Animal Models

The successful reanimation of human hearts using the Visible Heart® approach described in this chapter requires a level of cardiac health not always present in the available specimens (those deemed nonviable for transplant). Additionally, it is considered that the therapies for a specific category of pathologies often cannot be adequately or ideally tested by using "healthy" swine hearts as a model (e.g., severe aortic stenosis, dilated cardiac myopathy, or complex cardiac arrhythmias). In order to test therapies for these pathologies, a number of acute animal models have been created to mimic the anatomy and morphology of various human disease states. One example of this has been the development of various models for severe aortic stenosis, e.g., with the specific aim of determining how large calcific deposits on the leaflets affect the deployment and function of devices. To approximate severe stenosis of the aortic valve, we have: (1) directly

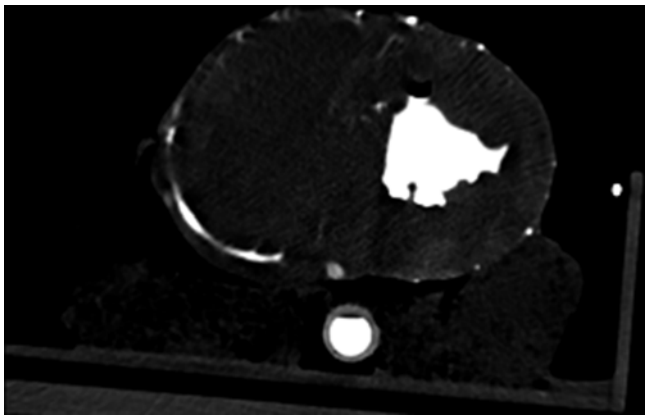

Fig. 41.10 Contrast-enhanced CT image of an isolated swine heart. The right coronary artery, aorta, and left ventricular endocardium are enhanced

adhered plastic models of calcification to the leaflets to reduce leaflet motion and (2) partially adhered the leaflet commissures to reduce the effective orifice areas of these valves. To date, such a model has allowed for expanded procedural testing of these devices (e.g., from balloon valvuloplasty to device deployment), providing useful insights into device performance as well as the potential interaction of deployed devices and the calcific deposits relative to the native anatomy. Another example has been the chronic use of high rate pacing to force the heart to remodel and dilate, mimicking the shape and function of patients with end-stage heart failure that often require cardiac resynchronization therapy. The ability to deliver, implant, and ensure capture of left-sided pacing leads in the relevant cardiac vascular anatomy has allowed designers to fine-tune lead and delivery system performance before entering into preclinical or first in man testing.

With the understanding that testing cardiac devices in relevant anatomies is key for better prediction of in vivo performance, there is ongoing research to further develop models, specifically models designed to simulate certain pathological states to test devices and delivery systems.

41.12 Future Directions

As anatomical resources develop and functional in vitro cardiac systems such as the Visible Heart® library and methodologies continue to evolve, so will the research possibilities within the realm of anatomical visualization and in vitro reanimation. Further, successful collaborations with the University of Manchester (UK) and Washington University (St. Louis, MO, USA) have been cultivated to determine the particular anatomical structure of the cardiac conduction system [38, 39]. Additionally, continued imaging should provide further anatomical information on cardiac disease states highlighting how disease management could, in turn, be effecting reverse remodeling on a cellular scale as well as a global scale of cardiac anatomy. Currently, all collected datasets (videoscopic, CT, echocardiographic, and MRI) are being used to create a digital database of human anatomies by rendering 3D computational models using software packages such as Mimics (Materialise, Leuven, Belgium); such datasets are being used to create physical representations of certain specimens via 3D printing [12]. Along with the plastination of select specimens, our work in creating real-life and computational 3D models (e.g., for both object printing and computation simulations) will pave the way for ongoing investigations and provide anatomically correct models for investigations related to device design and/or for educational purposes.

In addition, our laboratory is continually improving the Visible Heart® methodologies with systems designed to optimize the physiological function and control of the heart to improve the reproducibility, longevity, and utility of investigations. New cardioplegia and perfusate solutions are being tested as means to better protect the heart from ischemia and edema (some may be delivered as a pretreatment to specimens before extraction). Further, there is a continuing need to modify the setup/apparatus itself to better accommodate various delivery system designs (such as subclavian and femoral access systems). It should also be noted that the use of Visible Heart® methodologies to augment chronic studies has allowed for the validation of surgically created anatomies and the direct visualization of chronic device implants that were not previously possible. We consider that the utilization of both fixed specimens and Visible Heart® methodologies for device evaluation should be used in a complementary fashion with other techniques that utilize in vivo or in vitro methods to test the reliability, durability, biocompatibility, and/or other design parameters of newly developed transcatheter-delivered devices [30]. There is little doubt that the continued testing of novel cardiac prostheses via in vitro and in vivo studies will provide scientists, engineers, and/or clinicians working in this field with the necessary tools to drive the required research and development of the next generation of transcatheter-delivered cardiac devices.

41.13 The Atlas of Human Cardiac Anatomy

As novel therapies become clinically available and are implanted by more and more physicians, individuals will require continued education in the techniques required to navigate and deploy such devices. In response to this need, our laboratory has created a free access website, The Atlas of Human Cardiac Anatomy (www.vhlab.umn.edu/atlas), which can be utilized by cardiac device developers and clinical

implanters to gain insights on the relative variability in functional cardiac anatomy [12]. This website uniquely includes downloadable movie clips of functional cardiac anatomy; comparative imaging using echo, fluoroscopy, and MRI; and digital reconstruction images obtained from the human hearts of organ donors whose hearts were deemed not viable for transplant.

41.14 Summary

In summary, the study of fixed and reanimated human hearts, using the various methodologies described here, provides an individual with novel insights on normal and pathological human cardiac anatomies. Additionally, one can better visualize anatomical alterations that occur with specified pathologies and/or those that may occur following the deployment of devices within the heart. More specifically, the Visible Heart® methodologies to reanimate large mammalian hearts have provided a unique perspective on functional cardiac anatomies. By reanimating hearts using a clear perfusate, we are able to visualize functional anatomies with endoscopes placed directly within various heart chambers and/or within the vessels of the heart. Such anatomical knowledge is critical for device designers and developers, as well as clinicians who utilize these less invasive cardiac repair approaches for patients with acquired or congenital structural heart defects. Furthermore, when direct visualization is simultaneously coupled with clinically employed imaging modalities, it provides critical insights that can be used to more quickly and precisely advance such technologies. We consider that the utilization of both fixed specimens and Visible Heart® methodologies for device evaluation should be used in a complementary fashion with other techniques that utilize in vivo or in vitro methods to test the reliability, durability, biocompatibility, and/or other parameters of newly developed transcatheter devices. The continued testing of novel cardiac devices via in vitro and in vivo studies will provide scientists and engineers working in this field with tools to drive the required research and development of the next generation of cardiac devices.

References

1. Anderson RH, Becker AE (1993) The heart: structure in health and disease. Gower Medical Pub, London
2. Weinhaus AJ, Roberts KP (2009) Anatomy of the human heart. In: Iaizzo PA (ed) The handbook of cardiac anatomy, physiology, and devices, 2nd edn. Humana Press, Totowa
3. Loukas M, Sullivan A, Tubbs RS et al (2010) Chiari's network: review of the literature. Surg Radiol Anat 32:895–901
4. Maselli D, Guarracino F, Chiaramonti F et al (2006) Percutaneous mitral annuloplasty: an anatomic study of human coronary sinus and its relation with mitral valve annulus and coronary arteries. Circulation 114:377–380
5. Anderson SE, Quill JL, Iaizzo PA (2008) Venous valves within left ventricular coronary veins. J Interv Card Electrophysiol 23:95–99
6. Bateman MG, Iaizzo PA (2011) Comparative imaging of cardiac structures and function for the optimization of transcatheter approaches for valvular and structural heart disease. Int J Cardiovasc Imaging 27:1223–1234
7. Anderson RH, Cook AC (2002) Attitudinally correct nomenclature. Heart 87:503–506
8. Tajik AJ, Seward JB, Hagler DJ et al (1978) Two dimensional real-time ultrasonic imaging of the heart and great vessels. Mayo Clin Proc 53:271–303
9. Edwards WD, Tajik AJ, Seward JB (1981) Standardized nomenclature and anatomic basis for regional tomographic analysis of the heart. Mayo Clin Proc 56:479–497
10. Thomas AC, Davies MJ (1985) The demonstration of cardiac pathology using perfusion-fixation. Histopathology 9:5–19
11. Kilner PJ, Ho SY, Anderson RH (1989) Cardiovascular cavities cast in silicone rubber as an adjunct to post-mortem examination of the heart. Int J Cardiol 22:99–107
12. http://www.vhlab.umn.edu/atlas. Accessed 14 Dec 2014
13. Quill JL, Hill AJ, Laske TG et al (2009) Mitral leaflet anatomy revisited. J Thorac Cardiovasc Surg 137:1077–1081
14. Quill JL, Geesling AG, Iaizzo PA (2009) Transcatheter aortic valve deployment: interactions between native leaflets and coronary ostia. J Med Devices 3:027530
15. Ton-Nu T, Levine RA, Handschumacher MD et al (2006) Geometric determinants of functional tricuspid regurgitation: insights from 3-dimensional echocardiography. Circulation 114:143–149
16. Plass A, Valenta I, Gaemperli O et al (2008) Assessment of coronary sinus anatomy between normal and insufficient mitral valves by multi-slice computer tomography for mitral annuloplasty device implantation. Eur J Cardiothorac Surg 33:583–589
17. Tops L, Wood D, Delgado V et al (2008) Noninvasive evaluation of the aortic root with multislice computed tomography. J Am Coll Cardiol Imaging 1:321–330
18. Salton CJ, Chuang ML, O'Donnell CJ et al (2002) Gender differences and normal left ventricular anatomy in an adult population free of hypertension. J Am Coll Cardiol 39:1055–1060
19. Eggen MD, Bateman MG, Iaizzo PA (2011) Methods to prepare perfusion fixed cardiac specimens for multimodal imaging: the use of formalin and agar gels. J Med Devices 5:027539
20. Eggen MD, Swingen CM, Iaizzo PA (2009) Analysis of fiber orientation in normal and failing human hearts using diffusion tensor MRI. In: 2009 IEEE international symposium on biomedical imaging: from nano to macro, pp 642–645
21. Messika-Zeitoun D, Serfaty J-M, Brochet E et al (2009) Multimodal assessment of the aortic annulus diameter. J Am Coll Cardiol 55:186–194
22. Tsang W et al (2012) Accuracy of aortic annular measurements obtained from three-dimensional echocardiography, CT and MRI: human in vitro and in vivo studies. Heart 98:1146–1152
23. Richards AL, Cook RC, Bolotin G et al (2009) A dynamic heart system to facilitate the development of mitral valve repair techniques. Ann Biomed Eng 37:651–660
24. Nanthakumar K, Jalife J, Masse S et al (2007) Optical mapping of Langendorff-perfused human hearts: establishing a model for the study of ventricular fibrillation in humans. Am J Physiol Heart Circ Physiol 293:H875–H880
25. Langendorff O (1895) Untersuchungen am uberlebenden Saugenthierherzen [Investigations on the surviving mammalian heart]. Pflugers Arch 61:291–332
26. Araki Y, Usui A, Kawaguchi O et al (2005) Pressure–volume relationship in isolated working heart with crystalloid perfusate in swine and imaging the valve motion. Eur J Cardiothorac Surg 28:435–442
27. de Weger A, van Tuijl S, Stijnen M et al (2010) Direct endoscopic visual assessment of a transcatheter aortic valve implantation and

performance I the physioheart, an isolated working heart platform. Circulation 121:e261–e262
28. Chinchoy E, Soule CL, Houlton AJ et al (2000) Isolated four-chamber working swine heart model. Ann Thorac Surg 5:1607–1614
29. Hill AJ, Laske TG, Coles JA Jr et al (2005) In vitro studies of human hearts. Ann Thorac Surg 79:168–177
30. Eggen MD, Bonner MD, Williams ER, Iaizzo PA (2014) Multimodal imaging of a transcatheter pacemaker implantation within a reanimated human heart. Heart Rhythm (images), doi:10.1016/j.hrthm.2014.03.052. PMID: 24732365
31. Michaëlsson M, Ho SY (2000) Congenital heart malformations in mammals: an illustrated text. Imperial College Press, London
32. Sigg DC, Coles JA, Oeltgen PR et al (2002) Role of δ-opioid receptor agonists on infarct size reduction in swine. Am J Physiol Heart Circ Physiol 282:H1953–H1960
33. Quill JL, Laske TG, Hill AJ et al (2007) Direct visualization of a transcatheter pulmonary valve implantation within the Visible Heart®—a glimpse into the future. Circulation 116, e548
34. Iaizzo PA, Hill AJ, Laske TG (2008) Cardiac device testing enhanced by simultaneous imaging modalities: the Visible Heart®, fluoroscopy, and echocardiography. Expert Rev Med Devices 5:51–58
35. Eggen M, Swingen C, Matta P et al (2009) Design of a novel perfusion system to perform MR imaging of an isolated beating heart. J Med Devices 3:027536
36. Eggen MD, Bateman MG, Rolfes CD et al (2010) MRI assessment of pacing induced ventricular dyssynchrony in an isolated human heart. J Magn Reson Imaging 31:466–469
37. Richardson E, Hill AJ, Skadsberg ND et al (2009) The pericardium. In: Iaizzo PA (ed) The handbook of cardiac anatomy, physiology, and devices, 2nd edn. Humana Press, Totowa, pp 125–136
38. Dobrzynski H, Li J, Tellez J et al (2005) Computer three-dimensional reconstruction of the sinoatrial node. Circulation 111:846–854
39. Chandler N, Aslanidi O, Buckley D et al (2011) Computer three-dimensional anatomical reconstruction of the human sinus node and a novel paranodal area. Anat Rec 294:970–979

Current Status of Development and Regulatory Approval of Cardiac Devices

42

Stephen A. Howard, Michael G. Bateman, Timothy G. Laske, and Paul A. Iaizzo

Abstract

Medical devices are rapidly advancing and changing the medical field. Progress has been demonstrated in many fields such as minimally invasive surgical techniques for valve replacement and 3D cardiac mapping of arrhythmias. These medical device advances allow physicians to help more patients quicker and more efficiently. The field of cardiac device development can be considered as relatively new, beginning in the early 1950s, and today new technologies in this field are presented at ever increasing rates. Many times, these advances come from an unmet clinical need. In some ways, physicians are unable to treat (or are at best ineffectively treating) certain types of patients in this aging society. Motivated by these needs, medical device designers—scientists, physicians, patients, or simply individuals with good ideas—choose to undergo the rigorous, yet rewarding, path of medical device development.

The development path follows a certain route from device conception, intellectual property generation, and testing to regulatory approval. Since cardiac medical devices are created to help patients, they must also undergo stringent testing for durability, biocompatibility, and manufacturability. To complete these assessments, both animal and clinical testing can be utilized, especially with regard to valve replacement devices. Once an adequate amount of data pertaining to the safety and efficacy of the device has been collected, it will then be sent to a regulatory body to gain approval to market the device.

Keywords

Cardiac device design • Cardiac device development • Device ideation • Risk mitigation • Intellectual property • Device testing • Regulatory approval

Abbreviations

DFM	Design for manufacturability
FDA	Food and Drug Administration
FMEA	Failure mode and effect analysis
HDE	Humanitarian device exemption
IDE	Investigational device exemption
IFU	Instructions for use
IP	Intellectual property
USPTO	United States Patent and Trademark Office
VOC	Voice of customer

S.A. Howard, PhD (✉) • M.G. Bateman, PhD • T.G. Laske, PhD
Medtronic, Inc., Mounds View, MN 55112, USA
e-mail: stephen.howard@medtronic.com

P.A. Iaizzo, PhD
Department of Surgery, University of Minnesota, Minneapolis, MN, USA

42.1 Introduction

All it takes is a napkin drawing or a rough shape crafted with clay. Such humble beginnings can spark an idea or revolution for the way that cardiac care is administered. Ideas can blossom into intricate high-tech medical devices that push

P.A. Iaizzo (ed.), *Handbook of Cardiac Anatomy, Physiology, and Devices*, DOI 10.1007/978-3-319-19464-6_42

the envelope of design and advance the field of medicine. These are exciting opportunities, yet the journey of creating a medical device can be daunting. However, for those who are successful in developing such devices, there can be great rewards. This is the reason for so many entrepreneurs entering the medical device space!

When you consider what it takes to fully create, develop, manufacture, and market a cardiac device, there are many points to discuss. First and foremost, the device needs to serve an unmet need (whether or not it is apparent). Within the cardiac space, this can range from the inability to measure a particular pressure to finding a way to successfully repair or replace failing myocardium. Any cardiac device must be technically feasible, and it requires that issues of design, quality, manufacturability, regulation, cost, and reimbursement must be considered during the design process. In many cases, the earlier these areas are considered in the design space, the more effectively the device can be brought to market. Even if a device is the best idea in the world and can cure a disease, if you cannot successfully make it or if no one can afford to buy it, then the product is doomed to fail.

42.2 Anatomy of a Cardiac Device

For a product to be viable, there are some key characteristics that must be incorporated or considered in the design. These characteristics demonstrate that the device has been tested and manufactured correctly, and they also take into consideration the risks inherent to the device. This next section will discuss the different design considerations that need to be developed while creating a medical device. These will drive toward a device that functions the way it is required and will do as little harm to the patient as possible. These topics on design characteristics can be used in other areas of medical product design, but, for the sake of brevity, this chapter will focus on cardiac devices.

42.2.1 Functionality

Consumers—including physicians, patients, and buyers—all have certain expectations of a cardiac device. When a physician uses a device, he/she expects that it will function in the manner in which it is intended. This may seem elementary, but the idea that the device must always work as specified is integral to the design, and the first device must work the same as the one thousandth device. To be successful, a new product must elicit *functionality* above and beyond the currently available solutions and techniques. The functionality of a given cardiac device ideally also encompasses an ability to perform the desired tasks without compromising any other biological process. For example, an atrial septal occluder device should not impede the function of the tricuspid or mitral valve, nor should it increase the potential risks of embolism and stroke which it is trying to mitigate. These specifications are often outlined by regulatory committees such as the International Organization for Standardization (ISO).

For therapeutic devices deployed in the left atrium, the functionality of the device also encompasses the delivery of such therapies. For instance, left atrial cardiac ablation requires a transseptal puncture to be performed before the device can be inserted into the left atrium. The delivery path is such that it must create a hole in the interatrial septum and thus provide an access point to get to the left atrium. If the hole is misplaced, or if during the puncture the needle is advanced too far, it can cause unwanted complications of either cardiac tamponade or aortic perforation. Neither one of these situations is desired and, as such, must be considered while thinking about the left atrial ablation therapy (see Sect. 42.3.4 on risk mitigation). To ignore this portion of the procedure may result in unforeseen issues with the procedure which may or may not have been caused by the delivery of the device. In many cases, the delivery of a device has a larger impact on the ability to perform the procedure. For some mitral valve repair procedures, the location of the puncture in the atrial septum is paramount to having a quick and successful procedure [1]. In summary, the device being developed must be thought of as a *device delivery procedure* and include everything involved with its successful use. This approach takes into consideration the system as a whole instead of a single part; the system must be considered as a whole; otherwise, issues may occur due to the unforeseen interactions between parts of the procedure.

Another aspect of functionality is related to unforeseen uses or the *off-label* use of devices by physicians. An off-label use of a device is one where the manufacturer of the device has clearly specified the use conditions in which such a device can be utilized, yet the physician has elected to use it in another fashion or in a patient in which the device is not intended to be used. An interesting thing to note is that the physicians have a fair bit of freedom to use the cardiac device however they see fit. Since they are ultimately responsible for the well-being of the patient, if they believe that a cardiac catheter would better serve the patient in a manner other than what is listed or suggested by the company in their instructions for use (IFU), they can and may decide to use the device however they choose. In other words, in most cases, they will use the devices as intended, but may also use them outside of the bounds of the IFU if they believe it is in the best interest of the patient.

Nevertheless, an off-label use of devices puts medical device companies in a peculiar position. On the one hand, the company likely enjoys the benefits of their product helping more people than was originally intended, as well as possibly

higher sales. On the other hand, the action of using the device in such an off-label fashion cannot be condoned, marketed, or suggested by the company without potential repercussions for promoting the device to be used in such a way that has not been tested or cleared through regulatory channels.

42.2.2 Biocompatibility

In 1987, Williams described how the biocompatibility of a material can be qualitatively evaluated to assess its relative performance when implanted. He said that biocompatibility can be defined as the ability of a material to perform with an appropriate host response under specified conditions [2]. The succinctness of the term *biocompatibility* can be misleading when applying the principle to cardiac devices. Often within a single medical device, there may be a multitude of different materials that are utilized. For example, the WATCHMAN™ left atrial appendage (LAA) closure device (Boston Scientific, Marlborough, MA, USA) is made of a collapsible nitinol structure with a polyethylene terephthalate (PET) mesh covering which is permanently implanted into the patient, whereas the delivery system is made of another polymer that will be in contact with the patient for <24 h. This means that the delivery system must not elicit acute immune responses within the patient including (but not limited to) allergic reactions. The WATCHMAN does not need to be biologically inert, but it must not cause an undue biological response from either the PET or the nitinol. The purpose of the device is to block the LAA to mitigate the formation of a blood clot within the LAA, followed by the subsequent release of emboli into the bloodstream. Thus, the requirement for the device is that it will effectively section off the LAA and endothelialize, thereby creating a biologic barrier between the left atrium and the LAA. Although this is a biological response due to a foreign object in the heart, it can still be deemed biocompatible since it will elicit this appropriate response from its host and will not be detrimental to overall function (Table 42.1).

The mechanisms related to how the host or patient may respond to different components of a cardiac device must be extensively evaluated to ensure that appropriate materials are selected for the final device design. This evaluation can be complicated by the fact that it is hard to replicate the range of human immune responses that may exist in vitro. To address this, all cardiac devices must also undergo rigorous animal testing, although it is important to note that animal testing can sometimes provide misleading results on species-specific bioreactivity. An example of this can be seen in the design and development of the Braunwald–Cutter heart valve ball and cage prostheses (Fig. 42.1), whereby cloth-covered cage struts were designed to encourage endothelialization and subsequently decrease any chance of thrombolytic events [3].

Table 42.1 Potential patient–device interactions causing clinical complications [2]

• Adverse local tissue interactions:
– Inflammation – Toxicity – Carcinogenic response – Calcification – Embolization or lymphatic spread of material fragments
• Induced device migrations: encapsulation or foreign body response
• Inappropriate or altered healing responses
• Associated infections
• Thrombosis
– Thrombotic occlusion – Thromboembolism

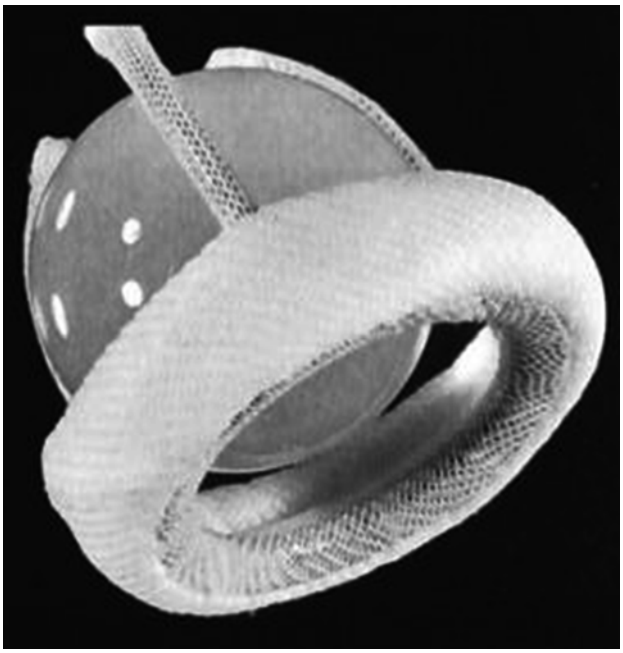

Fig. 42.1 Braunwald–Cutter valve

Extensive testing in the mitral position of pigs, sheep, and calves showed promising results; thus, the device was approved for human clinical trials. However, the device did not elicit the same host responses when implanted in humans; rather, it resulted in aggravated wear on the cloth cage struts and, more critically, the formation of debris embolization.

It should also be emphasized that host responses are not limited to immune reactions. For example, implanted tissue heart valves remain susceptible to accelerated prosthesis leaflet calcification. More specifically, it has been reported that this type of calcification is initiated by reactions between the extracellular fluid and the leaflet membranes, creating calcium phosphate mineral deposits [4]. As a result, much research is ongoing to enhance leaflet materials and minimize bioreactivity, including calcification inhibitors on the

valves that limit mineral deposition on the implanted materials. Furthermore, the materials used in a device can display unexpected interactions with the host, as evidenced by the earliest versions of the Starr–Edwards caged-ball mechanical heart valve. The valve design used a silicone ball that was found to absorb lipids from the blood and thus swell [4]. In addition to resultant poor valve function, this also caused the silicone balls to become brittle; in turn, this increased the possibility of ball fracture and consequent embolization of small fragments into the arteries downstream of the valve position.

42.2.3 Durability

Along with the biocompatibility, a device must be *durable* enough to withstand the mechanical loads placed upon it. These forces can be exerted upon the device by implantation, cardiac motion, or external events such as getting hit in the chest or falling on the ground (specifically for implantable devices). Potential situations like these must be considered when designing the device, to ensure it has the robustness needed to withstand such environments as well as an active lifestyle.

Major factors that any design engineer must take into consideration are the repetitive movements and strains that will be placed on a device within a patient's body. If you were to imagine the environment in which a coronary stent is placed, the arteries will have a cyclic pressure placed on them which, in turn, will flex and relax the stent with each heartbeat. This requires the stent's material to either: (1) oscillate with the artery while being durable enough to withstand flexing for the lifetime of the stent or (2) provide enough opposing force to the artery that it does not move during these times of increased pressure.

Cardiac pacing and defibrillation leads are also exposed to repetitive mechanical stresses that can cause faults or failures in their integrity. Two individual incidents were observed within defibrillation leads from two separate companies—St. Jude Medical (St. Paul, MN, USA) and Medtronic, Inc. (Minneapolis, MN, USA)—that were competing to get a small defibrillation lead on the market. The two companies produced small-diameter leads, the Riata (St. Jude Medical) and Sprint Fidelis (Medtronic, Inc.), that gained FDA approval and were then appropriately implanted clinically [5]. Before the release of these smaller leads, >8F defibrillation leads were the standard of care, but in 2002, St. Jude Medical released their 7.6F Riata defibrillation lead. In response, Medtronic, Inc., released their 6.7F Sprint Fidelis in 2004, shortly followed by the 6.3F Riata ST by St. Jude Medical. The perception was that a smaller lead would decrease the blockage caused within the venous system at the level of the subclavian vein. However, it was found that these systems were unable to perform at adequate levels of durability within the body [5]. Both companies ended up having issues where their leads broke or eroded to the point where the conductor wires could penetrate and cause misreading of the cardiac signals and potentially lead to excessive shocks being delivered to the patient (or even worse, no shocks were delivered when they were needed).

In 2007, Medtronic, Inc., sent a letter to physicians informing them that they had seen failures in the field both at the distal portions of these leads and at points near the anchoring sleeve tie-down. Further, they reported that the distal failures were significantly affected by the bending of the lead body due to tortuous anatomy in the veins. The failures at the tie-down location were potentially caused by the way physicians implanted and secured the leads within the body. Each of these failure modes suggested that the way in which the lead was implanted could make a significant impact on the longevity of these devices and their potential for failure. Ultimately in late 2007, Medtronic, Inc. issued a voluntary market suspension that the FDA formally considered to be a recall. During this time, St. Jude Medical was also seeing similar issues with their leads. They reported that portions of their leads were being eroded to the point where the wires were being externalized in both styles of the Riata leads. It was also reported that the primary reason for this externalization was due to abrasion of the lead insulation with either the anatomy (e.g., tricuspid valve) or the internal components of the lead (e.g., the pacing/sensing wires). In one study, they found that a common defect was due to the internal abrasion of either the pace/sense coils or the shocking coils against the silicone insulation. This would be in response to the repetitive motion of the lead and the ability for the internal components to move relative to the external insulation. This caused what they deemed to be an inside-out abrasion, where these wires were wearing away at the insulation and become externalized and readily visible under fluoroscopy [6]. Due to these failures, St. Jude Medical ended up removing the Riata family of leads from the market in 2010 and recalling them in 2011. Since these recalls, the defibrillator lead market has stayed at >8F, due to the perception that smaller leads could be associated with potential failures in patients.

Both of these cases are prime examples for why device durability testing is essential for the development of robust cardiac devices. Notice that it is not always a matter of how the device will react within the body (which seemed to be the case for the Riata leads), but also how the devices are implanted that may lead to potential failure modes. Ultimately, if a cardiac device is not tested properly in *relevant use* conditions, certain factors can be overlooked and may ultimately end up negatively impacting patients.

42.2.4 Design for Manufacture

The ability to put together a device, or *manufacturability*, is something that should not be overlooked during the design processes. By incorporating early feedback about manufacturing the product, the risks of not being able to build the device efficiently enough or to produce adequate quantities to fulfill demand will be greatly reduced. Failure in either case could cause the product to be stifled, no matter how successful or clinically helpful it is. As such, design for manufacturability (DFM) has become a common practice in the cardiac device industry, a practice that emphasizes how a successful design should ensure the highest-quality products while decreasing manufacturing costs. This is accomplished by making manufacturing cost estimates to proactively guide and prioritize cost reduction efforts involved with design. Consequently, DFM should have significant effects on product lead times, development costs, and ultimate product quality. As such, DFM specifically requires input from a multidisciplinary team, including manufacturing engineers, cost accountants, and production personnel, in addition to the design engineers [7]. Yet, when applying these principles to cardiac device design, it is imperative to understand that the quality of care impacted by the device must not be compromised by the need for a more cost-effective manufacturing process. One needs to consider that production costs can be controlled by using existing technologies and established manufacturing techniques. There are many methods for ensuring that the requirements for manufacturing are being taken into consideration, and there are several numerical methods of design and testing (also known as *in silico testing*) that can be used to streamline the design for the manufacturing process.

42.3 Development Process

There are often two types of development referred to by designers—iterative and disruptive. Those that fall into the *iterative* category are devices that generally are perceived as logical next steps in the development chain. For example, this would include the addition of a third and fourth electrode to a left-sided lead that would give the physician more vectors to choose from when programming a pacemaker, as discussed in Chap. 30. The ideas and devices that are considered to be *disruptive* are those that medical industry professionals would consider as *game changers*. These are devices like transcatheter-delivered cardiac valves. The option prior to these transcatheter valves was open-heart surgery, which often involved placing the patient on cardiac bypass and fully stopping the heart; this procedure limited the population of patients who could receive the treatment to those that were able to physically undergo an invasive surgery and required weeklong recovery periods in the hospital. In other words, these devices have effectively provided a means to treat more of the patient populations which were underserved by prior medical management.

Although there may be a valid unmet clinical need, oftentimes there are points along the product development pathway that may ultimately put a halt to a device or therapy. This can be as simple as the product not working as intended or a business decision to not pursue a particular therapy because it does not align with their internal objectives. This, along with other reasons, is generally why larger companies will often focus their efforts on incremental improvement of devices as opposed to disruptive technologies. The incremental improvements are much more predictable and lower risk, since the market is already known and the needs often come directly from their voice of customer (VOC). Disruptive technology offers a greater amount of risk and, conversely, often a higher reward. This volatility of the device can be a deterrent for larger, publicly held companies that rely on stability, but it provides an opportunity for smaller companies willing to take the risk.

Whether it is an iterative or disruptive technology, the development process generally follows a similar pathway (also utilized in nonmedical device development), with the hope of producing a marketable product. Often, a problem is identified within the field, and to better understand the clinical needs, the designers must empathize with those experiencing the problem. This can be the physician, patient, payers, or any other stakeholders. While studying and understanding these situations, the designers gain invaluable insights as to the root cause(s) of the clinical problem or need, as well as what confounding factors are present. Then, by defining which portion of the issue they are trying to address, designers can begin to hone in on a potential solution. In turn, this will spark ideas and a multitude of solutions (partial or complete) will be generated. These solutions (as you will see in Sect. 42.3.3) will be prototyped and selected based on technical and market feasibility. Promising options will then be tested for usability and functionality; if an acceptable option is produced, the design will be frozen to move on to preclinical animal testing and eventual clinical testing (Fig. 42.2) (see Chap. 43). The generalized overarching progression of how cardiac devices develop from concept to market will be presented in the following sections.

42.3.1 Six-Phase Approach to Device Development

There are many ways that device development can be approached, but often they follow a similar pattern: (1) generate an idea, (2) prove it to be feasible, (3) test the idea, (4) market the idea, (5) and make sure that it does not cause unfavorable

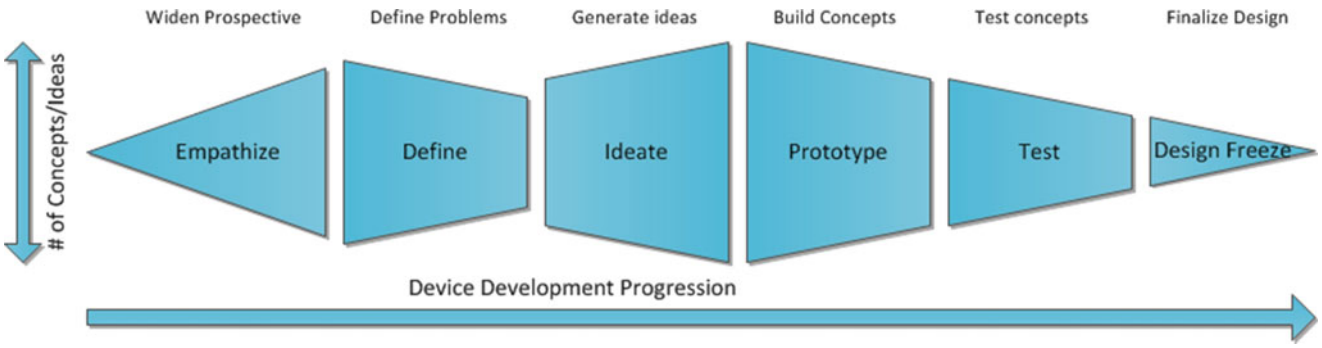

Fig. 42.2 Flowchart of the design thinking process

issues in the field. This is obviously oversimplifying things, and each of these steps requires a vast amount of work to "get it right." Despite the simplification, all of these steps are essential to fully develop and market a cardiac device. This section will describe a more commonly used phase–gate system that breaks up the process into six phases of development, as shown in Fig. 42.3. Importantly, throughout each of these phases, a number of different elements need to be checked and rechecked in order to create a successful device.

As the development process advances along the phases, the subsequent tasks are generally associated with higher costs. For instance, the first phase of the development process is *device conception*, in which a clay model or a sketch of the product may be the only thing required, along with asking some key stakeholders whether or not the idea is worth the time and effort. This requires very little monetary investment. The next phases require creating animations and prototypes and testing of these advanced concept devices; these phases will incur greater costs. Prior to market release, at a minimum, preclinical and even some clinical testing will be necessary, which may require the investment of millions of dollars and multiple years of study before finally being able to market and realize profit from the device.

Phase 0 is the *planning phase* during which much of the groundwork is completed, including developing prototype devices, creating a product platform, assessing market opportunities (determining if it will be worth pursuing financially), and identifying product constraints associated with intellectual property (see Sect. 42.3.2). The decision to move on to the next phase often requires insights related to perceived market value versus return on investment, an evaluation that is required to bring any device to the market.

Phase 1 is considered the *concept development phase*. This is when the development/refinement process, as well as benchtop testing, of the device begins. For example, feasibility studies are performed to determine whether the product is technically possible to manufacture and create, as well as to estimate the potential market size. Ultimately, the market

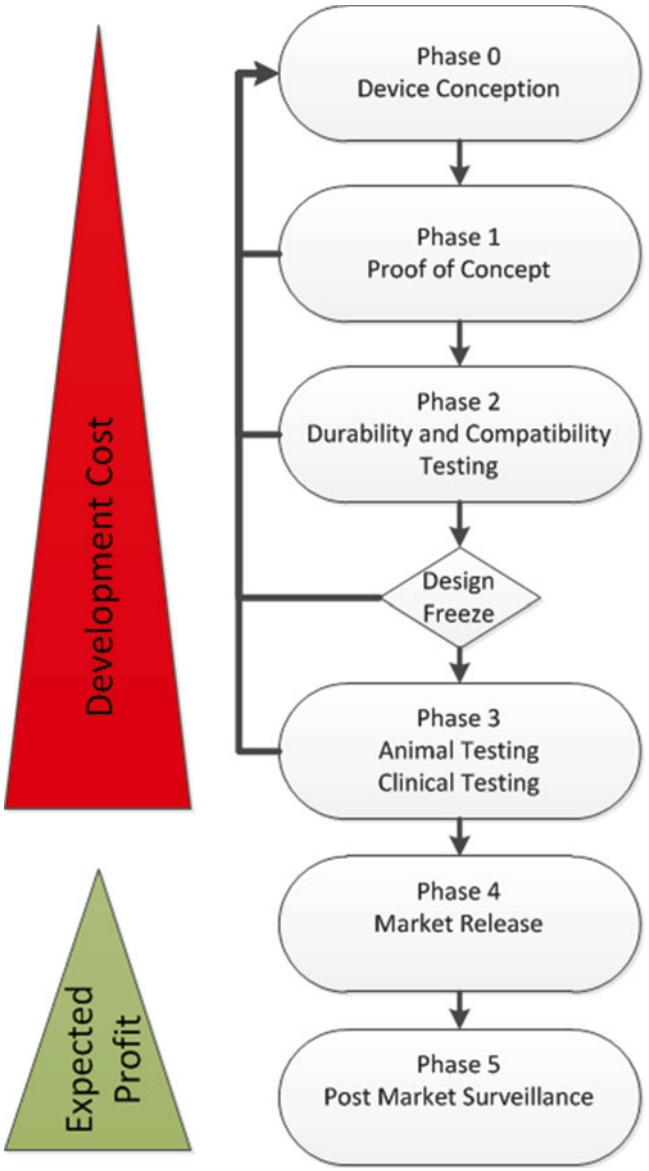

Fig. 42.3 Flowchart of the device development process. The six phases of device design are shown, as well as the associated cost and profit factors related to marketing a medical device

size will determine the profitability of the device. It should be noted that there remains a special need for pediatric-sized cardiac devices, partly because they are often considered nonprofitable to manufacture at small volumes and are thus generally developed as a humanitarian effort.

Phase 2 (*durability and compatibility testing*) occurs after the device design meets the previous criteria from Phase 1. This is where further benchtop tests are performed for both accelerated failure and required function of the devices. In vitro work or acute animal studies can also be initiated to assess potential biocompatibility. The end of Phase 2 generally involves a design freeze where nothing can be changed on the device without going back to Phase 1 or 0. At this point in time, the design engineers, in partnership with the entire development team, must determine the most optimal design and cease all design work and begin the preclinical and clinical testing.

Phase 3 (*animal and clinical testing*), which is initiated after the design freeze, assures that testing will provide an accurate assessment of the device function within a living organism. Testing often includes chronic implantation in appropriate animal models, which is then followed by regulatory approvals before the onset of clinical trials in humans. Yet, even subsequent to a success clinical trial, final approval for market release of the product is sought.

Phase 4 is initiated when the product is actually *market released*. Usually, this is the phase of the overall process where the company expects to see a return on investment. Yet profitability is contingent on successful clinical trials, approval of the device for market release by the regulatory body of the country, and the ability of the company to commercialize and market the device, as well as receive payment (reimbursement) for sales.

Phase 5 is considered to be the *post-market assessment*. Even though a product is fully marketed and approved by a regulatory agency, the company is still required to perform follow-up studies to ensure that the device does not cause any unforeseen issues with patients over time. This acts as a safeguard to the patients that are being served by the device. In some cases, even though stringent testing in animal and human trials has been performed, there may be unexpected issues with the longevity of the device or unanticipated failures. This also provides the company with additional information for future improvement of the device. Assessment that can be performed in this phase includes postmortem studies, where the company may receive the explanted device and then analyze its status/condition.

42.3.2 Intellectual Property

Before finalizing any design, one aspect that must be taken into consideration is the intellectual property (IP) associated with the device idea. Generally, IP refers to a work or invention to which one has rights. This is often associated with patents, copyrights, trademarks, or trade secrets. In all of these cases, there are specific actions that need to take place to protect the creator of the idea, so they can utilize their ideas without others unduly copying or inappropriately using their works or inventions.

Ultimately, a major part of the product design process is to maintain ownership or licensing agreements of IP relative to the technologies being developed. A *trademark* is a name or symbol that is associated with a product or brand in which a company (and only that company) has full rights to use that name or symbol. This prevents others from using the name and associated marketing as a means of promoting their products or services. Similarly, a *copyright* may be granted for any written and/or graphical materials to an individual or group of individuals to protect their work and reduce the risk of plagiarization [8]. Another method to protect an idea or product is to keep it a *trade secret*. Simply put, this is the act of not divulging any information regarding how a product is made, operates, or performs (e.g., a device running on proprietary software or novel circuitry) while banking on the notion that no one can reverse engineer the product and thus replicate it. Yet it should be noted that anyone successful in reverse engineering a product may then duplicate the product or procedure (even without knowing the trade secret) with no legal consequences [8].

Within the medical device arena, a primary way of protecting IP is to file and obtain a device *patent* with broad claims. A patent is a legal document that explicitly describes how a device works or how a procedure is completed, providing enough information that anyone within the field could duplicate the device or process. In the USA, patents provide legal protection for 20 years, thus guaranteeing exclusive marketing rights during that period. However, upon expiration, the device can be copied by competitors without legal recourse [8]. With the long life span of patents, there is often little concern of the patent expiring due to the speed at which devices are developed or improved, as newly created and updated products will likely hold new patent protection. For this reason, it is vital for any product developer to have a solid understanding of how to read patents in order to avoid patent infringement upon the development and release of their own device. Typically, patents are classified according to device type and use and will first provide the filing number(s), inventor(s), and the date filed. Next, a description of the device/process is presented, generally involving sketches and other images of IP. The most pertinent information is contained within the claims section, which specifically describes what part of the IP is novel and hence what is officially patented and protected by the law. The claims section is generally the portion that legal teams will address when reviewing a patent case.

To obtain a patent, the United States Patent and Trademark Office (USPTO) requires that the idea must be novel, useful, and nonobvious. As such, the idea must fall into one of the categories of a process, machine, article of manufacture, composition of matter, or improvement of any of the previous items [9]. The USA has recently changed to a first-to-file patent system, which is similar to the current European patent procedure. Previously, the USPTO granted ownership of a patent to individuals who were the first to invent. This would mean that documentation was vitally important with dates and signatures referencing the date of the initial invention of the idea. While this method has its merits, the USA decided to move to a first-to-file system which means the patent is awarded to the individual or group of individuals who were the first to file a patent on that particular process, machine, and/or patentable idea.

In general, in order to determine if an idea is patentable, one must first search existing patents to see if it has already been invented. In many cases, finding and utilizing patent information can benefit medical device designers. According to the European Patent Office, there are a number of reasons and ways to use patents to your benefit including to "find out what currently exists and build on it," "keep track of who's doing what," and/or "avoid infringing on other people's patent rights" [10]. To find pertinent patents relative to the cardiac device you hope to develop, there are many online databases that can be searched for specific information. A few examples of such databases include the European publication server [11], FreePatentsOnline [12], and Google [13].

42.3.3 Device Ideation

While a "new" medical device is still in the early conceptualization phase, it is important to fully investigate the potential landscape of the design space. This is often referred to as *brainstorming* and is an easy way to obtain a multitude of device options to solve the underlying problem(s). A good approach to a brainstorming session is to understand that any idea is a good idea, which is similar to the idea employed in acting/improvisation comedy of "yes, and…." This statement is seemingly insignificant, but it emphasizes the idea that you need to build upon the ideas of others. If one actor says that they are just coming home from the circus, their counterpart must go along with the premise that it is where they came from and add upon the story. If the counterpart were to say "no, that is not what you did," they effectively stopped all progression in the scene and added nothing of value. In the same way, during a brainstorming session, even though an idea suggested by a colleague may be completely impossible, it is important to run with the idea instead of shooting it down outright. For example, even though it is currently impossible to physically levitate the patient during open-heart surgery, the notion that you could gain access to both the front and the back of the patient without flipping them may spark an idea of how to support patient management during a procedure. In that sense, it is important to maintain these "off-the-wall" ideas because often they can lead to alternative solutions to the problem that was not previously considered.

Once the ideas are compiled, then a session to down-select to the best options or routes is required. Often for a smaller project, 4–10 options may be initially considered, and prototyping can begin on each of them. Generally during this time, the resources are limited, so "quick and dirty" prototypes are often the way to go. The purpose is not to obtain fully working prototypes that portray all of the intended features, but to create rough models (i.e., out of clay or cardboard) that may help one to understand a proposed feature. In many ways, the act of prototyping over the past decade has seen some huge changes. Often when someone says prototyping, a common conception is an engineer sitting in his garage and building a model of a device. However, in recent years, this has transformed to that same engineer, although still likely to work in his garage, creating a CAD model of possible designs and sending it to a 3D printer to have the part(s) actualized from the computer. Due to technologies such as 3D design software and 3D printers, prototyping offers even more possibilities for generating ideas. Note that the New Product Design and Business Development course at the University of Minnesota has required, for several years, that all design teams utilize 3D technology to create at least one of their prototypes.

Whether designers decide to 3D print or build their initial prototypes, they can begin to down-select from these concepts and refine their ideas, to understand the best path forward for their design space. One of the primary purposes of Phase 0 is to develop *proof of concept* and to confirm that the idea can be constructed and eventually manufactured into a viable product.

After proof of concept has been attained and market potential assessed, the design team should select a handful of devices from their initial mock-ups that will be fully prototyped and can be shown to customers for feedback. This is generally a part of Phase 1, where feedback is obtained by collecting the VOC from a large sample size of potential users with varied backgrounds and clinical experiences. The VOC can be obtained through direct questioning, observation, and/or discussions (or use of a prototype) with the customer. The "customers" that will be addressed may consist of many different groups of individuals, including: (1) those who will use the device, (2) those who may be on the receiving end of the device, (3) those who would purchase or pay for the device (reimbursement, insurance companies), and (4) those who could potentially profit from the successful device (investors). These groups of individuals will often

aid in the design process and hopefully improve the overall design of the product, to fully meet the expectations of all the primary customers. For instance, a user may want the device to be easy and intuitive to use, while the payer's focus is on expense and potential benefit to the patient in order to ultimately reduce healthcare costs (e.g., including a reduction in the number of required future procedures). Those who expect to profit from the product (e.g., a company's chief financial officer) may demand that the costs of product development are minimized. Hence, all of these design criteria and concerns must be proactively considered and addressed by the design team, if their desire is to create a product that satisfies the majority of their potential customers.

42.3.4 Risk Mitigation

An important fact to remember is that there are no cardiac devices without risks. These risks may be simple, such as an implantable device recording for longer than required for each time segment, in turn causing the battery to deplete faster and require more frequent replacement. The risks can be as significant as a turbine in a ventricular assist device being stressed to the point where it fractures and sends fragments into the bloodstream. Obviously, neither of these situations is favorable, but, at the same time, one is certainly more acceptable than the other based on the risk that it poses to the patient.

In addition to brainstorming, it follows that all of the potential device defects and failures need to be tracked and accounted. Note that early on in the development process, one needs to consider the risks and benefits of employing any new procedure that utilizes a newly developed device (Fig. 42.4). In order to complete the risk analysis on a device, one typically employs a failure mode and effect analysis (FMEA), generally defined as a procedure in product development and operations management for identifying potential failure modes within a system, including classification of the severity and likelihood of failure. It is considered that any successful FMEA activity helps the research and development team to identify potential failure modes based on past experiences with similar products or processes. This, in turn, enables the team to eliminate such failures with minimum effort and resource expenditure, thereby reducing development time and cost. Complete FMEA on a new prosthetic valve typically creates a 150-page spreadsheet of potential problems, including everything from leaflet material breakdown to misalignment of the prosthesis within a heart. Each identified failure mode must be assessed for how likely it will happen and how severe the impact on the patient could potentially be. If one particular failure mode could feasibly occur in 1 out of every 100,000 patients and have minimal impact on the patient's health, it will not create a drastic design change. However, if within the same occurrence rate a patient may potentially die from the resulting complications, such a failure mode would need to be addressed.

42.3.5 Device Testing

When a cardiac device design moves from Phase 0 into Phase 1 of the design process, a series of testing regimens are initiated to ensure that the device meets the standards set forth by various international governing organizations. These testing methodologies are not only required for the successful market release of a new cardiac device, but they also provide insights into the design and development of the device and/or subsequent devices. For example, the testing results

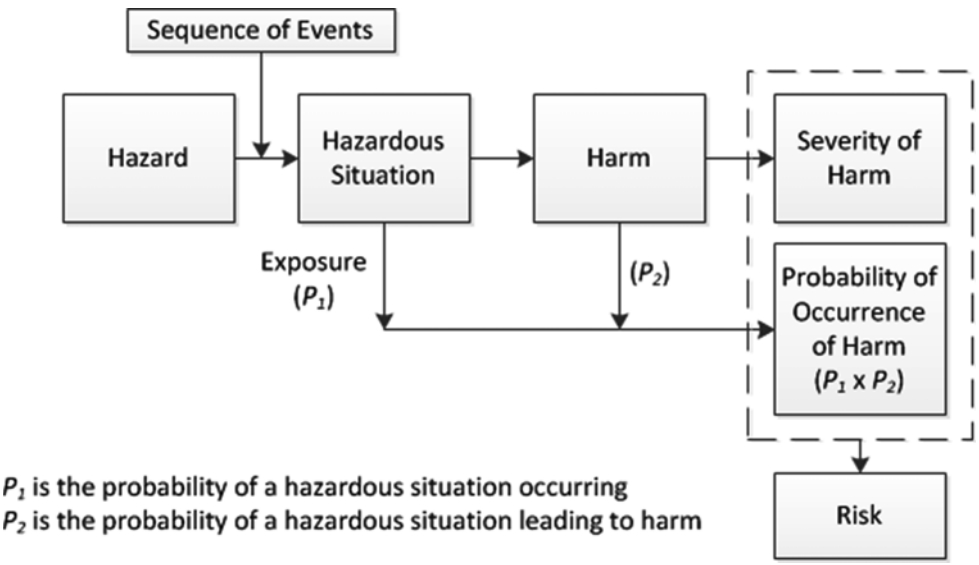

Fig. 42.4 Example flowchart for performing risk estimations

from a cardiac ablation catheter can elicit information to the design team on which portions of anatomy need to be ablated to treat the underlying arrhythmia more effectively. Based on this information, an anatomically shaped catheter like the Arctic Front Advance cryoballoon (Medtronic, Inc.) can be developed to address circumferential ablation needs for the pulmonary vein ostia.

Cardiac device testing can take many forms and often starts with basic static benchtop testing without the use of native biological tissues. In place of biological tissues, surrogate materials can be used as tissue analogues such as silicone, nylon, sponge, or foam [8]. For example, mock silicone substrates approximating the anatomy of a human left atrium and pulmonary veins can be created to investigate the ability for ablation catheters to reach key arrhythmogenic locations within the left atrial anatomy. This is not only a more repeatable procedure due to a decrease in substrate variability, but it is also more cost-effective than obtaining live tissue or live animals to perform such initial basic testing. However, these techniques may not provide necessary insights into specific tissue interactions and/or biocompatibility, which are primary concerns when developing catheters that must be placed and manipulated within a human body.

In the case of cardiac pacemakers and defibrillators, all current therapies involve devices, delivery systems, and monitoring tools that are inserted into the body and exposed to a harsh biological environment. Some of these products (e.g., delivery systems and introducer sheaths) will only be in contact for a short period of time, yet the pacemaker and the cardiac lead may remain in the patient for the rest of his/her life. Note that specific concerns regarding biocompatibility are discussed at length in Sect. 42.2.2 of this chapter. In general, the potential for device rejection can be assessed with in vitro immunological responses to the device; a strong immunological response would be indicative of a possible problem relative to biocompatibility and thus a possible device rejection. However, today most pacemakers and leads are constructed from well-studied materials with known levels of biocompatibility as well as several years of clinical experience. As such, adverse reaction testing is predominantly assessed during chronic animal studies if new materials are used, and adequate data on the materials cannot be leveraged during regulatory submissions to agencies like the FDA.

Another important factor to consider when designing medical devices is the combined effect that temperature and pressure may have on the device. For instance, the polymers and metal wires inside a deflectable delivery sheath will have altered properties after being subjected to human body temperatures while being submerged in a fluid (blood) for prolonged periods of time. In some cases, these altered properties can be advantageous depending on how the device is designed. The informed engineer may choose to design the device, a percutaneous delivery system, for example, to be stiff when entering into the vein/artery, thus allowing for easier placement, and then become more malleable inside the body, as the temperature increases, so as not to cause internal damage to the vasculature.

It is important to consider that before embarking upon the expensive animal testing protocols, which are required to prove the efficacy of a potential replacement valve technology, there is exceptional value in testing the device in reanimated beating heart models. Described at length in Chap. 41, such an approach allows researchers to employ an isolated, living heart as a model to visualize what occurs inside the heart during device deployment and/or how the device may interact with the myocardium throughout all the phases of the cardiac cycle. Additionally, the reanimation of human donor hearts, deemed not viable for transplant, allows for the visualization of specific valve interaction with the varied endocardial anatomy of human hearts, both healthy hearts and those with indications of heart valve disease.

Once in vitro testing techniques have been properly utilized and the device design has been locked in, the development process moves into Phase 3, whereupon the device must be proven safe in appropriate preclinical testing. Generally, this requires extensive testing on animal models (acute and/or chronic) before it can progress into a human clinical trial. With this, a well-written preclinical testing protocol defines that in order to predict the safety and performance of clinical use, a sufficient number of animals of the same species must be used (preferably the same gender and age). In addition, the animals should have both experimental and control valves implanted in them in each position, as indicated by the IFU. The number of animals to be studied may be best determined based upon the risk analysis of the device and the required statistical significance of the experimental design. The duration of the experiment is typically specified in accordance to the parameter(s) under investigation, and each animal must undergo a macroscopic and microscopic postmortem examination. Once the preclinical animal testing is performed using good laboratory practices, a third-party observer (outside auditor) typically will produce a report summarizing all data collected and making a recommendation regarding the clinical safety and performance of the device.

42.3.6 Clinical Testing and Regulatory Approval

Once a cardiac device has been proven safe and efficacious during rigorous animal testing, device developers will then embark upon human clinical trials before it can be properly market released. Current regulatory processes in the USA and European Union differ significantly in the requirements

and guidelines laid out for clinical testing and market approval. However, both regulatory committees share the same fundamental principles and apply frameworks designed to ensure the safe and effective release of medical devices into the market. This section will briefly highlight features of both approval processes, and additional details about the clinical trial process can be found in Chap. 43.

From a legal standpoint, human clinical testing of an unapproved cardiac device in the USA that poses a significant risk to the patient population cannot be initiated without preapproval from the Food and Drug Administration (FDA) in the form of an investigational device exemption (IDE). The IDE is designed to provide the FDA with relevant data on device design and preclinical testing, as well as the intended study protocol. A device company must also apply for an IDE if they wish to expand the indication of an existing device. These clinical investigations may begin at an approved site 30 days after the FDA receives the IDE application, assuming that in-house Institutional Review Board approval has already been obtained and that the FDA has not notified the sponsor that the investigation may not begin [14].

To date, FDA approval is contingent on various factors and based upon the intentions of the device; the rigor associated with the approval process increases with the classification of the device. These device classifications are briefly defined as:

- Class I devices which pose the lowest risk to the patient and include noninvasive devices such as surgical bandages and tongue depressors. These devices are placed under the general rules applied to all medical devices and nothing more. Controls include prohibitions against adulteration and misbranding, requirements on establishing registration and device listing, adverse event reporting, and good manufacturing practices [15].
- Class II devices, such as cardiac catheters, are deemed to pose a high enough risk that regulation through the general controls alone is not sufficient. The majority of class II devices require a premarket notification in the form of a 510(k), to provide data demonstrating that the described device is "of substantial equivalence" to an existing product with regard to its safety and effectiveness. Although a 510(k) can be substantiated through preclinical testing, approximately 10 % of applications include clinical data [14].
- Class III devices which are used to support and sustain human life and would also present a high risk of injury or fatality if the device fails (i.e., implanted cardiac valves). Almost all class III devices require premarket approval by the FDA before they can be legally marketed, thus requiring clinical data demonstrating that the devices are safe and effective in the target population [14]. As such, all types of cardiac replacement valves fall exclusively into this category. Since the valve aids in sustaining human life and device failure could be fatal, the valve must be tested to ensure that it meets the testing required for class III devices.

Another approach for device regulatory approval is the humanitarian device exemption (HDE). This is a regulatory pathway for the accelerated market release of class III devices, an exemption which is intended for devices that address diseases or conditions that affect fewer than 4000 patients a year in the USA. Nevertheless, approval of an HDE requires the sponsor to prove that the device is safe and effective and that all possible risks associated with it are outweighed by the foreseen benefits. Typically, such approval requires smaller clinical trials in fewer institutions, allowing smaller companies to develop class III devices beyond preclinical investigations.

The idiosyncrasies of clinical trial requirements, development, and completion are described in Chap. 43. In summary, gaining market approval in either the USA or the European Union can be a lengthy, expensive, and time-consuming endeavor. Before embarking on the development of a cardiac device, an understanding of these pathways and the intricacies of each regulatory body will help the designer complete the process in the most timely and cost-effective manner possible. To date, the differences between the US and the European Union regulatory bodies result in a large portion of pilot clinical trials and early device testing occurring outside of the USA. Thus, the typical cardiac device is introduced into general clinical practice in the USA 1–3 years after its market release in the European Union [14]. For more details on the design and execution of clinical trials for cardiac devices, the reader is referred to Chap. 43.

42.4 Summary

The key principles for designing any medical device generally hold true for all cardiac devices. A generalize path is to (1) critically define the clinical problem; (2) sketch concepts, develop animations, and build prototype; (3) test the concepts and perform benchtop testing; (4) conduct preclinical studies; (5) initiate clinical trials as needed; and ultimately (6) obtain regulatory approval prior to full market launch of the device. Throughout this process, there are a multitude of factors that need to be considered and taken into account when determining the requirements of the device. These factors include its planned function, biocompatibility, manufacturability, and marketability, to name a few. Although difficult to manage at times, these considerations will be vital for creating a successful product. Any development process for a medical/cardiac device requires a great deal of

upfront effort to ensure that the product will thrive. In today's world, this process relative to cardiac devices can take many years, even up to a decade before a device receives approval to be used in a patient and/or before any real profit may be realized. As such, the cardiac device industry can be a very difficult environment for a start-up, yet it can be exceedingly rewarding not only financially but also due to the fact that the product can directly and indirectly affect millions.

When you consider the breadth and depth of the cardiac medical device field, it is encouraging to observe how it continues to rapidly develop and expand the industry and, in turn, provide innovative and revolutionary clinical technologies. Although many therapies are conceived from a need within the operating room or cardiac catheterization laboratory, their design and development will lead to future novel procedures and techniques that continue to improve treatment for patients with various pathologies. There is little doubt that these innovative improvements will continue to extend and enhance the overall quality of life for millions of patients worldwide.

References

1. Altioke E, Becker M, Hamada S, Reith S, Marx N, Hoffmann R (2011) Optimized guidance of percutaneous edge to edge repair of the mitral valve using real-time 3-D transesophageal echocardiography. Clin Res Cardiol 100:675–681
2. Williams DF (1987) Definitions in biomaterials: proceedings of a consensus conference of the European Society for Biomaterials, Chester, England, March 3–5, 1986. Elsevier, Amsterdam and New York
3. Schoen FJ, Goodenough SH, Ionescu MI et al (1984) Implications of late morphology of Braunwald-Cutter mitral heart valve prostheses. J Thorac Cardiovasc Surg 88:208–216
4. Schoen FJ, Levy RJ (2005) Calcification of tissue heart valve substitutes: progress toward understanding and prevention. Ann Thorac Surg 79:1072–1080
5. Ellis CR (2013) The extinction of small caliber transvenous ICD leads: downsizing in a race to a recall. Heart Rhythm 10:191–192
6. Hauser RG, McGriff D, Retel LK (2012) Riata implantable cardioverter-defibrillator lead failure: analysis of explanted leads with a unique insulation defect. Heart Rhythm 9:742–749
7. Myken PSU, Bech-Hansen O (2009) A 20-year experience of 1712 patients with the Biocor porcine bioprosthesis. J Thorac Cardiovasc Surg 137:76–81
8. Ulrich KT, Eppinger SD (1995) Product design and development. McGraw-Hill, New York
9. The United States Patent and Trademark Office website www.uspto.gov. Accessed 10 Aug 2014
10. Zenios SA (2010) Biodesign: the process of innovating medical technologies. Cambridge University Press, Cambridge
11. The European Patent Office website www.epo.org. Accessed 10 Aug 2014
12. European Publication Server https://data.epo.org/publication-server/?lg=en. Accessed 17 Dec 2014
13. Google Patents website www.google.com/patents. Accessed 17 Dec 2014
14. Kaplan AV, Baim DS, Smith JJ et al (2004) Medical device development: from prototype to regulatory approval. Circulation 109:3068–3072
15. Chai JY (2000) Medical device regulation in the United States and the European Union: a comparative study. Food Drug Law J 55:57–80

Clinical Trial Requirements for Cardiac Devices

43

Jenna C. Iaizzo

Abstract

Early medical device concepts that show promising safety and/or efficacy results in preclinical trials, bench top testing (including accelerated wear testing), a virtual prototyping environment, and/or computation modeling studies will eventually be implanted in humans. Currently in the United States, the required time to develop a new cardiac device and gain approval for market release is highly dependent on the time it takes to perform proper clinical trials, i.e., to receive the needed clearance or approval from the Federal Drug Administration.

Keywords

Clinical trial • Cardiac devices • Regulatory agency • Food and Drug Administration

Abbreviations

CE	Conformité Européenne or European Conformity
CEC	Clinical Events Committee
CFR	Code of Federal Regulations
DSMB	Data Safety Monitoring Board
EC	Ethics Committee
EOA	Effective orifice area
FDA	Federal Drug Administration
GCP	Good Clinical Practice
GLP	Good Laboratory Practice
GMP	Good Manufacturing Practice
IDE	Investigational Device Exemption
IRB	Institutional Review Board
ISO	International Organization for Standardization
OPC	Objective performance criteria
PMA	Premarket approval

J.C. Iaizzo, MBA (✉)
Medtronic, Inc., Minneapolis, MN 55428, USA
e-mail: jiaizzo@gmail.com

43.1 Introduction

Clinical trials play a crucial role in the process of bringing medical devices, specifically cardiac devices, to the market and for providing continued scientific clinical data after commercialization (Fig. 43.1). Prior to executing a clinical trial, researchers, scientists, and engineers cannot predict how the newly developed devices will perform in a human body. Furthermore, most cardiac devices are typically class III life-sustaining devices that are implanted in patients with life-threatening conditions, but there is a broad spectrum of the patients receiving these therapies that will likely have many other clinical complications; in some cases, these complications may adversely affect the potential success of novel technologies. Therefore, carrying out a carefully designed and comprehensive clinical trial provides an significant opportunity to examine the outcomes of the new cardiac device in humans and, in turn, the resultant clinical data gives patients, physicians, and the entire scientific community the information needed to potentially use the new device. Yet today, the primary purpose of a clinical trial is to provide valid scientific data about the safety and/or efficacy of a device, resulting in clinical evidence for future use or retraction of a therapy.

P.A. Iaizzo (ed.), *Handbook of Cardiac Anatomy, Physiology, and Devices*, DOI 10.1007/978-3-319-19464-6_43

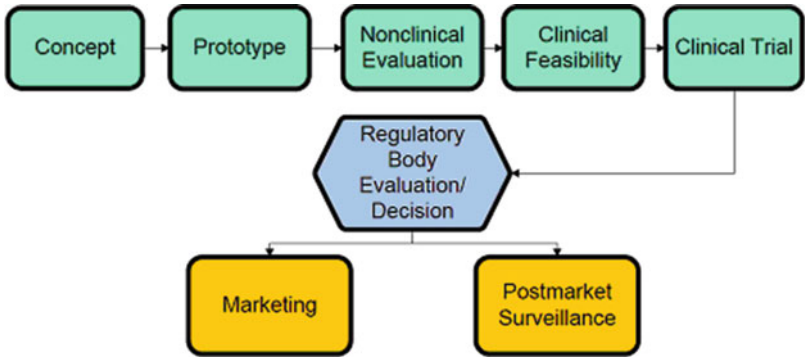

Fig. 43.1 Timeline of medical device development ©2013 Heart Valves: From Design to Clinical Implantation, Clinical trial requirements for cardiac valves, Iaizzo JC, Lovas ATF. With kind permission of Springer Science+Business Media, New York

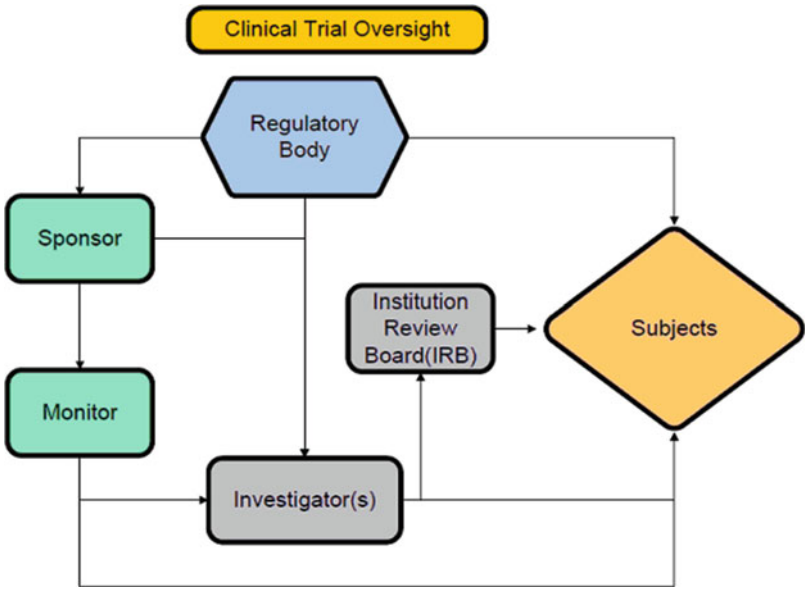

Fig. 43.2 Clinical trial oversight ©2013 Heart Valves: From Design to Clinical Implantation, Clinical trial requirements for cardiac valves, Iaizzo JC, Lovas ATF. With kind permission of Springer Science+Business Media, New York

With the diversity of cardiac devices, there are various types of clinical trials that can be defined, from trials where a novel valve technology is being used for the first time (*first in human* studies) to post-market trials in which a cardiac therapy has obtained regulatory approval but is studied further to examine long-term effects, pursue additional indications, and/or to obtain more specific information about the overall therapy. In other words, clinical evidence is vital not only to demonstrate the safety and efficacy of a device/therapy in humans but also to further examine how well the device works compared to standard of care, other devices, and/or concomitant treatments. In the specific case of a newly developed heart valve, studies will often be designed to compare the new valve against the native valve, other heart valve devices, and/or the current standard of care treatments. Using the example of planning a clinical trial for a new heart valve, this chapter provides a general summary of the present state of clinical trials, including an overview of (1) the current stance of regulatory bodies that oversee trials, (2) specific features of a trial design, and (3) the many considerations involved in the proper implementation of heart valve clinical trials.

Regarding the design of a clinical trial, the following groups/individuals may be identified, each with their specific role(s) (Fig. 43.2):

***Sponsor*(*s*)**: The developer of the technology seeking approval for market release.

***Investigator*(*s*)**: Non-biased individuals that will implant/deploy the novel technology and will also be responsible for individual patient follow-ups. In some cases, investigators can also develop their own field clinical trial(s).

***Monitor*(*s*)**: Individuals responsible to ensure that the trial is performed in an ethical and proper fashion. They usually work for the sponsor and make frequent visits to participating institutions to review data and regulatory documents.

Regulatory bodies also have their own process for auditing sponsors and investigators through their Bioresearch Monitoring group(s).

***Institutional Review Board* (*IRB*)/*Ethics Committee* (*EC*)**: The overseeing body at a given institution that is ultimately responsible for ensuring that the clinical protocol is appropriate and that the institutional investigators perform the study in a proper and ethical manner. These boards may have different names according to the institutional structure.

Subjects: Individual patients who were deemed appropriate to be enrolled (meeting all inclusion criteria and none of the exclusion criteria) into the planned clinical trial and who provided informed consent to participate.

43.2 Regulatory Bodies

Regulations and the regulatory bodies that govern both cardiac devices and clinical trials play important roles in how new technologies reach the market. A solid partnership between a sponsor and a regulatory body, aided by clear communication, can affect whether the technology can reach the market in an expeditious manner. Regulatory bodies are important, as they ensure consistency in clinical trials and that they are run properly in order to provide the supportive scientific evidence required. Specifically, there are numerous regulatory bodies that provide oversight for cardiac device clinical trials throughout the world. A brief overview of the regulatory bodies from three different countries follows, yet our discussion focuses mainly on the Food and Drug Administration (FDA) in the United States.

43.2.1 Food and Drug Administration (United States)

The FDA is responsible for regulating medical devices and therefore oversees the associated clinical trials exclusively within the United States. The FDA's mission statement consists of two primary parts: (1) promoting public health by promptly and efficiently reviewing clinical research and taking appropriate action on marketing of regulated products in a timely manner and (2) protecting public health by ensuring a reasonable assurance of safety and effectiveness of devices intended for human uses [1]. The Center for Devices and Radiological Health (CDRH) is the branch that oversees medical devices. Cardiac devices that incorporate other therapies (i.e., pharmacological agents) will need to confirm if they will work through CDRH and/or the Center for Drug Evaluation and Research (CDER).

In the United States, there are three regulatory classes of devices based on the considered levels of risk involved. All class I–III devices are subject to general controls, meaning the FDA reviews factors such as labeling, registrations, etc. Class I devices have the lowest amount of risk and regulatory controls (devices such as elastic bandages and surgical gloves). Class II devices must meet specific performance standards in addition to all class I requirements (devices such as surgical drapes). Most stringently, class III devices require premarket approval (PMA) to ensure their safety and efficacy. As such, class III devices are considered as the riskiest category of devices and include devices such as implantable pacemakers and heart valves.

It should be noted that the FDA regulations for medical device products are detailed in Title 21 of the Code of Federal Regulations (CFR). The most applicable parts of CFR 21 that apply to cardiac devices and clinical trials include Part 812 (Investigational Device Exemption, or IDE) and Part 814 (PMA). Most new and novel cardiac devices are required to undergo IDE clinical trials before receiving FDA approval. As the regulatory landscape is typically in constant flux, it is crucial to reference and follow current guidance and regulations set forth by the respective governing regulatory body.

In the example of heart valves, there is specific guidance in documents like the FDA's Heart Valves—IDE and PMA Applications Draft Guidance; these documents state that "a replacement heart valve is a device intended to perform the function of any of the heart's natural valves" [2]. A replacement heart valve is defined as a pre-amendment-type device, that is, a device marketed prior to passage of the Medical Device Amendments to the Federal Food, Drug, and Cosmetic Act (the Act).

Furthermore, this FDA draft explains that clinical trials are necessary to evaluate most new replacement heart valve designs, and it also recommends that clinical investigations are executed by following the methods described in ISO 5840:2005 or an equivalent document. Specifically, the document ISO 5840:2005 is a guide for cardiovascular implants and valve prostheses provided by the International Organization for Standardization (ISO) [3]. When developing a clinical database and trial strategy, the appropriate FDA guidance should be referenced.

43.2.2 Other Regulatory Bodies

In Europe there are various *notified bodies* that provide oversight of clinical trials. The most prevalent regulatory oversight applies to the 27 countries in the European Economic Area; these are countries required to obtain a *CE mark* (Conformité Européenne or European Conformity). Importantly, the criteria to receive a CE mark in Europe are notably different than those for securing FDA approval. As mentioned previously, to receive approval for a new technology in the United States, the manufacturer must demonstrate the device to be reasonably safe and effective. To receive approval to release a device to market in the European Union, the manufacturer must demonstrate that the medical

device is safe and that it performs in a manner consistent with the manufacturer's intended use [4]. Interestingly, given these differences in geographic regulatory approval, most manufacturers typically seek approval in Europe or other countries before the United States. Moving into other countries poses different obstacles which may influence the intended quality and importance of every clinical trial completed for the new device.

43.2.3 Good Clinical Practice Oversight

Similar to the importance of following Good Manufacturing Practice (GMP) and Good Laboratory Practice (GLP) when prototyping cardiac devices, it is important to follow guidelines for how to appropriately conduct clinical studies that could affect the safety and well-being of human participants. Good Clinical Practice (GCP) was developed by a collaborative group of regulatory authorities worldwide, including the European Union, Japan, and the United States by the International Conference on Harmonisation. Effective in 1997, GCP provides international assurance that data and results of clinical investigations are credible and accurate and that the rights, safety, and confidentiality of participants in clinical research studies are respected and protected. More specifically, GCP consists of 13 principles which are detailed in Table 43.1.

Table 43.1 13 Principles of good clinical practice [5]

Ethics
1. Ethical conduct of clinical trials
2. Benefits justify risks
3. Rights, safety, and well-being of subject prevail
Protocol and science
4. Nonclinical and clinical information supports the trial
5. Compliance with a scientifically sound, detailed protocol
Responsibilities
6. Institutional Review Board/Independent Ethics Committee approval prior to initiation
7. Medical care and decisions by qualified physicians
8. Each individual qualified (education, training, experience) to perform his/her tasks
Informed consent
9. Freely given from every subject prior to participation
Data quality and integrity
10. Accurate reporting, interpretation, and verification
11. Protects confidentiality of records
Investigational products
12. Conform to Good Manufacturing Practice and used per protocol
Quality control/quality assurance
13. Systems with procedures to ensure quality of every aspect of the trial

43.3 The Generalized Clinical Trial Cycle/ Process

Addressing all aspects of a clinical trial in depth is an enormous undertaking and beyond the scope of this chapter; thus, the following sections will highlight some of the foundational methods and processes of a typical heart valve clinical trial which can generally be translated to the complexities of other cardiac devices. As you can see in Table 43.2, there are many tasks that need to be addressed with the development and execution of a clinical trial. It is important to note that some of these tasks may occur simultaneously.

43.3.1 Features of a Trial Design for a Newly Developed Cardiac Device

It is pertinent to research and understand all current published information and relevant heart valve trial data prior to planning and executing a clinical trial. There is much to be gained from studying the details of previous trial designs, as well as the subsequent outcomes associated with those trials. In regards to gaining FDA approval for any cardiac device, the importance of clinical evidence cannot be stressed enough. In the beginning stages of planning a clinical trial design, associated publications and previous research may help shape important components for the new trial, such as: patient inclusion/exclusion criteria, statistical designs employed in such trials, and/or the general patient populations to be studied.

Table 43.2 Standardized clinical research process

1.	Prepare a clinical plan
2.	Recruit investigators
3.	Prepare protocol
4.	Prepare case report forms
5.	Prepare informed consent form
6.	Perform investigator site visit
7.	One-on-one investigator reviews, including clinical plan, protocol, case report forms, and informed consent form
8.	Obtain an investigator agreement
9.	Obtain IRB approvals for each participating institution
10.	File an IDE
11.	Obtain IDE approval
12.	Perform periodic investigator meetings
13.	Conduct the clinical study, i.e., a multicenter study
14.	Monitor the multicenter study
15.	Conclude study
16.	Compile data from each institution
17.	Analyze overall collected data
18.	Write final clinical report

A well-controlled clinical investigation includes a clear objective and defined methods of analysis. More specifically, the objectives should address the proposed medical claims for the investigational device and these objectives should be refined to explicitly address the safety and efficacy of the heart valve in a defined population. Next, it is important to structure a trial so there can be a valid comparison to controls. For example, in current transcatheter valve therapy trials, the new therapy (transcatheter valves) is directly compared to a standard open-heart valve surgery. A control group gives the results a meaningful comparison to an existing therapy or treatment, which is important to the scientific community and may be crucial for future marketing. Often, an appropriate control group can be identified by performing a careful and thorough literature search or seeking out the key opinion leaders in the related field. Furthermore, performing early research on the specific disease or conditions that the heart valve will treat is equally important, in order to understand the natural progression of the disease or condition and the current benefits or limitations of other treatments. It should be noted this step is often completed in earlier phases of device prototyping, but it is recommended that designers review the research once again just prior to planning the clinical trial. Finally, literature searches on similar treatments/heart valves can also assist in identifying the appropriate disease populations and justifying the inclusion and exclusion criteria for the trial.

When the patient population and treatment/control cohorts are clearly identified, one needs to consider the next set of factors that impact the ultimate design. First, the type of trial design must be determined, whether it is randomized, blinded, or double blinded. Each of the designs may strengthen the significance of the trial results, while also minimizing bias and providing comparability of groups. Well-defined trial endpoints are of great significance for the overall success of a clinical trial. For example, typical heart valve trial endpoints should encompass both safety and efficacy measures. Note that adverse events often comprise the safety endpoint for a given trial. Typically, effectiveness endpoints are found in the form of the presence or absence of a clear, definite effect on a patient, e.g., death or the resultant effective orifice area (EOA). Table 43.3 provides a list of key steps to consider in designing a clinical trial for the development of a new heart valve technology.

An often overlooked aspect of the early execution or startup of a clinical trial is a high degree of physician involvement or engagement. While physicians play a major role throughout the execution of the trial, it is important to gain physician insights into the overall design and planning of a clinical trial early on in the process. Being that physicians are ultimately the users of the heart valve being studied, their clinical knowledge can be valuable in creating a well-designed and thorough clinical trial.

43.3.2 Reimbursement and Payer Information

While the process for development of clinical trials is essential to understanding the appropriate use of medical interventions of all types, it is also important for payers to understand potential coverage for the device. When designing a clinical trial, it is recommended that one reads the National Coverage Determination for Routine Costs in Clinical Trials (310.1) provided by Centers for Medicare and Medicaid Services [6].

Table 43.3 General steps in the development of a clinical study design

• Develop study objective which includes research objective, device claims, and pilot of feasibility study
– Note that the study objective should be phrased as a research question posed to address medical claims for the device – Refine the research question to specifically address the safety/effectiveness of the device in a well-defined patient population for one or more outcomes – Perform a pilot or feasibility study; if claims are inadequately known, conduct a pilot or feasibility study on a small subgroup of patients or subjects. As such, the pilot study objectives are to identify claims more precisely, test study procedures, and/or obtain estimates of properties of outcome and/or other variables
• Properly identify and select variables/parameters • Define study population(s) and appropriate clinical controls
– Prior to study, define rigorous inclusion/exclusion criteria – Define subset of the general population representing the target population for the device
• List all parameters of the specific study design • Define study masking (i.e., your bias control) • Define number of study sites and potential investigators
– Fit the needs for a sufficient number of eligible patients in a timely fashion – Center must be capable of processing patients – Engage competent staff members who work well on the trial – Identify investigators willing to recruit patients and conduct the study as specified in the protocol – All center individuals need be qualified to perform trial parameters
• Determine proper patient sample size, i.e., the study is properly statistically powered

43.3.3 Clinical Trial Site Selection

By definition, investigational sites include all centers implanting the cardiac device that submit data as part of the investigation. The initial selection of the proper hospitals/institutions and physicians to participate in a given clinical trial is a crucial step toward executing a successful clinical research trial. After time and money are invested in creating the trial design and protocol, the actual execution can affect the outcome of the trial. Therefore, all possible steps should be taken to eliminate extraneous variables such as reeducation or elimination of a site that does not abide by the set protocol. Furthermore, the selection of appropriate physicians to participate in a clinical research trial is another variable to carefully examine before proceeding with the trial. It is critical to qualify the experience of the physicians relative to their ability to utilize novel or investigational therapies similar to the device you are investigating. It would be strategic to identify and recruit physicians already well established in the related therapy or device and those that are familiar with conducting complex clinical trials. These physicians will become the trial investigators responsible for the precise execution of the protocol at each institution or site. Not only should the physician investigators have adequate experience with clinical trials, but it is important to ensure that the institution's support staff is knowledgeable and skilled in their execution as well. It is good practice to check the institution's previous clinical trial performance. Finally, it is essential to make sure the physician investigators have not been disbarred, banned, or excluded from participating in any type of clinical trial.

Another pertinent variable to consider when selecting sites is the actual geographic location. The clinical trial design and projected subject population(s) are helpful when identifying the amount of sites needed in the trial. As such, typically large metropolitan area hospitals are chosen to participate in clinical trials from the perspective that they should be able to quickly recruit the desired patients. However, there are regional hospitals that receive a high amount of referrals; thus, these hospitals may be able to effectively contribute to enrollment in clinical trials. Ensuring that an investigational site has an adequate potential patient population is important, given the amount of time it takes to train the personnel at a site and activate them as a part of the trial. It is interesting to note that a very small percentage of American senior citizens participate in clinical trials, although the elderly bear a disproportionate burden of disease in the United States [7]. Sites that have experience working with and successfully recruiting the appropriate patient populations can be immensely helpful in enrolling subjects in a timely manner to complete a trial.

The potential for conflicts of interest is also something to manage when choosing clinical sites for a trial. More specifically, cardiac device clinical trials typically involve a high level of physician engagement in the trial and the technology/therapy being tested. Therefore, to legitimize their participation, it is critical to rule out any potential bias with regard to how the trial is run and the quality of the data being captured. It should be noted that many sponsors and clinical sites have built-in regulations or processes to cover any potential conflicts of interest.

43.3.4 Clinical Trial Execution

Throughout the execution of a clinical trial, there are multiple activities happening simultaneously that need to be managed (also dependent on design of the trial). For example, most subjects in the trial will require follow-up visits. Specifically for heart valve trials, it is important to design a trial with multiple follow-up visits in order to capture long-term data on the subject population(s). With clinical evidence being the primary end product of a clinical trial, it is crucial to ensure that institutions capture valid and accurate data in a highly efficient manner. Recently, there have been several technological advances to make capturing trial data more efficient and user-friendly for the hospital/sites. The trial data is captured on what most clinical trial sponsors called *case report forms*. Historically, the hospitals/sites would complete hard copy forms and send them back to sponsor(s); this could be quite cumbersome especially with monitoring and processing the data to ensure accuracy. Currently, nearly all trial data are collected electronically (sites enter data directly into an online case report form, and the sponsor can see the data in real time). Therefore, as new trials are rolled out and more heart valves are being studied, it will be critical to keep up with the ever-evolving technologies that are being developed and deployed to ensure the integrity, quality, and efficiency of clinical trials.

An interesting trend in recent transcatheter heart valve trials is the development and utilization of screening committees. For example, a screening committee for a heart valve transcatheter trial would typically be compromised of well-established, objective cardiac surgeons and interventional cardiologists. As such, it is imperative that these individuals also be familiar with the details of heart valve technologies and the trial design. Furthermore, it is important that the screening committee be knowledgeable about the patient population which the trial is enrolling as well as the specific inclusion/exclusion criteria. The screening committee could also be used to assist in determining and identifying the appropriate patients for a properly designed trial. It is critical to recruit an overall subject population that is highly consistent; this is especially important when multiple clinical sites/hospitals are participating in the trial.

Assuming the trial has progressed to the point of near completion, there are several other factors to consider.

For example, all subjects should be accounted for in the final clinical report. It is recommended that complete subject accounting, on a per subject basis, for each cohort is provided. Therefore, the report should include: (1) the total number of subjects expected for follow-up, (2) number of subjects discontinued because of death or device removal, and (3) number of subjects that were actually evaluated at each preplanned time point.

Depending on the type of trial and the primary endpoints listed in the protocol, submitting for regulatory approval may happen before the trial is fully complete. For example, in an IDE study with primary endpoints at 1 year of subject follow-up, an application for PMA may be submitted and granted prior to the end of all subject follow-up. Nevertheless, this will depend on the accepted trial design. It should be noted that the FDA expects long-term data for most IDE heart valve trials. Therefore, in some trials, the specific heart valve may be commercialized prior to the end of all follow-up visits, but regular reports continue to be submitted to regulatory bodies containing the long-term data. Finally, the overall timeline for submission for regulatory approval will ultimately depend on the statistical methods and analytical processes laid out in the final trial protocol. It is important that this section of the device trial protocol be carefully followed, as it is agreed upon by the FDA or regulatory body prior to initiation.

Excerpts from the Draft Guidance for Industry and FDA Staff Heart Valves—IDE and PMA Applications are outlined below to provide clear direction from FDA's perspective on the conduct of a heart valve clinical trial [2]. Again, it is important to reference the appropriate FDA guidance that your cardiac device may fall under.

43.3.5 Data Collection Within the Clinical Trial

As clinical evidence to support the use of the investigative heart valve is the ultimate product of conducting a clinical trial, the remainder of this chapter will focus on the collection of data and various regulations one needs to consider related to clinical evidence. FDA guidance provides detailed insight into what is expected in a data collection plan and therefore should be referenced frequently throughout development of the protocol. Listed below is an important narrative from the FDA Guidance document that one should understand prior to data collection:

> The sponsor who discovers that an investigator is not complying with the signed agreement, the investigational plan, requirements in 21 CFR Part 812 or other applicable FDA regulations, or any conditions of approval imposed by the reviewing investigational review board or FDA is responsible for promptly securing the investigators compliance or discontinuing shipment of the device to the investigator and terminating the investigator's participation in the investigation (21 CFR 812.46(a)). Your protocol must ensure that the investigation is scientifically sound by ensuring consistency between the indication studied and the subject inclusion and exclusion criteria (21 CFR 812.25(b)). In all study designs, you should ensure that investigators collect the appropriate information. Specifically, you should ensure that the clinical data collection forms used by the investigators and institutions are consistent with the clinical protocol. You should also ensure that informed consent document(s) is consistent with the clinical protocol [2].

43.3.6 Data Collected for Each Subject Enrolled into a Clinical Trial

Each subject enrolled in the study should be followed and appropriate data collected according to the study protocol. Additionally, follow-up data should be collected for each subject until the entire study is terminated for all subjects; this follow-up data is typically collected during office, clinic, or hospital visits. It is recommended that telephone follow-up should be used only to verify death or loss to follow-up. Being data should be collected until the entire study is terminated for all patients, the follow-up period may be significantly longer than stated in the original study protocol for most patients. Accordingly, an informed consent must be received for the planned follow-up period from all subjects (21 CFR 50.25(a)(1)). Therefore, any subject not willing to fully participate in the study, which includes the follow-up period, should not be enrolled [2]. Most institutions have a thorough consent process, as governed by regulatory bodies and their own IRBs. This consenting process will ensure that subjects being enrolled in the trial will complete all follow-up visits; however, trial attrition still occurs. There is the potential that some patients will enroll in a clinical trial to obtain the latest technologies, with little or no intent of being part of post-monitoring.

The FDA's guidance goes into more detail about the specific data they would like to see collected, as it will help ensure consistency across populations receiving heart valves (Table 43.4). For example, follow-up data for most heart valve trials should include the normal ranges for the clinical laboratory blood tests evaluated, according to the normal

Table 43.4 Echocardiographic hemodynamic data (stratified by valve size for each patient enrolled)

• Peak pressure gradients
• Mean pressure gradients
• Effective orifice areas
• Existence and/or relative degree of valvular regurgitation
• Native valve's effective orifice area index
• Native valve's performance index
• Resting cardiac output
• Average cardiac index

ranges used by the laboratories that conduct the testing. Plasma free hemoglobin is preferable to serum lactate dehydrogenase, haptoglobin, and reticulocyte count for the evaluation for hemolysis because it is considered that plasma free hemoglobin has higher clinical sensitivity for the detection of hemolysis than the other three laboratory tests. The diagnostic preoperative data collected should include the normal ranges for the clinical laboratory blood tests that are evaluated, with the normal ranges being determined by the laboratories used [2]. As detailed, it should be apparent the amount of data and work institutions will undertake to participate in new heart valve trials.

Typically, enrolled patients will be followed subsequent to the procedure by their personal cardiologists (not the implant surgeon/interventionalist), and often there will be preclinical data available for a given patient as well. Therefore, the study investigators should work in conjunction with the patients' physicians to collect all appropriate data from the correct time periods. This may be better accomplished if the study investigator or the sponsor obtains contact information for the following physician, so he/she can be advised of the actual study protocol. It is important to note that only study procedures (out of the standard of care scope) should be performed by investigators trained on the trial protocol.

As there is increasing interest in all valve positions, FDA guidance has started to address specific details for these different positions. It is recommended for trials that involve replacement of pulmonic valves and/or pulmonic-valved conduits that one should calculate the effective valve orifice area, since the cone shape of the right ventricular outflow tract makes echocardiographic measurements of the right ventricular outflow tract diameters very difficult. This measurement, if identified within a clinical design, may lead to potentially inaccurate calculations, i.e., if one employs a continuity equation method for the pulmonic valve EOA. Similarly, for replacement pulmonic valves and pulmonic-valved conduits, the FDA does not recommend calculation of EOA indexes and performance index data, which are determined using EOA data [2].

43.3.7 Clinical Trial Follow-Ups

In general, each subject entered into the study should be followed and appropriate data collected according to the study protocol, and associated follow-up data should be collected for *each* subject until the *entire* study is terminated for *all* subjects. Unfortunately, this is not always the case; therefore, it is important to plan for potential attrition in the statistical plan by having an adequate population enrolled greater than the minimum number of patients needed for an appropriate analysis. It is helpful to determine the appropriate subject population by referring to the term *follow-up in patient-years*. For example, the recommended follow-up of 800 patient-years is statistically derived as follows. Single sample one-sided hypothesis testing can be used to demonstrate that each of the complication rates associated with the investigational device is less than 2 times the objective performance criteria (OPC) for that complication. The appropriate null hypothesis is that the true rate associated with the investigational device is 2 or more times its OPC. To reject this null hypothesis is to accept the alternative hypothesis that the true rate associated with the investigational device is less than 2 times its OPC [2].

Generally, in order to provide a clinically sufficient amount of data on the investigational heart valve technology, it is generally recommended by the FDA that all subjects be followed for 1 year or more. If a clinical investigation is for one valve position, it is recommended that at least 300 subjects are followed for 1 year or more, for a total of 800 patient-years of follow-up. If the study is for two valve positions (i.e., aortic and mitral), it is recommended that at least 150 subjects are followed for 1 year or more for each valve position, for a total of 400 patient-years of follow-up per valve position. It is generally recommended that one conducts a valve technology clinical study at eight or more primary centers, with 30+ subjects implanted at each center for a one-position study and 15+ subjects implanted at each center for a two-position study [2]. As noted within the FDA recommendations, using fewer than eight primary centers can introduce unanticipated bias into these complex clinical trials.

Some heart valve technologies may be implanted or deployed in more than one of the four heart valves. Therefore, it has been specifically recommended by the FDA that, for one-position and two-position studies, trials be designed for the subsequent implanting of 15+ subjects for each size and each position of valve. In other words, if a study assesses the potential for both aortic and mitral replacement with a given technology, the study should enroll 15+ subjects at the aortic position and an additional 15+ subjects at the mitral position, for each valve size. It should be noted that this recommendation of 15 subjects implanted per size per position criterion is based on statistical calculations for echocardiographic EOA data; these calculations showed that in order to assure a sufficiently narrow 95 % confidence interval, the minimum number of subjects implanted with each valve size was 15. If you were to design a trial in which you hoped to omit any valve size, the FDA specifically recommends that you explain how the data you plan to collect would still remain representative of all the sizes that you intend to market. With the rapid development of cardiac imaging capabilities, any well-designed clinical trial on a valve technology will also require follow-up image assessments (Table 43.5).

43.3.8 Complications and Complication Rates

The types of complications to expect from patients treated with newly developed valve technologies include valve thrombosis, major hemorrhage, perivalvular leak, and/or stroke. For the initial three complications, the rate of occurrence with current technologies is typically less than 1.2 % per patient-year (i.e., within 800 patient-years) for aortic and mitral positions combined [2]. Therefore, such rates typically must be matched or exceeded by the novel technology. It is generally recommended for valve technologies that the complication data include hemorrhages resulting from all causes (all-cause hemorrhage) rather than just hemorrhages related to anticoagulant therapy (anticoagulant-related hemorrhage). Additionally, it is typical that the complication data include all-cause reoperations, valve-related reoperations, explants, all-cause deaths, and valve-related deaths.

The clinical trial sponsors are ultimately responsible for ensuring proper monitoring of the investigation and must select non-biased monitors qualified by appropriate training and experience. For example, the FDA generally suggests that each trial sponsor (designer) establishes a Data Safety Monitoring Board (DSMB) to review adverse events and recommend study termination if safety concerns are warranted. Nevertheless, the DSMB should establish criteria for recommending study termination for safety reasons before the study begins and should meet at least two times during the study to monitor adverse events. Furthermore, it is recommended that the DSMB should include members who are independent from the study sponsors and investigators; additionally, two or more members should be physicians including a cardiothoracic surgeon and a cardiologist. Additionally, if the study involves statistical analyses, one member should be a qualified statistician.

It is also recommended that the sponsor establish a Clinical Events Committee (CEC) in order to adjudicate adverse events as being valve technology related or not and to classify the severity of an elicited adverse event. Similar to the DSMB, the CEC should have members who are independent from the study sponsors as well as selected clinical investigators. It is important to charter CEC and DSMB committees for a trial, as they add independent validation to the credibility of the research. As the execution of the study proceeds and endpoints are reached, the CEC and DSMB committees will be commissioned to adjudicate the data which will be necessary for the PMA submission. Table 43.6 outlines the recommendations for what should be included in a PMA submission.

A PMA should include the actual number of all noted adverse events. In addition, it is generally recommended that

Table 43.5 Reports included as follow-up data

• Echocardiograms
• Cardiac catheterizations
• Other cardiovascular imaging procedures, including CT and MR scans
• Chest X-rays

Table 43.6 FDA recommendations for a final premarket approval report

• Summary of patients/subjects not completing the study (stratified by lost to follow-up, death, or explant)
• Specific locations of all investigational sites in which procedures were performed
• Relative comparison of preoperative and postoperative NYHA functional class (presented as the percentage of subjects in each class at baseline, at each follow-up time point, and as the percentage of subjects at each follow-up time point who improved, worsened, or did not change in class)
• Pre-implant/procedure effective orifice area of the given heart valve
• Number of implanted patients/subjects stratified by the given investigational sites, replacement/repair valve positions (e.g., aortic, mitral, or double valve), and/or employed valve sizes
• Number of treated patients/subjects followed to 1 year post-procedure, stratified by investigational site, valve treated (e.g., aortic, mitral, or double valve), and/or employed valve sizes
• Follow-up duration information (total and by valve position) including mean follow-up times, standard deviations, range of follow-up, and cumulative follow-up in patient-years
• Any identified confounding factors (e.g., by hazard regression analysis applied to identify risk factors, gender, age at implant, preoperative NYHA functional classification, previous valve surgery, concomitant coronary artery bypass surgery, implant position, and implant size) which might affect the incidence of reoperation, explant, and/or death
• Patient compliance data for follow-up visits (e.g., NYHA functional classification data, echocardiographic data, and/or clinical laboratory results)
• Complete list of complications by patient identification number
• Summary of any and all subject complaints received
• All case report forms (i.e., for a 10 % random sampling of the subject population)
• All copies of case report forms for each and every subject not completing the study
• Explant analysis data obtained for each and every case (i.e., when a valve was explanted or an autopsy was performed)
• All death reports, including autopsy reports when available, especially when the cause of death was classified as non-valve related

the trial sponsor expresses early complication rates as the number of adverse events divided by the total number of subjects [2]. A sponsor should also include linearized late complication rates; these rates are calculated as the number of late adverse events divided by the total number of late patient-years.

With the rapidly changing regulatory environment and concerns for ensuring safety of cardiac valves, the clinical trial process will continually evolve. It is important to keep up to date on additional requirements and landmark trials that are testing devices similar to the new heart valves being developed today. The FDA provides valuable resources on their website along with a repository for most clinical trials that are occurring in the United States (www.clinicaltrials.gov).

43.4 Summary

Clinical trials are an important and critical step in bringing new technologies, such as cardiac devices, to the market. As detailed above, there are many facets involved in the development and execution of a clinical trial. This chapter provides a high-level overview of these aspects, which may vary from product to product. Setting up a calculated trial and executing it proficiently will affect the ability to successfully market a cardiac device. The clinical trial requirements and regulatory and reimbursement landscape are vast and constantly changing. When designing a clinical trial, it is important to keep in mind the various regulatory requirements, the importance of GCP, the selection of participating institutions, data collection, endpoints, and overall execution of the trial. With such a heavily regulated environment as well as the intricacies of cardiac devices, ensuring proper conduct to ensure high quality data is crucial. This chapter provides a general overview of the present state of human heart valve clinical trials, including: (1) the current positions of regulatory bodies that oversee trials, (2) specific features of a trial design, and (3) considerations involved in the proper implementation of trials.

References

1. U.S. Food and Drug Administration (2010) What we do. U.S. Department of Health & Human Services. http://www.fda.gov/AboutFDA/WhatWeDo/default.htm. Accessed 17 Dec 2014
2. U.S. Food and Drug Administration (2010) Draft guidance for industry and FDA Staff Heart Valves—Investigational Device Exemption (IDE) and Premarket Approval (PMA) Applications Draft Guidance. http://www.fda.gov/downloads/medicaldevices/deviceregulationandguidance/guidancedocuments/ucm198043.pdf. Accessed 17 Dec 2014
3. International Organization for Standardization (ISO), ISO 5840:2005, "Cardiovascular Implants - Cardiac Valve Prostheses" (ISO 5840)
4. Kaplan AV, Baim DS, Smith JJ et al (2004) Medical device development: from prototype to regulatory approval. Circulation 109:3068–3072
5. U.S. Food and Drug Administration (2011) Good Clinical Practice 101: an introduction. http://www.fda.gov/downloads/training/cdrhlearn/ucm176414.pdf. Accessed 17 Dec 2014
6. Centers for Medicare & Medicaid Services (2012) Medicare clinical trial policies. https://www.cms.gov/ClinicalTrialPolicies. Accessed 17 Dec 2014
7. Centers for Medicare & Medicaid Services (2012) National Coverage Determination (NCD) for Routine Costs in Clinical Trials (310.1) – Current Policy – July 2007 NCD. Medicare Clinical Trial Policies. http://www.cms.gov/medicare-coverage-database/details/ncd-details.aspx?NCDId=1&ncdver=2&bc=BAABAAAAAAAA&. Accessed 17 Dec 2014

Cardiac Devices and Technologies: Continued Rapid Rates of Development

44

Paul A. Iaizzo

Abstract

The primary goals of this last chapter are to: (1) make note of the technologies mentioned earlier in this book, (2) describe some important changes in healthcare and global markets that could have an impact on the use rate of technologies being developed, and (3) discuss several other future opportunities in the cardiac device arena. It should be noted that the chapters of this third edition were updated, and new ones were added to specifically describe recent critical advances in cardiac device technologies and/or clinical applications. There are also other areas of importance in cardiac treatment such as biological approaches to disease management (stem cell therapy), genomics (diagnostics and gene therapy), proteomics, and/or tissue engineering, all of which may have a major impact on the future of cardiac clinical care; however, detailed discussions of these approaches are beyond the scope of this book.

Keywords

Medical device development • Implantable therapies • Catheter-delivered devices • Endocardial ablation devices • Device coating agents • Telemedicine • Implantable sensors Cardiac imaging • Surgical tools • Less invasive surgery

44.1 Introduction

Since the second edition of this book was published in 2009, much has changed in the field of cardiac devices. In response, several new chapters were added, and others were expanded in this third edition, so to accommodate the rapid growth and innovation in this field. In many of these chapters, the authors provided histories of cardiac device development and fairly thorough discussions of currently employed devices and/or assessment technologies. To appreciate how rapidly innovations in the area of cardiac disease continue to progress, one can simply perform a search on the United States Patent and Trademark Office website (www.uspto.gov). This search produces an impressive number of companies and/or individuals that are attempting to secure intellectual property protection in this clinical category. More specifically, Table 44.1 summarizes the number of published *patent applications* identified in October of 2015, 2008, and 2004, citing the following keywords: cardiac, cardiac surgery, cardiology, cardiac electrophysiology, cardiovascular stents, and cardiac repair.

Note that this list likely does not include all issued patents, as some may be foreign and many of these patents detail prospective future products. For example, in searching the same database mentioned above (at time of print for this book), the key word CARDIAC produces 93,942 *issued patents* in 2015 since 1976, compared to 49,017 patents issued in 2008 and 37,410 in 2004. This rapid increase includes only US patent applications, yet the same is true for the number of new international patent submissions. There are several other resources to locate information on emerging

P.A. Iaizzo PhD (✉)
Departments of Surgery and Integrative Biology and Physiology, Carlson School of Management, Lillehei Heart Institute, Institute for Engineering in Medicine, University of Minnesota, 420 Delaware St. SE, B172 Mayo, MMC 195, Minneapolis, MN 55455, USA
e-mail: iaizz001@umn.edu

P.A. Iaizzo (ed.), *Handbook of Cardiac Anatomy, Physiology, and Devices*, DOI 10.1007/978-3-319-19464-6_44

Table 44.1 Patent applications for various key words

	Number of patent applications		
Keyword	2015	2008	2004
Cardiac	93,942	46,946	18,920
Cardiac surgery	5,404	2331	1015
Cardiology	14,798	3961	1480
Cardiac electrophysiology	869	213	79
Cardiovascular stents	313	137	52
Cardiac repair	224	127	32

Source: United States Patent and Trademark Office website (www.uspto.gov)

cardiac devices, such as the Food and Drug Administration website (http://www.fda.gov), the Google™ patent search website (https://www.google.com/?tbm=pts&hl=en&gws_rd=ssl), and various other websites. It is important to note that, relative to medical devices, not all countries uphold patent protection to the same international standards; this is a major issue to consider as a corporation looks to expand globally. Discussion of these implications is beyond the scope of this text, but those developing cardiac devices need to be critically aware of this reality. For example, it was recently noted by Shara Aranoff, former Commissioner and Chairman of the US International Trade Commission [1], that "Over the past 20 years, the number of patent infringement disputes filed annually at the U.S. International Trade Commission (ITC) has more than tripled. Although typically associated with smartphones and semiconductor chips, the ITC has also seen quite a few disputes involving medical devices. Important trends are emerging in medical device patent litigation at the ITC."

Many novel ideas that eventually lead to new products, therapies, and/or training protocols often first occur through "basic" cardiac research or clinical patient management. Hence, in order for emerging technologies to continue to advance at a rapid rate, it is imperative that laboratories performing basic research in cardiac-related technological areas continue to receive necessary support. Furthermore, prototype testing and clinical trials are essential to insure that the best possible technologies are developed and eventually made available for general use. Yet, it is important to note that many critical lessons can be learned from trials that employ misdirected devices or technologies.

When considering the design of a medical device, there are typically a number of key processes or steps involved:

- A device sketch (e.g., on a cocktail napkin, iPad, or smartphone during a meeting with a clinician, with a signed nondisclosure agreement)
- Detailed drawings and intellectual property disclosures
- A critical study of the associated normal and pathologic anatomies
- The creation of an impressive animation of device design, its function, and/or its clinical delivery/placement
- Device prototype development (rapid, working, polished prototypes and/or computer simulations)
- Bench testing (safety, wear, and biocompatibility testing)
- Redesign: set on a final design freeze
- Preclinical research: animal testing
- Redesign (if needed) or initiation of clinical testing
- Simulation systems of device implantation
- Market release and/or corporate acquisition

Some devices can be employed as life-saving measures prior to approval for market release, if a *Humanitarian Device Exemption* is obtained. For more details on the design process, the reader is referred to Chap. 42.

As cardiac devices become more beneficial and help people live longer lives, we foresee that there will be a need to design devices that: (1) have even higher reliability and longevity; (2) can be upgraded, extracted, and/or replaced; and/or (3) allow for easy data retrieval (i.e., "big data" obtained remotely). More specifically, the retrieval of data and/or the reprogramming of implantable cardiac systems (sensor/pacing/defibrillation) should be accomplished with minimal need for patient training or education; they should function as seamlessly and simply as possible (*you just implant them!*). As these systems evolve, there will be growing interest from healthcare payers as well as the physicians and/or hospitals that monitor patients. Furthermore, data would ultimately and automatically be interfaced with *electronic health records* which are becoming commonplace in the USA and many global markets. Importantly, the increased use of home monitoring may be perceived as the only possible way to manage the growing amount of "big data" collected from the "baby boomer" patients receiving such therapies. This approach in turn may result in: (1) improved care, (2) greater levels of patient confidence, (3) better understanding of disease-specific therapies, and/or (4) overall cost savings for both the healthcare industry and consumers. It should also be noted that currently there are patient-owned medical records, as mandated in a Presidential order in 2004. Furthermore, with the passing of the *Affordable Care Act* in the USA, the future of cardiac device coverage will be affected, but at this time it is still not clear how and/or to what degree. To learn more about these policies, the reader is referred to http://www.hhs.gov/healthcare/facts/timeline/index.html. The Affordable Care Act was passed by Congress and then signed into law by President Obama on March 23, 2010; on June 28, 2012, the Supreme Court rendered a final decision to uphold the healthcare law. Important features of the Act include the following:

1. *Coverage*
   - Ends preexisting condition exclusions for children: health plans can no longer limit or deny benefits to children under 19 due to a preexisting condition.
   - Keeps young adults covered: individuals under 26 of age may be eligible for coverage under their parents'

health plan.
- Ends arbitrary withdrawal of insurance coverage: insurers can no longer cancel coverage just because an individual makes an honest mistake.
- Guarantees right to appeal: individuals have the right to ask their insurance provider to reconsider denial of payment.

2. *Costs*
   - Ends lifetime limits on coverage: lifetime limits on most benefits are banned for all new health insurance plans.
   - Reviews premium increases: insurance companies must publicly justify any unreasonable rate hikes.
   - Helps individuals get the most from their premium dollars: dollars spent on premiums must be spent primarily on healthcare, not administrative costs.
3. *Patient Care*
   - Covers preventive care at no cost: individuals may be eligible for recommended preventive health services without a copayment.
   - Protects choice of doctors: individuals may choose their own primary care doctors from the plan's network.
   - Removes insurance company barriers to emergency services: individuals can seek emergency care at a hospital outside of the health plan's provider network.

Within the last several years, we have again witnessed a fair number of cardiac device recalls due to the so-called *inherent failures*. However, this may be not so surprising, as the sophistication of these devices continues to increase and more and more clinicians have started to implant them. Nevertheless, it needs to be emphasized that human cardiac anatomy is highly variable and dynamic (ever changing, with reverse remodeling occurring with improved outcomes and survival); thus, we need to consider that the implant environment continues to change post-therapeutically (post-implant) and is a highly caustic environment. The human body has innate healing and foreign body response systems.

Despite the occurrence of failed devices, all designs were required to pass rigorous bench testing, animal trials, and human clinical trials before approval for market release. It is of interest to note that each company often designs their own bench testing equipment because, in most cases, the device designs are novel or unique. In fact, many times this testing equipment also becomes proprietary. Therefore, it is likely that bench testing of cardiac devices with high sales volumes will become regulated by governments sometime in the near future.

To provide greater perspective on the design and testing challenges facing the cardiac device industry, perhaps an example will suffice. A pacing lead moves approximately 100,000 times every day (or 37,000,000 times annually), and this can occur in multiple locations and with numerous degrees of freedom. Furthermore, when considering failure of the lead insulation alone, we must expect failures due to abrasions, the association with the fibrous device pocket, the potential for lead-to-lead interactions, anatomical considerations (bones, ligaments, etc.), and/or other complications. It is also interesting to note that some features of lead implantation (e.g., design of the anchoring sleeves) have received little attention or study, yet this may greatly influence the potential for lead failures. For a detailed review on the bench testing of cardiac valves, the reader is referred to Kelley et al. [2].

Again, several new chapters were added to this edition of the textbook, and others were updated to provide the reader with additional information on bench top (in vitro), preclinical, and clinical testing/research (e.g., Chaps. 27 and 41–43).

44.2 Resuscitation Systems and Devices

Even before the cardiac patient enters the emergency and/or operating room, there are many new technologies being developed to aid in resuscitation. Such innovations range from improvements of existing tools (e.g., automated application of cardiopulmonary resuscitation, the use of active compression–decompression devices) to novel mechanisms that accomplish better patient outcomes (e.g., impedance threshold valve, cerebral cooling, and inducing mild hypothermia). Furthermore, automated external defibrillators have become commonplace in the USA, with units being purchased for use in schools, health clubs, emergency vehicles, shopping malls, and even personal homes. Recent clinical trials describe the success of these emerging technologies (see Chap. 38).

44.3 Implantable Therapies

Advances in microtechnology have now made it possible to create implantable therapies that can be life saving, e.g., implantable defibrillators to detect and treat thousands of episodes of sudden cardiac fibrillation. For example recently, there has been a drive to implant vagal nerve stimulators for several proposed therapies including heart rate control, blood pressure control, dietary control, and/or even the reversal of depression. The need for such devices will likely increase at an exponential rate and will be directed specifically to all types of cardiac complications.

44.3.1 Left Atrial Appendage/Atrial Fibrillation Therapy

There are growing numbers of treatment for the side effects of atrial fibrillation which, in some patients, leads to crip-

pling strokes. The focus of these devices is to modify the role of the left atrial appendage in pathologies associated with atrial fibrillation. More specifically, this tiny alcove of the heart has been described to service as a "starter heart" for the human embryo; it can be a site for blood to pool and subsequently form clots that can be expelled out of the heart and into the brain, causing strokes. Today, it is estimated that atrial fibrillation affects five million people worldwide and is considered to be responsible for up to 25 % of all strokes. It has been reported that, due to aging of the population, the number of patients with atrial fibrillation will likely increase by approximately 2.5-fold by the year 2050 [3].

At present, one of the most common treatments for atrial fibrillation is the administration of anticoagulant drugs; note that there are several new drugs available in addition to coumadin. From a device perspective, suggested approaches to treat this problem include tissue clamps, screens, and other methods to seal off the appendage; many of these approaches are being studied through ongoing clinical trials. Nevertheless, ablation is a critical tool for treating atrial fibrillation, and for more details the reader is referred to the new chapter in this textbook (Chap. 29), as well as Chap. 32 on the mapping of such arrhythmias.

44.3.2 Cardiac Remodeling

Chronic cardiac remodeling is a well-known response of dilated cardiomyopathy and is thought to play a central role in disease progression [4–6]. Associated heart chamber dilation and/or wall thinning will elevate overall wall stress which is considered to trigger the local release of neurohormones, thereby adversely affecting myocardial molecular biology and physiology [7]. Therapeutic approaches to treat heart failure have been described primarily as a means to inhibit or even induce reverse remodeling (e.g., beta-adrenergic blockade). More recently, mechanical unloading using left ventricular assist devices (see Chap. 39), extracorporeal pumps (Chap. 33), or portable whole heart support systems (e.g., EXCOR®, Berlin Heart, Berlin, Germany) have been employed as alternatives. Such interventions can profoundly unload a heart, leading to reverse remodeling and thus improved physiological performance [4]. The design of such pump systems has been ongoing, and the goal has been to transition from external (or partially external) to fully implantable pumps (e.g., external to internal pumps with small rechargeable battery packs). Furthermore, when system developers changed from pulsatile to continuous pumps, pump size was reduced by ~1/7, pump weight was reduced by ~1/4, and they were also quieter and more reliable (e.g., fewer moving parts); see Chap. 39 for further details.

44.4 Catheter-Delivered Devices

Since the first edition of this textbook in 2005, there has been a boom in the delivery of specialized cardiac devices that can be introduced intravascularly or via intracardiac methods. Such devices include stents, septal occluder devices, valves, leads, implantable pacemakers, and ablation tools (see Chaps. 8, 28, 30, and 35). Currently, the field of transcatheter-delivered valves is one of great interest and high competition within the medical device industry (Chap. 36). In addition, the team approach for the clinical delivery of such systems is becoming widespread, with cardiologists and cardiac surgeons working together in hybrid catheter lab/operating rooms to perform multi-tiered treatments on patients (e.g., implanting pacing/defibrillation systems, valves, and/or bypass grafts). As the number of these *centers of excellence* continues to increase to perform such procedures, it is likely that older individuals will be receiving implantable devices and/or other cardiac therapies. It should be noted that there are also cardiac catheters on the market to deliver stem cell or gene therapies (see Chap. 40).

44.4.1 Stents

An intraluminal coronary artery stent is a small wire mesh tube that is placed within a coronary artery to keep the vessel patent (open). Stents are commonly deployed: (1) during a coronary artery bypass graft surgery to keep the grafted vessel open, (2) after balloon angioplasty to prevent reclosure of the blood vessel, and/or (3) during other heart surgeries. For delivery, a stent is collapsed to a small diameter and put over a balloon catheter. Typically with the guidance of fluoroscopy, the catheter and stent are moved into the area of the blockage. When the balloon on the delivery catheter is inflated, the stent expands, locking it in place within the vessel and thus forming a scaffold which holds the artery open. Stents were originally intended to stay in the vessel permanently, keeping it open to improve blood flow to the myocardium and thereby relieving symptoms (usually angina). Note that a stent may be used instead of angioplasty. The type of stent to be deployed depends on certain features of the artery blockage, i.e., size of the artery and where the blockage is specifically located. Today bioabsorbable stents are being deployed. Often stents need to be placed at vessel bifurcations, and thus special techniques and/or stents need to be deployed. For example, a *provisional technique* is a generally accepted procedure for treating a bifurcation in a coronary artery. The main branch is stented first, with the stent deployed to a diameter matching the distal side of the target vessel. This is then followed by a *proximal optimization technique* which addresses the malapposition of stent

struts resulting from sizing the stent using the distal side of the target vessel. Lastly, the use of a final *kissing balloon technique*, in which two balloons are simultaneously deployed into the main branch and side branch, is used in order to restore patency to the jailed side branch and obtain better strut apposition at the bifurcation (see: http://www.vhlab.umn.edu/atlas/device-tutorial/stents). It should be noted that at the Transcatheter Cardiovascular Therapeutics (TCT) meetings held in 2014 and 2015, a special session was dedicated to the discussion of various stenting techniques that can be utilized in various clinical situations (see: http://www.crf.org/tct).

44.4.2 Catheter-Delivered Leads or Pacemakers

One of the continuing challenges in the area of intracardiac lead development is to downsize lead diameters and, at the same time, minimize the possibility of fractures or failures. Similarly, there is growing practice in the placement of leads within the cardiac veins, as well as in the development of tools for cannulation of the coronary sinus. For a detailed discussion of left-sided leads and resynchronization therapy, the reader is referred to Chap. 31.

Although pacing systems with leads have been utilized since the inception of cardiac pacing, recent advances in miniaturization technology and battery chemistry have made it possible to develop a self-contained pacemaker small enough to be implanted entirely within the heart, while still aiming to provide similar battery longevity to conventional pacemakers. In general, leadless pacemakers (or transcatheter-delivered pacemakers) are self-contained devices designed to be implanted within the chambers of the heart directly at the desired site of pacing. By eliminating the need for a subcutaneous device pocket and insertion of a permanent lead within the vasculature, some of the complications associated with traditional pacing systems can be avoided, including pocket infection, erosion and/or hematoma as well as lead dislodgement, fracture and/or infection. For more details on these devices, see Chap. 30.

44.5 Implantable Sensors

Device and battery technologies continue to decrease in size and, at the same time, exhibit improved efficiency. Also, there have been rapid advances in printable and/or flexible micro-electronics. In turn, this creates increasing opportunities for novel approaches to long-term assessment of various physiological parameters from unique aspects of the entire cardiovascular system. Numerous innovations for the management and collection of "big data" have arisen in the field of medicine, including implantable computers and sensors, wireless data transmission, and web-based repositories for collecting and organizing information.

One such device, the Reveal LINQ™ Insertable Cardiac Monitor (Medtronic, Inc., Minneapolis, MN, USA), is an implantable monitoring system that records subcutaneous electrocardiograms and is indicated for human clinical use for: (1) patients with clinical syndromes or situations at increased risk of cardiac arrhythmias, and (2) patients who experience transient symptoms that may suggest a cardiac arrhythmia [8]. A common use of the system is for unexplained syncope (fainting), in which case the implanted device can capture episodes with impaired cardiac output, including bradycardias (unusually low heart rates), asystoles (long periods without a heartbeat), or tachycardias (unusually high heart rates). The Reveal LINQ is intended to continuously sense and collect unique and valuable information such as heart rate, physical activity, and body temperature from a sensor injected under the patient's skin. Subsequently, physicians can access these data via a controlled website at any time and review screens that present summaries from the latest downloads, trend information, and/or detailed records from specified times or problem episodes. Interestingly, these human clinical devices have been recently deployed in captive and free-ranging wildlife to aid in the characterization of normal physiology and the interaction of animals with their environment, including reactions to humans (Fig. 44.1) [9].

44.6 Procedural Improvement

With pressure on the healthcare system to continually reduce treatment costs and better document the outcome benefits of a given therapy, much effort will continue to be focused on procedural improvements for cardiac care.

44.6.1 Cardiac Imaging

Our ability to image internal and external features of the heart continues to improve at a rapid rate and, as indicated in Chaps. 22 and 24, the sophistication of such systems can be quite extreme. Yet, as the cost of computer hardware decreases and capabilities increase, opportunities to downsize and develop such technologies for widespread use continue to become more and more feasible.

44.7 Training Systems

As technologies have become more advanced, so has the need to teach students, residents, and physicians on how to use them. There are numerous education programs, conferences,

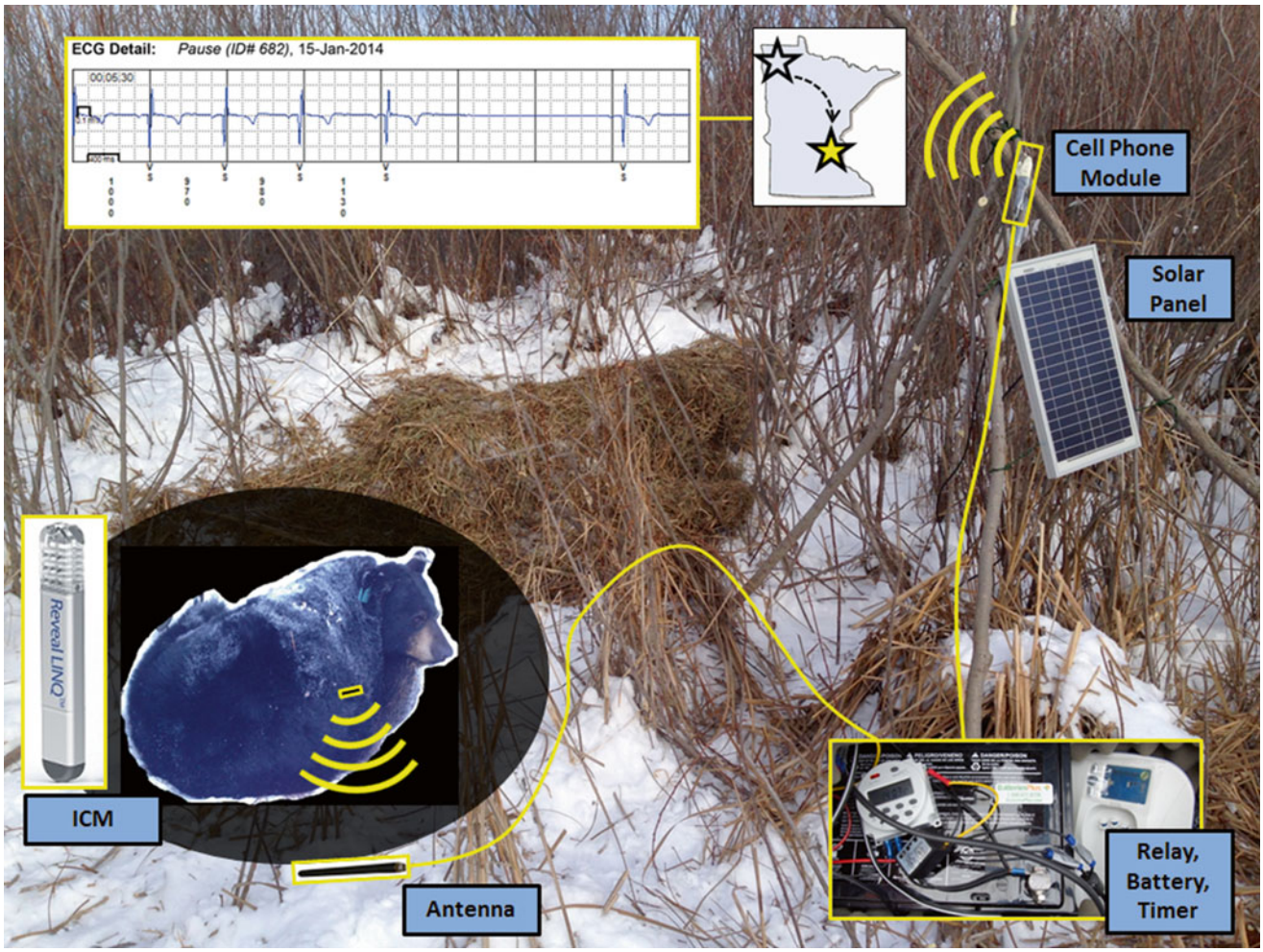

Fig. 44.1 The use of a wireless telemetry system at a bear den. The insertable cardiac monitor (Reveal LINQ™, Medtronic Inc., Minneapolis, MN, USA) communicated with a relay station housed in a waterproof container via an antenna buried under the bear. Transmissions to an Internet site were via a cellular module attached to a timber tripod fabricated at the site. The system was powered by 12 V batteries charged by a solar panel [9]. *ICM* insertable cardiac monitor

websites, teleconferences, and special courses offered. For example, our laboratory has developed a free access website dedicated to the education of functional cardiac anatomy, imaging, 3D models, and device deployment (see http://www.vhlab.umn.edu/atlas/).

44.8 Summary

Within this book, several devices utilized for cardiac electrophysiology, interventional cardiology, and cardiac surgery were discussed. The development of such innovative technologies continues to mature at a rapid rate and includes: (1) resuscitation systems and devices, (2) implantable therapies (pacemakers, implantable cardioverter defibrillators, stents, septal occluders, valves, annular rings, fibrin patches, etc.), (3) delivery systems/invasive therapies (angioplasty, ablations, catheters, etc.), (4) procedural improvements (noninvasive mapping systems, 3D echocardiography, magnetic resonance imaging, training simulators, etc.), (5) less invasive surgical approaches (off-pump, robotics, direct aortic transcatheter valve placements, etc.), (6) post-procedural follow-up/telemedicine (electrical, functional, adverse events, etc.), and (7) training tools. There is no doubt that continued improvement of these technologies, as well as advances in rehabilitation and other support services (patient education, training, home monitoring, etc.), will extend and/or save lives and enhance the overall quality of life for individuals with cardiovascular disease. Many of these developments are currently available, and the challenge for healthcare providers in the coming years will be to provide the best possible care in the most cost-effective way. Perhaps we will see the day of the family house call once again, where the healthcare provider visits the home and assesses and monitors all family members living there during a single visit (ECGs, electronic auscultations, pressure assessments, echocardiography, device reprogramming, blood and

genetic analyses, etc.). It should be noted that it was not that long ago, in the 1960s, that medical students were still instructed on how to perform a "traditional house call."

In conclusion, it is exciting to think about the technologies that have been employed thus far as well as those that are being developed that will positively affect the overall healthcare of the cardiac patient. It continues to be an exhilarating era to be working in the field of cardiovascular sciences.

References

1. Aranoff S (2014) The National Law Review. 29 October 2014. http://www.natlawreview.com/author/shara-aranoff
2. Kelley TA, Marquez S, Popelar CF (2013) In vitro testing of heart valve substitutes. In: Iaizzo PA, Bianco RW, Hill AJ, St Louis JD (eds) Heart valves: from design to clinical implantation. Springer, New York, pp 283–320
3. Santini M, Ricci RP (2006) The worldwide social burden of atrial fibrillation: what should be done and where do we go? J Interv Card Electrophysiol 17:183–188
4. Cohn JN, Ferrari R, Sharpe N (2000) Cardiac remodeling–concepts and clinical implications: a consensus paper from an international forum on cardiac remodeling. J Am Coll Cardiol 35:569–582
5. Anversa P, Olivetti G, Capasso JM (1991) Cellular basis of ventricular remodeling after myocardial infarction. Am J Cardiol 68:7D–16D
6. Saaverda WF, Tunin RS, Paolocci N et al (2002) Reverse remodeling and enhanced adrenergic reserve from passive external support in experimental dilated heart failure. J Am Coll Cardiol 39:2069–2076
7. Francis GS (2001) Pathophysiology of chronic heart failure. Am J Med 110:37S–46S
8. REVEAL LINQ™ LNQ11 Insertable Cardiac Monitor Clinician Manual. http://manuals.medtronic.com/wcm/groups/mdtcom_sg/@emanuals/@era/@crdm/documents/documents/contrib_185856.pdf
9. Laske TG, Garshelis DL, Iaizzo PA (2014) Big data in wildlife research: remote web-based monitoring of hibernating black bears. BMC Physiol 14:13

Website Sources (All Websites Were Accessed on December 27, 2014)

http://www.uspto.gov
http://www.fda.gov/
http://www.google.com/patents?
http://www.hhs.gov/healthcare/facts/timeline/index.html
http://www.vhlab.umn.edu/atlas/
http://www.vhlab.umn.edu/atlas/device-tutorial/stents
http://www.crf.org/tct
http://www.crest.umn.edu/

Index

P.A. Iaizzo (ed.), *Handbook of Cardiac Anatomy, Physiology, and Devices*, DOI 10.1007/978-3-319-19464-6